ANNUAL MEETING OF THE AMERICAN SOCIETY OF BIOMECHANICS

PENN STATE UNIVERSITY, AUGUST 26-29, 2009

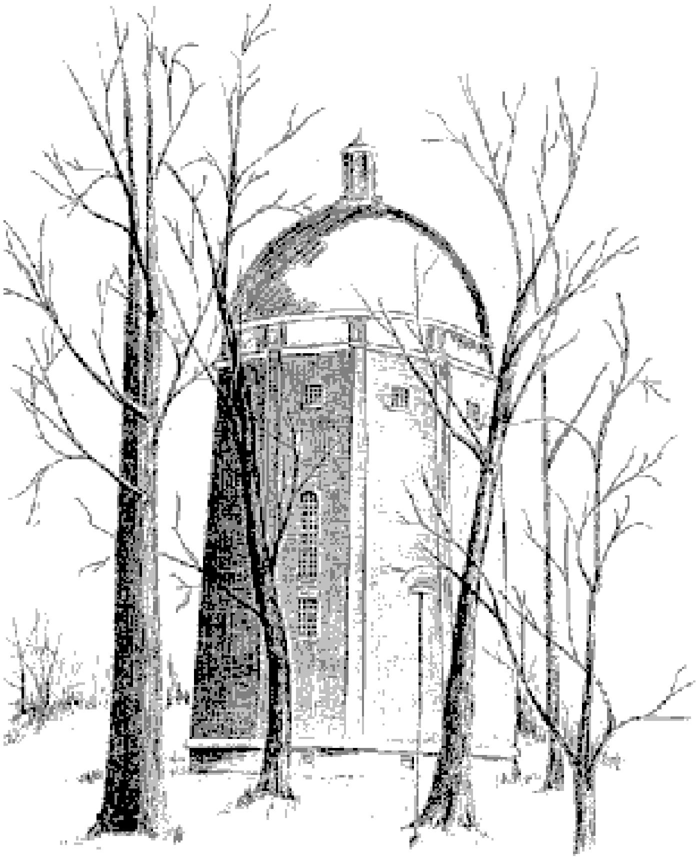

PROGRAM

WELCOME

Message from Conference Chairs

It is our great pleasure to welcome you all to The Pennsylvania State University for the Annual Meeting of the American Society of Biomechanics. It has been 30 years since this conference was last at Penn State, in that time the size of the conference has grown but we hope we can still offer all of you a warm and friendly welcome.

John Challis
Meeting Chair

Jinger Gottschall
Meeting Chair

Steve McCaw
Program Chair

Message from the President

Welcome to the 32nd Annual Meeting of the American Society of Biomechanics. It is especially meaningful to preside over this meeting at Penn State, my own alma mater and the birthplace of graduate education in biomechanics. The Program and Meeting Chairs have been working incredibly hard over the past year in planning a meeting that is scientifically diverse and stimulating, with plenty of opportunity to reconnect with friends and colleagues.

The rest is up to you - Enjoy!

Irene Davis
ASB President

Map

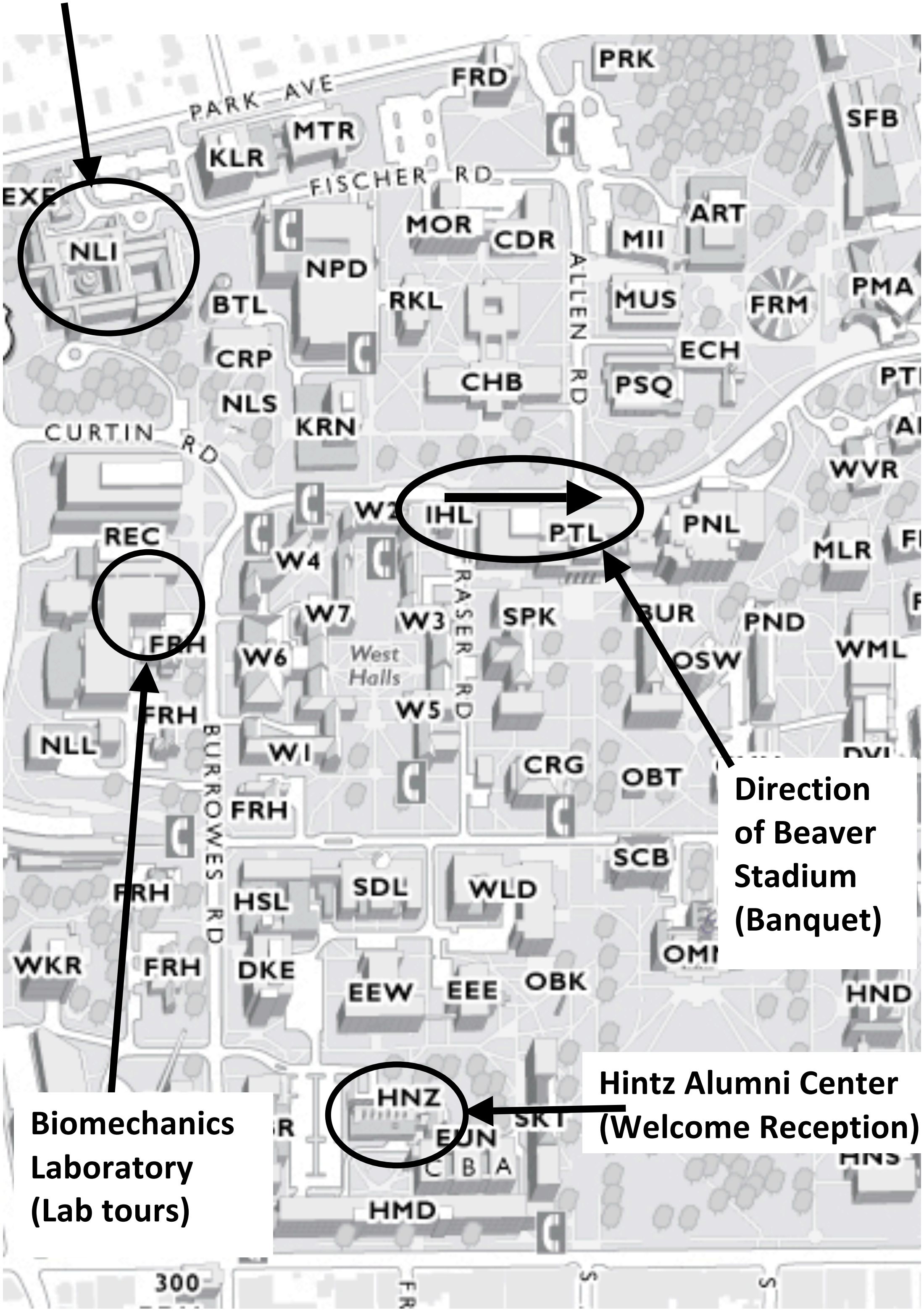
PARK AVE
FISCHER RD
CURTIN RD
ALLEN RD
FRASER RD
BURROWES RD
PRK
FRD
SFB
MTR
KLR
EXE
ART
MOR
CDR
MII
NLI
NPD
PMA
MUS
FRM
BTL
RKL
ECH
CRP
CHB
PSQ
NLS
KRN
WVR
W2
IHL
PTL
PNL
REC
W4
MLR
W7
W3
SPK
BUR
PND
FRH
W6
West Halls
OSW
WML
W5
NLL
WI
CRG
OBT
FRH
SCB
HSL
SDL
WLD
OMI
WKR
DKE
EEW
EEE
OBK
HND
HNZ
SKT
EUN
HNS
C B A
HMD
300

Nittany Lion Inn (conference venue)

Direction of Beaver Stadium (Banquet)

Biomechanics Laboratory (Lab tours)

Hintz Alumni Center (Welcome Reception)

Presenter Instructions

Information for Poster Presentations

The poster boards will be 48” x 48”. Posters printed on a single large sheet of paper are preferred. It is recommended that your poster be 36” (91 cm) wide x 46” (117 cm) high in portrait mode. Pins will not be permitted on the poster boards. Instead, Velcro will be used and this will be available in the exhibit rooms. Posters may be mounted at 7:45 AM and must be removed by 7:00 PM. It is recommended to hang your poster no later than 8:30 AM and remove no earlier than 6:15 PM. Presenters should stand by odd numbered posters only for the first 45 minutes (4:45 until 5:30 PM), and stand by the even number posters only for the second 45 minutes (5:30 until 6:15 PM).

Information for Podium Presentations

Each presentation podium will be equipped with a laptop computer that is connected to the projection and sound system. All presentations must be loaded onto and delivered using the provided computer. Because of time constraints, there will not be enough time for each presenter to connect their own computer.

Location: Our “Ready Room” will be the Mount Nittany Room. It is located on the ground floor next to Board Room 2 (see map on next page).

Times: Wednesday through Friday 12pm-2pm OR 4pm – 6pm
Please attend on the day before your presentation.

What to Do: Please bring your presentation on a USB Drive to this location to load it and confirm that it will work on the presentation computers. Your files will be copied to our system at that time.

Assistance: Technical assistance will be available in the Ready Room. However, priority will be given to the loading of presentations. If your presentation file does not work properly on the provided computers, the computers will be available for troubleshooting at the end of the Ready Room session.

Presenter Frequently Asked Questions (FAQs)

Q: Where is the Ready Room located?
A: It is on the ground floor (downstairs), in the Mount Nittany Room near Board Room 2.

Q: What do I do if I cannot make the Ready Room hours on Wednesday for my Thursday presentation?
A: If your flight will not get you to State College until after 6pm on Wednesday, the day before your Thursday presentation, please contact Nick Giacobe (nxg13@psu.edu) to arrange an alternate time.

Presenter Instructions

Q: Can I use a Macintosh computer for my presentation?

A: We have selected a Windows environment for all computers in the ready room, and in the lecture rooms. Macintoshes will not be available.

Q: Can I use my own computer (i.e. codecs, special software, etc) for my presentation?

A: No. Unfortunately, there is insufficient time between presenters to allow for computer swapping at the podium.

Q: Will I be able to use the computer's audio during my presentation?

A: Yes, it will be pre-connected. You will be able to control the volume from the computer.

Q: Can I use my own mouse/pointing device during the presentation?

A: Yes, but only if it does not require the installation of drivers (i.e. it must be a standard HID interface).

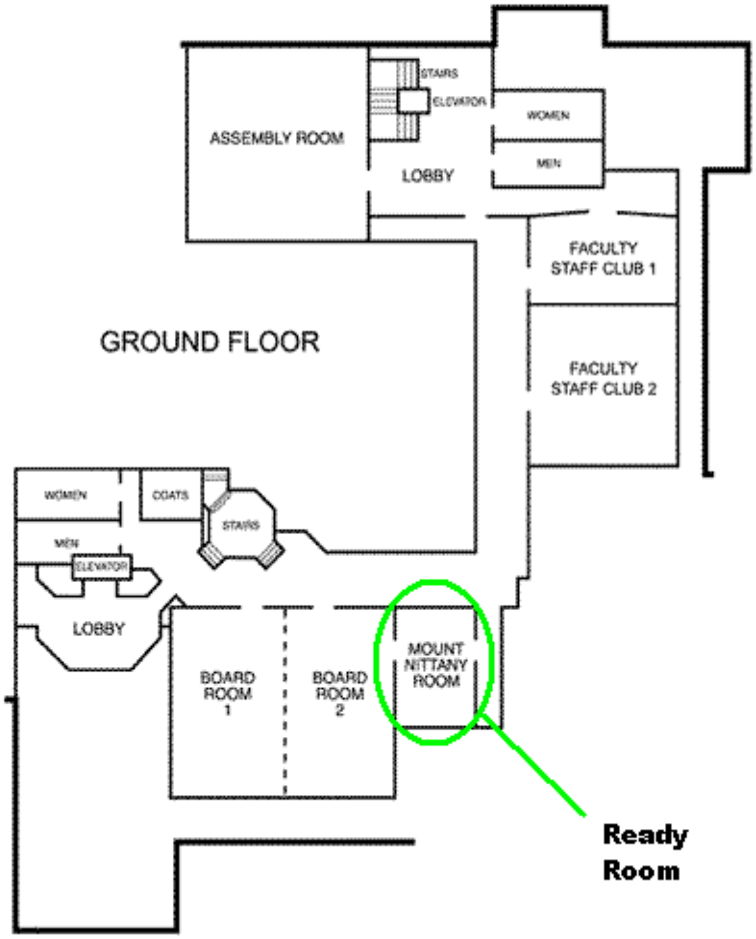
STAIRS
ELEVATOR
ASSEMBLY ROOM
WOMEN
MEN
LOBBY
FACULTY STAFF CLUB 1
GROUND FLOOR
FACULTY STAFF CLUB 2
WOMEN
COATS
STAIRS
MEN
ELEVATOR
LOBBY
BOARD ROOM 1
BOARD ROOM 2
MOUNT NITTANY ROOM
Ready Room

Meeting Floor Plan

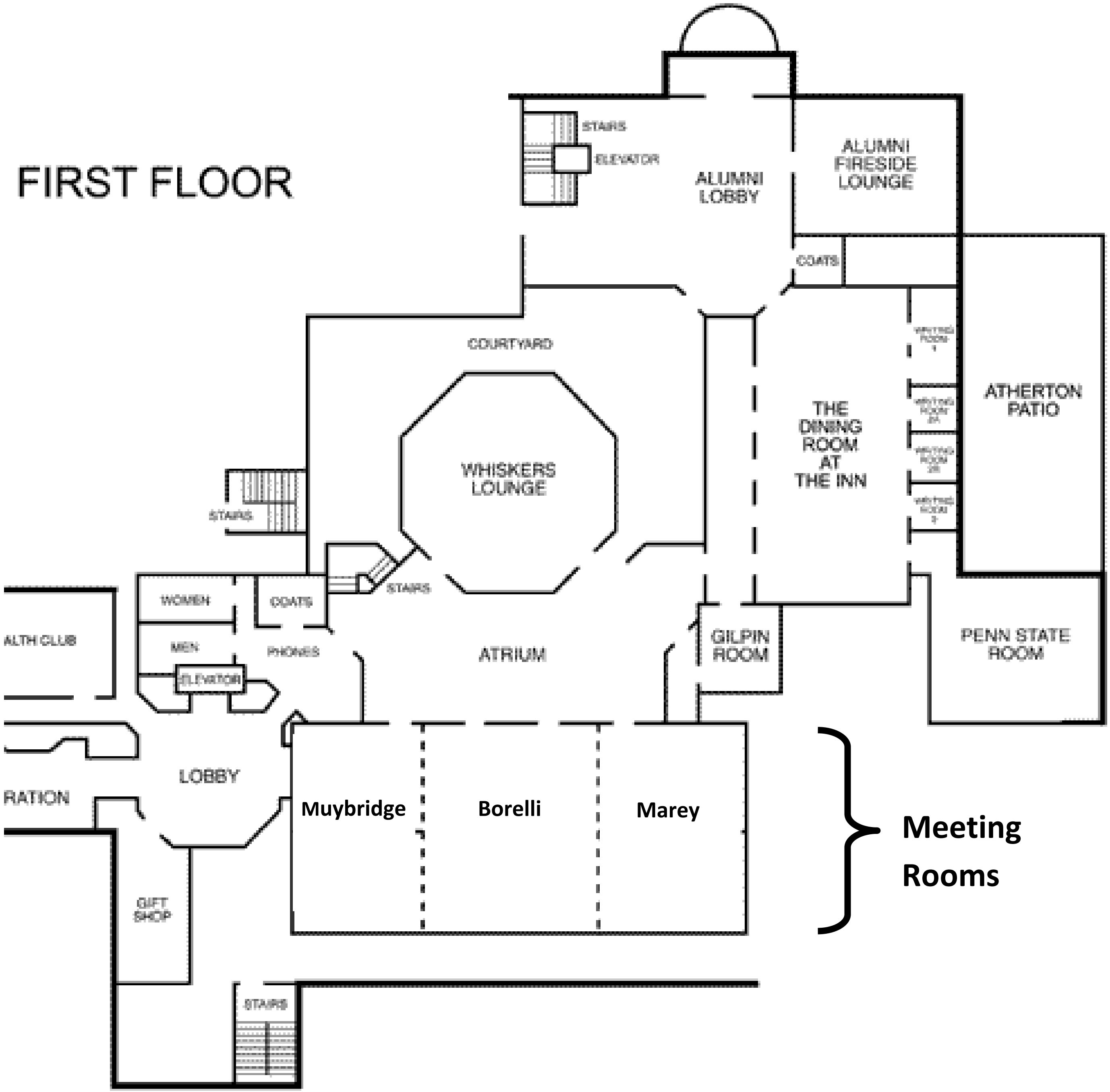
FIRST FLOOR
STAIRS
ELEVATOR
ALUMNI LOBBY
ALUMNI FIRESIDE LOUNGE
COATS
COURTYARD
WRITING ROOM 1
WRITING ROOM 2A
WRITING ROOM 2B
WRITING ROOM 3
ATHERTON PATIO
THE DINING ROOM AT THE INN
WHISKERS LOUNGE
STAIRS
WOMEN
COATS
STAIRS
ALTH CLUB
MEN
PHONES
ELEVATOR
ATRIUM
GILPIN ROOM
PENN STATE ROOM
LOBBY
RATION
Muybridge
Borelli
Marey
Meeting Rooms
GIFT SHOP
STAIRS

Meetings Instructions

Poster Presentations

Presenters should stand by odd numbered posters only for the first 45 minutes (4:45 until 5:30 PM), and stand by the even number posters only for the second 45 minutes (5:30 until 6:15 PM). In the Alumni Lounge posters are numbered 1 to 66, in the Assembly Room 67 to 117, and in the Faculty Staff Club 118 to 192.

Podium Presentations

Each presenter is allotted 15 minutes; 10 minutes for the presentation, three minutes for questions, and two minutes for the transition between speakers. Please approach a microphone to ask a question.

Coffee Breaks

During the coffee breaks, beverages and snacks will be provided in the Assembly Room and the Faculty Staff Club.

Lunch

There are multiple sites where lunch will be served. If one spot is busy please move to another site, there will be people available to offer you direction.

Banquet

The banquet will be Friday evening. It will be held in the club area of Beaver Stadium. Buses will leave for the stadium from 6:15 PM onwards, and will be available for return from 9:30 until 10 PM. The stadium is just over a mile to walk, you simply need to follow Curtin Road east. From 7 PM until 9 PM the All-Sport Museum within the stadium will be available for a self-guided tour.

Internet Access

There is a public access wireless network in the Nittany Lion Inn. No user id or password is required.

ACKNOWLEDGEMENTS

The organizers would like to thank the following for their generous support,

Department of Kinesiology, Penn State University
Department of Industrial Engineering, Penn State University
Department of Mechanical and Nuclear Engineering, Penn State University
Department of Orthopaedics & Rehabilitation, Penn State University
The College of Health and Human Development, Penn State University
The College of Engineering, Penn State University
National Institutes of Health
Nike Corporation.

The American Society of Biomechanics would like to acknowledge their two corporate sponsors,

TekScan	(http://www.tekscan.com/)
Phoenix Technologies, Inc.	(http://www.phoenix.com/)

The following kindly reviewed abstracts for this meeting,

Nadya Amor
Don Anderson
Allison Arnold
Bradford Bennett
Rhonda Boros
Thomas Brown
Sachin Budhabhatti
Tamara Bush
John Challis
Young-Hui Chang
Ajit Chaudhari
Li-Shan Chou
Trey Crisco
Richard Debski
Glenn Fleisig
Jinger Gottschall
D. C. Grieshaber
Joseph Hamill
Tammy Donahue
Walter Herzog
Michael Hirsh
Katherine Holzbaur
Richard Hughes
Yih-Kuen Jan
Lindsay D. Johnson
Andrew Karduna
Suzanne Konz
Rodger Kram
Laurel Kuxhaus
Kevin Laudner
Michele LeBlanc
William Ledoux
Zong-Ming Li
Rick Lieber
Ann Livengood
Craig McGowan
Todd McLoda
Jill McNitt-Gray
Chris Miller
Clare Milner
David Nuckley
David Pearsall
Stephen Piazza
Danny Pincivero
Shirley Rietdyk
Stacie Ringleb
Brandi Row
Jason Scibek
Robert Siston
Cecile Smeesters
Jeremy Smith
Darryl Thelen
Brian Umberger
K. Vrongistinos
Henry Wang
Samuel Ward
John Williams
Vanessa Yingling
Bing Yu
Joseph Zeni Jr
Ronald Zernicke

Wednesday, August 26th, 2009

11:00-6:00	Registration and Poster Placement
12:00–4:00	Laboratory Tours Biomechanics Laboratory (see map for location)
12:00-2:00	Topic: Tutorial I Sam Slobounov (Penn State University) Incorporating Virtual Reality and Brain Imaging Technologies: Implications for Rehabilitation **Marey Room**
2:00-4:00	Topic: Tutorial II Dan Ferris (University of Michigan) Building a Robotic Lower Limb Exoskeleton **Borelli Room**
4:00-6:00	ASB Executive Meeting **Marey Room**
6:00-7:30	Welcome Reception Hintz Alumni Center (see map for location)

Thursday, August 27th, 2009
8:00-9:15 AM

	Topic: Methods & Imaging ***Chair***: Robert Siston ***Student Co-chair*** **Marey Room**	**Topic**: Aging ***Chair***: Michael Madigan **Borelli Room**	**Topic**: Upper Extremity ***Chair***: Karen Troy ***Student Co-chair*** **Muybridge Room**
8:00	Validation of a single camera 3D motion tracking system *O'Connor, Armstrong, Weinhandl, Kusik & Barrows* University of Wisconsin-Milwaukee	Effect of tactile paving on gait parameters in older adults *Thies, Kenney & Howard* University of Salford	Associations between force steadiness & tests of hand function across the adult life span *Marmon, Pascoe & Enoka* University of Colorado
8:15	Load dependent variations in knee kinematics measured by dynamic MR *Westphal & Thelen* University of Wisconsin-Madison	Plantarflexor moment arm correlates with preferred gait velocity in healthy elderly subjects *Lee & Piazza* Pennsylvania State University	The effects of single- vs. double-row supraspinatus surgical repair on cyclic and failure loading *Pincivero, Marbaugh, Levine, Iagulli, Rabenold, Frangiamore & Goel* University of Toledo
8:30	Semi-automated tendon identity tracking in MR images *Jensen, Goetz, Thedens, Baer, Lawler & Brown* University of Iowa	The relationship between balance and cognition in parkinson's disease *Nocera, Vallabhajosula, Amano & Hass* University of Florida	The influence of fifteen muscles on distal radioulnar joint loading: a biomechanical model *Bader, Boland, Uhl & Pienkowski* University of Kentucky
8:45	Expanding the potential of cine pc MRI in tracking musculoskeletal motion *Behnam, Wilson & Sheehan* National Institutes of Health	Invariant density analysis of postural sway and prospective fall risk in community-dwellering elderly *Hur, Kang, Lipsitz & Hsiao-Wecksler* University of Illinois at Urbana-Champaign	Etensor strength, surgical tensioning and pinch force following brachioradialis to fpl tendon transfer: a simulation study *Mogk, Johanson, Hentz, Holzbaur & Murray* Rehabilitation Institute of Chicago
9:00	Aplication of musculoskeletal models to aging: obtaining subject-specific measures of muscle volume using MRI *Hasson, Miller, Foulis, Kent-Braun & Caldwell* University of Massachusetts Amherst	The effects of Morton's extension inserts on plantar loading patterns, pain and function in individuals with hallux rigidus *Morris, Tome, Patel, Baumhauer, & Nawoczenski* Ithaca College	Modeling muscle contributions to multijoint mechanics *Hu, Murray & Perreault* Northwestern University
	COFFEE AND EXHIBITS **Assembly Room and Faculty Staff Club**		

Thursday, August 27th, 2009
9:45-11:00 AM

	Topic: Motor Control ***Chair***: Alaa Ahmed ***Student Co-chair*** **Marey Room**	**Topic**: Gait ***Chair***: Jinger Gottschall **Borelli Room**	**Topic**: Orthopaedics ***Chair***: Neil Sharkey ***Student Co-chair*** **Muybridge Room**
9:45	Modulation of force structure via visual scaling of fast time scale processes *Hu & Newell* The Pennsylvania State University	The effects of sprint speed on apparent stiffness in uni-lateral trans-tibial amputee sprint runners *McGowan, Grabowski, McDermott, Kram & Herr* University of Texas	Meniscal modeling in a discrete element analysis of the knee *Anderson, Iyer, Segal & Brown* University of Iowa
10:00	Effects of head position and impact direction on neck muscle response to perturbations *Vasavada, Trask, Knottnerus & Lin* Washington State University	The relationship between muscle strength and gait asymmetry in unilateral, trans-tibial amputees *Lloyd & Royer* University of Calgary	Altered 3-d quadriceps moment arms in patellofemoral pain *Wilson, Behnam & Sheehan* National Institutes of Health
10:15	High actuator gains are necessary to control a fast fingertapping motion optimally *Theodorou & Valero-Cuevas* University of Southern California	A computer simulation model for predicting optimal prosthesis inertial parameters *Theroux-Jones, Royer & Umberger* University of Delaware	Performance of a hip protector depends on its position during a fall *Choi, Hoffer & Robinovitch* Simon Fraser University
10:30	Gravity dominates unconstrained, three-dimensional reaching in rhesus monkeys *Jindrich, Courtine, Liu, McKay, Moseanko, Bernot, Roy, Zhong, Tuszynski & Edgerton* Arizona State University	Contributions of leg muscles to the axial knee joint contact force during normal walking *Sasaki & Neptune* Boise State University	Evaluation of synthetic composite tibias for fracture testing *Quenneville, Fraser & Dunning* The University of Western Ontario
10:45	Afferent regulation of locomotor cpg contributes to movement stabilization: a simulation study *Klishko, Markin, Shevtsova, Lemay, Rybak & Prilutsky* Georgia Institute of Technology	Re-interpreting detrended fluctuation analyses of stride-to-stride variability in human walking *Dingwell & Cusumano* University of Texas	Greater trochanter reattachement: experimental evaluation of cable tension & displacement during walking *Duke, Laflamme, Brailovski, Bourgeois, Toueg, Levasseur & Petit* Sacre Coeur Hospital
	COFFEE AND EXHIBITS **Assembly Room and Faculty Staff Club**		

Thursday, August 27th, 2009
11:30-12:45 AM

	Topic: Sport ***Chair:*** Rick Hinricks ***Student Co-chair*** **Marey Room**	Topic: Muscle ***Chair:*** Sylvia Blemker **Borelli Room**	Topic: Hand ***Chair:*** Joe Sommer ***Student Co-chair*** **Muybridge Room**
11:30	Effect of Loading Condition on Traction Coefficient between Shoes and Artificial Turf Surfaces *Kuhlman, Sabick, Pfeiffer, Cooper & Forhan* Boise State University	Effects of tendon morphology on muscular work and efficiency *Gidley & Umberger* University of Massachusetts	MRI-compatibile loading devices for measurement of tendon and median nerve motion within the carpal tunnel *Goetz, Baer, Jensen, Thedens, Lawler & Brown* University of Iowa
11:45	Peak traction coefficients of cleated athletic shoes at various angles of internal rotation on artificial turf *Cooper, Pfeiffer, Sabick, Kuhlman, Simonson & Shea* Boise State University	Thigh-calf and heel-gluteus contact forces in high flexion (experimental results) *Pollard* National Institute for Occupational Safety & Health	A probabilistc biodynamic model for finger tendon force estimation clarifies the roles of the flexors *Li & Zhang* University of Pittsburgh
12:00	Barrier clearance in the 3000m steeplechase *Ingebretsen, Hunter, Cunningham & Willis* Brigham Young University	Reductions in stretch shorten cycle force enhancement with increased coupling time during maximal knee extensions *Pain, Begon & Forrester* Loughborough University	Biomechanical evaluation of the change in thumb extension following relocation of the extensor pollicis longus tendon *Nicewonder, Chloros, Wiesler & Tanaka* Virginia Tech – Wake Forest University
12:15	Foot strike contact location and foot loading during the development of running in children age 3 to 11 years *Mientjes, Pisciotta & Lafortune* Nike Sport Research Lab	Gait retraining to reduce the knee adduction moment through real-time feedback of dynamic knee alignment *Barrios & Davis* University of Delaware	A new device for measuring flexor tendon forces and grip force: a cadaver model *Park, Freivalds, Sharkey & Lowe* Pennsylvania State University
12:30	The effect of gender & perceived threat on the reaction & movement times of young adults performing a simulated sport-protective response *Lipps, Eckner, Richardson & Ashton-Miller* University of Michigan	Effects of novel physiological-based functional electrical stimulation patterns on post-stroke gait *Kesar, Perumal, Reisman, Rudolph, Higginson & Binder-Macleod* University of Delaware	Grip force fluctuations are more than just noise *Rácz & Valero-Cuevas* University of Southern California
	LUNCH		

Thursday, August 27th, 2009
Afternoon

	Topic: Awards ***Chair:*** Rodger Kram **Borelli Room**	
2:00	The influence of prior hamstring injury on musculotendon morphology & muscle contraction mechanics *Silder & Thelen* University of Wisconsin-Madison	Young Scientist Pre-Doctoral Award
2:15	3D synergies in handwriting *Shim, Hooke, Karol & Park* University of Maryland	Young Scientist Post-Doctoral Award
2:30	Orderly recruitment of motor units by optical stimulation in transgenic mice *Llewellyn, Thompson, Deisseroth & Delp* Stanford University	Finalist *Journal of Biomechanics* Award
2:45	Loss of isometric tension in myofibrils undergoing activated stretches *Panchangam & Herzog* University of Calgary	Finalist *Journal of Biomechanics* Award
3:00	Mechanical loading of in situ chondrocytes in a lapine retropatellar cartilage after anterior cruciate ligament transection *Han, Seerattan & Herzog* University of Calgary	Finalist *Clinical Biomechanics* Award
3:15	Patellofemoral kinematic differences exist between high-load and low-load conditions in patients with patellofemoral pain *Draper, Besier, Santos, Fredericson, Beaupre, Delp & Gold* Stanford University	Finalist *Clinical Biomechanics* Award
3:30	**COFFEE AND EXHIBITS** **Assembly Room and Faculty Staff Club**	
3:45	Topic: Keynote ***Chair:*** Neil Sharkey **Borelli Room**	
	"The Neuromechanical Foundations of Handedness"	

Thursday, August 27th, 2009
4:45-6:15 PM

POSTERS

Presenters should stand by odd numbered posters only for the first 45 minutes (4:45 until 5:30 PM), and stand by the even number posters only for the second 45 minutes (5:30 until 6:15 PM).

Topic	Poster Numbers	Location
Sports	1 - 25	Alumni Lounge
Running	26-32	Alumni Lounge
Landing	33-47	Alumni Lounge
Skeletal Tissue	48-62	Alumni Lounge
Aging	67-82	Assembly Rooms
Mechanics	83-108	Assembly Rooms
Animal	109-113	Assembly Rooms
Muscle	118-140	Faculty Staff Club
Upper Extremity	141-179	Faculty Staff Club

Topic: Sports
Location: Alumni Lounge

1 The effect of hip strengthening on running and squatting mechanics in female runners
Willy & Davis - University of Delaware

2 The effect of squat load and depth on patellofemoral joint kinetics
Cotter, Devor, Jamison & Chaudhari - The Ohio State University

3 On gender differences in the reaction times of sprinters at the 2008 Beijing Olympics
Lipps, Eckner, Richardson, Galecki & Ashton-Miller - University of Michigan

4 Effects of a simulated soccer match on cutting knee dynamics and reaction time
Collins, Smith, Ebersole & O'Connor – University of Wisconsin-Milwaukee

5 Frequency analysis of ski chatter in slalom skiing: comparison of inside and outside ski responses
Smith, Lappi & Reid - Norwegian School of Sport Sciences

6 Force measurement during ice hockey forward skating
Stidwill, Pearsall, Dixon & Turcotte - McGill University

7 The effects of testing technique on the performance of chest protectors in Tae Kwon Do
Tsui & Pain - Loughborough University

8 Assessment of a potential ACL injury risk protocol
Weinhandl, Armstrong, Earl, Kusik, Barrows & O'Connor - University of Wisconsin-Milwaukee

9 Joint-specific power absorption during eccentric cycling
Elmer, Madigan & Martin - University of Utah

Thursday, August 27th, 2009
4:45-6:15 PM

continued Topic: Sports
***Location*: Alumni Lounge**

10	Ground contact time in steeplechase hurdling *Willis & Hunter* - Brigham Young University
11	The effect of approach in volleyball spike jump for female athletes Hsieh - California State University, Chico
12	Specificity in the strength and power profiles of elite athletes Forrester & Pain - Loughborough University
13	A comparison of base running techniques in baseball Ficklin, Dapena & Brunfeldt - Indiana University
14	The influence of cricket leg guards on running times and stride parameters Webster & Roberts - Loughborough University
15	Partial external soft tissue vibration damping decreases local oxygen consumption Coza, Nigg, Dunn & Anderson - University of Calgary
16	Maximizing velocity in the hammer throw Hunter, Robinson & Clyde - Brigham Young University
17	Biomechanical parameters and mile performance Tukuafu, Hunter, Cunningham & Willis - Brigham Young University
18	Kinematics estimation sing a global optimization with closed loop constraints Begon, Fohanno & Colloud - Université de Montréal
19	3-D inverse dynamics analysis of martial arts circular kick Saxby & Robertson - University of Ottawa
20	Kinematic description of three types of softball pitches using a unique glenohumeral model Miller, Richards, Kaminski & Royer - University of Delaware
21	Movement classification for studies on player-surface interaction El Kati, Forrester & Fleming - Loughborough University
22	Shoulder rotational properties of throwing atheletes Zheng & Eaton - UNC Charlotte
23	An analysis of characteristics of ground reaction forces according to circle motion in gymnastics the pommel horse Kim, Park & Jean - Dankook University
24	Kinematic analysis on the motion of jump lotus kick 540° in Wushu Kang, Park & Jeon - Dankook University
25	Influence of inertial estimates on elbow joint moments during pitching Wicke, Keeley & Alford - Texas A&M-Commerce

Thursday, August 27th, 2009
4:45-6:15 PM

	Topic: Running ***Location***: Alumni Lounge
26	The influence of force loading patterns on heel pad properties *Gales & Challis* - The Pennsylvania State University
27	Segment coordination response to alterations in foot strike pattern *Gruber, Russell, Miller, Chang & Hamill* - University of Massachusetts
28	Is midfoot striking during running advantageous over rearfoot or forefoot striking? *Altman & Davis* - University of Delaware
29	Influence of thong flip-flops on running kinematics in preschoolers *Shroyer, Robinson & Weimar* - Auburn University
30	Joint contributions to support moment during running and hopping in a runner with achilles tendinopathy: an interlimb comparison *Chang, Popovich, Jr. & Kulig* - University of Southern California
31	Changes in joint kinematics and asymmetry throughout a run to fatigue in healthy female runners *Brown, Zifchock, Miana & Hillstrom* - Hospital for Special Surgery, New York
32	The influence of pelvic control on running mechanics *Jamison & Chaudhari* - The Ohio State University

	Topic: Landing ***Location***: Alumni Lounge
33	Prophylactic ankle stabilizers affect ankle but not knee or hip joint energetics during drop landings *Gardner, Barlow & McCaw* - llinois State University
34	The relation between knee separation distance and lower extremity kinematics during a drop land: implications for clinical screening *Havens, Sigward, Cheng, Pollard & Powers* - University of Southern California
35	The influence of relative hip and knee extensor strength on lower extremity biomechanics during a drop land task *Stearns & Powers* - University of Southern California
36	Differences of tibiofemoral kinematics between ACL-intact and ACL-deficient knees in an in vitro simulated pivot landing - *Oh, Kreinbrink, Antle, Wojtys & Ashton-Miller* University of Michigan
37	Impact forces during ballet: implications for injury *Boros & Skelton* - Texas Tech University
38	Optimising ballet floor design to assist in injury prevention *Fleming* - Loughborough University
39	Using ankle, knee & hip peak angular velocities to predict lower extremity work during drop landings *Barlow, Gardner & McCaw* - Illinois State University
40	Can risk factors for knee injury during landing be reduced by simple verbal instruction? *Milner, Srivatsan, Zhang & Fairbrother* - University of Tennessee, Knoxville
41	The effects of different fatiguing protocols on landing mechanics and knee kinesthetic sense *Afifi & Hinrichs* - Arizona State University

Thursday, August 27th, 2009
4:45-6:15 PM

continued Topic: Landing
Location: Alumni Lounge

42	Asymmetry in joint work of healthy participants during landing *Wortley, Zhang & Carson* - The University of Tennessee, Knoxville
43	The influence of gender & maturation on landing strategies: implications for ACL injury *Sigward, Pollard, Cheng, Lee & Powers* - University of Southern California
44	The effects of strength training on knee biomechanics during a drop jump in males *Sorensen, Dai, McIntyre & Gillette* - Iowa State University
45	Comparison of testing protocols of ankle sprain mechanism: inversion drop test & landing on an inverted surface *Chen, Zhang , Wortley, Milner & Bhaskaran* - The University of Tennessee, Knoxville
46	Biomechanical characteristics of drop landing on an inverted surface with ankle brace *Zhang, Chen & Wortley* - The University of Tennessee, Knoxville
47	The influence of jump landings on dynamic stability *Liu & Heise* - University of Delaware

Topic: Skeletal Tissue
Location: Alumni Lounge

48	Treadmill running and tower climbing exercise produce genotype dependent responses in the femurs of C57BL/6J (B6) and DBA/2J (D2) aged inbred mice *Gdovin, Sharkey & Lang* - The Pennsylvania State University
49	The effect of atorvastatin calcium on the cortical bone strength of corticosteroid treated rabbits *Handal, John, Booker, Khurana, Saing & Samuel* - Albert Einstein Medical Center
50	Geomata: a robust and intuitive software application for extracting anatomical boundaries from medical images *Bennetts & Erdemir* - Cleveland Clinic
51	Semi-automatic 3D virtual reconstruction of simulated comminuted articular fractures *Thomas, Anderson, Willis, Marsh & Brown* - The University of Iowa
52	Tension pattern of the cruciate ligament fibers during rolling and sliding *Wang, Li, O'Farrell, Harner & Zhang* - University of Pittsburgh
53	A comparison of prodisc and charite TDR designs under alternative wear testing standards *Goreham-Voss & Brown* - University of Iowa
54	The need for a bail-out plan: screw options for osteoporotic bone *Hartsell & Cooper* - Smith & Nephew, Inc
55	Use of design of experiment approach to predict force - displacement relationship for the subject-specific model of lateral meniscus *Kia, Guess, Mishra & Thiagarajan* - University of Missouri – Kansas City
56	Orientation-dependent impingement contact mechanics for hard-on-hard total hip bearings *Elkins, Pedersen,Callaghan & Brown* - University of Iowa
57	Structural properties of diabetic and normal plantar soft tissue *Pai & Ledoux* - VA RR&D Center of Excellence for Limb Loss Prevention & Prosthetic Engineering, Seattle

Thursday, August 27th, 2009
4:45-6:15 PM

continued Topic: Skeletal Tissue
Location: Alumni Lounge

58	The effects of lateral ligament sectioning on the stability of the ankle and subtalar joint *Ringleb, Dhakal, Anderson, Bawab, Paranjape & DeMaio* - Old Dominion University
59	Correlation between bone mineral density and fixation strength of orthopedic bone plates *Cartner, Zheng, Ricci & Tornetta* - Smith & Nephew, Inc.
60	Achieving greater bone-plate compressive forces in fracture fixation *Cartner, Ricci & Tornetta* - Smith & Nephew, Inc.
61	In vivo tracking of tendon elongation using ultrasound *Karimpoor, Screen & Morrissey* - Queen Mary University of London
62	An investigation of pubovisceral muscle enthesial loading at the end of the second stage of labor *Kim, Ashton-Miller & DeLancey* - University of Michigan

Topic: Aging
Location: Assembly Room

67	Age-related differences in balance after task-specific training *Bieryla & Madigan* - Virginia Tech
68	Effects of aging-related losses in muscle strength on the feasible region for balance recovery *Kadono & Pavol* - Oregon State University
69	Effect of visual perturbations and dual task on treadmill walking of older and younger adults *Beschorner, McGowan, Redfern, Sparto & Cham* - University of Pittsburgh
70	A three-dimensional kinematic and kinetic comparison of overground and treadmill walking in healthy elderly subjects *Watt, Franz, Jackson, Dicharry, Riley & Kerrigan* - University of Virginia
71	Center of mass position during repeated exposure to forward and backward slipping *Coley & Cham* - University of Pittsburgh
72	Effect of vibrotactile trunk tilt feedback on postural stability in older adults *Ursu, Jiang, & Sienko* - University of Michigan
73	Center of pressure sway parameters considered jointly better differentiate older adult fallers from non-fallers *Bigelow & Berme* - University of Dayton
74	Control of submaximal center of pressure movements in healthy women: effects of age and movement type *Hernandez, Ashton-Miller & Alexander* - University of Michigan
75	Preliminary investigation of balance recovery from a trip in overweight and normal weight older adults *Matrangola, Bieryla & Madigan* - Virginia Polytechnic Institute & State University
76	Effects of age & walking speed on metabolic cost & lower extremity joint kinematics during gait in healthy adults *Peterson & Martin* - Pennsylvania State University
77	The effects of gender & obesity on trunk inertial parameters in old & elderly adults *Chambers, Sukits, McCrory & Cham* - University of Pittsburgh
78	Effects of a single step requirement on balance recovery maneuvers in young & older adults *Dinn & King* - University of Missouri – Kansas City

Thursday, August 27th, 2009
4:45-6:15 PM

continued Topic: Aging

Location: Assembly Room

79	Temporal changes in gait in healthy older individuals during prolonged treadmill walking *Bechard, Birmingham, Jones, Giffin, Zecevic & Jenkyn* - The University of Western Ontario
80	Response of the knee adduction moment to changes in gait speed: peak versus impulse *Maly & Robbins* - McMaster University
81	Age-related changes in dynamic stability & avoidance strategies when stepping over an obstacle in a dual task paradigm *Paquette & Vallis* - University of Guelph
82	Effects of backward walking on balance and lower extremity walking kinematics in healthy young and older adults *Dufek, Mercer, Aldridge, Melcher & Gouws* - University of Nevada, Las Vegas

Topic: Mechanics

Location: Assembly Room

83	Electromyographic responses to aging in children with cerebral palsy *Laurer, Pierce, Tucker, Barbs & Prosser* - Temple University
84	PCL treatment influences sensitivity to joint line changes in total knee arthroplasty *Hast, Walker & Piazza* - The Pennsylvania State University
85	Effect of force redirection on upper limb net joint moments during wheelchair propulsion *Munaretto, McNitt-Gray, Flashner & Requejo* - University of Southern California
86	The use of an accelerometer to determine vestibulospinal function: the NIH toolbox project *Lin, Steed, Marchetti, Musolino, Redfern & Whitney* - University of Pittsburgh
87	Changes in wrist moment arms of the first dorsal extensor compartment following simple distal radius malunions *Scallon, Bednar, Ladd & Murray* - Northwestern University
88	Biomechanics of the sit to stand in people with multiple sclerosis *Bowser, Rourke, White & Simpson* - University of Georgia
89	Assessment of the pressore steptm system as an extended wear weightbearing activity monitor for use with orthopaedic patients *Williams, Allen, Wu, Rudert & Pedersen* - University of Iowa
90	Cumulative knee loading relates to pain intensity & knee extensor torque in people with knee osteoarthritis *Maly & Robbins* - McMaster University
91	Influence of asymmetry of lower extremity force on center of mass velocity during a sit to stand task among subjects with hip fracture *Kneiss, Yelle & Houck* - Ithaca College-Rochester
92	Sensory feedback from ankle extensor afferents improves locomotor output in human SCI *Wu, Gordon, Kahn & Schmit* - Rehabilitation Institute of Chicago
93	Effect of foot and ankle muscle strength in participants with PTTD compared to healthy controls *Fetzer, Hilton & Houck* - Ithaca College-Rochester
94	Gait training and knee hyperextension *Teran-Yengle, Segal, Johnston, Singh, Torner, Walace & Yack* - The University of Iowa

Thursday, August 27th, 2009
4:45-6:15 PM

continued Topic: Mechanics

Location: Assembly Room

95	Pilot study of gait symmetry effects following hip fracture rehabilitation *Rodgers, Geigle & Miller* - University of Maryland
96	Balance adjustment during obstacle crossing in patients with total hip arthroplasty *Chiu & Chou* - University of Oregon
97	Passive resistance to knee motion following total knee arthroplasty *Byrne & Prentice* - Memorial University of Newfoundland
98	Mechanical properties of an elastomer insert ankle foot orthosis *Talaty, Seale, & Siegler* - Drexel University
99	Load transfer and symmetry in gait during double support in acquired brain injury and healthy controls *Yarossi, Nolan, Savalia, Forrest & Elovic* - Kessler Foundation Research Center
100	Robotic outcomes in persons with rotator cuff tears *Finley, Conroy, Jones-Lush & Bever* - University of Indianapolis
101	Improving dynamic stability during the compensatory stepping response of a transfemoral amputee *Crenshaw, Kaufman & Grabiner* - University of Illinois at Chicago
102	Locomotor training: the effects of treadmill speed and body weight support on lower extremity joint kinematics *Lathrop, Morin, Worthen-Chaudhari, Chaudhari, Basso, Schmiedeler & Siston* - The Ohio State University
103	Does acute whole body vibration training improve physical performance for people with knee osteoarthritis? *Salmon & Tillman* - University of Florida
104	Surgical recession of the gastrocnemius does not influence plantar pressure *Chimera, Castro & Manal* - University of Delaware
105	Stand-to-sit movement after bi-compartmental knee replacement *Wang, Dugan, Frame & Rolston* - Ball State University
106	Joint moment contributions to swing knee extension acceleration during gait in subjects with spastic hemiplegic cerebral palsy *Goldberg, Requejo & Fowler* - University of California, Los Angeles
107	Reliability and repeatability of self-selected wheelchair transfer techniques *Lin, Koontz & Kankipati* - Department of Veterans Affairs, Pittsburgh, PA
108	Scapular-humeral kinematics during wheelchair propulsion *Raina, McNitt-Gray & Requejo* – University of Southern California

Topic: Animal

Location: Assembly Room

109	Effects of multiple-group muscle weakness on the retro-patellar cartilage in rabbits *Youssef, Seerattan, Leonard & Herzog* - The University of Calgary
110	Validation of an experimental device simulating the stance phase of a canine hindlimb at trot: an in vitro kinematics study *Lussier, Clément, Jaafar, van Petit & Hagemeister* - University of Montreal

Thursday, August 27th, 2009
4:45-6:15 PM

continued Topic: Animal

Location: Assembly Room

111	Exercise effects via treadmill running and tower climbing on femoral bones of C57BL/6J and DBA/2J adult female mice *Preston, Sharkey & Lang* - The Pennsylvania State University
112	Effects of exercise in trabecular and cortical bone of osteopenic rats: a biomechanical study *Zamarioli, Simões, Chagas, Volpon & Shimano* - Laboratory of Biomechanics – Faculty of Medicine of Ribeirão Preto
113	Changes in muscle-skeletal system after spinal cord injury: a biomechanical study in paraplegic rats *Zamarioli, Maranho, Okubo, Falcai, Volpon & Shimano* - Faculty of Medicine of Ribeirão Preto

Topic: Muscle

Location: Faculty Staff Club

118	Conservation of limb function after peripheral nerve injury in rat locomotion *Bauman & Chang* - Georgia Tech
119	Lower extremity muscle volumes can be accurately obtained from high resolution MRI *Sepulveda, Kingsbury, Eng, Lieber & Ward* - University of California, San Diego
120	Isometric force production requires asymmetric muscle-tendon length trajectory *Sawicki & Roberts* - Brown University
121	Muscle forces in the lower limb predicted by static and dynamic optimization *Miller, Umberger & Caldwell* - University of Massachusetts
122	Power augmentation in a compliant muscle-tendon system *Sheppard, Sawicki & Roberts* - Brown University
123	Isokinetic plantar flexion torque increases after open gastrocnemius recession *Chimera, Castro & Manal* - University of Delaware
124	Architectural parameters of the tricep brachii during isometric contractions *Kutz, Fiolo, Infantolino & Challis* - The Pennsylvania State University
125	Comparison of rotator cuff muscle architecture between humans and selected vertebrate species *Kwan, Eng, Ward* - University of California San Diego
126	Are ultrasound measures of muscle thickness representative of muscle activation in the abdominal wall? *Brown & McGill* - University of Waterloo
127	Seat tube angle affects rectus femoris activation when riding in an aerodynamic position *Silder, Gleason & Thelen* - University of Wisconsin-Madison
128	Quadriceps activation at different hip and knee joint angles *Winter & Burnley* - Aberystwyth University
129	Knee extensor torque reduction during constant perceived exertion isometric contractions *Mukherjee & Pincivero* - The University of Toledo
130	Muscle forces during mastication *Vilimek & Goldmann* - Czech Technical University in Prague
131	A novel approach for experimental derived muscle parameters of the soleus muscle *Binder-Macleod, Manal & Buchanan* - University of Delaware

Thursday, August 27th, 2009
4:45-6:15 PM

continued Topic: Muscle
Location: Faculty Staff Club

132 Estimating dynamic muscle forces of torso during flexion movement
Gottipati & Plaut - Virginia Polytechnic Institute & State University

133 Fascicle lengths in the first dorsal interosseous muscle
Ellis, Casey, Infantolino & Challis - The Pennsylvania State University

134 The influence of running speed on the extensor paradox observed in adult runners
Lambert, Kwon & Kwon - Texas Woman's University

135 Maximal knee extension stretch shorten cycles on an isovelocity dynamometer to examine active force ehancement
Pain, Begon & Forrester - Loughborough University

136 Deep hip muscle activation during a squat exercise
Decker, Krong, Peterson, Anstett, Torry, Giphart, Shelburne & Philippon - Steadman-Hawkins Research Foundation

137 Force-length profiles for the triceps brachii
Fiolo, Kutz, Infantolino & Challis - The Pennsylvania State University

138 Motor asymmetry reduction in older adults revealed by interlimb transfer
Wuebbenhorst & Sainburg- The Pennsylvania State University

139 Can an external muscle stimulus help the learning of complex gross coordinate motion?
Shin, Park & O'Sullivan - Seoul National University

140 Upper limb muscle volume characterization in older adult subjects
Vidt, Daly, Marsh & Holzbaur - Wake Forest University

Topic: Upper Extremity
Location: Faculty Staff Club

141 Interlimb coordination differences in left- and right-handers.
Przybyla & Sainburg - The Pennsylvania State University

142 A method to quantify the influence of radial head fracture location on elbow kinematics
Kuxhaus, Brogdon, Druschel, Schimoler, Marchessault, Baratz & Miller - Allegheny General Hospital

143 A method for alignment of the glenoid implant based on sphere fitting
Lewis & Armstrong - Penn State Hershey

144 Development of an analytical model for rotator cuff repairs
Aurora, van den Bogert & Derwin – Lerner Research Institute

145 Theoretical analysis of the muscle loading in a thumb in response to increased joint stiffness
Wu, Li, Cutlip & An - National Institute for Occupational Safety & Health, Morgantown, WV

146 The effect of TFCC injury on ECU function and friction
Domire, Karabekmez, Duymaz, Rutar, Amadio & Moran - Mayo Clinic

147 Inverse optimization of digit forces in multi-finger prehension based on analytical determination of the objective function
Niu, Tereknov, Pesin, Latash & Zatsiorsky - The Pennsylvania State University

148 A quantitative analysis of the relationship between scapular orientation & shoulder strength
Picco, Fischer & Dickerson - University of Waterloo

Thursday, August 27th, 2009
4:45-6:15 PM

	continued Topic: Upper Extremity ***Location*: Faculty Staff Club**
149	The effects of noise on the control of a planar model of reaching *Nguyen & Dingwell* - University of Texas at Austin
150	A method for quantifying active thumb circumduction motion in children *Bruening, Cooney & Lubahn* - Shriners Hospitals for Children, Erie PA
151	Revisiting finger flexor excursions with current modeling techniques *Kociolek & Keir* - McMaster University
152	The relationship between hand dexterity and hand muscle structure *Hsu, Halayko, Kim & Shim* - University of Maryland
153	Muscle fatigue affects task performance during repetitive upper extremity movements *Gates, Smallwood & Dingwell* - University of Texas
154	EMG analysis of abductor policis longus, extensor carpi ulnaris & flexor carpi ulnaris during forearm prono-supination *Bader, Boland, Stone, Uhl & Pienkowski* - University of Kentucky
155	A strain-energy approach to simulating slow finger movements and changes due to loss of musculature *Kurse & Valero-Cuevas* - University of Southern California
156	Hand force estimation strategies for field application *Stevenson, Reid, Godwin & Sadler* - Queen's University
157	Effect of modulation of the internal forces on digit coordination during multi-finger object prehension *Martin, Latash & Zatsiorsky* - The Pennsylvania State University
158	Catch like property in human adductor pollicis muscle *Fortuna, Vaz & Herzog* - Federal University of Rio Grande do Sul
159	Frictional properties of the hand skin *Uygur, de Freitas & Jaric* - University of Delaware
160	Finger enslaving in a three-dimensional pressing task *Kapur, Friedman, Zatsiorsky & Latash* - Pennsylvania State University
161	Activation of the shoulder musculature during a sustained submaximal abduction isometric contraction. *Timmons, Adler & Boguszewski* - The University of Toledo
162	In-vitro estimation of finger joint reaction forces during isometric force generation *Lee & Kamper* - Rehabilitation Institute of Chicago
163	Clavicle kinematics following change in length of the sternoclavicular ligaments *Szucs & Borstad* - The Ohio State University
164	Relationship between clinical & biomechanical measures of hand function *Amano, Alberts, Richardson, Doidge, Joyner & Hass* - University of Florida
165	Characterization of the flexor digitorum superficialis as a predictor of grasping strength *Shain, Kim ,& Craelius* - Rutgers University
166	The effects of suprascapular nerve block on humeral head translation *San Juan, Kosek & Karduna* - University of Oregon
167	Effect of the t-poles & conventional hiking poles on the foot VGRF and the joint moment of the upper extremity joints *Singhal, Yoon, Casebolt & Kwon* - Texas Woman's University

Thursday, August 27th, 2009
4:45-6:15 PM

continued Topic: Upper Extremity
Location: Faculty Staff Club

168	An analysis of the finger joint moments in a hand at the maximal isometric grip: effects of friction & cylinder diameter *Wu, Dong, McDowell & Welcome* - National Institute for Occupational Safety & Health
169	Influence of glenoid inclination on rotator cuff moment arms: a computational study *Langenderfer, Baldwin & Rullkoetter* - Central Michigan University
170	Prehension synergy: the changes in synergistic digit actions under systematcially manipulated conditions of task constraints *Park, Kim & Shim* - University of Maryland
171	Shoulder rotator muscle fatigue and EMG during repeated maximal effort exercise *Hess, Calhoun & Pincivero* - The University of Toledo
172	Scapulothoracic motion & muscle activity during the raising & lowering phase of an overhead reaching task *Ebaugh & Spinelli* - Drexel University
173	Variance in upper extremity muscle activity during cyclic pushing tasks *Hodder, Gruevski & Keir* - McMaster University
174	Evaluation of glenohumeral muscles during provocative tests designed to diagnose slap lesions *Wood, Sabick, Pfeiffer, Kuhlman, Christensen, Curtin, Nilsson & Shea* - Boise State University
175	Humeral retroversion in biomedical perspective: ranges of variation in human populations and the role of activity patterns in their developmental determinants *Eckhardt & Kuperavage* - The Pennsylvania State University
176	Modifications in joint kinetics during manual wheelchair propulsion over time *Coghlan, McNitt-Gray, Requejo, Mulroy & Ruparel* - University of Southern California
177	The associations between biomechanical impairments and hand function in people with rheumatoid arthritis *Baker & Rogers* - University of Pittsburgh
178	An anatomic coordinate system of the trapezium using curvature *Rainbow & Crisco* - Brown University
179	Power grip force is modulated in dynamic arm movement *Gao, Lin & Marzilli* - University of Texas Southwestern Medical Center

Friday, August 28th, 2009
8:00-9:15 AM

	Topic: Tendon & Ligament **Chair**: Tom Brown ***Student Co-chair*** **Marey Room**	Topic: Locomotion Energetics **Chair**: Brian Umberger **Borelli Room**	Topic: Spine **Chair**: Paul Ivanic ***Student Co-chair*** **Muybridge Room**
8:00	The effect of cyclic loading on the coefficient of friction differs by gender in the articular cartilage of murine knee joints *Drewniak, Jay, Fleming & Crisco* Brown University	Metabolic response in functional electrically stimulated pedaling with the lower leg muscles *Hakansson & Hull* University of Delaware	Comparing load and posture on industrial based lifting tasks: effects of gender, spinal load magnitude & postural asymmetry *Nairn, Parkinson, Callaghan & Drake* University of Windsor
8:15	Individuals with patellofemoral pain demonstrate higher patellofemoral joint stresses compared to those who are pain-free: evaluation using finite element analysis *Farrokhi & Powers* University of Southern California	Foot-strike pattern selection to minimize muscle energy expenditure during running: a computer simulation study *Miller, Russell, Gruber & Hamill* University of Massachusetts, Amherst	Development and validation of a non-invasive spinal motion measurement system *Stinton, Shapiro, Mullineaux, Shaffer, Cassidy & Pienkowski* University of Kentucky
8:30	Mechanical properties of the anterior cruciate ligament after corticosteroid administration *Okubo, Zamarioli, Falcai, Volpon & Shimano* University of São Paulo	Elastic leg exoskeleton reduces the metabolic cost of hopping *Grabowski & Herr* Massachusetts Institute of Technology	Is muscle co-activation a predisposing factor for low back pain development during standing? *Nelson-Wong & Callaghan* University of Waterloo
8:45	The depth of the medial tibial plateau is an important anterior cruciate ligament injury risk factor *Hashemi, Chandrashekar, Gill, Slauterbeck, Schutt, Dabezies, Mansouri & Beynnon* Texas Tech University	Changes in kinematics, metabolic cost & external work done during walking with a propulsive force *Zirker, Bennett, Friedman, Mehdi & Abel* University of Virginia	An in-vitro biomechanical evaluation of posterior lumbar dynamic stabilization systems: universal clamp and wallis *Shaw, Ilharreborde, Berglund, Zhao, Gay & An* Mayo Clinic
9:00	Low stress tendon fatigue: mechanical and structural findings *Parent & Langelier* Université de Sherbrooke	Effects of age and walking speed on coactivation during gait *Peterson & Martin* Pennsylvania State University	Is there a low back cost to hip-centric exercise? examining the l4/l5 joint compression during movements prescribed to overload the hips *Frost, Beach, Fenwick, Callaghan & McGill* University of Waterloo

COFFEE AND EXHIBITS

Assembly Room and Faculty Staff Club

Friday, August 28th, 2009
9:45-11:00 AM

	Topic: Knee ***Chair***: Irene Davis ***Student Co-chair*** **Marey Room**	**Topic: Muscle and Tendon** ***Chair***: Huub Maas **Borelli Room**	**Topic: Upper Extremity** ***Chair***: Andy Karduna ***Student Co-chair*** **Muybridge Room**
9:45	Injury prevention training results in biomechanical changes consistent with decreased knee loading in female athletes during landing *Pollard, Sigward & Powers* University of Southern California	Non-uniform distribution of sarcomere lengths along a muscle fiber *Infantolino & Challis* The Pennsylvania State University	Forward dynamic simulation of an upper extremity movement using computed muscle control *Daly, Vidt & Holzbaur* Wake Forest University
10:00	Effect of off-loader braces and degree of valgus correction on clinical outcome for persons with medial knee OA *Russell & Ramsey* University at Buffalo	A phenomenological model of shortening induced force depression during muscle contractions *McGowan, Neptune & Herzog* University of Texas at Austin	Glenohumeral joint contact forces during wheelchair activities *Morrow, An & Kaufman* Mayo Clinic
10:15	Longitudinal Sex Differences In Knee Abduction In Young Athletes *Ford, Shapiro, Myer, van den Bogert & Hewett* Cincinnati Children's Hospital	Postactivation potentiation and decreased motor unit firing rate during submaximal contractions of the tibialis anterior *Inglis, Howard, MacIntosh, Gabriel & Vandenboom* Brock University	Influence of indenter size and wrist posture on transverse carpal ligament stiffness *Holmes, Howarth, Callaghan & Keir* McMaster University
10:30	Articular loading during walking in subjects with ACL deficiency *Manal, Snyder-Mackler & Buchanan* University of Delaware	The magnitude & the time dependent structure of force fluctuations are muscle-length dependent *Winter & Challis* Aberystwyth University	Recovery of scapula kinematics & shoulder muscle activation following an isometric fatigue task *Borstad, Kynyk, Lower, Sellers, Szucs & Navalgund* The Ohio State University
10:45	Comparison of tibial translations during soft and stiff landings in healthy adults: a biplane fluoroscopy study *Peterson, Krong,Giphart, Shelburne, Steadman & Torry* Steadman Hawkins Research Foundation	A biomechanical comparison of the side-to-side and pulvertaft tendon transfer repair techniques *Brown, Hentzen, Kwan, Ward, Friden & Lieber* University of California San Diego	Cycle to cycle variability in a repetitive upper extremity task *Keir, Brown & Holmes* McMaster University

COFFEE AND EXHIBITS

Assembly Room and Faculty Staff Club

Friday, August 28th, 2009
11:30-12:45 PM

	Topic: Computational Biomechanics ***Chair***: Martin Tanaka ***Student Co-chair*** **Marey Room**	**Topic: Running** ***Chair***: Ewald Hennig **Borelli Room**	**Topic: Aging** ***Chair***: Monica Maly ***Student Co-chair*** **Muybridge Room**
11.30	Adaptive surrogate modeling for cost-effective determination of nonlinear tissue properties *Halloran, Frampton & Erdemir* The Cleveland Clinic	Dynamic arch development: midfoot contact area and loading during running in children age 3 to 11 years *Mientjes, Pisciotta & Lafortune* Nike Sport Research Lab	Influence of age & gait speed on required coefficient of friction independent of step length *Anderson & Madigan* Virginia Polytechnic Institute & State University
11.45	Pelvic motion during seated pedaling facilitates intersegmental energy transfer *Gleason, Silder & Thelen* University of Wisconsin - Madison	In vivo knee cartilage contact during downhill running *Anderst, Thorhauer & Tashman* University of Pittsburgh	Modulating step length during walking by young and old adults *DeVita, Copple, Patterson, Rider, Long, Steinweg & Hortobagyi* East Carolina University
12.00	The use of subject-specific anatomic parameters in an EMG-driven musculoskeletal model results in improved knee joint moment predictions when compared to generic & scaled models *Tsai & Powers* University of Southern California	Using forward dynamic simulations of high speed running to assess hamstring strain injury potential *Chumanov, Heiderscheit & Thelen* University of Wisconsin-Madison	A shoe-based method for randomly perturbing the stance phase of gait and its effect on step width *Kim, Richardson, Nnodim, Takemura & Ashton-Miller* University of Michigan
12.15	Computational simulation of ankle contact mechanics following focal defect resurfacing with a metallic implant *Anderson, Tochigi, Rudert, Vaseenon, Amendola & Brown* University of Iowa	The probability for tibial stress fracture increases with running speed despite a reduction in the number of loading cycles *Edwards, Taylor, Rudolphi, Gillette & Derrick* Iowa State University	Are feedback related adjustments to step width affected by performance of the Stroop Test? *Hurt, Rosenblatt & Grabiner* University of Illinois at Chicago
12.30	A large scale optimization approach to generate subject-specific knee joint models *Borotikar & van den Bogert* Cleveland Clinic	Mechanics of unilateral trans-tibial amputee sprint runners *Grabowski, McGowan, Herr, McDermott & Kram* Massachusetts Institute of Technology	Lower extermity muscle strength and gait variability in older adults *Shin, Valentine, Evans & Sosnoff* University of Illinois at Urbana-Champaign
	LUNCH		

Friday, August 27th, 2009
Afternoon

2.00	Topic: **Hay Lecture** ***Chair:*** Vladimir Zatsiorsky ***Introduction***: Jill McNitt-Gray ***Presentation***: Tom Buchanan **Borelli Room**
	Doris Miller (University of Western Ontario) "Ups and downs of the competitive diving"
3:15	**COFFEE AND EXHIBITS** **Assembly Room and Faculty Staff Club**
3:45	Topic: **Keynote Lecture** ***Chair:*** Irene Davis **Borelli Room**
	Kiisa Nishikawa (Northern Arizona University) "How do they do it? Specializations of toads for extremely rapid prey capture"

Friday, August 28th, 2009
4:45-6:15 PM

POSTERS

Presenters should stand by odd numbered posters only for the first 45 minutes (4:45 until 5:30 PM), and stand by the even number posters only for the second 45 minutes (5:30 until 6:15 PM).

Topic	Poster Numbers	Location
Balance	1 – 30	Alumni Lounge
Walking	31-65	Alumni Lounge
Methods	67-104	Assembly Room
Motor Control	105-115	Assembly Rooms
Computational Biomechanics	118-132	Faculty Staff Club
Injury	133-144	Faculty Staff Club
Ergonomics	145-158	Faculty Staff Club
Spine	159-186	Faculty Staff Club
Cardiovascular	187-188	Faculty Staff Club

Topic: Balance
Location: Alumni Lounge

1 Dynamic postural stability in pregnant fallers, non-fallers and nonpregnant controls
McCrory, Chambers, Daftary & Redfern - West Virginia University

2 Kinematic responses to galvanic stimulation of the human vestibular system during locomotion
Steed, Roche & Redfern - University of Pittsburgh

3 Recovery gait following an unexpected slip
Timcho, Chambers & Cham - University of Pittsburgh

4 Are restricted, repetitive behaviors and postural control linked in autism spectrum disorders?
Hass, Fournier, Selbst, Benefield, Lewis & Radonovich - The University of Florida

5 Quiet standing and quiet sitting in young children with autism spectrum disorders
Fournier, Radonovich, Selbst, Benefield & Hass - The University of Florida

6 Emotional influences on the center of pressure trajectory during gait initiation
Joyner, Gamble, Fournier, Hass & Janelle - University of Florida

7 Preliminary investigation of slip and trip propensity in overweight and normal weight adults
Matrangola, Anderson & Madigan - Virginia Polytechnic Institute & State University

8 The influence of turning strategy on dynamic postural stability in person with early stage parkinson's Disease
Song, Ferris, Sigward, Fisher, Petzinger, Parent & Salem - University of Southern California

9 Five-toed socks decrease static postural control among health individuals as measured with time-to-boundary analysis *Shinohara & Gribble* - University of Toledo

10 Modeling and simulation of balance recovery responses to tripping
Shiratori, Coley, Cham & Hodgins - Carnegie Mellon University

Friday, August 28th, 2009
4:45-6:15 PM

continued Topic: **Balance**
Location: Alumni Lounge

11	Effect of balance recovery task difficulty on stepping velocities for forward, sideways and backward loss of balance directions *Telonio & Smeesters* - Université de Sherbrooke
12	Effects of age and instructions limiting the number of steps on the threshold of balance recovery *Cyr & Smeesters* - Université de Sherbrooke
13	Recovery from postural perturbations without stepping following localized muscle fatigue *Davidson, Madigan, Nussbaum & Wojcik* - University of Colorado Denver
14	The effect of lumbopelvic posture on pelvic floor muscle activation and intravaginal pressure generation in continent women *Capson, Nashed & McLean* - Queen's University
15	The interaction between posture and cognition during a manual fitting task *Seaman, Ponto, Keough, Ryu & Haddad* - Purdue University
16	Predicting an imminent fall using 3D trunk acceleration *Cain, Crenshaw, Kaufman & Grabiner* - University of Illinois at Chicago
17	Comparison of an automatic and voluntary task in early Parkinson's disease *McVey, Stylianou, Lyons, Pahwa, Luchies & Cheney* - The University of Kansas
18	Postural sway changes in mild to moderate Parkinson's disease *Stylianou, Luchies, McVey, Lyons & Pahwa* - The University of Kansas
19	The effect of boundary shape and minimal selection on single limb stance postural stability *Joshi, Bazett-Jones, Earl & Cob* - University of Wisconsin-Milwaukee
20	Recovery limb positioning and trip recovery success *Roos, McGuigan & Trewartha* - The University of Texas at Austin
21	Trip recovery strategy selection in younger and older adults and the associated physical demands *Roos, McGuigan & Trewartha* - The University of Texas at Austin
22	Magnitude of potential vulnerability to balance control after a transition to standing *DiDomenico & McGorry* - Liberty Mutual Research Institute for Safety
23	Dynamic stability assessed with frequency analysis compared to spatiotemporal analysis *Heise, Liu, Smith, Allen & Hoke* - University of Northern Colorado
24	Body center of pressure control during gait initiation in transtibial amputees *Fink, Yen, Auyang & Chang* - Georgia Tech
25	Effects of increased task difficulty on performance variable stabilization during human locomotion *Auyang & Chang* - Georgia Tech
26	Automatic detection of slip-induced backward falls *Liu & Lockhart* - University of Houston
27	Proactive balance control: kinematic analysis of a reach task *Mukherjee & Armstrong* - The University of Toledo
28	Comparison of total hip arthroplasty and a hip resurfacing during quiet standing *Bouffard, Therrien, Nantel, Lavigne, Venditolli & Prince* - Marie Enfant Rehabilitation Center
29	Differences in upper body posture and postural muscle activation in females with larger breast sizes *Bennett, Kuhlman, Sabick, Pfeiffer & Laverson* - Boise State University
30	Postural control response to stance on a compliant surface *Haworth, Strang, Hieronymus & Walsh* - Miami University

Friday, August 28th, 2009
4:45-6:15 PM

	Topic: **Walking** ***Location***: Alumni Lounge
31	An evaluation of functional asymmetry at non-preferred walking speeds *Smith, Rice & Seeley* - Brigham Young University
32	Vertical displacement of the center of mass during spring-loaded crutch ambulation *Dunn & Seeley* - Brigham Young University
33	Time-normalization techniques for gait data *Helwig, Hong & Hsiao-Wecksler* - University of Illinois at Urbana-Champaign
34	Interaction between mass and alignment on knee adduction movement in patients with knee osteoarthritis *Moyer, Birmingham, Kean, Jones, Jenkyn, Chesworth & Giffin* - University of Western Ontario
35	Changes in ankle kinematics to preserve an invariant roll-over shape *Wang & Hansen* - Northwestern University
36	Electrical stimulation of the semitendinosus during terminal swing increases knee flexion excursion during early stance *Hernandez, Lenz & Thelen* - University of Wisconsin-Madison
37	Lower extremity coordination in obese women *Russell, Gruber, van Emmerik & Hamill* - University of Massachusetts Amherst
38	KInematic adaptations of the forefoot and hindfoot during cross-slope walking *Damavandi, Dixon & Pearsall* - McGill University
39	Kinectics of a weighted challenge in individuals with knee osteoarthritis *Kubinski & Higginson* - University of Delaware
40	Varus knee torques in high-heeled stair descent *Stevermer, Nelsen & Gillette* - Iowa State University
41	Lower extremity joint moment during carrying tasks in children Gillette, *Stevermer, Miller, Edwards & Schwab* - Iowa State University
42	The robotic gain simulator: the effect of EMG to force *Aubin & Ledoux* - VA RR&D Center of Excellence for Limb Loss Prevention & Prosthetic Engineering, Seattle
43	Midtarsal kinematics defined using finite helical axes analysis *Okita, Meyers, Challis & Sharkey* - The Pennsylvania State University
44	Plantar flexor reflex response to a perturbation during human walking maintains ankle joint torque pattern *Kao, Lewis & Ferris* - University of Michigan
45	Gait strategy changes with walking speed to accommodate biomechanical constraints *Kang, Yeom & Park* - KAIST, Korea
46	The role of tibialis posterior on foot kinematics during walking *Pohl, Rabbito & Ferber* - University of Calgary
47	Children with cerebral palsy require more strides to dissipate disturbances present in their walking pattern Kurz, Corr & Stuberg - University of Nebraska Medical Center
48	Individual limb work is influenced by ankle-foot-orthotics worn by children with cerebral palsy *Kurz, Stuberg & Ginsburg* - University of Nebraska Medical Center

Friday, August 28th, 2009
4:45-6:15 PM

	continued Topic: Walking ***Location***: Alumni Lounge
49	Differences in frontal plane stability during treadmill and overground walking *Rosenblatt & Grabiner* - University of Illinois at Chicago
50	Compensatory changes in the uninvolved knee after gait training with real-time feedback in adults with knee osteoarthritis *Singh, Segal, Johnston, Teran-Yengle, Torner, Walace & Yack* - The University of Iowa
51	Effective rocker shapes for walking, swaying and standing *Wang & Hansen* - Northwestern University
52	Sensitivity analysis of loading conditions on mechanical stiffness measurements of a passive dynamic ankle foot orthoses *Takahashi & Stanhope* - University of Delaware
53	Biplane fluoroscopy analysis of knee kinematics during gait *Krong, Peterson, Giphart, Shelburne & Torry* - Steadman-Hawkins Research Foundation
54	Effect of total hip arthroplasty on contribution of individual joints to dynamic effect of total hip arthroplasty on contribution of individual joints to dynamic support during walking *Chou, Amali & Lugade* - University of Oregon
55	The immediate bilateral effects of unilateral knee bracing for the treatment of knee osteoarthritis: preliminary results *Zifchock, Backus, Bogner, Pavlov, Mandl, Chen, Garrison, Brown, Cordasco, Williams, Hunter, Bedi & Hillstrom* - Hospital for Special Surgery, New York
56	Effect of walking speed on plantar loading and foot kinematics in subjects with stage II posterior tibial tendon dysfunction *Neville, Flemister & Houck* - SUNY Upstate Medical Center
57	Kinematic and EMG comparison of gait in normal gravity and microgravity *De Witt, Edwards, Perusek, Lewandowski & Samorezov* - Wyle Integrated Science & Engineering Group
58	The origins of bipedal locomotions inferred from geometric cross sectional properties of ancient african femora *Kuperavage & Eckhard* - Pennsylvania State University
59	Distinguishing between mechanical pathology and compensation using gait analysis in people with knee osteoarthritis *Maly & Costigan* - McMaster University
60	Temporal and frequency characteristics of trunk and hip muscle activity patterns in early walkers with and without cerebral palsy. *Prosser, Lee, Barbe, VanSant & Lauer* - Temple University
61	Evaluation of asymmetry in ground reaction forces and muscle activity during the stance phase of gait in asymptomatic subjects *Burnett, Campbell-Kyureghyan, Kar & Quesada* - University of Louisville
62	Comparison of ankle and foot joint kinetics after heel-off between individuals with posterior tibial tendon dysfunction and controls *Van Vlack, Tome, Neville, Flemister & Houck* - Ithaca College-Rochester
63	Footwear is an Important determinant for medial-lateral stability during hill transitions in walking humans *Stern & Gottschall* - The Pennsylvania State University
64	At similar slopes, stair walking is a safer alternative to ramp walking *Sheehan & Gottschall* - The Pennsylvania State University
65	Transitioning to the next level: foot position and hip muscle activity during stair walking *Gascon & Gottschall* - The Pennsylvania State University
65	The effect of body weight support on the ankle-foot roll over shape *Morin, Lathrop, Worthen-Chaudhari, Basso, Schmiedeler & Siston* - The Ohio State University

Friday, August 28th, 2009
4:45-6:15 PM

Topic: Methods

***Location*: Assembly Room**

67	Ground reaction force measurements for multi-segment foot models *Bruening, Cooney & Buczek* - Shriners Hospitals for Children, Erie PA
68	Ground reaction force is a temporal predictor of anterior tibial translation during drop landing in healthy adults *Peterson, Krong, Giphart, Steadman, Torry & Shelburne* - Steadman Hawkins Research Foundation
69	Modeling of custom foot orthotics *Trinidad, Krishnamurty & Hamill* - University of Massachusetts Amherst
70	Comparing Cardan rotation angle and finite helical axis representations of talocrural and subtalar in vivo kinematics *Sheehan* - National Institutes of Health
71	The relationship between intravaginal and urethral pressure during voluntary contraction and during coughing in continent women *McLean & Madill* - Queen's University
72	Influence of microstructure on the mechanical properties of vertabral bone assessed by quantitative computed tomography – study on synthetic – model *Levasseur, Ploeg & Petit* - Hôpital du Sacré de Montréal
73	On the appropriateness of estimating intramuscular myoelectric signals from surface electrodes for the rotator cuff *Brookham, Waite & Dickerson* - University of Waterloo
74	Design and development of a dynamic knee simulator for in-vitro knee biomechanics research *Cassidy, Ens & Chandrasheka* - University of Waterloo
75	The effect of lower limb instrumentation on kinetics and kinematics during stair climbing *Beath & Durkin* - University of Waterloo
76	Rethinking maximum voluntary exertion techniques to avoid muscle fatigue while reducing experimental setup time: a shoulder example *Chopp, Fischer & Dickerson* - University of Waterloo
77	Intersegmental dynamics of swing are refined over time to accommodate changes in leg inertia *Smith, Villa, Orpet & Heise* - University of Northern Colorado
78	Vibration platform oscillation characteristics using high speed 3-D motion capture *Branscomb, Smith & Bressel* - Utah State University
79	Characterization of head motion in the MR environment *Andrews-Shigaki, Robinson, Zaitsev, Chang & Ernst* - University of Hawaii at Manoa
80	Partitioning gait data into temporal and intensity differences *Helwig, Hong & Hsiao-Wecksler* - University of Illinois at Urbana-Champaign
81	The validity of different occlusal indicators *Forrester, Pain, Toy & Presswood* - Loughborough University
82	Measuring the propagation of a mechanical wave through soft tissue with a 3D motion capture system *Pérez-Jiménez & Pain* - Loughborough University
83	Piecewise linear approximation to filter force plate signals *Cannella, Mehta & Silfies* - Drexel University
84	Accuracy of optical and electromagnetic tracking systems during dynamic motion *Lugade, Erickson, Fujimoto, Chen, San Juan, Karduna & Chou* - University of Oregon
85	Repeatability of In-vivo motion analysis: optical vs. electromagnetic tracking systems *Chen, Fujimoto, Ewers, Amasay, San Juan, Lugade, Erickson, Chou & Karduna* - University of Oregon

Friday, August 28th, 2009
4:45-6:15 PM

continued Topic: Methods
Location: Assembly Room

86	Influence of pelvis cluster configurations on estimating joint parameters in gait analysis: a pilot Study *Ramanujam, Terry & Forres* - Kessler Foundation Research Center
87	Reliable knee positioning for weight-bearing MRI *Dubowsky, Gade, Allen & Barrance* - Kessler Foundation Research Center
88	Test-retest reliability of in-shoe lateral heel pressure measurements during gait *Leitch, Birmingham, Giffin, Jones & Jenkyn* - University of Western Ontario
89	A device to quantify cyclic compressive loads applied to soft tissue for in-vivo animal models *Cunningham & Butterfield* - University of Kentucky
90	Ankle shock while running on a treadmill: a requisite stride number *Waddell, Brewer & Cappaert* - University of Mississippi
91	Capturing wheelchair propulsion kinematics using inertial sensors *Hooke, Morrow, An & Kaufman* - Mayo Clinic
92	Assessing the fit of constitutive models to experimental stress-strain data *Morrow, Donahue, Odegard & Kaufman* - Mayo Clinic
93	The effects of model degrees of freedom and marker weight on resultant hip kinematics in OpenSim *Thompson, Chaudhari & Siston* - The Ohio State University
94	A combinatorial approach to automated patient-specific finite element meshing *Ramme, Magnotta & Grosland* - The University of Iowa
95	Feature based all hexahedral mesh generation in orthopaedic biomechanics *Shivanna, Tadepalli, Magnotta & Grosland* - The University of Iowa
96	Method for verifying mechanical properties of proximal tibia trabecular bone derived from CT data *Alipit & Racanelli* - Stryker Orthopaedics
97	Repeatability of ankle joint kinematic data at heel strike using the Vicon plug-in gait model *Wright, Seitz, Arnold & Michener* - Virginia Commonwealth University
98	Finite element analysis based design optimization for prosthetic socket *Gao, Wang & Le* - University of Texas Southwestern Medical Center
99	A comparison of shoulder joint angle reduction methods *Oyama, Leigh & Yu* - The University of North Carolina at Chapel Hill
100	A novel portable visuomotor manual reaction time test *Kim, Eckner, Richardson & Ashton-Miller* - University of Michigan
101	Time-lapse microtomography of trabecular bone deformation using flat panel X-Ray sensor *Jirousek* - Academy of Sciences of the Czech Republic
102	Two methods to determine muscle forces and joint contact force: comparison to experimental muscle activity *Richards, Zeni, Jr. & Higginson* - University of Delaware
103	Volitional MVC EMG normalization tasks between days *MacLeod, Chimera, Manal & Buchanan* - University of Delaware
104	Comparison of warm-up periods for treadmill running *Fellin & Davis* - University of Delaware

Friday, August 28th, 2009
4:45-6:15 PM

Topic: Motor Control

Location: Assembly Room

105	Comparison of gleno-humeral kinematics obtained using bone pins and skin mounted markers – a preliminary validation study *Rao, Miana, Lenhoff, Backus, Vanadurongwan, Chen, Brown, Coleman, Cordasco, Altchek, Fealy, Imhauser, Karduna, Warren, Wright, Zifchock & Hillstrom* - New York University
106	Passive sensitivity determines goal-level variability in a shuffleboard task *John, Dingwell & Cusumano* - Pennsylvania State University
107	Stochastic control models explain how humans exploit redundancy to control stepping variability during walking *Dingwell, John & Cusumano* - University of Texas
108	Biomechanics of transport of a fragile object *Gorniak, Zatsiorsky & Latash* - Pennsylvania State University
109	Multi-muscle synergies in a dual task *Klous, dos Santos & Latash* - Pennsylvania State University
110	Temporal effects of galvanic vestibular stimulation on gait as measured by accelerometers *Roche, Steed & Redfern* - University of Pittsburgh
111	Relationships between spastcity of the knee extensors and muscle mass in children with cerebral palsy *Pierce, Prosser, Lee & Lauer* - Widener University
112	Consistent hopping performance through different joint-level strategies *Yen & Chang* - Georgia Tech
113	A theoretical study of the effect of elbow muscle co-contraction level on forearm steadiness *Gordon & Ashton-Miller* - University of Michigan
114	Effect of target size on whole body inter joint synergies: an uncontrolled manifold analysis *Karol & Shim* - University of Maryland
115	Muscle recruitment order in various reaction time tests *Pain, Gu & Hiley* - Loughborough University

Topic: Computational Biomechanics

Location: Faculty Staff Club

118	Mechanical properties of orbital fat and its encapsulating connective tissue *Chen & Wei* - University of Southern California
119	Single level fusion in a C2 cervical spine finite element model *Kallemeyn, Smucker, Fredericks, Shivanna & Grosland* - The University of Iowa
120	An EMG assisted biomechanical model of lumbar spine with passive components *Shu, Burnfield & Mirka* - Madonna Rehabilitation Hospital, Lincoln, NE
121	Arm motion coupling during locomotion-like actions: an experimental study and a dynamic model *Shapkova, Terekhov & Latash* - The Pennsylvania State University
122	Validation of an experimental device simulating the stance phase of a canine hindlimb at trot in the cranial cruciate deficient stifle: an in vitro kinematics study *Lussier, Clément, Jaafar, Petit & Hagemeister* University of Montreal

Friday, August 28th, 2009
4:45-6:15 PM

continued Topic: Computational Biomechanics
Location: Faculty Staff Club

123 Telescoping action improves the fidelity of an inverted pendulum model in diplegic cerebral palsy gait
Buczek, Cooney, Walker, Rainbow & Sanders - National Institute for Occupational Safety & Health, Morgantown WV

124 An EMG driven model to estimate ACL forces during normal walking
Shao, Manal & Buchanan - University of Delaware

125 The study of menisci effect on tibio-femoral kinematics in a computational knee joint
Kia, Guess & Paiva - University of Missouri – Kansas City

126 Integration of vibrotactile feedback in a 3D model of human balance
Ersal, Vichare & Sienko - University of Michigan

127 Biomechanical animations communicate emotion during walking
Wei, Keen, Herzog, Crane & Gross - University of Michigan

128 An analytical approach to evaluating uncemented total hip replacement intraoperative proximal femur fracture risk
Schmidt, Shields, Fuchs, Racanelli & Wang - Stryker Orthopaedics

129 Study of muscle torque sharing patterns in isometric plantar flexion by an EMG-driven biomechanical model
Oliveira & Menegaldo - Federal University of Rio de Janeiro

130 A method to determine whether a musculoskeletal model can resist arbitrary external loadings within a prescribed range *Chu & Hughes* - University of Michigan

131 Uncertainties in tissue mechanical response with increased cell density: microstructural and homogeneous models revisited *Bennetts, Chokhandre & Erdemir* – The Cleveland Clinic

132 Identification of footwear insole material response for optimal reduction of plantar heel pressure
Chokhandre, Erdemir & Cavanagh - The Cleveland Clinic

Topic: Injury
Location: Faculty Staff Club

133 Comparing knee kinematics during gait using biplane fluoroscopy and optical marker-based methods
Krong, Peterson, Giphart, Shelburne & Torry - Steadman-Hawkins Research Foundation

134 Linear head accelerations resulting from short falls onto the occiput in children
Heller, George, Yamaguchi, McGowan & Prange - Exponent Failure Analysis Associates

135 Correlating femoral shape with patellar kinematics to uncover the mechanisms of maltracking in patellofemoral pain *Sheehan, Wilson, Harbaugh & Alter* - National Institutes of Health

136 Severity of head impacts resulting in mild traumatic brain injury
Beckwith, Chu, Crisco, McAllister, Duma, Brolinson & Greenwald - Simbex

137 The relationship between MB loading asymmetry and knee function prior to total knee arhroplasty
Christiansen & Stevens-Lapsley - University of Colorado Denver

138 Injury tolerance criteria for short duration axial loading of the tibia
Quenneville, McLachlin, Fraser & Dunning - The University of Western Ontario

Friday, August 28th, 2009
4:45-6:15 PM

	continued Topic: Injury ***Location***: Faculty Staff Club
139	Anticipatory effects on frontial plane hip kinematics during cutting movements *Mizell, Hass, Siders & Tillman* - University of Florida
140	Theoretical predictions of human upper extremity buckling behavior under impulsive end-loading: effects of gender and extensor muscle stretch behavior *Lee & Ashton-Miller* - University of Michigan
141	Misstepping and hip fractures in the osteoporotic elderly *Uygur, Richards, Jaric, de Freitas & Barlow* - University of Delaware
142	Comparison of functional and isokinetic fatigue protocols: injury research implications *Douex & Kaminsk* - Univeristy of Deleware
143	Patellofemoral joint kinetics during forward step-up, lateral step-up and forward stepdown exercises *Chinkulprasert, Vachalathiti & Powers* - Mahidol University
144	Occupant kinematics in locomotive low-speed impacts *Serina, Peterson, White & Desautels* - Talas Engineering, Inc.

	Topic: Ergonomics ***Location***: Faculty Staff Club
145	Balance control during material handling over a slippery surface *Catena, DiDomenico & Dennerlein* - Harvard School of Public Health
146	Lower body kinematics while walking across a sloped surface *Breloff, Wade & Waddell* - Univerisity of Oregon
147	Endurance time is joint-specific: a modeling and meta-analysis investigation *Avin & Law* – The University of Iowa
148	Safe patient handling: a kinematic analysis of device-assisted versus no versus sit-to-stand motion *McBride, Hueftle, Krause, Buster, Burnfield, Bashford & Taylor* – Madonna Rehabiliation Hospital
149	Fatigue effects on slip risk while wearing fire-protective equipment *Sukits, Montgomery, Kong, Hostler, Suyama, Cham & Chambers* – University of Pittsburgh
150	Upper extremity muscle fatigue that induces muscle imbalances does not increase movement instability *Gates & Dingwell* – University of Texas, Austin
151	Safety margin in ramp torque production task with a circular object *Huang & Shim* – University of Maryland
152	An ergonomic investigation of speed fastening work rates *Gooyers & Stevenson* - Queen's University
153	Comparison of use of backrest and forearm support with a standard workstation and a workstation with a board attachment *El Sagheir & Dumas* - Queen's University
154	Biomechanical evaluation of supported standing with diagonal *Abdoli-Eramaki, Damecour, Ghasempoor & Bouchard* - Ryerson University

Friday, August 28th, 2009
4:45-6:15 PM

continued Topic: Ergonomics

Location: Faculty Staff Club

155	Predicted acceptable load transfer through the ribcage while leaning on the dynamic trunk support *Abdoli-Eramaki, Damecour, Ghasempoor & Bouchard* - Ryerson University
156	The effect of prolonged vibration exposure on the tensile mechanical properties of single layers of the annulus fibrosus *Gregory & Callaghan* - University of Waterloo
157	A comparison of lower extremity fatigue between leather and rubber boots in professional firefighters *Wade, Garten, Breloff & Acevedo* - Auburn University
158	Pressures applied to anatomical landmarks of the knee while kneeling postures *Moore, Porter & Mayton* - National Institute for Occupational Safety & Health, Pittsburgh

Topic: Spine

Location: Faculty Staff Club

159	Using a robotic treadmill trainer to measure changes in rat locomotion following spinal cord injury *Neckel, Dai, Laracy & Bregman* - Georgetown University
160	Sex differences in posture and kinematics of the human head and neck *Zheng, Jahn & Vasavada* - Washington State University
161	An heirarchical viscoelastic ligament failure model *Lucas, Salzar & Bass* - Exponent, Inc.
162	The efficacy of stability ball accommodation training on trunk posture, muscle activation levels and discomfort ratings during seated office *Jackson, Gregory, Banerjee, & Callaghan* - University of Waterloo
163	Use of a geared wheelchair wheel for facilitating manual ramp ascent: effects on trunk muscular demand *Howarth, Polgar, Dickerson & Callaghan* - University of Waterloo
164	Changes in posture do not affect the functional range of motion for the porcine cervical spine under shear loading *Howarth, Gallagher & Callaghan* - University of Waterloo
165	The effects of anterior shear displacement rate on the viscoelastic properties of the porcine cervical spine *Gallagher, Howarth, Callaghan* - University of Waterloo
166	Influence of automobile seat lumbar support prominence on spine and pelvis postures: a radiological investigation *De Carvalho & Callaghan* - University of Waterloo
167	Intervertebral disc biomechanics adjacent to fusion *Ellingson, Mehta, Huelman & Nuckley* - University of Minnesota
168	Effect of technique on knee, hip and L/S net moments in the parallel back squat *King, Hannon & Shoup* - Ithaca College
169	Validity of surface EMG electrode placement for trunk musculature *Mehta, Cannella, Ebaugh & Silfies* - Drexel University
170	Whiplash injury prevention with active head restraint *Ivancic, Sha & Panjab* - Yale University

Friday, August 28th, 2009
4:45-6:15 PM

continued Topic: Spine
Location: Faculty Staff Club

171 Strain in thoracolumbar spine during cyclic loading at two frequencies
Yalla, Campbell-Kyureghyan, Cerrito & Voor – University of Louisville

172 Females exhibit shorter paraspinal reflex latencies than males
Miller, Slota & Madigan - Virginia Tech-Wake Forest SBES

173 Evaluation of lumbar lordosis with and without high-heeled shoes
Russell, Muhlenkamp & Hoiriis - Life University

174 Trunk and leg muscle EMG and perceived exertion during resisted trunk rotation exercise
Marbaugh, Goel, Dick, & Pincivero - The University of Toledo

175 The effect of follower load on lumbar spine facet joint forces and intervertebral disc pressures
Popovich Jr., Welcher, Cholewicki, Tawackoli & Kulig - University of Southern California

176 Differences in wear resulting from perturbations of the ISO standard for total disco replacement
Goreham-Voss & Brown - University of Iowa

177 Cervical laminoplasty construct stability: experimental and finite element investigation
Tadepalli, Gandhi, Fredericks, Smucker, & Grosland - University of Iowa

178 Effect of initial methotrexate concentration on the elution and mechanical properties of vertebroplastic bone cement *Handal, Schulz, Pahys, Williams, Kwok & Samuel* - Albert Einstein Medical Center

179 Fatigability of trunk muscles when simulating pushing movement during treadmill walking
Peng, Lin, Lien & Chiou - Graduate Institute of Rehabilitation Science, Chang Gung University

180 Pelvic and shoulder rotations of idiopathic scoliotic adolescents during walking
Briand, Charbonneau, Labelle & Prince - University of Montreal

181 Relative contributions to disc degeneration progression is higher by degenerative tissue matrix than annular fibers laxity: a finite element analysis in pure compression *Hussain, Gay, An, Triano & Tepe* - Logan University

182 Effect of golf swing styles on resultant joint movements of low body joints and L4/L5
Shin & Hur - University of Illinois at Urbana-Champaign

183 Effect of active head restraint on residual neck instability due to rear impact
Ivancic, Sha, Lawrence & Mo - Yale University

184 Effects of seated whole-body vibration on spinal stability control: stiffness and reflex
Slota & Madigan - Virginia Tech

185 Motion effects of manual manipulations on cervical lateral flexion
Rutledge, Vorro, Gorbis & Bush - Michigan State University

186 Intradiscal pressure changes with posterior lumbar dynamic stabilization systems: universal clamp and walls
Shaw, Ilharreborde, Berglund, Zhao, Gay & An - Mayo Clinic

Friday, August 28th, 2009
4:45-6:15 PM

Topic: Cardiovascular

Location: Faculty Staff Club

187	Biomechanical analysis of dynamic respiratory deficits in axial dystonia *Razzook, Stanley, Drinkard, Alter, Woolstenhulme, Lebiedowska & Damiano* - National Institutes of Health, Bethesda
188	The role of calcium interaction with titin immunoglobulin domain in cardiac muscle *DuVal & Herzog* - University of Calgary

Saturday, August 29th, 2009
8:30-9:45 AM

	Topic: Comparative Evolution ***Chair***: Kiisa Nishikawa ***Student Co-chair*** **Marey Room**	Topic: Muscle ***Chair***: Darryl Thelen **Borelli Room**	Topic: Methods ***Chair***: Kurt Manal ***Student Co-chair*** **Muybridge Room**
8:30	Do humans stabilize running like robots? *Qiao & Jindrich* Arizona State University	Does aponeurosis morphology affect injury susceptibility in skeletal muscle? *Rehorn & Blemker* University of Virginia	A method for quantifying pipette ergonomics *Zhao, Berglund, Blazeski, Tung & An* Mayo Clinic
8:45	Evidence for passive stabilization during single-limb stance in flamingos *Ting & Chang* Emory University & Georgia Institute of Technolog	Series elastic elements limit muscle lengthening rates in eccentric contractions *Roberts & Azizi* Brown University	A method for prediction of seated spinal curvature *Leitkam & Bush* Michigan State University
9.00	Sequential disruption of the crural fascia results in loss of stability during locomotion *Stahl & Nichols* Georgia Institute of Technology & Emory University	Optimization of muscle wrapping objects using simulated annealing *Gatti & Hughes* University of Michigan	A new method designed to quantify sensorimotor integration in the lower extremity *Lyle, Valero-Cuevas & Powers* University of Southern California
9.15	Quantifying human knee anthropometric differences between ethnic groups & gender using shape analysis techniques *Schmidt, Reyes, Fischer, Geesink, Nolte, Racanelli & Reimers* Stryker Orthopaedics	History effects of antagonist coactivation at constant muscle length *Maas & Huijing* Faculteit Bewegingswetenschappen	Dimensional accuracy of an automated ankle foot orthosis fit and manufacturing process *Schrank & Stanhope* University of Delaware
9:30	Hypothesis test and rejection in evolutionary biomechanics: reconstruction of body size (stature and mass) in LB1 from flores Indonesia *Weller, Kuperavage & Eckhardt* The Pennsylvania State University	In-vivo tomographic elastography using skeletal muscle noise *Sabra & Archer* Georgia Institute of Technology	Simulation of gait using a 3d musculoskeletal model *Ackermann & van den Bogert* Cleveland Clinic
	COFFEE AND EXHIBITS **Assembly Room and Faculty Staff Club**		

Saturday, August 29th, 2009
10:00-11:15 AM

	Topic: Sport ***Chair***: Michelle Sabick ***Student Co-chair*** **Marey Room**	**Topic**: Gait and Posture ***Chair***: Kevin Ford **Borelli Room**	**Topic**: Bone ***Chair***: Don Anderson ***Student Co-chair*** **Muybridge Room**
10:00	Upper extremity motion sequence in javelin throwing *Liu, Leigh & Yu* Beijing Sport University	Transfer of dynamic learning across postures *Ahmed & Wolpert* University of Colorado at Boulder	Reduced impact loading following gait retraining over a 6 month period *Davis, Crowell,Fellin & Altman* University of Delaware
10:15	Relationships between selected javelin technique variables & throwing performance *Leigh, Liu & Yu* The University of North Carolina at Chapel Hill	Postural feedback scaling describes the postural abnormality of Parkinsonian patients *Kim, Horak, Carlson-Kuhta & Park* KAIST	Validating the enhanced daily load stimulus model using the bedrest analog of spaceflight *Genc, Humphrey, Rice, Englehaupt, Novotny, Gopalakrishnan, Ilaslan, Licata & Cavanagh* Case Western Reserve University
10:30	The effects of detraining on stabilometric performance in volleyball players *Dai, Sorensen & Gillette* Iowa State University	Postural sway dynamics and falls risk in type 2 diabetes *Morrison, Colberg, Parson & Vinik* Old Dominion University	Mechanical loading causes an acute and temporary decrease in the stiffness of mouse tibiae *Bhatia & Troy* University of Illinois at Chicago
10:45	Gender differences in head impact acceleration in collegiate ice hockey *Brainard, Beckwith, Chu, Crisco, McAllister, Duhaime, Maerlender, Duma, Brolinson & Greenwald* Simbex	Influence of foot-floor friction coefficient on the passive response to slip during walking *Mahboobin, Cham & Piazza* University of Pittsburgh	The role of juxta-articular bony compliance on intra-articular impact stresses *Goreham-Voss, Tochigi, Rudert & Brown* University of Iowa
11:00	Inside/outside force ratio and ski chatter in slalom skiing *Lappi, Reid, Haugen & Smith* Norwegian School of Sport Sciences	Quantifying coordination during recovery from a tripping task *Rosenblatt, Hurt & Grabiner* University of Illinois at Chicago	The geometry of the tibial plateau and tibiofemoral kinematics: a biomechanical analysis *Hashemi, Chandrashekar, Gill, Slauterbeck, Schutt, Dabezies, Mansouri & Beynnon* Texas Tech University
	COFFEE AND EXHIBITS **Assembly Room and Faculty Staff Club**		

Saturday, August 29th, 2009
11:30-12:45 AM

	Topic: Ergonomics ***Chair***: Peter Keir ***Student Co-chair*** **Marey Room**	Topic: Rehabilitation ***Chair***: Margaret Finley **Borelli Room**	Topic: Motor Control ***Chair***: Jae Kun Shim ***Student Co-chair*** **Muybridge Room**
11:30	Transmission of whole body vibration in children while standing *Bressel, Smith & Branscomb* Utah State University	Development of a low cost robotic gait trainer *Bradford & Pidcoe* Virginia Commonwealth University	Sense of effort during single- and multi-finger force production *Gregory* U.S. Military Academy
11:45	Knee positioning influences whole body 3-D vibration transmission *Smith, Bressel, Branscomb & Snyder* Utah State University	Biomechanical asymmetry before and after total knee arthroplasty in subjects with and without back pain *Campbell-Kyureghyan, Burnett, Topp & Quesada* University of Louisville	Sources of two components of variance in multifinger cyclic force production tasks Kariyamaanikam, *Friedman, Zatsiorsky & Latash* Penn State University
12:00	Changes in scapular kinematics pre and post workday *Ettinger, Kincl & Karduna* University of Oregon	Effect of selective muscle weakness on range of motion of glenohumeral joint *Shah, Novotny & Higginson* University of Delaware	Prehension stratigies for grasping objects with complex geometry *Slota, Latash & Zatsiorsky* Pennsylvania State University
12:15	Developing an empirical spatial shoulder muscle activity map *Belbeck, Chow & Dickerson* University of Waterloo	Upper extremity kinetic model of functional arm reaching in stroke *Liu, Rodgers, Waller, Kepple & Whitall* University of Maryland	Simple finger movements require complex coordination of excursions and forces across all muscles *Kutch, Kurse, Hoffmann, Theodorou, Hentz, Leclercq, Fassola & Valero-Cuevas* Southern California
12:30	Biomechanical evaluation & redesign of an accessory unit for exercise in manual wheelchair users *Hofmann & Troy* University of Illinois at Chicago	Reliability of muscle fibre conduction velocity in the tibialis anterior *McIntosh & Gabriel* Brock University	Flexion-withdrawal reflexes in the upper-limb adapt to the position of the limb *Riley, Krepkovich, Mayland, Murray & Perreault* Rehabilitation Institute of Chicago
	LUNCH		

Saturday, August 29th, 2009
Afternoon

2:00	Topic: Borelli Award ***Chair:*** John Challis ***Introduction***: Richard Hughes ***Presentation***: Rodger Kram **Borelli Room**
	James Ashton-Miller (University of Michigan) "The Borelli Lecture"
3:15	**COFFEE BREAK** **Assembly Room and Faculty Staff Club**
3:45	Topic: ISB Sponsored Keynote ***Chair:*** Walter Herzog **Borelli Room**
	Ewald Hennig (University Duisburg-Essen) "Athletic Footwear for Injury Prevention and Performance Enhancement"
4:45	Topic: Awards and Closing Ceremony ***Chair***: Irene Davis **Board Room**
5:30	**ASB Exectutive Meeting**

Keynote Biographies

Keynote - “The Neuromechanical Foundations of Handedness“

Robert Sainburg, is a faculty member at Penn State University with appointments in Kinesiology and Neurology. Bob has been involved in research in motor control for over 20 years, applying biomechanics and employing novel experimental techniques to the analysis of handedness. Bob was trained as an occupational therapist, before obtaining both a masters and doctoral degree from Rutgers University in neuroscience. His training was completed by a three post-doc in neurobiology at Columbia University. Bob held a faculty position at SUNY Buffalo in the Departments of Occupational Therapy, Physical Therapy, Exercise and Nutrition Sciences.

Bob’s specific research interest is the neural mechanisms underlying control of multi-joint arm movements in humans. He combines both psychophysical experiments and biomechanical simulations to determine the neural processes responsible for coordinating the complex mechanics of the musculoskeletal system. Studies in patients with neurological lesions are conducted to determine the contributions of specific neural structures to control.

Bob recently gave the Pattishall Research Lecture, which is delivered each year by the most recent recipient of the Pattishall Outstanding Research Achievement Award. He is the Executive Editor of the Journal of Motor Behavior, and co-director of the Interdisciplinary Graduate Program in Neuroscience at Penn State.

James G. Hay Memorial Lecture - “Ups and downs of the competitive diving”

Doris I. Miller, Professor Emerita, University of Western Ontario, has been actively involved in sports biomechanics research throughout her career focusing upon computer simulation and modeling, lower extremity amputee running and competitive diving. Her assignment as diving coach at the University of Saskatchewan initially peaked her interest in biomechanics and led her to pursue a Ph.D. at Penn State in that specialty. Her doctoral dissertation (1970) involved a 3-D computer simulation and graphic display of dive flight. She has held faculty appointments at the universities of Toronto, Saskatchewan, Washington and Western Ontario. Dr. Miller was involved with USA Diving from 1983 to 2009, providing reports on competition performances, participating in coach education seminars and receiving the Paragon, United States Diving Service and Glenn McCormick Memorial awards. In addition to her publications in peer-reviewed journals, she has given invited presentations at national and international conferences. She has been editor of Exercise and Sport Sciences Reviews, editorial consultant for the Journal of Biomechanics, and on the editorial boards of the Journal of Applied Biomechanics and Sports Biomechanics. She is a Founding Member of ISB, ASB and CSB; a fellow of the American Academy of Kinesiology and Physical Education, ISBS (Dyson Lecturer), CSB (Career Award); Emeritus Member of ASB (6th president) and Honorary Member of ISB.

Keynote Biographies

Keynote – "How do they do it? Specializations of Toads for Extremely Rapid Prey Capture"

Dr. Kiisa Nishikawa is a Regents' Professor in the Department of Biological Sciences at Northern Arizona University. She received her Ph.D. in Zoology from the University of North Carolina. She was a postdoctoral fellow in the Department of Anatomy and Neurobiology at Dalhousie University and a Miller Postdoctoral Fellow in the Museum of Zoology at the University of California at Berkeley. Her research interests include evolution of brain and behavior, biomechanics, muscle contraction, and neuromuscular control of ballistic movements. Twenty years of research in her laboratory has demonstrated that, among vertebrates, toads are uniquely adapted for ballistic prey capture. They achieve movement velocities more than 100 times greater than those of other anurans. In her presentation, Dr. Nishikawa will discuss adaptations of toads that contribute to extreme movement velocities and muscle power output, including anatomical substrates for catch and trigger mechanisms, muscle activation patterns, and muscle physiology.

Borelli Award Winner

James A. Ashton-Miller, Ph.D., is The Albert B. Schultz Collegiate Research Professor and a Distinguished Research Scientist affiliated with the Departments of Mechanical Engineering, Biomedical Engineering, and Internal Medicine, and the Institute of Gerontology, at the University of Michigan, Ann Arbor.

Dr. Ashton-Miller received his BSME from the University of Newcastle-upon-Tyne in England, an MSME from MIT, and a PhD from the University of Oslo, Norway in 1982. After working at the University of Illinois at Chicago he was recruited to the University of Michigan in 1983.

His research has principally addressed the etiology of unintentional injuries in the population, partly because they cost the country billions of dollars in direct and indirect costs each year. This includes research on the etiology of back injuries; neuromuscular aging, balance and falls in the elderly; the pathomechanics of ACL injuries in athletes; and the etiology of birth-related injuries in women.

Professor Ashton-Miller directs the Biomechanics Research Laboratory and is Associate Director of the Bone and Joint Injury Prevention and Rehabilitation Center at the University of Michigan that was started with a $5m donation. He has authored over 170 peer-reviewed papers, 15 book chapters and mentored 23 doctoral theses. He and his students have received over a dozen national and international awards for their research. He has served as a member of several NIH study sections in the field of aging, was elected president of the American Society of Biomechanics in 2001, and in 2008 served as Meeting Chair for the North American Congress of Biomechanics. He consults to the NCAA and a number of Fortune 500 companies.

Keynote Biographies

ISB Sponsored Keynote – “Athletic Footwear for Injury Prevention and Performance Enhancement”

Dr. Ewald Hennig was born, raised, and educated in Germany, studying physics and completing his graduate studies in applied physics at the J. W. Goethe University in Frankfurt. From 1981 to 1984 he worked and studied at the biomechanics department of the Pennsylvania State University and was awarded a Ph.D. degree in 1984. After returning back to Germany he first was an assistant professor at the University of Konstanz and in 1987, he became full professor for biomechanics at the Department of Movement and Sport Sciences of the University Duisburg-Essen.

Dr. Hennig holds several patents for biomedical and biomechanical instrumentation, one of which is licensed to Novel Inc. (Germany) for the manufacturing of pressure distribution devices. His research interests include lower extremity biomechanics, casual and athletic footwear, the role of skin receptors for balance control, obesity problems in adults and children, and diabetic foot studies. He has published over 350 papers, abstracts, and chapters in books.

In his leisure time, Dr. Hennig enjoys reading, hiking, running, biking, and skiing. He also loves travelling and visiting friends in many parts of the world.

For more than 20 years his laboratory has been involved in the testing of running shoes for a government supported consumer agency. A description of the testing procedures, results and the changes in running shoe biomechanics during the last 20 years will be presented in the keynote lecture. Whereas the focus of running shoe research is mainly the reduction of overuse injuries, performance criteria are predominant in the design of soccer shoes. Soccer players prefer light weight but stable shoes, offering adequate traction for explosive movements on the field. His laboratory has been involved for more than ten years in analyzing the modern game of soccer and in the testing of performance aspects of soccer shoes. Results will be presented that soccer shoes designs can help to enhance performance of players by adequate traction and a reduction in shoe weight. Maximum kicking speed and - even more important - kicking accuracy can be influenced by soccer shoe design. The comparison of the prevention and performance perspective shall highlight the importance and value of biomechanical research for better athletic footwear.

PROGRAM OVERVIEW

Wednesday, August 26th 2009

11:00 - 06:00	**Registration and Poster Placement**
12:00 – 04:00	**Lab Tours**
12:00 - 02:00	**Tutorial I**
02:00 – 04:00	**Tutorial II**
04:00 – 06:00	**ASB Executive Meeting**
06:00 – 07:00	**Reception – Hintz Alumni Center**

Thursday, August 27th 2009

07:00-8:00	**Registration and Poster Placement**		
08:00-08:15	**Methods Imaging**	**Aging**	**Upper Extremity**
09:15-09:45	**COFFEE AND EXHIBITS**		
09:45-11:00	**Motor Control**	**Gait**	**Orthopaedics**
11:00-11:30	**COFFEE AND EXHIBITS**		
11:30-12:45	**Sport**	**Muscle**	**Hand**
12:45-02:00	**LUNCH**		
02:00-03:30	**Awards Lectures**		
03:30-03:45	**COFFEE AND EXHIBITS**		
03:45-04:45	**Keynote Lecture by Bob Sainburg**		
04:45-06:15	**Posters and Exhibits**		
06:15-07:15	**Mentoring Roundtable**		

Friday, August 28th 2009

07:00-08:00	**Past Presidents Breakfast + Poster Placement**		
08:00-09:15	**Tendon/Ligament/Cartilage**	**Locomotion Energetics**	**Spine**
09:15-09:45	**COFFEE AND EXHIBITS**		
09:45-11:00	**Knee**	**Muscle**	**Upper Extremity**
11:00-11:30	**COFFEE AND EXHIBITS**		
11:30-12:45	**Computational Biomech.**	**Running**	**Aging**
12:45-02:00	**Lunch**		
02:00-03:15	**Hay Lecture – Doris Miller**		
03:30-03:45	**COFFEE AND EXHIBITS**		
03:45-04:45	**Keynote Lecture by Kiisa Nishikawa**		
04:45-06:15	**Posters and Exhibits**		
06:30-09:00	**Banquet – Beaver Stadium (walk-able, buses will also leave from Nittany Lion Inn)**		

Saturday, August 29th 2009

07:00-08:00	**5K Lab Challenge**		
08:30 -09:45	**Methods Imaging**	**Aging**	**Upper Extremity**
09:45-10:00	**COFFEE**		
10:00-11:15	**Motor Control**	**Gait**	**Orthopaedics**
11:15-11:30	**COFFEE**		
11:30-12:45	**Sport**	**Muscle**	**Hand**
12:45-02:00	**Lunch and ASB Business Meeting**		
02:00-03:15	**Borelli Lecture – James Ashton-Miller**		
03:30-03:45	**COFFEE**		
03:45-04:45	**ISB Sponsored Keynote Lecture by Ewald Hennig**		
04:45-05:30	**Closing Ceremony and Awards Ceremonies**		
05:30-07:00	**ASB Executive Board Meeting**		

ANNUAL MEETING OF THE AMERICAN SOCIETY OF BIOMECHANICS
PENN STATE UNIVERSITY

AGE-RELATED DIFFERENCES IN BALANCE AFTER TASK-SPECIFIC TRAINING

Kathleen A. Bieryla and Michael L. Madigan
Virginia Tech, Blacksburg, VA, USA
email: kbieryla@vt.edu, web: http://www.biomechanics.esm.vt.edu

INTRODUCTION

Falls are a leading source of injury and death in adults over the age of 65 [1]. Numerous exercise interventions have been proposed to help reduce falls in older adults, but do not consistently result in a decrease in falls [2]. This may be due to the fact that the vast majority of these exercises are general in nature and not specifically focused on the motor and sensory skills directly involved in preventing falls. Task-specific training is an alternative intervention approach that may prove beneficial in preventing falls in older adults. However, it is unclear how increased age may influence any beneficial effects from task-specific training.

Based upon this, the main purpose of this study was to investigate how age influences the beneficial effects of task-specific training on balance. It was hypothesized task-specific training would improve balance in both young and older adults, but older adults would experience less improvement and poor retention of these improvements compared to young adults.

METHODS

Six young (mean age 22.8 ± SD 2.6 years) and six older (73.2 ± 2.2 years) adults were recruited to participate in the study from the university population and surrounding community, and informed consent was obtained prior to participation. A single subject experimental design was used where participants served as their own controls using multiple baseline measurements prior to the task-specific training intervention. The experiment consisted of four baseline tests, each separated by one week, four weeks of training, and three follow-up tests up to three months later.

Testing and training were performed on a pneumatic instrumented moving platform (PIMP) (Figure 1). At the start of each test, participants stood on the PIMP relaxed while looking straight ahead. Prior to the first baseline test, each participant's maximum displacement that could be withstood without stepping was determined. Each baseline and follow-up test consisted of six trials using this maximum displacement (including three forward and three backward translations). Training consisted of three sessions per week for four weeks, and 50 trials per session. Throughout the training, the direction of the PIMP was varied randomly and distance traveled of the PIMP was varied based on the participant's performance.

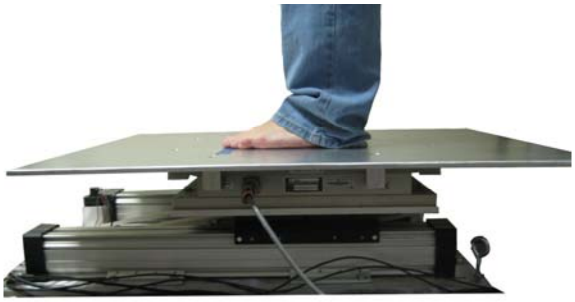

Figure 1: Experimental set-up of the PIMP. The PIMP translated a maximum of 0.15 m forward and 0.25 m backward at an average velocity of 0.45 m/s. A force platform is integrated with the PIMP and used to quantify balance.

During all testing sessions, ground reaction forces were sampled at 1000 Hz from a force platform mounted on the PIMP, and the center of pressure (COP) was determined. Balance was quantified using the time to stabilization of the center of pressure (TTS COP) [2]. TTS COP was defined as the time for the COP velocity to return below a threshold velocity that was common across all participants. This threshold was based upon the mean and standard deviation of COP data prior to PIMP movement from all participants. A two-way mixed-model ANCOVA was conducted on TTS COP with age (young or old) and session (before training, 1 wk. post-training, 1 mo. post-training, 3 mo. post-training) as independent variables, and absolute value of PIMP displacement as a covariate. In the event of an age x session interaction, post hoc Student's *t* tests were conducted. Translation direction did not have an effect on TTS COP, and therefore was not included in the analysis.

RESULTS AND DISCUSSION

TTS COP exhibited a significant age x session interaction (p=0.001) indicating differences in how task-specific training influenced young and older adults (Figure 2).

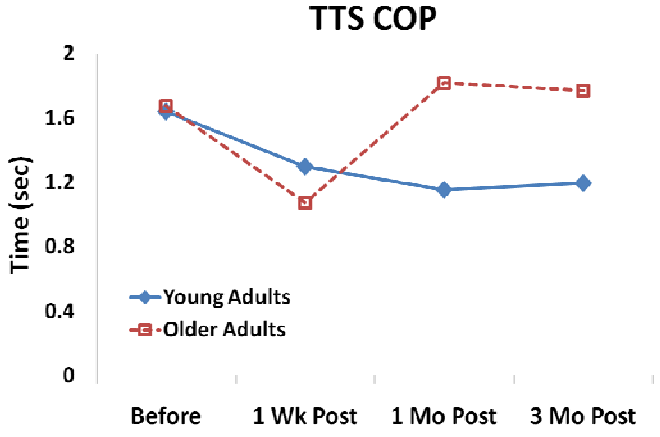

Figure 2: Mean TTS COP values for young and older adults before training, one week, one month, and three months post-training. Solid blue line represents young adults; dotted red line represents older adults.

Both young and older adults decreased their TTS COP after four weeks of training an average of 20.8% and 34.5%, respectively ($p<0.05$). One month post-training, young adults were able to maintain this reduction (mean value was 25.7% lower than before training; $p<0.05$) while older adults were not (mean value was 9.0% higher than before training; $p>0.05$). Three months post-training, young adults maintained improvements from training (mean value was 20.7% lower than before training; $p<0.05$).

Based upon the assumption that decreases in COP TTS correspond to improved balance, our results support the hypothesis that task-specific training would improve balance in both young and older adults. Repeated exposure to a postural perturbation alters sensory information processing [3]. By training participants on the PIMP, improvements in balance were possibly due to accessing stored information obtained due to repeated practice. Pai et al. (2007) also demonstrated older adults have the ability to improve balance recovery skills similar to young adults after a single session of repeated exposures to a simulated slip [4].

While young adults were able to retain the improvements up to three months post-training, older adults were unable to retain the improvements one month post-training. One explanation may be age-related declines in the central nervous system. Improvements in balance after training may involve a shift from longer reflex pathways starting at the spinal cord to shorter reflex pathways in the cortical and subcortical region [3] which older adults were not able to form with four weeks of training.

With the current training protocol, both young and older adult were able to improve their balance with task-specific training, but older adults did not maintain these improvements. This suggests the training protocol used here was sufficient to improve balance in older adults one week later, but not for one month later. As such, more training is likely needed for older adults by either increasing the number of trials performed each day of training, the number of training days per week, or the number of weeks of training.

CONCLUSIONS

An improvement in balance was seen after four weeks of task-specific training in both young and older adults. This improvement was retained for three months in young adults but was not maintained for one month in older adults.

Although the results showed beneficial effects of task-specific training on balance, future studies should determine the optimal training to allow for improvements to be retained in older adults.

REFERENCES

1. CDC. *Web-based Injury Statiscs Query and Reporting System* (WISQARS) [Online] 2007.
2. Lord SR, et al. *J Am Geriatr Soc* **43**, 1198-206, 1995
3. Vearrier LA, et al. *Gait Posture* **22**, 153-163, 2005.
4. Pai YC, et al. *Phys Ther* **87**, 1478-1491, 2007.
5. Pavol MJ, et al. *J Gerontol A Biol Sci Med Sci* **57**, M496-503, 2002.

ACKNOWLEDGEMENTS

KAB was supported by an American Association of University Women Selected Professions Fellowship.

ALTERED 3-D QUADRICEPS MOMENT ARMS IN PATELLOFEMORAL PAIN

Nicole A. Wilson, Abrahm J. Behnam and Frances T. Sheehan
Functional & Applied Biomechanics Section, Rehabilitation Medicine, National Institutes of Health
email: gavellif@cc.nih.gov

INTRODUCTION

Current literature suggests a multifactorial etiology for patellofemoral (PF) pain that is associated with abnormal patellar kinematics (maltracking) [1,2]. However, the factors that initiate the shift from healthy to pathologic knee biomechanics have yet to be determined. Since the patella can move in all six degrees-of-freedom, patellar maltracking can manifest as changes in both patellar orientation (rotation) and displacement (translation). Recent studies have shown that lateral patellar subluxation, patellar flexion, tilt, and negative spin (superior patellar pole rotates medially) are prominent markers of maltracking in PF pain [1,2]. These maltracking changes could be due to a disrupted force balance at the knee, improper muscle activation patterns, or altered PF bone shape. For example, it is commonly hypothesized that weakness and/or delayed activation in the vastus medialis (VM) muscle results in lateral patellar subluxation and tilt [3]. However, unlike PF translations, force imbalance is not necessarily the cause of rotational maltracking patterns. Changes in the quadriceps' moment arms could also result in PF rotational maltracking. Furthermore, moment arm dysfunction has been identified in other pathologies [4]. The purpose of this study was to evaluate the role of the quadriceps' moment arms in PF pain by comparing the relative moments, with respect to the patellar center of mass, of each quadriceps component in healthy knees to those in knees with PF pain and maltracking.

METHODS

Twenty two asymptomatic knees with no prior history of knee problems or pain, and 12 knees with clinically-diagnosed PF pain and maltracking were placed supine in a MR imager (1.5 T, GE Medical Systems, Milwaukee, WI, USA or 3.0 T, Philips Medical Systems, Best, NL) [5]. Kinematics were not significantly different between the two imaging systems. During cyclic knee flexion/extension, and using a 2D sagittal-oblique imaging plane (perpendicular to the femoral epicondylar line and bisecting the patella), a 3-D dynamic cine-phase contrast (PC) MR image set (x,y,z velocity and anatomic images frames) was acquired [5]. Two additional cine-PC sets (Figure 1a) were acquired using coronal-oblique imaging planes (parallel to the quadriceps tendon). Dynamic cine images were also acquired in three axial planes to establish anatomical coordinate systems (Figure 1b). The kinematics of each bone were quantified through integration of the velocity data [5]. All points of interest were visually identified in a single frame of the dynamic images and tracked through the motion

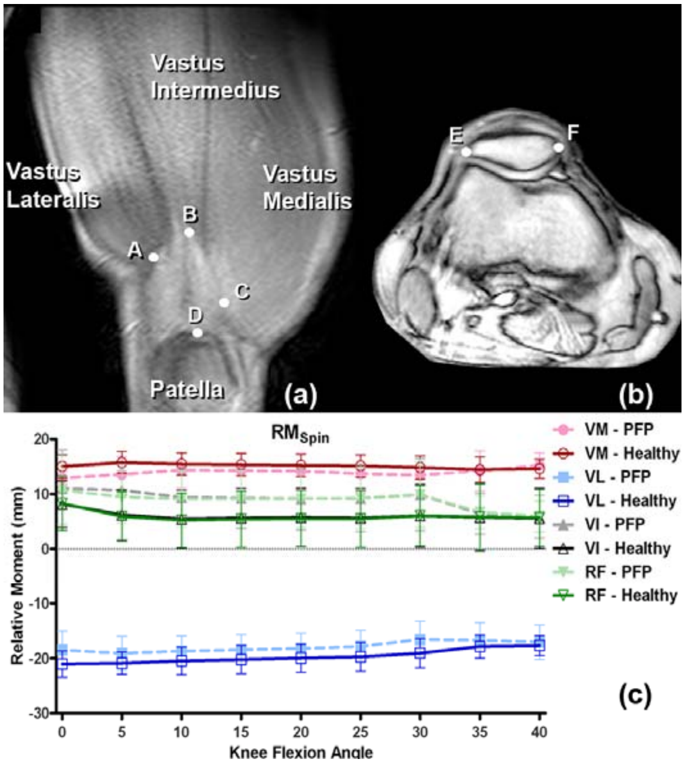

Figure 1: (a) Anatomic coronal-oblique PC image. White dots show the myotendinous junctions of the *(A)* VL; *(B)* VI; and *(C)* VM. *(D)* Represents the patellar insertion of the VI / RF tendon. **(b)** Axial dynamic image at full extension. Insertions of *(E)* VL and *(F)* VM portions of quads tendon on the patella. **(c)** Mean **Relative Moment – RM$_{Spin}$** (positive indicates superior pole rotates laterally) between 0° and 40° knee flexion. Asymptomatic mean: open symbol, solid line. PF pain mean: filled symbol, dashed line. Error bars: standard deviation.

cycle based on each bone's kinematics. For each component of the quadriceps muscle, the myo-tendinous junctions (MTJs) were identified in the first frame of the coronal PC series and tracked in a similar manner. The tendon insertion onto the patella was the midpoint of the most proximal edge of the patella (Figure 1a) for the rectus femoris (RF) and vastus intermedius (VI), and the most lateral and medial patellar points (Figure 1b) for the vastus lateralis (VL) and VM. Tendon lines-of-action were defined as the unit vector between the respective MTJ and the tendon insertion on the patella.

The relative moment (**RM**, 3D vector) represents the coefficients of the muscles in moment equilibrium equations. **RM** was used to assess the contribution of each quadriceps muscle in the three planes of motion. **RM** was defined as the cross product of the tendon line of action and a line connecting the line of action with the patellar center of mass and was composed of: flexion/extension ($\mathbf{RM_{F/E}}$), tilt ($\mathbf{RM_{Tilt}}$) and spin ($\mathbf{RM_{Spin}}$). The moment of each muscle could then be calculated by multiplying scalar force by **RM**. Two-way ANOVA ($\alpha=0.05$) was used to compare **RM**s between groups and Pearson's r was used to identify associations between **RM**s and patellofemoral kinematics.

RESULTS

The VM and VL primarily control patellar spin and tilt (Table 1: both muscles have the largest magnitude **RM** in these directions). $\mathbf{RM_{Spin}}$ and $\mathbf{RM_{Tilt}}$ for the VM and VL are similar in magnitude, but opposite in direction. Patellar flexion is primarily controlled by the VI and RF. In PF pain, **RM**s were altered in every muscle. For example, the absolute magnitude of $\mathbf{RM_{Spin}}$ decreased 9.6% and 8.4% for the VL and VM, respectively (Figure 1c). $\mathbf{RM_{F/E}}$ was highly correlated with patellar extension for all muscles in knees with PF pain ($r \geq 0.90$), but only for the VI and RF in asymptomatic knees ($r \geq 0.91$). For the VL and VM, $\mathbf{RM_{Tilt}}$ was highly correlated with patellar tilt in asymptomatic knees (r = 0.85 and 0.94, respectively), but in knees with PF pain the association was less strong (r = 0.75 and 0.81, respectively). $\mathbf{RM_{Spin}}$ was not correlated with patellar spin in either group.

DISCUSSION

This is the first study to characterize the relative moments of the individual quadriceps *in vivo* in both healthy subjects and subjects with PF pain. While changes in **RM** *were* seen for every muscle in subjects with PF pain, **RM** alterations were not the direct cause of rotational maltracking [1,2]. The changes in the quadriceps moment arms actually opposed maltracking patterns seen in patients with PF pain. Therefore, it is likely that a force imbalance leads to both the translational and rotational kinematic alterations seen in PF pain.

The lack of association between $\mathbf{RM_{Spin}}$ and patellar spin suggests that other factors may control patellar spin (e.g. passive constraint from the femoral sulcus). Whereas, the $\mathbf{RM_{F/E}}$ in patients with PF pain suggests that all muscles are recruited to create a PF extension moment.

The VM plays an important role acting as the antagonist for the VL based on the balance in $\mathbf{RM_{Tilt}}$ and $\mathbf{RM_{Spin}}$. The current results show that in patients with PF pain changes in the **RM** generally increase the VM's capacity to offset the VL. This suggests that kinematic alterations seen in PF pain are coupled with moment arm changes which favor normal PF kinematics. However, VM weakness will limit the ability of the VM to offset the VL (joint moment = force x moment arm) despite moment arm changes favoring normal PF kinematics. Therefore, direct knowledge of the force contributions from each quadriceps muscle is required for complete description of the etiology of patellar maltracking.

REFERENCES

1.Sheehan FT, et al. *J Orthop Res*, 2008 [epub].
2.Wilson NA. *J Bone Joint Surg* **91**, 558-566, 2008.
3.Makhsous M. *Med Sci Sport Ex* **36**, 1768-75, 2004.
4.Gage JR, et al. *J Pediatr Orthop* **10**, 265-274, 2001.
5.Sheehan FT, et al. *J Biomech* **31**, 21-26, 1998

Table 1: Mean (SD) quadriceps relative moments (**RM**) at 10° of knee flexion. Positive directions of motion are patellar flexion, medial tilt, and positive spin. * $p<0.05$, ** $p<0.01$

	VL		**VM**		**VI**		**RF**	
	Healthy	**PF Pain**	**Healthy**	**PF Pain**	**Healthy**	**PF Pain**	**Healthy**	**PF Pain**
$\mathbf{RM_{F/E}}$	0.3 (0.9)	-0.2 (1.3)**	0.3 (0.9)	-0.2 (1.2)**	-5.4 (2.9)	-5.7 (2.4)*	-2.7 (2.8)	-2.5 (2.6)
$\mathbf{RM_{Tilt}}$	-5.8 (2.5)	-5.9 (2.1)	5.0 (2.4)	5.3 (2.4)	0.7 (2.0)	1.9 (1.7)**	0.5 (1.2)	1.3 (1.1)**
$\mathbf{RM_{Spin}}$	-20.5 (2.5)	-18.7 (2.8)**	15.5 (2.0)	14.3 (3.2)**	5.4 (5.3)	9.4 (5.4)**	5.2 (5.0)	9.1 (5.1)**

SENSE OF EFFORT DURING SINGLE- AND MULTI-FINGER FORCE PRODUCTION

Robert Gregory
Center for Physical Development Excellence, U.S. Military Academy, West Point, NY
E-mail: robert.gregory@usma.edu, Web: http://www.usma.edu/dpe

INTRODUCTION

The musculoskeletal system is the physiological entity that allows us to move within our environment. The voluntary muscles drive the system's kinematic behavior. Therefore, a thorough understanding of how these muscles behave is of great importance in analyzing the performance of the musculoskeletal system. Because of this, it is essential to effectively describe the muscular effort expended (or the metabolic cost associated with producing muscle tension) during a wide range of human activities [1].

The concept of muscular effort as it pertains to the biomechanics and motor control of human movement, however, is not clearly defined. In particular, there has been very little research in which effort ratings have been used to investigate the biomechanics and motor control of hand function. While previous studies have examined perception of finger forces during force matching tasks [2,3,4], only one study [5] has been conducted to directly examine the relationship between finger force production and sense of effort. This study compared sense of effort between unilateral and bilateral isometric finger force production tasks; it demonstrated that there was a relatively linear relationship between sense of effort and force production during unilateral and bilateral finger pressing tasks and that effort was increased during bilateral as compared to unilateral tasks.

Because precise force control during skilled manual activities (e.g., writing, grasping) requires an accurate sense of effort, it is necessary to relate judgments of muscular effort to biomechanical quantities. Therefore, the purpose of this study was to investigate sense of effort during unilateral isometric single- and multi-finger force production tasks. It was hypothesized that sense of effort is increased during multi-finger as compared to single-finger force production tasks.

METHODS

Twelve healthy, right-hand dominant individuals (6 males, 6 females) between 20-40 years of age participated in this study.

After undergoing informed consent procedures, all subjects participated in a warm-up protocol that consisted of 5 min of arm cranking exercise on an upper body ergometer and 5 min of hand/wrist stretching exercises. Following a familiarization protocol that involved force production at both submaximal and maximal effort levels, the subjects performed unilateral isometric finger force production tasks using four single (index [I], middle [M], ring [R], or little [L] fingers)- and three multi (I and M fingers; I, M, and R fingers; and, I, M, R, and L fingers)-finger combinations. The subjects produced forces that corresponded to effort levels of 2, 4, 6, 8, and 10 on the OMNI Scale of Perceived Exertion (0 = no effort, 10 = maximal effort) [6] while pressing on force sensors (ELF B201-M; Tekscan, Inc.; South Boston, MA) located on a horizontally-oriented surface in front of the subjects. Each trial was 6 s in duration; the first 3 s allowed the subject to ramp up to the force that corresponded to the specified effort level, and the last 3 s were averaged to calculate a representative force value for the trial. The 35 conditions (7 finger combinations × 5 effort levels) were presented in random order. Each trial was separated by a period of 2 minutes to minimize the effects of fatigue.

The finger force data were collected at a sampling rate of 100 Hz. The data was filtered using a 4th order Butterworth filter with a cutoff frequency of 6 Hz. A two-way within-within subjects factorial ANOVA was used to assess the effects of finger combination and effort level on finger force (absolute and normalized to MVC strength). In addition, the force deficit between the single-finger and multi-finger force production tasks was calculated.

RESULTS AND DISCUSSION

Absolute finger force significantly increased as a function of effort level across all single- and multi-finger pressing tasks ($F_{4,8} = 23.46$, $P<0.0005$; see Table 1). In addition, there was a significant increase in relative finger force as a function of effort level across all single- and multi-finger pressing tasks ($F_{4,8} = 584.94$, $P<0.0001$; see Table 1). However, there was no difference in relative finger force across all effort levels as a function of task ($F_{6,6} = 1.41$; $P=0.34$).

Finger force deficit significantly increased as a function of effort level across all multi-finger pressing tasks ($F_{4,8} = 16.14$; $P<0.001$). The mean force deficits ranged between 5.4-26.4 N, 7.2-54.0 N, and 11.8-70.2 N for the IM, IMR, and IMRL finger combinations, respectively. Also, there was a significant increase in finger force deficit as the number of involved fingers increased across all effort levels ($F_{2,10} = 14.13$; $P<0.001$).

The increase in absolute finger forces and finger force deficit as a function of effort level was to be expected, since increases in force production are accompanied by increases in sense of effort [1,5,6]. However, relative finger force production did not vary as a function of task across all effort levels; this finding was not expected, since sense of effort has been shown to increase as the number of structural units involved in a task increases [2,3].

CONCLUSIONS

There was a relatively linear relationship between sense of effort and finger force production during unilateral single- and multi-finger pressing tasks. In addition, the force deficit during multi-finger pressing tasks increased linearly as a function of effort level. However, the sense of effort did not differ as the number of fingers involved in the pressing task was varied; this was reflected in the finding that there was no difference in the relative finger force across all effort levels as a function of task. By determining the relationship between force and sense of effort (the slope of the function relating force to effort), it should be possible to evaluate changes in effort as a function of movement task conditions. This could be a boon for both basic and clinical research.

REFERENCES

1. Andrews JG. *Med Sci Sports Exerc* **15**, 199-207, 1983.
2. Li S. *Neurosci Lett* **409**, 239-243, 2006.
3. Li S, Leonard CT. *Exp Brain Res* **172**, 301-309, 2006.
4. Park WH, et al. *Exp Brain Res* **182**, 169-177, 2007.
5. Gregory RW. *Med Sci Sports Exerc* **40**, S444, 2008.
6. Robertson RJ. *Perceived Exertion for Practitioners*. Human Kinetics, Champaign, IL, 2004.

Table 1: Absolute and relative forces (mean ± SD) for the one (I, M, R, or L)-, two (I and M)-, three (I, M, and R)-, and four (I, M, R, and L)-finger combinations as a function of effort level.

Finger Combination	Force	Effort Level				
		2	4	6	8	10
I	Abs (N)	8.8±4.8	15.6±5.6	27.4±12.5	35.4±11.7	60.2±15.9
	Rel (% MVC)	13.6±7.8	25.6±12.4	45.8±30.3	59.2±22.0	100.0±0.0
M	Abs (N)	7.0±4.1	13.8±6.2	20.8±6.8	28.4±7.8	43.4±14.4
	Rel (% MVC)	16.4±12.9	30.6±14.6	48.7±16.1	68.7±17.8	100.0±0.0
R	Abs (N)	7.0±3.9	10.4±4.7	19.4±7.2	22.4±9.0	38.6±12.2
	Rel (% MVC)	16.6±9.7	26.1±14.2	50.4±16.0	58.2±23.5	100.0±0.0
L	Abs (N)	4.8±2.7	9.0±4.1	13.2±5.7	21.6±6.5	28.2±9.5
	Rel (% MVC)	17.2±11.6	30.9±17.9	46.2±20.4	79.5±24.3	100.0±0.0
IM	Abs (N)	10.4±4.1	17.8±6.0	28.0±9.9	45.8.2±14.6	77.2±25.4
	Rel (% MVC)	12.9±6.3	23.8±10.0	36.7±15.5	60.1±13.9	100.0±0.0
IMR	Abs (N)	15.6±7.5	22.0±9.3	37.4±14.3	46.2±14.9	88.2±20.9
	Rel (% MVC)	17.1±10.1	23.9±11.2	40.7±16.2	51.7±13.9	100.0±0.0
IMRL	Abs (N)	15.8±7.1	24.2±9.9	41.0±15.0	55.4±15.6	100.2±21.6
	Rel (% MVC)	15.0±7.9	23.5±12.6	40.5±18.6	55.3±14.4	100.0±0.0

LOCOMOTOR TRAINING: THE EFFECTS OF TREADMILL SPEED AND BODY WEIGHT SUPPORT ON LOWER EXTREMITY JOINT KINEMATICS

[1] Rebecca L. Lathrop, [1]Brooke Morin, [1]Lise Worthen-Chaudhari, [1]Ajit M.W. Chaudhari, [1]D. Michele Basso,
[2]James P. Schmiedeler, and [1]Robert A. Siston
[1]The Ohio State University, Columbus, OH, USA, [2]University of Notre Dame, Notre Dame, IN, USA
email: lathrop.16@osu.edu

INTRODUCTION

Body Weight Supported Treadmill Training (BWSTT) is a rehabilitation method that can help individuals with incomplete Spinal Cord Injuries (SCIs) regain the ability to walk. In BWSTT, patients are supported by a harness above a treadmill while therapists provide manual assistance to help approximate normal gait. Recovery of function is achieved by reorganization of neural pathways in the spinal cord, and depends on task-specific rehabilitation. To be effective, BWSTT must simultaneously provide elements of both weight-bearing and rhythmic movements; providing one without the other has been shown ineffective for recovery of walking ability after SCI [1].

Despite the need to replicate normal gait characteristics, techniques for selecting key training parameters, such as treadmill speed and percentage of body weight support (BWS), have not been established. Previous studies (eg. [2]) have explored the effect of BWS on lower extremity kinematics at constant speeds, but not the combined effect of BWS and speed. In this study, we determined the effect of altering treadmill speed and BWS on stance phase duration, peak knee angles, and peak ankle plantar and dorsi flexion angles.

METHODS

We obtained informed consent from four healthy subjects (3 male, 25.25 ± 3.3 y). Subjects performed a ten meter over ground walk to determine self-selected (SS) walking speed. Reflective markers were then placed on their skin using the Point-Cluster Technique [3].

Subjects walked on a split belt instrumented treadmill (Bertec Corp., Columbus, OH) at three speeds (SS, 0.5 x SS, and 1.5 x SS) and four levels of BWS (0%, 30%, 50%, and 70%). Conditions were randomized for each subject. Ground reaction forces were collected at 200 Hz and low-pass filtered with a fifth order Butterworth filter (10 Hz cutoff frequency). Body weight support was provided by a medical harness and a closed-loop pneumatic force control system (Vigor Equipment, Stevensville, MI; Tescom, Elk River, MN). Kinematic gait data were collected using a seven camera VICON motion analysis system (Vicon Mx cameras, Vicon, Inc.).

Kinematic data were processed in Vicon Nexus and OpenSim (Stanford University, Stanford, CA). We determined knee and ankle angles using the inverse kinematics tool in OpenSim, which uses a least squares approach to minimize the difference between experimental marker location and virtual markers on the model while maintaining joint constraints [4].

We determined the effects of BWS and treadmill speed on stance phase duration, knee angle, and ankle angle using a 3 x 4 repeated-measures analysis of variance (ANOVA). Duration of stance was defined as the percent of the gait cycle taken up by stance. Post-hoc tests were performed, using a Bonferroni adjustment for multiple comparisons, for factors that were significantly changed at the $p<0.05$ level. Statistical tests were performed with a statistical software package (SPSS Inc, Chicago, IL).

RESULTS AND DISCUSSION

The repeated measures ANOVA revealed that all variables of interest were significantly affected ($p<0.001$) by increasing BWS at a constant speed, by altering treadmill speed at a constant level of BWS, and by the interaction effect of altering treadmill speed and BWS.

When either speed or BWS increased, the stance duration decreased (Figure 1a). This trend was compounded when both speed and BWS increased together. Mean stance duration for the baseline condition (0% BWS, SS speed) was 61.99% ± 1.18. The mean stance duration for 70% BWS, 1.5 x SS was 48.77% ± 5.10, suggesting that a flight phase occurred for some subjects at this condition. Nine of eleven combinations of BWS and treadmill speed resulted in a significantly different ($p<0.001$) stance duration when compared to the baseline condition.

Maximum knee flexion angles increased with increasing BWS and with increasing treadmill speed (Figure 1b) and were significantly different from the baseline condition in five of the eleven conditions. Hyperextension occurred for some subjects at the 30% BWS condition, but did not occur for any other conditions.

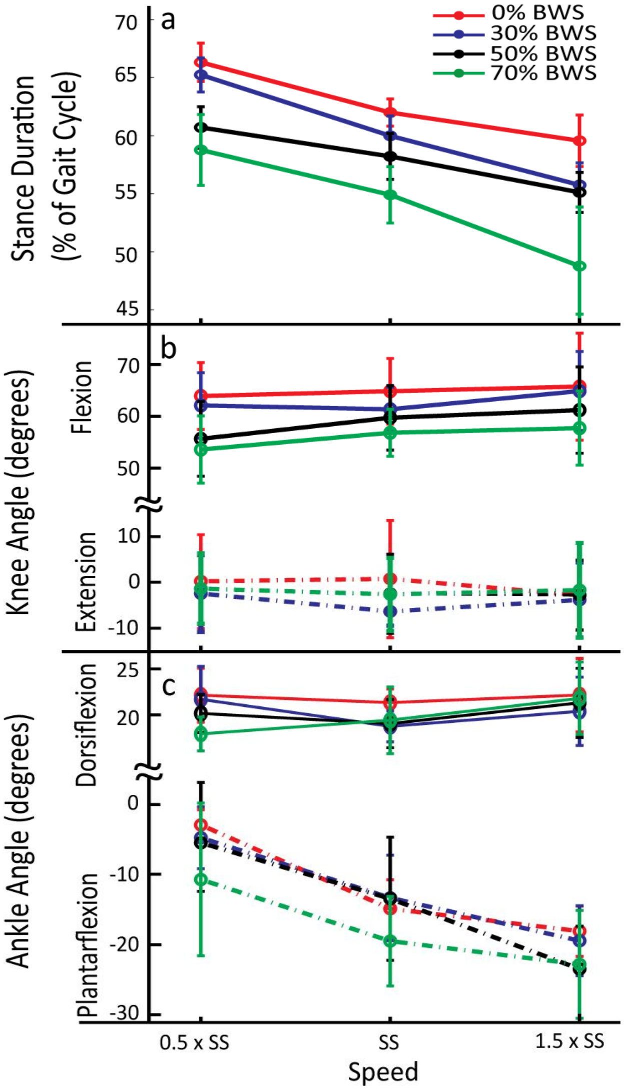

Figure 1: Mean and standard deviations for a) percent of stance, b) maximum and minimum knee flexion angle and c) maximum ankle dorsiflexion and plantarflexion angles at three treadmill speeds and four levels of body weight support.

Ankle plantar flexion experienced larger changes than did ankle dorsiflexion (Figure 1c). Plantar flexion increased in magnitude as treadmill speed increased and also as BWS was applied. Less than a 5^{o} difference was observed for dorsiflexion with the application of BWS over all treadmill speeds. Six of the eleven training conditions produced significantly different peak plantarflexion angles when compared with the baseline condition, but only two training conditions produced significantly different peak dorsiflexion angles.

CONCLUSIONS

Because BWSTT seeks to replicate normal gait, understanding the effects of speed and BWS on kinematics is an important step in selecting training parameters. While we found statistically significant changes in all gait characteristics due to changes in BWS and treadmill speed, it is interesting to note that we observed larger changes in the magnitude of ankle plantar flexion due to changes in speed than changes in BWS. Also, small dorsiflexion angle differences noted across conditions indicate that altering speed and BWS may not significantly influence this motion during locomotion in controls. Additional analysis of ankle motion is required.

In order to optimize BWSTT parameters for functional locomotor recovery, further work is required to investigate biomechanical mechanisms underlying these altered joint kinematics demonstrated during BWS conditions over a range of speeds.

REFERENCES

1. Hutchinson, K.J., et al., *Brain*, 2004. **127**(Pt 6): p. 1403-14.
2. Finch, L., H. Barbeau, and B. Arsenault, *Phys Ther*, 1991. **71**(11): p. 842-55; discussion 855-6.
3. Andriacchi, T.P., et al., *J Biomech Eng*, 1998. **120**(6): p. 743-9.
4. Delp, S.L., et al., *IEEE Trans Biomed Eng*, 2007. **54**(11): p. 1940-50.

CORRELATING FEMORAL SHAPE WITH PATELLAR KINEMATICS TO UNCOVER THE MECHANISMS OF MALTRACKING IN PATELLOFEMORAL PAIN

Frances T. Sheehan, Nicole A. Wilson, Calista M. Harbaugh, Katharine Alter
Functional & Applied Biomechanics Section, Rehabilitation Medicine, National Institutes of Health
email: gavellif@cc.nih.gov

INTRODUCTION

Patellofemoral (PF) pain is widely accepted as one of the most common pathologies involving the knee, yet the etiology of this pain is still an open debate. It is commonly thought that idiopathic pain arises from elevated joint contact stresses due to PF maltracking / malalignment. The latter likely results from imbalanced forces acting on the patella, which may partially arise from pathological femoral shape. However, no studies have explored the relationship between PF shape and kinematics ("tracking") in a population of patients with clinically-diagnosed PF pain and maltracking. Thus, the effects of femoral shape on patellar kinematics are unknown. Therefore, the objective of this study was to correlate PF bone shape and kinematics, based on dividing the patients with PF pain into kinematically distinct subgroups.

METHODS

Two cohorts participated in the IRB-approved study. The first consisted of 30 knees (19 subjects) clinically diagnosed with PF pain and maltracking ("maltrackers"). The second cohort was an asymptomatic population, consisting of 37 knees (28 subjects). No significant differences in demographics existed between cohorts.

For all subjects, two sets of magnetic resonance (MR) images were acquired. The first was a high resolution 3D sagittal gradient recalled echo (GRE) series. The second was a full dynamic image set, including sagittal-oblique fast-PC MR images (x,y,z velocity and anatomic images over 24 time frames) and axial fastcard images (anatomic images only). Subjects cyclically extended/flexed their knee from maximum attainable flexion to full extension and back during all dynamic acquisitions.

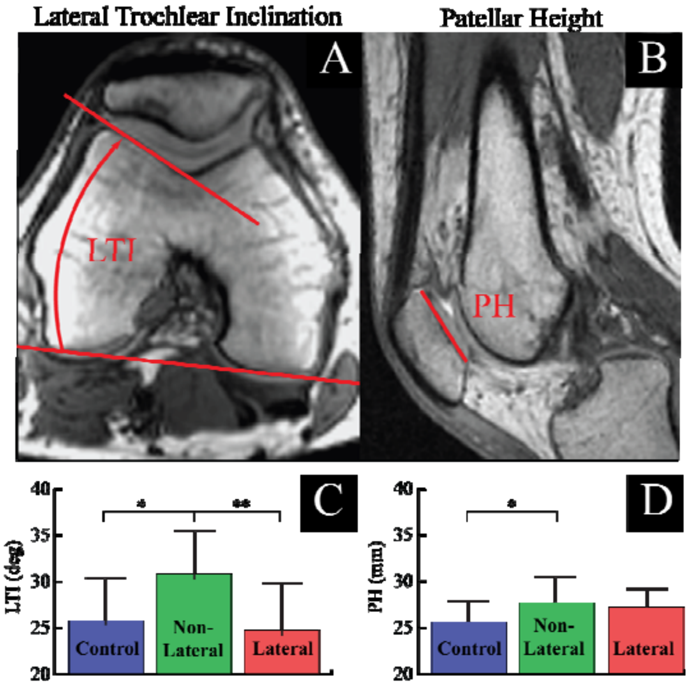

Figure 1: (A) Lateral trochlear inclination angle: the angle between the lateral edge of the femoral sulcus and the posterior edge of the femur at the level of the femoral epicondyles. (B) Patellar height: the length of the posterior edge of the patella at the tallest section of the patella. (C&D) Mean (+SD) of A & B, respectively for all three groups. (* $p<0.05$, ** $p<0.01$)

PF kinematics were defined relative to an anatomical coordinate system (identified in a single time frame, based on the dynamic anatomic images) using 3 translations: medial, superior and anterior and 3 rotations: flexion, medial tilt and varus (positive directions are listed). The kinematics were reduced to two variables: value (the magnitude of each kinematic variable at 10° of knee extension) and slope (the linear best fit of each variable with knee angle) [1]. Subgroups were created by dividing the cohort with PF pain into two groups based on PF medial displacement [2]. Patients with a value of PF placement that was medial of the asymptomatic average (≥ -0.45 mm) with a medial displacement slope ≤ 0.25 mm/° were defined as "non-lateral maltrackers" (n=13). All others were defined as "lateral maltrackers" (n=17).

The sagittal GRE images were aligned based on anatomical references and then an axial image set was created. Eleven measures of PF shape were taken from the 3D GRE sagittal and axial images, but the primary focus of current study was the lateral trochlear inclination angle and patellar height (LTI and PH, Figure 1).

RESULTS

LTI was 20.0% (p=0.008) and 11.3% (p=0.016) greater in non-lateral maltrackers, compared to lateral maltrackers and asymptomatic subjects, respectively (Figure 1). Patellar height was 7.6% greater in non-lateral maltrackers, compared to the asymptomatic population (p=0.020).

Both maltracking groups demonstrated differences in kinematics compared to the asymptomatic average. Non-lateral maltrackers had increased patellar flexion and the lateral maltrackers had increased lateral and superior displacement, increased flexion, lateral tilt and valgus rotation. A moderate correlation between LTI and PF lateral tilt was found for both non-lateral maltrackers (Table 1, r = 0.55) and asymptomatic subjects (r = 0.61). Interestingly, LTI was strongly inversely correlated with superior displacement (r = -0.70) for lateral maltrackers. Patellar height was moderately correlated with superior displacement (r = 0.56) and extension (r = -0.68) for non-lateral maltrackers.

DISCUSSION

A key aspect of this study is that it not only defines differences in femoral shape between populations, it begins to explain potential sources of maltracking by correlating femoral shape with PF kinematics. Specifically, the associations between PF shape and kinematics are different for the lateral and non-lateral maltrackers, indicating a different reliance on the femoral sulcus for restricting patellar motion at or near full extension.

In the lateral maltrackers, lateral patellar tilt and translation were not correlated with femoral shape. This was likely due to the increased PF superior position (patella alta), which removed the patella from the sulcus groove early in terminal extension. Thus, femoral shape was not a controlling factor in terminal extension and soft tissue imbalance dominated PF kinematics. The inverse correlation between LTI and superior patellar displacement in this group potentially arose from the influence of kinematics on femoral shape. Specifically, in the presence of patella alta, the patellar disengaged earlier in terminal extension, which produced less mechanical stress on the proximal femoral sulcus. These lower stresses may have fostered bone remodeling, which resulted in a lower LTI [3]. For the non-lateral maltrackers, the lack of patella alta and larger patellar height allowed the patella to remain engaged with the femoral groove further into terminal extension. Thus, the correlation between LTI and lateral patellar was expected.

The two maltracking subgroups often demonstrated mean values for femoral shape on opposite sides of the asymptomatic mean (Figure 1). Thus, analysis of the maltracking population as a whole would have masked differences found between subgroups. The ability to better categorize patients with PF pain will likely improve treatment by providing a more specific etiology of maltracking in individual patients. Differences in femoral shape may support clinical tool development for predicting maltracking patterns in PF pain without dynamic imaging.

REFERENCES

1. Sheehan FT, et al. *J Orthop Res*, 2008 [epub].
2. Sheehan FT. *Clin Orthop Rel Res*, 2009 [in press].
3. Amis AA. *J Bone Joint Surg* **90**, 864-69, 2008.

Table 1: Pearson's Correlation Coefficients (r) for LTI and PH with PF Kinematics (*p≤0.05 **p≤0.001)

Cohort	Parameter	Displacement			Rotation		
		Medial	Superior	Anterior	Flexion	Medial Tilt	Varus
Non-Lateral	LTI	0.13	-0.32	-0.46	-0.33	**0.55***	0.11
Lateral	LTI	0.26	**-0.70***	-0.22	0.07	0.42	-0.17
Control	LTI	**0.35***	-0.25	0.20	-0.17	**0.61****	0.21
Non-Lateral	PH	0.00	**0.56***	0.09	**-0.69***	0.11	0.48
Lateral	PH	0.31	0.09	0.02	-0.21	-0.13	0.07
Control	PH	0.07	0.27	0.34	0.04	0.16	-0.14

A COMPUTER SIMULATION MODEL FOR PREDICTING OPTIMAL PROSTHESIS INERTIAL PARAMETERS

[1] Marisa Theroux-Jones, [1] Todd Royer, [2] Brian Umberger
[1] University of Delaware, Newark, DE, USA, [2] University of Massachusetts, Amherst, MA, USA
Email: marisatj@udel.edu

INTRODUCTION

Persons with unilateral below-knee amputation face problems both with an asymmetrical gait and a higher energy cost during walking [1]. An asymmetrical gait may lead to deterioration of the knees and lumbar spine [2], and an elevated energy cost can lead to premature fatigue. Current design philosophy is to make prosthetic limbs as lightweight as possible. The considerable difference in mass and moment of inertia that exists between the intact and prosthetic limbs is likely a major cause of gait asymmetry in amputees. Increasing the mass of the prosthesis could improve gait symmetry, but might also increase energy cost. Selles et al. [3] noted theses trade-off in prosthesis design, but did not report an optimal balance between these competing factors.

A simulation model that allows prosthesis inertial properties to be varied could be used as a tool to test the feasibility of restoring gait symmetry to amputees. Such a model could also potentially minimize the amount of trial-and-error testing needed in applying the current results. Therefore, the aim of this study was to utilize a computer simulation model and numerical optimization algorithm to test the feasibility of determining an inertial setup of the prosthetic limb that would restore gait symmetry, without increasing the demands of walking.

METHODS

Lower limb motion during the swing phase of walking was modeled using two rigid segments representing the thigh and combined stump/prosthesis. The hip joint was fixed in space and the two segments articulated at the knee joint. The equations of motion and corresponding Matlab code were generated using Autolev. Initial and final angles and angular velocities for the simulations were obtained from able-boded subjects [2], but the inertial properties of the limb segments were based on amputee subjects [1]. This arrangement allowed us to test whether the inertial properties of the prosthesis could be varied to restore normal gait symmetry, while also keeping the effort required to swing the leg low.

A simulated annealing optimization algorithm was used to determine the amount of mass that should be added to the prosthetic limb, and the location below the knee at which this mass should be added, to restore normal gait symmetry. The added mass was limited (0.0-1.7 kg) so that the prosthesis and stump mass would not exceed that of the intact limb, and the location of the added mass was limited to between the knee joint and the bottom of the foot. In addition to optimizing the mass magnitude and location, the hip and knee joint torques were optimized, using the able-boded values [2] for the initial guess. Thus, the optimization problem was to find the added mass magnitude and location, as well as the hip and knee joint torques, that matched the final joint angles and angular velocities, while requiring the least effort. The effort required to swing the limb, used as a proxy for energy cost, was quantified as

$$effort = \int_{t_o}^{t_f} \sqrt{T_H^{\ 2} + T_K^{\ 2}}\, dt$$

where t_o is the initial time, t_f is the final time of the swing phase, T_H is the hip torque, and T_K is the knee torque.

RESULTS AND DISCUSSION

The optimal arrangement predicted by the simulation model was to add a mass of 0.91 kg at a location of 0.28 m below the knee (i.e. below the midpoint of the shank). This added mass represents slightly greater than half of the maximum amount of mass that could be added to the prosthesis in the optimization framework. Thus, the total mass of the prosthetic limb (4.13 kg) was still lighter than the intact limb (4.91 kg). The amount of added mass and its location shift the center of mass of the entire shank segment more distally, from 0.16 m to 0.19 m below the knee joint, and increased the moment of inertia of the shank from 0.18 kg-m^2 to 0.25 kg-m^2. The optimized values are closer to the center of mass and moment of inertia for the intact limb, 0.25 m and 0.42 kg-m^2, respectively.

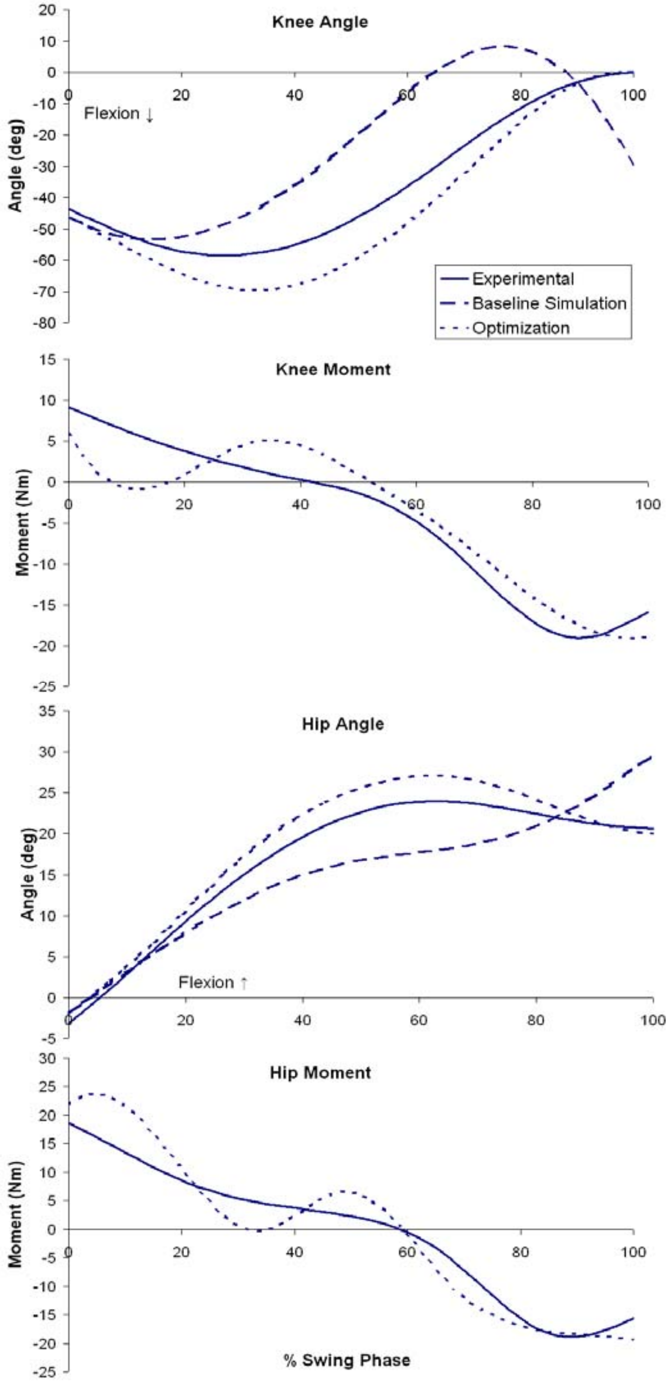

Figure 1: Graph of hip and knee angles and moments showing experimental data from a normal subject, baseline simulation results with no added mass, and optimization results with the added mass

In Figure 1, the baseline simulation without any added mass shows that the inertial characteristics of the prosthesis resulted in substantially different movements of the leg, compared to the experimental condition. Following the optimization, gait symmetry was restored and the kinematics were in good agreement with the experimental data. This was accomplished with a cost that was lower (effort = 88.2) than the value obtained from the data in able-bodied subjects [2] (effort = 104.7), indicating that near-normal leg swing can be restored, without increasing the demands of swinging the limb.

The model predictions are to increases both the mass and moment of inertia of the prosthesis, but not so much that they match the values for the intact limb. The resulting motion is returned to normal, and therefore both the effort and asymmetry are reduced by increasing moment of inertia. While this optimization suggests the optimal prosthesis set-up would be lighter than an intact limb, it still would require adding nearly 1 kg to the mass of current designs. According to prosthesis technicians and amputee patients [1], however, adding mass to a prosthetic leg is undesirable. The suggestion of adding a significant amount of mass to the leg will probably be met with great scepticism. However, it may be possible to obtain nearly as good results by placing less mass at a greater distance from the knee joint, which might be viewed more favourably.

The follow-up to this study will be empirical testing of the predictions made by the simulation model. Improvements in the model may also be called for, as a number of simplifications are currently involved. The present results may not revolutionize lower limb prosthesis designs, however, they do call for the careful consideration of mass and mass distribution to aid in the restoration of gait symmetry.

REFERENCES

1. Mattes SJ, et al. *Arch Phys Med Rehabil*, **81**, 561-568, 2000.
2. Sanderson DJ, et al. *Gait and Posture*, **6**, 126-136, 1996.
3. Selles RW, et al. *Arch Phys Med Rehabil*, **84**, 569-577, 2003.

IN-VIVO TOMOGRAPHIC ELASTOGRAPHY USING SKELETAL MUSCLE NOISE

Karim G. Sabra, Akibi Archer
email: karim.sabra@me.gatech.edu

INTRODUCTION

Measuring the in-vivo viscoelatic properties of skeletal muscles allows for objectively monitoring human motor functions. Elastography techniques have been developed to estimate the viscoelastic properties (e.g. muscle stiffnesss) of skeletal muscles by measuring the velocity *c* (m/s) and attenuation of low-frequency mechanical vibrations (e.g. shear waves) propagating along the tested muscles [1]. These mechanical vibrations are typically generated using an external mechanical (e.g. vibration probe) or radiation source (e.g focused ultrasonic beams). However low frequency vibrations (<100Hz), also called muscle noise, are naturally generated during voluntary contractions by the skeletal muscles themselves due to synchronous dimensional changes of the muscle fibers and overall change of the muscle-tendon geometry [2]. Recordings of these vibrations, e.g. using skin-mounted accelerometers (Fig. 1.a-b) are called surface mechanomyograms (S-MMG). A low-cost and non-invasive passive elastography technique was developed to estimate the stiffness of skeletal muscles by computing the cross-correlations of S-MMGs recorded between a pair of sensor (Fig 1.c) in order to estimate the propagation velocity *c* of the natural mechanical vibrations along the muscle, thus without requiring an external mechanical or radiation excitation. Moreover, when using an array of skin-mounted sensors overlaying the muscle (Fig 1.a), passive elastography can provide simultaneous measurements of the muscle's viscoelastic response between several sensor pairs (Fig 1.c), similarly to a CT scan. The purpose of this project is to construct in-vivo tomographic measurements of the stiffness's variations along the biceps brachii's axis during isometric elbow flexions using passive elastography (Fig 1.d).

METHODS

Four healthy male subjects underwent testing that involved performing two series of four 5s long isometric contractions at 20%, 40%, 60%, 80% of the maximimum voluntary contraction (MVC) level using the Biodex System 3, level. The subject's arm was placed horizontally in a 90 degrees supinated flexion position and was immobilized using a supporting stand to minimize motion artifacts. S-

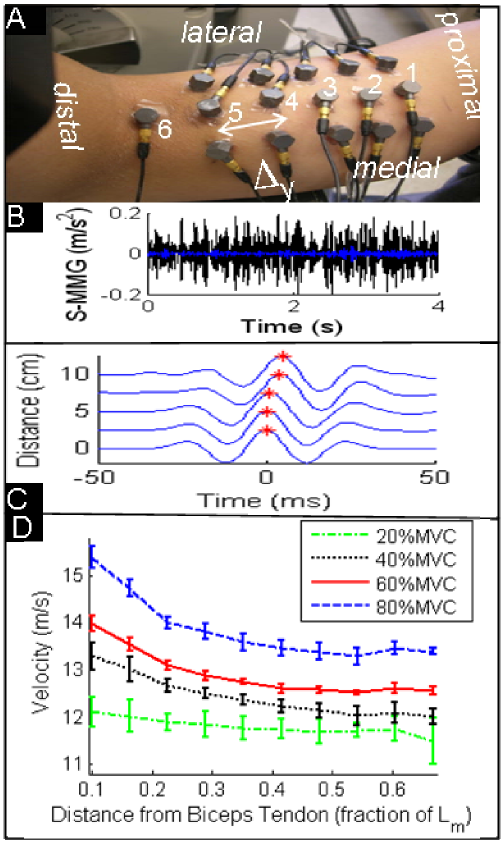

Figure 1: **A**) Experimental set-up for isometric biceps contraction. Accelerometers #1-#6 are located along the biceps axis. **B**) Surface mechanomyogram recording at 60%MVC (black line) contraction level and at rest (blue line) on accelerometer #1. **C**) Examples of stacked normalized cross-correlation time functions for increasing sensor separation distance between accelerometer #1-#5, using accelerometer #1 as a reference (see Eq. 1). **D)** Variations of the longitudinal propagation velocity of S-MMG along the biceps brachii, obtained from passive elastography, during isometric elbow flexion from 20% to 80% MVC for one subject. The longitudinal distance (horizontal axis) is measured from the distal biceps tendon and normalized by the estimated length L_m of the biceps brachii long head muscle

MMG were recorded (10kHz sample rate) over the biceps brachii muscle using an array of miniature skin-mounted single-axis accelerometers (weight=2g, diameter=1cm, sensitivity=100 mV/g) aligned along the biceps axis. The longitudinal grid spacing Δ_y (Fig 1.a) was determined as 13% (±4%) of the estimated length (L_m=17.6cm±2.7cm, N=4) of the biceps brachii long head muscle of each subject [4] so that the sensor grid covered the region between 7% and 70% of L_m where the coordinate origin is set at the distal end (0% of L_m). Following the procedure described in Sabra et al. (2007b), S-MMG were then filtered in the high-frequency band B=[25-65Hz] to minimize the effects of motion artifacts and force tremor (Fig 1.b) [2]. Since high-frequency S-MMG (f>25Hz) are dominated by local muscle fiber activity [2], they were found to propagate predominantly along the biceps axis likely due to the fusiform architectural organization of muscle fibers. Hence the cross-correlation time function of the S-MMG records was only computed between all pairwise combination of the sensors #1 to #6 located directly above the main axis (Fig 1.a) in order to determine the inter-sensor travel time as defined by the peak maximum (see red cross on Fig 1.c) [3]. Assuming that the muscle tissues are locally homogenous and given the know sensor spacing, all these travel-times measurements were used to invert for the local velocity of natural mechanical vibrations using a standard travel-time tomography inversion scheme for straight paths.

RESULTS AND DISCUSSION

Figure 1.d displays typical variations, for one subject, of the estimated longitudinal velocity profile $c(d)$ of the coherent S-MMG along the biceps axis as obtained from travel-times tomography for increasing contraction levels. The longitudinal distance d from the distal biceps tendon was normalized by the estimated length (L_m) of the biceps brachii long head muscle to ease inter-subject comparisons. First, a linear relationship was recovered between the mean value of the estimated muscle stiffness (proportional to c^2 [1]) computed in the muscle belly's region ($0.4L_m < d < 0.65L_m$) over all subjects, and the contraction level (%MVC) such that $< c^2 >= a\ MVC + b$, where a=0.59, b=123 (determination coefficient R^2= 0.986, P<0.01). Second, the estimated local velocity in the distal region of the biceps brachii ($d<0.2L_m$) was found to be significantly higher (P<0.01) than in the proximal region ($d> 0.5L_m$), especially at higher contraction level (e.g. by up to 15% at 80%MVC) thus indicating a non-uniform stiffening of the biceps during isometric elbow flexion.

These measurements of biceps stiffness (proportional to c^2 [1]) obtained from passive elastography are strongly correlated with the produced torque output during isometric contractions and in quantitative agreement with results from previous active elastography experiments on the biceps during similar efforts [1]. Furthermore the non-uniform stiffening of the biceps during isometric elbow flexion likely results from the presence of an internal aponeurosis spanning the distal third of the longitudinal axis of the biceps, and which is known to be structurally similar to tendons and ligaments is thus stiffer (i.e., less compliant) than muscle fibers [4].

CONCLUSIONS

The passive elastography results demonstrate that the local viscoelastic properties of skeletal muscles can be estimated from their natural vibrations generated during voluntary contraction. Furthermore, using a multichannel sensor array, passive elastography allows to easily construct tomographic profiles of muscle stiffness, while conventional active elastography techniques would require a large number of vibration sources or repeated measurements to do so. Finally, the development of passive elastography could lead to simpler, low-cost and objective monitoring of physical therapy treatments for the rehabilitation of neuromuscular disorders such as muscle spasticity

REFERENCES

1.Greenleaf J.F. et al. (2003), *Ann. Rev. of Bio.* Eng. 5: 57-78.

2. Orizio C.(1993). *Crit. Rev. Bio. Eng.* 21:201-243.

3.Sabra et al. (2007). *App. Phys. Lett.* 90:L07-01965R

4.Papas et al. (2002). *J. of App. Physio.* 92:2381-2389.

KINEMATIC ADAPTATIONS OF THE FOORFOOT AND HINDFOOT DURING CROSS-SLOPE WALKING

Mohsen Damavandi, Phil Dixon and David Pearsall
Department of Kinesiology and Physical Education
McGill University, Montreal, QC, Canada,
email: david.pearsall@mcgill.ca, web: http://www.mcgill.ca/edu-kpe/

INTRODUCTION

Biomechanics research in gait has focused largely on level walking, with less attention paid to transversely inclined (cross-sloped) surfaces [1–3]. Despite cross-slopes being a regular feature of our environment, little is known about specific inter-segmental foot adaptations necessary to maintain both balance and forward locomotion.

Substantial left to right asymmetrical changes in the kinematics and kinetics of the hip, knee and ankle joints have been recently reported [4], even with modest cross-slopes angles. While for young adults cross-slope may not be a significant challenge, the asymmetrical demands of cross-slope walking could pose great functional muscular-skeletal and balance obstacles for special populations (elderly, amputees, *etc*). From the above study, it is hypothesized that forefoot-hindfoot (FF-HF) kinematics also will be different between level and cross-slope walking.

METHODS

Ten healthy adult males with no previous orthopedic ailment participated in the study. Participants were fitted with 39 reflective markers placed over bony landmarks according to the Oxford Foot Model [5] (Figure 1). A 7m inclinable walkway with an embedded force plate (AMTI, model OR6-5-1000, Watertown, MA, USA) was used. Participants were habituated to the walkway area and then performed a minimum of six self-selected speed walking trials on the flat (0º) and inclined (10º) conditions. Kinematic adaptations of FF-HF were compared between level walking (LW), up-slope inclined walking (IWU), and down-slope inclined walking (IWD) for the right foot only. Kinematic data were collected at 240 Hz using an eight camera Vicon^{TM} system (Vicon, Los Angele, USA). The data were filtered with a fourth-order zero-phase lag Butterworth filter having a cutoff frequency of 8 Hz in MatLab® (v2008b, The Mathworks Inc., Natick, MA, USA).

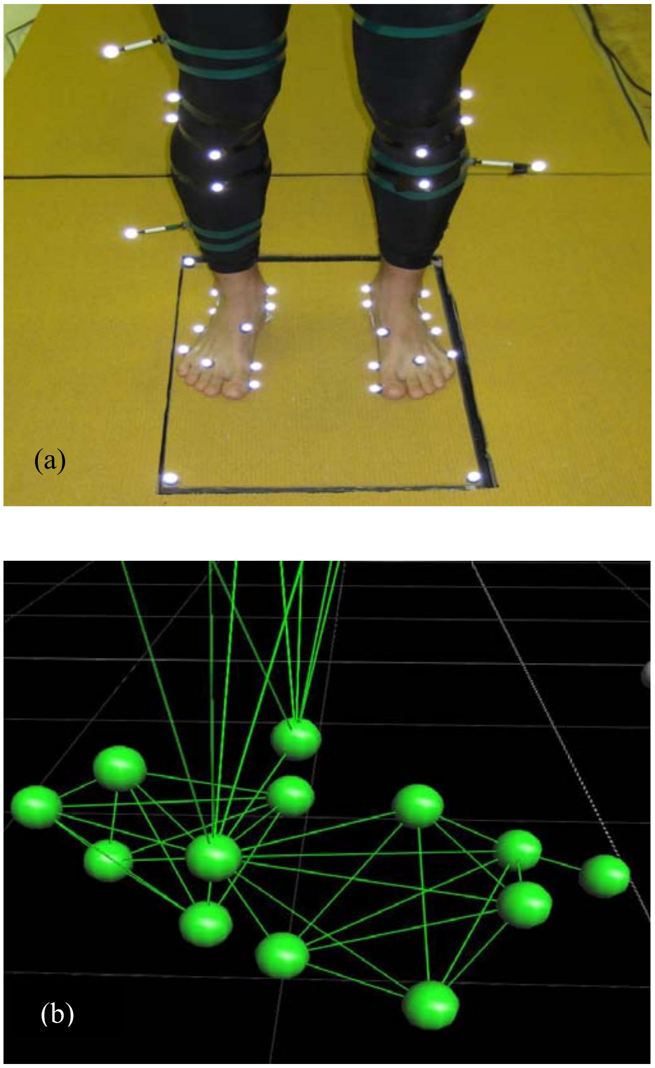

Figure 1: Anterior view (a) of marker placement based on Oxford Foot Model. Lateral view (b) of right foot rendered in Vicon environment.

For statistical analysis of the motion patterns of the FF and HF, the stance phase was evaluated at three events determined from the vertical ground reaction force (GRF). The events were taken at the first and second maximum GRF values (MaxFz1 and MaxFz2, respectively) and at the minimum GRF between them (MinFz). The three-dimensional (3D) kinematics of FF-HF were analyzed using a between subject MANOVA for repeated measures using SPSS^{TM} (SPSS for Windows, version 16.0). This was followed by a Bonferroni post-hoc test if a statistical difference was observed ($\alpha = 0.05$).

RESULTS AND DISCUSSION

The abduction/adduction of FF with respect to HF was significantly different at MaxFz2 and MinFz ($p < 0.001$ and $p = 0.005$, respectively) (Figure 2). For MaxFz2, post-hoc analysis revealed differences between LW and both slope conditions (IWU, $p = 0.043$; IWD, $p = 0.004$), and between IWU and IWD ($p = 0.000$). For MinFz, differences were observed between IWD and the two other conditions (IWU, $p = 0.006$; LW, $p = 0.041$).

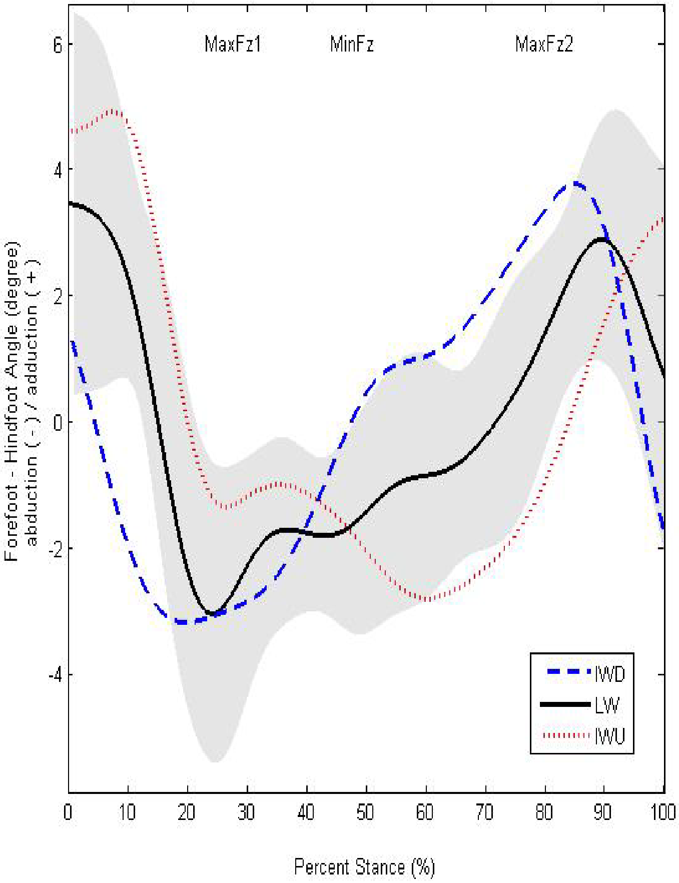

Figure 2: Overall mean trials of forefoot-hindfoot abduction/adduction in flat and inclined conditions. Gray area indicates the standard deviation of level walking trials.

FF-HF kinematics during level walking has been reported in previous studies [6]. This study shows that compared to horizontal walking, cross-slope walking requires adaptations of the FF-HF. In general, results suggest that subjects modified their transverse plane kinematics in order to minimize and conform to the ground height difference between the LW, IWU and IWD foot induced by the cross-slope.

CONCLUSIONS

The mechanisms by which the body enables cross-slope walking, specifically in order to prevent slipping, can be seen in the alteration of the FF-HF kinematics. Variations in the relative motions of the foot segments need to be considered in the design of lower limb prostheses and in orthopaedic and neurological rehabilitation.

REFERENCES

1. DeGarie L and Pearsall DJ. *Proceedings of the XIth Congress of the Canadian Society for Biomechanics*, Montreal, 111, 2000.
2. Nicolaou et al. *Proceedings CD of the IVth World Congress for Biomechanics*, Calgary, Canada, 2002.
3. Pearsall DJ, et al. *International Society for Posture & Gait Research*, Burlington, Vermont, 2007.
4. Dixon CD and Pearsall DJ. *J Appl Biomech*, in press.
5. Carson MC, et al. *J Biomech* **34**, 1299-1307, 2001.
6. Chang R, et al. *J Biomech* **41**, 3101-3105, 2008.

Emotional Influences on the Center of Pressure Trajectory during Gait Initiation

Jessica Joyner, Kelly Gamble, Kim Fournier, Chris J. Hass, and Christopher Janelle
Department of Kinesiology and Applied Physiology, University of Florida
Email: kmgamble@hhp.ufl.edu, Web: http://www.hhp.ufl.edu/apk/ces/affil/pp/index.php
Web: http://www.hhp.ufl.edu/apk/ces/affil/nm/index.php

INTRODUCTION

A growing body of literature supports the long held notion that human emotion and motor actions are largely intertwined. In general unpleasant emotions prime avoidance behaviors, whereas pleasant emotions prime approach behaviors [1]. Additionally, research has shown that emotions modulate the force and speed of single joint hand and arm movements [2, 3]. However, important questions remain concerning how emotion influences whole body movements, such as gait initiation.

The purpose of the current study was to determine the impact of emotional state on the preparatory phase (center of pressure (COP) displacements and velocities) of gait initiation in healthy young adults. Given that gait initiation in our experimental task was an approach behavior, we hypothesized that exposure to pleasant pictures would facilitate gait initiation as indexed by increased displacement and velocity of the COP trace in effort to propel the person in the forward direction when moving toward the projected image. Conversely, exposure to unpleasant pictures, which prime avoidance behaviors and hinder approach-related behavior, should impede gait initiation as indexed by reduced COP displacement and velocity.

METHODS

Fifteen females (age = 20.53 ± 1.69 years), free of any lower extremity injuries, participated in this study. Participants completed two practice trials and 20 gait initiation trials. As is common in the affective sciences, pictures selected from the International Affective Picture System (IAPS) were used to manipulate emotional states during each gait trial. The IAPS provides standardized emotional stimuli, and serves as a worldwide measurement standard for the study of emotion [4]. Presented stimuli included 15 digitized photographs including 5 unpleasant (attacking people), 5 pleasant (erotic couples) and 5 neutral (neutral faces) pictures. Five trials were completed with no picture (blank) as a control condition. Pictures (36 x 50 cm) were presented on a 2m x 1.5m screen located 6 m in front of participants. See Figure 1 for experimental set-up. Each trial began with the presentation of a fixation cross on the video screen for 2 s, which was replaced by an IAPS image for 2-4s. Participants were instructed to look at the picture for the entire time it was on the screen. Participants immediately initiated walking with their preferred limb at picture offset and continued walking for several steps at their self-selected pace. Magnitude and velocity of the COP displacement in the mediolateral (ML) and anteroposterior (AP) directions during the 3 periods of the COP trace (S1, S2, S3) were compared across picture type.

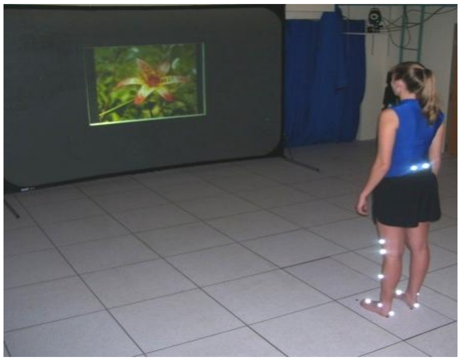

Figure 1. Experimental setup. Location of screen relative to participants' initial start position for each trial.

RESULTS AND DISCUSSION

Three separate multivariate analysis of variances (MANOVA) were conducted to determine the effect of valence (pleasant, unpleasant, neutral, blank) on the dependent variables during the 3 COP trace periods. The MANOVA revealed a significant effect of valence (*p* = .002) for the variables in the S1 region of the COP curve. Analysis of variance (ANOVA) was conducted on each dependent variable as a follow-up test. Valence category differences were significant for AP COP displacement (*p* = .05), AP COP velocity (*p* = .007), and ML COP velocity (*p* = .05). The Bonferroni post hoc analysis revealed a significant reduction in the AP COP displacement following exposure to the unpleasant pictures relative to the pleasant pictures and control condition (See Figure 2). A significant reduction in the AP COP velocity was also observed following exposure to unpleasant pictures relative to all other conditions (See Figure 3). Finally, the ML COP velocity was significantly reduced following exposure to unpleasant relative to the neutral pictures (See Figure 4). No significant differences were found in the S2 or S3 region of the COP trace.

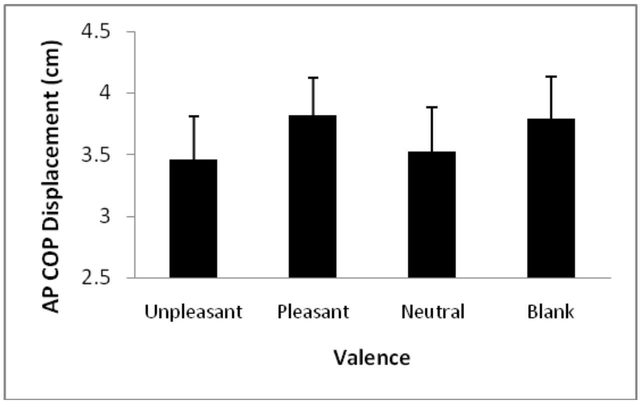

Figure 2: AP COP displacement during the S1 phase of gait initiation

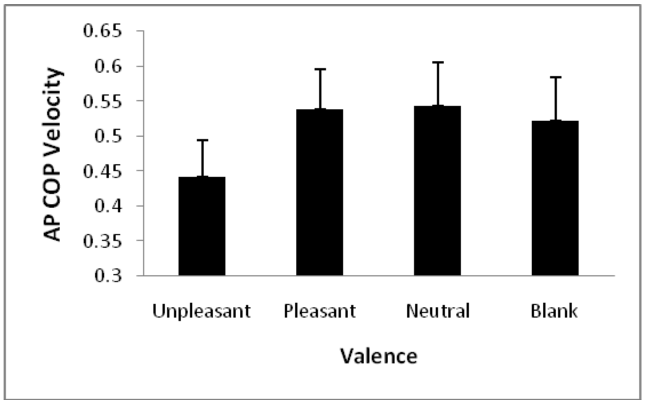

Figure 3: AP COP velocity during the S1 phase of gait initiation

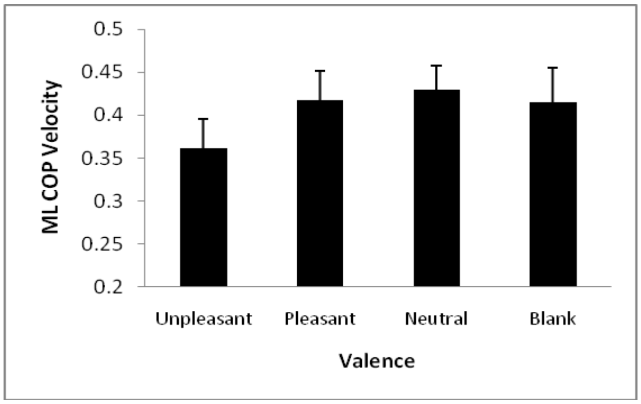

Figure 4: ML COP velocity during the S1 phase of gait initiation

As hypothesized, exposure to unpleasant emotional pictures impeded participants' initiation of gait. Backward movement of the COP trace (i.e., anteroposterior direction) during S1 produces the forward momentum required to initiate gait. As such, these data provided seminal evidence that the induction of unpleasant emotion both diminishes and slows the backward COP movement needed for efficient gait initiation. Contrary to prediction, the exposure to pleasant pictures did not facilitate gait initiation relative to the neutral pictures and control condition.

CONCLUSION

In conclusion, our findings permit strong inference that emotional state systematically modulates whole body movements, such as gait initiation. Additionally, the data indicate that unpleasant affective states (i.e., threat) can interfere with efficient gait initiation, having important implications for populations with postural and gait difficulties. Implications and future directions are discussed.

REFERENCES

1. Chen M and Bargh JA. *Personality and Social Psychology Bulletin* **25**, 215-224, 1999.
2. Coombes SA, et al. *Emotion* **7**, 275-284, 2007.
3. Coombes SA, et al. *Emotion* **8**, 104-113, 2008.
4. Lang PJ, et al. *International affective picture system (IAPS): Instruction manual and affective ratings* (Tech. Rep. No. A-6). University of Florida, Gainesville, FL.

RELIABLE KNEE POSITIONING FOR WEIGHT-BEARING MRI SCANS

[1, 2] Sarah R. Dubowsky, Ph.D., [2] Venkata Gade, M.S., [2] Jerome Allen, M.S., [1, 2] Peter J. Barrance, Ph.D.
[1] University of Medicine & Dentistry of New Jersey/New Jersey Medical School, Newark, NJ, [2] Rehabilitation Engineering Analysis Laboratory, Kessler Foundation Research Center, West Orange, NJ
email: sdubowsky@kesslerfoundation.net; web: http://www.kmrrec.org/rehabengineering/

INTRODUCTION

Osteoarthritis (OA), characterized by progressive joint degradation, is a debilitating disease that results in pain, stiffness, and lack of mobility. The knee is the most common site for the development of OA, and local biomechanical risk factors such as an anterior cruciate ligament tear may be linked to the initiation and progression of OA by resulting loading changes on the tibiofemoral plateau.

To quantify changes in positioning at the knee *in-vivo*, consistent knee flexion over multiple scans, as well as minimization of motion during scanning, become crucial. We have developed a system that uses an MRI compatible knee angle sensor (ShapeSensorMRI, Measurand, Inc., Frederickton, NB), to provide visual feedback to a participant during weight-bearing imaging in a vertically open MRI scanner (FONAR Corporation, Melville, NY). The aims of the current study were to: 1.) test the real-time knee angle feedback system for MRI compatibility and participant ease of use; 2.) test the reliability of this system in achieving consistent knee position over repeated scans, as evaluated from independent measures derived from the MRI images; and 3.) test the effectiveness of real-time feedback in maintaining a knee position for the duration of an MRI scan.

METHODS

A healthy male subject (31 yrs) gave informed consent to participate in the MRI scanning described in this study. These images were acquired during data collection for a study on the effect of weight-bearing on knee positioning and contact, approved by the Institutional Review Board at Kessler Foundation Research Center.

The ShapeSensorMRI was placed on the leg using double-sided tape. A custom receiving coil, developed by FONAR engineering staff, was then placed around the knee, and held in place with Velcro straps attached to the upper thigh (Fig. 1).

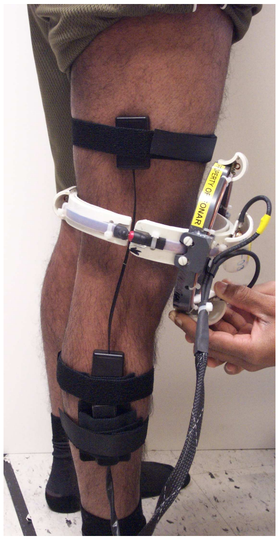

Figure 1: Custom Coil and ShapeSensorMRI Set-Up.

Data collection: A 3D steady state GRE free precession scan sequence was used, with a pixel spacing of 0.9766 mm, slice thickness of 1.5 mm, and field of view of 250 mm. Each scan lasted 2:16 min, and the scanning order, described below, was chosen randomly. The data collection protocol was as follows: For each scan (unless noted otherwise), the subject was provided real-time feedback from the ShapeSensorMRI on a television screen, in order to maintain a targeted knee flexion angle (KFA) of 20º for the duration of the scan. The subject rested at approximately neutral flexion between every scan, requiring retargeting of the KFA each time. The knee sensor's output was sampled at 100 Hz for each trial. A total of 7 scans were collected in the following order (starting on the left side): 1.) With the scan table vertical (90º), the subject was fully weight-bearing, (L90); 2, 3, 4.) With the scan table at 20° from horizontal, the subject was scanned in low weight-bearing (L20). The L20 scan was repeated twice for purposes of image parameter optimization; the three trials were labeled L20 Trial I, II, and III. The sensor and coil were then moved to the right leg for the remaining scans: 5.) R20; 6.) R90-Trial I, and 7.) R90 with visual feedback removed after reaching the target (R90-Trial II).

Analysis: ShapeSensorMRI output was analyzed to evaluate the subject's performance in maintaining the sensor-measured KFA over the scan period. To assess the consistency of the actual tibiofemoral positioning achieved, KFA was also computed using independent measures derived from the MRI images. This method used 3D geometric modeling and surface matching of bones to accurately transfer coordinate systems between sequential scans [1]. Bone surface models were reconstructed from a single operator's digitization on the sequential images using a graphics tablet (Wacom, Japan). The accuracy of the technique was previously reported as ±1.5º [2]. Three separate image-based analyses were performed to explore the consistency of actual KFA across the repeated trials. Each analysis required four scans to calculate KFA outputs (L90, L20, R20, R90). The mathematical algorithm to calculate image-based KFA's was dependent on the digitization of the L20 scan; therefore the permutations of scans used for each analysis were: Analysis 1 used scans 1, 4, 5, 6; Analysis 2: 1, 2, 5, 7; and Analysis 3: 1, 3, 5, 7.

RESULTS AND DISCUSSION

The system was effective in providing real-time feedback to the participant during weight-bearing MRI scanning, and the participant was able to target the knee angle consistently (Table 1). Contrary to our expectation, removal of feedback had no effect on the standard deviation of the targeting error.

Table 1: Reliability in targeting a 20° KFA over multiple scans using ShapeSensorMRI.

Scan Number	Average (deg)	StDev (deg)
1. L90	19.94	0.26
2. L20 – Trial I	19.80	0.29
3. L20 – Trial II	19.59	1.05
4. L20 – Trial III	19.78	0.38
5. R20	18.84	0.97
6. R90 – Trial I	19.07	0.23
7. R90 – Trial II	18.62	0.25

The results of the image-based analyses (Table 2) indicated the following: 1. All angles are considerably different from the targeted KFA (20º). Discrepancies between externally measured and image based KFAs are expected, since hip and ankle joint centers are not visible in the MRI scans. 2. Knee angles for L20 were consistent across the three scans (Analyses 1, 2, 3), indicating the true bone positions were consistently reproduced in repeated trials. 3) Image based KFA's at R20 and R90 are similar to each other, indicating consistent reproduction of knee angles for high and low weight-bearing conditions. However, there is considerable discrepancy between image based KFA's measured in L20 and L90. One possible explanation was an observed impingement of the custom coil that may have impeded the ShapeSensorMRI from bending, requiring the subject to flex more to match the targeted KFA. 5) Comparing R90 Analyses 1, 2, & 3 shows little effect of the removal of feedback.

Table 2: KFA's computed from MRI scan sequences and image-based analysis.

	Analysis				
	1	2	3	Avg	StDev
L90	28.58	26.84	26.72	27.38	1.04
L20	32.82	32.41	33.53	32.92	0.57
R20	25.08	26.85	26.79	26.24	1.01
R90	24.51	25.71	25.49	25.24	0.64
Avg	27.75	27.95	28.13		
StDev	3.83	3.02	3.65		

CONCLUSIONS

An MRI-compatible real-time feedback system was successfully used to facilitate repeatable knee positioning during scanning. Our initial results indicate that the ShapeSensorMRI can be used to reproduce a given KFA consistently, and that analyzing the angles by digitizing each scan yields repeatable results. More subjects will be needed to verify this, particularly in light of the higher KFA's recorded for one of the conditions. Lastly, while we anticipated that there would be increased target-angle deviation when the subject had no real-time feedback, no such effect was observed. Based on our other testing of the effects of feedback, we expect that this will indeed lead to reduced motion during scanning in some subjects.

REFERENCES

1. Barrance PJ, et al. *Proceedings of ASME 2006 SBC*, Amelia Island, FL, US. BIO2006-157507.
2. Barrance PJ, et al. *Proceedings of the ASB 2007 Annual Conference*, Stanford, CA, US. P1-10.

ACKNOWLEDGEMENTS

The contents of this abstract were developed under two grants from the Department of Education, NIDRR H133G080136 and H133P070007. However, those contents do not necessarily represent the policy of the Department of Education, and you should not assume endorsement by the Federal Government. Support for the work was also provided by the Kessler Foundation.

A COMPARISON OF SHOULDER JOINT ANGLE REDUCTION METHODS

Sakiko Oyama[1,2], Steve Leigh[2], and Bing Yu[2]
[1]Department of Exercise and Sports Science, [2]Center for Human Movement Science,
Division of Physical Therapy
The University of North Carolina at Chapel Hill
email: oyamas@email.unc.edu

INTRODUCTION

Joint angles are commonly used in biomechanical analyses of movement abnormalities, injury risk factors, and technique. They can be reduced from three-dimensional (3-D) coordinate data, which are obtained using a variety of instruments and techniques. Furthermore, there are multiple ways to reduce joint angles from 3-D coordinate data. Two common methods of calculating joint angles are the projection angle method and the Euler angle method. It is important that joint angles accurately and consistently represent human movement for researchers to draw valid conclusions from meaningful evaluations, for comparing different data sets, and for using the joint angles in further analyses, such as inverse dynamics.

The purpose of this study was to compare shoulder joint angles reduced using the projection angle method with shoulder joint angles reduced using the Euler angle method.

METHODS

Two High Definition, video camcorders were used to record the mens and womens javelin finals at the 2008 US Olympic team trials. The camcorders were aligned so their optical axes were perpendicular and operated at 60 frames/second. The legal trial with the longest official distance from the 12 female and 12 male javelin throwers competing were included in the data analysis. Twenty-one body landmarks, and the tip, tail, and center of mass of the javelin were manually digitized in both camcorder views for each throw [1]. Three-dimensional coordinate data were obtained using the Direct Linear Transformation procedure [2]. Each trial was time normalized from the instant of right foot touchdown to the instant of release.

Three different methods were used to reduce three sets of shoulder angles (horizontal adduction, abduction, and external rotation angles), from the coordinate data. Shoulder angles in set one were calculated as projection angles between the throwing arm and the trunk segments. Shoulder angles in sets two and three were calculated as Euler angles between the throwing arm and trunk segments. Set one employed an Euler angle rotation sequence of (1st) horizontal adduction, (2nd) abduction, and (3rd) external rotation (Model 1). Set two employed an Euler angle rotation sequence of (1st) abduction, (2nd) horizontal adduction, and (3rd) external rotation (Model 2).

The coefficient of multiple correlation (CMC) and the mean absolute difference were calculated between the angles in set one and set two, and between the angles in set one and set three. The group means and standard deviations of the CMCs and the mean absolute differences for each of the corresponding joint angles were calculated.

RESULTS AND DISCUSSION

The group means and standard deviations of the CMCs and the mean absolute differences between sets one and two, and one and three are displayed in Table 1.

In absence of a true gold standard to calculate 3-D joint angles, we cannot determine the most accurate joint angle calculation method. However, evaluating the agreement of the magnitudes and patterns of the shoulder joint angle time histories allows us to assess comparability of the different data reduction methods. The results of this study demonstrate that the patterns of joint angles calculated using the projection angle method and Model 1 of the Euler angle method were very similar, as indicated by the high CMCs (range: 0.976-0.998). The joint angle patterns calculated using Model 2 of the Euler angle method had less agreement with the patterns from the projection angle method. This is especially obvious when looking at the abduction (CMC: 0.755) and horizontal adduction (CMC: 0.663) data.

The absolute error between the projection angle data and the Euler angle data was highest for the abduction angles for both Model 1 (10±3°) and Model 2 (13±6°). The accuracy of this angle in Euler angle calculations is primarily dependent on the rotation order used. Interestingly, the absolute error value for abduction in Model 1 was lower than for Model 2. Abduction was the 1st and 2nd rotation in Model 2 and Model 1, respectively. Additionally, the absolute error between the projection and Euler horizontal adduction angles was much lower for Model 1 (1±0°) compared with Model 2 (13±5°). These results indicate that the joint angle time histories calculated using Model 1 have better agreement with the projection angle method, compared with Model 2.

An advantage of using an Euler angle sequence to calculate joint angles is that the joint angles can be expressed as three independent angles that are anatomically relevant. Projection angle calculations involve nine direction cosines that are redundant, and the angles may not be readily interpretable. A disadvantage of using an Euler angle method is that calculation can be affected by singular positions, especially when the joint moves through a large range of motion. Choosing the reference system that minimizes the occurrence of singular points during the movement of interest may be important when using an Euler angle reduction method.

The shoulder joint angles and sequences of joint rotations in Models 1 and 2 of this study are relevant for analyzing throwing motions. The Model 1 calculates the angle with the greatest range of motion as the 1st rotation. The angles calculated using this rotation sequence have good agreement in pattern and magnitude with the angles calculated using a projection method, thus seems to be a strong method for reducing shoulder joint angles for the analysis of throwing motions. The order of rotation of Model 2 was abduction followed by horizontal abduction. From an anatomically neutral position, abduction must occur before horizontal abduction is possible. However, the angles calculated using this rotation sequence have less agreement with those calculated using a projection method, thus seems to be a poorer choice for reducing shoulder joint angles for analyzing throwing motions.

CONCLUSIONS

The Euler angle sequences used in this study are relevant for analyzing throwing motions. A rotation order of horizontal adduction, abduction, and external rotation produces comparable joint angle patterns and magnitudes to those calculated using a projection angle method. This reduction method is a strong choice for analyzing shoulder joint angles in throwing motions.

REFERENCES

1. Abdel-Aziz YI and Karara HM. *ASP Symposium on Close Range Photogrammetry*, ASP, Falls Church, VA, 1971.
2. Hay JG and Yu B, *J Sports Sciences*, **13**, 125-140, 1995.

ACKNOWLEDGEMENTS

This study was financially supported by USA Track and Field, the Graduate School at the University of North Carolina at Chapel Hill, and the International Society of Biomechanics.

Table 1: Means and standard deviations of coefficient of multiple correlations (CMC) and absolute difference between the joint angles calculated using projection angle and Euler angle sequence Model 1 and 2.

	External Rotation		Abduction		Horizontal Adduction	
	CMC	Absolute Difference	CMC	Absolute Difference	CMC	Absolute Difference
Model 1	0.988 ± 0.009	6° ± 2°	0.761 ± 0.100	10° ± 3°	0.998 ± 0.003	1° ± 0°
Model 2	0.992 ± 0.005	5° ± 1°	0.755 ± 0.136	13° ± 6°	0.663 ± 0.119	13° ± 5°

CYCLE TO CYCLE VARIABILITY IN A REPETITIVE UPPER EXTREMITY TASK

Peter J. Keir, Melissa M. Brown and Mike W. Holmes
McMaster Occupational Biomechanics Laboratory, Department of Kinesiology
McMaster University, Hamilton, Ontario, Canada (pjkeir@mcmaster.ca)

INTRODUCTION

In the search for mechanisms and risk factors for occupational injuries to the upper extremity, many facets of the work task have been evaluated. High repetition and high force, especially in combination are known risk factors for the development of disorders [1]. Traditionally, measures have been averaged or summed over the entire shift or task. More recently, it has been suggested that injury or pain may be associated with the cycle to cycle variability of a task [2]. The purpose of this study was to re-examine the effect of force and repetition on muscle activity during a pushing task with and without grip, on a cycle by cycle basis.

METHODS AND PROCEDURES

Ten male and 10 female participants performed a series of bimanual horizontal pushing tasks with and without simultaneous gripping. The set-up included two parallel tracks with a grip dynamometer on the right side and a post on the left (Fig. 1). Handle position was monitored using linear potentiometers. A combination of three force levels (1 kg, 2 kg, and 4 kg on each side), three frequencies (4/min, 8/min, and 16/min) and two grip conditions (30% maximum grip and self-selected) were performed in 120 s trials [3].

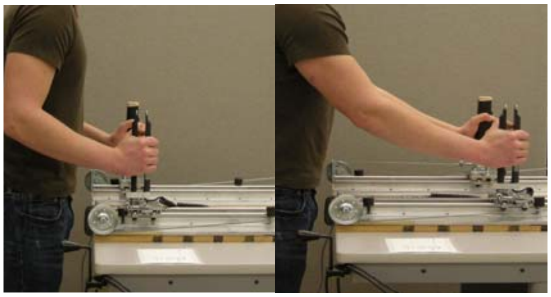

Figure 1: Dual pushing task. Grip force was measured on the right.

EMG was collected from 8 muscles: posterior deltoid, anterior deltoid (AD), biceps brachii, triceps brachii, extensor digitorum, extensor carpi radialis, flexor digitorum superficialis and flexor carpi radialis. Grip force, displacement and EMG were sampled at 2048 Hz. Raw EMG was linear enveloped at 3 Hz. For each muscle, EMG was normalized to maximum voluntary exertion (MVE) and averaged (AEMG).

For each full trial, cycle, and cycle component (Fig. 2), push distance, time, AEMG, and muscular rest were calculated. Variability was examined using the standard deviations (SD) of each component and the coefficient of variation (COV = SD/mean) for time and AEMG. In addition, the AEMG work/rest ratio was calculated.

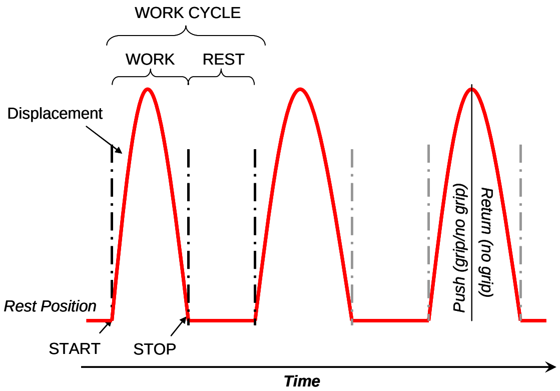

Figure 2: Definitions for cycle-to-cycle analysis. Only potentiometer data shown.

RESULTS and DISCUSSION

Although each cycle was initiated with a metronome, considerable variability was found in the cycle components. Variability (using SD) in work time was lowest in the high frequency condition (16/min) with and without grip. Gripping intensified this effect and resulted in lower work SD in the high load condition. Rest and cycle time variability had no relationship to frequency or force. The COV adjusts the SD for the duration of each phase and indicated a similar relationship for work time but, for most conditions, indicated very small COV during rest, especially at 4 and 8 cycles/min.

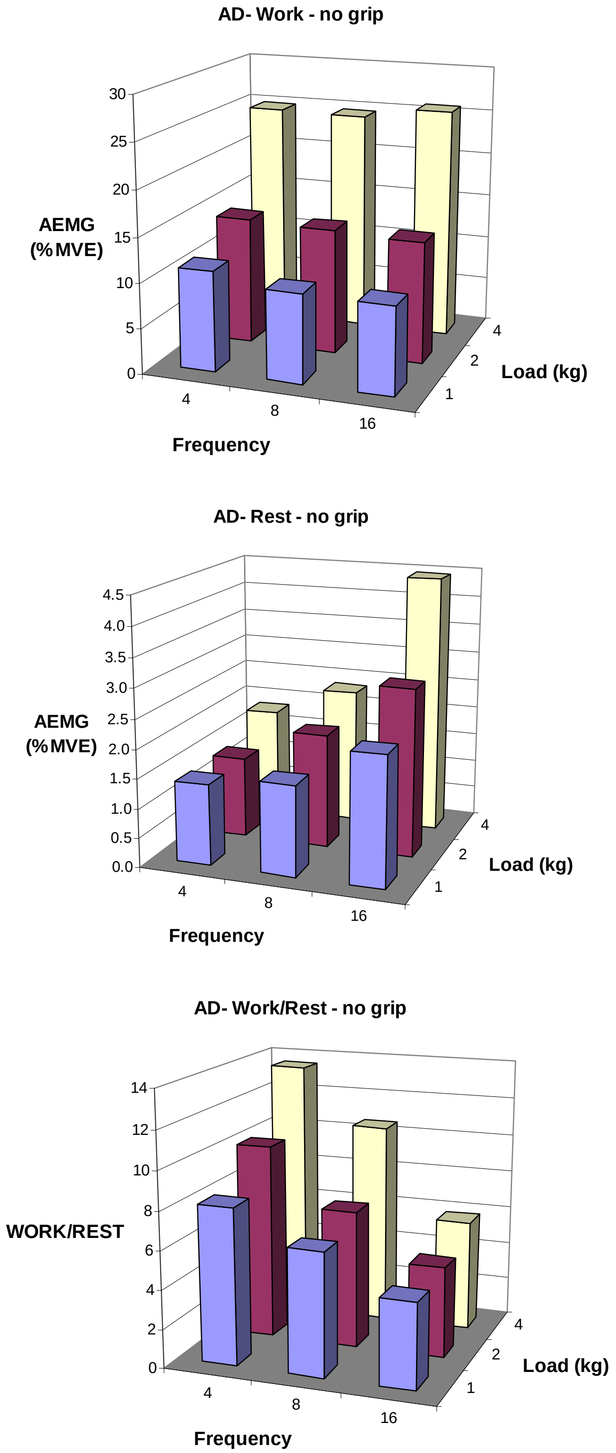

Figure 3: Mean anterior deltoid (AD) muscle activity versus load and frequency in work and rest phases of the cycle. Top – work phase (AEMG in %MVE). Middle – Rest phase (AEMG in %MVE). Bottom – Work/Rest AEMG Ratio.

In terms of AEMG, the anterior deltoid responded to the force required reaching about 25% MVE with the highest load but was invariant to frequency during the work phase (push + return) (Figure 3 - top). The same pattern of activity was seen with the grip. During the rest periods (non-work), the mean AEMG was less than 4.5% but was dependent on both force level and frequency (Figure 3, middle). The increase in activity with frequency and load may reflect anticipation of the next cycle or an inability to achieve rest between pushes.

It has been suggested that EMG variability, defined as RMS EMG (work) divided by RMS EMG (rest), is an important variable with respect to pain, experience and development of work related disorders [2]. Plotting this cycle to cycle ratio reveals a perspective novel to either work or rest alone (Figure 3 - bottom). Thus the work/rest ratio has a shape that reflects a relationship inverse to the rest activity but relatively independent of the work activity. This pattern was not evident when the entire trial was analyzed as a whole [3]. By examining the activity in this manner, it can be seen that the work phase is invariant to frequency but the rest activity, and the task overall, is dependent on both load and frequency.

Simultaneous gripping and pushing are common in the workplace and detailed examination of the muscular response to loading and frequency parameters will provide further insights to potential injury mechanisms. Examining tasks on a cycle to cycle basis, particularly with respect to variability of EMG, time, and kinematics, holds promise for elucidating the nature of disorder development in the upper extremity.

REFERENCES

1. Silverstein, B.A. et al. *Br J Indust Med*, 43(11), 779-784, 1986.
2. Madeleine, P. et al. *Ergonomics*, 51(7), 1078-1095, 2008.
3. Brown, M.M. *M.Sc. Thesis*, McMaster University, 2008.

ACKNOWLEDGEMENTS

This study was funded in part by AUTO 21 (A201-AHS) & NSERC Discovery grant #217382-04.

FOOTWEAR IS AN IMPORTANT DETERMINANT FOR MEDIAL-LATERAL STABILITY DURING HILL TRANSITIONS IN WALKING HUMANS

Keith A. Stern and Jinger S. Gottschall
Department of Kinesiology, The Pennsylvania State University
29 Recreation Building, University Park, PA

INTRODUCTION

Walking on sloped surfaces increases the risk of falls in the elderly [1], the leading cause of unintentional injury in the United States. However, it is nearly impossible for individuals to avoid surface transitions when walking either inside or outside during daily life. An appropriate biomechanical response to reduce the risk of falling during these transitions is to change your base-of-support by altering medial-lateral step width [2]. Furthermore, the proper control of step width requires cutaneous feedback from the plantar surface of the foot [3]. Since footwear can cause changes in gait patterns as well as affect cutaneous feedback, [3,4,5] many people may be experiencing reduced feedback as a result of thick cushioning in their shoes. Although individuals at risk for falling may require cushioned insoles to reduce loading forces, a prescribed textured foam insole may provide support without reducing cutaneous feedback. We hypothesize that textured foam insoles will decrease step width and muscle activity as compared to regular shoes. Conversely, similar to icing the plantar portion of the foot, thick cushioned insoles will increase step width and muscle activity as compared to regular shoes.

METHODS

Five healthy college-aged participants, 4 men and 1 woman, completed the protocol.

We placed reflective markers over the posterior calcaneus (heel) and the first metatarsal (toe) to be recorded using a six camera photogrametry system. Electromyography surface electrodes were placed over the soleus muscles to record muscle activity.

Participants completed five walking conditions on a 15 degree ramp: Level, Level → Uphill, Uphill → Level, Level → Downhill, and Downhill → Level (Figure 1). The walking trials were repeated for each of the following footwear conditions: personal athletic shoes, personal athletic shoes with foam insoles, personal athletic shoes with textured insoles, barefoot, and iced. For each trial, we measured the medial-lateral distance between the left and right heels as well as muscle activity for the soleus. Lastly, we compared these kinematic and muscle variables across conditions using paired t-tests ($p<0.05$).

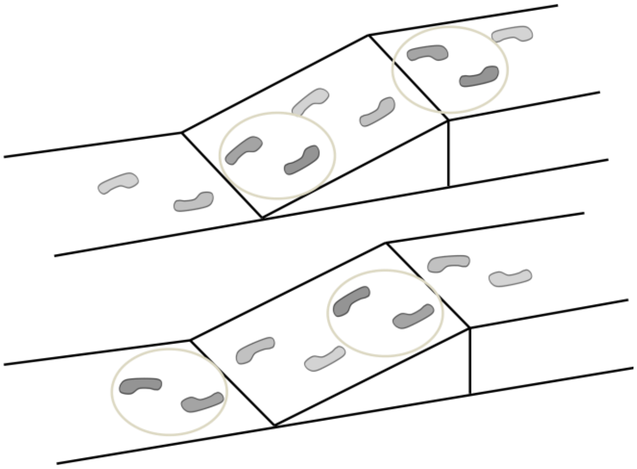

Figure 1: Uphill and downhill step positions. Circled footprints represent the measured step widths at Level → Uphill, Uphill → Level, Level → Downhill, and Downhill → Level (clockwise from top left).

RESULTS AND DISCUSSION

To summarize, medial-lateral step width and soleus activity were greater during the conditions utilizing the foam insoles compared to the conditions with regular and textured insoles.

Specifically, the soleus, which aids in postural stability, was 32% higher using the foam insoles as compared to regular shoes during level walking.

Furthermore, during the foam insole conditions, heel step width was significantly higher in all transition steps and level walking. Potentially, the participants walked with a larger base of support to increase medial-lateral stability due to decreased sensory feedback. Conversely, as seen in Table 1, during the textured insole conditions, heel step width was significantly smaller than foam insoles ($p<0.05$, Downhill → Level $p<0.07$). Possibly, the participants were able to maintain this energetically economic step width due to the increased sensory feedback provided by the textured insole.

During the Uphill → Level and Downhill → Level trials, we assumed that step width would not differ from that of level walking since both feet are on a level surface. However, in the foam insole and ice conditions, the participants' step width increased by 19.5% to 42.5%. Whereas, during the textured insole and barefoot conditions step width only differed by 2.3% to 13% from level walking.

CONCLUSIONS

Our results demonstrated that foam insoles led to a larger step width thereby causing a possible reduction in medial-lateral stability as compared to regular shoes. Textured insoles did not significantly improve medial-lateral stability as compared to regular shoes; however, unlike foam insoles, medial-lateral stability did not decrease with the additional textured insole. Therefore, we surmise that a foam insole with a textured surface could offer additional cushioning to regular shoes without compromising cutaneous feedback.

ACKNOWLEDGEMENTS

We thank Nori Okita and Denny Ripka for their assistance in the experimental set up, as well as Zac Dunkle, Andy Harkins, Matt Hinkley, John Nicotera, Jessi Ritegno, Molly Ritter, and Sarah Taylor for their help collecting and processing data.

REFERENCES

1. Prentice, SD, et al. *Gait and* Posture **20**, 255-265, 2004.
2. Maki, BE, et al. *J. of Electromyography and Knesiology* **18**, 243-254, 2008.
3. Robbins S, Waked E, McClaran J. *Age and Ageing* **24**, 67-72, 1995.
4. Nurse MA, et al. *J. of Electromyography and Kinesiology* **15**, 496-506, 2005.
5. Waked E, Robbins S, McClaran J. *J. of Testing and Evaluation* **25**, 143-148, 1997.

Table 1: Mean heel step width and soleus muscle activity for all subjects, normalized to level walking in regular shoes and bare feet. Bold values represent significant ($p<0.05$) differences from Level Regular, and asterisks (*) represent significant ($p<0.05$) differences between footwear conditions.

Mean Normalized Medial-Lateral Step Width at Heel						
Condition:	Regular	Foam	Textured		Barefoot	Ice
Level	100.00	**133.36***	**87.65***		100.00	100.91
Level → Uphill	95.00	**126.27***	104.20*		117.81	112.57
Uphill → Level	**110.35**	**131.23***	98.02*		97.71	119.58
Level → Downhill	**118.98**	**134.16***	118.88*		102.23	98.20
Downhill → Level	**109.79**	**142.59**	**110.10**		113.17	126.36
Mean Normalized Soleus Muscle Activity						
Condition:	Regular	Foam	Textured		Barefoot	Ice
Level	100.00	**131.91***	101.21*		87.01	92.89
Level → Uphill	**180.38**	**204.26**	**221.45**		**179.23**	**174.77**
Uphill → Level	109.35	113.73	104.90		109.61	103.84
Level → Downhill	100.78	107.92	107.23		86.26	94.05
Downhill → Level	**124.68**	**154.87**	**160.05**		149.37	160.85

SINGLE LEVEL FUSION IN A C27 CERVICAL SPINE FINITE ELEMENT MODEL

Nicole Kallemeyn, Joseph Smucker, Douglas Fredericks, Kiran Shivanna, Nicole Grosland
The University of Iowa, Iowa City, IA
email: nicole-grosland@uiowa.edu, web: http://www.ccad.uiowa.edu/mimx

INTRODUCTION

Spinal fusion is one of the most common procedures performed on the cervical spine. A fusion procedure consists of removing a degenerated intervertebral disc and inserting some form of graft material into the disc space to restore/maintain disc height and appropriate lordotic curvature of the cervical spine.

The long term goal of this procedure is to establish a completely fused and stable region across the space formally occupied by the intervertebral disc. Long term adjacent level degeneration after spinal fusion surgery has been documented in many clinical studies [1]; however, the etiology is not fully understood. A biomechanical hypothesis of the causes of adjacent level degeneration after fusion is that it is due to an altered stress environment and motion redistribution throughout the cervical column [2].

In vitro studies can be used to examine changes in axial stiffness and failure characteristics in an implanted spine, but are limited to studying the external responses. Finite element analysis has the ability to study internal changes (e.g. stress) in adjacent levels due to fusion, as well as the effects of the external response.

In this study, a single level C45 fusion was simulated within an intact C27 finite element model. The hybrid loading method was used to evaluate the effects of the fusion on the adjacent levels.

METHODS

The finite element model was developed using our previously reported meshing techniques for the cervical spine [3], and was validated using experimental data from the same specimen which was used for model development. The intact C27 model (Figure 1) of the cervical spine was analyzed in flexion-extension, lateral bending, and axial rotation moments up to ±1.0 Nm.

Fusion was simulated by making the C45 intervertebral disc properties similar to that of bone. The model was analyzed again in flexion-extension, lateral bending, and axial rotation by increasing the moment until the primary C27 motion matched that of the intact C27 motion.

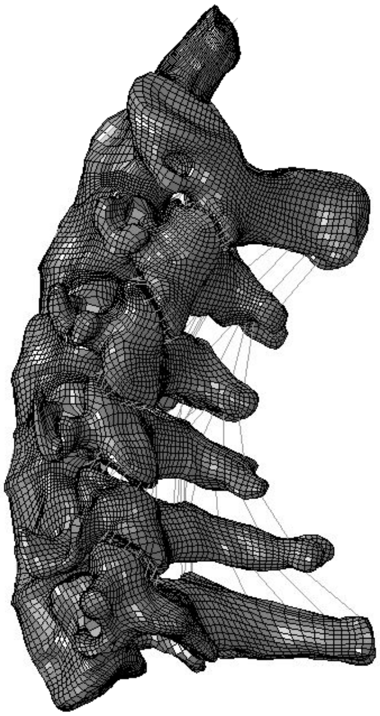

Figure 1. C27 finite element mesh.

Changes in motions, vertebral body stresses, and disc stresses were calculated at all levels in both cases to determine the relative effect of fusion on these parameters using the hybrid loading protocol.

RESULTS AND DISCUSSION

The fused model required moments greater than 1.0 Nm to obtain the same overall motion as the intact case for each mode of loading.

Increases in motion at each non-fused level varied from 15% at level C67 in right lateral bending, to 39% in level C67 in left axial rotation (Figure 2).

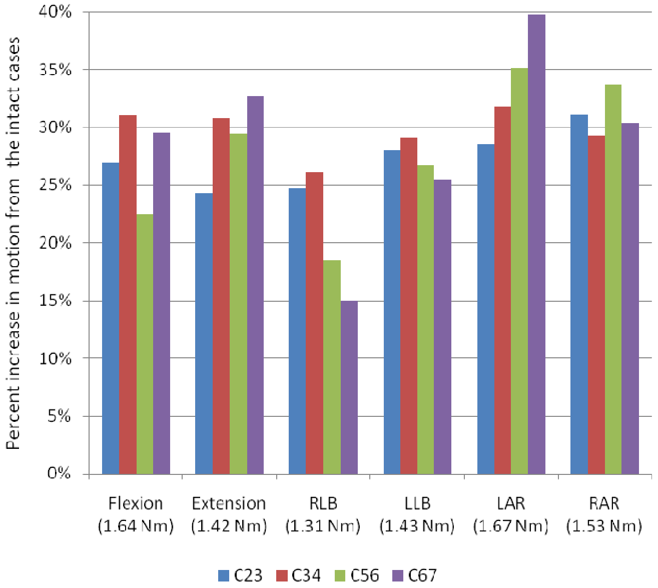

Figure 2. Percent increase in motion following C45 fusion.

Stresses in the vertebral bodies and intervertebral discs were compared for the fused and intact models. The von Mises stresses in the anterior regions of the vertebral bodies increased between 9 and 79% in all cases with the exception of C4 during extension and lateral bending, and for C5 in right lateral bending. In these cases, the stresses either remained the same or slightly decreased due to changes in load sharing within the fused C45 segment.

Stresses in the non-fused intervertebral discs were also compared (Figure 3). For flexion and extension, the von Mises stresses were analyzed in the anterior portion of the discs. In left lateral bending and left axial rotation, the left portion of the annulus was analyzed, and in right lateral bending and right axial rotation, the right portion of the annulus was considered.

CONCLUSIONS

This study examined the effects of simulated fusion on adjacent levels using the hybrid loading protocol. After fusion, adjacent levels in the spine experienced increases in intervertebral motions to compensate for the fused level. In addition, stresses in the vertebral bodies and discs of the non-fused levels also increased. Sustained changes such as those described have the potential to lead to degeneration and osteophyte growth. Increases in motions and stresses at adjacent levels (for all loading modes except extension) were found in another cervical spine multilevel (C37) finite element study of fusion [4]. Other fusion studies have quantified increases in adjacent level stresses for various surgical techniques and graft materials [5-6]. These findings may help to explain clinical observations of adjacent level degeneration following cervical spine fusion.

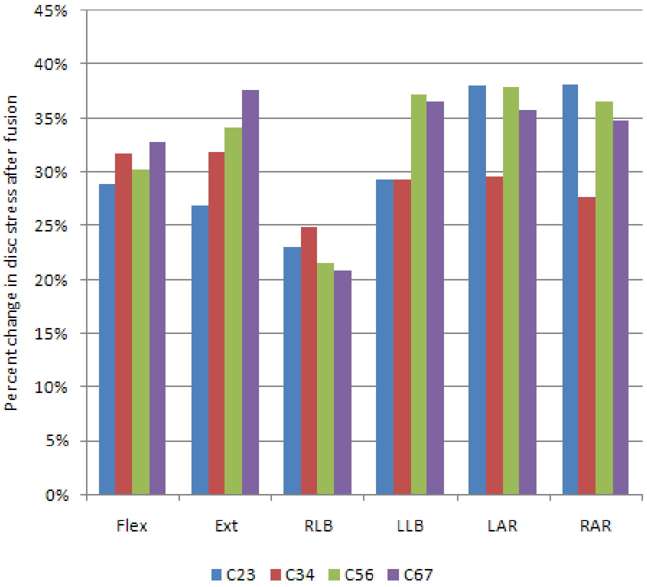

Figure 3. Percent increase in disc stresses after C45 fusion.

REFERENCES

1.Bartolomei JC, et al. *Neurosurg Clin North Am*, **16**, 575-587, 2005.
2.Panjabi MM. *Clinical Biomechanics* **22**, 257-265, 2007.
3.Kallemeyn NA, et al. *Computer Methods and Programs in Biomedicine*, accepted, 2009.
4.Lopez-Espina CG, et al. *Spine* **31**, 972-978, 2006.
5.Kumaresan S, et al. *Bio-Medical Materials and Engineering*, **7**, 221-230, 1997.
6.Maiman DJ, et al. *Bio-Medical Materials and Engineering*, **9**, 27-38, 1997.

Effect of Loading Condition on Traction Coefficient between Shoes and Artificial Turf Surfaces

Seth M. Kuhlman, Michelle B. Sabick, Ronald Pfeiffer, Benjamin Cooper, Jackie Forhan
Center for Orthopaedic and Biomechanics Research
Boise State University
Boise, ID 8372

INTRODUCTION

Characterization of the shoe-sports surface interface has become an increasingly popular topic among researchers as seen by the proliferation of journal articles published within the past five years [1-6]. It has been hypothesized that an increase in traction increases musculoskeletal loads and concomitantly injuries [7]. Therefore, traction has been quantified on both artificial and natural surfaces, in rotational and translational motions, and across varying loading conditions.

Though research has been ongoing since the 1970's, the majority of the early testing methodologies used are not relevant [7] and most are not up to date with technologies currently available for both data acquisition and data analysis. One of the key weaknesses of many existing studies is the use of vertical compressive forces that are lower than those created by an athlete in realistic situations[8]. Vertical loads ranging from as low as 67 N and up to 1055 N have been used, often without much justification[1, 3, 4, 8-10].

The purpose of this paper is to quantify the effect of varying vertical load on the shoe-turf traction characteristics on an actual artificial turf installation.

METHODS

In determining the performance characteristics of turf surfaces, researchers have generally reported static and dynamic traction forces or coefficients based upon the model of Coulomb friction, even though many of the assumptions of Coulomb friction are violated in the case of turf-shoe interactions. The following definitions were used to determine the dynamic, static and peak traction variables.

1. Static Traction Coefficient- Ratio of the horizontal force resisting motion and the normal force at the instant before motion occurs.
2. Dynamic Traction Coefficient- Ratio of the horizontal force resisting motion and the normal force while the object is moving at a constant velocity. The dynamic traction coefficient was computed as the average of the traction coefficient over a 2 cm distance while sliding at a constant velocity.
3. Peak Traction Coefficient– The peak value of the ratio of the horizontal force resisting motion and the normal force during the entire trial.

Variations in traction characteristics due to changes in the vertical load applied were quantified using four different sport shoes on FieldTurf (FieldTurf Inc., Montreal, Quebec). Four shoe types were selected to encompass the range of different styles currently available to football players. The specific shoes tested were: Adidas Scorch 7 Fly Low, Nike Air Zoom Super Bad, Reebok 4 NFL Speed III, and Nike Air Zoom Super Speed. All shoes tested were men's size 12 and were kept complete and in original sale condition for testing. Each shoe was fitted with a rigid steel foot and ankle shaft with the remaining void in the shoe filled with an acrylic resin fortified grout. The foot position was chosen to engage all the shoe cleats as would occur under the condition of a hard stop by an athlete.

All testing was done in the Boise State University (BSU) Caven-Williams indoor practice facility with the BSU TurfBuster. Each shoe was tested in 8 different loading conditions ranging from 222 N to 1780 N in 222 N increments. All shoes were tested at a horizontal velocity of 10 cm/second over a 20 cm displacement. Data were collected at a rate of 250 Hz and post-processed using Matlab software. After determining the individual magnitudes of static, dynamic, and peak traction coefficients, the results were averaged together over three trials. A one-way ANOVA was performed to determine any differences across the shoes with a Tukey post-hoc analysis. For comparison within each shoe and across the load conditions a repeated measures ANOVA procedure was performed with a pair-wise T-Test post-hoc using a Bonferroni sliding scale adjustment for multiple comparisons.

RESULTS

The primary results for the traction characteristics are displayed in Figure 1. For all four shoes tested there was a distinct change in the slope of the traction coefficient vs. load slope between 666 N and 888 N. For all three variables, static, dynamic, and peak traction coefficients there were no significant differences between the shoe styles below 666 N except for a difference between the SuperBad and SuperSpeed shoes at 222 N in dynamic and peak traction. At 888 N and above there were multiple differences between shoe styles with the majority of the differences involving the SuperBad and SuperSpeed shoes ($p < 0.05$).

Within each shoe comparisons were made between loads of 888 N and above. Between the loads of 888 N and 1332 N there were no statistical differences in any of the traction variables or shoes. The only differences found were between highest and lowest loads, i.e. between 1779 N and 888 N.

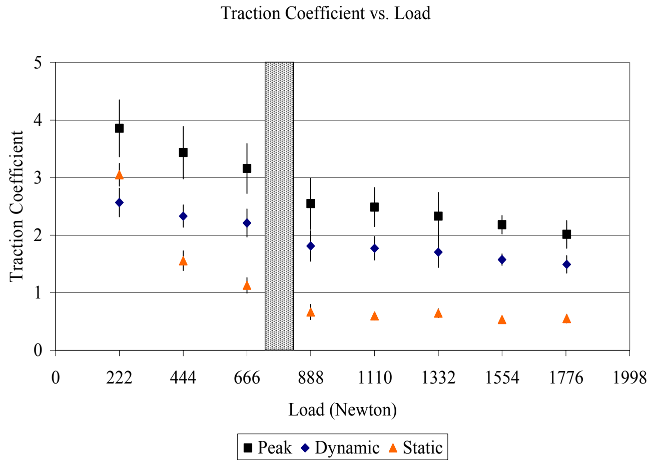

Figure 1: Average traction coefficient vs. vertical load condition for Static, Peak, and Dynamic traction variables

DISCUSSION

The statistical results of the comparisons across the four cleat styles show a distinct difference in shoe performance at loads below 666 N and above 888 N. In the lower load range the shoes perform almost identically implying a non-realistic load condition which is supported by McNitt [8]. Above 888 N however the differences in shoe design begins to emerge as seen by the many statistical differences among the shoes.

While there were performance differences seen across the shoes at all loads of 888 N and above there were only statistical differences within each shoe at a load of 1554 N and 1779 N. Implying that each shoe has no performance difference in traction characteristics in loads representing one bodyweight (up to 1332 N or 300 lbs). Above the one bodyweight range the shoes themselves begin to react differently to the turf surface. Further testing will be conducted to expand the current findings to multiple artificial and natural turf surfaces.

References

1.Livesay, G.A., et al., *Peak Torque and Rotational Stiffness Developed at the Shoe-Surface Interface.* Am J Sports Med. **34**(3): p. 415-422. 2006.
2.Naunheim, R., et al., *A Comparison of Artificial Turf.* J TRAUMA. **57**(6): p. 1311-1314. 2004.
3.Shorten, M., et al. *Shoe-Surface Traction of Conventional and In-Filled Synthetic Turf Football Surfaces*. in *XIX International Congress on Biomechanics*. 2003.
4.Cawley, P.W., et al., *Physiologic Axial Load, Frictional Resistance, and the Football Shoe-Surface Interface.* FOOT ANKLE INT. **24**(7): p. 551-556. 2003.
5.Childs, S.G., *The Pathogenesis and Biomechanics of Turf Toe.* ORTHOP NURS. **25**(4): p. 276-280. 2006.
6.Villwock, M.R., et al., *Football Playing Surface and Shoe Design Affect Rotational Traction.* Am J Sports Med: p. -. 2009.
7.Nigg, B., *The validity and relevance of tests used for the assessment of sports surfaces.* MED SCI SPORT EXER. **22**(1): p. 131-139. 1990.
8.McNitt, A.S., et al., *Development and Evaluation of a Method to Measure Traction on Turfgrass Surfaces.* J TEST EVAL: p. 99-107. 1997.
9.Villwock, M.R., et al. *Football Playing Surface Components May Affect Lower Extremity Injury Risk*. in *North American Congress on Biomechanics*. 2008. Ann Arbor, MI.
10.Villwock, M.R., et al. *Football Shoe Design May Affect Lower Extremity Injuty Risk*. in *North American Congress on Biomechanics*. 2008. Ann Arbor, MI.

ACKNOWLEDGEMENTS

This research was funded by the National Football League. The authors thank Intermountain Orthopaedics for sponsoring a graduate fellowship.

AT SIMILAR SLOPES, STAIR WALKING IS A SAFER ALTERNATIVE TO RAMP WALKING

Riley C. Sheehan and Jinger S. Gottschall
Department of Kinesiology, The Pennsylvania State University
University Park, PA 16802 USA
Email: rcs241@psu.edu, http://www.biomechanics.psu.edu/nml/

INTRODUCTION

According to the CDC, falls are the leading cause of injury-related deaths in older adults. With more than one-third of adults over the age of 65 falling at least once a year [1], it is important to understand the fall risks associated with different locomotor tasks. Depending on the task, such as stair walking and ramp walking, the variables utilized to assess fall risks differ.

Falls often occur because of medial-lateral (ML) instability, anterior-posterior (AP) instability, or improper toe clearance. For healthy individuals walking on a level surface, increasing step width (SW) is a strategy used to manage ML instability [2]. Similarly, AP instability, due to increased shear forces [3], is mitigated by spending a greater percentage of the gait cycle in stance. Lastly, increases in the activation of the tibialis anterior (TA) during swing indicates the increased importance of toe clearance during walking [4].

The purpose of this study was to compare the risk of falling associated with the ascent and descent of ramps and stairs. We expected the gait pattern of ramp walking to exhibit changes indicative of maintaining ML and AP stability, as well as proper toe clearance. Specifically, we hypothesized that SW and percentage of time in stance would increase on the ramp. In addition, because of the elevated risk of tripping during ramp walking, we hypothesized that TA activity would also be greater during swing.

METHODS

Seven healthy, college-aged men (age = 22 ± 2 yr) completed the protocol of level, ramp and stair walking (Figure 1). A motion analysis system tracked the position of markers on the first metatarsal of each foot. Electromyography data of the TA were collected using surface electrodes. Five successful trials for each condition were captured and the values averaged. All data were measured for one stride from left toe-off to left toe-off. The uphill conditions were: level to step 1 (L→1), level to step 2 (L→2), step 1 to step 3 (1→3), step 3 to plateau (3→P), and step 2 to plateau (2→P). The downhill conditions were: plateau to step 3 (P→3), plateau to step 2 (P→2), step 3 to step 1 (3→1), step 1 to level (1→L), and step 2 to level (2→L).

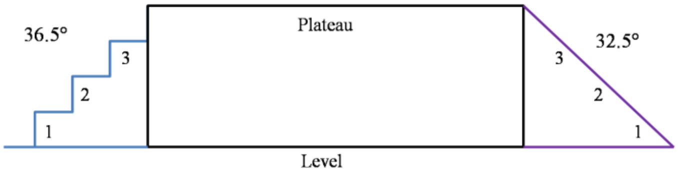

Figure 1: Stair/Ramp Apparatus (not to scale).

SW was defined as the mean lateral distance between the first metatarsals during double support. Percent time in stance was defined as the time from foot-strike to toe-off of the left foot divided by the stride time. The mean activity of the TA was calculated during the swing phase of each stride. All values were normalized to measurements made during level walking. The ramp and stair values were compared using a paired t-test for each condition with significance of $p < 0.05$.

RESULTS AND DISCUSSION

Contrary to our hypothesis, there was no significant difference in SW between ramp walking and stair walking. However, when compared to level walking, the uphill conditions for both the ramp and stairs showed narrower SW. This change most likely accommodates the increased need for propulsion [5]. Conversely, the downhill conditions showed larger SW than level walking, indicating a greater need for ML stability (Figure 2).

We observed a greater time in stance for ramp walking when compared to stair walking (Figure 3). This result may indicate the need for propulsion going uphill and the need to maintain AP stability going downhill. It is also possible that the greater time in swing on the stairs, a result of the shorter time in stance, could be explained by the need for additional time to properly place the foot.

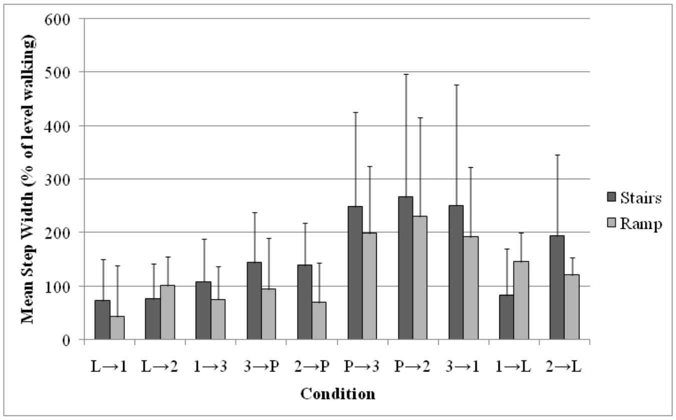

Figure 2: Step Width
There was no significant difference in SW between the stairs and the ramp. However, SW was consistently less when walking uphill than downhill ($p<0.05$).

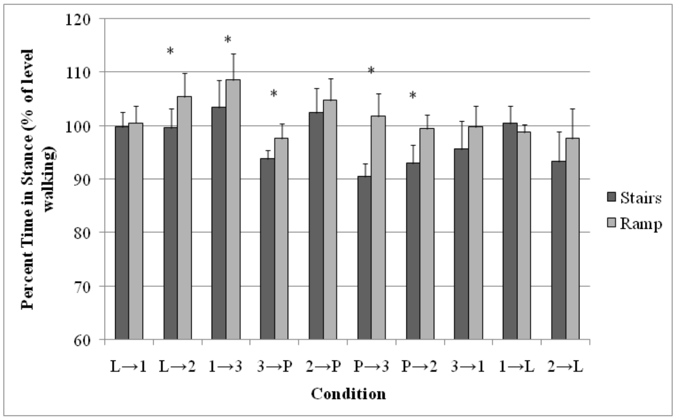

Figure 3: Percent Time in Stance
The time in stance on the ramp was on average 5.4% greater than on the stairs. For the significant conditions, the average was 6.5% greater with the greatest change of 11% occurring on the P→3 condition (* indicates significance).

The downhill P→2, 3→1, and 2→L conditions on the ramp showed greater TA activity (Figure 4). However, we are unsure if we can attribute this result to toe clearance. It is more likely that the difference in TA activation is explained by the unique gait patterns for ramp and stair walking. During downhill ramp walking, like level walking, participants use the typical heel strike to toe-off gait pattern. However, when walking on stairs, participants utilize a toe-strike to toe-off pattern. When the ankle is extended, TA activity is not necessary or expected.

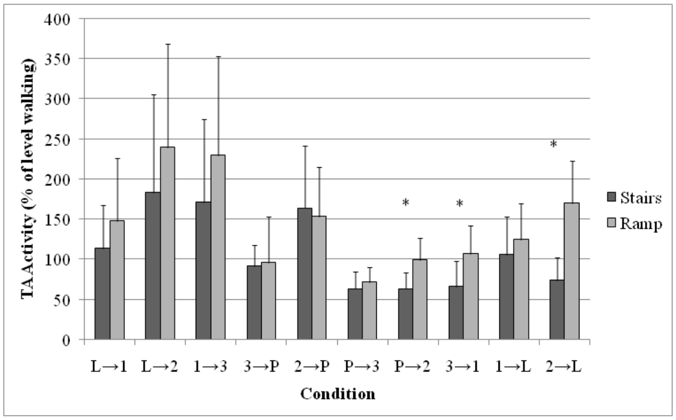

Figure 4: Mean TA Activity during Swing
The mean TA activity during swing on the ramp was on average 32% greater than on the stairs. For the significant conditions, the average was nearly 46% greater with the 2→L condition showing a 72% increase (* indicates significance).

CONCLUSION

Our data demonstrate that ramp and stair walking provide different challenges to ML and AP stability in addition to toe clearance. The results of this study suggest that, at similar slopes, stair walking appears to be a safer method of changing elevation than ramp walking.

In the future, we hope to further identify additional risk factors for falling during ramp and stair walking. We also plan to expand this research to other walking tasks and participant populations.

ACKNOWLEDGEMENTS

We thank Nori Okita, Denny Ripka, and the undergraduate assistants for their help.

REFERENCES

1.http://www.cdc.gov/HomeandRecreationalSafety/Falls/adultfalls.html
2. Brach JS, et al. *J Neuroeng Rehabil* **2**, 21, 2000.
3. Redfern MS, et al. *Gait Posture* **6**, 119-25, 1997.
4. Winter DA. *The Biomechanics and Motor Control of Human Gait*, 1991.
5. Erdimir A, and Piazza, SP. *Gait Posture* **15**,212-9, 2002.

ARE RESTRICTED, REPETITIVE BEHAVIORS AND POSTURAL CONTROL LINKED IN AUTISM SPECTRUM DISORDERS?

Chris Hass, Kimberly Fournier, Jacquelyn Selbst, Hope Benefield, Mark Lewis and Krestin Radonovich
Applied Neuromechanics Laboratory, The University of Florida, Gainesville, FL
email: cjhass@hhp.ufl.edu

INTRODUCTION

Restricted interests and repetitive stereotyped behaviors (RRBs) encompass one of the core diagnostic areas of autism spectrum disorders (ASD). RRBs are believed to be a heterogeneous group of behaviors that may vary according to both age and level of functioning [1]. Motor clumsiness has been reported to be predictor of repetitive behavior in individuals with pervasive developmental disorders; however the relationship between motor control and repetitive behaviors remains to be fully defined [2].

In an effort to help further define this relationship, we compared motor control and RRBs in children with ASD and typically developing children (TD). Using measures previously used in the literature to assess motor control [3] and RRBs [4], we compared the center of pressure (COP) sway area during quiet stance with intensity and frequency scores on the Revised Repetitive Behaviors scale (RBS-R) [5].

METHODS

The presence of repetitive behaviors was determined in 30 children diagnosed with ASD (3.7 to 15.7 yrs) and 29 TD children (2.4 to 15.9 yrs). The RBS-R is an empirical rating scale used to assess the presence and severity of repetitive behaviors (Stereotyped Behavior, Self-Injurious Behavior, Compulsive Behavior, Ritualistic Behavior, Sameness Behavior and Restricted Behavior). The scale provides 2 separate scores for each of the 6 subscales and overall total. One score is an *intensity* score, a sum the ratings for each item and the other score is a *frequency* score, a sum of the number of items endorsed or scored as present.

In addition, children performed quiet stance trials where they were asked to stand as still as possible with their feet comfortably apart (a self–selected stance width) and with their arms comfortably at their side for 15 seconds. Foot positioning was marked on the initial trial and used for all subsequent trials. Children performed four experimental trials.

Ground reaction forces (GRF) were recorded (360 Hz) from a forceplate (Type 4060–10, Bertec Corp., Columbus, OH) embedded level with the floor. Ground reaction forces and moments collected from the forceplate were processed and the location of the COP was calculated. Once the COP was calculated, the sway area was determined by multiplying the peak displacements in the mediolateral and anteroposterior directions. An individual's data from the four experimental trials were averaged to provide one representative datum for Sway Area which was then submitted for statistical analyses.

We had three primary questions of interest: 1. Is the magnitude of postural sway greater in children and adolescents with ASD compared to those typically developing? 2. Are RBS-R scores related to the magnitude of postural sway?; and 3. Is this relationship more pronounced in ASD.

RESULTS

Children and adolescents with ASD consistently produced greater postural sway in both the antero posterior and mediolateral direction leading to greater sway area ($P<0.05$) compared to their age matched peers (Figure 1). Not surprisingly, children and adolescents with ASD exhibit significantly greater frequencies and intensities of repetitive and restricted behaviors (Table 1).

Overall in the population of 59 children and adolescents, our measure of postural control (sway area) was significantly correlated with the both the overall RBS-R frequency and intensity scores (r=.52, p<0.001 and r=.54, p<0.001) as well as 5 out of the 6 subscale scores (r range of .37 to .65, all p<0.01). The magnitude of sway was not related to the scores related to self injurious behavior.

However, when you look at these relationships within groups, it appears that RBS-R scores are only related to postural control in the group with ASD. In ASD, sway area was significantly correlated with the frequency and intensity of strereotyped behavior (r=.56;r=.39), compulsive behaviors (r=.31;r=.45), and RBS-R overall (r=.31;r=.37); intensity of ritualistic behavior (r=.4,) and intensity of restricted behavior (r=.55). Conversely, in typically developing children, the magnitude of postural sway was only related to the frequency and intensity of self injurious behavior (r=.71, p<0.001 and r=.70, p<.0.001) RBS-R scores.

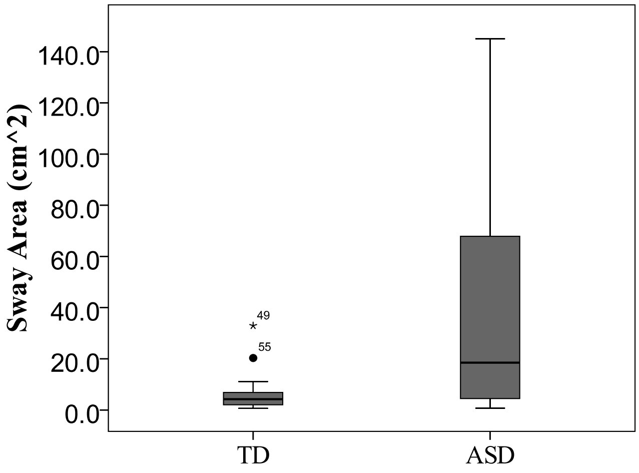

Figure 1. Box plot for COP sway area.

DISCUSSION

Our results support previous reports that RRBs are related to gross motor performance. However, we are the first to show a relationship between these behaviors and postural control. Both the overall intensity and frequency scores were significant predictors of COP sway areas in ASD. Of interest are the significant individual intensity and frequency subscore predictors. RRBs can be loosely classified into lower-level (more repetitive motor behaviors) and higher-level behaviors (circumscribed interests, resistance to change, rigid routines and rituals) suggesting different neuropsychological mechanisms. It seems the intensity of both higher-level and lower-level behaviors are significantly related to deficits in postural control, whereas only the frequency of lower-level behaviors seem to be related to deficits in postural control.

CONCLUSIONS

The increased postural sway and the apparent link between RRB's, a core feature of ASD, and postural control suggests future research is warranted in this area. Intervention trials aimed at improving postural control are underway in attempt to improve treatment of ASD.

REFERENCES

1.Esbensen, A. et al. (2009). *Journal of Autism and Developmental Disorders*, ***39***, 57-66.
2. Carcani-Rathwell, I. et al. (2006). *Journal of Child Psychology and Psychiatry **47***), 573-81.
*3.*Minshew, N. J. (2004). *Neurology*, ***63***, 2056-61.
4. Cuccaro, M. et al. (2007). *Child Psychiatry and Human Development **37***, 347-60.
5. Bodfish, J. et al. (2000). *Journal of Autism and Developmental Disorders*, ***30***, 237-43.

ACKNOWLEDGEMENTS

Autism Speaks #CH/1964/01-201007-065-00-00-01

Table 1. Group scores (M ± SD) for the RBS-R intensity and frequency scale scores.

	Intensity		Frequency	
RBS-R Scales	**TD (n=29)**	**ASD (n=30)**	**TD(n=29)**	**ASD (n=30)**
1 Stereotyped	0.6 ±1.3	6.1 ± 3.7	0.4 ± 0.8	3.7 ± 1.7
2 Self-Injurious	0.1 ± 0.4	2.9± 3.2	0.1 ± 0.4	2.1 ± 2.1
3 Compulsive	1.0 ± 2.9	5.6 ± 3.8	0.7± 1.4	3.4 ± 1.9
4 Ritualistic	0.9 ± 2.2	6.7 ± 4.0	0.7 ± 1.2	3.7± 1.8
5 Sameness	0.8 ± 2.0	9.1 ± 6.5	0.6 ± 1.3	5.5 ± 2.6
6 Restricted Interest	0.3 ± 1.1	4.5 ± 3.3	0.2 ± 0.5	2.5 ± 1.3
Total Score	3.8 ± 9.0	34.9 ± 17.4	2.7 ± 4.7	20.9 ± 7.4

BIOMECHANICAL EVALUATION OF SUPPORTED STANDING WITH DIAGONAL REACH

[1] Mohammad Abdoli-E, [2]Caroline Damecour, [1]Ahmad Ghasempoor, and [2]Joan Stevenson
[1] Ryerson University, Toronto, ON, Canada. email: m.abdoli@ryerson.ca
[2] Queens University, Kingston, ON, Canada.

INTRODUCTION

Low back pain has been reported in association with forward bent and twisted trunk postures in standing[1]. To reduce loading on the spine, assistive devices, such as the Personal Lift Assistive Device have been investigated and shown to be helpful[2]. The Dynamic Trunk Support (DTS) is an alternate type of device that is external, similar to a chair postures (Figure 1). The DTS is designed to provide continuous partial support which makes it suitable for both static and dynamic trunk postures depending on the type of work activity. The objective of the DTS is to reduce compressive lumbar spine loading as well as postural trunk muscle work rather than eliminate through passive positioning. The contact point is the upper ribcage which maximizes the distance where weight is transferred and the lumbar spine. In a previous study, the DTS reduced back and hip extensor muscle activity by an overall average of 60% with static forward flexed trunk angles in 10 degree increments between 10 and 40 degrees[3]. In comparison, leaning against a desk resulted in no change in muscle activity[3]. The purpose of this study is to test the biomechanical effects with dynamic trunk postures that are associated with extreme reaching.

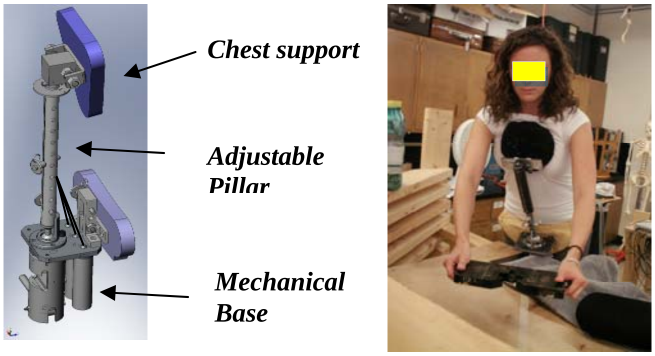

Figure 1: The Dynamic Trunk Support has 3 components; mechanical base, pillar and support. The mechanical base is designed to move in 3 directions. The support transfers weight through the upper 3 ribs and upper half of the sternum.

METHODS

Ten females, with an average age of 30.5 years (SD 9.2) and who gave informed consent, lifted a 5kg three times with 2 hands to a fixed distance (57cm) on a 45-degree diagonal to the left at the height of the pelvis under three conditions: no support, leaning on the desk (normalized to the height of the anterior pelvic crest) and leaning on the DTS with the contact point at the upper half of the sternum). A Fastrak^{TM} (Polhemus, Colchester, VT, US) human motion system was used to continuously collect changes in the position of the trunk, right arm, and right lower extremity. The trunk was divided into three sections. The absolute trunk angles in three dimensions that match with the peak upper thoracic flexion angle are compared. These angles correspond to the maximal reach distance. An 8 channel EMG (Bortec Biomedical, AB, CAN) was used to collect muscle activity from bilateral L5 erector spinae, gluteus maximus and right hamstring. The right upper and lower trapezius muscle was also monitored but results aren't presented here. Muscle activity was calibrated to maximal voluntary contraction with peak values compared. An AMTI force platform (AMTI, Watertown, MA, US) was used to record changes in center of pressure. Moments were calculated using an upwards link segment model. Repeated measure ANOVA tested for differences.

RESULTS

Leaning on a support resulted in a significant reduction of forward flexion of the upper and lower with a 10 degree reduction of the average. Leaning on the desk resulted in a significant reduction in lumbar spine and pelvis rotation (approx 7-10 degrees). Leaning on the DTS resulted in no change to rotation but a small decrease in peak side flexion (Figure 2). Muscle activity was significantly reduced for supported reaching in comparison to no support with a 17% average average reduction while leaning on the DTS and 28% reduction while leaning on the desk (Table 1).

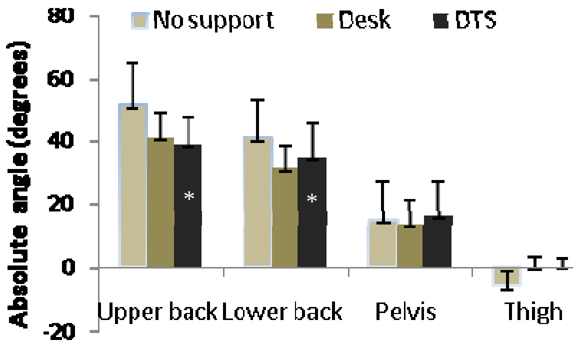

a) flexion

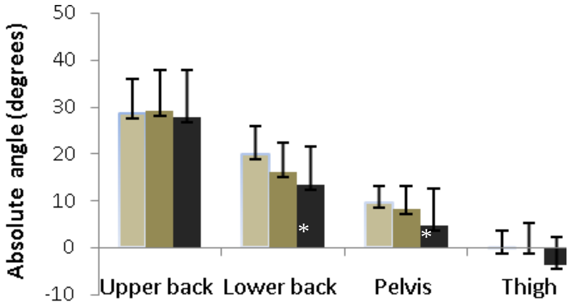

b) side flexion

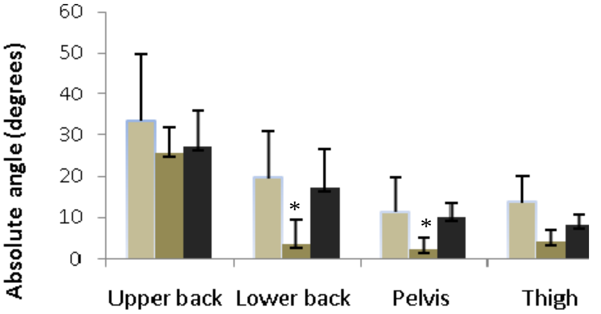

c) rotation

Figure 2: Absolute angles at maximal reach distance corresponding to picking up weight; flexion (a), side flexion (b) and rotation (c).

The changes in center of pressure position at maximal reach were significantly different between conditions with only a small change occurring while leaning on the DTS (Figure3).

	LES		Gluteus Max		Hamstring	
No support	34.5	(12.5)	10.6	(3.6)	11.1	(7.4)
Desk	25.0	(8.1)	8.8	(3.2)	8.8	(3.9)
DTS	28.4	(10.6)	8.0	(3.0)	9.4	(4.2)
	p=0.001		p=0.03			

Table 1: EMG on right side in %MVC.

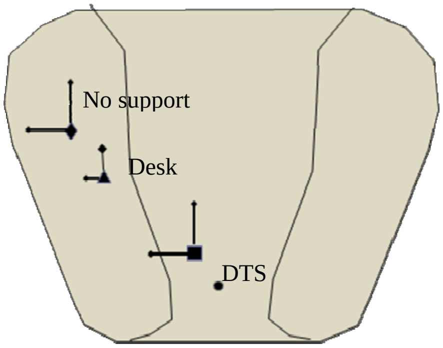

Figure 3: Changes to center of pressure position at maximal reach.

Leaning on the desk, reduces the 3-dimensional moment on the hip however it increases the lumbar spine rotation moment. Leaning on the DTS, reduces both spinal and hip moments without increasing the spinal rotation moment (Table 2).

	No support	Desk	DTS
L4/L5			
Flexion moment (Nm)	166.69 (3.79)	156.04 (4.06)	152.88 (3.1)
Lateral moment (Nm)	172.98 (4.13)	158.95 (3.86)	163.54 (4.1)
Twist moment (Nm)	17.21 (1.38)	18.51 (1.23)	14.94 (2.1)
Hip			
Flexion moment (Nm)	152.36 (3.32)	130.87 (2.23)	114.51 (2.39)
Lateral moment (Nm)	156.75 (3.96)	139.36 (3.83)	118.75 (3.25)
Twist moment (Nm)	16.58 (1.49)	18.49 (1.03)	15.36 (1.15)

Table 2: 3D moments for hip and L4/5. Repeated measure ANOVA presenting the main effects that were significant for at least one of the dependent variables (0.001).

DISCUSSION

Both supported postures reduced the postural muscle activity of the trunk suggesting that the longer reach distance associated with leaning forward is an important variable for consideration with standing work. Using the DTS for support appears to be favorable since it does not result in additional rotational moment at the lumbar spine which could contribute to an increased risk for back injury.

REFERENCES

1. Kerr et al., 2001, Am.J.Public Health, vol. 91, no. 7, pp. 1069-1075
2. Abdoli-E, et al. 2008, Clin.Biomech. 23, no. 3, 372-380
3. Tissot F. et al. S. 2005. Ergonomics 48(3):249-269.
4. Damecour C et al. ACE, (2008).

PARTIAL EXTERNAL SOFT TISSUE VIBRATION DAMPING DECREASES LOCAL OXYGEN CONSUMPTION

[1]Aurel Coza, [1]Benno M. Nigg, [2]Jeffrey F. Dunn and [3]Brady Anderson

[1]Human Performance Lab, University of Calgary, Calgary, Canada[2]Experimental Imaging Centre and
Dept of Radiology, University of Calgary, Calgary, Canada; [3] adidas AG, Herzogenaurach, Germany
email: acoza@kin.ucalgary.ca

INTRODUCTION

Soft tissue exposure to vibrations was shown to increase the muscle activity [1]. External soft tissue vibration damping, using compression apparel, was associated with an increase of the damping coefficient of the soft tissue compartments of the leg and a decrease of the muscle activity during vibrations exposure [2]. It is assumed, but not known, that a decrease in muscle activity induced by apparel could also decrease the energy used by the muscles to dampen soft tissue vibrations, thus leaving more energy available for the task at hand.

Therefore, the aim of this study was to quantify the effects of external soft tissue vibration damping on local muscle energy consumption.

METHODS

Eight subjects were selected for this study. All subjects were free of injuries at the time of the study.

The subjects were exposed to two testing conditions using control and compression apparel. Prior to testing, the subjects were instructed to repeatedly stand on toes (40 repetitions/minute) while standing on a vibration platform operating at a frequency of 16 Hz and an amplitude of 12 mm.

A pressure cuff was placed on the right thigh and rapidly inflated at 280 mmHg at the beginning of each testing trial. The pressure was maintained for 90 seconds for each trial. Three trials were performed for each condition. Each trial was followed by a 3 minute break (no pressure).

3D accelerometers were placed on the vibration platform and on the triceps surae in order to record the input (platform) and the transmitted vibration (triceps surae) respectively.

A Near Infrared Spectrometer (NIRS) optode (NIRO 200, Hamamatsu Photonics, Japan) was placed on the gastrocnemius medialis muscle in order to quantify changes in tissue oxyhemoglobin (HbO_2) concentration during arterial occlusion.

The vibration transmission coefficient (Tc) was computed as the ratio between the input vibration energy (vibration platform) and the soft tissue vibration energy (triceps surae). The energy of the vibration was computed from the individual power spectra of the acceleration signals by summing over all the discrete powers in the 5-50 Hz frequency range.

Oxygen consumption rate (VO_2) was determined by linearly fitting the linear portion of the HbO_2 concentration data (usually the first 30 seconds after the onset of exercise and cuff inflation) and expressing the result as the slope of the best fit line.

The absolute Tc and VO_2 values can not be compared across subjects due to the variability in tissue volume interrogated by the NIRS; therefore, the relative transmission coefficient (rTc) and relative oxygen consumption rate (rVO_2) were computed as the percentage change when comparing the control to the apparel condition.

RESULTS AND DISCUSSION

The HbO_2 concentrations during the first 60 seconds after the onset of exercise for the apparel and control condition are shown in figure 1. The slopes for the apparel and control condition are distinguished.

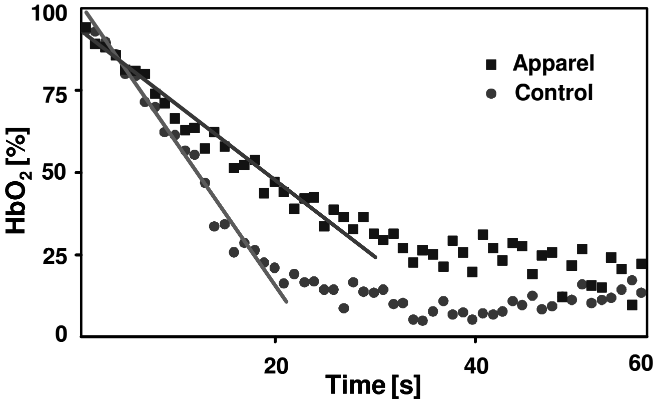

Figure 1: Oxyhemoglobin concentration for the apparel and control condition during the first 60 seconds after the onset of exercise.

A strong correlation (r^2=0.84) between the relative oxygen consumption rate (rVO_2) and the relative transmission coefficient (rTc) was observed (Fig 2).

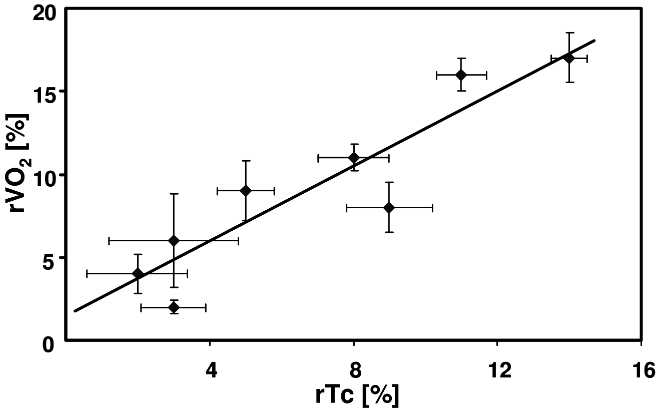

Figure 2: Relative transmissibility factors (rTc) vs. relative oxygen consumption rate (rVO_2) when changing from control to apparel condition.

A higher rTc value means a larger difference between the Tc-control and Tc-apparel (i.e. high apparel damping effects). A higher rVO_2 value represents a large difference between the VO_2-control and VO_2-apparel (i.e. a lower oxygen consumption rate for the apparel condition compared to control). A positive correlation between the two variables (rTc and rVO_2) indicates that the higher the external damping the higher the difference between the control and apparel oxygen consumption rate. Thus the apparel seems to decrease the oxygen consumption rate when compared to the control situation. Furthermore, the decrease in the oxygen consumption rate linearly correlates with the increase in the damping effects of the apparel.

Since both the transmissibility coefficient and the oxygen consumption rate are a measure of the energy of the system, a linear relationship between the two is generally expected. However, the oxygen consumption rate seems to increase more rapidly than the transmissibility.

Extrapolating these results to a less controlled setup (e.g. running) one could expect that apparel can have an impact on the muscle energy consumption by means of external soft tissue vibration damping. However, this is a local effect and although this has the potential to locally decrease the oxygen consumption, the mechanisms involved in this process are not fully understood and require further investigation.

CONCLUSION

This study has shown that:

(a) external damping of soft tissue vibrations (apparel) decreased the local oxygen consumption rate.
(b) there is a linear relationship between the vibration energy transmitted to the muscles and the effect on oxygen consumption rate.

REFERENCES

*1.*Nigg, BM and Wakeling, JM *Ex. and Sport Sci. Rev.*, 29(1): 37-41, 2001.
*2.*Coza A and Nigg BM, *NACOB,* Ann Arbor, MI, Abstract 253, 2008.

ACKNOWLEDGEMENTS

This study was financially supported by adidas AG and the da Vinci Foundation.

INSIDE/OUTSIDE FORCE RATIO AND SKI CHATTER IN SLALOM SKIING

Marjaana Lappi, Robert C. Reid, Per Haugen, Gerald Smith
Norwegian School of Sport Sciences, Oslo, Norway
email: marjaanalappi@gmail.com

INTRODUCTION

Although skiers must move laterally to balance against the ground reaction forces (GRF) during turning, they can control the force distribution between the inside and the outside ski through fine-tuning of lateral balance [1]. This force distribution is important for performance, yet it is a topic of debate in coaching circles.

Traditional philosophies describe a lateral balance where the GRF loading occurs predominantly on the outside ski. However, with recent developments in equipment, philosophies have emerged promoting a more even distribution. While this may reduce ski-snow friction when carving, it may also result in greater skidding and chatter. The purpose of this study was to describe and compare ground reaction forces in slalom skiing between two courses typical of competition.

METHODS

Nine male Norwegian skiers (body weight 859 ± 71 N) and FIS ranked between 165 and 705 (2007/08) were tested over 3 consecutive days. Kinetic characteristics were analyzed for 2 rhythmical course settings with linear distances of 10 and 13 m between gates. The middle 10 turns of each trial were analyzed to determine GRF using 50 Hz plantar pressure insoles (Novel GmbH, Germany) and associated data logging instrumentation shown in Figures 1 & 2.

Right and left turns were separately analyzed due to differences in the side-to-side slope gradient. Inside/Outside force ratio was calculated based on force impulse during each turn. The mean residual between raw force measurements and a smoothed force-time curve (cut-off frequency 5 Hz) was used to quantify chatter for each ski. Repeated measures ANOVA was used to compare turn directions and courses and Pearson's correlation to assess the relationship between chatter and force distribution.

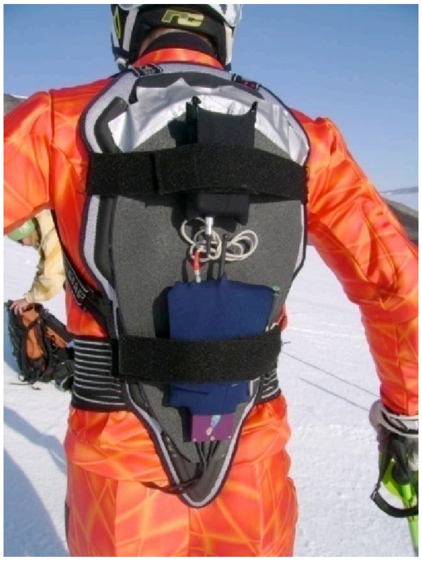

Figure 1. Data logging was accomplished with a portable acquisition system carried in a small backpack. Cables to the insole system were routed underneath a skier's standard suit.

Figure 2. Data were collected under simulated race conditions during a glacier training camp with hard snow surface conditions comparable to competition.

RESULTS AND DISCUSSION

Inside ski forces averaged about half to two-thirds of outside ski forces. This can be seen in the example trial shown in Figure 3. Inside/Outside ratios were on average greater for right-hand turns on both courses, but these differences were not statistically significant (Table 1). That right turns tended to have loading forces more evenly distributed between skis was perhaps due to the slight side-to-side gradient difference or perhaps due to leg dominance.

The inside ski of turns tended to chatter more than the outside ski in the tight turns of the 10 meter course. This larger mean chatter may be due to the shorter turn radius required of the inside ski.

Better performance was related to greater outside ski force distribution (lower ratio), as performance times correlated well with the Inside/Outside Force Ratio on both courses ($r = 0.81$, $p < 0.02$ for the 10 m course and $r = 0.73$, $p < 0.05$ for the 13 m course, n=8). No significant correlation was found between chatter and ski force distribution.

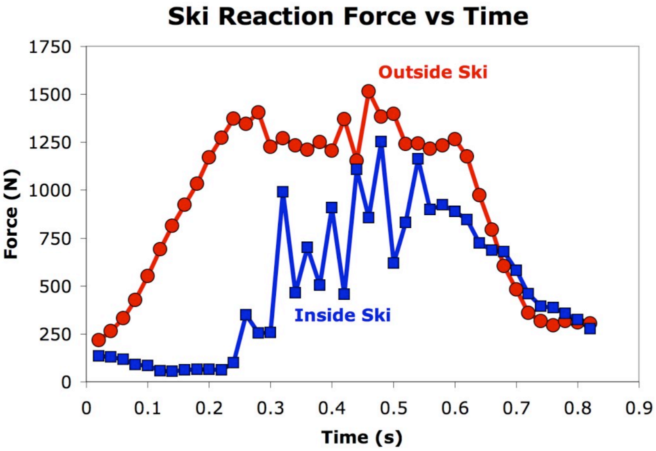

Figure 3. Representative ski reaction force curves during a single slalom turn. The ski to the outside of the turn typically had greater force than the inside ski. The rapid changes of force seen for the inside ski of this turn reflect "chattering" of the ski on the surface.

CONCLUSION

This study presents a novel approach to evaluating common slalom technique problems associated with ski force distribution and chattering of skis. Magnitude of chattering was not clearly related to the inside/outside force distribution. Technique training with such force measuring systems could potentially assist coaches in identification of problems associated with the ski force distribution between inside and outside skis.

REFERENCES

1. LeMaster R. *The Skier's Edge*. Human Kinetics: Champaign, IL.

ACKNOWLEDGEMENTS

We would like to thank the Norwegian Olympic and Paralympics Committee and the Norwegian School of Sport Sciences for funding support and Edge for participating in the study.

Table 1: Means ± SD Inside/Outside Force Ratio, Chatter Inside, Chatter Outside and Inside/Outside Chatter Ratio (n=9).

Course:	**10 meter**		**13 meter**		**Course Compare**
Turn Direction:	**Left**	**Right**	**Left**	**Right**	**L / R (p)**
Inside/Outside Force Ratio	0.59 ± 0.22	0.67 ± 0.13	0.54 ±0.21	0.63 ± 0.14	.077 / .096
Chatter Inside (N)	23 ± 7	24 ± 4	17 ± 5	17 ± 4	.0006 / .001
Chatter Outside (N)	15 ± 4	17 ± 4	16 ±4	16 ±3	.559 / .645
Inside/Outside Chatter Ratio	1.72 ± 0.27	1.86 ± 0.27	1.16 ± 0.25	1.20 ± 0.23	.0004 / .0003

EFFECTS OF A SINGLE STEP REQUIREMENT ON BALANCE RECOVERY MANEUVERS IN YOUNG AND OLDER ADULTS

Ghassan G. Dinn and Gregory W. King

Department of Civil and Mechanical Engineering, University of Missouri – Kansas City, Kansas City, MO, USA, kinggr@umkc.edu

INTRODUCTION

Step responses are often needed to prevent falls following large balance disturbances [1]. Numerous researchers have studied age effects on step responses using forward lean-and-release balance perturbations (e.g. [2,3]). To simplify testing and data analysis, these studies often require participants to take a single step in response to the balance perturbation. Compared to a step response without this constraint, instructions limiting the number of steps do not impact balance recovery among young adults [4]. However, age reduces the ability to recover balance with a single step [5]; therefore requiring older adults to take single steps may elicit unnatural responses in this population.

The goal of this study was to compare step responses with and without the single step requirement in young (YA) and older adults (OA). We hypothesized that: (1) OA, compared to YA, would use a step response with reduced landing phase ankle joint force; and (2) the single step requirement would cause OA, but not YA, to use larger landing phase ankle joint force in comparison to step responses without the single step constraint.

METHODS

Participants. Twelve healthy YA (mean age 25 ± 3.0 years) and thirteen healthy OA (mean age 71 ± 2.8 years) male participants were recruited and screened for major musculoskeletal, cardiovascular, and neurological disorders. Participants provided informed consent as approved by the institution's human subjects committee.

Tasks. Participants performed ten step responses facilitated by forward lean-and-release balance perturbations. No instructions were given to participants during the first five trials (instruction group #1). During the last five trials, participants were instructed to take a single step with the dominant limb (instruction group #2).

Measurements. Reaction forces and moments were sampled at 1 kHz from force plates (AMTI, Watertown, MA, USA) placed under initial left and right foot stance positions; and under the step foot landing position. Foot and shank positions were sampled at 120 Hz with a Vicon motion capture system (Vicon, Los Angeles, CA, USA) tracking reflective markers placed bilaterally on the second metatarsal, calcaneous, lateral malleolus, tibia, and femoral epicondyle. Manual foot and shank anthropometric measures were taken by the investigators with a measuring tape and callipers.

Data Analysis. An inverse dynamics algorithm was used to determine ankle joint dynamics during the landing phase of each response. Model inputs included force plate, motion capture, and anthropometric data. Model outputs included ankle joint force profiles, which were used to calculate maximum landing phase ankle joint forces in the proximal-distal (PD), medial-lateral (ML), and anterior-posterior (AP) directions.

Statistical Analysis. Statistical analysis was performed with SPSS (SPSS, Inc., Chicago, IL, USA). A multivariate analysis of variance (MANOVA) was performed on all outcome variables, with instruction group (GRP) as the within-subject factor and age group (AGE) as the between-subject factor. Follow-up univariate tests were performed on individual variables demonstrating a significant main effect or interaction. Comparisons with p-values <0.05 were considered statistically significant.

RESULTS and DISCUSSION

The MANOVA revealed a significant overall AGE effect on maximal ankle joint landing force ($p<0.05$). Follow-up univariate tests on this result revealed significant AGE effects on maximal ankle force in the proximal (age-related decrease: $p<0.05$) and posterior (age-related decrease: $p<0.01$) directions. The MANOVA failed to reveal a significant AGE x GRP effect ($p = 0.09$); however, individual univariate tests revealed a significant GRP effect on maximal posterior force (larger for single step condition: $p<0.05$). Follow-up paired t-tests within each AGE group revealed that this effect occurs in OA ($p<0.023$) but not YA ($p = 0.438$). Results are summarized in **Figure 1**.

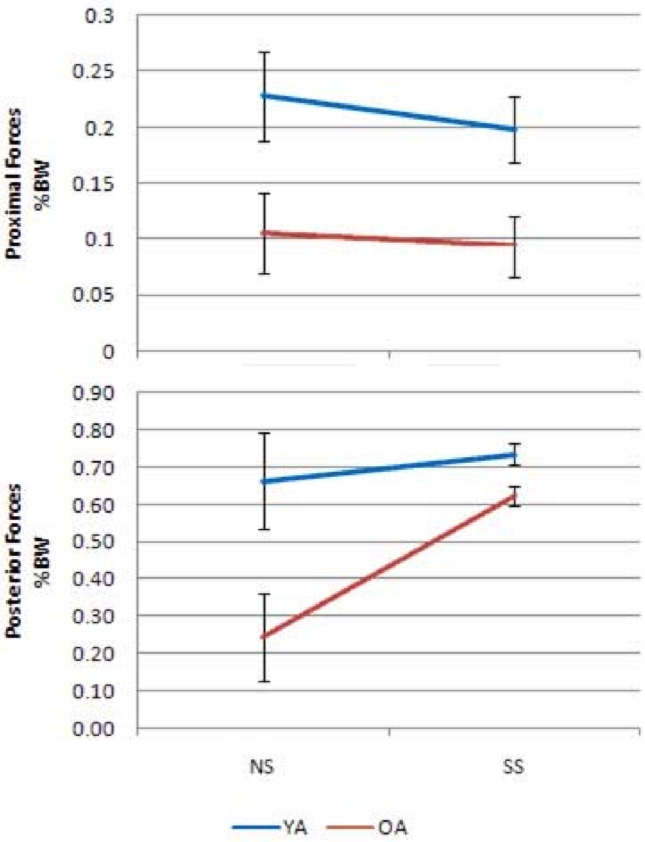

Figure 1: Maximal ankle joint landing forces for Natural Step (NS) and Single Step (SS) conditions.

These results suggest that OA, compared to YA, use smaller ankle joint forces when stepping to arrest a fall. This supports our first hypothesis that an age-related decline would be observed in landing phase ankle forces. This effect occurred in the proximal and posterior directions, suggesting an age-related decrease in the braking forces associated with the stepping maneuver. This effect is likely related to the tendency of OA to take multiple steps, which are smaller in magnitude and often not sufficient to arrest the body's forward momentum [6].

The non-significant AGE x GRP interaction suggests a similar overall GRP effect in each AGE group. This does not support our second hypothesis that OA, but not YA, would generate larger landing forces with a single step requirement. However, we observed a significant GRP effect when considering only maximal posterior ankle force, suggesting larger forces for the single step condition. Follow-up testing revealed that this effect only occurred in OA, suggesting that OA may alter their strategy based on stepping instructions. Although not specifically quantified here, OA may have used larger step lengths to ensure a successful recovery [5], a strategy likely associated with larger biomechanical demands [2]. The absence of this tendency in YA is consistent with studies demonstrating no instructional effects in YA [4].

CONCLUSIONS

This study demonstrates an age-related decrease in ankle joint landing forces used during a balance-restoring step response. Overall, instructions limiting the number of steps did not have an effect on ankle joint forces in YA or OA. However, OA appear to use larger maximal posterior ankle force when asked to take a single step, an effect not observed in YA. This suggests that imposing a single step requirement may elicit unnatural responses among OA during step response balance testing paradigms.

REFERENCES

1.Luchies CW, et al. *J Am Geriatr Soc* **42**, 506-512, 1994.
2.King GW, et al. *Gait Posture* **22**, 219-224, 2005.
3.Thelen DG, et al. *J Gerontol A Biol Sci Med Sci* **52**, M8-13, 1997.
4.Cyr MA, et al. *J Biomech* **40**, 2857-2864, 2007.
5.Wojcik LA, et al. *J Gerontol A Biol Sci Med Sci* **54**, M44-50, 1999.
6.Schulz BW, et al. *Gait Posture* **22**, 198-209, 2005.

A PHENOMENOLOGICAL MODEL OF SHORTENING INDUCED FORCE DEPRESSION DURING MUSCLE CONTRACTIONS

[1]Craig P. McGowan, [1]Richard R. Neptune and [2]Walter Herzog
[1]Department of Mechanical Engineering, University of Texas at Austin, Austin, TX, USA
[2]Faculty of Kinesiology, University of Calgary, Calgary, AB, Canada
email: cpmcgowan@mail.utexas.edu, web: www.me.utexas.edu/~neptune/

INTRODUCTION

History dependent effects on muscle force development such as shortening induced force depression have long been known to exist in skeletal muscles. These effects have been identified in individual muscle fibers [1], whole muscles *in situ* [2], whole muscles *in vivo* [3] and whole muscle groups *in vivo* [4]. However, the experimental protocols required to identify history dependent effects do not readily permit the evaluation of how they influence cyclic movements in locomotor tasks such as walking.

Computer modeling and simulation provide a theoretical framework for examining how intrinsic muscle properties influence movement performance. Currently, few muscle models exist that attempt to include history dependent effects. Therefore, the first step towards understanding the influence of history dependent effects on complex movements must be to develop a muscle model that reliably reproduces experimental data when the experimental conditions are simulated. The specific aim of this study was to develop a Hill-type muscle model and simulations of whole muscle in situ experiments that reproduce the timing and magnitude of shortening induced force depression previously measured in cat soleus muscles [2].

METHODS

The muscle model and simulations were developed using SIMM (MusculoGraphics, Inc). The experimental muscle ergometer was modeled with two blocks mounted horizontally on a frictionless surface with a muscle governed by Hill-type intrinsic properties mounted between them. One block was fixed while the other block underwent prescribed linear motion in which velocity was controlled. Values for the optimal muscle fiber length (36 mm), tendon slack length (74 mm, including aponeurosis), maximum shorting velocity (3.3 lengths/sec) and maximum isometric force (22.4 N) were set to the approximate average values for a cat soleus muscle.

Simulations were developed to match the protocol from the experimental study [2]. Briefly, the experiment was designed to compare the isometric force following a constant velocity contraction with the isometric force of a muscle that did not shorten. To account for force-length effects, all contraction ended at the same length (4mm less than optimal). Two sets of experiments were conducted to examine the effects of shortening length and shortening velocity. In the first set of experiments, shortening velocity was held constant (4 mm/s) and the initial muscle length was varied such that the muscle shortened over different lengths (2, 4, 6, 8 and 10mm). In the second set of experiments, the muscle shortened a fixed amount (8 mm) at a range of constant velocities (4, 8, 16, 32, 64 and 256 mm/s).

Previous research has shown a strong correlation between muscle work during shortening and shortening induced force depression [2]. Therefore, in our model the magnitude of force depression was calculated based on cumulative muscle work, assuming a linear relationship derived from previous experimental data [2]. In addition to magnitude, experimental studies have also identified a transient component to force depression which affects the rate at which force returns to a steady state level following shortening. We modeled the transient recovery after Corr and Herzog [5] who developed an exponential recovery function and showed it was moderately correlated with muscle work. Finally, consistent with experimental results, force depression in the simulations persists until muscle activation drops to zero.

RESULTS AND DISCUSSION

The results of the simulations were in excellent agreement with the experimental data. The constant velocity experiments exhibited both an increase in steady-state force depression and a decrease in the rate of force recovery with increasing length change (Fig 1A). The variable velocity experiments exhibited a decrease in steady state force depression and an increase in rate of force recovery with increasing shortening velocity (Fig 1B).

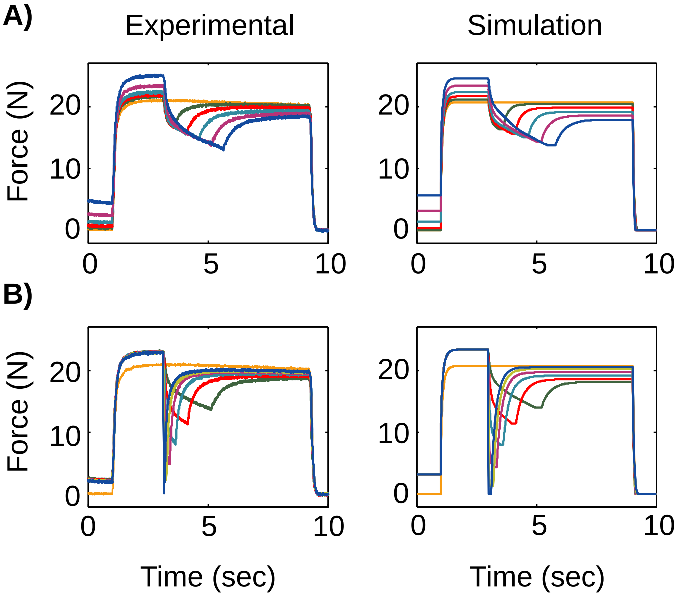

Figure 1. The simulations of *in situ* experiments (right) were accurately able to reproduce the experimental data (left) showing the effects of changing A) length and B) shortening velocity on history dependent force depression.

In addition to accurately describing history dependent force depression, our simulations also revealed a good agreement between experimental and simulated force-length and force-velocity effects. During the longest constant velocity shortening trials (8 and 10mm) the initial length of the muscle was 10-15% greater than optimal and passive force contributed to both the passive (0-1 sec) and initial isometric forces (1-3 sec). The increase due to this passive contribution was similar between the experimental and simulated data.

The maximal shortening velocity of the cat soleus is between 3 and 4 lengths/sec, thus our value of 3.3 lengths/sec is well within the biological range. During both the constant velocity and variable velocity conditions, the magnitude of force decrease due to shorting velocity was very similar between experimental and simulated data.

Despite the good agreement between experimental and simulated muscle force, there were some limitations to the current model. First, the simulated muscle forces tended to reach maximal values more quickly than the experimental forces and the simulations did not have as gradual of a curvature as isometric force was reached (~1-2 sec). This is most likely due to differences in the series elastic compliance used in the model. The free tendon of the cat soleus is very stiff, however the aponeurosis and muscle tissue itself are likely much more compliant. In the current simulations, we account for the aponeurosis in the series elastic compliance, but not the muscle tissue. Thus, it is likely that the value we selected to represent the net series elastic compliance may have been too stiff. The second limitation in the current model was that the algorithm used to identify the end of shortening relied on calculating the fiber acceleration and thus could not detect the end of shortening until a frame past when it occurred. This limitation had the effect of producing a “flat spot” just before the transient period of force recovery began. However, we feel these limitations are relatively minor and should not have a substantial impact on interpreting the influence of shortening induced force depression on cyclic movements.

CONCLUSIONS

The results of our study show that a relatively simple phenomenological muscle model can accurately reproduce experimentally measured shortening induced force depression. In future studies, the model will be incorporated into more complex musculoskeletal models to examine the influence force depression has on cyclic movements such as walking or pedaling.

REFERENCES

1. Edman et al. *J. Physiol. Lond.* 281, 139-155, 1978.
2. Herzog et al. *J. Biomech.* 33, 659-668, 2000.
3. DeRuiter et al. *J. Physiol.* 507, 583-591, 1998.
4. Lee et al. *J. Appl. Physiol.* 87, 1651-1655, 1999.
5. Corr and Herzog, *J. Appl. Physiol.* 99, 252-260, 2005.

EFFECTS OF BACKWARD WALKING ON BALANCE AND LOWER EXTREMITY WALKING KINEMATICS IN HEALTHY YOUNG AND OLDER ADULTS

Janet S. Dufek, John A. Mercer, Jennifer M. Aldridge, Geoffrey G. Melcher and Philana-Lee Gouws
Department of Kinesiology and Nutrition Sciences, University of Nevada, Las Vegas, Las Vegas, NV, USA
email: jdufek@unlv.nevada.edu, web: http://kinesiology.unlv.edu.

INTRODUCTION

Falls are a leading cause of morbidity in the United States, especially among the older adult population. More than one-third of adults in the U.S. who are 65 years of age and older experience a fall each year [1]. Among older adults, falls are the leading cause of injury deaths and the most common cause of nonfatal injury and hospital admission for trauma [2]. We questioned whether a backward walking intervention would augment stability and enhance range of motion of the lower extremity joints during forward walking, thus potentially leading to fall reduction. The purpose of the study was to compare overall system balance and lower extremity kinematic patterns during walking between healthy younger and healthy older adults following a four-week intervention of backward walking. We hypothesized that the intervention would significantly improve balance for the older adult population. We further hypothesized that lower extremity kinematic patterns (range of motion values) would more closely approximate patterns exhibited by young adults following the intervention.

METHODS

Ten healthy young adults (21.9±2.8 yrs; 175.3±10.5 cm; 70.4±11.5 kg) and 10 healthy, non-faller older adults (69.8±7.7 yrs; 167.8±11.8 cm; 70.7±15.2 kg) volunteered to participate. After providing institutionally approved written informed consent, all participants completed a balance pre-test which consisted of five stability tests performed on a balance platform (Bertec; 3000 Hz): 1) normal stance, eyes open (N-EO), 2) normal stance, eyes closed (N-EC), 3) perturbed stance, eyes open (P-EO), 4) perturbed stance, eyes closed (P-EC), and 5) limits of stability (LOS). The perturbed stance condition was defined as that obtained while standing on a 3 cm thick piece of foam. The average of three balance trials for each test was used for subsequent analysis. Participants were instrumented with 16 lower body reflective markers (Plug-in-Gait model). A 12-camera motion capture system (Vicon, 120 Hz), calibrated per manufacturer's instructions, was used to obtain kinematic data during both forward (n=5) and backward (n=5) walking trials at preferred velocity (pre-test). A four-week backward walking exercise intervention (10-15 min/day; 3 days/wk) followed. At the end of the second (mid) and fourth (post) week of backward walk training, balance tests were repeated following the same procedures as during the pre-test. Kinematic assessment was conducted during pre and post testing sessions only. Five dependent variables (individual balance test scores) were evaluated using 2 (group) x 3 (session) mixed model analyses of variance ($\alpha=0.05$). A low pass Butterworth filter (fc=6 Hz) was used to smooth the kinematic position data prior to calculation of derivatives. Seven kinematic dependent variables including sagittal plane lower extremity joint range of motion (ROM), maximum lower extremity joint angular velocity and knee joint coronal plane (varus-valgus) ROM values were evaluated during the support phase of forward and backward walking using 2 (group) x 2 (session) mixed model analyses of variance ($\alpha=0.05$).

RESULTS AND DISCUSSION

There were no significant group x session interactions observed for any of the balance variables. Group (young vs. old) was significantly different for P-EO ($F_{1,18}=6.02$; p=0.0246), P-EC ($F_{1,18}=10.15$; p=0.0051) and LOS. Session (pre, mid, post) was significantly different ($F_{2,18}=5.02$; p=0.0102) for P-EC. Balance test results are summarized graphically in Figures 1-2.

There were no significant group x session interactions observed for any of the kinematic parameters. There were no significant differences between groups in lower extremity kinematics during the support phase of forward walking. Both groups significantly increased backward walking velocity across the intervention period ($F_{1,18}$=33.22; p<0.0001). During backward walking, older adults exhibited significantly greater ROM at the ankle ($F_{1,18}$=7.36; p=0.0143) vs young adults. In addition, there was a significant difference observed between groups for knee joint varus-valgus ROM, with older adults exhibiting greater ROM ($F_{1,18}$=11.51; p=0.0032). Maximum angular velocity of the ankle joint was observed to be different between test sessions ($F_{1,18}$=14.33; p=0.0014) with both groups exhibiting increased maximum angular velocity of the ankle following the intervention.

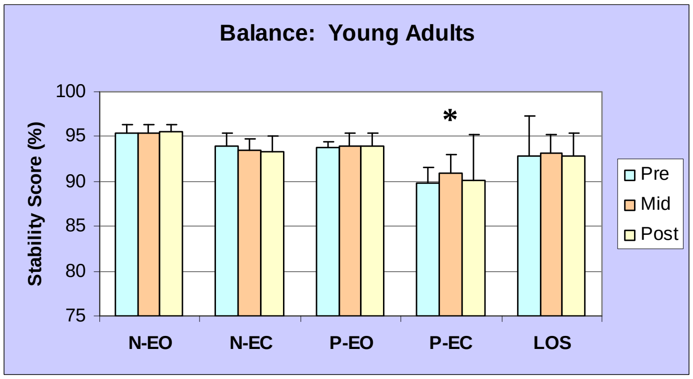

Figure 1. Balance scores for young adults across test sessions. * p<0.05 among test sessions.

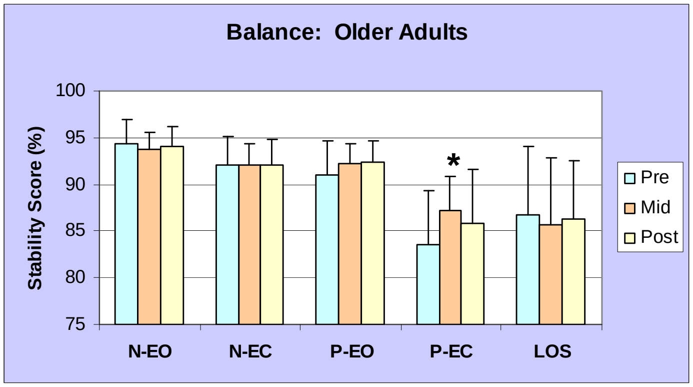

Figure 2. Balance scores for older adults across test sessions. * p<0.05 among test sessions.

We anticipated differences between groups in balance and kinematic measures. Results refuted our hypothesis that there would be differences in forward walking kinematics between groups. We did observe differences in balance outcomes as a result of the backward walking intervention. Differences were observed for the most challenging balance task (P-EC) with both groups exhibiting significantly improved stability following backward walking. Older adults also exhibited a trend toward improvement in balance for P-EO (Figure 2). We also sought to determine if differences in lower extremity forward walking kinematic characteristics would exist for older adults following the backward walking intervention. Since there were no observed differences in lower extremity kinematics during forward walking between groups, results can speak only to the potential benefits of backward walking on improving balance characteristics.

Observed differences in ankle joint kinematics following the intervention for both young and older adults does deserve greater attention. It is known that toe clearance during the swing phase of gait decreases with age [3]. A change in ankle joint kinematics that might be induced as a result of walking backward could be of benefit relative to reducing fall occurrence for older adults and other populations at risk for falls and deserves further study. In addition, additional exercise prescriptions may induce differential responses.

CONCLUSIONS

Results of the study suggest that backward walking may enhance stability during a challenging balance task for healthy younger and older non-faller populations. The implications of this intervention for those at risk for falls may be even more remarkable. Additional research is warranted to examine this possibility.

REFERENCES

1. Hausdorff, JM et al. Gait variability and fall risk in community-living older adults: A 1-year prospective study. *Archives of Phys Med Rehabil.* **82,** 1050-1056, 2001.
2. Centers for Disease Control and Prevention (CDC). Falls among older Adults: An overview. http://www.cdc.gov/ncipc/factsheets/adultfalls.htm Retrieved on April 12, 2007.
3. Mills PM et al. Toe clearance variability during walking in young and elderly men. *Gait & Posture* **28,** 101-107, 2008.

ACKNOWLEDGEMENTS

Partially funded by Bertec Corporation, Columbus, OH and the President's Research Award, University of Nevada, Las Vegas, Las Vegas, NV.

A THREE-DIMENSIONAL KINEMATIC AND KINETIC COMPARISON OF OVERGROUND AND TREADMILL WALKING IN HEALTHY ELDERLY SUBJECTS

[1] Jaclyn R. Watt, [1]Jason R. Franz, [1]Keith Jackson, [1]Jay Dicharry,
[1]Patrick. O. Riley and [1]D. Casey Kerrigan
[1]Department of Physical Medicine and Rehabilitation, University of Virginia, USA
email: dck7b@virginia.edu

INTRODUCTION

Instrumented treadmills offer a number of advantages for the biomechanical analysis of elderly gait, yet it is unclear how closely treadmill gait approximates overground gait. Although studies have indicated that the kinematics and kinetics of overground and treadmill gait are very similar in young adults [1-3], very few studies have investigated treadmill walking in the elderly. In order to validate the use of instrumented treadmills with an elderly population, the differences between treadmill and overground gait in the elderly must be understood. The purpose of this study, therefore, was to compare the three-dimensional kinematics and kinetics of treadmill gait to overground gait in a group of healthy elderly subjects.

METHODS

Three-dimensional kinematic and kinetic data for eighteen healthy, nondisabled elderly subjects, age 65 to 81 years (mean, 70.3yrs), were collected for speed-matched overground and treadmill walking conditions. Ground reaction force signals from an AMTI compound instrumented treadmill (AMTI, Watertown, MA, USA) and stationary in-ground force plates were collected and synchronized with kinematic data from a ten camera VICON 624 motion analysis system (Figure 1).

Each subject first walked 15 m overground at his or her self-selected comfortable walking speed until at least three complete gait cycles were collected for each lower limb. The average walking speed of two randomly selected overground trials for each subject was determined to establish speed for subsequent treadmill walking trials. Subjects then walked on the side-by-side treadmill force plate units for a two minute acclimation period followed by a 30 second data collection period.

Motion capture and GRF data were processed using VICON Plug-in Gait to calculate joint kinematics, joint kinetics, and temporospatial parameters (VICON, Centennial, CO, USA). Data obtained from the instrumented treadmill were pre-processed using in-house algorithms implemented in LabView (National Instruments, Austin, TX, USA). Maximum and minimum kinematic and kinetic values at characteristic peaks were obtained from each subject's average curves. The differences between each subject's overground and treadmill maxima and minima were evaluated using paired-samples *t*-tests.

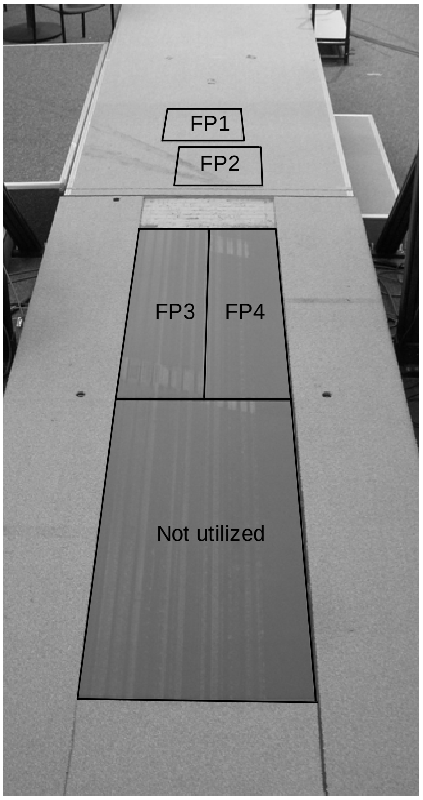

Figure 1. Location of individual force plates on the raised walkway. FP3 and FP4 are imbedded in the split belt treadmill. Overground trials used any of the four plates while treadmill trials used FP3 and FP4.

RESULTS AND DISCUSSION

This comparison of treadmill to overground gait in elderly subjects revealed the adoption of both a quicker cadence and shorter stride length during treadmill walking (Table 1). The majority of absolute kinematic maxima and minima were reduced for treadmill walking, implying a larger range of motion for overground gait. While the overall patterns of the three-dimensional joint moments at the hip, knee, and ankle were similar for treadmill and overground walking, significant reductions in sagittal and coronal plane hip and knee joint moments were observed during treadmill walking. Also, treadmill gait showed significant reductions in ankle and hip power generation and power absorption at the knee during push-off.

Compared to our previous study of young adults [1], temporospatial differences between treadmill and overground walking were much greater in the elderly than in the young adult population (Table 1). Similar reductions in joint angles and moments and also hip power generation and knee power absorption were observed in young adults during treadmill walking, but to a lesser extent than was seen in the elderly subjects. Although a two minute accommodation period was used and subjects reported feeling comfortable prior to data collection, possible inexperience of the elderly subjects with treadmill use may have contributed to the gait related changes that were observed.

CONCLUSIONS

Most of the differences observed between treadmill and overground walking are likely due to changes in temporospatial parameters that may be linked to treadmill unfamiliarity. Because of this, we believe that instrumented treadmill use for research or training purposes in the elderly is appropriate, but that accommodation to treadmill ambulation may likely be more difficult than is observed in young adults.

REFERENCES

1. Riley, P. O., et al. *Gait Post.* **26**, 17-24. 2007.
2. Murray, M. P., et al. *J. Appl. Phys.* **59**, 87-91. 1985.
3. Matsas, A., et al. *Gait Post*. **11**, 46-53. 2000.

ACKNOWLEDGEMENTS

This study was funded in part by a grant from the National Institute of Health (R01 AG027192).

Table 1. Mean (SD) temporospatial characteristics for both young and elderly subjects for treadmill and overground walking, with *p*-values reported for the elderly subjects. SD = standard deviation.

	Young (Mean 23.4 yrs, SD 4.3)		Elderly (Mean 70.3 yrs, SD 4.8)		
	Treadmill	Overground	Treadmill	Overground	*p*
Speed (m/s)	1.40 (0.16)	1.45 (0.17)†	1.25 (0.21)	1.27 (0.20)	0.069
Cadence (steps/min)	113.43 (7.83)	113.48 (7.78)	116.88 (10.63)	110.10 (7.60)	0.009*
Stride Time (s)	1.06 (0.07)	1.07 (0.07)	1.04 (0.09)	1.10 (0.08)	0.009*
Stride Length (m)	1.49 (0.13)	1.53 (0.13)†	1.30 (0.24)	1.39 (0.19)	<0.001*

† Significant difference in the young adult study ($p < 0.05$) [1].
* Significant difference in the elderly adult study ($p < 0.05$).

CUMULATIVE KNEE LOADING RELATES TO PAIN INTENSITY AND KNEE EXTENSOR TORQUE IN PEOPLE WITH KNEE OSTEOARTHRITIS

[1]Monica R. Maly and [2]Shawn M. K. Robbins
[1]School of Rehabilitation Science, McMaster University, Hamilton, ON, Canada, mmaly@mcmaster.ca
[2]School of Physical Therapy, The University of Western Ontario, London, ON, Canada, smrobbin@uwo.ca

INTRODUCTION

The peak knee adduction moment (KAM) has received much attention as a proxy for medial loading in knee osteoarthritis (OA). One limitation, however, is that the peak KAM represents exposure to loading during a single stride and therefore does not represent loading experienced throughout daily activity. The mechanical properties of articular cartilage in response to load vary in a time-dependent manner [1]. Furthermore, two individuals may have the same peak KAM but one could be twice as physically active as the other.

Representing the total exposure to knee loading, accounting for magnitude, abnormality and repetition may be useful in understanding clinical outcomes in knee OA. Cumulative loading represents a total exposure to loading, reflecting both the nature and repetition of loads [2]. It shares a dose-response relationship with osteoarthritic changes in the spine [3]. Although cumulative load is a recognized mechanism in low back injury [4], it has not been studied in knee OA. The purpose of this study was to compare relationships between the peak KAM and cumulative knee loading (CKL) with pain and knee extensor torque in knee OA.

METHODS

A convenience sample of 7 adults with radiographic knee OA was recruited through an orthopaedic clinic (age 53 ± 9 years, body mass index 29 ± 4 kg/m^2, 1 women).

Pain intensity was captured on the P4 questionnaire, which asks participants to rate pain intensity (0=no pain, 10="pain as bad as it can be") in the morning, afternoon, evening and with activity. Mean peak knee extensor torque of the OA knee was measured on the Biodex System 3 isokinetic dynamometer (Biodex Medical Systems, New York, USA). After submaximal practice, participants completed 5 concentric maximal knee extensor contractions at 60°/s. The mean peak values were normalized to body mass. Torque measurements were not collected on one participant due to drop-out.

Daily CKL was the product of the stance KAM impulse and mean number of steps per day. The KAM impulse was calculated using gait data from 8 cameras (Motion Analysis Corp., Santa Rosa, USA) with a sample rate of 60 Hz and a synchronized floor-mounted force plate (AMTI, Watertown, USA) with a sample rate of 1200 Hz. A Helen-Hayes marker configuration was used, with 21 reflective markers. Participants stood on the force plate to provide a reference frame. Participants actively flexed, extended, abducted and adducted the hip to calculate functional hip centres. The KAM waveform was extracted. The stance phase was integrated, using the trapezoidal rule in a custom Matlab program (Mathworks Inc., Natick, USA). The mean KAM impulse from 5 trials was calculated but was not normalized to mass or height to represent the absolute load borne through the medial compartment. The mean number of steps taken daily (steps/day) was measured with a uni-dimensional accelerometer (ActiGraph, Fort Walton Beach, USA) with an epoch of 60 seconds. The epoch represents the period for which a sum of the number of steps is written to memory. Participants wore the accelerometer for 7 consecutive days over the midline of the affected thigh.

Pearson correlation coefficients were calculated between P4 scores and mean peak extensor torque/mass with the peak KAM, CKL, impulse and steps/day.

RESULTS

A broad range of values was noted in pain, extensor torque, peak KAM and CKL, as well as the knee adduction moment impulse and steps/day. Pain and peak KAM values appeared typical for a sample with knee OA. Steps/day revealed very low levels of physical activity (Table 1).

Table 1: Descriptive statistics for pain, extensor torque, peak adduction moment and cumulative knee loading variables.

Variable	Mean (SD)	Range
P4 Pain Score (/40)	16.7 (5.2)	9 – 23
Peak Knee Extensor Torque (Nm)	140.2 (48.3)	61.4 – 180.7
Peak Knee Extensor Torque/Mass (Nm/kg)	1.22 (0.68)	0.83 – 1.98
Peak Knee Adduction Moment (Nm/kg)	0.55 (0.12)	0.45 – 0.79
Cumulative Knee Load (KNm*s)	77.5 (41.8)	30.0 – 132.9
Knee Adduction Impulse (Nm*s)	23.0 (9.9)	12.9 – 39.4
Steps/day	3382 (1488)	1920 – 6118

Correlates with Pain

Pain shared a weak relationship with the peak KAM (r=0.18). However, relationships between pain and the CKL (r=-0.30) or knee adduction impulse (r=-0.31) were moderate. Pain shared no relationship with the number of steps/day (r=0.00).

Correlates with Knee Extensor Torque/Mass

Knee extensor torque normalized to body mass had no relationship with the peak KAM (r=0.04, Figure 1) and a weak relationship with CKL (r=0.18). However, knee extensor torque normalized to body mass related to the knee adduction impulse (r=0.32, Figure 2). No relationship was found between extensor torque/mass and the number of steps/day (r=-0.13).

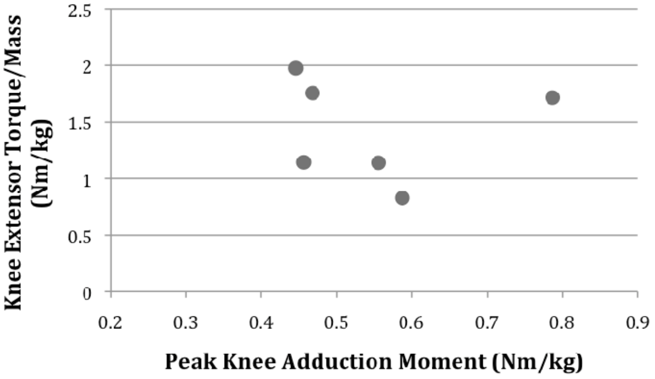

Figure 1: No relationship (r=0.04) between the peak knee adduction moment and extensor torque normalized to mass.

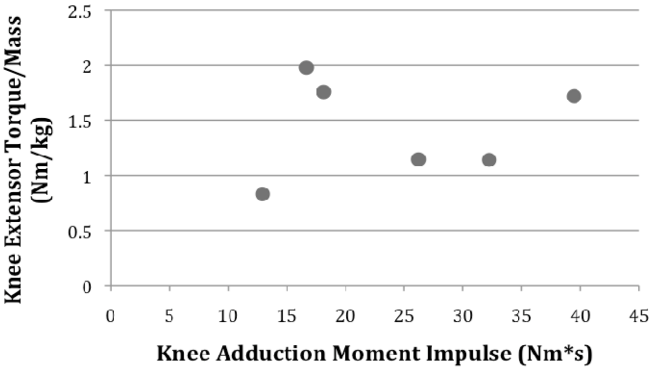

Figure 2: Knee adduction impulse related to extensor torque normalized to mass (r=0.32).

DISCUSSION AND CONCLUSIONS

Pain intensity and knee extensor torque showed stronger relationships with exposure to medial loading (CKL and impulse) than peak loading. Previous work [5] has also shown stronger relationships between pain and impulse versus peak. This study adds by relating knee extensor torque to loading characteristics. Thus, exposure to loading variables show promise in understanding the mechanical pathology underlying knee OA.

This sample had very limited exposure to walking, well below recommendations for physical activity and normative values for healthy adults [6]. The effectiveness of walking programs in knee OA may simply reflect physical re-activation. Because the number of steps/day did not relate to pain intensity or knee extensor torque, it appears that pain and weakness may not contribute to physical inactivity. However, the small sample and limitations of accelerometry to capture modes of physical activity other than walking and running are limitations. Nevertheless, the factors that limit walking activity in people with knee OA deserve attention.

REFERENCES

1. Flachsmann et al. *J Orthop Res* **19**, 1131-1139, 2001.
2. Kumar. *Spine* **15**, 1311-1316, 1990.
3. Seidler et al. *Occup Environ Med* **58**, 735-746, 2001.
4. Norman et al. *Clin Biomech* **13**, 561-573, 1998.
5. Thorp et al. *Arthritis Rheum* **57**, 1254-1260, 2007.
6. Bohannon et al *Phys Ther* **87**, 1642-1650, 2007.

ACKNOWLEDGEMENTS

Fowler Kennedy Sports Medicine Clinic Internal Funding Competition and the Natural Sciences & Engineering Council of Canada #353715-2008.

INVARIANT DENSITY ANALYSIS OF POSTURAL SWAY AND PROSPECTIVE FALL RISK IN COMMUNITY-DWELLERING ELDERLY

Pilwon Hur[1], Hyun Gu Kang[2,3], Lewis A. Lipsitz[2], and Elizabeth T. Hsiao-Wecksler[1]

[1] Mechanical Science & Engineering, University of Illinois at Urbana-Champaign, Urbana, IL
[2]Institute for Aging Research, Hebrew SeniorLife; Harvard Medical School; Beth Israel Deaconess Medical Center, Boston MA; [3]Biomedical Engineering, Boston University, Boston MA

E-mail: ethw@uiuc.edu Web: www.mechse.uiuc.edu/research/hsiao-wecksler/

INTRODUCTION

Falls are one of the most common health concerns facing elderly persons today. About one-third of community-dwelling persons over the age of 65 and nearly one-half of institutionalized persons will fall each year.

Most prior studies have examined fall risk factors based on statistical descriptions of the current behavior of subjects. For instance, traditionally, center of pressure (COP) data have been analyzed using measures that describe the shape or speed of the trajectory. However, these traditional COP parameters represent only the present body sway behavior during the data collection, not in the future. Even though present behavior states may be associated with future falls, there is no *a priori* reason to expect that these traditional measures fully represent the future behavior of COP. That is, traditional measures in themselves are not designed for predicting future events.

A Markov-chain model can be used to determine how the COP behavior will evolve to a stationary distribution, called the Invariant Density. This invariant density analysis (IDA) procedure for examining COP behavior has been found to be successful at distinguishing and providing physiological insight into age-related differences in postural control behavior in a cross-sectional study on healthy young, middle-aged, and elderly adults [1]. In the current study, we propose to validate whether IDA parameters, which predict future states of COP, have the ability to predict fall risk of an elderly cohort of community-dwelling men and women.

METHODS

Experiment

Data were analyzed from the MOBILIZE Boston Study, an ongoing population-based study of 765 community-dwelling older adults [4]. We used data from the first 600 participants. After excluding for insufficient falls follow-up and unacceptable IDA noise level (≥0.5mm), 304 adults were categorized as non-recurrent fallers (< 2 falls) and 140 adults were categorized as recurrent fallers (≥ 2 falls) based on their prospective falls calendars and follow-up phone calls during the first year of study. Anterior-posterior (AP) and medial-lateral (ML) COP data were collected at baseline. Subjects were asked to stand quietly on a force plate for five 30s trials with their eyes open. COP data were sampled at 240 Hz.

COP analysis

IDA is an analysis tool for COP data using a Markov-chain model. IDA assumes that COP data are stochastic, and future COP movement depends only on the present location of the COP. A "state" is defined as the distance from the centroid of the COP stabilogram to the COP current position. (The width of each state ring is 0.2 mm, as determined by the force platform noise level.) The long term movement of the COP is determined by the invariant density, which is an eventual distribution of probability of finding the COP at any given distance away from the center. Invariant density can be computed as the left eigenvector of the transition matrix, which describes the transition probability of the COP from one state to another. Therefore, analyzing the invariant density can give insight to the future behavior of the COP.

Invariant density is characterized by five parameters.

1. *Ppeak*: Identifies the largest probability of the invariant density.
2. *MeanDist* ($\sum_{i\in I} i\pi(i)$): Weighted average state (or average location) that contains the location of the COP. (*I* is the set of all states).
3. *D95*: 95% of the COP data are contained within and below this and all previous states.
4. *EV2*: The second largest eigenvalue of the transition matrix, which corresponds to the rate of convergence of the invariant density.
5. *Entropy* ($-\sum_{i\in I} \pi(i)\log_2 \pi(i)$): Describes the randomness of the system; i.e., low entropy corresponds to a more deterministic system and high entropy refers to a more stochastic system.

In order to compare the IDA parameters to common measures of COP, we also evaluated fall status in terms of traditional descriptive statistical COP measures (TRAD, [2]) and another stochastic-based COP analysis method, Stabilogram Diffusion Analysis (SDA, [3]).

Statistical analysis

One-way analysis of variance (ANOVA) was used to test for differences between non-recurrent (NF) and recurrent fallers (RF), with α = 0.05 (SPSS Inc., Chicago, IL; v15).

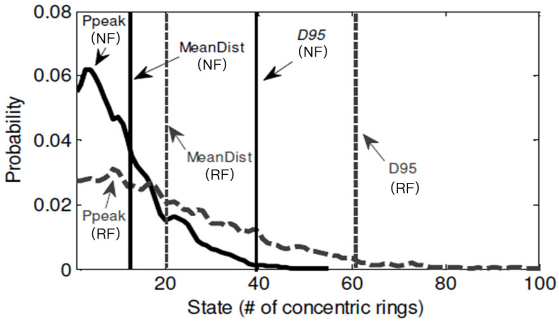

Figure 1. An example plot of the invariant densities of both NF (solid) and RF (dashed) showing the eventual distribution of probability that the COP will be found in a particular state

RESULTS/ DISCUSSION

Significant differences in COP measures were found between recurrent fallers (RF) and non-recurrent fallers (NF) (Table 1).

All IDA measures except *EV2* successfully distinguished recurrent fallers from non-recurrent fallers (Table 1). Only a few SDA and TRAD measures could make this distinction.

Table 1. IDA, SDA, and TRAD parameters with statistically significant differences between NF and RF. Mean±SE

	NF n=304	RF n=140	P
IDA			
Ppeak	0.047±0.0001	0.043±0.001	0.007
MeanDist	3.53±0.06	3.98±0.14	0.001
D95	8.43±0.15	9.56±0.33	<0.001
EV2	0.9992 ± 10^{-5}	0.9993 ± 10^{-5}	0.072
Entropy	5.33±0.025	5.47±0.038	0.001
SDA			
AP_crit dist	20.18±0.92	26.32±2.54	0.005
Rad_crit dist	31.64±1.46	38.90±3.74	0.030
TRAD			
MaxDistRad	14.51±0.24	15.41±0.39	0.043
SD_Rad	5.62±0.09	5.98±0.16	0.042
Range_AP	23.20±0.38	24.68±0.61	0.033
Power_AP	130.90±4.84	153.74±9.62	0.019

Smaller *Ppeak*, larger *MeanDist* and *D95* imply that COP of RF are more likely to stay away from the centroid and tend to wander around wider and more randomly than NF. Larger *Entropy* implies that the COP of RF follow more stochastic paths. This can be interpreted as RF having less degree of active control to keep the COP trajectory closer to the centroid. Finally, even though there were no statistical differences in *EV2* between groups, RF tended to have larger *EV2*, indicating that the COP of RF may converge more quickly to a steady-state behavior than for NF.

In conclusion, the COP of RF were found to fluctuate in a more random behavior than NF. IDA measures provide additional information about balance dynamics that are not captured by traditional COP measures and may provide insights into potential mechanisms of falls.

REFERENCES

1. P Hur et. al. *ASME Summer Bio Conf*, Lake Tahoe, CA. August, 2009
2. TE Prieto et. al. *IEEE Trans Biomed Eng* 43, 1996
3. JJ Collins & CJ De Luca. *Exp Brain Res* 95, 1993
4. SG Leveille et al. *BMC Geriatr* 8:16, 2008

ACKNOWLEDGEMENT

HRCA/Harvard Research Nursing Home Program Project, funded by NIH (AG004390)

MODELLING OF CUSTOM FOOT ORTHOTICS

Lieselle Trinidad[1], Sundar Krishnamurty[1], Joseph Hamill[2]
[1]Department of Mechanical and Industrial Engineering, [2]Department of Kinesiology,
University of Massachusetts Amherst, Amherst, MA
e-mail: skrishna@ecs.umass.edu

INTRODUCTION

This paper presents the application of simulation-based design approach to Custom Foot Orthotics (CFOs). Specifically, this paper describes a surrogate or meta modeling technique for use in engineering modeling, analysis and design of CFOs.

Although orthotics have become widely used and accepted as devices for the prevention of and recovery from injuries, the design process continues to be based on empirical means. A deeper understanding of the therapeutic effects of a CFO and its design for optimal performance can be achieved through systematic simulation-based engineering modeling and analysis studies. Previously, we have presented a methodical approach to engineering modeling and analysis using Finite Element Analysis (FEA) [1]. Salient steps in this development of accurate CFO models included the creation of FEA models for complicated nonlinear material properties, as well as processes for the modeling and replication of complex three-dimensional CFO geometries.

This paper further extends our work on modeling and analysis [1] and introduces the concepts surrogate or meta modeling for engineering design optimization of CFOs. The primary motivation for this work is the recognition that FEA models can be computationally intensive, often requiring multiple hours or days to run a single simulation. Alternatively, the use of metamodels to simulate the performance of the complex FEA results can serve as effective and efficient mechanism to execute design optimization through multiple analysis iterations and to facilitate the selection of the most optimal CFO for individual subjects.

Metamodels (or Surrogate models) are models of analysis models that are one level of abstraction away from an original design or analysis model that can serve as predictive models in engineering design. While they are simplifications, they can be developed to maintain the important characteristics of the original model, while simultaneously increasing the speed of computing and making the process more efficient [2].

METHODS AND PROCEDURES

A most widely used surrogate modeling technique in engineering design is the response surface models (RSM) [3]. It is an approximation method to predict and estimate the values of unknown real valued function, given the values of the function at other known points. Using a least square regression fitting method of surrogate modeling, RSM can then be used in place of the costly original analysis model [4].

1) Modeling, Analysis, and Design of CFOs

Previous research [1] detailed a simulation-based design procedure for the systematic design of CFOs. Findings showed that when properly employed, the models have the potential to replace the empirical tables currently used for designing CFOs. Further extending this simulation-based approach to include predictive models will enable optimal design of CFOs based on an individual person’s body weight, activities, loading conditions, etc. Therefore, these simulation-based modeling, analysis and corresponding results offer a promising new approach to optimal design of CFOs.

2) Approximations using RSM

RSM process was applied to the experimental data from the FEA model of CFOs research from a previous study [1]. A finite element model was created and the applied load versus the deflection of the arch area using three weight classifications was analyzed. However, while FEA models enable assessment of performances at select, discrete data points, such as the three weight classifications, further modeling becomes necessary to use the results in optimal CFO designs based on a patient's body weight, activities, loading conditions, etc. Accordingly, the data results were used to build a second-order response surface model (RSM). The data set is listed in Table 1 from our previous study.

Thickness (mm)	**Mass (kg)**	**Deflection (mm)**
2	45	1.31
2	102	3.62
3	45	0.6
3	102	1.4
3	140	4.59
4	45	0.35
4	102	0.78
4	140	2.27
5	45	0.22
5	102	0.49
5	140	1.38

Table 1. Data set from FEA of custom foot orthotics research from [1]

The inputs to the meta model were specified as the orthotic thickness (x_1) and the subject's mass (x_2). The output data were specified as the arch deflection values. The RSM model of the data was determined from the three orthotic thickness categories (3mm, 4mm, and 5mm) and the three masses (45 kg, 102 kg and 140kg).

RESULTS AND DISCUSSION

The resulting second order RSM using quadratic polynomial regression is shown below.

$$[-0.55562+0.88547x_1+0.014145x_2+0.0040291x_1x_2-0.23625x_1^2-6.3712e\text{-}005x_2^2]$$

This RSM model is continuous, differentiable, and lends itself to exploring the characteristics of the output (arch deflection) as a function of the inputs (orthotic thicknesses and weights). More importantly, this model forms the basis for design optimization and can be used to minimize arch deflection by choosing the optimum orthotic thickness, given an individual's weight. A key challenge in the use of such RSM models is their accuracy and robustness. Here, the root mean square error (RMSE) can be used as an indicator of the accuracy of the model. RMSE from this model is found to be less than 2 (1.5), indicating that the meta model does not deviate too far from the FEA model values indicating high accuracy.

CONCLUSIONS

RSM models are easy and straight forward to use in practical situations. They will be flexible and adaptive to include other design considerations, such as the activity factor, as well to account for active or passive use (standing, walking, or running). Thus, with the new and enhanced modeling capabilities, CFOs can be custom designed and developed with the optimal design characteristics for each individual customer. Such a model could also facilitate the assessment of the robustness of resulting designs, by enabling visual inspection of the impact of small changes in the input conditions on the overall performance of the CFOs.

REFERENCES

1. Trinidad, L. (2008). *NACOB*, Ann Arbor, MI, Abstract 370.
2. Hazelrigg, G.A., (1999). *ASME J Mech Design*, 121, 336-341.
3. Shao, T., & Krishnamurty, S., (2006). *ASME*. Philadelphia, PA, DETC2006-99493.
4. Shao, T., (2007). (PhD Dissertation, University of Massachusetts Amherst, MA.
5. Simpson, T. W. et al. (1998). *AIAA*, 98-4755.

DISTINGUISHING BETWEEN MECHANICAL PATHOLOGY AND COMPENSATION USING GAIT ANALYSIS IN PEOPLE WITH KNEE OSTEOARTHRITIS

[1]Monica R. Maly and [2]Patrick A. Costigan
[1]School of Rehabilitation Science, McMaster University, Hamilton, ON, Canada, mmaly@mcmaster.ca
[2]School of Kinesiology and Health Studies, Queen's University, Kingston, ON, Canada, pat.costigan@queensu.ca

INTRODUCTION

The external knee adduction moment during gait has been implicated in the initiation of chronic knee pain [1] and radiographic progression of knee osteoarthritis (OA) [2]. Gait analysis yields thousands of data points beyond the knee adduction moment that likely contain information important to detecting and treating this disease. Principal components analysis (PCA) reduces the large gait data set to only important, uncorrelated variables and has proven useful in distinguishing between severities of knee OA [3]. However, this statistical approach may limit other interpretations. For example, PCA has not distinguished between characteristics that represent mechanical pathology, which lead to disease progression, versus those that represent compensation, which reduce or counteract pathological aspects of knee OA. Much interest has been invested in potential gait compensations, such as foot rotation and trunk lean. However, to-date no systematic approach has been used to identify gait compensations in people with knee OA. As preliminary step, correlates with structural disease markers such as mal-alignment likely identify pathological gait characteristics; while correlates of behavioural modification markers, such as self-efficacy can identify purposeful gait compensations. This study aims to distinguish between gait characteristics that represent mechanical pathology versus compensation among people with knee OA.

METHODS

An OA group of 54 adults with radiographic knee OA participated (age 68 ± 9, body mass index 29 ± 5 kg/m^2, 32 women). A control group (CON) of 52 symptom-free older adults with clear radiographs participated (age 64 ± 6, body mass index 26 ± 4 kg/m^2, 27 women).

Anatomical knee alignment was used as a marker of OA pathology using standardized coronal knee radiographs. Participants stood barefoot, positioned so that a transverse line through the femoral condyles was in the coronal plane. Anatomical angle was the angle between the tibial and femoral shafts and varus was designated positive.

Self-efficacy for physical tasks was assessed as a marker of OA compensations using the Arthritis Self-Efficacy Scale. Self-efficacy is the belief one has the capacity to execute actions required to satisfy specific demands [4]. Compromised self-efficacy coincides with the implementation of compensations in people with knee pain [5].

Gait data was collected using the Queen's Gait Analysis in Three Dimensions (QGAIT) system. Data was collected with an Optotrak optoelectronic system (Northern Digital, Waterloo, Canada) and a force plate (AMTI, Massachusetts, USA). Six infrared emitting diodes (IREDs) were used: Four IREDs were placed over anatomical landmarks (greater trochanter, lateral femoral condyle, fibular head, lateral malleolus) and two IREDs on anteriorly projecting probes attached to thigh and shank. Five walking trials were sampled at 100 Hz.

Three-dimensional positive and negative peaks, timings, ranges and stance averages for gait variables were averaged across 5 trials. Multivariate analysis of covariance (MANCOVA) compared the means for OA and CON with gait speed as a covariate. We entered data into the MANCOVA in 5 blocks: knee angles, knee forces, knee moments, hip forces, hip moments. Post hoc tests identified which variables were different between groups. Finally, gait characteristics unique to the OA group were correlated (Pearson) with each of alignment and self-efficacy scores.

RESULTS

After controlling for gait speed, 25 gait variables were unique to OA compared to CON. Of these 25, six were related to anatomical alignment and eight related to self-efficacy for physical tasks (Table 1).

Table 1: Relationships between unique knee OA gait characteristics and anatomical alignment and self-efficacy.

Distinctive Knee OA Gait Characteristics	**Anatomical Alignment**	**Self-Efficacy**
Knee Kinematic Variables		
Peak Knee Adduction Angle (°)	0.57*	0.14
Peak Knee Abduction Angle (°)	0.55*	0.07
Average Stance Knee Adduction-Abduction Angle (°)	0.75*	0.18
Peak Knee Extension Angle (°)	0.09	-0.58*
Range Knee Flexion-Extension Angle (°)	-0.34	0.49*
Average Stance Knee Flexion-Extension Angle (°)	0.04	-0.48*
Peak Knee External Rotation Angle (°)	-0.07	-0.33
Range Knee Internal-External Rotation Angle (°)	0.12	0.16
Knee Kinetic Variables		
Peak Knee Posterior Force (N/kg)	0.22	-0.35*
Time to Peak Knee Posterior Force (%)	0.12	-0.05
Time to Peak Knee Anterior Force (%)	-0.13	0.30
Peak Knee Distal Force (N/kg)	0.17	-0.48*
Range Knee Proximal-Distal Force (N/kg)	-0.21	0.49*
Average Stance Knee Proximal-Distal Force (N/kg)	0.32	-0.35
Time to Peak Knee Flexion Moment (%)	0.12	-0.30
Peak Knee Extension Moment (Nm/kg)	0.10	-0.32
Time to Peak Knee Extension Moment (%)	-0.09	-0.03
Range Knee Flexion-Extension Moment (Nm/kg)	-0.09	0.40*
Hip Kinetic Variables		
Peak Hip Anterior Force (N/kg)	-0.45*	0.32
Range Hip Anterior-Posterior Force (N/kg)	-0.28	0.47*
Peak Hip Medial Force (N/kg)	0.58*	0.25
Average Stance Hip Medial-Lateral Force (N/kg)	0.75*	-0.10
Peak Hip Proximal Force (N/kg)	-0.02	-0.03
Time to Peak Hip Proximal Force (%)	-0.17	-0.17
Peak Hip Adduction Moment (Nm/kg)	-0.28	0.23

*p<0.001(Bonferroni correction for multiple comparisons)

In general, anatomical knee alignment related to gait measures reflecting dynamic frontal plane knee alignment and forces acting at the hip (Figure 1A). By comparison, self-efficacy scores related to sagittal plane knee angles (Figure 1B), forces acting at the knee, the range knee flexion-extension moment and the range hip anterior-posterior force.

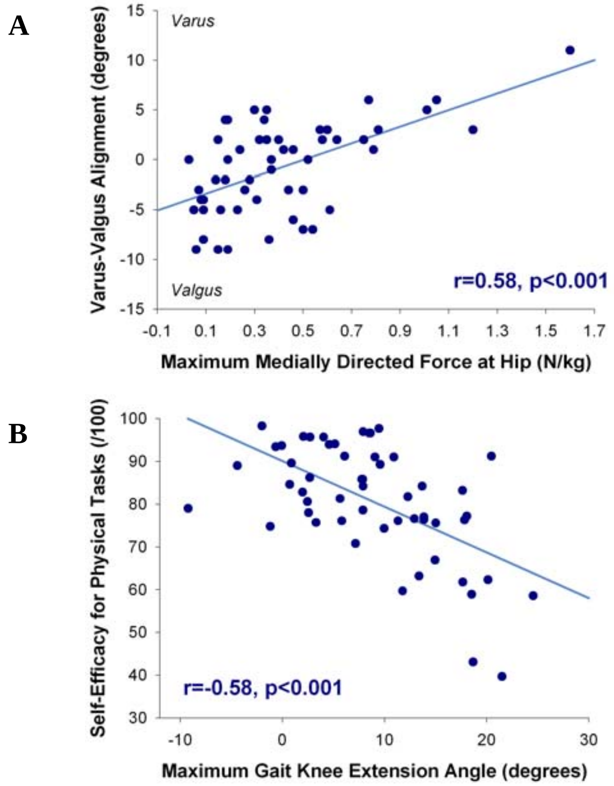

Figure 1: Anatomical knee alignment related to characteristics that reflected knee OA pathology, such as hip joint forces (A) while self-efficacy related to characteristics that reflect compensations, such as reduced knee range of motion (B).

DISCUSSION AND CONCLUSIONS

Of the gait characteristics unique to knee OA, this technique completely segregated pathological from compensatory characteristics through correlates of mal-alignment versus self-efficacy. Pathological factors extended beyond the knee, emphasizing the need to consider the lower extremity kinetic chain. Self-efficacy, which reflects the ability to mobilize motivation and cognitive resources to complete specific tasks, proved useful in identifying potential compensatory strategies. These compensatory characteristics, in general, appeared to represent a "careful" approach to walking performance.

REFERENCES

1. Amin et al. *Arthritis Rheum* **51**, 371-376, 2004.
2. Miyazaki et al. *Ann Rheum Dis* **61**, 617-672, 2002.
3. Astephen et al. *J Biomech* **41**, 868-876, 2008.
4. Bandura. *Psychol Health* **13**, 623-649, 1998.
5. Maly & Cott, *Arthritis Care Res* (in press).

ACKNOWLEDGEMENTS

Canadian Institutes of Health Research #99034 and Natural Sciences & Engineering Council of Canada #353715-2008

ORIENTATION-DEPENDENT IMPINGEMENT CONTACT MECHANICS FOR HARD-ON-HARD TOTAL HIP BEARINGS

[1]Jacob M. Elkins, [1]Douglas R. Pedersen, [1,2]John J. Callaghan, [1]Thomas D. Brown
[1]Department of Orthopaedics and Rehabilitation, University of Iowa, Iowa City, IA
[2]Veterans Affairs Medical Center, Iowa City, IA
email: jacob-elkins@uiowa.edu

INTRODUCTION

Dislocation is a serious problem in total hip joint replacement, and now ranks number one in terms of reasons for THA revisions [1]. Neck-on-liner impingement is a direct precursor of dislocation. Larger femoral heads increase the stable range of motion but also lead to a greater volume of wear particles in traditional metal on polyethylene constructs. To partially address this concern, interest in hard-on-hard bearings, such as metal-on-metal (MOM) and ceramic-on-ceramic (COC) has reemerged. However, the use of these couples leads to new worries regarding impingement mechanisms: catastrophic failure for COC as well as debris generation and metal-ion hypersensitivity in the case of MOM. To investigate the very high contact stresses present during impingement of hard-on-hard constructs, a 3D dynamic contact finite element (FE) model was developed. Sit-to-stand maneuvers, commonly associated with dislocation, served as a representative kinetic/kinematic challenge.

METHODS

A finite element model of a MOM implant was developed from manufacturer-provided surface geometry files (IGES), pre-processed using PATRAN (v. 8.5) and TrueGrid (v 2.3). The FE models consist of 3 parts: Femoral component (28mm head diameter), liner (28-46mm diameters) and metal backing. Based on convergence studies, the femoral head was meshed with 8,192 continuum elements, and the femoral neck with 5120 continuum elements. Since the distal femoral component was not involved in impingement, for computational economy this region was meshed more coarsely (2112 elements), and was assumed to behave as a rigid body. The meshing of the liner was also based on convergence studies, involving 4116 continuum elements. The metal backing (also 4116 elements) was assumed rigid and fully constrained by the bony acetabulum.

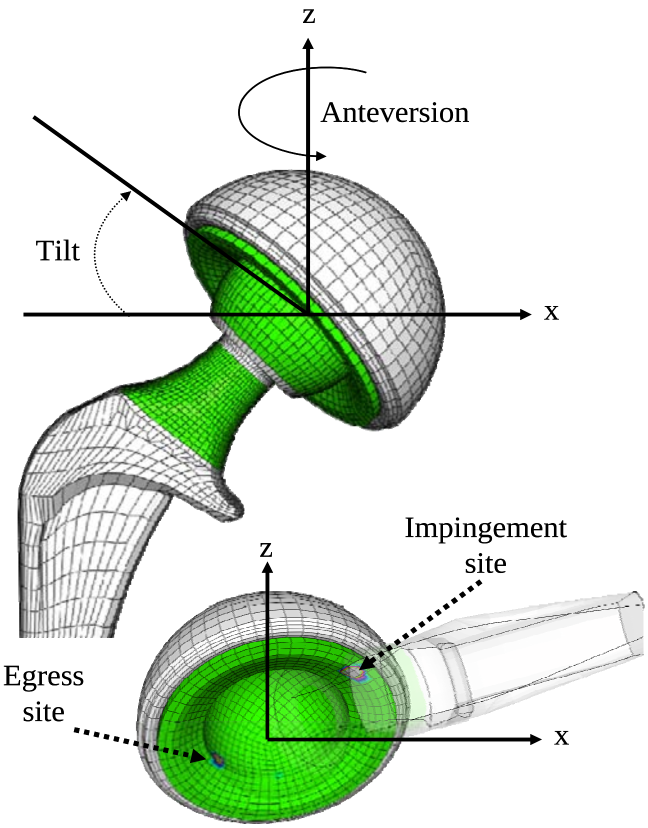

Figure 1: (top) Finite element model demonstrating cup placement orientation, (bottom) rotated model showing impingement and egress sites

The CoCr femoral head, neck and liner were modeled as linearly elastic (Modulus 210GPa, Poisson’s ratio 0.3).

Model input kinematics and kinetics were derived from motion data from 10 subjects performing a sit-to-stand challenge [2]. The motion sequence was discretized into 55 steps, with rotational degrees of freedom and joint reaction forces applied to the femoral head center.

Solutions were obtained using Abaqus Explicit (v. 6.7.1). Reaction forces and moments were collected from the acetubular center. Stresses and contact pressures were extracted for the liner at the egress and impingement sites (Fig. 1), as well as the femoral neck and head. Twenty-five distinct cup orientations were investigated.

RESULTS AND DISCUSSION

Range of motion before dislocation for the 25 cup orientations during the sit-to-stand maneuver were consistent with previous analyses [3]. Von Mises stresses and contact pressures for the individual FE runs were interpolated continuously (Figs 2, 3).

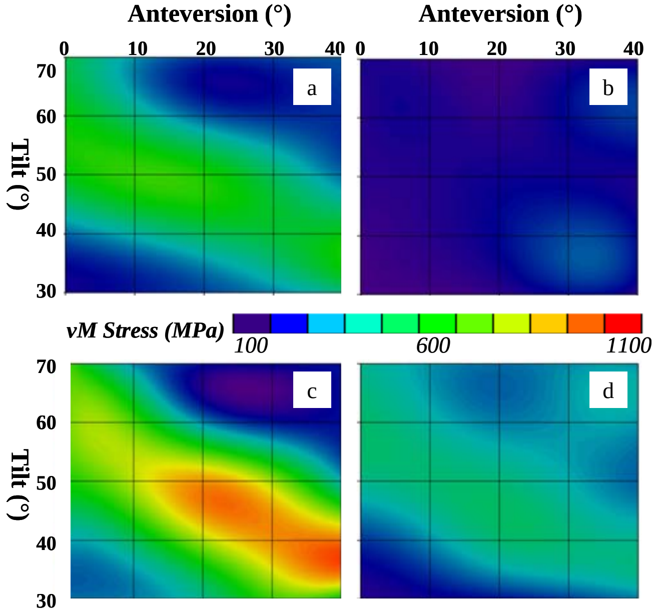

Figure 2: Peak von Mises stresses as a function of cup orientation (continuous interpolation based on 25 discrete samplings) for (a) liner egress site; (b) liner impingement site; (c) femoral neck and (d) femoral head

Since different cup orientations had different ROMs, maximum values for stresses and pressures were all reported at a constant value (6 mm) of femoral head subluxation.

For all analyses, stresses and pressures in the liner were greater at the egress site than the impingement site. Stresses and pressures were greatest overall in the femoral neck region owing to the smaller calculated contact area of the neck compared to the contact zone of the liner due to localized differences in regional mesh densities. There was a mild trend for stresses and contact pressures to be higher at a combination of high cup anteversion and lower degrees of cup tilt.

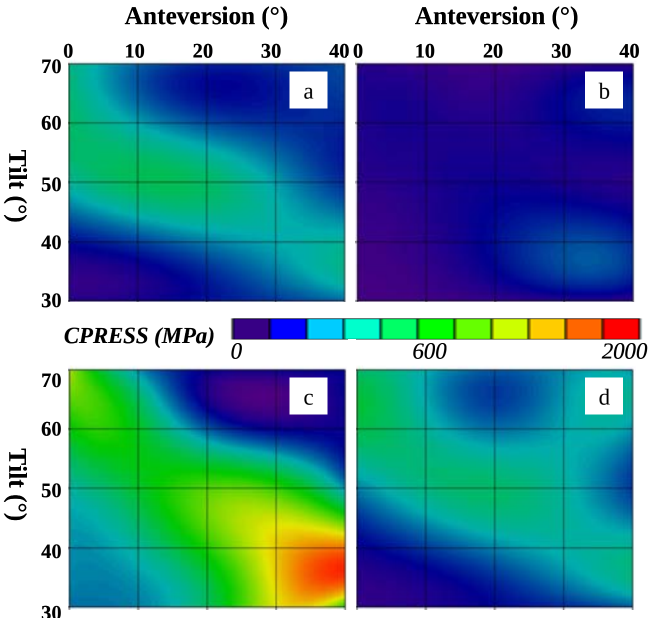

Figure 3. Peak contact pressure as a function of cup orientation (continuous interpolation from 25 discrete samplings) for (a) liner egress site; (b) liner impingement site; (c) femoral neck and (d) femoral head

Brief yet very high levels of stresses develop during mechanical impingement. In some instances these approached and even exceeded the yield stress for orthopaedic CoCr (800MPa, ASTM 2000), raising concerns about material failure and/or release of particulate or excessive metallic ion levels from chronic impingement, for untoward surgical placement of implant components.

CONCLUSIONS

Impingement of MOM implants makes for the possibility of stresses exceeding the material failure limits. This can have dire consequences, regardless of dislocation: debris generation, hypersensitivity reactions, aseptic lymphocytic vascular pseudotumors formation, impeded bony ingrowth, and cup dissociation. Knowledge of this may better inform surgical placement of MOM implants.

REFERENCES

1.Bozic, KJ, et al. *JBJS* **91**, 128-133, 2009.
2.Nadzadi, ME, et al. *J Biomech* **36**, 577-591, 2003.
3.Nadzadi, ME, et al. *J Biomech* **17,** 32-30, 2002.

ACKNOWLEDGEMENTS

Financial support was provided by the Department of Veterans' Affairs Medical Research Program and NIH AR53553

RESPONSE OF THE KNEE ADDUCTION MOMENT TO CHANGES IN GAIT SPEED: PEAK VERSUS IMPULSE

[1]Monica R. Maly and [2]Shawn M. K. Robbins
[1]School of Rehabilitation Science, McMaster University, Hamilton, ON, Canada, mmaly@mcmaster.ca
[2]School of Physical Therapy, The University of Western Ontario, London, ON, Canada, smrobbin@uwo.ca

INTRODUCTION

The external knee adduction moment during gait is a proxy for the distribution of load between the medial and lateral compartments of the knee. Peak values from this moment have been implicated in the initiation of chronic knee pain [1] and radiographic progression of knee osteoarthritis (OA) [2]. Factors that influence the knee adduction moment include mechanical alignment of the lower limb and overall body weight. Some studies have also demonstrated a relationship between gait speed and the peak knee adduction moment [3], though this relationship has not been consistently reported [4]. Understanding the effect of gait speed on the knee adduction moment is important because gait speed is easily modified and therefore could be a treatment strategy to modify joint loading [5].

Despite previous emphasis on the peak, researchers have found that the knee adduction moment impulse, which reflects both the duration and magnitude of medial loading during a stride, is also important in radiographic and symptomatic knee OA [4]. However, the knee adduction moment impulse has not been examined with the participants ambulating at different speeds. It is unclear how the impulse would change with increasing gait speed. Any increase in amplitude might be negated by the anticipated decrease in the stance time with a faster gait speed. Thus, the purpose of this study was to examine changes in the knee adduction moment, including the peak and impulse, in response to controlled changes in gait speed, in healthy participants during over ground ambulation.

METHODS

A convenience sample of 32 healthy adults participated (age 32 ± 8 years, body mass index 25 ± 4 kg/m^2, 18 women).

The knee adduction moment was calculated using 8 cameras (Motion Analysis Corp., Santa Rosa, USA) with a sample rate of 60 Hz and a synchronized floor-mounted force plate (AMTI, Watertown, USA) with a sample rate of 1200 Hz. A Helen-Hayes marker configuration was used, with 21 reflective markers. Participants stood on the force plate to determine body mass and provide a reference frame. Participants actively flexed, extended, abducted and adducted the hip to calculate functional hip joint centres.

Three gait speed conditions were examined in the following order: self-selected, slow and fast. For the self-selected condition, participants ambulated barefoot across a 6 metre capture area. The time required for each participant to ambulate the 6 metres was recorded using a stopwatch (Sportline 220, Sportline Inc., New York, USA). For the slow condition, participants completed the six metres in a 15% longer time period than the self-selected speed. For the fast condition, participants ambulated 15% faster compared to the self-selected speed. For all conditions, a successful trial was defined as completing the six metres within ±5% of the target time. Then, kinematic and kinetic variables were calculated with commercial software using a fixed tibial coordinate system (Orthotrak 6.2.4, Motion Analysis Corp., Santa Rosa, USA). Data were not normalized to stride.

To ensure appropriate gait speeds were achieved, forward progression speed of the sacral marker was reviewed. Trials were excluded if gait speed was not within 2.5% of the target. Five trials were averaged for the self-selected condition and 3 trials were averaged for the slow and fast conditions.

A one-way repeated measures analysis of variance (ANOVA) was used to identify differences in gait speed and between conditions in the stance peak and impulse of the knee adduction moment waveform, ($p < 0.05$). Adjusted p values, using Greenhouse-Geisser values, were examined if the assumption of sphericity was not tenable as demonstrated by Mauchly's Test of Sphericity (p <

0.05). The sphericity assumption maintains that the pair-wise comparisons have equivalent variances. Tukey's Honestly Significance Difference test was used to make pair-wise comparisons between the condition means.

RESULTS

Gait speed data violated the sphericity assumption. Thus, an adjusted repeated measures ANOVA was analyzed and revealed that mean gait speeds during self-selected (1.39 ± 0.15 m/s), slow (1.19 ± 0.13 m/s) and fast (1.60 ± 0.17 m/s) conditions were different ($p<0.05$).

Data for the mean peak knee adduction moment in each condition violated the sphericity assumption. An adjusted repeated measures ANOVA revealed differences in the peak between the conditions ($p<0.05$). There was a greater peak during the fast condition compared to the slow condition. The peak for the self-selected condition was not different than the slow or fast conditions (Table 1).

Data for the mean knee adduction moment impulse met the sphericity assumption. A difference existed between conditions for impulse ($p<0.05$). The impulse for the slow condition was greater than both the self-selected and fast conditions. There was no difference in the impulse between the self-selected and fast conditions (Table 1).

Table 1: The knee adduction moment impulse and peak mean values during self-selected, slow and fast gait speeds among 32 healthy adults.

Variable	Self-selected Speed Mean (SD)	Slow Speed Mean (SD)	Fast Speed Mean (SD)
Impulse (Nm*s)	8.97 (3.93)	10.14 (4.72)	8.83 (4.00)
Peak (Nm)	30.05 (10.97)	27.63 (10.08)	32.28 (13.18)

By examining data non-normalized to stride, differences between speeds in the peak and impulse revealed information important to understanding the medial loading environment (Figure 1).

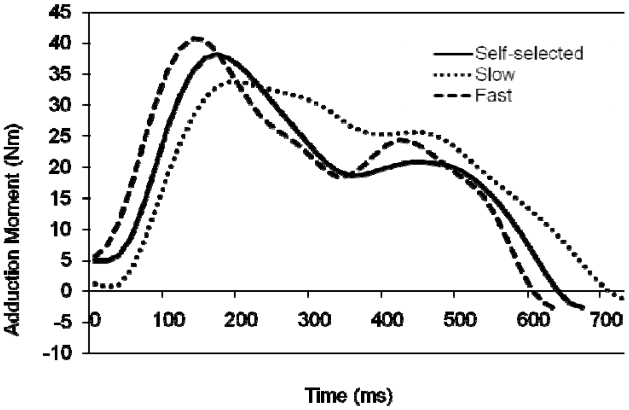

Figure 1: External knee adduction moment for the self-selected, slow and fast gait speeds in one participant.

DISCUSSION AND CONCLUSIONS

Gait speed altered the knee adduction moment and therefore the distribution of loading across the medial and lateral knee compartments. Speed-related changes in the peak and impulse occurred in opposite directions, suggesting these variables represent different aspects of medial loading. The impulse was more sensitive than the peak to changes in gait speed. The impulse was time-dependent and reflected total loading of the medial compartment during one stride. An increase in gait speed by 15% from the self-selected to fast condition did not alter the impulse. Thus, slowing gait speed below self-selected speed had a greater influence on the impulse than increasing gait speed. Meanwhile, the peak reflected the maximum medial load. A 30% increase in gait speed (from slow to fast condition) was required to increase the peak.

Slowed gait speed has been recommended as a potential intervention for knee OA [5]. These findings highlight that while slowed gait speed results in a lower peak load, a concurrent increase in impulse may result in a greater total load exposure.

REFERENCES

1. Amin et al. *Arthritis Rheum* **51**, 371-376, 2004.
2. Miyazaki et al. *Ann Rheum Dis* **61**, 617-672, 2002.
3. Kirtley et al. *J Biomed Eng* **7**, 282-288, 1985.
4. Thorp et al. *Bone* **39**, 1116-1122, 2006.
5. Mundermann et al, *Arthritis Rheum* **50**, 1172-1178, 2004.

ACKNOWLEDGEMENTS

Natural Sciences & Engineering Council of Canada #353715-2008

PREDICTED ACCEPTABLE LOAD TRANSFER THROUGH THE RIBCAGE WHILE LEANING ON THE DYNAMIC TRUNK SUPPORT

[1] Mohammad Abdoli-E, [2]Caroline Damecour, [1]Ahmad Ghasempoor, and [1]Julie Bouchard
[1] Ryerson University, Toronto, ON, Canada. email: m.abdoli@ryerson.ca
[2] Queens University, Kingston, ON, Canada.

INTRODUCTION

The Dynamic Trunk Support (DTS) is a forward placed support designed to reduce postural muscle activity when standing with the trunk bent forward. Weight is transferred by leaning through the support plate that fits to the upper half of the sternum and anterior portion of the upper 4-6 ribs (Figure 1, A). To date, laboratory testing has demonstrated the effectiveness of the DTS in reducing lumbar spine compression loading(1,2). In preparation for field studies, we need to predict weight tolerance through the ribcage in order to determine support parameters (i.e. amount of support provided by the mechanism at the base of the device). So far, participants have used a 10-point visual analog scale (VAS) anchored by no compression and extreme compression to rate the sensation of compression through the upper rib cage. While this value has been a valuable indicator for use in preliminary investigations of the trade-off between compression through the ribcage and gains in reduced discomfort, reduced muscle activity and reduced spine loading; the scale does not help with setting mechanical parameters. To do this, a revised 10-point VAS was used based on Borg descriptors with 10 set as the maximal accepted value (MAV).

METHODS

Ten females participants rated their preference for support plates with different combinations of shapes (heart, round and square), vertical size (115mm, 152.5mm) and width normalized to the 5th, 50th and 95th percentile female[4]. The XSENSOR (Sensor technology, CA) was used to map pressure. The padding thickness was unchanged. To determine the MAVs, a harness was placed around the ribcage and attached to a hand-held dynamometer in front (Figure 1-B). After several practice pulls, the MAV for short term use defined as less than 1 minute was recorded followed by 3 repetitions, in random order, in increments equal to 15% MAV were tested for subjective ranking. A second session, on a separate day, was completed with the MAV, defined as an 8-hour shift for full day.

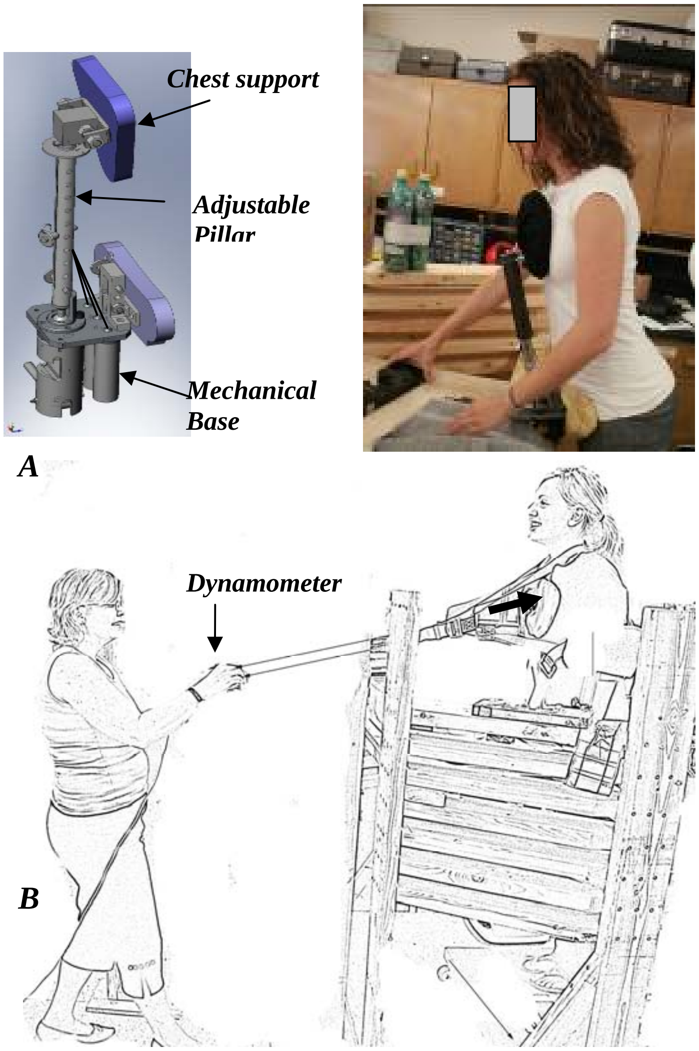

Figure 1. Subjective rating of actual compression in reference tolerance for short term (top) and full work shift (bottom).

RESULTS:

Eighty percent preferred the round shape but dimension preference varied. The anticipated MAV for full day is approximately 33% of the short term MAV. Both scales present with a similar linear relationship (Figure 2).

DISCUSSION:

The results indicate that a larger sample group is needed to determine aggregate preferences for size and shape of support plates. The VAS anchored by MAV and using Borg descriptors appears to correlate with actual compressive loading and therefore could be used in field studies as an indicator for compression loading. A limitation is that this homogenous group may not represent the workplace and full day MAVs are based on predicted values regardless of previous work experience.

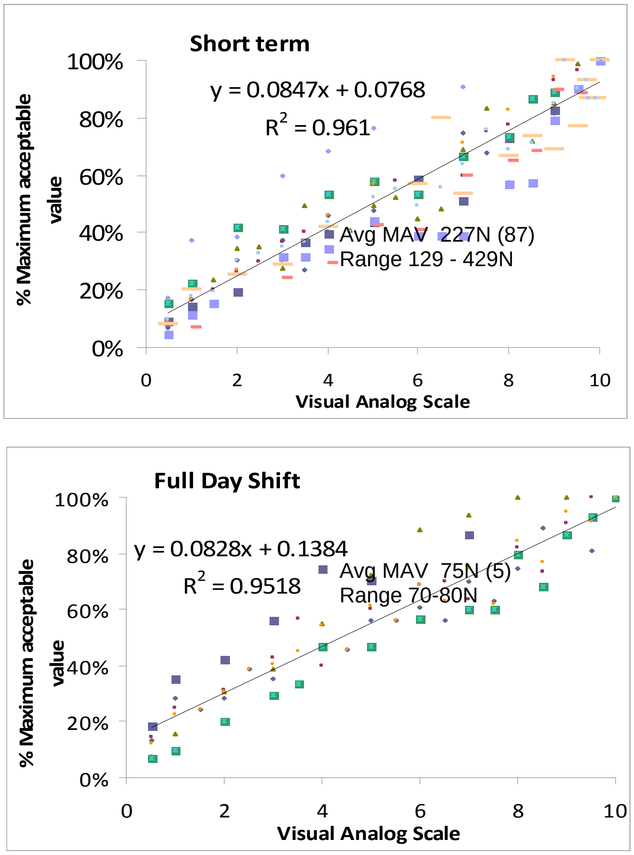

Figure 2. Subjective rating of actual compression in reference tolerance for short term (top) and full work shift (bottom).

REFERENCES:

[1]. Damecour C. et al. (2008). Comparison of two heights of forward placed trunk supports with standing work. (in process)

[2]. Damecour C. et al. (2009). The effects of reaching forward at terminal diagonal reach. Conference proceedings, Ontario Biomechanics Conference.

[3]. Adultdata Handbook (1995).

UNCERTAINTIES IN TISSUE MECHANICAL RESPONSE WITH INCREASED CELL DENSITY: MICROSTRUCTURAL AND HOMOGENEOUS MODELS REVISITED

Craig Bennetts, MS, Snehal Chokhandre, MS, Ahmet Erdemir, PhD

Computational Biomodeling Core, Department of Biomedical Engineering
Lerner Research Institute, Cleveland Clinic, Cleveland, OH
e-mail: erdemira@ccf.org, web: http://www.lerner.ccf.org/bme/cobi

INTRODUCTION

Finite element analysis, using models of single cells embedded in an extracellular medium, has provided new insights into cellular loading in cartilage [1] and meniscus [2]. Commonly, these models are driven by stress-strain state obtained by simulating tissue deformations with constitutive models representing homogeneous materials. A major assumption of this process is that the stress-strain behavior of the homogeneous tissue model is equivalent to the nominal stress-strain response of the cellular level model. While the extent of violating this assumption may be considered negligible for a single cell in a given volume [1], reportedly higher cell densities [3] may considerably increase uncertainty in simulation results. Therefore, the objective of this study is to quantify the mismatch in elastic response of cartilage models; based on a homogeneous tissue model and with increasing cell densities. Multiscale coupling approaches targeting prediction of cell deformations from tissue and/or organ level loading will likely benefit from this investigation while balancing computational demand with accuracy requirements.

METHODS

The effect of cell density on the mechanical response of a 100 μm by 100 μm square was examined by conducting finite element analysis on three plane strain models (Figure 1): i) homogeneous model with extracellular matrix only, ii) with a single cell at center, and iii) with three cells distributed randomly within the area [3]. During random placement, a minimum pericellular-to-pericellular spacing of 25 μm and a minimum pericellular-to-tissue-edge spacing of 12.5 μm were enforced. The cells have radii of 5 μm, surrounded by a layer of pericellular matrix with a thickness of 2.5 μm [1]. Linearly elastic materials were used for all regions, with properties estimated from Guilak and Mow [1]. The extracellular matrix had a Young's modulus of 1.0 MPa and a Poisson's ratio of 0.125. For the pericellular matrix these were 0.5 MPa and 0.125; for the cell, 0.001 MPa and 0.25. All models were meshed with quadrilateral elements using TrueGrid (XYZ Scientific Applications, Inc., Livermore, CA).

On each model, two different simulation conditions were performed using Abaqus (Simulia, Providence, RI): i) a non-confined uniaxial compression, and 2) a simple shear. For compression, the top edge was moved downwards to a final displacement of 15 μm (nominal compressive strain of 0.15). For shear, the top edge was displaced by ~30 μm sideways to obtain a final nominal shear strain of 0.30. In each case, nominal stress was calculated as the sum of reaction forces divided by area of action (100 μm x unit out-of-plane thickness). Nominal strain was the displacement normalized by model height (100 μm). Finite element analysis also provided the local stress distribution.

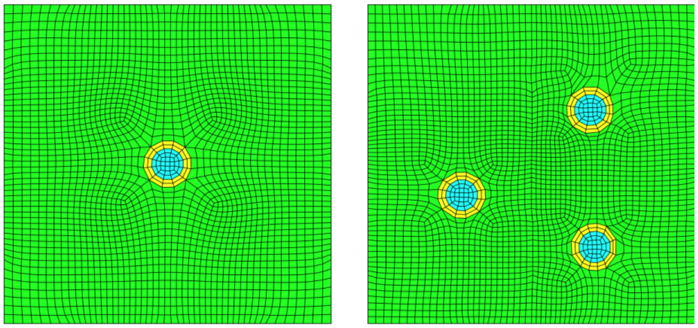

Figure 1: Single-cell and three-cell models illustrating the extracellular matrix, pericellular medium, and cells.

RESULTS AND DISCUSSION

It is not surprising that as generally softer cells were placed inside the extracellular medium, the overall mechanical response became less stiff (Figure 2). At a given nominal compressive strain, overall compressive stress was 3.0% to 3.6% lower for the single-cell model predictions, when compared against the homogeneous extracellular matrix model. It was decreased by 8.5% to 9.7% for three-cell model. Percentage error increased as nominal compressive strain became larger. For shear loading, single-cell model predicted 4.0% to 4.6% lower nominal shear stress. Comparisons between three-cell model results and those of the homogeneous extracellular matrix model revealed decreased stress values, from 8.9% to 10.2%. Under shear loading, the percentage error was higher at small strains. While error predictions for single cell agree well with previously reported discrepancies [1]; three cell model illustrates the amplification of such errors due to higher number of cells in a region of interest. One should note that the error estimates will likely be influenced in a three-dimensional representation under combined loading; with a detailed representation of the extracellular matrix architecture and tissue mechanics, e.g. biphasic materials.

Identification of cell deformations from body level loading is vital to relate cell vitality and cell mechanobiology to human movement. It is clear that cell deformations and stresses depend on their surrounding medium (Figure 3). In macroscopic modeling of the mechanical deformations in joints and organs, homogeneous representations of tissues are rather attractive due to computational cost. At desired regions in the tissue, a microscopic finite element representation can predict cell deformations by post-processing the stress-strain predictions of the macroscopic model. This study portrays that an increasing level of error in prediction of cell deformations is likely, based on mismatches in predictions of homogeneous and microstructural representations, and depending on cell density and macroscopic strain level. If such inaccuracies cannot be afforded, one may choose direct coupling of macro/micro models using computational homogenization techniques [4], with the expense of an increased computational demand. Alternatively, homogeneous constitutive models, representative of underlying cell distribution and mechanics, can be developed [5].

REFERENCES

1. Guilak F and Mow VC *J Biomech* **33**, 1663-1673, 2000.
2. Gupta T and Donahue TLH *Acta Biomaterialia* **2**, 483-492, 2006.
3. Gilmore RSC and Palfrey AJ *J Anat* **157**, 23-31, 1988.
4. Breuls RGM, et al. *J Biomech Eng* **124**, 198-207, 2002.
5. Wu and Herzog *Annals of Biomed Eng* **28**, 318-330,2000.

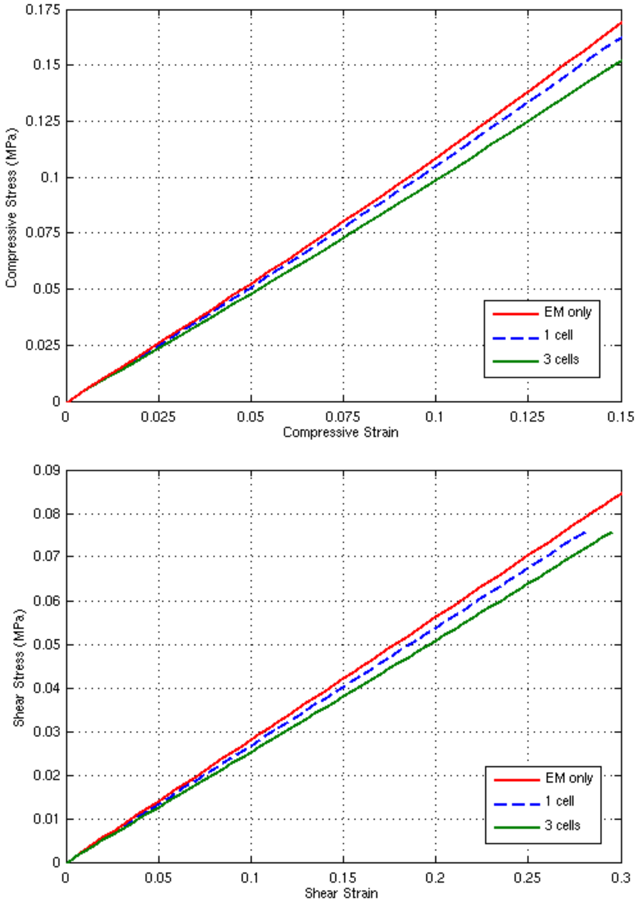

Figure 2: Nominal mechanical response of models under uniaxial compression (top), and in simple shear (bottom). EM: extracellular matrix.

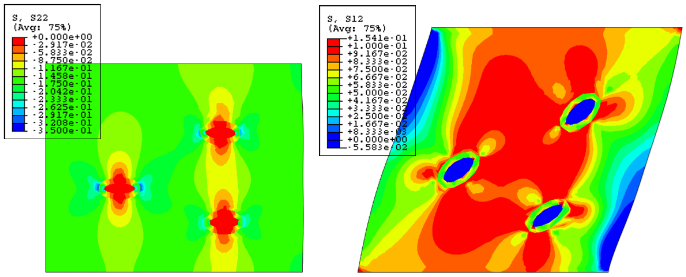

Figure 3: Localized uniaxial stresses along compression axis for compression (left), and shear stress distribution for simple shear (right). Three-cell model predictions are shown.

INTERVERTEBRAL DISC BIOMECHANICS ADJACENT TO FUSION

Arin M. Ellingson, Hitesh P. Mehta, Justin H. Huelman, and David J. Nuckley
Musculoskeletal Biomechanics Research Laboratory, University of Minnesota
e-mail: dnuckley@umn.edu, web: http://mbrl.umn.edu

INTRODUCTION

Chronic low back pain is the most prevalent musculoskeletal impairment in the U.S. afflicting between 15% and 65% of the population [1]. Classical surgical treatment for discogenic low back pain involves lumbar interbody fusion. While many procedures exist, they share common complications of progressive degeneration of discs adjacent to the fusion. The etiology of this adjacent disc disease is poorly understood; however, changes in local spine biomechanics have been implicated [2-4]. Fusion effects on the adjacent disc and disc two levels away have not been reported. *Thus, the purpose of this study was to examine the lumbar spine after fusion to determine the biomechanical effects one and two levels away from the fusion.*

METHODS

Seven human cadaveric lumbar spines (L3-S1), exhibiting equal sex distribution and an average age of 61 years (range 43-70 years), were acquired from the UM bequest program. The osteoligamentous tissues were embedded in polymethylmethacrylate (PMMA) and tested in a six-axis Spine Kinetic Simulator (8821 Biopuls, Instron, Norwood, MA). Pure moments of up to 8 Nm in flexion/extension, right and left lateral bending, and right and left axial rotation were applied sinusoidally in moment control while minimizing shear forces at the bottom of the construct. Similarly, cyclic compression loading was applied up to 500 N. Segmental range of motion (ROM), stiffness, hysteresis, and neutral zone were measured using six-axis load data and a 3D visual motion analysis 5-camera system (Vicon MX-F40NIR, Vicon Motion Systems, Centennial, CO). Pressure across L3-L4 was measured with a custom pressure transducer, which utilized a 200 psi miniature pressure transducer (Model 060-200, Precision Measurement Co., Ann Arbor, MI) inserted within a 13 gauge needle and backfilled with silicone. Specimens were sequentially tested through the following cases: (1) intact, (2) fused at L5-S1, and (3) with a two level fusion spanning L4-S1. ANOVA techniques were used with paired t-test contrasts to elucidate specific differences between the groups using Bonferroni correction and an alpha acceptance of 0.05.

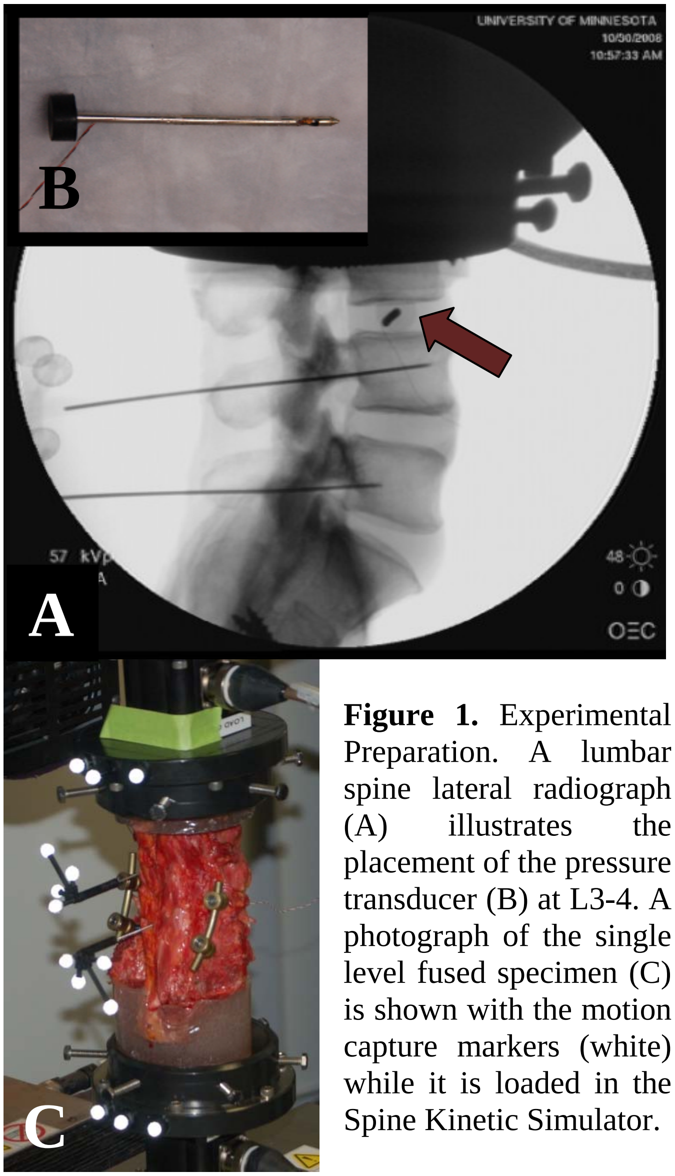

Figure 1. Experimental Preparation. A lumbar spine lateral radiograph (A) illustrates the placement of the pressure transducer (B) at L3-4. A photograph of the single level fused specimen (C) is shown with the motion capture markers (white) while it is loaded in the Spine Kinetic Simulator.

RESULTS AND DISCUSSION

The range of motion and stiffness data collected for the intact lumbar spine are similar to those collected using analogous methods of load application [5]. The entire spinal construct (L3-S1) exhibits significantly increased stiffness (p=0.0107) and decreased range of motion (p<0.0362) in the sagittal plane with each successive fusion. Lateral bending displayed significant differences between the two level fusion and each of the other cases for stiffness (p<0.0013) and range of motion (p<0.0097). Finally, for the total construct (L3-S1) in axial rotation, the stiffness was significantly distinct (p<0.0059) in spite of non-significant changes in range of motion.

The L3-4 spinal level was specifically evaluated with regard to its biomechanical changes including intradiscal pressure. Fusion two levels removed from the spinal level of interest demonstrated non-significant changes in range of motion, stiffness, neutral zone, and hysteresis (Figure 2). Furthermore, the L3-4 intradiscal pressure was found to be similar between the intact case and the case with a fusion two levels away. A fusion procedure immediately adjacent to the level of interest produced significantly larger flexion and extension stiffness in that level of interest as well as flexion intradiscal pressure (p=0.0034). Axial compression resulted in significantly (p=0.0009) increased intradiscal pressure with a fusion immediately adjacent to the level tested (Figure 3).

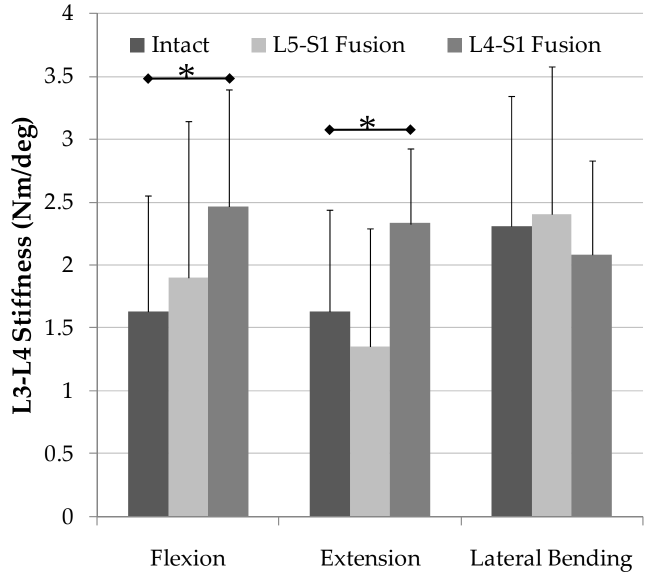

Figure 2. L3-L4 Spinal stiffness as a function of fusion. Only adjacent fusion affects spinal stiffness in flexion *(p=0.0492) and extension *(p=0.0500).

Limitations of the current research include large intra-specimen variability (disc health) which affected biomechanics and disc pressure, the lack of a follower load, and the cadaveric nature of the tests—without active musculature. Despite these, our data demonstrate that the biomechanical compensation of the spine after fusion affects the discs immediately adjacent to the fusion significantly, but those even two levels away are less affected.

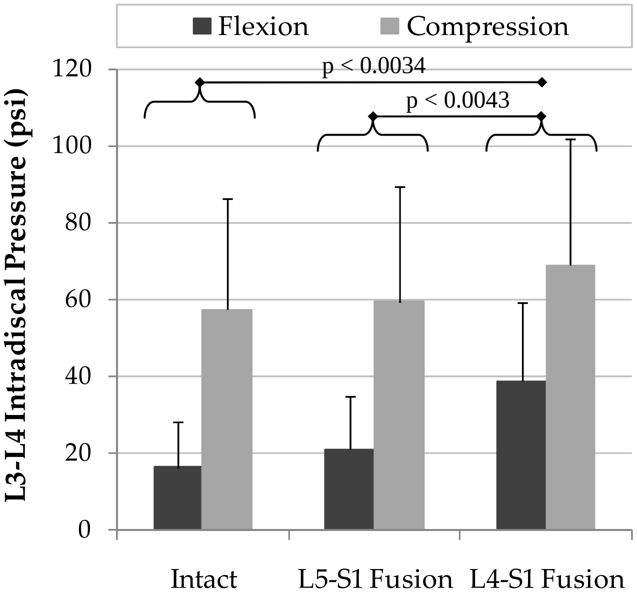

Figure 3. Intradiscal pressure as a result of flexion and compression loading with no fusion, fusion two levels away, and adjacent level fusion.

CONCLUSIONS

This study reveals biomechanical changes within the disc due to fusion surgery. Adjacent fusion significantly increases disc stiffness and pressure compared with fusion two levels away. Increased pressures likely precipitate the degenerative changes which have been shown to follow. Thus, mitigation of the rigid (fusion) boundary condition in the spine may reduce the effects of this degenerative cascade and prevent the recurrence of low back pain in these patients.

REFERENCES

1. Andersson GB. *Lancet* **354** (9178): 581-5, 1999.
2. Cunningham, BW, et al. *Spine* **22** (22): 2655-63, 1997.
3. Nunley, PD, et al. *Surgical Neurology* **70**: 247-51, 2008.
4. Weinhoffer, SL, et al. *Spine* **20** (5): 526-31, 1995.
5. Panjabi MM, et al. *Spine* **32** (12): 1311-19, 2007.

ACKNOWLEDGEMENTS

This research was funded by Disc Dynamics Inc.

GEOMATA: A ROBUST AND INTUITIVE SOFTWARE APPLICATION FOR EXTRACTING ANATOMICAL BOUNDARIES FROM MEDICAL IMAGES

Craig Bennetts, MS, Ahmet Erdemir, PhD

Computational Biomodeling Core, Department of Biomedical Engineering
Lerner Research Institute, Cleveland Clinic, Cleveland, OH
bennetc2@ccf.org, erdemira@ccf.org, http://www.lerner.ccf.org/bme/cobi

INTRODUCTION

Defining the surface geometry of anatomical structures from medical images is a necessary preliminary step for finite element analysis. Most automated segmentation techniques fail to provide satisfactory results due to their lack of general applicability to different imaging modalities. Manual segmentation is often tolerated when a limited number of models need to be generated, but becomes prohibitive at high volumes or in time sensitive situations. These limitations and the availability of image segmentation libraries spurred prototyping of various image processing tools [1]. Semi-automated methods with simplified interfaces has been developed with the intentions of robust and expedited segmentation [2]. However, these approaches still require an understanding of the underlying algorithms to appropriately set required segmentation parameters.

The goal of this study is to develop a novel software package that provides a simple and intuitive interface, free from complicated segmentation parameters and powered by a robust semi-automated segmentation algorithm, called Grow Cut [3]. This application is intended to accelerate the generation of geometric models of tissue anatomy for finite element analysis.

METHODS

The software was written in C++, using OpenGL [4] for image visualization and FLTK [5] for the graphical user interface. These software libraries are open source and provide cross-platform support, therefore promoting future development and adoptability. The interface is simple, having only a few, straightforward tools to assist in image segmentation. The most frequently used functions (e.g. selection of region of interest, boundary output) are accessible from a pop-up menu (Figure 1), eliminating the need to leave the image workspace and thereby likely to improve operational efficiency and usability.

The Grow Cut segmentation algorithm was implemented to provide the core functionality of the application [3]. It is an interactive multi-label, N-D image segmentation algorithm, which evolves by cellular automata. The user designates pixels as either foreground or background, by interactively “painting” over a small subset of pixels on the image slice. In this selection, which can also be referred as seeding, the user incorporates the variability of intensities present within each region. The brush size is adjustable to accommodate small or large features. Application of the algorithm starts the growth of selected regions within a 2D slice, claiming pixels of highest similarity in intensity to those at the edge of the growing region. Following convergence, the results can be modified by redefining inappropriately labeled pixels and reapplying the algorithm. At the boundary between foreground and background regions is the contour for the segmented structure of interest. A user-defined number of evenly spaced boundary point coordinates can be exported from a boundary. By processing each image slice of a full image set, the user may obtain contours describing the entire surface of the tissue.

RESULTS AND DISCUSSION

The general applicability of the software is illustrated, showing the segmentation of the femoral head from computed tomography (CT) (Figure 1), magnetic resonance imaging (MRI) (Figure 2) and color photos (Figure 3). All images were obtained from the male subject of the Visible Human Data Set [6].

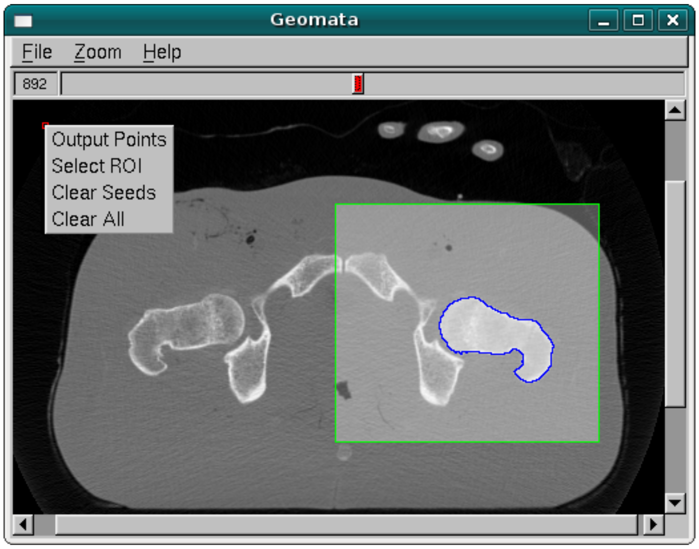

Figure 1. Segmentation of the femoral head from a CT scan. The pop-up menu provides basic functionality for selecting region of interest and writing boundary points to a file.

Geomata successfully extracted anatomical boundaries from relatively homogeneous images obtained from CT and also resolved harder segmentation problems commonly associated with MRI and color pictures. In the latter cases, the high contrast in images results in highly varying foreground/background information. Such inhomogeneities are known to complicate the segmentation process.

Capabilities of Geomata, provided by a powerful segmentation algorithm and a minimalistic user interface, allow robust and intuitive identification of tissue geometries. In the future, the Grow Cut segmentation algorithm will be extended to operate in 3D, which will further reduce the amount of time required for user interaction and the extraction of surface geometry.

REFERENCES

1. Caban JJ et al. *J Digital Imaging* **20**, 83-93, 2007.
2. Yushkevich PA, et al. *Neuroimage* **31**, 1116-1128, 2006.
3. Vezhnevets V and Konouchine V,“GrowCut” - Interactive Multi-Label N-D Image Segmentation By Cellular Automata, *GraphiCon*, Novosibirsk, Russia, 2005.

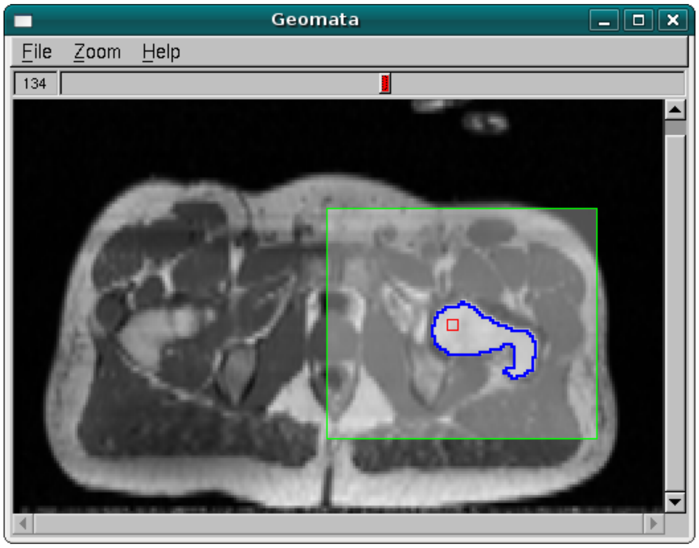

Figure 2. Segmentation of the femoral head from MRI. The algorithm has to capacity to perform adequately on low resolution, high contrast images.

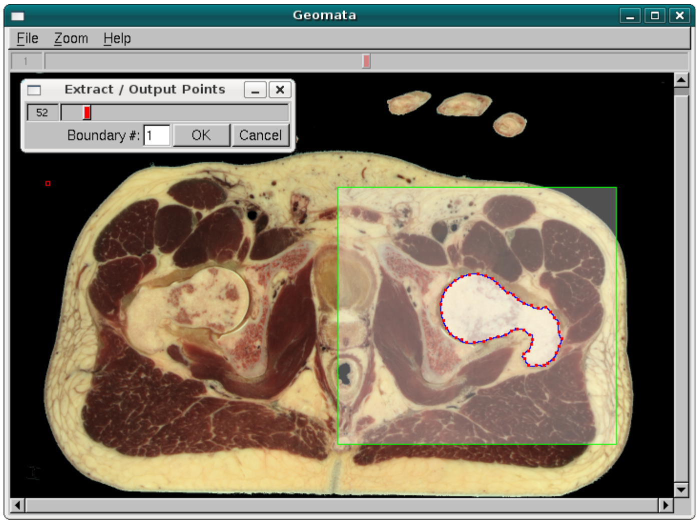

Figure 3. Segmentation of the femoral head from a color picture showing boundary points. The point extraction window allows user to change number of points on the boundary.

4. http://www.opengl.org, accessed on 04/01/2009.
5. http://www.fltk.org, accessed on 04/01/2009.
6. http://www.nlm.nih.gov/research/visible/visible_human.html, accessed on 04/01/2009.

ACKNOWLEDGMENTS

This study was partially funded by NIH grants 2R01HD037433 (PI: Peter R. Cavanagh) and 1R01EB006735 (PI: Antonie J. van den Bogert).

INFLUENCE OF AGE AND GAIT SPEED ON REQUIRED COEFFICIENT OF FRICTION INDEPENDENT OF STEP LENGTH

Dennis E. Anderson and Michael L. Madigan
Kevin P. Granata Musculoskeletal Biomechanics Lab, Department of Engineering Science and Mechanics,
Virginia Polytechnic Institute and State University, Blacksburg, VA
email: dennisa@vt.edu, web: www.biomechanics.esm.vt.edu

INTRODUCTION

Falls are a major cause of injury and death in both the elderly and occupational settings, and slips are a major cause of falls [1]. The required coefficient of friction (RCOF) has been used as an indicator of the risk of slips as it indicates the minimum friction necessary to prevent the foot from slipping [1]. RCOF increases with step length independent of gait speed [2]. RCOF may also depend on age: older adults show lower RCOF during stair descent when compared to younger adults [3], although in a study of gait on level surfaces no significant age differences were found [4]. However, this study used self-selected walking conditions, and the older adults in the study walked at significantly slower speeds and took significantly smaller steps than the younger adults. Thus, it is unknown if there are age differences in RCOF independent of speed and step length. The purpose of this study was to examine the effects of age and speed on RCOF during gait on level surfaces, and separate age and speed effects from the effects of step length.

METHODS

Forty healthy adults participated in gait testing including 20 young adults (mean age 23.9±3.3 years) and 20 older adults (mean age 80.3±4.0 years). Each age group included 10 males and 10 females. Informed consent was obtained prior to participation. Participants walked down a walkway under four gait conditions, and stepped on a six degree-of-freedom force platform (Advanced Mechanical Technology Inc., Watertown, MA) placed in the center of a walkway with their right foot. Ground reaction forces were collected at 1000 Hz for each trial. A VICON 460 motion analysis system (VICON Motion Systems Inc., Lake Forest, CA) was used to record the positions of reflective markers placed on the left and right heel and right ASIS at 100 Hz.

All four gait conditions involved controlled gait speed, and two conditions controlled step length as well (Table 1). Speed was controlled by having participants keep pace with a moving belt placed alongside the walkway. Step length was controlled by having participants step on markings on the walkway. Gait conditions were presented to each participant in a random order. Three trials were collected for each condition. For each trial, speed and step length were determined from marker data.

A single trial was selected for analysis for each participant and gait condition. The trials were selected such that there were no significant speed differences between gait conditions with the same target speed (e.g. SF and SS, FF and FS) nor between age groups within gait conditions. Similarly, trials were selected so there were no significant differences in step lengths between gait conditions SS and FS, nor between age groups within these conditions.

The RCOF was determined by dividing the anterior-posterior shear force by the normal force throughout stance phase (Figure 1). The peak (minimum)

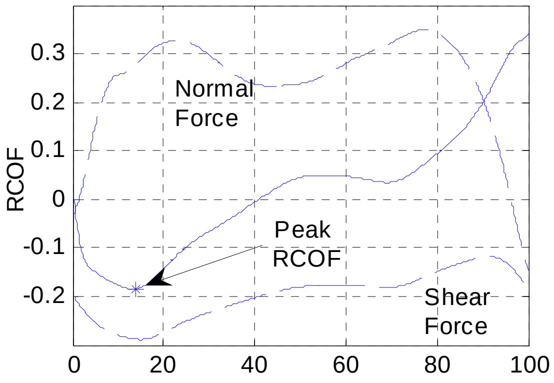

Figure 1: RCOF (solid line) is calculated throughout the stance phase as shear over normal ground reaction forces (dashed lines). Peak RCOF occurs in early stance phase.

RCOF during early stance phase was used for further analyses because it represents the minimum magnitude of coefficient of friction that will prevent the foot/heel from slipping forward.

Two-way repeated measures ANOVAs were used to investigate the effects of age and speed on RCOF within both controlled and uncontrolled step length conditions. A two-way repeated measures ANOVA was also used to investigate the effects of age and speed on step length within the uncontrolled step length conditions. All analyses were performed in JMP (SAS Institute Inc., Cary, NC, USA).

RESULTS AND DISCUSSION

In gait conditions SF and FF, in which step length was not controlled, RCOF (Table 2) was lower in older adults ($p = 0.015$) and increased with increased speed ($p < 0.001$). However, older adults exhibited smaller step lengths ($p = 0.026$), and RCOF was affected by step length ($p<0.001$). Therefore, these age differences in RCOF were confounded by differences in step length.

In gait conditions SS and FS, in which step length was controlled, RCOF (Table 2) was not significantly different between age groups ($p =0.671$), and decreased with increased speed ($p =0.049$). For these conditions, there were no age differences in speed ($p = 0.151$) or step length ($p = 0.133$).

The results show that when step length is controlled, there is no age difference in RCOF. In addition, increasing gait speed while not controlling step length increased RCOF (as in [2]), but increasing gait speed while controlling step length decreased RCOF. This speed effect may be due to greater increases in normal force than shear force when walking at a higher speed with the same step length.

Table 2: Mean (SD) RCOF by age group for the four gait conditions tested.

Gait Condition	RCOF	
	Older	Younger
SF*	0.166 (0.025)	0.201 (0.022)
FF*	0.195 (0.040)	0.227 (0.027)
SS	0.188 (0.033)	0.175 (0.025)
FS	0.169 (0.041)	0.170 (0.036)

* Significant age group differences ($p < 0.05$).

CONCLUSIONS

- RCOF during level gait does not appear to depend on age independent of gait kinematics (speed and step length).
- RCOF during level gait decreases with increased speed when step length is held constant.

REFERENCES

1. Redfern MS, et al. *Ergonomics* **44**, 1138-1166, 2001.
2. Cooper RC, et al. *Gait Posture* **27**, 547-551, 2008.
3. Christina KA and Cavanagh PR. *Gait Posture* **15**, 153-158, 2002.
4. Lockhart TE, et al. *Ergonomics* **46**, 1136-1160, 2003.

ACKNOWLEDGEMENTS

This work was supported by Award Number F31AG030904 from the National Institute on Aging. The content is solely the responsibility of the authors and does not necessarily represent the official views of the National Institute on Aging or the National Institutes of Health.

Table 1: The four gait conditions tested. Speed condition was either slow or fast, and step length condition was either freely chosen or controlled. Mean (SD) values obtained are presented.

Gait Condition	Speed		Step length	
	Condition	Mean (SD) Value (m/s)	Condition	Mean (SD) Value (m)
SF	Slow	1.180 (0.026)	Free*	Y: 0.672 (0.028) O: 0.630 (0.043)
FF	Fast	1.523 (0.031)	Free*	Y: 0.785 (0.044) O: 0.741 (0.048)
SS	Slow	1.184 (0.034)	Set	0.650 (0.005)
FS	Fast	1.526 (0.045)	Set	0.653 (0.010)

*Significant age group differences in step length ($p < 0.05$).

EVALUATION OF SYNTHETIC COMPOSITE TIBIAS FOR FRACTURE TESTING

[1] Cheryl E. Quenneville, [2]Gillian S. Fraser and [1]Cynthia E. Dunning
[1]The Jack McBain Biomechanical Testing Laboratory, Department of Mechanical & Materials Engineering, The University of Western Ontario, London, Ontario, Canada, [2]General Dynamics Land Systems Canada, Engineering Design & Development, London, Ontario, Canada
e-mail: cdunning@uwo.ca

INTRODUCTION

Composite synthetic bones are widely used in orthopaedic research. They offer many advantages over post mortem human specimens, including low inter-specimen variability in both geometry and material properties, ready availability, and ease of handling, storage and disposal. Fourth generation models of Sawbones® (Pacific Research Laboratories, Inc., Vashon, WA, USA) are made using a short glass fiber reinforced epoxy resin injected around a core of rigid polyurethane foam. These composite bones have been previously validated to replicate natural bone response under bending loading at a quasi-static rate [1].

Fracture studies for the purpose of injury prediction are an important area of research that could benefit from the advantages of synthetic bones. For them to be an appropriate surrogate, the fracture strength and patterns need to be consistent with the natural human response, as previously examined [2,3]. The purpose of this study was to evaluate the current generation of Sawbones® tibias for fracture tolerance when exposed to short duration impacts.

METHODS

Impact testing was conducted on nine large Sawbone® tibias (Model 3402). Eight of the specimens were the manufacturer's standard model, with an open canal and hole in the distal cortex. The ninth bone had the canal filled with polyurethane foam and the distal hole patched with epoxy resin by the manufacturer. Each tibia was supported vertically, aligned based on the anterior ridge of the tibia and the center of the medial malleolus, and potted in cement proximally.

Each specimen was instrumented with triaxial stacked strain gauge rosettes (C2A-13-125WW-350, Vishay Micro-Measurements, Raleigh, NC, USA) along the anterior surface. A laser line was projected along the anterior ridge of each bone, and the centre gauge of each rosette was aligned with the laser. Three rosettes were located distally, separated by 6mm gaps. A fourth rosette was located 1cm from the surface of the cement at the proximal end. Each gauge was independently wired into a quarter-bridge completion circuit (SCXI 1314, National Instruments, Austin, TX, USA).

An apparatus designed to apply axial impact loads to the tibias was used [4]. Each potted tibia was secured proximally to a bracket on linear bearings. The distal end of the tibia rested against an artificial talus made of polyethylene that was attached to a load cell mounted on a second bracket on bearings (Figure 1). A projectile of variable mass was propelled 40cm through a tube by pressurized air to strike the distal bracket. The projectile velocity and load imparted to the tibia along with all strain gauge signals were collected using a custom-written LabVIEW® (National Instruments, Austin TX, USA) program at a sampling frequency of 15kHz.

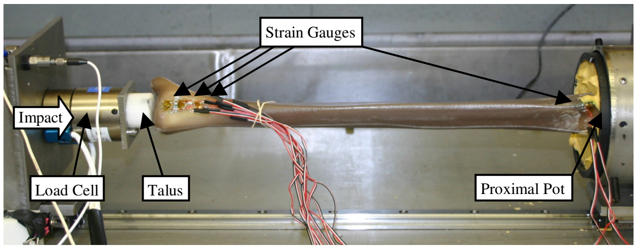

Figure 1: Instrumented tibia in the impacting apparatus. Three strain gauge rosettes were attached distally and one proximally.

Since impact force is specimen-dependent, and could therefore not be used as the input target for testing, desired kinetic energy levels were targeted. To vary the momentum, and allow examination of this variable in fracture tolerance, four standard specimens were tested using a 3.9kg projectile mass and four standard specimens plus the canal-filled specimen were tested using a 6.8kg projectile mass. Energy values for the impacts were based on preliminary tests, and were increased in 20J steps to average three strikes before failure, minimizing cumulative damage effects. Failure was defined as the specimen being in at least two separate pieces. Results were analyzed using paired t-tests ($\alpha=0.05$).

RESULTS

Failure occurred in all specimens, with damage concentrated in the distal region. Damage occurred in two manners concurrently: delamination of the epoxy resin from the polyurethane foam, as well as breaking apart of sections of the bone. The 3.9kg mass caused average peak forces of 4702±509N, and the 6.8kg mass caused average peak impact forces of 5718±642N (Figure 2). These were significantly different ($p=0.05$). The specimen with the canal filled fractured at a peak force of 5761N, which was not different than the standard specimens ($p=0.95$). Average impact momentums of 22.0±0.1Ns and 31.6±2.1Ns, and kinetic energies of 61.9±0.4J and 73.8±9.8J occurred for the light and heavy masses, respectively. Momentum was significantly different between projectile masses ($p=0.03$); as was kinetic energy at fracture ($p=0.03$).

Strain data were averaged for the 40J tests. The highest strains were recorded at the distal-most gauge level (averaging 4000με), and decreased proximally. There were no differences in strain between the masses at any gauge level ($p>0.11$).

DISCUSSION

This study subjected synthetic composite tibias to short duration axial impact loads. The cortical analog used in these models has previously been investigated [5], and fracture toughness was found to fall within the natural range of human bone. In the current study separation of the epoxy resin from the polyurethane foam during failure was common, and not representative of natural bone fractures.

Impact force at failure was found to be highly reproducible, but not affected by reinforcement of the distal canal. It had been postulated that the hole in the distal cortex would act as a stress concentrator, but this does not appear to be the case. To examine the role of other factors in addition to force, two projectile masses were used. Increased mass resulted in increased momentum, energy, and force to cause failure. This demonstrates the effect of test conditions on the fracture tolerance.

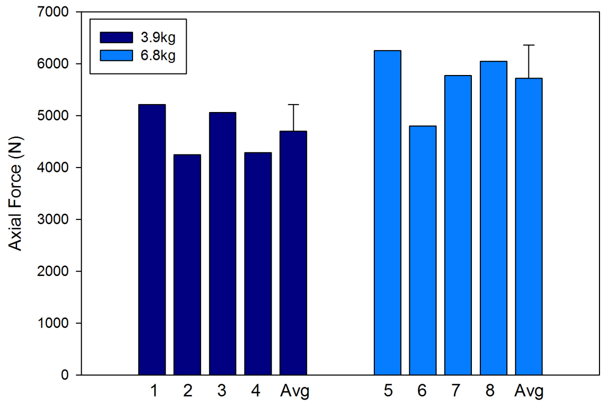

Figure 2: In the standard specimens tested, the 3.9kg mass caused average forces of 4702±509N and the 6.8kg mass caused average forces of 5718±642N, with failures between 4244-6251N.

Past research on lower limb injury following impact loading has focused primarily on quantifying fracture forces [2,3]. As such, there is little comparative data for the output variables of energy, momentum, and bone strains. With regards to force, previous lower limb fractures occurred for forces ranging between 3.8-13.0kN [2,3]. These values are higher than those attained in the present study, and suggest that these models do not represent cadaveric bone. A convex geometry of the distal articular surface noted on the synthetic tibias resulted in mostly point-loading, and could be a contributing factor in the lower fracture force.

This study has quantified the fracture response of fourth generation composite bones. The specimens demonstrated low inter-specimen variability, but lower fracture strength than previous studies. There was also unnatural delamination of the cortical shell during failure. This suggests they may not be representative of the natural response of bone under these testing conditions.

REFERENCES

1. Heiner AD. *J Biomech* **41**, 3282-3284, 2008
2. Funk JR et al. *J.Biomech.Eng.* **124,** 750-757, 2002
3. Yoganandan N et al. *Society of Automotive Engineers* 962426, 1996
4. Quenneville CE et al. *North American Congress on Biomechanics,* Abstract 145, 2008
5. Chong ACM et al. *J Biomech Eng* **129**, 487-493, 2007

RECOVERY FROM POSTURAL PERTURBATIONS WITHOUT STEPPING FOLLOWING LOCALIZED MUSCLE FATIGUE

[1] Bradley Davidson, [2]Michael Madigan, [2]Maury Nussbaum, and [3]Laura Wojcik
[1]University of Colorado Denver, [2]Virginia Tech, [3]Packer Engineering
email: bradley.davidson@ucdenver.edu

INTRODUCTION

Falls from heights continue to be problematic, recently accounting for 14.2% of reported occupational fatalities in the US [1]. Several investigations have demonstrated changes in postural sway following localized muscle fatigue (LMF) [2,3]. Since a link between increased postural sway and falling has been established (albeit among older adults) [4], these findings may indicate that LMF contributes to the risk of falling. Quiet standing is a relatively easy task for most individuals, and workplace related falls may be precipitated by postural perturbations. Wilson et al. [5] reported a LMF-induced shift in strategy during a perturbation; however, this is not indicative of changes in ability to recover with LMF. Therefore, the goal of this investigation was to assess the effects of LMF on measures of balance recovery (BR) following a postural perturbation. Both young and older adults were included, and two different muscle groups were fatigued. We hypothesized that LMF would increase center of mass (COM)-based variables and would decrease the maximum perturbation that could be withstood without stepping.

METHODS

Thirty-two participants were recruited including 16 young (19.4±1.4 years) and 16 older adults (62.2±5.1 years). Participants performed two sessions, separated by one week, during which they underwent a series of postural perturbations before and after LMF. In one session the ankle plantar flexors were fatigued; in the other session the lumbar extensors were fatigued [6]. Perturbations were administered with 13 kg padded pendulums (Figure 1) and perturbation magnitude was defined as the linear momentum just before impact. Each series of perturbations consisted of equal numbers of randomly-ordered anterior directed (AD) and posterior directed (PD) perturbations. Only results for AD perturbations are reported here.

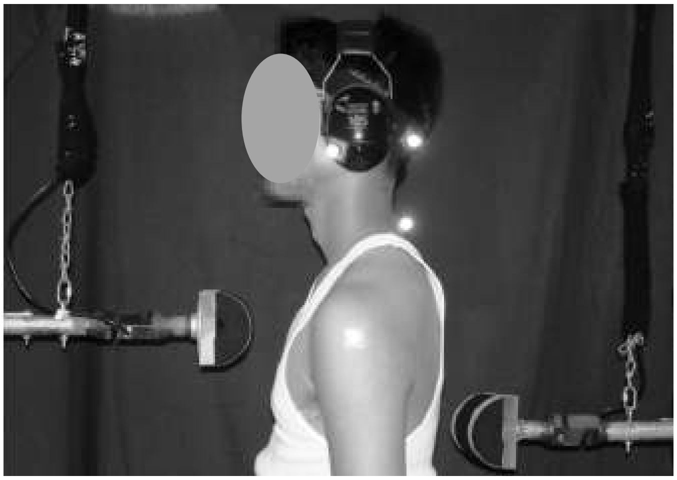

Figure 1: Pendulums positioned in the front and back of the participant.

The experiment began with an initial series of 20 perturbations (10 N·s AD, 7 N·s PD) to allow any adaptation in BR to occur prior to investigating the effects of LMF. Next, a series of increasing magnitude AD and PD perturbations beginning at 6 N·s and 5 N·s, respectively, were applied. Following a successful recovery without stepping, the magnitude was increased by 2 N·s for AD and 1 N·s for PD perturbations. If a step occurred, the same magnitude was repeated. If two stepping responses occurred for a given magnitude, the previous magnitude was recorded as the maximum perturbation withstood without stepping. Sixteen constant-magnitude perturbations were then administered at 4 N·s and 2 N·s below the maximum AD and PD perturbations, respectively, and used to investigate the effects of fatigue and age on COM kinematics.

Positions of 16 anatomical markers were sampled at 100 Hz and low-pass filtered at 5 Hz. An anthropometrically correct six-segment kinematic model (feet, shanks, thighs, pelvis, torso/arms, and head) was used to approximate the COM trajectory. Measures of BR included the maximum perturbation that could be withstood without stepping, and descriptors of the COM trajectory including peak displacement relative to initial position, time-to-peak displacement, peak AD velocity, time-to-peak velocity, minimum time-to-boundary, and time-to-return to within 20% of peak displacement. COM-based displacement measures were normalized by ankle-to-toe length and velocity measures were normalized by multiplying by participant mass to account for inertial effects.

A repeated measures analysis of variance was used to examine the effects of fatigue (unfatigued, fatigued), muscle (ankle plantar flexor, lumbar extensor), and age (young, older) on BR measures. Covariates included perturbation magnitude and COM kinematics at the instant of pendulum contact. Effect size was quantified using Hedge's g.

RESULTS AND DISCUSSION

Statistical tests revealed no interactive effects, and no effects of muscle group for any of the dependent variables. Four of the six COM-based measures were affected by LMF including a 2.7% increase in peak COM displacement ($p<0.001$, Hedge's $g=0.32$), a 4.1% increase in time-to-peak COM peak displacement ($p<0.001$, $g=0.47$), a 0.6% increase in peak COM velocity ($p=0.011$, $g=0.22$), and a 3.5% increase in time-to-return within 20% of peak COM displacement ($p=0.002$, $g=0.28$). The maximum perturbation that could be withstood without stepping decreased 3.6% and exhibited a moderate effect size ($g=0.43$), but did not reach statistical significance ($p=0.086$).

The maximum perturbation that could be withstood without stepping was 17.8% lower among the older adults ($p=0.029$, $g=0.57$). Older adults exhibited an 8.6% higher peak COM velocity ($p=0.006$, $g=0.31$) and a 4.6% lower time-to-peak COM velocity ($p=0.042$, $g=0.23$).

Overall, our results showed that COM excursion during BR increased after LMF. COM-based measures exhibited greater excursions with LMF. Both peak COM displacement and time-to-return within 20% of the peak displacement indicated that the perturbed COM not only moved closer to the base-of-support boundary, but was displaced for a longer period of time following LMF. Increases in the peak COM velocity and time-to-peak COM displacement corresponded with an increase in peak angular momentum and a delay in reversing the direction of momentum, respectively. When considered together, these changes imply a greater likelihood of stepping and possibly a decrease in the ability to recover without stepping. Consistent with this interpretation, the maximum perturbation that could be withstood without stepping tended to decrease with LMF (effect size $g=0.47$). However, the increment in perturbation magnitude used to identify this maximum perturbation may have, in retrospect, been too large to detect small effects of LMF.

In summary, the results indicate that LMF impaired BR in both age groups in a similar manner. These changes occurred during submaximal perturbations, and may imply a higher likelihood of requiring an alternate strategy (such as stepping) with slightly larger perturbations.

REFERENCES

1. BLS. Report from US Dept of Labor , 2005
2. Corbeil P, et al. *Gait Posture* **18**, 92-100, 2003.
3. Lundin T, et al. *J Appl Biomech* **9**, 191-201, 1993.
4. Maki B, et al. *J Gerontol* **49,** M72-84, 1994.
5. Wilson E, et al. *Gait Posture* **23**:348-354, 2006.
6. Davidson B, et al. *Gait Posture* **29**, 552-557, 2009.

ACKNOWLEDGEMENT

This research was supported by R01 OH07882-02.

Table 1: Least squares mean ± SE for each measure categorized by fatigue level and age group.

Balance Recovery Measure	Young		Older	
	unfatigued	fatigued	unfatigued	fatigued
max. perturbation magnitude (N·s) †	7.41±0.14	7.38±0.14	6.31±0.14	5.88±0.14
peak displacement (%) *	26.1±0.3	26.6±0.3	25.2±0.3	25.9±0.3
time-to peak displacement (msec) *	591.0±7.9	608.4±8.4	538.1±8.5	567.2±8.1
peak velocity (N·s) ***,†**	16.57±0.08	16.65±0.08	17.96±0.08	18.09±0.08
time-to peak velocity (msec) †	145.8±0.8	146.7±0.9	139.5±0.9	139.5±0.8
min. time-to-boundary (msec)	572.3±10.2	57.09±10.7	587.9±10.5	585.6±9.9
return to 20% (msec) *	1336±27	1334±28	1295±29	1369±28

* significant effect of fatigue, † significant effect of age

MEASURING THE PROPAGATION OF A MECHANICAL WAVE THROUGH SOFT TISSUE WITH A 3D MOTION CAPTURE SYSTEM

Idafe Pérez Jiménez, Matthew T.G. Pain
School of Sport & Exercise Sciences, Loughborough University, UK
email: I.Perez-Jimenez@lboro.ac.uk

INTRODUCTION

The shape of a body segment can change due to movement or interactions with other segments and external objects. In an impact, a mechanical wave propagates through body segments. Soft tissue deformation has been reported to account for up to 70% of the energy lost in some of these segments [1]. The surface contracts and expands under the influence of this wave, whose characteristics will be dependent on the mechanical properties of underlying tissues and on the excitation itself. Measuring surface area changes can provide information on energetic interactions and on the properties of the tissues through which the wave is propagating.

Moreover, an accurate determination of areas and volumes of body segments, and how they change, is an important tool for several other areas of biomechanics research, such as the determination of inertia parameters. An experimental technique was developed to perform a detailed analysis on the changes in area and volume with time of a moving segment, particularly during impacts.

METHODS

Instrumentation: A Vicon motion capture system with nine T020 and two MX13 cameras was employed to detect 3 mm and 5 mm hemispherical reflective markers. Working frequency was set at 700 Hz.

Evaluation: The reliability of the technique used to measure areas was first evaluated using 130 markers on a rigid cylinder, with five static and five dynamic trials. Areas calculated directly (520±18 cm^2) were compared to those calculated from marker positions. The consistency of results was also assessed. The calculation of volumes using markers was assessed by comparing these volumes with those measured through an immersion method, in objects with different degrees of deformation.

Observation of impacts: The lower leg of a subject was covered with eighty-nine 5 mm hemispherical markers (Figure 1). Trials were recorded with subjects instructed to stand static (to evaluate consistency of measurements) and to perform, on a force plate, a controlled two-footed drop landing, a stamp a running stride, and bounces. Five trials of each type were recorded.

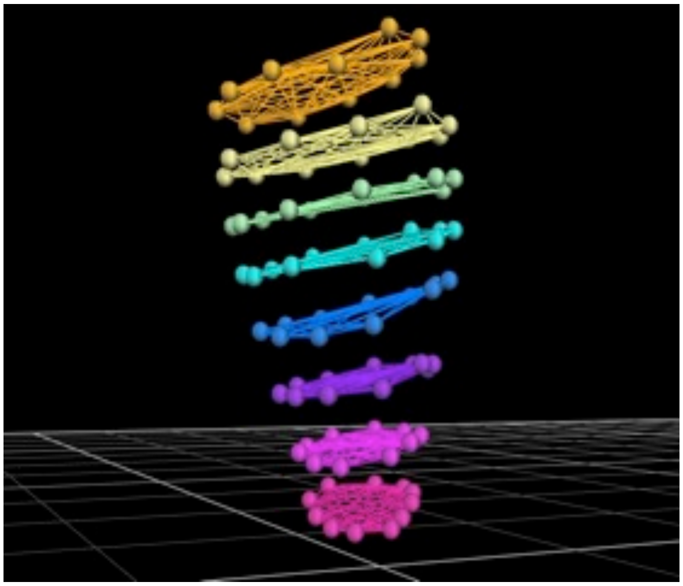

Figure 1: View from behind of the marker set on the lower leg. Column 6 is shown in the middle.

RESULTS AND DISCUSSION

Mean standard deviation of areas between markers for static trials on the rigid cylinder was 0.09% of the mean area. For dynamic trials the SD amounted to 0.12% of the mean area. This values can be considered low and hence imply a very consistent measurement of areas.

The area calculated for the cylinder was 515±1 cm^2, which lies within the margin of error of the direct method calculation. There was no significant difference between areas calculated in static and dynamic trials ($p<0.05$). The difference between measured and calculated volumes ranged between +1.3% and -12.4% and was very dependant on the deformation of the object.

For static trials, with the subject standing at rest, the mean area between each set of three first neighbor markers was 651.9 ± 4.2 mm^2, which results in a SD of 0.65%. The greatest individual area SD was 1.83%. The difference between the rigid object and the subject arises because the subject is never completely still, but the low SD still allows resting areas to be used for comparison. The mean distance between first neighbor markers in static trials on the subject was 42.21 ± 14.77 mm. The significant variation of distances responds to the fact that the dimensions of the lower leg change noticeably between different areas (see Figure 1).

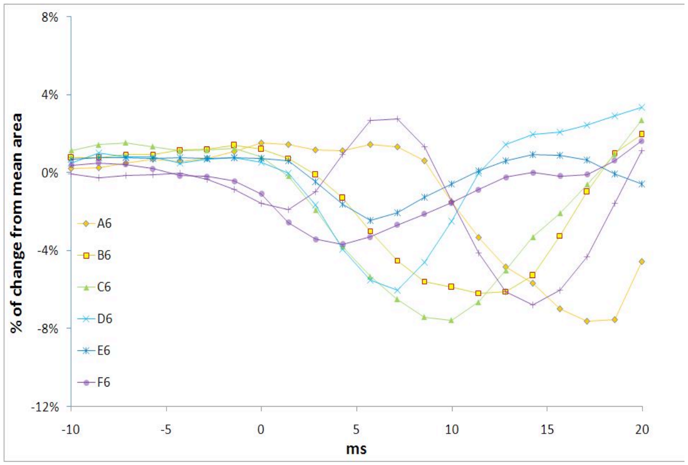

Figure 2: Deformation of sectors in column 6, corresponding to the back of the lower leg. Height of sectors labeled A-F top to bottom.

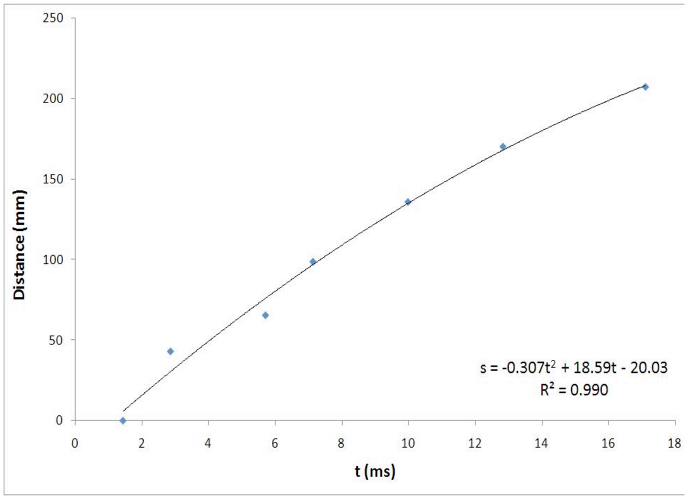

Figure 3: Distance to lowest sector versus time to reach maximum deformation due to impact, and a quadratic fit of the points.

During the drop landing, when the subjects managed to remain standing straight and minimized ankle and knee flexion, area variations were predominantly due to the impact. Figure 2 shows the changes in area for a column of sectors in the back of the lower leg. The first contraction and expansion have a similar phase, showing that this method can provide information on the mechanical behavior of soft tissue under impacts.

Figure 3 represents the time at which each sector shows maximum contraction after the impact, against the distance between the middle of that sector and the lowest one. This allows a rough estimation of the velocity of the wave front. For this subject and this set of trials the initial velocity was found to be 18.59 m·s^{-1} using a quadratic fit and 12.99 m·s^{-1} using a linear one. This calculation should however be regarded with care, since, typically, only one frame separated the maximum contraction of consecutive sectors. There is, on the other hand, enough data available to use wave mechanics and examine the frequency and amplitude calculations of intra-segmental motion.

CONCLUSIONS

A method has been developed to measure the changes in area and volume of segments. The accuracy and precision of the data obtained allows the detection of variations in area and volume of soft tissue due to impacts in intra-segmental motion. This provides data for a wave mechanics analysis of the excitation, which itself will provide information on the mechanical properties of the soft tissue underlying the measured surface. However, several practical problems arise from applying the method to real situations, such as deformations due to the movement itself, also an area of interest. A higher working frequency would also be desirable to fine-tune the timing, due to the velocity with which the wave propagates and the small distances involved.

REFERENCES

1. Pain, MTG & Challis, JH. *J Appl Biomech,* **18** (3), 231,42, 2002.

COMPUTATIONAL SIMULATION OF ANKLE CONTACT MECHANICS FOLLOWING FOCAL DEFECT RESURFACING WITH A METALLIC IMPLANT

Donald D. Anderson, Yuki Tochigi, M. James Rudert, Tanawat Vaseenon,
Annunziato Amendola, and Thomas D. Brown

Department of Orthopaedics and Rehabilitation, University of Iowa, Iowa City, IA, USA
e-mail: don-anderson@uiowa.edu URL: http://poppy.obrl.uiowa.edu

INTRODUCTION

Focal resurfacing of persistent osteochondral defects (OCDs) with a metal implant is a promising new treatment option for certain patients. The superior dome of the talus is a common site for this pathology, but the geometric complexity of the talar articular surface presents challenges to successful implant design, selection, and surgical placement.

The purpose of this study was to document the effect of small perturbations of implantation parameters upon ankle contact mechanics after focal resurfacing of the talar dome with a metal implant.

METHODS

Finite element (FE) simulations of loading of the intact ankle, the ankle after the introduction of a 15 mm cylindrical defect to the medial edge of the talar dome, and the ankle with a focal resurfacing implant (Figure 1) were performed. The effects of various implantation parameters (implant height, rotation about its post axis, and valgus/varus tilt) were studied over a simulated motion cycle.

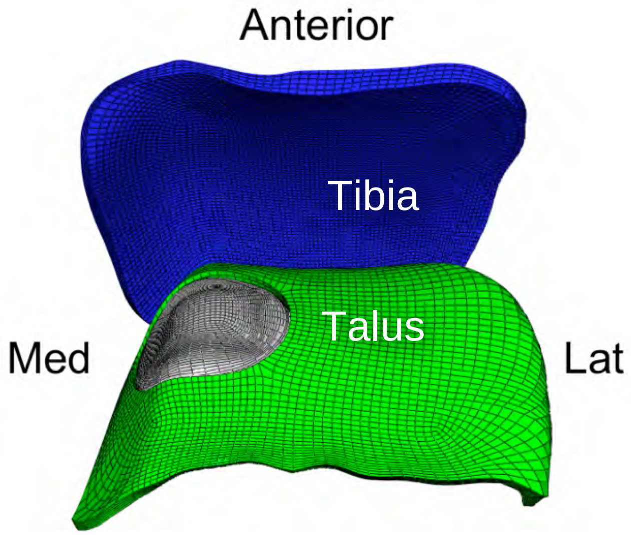

Figure 1. This antero-superior view of the ankle (joint is opened for visualization) shows the FE contact model, with a focal resurfacing metal implant placed medially upon the superior surface of the talus.

The ankle contact FE modeling approach was based on previous work [1], with bone being treated as rigid, and cartilage as a linear elastic material ($E=12MPa$; $\nu=0.42$). The resurfacing implant was included as an additional rigid surface. Contact was modeled between cartilage surfaces, as well as between the superior cap surface and the opposing tibial surface, and between the cap sides and the adjacent talar cartilage surface.

A 300 N axial load was applied across the ankle joint. Then the tibia was rotated (under load) about the talus through a functional arc of flexion/extension (±10°), with the talus free to rotate in response to tibio-talar articulation.

Complementary static loading experiments [2] were performed in seven fresh-frozen cadaver ankles, before and after creation of a 15 mm cylindrical OCD on the medial edge of the talar dome, in part to validate the FE model. Ankle contact stresses were measured using a high-resolution sensor (TekScan) [3]. The defect was then resurfaced with a metallic implant (HemiCAP; Arthrosurface Inc.), supplemented with a custom implant-bone interface fixture that allowed very fine control (0.25 mm increments) of implantation height. Contact stress measurements were repeated at implant heights from -0.5 to +0.5 mm with respect to an as-implanted reference.

RESULTS AND DISCUSSION

With the untreated defect, experimentally there was a 20% reduction in the ankle contact area and a 40% increase in peak contact stress, plus a pronounced shift in the highest-loaded region. Following flush resurfacing with the implant, contact area recovered to 90% of intact, but peak contact stresses remained

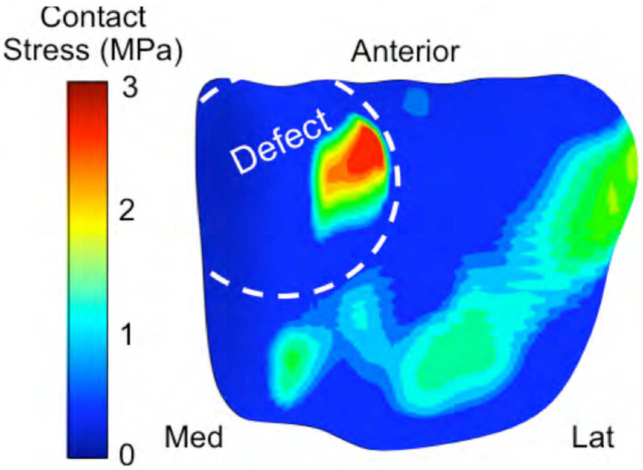

Figure 2. This view of the inferior aspect of the tibia shows the elevated contact stress over a resurfacing metal implant placed 0.25 mm proud with respect to the surrounding cartilage, as computed by the FE model.

elevated. When the implant was 0.25 mm proud, there was a 120% elevation in peak contact stress atop the metal cap (Figure 2). FE-computed contact stresses and trends agreed closely with experiments.

Whereas simulations in the intact state showed smooth and regular motion across the duty cycle, in the presence of an unfilled defect, there was dramatically increased external rotation with ankle plantarflexion (3.4° of external rotation as plantarflexed from neutral to 10° in the defect state, versus 1.0° of internal rotation in the intact state – Figure 3). There was also a striking elevation in cartilage stress on the talar dome directly adjacent to the defect at the higher angles of plantarflexion, reflecting an absence of buttressing of cartilage at the defect lip. The implantation of a resurfacing device substantially restored the natural kinematics, but did not uniformly restore stresses to levels in the intact ankle.

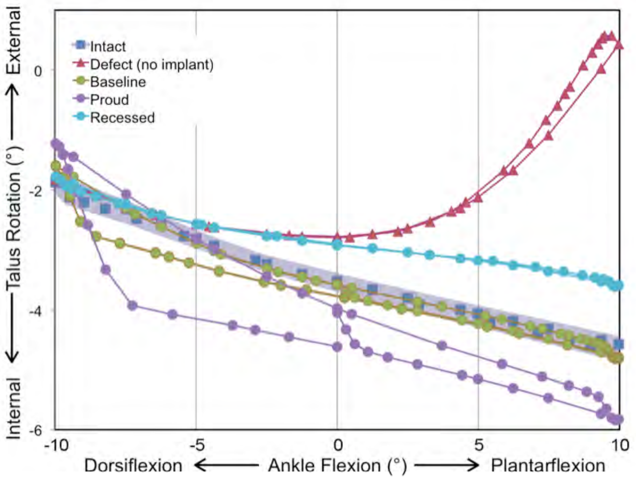

Figure 3. Coupled talar internal rotation associated with plantarflexion of the ankle was greatly disrupted when an unfilled talar OCD was modeled. A focal resurfacing implant restored the normal talar kinematics.

CONCLUSIONS

Focal resurfacing with a metal implant appears to be a viable strategy to restore normal joint mechanics in ankles with a large talar OCD. However, given that implant-on-cartilage contact stresses were highly sensitive to proudness and malpositioning, very precise implantation is necessary. Over time, active tissue remodeling may compensate for small incongruities in the implant-to-cartilage interface. The FE approach holds substantial attraction for studying other resurfacing options, such as osteochondral plugs or other implant designs.

REFERENCES

1. Anderson DD, et al. *Biomech Model Mechanobiol*. **5**:82-9, 2006.
2. Tochigi Y, et al. *J Bone Joint Surg [Am]*. **88**:2704-13, 2006.
3. Brown TD, Rudert MJ, Grosland NM. *Clin Orthop Relat Res*. **423**:52-8, 2004.

ACKNOWLEDGEMENTS

This work was supported by a research grant from Arthrosurface Inc. (Franklin, MA), and by NIH/NIAMS Grant P50 AR055533.

A METHOD FOR QUANTIFYING PIPETTE ERGONOMICS

Kristin Zhao, Lawrence Berglund, Adriana Blazeski, Wen-Lin Tung, and Kai-Nan An
Biomechanics Laboratory, Division of Orthopedic Research, Rochester, MN
email: zhao.kristin@mayo.edu

INTRODUCTION

Work involving pipetting has been associated with elevated rates of musculoskeletal disorders of the hand and wrist. From an ergonomic perspective, force, posture and repetition are recognized as major contributing factors to these potential disorders. Biomechanical investigations of muscle activations (electromyography) and the strain imposed on the hand-arm-shoulder musculature have been performed to compare various designs of pipettes and conditions of the task [1,2]. In general, the resistance of the plunger and the deviation of the extremity from an ergonomically-favorable position have been found to minimize the strain. The plunger resistance depends not only on the design, but also the viscosity of the fluid. Furthermore, the precision of the task could also influence the muscle force and activity.

This purpose of this work is to present a method for assessing the biomechanics of the hand while pipetting with a manual pipette. The methodology is presented along with the data from nine subjects. Biomechanical data quantifying the mechanics of the pipette, as well as the effect of pipette design on posture and joint loading, can lead to improved pipette designs that will potentially reduce the incidence of hand and wrist pathologies.

METHODS

Phase 1: Pipette mechanics

Plunger mechanics (normal and overshoot) and ejector mechanics were obtained on a material testing machine (Figure 1). A 25 lb load cell (Transducer Techniques, Temecula, CA) was used in conjunction with the load cell installed on the test machine to minimize the noise observed in the experimental data. Load and displacement data were recorded for each test using MTP (Natick, MA) software supplied with the MTS (MTS Corporation, Eden Prairie, MN) software operating system.

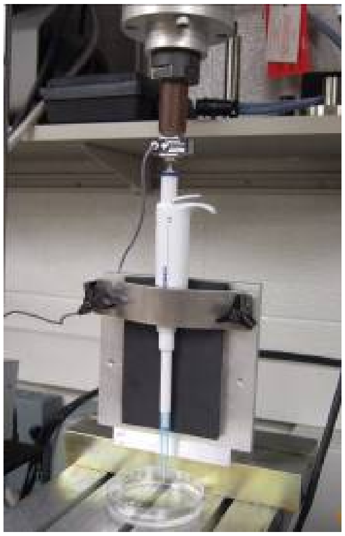

Figure 1: Testing of plunger mechanics in material testing machine.

The pipette was tested at multiple loading rates, two liquid viscosities, and three liquid volume conditions. Two rates of loading were tested, representing slow (5mm/sec) and fast (30mm/sec) action. These rates were determined by observation of normal use of pipettes (obtained by video analysis). Two different fluids of different viscosities were used, Sigma Triton X-100 surfactant (Brookfield, viscosity 240 cps at 25 C, cps=centipoise) for high viscosity and distilled water (1 cps) for low viscosity. The three liquid volumes (10, 100, and 1000µL) required three different pipettes. In each condition, three trials were collected, followed by a single trial with just air in the pipette. Load versus displacement curves were obtained for each trial. Data were obtained at 50 Hz for the 5mm/sec rate and 350 Hz for the 30mm/sec rate.

Forces required to eject the tips from the pipette were recorded in a similar manner on the MTS. After the tip was inserted onto the pipette, the pipette was placed on a jig on the test machine and the injector tip pushed with the indenter on the load cell at 5 mm/sec until the tip was ejected. The data was recorded at a rate of 200 Hz.

Phase 2: Subject measurements

Nine experienced pipette users were recruited for study involvement according to IRB guidelines. Subjects were asked to pipette at a slow rate (5mm/sec) using the 1000µL pipette with low viscosity fluid. The top surface of the plunger and ejector were fitted with paper-thin pressure sensors (Tekscan, Inc.) for use in detecting the various phases of the pipetting trials. Electromagnetic sensors (Liberty, Polhemus Inc.) were fixed and reinforced with tape to the pipettes and the subject's lower arm, dorsal side of the hand, and the thumb metacarpal and first and second phalanges (Figure 2).

Anatomical coordinate systems were set up on each segment of interest, and points were also tracked on the pipette for use in locating the long axis (plunger axis) of the pipettes for determining the moment arm (to the CMC joint). In addition, a point on the distal, palmar side of the tip of the thumb was located for tracking the displacement of the thumb in 3D space.

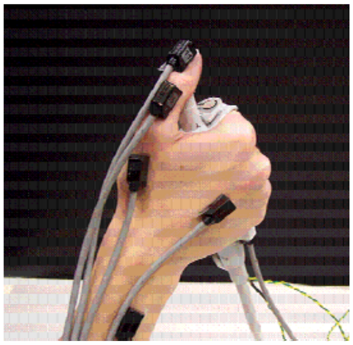

Figure 2: Subject setup including electromagnetic and pressure sensors.

All subjects were asked to use the pipette in a standardized manner. They were asked to draw in water, dispense the water, and finally eject the tip. Dynamic translation and rotation data were synchronously obtained from all of the sensors at 100 hz during the trials. Joint rotations were determined at each time point for each joint (PIP, MCP, CMC) using a helical axis decomposition method. CMC joint moment arms were determined at each time point as the perpendicular distance from the position of the CMC joint to the long axis (plunger axis) of the pipette. Three trials were performed.

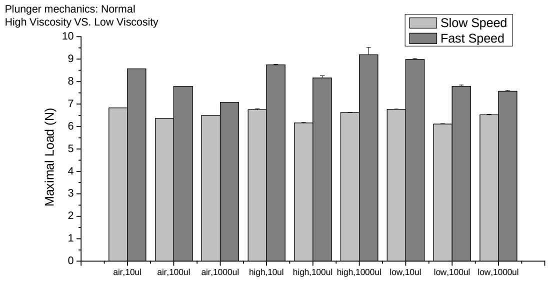

Figure 3: Comparison of maximal plunger load across all fluid viscosities, and slow and fast speed.

RESULTS AND DISCUSSION

The following graphs depict representative data that were obtained using the methods described. The maximal plunger load as a function of fluid viscosity and speed is presented (Figure 3).

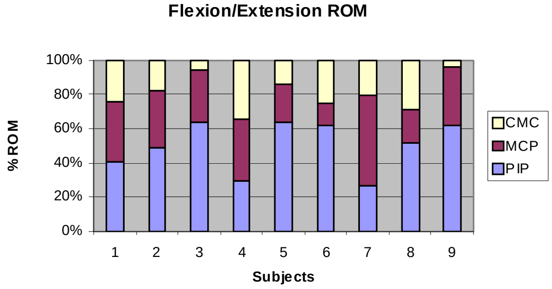

Figure 4: Joint ranges of motion during the plunging phase of the movement.

With knowledge of the plunger mechanics and joint positions obtained from the subjects (Figure 4), moment at the CMC joint can be approximated (Figure 5).

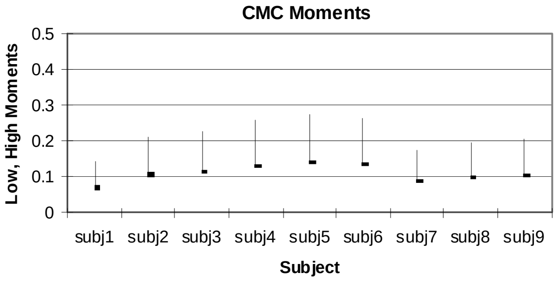

Figure 5: Potential CMC moments experienced by each subject during the plunging phase of motion.

Ergonomic investigations of manual pipetting can be used to assess pipette design parameters and their effect on musculoskeletal parameters such as joint loading. This will help lead to improved pipette designs or usage instruction that will potentially reduce the incidence of hand and wrist pathologies.

REFERENCES

1. Asundi, KR et al. *Human Factors* **47**(1), 67-76, 2005.
2. Fredriksson, K. *Ergonomics*. **38**(5),1067-73, 1995.

ACKNOWLEDGEMENTS

This study was supported by Socorex Isba S.A. – Switzerland.

INJURY TOLERANCE CRITERIA FOR SHORT DURATION AXIAL LOADING OF THE TIBIA

[1] Cheryl E. Quenneville, [1]Stewart D. McLachlin, [2]Gillian S. Fraser and [1]Cynthia E. Dunning
[1]The Jack McBain Biomechanical Testing Laboratory, Department of Mechanical & Materials Engineering, The University of Western Ontario, London, Ontario, Canada, [2]General Dynamics Land Systems Canada, Engineering Design & Development, London, Ontario, Canada
e-mail: cdunning@uwo.ca

INTRODUCTION

Axial loading of the lower leg during short-duration impulsive events, such as ejection seat and parachute landings, or in-vehicle landmine blasts, can cause significant lower limb injuries. To date, most of the research investigating the axial injury tolerance levels of the lower limb has been conducted by the car crash industry [1]. The aforementioned short duration events achieve higher forces over less time than car crashes, and as such, investigation into the applicability of the current injury criterion is required.

The current standard used for assessing risk from these types of events has been specified for anti-vehicular (AV) landmine blasts [2] as a maximum axial force level of 5.4kN. However, factors other than force, such as energy, momentum or impulse, may be important for these scenarios. The purpose of this study was to investigate the injury tolerance of the tibia to axial impacts representative of short-duration (<10ms) events, and the appropriateness of the current force-only standard.

METHODS

Impact testing was conducted on seven pairs of fresh-frozen isolated cadaveric tibias from male donors (mean age: 48±5 years). Paired specimens were used to allow side-by-side comparison of the force-momentum-energy relationships examined by the loading protocols. Each tibia was supported in a vertical orientation, aligned based on the anterior ridge of the tibia and the center of the medial malleolus, and potted in cement proximally.

An impacting apparatus designed to apply axial loads to the tibias was used. Each potted tibia was secured proximally to a bracket on linear bearings. The distal end of the tibia rested against an artificial talus made of polyethylene attached to a second bracket on bearings that was instrumented with a load cell. A projectile of variable mass was propelled through a tube by pressurized air to strike the distal bracket. The projectile velocity and load imparted to the tibia were collected at a sampling frequency of 15kHz.

Since impact force is specimen-dependent, and could therefore not be used as the input target for testing, kinetic energy levels were targeted. Preliminary tests were conducted on two pairs of specimens in energy increments of 50J (Protocol 1). To allow examination of momentum as an injury risk factor, one specimen from each pair was impacted using a 3.9kg mass and the contralateral with a 6.8kg mass. Failure occurred in the 150–250J range, and so the remaining five pairs of specimens were impacted in energy increments of 100J (Protocol 2), starting at 150J. Results were analyzed using paired t-tests to determine differences between the masses (α=0.05). A best subsets regression analysis was performed to determine the variables and equation that predicted injury risk. A Weibull model was used to establish a probability of injury curve.

RESULTS

Fractures were achieved in all specimens, with damage being concentrated in the distal region. The 3.9kg mass caused average peak impact forces of 12563±1982N, compared to 12581±2277N for the 6.8kg mass (Figure 1). There were no differences in peak force between the two masses (p=0.98), or between Protocol 1 and 2 (p=0.80). Impact impulses averaged 17.6±3.7Ns. Average impact momentums of 43.0±4.4Ns and 57.1±3.6Ns, and kinetic energies of 239±45J and 241±30J occurred for the light and heavy masses, respectively. Momentum to cause fracture was different between masses ($p<0.001$), and lower than found in previous studies [1]. Kinetic energy had no differences between masses ($p=0.94$), and was in the same range as those found in previous studies [1], even though the current study achieved higher forces.

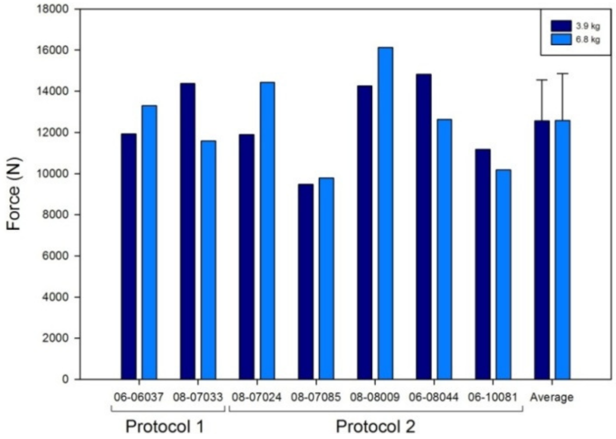

Figure 1: The 3.9kg mass caused average forces of 12563±1982N, and the 6.8kg mass caused average forces of 12581±2277 N, with no fracture force below 9481N.

To determine the most appropriate survival equation, the effects of each variable were tested using a best subsets regression. Variables that were examined included projectile mass, velocity, momentum, kinetic energy, axial force, specimen age, height, and body mass. From these factors, the best model ($R^2=0.73$, adj. $R^2=0.69$) included the natural log of axial force (in Newtons), kinetic energy (in Joules), age (in years), and height (in centimeters) as significant independent variables. This yielded the risk equation:

$$Injury\ risk = -2.123 - 0.666 * \ln(F) + 0.0104 * KE + 0.0397 * Age + 0.026 * Height$$

A Weibull analysis was performed to develop a survivability curve based on this equation. One was also developed based on axial force, to allow comparison with previous equations (Figure 2). This found that 10% risk of failure corresponded to a load of 7.9kN ($R^2 = 0.86$).

DISCUSSION

This study subjected pairs of isolated cadaveric tibias to axial impact loads representative of short duration loading events. Testing of isolated bones reduces the complexity found in full lower limb testing, allowing the separation of tibia injury risk from lower-leg injury risk. However, this gives no indication of risk to the talus and calcaneus, which are often injured during these events.

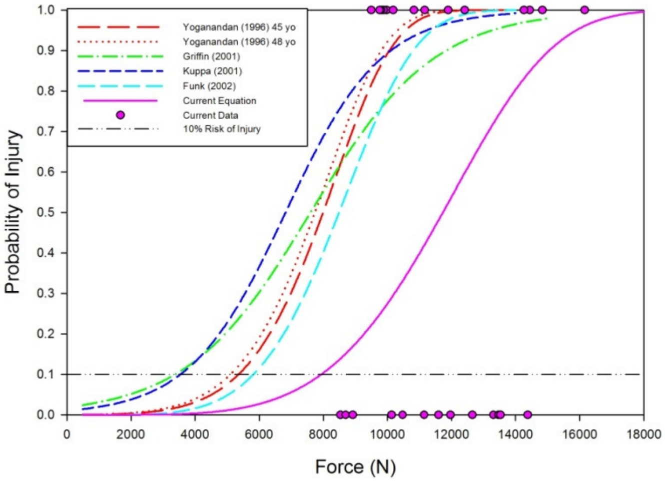

Figure 2: Previous injury probability curves, compared to the current equation developed from the data points shown and a Weibull analysis.

The peak forces in the present study were higher than those attained in previous studies of whole, below-the-knee specimens under conditions simulating car crash injuries [1]. This suggests that the previous limit may be too conservative for short duration impacts of the isolated tibia. It is also possible that higher forces were tolerated due to the decreased loading duration in the current impact events, indicating that impulse could be an important factor in the injury tolerance of the tibia as has been suggested for other areas of the body, such as the head [3]. Fracture did not appear to be controlled by a specific momentum level, but energy was found to be an important factor in injury risk assessment, in addition to force.

This study isolated the fracture tolerance of the cadaveric tibia under short duration axial loading. It is the first of its kind to propose the use of energy as a secondary injury criterion for the lower leg, and a new force standard of 7.9kN has been proposed for short duration axial loading.

REFERENCES

1. Yoganandan N et al. *Society of Automotive Engineers* 962426, 1996
2. NATO *HFM-090 Task Group 25 Report*, 2007
3. Yoganandan N et al. *IUTAM Symposium,* Dublin, 2006

EFFECT OF SELECTIVE MUSCLE WEAKNESS ON RANGE OF MOTION OF GLENOHUMERAL JOINT

Shridhar Shah, John Novotny and Jill Higginson
Department of Mechanical Engineering, University of Delaware
email: shridhar@udel.edu, novotny@udel.edu, higginson@udel.edu

INTRODUCTION

The human arm is a redundant system, with multiple muscles actuating 3 degrees of freedom at the glenohumeral joint. Aging is associated with significant strength decrements and has adverse effects on functional range of motion [3]. However, weakness in one muscle can be compensated by another muscle to some extent to maintain the ability to perform activities of daily living. Using simulations, we studied the effect of selective muscle weakness on range of motion in different planes of elevation, while accounting for muscle compensation. The objective of this study was to quantify the effect of selective muscle weakness on range of motion, determine appropriate muscle excitation patterns, and identify which muscles can provide compensation.

METHODS

A musculoskeletal model of the upper extremity with five degrees of freedom and 26 muscles crossing the shoulder complex and elbow joint was used. The five degrees of freedom were: thoraco-humeral elevation angle, elevation plane angle, humeral rotation, elbow flexion-extension and wrist pronation-supination. This model was obtained by modifying a more comprehensive model of the upper extremity with 15 degrees of freedom and 50 muscle elements [2]. The muscle activation dynamics were modeled as a first-order differential equation. Muscle force production was represented as a Hill-type muscle. The shoulder model was created using SIMM (Musculographics Inc.) software. The equations of motion were generated using SD/Fast software. The Dynamics Pipeline module in SIMM was used to generate forward simulation code in C language.

A parallel version of simulated annealing was implemented on a computer cluster (128 AMD Opteron270 processors, 2000 MHz) to predict the excitation patterns that would produce a motion that matched the experimental kinematic data. The algorithm tried to minimize the difference between measured and simulated kinematic data with limited muscle co-activation [1].

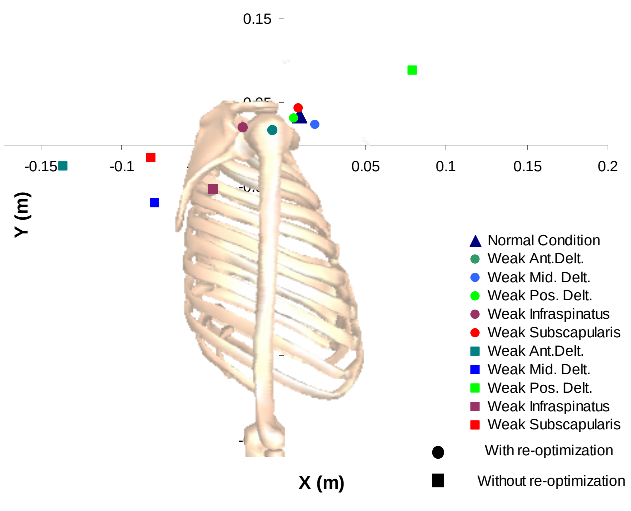

Figure 1: The position of distal end of humerus in X-Y plane for different perturbations after one second simulation of abduction in 0 degree elevation plane. The square markers show the effect of weakness in muscles without considering compensation strategies while the circular markers represent end position after re-optimization accounting for compensation by healthy muscles.

The simulation required kinematic data for five degrees of freedom. The kinematic data was collected on one male subject (21 years old, 73 kg and 1.72 m) using 8 Motion Analysis cameras at 60 Hz (Motion Analysis Corporation). The subject was asked to lift the arm approximately in 90, 30, 0 and -30 degrees of planes of elevation.

Four simulations were generated for shoulder abduction with the arm in -30, 0, 30 and 90 degrees of planes of elevation. Duration for each simulated arm elevation was 1 second. For each condition, simulations were generated with normal strength and 10 weakened states. Five muscle elements (three heads of Deltoid, Infraspinatus and Subscapularis) were perturbed by reducing their strength by 50% and simulated with and without re-optimization. The purpose of re-optimization was to determine new excitation patterns which may result due to weakness in a muscle. The results of these simulations were recorded in terms of XYZ position of the distal end of the humeral head. The results after optimization were compared with normal and weakened conditions.

RESULTS AND DISCUSSION

By simulating selective muscle weakness without re-optimization, we find the effects of each muscle on range of motion (Figure 1). The results illustrate that middle deltoid plays an important role in elevation of the arm while stabilizing its posterior motion, anterior deltoid and subscapularis resist motion in the posterior direction while posterior deltoid stabilizes the arm motion in the anterior direction. Middle deltoid and subscapularis also prevent external rotation while infraspinatus and posterior deltoid resist interior rotation of the humerus.

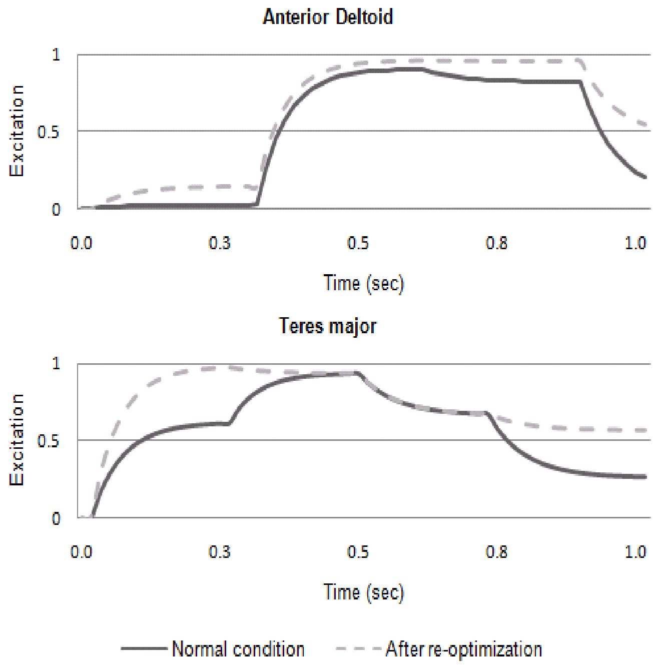

Figure 2: Comparison of excitation pattern of anterior deltoid and teres major for normal condition and after re-optimization for subscapularis weakness.

Following re-optimization, range of motion can be recovered. The final state of the distal end of the humerus with weak muscles was within ±3.5cm of the normal condition. Clearly, a subset of healthy muscles can compensate for weakness in a single muscle. The comparison of excitation patterns of normal condition with excitation patterns of weak state after re-optimization is a useful tool to identify the compensatory strategy (Table 1). Table 1 shows significant increases or decreases in excitation of healthy muscles as part of each compensation strategy. For example, an increase in excitation after of teres major and anterior deltoid was observed after re-optimization as part of a compensation strategy for weak subscapularis (Figure 2).

From this study, we gained insight about the role of muscles over a large range of motion, which may have clinical implications. By determining which upper extremity muscles play major roles in compensation, clinicians can choose which muscles to target for strength training and rehabilitation programs.

Table 1: Change in excitation patterns due to compensation by healthy muscles (for should abduction in 0 degree elevation plane).

Weak Muscle	**Increase in Muscle Excitation**	**Decrease in Muscle Excitation**
Anterior deltoid	Ant. deltoid, Pectoralis major, Biceps	Pos. deltoid
Middle deltoid	Ant. deltoid, Supraspinatus, Infraspinatus, Subscapularis	Teres minor, Teres major, Long head of bicep
Posterior deltoid	Supraspinatus, Pectoralis major	Ant. deltoid, Teres major
Infraspinatus	Supraspinatus, Biceps	Ant. deltoid, Mid. deltoid, Teres major
Subscapularis	Teres major, Ant. deltoid	Pos. deltoid, Infraspinatus

REFERENCES

1. Higginson, JS, et al. *Journal of Biomechanics* **38(9):** 1938-1942, 2005.
2. Holzbaur KR, et al. *Ann. Biomed. Eng.*, **33(6)**: 829-40, 2005.
3. Hughes RE, et al. *Am J Sports Med.*, **27(5)**: 651-7, 1999.

THE EFFECTS OF TESTING TECHNIQUE ON THE PERFORMANCE OF CHEST PROTECTORS IN TAE KWON DO

F. Tsui and M.T.G. Pain
Loughborough University, Loughborough, UK
E-mail: F.Tsui@lboro.ac.uk, Web: www.lboro.ac.uk

INTRODUCTION

In WTF competition Tae Kwon Do (TKD), points are scored by delivering forceful blows to the torso and head. As such, each competitor is required to wear head and chest protection. While there have been many advances in head protection from helmet studies motivated by American football and ice hockey, limited research exists on chest protectors, or 'hogus' as they are called in TKD. Even more limited are the methods that have been developed to assess their effectiveness.

The British Standards requires that trunk protectors be placed on a rigid anvil and tested with a rigid impactor. However, this type of test is severely limited. Pain et al. (2008) showed that rugby shoulder pads tested in a similar fashion deformed in a point-elastic manner and only tested the pad's material properties. Even during a tackle, force was only reduced over the bony bits of the acromio-clavicular joint and showed no change over the surrounding soft tissue. Thus, the pad performance was dependent on the properties of the colliding bodies as they were in series. This test also failed to account for the actual injury mechanisms that the pads were trying to prevent. The following explores how different testing techniques can affect the performance of a TKD hogu.

METHODS

Individual hogu performances were assessed using the 'Standard' method and 'Kicking' method. Surface forces were measured at 500 Hz using two Tekscan F-Scan sensors (Boston, MA), while the transmitted forces were collected differently in each test. The ratio between peak surface and transmitted forces were labeled as the Protective ratio or 'P-ratio'. In total, four hogus were tested; three were commercially available (Adidas, Adidas Electronic, Kwon), while the fourth was made from inserting medium-grade Confor foam (C-45) into the shell of the Adidas Electronic hogu.

The 'Standard' method re-created the tests outlined by the British Standards. The hogu was placed on a force plate (Kistler 2981B12) set at 2000 Hz, while a modified 2.75-kg shot put was released from a height of 0.45 m by an electromagnet to produce an impact energy of 12 J. The impact location was controlled by the placement of the foot sensors.

In the 'Kicking' method, two expert martial artists performed rear-leg roundhouse kicks to the instrumented hogus worn by BOBXL (Century Fitness), a martial arts training dummy (Figure 1a). Its base was set flush against a wall and a high-density foam was inserted between its back and the wall to minimize rocking of the overall unit. 11 Vicon MX cameras operating at 250 Hz were used to capture 11 opto-reflective markers to obtain joint kinematics for the hip, knee, ankle and foot. Impact force data were captured by a miniature force plate strapped to BOBXL's chest (Figure 1b). This plate was 150 mm x 100 mm and consisted of four tri-axial force transducers (Piezotronics) recording at 2000 Hz. Force and motion data were both captured by Vicon Nexus software.

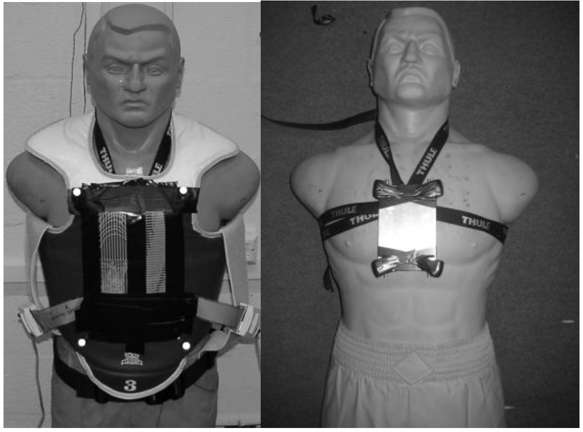

(a) (b)

Figure 1. (a) instrumented hogu on BOBXL; (b) mini force plate strapped to BOBXL's chest.

RESULTS AND DISCUSSION

Overall, hogu performance in the ‘Standard’ test (Table 1) did not mimic the ‘Kicking’ test (Table 2). For a given pad, the former produced higher surface and transmitted forces, higher P-ratios and lower contact times than the latter. This was attributed to the rigid nature of the anvil and impactor and not the kicks themselves as foot velocities were near the peak linear foot velocities of 13-18 m/s reported for other elite martial artists (Lai & Wei, 2002). Impact forces were also similar to the literature but could not be compared due to disparities in methodology. Higher contact times in kicks were explained by the visco-elastic nature of both the foot and BOBXL.

Table 1. Hogu Performance for ‘Standard’ Method.

Pad	Tekscan		Force Plate		P-Ratio
	Force (kN)	CT (ms)	Force (kN)	CT (ms)	
Adidas	2.40 ± 0.18	21.4	2.78 ± 0.10	20.2	1.16
Adidas Electronic	2.08 ± 0.16	24.2	1.75 ± 0.08	24.5	0.84
Kwon	2.75 ± 0.22	17.8	3.56 ± 0.35	12.8	1.30
Confor	1.66 ± 0.11	47.8	1.15 ± 0.06	46.0	0.70

For all kicks, the pads performed quite consistently, while the performance in the ‘Standard’ method was dependent on the hogu. In particular, the Kwon and Adidas increased in force as the impacts were transmitted through the pad (i.e. P-ratio >1). This was likely due to the: a) material deforming too quickly to attenuate the rigid impact, as supported by the lower contact times; and, (b) under-sampling due to multi-plexing and low sampling frequency of the sensors. While sensor performance was a concern, it was present for all trials suggesting that the relative difference between P-ratios would likely remain similar (i.e. Confor still better than Kwon).

The relationship between P-ratios were consistent except for the Adidas Electronic hogu, which did well in the ‘Standard’ method but scored poorly during kicks. Two possible explanations were that the materials in this hogu: a) provided adequate local resistance, but transmission increased since the foot was more massive with a larger contact area; and/or, b) were strain-rate dependent since, at impact, the shot put was travelling at ~2.95 m/s versus 12+ m/s for the majority of all kicks.

CONCLUSIONS

Current performance tests of hogus are merely an examination of their material properties and do not reflect their performance during typical use. As such, it is important to develop a performance test which stresses the hogu as it would be used in competition.

REFERENCES

1. Pain, MTG et al. *J Sports Sci*, **26** (8), 855-862, 2008.
2. British Standards, BS EN13277-3:2000.
3. Lai, WB & Wei, X. *ISBS*, Cáceres, Spain, 2002.

Table 2: Hogu performance for the ‘Kicking’ method for both subjects. CT represents contact time.

Subject 1. Age: 36, Mass: 93.6 kg, Height: 1.74 m

Pad	Foot Velocity (m/s)	Tekscan		Force Plate		P-ratio
		Force (kN)	CT (ms)	Force (kN)	CT (ms)	
Adidas	12.19 ± 0.50	1.92 ± 0.33	41.6 ± 2.8	1.02 ± 0.22	42.4 ± 5.2	0.53 ± 0.09
Adidas Electronic	12.00 ± 0.55	1.63 ± 0.34	40.8 ± 4.1	0.90 ± 0.20	45.0 ± 1.7	0.57 ± 0.17
Kwon	11.76 ± 0.58	1.52 ± 0.29	82.6 ± 26.8	0.86 ± 0.22	59.4 ± 4.7	0.57 ± 0.16
Confor	12.13 ± 0.45	1.52 ± 0.48	91.7 ± 22.1	0.69 ± 0.21	48.2 ± 5.6	0.46 ± 0.07

Subject 2. Age: 25, Mass: 82.4 kg, Height: 1.84 m

Pad	Foot Velocity (m/s)	Tekscan		Force Plate		P-ratio
		Force (kN)	CT (ms)	Force (kN)	CT (ms)	
Adidas	13.59 ± 0.47	1.95 ± 0.41	42.6 ± 2.5	1.24 ± 0.18	36.0 ± 2.1	0.65 ± 0.15
Adidas Electronic	14.76 ± 0.32	1.41 ± 0.27	49.8 ± 20.4	1.02 ± 0.12	31.6 ± 3.5	0.74 ± 0.12
Kwon	14.21 ± 0.55	1.59 ± 0.48	105.4 ± 19.8	1.13 ± 0.16	31.2 ± 4.8	0.78 ± 0.28
Confor	14.47 ± 0.53	1.74 ± 0.42	108.2 ± 3.9	0.87 ± 0.28	34.8 ± 3.6	0.53 ± 0.20

KINEMATIC AND EMG COMPARISON OF GAIT IN NORMAL G AND MICROGRAVITY

[1]John K. De Witt, [2]W. Brent Edwards, [3]Gail P. Perusek, Beth E. Lewandowski[3] and [4]Sergey Samorezov

[1]Wyle Integrated Science and Engineering Group, Houston, TX, USA; [2]The Iowa State University, Ames, IA, USA; [3]NASA Glenn Research Center, Cleveland, OH, USA; [4]ZIN Technologies, Cleveland, OH, USA.
email: john.k.dewitt@nasa.gov

INTRODUCTION

Astronauts regularly perform treadmill locomotion as part of their exercise prescription while they are on board the International Space Station. Although locomotive exercise has been shown to be beneficial for bone, muscle, and cardiovascular health, astronauts return to Earth after long-duration missions with net losses in all three areas [1]. These losses might be partially explained by fundamental differences in locomotive performance between normal gravity (NG) and microgravity (MG).

During locomotive exercise in MG, the subject must wear a waist and shoulder harness that is attached to elastomer bungees. The bungees are attached to the treadmill, and provide forces that are intended to replace gravity. However, unlike gravity, which provides a constant force on all body parts, the bungees provide a spring force only to the harness. Therefore, exercise in MG has two fundamental differences from exercise in NG: 1) forces returning the subject to the treadmill are not constant, and 2) forces are applied to the axial skeleton only at the waist and shoulders. The effectiveness of the exercise may also be affected by the magnitude of the gravity replacement load. Historically, astronauts have difficulty performing treadmill exercise with loads that approach body weight (BW) because of discomfort and inherent stiffness in the bungee system.

The unique requirements for locomotion in MG could cause differences in performance between gravitational locations. These differences may help to explain why long-term effects of treadmill exercise training in MG may differ from those found in NG. The purpose of this investigation was to compare locomotion in NG and MG to determine if differences in kinematic or muscular activation pattern occur between gravitational environments.

METHODS

Five subjects (2M, 3F) completed treadmill walking at 1.34 $m \cdot s^{-1}$ and running at 3.13 $m \cdot s^{-1}$ in NG and MG. NG trials were collected on a laboratory treadmill at NASA Glenn Research Center. MG trials were collected during parabolic flight on a C-9 aircraft at NASA Johnson Space Center. The external load (EL) was provided by bungees during MG trials. Trials were completed under low EL (56.2 ± 6.3% BW) and high EL (87.3 ± 6.6% BW) conditions.

Kinematic data were collected with a video motion capture system (SMART Elite, BTS Bioengineering SpA, Milan, Italy) at 60 Hz. The 3-D positions of markers on the lower extremity and trunk were recorded, rotated into a treadmill reference frame, and projected onto the sagittal plane. All subsequent kinematic calculations were completed in 2-D.

Telemetered electromyography (EMG) (Myomonitor III Wireless EMG System, Delsys Inc., Boston, MA) was used to obtain data on activation of the tibialis anterior, gastrocnemius, rectus femoris, semimembranosus, and gluteus maximus. Before any motion trials were conducted, subjects performed maximal voluntary isometric contractions of each muscle to standardize electrode placement. All motion capture and EMG data were synchronized via a global analog pulse that was recorded simultaneously by each hardware device.

Hip, knee, and ankle joint range of motion (ROM) and flexion and extension extremes were computed using the angles between adjacent segments, with markers defining their long axes. EMG data were rectified and filtered and then examined to quantify the time of initial activation and the total activation duration of each stride using the methods of Browning et al. [2]. Multiple strides were analyzed for each gravitational environment, and trial means were computed. Effect sizes (ESs) and their 95% confidence intervals (CIs) were computed for joint kinematic and EMG scores.

RESULTS and DISCUSSION

When all factors tested were combined (EL, locomotive mode), 96 comparisons were made. Because our intent was to identify differences between gravitational environments, we have limited our presentation to variables in which the 95% confidence interval for the effect size did not include 0 (see Table 1, Figure 1).

Hip ROM during walking was larger in MG with low EL, and the hip achieved greater flexion during MG than NG. Maximum dorsiflexion was larger in NG than MG during walking with high EL. The gastrocnemius was activated earlier in the stride in MG during high EL.

Hip ROM was the only kinematic measure that was different for the two gravitational environments during running. Subjects achieved greater hip flexion in MG. In each running condition, the gluteus maximus and semimembranosus were activated later in the stride in MG.

Although we tested only a small sample, we have detected some differences between locomotion in MG and NG that centralize about the hip, with the exception of ankle kinematic and musculature effects found during walking with high EL. Returning astronauts have been found to have a net decrease in bone mineral density at the hip after long-term spaceflight [1]. Interestingly, hip ROM seems to be greater in MG than in NG. This increase in ROM may be an adaptation to accommodate the EL, but also acts to reduce the countermeasure efficacy.

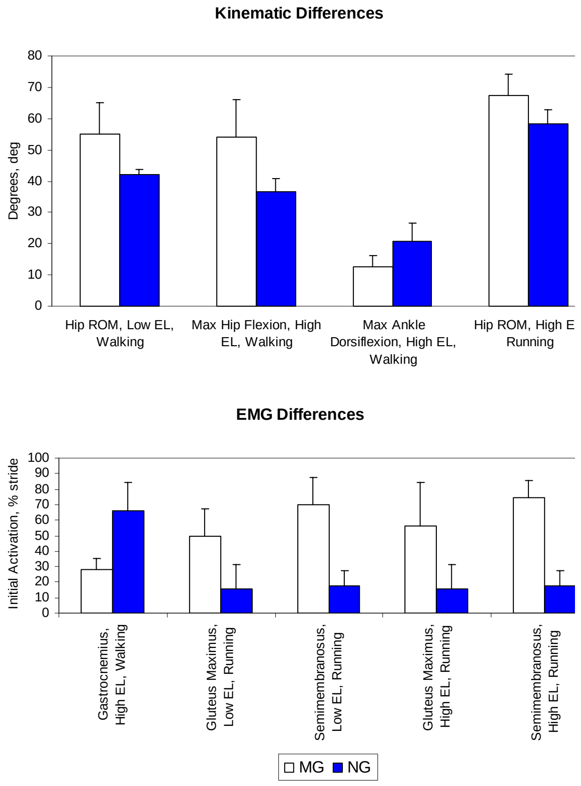

Figure 1: Differences between MG and NG for kinematic (upper) and EMG (lower) dependent variables.

Our data suggest that kinematics and muscle activation may be different in MG and NG during running, and this could influence responses to training. It may also help us better understand why musculoskeletal deconditioning occurs during space flight. Future research with larger numbers of subjects is necessary to better quantify kinematic and EMG differences between MG and NG.

REFERENCES

1. LeBlanc AD, et al. *J Musculoskelet Neuronal Interact* **7**, 33-47, 2007.
2. Browning RC, et al. *Med Sci Sports Exerc* **39**, 515-525, 2007.

Table 1: Effect sizes (ESs, MG vs NG) and their 95% CIs for kinematic and EMG dependent variables.

Walking	ES	95% CI	Running	ES	95% CI
			Low EL		
Hip ROM	**1.62**	[0.19,3.05]	Gluteus Maximus Initial Activation	**1.80**	[0.33,3.26]
			Semimembranosus Initial Activation	**3.35**	[1.43,5.28]
			High EL		
Gastrocnemius Initial Activation	**–2.48**	[–4.13,–0.83]	Hip ROM	**1.41**	[0.03,2.80]
Maximal Hip Flexion	**1.73**	[0.28,3.18]	Gluteus Maximus Initial Activation	**1.64**	[0.21,3.07]
Maximal Ankle Dorsiflexion	**–1.48**	[–2.88,–0.08]	Semimembranosus Initial Activation	**5.04**	[2.51,7.57]

THE EFFECT OF BODY WEIGHT SUPPORT ON THE ANKLE-FOOT ROLL-OVER SHAPE

[1] Brooke Morin, [1]Rebecca L. Lathrop, [1]Lise Worthen-Chaudhari, [1]D. Michele Basso, [2]James P. Schmiedeler and [1]Robert A. Siston
[1]The Ohio State University, Columbus, OH, USA, [2]University of Notre Dame, Notre Dame, IN, USA
email: Morin.29@osu.edu , web: http://www.mecheng.osu.edu/nmbl/

INTRODUCTION

Body weight supported treadmill training (BSWTT) has emerged in the past two decades as method of gait rehabilitation for neurological injuries such as incomplete spinal cord injury and stroke. During this therapy, patients placed over a treadmill have a portion of their body weight supported with a harness, and trained therapists provide manual assistance as necessary to promote upright posture and lower-extremity trajectories associated with normal gait [1]. Despite its prevalence, much is still unknown about the effects on gait of key BWSTT parameters, such as the percentage of body weight support (BWS).

Successful rehabilitation depends on accurately replicating the forces and motions present during normal locomotion. A single measure that expresses the relationship between these terms is the ankle-foot (AF) roll-over shape, defined as the circular arc formed when the center of pressure (COP) is transformed into a shank-based coordinate system [2]. This shape is suggested to be clinically invariant under a variety of walking conditions [e.g., 2,3]. Thus, changes in the AF roll-over shape with BWS may indicate that the relationship between the forces and motions associated with normal walking is altered during BWSTT. This study seeks to determine the effect of BWS on the radius of the AF roll-over shape and the anterior and superior locations of its center.

METHODS

Nine neurologically unaffected subjects, 5 male and 4 female, participated in this study. The means and standard deviations of their heights and ages were 1.73 ± 0.09 m and 23.11 ± 2.47 years, respectively. Informed consent was obtained.

At the beginning of the study, the subjects walked overground at a comfortable speed, which became their self-selected speed for the duration of the trials. Four reflective markers were then placed on their left lateral mallelous, calcaneus, 5th metatarsal, and lateral epicondyle. Subjects walked on a split-belt instrumented treadmill (Bertec Corp., Columbus, OH) at their self-selected speed with four levels of BWS (0%, 30%, 50%, and 70%). Conditions were randomized for each subject. Ground reaction forces were collected at 200 Hz. A medical harness and a closed-loop pneumatic force control system (Vigor Equipment, Stevensville, MI;

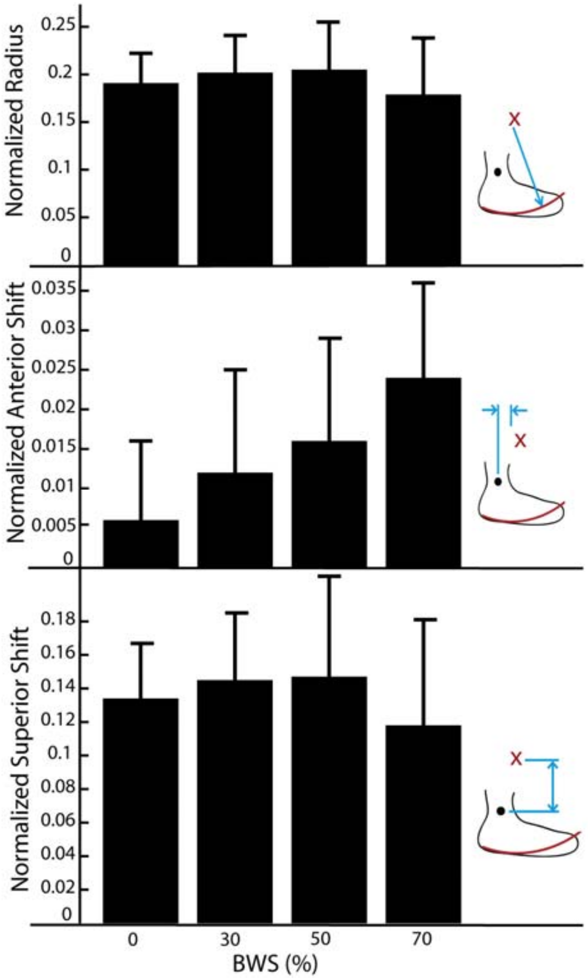

Figure 1: Mean roll-over shape parameters with increasing BWS. Each parameter, (a) radius, (b) anterior shift, and (c) superior shift, is normalized by subject height. The error bars represent one standard deviation.

Tescom, Elk River, MN) provided BWS. Kinematic gait data were collected using a seven camera VICON motion analysis system (Vicon Mx cameras, Vicon, Inc.). Data collection continued for approximately 20 seconds at each level of BWS to allow the gait to reach steady state. We analyzed nine consecutive steady-state gait cycles per condition for each subject.

We calculated the AF roll-over shapes by fitting a circle to the COP data after transforming it into a shank-based coordinate system [2]. The radius of this circle and the anterior and superior locations of its center were normalized by subject height (H). We investigated the effect of BWS on these normalized quantities using a repeated measures analysis of variance (ANOVA) and performed post-hoc tests using the Bonferoni correction factor.

RESULTS AND DISCUSSION

The radius, anterior location, and superior location of the AF roll-over shape were influenced by BWS ($p<0.001$) (Figure 1). Post-hoc tests indicated that the anterior shift changed significantly between all BWS values and that all parameters changed significantly between 30% and 70% BWS (Table 1). Additionally, the variability in the radius and the superior shift increased with increasing BWS. Further investigation of individual subject responses to changes in BWS showed that different subjects employed different strategies to compensate for increased BWS, which may explain the observed increase in parameter variability.

The roll-over shape center shifts anteriorly with increased BWS at each level. Previous modeling results of asymmetrical gaits for transtibial prosthesis users illustrated that an anterior shift of the prosthesis alignment results in reduced joint torque and larger stride lengths [4]. Similarly, with increasing amounts BWS, our subjects may have shifted their weight anteriorly and adjusted their torques and stride length. The mechanisms resulting in this anterior shift are a topic of future study.

Hansen et al. suggested that an anterior shift of the roll-over shape center of less than 0.005H was not meaningful in a clinical setting [2]. However, our data demonstrate changes in all three parameters between 0.01H and 0.03H. These changes may be clinically meaningful, but further work is necessary to determine the threshold beyond which changes in the roll-over shape are clinically relevant.

CONCLUSIONS

This study investigates the effects of increasing BWS on the AF roll-over shape as a means to measure how well normal walking forces and motions are replicated in BWSTT. In contrast to previous work that identified it as an invariant of normal walking, our findings indicate that the AF roll-over shape radius and center location change with increased BWS in neurologically unaffected subjects. The true clinical utility of this result can only be determined through comparison with the AF roll-over shapes of neurologically impaired subjects obtained under similar training conditions.

REFERENCES

1.Behrman AL, et al. *Phys Ther*, **80**, 688-700, 2000.
2.Hansen AH, et al.*Clin Biomech* **19**,407-414, 2004.
3.Hansen AH, et al. *JRRD* **42,** 381-390, 2005.
4.Srinivasan S, et al. *J Biomech Eng* **131**, 031003 2009.

Table 1: Change in mean roll-over parameters normalized by height for a given pair of BWS values. For instance, (0,30) is the change in means between 0% and 30% BWS. A "*" indicates statistical significance, which, due to multiple comparisons, occurs with p <0.008.

BWS	**Radius/Height**		**Anterior Shift/Height**		**Superior Shift/Height**	
	Change	p-value	Change	p-value	Change	p-value
0,30	-0.011	0.044	-0.006	<0.001 *	-0.011	0.056
0,50	-0.014	0.041	-0.010	<0.001 *	-0.012	0.079
0,70	0.012	0.099	-0.017	<0.001 *	0.017	0.029
30,50	-0.003	0.652	-0.004	0.001 *	-0.001	0.826
30,70	0.023	0.001 *	-0.012	<0.001 *	0.027	<0.001 *
50,70	0.026	<0.001 *	-0.008	<0.001*	0.029	<0.001 *

SEMI-AUTOMATIC 3D VIRTUAL RECONSTRUCTION OF SIMULATED COMMINUTED ARTICULAR FRACTURES

[1]Thaddeus P. Thomas, [1]Donald D. Anderson, [2]Andrew R. Willis,
[1]J. Lawrence Marsh, and [1]Thomas D. Brown
[1]Department of Orthopaedics and Rehabilitation, The University of Iowa, Iowa City, IA
[2]University of North Carolina at Charlotte, Charlotte NC
email: thaddeus-thomas@uiowa.edu

INTRODUCTION

High-energy comminuted peri- and intra-articular fractures involving multiple bone fragments pose a substantially more difficult surgical challenge to reconstruct than do more commonplace low-energy fractures. It can be difficult for the surgeon even to ascertain how the bony fragments should fit back together to restore the original anatomy: an activity that in essence involves solving a three-dimensional (3D) puzzle. In addition, the further the fragments are displaced, and the more they are interspersed, the more challenging it is to know in what sequence they might best be repositioned, so as to minimize additional surgical trauma to already severely injured surrounding soft tissues. These issues are especially important given the purported benefits of less invasive surgical techniques.

Virtual reconstruction with 3D puzzle solving methods can provide objective descriptors of comminuted articular fracture severity, and can serve as a valuable blueprint for surgical reconstruction. The complexities of natural bone specimens confound the development of this technology, and conventionally acquired clinical CT scan data afford less-than-ideal spatial resolution of fragment surfaces. Toward clinical application, algorithmic developmental work on 3D puzzle solving benefits from more precise data. Therefore, the purpose of this work was to develop a platform that utilized test specimens whose fragment geometries were precisely quantifiable so that a novel method for fracture reconstruction could be tested. It was hypothesized that an accurate fracture reconstruction would be possible by matching fragment periosteal surfaces to an intact (or mirrored contralateral) template using a semi-automated algorithm.

METHODS

A methodology for generating fragmentation-dispersal patterns typical of comminuted orthopaedic fractures in non-biologic replicas of normal tibial geometry was developed. This well-behaved platform provides an ordered progression in complexity to guide ongoing algorithmic developments in the 3D puzzle solver (Figure 1).

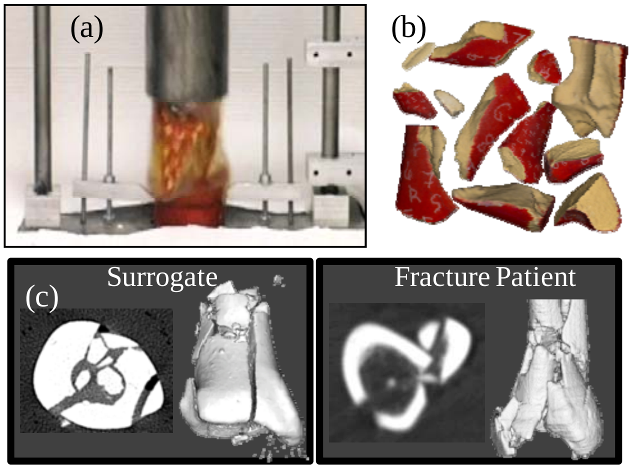

Figure 1. An instrumented drop tower (a) was used to create the comminuted fracture (b), similar to clinically observed (c).

Five identical replicas of human distal tibia anatomy, derived from CT, were machined from blocks of high-density polyurethane foam [1]. This material exhibits mechanical and fracture behavior comparable to that of human cortical bone, and when suitably doped with $BaSO_4$, it displays similar x-ray and CT appearance [2]. A talus analog molded of polymethyl methacrylate provided an anatomically corresponding proximal surface for tibio-talar contact, and a flat distal side for flush impactor contact. These test specimens were then encased together in a gelatin to simulate the surrounding soft tissues of the distal shank.

Fracture impacts were delivered using an instrumented drop tower. A heavy steel cylinder of parametrically selected mass was released at a selected height to deliver nominally 200 Joules of kinetic energy (Fig 1.a). Pre- and post-fracture fragment geometries were separately obtained using laser (Fig 1.b) and CT scans (Fig 1.c).

The reconstruction algorithm began with periosteal surface identification. Since the tibia analog's outer surface was colored red before impact, it could be segmented from the fragment's fractured surface using an automatic texture classification program. The tibia was then methodically reconstructed by matching fragment and intact periosteal surfaces using Geomagic Studio Software. This technique started by aligning the fragment with the largest surface area to the intact template using an iterative closest point algorithm (ICP). The algorithm proceeded by individually aligning the remaining fragments, from largest to smallest. The accuracy and speed of alignment was improved by iteratively reducing the ICP algorithm's searchable area over the template once a fragment was placed. The accuracies of the puzzle solutions were then quantified by calculating distances between the intact and the reconstructed surfaces.

RESULTS AND DISCUSSION

The fracture morphologies generated by this protocol simulated clinical fracture cases (Fig 1.c). The replica tibias were fractured into 8 to 14 discrete fragments of varying sizes, with 2-4 of those being articular. Post-fracture fragment volumetric comparison showed that approximately 95% of the pre-fractured volume was recovered as manipulably-sized fragments. Figure 2 illustrates the puzzle solutions obtained for the 5 tibias. Computational surface alignment yielded precise geometric reconstructions, with alignment accuracy ranging from 0.03 to 0.2 mm.

Intra-operative navigation tools exist to aid in the reconstruction of long-bone fractures, but these systems require a high degree of user interaction and are of limited value for the complex geometries of comminuted articular fractures. 3D puzzle solving methods can help to fill this need, providing a pre-surgical blueprint for reconstruction.

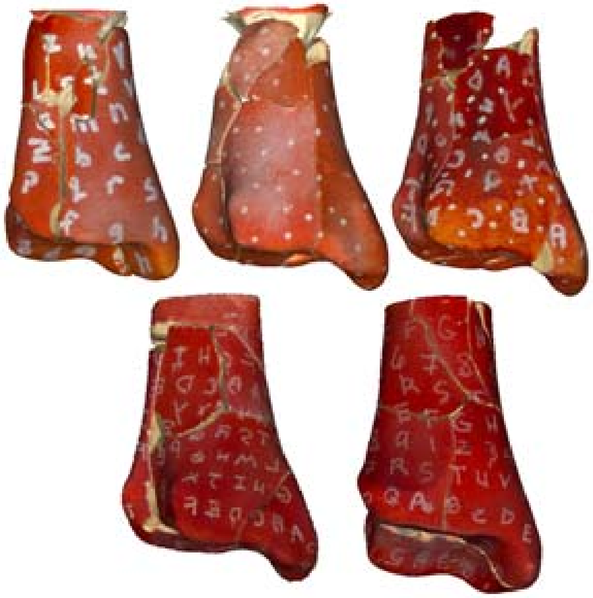

Figure 2: Reconstruction results for 5 replicas

The methodology for recreating comminuted fracture geometries in a suitable surrogate material presented here provided idealized data that facilitated the advancement of a semi-automated periosteal alignment algorithm. With its impressive accuracy and potential to be fully automated, this algorithm is likely to one day be an integral part in the virtual reconstruction of actual clinical cases. Of course many challenges remain to be addressed before this is possible. With further advancement, this nascent technology has the potential to significantly enhance the way in which surgeons reconstruct comminuted intra-articular fractures.

REFERENCES

[1] Anderson DD; Frank MC; McKinley TO; Brown TD. *54th ORS*, #998, 2008.

[2] Beardsley CL; Bertsch CR; Marsh JL; Brown TD. *J Biomech*, (**35**):331-338, 2002.

ACKNOWLEDGMENTS

Funded by the NIH (P50AR055533 and R21AR054015), the AO Foundation, Switzerland, and by a MRIG from the Roy J. Carver Charitable Trust at The University of Iowa. Distal tibia replicas were machined in the Rapid Manufacturing and Prototyping Laboratory at Iowa State University, courtesy of Dr. Matthew Frank.

ELECTRICAL STIMULATION OF THE SEMITENDINOSUS DURING TERMINAL SWING INCREASES KNEE FLEXION EXCURSION DURING EARLY STANCE

Antonio Hernández, Amy L. Lenz and Darryl G. Thelen
University of Wisconsin-Madison
email: ahernand@cae.wisc.edu, web: http://www.engr.wisc.edu/groups/nmbl/

INTRODUCTION

Tight hamstrings are often implicated and targeted for treatment in children who exhibit crouch gait, a gait disorder characterized by excessive hip and knee flexion during stance. Computer simulations have provided insights into the biomechanical influence that the hamstrings have on lower extremity motion during gait [1-3], but must be validated before they can be used for guiding treatment strategies. Electrical stimulation protocols have recently been introduced to test model predictions under tightly controlled conditions [4-5]. In this study, we synchronized electrical stimulation to a gait cycle to measure medial hamstring (ST, the semitendinosus) function during walking. We tested the hypothesis that ST stimulation introduced during terminal swing would increase knee flexion in early stance. We also evaluated the influence that hamstring stimulation had on hip flexion to better understand coupling between the joints.

METHODS

Eight healthy young adults (30±6y, 1.76±0.07m, 77±22kg) participated. Subjects performed 90s walking trials on a split-belt instrumented treadmill at a preferred speed. A real-time controller monitored the subject's heel strike times. This information was used to deliver short-duration electrical stimuli starting at either 90% (terminal swing) or 0% (early stance) of the gait cycle. The ST muscle was stimulated in approximately 10 randomly selected strides per trial. An individual stimulus consisted of four 300μs current (≤50mA) pulses delivered over 90 ms via surface electrodes.

EMG signals were recorded and used to determine the onset of stimulation. Whole body kinematics were simultaneously recorded using a passive motion capture system, and used to compute three dimensional lower extremity joint angles. The stimulation-induced movement was defined as the change in the joint flexion excursion (that starts in terminal swing and ends prior to mid-stance) of the stimulated strides relative to the previous, non-stimulated strides (Fig. 1). These changes were compared between the two stimulus times via paired t-tests.

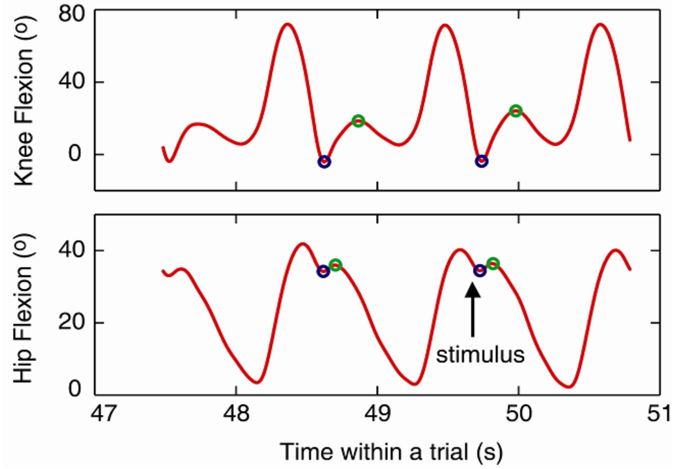

Figure 1: Knee and hip flexion excursions during the late swing-to-early stance transition. **o** = low value and **o** = high value of joint flexions.

RESULTS

Increases in knee flexion excursion (due to increased flexion following the stimulus) averaged 3^o across subjects when the stimulus was introduced during terminal swing, compared to 1^o when the stimulus was introduced during early stance. The hip flexion excursion changes averaged 0^o across subjects for stimulation applied during terminal swing or early stance. Two subjects displayed a small yet significant reduction in hip flexion excursion for stimulation during terminal swing. In these two subjects, the changes in knee flexion excursion were not significantly different from the non-stimulated trials.

DISCUSSION

A computer model of our experimental paradigm predicts that early stance knee flexion should increase as a result of hamstring stimulation, more so if the stimulus is applied during terminal swing than at heel contact. This prediction is generally consistent with our measurements. The gait model also suggests that the influence of hamstring stimulation on hip flexion should be smaller than at the knee. This is also generally consistent with our experiments, in that we could not detect a difference in average hip flexion for 5 of the 7 subjects. However, two subjects did exhibit increased hip extension during stance. Interestingly, these same subjects did not exhibit a significant change in knee flexion as a result of stimulation. These results suggest that hip extension may be induced when the knee trajectory is constrained, perhaps as a result of joint stiffenss due to action of other muscles. Such observations may be important to consider when using models to investigate the gait of individuals with pathologies, who often exhibit abnormal joint stiffness.

We conclude that stimulating the hamstrings during terminal swing can induce knee flexion during stance, but that the magnitude is variable between subjects and seems coupled to the muscle's function at the hip.

REFERENCES

1. Arnold et al., *J Biomech* **40**, 3314-3324, 2007.
2. Hicks et al. *J Biomech* **41**, 960-967, 2008.
3. Arnold et al. *J Biomech* **38,** 2181-2189, 2005.
4. Stewart C et al. *Gait Posture* **28**, 372-377, 2008.
5. Hernández A. et al. *J Biomech* **41**, 137-44, 2008.

ACKNOWLEDGEMENTS

NIH AG20013. Amy Silder assisted with data collection.

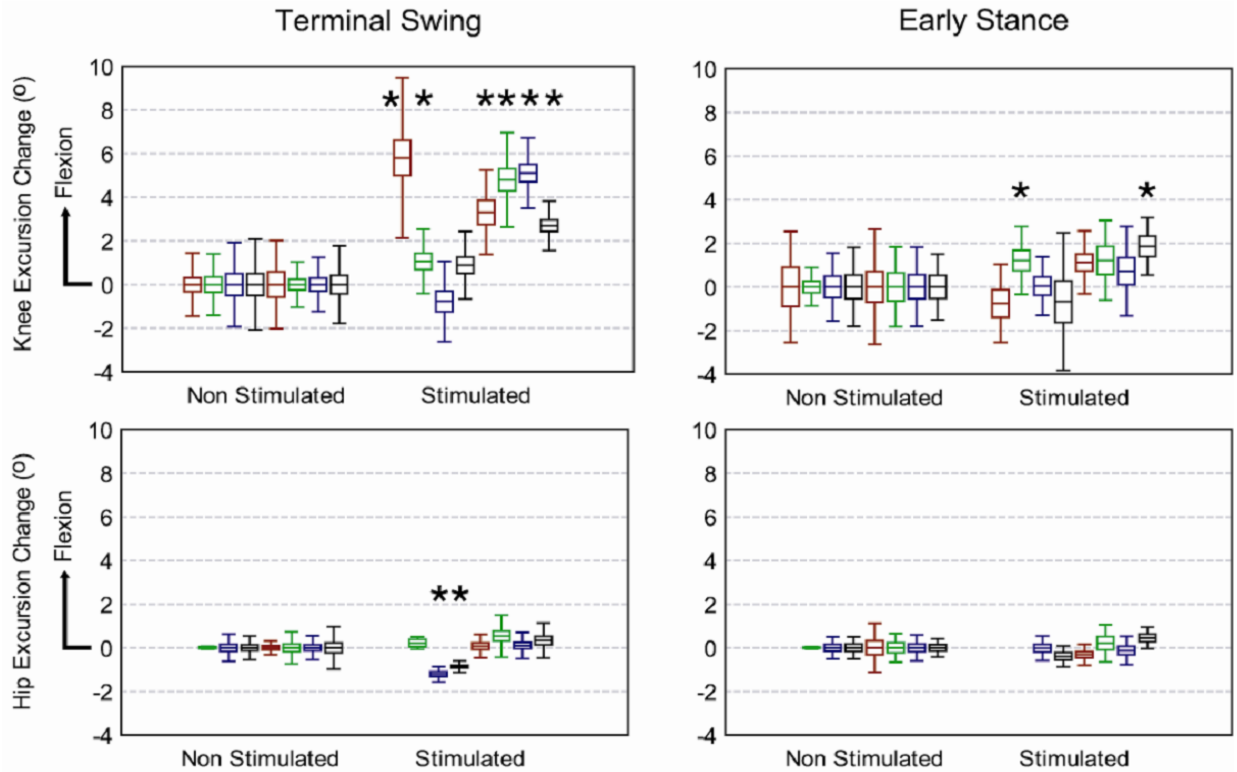

Figure 2: Experimental (stimulated) and predicted knee and hip angle excursion changes relative to non-stimulated strides. The excursions of non-stimulated strides have been zeroed as they represent a baseline level for the comparison of the means. ⋆= statistically significant result, ◊ = change predicted by the simulation.

A NOVEL APPROACH FOR EXPERIMENTAL DERIVED MUSCLE PARAMETERS OF THE SOLEUS MUSCLE

Benjamin I. Binder-Macleod, Kurt Manal, Thomas S. Buchanan
Department of Mechanical Engineering, University of Delaware, Newark, DE
email: manal@udel.edu, web: http://www.cber.udel.edu/

INTRODUCTION

A muscle's architecture influences the force it can produce and where on the length tension curve it operates. Being able accurately describe a muscle would be of great advantage for clinical research and critical for those who are creating musculoskeletal models.

The soleus is one of the strongest muscles in the body and along with the gastrocnemii produce approximately 90% of the plantarflexion moment at the ankle. The soleus plays a critical role for maintaining posture, balance, and gait [1]. At high knee flexion (> 100°) the gastrocnemii become shortened and are unable to produce significant force. With the knee in this position the plantarflexion moment would be primarily the product of the soleus. The force produced by the soleus can then be approximated from the plantarflexion moment and moment arm of the Achilles tendon. The force along with fiber length and pennation angle through the range of ankle motion would allow for the characterization of the soleus muscle architecture and force-length relationship.

The purpose of this paper is to present a novel approach, which utilizes ultrasound, to characterize the architecture of a muscle and present a study of the soleus describing its isometric force, fiber length, and pennation angles through normal range of motion.

METHODS

8 healthy male subjects (23.1 ±2.3 yrs, 1.8 ±.06 meters, 80.8 ±11.6 kgs) participated in the study. The experimental protocol was approved by the Human Subjects Review Board at the University of Delaware. All subjects submitted written informed consent prior to testing.

Muscle parameter measurements were taken with the subjects in a kneeling position (Figure 1) in an isokinetic dynamometer (Biodex System 3, Shirley, NY). Plantarflexion moments at maximum voluntary contraction (MVC) and ultrasound images (Aloka SSD-5000, Tokyo, Japan; 60 mm linear probe, B-mode, 10 MHz) of the belly of the soleus muscle were recorded simultaneously at 5 degree increments from 25° dorsiflexion to 20° plantarflexion. Knee angles were maintained at a flexion angle of 120° to 125° to minimize the contribution of the gastrocnemii to the plantarflexion moment. The Achilles tendon moment arm was found using a hybrid method combining a 7 camera motion analysis system (Qualysis AB, Gothenburg, Sweden) and ultrasound images [2].

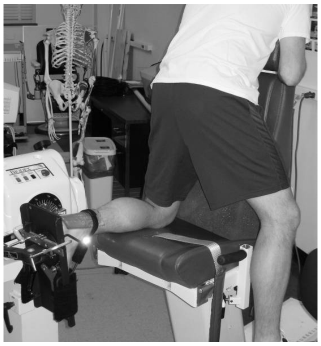

Figure 1: Subject positioning

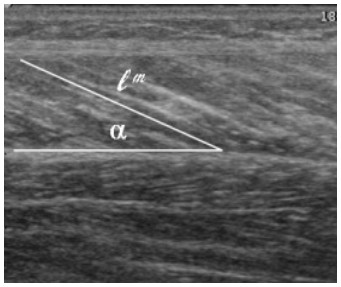

Figure 2: Ultrasound image with pennation angle (α) and fiber length (l^m) highlighted

Pennation angles and fiber lengths were determined using ultrasound console functions at each ankle angle (Figure 2). The optimal fiber length for each subject was defined as the fiber length at the ankle angle which produced the maximum force. Fiber lengths and forces at all angles were normalized to the maximum force and optimal fiber length and then plotted.

RESULTS AND DISCUSSION

Table 1 reports the compiled muscle parameters measured the soleus muscle. Specifically, we report the values between 25° dorsiflexion to 20° plantarflexion. The results show a variety of interesting trends. The moments, forces, and fiber lengths all decrease with increasing plantarflexion angle. The moment arms and pennation angles increase with increasing plantarflexion angle. Peak force was produced with the ankle in twenty degrees dorsiflexion with a corresponding optimal fiber length of 38 mm. This is interesting because optimal fiber length corresponds to the ankle angle at which maximum moments are required during gait. Our pennation angles and fiber lengths show consistent trends with data reported by others [3]. The moments however between studies are significantly different. This discrepancy is believed to be from different positioning of the subjects in each study.

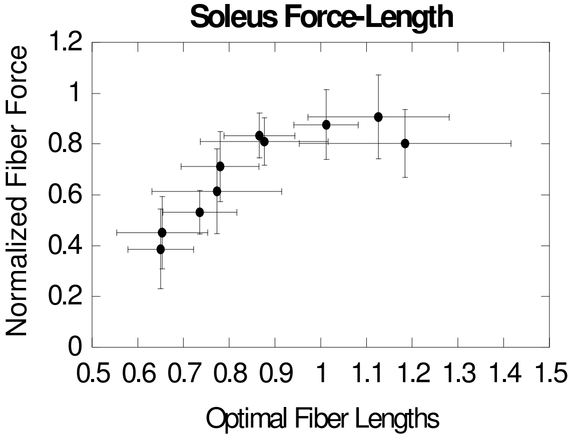

Figure 3: Normalized fiber force and length with vertical and horizontal bars showing standard deviations.

Figure 3 illustrates the normalized force-length relationship for the soleus muscle. The operational range for normalized fiber length is .65 to 1.18. The soleus is weakest at around 20 degrees plantarflexion producing only about 38.7% of the maximum force.

CONCLUSIONS

The objective of this paper set out to describe the architectural parameters of the soleus. Previous works reporting these measures have used MRI in their approach which can be quite costly and time consuming and thus is not ideal when attempting to characterize the muscle architecture for many subjects. The method presented herein uses ultrasound which is much less expensive and timely. Care should be taken when comparing moments between studies in which different positioning is used. We selected the kneeling position in an effort to isolate the soleus. With the exception of the moment our results are consistent with other methods. The parameters and force tension relationship reported of the soleus should benefit future studies of how the soleus and other plantarflexor muscles of the ankle contribute to posture and gait.

REFERENCES

1.Perry A, *Gait Analysis*, McGraw-Hill, Inc., New York, 1992.
2.Cowder J, et al., *ASME Summer Bioengineering Conference*, 2008.
3.Maganaris CN, *Acta Physiol Scand.* **172**:279-285, 2004

Table 1: Muscle parameters through ankle range of motion from 25° dorsiflexion(-) to 20° plantarflexion(+)

Ankle Angle (deg)	**-25**	**-20**	**-15**	**-10**	**-5**	**0**	**5**	**10**	**15**	**20**
Moment (Nm)	63.4 ±38.2	66.1 ±35.3	66.8 ±36.3	66.8 ±33	62.9 ±26.7	55.6 ±28.6	45.1 ±18.6	42.5 ±15.6	33.7 ±14.9	27.2 ±10
Moment Arm (mm)	38.4 ±4.6	38.6 ±5.3	39.3 ±5.1	40.6 ±5.7	40.8 ±5	41 ±5.9	42.1 ±5.8	42.7 ±6.5	42.5 ±5.1	42.1 ±5.8
Fiber length (mm)	39.8 ±5.7	38.1 ±3.9	34.4 ±4	29.9 ±6.2	29.5 ±5.2	26.1 ±4.6	25.7 ±3.1	24.7 ±2.4	20.9 ±1.8	20.9 ±1.9
Fiber Pennation (deg)	20 ±3.8	22.9 ±4	24.5 ±4.9	27.5 ±4.1	27.3 ±5.3	28.5 ±5.3	31.9 ±5	32.4 ±7	36.2 ±5.2	36.9 ±4.9
Tendon Force (N)	1894 ±611	1945 ±452	1899 ±737	1859 ±587	1697 ±395	1484 ±473	1186 ±228	1065 ±246	787 ±309	648 ±215
Muscle Force (N)	2005 ±841	2111 ±738	2038 ±789	1965 ±644	1864 ±523	1672 ±603	1383 ±333	1229 ±288	975 ±385	808 ±250

Effects of Multiple-Group Muscle Weakness on the Retro-patellar Cartilage in Rabbits

Aliaa Rehan Youssef, Ruth Seerattan, Tim Leonard, Walter Herzog
The University of Calgary, Human Performance Lab
email: ayoussef@kin.ucalgary.ca

INTRODUCTION

Osteoarthritis (OA) is one of the most prevalent chronic musculoskeletal disorders in North America. The etiology of OA is thought to be multi-factorial. Studies have mainly focused on the changes occurring following intra-articular derangement such as ligament transection. Little is known on how changes in periarticular structures, such as skeletal muscles, may affect the fully intact joint. Muscle weakness is an acknowledged associate of joint degeneration and OA. There is evidence that muscle weakness might be an independent contributor to the initiation and development of OA [1]. Recently, degeneration of the retro-patellar cartilage was evident after induced quadriceps muscle weakness [2]. The muscle weakness induced in that study was restricted to a single muscle group, the knee extensors. Although such muscle weakness can occur due to muscle or peripheral nerve injury, it likely does not represent a large population. On the contrary, general muscle weakness, affecting all limb muscles occurs to a great extent in many sub-populations, for example the elderly. Therefore, the purpose of this study was to investigate micro-structural changes in the rabbit knee cartilage following a period of systematic knee extensor and ankle plantar flexor muscle weakness. We hypothesized that multiple group muscle weakness is associated with degenerative changes in the knee cartilage, thereby, providing evidence that muscle weakness might be an independent risk factor for joint degeneration leading to OA.

METHODS

Ten skeletally mature, 11-month-old, female New Zealand white rabbits were divided randomly into sham control (n=5) and experimental (n=5) groups. The experimental group received 3.5 units/kg botulinum type-A toxin (BTX-A) (*Botox, Allergan Inc, Canada*) injections into the quadriceps muscles and 1.75 units/kg into the plantar flexor muscles. The sham control animals received injections of 0.9% sodium chloride solution using an identical procedure and an equal injection volume. After four weeks, quadriceps weakness, quadriceps and plantar flexor muscles atrophy and degenerative changes in the retro-patellar cartilage were measured.

Knee extensor weakness was quantified as the maximum isometric knee extensor torque at three different knee angles (80°, 100° and 120°). Immediately after sacrifice, ***quadriceps atrophy*** was determined by measuring the difference in the wet mass between corresponding hind limbs. Cartilage was stained with India-Ink and ***gross morphology*** was graded [3]. The ***degenerative changes*** in the retro-patellar cartilage were assessed by histological analysis using the Mankin grading system [4]. Statistical analyses were done using non-parametric tests ($\alpha=0.05$).

RESULTS

Isometric knee extensor torque averaged across all knee angles tested were significantly smaller ($p<0.01$) in the experimental (85%±9) compared to the control group (-7%±10) (Figure 1).

Atrophy was significantly greater in the experimental rabbits compared to the control group rabbits (Figure 2, $p<0.01$). The relative difference in the quadriceps total mass between the corresponding hind limbs of the experimental rabbits was 36%±10, whereas it was -0.15%±2 in the control group rabbits. The relative difference in total mass of the plantar flexors was 34%±6 in the experimental and -0.35%±9 in the control group rabbits (Figure 3, $p<0.01$).

Gross Morphology grades of the retro-patellar cartilage were statistically the same between the corresponding hind limbs within each group as well as between the two study groups. This was also true for the degenerative changes graded by the ***Mankin scores*** (Figure 4, $p>0.05$)). The tibiofemoral cartilage gross morphology and histology are being analyzed.

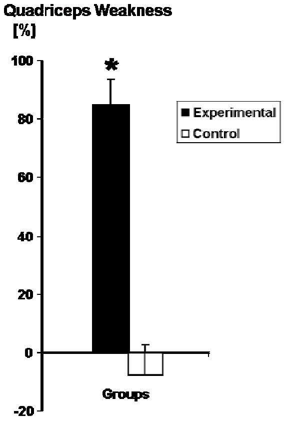

Figure 1: Quadriceps percent weakness of the experimental and the sham control rabbits, averaged across all knee angles tested. Group means and SD are shown. (*$p < 0.01$)

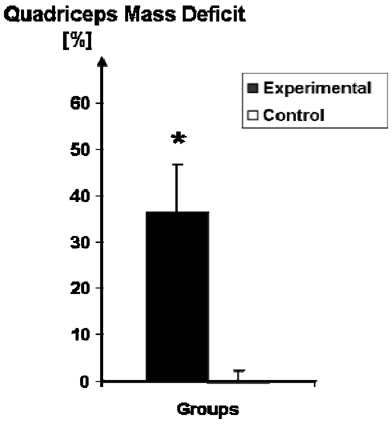

Figure 2: Quadriceps percent mass deficit of the experimental and the sham control rabbits. Group means and SD are shown. (*$p < 0.01$)

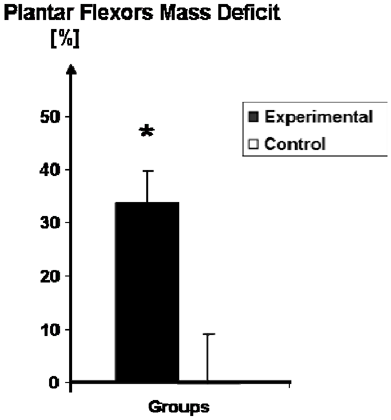

Figure 3: Plantar flexors percent mass deficit of the experimental and the sham control rabbits. Group means and SD are shown. (*$p < 0.01$)

DISCUSSION

The results of decreased isometric torque and increased muscle mass deficit confirmed the development of muscle weakness following Botox injections. Cartilage gross morphology and histology grades of the retro-patellar cartilage were the same for the two study groups, which is in contrast to previous findings of isolated quadriceps weakness [2]. There are many possibilities to explain the differences between the model of isolated muscle weakness and full hind limb weakness. Most likely, but unproven, is the idea that hind limb use differed substantially between the two models. For isolated quadriceps weakness, it is known that rabbits were weight bearing during the experimental protocol, although with reduced vertical ground reaction forces[5]. Unfortunately, such data are not available for the full hind limb weakness model. Another possible explanation is that animals in this study received a higher volume of Botox. BTX-A is a diffusible substance [6] and could have entered the knee joint. Botox has been shown to have a chondroprotective effect [7], thus possibly explaining the current results.

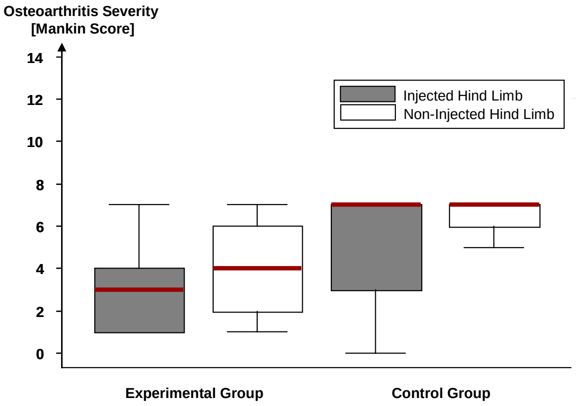

Figure 4: Box plots of the Mankin scores from the injected and the non-injected hind limbs of the study groups.

REFERENCES

1. Slemenda C, et al. *Arthritis Rheum* 1998; 41: 1951-1959.
2. Rehan Youssef A, et al. *Osteoarthritis Cartilage* (Accepted).
3. Yoshioka M, et al. *Osteoarthritis Cartilage* 1996; 4: 87-98.
4. Mankin H, et al. *J Bone Joint Surg* Am 1971; 53: 523-537.
5. Longino D, et al. *J Orthop Res* 2005; 23: 1411-1418.
6. Borodic G, et al. *Mov Disord* 1994; 9: 31-39.
7. Namazi H. et al. *Int Immunopharmacol* 2006; 6: 1743-1747.

ACKNOWLEDGEMENTS

CIHR, CRCP, AHFMR OA team grant, The Egyptian Ministry of Higher Education.

THE RELATIONSHIP BETWEEN BALANCE AND COGNITION IN PARKINSON'S DISEASE

Joe Nocera, Srikant Vallabhajosula, Shinichi Amano, Chris Hass
University of Florida, Applied Neuromechanics Laboratory
jnocera@ufl.edu

INTRODUCTION

Parkinson's disease (PD) has traditionally been designated as a motor disorder characterized by tremor, rigidity, akinesia, and postural instability. However, non-motor symptoms, specifically cognitive impairment, is often concomitant with the disease process further complicating quality of life for the patient [1]. The cognitive deficits demonstrated in PD impact a variety of domains; most notably executive function and working memory.

Recently studies have demonstrated that cognitive impairment may be closely linked to specific subsets of motor symptoms within the clinical spectrum of Parkinson's disease. In particular, motor symptoms not influenced by dopminergic stimulation, including postural instability, have been associated with accelerated cognitive decline [2]. To date however, studies examining this relationship have relied mainly on subjective motor measures provided by Unified Parkinson's Disease Rating Scale (UPDRS). Unfortunately, clinical measures, such as the UPDRS, frequently used to assess postural stability are too simplistic and fail to capture the essence of postural instability in this population [3]. Therefore, to further understand to impact of motor symptoms on cognitive status, motor function must be objectively quantified. A clear understanding of the relationship between postural instability and cognition is important to not only understanding the disease process itself but also for designing and implementing appropriate interventions.

Therefore, utilizing center of pressure (COP) sway area as a measure of postural instability and standard neuropsychological measures to evaluate cognition, this study investigated the relationship between postural instability and cognition in PD.

METHODS

Twenty individuals with PD participated (age: 63 ± 2; Modified Hoehn & Yahr stage of 1 to 3). All biomechanical and neuropsychological testing was performed in the Applied Neuromechanics Laboratory, Center for Exercise Science at the University of Florida, Gainesville, Florida.

Ground reaction forces (GRF) were recorded (360 Hz) from one forceplate (Type 4060–10, Bertec Corp., Columbus, OH) embedded level with the laboratory floor. GRF and moments were then used to calculate the COP.

During quiet stance trials, participants were asked to stand with their feet comfortably apart (a self–selected stance width) with both feet on the adjacent forceplate. Foot positioning was marked on the initial trial and used for all subsequent trials. Participants were asked to stand as still as possible for 20 seconds with their arms comfortably at their side. Participants performed four experimental trials. Trials where voluntary movements were observed were rejected and additional trials were performed.

Once the COP was calculated, the peak displacements in the mediolateral and anteroposterior directions were determined and the COP sway area was calculated.

In a quiet room, standard neuropsychological tasks were utilized to evaluate both executive function and working memory and included:

1. Digit Span backward: Participants recalled an increasingly long string of digits in the reverse order of presentation. Digit backward span is commonly utilized as an evaluation of working memory [4].
2. Color-word Interference Test: Participants say the color in which another color word is printed in (e.g., for BLUE printed in red ink, the answer is

‘red’). This is a commonly-used executive function task [4].

3. Letter Verbal Fluency: Participants produce as many words (F, A, or S) as they can that begin with that letter in 60 seconds. This is generally considered a measure of a verbal component of executive function [4].
4. Semantic Verbal Fluency: Participants produce as many words as they can that fit a particular category (animals) in 60 seconds. This is generally considered a measure of a verbal component of executive function [4].

To establish the inter-relationships between the different variables, correlations between COP sway area, digit span backward, color-word interference test, letter verbal fluency, semantic verbal fluency were examined using Pearson product. An alpha level of 0.05 was used for all tests. All analyses were conducted with SPSS (16.0 for Windows, Chicago, Il, USA).

RESULTS AND DISCUSSION

Significant negative correlation were demonstrated between three of the four cognitive measures; digit span backward (r = -.4601, *p* < .05), color-word interference test (r = -.4602, *p* < .05), letter verbal fluency (r = -.5162, *p* < .05), semantic verbal fluency (r = -.1420, *p* > .05).

The results demonstrate that as cognitive scores (executive function and working memory) decrease COP sway area and thus postural instability increases. Similar with previous research, this study suggests that cognitive impairment may correlate with motor severity. For example, Levy et al. found that both bradykinesia and axial symptoms were associated with an increased incidence of dementia [5]. Additionally, Aarsland and colleagues noted akinetic dominant PD is a risk factor for dementia. Cognitive impairment is common and has devastating implications on the quality of life for patients with PD. Thorough motor examinations may provide insight into those patients that may be at risk for developing dementia and who may be a candidate for early and preventative therapy.

CONCLUSIONS

Results of this study provide further evidence that motor function, specifically postural control may be negatively influenced by cognitive dysfunction in PD.

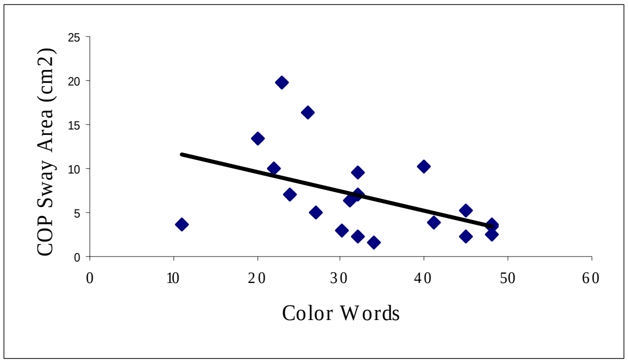

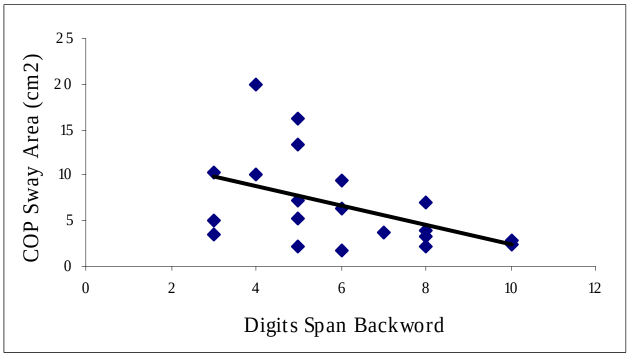

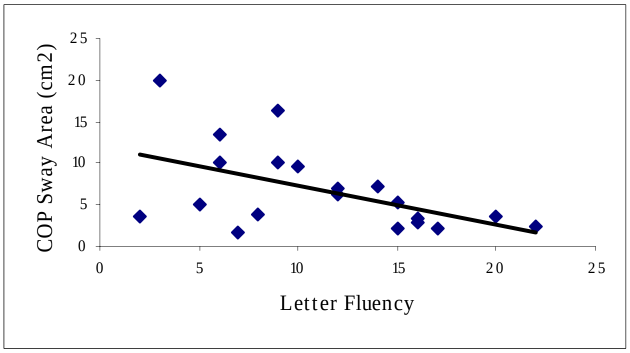

REFERENCES

1. Caballol N, et al. *Mov Disord* 22, S358-366, 2007.
2. Aarsland D et al. *The Rate of Cognitive Decline in Parkinson Disease. Arch Neurol* 61, 1906-1911, 2004.
3. Adkin AL, et al. *Mov Disord* 18(5), 496-502. 2003.
4. Delis DC et al. *The Delis-Kaplan Executive Function System.* San Antonio, TX: The Psychological Corporation.
5. Levy G et al, *Arch Neurol* 55, 539-544, 2000.

ACKNOWLEDGEMENTS

This work was supported by NIH grant 5R03HD054594-02

TRANSITIONING TO THE NEXT LEVEL: FOOT POSITION AND HIP MUSCLE ACTIVTY DURING STAIR WALKING

Sarah S. Gascon and Jinger S. Gottschall
The Pennsylvania State University, NeuroMotion Laboratory
email: ssg146@psu.edu, web: www.biomechanics.psu.edu/nml/

INTRODUCTION

Stairs are everywhere. And although using stairs is a common and simple task, anyone can be seriously injured when traveling up or down stairs. In fact, according to the National Safety Council, accidents during stair walking are ranked as high as second among the primary causes of unintentional injuries [1].

In order to maintain lateral stability during walking in the natural environment, we continually modify foot placement in an effort to modulate our base of support. The base of support can be improved with increased lateral step width and increased external foot rotation. We define step width as the lateral distance between the two calcanea (heels) during double support stance and external rotation as the lateral distance between the two halluces (toes) with respect to the line of progression during stance [2]. Thus, the measurement of step width and external rotation provides functional insight regarding lateral stability.

The hip adductors and hip abductors aid in the control of foot placement during level walking. The adductor longus (ADL) is active during terminal swing for the control of foot placement and single support stance for pelvic stabilization [3]. The tensor fascia latae (TFL) is active during the first third of stance in order to steady the pelvis and during the first half of swing in order to promote foot clearance [3]. Currently, there is no published data documenting how the muscle activity of these two muscles is modified during up or down stair walking.

The purpose of the present study was to determine if foot placement and hip muscle activity are modified during transitions between level and stair walking. We hypothesized that, compared to level walking, lateral step width, measured at the heel, and external foot rotation, measured at the toe, would be larger during the transition strides between level and stair surfaces. Likewise, in order to accomplish this wider foot placement, we hypothesized that mean abductor muscle activity would be less while mean tensor fascia activity would be greater than level walking during the transition strides.

METHODS

Six men and six women completed the protocol. All of the walking trials were completed at a self-selected velocity on a 25 m walkway. We utilized a custom-built portable apparatus composed of four stairs (20.32 cm rise x 27.94 cm run) continuous with a 3.66 m plateau.

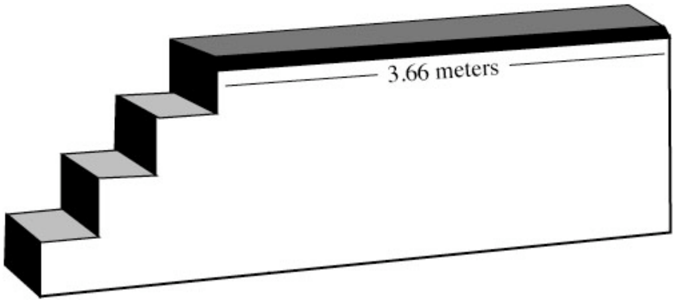

Figure 1. Portable stair apparatus.

In addition to level walking, we collected 5 stair walking trials for each of the following 6 conditions; transition from floor to up stair (L-UP), up stair only (UP), transition from up stair to plateau (UP-L), transition from plateau to down stair (L-DN), down stair only (DN), and transition from down stair to floor (DN-L).

We collected kinematic data with a six-camera, passive marker 3D photogrammetry system and electromyography signals using a wired amplifier system. Prior to data collection, we placed retroreflective markers on the first metatarsal (toe) and posterior calcaneus (heel) of both shoes for each participant. In addition, we placed surface electrodes on the tensor fascia latae (TFL) and adductor longus (ADL) muscles.

Foot placement and muscle activity were analyzed across all conditions using a repeated measures design (ANOVA) and Newman-Keuls post hoc tests. Significance was defined as $p \leq 0.05$.

RESULTS AND DISCUSSION

In support of our hypothesis, compared to level walking, step width and external rotation were larger during all down stair conditions and step width was larger during the transition from level walking to up stair walking. Interestingly, external rotation was smaller during the up stair conditions, possibly as an effort to maximize propulsion [4].

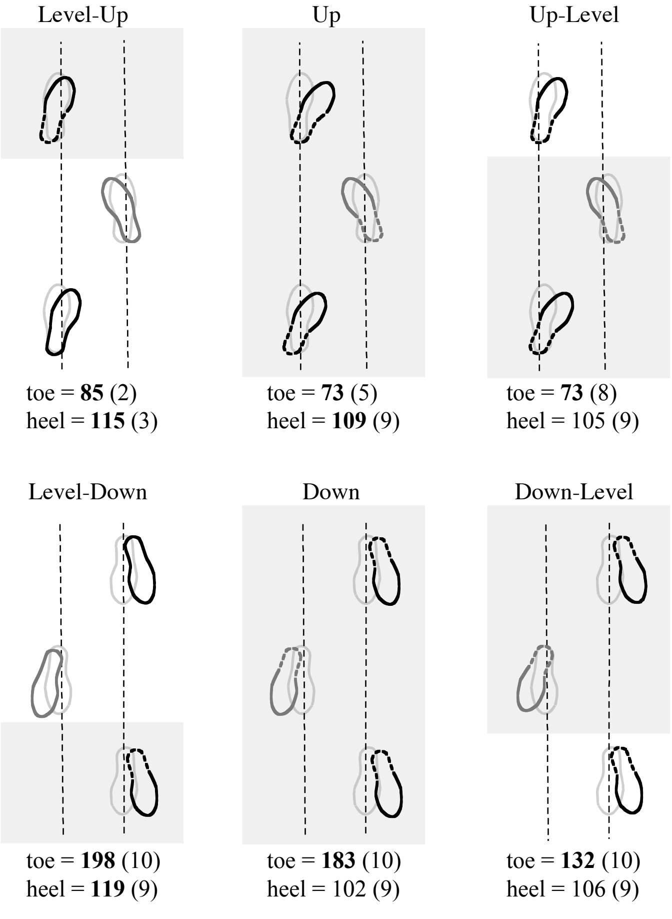

Figure 2. Schematic representation of toe and heel placement as a percentage of level walking. The values are mean *(standard deviation)* for the 6 participants. The bold values indicate a statistically significant difference ($p < 0.05$) compared to level walking. The shaded areas represent the stairs. The transparent shoe prints represent the level walking placement and the superimposed black (left foot) and grey (right foot) shoe prints represent how the placement changed during each stair condition. Please note that the dashed heel print represents steps where the forefoot contacted the ground first to initiate stance.

ADD	*swing*	*stance*
L-UP	**200** *(22)*	**186** *(32)*
UP	**257** *(31)*	**192** *(28)*
UP-L	**237** *(25)*	**147** *(21)*
L-DN	**77** *(18)*	**141**_(26)_
DN	**77** *(21)*	**159** *(17)*
DN-L	**85** *(27)*	**146** *(16)*

TFL	*swing*	*stance*
L-UP	104 *(42)*	**243** *(51)*
UP	**163** *(41)*	**166** *(64)*
UP-L	**144** *(55)*	106 *(68)*
L-DN	107 *(52)*	**124** *(57)*
DN	**132** *(52)*	**139** *(60)*
DN-L	**128** *(51)*	97 *(34)*

Table 1. Adductor longus (ADD) and tensor fascia latte (TFL) data during swing and stance for each of the six experimental conditions as a percentage of level walking. The values are mean *(standard deviation)* for the 6 participants. The bold values indicate a statistically significant difference ($p < 0.05$) compared to level walking.

CONCLUSIONS

To summarize, in comparison to level walking, during the up stair walking conditions, step width was larger while external rotation was smaller. During the down stair walking conditions, both step width and external rotation were larger. These results illustrate that the transition from level to stair surfaces did, in fact, challenge lateral stability. In order to maintain stability, the participants increased their base of support with a wider step width and decreased adductor activity.

REFERENCES

1. www.nsc.org
2. Kaufman KR, et al. *J Biomech* **34**, 907-15, 2001.
3. Winter DA. *The Biomechanics of Human Gait,* 1991 .
4. Erdemir A, Piazza SJ. *Gait Posture* **14**, 212-9.

MENISCAL MODELING IN A DISCRETE ELEMENT ANALYSIS OF THE KNEE

Donald D. Anderson, Krishna S. Iyer, Neil A. Segal, and Thomas D. Brown
– for the Multicenter Osteoarthritis Study Group –

Department of Orthopaedics and Rehabilitation, University of Iowa, Iowa City, IA, USA
e-mail: don-anderson@uiowa.edu URL: http://poppy.obrl.uiowa.edu

INTRODUCTION

Discrete element analysis (DEA) is a means for estimating articular joint contact stress, using bone surface geometries derived from CT or MRI [1]. The utility of DEA in studying knee joint contact stress from a cohort of 60 subjects from the Multicenter Osteoarthritis (MOST) study, an investigation of the incidence and progression of knee osteoarthritis in a cohort of 3026 men and women, was previously established [2] (Figure 1).

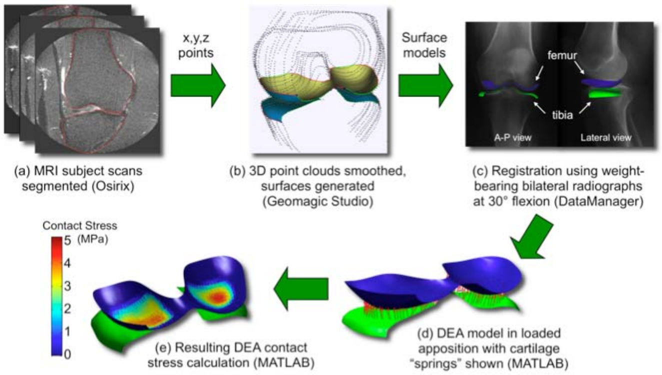
x,y,z
points
Surface
models
femur
tibia
A-P view
Lateral view
(a) MRI subject scans segmented (Osirix)
(b) 3D point clouds smoothed, surfaces generated (Geomagic Studio)
(c) Registration using weight-bearing bilateral radiographs at 30° flexion (DataManager)
Contact Stress
(MPa)
5
4
3
2
1
0
(e) Resulting DEA contact stress calculation (MATLAB)
(d) DEA model in loaded apposition with cartilage "springs" shown (MATLAB)

Figure 1. This schematic outlines the approach implemented for population-wide investigations of habitual contact stress exposure.

In that previous work, the meniscus was not included in the knee models.

The meniscus plays an important role in stress transfer across the knee joint. DEA models, as conventionally implemented, have not incorporated intervening tissues between contacting cartilage surfaces. However, in principle, the meniscus can reasonably be treated as simply another deformable in-line structure, using the same DEA concepts. This of course requires meniscal geometry (available from MR images) and appropriate modification to the underlying formulation of DEA equations being solved.

In the present study, the feasibility of incorporating a meniscus in a knee DEA model was evaluated in a group of MOST subjects for whom the meniscal geometry was amenable to segmentation from MR images. Computed contact stress distributions with the meniscus included were compared to those computed without a meniscus.

METHODS

The basic DEA implementation constructs a system of linear compressive elements at closest-point vertex pairings between the tibia and the femur, with the spring constants reflecting local effective stiffness, based upon the elastic modulus, Poisson's ratio, and thickness of the cartilage. When menisci are included, the local effective stiffness can instead be taken as a series composite of the local meniscus and local cartilage stiffnesses, with deformations distributed between the two tissues according to their respective individual stiffness values.

$$(1/k_{\text{composite}}) = (1/k_{\text{cartilage}}) + (1/k_{\text{meniscus}})$$

The local meniscus stiffness can be derived from its material properties and its thickness (h_{meniscus}) at any given point in the structure.

$$k_{\text{meniscus}} = \frac{E_{\text{meniscus}}\,(1-\nu_{\text{meniscus}})}{(1+\nu_{\text{meniscus}})\,(1-2\nu_{\text{meniscus}})\,h_{\text{meniscus}}}$$

The meniscal thickness distribution was computed first, using a closest point algorithm between superior and inferior meniscal surfaces. Those tibia-femur vertex pairings having an intervening meniscus segment were next identified. The meniscus was assumed to not move with respect to the tibia during a simple quasistatic loading at a fixed knee flexion angle. The meniscal thickness to be associated with a given tibiofemoral vertex pairing was obtained by then indexing the closest point on the inferior surface of the meniscus with the tibia. A combined stiffness matrix was then constructed using the paired meniscal and cartilage thicknesses, and the correspondingly modified DEA equations are solved to calculate contact stress.

In order to assess the feasibility of meniscus inclusion in a knee DEA model, the menisci were subsequently segmented for twenty-four of the MOST study knees for which the menisci could be reasonably discriminated on MR images. Linear elastic compressive material properties ($E_{cartilage}$ = 12MPa, $\nu_{cartilage}$ = 0.42; $E_{meniscus}$ = 80MPa, $\nu_{meniscus}$ = 0.3) were assigned for the materials. The meniscal DEA formulation was then applied, with the same displacements applied as for the models without menisci, yielding alternative contact stress values for comparison.

RESULTS AND DISCUSSION

The computed contact stress distributions extended over a larger area, as expected, when the knee DEA formulation was modified to include a meniscus (Figure 2). There were only minor reductions in the computed maximum contact stress values, which still occurred centrally on the joint surfaces. Given that the model was run in displacement control, this result was not totally unexpected. The inclusion of menisci resulted in model run times similar to those without menisci.

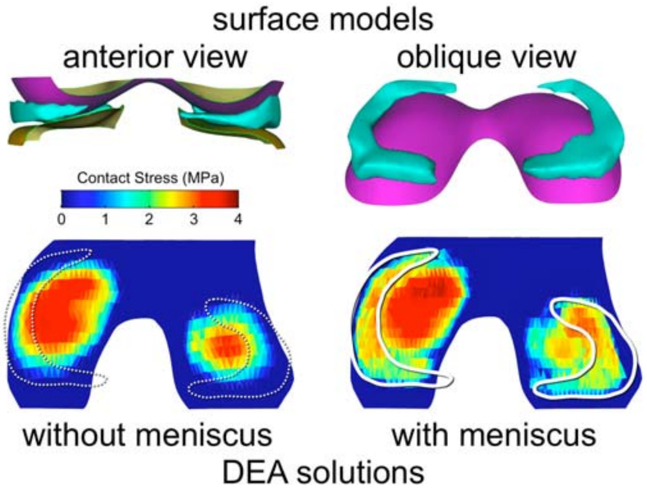

Figure 2. The inclusion of a meniscus resulted in a broader distribution of contact stress over the articular surface, but the maximum computed values were comparable, and still centrally located.

This exploration of feasibility assumed that the menisci do not move relative to the tibia when loaded. The implementation remains to be validated experimentally. These limitations clearly must be addressed in future (ongoing) work.

CONCLUSIONS

Based upon pilot work aimed at identifying local mechanical risk for incident symptomatic knee OA, the presented subject-specific implementation of DEA has shown itself as a feasible method for exploring the associated articular joint mechano-pathology. A viable approach to including a meniscus in knee joint DEA models has been developed and implemented. These methods open the way for more widespread use of subject-specific determination of risk for OA attributable to habitual contact stress exposure.

REFERENCES

1. Li G, Sakamoto M, Chao EY. *J Biomech* **30**:635-8, 1997.
2. Anderson, D, Segal N, Torner J, Brown T. *Am. Soc Biomech Conf*, California, 2007.

ACKNOWLEDGEMENTS

The assistance of Ms. Jennifer Baker in tracing of geometries from MRI scans is gratefully acknowledged. This research was funded by grants from the University of Iowa BSFP, and from the NIH: University of Iowa (AR48939 and AG18832); Boston University (AG18820); University of Alabama (AG18947); University of California San Francisco (AG19069); Association of Academic Physiatrists (5K12HD001097-08).

Does Acute Whole Body Vibration Training Improve Physical Performance for People with Knee Osteoarthritis?

Jay R. Salmon and Mark D. Tillman
University of Florida
jsalmon@ufl.edu   mtillman@hhp.ufl.edu

INTRODUCTION

Osteoarthritis (OA), is the most common form of arthritis, and the most prevalent joint disorder worldwide [1]. Abnormal biomechanics in the knee joint may initiate the disease process leading to OA. Additionally, knee pain associated with OA can further alter the mechanics of the lower extremity leading to difficulty in the performance of activities of daily living (ADLs).

Traditional therapies for knee OA consist primarily of pharmacologic and surgical treatments. Each of these presents difficulties, especially when treating the elderly, the main population affected by knee OA. Other forms of managing knee OA, such as exercise, offer numerous advantages. Furthermore, there appears to be a need for additional viable, nonpharmacologic modalities to treat knee OA.

Previous studies have shown whole body vibration (WBV) to be effective in increasing muscle strength and power, improving balance and mobility, improving circulation, and altering certain hormone levels (e.g. growth hormone, IGF-1, cortisol, and testosterone) [2]. Additionally, WBV offers particular advantages as an intervention for special populations.

The purpose of this study was to test the hypothesis that a single session of WBV training (WBVT) would improve the physical performance of individuals with knee OA in three tests designed to simulate ADLs: the Timed-Up-and-Go Test (TUG), a step test, and a 20 meter walk test.

METHODS

Seventeen individuals with symptomatic knee OA, for whom it was safe to perform WBVT, were recruited from orthopedic clinics, fitness centers, care centers, and the community surrounding the university campus.

A Power Plate vibration platform (2004 model Power Plate Personal) was used in all WBV training sessions. Participants stood on the platform with knees slightly flexed and received tri-planar (mostly vertical), sinusoidal WBV at 35 Hz and 4-6 mm displacement, 10 times in 60 second increments with 60 second rest periods in between each bout of WBV. The total exposure time was 10 minutes (Figure 1).

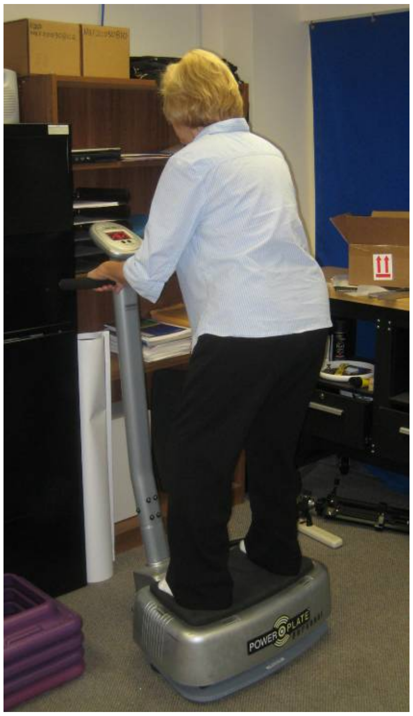

Figure 1: Participants stood on the vibration platform with knees slightly flexed as shown above.

Outcome measures included the time (in seconds) required to complete the following tests: 1) TUG, 2) step test, 3) 20 meter walk test, as well as knee pain levels as measured using a 10 cm visual analog scale (VAS) immediately following each test. The outcome measures were recorded at the following intervals: pre-intervention, five minutes post-intervention, and one hour post-intervention.

Separate one-way ANOVA were performed for each outcome variable across the three testing intervals ($\alpha = .05$). Pearson correlations were performed to examine the linear correlation of VAS scores on times to complete the three functional tests, respectively.

RESULTS AND DISCUSSION

Main effects were detected for both time to complete the step test (F(2,28) = 6.243, *P* = .006) and time to complete the walk test (F(2,28) = 4.370, *P* = .022). Post-hoc analyses revealed that the time to compete the step test five minutes after WBVT improved significantly (*P* = .042) from the pre-test, while the improvement from pre-test one hour after WBVT failed to reach significance (*P* = .085). There was no significant change in time to complete the step test from five minutes after WBVT to one hour after WBVT (*P* >.05) (Figure 2). Post-hoc analyses of the times to complete the walk test, however, failed to show any significant changes (*P* >.05). No significant changes following WBVT were found for the TUG, nor for the pain levels following any of the tests (*P* >.05). A moderate correlation (r = .465, *P* = .001) was found between the VAS scores and the time to complete the step test across all trials. No other significant correlations were found (*P* >.05).

We found that WBVT was well-tolerated in nearly all participants, and our results showed that an acute bout of WBVT was effective in improving the ability of individuals with knee OA to perform a step test designed to simulate the task of going up and down stairs. While it is beyond the scope of this study to ascertain the exact mechanism by which physical performance was improved, a review of previous studies [2] and our failure to find an accompanying significant decrease in pain levels suggests that the improved performance is likely due to beneficial effects of WBVT on the neuromuscular system, such as improved balance and increased muscular strength and power. It should be noted, however, that while not reaching significance, we did find that pain levels following the step test decreased on average 28% five minutes after WBVT. Together with the moderate correlation between pain levels and step test performance, there is some evidence that pain reduction may have contributed to improved performance. Overall, our findings suggest that WBVT may be an effective nonpharmacologic modality to treat some knee OA symptoms, although further investigation is needed.

REFERENCES

1. Reginster JY. *Rheumatology (Oxford)* **41**, 3-6, 2002.
2. Prisby RD, et al. *Ageing Res Rev* **7**, 319-329, 2008.

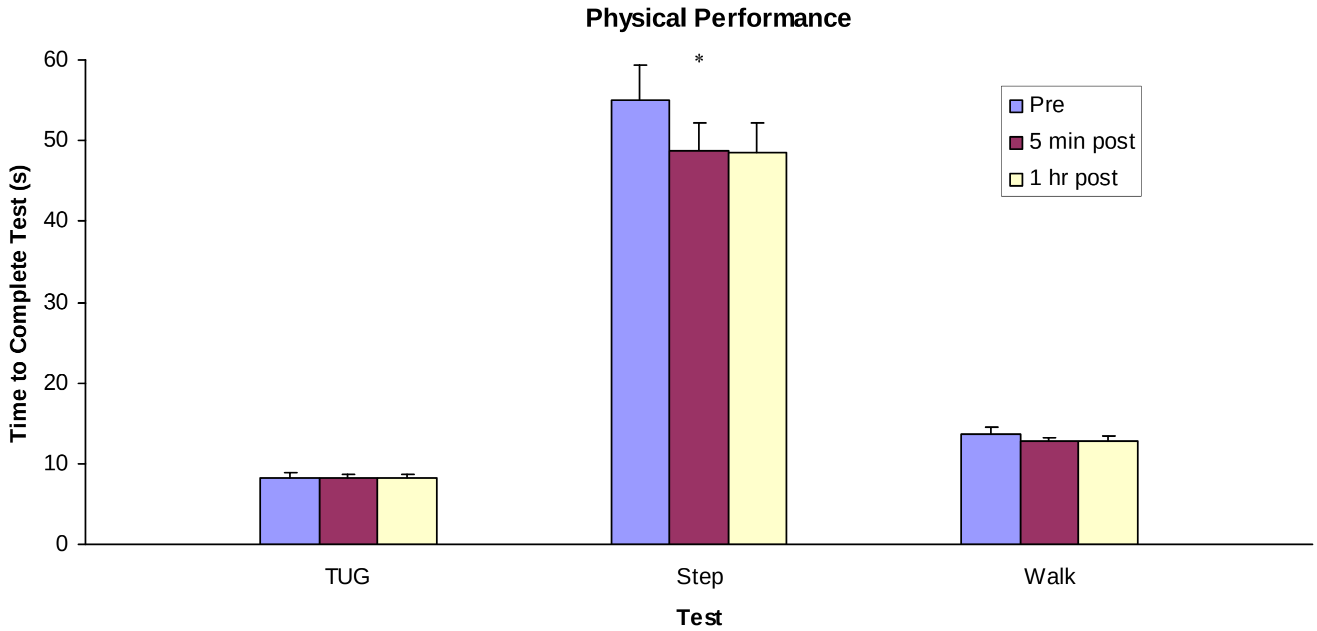

Figure 2: Mean and standard error (SE) before, 5 minutes after, and 1 hour after WBVT for the following tests: TUG, step, and walk. * - 5 min post values are significantly lower than pretest values (*P* <.05).

JOINT CONTRIBUTIONS TO SUPPORT MOMENT DURING RUNNING AND HOPPING IN A RUNNER WITH ACHILLES TENDINOPATHY: AN INTERLIMB COMPARISON

Yu-Jen Chang, John M. Popovich, Jr., Kornelia Kulig
Jacquelin Perry Musculoskeletal Biomechanics Research Laboratory, Division of Biokinesiology and Physical Therapy, University of Southern California, Los Angeles, CA.
email: changyuj@usc.edu, web: http://pt2.usc.edu/labs/mbrl/

INTRODUCTION

The ankle is the primary contributor to support moment during running and hopping [1, 2]. We hypothesized that this contribution will be decreased in the presence of Achilles tendinopathy and that the alterations in contribution will be task dependent. This study aims to compare differences in joint contributions to support moment between the involved and non-involved leg in a subject with unilateral Achilles tendinopathy during running and hopping tasks.

METHODS

One experienced male runner (56 y/o) with chronic right side Achilles tendinopathy participated in this study. The condition was identified clinically and the pathology was confirmed using ultrasonography (Figure 1). Lower extremity kinematics (Vicon 612 motion analysis system, Oxford, UK; 250 Hz), and kinetics (AMTI force plate, Watertown, MA; 1500 Hz) were obtained during running, single-legged hopping and double-legged hopping. The running speed was controlled at 4 m/s ±5% for all trials (N=6). Single- and double- legged hopping (N=20) frequency was set at 2.2Hz using a metronome.

The vertical ground reaction force was recorded, and the sagittal plane hip, knee, and ankle joint moments were computed using standard inverse dynamics equations. The support moment was calculated by the summation of the sagittal extensor moments [3].

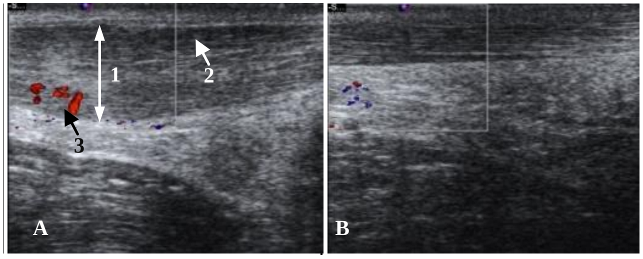

Figure 1. Ultrasound image of the involved Achilles tendon (A). Achilles tendinopathy was characterized by 1) focal thickening of the tendon; 2) hypoechoic region; and 3) neovascularization compared to uninvolved tendon (B).

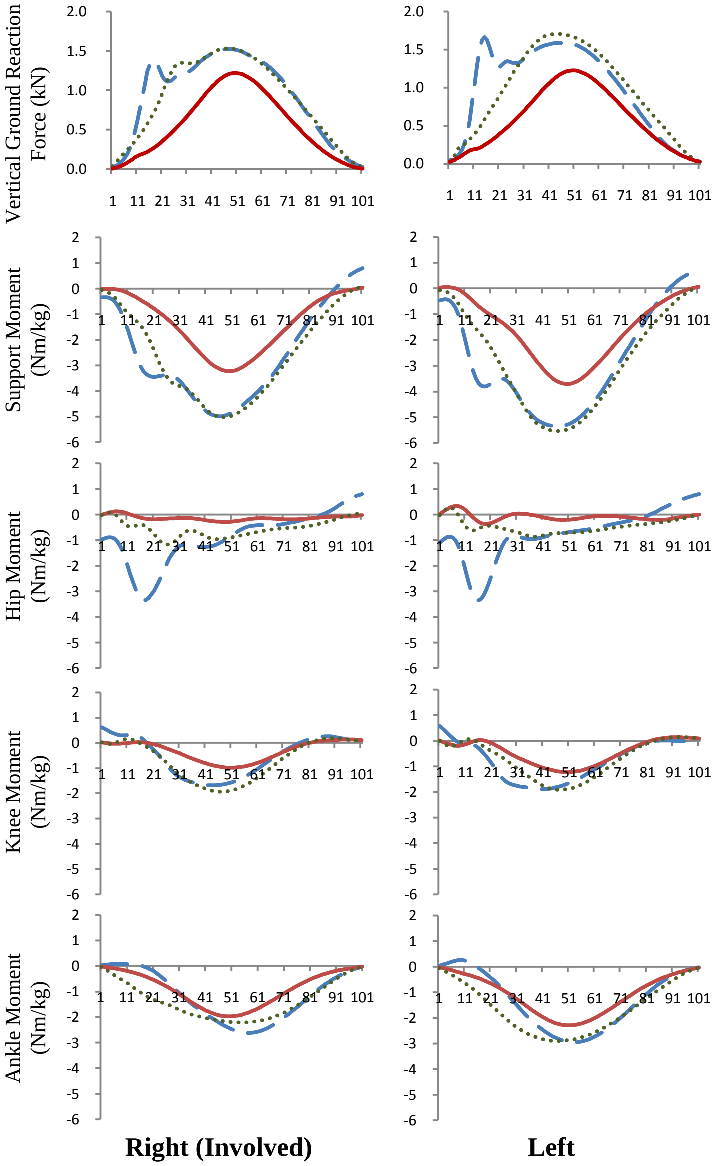

Figure 2. Vertical ground reaction force, support moment, and sagittal moments for the hip, knee, and ankle joints during running and hopping during normalized ground contact phase. Dashed-line: running; dotted-line: single-legged hopping; solid line: double-legged hopping. Negative moment denotes extensor for support moment, hip and knee, and plantarflexor for ankle.

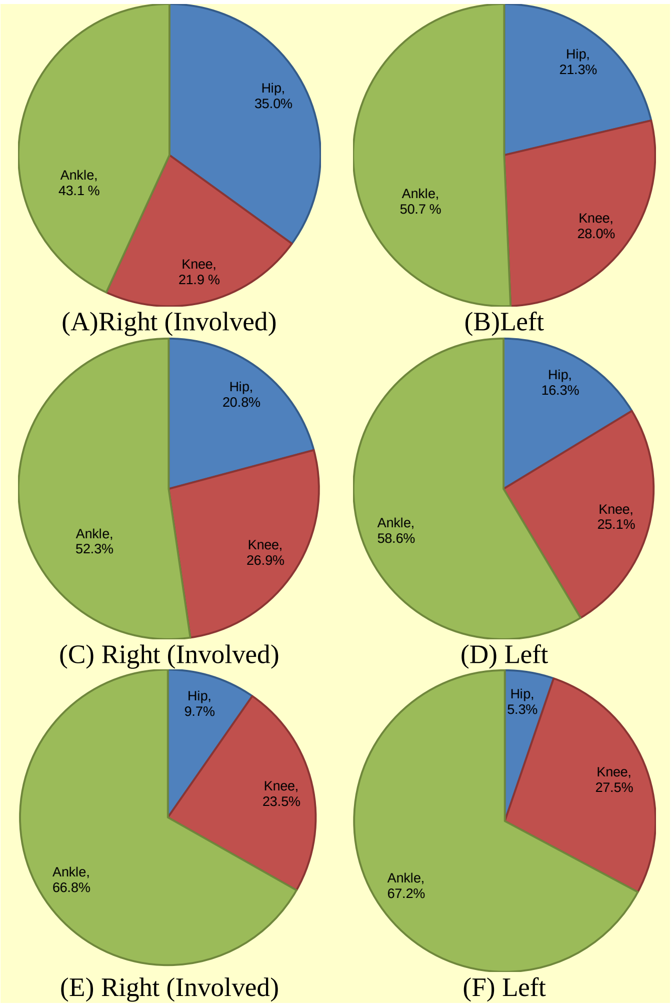

(A)Right (Involved) (B)Left

(C) Right (Involved) (D) Left

(E) Right (Involved) (F) Left

Figure 3. Percent contribution to support moment during ground contact phase of running (A, B); single-legged hopping (C, D); and double-legged hopping (E, F).

The averaged percent contribution to support moment for each joint was calculated by dividing the net sagittal joint moment by the support moment, respectively.

RESULTS AND DISCUSSION

The peak vertical ground reaction force (active peak) was lower for the involved leg during running and single-legged hopping, but there were no differences between sides during the double-legged hopping task (Table 1). The peak support moment exhibited a similar pattern; the results showed a lower peak support moment on the involved side for all three movement tasks, which might be driven by the ankle joint as its joint moments were consistently lower on the involved side among task (Table 1, Figure 2).

The ankle joint is the primary contributor to support moment across tasks (Figure 3). Although, when the ankle contribution during running was diminished on the involved side, other joints, especially the hip, increased their contribution to support moment. This phenomenon of re-distributing the ankle joint's contribution was also observed, though to a lesser extent, during single-legged hopping (Figure 3-C, D), but this was not obvious during the double-legged hopping (Figure 3-E, F).

Following injury, the mechanical properties of soft tissues are altered [4]. A degenerated tendon is more compliant than a healthy tendon, which might lead to a more compliant joint and result in lesser contribution to support moment. This study observed that the involved ankle joint contributed less to the support moment during the ground contact phase of habitual running, as well as during un-practiced hopping, though the contribution pattern was less pronounced. Yet, this finding was not observed when a synchronous double limb activity was performed. This implies that the involved joint was capable of contributing to the support moment, but either the additional moment demands of unipedal support or adaptive learned movement strategies resulted in altered joint contributions to support moment in the presence of long standing pathology.

REFERENCES

1. Günther M & Blickhan R. *J Biomech* **35**, 1459-1474, 2002.
2. Farley CT & Morgenroth DC. *J Biomech* **32**, 267-273, 1999.
3. Winter DA, *J Biomech* **13**, 923-927, 1980.
4. Arya S & Kulig K. *J Appl Physiol* In review.

Table 1. Averaged peak vertical ground reaction force, support moment, and hip, knee, and ankle joint moment values for three tasks.

	Right (Involved)			Left		
	Running	Single Leg Hopping	Double Leg Hopping	Running	Single Leg Hopping	Double Leg Hopping
Vertical Ground Reaction Force (kN)	1.53	1.54	1.23	1.58	1.73	1.23
Support Moment (Nm/kg)	4.99	5.04	3.24	5.36	5.59	3.72
Hip Moment (Nm/kg)	3.36	1.35	0.31	3.36	0.94	0.39
Knee Moment (Nm/kg)	1.68	1.95	0.98	1.89	1.93	1.23
Ankle Moment (Nm/kg)	2.62	2.22	1.98	2.96	2.91	2.29

FORWARD DYNAMIC SIMULATION OF AN UPPER EXTREMITY MOVEMENT USING COMPUTED MUSCLE CONTROL

[1] Melissa Daly, MS, [1] Meghan Vidt and [1]Katherine R.S. Holzbaur, PhD
[1] Virginia Tech/Wake Forest School of Biomedical Engineering and Sciences, Wake Forest University Baptist Medical Center, Winston-Salem, NC 27157
email: mdaly@wfubmc.edu, web: http://www.sbes.vt.edu/kholzbau/MoBL/

INTRODUCTION

Dynamic simulation is a powerful tool for investigating the role of motor control in the production of human movement. It can allow researchers to investigate the role of individual muscles in healthy and pathologic movement in a way that cannot be achieved experimentally, and permits the simulation of potential clinical interventions so functional outcomes can be predicted. Computed muscle control (CMC) is an efficient method of generating muscle excitations needed to produce a specific kinematic trajectory using static optimization along with feedforward and feedback controls [1]. While CMC has been validated for use in the lower limb [2], its appropriateness for use in the upper limb has yet to be tested. The goal of this study is to determine if CMC generates appropriate muscle excitations for an upper limb task, specifically a forward reaching movement in the horizontal plane.

METHODS

Three healthy nonimpaired young adults were asked to perform a forward reaching movement with their dominant arm. Subjects provided written informed consent. The arm was initially held with the shoulder abducted to 90 degrees with the elbow fully flexed, and the subjects were asked to reach forward in the horizontal plane to full elbow extension and return to the beginning posture. Two trials for each subject were performed. Kinematics were recorded over a seven second reach using a seven camera Hawk system (Motion Analysis Corp., Santa Rosa, CA). EMG data were collected from the triceps, biceps and deltoid muscles using 2 cm surface electrodes (BIOPAC Systems Inc., Goleta, CA). The EMG data was filtered using a 39th order high pass Hamming-window based linear-phase filter with a cutoff frequency of 0.2 Hertz, rectified, and enveloped for each trial using a custom Matlab program (The Mathworks Inc., Natick, MA). The signals were then normalized to EMG collected during a maximum isometric contraction for each muscle of interest.

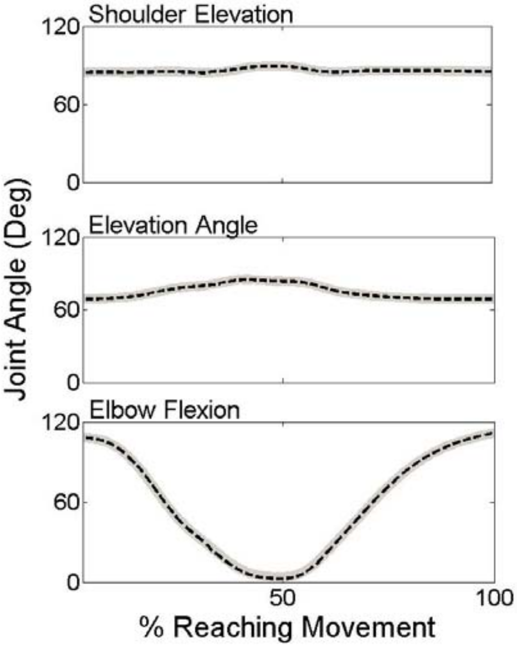

Figure 1: Simulated kinematics (dashed line) closely match observed kinematics (gray line) for subject 2.

An upper limb model based on a previously described kinematic model of the upper limb [3] was implemented in OpenSim [4] and used in the analysis, including five degrees of freedom (forearm rotation, elbow flexion, shoulder rotation, shoulder elevation and shoulder elevation angle), 32 muscles crossing the shoulder, elbow and forearm, and appropriate inertial parameters for the segments [5;6]. Computed muscle control [1] was used to compute muscle excitations that would drive a forward dynamic simulation to track the measured joint kinematics. The joint kinematics resulting from the simulations were compared to the measured kinematics. In addition, the predicted muscle activations were compared to the normalized and rectified EMG for biceps, triceps, and deltoid.

RESULTS AND DISCUSSION

The CMC algorithm accurately tracked all of the joint angles for each subject with only small deviations (± 0.42 degrees) from the experimental kinematics (for examples at the elbow and shoulder see Figure 1). The timing of muscle activations was similar to those recorded experimentally. For all three subjects, deltoid was activated throughout the motion to hold the arm in abduction. Triceps was primarily activated during elbow extension in the first part of the reach, while biceps was activated during the flexion in the second phase of the movement. The predicted activations capture these salient features of the activation timing (Figure 2). Simulated activations were not smooth over the time of the movement; investigations into the source of this anomaly are ongoing.

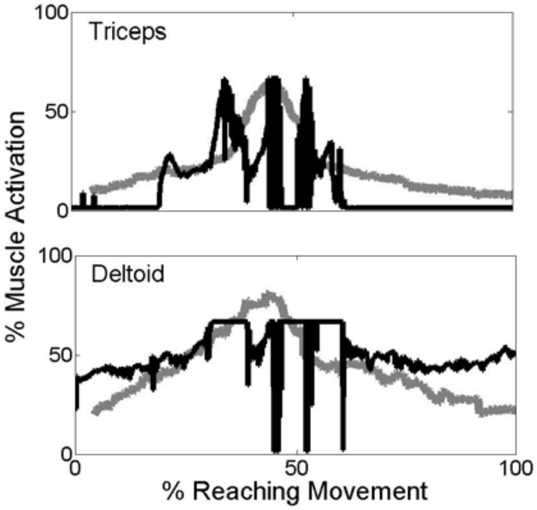

Figure 2: Predicted (gray line) and measured (black line) timings for deltoid and triceps for subject 1. Predicted muscle activations approximate timings seen with EMG.

One second of movement took approximately 4 hours to solve with the CMC algorithm with this model and this movement, while for a model of the lower limb one second of simulation of a gait movement took approximately 20 minutes [2]. This increase is likely due to increased complexity of the upper limb model, including complex muscle paths, wrapping surfaces, and joint descriptions that incorporate constraints. While results are promising, the use of this algorithm for upper limb motions should be further validated with additional subjects for this movement. In addition, CMC may not produce appropriate activations for all movements, or for all subjects; for example, for subjects with a neuromuscular pathology, CMC may not adequately capture changes in motor control. Additional validation of this approach for different subject populations and tasks should be performed.

CONCLUSIONS

CMC is able to adequately track the experimental kinematics and calculate appropriate muscle activation patterns for an upper limb reaching movement. Additional validation of this approach is ongoing to ensure accurate predictions are made. The use of CMC must be validated for other populations of subjects and for more complex movements.

REFERENCES

1. D. G. Thelen, F. C. Anderson, and S. L. Delp, *J. Biomech.*, **36**, no. 3, pp. 321-328, Mar.2003.
2. D. G. Thelen and F. C. Anderson, *J. Biomech.*, **39**, no. 6, pp. 1107-1115, 2006.
3. K. R. Holzbaur, W. M. Murray, and S. L. Delp, *Ann. Biomed. Eng*, **33**, no. 6, pp. 829-840, June2005.
4. S. L. Delp, F. C. Anderson, A. S. Arnold, P. Loan, A. Habib, C. T. John, E. Guendelman, and D. G. Thelen, *IEEE Trans. Biomed. Eng*, **54**, no. 11, pp. 1940-1950, Nov.2007.
5. M. A. Harrington, Jr., T. S. Keller, J. G. Seiler, III, D. R. Weikert, E. Moeljanto, and H. S. Schwartz, *J. Biomech.*, **26**, no. 4-5, pp. 417-426, Apr.1993.
6. J. T. McConville, T. D. Churhill, I. Kaleps, C. E. Clauser, and J. Cuzzi, AFAMRL-TR-80-119 Wright-Patterson Air Force Base, Yellow Springs, OH: Air Force Aerospace Medical Research Laboratory, 1980.

ACKNOWLEDGEMENTS

Wendy Murray. Ayman Habib, Craig Goehler for help with the simulations. Anthony P. Marsh, Zhelyazko Tumber, Lisa Johanson for help with the EMG data collection and processing. Finally, RIC collaborative project pilot funding.

Comparison of Rotator Cuff Muscle Architecture between Humans and Selected Vertebrate Species

Alan Kwan[1], Carolyn M. Eng[2], Samuel R. Ward[1],
[1]Department of Radiology, University of California San Diego, San Diego, CA
[2]Department of Anthropology, Harvard University, Boston, MA

email: srward@ucsd.edu, web: http://muscle.ucsd.edu

INTRODUCTION

One of the most common causes of pain and disability in the upper extremity is injury or disease in the shoulder, specifically in the rotator cuff muscle group. Although a variety of animal models have been used to study rotator cuff disease, there have been no formal reports comparing the organization of the musculature in these different species. Therefore, the goal of this study was to characterize and compare architectural data between the human rotator cuff muscles and those of several species commonly used in rotator cuff research.

METHODS

Eight animals commonly used in rotator cuff research were selected for the study: mouse (*Mus Musculus*), Sprague-Dawley rat (*Rattus norvegicus*), New Zealand White rabbit (*Oryctolagus cuniculus*), dog (*Canis familiaris*), Yucatan mini-pig (*Sus Scrofa*), sheep (*Ovis aries*), goat (*Capra hircus*), and cow (*Bos taurus*). Shoulders were harvested and fixed in 10% buffered formaldehyde. After fixation, the shoulders were stored in phosphate buffered saline (PBS). The outer layers of skin, fat, and overlying muscles were dissected away until the muscles of interest were exposed. The rotator cuff muscles were then excised for further analysis.

Muscle architectural measurements were made on the four rotator cuff muscles according to methods previously described (Lieber *et al.* 1990). The specific muscles studied were Supraspinatus (Sup), Infraspinatus (I), Teres minor (TM), and Subscapularis (Sub). Briefly, muscle mass (m), muscle length (L_m), and fiber length (L_f) were measured for each muscle. Fiber bundles from two to four predetermined regions were microdissected and sarcomere length (L_s) for each fiber bundle was measured using laser diffraction using the first to first order diffraction pattern (Lieber *et al.*, 1994) to calculate normalized fiber length (L_{fn}) and physiological cross-sectional area (PCSA) as previously illustrated (Lieber *et al.* 1994).

Scaling of muscle architecture with body mass across species was examined using linear regression of log transformed variables. Animal mass was treated as the independent variable and the architectural variable (PCSA or L_{fn}) was the dependent variable. The coefficient and the exponent of the exponential equation, $y=aM^b$ (where y is the architectural variable, a is the coefficient, M is the animal mass, and b is the scaling exponent) were used to compare scaling relationships among the rotator cuff muscle.

RESULTS AND DISCUSSION

PCSA varied in all muscles within and between each species. However there were similarities in an individual muscle's contribution to total rotator cuff PCSA between species. In the dog, rat, mouse and rabbit models, the subscapularis had the largest PCSA, contributing 45%, 47%, 48%, and 41% respectively to total rotator cuff PCSA, which is comparable to the human subscapularis which contributes 42%. The other muscles of the rotator cuff for these species also shared similar percentages to the human rotator cuff muscles. The goat, sheep, pig and cow were similar to each other with the infraspinatus having the largest PCSA (39%, 40%, 39%, 50%, relatively, of total rotator cuff PCSA) but less similar to human relative to the species mentioned above (Figure 1).

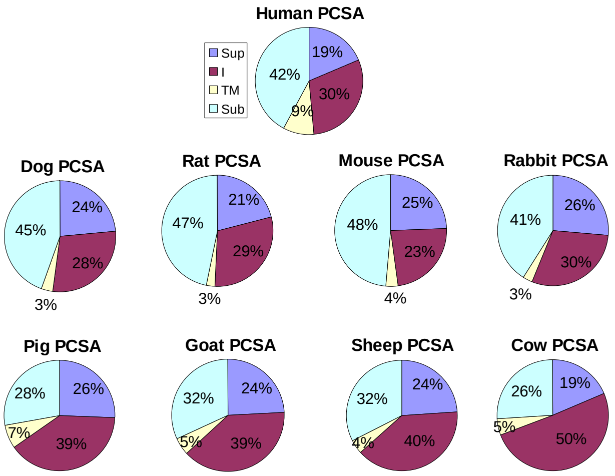

Figure 1. Percent contribution of each muscle to total rotator cuff PCSA: Supraspinatus (Sup), Infraspinatus (I), Teres Minor (TM), Subscapularis (Sub).

Log transformed data revealed normalized fiber length and PCSA all scale linearly with body mass ($0.86 \leq R^2 \geq 0.99$) (Figure 2, Table 1). Analysis of the scaling exponents suggests geometric scaling rules between species.

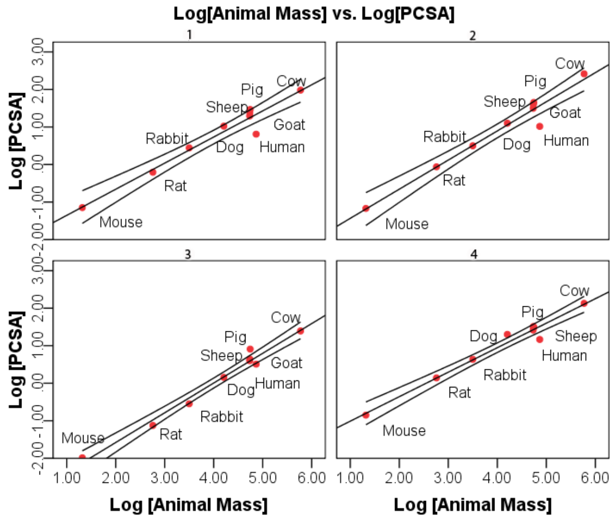

Figure 2. Relationship of muscle PCSA to body mass. Each rotator cuff muscle PCSA scales linearly to body mass. (1-Supraspinatus, 2-Infraspinatus, 3-Teres Minor, 4-Subscapularis)

CONCLUSIONS

Although none of these animals is an ideal match to the muscular anatomy of the human shoulder, our data shows that the relative PCSA of the rotator cuff muscles of the smaller animals, dog, rabbit, rat and mouse more closely match those of the human. Architectural properties such as fiber length and PCSA scaled geometrically with animal mass across all species. The use of animals in research has helped further the understanding of human disease. These data will be useful in selecting the appropriate animal model for future studies involving the rotator cuff.

REFERENCES

1. Lieber *et al.* (1990). *J. Hand Surg.* **15A**, 244-250.
2. Lieber *et al.* (1994). *J. Neurphysiol.* 71, 874-881.

Table 1. Regression exponents and coefficients for L_{fn} and PCSA relative to body mass.

	L_{fn}			PCSA		
Muscle	**b**	**a**	**R^2**	**b**	**a**	**R^2**
Supraspinatus	0.339±0.017	0.168±.073	0.983	0.696±0.061	-2.050±0.259	0.949
Infraspinatus	0.295±0.032	0.182±0.136	0.925	0.776±0.061	-2.209±0.260	0.958
Teres Minor	0.303±0.047	-0.039±0.200	0.856	0.792±0.044	-3.163±0.189	0.978
Subscapularis	0.325±0.043	-0.081±0.184	0.890	0.652±0.042	-1.662±.180	0.971

STRUCTURAL PROPERTIES OF DIABETIC AND NORMAL PLANTAR SOFT TISSUE

[1,2]Shruti Pai and [1,2,3]William R. Ledoux
[1]VA RR&D Center of Excellence for Limb Loss Prevention and Prosthetic Engineering, Seattle, WA 98108, and Departments of [2]Mechanical Engineering and [3] Orthopaedics and Sports Medicine, University of Washington, Seattle, WA 98195
email: wrledoux@u.washington.edu, web: www.amputation.research.va.gov

INTRODUCTION

Approximately 20.8 million Americans were estimated to have diabetes in 2005 [1]. A serious complication of diabetes is plantar ulceration, which can often lead to amputation of the affected limb [2]. To develop better treatment options, an understanding of the differences between healthy and diabetic plantar tissue properties is needed. Unconfined compression tests are typically used for determining the plantar tissue material properties [3, 4]. However, this method assumes a frictionless boundary condition at the tissue-platen interface that has yet to be experimentally confirmed. It is more physiologically accurate and experimentally repeatable to constrain the tissue at both ends to emulate the bone and skin constraints that occur *in vivo*. Thus, this study examines the structural rather than material properties of the plantar soft tissue.

The purpose of this study is to characterize the compressive properties of the plantar tissue beneath the heel (i.e., the subcalcaneal tissue) in both diabetic and normal (i.e., non-diabetic) specimens. Knowledge of the physiologic compressive properties is critical to understanding possible mechanisms of ulcer formation in diabetic patients.

METHODS

Specimens were obtained from two fresh frozen cadaveric feet; one non-diabetic (caucasian male, 78yrs) and one diabetic donor (caucasian male, 55yrs, diagnosed for 42 yrs), which were purchased from the National Disease Research Interchange. Institutional Review Board approval was obtained for this study from the Human Subjects Division at the University of Washington.

The plantar soft tissue was dissected free from the calcaneus, cut into cylindrical specimens using a 2.54cm diameter punch, and further dissected from the skin using a scalpel (Figure 1). Each specimen was then placed in an environmental chamber between two platens covered with 220 grit sandpaper. The setup was attached to an ElectroForce 3200 materials testing machine. The chamber was designed to heat a water bath below the platen and create a moist environment near 100% humidity and at 35°C to approximate conditions *in vivo*. The bottom platen was raised to apply a 0.1N compressive load and specimen initial thickness was measured (Table 1).

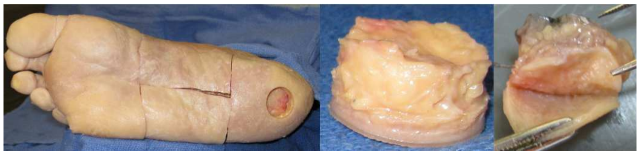
(a) **(b)** **(c)**

Figure 1: Specimen detail showing (a) location of subcalcaneal specimen, (b) close up of specimen prior to skin dissection, and (c) skin removal from specimen.

Table 1: Specimen information

	Donor Weight (N)	Specimen Weight (g)	Initial Thickness (mm)
Diabetic (D)	801	5.4	9.9
Normal (N)	702	6.2	12.4

The target load, based on specimen cross-sectional area, donor weight, and normative ground reaction force and contact area [5], was used to determine the target displacement. In load control, the specimen underwent ten 1Hz sine waves from 10N to the target load; the maximal absolute displacement was noted as the target displacement.

A series of three triangle waves were used to estimate the peak stress, peak strain, modulus (the slope of the curve after the inflection point), and energy loss (the area between the loading and unloading curves) for each specimen. Five different frequencies near the physiologic range were used (1, 2, 3, 5, and 10Hz) to test the frequency dependence of the subcalcaneal plantar tissue. Given the small sample size, it was not possible to do any statistical tests at this time.

RESULTS AND DISCUSSION

The diabetic specimen had a greater elastic modulus and energy loss at all testing frequencies compared to the normal specimen (Figure 2 and Table 2). These findings agree with previous demonstrations of increased energy absorption in diabetic heel pads [6] and increased stiffness in older diabetic plantar tissue [7]. Peak stress was also greater in the diabetic specimen, but that is likely a function of the increased peak strain (each specimen had a unique initial thickness and target displacement.)

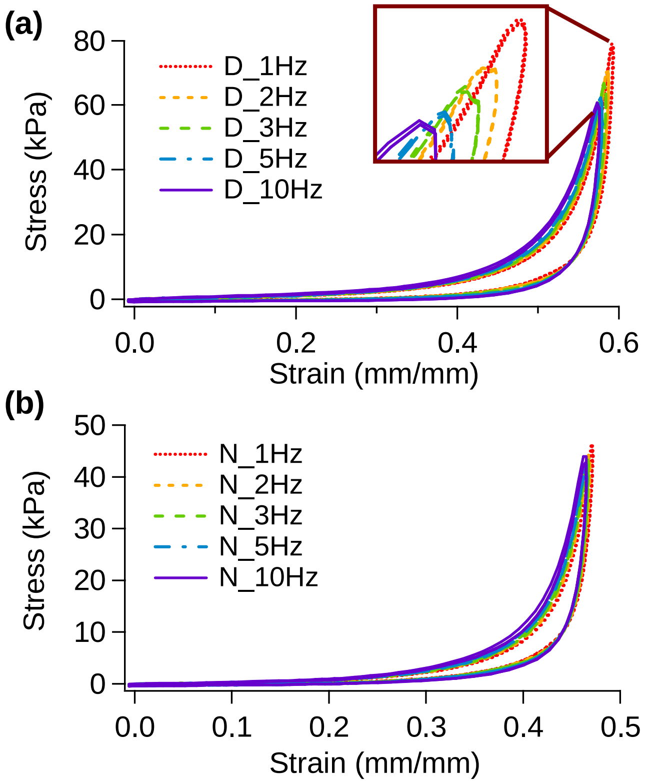

Figure 2: Stress versus strain response for the (a) diabetic, and (b) non-diabetic specimens at the five different frequencies

The structural properties for both specimens showed some dependence on testing frequency. Notably, the peak stress decreased with increasing frequency for the diabetic specimen (Table 2). This finding is contrary to previous findings [3, 8] and is believed to be an artifact of slight differences in peak strain. For example, with the diabetic specimen a difference in peak strains of 1.7% between the 1Hz and 10Hz tests resulted in a 18kPa difference in peak stress (Table 2). These results highlight the need for sensitive testing equipment; it is experimentally very difficult to obtain the target strains for such small displacements at high testing frequencies.

Table 2: Parameters for different frequencies for diabetic (D) and normal (N) specimens.

Test (Hz)		Peak stress (kPa)	Peak strain (%)	Modulus (kPa)	Energy loss (%)
1	**D**	78	59.3	603	56.7
	N	46	47.1	428	45.8
2	**D**	70	58.7	566	61.1
	N	44	46.8	436	50.4
3	**D**	66	58.4	527	66.2
	N	43	46.7	454	53.7
5	**D**	62	57.9	541	70.4
	N	42	46.5	488	57.9
10	**D**	60	57.6	607	79.1
	N	43	46.5	546	65.7

Future aims of this study, currently in progress, are to increase the number of specimens and to look at different specimen locations (e.g., the metatarsal heads, the hallux and the lateral midfoot) that also bear load and are prone to ulceration in patients with diabetes. Strategies for improving the ability of the materials testing machine to reach the target displacement at high frequencies are also being developed.

REFERENCES

1.CDCP. *Nat Diab Fact Sheet*. Atlanta, GA: 2005.
2.Van Schie CH, *Int J LE Wnds* **4**(3), 160-70, 2005.
3.Ledoux WR, *J Bmch* **40**(13), 2975-81, 2007.
4.Miller-Young JE, *J Bmch* **35**(12), 1523-31, 2002.
5.Ledoux WR, *Gait Posture* **15**, 1-9, 2002.
6.Hsu TC, *Diabet Med* **17**, 854-59, 2000.
7.Zheng YP, *Ult Sound Med Bio* **26**, 451-56, 2000.
8.Hsu CC, *Ult Sound Med Bio* **31**, 1423-29, 2005.

ACKNOWLEDGEMENTS

This work is being supported by NIH grant 1R01 DK75633-03 and the Department of Veterans Affairs, RR&D Service.

VARIANCE IN UPPER EXTREMITY MUSCLE ACTIVITY DURING CYCLIC PUSHING TASKS

Joanne N. Hodder, Kristina M. Gruevski and Peter J. Keir
McMaster Occupational Biomechanics Laboratory, McMaster University, Hamilton, ON
email: hodderjn@mcmaster.ca

INTRODUCTION

Fifty percent of industrial manual materials handling tasks involve pushing or pulling tasks but little research has examined them [1, 2]. Previously, these tasks have been examined by hand forces, foot centre of pressure and trunk electromyography (EMG)[2]. Typically, tasks (trials, jobs) have been evaluated as a whole, however, there has been a recent interest in the cyclic aspects of tasks [3]. Madeleine et al (2008) subdivided trials into work to rest ratios of kinematic and average EMG (AEMG) data. They noted lower work to rest ratio variability in muscle activity in the presence of pain [3]. Additionally, tasks with external constraints on time or posture have been seen to increase muscle activity to perform that task [3]. The purpose of this study was to examine the effect of externally modulated and self paced task frequencies on uni- and bimanual pushing tasks using a novel cycle to cycle approach.

METHODS

Fifteen females (23.8 ± 7.7 years, 163.8 ± 5.8 cm, 61.2 ± 11.2 kg) participated after giving informed consent. Participants performed a series of pushing tasks which included, unilateral, bimanual and reciprocating on a dual track apparatus which had two handles that moved independently, or be tethered together. Five pushing tasks were performed (Table 1). These tasks were each performed at 15 and 30 cycles per min (cpm), and a self selected pace, for a total of 15 tasks.

Table 1: Summary of pushing tasks performed.

Task	Frequency		
	15/min	30/min	Self
Bimanual Tethered	x	x	x
Bimanual Un-Tethered	x	x	x
Reciprocating	x	x	x
Reciprocating Cont.	x	x	x
Unilateral	x	x	x

A mass of 2 kg was applied to each handle. Eight channels of electromyography (EMG) included the anterior deltoid (AD), middle deltoid (MD), posterior deltoid (PD), pectoralis major (PM), right and left trapezuis (RT & LT), right and left external oblique (REO & LEO). Linear potentiometers, located on both tracks recorded the displacement of each handle.

Full trial means, peaks, minimums and standard deviations (SD) were calculated for each muscle and potentiometer. Muscle activity was normalized to maximum voluntary excitation. Tasks were further analyzed on a cycle by cycle basis, subdivided into work (with push and return phases) and rest cycles. Coefficients of variation (COV= SD/mean), and crest factors (CF= peak/mean), were calculated for the overall tasks, and each phase of the cycle (work, rest, push and return). A repeated measures ANOVA was used for analysis.

RESULTS AND DISCUSSION

Overall, significant differences in muscle activity were found due to task, frequency and their interaction. In particular, upper extremity muscle activities were significantly lower in the 15 cpm trials than in the 30 cpm and self selected paces. COV for all upper extremity muscles were the largest at 15 cpm, except for the continuous task.

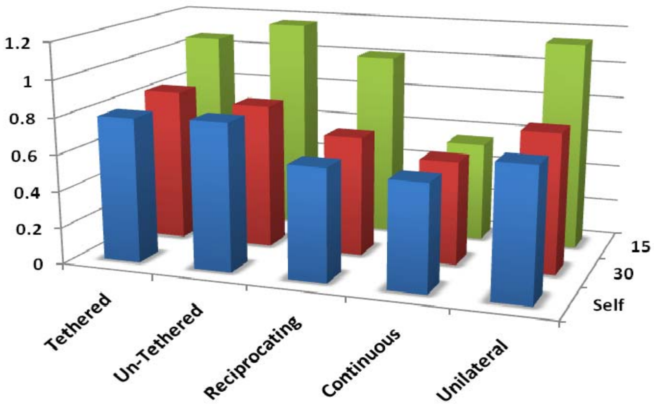

Figure 1: COV of anterior deltoid for entire trial.

Similar patterns were also seen for the 30 cpm and self selected frequencies, and were paralleled with CFs. These results reflect the increased variability (or range) introduced by the rest in the slower trials and notably absent in the more continuous trials.

A goal of the current study was to analyze specific aspects of the cycle. Cycles were defined in terms of work and rest. Work periods were subdivided into push and return phase (Fig. 3). Work was defined at the time in which the right handle was moving with forward being the "push" phase and negative displacement being the "return" phase.

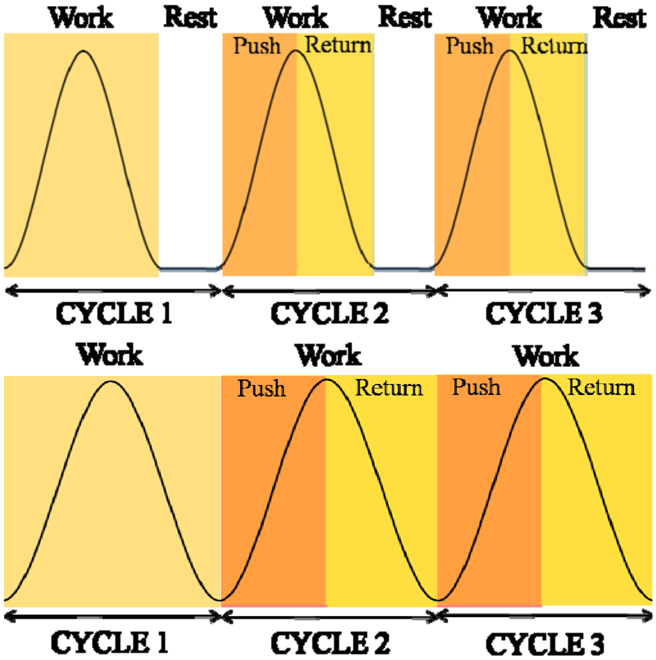

Figure 2: Schematic of the trials with rest (top) and trials without rest (bottom).

Although time was constrained with a metronome to start pushing, no signal was given to begin the return phase. Work time was most variable at 15 cpm, as participants took a longer return phase than other frequencies. Interestingly, there were very few rest phases found in many of the 30 cpm and self selected trials.

Cycle to cycle analysis of muscle activity revealed different statistical differences than were found across the trial as a whole. When examining the work phase, unlike the full trial means, the PM was the only muscle that demonstrated a significant effect of task, frequency and the interaction of both. The PM, RT, LT, REO and LEO muscle activities during the return phase had significantly greater activity for both 30cpm and self selected paces. As expected, shoulder muscle activity was greatest in the push phase at all frequencies.

The COV for each phase also differed from the full trials. For example, the AD had lower COV during both reciprocating and continuous tasks (Fig. 3). The lack of variability seen overall during continuous tasks may not just be due to the lack of rest in these trials, but as well due to the reciprocating technique itself.

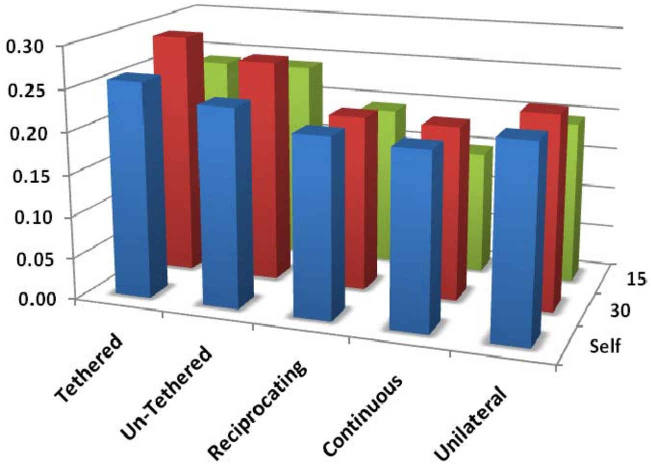

Figure 3: COV of anterior deltoid of push phase.

When examining repetitive work, overall trial means may not provide a complete analysis of the task. Recently, Madeline et al (2008) examined repetitive tasks on a cycle to cycle basis and found work to rest ratios were less variable in participants experiencing pain compared to those without pain [3]. In addition, variability of different aspects of the task may provide additional insights to experience and injury. The current investigation aimed to further develop cycle to cycle analysis using a novel approach of assessing specific cycle phases and their variability.

REFERENCES

1.Baril-Gingras & Lortie. *Ergo* **58**, 905-925, 2005.
2.Granata & Bennett. *Human Factors* **47**(3), 536-549, 2005.
3.Madeleine, et al. *Ergo* **51**(7), 1078-1095, 2008.

ACKNOWLEDGEMENTS

This study was funded by NSERC Discovery Grant # 217382-04.

THE EFFECTS OF MODEL DEGREES OF FREEDOM AND MARKER WEIGHT ON RESULTANT HIP KINEMATICS IN OPENSIM

[1] Julie A. Thompson, [1,2]Ajit M.W. Chaudhari and [1,2]Robert A. Siston
Departments of [1]Mechanical Engineering and [2]Orthopaedics, The Ohio State University
email: thompson.1288@osu.edu

INTRODUCTION

Dynamic simulations of movement are useful tools for studying how the neuromuscular and musculoskeletal systems interact to produce coordinated movement. These simulations commonly use motion capture data as input, but frequently the complexity of the model, including parameters such as the degrees of freedom (DOF) of certain joints, is chosen by the user and may not match the same degrees of freedom used by the motion-capture software.

OpenSim is an open-source software package that was developed for the purpose of creating and analyzing musculoskeletal models and dynamic simulations of movement [1]. The software computes kinematics using a least squares approach to minimize the difference between experimental marker location and virtual markers on the model while maintaining joint constraints [1]. However, this approach presents a challenge when creating musculoskeletal simulations from gait data. Since there is no set of established "rules" on how to weigh the markers, what is the effect on resultant kinematics of choosing different weights?

The purpose of this study was to use a simple model, looking only at the motion of the hip, to investigate how marker weights and choice of model DOF affect kinematics and to compare the kinematics with the same results from a common motion capture analysis technique.

METHODS

Gait data was obtained for 1 healthy subject while walking at a self-selected speed in our motion analysis laboratory using a Vicon motion capture system. The experimental kinematics of the femur were measured using the Point-Cluster Technique [2], and a functional hip joint center (fHJC) was obtained by having the subject trace out a star-arc pattern with a straight leg [3].

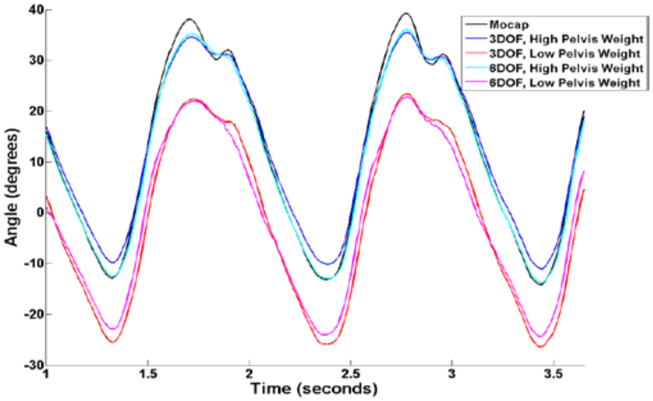

Figure 1: Hip flexion angle for differential marker weighting on 3-degree-of-freedom hip and 6-degree-of-freedom hip.

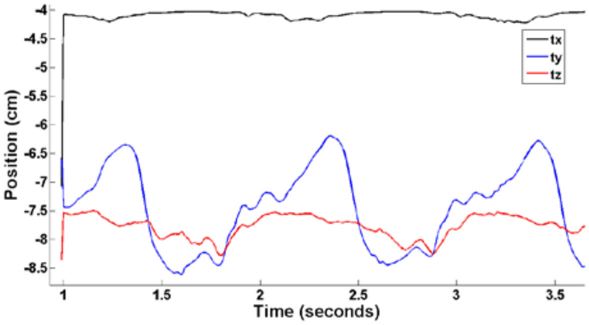

Figure 2: Hip translations in the sagittal (tx), frontal (ty), and transverse (tz) planes.

Using custom scripts in Matlab and Vicon Bodybuilder, joint angles between the femoral coordinate system and the pelvic coordinate system were calculated using a standard Euler method (Mocap results).

A generic musculoskeletal model of only the pelvis and left femur was scaled in OpenSim using static calibration data obtained in the gait laboratory. We systematically adjusted the static pose weights for the markers on the pelvis, greater trochanter, femur, and a virtual marker that represented the fHJC.

The inverse kinematics problem was then solved using the same weights as the scaling procedure, including 4 markers that represent the centroid and principal axes of the cluster of 10 femoral markers. 28 solutions of the inverse kinematics problem were calculated; 16 with equal weighting on all markers of 1, 10, 100, or 1000 and 12 with differential weighting. For differential weighting, the pelvis marker weights were fixed at 1 or 1000 while the markers on the leg were varied. 8 of the equal weight trials used the fHJC while the other 8 did not. We used a 3 DOF hip model for 14 of the trials, which is commonly used in OpenSim, then released the translational constraints for the other 14 (6 DOF model). The resultant maximum and minimum hip angles in the sagittal, frontal, and transverse planes (OpenSim results) were compared amongst trials and with the Mocap results.

RESULTS AND DISCUSSION

Resultant kinematics did not change in a given model when all markers were given equal weighting (Trials 1-16, Table 1). For a given series of trials (e.g. 1-4) all angles were within one-tenth of a degree. However, differential weighting led to large differences. The resultant OpenSim kinematics were closest to the Mocap results when the pelvis markers were weighted highly (Figure 1). Hip flexion angles matched most closely when using the fHJC than when not using it, which may have been expected.

While using a 6 DOF hip model in OpenSim resulted in kinematics that more closely matched the Mocap results than a 3 DOF hip model, we noticed large translations of the femoral head (Figure 2). The average sagittal plane (tx) translation was 1.4 mm, after the femoral head jumped anteriorly about 3 cm. The average frontal plane (ty) translation was 2.17 cm and the average transverse plane (tz) translation was 8.9 mm. The 6 DOF hip model with differential weighting and a high pelvis weight resulted in kinematics that most closely matched the Mocap results for hip flexion and adduction. No trial was able to closely replicate internal/external rotation.

CONCLUSIONS

The purpose of this study was not to determine whether OpenSim or motion capture provided the “right” or “wrong” kinematic result. Instead, this work illustrates the need for researchers to carefully establish marker weights in OpenSim and to select the appropriate model specific to the questions he or she seeks to answer.

REFERENCES

1. Delp, S.L., et al. *IEEE Transactions on Biomedical Engineering* **54**, 1940-1950, 2007.
2. Andriacchi, T.P., et al. *Journal of Biomechanical Engineering* **120**, 743-749, 1998.
3. Camomilla, V., et al. *Journal of Biomechanics* **39**, 1096-1106, 2006.

ACKNOWLEDGEMENTS

The authors thank Jeff Reinbolt for all of his helpful advice and suggestions concerning OpenSim.

Table 1: Summary of the effect of marker weight and model degrees-of-freedom on peak hip angles.

Trial	Hip DOF	Marker Weights				Hip Flexion (°)		Hip Adduction (°)		Hip Rotation (°)	
		Pelvis	HJC	Femur	Cluster	Max	Min	Max	Min	Max	Min
1-4	3	1,10,100,1000	1,10,100,1000	1,10,100,1000	1,10,100,1000	29.3	-20.8	14.0	-9.4	24.9	8.3
5-8	6	1,10,100,1000	1,10,100,1000	1,10,100,1000	1,10,100,1000	33.9	-14.4	12.2	-7.2	21.6	3.7
9-12	3	1,10,100,1000	No	1,10,100,1000	1,10,100,1000	28.0	-22.1	14.2	-10.0	24.3	8.1
13-16	6	1,10,100,1000	No	1,10,100,1000	1,10,100,1000	27.7	-20.3	12.2	-7.0	16.0	-2.0
17	3	1	10	10	10	24.5	-25.6	15.6	-11.7	20.6	1.5
18	3	1	100	100	100	23.5	-26.4	16.0	-12.2	19.2	-0.2
19	3	1	1000	1000	1000	23.4	-26.4	16.0	-12.2	19.0	-0.4
20	3	1000	1	1	1	37.8	-7.5	12.3	-5.6	27.0	16.6
21	3	1000	10	10	10	37.6	-7.9	12.3	-5.7	27.0	16.5
22	3	1000	100	100	100	35.5	-11.1	12.5	-6.5	26.6	15.2
23	6	1	10	10	10	32.7	-15.2	12.1	-7.3	21.5	3.0
24	6	1	100	100	100	32.4	-15.3	14.8	-3.9	20.7	4.0
25	6	1	1000	1000	1000	22.7	-24.4	12.8	-11.7	42.1	20.5
26	6	1000	1	1	1	36.8	-13.6	12.4	-7.0	22.4	5.1
27	6	1000	10	10	10	36.7	-13.8	12.3	-7.0	22.1	4.9
28	6	1000	100	100	100	36.0	-13.9	12.3	-7.0	21.9	4.7
Mocap						39.2	-14.2	12.4	-7.5	5.4	-12.7

EVALUATION OF GLENOHUMERAL MUSCLES DURING PROVOCATIVE TESTS DESIGNED TO DIAGNOSE SLAP LESIONS

[1]Vanessa Wood, [1]Michelle Sabick, [1]Ron Pfeiffer, [1]Seth Kuhlman, [1]Jason Christensen,
[2]Mike Curtin, [2]Kurt Nilsson, and [2]Kevin Shea
[1]Center for Orthopaedic & Biomechanics Research, Boise State University,
[2]Intermountain Orthopaedics

INTRODUCTION

Despite considerable advances in the understanding of glenohumeral (GH) biomechanics and glenoid labral pathologies, arthroscopy remains the only definitive means of SLAP lesion diagnosis [3]. Unfortunately, natural GH anatomic variants limit the reliability of radiographic implications [2]. Accurate clinical diagnostic techniques would be advantageous due to the invasiveness, patient risk, and financial cost associated with arthroscopy. More than 20 provocative tests designed to elicit labral symptoms as a diagnostic sign have shown promising accuracy by their respective original authors, but follow-up studies generally fail to reproduce those findings. The purpose of this study was to compare the behavior of GH joint stabilizing muscles in seven promising provocative tests. Electromyography (EMG) was used to characterize the activation of GH joint stabilizing muscles, with particular interest in the long head biceps brachii (LHBB) behavior, as activation of the LHBB and subsequent tension in the biceps tendon should illicit labral symptoms in SLAP lesion patients [2].

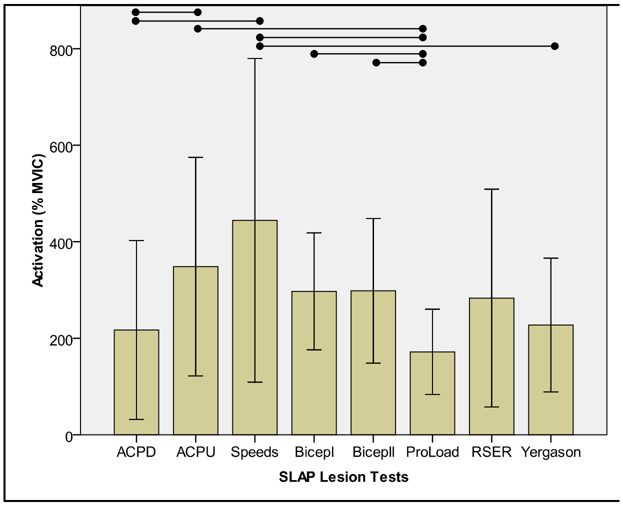

Figure 1: Muscle activation of the SLAP tests.

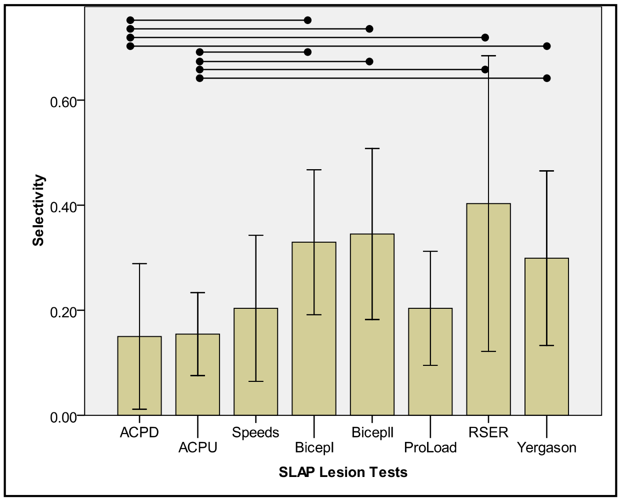

Figure 2: Muscle selectivity of the SLAP tests.

METHODS

A cohort of 21 healthy volunteers without a history of shoulder pathology was recruited for this study (11 females, 10 males). The tests analyzed were Active Compression palm up and palm down (ACPU and ACPD) [8], Speed's [1], Pronated Load (ProLoad) [9], Biceps Load I (Bicep I) [6], Biceps Load II (Bicep II) [5], Resisted Supination External Rotation (RSER) [7], and Supination Sign (Yergason's) [10]. The tests were modified to be performed on a Biodex System II Dynamometer (Biodex Medical Systems, Shirly, NY) to improve reproducibility. EMG was used to record muscle activity for muscles surrounding the right GH joint, the long and short heads of the biceps brachii (LHBB and SHBB), anterior deltoid (DELT), pectoralis major (PECT), latissimus dorsi (LAT), infraspinatus (INFRA), and supraspinatus (SUPRA). Due to the location of the SUPRA deep to the trapezius, a single 44-gage fine-wire indwelling electrode was inserted to monitor its activity, and for the remaining muscles bipolar Ag-Ag-Cl surface electrodes were positioned over the muscle belly and parallel with the orientation of the muscle fibers. EMG data were recorded at 1250 Hz (Noraxon USA, Inc, Scottsdale, AZ) and filtered with custom MATLAB software. The subjects performed three trials of each test, and the test data were normalized to a percentage of effort based on

MVIC data. Muscle activity for each test was characterized by two variables, activation and selectivity. Muscle activation was defined as the muscle's peak normalized EMG amplitude. Muscle selectivity was defined as the ratio of muscle activation for the muscle of interest over the sum of all seven muscles' peak activations. A repeated measures analysis of variance (ANOVA) was performed to identify significant differences among tests for each muscle. A pair-wise t-test post-hoc analysis was performed to compare results between tests using a p-value sliding scale Bonferroni adjustment [4]. A paired-sample t-test was used to assess variances in behavior (p=0.05) between male and female groups.

RESULTS

Each test elicited a variance in muscle activation and selectivity (p=.000). Each muscle demonstrated significant differences in muscle activation and selectivity for at least one of the pairs of tests with the exception of the LAT for both variables and the INFRA for selectivity. Specifically the LHBB had a significant difference (p=.000) in activity between tests (Figure 1). The LHBB had the greatest activation for ACPU, Speed's, Bicep I, and II without distinguishable differences in performance between them. ACPD and Yergason's and Bicep I and II were statistically equivalent in eliciting LHBB activation. Both ACPU and Speed's caused greater LHBB activation than ACPD, ProLoad, and Yergason's. Bicep I and II caused greater LHBB activity than ProLoad, while ACPD had the weakest performance. LHBB selectivity results for the tests proved similar to those for muscle activation, where each test produced a variance in muscle selectivity (p=.000) (Figure 2). Bicep I and II produced the greatest LHBB selectivity of the group, performing better than ACPU, ACPD, ProLoad, and Speed's. Yergason's was also highly selective, performing better than ACPU and ACPD respectively. Bicep I and II, ACPU and ACPD, and Speed's and ProLoad were equivalent in selectively activating the LHBB, while ACPU and ACPD had the worst LHBB selectivity of the group. RSER did not have significant LHBB behavior, and no differences were seen between male and female groups (p >.05).

DISCUSSION

ACPU, Speed's, and Bicep I, and II elicited the largest LHBB activity, suggesting that during these tests more tension was applied to the bicep tendon. Bicep I and II were highly selective for the LHBB, which should reduce the number of potential sources for confounding results. Therefore in this study ACPU, Speed's, and Bicep I, and II had the greatest potential for clinical SLAP lesion detection. Interestingly, these four tests shared design patterns relating to location of the applied load, forearm orientation, joint position, and line of pull, and these characteristics may prove valuable for optimizing SLAP test design and performance. Each test required active resistance to a load that was applied perpendicular to the palm of the subject's hand. The load was resisted by either an isometric contraction (ACPU, Bicep I, and II) or by an isokinetic contraction (Speed's). The forearm was supinated in all cases due to either the 'palm up' position (ACPU and Speed's) or the 'curl' position (Bicep I and II). Each test applied the load in one of two joint positions that placed the LHBB and biceps tendon in a direct line of pull of the superior labrum. For ACPU and Speed's, the shoulder was flexed to a maximum of 90° with the elbow fully extended, and for Bicep I and II the shoulder was abducted at or above 90° with the elbow flexed at 90°. These unique test characteristics should be further evaluated to determine their role in SLAP test performance.

REFERENCES

1. Bennett, W.F., *Specificity of the Speed's Test: Arthroscopic Technique for Evaluating the Biceps Tendon at the Level of the Bicipital Groove.* Arthroscopy, 1998. **14**(8): p. 789-796.
2. DaSilva, J.J., A.G. McNickle, and B.J. Cole, *Arthroscopic Superior Labrum Anterior to Posterior Repair.* Operative Techniques in Orthopaedics, 2008. **18**(1): p. 53-61.
3. Dessaur, W. and M. Magarey, *Diagnostic accuracy of clinical tests for superior labral anterior posterior lesions: a systematic review.* Journal of Orthopaedic and Sports Physical Therapy, 2008. **38**(6): p. 341-352.
4. Holm, S., *A simple sequentially rejective multiple test procedure.* Scandinavian Journal of Statistics, 1979. **6**: p. 65-70.
5. Kim, S.-H., et al., *Biceps Load Test II: A Clinical Test for SLAP Lesions of the Shoulder.* The Journal of Arthroscopic and Related Surgery, 2001. **17**(2): p. 160-164.
6. Kim, S.-H., K.-I. Ha, and K.-Y. Han, *Biceps Load Test: A Clinical Test for Superior Labrum Anterior and Posterior Lesions in Shoulders With Recurrent Anterior Dislocations.* The American Journal of Sports Medicine, 1999. **27**(3): p. 300-303.
7. Myers, T.H., J.R. Zemanovic, and J.R. Andrews, *The Resisted Supination External Rotation Test: A New Test for the Diagnosis of Superior Labral Anterior Posterior Lesions.* The American Journal of Sports Medicine, 2005. **33**(9): p. 1315-1320.
8. O'Brien, S.J., et al., *The Active Compression Test: A New and Effective Test for Diagnosing Labral Tears and Acromioclavicular Joint Abnormality.* The American Journal of Sports Medicine, 1998. **26**(5): p. 610-613.
9. Wilk, K.E., et al., *Current Concepts in the Recognition and Treatment of Superior Labral (SLAP) Lesions.* Journal of Orthopaedic and Sports Physical Therapy, 2005. **35**: p. 273-291.
10. Yergason, R.M., *Supination Sign.* 1995.

ASYMMETRY IN JOINT WORK OF HEALTHY PARTICIPANTS DURING LANDING

Michael Wortley, Songning Zhang, and Daniel Carson
The University of Tennessee, Knoxville
e-mail: mwortley@utk.edu

INTRODUCTION

It has long been known that human movements are not perfectly symmetrical, but 2-D methodologies often necessitated that bilateral symmetry be assumed. Some studies have investigated the symmetry of populations that could not be assumed to be symmetrical, such as patients with unilateral arthritis or joint replacements [1], but few studies have examined the symmetry of healthy populations. In studies that have used healthy subjects, studies employing a single subject design have concluded that there were asymmetries present while studies which have pooled the measurements of a group of subjects have often concluded that the subjects were symmetrical [2]. Due to the variety of movements studied and methodologies used in these studies, there currently is no consensus on what is considered normal symmetry in able-bodied people.

Bilateral landing is well suited to the study of asymmetry because it is a simple, reproducible movement in which perfect symmetry is the default assumption. The work done at each joint is primarily eccentric, and since joint work is additive it lends itself well to computing symmetry index variables. Therefore, the purpose of this study was to describe the symmetry of healthy participants during drop landing using joint work as the criteria.

METHODS

Sixteen right-leg dominant recreational athletes (8 male, 8 female, 22±3.6 years, 180.0±8.0 cm, 70.7±12.6 kg) with no history of major lower extremity injury were recruited for this study. All participants had a measured leg length discrepancy of less than 1 cm [3]. During data collection, participants performed a maximum vertical jump (MVJ), followed by 5 drop landings from an overhead bar at each of two heights (30cm and 60cm). A 7-camera motion analysis system (Vicon) was used to record 3D kinematics at 240 Hz. Two force platforms (AMTI) recorded the ground reaction forces at 1200 Hz. Joint power was computed in component form for the ankles, knees, and hips of each leg using Visual-3D software (C-Motion, Inc), and the sagittal plane component of the joint powers (P_J) were integrated to compute joint work.

Landing was considered to begin the first moment either foot touched the force platform (t_i) and end the moment the center of mass reached its lowest point (t_f). The work done by each joint was summed to compute the total work done by the right leg (TW_R) and left leg (TW_L). The symmetry index (SI_{TW}) was determined using Equation 1 [4].

$$SI_{TW} = \frac{(TW_R - TW_L)}{(TW_R + TW_L)} \qquad \textbf{(1)}$$

In order to see how the amount of work done by each leg varied through time, the work was computed in discrete intervals for right leg (DW_R) and left leg (DW_L) using Equation 2. The peak value of [$DW_R(t)$ - $DW_L(t)$] was ΔW_{peak}, and the time at which that occurred was $t_{\Delta Wp}$. A symmetry index at $t_{\Delta Wp}$ ($SI_{\Delta Wp}$) was calculated using Equation 3.

$$DW(t) = \sum_J \int_{t-\left(\frac{1}{240}\right)}^{t} P_J \, dt \, , t_i < t \le t_f \qquad \textbf{(2)}$$

$$SI_{\Delta Wp} = \frac{\Delta W_{peak}}{[DW_R(t_{\Delta Wp}) + DW_L(t_{\Delta Wp})]} \qquad \textbf{(3)}$$

TW_R and TW_L were compared to one another in a 2x2 (side x landing height) repeated-measures ANOVA ($p < 0.05$). SI_{TW}, ΔW_{peak}, $t_{\Delta Wp}$, and $SI_{\Delta Wp}$ were compared between landing heights using a one-way ANOVA. Regression models were fitted to SI_{TW} and $SI_{\Delta Wp}$ beginning with a fully saturated model containing landing height, MVJ, gender, mass, and the difference in touchdown time between the right and left legs (ΔT_{TD}) as explanatory variables. The least significant terms were removed sequentially until a final hierarchical model with all remain terms significant at an $\alpha = 0.05$ level was found.

RESULTS AND DISCUSSION

MVJ of the participants ranged from 25.7 to 68.1 cm, and ΔT_{TD} ranged from -8.4 to 16.8 ms, with positive values indicating that right foot touched down first.

TW_R and TW_L were significantly different from one another within subjects ($p<0.0001$, Table 1), and the landing height had no effect on this relationship (side x landing height p=0.9629). Using SI_{TW} as a criteria, the participants were significantly more asymmetric when landing from 30 cm than from 60 cm (p=0.0002). However, referring to Table 1 and equation 1, it is clear that the lower SI_{TW} at 60 cm was not due to a reduced difference between TW_R and TW_L, but due to the greater amount of work that must be done to land from the higher height.

Table 1: Mean values of total work done by the left and right legs and symmetry index (mean ± STD).

Landing Height	TW_R (J)†	TW_L (J)	SI_{TW}
30 cm	-147.5 ± 48.4	-92.5 ± 19.4	0.22 ± 0.10‡
60 cm	-251.8 ± 74.1	-196.0 ± 44.7	0.12 ± 0.08

† - Significantly greater than TW_L ($p<0.0001$)
‡ - Significantly greater than 60 cm (p=0.0002)

Mean values of ΔW_{peak} and $t_{\Delta Wp}$ were 4.5 ± 3.1 J and 56.2 ± 12.6 ms for landings form 30 cm, and 7.8 ± 4.1 J and 41.1 ± 15.1 ms for landing from 60 cm. Both variables were significantly different between landing heights ($p<0.0001$ for ΔW_{peak} and p=0.0002 for $T_{\Delta Wp}$). $SI_{\Delta Wp}$ was not significantly different between landing heights (mean 0.38 ± 0.16, p=0.57), indicating that at time $t_{\Delta Wp}$ participants performed 38% more work with the right leg than the left leg regardless of the landing height.

The final regression model for SI_{TW} ($R^2 = 0.67$, $p<0.0001$) contained terms for landing height, MVJ, ΔT_{TD}, and a MVJ x ΔT_{TD} interaction. In participants with a greater MVJ, SI_{TW} was very sensitive to changes in ΔT_{TD}, but this effect was not present for subjects with a small MVJ (Figure 1). This suggests that greater leg strength may allow participants to land with greater asymmetry.

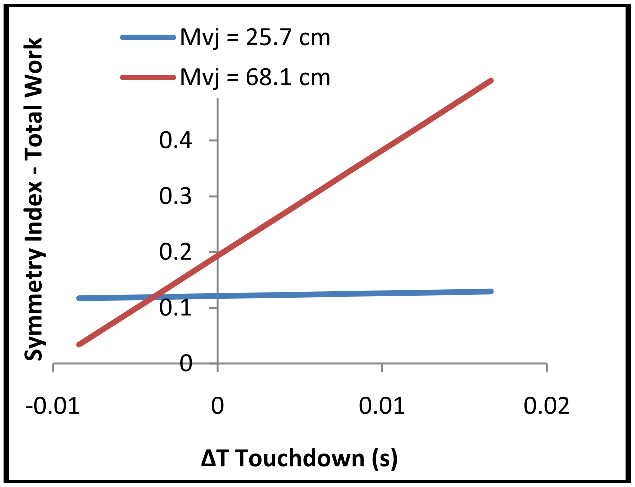

Figure 1: Interaction plot showing how SI_{TW} is related to M_{VJ} and ΔT_{TD}.

The final regression model for $SI_{\Delta Wp}$ ($R^2 = 0.56$, $p<0.0001$) contained only ΔT_{TD} as a significant factor such that $SI_{\Delta Wp}$ increased linearly as ΔT_{TD} increased. Asymmetry at time $t_{\Delta Wp}$ appears to be closely related to the initial conditions of landing.

CONCLUSIONS

Although the participants had no expectation of asymmetry, they did exhibit systematic asymmetry in the pattern of work performed during landing. All participants had a moment of peak asymmetry approximately 50 ms after touchdown that was closely related to the difference in contact times between the feet. After that point, participants with greater vertical jumping ability tended to remain asymmetrical while the participants with less jumping ability tended towards greater symmetry. More research is needed to determine if this is a natural characteristic of the way healthy people land or an artifact of landing in the lab environment.

REFERENCES

1. Milner, CE. *Gait Posture* **28,** 69-73, 2008.
2. Schot, PK, et al. *Med Sci Sports Exerc* **26,** 1153-9, 1994.
3. Beattie, P, et al. *Phys Ther* **70**, 150-7, 1990.
4. Borden, LS, et al. *Gait Posture* **9,** 24-30, 1999.

FATIGUE EFFECTS ON SLIP RISK WHILE WEARING FIRE-PROTECTIVE EQUIPMENT

[1]Alison L. Sukits, [1]Jenna D. Montgomery, [2]Pui Wah Kong, [2]David Hostler, [2]Joe Suyama, [1]Rakié Cham,
[1]April J. Chambers
[1]Department of Bioengineering, University of Pittsburgh, Pittsburgh, PA, USA
[2]Department of Emergency Medicine, University of Pittsburgh, Pittsburgh, PA, USA
email: Alison.L.Sukits@gmail.com, web: http://hmbl.bioe.pitt.edu

INTRODUCTION

In 2006, over 10,000 firefighter injuries resulted due to slips and falls, accounting for approximately 25% of all fireground injuries [1]. Fire-protective equipment has been shown to negatively impair postural balance by increasing sway length and sway area [2].

After experiencing a slip or anticipating a slippery surface, subjects have been shown to alter their gait. Several ways this is accomplished is by reduced stance duration, normalized stride length, and angular foot velocity at heel contact [3]. Additionally, subjects alter their gait by reducing their peak required coefficient of friction (RCOF) after a slip or when anticipating a slippery surface. These changes have been shown to reduce slip risk [3-6].

Fatigue has also been shown to alter gait and slip risk. Specifically, previous research has found that following induced quadriceps fatigue, subjects increased their RCOF, thus increasing their slip risk [4,5]. It was found that this increased risk of slipping may result in a higher incidence of falls due to fatigue [5]. Additionally, studies have shown that postural sway increases after fatigue, leading to increased fall risk [7,8].

It is possible that combining fatigue and fire-protective equipment will result in even greater disturbances in balance and gait. The goal of this study was to determine the effect of fatigue on slip risk while wearing fire-protective equipment.

METHODS

Six male subjects (mean age 28.2 ± 6.4 years, height 1.77 ± 0.06 m, mass 83.3 ± 5.4 kg), screened for adequate physical abilities, participated in this study. Each wore a heart rate monitor and fire protective gear including: fire resistant pants and coat, steel toe boots, Nomex hood, heavy gloves, polycarbonate helmet, self-contained breathing apparatus, and facemask.

Subjects, carrying a 6.8 kg bar to mimic an axe, walked at a self-selected pace across a vinyl tile walkway. Ground reaction forces and whole body motion were sampled at 1080 and 120 Hz, respectively. The subjects performed five baseline dry walking trials (BD). Without the subjects' knowledge, a glycerol solution (glycerol-water ratio of 75:25) was applied at the left/leading foot-floor interface, generating an 'unexpected slip'.

Subjects were then randomized into two groups, fatigue or rest. Subjects in the fatigue group experienced a 20 minute fatigue protocol. Fatigue consisted of carrying the bar up and down two flights of stairs, dragging a 29 kg dummy backwards, performing a 12 lb bucket pull for one minute at 90 bpm, and resting for two minutes. Repetitions were performed for the 20 minute period. All subjects exceeded 85% of age predicted heart rate maximum during the fatiguing period. Following fatigue, subjects performed 10 recovery dry walking trials (RDF). This was followed by an 'unexpected slip' on the 11th trial. Subjects then underwent a 20 minute seated rest period. Another 10 recovery dry trials (RDR) and a third slip on the 11th trial were collected. Subjects in the rest group underwent the same protocol except they experienced the rest period first and the fatigue period second.

The variable of interest was peak RCOF for BD, RDF and RDR. Peak RCOF was calculated using the ratio of force in the anterior-posterior direction to the normal force. The maximum value during 10-30% of the stance was selected for analysis [6].

A within-subject ANOVA was performed with the independent variable of condition (baseline, fatigue, rest) and dependent variable RCOF. An alpha value of 0.05 was used.

RESULTS AND DISCUSSION

Condition was significant for peak RCOF (p=0.0006). Following rest or fatigue, subjects were able to significantly decrease their peak RCOF compared to baseline walking (Figure 1). Additionally, peak RCOF values after rest were significantly lower than after fatigue.

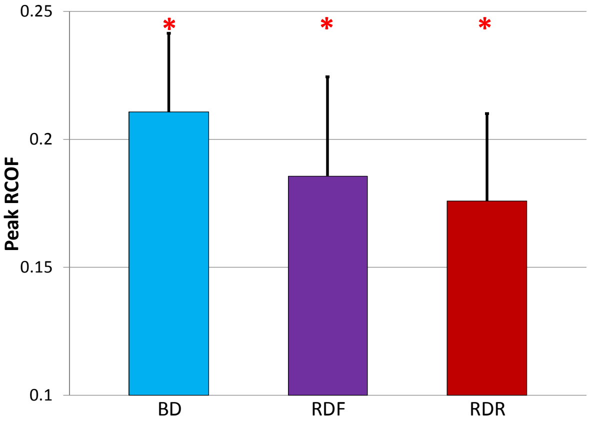

Figure 1: Mean peak RCOF for each condition. Standard deviation bars are provided. * Denotes significance between all conditions.

It is difficult to distinguish between anticipation and fatigue. Previous research has shown that following a slip subjects alter their gait when anticipating a slippery surface. Specifically, subjects lower their peak RCOF. This is thought to lower the risk of experiencing another slip. [3-5]. Similarly, it was found here that subjects lowered their peak RCOF following the first slip regardless of fatigue group. This reduction puts them at a lower risk of slipping. [3].

Interestingly, there was a significant difference between rest and fatigue. Following fatigue, although subjects lowered their peak RCOF compared to BD, they were not able to lower it as much as following rest. These findings suggest that even with the potential presence of slip anticipation, fatigue effects may prevent firefighters from maximally reducing their risk of slipping. An increased risk of slipping following fatigue has been noted previously. Parijat et al. found that RCOF increased following fatigue. This increase in RCOF translates to an increase in slip risk [4,5].

It is important to note that our fatigue protocol consisted of full-body fatigue similar to an occupational setting whereas, Parijat et al. only fatigued the quadriceps group [4,5]. Additionally, a potential limitation of our experimental design is the challenge of teasing out fatigue and anticipation effects. It is also possible that we are limited by a small sample size and unknown effects of fire-protective equipment during gait and slipping [2]. With the results presented, RCOF values indicate that following fatigue, subjects were at a higher risk of slipping.

CONCLUSION

It was found that subjects lowered their peak RCOF following the first slip. This reduction puts them at a lower risk of slipping. Following fatigue, subjects were not able to lower peak RCOF as much as following rest. These findings suggest that even with the potential presence of slip anticipation, fatigue effects may prevent firefighters from maximally reducing their risk of slipping.

REFERENCES

1. Karter, M.J. et al. *NFPA Journal*. 2007; 101(6):84-89.
2. Punaxallio A. et al. *Aviat Space Environ Med*. 2003; 74 (11):1151-1156.
3. Cham, R et al. *Gait and Posture*. 2002; 15:159-171.
4. Parijat P, et al. *Gait and Posture*. 2008; 28(4):568-573.
5. Parijat P, et al. *Ergonomics*. 2008; 51(12): 1873-1884.
6. Redfern M, et al. *Ergonomics*. 2001; 44(13):1138-1166.
7. Hsiao H, et al. *Ergonomics*. 2001; 44(5): 537-61.
8. Nardone A, et al. *Electroencephalogr Clin Neurophysiol*. 1997; 105(4): 309-20.

CENTER OF MASS POSITION DURING REPEATED EXPOSURE TO FORWARD AND BACKWARD SLIPPING

Brooke Coley[1] and Rakié Cham[1]

[1]Human Movement and Balance Laboratory, Department of Bioengineering
University of Pittsburgh, Pittsburgh, PA, USA
Email: bcc4@pitt.edu, web: www.hmbl.bioe.pitt.edu

INTRODUCTION

Center of mass (COM) control is critical to the maintenance of balance when perturbed. In contrast to an exposure to an unexpected balance perturbation, i.e. a slip, proactive postural adjustments, e.g. repositioning of the COM, are made when the perturbation is anticipated in an attempt to increase stability and to reduce the likelihood of falling [4]. It is known that older adults are capable of increasing their stability through proactive postural adjustments to the COM state when repeatedly exposed to a slipping perturbation [6,7]. Other studies have also described COM adaptations in young adults to be impacted by both experience with and knowledge of a slip perturbation [4,5].

To date, potential associations between (healthy) aging and the ability to generate proactive postural adjustments when balance is challenged during a novel gait task has not yet been investigated. Successful balance maintenance during walking requires the ability to adjust postural responses to various environmental and task constraints. Changing the direction of locomotion is one way to vary task constraints and research supports that forward and backward walking are run from the same motor program [2,8]. This facilitates comparison between familiar (forward gait) and novel (backward gait) walking activities to describe abilities to generate postural responses when balance is challenged. The purpose of this study is to investigate differences in anticipatory postural strategies when repeatedly exposed to slipping perturbations between the two gait activities. Adaptations to whole body COM position with respect to the ankle of the slipping foot fifty milliseconds pre-slip will be compared for both young and older adults in an unexpected and when repeatedly exposed to the same slip perturbation.

METHODS AND PROCEDURES

Eleven young (22-35 years old) and eight healthy older (65-74 years old) subjects, screened for neurological and musculoskeletal abnormalities, were recruited for participation. Subjects were first asked to walk on known dry floors to retrieve baseline forward and backward gait characteristics. In each walking direction, presented in a random order, the slipping protocol included 2 conditions: (1) unexpected slip (subject unaware of the slippery condition and expecting a dry condition) (2) 5 repeated slips (subject aware of the slippery condition). Only the 1st and 5th repeated slips were included in this analysis. The slips were induced at foot contact with a glycerol solution. Whole body motion data were collected at 120 Hz. Segment masses and moments of inertia were determined as per deLeva [1]. Anterior-posterior (AP), medial-lateral (ML) and vertical COM position with respect to the ankle at foot contact were the dependent variables in a mixed model ANOVA with subject as a random effect; trial within direction (unexpected slip (UWS), repeated slip 1 (RWS1) and repeated slip 5 (RWS5)), age group (young/older), direction (forward/backward gait), and the interaction of these terms as fixed effects. Significance was set at $\alpha = .05$.

RESULTS

The ML-COM position was significantly correlated with the interaction of age and direction ($p<.005$, Figure 1a). A reduction in the ML distance between the ankle and the COM was observed in the backward direction for older adults. A significant age x trial within direction effect on AP-COM was also found ($p<.05$, Figure 1b). Specifically, older adults decreased the distance between their ankle and AP-COM position by 24% by the 5th repeated slip compared to only 3% in younger adults. Trial within direction played a significant role in the vertical positioning of the COM ($p<.001$) (Figure 1c). Posthoc results showed the vertical COM to be located more superiorly in repeated slips 1 and 5 compared to the unexpected slip. Young and older adults similarly changed the vertical location of their COM with respect to the ankle. Vertical COM position was different between directions independent of age. The vertical COM averaged across groups was 82.7 cm and 76.7 cm in the forward and backward directions, respectively.

DISCUSSION AND SUMMARY

Older adults differed from younger adults in that they moved their ML-COM closer to the body in the backward direction and continued to decrease AP-COM position with repeated exposure in both directions. This may be due to the precautionary gait (i.e., shorter step length and decreased foot-floor angle) in anticipation of the slippery condition [4, 6]. Further analysis is necessary to determine whether natural differences in walking posture (i.e., slightly leaning forward while walking backward) play a role in the significance found in vertical COM position between directions.

Older adults were affected by task novelty as well as repeated exposure to the perturbation. The results indicate that older adults adapt the AP-COM similarly regardless of direction continuously attempting to reach an optimal strategy with repeated exposure. However, older adults were impacted by task novelty in the ML-COM responses. This may indicate ML-COM stability to be a focal point of proactive postural adjustments to maintain balance when unfamiliar with the gait task.

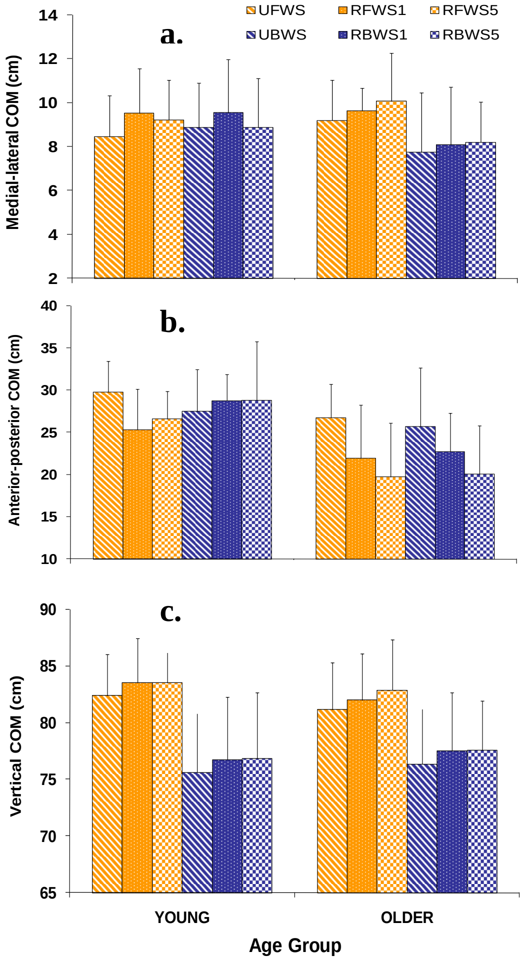

Figure 1. (a) Medial-lateral (b) anterior-posterior and (c) vertical COM position with respect to the ankle in young and older adults where orange indicates forward walking (F) and blue backward walking (B) trials. Trials within each direction are pictured with diagonal lines (U(F/B)WS - unexpected slip), dots (R(F/B)WS1 - repeated slip 1) and checkerboard (R(F/B)WS5 - repeated slip 5) patterns. Error bars represent standard deviations.

REFERENCES

1. deLeva P, *J Biomech* 29, 1223-30, 1996.
2. Duysens J, *J Neurophysioly* 76, 301-10, 1996.
3. Heiden TL, *Gait Posture* 24, 237-46, 2006.
4. Marigold DS, *J Neurophysiol* 88, 339-53, 2001.
5. Pai YC, et al. *Phys Ther* 87, 1478-91, 2007.
6. Pavol MJ, *J Gerontol Med Sci* 57A, M496-503, 2002.
7. Pavol MJ, *J Gerontol Med Sci* 59A, 484-502, 2004.
8. Winter DA, *J Mot Behav* 21, 291-305, 1989.

ACKNOWLEDGEMENTS

This study has been supported in part by F31 AG025684-03 NIH Ruth L. Kirschstein Award.

MIDTARSAL KINEMATICS DEFINED USING FINITE HELICAL AXES ANALYSIS

[1,3]Nori Okita, [3]Steven A. Meyers, [1]John H. Challis, and [1,2]Neil A. Sharkey
Departments of [1]Kinesiology, [2]Orthopaedics and Rehabilitation, and [3]Mechanical and Nuclear Engineering, The Pennsylvania State University, University Park, PA 16802, USA
Email: nas9@psu.edu; URL: http://www.biomechanics.psu.edu

INTRODUCTION

The midtarsal joint of the normal foot has been observed to display bimodal behavior during the stance phase of walking. The forefoot is reasonably flexible during weight acceptance to conform to terrain; upon heel rise and thereafter it increases stiffness to propel the body forward. This changeover from a flexible to a stiff construct is often referred to as the midtarsal joint locking mechanism, and the most logical and frequent explanation for its existence is non-synchronous migration of talonavicular and calcaneocuboid joint axes [1].

Recently Okita et al. [2] observed increased excursion of the midtarsal joints in concert with subtalar inversion and rapidly increasing forces in the plantarflexors during the last 40% of the stance phase, suggesting the existence of transverse tarsal joint locking mechanism.

The purpose of the current study was to characterize the internal midtarsal kinematics during simulations of normal gait using finite helical axes.

METHODS

Ten normal fresh frozen donated cadaver extremities (5M/5F, 59.2 ± 14.2 years) were evaluated. Dynamic simulations of the stance of gait were conducted by employing a robotic dynamic activity simulator at 1/20th the velocity of typical walking [3]. Tibia, talus, calcaneus, navicular, and cuboid were instrumented with marker clusters composed of four retro-reflective markers (6 mm dia.) connected by carbon fiber rods (0.16 mm dia.). Marker trajectories were recorded at 100 Hz using a seven-camera passive 3D photogrammetry system (Motion Analysis Corp, Santa Rosa, CA) with a typical 3D reconstruction residual of 0.3 mm. For each specimen, the simulation parameters were optimized by adjusting sagittal plane tibia kinematics and six muscle actuations (TA:Tibialis Anterior, TP:Tibialis posterior, PER:Peroneus longus, FHL:Flexor hallucis longus, FDL:Flexor digitorum longus, and TS:Triceps Surae) until target ground reaction forces (AMTI, Newton, MA) were attained. Data collection trials were repeated three times.

The marker data were smoothed using a dual-pass 4th-order Butterworth filter at 2 Hz cutoff frequency, and a least squares method [4] was employed to obtain homogeneous coordinate transformation matrices for each bone.

Finite helical axis parameters were obtained using the relative transformation of the distal bone with respect to the proximal bone [5]. Average unit vectors ($\underline{\mathbf{n}}$) along the helical axis between two bones for each specimen were obtained by dividing the ensemble average of the joint angles ($\varphi\underline{\mathbf{n}}$) with the angle of rotation (φ) about the helical axis. The across specimen average was obtained in similar manner.

RESULTS AND DISCUSSION

Qualitatively, bimodal behavior of the foot was observed. Figure 1 shows the superior, posterior, and medial view of the time progression of the unit vectrors of the helical axes for the a) transverse tarsal joints and b) calcaneotalar and cubonavicular joints.

In general, the orientation of the helixal axes changed throughout the stance phase. Prior to the foot flat at approximately 35% of stance phase, the joint axes, especially calcaneocuboid (Figure 1a), were rather randomly orientated in all planes, indicating the flexibility (laxity) of the joints, thereafter all unit vectors became more organized as the foot stiffened. The rotation axes between the given pair were non-parallel in at least in one plane at a given instant. Inflection of the axis orientation can be seen in most of profiles at approximately 25% and 65%, and 80%.

The correlation between the changes in helical axes directions and muscle and ground reaction force profiles are clearly seen in this study. Joints were loose during weight acceptance without plantarflexor muscle activity and with most of the ground reaction forces concentrated in the hindfoot. Inflections of the axes orientations at 25%, and 65% seem to be a delayed response to the first TS and TP activations at 20% and second TP activation at 60%, respectively. The inflection at 80% (especially in the cubonavicular joint) corresponded to the second ground reaction force peaks and peaks of all muscles except for the TA at 80%.

The foot is under considerable loading in late stance due to high ground reaction and muscle forces, resulting in a change of joint axes orientations resulting in increased geometrical constraint. Even with this increased constraint, some joints had notable excursions [2].

CONCLUSIONS

The orientations of the helical axes were seen to correspond well to externally applied forces.

Joint stiffness is controlled by the combined effects of muscle, and ground reaction forces, ligaments, and anatomical/geometrical constraints. It appears that the foot is utilizing all of the above effectively, allowing for the gradual change and/or maintenance of stiffness during different phases of stance.

The current data partially support the idea of a transverse tarsal joint locking mechanism. The talonavicular and calcaneocuboid joint axes remained non-parallel after foot flat as the stiffness of the foot increased, matching the classic description as presented in the literature [1]. However, prior to this stiffening stage, joint axes were not parallel to each other; they were rather randomly oriented due to the minimal constraints posed at the joints.

REFERENCES

1. Elftman H, Clin Orthop16, 41-46, 1960.
2. Okita N, et al. Transactions of the Orthopaedic Research Society, Las Vegas, NV, #394, 2009.
3. Hoskins AH PhD Dissertation The Pennsylvania State University, 2006.
4. Challis JH, J Biomech 28, 733-737, 1995.
5. Spoor CW & Veldpaus FE, J Biomech 13, 391-393, 1980.

a) talonavicular (--) and calcaneocuboid (--) joints

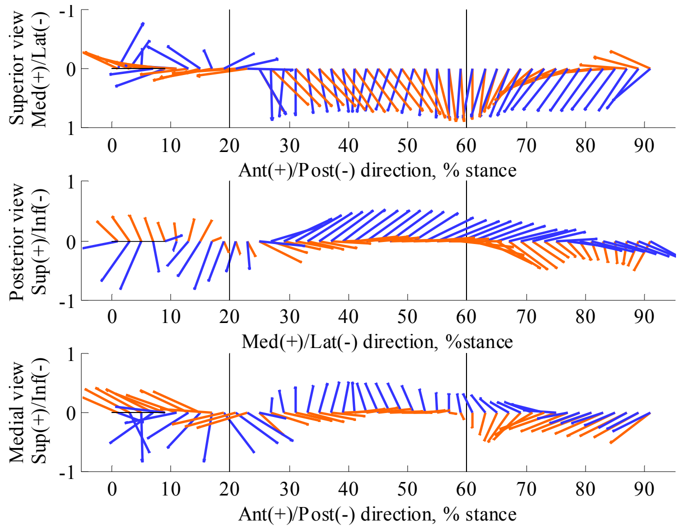

b) calcaneotalar (--) and cubonavicular (--) joints

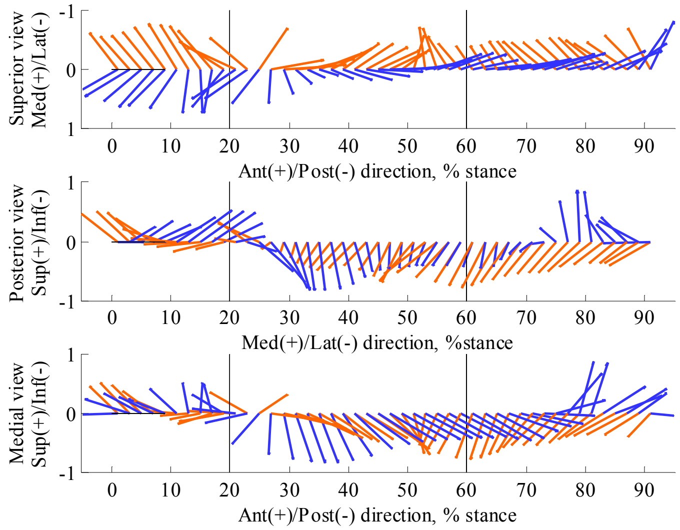

Figure 1: Progression of helical axis orientation during stance phase of gait for a) transverse tarsal joints, and b) calcaneotalar and cubonavicular joints. Mean profiles from ten specimens are shown. From the top to bottom in each group, superior, posterior, and medial views for a left foot is shown with the same scaling in all axes. Approximate muscle activations are indicated by the vertical lines at 20% for the TS and first TP activation, and at 60% for the second TP activation. Vertical ground reaction force and all muscles except for the TA peaked at 80% (in agreement with clinical data). Foot flat was observed between approximately 35~65% of stance.

ACKNOWLEDGEMENTS

NIH (5R03HD050532-02).

TRUNK AND LEG MUSCLE EMG AND PERCEIVED EXERTION DURING RESISTED TRUNK ROTATION EXERCISE

[1,2]Kelly R. Marbaugh, [2]Vijay K. Goel, [2]David Dick, [1]Danny M. Pincivero
[1]Human Performance and Fatigue Laboratory, Department of Kinesiology, [2]E-CORE, Department of Bioengineering, The University of Toledo
Email: danny.pincivero@utoledo.edu

INTRODUCTION

Due to the high prevalence of low back pain in otherwise healthy adults (1), modalities designed to strengthen and condition the trunk muscles have been primarily limited to actions involving sagittal plane trunk movements. As axial trunk rotation is often cited as a contributory mechanism to low back injury, few devices currently exist to assist exercise-related development of trunk rotation strength. The objectives of the present study were to develop, and provide initial validation of, a working prototype exercise device designed to provide graded resistance to standing trunk rotation. The initial level of validation was obtained by examining trunk and leg muscle activation, via the electromyogram (EMG), and ratings of perceived exertion (RPE).

METHODS

Prototype development

A fourth generation working prototype device (patent pending, 2) designed to provide resistance to trunk and pelvic axial rotation is pictured in Figure 1. The device provides adjustable resistance to 2 independently controlled attachments that secure a user's upper trunk and pelvic regions, while the user in a weight bearing position.

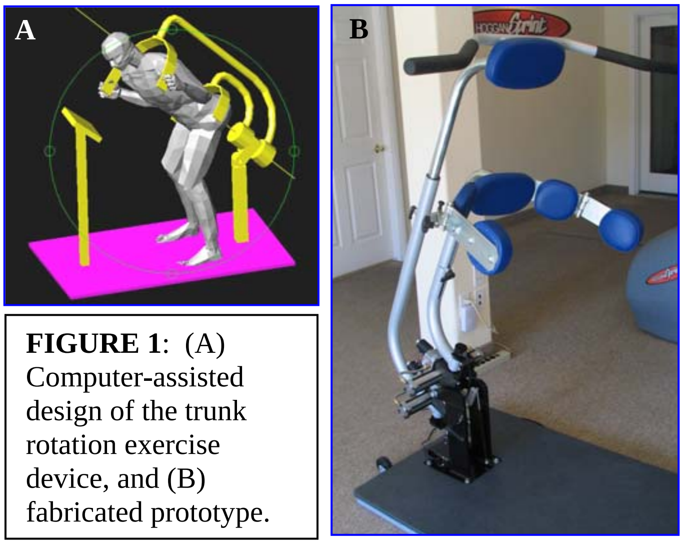

FIGURE 1: (A) Computer-assisted design of the trunk rotation exercise device, and (B) fabricated prototype.

The resistance to rotation is independently computer-controlled to the upper and lower attachments, and is provided by hydraulic linear actuators operating with a rack-and-pinion mechanism. The device was designed to provide 11 levels of resistance, in 1 point increments. Rotational potentiometers were embedded within the base of each rotational attachment, which allowed a total excursion of 140 degrees of rotation. The sagittal orientation of the resistance attachments was adjustable (continuous) from the upright position to 45 degrees of forward lean.

Human validation study

Seven healthy young adults (5 men, 2 women, 23.0 ± 3.4 years, 73.5 ± 8.4 kg, 174.2 ± 7.0 cm,) with no history of low back or lower leg injury, neurological or cardiopulmonary conditions participated in two evaluation sessions, separated by approximately 1 week. Subjects performed 3 full cyclical trunk rotations on the device at each of the 11 resistance levels (0-10), in a random order, at a set cadence (20 cycles per minute), with 2 minutes of rest separating each bout. During the exercise bouts, muscle EMG was recorded at 2000 Hz (20-500 Hz bandpass filtered via pre-amplified bi-polar bar surface electrodes (Delsys Inc.) from the following muscles, bi-laterally: rectus abdominis (RA), external abdominal oblique (EO), internal abdominal oblique (IO), paraspinal muscles at T9, L3, and L5, latissimus dorsi (LD), vastus medialis (VM), vastus lateralis (VL), rectus femoris (RF), medial hamstring (MH), adductors (AD), gluteus medius (Gmed) and gluteus maximus (Gmax). The raw EMG data were full-wave rectified, low pass filtered (6 Hz), and integrated (IEMG) over the portion of each movement cycle that corresponded to the prime mover action of each muscle. The IEMG data were subsequently normalized to a percent of the data obtained at the greatest resistance level. Immediately following each bout of 3 cycles at each resistance level, subjects provided a numerical rating of their perceived exertion, via the Borg category-ratio (CR-10) scale. Figure 2 illustrates a sample tracing the processed EMG data over a series of rotation cycles at one subject at a resistance level of 8.

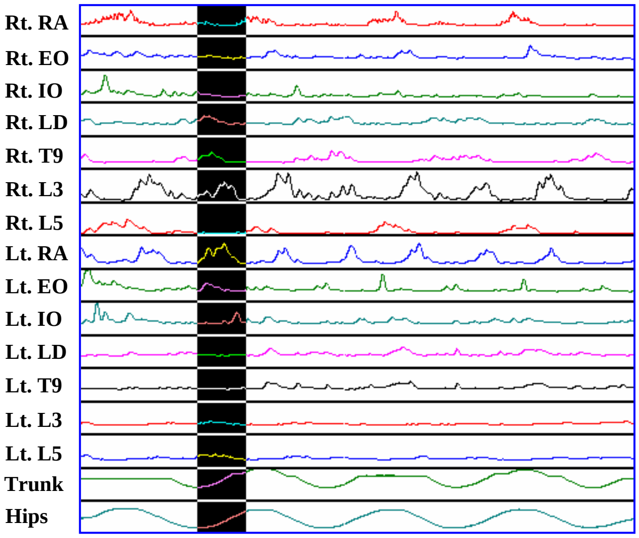

FIGURE 2: Sample tracing of processed surface EMG tracings from the trunk muscles during cyclic exercise on the trunk rotation device. The highlighted region indicates a rightward rotation.

RESULTS AND DISCUSSION

The results demonstrated a significant ($p<0.05$) increase in ratings of perceived exertion across the resistance levels (Figure 3).

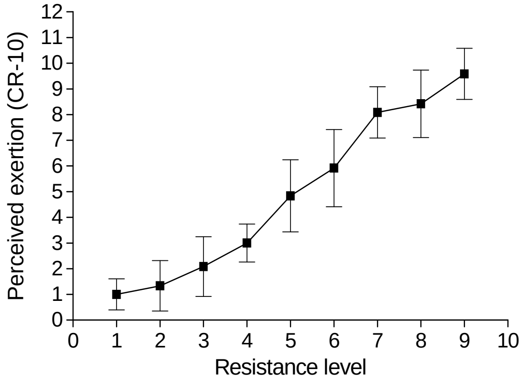

FIGURE 3: Ratings of perceived exertion, as a function of resistance level during trunk rotation exercise.

With respect to the normalized IEMG data, significant ($p<0.05$) increases were observed for most muscles beyond resistance level 4, when considering their primary motion, as a function of resistance level (Figure 4).

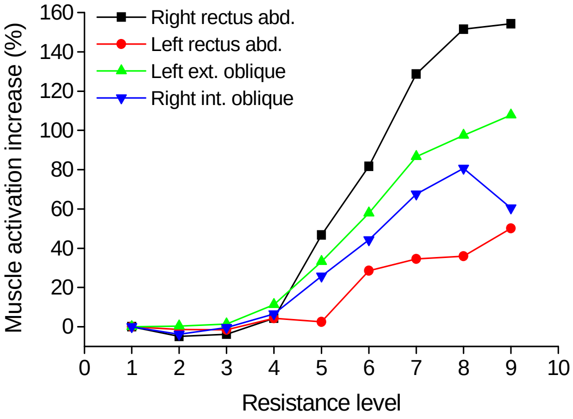

FIGURE 4: Normalized IEMG data of the abdominal muscles during rightward rotations, as a function of device resistance level.

CONCLUSIONS

The major findings of the present study demonstrate that the newly designed trunk rotation exercise device was effective at progressively recruiting the trunk rotator muscles that are active in the intended motions. As confirmed by the expected increase in perceived exertion, current investigations are addressing the efficacy of using such a device for sport-specific training and performance enhancement.

REFERENCES

1.Manning DP, et al. *Spine*, **9**, 734-739, 2008.
2.www.turningpointeffect.com

ACKNOWLEDGEMENTS

The authors acknowledge support from The Turning Point, LLC and Hoggan Health Industries.

PCL TREATMENT INFLUENCES SENSITIVITY TO JOINT LINE CHANGES IN TOTAL KNEE ARTHROPLASTY

[1]Michael W. Hast, [2]Clinton D. Walker and [1,3,4]Stephen J. Piazza
Departments of [1]Mechanical & Nuclear Engineering, [3]Kinesiology, and [4]Orthpaedics & Rehabilitation
The Pennsylvania State University, University Park, PA
[2]Stryker Orthopaedics, Mahwah, NJ
email: piazza@psu.edu

INTRODUCTION

To restore natural knee kinematics during total knee arthroplasty (TKA), a surgeon must attempt to properly balance ligament tensions while trying to maintain natural knee motions. Implants are usually designed with the expectation that the gap between cut bone surfaces is equal in flexion and extension. However, it is not uncommon for the flexion gap to be larger than the extension gap because of excessive collateral ligament laxity. A surgeon may address this gap inequality by increasing tibial bearing thickness while shifting the femoral component proximally. This ligament balancing technique results in an elevated "joint line", so called because the articular interface is moved proximally relative to its original natural position.

Treatment of the posterior cruciate ligament (PCL) is also an important consideration for surgeons performing TKA. Radiographic evidence has shown that the choice between cruciate-retaining (CR) and posterior-stabilizing (PS) designs does not inherently change the joint line location [1]. It is unclear, however, how elevations of the joint line affect soft tissues such as the PCL because their attachment sites do not shift with the joint line.

Computer simulation can be an effective tool for examining the effects of joint line elevation, as implant placements can be varied while all other properties of the knee are kept constant. The purpose of this study was to use a computational model to investigate the sensitivity of CR and PS TKA kinematics and kinetics to proximal shifts of the joint line.

METHODS

A 12-degree-of-freedom forward-dynamic model replicated a cadaveric 'Oxford Rig,' which performed controlled knee flexions from 20°-120°. Anatomy of the lower extremity was based on the model described by Delp [2], and a 30 kg mass was placed at the pelvis to simulate body weight.

Knee flexion was controlled by a lumped quadriceps actuator with the same line of action as vastus intermedius. The quadriceps force necessary to lower the pelvis at a constant rate was determined using a proportional-derivative controller. The PCL was modeled with 10 fibers with slack lengths and attachment points of the fibers based on the findings of Makino et al [3]. Other ligaments and passive muscles that cross the knee were modeled with force-length and force-velocity relationships.

PS and CR versions of the same total knee replacement design (Scorpio; Stryker Orthopaedics) were compared in the simulation. Positions of the femoral and tibial implants were shifted proximally in 1 mm increments up to 6 mm to simulate elevations of the joint line. Contact between the implants was modeled using a rigid body spring model [4]. Tibiofemoral contact points were defined by locating the center of pressure on the medial and lateral condyles. Knee joint angles were computed following the convention of Grood and Suntay [5].

RESULTS AND DISCUSSION

Proximal shifts in joint line affected the kinematics of CR and PS designs differently (Figure 1). For the CR knee with no joint line elevation, contact points were relatively stationary from 20°-120° of flexion. The CR knee exhibited increasing posterior movement of the contact points (‘femoral rollback’) as the joint line became more elevated. For 6 mm elevation, the tibiofemoral contact points for the CR knee approached the posterior lip of the tibial implant at 120° of flexion. In contrast, the PS knees exhibited similar degrees of rollback for all joint line elevations.

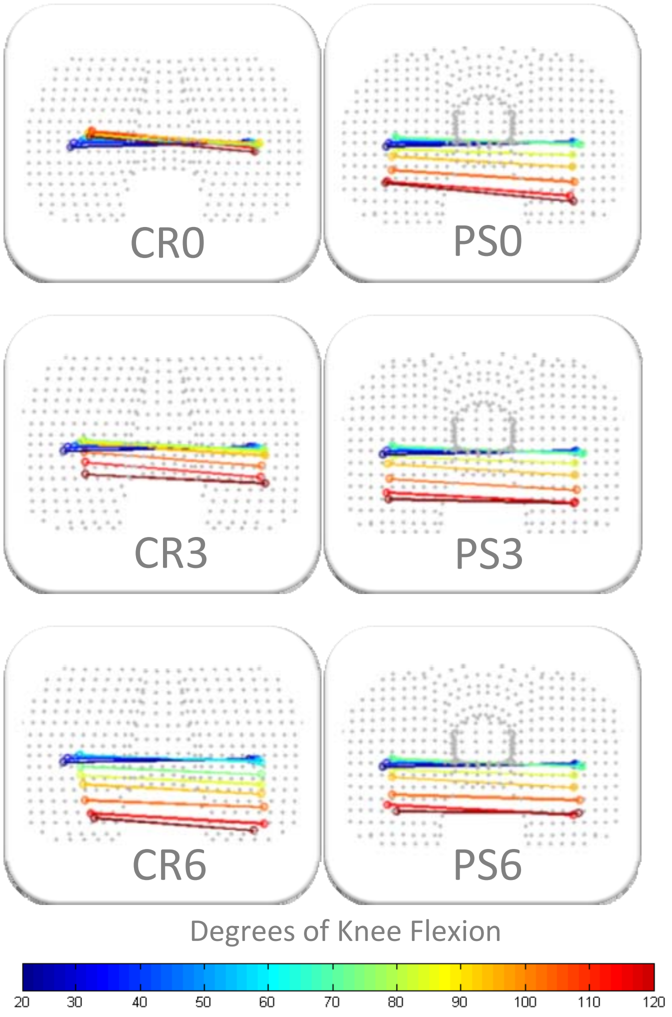

Figure 1: Locations of contact points in 10° increments between 20° and 120° flexion for CR and PS knees at 0 mm, 3 mm, and 6 mm of joint line elevation. A superior view of a right tibial component is shown.

Tibiofemoral (TF) contact forces were similar for CR and PS knees between 20° and 70° of knee flexion (Figure 2). At angles higher than 70°, however, TF forces were generally higher for the CR knee than for PS. The magnitude of TF contact forces were sensitive to increases in joint line elevation for the CR knee, primarily due to tension in the PCL that increased with elevation. At 120° of flexion, TF contact force in the CR knee with 6 mm of joint line elevation was approximately double that force seen when the joint line was unchanged. Because the PCL is removed in PS TKA, tibiofemoral forces in the PS knee were not insensitive to increased joint line elevation.

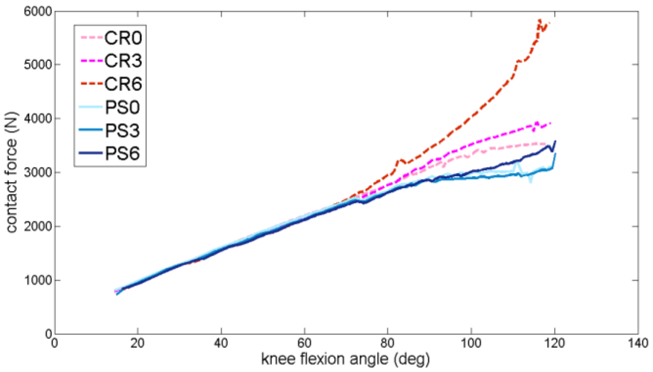

Figure 2: Tibiofemoral contact force magnitude plotted against knee flexion angle for CR and PS knees at 0, 3, and 6 mm of joint line elevation.

CONCLUSIONS

Investigations of the influence of joint line elevation are important for improving the functional outcome of total knee replacements following TKA. In this study, simulated kinematics and kinetics of a CR design appeared to be more sensitive to changes in the joint line. Conversely, the corresponding PS design provided consistent motions and TF contact forces, regardless of joint line elevation.

REFERENCES

1. Cope MR, et al. *J. Arthroplasty* **17** 206-208, 2002.
2. Delp SL, et al. *IEEE Trans. Biomed Eng.* **37** 757-767, 1990.
3. Makino A, et al. *Arthroscopy* **22** 684.e1-5,2006.
4. Li G, et al. *J. Biomech* **30** 635-638, 1997.
5. Grood ES, Suntay WJ *J. Biomech Eng* **105** 136-144, 1993.

ACKNOWLEDGMENTS

Supported by Stryker Orthopaedics.

COMPARING CARDAN ROTATION ANGLE AND FINITE HELICAL AXIS REPRESENTATIONS OF TALOCRURAL AND SUBTALAR IN VIVO KINEMATICS

Frances T. Sheehan
Functional & Applied Biomechanics Section, Rehabilitation Medicine, National Institutes of Health
email: gavellif@cc.nih.gov

INTRODUCTION

The joints of the rear-foot are subjected to the highest stresses and are the most commonly injured, as compared the other joints in the human body. Yet, little is known about the *in vivo* kinematics of the talocrural and subtalar joints. The data available for these joints have typically been presented in terms of the finite helical axis (FHA) and are most often acquired through static cadaver experiments. The FHA representation has been favored over Cardan rotation angles because it lent itself to the measurement tools available, did not have the potential for data singularities and lacked sequence dependency. Thus, the primary purpose of this study was to fully quantify the kinematics of the subtalar, talocrural, and calcaneal-tibial joints in 25 healthy ankles during a volitional task. Using these data, the utility of representing kinematics using the FHA was compared to the Cardan rotation representation. As part of this comparison, the sensitivity of the rotation angles to the selection of the rotation sequence was determined.

METHODS

Twenty healthy subjects participated in this IRB approved study. Time permitting, both ankles were studied. In total data for 25 ankles were collected (age = 26.2 ± 4.5 years; weight = 71.1 ± 13.3 kg; height = 173.6 ± 7.2 cm, 6F/19M).

Subjects were placed supine in a 1.5T MR imager (LX; GE Medical Systems, Milwaukee, WI, USA), after obtaining informed consent. A specialized ankle loading device was used to apply load during plantarflexion (PF), defined as the rotation of the calcaneus about the tibial medial-lateral (M-L) axis. This loading device allowed 3 degrees of rotational freedom at the ball of the foot. Zero degrees of tib-foot PF was defined as when the long axis of the tibia was perpendicular to the plantar surface of the foot. While subjects cyclically plantarflexed and dorsiflexed their ankle at 35 cycles/min, aided by an auditory metronome, fast-PC MR images were collected (anatomic and x, y, z velocity images, temporal resolution =72 ms, imaging time=2:48). The imaging parameters were consistent with prior studies [1]. The sagittal-oblique imaging plane contained the soleus musculotendon junction, tibia, calcaneus, and talus (Figure 1). The 3D time-dependent orientation and displacement of the tibia,

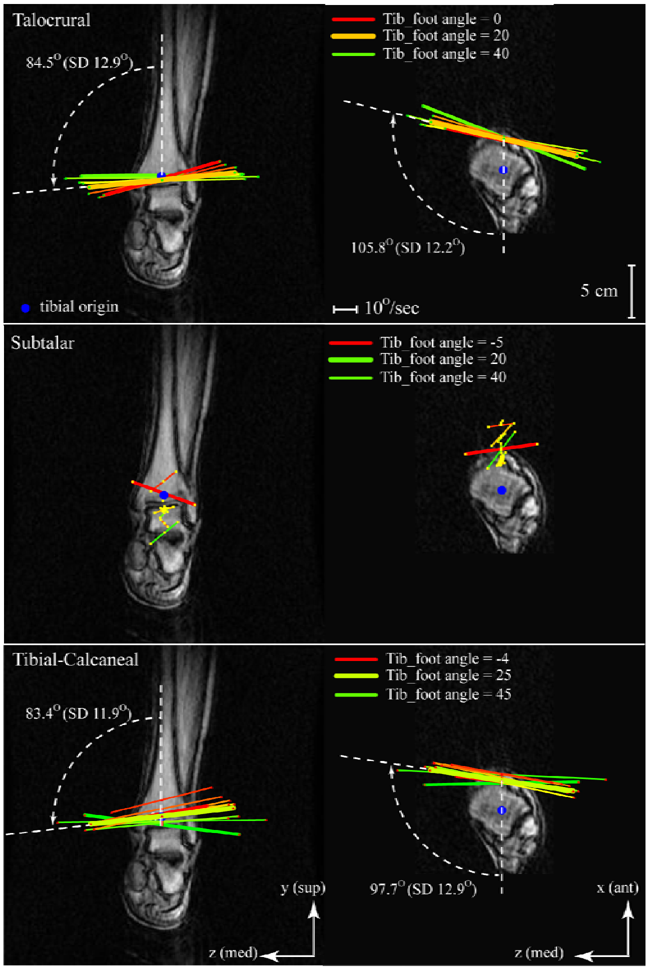

Figure 1: The average FHA overlaid on the left foot images of one subject. Maximum dorsiflexion = dark red, maximum PF = dark green. The FHA is shown to scale and all images are of the same scale (280 mm^2). Thus, the length of each FHA represents the amount of rotation occurring at that tib-foot angle. Blue circle = tibial origin. The FHA is shown at 5° increments of tib-foot angle, for clarity.

talus, and calcaneus were derived through integration of the velocity data [2]. From these data the FHA was determined along with the Cardan rotation angles (zyx-body fixed sequence). Since the FHA is undefined as the angular velocity goes to zero, it was not reported for angular velocities less than 0.25 rad/s. Mean Cardan rotation angles were calculated for the entire population at each tib-foot angle and converted into a series of orientation matrices. Then all 12 non-repeating Cardan rotation angle sequences were calculated for the "mean" matrices. For clarity, only tib-foot PF was reported.

RESULTS

The talocrural and tibial-calcaneal FHAs had similar directions, which were predominantly M-L (Figure 1). The tibial-calcaneal joint displayed the expected supination pattern of plantarflexion with internal rotation and inversion as did the talocrural joint. The PF and inversion directions were fairly consistent throughout the arc of motion, but the axes became less internally directed as the foot plantarflexed. The average direction of the subtalar FHA did not represent the data well, as its direction changed sign in all three planes at least once during ankle plantarflexion for the majority of subjects. The average translation (SD) along the FHA over the arc of motion was -0.5 (1.4), -0.3 (1.4) and -0.6 (1.4) for the talocrural, subtlar and tibial-calcaneal joints, respectively. The total rotation about the FHA (SD) through the arc of motion, averaged across subjects, was 31.7º (11.3º), 15.1º (9.7º) and 29.1º (8.5º) for the talocrural, subtalar and tibio-calcaneal joints, respectively. The high variability reflects the different ranges of tib-foot angle achieved by each subject.

The zyx-Cardan rotation angles agreed with the FHA data, but better represented subtalar kinemetics. Across the arc of motion, most ankles demonstrated talocrural and calcaneal-tibial supination, except for five (two with talocrural external rotation, one with external calcaneal-tibial rotation and one with calcaneal-tibial eversion). Subtalar kinematics were the most variable, with three ankles demonstrating pronation. Five, ten and fourteen ankles demonstrated subtalar dorsiflexion, external rotation and eversion, respectively. The tibial-calcaneal and subtalar joints had the largest and smallest translations, respectively.

The selection of Cardan rotation sequence had little effect on the conversion of the direction cosine matrix to rotation angles. The sensitivity to sequence selection ranged from 0.1º to 0.9º; smaller than the inter-subject variability [1].

DISCUSSION

Since the subtalar kinematics are not well defined by the FHA, the Cardan rotation angles are a better descriptor of rear-foot kinematics. Unlike the FHA, Cardan rotation angles are defined when there is zero angular velocity and the initial joint attitude can be incorporated within these angles. The latter may be critical when defining pathologies. Further, the sensitivity to sequence selection was quite small. Thus, rear-foot kinematics are independent of the Cardan rotation sequence. This small sensitivity is likely due to rotation angles that do not exceed a range from -45º to 10º. During an activity with larger rotations in more than one plane (e.g., the hip or shoulder) this finding will likely not hold. Yet, for the ankle joint, the choice of Cardan rotation sequence clearly does not alter the final rotation angles. On the other hand, translations can only be fully understood using knowledge of the FHA location. For example, the large translation of the calcaneus origin can be attributed almost entirely to its origin being at a distance from the calcaneal-tibial FHA.

The use of Cardan rotation angles also clarified the relationship between the motion at the tibial-calcaneal and talocrural joints. Due to the variability of subtalar motion across subjects, the relationship between motion at the tibial-calcaneal and talocrural joints was inconsistent. Thus, assuming any knowledge of subtalar or talocrural motion, based on tibial-calcaneal motion, is not feasible.

REFERENCES

[1] Rebmann & Sheehan. *JMRI* **17,** 206-213, 2003.
[2] Sheehan, F. T. *J Biomech* **40,** 1038-1047, 2008.

THE EFFECTS OF NOISE ON THE CONTROL OF A PLANAR MODEL OF REACHING

[1] Hung Nguyen and [2]Jonathan Dingwell
[1]Department of Mechanical Engineering, University of Texas at Austin
[2]Nonlinear Biodynamics Laboratory, Department of Kinesiology, University of Texas at Austin
Email: jdingwell@mail.utexas.edu, web: http://www.edb.utexas.edu/faculty/dingwell/index.html

INTRODUCTION

Noise can emanate from internal neuromuscular signal or from external sources. These perturbations to the joint torque can alter the trajectory of the motion and affect end point accuracy. In reaching, noise at the elbow and shoulder can impart different effects on the end point performance. In similar redundant tasks, people explore the variability in the musculoskeletal system to compensate for these noisy signals while still achieving the desired trajectory [1]. Here, we provide an analytical analysis of how motor noise at the shoulder and elbow joint independently change the trajectory and accuracy of a reaching task. The results provide important insights on how to implement a control architecture that would optimally minimize motor noise. Based on previous studies [1], we expect the motor noise at the elbow to have a more significant effect on the endpoint accuracy in reaching task than the shoulder. If the error is more critical at the elbow, we expect that controlling the elbow would significantly reduce the error.

METHODS

A 2-dof torque-driven model (similar to [2]; fig.1b) was used in the simulations. During each cycle, the arm model performs a straight-line reaching motion and returns to its initial state. A measure of the endpoint position after each cycle was used to analyze the performance of the reaching task. Signal-dependent noises [3] were independently added to the torques at the elbow and shoulder to quantify how they affected the end point accuracy.

While noises are persistent in movement, humans do use some control mechanism to minimize its effect on the end point accuracy. Simple proportional controllers (fig.1b) were implemented at the shoulder and elbow joints to quantify the independent and combined effects of these controllers on the end point location. Eight different combinations of noise and controller were simulated (Table 1).

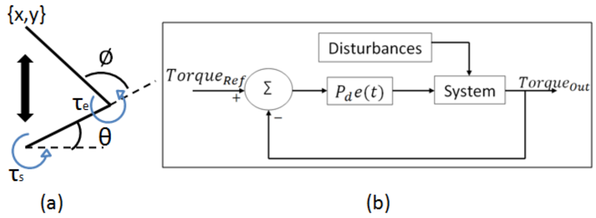

Figure 1: Schematic of the reaching model (a) and proportional controllers which applied torques at the elbow and shoulder (b). The difference between the output torques and the desired torques at the joints is denoted by $e(t)$ and the gain by P_d.

Simulations were implemented in Matlab (MathWorks ®). Each condition was simulated for 20 trials and the average values were recorded. Anthropometric data were obtained from Winter [4] with H=1.80m and M=90.5kg.

RESULTS AND DISCUSSION

Average end point errors are shown in fig.2. Under the same magnitude of signal dependent noises, noise added to the elbow had a larger impact on the trajectory of the motion as well as the end point accuracy (10.08 vs. 3.93 cm). The effect of the shoulder noise on the end point accuracy was dampened by the inertial load of the elbow during movement. However the effect of the elbow motor noise was transmitted to the end point with minimal resistance from the shoulder. In simulations where noises were added only to the elbow, the addition of a controller at the elbow joint improved performance by 72% (from 10.08 to 2.84 cm). When noises where only added to the shoulder, the controller improved the performance of the end point accuracy by 81% (from 3.93 to 0.74 cm).

Table 1: The mean distance errors (cm) of different noise and control schemes. Subscripts (noise, con) indicate the noise and controller inserted or applied at each joint (E: elbow, S: shoulder, SE: noise and shoulder, NO: none).

	S_{noise}	E_{noise}	SE_{noise}
No_{con}	3.93 (±2.57)	10.08 (±8.68)	11.40(±7.12)
S_{con}	0.74 (±0.51)		10.34(±7.26)
E_{con}		2.84 (±1.41)	4.44(±2.76))
SE_{con}			2.83(±1.97)

When noises were added simultaneously to both the elbow and shoulder without implementing any control, the effects of these raw noises on the end point errors were not additive (Table 1). Thus couplings in the model act as dampers to the noise inserted at the individual joints. We implemented separate controllers at each joint to analyze which controlling scheme would yield greater improvements for end point accuracy. With only a shoulder controller, the average end point accuracy improved by 9% (from 11.40 to 10.34 cm). With only an elbow controller, the end point accuracy improved by 61% (from 11.40 to 4.44 cm). When controllers were implemented at both the shoulder and the elbow simultaneously, the end point accuracy improved by 75% (from 11.40 to 2.83 cm). Thus when distal noises are active, using a proximal controller has very little effect on performance.

Comparing across controllers in the presence of noise at both the elbow and shoulder, we found on average the elbow controller improved the end point accuracy by 57% (from 10.34 to 4.44 cm) over the shoulder controller, while having controllers at both joint improved the accuracy of the end point trajectory by 36% (from 4.44 to 2.83 cm) over having the controller only at the elbow. While implementing controllers at both joints yielded the best performance, the result from elbow only control suggests that using both controllers is not cost efficient.

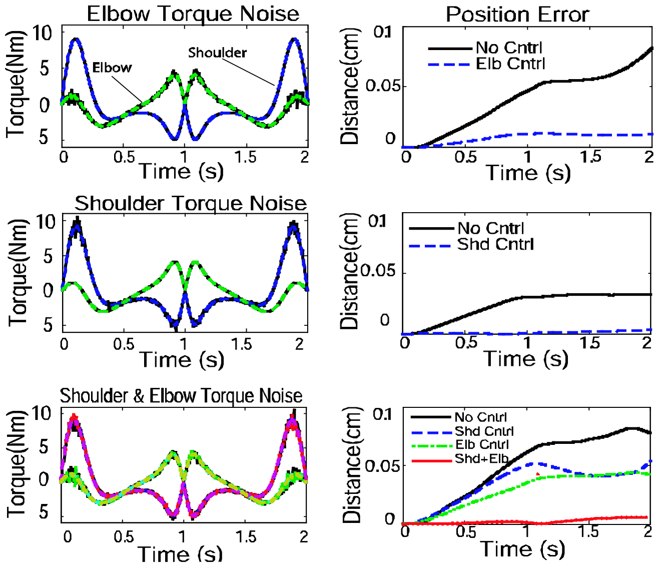

(a) (b)

Figure 2: Average torque (a) and position error (b) during the reaching movement for 20 trials.

CONCLUSIONS

The model provides analytical evidence of how motor noises affect the end point accuracy. Distal motor noise has the most significant impact on performing task; therefore, this is critical when designing controllers to improve the performance in reaching tasks. If a system can tolerate noise in some components while tightly controlling noise in other areas, this can lead to simpler control mechanism that would not compromise the task goal [1].

REFERENCES

1.Cusumano JP, et al. *Bio Cybern* **94**, 369-79, 2006.
2.Scheidt RA, et al. *J Neurophysiol* **93**, 3200-12, 2005
3.Hamilton AF, et al. *Exp Brain Res* **157**, 417-30, 2004.
4.Winter, D.A. *Biomechanics and motor control of human movement*, John Wiley & Sons, Ontario, Canada.

RELATIVE CONTRIBUTIONS TO DISC DEGENERATION PROGRESSION IS HIGHER BY DEGENERATIVE TISSUE MATRIX THAN ANNULAR FIBERS LAXITY: A FINITE ELEMENT ANALYSIS IN PURE COMPRESSION

[1]Mozammil Hussain, [2]Ralph E. Gay, [3]Kai-Nan An, [4]John J. Triano, [1]Rodger Tepe

[1]Division of Research, Logan University, Chesterfield, Missouri, USA
[2]Department of Physical Medicine and Rehabilitation, Mayo Clinic, Rochester, Minnesota, USA
[3]Department of Orthopedic Research, Mayo Clinic, Rochester, Minnesota, USA
[4]Canadian Memorial Chiropractic College, Toronto, Ontario, Canada
E-mail: mozammil.hussain@logan.edu

INTRODUCTION

Mechanical compression initiates progression of degeneration within intervertebral discs. Compressive forces (up to 70-80%) from one motion segment to another are transmitted to the disc, whereas tissue matrix and annular fibers of the disc share this compressive load to be transmitted. In response to external compression, the disc tissue matrix (fluid and proteoglycans) contributes to compressive load-bearing capabilities and develops hydrostatic pressure, whereas tensile loads are transmitted to the annular fibers which causes disc bulging. Therefore, the disc composite structure, consisting of tissue matrix and annular fibers together provides mechanical strength to the disc, but in different ways. Despite several experiments showing disc degeneration (DD) analysis, an understanding of the relative contributions of tissue matrix and annular fibers to the overall disc biomechanical response during DD is unknown. Also unknown is how degenerative change in only one of the tissue components affects disc biomechanics.

Due to anisotropic properties imparted by annular fibers to the disc, measurement of annular stress patterns using *in vitro* strain gauge techniques is difficult. Also, it is difficult to simulate degenerative changes only in one of the disc components utilizing either *in vivo* or *in vitro* methods. Finite element (FE) methods overcome some of these limitations. Using a FE model, the focus of the current study is to investigate the relative contributions of tissue matrix (healthy or degenerated) and annular fibers (healthy or degenerated) in governing disc behavior.

METHODS

A previously validated three-dimensional FE model of a C5-C6 motion segment without posterior elements was used [1]. The vertebra-disc-vertebra unit consisted of cortical bone, cancellous bone, endplates, annulus fibrosus (AF), and nucleus pulposus (NP). Regional geometry variations within the disc were performed by subdividing both AF and NP into four quadrants each – anterior, posterior, and right and left lateral. The tissue matrix between outer AF and NP boundaries was embedded with four concentric lamellae of collagen fibers along with a fiber lamella at each of the AF outer and AF-NP boundaries, thereby modeling a total of six concentric fiber lamellae. Each lamella was modeled with two fiber layers oriented at an equal and an opposite angle to the transverse plane, forming a criss-cross pattern. The fiber layer orientation angles of each lamella were increased in the order of 5° magnitude from innermost to outermost lamella: ±40° (innermost lamella), ±45°, ±50°, ±55°, ±60°, and ±65° (outermost lamella). This model represented the morphology and material properties of the healthy disc that was adopted from the literature.

With DD progression, tissue matrix transforms into a dehydrated stiff structure, while the fibers lose their elasticity. In order to represent these degenerative changes, two grades of DD, moderate and severe, were introduced into the healthy disc. In the moderate stage of DD, material properties (elastic modulus and Poisson's ratio) of only NP were changed (equivalent to the AF properties), whereas both AF and NP properties (elastic modulus was doubled as compared to the moderate degeneration) were varied in severely degenerated disc. The elasticity of the annular fibers was decreased by 10% and 30% in moderate and severe

DD, respectively. For a better understanding of degenerative changes in the disc tissue matrix and annular fibers, three different types of degenerative tissue material properties were included in the healthy disc to simulate the moderate and severe stages of DD: elasticity changes in the tissue matrix alone, elasticity changes in the annular fibers alone, and elasticity changes in both tissue matrix and annular fibers. Although morphological changes such as decrease in disc space and NP area also occur with DD, these degenerative changes were not included in the current study, as our objective was to analyze the disc biomechanics with respect to only degenerative material property changes in tissue matrix and/or annular fibers. An axial compressive load of 50 N (equivalent to upper body weight) was simulated on the superior surface of the top vertebra, and the inferior surface of the bottom vertebra was constrained in three planes. For the three models (healthy, moderate, and severe) with three different degenerative material property changes (tissue matrix alone, annular fibers alone, and both tissue matrix and annular fibers), the axial compressive stresses in AF tissue matrix and von-Mises stresses in annular fibers were computed for anterior, posterior, and right and left lateral regions of the AF. Moderate and severe DD were normalized with respect to healthy disc. Finite element software (ABAQUS) was used to perform the analysis.

RESULTS AND DISCUSSION

Degenerative changes in tissue matrix and annular fibers increased tissue matrix stresses (Figure 1), and decreased annular fiber stresses (Figure 2). Therefore, reduction in annular fiber stresses was compensated by higher tissue matrix stresses. When degenerative elasticity was introduced in the tissue matrix alone, both matrix and fiber stress changes were higher than the corresponding stress changes when degenerative elasticity was introduced in the annular fibers alone. These stress changes were highest when severe degenerative elasticity was modeled together in tissue matrix and annular fibers. Slight decrease in tissue matrix stresses during moderate DD may represent instability associated with an abnormal increased segmental flexibility. Higher stress concentration in tissue matrix was observed in the anterior-lateral AF regions with compensatory lower fiber stresses in those regions. Outer fiber lamellae were more stressed than the inner fiber lamellae. The difference in matrix stresses between lateral regions may be due to a negligible coupled moment, arising from a slight asymmetric compressive loading. The current conclusions may vary for distraction and other moment loadings. Future degenerative disc compression studies should be considered to verify the current findings.

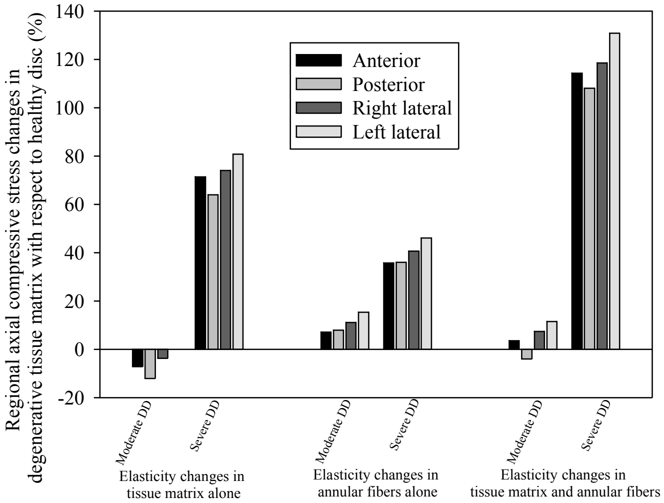

Figure 1: Regional tissue matrix stress changes in AF due to degeneration in tissue matrix and/or annular fibers compared to healthy disc

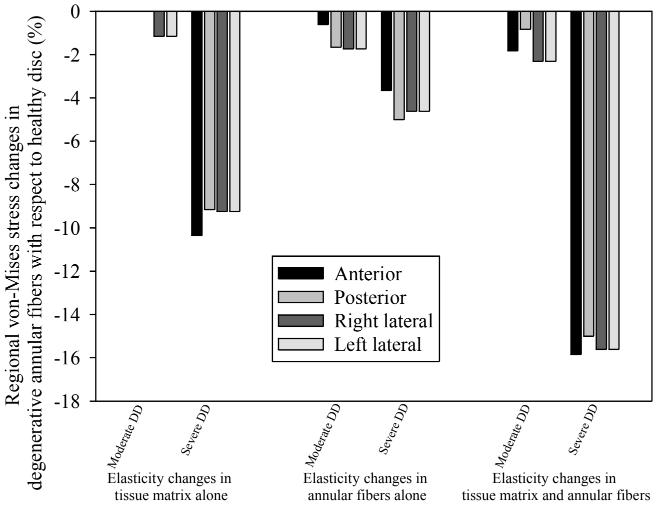

Figure 2: Regional annular fiber stress changes due to degeneration in tissue matrix and/or annular fibers compared to healthy disc

REFERENCES

1. Hussain, M and Tepe, R (2008). *Summer Bioengineering Conference (ASME)*, Marco Island, Florida.

INFLUENCE OF PELVIS CLUSTER CONFIGURATIONS ON ESTIMATING JOINT PARAMETERS IN GAIT ANALYSIS: A PILOT STUDY

Arvind Ramanujam[1], Kevin Terry[1,2] and Gail Forrest[1,2]
[1]Kessler Foundation Research Center, West Orange, NJ;
[2]University of Medicine and Dentistry of New Jersey, Newark, NJ;
email: aramanujam@kesslerfoundation.net, web: www.kesslerfoundation.net

INTRODUCTION

In gait analysis, techniques used to determine joint parameters are prone to errors arising from palpation, soft tissue artefact and marker dropouts. Possible reasons for marker dropouts include poor calibration, ambient reflections or marker occulsion by limbs of patients. Stereo-photogrammetry and marker clusters associated with body segments of interest have previously been used to accurately estimate the instantaneous position of certain anatomical landmarks (AL) [1-3]. One such study investigated the sensitivity of hip joint kinematics based on different thigh cluster configurations [1].

Common full body marker sets that are used in routine gait analyses include the Helen-Hayes (H-H) marker set, the modified H-H marker sets or a derivation of H-H set. These marker sets place a lot of emphasis on accurate placement of the bilateral anterior superior iliac spine (ASIS) markers, when using regression equations to determine joint centers. During pathological gait such as stroke, often the ASIS marker is occluded due to hemiparesis of the more affected limb. Filling these occluded gaps in marker trajectory with extensive dropouts has always been a challenging task. The objective of this pilot study was to investigate the accuracy and reliability of four pelvic cluster configurations on estimating the ASIS marker and its influence on joint kinematics.

METHODS

Able bodied gait data was collected at 120Hz using a Vicon motion capture system from one participant who provided informed consent. Markers were placed on AL as defined by Plug-in-Gait (VICON, Oxford Metrics, Oxford, UK). Four alternative markers not included in the Plug-In-Gait (LPEL1, LPEL2, RPEL1, RPEL2) were placed on the lateral bony aspect of the pelvis *(anterior iliac crest)* in close proximity to the ASIS (~4cm apart) (Figure 1). Anthropometric measurements were recorded manually. Data collection included a static trial and ten gait trials. Data was filtered (6 Hz low pass butterworth filter) and normalized to percent gait cycle (Matlab 7.6, The MathWorks, Natick, MA). All data collection and analyses using the Plug-in-Gait model were performed by the same investigator.

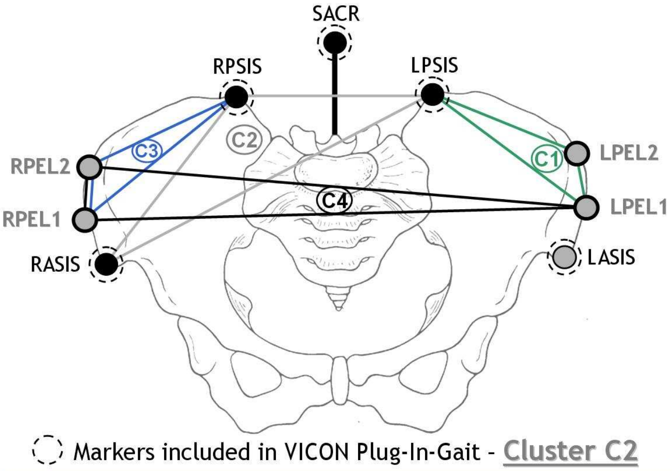

Figure 1: Pelvic cluster configurations for LASIS.

The *replace4* bodybuilder macro (VICON) was used over the ten gait trials to estimate the left ASIS marker (as a virtual marker) using each of four pelvic clusters (Figure 1): (C1) Ipsilateral cluster (LPEL1, LPEL2, LPSIS); (C2) Bilateral posterior cluster (LPSIS, RPSIS, RASIS); (C3) Contralateral cluster (RPEL1, RPEL2, RPSIS); (C4) Bilateral anterior cluster (LPEL1, RPEL1, RPEL2). The results were then compared to the actual ASIS location and the calculated joint parameters.

RESULTS AND DISCUSSION

The four pelvic cluster configurations determined 3D-differences in joint parameter estimations. The 3D-Mean absolute error (MAE) in predicting the ASIS marker was largest for C3 (14.45±1.63mm), and smallest for C1 (2.46±1.3mm) and C4 (2.79±0.62mm) (Figure 2A). Also, the MAE in the superior-inferior direction was the highest across all clusters (12.62±12.77mm). 3D-MAE estimates for the lower-extremity joint centers showed a similar trend (Figure 2B). The hip joint center (HJC) had the maximum 3D-MAE of all the joint centers (6.35±7.05mm) with minimal errors at the knee (KJC: 1.37±1.41mm) and ankle (AJC: 0.56±0.65mm) joint centers. Correlations between MAE for estimating the ASIS and (1) HJC, (2) KJC, (3) AJC predicted a positive linear correlation of r=0.86, r=0.48 and r=0.27, respectively, indicating a decrease in MAE from proximal to distal segments (Figure 3). Similar errors were seen in the joint kinematics (Table 1).

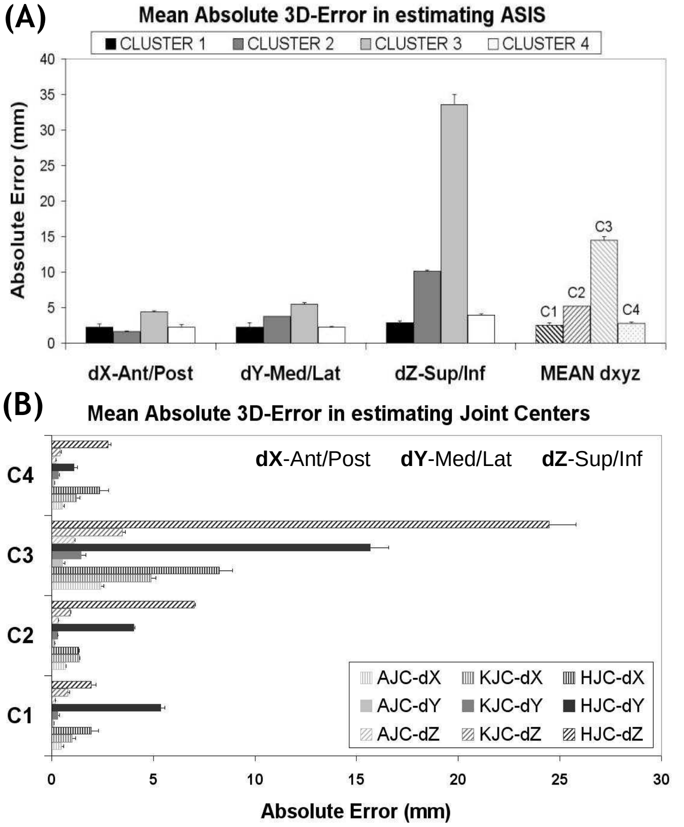

Figure 2: Mean absolute 3D-error estimates for (A) ASIS; (B) Joint Centers.

The dependencies of the joint center calculations on the ASIS and the resulting errors observed in joint kinematics, places emphasis on accurate estimation of the ASIS marker. Marker occlusions at the pelvis should be accounted for with accuracy and precision using suitable reconstruction techniques. Clusters C1 and C4 provided the most accurate estimates for the ASIS locations with minimal errors. The majority of the markers used in clusters C1 and C4 were on the ipsilateral side and/or the anterior aspect of the pelvis, closest to the ASIS. Either of these factors could have potentially contributed towards reducing errors in ASIS estimations and joint centers.

Table 1: Lower extremity MAE in joint kinematics.

3D Angles		**C1**	**C2**	**C3**	**C4**
Ankle angles	MAE	0.27º	0.42º	1.46º	0.30º
	(±SD)	(0.17)	(0.02)	(0.24)	(0.18)
Knee angles	MAE	0.42º	0.40º	1.71º	0.33º
	(±SD)	(0.17)	(0.03)	(0.28)	(0.15)
Hip angles	MAE	1.25º	2.37º	7.91º	1.14º
	(±SD)	(0.39)	(0.07)	(1.26)	(0.31)

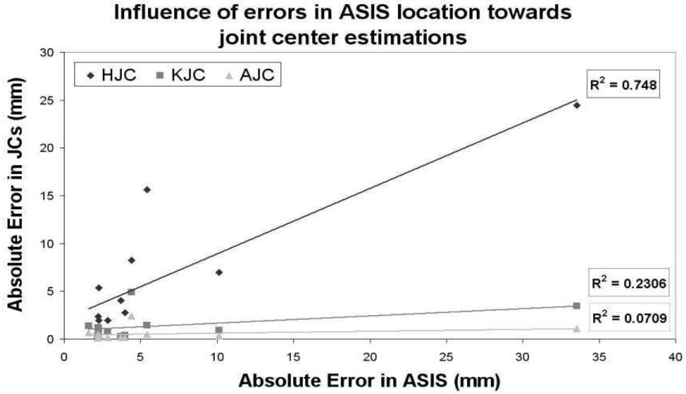

Figure 3: Linear correlations between ASIS and Joint Center error estimates.

CONCLUSIONS

The pelvis is considered to be a rigid body segment; however, the reliability of using pelvic clusters and its errors in predicting missing ASIS markers is dependent on its relative location on the pelvis. Also, the accuracy of these pelvic clusters may vary depending on pathology and dynamic activity (i.e. alternating or synchronous sequences). In stroke gait, due to lack of arm movement on the paretic side, the use of cluster C4 that includes two anterior pelvic markers (RPEL1, RPEL2) from the non-paretic side and one from the paretic side (LPEL1) is a possible solution with minimal predictive errors in joint parameters. It is thus important to use an optimal cluster configuration for marker predictions based on population and activity. Further research will investigate these differences on a larger *n* size.

REFERENCES

1.Schache AG, et al. *Gait Posture* **27**, 60-69, 2008.
2.Stagni R, et al. *J Biomech* **33**, 1479-1487, 2000.
3.Schwartz MH, et al. *J Biomech* **38**,107-116, 2000.

PELVIC MOTION DURING SEATED PEDALING FACILITATES INTER-SEGMENTAL ENERGY TRANSFER

[1] Kyle Gleason, [2]Amy Silder and [1-3] Darryl G. Thelen
Departments of [1]Mechanical Engineering, [2] Biomedical Engineering, and [3]Orthopedics and Rehabilitation, University of Wisconsin - Madison
email: kpgleason@wisc.edu

INTRODUCTION

Musculoskeletal simulations of pedaling typically assume that the pelvis is stationary [1,2]. While such models have provided insights into muscular coordination [3], they cannot account for energy transfer between the upper and lower body that arises from hip translation [4]. A previous study using bone pins showed that some hip motion does arise naturally during seated pedaling, but that it cannot be tracked accurately using markers over the trochanter or anterior superior iliac spine [5]. We recently showed that a triad of markers located on posterior landmarks can be used to obtain estimates of hip motion that are relatively consistent with bone pin data (Fig. 1). In that study, the pelvis was shown to roll and internally rotate from 2-3 deg toward the downstroke limb [5]. The objective of this study was to examine the amount of energy transferred to the limb via this hip motion. A second objective was to incorporate a moving pelvis into a musculoskeletal simulation of pedaling, to better understand energy transfer via the hip joint reaction force throughout a pedal stroke.

METHODS

Five experienced cyclists (4 male, 1 female) pedaled on a stationary adjustable bike, which was set to a 73 deg seat tube angle with the relative seat and handlebar positions set to match their own bicycle. Subjects pedaled in a drops hand position at a constant cadence of 90 rpm. The resistance of a fluid trainer was set to achieve a power output (120-245 W) that an individual subject could maintain for a 40k distance. Whole body, crank and pedal kinematics were recorded using a passive motion capture system. Sagittal plane pedal force data was simultaneously collected using custom instrumented pedals.

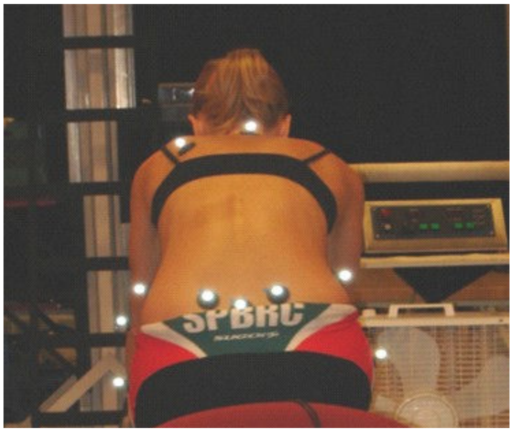

Figure 1: A triad of posterior markers over the posterior iliac spine and sacrum was used to track three dimensional pelvic motion.

A whole body linked segment musculoskeletal model [6] was scaled to each subject based on height, body mass and segment lengths. An inverse kinematics routine was then used to compute the joint angles that optimally matched the marker positions at each frame in a trial. Inverse dynamics analysis was performed to compute the three dimensional joint moments and net power at the hip, knee and ankle and crank. These power curves were integrated over each crank cycle, and averaged to estimate the net work done at each joint. Crank work was computed in a similar manner. Net hip transfer work, from the upper to lower body segments, was estimated as the difference between the crank work and net work done at the lower extremity joints.

A three-dimensional forward dynamic simulation of pedaling was created to better to understand the affect of pelvis motion on power generation in pedaling. In the simulation, the pelvis was prescribed to follow experimental kinematic trajectories. Lower extremity muscle excitations were computed to drive the closed loop model to track measured crank and pedal angles [6]. The hip joint reaction force and translational velocity was used to compute hip translational power throughout a pedal stroke.

RESULTS AND DISCUSSION

All subjects exhibited a net positive flow of energy from the upper body to lower extremities. This hip transfer work ranged from 2.8-15.2 J during a pedal stroke, which accounted for an average of 6.6% (range 2 to 13%) of work done on the crank. A simulation of pedaling demonstrates that most of this positive hip transfer work occurs during the second half of the downstroke, when the hip joint reaction is high and the hip is translating forward and downward [5]. Interestingly, the hip power curve demonstrates that there are smaller negative power bursts at the top of the crank cycle and during the upstroke. Negative power at the top may represent energy transfer from the decelerating limb to the upper body, which is subsequently released during the downstroke. However, negative power during the upstroke of the crank cycle may represent energy transfer to the upper body that is later released in the contralateral limb. Additional simulations of subject-specific pedaling are needed to ascertain how general these patterns are. We conclude that hip translation can facilitate inter-segmental energy transfer, and that accounting for such affects in models may provide additional insights into the muscular coordination of pedaling.

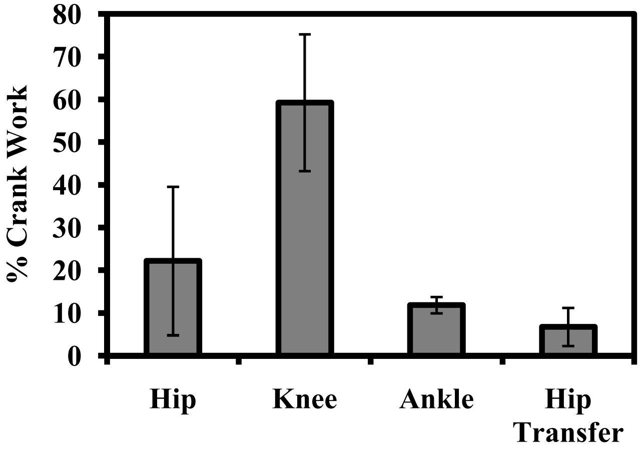

Figure 2: Percent crank work distribution done via lower extremity joints and the upper body via energy transfer through hip translation.

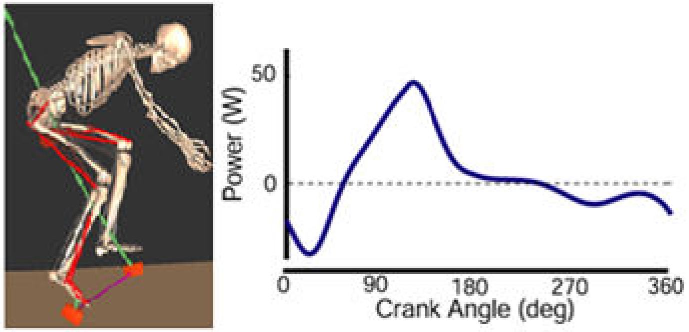

Figure 3: A three-dimensional forward dynamic simulation was used to simulate pedaling with a moving pelvis. Shown is the estimated hip transfer power arising from hip translation.

REFERENCES

1.Fregly, B. J., et al. *J of Biomechanical Engineering*, 122: 446-452, 2000.
2.Raasch, C. C. et al. *J of Biomechanics*. 30: 595-602, 1997.
3.Zajac, F. E., et al. *Gait and Posture,* 16: 215-232, 2002.
4.Martin, J. C., et al. *J. of Applied Biomechanics,* 114: 276-291, 1998.
5.Neptune, R. R., Hull, ML. *J of Biomechanics,* 28:423-437, 1995.
5.Sauer, J. L., et al. *Med. Sci. Sports Exrc*., 39:2204–2211, 2007.
6.Thelen, D. G. et al. *J of Biomechanics.,* 36:321-328, 2003.

ACKNOWLEDGEMENTS

Rick Neptune, PhD

A METHOD FOR QUANTIFYING ACTIVE THUMB CIRCUMDUCTION MOTION IN CHILDREN

Dustin A. Bruening, Kevin M. Cooney, John D. Lubahn
Shriners Hospitals for Children, Erie PA
email: dbruening@shrinenet.org

INTRODUCTION

Defects of the thumb, such as hypoplasia, trigger thumb, triphalangeal thumb, and syndactyly or polydactyly, represent approximately 16% of all upper extremity congenital anomalies [1]. Quantitative measurements of thumb function, such as those needed to evaluate surgical outcomes, have been difficult to establish due to the complex nature of thumb motion [2]. Motion analysis has been proposed as an alternative to traditional passive goniometric methods [3, 4] as it can be used to capture active movements. However, motion analysis may be difficult to use with certain populations. For example, Su et al. [4] created an algorithm to determine the workspace, or functional area within which the thumb operates. This was defined by two circumduction motions, one with the thumb fully extended and one with the MCP and IP joints flexed. The workspace was defined as the quasi-conical surface area between the two 'circles'. The method was tested only on normal adults, and in applying this method to children, both normal and those with anomaly, we found that the complicated motions required by the method are difficult for young children and impaired patients to perform. Furthermore, many children that we desire to evaluate do not have motion at the MCP or IP joints, a requirement to determine the area workspace. For these reasons, we desired an alternative method to evaluate thumb motion, and particularly the circumduction pattern, in pediatric populations. The purposes of this study, therefore, were to develop such an algorithm and to establish baselines of normal motion in pediatric subjects.

METHODS

Nine pediatric subjects with normally developing thumbs participated in the study (ages 2-18, mean 9.5). Both thumbs were tested on 5 of the 9 subjects, bringing the total to 14 thumbs. The length of each thumb, from the radial styloid to the thumb tip, was first measured. Each subject's wrist and hand were then placed into a custom wooden jig to keep wrist motion to a minimum. A 4-mm diameter retro-reflective marker was placed on the nail bed near the thumb tip and a three-marker cluster was placed on the radius. Subjects were instructed to keep the thumb extended (at the IP joint) while moving the tip in a large circle. For younger children, various techniques (toys, etc.) were employed to guide the thumb tip trajectory. Marker trajectories were captured at 120 Hz. using a 10-camera Vicon 612 motion analysis system.

Data processing was performed using custom Labview and Matlab software. Marker trajectories were low-pass filtered at 3 Hz. The marker cluster was used to construct a local coordinate system fixed to the radius and the thumb tip trajectory was expressed in this local coordinate system to account for extraneous movements of the arm and hand within the laboratory coordinate system.

Su et al. calculates a perimeter based on a single circular movement. In our experience, younger subjects require several motions to fully capture the end ranges of motion. To incorporate the end ranges of several circles, we used a convex hull algorithm to enclose the entire data set. First, the data was fit to a least-squares plane using singular value decomposition (SVD). Then, a two-dimensional convex hull was fit to the cluster of points. The hull indices were then used in the original 3-dimensional data set to create the enclosed circular perimeter. The length of the perimeter was calculated as the Euclidean distance between each successive hull indexed point. The perimeter values were then correlated to the measured thumb length.

RESULTS AND DISCUSSION

The algorithm was successful in capturing the end ranges of motion from several circular motions so that precise curves are not required (Figure 1). As the thumb passes the palm there is a concavity in the trajectory. This concavity does not necessarily reflect end range of motion, and if follwed in the perimeter calculation, could result in erroneously greater perimeters when the concavity increases. In the present algorithm, the concavity is enclosed by a straight line between the end ranges of motion before and after it.

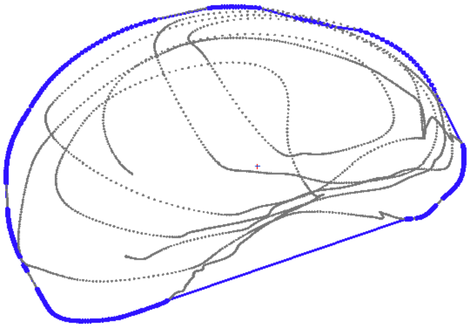

Figure 1: Sample circumduction motion in a 6 yr. old subject. Trajectory points are shown in gray, while convex hull nodes, and linear interpolations, are shown in blue.

The perimeter showed a good correlation (R=.90) with thumb length, although some bilaterally tested subjects had slightly different perimeter values between sides. This variability may be a limitation in all active range of motion thumb studies. The correlation is also sensitive to errors in thumb length measurements.

Overall, however, the algorithm captured the motion of interest in a difficult population. By including, and enclosing, all possible trajectory points, we were able to capture the full range of motion of pediatric subjects. In subjects with good cognition and dexterity, and where IP and MP motion is available, the current method is also compatible with Su et al in calculating an active thumb workspace.

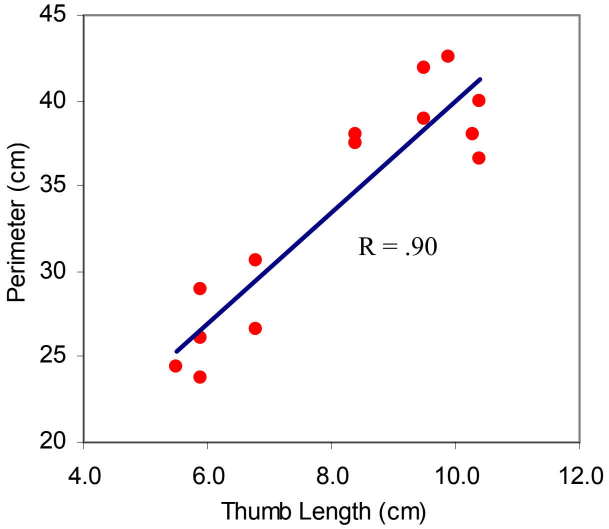

Figure 2: Scatterplot of thumb length and perimeter.

REFERENCES

1. Kleinman, W.B., Hand Clin, 1990. **6**(4): p. 617-41.
2. Staines, K.G., et al., Plast Reconstr Surg, 2005. **116**(5): p. 1314-23; discussion 1324-5.
3. Chang, L.Y. and N.S. Pollard, IEEE Trans Biomed Eng, 2008. **55**(7): p. 1897-906.
4. Su, F.C., et al., J Biomech, 2003. **36**(7): p. 937-42.

THE INFLUENCE OF JUMP LANDINGS ON DYNAMIC STABILITY

[1] Kathy Liu and [2]Gary Heise
[1] Biomechanics and Movement Sciences, PhD Student, University of Delaware, Newark, Delaware
[2] Biomechanics Laboratory, University of Northern Colorado, Greeley, Colorado
email: kathyliu@udel.edu

INTRODUCTION

Dynamic stability is the ability to transition from a dynamic movement to a stable, static condition over one's base of support. Time-to-stability (TTS), based on the diminishing fluctuations of ground reaction forces and COP trajectories, is often used to assess this transitional ability [1]. Experiments designed to assess dynamic stability between different athletic populations [2] and individuals with and without ankle instability [3] are examples of past research efforts.

TTS is often assessed after someone lands on one foot from a forward hop or from a forward-directed vertical jump [2,3]. The influence of different landing directions has received little attention. Recently Wikstrom et al. [4] examined the difference in dynamic stability between hops from different directions by evaluating a postural stability index, not TTS. The index score based on the medial-lateral (ML) ground reaction force was the only measure to show differences between hop directions.

The purpose of the present investigation was to assess the influence of landing direction on TTS, a measure more commonly used among researchers assessing dynamic stability. Specifically, hops from four different directions were examined while each orthogonal component of the ground reaction force was used to calculate TTS measures.

METHODS

Twenty healthy, recreationally active participants (9 men and 11 women, age = 28 ± 4 yrs, body mass = 73.3 ± 21.5 kg, height = 173.4 cm ± 10.5 cm) volunteered for this study. Participants were asked to complete four hopping tasks onto an AMTI force plate. They used no footwear and landed on their dominant foot which was identified by asking what foot they would use to kick a ball. The four hopping tasks were: a forward hop at 100% of their leg length (F), a laterally directed hop (L), a medially directed hop (M), and a backwards hop (B). The hopping tasks were assigned in a randomized order and the mean of three trials for each condition was used in statistical analyses.

Ground reaction force (GRF) data were collected at 100 Hz for 10 seconds after landing. TTS was calculated using a sequential estimation technique applied to components of the GRF in the medial-lateral, anterior-posterior, and vertical directions (Fx, Fy, and Fz, respectively) [1]. Three separate repeated measures analysis of variance were used to assess differences in hop direction. Post hoc within-subject contrasts were completed if statistical significance was found ($\alpha = .05$).

RESULTS AND DISCUSSION

There were statistically significant differences in landing direction for each measure of TTS. For Fx, the medial-lateral force, the F and B directions resulted in lower times than the M and L directions (see Figure 1). The opposite result was identified for Fy, the anterior-posterior force; the M and L directions had lower TTS values than the F and B directions (see Figure 1). When considering the vertical force, Fz, the F direction had a lower time than the other three directions.

When using GRF data for TTS, hop direction is a clear influence. The mean TTS values for Fz-based calculations were between 2.0 and 3.0 sec, whereas TTS based on horizontal ground reaction forces resulted in values near 1.0 sec or near 4.0 sec depending on hop direction (see Figure 1). Direct comparison of our results with previous work is difficult because of different protocols and different measures on dynamic stability.

As stated, Wikstrom et al. [4] showed differences in a stability index measure based on medial-lateral force, but no difference when using the anterior-posterior or vertical ground reaction force. They also did not examine a backward hop, but used two "diagonal" directions which were between a forward hop and a lateral hop. In addition, Gerbino et al. [2] reported center acquisition times, a measure similar to TTS, for a "side weight shift" between 3.0 and 4.0 sec which is similar to the higher values reported in the present study.

The multiple directions of hops investigated in the present study are often neglected in dynamic stability research. The large differences in TTS reported here suggest that a more complete profile of dynamic stability should include hops or jumps from more than one direction. Since ankle injuries happen most often in landing from a jump, future work should focus on the dynamic stability of multiple directions of hops. In addition, future research should also focus on mechanisms responsible for dynamic stability and how proprioceptive reactions to landings occur at the ankle.

CONCLUSIONS

Time to stability measures, calculated from the orthogonal components of the ground reaction force, are highly dependent on hop direction. These results suggest that researchers investigating ankle instability and other compromises to a person's stability should take into account multiple directions of landing when assessing dynamic stability.

REFERENCES

1. Colby, S, et al. *Journal of Orthopaedic & Sports Physical Therapy,* **29(8)**, 444-454, 1999.
2. Gerbino, PG et al. *Gait & Posture*, **26(4)**, 501-507, 2007.
3. Wikstrom, EA et al. *J Athletic Training* **41**, 245-250, 2004.
4. Wikstrom, EA, et al. *J Science Med Sport* **11**, 106-111, 2008.

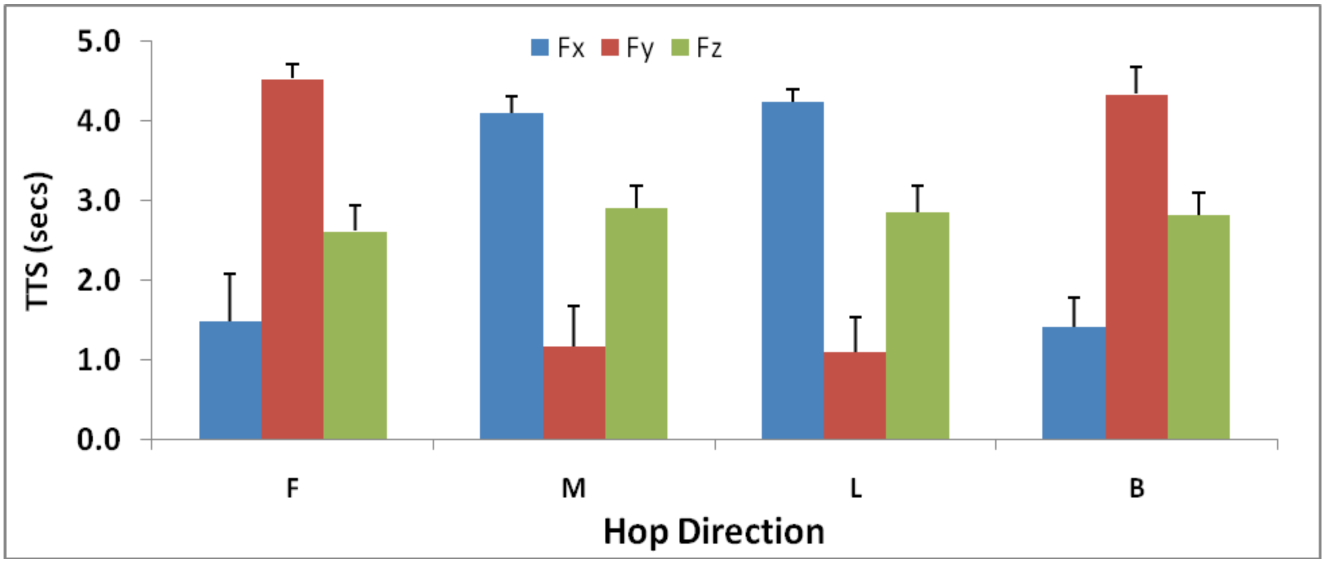

Figure 1. Mean time-to-stability values for all hop directions Forward, Medial, Lateral, Backward using sequential averaging technique of Colby et al. (1999) applied to Fx, Fy, and Fz. Error bars represent SD among 20 subjects. Statistically significant differences between hop directions are identified in the text.

REVISITING FINGER FLEXOR EXCURSIONS WITH CURRENT MODELING TECHNIQUES

Aaron M. Kociolek and Peter J. Keir
Occupational Biomechanics Laboratory, McMaster University, Hamilton, ON, Canada
Email: kociolam@mcmaster.ca

INTRODUCTION

The pathophysiologies of many distal upper extremity work-related musculoskeletal disorders are uncertain. Differential motion between the extrinsic finger flexor tendons is thought to contribute in the development of hand/wrist tenosynovitis and carpal tunnel syndrome due to increased frictional work. Armstrong and Chaffin [1] developed anthropometric-based regression equations to estimate flexor digitorum profundus (FDP) and flexor digitorum superficialis (FDS) tendon excursions with wrist and finger joint displacements from four cadaveric specimens. Treaster and Marras [2] used the equations to predict FDP and FDS cumulative tendon excursions during keyboarding. The equations have also been used in a two-dimensional model to estimate frictional work at the tendon sheath [3]. However, there is a need to evaluate this approach with empirical data and current modeling techniques.

Holzbaur et al. [4] recently developed a three-dimensional biomechanical model of the upper extremity with 15 degrees of freedom and 50 muscle actuators to simulate movement at the shoulder, elbow, forearm, wrist, thumb and index finger. However, several additions are needed to assess FDP and FDS tendon excursions. Efforts to model joint displacements of the third, fourth and fifth digits with anatomically correct extrinsic finger flexors are needed to calculate differential tendon motion (and to develop an analytical model for frictional work). The purpose of this study was to develop a biomechanical hand model with accurate extrinsic finger flexor tendon excursions.

METHODS

Software for Interactive Musculoskeletal Modeling (SIMM) by MusculoGraphics Inc. (Santa Rosa, CA) was used to further refine an existing hand model (Figure 1). The Holzbaur et al. [4] upper extremity model served as a starting point, which has representations of the carpals, metacarpals and phalanges scaled as a 50th percentile male. Metacarpophalangeal (MCP) joints of the third, fourth and fifth digits were modeled as universal joints to simulate flexion/extension and abduction/adduction. Proximal and distal interphalangeal (DIP and PIP) joints were modeled as hinges to simulate flexion/extension. Since detailed descriptions of the MCP and IP joint rotation axes did not exist for the third, fourth and fifth digits, cylinders were fit at the bone surfaces to characterize movement. This method was also used for the MCP and IP joints of the second digit [4]. Also, range of motion parameters were set equivalent to those existing for the second digit [4].

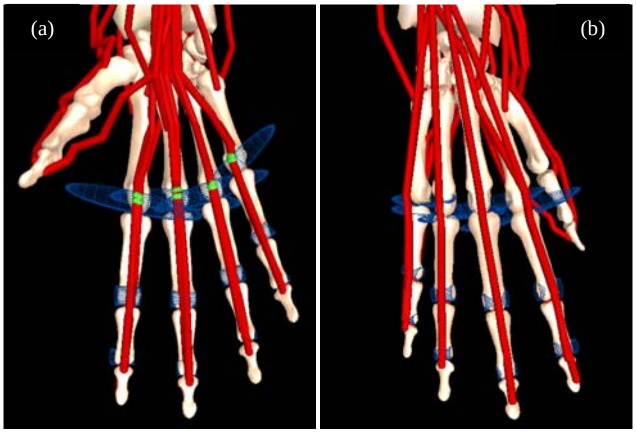

Figure 1: Hand model in (a) palmar and (b) dorsal views illustrating muscle-tendon geometry (red cords) and wrapping surfaces (blue shapes).

Eight extrinsic finger flexors were included in the model. The muscle–tendon paths were described with a series of points in the bone local coordinate systems. Points that constrain the paths of the FDP and FDS (such as annular pulleys) were added to improve the anatomical accuracy of the hand model. Wrapping surfaces were also added at the MCP and IP joints to simulate accurate tendon excursions. Muscle-tendon excursions of the FDP and FDS were calculated with MCP and IP flexion/extension and compared to regression outputs from Armstrong and Chaffin [1] for a 50th percentile male.

RESULTS AND DISCUSSION

Generally, modeled tendon excursions of the FDP and FDS were small compared to regression with MCP flexion/extension (Figure 2a). The modeled FDP and FDS tendon excursions were 85.3±1.6% and 80.3±1.2% compared to regression respectively (Table 1). Modeled tendon excursions of the FDP and FDS generally agreed with regression through PIP and DIP flexion (Figure 2b). Modeled FDP and FDS tendon excursions with PIP flexion were 97.3±1.2% and 99.1±1.0% of the regression respectively (Table 1). Modeled FDP tendon excursions were 100.1±1.7% with DIP flexion compared to regression (Table 1).

The modeled FDP and FDS tendon excursions were not always linear, which resulted in deviations from regression near the extremes of joint displacement. This was particularly evident for FDP and FDS tendon excursions with PIP joint displacements. However, experimental tendon excursions are unlikely to be perfectly linear since the joint center locations change with joint displacements.

Although some differences were observed between modeled and calculated FDP and FDS tendon excursions, there is limited empirical data describing tendon kinematics. The anthropometric-based regression equations developed by Armstrong and Chaffin [1] were derived from four cadaveric specimens. Research is in progress to obtain anthropometric measurements and tendon excursions *in vivo* with MCP, PIP and DIP joint displacements using ultrasound and motion capture. Efforts to model individual tendon excursions with joint displacements will follow.

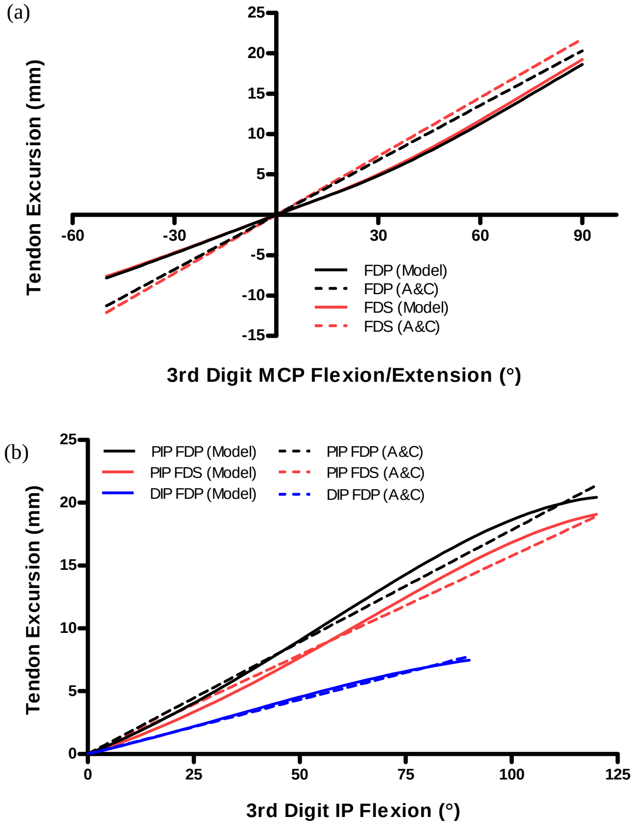

Figure 2: Tendon excursions of the FDP and FDS with third digit (a) MCP and (b) PIP and DIP joint displacement. Positive values are joint flexion. Negative values are joint extension. A&C is an abbreviation for Armstrong and Chaffin [1].

REFERENCES

1. Armstrong TJ and Chaffin DB *J Biomech* **11**, 119-128, 1978.
2. Treaster DE and Marras WS *Clin Biomech* **15**, 499-503, 2000.
3. Moore A, et al. *Ergonomics* **34**, 1433-53, 1991.
4. Holzbaur K, et al. *Biomed Eng* **33**, 829-840, 2005.

ACKNOWLEDGEMENTS

This study was funded by NSERC Canada (grant # 217382-04).

Table 1. Tendon excursions of the extrinsic finger flexors with joint flexion/extension (mm/100°).

		Third Digit			Fourth Digit			Fifth Digit		
		MCP	PIP	DIP	MCP	PIP	DIP	MCP	PIP	DIP
FDS	Modeled	19.2	15.8	0.0	18.7	15.1	0.0	17.9	14.1	0.0
	Armstrong and Chaffin [1]	24.2	15.8	0.0	23.4	15.3	0.0	21.9	14.3	0.0
FDP	Modeled	18.9	17.4	8.8	18.6	16.6	8.2	17.6	16.1	7.8
	Armstrong and Chaffin [1]	22.6	17.8	8.8	21.7	17.3	8.3	20.3	16.4	7.7

DEVELOPMENT OF A LOW COST ROBOTIC GAIT TRAINER

[1] J. Cortney Bradford, [1]Peter E. Pidcoe
[1]Department of Physical Therapy, Virginia Commonwealth University, Richmond, VA
email: bradfordjc@vcu.edu

INTRODUCTION

Stroke is one of the leading causes of disability in the United States with 750,000 individuals affected each year (1). A major residual effect of stroke is impaired walking ability. While 70-80% of adults who survive a stroke will regain the ability walk short distances, less than 50% are able to achieve even limited community ambulation (2). Each year the cost of stroke is nearly $30 billion in direct medical costs and nearly $20 billion in lost productivity (3). Residual disability from stroke has high social and economic impact. Restoration of gait is a major goal of rehabilitation for persons with stroke.

The current focus for gait restoration due to paralysis associated with stroke is on task specific, repetitive rehabilitation techniques. This means that in order to relearn a normal walking gait pattern the patient must practice walking. Body weight supported treadmill training is a task specific therapy that has been shown to improve gait in hemiparetic stroke subjects (4), however it has failed to become widely used because of the high staffing costs required to perform the treatment (5).

More recently, the field of robot-assisted motor rehabilitation has emerged and is rapidly developing. In this type of training, a machine guides the lower extremities in a normal gait pattern while the body weight of the subject is supported. In a recent review of robotic-assisted gait training devices used in post stroke rehabilitation, the authors found that robotic gait trainers were as effective as body weight supported treadmill training (6). One major disadvantage of these robotic gait trainers is the actual cost of the device. While the number of staff required to perform the therapy is reduced, these devices can be very expensive and often too expensive for widespread clinical application.

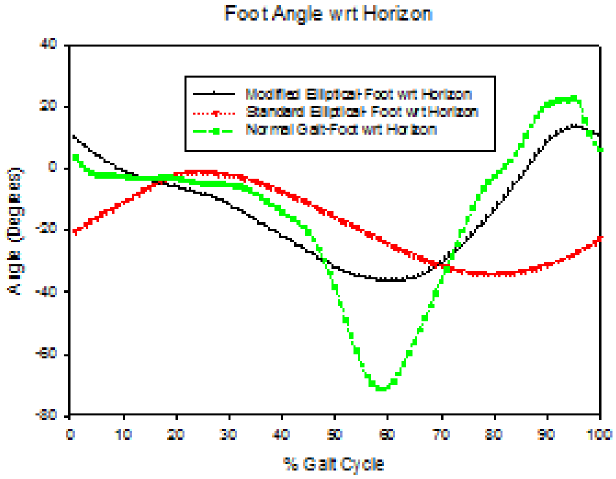

Figure 1: Foot angles with respect to horizon during ambulation on the modified and non-modified elliptical trainer and during normal gait.

Our solution to this problem was to create a low-cost robotic device that has the ability to simulate normal gait. The platform for our design is a commercially available elliptical trainer ($600) which has been modified and coupled with a body-weight support system.

METHODS

The elliptical based robotic gait trainer (EBRGT) was developed from a commercially available elliptical trainer. Elliptical trainers provide a lower extremity motion that simulates walking or running. The foot is moved in an elliptical pattern on a leaf spring shaped ski. This provides some shock attenuation and ankle movement, however, the ankle joint stays in a neutral to plantar-flexed position throughout the gait cycle with this design. This is depicted by the red line in Figure 1. This pattern is different from normal gait, depicted by the green line in Figure 1.

To create the EBRGT, the footplates of the elliptical trainer were modified to allow sagittal plane ankle articulation in a controlled trajectory that mimics normal gait. First a rigid platform was attached at one end to the ski. The other end was attached directly to the peg supporting the back end of the ski. This was done so that the impact absorbing quality of the leaf spring ski could still be exploited, but also provided a rigid surface to mount the mechanical components for the modification.

A new footplate was created and attached to the rigid platform via a single axis bearing, allowing sagittal plane articulation. Footplate motion was driven by an AC servo motor, coupled with a worm gear box and mechanically linked to the footplate via a belt drive. These modifications were made to both the left and right side of the elliptical trainer.

The motion of each footplate was controlled by a separate single axis controller. To link the motion of the left and right footplate, each controller received feedback from a common optical encoder mounted on the axis of the elliptical trainer flywheel. Figure 2 illustrates the control schematic. Recall that the flywheel drives the motion of both skis, with the left and right ski being 180 degrees out of phase. The motion of the footplate was controlled as follows: The user drives the motion of the elliptical by applying force to the footplates. This causes the flywheel to start turning. The encoder provides feedback about the position of the flywheel to the controllers and the position of the footplate (orientation in the sagittal plane) is adjusted based on the position of the flywheel. Specific events in a normal gait cycle have been synchronized to the position of the flywheel on the elliptical.

RESULTS AND DISCUSSION

The design of the EBRGT allows active control of the orientation of the footplate in the sagittal plane. In a previous iteration of the design, we were able to achieve a sagittal plane articulation of the footplate similar to an average normal gait pattern using only a passive mechanical modification to the elliptical. Figure 2 illustrates the footplate pattern for an entire gait cycle for three different conditions: elliptical with passive mechanical modifications, elliptical before modifications, and level surface walking. Note that the modified elliptical pattern (black) more closely resembles normal gait (green), as compared to the non-modified elliptical pattern (red). The new active system allows for the footplate to follow a pattern that mimics normal gait, while still allowing the pattern to be adjusted for each user.

CONCLUSIONS

The EBRGT may be a low-cost solution for robotic gait training in a population suffering gait deficits secondary to stroke. Studies are in progress to test the effectiveness of the EBRGT as a gait rehabilitation tool for patients with gait deficits secondary to stroke.

REFERENCES

1. Williams GR, et al. *Stroke* **30**, 2523-2528, 1999.
2. Friedman PJ. *Int Disabil stud* **12**, 119-122, 1990.
3. Mayo N. *Phys Med Rehabil* **7**, 1-25, 1993.
4. Sullivan KJ, et al. *Phys Ther* **87**(12), 1-23, 2007.
5. Morrison SA, et al. *JNPT* **31**, 50-54, 2007.
6. Mehrholz J et al. *Cochrane Database of Systematic Reviews* **4**, Art No:CD006185, 2007.

ACKNOWLEDGEMENTS

This project was funded by an A. D. Williams research award.

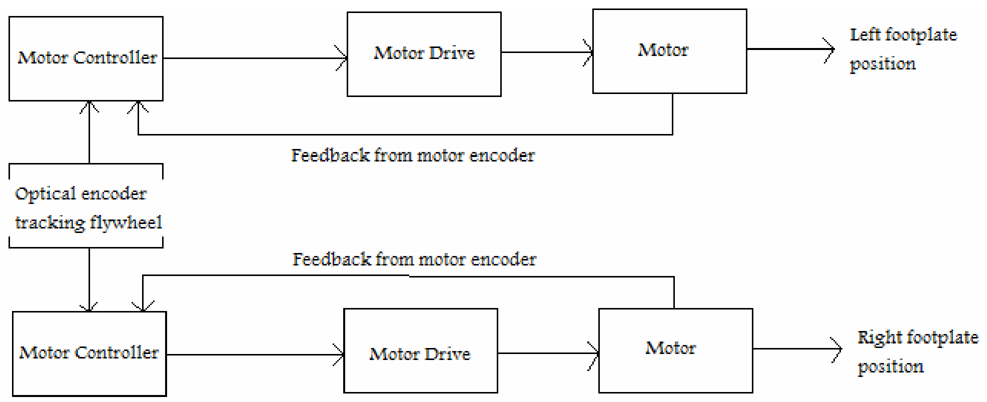

Figure 2: EBRGT control block diagram.

THE RELATION BETWEEN KNEE SEPERATION DISTANCE AND LOWER EXTERMITY KINEMATICS DURING A DROP LAND: IMPLICATIONS FOR CLINICAL SCREENING

Kathryn L. Havens, Susan M. Sigward, Wei-Cheng Cheng, Christine D. Pollard, Christopher M. Powers
Jacquelin Perry Musculoskeletal Biomechanics Research Laboratory
Division of Biokinesiology and Physical Therapy
University of Southern California, Los Angeles, CA, USA
email: khavens@usc.edu, web: www.usc.edu/go/mbrl

INTRODUCTION

Prospectively, three-dimensional knee abduction (valgus) angle during a drop land was found to be a predictor of anterior cruciate ligament injury risk in female athletes. [1] As a result, techniques have been developed to screen athletes for excessive frontal plane knee motion during drop land tasks in attempt to identify those at increased risk for injury.

Due to the time and expense related to assessment of three-dimensional joint kinematics, techniques assessing the extent to which the knees collapse medially have been adopted clinically. Techniques typically include measures of knee separation distance in the frontal plane during landing. While these measures have been used in several research studies to identify gender differences and to assess the effects of training, [2,3,4] it is not clear how they relate to abduction of the knee. Given the potential for transverse and frontal plane motion of the lower extremity to influence measures of knee separation distance, it is possible that these clinical assessments do not accurately represent knee frontal plane kinematics.

The purpose of this investigation was twofold: 1) to determine the relation between minimum knee separation distance and bilateral knee abduction angles and, 2) to determine the association between minimum knee separation distance and bilateral lower extremity transverse and frontal plane angles.

METHODS

Subjects consisted of 25 healthy, females athletes (ages 11 to 23 yrs) with no history of previous knee injury. Average height was 162.4 cm and average weight was 57.67 kg.

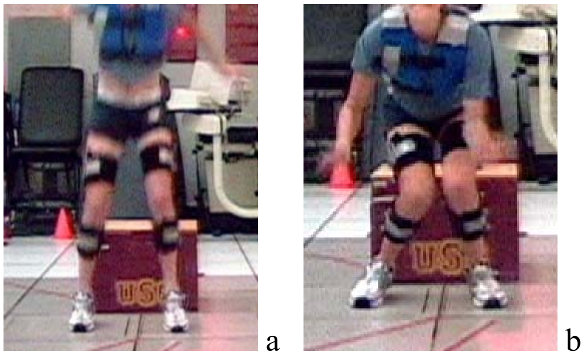

Figure 1: Deceleration phase of a drop land, at foot contact (a) and maximum knee flexion angle (b)

Subjects performed a bilateral drop land from a 36 cm platform followed by a maximum vertical jump. Three-dimensional kinematics were collected using an 8 camera Vicon motion analysis system (250 Hz). Visual3D™ software (C-Motion, Inc., Rockville, MD, USA) was used to quantify three dimensional, 6 degree-of-freedom hip, knee, and ankle kinematics.

All data were analyzed during the deceleration phase of landing, defined as the time between foot contact and maximum knee flexion angle (Figure 1). Minimum knee separation distance was calculated as the distance between the right and left lateral femoral epicondyles in the frontal plane. Lower extremity transverse and frontal plane angles were identified bilaterally at the time of minimum knee separation. Right and left angular data were averaged to account for the contribution from each lower extremity to the knee separation distance. Data were average across three trials.

The independent variable of interest was minimum knee separation distance. Dependent variables included the average knee and hip frontal and transverse plane, and ankle frontal plane angles of both limbs.

Linear regression was used to determine the association between minimum knee separation distance and bilateral average knee frontal plane angle. Stepwise multiple regression was used to identify the best predictors of minimum knee separation distance during a drop land. Statistical analyses were performed using SPSS software (Chicago, IL). Significance levels were set at $P \leq 0.05$.

RESULTS

Bilateral average knee frontal plane angle was a significant predictor of minimum knee separation distance ($R=0.573$, $R^2=0.328$, $P=0.003$; Figure 2). The association was negative, indicating that greater knee abduction angles were associated with smaller knee separation distances.

Figure 2. **Knee separation distance vs. Knee frontal plane angle**

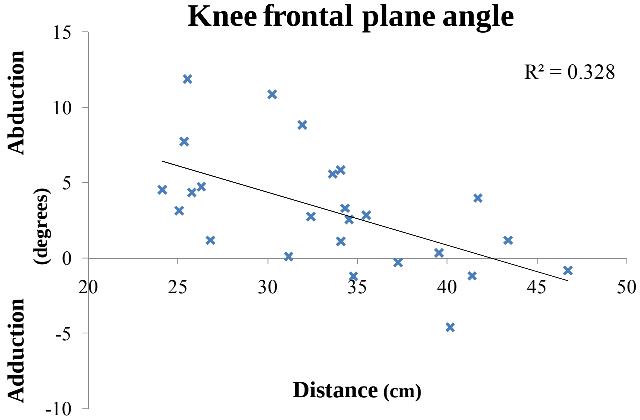

Figure 3. **Knee separation distance vs. Hip frontal plane angle**

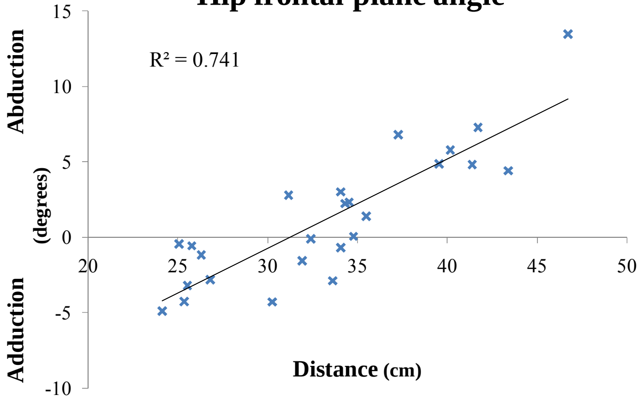

Of the dependent variables, average bilateral hip frontal plane angle was the only predictor of minimum knee separation distance ($R= 0.861$, $R^2 = 0.741$, $P < 0.001$; Figure 3). In general, greater hip abduction angles were associated with greater knee separation distances.

DISCUSSION

Bilateral average knee frontal plane angle explained only 33% of the variance in minimum knee separation distance, suggesting that it is not a good indicator of knee abduction angle during a drop land. Minimum separation distance appears to be a better indicator of bilateral average hip frontal plane angle as it was the only predictor of knee separation distance to enter into the regression equation, explaining 74% of the variance.

CONCLUSIONS

Measures of knee separation distance during bilateral landing tasks appear to provide information regarding medial collapse of the lower extremities. However, they are more indicative of frontal plane hip motion. Caution must be taken when relating these measures to knee abduction angles.

REFERENCES

1. Hewett TE, et al. *Am J Sports Med* 33, 492-501, 2005
2. Ford KR, et al. *Am J Sports Med* 33, 1745-50, 2005
3. Barber-Westin SD, et al. *Am J Sports Med* 33, 1-8, 2005
4. Noyes FR, et al. *Am J Sports Med* 33, 197-207 2005

ACKNOWLEDGEMENTS

This study was funded by the National Institutes of Health (R01 AR053073-02).

INFLUENCE OF ASYMMETRY OF LOWER EXTREMITY FORCE ON CENTER OF MASS VELOCITY DURING A SIT TO STAND TASK AMONG SUBJECTS WITH HIP FRACTURE

[1,2] Janet Kneiss, [1]Ryan Yelle and [1,2] Jeff Houck
[1]Ithaca College-Rochester, Rochester, NY, [2] University of Rochester Medical Center, Rochester, NY
email: Janet_Kneiss@URMC.Rochester.edu

INTRODUCTION

Physical decline after a hip fracture is associated with changes in movement strategies that affect functional status. Recent studies of subjects post hip fracture demonstrate greater force (vertical ground reaction force[vGRF]) of the uninvolved limb during the rising phase of a sit to stand (STS) task[1]. Yet, how the preference of subjects post hip fracture for the uninvolved side influences center of mass (CM) defined movement strategies during a STS task is unclear. Healthy elderly subjects compared to subjects with mobility limitations are characterized by: higher horizontal CM velocity, and decreased sit to stand time. [2,3] Subjects with mobility limitations use CM horizontal velocities lower than 0.4 m/s during a STS task. The lower CM horizontal velocity is thought to be an adaptation to maintain stability as the individual moves the CM over the base of support[2]. In contrast, CM vertical velocity may be lower in the presence of strength deficits and learned preference for the uninvolved limb (higher vGRF of the uninvolved limb) [4]. The purpose of this study was to compare CM velocity (horizontal and vertical) and vGRF(involved/uninvolved) during the rising phase of a STS task in subjects post hip fracture.

METHODS

Fourteen individuals with hip fracture (5 male, 9 female; age=78 ± 6) and 15 elderly controls (3 male, 12 female; age=69 ± 10) volunteered for this study. Surgical procedures for hip fractures included hemiarthoplasty (8) and ORIF (6). Subjects were between 2-12 months post hip fracture and were currently discharged from care.

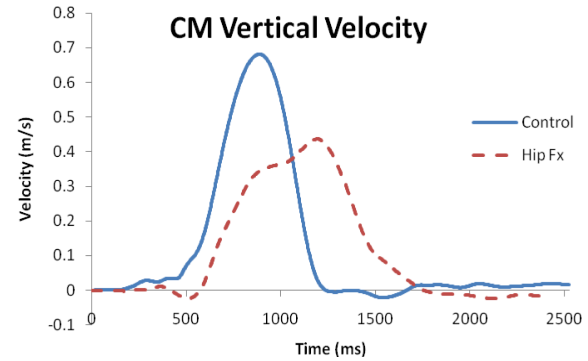

Figure 1: Example of CM vertical velocity for an elderly control (solid line) and hip fracture subject (dotted line).

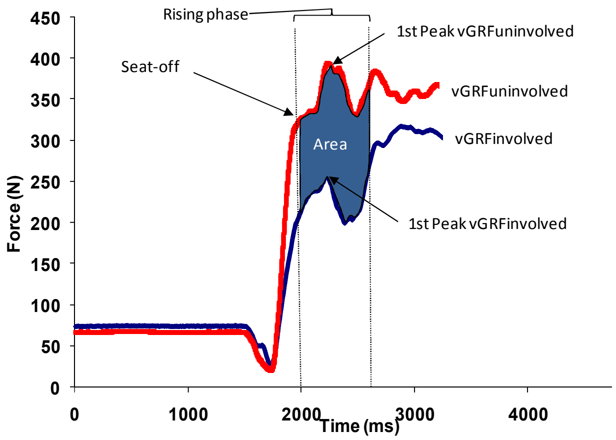

Figure 2: The unilateral measures of vGRFinvolved/uninvolved were determined from the left and right force plates. Symmetry during the rising phase was calculated as the area between the vGRFinvolved and uninvolved throughout the rising phase.

An Optotrak Movement Analysis System (Northern Digital, Inc, Waterloo, CANADA) and force plate (Kistler, Amherst, NY) integrated with The Motion Monitor software (Innsport, Inc, Chicago, IL, USA) was used to measure ground reaction force. To assess lower extremity force, four force plates were used to record GRF under each leg (unilateral), the trunk (bilateral) and the seat (bilateral) at a sampling rate of 1000 Hz during a STS task. The STS task was performed 3 times without hands. The rising phase was determined from seat off (start of rising phase) to the point of level body weight (end of rising phase). The vertical and horizontal GRF, were divided by mass, and integrated with respect to time, to determine CM (horizontal and vertical) velocity during the rising phase of the STS task (Figure 1). Gravity was taken into account in determining vertical CM velocity. Preference for the uninvolved limb was defined as the AREA between the vGRF of the involved versus uninvolved side during the rising phase (Figure 2). Peak horizontal and vertical velocity of the CM, AREA, and peak vGRF during the rising phase were compared between the controls and subjects post hip fracture using two sample t – tests. Pearson Product Moment correlations were used to explore the univariate correlations among variables.

RESULTS AND DISCUSSION

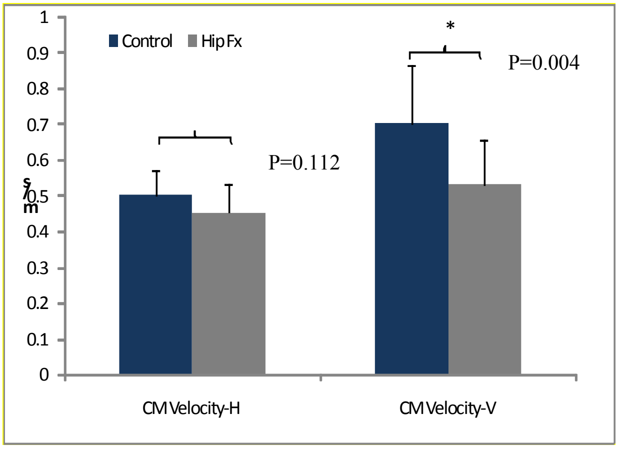

Figure 3: CM velocity horizontal and vertical for both hip fracture and control subjects. P-values are results of a 2 sample t-test.

The new findings of this study show that subjects with hip fracture exhibit significantly lower vertical CM velocities (p=0.004, HF = 0.45m/s ± .08 vs Cont = .50m/s± .07) during a sit to stand task (rising phase) while maintaining similar horizontal CM velocities compared to controls (p=0.11, HF = 0.53m/s ± .12 vs Cont = .70m/s± .16) (Figure 3). Additionally, subjects with hip fracture tended to rise with a preference for the uninvolved side (Area:p=0.008, HF = 1.25 N*s/Kg ± .85 vs Cont =0.53N*s/Kg ± .22), relying 20-30% less on their involved limb (Peak (vGRF) involved:p=0.009, HF = 5.37 N/Kg ± .84 vs Cont = 6.43 N/Kg ± 1.18) compared to their uninvolved limb (Peak (vGRF) uninvolved:p=0.79, HF = 6.62 N/Kg ± 0.67 vs Cont = 6.52 N/Kg ± 1.33). A moderate correlation was observed between CM velocity vertical and Area (p=.005: r=.703) for the hip fracture group. The reliance on the uninvolved side has a much stronger influence on CM velocity vertical than the horizontal. Theoretically the lower CM velocity may result from a learned movement strategy to slow down CM velocity vertical in order to minimize falls risk. A higher CM velocity vertical in the presence of 20-30 % vGRF asymmetry may push the CM close to the limits for maintaining balance. Therefore a slower CM velocity vertical may be a compensation to decrease falls risk post hip fracture, explaining the correlation between AREA and CM velocity vertical. Strength deficits may also contribute and are amenable to progressive resistance training. New training programs seeking to return subjects post hip fracture to pre-morbid status may consider evaluating these alterations of lower extremity force and CM velocity.

CONCLUSIONS

Hip fracture subjects transitioned from sit to stand with decreased vertical CM velocity and higher vGRF on the uninvolved side despite being discharged from rehabilitative care. Decreases in vertical (rather than horizontal) CM velocities may represent compensatory movement strategies associated with falls risk in subjects post hip fracture.

REFERENCES

1. Portegijs E, Sipila S, Rantanen T, Lamb SE. Leg extension power deficit and mobility limitation in women recovering from hip fracture. *American Journal of Physical Medicine & Rehabilitation* 2008;87:363-70.
2. Hughes MA, Schenkman ML. Chair rise strategy in the functionally impaired elderly. *Journal of Rehabilitation Research & Development* 1996;33:409-12.
3. Pai YC, Patton J. Center of mass velocity-position predictions for balance control.[erratum appears in J Biomech 1998 Feb;31(2):199]. *Journal of Biomechanics* 1997;30:347-54.4.
4. Magaziner J, Hawkes W, Hebel JR, et al. Recovery from hip fracture in eight areas of function.[see comment]. Journals of Gerontology Series A-Biological Sciences & Medical Sciences 2000;55:M498-507.

ACKNOWLEDGEMENTS

The authors are grateful for support from the National Institute of Aging; Center for Research Translation,Grant#:1P50AR054041-02)

PLANTARFLEXOR MOMENT ARM CORRELATES WITH PREFERRED GAIT VELOCITY IN HEALTHY ELDERLY SUBJECTS

[1] Sabrina S.M. Lee and [1,2,3] Stephen J. Piazza
Departments of [1]Kinesiology, [2]Mechanical & Nuclear Engineering, and [3]Orthopaedics & Rehabilitation,
The Pennsylvania State University, University park, PA, USA
email: piazza@psu.edu

INTRODUCTION

Walking ability is a fundamental determinant of quality of life that is known to decline with advancing age. Gait velocity begins to decline at 12% to 16% per decade after the age of 70 [1] mainly through a reduction in step length [2]. Reduced walking velocity has been attributed to age-related reductions in lower extremity strength and power [3,4].

Decreased walking velocity in older adults is accompanied by decreased ankle plantarflexion range of motion, plantarflexor moment, and plantarflexor power during gait [3,4]. Judge et al. found that older adults walk faster by generating greater hip flexor power, suggesting (a) that ankle plantarflexor power cannot be increased and is thus a limiting factor in determining walking speed; and (b) that different strategies might be employed at fast and preferred walking speeds in older adults.

It is reasonable to expect that age-related decreases in triceps surae cross-sectional area contribute to reduced plantarflexor moment- and power-generating capacity, but other musculoskeletal architecture parameters have the potential to influence moment and power and thus gait velocity. Plantarflexor moment arm and muscle fascicle length are two such parameters whose influence on gait velocity has not yet been studied.

The purpose of this study was to investigate the influence of plantarflexor moment arm and plantarflexor fascicle length on both preferred and maximum gait velocity in a group of healthy elderly subjects.

METHODS

Fascicle length, pennation angle, and plantarflexion moment arm of the lateral gastrocnemius muscle were measured in 10 elderly adult males (76.1 ± 5.4 y, 174.1 ± 5.2 cm, 87.3 ± 13.6 kg). Subjects received a screening questionnaire to exclude those with a history of stroke, heart attack, arthritis, and joint surgery. None of the subjects reported any muscular or joint injuries in the year prior to testing. All subjects gave informed consent prior to testing and all procedures were approved by the Institutional Review Board of the University.

Fascicle length and pennation angle were determined from images captured using B-mode ultrasonography (Aloka 1100; transducer: SSD-625, 7.5 MHz). Images of the central region of the muscle were obtained while the subjects were standing in anatomical position.

Plantarflexor moment arm was calculated from tendon excursion measured from ultrasound images and measured foot rotations. In these tests, the foot was rotated manually by an experimenter from approximately 5º dorsiflexion to 20º plantarflexion using a potentiometer-instrumented rotating foot platform while a second experimenter captured ultrasound images of the musculotendinous junction. During these tests, the subject was seated with the knee fully extended and the subject plantarflexed maximally against the foot platform in order to minimize artifact resulting from variation in tendon tension during movement [5]. Moment arm was estimated as the slope of the line fit to the tendon excursion versus ankle angle data.

Preferred walking speed was determined using the Six-Minute Walk Test [6], in which the subject was asked to walk at a preferred pace for six minutes along a level walkway between two cones spaced 50 m apart. Maximum walking velocity was assessed during tests in which subjects were asked to walk 4 m as fast as possible.

RESULTS

A moderate and significant correlation ($R^2 = 0.48$, $p = 0.026$) was found between plantarflexion moment arm and preferred walking velocity but no significant correlation ($R^2 = 0.13$, $p = 0.312$) was found between plantarflexion moment arm maximum velocity (Figure 1). No significant correlations were found between lateral gastrocnemius fascicle length and preferred walking velocity ($R^2 = 0.20$, $p = 0.193$) or maximum walking velocity ($R^2 = 0.10$, $p = 0.382$) (Figure 2). Neither walking velocity (preferred or maximum) nor plantarflexor moment arm was found to correlate with body height (all $R^2 \leq 0.21$; $p > 0.05$).

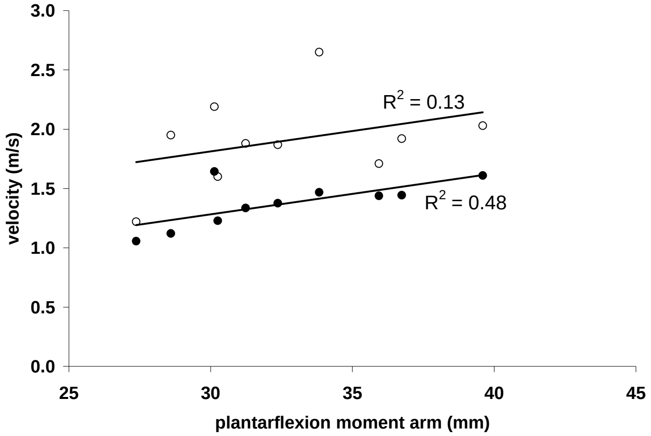

Figure 1. Preferred walking velocity (filled circles) and maximum velocity (open circles) plotted versus plantarflexion moment arm.

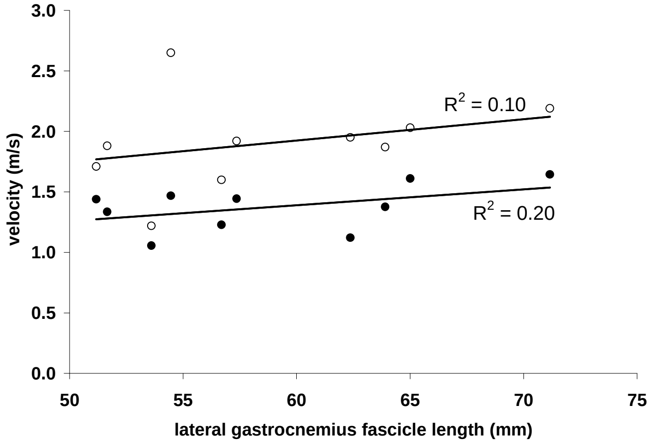

Figure 2. Preferred walking velocity (filled circles) and maximum velocity (open circles) plotted versus lateral gastrocnemius fascicle length.

DISCUSSION

Preferred walking velocity was found to correlate with plantarflexor moment arm, but this was not the case for maximum walking velocity. This finding suggests that age-related reduction in step length at the preferred velocity depends to some extent on the mechanical advantage of the plantarflexor muscles but that this dependence vanishes when subjects are asked to walk fast, perhaps because of increasing reliance on another mechanism, such as the hip flexors, to increase step length [3].

Bean et al. [6] found Six-Minute Walk Test performance to correlate moderately with ankle power ($R^2 = 0.37$) and ankle strength ($R^2 = 0.24$) in isokinetic and isometric dynamometer tests in a mobility-limited population. Our findings suggest that plantarflexor moment arm is an even better predictor of preferred gait speed, perhaps because maximal moments are were not generated during preferred walking in our healthy elderly subjects. A likely mechanism is that a larger plantarflexion moment arm permits a subject to take a longer step and that the importance of having a sufficient moment arm is increased when muscle mass is lost with aging.

CONCLUSIONS

Plantarflexor moment arm is moderately correlated with walking velocity in healthy elderly subjects. This finding that mechanical advantage is a potentially important determinant of locomotor ability in the elderly will help with designing and targeting interventions intended to preserve mobility in this population.

REFERENCES

[1] Hinman JE et al. *Med Sci Sports Exerc* **20**, 161-166, 1988.

[2] Crowninshield RD et al. *Clin Orthop* **132**, 140-144, 1978.

[3] Judge JO et al. *Journal of Gerontology* **51A**, M303-M312, 1996.

[4] Winter DA et al. *Phys. Ther.* 70, 340-347, 1990.

[5] Maganaris CN et al. *J. Physiol.* 510, 977-985, 1998.

[6] Bean et al. *J Gerontology A Biol Sci Med Sci* **57**, M751-756, 2002.

ACKNOWLEDGEMENTS

The authors would like to thank Emre Ak, Nancy Campbell, Amanda Mesa, Kathleen Mulvaney, and Tom Novack for their assistance in data collection.

TEMPORAL EFFECTS OF GALVANIC VESTIBULAR STIMULATION ON GAIT AS MESURED BY ACCELEROMETERS

Jennica L. Roche, Daniel P. Steed and Mark S Redfern
Human Movement and Balance Laboratory, Department of Bioengineering
University of Pittsburgh, PA, USA
Email: jlr59@pitt.edu, Web: http://hmbl.bioe.pitt.edu/

INTRODUCTION

Balance and stability in human postural control is a complicated phenomenon. Regulated by the integration of vestibular, visual, and proprioceptive sensory feedback, it can often be difficult to tease out the contributions from each input. The primary aim of this project is to contribute to the understanding of the impact of vestibular signals through the use of galvanic vestibular stimulation (GVS) as the method of vestibular perturbation. Specifically, understanding the timing the vestibular contribution will offer a better explanation to its effect.

Hlavacka et al. examined the effects of GVS on COP during stance using a stimulus profile similar to a cosine-bell wave form with a peak amplitude of 1mA; they observed a response delay of approximately one second after GVS trigger [1]. Further studies, including Britton et al., have observed a latency to GVS in the electromyographic response of ~110 to 140ms [2]. These time responses have not been explicitly explored in gait; however, it has been found that in lower body control, especially foot placement, that vestibular input is phase dependent. Bent et al. reported GVS at heel contact (HC) creates the largest response deviations [3]. Additionally, upper body response is believed to be based on the transition into a dynamic state and not directly phase related [3, 4].

METHODS

The study consisted of nine young, healthy adults (2F, 7M; mean age 25 ± 3.7 years) who were screened to be free of any neurological and vestibular disorders.

After the skin was abraded (NuPrep^{TM} gel), cleansed, and coated (TENS Clean-Cote® whipe), two self-adhering Superior Silver® stimulating electrodes (3.17cm diameter) were affixed over each subjects' mastoid processes in a binaural-bipolar configuration. The GVS current was composed of two five second square pulses with alternating polarity and an amplitude of 1mA. The two pulses were applied by a linear stimulus isolator (model A395R-A, World Precision Instruments, Inc), and separated by one second of rest. For any trial where the GVS was applied, only data from the first five seconds of the current were analyzed.

Three triaxial accelerometers (SparkFun, Freescale MMA7260Q, ±6g) were adhered to the top of the head, back of the thorax between the scapula, and back of the pelvis between the right and left posterior superior iliac spines using double-sided tape. Each accelerometer allowed for the collection of three dimensional accelerations in each segment, up to six gravitational units (g) (typical sensitivity = 200mV/g; XY bandwidth response = 350 Hz; Z bandwidth response = 150Hz). Accelerometers were connected to the CPU via a NI USB-6211 data acquisition device, collected at 160Hz.

A total of seven conditions of trials with a repetition of three were collected. The trials were composed of: three GVS conditions (none/R^+/R^-), two eye conditions (open [EO]/closed [EC]), and two GVS trigger conditions (heel contact [HC]/mid-stance [MS]). The trigger condition is relative to the HC of the right foot. The MS and EO trials were a part of a larger study and were not examined here.

DATA PROCESSING

The raw voltages were extracted from the accelerometers; an average was taken over the EO, static trial and then subtracted from all data points. The middle three strides were selected from each of the three control trials for each subject based on HC as detected by the footswitches. The stride before GVS trigger, from each of the subjects' GVS trials, was also included as a control stride; these select strides were averaged as a baseline of normal accelerations. Deviation from normal acceleration was defined as the first point at which the difference between the trial data and the control mean was greater than two times the standard deviation of the control strides for twenty or more points.

RESULTS

Overall, an initial deviation of the segmental accelerations occurred within the first stride after GVS. On average, the deviations centered about the first heel contact following the activation of the stimulus. This time point is approximately 500ms after the stimulus. Figure 1 below displays a typical acceleration plot depicting the initial deviation near fifty percent of a stride.

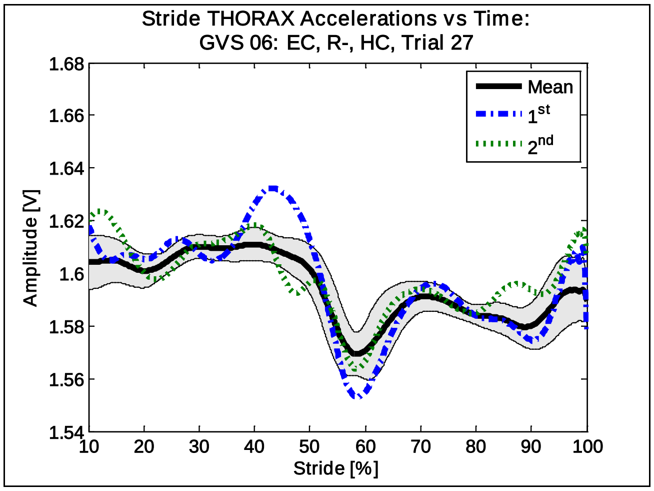

Figure 1: Typical filtered, thorax acceleration plot, where the blue line (-·-) is the first stride after stimulus initiation and the green line (--) is the second stride following GVS.

Table 1 below displays the averaged results of the deviation points with respect to the percentage of the gait cycle across subjects. The within subject variability is much smaller than the values presented here, especially in the thorax accelerations with values ranging from approximately 1% to 25%. All trials beginning with values already greater than two standard deviations from the control mean were excluded from the calculations. Values about 100% represent point in the second stride after the GVS trigger.

Table 1: Average GVS Deviation Time in Gait Cycle

Stim. Type	**Segment**	**Initial Deviation (% Stride)**
R^+	**Head**	63.1±43.8
	Thorax	55.3±38.7
	Pelvis	43.2±27.4
R^-	**Head**	62.2±35.2
	Thorax	56.0±33.9
	Pelvis	41.9±31.2

DISCUSSION

The findings of this research indicate that the initial deviation from normal accelerations in gait can be seen as early as 15-25% into the stride following the GVS within subject. The timing as seen from the acceleration data precedes that of which can be seen from the motion capture data from the same study; it was reported that kinematic deviation initiated at 1.2 seconds after GVS [5]. Moreover, the clustering of the deviation times about the HC of the first step is consistent with the current literature, because it is a point of dynamic transition [4]. Additionally, when vision and proprioceptive feedback from the swing leg are lacking, the balance system would have received increased contributions from the vestibular system to maintain stability. The incorrect vestibular inputs due to GVS may have caused the deviation from the normal acceleration pattern [6].

It is logical that the initiation of the acceleration deviation does not occur earlier than observed for several reasons. As shown by Brittion et al., the neurological transfer time required to process the vestibular input and activate the muscles should be no less than 100ms [2]. Also, as explained by Bent et al., the postural stability and foot trajectory has already been set by the proprioceptive feedback from the previous double stance phase.

Due to the large variability in the timing and small differences being identified in the accelerometer output, it is recommended that the timing effects of GVS be further explored with more sensitive equipment and a larger subject pool.

REFERENCES

1. Hlavacka et al. *Brain Res Bull* **40**, 431-435, 1996.
2. Britton et al. *Exp Brain Res* **94**, 143-151, 1993.
3. Bent et al. *Exerc.Sports Sci Rev.*, **33.3**, 107-113, 2005.
4. Bent et al. *J Neurophysiol* **92**, 1269-1275, 2004.
5. Steed et al. *U of Pittsburgh MS Thesis*, 2009.
6. Cenciarini et al. *J Neurophysiol* **95.** 2733-2750, 2006.

ACKNOWLEDGEMENTS

Subjects were screened at the Eye & Ear Institute, University of Pittsburgh Medical Center. Partial funding was provided by Robert Bosch LLC.

Effect of Visual Perturbations and Dual Task on Treadmill Walking of Older and Younger Adults

[1] Kurt Beschorner, [1]Ryan McGowan, [1]Mark Redfern, [1]Patrick Sparto and [1]Rakié Cham
[1]Department of Bioengineering, University of Pittsburgh
email: keb52@pitt.edu

INTRODUCTION

The ability to process and integrate sensory information is critical to maintaining balance during everyday activities, especially during transition between different sensory environments (e.g. walking from a narrow corridor to large lobby). In order to maintain balance during sensory perturbations, the body adjusts the relative contributions of the different sensory systems, an effect commonly known as sensory re-weighting [1]. Previous research has indicated that older adults may have more difficult time suppressing inaccurate sensory information [2-4]. Older adults have been shown to be particularly sensitive to visual perturbations during standing [4], indicating that older adults may be more visually dependent.

The purpose of this study is to observe the effects of visual perturbations on the walking balance of older and younger adults. Additionally, adaptation effects resulting from a repeated exposure to these perturbations will be examined. Finally, this study will also observe dual task effects on walking balance when exposed to visual perturbations.

METHODS

For this study, 8 younger adults (mean age: 24.0 y, range: 22-30 y.) and 5 older adults (mean age 78.5 y, range: 75-80 y.) participated. The subjects were consented and the study was approved by the Institutional Review Board.

Subjects were immersed in a custom-built virtual reality environment with visual information being projected on three screens surrounding the subject and providing a full 180° view. The subjects walked on a treadmill with a velocity set at either 1 or 0.8 m/s based on the natural walking speed of the subject. The visual environment was modeled as a long hotel hallway, and generated using Unreal Tournament 2004 with the CaveUT mutator used to display the scene in a multi-screen environment. The velocity of this optic flow relative to the speed of the treadmill could be controlled using the data collection software. A sensor was placed on the subject's back at the height of the T10 vertebrae to measure the position of this marker.

A total of eight treadmill walking trials were collected in randomized order. Each trial lasted 3 minutes. These trials consisted of two different dual task conditions (no dual task, dual task) by four different optic flow conditions. In the dual task conditions, subjects were asked to distinguish between high and low tones that were played into their ear. They were instructed to push a button as quickly as possible after hearing the high tone. No response was required after hearing the low tone. The four optic flow conditions were the following: baseline in which the optic flow was congruent with the speed of the treadmill (same direction and speed); a sinusoidal condition where a sinusoid was superimposed on the baseline condition; a step condition where the optic flow was stepped down from the treadmill velocity to 0 (gave the appearance of not moving) and then back to the treadmill velocity in 20s intervals; and a reverse/forward condition where the optic flow reversed directions (between congruent and anti-congruent with walking speed) in 20s intervals. The sinusoidal, step and reverse/forward perturbations were repeated during the entire walking trial (3 minutes). The largest responses were seen in the reverse/forward conditions, which were further analyzed.

Typically, subjects reacted to the reverse/forward condition by moving anteriorly towards the front of the treadmill while the scene was moving anti-congruent to the treadmill and then moved posteriorly towards the back of the treadmill when the scene velocity switched back to be congruent with the treadmill velocity (Fig. 1). Therefore, the primary measure, termed anterior excursion, was the maximum anterior displacement as a percentage of the total possible anterior displacement. The total possible anterior displacement was the difference between the furthest anterior point that subjects could reach due to slack in the harness and the location of the subject at the start of the perturbation (Fig. 1). The perturbations in which the subjects started in the front 40% and therefore had little additional room to move forward (13 out of 88 perturbations) were not considered in this analysis. An ANOVA analysis was performed using the combined baseline and reverse/forward data to determine the effects of the optic flow condition, age group and their interaction on the anterior movement percentage. An additional ANOVA analysis was performed using just the data from the reverse/forward condition to determine the primary and interaction effects of age group, dual task, exposure to the same visual perturbation in a previous trial (between trial habituation), exposure to the stimulus within a trial (within trial adaptation) and the interaction effects of these fixed factors. In addition, subject was considered a random factor.

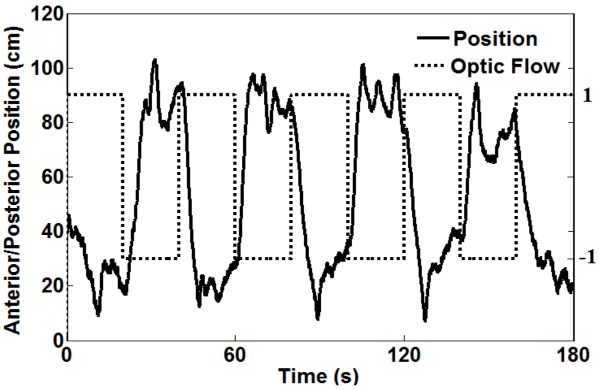

Figure 1: Anterior/posterior movement (solid line) for a reverse/forward optic flow (dashed line).

RESULTS AND DISCUSSION

Subjects had a significantly larger anterior movement percentage during the reverse/forward trials (Mean: 42.6%) compared with the baseline trial (Mean: 24.5%) ($p<0.01$). In addition, older adults (Mean: 45%) were found to have larger anterior movement percentages than younger adults (Mean: 27.6%) ($p<0.05$) and a significant age group x trial type interaction effect was found ($p<0.01$) indicating that the trial type affected the age groups differently.

While analyzing just the reverse/forward trials, the primary factors affecting the anterior movement percentage were dual task ($p<0.01$, Fig. 2), between trial habituation ($p<0.05$, 1st exposure mean: 42.6%; 2nd exposure mean: 26.7%), and age group ($p<0.05$). Specifically, the older subjects experienced a larger response to the perturbation in the reverse/forward trials than the younger subjects. An interaction effect between age group and repetition number was also observed ($p<0.05$). Younger subjects exhibited a slight increase in response while older subjects exhibited a slight decrease in response.

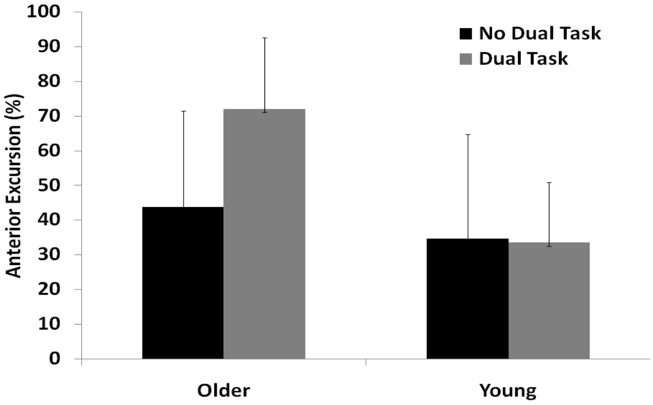

Figure 2: Effect of age group and dual task on anterior excursion.

CONCLUSIONS

This study showed that the older adults had a stronger response to an optic flow perturbation, indicating that the older adults may be more visually dependent on their surrounding environment. The older adults, however, may have also been able to show some adaptation and habituation as they experience repeated exposures to the stimulus. This dependence on vision while walking, may make them at risk for falls when visual information is either unavailable or unreliable.

ACKNOWLEDGEMENTS

Funding and support was provided by the Pittsburgh Claude D. Pepper Older Americans Independence Center (NIH P30 AG024827)

REFERENCES

1. Peterka and Loughlin, P.J., 2004, *J. Neurophysiol.* **91**, pp. 410-23.
2. Teasdale et al., 1991, *Exp. Brain Res.* **85**, p. 691-6.
3. Hay et al., 1996, *Exp. Brain Res.* **108**, p. 129-39.
4. O’Connor, et al., 2008, *Gait Posture* **28**, pp. 385-91.

VERTICAL DISPLACEMENT OF THE CENTER OF MASS DURING SPRING-LOADED CRUTCH AMBULATION

Travis R. Dunn and Matthew K. Seeley
Brigham Young University, Provo, UT, USA
email: pahoran2001@yahoo.com

INTRODUCTION

Approximately 600,000 Americans use crutches each year [1]. A relatively novel spring-loaded crutch design is now being marketed (Figure 1A). The manufacturer (Millennial Medical Inc, Logan, UT, USA) of this crutch design has speculated that because a spring located in the crutch post compresses during crutch-ground contact, crutch length decreases, and less vertical displacement of the whole-body center of mass (COM) may occur during each crutch-ground contact phase of crutch ambulation. Although this idea is somewhat intuitive, it has not yet been evaluated objectively. Decreasing vertical displacement of the COM during crutch ambulation may be important, as it could decrease mechanical work that is performed on the COM and contribute to decreased metabolic energy expenditure during crutch ambulation; increased metabolic energy expenditure is a major challenge for habitual crutch users [2].

The primary purpose of this study was to objectively evaluate the idea that COM vertical displacement during the crutch-ground contact phase of crutch ambulation is less during spring-loaded crutch ambulation, relative to traditional crutch ambulation. We formulated two hypotheses related to this purpose: (1) COM vertical displacement during crutch-ground contact would be less during spring-loaded crutch ambulation than during traditional crutch ambulation; and (2) COM vertical displacement during spring-loaded ambulation would be negatively correlated to subject body mass. The second hypothesis was based upon the premise that increased body mass would increase spring compression and further decrease COM vertical displacement during spring-loaded crutch ambulation. Additionally, in an attempt to better understand other source(s) of potential differences in COM vertical displacement, we observed several other basic kinematic variables that could influence COM vertical position during crutch ambulation; these included sagittal-plane elbow, hip, knee, and ankle joint angle.

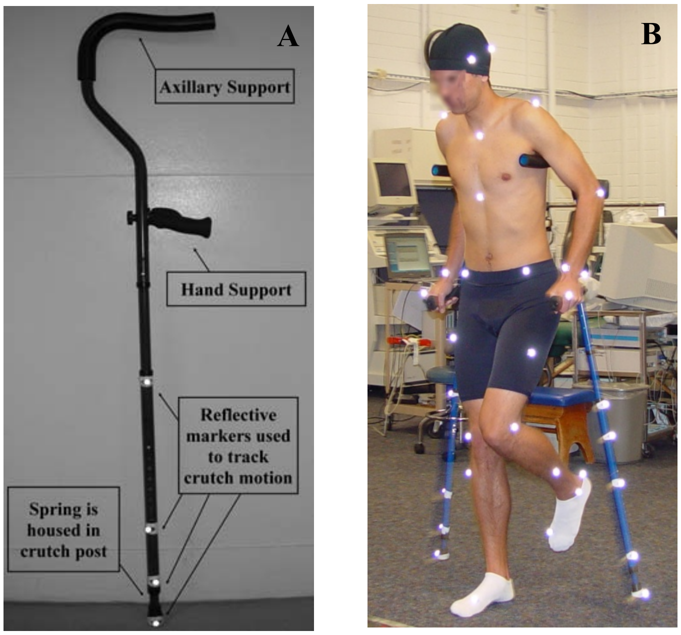
A
Axillary Support
Hand Support
Reflective markers used to track crutch motion
Spring is housed in crutch post
B

Figure 1A. The spring-loaded crutch design that was tested during the present study; **B.** the marker set that was used during the present study.

METHODS

Eighteen healthy subjects (10 females; 8 males; age = 23 ± 2 yrs; height = 1.72 ± 0.10 m; mass = 68.6 ± 14.5 kg) gave informed consent and participated in this study. Subjects were fitted to crutches in a uniform manner using accepted standards. Subjects then became familiar with each crutch type by ambulating for approximately 100 meters with each crutch type. Thirty-five reflective markers were applied to each subject according to the VICON Plug-In Gait model (Figure 1B). Subjects performed three ambulation trials with each crutch type at a standardized speed (0.97 ± 0.05 m/s). The crutch order was randomized and videography (VICON, Centennial, CO, USA; 60 Hz) was used to measure the spatial position of the reflective markers. Whole-body COM position and the aforementioned joint angles were calculated using VICON Nexus software. A custom algorithm was written in Matlab to evaluate the dependent variables only during the crutch-ground contact phase of crutch ambulation. Related to Hypothesis 1, paired *t*-tests (p = 0.05) were utilized to compare COM vertical displacement and joint angles between spring-loaded and traditional crutch ambulation. Significance levels for these comparisons were adjusted using the false discovery rate procedure [3]. Related to Hypothesis 2, a Pearson product moment correlation coefficient was calculated in order to evaluate a potential relationship between subject mass and vertical COM displacement.

RESULTS AND DISCUSSION

Means, standard errors, and *p* values corresponding to the paired *t*-tests are presented in Table 1. No significant between-crutch difference existed for COM vertical displacement. Similarly, following adjustments for multiple comparisons, no significant between-crutch difference existed for any observed joint angle. No significant correlation ($r^2 = -0.37$; $p = 0.13$) was found between body mass and COM vertical displacement (Figure 2).

The data failed to support both of our hypotheses. Regarding Hypothesis 1, and contrary to previous speculation, there is no difference for COM vertical displacement between spring-loaded and traditional crutch ambulation. We did objectively observe spring compression during crutch ambulation, as was expected. However, the apparent resulting decrease of crutch length does not significantly alter the vertical displacement of the COM while it moves forward, past the crutch-ground contact location. This is important, as it indicates that similar magnitudes of mechanical work are performed on the COM during spring-loaded and traditional crutch ambulation. This observation supports metabolic data recently collected in our lab that indicated metabolic costs are similar for spring-loaded and traditional crutch ambulation. The present data also contradicted Hypotheses 2, which predicted a negative relationship between subject mass and COM vertical displacement during spring-loaded crutch ambulation. This observation further supports the notion that spring compression that occurs during spring-loaded crutch ambulation probably does not significantly influence COM vertical displacement. Perhaps an evaluation of other kinematic measures would indicate how the body compensates for the increased compliance of the spring-loaded crutch.

Table 1. Results from paired *t*-tests. $COM\Delta_Z$ indicates COM vertical displacement; MEA, MHA, MKA, and MAA indicate mean elbow, hip, knee, and ankle angles during crutch-ground contact.

	Spring	Traditional	*p*
$COM\Delta_Z$	2.47 ± 0.29	2.77 ± 0.19	0.24
MEA	37.0 ± 2.0	34.0 ± 1.5	0.02
MHA	24.9 ± 2.2	25.2 ± 2.1	0.75
MKA	50.3 ± 2.2	49.8 ± 2.8	0.72
MAA	0.9 ± 1.5	1.2 ± 1.4	0.81

CONCLUSIONS

There is no difference in the magnitude of whole-body COM vertical displacement during spring-loaded and traditional crutch ambulation. This indicates that mechanical work performed on the COM during crutch ambulation is also similar between spring-loaded and traditional crutches. Also, there is no statistical difference between spring-loaded and traditional crutch ambulation for various sagittal-plane joint kinematics.

ACKNOWLEDGEMENTS

We wish to acknowledge and thank Millennial Medical Incorporated and The Mary Lou Fulton Endowment for the College of Health and Human Performance at Brigham Young University for funding this study.

REFERENCES

1. Russell J et al., *Cntr Disease Control Prev* 292, 1-10, 1997.
2. Fisher & Patterson, *Arch Phys Med Rehab* 62, 250-256, 1981.
3. Curran-Everett D, *Am J Physiol*, 279, R1-R8, 2000.

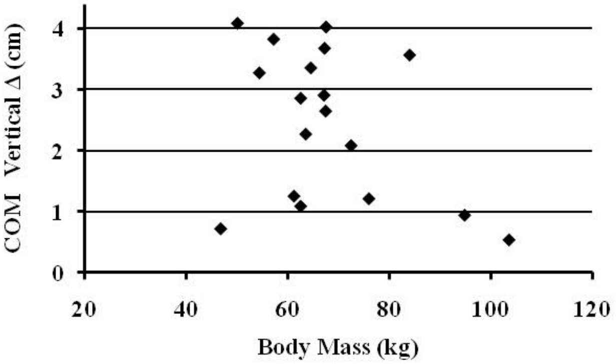

Figure 1. A scatter plot showing the relationship between body mass and COM vertical displacement during spring-loaded crutch ambulation.

COMPARISON OF AN AUTOMATIC AND VOLUNTARY TASK IN EARLY PARKINSON'S DISEASE

[1]Molly McVey, [1,2]Antonis Stylianou, [3]Kelly Lyons, [3]Rajesh Pahwa, [1,2]Carl Luchies, and [4]Paul Cheney
[1]Mechanical Engineering, The University of Kansas, Lawrence, KS, USA luchies@ku.edu
[2]Landon Center on Aging, [3]Parkinson's Disease and Movement Disorder Center, [4]Molecular and Integrative Physiology; The University of Kansas Medical Center, Kansas City, KS, USA

INTRODUCTION

The motor deficits associated with Parkinson's disease (PD) are well known and include akinesia/bradykinesia, resting tremor, rigidity, and postural instability. Although all of these deficits presumably stem from circuit dysfunction in the basal ganglia due to a loss of dopamine neurons, the underlying neural mechanisms are not well understood. The basal ganglia are known to be involved in making the necessary postural adjustments to maintain balance during voluntary movement [1]. The basal ganglia may also play a role in the automatic step response to a balance disturbance (balance recovery) since impairments in this task have been demonstrated in individuals with PD [2].

Previous studies have identified impairments caused by PD in both voluntary tasks (e.g. gait initiation) and automatic tasks (e.g. balance recovery). However, the balance recovery studies have primarily focused on persons with PD who already exhibit clinical signs of postural instability. Recently, several differences in balance recovery have been identified in persons with early PD and no clinical signs of postural instability [3]. The focus of this study was to determine if the same effects of early PD are also observed in gait initiation. We hypothesized that we would see similar effects of PD in the two tasks (differences in weight shift time, ankle angle, and COP movement).

METHODS

Participants: 10 subjects with Parkinson's disease (PD) and 11 healthy controls (HC) (PD: age 63.2 ± 8.9 years, H&Y 2; HC: age 68.0 ± 9.6 years) completed the study. The analysis reported here is based on a subgroup of 10 PD and 10 HC in the balance recovery task and a subgroup of 7 PD and 11 HC in the gait initiation task.

Tasks: In both tasks, the participant began each trial by standing quietly with feet a shoulder width apart. In the Gait Initiation (GI) task, the participant stood with arms relaxed at the sides and was instructed to initiate forward walking in response to a visual cue. The participant was allowed to self-select the foot used for the first step and the walking speed. Three trials were conducted. In the Balance Recovery (BR) task, the participant stood with arms crossed at the chest wearing a rigid waist harness attached via a cable to a weight-drop mechanism (dropped weight = 20% BW, pull distance = 8.7% waist height), which delivered a posterior waist pull. The participant was asked to respond naturally to the balance disturbance. A safety harness was used to ensure participant safety.

Data Collection: Force plate data were collected using three AMTI (Advanced Medical Technology Inc.; Watertown, MA) six-component force plates and EMG data were collected using bipolar surface electrodes (Noraxon; Scottsdale, AZ) from the tibialis anterior (TA) with a sampling frequency of 1080 Hz. Kinematic data were collected at 120 Hz using reflective markers and a six camera Vicon 512 (Vicon Peak; Lake Forest, CA) motion analysis system. Markers were placed bilaterally on the 2nd toe, ankle, heel, calf, and knee. All responses were video taped.

Data Analysis: Stimulus onset was defined as the onset of the light in the GI task and onset of the waist pull force in the BR task. Liftoff and landing were defined by the movement of the heel marker in the GI task and by force plate unloading/loading in the BR task. Temporal parameters included reaction time (stimulus onset to first TA onset), weight shift time (reaction time to liftoff), and step duration (time between liftoff and landing). Kinematic parameters included step length (distance traveled by the heel marker between liftoff and landing), step height (maximum vertical displacement of the heel marker between liftoff and landing), and ankle plantarflexion (PF)/dorsiflexion (DF) angle. Ankle angle was calculated at liftoff and landing. COP parameters included the anterior-posterior (AP) and medial-lateral (ML) displacement of the center of pressure (COP) at liftoff and landing of the first step. All data were processed with MATLAB (Mathworks, Natick, MA, USA). T-tests ($p<0.05$) were used to assess group differences using SPSS (SPSS Inc., Chicago, IL, USA).

RESULTS AND DISCUSSION

In the BR task, significant differences were found between groups in weight shift time, ankle angle at liftoff, and COP displacement at landing. No significant differences were found in any of the other parameters. In the GI task, no significant differences were found between groups in any of the parameters (Table 1). In BR, the PD group had a longer weight shift time than HC, were in DF at liftoff while the HC were in PF, and the COP was further forward than HC at landing. In GI, both groups had similar weight shift times, were in DF at liftoff, and the COP displacement at landing was similar.

Study limitations include the differences across the two tasks in movement direction (anterior in GI, posterior in BR) and stimulus type (visual in GT and somatosensory in BR).

CONCLUSIONS

The results of this study suggest that in early PD, the first step in the voluntary gait initiation task is not impaired as is the first step of the automatic balance recovery task. This suggests that in the early stages of the progression of Parkinson's disease, the underlying neural mechanisms of the basal ganglia may affect voluntary tasks differently than automatic tasks.

REFERENCES

1. Kandel ER, et al. *Principles of Neural Science,* McGraw-Hill, New York, NY.
2. Jacobs JV, et al. *Neuroscience* **141**, 999-1009, 2006.
4. McVey MA, et al. *Proceedings of the Summer Bioengineering Conference,* Marco Island, United States, Abstract 192822, 2008.

.

ACKNOWLEDGEMENTS

Assistance from Michael Haines and Laura Zahner and support from the Self Graduate Fellowship and the Landon Center on Aging are acknowledged.

Table 1: Results in Balance Recovery (Automatic Response) and Gait Initiation (Voluntary Response) *Indicates a p-value < 0.05. ML = medial-lateral, AP = anterior-posterior; a + angle indicates PF, - DF

	Balance Recovery		Gait Initiation	
	HC	**PD**	**HC**	**PD**
Temporal Parameters (ms)				
Reaction Time	124 (19)	123 (17)	161 (65)	173 (47)
Weight Shift Time	222 (54)*	500 (304)*	922 (135)	914 (121)
Step Duration	113 (51)	153 (33)	464 (24)	462 (62)
Kinematic Parameters				
Step Length (mm)	8.2 (3.7)	10.2 (4.6)	24.4 (3.6)	25.0 (6.2)
Step Height mm)	1.4 (2.0)	1.8 (2.5)	3.3 (1.2)	3.7 (1.8)
Liftoff Angle (°)	1.5 (3.8)*	-4.1 (3.6)*	-6.6 (2.4)	-7.3 (3.6)
Landing Angle (°)	-1.3 (4.0)	-5.1 (5.2)	-17.2 (16.8)	-26.0 (13.6)
COP Displacement (mm)				
ML at Liftoff	128 (19)	125 (34)	41 (27)	25 (20)
AP at Liftoff	29 (25)	64 (49)	-34 (26)	-26 (18)
ML at Landing	129 (22)	127 (33)	105 (27)	96 (27)
AP at Landing	42 (17)*	71 (37)*	16.8 (33)	30 (38)

PATELLOFEMORAL KINEMATIC DIFFERENCES EXIST BETWEEN HIGH-LOAD AND LOW-LOAD CONDITIONS IN PATIENTS WITH PATELLOFEMORAL PAIN

[1]Christine Draper, [1]Thor Besier, [1]Juan Santos, [1]Michael Fredericson,
[1,2]Gary Beaupre, [1]Scott Delp, and [1]Garry Gold
[1]Stanford University, Stanford, CA, [2]VA RR&D Center, Palo Alto, CA
email: cdraper@stanford.edu

INTRODUCTION

Patellofemoral pain is a common knee disorder accounting for 25% of knee injuries seen in some sports medicine clinics [1]. Despite the incidence of this disorder, accurate diagnosis and effective treatment remain challenging.

Approximately 50% of patients with patellofemoral pain are diagnosed with abnormal motion, or maltracking, of the patella that is thought to lead to pain [2]. This diagnosis is typically performed by observing the motion of the patella during seated knee extension with no externally applied load to the joint. Pain typically arises during highly-loaded activities and it remains unclear how accurately patellofemoral joint kinematics measured during unloaded joint motion reflect joint kinematics during functional tasks.

The goal of this study was to compare upright, weight-bearing patellofemoral joint kinematics to supine, low-load patellofemoral joint kinematics.

METHODS

We examined the patellofemoral joints of 12 subjects with patellofemoral pain (8M, 4F). Subjects were between 20-32 years of age and had no prior surgery or traumatic knee injuries. Single-slice, spiral real-time MR images [3] of their knees were obtained during supine, knee flexion/extension with no externally applied load (low-load) and during an upright, weight-bearing squat. The supine, low-load images were obtained using a 1.5T Signa CV/i scanner (GE Healthcare) and the following scan parameters: FOV: 24cm, pixel size: 1.1mm, frame rate: 10 fr/s, 70 interleaves, readout trajectory: 2.4ms. The weight-bearing images were obtained using a 0.5T Signa SP open-MRI scanner (GE Healthcare) fit with a backrest to stabilize subjects in an upright position. The following scan parameters were used: FOV: 16cm, pixel size: 1.88mm, frame rate: 6 fr/s, 6 acquisitions/frame, readout trajectory: 16ms. In both scanners a body coil was used for RF transmission and a surface coil was used for signal reception. Subjects performed knee flexion/extension from 0° to 30° of knee flexion and back at a rate of 6°/s. An oblique-axial image through the widest portion of the patella was acquired (Figure 1).

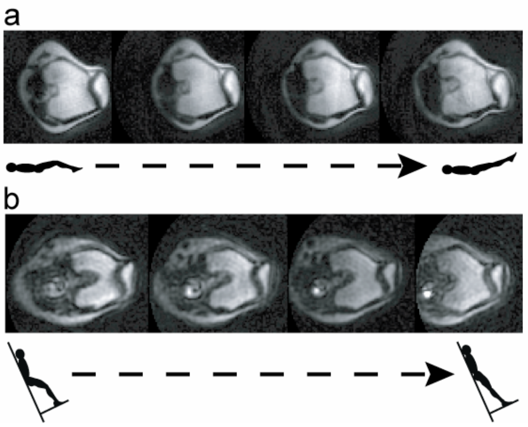

Figure 1: Real-time MR images of patellofemoral joint during (a) supine, low-load knee extension and (b) upright, weight-bearing knee extension.

Patellofemoral joint kinematics were measured by identifying bony landmarks on all real-time images. Bisect offset describes the medial/lateral position of the patella and is the percentage of the patella lateral to the midline of the femur. Patellar tilt is the measure of the angle formed by lines joining the posterior femoral condyles and the maximum width of the patella (Figure 2).

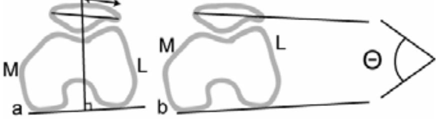

Figure 2: Diagram of (a) bisect offset (BO) and (b) patellar tilt (Θ) measurements

RESULTS AND DISCUSSION

Due to the variability in patellar motion, the subjects were separated into two groups based on weight-bearing joint kinematics: a) those with normal patellar tracking and b) those with maltracking relative to pain-free controls [4]. Six of the subjects (4M, 2F) exhibited excessive lateral translation of the patella (Bisect offset > 64% at full extension) and seven subjects (5M, 2F) exhibited excessive lateral tilt (Tilt > 9° at full extension).

a: Normal Patellar Translation

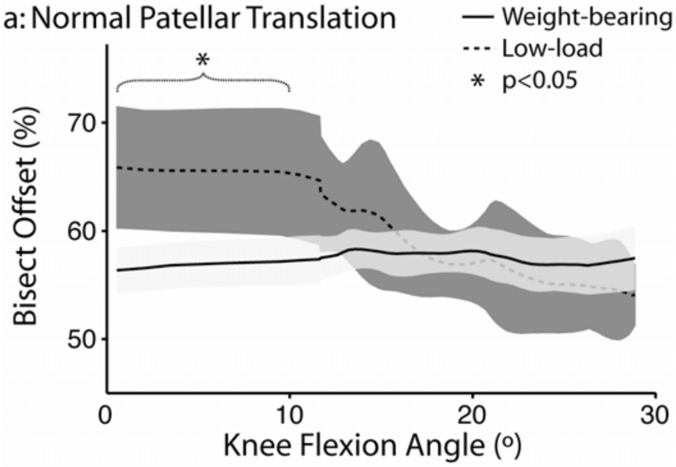

b: Excessive Lateral Patellar Translation

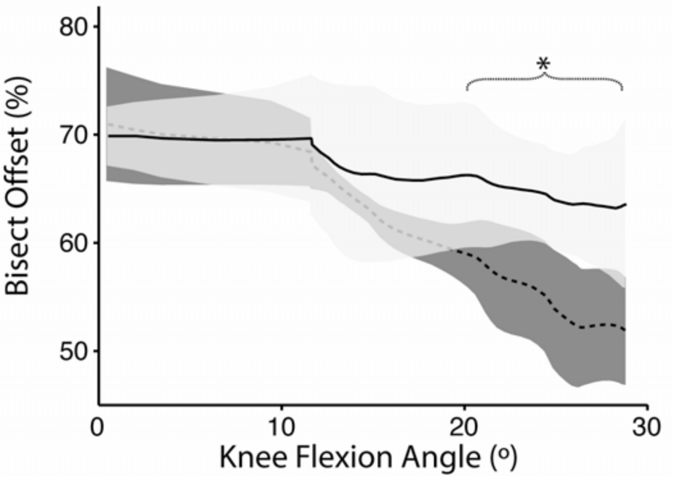

Figure 3: Relationship between bisect offset and knee flexion angle during low-load and weight-bearing knee extension. (a) Subjects without excessive lateral translation of the patella (n=6). (b) Subjects with excessive lateral translation of the patella (n=6). Larger bisect offset indicates that the patella is more lateral relative to the femur.

We detected significant differences in bisect offset between low-load knee extension and weight-bearing knee extension in both groups (p=0.001); however, the range of knee flexion angles over which these differences occur varied. In subjects with normal patellar translation, bisect offset during low-load knee extension was increased by an average of 9% compared to weight-bearing bisect offset between knee flexion angles of 0-10° (Figure 3a). In subjects with excessive lateral translation of the patella, bisect offset during low-load knee extension was on average 9% smaller than weight-bearing bisect offset between knee flexion angles of 20-30° (Figure 3b). Patellar tilt varied between loading conditions only in the group with excessive lateral patellar tilt. In this group, patellar tilt during low-load knee extension was on average 5° smaller compared to tilt during weight-bearing between knee flexion angles of 20-30°.

CONCLUSIONS

These results indicate that patellofemoral joint kinematics measured during supine knee extension with no externally applied load may not reflect the kinematics occurring during upright, weight-bearing movement. These results have implications in the study of joint mechanics as well as in the diagnosis and treatment of patellofemoral pain.

Maltracking of the patella is typically defined during seated knee extension. However, due to the effect of joint load on the medial/lateral translation of the patella, some patients with normal weight-bearing patellar tracking may appear to have excessive lateral patellar translation during low-load knee extension and might be misdiagnosed. Assessment of patellar maltracking during weight-bearing knee extension may be more appropriate.

REFERENCES

1.Devereaux MD and Lachmann SM. *Br J Sports Med* **18**, 18-21, 1984
2.Dehaven KE, et al. *Am J Sports Med* 7, 5-11,1979
3.Santos JM, et al. *Conf Proc IEEE Eng Med Biol Soc* **2**, 1048-1051, 2004.
4.Draper CE, et al. JOR (in press)

ACKNOWLEDGEMENTS

VA Rehabilitation R&D Service (#A2592R), NIH (EB002524-01, EB005790-01).

POSTACTIVATION POTENTIATION AND DECREASED MOTOR UNIT FIRING RATE DURING SUBMAXIMAL CONTRACTIONS OF THE TIBIALIS ANTERIOR

J. Greig Inglis, Jon Howard, Kyle MacIntosh, David A. Gabriel and Rene Vandenboom
Brock University, St. Catharines, Ontario, L2S 3A1, CANADA
email: greig.inglis@BrockU.ca

INTRODUCTION

Muscle force development during voluntary contractions is very history dependent. A classic example of this is the depression in force that occurs during prolonged activity, i.e. fatigue. A lesser known example is the increase in force observed consequent to brief (unfatiguing) activity, an outcome referred to as postactivation potentiation (PAP). In both fatigue and PAP, intracellular mechanisms modulate the intrinsic force-generating ability of individual muscle fibers within the motor unit population. During activity, these respective processes may coexist and the muscle force may indeed reflect the balance between these competing phenomena [1].

The influence of PAP on motor unit activation is not understood. In principal, PAP could down-regulate the motor unit discharge rate required to attain a given force or power output. Indeed, Adams and De Luca [2] reported an early and transient reduction in the discharge rate of select motor units within fatigued vastus lateralis muscle. The origin of this response, i.e., fatigue or PAP, was not, however, identified. On the other hand, Klein et al. [3] noted that motor unit discharge rates were reduced when PAP was observed in triceps brachii muscle during submaximal isometric contractions.

Given the uncertainty regarding the etiology of reduced motor unit discharge rates, we sought to clarify the role of PAP on this parameter. To this end, we compared motor unit discharge rates of unfatigued tibialis anterior muscle during submaximal contractions in the potentiated and unpotentiated state.

METHODS

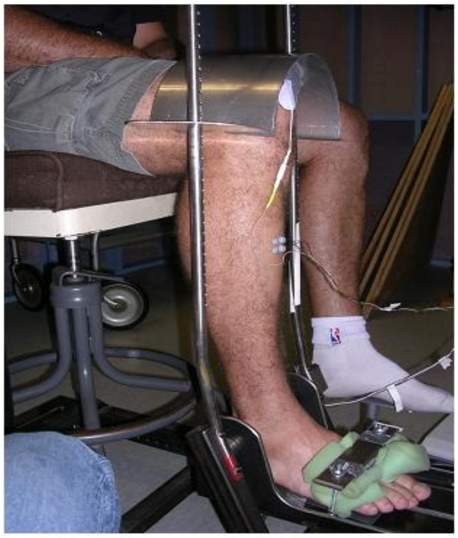

Figure 1: The testing chair and lower-leg testing unit designed

Ten healthy college aged subjects were recruited with no history or neurological or neuromuscular disorders. The subjects visited the Electromyographic Kinesiology lab at Brock University on three separate occasions. The first visit was a familiarization, the second involved data collection without indwelling electrodes and the final visit involved all aspects of the study, including indwelling electrode data collection.

Day 1:

Day 1 consisted of subject initiation to the laboratory environment where they were introduced to the equipment and informed of all aspects of the study. Subjects then signed an informed consent document, and were asked to assume a supine position to locate the most proximal motor point on the tibialis anterior. The skin surface was cleaned and mildly abraded in preparation for placement of the surface electrodes. Once the surface electrodes were placed on the skin, the subject was moved to a testing chair for the remainder of the testing session (Figure 1). Baseline measurements were taken that included maximum voluntary contraction (MVC) of the dorsiflexors and a maximal motor response

(M_{max}) was elicited by electrical stimulation of the peroneal nerve.

Day 2 and 3:

Day 2 and 3 consisted of the identical subject preparation for data collection as was seen in Day 1. Once the surface electrodes were placed and the subject was moved to the testing chair, both MVC and M_{max} were again determined (this was done post needle placement on Day 3). Subjects were given a rest period (ten minutes) and three twitches were evoked to elicit M_{max} followed by a five second contraction equal to 50% of MVC and another three M_{max} twitches (Unpotentiated condition). The subjects were again given a ten minute rest period. Another three twitches to elicit M_{max} were given, followed by a ten second contraction equal to 100% of MVC. Immediately following the 100% MVC, three twitches to elicit M_{max} were given followed by a five second contraction equal to 50% of MVC (Potentiated condition). This was followed by another three twitches to elicit M_{max} and a rest period. Finally, after another ten minutes of rest, three twitches which elicited M_{max} were given and followed by a five second contraction equal to 50% of MVC, which was also followed by three M_{max} twitches (Unpotentiated condition).

Days 2 and 3 were identical, except on Day 3, the indwelling electrode was additionally used to record motor unit activity.

Statistical Analysis:

All data were analyzed using the *a priori* planned comparisons (single-degree of freedom *F*-tests).

RESULTS AND DISCUSSION

M-wave

The peak-to-peak amplitude of M_{max} exhibited no statistically significant differences among all conditions ($p's>0.05$).

MPF

The frequency content of surface electromyographic (sEMG) activity showed no statistically significant differences ($p's>0.05$) in Mean Power Frequency (*MPF*) between pre- and post-unpotentiated conditions. However, when comparing both (pre/post) unpotentiated conditions to the potentiated condition there was a statistically significant decrease (Pre 58.1 ± 8.5, Post 62.2 ± 8.3, Potentiated 53.6 ± 8.6; 13.8% change; $p=0.005$).

Firing Rates:

The results of the firing rates derived from indwelling recordings followed the same pattern as was seen with the sEMG *MPF* data. The pre/post unpotentiated data showed no significant differences between the two conditions ($p>0.05$). However, similar to the *MPF* data, the potentiated compared to unpotentiated conditions resulted in a statistically significant decrease in firing rate (Pre 20.3 ± 2.4, Post 20.0 ± 3.7, Potentiated 18.3 ± 3.0; 9.9% decrease; $p=0.004$).

The *RMS* data supported the findings for the M_{max}, as it remained constant throughout all trial conditions. The stability of M_{max} suggests that the differences seen in firing rate could not be attributed to muscle fatigue. These findings accompanied with the frequency and firing rate data (surface and indwelling, respectively) indicate that the potentiation of the muscle caused a decrease in motor unit firing rates compared to the same unpotentiated muscle.

CONCLUSIONS

Based on the data presented, we can support the findings of De Luca et al. [4] who also observed a decrease in firing rates, which they speculated were due to potentiation. This research protocol set out to specifically target the potentiation of the muscle and the subsequent response. This study demonstrated that potentiation does decrease firing rates when the motor response is unchanged in subjects with no neuropathies.

REFERENCES

1. Krarup (1981) *J Physiol* **311***, 389 – 400.*
2. Adams and De Luca, et al. (2005). *J Appl Neurophysiol* **99**, 268 – 280.
3. Klein et al. (2001) *Neurosci Letters* **316**, 153-156.
4. De Luca, et al. (1996). *J Neurophysiol* **76**, 1503-1516.

ACKNOWLEDGEMENTS

This research was supported by NSERC grants (DG)(RV)

Treadmill Running and Tower Climbing Exercise Produce Genotype Dependent Responses in the Femurs of C57BL/6J (B6) and DBA/2J (D2) Aged Inbred Mice

[1] Peter Gdovin, [1]Neil A. Sharkey, and [1]Dean H. Lang
[1]Biomechanics Laboratory, Department of Kinesiology, The Pennsylvania State University
email: tcl133@psu.edu

INTRODUCTION

We are interested in gene-environment interactions that influence skeletal performance. By focusing efforts on defining interactions between genes and environmental loading, therapeutic interventions may someday be designed to target specific genotypes where differential responses are anticipated. To begin to examine these issues we hypothesized that the two principal types of exercise, aerobic training and strength training will both produce differential skeletal responses in D2 and B6 inbred strain of mice.

METHODS

B6 and D2 inbred female mice were subjected to treadmill running or tower climbing at 480 days of age. Ninety mice were used in a 2 x 3 experimental design with strain (B6 vs. D2), and treatment (treadmill running or tower climbing vs. control) as independent factors resulting in six groups with 13 mice per group. Treadmill running is more closely identified as an aerobic exercise while tower climbing is a more resistance type of exercise. Those mice in the aerobic exercise treatment group underwent treadmill running 30 min/day, five days a week, over a five week period with increasing speed and incline peaking at 15 m/min on a twenty five degree incline for the duration of week 5. Mice in the resistance training group were required to climb a one meter tall tower to drink from water bottles placed at the top. Mice remained in these towers 24 hours per day for five weeks. All procedures complied with and were approved by the Pennsylvania State University Institutional Care and Use Committee.

At the conclusion of the intervention the femurs were harvested and frozen at -20C until examined. Femoral shafts were loaded to failure in three-point bending using an MTS 858 Mini-Bionix apparatus (MTS Systems, MN, USA) and structural properties were derived from load-displacement data. The

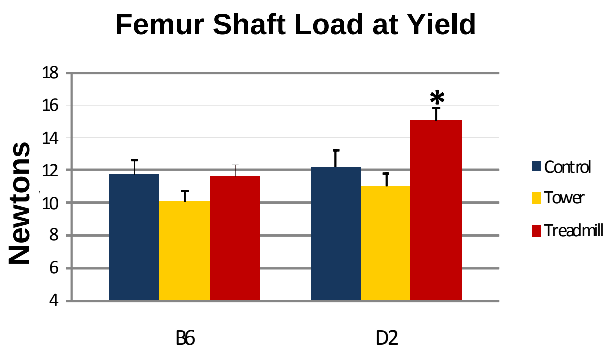
Femur Shaft Load at Yield

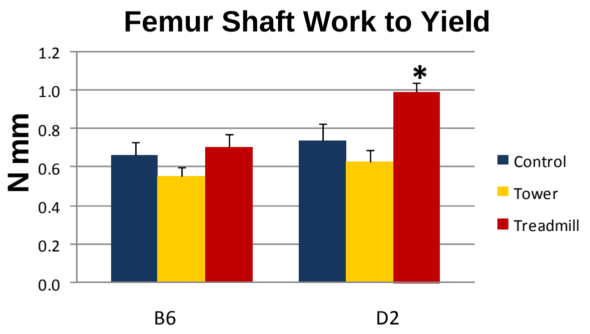
Femur Shaft Work to Yield

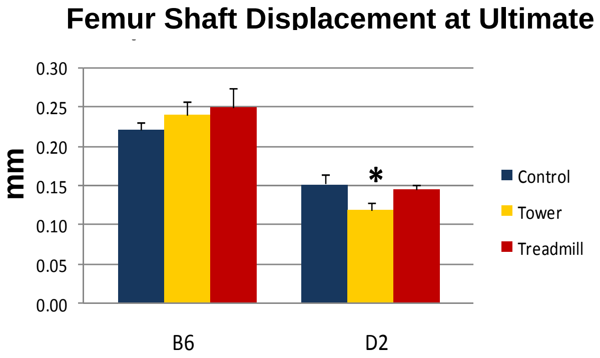
Femur Shaft Displacement at Ultimate

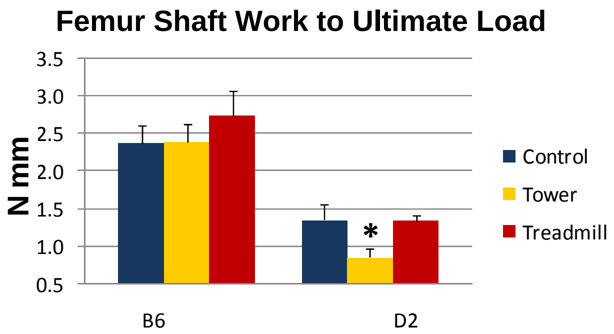
Femur Shaft Work to Ultimate Load

Figures 1-4: These four figures illustrate the significant differences between the B6 and D2 mice.

effects of the exercise intervention were evaluated within each mouse strain separately. Exercise treatment group differences were evaluated using a one-way ANOVA. Post-hoc multiple comparisons were made using a 2-sided Dunnett test where treadmill running and tower climbing were compared to controls. Differences at the 95% confidence level were considered significant, while those at 90% were considered suggestive.

RESULTS AND DISCUSSION

Genetic strain had a significant effect on many of the skeletal measures (data not presented). Of primary interest were those skeletal measures that displayed significant effects as function of exercise treatment. Exercise effects were examined within each strain separately. The mechanical performance of femurs from D2 mice were significantly affected by exercise whereas B6 femur did not exhibit any significant differences due to exercise treatment. (Table 1)

In D2 mice, treadmill running significantly increased yield load and work to yield and produced a suggestive increase in displacement at yield compared with controls. In contrast, tower climbing reduced the mechanical properties of the femoral shaft in D2 mice with a decrease in displacement at ultimate load and work to ultimate load. Figures 1-4 illustrate the treatment effects of treadmill running and tower climbing compared to controls within each strain separately. These results indicate that in D2 mice treadmill running produced significantly stronger bones at yield whereas tower climbing significantly reduced mechanical properties at ultimate load. Although not statistically significant, the B6 treadmill mice took longer to fail and absorbed more energy than B6 controls.

CONCLUSIONS

Clearly, these results indicate that the skeletal effects of physical activity and exercise are extremely dependent on both genetics and type of exercise. These data emphasize the importance of gene by environment interactions. Future research may provide the foundation on which to build effective means of assessing fracture risk due to osteoporosis and thereby enabling more early intervention. A more thorough understanding of genetic control will also enhance our abilities to decipher the molecular and physiological mechanisms affecting skeletal health and could lead to new treatment options that effectively target patient-specific deficits.

Table 1: Femur Shaft Mechanical Properties from Three-point Bending Test

Femur Shaft Mechanical Properties from Thee-point Bending and Shear Test							
Main Effects		Treatment Effects within Each Strain Separately					
		B6			D2		
Variable	Values	Control	Tower	Treadmill	Control	Tower	Treadmill
Yield Load (N)	Mean	11.75	10.07	11.58	12.23	11.07	*15.10
	SE	0.87	0.63	0.76	1.03	0.74	0.68
	p-value		ns			p = 0.002	
Displacement at Yield Load (mm)	Mean	0.100	0.099	0.110	0.108	0.102	^0.122
	SE	0.005	0.005	0.009	0.005	0.005	0.004
	p-value		ns			p = 0.006	
Work to Yield Load (Nmm)	Mean	0.66	0.55	0.70	0.74	0.63	*0.99
	SE	0.07	0.05	0.07	0.09	0.06	0.05
	p-value		ns			p = 0.001	
Displacement at Ultimate Load (mm)	Mean	0.220	0.239	0.250	0.152	*0.118	0.146
	SE	0.010	0.017	0.024	0.012	0.010	0.005
	p-value		ns			p = 0.024	
Work to Ultimate Load (Nmm)	Mean	2.37	2.39	2.75	1.35	*0.85	1.35
	SE	0.24	0.25	0.33	0.20	0.12	0.07
	p-value		ns			p = 0.007	

Group differences from ANOVA for exercise treatment. P-values for treatment main effect; ns: not significant; * indicates $p < 0.05$ and ^ $p < 0.10$ for pairwise comparisons of individual treatment (treadmill running or tower climbing) compaired to controls (Dunnett test).

EXERCISE EFFECTS VIA TREADMILL RUNNING AND TOWER CLIMBING ON FEMORAL BONES OF C57BL/6J AND DBA/2J ADULT FEMALE MICE

[1]Preston, H M, [1]Sharkey, N A and [1]Lang, D H
[1]Biomechanics Laboratory, Department of Kinesiology, The Pennsylvania State University
e-mail: hmp131@psu.edu

INTRODUCTION

It is widely accepted that bone is able to adapt to changes in its loading environment by altering its mechanical properties. The details of this adaptation are still being explored, including the attempted elucidation of the genes involved. However, the response of bone to mechanical demand is very complex in regard to the genetic interactions within bone as well as potential indirect influences on bone via genes that affect such things as behavior, muscle force and body weight. The main focus of our study was to further explore gene-environment interactions relative to bone adaptation. Increasing our understanding of these interactions may someday enable more individualized interventions dependent on a person's genotype when preventing and treating bone disease such as osteoporosis. An inbred mouse strain provides a useful model for exploring environmental influences due to the ability to generate animals with a high level of genetic similarity. Two different inbred mouse strains with known differences in skeletal phenotypes, C57BL/6J (B6) and DBA/2J (D2), were exposed to two different methods of mechanical loading. An aerobic based exercise intervention, treadmill running, and a more resistance based intervention, tower climbing. We hypothesized there would be a differential skeletal response relative to exercise type within each strain.

METHODS

Ninety 180 day old female mice equally divided between B6 and D2 inbred strains were exposed to treadmill running, tower climbing or served as controls (15 in each group). The treadmill runners were put onto a rodent treadmill 5 days per week for 5 weeks and the speed, incline and duration were gradually increased. During the final week, a target speed of 15 m/min at a 25 degree incline for 30 minutes was reached. The tower climbers were housed in a cage attached to a 4 ft tall mesh wire tower with water bottles placed at the top of the tower. Tower climbers remained in the towers 24 hours per day for a 5 week period. To train the mice during the first week, the water bottles were put at the bottom of the tower and gradually raised to the top. The mice then climbed to the top of the towers to drink for the remaining weeks of the intervention. The mice were sacrificed two hours after the last day of exercise and the right femur was harvested and frozen at –20C until tested. All procedures complied with and were approved by the Pennsylvania State University Institutional Care and Use Committee. After taking several gross morphological measurements, the cortical mid-shaft was evaluated prior to mechanical testing using micro-computed tomography (Scanco Medical, Zurich, Switzerland). The femur was then loaded to failure in three-point bending and the femoral neck was loaded to failure in a shear test using a MTS 858 Mini-Bionix apparatus (MTS Systems, MN, USA). Structural properties were derived from the load-displacement data. Material properties were estimated using the resulting cross-sectional and structural data. An ANOVA was used to evaluate the effects of exercise type within each strain on all structural, material and morphological variables. A 2-sided Dunnett was used for post hoc multiple comparisons. Significance was determined using a 95% confidence level.

RESULTS

We were primarily interested in the effects of exercise treatment within each strain. The B6 mice displayed numerous treatment effect differences. Treadmill running resulted in significantly greater values for load at yield, shear ultimate load (of the femoral neck) and cortical thickness at the lateral mid-diaphysis (Table 1). Tower climbing resulted in significantly greater values for head diameter, displacement at yield and strain at yield (Table 2). Both treadmill running and tower climbing significantly increased work to yield in the B6 mice as well. However, controls had significantly higher values when compared to tower climbers for displacement, work, and strain at ultimate load as well as post yield displacement and post yield work at ultimate load and post yield displacement at failure. There were also significant differences between the control mice and the treadmill runners for coronal width and medullary area within the D2 strain with treadmill runners having smaller values than the controls. D2 mice also had significant differences for shear ultimate load and work with control mice having larger values than the tower climbers.

Table 1: Treadmill Running Effects for B6 Mice. Mean, standard error (SE) and significant p-values for Treadmill versus Control are shown.

Treadmill Effect for B6 Mice		Treatment	
Variable	**Values**	**Treadmill**	**Control**
Load at Yield (shaft)	**Mean**	12.944	11.515
	SE	0.459	0.347
	p-value	0.054	
Work to Yield (shaft)	**Mean**	0.713	0.582
	SE	0.040	0.024
	p-value	0.049	
Load at Ultimate (neck)	**Mean**	17.063	15.502
	SE	0.455	0.452
	p-value	0.044	
Cortical thickness at lateral mid-dipahysis	**Mean**	0.651	0.630
	SE	0.005	0.006
	p-value	0.020	

Table 2: Tower Climbing Effects for B6 Mice. Mean, standard error (SE) and significant p-values for Tower versus Control are shown.

Tower Effect for B6 Mice		Treatment	
Variable	**Values**	**Tower**	**Control**
Strain at Yield (shaft)	**Mean**	0.019	0.017
	SE	0.001	0.000
	p-value	0.022	
Work to Yield (shaft)	**Mean**	0.742	0.582
	SE	0.049	0.024
	p-value	0.014	
Displacement at Yield (shaft)	**Mean**	0.103	0.092
	SE	0.003	0.002
	p-value	0.019	
Head Diameter	**Mean**	1.526	1.464
	SE	0.010	0.016
	p-value	0.022	

DISCUSSION

These results provide further evidence that genetic background imparts differences in the response to mechanical stimuli. Differential intervention effects across the two inbred strains were confirmed, with B6 mice being more responsive than D2 mice. Both types of exercise had a positive effect on yield mechanical properties in the B6 mice. Treadmill running increased load at yield and work to yield at the mid-diaphysis and the load at ultimate load was also increased at the femoral neck. Tower climbing increased displacement at yield, work to yield and strain at yield at the mid-diaphysis. These results indicate a beneficial skeletal response to exercise within the B6 strain.

Strain and exercise type had an effect on skeletal morphology as well. Tower climbers within the B6 strain had significantly larger head diameters, demonstrating a positive skeletal response to the more resistance type of exercise intervention. Treadmill running increased the cortical thickness at the lateral mid-diaphysis within the B6 mice and decreased the medullary area in the D2 mice (indicating increased endocortical bone formation). Thus, aerobic based exercise resulted in positive morphological changes within both strains. The coronal width in the D2 mice, however, was less in the treadmill runners as compared to the controls.

Tower climber values were less at ultimate load than the controls for mechanical properties of the femoral mid-diaphysis within the B6 mice and of the femoral neck within the D2 mice. These results suggest that tower climbing may inhibit the maximum mechanical capacity at both the mid-diaphysis and femoral neck depending on strain. In summary, within the B6 strain, exercise positively increased yield mechanical properties at the mid-diaphysis, ultimate mechanical properties at the femoral neck and morphological parameters at both the mid-diaphysis and neck. Treadmill running also positively affected bone formation at the mid-diaphysis within the D2 mice.

CONCLUSION

These data provide evidence that there are skeletal responses to exercise relative to genetic strain and treatment type in adult mice.

UPPER EXTREMITY MUSCLE FATIGUE THAT INDUCES MUSCLE IMBALANCES DOES NOT INCREASE MOVEMENT INSTABILITY

[1]Deanna H. Gates and [2]Jonathan B. Dingwell

[1] Department of Biomedical Engineering, University of Texas, Austin, TX, USA
[2] Nonlinear Dynamics Laboratory, Dept. of Kinesiology, University of Texas, Austin, TX, USA
Email: jdingwell@mail.utexas.edu, Web: http://www.edb.utexas.edu/faculty/dingwell/

INTRODUCTION

Asymmetric motions are common in the workplace [1] and may cause differential repeated loading of joints and muscles. The diverse demands on the muscles surrounding a joint may cause them to fatigue at different rates and to different degrees [2]. Muscle fatigue leads to decreased force production [3]. This could create a force imbalance around the joint, which could lead to abnormal stress distributions [4] within the underlying tissues, resulting in inflammation. Strength imbalances could also lead to movement instability, which could further increase injury risk. The purpose of this study was to determine if local fatigue of the shoulder flexors could generate a muscle strength imbalance about the shoulder and if this would impact the body's ability to maintain stability of the shoulder motion during a repetitive work task.

METHODS

20 healthy right-handed (25 ± 2 years) subjects sat in an adjustable chair with seat belts to help them maintain constant posture. They then pushed a low weight (10% MVC) back and forth along a low friction horizontal track in time with a metronome for 5 minutes (Pre-Test; Fig. 1A-B). Subjects then performed either a repetitive lifting task designed to fatigue the shoulder *flexors* for 3 minutes (LIFT; Fig. 1C) or the same sawing task with 25% MVC for 4 minutes (SAW; Fig. 1B). They then performed the same sawing task for an additional 5 minutes (Post-Sawing). 3-D movements of the arm and trunk were recorded continuously at 120 Hz using VICON. The three rotational angles of the shoulder were calculated using Euler angles. EMG data were collected at 1080 Hz from 9 arm and trunk muscles. Maximum force measurements (MVCs) were taken at various points throughout the trial (Fig. 1A). These included shoulder flexion, extension, internal rotation, and external rotation strength. EMG instantaneous mean power frequencies (IMPF) were calculated to quantify muscle fatigue [5].

Local dynamic stability [6] was quantified using short-term local divergence exponents (λ_s*) which indicate the rate of divergence of neighboring trajectories. Positive exponents indicate local instability, with larger exponents indicating greater instability [6]. λ_s* was calculated for the shoulder, elbow and wrist pre and post-fatigue. λ_s* values were compared using 2-factor (Pre/Post x Lift/Saw) within subjects ANOVAs. MVC values were first normalized to % maximum MVC and compared using 2-factor (Time Point (1-4) x Lift/Saw) within subjects ANOVA.

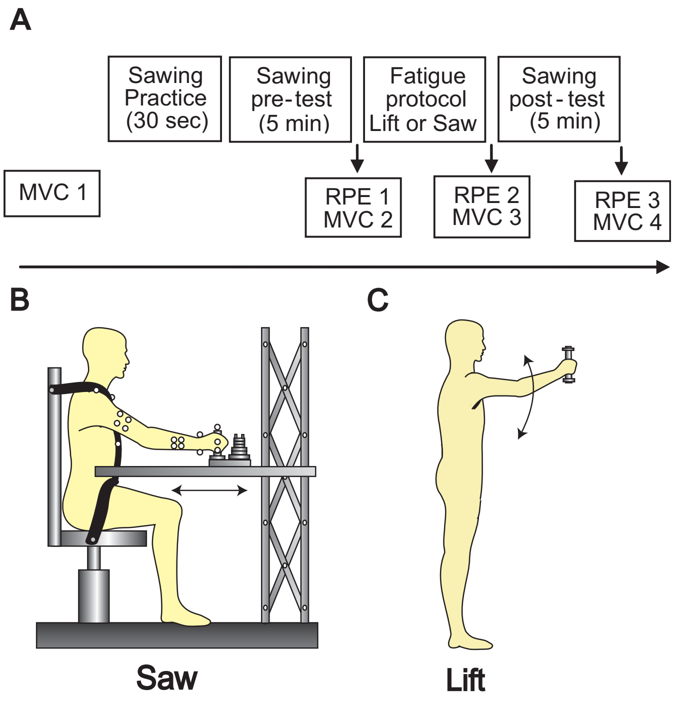

Figure 1: Experimental procedure

RESULTS AND DISCUSSION

Subjects exhibited significant muscle fatigue. This is evident in the decreases in IMPF (Fig. 2) and muscle strength. Strength decreases in shoulder flexion, extension, and internal, external rotation were all significant ($p < 0.006$). The muscle strength also became slightly more unbalanced as a result of targeted fatigue of the shoulder flexors (Fig 3). λ_s* tended to decrease for shoulder and elbow movements (Fig. 4). This decrease was only significant for shoulder motion after the lifting task ($p = 0.035$).

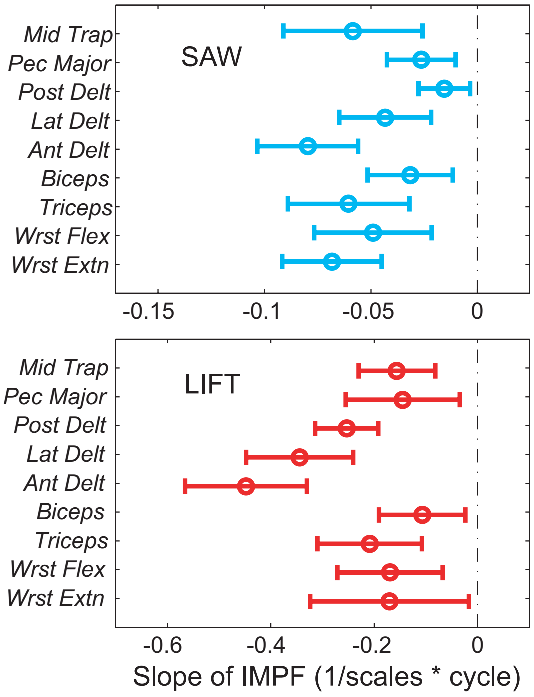

Figure 2: The instantaneous mean power frequency of the EMG decreased over the fatigue task in all muscles tested.

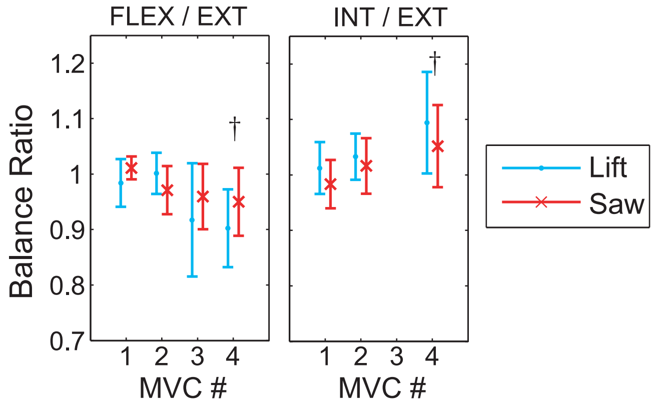

Figure 3. The ratio of shoulder flexion to extension strength decreased after the lifting task ($p < 0.05$), while the ratio of internal to external strength increased ($p < 0.05$). No changes in muscle balance were seen after the sawing task.

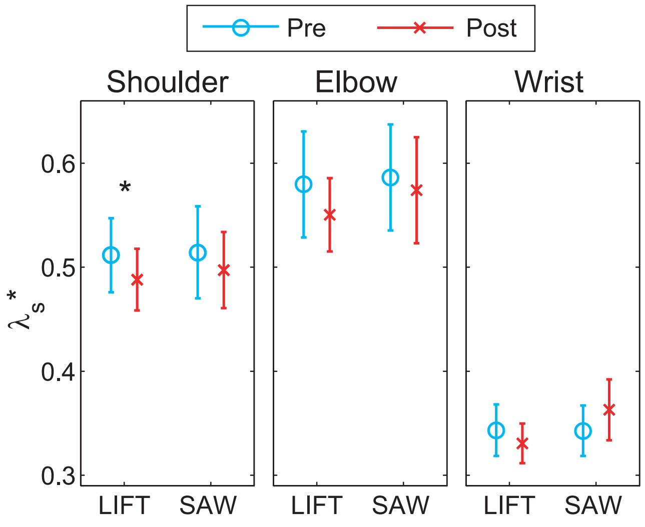

Figure 4: Movements at the shoulder became more stable after fatigue. This change was significant after lifting ($p = 0.035$) but not sawing ($p = 0.241$).

CONCLUSIONS

Subjects performed consistently accurate movements before and after fatigue (Not shown). Fatigue led to decreased muscle strength and increased muscle imbalance. Fatigue also led to increased movement stability. This result suggests that after subjects fatigued, they may have needed to apply greater control to their shoulder movements. Therefore, subjects can compensate for muscle fatigue while performing multi-joint redundant tasks, in ways that maintain both movement stability and task precision.

REFERENCES

1. Marras, W.S. et al. (1993) *Spine* 18 (5): 617-28.
2. Kumar, S. (2001) *Ergonomics* 44(1): 17-47.
3. Basmajian, J. and DeLuca, C. (1995) *Muscles Alive* 5th Ed.
4. Gorelick, M. et al. (2003) *Appl Ergon* 34(4): 317-25.
5. Hostens, I. et al. (2004) *J Electromyogr Kinesiol* 14: 205-215.
6. Dingwell, J. and Marin, L. (2006) *J Biomech* 39(3): 444-52.

ACKNOWLEDGEMENTS

NIH Grants # 1-R21-EB003425-01A1 and # 1-R03-HD058942-01.

AN EMG DRIVEN MODELTO ESTIMATE ACL FORCES DURING NORMAL WALKING

Qi Shao, Kurt Manal and Thomas S. Buchanan
Center for Biomedical Engineering Research
University of Delaware, Newark, DE, USA
email: shao@udel.edu, web: http:// www.cber.udel.edu

INTRODUCTION

The ACL is the most frequently injured knee ligaments. To develop better surgical procedures and rehabilitation regimens for ACL deficient patients, it is of great importance to know internal knee-ligament loading. A few numerical models have been used to calculate ACL forces during gait [1, 2]. However these models were not driven by measured muscle activations, which may vary from patient to patient.

In this paper we describe an EMG-driven model that incorporates a knee-ligament model, and we apply this approach to estimate ACL forces during normal gait.

METHODS

Five young healthy subjects who gave informed consent were included in this study. EMGs, joint positions and force plate data were collected from four walking trials. EMGs were collected from the major muscle groups of the right leg (MG, LG, Sol, TA, RF, VM/VL/VI, BFL/BFS, SM/ST) using surface electrodes. MVC trials were collected for normalization of EMG. The subjects were required to strike force plate 1 using their right foot and force plate 2 using their left foot. In this study we simulated the stance phase of the walking trials.

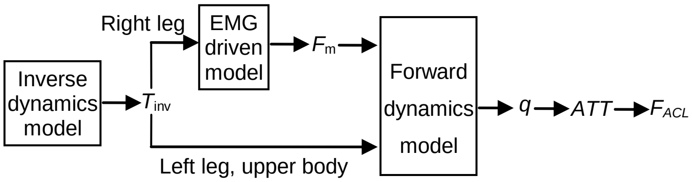

Figure 1: Flow chart of using the forward dynamics model to estimate ACL force.

We calculated ACL forces through a two-step procedure (Figure 1).

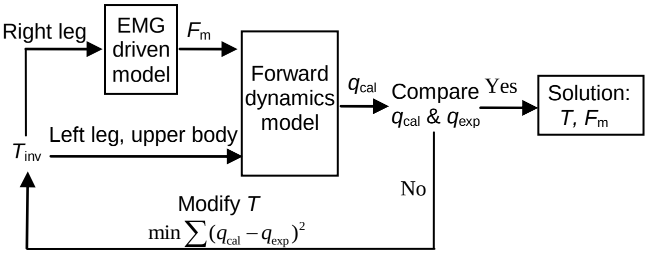

Figure 2: Flow chart of the forward dynamics model.

First, a forward dynamics model of the whole body was developed to calculate muscle forces, joint torques and joint angles, and the model was verified by successfully replicating experimental joint angles. The musculoskeletal model was constructed using SIMM (Motion Lab Systems, Inc., Baton Rouge, LA). It included 11 segments: femur, tibia/fibula, patella, talus, and calcn of both limbs, back. Here the back segment included the mass and inertial properties of the pelvis, torso, head, and arms. This model had 9 DOF in sagittal plane: horizontal and vertical position of pelvis, pelvis rotation, hip, knee and ankle extension/flexion of both limbs. The equations of motion were solved using SD/FAST (Symbolic Dynamics, Inc., Mountain View, CA). Muscle forces, Fm, calculated from an EMG-driven model [3, 4] were used to drive the model spanning the right ankle and knee joint. For the other joints, the model was driven by the joint torques calculated using inverse dynamics, T_{inv}. T_{inv} were calculated using dynamic optimization of the inverse dynamics model, with an emphasis on reducing residual forces and torques at the pelvis. F_m were calculated through our EMG-driven model to match the calculated T_{inv}. Ground reaction forces during the simulation were prescribed to the experimentally recorded values. Since T_{inv} may not necessarily drive a successful forward simulation as shown by others [5, 6], we used an optimization to find a solution of joint torques, T, that could successfully reproduce experimental kinematics during forward simulation (Figure 2). T_{inv} were used as initial values during the optimization. After solution was obtained, it could be used to drive a forward simulation and track the experimental kinematics.

Second, the forward dynamics model was incorporated with a knee-ligament model. The muscle forces and joint reaction forces/torques calculated from the previous step were used as inputs for the forward dynamics model. At each time step, we used SD/FAST to solve the translations between femur and tibia that could hold the segments in the calculated joint positions. The knee-ligament model was then used to calculate ligament forces. In the knee-ligament model, each knee ligament was composed of a number of bundles [2], and each ligament bundle was modeled as a nonlinear elastic element, described by a nonlinear force-strain relationship [7]. After the translations between femur and tibia were calculated, the ligament length was determined, and the ligament force was calculated using the force-strain relationship.

RESULTS AND DISCUSSION

The forward dynamic right knee and ankle joint moments calculated from the EMG-driven model matched the inverse dynamic joint moments (Figure 3). The calculated right hip, knee and ankle joint angles matched the measured angles (Figure 4). There were two ACL force peaks near LTO and RTO (Figure 5).

CONCLUSIONS

We have developed a forward dynamics model that uses EMGs as input to estimate ACL forces during normal stance phase. It successfully tracked measured kinematics. The model could also be implemented to calculate the translations between femur and tibia. The calculated result of two ACL force peaks near LTO and RTO was consistent with previous studies [1, 2], and could be explained by the onset of two GRF peaks during stance phase.

In future studies we will compare our simulation results with the results from *in vivo* studies, and apply this model to patients with pathologies, which could provide insight of patients' knee ligament loading to clinicians. We will also explore differences in ligament biomechanics associated with different rehabilitation protocols.

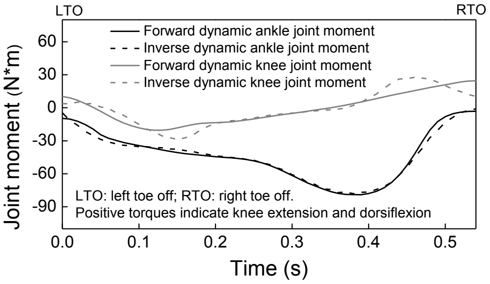

Figure 3: Forward and inverse dynamic joint moment profiles.

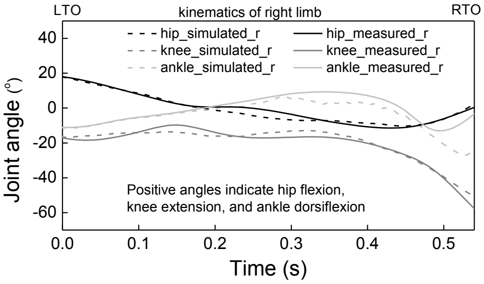

Figure 4: Simulated joint kinematics and measured kinematics.

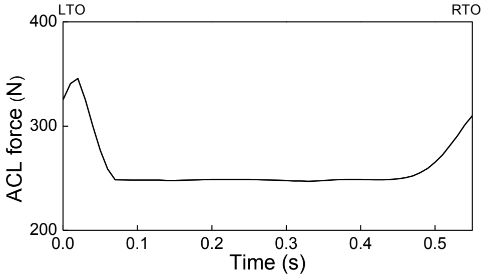

Figure 5: ACL force profile during stance phase.

REFERENCES

1.Collins JJ. *J Biomech*, 28, 251–267, 1995.
2.Shelburne KB, et al. *J Biomech*, 37, 797–805, 2004.
3.Buchanan TS, et al. *J Appl Biomech*, 20, 367-395, 2004.
4.Shao Q and Buchanan TS. *J Biomech*, 41, 3097-3100, 2008.
5.Chao EY and Rim K. *J Biomech*, 6, 497-510, 1973.
6.Seth A and Pandy MG, *J Biomech*, 40, 356-366, 2007.
7.Blankevoort L et al. *J Biomech*, 24, 1019-1031, 1991.

ACKNOWLEDGEMENTS

NIH R01-HD38582, R01-AR46386 and R01-AR48

Comparison of Ankle and Foot Joint Kinetics after Heel-Off Between Individuals with Posterior Tibial Tendon Dysfunction and Controls

[1]Kelly Van Vlack, [1]Josh Tome, [2]Chris Neville, [3]A. Sam Flemister, [1]Jeff Houck
[1]Ithaca College-Rochester, Rochester, NY, [2]SUNY Upstate Medical Center, Syracuse, NY, University of Rochester Medical Center, Rochester, NY
email: jhouck@ithaca.edu

INTRODUCTION

Posterior tibial tendon dysfunction (PTTD) is associated with loss of muscle function and acquired flatfoot deformity.[1,3,4,] These deficits are associated with decreased ankle power at push off.[4] Kinematic studies suggest that the decreased ankle power at push off is not accompanied by significant changes in kinematic ***patterns*** of the 1st metatarsal[1] or forefoot[3] in plantar flexion. This suggests that angular velocity of the forefoot may be normal, and that midfoot power ***generation*** may also be normal. Simplified kinetic foot models (two segment – forefoot, hindfoot) are able to reveal whether the forefoot power ***generation*** at push off, identified in previous studies,[2] is maintained or decreased due to deficits in muscle control as a result of PTTD and/or loss of midfoot stability as a result of acquired flatfoot deformity. The purpose of this study was to compare midfoot and ankle kinetics (moment, angular velocity and power) between individuals with stage II PTTD and matched controls at the push off phase of stance.

METHODS

Thirteen individuals with PTTD (3 male, 10 female; age=57 ± 10; body mass index = 31 ± 6) and 9 control participants (1 male, 8 female; age= 54± 7; body mass index = 32 ± 3) volunteered for this study. The Foot Function Index average score of 27 ± 12 % for the individuals with PTTD suggested moderate limitations in function and pain. The arch height index, used to document the medial longitudinal arch, was significantly lower ($p < 0.01$) in the individuals with PTTD (PTTD = 0.308 ± .019 vs Control = 0.350 ± 0.015) verifying the presence of a lower arch and suggestive of acquired flatfoot.

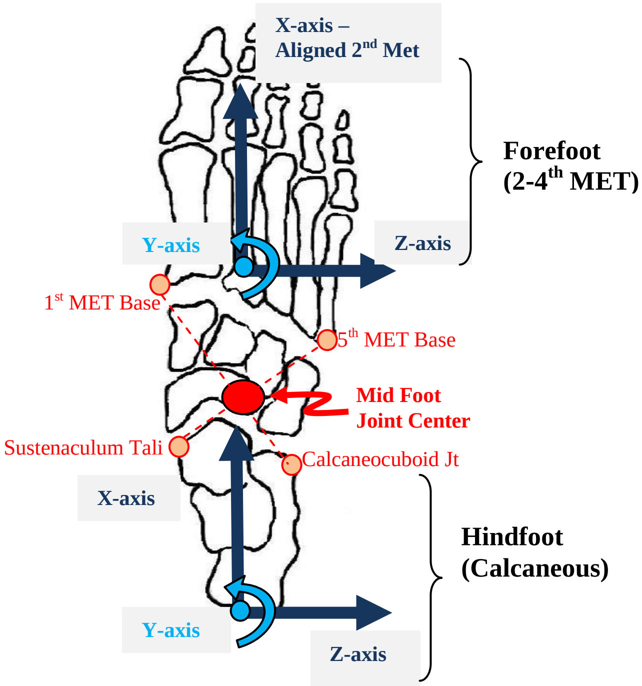

Figure 1: The midfoot joint center, forefoot segment (markers placed on 2-4 metatarsals [MET]) and hindfoot (calcaneous) are shown.

An Optotrak Movement Analysis System (Northern Digital, Inc, Waterloo, CANADA) and force plate (Kistler, Amherst, NY) integrated with The Motion Monitor (Innsport, Inc, Chicago, IL, USA) was used to measure movement and force data from a multi-segment foot model during walking.[1] Walking speed was controlled at 1.0 m/s using timing gaits. Force data was collected at 1000 Hz and kinematic data at 60 Hz. The two segment kinetic foot model (**Figure 1**) consisted of the forefoot and hindfoot. The forefoot was defined by placing 3 infrared emitting diodes (IRED's) on the 2-4th metartarsals. The hindfoot was defined by placing a triad of three IRED's on the skin over the lateral calcaneous. The midfoot joint center was the midpoint between the sustentaculum tali, 1st metatarsal base, calcaneocuboid joint, and 5th metatarsal base. On dried skeletons this joint center approximated the lateral aspect of the talonavicular joint (**Figure 1**). An inverse dynamics solution was calculated for each segment (Forefoot, Hindfoot) at the point of peak ankle plantarflexion angular velocity of walking. At this point of stance the heel is off the ground and the center of pressure is located between the 2nd and 4th metatarsal heads. Two sample t tests were used to compare the moments, angular velocity and powers (midfoot and ankle) at this point of stance between PTTD and controls.

RESULTS AND DISCUSSION

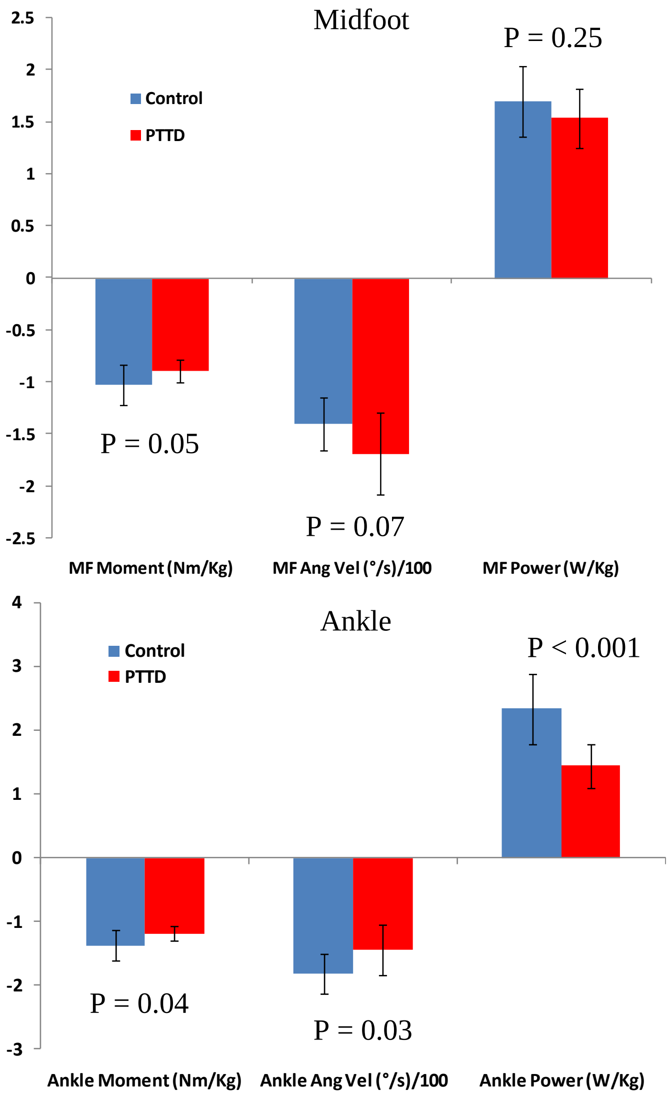

Figure 2. The midfoot (top) and ankle (bottom) joint moments, angular velocity(scaled for graphing) and powers. "-" values for moments and angular velocity indicate plantar flexion. P values are the result of two sample t-tests.

The new findings of this study show minimal differences in the midfoot kinetics and significant differences in ankle kinetics of individuals with PTTD compared to controls (**Figure 2**). Individuals with PTTD maintained their midfoot power generation despite a significantly lower ankle power generation. The midfoot moment of the PTTD group showed significantly lower plantar flexion moments. However, this lower moment was associated with a higher forefoot angular velocity, resulting in no difference in the midfoot powers. The individuals with PTTD maintained their midfoot power despite lower ankle powers and acquired flatfoot deformity. Maintenance of the midfoot power generation may indicate compensation via active mechanisms (ie, muscle control) to preserve foot rigidity at push off. Further, the ankle power may partially depend on the ability of subjects to stabilize their midfoot. The ankle power generation was 30 % less in the PTTD group, suggesting that push off is impaired. Clinically, this lower ankle power suggests that a solid ankle foot orthosis, which is in common use, may further restrict ankle plantar flexor function, causing further loss of power. As long as midfoot power is maintained, other alternatives like jointed ankle designs should be considered for individuals with PTTD to minimized deficits in ankle power.

CONCLUSIONS

The presence of PTTD and acquired flatfoot deformity minimally influenced midfoot kinetics. However, ankle kinetics demonstrated large differences attributable to PTTD and acquired flatfoot deformity.

REFERENCES

1. Houck, J, Neville, C; Tome, J., Flemsiter, A. Ankle and Foot Kinematics in Subjects with stage II PTTD during the Stance Phase of Gait. Foot & Ankle International (In Press)
2. MacWilliams BA, Cowley M, Nicholson DE. Foot kinematics and kinetics during adolescent gait. *Gait & Posture*. 2003;17: 214-24.
3. Ness ME, Long J, Marks R, Harris GF. Foot and Ankle Kinematics in Subjects with Posterior Tibial Tendon Dysfunction. *Gait & Posture*. 2008;27: 331-339.
4. Ringleb SI, Kavros SJ, Kotajarvi BR, Hansen DK, Kitaoka HB, Kaufman KR. Changes in gait associated with acute stage II posterior tibial tendon dysfunction. *Gait & Posture*. 2007;25: 555-64.

ACKNOWLEDGEMENTS

The authors are grateful for support from the National Institute of Arthritis and Musculoskeletal and Skin Diseases(Grant #:1R15ARO54507-01A1

THE EFFECT OF CYCLIC LOADING ON THE COEFFICIENT OF FRICTION DIFFERS BY GENDER IN THE ARTICULAR CARTILAGE OF MURINE KNEE JOINTS

[1]Elizabeth Drewniak, [2]Gregory Jay, [1]Braden Fleming, and [1]Joseph Crisco
[1]Bioengineering Laboratory, Department of Orthopaedics, Alpert Medical School of Brown University,
[2]Department of Emergency Medicine, Alpert Medical School of Brown University
email: Joseph_Crisco@brown.edu

INTRODUCTION

For the past several decades, many researchers have focused on biotribology in attempts to better understand osteoarthritis (OA). Various techniques have been used to examine the biotribological properties of articular cartilage (AC), including the coefficient of friction (CoF). Investigators have measured the coefficient of friction in a variety of species across several joints. Numerous methods have been developed to measure CoF of AC such as pendulums, custom systems like arthrotripsometers, the rubbing of cartilage plugs, and atomic force microscopy (AFM) [1]. In addition to investigating the frictional properties of cartilage, some groups have studied the effects of cyclic loading of cartilage plugs on CoF [2, 3].

The goal of this work was to investigate the effects of cyclic loading on the coefficient of friction of the articular cartilage of intact murine joints. This work was accomplished using intact knee joints from 10-week-old BL6 mice as the fulcra of two pendulum systems. A passive pendulum system was used to measure the CoF. Cyclic loading utilized an active pendulum with a DC motor and a series of linkages that allowed for both shear and compressive forces. We hypothesized that cyclic loading would increase the coefficient of friction of the AC in murine knee joints.

METHODS

Both hind limbs from six male and six female BL6 10-week-old mice were excised post-euthanasia. Skin, musculature, and connective tissue were removed from the freshly harvested limbs. The joint capsule was left intact. The proximal femur and distal tibia of each joint were rigidly fixed in 6.35 mm square tubes with urethane potting compound (Smooth-ON, Easton, PA). Each intact knee was then mounted in a passive pendulum system. The tibia was fixed to a base with two set screws and the pendulum arm was fit to the proximal end of the femur, creating a resting angle of ~70º (Figure 1a).

Following specimen preparation, the CoF of the knee AC of all specimens was measured. To find CoF, the knee was set at an initial angle of 12 ± 2º, released, and allowed to oscillate freely. Reflective markers were placed on the arm of the pendulum and the base of the apparatus. Motion was tracked with Qualisys AB cameras and software (Gothenburg, Sweden). Three trials were recorded for each specimen and oscillation data was processed with Visual3D (C-Motion, Inc., Germantown, MD) and custom MATLAB code (MathWorks, Inc., Natick, MA), which calculated CoF values for each joint using a Stanton linear decay model [4]. Within each pair, one joint was randomized as the experimental knee and loaded into an active pendulum system for cyclic loading (Figure 1b) at a frequency of ~1.5 Hz. CoF measurements were repeated at t = 2.5 min, 15 min, 30 min, 45 min, 1 hr, and 2 hr. The experimental limb was then placed unloaded in media for 12 hours. CoF measurements were then repeated at t = 0 hr, 2.5 min, 15 min , 30 min, 45 min, 1 hr, 2 hr, 4 hr, 24 hr, resulting in 26 cumulative hours of cyclic loading. The remaining joint from each pair served as the contra lateral control, and was placed unloaded in cultured media throughout testing. CoF of the contra-lateral control joint was measured at t = 0 hr and immediately following the last CoF measurement of the experimental limb.

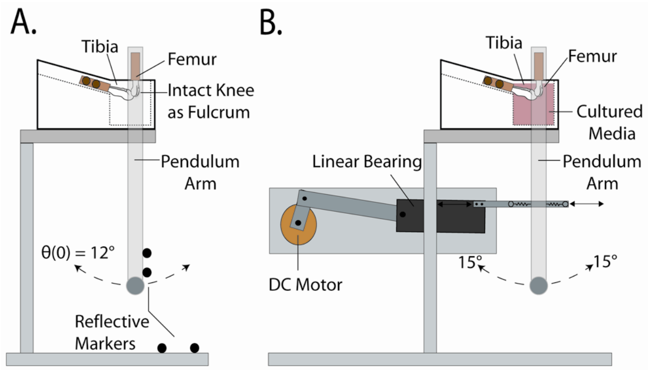

Figure 1: Schematic of the (A) passive pendulum used for CoF measurements and (B) active pendulum system used for cyclic loading.

Mean (±SD) CoF values were calculated for all joints at each time point. Differences between initial CoF values and t = 24 hr were evaluated with a paired t-test. Differences between gender at t = 24 hr were compared with a t-test (SigmaStat3.5, Systat Software, Inc., San Jose, CA). A significant value of $p<0.05$ was set *a priori*.

Custom MATLAB code was used to examine the path lengths of the pendulum arm in the x- (flexion/extension) and y-directions (medial/lateral) during oscillation.

RESULTS AND DISCUSSION

Twenty-six cumulative hours of cyclic loading significantly increased CoF values of the female mouse knee AC ($p<0.009$), while cyclic loading did not significantly increase CoF values of male mouse knee AC ($p=0.560$) (Table 1). Contra lateral control CoF values remained constant over the course of the experiment. Pendulum path length showed no correlation with CoF values, time, or gender.

Table 1: Mean (±SD) coefficient of friction (CoF) values for articular cartilage of both males and females prior to cyclic loading (t = 0 hr) and immediately following all testing (t = 24 hr).

Gender	t = 0 hr	t = 24 hr
Male	0.0387 (0.0129)	0.0417 (0.0204)
Female	0.0329 (0.0087)	0.1180 (0.0476)

The purpose of this work was to investigate the effects of cyclic loading on the coefficient of friction of the AC of intact murine knee joints. While the use of mice for biomechanical studies poses design and handling challenges due to their small size, it also provides many benefits when dealing with various orthopaedic disorders, including osteoarthritis, because of its transgenic capabilities.

Two previous studies used varying techniques to assess the frictional properties of cartilage plugs under cyclic loading [2, 3]. Both studies showed the same general trend of increasing CoF values over the course of testing; hence we anticipated the same trends. While the CoF of the female AC rose, it took much more time to finally increase compared to the previous studies. The CoF of the male AC did not experience a similar increase. Because our system allows for unconstrained motion of the intact joint, it more closely emulates *in vivo* conditions than do cartilage plugs.

An unexpected finding from this work was that gender of the mouse had an effect on the response to cyclic loading. While we expected low variability across genders because the mice were part of the same colony, these results support the widely known fact that female gender is a risk factor for OA.

REFERENCES

1. Mow VC & Huiskes R. Basic Orthopaedic Biomechanics and Mechano-Biology, 3rd ed., Lippincott Williams & Wilkins, Philadelphia, PA
2. Forster H and Fisher J. *Proc IMechE [H]* **213**, 329-345, 1999.
3. Park S, et al. *J Biomech* **37**, 1679-1687, 2004.
4. Crisco JJ, et al. *Proc IMechE [H]* **221**, 325-333, 2007.

ACKNOWLEDGEMENTS

Funding sources: NIH AR050180, NIH P20-RRO24484, RIH Orthopaedic Foundation, Inc., and University Orthopedics, Inc. The authors also thank Ling Zhang.

COMPARING LOAD AND POSTURE ON INDUSTRIAL BASED LIFTING TASKS: EFFECTS OF GENDER, SPINAL LOAD MAGNITUDE AND POSTURAL ASYMMETRY

Brian C. Nairn[1], Robert J. Parkinson[2], Jack P. Callaghan[3], Janessa D.M. Drake[1]
[1]Department of Kinesiology, University of Windsor, Windsor, Ontario,
[2]Giffon Koerth Forensic Engineering, Toronto, Ontario
[3]Department of Kinesiology, University of Waterloo, Ontario
E-mail: jdrake@uwindsor.ca

INTRODUCTION

Injury potential and the effects of coupled postures with various load magnitudes is a matter of interest for manual material handlers. Drake and Callaghan [1] quantified passive lumbar axial twist motion *in vivo* combined with various flexion/extension postures. The coupling of flexion/extension was shown to modulate the axial twist range of motion [1]. These changes in motion can alter the load distribution and failure mechanisms among tissues of the low back [1,2], potentially increasing the risk for injury. From an analysis of over 400 repetitive lifting industrial jobs' load magnitude, trunk flexion angle, and twist velocity were identified as risk factors for low back injury [3]. Also, increases in lateral shear and compression forces have been correlated to decreases in lift origin height and increases in asymmetrical posture [4]. Regarding gender, the cross-sectional areas of erector spinae, internal and external oblique, psoas major, and quadratus lumborum have been found to be larger in males compared to females which can change the load and loading pathways on each muscle [5]. However, gender has been shown to have less of an impact on spinal loads than postural asymmetry and load weight [6]. Females are increasingly performing manual materials handling tasks and may be at an increased risk to low back injury [5]. Also, many industrial settings use fixed loads and origin and destination heights throughout these tasks. Therefore, the purpose of this study was to quantify the trunk angle and trunk muscle activation in men and women during symmetrical and asymmetrical lifting tasks.

METHODS

Ten participants (5 male and 5 female) performed multiple lifting trials with an instrumented lifting apparatus. Two loads (7.6 kg and 9.7 kg) were lifted from three floor positions to three 1.2 m high shelf positions. The floor and shelf locations were directly in front of the participants (centre) and at approximately 1 m to the left and right of centre. The three lifting tasks used in this study were: left floor to right shelf, right floor to left shelf, and centre floor to centre shelf. The lifts were presented to the participants in a random order. The participants were required to rest between trials to prevent fatigue. Lifting speed and technique were not controlled for, and participants were free to move in any way so long as they remained on the 0.9 m^2 force plate.

Electromyography (EMG) was collected and processed from five muscles bilaterally: rectus abdominis (RRA, LRA), internal oblique (RIO, LIO), external oblique (REO, LEO), latissimus dorsi (RLD, LLD), and the erector spinae at the L3 level (RL3, LL3). Maximum voluntary contractions were performed in order to normalize the EMG. Joint angles of the spine were measured using a Lumbar Motion Monitor (LMM, Biomec Inc., Cleveland, USA). Peak EMG and peak three-dimensional spine angles were quantified for each trial. The six individual spine angles were combined to form three angles of flexion-extension, right-left lateral bend, and right-left axial twist. This removed the impact of the angle polarity in subsequent comparisons.

RESULTS AND DISCUSSION

There were no statistical differences in EMG across gender, lift task, or load. The average EMG per channel ranged from a low in the rectus abdominis muscles (RRA 11.6 ±8.9 %MVC, LRA 11.5 ±7.5%MVC) to a high in the erector spinae muscles (RL3 59.2 ±6.4%MVC, LL3 62.2 ±8.8%MVC).

The EMG activation pattern is shown in Figure 1. The flexion-extension angles were different between the centre lifts (66.3 ±11.3°) and the left/right floor to right/left shelf lifts (58.2 ±12.5°, *P*=0.0007), but did not differ with load or gender (*P*>0.052). There were no statistical differences in the lateral bend angles (11.5 ±3.3°, *P*>0.140). There were two main effects, lift type (*P*<0.0001) and load (*P*=0.035), on right-left twist angles. The twist angles were 36.8 ±3.9°, 30.1 ±7.0°, and 17.0 ±8.1° for the left floor -right shelf, right floor -left shelf, and centre floor -centre shelf lifts respectively (Figure 2). The twist angles were larger for the 9.7 kg load (28.6 ±10.4°) than the 7.6 kg load (26.0 ±11.3°).

Despite differences in the trunk flexion-extension and twist angles with lift and load, there were no differences found in the muscle activation levels. In part, this could be due to the small sample size in this study. There appears to be a trend for higher abdominal activation in females for heavier loads and asymmetrical lifts, whereas males modulate their back activation for these same lifts. It is possible that additional muscles are used when the lift changes from a symmetric to an asymmetric type. The addition of the mid-back and hip EMG (i.e. gluteus medius) may provide insight into the repeated identification of combined postures and load magnitude as risk factors for low back pain. A recent study by Nelson-Wong et al. [7] found that bilateral gluteus medius activity was a predictor for previously asymptomatic individuals to develop low back pain over a two-hour standing task.

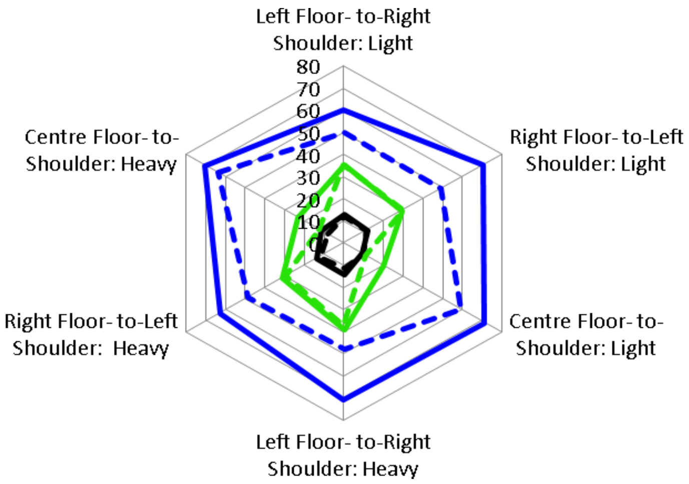

Figure 2: The average peak trunk angles in degrees for females (solid) and males (dashed) for each of the lifting conditions.

This study was the first part of a larger study aimed at deciphering the relationship between load magnitude and posture on the risk of injury. Using an EMG-driven spine model may reveal that joint loading is modified by load and symmetrical-asymmetrical lifting in a similar manner to trunk angle.

ACKNOWLEDGEMENTS

We would like to thank the Centre of Research Expertise for the Prevention of Musculoskeletal Disorders (CRE-MSD) for their financial support.

REFERENCES

1. Drake JDM, Callaghan JP. *Clin Biomech*, **23**, 510-19, 2008.
2. Drake JDM, et al. *Clin Biomech*, **24**, 1-9, 2009.
3. Marras WS, et al. *Spine*, **18**, 617-628, 1993.
4. Davis KG, et al. *Ergonomics*, **48**, 1031-46, 2005.
5. Marras WS, et al. *Clin Biomech*, **16**, 38-46, 2001.
6. Marras WS, et al. *Spine J*, **3**, 93-99, 2003.
7. Nelson-Wong E, et al. *Clin Biomech*, **23**, 545-53.

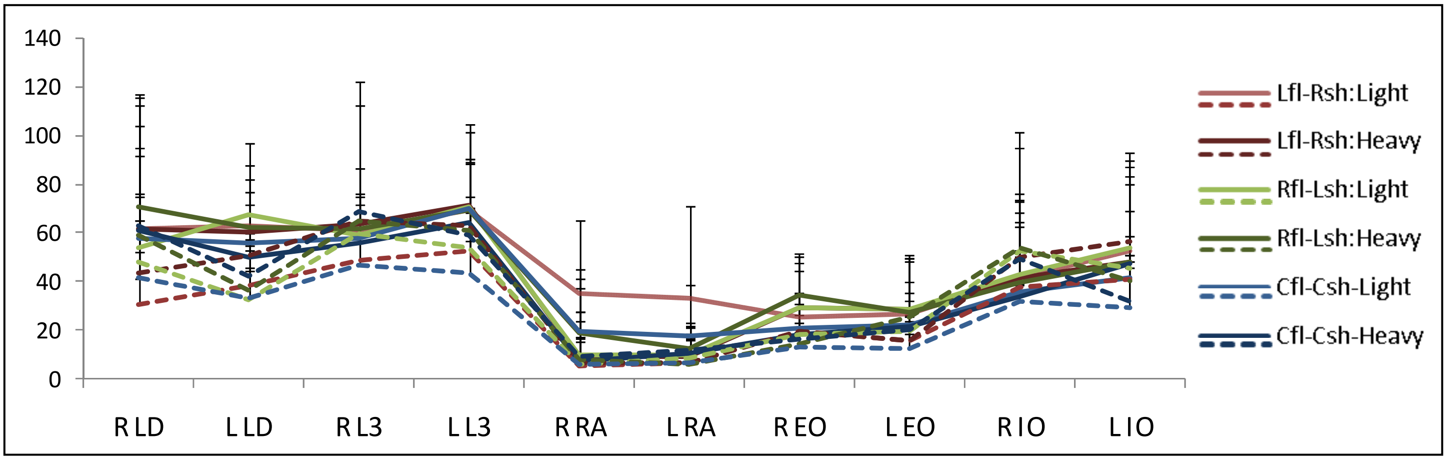

Figure 1: The average peak EMG for females (solid lines) and males (dashed lines) for each of the lifting conditions: left floor to right shelf (Lfl-Rsh), right floor to left shelf (Rfl-Lsh), and centre floor to centre shelf (Cfl-Csh).

VIBRATION PLATFORM OSCILLATION CHARACTERISTICS USING HIGH SPEED 3-D MOTION CAPTURE

Jaimie Branscomb, Gerald Smith, and Eadric Bressel
Biomechanics Laboratory, Utah State University, Logan, UT, USA
email: jaimie.b@aggiemail.usu.edu

INTRODUCTION

Review papers dealing with whole body vibration (WBV) training contain numerous inconsistent outcomes [1, 2, 3]. While some of these inconsistencies may be due to procedural differences, a less obvious source of variability may be inherent in some of the vibration instrumentation used in the studies. Few WBV studies provide detailed information concerning the vibration characteristics of the instrumentation beyond what may be provided by manufacturers. Accelerometry measured characteristics are typically reported but often these are one-dimensional, vertically oriented data with little information concerning horizontal plane vibration and its potential effect on subject responses to vibration treatment.

Three-dimensional motion analysis instrumentation has only recently increased speed and resolution capabilities to where high frequency vibration can be reliably detected. This project made use of such instrumentation to compare vibration platform motion characteristics with the specifications listed by manufacturers.

METHODS

Two commercial vibration platforms were used in this study testing 3-D motion characteristics through a range of frequencies and loading conditions. Initial testing was performed in an unloaded condition while comparison loaded data were obtained as a subset of another study concerning vibration attenuation with adult subjects. Manufacturer specifications are also reported for each device.

The FreeMotion iTonic vibration platform allows user control of frequency and amplitude with nominal settings of 25 Hz, 30 Hz and M on a frequency dial and amplitudes of High and Low on a second dial. The Pneu-Vibe Pro vibration platform from PneMex Inc. allows user control of frequency and amplitude through a control box with continous settings of frequency between 10 and 60 Hz and a switch changing amplitude between high and low. Three conditions were tested for the machines: nominal frequencies of 25 Hz, 30 Hz and M or 55 Hz for iTonic and Pneu-Vibe respectively. Low amplitude was used in each case.

A Vicon MX system with seven T-20 cameras sampling at 500 Hz tracked the three-dimensional trajectories of low mass retro-reflective markers placed on corners of the vibration plates using double-sided tape. 3-D position data from each reflective marker were computed and subsequently analyzed cycle-by-cycle using Microsoft Excel. Twenty cycles of vibration data were extracted for each condition. Mean peak-to-peak amplitude in each direction was determined as the average across the 20 cycles.

RESULTS AND DISCUSSION

Typical vibration characteristics for both machines are illustrated in Figures 1 – 3. In the unloaded condition, iTonic vibrations were systematically higher in frequency than nominal: about 28 and 33 Hz for the 25 and 30 Hz settings. M frequency corresponded with about 42 hz. For the Pneu-Vibe machine vibration frequencies were more complex with vertical motion occurring at twice the frequency of horizontal oscillation (Figure 1A) for the nominal 25 Hz setting. At other frequency settings, Pneu-Vibe was systematically low (24 Hz and 53 Hz for the nominal 30 and 55 Hz settings). Under loaded conditions, Pneu-Vibe was more consistent with systematically low frequencies (19, 25 and 53 Hz for the 25, 30 and 55 Hz settings). When loaded, iTonic exhibited similar frequency to unloaded.

Motion characteristics of the platforms were complex with both vertical and horizontal movements. Peak-to-peak amplitude was relatively consistent for the iTonic machine across frequency but changed dramatically for the Pneu-Vibe. This was especially strong for the 55 Hz condition (Figure 2) where vertical amplitude was about 5 mm. Similar large amplitude oscillation was observed for the device under loaded conditions.

CONCLUSIONS

Both Pneu-Vibe and iTonic vibration platforms differed in frequency by more than 10% from nominal settings of 25 and 30 Hz. The iTonic machine was systematically higher than nominal in frequency but was very consistent in this characteristic with changes due to loading. While repeatable, Pneu-Vibe had a complex movement pattern with horizontal and vertical frequencies different in the unloaded condition.

Peak-to-peak amplitude of the Pneu-Vibe machine changed with frequency and reached as much as 5 mm. In contrast, amplitude of vibration for iTonic was relatively consistent across frequencies. For controlled vibration dosage in therapy or training, such differences may be important considerations.

REFERENCES

1. Dolney D & Reyes GFC. *Curr Sports Med Rep* **7,** 152-157, 2008.
2. Jordan MJ et al. *J Strength Cond Res* **19,** 459-466, 2005.
3. Cardinale M & Wakeling J. *Br J Sports Med* **39,** 585-589, 2005.

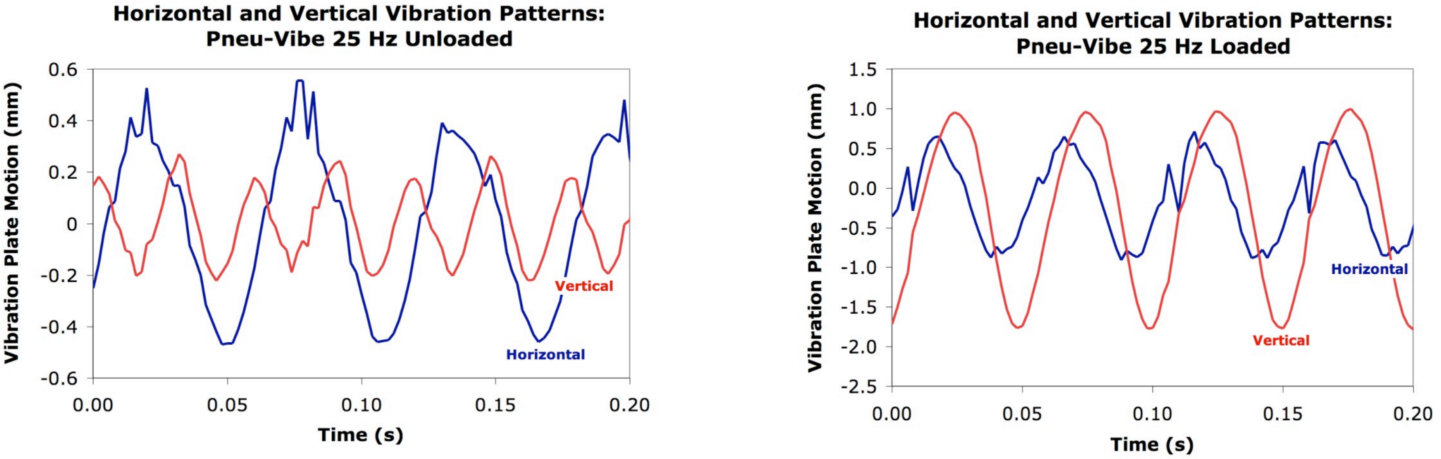

Figures 1A and 1B: Movement patterns for the Pneu-Vibe machine at a nominal frequency of 25 Hz in unloaded (left) and loaded (right) conditions. Note that unloaded, the vertical frequency was double the horizontal frequency (about 34 and 17 Hz) but once loaded to body weight the horizontal and vertical vibrations were of the same frequency but somewhat out of phase. In addition, peak-to-peak amplitudes changed with loading condition.

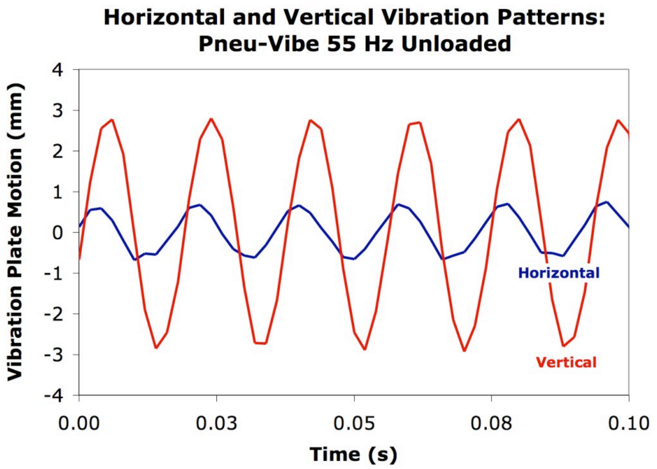

Figure 2. Movement patterns for the Pneu-Vibe machine near its maximum frequency. Despite the same amplitude setting as used with lower frequencies (Figure 1), vertical motion was considerably greater.

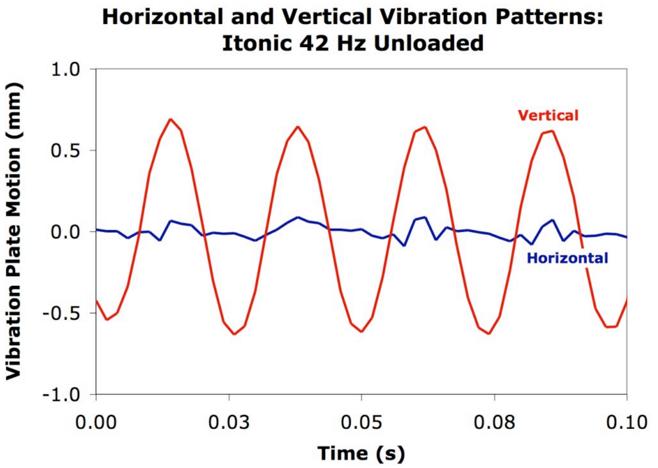

Figure 3. Movement patterns for the iTonic machine at its maximum frequency of about 42 Hz. At this frequency little horizontal motion was evident in the unloaded condition shown in the graph or when loaded to body weight.

Modeling and Simulation of Balance Recovery Responses to Tripping

Takaaki Shiratori[1] Brooke Coley[2] Rakié Cham[2] Jessica K. Hodgins[1]
[1] Robotics Institute, Carnegie Mellon University, PA, USA
[2] Department of Bioengineering, University of Pittsburgh, PA, USA
E-mail: siratori@cs.cmu.edu Web: http://www.engr.pitt.edu/hmbl

INTRODUCTION

Falls induced by tripping are harmful for older adults, and cause severe injury, hospitalization, and disability. Appropriate postural response strategies are necessary to avoid these accidents [1, 2, 3, 4]. Thus, experimental gait studies have been key in describing these responses. However, the causes of failed recovery attempts are difficult to determine from experiments alone. Computational modeling and simulation techniques can complement experimental approaches to gain a greater understanding of trip-initiated postural responses and causes of falls. The current work presented here describes our preliminary efforts to model balance recovery strategies triggered by tripping using physical simulation to understand the effects of specific parameters of the postural response on the dynamics of the response.

METHODS

Capturing Balance Recovery Responses to Tripping

Nine young (21-35 year old) and six older (65-75 years old) healthy adults, screened for neurological and musculoskeletal abnormalities, were recruited for participation in this study. First, range of motion test was recorded to construct the kinematic structure of each subject and to convert marker position data to joint angle data with Vicon iQ. Next, subjects were asked to walk onto a known dry floor to retrieve baseline gait characteristics. Subjects were then informed that in the next set of trials, at some point they would experience a trip. Subjects had no knowledge of the exact timing at which it would occur. Three trips were randomly inserted into 5 unperturbed trials. All subjects were harnessed to prevent hitting the floor in the event of an irrecoverable loss of balance. Whole body motion data were collected at 120 Hz. The trips were triggered at heel contact of the leading/right foot to catch the trailing/left foot in mid-swing. Only the first (unexpected trip) is used for further analysis.

Simulating Responses to Tripping

To model the dynamics of tripping responses, which were categorized as elevating or lowering strategies [1], physical controllers were designed with finite state machines (FSM) to determine the desired position and gains of each controlled joint for each state using proportional derivative (PD) controller:

$$\tau = k_p(\theta_d - \theta) - k_d\dot{\theta},$$

where θ_d is desired joint position, θ and $\dot{\theta}$ are the current joint angle and angular velocity, and k_p and k_d are spring and dumper gains, respectively. The parameters were set for each state in FSM. The simulation was initialized just before the trip occurred using the joint angles and velocities recorded experimentally. Tripping was simulated in 2D (sagittal plane), and all the parameters were manually set so that resulting motions were as close to motion capture data as possible. The posture of the upper body was maintained to be that recorded at the onset of the trip with high gains Tripping/collision forces were modeled using the data published by Pijnappels et al. [3].

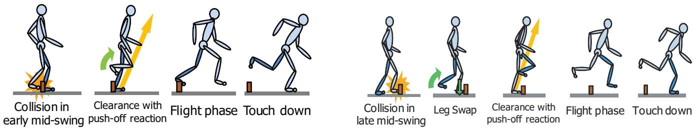
Collision in early mid-swing
Clearance with push-off reaction
Flight phase
Touch down
Collision in late mid-swing
Leg Swap
Clearance with push-off reaction
Flight phase
Touch down

Figure 1. Tripping strategies. Left: elevating strategy, and right: lowering strategy.

The controller for an elevating strategy had four states: *Passive Reaction*, *Clearance*, *Flight Phase*, and *Touch Down* (top of Figure 1). In Passive Reaction, the support leg maintained the torso attitude, and the swing leg was moving forward to prepare for stance. Tripping forces were applied to the swing toe. The durations of the passive reaction reported in in [2] were used to change the state to Clearance. In Clearance, flexion torques were applied to the swing leg to clear the obstacle, while extension torques were applied to the support leg to perform a push-off reaction. The compensation torque was also applied to the support ankle to achieve Flight Phase. When the support leg left the ground, the state became Flight Phase. In

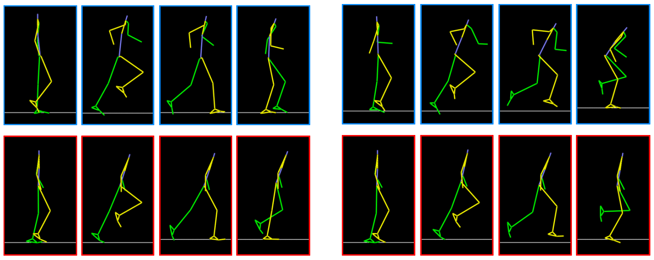

Figure 2. Results of simulating the elevating strategy with Double Support (left) and Flight Phase (right). Top: motion capture data and bottom: simulated motion. Yellow and green legs were tripped and non-tripped legs, respectively.

Flight Phase, extension torques were applied to the front leg for ground contact, and flexion torques were applied to the rear knee. In Touch Down, torques to maintain the torso attitude were applied to the joints of the support leg, and flexion torques were applied to the swing leg to move forward.

The controller for a lowering strategy had five states: *Passive Reaction*, *Leg Swap*, *Clearance*, *Flight Phase*, and *Touch Down* (bottom of Figure 1). Passive Reaction in the lowering strategy was the same as that in the elevating strategy. In Leg Swap, extension torques were applied to the swing leg for ground contact, and the support leg kept the stance posture. Once the swing leg touched the ground, the state became Clearance. In Clearance, flexion torques were applied to the non-tripped leg to become a swing leg and to clear the obstacle. The tripped leg became a support leg, and extension torques were applied for a push-off reaction. Flight Phase and Touch Down were the same as those in the controller of the elevating strategy.

RESULTS AND DISCUSSION

Out of 15 subjects total, seven performed an elevating strategy and eight performed a lowering strategy. In addition to the flight phase described by Pijnappels et al. [3], we observed some subject recovery strategies to include a double support phase. This double support phase was observed when walking speed was slow (∼1.0 m/s). Eight subjects (four performing elevating strategy, four performing lowering strategy) exhibited this double support phase. Since the double support phase was observed in several subject recovery strategies during slow speed walking, Double Support was used in these simulations instead of Flight Phase if walking speed was slow or if flight phase could not be achieved. When both legs touched the ground, the state became Double Support, and flexion torques were applied to the rear leg for the step.

The simulation results for both the elevating and lowering strategies were compared with motion capture data (Figures 2 and 3). Qualitatively, they were similar to the actual motions. Acceptable matches of the trajectories and height of the tripped/non-tripped foot were also produced (Figure 4).

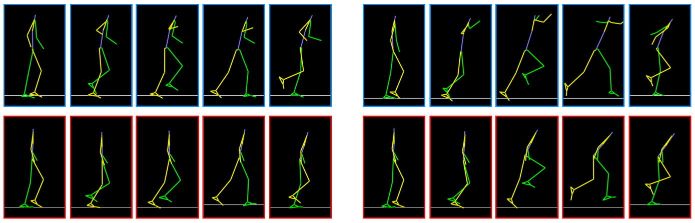

Figure 3. Results of simulating the lowering strategy with Double Support (left) and Flight Phase (right). Top: motion capture data and bottom: simulated motion. Yellow and green legs were tripped and non-tripped legs, respectively.

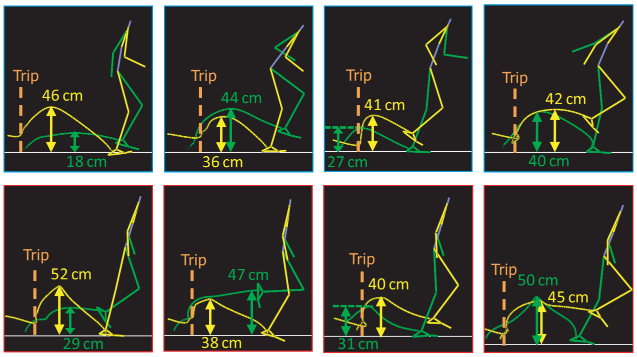

Elevating with Double Support

Elevating with Flight Phase

Lowering with Double Support

Lowering with Flight Phase

Figure 4. Comparison of foot trajectories and height between motion capture data and simulated motion. Top: motion capture data and bottom: simulated motion. Yellow and green lines were trajectories of tripped and non-tripped feet, respectively.

CONCLUSION

Responses to tripping were physically simulated based on motion capture data of tripping. In the future, we will collect more data to further develop and validate the simulation models. We will also extend our 2D simulation to 3D including arm movements. Finally, the long term goal of this work is to use the simulations to gain a better understanding of trip-triggered failed postural recovery responses in older adults.

REFERENCES

[1] Eng J.J., et al., *Experimental Brain Research*, 102:339–349, 1994.
[2] Schillings A.M., et al., *J. Neurophysiology*, 83:2093–2102, 2000.
[3] Pijnappels, M., et al., *J. Biomechanics*, 37:1811–1818, 2004.
[4] Pijnappels, M., et al., *J. Biomechanics*, 38:627–634, 2005.

ACKNOWLEDGEMENTS

This study has been supported in part by F31 AG025684-03 NIH Ruth L. Kirschstein Award and by NSF Quality of Life Technology Center.

THE INFLUENCE OF RELATIVE HIP AND KNEE EXTENSOR STRENGTH ON LOWER EXTREMITY BIOMECHANICS DURING A DROP LAND TASK

Kristen M. Stearns, Christopher M. Powers
Jacquelin Perry Musculoskeletal Biomechanics Research Laboratory
Division of Biokinesiology and Physical Therapy
University of Southern California, Los Angeles, CA, USA
email: lemly@usc.edu, web: www.usc.edu/go/mbrl

INTRODUCTION

Tears of the anterior cruciate ligament (ACL) are 4-6 times more likely to occur in females, as compared to males [2]. While the cause for this discrepancy in ACL injury rates is unknown, specific biomechanical profiles have been identified that may place females at greater risk of injury. For example, females demonstrate increased valgus moments at the knee, which have been directly linked to an increased risk of ACL injury [2]. Additionally, females tend to demonstrate decreased hip and knee flexion, increased knee extensor moments, and decreased energy absorption at the hip during landing [1,2].

One possible explanation for these gender specific differences in landing strategies may be related to weakness of the hip muscles, which provide dynamic stability during landing. In particular, weakness of the hip extensors relative to the knee extensors may cause an over-reliance on the knee musculature and associated passive structures (i.e. ligaments) to absorb impact forces during landing [3,4,5]. The purpose of this study was to investigate the influence of hip extensor muscle strength relative to knee extensor muscle strength on lower extremity biomechanics during landing.

METHODS

Eight healthy females, free from lower extremity pathology or previous injury, participated in 2 data collection sessions: 1) kinematic and kinetic assessment during a drop landing task from a 14 in box, and 2) isometric strength testing of hip and knee extension using a Cybex Isokinetic dynamometer. All data was collected from the dominant lower extremity, defined as the leg with which the subject would prefer to kick a ball.

Lower extremity kinematics and ground reaction forces were collected using an 8-camera Vicon Motion Analysis System (Vicon 612, Oxford, UK; 250 HZ) and 2 floor-embedded force plates (AMTI, Watertown, MA; 1500 Hz). Peak knee valgus moments, peak hip and knee flexion angles, and hip energy absorption were calculated during the deceleration phase of the drop land, as defined by the time from initial foot contact on the force plate to peak knee flexion angle.

For the strength testing, subjects performed 3 maximum isometric contractions of 5 seconds duration for both hip and knee extension. The average isometric torque produced during the best repetition was used to calculate the hip/knee extensor strength ratio (HKR). A strength ratio greater than 1 indicated that hip extensor muscle strength was greater in magnitude than knee extensor muscle strength, while a strength ratio less than 1 indicated that isometric knee extensor muscle strength was greater in magnitude than hip extensor muscle strength. The 6 subjects were then divided into 2 groups based on the results of their strength results. Three of the subjects had a HKR greater than 1, and 3 subjects had a HKR less than 1.

Comparisons of kinematic and kinetic variables between the 2 groups were made using independent samples t-tests. In addition, linear regression analysis was performed to determine the relationship between the HKR and the peak valgus moment.

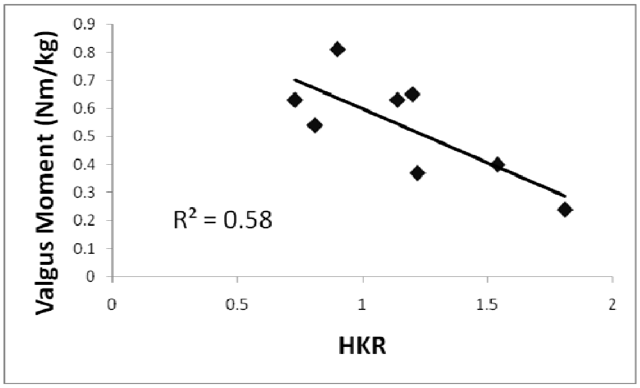

Figure 1: Peak knee valgus moments plotted against the HKR for all 8 subjects included in the study. Linear regression produced an $R^2 = 0.58$

RESULTS

Table 1 provides a summary of the average data averaged for the 2 groups of subjects. The 5 subjects in the high HKR group (i.e. HKR > 1), had an average ratio of 1.38 ± 0.3, while the 3 subjects in the low HKR group (i.e. HKR < 1), had an average ratio of 0.81 ± 0.1. When compared to the low HKR group, subjects in the high HKR group had lower peak knee valgus moments, greater peak hip and knee flexion angles and greater energy absorption at the hip. Linear regression of the HKR on the peak knee valgus moment for all the subjects resulted in a R^2 value of 0.58 ($p<0.05$), indicating that 58% of the variance in peak knee valgus moment could be explained by the HKR.

DISCUSSION

Although our study included only a small number of subjects, distinct differences in landing strategies were noted between the two groups. In general, individuals with a lower HKR tended to land using a biomechanical pattern thought to increase knee loading (i.e. diminished sagittal plane motion and increased frontal plane moments). Conversely, subjects with high HKR's demonstrated improved energy absorbed at the hip and a biomechanical strategy thought to be less "at risk" for knee injury. The results of the linear regression analysis support the premise that strength of the sagittal plane musculature is associated with frontal plane knee moments.

CONCLUSIONS

These results indicate that the relative strength of the hip extensors, compared to the knee extensors, may influence hip and knee biomechanics during landing. Our results suggest that interventions aimed at strengthening the hip extensors may improve the lower extremity biomechanics associated with knee injury in female athletes, however additional research would be needed to test this hypothesis.

REFERENCES

1. Decker MJ, et al. *Clin Biomech* **18**, 662-669, 2003.
2. Hewett TE, et al. *Am J Sports Med* **33**, 492-501, 2005.
3. Schmitz RJ, et al. *Clin Biomech* **22**, 681-688, 2007
4. Pollard CP, et al. *Clin J Sport Med* **17**, 38-42, 2007.
5. Zazulak BT, et al. *JOSPT* **35**, 292-299, 2005

ACKNOWLEDGEMENTS

This study was supported by the Foundation for Physical Therapy (PODS I).

Table 1: Summary of the HKR and biomechanical variables calculated over the deceleration phase of the drop land for the subjects with the high and low HKR.

Group	HKR	Knee Valgus Moment (Nm/kg)	Peak Knee Flexion Angle (Degrees)	Peak Hip Flexion Angle (Degrees)	Hip Energy Absorption (Watts/kg)
High HKR (n=3)	1.38 ± 0.3	0.45 ± 0.09	87.6 ± 8.6	73.8 ± 5.5	160.18 ± 14.5
Low HKR (n=3)	0.81 ± 0.1	0.66 ± 0.14	81.9 ± 11.5	68.0 ± 9.5	110.6 ± 45.4

INTERACTION BETWEEN MASS AND ALIGNMENT ON KNEE ADDUCTION MOMENT IN PATIENTS WITH KNEE OSTEOARTHRITIS

[1]Rebecca Moyer, [1]Trevor Birmingham, [1]Crystal Kean, [1]Ian Jones, [1]Thomas Jenkyn,
[1]Bert M Chesworth, [1]J Robert Giffin
[1]Wolf Orthopaedic Biomechanics Laboratory, Fowler Kennedy Sport Medicine Clinic,
University of Western Ontario, London, ON
Email: rmoyer@uwo.ca

INTRODUCTION

Knee osteoarthritis (OA) is a leading cause of pain, disability and health care use. The need to better understand risk factors, and their mechanisms, for progression of the disease is paramount. There is some evidence to suggest that the effect of BMI on the development and/or progression of knee OA depends on lower limb alignment [1,2,3].

Although the results of clinical studies evaluating this potential interaction have been inconsistent, authors have consistently suggested that the likely mechanism is due to increased focal loading of the medial compartment of the knee.

The external adduction moment about the knee during walking is a valid proxy for the dynamic load on the joint's medial compartment [4]. The magnitude of the knee adduction moment (KAM) is a potent risk factor for progression of OA [5]. Body mass and varus alignment of the lower limb contribute to the KAM and are the targets of various treatment strategies.

The purpose of the present study was to evaluate the interaction between mass and alignment when predicting the KAM in patients with knee OA. We hypothesized that the effect of body mass on the KAM would be moderated by the extent of limb malalignment.

METHODS

354 patients with knee OA were recruited from a cohort of patients being screened for participation in a prospective study of osteotomy procedures. Patients underwent 3-D gait analysis using an 8-camera motion capture system and modified Helen Hayes markers set (Eagle EvaRT; MAC, Santa Rosa, CA) synchronized with a single floor-mounted force plate (AMTI, Watertown, MA).

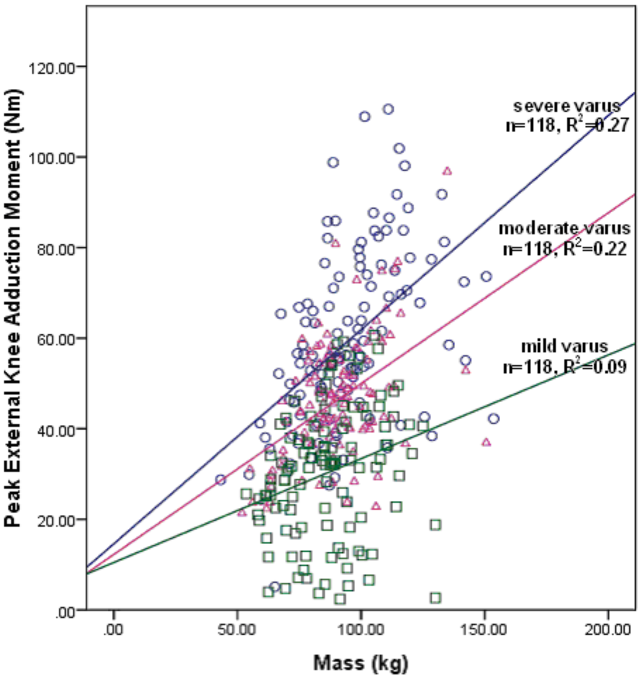

Figure 1: Scatterplot illustrating the relationship between mass and knee adduction moment for patients with different extents of malalignment.

The peak KAM (Nm) was calculated from the kinematic (60Hz) and kinetic (1200Hz) data using commercial software (Orthotrak 6.2.4; MAC, Santa Rosa, CA) and custom post-processing techniques. Gait speed, toe out and lateral trunk lean were also determined. Body mass (kg) and height (m) were measured prior to gait testing. Frontal plane alignment was quantified using the mechanical axis (hip-knee-ankle) angle (deg) measured from standing long-cassette radiographs.

We tested for effect modification by entering the interaction term (mass*mechanical axis angle) into a linear regression model predicting peak knee adduction moment (Equation 1).

(Equation 1)
KAM = height + speed + toe-out + trunk-lean + mass + alignment + mass*alignment

We then split the sample into three subgroups based on tertiles for mechanical axis angle and evaluated the relationship between mass and knee adduction moment for each subgroup using simple linear regression.

RESULTS AND DISCUSSION

The interaction term (mass*mechanical axis angle) significantly ($p=0.04$) contributed to a model predicting the KAM while controlling for height, gait speed, toe out, trunk lean, mass and mechanical axis angle (Total $R^2=0.67$). In patients with severe varus alignment (≥9deg) KAM increased 0.47 Nm for every 1kg increase in mass. In patients with moderate varus alignment (4.80 to 8.99deg) KAM increased 0.38 Nm for every 1kg increase in mass. In patients with mild varus alignment (≤4.79deg) KAM increased 0.23 Nm for every 1kg increase in mass (Figure 1, Table 1).

CONCLUSIONS

These findings illustrate that there is a significant interaction between mass and alignment when using these two variables to predict medial compartment loading during walking in patients with knee OA. As we hypothesized, the effect of body mass on the KAM depends on the extent of limb malalignment. Those with greatest malalignment exhibit the greatest association between mass and peak knee adduction moment. Individuals with both increased mass and increased malalignment may benefit most from earlier intervention strategies intended to decrease dynamic knee joint loads.

REFERENCES

1. Felson DT, et al. *Arthritis and Rheumatism* **50**(12), 3904-3909, 2004.
2. Sharma L, et al. *Arthritis and Rheumatism* **43**(3), 568-575, 2000.
3. Niu J, et al. *Arthritis and Rheumatism* **61**(3), 329-335, 2009.
4. Andriacchi TP and Mundermann A. *Current Opinion in Rheumatology* **18**, 514-518, 2006.
5. Miyazaki T, et al. *Annals of the Rheumatic Diseases* **61**, 617-622, 2002.

Table 1: The un-standardized regression coefficient values with 95% confidence intervals for each of the three subgroups.

Alignment (deg)	β	95% CI
Severe Varus (n=118)	0.47	0.33-0.62
Moderate Varus (n=118)	0.38	0.25-0.5
Mild Varus (n=118)	0.23	0.09-0.37

EFFECT OF FORCE REDIRECTION ON UPPER LIMB NET JOINT MOMENTS DURING WHEELCHAIR PROPULSION

Joseph M. Munaretto [1], Jill L. McNitt-Gray [1,2,3], Henryk Flashner [4], and Philip S. Requejo[5]
[1]Department of Biomedical Engineering, [2]Kinesiology, [3]Biological Sciences
[4]Aerospace and Mechanical Engineering, University of Southern California, Los Angeles, CA
[5]Pathokinesiology Laboratory, Rancho Los Amigos National Rehabilitation Center, Downey, CA
E-mail: munarett@usc.edu

INTRODUCTION

The force applied by the wheelchair user during manual wheelchair (MWC) propulsion often has a radial component that does not contribute to torque generation about the axis of the wheel. The mechanical cost on the body as well as effect on the pushrim while varying force direction has been simulated [1] using an inverse dynamic model. As shown for other multijoint goal directed tasks [2, 3], redirection of the reaction force relative to the body segments redistributes the net joint moments across the joints. While redistribution of the mechanical demand across the upper extremity may be advantageous to avoid overloading of individual musculoskeletal components, the same propulsive torque needs to be applied to the wheel to accomplish the task objective.

In this study, we determined the range of net joint moment cost profiles needed to perform the same MWC task by using an experimentally validated 2D inverse dynamic model. Propulsion force was varied in direction, while torque applied to the pushrim was constrained to the experimentally measured condition. The net joint moment cost profiles of two subjects performing the MWC task were compared to illustrate how the mechanical demand imposed on the individual may vary when satisfying the same task objectives.

METHODS

Two wheelchair users volunteered to participate in this study in accordance with the Institutional Review Board. The subjects propelled at self-selected speeds for 10 seconds. Reflective markers were used to monitor the 3D motion of the hand, forearm, upper arm, and trunk segments (VICON, 50 Hz). The force applied to the wheelchair during propulsion was measured using force transducers (2500 Hz) mounted along the spokes of the wheel. Kinematics were projected into the sagittal plane and translated so that the origin lied at the center of the wheel.

A two segment, two dimensional inverse dynamic model of the human body was created using MATLAB. Segments for the forearm and upper arm were represented as rigid bodies and segment kinematics were determined from experimental marker data. The measured reaction force was assumed to act at the distal end of the forearm (wrist marker).

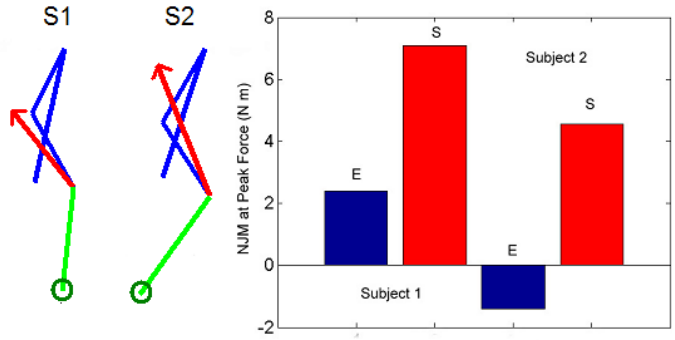

Figure 1: Kinematics and NJM at peak push force

The location of the wrist/pushrim reaction force on the pushrim was determined from the location of the wrist on the wheel

$$\theta_{Wheel} = \tan^{-1}\left(\frac{y_W}{x_W}\right)$$

where x_W and y_W are the Cartesian coordinates of the wrist. In this case, top dead center (TDC) would be 90°. The torque applied to the wheel was calculated as

$$\tau_z(t) = F_y(t)\cos\theta_{Wheel}(t) - F_x(t)\sin\theta_{Wheel}(t)$$

where F_x and F_y are the components of the reaction force in the global frame acting on the wheel. The torque does not account for wheel radius, and is defined so that a propulsive torque is negative (clockwise).

Next, the direction of the force acting on the subject in the global reference frame, θ_F, was allowed to vary covering all angles that could produce a negative wheel torque (propulsive). At each angle and instant in time, the resultant force magnitude needed to generate the measured torque was determined as

$$F_{mag}(t) = \frac{\tau_z(t)}{\sin(\theta_{Wheel}(t) - \theta_F)}$$

From the computed resultant force and direction, horizontal and vertical components were computed for each force angle simulation.

For each force angle, the sum of absolute net joint moments (NJMs) at the elbow and shoulder was computed using the inverse dynamic model and measured kinematics. To better physically relate the direction of the push force, force angle was represented relative to the forearm with positive indicating the force acting behind the forearm.

RESULTS AND DISCUSSION

At peak push force (and entire cycle), Subject 2 acts more forward on the pushrim than Subject 1 (Figure 1). The push force acts on the body in front of the forearm for Subject 1, but behind the forearm for Subject 2. The NJM at the elbow is flexor for Subject 1 but extensor for Subject 2.

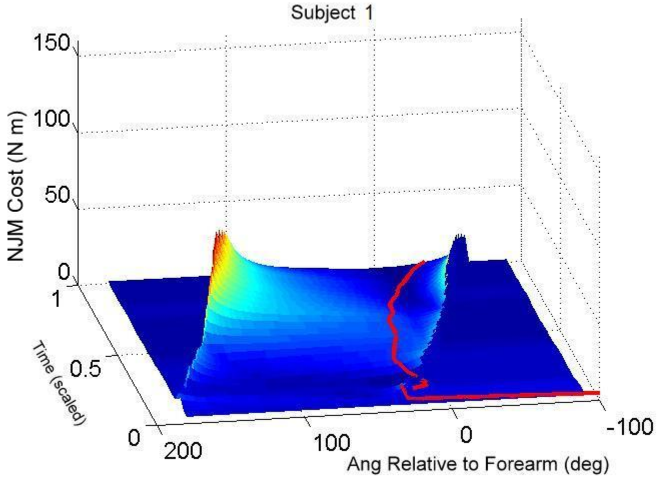

Figure 2: Sum of absolute NJM of shoulder and elbow at varying force angles for Subject 1

For Subject 1, low NJM costs are found at positive force angles (behind the forearm) but move to slightly negative force angles with time (Figure 2). For Subject 2, low NJM costs are located at slightly negative force directions relative to forearm, which become slightly more negative with time (Figure 3).

NJM costs for both subjects' experimental movements lie near the minima on their respective cost surfaces (red lines). The optimal force directions lie on opposite sides of the forearm, creating different NJM at the elbow and due to the different human / wheel kinematics (Figure 1). These results emphasize the need to assess observed technique in within the context of individual cost-functions.

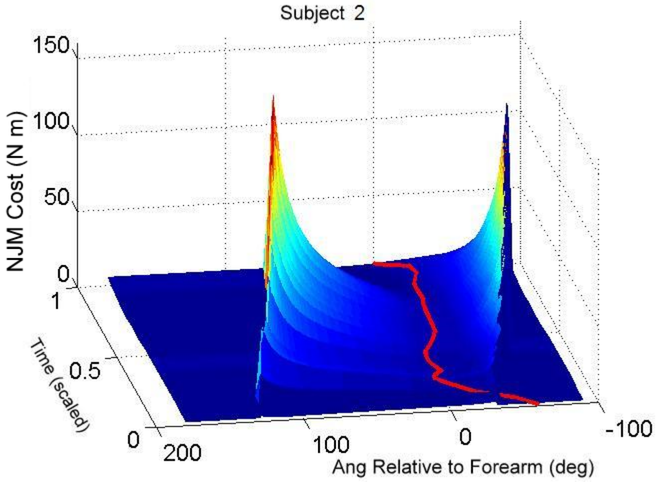

Figure 3: Sum of absolute NJM of shoulder and elbow at varying force angles for Subject 2

CONCLUSIONS

Constraint of force magnitude based on torque generation requirements provides a realistic framework for simulating propulsion kinetics. Future work will explore more complex and clinically-motivated subject-specific cost functions.

REFERENCES

1.Rozendaal LA, et al. *J Biomech*, **36**(2): 239-247, 2003.
2.McNitt-Gray JL, et al. *J Biomech*, **34**(11): 1471-1482, 2001.
3.Mathiyakom W, et al. *Clinical Biomechanics* **20**(1): 105-111, 2005.

TIME-LAPSE MICROTOMOGRAPHY OF TRABECULAR BONE DEFORMATION USING FLAT PANEL X-RAY SENSOR

Ondrej Jirousek
Department of Biomechanics, Institute of Theoretical and Applied Mechanics,
Academy of Sciences of the Czech Republic, v.v.i, Prague, Czech Republic
email: jirousek@itam.cas.cz, web: http://www.itam.cas.cz

INTRODUCTION

For investigation of morphological and material properties of materials with complex inner structure, such as trabecular bone several aspects influencing the overall material properties play an important role. Microstructural arrangement of individual trabeculae greatly influences overall mechanical properties of the bone [1].

In recent years 3-D imaging techniques were established which enables direct measurement of structural properties of materials with complex inner structure [2, 3]. These techniques can be used not only to measure the morphological properties of the material, but they can be successfully applied to measure its mechanical performance. To capture the 3-D deformation it is possible to use microfocus Computed Tomography applied to a sample which undergo deformation. In the case of time-lapse tomography of trabecular structure a bone sample is fixed in a special loading device enabling load application in increments and subsequent scanning.

The deformed inner structure of the sample is then reconstructed during the deformation process. This enables to capture the strains in the individual trabeculae and to measure the highly localized strains within each trabecula. Results obtained from the real–time microtomography can be used to compare post-yield behaviour of trabecular bone or to validate micro–FE models created from the micro–CT scans of the undeformed sample. Real–time tomography can also provide useful information in the design of tissue scaffolds where maximization of mechanical strength with optimization of flow and diffusion properties of the scaffold is essential for sufficient cell ingrowth.

METHODS

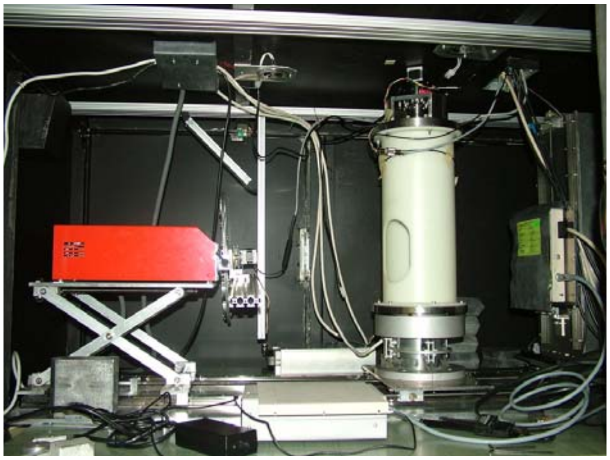

Figure 1: Experimental setup: X-ray source (left), loading device (middle), flat panel detector (right).

Two samples of trabecular bone were extracted from proximal femur using water-cooled IsoMet 1000 precision saw (Buehler, Inc.). Cylindrical samples 10mm high and 10 mm in diameter were extracted in the direction respecting the trabecular structure. Another sample was extracted for the nanoindentation purposes from the same region. The surface of the sample was polished down to submicron precision using diamond paste and diamond particle suspension. Minimal sample dimensions respect in both cases recommended minimal values with respect to the maximal pore size. A special attention is paid to the proper boundary conditions.

High resolution tomographic images of the sample are obtained using X-ray tungsten microfocus tube (Hamamatsu photonics) with 5 µm spot size (divergent cone beam) and flat-panel X-ray sensor ((Hamamatsu photonics) with active area 120 mm x 120 mm. The loading device with the mounted sample is placed on a rotating table controlled by stepper motors. The load is applied gradually in 1% strain increments and complete tomography of the sample is taken in 180 projections per increment. The overall strain applied to the sample was 10 %.

From the projections obtained at different strain levels (0.01, 0.02 ... 0.1) cross–sectional slices were reconstructed using cone–beam inverse Radon transformation. From the volumetric images it is possible to calculate strains in any cross–section using image correlation techniques. The deformed structure of trabecular bone in three selected strain levels is shown in Fig. 2.

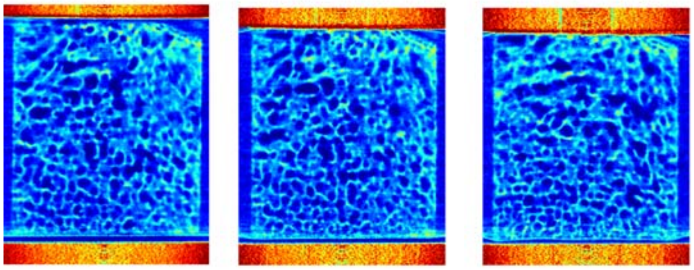

Figure 2: Reconstruction of the deformed sample in the median plane for selected strains.

Measurement of intrinsic material properties at microscale can be performed by means of nanoindentation. Nanoindenter equipped with Berkovich (three-sided pyramid) diamond probe was used to determine the material properties at trabecular level [4]. Constitutive material model for each sample was obtained by means of simulating the nanoindentation using the finite element method and fitting the response curve to obtain material properties. Two plasticity criteria were compared. The first criterion was simple von Mises criterion, where only the yield stress σ_y and post-yield modulus E_t was identified. The second criterion was four-parameter elasto-plastic constitutive equation based on Drucker-Prager plasticity criterion which is able to capture the pressure-dependent inelastic behavior. In this case, internal friction angle α, cohesion c and dilatation angle θ were identified by fitting the force-deflection curve obtained from the FE simulation to the curve obtained experimentally.

The indentation FE model was developed and solved as an axisymmetric contact problem. The Poisson's ratio is assumed to be known quantity in the FE simulations and the parameters are identified using an iterative approach. Identified material models were used in FE simulation of the experiment, where reconstructed microstructure was loaded by the corresponding displacement boundary conditions. From the FE model, apparent stress is calculated as reaction forces at the end of the sample divided by the cross-sectional area and response in terms of the force-displacement curve is obtained and compared to the measured one.

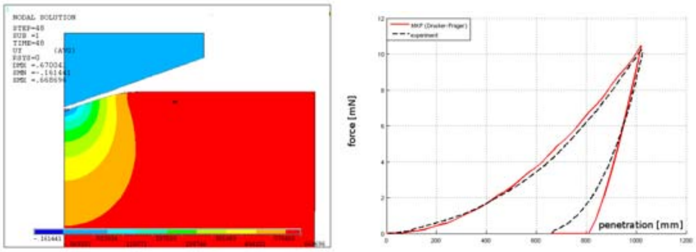

Figure 3: Fitting material properties from the FE simulation of nanoindentation experiment.

CONCLUSIONS

Combination of the nanoindentation and microstructural FE models of high resolution is a promising technique to study pre and post-yielding behaviour of materials with complex inner structure. Techniques described in the paper enable to generate FE models of the inner structure based on the computer tomography data and to provide these models with proper constitutive equation based on nanoindentation results. Two different material models for the trabeculae were identified in FE simulation of the nanoindentation and used in subsequent analysis of the deformation behavior of the trabecular microstructure.

Apparent stress-strain curves were computed from the FE simulations and compared to the experimentally determined ones. It was found that the Drucker-Prager plasticity is more suitable criterion for the trabecular bone since it is able to capture its pressure-dependant behavior. Results from the FE simulation of the sample compression show promising results when compared to experimentally determined values obtained from the tomographic measurements.

REFERENCES

1. Wagner H. D., et al. *Journal of Biomechanics*, **25**, 1311–1320, 1992.
2. Mathieu LM, et al. *Biomaterials*, **27**, 905–916, 2006.
3. Jones AC, et al. *J Mater Sci: Mater Med*, **15**, 529–532, 2004.
4. Oliver, W.C., Pharr, G.M., *Journal of Material Research*, **7**, 1564-1583, 1992.

ACKNOWLEDGEMENTS

This work has been supported by the Grant Agency of the Czech Republic (grant No. 103/07/P483) and the Grant Agency of the Academy of Sciences of the Czech Republic (grant No. AV0Z2071052).

CHANGES IN SCAPULAR KINEMATICS PRE AND POST WORKDAY

[1]Luke Ettinger, [2] Laurel Kincl, [1]Andrew Karduna
University of Oregon [1]Department of Human Physiology, [2] Labor Education and Research Center
email: lettinge@uoregon.edu, web: http://biomechanics.uoregon.edu/obl/

INTRODUCTION

Shoulder impingement syndrome is the most commonly diagnosed musculoskeletal disorder of the shoulder complex [1]. It has been found that of the 3 scapular rotations, upward rotation was the only movement to significantly affect the clearance of the rotator cuff tendons within the subacromial space [2]. Shoulder impingement syndrome has been found to occur frequently in workers requiring repetitive arm motions such as dental hygienists. While working, dental hygienists may require their shoulders to be elevated above 60 to 90 degrees for long periods of time [3]. It is believed that repetitive tasks may alter normal shoulder kinematics and cause compensatory shoulder motions to adjust for deficits caused by fatigue [4]. We hypothesized that workday fatigue would cause increases in scapular upward rotation from normal glenohumeral kinematics [4]. To the best of our knowledge there have been no published studies comparing 3D scapular kinematics between pre and post workdays in any population. Additionally, no studies of this nature have been conducted within the workspace of the desired population.

METHODS

Four healthy female dental hygienists participated in this study (mean age, 35 years). All subjects worked full time (40+ hours per week) and all data were collected before and after a full 8 hour workday at the clinic the hygienist was employed. Kinematic data were collected via the Polhemus Fastrack magnetic tracking system with three receivers: thorax, scapula and humerus (Figure 1). The thoracic receiver was attached using double side adhesive tape to the manubrium inferior to the jugular notch. The scapular receiver was attached using a scapula tracker jig and Velcro strips on the scapular spine and acromion process [2]. The humeral receiver was placed over the deltoid tuberosity using a molded cuff. Bony landmarks were digitized using the stylus during the calibration phase of our experimental protocol. For all trials, data were collected at a rate of 40 Hz.

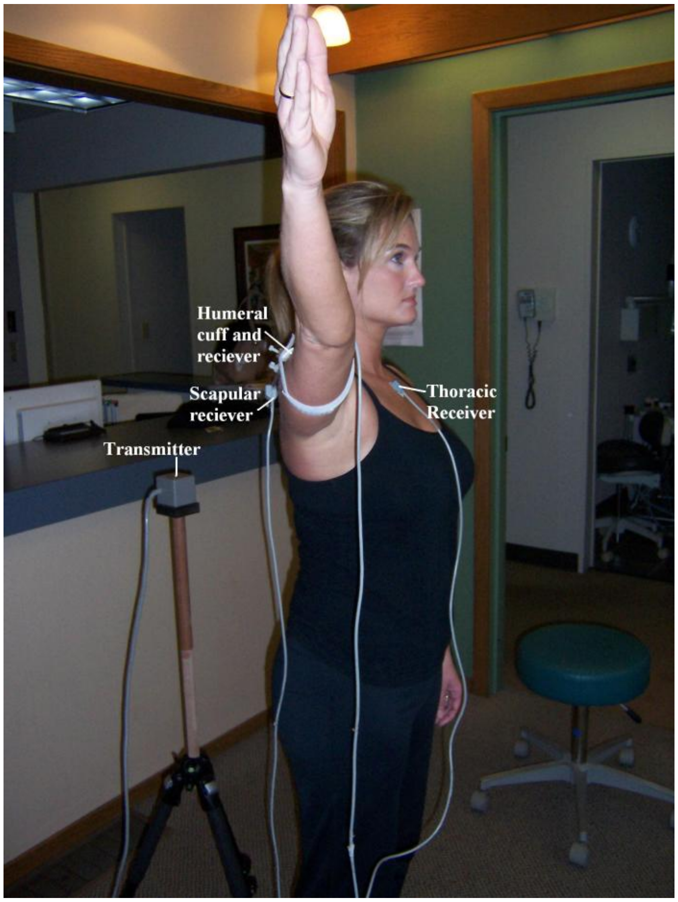

Figure 1: Experimental setup and attachment of sensors.

During calibration and data collection trials, subjects were in a standing position. The arbitrary axis systems defined by the Polhemus were converted to anatomically appropriate axis systems based on the recommendations of the International Society of Biomechanics (ISB) Committee for Standardization and Terminology [5].

Each subject preformed three unconstrained arm elevation movements with their dominant arm.

Arm movements were preformed in the scapular plane (30° from frontal plane). The speed of the movement was controlled by having the subject achieve maximal humeral elevation in 4 seconds and returning their arm to their side using the same path in an additional 4 seconds. Data were collected twice, once in the morning before work and once immediately following the work day. An average of the three arm elevations trials was made; from these data, humeral elevation and scapular upward rotation were interpolated in 5 degree increments during the humeral elevation path.

RESULTS AND DISCUSSION

Using the pre and post workday data for each subject, we plotted scapular upward rotation with respect to the thorax to humeral elevation with respect to the thorax (Figure 2). From all subjects, an observable increase in scapular upward rotation was noted after the workday. From both subjects 1 and 2 it appeared that the increase in scapular upward rotation was more profound towards the peak of humeral elevation post workday. Intuitively this makes sense, as increased humeral elevation demand typically requires more scapular involvement. These preliminary findings are consistent with our hypothesis that scapular upward rotation would increase post workday due to a compensatory fatigue mechanism. However, more subjects are needed to confirm these preliminary results.

ACKNOWLEDGEMENTS

Funding for this project was possible through a NIOSH grant 5R01OH008288.

REFERENCES

1. Fu FH, et al. *Clin Orthop* (269): p.162-73, 1991
2. Karduna AR, et al. *J Shoulder Elbow Surg* 14(4): p. 393-9, 2005
3. Svendsen, S.W., et al., *Arthritis and Rheumatism*, 50(10): p. 3314-22, 2004.
4. K. McQuade, et al. *Clinical Biomechanics* 10: p. 144–8, 1995.
5. Wu, G., et al. *J Biomech*, 38(5): p. 981-992, 2005.

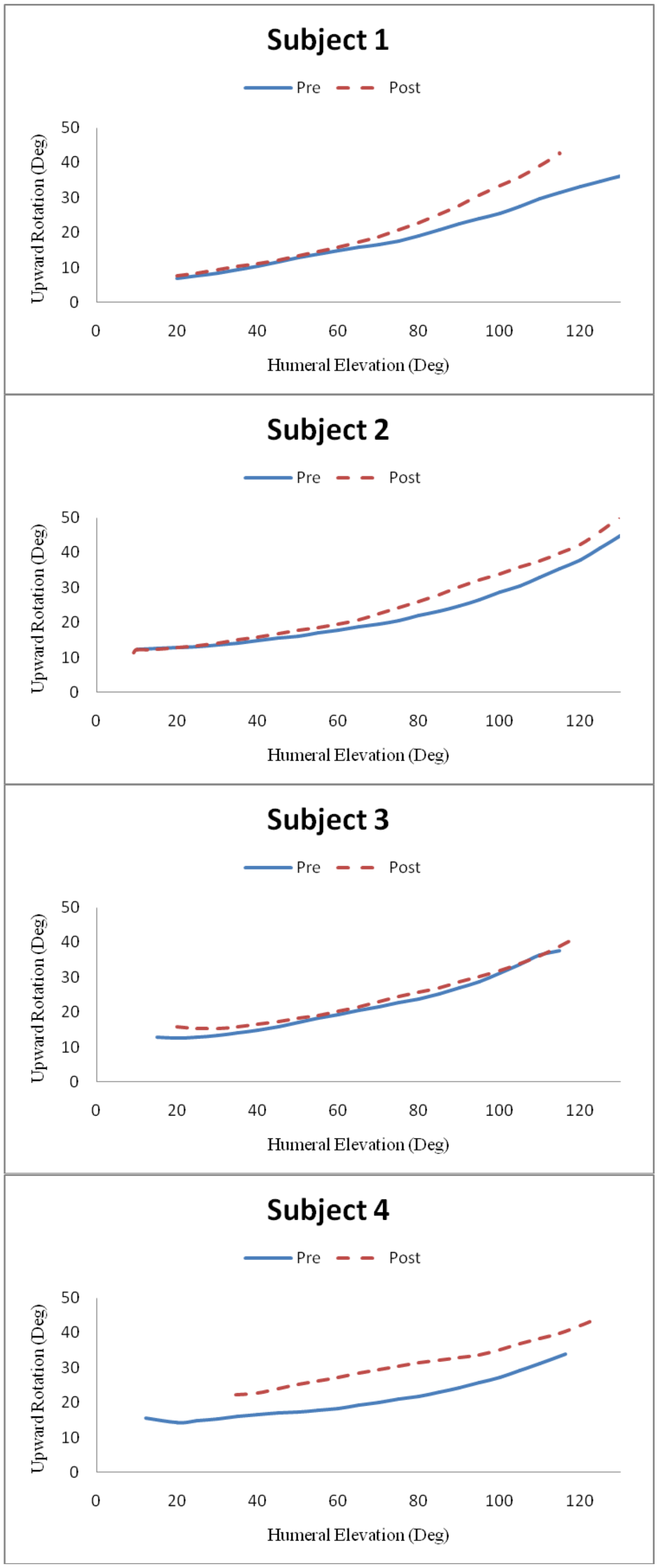

Figure 2: Changes to scapular upward rotation as a result of workday fatigue.

POWER AUGMENTATION IN A COMPLIANT MUSCLE-TENDON SYSTEM

Peter Sheppard, Gregory S. Sawicki and Thomas J. Roberts
Dept. of Ecology and Evolutionary Biology, Brown University, Providence, RI, USA
email: Peter_Sheppard@brown.edu

INTRODUCTION

In a compliant muscle-tendon (MT), peak power output can exceed that of the muscle alone during contractions against inertial loads. In the early stages of the contraction, the series tendon is stretched, storing energy; in the later stages, this stored strain energy is released and aids in the acceleration of the mass. This stretch and recoil of the tendon essentially decouples in time the production of the mechanical work by the muscle and the delivery of this work to the load [**1**]. A theoretical study exploring this phenomenon estimated that maximum achievable power amplification should approach twice that of peak isotonic power [**2**]. However, few *in vitro* studies have been undertaken to examine real-world muscle-tendon performance during contraction against an inertial load. The goal of this study was to determine the maximal possible power amplification for muscle-tendon operating against varying inertial loads. We hypothesized that peak power output during contractions against an inertial load would exceed peak isotonic power of muscle alone, and that magnitude of power amplification would be load dependent.

METHODS

We tested four bullfrog plantaris muscle-tendons *in vitro*. We attached a nerve-cuff to the sciatic nerve and stimulated the muscle using a 4V 100 ms pulse train (.2 ms pulses, 100 pps). For each preparation, we used a muscle ergometer to simulate an inertial load lever system (**Figure 1**). Ergometer length was controlled using a feedback system involving real-time force samples (1000 Hz) from the muscle ergometer. These force values were used in conjunction with the equations of motion of the simulated mechanical system to calculate change in lever position, which was then used to control ergometer position. Nine simulated loads were tested, ranging from a normalized weight (W) of ~0 to 1.0*MT F_{max}. We recorded MT force and length from the ergometer and muscle fiber length from surgically implanted sonomicrometry crystals. To calculate contractile element (CE) length we multiplied muscle fiber length by a gearing factor (~1.5) to account for the effects of muscle pennation. Power was calculated as the product of force and velocity. We integrated the positive regions of the power curves and divided by muscle

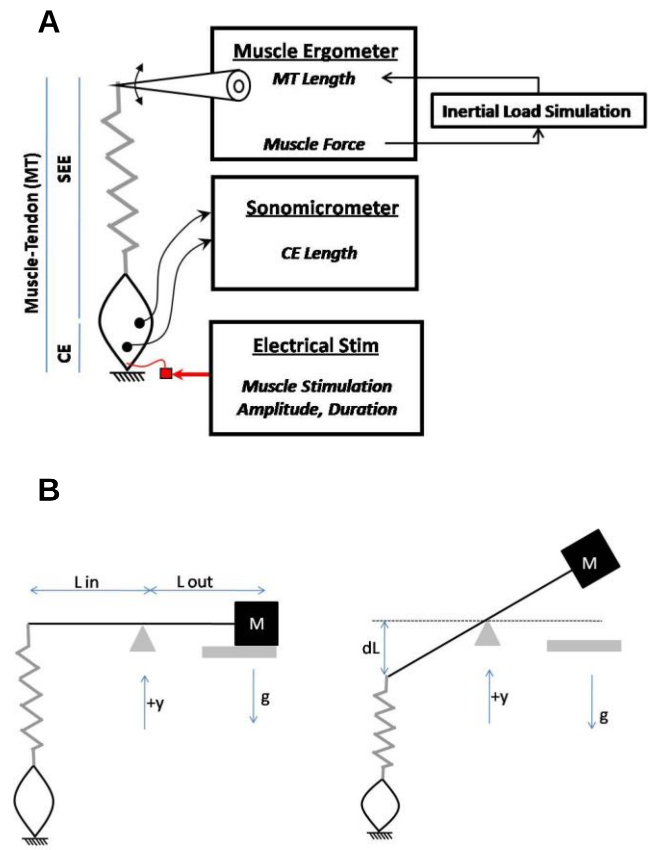

Figure 1. A diagram of the experimental setup (A) and the inertial-mass simulation used to control the ergometer position during contraction (B). MT force was sampled in real-time from the muscle ergometer and fed into the inertial load simulation, where the change of position (dL) was calculated using equations of motion. Position of the muscle ergometer was then controlled based on dL. Lin/Lout =1 and g = 9.8 m/s^2.

mass to obtain mass-specific MT and CE positive work. Peak isotonic power was calculated from an experimentally determined force-velocity curve using a standard "after-load" protocol. We computed a power amplification ratio by dividing the peak MT power from each contraction on a simulated load by the peak isotonic power.

RESULTS AND DISCUSSION

Both the power ratio and positive work output varied significantly within the range of inertial loads explored ($p<0.0001$). A peak power ratio of 1.81 ± 0.19 (unitless) was achieved at W = 0.5 (**Figure 2, black)**. The peak isotonic power of the muscle alone was 235 ± 5.5 W/kg. Total positive work output was also greatest at this intermediate load (W = 0.5) and was 20.8 ± 2.9 J/kg (**Figure 2, red**).

The sample contraction (W = 0.5) shown in **Figure 3** illustrates the mechanism of power amplification. Energy storage can be visualized by comparing CE and load power traces (**Figure 3, C**). In the first half of the contraction, the CE produces power before any movement of the load (**Figure 3, B**). This work is stored as elastic strain energy within the stretched tendon. In the second half of the contraction, elastic strain energy is released, allowing power delivered to the load to exceed power produced by the muscle CE.

CONCLUSIONS

These results indicate that during the acceleration of an inertial load, compliant muscle-tendon systems can produce power outputs that exceed the muscle's peak isotonic power. Additionally, this capacity for power amplification is load dependent. There is an optimal inertial load for maximally exploiting muscle-tendon compliance. At W = 0.5, a balance between the tendon's ability to absorb muscular work and release this work to the load is achieved. This load not only resulted in the peak power ratio, but also the maximal positive work output by the muscle. Further studies might examine real-world behaviors where such power amplification is seen, such as frog jumping, to see if systems in nature have evolved to operate near optimal inertial loads.

REFERENCES

1. Roberts, T.J. et al. *J Exp Biol* **206**, 2567-2580, 2003.
2. Galantis, A. et al. *Proc. R. Soc. Lond. B* **270**, 1493-1498, 2003

ACKNOWLEDGEMENTS

Supported by NIH F32AR055847 to GSS and NSF IO0642428 to TJR

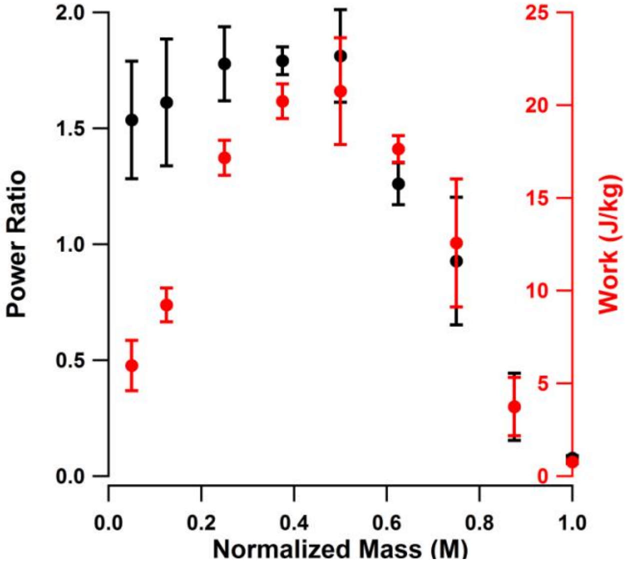

Figure 2. The mean ± SD of power ratio (black) and positive work output (red) for each of the inertial loads from the four preparations.

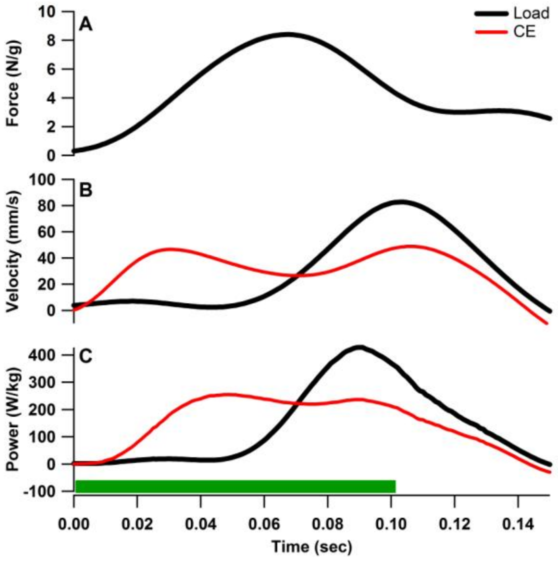

Figure 3. Representative (**A**) force (N/g), (**B**) load and CE velocity (mm/s), and (**C**) load and CE power (W/kg) versus time (sec) curves for ideal inertial load conditions (W = 0.5). The green bar represents the duration of muscle stimulation.

DOES APONEUROSIS MORPHOLOGY AFFECT INJURY SUSCEPTIBILITY IN SKELETAL MUSCLE?

[1] Michael Rehorn, and [1,2]Silvia S. Blemker
[1]Department of Biomedical Engineering University of Virginia, [2]Department of Mechanical and Aerospace Engineering University of Virginia
email: mrr6r@virginia.edu

INTRODUCTION

In athletes, some muscles are injured more commonly than others; however, the factors making some muscles more injury prone are not well understood [1]. The overall goal of this work is to determine if there are characteristics of a muscle's morphology that could increase the muscle susceptibility to injury. In the hamstrings, the biceps femoris longhead is injured more frequently than the other hamstrings, particularly along the proximal myotendinous junction (MTJ) [2]. We hypothesize that injuries occur at the proximal myotendinous junction because this region undergoes large localized strains.

What would give rise to localized strains along the proximal myotendinous junction? The biceps femoris longhead has a broad distal aponeurosis shared with the biceps femoris shorthead and a narrower proximal aponeurosis. We hypothesize that this differential fiber attachment area between the distal and proximal regions of the muscle gives rise to regions of high localized strain along the proximal myotendinous junction. Stiffness properties of the aponeurosis may also affect the strain distribution in the muscle. The goals of this work were to: (*i*) build a finite element model of the biceps femoris longhead to predict the strain distribution in the muscle, and (*ii*) build a simplified finite element model to determine how the morphology of the aponeuroses affects the strain distribution in the muscle.

METHODS

We created a three-dimensional (3D) finite element model of the biceps femoris longhead from reconstructed magnetic resonance data (Fig. 1A) [3]. To explore the effects of aponeurosis morphology on the tissue strains, we created a series of simplified finite element models that have similar tendon and fiber lengths to the biceps femoris model. These models were all 9*cm* thick (Fig. 1C) and had an average fiber length of 10*cm*. To study the effects of differential fiber attachment areas, we varied the ratio of proximal tendon width to distal tendon width (P_W/D_W, Fig. 1C). We also studied the effects of the aponeurosis cross-sectional area by varying the proximal aponeurosis thickness (P_T) and distal aponeurosis thickness (D_T). We called the model in which the aponeurosis morphology was most similar to the biceps model the "baseline model" –in this model the P_W/D_W ratio was 0.14, and tendon thicknesses were 8*mm*.

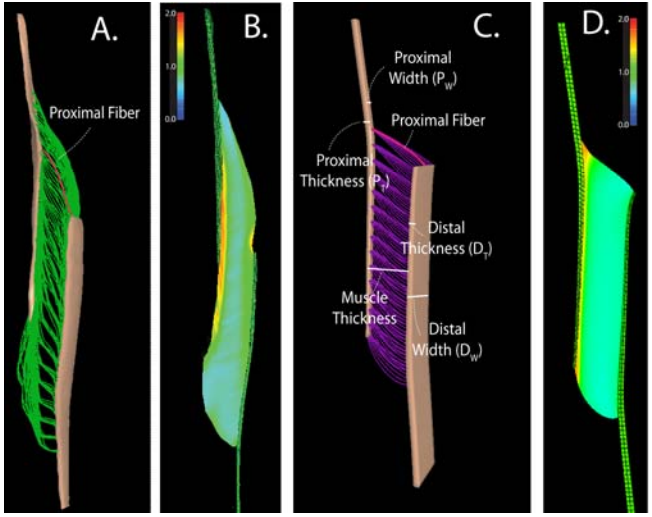

Figure 1. Complex and simplified finite-element models. A finite element of the biceps femoris model was constructed (A) to analyze along-fiber stretch distribution (B). A simplified model of a muscle was constructed to test the effects of varying certain parameters (C) on the along-fiber stretch in the muscle (D).

In all the models, muscle and tendon tissue were modeled as a transversely isotropic, hyperelastic material [4]. This constitutive model has been shown previously to predict strain distributions that match dynamic imaging measurements [4]. In all simulations, an eccentric contraction was modeled by applying a 2*cm* length change while increasing activation from 10% to 50%. We chose this eccentric contraction condition because injuries

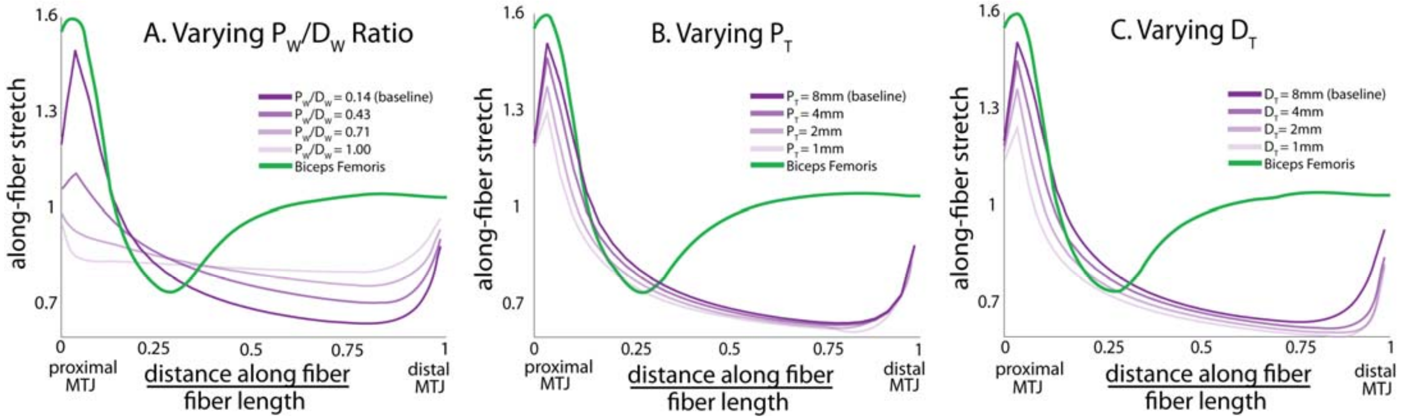

Figure 2. Along-fiber strains for the biceps femoris model and simplified models. The along-fiber strains are plotted vs. the distance from the proximal attachment. The along-fiber strains were analyzed for varying the ratio of the proximal aponeurosis width to distal aponeurosis width (A.), varying proximal aponeurosis thickness (B.), and varying distal aponeurosis thickness (C.). The strains from a proximal fiber in the biceps femoris model are overlaid on each plot. See Fig. 1C for illustration of parameters.

most commonly occur during eccentric loading conditions. The variation in along-fiber stretch throughout a proximal fiber of each muscle was analyzed (Fig 1B and D). The along fiber stretch was defined as $\sqrt{(\mathbf{a_o}\cdot\mathbf{C}\cdot\mathbf{a_o})}$ ($\mathbf{a_o}$=fiber direction, $\boldsymbol{C}$=right Cauchy-Green tensor) [5].

RESULTS AND DISCUSSION

The biceps femoris model predicted large strain localized along the proximal myotendinous junction (Fig 1B). The region of the tissue nearest the proximal aponeurosis undergoes lengthening of nearly 60% while other regions of the muscle are shortening. The baseline simplified model predicted similar strains and strain distributions as the biceps femoris model, especially along the proximal myotendinous junction (Fig 1D). The fiber in the biceps femoris model experiences some lengthening near the distal myotendinous junction, while the fiber in the simplified model shortens in this region (Fig. 2A). This discrepancy is likely due to the curvature of the biceps femoris muscle that is not represented in the simple models.

Varying the ratio of proximal tendon width to distal tendon width had the most dramatic effect on the strains in the simplified model (Fig. 2A). As the width of the proximal tendon began to approach that of the distal tendon, the magnitude of the maximum strain in the fiber decreased from 50% stretch (P_W/D_W ratio of 0.14) to 3% shortening (P_W/D_W ratio of 1.0). For both the proximal and distal aponeuroses, decreasing the thickness (and thereby effectively decreasing the stiffness) resulted in more uniform strains. However, the effect of the thicknesses was not as dramatic as the widths. An 8-fold variation in the thicknesses decreased the peak strains by roughly 15% (Fig. 2B and C).

CONCLUSIONS:

The finite element model of the biceps femoris predicted high localized strains along the proximal myotendinous junction during eccentric contractions, which is precisely where this muscle is most commonly injured. This result supports the prevailing hypothesis that muscles are injured in regions of high localized strains. Our next step is to validate the strain predictions from this model with *in vivo* dynamic imaging data [6].

The simplified models provided insight into which features of the muscle morphology can give rise to large localized strains along the proximal myotendinous junction. As a result of this analysis, we suggest a new hypothesis that muscles that have a discrepancy in the area of fiber attachment (e.g., fibers that originate along a narrow aponeurosis and insert in a broad aponeurosis) are more susceptible to regions of large localized strain and potential strain injuries.

REFERENCES

1. Orchard J., *NZJSM.,* 92-98, 2002.
2. Silder A, et al. *Skeletal Radiology*, 37(12), 1101-1109, 2008.
3. Rehorn, et al. *ASME Summer Bioengineering Meeting*, Lake Tahoe, CA, 2009.
4. Blemker S.,et al. *J Biomech.*,38(4),657-665,2005.
5. Holzapfel G., *Nonlinear Solid Mechanics: A Continuum Approach for Engineering*, Wiley & Sons, 2000.
6. Zhong X, et al. *J. Biomech*., 41(3), 532-540, 2008.

ACKNOWLEDGEMENTS

Darryl Thelen, Amy Silder, and NIH grant R01 AR 056201

THE USE OF AN ACCELEROMETER TO DETERMINE VESTIBULOSPINAL FUNCTION: THE NIH TOOLBOX PROJECT

[1]Chia-Cheng Lin, [2]Daniel P. Steed, [3]Gregory F. Marchetti, [4]Mark C. Musolino,
[2]Mark S. Redfern, [1]Susan L. Whitney
[1]Department of Physical Therapy and [2]Department of Bioengineering,
University of Pittsburgh, Pittsburgh, PA, USA
[3]Rangos School of Health Sciences, Duquesne University, Pittsburgh, PA
[4]Crossroads Consulting LLC, Johnstown, PA, USA
email: chaicheng@gmail.com, web: http://hmbl.bioe.pitt.edu/home.htm

INTRODUCTION

The overall goal of this project was to develop a tool to be used by non-specialty trained personnel to quantify standing balance, particularly as it relates to vestibulospinal function. Accelerometers may be able to be used across the life span to record sway under varying sensory conditions [1]. In addition, recent evidence suggests that accelerometers can be used to identify older adults who are at risk for falling [2]. Our goal in this pilot study was to determine if an accelerometer can accurately record postural sway during standing for healthy young adults. This project is part of a larger effort (the NIH Toolbox Project) to develop an inexpensive system that can help investigators determine if the vestibular system is functioning properly.

METHODS

Ten young volunteers (3M, 7F; mean age 26.9 ± 5.51 years, height 66 ± 3.20 inch) participated and performed the following 6 standing trials twice: eyes open or closed while standing on a solid surface or on 2 different types of high density foam pads. Subjects stood with feet together and arms crossed in front of the chest. Instructions were standardized and subjects stood in position for 90s. The first 5 seconds and the final 25 seconds of each trial were truncated and not used in this project.

A custom-designed, custom-built accelerometer system was developed using a dual-axis accelerometer (ADXL213AE, ±1.2 g, Analog Devices, Inc.) that was pre-mounted on a breakout board (SparkFun Electronics). Acceleration data was wirelessly transmitted from the sensor to the collection station via Bluetooth®. A custom LabVIEW code (Crossroads Consulting, LLC) imported the acceleration at 100 Hz, and filtered using a 4th order, 5 Hz low-pass filter, sway was quantified using root-mean-square (RMS), peak-to-peak, and path length of the accelerometer data.

The system, composed of battery, sensor, and transmitter modules, was fixed to a belt using Velcro (Figure 1). The Velcro belt was secured around the subjects' pelvis and the sensor module was attached to the belt so that the axes of the accelerometer were approximately aligned with the anteroposterior and mediolateral axes of each subject.

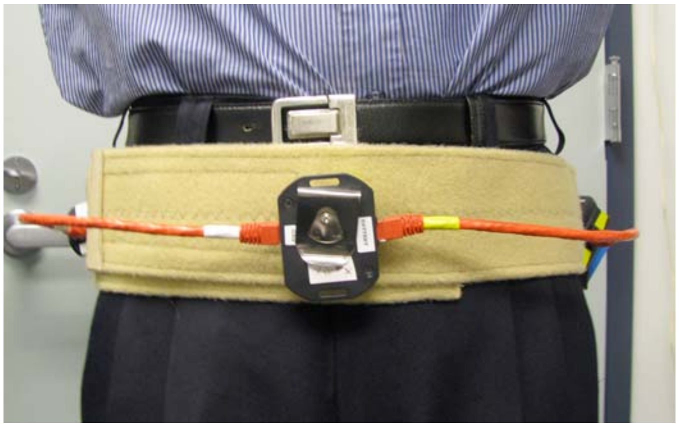

Figure 1: Accelerometer measurement system. Left: transmitter, middle: sensor, right: battery

Statistical analysis: Descriptive statistics (mean, SD) of performance were calculated across two testing sessions for each sway parameter within each test condition (Figure 2). Estimates of reliability across two testing sessions were determined using the Intraclass Correlation Coefficient (ICC) based on a two-way mixed effects model of consistency.

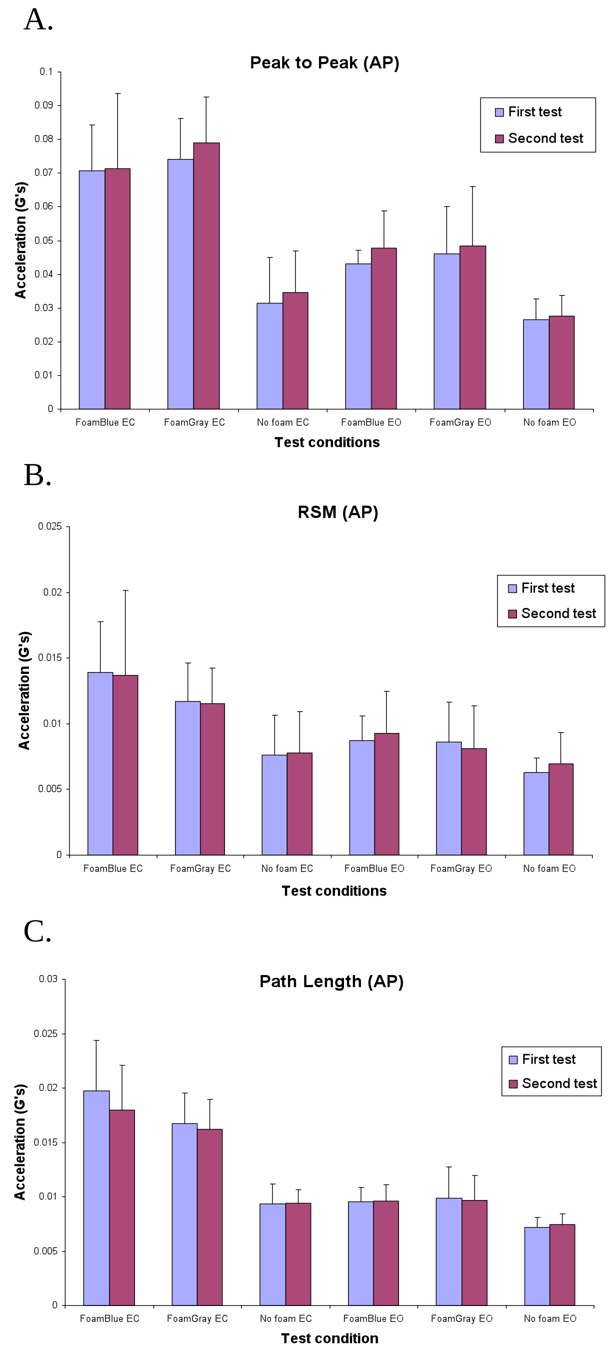

Figure 2: A. Peak to Peak B. RMS C. Path Length. EC: eyes closed; EO: eyes open.

RESULTS AND DISCUSSION

Between-session reliability was good to excellent on a firm surface with eyes closed across all sway parameters (ICC = 0.64-0.83). Across all test conditions, between session reliability appeared higher with the path length parameter (ICC = 0.58-0.82) with the exception of eyes closed on gray foam (ICC = 0.29). Peak to peak and RMS sway parameters demonstrated lower between session reliability estimates except on firm surfaces with eyes closed. There were no differences noted between sessions.

The low variability in the data may have affected the reliability statistic, yet the ICC's were reasonable. It appears that reliability of the 6 tests appear to be moderate to good. Our group will continue to attempt to determine how to make the human performance more repeatable between sessions by attempting to further standardize the verbal instructions to the subject. Advantages of the new use of the off the shelf technology include significant cost savings and the wireless ability to collect the data.

SUMMARY

The new use of the accelerometer appears to be effective as an inexpensive, reliable measure of postural sway.

REFERENCES

1.Mathie MJ et al. *Physiol Meas* **25(2)**, R1-20, 2004.
2.O'Sullivan M et al. *Age Ageing* Feb 28, 2009.

ACKNOWLEDGEMENTS

Funded with Federal funds from the Blueprint for Neuroscience Research, National Institutes of Health, under Contract HHS-N-260-2006 00007-C.

TWO METHODS TO DETERMINE MUSCLE FORCES AND JOINT CONTACT FORCE: COMPARISON TO EXPERIMENTAL MUSCLE ACTIVITY

[1] Chris Richards, [2]Joseph Zeni, Jr and [1]Jill Higginson
[1]University of Delaware, Department of Mechanical Engineering, Newark DE
[2]University of Delaware, Department of Physical Therapy, Newark, DE
email: cjrich@udel.edu

INTRODUCTION

Accurate measurements of muscle and joint contact forces are not possible without invasive, in-vivo techniques. Musculoskeletal modeling has enabled researchers to estimate these forces and contributions to walking. Previous studies have found that static and dynamic optimization give similar results for healthy young adults [1]. While both methods are capable of calculating muscle forces, few studies have validated the muscle force output with experimentally acquired muscle activity, and no previous studies to our knowledge have simultaneously compared the two methods to experimental muscle activity [2]. The purpose of this study was to compare the results of forward dynamic optimization, static optimization and experimental muscle activity. Determining the physiological validity of these optimization techniques will assist in the estimation of joint forces which may be especially important for investigations of diseases that may be mechanically initiated, such as osteoarthritis.

METHODS

Walking data was obtained from a random single healthy subject without neurological or orthopedic impairments who was part of a larger project. Retroreflective markers were applied using a Helen Hayes marker set. Electromyographic (EMG) data from the vastus lateralis and semimembranosus were obtained using surface electrodes (Noraxon, Scottsdale, AZ). EMG data was sampled at 1080 Hz. Three dimensional kinematic data were collected using eight infrared cameras at 60 Hz (Motion Analysis, Santa Rosa, CA). The subject walked at a self-selected speed (1.25 m/s) on a custom built, split-belt treadmill with dual integrated force plates (Bertec Corp., Columbus, OH). Ground reaction force and center of pressure data was sampled at 1080 Hz. A single 30 second walking trial was obtained. Joint angles were calculated from Euler transformations and joint moments and joint reaction forces were calculated using inverse dynamic techniques.

Dynamic Optimization

OpenSim was used to generate a three-dimensional, subject-specific, forward dynamic simulation of the walking trial. A generic three-dimensional model provided in the software was used, which consists of 23 degrees of freedom (DOF) and 54 muscles. Based on marker placements, the model was scaled to match anthropometric measurements of the subject. Through OpenSim's CMC algorithm with experimental kinematic (marker position) and kinetic (GRF) data as inputs, muscle forces that reproduced the subject's gait were calculated.

Static Optimization

A custom-written MATLAB code was used to solve a static optimization problem at each time step. Experimental joint torques were used as the inputs for the model, and muscle forces were calculated using a given cost-function (the sum of the muscle stresses squared). Forty-eight muscles were used in the optimization, including bi-articular muscles of the hip, knee and ankle.

Knee joint contact forces were calculated for both optimization methods using the vector sum of the muscle forces and joint reaction forces along the longitudinal axis of the femur. Knee joint contact force was normalized to body weight. Raw muscle forces were compared between the optimization techniques. EMG signals and muscle forces were also normalized to peak value during the trial. These normalized values were used to compare the simulation computed muscle activation to experimental data.

RESULTS AND DISCUSSION

Peak muscle forces for the quadriceps and hamstrings were higher in the dynamic optimization (Figure 1). As a result, higher knee joint contact forces were calculated with the dynamic optimization. Peak compression force was 4.29 BW and 3.05 BW using the dynamic and static optimization routines, respectively.

Muscle force onset and time to peak were very similar in the dynamic and static optimizations (Figure 1). Muscle force patterns from both routines matched the experimentally acquired EMG signal over the majority of the stance phase (Figure 2). Peak muscle forces corresponded closely to peak muscle activity.

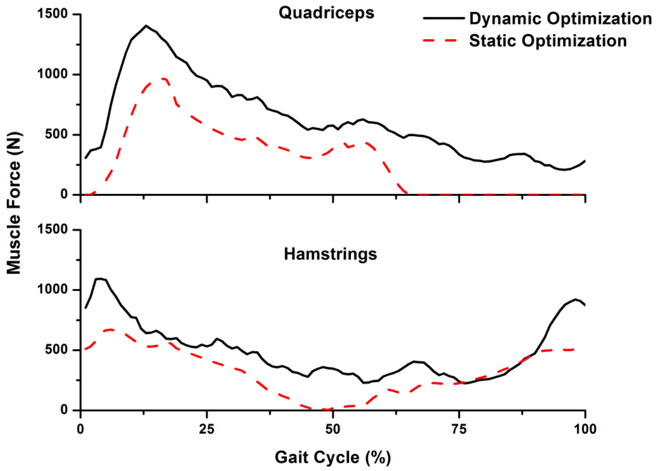

Figure 1. Computed muscle forces from dynamic and static optimization normalized over one gait cycle.

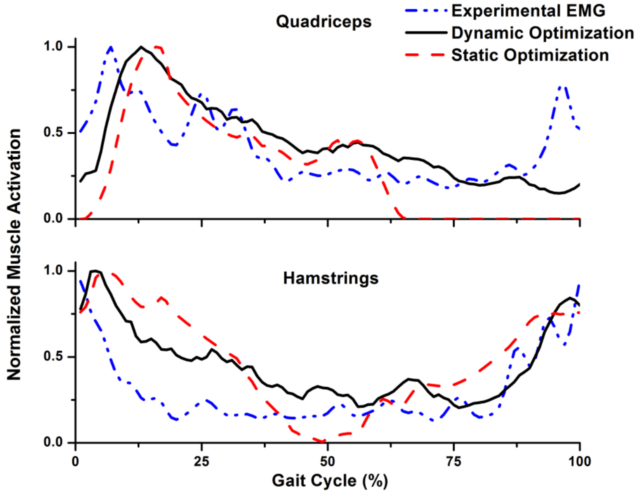

Figure 2. Optimized muscle activations and experimental EMG normalized to peak values during the trial.

CONCLUSIONS

Dynamic and static optimization provided patterns of muscle forces that were very similar to each other and to experimental muscle activity. Dynamic optimization routines produced higher muscle forces and higher knee joint contact forces than static optimization.

Differences in the magnitude of muscle forces between dynamic and static optimization is likely attributable to different methodology of the techniques. Both techniques utilized the same cost function and had similar constraints of maximal muscle forces. However, dynamic optimization matched kinematics over the whole gait cycle, while static optimization reproduced joint moments at each time step, irrespective of the previous or forthcoming time step.

Without in-vivo measurement of joint contact forces it is not possible to say which optimization routine produced more accurate forces. However, the results from this study are comparable to previous research using in-vivo techniques. During walking, joint compression forces exceeded 2.5 BW [3]. Taylor et al. found mean knee joint compression forces of 2.8 BW during treadmill walking, with a range of up to 3.3 BW [4]. These values are similar to those calculated via static optimization and differences may be attributable to variation in the self-selected walking speed.

While this study has demonstrated that dynamic and static optimization techniques can successfully reproduce the pattern of muscle activation, future work in our lab will validate the techniques in a larger sample which includes impaired populations.

REFERENCES

1. Anderson, FC and Pandy, MG. *J Biomech*, **34**(2), 153-61, 2001.
2. Anderson, FC and Pandy, MG. *J Biomech Eng*, **123**(5), 381-90, 2001.
3. Mundermann, A, et al. *J Orthop Res*, **26**(9), 1167-72, 2008.
4. Taylor, SJ and Walker, PS. *J Biomech*, **34**(7), 839-48, 2001.

ACKNOWLEDGMENTS

This work was funded by NIH P20-RR16458. The authors would like to thank Nicole Zahradka for her assistance with data processing.

IDENTIFICATION OF FOOTWEAR INSOLE MATERIAL RESPONSE FOR OPTIMAL REDUCTION OF PLANTAR HEEL PRESSURE

Snehal Chokhandre, MS[1], Ahmet Erdemir, PhD[1], Peter Cavanagh, PhD, DSc[2]

[1]Computational Biomodeling Core, Department of Biomedical Engineering, Lerner Research Institute, The Cleveland Clinic , Cleveland, OH
[2]Department of Orthopaedics and Sports Medicine , University of Washington , Seattle, WA
e-mail: chokhas@ccf.org, web: http://www.lerner.ccf.org/bme/cobi

INTRODUCTION

Reduction of heel pressures is important to relieve plantar heel pain, to prevent heel ulceration in people with diabetes, and to promote comfort [1]. Using finite element analysis and mechanical responses of commonly available insole materials, Goske et al. [2] showed that insole conformity and thickness are the most important parameters in reducing high heel pressures. While the mechanical response of the insole material was not found to be as influential, the insole materials evaluated in their study were limited to a narrow range of deformation characteristics. It is possible that the material properties of an insole can be optimized to further the benefits of fully conforming and thick insole designs. Therefore, our goal is to find an optimal insole material response to relieve heel pressure maximally. If successful, our approach could guide the design of new footwear materials.

METHODS

A two-dimensional plane strain finite element model of the heel pad and footwear from an earlier study by Goske et al. [2] was used (Figure 1). The model was capable of predicting peak heel pressures for different insole material coefficients. A vertical compressive load of 678 N was used to simulate the first step of walking.

The mechanical response of the insole material was represented by a hyperfoam material model [3]. The strain energy function was:

$$U=\frac{(2\mu)}{\alpha^2}\left[\lambda_1^{\alpha}+\lambda_2^{\alpha}+\lambda_3^{\alpha}-3+\frac{1}{\beta}\left(J_{el}^{(-\alpha\beta)}-1\right)\right] \qquad (1)$$

where:

$$\beta=\frac{\nu}{(1-2\nu)} \qquad (2)$$

μ is the shear modulus, α specifies the large strain behavior (shape of stress-strain curve), ν is the effective Poisson's ratio and β relates to the volumetric response (indicating degree of compressibility). $\lambda_{(1\text{-}3)}$ are the principal stretches.

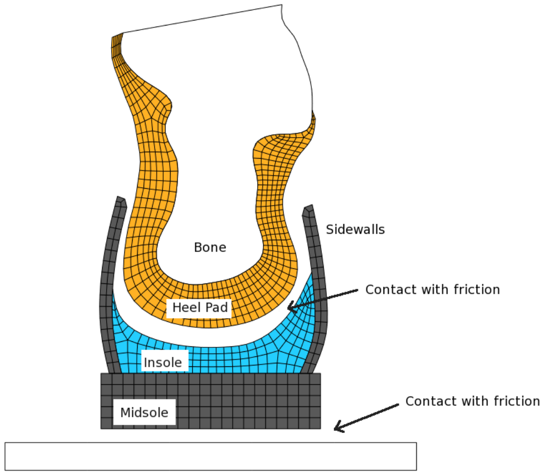

Figure 1: Finite element model of the heel pad and footwear [1].

The optimal insole parameters were found by iteratively changing μ, α and ν to minimize peak heel pad pressures predicted from the finite element model. The finite element analysis was conducted in Abaqus (Abaqus, Inc., Providence, RI) . Iterations were handled through a gradient-based optimization protocol using Matlab (The Mathworks, Inc., Natick, MA), where μ, α and ν were the optimization variables (bound to be $>$ 0) and the peak pressure was the objective. The best design proposed by Goske et al. [2] for favorable pressure relief was used as a starting point to identify an optimal insole material. Their design incorporated a 12.5 mm thick, full conforming insole, made out of Microcel Puff

Lite. Following optimization, the stress-strain response of the initial material (Microcel Puff Lite) and the optimized material were calculated for uniaxial compression (confined), simple shear, and volumetric compression [3].

RESULTS AND DISCUSSION

Predictions of peak pressures for barefoot and Microcel Puff Lite conditions are provided in Table 1, along with the performance of the optimized material. A combination of Microcel Puff Lite and a full conforming insole with a thickness of 12.5 mm resulted in a 41.3 % reduction compared to barefoot condition. The optimized material resulted in a 15% reduction in the peak pressure compared to Microcel Puff Lite. This was accomplished by decreasing the initial shear modulus (μ) and increasing the compressibility of the material. The latter was suggested by the drop in the Poisson's ratio. These changes were also evident in the mechanical response of the optimized material when compared against that of Microcel Puff Lite (Figure 2). The optimized material was softer, less resistant to shear and more compressible than Microcel Puff Lite.

Table 1: Material coefficients and predicted plantar heel pressures for barefoot and insole conditions.

	μ (MPa)	α	ν	Peak Pressure (MPa)
Barefoot	-	-	-	0.435[2]
Microcel Puff Lite	1.220	48.28	0.0280	0.255[2]
Optimized	0.217	48.68	0.0001	0.216

CONCLUSION

A highly compressible and softer foam material, used in combination with a full conforming and thick insole design, will likely lead to an optimal reduction in plantar pressures. It is possible that open foam insole materials may exhibit such characteristics and potential candidates can be found from studies characterizing insole material response, e.g. Petre et al. [4]. Further investigations are warranted to explore the manufacturability of such designs and evaluate their real life performance.

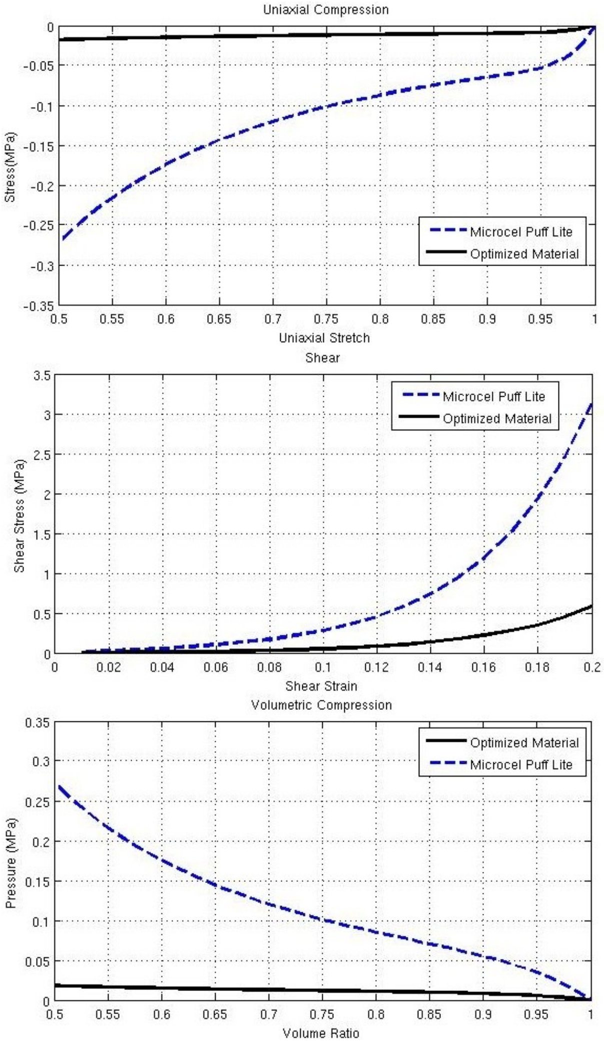

Figure 2 : Mechanical response of Microcel Puff Lite against the response of the optimized insole material.

REFERENCES

1. Fowler E et al., *Ostomy Wound Management ,* **54**, 42-57, 2008.
2. Goske et al. *Journal of Biomechanics,* **39***,* 2363-70, 2006.
3. *Abaqus Analysis User's Manual* ,Version 6.7.1, 2007.
4. Petre, M et al. *Comp. Methods in Biomechanics and Biomedical Engineering,* **9**, 231-42, 2006.

ACKNOWLEDGEMENTS

This study is funded by a National Institutes of Health grant, 2R01HD037433 (PI: Peter R. Cavanagh).

A PROBABILISTC BIODYNAMIC MODEL FOR FINGER TENDON FORCE ESTIMATION CLARIFIES THE ROLES OF THE FLEXORS

[1] Kang Li, [1,2,3]Xudong Zhang
[1]Departments of Orthopaedic Surgery, [2]Mechanical Engineering & Materials Science,
[3]Bioengineering, University of Pittsburgh, PA, USA, email: xuz9@pitt.edu

INTRODUCTION

Previous deterministic finger biomechanical models predicted that the flexor digitorum superficialis (FDS) was silent whereas the flexor digitorum profundus (FDP) was the only active flexor during finger flexions [1-2]. Experimental studies in vivo, however, recorded activities of both flexors [3-5]. This study proposes a probabilistic biodynamic model for estimating the muscle-tendon forces in the index finger during flexion. Our hypothesis is that accommodating variability of musculoskeletal parameters in a model will result in better population-based predictions of the muscle-tendon forces, and specifically will clarify the roles of the flexors (FDP and FDS) in finger movement.

METHODS

The index finger is modeled as a 3-segment and 4-DOF linkage system actuated by 11 muscle-tendon units with flexion/extension at distal interphalangeal (DIP), proximal interphalangeal (PIP) and metacarpophalangeal (MCP) joints and zero abduction/adduction angle at its MCP joint. This system is subject to the moment equilibrium condition, $\tau(t) = M(t)\cdot F(t) + \tau_{passive}(t)$, where $F(t)$ is the muscle-tendon force, $M(t)$ represents the moment arms of these forces, and $\tau_{passive}(t)$ is the passive torque. The $\tau_{passive}(t)$ is assumed effective only for MCP flexion/extension and follows a polynomial torque-angle relationship $a_3\theta^3 + a_2\theta^2 + a_1\theta + a_0$ [7], where a_3, a_2, a_1, and a_0, are the coefficients of the polynomial and θ is the joint angle. The force constraints reflecting the interconnected nature of multiple finger tendons [1] are included in the model. The muscle-tendon forces can be estimated by solving a nonlinear optimization problem with the objective function of minimizing the muscle stress, defined as the quotient of the muscle force divided by its physiological cross sectional area (PCSA). Force predictions by the above dynamic model depend on model parameters including moment arms, PCSAs, and passive torques.

In previous deterministic models, moment arms of extensors and PCSA values are assumed constant across subjects for the entire range of motion (Figure 1a); moment arms of flexors and passive torques are assumed constant across subjects for a given posture (Figure 1b).

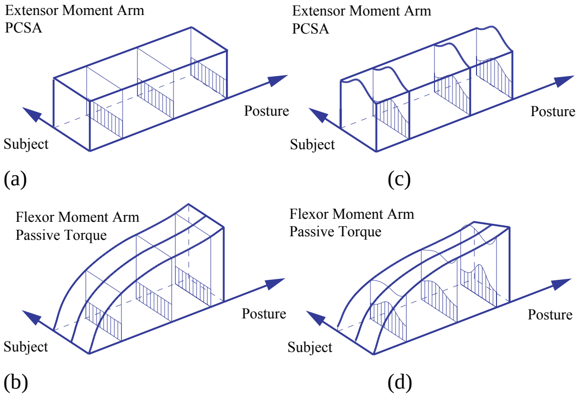

Figure 1. Uniform, posture-independent (a) and posture-dependent (b) distributions of parameters commonly used in deterministic models; more realistic posture-independent (c) and posture-dependent (d) distributions in the proposed model.

The current model recognizes the variability in these parameters and models them as random variables using Monte-Carlo methods (Figure 1 c,d) as follows. The moment arms m of the flexors and extensor tendons (ES: extensor slip and TE: terminal tensor) are estimated as $m = r$ for extensors, and $m = d + y \cdot g(\theta)$ for flexors [6], where d is the distance between long axis of the bone and the tendon, y is the distance from the joint center to sheath, $g(\theta)$ is a function of θ. We model the r, d, y parameters as well as the PCSA values of the two flexors, and the four coefficients of passive torque, a_3, a_2, a_1, and a_0, as independent random variables following a normal distribution. The means of these parameters are from [1,6,7] and the variances of the parameters are chosen to be one-tenth of the means. The length and thickness of each segment are also modeled as the random variables with the mean and standard deviation derived from a pre-established database [8]. Two thousand samples are generated for each of the random variables and served as the input to the biodynamical model described above. Parameters of other muscle-tendon units in this model are calculated based on the methods from [1]. The proposed probabilistic model is tested on an experimentally measured index finger movement from a pre-established database [8]. Identical joint kinematic data are used in all instantiations of the simulation.

RESULTS AND DISCUSSION

The predicted flexor forces (Figure 2) display a pattern that qualitatively agrees with what was recorded in an in-vivo study [5]. The predicted FDP force declines in the initial phase of the movement (the first 0.4s) and then increases to sustain the motion and dominated the movement after the initial phase. The FDS dominates the movement in the initial phase and decreases significantly before the FDP dominates the movement. This FDS force-time pattern in the initial phase also agrees with previous observations [3]. An inspection of the individual flexor force profiles reveals that another type of force pattern reported in [5] could be simulated. Both the FDP and FDS forces formgamma distributions at a given time or posture (Figure 3). When the FDP dominates the movement, the FDS is no longer silent (Figure 2). The probability for FDS not being silent (FDS force >0. 01N) ranged from 36.4%~56.7%.

CONCLUSIONS

We demonstrated that the proposed model was able to unveil the active, intricate roles of the FDP and FDS during finger flexion, which previous deterministic models failed to show [1-3]. The results clarified the controversy surrounding the roles of the flexors in finger movement dynamics and demonstrated the efficacy of probabilistic models in predicting more realistic muscle-tendon forces for a population.

Compared to previous stochastic biomechanical modeling work [9,10], this study features a novel method to incorporate both the inter-person and movement-dependent variabilities of musculo-skeletal parameter. Capturing these variabilities is critical for the implementation of stochasticity in dynamical modeling. Previous models have neglected the fact that the moment arms are not only subject-specific but also posture-dependent. Such an oversimplification may only be adequate for static biomechanical modeling.

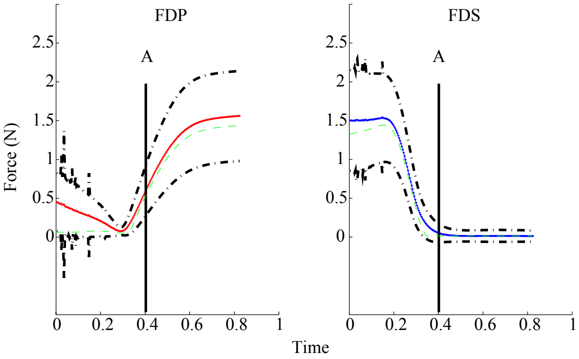

Figure. 2. The predicted FDP and FDS force distributions during the movement: the time-varying mean (solid line) and ±1 standard deviation (between the two dash-dot lines). The vertical solid lines denote the time point before which the FDS dominated the movement and after which the FDP dominated the movement. The dashed line is the force profile predicted by a deterministic model.

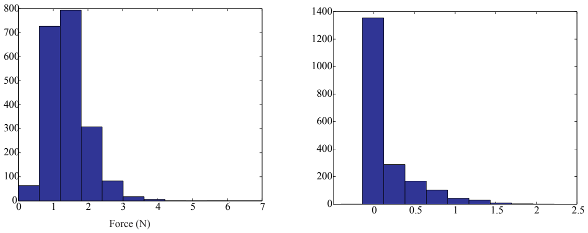

Figure. 3. The FDP and FDS force distributions at a randomly selected posture when the FDP was the major flexor.

REFERENCES

1.Brook et al. Med Eng Phys, **17**, 54-63, 1995
2.Sancho-Bru et al. J Biomech, **34**,1491-1500, 2001
3.Dennerlein et al. J Orthop Res, **17**,178-184, 1999
4.Kuo et al. J Biomech, **39**, 2934-2942, 2006
5.Nikanjarn et al. Hum Mov Sci, **26**, 1-10,2007
6.An et al. J. Biomech, **16**,419-425,1983
7.Kamper et al. J Biomech **35**, 1581-1589, 2002
8.Braido et al. Hum Mov Sci **22**, 661-678, 2004
9.Hughes et al. Med Biol Eng Comput, **35**, 544-548, 1997
10.Langenderfer et al. Ann Biomed Eng, **34**, 465-476, 2006

THE RELATIONSHIP BETWEEN HAND DEXTERITY AND HAND MUSCLE STRUCTURE

Jeffrey Hsu, Daniel W. Halayko You-Sin Kim, Jae Kun Shim
Department of Kinesiology, University of Maryland, College Park
email: jefhsu@umd.edu web: http://www.sph.umd.edu/KNES/faculty/jkshim/

INTRODUCTION

Interactions with the external environment require a skilled and proficiently functioning hand that can perform complex actions, such as pressing, grasping, writing and typing. Adequate finger strength and coordination are crucial in hand function. Hand-finger movements are controlled by multiple muscles which can be differentiated by location. Intrinsic hand muscles originate and insert within the hand. Extrinsic hand muscles originate in the forearm and insert into the hand. The overall function of the intrinsic hand muscles is considered to be fine motor control, while the extrinsic hand muscles function is gross motion performance and major hand forces production [1]. Different anatomical points of attachment of the muscles allows for different extrinsic and intrinsic contributions at different force application points [2]. For example, producing a force at the distal phalanges (DP) will elicit intrinsic extrinsic muscles as the focal force generators [3] while producing a force at the proximal interphalanges (PIP) will elicit intrinsic muscles as the focal generators.

The purpose of this preliminary study is to examine the relationship between finger coordination and strength, and intrinsic and extrinsic muscle volume. This study intends to use structural magnetic resonance imaging (MRI) to examine the muscle structure.

METHODS

Six right handed young adults (2M, 4F 23.4 ± 4.6) participated in this study. All subjects were sedentary as defined by the U.S. Surgeon General's recommendation for physical activity. Professional typists and musicians were excluded from this study.

MAGNETIC RESONANCE IMAGING

A 1.5T MRI system (Signa HDe 1.5 T, General Electric Healthcare) was used. The 8-channel head coil was used to scan the forearm and hand.

All subjects received two MRI scans- one of the right forearm and one of the right hand. Subjects lied on the right side of the body with the right shoulder fully extended (i.e., superman position). For actual imaging, the following sequences were obtained using a 4-channel HD wrist array coil with a 3-inch internal diameter: transverse T1-weighted spin-echo (TR/TE, 6/1.9; matrix, 1024 x 1024; field of view, 25 x 25 cm; number of acquisitions, ~175; slice thickness, 1 mm) on the dominant limb's hand and T1-weighted spin-echo (TR/TE, 5.8/1.9; matrix, 1024 x 1024; field of view, 40 x 40 cm; number of acquisitions,~150; slice thickness, 2mm).

Analyze 8.1 (Analyze, KY) was used to separate muscle and non-muscle tissue. Bones, tendons, ligaments, skin, subcutaneous and intramuscular fat, and muscle were each assigned an intensity value based upon the individual tissue's gray scale value. The extrinsic hand muscles (EM) were defined as muscle tissue in the forearm (between the proximal ulna and distal radius). The intrinsic hand muscles (IM) were defined as muscle tissue in the hand (between the distal radius and the distal phalanx).

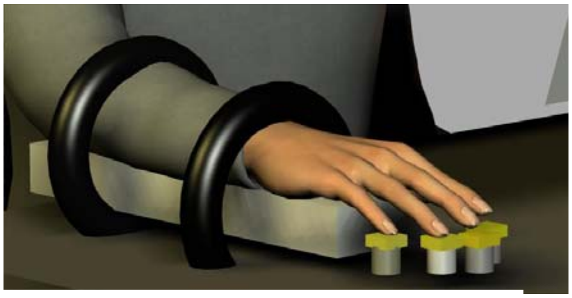

Figure 1. MVT experimental setup

HAND DEXTERITY

Jebsen Taylor Hand Function (JTHF): The seven-item JTHF test was administered to each subject. Standard materials and procedures were followed.

MAXIMUM VOLUNTARY TORQUE (MVT)

Four-one dimensional force transducers were secured on a wooden board (Figure 1). The position of the sensors was adjusted to fit the individual hand anatomy of the subjects. Subjects produced an isometric force on an insulating thimble, which was mounted on the transducers, by pressing. Subjects produced four-finger (index, middle, ring, and little fingers) maximum voluntary forces from the PIP and DP. MVT about the metacarpophalangeal (MCP) joints were calculated as the product of maximum voluntary force and the distance between the MCP and the force application point. MVT were measured and calculated for PIP (MVT_P) and DP (MVT_D).

RESULTS

The results (Figure 2) showed that the MVT_D is correlated with EM volume (r =0.88, $p<0.05$) while MVT_P is correlated to IM volume (r = 0.77, $p<0.05$). There was no significant correlation between EM volume and Writing performance (r = -0.31), and IM volume and Writing (r = 0.71). There was a negative correlation between Writing and distal MVT (r = -0.66), and Writing and proximal MVT (r = -0.50). All other JTHF tasks showed no correlation with strength or muscle volume.

CONCLUSIONS

The results suggest that MVT increases with muscle volume. Despite being statistically insignificant, there appears to be a trend where, hand dexterity decreases with increasing strength. The conclusion supports the "strength-dexterity tradeoff hypothesis” previously reported in another cross-sectional study [4]. However, a previous longitudinal study, where strength training intervention was applied, suggested the “strength-dexterity equivalence hypothesis[5]”.

REFERENCES

1. Long (1970) *J Bone Joint Surg Am*, **52**, 853-67
2. Li et al (2000) *Clin Biomech*,**15**, 203-11
3. An et al (1985) *J Orthope Res*,***3***,*201-11*
4. Shinohara et al (2003) *J Appl Physiol*,**95**, 1361-69
5. Shim et al (2008) *Motor Control* **12**, 311-29

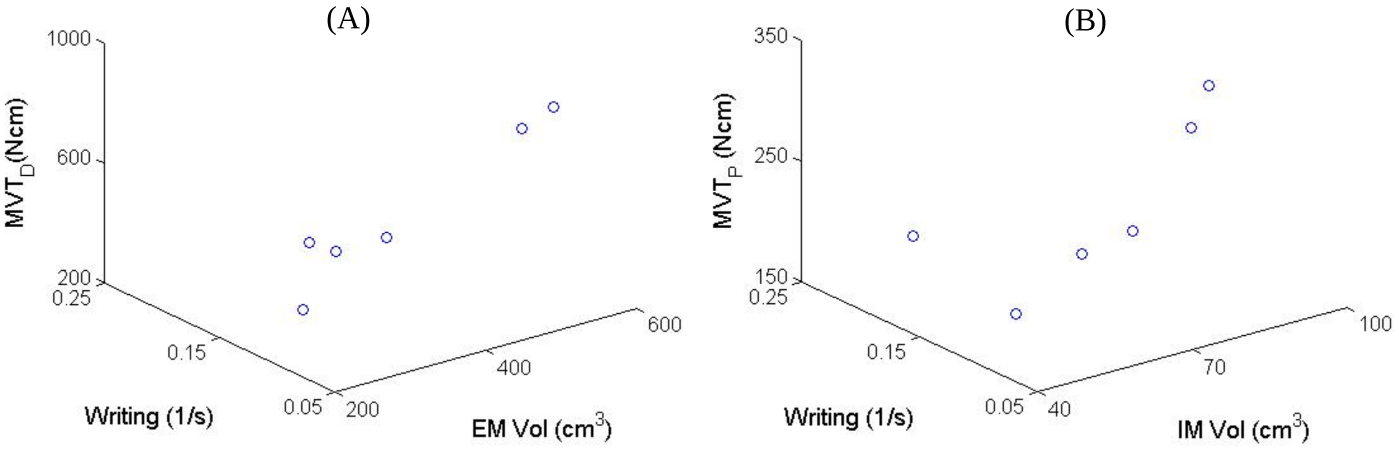

Figure 2. Relationship between four finger MVT, muscle volume and writing performance. (A) MVT produced at the DP (MVT_D), writing and extrinsic muscle volume (EM Vol) (B) MVT produced at the PIP (MVT_P), writing and intrinsic muscle volume (IM Vol).

EFFECT OF TECHNIQUE ON KNEE, HIP, AND L5/S1 NET MOMENTS IN THE PARALLEL BACK SQUAT

Deborah King, Joseph Hannon and Eric Shoup
Department of Exercise and Sport Sciences, Ithaca College
email: dking@ithaca.edu, web: http://www.ithaca.edu/ess

INTRODUCTION

The parallel back squat is a common strength exercise used in rehabilitation, sports, and general conditioning [1]. The literature proposes that proper technique is required to reduce the risk of knee and back injuries [1,2,3]. Guidelines for proper technique typically promote keeping the shins as vertical as possible to reduce shear stress on the knees [1].

Fry, et al. physically restricted lifters' forward knee motion by placing a board even with the toes in a back squat in comparison to unrestricted knee motion [4]. Static sagittal plane knee torque at the bottom of the squat was significantly greater in the unrestricted squat (knees allowed more anteriorly) and static sagittal plane hip torque was significantly greater in the restricted motion squat [4]. The greater hip torques in the restricted squat were accompanied by greater anterior trunk lean which is commonly associated with greater low back torque and forces. Fry et al. concluded that proper lifting must involve an optimal environment for all joints [4].

The purpose of this study was to investigate the differences in lower extremity net muscle moments during two variations of the parallel back squat under dynamic conditions that did not involve imposing a physical restriction on the lifters movement patterns. Specifically the purpose was to compare knee, hip, and L5/S1 net muscle moments during a modified power squat with the focus on sitting back and keeping the shins vertical versus a modified Olympic squat with the focus on pressing the knees forward and keeping the back vertical.

METHODS

Ground reaction force and 3D lower extremity kinematics were measured from the right leg of 16 male collegiate athletes using a force plate and 3D video analysis, respectively. All athletes were currently engaged in strength programs that involved squats as part of their training. A one repetition maximum was determined from sub maximum testing using a standard prediction equation [5]. Each subject also received standard instruction and practice in both techniques. The modified Olympic technique required the subject to focus on keeping the back vertical and pressing the knees forward over towards their toes. The modified power technique required the subject to break at their hips and focus on sitting back and keeping their shins vertical.

During testing, thirteen retro-reflective markers were placed on select anatomical landmarks to define foot, lower leg, thigh, pelvis and lumbar segments. Force and video data, from three cameras, were recorded during three squats of each technique. The weight was set to 75% of the predicted 1 RM. Net muscle moments for the ankle, knee, hip, and L5/S1 were calculated using standard inverse dynamic procedures. Paired t-tests were used to test for significant differences at the alpha = 0.05 level.

RESULTS AND DISCUSSION

During the modified Olympic squat, the knee was flexed on average 10 degrees more than during the modified power squat ($p=0.003$) with the knee joint center 0.04 m farther in front of the ankle than in the modified power squat; though, this distance was not significant ($p=.097$). The hip angle was not significantly different between the two techniques, however, the hip joint was significantly closer, anteriorly, to the ankle, 0.04 m, in the modified Olympic squat compared to the modified power squat ($p=.047$). The knee and hip angles in both of these techniques were not as flexed as either the restricted or unrestricted conditions of the Fry et al. study [4] indicating that the shins and back tended to be more vertical in both techniques of this study as compared to the techniques used in the Fry et al.

study. Lower extremity joint angles are provided in Table 1.

Peak knee extension moment was on not significantly greater in the modified Olympic squat (p = 0.068); though all but two subjects had higher knee extension moments in the modified Olympic Squat. Average sagittal plane joint moments are provided in Table 2. The two subjects who did not have higher knee extension moments in the modified Olympic squat displayed few differences in knee joint angular kinematics between the two squats. The knee extension moments calculated for the modified Olympic squat were similar in magnitude to those reported by Fry et al. for the restricted squat where the subjects' knees came even with their toes [4]. In our study, while the position of the knees relative to the toes was not measured, based on joint kinematics typical segment lengths, the knees of our subjects on average were just behind or even with the toes in the modified Olympic squat. Peak knee adduction moment was significantly greater, on average 12 Nm, during the Olympic squat (p=0.004).

There was no significant difference in hip or L5/S1 extension torque between the two squat techniques, which given the similarity in hip joint angular kinematics displayed by the subjects is not surprising, even though the hips were farther back in the modified power squat as compared to the modified Olympic Squat. Neither the arch of the back nor the upper trunk angle was measured in this study. It is possible that the curvature of the spine differed between the two techniques. Future studies should record the posture of the spine in addition to trunk tilt.

Peak hip abduction moment was significantly less, on average 14 Nm, during the modified Olympic Squat as compared to the modified power squat (p = 0.029) and peak hip internal rotation moment was significantly greater for the modified Olympic squat, on average 6 Nm (p = 0.002). While statistically significant with moderate effect sizes 0.4 to 0.5, given the small magnitudes of these moments it is unlikely these differences are clinically meaningful.

CONCLUSIONS

Lifters in this study were instructed in two squat techniques: a modified Olympic technique emphasizing a vertical back posture and a modified power technique that emphasized a vertical shin position. There were significant differences in observed knee angles and anterior hip positioning between the two techniques; though there was minimal difference in trunk lean as measured at the pelvis. The modified Olympic technique tended to have higher knee joint moments; though this trend was not significant. Peak knee, hip, and L5/S1 extension moments were not significantly different between the two techniques.

REFERENCES

1. Chandler, TJ and MH Stone. *Strength Cond J.* **13**, 51-60, 1991.
2. Dunn, B, et al. *Strength Cond J.* **6**, 10-22, 1984.
3. McLaughlin, TM et al. *Res Q Exerc Sport* **49**, 175-188, 1978.
4. Fry, AC, et al. *J Strength Cond Res* **17**, 629-633, 2003.

**Table 1. Average (± SD) Lower Extremity Relative Joint Angles for Each Squat Technique. ***significant difference at α = 0.05 between techniques. Angles represent relative angles between adjacent segments.

	Ankle (deg)	**Knee (deg)**	**Hip (deg)**
Modified Olympic	90.5 ± 5.8	87.7 ± 18.0	101.0 ± 13.0
Modified Power	93.7 ± 8.8	97.8 ± 21.2	97.9 ± 13.3
p-value	*0.151*	*0.006**	*0.245*

Table 2. Average Sagittal Plane (± SD) Peak Net Muscle Moments for Each Squat Technique. Moments are internal net muscle moments.

	Knee* (Nm)	**Hip* (Nm)**	**L5/S1* (Nm)**
Modified Olympic	120.6 ± 47.8	218.0 ± 40.9	487.1 ± 92.2
Modified Power	103.1 ± 42.9	209.7 ± 51.3	477.5 ± 109.5
p-value	*0.068*	*0.250*	*0.366*

LOWER EXTREMITY COORDINATION IN OBESE WOMEN

Elizabeth M. Russell, Allison H. Gruber, Richard E.A. van Emmerik, Joseph Hamill
Biomechanics Laboratory, University of Massachusetts Amherst
email: erussell@kin.umass.edu web: www.umass.edu/biomechanics/

INTRODUCTION

There exists a relationship among the timings of lower extremity segments and pathology. Lower extremity coupling/interaction patterns between the rearfoot and leg may have implications for injury at the knee joint. Rearfoot eversion can alter the kinematics and kinetics farther up the chain in the lower extremity and possibly risk injury to bone and/or soft tissue. Obese persons have greater rearfoot eversion ranges of motion than non-obese [1]. Examining the coordinated motion of the lower extremity segments in space and time gives insights that traditional time series plots of joint angles cannot. Obesity is also the primary, modifiable risk factor for soft tissue knee injuries such as osteoarthritis [2] and it is possible that the coupling relationships between the rearfoot and leg may be related to this soft tissue injury.

Pohl et al. [3] investigated these coordination relationships in walking and found that prolonged tibia external rotation occurred as the rearfoot began to invert. These opposing motions between the articulating rearfoot and leg segments may differ between obese and non-obese individuals and have important implications for lower extremity injury. The purpose of this study was to explore inter-limb kinematic coordination in obese women. We hypothesized that greater eversion range of motion in the obese group would alter the rearfoot-leg coordination patterns between obese and non-obese.

METHODS

Ten obese (age 25.3 ± 9.8 years; BMI 33.09 kgm^{-2}) and ten non-obese (age 25.1 ± 3.8; BMI 22.66 kgm^{-2}) women gave written consent to participate in the study. All participants were free of injuries.

Kinematic (240 Hz) and ground reaction force (1200 Hz) data were collected as subjects walked at a self-selected pace ten times across a force platform. Kinematic data were low-pass filtered and interpolated to 101 data points. Rearfoot eversion/inversion and leg rotation segment angles were calculated in the global coordinate system. All angles were referenced to a standing posture.

A modified vector coding approach assessed the coordination between the segments. Angle-angle plots of the leg relative to the rearfoot were constructed and inter-segment coordination was inferred from the vector angle (θ) between two adjacent time points relative to the horizontal.

$$\theta_i = \left| \tan^{-1}[(y_{i+1}-y_i)/(x_{i+1}-x_i)] \right|$$

Vector angles of 45° and 135° indicated in-phase and anti-phase coordination, respectively. Angles of 90° and 0°/180° indicate exclusively rearfoot and leg movement, respectively. Vector angles were averaged using circular statistics across each third of stance. Rearfoot and leg ranges of motion were the difference between max and minimum values.

To examine continuous inter-limb coordination between segments rotations, zero-lag cross correlations were calculated across time series angular displacement curves. Fisher's Z-Transformation was applied to these values for statistical analyses. Multi-variate ANOVA's ($p<0.05$) assessed differences between groups and tertiles of stance and effect sizes (ES) assessed differences between groups.

RESULTS

The obese group walked significantly slower than the non-obese group (1.33±0.08 vs.1.46±0.12 m·s^{-1}) (p=0.017) by decreasing step length (0.75±0.1 vs. 0.80±0.1 m) and frequency (106.6±4.8 vs. 109.7±4.4 steps/s).

Range of motion was greater in the obese group for the rearfoot (13.1°±4.2 vs. 10.5°±2.6; p<0.01) and leg (19.3°±4.9 vs. 16.9°±4.2; p<0.01) (Fig. 1). Foot eversion occurred with leg internal rotation in early stance and external rotation in late stance.

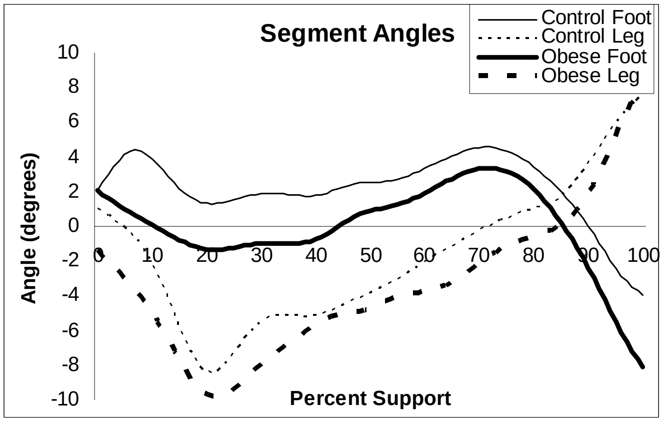

Figure 1: Rearfoot inversion (+)/eversion (-) and leg external (+)/internal (-) rotation.

Cross correlations were low except during late stance when large opposing rotations of rearfoot eversion and leg external rotation occurred (Table 1).

Table 1. Cross correlations between rearfoot and leg excursions. In both tables, * indicates significant differences between groups and numbers indicate significant differences from other tertiles of stance.

	Early stance	Mid stance	Late stance
Control	0.44 ± 0.54^{3}	0.36 ± 0.61^{3}	$-0.76 \pm 0.53^{1,2}$
Obese	0.34 ± 0.62^{3}	0.29 ± 0.55^{3}	$-0.91 \pm 0.11^{1,2}$

Across the stance phase, the vector coding showed no differences between the obese and control coordination patterns ($p=0.742$, ES=0.48), but there were differences between the groups at mid stance (Table 2, Fig 2).

Table 2: Vector coding analysis of coordination patterns between the foot and leg.

	Early stance	Mid stance	Late stance
	ES = 0.32	ES = 0.75	ES = 0.04
Control	$37.17°^{3}$	$28.14°\,*^{3}$	$117.41°^{1,2}$
Obese	$22.30°^{2,3}$	$44.99°\,*^{1,3}$	$117.71°^{1,2}$

CONCLUSION

The combination of increased rearfoot and leg range of motion in the obese group altered the coordination patterns between the groups, despite similar shapes of segment angle plots. Large negative correlations for the opposing rotations of the rearfoot and leg in late stance suggest that the strongest temporal, coupled coordination occurs before toe-off.

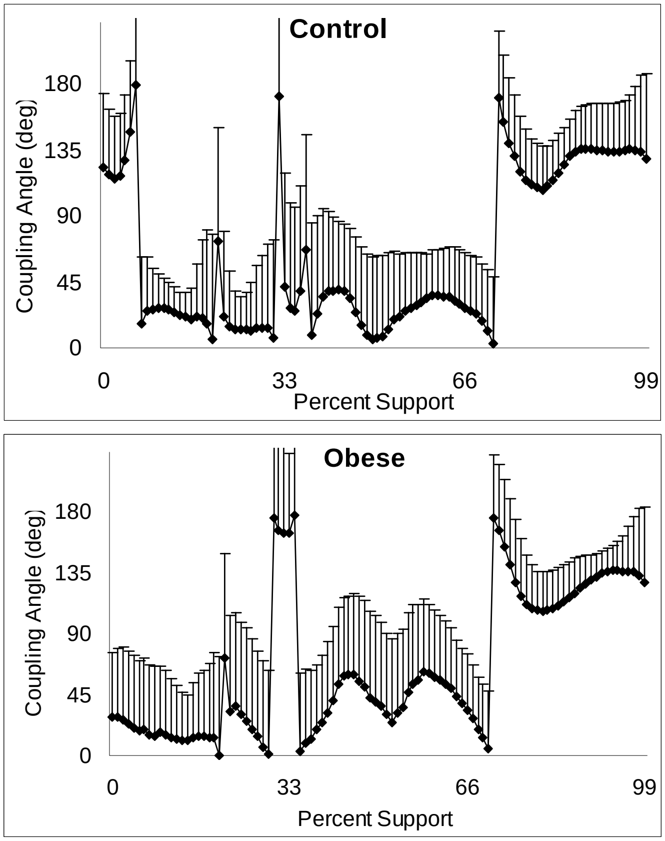

Figure 2: Mean vector coding angles and standard deviation bars

The vector coding approach gives a more detailed assessment of the coordination. Overall, during early stance, the foot eversion with leg internal rotation produced a moderately in-phase coordination of the two segments, however the control group showed greater inversion during early stance. During mid-stance the obese group displayed in-phase coordination while the control group had greater proximal segment motion. During late stance, a more anti-phase coordination pattern predominated between the rearfoot and leg. Asynchronous timing between these segments may be a risk factor for chronic lower-extremity injury [4]. These opposing motions may place stress on soft tissue and have detrimental impact on the tissue and ligaments at the ankle and superior joints.

REFERENCES

1. Messier SP, et al. *Foot Ankle* **15**, 29-34, 1994.
2. Felson DT, et al. *Ann Intern Med* **109**, 18-24, 1988.
3. Pohl MB, et al. *Gait Posture* **25**, 295-302, 2007.
4. Hamill J, et al. *Med Sci Sports Exercise* **24**, 807–13, 1992.

THE EFFECT OF HIP STRENGTHENING ON RUNNING AND SQUATTING MECHANICS IN FEMALE RUNNERS

[1]Richard Willy, MPT and [1,2]Irene S. Davis, PhD, PT
[1]University of Delaware, Newark, DE, [2]Drayer Physical Therapy Institute, Hummelstown, PA, USA
Email: rwilly@udel.edu

INTRODUCTION

Excessive hip adduction and internal rotation during running has recently been associated with a number of running-related injuries including patellofemoral pain syndrome and iliotibial band syndrome [1,2]. This pattern is especially noted in females. Hip strengthening is often advocated for these individuals to improve their mechanics and reduce their symptoms. It has been shown that these programs improve strength [3] and reduce symptoms [4]. However, it is not clear whether strengthening the hip results in a change in movement patterns during functional activities.

Only one study has examined the effect of hip strengthening on running mechanics [5]. The study involved active females with normal hip mechanics. A small but significant increase (1.4°) in peak hip adduction excursion during running was noted. The change in the opposite direction may have been due to between-day error resulting from marker placement. Strengthening alone may not result in meaningful improvements in hip kinematics. It is also plausible that subjects with normal hip mechanics do not have much capacity for improvement.

Therefore, the purpose of this study was to examine the effect of a hip strengthening program on both running and squatting mechanics in females with excessive peak hip adduction during running. It was hypothesized that hip adduction would not be improved during running. However, as the program included single leg squat exercises, a decrease in hip adduction during this activity was expected.

METHODS

An *a priori* power analysis revealed that 10 subjects per group were required to adequately power this investigation. To date, 5 subjects (23.1 years ±3.5) and 4 controls (22.4±2.1) have been analyzed. All subjects were healthy and running at least 6 miles week. For inclusion, peak hip adduction during running had to be $\geq 20°$, which was 1 sd above the mean of a normative database of healthy runners.

Baseline data were collected on all subjects. 35 retroreflective markers were utilized to analyze running kinematics (VICON, Oxford, UK). Anatomical marker placement was recorded via a marker placement device, which has been shown to improve day-to-day reliability [6]. Data were first collected during a single leg squat. Subjects were asked to squat to at least 45° knee flexion for 5 consecutive repetitions. Hip adduction and internal rotation were analyzed at the point of 45° knee flexion. Next, participants ran at 3.35 m/sec on an instrumented treadmill (AMTI, Watertown, MA). Following a 5 minute warm-up, kinematic and kinetic data were sampled at 200 Hz and 1000 Hz, respectively. 3-D joint angles were calculated with Visual 3-D software (C-Motion Bethesda, MD). Customized software (National Instruments, Austin, TX) was utilized to extract variables of interest.

Peak hip abduction and external rotation strength values were collected via a handheld dynamometer (Nicholas, Lafayette, IN). The dynamometer was stabilized against the subjects with straps to eliminate the potential effect of examiner strength. Strength values were normalized to body weight and limb length. The peak of three maximal effort trials was used for analysis.

Subjects in the strength training group (STR) completed a 6-week, 3x/week hip strengthening protocol aimed at the hip abductors and external rotators. Exercises were progressed weekly under the supervision of a physical therapist. They included both supine and standing exercises. Standing exercises included single leg squats and were performed in front of a mirror in order to monitor proper lower extremity alignment. Subjects in the control group (CON) did not engage in any strength training. Following the 6-week intervention or control period, all subjects returned for a final hip strength measurement and motion analysis session. The marker placement device was used to place the anatomical markers using the positions recorded during the first visit. The analysis of running and squatting kinematics were repeated. Meaningful changes were operationally defined as ≥ 15%.

RESULTS

Hip strengthening resulted in a 45.3% increase in hip abduction strength and a 29.1% gain in hip external rotation strength (Fig. 1). No changes were noted in the CON group for either measure.

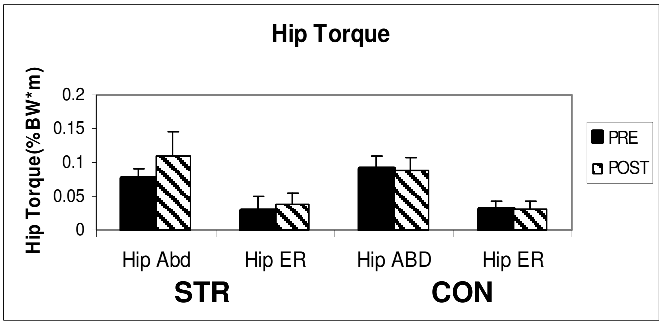

Fig. 1: Comparison of hip torque, pre- and post-intervention.

During the single leg squat, hip adduction was decreased by 7.5°±6.3 (-85.4%) in the STR group (Fig. 2). Hip internal rotation was not changed. No changes were seen in either measure in the CON group.

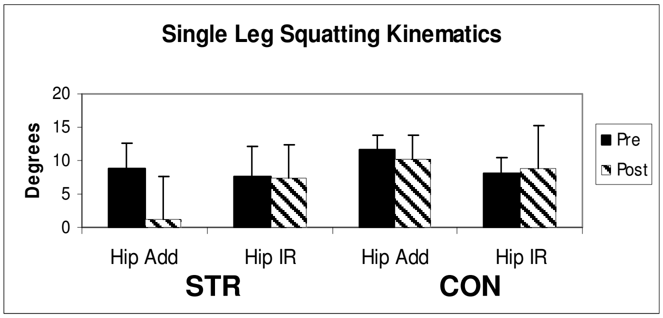

Fig. 2: Single leg squatting kinematics, pre- and post-strengthening for the STR and CON groups.

As expected, there were no changes in hip kinematics during running as a result of the strengthening program (Fig. 3). No changes were noted in the CON group as well.

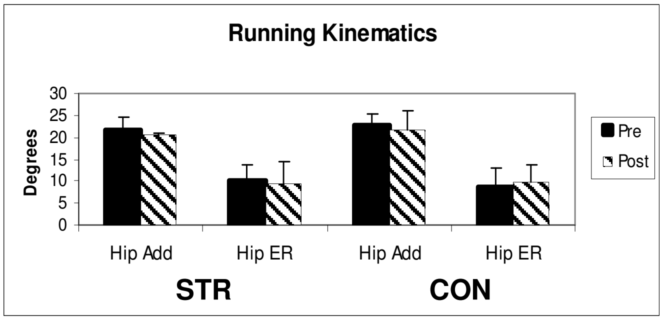

Fig. 3: Hip kinematics during running, pre- and post-strengthening for the STR and CON groups.

DISCUSSION

It appears that the 6-week intervention produced a marked gain in hip strength. In addition to the hip abductor and external rotator strengthening exercises, subjects also performed single leg squats. This single leg squat training likely explains the improvements seen in the single leg squat. Perhaps more importantly, subjects were instructed in proper alignment during this activity and were able to monitor themselves in a mirror as they performed their squat training. This feedback may be considered neuromuscular training that is specific to single leg squatting. The incorporation of this neuromuscular retraining may have contributed the most to the reductions in peak hip adduction values during single leg squatting.

While hip strength was notably increased, hip mechanics during running were completely unaffected by the strengthening program. While these runners were healthy, the peak hip adduction they exhibited was similar to that of runners with patellofemoral pain syndrome and iliotibial band syndrome. Hip strengthening, including single leg squats, is often part of treatment for these injuries. It is unlikely that this standard approach will improve abnormal running mechanics in these patients.

It has recently been shown that neuromuscular re-education, using real-time feedback during running, can significantly reduce abnormal hip mechanics [7]. This was accomplished in the absence of a strengthening program. Therefore, if the goal of an intervention is to improve mechanics, it appears that neuromuscular re-education is needed and strength training alone is inadequate.

CONCLUSIONS

These preliminary data suggest that hip strengthening alone does not result in meaningful changes in hip kinematics during running.

REFERENCES

1. Noehren B, et al. *Clin, Biom*. **22:**951-956,2007.
2. Willson JD, Davis IS. *Clin, Biom*. **23:**203-11,2008.
3. Mascal CL et al. *J Orthop Sports Phys Ther.***29**:642-60, 2003.
4. Nakagawa et al. *Clin. Rehabil*. **22:**1051-60, 2008.
5. Snyder KR et al. *Clin. Biom.* In press.
6. Noehren B, Davis IS. *Proc. of NACOB*, 2008
7. Noehren B et al. Proceedings CSM meeting, APTA, 2007.

ACKNOWLEDGEMENTS

Support for this project was provided by the Foundation for Physical Therapy, Drayer Physical Therapy Institute, NIH 1 S10 RR022396, DOD W911NF-05-1-0097.

BIOMECHANICAL ANIMATIONS COMMUNICATE EMOTION DURING WALKING

Lan Wei, Brendan Keen, Christine Herzog, Elizabeth Crane and Melissa Gross
School of Kinesiology, University of Michigan, Ann Arbor, MI 48109-2013
email: mgross@umich.edu, web: http://www.umich.edu/~mgross

INTRODUCTION

Emotion can be recognized in human movements from video displays showing only joint center motions [1,2]. These video displays are not derived from biomechanical models, and so limit the ability to integrate kinematic data with perceptual studies of emotion recognition. Although joint center displays generated from motion capture data have been used to study gender and person identification [3,4], biomechanical animations have not yet been validated in emotion recognition studies. Because view perspective has been shown to affect emotion, gender and person recognition [3-5], validation studies of emotion recognition using biomechanical displays should include different view perspectives.

The purpose of this study was to determine: (1) if emotions could be recognized from animated displays of gait data, (2) if emotion recognition rates were comparable to those obtained with video displays, and (3) if view perspective affected emotion recognition in animated displays.

METHODS

In a previous study [6], motion capture data were collected from 42 individuals during walking with five emotions: angry, joyful, content, sad and neutral. Sixty observers were shown side-view videos of the walking trials and then selected one of ten emotions they thought the walker was feeling. The 10 trials with the highest mean recognition rates for each emotion were included in this study. These 50 trials (5 emotions x 10 walkers) were generated by 32 walkers (44% male; 20.2 ± 2.8 yrs).

A single gait cycle from each walking trial was selected for analysis. Data from the right arm and right leg were not captured in the previous study, so left-side marker data were time-shifted and reflected to create marker data for the right-side limbs. The limbs were modeled with virtual markers placed at the joint centers of the shoulder, elbow, wrist, hip, knee, and ankle, and on the heads of the 3rd metatarsals and metacarpals and the heels. The trunk was modeled with virtual markers placed on the spine at the levels of C5, T6 and L3, and at the center of the head. Gait cycles were time normalized, and the endpoints were adjusted so that data at 0 and 100% of the cycle were the same.

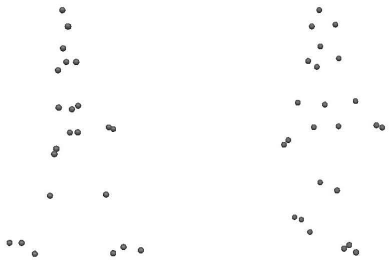

Figure 1: Side (left) and oblique (right) views of virtual markers in animated displays.

Animated displays of the virtual markers during the walking trials were exported from Visual3D as movie files displayed from side or oblique (45 deg between side and front) views (Figure 1). The walking speed, distance covered, and the number of gait cycles were the same in the video and animated displays of each walking trial. Each walking trial was looped so that it displayed three times in succession. The 100 videos (2 views x 50 walking trials) were ordered into three random sequences.

Observers (n=27; 59% female; 19.9 ± 1.6 yrs) viewed each of the 100 videos and selected one of ten emotions that they thought the walker was feeling. The mean recognition rate was calculated for each emotion and view. A Chi-square test was used to determine if the distribution of observer responses was different from chance. A mixed model with random walker and observer effects, and fixed effects of walker gender, observer gender, sequence, emotion and view was used to test for differences between means ($p < .05$).

RESULTS AND DISCUSSION

Observers were able to recognize the emotions felt by the walkers at levels that exceeded chance (10%) for all emotions and displays (Fig. 2). Side-view recognition rates were 33, 42, 53 and 25% less for animated than for video displays for angry, content, joyful and sad emotions, respectively. View interacted with emotion for the animated displays so that recognition was better with the side view for sad (9%) and with the oblique view for joy (32%). Recognition rates were not different among any displays for neutral trials. Recognition rates were not affected by video sequence, walker gender or observer gender.

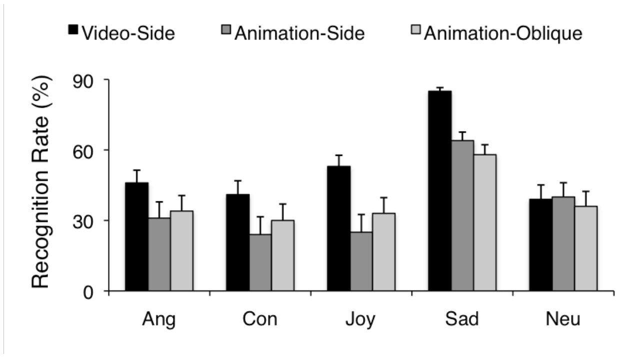

Figure 2: Recognition rates for video and animated displays of walking trials for each target emotion.

The lower recognition rates with the animated displays were associated with greater confusion with neutral (Table 1). For content and joyful trials, decreased recognition with the animated displays was also associated with an increase in confusion between content and joy. Recognition rates for the non-target emotions were less than chance for all emotions and views except for disgust in angry.

Our results indicate that emotions felt by walkers were recognized with the animated displays but at rates less than video displays of the same walking trials. View affected recognition for two of the five target emotions. Our results demonstrate that animated displays generated from biomechanical models of the body can be used to test hypotheses related to emotion assessment during movement. Because the data used to create the animations can be used to calculate kinematics, our method can be used for future studies of the bodily expression of emotion in healthy individuals and individuals with affective disorders.

REFERENCES

1. Atkinson AP, et al. *Perception* 33, 717-746, 2004.
2. Roether CL, et al. *Current Biology* **18**, R329-330, 2008.
3. Troje NF, et al. *J Vision* **2**, 371-387, 2002.
4. Troje NF, et al. *Perception & Psychophysics* **67**, 667-675, 2005.
5. Gross MM, et al. *Proc. International Society for Research on Emotion,* Atlanta, GA, 2006.
6. Crane EA, et al., Emotion-related movement style during walking. *Submitted*.

ACKNOWLEDGEMENTS

Funded by NSF Grant (044430) to M. Gross.

Table 1: Mean recognition rates (%) for side-view video and animated displays.

Trial	Display	Angry	Content	Joyful	Sad	Neutral	Awe	Fear	Surprise	Disgust	None
Angry	Video	**46.2***	5.0	9.0	0.3	9.4	3.0	7.0	5.7	12.0	2.3
	Anim	**31.1**	4.8	9.3	5.9	13.0	0.4	10.4	4.8	16.3	4.1
Content	Video	4.7	**41.1***	9.4	8.0	22.1	4.0	2.0	1.0	5.4	2.3
	Anim	4.4	**24.4**	18.9	6.3	33.7	5.2	0.4	2.2	3.0	1.5
Joyful	Video	10.4	10.1	**52.7***	0.7	6.4	6.0	1.7	5.7	4.0	2.3
	Anim	15.9	13.7	**24.8**	5.9	14.4	5.6	5.6	2.6	7.4	4.1
Sad	Video	1.7	1.0	0.3	**84.6***	3.7	0.3	3.4	0.3	3.4	1.3
	Anim	0.7	9.7	1.1	**63.9**	8.2	2.2	7.4	2.6	3.0	1.1
Neutral	Video	6.0	21.7	4.0	12.7	**39.0**	3.7	4.0	1.3	4.7	3.0
	Anim	2.6	28.1	7.4	3.0	**39.6**	3.7	7.4	1.9	4.4	1.9

*p < .001

THE EFFECTS OF SPRINT SPEED ON APPARENT STIFFNESS IN UNI-LATERAL TRANS-TIBIAL AMPUTEE SPRINT RUNNERS

[1]Craig McGowan, [2]Alena Grabowski, [3]William McDermott, [4]Rodger Kram, and [2]Hugh Herr.
[1]University of Texas, Austin, [2]Massachusetts Institute of Technology, [3]The Orthopedic Specialty Hospital, Salt Lake City, UT, [4]University of Colorado, Boulder
email: cpmcgowan@mail.utexas.edu

INTRODUCTION

Recent research suggests that the ability to generate force limits top speed in humans with intact limbs [1, 2]. A number of high-speed sprint running studies have shown that as sprinters increase velocity, peak vertical ground reaction forces increase in magnitude and occur earlier during the stance phase (Fig. 1A) [e.g., 3]. This leads to an increase in eccentric stiffness, which describes the relationship between force and center of mass displacement from foot contact to peak force (Fig 1B)[4]. Preliminary data have shown a strong correlation between eccentric stiffness and stance averaged vertical ground reaction force, a key determinate for top running speed [1]. While eccentric stiffness increases with speed, the rate of force decline and concentric (unloading) stiffness, remain unchanged.

Recent data from an elite bi-lateral amputee, who uses running-specific prostheses designed to mimic the spring-like characteristics of biological limbs during running, shows that he achieves top speeds using different mechanical means than intact sprinters [3, 5]. Specifically, at top speed, peak vertical ground reaction forces are much lower for this bi-lateral amputee than for performance-matched intact sprinters [5], and unlike intact athletes, eccentric stiffness is nearly independent of running speed.

To better understand the mechanical effects of running-specific prostheses compared to intact limbs, we measured temporospacial and ground reaction force (GRF) variables of uni-lateral trans-tibial amputee sprinters over their full range running speeds. Uni-lateral amputees provide a unique opportunity because each amputee's intact limb serves as a control for comparing of the biomechanics between the biological limb and the residual plus prosthetic limb.

We hypothesized that eccentric stiffness would increase with increasing speed in the intact leg but would be independent of speed in the prosthetic leg, and that concentric stiffness would be independent of speed in both legs.

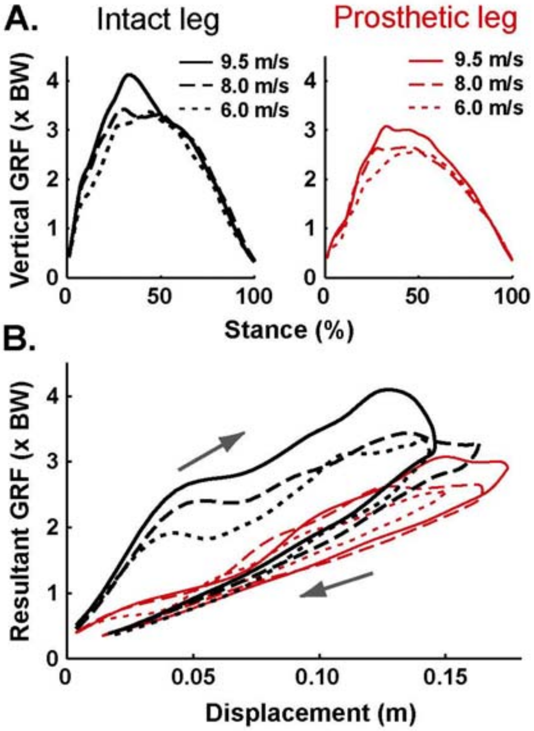

Fig 1. Representative traces from a single subject at three speeds. A) Stance normalized vertical GRF. B) Resultant GRF plotted against center of mass displacement. Eccentric stiffness is calculated from toe-on to peak force and concentric stiffness is calculated from peak displacement to toe-off.

METHODS

Six otherwise healthy unilateral trans-tibial amputee elite Paralympic sprinters (4 M, 2 F) participated in the study. All subjects gave informed written consent according to the approved Intermountain Healthcare IRB protocol. All of the experiments were conducted at the Biomechanics Laboratory of the Orthopedic Specialty Hospital .

Subjects performed a series of discontinuous constant speed running trials consisting of short running bouts of at least 10 strides. Data were collected on a custom-built, high-speed, 3D force sensing motorized treadmill (Athletic Republic, Park City, UT) at 1600 Hz and were filtered with a critically damped filter implemented using Visual 3D software. Subjects began each series of trials at 3 m/s and speeds were increased in 1 m/s increments until they reached ~ 75% of their maximal running speed. Speed was then increased in 0.2-0.5 m/s increments until subjects reached their top speed, determined as the speed at which they could no longer maintain their horizontal position on the treadmill. Subjects were given as much time between trials as needed for full recovery.

Instantaneous stiffness was calculated using a modified spring-mass model assuming a constant horizontal and angular velocity. Stiffness was calculated as the ratio of the resultant GRF and the resultant displacement of the center of mass. Eccentric stiffness was calculated from toe-on to peak force, while concentric stiffness was calculated from peak leg displacement to toe-off (Fig. 1B).

RESULTS AND DISCUSSION

The results of our study support our hypotheses. Eccentric stiffness increased significantly with increasing speed in the intact leg, but was independent of speed in the prosthetic leg (Fig. 2A). Additionally, eccentric stiffness was greater in the intact leg compared to the prosthetic leg at speeds of 7 m/s and higher. Concentric stiffness was independent of speed in both legs, and not significantly different from eccentric stiffness in the prosthetic leg (Fig 2B). Consistent with previous preliminary results, there was a significant correlation between stance averaged vertical GRF and eccentric stiffness.

Our results suggest that the stiffness of the prosthetic leg is dominated by the passive mechanical properties of the prosthesis and cannot be modulated in response to speed in the same fashion as the biological leg. The correlation between eccentric stiffness and average vertical GRF suggests that a fixed stiffness prosthesis may limit the ability to produce high vertical GRF, especially at high speeds. Thus, in order to achieve similar top speeds as intact sprinters, athletes with prostheses must alter other aspects of running mechanics such as contact length or step frequency.

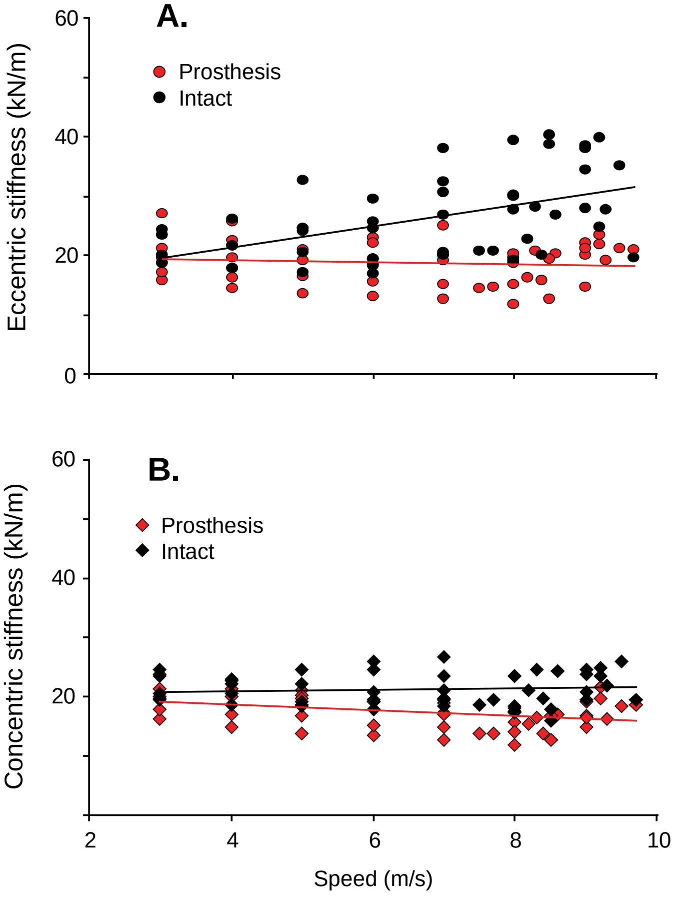

Fig. 2 A) Eccentric and B) concentric stiffness vs speed.

REFERENCES

1. Weyand PG, et al. *J Appl Physiol* **89,** 1991-1999, 2000.
2. Usherwood JR and Wilson AM. *Nature* **438**, 753-754, 2005.
3. Bruggemann G-P et al. *Sports Technol* **1,** 220-227, 2008.
4. Luhtanen P and Komi PV. *Eur J Appl Physiol* **44**, 279-289.
5. Weyand PG et al. *J Appl Physiol* In Press, 2009.

ACKNOWLEDGEMENTS

The authors wish to thank Stephanie Koenig, Steve Swanson, and The Orthopedic Specialty Hospital.

HUMERAL RETROVERSION IN BIOMEDICAL PERSPECTIVE: RANGES OF VARIATION IN HUMAN POPULATIONS AND THE ROLE OF ACTIVITY PATTERNS IN THEIR DEVELOPMENTAL DETERMINANTS

Robert B. Eckhardt and Adam J. Kuperavage
Laboratory for the Comparative Study of Morphology, Mechanics and Molecules
Department of Kinesiology, The Pennsylvania State University, University Park, PA, USA
email: eyl@psu.edu

INTRODUCTION

The LB1 skeleton is the most complete individual in a collection of small, incomplete skeletons that were recovered from Flores, an island of 14,200 km^2 that is located east of the Wallace Line in Indonesia. Originally limited morphological characterizations [1] were supplemented [2] by details of additional postcranial remains. These included description of a humerus with damage to its proximal end. The initial estimate of the extent of LB1/50 humeral torsion was 110º, which was stated to be well outside the range given for living humans as 141º to 178º, implying that the extent of humeral rotation reflects only phylogenetic information, and that this and other reportedly unique morphological features required recognition of a new human species, "Homo floresiensis*.*" In the alternative hypothesis that our research group formulated in response to these contentions, Jacob, et al. [3] noted that torsion of the humerus is in part ontogenetic, in response to the dynamic forces exerted by shoulder rotators on the growing bone. Reported here are the results of investigations that build upon and extend those that we have published previously [3].

METHODS

In the anthropological literature, the basic reference condition is assumed to be that for quadrupedal mammals having a humeral head facing posteriorly, with deviation of the humeral head from this position to facing more medially being reported as increased torsion. In the human clinical and sports literature, humeral head position is referred to as humeral retroversion, with the humeral head facing inward thus constituting the default condition (0º retroversion), so that increasing posterior deviation is reported as greater retroversion. Consequently,

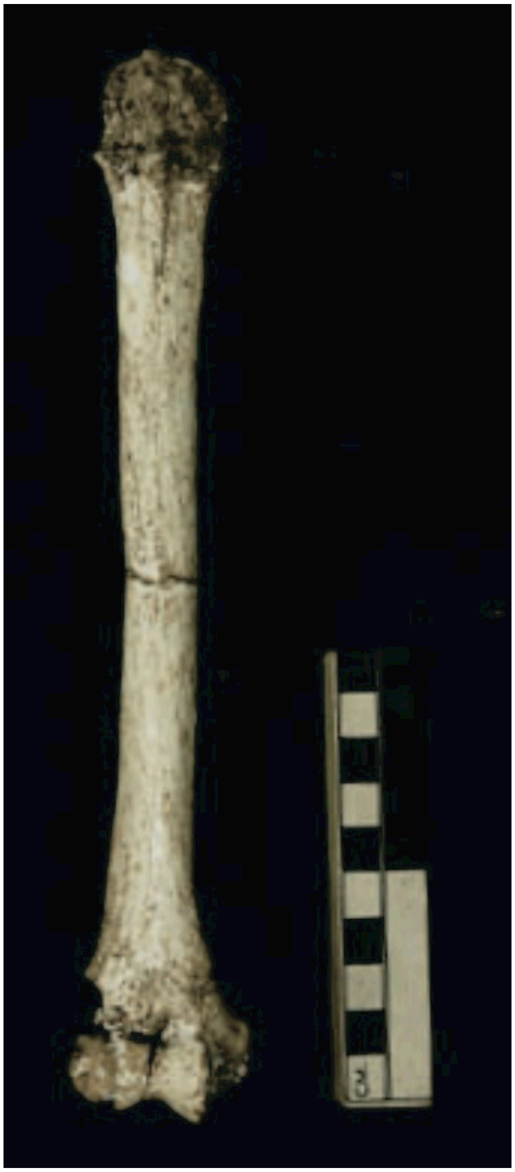

Figure 1: LB1/50 humerus, anterior aspect. Note near absence of deltoid tuberosity as well as minimal difference between subdeltoid and supradeltoid widths of the shaft. These indicators of markedly weak muscle development are consistent developmentally with a very low degree of humeral torsion.

large retroversion angles correspond to small torsion angles.

Two sources of data were used in this study: 1) more extensive review of the published literature on humeral torsion in various human subpopulations, particularly those groups that might manifest the influences on development of humeral torsion as a result of participation in certain sports and other vigorous physical activities; 2) radiographic and CT (computerized tomographic) scans on athletes participating in sports (such as baseball) that might increase developmental stresses on humeral development, as well as patients with abnormalities of development that would be expected to affect development of the upper limb skeleton. Radiographic and CT data from the literature were reviewed; these are supplemented here with data collected at the General Clinical Research Center, the Pennsylvania State University College of Medicine, in cooperation with members of our Laboratory, using a Siemens model Sensation 40 with scanning protocol of 1.5 mm x 0.75 mm.

RESULTS AND DISCUSSION

A 95% confidence interval for an expanded sample of 293 humans from 15 recent worldwide human populations now shows that humeral torsion angles range from below 115º to approximately 180º, while restudy of LB1/50 reported a humeral torsion angle of 120º [4]. From our studies [3], extended here, it can be concluded that the Liang Bua Cave skeletal sample, as represented by the LB1 humerus, does not present evidence from the extent of humeral torsion that requires recognition of a new species of human.

Furthermore, studies of individuals, whether participants in selected sports, show that humeral torsion, rather than being a static attribute that encodes only phylogenetic information, actually is developmentally dynamic in its morphological expression. Because the lateral rotators insert within the proximal epiphysis whereas most of the medial rotators act distally on the shaft, forces working in opposite directions during development normally add approximately 32º of secondary torsion. The extent of this secondary (developmental) torsion depends on a variety of factors. For example, in college baseball players, the mean humeral retroversion in the dominant (pitching) arm was 36.6º ± 9.8º, while in the non-dominant arm it was 26º ± 9.4º [5]. In contrast, Israeli patients with Laron syndrome, characterized by weak development of muscles and their attachment sites, show reduced humeral torsion [6]. Our studies on patients with diagnostically similar developmental abnormalities to the Israeli sample, extend and support this recently reported work [6],

CONCLUSIONS

This study documents the scientific potential of evolutionary biomechanics, in which studies of human form (morphology) become far more informative through the combination of temporal depth of observations with experimental analyses in living subjects. Our objective is to replace static, descriptive, dichotomous perspectives with much deeper, broader, and more dynamic comparative frameworks for analysis. Our Laboratory group emphasizes the generation of testable hypotheses about human form, function, and evolution within the explicitly rigorous frameworks characteristic of biomedical science.

REFERENCES

1. Brown, P., et al. *Nature* **431**, 1055-1061, 2004.
2. Morwood, MJ, et al. *Nature* **437**, 1012-1017, 2005.
3. Jacob, T, et al. *Proc Natl Acad Sci, USA* **103**, 13421-13426, 2006.
4. Larson, SG, et al. *J Hum Evol* **53**, 718-731, 2007.
5. Reagan, KM, et al. *Am J Sports Med* **30**, 354-360, 2002.
6. Hershkovitz, I, et al. *Am J Phys Anthrop* **134**, 198-208.

EFFECTS OF AGING-RELATED LOSSES IN MUSCLE STRENGTH ON THE FEASIBLE REGION FOR BALANCE RECOVERY

Norio Kadono and Michael Pavol
Department of Nutrition and Exercise Sciences, Oregon State University, Corvallis, OR
email: mike.pavol@oregonstate.edu

INTRODUCTION

Backward falls are a concern for older adults. They are the hardest falls to prevent and can lead to serious injury, including hip fracture. It is therefore important to understand the factors that adversely influence the ability to prevent a backward fall. One such factor may be aging-related losses in muscle strength. Muscle strength decreases with older age, and weaker lower extremity muscles have been associated with lesser balance control among older adults [1]. Conceivably, aging-related losses in muscle strength might impair the ability to support the weight of the body and stop its downward motion following a recovery step. Yet in one study, older adults who fell following an induced trip were stronger than those who did not [2]. At present, it remains unknown to what extent aging-related losses in muscle strength affect the ability to recover from a backward balance loss. This study used a mathematical modeling approach, along with a modification of the concept of the feasible region for balance recovery [3], to investigate the effects of aging-related losses in muscle strength on the ability to restore static balance after a recovery step from a backward balance loss.

METHODS

A six-link, sagittal-plane model was developed to simulate the balance recovery motions of young and older adults after touchdown of a backward recovery step. The links of the model represented the front and rear feet, rear leg, rear thigh, head-arms-torso, and front thigh-and-leg. The rear foot, representing the foot that took the recovery step, was fixed to the ground and the front foot was constrained to slide along the ground. The rear limb was actively controlled through a set of 10 Hill-type musculotendon actuators that included uniarticular flexor and extensor actuators across the ankle, knee, and hip and biarticular rectus femoris, hamstrings, and gastrocnemius actuators. The front limb of the model moved passively. Angle-dependent passive joint moments were used to enforce the anatomical range of motion at each joint.

Each musculotendon actuator consisted of a contractile element (*CE*), a passive elastic (*PE*) element, and a series elastic (*SE*) element, acting between assumed points of origin and insertion. The *CE* was controlled by a dimensionless neural excitation signal and incorporated time-dependent excitation-activation dynamics, a length-tension relationship, and a force-velocity relationship. The *PE* and *SE* elements were modeled as nonlinear springs. A set of 11 parameter values determined the characteristics of each musculotendon actuator.

Two sets of musculotendon parameter values were derived to represent the respective lower extremity strength characteristics of young and older adults. Parameter values for young adults were derived from published sources. Aging-related losses in muscle strength were simulated by decreasing the *CE* maximum isometric force by 25%, decreasing the ratio of Type II to Type I fibers by 30%, increasing the *CE* deactivation time constant by 20%, and increasing *PE* and *SE* stiffness by 8%.

Feasible regions for balance recovery were determined for the models of young and older adults using repeated optimizations. In each optimization, the backward velocity of the body center of mass (*COM*) and the downward velocity of the hips were initialized to 15% body height/s, representative of the state at step touchdown for successful recoveries from a forward slip during a sit-to-stand [4]. Either the initial COM horizontal position (X_{COM}) or the initial hip height (Z_{HIP}) was chosen. Then, either the maximum or minimum value of the other variable was found from which static balance could be restored. The simulated annealing algorithm was used for this optimization. “Control” variables were the initial joint angles and velocities, initial *CE* activation levels, and the neural excitation signals to the actuators. Initial angles and velocities were constrained to anatomical ranges. Neural excitation signals were parameterized by the start time, magnitude, and stop time of five periods of constant excitation. These periods of constant excitation were connected by linear changes in excitation. The cost function to be minimized was of the form:

$$I_{COST} = kf_0 + \sum g_m + \sum h_n$$

where the f_0 was an initial X_{COM} or Z_{HIP}, the k was +1 to minimize f_0 and -1 to maximize f_0, the g_m were penalty values associated with violating the continuous constraints on the ground reaction forces during the movement, and the h_n were penalty values associated with violating the constraints on the final state. The penalty functions required the six-link model to perform the body-stabilizing motions during the simulation in a manner that young and older adults could in real life and to bring itself to a statically stable, near-stationary state at the end of the simulation. A fourth-order Runge-Kutta method with adaptive step sizes was used to integrate the equations of motion of the model during the forward dynamic simulations. The duration of each simulation was 1 second.

RESULTS AND DISCUSSION

As hypothesized, the feasible region for balance recovery was smaller in area for older adults than for young (Figure 1). The differences between regions were primarily in the range of X_{COM} from which static balance could be restored. The feasible region for older adults did not extend as far anteriorly or posteriorly as that for young adults, with the largest differences observed at lower hip heights. The forward boundary for older adults at a Z_{HIP} of 50% body height (Bh) was 25% foot length (fl) less anterior than that for young adults and the rear boundary for older adults at a Z_{HIP} of 45% Bh was 12% fl less posterior than that for young adults. In contrast, there were negligible differences in the predicted ranges of Z_{HIP} from which young and older adults could restore static balance at X_{COM} common to both regions.

Although a low hip height at step touchdown was previously found to be a primary predictor of backward falls [4], the present results suggest that typical aging-related losses of muscle strength do not notably impair the ability to recover balance at low hip heights. Instead, aging-related losses of muscle strength appear to reduce the range of stepping foot placements for which balance recovery is feasible. Older adults are less able than young to recover from a backward balance loss if they take a very short or very long step.

CONCLUSIONS

Aging-related losses in muscle strength can impair the ability to recover from a backward balance loss if too short or too long a recovery step is taken. However, if a medium-length step is taken, older adults can show the same ability to recover balance as young adults. Therefore, the present results suggest that training of the stepping response might prove to be more effective than strength training in preventing backward falls by older adults.

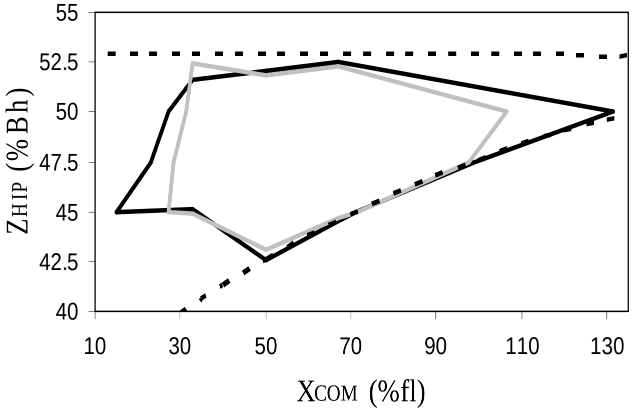

Figure 1: The feasible regions of balance recovery showing the initial states from which young (black line) and older (gray line) adults could restore static balance. The dashed lines represent the anatomical constraints on the initial state. X_{COM} = center of mass position anterior to the rear heel. Z_{HIP} = hip height. fl = foot length. Bh = body height.

REFERENCES

1. Daubney ME, et al. *Phys Ther* **79**, 1177-1185, 1999.
2. Pavol MJ, et al. *J Am Geriatr Soc* **50**, 256-262, 2002.
3. Pai YC, et al. *J Biomech* **30**, 779-786, 1999.
4. Pavol MJ, et al. *J Biomech* **40**, 1318-1325, 2007.

ACKNOWLEDGEMENTS

Funded by the Ringe Faculty Excellence Fund for Life Quality and Longevity and the OSU Center for Healthy Aging Research.

CHANGES IN WRIST MOMENT ARMS OF THE FIRST DORSAL EXTENSOR COMPARTMENT FOLLOWING SIMPLE DISTAL RADIUS MALUNIONS

[1]Gregory L. Scallon, [3,4]Michael S. Bednar, [5]Amy L. Ladd, and [1,2,4] Wendy M. Murray
Depts. of [1]Biomedical Engineering and [2]PM&R, Northwestern University; [3]Dept. of Orthopaedic Surgery and Rehabilitation, Loyola University; [4]Edward Hines Jr. VA Medical Center; [5]Dept. of Orthopaedic Surgery, Stanford University
email: w-murray@northwestern.edu

INTRODUCTION

Distal radius fractures comprise over 10% of classified fractures seen in US and European Emergency Departments [1]. If all displaced fractures were treated exclusively with closed reduction (non-invasive realignment), it is postulated that 60% would later fuse into the deformed, unreduced state, yielding a malunion [2]. Even with current management techniques, 27% of these displaced fractures lose their reduction [3]. Thus, open reduction (invasive realignment) or even osteotomy (surgically fracturing the fused bone) is frequently warranted to correct deformity. Increasing anatomical deformity in a distal radius malunion is associated with loss of grip strength, range of motion, and unfavorable cosmetic assessment [4]. However, the severity of the deformity that requires surgical intervention is not well defined.

This work aims to improve understanding of the role biomechanics plays in decreased function following distal radius malunions. Significant changes in wrist moment arms of muscles of the first dorsal extensor compartment have been observed in a cadaver study that simulated complex malunions involving significant dorsal angulation, radial inclination, and radial shortening [5]. We simulated a range of simpler distal radius malunions in order to elucidate how malunion severity influences the wrist moment arms of the muscles of the first dorsal extensor compartment.

METHODS

We simulated a broad range of simple distal radius malunions using a biomechanical model of the upper limb [6]. A transverse cut was made 3.3 cm proximal to the radial styloid process, creating an extra-articular "fracture" in the radius. Three degrees of freedom—dorsal angulation, radial inclination, and radial shortening—were introduced by a fracture "joint" describing the rigid body transformation from the proximal radius to the distal fracture segment (Fig. 1). The "range of motion" for each degree of freedom ranged from the normal anatomy of the distal radius to 14.1° radial inclination, 25.9° dorsal anguation, and 7.2 mm radial shortening, respectively. Positioning all three degrees of freedom at their extreme values simulated the complex malunion evaluated in the previous cadaver study [5].

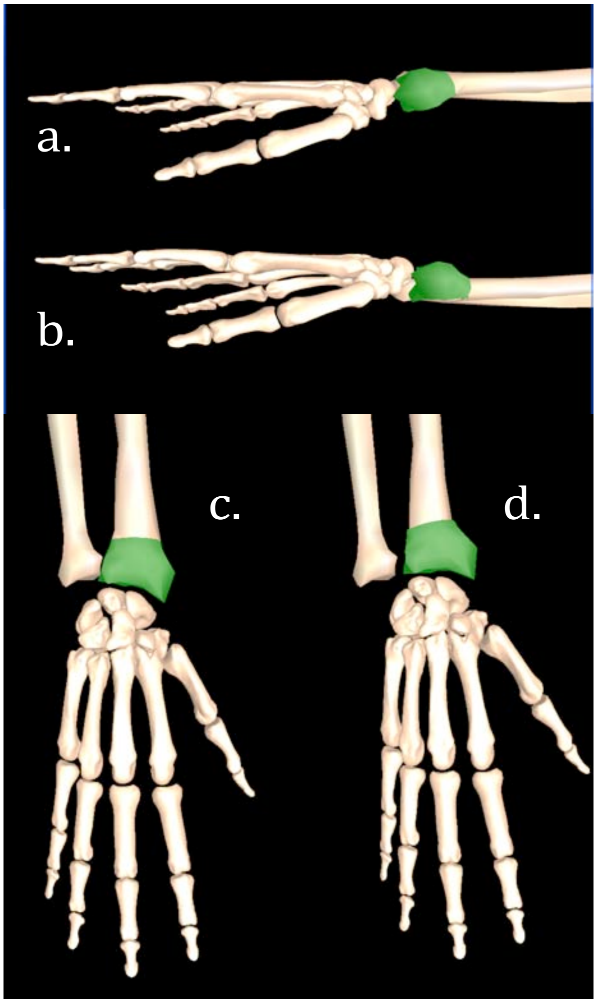

Figure 1. Model used in normal wrist configuration (a,c) and with 25.9° of dorsal angulation (b) and 14.1 ° of radial inclination (d).

Flexion and deviation moment arms of the muscles of the first dorsal extensor compartment, extensor pollicis brevis (EPB) and abductor pollicis longus (APL) were estimated at neutral flexion and deviation. The change in moment arm produced by each simple malunion was normalized by the change in moment arm caused by the complex malunion.

RESULTS AND DISCUSSION

Overall, isolated radial inclination had a more substantial effect on wrist flexion moment arms than deviation moment arms (Fig. 2). Radial inclination of 14.1° decreased flexion moment arm of EPB by 74.8% of the decrease caused by the complex malunion. For the APL, radial inclination of 14.1° decreased flexion moment arm 122% of that caused by the complex malunion.

In contrast, isolated dorsal angulation had a greater effect on deviation moment arms than flexion moment arms. Dorsal angulation of 25.9° increased the wrist deviation moment arm of EPB by 123% of the increase caused by the complex malunion. For the APL, dorsal angulation of 25.9° increased flexion moment arm 98.9% of that caused by the complex malunion.

As secondary effects, radial inclination increased deviation moment arms of both muscles (< 50% of complex malunion, Fig. 2B), and dorsal angulation decreased flexion moment arms of both muscles (< 50%). There were no observed effects of radial shortening on EPB or APL wrist moment arms.

To validate the simulations, changes in flexion and deviation moment arms of the EPB and APL were compared to the anatomical model of the complex malunion [5]. The simulated complex malunion produced the trends described in the cadaver study.

CONCLUSIONS

Both radial inclination and dorsal angulation decreased flexion moment arms and increased deviation moment arms. However, the changes were not additive and, at the extreme values, isolated radial inclination and dorsal angulation caused greater moment arm changes than the complex malunion. These results suggest that isolated malunion deformities may have comparable or more pronounced effects on the mechanical actions of the first dorsal extensor compartment than combinations of these deformities. Thus, surgical intervention may be necessary in malunions that exhibit only one degree of radiographic deformity.

REFERENCES

1. Melton III LJ, et al. *Osteoporosis International* **9**, 29-37, 1998.
2. Mackenney PJ, et al. *J Bone Joint Surg Am* **88**, 1944-1951, 2006.
3. Cooney III WP, et al. *J Bone Joint Surg Am* **62**, 613-619, 1980.
4. McQueen M, et al. *J Bone Joint Surg Am* **70**, 649-651, 1988.
5. LaRoque ES, et al. *J Bone Joint Surg Am* **90**, 1979-1987, 2008.
6. Holzbaur KR, et al. *Ann Biomed Eng* **33**, 829-840, 2005.

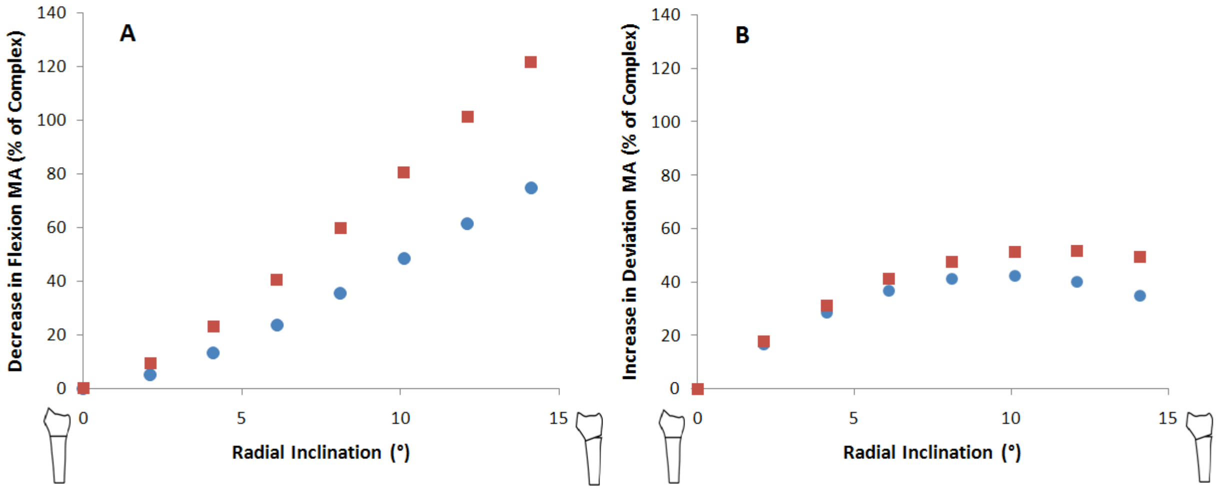

Figure 2. Effects of isolated radial inclination on muscle moment arms of the first dorsal extensor compartment. (A) Decrease in flexion moment arms for the EPB (blue circles) and APL (red squares). Increase in deviation moment arms (B). Zero degrees represented no deformity.

LINEAR HEAD ACCELERATIONS RESULTING FROM SHORT FALLS ONTO THE OCCIPUT IN CHILDREN

[1]Michelle F. Heller, [1,3]Juff George, [2]Gary T. Yamaguchi, [1,3]Joseph C. McGowan and [1]Michael T. Prange
[1] Exponent Failure Analysis Associates, Philadelphia, PA, [2] Phoenix, AZ
[3]Drexel University School of Biomedical Engineering
email: mheller@exponent.com, web: www.exponent.com

INTRODUCTION

Childhood falls are a common occurrence and account for approximately 2.8 million emergency department visits each year. Although short falls most often do not result in serious injury[1], they do have the potential to cause serious head injuries or death[2]. Quantifying the characteristics of falls that lead to injury in children of various ages may lead to a greater understanding of the biomechanical implications of such events and may increase awareness among parents of the potential danger of a short fall. Such awareness could prompt caregivers to seek more timely medical attention should a household fall occur. The purpose of this research was to measure and compare the head response from impacts after falls from various heights and onto various surfaces.

METHODS

To simulate falls of toddlers and young children, two anthropomorphic test devices (ATDs) were used during the testing. A 1-year-old Child Restraint/Air Bag Interaction (CRABI 12-month-old, Denton ATD, Inc., Milan, OH) and a 3-year-old Hybrid III (Denton ATD, Inc., Milan, OH) were used. Instrumentation was placed at the center of gravity (CG) of each of the ATD's heads to measure the linear head accelerations along the three orthogonal axes. Both the 1-year-old and 3-year-old ATDs were suspended supine from a single point of support with the head angled slightly downward (Figure 1). Using a pneumatic release, the ATDs were dropped such that the back of their head contacted the ground first. The measured drop heights represent the distance from the ATD head to the impact surface. The ATDs were dropped from three heights of 0.8 m, 1.2 m, and 1.5 m (2.5 ft., 4 ft., and 5 ft.) onto two surfaces (concrete, carpet with foam carpet padding). Each age, surface, and height combination was conducted at least three times. The data were filtered using standard methods for impact data (CFC 1000). Peak linear head accelerations in each of the three directions and the resultant were determined, and the head injury criterion (HIC_{15}) was calculated for each trial. Effects of surface, height, and age on peak head acceleration and HIC were determined utilizing a three-way analysis of variance.

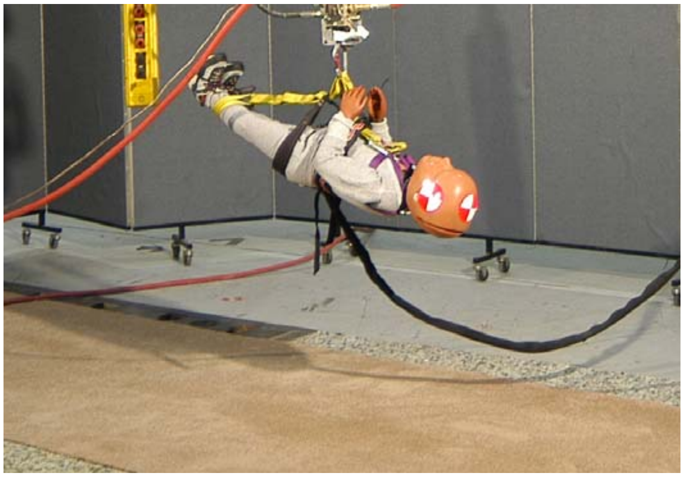

Figure 1: Three-year-old dummy being dropped from 0.8 m onto carpet with padding.

RESULTS AND DISCUSSION

The investigated falls resulted in occiput-to-ground contact velocities ranging from approximately 3.8 to 5.5 meters per second. The averaged peak resultant linear head accelerations and averaged HIC_{15} for the 1-year-old and 3-year-old ATDs are summarized in Figures 2 and 3.

Consistent with expectation, peak head linear acceleration and HIC_{15} increased with increased fall height, age, and impact surface stiffness ($p<0.001$). The linear acceleration and HIC caused by a 1.5 m fall onto carpet in the three year old is less than that caused by a 1.2 m fall onto concrete.

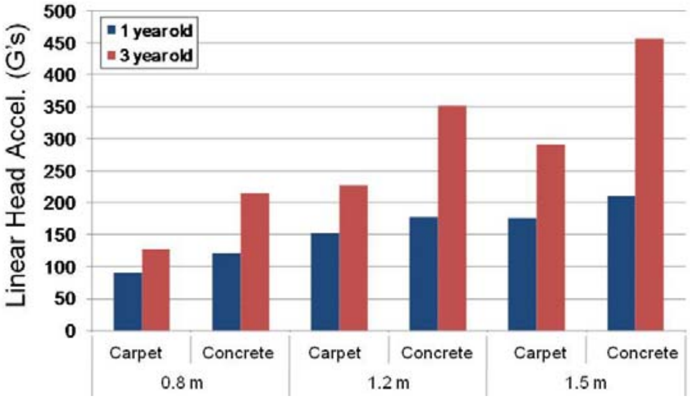

Figure 2: Averaged 1-year-old and 3-year-old peak head linear acceleration data when dropped onto occiput for all conditions.

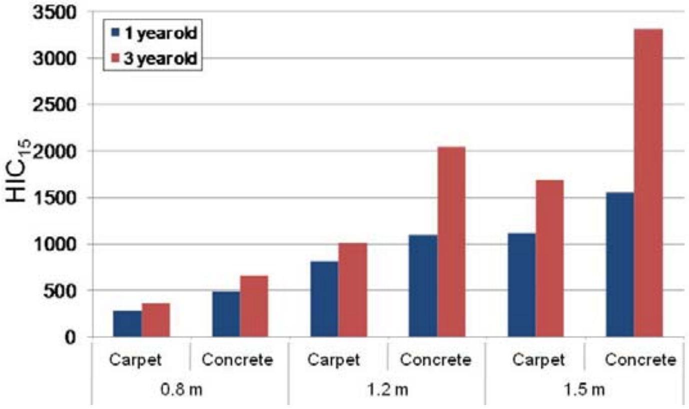

Figure 3: Averaged 1-year-old and 3-year-old HIC$_{15}$ when dropped onto occiput for all conditions.

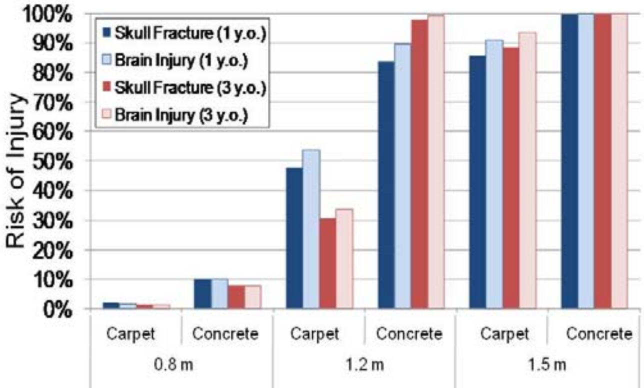

Figure 4: Risk of AIS≥4 brain injury and skull fracture in 1- and 3-year-old children [3].

To estimate injury risk associated with these configurations, the HIC$_{15}$ value for each trial was used to calculate the average corresponding risk of AIS≥4 brain injury in the 1- and 3-year-old populations (Figure 4) [3]. As shown in Figure 4, the 0.8 m (2.5 ft) falls on carpet and concrete resulted in minimal risk of brain injury and skull fracture (≤10%). A moderate risk of head injury (30%-55%) was associated with the head accelerations from a 1.2 m (4 ft) fall onto a carpet surface. Falls from 1.5 m (5 ft) onto carpet and concrete and falls from 1.2 m (4 ft) onto concrete produced a high risk of brain injury and skull fracture (>80%). As shown in Figure 3, five conditions (all but 0.8 m carpet) resulted in HIC$_{15}$ values above the Injury Assessment Reference Value (IARV) used in automotive safety testing in both the 1-year-old and 3-year-old ATD[3].

Although falls from relatively short heights do have the potential to cause brain injuries in small children, it is well known that children often fall from similar heights while sustaining only minor injuries. Fall orientation plays a large role in determining the risk of head injury in a short fall. This study focused on a severe scenario where the head was the first point of contact with the ground. Lower accelerations would occur if a child would strike another part of his/her body such as their buttocks, chest, or extremities prior to head contact from the heights investigated [4].

CONCLUSIONS

Depending on the circumstances including a child's age, fall orientation, fall height, and landing surface, even falls from short distances may result in serious injuries in 1- and 3-year-old children.

REFERENCES

1. Borse N.N. et al. *CDC Childhood Injury Report*, Atlanta, GA: CDC, NCIPC, 2008.
2. Plunkett J. *Am J Forensic Med and Pathol*, **22**(1), 1-12, 2001.
3. Mertz H.J. et al. *Stapp Car Crash Journal*, **47**, 155-188, 2003.
4. Bertocci G.E. et al. *Arch Pediatr Adolesc Med*, **157**, 480-486, 2003.

ACKNOWLEDGEMENTS

This work was funded by Exponent Failure Analysis Associates.

GENDER DIFFERENCES IN HEAD IMPACT ACCELERATION IN COLLEGIATE ICE HOCKEY

[1]Lindley L. Brainard, [1]Jonathan G. Beckwith, [1]Jeffrey J. Chu, [3]Joseph J. Crisco, [4]Thomas W. McAllister, [4]Ann-Christine Duhaime, [4]Arthur C. Maerlender, [5]Stefan Duma, [6]Gunnar Brolinson and [1,2]Richard M. Greenwald

[1]Simbex, Lebanon, New Hampshire, [2] Thayer School of Engineering, Dartmouth College, Hanover, New Hampshire, [3]Alpert School of Medicine of Brown University/Rhode Island Hospital, Providence, Rhode Island, [4]Dartmouth Medical School, Lebanon, New Hampshire, [5]Virginia Tech, Wake Forest Center for Injury Biomechanics, Blacksburg, Virginia, [6]Edward Via College of Osteopathic Medicine, Blacksburg, Virginia
Email: lbrainard@simbex.com, Web: http://www.simbex.com

INTRODUCTION

In 2003, the Center for Disease Control and Prevention concluded that over 1.2 million instances of sports related mild traumatic brain injury (mTBI), or concussion, are reported annually in the United States, with the actual number of injuries probably much higher due to under-reporting [1]. Athletes participating in helmeted sports at the collegiate level are frequently exposed to direct head impacts, creating a unique cohort of subjects to study the relationship between impact exposure and concussion. Epidemiological studies of collegiate athletes have suggested concussion rates for females are higher than their male counterparts [2]. There are no data available comparing head impact exposures between male and female athletes. Head Impact Telemetry (HIT) technology (Simbex, Lebanon NH) was developed to measure the location and severity of head impacts sustained during helmeted team sports without affecting play. This technology previously has been used to quantify head impacts sustained by junior level male hockey players [3] and provides an ideal method for exploring the role of gender with respect to mTBI. This study aims to quantify the differences in severity and location of head impacts experienced by male and female collegiate ice hockey players.

METHODS

On-ice head impact data from 3 NCAA Division I hockey teams (one male, two female) were collected from every practice and competition, defined as contact sessions, during the 2008-2009 season. Participating athletes wore helmets equipped with 6 single-axis accelerometers which measure and record head impacts in real-time [4]. Data collected from the helmets were post-processed to compute linear and angular acceleration of the head as well as impact location. All impacts were categorized into one of five location groups (Top, Left, Right, Back and Front). Two-sample t-tests ($\alpha = 0.05$) were conducted to assess differences by gender for impact frequency, impact location, and maximum recorded peak linear and angular acceleration.

RESULTS AND DISCUSSION

A total of 9,790 impacts were collected from 41 female and 10 male hockey players. Female and male athletes participated in 111 ± 17 and 95 ± 5 contact sessions, respectively, where the mean number of impacts sustained by female subjects during each session was significantly lower than males (1.5 ± 0.7 vs 3.2 ± 1.4, $p < 0.001$). Male

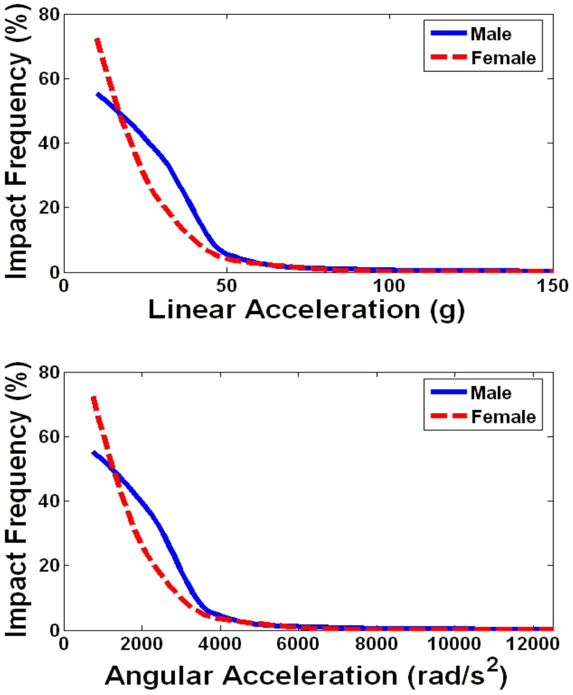

Figure 1: The frequency of more severe impacts was higher in male hockey players than in female hockey players.

hockey players had higher resultant linear and angular head accelerations than female hockey players (Figure 1). Distributions of impacts by peak linear and peak angular acceleration were not normally distributed, with 95% of all impacts less than 50g and 5,183 rad/s^2 for males, and less than 45g and 3,786 rad/s^2 for females. The top 1, 2, and 5 percentiles of all impacts, for both linear and angular acceleration, were significantly higher ($p < 0.001$) for males than females (Table 1).

Multiple t-tests were performed to compare impact locations by gender. The frequency of impacts by location was the same between male and female subjects ($p > 0.22$) for all locations except the top of the head, where males received fewer impacts than females (Figure 2). The highest percentage of impacts for both men and women occurred to the front and back of the head (Front - 32%M, 28%F; Back - 36%M, 33%F), while impacts to the Top (3%M, 9%F) were relatively infrequent, compared to the other locations.

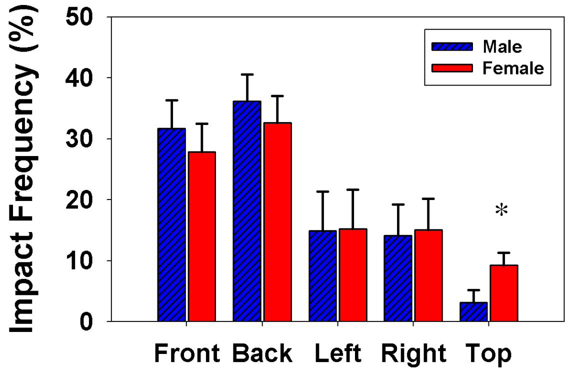

Figure 2: Frequency of head impacts by location for male and female collegiate hockey players. (* $p < 0.05$)

The differences in impact frequency and magnitude between male and female hockey players could reflect differences in speed, body weight, and allowable contact in the respective games. The similarity of impact location distribution between gender may simply be a characteristic of the sport of hockey. It is important to note that these impact data do not necessarily correlate with resultant anatomic or functional tissue injury or symptomatology, which likely depends on a complex interaction between host and biomechanical factors, including brain mass and physiology.

CONCLUSIONS

Male athletes sustained higher numbers of head impacts per session with higher head acceleration than their female counterparts. The relationships among head impact biomechanical variables and the incidence and severity of concussions are unknown. Understanding the intrinsic and extrinsic risk factors that differentiate head impact biomechanics experienced by male and female athletes may lead to increased understanding of the mechanisms causing concussion and other long-term effects, which in turn could lead to improved standards, equipment design and guidelines for diagnosing and treating concussions on an individual basis.

REFERENCES

1.Gerbeding JL et al. *Center for Disease Control and Prevention.* 1-5, 2003.
2.Agel, J et al, *Journal of Athletic Trainers.* 42(2), 249-254, 2007.
3.Mihalik, JP et al. *Journal of Sports Engineering and Technology.* 222(Part P.), 45-52, 2008.
4.Crisco, JJ et al. *Journal of Biomechanical Engineering* 126, 849-854, 2004.

ACKNOWLEDGEMENTS

Research for this study was funded by the National Center for Medical Rehabilitation Research at the National Institute of Child Health and Human Development at the National Institutes of Health (Grant R01HD48638) and the National Operating Committee on Standards for Athletic Equipment (Grant 04-07).

Table 1: Male hockey players sustained head impacts with higher peak linear and angular acceleration than female hockey players. The top 1, 2 and 5 % of all impacts were higher for males than females (*$p < 0.001$).

	Male Hockey (Total Impacts = 3,052)				**Female Hockey (Total Impacts = 6,747)**			
	Linear Acc. (g)		**Angular Acc. (rad/s^2)**		**Linear Acc. (g)**		**Angular Acc. (rad/s^2)**	
	Mean	Range	Mean	Range	Mean	Range	Mean	Range
***Top 1 %**	128±20	≥ 101	13069±1931	≥ 10250	93±22	≥ 72	8204±2193	≥ 6382
***Top 2 %**	108±26	≥ 78	11007±2556	≥ 7975	80±20	≥ 62	6928±2011	≥ 5183
***Top 5 %**	80±29	≥ 50	8373±2742	≥ 5183	63±19	≥ 45	5395±1812	≥ 3786

SEGMENT COORDINATION RESPONSE TO ALTERATIONS IN FOOT STRIKE PATTERN

Allison H. Gruber, Elizabeth M. Russell, Ross H. Miller, Ryan Chang, Joseph Hamill
Biomechanics Laboratory, University of Massachusetts, Amherst, MA
Email: agruber@kin.umass.edu Web: www.umass.edu/biomechanics/

INTRODUCTION

The timing and magnitude of segment rotations during running have been investigated as possible mechanisms for lower extremity injury. The relative timing, or coordination, of foot and shank rotations is mechanically linked due to the anatomy of the subtalar joint. Bates et al. suggested a disruption in timing between calcaneal eversion and internal tibial rotation may cause excessive knee joint stress [1]. Compared to the rearfoot (RF) strike pattern, the forefoot (FF) strike pattern has been characterized by greater rearfoot inversion at touchdown forcing the rearfoot to rotate through greater eversion excursion and excursion velocities [2]. Greater eversion excursion has been found to correlate with greater tibial internal rotation excursion; a mechanism that may increase stress to the soft tissue of the knee [3]. Due to these factors, those who naturally run with a FF strike pattern may be predisposed to knee injury. Runners may be instructed to switch strike patterns depending on the type of injury to which they are predisposed.

Dynamical systems techniques, such as vector coding, quantify the continuous spatial coordination between segment rotations and may reveal a richer set of kinematic information than more traditional discrete analyses. Therefore, the purpose of this study was to quantify adjustments in shank and foot coordination via a modified vector coding technique when runners change from their preferred to an alternate strike pattern.

METHODS

Ten natural RF strike runners (6 males, 4 females, age = 28±4 yrs, mass = 67.86±9.36 kg, height = 1.72±0.12 m) and 4 natural FF strike runners (4 females, age = 27±6 yrs, mass = 63.79±9.74 kg, height = 1.68±0.05 m) participated in this study. RF strike was defined as landing on the heel. FF strike was defined as landing on the forward section of the foot or toes without the heel making contact with the ground. Each subject gave approval for participation in accordance with University IRB policy.

Reflective markers were placed on the leg and foot of the right limb. Three-dimensional (3D) motion was recorded with an eight camera motion capture system operated at 200 Hz. Subjects ran on a treadmill at their preferred running speed (RF runners = 3.02 ±0.45 m/s, FF runners = 2.91±0.21 m/s) with their preferred and the alternate strike pattern for 5 minutes. Kinematic data during the last minute of each condition was used to calculate 3D lower extremity segment angles using a right-hand orthogonal Cardan Xyz rotation sequence. Segment angles were referenced to the lab coordinate system. Phase angles (γ) were derived by a vector drawn between two adjacent time points on an angle-angle plot of shank internal/external (IR/ER) segmental rotation and foot segment inversion/eversion (INV/EV)[5].

$$\gamma_i = \tan^{-1}[(y_{i+1}-y_i)/(x_{i+1}-x_i)]$$

Phase angles were drawn relative to the right horizontal and categorized into one of four coordination patterns (Table 1) [6]. Mean phase angles were determined by circular statistics and averaged over early (1-33%), mid (34-66%), late stance (67-99%). Effect sizes (ES) were calculated to assess differences between groups.

Table 1: Phase angle categories

Coordination Pattern	Coupling Angle Definition
Anti-phase (i)	$112.5^\circ \le \gamma < 157.5^\circ$ $292.5^\circ \le \gamma < 337.5^\circ$
In-phase (ii)	$22.5^\circ \le \gamma < 67.5^\circ$ $202.5^\circ \le \gamma < 247.5^\circ$
Exclusive shank segment rotation (iii)	$0^\circ \le \gamma < 22.5^\circ$, $157.5^\circ \le \gamma < 202.5^\circ$, $337.5 \le \gamma \le 360^\circ$
Exclusive foot segment rotation (iv)	$67.5^\circ \le \gamma < 112.5^\circ$ $247.5^\circ \le \gamma < 292.5^\circ$

RESULTS AND DISCUSSION

Rearfoot Running When running with a rearfoot strike pattern, FF runners exhibited greater maximum INV (ES=0.7) and foot excursion (ES=0.9) than RF runners. Rearfoot running resulted in greater maximum foot EV (RF ES=0.7; FF ES=1.3) and increased shank IR (RF ES=0.3; FF ES=0.3) for both groups. The pattern of coordination was different between groups indicated by differences in mean phase angle for mid (ES=0.9) and late stance (ES=0.7) (Figure 1a). Both groups began with an in-phase coordination pattern but FF runners had an abrupt shift in coordination while the shift for RF runners was more gradual. RF runners had anti-phase and exclusive foot segment rotation coordination patterns for mid and late stance respectively whereas FF runners had exclusive shank segment rotation and in-phase coordination patterns.

Forefoot Running There was no difference in segment angles, excursion, or coordination patterns between groups when running with a forefoot strike pattern. RF runners altered their coordination pattern from anti-phase to exclusive foot rotation during mid stance compared to the rearfoot running condition (ES=1.2). FF runners also altered coordination from in-phase in rearfoot running to exclusive foot segment coordination in mid stance during forefoot running (ES=0.8) (Figure 1b).

CONCLUSION

All subjects experienced greater maximum foot EV during the rearfoot running condition which may contribute to increased stress to the knee. Forefoot running resulted in foot EV without shank IR (exclusive foot rotation) which is not consistent with the segment interaction suggested by Bates et al [1]. Rearfoot and forefoot strike patterns had fundamentally different coordination patterns. RF runners were able to match the coordination pattern of the FF runners during the forefoot strike pattern but FF runners were not able to match the coordination pattern of RF runners during the rearfoot strike pattern. These differences may not have been realized with traditional kinematic analysis.

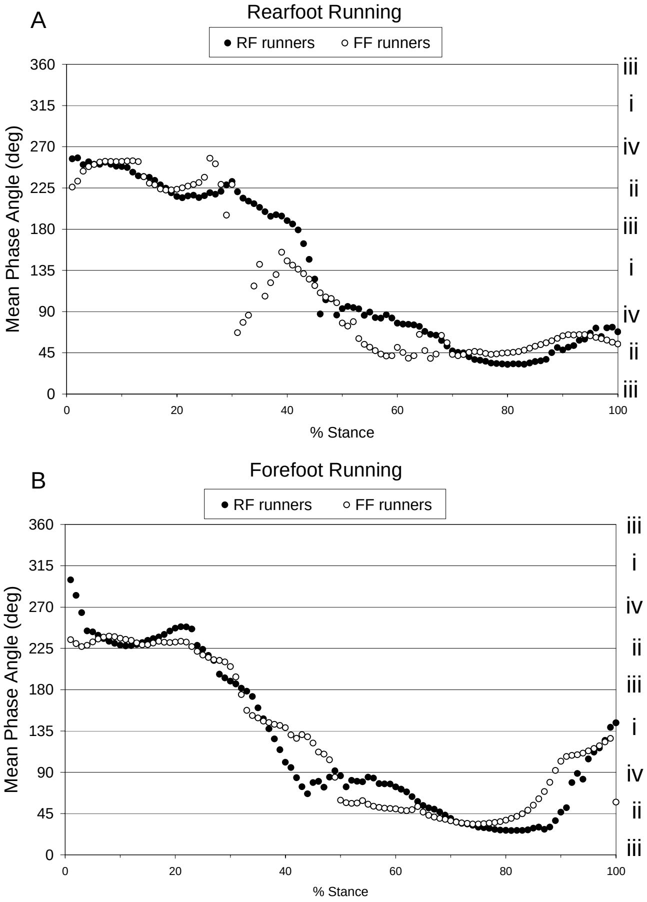

Figure 1: Mean phase angle between foot EV/INV and shank IR/ER during (A) rearfoot running and (B) forefoot running. Refer to Table 1 for coordination pattern definitions of (i) anti-phase, (ii) in-phase, (iii) exclusive shank rotation, and (iv) exclusive foot rotation.

REFERENCES

1. Bates BT, et al. *Running*, 1978; Fall: 24-31.
2. Stackhouse, et al. *Clin Biomech*, **19**, 64-70, 2004.
3. McClay I, Manal K. *Clin Biomech*, **13**, 195-203, 1998.
4. Oakley T, Pratt DJ. *Clin Biomech*, **3**, 159-165, 1988.
5. Heiderscheit et al. *J App Biomech*, **18**, 110-`21, 2002.
6. Chang R, et al. *J Biomech* **41**, 3101-`05, 2008.

A LARGE SCALE OPTIMIZATION APPROACH TO GENERATE SUBJECT-SPECIFIC KNEE JOINT MODELS

[1, 2] Bhushan S. Borotikar, [1]Antonie J. van den Bogert
[1] Department of Biomedical Engineering, Cleveland Clinic, Cleveland, OH, [2]Department of Chemical and Biomedical Engineering, Cleveland State University, Cleveland, OH
Email: borotib@ccf.org, Web: http://www.lerner.ccf.org/bme/bogert/

INTRODUCTION

When considering the use of computational joint models in clinical applications such as injury prevention or treatment planning, it becomes important that the model represents the joint mechanics of a specific subject [1]. While geometry of the joint structures (ligaments and articular surfaces) can be measured non-invasively by imaging techniques, this is not the case for their mechanical properties. Only indirect information is available via whole joint mechanical testing.

It has been previously shown that knee joint mechanics is relatively insensitive to cartilage load-deformation properties [2]. Ligament resting lengths, on the other hand, are a critical parameter which can not be measured from imaging data with sufficient accuracy. Here we present a novel efficient optimization method that can find model parameters for a 3D knee joint model from a large set of whole joint load-deformation measurements.

METHODS

Mechanical testing was performed on five cadaveric knee specimens using a six degree of freedom motion platform (R2000, Parallel Robotic Systems Corp., Hampton, NH) and an in-house developed software interface in LabVIEW (National Instruments Corp., Austin, TX). Tibiofemoral rotation and translation were measured in each specimen at four flexion angles (0^0, 15^0, 30^0, and 45^0) during application of internal-external moment ($\pm$5Nm in steps of 1Nm), varus-valgus moment ($\pm$10Nm in steps of 2.5Nm) and anterior-posterior drawer force ($\pm$100N in steps of 10N), a total of 192 loading conditions including 40 neutral loading conditions recorded in between the switchover from one loading direction to another.

Each specimen was imaged using MRI (OrthOne 1.0T scanner, ONI medical systems, Wilmington, MA). Computational tibiofemoral knee joint models were generated using the modeling techniques and parameters already discussed in [1]. Plastic screws were embedded in medial and lateral epicondyles of the tibia and the femur of each specimen to ensure minimal error between the coordinate systems of the experiment and the corresponding joint model. The model was implemented using existing software for 3D quasi-static joint modeling [3].

Our optimization goal was to find the 12 ligament line element resting lengths that minimize the difference between the simulated and measured tibiofemoral kinematics (3 translations and 2 rotations for each loading condition). The original joint model software [3] was designed to solve the equilibrium positions and orientations of the moving rigid bodies and particles with respect to the ground rigid body as an output. To customize the model for our optimization approach, the joint model software was accessed via the MATLAB MEX-function interface to provide the force imbalance (*GF*) of the bodies as an output for the applied external loading condition (*i*) and initial rigid body positions as an input such that,

$$C_i = GF\,(K_i) \qquad (1)$$

where K_i = model position/orientation variables for moving rigid bodies (or particles) at *i*. Analytical derivatives of *GF* with respect to K_i were obtained from the joint model [3]. The objective function that quantifies the model difference with respect to the experiments is given by:

$$f(X) = \sum_{i=1}^{n} (Si - Mi)^2 \qquad (2)$$

where $X = (K_1,\ldots,K_n,P_1,\ldots,P_m)$, P_i = unknown model parameter (resting lengths), M_i = measured kinematic variables for loading condition *i*, and S_i = corresponding kinematic variables in the model, a subset of K_i. This is a large-scale constrained optimization problem which was solved by the TOMLAB/SNOPT solver (http://tomopt.com) to minimize the objective function (2) while satisfying the constraints $C_i = 0$.

In our problem, n = number of loading conditions = 192, m = number of unknown model parameters = 12, M_i = 5 for each loading condition i, and $K_i = C_i$ = 23 for each loading condition i. This required the SNOPT algorithm to solve for (192*23) + 12 = 4428 parameters. We started the optimization with an initial guess of X where all the K_i variables satisfied the static equilibrium conditions $C_i = 0$ for an initial guess of model parameters P_i based on ligament lengths as seen in MRI scans. Results from the first specimen are presented.

RESULTS

The optimization terminated with objective function (2) having an RMS value of 3.4 mm for translations and 6.5° for rotation. Figures 1 and 2 show the model optimization results in comparison with the experimental data for selected kinematic variables. In figure 1, prominent peaks correspond to the internal-external loading conditions whereas in figure 2, the peaks can be identified in the anterior-posterior loading conditions. Kinematics are reported as femur moving with respect to tibia.

DISCUSSION

As can be seen from the figures, the model still appears stiffer than the experiments in the regions where the kinematic parameter is the primary response (peaks) to the isolated loading condition. Incorporating ligament stiffness as optimization parameter might help the model to be more accurate. The model behavior in the secondary response parameter corresponding to the isolated loading condition (e.g. anterior translation in response to rotation torque) does not appear to be in qualitative agreement with the experiments. Sensitivity analysis pointed towards ligament insertion points being responsible. With a rich multi-dimensional load-deformation dataset such as we have used, we expect it will be feasible to improve the model by including the ligament stiffness and ligament insertion points as optimizing parameters along with the ligament resting lengths.

The model optimization presented here required 10 hours of computation time. A traditional small scale unconstrained optimization in which only the ligament resting length parameters are optimized would take approximately 58 to 60 hours to reach the same level of optimality because at each parameter guess, equilibrium must be solved at all loading conditions. This introduces high computational cost and potential convergence problems.

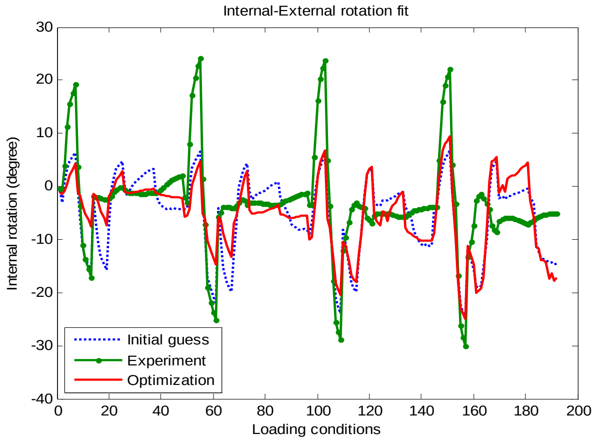

Figure 1: Comparison between the optimized model and measured Internal-External rotations.

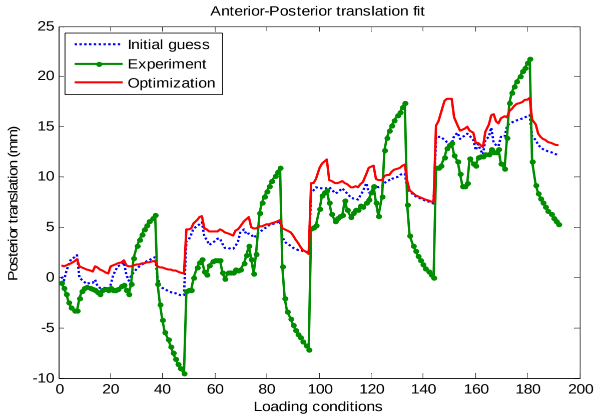

Figure 2: Comparison between the optimized model and measured Anterior-Posterior translation.

REFERENCES

1. Borotikar BS et al. *Proceedings of 30th Annual Meeting of ASB*, Blacksburg, VA, Abstract 328, 2006.
2. Blankevoort L, Huiskes R. *J Biomech* **29**, 955-961, 1996.
3. Kwak SD et al. *Comp Meth Biomech Biomed Engg* **3**, 41-64, 2000.

ACKNOWLEDGEMENTS

This study is supported by an ISB Dissertation grant and NIH grant R01 AR049735. We also gratefully acknowledge the help and support from Dr. Blankevoort and thank Columbia University for providing the source code for the joint model software.

THE INFLUENCE OF FORCE LOADING PATTERNS ON HEEL PAD PROPERTIES

[1,2] Daniel J. Gales and [1]John H. Challis
[1] Biomechanics Laboratory, Department of Kinesiology, The Pennsylvania State University, University Park, PA, USA
[2] Lock Haven University of Pennsylvania, Lock Haven, PA, USA
E-mail: djg153@psu.edu

INTRODUCTION

Research examining the temporal characteristics of gait have reported that the stride time intervals during walking [1] and running [2] demonstrate long term correlations. Therefore, the stride interval times are not normally distributed but have fractal like properties. Jordan et al. [2] showed that long term correlations are present in the vertical ground reaction forces in subject running. Research examining the influence of time intervals on the properties of human pad indicated that physiologically realistic time intervals between loadings do influence the properties of the human heel pad, conferring some advantage in its ability to attenuate the forces associated with loadings [3].

No study to date has reported the mechanical properties of the human heel using time series force loading profiles which reflect actual ground reaction patterns. Therefore the purpose of this study was to compare the mechanical properties of heel pads in cadaver specimens using a servo-hydraulic compression device with time series force loading profiles which reflect the vertical ground reaction forces experienced in vivo.

METHODS

To obtain realistic loading patterns for the cadaver heel pads eleven injury free runners were recruited; each ran on an instrumented treadmill at their preferred running speed for eight minutes. The treadmill had two force plates under the belt; these plates permitted determination of the vertical ground reaction forces. The force profile for one representative subject was used as the force profile when the cadaver heel pads were tested. Examination of the impact peak ground reaction forces using the Detrended Fluctuation Analysis [4] showed the presence of long-term correlations.

Eight fresh-frozen cadaver feet were thawed to room temperature before completing all procedures. All tissues superior to a 45 mm horizontal line marked on the foot above the uncompressed heel were removed using blunt dissection. Heel pads remained fixed to the calcaneus and the foot and toes and overlying skin remained intact throughout the testing procedures.

Dynamic mechanical testing of the heel pads was completed using a servo-hydraulic material test system (MTS model 858). The MTS was operated in force control mode and programmed to compress these specimens 400 times to a maximum impact peak force based on subject data, scaled to body weight of each cadaver. Each heel pad was subjected to four impact peak VGRF conditions: minimum in the experimental time series, mean, maximum, and actual (fractal). Therefore, for example, for the minimum condition the heel pads experienced an impact peak force which corresponded to the minimum impact peak force recorded in the experimental data; while in the fractal condition the heel pad experienced loadings which varied in the same way loadings vary during the actual running footfalls (in a fractal pattern). The MTS was programmed to mimic the impact peaks of the representative subject in both the magnitude of the impact peak and the frequency of loading. For all conditions applied force and pad displacement were collected at 10,000 Hz, from which the heel pad deformation, hysteresis, and stiffness at 50% body weight were computed. To avoid potential differences in heel pad properties created during initial loadings the first 10 compressions were ignored.

Statistical comparisons were made between footfalls in the fractal sequence which had the same force levels in the other conditions. For example, if footfall 100 in the fractal condition had the maximum force then the metrics of heel pad properties were compared with the metrics determined during the maximum condition for the same footfall.

RESULTS AND DISCUSSION

Mean and standard deviation maximum forces for each condition were: minimum (680.5 ± 108.4 N), mean (769.4 ± 126.8 N), maximum (885.9 ± 142.0 N), and fractal (770.0 ± 121.8 N). It was anticipated that there would be differences between force conditions. An ANOVA comparing the maximum forces indicates significant differences ($p < 0.001$) between all conditions excluding the comparison between the fractal and mean conditions.

The maximum deformation and stiffness at body weight results indicate significant differences ($p< 0.001$) between all conditions (Table 1). Under the fractal loading condition, the heel pad produced less deformation than the maximum and mean conditions and less stiffness than the mean and minimum conditions (Table 1). These data suggest that the fractal condition provides a firmer impact (greater stiffness and less heel pad deformation) compared to the maximum condition. In addition, the fractal condition produced significantly different results when compared to the mean condition.

Similar to the deformation and stiffness results, hysteresis results indicate significant differences between all conditions with hysteresis increasing with increasing forces (Table 1). Under the fractal condition, hysteresis results indicate significantly less hysteresis compared with the maximum and mean force conditions.

These results indicate that the variations seen in heel pad loadings due to physiologically realistic forces do influence the properties of the human heel pad. It would seem that given that the typical loading patterns on the heel pad are fractal this confers some advantage on the ability of the heel pad in its ability to attenuate the forces associated with loadings.

REFERENCES

1. Hausdorff JM, et al. J Appl Physiol **78**, 349-358, 1995.
2. Jordan K, et al. *Hum Mov Sci* **26**, 87-102, 2007.
3. Gales DJ and Challis JH. *NACOB Meeting*, Ann Arbor, Abstract 638, 2008.
4. Peng CK, et al. *Phys Rev E* **49**, 1685-1689, 1994.

Table 1: Mean and standard deviation of heel pad properties for final 390 compressions of cadaver specimens for each experimental condition. All metrics were significantly different ($p < 0.001$) between conditions.

Condition	**Maximum deformation (mm)**	**Hysteresis (%)**	**Deformation at 50% BW (mm)**	**Stiffness at 50% BW ($N.m^{-1}$)**
Minimum	4.5 ± 1.6	54.2 ± 5.3	4.5 ± 1.6	52.0 ± 23.2
Mean	4.5 ± 1.3	55.7 ± 6.2	4.5 ± 1.3	50.1 ± 19.0
Maximum	4.6 ± 1.4	55.9 ± 6.3	4.6 ± 1.4	48.9 ± 18.6
Fractal	4.6 ± 1.4	54.8 ± 5.0	4.6 ± 1.4	49.1 ± 18.8

EXPANDING THE POTENTIAL OF CINE PC MRI IN TRACKING MUSCULOSKELETAL MOTION

Abrahm J. Behnam, Nicole A. Wilson and Frances T. Sheehan
Rehabilitation Medicine, National Institutes of Health
email: gavellif@cc.nih.gov

INTRODUCTION

The rising cost of musculoskeletal pathologies, disease and injury create a pressing need for accurate and reliable methods to quantify 3D musculoskeletal motion. For this reason, there has been a renewed interest in this area over the past few years [1-3]. Unfortunately, the majority of the current techniques available for studying skeletal kinematics are fluoroscopic in nature, which expose the patient to ionizing radiation and are incapable of measuring muscle function. Ultrasound eliminates the need for ionizing radiation and can track muscle motion, yet remains primarily 2D and cannot accurately track 3D skeletal kinematics. Cine-phase contrast (PC) MRI remains the only imaging technique with the ability to non-invasively track 3D musculoskeletal motion during volitional activity, but current scan times are long (~2.5 minutes). Minimizing these scan times will broaden the spectrum of potential patients that can be studied. Therefore, the purpose of this study was to validate the use of cine-PC MRI for quantifying musculoskeletal motion on a 3.0T platform and to determine if scan time can be reduced.

METHODS

The ability to track 3D musculoskeletal motion was assessed by quantifying the accuracy and precision of cine-PC MRI, using the 3.0T platform. To quantify accuracy a motion phantom, similar to one previously described [4], was constructed. The phantom moved a sample box containing 1:10 of CuSo4 in a 0.6% agarose gel solution, mimicking the T1 MRI properties of bone. Four holes were milled in the box and plastic rods were inserted through the holes to create MRI signal voids (fiducials). The motion phantom was placed in a 3.0T Philips MR scanner (Philips Medical Systems, Best, NL) and aligned with the scanner's axial plane. Standard 2-element flexible coils were placed left-right (LR) and anterior-posterior (AP) of the phantom, respectively. A pole extended from the phantom, which a single researcher used to move the sample box in a circuitous path at 30 cycles/min (guided by an auditory metronome). Movement was confined to the axial plane [4].

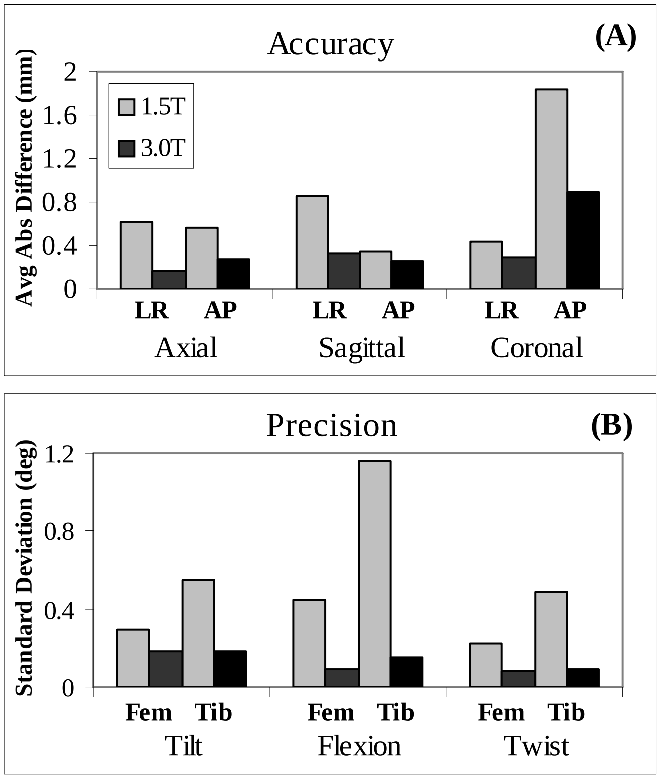

Figure 1: Comparison of in-plane accuracy and precision between 1.5T [6] and 3.0T platforms for two data averages.

Cine-PC images were acquired in all three cardinal planes using two data averaging and no data averaging (scan time = 2.06 and 1.08 minutes, respectively). All other imaging parameters [TR (6.8 msec), TE (3.4 msec), spatial resolution ($0.47mm^2$), flip angle (20 deg), temporal resolution = 81.6 msec] remained constant. Because phantom motion was confined to the axial plane, there were large out-of-plane motions when data was acquired in the sagittal and coronal planes. The corresponding out-of-plane directions were the RL and AP-directions. Regions of interest (ROIs) were visually identified within the boundaries of the sample box in the first frame. Their trajectories were then computed in 3D space through integration of the velocity data.

For comparison, high spatial and temporal resolution cine images (no velocity) were acquired in the axial plane [TR (4.1 msec), TE (1.2 msec), spatial resolution (0.25mm^2), temporal resolution = 4.1 msec]. Using these images, the centroid of each fiducial was visually identified in each frame using ImageJ (NIH, Bethesda, MD). Accuracy was defined as the average absolute difference in the ROI's trajectory calculated through: (1) integration of the velocity data and (2) visual tracking of the fiducials.

To quantify precision, a 3D dynamic cine-PC MR image set (x,y,z velocity and anatomic images using a sagittal-oblique imaging plane) was acquired during cyclic knee flexion/extension in 12 healthy subjects, placed supine in the same 3.0T MR imager [4]. Cine images were also acquired in three axial planes to establish anatomical coordinate systems. Kinematics of the femur, tibia and patella were quantified via integration of velocity data. Precision (the variability associated with tracking *in vivo* skeletal motion using velocity integration) was defined as the standard deviation of the kinematics, derived in 10 independent analyses of the same image set. The mean precision was calculated for the femur and tibia across subjects.

RESULTS

Using cine-PC on the 3.0T platform (2 data averages) reduced imaging time by 25% (42 seconds) over the 1.5T platform and improved accuracy, on average by 50% (0.41 mm, Figure and Table 1A). No data averaging reduced imaging time by 47% (100 seconds) over the 1.5T platform with improved accuracy (38% or 0.33 mm). Precision improved on average by 72% for both the femur and tibia for *in vivo* skeletal motion (Figure and Table 1B).

DISCUSSION

Given the variety of techniques that quantify skeletal motion *in vivo*, cine-PC MRI is ideal for this task due its ability to simultaneously quantify 3D skeletal and muscular motion. In addition, it is non-invasive and non-ionizing. The 3.0T platform further enhances cine-PC MRI by improving scan time, accuracy and precision. On the 3.0T platform, it is possible to reduce scan time to 1 minute while maintaining superior accuracy and precision [2].

For most musculoskeletal cine-PC MRI studies, using proper imaging alignment can create small out-of-plane rotations and translations (e.g. ~4.5^o and ~5.1 mm for the knee). Yet, motion phantom excursions in the AP and RL directions are 25 mm and 18 mm, respectively [4]. Therefore, the phantom harshly represents the accuracy of tracking in vivo skeletal motion and the sagittal and axial plane data (accuracy < ~0.4 mm in all directions) is the best representation of realistic *in vivo* motion. Large out-of-plane motions, similar to the coronal plane data, were only seen in a few of the worst patellofemoral maltrackers [5].

With scan time reduced to only one minute and dramatic improvements in both accuracy and precision, 3.0T cine-PC MRI is a robust technique for tracking *in vivo* musculoskeletal motion. The reduced scan time of 1 minute broadens the potential patient population to include those with limited movement abilities.

REFERENCES

1. Fregly BJ et al. *J Biomech Eng* **127**, 692-9, 2005.
2. Tashman et al. *J Biomech Eng* **125**, 238-45 2003.
3. Shih YF et al. *Am J Sports Med* **32**, 1209-7, 2004.
4. Sheehan et al. *J Biomech* **31**, 21-26, 1998.
5. Sheehan et al. *J Orthop Res* **466**, 450-8, 2008.
6. Sheehan et al. *J MRI* **17**, 206-213, 2003

Table 1A: Accuracy (mm) for phantom motion.

	2 Averages		**No Averages**	
	Left-Right	**Posterior-Anterior**	**Left-Right**	**Posterior-Anterior**
Axial	*0.16	*0.28	*0.57	*0.38
Sagittal	0.33	*0.25	0.36	*0.14
Coronal	*0.29	0.89	*0.36	0.85

* in-plane directions of motion.

Table 1B: Precision (°) for in vivo skeletal motion.

	Flexion	**Int / Ext Rotation**	**Varus / Valgus**
Femoral Displacement	0.09	0.18	0.08
Tibial Displacement	0.15	0.18	0.09

ANTICIPATORY EFFECTS ON FRONTAL PLANE HIP KINEMATICS DURING CUTTING MOVEMENTS

[1]Ryan Mizell, [1] Chris J. Hass, [1] Ronald Siders, and [1] Mark D. Tillman
[1]University of Florida
email: rmizell@ufl.edu

INTRODUCTION

The anterior cruciate ligament (ACL) prevents anterior displacement of the tibia with respect to the femur [1]. Occurring primarily under noncontact conditions, females tear their ACL four to six times more frequently than males [2]. Injury to the ACL primarily occurs during a unilateral stance phase where the support leg is internally rotated and adducted at the hip, internally rotated and abducted at the knee, and an everted ankle [3]. This dangerous alignment is usually produced during the early decelerative phase of one leg landings, planting and cutting, or sudden stops [3].

Although researchers have made gender comparisons during anticipated conditions *or* under unanticipated conditions, there have been no published studies comparing cutting maneuvers between genders during anticipated *and* unanticipated conditions. Therefore, the purpose of this study was to compare frontal plane kinematics of the hip at initial contact (IC) and peak of early decelerative phase (Peak) during anticipated and unanticipated conditions.

We hypothesized that the unanticipated condition would produce a potentially more dangerous alignment regarding ACL function to the anticipated conditions.

METHODS

For this study, 18 participants (11 males and 7 females) were recruited. Three dimensional motion analysis was performed using a Vicon MX system collecting data at 240 Hz and a Bertec force plate collecting at 2400 Hz.

Prior to participating in the study, all participants read and signed an Informed Consent form. For this experiment, participants performed a side cut, run, or crossover cut under anticipated and unanticipated conditions. To be analyzed, each trial had to meet the following criteria: the cutting angle between 35° to 60°, the right foot on the force plate, an approach speed of 5.5 to 7.0 meters per second (m/s), and performance of correct cutting movement. The speed of each participant was monitored by Basler electronic timing gates, and cones were placed on the floor to insure that the movement was performed at the correct angle.

The trials were performed under two conditions: anticipated and unanticipated. For the anticipated condition, the participant was informed which maneuver to perform prior to the approach towards the force plate. For the unanticipated condition, the participant was given a signal from a light system during the approach towards the force plate. The timing of the signal was specifically calibrated to each participant prior to beginning the testing. Each participant performed 30 random trials consisting of five trials each of left, straight, or right under the two conditions.

Vicon Nexus software was used to quantify joint kinematics. Stance phase was defined as the time when vertical GRF was greater than 10 N. Each trial was time normalized to 100% of stance phase and was linear interpolated to 101 data points.

Two separate 2 (gender) x 2 (direction) x 2 (condition) ANOVA were performed on the frontal plane joint angles of the hip at IC and at the Peak. The early decelerative phase was defined as initial contact to 20% of stance phase [3].

RESULTS AND DISCUSSION

Results indicated that gender differences exist in frontal plane kinematics of the hip at IC ($F = 12.53$, $p = .003$) and at Peak ($F = 12.11$, $p = .003$) during cutting maneuvers (Figure 3). Also, frontal plane kinematics differed at IC ($F = 41.74$, $p < .001$) and at Peak (F = 46.90, p < .001) for the direction of movement (Figure 2). Interestingly, no significant differences for the anticipated and unanticipated conditions at IC (F < .01, p = .993) or peak (F < .01, p = .983) (Figure 3).

There were significant differences for gender of frontal plane joint angles at IC and at Peak. At IC, males displayed more hip abduction than females (Figure 2). At Peak, males displayed abduction where females displayed hip adduction (Figure 2). Since movements of the hip can influence movement at the knee, these gender differences may relate to a potential factor in the injury rate discrepancy between males and females. By adducting the hip, female athletes may place the knee in a position more likely to be abducted at Peak. Knee abduction has been documented as a potentially dangerous alignment for ACL tears in males and females [4].

In addition, there were directional differences at IC and at Peak (Figure 3). At IC, the hip was significantly more abducted during a side cut than a crossover cut. At Peak, the side cut produced hip abduction, but the crossover cut produced hip adduction. Similar to the gender differences, hip adduction can lead to knee abduction [4].

Although significant differences were not observed when comparing conditions, subjective inspection seems to indicate that lacking anticipation affected the genders differently (Table 1). Males tended to decrease abduction when performing the side cut, while females tended to increase abduction. However, males tended to increase abduction, while females tended to increase adduction during the crossover cut. Increased in adduction during the crossover cut could produce a more dangerous alignment.

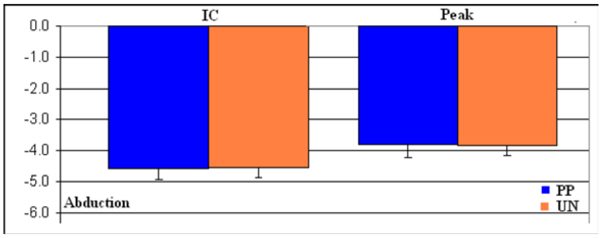

Figure 1: Condition comparisons of hip frontal plane kinematics during cutting at IC and Peak.

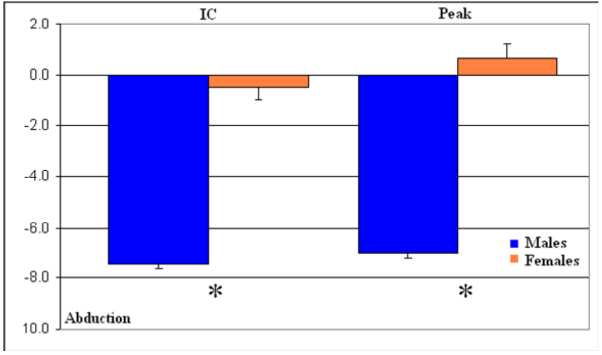

Figure 2: Gender comparisons of hip frontal plane kinematics during cutting at IC and Peak (* significant at p < .05).

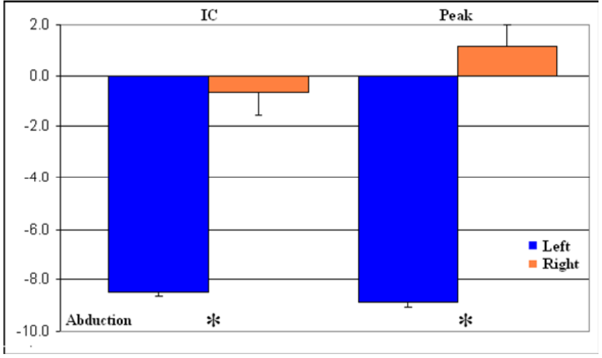

Figure 3: Directional comparisons of hip frontal plane kinematics during cutting at IC and Peak (* significant at p < .05).

REFERENCES

1. Girgis FG, et al. *Clin Orthop* **106**, 216-231, 1975.
2. Arendt EA, et al. *AJSM*, **23**, 694-701, 1995.
3. Boden BP, et al. *Othoped*, **23**, 573-578, 2000.
4. Hewett TE, et al. *AJSM*, **33**, 492-501, 2005.

Table 1: Frontal plane joint angles of the hip during different directions and conditions of cutting movements at IC and Peak. Preplanned (PP) Unanticipated (UN)

	Initial Contact				**Peak of Early Decelerative Phase**			
	Left		Right		Left		Right	
	PP	UN	PP	UN	PP	UN	PP	UN
Males	-11.3 ± 4.6	-10.7 ± 6.2	-3.8 ± 4.9	-4.0 ± 5.0	-12.1 ± 4.5	-10.6 ± 6.5	-1.8 ± 5.6	-3.5 ± 5.3
Females	-3.7 ± 3.9	-5.9 ± 6.9	3.1 ± 5.0	4.8 ± 3.6	-3.8 ± 6.1	-6.7 ± 8.9	5.2 ± 5.8	8.0 ± 2.8

RELATIONSHIP BETWEEN CLINICAL AND BIOMECHANICAL MEASURES OF HAND FUNCTION

[1] Shinichi Amano, [2]Jay Alberts, [2]Sarah Richardson, [1]Douglas Doidge, [1]Jessica Joyner, and [1]Chris Hass
[1]University of Florida, [2]Cleveland Clinic
E-mail: samano@ufl.edu

INTRODUCTION

Impaired upper extremity and hand function are major debilitating factors for the performance of activities of daily living (ADL) in aging and disabled populations. Typically, function has been evaluated clinically using standardized performance tests such as the Box and Block test (BBT) and coin rotation tasks. While informative, these tests measure hand function in global terms and in isolation of functional motor performance. In general, clinical tests of manual function are more concerned with movement quantity as opposed to movement quality. Conversely, the precise control of muscle forces is an elementary component of skilled movement production and its quantitative assessment provides insight into the control and coordination of voluntary hand movements. Further, Kilbreath et al. revealed that approximately 54% of ADL's involve bimanual tasks [1]. Thus, a more specific and functionally relevant assessment protocol may be needed.

The purpose of this study is to compare performance on the clinical unimanual tasks that are commonly used to assess manual dexterity to a more objective, functionally relevant and quantifiable bimanual dexterity paradigm. The paradigm was designed to replicate the performance of many ADLs (i.e. opening a container or buttoning a shirt) in which one hand functions to stabilize the object while the other hand performs some manipulation of the object. The bimanual dexterity system is equipped with force\torque transducers to measure grasping forces produced by both hands simultaneously.

METHODS

Eighteen right-handed (RH), 12 left-handed (LH), and seven ambidextrous (AM) healthy college students, between ages of 18 to 30, participated in this study. Handedness was assessed by a modified version of the Edinburgh Handedness Inventory [2]. Participants were asked to be seated comfortably and to perform both unimanual and bimanual movement tasks. The unimanual tasks consisted of the BBT, a coin rotation task (turning a nickel with thumb, forefinger, and middle), and a lock rotation task (turning a combination lock with a precision grip). Participants were instructed to complete each task as fast as possible and performed the tasks using both their dominant and non dominant hand. The dependent measure for the BBT was the number of the blocks transferred in one minute. For coin rotation and lock rotation tests, the time that participants needed to complete 10 turns was recorded. The average of all three trials was used for statistical analysis.

In the bimanual task, participants were asked to simultaneously grasp the two stacked transducers (Figure 1) with a precision grip, and to separate the top transducer from the bottom one, with one hand on the top and the other hand on the bottom. The transducers were connected via an 8-Newton electromagnetic force. Participants performed this task four times with their dominant hand serving as the manipulating hand (upper transducer) and four trials with their non-dominant hand serving as the manipulating limb. Order of the four trial block was randomized across hands. Movement time (MT), the time interval between the onset of grip force and the time at which the separation of devices occurs, was measured and used with unimanual task scores for statistical analysis.

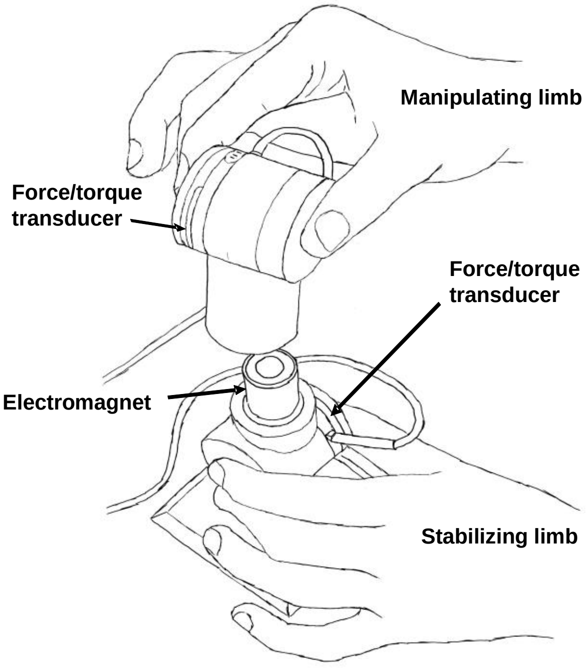

Figure 1: Illustration of bimanual dexterity device. The lower limb serves to stabilize the object while the upper limb acts to manipulate and separate the two objects.

RESULTS AND DISSCUSSION

Performance on the clinical tests and the functional bimanual task were related. Specifically, performance of coin rotation tasks with the dominant hand was significantly related to movement time when the dominant hand was on the upper transducer (RH: r=.515, p=.01, LH: r=.477, p=.04). Although the scores of BBT were not related to MT in both groups, MT and the scores of lock rotation task when using the dominant hand were found to be significantly correlated (RH: r=.395, p=.05, LH: r=.624, p=.01). However, when participants used their non-dominant hand, none of unimanual task scores were significantly correlated with bimanual task performance. The descriptive statistics are listed in Table 1.

Our results indicate that bimanual task performance (MT) clearly correlated well with commonly used functional unimanual tasks when participants used their dominant hand to lift the upper transducer. This suggests the bimanual task measurement used here appears to be valid for estimating upper extremity function. However, careful consideration seems to be required since grip strength is also likely to influence our outcome measures. In this study, we also measured participants' grip strength and compared it to the upper device MT. We found strong correlation between them when participants used their dominant hand to grasp the upper device (RH: r=-.536, p=.01, LH: r=-.548, p=.03). Since the magnet resistance was applied to the transducers in the bimanual task measurement, participants needed to generate enough grip force to lift the upper transducer. Therefore, we need to consider both force modulation and manual dexterity when we study bimanual task performance. Since our bimanual task performance measure correlated with standardized performance tests, and since the force transducers we used can quantify kinematic and kinetic data simultaneously, it has potential to be a more comprehensive measure of manual dexterity than current clinical measures of dexterity.

REFERENCES

1. Kilbreath SL, et al. *Aust J Physiother* **51(2)**, 119-122, 2005
2. Oldfield RC *Neuropsychologia*, **9**, 97-113, 1971

Table 1: Means (SD) of unimanual dexterity scores and bimanual task performance

	BBT (# blocks)		**Coin Rotation (s)**		**Lock Rotation (s)**		**Movement Time (s)**	
	Dominant	Non-Dominant	Dominant	Non-Dominant	Dominant	Non-Dominant	Dominant	Non-dominant
Right-handed	69.6 (9.0)	65.0 (7.9)	6.8(1.2)	8.2(2.3)	9.7(1.9)	11.2 (2.8)	0.69 (0.33)	0.71(0.35)
Left-handed	67.2 (7.1)	66.0(7.2)	7.6(1.5)	8.6(3.5)	12.9(3.1)	12.1(2.2)	0.79 (0.39)	0.79(0.35)

SIMULATION OF GAIT USING A 3D MUSCULOSKELETAL MODEL

Marko Ackermann and Antonie J. van den Bogert
Department of Biomedical Engineering, Cleveland Clinic
email: bogerta@ccf.org, web: http://www.lerner.ccf.org/bme/bogert

INTRODUCTION

Predictive simulation of gait has many applications ranging from the design of assistive devices to the planning of surgical interventions. Unfortunately, the traditional method to solve the resulting optimal control problem, the shooting method, is computationally very expensive. This, associated with the high complexity of current models of the musculoskeletal system, prevents the wider use of predictive simulation of gait in clinical applications. For instance, Anderson and Pandy (2001) reported a computational time of 10000 hours to simulate gait for a 3D model using the shooting method [1].

Direct collocation (DC) has been proposed as a computationally more efficient alternative to the shooting method [2]. We have shown that DC is particularly suited to solve the two point boundary value problem arising from the periodicity constraints in gait using a 2D musculoskeletal model [3]. In this paper we assess the accuracy and computational efficiency of DC when used to simulate gait with a state of the art 3D model.

METHODS

The 3D musculoskeletal model was adapted from [4] and consisted of 8 segments (pelvis, thighs, shanks, feet and wobbling trunk mass) actuated by 86 Hill-type muscle models. Foot-ground contact was modeled by 92 elements distributed over the foot sole with nonlinear spring-damper properties and friction. The model has 214 states $\boldsymbol{x}$ (generalized coordinates and velocities, muscle contractile element lengths and muscle activations) and 86 controls $\boldsymbol{u}$ (muscle excitations).

The optimal control problem was formulated as: for a given gait speed v find trajectories $\boldsymbol{x}(t)$ and $\boldsymbol{u}(t)$ and stride period T that minimize a cost function J subject to constraints due to system dynamics

$$\dot{\boldsymbol{x}} = \boldsymbol{f}(\boldsymbol{x},\boldsymbol{u}) \tag{1}$$

and periodicity

$$\boldsymbol{x}(T) = \boldsymbol{x}(0) + vT\ \hat{\boldsymbol{x}}, \qquad \boldsymbol{u}(T) = \boldsymbol{u}(0), \tag{2}$$

where $\hat{\boldsymbol{x}}$ is the state space unit vector for forward translation.

The optimal control problem was transformed into a Nonlinear Programming Problem (NLP) using direct collocation [5]. Unknowns were T and states and controls at each node k. System dynamics was discretized using the trapezoidal scheme as

$$\frac{\boldsymbol{x}_{k+1} - \boldsymbol{x}_k}{t_{k+1} - t_k} = \frac{\boldsymbol{f}(\boldsymbol{x}_k,\boldsymbol{u}_k) + \boldsymbol{f}(\boldsymbol{x}_{k+1},\boldsymbol{u}_{k+1})}{2}. \tag{3}$$

The method was evaluated on a tracking problem, with cost function consisted of two terms, the first measuring the "distance" between simulated and normative, experimental data, and the second measuring muscle "effort":

$$J = \frac{1}{m(n-1)} \sum_{j=1,k=1}^{m,n-1} \left(\frac{y_{j,k} - \bar{y}_{j,k}}{\sigma_{j,k}} \right)^2 + w \sum_{i=1,k=1}^{86,n-1} \frac{V_i a_{i,k}^2}{V(n-1)} \tag{4}$$

where n is the number of nodes, a is the muscle activation, V is the muscle volume, $\bar{y}$ is reference experimental data (vertical, medial-lateral and posterior-anterior ground reaction forces, position of the pelvis CM and hip, knee and ankle angles), y is the corresponding simulated quantity, σ is a corresponding scaling factor, m is the number of states and grfs considered in the first term, and w is a weight factor.

A walking speed of 1.1m/s was imposed, bilateral symmetry was assumed, and the weight factor in (4) was set to w=1. The NLP was solved by using SNOPT (tomopt.com/tomlab), a sparse sequential quadratic programming solver. The primordial initial guess was obtained by successive unconstrained optimizations where a term was added to the cost function (4) containing the mean squares of the dynamic constraint violations (3) multiplied by a weight factor. The weight factor was gradually increased until dynamic constraints' violations were small enough to allow convergence of the dynamically constrained optimization.

Accuracy was first assessed by mesh refinement, with solutions obtained for 25, 50 and 100 nodes. For further validation, the initial conditions and states from the DC solutions were used as inputs for conventional integration with variable integration step (Matlab ODE23), and results were compared.

RESULTS AND DISCUSSION

Figure 1 shows the solution for three representative variables, right vertical ground reaction force, right hip flexion and right Soleus activation for the three mesh densities. All DC solutions are very similar while the 50-node and the 100-node solutions are virtually identical, which is also indicated by the very similar values of the corresponding optimal cost function values (Tab.1).

The comparison with forward integration results (red lines in Fig.1) shows a significant divergence for the 25-node solution, a small one for the 50-node solution and an excellent agreement between the 100-node DC solution and the corresponding forward integration results. This is also illustrated by the decreasing differences at the end of the simulation as the mesh is refined (Tab.1). The comparison shows that an accurate solution in terms of agreement with forward integration results (100-node solution) can be reproduced using much coarser meshes (50 or even 25 nodes). It also indicates that a 50-node discretization is probably appropriate for most simulations using this model.

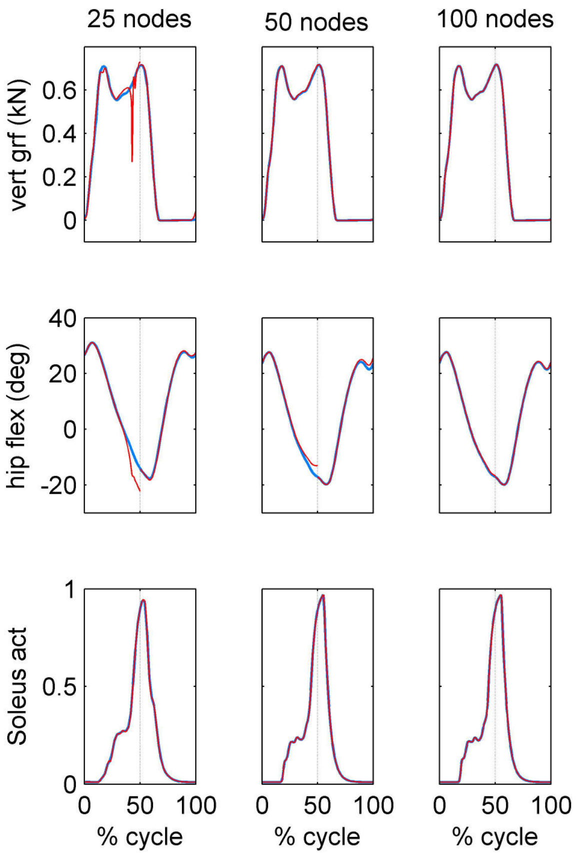

Figure 1: Blue curves are solutions using DC and 3 different mesh densities, 25, 50 and 100 nodes. Red lines are the corresponding results of forward integration using the neural excitations and initial conditions from the DC solutions.

The computation time, including the generation of a feasible initial guess and multiple restarts of the optimizations, was in the order of one week on a personal computer. This compares very favorably to the computational cost reported in other predictive gait simulation studies, most remarkably to the 10000 hours in [1], which used the shooting method and a musculoskeletal model of similar complexity.

This study shows that direct collocation is an accurate and computationally more efficient alternative to other methods for predictive simulation of gait using realistic, complex musculoskeletal models. While we tested our algorithms on a tracking problem, we expect similar performance on predictive gait optimizations, based on experience with 2D models [3].

Table 1: cost function value J and mean of absolute differences at the end of the simulation between the DC solution $\boldsymbol{x}(T/2)$ and the forward integration result $\boldsymbol{x}^{i}(T/2)$.

nodes	*cost function* (J)	*mean* $\lvert\boldsymbol{x}(T/2)-\boldsymbol{x}^{i}(T/2)\rvert$
25	0.1552	0.047
50	0.0974	0.016
100	0.0973	0.004

REFERENCES

1. Anderson FC and Pandy MG. *J Biomech Eng* **123**, 381-390, 2001.
2. Kaplan ML and Heegaard JH. *J Biomech* **34**, 1077-1083, 2001.
3. Ackermann M and van den Bogert AJ. *NACOB 2008*, Ann Arbor, MI, USA, abstract 78, 2008.
4. McLean SG et al. *Clin Biomech* **19**: 828-838.
5. Betts JT. *Practical methods for optimal control using nonlinear programming*, SIAM, 2001.

ACKNOWLEDGEMENTS

This work was supported by the NIH grant R01 EB006735.

SHOULDER ROTATIONAL PROPERTIES OF THROWING ATHELETES

[1] Nigel Zheng, and [2]Koco Eaton
[1]Mechanical Engineering, UNC Charlotte, NC, [2]Tampa Bay Rays, Tampa. FL
email: nzheng@uncc.edu, web: http://www.coe.uncc.edu/~nzheng

INTRODUCTION

Shoulder pain is a frequent phenomenon among baseball pitchers, regardless of age or level of play. Pain experienced during throwing results in an inability to throw with velocity, causing a dead arm syndrome. The cause of pain and injury may be due to overuse of the pitching arm, inadequate rest and poor pitching mechanics. Shoulder rotational laxity is often checked and compared bilaterally. However, current exam may not be adequate to catch any signs of potential injuries. Computer assisted exam may provide us more detailed and quantitative shoulder rotational properties. The purpose of this study is to quantify the shoulder rotational properties, such as the shoulder rotational flexibility, and compare shoulder rotational properties of throwing athletes between dominant and non-dominant shoulder and with and without arm injury history.

METHODS

One hundred baseball pitchers from professional and collegiate teams were recruited for the study. After having signed IRB approved consents and filled out injury questionnaires, they were examined using a custom-made wireless device. The wireless system was calibrated and validated with errors less than 1 ^{o} for orientation and 1 N for force measurement. The arm orientation and force applied during testing were recorded at 100 Hz. Subjects were tested on both shoulders in external and internal rotations (Fig.1). Five trials were collected for each condition and a total of 20 trials were collected from each subject. A 15-second pause was taken between trials. The resistance onset angle (ROA) and end-point angle (EPA) were determined when the rotational force applied reached 2 N and 40 N, respectively (Fig. 2). Both free range of motion (fROM) and end range of motion (eROM) were determined. The shoulder rotational flexibility (SRF) was determined as the amount of rotation caused by a unit rotational torque. The rotational torque was calculated using the forearm mass, length, orientation and the force applied. Bilateral differences were compared among three groups (players without injury history, with surgery history and with injury history but no surgery) using multivariate analysis with alpha set at 0.05 (SPSS, Chicago, IL).

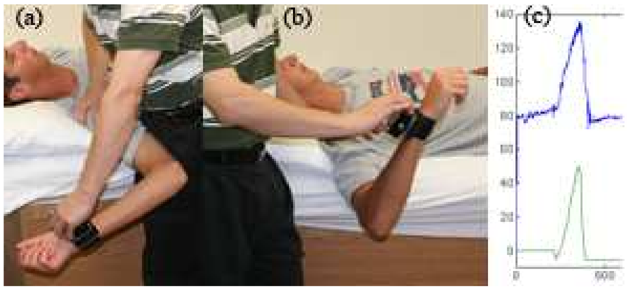

Figure 1: Shoulder rotational tests (a) external, (b) internal, (c) shoulder rotational angle in degrees (top) and applied force in N (bottom).

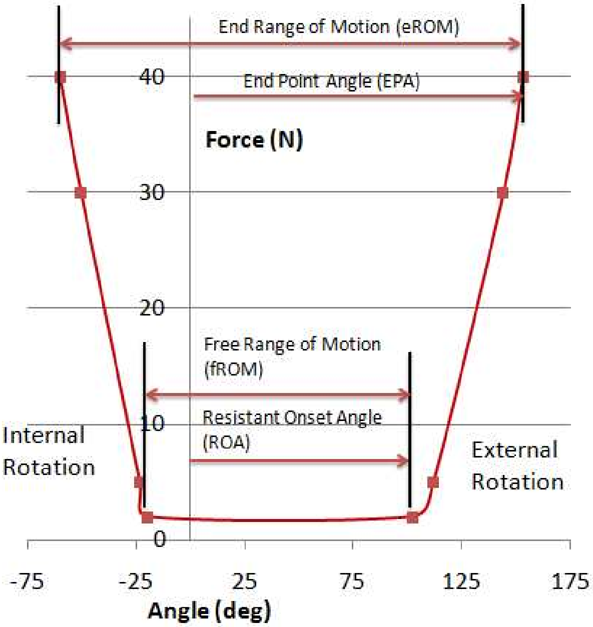

Fig. 2 Variables of shoulder rotational properties.

RESULTS AND DISCUSSION

All subjects filled out injury questionnaires. Ten were injured at the time of test and did not

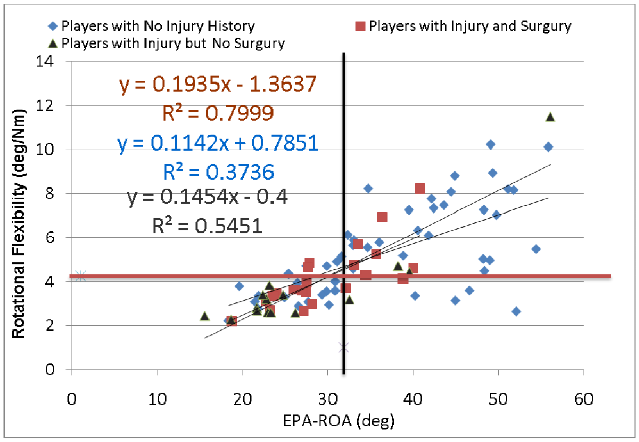

External Rotation

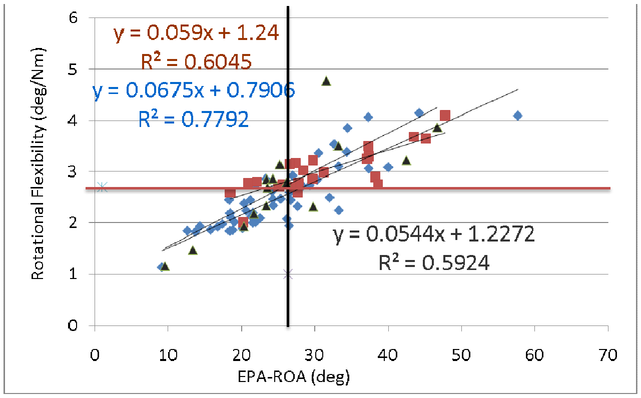

Internal Rotation

Figure 3: Shoulder Rotational Flexibility vs. angle change under loading (EPA-ROA) in uninjured (◆), injured with surgery (■) without surgery (▲). The black and red lines shows the median values.

participate in the laxity test. Twenty three had surgeries performed on their throwing arm. Fifteen had throwing arm injuries in the past year but did not have surgery. Table 1 lists means and standard deviations of shoulder rotational variables. The dominant arm had significantly lower internal ROA (p=.000), internal EPA (p=.000) and internal SRF (p=.003), but significantly higher external ROA (p=.000), external EPA (p=.000) and external SRF (p=.002) than the non-dominant arm. There were no significant differences in fROM and eROM between the dominant and non-dominant arms. For the throwing arm, most subjects with surgery history had internal SRF above the median (Fig. 3). Most subjects with injury history had external SRF below the median. Although not significant (p=0.09) the injured group had greater external SRF of the throwing arm (1.02±0.5°/Nm). No significant differences were found among three groups for the throwing arm. However, when the bilateral differences were compared, the players with surgery history had greater bilateral differences in fROM (11±4°, p=0.02) and eROM (7.5±3°, p=0.06) than the players without injury history. For the group without injury, the bilateral differences matched well with previously reported data [1]. Posterior contracture is related to the internal rotation deficit of the throwing arm. Further research is in progress to relate shoulder rotational properties and pitching mechanics.

CONCLUSIONS

Significant bilateral differences exist in shoulder rotational properties of throwing athletes, except for fROM and eROM. Both groups with injury history and surgery history had different rotational flexibility either for internal rotation or for external rotation. Greater external SRF may be related to throwing arm injuries, both on the elbow and shoulder. Findings of this study may lead us to effective preventive measures of throwing arm injuries.

REFERENCES

1. Borsa, PA et al, *Med. Sci. Sports Exer.* 2006

ACKNOWLEDGEMENTS

This study is funded by a Clinical Research Grant from the Major League Baseball.

Table 1: Means±Standard Deviation of Shoulder Rotational Variables.

	Dominant		**Non-dominant**		**Range of Motion**		
	Internal	**External**	**Internal**	**External**		**fROM**	**eROM**
ROA(deg)	50 ± 15	97 ± 13	61 ± 15	85 ± 14	**Dominant**	147 ± 21	209 ± 20
EPA(deg)	70 ± 12	133 ± 16	90 ± 12	117 ± 14	**Non-dominant**	146 ± 23	206 ± 20
SRF(°/Nm)	2.7 ± 0.7	4.8 ± 2	3 ± 0.9	4.1 ± 1.5			

EFFECT OF OFF-LOADER BRACES AND DEGREE OF VALGUS CORRECTION ON CLINICAL OUTCOME FOR PERSONS WITH MEDIAL KNEE OA

[1]Mary E. Russell and [2]Dan K. Ramsey
[1]Department of Mechanical Engineering, University at Buffalo, NY
[2]Department of Exercise and Nutrition Sciences, University at Buffalo, NY

INTRODUCTION

Medial compartment knee osteoarthritis (MKOA) is a complex process that is associated with genu varum, quadriceps weakness (1) and medial compartment joint laxity (2) that predisposes one to episodes of instability (3). The goal for conservative management is to control pain and improve function and health related quality of life. Unloader braces offer a reasonable alternative for pain relief and improved function without the surgical risk of osteotomy. Research suggests instability resulting from substantial frontal plane joint laxity is controlled mechanically via the brace and that a neutral brace alignment may afford the same benefit as valgus correction (4). However, the braces in that study were fabricated with the knee unloaded and the order in which brace alignment was tested was not randomized, potentially biasing the results towards neutral. Therefore, the purpose of this study was to ascertain the degree to which valgus unloader knee braces control instability, improve pain relief and function, and influence kinematic and kinetic patterns during gait among patients with medial knee OA (MKOA) and genu varum.

METHODS

Eight patients with moderate to severe MKOA and genu varum were recruited and fitted for a custom GII Select Unloader Brace (OSSUR Americas, Foothill Ranch CA). A cast of the involved limb was taken with the patient in weightbearing and a brace was fabricated specific to each individual's leg shape and alignment. Skeletal alignment was measured from standing weight bearing radiographs and quadriceps strength was assessed isometrically. Pain, instability and functional status were assessed using the self-report Knee Outcome Survey- Activities of Daily Living Scale (KOS-ADLS) and Knee Osteoarthritis Outcome Score (KOOS). Gait analysis was performed to assess kinematic and kinetic patterns under three conditions, knee unbraced (baseline), followed by two randomized brace settings with the knee in neutral (regular knee alignment) and 4° valgus. A two week washout period separated brace conditions. Data from six healthy age and gender matched controls were compared. Table 1 illustrates their demographics. Repeated-measures ANOVA with *post hoc* pairwise comparisons were used for comparing brace settings. Independent t-tests were used to assess differences between groups. Alpha was set at $p < 0.05$.

Table 1: Subject demographics

Group	**♂ n = 5, 3**	***♀ n = 3, 3***
MKOA	51.6 ± 8.1 yrs, BMI 31.1 ± 6.7 kg/m2	52.0 ± 7.5 yrs, BMI 27.8 ± 1.8 kg/m2
Control	55.0 ± 9.6 yrs, BMI 28.2 ± 1.5 kg/m2	51.0 ± 6.6 yrs, BMI 24.3 ± 3.4 kg/m2

MKOA: Tested @ baseline, neutral and valgus.
Control: Tested once

Table 2: Subjects radiographic data

	OA	**Control**
Mechanical axis (°)	174 ± 4	179 ± 2
Weight bearing line (%)	0.2 ± 0.2	0.4 ± 0.1
Medial joint space (mm)	2.0 ± 0.9	5.1 ± 1.7
Lateral joint space (mm)	7.2 ± 1.1	6.3 ± 1.1

RESULTS AND DISCUSSION

The MKOA group demonstrated significant medial joint space narrowing and malalignment (weight-bearing line < 50% denotes varus, Table 2). Patients had significant quadriceps strength deficits (Figure 1a). Symptoms, pain, function and knee instability from self-report questionnaires scored worst when unsupported (Figure 1b) and pain, symptoms, and function scored highest with the neutral brace compared to the valgus but remained lower than healthy controls (Figure 1b). Knee flexion excursions (RoM) during weight acceptance was impaired compared to controls in all brace settings but RoM significantly increased with the brace aligned in valgus (Figure 2a). A trend towards improved knee stability was observed with neutral alignment affording better results (Figure 2b and Table 3). Peak knee adduction moments were unaffected by either brace setting and remained significantly higher compared to controls (Figure 3a and b).

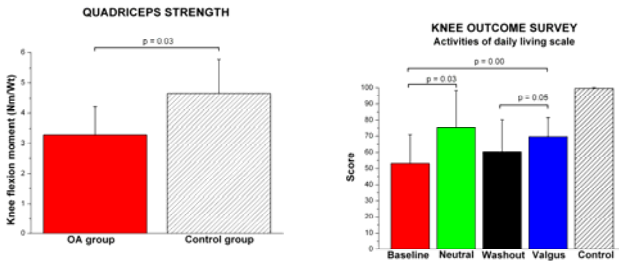

Figure 1: a) Quadriceps strength **b)** KOS self report questionnaire assessing pain and function.

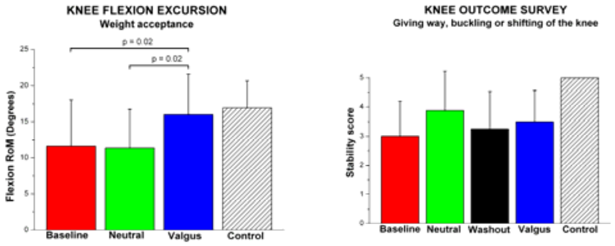

Figure 2: **a)** Knee flexion excursions from initial contact to peak knee flexion. **b)** Knee stability derived from KOS self-report questionnaire.

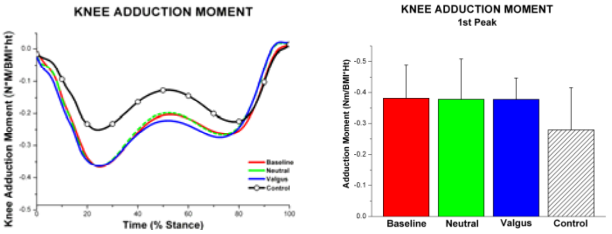

Figure 3: **a)** Adduction moments during the stance phase of gait **b)** First peak knee adduction moment during weight acceptance

CONCLUSIONS

Our results could impact the treatment of a large number of patients with symptomatic medial knee OA since osteotomy is often rejected. By stabilizing the knee, neutral alignment performed as well or better than valgus alignment in reducing pain and disability. The overall preference for neutral alignment maybe the result that braces are reportedly difficult to wear for extended periods because of the degree of force they impart to the limb to alter alignment. To ascertain whether the trend in improved stability is significant, a larger sample size is warranted. Further study is also necessary to identify whether neuromuscular activity is reduced as a result of bracing. Evidence suggests that by stabilizing the knee mechanically, less muscle activity is required and is part of the pain relief mechanism.

Given the encouraging evidence that off-loader bracing maybe effective in mediating pain relief in conjunction with knee OA and malalignment, their use should be considered before joint realignment or replacement surgery. With the number of patients with varus deformities and knee pain predicted to increase as the population ages, a reduction of patient morbidity for this widespread chronic condition could have a positive impact on healthcare costs and the economic productivity and quality of life of the affected individuals. The benefits lie with the potential for increased use of the brace as a method to reduce pain and delay or prevent more invasive interventions.

REFERENCES

1. Lewek MD. J Orthop Res. 22:110-115, 2004.
2. Lewek MD. Osteoarthritis Cartilage. 12:745-751, 2004.
3. Fitzgerald GK Arthritis Rheum. 51:941-946, 2004
4. Ramsey DK. J Bone Joint Surg Am 2007 89(11):2398-407.

ACKNOWLEDGEMENTS

Össur Americas for providing Select Unloader braces.

Table 3: Response to KOS-ADLS question of giving way, buckling or shifting of knee

	OA Subjects							
	Baseline	*%*	*Neutral*	*%*	*Washout*	*%*	*Valgus*	*%*
No giving way, buckling, or shifting of knee	**1**	**12.5**	**4**	**50**	**2**	**25**	**2**	**25**
Have symptom but doesn't affect my activity	**1**	**12.5**	**1**	**12.5**	**1**	**12.5**	**1**	**12.5**
symptom affects activity slightly	**4**	**50**	**1**	**12.5**	**2**	**25**	**4**	**50**
symptom affects activity moderately	**1**	**12.5**	**2**	**25**	**3**	**37.5**	**1**	**12.5**
symptom affects activity severely	**1**	**12.5**	**0**	**0**	**0**	**0**	**0**	**0**
symptom prevents me from all daily activity	**0**	**0**	**0**	**0**	**0**	**0**	**0**	**0**

BIOMECHANICAL ANALYSIS OF DYNAMIC RESPIRATORY DEFICITS IN AXIAL DYSTONIA

Alexander R. Razzook, Christopher J. Stanley, Bart Drinkard, Katharine Alter, Joshua Woolstenhulme, Maria Lebiedowska, and Diane L. Damiano
Rehabilitation Medicine Department, National Institutes of Health, Bethesda, MD
email: arazzook@cc.nih.gov, web: http://pdb.cc.nih.gov

INTRODUCTION

Dystonia is defined as a movement disorder in which involuntary sustained or intermittent muscle contractions cause twisting and repetitive movements, abnormal postures or both [1]. Axial dystonia affects the trunk region, potentially involving muscles that control lung volume and breathing. Our study reports on a patient who had normal breathing function while standing at rest, but reported debilitating shortness of breath while walking that could be alleviated with sensory tricks. The purpose of this study was to evaluate the dynamic physiological causes of the patient's reported shortness of breath and determine if there was a biomechanical basis for the patient's symptoms. The hypothesis that dystonia restricts the patient's lung volume by pulling him into a flexed and rotated trunk posture during walking.

METHODS

A Vicon 612 motion capture system (Vicon Motion Systems, Lake Forest, CA) was used to capture 3D full body gait kinematics during quiet standing, overground and treadmill walking for a 60 year old male (1.78m, 90.9kg). An additional 32 markers were placed on the patient to measure chest wall motion as described by Ferrigno et al. (Figure 1) and form the vertices of each compartment [2]. Surface EMG electrodes were placed on the rectus abdominus, external oblique, and erector spinae muscles (Motion Labs Systems, Baton Rouge, LA). The speed of the treadmill was set to the subject's over ground self-selected walking velocity. Kinematics, total chest wall volume (TCW) and compartment chest wall volumes (CCW) were calculated during the movement trial using Visual3D (C-Motion, Inc., Rockville, MD).

A MedGraphics CPX Ultima metabolic cart (St. Paul, MN) was used to measure lung function. A resting respiratory trial was collected to determine if the patient had a structural lung problem, and a pulmonary function test (PFT) assessed the patient's lung function and capacity. Forced vital capacity (FVC) from the PFT was used to calibrate the range of volumes measured by the chest markers. The relative volume for each of the nine compartments was calculated from the FVC range and divided by the total chest wall volume to determine a percent contribution to total chest wall volume.

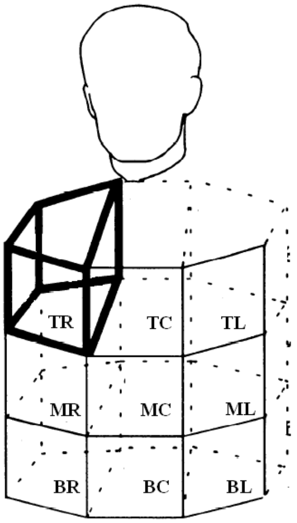

Figure 1: Compartment volumes adapted from Ferrigno et al [2].

The percentage contribution of each compartment to TCW was calculated from the maximum and minimum tidal volume. For the PFT, percentage contribution of each compartment to TCW was calculated by looking at the maximum TCW relative to the minimum TCW.

RESULTS AND DISCUSSION

Results from the clinical gas exchange tests and PFT indicated that the patient has normal lung function during standing and ruled out restrictive or obstructive lung disease. The patient's tidal volume (V_t), respiratory rate (RR), and oxygen saturation were normal during quiet standing.

The gait study demonstrates atypical EMG muscle activity including prolongation and intensity of activation in abdominal muscles on the right during walking activities. The patient walks with trunk flexion (20°+), lateral tilt (10°), and rotation to the right (6°). The posture is consistent with the EMG activation pattern, suggesting that dystonia is a cause for his symptoms. With walking, this patient does not demonstrate the normal compensations of: increased V_t and increased RR. He compensates for the increased metabolic demand solely by increasing his RR (Table 1).

The dystonic posture was thought to decrease the available lung volume, resulting in either (1) a decreased TCW paradigm, or (2) a volume substitution paradigm in which the left side of the chest would compensate for the functional reduction of volume on the right.

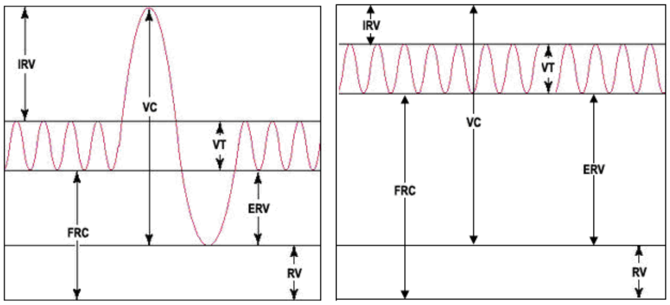

Figure 2: (left) Typical lung volume measures; (right) Depiction of patient's normal V_t at hyperinflation.

The contribution of the right side compartments to the total chest volume decreased during walking from standing (Table 2). This decrease was compensated by an increase in the left side compartments' contribution to the total chest volume, indicating the substitution paradigm. The motion capture chest volume data shows that the patient breathes at volumes near maximum FVC during standing and walking despite a relatively normal V_t. These results suggest that the patient breathes with hyper-inflated lungs. This type of breathing requires a higher metabolic cost, as seen in his VO2 consumption (62% of predicted V02 Max) during walking (Table 1).

Table 2: Percent contribution of chest compartments to total chest wall volume; 9 compartments for each condition sum to 100%

	TR	TC	TL
PFT	7%	10%	7.6%
Standing	15.7%	13.4%	16.1%
Walking	-2.4%	9.6%	29.4%
	MR	**MC**	**ML**
PFT	9.5%	9.3%	11.4%
Standing	7.2%	6.3%	6.9%
Walking	3.7%	3.8%	11.5%
	BR	**BC**	**BL**
PFT	15.8%	19.4%	9.9%
Standing	10.8%	12.2%	11.4%
Walking	2.9%	14.9%	26.7%

CONCLUSIONS

Despite the patient's normal resting PFTs, he demonstrated a functionally restrictive ventilation pattern during walking. The patient's dystonia caused abnormal abdominal muscle contraction, affecting trunk posture and limiting chest wall volume during walking.

This abstract demonstrates the unique utility of combining respiratory and biomechanical analyses in dynamic activities. This analysis may provide a dynamic alternative to static plethysmography, and could be valuable in other populations with rib and trunk deformities, scoliosis, myopathies, or incomplete paresis from spinal cord injury.

REFERENCES

1.Fahn et al. *Adv in Neur* **78**, 1-10, 1998.
2.Ferrigno et al. *Journal of Applied Physiology* **77**, 3, 1224-1231, 1994.

ACKNOWLEDGEMENTS

The authors would like to acknowledge Scott Selbie of C-Motion for assistance in data analysis.

Table 1: Differences in Oxygen Consumption (V02), Carbon Dioxide Production (VC02), Respiratory Rate (RR), Tidal volume (V_t) and Ventilation (VE).

Condition	VO2 (mL/min)	VCO2 (mL/min)	RR (br/min)	V_t BTPS (mL)	VE BTPS (L/min)
Standing	535.4 (34.6)	449.9 (18.4)	15.1 (1.0)	1048.2 (65.2)	15.8 (.4)
Walking	1760.9 (186.8)	1398.1 (169.5)	45.9 (7.5)	1060.6 (273.3)	46.7 (3.6)

TEMPORAL CHANGES IN GAIT IN HEALTHY OLDER INDIVIDUALS DURING PROLONGED TREADMILL WALKING

[1] Daniel J Bechard, Trevor Birmingham, Ian Jones, Robert Giffin, Aleks Zecevic and Thomas Jenkyn
[1]Wolf Orthopaedic Biomechanics Laboratory, Fowler Kennedy Sport Medicine Clinic, the University of Western Ontario
e-mail: dbechard@uwo.ca

INTRODUCTION

Previous researchers have suggested that changing various gait kinematics can significantly influence mechanical loading of the knee [1-3]. Specifically, the magnitude of toe out [1] of the stance limb and/or lateral trunk lean over the stance limb [2] have been shown to be associated with the external adduction moment about the knee during walking, a valid and reliable proxy for the dynamic load on the medial compartment. It is unclear, however, whether such gait kinematics simply represent normal variation between individuals in the way they walk, or are truly compensatory mechanisms in response to various factors such as fatigue, pain, or disease. Similarly, the stability of toe out and lateral trunk lean measures during prolonged walking for healthy individuals is currently unknown. Therefore, the purpose of the present study is to evaluate toe out and lateral trunk lean measures during prolonged walking in healthy older adults.

METHODS

To date, four subjects with no previous health concerns related to mobility were asked to complete 60 minutes of walking on a dual force plate instrumented treadmill (hp Cosmos, Kistler Instrument Corp., Amherst, U.S.A.) surrounded by four high resolution cameras (Motion Analysis Corp., Santa Rosa, U.S.A.).

All subjects were instrumented with a modified Helen Hayes marker set. Treadmill walking speed for each subject was determined by calculating his/her over ground walking speed. A random trial was averaged using the sacral marker.

To ensure familiarization to the treadmill and surroundings prior to beginning the session, the subject was asked to walk on the treadmill for at

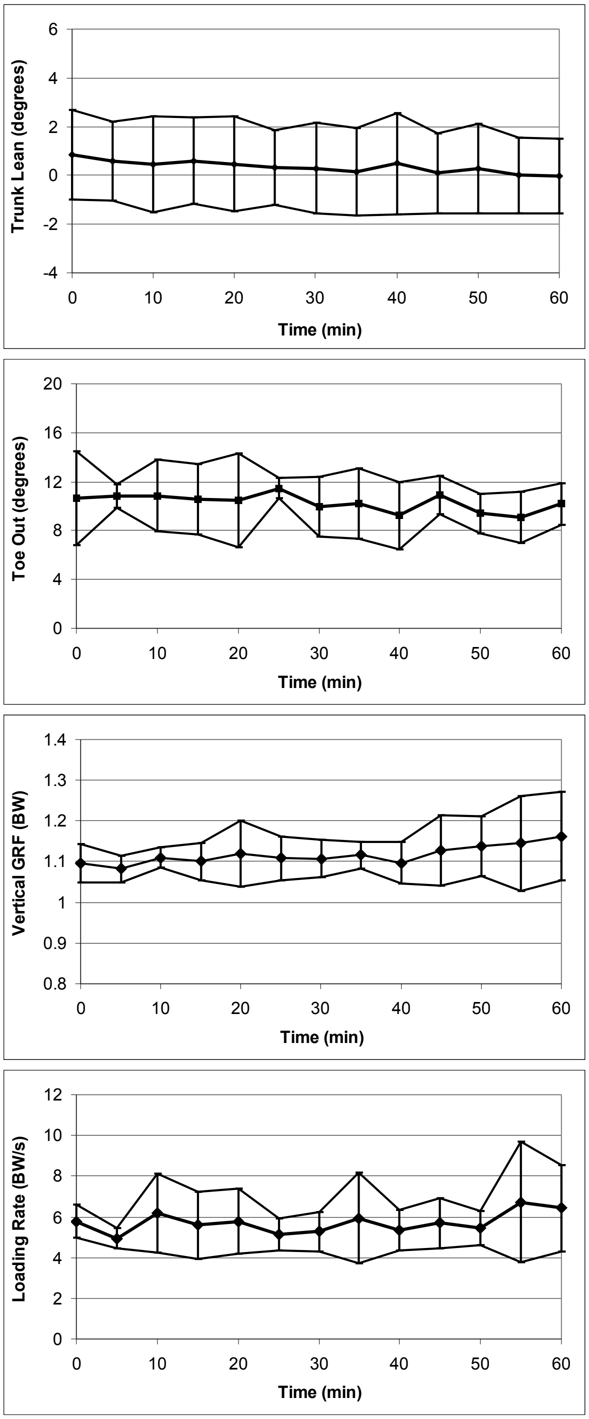

Figure 1: Mean (±SD) Trunk lean, toe out, vertical GRF, and loading rate over time.

least six minutes. A rest period was given if needed. The subject increased walking speed at his/her own preferred pace. Data collection commenced when the treadmill speed met that of the over ground calculated walking velocity. Data collection during 15 second intervals was completed every 5 minutes for 60 minutes. Three successive right foot strikes were cropped and averaged. Data reduction and post processing was completed using EVaRT, Orthotrak (Motion Analysis Corp., Santa Rosa, U.S.A.) and custom software. Primary variables of interest were the maximum toe out angle and lateral trunk lean during stance. Vertical Ground Reaction Force (GRF) and loading rate were also evaluated.

Data were analyzed using a one way repeated measures ANOVA for all variables to determine if a change occurred with respect to time. Statistical significance will be reported at $p < .05$.

RESULTS AND DISCUSSION

Subject demographics are reported in Table 1. Gait variables over 60 minutes are shown in Figure 1. Relatively small changes in all variables were observed over time. Maximum trunk lean occurred at the 0 minute mark (0.85±1.84 degrees) with minimum occurring at 60 minutes (-0.03±1.54 degrees). Maximum toe out occurred at the 25 minute mark (11.48±0.82 degrees) with minimum occurring at 55 minutes (9.04±2.10 degrees). Maximum VGRF occurred at 60 minutes (1.16±0.11 BW) while minimum occurred at 5 minutes (1.08±0.03 BW). Maximum loading rate occurred at 55 minutes (6.7±2.96 BW/s) with minimum occurring at 5 minutes (4.9± 0.51BW/s). With the present sample size, no significant changes occurred in any variables with respect to time.

CONCLUSIONS

These preliminary findings suggest that healthy older adults with no previous history of disability affecting mobility do not significantly change trunk lean or toe out over prolonged walking.

With a greater sample size, this investigation will lay the ground work for subsequent studies comparing subjects with and without disease.

REFERENCES

1. Jenkyn T. *J Biomech* **41**, 276-283, 2008.
2. Hunt M. *Arthritis and Cartilage* **16,** 591-599, 2008.
3. Mundermann A. *Arthritis & Rheumatisms* **50**, 1172-1178, 2004.

Table 1. Demographic information

	Sex	**Age (years)**	**Mass (kgs)**	**Height (m)**	**BMI**	**Gait Speed (m/s)**
Average ± SD	2M 2F	48.5 ± 10.0	67.7 ± 13.1	1.71 ± 0.05	23.0 ± 3.6	1.25±0.13

IS MIDFOOT STRIKING DURING RUNNING ADVANTAGEOUS OVER REARFOOT OR FOREFOOT STRIKING?

[1]Allison R. Altman and [1,2]Irene S. Davis
[1]Dept. of Physical Therapy, University of Delaware, [2]Drayer Physical Therapy, Hummelstown, PA
email: aaltman@udel.edu

INTRODUCTION

The majority of runners strike the ground with their heel first, indicating that they are rearfoot strikers (RFS). However, 25% of runners either land with a midfoot strike (MFS), making contact with a flat foot, or with a forefoot strike (FFS), striking the ground with the ball of their foot [1]. It has been shown that RFS display characteristics of the heel strike transient in their vertical ground reaction forces (GRF) [2]. This causes distinct impact peaks (IP), which can be associated with relatively high instantaneous and average vertical loading rates (IVLR and AVLR, respectively), and peak positive tibial acceleration (PPA). When increased, this can place the runner at risk for tibial stress fractures [3]. While a FFS pattern reduces these loading variables, it increases the demand on the plantarflexion musculature [2]. This makes these runners more susceptible to Achilles tendinitis. In addition, the ground contact force is concentrated under the ball of the foot, increasing the risk for metatarsalgia.

It is possible that running with a MFS pattern provides a compromise between these two extremes, and may reduce the risk of these injuries. Barefoot runners adapt a MFS pattern in order to reduce the impact loading [4]. These runners anecdotally report fewer injuries since going barefoot [5]. However, studies of MFS running are missing from the literature.

Therefore, the purpose of this study was to compare MFS to RFS and FFS running mechanics. We hypothesized that loading variables, IVLR, AVLR, IP and PPA MFS will fall between those of RFS and FFS in a group of natural RFS.

METHODS

This is an ongoing study of which five healthy runners have been recruited to date. Subjects were all healthy RFS runners, logging at least 10 miles per week. All rated their treadmill comfort greater than 8/10 on a treadmill comfort scale. A tri-axial accelerometer (PCB Piezotronics, DePew, NY) was tightly affixed to the distal tibia with tape and overwrap. Subjects ran on an instrumented treadmill (AMTI, Watertown, MA). They began their warm-up by walking on the treadmill for 2 minutes. Subjects were then asked to choose a speed they felt they could easily maintain running for 15 minutes. They ran for 5 minutes with their natural RFS pattern, followed by 5 minutes with a MFS pattern and finally 5 minutes with a FFS pattern. They were provided a 1-minute walk period in between each condition. Based on preliminary studies, 5 minutes seemed to be adequate time for subjects to adopt the new strike pattern comfortably. Five consecutive strides for each condition were recorded at the end of each 5-minute period. Ground reaction force and tibial accelerometer data were collected at 1000 Hz, using Nexus (VICON, Oxford, England). Custom code (LabVIEW, National Instruments, Austin, TX) was used to extract AVLR, IVLR, IP, and PPA the data. AVLR was the average vertical load rate determined as the slope between points at 20% and 30% of the curve from footstrike to IP. IVLR was the derivative of the vertical GRF just prior to IP. If no IP was present, as is common for FFS, the IVLR was taken at 13% of stance [6]. IP, was the first peak in the vertical GRF, again, if not present, the value at 13% was extracted. Finally, PPA was the maximum peak positive tibial acceleration along the long axis of the tibia.

Due to the currently low subject numbers, data will be compared qualitatively. A difference of 10% was considered meaningful.

RESULTS AND DISCUSSION

Three male and 2 female subjects have completed the study to date. On average, they were 26.8 (4.8) years old, weighed 75.8 (22.3) kg, and were 1.78 (0.17) m tall. All subjects rated their treadmill comfort at 10/10. Self-selected speeds ranged from 2.4-3.3 m/s.

The mean vertical GRF curves for each strike pattern are seen in Figure 1. Note that the patterns are similar between the RFS and MFS patterns. As expected, the FFS pattern was missing a distinct impact peak.

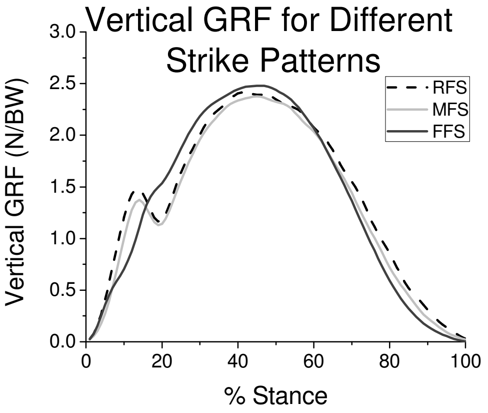

Figure 1. Vertical GRF for rearfoot, midfoot, and forefoot strike patterns. Note the progressively decreased impact peak between the rearfoot, midfoot and forefoot strike patterns.

When analyzing the group mean data for each of the variables of interest, again the MFS values were similar to the RFS values, but different than the FFS values (Figure 2). In all cases, the FFS pattern is associated with lower impact loading.

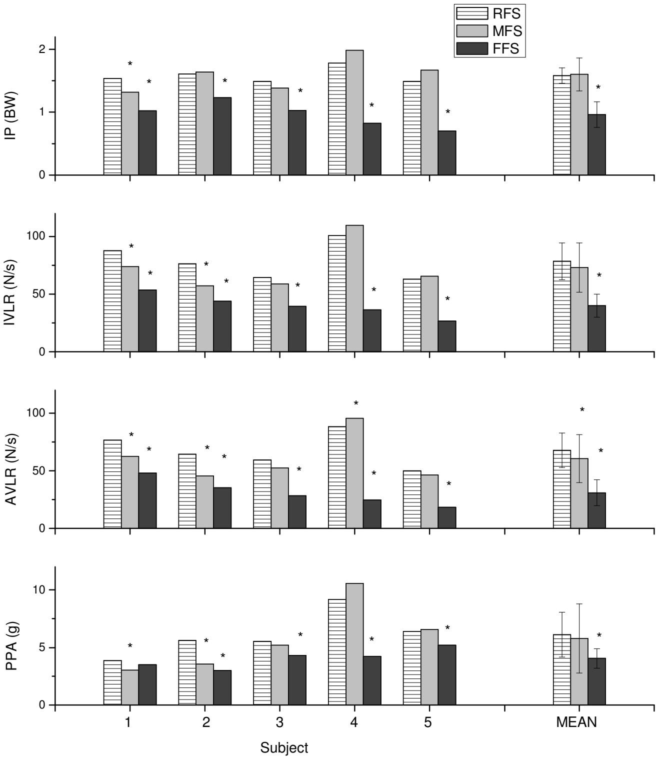

Figure 2. Individual and mean data for the discrete variables of interest. *Indicates >10% difference.

However, a closer look at the individual data reveals some interesting findings about the MFS pattern. Subjects 1-3 demonstrate the expected pattern of forces, with the highest associated with the RFS, the lowest with the FFS, and the MFS falling in between.

The findings for PPA were less consistent. PPA has been shown to be strongly correlated to vertical loading rates [7]. However, PPA values can be influenced by error associated with accelerometer placement, including location, orientation and tension of the overwrap. This error is not present in the force data. To improve consistency in placement, a single investigator attached the accelerometer for all subjects. However, this likely does not remove all of the error associated with this measure

Subject 4 and 5 demonstrated an increase in most of their impact loads with a MFS pattern. It is possible that these subjects were not comfortable running with the MFS pattern. Both MFS and FFS running was novel to these subjects, however, MFS was the more difficult one to use. In addition, while subjects were asked to run with a flat footstrike, most tended to land with their toes slightly up. This may explain why the MFS was more like the RFS than the FFS. Unfortunately, center of pressure data are not available to calculate the precise strike index associated with the MFS pattern.

This information might be useful in counseling runners with injuries about footstrike patterns. A modification from a RFS to a FFS results in a marked change of kinematics and kinetics [2]. On the other hand, changing from a RFS to a MFS appears to produce more subtle differences. These small changes over many footstrikes, may be enough to reduce a runner's risk for a repeated injury.

CONCLUSIONS

Based upon these very preliminary results, it appears that MFS running is more similar to the RFS pattern than the FFS pattern. However, a MFS pattern appears to be associated with a reduction in impact loading from the RFS pattern.

REFERENCES

1. Hasegawa H et al. *J Strength Cond Res.* **21(3)**, 888-893, 2007.
2. Williams DS, et al. *J App Biomech* **16,** 210-218, 2000.
3. Milner CE, et al. *MSSAAAE* **38(2),** 323-328, 2006.
4. Squadrone R, et al *J Sp Med Phys Fit* **49(1)**, 6-13, 2009.
5. Robbins et al, *MSSE* 19(2):148-156*,* 1987
6. Willy RW et al. *NACOB* 2008.
7. Lafortune MA et al. *J Biomech* **28(1)**, 113-117, 1995.

ACKNOWLEDGEMENTS

DOD W911NF-05-1-0097

DYNAMIC STABILITY ASSESSED WITH FREQUENCY ANALYSIS COMPARED TO SPATIOTEMPORAL ANALYSIS

[1]Gary D. Heise, [2]Kathy Liu, [1]Jeremy Smith, [1]Amanda Allen and [1]Maryann Hoke
[1]Biomechanics Laboratory, University of Northern Colorado, Greeley, Colorado
[2] Biomechanics and Movement Sciences, University of Delaware, Newark, Delaware
email: gary.heise@unco.edu, web: http://www.unco.edu/nhs/ses

INTRODUCTION

Static postural stability is often assessed by analyzing the displacement of the center of pressure (COP) while a person stands quietly on a force platform [1]. COP frequency has been a focus of researchers because this approach is thought to be more physiologically meaningful. For example, various control strategies have been associated with different frequency bands of COP displacement during static postural assessments [2].

Dynamic stability describes the process of transitioning from movement to a quiet, standing posture. Time-to-stability (TTS), based on the diminishing fluctuations in ground reaction forces and COP trajectories, is often used to assess this transition [3]. Although TTS has been used to evaluate ankle instability and landing direction, it lacks information about how forces and the COP may change while a person transitions to a stable state. Similar to assessments of static posture, frequency analysis of the COP might provide further insights into how an individual attains stability.

The primary purpose of this study was to evaluate the frequency content of the COP displacement-time series as a person lands one-footed from four different hop directions and becomes stable. Secondly, a comparison was made with spatiotemporal measures of the COP.

METHODS

Twenty healthy, recreationally active men (n=9) and women (n=11) volunteered for this study (overall mean age = 28 ± 4 yrs, mean body mass = 73.3 ± 21.5 kg, mean body height = 173.4 cm ± 10.5 cm). Participants were asked to complete four hopping tasks onto an AMTI force platform (barefoot, landing with dominant leg). The four hopping tasks were: after two steps, a forward hop from 100% of their leg length (F); a lateral hop from the side (L); a medial hop from the side (M); and a backwards hop (B). The latter three hops were taken from the edge of the platform and all tasks were performed in a random order.

Ground reaction force data were collected at 100 Hz for 10 s after landing. COP coordinates were calculated and dependent measures were determined following the procedures of Prieto et al. [1]. Mean velocities of the COP in both the anterior-posterior (AP-MVELO) and medial-lateral (ML-MVELO) directions were calculated (spatiotemporal measures). A rotational frequency measure (MFREQ) was calculated, which is proportional to the ratio of the overall mean velocity to the mean distance of the COP. This is considered a “time-domain hybrid” measure. In the frequency domain, the initial 5 s of the AP and ML COP displacement-time series were subjected to a Fast Fourier analysis. The resulting power-frequency spectrum was integrated and the frequencies for AP and ML directions which corresponded with 95% total power were identified (AP-95FREQ, ML-95FREQ). Separate repeated measures analysis of variance tests were used to determine differences in hopping direction for all measures. The probability of a Type I error was set at 0.05.

RESULTS AND DISCUSSION

Only one difference in hop direction was found among the dependent variables (see bottom panel of Figure 1 and caption). Although not statistically tested, the ML components of MVELO and 95FREQ were less than the corresponding AP components for each hop direction (see top and bottom panels of Figure 1).

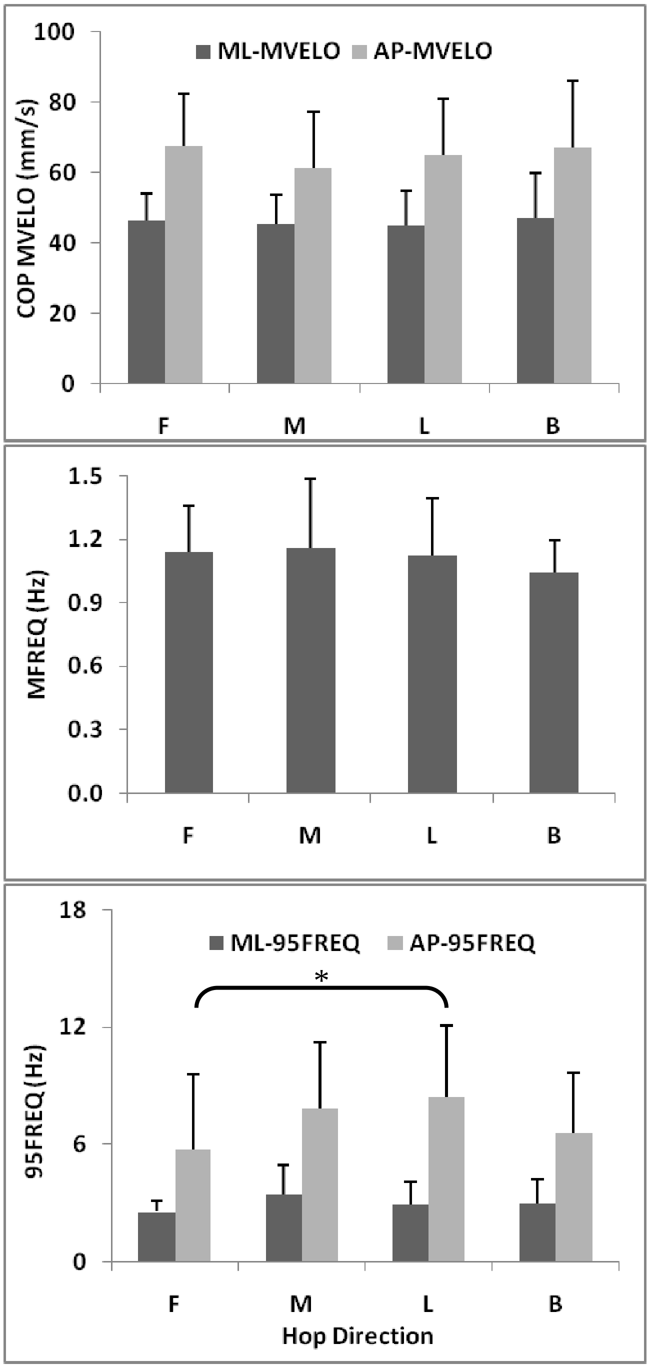

Figure 1: Means and SDs for MVELO (top), MFREQ (middle), and 95FREQ (bottom) for each hop direction (F=forward; M=medial; L=lateral; B=backward). AP-95FREQ (bottom) for the forward direction is significantly less than the lateral direction. * p < .05.

==================================

MVELO and MFREQ values are considerably higher than what has been reported for two-legged, static postural conditions [1]. Larger MVELO values in the AP direction, as compared to the ML direction, were expected for one-legged stance because a person's base of support is smaller in the ML direction. The hybrid measure, MFREQ which used overall mean COP velocity and distance, did not discriminate between hop directions. Because this measure relates the size of the stabilogram to COP velocity [1], its application to one-legged stability applications appears limited.

Frequency analysis resulted in high variability (see bottom panel of Figure 1) and a limited ability to distinguish among hop directions. Previous research in our lab showed that a sequential averaging technique for calculating TTS based on AP, ML, and vertical components of the ground reaction force was effective in identifying differences between hop directions [5]. 95FREQ has been described as an estimate of the extent of the COP frequency content [1]. Others have investigated the power present in various frequency bands [6], but the maximum frequency considered was 3 Hz. In our study, power was clearly present above 3 Hz (bottom panel of Figure 1) and so for dynamic stability conditions, the typical frequency bands associated with postural control must be examined systematically.

CONCLUSIONS

One difference in hop direction was found for a frequency-based measure (AP-95FREQ) whereas no differences were found in spatiotemporal measures. Frequency analysis of COP displacements must be examined more systematically in order to determine its effectiveness in assessing dynamic stability.

REFERENCES

1. Prieto TE, et al. *IEEE Trans Biomed Eng* **43**, 956-966, 1996.
2. Callavalle, AR, et al. *Eur J Appl Physiol* **104**, 643-649, 2008.
3. Wikstrom, EA, et al. *J Athletic Training* **39**, 247-253, 2004.
4. Wickstrom, EA et al. *J Sci Med in Sport*, 11, 106-111, 2008.
5. Liu, K. *The Influence of Ankle Taping and Landing Direction on Dynamic Stability*, M.S. Thesis, 2008.
6. Nagy, E, et al. *Eur J Appl Physiol*, **100**, 97-104, 2007.

THE EFFECT OF SQUAT LOAD AND DEPTH ON PATELLOFEMORAL JOINT KINETICS

Joshua A. Cotter[1], Steven T. Devor[1], Steven T. Jamison[2], and Ajit Chaudhari[2]
Health and Exercise Science Program[1] and Department of Orthopaedics[2] The Ohio State University
E-mail: cotter.38@osu.edu, Web: http://www.sportsmedicine.osu.edu

INTRODUCTION

The squat exercise is prescribed in a wide variety of environments ranging from physical rehabilitation to strength programs for professional athletes. Although widely used, there is dispute among professionals as to what depth should be prescribed, or even if a squat exercise should even be utilized in a program.

Patellofemoral pain is one of the most common disorders of the knee. Overuse and chronic overloading of the patellofemoral joint have been correlated with patellofemoral pain [1]. It is therefore important to better understand the forces that are produced through the patellofemoral joint at different squat loads and depths that are often prescribed.

In general, with increasing depth of the squat exercise, a decrease in load is required to allow the movement to take place. This necessitates assessing strength levels at each individual depth.

The purpose of this study was to investigate the relationship between differing squat depths and loads on peak knee moments and patellofemoral joint reaction force (PFJRF). We hypothesized that the decreasing loads required as squat depth increases will result in a constant PFJRF.

METHODS

Twelve subjects participated in the study after providing IRB-approved informed consent. All subjects had experience with resistance training for at least one year, had no previous leg surgeries, could squat without pain, and were able to perform a deep squat with good technique.

Testing for 1 repetition maximum (RM) was performed on each subject at depths of above parallel (~ 90°), parallel (~110°), and below parallel (~135°). At a subsequent session 2-6 days later, subjects performed 13 different squat trials utilizing the three depths with loads consisting of unloaded, 50% 1RM, and 85% 1RM. During the second session, trials were captured with both digital video of the sagittal plane and with motion capture. Squat depths were monitored and communicated to the subject by a light that signaled the subject was at the desired depth. Once at the correct depth, the subject paused in the bottom position for one second before rising out of the squat.

An eight camera Vicon MX-F40 system, two Bertec 4060-10 force plates, and Vicon Nexus software were used to record the squat trials. Retro-reflective markers were attached with two-sided adhesive tape to the subject's legs utilizing a modified Point-Cluster technique [2, 3]. Custom scripts in Matlab and Vicon Bodybuilder were used to calculate knee kinematics and kinetics.

PFJRF was calculated using a biomechanical model requiring the tibiofemoral moment (M_{tf}) and the tibiofemoral joint angle as input variables. An effective lever arm (L_{eff}) for the quadriceps was calculated using linear and non-linear equations where x is the tibiofemoral joint angle:

<95°: $L_{eff} = -0.0028x^2 + 0.036x + 41$
85 – 100°: $L_{eff} = 1.26x - 98.5$
>100°: $L_{eff} = -0.0042x^2 + 0.86x - 17$

Equations were fit to the data (R^2 = .99, 1.00, and 1.00 respectively) of Gill and O'Connor [4]. Quadriceps force (F_q) was then calculated by dividing the tibiofemoral moment by the effective lever arm ($F_q = M_{tf}/L_{eff}$).

PFJRF was calculated as the product of the quadriceps force and a constant *k* representing the ratio of PFJRF/F_q ($PFJRF = k \cdot F_q$). The constant *k* was determined for each tibiofemoral joint position by using a non-linear equation ($k = 0.000064x^2 + 0.014x + 0.37$) fit to the data ($R^2 = 1.00$) of Gill and O'Connor [4].

An analysis of variance for repeated measures was used to compare peak knee moments and peak patellofemoral joint reaction force between squatting depths and loads.

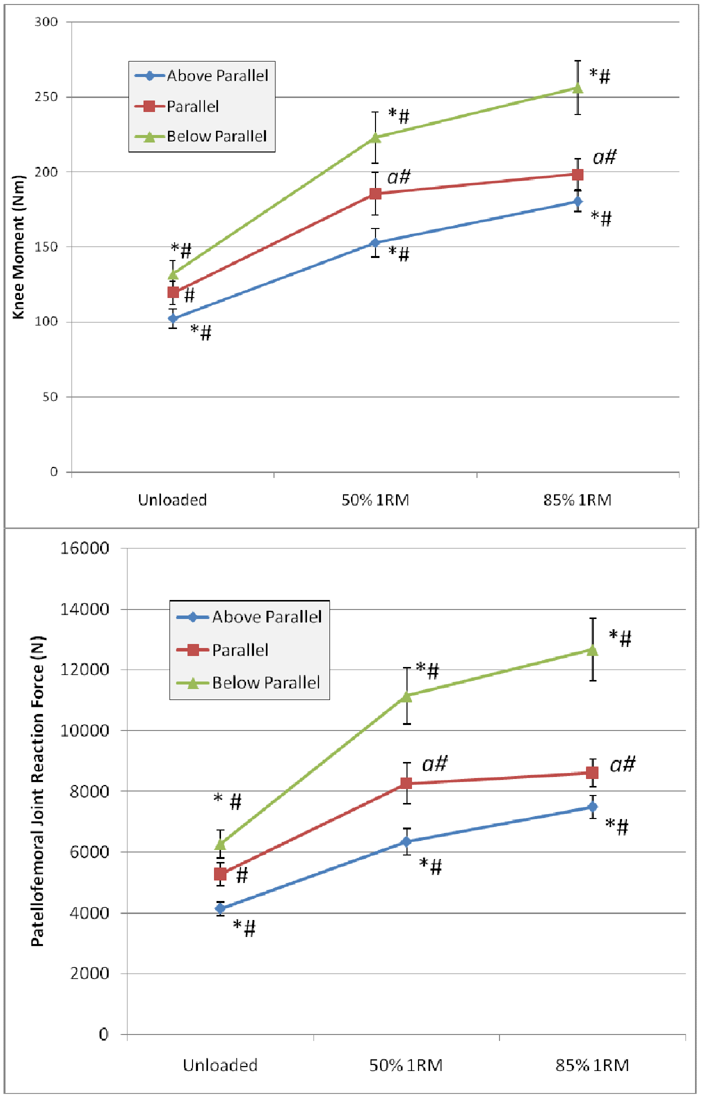

Figure 1: Peak knee moments (Top) and peak patellofemoral joint reaction forces (Bottom) while performing unloaded, 50% 1RM, and 85% RM squats at above parallel, parallel, and below parallel depths. Error bars represent ±1 SE. * represents significant differences between all loaded trials at each respective depth ($p < .05$). # represents significant differences between depths at each respective load ($p < .05$). *a* represents significant differences from the unloaded trial for its respective depth ($p < .05$).

RESULTS AND DISCUSSION

Peak knee moments were significantly different between all depths at each respective load (Figure 1 - Top). Increasing loads from unloaded to 50% to 85% 1RM increased peak knee moments for above parallel squats and below parallel squats. There was no difference in moments between 50% 1RM and 85% 1RM with the parallel squat. Average depths were 92.8 degrees for the above parallel squat, 117.81 degrees for the parallel squat, and 133.8 degrees for the below parallel squat.

PFJRF mimicked the relationships seen with the peak knee moments. Peak PFJRF were significantly different between all depths at each respective load (Figure 1 - Bottom). Increasing loads from unloaded to 50% to 85% increased PFJRF for above parallel and below parallel squats. There was no difference in PFJRF between 50% 1RM and 85% 1RM with the parallel squat.

CONCLUSIONS

Although decreasing loads are generally necessary with deeper squat depths, decreasing the load proportionately to the change in 1RM is not enough to offset the increases in PFJRF typically seen with increasing knee flexion. These results suggest that decreases in load with increased depth in the back squat may not be enough to protect the patellofemoral joint while utilizing this exercise at deeper depths. Future research needs to better define the loading conditions on the patellofemoral joint (magnitude and cycles) that are injurious. In addition, proper loading schemes for differing squat depths should be investigated to find a balance between eliciting a proper training response while limiting the potential for injury at the patellofemoral joint.

REFERENCES

1.LaBella C. *Primary Care* **31**, 977-1003, 2004.
2.Andriacchi TP, et al. *Journal of Biomechanical Engineering* **120**, 743-9, 1998.
3.Dyrby CO and Andriacchi TP. *Journal of Orthopaedic Research : Official Publication of the Orthopaedic Research Society* **22**, 794-800, 2004.
4.Gill HS and O'Connor JJ. *Clin Biomech (Bristol, Avon)* **11**, 81-89, 1996.

The Geometry of the Tibial Plateau and Tibiofemoral Kinematics: A Biomechanical Analysis

J. Hashemi[1], N. Chandrashekar[2], B. Gill[1], J. Slauterbeck[3], R. Schutt[1], E. Dabezies[1], and B. Beynnon[3]
[1]Texas Tech University (HSC); [2]University of Waterloo; [3]University of Vermont
email: javad.hashemi@ttu.edu, web: http://www.me.ttu.edu/Hashemi

INTRODUCTION

The geometry of the tibial plateau is complex and asymmetric. The subject to subject differences in tibial plateau geometry could play a crucial role in the biomechanical response of the tibiofemoral joint to loads. Prior research has characterized the geometry of the tibial plateau with a single posterior slope obtained from a lateral x-ray. However, we have shown that it is more accurate and comprehensive to characterize the geometry of the tibial plateau using medial slope (MTS), lateral slope (LTS), coronal slope (CTS) as well as the depth of the medial tibial plateau (MTD) through MRI measurements.[1] In this paper we present the range of measurements and how they could influence anterior tibial translation and internal/external rotation of the tibiofemoral joint.

METHODS

In a blinded study, the MTS, LTS, CTS, and MTD of the bony portion of the tibial plateau were measured using sagittal and coronal MRI images. The MRIs were obtained from 33 female and 22 male subjects. Student t-tests were performed to test for the significance of differences between sexes. Paired t-tests were performed to assess side to side differences between MTS and LTS within subjects.

RESULTS AND DISCUSSION

For the male subjects, the MTS ranged between –3.0° and +10.0° while the LTS ranged between 0.0° and +9.0°. For the female subjects, the corresponding ranges in MTS and LTS were 0.0° to +10.0° and +1.0° to +14.0°, respectively. The CTS ranged between 0.0° and +6.0° for the males and -1.0 ° to 6.0° for the females. The MTS for the females (mean; 5.9 degrees) was significantly greater than that of the males (mean; 3.7°: p = 0.01). Similarly, the LTS for the females (mean; 7.0 degrees) was significantly greater than that of the males (mean; 5.4° p = 0.02). There was a significant difference (pair-wsie comparison) between the MTS and the LTS values when considering the males and females as separate groups as well as the pooled population (all p<0.05). Finally, the CTS for females (mean; 2.5 degrees) was significantly less than that of the males (mean; 3.5° p = 0.03). The depth of subchondral bone concavity of medial compartment of the tibia ranged from 1.4 mm to 4.2 mm (2.7+/-0.76) for females and from 1.2 to 5.2 (3.1+/-0.99) for males. There was no difference in the depth of concavity of the medial compartment between the males and females (p = 0.1); however the statistical power associated with this comparison was low (34%).

Comparison of joint reaction forces in two subjects with different CTS values is given in Figure 1. The knee in Figure 1a has a contact force with a lateral directed component presented by the horizontal solid red arrow and the knee in Figure 1b has contact force with a small or zero lateral component. Thus the subject in 1a will be more susceptible to lateral movement resulting in abduction of the knee (less dynamic valgus).

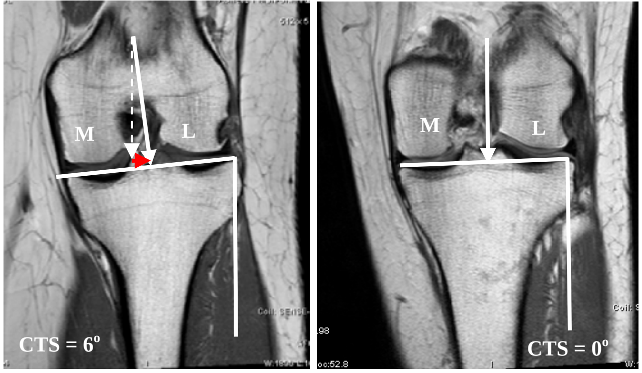

(a) (b)

Figure 1. JCF for two subjects with different CTS (a) CTS=6° and (b) CTS = 0°.

Comparison of joint reaction forces in two subjects with different tibial slopes is presented in Figures 2 and 3 with the knee near full extension. Subject #1 in Figure 2 has an MTS of 10° and an LTS of 10 °. Subject # 2 in Figure 3 has an MTS of 0° and an LTS of 4°. Solid lines represent slopes and solid arrows the corresponding compressive joint forces. Note that the knee in 2(a) and 2(b) has larger anterior directed components that act on both medial and lateral compartments when compared to the subject in 3(a) and 3(b).

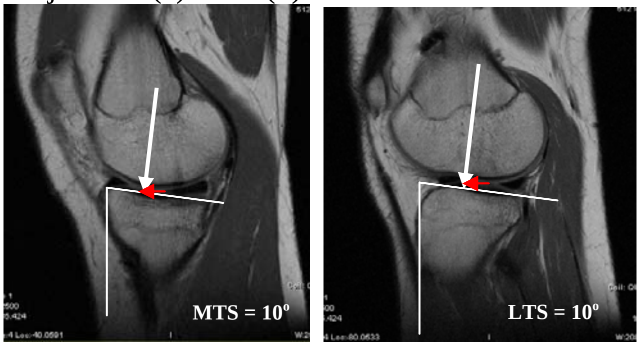

(a) (b)

Figure 2. JCF for subject 1: (a) medial side and (b) lateral side.

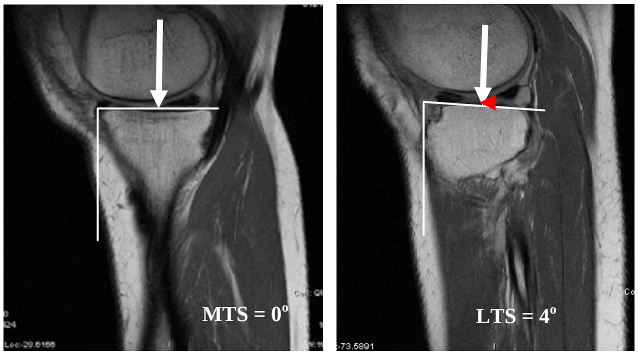

(a) (b)

Figure 3. JCF for subject 2: (a) medial side and (b) lateral side. Note differences compared to Figure 2.

Comparison of joint reaction forces in two subjects with negative differences between MTS of 3° and LTS of 9° (Figure 4) and positive differences between MTS of 6° and LTS of 1° (Figure 5) is presented. Solid lines represent slopes and the forces that act on the medial and lateral plateaus. The horizontal arrows in Figure 4(a) and 4(b) show opposite directions of application resulting in a tendency for internal rotation of the tibia. The horizontal arrows in 5(a) and 5(b) both act posteriorly but the lateral component is larger resulting in a tendency for external rotation.

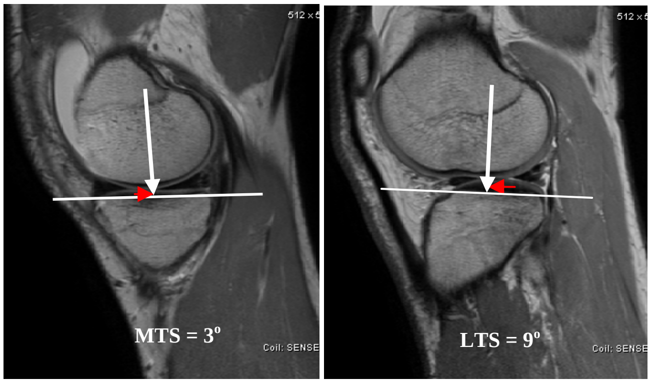

(a) (b)

Figure 4. JCF for a subject with negative difference between MTS and LTS: MTS < LTS.

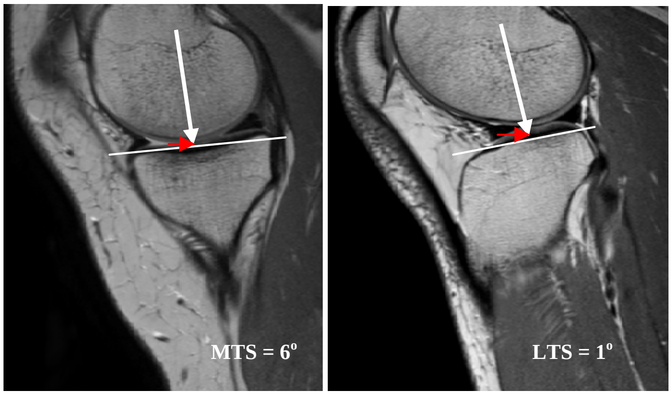

Figure 5. JCF for a subject with positive difference between MTS and LTS: MTS > LTS.

CONCLUSIONS

The geometry of the tibial plateau plays a crucial role in the biomechanical behavior of the tibiofemoral joint. According to our theoretical analysis, subjects with steeper lateral to medial CTS (Figure 1) will possibly be less susceptible to dynamic valgus. Subjects with steep MTS and LTS are potentially more susceptible to anterior tibial translation. Subjects with steeper LTS than MTS will be more susceptible to internal rotation while subjects with steeper MTS than LTS will be susceptible to external rotation.

Furthermore, the geometry of the tibial plateau could influence anterior cruciate ligament loading/injury, susceptibility to osteoarthritis, and uni-compartmental or total knee reconstruction.

REFERENCES

1. J. Hashemi, et al., The Geometry of the Tibial Plateau and its Influence on the Biomechanics of the Tibiofemoral Joint, *Journal Bone and Joint Surgery (JBJS)* 2008 Dec;90(12):2724-34.

VALIDATING THE ENHANCED DAILY LOAD STIMULUS MODEL USING THE BEDREST ANALOG OF SPACEFLIGHT

Kerim O. Genc[1,2], Brad T. Humphreys[3], Andrea J. Rice[2], Ricki K. Englehaupt[4], Sara C. Novotny[2], Raghavan Gopalakrishnan[4], Hakan Ilaslan[6], Angelo A. Licata[4,5,7], and Peter R. Cavanagh[2]
[1]Department of Biomedical Engineering, Case Western Reserve University, Cleveland, OH, [2]Department of Orthopaedics and Sports Medicine, University of Washington, Seattle, WA, [3]ZIN Technologies, Cleveland, OH, [4]Department of Biomedical Engineering, Lerner Research Institute, [5]The Center for Space Medicine, [6]Department of Diagnostic Radiology, Imaging Institute, and [7]Department of Endocrinology, Diabetes and Metabolism, Endocrinology & Metabolism Institute, Cleveland Clinic, Cleveland, OH; email: genck@u.washington.edu

INTRODUCTION

Carter, Whalen and colleagues [1,2] hypothesized that the effects of mechanical stimuli on bone homeostasis can be modeled with an empirical relationship called the daily load stimulus (DLS), which results from multiple individual loading events of various magnitudes and is expressed as follows:

$$DLS = \left[\sum_{j=1}^{k} n_j \left(Gz_j \right)^m \right]^{1/2m} \qquad \text{(Eq. 1)}$$

Gz = Peak magnitude of vertical component of ground reaction force (GRF)
j = Number of loading conditions
n= Number of loads in each j^{th} loading condition
k = Number of different loading conditions
m = Weighing factor {e.g. 4}

Thus far, researchers have only been able to determine the value of the exponent m through indirect methods and approximations to animal data. A value of 4 has been typically used.

Genc et al. [3] proposed an enhanced DLS model (EDLS) which is based on Eq. 1, but takes into account the effects of recently developed theories on saturation from repeated mechanical stimuli, rest insertions, and standing on the osteogenic potential of bone

Although Whalen et al. [4] were able to monitor GRF loading from normal daily activity, a direct examination of the EDLS has not been possible because no longitudinal studies of bone density which carefully control the loads applied to the musculoskeletal system have yet been performed. Prolonged bedrest, a frequently used analog to study musculoskeletal changes that occur during long-duration spaceflight, has potential as a method of validating the EDLS model. This is because diet and other factors are well controlled, and every external mechanical input into the musculoskeletal system can be controlled and monitored throughout the bedrest period (typically 30-90 days).

The purpose of the current study was to quantify typical daily loads experienced by the lower extremities of selected free-living volunteer subjects and to plan individualized exercise prescriptions based on the EDLS theory as countermeasures to prevent bone loss during an 84-day bedrest experiment. The specific aim of this study is to validate the EDLS model and directly determine the best value of the exponent m. To do this, we report here the pre- and post-bedrest volumetric bone mineral density (vBMD) changes acquired from quantitative computerized tomography (QCT) from the first 11 subjects in an ongoing experiment which will enroll 22 total subjects.

METHODS

Eleven subjects (6 male, 5 female), who were not habitual exercisers, were randomized to control (n=6) or treatment (exercise; n=5) groups and confined for 12 weeks to 6-degree head-down bedrest in the Clinical Research Unit at the Cleveland Clinic. During this time, the treatment group underwent individualized daily treadmill exercise programs in the Zero Gravity Locomotion Simulator (ZLS) [5] designed to replace their daily mechanical load stimulus experienced during free-living. Control subjects were suspended in the ZLS on the same schedule but did not exercise. Exercise was prescribed in equal, alternating epochs of activity and rest, which did not exceed a 5-minute duration, to mitigate the saturation effects said to occur with continuous repeated cyclical loading from activities such as walking or running [3].

In a method similar to Whalen et al. [2], the relative ratio of the mean EDLS before and during bedrest was used as a predictor of relative bone density before and after bedrest (Eq. 2).

$$\frac{\text{vBMD Post - Bedrest}}{\text{vBMD Pre - Bedrest}} = \frac{\text{Mean Bedrest EDLS}}{\text{Mean Pre - Bedrest EDLS}} \quad \text{(Eq. 2)}$$

RESULTS

Average vBMD from QCT data of all measurement categories indicated that during bedrest, control subjects had an EDLS ratio (Eq. 2) of zero and a vBMD ratio of 0.96 ± 0.03 (a vBMD loss of 4.44 ± 3.2%), whereas subjects who exercised, with a mean EDLS ratio of 0.99 ± 0.04, had a mean vBMD ratio of 1.01 ± 0.04 (a vBMD gain of 0.67 ± 4.0%) (Table 1, Figure 1). Both groups showed large inter-subject variability.

A mission to Mars is expected to be ~3 years in duration and linearly extrapolating the present results to a Mars mission suggests an average vBMD loss of 38.7% in crewmembers who do not perform any sort of exercise countermeasure and a gain of 7.98% in those who do (Figure 1).

DISCUSSION

Exercise prescriptions for bedrest subjects based on an approach that maintains an EDLS ratio as close as possible to 1 (Eq. 2) appears to have been successful, on average, thus far in attenuating bone loss compared to controls (Figure 1).

The bedrest study is ongoing, the data set is currently small, and statistical inference is not yet possible. Once the study is complete (n = 22 total), it will be possible to directly validate the estimated value of the exponent m by adjusting its value in the EDLS such that both the EDLS and vBMD ratios are equal.

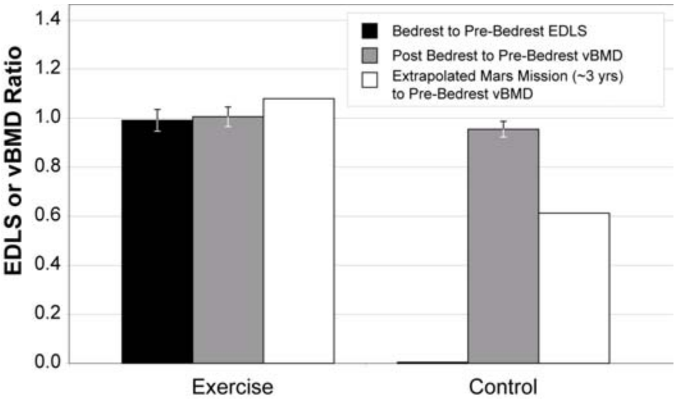

Figure 1: EDLS, bedrest vBMD and extrapolated Mars mission vBMD ratios for bedrest exercise (n = 5) and control (n = 6).

The EDLS model has the potential to improve the prescription of exercise countermeasures and prevent bone loss in crewmembers during spaceflight and on excursions to other planetary surfaces.

REFERENCES

1. Carter DR, et al. *J Biomech* **20**, 785-94, 1987.
2. Whalen RT, et al. *J Biomech* **21,** 825-37, 1988.
3. Genc et al. *Proceedings of the American Society of Biomechanics,* Palo Alto, United States, Abstract 179, 2007.
4. Whalen RT, et al. *Physiologist*, **36,** S139-40, 1993.
5. Genc et al. *Aviat Space Environ Med*, Nov **77**(11), 1117-24, 2006.

ACKNOWLEDGEMENTS

This work is supported by NASA grant NNJ05HE72G, by the National Space Biomedical Research Institute through NASA NCC 9-58 and in part by the National Institutes of Health, National Center for Research Resources, CTSA 1UL1RR024989, Cleveland, Ohio.

Table 1: Percent change in volumetric bone mineral density (vBMD) in exercise and control bedrest subjects

Subject	% vBMD changes from QCT			
	Femoral Neck	**Greater Trochanter**	**Intertrochanteric Space**	**Total Hip**
Exercise	-0.1 ± 2.4	-1.7 ± 4.5	3.1 ± 5.2	1.4 ± 4.0
Control	-4.4 ± 4.2	-4.0 ± 3.3	-4.5 ± 2.6	-4.9 ± 2.7

VOLITIONAL MVC EMG NORMALIZATION TASKS BETWEEN DAYS

[1] Toran MacLeod, [1]Nicole Chimera, [1]Kurt Manal, [1]Thomas S. Buchanan
[1]Center for Biomedical Engineering Research, University of Delaware, Newark, DE USA
email: macleod@udel.edu, web: http://www.cber.udel.edu/

INTRODUCTION

Using different normalization techniques has been shown to affect clinical interpretation [1]. The ideal normalization task is quick and reliable between subjects and data collections first, and it is also similar in motion to the trial being normalized second. The magnitude of the EMG signal from the normalization task is also important, especially for neuromusculoskeletal modeling [2], where the normalized signal is expected to be less than 1.0. A larger neural activation during the normalization task in comparison to a movement like running is often not possible.

Isometric maximal voluntary contractions (MVC) near the midpoint of the joint range of motion are often used as a normalization task. Others have suggested using isokinetic MVCs as an EMG normalization task because of the similarity in muscle action [3]. To normalize a running trial, a single concentric isokinetic MVC used as a normalization task may be close to ideal, because it is easy to obtain, similar in motion, and may have a larger raw EMG in comparison to isometric or eccentric contractions [3]. The best method for normalization at this point is not clear.

Possible between day variability in a normalization task EMG could affect comparisons between studies, within intervention, or pre-post comparisons [1]. The reliability of a single isokinetic MVC peak EMG used as a normalization task is unknown. To answer this question an experiment was carried out to compare isometric and isokinetic normalization tasks across days and subjects. These data will help to determine which normalization task is most ideal.

METHODS

Active male subjects (n=5) that were familiar with performing maximal voluntary contractions volunteered for the study. The protocol consisted of three separate days of testing and subjects repeated the same tasks on each day.

EMG data were collected (1000 Hz) from vastus lateralis (VL) and vastus medialis (VM) of a randomized leg with surface electrodes (Motion Laboratory Systems, Baton Rouge, Louisiana). Electrode placement and alignment followed standardized guidelines [4]. Further, care was taken to position the electrodes in the same place between collection days by marking the location with a pen to decrease the error related to between day EMG data collection and focus on variability of the normalization task.

All MVC testing was conducted on a Biodex System 3 Pro dynamometer (Biodex, Shirley, NY, USA). Each subject performed two trials of maximal knee extension at two angles (70 and 90 deg.) of knee flexion for the isometric protocol (isom) and two trials at four speeds (60, 180, 240 and 300 deg./s) of maximal isokinetic concentric knee extension (isok). Subjects randomly performed the sequence of trials. A resting trial was collected in between each active trial to minimize fatigue. In addition, subjects performed five running trials at 4.0 m/s, immediately after the Biodex protocol. The vertical component of the ground reaction force from a force platform (AMTI, Watertown, MA) was used to determine stance phase.

Raw EMG and force data were post-processed within analysis software (V3D, C-Motion Inc., Gaithersburg, MD, USA). EMG data had any DC offset corrected first, then were high-passed above 20 Hz through a phase corrected fourth order Butterworth bidirectional filter. A linear envelope was created using full wave rectification and a fourth order low-pass Butterworth filter at 20 Hz. The mean of the resting trials were then removed. For the normalization tasks peak EMG activity was defined as the single largest value of muscle activation.

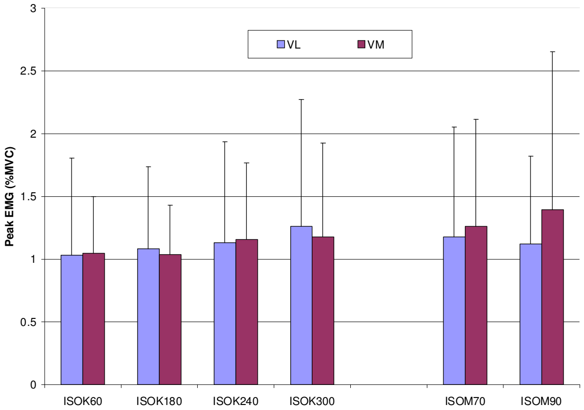

Figure 1: Stance phase peak EMG mean and standard deviations comparing normalization tasks across days and subjects for two quadriceps muscles (VL and VM)

Stance phase EMG data collected during the running trials were normalized to the peak EMG value of the six different normalization tasks. Peak normalized EMG values during stance phase were averaged across the five running trials. This was repeated for the six different normalization tasks. Subject data were then pooled to compute averages and standard deviations for each of the normalization tasks. These data were then used to compare the variance (standard deviation) in peak EMG values during running using different normalization tasks between days.

RESULTS AND DISCUSSION

Variability within the EMG normalization task used to compare between days could hide or accentuate clinically significant differences. Standard deviation from the mean could be accounted for by running trial and intersubject variability. Without variability in normalization tasks the standard deviation would be the same across tasks. However, stance phase peak normalized EMG (%MVC) means and standard deviations tended to increase for both muscles as isokinetic speed increased, and continued to be larger and more variable as the isometric knee angle increased (Figure 1). These results indicate that the two slower isokinetic normalization tasks are less variable, and are a more reliable method for EMG normalization.

The normalized EMG, for all tasks, were greater than 1.0 indicating that the normalization task peak EMG were smaller than those during stance phase. Normalized EMG during running are often larger than 1.0, so these results were not unexpected. However, the two slower isokinetic MVC normalization tasks had the smallest peak normalized EMG during stance and were closest to 1.0.

CONCLUSIONS

The optimal normalization task used for EMG is quick to perform and is reliable between collections. Large standard deviations were found in peak stance phase EMG using all normalization tasks. Clinical differences may not be detected if variability in the normalization task does not reveal real differences [1]. These data indicate that peak EMG from two muscles of the quadriceps will vary greatly because of the unreliability of commonly used normalization methods.

Others have come to the conclusion that clinical differences may be detected best when using an isometric MVC normalization task [1]. The results of this study indicate that the isometric MVC normalization task has greater variability in comparison to two slower isokinetic MVCs. Variability within the normalization task warrants further attention. Based on the current findings it is proposed that an isokinetic concentric contraction of either 60 or 180 deg./s be used because the task satisfies most of the requirements of the ideal normalization method.

REFERENCES

1.Benoit DL, et al. *Gait & posture* **18**, 56-63, 2003.
2.Buchanan TS, et al. *Journal of applied biomechanics* **20**, 367-95, 2004.
3.Burden AM, et al. *J Electromyogr Kinesiol* **13**, 519-32, 2003.
4.Hermens HJ, et al. *J Electromyogr Kinesiol* **10**, 361-74, 2000.

ACKNOWLEDGEMENTS

Supported by NIH R01-AR046386-06

POSTURAL SWAY CHANGES IN MILD TO MODERATE PARKINSON'S DISEASE

[1,2]Antonis Stylianou, [1,2]Carl Luchies, [1]Molly McVey, [3]Kelly Lyons, [3]Rajesh Pahwa
[1]Mechanical Engineering, The University of Kansas, Lawrence, KS, USA email: luchies@ku.edu
[2]Landon Center on Aging, [3]Parkinson's Disease and Movement Disorder Center, The University of Kansas Medical Center, Kansas City, KS, USA

INTRODUCTION

Postural control impairment is one of the most debilitating problems in patients with Parkinson's disease (PD), leading to increased risk of falling, fractures, and psychological fear of falling. The consequence is a significant reduction in their quality of life and life expectancy [1]. Most studies of postural sway parameters in PD were done on PD groups of moderate to high severity so very little is known about the initial changes in postural sway control in PD.

Force plate posturography is extensively used to quantify postural sway characteristics by analyzing the motion of the center of pressure (COP). Several studies investigated the differences in sway parameters between PD and age matched controls with mixed results [2]. Some studies found less variability for PD while others found an increase. The contradictory results can be explained by the differences in PD severity levels of the study populations and by differences in testing protocols.

In this study we investigated the sway path length characteristics between mild to moderate PD (H&Y 1.5-3), age matched and young control subjects.

METHODS

Nineteen PD patients (mean age = 65 years, SD = 9.7 years, range = 49-82 years) who were previously diagnosed with idiopathic Parkinson's disease and receiving treatment at the Parkinson's Disease & Movement Disorder Center at the University of Kansas Medical Center participated. All PD subjects had mild to moderate PD without musculoskeletal or significant balance problems not associated with Parkinson's. Fourteen elderly healthy controls (EH), (mean age = 67.8 years, SD = 9.6 years, range = 48-79 years) and ten young healthy controls (YH), (mean age = 23.9 years, SD = 2.5 years, range = 19-28 years) also participated.

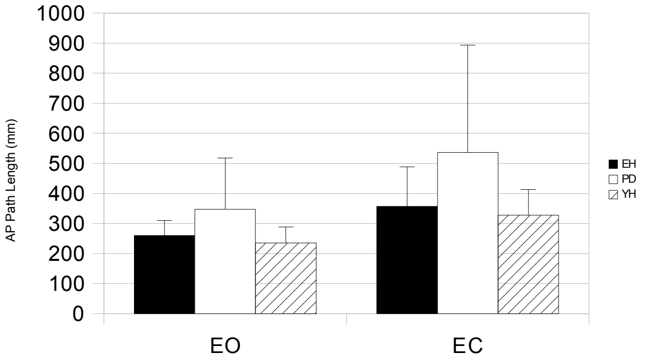

Figure 1: Mean (SD) of the AP sway length.

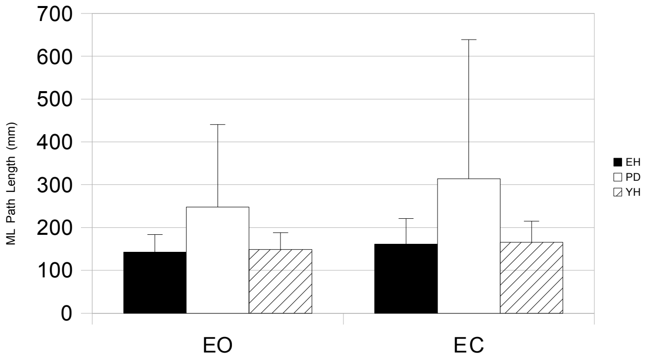

Figure 2: Mean (SD) of the ML sway path length.

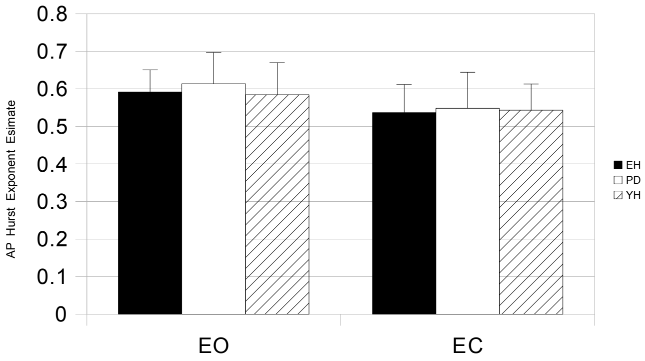

Figure 3: Mean (SD) of the Hurst exponent in the AP direction.

Control subjects were all physically active and free of any musculoskeletal or neurological disorders. All procedures were approved by the Institutional

Review Board of the University of Kansas Medical Center.

Postural sway during quiet standing, was measured using force plates (Advanced Medical Technology Inc. Watertown, MA) for three 30 second trials with eyes open and three trials with eyes closed. Force plate data were sampled at 1080 Hz using a Vicon 512 system (Vicon Peak, Lake Forest, CA). The subjects were instructed to maintain an upright posture with arms relaxed at their sides and with their feet shoulder width apart. The PD subjects were tested on the "on period" of their usual antiparkinsonian medication.

The following parameters were calculated to characterize postural sway: the sway path length in the AP and the ML directions, and the Hurst exponent in the AP and ML directions. Hurst exponents were calculated using Detrended Fluctuation Analysis [3]. Analysis was done in MATLAB (Mathworks, Natick, MA, USA), and statistical analysis was done in SPSS (SPSS Inc., Chicago, IL, USA).

RESULTS AND DISCUSSION

The AP sway path length was significantly greater for the eyes closed condition compared to the eyes open condition for all three subject groups: YH group (EO: 235.2 ± 53.7 mm, EC: 328 ± 84.9 mm, p = .010, a 28% increase), EH group (EO: 260.1 ± 49.7 mm, EC: 356.6 ± 132 mm, p = .015, a 27% increase) and for the PD group (EO: 347.3 ± 170.8 mm, EC: 536.8 ± 356.9 mm, p = .037, a 35% increase). Significant differences were observed only between the YH and PD group for the eyes open condition: PD > YH (p = .044). The results are shown in Figure 1.

For the ML sway path length, visual interaction was not statistically significant in any of the subject groups. Group differences were observed between the EH and the PD groups for both the eyes open and eyes closed conditions, (EO: PD > EH, p = .020, EC: PD > EH, p = .032). The results are shown in Figure 2.

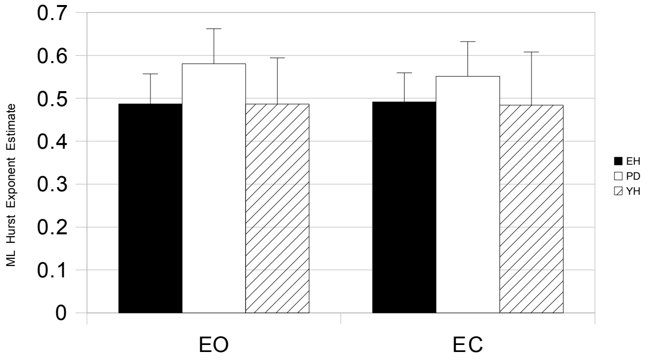

Figure 4: Mean (SD) of Hurst exponent in the ML direction.

Results of the Hurst exponent analysis are depicted in Figures 3 and 4. Significant changes due to visual condition were observed only in the PD group in the AP direction (EO: 0.6134 ± 0.0836, EC: 0.5482 ± 0.0963, a 12% decrease). Between group differences were observed between YH and PD in the ML direction for the eyes open condition, PD > YH, p = .039. The comparison between EH and PD yielded significant differences in the Hurst exponent in the ML direction for both visual conditions, for the EH group (EO: 0.4866 ± 0.0699, EC: 0.4913 ± 0.0681), and for the PD group (EO: 0.5802 ± 0.0816, EC: 0.5513 ± 0.0807) with PD > EH, p = .002 for eyes open and p = .013 for eyes closed.

CONCLUSIONS

Our results indicate that mild to moderate PD causes significant changes in sway characteristics for both the AP and ML directions, and that visual feedback effects in the PD group are similar with the two control groups. It is interesting that for the sway path length, both PD and aging caused an increase in the AP direction, with PD causing a significantly larger increase; but in the ML direction, only an increase due to PD was observed. At the same time in the ML direction, both YH and EH exhibit anti-persistent behavior evidenced by Hurst exponents below 0.5 whereas PD exhibit persistent behavior with Hurst exponents above 0.5.

REFERENCES

1. Adkin AL, et al. *Experimental Brain Research* **143**, 160-170, 2002.
2. Blaszczyk JW, et al. *Experimental Brain Research* **183**, 107-114, 2007.
3. Peng C, et al. *Chaos* **5**, 82-87, 1995.

THE EFFECTS OF STRENGTH TRAINING ON KNEE BIOMECHANICS DURING A DROP JUMP IN MALES

Christopher J. Sorensen, Boyi Dai, Patrick McIntyre, and Jason C. Gillette
Department of Kinesiology, Iowa State University, Ames, IA, USA
email: chriss40@iastate.edu, web: http://www.kin.hs.iastate.edu/

INTRODUCTION

In the United States there are approximately 175,000 primary Anterior Cruciate Ligament (ACL) reconstruction surgeries a year with an estimated cost of $11,500 each for a total of over $2 billion annually [1]. Results from movement studies and cadaver simulation studies [2] suggested that mechanisms that increase ACL strain are large proximal anterior shear force, small knee flexion angles, large valgus angles/moments, and large quadriceps EMG activity combined with small hamstring EMG activity during sudden deceleration movements.

The majority of previous studies looking at risk factors that lead to ACL injuries have been done using female subjects because females have a higher incidence rate. However, males still account for more total ACL injuries as there are a greater number of males involved in sports that regularly use the maneuvers mentioned above [3]. Therefore, the purpose of the current study was to see if 8 weeks of lower body resistance training would reduce the potential risk factors to ACL injuries during a drop jump in male subjects.

METHODS

Seven males (age 21.7 ± 1.6 yrs, height 1.83 ± 0.06 m, mass 84.2 ± 13.9 kg) from a basic weight training class at Iowa State University were recruited for this study. Subjects completed a pretest session, 8 weeks of lower body training, and a posttest session. Quadriceps and hamstring strength of the subjects' dominant leg was tested using a handheld dynamometer. For both tests the subjects sat in an upright position with their knees bent 90º and the subjects were asked to maximally extend or flex their knee for 3 seconds. Three trials of each test were completed. Reflective markers were then placed on the subject's dominant leg to collect kinematic data. The subject then performed 3 maximum vertical drop jumps. The drop jumps consisted of the subject standing on a 33 cm box with his feet 35 cm apart. The subject was then instructed to drop from the box with his dominant foot landing on a force platform and then immediately perform a maximal effort jump upon landing. Subjects were instructed to swing their arms during the jump as though they were rebounding a basketball. Motion capture and force data were collected at 160 Hz and 1600 Hz respectively.

During the training phase, subjects were asked to perform weight training sessions 3 times per week. They were to complete 3-4 exercises for the quadriceps and hamstring during each session. For

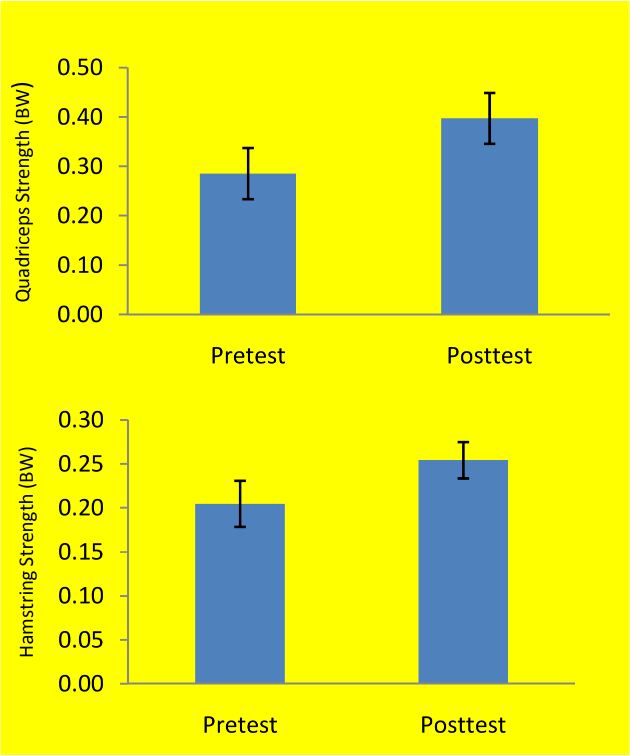

Figure 1: Quadriceps and hamstring strength before and after 8 weeks strength training

each exercise the subject completed 2-3 sets of 8-12 repetitions at a weight that they could complete all repetitions with proper technique. Exercises included dumbbell and barbell squats, dumbbell and barbell lunges, single leg dumbbell squats, machine leg curls and leg extensions, as well as stability ball leg curls.

Inverse dynamics were used to calculate the peak anterior tibial shear force (PATSF), knee flexion angle, abduction angle, extension moment, and adduction moment at PATSF. All parameters were transferred to local tibia coordinate system and expressed as internal loading. PATSF, hamstring and quadriceps strength were normalized to body weight (BW). Moments were normalized to BW and body height (BH). A two-tailed paired t-test was used to test for significance between pretest and posttest values (p-values<0.05 were considered significantly different).

RESULTS AND DISCUSSION

The total strength training session participation rate was 83% or 20 of 24 total sessions (8 weeks, 3 sessions/week). Quadriceps and hamstring strength increased significantly after 8 week strength training (p=0.01, Figure 1). The quadriceps strength increased from 0.29 ± 0.05 BW to 0.40 ± 0.05 BW, and hamstring strength ratio increased from 0.20 ± 0.03 BW to 0.25 ± 0.02 BW. No significant differences were observed for any of the biomechanical variables (p>0.05, Table 1).

Herman et al. [4] found that strength training alone was not able to change knee and hip kinematics and kinetics in female recreational athletes during a stop-jump task. Myer et al. [5] observed that both plyometric and balance training can reduce lower extremity valgus measures while some sagittal and frontal plane kinematic changes were both training and task specific. They suggested that neuromuscular training including plyometric and dynamic training should be included in ACL injury-prevention protocols. This study was consistent with the findings of Herman et al. [4] that strength training alone may not reduce ACL risk factors for males as well as females. Although lower extremity control patterns were found to be different between males and females and were proposed to be one of the potential causes of higher ACL injuries rates in females [6], it seems males and females have similar responses to strength training.

It has been suggested that control of the lower extremities during deceleration tasks depends on both strength capacity and neuromuscular patterns [4]. Although strength training could increase the muscular capacity to maintain the joint's stability, inappropriate neuromuscular control patterns may play a more important role in keeping joints in a safe condition and effectively using somatosensory feedback to adjust the control pattern according to the environment. However, strength training could increase the control capacity of joints and enhance the effects of neuromuscular training.

CONCLUSIONS

Lower body resistance training alone was able to increase quadriceps and hamstring strength but was not able to reduce ACL injury risk factors in males. Proper ACL injury prevention programs should include both strength and neuromuscular training.

REFERENCES

1.Gottlob CA, et al. *Clin Orthop* **367**, 272-282, 1999.
2.Yu B, and Garret WE. *Br J Sports Med* **41,** 47-51, 2007.
3.de Loess M, et al. *Scand J Med Sci Sports* **10**, 90–97, 2000.
4.Herman DC, et al. *Am J Sports Med* **36**, 733-740, 2008.
5.Myer GD, et al. *Am J Sports Med* **34**, 445-455, 2006.
6.Malinzak RA, et al. *Clin Biomech* **16**, 438-445, 2001.

Table 1: Average and Standard Deviation of Dependent Measures at Pretest and Posttest

	PATSF (BW)	Flexion Angle (Deg)	Abduction Angle (Deg)	Extension moment (BW*BH)	Adduction moment (BW*BH)
Pretest	0.17±0.10	36.28±11.91	2.07±4.39	0.05±0.03	-0.03±0.02
Posttest	0.19±0.08	39.16±7.41	2.88±4.65	0.06±0.02	-0.03±0.02

The Depth of the Medial Tibial Plateau is an Important Anterior Cruciate Ligament Injury Risk Factor

J. Hashemi[1], N. Chandrashekar[2], B. Gill[1], J. Slauterbeck[3], R. Schutt[1], E. Dabezies[1], and B. Beynnon[3]
[1]Texas Tech University (HSC); [2]University of Waterloo; [3]University of Vermont
email: javad.hashemi@ttu.edu, web: http://www.me.ttu.edu/Hashemi

INTRODUCTION

Identification of the risk factors that place an individual at increased risk for suffering anterior cruciate ligament (ACL) injuries has been the subject of extensive research during the past decades. However, the geometry of the tibial plateau has been largely ignored as a source of possible risk factors. Discovery of the ACL injury risk factors associated with the tibial plateau may 1) lead to delineation of the existing sex-based disparity in ACL injuries and 2) help develop strategies for the prevention of ACL injuries regardless of subjects' sex.

METHODS

The medial (MTS), lateral (LTS), and coronal (CTS) tibial slopes as well as the medial tibial depth (MTD) of concavity in 55 uninjured controls (33 females and 22 males) and 49 ACL-injured cases (27 females and 22 males) were measured using MRI images (Figure 1). A logistic regression model was used to determine the probability of ACL injury in a subject based on the measured covariates.

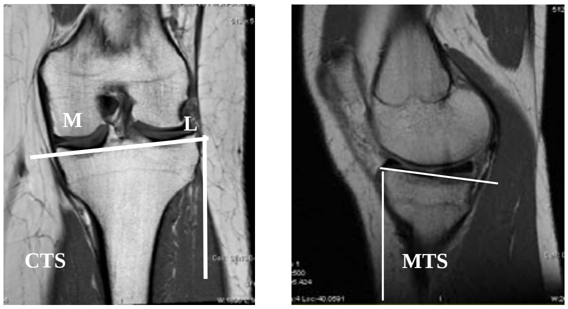

(a) CTS (b) MTS

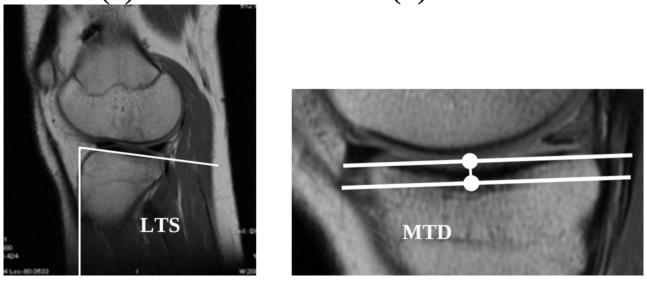

(c) LTS (d) MTD

Figure 1. (a) Coronal tibial slope (CTS), (b) Medial tibial slope (MTS), (c) lateral tibial slope (LTS), and (d) the medial tibial depth (MTD).

RESULTS AND DISCUSSION

Analysis of the combined data from the males and females found that the MTD value was lower and the posterior directed MTS and LTS values were greater in the ACL injured subjects compared to the controls ($p<0.0001$, $p = 0.018$, $p=0.0098$). There was no difference in the means of CTS value between the groups ($p=0.94$). Analysis of the data obtained from the males revealed the same findings: The mean of MTD values was lower, the means of the posterior directed MTS and LTS values were greater in the ACL injured subjects compared to the controls ($p=0.0008$, $p=0.0089$, $p=0.033$), and there was no difference in the CTS value ($p=0.74$). When considering the females as a group, the mean of MTD value was found to be lower ($p=.0004$), and there was a trend for the mean of posteriorly directed LTS value to be greater in the ACL injured subjects compared to the controls. In females, there was no difference in the mean values of MTS and CTS values between the ACL-injured and control groups.

Based on the combined data, the maximum likelihood estimate of the logit model was obtained to be

$$logit(p) = 1.100 - 1.121\,MTD + .159\,LTS + .169\,sex * MTS \qquad (1)$$

Where p denotes the estimated probability of ACL injury for given values of the risk factors in the model and the variable sex is defined to be 1 for male subjects and 0 for female subjects. Accordingly, for both sexes, the odds ratio (OR) for ACL injury for *c* unit change in one measured variable while keeping the other variables constant is

$$OR(variable) = e^{-1.12c} \qquad (2)$$

The *ORs* and their respective 95% confidence intervals are presented in Table 1. There was an inverse relationship between the risk of ACL injury and the MTD values. For instance, if *c* is decreased by 1mm (c= -1), the *OR*(MTD) will be 3.03; indicating that the odds of ACL injury increases 3.03 times with a one mm decrease in MTD at each level of MTS and LTS. The odds ratio increases exponentially when MTD decreases as a multiple of c. For example, when c is decreased by 2mm the odds of injury associated with this MTD measurement alone increase 9.4 times with a corresponding confidence interval ranging from 3.13 to 27.98. It is important to note that this *OR* does not include the effect of the risk factor LTS and only reports on the effect of MTD adjusted for the other risk factors in the model. To assess the impact of a one degree increase in LTS combined with a 1mm decrease in MTD, the *OR*s for the respective covariates are multiplied. Thus for females, since only LTS and MTD are contributors to the model, a degree increase in the posterior slope of the LTS and a 1 mm decrease in MTD, will result in an overall *OR* of 3.58 (1.17 x 3.03 = 3.58). Amongst the male subjects, for a given MTD and MTS, a one degree increase in LTS will result an increase in the odds of injury by 1.17 (95% C.I. 1.01 to 1.39). Thus for males, since MTS, LTS, and MTD are all contributors to the model, the overall *OR* will be 4.18 which is the product of respective ORs (1.17 x 3.03 x 1.18) for a 1mm decrease in MTD combined with 1 degree increases in each of the values of MTS and LTS.

Table 1. Odds ratios for MTS, LTS, and MTD.

Effect	**Point Estimate**	**95% Wald Confidence Limits**	
LTS	1.17	1.002	1.37
MTD	3.03	1.78	5.26
Sex*MTS	1.18	1.01	1.39

In order to expose the potential impact of tibial slopes in combination with depth of medial tibial concavity, we also prepared graphs of normalized LTS versus MTD (Figure 2). Again, we normalized the LTS and MTD of all subjects (injured and uninjured) with respect to their maximum values in the uninjured population (14°, and 5.2 mm respectively).

In the figure, the area of the plot is divided into four regions by two mutually orthogonal lines representing the normalized median values of the un-injured control population. In Figures 2, 75% of the injured subjects fall in the lower right quadrant (Region IV; high LTS, low MTD). Note that there are no injured subjects in Region I (low LTS and high MTD).

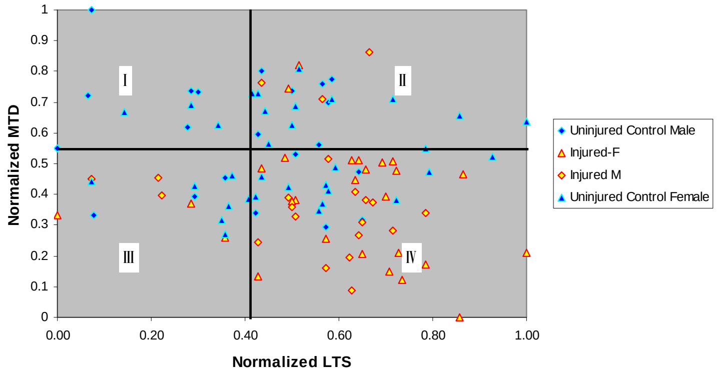

CONCLUSIONS

In this investigation we found that subjects with increased medial and lateral tibial plateau slopes combined with a decreased medial tibial depth are at increased risk of suffering an ACL injury. Our results suggest that MTD is an important risk factor for ACL injury followed by LTS and MTS. These tibial plateau measurements could all be considered as robust risk factors for ACL injury in the development of injury risk models.

REFERENCES

1. J. Hashemi, et al., The Geometry of the Tibial Plateau and its Influence on the Biomechanics of the Tibiofemoral Joint, *Journal Bone and Joint Surgery (JBJS)* 2008 Dec;90(12):2724-34.

INTEGRATION OF VIBROTACTILE FEEDBACK IN A 3D MODEL OF HUMAN BALANCE

Tulga Ersal, Vivek V. Vichare and Kathleen H. Sienko
Department of Mechanical Engineering, University of Michigan, Ann Arbor, MI
email: tersal@umich.edu

INTRODUCTION

Vibrotactile feedback has been experimentally shown to significantly improve postural stability in subjects with unilateral and bilateral vestibular loss during both single-axis [1] and multidirectional [2] perturbations of stance. The feedback device consists of an array of vibrating actuators (tactors) that map body tilt estimates onto the subject's torso; tactor rows and columns indicate tilt severity and direction, respectively. This study aims to integrate external vibrotactile feedback in a mathematical model of human stance in order to 1) gain insight into the effects of the device during multidirectional perturbations, 2) develop theoretical justifications for the experimental observations, and 3) enable subsequent optimization of the display design.

METHODS

The human body was modeled as a multibody system consisting of the legs, torso, arms, and head. The model was assumed to be connected to the support surface through the ankles. The legs were modeled as solid circular cylinders, the torso as a solid elliptic cylinder, and the head as a solid ellipsoid. The model was parameterized using the percent-of-total-weight and -height data available in the literature. The ankles and the hips were modeled as spherical joints, but the hip joints included additional vertical springs to allow for torso sway in the medial-lateral (M/L) plane. The knees were assumed to be locked.

The proprioceptive balance control mechanism was assumed to comprise two independent full-state-feedback controllers for the anterior-posterior (A/P) and M/L axes, respectively. The assumption of independence was supported by experimental evidence [3], and the full-state-feedback assumption had previously been used by other researchers [4, 5]. The proprioceptive sensory information was assumed to be without noise, but with delay. The feedback gains and delay were adjusted to achieve initial peaks and slopes of A/P and M/L tilt similar to the ones observed in the experiments. No feedforward or estimation mechanism was considered.

The vestibular control system was adopted from the linear feedback model of canals and otoliths given in [6] with the addition of an overall gain that could be adjusted to simulate different levels of vestibular loss. The vestibular control torque was added to the proprioceptive control torque at the ankles based on the rationale that for small perturbations "ankle strategy" is preferred [5].

The vibrotactile feedback device was modeled following the same algorithm used in the actual device. Specifically, the device gives feedback based on the measured torso sway plus one-half of its rate, thereby providing PD-type feedback. Three rows of tactors were used to code different sway magnitudes, while tactor columns were used to code tilt direction. In the model, each of the three rows was assumed to have a constant gain associated with it. Furthermore, two additional gains contributed to the overall gain in the A/P and M/L directions. The tactor gains were determined through numerical optimization to maximize their effect. Thus, best-case scenarios were evaluated. Three configurations varying in spatial resolution were experimentally tested and modeled, namely, 4, 8, and 16 column displays providing 90°, 45°, and 22.5° resolutions, respectively. These displays used a nearest-tactor strategy, meaning only the tactor closest to the direction of sway fired. A fourth display, 4I, allowed the tactors in a 4-column display to fire independently along the A/P and M/L axes. When the tactors did not align with cardinal directions, it was assumed that the human was capable of perfectly separating the tactor output into its cardinal components. This again implies that the best-case scenario was considered. The tactor output was filtered through a first order low-pass filter to create a smooth output. The model also included the delay associated with sensing and reacting to vibrotactile feedback.

Finally, the vibrotactile feedback was considered as an amplification factor for the integrated ankle torque. This allowed for the device to affect the balance through the existing control mechanism rather than being an additional torque source in and of itself.

RESULTS AND DISCUSSION

Simulations were run for the various discrete surface perturbations performed in the experimental sessions including: 180°, 270°, 45°, 191°, 225°, 11°, 326°, 90°, 360°, and 146°. The angles were measured clockwise from the anterior axis. A sample result for a 225° perturbation is shown in Figure 1 for the 4-column configuration; its shape is in good qualitative agreement with the experimental result, and it also predicts the time-to-peak and peak magnitudes fairly well. Table 1 highlights some of the percent reductions in root-mean-square (RMS) sway obtained with the various simulated displays.

Based on the simulation results, the following conclusions were drawn about the theoretical effects of the feedback device:

1. The device reduced the RMS sway, but it was more effective along the A/P axis than the M/L axis; a finding consistent with the experiments. That is arguably because the human is more stable in the M/L axis than in the A/P axis due to the mechanics of the body, which is apparent in the relatively lower feedback gains in the M/L axis in the model.
2. The device did not have a significant effect on the initial peak displacement along the A/P axis. Rather, it reduced the RMS sway by impacting the return trajectory. This was because the peak displacement was mainly affected by the proprioceptive controller due to the larger delays associated with the other controllers involved. Likewise, experimentally it was shown that the feedback reduced the time to return to upright following the initial peak displacement and the subsequent RMS sway (predominantly in the A/P direction).

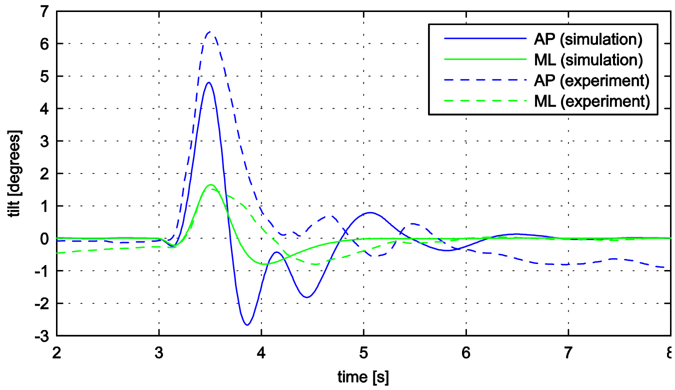

Figure 1. Sample experimental vs. simulated body tilt for a 225° perturbation and 4 columns

Table 1. Reduction in RMS sway in various directions

Dir		Reduction in RMS sway			
		4 col	8 col	16 col	4I col
180°	Total	19%	20%	20%	19%
	AP	19%	20%	20%	19%
	ML	1%	1%	1%	0%
270°	Total	11%	11%	11%	12%
	AP	0%	1%	1%	1%
	ML	11%	11%	11%	12%
225°	Total	17%	17%	18%	17%
	AP	18%	19%	19%	19%
	ML	3%	3%	10%	-6%
191°	Total	19%	19%	19%	19%
	AP	20%	19%	19%	19%
	ML	6%	7%	5%	12%

3. Although there may be some differences in trajectories, no significant difference was observed in the RMS sway among the different displays. This is likely because all tested configurations provided feedback along the A/P axis, for which the feedback had the greatest effect. Therefore, a 4-column display may provide sufficient resolution for augmenting native sensory cues during multidirectional surface perturbations for individuals with compromised vestibular function.

REFERENCES

1. Wall, C, et al., *Journal of Vestibular Research-Equilibrium & Orientation* **15**, 313-325, 2005.
2. Sienko, KH, et al., *Journal of Vestibular Research* **in press**, 2009.
3. Matjačić, Z, et al., *Journal of Biomechanics* **34**, 187-196, 2001.
4. van der Kooij, H, et al., *Biological Cybernetics* **80**, 299-308, 1999.
5. Kuo, AD, *IEEE Transactions on Biomedical Engineering* **42**, 87-101, 1995.
6. Nashner, LM, *Kybernetik* **10**, 106-110, 1972.

ACKNOWLEDGEMENTS

The experimental data collected in this study was supported by the National Institutes of Health (NIH NIDCD R01 DC6201) under the direction of Dr. Conrad Wall. The authors also gratefully acknowledge the contributions of Conrad Wall, Dave Balkwill, Dominic Piro, and Arthur Kuo.

MODELING MUSCLE CONTRIBUTIONS TO MULTIJOINT MECHANICS

[1,3]Xiao Hu, [1,2,3,4]Wendy Murray and [1,2,3]Eric Perreault
Departments of [1]Biomedical Engineering and [2]PM&R, Northwestern University, Chicago, IL
[3]SMPP, Rehabilitation Institute of Chicago, Chicago, IL; [4]VA Hines, Hines, IL
Email: x-hu@northwestern.edu

INTRODUCTION

Humans regulate arm mechanics to allow for stable interactions in a range of tasks. Understanding how this regulation occurs is an essential problem in motor control. At a fixed posture, regulation occurs largely through changes in muscle activation. These changes can be quantified by estimates of endpoint stiffness, which describes the relationship between displacements of arm posture, applied at the hand, and the corresponding endpoint forces [1]. There have been many empirical studies of endpoint stiffness regulation, but the underlying physiology remains poorly understood. As a result, quantitative models do not exist for exploring how changes in neural activation, as occur following motor learning or injury, influence regulation of arm mechanics.

For small, rapid perturbations, muscle mechanics are dominated by short-range stiffness (SRS) [2]. Since arm stiffness is usually measured using such perturbations, we hypothesized that it would be dominated by the SRS of active muscles. We recently developed a SRS model dependent only on muscle geometry and force [3]. Here we assess if this muscle model can be combined with a musculoskeletal model of the arm to predict how endpoint stiffness varies with changes in muscle activation. Such a combined model would allow for computational explorations of how changes in neural drive influence the regulation of human arm mechanics.

METHODS

Modeling

The musculoskeletal model used in this study was developed by Holzabaur et. al [4] and implemented in SIMM (Musculographics Inc.). It consisted of 3D representations of the shoulder and elbow, and included 18 shoulder muscles and 22 elbow muscles.

The SRS of all muscles was modeled as detailed by Cui et. al [3]. In summary, the model (Eq. 1) contains a force-dependent muscle stiffness (K^m, Eq. 2) in series with a tendon stiffness K^t. Because anatomical data for all tendons were not available, K^t was defined as described by [5] rather than [3] (Eq. (3)). Parameters defining muscle fiber length (l_0^m), maximum force (F_0^m) and tendon slack length (l_s^t) were obtained from the SIMM model [4]. γ is a dimensionless constant describing the scaling of SRS with force [3]. No parameters were fit to the experimental data presented below.

$$K = K^m K^t / (K^m + K^t) \qquad (1)$$

$$K^m = \gamma F^m / l_0^m \qquad (2)$$

$$K^t = 37.5 F_0^m / l_s^t \qquad (3)$$

The resulting musculoskeletal model was used to estimate endpoint stiffness during conditions matched to previous experiments [6], in which subjects exerted isometric forces against a rigid manipulator. Presented results are for the right hand positioned, ~30 cm in front of the shoulder. Optimization was used to distribute forces across muscles [7].

The estimated forces (F^m) were used to calculate muscle stiffness according to Eq. 2. Muscle stiffness can then be used to compute the joint stiffness (K^j) and endpoint stiffness (K^e) through the coordinate transformations in Eq. 4 [8], where θ is the joint angle vector and F^{end} is the endpoint force. J and G are Jacobians relating motions in joint space to muscle and endpoint space, respectively.

$$\begin{aligned} K^j &= J^T K^m J + \frac{\partial J^T}{\partial \theta} F^m \\ K^e &= \left(G^{-1}\right)^T \left[K^j - \frac{\partial G^T}{\partial \theta} F^{end} \right] G^{-1} \end{aligned} \qquad (4)$$

Experiment

In addition to the available endpoint stiffness data [6], we collected electromyograms (EMGs) from 8 muscles crossing the elbow and shoulder to evaluate how the optimization algorithm distributed muscle forces. These new experiments had postures and endpoint forces matched to those used previously [6]. EMGs are expressed as a percentage of the recorded EMGs during a maximum contraction.

RESULTS and DISCUSSION

Endpoint stiffness can be described graphically using an ellipse to show the directions along which the arm is most resistant to postural perturbations [1]. Stiffness ellipses measured for one subject and the corresponding model predictions are below (Fig. 1). Each ellipse is centered at a location proportional to the force direction and magnitude the subject was exerting. The model describes the experimental data well, but there is some discrepancy in the size of the modeled ellipses, especially for endpoint forces directed medially. Stiffness magnitude can be quantified by the area of the ellipse. The r^2 between the experimental and modeled areas was 0.72.

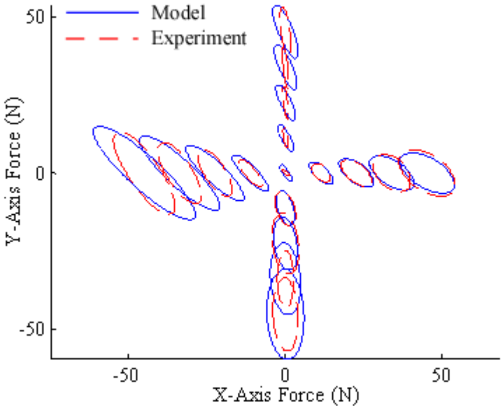

Figure 1: Modeled and experimental endpoint stiffness.

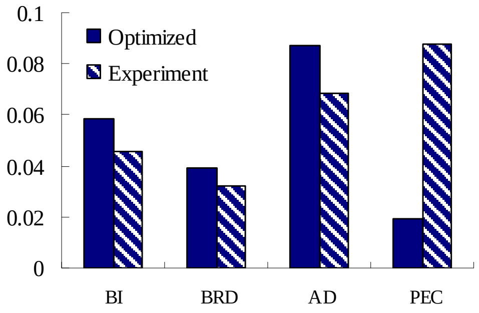

Figure 2: EMG and normalized force. Biceps (BI), BRD (Brachioradialis), Anterior Deltoid (AD) and Pectoralis major Clavicular head (PEC).

These size differences may be due to an inaccurate estimation of anterior deltoid (AD) activation in the model. Estimated muscle forces obtained by optimization and measured EMGs are shown for four muscles active during the generation of medial forces (Fig. 2). The optimization algorithm suggested that shoulder flexion is dominated by AD activation, whereas the EMGs show contributions from both AD and pectoralis (PEC). This difference may be due to sensitivity of the employed optimization to muscle moment arms. For the posture studied, the modeled moment arm (4.5 cm) was much greater than reported in an independent study [9] (1.9 cm). Decreasing the AD moment arm redistributed the estimated muscle activations to better match experimental EMGs and improve the accuracy of the modeled endpoint stiffness (Fig. 3). In the updated model, the r^2 between experimental and modeled stiffness areas increased to 0.84.

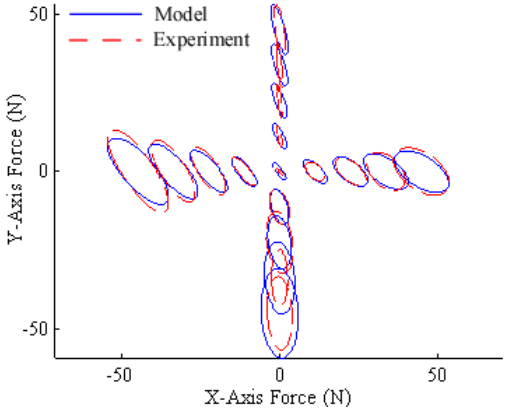

Figure 3: Influence of altered AD moment arm on endpoint stiffness.

In conclusion, we can characterize endpoint stiffness using a realistic musculoskeletal model coupled to a model of muscle SRS. This was accomplished without fitting any model parameters to the presented experimental data. The model generalized across subjects and postures (not shown) suggesting it can be used to assess how changes in muscle activation influence the regulation of endpoint stiffness under a wide range of conditions.

REFERENCES

1.Mussa-Ivaldi, FA, et al, *J Neuroscience* **5**, 2732-2743, 1985
2.Kirsch, RF, et al, *Biomed Eng, IEEE Trans* **41**, 758-770, 1994
3.Cui L, et al. *J Biomech* **41**, 1945-1952, 2008
4.Holzbaur KRS, et al. *Ann Biomed Eng* **33**, 829-840, 2005.
5.Zajac, FE *Crit Rev Biomed Eng* **17**, 359-411, 1989
6.Perreault, EJ, et al. *Exp Brain Res* **141**, 312-323, 2001
7.Crowninshield, RD. *Bull Hosp Jt Dis Orthop Inst* **42**, 164-70, 1983
8.McIntyre J, et al. *Exp Brain Res* **110**, 248-264, 1996
9.Kuechle DK, et al. *J. Shoulder Elbow Surg* **6**, 429-439, 1997.

ACKNOWLEDGEMENTS

This work was supported by NIH grants K25 HD044720. The authors would also like to thank Dr. C. Goehler for his simulation help.

PLANTAR FLEXOR REFLEX RESPONSE TO A PERTURBATION DURING HUMAN WALKING MAINTAINS ANKLE JOINT TORQUE PATTERN

Pei-Chun Kao[1], Cara L. Lewis[1], and Daniel P. Ferris[1]
[1]Human Neuromechanics Laboratory, University of Michigan, Ann Arbor, MI, USA
E-mail: kaop@umich.edu

INTRODUCTION

Appropriately gated reflexes play an important role in correcting gait perturbations and preventing falling (Nielsen and Sinkjaer, 2002). Many previous studies have documented large increases in ankle plantar flexor electromyographic (EMG) activity following a rapid dorsiflexion perturbation during human walking (Sinkjaer et al, 1996). In spite of numerous studies on this type of perturbation response, there is virtually no data on the mechanical effects produced by the reflex response.

Mechanical quantification of reflex responses during gait perturbation is critical to the advancement of accurate computer simulations of neuromusculoskeletal models. Appropriate reflex responses in the computer simulations would allow investigators to faithfully reproduce behaviors related to unexpected perturbations. While there are many advanced musculoskeletal models for computer simulations, programming reflex responses into the simulations requires knowing general principles governing how the nervous system scales reflex responses.

The purpose of this study was to mechanically quantify joint kinetics of reflex responses during an unexpected gait perturbation. Previous studies on motor adaptation to a robotic ankle exoskeleton found that subjects decreased soleus EMG amplitude by ~35% with 45 minutes practice walking with plantar flexor assistance (Gordon and Ferris, 2007). It seemed likely that turning off the robotic assistance unexpectedly after adaptation would cause a gait perturbation and result in a reflex response stabilizing the body.

METHODS

We used a pneumatically-powered ankle exoskeleton controlled by soleus muscle activation (i.e., proportional myoelectric control) to provide plantar flexor torque assistance (**Fig 1**). We recorded lower-body kinematics, ground reaction forces, muscle activity, and soleus H-reflex measurements at late stance during steady state and randomly perturbed steps as subjects walked on an instrumented treadmill at 1.25 m/s. Perturbations occurred at least10 steps apart and we averaged data from ~4 steps. We calculated joint kinetics using Visual 3D software.

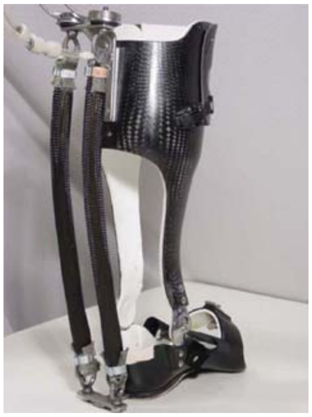

Figure 1. The robotic ankle exoskeleton had two artificial pneumatic muscles providing plantar flexor torque when activated. Each exoskeleton was custom made for each subject.

RESULTS AND DISCUSSION

During steady-state walking, the ankle exoskeleton provided a substantial plantar flexor moment (0.77±0.26 Nm/kg, mean±SD) (**Fig 2**) that was ~50% of the total ankle plantar flexor moment during push-off (1.50±0.12 Nm/kg). When the power was turned off, subjects reacted to the unexpectedly decreased exoskeleton assistance by increasing soleus EMG with a time lag of 60±29 (mean±SD) milliseconds after the ankle angle deviated from the steady state pattern. The rapid increase in soleus recruitment prevented the total ankle moment from differing from the steady state pattern (**Fig 2**). Subjects had significantly smaller ankle positive work (perturbed: 14.6±3.4 J; steady

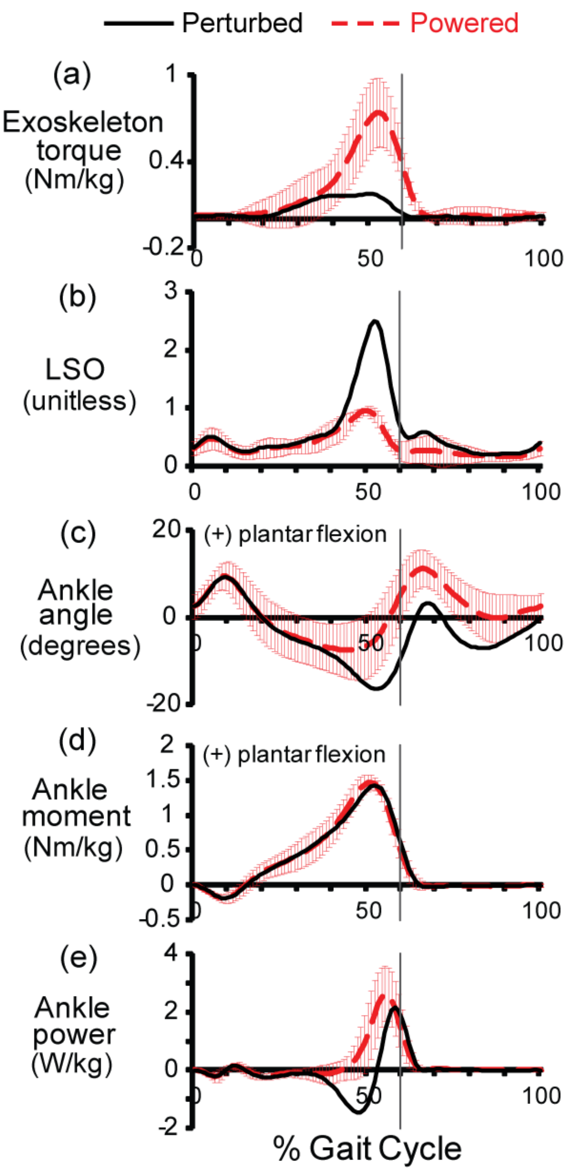

Figure 2. Gait dynamics during powered and perturbed steps. The error bars indicate ±1SD.

state: 24.5±3.4 J; *p*<0.0001) and greater negative work (perturbed: -17.4±4.7 J; steady state: -8.3±3.6 J; *p*<0.0001) during the perturbed steps compared to steady state.

In spite of the invariant ankle joint moment, the total support moment was substantially different during the perturbed steps compared to the steady state condition (**Fig 3**). The second peak of overall support moment was ~36% larger for the perturbed steps compared to the steady state steps (perturbed: 1.00±0.24 Nm/kg; steady state: 0.64±0.26 Nm/kg; *p*<0.0001).

The peak force of the contralateral leading leg after perturbation was ~15% greater than steady state walking (perturbed: 12.53±0.97 N/kg; steady state: 10.93±0.43 N/kg; *p*<0.0001). This result is consistent with observations of passive dynamic walking models with variations in trailing limb mechanical impulse.

During the perturbed steps, the normalized soleus H-reflex gain (H-reflex amplitude/background EMG) was not significantly different compared to the powered steps (*p*=0.17).

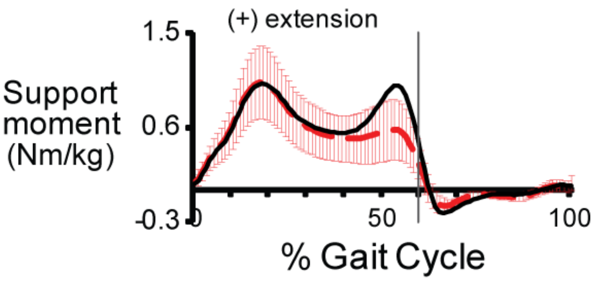

Figure 3. Overall support moment during powered and perturbed steps.

SUMMARY/CONCLUSIONS

This is the first study to show that the nervous system modulates reflex responses during human walking to maintain invariant ankle joint patterns relative to unperturbed gait. Our findings suggest that ankle joint moment patterns are maintained even when the overall support moment pattern changes during a gait perturbation. This may represent a general principle governing reflex responses to mechanical perturbations that could be easily implemented in computer simulations of neuromusculoskeletal models.

REFERENCES

1. Gordon and Ferris. J of Biomech, 2007.
2. Nielsen and Sinkjaer. J Electromyogr Kinesiol, 2002.
3. Sinkjaer T et al. J Neurophysiol, 1996.

ACKNOWLEDGMENTS

Supported by NIH grants R21 NS062119 and F32 HD055010

ASSESSMENT OF A POTENTIAL ACL INJURY RISK PROTOCOL

[1]Joshua Weinhandl, [2]Brian S. R. Armstrong, [1]Jennifer E. Earl, [2]Todd P. Kusik,
[2]Robb T. Barrows, and [1]Kristian M. O'Connor

[1] Department of Human Movement Sciences
[2] Department of Electrical Engineering
University of Wisconsin-Milwaukee, Milwaukee, WI, USA
E-mail: weinhan2@uwm.edu Web: www.chs.uwm.edu/neuromechanics

INTRODUCTION

Three-dimensional kinematics of the lower limb during dynamic activities have been shown to be predictive of ACL injury [1]. Motion tracking outside of a laboratory environment is a critical next step in applying ACL research findings to the general population. The Retro-Grate Reflector (RGR) is a new technology that allows for 3-D motion capture using a single camera [2]. An RGR target is constructed by applying artwork on the front and back of a transparent substrate, such as a glass or plastic plate (Figure 1).

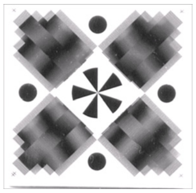

Figure 1: RGR target. Moiré patterns co-vary with out-of-plane rotations, permitting 6DOF tracking with a single camera system.

The kinematic information derived from RGR measurement has been shown to match measurements recorded with a multi-camera system [3]. The next phase of development is to use the RGR camera system outside of the laboratory environment, establishing a quick and easy 3-D testing protocol while maintaining an accurate description of the person's movement patterns. Therefore, the purpose of this study was to conduct a field testing protocol and to assess the dynamics of two tasks with the goal of detecting asymmetries.

METHODS

The data collection system consisted of a single Basler A501k (Ahrensburg, Germany) 1.3 MPixel camera and a portable computer. A custom-built high-power LED lighting system was used to provide illumination for the RGR target. The system was transported to an indoor gymnasium and members of the university women's soccer team participated during a normally scheduled off-season condition session. Operating with a single camera, set up of the RGR system for data collection required approximately 15 minutes.

For each subject, 3-D target poses were recorded for the thigh and shank. This was done separately for the left and right legs during two tasks; 1) a drop jump (DJ), and 2) a land-and-cut maneuver (CUT). Three trials were collected for each task and side, for a total of 12 trials. Both tasks were initiated from a 35-cm high box (Figure 2). Prior to data collection, a standing trial was collected for each side with the subject standing on the ground. All data were collected at 100 Hz. The total time to complete the data collection for each subject was ~7 minutes and 15 total subjects were collected in two hours.

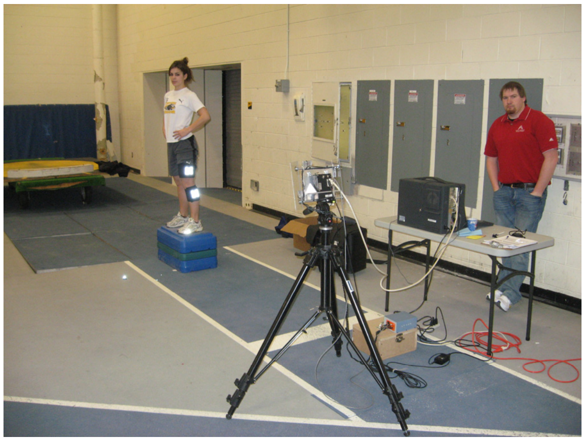

Figure 2: Experimental setup in an indoor gymnasium.

Target poses for the thigh and shank during the movement trials were expressed relative to the standing trial pose. Knee angles were calculated using a joint coordinate system approach [4]. Since the camera was not placed orthogonal to the plane of motion, a transformation between the camera-based coordinate system and the global coordinate system was estimated through an optimization procedure that minimized the correlation between sagittal and frontal plane joint angle time series for each movement trial. This approach was loosely based on previous work attempting to reduce cross talk in clinical gait data [5]. The mean difference between right and left joint angles as well as the R^2 values between the right and left time series were computed to evaluate symmetry during the two tasks for each subject. The mean differences and R^2 values were compared across tasks using a dependent t-test ($p<0.05$)

RESULTS AND CONCLUSIONS

The mean difference between right and left sides was not significant for either the DJ or CUT task (Table 1). While the group mean time series in the sagittal, frontal, and transverse planes matched closely between sides (Figure 3), individual subject correlations varied for both tasks. In the sagittal plane, the correlation between right and left time series was significantly less for the CUT task. However, the R^2 values were high for both tasks, suggesting symmetry in the sagittal plane. Asymmetries were detected in the frontal and transverse plane for both tasks, as evident by the lower correlations. In addition, the R^2 value in the frontal plane was significantly less for the DJ task compared to the CUT task. Therefore, the asymmetry between sides was larger during the DJ and it may be a better task for detecting asymmetries. In summary, through the use of the RGR technology we were able to conduct a 3-D field test that required minimal setup and was conducted with relative ease while maintaining an accurate description of the individuals' movement pattern.

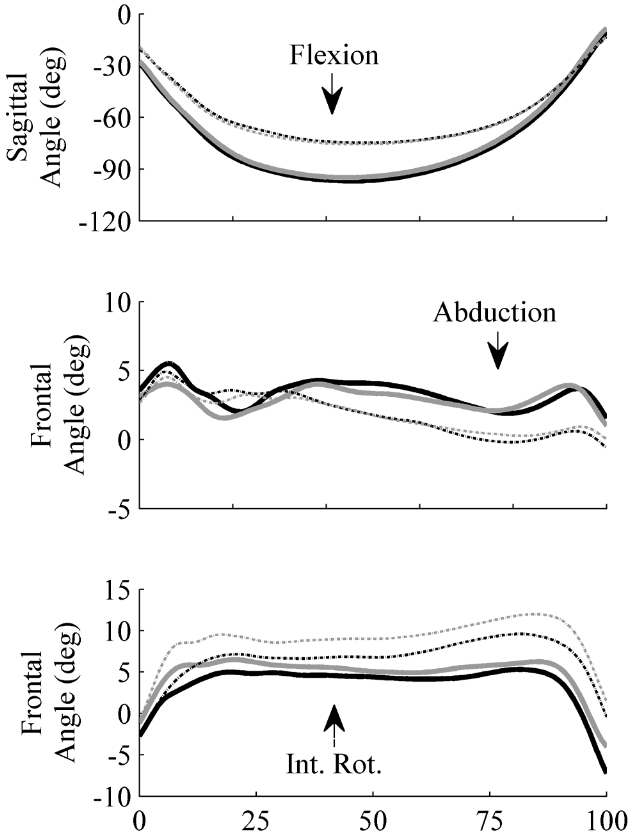

Figure 3: Knee angles in all three planes. The thick lines represent DJ (black=right, grey=left) and the thin lines represent CUT (black=right, grey=left).

REFERENCES

1. Hewett, TE et al. *Am J Sports Med*, **33**, 492-501, 2005.
2. Armstrong, BSR. In *Proc. 2002 Int. Conf. on Robotics and Automation*. IEEE, 2002.
3. O'Connor et al. *Proceedings of the American Society of Biomechanics*, Stanford, CA, 2007.
4. Grood & Suntay. *J Biomech Eng*, **105**, 136-144, 1983.
5. Rivest, L. *J Biomech*, **38**, 1604-1611, 2005.

ACKNOWLEDGEMENTS

The authors would like to thank the UWM Research Growth Initiative and the NIH (1R15AR056117-01) for their financial support of this project.

Table 1. Comparison of knee joint kinematics during the drop jump, and land-and-cut tasks.

	Sagittal		**Frontal**		**Transverse**	
	R/L diff	R^2	*R/L diff*	R^2	*R/L diff*	R^2
DJ	-1.9 (6.4)	0.99 (0.01)	0.3 (5.9)	0.30 (0.23)	-1.4 (8.6)	0.49 (0.39)
Cut	0.4 (9.6)	0.98 (0.02)	-0.1 (5.5)	0.54 (0.28)	-2.3 (8.5)	0.53 (0.32)
p-value	0.129	0.027	0.698	0.011	0.551	0.724

INFLUENCE OF INERTIAL ESTIMATES ON ELBOW JOINT MOMENTS DURING PITCHING

[1] Jason Wicke and [2]David Keeley
[1]Texas A&M-Commerce, [2]University of Arkansas
email: jason_wicke@tamu-commerce.edu

INTRODUCTION

Body segment parameters (BSP) such as mass, center of mass location and moment of inertia are required input parameters for estimating the forces and moments acting about a joint. These BSP can only be indirectly estimated, and are most often obtained via body segment models (BSM). With different BSM available, the outcome of the BSP estimates, and in turn, the joint kinetic calculations will likely differ.

The extent BSP estimates influence the joint kinetic calculations has been examined in both walking and lifting. Although minimal influence was found in walking [1], there was a significant influence in the lifting [2]. In both studies, faster limb motions were suggested to result in a greater sensitivity of the joint force and moment calculations to the BSP estimates.

During ballistic motions, such as throwing, it would therefore be expected that accurate BSP estimates are crucial to valid measures of the forces and moments acting about a joint. The goal of this study was to examine the extent to which BSP estimates from different BSM influence the forces and moments acting at the elbow during a baseball pitch.

METHODS

Seven male collegiate pitchers participated for this study (Age = 19.0 ± 0.7 years, height = 1.90 ± 0.1 m, weight = 91.4 ± 9.5 kg). Prior to testing, participants first signed an institutional-approved consent. Front and side images of the participants were taken, using digital cameras. These images were used to determine BSP via the Jensen [3] model. Next, anthropometric measures were taken in order to establish BSP from the DeLeva [4], Zatsiorsky [4] and Dempster [5] models.

Participants threw ten, two-seam fast ball pitches. The pitching motion was captured using three digital video cameras set at 300 Hz. Direct linear transformation was used to determine the three dimensional joint locations from the point of maximum shoulder external rotation to maximum shoulder internal rotation, distinguishing the forward pitching motion. Data was filtered using a 2nd order Butterworth filter with a cut-off frequency of 16.7 Hz.

Motion data was then combined with the BSP estimates from the four different models to determine the forces and moments acting about the elbow joint. The relationship between the change in BSP estimate (using Dempster as the baseline) and the change in the kinetic estimates were determined by using the slope between these two entities [1]. A repeated-measures analysis of variance was then used to determine whether significant differences in the BSP estimates from the different models as well as the average slopes of the forces and moments about the elbow.

Table 1: Mean ± SD for BSP estimates obtained from different models. * = $p < 0.05$, ** = $p < 0.01$. Note: Hand = hand + baseball.

	Hand Mass (kg)	FA Mass (kg)	Hand CM (m)	FA CM (m)	Hand I_{TVS} $(kg \cdot m^2)^{-2}$	FA_{TVS} $(kg \cdot m^2)$
Dempster	1.35 ± 0.13	3.22 ± 0.33	0.08 ± 0.01*	0.14 ± 0.01**	0.31 ± 0.01**	2.20 ± 0.38**
Jensen	0.70 ± 0.06**	1.67 ± 0.11**	0.08 ± 0.01*	0.11 ± 0.01**	0.17 ± 0.02**	3.16 ± 0.50
Zatsiorsky	1.35 ± 0.13	3.26 ± 0.34	0.13 ± 0.01	0.12 ± 0.01	0.56 ± 0.01	3.90 ± 0.67
DeLeva	1.35 ± 0.13	3.26 ± 0.34	0.13 ± 0.01	0.12 ± 0.01	0.54 ± 0.01	3.73 ± 0.64

RESULTS AND DISCUSSION

BSP estimates from the different models are shown in Table 1. The large difference in the hand and forearm mass estimates indicates that either the Jensen geometric model or using percent body mass, are not a good method of estimation. The Jensen and Dempster models were similar in the hand center of mass (and different from the other two models), but significantly different for the forearm. Large variations were found in the moments of inertia for both the hand and forearm between the Jensen, Dempster and other two models.

The average slopes of the forces and moments at the elbow, as a function of the Dempster values are shown in Table 2. A significant difference from the kinetic variables estimated at the elbow using the Dempster model was found by all other models. The moment calculations from the different models were not significantly different, likely due to the large standard deviations. Significant differences were found between all four models for estimating the horizontal and vertical forces acting that the elbow. These results suggest that the moment calculations are not as sensitive to BSP estimates than are the vertical and horizontal forces acting at the elbow. Alternate finding might result for examining the kinetics at the shoulder, or using individual of varying morphologies.

Table 2: Mean ± SD for slopes of the three models compared to Dempster. Note: all models significantly different ($p<0.05$) from Dempster across all variables, * = $p < 0.05$.

	M	**F_{vert}**	**F_{horiz}**
Jensen	1.39 ± 2.71	1.14 ± 0.78*	1.13 ± 0.77*
Zatsiorsky	2.73 ± 5.82	3.00 ± 2.46*	3.00 ± 2.46*
DeLeva	2.07 ± 3.49	2.13 ± 1.95*	2.13 ± 1.95*

Further investigations are needed to ensure that the best model for the specific motion and the demographics of the participants in the study. It is believed that geometric models provide the most individualized BSP estimates and therefore would likely result in the most appropriate model. However, this statement cannot be justified in this study.

CONCLUSIONS

This investigation examined the influence of BSP estimates on the kinetics at the elbow joint during pitching. Significant differences were found among the BSP estimates depending on the model used. These variations had a significant effect on the measures of the horizontal and vertical forces, but not on the moment about the transverse axis. These findings support previous studies [1,2] indicating that accurate inertial estimates are necessary in motions that are at higher speeds, such as running and throwing.

REFERENCES

1. Pearsall DJ & Costigan PA. *Gait & Posture **9**, 173-183, 1999*.
2. Plamondon A, et al. *Clin Biomech* ***11***, 101-110, 1996.
3. Jensen, RK. *J. Biomech* **11**, 349-358, 1979.
4. deLeva, P. *J. Biomech* **29**, 1223-1230, 1996.
5. Dempster, WT. *WADC Tech. Report, **TR-55-159***, Wright-Patterson Air Force Base.

IN VIVO TRACKING OF TENDON ELONGATION USING ULTRASOUND

[1] Mahta Karimpoor, Hazel Screen, and Dylan Morrissey
[1] School of Engineering and Materials Science, Queen Mary University of London
Mile End Road, E1 4NS, London, UK
Telephone: +44 (20) 7882 5435, fax: +44 (20) 8983 1007, email: mahta_kp@hotmail.co.uk

INTRODUCTION

Measuring tendon strains is of particular clinical importance since it enables understanding of mechanical properties of tendon [1]. This is achieved by looking at the changing position of Myotendenious Junction (MTJ) using ultrasound [1]. Ultrasound (US) has become a standard method to look at tendon behavior and disorders affecting tendons and nerves [2]. Oliveruira and colleagues [3] have developed cross correlation algorithm for estimation of MTJ displacement in sequence of US images at 5 frames/s sampling rate. However, this method is sensitive to noise channel and can be affected by speckle noise varying in intensity values. This can be solved by de-noising the image through optimizing signal oscillation using Total Variation minimization [4].

We have developed a method in MATLAB which applies cross correlation by an adaptive mask to track the related movement of MTJ on a sequence of de-noised binarized images.

METHODS

Six male subjects 26 (± 7.50) years old were recruited from the student body of Queen Mary, University of London. Each subject lay prone on an Isokinetic dynamometer and was then asked to push against the footplate with as much force as they could for 5 seconds. During this period an ultrasound probe (12L-RS 5.0-13.0 MHz wideband linear array probe) was placed on their skin at the MTJ, recording an US movie (AVI format) of MTJ movements at 25 frames per second. During isometric contraction, force was recorded by the dynamometer. Details of Isokinetic measurements are the same as described in Maganaris' paper [5].

The two visible white lines coming into the MTJ in each US image is referred to as Myotendinous Unit (MTU) in this study. The MTU components derived from US scan is affected by distortions facts such as speckle which causes confusion in cross correlation. Using Total Variation Minimization (TVM) introduced by Rudin, Osher and Fatemi [6] can overcome this problem by smoothing rapid changes in speckle noise while preserving the original signal. The effect of TV on the image is shown in Figure 1: Total Gradient Variation De-noising block. In order to detect the MTJ more accurately, shape of the MTU was extracted from the other structures in the image. This began with binarizing the image using a threshold value called gray-threshold. Morphological enhancement was then used to boost the enhancement. The MTJ's initial coordinate was identified manually in the first frame as initial reference. The related component of MTU which contains the MTJ was labelled to verify the MTU for the next frame. See Figure 1 (Extract MTU block). If the frame-rate remains high enough, the changing rate of MTU's position in frame sequences will be limited and cannot vary in big scale. Thus, if the next image frame is binarized, then there is a major intersection between MTUs of the two binarized frames. This information was used to locate the MTU for the next frame. After extracting MTU, a rectangular template matrix from the previous images was defined to cross-correlate with the extracted MTU of the next frame. The point at which maximum cross correlation occurs was considered as new position of MTJ. The new position of the MTJ was taken as the centre of next template matrix. This process was repeated iteratively for the remaining sequence of images. The final algorithm used to detect the MTJ location with the functions at each step is drawn in Figure 1. As the subjects contract the muscle, the angle of gastrocnemius muscle at the point of junction becomes bigger. As a result, fixed-size of template on each frame fails algorithm to find the proper place of MTJ. To prevent this, an adaptive algorithm is needed to define suitable rectangle for every template at each frame. This uses star-shape of template which needs to remain in fixed ratio of

"1" and "0" binary values compared to whole area of the image.

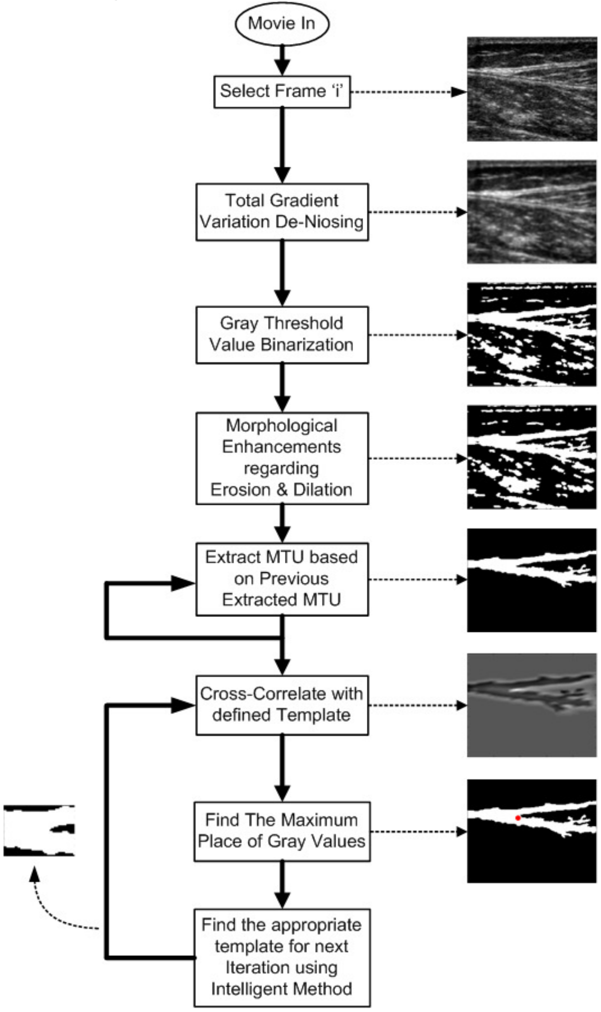

Movie In
Select Frame 'i'
Total Gradient Variation De-Niosing
Gray Threshold Value Binarization
Morphological Enhancements regarding Erosion & Dilation
Extract MTU based on Previous Extracted MTU
Cross-Correlate with defined Template
Find The Maximum Place of Gray Values
Find the appropriate template for next Iteration using Intelligent Method

Figure 1: Final algorithm used for MTJ tracking

RESULTS AND DISCUSSION

Figure 2.1 shows the plot of location of MTJ detected by algorithm against frame sequences. Figure 2.2 presents force-elongation curve resulting from information taken by dynamometer and MTJ displacement detected by the algorithm. As can be seen from the results, the algorithm successfully tracks MTJ movement during isometric contraction. The results have similar trends to force-elongation curve of the Achilles tendon in vivo. Tracking results have also been checked visually using a circle pointer at MTJ in each image to ensure the algorithm is properly tracked throughout contraction. TV and binarization are introduced as vital approaches in this study. Image Binarization enhances the template matching procedure by looking for the correct match in an image with limited values to '1's and '0's.

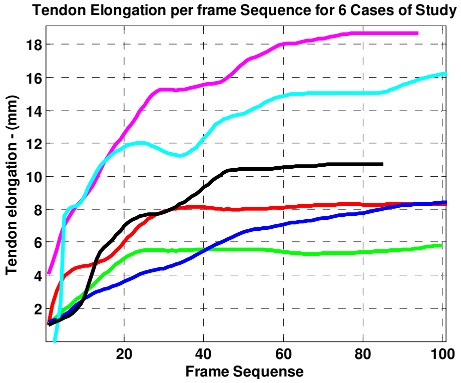

Figure 2.1: Tendon Elongation (location of MTJ) per frame sequence.

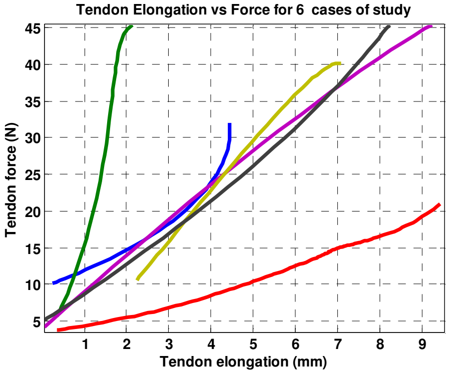

Figure 2.2: Force-elongation curve obtained from MTJ tracking using segmentation

CONCLUSIONS

The cross correlation technique used for feature detection together with segmentation and enhancement methods appears to be a successful approach for MTJ detection in ultrasound images.

REFERENCES

1.Maganaris CN, et al. In Vivo Human Tendon Mechanical Properties, Journal of Physiology,vol. 521.1,pp. 307-313, Sep. 1999.

2.Martinoli C, et al. Ultrasound of tendons and nerves, European Radiology, vol 12, pp 44-55, Jan 2002.

3.Oliveira L.F.D, et al. Estimation of myotendinous junction displacement using a cross correlation algorithm for ultrasound images, American Biomechanics Society, 2007.

4.Stephen Boyd, Convex Optimization. Cambridge University Press, 2004.

5.Maganaris cn, et al. Tensile properties of in vivo human gastrocnemius tendon. Journal of Biomechanics, vol 35, pp: 1639-1646. 2002.

6. Ruin Leonid I., et al. Nonlinear total variation based noise removal algorithms. Physica D, 256-268, 1992.

SEVERITY OF HEAD IMPACTS RESULTING IN MILD TRAUMATIC BRAIN INJURY

[1]Jonathan G. Beckwith, [1]Jeffrey J. Chu, [2]Joseph J. Crisco, [4]Thomas W. McAllister,
[5]Stefan M. Duma, [6]P. Gunnar Brolinson, and [1,3]Richard M. Greenwald
[1]Simbex, NH, [2]Alpert Medical School of Brown University/Rhode Island Hospital, RI, [3]Thayer School of Engineering, Dartmouth College, NH, [4]Dartmouth Medical School, NH, [5]Virginia Tech-Wake Forest Center for Injury Biomechanics, VA, [6]Edward Via College of Osteopathic Medicine, VA
email: jbeckwith@simbex.com, web: http://www.simbex.com

INTRODUCTION

In 1999, the National Institutes of Health Consensus Development Panel declared the incidence of mild traumatic brain injury (mTBI), or concussion, had reached epidemic proportions and concluded that reducing incidence, severity, and post-injury symptomology of mTBI should be a national research priority. Since that time, new evidence has been presented further suggesting a link between mTBI history and the likelihood of developing mild cognitive impairment, clinical depression, and early onset of Alzheimer's disease [1].

Sporting fields, particularly contact sports such as American-style football, are unique living laboratories for exploring human response to impact. Recently, in an attempt to determine the characteristics of head impacts leading to mTBI, the National Football League (NFL) reconstructed 31 contact events, identified through video analysis, providing impact severity measures for 25 concussive and 33 subconcussive impacts [2]. While insightful, practical constraints of laboratory reconstruction limit the scale of data collection and the ability to draw definitive conclusions.

Head Impact Telemetry (HIT) technology (Simbex, NH) was created to record the biomechanical response to impact on human subjects while participating in helmeted sports [3]. By providing historical records of impact, including those associated with mTBI, these data can be used to evaluate established injury thresholds, validate existing hypotheses, or generate new hypotheses regarding the mechanisms of brain injury. The purpose of this initial study was to examine impact severity measures obtained with the HIT System that were associated with the clinical diagnosis of mild traumatic brain injury.

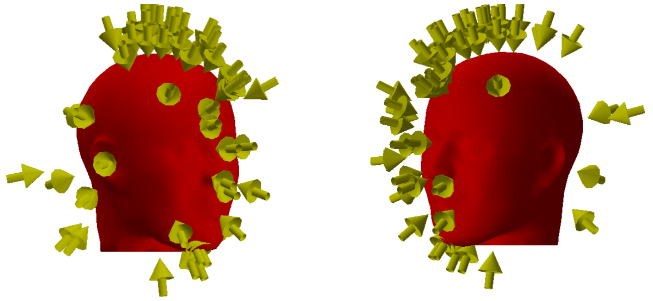

Figure 1: Location of 55 impacts recorded with the HIT System that resulted in diagnosis of mTBI

METHODS

Over a four year period, spring 2005 through fall 2008, 901 players from 8 collegiate and 6 high school football teams wore instrumented helmets during organized practices and games. Subjects were selected on a voluntary basis and included representatives from all position groups.

Helmets were equipped with an additional in-helmet unit (Riddell, OH) that positioned six single-axis accelerometers (Analog Devices, MA) against a player's head providing isolated head acceleration measures [3]. When any accelerometer exceeded a 14.4g threshold, 40 ms of data were recorded, time stamped, and processed for impact location and peak head CG linear and angular acceleration [3]. Linear acceleration time-series data were used to calculate time-weighted injury severity metrics, Gadd Severity Index (GSI) and Head Injury Criterion (HIC_{15}), used by the sports and automotive industries.

Instances of mTBI, defined as an alteration in mental status resulting from a blow to the head or body which may or may not involve loss of consciousness, were diagnosed and treated by medical staff at each institution. Each case was independently reviewed, verified, and classified using the American Academy of Neurology (AAN) grading scale. Injuries were synchronized with a single recorded impact by cross referencing the impact time-stamp with on-field reports by team personnel, and, when available, confirmed with video footage.

RESULTS AND DISCUSSION

71,390 impacts were recorded from 52 athletes diagnosed with mTBI. Three subjects sustained two injuries providing 55 recorded concussive impacts. All but 5 cases were designated as Grade 2, with symptoms resolving in less than 21 days for all but one subject (range: 15 min - 59 days). Median age, height, and weight of the concussed athletes at time of injury was 18.9 yr ± 2.3, 182 cm ± 6, and 91 kg ± 15 respectively with all position groups represented.

Average peak linear and angular acceleration for concussive impacts were 107 g ± 31and 7,079 rad/s^2 ± 3,408. HIC$_{15}$ and GSI had a higher relative variance with mean values of 272 ± 213 and 360 ± 271, respectively. 469 subconcussive impacts (0.6%) exceeded the peak linear acceleration concussive mean, of which 25 (0.03%) had peak acceleration values greater than the highest recorded concussive impact. 51% of all concussive impacts occurred to the front of the head, 22% to the top, 20% to the side (left and right), and 7% to the back (Figure 1). While concussive impacts occurred at similar frequencies as subconcussive impacts to the top (16%) and sides (18%) of the head, the rates of subconcussive impacts to the front (38%) and back of the head (28%) were lower and higher than concussive impacts to the same locations respectively.

Two-sample t-tests ($\alpha = 0.05$) indicated linear acceleration, angular acceleration, and GSI for concussive impacts are statistically similar to values previously reported by the NFL [2], with on-field HIC$_{15}$ values being slightly lower (Table 1). Probability curves were generated using logistic regression with the concussed player's subconcussive impacts as controls (Figure 2). Results from this analysis suggests previously reported estimates of concussion probability, based on single severity measures, are overestimated due to undersampling of subconcussive events. While it is encouraging that these findings agree with historical studies, current injury severity measures appear to not adequately predict mTBI. Further analysis is required to identify alternative measures, potentially based on individual or cumulative impact history, that improve predictive power.

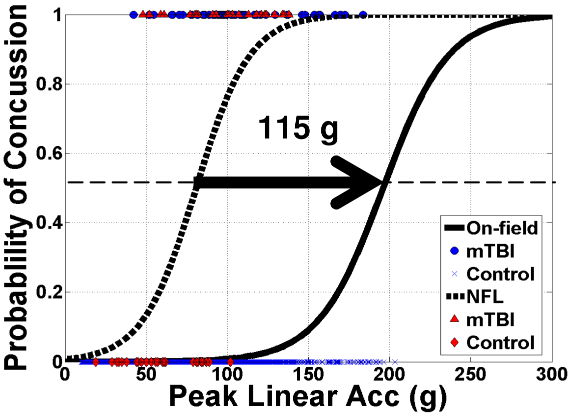

Figure 2: Probability of concussion based on peak linear acceleration. The shift in logistic regression is due to the significant number of high level accelerations that don't result in a concussion.

REFERENCES

1. Guskiewicz K, et al. *Med Sci Sports Exerc*. 39(6): 903-909, 2007.
2. Pellman E, et al. *Neurosurgery*. 53:799-814, 2003.
3. Greenwald R, et al. *Neurosurgery*. 62:789-798, 2008.

ACKNOWLEDGEMENTS

This work was supported in part by award R01HD048638 and R01NS055020 from the National Institute of Health, R01CE001254 and 5R49CE000196 from the Centers for Disease Control and Prevention, and NOCSAE 07-04. We acknowledge the researchers/institutions from which the data were collected: Lindley Brainard, Simbex, Kevin Guskiewicz PhD, ATC and Jason Mihalik PhD, Univ of North Carolina, Mike Goforth ATC and Steve Rowson MS, Virginia Tech, Dave Dieter, Edward Via Virginia College, Russell Fiore ATC and Beth Therrian MS, Brown Univ, Steve Broglio PhD, ATC Univ of Illinois, Scott Anderson ATC and Brock Schnebel MD, Oklahoma Univ, Ron Gatlin ATC, Casady HS, Jeff Frechette ATC and Scott Roy ATC, Dartmouth College, Brian Lund ATC and Dean Kleinschmidt ATC, Univ of Indiana, Mickey Collins PhD, UPMC – Center for Sports Medicine, Ann-Christine Duhaime, MD and Arthur Maerlender PhD, Dartmouth Medical School

Table 1: Descriptive statistics of concussive impacts recorded during competition relative to those obtained through laboratory reconstructions (* denotes $p > 0.05$).

	On-Field Measurement (n = 55)				**NFL Reconstruction (n = 25)**			
	Lin Acc (g)*	**Ang Acc (rad/s^2)***	**HIC$_{15}$**	**GSI***	**Lin Acc (g)**	**Ang Acc (rad/s^2)**	**HIC$_{15}$**	**GSI**
Mean	107	7,079	272	360	98	6,432	381	474
SD	31	3,408	213	271	28	1,813	197	252
Max	172	15,485	940	1,116	138	9,678	730	866
Min	42	470	21	27	48	2,615	77	94

EFFECTS OF A SIMULATED SOCCER MATCH ON CUTTING KNEE DYNAMICS AND REACTION TIME

Joseph D. Collins, J. Carson Smith, Kyle T. Ebersole, and Kristian M. O'Connor

Department of Human Movement Sciences
University of Wisconsin-Milwaukee, Milwaukee, WI, USA
E-mail: collins2@uwm.edu Web: www.chs.uwm.edu/neuromechanics

INTRODUCTION

Anterior cruciate ligament (ACL) injuries are one of the most expensive and debilitating in sports, with the females having a higher incidence. It has been shown that more injuries occur later in soccer games than in the beginning, suggesting a possible fatigue effect [1]. However, few studies have examined the role of a whole-body functional fatigue on injury risk, and one that did found minimal changes in knee dynamics post-fatigue [2]. This may be because measures were taken during an anticipated cutting maneuver. Past literature has shown an increase in knee joint loading during an unanticipated sidestepping maneuver compared to one that was preplanned [3]. Additionally, it has been shown that performance was impaired on an Eriksen-Flanker decision-making task following a 30-minute bout of moderate intensity cycling [4]. A worst-case scenario for injury risk may be presented when fatigue and decision-making are combined. It is possible that the mechanism by which cutting mechanics are altered post-fatigue is supraspinal: via deficits in an athlete's ability to make quick and accurate decisions, regardless of alterations occurring in the muscle itself. This prediction was evidenced in a study, which implemented a short, high-intensity fatigue protocol and measured knee dynamics during a single leg landing [5]. However, this study did not address the physiological effects of longer term sustained activity such as in a soccer game. Therefore, the purpose of this study was to investigate fatigue and decision-making effects on cutting knee dynamics. It was hypothesized that the effect of fatigue would be exacerbated for unanticipated trials.

METHODS

Ten female soccer players performed running and cutting maneuvers while three-dimensional kinematic and kinetic data were collected before and after a 60-minute soccer-specific exercise protocol [2]. Subjects performed 15 unanticipated trials (5 run, 5 stop and 5 cut) and five additional anticipated cutting trials during each session. The twenty total trials were presented in a random order (only the ten cutting trials were analyzed). The kinematic data were collected using a seven-camera Motion Analysis Eagle system (200 Hz), and force data were collected with an AMTI force platform (1000 Hz). Touchdown angle, range of motion (ROM), and peak moments were assessed in all three planes. Participants also completed an Eriksen-Flanker reaction time task to assess choice reaction time and error rates separate from the cutting movement execution. Statistical analyses included 2×2 (fatigue × anticipation) repeated measures ANOVAs to assess cutting knee dynamics and 2×2 (fatigue × congruency) ANOVAs to assess reaction time and accuracy for the Eriksen-Flanker test ($p<.05$).

RESULTS AND CONCLUSIONS

There were differences in knee dynamics for the cutting task due to both fatigue and anticipation, but there were no interaction (fatigue x anticipation) effects for any variable (Table 1 and Figure 1). The transverse plane ROM was increased for post-fatigue trials, which is consistent with past research utilizing the same fatigue protocol [2]. There were also trends in the sagittal plane for both ROM and peak moment, which could suggest decreased muscular effort with fatigue. Both sagittal and frontal planes ROM were greater for unanticipated trials compared to preplanned ones. There were also increases in peak moments measured in the frontal and transverse planes for unanticipated trials (Table 1). These results are consistent with literature suggesting that unanticipated trials allot the athlete less time to make the necessary postural modifications and therefore elicit greater peak knee moments [3]. There were no significant fatigue effects for either reaction time or accuracy for the Eriksen-Flanker task. However, for congruent trials reaction time was 50±11.8 ms faster and accuracy increased by 4±0.8%. The better performance on the congruent trials is consistent in the literature; however the lack of fatigue effect differs from previous literature [4]. The lack of a significant interaction in the cutting dynamics and lack of a decrement in the reaction time task both suggest that decision-making performance may not be a factor that explains the rise in ACL injuries rates later in soccer games.

REFERENCES

1. Hawkins, R.D. et al. *British J Sports Med*, **35**, 43-47, 2001.
2. Sanna, G. et al. *Clin Biomech*, **23**, 946-954, 2008.
3. Besier, T.f. et al. *Med Sci Sports Exer*, **33**, 1176-1181, 2001.
4. Hillman, C.H. et al. *Int J Psychophysiol*, **48**, 307-314, 2003.
5. Borotikar, B.S. et al. *Clin Biomech*, **23**, 81-92, 2008.

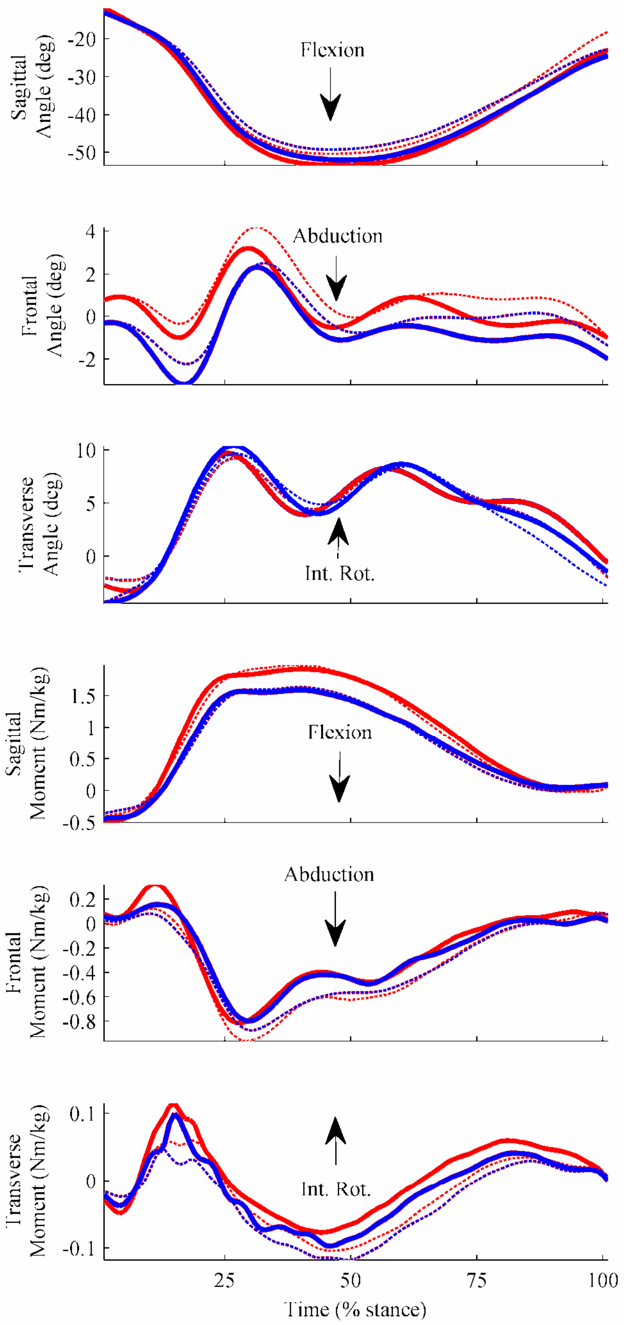

Figure 1. Knee angles and moments in all planes. Red lines represent pre-fatigue and blue represent post-fatigue. Thin lines represent anticipated cuts and thick represent unanticipated cuts.

Table 1. Group mean knee touchdown angles, ROM, and peak moments.

	Sagittal			Frontal			Transverse		
	TD (°)	ROM (°)	Moment (Nm)	TD (°)	ROM (°)	Moment (Nm)	TD (°)	ROM (°)	Moment (Nm)
Pre_Ant	-12.7 (4.4)	-38.4 (4.7)	2.03 (1.1)	0.72 (3.7)	-2.7 (2.7)	0.28 (0.23)	-2.1 (7.1)	12.2 (3.8)	0.12 (0.07)
Pre_Un	-12.2 (5.3)	-41.9 (4.2)	2.05 (1.1)	0.71 (3.8)	-3.3 (2.8)	0.43 (0.26)	-2.4 (7.9)	13.6 (5.0)	0.18 (0.11)
Post_Ant	-12.9 (4.6)	-36.7 (4.4)	1.69 (0.92)	-0.26 (3.3)	-3.0 (2.6)	0.23 (0.16)	-4.4 (11.2)	15.4 (5.6)	0.09 (0.05)
Post_Un	-13.0 (4.1)	-39.8 (8.0)	1.68 (0.89)	-0.33 (3.4)	-3.8 (2.4)	0.34 (0.19)	-4.6 (11.4)	16.0 (6.0)	0.15 (0.1)
Anticipation	P=.683	P=.004*	P=.897	P=.806	P=.041*	P=.002*	P=.707	P=.152	P=.028*
Fatigue	P=.602	P=.055	P=.058	P=.129	P=.412	P=.333	P=.341	P=.016*	P=.105

THE EFFECT OF BOUNDARY SHAPE AND MINIMA SELECTION ON SINGLE LIMB STANCE POSTURAL STABILITY

[1]Mukta Joshi, [1]David M Bazett-Jones, [1]Jennifer E Earl, and [1]Stephen C Cobb
[1]Neuromechanics Laboratory, University of Wisconsin-Milwaukee

INTRODUCTION

Postural stability computed using stabilometry is a common method of quantifying balance. Traditionally used measures of postural stability, such as COP displacement, either do not account for the rate of COP change and/or fail to account for the position of the COP with respect to an individual's stability limits. Time to Boundary (TTB) is a novel approach to quantify postural stability that takes the above spatiotemporal characteristics of COP into account [1, 2].

Although TTB is proving to be an important measure of bilateral [3] and single limb [4] stance position postural stability, two factors involved in computing the measure, the definition of the stability limits and the number of minima utilized to represent an individual's postural stability, have yet to be completely investigated. With respect to stability limit definition, the foot is typically modeled as a rectangle with anteroposterior (AP) limits defined as the length of the foot and mediolateral (ML) limits defined as the widest portion of the foot. For bilateral stance position testing, however, the use of a multi-segmented polygon as opposed to a rectangle has been recommended because the data may be more intuitive if the boundary is representative of the support formed by the participant's feet [5]. Although the same argument could be made for single-limb stance position testing, the effect of boundary shape has not been investigated. With respect to minima selection, some investigations have utilized the means of all of the trial minimas [3] while others included only the 10 absolute trial minima [4]. The effect of using 10 vs multiple discrete points to represent an individual's postural stability, however, has not been determined.

The purpose of the current study, therefore, was to investigate the effect of stability limit definition and minima selection on TTB measures computed during single-limb stance position testing.

METHODS

24 apparently healthy participants (12 m; age: 21.3 ± 2.4 yrs; mass: 71.8 ± 14.5 kg; height: 169.2 ± 14.1 cm) were recruited. Single-limb stance position postural stability was assessed during eyes open and eyes closed conditions. All participants wore the same style sandal (Hana, Maui and Sons, Pacific Palisades, CA) and foot position on the force plate was standardized using a using a 90° angle (a Framing Wizard, Swanson Tools) (Figure 1)

Postural stability trials consisted of a 30 s trial during an eyes open condition in a left single-limb stance position.

Following the balance trials, a custom written program (Matlab, v. 7.6.0, The MathWorks Inc, Natick, MA) was used to compute TTB using the mean of all minimas during a trial and the mean of only the 10 absolute minima. The program also computed TTB with rectangle (Figure 1a) and trapezoidal (Figure 1b) defined stability limits.

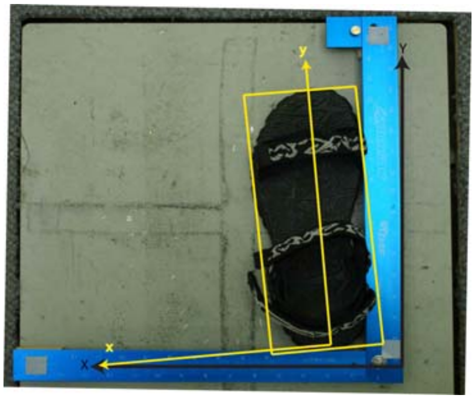

Figure 1a: Length of the rectangle was equal to the length of the sandal and width was the maximum width of the sandal.

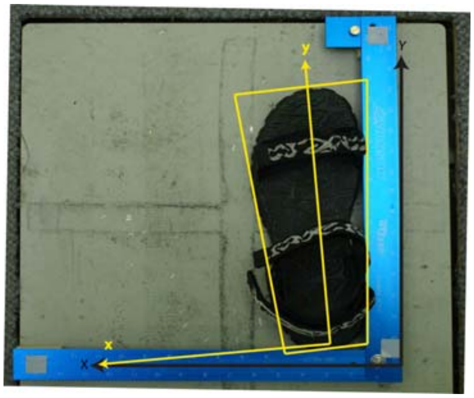

Figure 1b: The trapezoid widths were defined as the maximum widths of the forefoot and rearfoot portions of the sandal.

The effect of minima selection on AP and ML postural stability was investigated using the Wilcoxon Rank Test (SPSS v. 16.0, Chicago, IL). Dependent t-tests, were utilized to investigate the effect of stability limit shape on ML postural stability. The significance level for all analyses was established at $\alpha \leq 0.05$.

RESULTS AND DISCUSSION

Wilcoxon test results revealed no significant differences in the AP ($z = -0.201$, $p = 0.841$) and ML ($z = -0.186$, $p = 0.852$) TTB computed between using all versus 10 absolute minima.

The paired-samples t test did not reveal significant difference in ML ($t(23) = -0.956$, $p = 0.349$) TTB computed using rectangular versus trapezoidal stability boundary limits (Table 1).

Table 1: Mean (SD) ML eyes open condition TTB.

Stability Boundary Shape	Time-to-Boundary (s)
Rectangular	3.02(1.01)
Trapezoidal	3.79(4.11)

Based on the results of the study we conclude that rectangular versus trapezoidal boundary shape may not significantly affect eyes open single-limb stance ML TTB scores in apparently healthy participants. Furthermore, quantifying postural stability as the mean of all TTB minima versus the mean of 10 absolute minima may not provide different information regarding an individual's single limb balance.

REFERENCES

1. van Emmerik REA, et al. *J Appl Biomech* **16**, 394-406, 2000.
2. Hertel J et al. *J Appl Biomech* **22**, 67-73, 2006.
3. Van Wegen, EEH, et al. *Motor Control* **3**, 254-269, 2001.
4. Hertel J, et al. *Gait Posture* **25**, 33-39, 2007.
5. Haddad J et al. *J Appl Biomech*, **22**, 155-161, 2006.

PEAK TRACTION COEFFICIENTS OF CLEATED ATHLETIC SHOES AT VARIOUS ANGLES OF INTERNAL ROTATION ON ARTIFICIAL TURF

[1] Ben Cooper, [1]Ronald Pfeiffer, [1]Michelle Sabick, [1]Seth Kuhlman, [1]Shawn Simonson, and [2]Kevin Shea
[1]Center for Orthopaedics & Biomechanics Research, Boise State University, [2]Intermountain Orthopaedics
email: bejamincooper@u.boisestate.edu

INTRODUCTION

As an alternative to natural grass playing fields, the installation of artificial turf surfaces has grown exponentially over the past several decades. Despite the growing popularity of artificial turf, little is known about the interaction between the player's shoe and the turf surface. Previous research has cited the difficulty in maximizing performance (high traction), yet minimizing the risk of injury (low traction) [2]. Due to numerous factors that affect the turf-shoe interaction, determining safe traction ranges for artificial turf is very difficult. However, the first step needs to be taken to determine the safe range between performance and risk of injury for traction.

The purpose of this study was to investigate variances in peak traction coefficients based on a particular cleated athletic shoe on artificial turf at various angles of internal rotation during a linear translational motion. It was hypothesized that a variety of cleated athletic shoes at various angles of internal rotations would not exhibit different peak traction coefficients. Secondly, there would be no difference in peak traction coefficients within a cleated athletic shoe at the various angles of internal rotation.

METHODS

Four U.S. Men's size 12 cleated athletic shoes were used: Reebok 4 NFL Speed III Low (detachable studs), Nike Super Speed D3/4 (detachable studs), Nike Air Zoom Super Bad (molded studs) and Adidas Scorch 7 Fly Low (molded studs). The studs' bottom surface areas for each shoe were calculated. The Boise State University Turf Buster, a pneumatic and computerized device, was used to simulate a deceleration motion with the shoe. Testing was performed on FieldTurf®. Each cleated athletic shoe was set at various angles (0º, 30º, 60º, 90º) of internal rotation, and experienced linear translational motion while data was being collected. The following definition was used to determine the peak traction coefficient variable: *The peak value of the ratio of horizontal to vertical forces throughout the translation of the shoe. This value represents the greatest traction coefficient experienced during the shoe's translation*.

Repeated measures univariate analysis of variances (ANOVAs) was used to compare the means of the peak traction coefficients between each angle of internal rotation across all of the shoes and within each individual shoe. A Holm's Sequential Selective Bonferroni Method post-hoc was performed on significant findings.

RESULTS

Significant differences were found within cleated athletic shoe at various angles of internal rotation across all peak traction coefficients (p=0.000).

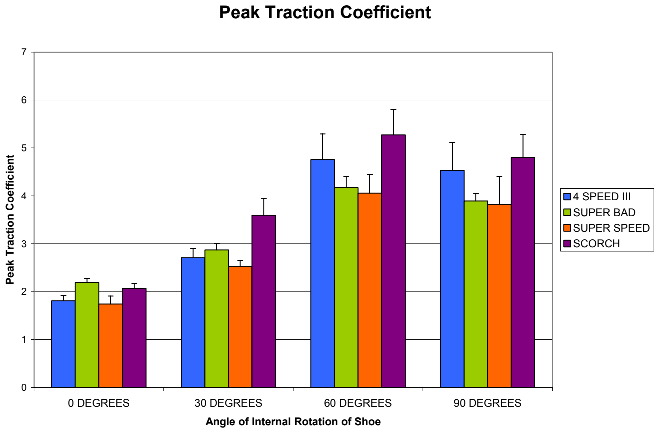

Figure 1. Comparisons of Peak Traction Coefficients Between Cleated Athletic Shoes and Across Angles of Internal Rotation

There were no significant differences between cleated athletic shoes on artificial turf.

Correlations between peak traction coefficients and the representative stud bottom surface area of each shoe were found to have no relationship between each other, R = 0.0257 (Table 1) (Figure 2).

Cleat Specifications				
Shoe Name	# of Cleats: Front	Rear	Total	Stud Area (cm^2)
4 Speed III	5	2	7	6.65
Super Bad	5	4	9	11.05
Super Speed	5	2	7	5.50
Scorch	9	4	13	9.22

Table 1. Cleat Specifications

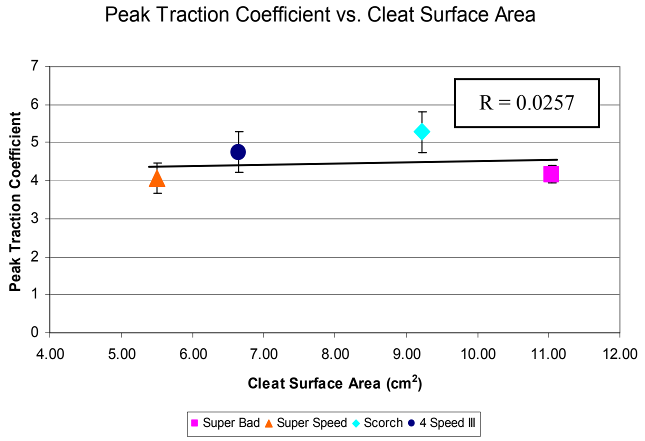

Figure 2. Peak Traction Coefficient vs. Cleat Surface Area

DISCUSSION

A pattern emerges across the peak traction coefficient plot (Figure 1). The values increased from 0º – 60º and then decreased from 60º – 90º. Statistically, there was no difference found from 60º – 90º. Based on bottom surface area of the cleats alone, there is no reason for peak traction coefficients to increase with increases in the angle of internal rotation. One explanation for this could be due to the fact the majority of the cleats are exposed to the turf material in the direction of the applied force, creating a phenomenon we have termed the "trench effect". The "trench effect" occurs when the studs from the shoe dig into the turf surface and create small canals in the material. As other studs pass through the previous studs' path in the turf material there is less resistance, thus making multiple studs along the same path less effective (Figure 3).

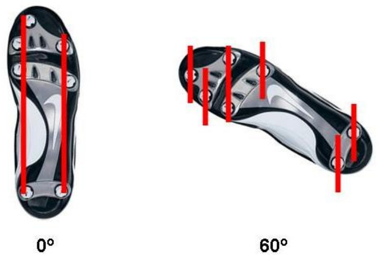

Figure 3. Trench Effect

As the shoe rotates from 0º – 60º, more studs are exposed and open to create unique paths in the turf material. This should increase the resistance, and ultimately the horizontal force necessary for linear translation.

CONCLUSIONS

The athlete's performance and safety are the two most important factors in sport. Maintaining the optimal level of performance without compromising the safety is the balancing act coaches, turf managers, and researchers struggle with daily. Determining the most favorable traction coefficient range is a complex task.

This study investigated the peak traction coefficients of cleated athletic shoes at various angles of internal rotation. Comparisons were made between the various angles of internal rotation within a cleated athletic shoe, as well as cleated athletic shoes across angles of internal rotation. Based on the results from this study, the type of cleated athletic shoe does not necessarily affect the peak traction coefficient. This contradicts some of the previous studies investigating differences in traction coefficients between cleated athletic shoes [1,3]. Another important finding was that the angle of internal rotation for the shoe had an affect on peak traction coefficients. A plausible explanation for this is the "trench effect".

With so few studies investigating linear translational traction and not enough consistency in the test methods, results between research groups becomes nearly impossible to compare to one another. Furthermore, the ultimate goal is to determine acceptable traction coefficient ranges that provide needed performance levels while minimizing the likelihood of injuries.

ACKNOWLEDGEMENTS

Thanks to Intermountain Orthopaedics for sponsoring graduate fellows. Without their support, none of this would be possible.

REFERENCES

1.Lambson, RB, et al. *Amer J Sport Med* **24**, 155 – 159, 1996.
2.Shorten, et al. Paper presented at the XIX International Congress of Biomechanics. 2003.
3.Torg, JS, et al. *Phy Sports Med* 1, 39 – 43, 1973.

LOWER EXTREMITY MUSCLE VOLUMES CAN BE ACCURATELY OBTAINED FROM HIGH RESOLUTION MRI

Genaro S. Sepulveda[1], Trevor Kingsbury[1], Carolyn M. Eng[2], Richard L. Lieber[1,2], Samuel R. Ward[1,2,3]

Departments of [1]Bioengineering, [2]Orthopaedic Surgery, and [3]Radiology, University of California, San Diego
and Veterans Affairs Medical Center, La Jolla, CA 92093 USA
Email: srward@ucsd.edu, Web: http://muscle.ucsd.edu

INTRODUCTION

Magnetic resonance imaging provides distinct advantages over other non-invasive imaging modalities (such as ultrasound (US) and computed tomography (CT)), by offering high contrast of muscle, fat, and connective tissue, clarifying the delineation of muscle borders. MRI allows data to be acquired without exposing the subject to ionizing radiation, and a larger field of view allows for the acquisition of whole muscles and limbs. However, there are relatively few data in the literature validating the use of MRI to measure muscle volumes. Therefore, we directly compared cadaver-based and MRI-based data to quantify the accuracy of MRI-derived volume measurements.

METHODS

Eleven cadaveric legs were scanned using fast spoiled gradient echo pulse sequence (FSPGR) with high spatial resolution (1mm^3) on a GE 3T Signa MR imaging system. From the MR images, psoas major (PM), iliacus (Il), gluteus maximus (Gmax), gluteus medius (Gmed), rectus femoris (RF), vastus lateralis (VL), vastus intermedius (VI), vastus medialis (VM), adductor longus (AL), adductor brevis (AB), adductor magnus (AM), biceps femoris short head (BFS), biceps femoris long head (BFL), semitendinosus (ST), semimembranosus (SM), tibialis anterior (TA), medial gastrocnemius (MG), lateral gastrocnemius (LG), and soleus (Sol) were manually segmented in the three cardinal planes (e.g. Figure 1) to calculate volume using Analyze v.7.0 (Analyze Direct, Lenexa, KS). Because some muscle groups are difficult to separate, even during dissection, a selection of muscles were manually segmented as muscle groups: VL, VM, VI as vasti (Vas); MG and LG as gastrocnemius (Gas); BFS and BFL as biceps femoris (BF); Il and PM as iliopsoas (IP); and AL, AB, and AM as adductors (Add).

After scanning and image processing, legs were dissected and volumes were determined as described previously [1]. The degree of exact agreement between dissection- and MR-based volume measurements was determined using the Intraclass Correlation Coefficient (ICC). Relative error between measurement techniques was calculated using percent difference. P values < 0.05 were considered significant and all values are reported as mean ± standard error unless otherwise noted.

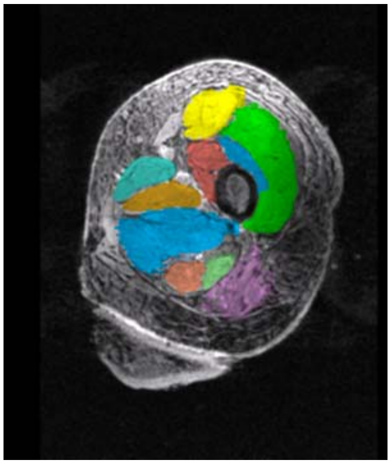

Figure 1. Segmentation of the mid-thigh in the axial plane. Colors are assigned to differentiate among muscles.

RESULTS & DISCUSSION

The MRI-derived volume measurements displayed an excellent linear correlation with dissection volumes (ICC = 0.962) when all 219 muscles were considered together, resulting in an average relative error of 17.94 ± 2.80% (Figure 2).

In the case of individual muscles, there was a wide range of accuracy (Table 1). MRI was extremely accurate in some muscles (e.g. AM: ICC 0.984, % diff 7.48%), while it was not accurate in others (e.g.

VM: ICC 0.768, % diff 34.28%). When these less accurate muscle were combined into natural muscle groups, there was an improvement in accuracy (Vasti: ICC 0.989, % diff 5.76%; Gas: ICC 0.971, % diff 11.10%; BF: ICC 0.955, % diff 11.84%; IP: ICC 0.948, % diff 8.85%; Add: ICC 0.989, % diff 5.99%).

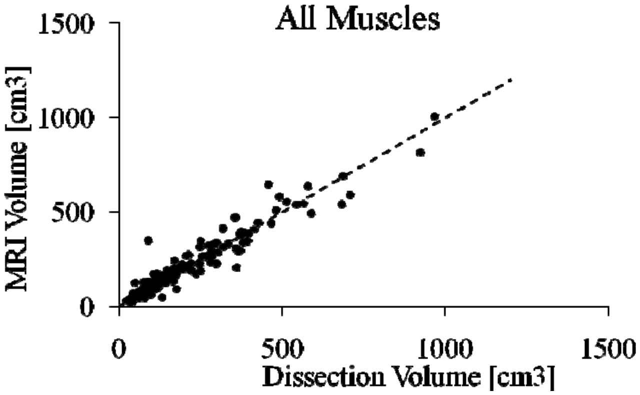

Figure 2. Scatter plot of muscle volume calculated from MRI segmentation (MRI Volume) versus dissected muscle volume (ICC = 0.962). Dashed line shows unity.

These data demonstrate that the accuracy of MRI-based volumes is dependent on the ability to distinguish between adjacent muscles. Muscles such as RF, AM, and Sol have consistently clear boundaries, and therefore, are more accurately measured. When segmenting muscles with unclear boundaries (i.e. VL, VM, and VI), selecting them within a larger muscle group (Vas) produces noticeably more accurate volume measurements. Because of this, MRI-derived volume should be interpreted with caution.

In general, high resolution MRI can be used to accurately measure lower extremity muscle volumes when intermuscular boundaries are discernable, and to produce graphical renderings of human anatomy that contain volume information.

REFERENCES

1. Eng, CM et al. *J. Biomech.* **40**: 3261-3266. 2007

Table 1. Relative errors and ICCs for individual muscle volume calculations.

Muscle	PM	Il	Gmax	Gmed	RF	VL	VI	VM	AL	AB	AM	BFS	BFL	ST	SM	TA	MG	LG	Sol
%Difference	20.21%	11.67%	11.22%	19.42%	7.29%	17.21%	33.16%	34.28%	11.75%	12.81%	7.48%	19.81%	27.67%	21.71%	18.27%	14.51%	11.95%	17.36%	9.20%
ICC	0.893	0.956	0.969	0.853	0.985	0.849	0.884	0.768	0.963	0.965	0.984	0.733	0.874	0.886	0.943	0.916	0.964	0.971	0.967

CHARACTERIZATION OF THE *FLEXOR DIGITORUM SUPERFICIALIS* AS A PREDICTOR OF GRASPING STRENGTH

Adam Shain MS, Nam Hun Kim PhD, and William Craelius PhD
Rutgers University, Dept of Biomedical Engineering, New Brunswick, NJ
email: ashain83@gmail.com

INTRODUCTION

The activity of forearm musculature during grasp has been studied by a variety of testing modalities in order to assess muscular conditions, predict grasping strength and control powered prosthetics. Of all testing modes Force Myography (FMG) is the only one that has demonstrated simultaneous multifunctional and multi degree of freedom control of prosthetic hands with sensors placed over the surface of the skin [1,2]. These studies, however, were not able to identify magnitudes of individual muscle activation for control of volitional movement. In the present study a new testing modality is introduced, targeted Force Myography (tFMG).

METHODS

tFMG detects the change in radial pressure and stiffness of a single muscle during contraction through the voltage response of a single force sensing resistor (FSR) strapped above the muscle body intrinsically combined with the overall change in radial pressure of the harnessed body segment. In this study tFMG of the *flexor digitorum superficialis* is assessed during power grasp. This was achieved through the development of inexpensive testing fixtures and methods in order to linearize and calibrate the voltage response curves of FSRs, making them an accurate and reliable tool in the assessment of grip force and forearm pressure.

RESULTS AND DISCUSSION

In determining correlation, the resting value was ignored because the tFMG value is arbitrary and based on raw force results. The force levels of every subject show a linear correlation at low to moderate force levels.

The normalized results of tFMG of the FDS and grasping strength (%MVC) were then compared and a clear linear relationship is observed. A best fit line of
%FMG= .95 x %MVC – 2.2,
$r^2 = 0.92$
error = 7.1 % MVC ± 5.3.

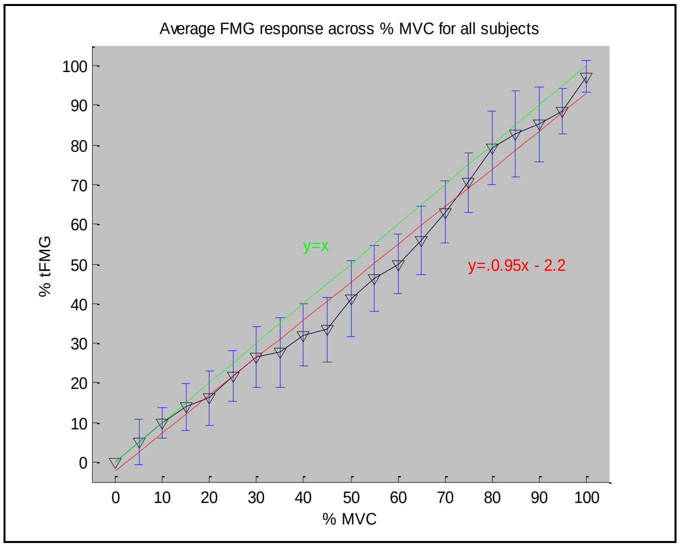

Figure 1: The moving average of all subjects' data reveals the behavior of the overall normalized data. The moving average follows the best fit line very well, staying within one σ at all times but the average of all the subject falls consistently below a pure linear relationship between % MVC and % tFMG.

Although there may be a significant variation to the overall fit line of the FDS's behavior during isometric contraction, intra-subject repeatability is higher. The individual slopes ranged from 1.21 to .87 with an average of .99 but the correlation of determination ranged from 0.90 to 0.98 with an average fit of 0.94 ± 0.03. This result is more important than overall fit; it indicates that this method could be used to create a fit line from a subject's perceived MVC and a minimal effort for real-time control of a prosthetic device.

CONCLUSIONS

It is demonstrated that the tFMG of the FDS recorded by a single FSR is adequate for determining the level of force activation. Although the variation may seem unacceptable when inter-subject data is compared, the more important behavior of intra-subject correlation is high. These results show that the improved testing methods are accurate and reliable but more importantly can be interpreted without knowledge of the actual grasping force, all which is required is an MVC and a very minimal contraction. The work presented here can easily be incorporated into future development of a multi-functional, multi-degree of freedom prosthetic limb with proportional control.

REFERENCES

1. Abboudi, R.L., et al. *IEEE Trans Rehabil Eng* **7**, 121-129, 1999.
2. Curcie, D.J., et al. *IEEE Trans Neural Syst Rehabil Eng* **9**, 69-75, 2001.

ESTIMATING DYNAMIC MUSCLE FORCES OF TORSO DURING FLEXION MOVEMENT

Pranitha Gottipati and Raymond H. Plaut
Kevin P. Granata Musculoskeletal Biomechanics Laboratory
Virginia Polytechnic Institute and State University, Blacksburg, VA, USA
E-mail: pranitha@vt.edu Web: www.biomechanics.esm.vt.edu

INTRODUCTION

Most of the dynamic movements of the upper human body involve flexion-extension and twisting. These movements are possible with the help of various torso muscle recruitments. A number of studies have shown that these recruitments are necessary for a stable dynamic movement. Some studies have used optimization techniques to estimate muscle activations while ensuring linear stability [1, 2]. While these studies are done in an isometric sense or with small perturbations in a dynamic sense, studies such as Zeinali-Davarani et al. [5] analyzed large-angle movements of a 3-dimensional system. In the present study, dynamic muscle force vectors are estimated during a time-dependent dynamic task using stable kinematic vectors. The goal of this study is to build a mathematical model of flexion movements of the torso and to estimate the dynamic forces in the muscles.

METHODS

The spine is modeled in the sagittal plane with 6 rigid bodies: 5 lumbar vertebrae and a trunk stacked upon a fixed pelvis. The model has 18 degrees of freedom. Each rigid body has 3 degrees of freedom: two are translational (y-translation corresponding to anterior-posterior movement and z-translation corresponding to vertical movement) and one is rotational (x-rotation corresponding to sagittal plane rotation). The intervertebral discs (IVDs) are modeled as 3 springs and 3 dampers associated with the 3 degrees of freedom, thus accommodating their viscoelastic behavior.

The shearing and translations of the IVDs are measured as described in Cholewicki and McGill [1]. The potential energy due to the IVD springs and the damping energy due to the IVD dampers represent the effects of the IVD forces.

The kinematic vectors for the model are estimated from measured experimental data of flexion and extension movements [3]. The data obtained from experiments provide the sagittal lumbar angle and the thoracic angle. The lumbar angles of each lumbar vertebra are estimated from the total lumbar angle using the method described by McGill and Norman [4]. The translations of each vertebra and the thorax are calculated as a polynomial function (equation 1) of the sagittal angle of the corresponding body. The velocity and acceleration vectors are obtained using finite differences.

$$\begin{aligned} y_i &= 0.0022 \times \theta_i^2 + 0.005 \times \theta_i - 0.002 \\ z_i &= 0.1 \times y_i + 0.01 \end{aligned} \qquad (1)$$

where θ_i is the lumbar angle of the i^{th} vertebra.

The muscle model that is adopted here is the one used by Cholewicki and McGill [1] with 90 torso mucles. It is a Hill-type muscle model and consists of a force generator in parallel with a spring and a damper. The force due to this muscle model is given as [2]

$$f_m = f_\circ \cdot \alpha(t) \cdot \left(q \cdot \left(\frac{L_m(t) - L_{mo}}{L_{mo}} \right) + c \cdot \frac{L_m{}'(t)}{L_{mo}} + 1 \right) \qquad (2)$$

where f_o = maximum muscle force, defined as the maximum muscle stress of F = 46N/cm^2 multiplied by the muscle cross-sectional area, $\alpha(t)$ = muscle activation, q = dimensionless intrinsic muscle stiffness gain, c = intrinsic muscle damping gain, L_m = muscle length, and L_{mo} = muscle rest length.

The dynamic equations of motion of the torso are developed using Lagrange's equations. The system has a total of 18 degrees of freedom and the equations of motion are given by

$$\frac{d}{dt}\left(\frac{\partial T}{\partial \dot{q}_i}\right) - \frac{\partial T}{\partial q_i} + \frac{\partial V}{\partial q_i} + \frac{\partial D}{\partial \dot{q}_i} = Q_i \qquad (3)$$

where T = kinetic energy, V = potential energy due to gravity and IVD springs, D = Rayleigh's dissipation function due to IVD dampers, q_i = generalized coordinates, and Q_i = generalized forces due to muscle forces.

Once the kinematic data are substituted in the equations of motion, equation 3 gives 18 linear equations with 90 unknowns in the muscle activations. Constrained optimization is used to find the unknown muscle activations. The muscle activations are chosen such that the metabolic power (cost function) is minimized while satisfying the developed indeterminate dynamic equations. The muscle activations are bound to the domain [0, 1). The cost function $p(\alpha_o)$ [2] is given by

$$p(\alpha_o) = m\left[37\sin\left(\frac{\alpha_o \cdot \pi}{2}\right) + 55.5\left(1 - \cos\left(\frac{\alpha_o \cdot \pi}{2}\right)\right)\right]$$

This program produces muscle activation discretely at each time step of the flexion cycle.

RESULTS AND DISCUSSION

The dynamic muscle forces are estimated for one flexion movement, with the flexion angle ranging from 0^0 to 60^0. To date, preliminary analysis is done on two sets of data and the following trends have been observed. The results show that three groups of muscles provide the major influence on the flexion movement: the erector spinae, the multifidus muscles, and the Obliques (External and Internal). The latissimus dorsi and the quad lumborum muscles have very negligible influence on the flexion movement; the forces exerted by these muscles are one order of magnitude less than the forces exerted by the other muscles. The highest activation levels of the multifidus muscles are observed at 32^0 of flexion with force magnitudes of 110N (figure 1). The illiocostallis lumborum muscles of the erector spinae group exerted the largest magnitudes of forces at the end of the flexion. The force at the end of the flexion is ten times than the force at the standing posture. However the longissimus thoracis muscles of the erector spinae have higher activation levels at 32^0 flexion angle compared to illiocostallis lumborum muscles with force magnitudes of 100N. At about 50^0 of flexion these muscle groups are completed activated and forces of 300N in magnitude are exerted (Figure2).

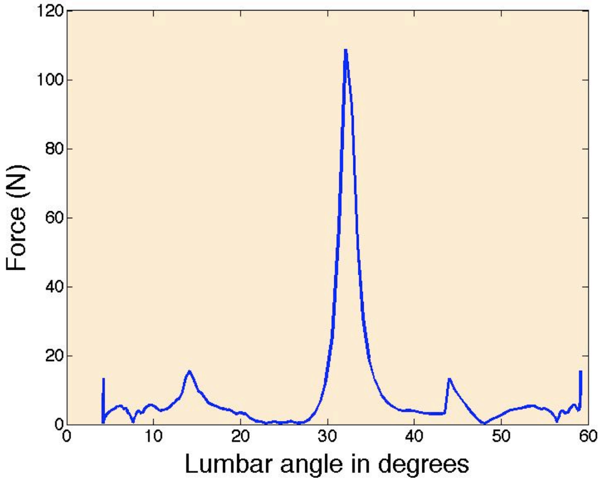

Figure 1: Forces of a mutlifidus muscle vs lumbar flexion abgle in sagittal plane.

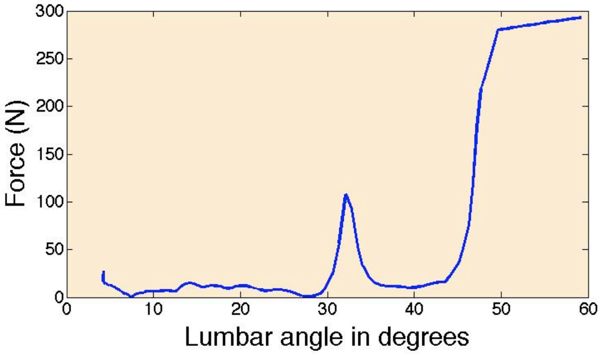

Figure 2: Forces of a Longissimus thoracis muscle vs lumbar flexion abgle in sagittal plane.

REFERENCES

1.Cholewicki J, McGill SM (1996). *Clin Biomech,* **11,** 1-15.
2.Franklin TC, Granata KP (2007). *J Biomech,* **40,** 1762-7.
3.Granata KP, Gottipati P (2008). *Ergonomics*, **51**(8), 1258-71.
4.McGill SM, Norman RW (1986). *Spine,* **11,** 666-8.
5.Zeinali-Davarani S, et al. (2008). *IEEE Trans Neural Syst Rehabil Eng,* **16,** 106-18.

THE ROLE OF CALCIUM INTERACTION WITH TITIN IMMUNOGLOBULIN DOMAIN IN CARDIAC MUSCLE

[1] Michael DuVall and [2]Walter Herzog
[1]Biological Sciences Dept., University of Calgary, [2]Kinesiology Dept., University of Calgary
email: mmduvall@ucalgary.ca

INTRODUCTION

In North America, cardiac diseases such as heart attacks and myopathies are on the rise. Fundamental muscle research has become a powerful tool to understanding these conditions and searching for ways to treat or prevent cardiac diseases. In an attempt to contribute to work in this area of research, we have focused on the smallest structurally intact component of striated muscle, the myofibril. Myofibrils are sub-cellular organelles consisting of linear strands of sarcomeres. Active myofibril force originates in the contractile filaments, actin and myosin, while passive force in myofibrils can be attributed virtually exclusively to the structural protein titin, also known as connectin [1]. Titin acts as a calcium dependent molecular spring that prevents sarcomeres in the myofibril from over-extending during muscle elongation. The calcium dependent elasticity of titin has been exclusively attributed to the PEVK domain, however this mechanism has only been able to explain a tiny contribution of the passive force regulation observed in myofibrils [2]. We propose that other domains in titin might hold the key to explaining titin's remaining passive force regulation. The purpose of this study was to identify the potential for passive force regulation of the Ig domain of titin. By focusing attention on the Ig domains, a novel role may be proposed involving calcium binding that would prove important for understanding how this elastic region may function in damaged and intact titin proteins.

METHODS

T1 I27 plasmid from human cardiac titin was used to recombinantly produced Ig-27 proteins [3]. The T1 I27 plasmid consists of 8 Ig-27 domains linked in series by two amino acids. The plasmid was inserted into the genome of chemically competent Escherichia coli of the C41(DE3) strain under optimal protein

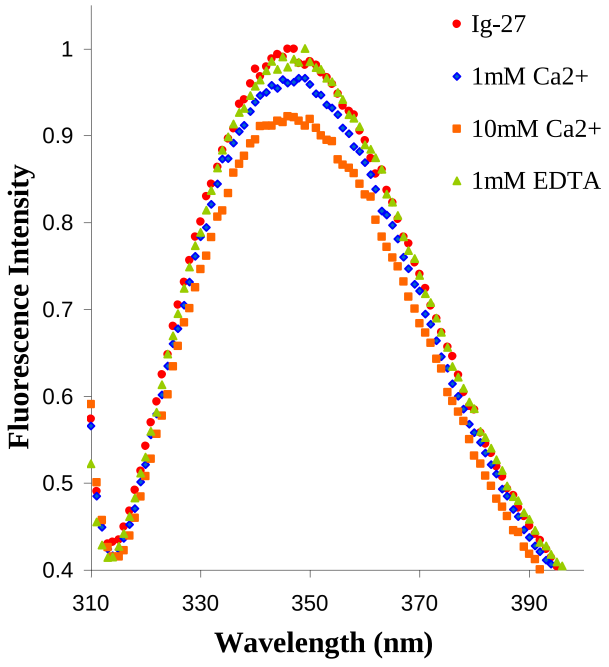

Figure 1: Fluorescence emission spectrum for titin Ig-27 domains excited at 295nm with the addition of calcium (Ca2+) and a calcium chelating agent (EDTA).

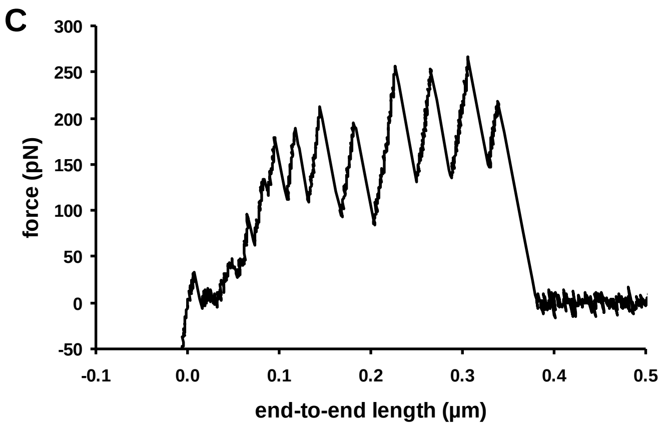

Figure 2: Force extension curve of titin Ig-27 constructs using AFM, revealing 8 saw tooth like unfolding events.

expression conditions. Nickel charged column chromatography was performed using a Histidine tagged sequence under specific imidazole wash conditions. Absorbance and fluorescence spectroscopy analysis was conducted on tryptophan fluorescence using a Hitachi F-2000 wavelength scanning spectrofluorimeter at 295nm.

RESULTS AND DISCUSSION

Using fluorescence spectroscopy analysis, it was seen that there was an observable degree of change in the microenvironment of the Ig-27 domain when a physiological level of calcium was introduced (Figure 1). The proposed calcium sensitivity arose from observations of π electron delocalization in the aromatic group of tryptophan. When 1mM calcium was added, there was a depression in the fluorescence intensity of the single tryptophan in each Ig-27 domain. Furthermore, the addition of excess (10mM) calcium resulted in a subsequent depression, proportionally similar to that caused by 1mM calcium. With the subsequent addition of EDTA, a calcium chelating agent, the fluorescence intensity improved to near original levels indicating reversibility to the calcium interaction we observed. Calculations were done to standardize trials from different Ig-27 samples, as well as to account for dilution effects in order to eliminate any differences between tests.

Important to note is the 3-dimensional location of the single tryptophan in each of the eight Ig-27 domains. As the tryptophan is buried in the physical structure, the application of a quenching agent (Ca2+) resulted in a smaller decline in fluorescence intensity than would have occurred if the tryptophan was located on the surface. This makes little difference to the plausibility of Ig-27 acting as a calcium dependent protein, but shows the importance of having sensitive detection procedures that can account for buried amino acids [4].

Tryptophan fluorescence analysis suggests that calcium binds to the Ig-27 domain resulting in a conformational change potentially affecting the stiffness of the Ig molecule. This change in stiffness can help explain some of the passive force regulation capability of titin in myofibrils, which would have important implications for understanding damaged or diseased myofibrils. Further work in our lab has involved atomic force microscopy (AFM) studies that serve to identify the forces associated with unfolding events when the Ig-27 domain is pulled apart. This work has proven to be a monumental starting point for determining if the calcium binding we have encountered translates into a change in the stiffness of titin Ig-27 domains. As seen in Figure 2, the 8 consecutive Ig-27 domains we have studied resulted in 8 unfolding events at forces greater than 100pN. They have been noted to unfold in a saw tooth pattern during extension, which will serve as our basis for comparison when calcium is added into the immediate environment.

CONCLUSIONS

The calcium sensitivity we have encountered for titin Ig-27 domains via tryptophan fluorescence studies has not been documented before. This novel entropic spring within titin may be a further source of comparison between damaged and intact titin proteins to better understand passive force regulation in cardiac muscle and the changes in passive properties associated with specific myopathies resulting in cardiac failure.

REFERENCES

1.Joumaa V, et al. *Am J Physiol Cell Physiol* **294**, 74-78.
2.Labeit D, et al. *Proceedings of the National Academy of Science,* United States, Abstract 100, 2003.
3.Steward A, et al. *Prot. Sci.* **11**, 2179-2183.
4.Lakowicz JR, *Principles of fluorescence spectroscopy*. 3rd ed. Baltimore Press

ACKNOWLEDGEMENTS

I would like to thank Marjolein Blaauboer for beginning the pioneer AFM work on titin Ig-27 domains in our lab.

Characterization of Head Motion in the MR Environment

[1] Brian Andrews-Shigaki, [2] Emily Robinson, [3] Maxim Zaitsev, [2] Linda Chang and [2] Thomas Ernst
[1] Department of Molecular Biosciences and Bioengineering, University of Hawaii at Manoa
[2] Department of Medicine, University of Hawaii at Manoa
[3] Department of Diagnostic Radiology, University Hospital Freiburg, Germany
email: bas@hawaii.edu web: http://www.hawaii.edu/mri

INTRODUCTION

Magnetic Resonance Imaging (MRI) and spectroscopy (MRS) scans are susceptible to subject motion. Therefore, methods for adaptive motion correction are needed (Figure 1). MR-based and external tracking systems are in development, particularly those for brain scans. While movement characteristics of motion disorders are well documented, little is known about the properties of head motion in the restricted MR environment. Knowledge of possible head movements will aid in the development of motion compensation systems. The purpose of this study is to determine if similar tremor frequencies found in movement disorders and significant velocities are reproducible in the restricted MR environment.

METHODS

Four participants (male, ages 27 – 36 years) performed a series of 8 pre-determined head movement patterns within an MRI head coil. These patterns included slow and fast left-right lateral oscillations (intentional tremor), slow and fast superior-inferior oscillations, fast motion from approximately 45 degrees off center left to right lateral and hold, fast motion from 45 degrees superior to inferior and hold, center position cough, and center position without motion. An infrared stereovision system (A.R.T. Track3, Germany, Figure 2) was installed in an MR scanner room and used to track head motion in a quadrature head coil (Siemens Trio), using 4 infrared reflective markers mounted on customized mouthpieces (Figure 3). Six degrees of freedom data (X, Y, Z translations and rotations) were collected over 10 s at 60 Hz. The homogeneous transform between A.R.T. tracking and MRI coordinate spaces was determined by performing a calibration using a structural phantom with attached tracking bodies [1]; all

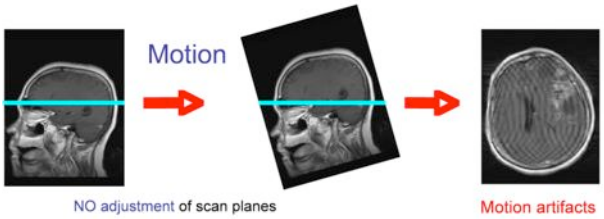

Figure 1: Motion during MRI scanning causes motion artifacts in reconstructed images.

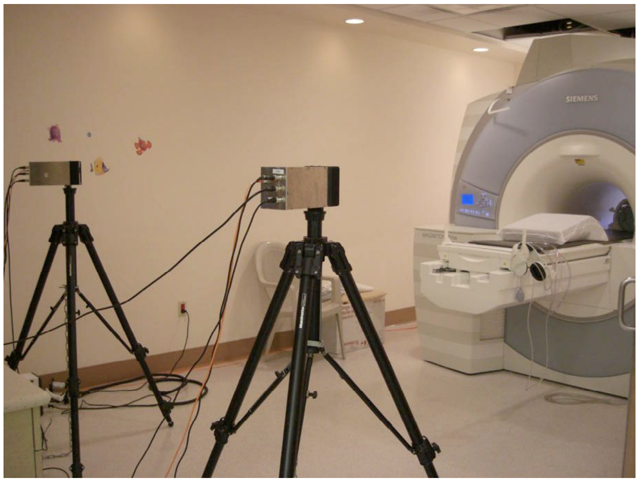

Figure 2: A.R.T. Track3 stereovision system and Siemens 3T scanner located in the MRI room.

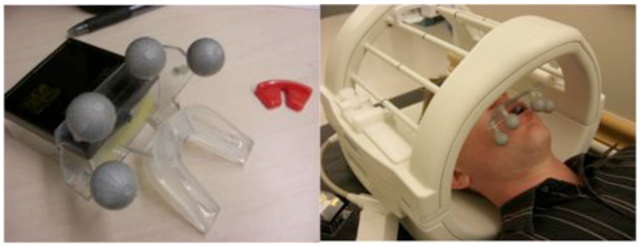

Figure 3: Custom mouthpiece / bite-bar for use in the MR environment.

values reported are relative to MRI isocenter. Collection and analysis of tracking data were performed using custom C++ and MATLAB functions [1].

RESULTS

Major results of the motion study are summarized in Table 1. *Slow oscillatory movements (left-right lateral* or *superior-inferior),* performed at an average frequency of 0.4 Hz, resulted in typical velocities of 0.1 m/s and 75 degree/s (about the Z/superior-inferior axis). *Fast oscillations* (as fast as possible voluntary tremors left-right lateral or superior-inferior) showed power in a frequency range of 3 to 11 Hz *(Figure 4, Table 1)*. Typical maximum velocities were 0.05 - 0.1 m/s and 50 - 90 degree/s, and average maximum accelerations were approximately 0.3 *g* and 2000 degree/s^2 (*Figure 5). Sharp transient movements* resulted in average maximum velocities of 0.57 m/s and 300 degree/s (*left-right lateral*), and 0.21 m/s and 400 degrees/s (*superior-inferior*). Average accelerations were approximately 0.5 - 1 *g* and 3000 degree/s^2, with maximum g-forces up to 2.0 *g* (on a single axis).

Simulated "coughing" led to translational values of 0.02 - 0.03 m/s and 0.1 *g*, and rotational velocity of about 10 degree/s.

DISCUSSION

Voluntary tremors involved frequencies similar to those observed in movement disorders (4 – 12 Hz) [2,3]. Although MR coils substantially restrict head movements, significant rotational and translational velocities can be achieved during fast head movements. Accelerations appear to be limited at 1 to 2 *g,* but velocities may reach close to 1 mm/ms and 0.5 degree/ms. Velocities during simulated coughing were surprisingly small. These movements may induce motion artifacts even for fast MR acquisitions in the 10 ms range.

REFERENCES

1. M. Zaitsev, et al., NeuroImage 2006; **31**:1038-1050
2. J. Jankovic, E. Tolosa. Lippincott Williams & Williams, 5th, 2007;24:298-315
3. N. Zasler, D. Katz, R. Zafonte, Demos Medical Publishing, 2007; 27:469-481

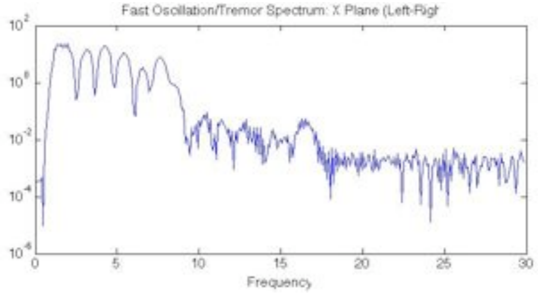

Figure 4: Fast left-right lateral (tremor) frequency spectrum.

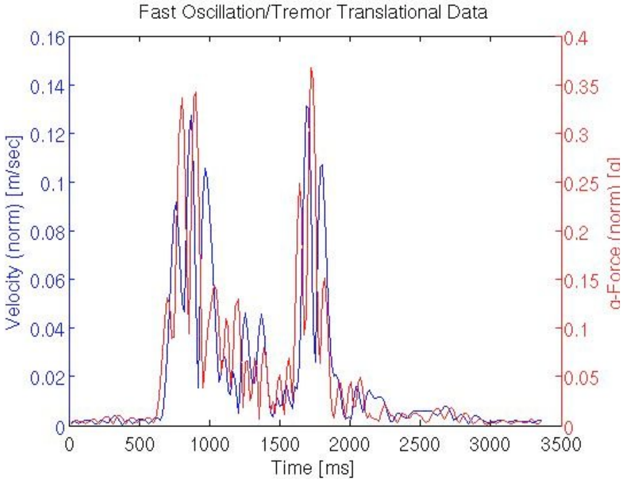

Figure 5: Fast left-right lateral (tremor) velocities (blue) and g-forces (red).

Summary of Motion Data					
		*Velocities***		*g-Force****	*Freq.*
	X (*) [m/s]	*Y (*) [m/s]*	*Rz (*) [0/s]*	*(*) [g]*	*[Hz]*
Slow L-R Osc.	0.14 (0.014)	0.07 (0.007)	74 (6)	0.1 (0.02)	0.3 - 0.5
Fast L-R Osc.	0.12 (0.027)	0.04 (0.007)	52 (10)	0.3 (0.06)	3.3 - 11
Sharp L to R	0.57 (0.086)	0.24 (0.052)	312 (47)	0.7 (0.12)	---
Cough	0.02 (0.003)	0.03 (0.008)	9 (2)	0.1 (0.02)	---
	Z (*) [m/s]	*Y (*) [m/s]*	*Rx (*) [0/s]*		
Slow S-I Osc.	0.11 (0.005)	0.11 (0.015)	171 (8)	0.2 (0.04)	0.3 - 0.9
Fast S-I Osc.	0.07 (0.003)	0.09 (0.019)	90 (2)	0.3 (0.05)	4.6 - 8.6
Sharp S to I	0.21 (0.008)	0.26 (0.011)	409 (9)	0.5 (0.04)	---

L-R = Left-Right Lateral, S-I = Superior-Inferior, Osc. = Oscillation
* +/- Standard Error
** Average Maximum Values
*** g-Forces represented in translational magnitude (norm)

Table 1: Summary of average maximum velocities, g-forces and range of frequencies.

THE ORIGINS OF BIPEDAL LOCOMOTION INFERRED FROM GEOMETRIC CROSS-SECTIONAL PROPERTIES OF ANCIENT AFRICAN FEMORA

Adam J. Kuperavage and Robert B. Eckhardt
Laboratory for the Comparative Study of Morphology, Mechanics and Molecules, Department of Kinesiology, Penn State University, University Park, PA, 16802 USA
email: ajk186@psu.edu

INTRODUCTION

The human lineage has been separate from other nonhuman primates for approximately 6 to 8 million years (Ma) [1, 2]. Beginning in 1981, Ruff and his colleagues [3] have published a series of papers showing that average bone strength (as measured through analysis of diaphyseal geometric cross-sectional properties) has been declining in the human lineage for the past two to three million years. Their data spans from recent populations of humans back to four million years ago, AL 288-1 (“Lucy”) [4].

The data presented here extends the comparison back by yet another two million years, or 50% more than the previously documented evidence relevant to the evolution of upright posture and bipedal locomotion in humans. The 6 Ma old *Orrorin tugenensis* femora represent the oldest femoral fragments pertinent to reconstructing posture and locomotion, and are at a temporal point near the divergence of a human lineage from its more ape-like ancestors (dating references are summarized in [5]). The unusually favorable conditions of fossilization have retained internal structural features, allowing for imaging of the diaphyseal cross-sections through computerized tomography (CT). We describe here the geometric properties of the diaphyseal cross-sections of the two partially intact fossilized femora, BAR 1002’00 and BAR1003’00, designated as the taxon *Orrorin tugenensis*.

METHODS

CT was used to image the internal distribution of cortical bone of BAR 1002’00 and BAR 1003’00. Each femur was scanned air helically with a Marconi Twin Flash CT Scanner at 1 mm increments proximally to distally about the long axis of the femur. Field of view was (222x222) mm^2, with a matrix of (512)^2 pixels yielding planar resolution of 0.434 mm/pixel. The series of CT images for each of the specimens were imported into Amira 4.1.1 software, in which 3D reconstructions were made. The geometric properties were measured from cross-sections perpendicular to the long axis of the bone at increments of 15% of diaphyseal length, proceeding distally to proximally. The CT scans were made in

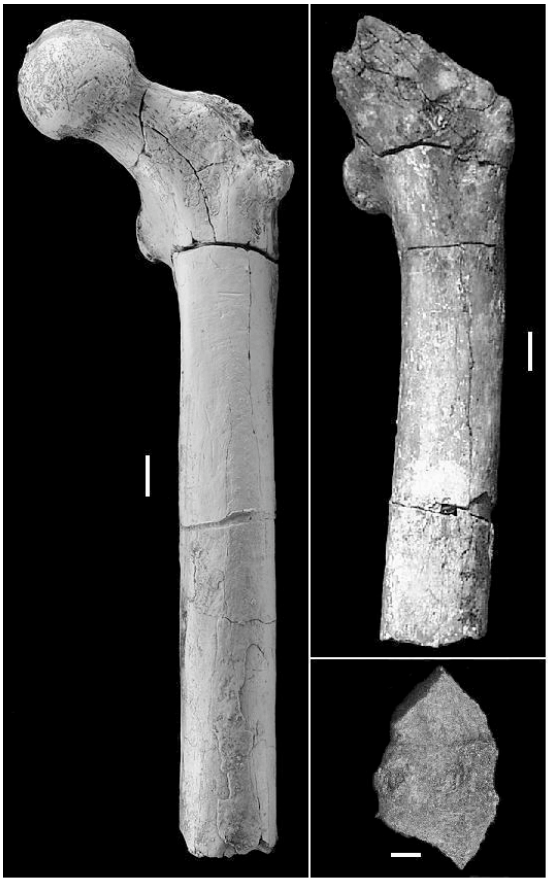

Figure 1: *Orrorin tugenensis* femora. Left: BAR 1002’00, Upper Right: BAR 1003’00, Lower Right: BAR 1215’00. The white bars indicate 1 cm scale.

1 mm increments, with a resultant volume unit (voxel) size of 0.434 x 0.434 x 1 mm^3. Differences in density are expressed in Hounsfield units (HUs), each of which corresponds to 0.1% of the attenuation coefficient difference between water and air. Each voxel is assigned a numeric value ranging from -1000 to 3095 HU. The true boundaries of the cross-sections within the blurred region on the image were determined through the Full-Width at Half-Maximum (FWHM) principle [6]. The potential FWHM error is < ± 1 pixel for each gradient. Geometric properties of cross-sections were then determined using the MomentMacro (technical details are available on the website of C. B. Ruff) in ImageJ software, which we used to calculate cross-sectional areas (CA; mm^2), total areas (TA; mm^2), medullary areas (MA; mm^2), section moduli (SM, mm^3), principal second moments of area (Imin and Imax; mm^4), and polar moments of area (mm^4).

RESULTS AND DISCUSSION

Due to the incompleteness of our specimens, we were able to measure only sections from 35% to 80% for BAR 1002'00 and from 50% to 80% for BAR 1003'00 (the cross-sectional properties at 80% of diaphyseal length are given in Table 1). These section percentages are approximations because of damage to both proximal and distal ends of the bones. The overall pattern, other than for MA, is consistent with the external dimensions of the two fossils, with BAR 1003'00 being moderately larger in diameter and appearing generally more robust in its proportions. The two individuals were from the same site (hence same place and approximate time) and differ appreciably in size.

CONCLUSIONS

The data presented here are consistent with previous findings, which indicate a steady decline in diaphyseal robusticity in *Homo* from the early Pleistocene to modern humans [4]. They also overlay and extend findings reported separately in [7]. The diaphyseal cross-sections of BAR 1002'00 and BAR 1003'00 exhibit markedly high percentages of cortical area compared to the modern human sample. However, their relatively thicker cortical areas do not translate into higher bending resistance (Imax and Imin) or torsional rigidity (J) in comparison to modern human sample. This observation about inferred functional properties probably results from the relatively smaller size of BAR 1002'00 and BAR 1003'00 compared to femora of later humans.

REFERENCES

1. Eckhardt, RB, *Sci Amer* **226**, 94-103, 1972.
2. Begun, DR, Science **303**, 1478-1480, 2004
3. Ruff, CB and Hayes, WC, *Amer J Phys Anthrop* **60**, 359-381, 1983.
4. Ruff, CB *Amer Sci* **94**, 508-514, 2006.
5. Galik, K et al., *Science* **305**, 1450-1453, 2004.
6. Ohman, JC et al., *J Hum Evol* **25**, 217-227, 1997.
7. Kuperavage, AJ, and Eckhardt, RB, *J Mech Eng,* in press.

Table 1: Comparisons of cross-sectional properties at 80% of diaphyseal cross-section length.

Specimen	CA	TA	MA	SM	Imax	Imin	Imax/Imin	J
BAR 1002' 00	351.1	439.5	88.4	2208.0	19845	11024	1.8	30868
BAR 1003' 00	347.3	436.6	89.4	2286.7	19122	11086	1.72	30207

CHANGES IN KINEMATICS, METABOLIC COST AND EXTERNAL WORK DONE DURING WALKING WITH A PROPULSIVE FORCE

Chris A. Zirker, Bradford C. Bennett, Douglas I. Friedman, Rafat E. Mehdi, Mark F. Abel
University of Virginia, Charlottesville, VA, USA
email: chriszirker@virginia.edu

INTRODUCTION

It is well understood that many factors can change the metabolic cost of walking although the biomechanical mechanism is sometimes unclear. Gottschall and Kram [1] demonstrated that by applying a horizontal force at the center of mass of a healthy adult, the metabolic cost of walking can be reduced. We explore how an assist force changes gait kinematics and the external work that accompany the reduced metabolic cost in order to better understand this process.

METHODS

Subjects performed five walking trials on a level treadmill at their self-selected comfortable walking speed (CWS) while kinematic and metabolic data were collected. Subjects wore a full body marker set of 38 markers and a facemask to measure gas exchange. Three-dimensional kinematic data were collected using an 8-camera Vicon Motion Analysis System at 120 Hz while metabolic data was collected via the Oxycon Mobile wireless portable ergospirometry system.

Subjects were a convenience sample of 10 healthy adult males without known musculoskeletal, neurological, cardiac, or pulmonary pathology [age = 32.8±13.2, height = 1.8±.07 m, mass = 77.5±12.0 kg]. Consent was approved and obtained for all subjects. In all trials, steady state metabolic rate was determined by monitoring real-time VO2/kg consumption until two minutes of constant rates were observed. Subjects performed an unassisted "warm up" trial, three trials in random order with horizontal assistive forces applied equal to 4%, 8%, and 12% of their body weight, and a final "cool down" unassisted trial. Each trial was preceded by a rest period long enough for resting steady state metabolic rate to be reached. Constant assist forces were applied through a waist belt strapped roughly around the subject's center of mass. After the experiment, subjects filled out a brief questionnaire asking about the experience of walking with an assist force.

Kinematic data were exported from Vicon and analyzed in MATLAB to find stride length, time spent in double support, recovery factor, relative phase, external work (Wext), and PE/KE as described by Bennett et al [2]. Center of mass (COM) data was filtered with a bidirectional zero-lag low-pass second order Butterworth filter with a cutoff frequency of 8 Hz. Differences between measures were determined using repeated measures ANOVA with Tukey's post hoc test. No significant differences were found for any measure between "warm up" and "cool down" for any measures, so data from the two were averaged to give the "normal" condition.

RESULTS AND DISCUSSION

During assisted trials, the metabolic cost of walking at CWS was shown to reduce by on average 23.7±6.3% of normal walking for 4% assistance force, 34.7±6.9% for 8% assistance, and 19.1±12.8% for 12% assistance ($p > .001$ for all).
Stride length was found to decrease as assist force increased ($p<.026$). There was a trend of decreasing time in double support with increasing assist force. Hip excursion and ankle excursion were both found to decrease while knee excursion increased with increasing assist force ($p < .01$). See table 1 for a summary of these results.

Relative phasing between potential and kinetic energy of the COM during walking showed that phase angle increased as assist force increased ($p<.005$). Recovery factor improved slightly at 4% ($p=.044$) and 8% ($p=.058$) assist force but not at 12% ($p=.972$). There were no significant differences in the PE/KE ratio between trials, although excursion of kinetic energy and potential energy both increased.
Four of ten subjects reported preferring 4% assist, five preferred normal walking, while only one

preferred 8%. Nine of ten subjects reported 12% as being the most uncomfortable trial.

Many of the kinematic changes observed were similar to those seen in downhill walking. The decrease in stride length with increased assist force may occur due to increased shear ground reaction forces required for braking as is seen in downhill walking [3]. Increased knee flexion during stance with increased assist force is also qualitatively similar to the knee flexion seen in walking down a steeper descent [3]. While the hip, knee and ankle joints did all demonstrate changes in excursion across HAF trials, these changes were small and subjects' general gait patterns and form were preserved.

Our measured reductions in metabolic cost are similar to but less than those found by Gottschall and Kram [1]. This could be because their subjects performed a standing rest while ours rested seated or because our subjects walked at CWS rather than a uniform speed. We found 8% assist to be the most metabolically efficient although 4% assist has the highest recovery factor and best phasing between PE and KE. 8% assist also showed an increase in Wext despite the decrease in metabolic cost. This could be explained by the assist force contributing positive work towards KE and PE excursion, possibly by providing propulsion as well as raising the COM as it pivots over the stance leg. These results highlight that changes in recovery factor, total external work and COM motion are not driving the observed reduction in metabolic cost.

CONCLUSIONS

These findings have important therapeutic implications for both rehabilitation and the development of assistive devices. When treating patients with disorders which cause them to fatigue rapidly, usage of an assist force in conjunction with treadmill exercises could increase the time patients remain active during therapy sessions. Because lower levels of assist force corresponded with improved recovery factor and relative phase, usage of small assist forces during gait training exercises may aid in improving form. It may also be useful as a reconditioning exercise for patients with severe lower limb weakness. Future work should examine if subjects with gait disorders demonstrate similar improvements and if these results can be replicated in over-ground walking.

REFERENCES

1.Gottschall JS and Kram R. *J.Appl.Physio,*. **94**, 1766-1772, 2003
2.Bennett BC, et al. *Arch.Phys.Med.Rehabil*. **86**, 2189-2194, 2005.
3.Cham R, Redfern MS. *Gait Posture*. **15(2),** 159-71, 2002.

ACKNOWLEDGEMENTS

We would like to thank Shawn Russell and Jason Franz for their assistance and advice.

Table 1: Summary of results.

	Normal	4%	8%	12%
% Reduction in Metabolic Cost	0.00%	23.70%*	34.66%*	19.05%*
Stride Length (m)	1.43	1.38*	1.35*	1.30*
% of Stride in Double Support	18.49%	17.48%	16.69%*	15.97%*
Recovery Factor	62.1	67.9*	67.6	63.0
Relative Phase (deg)	158.3	181.3*	199.4*	213.8*
W_{ext} ($J * kg^{-1} * m^{-1}$)	0.69	0.64	0.73	0.87*
PE/KE	1.16	1.13	1.13	1.12
Hip Excursion (deg)	47.6	43.5*	40.4*	35.5*
Knee Excursion (deg)	66.8	69.6*	71.5*	72.5*
Ankle Excursion (deg)	32.1	29.5*	26.7*	25.0*

SIMPLE FINGER MOVEMENTS REQUIRE COMPLEX COORDINATION OF EXCURSIONS AND FORCES ACROSS ALL MUSCLES

[1]Jason Kutch, [1]Manish Kurse, [1]Heiko Hoffmann, [1]Evangelos Theodorou, [3]Vincent R. Hentz,
[4]Caroline Leclercq, [5]Isabella Fassola, [1,2]Francisco Valero-Cuevas
[1]Brain-Body Dynamics Lab, Department of Biomedical Engineering, Viterbi School of Engineering
[2]Division of Biokinesiology & Physical Therapy, University of Southern California, Los Angeles, CA
[3]Stanford Medical School, Stanford, CA, [4]l'Institut de la Main, Paris, France,
[5]Keck School of Medicine, University of Southern California, Los Angeles, CA
email: kutch@usc.edu, web: http://bme.usc.edu/valero

INTRODUCTION

Producing accurate slow finger movements is critical to manipulation—and inaccurate finger movements are a hallmark of neurological diseases. Numerous studies have described the kinematics of able and pathological finger movements (e.g., (Dennerlein et al. 1998; Kamper and Rymer 2001; Littler 1973; Santello et al. 1998; Weiss and Flanders 2004)). This short report is, to our knowledge, the first complete simultaneous description of the force and excursion of all tendons that produce a coordinated finger flexion movement. We used computer-controlled motors to drive cadaveric index finger tendons to have direct access to the mechancial variables necessary to produce finger motion. This avoids the pitfalls of EMG and computational models, which cannot yet accurately estimate tendon excursion and force, or the role of skin and joint structures. This novel approach serves as the foundation for new research directions to understand the robustness of finger movement to neuromuscular dysfunction, and promote the design of novel robotic manipulators, prostheses and functional electrical stimulation schemes.

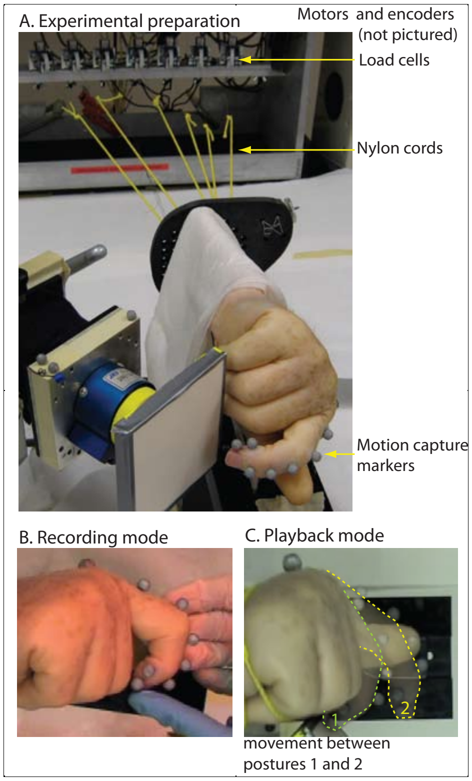
A. Experimental preparation
Motors and encoders (not pictured)
Load cells
Nylon cords
Motion capture markers
B. Recording mode
C. Playback mode
1
2
movement between postures 1 and 2

Fig. 1: Experimental preparation used to record a finger tapping movement and to play it back.

METHODS

Experimental preparation

We resected fresh frozen cadaver arms at the mid-forearm level and dissected them to reveal the proximal end of the insertion tendons of all seven muscles controlling the index finger (Valero-Cuevas et al. 2000): flexor digitorum profundus (FDP), flexor digitorum superficialis (FDS), extensor indicis proprius (EIP), extensor digitorum communis (EDC), first lumbrical (LUM), first dorsal interosseous (FDI), and first palmar interosseous (FPI). We fixed the specimen rigidly to a tabletop using an external fixator (Agee-WristJack, Hand Biomechanics Lab, Inc., Sacramento, CA), and we tied and glued (Vetbond Tissue Adhesive, 3M Inc., St. Paul, MN) the proximal tendons to Nylon cords attached to rotational motors, Fig. 1A. Motors were controlled using a LabVIEW Real-time controller (PXI-8183 National Instruments, Austin, TX) and custom-written software. The motors could be programmed to operate in three control modes: *force control* – a desired tendon force is maintained regardless of tendon excursion, *position control* – a desired excursion is produced, regardless of the required force, and *tunable spring control* – the applied force is proportional to the difference in excursion from a set-point. Encoders mounted on the motors recorded tendon excursion, while load cells mounted between motors and tendons recorded tendon force.

Experimental procedure

The experiment had two phases: recording and playback. In the recording phase, motors were operated in force control with a desired tendon tension of 5 N (same for all tendons). The experimenter moved the finger through a simulated tapping movement (Venkadesan and Valero-Cuevas 2008), while we recorded the resulting tendon excursions (Fig. 1B). In the playback phase, the motors were controlled as stiff tunable springs (spring constant 5 N/mm for all tendons), with the time history of recorded tendon excursions played back as spring-length set points. This control caused the finger to replicate the desired finger movement, which we played back ten times in series to measure repeatability.

RESULTS AND DISCUSSION

We found that producing the recorded tapping movement ten times in playback generated a consistent pattern of tendon excursions and tensions (Fig. 1C). Moreover, we found that, to replicate the movement, a complex pattern of excursion and forces emerged at all tendons (Fig. 2). Whereas simply pulling manually on one or two of the tendons generated a movement approximating tapping, the realistic movement requires specific excursions and forces. These requirements arise from the biomechanical constraints. For example, the time history of unique tendon excursions (where all tendons must retain a tonic tension and cannot go slack) is defined by the time history of joint angles by the equation

$$\dot{s}(t) = R^T(q(t))\dot{q}(t)$$

where the transpose of the (angle-dependent) moment arm matrix $R^T(q(t))$ maps uniquely from joint angle changes to tendon excursions. While the baseline tendon tensions are free parameters (i.e., level of co-contraction), we see that the relative changes in tendon tensions follow a complex patterns not completely coupled to the kinematics; likely because they are governed by complex strain energy changes resulting from the necessary eccentric and concentric contractions of our simulated muscles. Further study will examine the robustness of these coordination patterns to neuromuscular dysfunction.

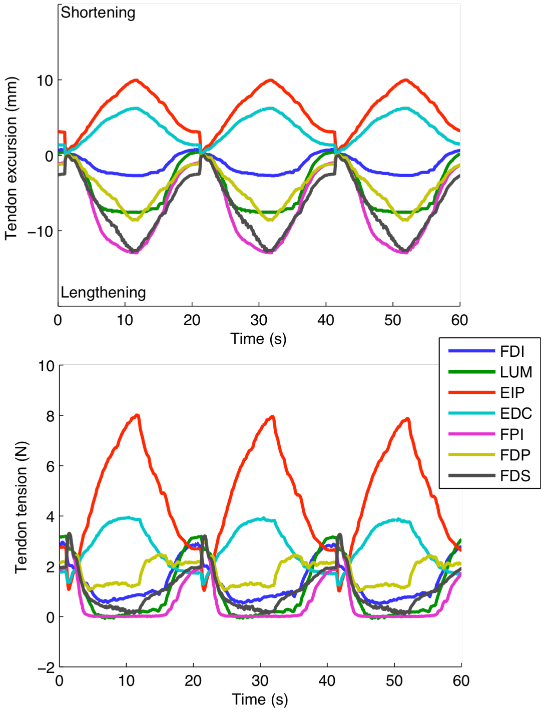

Fig. 2. Tendon excursions and tensions for the last three repetitions of the simple tapping movement.

CONCLUSIONS

We find that producing a repeatable tapping movement requires complex eccentric/concentric muscle contractions, suggesting that even simple natural movements are generated by the complex balance of activity in all muscles.

REFERENCES

1.Dennerlein JT, Mote CD, Jr., and Rempel DM. *Exp Brain Res* 121: 1-6, 1998.
2.Kamper DG, and Rymer WZ. *Muscle Nerve* 24: 673-681, 2001.
3.Littler J. *Hand* 5: 187-191, 1973.
4.Santello M, Flanders M, and Soechting JF. *J Neurosci* 18: 10105-10115, 1998.
5.Valero-Cuevas FJ, Towles JD, and Hentz VR. *J Biomech* 33: 1601-1609, 2000.
6.Venkadesan M, and Valero-Cuevas FJ. *J Neurosci* 28: 1366-1373, 2008.
7.Weiss EJ, and Flanders M. *J Neurophysiol* 92: 523-535, 2004.

ACKNOWLEDGEMENTS

NIH AR-050520, AR-052345 and NSF EFRI-COPN to FVC, and Dr. Jae Woong Yi.

SCAPULAR-HUMERAL KINEMATICS DURING WHEELCHAIR PROPULSION

Shashank Raina[1], Jill L. McNitt-Gray[1, 2, 3], Philip S. Requejo[2, 4]
[1]Depts. of Biomedical Engineering, [2]Kinesiology, [3]Biological Sciences, USC, LA, CA,
[4]Pathokinesiology Laboratory, Rancho Los Amigos National Rehabilitation Center, Downey, CA
Email:sraina@usc.edu

INTRODUCTION

For a wheelchair user, the shoulder joint and shoulder girdle take on a propulsive and weight bearing role as part of activities of daily living (ADL). The repetitive nature and mechanical demand imposed on the shoulder joint during ADL is often associated with acute and overuse injuries that can lead to secondary disabilities and a loss of independence and a decrease in quality of life in users with spinal cord injury [1]. Repetitive mechanical loading experienced by the shoulder joint tends to be highest in activities involving wheelchair propulsion, transfers, and lifts, contributing to fatigue of the surrounding musculature and potentially a decline in motor control which can lead to injury.

Integrity of the shoulder complex is dependent upon active and passive soft tissue to stabilize and control rotation of the shoulder joint and shoulder girdle. Weakness of surrounding musculature either due to fatigue or loss of innervations may lead to uncoordinated motion of scapula and humerus. The relative motion between the humerus and scapula is associated with pain believed to originate from compression of structures in the subacromial space (supraspinatus tendon, bicipital tendon and the subacromial bursae) [2]. Veeger et al.[3] using quasi-static analysis recorded the motion of the scapula, and predicted its motion based on the motion of the humerus, thorax and the applied force at the pushrim during a wheelchair pushing task. Koontz et al.[4]also studied the kinematics of the scapula under quasi-static conditions during a wheelchair push. The present study adds to this existing body of literature by quantifying scapular kinematics under dynamic conditions with low and high loading.

The purpose of this experiment was to determine how scapular-humeral kinematics are modified to accommodate physically demanding propulsion conditions. We hypothesized that an increase in the pushrim force during wheelchair propulsion will alter the scapular-humeral kinematics observed under preferred propulsion conditions.

METHODS

One 36 years old male wheelchair user with a T12 level injury and 16 years post injury was recruited from Rancho Los Amigos Rehabilitation Center. On the day of collection, informed consent was provided in accordance with the review board for human subjects. A wheelchair (WC) with aluminum frame was used to minimize magnetic interference during testing. The WC was positioned on a stationary ergometer with the rear wheels resting on two independent rollers. The wheelchair ergometer was calibrated for frictional force similar to over ground propulsion. A miniBIRD (Ascension Technology Corp.) magnetic tracking system was used to gather three dimensional kinematic data of the thorax, scapula, upperarm and forearm.

The participant performed two tasks. First, the participant propelled the test wheelchair at a self selected preferred speed for 10 seconds (Normal). To increase the force requirements of the propulsive task the participant was asked to maintain the preferred wheelchair velocity while additional load equivalent to an 8% grade was applied to the rollers of the ergometer.

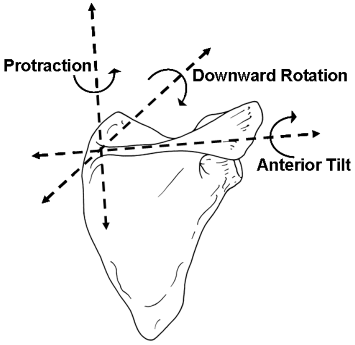

Figure 1: Depicts the motion of the scapula along the three axes.

Steady state propulsion data was collected after the wheelchair had reached the preferred wheelchair velocity. Protraction-retraction, medial-lateral rotation and anterior-posterior tilt of the scapula were defined using ISB standards (Fig. 1) and are represented in the thorax segment reference frame. Kinematic data was collected at 100 Hz and force was collected at 200 Hz using a SmartWheel® (Three Rivers Holdings LLC). Motion Monitor (Innovative Sports Training Inc.) and MatLab (MathWorks Inc.) software were used to analyze the data.

RESULTS

The participant was able to propel the wheelchair at a steady velocity under both normal and loaded conditions. The average peak force at the interface between the hand and pushrim during normal propulsion was 44N and the average peak force under the loaded condition was 105N. This increase in force was accompanied by a comparable increase in the moments at the shoulder and the elbow. During the loaded condition, more upward rotation, posterior tilting and protraction of the scapula was observed than during the normal condition (Table 1). The time of maximum upward rotation corresponded with the time of maximum rim force. The maximum protraction and posterior tilt were observed at the end on the propulsion phase under both conditions.

The change in subacromial space, defined as the distance between the acromion and the center of the shoulder joint (e.g. Mesker's Rotation Protocol) was greater during the loaded condition than in the normal condition and occurred at the top dead center (TDC) of the wheel. During the loaded condition, humeral head translated towards the acromion whereas during normal propulsion, the humeral head translated away from the acromion

	Normal		Loaded	
	Min (deg)	Max (deg)	Min (deg)	Max (deg)
A/P Tilt	-36.9	-8.5	-45.5	-13.8
Protrac/Retrac	24	43.7	24.5	46.2
Up/Down Rot	9.3	17.7	4.7	17.2

Table 1: Average range of motion of the scapula under both propulsion conditions. Posterior tilt is positive, Protraction is positive, and Downward rotation is positive.

DISCUSSION

In this study, the scapular-humeral kinematics during dynamic wheelchair propulsion changed when the magnitude of the pushrim force required to perform the task more than doubled. This increase in force required to maintain wheelchair velocity was accompanied by a comparable increase in the shoulder and elbow net joint moments and more upward rotation, posterior tilting and protraction of the scapula. The subacromial space decreased during the loaded condition and increased during the normal condition.

The trend of scapular motion is similar to what has been observed in other literature[5]. The absolute values of the scapular angles are comparable with Veeger et al[4]. As the arm moved through the propulsion cycle the scapula tilted posteriorly and into protraction for both loaded and normal condition. Although the scapula remained in anterior tilt throughout the motion, the amount of tilt reduced from the beginning to the end of the push phase. This motion moves the acromion away from the greater tuberosity and aids in avoiding impingement. The upward scapular rotation at the time of peak force under the loaded condition may be essential to accommodate the increase in force requirements.

Further study with more users is required to understand is these changes in mechanics are universal among the population and if they occur when using their own WC. A study of participants with cervical level injuries will allow us to understand differences in kinematics between the two populations.

REFERENCES

1. Ballinger DA, et al., *Arch Phys Med Rehabil*; 81(12):1575-81, 2000.
2. Sie IH, et al., *Arch Phys Med Rehabil*; 73(1):44-8, 1992.
3. Veeger HEJ, et al.,*Clin Biomech* ;8(2):81-90,1992.
4. Koontz A, et al., *Int J Ind Erg* 33:237-48, 2004.

FASCICLE LENGTHS IN THE FIRST DORSAL INTEROSSEOUS MUSCLE

Michael J. Ellis, Brendan J. Casey, Benjamin W. Infantolino and John H. Challis
Biomechanics Laboratory, Department of Kinesiology, The Pennsylvania State University, University Park, PA, USA
E-mail: mje5070@psu.edu

INTRODUCTION

In musculoskeletal models a common assumption is that the properties of whole muscle can be considered to behave like a scaled individual muscle fiber or sarcomere [1]. Indeed such a conceptualization of muscle is used even if the pennate structure of certain muscles is modeled [2]. Gross dissection of muscles indicates that this conceptualization of muscle does not accurately reflect many aspects of muscle architecture. It is still commonly assumed that the fascicles of human muscles stretch the entire length of the muscle from proximal to distal tendon [3]. There is limited evidence from anatomical studies that not all muscle fibers run from tendon to tendon, for example in cats [4], and in the long human muscles [5]. Many of these muscle fibers terminated within the muscle belly, and some were arranged in series with other fibers.

Understanding the force-length properties of muscle is important, for example, for the parameterization of musculo-skeletal models and can hold clinical significance, for example, in muscle tendon lengthening and transfer surgeries [6]. Therefore the purpose of this study was to determine for a muscle the distribution of lengths of the fascicles and tendon comprising the whole muscle. The implications of this distribution for the force-length properties of muscle will be addressed.

METHODS

From a selection of first dorsal interosseous (FDI) muscles obtained from cadavers one typical sample was selected for detailed analysis. All procedures concerning the handling of this cadaver material were conducted following university safety and ethical standards. The mass and length of the muscle with intact fascia were determined. The muscle was placed in 20% nitric acid to digest the overlying and connecting fascia. A trained operator dissected all of the muscle fascicles from the muscle with the aid of a Cannon RE-350 video visualizer (Cannon, New York, USA). Each fascicle was placed on a flat graduated surface and images of it recorded with a DVD recorder. Subsequent analysis of the fascicle and tendon dimensions were performed on the recorded fascicles images (Figure 1).

Once an image of a single muscle fascicle was obtained, the muscle belly length and the tendon lengths were measured using a custom MATLAB program (The MathWorks Natick, USA). The program has previously been validated for accuracy and repeatability using objects of known length. The accuracy of the measurement procedure was assessed to ±0.5 mm. In addition the length of the whole muscle's externally visible tendon was also measured, as was the length of the muscle belly. The fascicle lengths were compared to the overall length of the muscle.

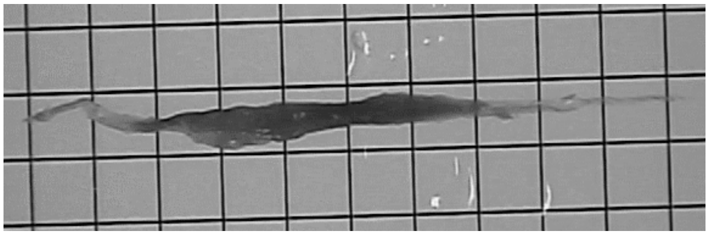

Figure 1: Image of a typical muscle fascicle with tendon intact. This was obtained from a video visualizer at a magnification of 12x. The grids are 5 mm squares.

RESULTS

A total of 70 fascicles were dissected from the sample FDI. They ranged in length from 8 mm to 40 mm, compared with a muscle belly length of 52.5 mm. The Anderson-Darling test was used to formally test if the lengths of the fascicles were normally distributed, which they were ($p > 0.05$;

Figure 2). The coefficient of variation, which provides a measure of the distribution of these data, was 25.3% (Table 1).

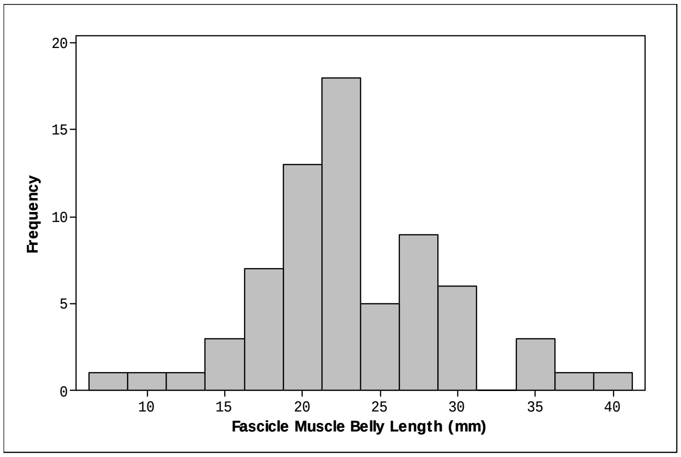

Figure 2: A histogram of the distribution of fascicle lengths.

Table 1: The muscle belly and tendon lengths of the fascicles (n=70) and the whole muscle.

Region	***Fascicle*** (mm)	***Whole Muscle*** (mm)
Belly	23.3 ± 5.9	52.5
Tendon	11.4 ± 9.3	8.1

The muscle fascicles did not run the entire length of whole muscle belly. The longest fascicle obtained from the specimen was 40 mm in length compared to the whole muscle belly length of 52.5 mm, while the shortest length was 8 mm.

Some of muscle fascicles had both proximal and distal tendons, others had only distinct proximal or distal tendons, and others had no distinct tendon. Those fascicles which had only one tendon or no tendon seem to be attached to other muscle fascicles in series.

DISCUSSION

The purpose of this study was to determine for a muscle the distribution of lengths of the fascicles comprising a muscle. The range of lengths was large but was normally distributed. Gordon et al. [7] determined the force-length properties of muscle and determined that fibers could produce muscle force until they had shortened to approximately 50% of their optimum length and lengthened by the same amount. In this study fascicle optimum length was not determined but its resting length but if the mean fiber length is assumed to be the optimum length then the operating width of the force length curve would be much greater than that observed by Gordon et al. [7] because of the long lengths of the some of the fascicles. Indeed the shape the curve may also vary because of the sum of contributions of fibers on different portions of their force-length curves.

That some fibers are serially arranged means that the operating range of a whole muscle can be greater than that implied by the lengths of the individual muscle fibers. This also has implications for the force-velocity properties of muscle because the maximum velocity of shortening is a function of the optimum length of a fiber [8], and would be greater for two fibers arranged in series.

There are some limitations in this study, in particular that only one muscle sample was analyzed, although these results are of interest despite this limitation. Greater automation of the data collection process will permit confirmation of these results for additional samples. These results have implications for the expression of both the force-length and force-velocity properties of muscle in whole muscle where the architecture of the muscle makes the situation more complex than is commonly assumed in some models of muscle.

REFERENCES

1. Zajac FE. CRC Rev Biomed Eng **17**, 359-411, 1989.
2. Otten E. *Exerc Sport Sci Rev* **16**, 89-137, 1988.
3. Koryak, Y. (2008). *Human Physiology* **34,** 102-112, 2008
4. Loeb GE, et al. *J Morphol* **191**, 1-15, 1987.
5. Heron MI, et al. *J. Morph* **216**, 35-46, 1993.
6. Lieber, R. and Friden, J. *Muscle & Nerve* **23**, 1647-1666, 2000.
7. Gordon AM, et al. *J Physiol* **184**, 170-192, 1966.
8. Hill AV. Proc *R Soc London B Biol Sci* **126**, 136-195, 1938.

MUSCLE FATIGUE AFFECTS TASK PERFORMANCE DURING REPETITIVE UPPER EXTREMITY MOVEMENTS

[1]Deanna H. Gates, [1]Rachel Smallwood, and [2]Jonathan B. Dingwell

[1]Department of Biomedical Engineering, University of Texas, Austin, TX, USA
[2]Department of Kinesiology & Health Education, University of Texas, Austin, TX, USA
E-mail: jdingwell@mail.utexas.edu Web: http://www.edb.utexas.edu/faculty/dingwell/

INTRODUCTION

Muscle fatigue may impair a person's ability to properly execute a task. At the muscle level, fatigue causes increased muscle latency [1]. Muscle fatigue may adversely affect the body's ability to successfully reproduce a movement [2]. However, others have shown no affect of fatigue on the end-point trajectories in multi-joint tasks [3-4], which suggests that subjects changed their neural control or coordination strategies to achieve the same overall task goal. The purpose of this study was to examine the effect of muscle fatigue on changes in performance and control of a repetitive upper extremity sawing task. The height of the task was set to shoulder level to impose an additional challenge on the subjects. The increased force variability and delayed reaction times associated with muscle fatigue [1, 4] suggest that task performance should deteriorate with fatigue: i.e., the magnitude of timing errors would increase. Alternatively, subjects could instead maintain overall task *performance* [4]: i.e., they would continue to achieve the task goal by changing their control strategy.

METHODS

12 healthy young right-handed subjects participated. Subjects sat in an adjustable chair and pushed a weight back and forth at shoulder height along a low friction horizontal track in time with a metronome until volitional exhaustion. The movement of a single marker placed on the top of the handle was recorded at 60 Hz using a Vicon motion analysis system.

Means and standard deviations of movement distance (D), speed (S), and timing errors (E) were computed to quantify overall task performance. Timing errors were calculated as the difference between the metronome and the maximum excursions of the hand [5]. Movement variability was also analyzed by recognizing that the primary *goal* of this task was to maintain time with the metronome, but many combinations of *D* and *S* achieve this goal. All (*D, S)* combinations which achieve the correct movement time define the "*goal equivalent manifold"* (GEM) for the task [5, 6] (Fig. 1). We then decomposed the variability in *D* and *S* into deviations tangent to (δ_T) and perpendicular to (δ_P) the GEM. The deviations δ_T make *no* contribution to the timing errors, while the deviations δ_P *do*. We hypothesized that temporal correlations in δ_T and δ_P would be different, reflecting different control strategies used to minimize timing errors. Principal components analysis was also performed to determine how well subjects aligned their movements with the GEM.

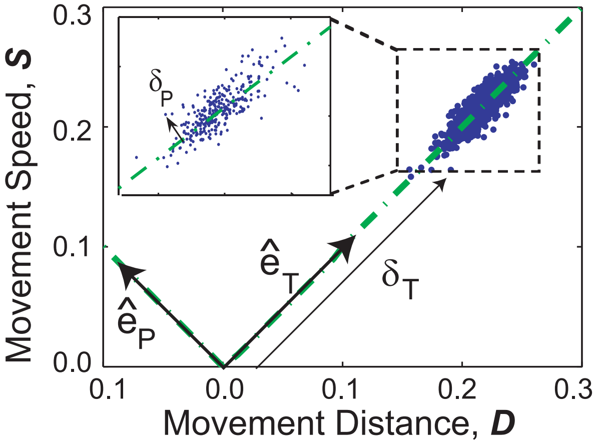

Figure 1: Illustration of the goal equivalent manifold (GEM) analysis.

Each time series was analyzed using detrended fluctuation analysis (DFA) [5, 7]. DFA produces a scaling exponent, α, that indicates how quickly deviations are corrected. Deviations that go *un*corrected lead to "persistent" correlations over consecutive movements. Thus, less "persistence" (smaller α) in a time series indicates more controlled process where deviations are corrected rapidly. DFA was performed on D, S, E, δ_P, and δ_T time series. Only the first and last 150 cycles were used to obtain 'Early' and 'Late' fatigue measures. Comparisons were made using a series of within subjects ANOVAs.

RESULTS AND DISCUSSION

Subjects performed the task for 11.2 ± 4.4 minutes. Subjects made shorter ($p = 0.001$) and slower ($p < 0.001$) movements post-fatigue, but maintained time with the metronome ($p = 0.44$). Subjects aligned themselves nearly, but not exactly, with the GEM (Fig. 3). On average, the angle between the subjects' movements and the GEM decreased post-fatigue ($p < 0.001$; Fig. 3). Persistent correlations were found for all time series. α decreased significantly for timing errors ($p = 0.001$). The correlations tangent to the GEM were significantly more persistent than those perpendicular to it ($p < 0.001$).

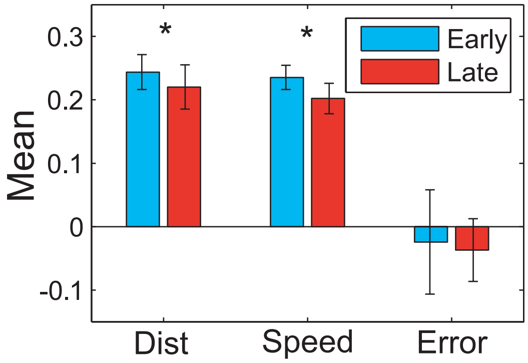

Figure 2. Subjects made shorter, slower movements post-fatigue ($p \leq 0.001$). Their timing errors did not change ($p = 0.44$).

CONCLUSIONS

Subjects maintained timing with the metronome by making shorter slower movements as they fatigued. Muscle fatigue caused the deviations timing errors to become less persistent. Thus, subjects altered their biomechanical movement strategies to maintain task performance. While people do shift their average behavior (i.e., new operating point along the GEM), they appear to maintain approximately the same overall control strategy with respect to the GEM.

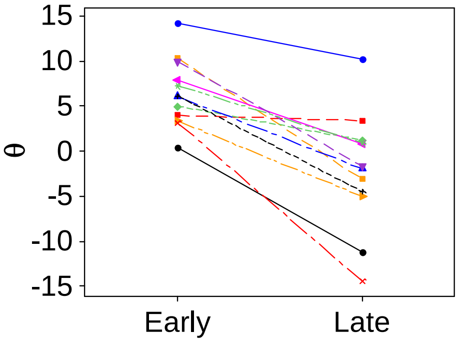

Figure 3. On average, the angle between the subjects' movements and the GEM decreased post-fatigue ($p < 0.001$).

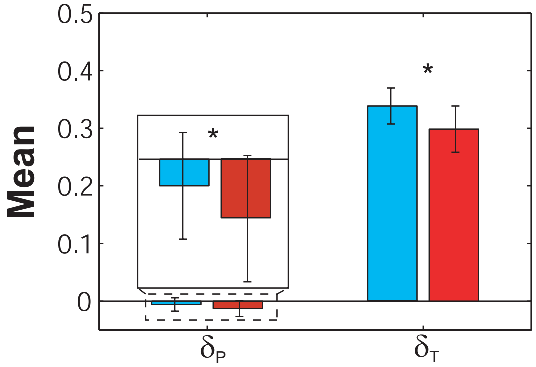

Figure 4. Subjects exhibited greater deviations perpendicular to the GEM post-fatigue ($p < 0.001$). They also had smaller deviations tangent to the GEM post-fatigue ($p<0.001$)

REFERENCES

1. Wilder, D., et al. (1996) *Spine* 21, 2628-39.
2. Jaric, S., et al. (1999) *Eur J Appl Physiol* 80, 467-71.
3. Cote, J. et al. (2002) *Exp Brain Res* 147, 394-8.
4. Selen, L., et al. (2007) *Exp Brain Res* 181, 99-108.
5. Gates DH & Dingwell JB. (2008) *Exp. Brain Res.* 187: 573-85.
6. Cusumano, J. & Cesari, P. (2006) *Biol Cybern*, 94, 367-79.
7. Hausdorff, J. et al. (1995) *J Appl Physiol* 78, 349-58.

ACKNOWLEDGEMENTS

NIH Grant # 1-R21-EB003425-01A1

MAGNITUDE OF POTENTIAL VULNERABILITY TO BALANCE CONTROL AFTER A TRANSITION TO STANDING

Angela DiDomenico and Raymond W. McGorry
Liberty Mutual Research Institute for Safety, Hopkinton, MA
email: angela.didomenico@libertymutual.com,
web: http://www.libertymutualgroup.com/researchinstitute

INTRODUCTION

Individuals are at an increased risk of a fall when the body is in an unstable position. Physical perturbations or volitional movements are one means of disturbing balance. The movement patterns required to perform postural transitions provide a challenge to the stable state of the human postural control system. Instability caused by sit-to-stand and sit-to-walk transitions have been investigated, primarily for the elderly and individuals with Parkinson’s disease [1]. However, a variety of additional postures are used during daily activities. Transitioning from these postures to a standing position may challenge multiple sensory systems required to integrate information in order to retain balance. In addition, maintaining awkward postures may result in muscle fatigue and the propensity toward postural instability, which may give rise to a fall or near fall incident [2]. The purpose of this study was to examine the effects of posture and duration within posture on balance measures following transition to a standing position.

METHODS

A full factorial repeated measures design was utilized for the experiment. Static posture and duration within posture were the two independent variables. Static postures included bent at waist, squatting, forward kneeling (hands and knees) and reclined kneeling (erect torso). The durations within posture were 30s, 60s, and 120s. Thirty male participants performed three replications of the 12 conditions (36 experimental trials). The age of the participants ranged from 18-67 years old with a mean (s.d.) of 43.6 (15.5) years. To minimize any confounding influences related to ordering, the presentation of the conditions was randomized after being blocked by replication.

During the trials, participants maintained one of the four static postures for a given duration. Participants transitioned to quiet standing at a self-selected velocity when alerted by an auditory signal. In addition, balance measures were calculated for a 60s baseline trial of quiet standing. Data was collected for a total of 20s, which included the time to transition (<5s). A minimum rest period of one minute was provided between trials to minimize cumulative fatigue effects.

Whole body motion analysis was performed with a passive motion capture system (Motion Analysis Corporation). The 3D trajectory data were collected at 100Hz and low-pass filtered using a fourth order Butterworth filter, 8Hz cutoff. Whole body center of mass (COM) position data were calculated as the weighted sum of 13 segments. Postural sway upon standing was recorded using two 40 cm x 60 cm force plates (Model # 9286AA, Kistler Instruments AG, Winterthur, Switzerland). Center of pressure (COP) position data was sampled at 1000Hz prior to low-pass filtering (zero lag fourth-order Butterworth, 5Hz cutoff). Balance measures for the period following a transition to standing included maximum COP velocity, COP range AP (antero-posterior), COP range ML (medio-lateral), maximum COM-COP inclination angle AP and maximum COM-COP inclination angle ML. Repeated measures analyses of variance using mixed models were performed to determine the effects of posture and duration in posture ($\alpha=0.05$).

RESULTS AND DISCUSSION

Initial analyses were performed to determine if the postures selected for investigation caused significant alterations to balance as compared to quiet standing (baseline). All balance measures were significantly larger than baseline (Table 1). The largest deviations were in max COP velocity.

Differences in the ML direction were larger than in the AP direction. Results indicated that the perturbation caused by these transitions did substantially affect balance.

Analyses of variance indicated no significant effect of duration within posture (p=0.0969 – 0.7003). Although there was a wide range of durations, all of them provided ample opportunity for the vestibular system to accommodate to the new posture. Durations were limited to two minutes to simulate everyday tasks, minimize discomfort to participants and minimize effects of muscular fatigue.

All balance measures were significantly affected by posture. Squatting and bent at waist did not produce significantly different effects on balance. The kneeling postures, however, had a more detrimental effect by increasing all measures, particularly the max COP velocity (Figure 1) and displacement (Figure 2) and inclination angle (Figure 3) in the ML direction. These postures affected more than one sensory system by creating substantial changes in the visual field, requiring rotation of the head in the global coordinate system, and challenging the lower body musculature. The need to integrate information from multiple systems may explain some of the resulting imbalance.

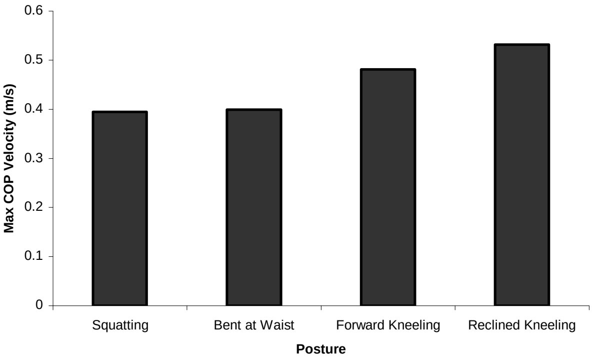

Figure 1. Max COP velocity after standing.

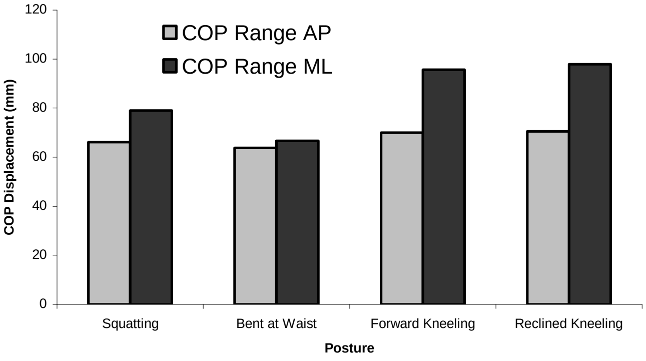

Figure 2.COP Range AP and ML after standing.

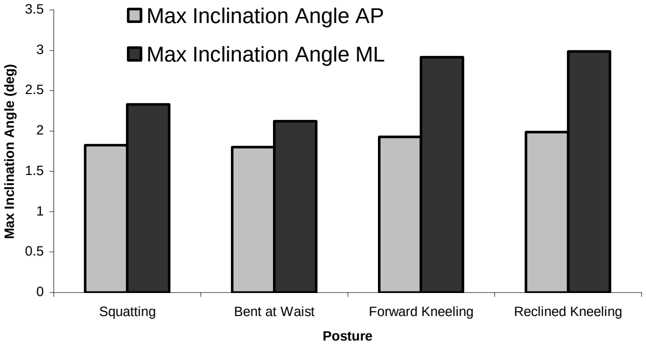

Figure 3. Max inclination angle AP and ML after standing.

CONCLUSIONS

Transitioning from one posture to another can create a perturbation that is detrimental to balance and may increase vulnerability to falls. Furthermore, the risk is dependent upon the posture maintained immediately prior to standing, with those requiring integration of sensory systems placing the largest burden on balance control.

REFERENCES

1. Buckley, TA, et al., *Movement Disorders* **23**, 1274-1280, 2008.
2. Chiou, S., et al., *Occupational Ergonomics* **1**, 81-93, 1998.

Table 1: Balance measures presented as a percentage of the corresponding baseline value during quiet standing.

Posture	Max COP Velocity	COP Range AP	COP Range ML	Max Inclination Angle AP	Max Inclination Angle ML
Bent at Waist	1214	194	562	194	254
Forward Kneeling	1466	214	806	208	348
Reclined Kneeling	1620	215	825	214	357
Squatting	1203	202	667	197	278

LOAD TRANSFER AND SYMMETRY IN GAIT DURING DOUBLE SUPPORT IN ACQUIRED BRAIN INJURY AND HEALTHY CONTROLS

[1]Mathew Yarossi, BS, [1,2] Karen J. Nolan, PhD, [1]Krupa K. Savalia, BS, [1,2]Gail F. Forrest, PhD
& [1,2]Elie P. Elovic, MD
[1]Kessler Foundation Research Center, West Orange, NJ, USA
[2]University of Medicine and Dentistry, New Jersey-NJ Medical School, Newark, NJ, USA
email: myarossi@kesslerfoundation.net; web: www.kesslerfoundation.net

INTRODUCTION

More than 8 million people in the United States are currently living with the effects of acquired brain injury (ABI), including traumatic brain injury and stroke. Individuals with ABI often have bilateral differences in limb loading and difficulty transferring weight to the affected limb causing disturbances in gait [1]. Asymmetrical limb loading during stance can potentially cause decreased velocity and increased incidence of falls, and may predispose the healthy leg to repetitive strain injuries. Previous research has examined the kinematics and temporal spatial aspects of gait asymmetry in ABI but has not specifically identified how load transfer affects gait. Symmetrical load transfer during double support should provide a more efficient transfer of momentum during gait, especially during weight acceptance on the paretic limb [2]. A more efficient transfer of load should also decrease double support time which has previously been identified to decrease energy cost and increase stability [3]. Therefore, the primary objective of this investigation was to examine the inter-limb differences in load transfer and symmetry during the double support phase of gait in individuals with ABI and healthy controls.

METHODS

Eight participants diagnosed with hemiplegia secondary to acquired brain injury, at least 19 months post injury, and eight age-matched healthy controls (HC) were recruited for participation (Table 1). Wireless pedobarography data was collected bilaterally using the Pedar-x Expert System while subjects performed a 2-minute walk. Data were analyzed for the first 18 seconds of the walking test. All data were analyzed using custom Matlab programming. Data were normalized to 100% of initial double support (IDS) and the corresponding terminal double support on the unloading leg. The normal force under each foot was calculated as a percentage of the total loaded force in body weights. A linear regression was then fit to the force of the loading leg over double support. Force on the loading leg was plotted against force on the unloading leg to determine the time point at which weight is distributed equally between both legs. This point also represents the time in which the majority of weight is transferred from the unloading leg to the loading leg and will be referred to as the weight transference point (WTP). Pairwise t-tests were used to determine differences between the ABI group and the HC group.

Table 1: Subject Demographics

Group	Gender	Age (yrs)	Height (kg)	Weight (kg)
ABI	9 M	51.6 ± 18.8	71.1 ± 3.7	89.2 ± 21.1
HC	4 M 4 F	51.8 ± 16.9	67.6 ± 3.1	75.6 ± 13.1

RESULTS AND DISCUSSION

Limb loading as function of total force was more linear bilaterally in the HCs (Table2; Figure 1 b,d). In the ABI group, healthy limb loading and contralateral affected limb unloading shows a linear transition of weight from one limb to the other (Figure 1 a,b). Affected limb loading as function of total force follows a less linear trend. This represents an inconsistent rate of loading of the affected limb, which may reduce momentum and lead to instabilities at this point of the gait cycle.

Table 2: Load Transfer and Symmetry Measures

	ABI Group		HC Group	
	Affected	Healthy	Right	Left
WTP (% IDS)	63.7 ± 18.8	49.7 ± 10.7	63.0 ± 16.9	61.7 ± 19.4
Max Force (% IDS)	41.6 ± 8.7	41.7 ± 13.8	50.7 ± 12.6	52.5 ± 9.03
R^2	.959 * ± .020	.973 ±.013	.989 * ± .010	.977 ± .022

(* = p ≤ 0.01)

During double support in the ABI group the WTP occurred ~10% earlier for unaffected foot loading than affected foot loading producing an asymmetrical gait pattern. A more rapid weight transfer in the ABI group may have negatively effect momentum and may impart medial-lateral forces creating instability. In the HC group there was less inter-limb difference indicating a more symmetrical loading during double support.

Healthy controls are at a more balanced position at the point of maximal loading when loading either limb. Individuals with ABI delay weight transfer on to the affected limb and are asymmetrically loaded at max loading. This asymmetrical load transfer onto the affected limb may create a necessity for compensation by other structures to maintain balance during double support.

CONCLUSIONS

Analyzing loading during gait as a function of the total force beneath both limbs produces greater information about balance and symmetry during double support. This simple analysis technique can be used as an evaluative tool for clinical intervention.

ACKNOWLEDGEMENTS

Kessler Foundation
NIDRR Grant # H133F070028
New Balance Athletic Shoe

REFERENCES

1. Mayer NH, et al. *Muscle Nerve Suppl.* **6**, S21-35, 1997.
2. Gok H, et al. *Clin Rehabil.* **17(2)**, 137-139, 2003.
3. Franceschini M, et al. *Clin Rehabil.* **17(4)**, 368-372, 2003.

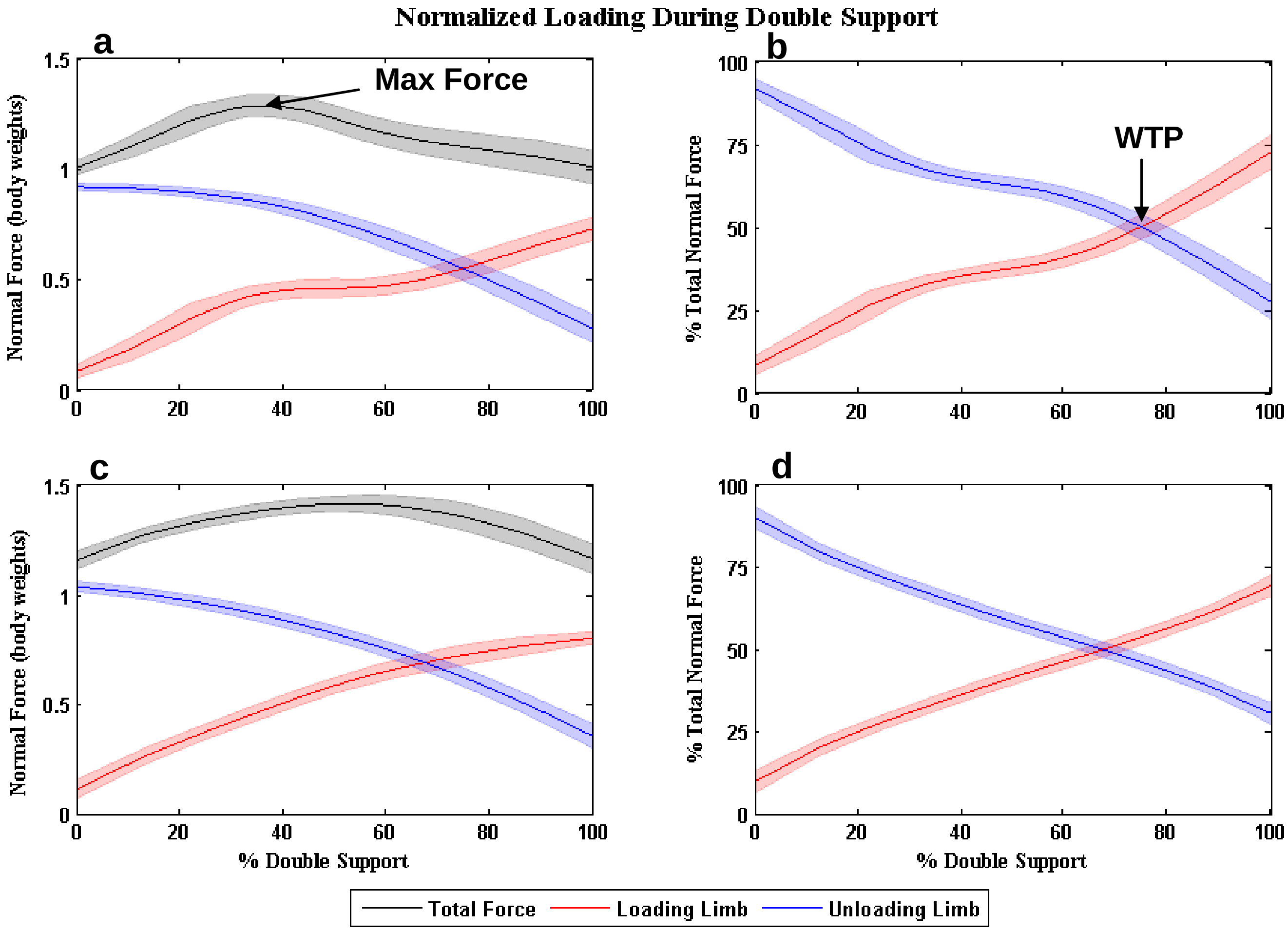

Figure 1: (a) ABI affected leg loading and healthy leg unloading and total force. (b) ABI normalized loading. (c) HC right leg loading and left leg unloading and total force. (d) HC normalized loading.

THE INFLUENCE OF FIFTEEN MUSCLES ON DISTAL RADIOULNAR JOINT LOADING: A BIOMECHANICAL MODEL

[1]Joseph Bader, [2]Michael Boland, [3]Timothy Uhl, [1,2]David Pienkowski
[1]University of Kentucky Center for Biomedical Engineering, [2]University of Kentucky Department of Orthopaedic Surgery, [3]University of Kentucky Department of Rehabilitation Sciences
Email: joseph.bader@uky.edu

INTRODUCTION

Optimal management of fractures, post-traumatic arthritis and instability of the distal radio-ulnar joint (DRUJ) requires an understanding of the forces generated across this joint as a function of the activities of daily living; however, such knowledge is currently incomplete. Therefore, this study sought to quantify the three dimensional forces acting across the DRUJ during pronation (P) and supination (S) through use of an anatomically determined vector based mathematical model of DRUJ loading. It then sought to determine the role that each individual muscle played in DRUJ loading.

METHODS

The origin and insertion of 15 muscles were marked on the upper extremity of nine fresh cadaveric specimens. Muscles examined included biceps brachii (BB), brachialis (BRA), brachioradialis (BRAR), supinator (SUP), extensor carpi radialis longus (ECRL), extensor carpi radialis brevis (ECRB), extensor indicis (EI), extensor policis longus (EPL), flexor carpi radialis (FCR), palmaris longus (PL), flexor carpi ulnaris (FCU), extensor carpi ulnaris (ECU), abductor policis longus (APL), abductor policis longus at the ulnar origin (APL), pronator teres (PT), and the pronator quadratus (PQ).

The positions of these muscles were digitally measured at various stages of P and S by using an electromagnetic 3D tracking sensor (Motion Star, Ascension Technologies, Burlington, VT). Data were collected for each of these fifteen muscles at each of 10° increments of simulated forearm pronosupination (PS) throughout the entire range of motion. Coordinates of the origin and insertion were used to determine the muscle's 3D vectoral orientation at each forearm position. A model consisting of 15 three-dimensional force vectors, one for each of the 15 muscles modeled, was created by combining two separate 2D models, one along the palmar-dorsal axis (shear force at the DRUJ), and a second along the radio-ulnar axis (transverse force at the DRUJ). Maximum muscle forces were determined based upon published tension fraction data [1] and physiological cross sectional area data [2]. Specimen motion ranged from 110° of pronation (P110) to 120° of supination (S120), but no single specimen exhibited that full range of rotation. A position was only analyzed if it was attained by at least 5 of the 9 specimens; therefore mean DRUJ forces were calculated only from the range of P80 to S90. A 3D transformation matrix was used to maintain a consistent set of anatomical reference axes for all angular positions. Forces at the DRUJ were calculated by summing the moments that each muscle provided to the forearm about the elbow. The resultant force acting at the DRUJ was determined from the shear and transverse forces.

The forces exhibited at each position were averaged for all specimens. The effect that each individual muscle had on DRUJ loading was found by removing that particular muscle from the model. Differences between the original model and the models with muscles removed were examined by using a paired t-test.

RESULTS AND DISCUSSION

The two muscles that exhibited the greatest increase in DRUJ loading at any one position and the two muscles that exhibited the greatest decrease in DRUJ loading were plotted against the original model (Figs. 1-3).

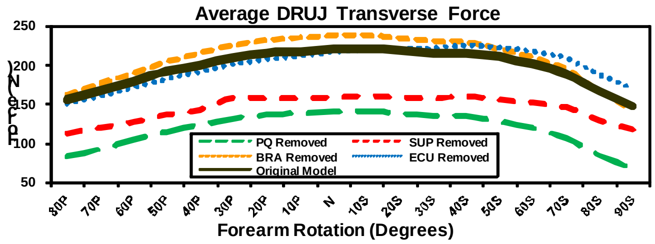

Figure 1: Effect of removing the PQ, SUP, BRA, and ECU on the average DRUJ transverse force during forearm rotation (n≥5).

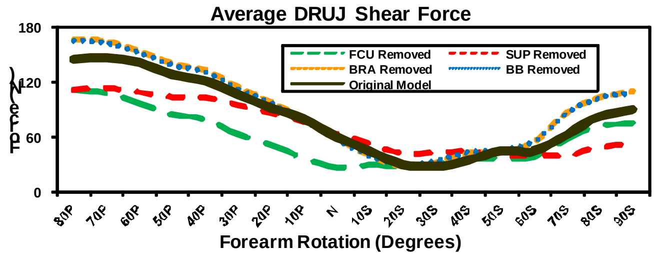

Figure 2: Effect of removing the FCU, SUP, BB, and BRA on the average DRUJ shear force during forearm rotation (n≥5).

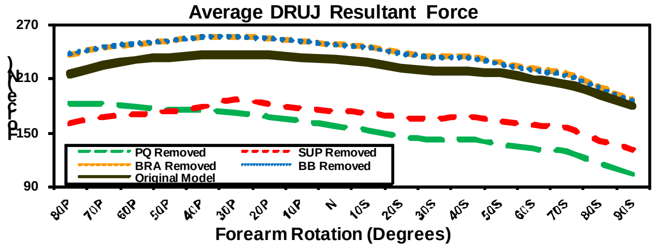

Figure 3: Effect of removing the PQ, SUP, BB, and BRA on the average DRUJ resultant force during forearm rotation (n≥5).

PQ and SUP caused the largest single position increase in transverse forces (82.4N and 62.1N) while BRA and ECU caused the greatest reduction in transverse forces (19.1N and 23.1N). FCU and SUP caused the largest single position increase in shear forces (44.6N and 38.2N) while BB and BRA reduced the shear forces the most (22.8N and 23.4N). SUP also had a significant reducing effect at 20S ($p=0.0185$) and at 30S ($p=0.0428$). The overall resultant DRUJ forces were increased the most by PQ and SUP (81N and 61.1N) while BB and BRA cause the greatest decrease in resultant DRUJ force (21.3N and 21.0N).

CONCLUSIONS

These results show that of all 15 muscles studied, the PQ was the greatest contributor to generating force across the DRUJ along the transverse axis, as well as to the resultant force. BRA contributed the most to offloading of the DRUJ along the transverse axis and 2nd most along the shear axis and resultant forces. BB contributed the most to DRUJ offloading along the shear axis and to resultant forces.

Removing a single muscle from the model does not seem to affect general trends of the model, only the magnitude. Along the transverse axis, all of the forces are greatest toward the middle of forearm rotation and decrease as the arm rotates in either direction. Along the shear axis, all forces are highest when the arm is in full pronation and the forces decrease toward their minimum around mid-supination before increasing. In the resultant plane, the forces were greatest in mid-pronation and decrease steadily to their minimum in full supination.

The data for BRA and BB is very similar for shear and resultant forces. This may be due to their similar axial placement on the proximal forearm. It may also be due to the fact that this was a maximal muscle force model and these are both large muscles with multiple roles in upper extremity movement. It is likely that the BB and BRA do not exert maximal muscle force during PS because this motion does not appear to be their primary function. It is worthy to note that simultaneous maximal contraction of all forearm muscles may not result in a maximal force across the DRUJ due to vectoral muscle force balancing. Collecting EMG data over the range of PS would help in scaling down the muscle forces during forearm rotation and help to create a more accurate model. However, the present study provides data that adds to our understanding of forearm muscle function and their cumulative result on distal upper extremity biomechanics.

REFERENCES

1.Brand PW, et al. *J Hand Surg [Am]* **6**, 209-219, 1981.
2.Murray WM, et al. *J Biomech* **33**, 943-952, 2000.

ACKNOWLEDGEMENTS

The research was funded in part by a grant from the University of Kentucky Department of Orthopaedic Surgery.

BALANCE CONTROL DURING MATERIAL HANDLING OVER A SLIPPERY SURFACE

[1,2]Robert D. Catena, [2]Angela DiDomenico and [1]Jack T. Dennerlein
[1]Harvard School of Public Health, [2]Liberty Mutual Research Institute for Safety
email: RC.biomechanics@gmail.com

INTRODUCTION

Although more workplaces are emphasizing workers' safety, certain jobs take the worker outside the controllable confines of the office or factory. Many outdoor manual material handlers (e.g. cargo loaders, delivery personnel) are required to contend with low friction (wet or icy) support surfaces in the line of duty. There is a particularly high occurrence rate of falls in industries requiring manual material handling (MMH) while outdoors [1]. Few balance control publications have endeavored to examine the effects of a slippery surface during material handling, and those that have, focused on gait. The goal of this research was to examine the differences between individuals that successfully and those that unsuccessfully perform a standing lateral load transfer over a novel slippery surface.

METHODS

Twenty healthy participants without substantial material handling experience completed a 180° standing load transfer. Specifically, participants would reach 90° laterally to a maximum "safe" distance, pick up a load of 5% body weight with both hands and transfer it 180° to the other side of the body. This was done over 3 surface conditions. After practice trials, 6 trials of a High-COF condition were conducted to determine a self-selected safe maximum load distance using a self-selected base of support. Those self-selected configurations were then re-assigned in a single trial of a Low-COF(1) condition. After practice trials with a low COF surface to make self-selected modifications to a new safe maximum load distance and base of support adjustments, 6 trials of Low-COF(2) were conducted. Low-COF(1) was the only condition when the participants were not given practice trials and not told of the surface condition before hand.

Balance was analyzed as the distance from the center of gravity to the edges of the base of support (COG-BOS). Balance control was analyzed as: the center of mass path deviation (COMpd), COG trajectory area (COGa), BOS adjustments, and lower extremity joint co-contractions. Finally, load transfer distances, load misplacements and losses of balance were tracked. Participants were given instruction not to completely lift a foot during the task. A step was the minimum threshold for loss of balance. Unsuccessful trials were not further analyzed. These trials entailed a loss of balance, misplacement of the load, or an inability to grab the load completely with both hands.

COM was calculated from individual segment masses using a 13-link model plus 1 box segment (after acquired). Segment masses and BOS were identified using a 12-camera motion capture system. The BOS was measured at each frame using four markers on each foot and accounting for toe and heel lifts. Eight lower extremity muscle activations normalized by maximum voluntary contraction were measured using surface electrode EMG. Each foot was positioned over a force plate (to measure utilized COF). The High-COF ($\mu \approx 0.86$) condition was created with standardized shoes on plywood surfaces. The Low-COF ($\mu \approx 0.14$) condition was created with Teflon tape on the bottom of the shoes over Teflon surfaces.

Nine of the 20 participants completed Low-COF(1) successfully. Therefore, 2 analyses were conducted: 1-way mixed model condition analyses on only the 9 participants that completed Low-COF(1) and 2-way mixed model analyses with 2 groups retrospectively divided by successful (SLC) and unsuccessful (ULC) attempt of Low-COF(1).

RESULTS AND DISCUSSION

1-way Condition Analyses for SLC:

Going from High-COF to Low-COF trials, the COG trended closer to the front and back of the BOS, but trended further away from the lateral edges of the BOS. The front and back of BOS may be more susceptible directions to fall in the slippery conditions, while sideways falls may be more likely in the non-slippery conditions. A possible alternative cause for these trends might be the wider stance that individuals adopted during most of a slippery trial. Unknown is whether wider stance is a cause of, or a co-result with differences in balance during the slippery condition. The COGa and COMpd both increased in Low-COF trials. Since these two variables were normalized respectively by BOS area and transfer distance, they could indicate either a decrease in balance control during slippery conditions or an adaptation to the slippery surface through greater modification of the COG during the trial (the latter being supported later in the abstract).

There was little change in lower extremity muscle co-contraction between surface conditions. There was a trend of decreased muscle co-contraction intensity around the ankle in Low-COF conditions, but was only significant for the ipsilateral foot during load drop off. There were no differences in muscle co-contractions about the hip/knee.

Table 1: Summary results for condition analyses

Variable	Results	P value
COG-BOS back side	High-COF > Low-COF	0.0051
COG-BOS pickup side	High-COF < Low-COF	0.0025
Stance width	High-COF < Low-COF	0.0001
COMpd	High-COF < Low-COF	0.0004
COGa	High-COF < Low-COF	0.0281
Ankle muscle intensity	High-COF > Low-COF	0.0083

*Group*COF Condition Analysis:*
While the COG trended further away from the BOS edges during pick-up and drop-off of the load in the SLC group, this was not so in the ULC group. The COG trended closer to the edges in the ULC group. There were similar interactions with stance width. Again, while the SLC group had wider stances in slippery conditions, the ULC group had narrowed stances in slippery conditions.

Muscle co-contraction intensity around the ankle also increased in the ULC group while it decreased in the SLC group during the Low-COF condition. Wider stances and higher utilized COFs used by the SLC group seem to indicate the major difference between the SLC group and the ULC group is that the SLC group may take advantage of the slipperiness of the surface by sliding their feet while ULC individuals do not, either because they do not know how to use this tactic or they are more conservative during the slippery condition. The "conservative" hypothesis is supported by increased ankle muscle activity during slippery conditions and no increase in COM path deviation in the ULC group compared to an increase by the SLC group during slippery conditions. We will investigate this possibility further by examining foot trajectories during the task for the two groups.

Table 2: Summary results for 2-way analyses

Variable	2-way interaction	P value
COG-BOS dropoff side	significant	0.0463
Stance width	significant	0.0001
COMpd	significant	0.0007
Ankle muscle intensity	significant	0.0049

A major limitation of this study was the specific task order rather than task randomization. We chose to do this so that Low-COF(1) would mimic an individual attempting a normal box transfer, as during High-COF(1), without knowing the slipperiness of the surface. By doing this we were not able to distinguish practice effects from condition effects. We have recently added a High-COF(2) at the end of the task protocol to examine this practice effect, but those data are currently not available. Another limitation is that only a single trial of Low-COF(1) was performed because it is novel only once, therefore we can only speculate as to what caused unsuccessful attempts at Low-COF(1).

CONCLUSIONS

1. The front and back of the BOS may be more susceptible directions of falling as stance is widened in slippery conditions. However, the likelihood of a loss of balance in any direction increases in individuals that unsuccessfully attempt a novel slippery surface box transfer.
2. Unsuccessful attempts at a novel box transfer task over a slippery surface may be due to a conservative, stiff posture rather than the possibly more appropriate relaxed and adaptable posture used by individuals that were successful.

REFERENCES

1. B.L.S., U.S. Department of Labor. 2006,

ACKNOWLEDGEMENTS

The Liberty Mutual – Harvard SPH Post-doctoral Fellowship Program funded this research.

SERIES ELASTIC ELEMENTS LIMIT MUSCLE LENGTHENING RATES IN ECCENTRIC CONTRACTIONS

Thomas Roberts and Emanuel Azizi
Dept. of Ecology and Evolutionary Biology, Brown University, Providence, RI, USA
email:roberts@brown.edu

INTRODUCTION

Series elastic elements can act to decouple the length changes of muscle contractile elements from the movements that occur at the body and joints. This decoupling has important functional consequences. For example, tendons can allow cyclical flexion-extension at a joint with nearly isometric muscles fibers to minimize muscular work [1,2]. By contrast, in some systems tendons can act to increase muscular work by storing CE work slowly and then releasing it rapidly to amplify muscle power [3]. These examples are familiar to most biomechanists. The role that tendons play in energy absorbing activities, when contractile elements function to dissipate mechanical energy, is less well understood. Measurements of muscle-tendon and muscle fascicle length changes *in vivo* suggest that the tendon can act as a mechanical buffer, limiting the rate of stretch of the contractile element[4]. We used an *in situ* muscle-tendon peparation to examine how the series elastic tendon influences contractile element velocity for ramp stretches at different lengthening velocities. We hypothesized that the rate of muscle fascicle lengthening would be reduced relative to that of the muscle-tendon unit (MTU) during eccentric contractions.

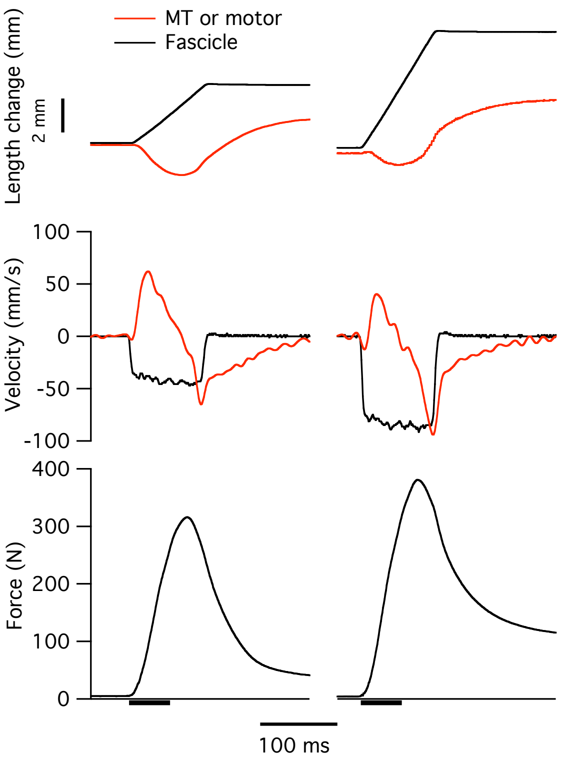

Figure 1. Sample contractions illustrate the decoupling of fascicle length changes (red) and MTU length changes (black). Left panels are for an intermediate rate of lengthening and the right panels are for a fast lengthening. Lengthening rate was varied by adjusting total motor excursion for a fixed period of time (100ms). Stimulation duration was 50ms for all conditions (bar). Positive velocities indicate shortening and negative velocities indicate lengthening.

METHODS

Lateral gastrocnemius muscles of wild turkeys were studied *in situ*. Animals were deeply anesthetized for all procedures. A muscle servomotor provided a measure of muscle force and length change in the whole muscle-tendon. Sonomicrometer crystals were implanted along muscle fascicles to measure fascicle length changes. The muscle nerve was stimulated with a supramaximal stimulus voltage. For each contraction, the motor applied a constant velocity ramp lengthening to the muscle-tendon. For all contractions, stimulus duration was 50ms and ramp duration was 100ms. Total excursion was varied to achieve a range of lengthening velocities. Sample contractions are shown in Figure 1.

RESULTS AND DISCUSSION

Fascicle length change patterns during eccentric contractions were qualitatively different from the length change imposed on the muscle-tendon unit by the servomotor. Sample contractions illustrate the typical pattern (Fig. 1). Under most conditions, fascicles shortened on average during MTU lengthening (Fig. 2). Peak instantaneous lengthening velocities of the muscle fascicles were more rapid than average values, but fell short of the lengthening velocity of the MTU.

Most fascicle lengthening occurred during the period following the ramp stretch, when the MTU was isometric (Fig. 1). During this period the tendon recoiled as muscle force declined during muscle deactivation. Peak instantaneous rates of muscle fascicle lengthening during this period were independent of ramp lengthening velocity (Fig. 3).

Eccentric muscle contractions tend to cause muscle damage. Our results highlight two possible benefits of the tendency of series elastic tendons to uncouple contractile element length changes from MTU length changes. First, the stretch of series elastic tendons may act to limit peak muscle forces. The force developed in a contraction is dependent on fascicle velocity, and the greatest forces are produced when fascicle actively lengthen. We found that the tendon limited fascicle lengthening velocity early in the contraction, which in turn limited peak forces. Second, peak fascicle velocities that occurred in the second half of the contraction were consistent and were determined by the intrinsic rate of relaxation of the muscle. This mechanism may provide a predictable loading regime to the muscle, independent of the highly variable loading that may be imposed by the environment.

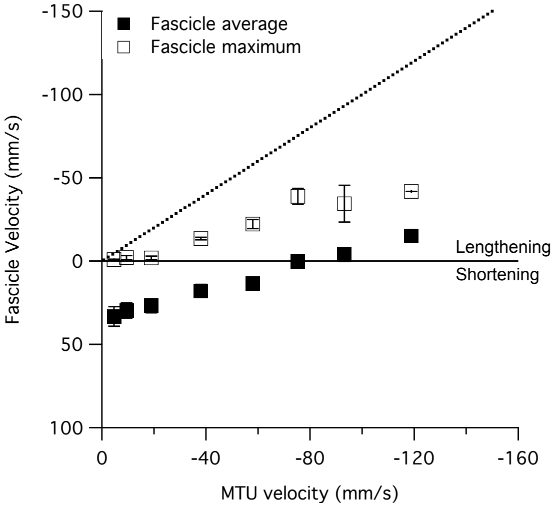

Figure 2. During the period of MTU lengthening, the average velocity of the muscle fibers (filled symbols) was much lower than the velocity applied to the MTU by the motor. The line of equality (dotted) represents the fascicle velocity expected if there were no effects of series elasticity or fascicle pennation. The effects of series elastic elements are apparent in that under most conditions, fibers shortened on average while the MT lengthened.

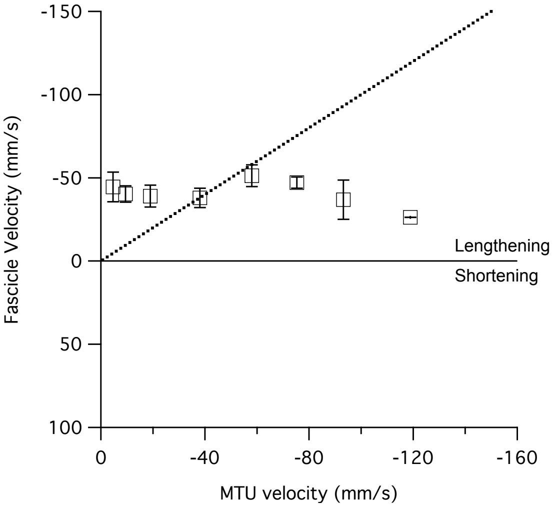

Figure 3. The peak instantaneous fascicle lengthening velocity during the period following the ramp lengthening, when the MTU was isometric, was independent of ramp lengthening velocity applied to the MTU.

CONCLUSIONS

The series elastic element can act to limit the maximal rate of muscle contractile element lengthening during an energy absorbing contraction. This mechanism may help to reduce muscle damage by limiting peak muscle forces and allowing for predictable, consistent rates of muscle contractile element lengthening.

REFERENCES

1. Roberts, T.J. et al. *Science* **275**, 1113-1115, 1997.
2. Fukunaga, T. et al. *Proc. R. Soc. Lond. B* **268**, 229-233, 2001.
3. Roberts, T.J. and R. L. Marsh, *J. Exp. Biol.* **206**, 2567-2580, 2003.
4. Reeves, N.D. and M. V. Narici, *J. Appl. Phys.* **95**, 1090-1096, 2003.

ACKNOWLEDGEMENTS

Supported by NIHF32054246 to EA and AR055295 to TJR.

IN VIVO KNEE CARTILAGE CONTACT DURING DOWNHILL RUNNING

William Anderst, Eric Thorhauer and Scott Tashman
University of Pittsburgh, Department of Orthopaedic Surgery
email:anderst@pitt.edu

INTRODUCTION

Altered contact mechanics following anterior cruciate ligament (ACL)-reconstruction may increase the risk for long-term joint degeneration[1,2]. Using a high-speed biplane x-ray system, the current study aimed to characterize in vivo knee cartilage contact during the dynamic loading activity of downhill running. Using the contralateral uninjured knee as a control, cartilage contact was measured serially following ACL-reconstruction. It was hypothesized that cartilage in ACL-reconstructed knees would be subjected to increased strain and the location of cartilage contact would be different in comparison to ACL-intact knees.

METHODS

Three subjects had 1.6 mm diameter tantalum beads implanted into their injured and asymptomatic contralateral knees during ACL-reconstructive surgery (3 beads in each femur and each tibia). Following surgery, sagittal 3T MRI scans and axial CT scans were performed on each leg. Cartilage and bones were segmented from the MRI scans and bones were segmented from the CT scans (Mimics Software, Ann Arbor, MI). Three-dimensional MRI and CT models were co-registered (Geomagic, Inc., Research Triangle Park, NC), creating identical anatomical coordinate systems on the left and right bones for each subject.

Subjects were tested within a biplane x-ray system while running downhill (10° slope) at 2.5 m/s three times following surgery (approx. 6, 12 and 24 months). Biplane x-rays were collected at 170 or 250 frames per second for 3 trials per leg for each test session. Implanted beads were tracked within the distortion corrected x-ray images with an accuracy of better than 0.10 mm[3]. Femur and tibia cartilage contact during single-support flexion was determined using this tracked data. Cartilage contact area, average cartilage strain and center of cartilage contact were determined for each compartment (medial/lateral) on each test date.

Cartilage contact areas were averaged within each compartment (i.e. medial contact area = (medial femur contact area + medial tibia contact area)/2) every instant of data collection. Cartilage strain was calculated as the amount of cartilage overlap indicated by the rigid cartilage models divided by the cartilage thickness for each point on the cartilage surface. The center of cartilage contact was determined at each instant by finding the weighted centroid of the contact area, using the amount of cartilage overlap as the weight factor. Joint rotations and translations were also calculated at each instant. All cartilage contact variables were interpolated every 1 degree of flexion. To facilitate analysis, comparisons were made between intact and ACL-reconstructed sides after averaging data across test dates at 5 degree increments of flexion, from 0 to 30 degrees.

RESULTS AND DISCUSSION

Average cartilage contact area in the intact medial compartment remained steady during flexion, ranging between 535 and 601 mm^2, while intact lateral compartment contact area decreased from 445 mm^2 at 0° flexion to 335 mm^2 at 30° flexion. Medial compartment contact area was larger than lateral compartment contact area throughout flexion in the intact knee. Following ACL-reconstruction, medial compartment contact area was generally lower than in the intact knee, while lateral compartment contact area was generally higher than in the intact knee. These differences between ACL-intact and ACL-reconstructed contact areas were most apparent at higher flexion angles. In the ACL-reconstructed knee, medial and lateral compartment contact areas were similar for all flexion angles (except 5°) (Figure 1).

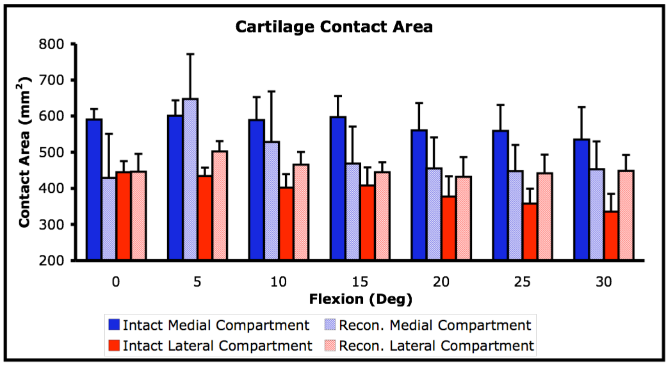

Figure 1: Cartilage contact area in the medial (blue) and lateral (red) compartments for the intact (solid) and ACL-reconstructed (shaded) knees. Standard deviation bars indicate among-day variability.

Medial compartment strain ranged between 14.5 and 18.7 percent, while lateral compartment strain ranged from 15.5 to 19.5 percent in the ACL-intact knees. In the ACL-reconstructed knees, medial compartment strain ranged from 15.0 to 19.3 percent, while lateral compartment strain increased from 14.5 percent at 0° flexion to 29.1 percent at 30° flexion (Figure 2). Increased cartilage strain identified in the lateral compartment may be an indication of increased risk for osteoarthritis (OA) development.

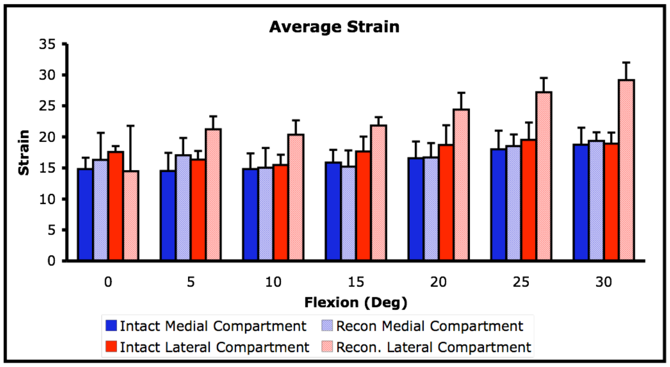

Figure 2: Average cartilage strain in the medial (blue) and lateral (red) compartments for the intact (solid) and ACL-reconstructed (shaded) knees. Standard deviation bars indicate among-day variability.

The path of the center of cartilage contact was more lateral on each cartilage surface following ACL-reconstruction. Additionally, at 0° flexion, the contact point on both the medial and lateral femur cartilage surfaces was more anterior following ACL-reconstruction (Figure 3). These modified contact paths on cartilage surfaces following ACL-reconstruction may increase risk for OA.

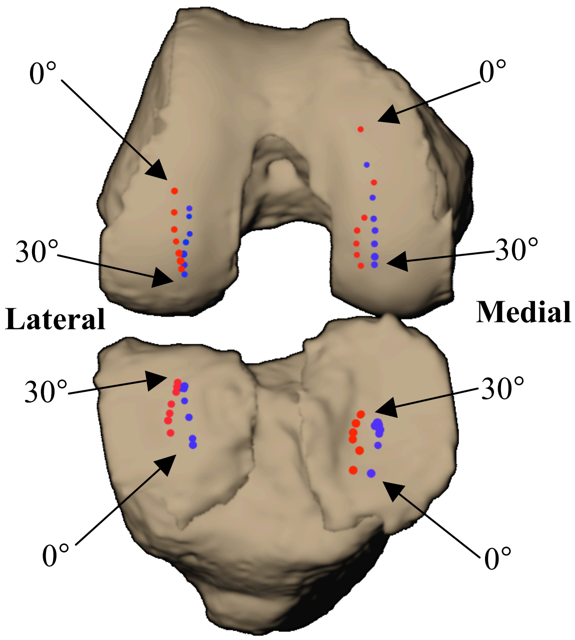

Figure 3: Center of cartilage contact region on the femur and tibia cartilage surfaces every in 5° increments, from 0° to 30° of flexion, during downhill running. Blue is intact contact center, red dots indicate ACL-reconstructed contact center. Figure indicates average contact location at each flexion angle for 6, 12 and 24 months post-surgery test dates.

CONCLUSIONS

This study presented, for the first time, in vivo cartilage contact mechanics during a dynamic loading task. This preliminary evidence indicates cartilage contact mechanics are modified following ACL-reconstruction. However, due to the low sample size, these conclusions should be interpreted with caution.

REFERENCES

1. Brandsson, et al. *Acta Orthop Scand* (2001).
2. Andriacchi, et al. *J. Biomech.* **38**, (2005).
3. Tashman, et al. *J. Biomed. Eng.* **125**, 238-245, 2003.

LOWER EXTERMITY MUSCLE STRENGTH AND GAIT VARIABILITY IN OLDER ADULTS

Sunghoon Shin, Rudy J. Valentine, Ellen M. Evans and Jacob J. Sosnoff
University of Illinois at Urbana-Champaign
email: jsosnoff@illinois.edu

INTRODUCTION

It is well established that with advanced age there are increases in motor variability including gait [1,2]. This age-related increase in gait variability is associated with increased risk of falls and other adverse events [3]. The mechanisms contributing to age-related increases in gait variability remain to be elucidated. It has been theorized that age-related increases in motor variability are also associated with muscular weakness [4]. Empirical support of this age, muscle weakness-variability theory has only been examined using manual motor tasks [4]. If gait variability is related to muscular strength of the lower extremities has not been established and is clearly important for ambulatory function in older adults. Consequently, the aim of this study was to examine the relationship between lower extremity muscle strength and gait variability in healthy older adults.

METHODS

Community-dwelling older adults (33 females and 21 males; height: 166.8 ±10.3 cm; weight 70.1 ± 6.2 kg; age: 70.1± 6.2 yrs) who were relatively healthy, reported no neuromuscular diseases and/or history of falls were assessed on the following outcomes: Muscle quality at the knee and ankle joints defined as force per unit leg lean mass with strength being determined from maximal isometric voluntary contraction (knee extension and flexion, ankle dorsiflexion and plantarflexion) using an isokinetic dynamometer (Humac Norm) and lean mass being assessed using dual energy x-ray absorptiometry (Hologic). Gait characteristics including mean and standard deviation of step length, stride length and step width from self-paced walking using a 7 m gait mat (CIR systems, Inc.). Step-wise linear regression were conducted to examine the relation between muscle quality and gait variability.

RESULTS AND DISCUSSION

Overall, knee muscle quality was negatively associated with step and stride length variability. Knee muscle quality was found to account for 11.3% and 12.5% in the variance of step and stride length, respectively. In contrast, ankle muscle quality was found to be negatively associated with step width variability. Ankle muscle quality accounted for 8.7% of the variance in step width.

The data suggests that older adults with lower muscle quality are more variable in their step length and width. The association between muscle quality, an index of functional muscle strength and gait variability is supportive of the hypothesis that there is a muscle weakness – variability association. This theory maintains that it is not chronological aging per se that drives increases in motor variability but rather deficits in neuromuscular function that are behaviorally manifested as muscle weakness [4]. Furthermore, the differential association between knee and ankle muscle quality to step length and width variability is congruent with the notion that mediolateral postural control is distinct from that of anterior-posterior postural control [5]. Moreover, it also suggests the possibility of designing unique interventions capable of differently improving step/stride length variability or step width variability.

REFERENCES

1. Newell KM, et al. Aging, complexity and motor performance. In J.E. Birren & K.W. Schaie (Eds.), *Handbook of the psychology of aging (6th Ed.)* (p 163-182). Amsterdam: Elsevier. (2006)
2. Grabiner PC, et al. Age-related changes in spatial and temporal gait variables. *Arch Phys Med Rehabil*. **82**, 31-5, 2001.
3. Brach JS, et al. Gait variability and the risk of incident mobility disability in community-dwelling older adults. *J Gerontol A Biol Sci Med Sci*. **62**,983-8, 2007
4. Sosnoff JJ et al Are age-related increases in force

variability due to decrements in strength? *Exp Brain Res.* ***174***, 86-94, 2006.

5.Winter DA, et al. Unified theory regarding A/P and M/L balance in quiet stance. J Neurophysiol. **75**, 2334-43, 1996.

.

Table 1: Stepwise linear regression coefficients with ankle and knee muscle quality predicting gait variability.

Gait parameters		**Unstandardized coefficients**		**Standarized Coefficients**	**t**	**p**
		B	Std.Error	Beta		
Step length	KIMQ	-.059	.023	-.337	-2.534	.014*
Stride length	KIMQ	-.094	.031	-.396	-3.049	.004*
Step width	AIMQ	-.045	.021	-.295	-2.183	.034*

* $p < .05$

KIMQ: Knee isometric muscle quality

AIMQ: Ankle isometric muscle quality

ISOMETRIC FORCE PRODUCTION REQUIRES ASYMMETRIC MUSCLE-TENDON LENGTH TRAJECTORY

Gregory S. Sawicki and Thomas J. Roberts
Dept. of Ecology and Evolutionary Biology, Brown University, Providence, RI, USA
e-mail: gsawicki@brown.edu

INTRODUCTION

During cyclic movements (e.g. running, walking) muscle fibers at distal joints produce force nearly isometrically and perform very little mechanical work. Elastic tendons in series with the muscle fibers store and return elastic energy in the interaction with the external environment to maintain steady speed [1, 2]. The goal of this study was to determine the muscle-tendon (MT) length trajectory required to maintain isometric, strut-like behavior of the muscle fibers in series with a highly compliant free tendon. We hypothesized that the MT length change pattern during a feedback controlled supramaximal isometric contraction would be asymmetric, reflecting the rapid rise and slower relaxation that is characteristic of muscle force production. Furthermore, we expected that peak muscle-tendon lengthening velocity during isometric contraction would exceed the peak muscle fiber shortening velocity observed during a 'fixed-end' (i.e. MT velocity = 0) contraction of the same duration.

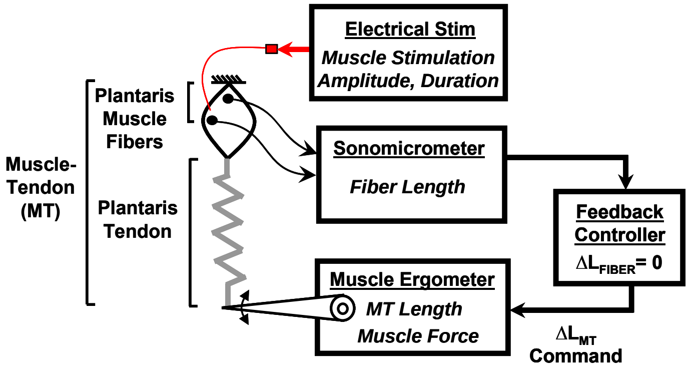

Figure 1. Schematic of the experimental apparatus. When the muscle was stimulated via the sciatic nerve (red arrow), a proportional integral derivative (PID) controller used sonomicrometer length feedback to generate a control signal for ergometer position. The PID control algorithm commanded the ergometer to adjust muscle-tendon (MT) length in order to keep muscle fibers isometric throughout the contraction. For example, upon stimulation, initial fiber shortening would be prevented by a feedback control signal to the ergometer to apply a rapid MT lengthening response.

METHODS

We isolated a bullfrog (*Rana catesbeiana*) plantaris muscle-tendon unit (plantaris muscle mass = 2.8 g, MT length = 64 mm; free tendon length = 30 mm) and surgically implanted a pair of sonomicrometry crystals (1 mm diameter) along the line of action of the plantaris muscle fibers. We attached a nerve-cuff to the sciatic nerve and the muscle-tendon to an ergometer under position control. Using a 4V, 50 ms pulse train (0.2 ms pulses, 100 pps), we supramaximally stimulated the muscle during two conditions. First, by keeping the ergometer position (and MT length) fixed we determined how much and how fast maximally stimulated plantaris muscle fibers would shorten against the series elastic plantaris tendon (i.e. 'fixed-end' contraction). Next, we used real-time feedback of plantaris fiber length from the sonomicrometery pair and an optimally tuned feedback controller on the ergometer to drive the MT through a length change pattern that prevented the plantaris fibers from shortening (i.e. we enforced isometric force production) (**Fig. 1**). For both conditions we set the rest length of the MT to correspond with the onset of passive force from an experimentally determined force-length curve (~1 N initial tension). We recorded (1) MT force and length from the ergometer and (2) muscle fiber length from the pair of surgically implanted sonomicrometry crystals.

RESULTS

In order to maintain muscle fibers isometric (**Fig 2., blue**), the ergometer applied a highly asymmetric MT length trajectory (**Fig 3., middle, blue**). The MT lengthened rapidly early in the contraction and then slowly shortened late in the contraction, mirroring the pattern of force development of the muscle fibers (**Fig 3., top, blue**). In contrast, during the 'fixed-end' contraction, muscle fibers shortened

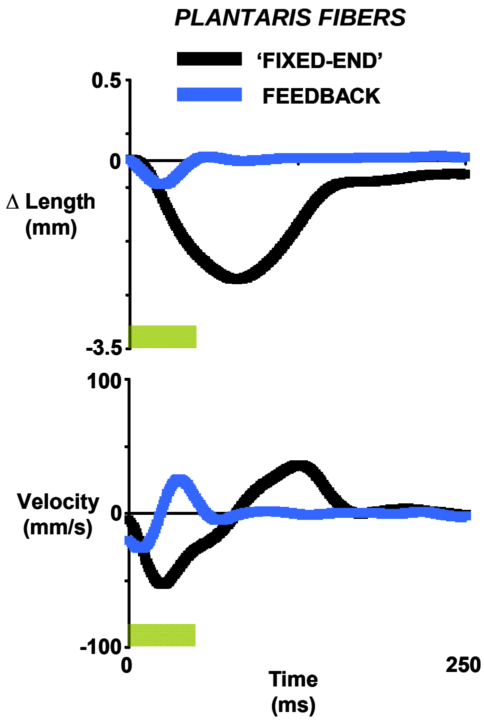

Figure 2. Length change (mm), and velocity (mm/s) versus time (ms) records from sonomicrometer crystal pair impanted in line with the plantaris muscle fibers during a 'fixed-end' (black) and feedback controlled (blue) contraction. The shaded green bars represent the period of supramaximal stimulation (50 ms). In the feedback condition, the muscle fibers remain nearly isometric. In the 'fixed-end' condition, the muscle-fibers shorten considerably against the series tendon.

considerably against the series elastic plantaris tendon (**Fig.2, top, black**). The peak MT lengthening velocity (+153 mm/s) required to maintain fibers isometric was nearly three times as fast as the peak muscle fiber shortening velocity (-52 mm/s) during the 'fixed-end' contraction and considerably higher than the maximum shortening velocity for plantaris fibers (~ -70 to -100 mm/s). MT peak force was markedly higher (+87%) in the feedback controlled isometric contraction when compared to the 'fixed-end' contraction (**Fig. 3, top**).

CONCLUSIONS

These results suggest that an asymmetric muscle-tendon length change pattern may be required for isometric force production in a compliant muscle-tendon. The results also highlight a potentially important trade-off. Because of the rapid MT lengthening that is required to maintain fibers isometric, it may be difficult to avoid muscle fiber shortening against the series tendon and costly muscle fiber positive work in a highly compliant muscle-tendon. On the other hand, a MT that is too stiff may limit the possibility for economical isometric force production and elastic energy storage and return. Further studies might explore the effects of varying series stiffness on the requirements for isometric force production in a muscle-tendon unit.

REFERENCES

(1) Roberts, T.J. et al. (1997). *Science,* 275(5303):1113-1115.
(2) Ishikawa, M. et al. (2005). *J Appl Physiol,* 99(2):603-608.

ACKNOWLEDGEMENTS

Supported by NIH F32AR055847 to GSS and NSF IO0642428 to TJR.

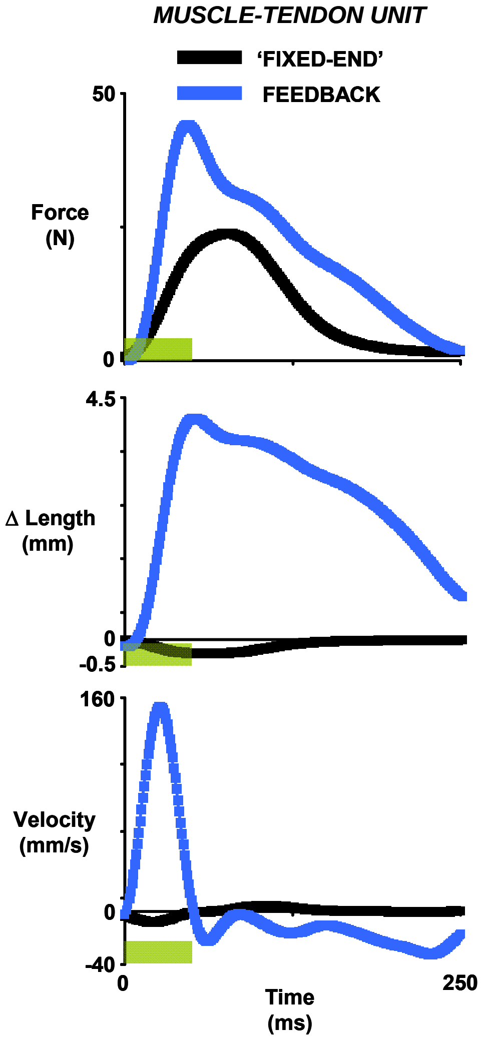

Figure 3. Force (N), length change (mm), and velocity (mm/s) versus time (ms) records for the whole muscle-tendon unit during a 'fixed-end' (black) and feedback controlled (blue) contraction. The shaded green bars represent the period of supramaximal stimulation (50 ms). In the feedback condition, the muscle-tendon is rapidly lengthened by the ergometer to keep muscle fibers isometric. In the 'fixed-end' condition, the muscle-tendon does not change length and the muscle fibers shorten against the series tendon.

The Effects of Suprascapular Nerve Block on Humeral Head Translation

Jun G. San Juan.[1], Peter Kosek[2], and Andy R. Karduna [1]
[1]University of Oregon, Eugene, OR, USA, [2]Pain Consultants of Oregon, Eugene, OR, USA
Email: bsanjuan@uoregon.edu, Web: http://biomechanics.uoregon.edu/obl/

INTRODUCTION

Shoulder impingement and rotator cuff tears are among the most common chronic shoulder injuries in the general population [1-3]. Although there are clearly underlying biological factors involved, many clinicians feel that abnormal mechanical forces may lead to a progression from impingement syndrome, or tendonitis, to rotator cuff tears. Since patient data are rarely available before the development of rotator cuff tears, it is not known whether abnormal decentralization of the humeral head is causal or compensatory in nature. Since the suprascapular nerve innervates both the supraspinatus and infraspinatus, which functions to centralize the humeral head, a suprascapular nerve block was utilized to achieve dysfunction of these muscles. The specific aim of this study is to examine the effects of a suprascapular nerve block on superior translation of the humeral head during dynamic shoulder abduction.

METHODS

Eight healthy subjects, 5 males and 3females (age 23 ± 3.3, weight 65.8 ± 13.8 kg, height 171.5 ± 6.2 cm) participated in this study. Subjects were asked to stand while performing normal shoulder elevations in the scapular plane prior to and following a suprascapular nerve block. Scapular plane orientation was defined as approximately 30-35 degrees anterior to the coronal plane. Prior to each collection the investigator positioned the arm in the correct plane, with the help of fluoroscopic (GE (OEC) 9800) image and returned the arm to the subject's side (Figure 1). Shoulder elevation trials were collected using fluoroscopy with subjects standing at a marked position, eyes facing forward, elbow in full extension, and slight forearm pronation. The range of motion was subject dependant, but all trials began with the arm at the subject's side. Shoulder elevation trials were collected prior to and after the suprascapular nerve block. To control the velocity of motion, an audible count of four seconds (eight seconds total) was used during both shoulder elevation and depression. Each set of trials consisted of two shoulder elevation and one shoulder depression in the scapular plane.

The suprascapular nerve block was performed by an anaesthesiologist (PK). An inch above the junction of the middle and outer third of the scapular spine, the suprascapular nerve was targeted at the scapular notch. After aspiration did not result in blood, lidocaine 1.5% 1 ml was injected. A total of 100 mg of lidocaine was injected to the subject's nerve. Ten minutes following initial injection, subjects was asked to stand, and the post block trial was collected.

In order to compare pre and post block trials, humeral elevation angles for both conditions were matched by calculating the humeral angle with respect to gravity. Humeral head translation was measured using a 2-D registration technique developed by Crisco et al. [4] The measured superior humeral head translation was calculated in each humeral elevation angle with respect to the resting position, which was defined as the 0° position, arm at the side. This method of measuring humeral head translation was previously validated by the investigator with a measured error of less than 0.5 mm. A one-way repeated measures analysis of variance (ANOVA) was used to examine mean differences between the two conditions (pre and post block).

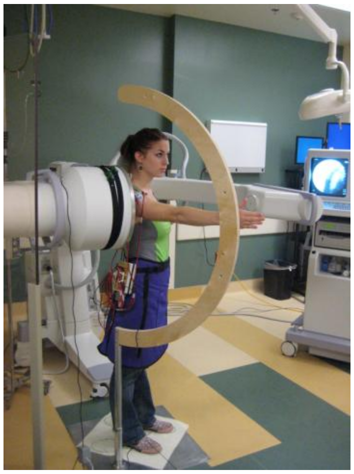

Fig. 1. Subject set-up during testing protocol.

RESULTS

There was no statistical difference between the measured humeral head translation before and after the suprascapular nerve block (p = 0.5). The pre-nerve block trials shows that only at 30 degrees of arm elevation is the humeral head superiorly migrated (0.5±3.1mm) compared to the initial position. On the other hand, the post-nerve block trials showed superior migration of the humeral head at 30 (1.4 ± 3.0mm) and 90 (1.1±3.7mm) degrees of humeral elevation (Figure 2).

DISCUSSION

The result of the current study shows that there is no difference in measured humeral head translation prior to and after suprascapular nerve block. This result is in accordance with a similar study by Werner et al. [5]. The pattern of increased in humeral head superior translation seen with rotator cuff patients, was not observed in the present study. This might suggest that decrease in muscle activation of the supraspinatus and infraspinatus has no effect on centralizing the humeral head in the glenoid during arm elevation. However, care should be taken when interpreting the results of this study due to the limited number of subjects. This is an ongoing research study and the investigators are planning on testing more subjects.

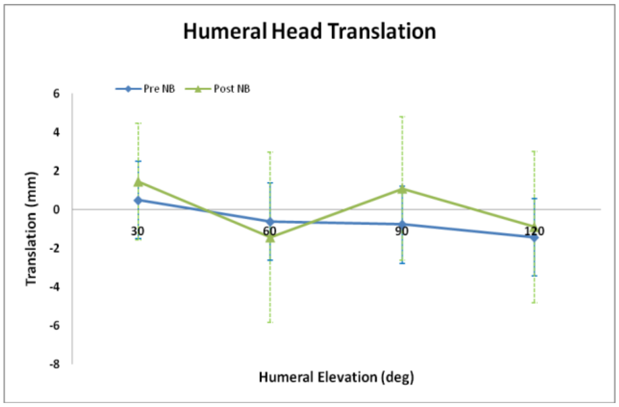

Fig. 2. Pre and post nerve block humeral head translation during shoulder elevation.

REFERENCES

1. Flatow, E.L., et al., *Am J Sports Med*, 1994. 22(6):779-88.
2. Ludewig, P.M. and T.M. Cook., *J Orthop Sports Phys Ther*, 2002. 32(6): p. 248-59.
3. Soslowsky, L.J., et al., *Orthop Clin North Am*, 1997. 28(1): p. 17-30.
4. Crisco et al., *J Biomech*. (1995) 28, 119-124.
5. Werner et al., *J Orthop Res*, 2006. 24(3): p. 491-500.

ACKNOWLEDGEMENTS

We would like to thank Diana Raponi for technical assistance with the fluoroscopy. Partial funding for this project was provided by a grant from NIOSH: 5R01OH008288.

APPLICATION OF MUSCULOSKELETAL MODELS TO AGING: OBTAINING SUBJECT-SPECIFIC MEASURES OF MUSCLE VOLUME USING MRI

[1]Christopher J. Hasson, [1]Ross H. Miller, [2]Steven A. Foulis, [2]Jane Kent-Braun, and [1]Graham E. Caldwell
[1]Biomechanics & Motor Control Laboratories, [2]Muscle Physiology Laboratory
University of Massachusetts Amherst; E-mail: cjhasson@kin.umass.edu

INTRODUCTION

Musculoskeletal models are widely used as aids to understanding human movement, such as walking or jumping [1]. In these modeling studies it is usual to scale the skeletal dimensions and muscular parameters to that of an average young male. On the other hand, few modeling studies have attempted to model the behavior of older individuals [2]. Such models should accurately reflect age-related changes in the mechanical properties of muscle.

The maximal isometric force capability (P_0) of the muscles in older individuals is generally decreased compared to younger adults [3]. P_0 is a critical parameter for musculoskeletal models, and is related to the volume of contractile tissue in a muscle. Magnetic Resonance Imaging (MRI) can be used to acquire *in vivo* muscle volumes [4]. After adjusting for architectural features by computing the physiological cross-sectional area (PCSA), subject-specific estimates of P_0 can be determined for individual muscles [5].

In healthy young male subjects there is relatively little non-contractile tissue (connective and adipose tissue) within muscle; therefore, PCSAs based on total muscle volumes may provide accurate estimates of the force-producing capability of a muscle for use in musculoskeletal models. On the other hand, older adults have an increased amount of non-contractile tissue within their muscles [6]. Failing to take this into account when modeling the behavior of older individuals may lead to over-estimations of the force producing capabilities of the older muscles.

The purpose of this study was two-fold: 1) to develop a user-friendly software analysis program to obtain *in vivo* measurements of muscle contractile volume from MRI data, and 2) to quantify age-related differences in the proportion of contractile and non-contractile muscle tissue in the ankle dorsi- and plantarflexor muscles.

METHODS

MRI images were taken of the left lower leg of 12 young and 12 older active and healthy male and female subjects (G.E. Sigma EchoSpeed Plus; 1.5 Tesla). Axial images were taken using a spacing of 4 mm (T1 weighted spin echo images; TR = 5000 ms, TE = 17 ms, pixel resolution 512x512, field of view 300 mm). Two sets of axial images of the leg were taken, one proximal, and one distal. Custom interactive software was written in MATLAB™ to identify muscle compartment cross-sectional areas (CSAs) and to separate contractile tissue from non-contractile tissue. For each subject, the proximal and distal sets of the lower-leg axial images were combined and then sorted according to slice location. This composite set of axial images was then loaded into the software for analysis. The perimeters of the dorsiflexors (DF), the soleus (SO), and the medial and lateral heads of the gastrocnemius (GA) were outlined in every other slice (Figure 1B).

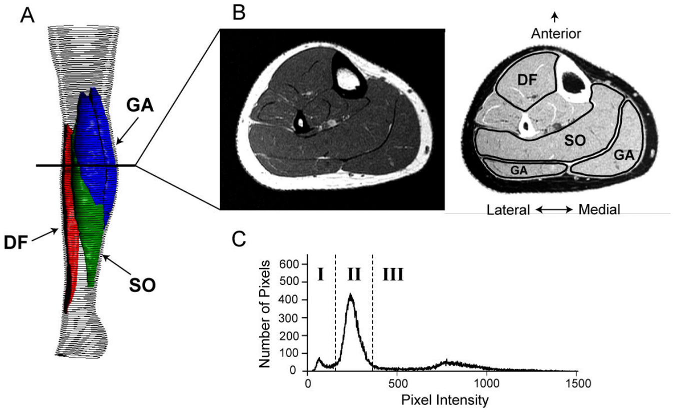

Figure 1. A: Example of reconstructed muscle volumes of the dorsiflexors (DF), gastrocnemius (GA), and soleus (SO). B: An axial MRI image illustrating the identification of the muscles of interest (left). Inverted image (right) C: Pixel intensity histogram showing the separation of cortical bone/tendon (I), muscle (II), and trabecular bone/adipose tissue (III).

A histogram representing the pixel intensities for the area within the leg boundary was created for each analyzed slice (Figure 1C). The lower pixel intensities represent cortical bone and tendon; the high intensities represent trabecular bone and adipose tissue; muscle tissue lies between these intensity regions. The pixel intensity thresholds for separation of these regions were initially chosen by identifying the peak intensity (representing muscle), and then finding where the slope to either side reaches zero. The interactive MRI analysis program then colored the corresponding MRI slice, based on the chosen thresholds. The thresholds were then manually adjusted until an optimal separation of contractile vs. non-contractile tissue was reached. The CSA of each muscle compartment in each analyzed slice (every other measured slice) was computed, multiplied by an 8 mm slice spacing (2 x 4 mm), and summed together to give muscle volumes. Separate three-way ANOVAs (age x gender x muscle [DF, GA, SO]) were performed with total and contractile tissue volumes as dependent variables. Signifance was set at $p < .05$.

RESULTS AND DISCUSSION

There were no age-related differences for total muscle volume ($p = .953$), however the older adults had smaller contractile tissue volumes ($p = .011$) (Figure 2, Table 1). Male subjects had larger total muscle volumes and contractile tissue volumes compared with the females ($p < .001$). Post-hoc analysis revealed consistent differences between all three muscles in both age groups in total and contractile tissue volume ($p < .01$ for all comparisons), such that the SO had the largest volumes, followed by the GA, and DF.

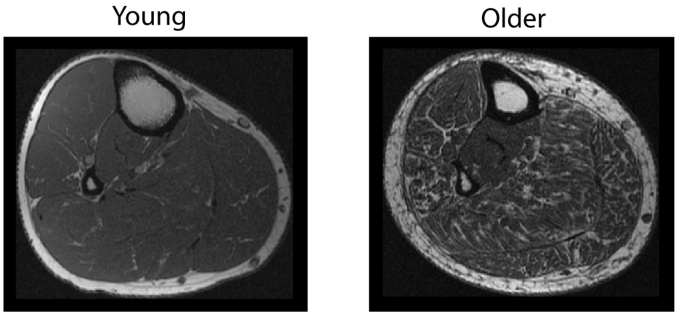

Figure 2. Comparison of young and older axial MRI slices midway through the lower leg (See Figure 1). Note significant increase in intramuscular adipose tissue (lighter intensities) in the older subject.

Our analysis revealed that there was no effect of age on total muscle volume, which includes the muscle volumes occupied by tendon and fat. However, the proportion of contractile tissue within the muscle compartments was significantly decreased in the older subjects, compared with the younger subjects (both males and females). This supports previous research showing a more than two-fold increase in non-contractile tissue with increasing age [6]. The observed differences between the volumes of the dorsi- and plantarflexor muscles (DF < GA < SO) were consistent in both age groups whether non-contractile tissue was included or excluded.

Table 1. Total muscle compartment and contractile tissue volumes. Values are Mean ± SD.

Group	Mus.	Total Vol. (cm^3)	Contractile Vol. (cm^3)	% Difference
Young Male	DF	276 ± 32	257 ± 28	-6.9
	GA	414 ± 80	397 ± 75	-4.1
	SO	443 ± 60	424 ± 53	-4.3
Young Female	DF	209 ± 48	191 ± 44	-8.6
	GA	342 ± 79	326 ± 79	-4.7
	SO	410 ± 65	390 ± 66	-4.9
Older Male	DF	306 ± 55	266 ± 44	-13.1
	GA	372 ± 60	306 ± 73	-17.7
	SO	540 ± 183	406 ± 164	-24.8
Older Female	DF	203 ± 36	169 ± 35	-16.7
	GA	267 ± 37	224 ± 35	-16.1
	SO	400 ± 70	349 ± 51	-12.8

CONCLUSIONS

An interactive software program was developed to obtain subject-specific measurements of the volume of contractile tissue within a muscle, excluding non-contractile (tendon and adipose) tissue. With aging there were significant increases in the amount of non-contractile tissue in the dorsi- and plantar-flexors. This should be considered when muscle volumes are used to estimate maximal isometric muscle force capabilities for modeling the behavior of older individuals.

REFERENCES

1. Pandy MG, et al. *Phonetica* **57**, 219-28, 2000
2. Thelen DG. *J Biomech* **125**, 70-7, 2003.
3. Bemben MG, et al. *Med Sci Sport Exerc* **23**, 1302-10, 1991.
4. Mitsiopoulos N, et al. *J Appl Physiol* **85**, 115-22, 1998
5. Gans C. *Exerc Sport Sci Rev* **10**, 106-207, 1982.
6. Kent-Braun JA, et al. *J Appl Physiol* **88**, 662-8, 2000.

ACKNOWLEDGEMENTS

Supported by NRSA 1F31EB005073 (CJH) and NIH R03AG026281 (GEC).

MODIFICATIONS IN JOINT KINETICS DURING MANUAL WHEELCHAIR PROPULSION OVER TIME

K.A. Coghlan[1], J.L. McNitt-Gray[1,2], P.S. Requejo[2,3], S. Mulroy[3], P. Ruparel[3]
[1]Department of Biomedical Engineering, USC, Los Angeles, CA,
[2]Department of Kinesiology, USC, Los Angeles, CA
[3]Pathokinesiology Laboratory, Rancho Los Amigos National Rehabilitation Center, Downey, CA
email: coghlan@usc.edu

INTRODUCTION

Wheelchair users must utilize their upper extremities for both locomotion, and everyday tasks such as driving, typing, and eating. The repetitive nature and mechanical demand imposed on the body during these activities of daily living is associated with shoulder pain[1]. Shoulder pain in wheelchair (WC) users can have a severe negative impact on quality of life. Furthermore, treatment of shoulder pain in wheelchair users is difficult since opportunities to rest the upper extremities are few. Prevention of shoulder pain therefore is a key to abating this problem.

Causal factors contributing to shoulder pain in WC users have not been clearly delineated. Understanding the mechanisms that lead to and exacerbate shoulder pain is an important step towards prevention of shoulder pain in this population. As an initial step, this study determines the changes in the mechanical demand imposed on the upper extremity during wheelchair propulsion over an 18 month period. Modifications in upper extremity mechanics will be interpreted in relation to clinical assessments and reported incidence of shoulder pain, as part of a larger, longitudinal study.

METHODS

Four WC users volunteered to participate in this study in accordance with the Institutional Review Board at the Ranchos Los Amigos National Rehabilitation Center, Downey, CA. Participants were male (average age 37.8 (+/- 1.9) years) with paraplegia from complete spinal cord injury (SCI), average 12.6 (+/- 3.6) years post SCI. All participants were free of shoulder pain that interferes with daily activities or requires medical intervention at the onset of the study.

Three dimensional push-rim propulsion forces were measured with a SmartWheel (Three Rivers Holdings, Mesa, AZ). The SmartWheel has strain gauges allowing the X, Y and Z axis forces and moments to be determined. A CODA (Charnwood Dynamics, Inc.) motion analysis system was used to collect three dimensional motion data.

Active markers were placed on the upper extremity and trunk to define the locations of the joint centers and the orientations of the hand, forearm, and upper arm segments. Subjects were tested in their own WC. The SmartWheel attaches to the axle of any WC with quick-release wheels.

A WC ergometer enabled data collection from multiple, consecutive propulsion cycles and provided a means of simulating propulsion over a range of surface conditions and inclines. Translational inertia present during actual propulsion was simulated on the ergometer using removable flywheels.

Participants were asked to propel at a self-selected velocity during three conditions: free, fast and simulated incline propulsion. Following a 20-second period of propulsion for accommodation, 10 seconds of data were collected for each of the three conditions. Prior to the simulated incline tests, the front of the WC ergometer was tilted up 4.57 degrees and the resistive load increased to match the necessary power requirements of an 8% incline, about 60 to 80W on a smooth surface. Participants were asked to perform the evaluation at initiation (baseline) and after 18 months (18-month period)

Push rim forces, upper extremity motion and wheelchair speed were monitored. A 3-D, 4-segment rigid body model of the upper extremities developed for a previous study was applied to the 3-

D motion data[2]. Net joint reaction forces and net joint moments for the wrist, elbow, and shoulder were calculated using inverse dynamics methods and compared between conditions.

RESULTS AND DISCUSSION

Comparison of mechanics between baseline and 18-months demonstrated significant modifications in reaction forces and joint kinetics in two of the four participants for the incline condition. No significant within-participant differences in force-time characteristics were observed during the self selected free and fast WC propulsion conditions.

Between-condition differences were attributed primarily to modifications in push-rim force-time profiles. In one case, modifications of the force-time characteristics were associated with significant increases in force production early in the propulsive phase (Fig. 1: Participant A). In another case, differences in force-time characteristics were associated with push rim force redirection (Fig. 1: Participant B). No significant differences in push-rim forces, joint kinetics, and kinematics were observed between baseline and 18 month post conditions for the other two participants under the incline conditions.

These preliminary results indicate that there exist significant differences in wheel chair propulsion strategies across participants over time. Continued tracking and integration with clinical assessments and longitudinal information regarding shoulder pain will assist in determining mechanical factors contributing to shoulder pain.

CONCLUSIONS

Modifications in mechanical demand imposed on the upper extremity occurred overtime. Observed differences in joint kinetics observed within an individual were attributed to differences in push rim force magnitude and direction in relation to the orientation of upper extremity segments. Future studies will investigate the relationship between changes in wheel chair locomotion strategies, presence or onset of shoulder pain, and the mechanical demand imposed during other activities of daily living.

REFERENCES

1. Campbell C.C, et al., *Clinical Orthopaedics & Related Research,* **140** (Jan, 1996).
2. Kulig, K.P., et al., *Clinical Orthopaedics & Related Research*, **354** (September 1998)

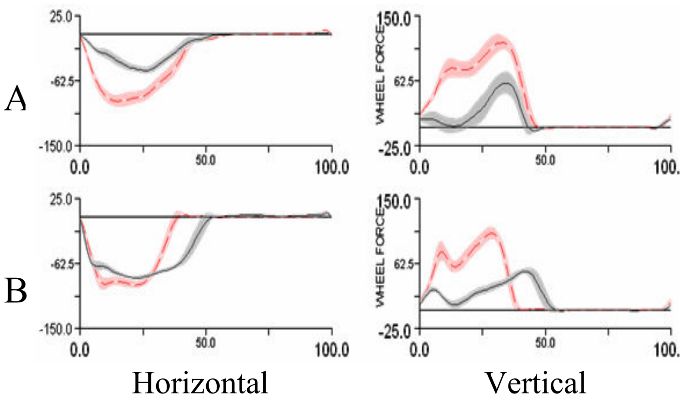

Figure 1: Mean (STD: shaded area) propulsive forces (N) at the hand/rim interface for participants A and B. The black (solid) curves represent the baseline data, while the red (dashed) curves represent the 18-month follow-up data.

ACKNOWLEDGEMENT:
Supported by NIH 5RO1HD049774.

Tension pattern of the cruciate ligament fibers during rolling and sliding

[1]Joon Ho Wang, [1]Kang Li, [1]Madelyn E. O'Farrell, [1]Christopher Harner [1,2,3]Xudong Zhang
[1]Departments of Orthopaedic Surgery, [2]Mechanical Engineering & Materials Science,
[3]Bioengineering, University of Pittsburgh, PA, USA, email: xuz9@pitt.edu

INTRODUCTION

Knowledge about the deformation and excursion of cruciate ligaments (ACL and PCL) in a functional knee is a key to understanding the mechanisms of cruciate ligament injuries and guiding the surgical treatments. Considerable efforts have been dedicated to studying the deformation of the cruciate ligaments and have provided valuable insights into their functions [1-5]. However, these studies lack either realistic kinematics or anatomically correct insertion site data. The purpose of this study is to examine the tension patterns of ACL and PCL in a fiber-by-fiber manner during a range of motion guided by in vivo knee kinematics. We hypothesized that tibia-femoral translation information is critical for accurate characterization of the tension patterns.

METHODS

Two fresh-frozen cadaver knees were thawed, and all soft tissues were stripped from the femur, tibia, and fibula beginning 6 cm from the joint line while keeping the fibula fixed to the tibia. Precision Nylon spherical markers (radius 9.525 mm) were rigidly affixed to the femur and the tibia, three on each bone without disrupting the soft tissue structures. High-resolution CT scans of the knees were then taken (slice spacing of 0.625 mm). Dissection of the knee specimens was then performed, during which the fibers of the cruciate ligaments were separated. In one knee, 13 fibers were identified from the ACL with 7 from the AM bundle and 6 from the PL bundle. In the other knee, 10 fibers were identified from the PCL with 5 in the AL bundle and 5 in the PM bundle. The femoral and tibial insertions of the fibers were marked using colored small head pins. A MicroScribe 3D Digitizer (Immersion Corp., CA) with a manufacturer-reported accuracy of ±0.2 mm was used to digitize the marked insertion points of the ACL and PCL fibers. The spherical marker surfaces were digitized such that 'point-cloud' representations of the surfaces were formed. Mimics software (Materialise, Belgium) was used to segment the bones and spherical markers separately from the CT scans and create 3D surface models of each. The insertion points of all the fibers of the ACL and PCL were mapped onto the 3D models (Figure 1). The fibers were represented by the straight lines connecting the corresponding points on the tibia and femur.

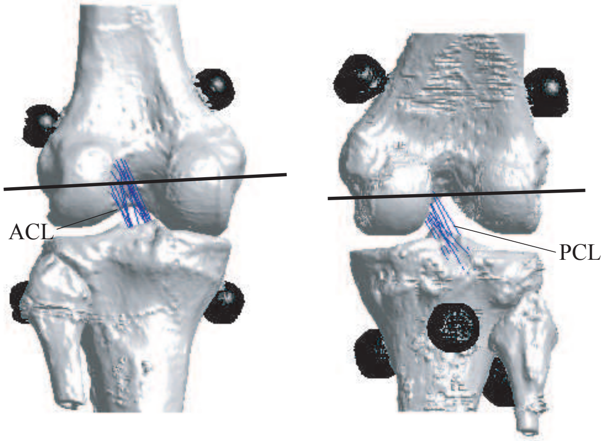

Figure 1: The bone models with multiple fibers (blue lines) of the cruciate ligaments. The thick solid lines are the flexion/extension axes.

A computer simulation was performed to drive the femur movement relative to the tibia with only flexion from 0-120° (rolling), and with both flexion and the medial-lateral (ML) and anterior-posterior (AP) translations (rolling and sliding). In the latter movement, the following relations between flexion and translations, derived from in vivo kinematic data, were applied:

AP_Translation=max (Flexion_angle*15/35, 15)
ML_Translation=max (Flexion_angle*6/35, 6)

The in vivo kinematic data suggest that the translations are linearly correlated with the flexion during normal range of movement and are bounded in deeper flexion.

The rolling in the simulation was guided by a flexion/extension axis determined from the following procedure. The procedure assumed that the posterior articulating portion of the femoral condyles is a concentric structure with a common axis. A series of parallel cross-sectional “cuts” of the medial and lateral femoral condyles were taken in the sagittal plane and fit to the posterior portion with circles. The centroids of these circles were then fit with a line. This line was deemed the axis of tibia-femoral flexion/extension.

RESULTS

Tibia-femoral translations significantly affected the tension patterns of the ACL (Figure 2). During rolling, the fibers of the AM and PL bundles became slack as the flexion angle increased. All of the fibers reached their maximum lengths at full extension. The mean (± standard deviation) zero force length was 41.7 (±2.9) mm for the AM fibers, and 41.7 (±3.5) mm for the PL fibers. The length decreased to 27.1 (±3.2) mm for the AM fibers and 21.6 (±2.1) mm for the PL fibers in deep flexion (120°). During rolling and sliding, the AM fibers became taut while most PL fibers were still slack before 90° of flexion. The maximum lengths of the fibers occurred at 45-80° for the AM fibers.

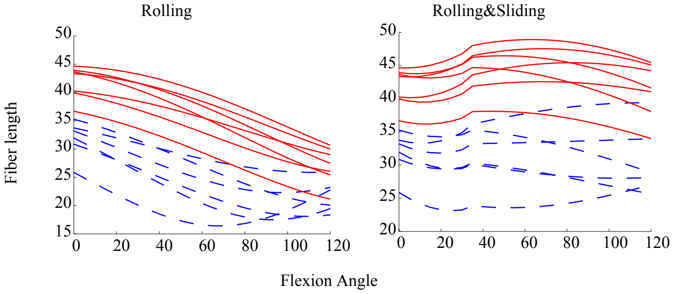

Figure 2: Fiber lengths of the ACL during rolling and rolling and sliding simulations. The solid line represents the fibers of the AM bundle and the dashed line represents the fibers of the PL bundle.

The tension patterns of the PCL were less affected by tibia-femoral translations (Figure 3). During rolling, both the AL and PM fibers were taut. The mean (± standard deviation) zero force length was 30.7 (±5.0) mm for the AL, and 30.7 (±2.8) mm for the PM. The lengths of the fibers of the AL bundle increased monotonically with increasing flexion and reached their maximum at maximum flexion. The fibers of the PM bundle had more complicated tension patterns. The length of the PM fibers increased initially. After reaching their maximum lengths at 65-120° of flexion, the lengths started to decrease. During rolling and sliding, the overall tension patterns did not change. But the maximum lengths of the fibers occurred at 80-90° for the PM bundle and 90-120° for the AL bundle.

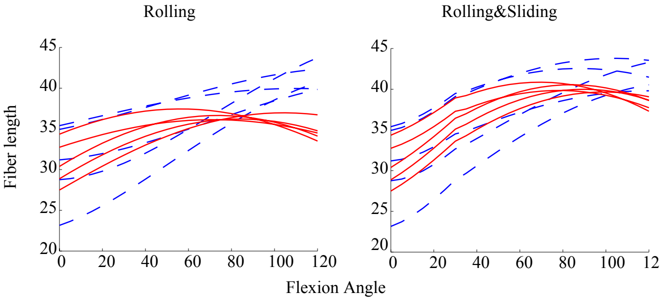

Figure 3: Fiber lengths of the PCL during rolling and rolling and sliding simulations. The solid line represents the fibers of the AL bundle and the dashed line represents the fibers of the PM bundle.

It was also observed that the fibers within the same bundle of the ACL or PCL showed similar tension patterns (Figures 2 and 3). However, some of the individual fibers of the PM bundle had significantly larger tension change, which suggests that a partial tear ligament injury may be more probable.

CONCLUSIONS

We investigated the tension patterns of individual fibers of cruciate ligaments using computer simulation that integrates in vivo and in vitro data. We showed that the fibers of the functional bundles of the ACL and PCL exhibited different tension patterns during movement.

We also demonstrated that tibia-femoral translation was a determinant of fiber tension patterns, which supported the notion that the inconsistencies observed in the previous studies were likely to be caused by the different movements used in the experiments.

REFERENCES

1. Fleming B et. al. Ann Biomed Eng, 32(3):318-28, 2004.
2. Garbelotti Jr SA et. al. Clinics, 62(5):619-626.
3. Noyes FR et. al. Arthroscopy 1994;10:371-82.
4. Jackson DW et. al. Arthroscopy 1993;9:224-7.
5. Cohen SB et. al. J. Knee Surgery 2004;17:211-3.

EFFECTS OF HEAD POSITION AND IMPACT DIRECTION ON NECK MUSCLE RESPONSE TO PERTURBATIONS

[1,2]Anita N. Vasavada, [1]Darrin Trask, [2]Anne Knottnerus and [1,2]David C. Lin
[1]Voiland School of Chemical Engineering and Bioengineering, [2]Dept. of Veterinary and Comparative Anatomy, Pharmacology and Physiology, Washington State University, Pullman, WA, USA
email: vasavada@wsu.edu, web: http://www.chebe.wsu.edu/Faculty/AVasavada.html

INTRODUCTION

Neck muscle reflexes are critical to restoring head posture following a perturbation to either the head or the body. For example, in a rear-end automotive impact, the neck muscles activate during head retraction. Occupant injuries are reported as more severe when the head is rotated [1]. This may be because reflex activity is altered with rotated postures and oblique impacts. The goal of this study is to examine the effect of head position and impact direction on neck muscle responses.

METHODS

Nine subjects (4 men, 5 women) were harnessed into a chair. Controlled perturbations (lasting ~100 ms) were applied to the top of the subject's helmet with a motor and impact force was recorded, after which the head was allowed to move freely. Subjects wore darkened swimming goggles and earplugs to minimize audio/visual cues and were instructed not to anticipate or resist the impact. Three perturbation conditions of 15 trials each were examined (Figure 1): (A) neutral head posture with the impact in the mid-sagittal plane; (B) head rotated 45° right with the impact in the mid-sagittal plane of the head; (C) head rotated 45° right with the impact from the front of the body. Comparing conditions B vs. A provides information about the effect of head position, whereas comparing conditions C vs. B provides information about impact direction.

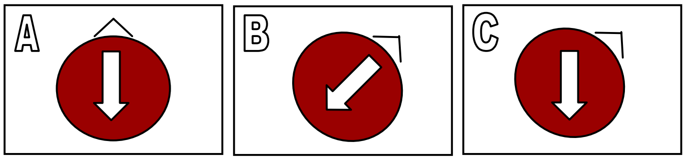

Figure 1: Testing conditions. Rectangle represents body, triangle represents front of subject's head, and arrows represent direction of impact.

Kinematics
Positions of infrared markers on the subject's head were recorded (Optotrak, Northern Digital, Inc.). Head rotational and translational kinematics were calculated in a coordinate system fixed to the initial head position in space.

Electromyography (EMG)
Neck muscle reflexes of the left and right sternocleidomastoid (LSCM, RSCM) were quantified with surface electromyography (Bagnoli-8, Delsys, Inc.). Data were bandpass filtered (50-450 Hz) and sampled at 1000 Hz. Normalized EMG integrals were calculated for a 100 ms interval before and after the perturbation. The incremental response was defined as the difference between post- and pre-impact integrated EMG.

Kinematic variables were averaged over all trials for each subject, and subject averages compared among conditions A, B and C using one-way repeated measures ANOVA. Because of the variability in EMG among subjects, one-way ANOVA was applied to each subject's EMG data individually. Significance level was set as $\alpha=0.05$.

RESULTS AND DISCUSSION

Forces applied to the subjects' heads (9 ± 2 N) were not significantly different in all three conditions.

Kinematics
In conditions A and B, the head kinematics were predominantly extension, whereas in condition C, there was a combination of extension and lateral bending (Figure 2). For the predominant motions (extension and lateral bending), the peak values were not statistically different between conditions A and B, but the peak values for condition C were statistically different from conditions A and B. That is, kinematics did not vary with head position but did vary with impact direction.

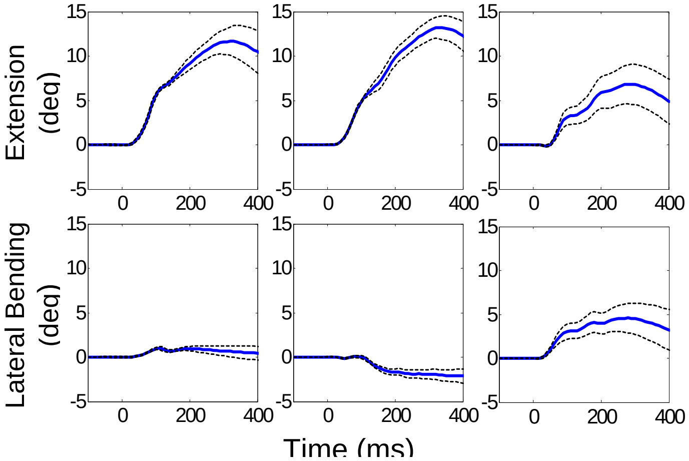

Figure 2: Head position traces of one subject, mean (solid) and standard deviation (dashed) of 15 trials.

Muscle Reflexes

Left Sternocleidomastoid. Baseline activity (required to hold the initial position) was significantly greater in conditions B and C than in A in all subjects (Figures 3 and 4). Baseline activity in C was also greater than in B in 6 of 9 subjects.

LSCM incremental response in condition B was not significantly different from A in 8 of 9 subjects; *i.e.*, head position did not significantly affect response. Incremental response in condition C was greater than B in only 4 of 9 subjects but greater than in A in 7 of 9 subjects; *i.e.*, impact direction may have a slightly greater effect than head position.

Right Sternocleidomastoid. Neither baseline muscle activity nor the response to the impact were statistically different among conditions A, B, and C (Figures 3 and 4). In other words, increased RSCM activity was not necessary to hold the right-rotated posture, nor was the muscle response affected by head position or impact direction.

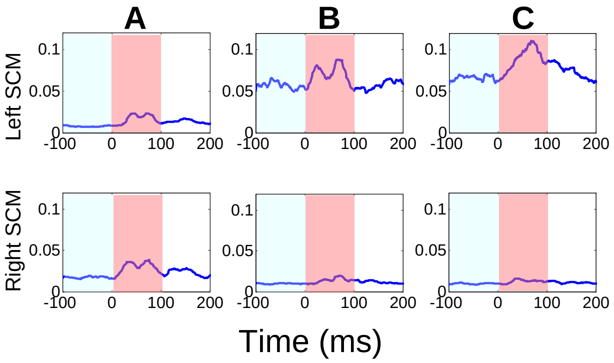

Figure 3: RMS EMG traces from one subject, 15 trials averaged (light shaded bar = 100 ms pre-perturbation, darker bar = 100 ms post-perturbation).

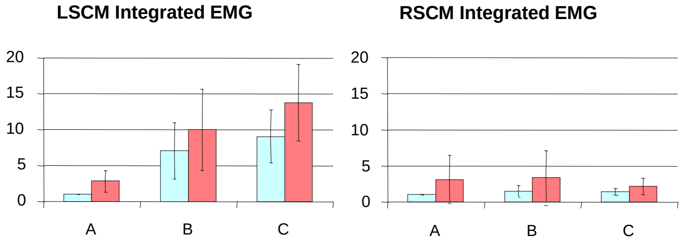

Figure 4: Integrated EMG, composite of all subjects. Data are normalized to baseline of condition A (light blue = pre-perturbation baseline, dark red = post-perturbation). Incremental response is (red – blue).

Two important neck reflexes are the vestibular reflex, which responds to head motion, and the stretch reflex, which responds to a change in muscle length. Evidence of both of these reflexes were present in most trials (note two peaks in Figure 3; the vestibular reflex had an earlier onset than the stretch reflex). Similar kinematics in conditions A and B implies similar vestibular inputs. Differences in muscle responses in A vs. B can still arise from differences in both baseline muscle activity and stretch (due to altered posture). The lack of statistically different LSCM incremental response in B vs. A implies that the baseline activity and altered muscle stretch due to rotated posture were not significant influences on the muscle response.

The different kinematics of conditions B vs. C should affect both the vestibular and stretch reflexes. Different incremental responses in the LSCM were expected in conditions B vs. C; however, only 4 of 9 subjects showed significant differences in incremental reflex responses.

CONCLUSIONS

For right-rotated head postures, the LSCM had more activity than RSCM both pre- and post-impact. Separately, both initial head position (affecting baseline muscle activity) and impact direction (affecting kinematics) did not lead to significant increases in incremental response in most subjects. However, the effect of both position and impact direction had a significant effect in incremental muscle response in most subjects.

REFERENCES

1. Sturzenegger, MG, et al. *Neurology* **44**: 688-693, 1994.

ACKNOWLEDGEMENTS

Supported by NSF-UBM #EF 0531870 and the Adler Foundation. We thank Gerald Lucas for design and construction of the experimental apparatus.

EFFECT OF TOTAL HIP ARTHROPLASTY ON CONTRIBUTION OF INDIVIDUAL JOINTS TO DYNAMIC SUPPORT DURING WALKING

Li-Shan Chou, Soroush Amali, and Vipul Lugade

Department of Human Physiology. University of Oregon. Eugene, Oregon 97403. USA.
email: chou@uoregon.edu, web: http://biomechanics.uoregon.edu/MAL

INTRODUCTION

Primary total hip arthroplasty (THA) is most commonly used for hip joint failure caused by osteoarthritis, a disease which affects 10% of the US population [1]. THA successfully replaces severely deteriorated hips and provides pain relief, enhanced mobility, comfort and independent living for many people who would otherwise be substantially disabled [2,3]. Studies assessing changes of gait function due to hip osteoarthritis and THA have primarily focused on kinematics and kinetics of the hip joint [4]. Investigation on the role of the ipsilateral knee and ankle joints in these gait compensation strategies is currently lacking. Furthermore, the surgical procedure has been recognized as the leading factor influencing total hip arthroplasty stability and post surgical functioning [5]. To our knowledge, a comparison study between the lateral and anterior THA approaches that evaluates the functional recovery and gait performance of patients has not been documented. Thus, the aim of this study was to describe the effect of THA on contribution of individual joints to the total support (extensor) moment of the involved limb during level walking.

METHODS

A total of 33 subjects, including 10 healthy adults (5 men, 5 women; mean age: 59.9 yrs) and 23 THA patients, participated in this study. THA patients were further classified by the type of surgery, the lateral (9 men, 2 women; mean age: 57 yrs) or anterior (8 men, 4 women; mean age: 56.9 yrs) approach. Surgical candidates were referred by two orthopaedic surgeons, each utilizing his preferred surgical approach (lateral or anterior). All patients had Zimmer hip implants, which included an acetabular component with a irradiated polyethylene liner (Trilogy Acetabular component, Zimmer Inc., Warsaw, IN) and femoral stem (Alloclassic SL Stem or Fiber Metal Taper; Zimmer Inc., Warsaw, IN) and metal head component. All patients underwent the same rehabilitation protocol, with the same therapist starting the night of surgery.

Testing for THA subjects occurred at presurgery, 6- and 16-weeks postsurgery. Healthy control subjects were tested twice within one month. Subjects were fitted with 29 retro-reflective markers as described previously and were instructed to walk barefoot along a 10 meter walkway at a self-selected speed. An 8-camera motion analysis system (Motion Analysis Corp., Santa Rosa, CA) was used to collect three-dimensional marker trajectory at 60 Hz. The ground reaction forces of both feet were collected with 2 force plates (Advanced Mechanical Technology, Inc., Newton, MA) at 960 Hz. The force data were time-synchronized to the video sampling to allow for computation of the joint moment using inverse dynamics.

The total support moment (Ms; Winter, 1980), as the summation of the net joint moments at the hip, knee, and ankle joints, represents the magnitude of the extensor synergy of the lower extremity during stance phase in order to prevent collapse of the lower limb while balancing and supporting the body. Therefore, individual joint moment contributions to the Ms (as % of Ms) were assessed at the occurrence of the first peak vertical ground reaction force to characterize lower limb supportive synergies in response to hip osteoarthritis and THA. This instant represents full weight acceptance during the single stance phase of the gait cycle. A mixed model analysis of variance with repeated measures was used to compare the effects of group and time period (SPSS Inc., Chicago, Ill.). Individual joint contributions were used as dependent measurements, with the significance level set at 0.05.

RESULTS AND DISCUSSION

Prior to surgery, all THA patients walked with a slower gait velocity ($P \leq 0.0305$) than controls. By 6 weeks postsurgery, only the anterior THA patients demonstrated an increased gait velocity when compared to presurgery, but remained different than controls. By 16 weeks postsurgery, the anterior THA patients continuously demonstrated improvements in gait velocity. Improvements in gait velocity were also observed in the lateral THA patients at this time as compared to presurgery.

No significant group and time effects were detected in values of the total support moment. However, THA group Ms values were found to be smaller than that of the controls, and demonstrated a trend to increase form presurgery to 16-week postsurgery. Furthermore, changes in contributions of individual joints to the Ms were observed for THA patients across testing periods (Figure 1). The hip contribution of the lateral THA group was significantly reduced at presurgery ($P=0.0018$) when compared to the controls. Significant improvement in hip contribution to the total Ms across testing time ($P \leq 0.019$) was detected in both THA groups. It seems that THA patients compensated the reduction in hip contribution with an increased ankle contribution. At 16-week postsurgery, the ankle contribution to the Ms of THA patients was significantly reduced as compared to presurgery, and approached to a level similar to the controls. No significant group or time effects were detected for the knee contribution.

CONCLUSIONS

A larger ankle plantarflexor contribution to Ms of THA patients may compensate for the diminished hip extensor contribution during level walking. The data from the current study suggest that maintenance of the Ms requires inter-dependent contributions of hip, knee and ankle joint moments.

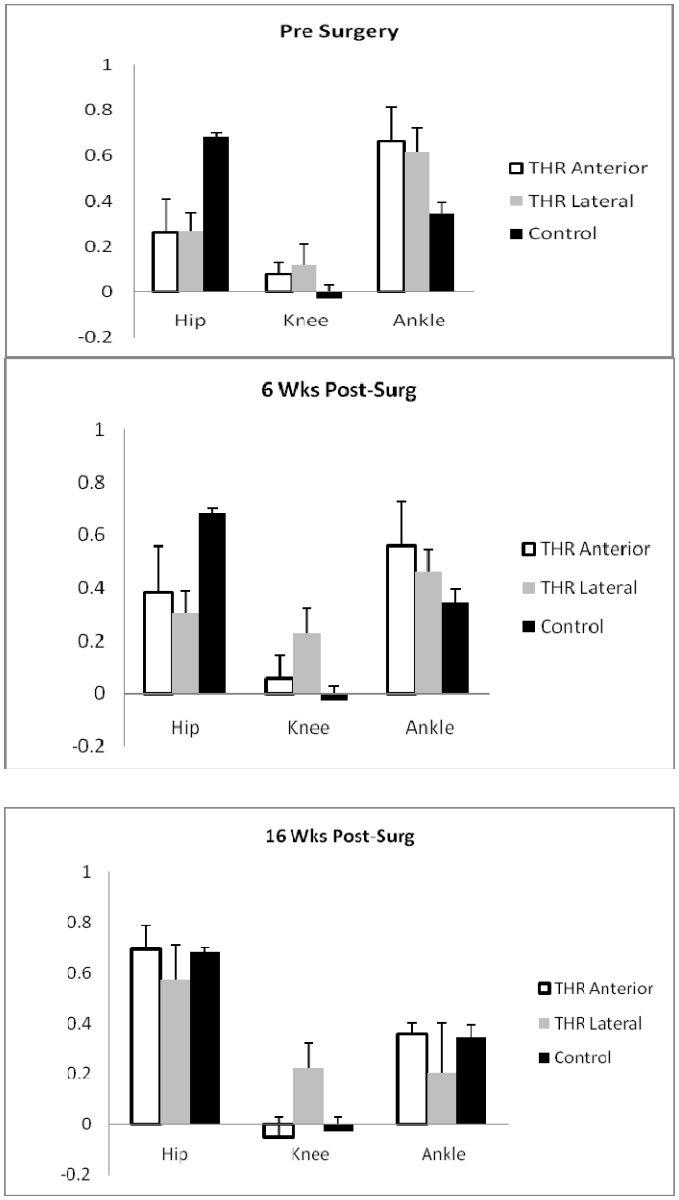

Figure 1. Ratios of individual joints' contribution to the total support moment (Ms) at presurgery, 6- and 16-week postsurgery.

REFERENCES

1. Jolles BM et al. J Rheumatol. 2004;31(9):1790-6.
2. Irving JF. *The Orthopedic Clinics of North America.* 2004;35(2):173-81.
3. Lawlor M et al., *Clin Rehabil.* 2005;19(5):465-74.
4. Perron et al., Clinical Biomechanics, 2000; 15:504-515.
5. DeWal H, et al. *Am J Orthop.* 2003;32(8):377-82.

STOCHASTIC CONTROL MODELS EXPLAIN HOW HUMANS EXPLOIT REDUNDANCY TO CONTROL STEPPING VARIABILITY DURING WALKING

[1] Jonathan B. Dingwell, [2] Joby John, [2] Joseph P. Cusumano
[1] Nonlinear Biodynamics Lab, Department of Kinesiology, University of Texas, Austin, TX
[2] Department of Engineering Science & Mechanics, Penn State University, State College, PA
E-mail: jdingwell@mail.utexas.edu Web: http://www.edb.utexas.edu/faculty/dingwell/

INTRODUCTION

Humans typically choose step length and frequency combinations that minimize energy cost [1]. While such optimizations predict *average* behavior, they do *not* explain the stride-to-stride *variability* that is always observed in walking. The human nervous system must either try to *overcome* this variability as a limiting constraint [2], or might instead *exploit* available system redundancies to try to optimize task performance [3]. Defining the essential *goal* of a task [3,4] can distinguish these alternatives.

One primary goal of walking on a motorized treadmill is to maintain, *on average* and *over time*, constant speed. However, variations in walking speed due to changes in stride length and/or stride time do occur and can be sustained over several consecutive strides. The main question addressed here is how do people *regulate* these variations?

METHODS

The primary requirement for walking on a treadmill with belt speed v is to not walk off the ends of the treadmill. This can be mathematically defined as:

$$\sum_{n=1}^{N}\left(L_n - v\cdot T_n\right) < K/2\,, \qquad (1)$$

where $L_n - v\cdot T_n$ is the net displacement walked for stride n and K is the length of the treadmill belt. Any sequence of $[L_n, T_n]$ that satisfy this inequality will accomplish the task. The simplest strategy can be formulated as the *Goal Function* [4]:

$$L_n - v\cdot T_n = 0 \quad \rightarrow \quad L_n/T_n = v\,. \qquad (2)$$

That is, subjects could attempt to maintain constant speed at each stride. Eq. 2 is not a “constraint”: it is not *required* by Eq. 1. It is rather only one possible hypothesized movement strategy. Thus, Eq. 2 defines a hypothesized “Goal Equivalent Manifold” (GEM) [4] for walking (Fig. 1). We hypothesized that humans minimize errors relative to this GEM.

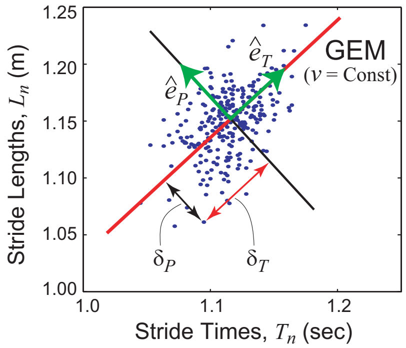

Figure 1: ***A:*** Decomposing $[T_n, L_n]$ into $[\delta_T, \delta_P]$.

Seventeen healthy volunteers (age 18-28) walked on a level treadmill (Woodway USA) at their preferred speed. 3D movements of their feet were recorded continuously for 2 trials of 5 min each and used to compute L_n and T_n for each stride, n.

We decomposed $[L_n, T_n]$ into deviations tangent to (δ_T) and perpendicular to (δ_P) the GEM (Fig. 1). Scalar δ_T deviations do *not* affect walking speed, but δ_P deviations directly define *errors* in walking speed. We computed standard deviations of each δ_T and δ_P time series. We used detrended fluctuation analysis (DFA) [5] to calculate stride-to-stride scaling exponents, α. Values of $\alpha > 0.5$ indicate statistical “persistence” (deviations go *un*corrected over consecutive strides). Values of $\alpha < 0.5$ indicate “anti-persistence” (deviations are corrected rapidly).

We then built a series of single-step stochastic control models based on the “minimum intervention principle” (MIP) [3]. The stride-to-stride walking dynamics were modeled as a nonlinear map:

$$\mathbf{x}_{n+1} = \mathbf{x}_n + G\mathbf{u}(\mathbf{x}_n) + N\,\mathbf{u}(\mathbf{x}_n) + \eta \qquad (3)$$

where $\mathbf{x}_n = [L_n, T_n]^T$ was the state for stride n, $\mathbf{u}(\mathbf{x}_n)$ was a vector of control inputs with gains G, N was multiplicative (motor output) noise, and η was additive (sensory and/or perceptual) noise. An unbiased stochastic optimal single-step controller was determined from the cost function:

$$C = \alpha e^2 + \beta p^2 + \gamma u_1^2 + \delta u_2^2 \qquad (4)$$

where the αe^2 term penalized the error relative to the GEM: $e = L_n - vT_n$. The βp^2 term penalized the distance, p, of the current state from the preferred operating point (POP), $[L^*, T^*]$. The last two terms penalized the control inputs, $\mathbf{u} = [u_1, u_2]^T$.

RESULTS AND DISCUSSION

Humans (HUM; Figs. 2-4) exhibited far greater variability for δ_T than δ_P variations, and statistical persistence ($\alpha > 0.5$) for δ_T, but *anti*-persistence ($\alpha < 0.5$) for δ_P deviations, precisely as predicted.

A strict MIP model [3] (G = I; $\beta = 0$) yielded dynamics significantly *different* from humans (Fig. 2). Adding a "preferred operating point" (POP; $\beta > 0$) on the GEM (analogous to optimizing energy cost) improved performance (Fig. 3), but still did not replicate the *anti*-persistence ($\alpha < ½$) seen in the δ_P deviations. However, a sub-optimal controller (OVC) that slightly *over*-corrected deviations away from the GEM ($G >$ I; $\beta > 0$) *did* exhibit anti-persistence in δ_P (Fig. 4), very similar to humans.

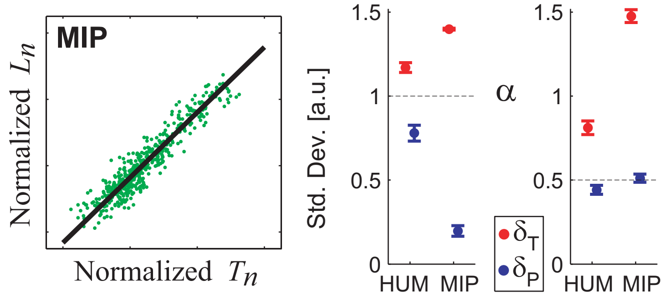

Figure 2: $[T_n, L_n]$ data for a typical trial for the pure MIP controller. Variability and DFA α exponents for δ_T and δ_P for humans (HUM) and the MIP model.

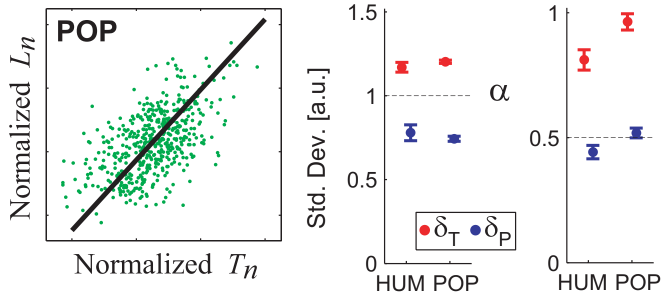

Figure 3: $[T_n, L_n]$ data for a typical trial for the optimal POP controller. Variability and DFA α exponents for δ_T and δ_P for humans (HUM) and the POP model.

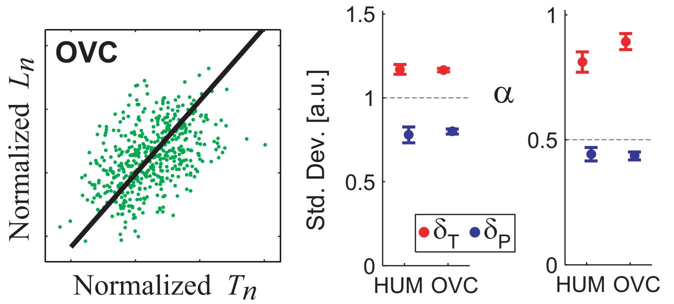

Figure 4: $[T_n, L_n]$ data for a typical trial for the OVC controller. Variability and DFA α exponents for δ_T and δ_P for humans (HUM) and the OVC model.

CONCLUSIONS

Here we present a novel decomposition of walking dynamics. We show that humans explicitly exploit available redundancy at *each* stride to maintain constant speed. Stochastic optimal control models demonstrated that healthy humans did *not* adopt precisely "optimal" strategies, but instead exhibited sub-optimal performance where they consistently *over*-correct small deviations in speed at each stride.

This "GEM-aware" control exploits inherent task redundancy to simultaneously achieve high task performance (low error) while allowing substantial motor variability. Humans achieve this control by allowing fluctuations that have no direct bearing on task performance to persist, while suppressing fluctuations that do. Our results reveal a new governing principal for regulating stride-to-stride variations in human walking that acts independently of, but in parallel with, minimizing energy cost.

REFERENCES

1. Zarrugh MY, et al. *Eur. J. Appl. Physiol.*, **33**: 293-306, 1974.
2. Harris CM & Wolpert DM, *Nature*, **394**: 780-784, 1998.
3. Todorov E., *Nature Neurosci.*, **7**: 907-915, 2004.
4. Cusumano JP & Cesari P, *Biol. Cybern.*, **94**: 367-379, 2006.
5. Peng C.-K. et al., *Nature*, **356**: 168-170, 1992.

ACKNOWLEDGEMENTS

Funded by Whitaker #RG-02-0354 (to JBD), NIH # EB007638 (to JBD), and NSF #0625764 (to JPC).

EFFECTS OF AGE AND WALKING SPEED ON METABOLIC COST AND LOWER EXTREMITY JOINT KINEMATICS DURING GAIT IN HEALTHY ADULTS

[1,2]Daniel S. Peterson, [1,3]Philip E. Martin
[1]Pennsylvania State University, University Park, PA [2]Steadman Hawkins Research Foundation, Vail, CO
[3]Iowa State University, Ames, IA; *dspeterson8@gmail.com

INTRODUCTION

Older adults exhibit higher metabolic cost of walking (C_w) than young adults across a range of walking speeds [1]. The underlying mechanism for this difference, however, is not fully understood. Recent studies have suggested stride length (SL) and step width (SW) variability may have a substantial effect on C_w [2,3], however the relationship between step variability and C_w in old and young has not been established clearly.

The purposes of this study were to determine 1) the effects of age and walking speed on SW and SL variability during gait, and 2) the relationship between these variables and C_w during gait.

METHODS

Subjects: Fourteen young (20-30 yrs) and 14 older (65-80 yrs) healthy active adults participated in this study.

Experimental Design: Participants walked on a treadmill for seven minutes at each of four speeds (0.89, 1.12, 1.34, and 1.57 $m \cdot s^{-1}$) in random order. 3D positions of reflective markers on the heel and 3rd metatarsal of the left and right feet were collected during each trial. Expired air was also collected for the determination of C_w.

Data Analysis: Foot position for each step was defined as the average location of the midpoint of the heel and 3rd metatarsal markers during single leg support. SW was computed as the mediolateral distance between right and left feet during consecutive stance periods. SL was determined by multiplying the time between consecutive same foot heel strikes by walking velocity (Figure 1). Step width variability (SWV) and stride length variability (SLV) were defined as the standard deviation of 350 consecutive SW and SL values, respectively, at each speed. SW, SL, SWV, and SLV were normalized to leg length.

An approximation of the rate of energy cost was calculated using both $\dot{V}O_2$ and $\dot{V}CO_2$ [4]. This value was normalized to body weight and divided by walking speed yielding metabolic cost per distance traveled ($J \cdot kg^{-1} \cdot m^{-1}$).

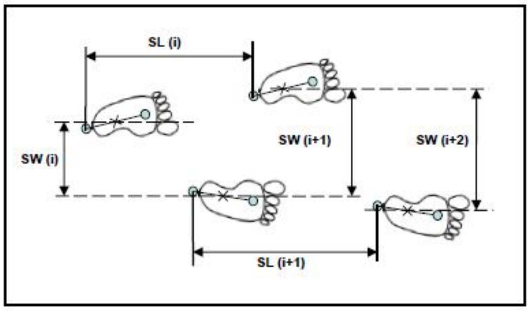

Figure 1: Example of stride width and stride length determination.

RESULTS

C_w was 23% higher for older adults with respect to young when averaged across walking speeds ($F_{1,26}$=29.86, p<0.001). No significant age effects were shown to exist on step width or stride length (SW: $F_{1,26}$=0.29, p=0.60; SL: $F_{1,26}$=0.39, p=0.54; Figure 2). Further, variability of both step width and stride length were also similar across age groups (SWV: $F_{1,26}$=0.79, p=0.38; SLV: $F_{1,26}$=0.03, p=0.87; Figure 3). When each of the four variables (SW, SL, SWV, and SLV) was correlated to C_w, few statistically significant relationships were observed.

DISCUSSION

Although older adults exhibited higher C_w when compared to young adults, SL, SW, SLV and SWV were all similar across age groups.

The lack of difference in kinematic variables is not entirely inconsistent with current literature, as results of studies looking at differences in step width variability between old and young adults have been equivocal. For example, Grabiner and colleagues [5,6] observed higher step width variability for older participants, whereas others [2,7] reported no age-related differences in step width variability.

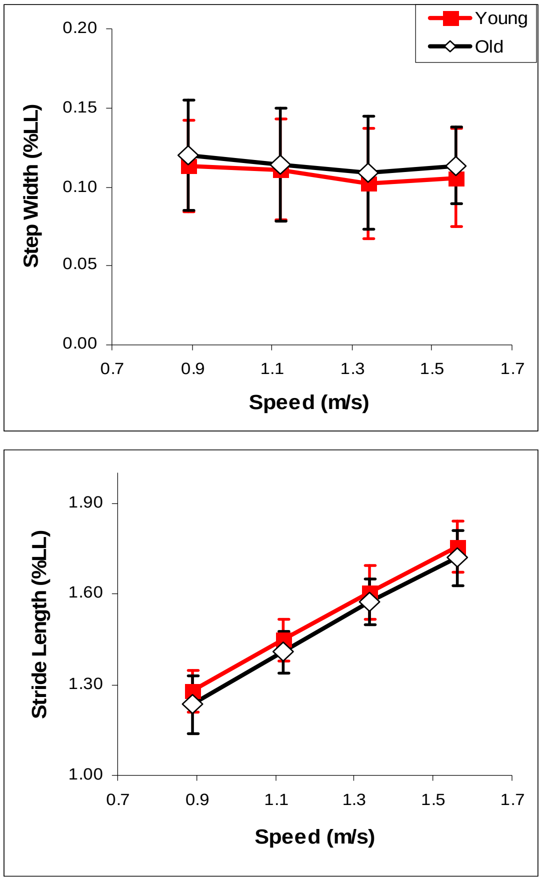

Figure 2: SW and SL across speeds in young and older adults.

Age effects on stride length variability have been equally mixed with studies showing both higher [2,6,7] and similar [5] variability in old with respect to young.

Though these studies generally give limited information on the physical activity levels of older and young participants, it is possible that health and physical activity status of subjects played a role in the discrepancy of their results. In the current study, older subjects were particularly active, participating in no less than three bouts of moderate physical activity per week. The high activity level of these older adults may have allowed them to retain kinematic profiles similar to younger adults.

CONCLUSION

Though C_w was higher in older adults in the current study with respect to young, step variability was similar for older and young participants. The lack of covariance of these variables across age groups, along with the limited relationships between step variability and C_w implies step variability does not reliably explain the higher C_w seen in healthy older adults.

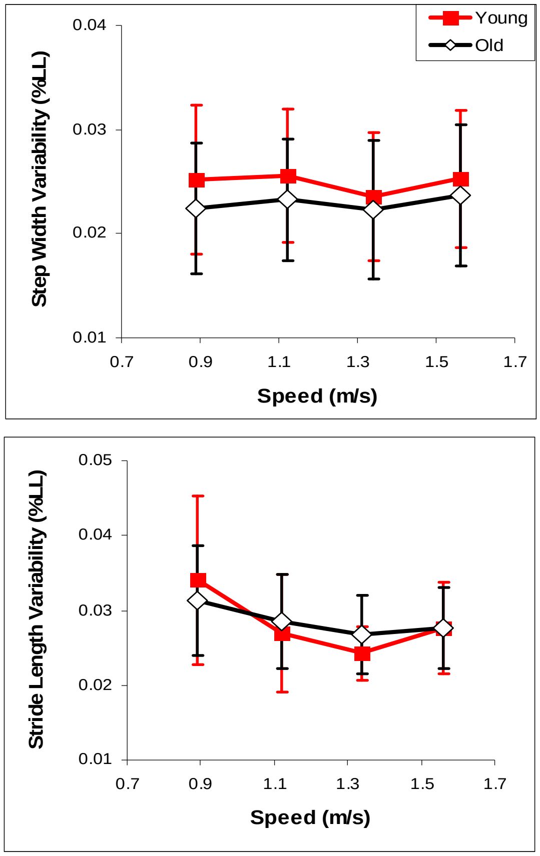

Figure 3: SW and SL variability across speeds in young and older adults.

REFERENCES

1. Mian OS et al. (2006). *Acta Physiol [Oxf]*. **186**(2):127-39.
2. Dean JC et al. (2007). *IEEE Trans Biomed Eng*. **54**(11):1919-26.
3. Donelan JM et al. (2001). *Proc Biol Sci*. **268**(1480):1985-92.
4. Brockway JM (1987). *Hum Nutr Clin Nutr*. **41**(6):463-71.
5. Owings TM & Grabiner MD (2004). *Gait Posture*. **20**(1):26-9.
6. Grabiner PC et al. (2001). *Arch Phys Med Rehabil*. **82**(1):31-5.
7. Kang HG & Dingwell JB (2007). *Gait Posture*. **27**(4):572-7.

Body Center of Pressure Control during Gait Initiation in Transtibial Amputees

Christopher Fink[1,2] Jasper T. Yen[1,3], Arick Auyang[1] and Young-Hui Chang[1,2,3]
[1]Comparative Neuromechanics Lab, School of Applied Physiology, Georgia Tech, Atlanta, GA, USA
[2]Prosthetics and Orthotics Program, School of Applied Physiology, Georgia Tech, Atlanta, GA, USA
[3]Bioengineering Program, Georgia Tech, Atlanta, GA, USA

INTRODUCTION

Gait initiation is an important activity of daily life and may even require a higher demand on the neuromuscular system than steady walking [1]. Each leg must transition from symmetrical function during stance into distinct roles of foot placement (lead limb) and body support (trailing limb) [2]. Although one can directly sense force under each foot, internal computations must be involved to sense a body center of pressure (COP), which usually lies outside of both areas of direct foot contact. This internal representation of body COP may be problematic for lower limb amputees due to the loss of sensorimotor control in the amputated leg. In particular, amputees often have difficulty with gait initiation [1].

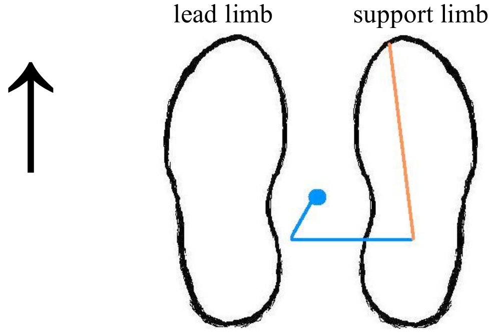

Fig 1. Schematic of stereotyped body COP movement during a normal gait initiation (non-amputee) showing double (blue) and single (orange) limb support.

We used an Uncontrolled Manifold (UCM) analysis [3] to study the consistency of body COP position resulting from the coordinated adjustments of force magnitudes and COP positions under each foot. Since we are only interested in how the body COP is affected by the combined control under both feet, we limited our study to the double limb support phase of gait initiation (Fig 1, blue). Just after double limb support, the trailing limb enters into a period of single limb support. This one-legged stance can be accomplished with a high degree of active balance (e.g., feedback control), or a high degree of dynamical predictability (e.g., feedforward control). We hypothesized that when a prosthesis is the trailing limb, unilateral amputees would stabilize body COP most at the end of double limb support to generate highly consistent and predictable dynamics prior to the ensuing single limb support on the prosthetic leg.

METHODS

Seven unilateral transtibial amputees (25-58 yrs, avg. 44.3 yrs) gave informed consent before participating in this study. All were in otherwise good health with no history of diabetes or vascular disease. During quiet stance, subjects were prompted in a randomized order to initiate gait with either their prosthetic leg or sound leg a particular leg (30 trials from each leg). We asked subjects to match the first step to a metronome beat with 150ms to first foot strike. We recorded foot base of support (Vicon) and ground reaction forces under each foot with 2 force plates (AMTI). Gait initiation began when static force changed by more than 32 N and double support ended when vertical force of trailing limb dropped to 32 N. Body COP position was calculated (MATLAB) from individual foot COP positions and magnitudes of force from each foot. Body COP positions were then time normalized to 100% of double support.

We derived a six parameter model for body COP position. We normalized 2 forces to body weight and 2 mediolateral (ML) and 2 anteroposterior (AP) COP positions to foot width and length, respectively.

We estimated the UCM (goal-equivalent task space) as the null space of the Jacobian relating the six parameters to body COP position. We ran the UCM analysis [see 3] at each 1% time slice for both performance variables: (i) ML position of the body COP; and (ii) AP position of body COP. We calculated Index of Motor Abundance (IMA) for each performance variable and limb leading condition. IMA>0 indicated subjects stabilized body COP position with coordinated adjustments of foot COP positions and forces [4,5].

RESULTS

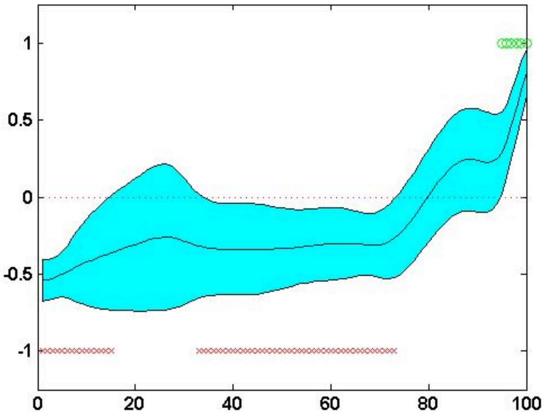

Fig 2. Mean IMA±SD for AP body COP position when leading with sound limb (N=7). IMA<0 (red x's) then switches to positive (green o's). N=7, $\alpha=0.05$.

UCM analysis revealed ML body COP position was stabilized ($p<0.05$) throughout double support with no effect of leading limb. For AP body COP position with sound limb leading, a long period of destabilization preceded stabilization at the end of double support (Fig 2-3). When the prosthesis led, AP body COP position was never stabilized.

DISCUSSION

ML body COP position was highly consistent over double support, without any effect of leading limb. This is not surprising considering since ML COP is highly sensitive to force magnitudes, which are easily controlled by both limbs.

Consistency of AP body COP position was highly dependent on lead limb. With sound limb leading, AP body COP position was highly consistent at the end of double support. This provides highly predictable dynamics for the subsequent single limb support by the prosthetic leg.

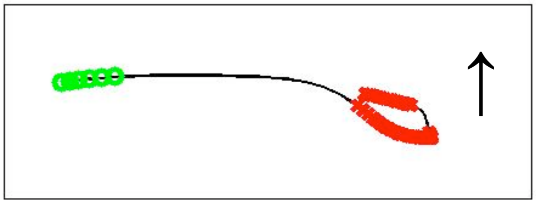

Fig 3. Representative double support phase of gait initiation. Sound (right) limb leading shows inconsistency (IMA<0, red) followed by highly consistent position (IMA>0, green). Arrow = AP movement direction.

Sensorimotor limitations in the prosthetic limb explain the need for stabilizing body COP movements at the end of double support. This creates predictable dynamics for one-legged stance on a prosthesis. When leading with prosthesis, single limb stance on the sound limb does not require predictable dynamics since there are no sensorimotor limitations to postural control. These findings may help guide training of recent amputees and future designs for actively controlled prostheses.

REFERENCES

1. Tokuno C, et al. *Gait and Posture.* **18**:158-169, 2003.
2. Vrieling A, et al. *Gait and Posture.* **27**:423-430, 2008
3. Scholz JP and Schöner G. *Exp Brain Res.* **126**: 289-306, 1999.
4. Auyang AG, Yen JT, and Chang YH. *Exp Brain Res.* **192**: 253-64, 2009.
5. Yen JT, Auyang AG, Chang YH. *Exp Brain Res*, accepted, 2009.

PIECEWISE LINEAR APPROXIMATION TO FILTER FORCE PLATE SIGNALS

Marco Cannella, Rupal Mehta and Sheri Silfies
Rehabilitation Sciences Reaserch Laboratory, Drexel University, Philadelphia PA
email: mc383@drexel.edu

INTRODUCTION

Variability in biological movement has been traditionally treated as random fluctuation and heavily filtered in the frequency domain. However Newell and Slifkin [1] revealed that the “variance of the movement dynamics is as reviling as the invariance in terms of unpaking the nature of the system organization”. Moreover the attempt to distinguish between deterministic and stochastic behavior of the postural sway has shown that the Center of Pressure (COP) time series is a typical nonstationary signal. This property of the signal limit the application of spectral techniques based on the Fourier transform [1].

We investigated the use of a Piecewise Linear Approximation (PWL) [2] to compensate for (a) the accuracy of the digital acquisition system and (b) for the threshold characteristic of the force plate in an attempt to preserve the stochastic characteristic of postural sway.

METHODS

Piecewise linear curves are often used to approximate complex boundary figures (sequence). Given a sequence f_n and a loss tolerance w, the PWL algorithm split the sequence into an upper ($f^+=f_n+w$) and lower ($f^-=f_n-w$) boundaries that define the error tunnel of the sequence f_n (figure 1).

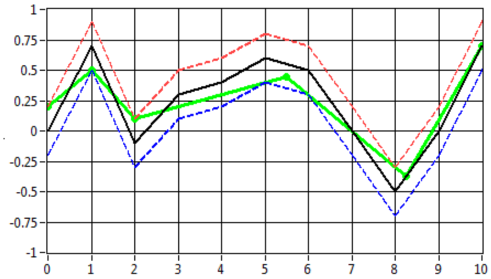

Figure 1: Piecewise Linear Approximation (green): original sequence (black), upper (red) and lower (blue) boundaries, .

Starting from one end of the tunnel the algorithm determines the longest single straight line within the boundary that approximate the sequence. The portion of the sequence approximated is deleted from the sequence itself and the algorithms starts again with the remaining portion of the sequence. This algorithm has been implemented in an OCCAM filter [4] to determine the strength of the noise in a deterministic signal. In compressing a noisy signal with a lossy compression algorithm, when the loss tolerance equals the strength of the noise the loss and the noise tend to cancel each other. The decompressed signal is the filtered signal [3]. OCCAM filter has been used in the present work to determine the strength of the noise (and consequently the tolerance w of the PWL approximation) produced by the digital acquisition system. To perform this analysis the force plate output was acquired with and without a 77kg weight (setup test). The result (figure 2) was found to be the same for both tests and all eight outputs of the force plate.

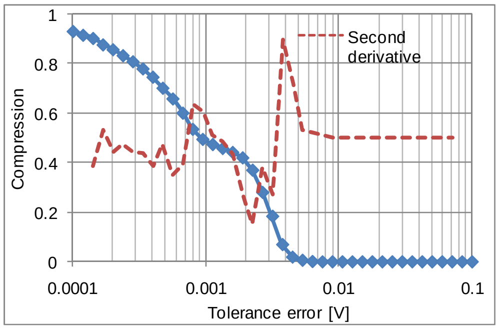

Figure 2: Compressed size versus allowed loss for the force plate output during the setup test. The peak of the second derivative (5mV) represents the loss that cancels the noise.

Postural sway of one of the author was acquired with a Kistler 9286AA force plate connected thought an external control unit (5233A2) to a NI PCI-6229 for digital acquisition. The eight outputs where filter at 500Hz, digitized at 3kHz (Raw Data). Three trials each of eyes open (EO) and eyes closed (EC) were collected for 60s. The eight channel were postprocessed with a PWL algorithm with the loss tolerance derived during the setup test (5mV). The result was multiplied by the respective sensitivity of the force plate to determine forces. Then the PWL was applied again to take into consideration the threshold of the force plate (0.125N for X and Y output and 0.25N for the Zs output).

For comparison with previously used method the same eight channels were filtered using a 33 points median filter and a 201 points mean filter (15Hz). Calculation of the COP was performed according to the Kistler's formulas spreadsheet. COP-based measures of postural steadiness were perform according to Prieto [4].

RESULTS AND DISCUSSION

Table 1 reports the results of COP-based measures with Eyes Open (EO) and Eyes Closed (EC) for the two different postprocessing of the force plate data.

Figure 3 shows a comparison between original output from the force plate, the filtered signal at 15Hz and the approach proposed with a Linear Piecewise Approximation.

CONCLUSIONS

The PWL within the amplitude domain offered similar performance to the commonly used digital filtering methods (median and mean filtering) with regard to commonly used parameter for describing postural sway.

However, better tuning of this technique with a recursive OCCAM filtering algorithm may reveal stochastic behavior of the COP trajectory and provide different information about motor behavior of the postural control system.

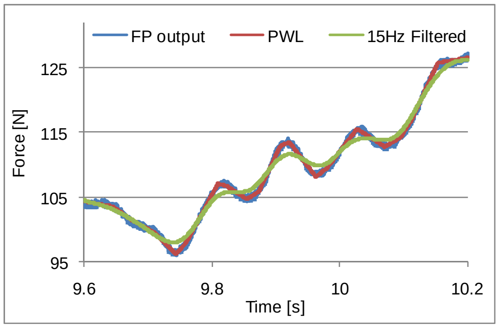

Figure 3: Original force plate signal (blue) filtered with a 15Hz mean filter (green) and approximated with a Piecewise Linear Algorithm (red).

REFERENCES

1. Riley M.A. and Turvey M.T. Journal of Motor Behaviour, 34(2), 99-125, 2002.
2. Imai H. and Iri M. Journal of Information Processing 9(3), 159-162, 1986.
3. Natarajan B.K. IEEE Transactions On Signal Processing 43(11), 2595-2605, 1995.
4. Prieto T.E. et Al. IEE Transaction On Biomedical Engineering, 43(9), 956-966, 1996.

Table 1: COP-based measures with Eyes Open (EO) and Eyes Closed (EC) for the two postprocessing techniques of quite standing force plate data along with results reported by Prieto (1996).

Measure	**15Hz Mean Filter**		**Piecewise**		***Prieto(1996)***	
	EO	**EC**	**EO**	**EC**	***EO(YA)***	***EC(YA)***
mean distance (mm)	3.07±0.92	3.04±0.40	3.06±0.92	3.04±0.40	*3.12±1.11*	*3.85±1.65*
mean distance ML (mm)	1.52±0.18	1.95±0.30	1.52±0.18	1.94±0.30	*1.5±0.77*	*1.66±0.95*
mean distance AP (mm)	2.39±1.01	1.93±0.22	2.38±1.02	1.93±0.22	*2.42±0.97*	*3.10±1.29*
rms distance (mm)	3.55±1.08	3.44±0.51	3.55±1.08	3.44±0.51	*3.56±1.20*	*4.39±1.81*
rms distance ML (mm)	1.96±0.21	2.45±0.45	1.95±0.21	2.45±0.45	*1.85±0.91*	*2.06±1.17*
rms distance AP (mm)	2.93±1.18	2.41±0.27	2.93±1.18	2.41±0.27	*2.95±1.08*	*3.82±1.54*
range (mm)	8.73±3.47	8.81±1.58	8.73±3.39	8.87±1.62	*14.3±4.34*	*18.0±7.14*
range ML (mm)	11.21±2.43	13.59±1.88	11.30±2.44	13.61±1.84	*8.48±3.89*	*9.79±5.42*
range AP (mm)	13.91±4.68	13.18±1.65	13.91±4.59	13.15±1.63	*13.3±4.27*	*17.7±6.97*
mean velocity (mm/s)	5.31±0.38	6.00±0.54	5.30±0.40	6.05±0.59	*6.90±1.79*	*8.89±2.86*
mean velocity ML (mm/s)	3.03±0.27	3.39±0.36	3.01±0.25	3.47±0.37	*3.82±1.19*	*4.43±1.65*
mean velocity AP (mm)	3.76±0.27	4.24±0.36	3.77±0.34	4.25±0.41	*4.92±1.34*	*6.72±2.18*
95% conf ellipse area (mm^2)	107±49	111±32	107±49	111±32	*99±66*	*162±140*

A COMPARISION OF LOWER EXTREMITY FATIGUE BETWEEN LEATHER AND RUBBER BOOTS IN PROFESSIONAL FIREFIGHTERS

Chip Wade[1], Ryan Garten[2], Scott Breloff [3], and Ed Acevedo[4]

[1]Department of Industrial and Systems Engineering, Auburn University, Auburn, AL, cwade1@auburn.edu
[2]Departments of Exercise and Sports Science, University of North Carolina Greensboro, Greensboro, NC.
[3]Univerisity of Oregon, Department of Human Physiology, Eugene, OR
[4]Departments of Health and Human Performance, Virginia Commonwealth University, Richmond, VA,

INTRODUCTION

Firefighters are confronted with a myriad of occupational challenges that increase the risk of injury and possibly death. These firefighting challenges are exacerbated by hazards (i.e., working on roofs, in smoky places, and on slippery surfaces) and the use of protective equipment (PPE), including fire-protective clothing and a self-contained breathing apparatus (SCBA). The National Fire Protection Association estimates that 80,800 firefighter injuries occurred in the line of duty in 2002. Results by type of duty indicate that 37,860 or 46.9% of all firefighter injuries in 2002 occurred during fire-ground operations. Overexertion and strain (32%), and falls, slips, and jumps (25.9 %) were the leading causes of fire-ground injuries (Karter AND Molis, 2003). The continuously changing work conditions, in association with increased physical exertion, require firefighters to maintain a high level of awareness and performance.

While all of the safety equipment and PPE provide for the welfare of the firefighter, a firefighter's boots play an equally critical role in working effectiveness and personal safety. The OSHA regulations and standards for appropriate foot and leg protection for fire brigades state that this must include either fully extended boots which provides protection for the legs or protective shoes or boots worn in combination with protective trousers. Firefighters use two types of boots that meet these requirements, a rubber boot and a leather boot. An argument can be made that although the rubber boot may provide greater protection from chemical hazards, the leather boot provides greater tactile sensitivity.

The purpose of this study is to examine changes in lower extremity fatigue in professional firefighters wearing rubber and leather boots participating in a fire simulation activity.

METHODS

Twelve professional firefighters (33 ± 6.8 years; height of 179 ± 6.47 cm; weight of 95.08 ± 21.47 kg), whom received, within the past 8 months a medical evaluation, including resting 12-lead EKG analysis, and clearance by a physician to participate in firefighting participated in this study. Each firefighter participated in two identical testing sessions [leather (5.37 ± 0.45 lbs) and rubber boots (6.45 ± 0.53 lbs)] on two separate days.

During each session, firefighters performed 2 sets of a three minute simulated firefighter stair climb wearing a 50 lb weighted vest to simulate their typical personal protective equipment, two 12.5 lb weights on the shoulders to simulate the weight of a high-rise pack (hose bundle), and a Vicon marker set (motion capture retro-reflective markers). The 12.5 lb weights were only worn during the stair climbs.

On each condition day (leather, rubber) the firefighter conducted 10 gait trials, followed by a balance assessment, followed by a seated MVC muscle fatigue test. Dependent measure for fatigue was torque production during the MVC seated test for: knee flexion/extension, and ankle plantar/dorsi flexion. The MVC procedure consisted of the firefighter conducting 2 sub-maximal contractions (at 50% of perceived maximal effort) prior to producing 3 repeated maximal contractions, on a CYBEX 6000 floor-based dynamometer. A 30-second break was given between MVC trials, with additional rest being provided during the change in dynamometer positioning for joint (ankle, knee) placement.

Following the initial testing protocol, the firefighter conducted a Simulated Firefighter Stair Climb (The Fire Service Joint Labor Management Wellness/Fitness Initiative - Candidate Physical Ability Test, 1999) for 3 minutes at a rate of 60 steps per/min. At the completion of the stair climb, the firefighter repeated the gait, balance, and MVC fatigue procedure. Following a 3 minute rest period, the complete procedure (gait, balance, MVC, stair climb) was repeated. A total of 3 cycles were completed.

RESULTS AND DISCUSSION

A series of repeated measures ANOVA analyses revealed a statistically significant between boots difference(s) for all MVC fatigue measures over time (Figure 1).

CONCLUSIONS

In general, while lower extremity muscle fatigue increases over time for both boot types, the results suggested that the leather boots contribute less to an increase in fatigue than that of the rubber. These findings have practical implications in the firefighting occupation when developing a safety and personal protective strategy. The implications lead to an assumption that given the varying degrees of advantages and disadvantages of each type of boot, the leather boot may have an advantage over rubber to a decrease in performance due to fatigue.

REFERENCES

Karter MJ. and Molis JL. (2003). NFPA Journal, Nov/Dec, 66-67.

Kincl et al. (2002). *Applied Occupational & Environmental Hygiene*, 17, 4, 256-266.

Figure 1. Lower extremity muscle fatigue (MVC) comparison between leather and rubber boots

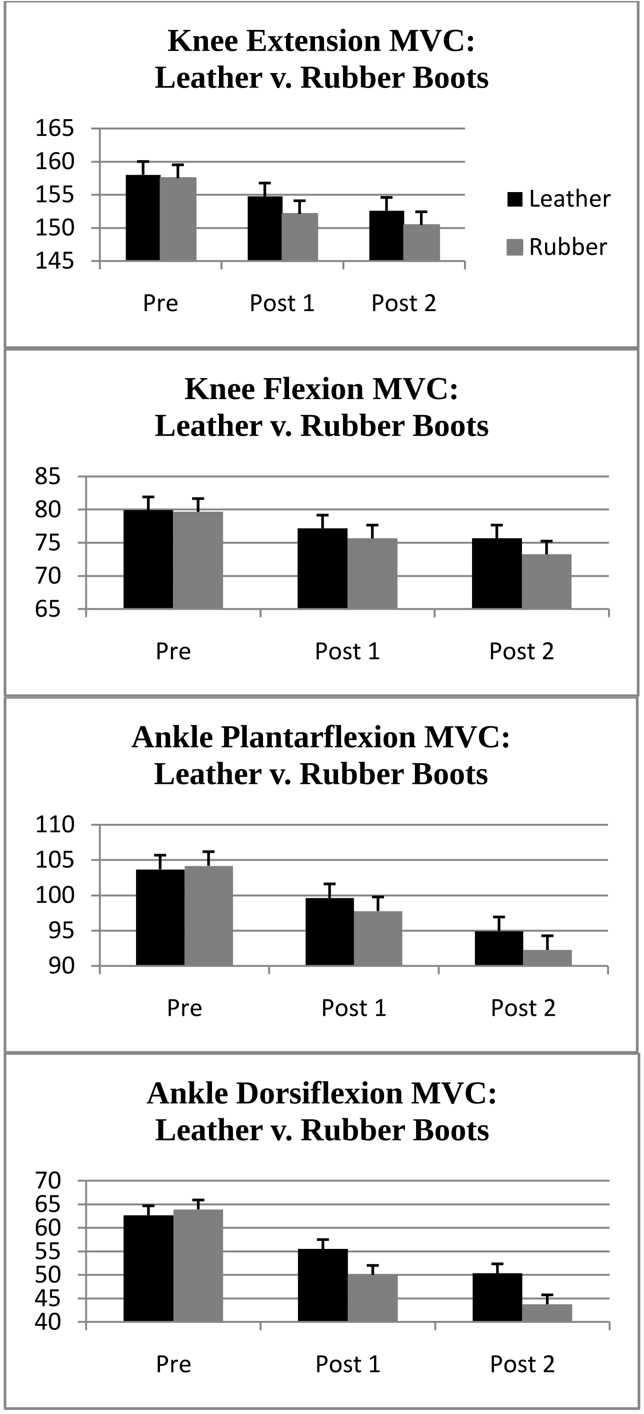

MECHANICS OF UNILATERAL TRANS-TIBIAL AMPUTEE SPRINT RUNNERS

[1]Alena Grabowski, [2]Craig McGowan, [1]Hugh Herr, [3]William McDermott and [4]Rodger Kram.
[1]Massachusetts Institute of Technology, [2]University of Texas, Austin, [3]The Orthopedic Specialty Hospital, Salt Lake City, UT, [4]University of Colorado, Boulder
email: alenag@mit.edu

INTRODUCTION

Over the range of sprint running distances (60-400m), a combination of energetics, muscular power, ground force generation, and fatigue resistance all influence performance. Absolute top speeds over short distances are primarily influenced by changes in contact length, step frequency, and force generation [1]. In general, previous research has shown that the ability to generate vertical force limits top speeds in humans with intact limbs [1, 2].

Running specific prostheses have been designed to mimic the spring-like behavior of biological limbs during running. Limited research exists that has examined the mechanical means by which amputees achieve top speeds [3-5]. Data from an elite bilateral amputee, using running-specific prostheses, show that he achieves top speeds using different mechanical means than intact sprinters [4, 5]. Specifically, at top speed his stance average vertical ground reaction forces are much lower and swing times are much faster than those of performance-matched intact sprinters [4]. The magnitude of force generation may be limited by the stiffness of running-specific prostheses. Additionally, faster swing times may result from the lighter mass of the combined residual leg plus prosthesis compared to an intact leg.

To better understand how running-specific prostheses affect biomechanics during sprinting, we measured the ground reaction forces (GRFs) and stride kinematics of unilateral trans-tibial amputee sprinters over a range of speeds up to top speed. To investigate whether prosthesis mass limits top speed, we also added mass to the prosthesis. We chose to study unilateral amputees because they provide unique insight since each amputee's intact leg serves as a control for comparing variables of interest between the intact leg and the residual plus prosthetic leg.

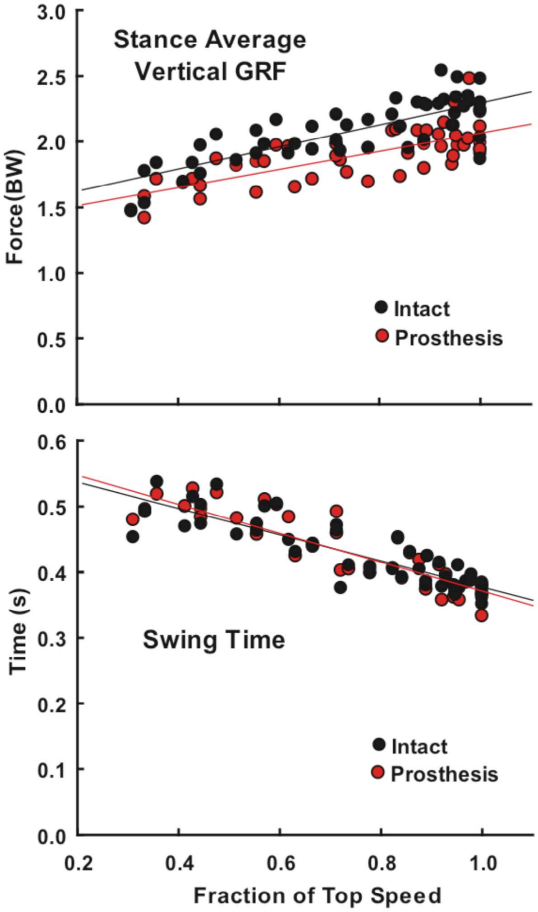

Figure 1. Stance average vertical GRFs ($R^2 = 0.55$, 0.62 for prosthesis and intact, respectively) and swing times ($R^2 = 0.80$, 0.77) for prosthetic versus intact limbs across speed, normalized to top speed.

We hypothesized that 1) stance average vertical GRFs would be greater and leg swing times would be longer for the intact compared to the prosthetic leg, and 2) adding mass to the prosthesis would not change stance average vertical GRFs, but would increase swing times of the prosthetic leg during sprinting.

METHODS

Six healthy unilateral trans-tibial amputee elite Paralympic sprinters (4 M, 2 F) participated and gave informed written consent according to the

Intermountain Healthcare IRB approved protocol. All experiments were conducted at the Biomechanics Laboratory of the Orthopedic Specialty Hospital.

After a 5-10 minute warm up, subjects performed a series of discontinuous constant speed running trials on a custom-built, high-speed, 3D force sensing motorized treadmill (Athletic Republic, Park City, UT). Each trial consisted of a short running bout that included at least 10 strides. Subjects began each series of trials at 3 m/s. We increased speed incrementally by 1 m/s until subjects approached their top speed. Then we increased speed in smaller increments until subjects reached their top speed, which was determined as the speed at which the subject put forth a maximal effort but could not maintain his/her position on the treadmill. Subjects were given as much time between trials as needed for full recovery. Subjects completed two additional top speed trials with masses of 100 and 300 grams added to their prosthesis. We increased mass by securing thin strips of lead distally to the blade of the prosthesis.

We collected ground reaction forces at 1600 Hz during all trials and filtered the data with a critically damped filter implemented using Visual 3D software. Using a custom Matlab program, we detected the instants of touch-down and toe-off using a 40 N threshold, and determined average vertical ground reaction force, contact length, swing time, aerial time, and step frequency from 10 consecutive steps on both the intact and prosthetic legs. Then we compared intact versus prosthetic leg variables using repeated-measures ANOVAs with Tukey HSD follow-up tests ($p<0.05$).

RESULTS AND DISCUSSION

We found that stance average vertical GRFs were 15% lower in the prosthetic leg compared to the intact leg across speed (Figure 1) and were significantly lower in the prosthetic leg compared to the intact leg at top speed (Table 1). However, swing times were not significantly different between prosthetic and intact legs across speed and at top speed (Figure 1, Table 1).

Top speed was not significantly affected by the addition of 100 or 300g to the prosthesis. Similar to our top speed results without added mass, subject's stance average vertical GRF's were significantly greater in the intact versus prosthetic legs, yet swing times were not different between legs at top speed with 100 or 300g (Table 1). The discrepancy in GRFs was larger with added mass on the prosthesis than without added mass.

Similar to previous studies, our results infer that running-specific prostheses limit the amount of force that can be generated at top speeds. Because swing times were not different between legs in unilateral trans-tibial amputee sprinters, they likely overcame the force deficiency in their prosthetic leg by significantly increasing step frequency in their intact leg to achieve top speeds (Table 1).

Future studies are warranted to examine the mechanisms underlying the mechanical differences, and the influence that mechanical differences have on sprint-running performance.

REFERENCES

1. Weyand PG, et al. *J Appl Physiol* **89,** 1991-1999, 2000.
2. Usherwood JR and Wilson AM. *Nature* **438**, 753-754, 2005.
3. Buckley JG. *Clin Biomech* **15,** 352-358, 2000.
4. Weyand PG et al. *J Appl Physiol* In Press, 2009.
5. Bruggemann G-P et al. *Sports Technol* **1,** 220-227, 2008.

ACKNOWLEDGEMENTS

The authors wish to thank Stephanie Koenig, Steve Swanson, and the Orthopedic Specialty Hospital.

Table 1: Stance average vertical GRF (vGRF), contact length (L_c), swing time (t_{sw}), aerial time (t_a), and step frequency (StepF) at top speeds for intact and prosthetic (Pros) legs with and without 300g added to the prosthesis. Data are Means ± SD. t_a is the time following each limb's stance phase. * indicates a significant difference between legs ($p<0.05$).

Condition	Leg	vGRF (BW)	L_c (m)	t_{sw} (s)	t_a (s)	StepF
Top Speed	Intact	2.19 ± 0.21	0.998 ± 0.095	0.370 ± 0.012	0.118 ± 0.007	4.31 ± 0.27
(8.8 ± 1.3 m/s)	Pros	2.02 ± 0.12*	1.039 ± 0.071	0.365 ± 0.017	0.133 ± 0.014	3.98 ± 0.18*
Top Speed, 300g	Intact	2.22 ± 0.23	1.016 ± 0.092	0.381 ± 0.004	0.127 ± 0.009	4.04 ± 0.19
(8.5 ± 0.9 m/s)	Pros	1.96 ± 0.15*	1.047 ± 0.088	0.378 ± 0.011	0.128 ± 0.012	3.96 ± 0.13

THE INFLUENCE OF PELVIC CONTROL ON RUNNING MECHANICS

Steve Jamison and Ajit Chaudhari
The Ohio State University
email: chaudhari.2@osu.edu, web: http://sportsmedicine.osu.edu

INTRODUCTION

It has been estimated that 74% of runners will experience an over-use running injury over the course of a season [1]. Despite this fact, running has grown in popularity in recent years, evidenced by increased numbers of running events, running clubs, and prevalence in the media.

Core strength and core stability have also received increased attention from coaches, trainers, therapists, physicians and researchers in recent years. Both strength and stability of the core appear to partially predict lower extremity injuries in athletes [2, 3], though the biomechanical link between core strength & stability and lower extremity injury remains unclear.

One potentially useful gauge of an individual's core stability is pelvic positional control while in a standing position. The purpose of this study was to test the hypothesis that decreased pelvic control during standing would correlate with biomechanical loadings that have previously been related to running over-use injuries.

METHODS

14 subjects (11 female, height=1.71±0.07m, mass=61.8±9.5kg) participated in this study after providing IRB approved informed consent. Each subject's pelvic positional control was measured using the LevelBelt device (patent pending). This device measures the angle of the pelvis in the medial-lateral (M/L) and anterior-posterior (A/P) directions while the subject transitions from a double leg stance to a single leg stance and back. The range of motion of the pelvis during this activity was used to quantify core stability while in a functional position. The test was done once for each leg, and the ranges of motion for the two legs were averaged.

Table 1: Correlations between medial/lateral LevelBelt score and biomechanical variables.

	R	*P*
Speed [m/s]	0.14	0.641
Peak Tibial Internal Rotation [deg]	0.66	0.010*
Peak Hip Adduction Angle [deg]	-0.67	0.008*
Hip Adduction Impulse [%bwh-s]	-0.49	0.075
Mean Resultant Knee Adduction Moment [%bwh]	0.50	0.071
Vertical GRF [%bw]	0.57	0.034*
Stance Width [%h]	0.62	0.017*

* significant (p<0.05) correlations

Biomechanical loadings during continuous overground running at a comfortable self-selected speed were determined in a motion capture laboratory (12.5m x 22m) with two Bertec 4060-10 force plates embedded in the floor and 8 Vicon MX-F40 cameras. A full-body marker set combining Plug-In-Gait for upper body [Vicon Motion Systems] and the Point-Cluster Technique for lower body [4] was used. Vicon BodyBuilder and custom Matlab scripts were used to calculate kinematics and kinetics during running.

Peak tibial internal rotation angle, peak hip adduction angle, hip adduction impulse, mean resultant knee adduction moments, and peak vertical ground reaction force were calculated for analysis. Hip adduction impulse was calculated as the integral of hip adduction moment over the stance phase (disregarding time points in which hip abduction moments were present). 3 trials were collected for each leg, and the biomechanical values for all trials with usable data were averaged.

Stance width during running was also calculated by determining the combined perpendicular distance between the lateral malleolus marker of each foot at foot strike to the line of forward progression.

Correlation coefficients and their statistical significance were calculated for each biomechanical loading parameter. Since this was a pilot study, no correction for multiple comparison was applied and a significance level of $\alpha=0.05$ was used.

RESULTS AND DISCUSSION

Several significant correlations were observed between M/L LevelBelt score and relevant biomechanical loading parameters (Table 1). Some were positive, including peak tibial internal rotation and peak vertical ground reaction force, indicating that increased pelvic positional control (i.e. lower M/L LevelBelt score) is related to reduced biomechanical risk for iliotibial band syndrome [5] and tibial stress fractures [6], respectively. However, peak hip adduction angle showed a significant negative correlation, indicating that increased pelvic positional control may be related to increased biomechanical risk for iliotibial band syndrome [5].

The correlation between M/L LevelBelt score and hip adduction impulse showed a trend towards a negative relationship, which would suggest that an increase in pelvic control (i.e. lower M/L LevelBelt score) results in increased biomechanical risk for iliotibial band syndrome [7]. On the other hand, the correlation between M/L LevelBelt score and mean resultant knee adduction moment showed a trend towards a positive relationship, which would suggest that an increase in pelvic control results in decreased biomechanical risk for patellofemoral pain [8].

As a possible explanation for the differences in biomechanics between those who have better pelvic positional control and those with worse pelvic positional control, we examined step width. As shown in Table 1, a significant positive correlation was observed between M/L LevelBelt score and stance width. This result suggests that those with worse pelvic positional control compensate by running with a wider stance.

One of the biggest limitations of this study is the difference in self-selected running speed between participants. The average speed of the group was 2.88±0.33m/s. While a self-selected speed was chosen to allow subjects to run as close to normally as possible, this may have created larger variation in the biomechanical loading parameters due to the known high correlation between moments and running speed. However, it is important to note that M/L LevelBelt score did not correlate with running speed (R=0.14), so pelvic control and speed may be independent factors influencing biomechanical loading during running.

CONCLUSIONS

The results of this study indicate a relationship between one measure of core stability, pelvic positional control, and biomechanical loading parameters that affect the risk of tibial stress fractures, patellofemoral pain, and iliotibial band syndrome. Future work in this area may provide additional scientific evidence for injury prevention programs to implement focused core stability training to prevent these injuries.

REFERENCES

1. MacMahon JM, et al. *XIX International Symposium on Biomechanics in Sports*. 2001.
2. Leetun DT, et al. *Medicine & Science in Sports & Exercise*, 2004. **36**(6): p. 926-934.
3. Zazulak BT, et al. *American Journal of Sports Medicine*, 2007. **35**(7): p. 1123-1130.
4. Andriacchi TP, et al. *Journal of Biomechanical Engineering*, 1998. **120**(6): p. 743-749.
5. Noehren, B, et al. *Clinical Biomechanics*, 2007. **22**(9): p. 951-956.
6. Grimston SK, et al. *International Journal of Sport Biomechanics*, 1991. **7**(3)p. 292-302.
7. MacMahon, JM, et al. *XVIII International Symposium on Biomechanics in Sports*. 2000.
8. Stefanyshyn, DJ, et al, *American Journal of Sports Medicine*, 2006. **34**(11): p. 1844-1851.

ACKNOWLEDGEMENTS

Funding for this study came from the Ohio State University Sports Medicine Internal Grants Program. Special thanks go to Chris McKenzie for his role in development of the LevelBelt & data interpretation and to Christine Glendon for her assistance with data processing.

RELIABILITY AND REPEATABILITY OF SELF-SELECTED WHEELCHAIR TRANSFER TECHNIQUES

[1,2]Yen-Sheng Lin, [1,2]Alicia M. Koontz and [1,2]Padmaja Kankipati
[1]Human Engineering Research Laboratories, Department of Veterans Affairs, Pittsburgh, PA
[2]Department of Rehabilitation Science and Technology, University of Pittsburgh, Pittsburgh, PA

INTRODUCTION

Individuals with spinal cord injury (SCI) rely heavily on their upper extremities (UE's) for activities of daily living such as wheelchair propulsion (WP), pressure reliefs, and transfers. The overuse of the upper limbs results in a high incidence of pain. The ability to transfer independently is key in maintaining functional independence. Extensive UE studies during WP have been published [1]; however very few studies have focused on UE biomechanics during transfers from a wheelchair to other surfaces. More recently, Gagnon et al. [2] reported 3D movement patterns of UE during level and non-level transfers. The data from Gagnon et al.'s study as well as our previous studies [3] indicates that the between-subject variability among SCI subjects is very large. This variability may be due to a number of factors such as upper limb strength, trunk balance, anthropometry (e.g., limb length, weight, etc.), and experience with transfers. These factors may also affect the intra-subject variability or in other words the ability of the subject to perform the same transfer, in the same way, each time to prevent the potential injuries caused by non-reproducible transfer. The purpose of this study was 1) to determine the intra-subject reliability of shoulder kinematics as well as hand reaction forces for self-selected transfer techniques between a homogenous group of unimpaired subjects (control subjects) and wheelchair users with SCI (case subjects); 2) compare movement strategies between the impaired and unimpaired groups;

METHODS

Subjects: Five men with paraplegia (age 40.02± 13.41 years old, weight 77.11±16.32 kg, level of injuries T4-L1) and thirteen unimpaired subjects (4 men/1 women, age 26.00±4.30 years old, weight 77.81±12.58 kg) provided informed consent for this study. The inclusion criteria of SCI subjects were C4 level or below that occurred over one year prior to the start of this study and able to transfer to/from a manual wheelchair independently, without self-reported pain or injury of UE that interferes with their ability to transfer.

Experimentation: A 7-camera 3D motion capture system (ViconPeak, Lake Forest, CA) measured the position of reflective markers placed on the back, chest, humerus, and forearm during the transfers. The cameras were positioned around a platform shown in Figure 1 that contains two force plates (Bertec Corporation, Columbus, OH) and a force sensing beam. All transfers began with the left arm on the bench and right arm on the force beam. Participants with SCI used their own wheelchair in the study. The case and control subjects were instructed to perform a lateral transfer from the wheelchair to the adjacent level tub bench; however the control subjects were required to refrain from using leg muscles during the transfers. Each transfer was performed five times.

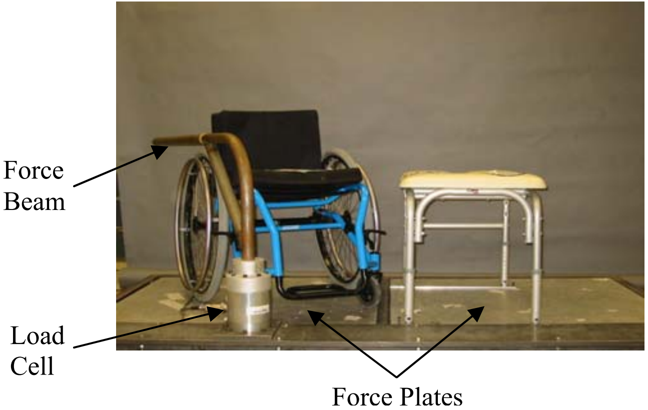

Figure 1: Experimental setup

Data Analysis: shoulder joint coordinate systems were based on the ISB recommendation for human joint motion. The shoulder flexion/extension and abduction and vertical reaction force were identified as outcome variables in each transfer trial. The maximum and minimum angles as well as peak vertical force were averaged over five trials for leading arm (i.e. arm reaching to new surface) and trailing arm (i.e. arm behind during move to new location) separately.

Statistical Analysis: The outcomes of intra-subject reliability were evaluated by intraclass correlation coefficients (ICC). ICCs were computed for each variable for both groups for varying number of trials (2, 3, 4 and 5 trials). A threshold parameter was considered reliable if ICC was larger than 0.6. The Mann-Whitney U non-parametric test was used for the comparisons between case and control groups. The level of significance was set at 0.05.

RESULTS AND DISCUSSION

Maximum extension angle of the trailing shoulder was found to be significantly lower for the case compared to the control group (p=0.01).This parameter was also found to be highly reliable in the case group (ICC=0.94) more than the control group (ICC=0.54) (Table 1). The possible scenario is that the force beam grabbed by trailing arm played a similar role with the hand rest in experienced SCI wheelchair users during transfer. The SCI subjects use the strategy with smaller trailing shoulder flexion angle to reduce the flexion moment known as a high risk factor to induce the shoulder impingement. Furthermore, the trailing arm forces showed the best reliability in both groups (Table 2) likely because the hand/arm is typically positioned closer to the body and slightly distal to the hip whereas more variation in leading hand placement is observed, that the maximum abduction of leading shoulder showed large variance in both groups. From the reliability analysis we found that similar intra-subject reliability over the threshold set initially was found for a large majority of variables (Table 1). The negative ICC value shown in the initial trials may be due to the limited sample considered in this study [4]. This study presented the reliability and repeatability analyses of leading and trailing as well as the comparison of SCI and control subjects. Future studies that include the shoulder joint loads are necessary to confirm this finding. More participants in SCI and control groups need to be considered to verify the reliability of transfer strategies.

REFERENCES

1. Cooper, R.A. et al. *American Journal of Physical Medicine & Rehabilitation*, 78(5), 435-446, 1999.
2. Gagnon, D. et al. *Clinical Biomechanics*, 23, 279-290, 2008.
3. Kankipati, P. et al. *Proceedings of the RESNA 2008 Annual Conference*, Arlington, VA, June 26-30, , 2008, CD-ROM.
4. Varnell, S.P. et al. *American Journal of Public Health*, 94(3), 393-399, 2004

ACKNOWLEDGEMENTS

Funding for this study was provided by the VA Rehabilitation Research R&D Services and the National Institute on Disability and Rehabilitation Research and the National Institute of Health, Center for Injury Research Control (VA-RR&D E3589V and B3079R NIDRR H133A011107, NIH R49/CCR310285-06).

Table 1. (Mean±SD) angle measured at the shoulder joints as well as intra-subject correlation coefficients (ICC) ranges, shown below the group averages, from the wheelchair to a target instrumented bench. (ǂ $p<.05$)

	SCI(N=5)		**Control(N=13)**	
	Leading UE	**Trailing UE**	**Leading UE**	**Trailing UE**
Shoulder				
Max Flexion	*53.73±12.69*	*44.70±4.86* ǂ	*46.33±9.26*	*50.77±8.51* ǂ
ICC range	*0.83-0.95*	*0.58-0.91*	*0.66-0.83*	*0.81-0.93*
Min Flexion	*28.90±5.89*	*23.01±6.57* ǂ	*14.11±6.99*	*30.24±10.27* ǂ
ICC range	*-0.06-0.59*	*0.83-0.97*	*0.49-0.85*	*0.87-0.96*
Max Abduction	*81.68±57.40*	*154.29±13.95*	*88.17±60.07*	*146.71±17.30*
ICC range	*0.40-0.95*	*-0.25-0.70*	*-0.28-0.31*	*0.75-0.93*

Table 2. Mean of peak reaction force (vertical component) as well as individually ICC ranges measured at the leading and trailing arms from wheelchair to a target instrumented bench in 5 trials.

	SCI (N=5)		**Control (N=13)**	
	Leading Arm	**Trailing Arm**	**Leading Arm**	**Trailing Arm**
Vertical				
Peak force ± SD (% BW)	*46.14±8.66*	*37.37±8.95*	*45.09±13.84*	*30.37±14.27*
ICC range	*0.91-0.96*	*0.98-0.99*	*0.61-0.92*	*0.99-1.00*

CONSISTENT HOPPING PERFORMANCE THROUGH DIFFERENT JOINT-LEVEL STRATEGIES

[1]Jasper Yen and [1,2]Young-Hui Chang
[1]Dept. of Biomedical Engineering, [2]School of Applied Physiology, Georgia Tech, Atlanta, GA, USA
email: jaspery@gatech.edu, web: http://www.ap.gatech.edu/Chang/Lab/CNLhome.html

INTRODUCTION

Cycle-to-cycle variability is an inherent aspect of locomotion. How is variability at the joint level organized to minimize variability at the task level of locomotion, such as variability of the ground reaction force? As suggested by [1], the following are three joint-level strategies that can minimize task-level variance (TASKV):

1.) Reduce total variance (TOTV) across all joints. This corresponds to overall noise reduction.
2.) Reduce only the fraction of overall noise that affects task variance, i.e. the task-relevant fraction (RELV). With redundant joints, there can be a fraction of overall noise that does not affect task variance [1, 2].
3.) Reduce sensitivity (SENS) of task variance to the task-relevant fraction of overall noise. In the case of joint torques acting on ground reaction forces, this may involve changing leg posture.

In a previous Uncontrolled Manifold study, we showed that to minimize variance of the vertical force generated against the ground, the task-relevant fraction of joint torque variance was minimized during human hopping in place at the preferred frequency [3]. Hopping was chosen because it represents a minimal locomotor paradigm with known task goals [4]. In this current study, we examined the three strategies of joint torque variance and how their roles changed when the task was constrained by increases in hopping frequency. We reasoned that the shorter ground contact times at faster hopping frequencies would influence the neuromechanical strategy and joint-level variance.

We hypothesized that different joint-level strategies would be used to maintain hopping performance across frequencies. That is, variance of vertical force impulse would remain constant across frequencies through compensatory changes in the variances and sensitivities of joint torque impulses.

METHODS

10 healthy subjects (ages 21 to 35 years) hopped on their right leg following the beat of an audible metronome set at 2.2, 2.8, and 3.2 Hz. For each hopping frequency condition, sagittal plane ankle, knee, and hip joint torques were calculated from kinematics and ground reaction forces in three 30-second trials recorded by a motion capture system (Vicon, UK; sampling rate 120 Hz) and a force plate (AMTI, USA; sampling rate 1080 Hz). Approximately 160 hops were analyzed for each subject and frequency condition.

During steady-state hopping, hop height is consistent from hop to hop [3], and subjects must generate a vertical force impulse against the ground equal to body weight divided by frequency. Force impulse variance must be minimized to keep a constant frequency. A 1-by-3 matrix (M) that maps ankle, knee, and hip joint torque impulses (τ) to vertical force impulse (F) was estimated [3].

$$F \approx M \times \tau^T \qquad (1)$$

For each subject and frequency condition, the joint torque impulse covariance matrix (C) was computed, and the trace of C is the total joint torque impulse variance (TOTV). The torque impulse variance that affected F variance is

$$\mathrm{NGEV} = M \times C \times M^T / (M \times M^T). \qquad (2)$$

The torque impulse variance that did not affect F variance per degree of freedom (GEV) is

$$\mathrm{GEV} = N \times C \times N^T / 2, \qquad (3)$$

where N is the 2-dimensional orthonormal null space of M. The fraction of TOTV that affected F variance is

$$\mathrm{RELV} = \mathrm{NGEV} / \mathrm{TOTV}. \qquad (4)$$

The sensitivity of F variance to RELV is

$$\mathrm{SENS} = \|M\|^2. \qquad (5)$$

We verified that force impulse variance (TASKV) was approximately equal to

$$\mathrm{TASKV} \approx \mathrm{TOTV} \times \mathrm{RELV} \times \mathrm{SENS} \qquad (6)$$

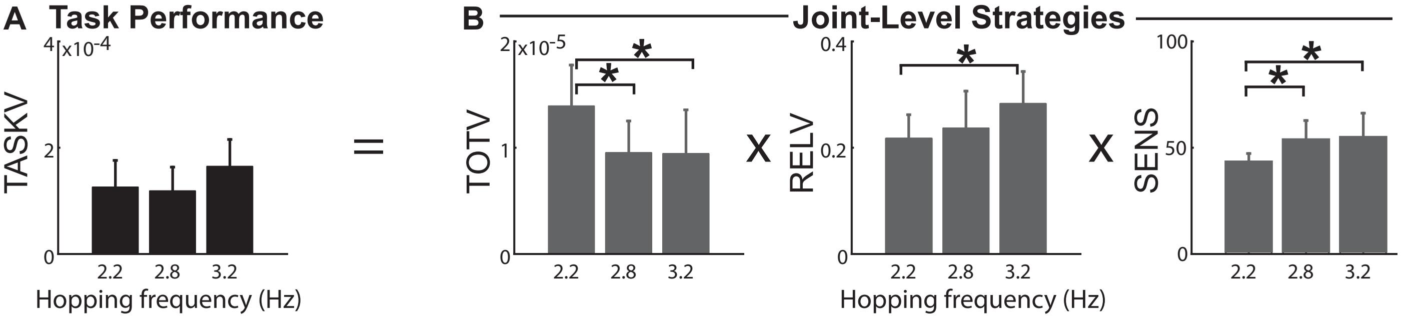

Figure 1: Normalized across-subject averages of force impulse variance (**TASKV**), total joint torque impulse variance (**TOTV**), force impulse-relevant fraction of TOTV (**RELV**), and force impulse sensitivity to RELV (**SENS**). TASKV = TOTV × RELV × SENS. TASKV did not change significantly across frequencies ($p > 0.05$) even though TOT, RELV and SENSV changed significantly across frequencies ($p < 0.001$).

RESULTS AND DISCUSSION

Task-level performance was consistent across hopping frequencies. There was no frequency effect on vertical force impulse variance (Fig. 1A, $p > 0.05$).

Even though task-level variance was consistent across hopping frequencies, variance at the joint-level changed. As hopping frequency increased, total torque impulse variance (TOTV) decreased, the force impulse-relevant fraction of total torque impulse variance (RELV) increased, and sensitivity of force impulse variance to joint variance (SENS) increased ($p < 0.001$, Fig. 1B).

The majority of the increase in sensitivity to torque impulse variance as frequency increased was an increase in ankle sensitivity (35±3 at 2.2 Hz; 48±9 at 3.2 Hz). This was a result of the more extended leg posture adopted at higher frequencies. Even though the torque impulse variance that affected force impulse variance (NGEV) was relatively small for all frequencies (Fig. 2), the force impulse-relevant fraction (RELV) increased with frequency. This may be a result of a decreased ability to structure torque impulse variance to maintain force impulse. To counteract the increases in sensitivity and force impulse-relevant fraction, total joint torque impulse variance (TOTV) was reduced. This reduction in overall noise may have been accomplished through co-contraction, as evidenced by higher joint stiffness values reported in other studies [4].

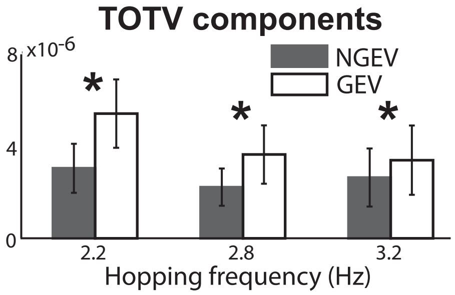

Figure 2: Normalized across-subject averages at each frequency condition of force-relevant (NGEV) and force-irrelevant (GEV) torque impulse variance. GEV was significantly greater than NGEV for all frequencies ($p < 0.05$).

CONCLUSIONS

We have shown that the human locomotor system changes its joint-level control strategies to preserve performance in response to an applied task constraint. The human locomotor system appears to have redundant strategies for achieving consistent performance, which are differentially and appropriately accessed depending on the conditions of the locomotor task. This may provide important insights for pathological gait when one or more of these joint-level strategies become hindered and the remaining strategies are more heavily relied upon to reduce gait variability.

REFERENCES

1. Cusumano JP, Cesari P. *Biol Cybern* **94**, 367-379, 2006.
2. Latash ML, et al. *Exerc Sport Sci Rev* **30**, 26-31, 2002.
3. Yen JT, et. al. *Exp Brain Res*, accepted, 2009.
4. Farley CT, et al. *J Appl Physiol* **71**, 2127-32, 1991.

ACKNOWLEDGEMENTS

The authors thank Arick Auyang for obtaining a portion of the data used in this study.

HYPOTHESIS TEST AND REJECTION IN EVOLUTIONARY BIOMECHANICS: RECONSTRUCTION OF BODY SIZE (STATURE AND MASS) IN LB1 FROM FLORES INDONESIA

Alex Weller, Adam J. Kuperavage, and Robert B. Eckhardt
Laboratory for the Comparative Study of Morphology, Mechanics and Molecules
Department of Kinesiology, The Pennsylvania State University, University Park, PA, 16802 USA
email: eyl@psu.edu

INTRODUCTION

The importance of size (stature and mass) required for motion in earlier human populations has been documented [1]. Mindful of the importance of such functional measures, previously our research group [2,3] challenged the hypothesis that specimen LB1, representing a sample of skeletons discovered on the 14,200 km^2 island of Flores, Indonesia, had been reconstructed convincingly as the holotype of a new human species, "Homo floresiensis." Among the features that had been used to support creation of this new taxon, and to distinguish it from other contemporaneous human populations, were some dimensions that are extreme, notably an endocranial volume of 380 ml and a stature of 106 cm. Here we test the null hypothesis that these values for brain size and body size accurately and necessarily characterize a new human species.

METHODS

Two sources of data were used in this study: 1) recently published stature and endocranial volume estimates for a series of skeletons (dated to a range of 940 to 2890 years bp) discovered at various sites on the small, rocky islands of Palau, a Pacific island group in Micronesia, northeast of Flores [4,5], and 2) our own independent estimates of the statures of limb bones based on the published dimensions (checked through our own direct studies of these specimens) of LB1 and LB8 from Flores, Indonesia. We used previously published regression equations derived from several series of recent human populations characterized by short statures [2].

RESULTS AND DISCUSSION

The recently published stature estimates [4,5] based on the Palau skeletal specimens range from 94 cm to 157 cm. For comparative context, the range of

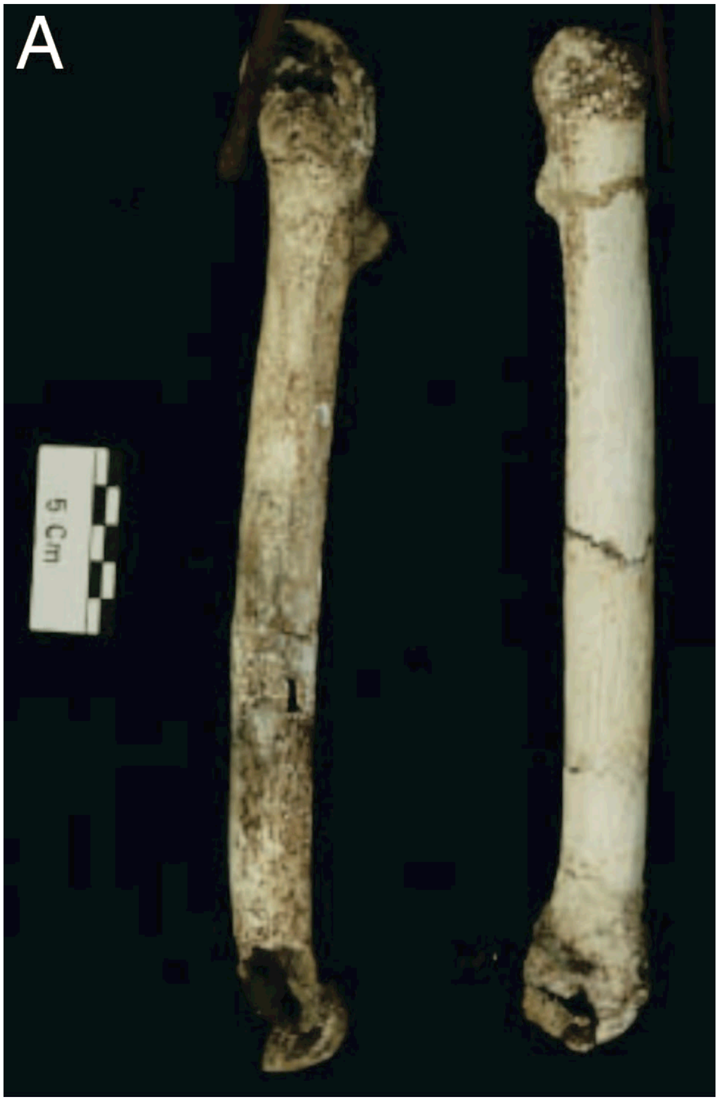

Figure 1: LB1 left and right femora, lateral views. Note particularly the contrasts in size and orientation of the lesser trochanters, which indicate lateral asymmetry, a common sign of abnormal development. As can be seen on other long bones of LB1, the relatively straight femoral shafts are consistent with rather weak muscle development.

stature observed in the Rampasasa human pygmies (N=76) living on Flores today is 1.33 m to 1.65 [3]; thus, the range of statures reconstructed for the Palau population sample encompasses not only LB1 from Flores, but also the most comparably representative human population presently living on that island. The overlaps in these data suggest the existence of stature differences lacking statistical or biological significance. We note further that the original stature estimates for LB1 employed inappropriate (African pygmy) reference samples for the regression and other predictive equations that were extrapolated for a geographically and ecologically far different (Pacific island) sample.

Unlike the situation in the Liang Bua Cave sample from Flores, which contains only a single skull that is characterized by unusual proportions and abnormal levels of asymmetry [3], the Palau samples [4,5] include multiple crania. Although preparation to free them from encrusted carbonate deposits continues, these crania exhibit endocranial volumes that approximate 1000 ml, which fall in the very low end of the observed range for extant normal populations of our species.

CONCLUSIONS

Reports of the discovery of the Flores skeletal remains [6,7] have occasioned unusually high levels of imagination to account for the reported data. Some of these speculations reported [8] have gone so far as to suggest that, based on scaling of body size to brain volumes found in placental mammals, a body mass appropriate to a human with a brain estimated to be as small as that reported for LB1 might scale to be as low as 16 kg. In contrast, reasonable extrapolations from the Palau skeletal remains produce a series of estimates for body mass centering on approximately 40 kg, again consistent with the living Rampasasa pygmy human population on Flores. Independent data on craniofacial and postcranial asymmetry, as well as the unusual proportions seen in the femora of LB1 (see Fig. 1) lend further bases for rejecting the hypothesis that the Flores skeletal remains must represent a new human species. At the same time, none of the available data, including DNA sequence analyses, provide support for rejection of the competing hypothesis [3] that LB1 represents a developmentally abnormal individual sampled from a population unsurprising for the region from which it was recovered. For all of these reasons, study of the LB1 skeleton offers an unusual possibility for gaining important insights into the structural and functional relationships among morphology (long bone dimensions plus markings, body mass), mechanics (power as well as other aspects of locomotion) and molecules (modern human DNA sequences).

REFERENCES

1. Wang, WJ and Crompton, RH, *J Biomech* **36**, 1237-1246, 2003.
2. Eckhardt, RB, et al. *Proceedings of the International Society of Biomechanics XXth Congress/American Society of Biomechanics 29th Annual Meeting*, Cleveland, OH, abstract, 2005.
3. Jacob, T, et al. *Proc Natl Acad Sci, USA* **103**, 13421-13426, 2006.
4. Berger, et al. *PLOS One* **3**, 1-10 (e1780), 2008.
5. Fitzpatrick, et al. *PLOS One* **3**, 1-12 (e3015), 2008.
6. Brown, P., et al. *Nature* **431**, 1055-1061, 2004.
7. Morwood, MJ, et al. *Nature* **437**, 1012-1017, 2005.
8. Niven, JE, *TREE*, doi:10.1016/j.tree.2006.11.009.

INTERSEGMENTAL DYNAMICS OF SWING ARE REFINED OVER TIME TO ACCOMMODATE CHANGES IN LEG INERTIA

Jeremy D. Smith, Samantha Villa, Ross E. Orpet, and Gary D. Heise
Biomechanics Laboratory, University of Northern Colorado, Greeley, CO
email: jeremy.smith@unco.edu

INTRODUCTION

Two recent studies [1, 2] investigated the effects of adding approximately 2 kg of additional mass distally to one leg during walking. A common purpose of these studies was to understand the effects of the inertia change over time. Noble and Prentice [1] found that individuals retained similar kinematic walking patterns after a brief period of accommodation to leg inertia changes. This was accomplished by increased muscle moment magnitudes at both the hip and knee. However, it was suggested that further insights into the accommodation process could be gained by investigating changes in intersegmental dynamics following the inertia change. Previously [1, 2], inverse dynamics assessments have focused only on changes in the muscle moment, but segment motions during walking arise not only from muscle contributions, but also from interactions among segments which depend on the motions and inertia of the segments, as well as more passive contributions from gravity [3]. Thus, the purpose of this study was to investigate the effects of changes in leg inertia on muscle, interaction, and gravity moments during the swing phase of walking. The effects of the inertia change were investigated over 1200 stride cycles.

METHODS

Two males and two females participated in this study (age = 22 ± 1 yrs, mass = 80.0 ± 16.0 kg, height = 1.76 ± 0.06 m). All participants were recreationally active and had prior experience walking on a treadmill. Participants walked on a treadmill at 1.5 $m\cdot s^{-1}$ under three loading conditions: a) pre-load, b) loaded and c) post-load. In both the pre-load and post-load conditions participants walked for five minutes on a treadmill in an unloaded state. In the loaded condition, 2 kg of lead shot, equally distributed between two packets, were added near the ankle of the right leg. Sagittal plane motion of the right leg was collected (60 Hz) during all walking trials.

The leg was modeled as three rigid segments (thigh, shank, and foot) interconnected by three revolute joints (hip, knee, and ankle). Segment inertia properties were determined using regression equations from the literature [4]. For the loaded condition, shank inertia properties were adjusted by modeling the added mass as a point mass located distally on the shank. An intersegmental dynamics approach was used to partition the net moment at each joint into muscle, interaction, and gravity components [3]. The first 300 strides during the pre-load and post-load conditions and the first 600 strides during the loaded condition were analyzed. Only the swing phase of each stride was analyzed since previous data [2] suggested that the inertial manipulation used in our study primarily alters the mechanics of swing. Absolute angular impulses of each moment component were computed by first rectifying each moment component and then integrating the resulting time series. To reduce stride-to-stride variability and the number of data points, data from five consecutive swing phases were averaged to create a single bin of data representing five strides as has been done previously [1].

RESULTS AND DISCUSSION

Absolute angular impulses at the hip and knee of muscle, interaction, and gravity moments increased after the load was attached to the ankle, and returned to baseline magnitudes after the load was removed. However, there appeared to be a brief period in which an overshoot occurred, particularly in the muscle and interaction moments, following load addition (Figure 1; focus on bin number 61-90). Gradually, moments settled into a steady state pattern. Following removal of the load there appeared to be another period of transition back to the baseline pattern (Figure 1; focus on bin numbers 181-190). This period of transition has been referred to as an after-effect by others [5]. The transition to a steady state pattern was longer in all subjects following the addition of mass (ranged from 45 to 250 strides across the four subjects) compared to the transition period following load removal (ranged from 10 to 50 strides across the four subjects). Our finding of a briefer transition following load removal was consistent with previous results [1].

The presence of an after-effect following load removal has been used by others [5] to suggest that the CNS's representation of the limb dynamics was altered by the change in limb inertia. Specifically, our data suggest that the increase in leg inertia was eventually accounted for by the CNS as seen during the steady-state response. Once the load was removed the moment patterns did not return immediately to baseline levels. Instead, the gradual return to baseline levels suggests that feedback information was most likely used to modify control of the limb during subsequent cycles. This interpretation is consistent with other interpretations based only on changes in the muscle moments [1].

The analysis used in our study also suggests that observed changes in muscle moments were most likely driven by changes in the interactions among segments after limb inertia changed. In general, it has been suggested [4] that muscle moments during walking counteract the effects of the interaction moments at each joint. As limb inertia increased in our study, so did the interaction moments at each joint. This increased the burden on the musculature to counteract the effects of the interaction among segments. Over a brief period, a more effective coordination between the interaction and muscle moments was produced, ultimately requiring less corrective action on the part of the musculature to control swing. Evidence of this improved coordination can be seen as a reduction in angular impulses at the hip and knee during the brief periods following a change in leg inertia.

REFERENCES

1. Noble, JW & Prentice, SD *Exp Brain Res* **169**, 482-495, 2006.
2. Smith, JD & Martin, PE *Hum Mov Sci* **26**, 412-425, 2007.
3. de Leva, P *J Biomech* **29**, 1223-1230, 1996.
4. Zernicke, RF, et al., *Adaptability of human gait*, Elsevier Science Publishers B.V., North-Holland, Netherlands, 1991.
5. Shadmehr, R & Mussa-Ivaldi, FA *J Neurosci* **14**, 3208-3224, 1994.

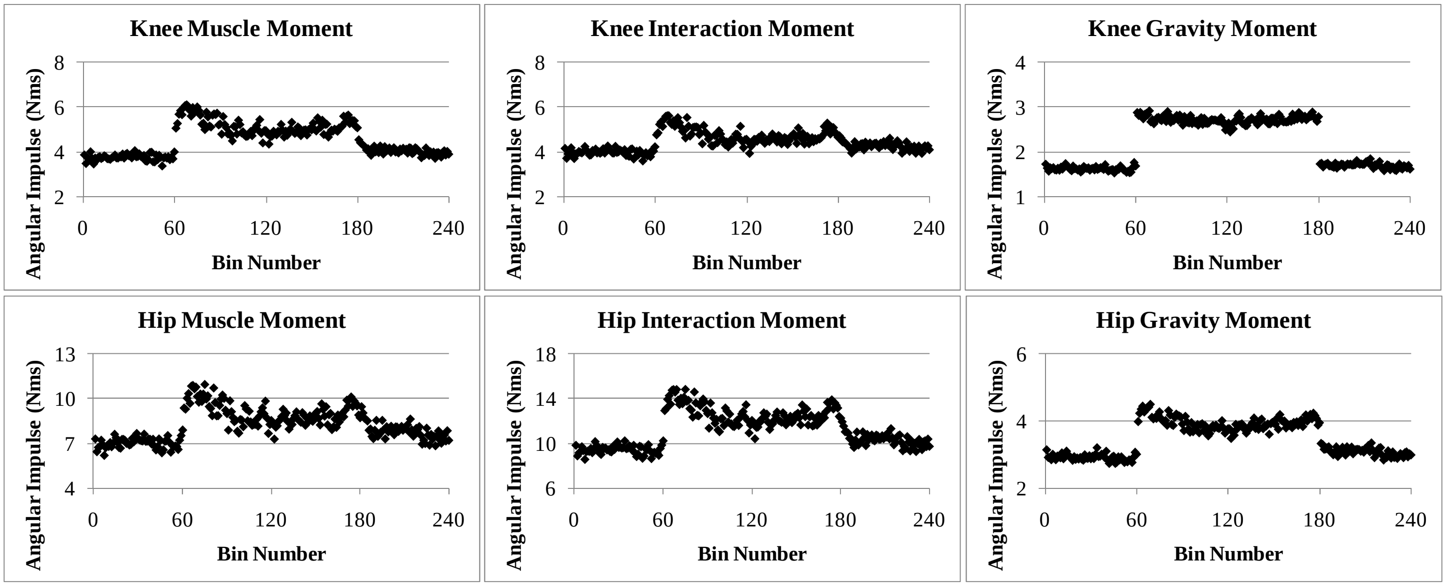

Figure 1: Absolute angular impulses of muscle, interaction, and gravity moments of the knee and hip during pre-load (bin numbers 0-60), loaded (bins 61-180), post-load (bins 181-240) conditions. Data are from one representative participant. Each bin represents the mean of five consecutive swing phases of the loaded leg. Absolute angular impulses increased immediately after the load was applied (bin 61). Over the next 150 strides (bins 61-90) absolute angular impulses gradually decreased to a lower magnitude, which remained relatively stable for the next 450 strides (bins 91-180).

RE-INTERPRETING DETRENDED FLUCTUATION ANALYSES OF STRIDE-TO-STRIDE VARIABILITY IN HUMAN WALKING

[1] Jonathan B. Dingwell, [2] Joseph P. Cusumano
[1] Nonlinear Biodynamics Lab, Department of Kinesiology, University of Texas, Austin, TX
[2] Department of Engineering Science & Mechanics, Penn State University, State College, PA
E-mail: jdingwell@mail.utexas.edu Web: http://www.edb.utexas.edu/faculty/dingwell/

INTRODUCTION

Step-to-step variations in gait cycle timing exhibit statistical persistence, as quantified by Detrended Fluctuation Analysis (DFA) [1,2]. Such statistical persistence is thought to be critical to "healthy" physiological function [2]. Indeed, human stride intervals become more uncorrelated (less persistent) in elderly subjects and patients with Huntington's disease [3]. This does not occur, however, in patients with peripheral neuropathy [4]. Here, we demonstrate that interpreting statistically persistent dynamics as "healthy," and uncorrelated or anti-persistent dynamics as "unhealthy" [2] is unfounded and reflects a fundamental misunderstanding of what the DFA algorithm actually quantifies [5].

Walking on a motorized treadmill requires one to maintain, *on average*, a constant speed. However, for any stride n, many combinations of stride length (L_n) and stride time (T_n) will achieve the exact same speed ($S_n=L_n/T_n$). Thus, walking at any constant speed does *not* require direct control of either L_n or T_n, but rather of S_n. We propose that DFA analyses directly reflect the degree to which each of these variables is (or is not) controlled, independent of any generic notions of "health" or "disease".

METHODS

Seventeen healthy volunteers (age 18-28) walked on a motor-driven treadmill (Woodway USA). Each subject completed two 5-min walking trials at each of five different speeds, ranging from 80% to 120% of preferred walking speed (PWS). 3D movements of their feet were recorded (Vicon, Oxford Metrics, UK) continuously and used to compute L_n, T_n, and $S_n=L_n/T_n$ time series for all strides for each trial.

Detrended Fluctuation Analysis (DFA) [1-3] was used to determine the degree to which each time series exhibited persistent or anti-persistent temporal correlations across successive strides. The DFA algorithm yields a scaling exponent, α (Fig. 1). $\alpha > 0.5$ indicates statistical "persistence" (i.e., deviations go *un*corrected over consecutive strides; Fig. 1(i)). $\alpha < 0.5$ indicates "anti-persistence" (i.e., deviations are corrected rapidly; Fig. 1(ii)).

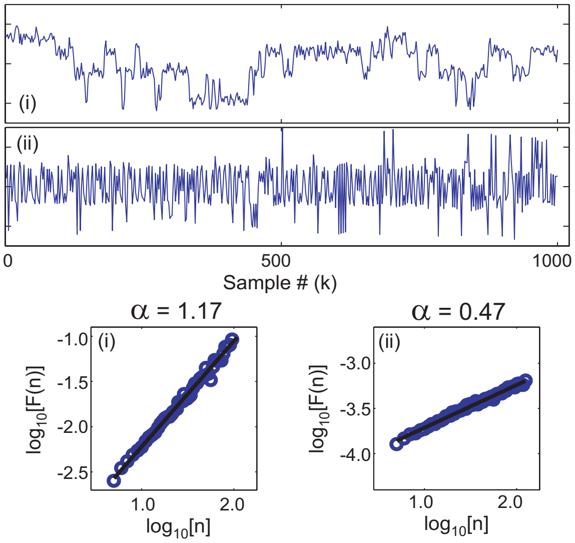

Figure 1: Example DFA output for two signals, both having unit variance. Signals exhibiting substantial drift (i) yield large values of $\alpha > ½$. Uncorrelated and/or anti-persistent signals (ii) yield smaller values: $\alpha \leq ½$.

To ensure our experimental results were not caused by the treadmill walking task itself, we created two types of "surrogate" data sets [6]. We generated 20 *randomly shuffled* surrogates [1,6] for each experimental [L_n, T_n] trial. This procedure maintained the exact same means and variances of the original L_n and T_n time series, but eliminated all temporal correlations. We also generated 20 *phase-randomized* surrogates [6,7] for each experimental trial. These surrogates additionally preserved the same statistical persistence in each original L_n and T_n time series. We computed net total distances walked to ensure no surrogate would have "walked off" the treadmill. We calculated new stride speed ($S_n = L_n/T_n$) time series for each [L_n, T_n] surrogate.

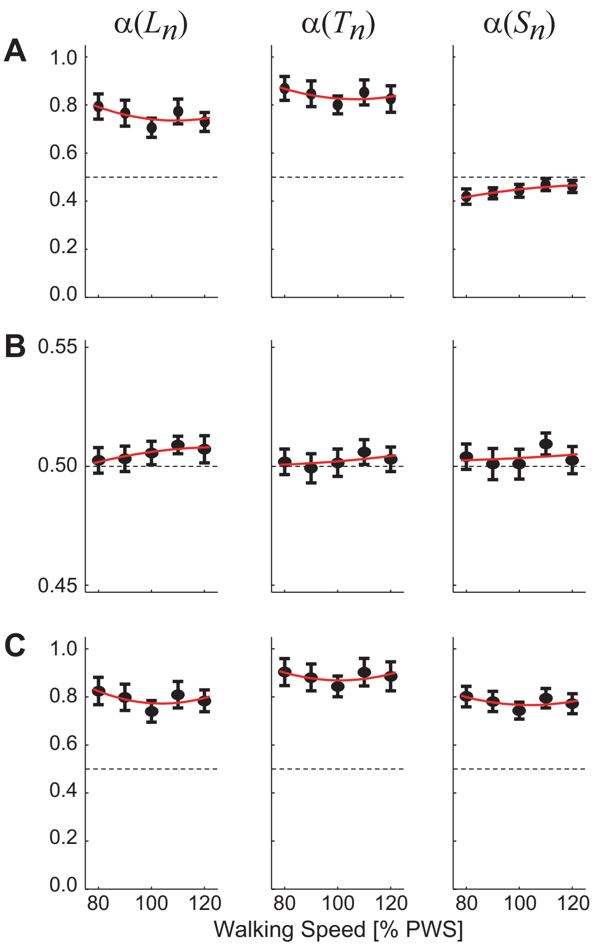

Figure 2: DFA α exponents for stride length (L_n), stride time (T_n), and stride speed ($S_n = L_n/T_n$) time series for (**A**) experimental human walking trials, (**B**) randomly shuffled surrogates (note the substantial difference in the vertical scale!), and (**C**) phase-randomized surrogates. Error bars are ±95% confidence intervals.

RESULTS AND DISCUSSION

As expected [1-4], human (Fig. 2A) T_n and L_n time series both exhibited significant statistical persistence (i.e., $\alpha > 0.5$). Conversely, S_n time series (Fig. 2A) exhibited consistent and statistically significant *anti*-persistence (i.e., $\sim 0.4 < \alpha < 0.5$) at all walking speeds. Thus, deviations in both T_n and L_n were allowed to persist, whereas deviations in S_n were rapidly reversed on the subsequent strides.

When the experimental T_n and L_n time series were shuffled in random order (Fig. 2B), the temporal correlations in all 3 time series were destroyed. By construction, the phase-randomized surrogates (Fig. 2C) yielded random time series that preserved the statistical persistence in both L_n and T_n. However, the statistical anti-persistence that was observed in the experimental S_n time series was replaced with strong statistical persistence ($\alpha >> ½$). Thus, the statistical anti-persistence seen in the experimental S_n time series did *not* result merely from dividing two independent statistically persistent time series.

CONCLUSIONS

It has been widely argued that statistically persistent fluctuations are a critical marker of healthy physiological function in general [2] and that uncorrelated or anti-persistent fluctuations are a sign of disease or pathology [1,2]. The present results strongly refute this interpretation. The subjects tested here (Fig. 2A) clearly cannot be both simultaneously "healthy" according to $\alpha(L_n)$ and $\alpha(t_n)$ and "unhealthy" according to $\alpha(S_n)$. Instead, our findings argue for an interpretation of these DFA exponents specifically within the nature of the control processes being studied. This interpretation is fully consistent with the fact that many different statistical processes can yield time series with a wide range of α values [5]. These findings were also directly supported by a simple mechanical model of walking with minimal feedback control that still exhibited a wide range of statistically persistent and anti-persistent walking behaviors [8].

REFERENCES

1. Hausdorff, J.M., et al. *J. Appl. Physiol*. 78, 349-358 (1995).
2. Goldberger, A.L. et al. *Proc. Natl. Acad. Sci. USA* 99, 2466-2472 (2002).
3. Hausdorff, J.M. et al. *J. Appl. Physiol*. 82, 262-269 (1997).
4. Gates, D.H. & Dingwell, J.B., *J. Appl. Physiol*. 102, 965-971 (2007).
5. Maraun, D., et al. *Nonlin. Processes Geophys*. 11, 495-503 (2004).
6. Theiler, J., et al. *Physica D* 58, 77-94 (1992).
7. Dingwell, J.B. & Cusumano, J.P. *Chaos* 10, 848-863 (2000).
8. Gates, D.H., Su, J.L. & Dingwell, J.B. *Physica A* 380, 259-270 (2007).

ACKNOWLEDGEMENTS

Funded by Whitaker #RG-02-0354 (to JBD), NIH # EB007638 (to JBD), and NSF #0625764 (to JPC).

Effect of the T-poles and conventional hiking poles on the foot VGRF and the joint moments of the upper extremity joints

Kunal Singhal, Sukhoon Yoon, Jeffrey B. Casebolt, and Young-Hoo Kwon
Biomechanics Laboratory, Texas Woman's University, Denton, TX
Email: ksinghal@twu.edu, ykwon@twu.edu

INTRODUCTION

Falls and fall related injuries are major source of concern in United States with more than one third elderly facing injury deaths due to falls [1,2]. Falls are the biggest cause of fractures among the elderly with the most common fractures being the hip followed by forearm, leg, ankle, pelvis, upper arm, and hand [3]. The elderly who experience a fall may develop a fear of falling, which may cause them to limit their activities [4]. This may eventually increase the risk of falling because of reduced mobility, strength and stability.

Previous studies reported that participation in a high intensity strength training program could increase dynamic stability in the elderly [5,6]. Assistive walking devices (AWD's), like crutch, canes, poles, etc., also help in improving the stability by increasing the base of support and would improve the activities of daily living (ADL). AWDs like poles, allow the weight to be transferred to upper extremity, thus reducing the loads on the lower extremity. This has a potential disadvantage in terms of increasing the joint loads on upper extremity joints. Thus, an effective AWD should not only reduce the burden on lower extremity but also minimize the increase in upper extremity burden.

One way to achieve this might be alteration in the design of the AWD. The current study concentrates on testing two such designs of walking poles, T-pole and conventional hiking poles. T-poles have different design with a telescopic style pole fixed to the hinge on vest. Because of different design and walking pattern employed there might be difference in the loads on the extremity joints as compared to the hiking poles.

The lower extremity loads were measured using the vertical ground reaction force (VGRF). The design of T-poles allows for greater changes in moment arm at upper limb and thus joint moments of the upper extremity joints (shoulder, elbow and wrist) were used as a measure of upper extremity joint load.

The purpose of the study was to compare the effects of two different types of walking poles (conventional hiking poles and new-design T-poles) on foot VGRF and joint moments of wrist, elbow and shoulder.

METHODS

Twenty healthy participants with an average age of 74.2 ± 5.5 years volunteered for the study. Exclusion criteria were determined by an independent physician. Participants were subjected to a medical screen in order to partake in the study and then randomly assigned to one of two groups: T-poles (N = 12) and Hiking poles (N = 8).

The participants were given sufficient walking exposure with poles for a period of 6 months. The groups walked three days per week for 45 min during a supervised walking session. Data were collected at the end of the 6-month period.

Gait analysis was performed in two different conditions: normal walking and pole walking. Ground reaction forces on the feet and poles were collected using 4 force plates (AMTI OR-6) while video data were captured from 8 digital camcorders (Panasonic AG-DVC20). Subsequent marker tracking and processing was done using Kwon3D Motion Analysis Suite Version 4.1 (Visol, Inc., Seoul, Korea; version XP 4.1). The upper extremity joint moments were computed through the inverse dynamics procedure using the pole GRF data and the motion data. The joint moment data were normalized to the body mass.

Relative reduction of the peak foot VGRF and the peak joint moments of the upper extremity joints were used as the dependent variables. Independent t-test was performed to compare the dependent variables between the subject groups with the type of pole being the independent variable. The significance level was set at $\alpha = 0.05$ and all analyses were performed with SPSS for Windows (SPSS Inc., Chicago, IL; version 14.0).

RESULTS

A significant difference was found in the breaking peak of the foot VGRF with the T-pole group showing a larger decrease as compared to hiking pole group (Table 1). No significant difference was observed in the propulsive peak of the foot VGRF. In the upper extremity joint moments, the T-pole group showed significantly smaller mean values at the elbow and shoulder than the hiking-pole group.

DISCUSSION

Based on results it is clear that T-pole owing to its design characteristics not only results in lesser VGRF acting on the lower limb joint, but also causes significantly lower joint moments at the upper limb joints as compared to hiking poles. Thus, in the elderly where there is a need to reduce the burden on lower extremity, T-pole will prove to be more conducive to increase or maintain the ADLs without increasing the upper extremity joint loads significantly.

Previous study [7], has found out an average reduction of 2.9% to 4.4% in VGRF, which is higher than what was found in the current study. This might be because the participants were healthy elderly and might not be relying on the poles to reduce their joint loads. Even though there is a difference in the data, overall trend shows that greater reduction in lower extremity joint loads, and lower upper extremity joint moments with T-pole as compared to hiking poles.

REFERENCES

1.CDC. www.cdc.gov/ncipc/wisqars, 2005.
2.Hausdorff JM, et al. Arch Phys Med Rehab, **82**, 1050-1056, 2001.
3.Bell, A, et al. Med J Australia, **173**, 176-177, 2000.
4.Vellas, BJ, et al. Age Ageing, **26**, 189-193, 1997.
5.Hess, JA, et al. J Manip Phys Th, **28**, 582-590, 2005.
6.Schlicht, J, et al. J Ger, **56A**, M281, 2001.
7.Willson, J, et al. Med Sci Sports Exerc, **33**, 142-147.

ACKNOWLEDGEMENTS

The authors of this paper would like to thank Martin van Breems for providing the poles.

Table 1: Mean relative reduction in VGRF and mean resultant joint moments of the upper extremity joints

	Resultant Joint Moment (Nm/kg)			**Change in Foot VGRF (%)**	
	Wrist	**Elbow**	**Shoulder**	**Breaking peak**	**Propulsive peak**
T-pole	0.09	0.11§	0.11§	-4.2§	-4
Hiking Pole	0.15	0.27	0.45	0.35	-2.02

Note: § Significantly ($p < .05$) different from the hiking pole.

EFFECTS OF TENDON MORPHOLOGY ON MUSCULAR WORK AND EFFICIENCY

Alexis D. Gidley and Brian R. Umberger
Department of Kinesiology, University of Massachusetts, Amherst, MA, USA
email: agidley@kin.umass.edu

INTRODUCTION

Muscles come in a variety of shapes and sizes, yet most fall into one of three major categories, based largely on relative tendon length and compliance [1]. One of these categories includes muscles with relatively long, highly compliant tendons. Muscles of this type are supposed to be especially well-suited for taking advantage of elastic energy-saving mechanisms, which has been discussed extensively in the literature [4]. However, it is difficult to fully appreciate the effects of tendon morphology on the metabolic cost of contraction, due to many differences in the muscles that have been studied and the protocols used in prior research.

Computer simulation models provide the ability to vary one or more parameters of interest, while holding all others constant, and thus could provide additional insight into the effects of morphology on muscle performance. Therefore, the purpose of this study was to determine the effects of tendon relative length and compliance on the energetics and efficiency of contraction, using a muscle modeling approach.

METHODS

A Hill-type muscle-tendon (MT) model [3], consisting of a contractile element (CE) and a series elastic element (SEE), was scaled to represent three major MT architectures [1]. The three configurations represented muscles with the following characteristics: 70% fiber, 30% tendon, 4% maximum tendon strain (70F30T4%); 40% fiber, 60% tendon, 2% maximum tendon strain (40F60T2%); and 20% fiber, 80% tendon, 6% maximum tendon strain (20F80T6%) [2]. All other model parameters were held constant across conditions. The muscle model used in this study [3] provided estimates of mechanical power output *and* the rate of metabolic energy expenditure.

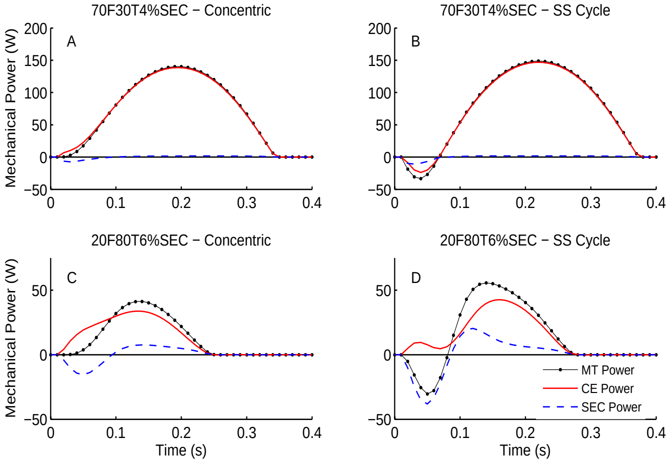

Figure 1: MT, CE, and SEE mechanical powers for simulated concentric and SS cycle contractions (70F30T4% & 40F60T2% models).

Mechanical work and efficiency for the three muscle types were evaluated in simulations where the CE was maximally activated with the MT attached to a 250 kg load [2]. Simulations were performed both with the load initially at rest (concentric condition) and with the load given an initial velocity eliciting a stretch-shorten cycle (SS cycle condition). Positive and negative mechanical work were determined by integrating the mechanical power curves for the MT, CE, and SEE. Metabolic cost was determined by integrating the metabolic power curve for the CE. Efficiency was computed as the ratio of positive MT work to metabolic cost. With this approach, any metabolic cost incurred during stretch is included in the efficiency calculation.

RESULTS AND DISCUSSION

For the concentric contractions, the amount of work done by the CE (and MT) was greatest for the 70F30T4% model and least for the 20F80T6% for all three models (Table 1). This is expected, as a greater relative CE length will allow force to be generated over a greater displacement, resulting in more work. The amount of energy stored and released in the SEE for the 70F30T4% and 40F60T2% models (Table 1) was a trivial proportion of the total work done (1-2%), but was a greater proportion (15%) for the 20F80T6% model (compare Figure 1A with 1C). The results for metabolic cost tended to mirror those for CE work (Table 1). Having a relatively longer CE (i.e., longer muscle fibers) allows for more work to be done; however, this also results in a greater volume of active muscle during contraction, and thus a higher metabolic cost. When the mechanical and metabolic data are combined, the efficiency for the 20F80T6% model was found to be slightly lower than in the other two models, which is due to the cost associated with stretching the long, compliant SEE in this model (Figure 1C). These 'initial' mechanical efficiencies are also higher than typical whole-body efficiency values (~0.25) [3].

Mechanical work values were greater in all three models for the SS cycle contractions than in the concentric contractions. However, the effects were not uniform across models. Positive MT work was 8% greater for the 70F30T4% model, 13% greater for the 40F60T2%, and 37% greater for the 20F80T6% model, than in the concentric contractions. Particularly for the 20F80T6% model, a considerable amount of the positive MT work was derived from the SEE (Figure 1D). For the 70F30T4% and 40F60T2% models, the metabolic costs incurred during the eccentric phases completely offset the additional work done, so that there was little or no change in efficiency (Table 1). In contrast, the efficiency in the 20F80T6% model was higher for the SS cycle contraction than in the concentric contraction. Notably, the efficiency for the 20F80T6% model was lower than the other two models for the concentric contractions, but exceeded the efficiency in the other two models for the SS cycle contractions. This is related to the fact that the CE never gets stretched in the 20F80T6% model (Figure 1D), and thus there is no energy dissipated in the CE during the SS cycle (Table 1). This muscle design does indeed appear to be especially well-adapted to the SS cycle [1,2], but this comes at the expense of performance in purely concentric contractions.

It is important to remember that the present results pertain only to one general set of conditions (e.g., one external load, full activation). More conditions will need to be considered in future work to test the generalizability of the results.

CONCLUSIONS

Based on specific changes made to CE and SEE properties in a muscle model, tendon relative length and compliance should have profound effects on both muscular work and efficiency. These model-based analyses should ultimately help us to better understand the structure-function relationships in muscle.

REFERENCES

1. Alexander, RM & Ker, RF *Multiple Muscle Systems*, 568-577, Springer-Verlag, New York, NY, 1990.
2. Caldwell, GE *J Applied Biomechanics* **11**, 1-24, 1995.
3. Umberger et al., *Computer Methods in Biomechanics and Biomedical Engineering* **6**, 99-111, 2003.
4. Schenau et al. *J Applied Biomechanics* **13**, 389-415, 1997.

Table 1: Mechanical work (J), metabolic cost (J), and efficiency for concentric and SS cycle contractions.

	CE work		**SEE work**		**MT work**		**Met Cost**	**MT Efficiency**
	POS	NEG	POS	NEG	POS	NEG		
Concentric								
70F30T4%	27.69	0.00	0.32	-0.32	27.69	0.00	59.46	0.47
40F60T2%	12.93	0.00	0.26	-0.26	12.93	0.00	28.41	0.46
20F80T6%	4.92	0.00	0.76	-0.76	4.92	0.00	11.35	0.43
SS cycle								
70F30T4%	29.51	-0.83	0.42	-0.42	29.94	-1.24	64.09	0.47
40F60T2%	14.21	-0.83	0.43	-0.43	14.64	-1.25	31.34	0.47
20F80T6%	5.47	0.00	1.72	-1.72	6.72	-1.25	12.70	0.53

A METHOD FOR ALIGNMENT OF THE GLENOID IMPLANT BASED ON SPHERE FITTING

Gregory Lewis and April Armstrong
Department of Orthopaedics and Rehabilitation, Penn State Hershey
email: aarmstrong@hmc.psu.edu

INTRODUCTION

Glenoid component loosening is an unresolved complication in total shoulder arthroplasty [1]. Surgical alignment of the glenoid implant is believed to have important effects on postoperative shoulder mechanics and implant longevity. Changes in orientation of only a few degrees have been shown in cadaver experiments and computer simulations to cause abnormal glenohumeral translations and joint reaction forces [2].

Unfortunately there is no widely accepted approach for aligning the glenoid component intra-operatively. Some surgeons aim to align the implant perpendicular to the scapular body. However, in healthy persons the 'version' angle of the glenoid relative to the scapular body varies by 20° [3], meaning that many patients will receive implants that are misaligned with their native anatomy.

In the present study we describe a method for aligning the implant in order to best reproduce the spherical shape of the patient's native glenoid surface. The accuracy of the method was assessed using three-dimensional computer models of scapulae created from CT scans. Two types of posterior glenoid wear commonly encountered in osteoarthritic patients receiving shoulder replacement were simulated.

METHODS

Sixteen cadaver scapulae without osteoarthritic changes were imaged using CT as previously described [4]. A three-dimensional geometric computer model was created for each scapula using Mimics software (Materialise, Belgium).

For each model, a series of point coordinates were sampled across the entire glenoid face and rim surface. A sphere having radius of 35 mm was fit to the face points using a nonlinear least squares algorithm. Additionally, a centerpoint of the glenoid surface was located based on the four extreme poles of the glenoid.

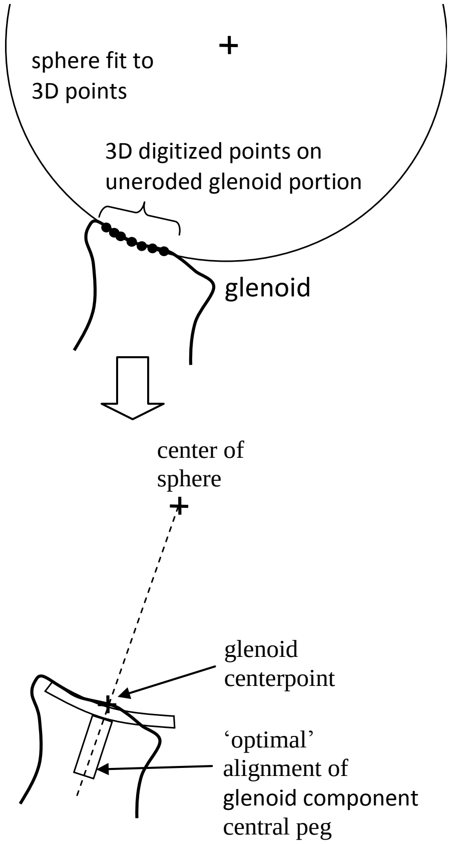

Figure 1: Glenoid implant alignment based on sphere fitting to uneroded portion of glenoid face (horizontal plane view).

The optimal 3D drill line was computed as the line passing through the center of the fit sphere and the glenoid centerpoint (Figure 1). Aligning the central peg of the glenoid component with this line will lead to best fit alignment of the component articular surface (having a 35 mm-radius curvature) with the native bone surface.

In cases of posterior glenoid wear commonly associated with osteoarthritis, the sphere may be fit to digitized points from the uneroded anterior portion of the glenoid face or rim. In each scapular model, two types of wear were simulated: (1) biconcave defect in which a portion of the face was eroded; and (2) global defect in which the entire face was abnormal but a portion of the anterior glenoid rim was intact. For biconcave defect the amount of uneroded face for sphere-fitting was varied from 10% to 100% (in increments of 10%) in the anterior-posterior direction, and similarly for type (2) the amount of available rim was varied from 10% to 50%. The resulting drill lines were compared to the optimal drill line computed using the entire glenoid face.

RESULTS AND DISCUSSION

For type (1) biconcave defects in which at least 40% of the glenoid face was uneroded and available for sphere fitting, the drill line estimates differed from the drill lines computed using the entire face by less than 5° in the transverse plane and 2° in the coronal plane for all 16 specimens (Figure 2). The transverse plane errors decreased to less than 3° for all specimens if at least 60% of the face was uneroded.

For type (2) global defects in which the anterior 50% of the glenoid rim was available for sphere fitting, errors were typically less than 5° in the transverse plane and 3° in the coronal plane.

These errors indicate that the proposed sphere fitting approach may enable accurate computer-assisted alignment of the glenoid component with the patient’s native anatomy, even in cases in which a portion of the glenoid is worn away. In practice the surgeon could digitize the glenoid surface and anatomical landmarks intra-operatively with a digitizing arm or similar tool, removing the need for creating a preoperative 3D scapular computer model. To address a primary limitation of the present study, the use of normal cadaver glenoids, we plan to implement the sphere-fitting method with models from preoperative CT scans of total shoulder replacement patients.

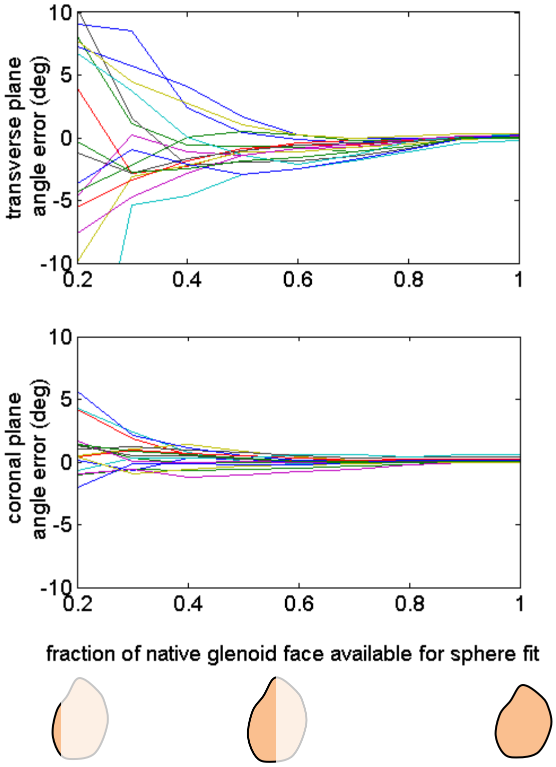

Figure 2: Angular errors, for each specimen, between the drill line computed from the entire glenoid face and the drill lines computed under simulated biconcave defects in which the uneroded portion of the face is used for sphere fitting.

REFERENCES

1. Bohsali KI, et al. *J Bone Joint Surg Am* **88**, 2279-2292, 2006.
2. Nyffeler RW, et al. *J Shoulder Elbow Surg* **15**, 625-629, 2006.
3. Churchill RS, et al. *J Shoulder Elbow Surg* **10**, 327-332, 2001.
4. Bryce CD, et al. *J Shoulder Elbow Surg* **17**, 825-832, 2008.

AN INVESTIGATION OF PUBOVISCERAL MUSCLE ENTHESIAL LOADING AT THE END OF THE SECOND STAGE OF LABOR

[1]Jinyong Kim, [1]James Ashton-Miller and [2]John DeLancey
[1]Department of Mechanical Engineering, [2]Department of Obstetrics & Gynecology
University of Michigan, Ann Arbor, Michigan, USA
Email: jinyongk@umich.edu, Web: http://me.engin.umich.edu/brl

INTRODUCTION

Maternal birth-related injuries are one of the most common causes of genital prolapse and incontinence in women [1]. A known risk factor is the stretch ratio in the maternal pubovisceral muscle (PVM) region of the levator ani muscle; this has been estimated to reach approximately 3.3 at the end of the second stage of labor [2]. This value is more than twice the value that non-pregnant striated muscle can achieve without injury [3]. Indeed, following difficult vaginal births, magnetic resonance imaging has been used to demonstrate avulsion of the left and/or right origin or 'enthesis' of the PVM [2, 4]. In this paper we used a simple finite element model to investigate the biomechanical factors that may underlie the pathomechanics of enthesial avulsion during vaginal birth.

METHODS

A three-parameter hyperelastic Mooney-Rivlin material model was chosen to describe the behavior the PVM and its enthesis. The strain energy density function, W, was defined as

$$W = C_{10}(I_1 - 3) + C_{01}(I_2 - 3) + C_{11}(I_1 - 3)(I_2 - 3)$$

where I_1 and I_2 are the stretch invariants of the right Cauchy-Green tensor. Material parameters for the model were taken from *in vitro* test results [5].

Simulations were performed by implementing the model into LS-DYNA (LSTC, Livermore, CA). The caudoposterior displacement of the PVM insertion during the second stage of labor [2] was used to load the model. The PVM insertion point was also considered to rotate anterocaudally with respect to its insertion, reflecting the perineal descent that occurs during birth [2].

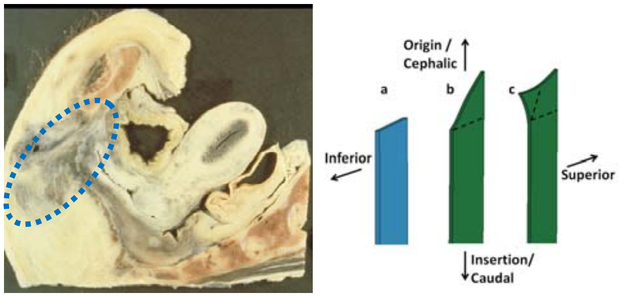

Figure 1: (Left) Sagittal section through a female cadaveric PVM enthesis. (Note that the rest of PVM geometry is distorted by embalming artefact.) (Right) Finite element meshes of alternative PVM models: (a) quadrilateral (control) case, (b) angled case, (c) angled and flared case.

Based on a sagittal section of a cadaver pelvis (Figure 1, Left), the PVM was simply modeled as a thin uniform band 5 mm thick. Given that the detailed morphology of the PVM enthesis has not been investigated, three plausible shapes were proposed (Figure 1). An angled case was modeled considering the fact that the PVM has an angled attachment to the posterior aspect of the pubic bone (Fig. 1, middle). Since flaring of the enthesis has been observed at many other attachment sites [6], we also investigated a structure with flaring on its inferior side (Fig. 1, right). These two models were compared with the control case of a simple quadrilateral structure (Fig. 1, left) in order to understand the effect of structural geometry on deformation. Finally, the enthesis itself was modeled by increasing the relative stiffness of the elements near the origin to reflect mineralization and higher Type 1 collagen content.

RESULTS AND DISCUSSION

While the first two geometric cases exhibited the largest maximum principal stresses on the inferior aspect of the enthesis, the angled case exceeded the quadrilateral case by a ratio of 3.2 to 1.94 (Figure 2). This phenomenon may be due to the increase in the relative anterocaudal rotation of the PVM origin with respect to its insertion. The effect of flaring appears to move the region of higher stress concentration caudally while also reducing the stress concentration at the enthesis. Of note is the fact that the stress concentration at the enthesis is higher in the middle than at either side. This result corroborates findings in other enthesial structures [7]. What is clear from these results is that avulsion is less likely to start at the superior margin than either the inferior margin or the mid-substance.

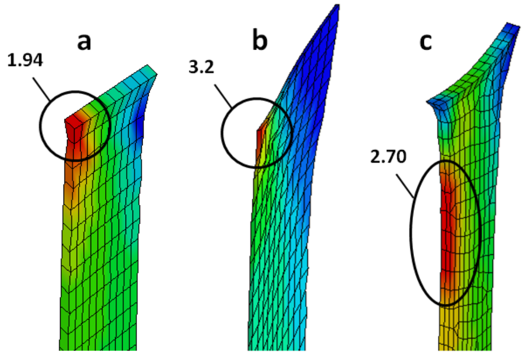

Figure 2: Contours of maximum principal stress in each of the three cases. Stresses are normalized by the remote maximum principal stress. Circles indicate regions of peak stress concentration.

For the latter two cases, normalized work done per a unit volume was computed at the highest stress concentration area (Figure 3, ordinate). The abscissa shows the relative stiffness of entheses compared to that of muscle. Figure 3 suggests that there exists an optimal range for the value of the ratio of the entheses and muscle stiffnesses. For both geometric cases, optimality is found when the enthesis stiffness is 1~2 times larger than the muscle stiffness, which is a reasonable finding given the histology of most entheses.

This is the first investigation of the biomechanical factors affecting avulsion of the PVM at its enthesis. Limitations include use of simplified 3-D PVM geometry and a 2-D isotropic model where a 3-D study evaluating stress transmission in the out-of-plane direction is really required. The model also does not yet reflect the variation in collagen fiber orientation across the enthesis. Since the second stage of labor lasts over an hour, the dissipation of stress over time may also be an important effect.

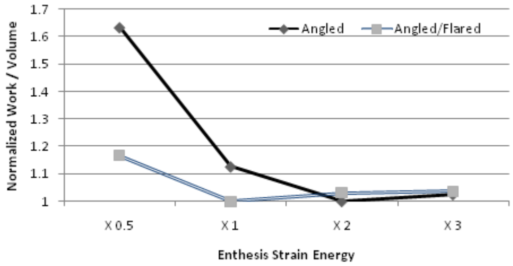

Figure 3: Reduction in stress/strain concentration with increasing enthesial zone stiffness.

CONCLUSIONS

1) Avulsion of the PVM enthesis is most likely to occur in its mid-substance or at the inferior margin, but not at its superior margin.
2) The risk of avulsion of the PVM at the end of the second stage of labor is affected by (a) enthesial geometry, and (b) the stiffness of the enthesis relative to the PVM itself.

REFERENCES

1. DeLancey JOL. *Am J Obstet Gynecol* **192**, 1488-1495, 2005.
2. Lien K, et al. *Obstet Gynecol* **103**, 31-40, 2004.
3. Brooks S, et al. *J Physiol* **488(Pt 2)**, 459-469, 1995.
4. Kearney R, et al. *Obstet Gynecol* **107**, 144-149, 2006.
5. Jing D, el al. *Proceedings of North American Conference on Biomechanics*, Ann Arbor, MI, Abstract 562, 2008.
6. Benjamin M, et al. *J Anat* **208**, 471-490, 2006.
7. Thomopoulos S, et al. *J Biomech* **39**, 1842-1851, 2006.

ACKNOWLEDGEMENTS

PHS grant P50 HD044406-06 (Project 1).

THE EFFECT OF FOLLOWER LOAD ON LUMBAR SPINE FACET JOINT FORCES AND INTERVERTEBRAL DISC PRESSURES

[1,2]John M. Popovich Jr., [2,3]Judson Welcher, [4]Jacek Cholewicki, [2]Wafa Tawackoli, and [1]Kornelia Kulig

[1] Biokinesiology & Physical Therapy, University of Southern California, Los Angeles, CA, USA
[2] Department of Surgery, Cedars-Sinai Medical Center, Los Angeles, CA, USA
[3] Biomedical Engineering, University of Southern California, Los Angeles, CA, USA
[4] Surgical Specialties, College of Osteopathic Medicine, Michigan State University, East Lansing, MI, USA
email: popovich@usc.edu, web: http://pt2.usc.edu/labs/mbrl/

INTRODUCTION

Recommendations for in-vitro biomechanical testing have been established and serve as general guidelines for testing spinal implants [1, 2]. As part of these guidelines, simulating muscle loads and anthropometric loading during in-vitro testing has been recommended as an integral part of the biomechanical testing process. The concept of applying a follower-type preload [3], a load that follows the curvature of the lumbar spine, is the current consensus in applying physiologic relevant loads. These external loads are experienced by anatomical tissues responsible for providing support to the spinal construct, including the intervertebral disc and facet joints. As such, quantifying the load to the spinal structures, with the application of a follower load, is important in understanding the consequences of load to the spinal tissues. Therefore, the purpose of this investigation was to determine the effect of applying a follower load to a human lumbosacral cadaveric specimen on facet joint forces and intradiscal pressure. We hypothesized that implementing a follower load will increase the load experienced by the facet joints and intervertebral disc.

METHODS

One fresh frozen human lumbosacral (L1-Sacrum) specimen (male, 78 y.o.) was used for the biomechanical study protocol. Fluoroscopic images were obtained to rule out gross morphologic deformity or pathology. The specimen was carefully dissected leaving only osteo-ligamentous anatomical structures. Wood screws were inserted into the L1 vertebra and the sacrum to assist in anchoring the specimen in two-part polyurethane potting solution. The distal ends of the specimen were submerged into the potting solution, such that the superior endplate of the L4 vertebra was parallel to the horizontal. The specimen was stored at -20°C prior to mechanical testing.

The potted specimen was thawed at room temperature and tightly secured into the mounting fixtures of an eight-axis Bose Kinematic Spine Tester (Bose Corporation, ElectroForce Systems Group, Eden Prairie, MN). Infrared light emitting diode 2x2 arrays were fixed to the vertebral bodies to record position using an optoelectronic motion analysis system (Optotrak 3020, Northern Digital, Inc., Waterloo, Canada). Bilateral facet joint capsules of the L4-L5 motion segment were incised 15mm to allow for placement of a thin-film pressure sensor (Flexiforce A201, Tekscan Inc., Boston, MA). The pressure sensor was placed in the joint and marked to insure similar placement throughout the testing protocol. Three needle pressure sensors (R.A. Denton, Inc., Rochester Hills, MI) were placed into the L4 intervertebral disc. The specimen was then instrumented with custom-designed components to allow for a follower-type preload.

Sagittal plane mechanical testing was performed before and after application of the follower load. The follower load provided approximately 378 N of preload that followed the lordotic path of the lumbar spine. The mechanical testing profile consisted of a continuous pure bending moment applied in the sagittal plane, testing flexion and extension of the lumbosacral specimen at a rate of 1°/sec until a ±10 Nm bending moment limit was attained. Five complete bending cycles were performed to condition the lumbosacral specimen. The specimen was sprayed with isotonic saline solution throughout mechanical testing to maintain adequate hydration.

Kinematic and kinetic data were recorded at a sampling rate of 50Hz. Data analysis was performed using Matlab version R2006a (The Mathworks, Inc., Natick, MA). The fourth bending cycle was used to calculate range of motion (ROM), facet load, and intervertebral disc pressure.

RESULTS AND DISCUSSION

Intervertebral angle, facet joint forces and intradiscal pressure during the entire fourth bending cycle are presented in Figure 1. Testing of this human lumbosacral specimen showed minimal changes in sagittal plane ROM with the application of the follower load, however peak facet forces and intradiscal pressure changed throughout the bending cycle. Peak ROM, facet force and intradiscal pressure are presented in Table 1.

CONCLUSIONS

Simulating anthropometric loading, by means of a follower load, during biomechanical in-vitro testing of the lumbosacral spine appears to change the loading behavior of the facet joints and intervertebral disc. Increasing the number of cadaveric samples and investigating facet joint surface kinematics may assist in better understanding this phenomenon.

REFERENCES

1. Wilke, H.J., et al. *European Spine Journal*, **7**, 148-154, 1998.
2. Goel, V.K., et al. *J Bone Joint Surg Am.* **88**, 103-109, 2006.
3. Patwardhan, A.G., et al. *Spine*. **24**, 1003-1009, 1999.

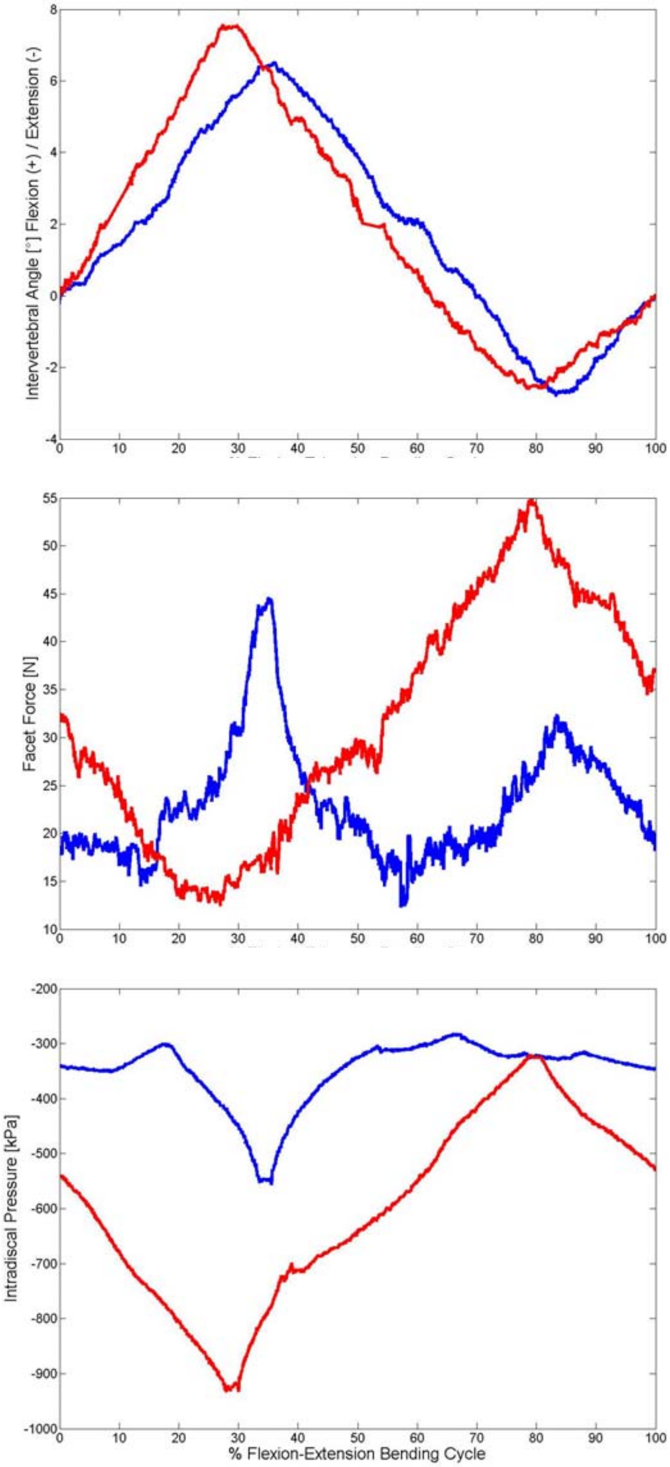

Figure 1. Intervertebral angle, facet force, and intradiscal pressure as a function of bending cycle.

— No Follower Load — Follower Load

Table 1. ROM, facet force, and intradiscal pressure at peak flexion and extension angles with and without follower load.

	Range of Motion (Degrees)		Facet Force (Newtons)		Intradiscal Pressure (kPa)	
	Flexion	**Extension**	**Flexion**	**Extension**	**Flexion**	**Extension**
Un-instrumented	6.52	-2.81	44.57	32.36	556.41	313.42
Follower Load	7.58	-2.62	13.03	54.96	914.98	326.74
% Difference	16.26%	-6.76%	-70.77%	66.38%	64.44%	4.25%

ARTICULAR LOADING DURING WALKING IN SUBJECTS WITH ACL DEFICIENCY

[1,2]Kurt Manal, [3]Lynn Snyder-Mackler and [1,2]Thomas S. Buchanan
[1]Department of Mechanical Engineering, [2]Center for Biomedical Engineering Research
[3]Department of Physical Therapy, University of Delaware
email: manal@udel.edu

INTRODUCTION

The knee adduction moment is often used as an indicator of knee joint loading. The magnitude of the moment has been shown to correlate with the severity and progression of knee osteoarthritis (OA) [1], and as such has become an outcome measure of great interest to those studying gait mechanics. The relationship between the knee moment and joint loading is not straightforward, particularly when agonist/antagonist muscle groups are co-activated. Co-activation is believed to be a neuromuscular strategy to help stabilize the knee and is used by individuals who are anterior cruciate ligament (ACL) deficient [2]. Individuals that suffer an ACL rupture, even if repaired, are at greater risk of developing knee OA than those never injured [3]. Increased co-contraction can elevate knee joint loading and therefore larger joint forces may be associated with the greater incidence of knee OA noted in this group of patients.

To evaluate articular loading requires a computational model that is sensitive to subject specific muscle activation patterns. This is important since different subjects may use different muscle activation patterns to stabilize their ACL deficient knee. In this paper we present results of an EMG-driven modeling approach to predict articular loading for a group of ACL deficient subjects during natural cadence walking. We hypothesized that the medial compartment loads would be greater than those in the lateral compartment. A secondary goal was to qualitatively compare our findings to other studies evaluating similarity in loading pattern and magnitude of load.

METHODS

Four ACL deficient subjects (2 male & 2 female) within 3 months of injury participated in this study. All subjects were young and athletic (mean age = 28.3 ± 15.3 years; height = 1.68 ± 0.11 meters & weight = 68.2 ± 9.9 Kgs). Standard motion analysis methods (ie., video cameras & force platform) and Visual3D (C-motion Inc.) were used to compute stance phase kinematics and kinetics for natural cadence walking. Medially and laterally offset segmental coordinate systems were constructed so that the frontal plane moment could be expressed about the approximate centers of the medial and lateral condyles. These moments were balanced by forces from muscles and soft tissue, and by contact forces acting on the medial and lateral compartments. The location of the contact forces within the medial and lateral compartments was fixed within subject but varied between subjects according to individual anthropometry.

Muscle forces were computed using an EMG-driven musculoskeletal model. Details of this model have been presented elsewhere [4]. Muscle activations for 10 muscles crossing the knee: semimembranosus (SM), semitendinosus (ST), biceps femoris longus (BFL), biceps femoris short head (BFS), medial and lateral gastrocnemii (MG & LG), rectus femoris (RF) and the vasti (VM, VL & VI) were recorded using surface EMGs (sampling rate = 1080 Hz). The EMGs and joint kinematics were used as inputs to a Hill-type muscle model to compute individual muscle forces. The muscle forces were applied to a moment balancing algorithm leaving only the contact forces or soft tissue loads as the unknowns. The contact forces for each trial were time normalized to 100 samples and normalized by bodyweight (BW) for data averaging. Three trials per subject were averaged in this manner.

RESULTS AND DISCUSSION

Consistent with our hypothesis was that ACL-deficient subjects had a larger medial contact force compared to the lateral. The peak average medial load was 2.47 (SD=0.56) BWs and 1.88 (SD=0.42) for the lateral compartment (Figures 1 & 2). The medial compartment exhibited a distinctive two-peak loading profile similar in shape and timing to the frontal plane moment. Peak loading occurred at approximately 80% of stance (Figure 1).

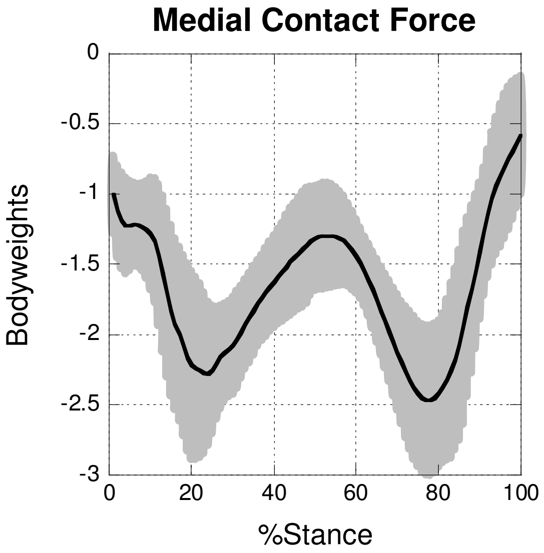

Figure 1. Average loading of the medial compartment during stance. The shaded region represents the standard deviation.

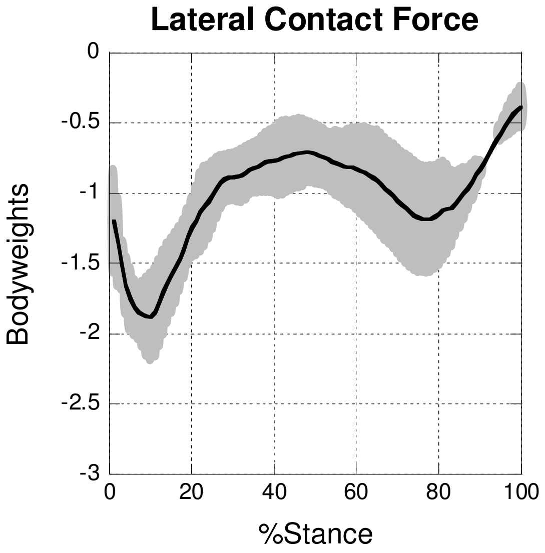

Figure 2. Average loading of the lateral compartment during stance. The shaded region represents the standard deviation.

Interestingly, the frontal plane moment typically exhibits an opposite pattern; the first peak is generally larger than the second. This suggests that inferring joint loading from the net moment may be too simplified an approach and that care should be taken if doing so. The lateral compartment also exhibited a two-peak pattern with the first peak greater than the second (Figure 2).

Many factors (e.g., methodology, patient characteristics, walking speed, etc.) make direct comparisons between our ACL-deficient subjects and those from other studies difficult. Nonetheless, several trends do emerge, most consistently when comparing patterns and timing for the medial compartment. Loading profiles for the ACL deficient subjects in our study were similar to patterns reported for an elderly individual fitted with an instrumented knee implant [5]. Both studies noted a double loading peak for the medial compartment. Lateral compartment loading in both studies was less than noted on the medial side. The lateral compartment for our subjects never became unloaded (ie., soft-tissue restraints were never in tension), consistent with findings reported by Zhao et al. [5]. This is in contrast to results obtained using a statically determinant model that predicted the lateral compartment was unloaded for approximately 40% of stance [6]. The same model predicted a double peak loading pattern for the medial compartment with peak forces of approximately 2 BWs.

CONCLUSIONS

The ACL-deficient subjects exhibited similar patterns of loading reported by others. Different however was the magnitude of the peak forces. The ACL-deficient subjects experienced greater medial and lateral loads compared to values reported for healthy individuals and an elderly subject with an instrumented knee. It is unclear if these differences were due to subject and/or methodological considerations or whether ACL-deficient subjects experience elevated joint loading during stance. Continued work to address this question is underway.

ACKNOWLEDGEMENTS

NIH RR016458, AR46386 & AR48212, S10RR022396

REFERENCES

1. Hurwitz W, et al., *J Orthop Res* **20**, 101-107, 2002.
2. Hurd et al., *J Orthop Res* **25,** 1369-1377, 2007.
3. Lohmander LS, et al., *Am J Sports Med* **35**, 1756-69, 2007.
4. Buchanan TS, et al. *J Appl Biomech* **20**, 367-395, 2004.
5. Zhao D, et al., *J Orthop Res,* **25**, 593-602, 2007.
6. Hurwitz et al., *J Biomech **31,*** 423-430, 1998.

FREQUENCY ANALYSIS OF SKI CHATTER IN SLALOM SKIING: COMPARISON OF INSIDE AND OUTSIDE SKI RESPONSES

[1, 2] Gerald Smith, [1] Marjaana Lappi, [1] Robert C. Reid
[1] Norwegian School of Sport Sciences, Oslo, Norway
[2] Utah State University, Logan, UT
email: Gerald.Smith@usu.edu

INTRODUCTION

Alpine ski racing involves a careful balancing of the forces acting on a skier to obtain an interaction with the environment which optimizes performance. Ski reaction forces are the largest of the external forces acting on a skier and are the most important for determining the path of the skier through a race course. However such reaction forces are difficult to measure under race-like conditions.

Several previous projects have built mobile force plates for attachment between skis and bindings [1,2]. Such devices require mounting on a unique pair of skis rather than on the finely tuned equipment to which a racer is accustomed. In addition they change ski stiffness, increase binding height along with increasing mass of the system all of which affect a skier's technique. Thus such equipment may alter the technique characteristics which are being studied. An alternative approach is to use instrumented insoles for measurement of pressure distributions between foot and boot using a skier's personal equipment. Reaction forces acting on skis can be estimated by summing across the insole surface.

In this study, snow reaction force characteristics during slalom turns were evaluated to better understand relationships of force distribution between skis and their interactions with the under-lying snow. In particular, ski "chattering" (which is low frequency, inconsistent grabbing of a ski during skidding) was characterized and related to loading distribution between inside and outside skis.

METHODS

Ski reaction forces were determined using Novel Pedar insoles placed between foot and boot bed. Pedar's mobile data logger recorded pressure distribution for right and left insoles at 50 Hz. Force from each sensor was summed to obtain a total force on each side vs. time.

High level Norwegian skiers (n=9, with FIS rankings between 165 to 705) were tested over 3 consecutive days during a September training camp on a glacier with nearly ideal, firm surface conditions. A rhythmical slalom course was set with 10 m spacing between gates. Ten turns (5 left, 5 right) near the middle of the course were analyzed. Right and left turns were not combined as there was a slight side-to-side slope gradient. The continuous force data for a run through the slalom course were separated turn by turn from transition point to next transition point. A typical force-time response is shown below in Figure 1. The five turns for each direction were separately analyzed but ultimately combined for a mean response of the skier on right or left turns.

Chattering characteristics were determined through a fourier analysis of the frequency amplitudes for the ski reaction forces. Mean amplitude in the 10-20 Hz range was determined for each turn. The response in this relatively low frequency range is distinct from other ski vibration of higher frequency.

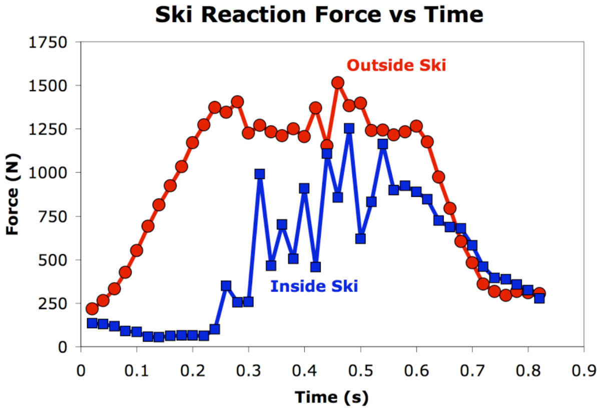

Figure 1. Representative ski reaction force curves during a single slalom turn. The outside ski typically had greater force than the inside ski. "Chattering" of the inside ski is apparent in the graph with rapid changes of force occurring while the ski was loaded during mid-turn.

RESULTS AND DISCUSSION

Ski reaction forces were considerably greater on the outside compared to the inside ski which had about two-thirds of outside forces. This is in good agreement with the force data described by Federolf [1]. Easily visible on force-time graphs, many skiers exhibited chatter of the inside ski. This effect was captured in the frequency distribution data (Figures 2A and 2B) in the 10 to 20 Hz range where inside ski amplitudes were 30 to 50% greater than outside ski amplitudes ($p < 0.01$).

Turn direction affected chattering characteristics for the outside skis (Figure 3). Right turns which were across the side-to-side gradient were associated with increased chatter compared to left turns with the gradient ($p = 0.009$). Inside skis had similar chattering for left or right turns which was greater than either direction outside skis.

Mechanical origins of chattering cannot be definitively determined from this study however these momentary discontinuities of force are likely due to shearing of snow under the ski [1]. Inside skis were typically loaded about two-thirds of outside skis, and would likely have less snow penetration making shearing of the snow layer under the edge, more likely. Also affecting penetration is ski edging angle where the inside leg geometry disadvantages ski edging compared to the outside leg. Finally, the inside ski must turn with a smaller radius of curvature (compared to the outside ski) making carving more difficult and skidding with potential chattering, more likely.

CONCLUSIONS

Ski chattering can be detected through spectral analysis of ski reaction force data. Greater chattering of inside skis was observed. This may be due in part to reduced loading of inside compared to outside skis in tight slalom turns.

REFERENCES

1. Federolf PA. *Finite Element Simulation of a Carving Snow Ski*. Swiss Federal Institute of Technology Zurich, 2005.
2. Klous M et al. *Lower extremity joint loading in carved ski and snowboard turns.* ISBS Proceedings, 91-94, 2007.

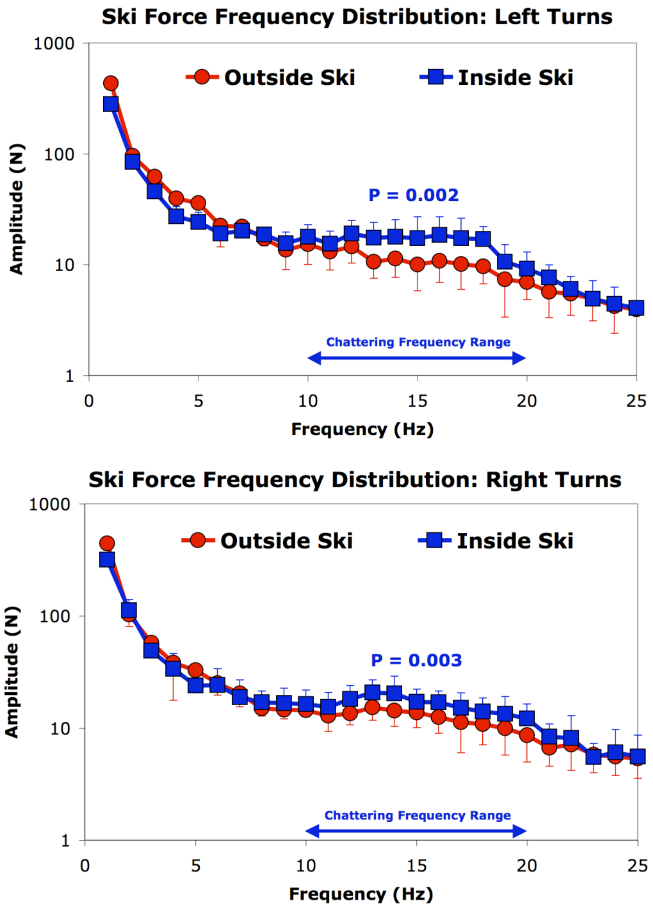

Figures 2A and 2B: Frequency spectrum for ski reaction forces during left and right turns. Chattering of the skis had frequencies in the range of about 10 to 20 Hz. Comparison of mean amplitudes in this range found significant differences for skis on the inside vs. outside of each turn.

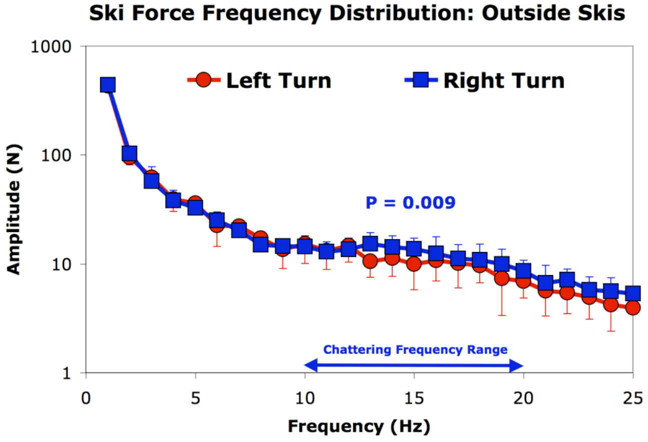

Figure 3. Frequency spectrum for ski reaction forces of the outside ski in left and right turns. Chattering was significantly greater for right turns perhaps due to a slight gradient across the direction of the slalom course.

DEVELOPMENT AND VALIDATION OF A NON-INVASIVE SPINAL MOTION MEASUREMENT SYSTEM

[1]Shaun Stinton, [2]Robert Shapiro, [2]David R. Mullineaux, [3]William Shaffer,
[3]R. Carter Cassidy and [1]David Pienkowski
[1]Biomedical Engineering, [2]Kinesiology and Health Promotion and [3]Orthopaedic Surgery, University of Kentucky
email: skstin2@uky.edu

INTRODUCTION

It has been estimated that 750,000 Americans suffer one or more spinal fractures each year due to osteoporosis [1]. Twenty-five percent of people who suffer a vertebral fracture will suffer another vertebral fracture within 5 years [2]. Spinal fractures cause considerable pain and disability to the patient and resulted in direct healthcare costs of $746 million in 1995 [1]. This expensive and debilitating problem will grow with the aging population and increasing prevalence of osteoporosis. It is probable that static (posture) and dynamic (gait) related abnormal loading of the spine interact with age-weakened tissue to produce a series of degenerative effects that culminate in disc degeneration and spine fractures.

To reduce the incidence and severity of spontaneous vertebral compression fractures, it is first necessary to identify motion and postural patterns that could lead to increased loading of the vertebrae resulting in fractures over time. Once a method for measurement of abnormal motion is developed and validated, human subjects could be tested to determine if abnormal motion is indeed predictive of vertebral fracture and whether preventative measures can be taken. The aim of this study is the first step of this process: development and validation of a spinal motion measurement system.

METHODS

Two cadaver torsos were tested: a 71 year old male (100 lbs) and 95 year old female (91 lbs). A spinal surgeon implanted bone pins (Synthes 4 mm Schanz screws) into 4 levels of the cadaver spines (T7, T12, L3, L5). The T7 level had 2 pins implanted. Retroreflective 4 mm marker triads were attached to the bone pins and additional marker triads were placed adhesively on the skin over the spinous process of the same vertebral levels. Markers were also used to define the pelvis and transverse processes (Figure 1).

The instrumented torso was attached to a testing fixture with metal bands that wrapped around metal bars on the fixture and through the obturator foramen of the pelvis. The fixture allowed for flexion/extension, lateral bending, and axial rotation. Trials of each motion were recorded for a single-cycle and five-cycles trials.

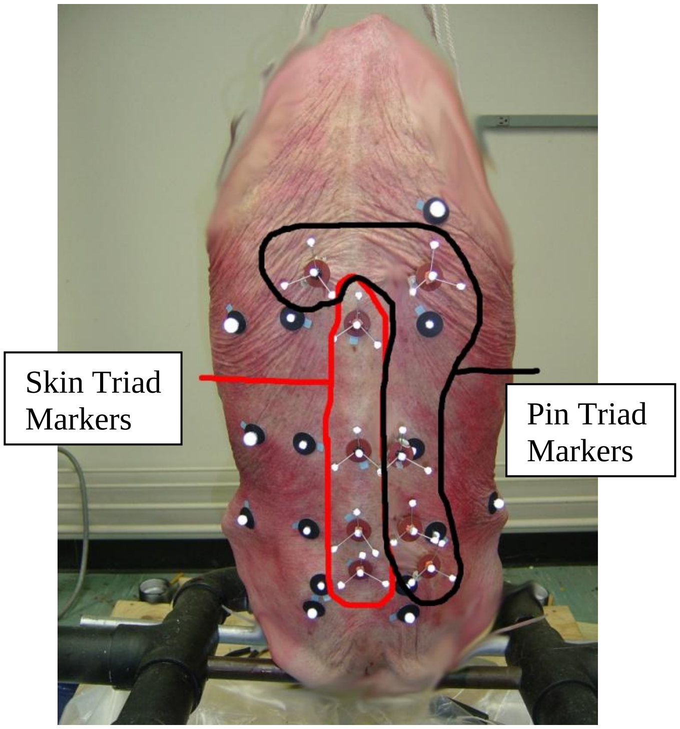

Figure 1: Cadaver torso attached to testing fixture instrumented with 51 retroreflective markers.

Seven Eagle-4 digital cameras with 2352x1728 pixel resolution (Motion Analysis Corp., Santa Rosa, CA) were used to record the 3D coordinates of the markers throughout the motion at 60 Hz using Cortex v1.0 software. The calibration error was determined to average 0.08mm and the residual error was 0.036mm.

Visual 3D software (C-Motion, Germantown, MD) was used to define a laboratory axis and local coordinate systems for each marker triad (skin and pin). These axes were used to calculate the 3D angles of each vertebra throughout the entire motion relative to the laboratory axis. The x, y, and z axes represent roll, pitch and yaw. The angles between the pin and skin triads were compared to determine the accuracy of using skin markers versus the gold standard of bone pins.

RESULTS AND DISCUSSION

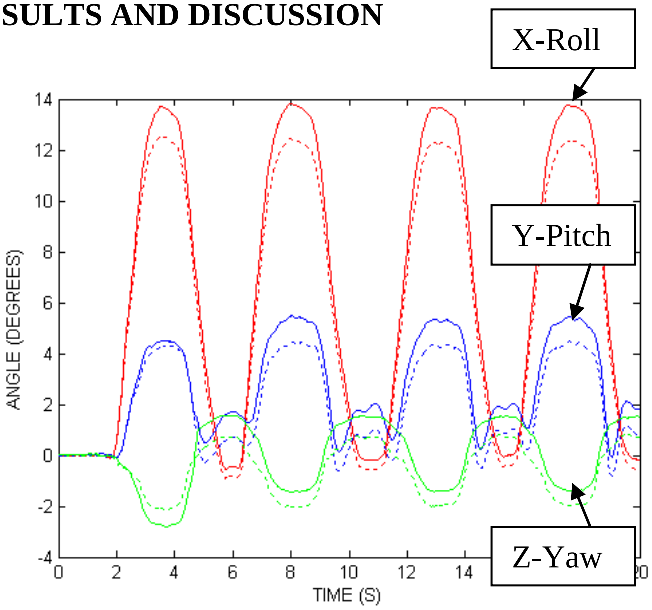

Figure 2: Joint angles of the T12 level in lateral bending for pin (solid lines) and skin (dashed lines) triads.

The results for all three rotations for the T12 level in the second cadaver during lateral flexion are given in Figure 2. The ranges of motion in flexion, lateral bending, and axial rotation were 14.4°, 5.6°, and 4.4° respectively. The maximum differences between the angle measured by the pin triad and the skin triad in the same motions were 1.4°, 1.05°, and 1.13°. The average errors were 0.73°, 0.72°, and 0.65°. The maximum errors occurred at the extreme of the motion. Better results were obtained in many cases, especially for upper levels (T7 or T12) and for flexion trials. In some cases the graphs of the skin and pin angles were coincident with differences less than half a degree around all axes. There are also trials with larger errors, generally in lower levels (L3 or L5) and in axial rotation.

With regard to the shape matching, the matching was good for all the different levels. In general, the upper levels (T7 and T12) showed smaller differences between the pin and skin triads than the lower levels (L3 and L5). The two pins implanted in the T7 level gave similar results for joint angle verifying that the use of bone pins as the standard to measure vertebral motion is reasonable. On average, the differences in the angles given by the two pin marker triads were less than 0.4° around all three axes.

CONCLUSIONS

It is hypothesized that biomechanical factors play a role in vertebral fracture along with osteoporosis. The first step in testing this hypothesis was to develop and validate a measurement system that can determine abnormal spinal motion. This research shows a potential method for this measurement and the accuracy to which the motion of the vertebrae can be determined. The results are promising in that skin markers provide an accurate representation of vertebral motion in cadaver torsos.

An algorithm could be used to account for skin sliding and could be used along with skin marker data in human subjects in a prospective study. In such a study the measured motion of an ‘at-risk for fracture’ group could be used to determine whether abnormal motion was predictive of fractures. Preventative measures such as targeted strength training, balance training, or orthotics could be used in the future to delay the onset of or even prevent future vertebral fracture in people designated as at-risk for fracture.

REFERENCES

1. Melton L 3rd. Epidemiology of spinal osteoporosis. *Spine* 1997:22(24);2S-11S.
2. Melton L 3rd, Chrischilles E, Cooper C, et al. Perspective. How many women have osteoporosis? *J Bone Miner Res* 1992:7;1005.

ACKNOWLEDGEMENTS

This research is funded by grants from the University of Kentucky’s Orthopaedic Surgery Department and the Kentucky Science and Engineering Foundation.

LOAD DEPENDENT VARIATIONS IN KNEE KINEMATICS MEASURED BY DYNAMIC MR

[1]Christopher Westphal and [1,2]Darryl Thelen
Departments of [1]Mechanical Engineering and [2]Biomedical Engineering
University of Wisconsin-Madison, Madison, WI, USA
email: cjwestphal@wisc.edu

INTRODUCTION

Musculoskeletal models that are used to simulate movement often represent the joints as kinematic constraints. For example, the knee has been modeled as a planar joint in which tibiofemoral and patellofemoral translations are a constrained function of the knee flexion angle [2]. Such an assumption may adequately describe normal low-load joint function, but cannot account for the load-dependent behavior of soft tissue (e.g. ligamentous) constraints. For example, others have computationally investigated the dependence of the knee extensor moment arm on quadriceps loading [3]. In addition, prior experimental studies have shown systematic variations in tibiofemoral kinematics in ACL deficient knees [1, 6].

The objective of this study was to assess whether measurable changes in tibio-femoral and patello-femoral kinematics could be induced in normal knees by varying joint loading during a simple knee flexion-extension task. To do this, we constructed a MR compatible loading device that could impose either an elastic or inertial load about the knee. This directly altered the timing of quadriceps activation within a knee flexion-extension cycle. Dynamic MR images were acquired and used to compute the three dimensional joint motion, which was compared between the two loading conditions.

METHODS

The dominant knee of four healthy subjects (ages 22-44y) were tested. Each subject performed cyclic knee flexion-extension at a rate of 30 cycles per minute through a ~35° range of motion within the bore of a scanner (Fig. 1). A MR compatible device with a geared loading assembly (13:1 gear ratio) was used to impose either an elastic (effective torsion spring stiffness of ~0.6 Nm/deg) or inertial load (effective inertia of ~5 kg-m^2) about the knee. Peak quadriceps loading occurred at maximum knee extension in the elastic case and at maximum knee flexion in the inertial condition (Fig. 1).

Cine phase contrast imaging was used to measure three-dimensional tissue velocities while the subjects performed the tasks. A sagittal-oblique imaging plane was defined that bisected the femur, tibia and patella, and was perpendicular to the femoral epicondyles [5]. Subjects repeated each loading condition three times, with each scan lasting 1min 48s. Scanning parameters were: spatial resolution = 0.9x0.9x6mm, VENC = 20cm/s, 256x256 matrix, TR/TE=11.9/5.2ms, and 40 reconstructed frames/cycle.

Regions of interest (ROI) and bone reference frames were defined for the femur, tibia, and patella in an initial frame (Fig. 2). At subsequent frames, linear least squares was used to compute the bone rigid body translational and angular velocities that best agreed with velocities of pixels within the ROI's. Forward-backward integration of the velocities was then used to track the three-dimensional bone motion throughout each cycle [4].

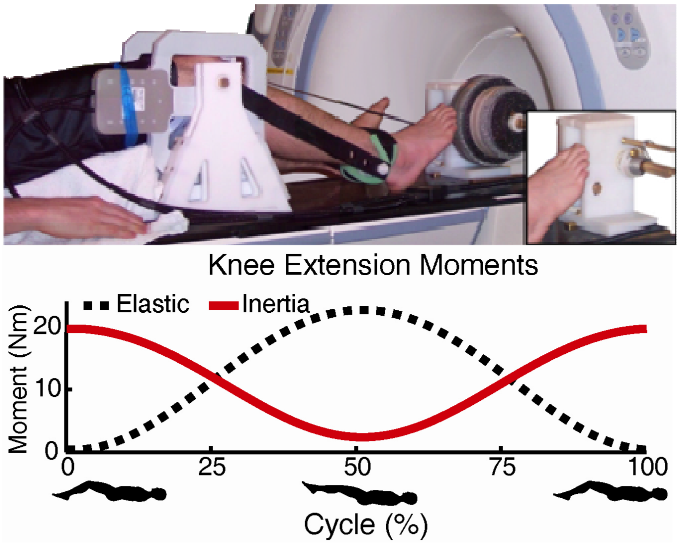

Figure 1. Knee flexion-extension was performed against inertia (shown) and elastic (see insert) loads in a MR scanner, resulting in quadriceps loading that was 180° out of phase.

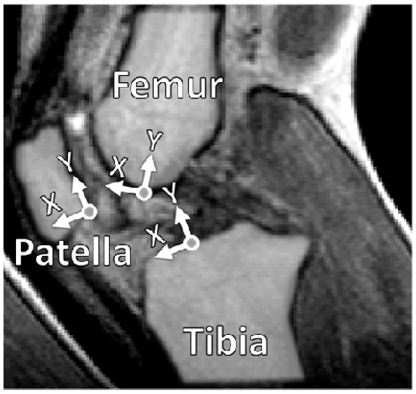

Figure 2. Bone reference frames fixed in the femur, tibia and patella were tracked by integrating three-dimensional velocity information that was acquired using cine-PC imaging.

RESULTS

Differences in knee kinematics were evident between the two loading conditions. Notably, the patella was more superiorly positioned and the tibia more anteriorly translated in the flexed knee under the inertial loading condition (Fig. 3). These differences resulted in the tibia undergoing an average of 3.4 mm greater anterior translation, relative to the femur, over a motion cycle under the elastic loading condition (Fig. 4).

DISCUSSION

We have shown in this study that measurable load-dependent changes in tibio-femoral and patello-femoral kinematics can be ascertained using dynamic MR imaging. The imaging sequence we used (cine-PC) required the subjects to perform multiple cycles of movement, thereby limiting us to loads that were <20% of maximum knee extension strength. Nevertheless even in these low load conditions, we observed systematic changes in knee kinematics that reflected the altered loading. In the inertial case, peak quadriceps loading occurred with the knee flexed which would act to pull the patella superiorly and tibia anteriorly. Such trends were evident in data for all four subjects. There are two potential applications of the testing paradigm. First, the data can be used to calibrate and validate subject-specific knee models. Model parameters could potentially be estimated using data from one load condition, and then model predictions could be then validated by comparing with data from another loading condition. Secondly, the empirical approach could be used to assess variations in knee kinematics in individuals with prior knee injuries. Together, enhanced knee models and simple ways of measuring *in vivo* joint kinematics could facilitate new insights into both normal and altered knee function.

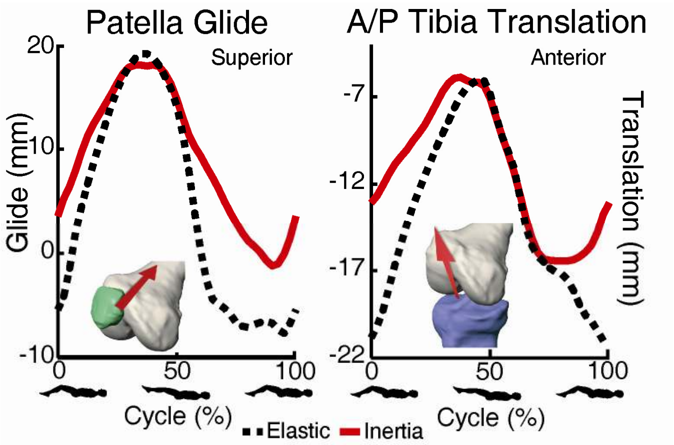

Figure 3. Over the motion cycle, the excursion of the patella glide and tibial translation is greater in the elastic loading condition.

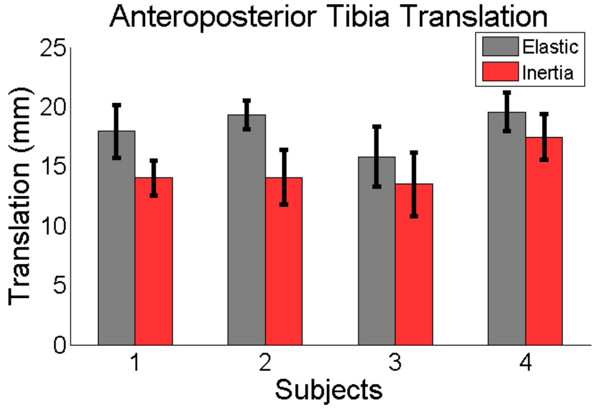

Figure 4. For all four subjects, greater anterior tibial translation was evident in the elastic loading condition, when compared to the inertial loading condition.

REFERENCES

1. Barrance et. al. *Clin Orthop Relate Res*, **454**, 74-80, 2007.
2. Delp et al. *IEEE Trans. On Biomed. Engr.* **37**, 757-767, 1990.
3. Pandy, MG, Shelburne, KB. *Clin Biomech*, **13,** 98-111, 1998.
4. Pelc et. al. *J Magn Reson Imaging*, **5**, 339-45, 1995.
5. Sheehan et. al. *J Biomech Eng*, **121**, 650-6, 1999.
6. Tashman et. al. *Am J Sports Med*, **32**, 975-83, 2004.

ACKNOWLEDGEMENTS

Scott Reeder, Amy Silder, and Kelli Hellenbrand

SENSORY FEEDBACK FROM ANKLE EXTENSOR AFFERENTS IMPROVES LOCOMOTOR OUTPUT IN HUMAN SCI

Ming Wu[1,2], Keith E. Gordon[1], Jennifer H. Kahn[1], Brian D. Schmit[1,2,3]

[1]Sensory Motor Performance Program, Rehabilitation institute of Chicago, Chicago, IL, USA
[2]Department of Physical Medicine & Rehabilitation, Northwestern University, Chicago, IL, USA
[3]Department of Biomedical Engineering, Marquette University, Milwaukee, WI, USA

INTRODUCTION

Limb load afferents modulate muscle activity during human walking. For example, after spinal cord injury (SCI), sensory feedback arising from mechanical loading of the ankle-foot enhances hip extensor activity during the stance phase of gait in air stepping[1]. The purpose of the current study was to use vibratory and electrical stimulation to identify the relative contributions of two major load sensing pathways of the ankle and foot: muscle afferents of the ankle plantar flexors and cutaneous afferents on the sole of the foot, to modulate locomotor patterns in human SCI. We hypothesized that both pathways would contribute significantly to ongoing locomotor activity.

METHODS

Six individuals with chronic incomplete SCI participated in this study. Subjects performed airstepping at 2.0 km/h. A driven gait orthosis, Lokomat (Hocoma, Zurich, Switzerland) prescribed a consistent kinematic pattern at the knees and hips during stepping.

Two separate experiments were performed to investigate the role of two specific load afferent pathways on locomotor patterns. In **experiment 1**, electrical stimulation was used to investigate the role of plantar flexor muscle afferents. In **experiment 2**, vibration was used to investigate the role of plantar surface cutaneous receptors. Four subjects participated in experiment 1 and 5 subjects participated in experiment 2 (3 subjects participated in both experiments at different days). In experiment 1, musculocutaneous stimulation was performed via a pair of self-adhesive electrodes (7×10 cm square; Dermatrode SR; American Imex Inc., Irvine, CA), placed over the calf muscle of right leg. Electrical stimulation was applied at 30 Hz, 20 pulses (0.67 s) at four different phases of the gait cycle (stance, swing, transition to swing and transition to stance) during robotic-assisted airstepping. Each trial consisted of 10 steps without stimulation, 10 sequential steps with stimulation applied during each cycle, followed by 10 steps without stimulation. Stimulation intensity was set at 2.0-2.5 motor threshold depending on the tolerance of the subject. Two repetitions of each stimulation sequence were applied in random order. In experiment 2, a similar protocol was used with vibration applied to the sole of the right foot during robotic-assisted airstepping using a custom deigned vibrator (250 Hz, duration = 0.67s).

Bilateral lower limb joint kinematics, kinetics, and electromyographic (EMG) activity from each subject were recorded. Hip and knee joint kinematics were measured using the joint sensors of the Lokomat. Kinetics were measured from 6-degree of freedom load cells attached to the leg attachment cuffs of the Lokomat.

All kinematic and kinetic data were smoothed using a 4th –order Butterworth low-pass filter with cut-off frequency at 5 Hz. Three-dimensional forces recorded from the load cells were used to calculate the total hip joint torque during stepping. For each subject, we created an average hip torque profile over a complete gait cycle using 29-30 steps recorded during passive airstepping. Then, we estimated the subjects' active hip moments by subtracting the passive hip torque profile from the total hip joint torque calculated for each condition. Peak hip torques were averaged across different trials and subjects (n = 4 for experiment 1 and 2) for each condition. The data from one subject in experiment 2 was excluded from the group average due to a unique torque pattern that was observed for this subject compared with other 4 subjects.

RESULTS AND DISCUSSION

A representative hip torque response from one subject when electrical stimulation was applied during the transition from stance to swing phase is shown in Fig. 1. During electrical stimulation, enhanced hip extension was observed during stance, with the peak extension torque occurring during the early stance phase of the gait cycle.

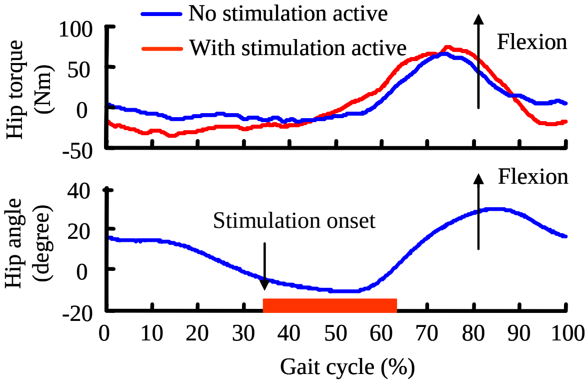

Figure 1: Typical hip torque responses from one subject with incomplete SCI during robotic-assisted airstepping. Torque responses were average from 5 steps with electrical stimulation and 30 steps with no stimulation active, respectively.

Across the group, enhanced hip extension torque was observed when the stimulation was applied during the stance to swing transition (Figure 2A). In contrast, with vibration only, modest changes in hip extension torque were observed across conditions (Figure 2B). No apparent change in hip flexion torque was observed for either electrical stimulation or vibration across conditions.

CONCLUSIONS

Results form this study suggest muscle load afferents are a primary contributor in modulating locomotor activity at the hip joint in human SCI. In addition the response to muscle load afferent stimulation was phase dependent. Such behaviors emphasize the contribution of sensory information, especially from ankle muscle load afferents, to the locomotor output in human SCI during treadmill walking. This knowledge may be especially helpful in identifying rehabilitation strategies for producing functional movements in human SCI.

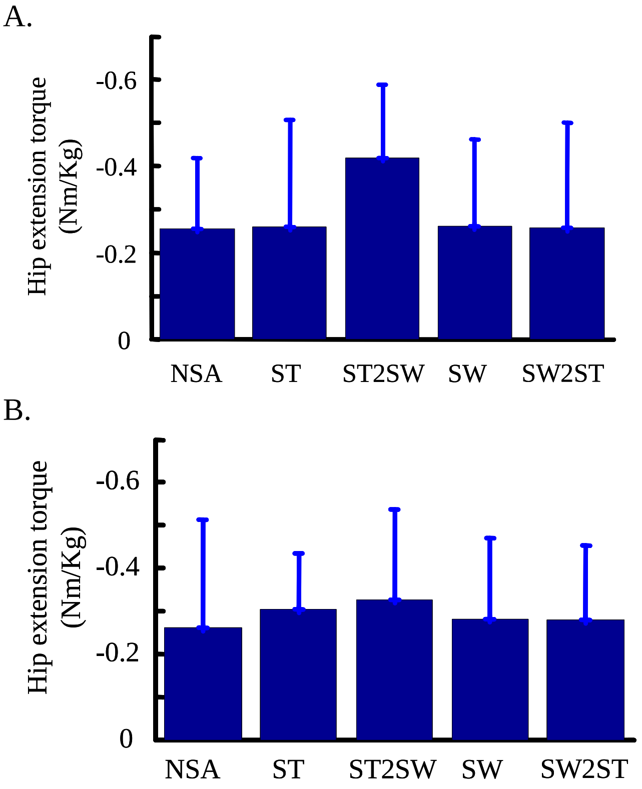

Figure 2: The peak hip extension torque responses triggered by electrical stimulation (A, n = 4) and vibration (B, n = 4) during 4 different stimulation phases, stance (ST), transition to swing (ST2SW), swing (SW), transition to stance (SW2ST), and no stimulation active (NSA). The data shown include the means and standard deviations (normalized by body weight of each subject) for 5 steps for each condition and 2 trials across different subjects.

REFERENCES

1. Gordon KE, et al. *J Neurophysiol* **101**: 2062-2067, 2009.

ACKNOWLEDGEMENTS

Drs. Wu and Gordon contributed equally to this study. This research was supported by Craig H. Neilson Foundation Fellowship 2787 and PVA Research Foundation Grant, 2552.

EFFECT OF FOOT AND ANKLE MUSCLE STRENGTH IN PARTICIPANTS WITH PTTD COMPARED TO HEALTHY CONTROLS

[1] Lindsay Fetzer, [1]Tiffany N. Hilton and [1]Jeff Houck
[1]Ithaca College-Rochester, Rochester, NY
email: jhouck@ithaca.edu

INTRODUCTION

Posterior tibial tendon dysfunction (PTTD) is associated with pain and loss of foot function. Subjects with stage II PTTD experience varying levels of strength deficits,[1] with ~ 40 % losing the ability to perform a unilateral heel rise. Hindfoot inversion is linked to midfoot stability through boney contact within the joints of the midfoot. Therefore, the inability to invert the hindfoot, associated with weakness of the posterior tibialis muscle, may result in midfoot instability and failure to heel rise. Acquired flatfoot deformity associated with PTTD may also contribute to the inability of subjects to stabilize the midfoot contributing to the inability to heel rise independent of hindfoot position. Finally, failure to heel rise may be caused by plantarflexor weakness that results from altered gait patterns and pain as a result of PTTD. The purpose of this study was to compare foot and ankle muscle strength among subjects with stage II PTTD that are able to perform a heel rise (strong), those unable to perform a heel rise (weak) and matched controls. The second purpose was to examine the relationship among hindfoot inversion strength, arch height and plantarflexion strength in subjects with stage II PTTD with varying levels of heel rise ability.

METHODS

Nineteen (12 women, 7 men) community-living men and women 40 years and older with stage II PTTD and fourteen (9 women, 5 men) control participants were recruited to participate in this study. Participants were asked to perform unilateral heel rises to determine the maximal number of times that they could achieve ≥80% rise height. Seven PTTD participants (2 male, 5 female; age=55 ± 8; BMI= 32 ± 5) were classified as "strong" (heel rise ≥ 5 repetitions) and 12 PTTD participants (5 male, 7 female; age=65 ± 13; BMI= 29 ± 5) were classified as "weak" (heel rise < 5 repetitions)[5]. All fourteen control participants (5 male, 9 female; age= 65± 11; BMI=27 ± 5) were able to complete ≥ 5 heel rise repetitions.

All data was collected during a single session. The peak torque of the plantar-flexor muscles was assessed with a Biodex Multi-joint System 4 Pro Isokinetic dynamometer (Biodex, Shirley, New York) at 3 speeds: isometric (0^o/sec), 60^o/sec and 120^o/sec. Isometric hindfoot inversion strength was measured using a force transducer (Model SML-200, Interface, Scottsdale, AZ) connected to a resistance plate and oscilloscope (TDS410A, Tektronix, Beaverton, OR). Between session reliability for this custom device is good (Intraclass correlation > 0.87) [6]. All strength measures were normalized to body weight. The arch index was measured in 10% and 90% of weight bearing and calculated using the dorsum height at 50% of foot length divided by the foot length from the base of the distal first metatarsal head to the heel [7].

Two way ANOVA's were used to compare groups (PTTD Strong, PTTD Weak, Control) and side (involved/Uninvolved) for strength and arch index variables. A logistic regression was used to evaluate the variables that most accurately predicted whether a participant was "strong" (n=21) or "weak" (n=12).

RESULTS AND DISCUSSION

There were no statistical differences between isokinetic ankle plantar flexion at any speed (**Table 1**). For isometric hindfoot inversion strength (**Figure 1**) both the PTTD weak group and PTTD strong group were significantly lower than controls (PTTD weak $p < 0.01$, PTTD strong $p = 0.028$). Acquired flatfoot deformity as indicated by the Arch Height Index was significantly lower in both the PTTD weak ($p < 0.001$) and PTTD strong groups ($p = 0.038$). The involved side of the PTTD weak group was significantly different than the uninvolved side ($p = 0.026$).

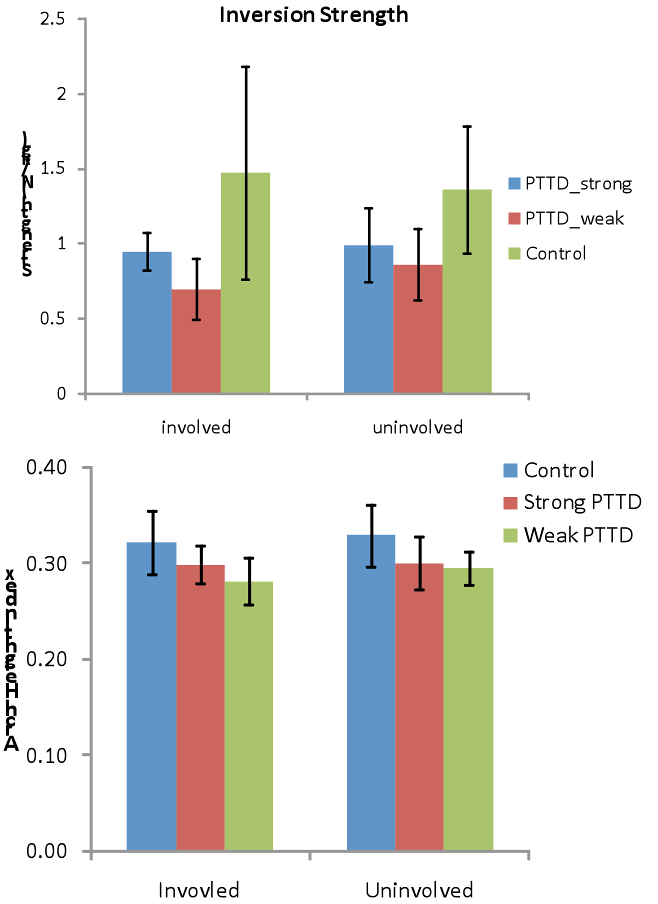

Figure 1: Peak isometric hindfoot inversion strength (Top) and Arch Height Index (Bottom) across groups. Error bars represent standard deviations.

Using logistic regression, the arch index at 90% of weight bearing and isometric hindfoot inversion strength accurately predicted 83 % of the PTTD weak subjects and 90 % of the PTTD strong and control subjects.

This data suggests that arch structure and isometric hindfoot inversion strength in subjects with stage II PTTD may play a significant role in determining the ability to perform a single leg heel raise. The role of ankle plantar flexion strength was not consistent across subjects. Some subjects that were unable to perform a single leg heel raise showed strong deficits in plantar flexion strength, while others showed no deficits. In several cases the deficits in strength (ankle plantarflexion and isometric inversion) occurred in both limbs, suggesting there was a carry-over effect to the uninvolved limb. This may occur because of alterations in gait that cause adaptations to occur bilaterally.

CONCLUSIONS

Arch structure and isometric inversion strength play a more consistent role in determining who can and can't perform a single leg heel raise than ankle plantarflexion strength.

REFERENCES

1. Flemister AS, Neville CG, Houck JR: The relationship between ankle, hindfoot, and forefoot position and posterior tibial muscle excursion. *Foot & ankle international* 2007; **28:** 448-55.
2. Ringleb SI, Kavros SJ, Kotajarvi BR, et al. Changes in gait associated with acute stage II posterior tibial tendon dysfunction. *Gait Posture.* Apr 2007; **25(4):** 555-64.
3. Shaffer MA, Okereke E, Esterhai JL, et al. Effects of immobilization on plantar-flexion torque, fatigue resistance, and functional ability following an ankle fracture. *Physical Therapy.* Aug 2000; **80 (8):** 769-780.
4. Houck JR, Nomides C, Neville CG, Flemister AS: The effect of stage II posterior tibial tendon dysfunction on deep compartment muscle strength: a new strength test. *Foot & ankle international* 2008; **29(9):**895-902.
5. Williams DS, McClay IS. Measurements used to characterize the foot and the medial longitudinal arch: reliability and validity. *Physical Therapy.* 2000; **80**:864-87

Table 1. Comparison of ankle plantar flexion strength across groups. No statistical differences were observed among groups.

Isokinetic Ankle Plantar Flexor Strength (Nm/Kg)						
	60°/s		**120°/s**		**0°/s**	
	Involved	**Uninvolved**	**Involved**	**Uninvolved**	**Involved**	**Uninvolved**
Control	0.64±0.22	0.64±0.24	0.46±0.15	0.46±0.17	1.25±0.33	1.26±0.31
Strong PTTD	0.60±0.19	0.58±0.19	0.46±0.20	0.49±0.23	0.96±0.29	1.00±0.22
Weak PTTD	0.44±0.24	0.51±0.22	0.39±0.16	0.39±0.14	0.81±0.21	0.85±0.19

DO HUMANS STABILIZE RUNNING LIKE ROBOTS?

Mu Qiao and Devin L. Jindrich
Department of Kinesiology and Center for Adaptive Neural Systems, Arizona State University
email: mqiao1@asu.edu, web: http://www.limblab.org/

INTRODUCTION

Over two decades ago, Raibert and colleagues built 2-D and 3-D legged robots capable of stable running based on the principle of symmetry and three simple control rules [1,2]. The control rules maintained running speed, height, and pitch angle. We tested whether humans stabilize running using strategies similar to those used by Raibert's robots. Specifically, we tested whether 1) humans control running height by modulating leg force (not stance duration) by determining whether the relationship between leg force and running height is linear, 2) humans control running speed by changing stance leg placement relative to a "neutral point" by determining the relationship between foothold placement and velocity increment within consecutive steps, and 3) whether humans control body attitude using hip torques.

We found that humans appear to use Raibert's robotic control laws to stabilize running. Leg force was linearly related to running height, and running speed was regulated by adjusting foothold placement relative to the neutral point (NP). Both hips generated moments which were linearly related to pitch angle and its time derivative.

METHODS

We used a VICON® 3-D motion tracking system, and two force platforms (Bertec) to record kinematics and Ground Reaction Forces. The platforms were obscured by a 120cm × 160cm, 2mm-thick rubber mat. 12 male participants (age = 29.2 ± 4.2years; body weight (bw) = 68.8 ± 8.8kg; body height (bh) = 175.5 ± 7.9cm) performed five trials in each of five running tasks: constant velocity running, acceleration, deceleration, stepping up and stepping down. COM trajectory was calculated with VICON's Plug-In-Gait model using anthropometric data collected from each participant.

RESULTS AND DISCUSSION

Humans showed significant correlations between mean leg force and running height across all trial conditions (Fig. 1). These relationships were particularly evident for acceleration (Fig. 2).

1. Mean Leg Force and Running Height

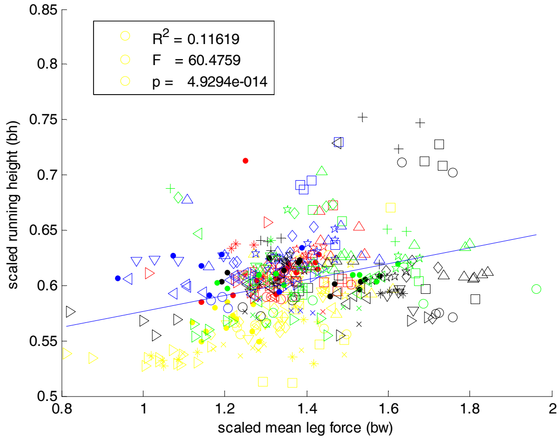

Figure 1: All participants' scaled mean leg force vs. scaled running height. Tasks shown are constant-velocity (red), acceleration (black), deceleration (blue), stepping up (yellow), and stepping down (green). Data from individual participants are represented by different symbols.

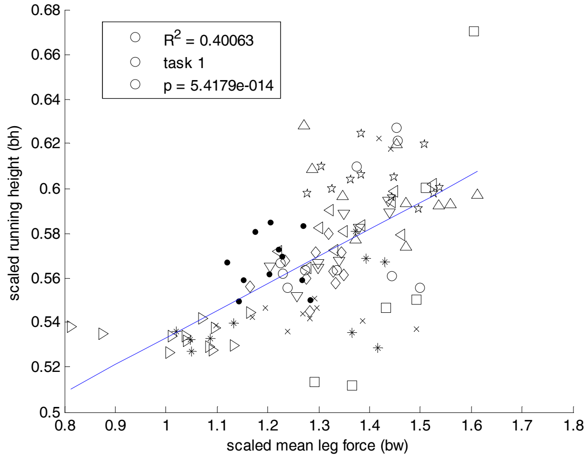

Figure 2: All participants' scaled mean leg force vs. scaled running height in the acceleration task.

In contrast, significant correlations between stance period and running height were not seen (Fig. 3).

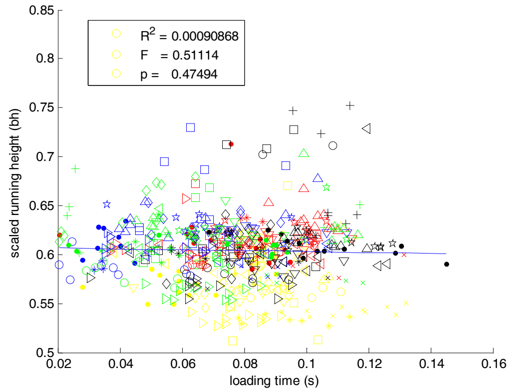

Figure 3: All participants' loading time vs. scaled running height.

2. Running Speed Control Strategy

The NP position is defined as one half of the product of touch down velocity and stance duration. Since the human foot does not make a point contact with the ground, we calculated the distance between the NP and the mid-stance COP position.

The distance between the mid-stance COP position and the NP showed a significant correlation ($p<0.01$).

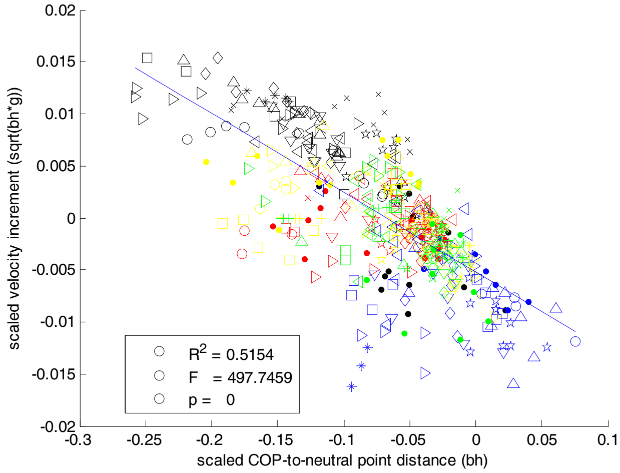

Figure 4: participants' scaled COP-to-NP distance vs. velocity increment.

3. Body Attitude Control

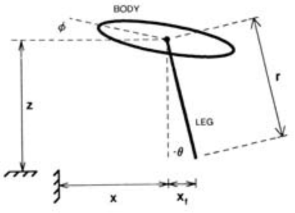

Figure 5: Schematic of body attitude.

Raibert's robots regulated body pitch angle and pitch velocity in stance phase according to the relationship

$$\tau = -k_p\left(\phi - \phi_d\right) - k_v\dot{\phi} \qquad (1)$$

where ϕ is body pitch orientation, ϕ_d is desired orientation, and k_p and k_v are constants. Body pitch angle was directly correlated with hip torque ($p<0.01$) as illustrated by typical trials (Figure 6).

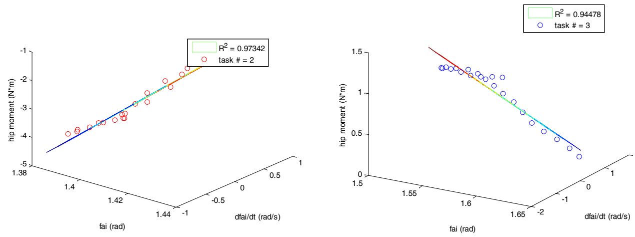

Figure 6: representative trials for attitude and hip moment relationship.

CONCLUSIONS

We found that humans appear to use control strategies to stabilize running that are similar to those used by dynamic running robots.

Height vs. Force Relationship: Running height was linearly related with mean leg force, but not with stance period. Humans thus maintained leg hopping height by adjusting force, not timing.

Running Speed: Humans adjusted leg touchdown position to place the COP in front of NP to decelerate while behind NP to accelerate. Humans thus maintained running speed by controlling foot placement.

Body Attitude Control: Body attitude (pitch) was regulated by the torque provided at both hips.

Although humans are morphologically more complex than Raibert's robots, the simple control laws successful for robot stability also appear to be employed by humans. These findings may be useful in designing real-time control systems for movement assisting device such as exoskeletons and powered orthotics and prosthetics, or for functional neuromuscular stimulation systems.

REFERENCES

1. Raibert, M. H. (1986). *Legged robots that balance*. Cambridge, Mass.: MIT Press.
2. Raibert MH (1986). Symmetry in running**.** *Science* **231:** 1292-1294

EMG ANALYSIS OF ABDUCTOR POLICIS LONGUS, EXTENSOR CARPI ULNARIS AND FLEXOR CARPI ULNARIS DURING FOREARM PRONO-SUPINATION

[1]Joseph Bader, [2]Michael Boland, [2]Joseph Stone, [3]Timothy Uhl, [1,2]David Pienkowski
[1]University of Kentucky Center for Biomedical Engineering, [2]University of Kentucky Department of Orthopaedic Surgery, [3]University of Kentucky Department of Rehabilitation Sciences
Email: joseph.bader@uky.edu

INTRODUCTION

Little is known about forearm biomechanics compared to joints such as the knee and hip. In order to develop a model to analyze the biomechanics of the forearm at locations such as the distal radioulnar joint, the function of forearm muscles must be analyzed and understood. Developing an accurate set of data to determine muscle function of various forearm muscles is necessary so that data placed into a biomechanical model is accurate as possible. This initial forearm muscle study examined the muscle function of the abductor policis longus (APL), extensor carpi ulnaris (ECU) and the flexor carpi ulnaris (FCU) during forearm rotation. Data was collected using indwelling electrode electromyography (EMG) and was collected in both the pronating and supinating direction.

METHODS

Data was collected using ten subjects in this IRB approved study. Two indwelling electrodes were placed in the right APL, ECU and FCU of each subject using a 25 Gauge needle. The needles were placed using published guidelines [1]. A grounding surface electrode was placed on the olecranon of the right shoulder. A 5 second baseline test was collected while the subject relaxed their arm. In order to scale the muscle activity between subjects, maximum EMG muscle activity of the muscle of interest was determined using published maximum voluntary isometric contraction exercises (MVIC) [2]. Each exercise was performed 3 times for 5 seconds with a 2 minute rest between each trial. The subject was then asked to hold the handle of an isokinetic dynamometer with the elbow at 90° of flexion (Figure 1). An abduction pillow was also placed under each subjects arm to standardize the testing and allow the subject to comfortably rest between trials. The handle of the dynamometer was placed in one of nine positions of forearm rotation: maximum pronation, 75° of pronation, 50° of pronation, 25° of pronation, neutral, 25° of supination, 50° of supination, 75° of supination and maximum supination. The subject was asked to grip the handle at the specified position and pronate their forearm as hard as they comfortably could for 5 seconds. This was done three times with a 2 minute break between each trial. The same procedure was then carried out at the same position while the subject supinated their forearm.

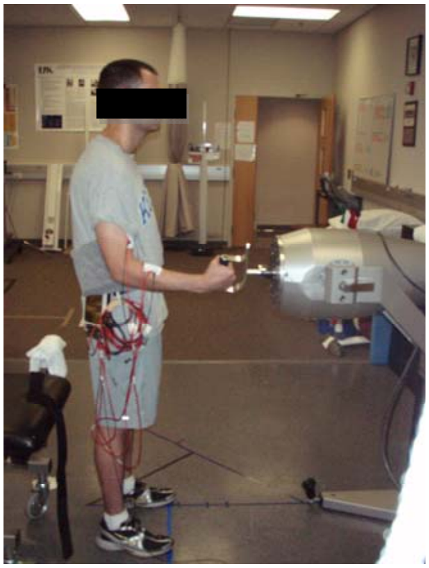
[redacted]

Figure 1: Instrumented subject holding dynamometer handle in testing position.

Data was collected at a rate of 2000 Hz. Once all data had been collected, the maximum value from the baseline test was subtracted from each muscle. The EMG data were then full wave rectified and low pass filtered. The root-mean-square (RMS) of the resulting linear envelope was then calculated. EMG values were normalized to the maximum RMS value. Ideally the highest value for a specific muscle would be from data collected from the MVIC trials, but this was not always the case. The normalized EMG values were then averaged for each of the three trials in both the pronating and supinating direction at each of the nine positions.

RESULTS AND DISCUSSION

EMG data from the APL (Figure 2) shows that the muscle was more active while supinating than pronating at each of the 9 positions. While pronating, APL muscle activity was greatest at 50° of pronation while supinating it was greatest at 50° of supination. The peak pronating signal was 46% of the largest APL signal observed while the peak supinating signal was 65%.

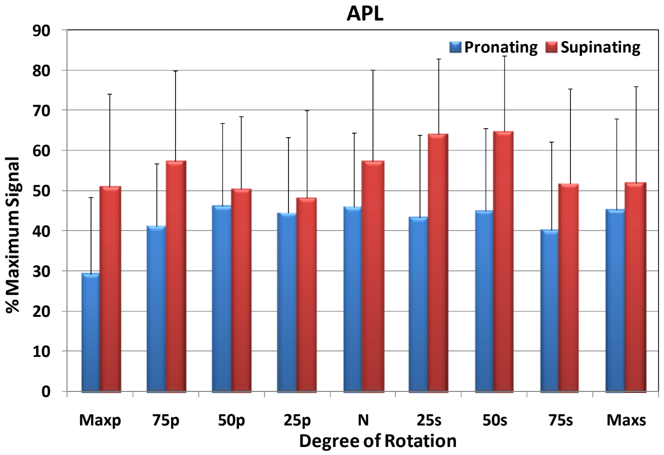

Figure 1: Pronating and supinating EMG activity for the APL for nine positions of forearm rotation.

EMG data from the ECU (Figure 3) shows that in pronated positions, the signal was greatest while the forearm was supinating. In supinated positions, the signal was greatest while the forearm was pronating. The greatest pronating signal occurred at maximum supination while the maximum supinating signal occurred at 50° of pronation. The peak pronating signal was 63% of the largest ECU signal observed while the peak supinating signal was 71%.

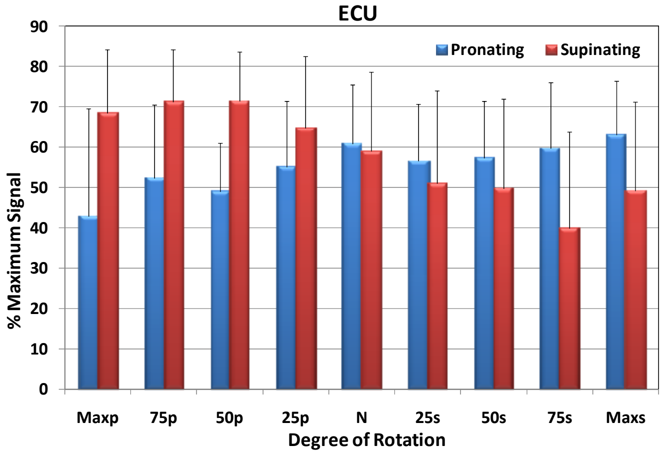

Figure 2: Pronating and supinating EMG activity for the ECU for nine positions of forearm rotation.

EMG data from the FCU (Figure 4) shows that in pronated positions, the signal was greatest while the forearm was supinating. In supinated positions, the signal was greatest while the forearm was pronating. The greatest pronating signal occurred at maximum supination while the maximum supinating signal occurred at maximum pronation. The peak pronating signal was 58% of the largest FCU signal observed while the peak supinating signal was 48%.

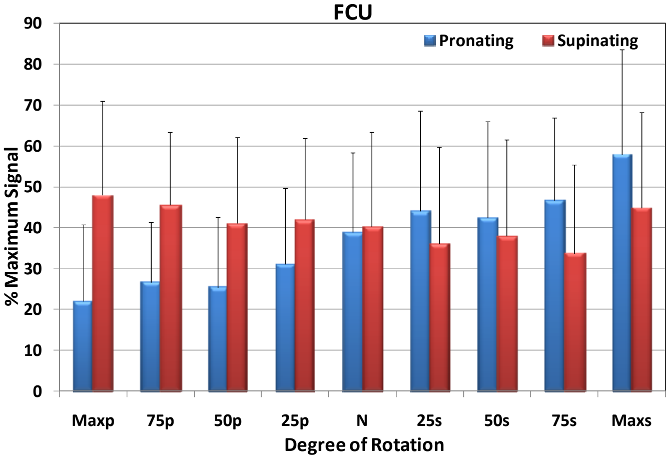

Figure 3: Pronating and supinating EMG activity for the FCU for nine positions of forearm rotation.

CONCLUSIONS

These results show that the APL is more active when the forearm is supinating than when it is pronating. The ECU and FCU are both more active in pronation positions when they are supinating and more active in supinating positions when they are pronating. This may indicate that the ECU and FCU play a role in slowing down forearm rotation as the maximum range of motion is approached in either direction.

REFERENCES

1. Perotto AO. *Anatomical Guide for the Electromyographer-The Limbs and Trunk 3rd ed.*, Charles C Thomas Publishing, Springfield, IL.
2. Kendall FP. *Muscles-Testing and Function with Posture and Pain 5th ed.*, Lippincott Williams, Baltimore, MD.

ACKNOWLEDGEMENTS

The research was funded in part by a grant from the University of Kentucky Department of Orthopaedic Surgery.

REDUCED IMPACT LOADING FOLLOWING GAIT RETRAINING OVER A 6 MONTH PERIOD

Irene S. Davis [1,2], Harrison Phillip Crowell [3], Rebecca E. Fellin[1] and Allison R. Altman[1]

[1] Dept. of Physical Therapy, University of Delaware, Newark, DE
[2] Drayer Physical Therapy Institute, Hummelstown, PA
[3] U.S. Army Research Laboratory, Aberdeen Proving Ground, MD

E-mail: mcclay@udel.edu

INTRODUCTION

The Healthy People 2010 initiative encourages people to engage in regular exercise throughout their lifetime. The American College of Sports Medicine is also promoting a new program, Exercise is Medicine, to encourage widespread physical activity. Running is one of the most popular fitness activities that Americans engage in. However, due to the repetitive nature of running, overuse injuries are common. Stress fractures are among the most serious overuse injuries a runner sustains. They are among the top 5 injuries that runners sustain. More alarming, they are reported to be associated with a 36% reinjury rate [1]. This may be attributed to the fact that the underlying causes of the injury were unaddressed.

Individuals who sustain a tibial stress fracture exhibit increased tibial shock, vertical impact peaks and vertical loadrates compared to healthy controls [2]. The rapid deceleration of the tibia at heel strike can lead to high strain rates in the bone, which are suspected of being a cause of stress fractures [3]. Therefore, reducing these loads during running may result in reducing stress fracture risk.

Recently, using real-time feedback from an instrumented treadmill, White et al. [4] reported an increased symmetry of loading in patients with a unilateral total hip replacement. In a pilot study, Crowell et al. [5] demonstrated that impact loads could be reduced in runners at risk for stress fractures. However, this needs to be examined on a larger scale. In addition, the long-term persistence of these changes has not been examined.

Therefore, the purpose of this study was to examine the effect of a gait retraining program using real-time feedback to reduce loading in runners at risk for tibial stress fractures. It was hypothesized that impact loading would be reduced and that the reductions would persist over a 6 month period.

METHODS

This is an ongoing study in which 4 females and 6 males, aged 24.1 (6.9) yrs, and running 25.5 (16.7) miles per week, have participated to date. All subjects were injury free, but exhibited tibial shock greater than 8.5 g during an initial screening. Baseline 3D ground reaction force and tibial accelerometer data were collected at 1050 Hz as subjects ran through the laboratory at 3.7 m/s (±5%). 5 acceptable trials were collected and analyzed.

Subjects first underwent an 8-session control period, where runtime was progressively increased from 15-30 minutes, but no feedback was provided. Kinetic data were then analyzed again. For the retraining sessions, a uniaxial accelerometer was attached to the distal medial tibia on the side that had the highest shock, noted in the baseline data collection. Visual feedback of their tibial shock was provided on a monitor (Figure 1) placed in front of them as they ran on the treadmill at a self-selected pace. Subjects were instructed to maintain their shock levels at 50% of their peak shock determined at baseline. A target was provided using a line placed on the monitor. With a brief practice, individuals were able to bring their tibial shock below the target value (Figure 1).

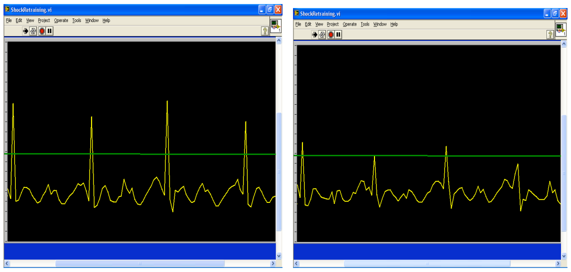

Figure 1. Tibial shock feedback. High baseline shock can be seen in the left panel. In the right panel, a 50% reduction in shock can be seen.

Runtime was progressively increased from 15 to 30 minutes over the 8-session program. Subjects were restricted from running outside the retraining sessions. Subjects received constant visual feedback for the first 4 sessions. The feedback was progressively removed over the remaining sessions such that subjects had only 3 minutes of feedback in their final session. Removal of feedback has been shown to be important for the persistence of novel skills [6].

Immediately after the last retraining session, kinetic data were collected again. Subjects were then instructed to gradually increase their mileage. They returned to the lab for a 1 and 6 month follow-up assessment. As the current number of subjects is low, the data will be presented descriptively. Variables of interest included the peak positive acceleration (PPA), the vertical impact peak (IPeak), and the average and instantaneous vertical loadrates (VALR, VILR).

RESULTS

Of the 10 subjects, 8 have completed their 1-month follow up and 7 have completed their 6 month follow up. Results for each variable of interest are presented in Figure 2 for the baseline data, the post control data and the 1 and 6-month follow-up data.

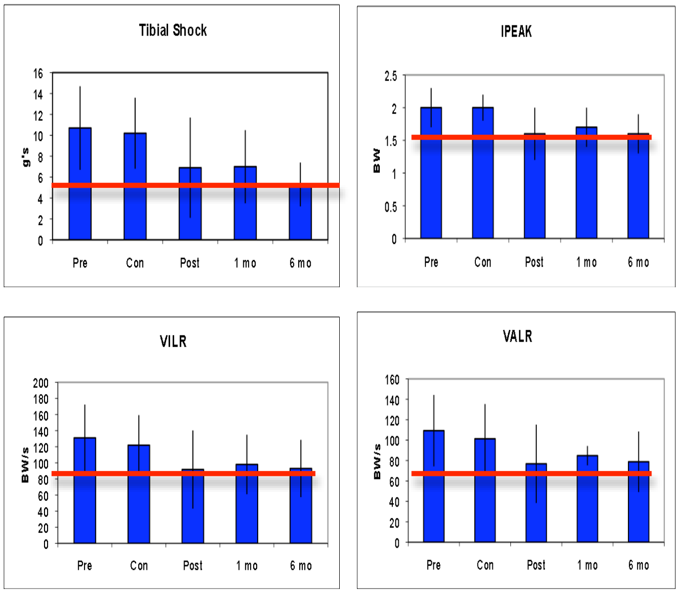

Figure 2. Impact loading variables at baseline, following the control period, following retraining, and at 1 and 6 months f-up. The lines indicate the normal value for these measures.

The effect size of the reductions (between baseline and post training) were as follows: PPA: 0.86, IPeak: 1.14, VILR:0.87, and VALR: 0.89

DISCUSSION

The overarching aim of this study was to determine if impact loading can be reduced with gait retraining using real-time feedback during running. Subjects served as their own controls, and thus a period of progressive treadmill running without feedback was included. No changes were noted following the control period, suggesting that running on the treadmill alone does not reduce impact loading. However, following the 8 sessions of retraining, reductions in the impact loading were associated with large effect sizes. This indicates a very strong effect of the intervention.

We were also very interested in the persistence of the changes beyond the training sessions. If mechanics return to their baseline values, then the risk of injury is again increased. We were encouraged by the results that showed essentially no difference between the values following the training, and at 1 and 6 months follow-up. We are continuing to follow-up with these subjects through 12 months. We believe that the systematic removal of feedback during the last 4 sessions of training may have contributed to persistence of the changes.

With the reductions noted with the retraining, the impact values all fell within normal values. The 35% reduction in tibial shock with retraining was markedly greater than that typically noted (10-12%) with footwear or orthotics [7]. This suggests that individuals may have a greater propensity to modify their own gait mechanics than do external devices.

CONCLUSIONS

Based on the results of these preliminary data, gait retraining, using real-time feedback can reduce impact loading in runners at risk for stress fractures. In addition, these reductions persist up to 6 months.

REFERENCES

1. Hauret ,KG et al. (2001). *Milit. Med*, **166**(9), 820-826.
2. Milner, CE et al. (2006). *MSSE* **38**, 323-328.
3. Fyhrie DP et al. (1998). *Ann. Biomed. Eng*., **26**(4), 660-665.
4. White, S (2005). *Arch. Phys. Med. Rehabil*. 86, 1958-63.
5. Crowell, HP et al. (2006). *Proc of 2006 ASB Mtg.*
6. Winstein, CJ et al. (1991) *Phys Ther* **71**(2):140-149
7. Butler RJ et al. (2006) *Am. J. Sports Med*. **34**(12):1998-2005.

ACKNOWLEDGEMENTS

DOD W911NF-05-1-0097, DOD X81XWH-07-1-0395, R01HD050679

GRAVITY DOMINATES UNCONSTRAINED, THREE-DIMENSIONAL REACHING IN RHESUS MONKEYS

D.L. Jindrich[1], G. Courtine[2], J. J. Liu[2], H.L. McKay[4], R. Moseanko[4], T.J. Bernot[4], R.R. Roy[2], H. Zhong[2], M.H. Tuszynski[4], V.R. Edgerton[2]
[1]Department of Kinesiology and Center for Adaptive Neural Systems, Arizona State University,
[2]Physiological Science & Brain Research Institute UCLA, Los Angeles, CA, [3]California Nat'l Primate Research Center, Davis, CA, [4]Neuroscience, UCSD and VA Medical Center, La Jolla, CA
email: devin.jindrich@asu.edu, web: http://www.limblab.org

INTRODUCTION

We studied the dynamics and motor control of arm movements by Rhesus monkeys during a food-retrieval task to identify the control strategies used for natural movements. Whereas many studies have investigated motor control during planar arm movements, fewer have focused on three-dimensional movements that must resist gravity. Gravity has also been argued to be less important as movement speed increases [1].

One potentially simple strategy for multi-joint movements involves controlling joint stiffness and allowing appropriate movements to evolve over time [2]. We therefore focused on two hypotheses:

1. Gravity dominates these unconstrained, three-dimensional reaching movements
2. Monkeys use joint stiffness-based control to execute nearly-reciprocal reach and retrieval movements.

We found that net joint moments primarily must resist gravity. In turn, gravity allows for reciprocal reach and retrieval movements using relatively simple joint stiffness control.

METHODS

While seated, monkeys reached, grasped, and retrieved grapes impaled on a post (Fig. 1). We recorded three-dimensional kinematics using 100 Hz video, calculated joint moments using inverse dynamics (iterative Newton-Euler algorithm), and decomposed them into moments due to gravity, segmental interactions, and moments produced by muscles and tissues of the arm.

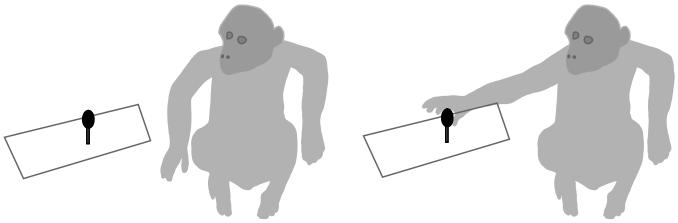

Figure 1. Diagram of reaching and grasping movements made by Rhesus monkeys.

RESULTS AND DISCUSSION

Gravity dominated unconstrained three-dimensional reach and retrieval movements made by Rhesus monkeys. Segment and interaction moments were less than half of the moments required to resist gravity for all joints except for shoulder flexion/extension, which was completely uncoupled from gravity in the angle convention used (Fig. 2).

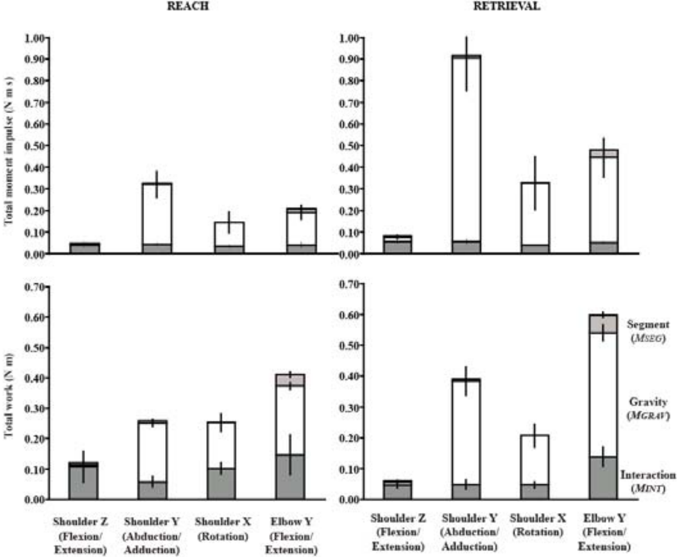

Figure 2. Total absolute moment impulses (top plots) and work (bottom plots) for primary shoulder and elbow degrees of freedom. Moment impulse was calculated by integrating the absolute value of each component of net moment with respect to time, and total work was calculated as the sum of

the absolute value of instantaneous work for each component of net moment. Consequently, these values represent the maximum amount of impulse or work that the moment component could contribute to the net impulse or work.

Observed linear relationships between joint moment and joint angle are consistent with the hypothesis that monkeys control stiffness during multi-joint movements (Fig. 3). Net Generalized Muscle Moments (M_{GM}) were correlated to joint angle, showing average individual-trial linear merit values above 0.9 for both reach and retrieval. Linear merit values calculate the variance explained by a linear relationship between variables without respect to the slope of the relationship [3].

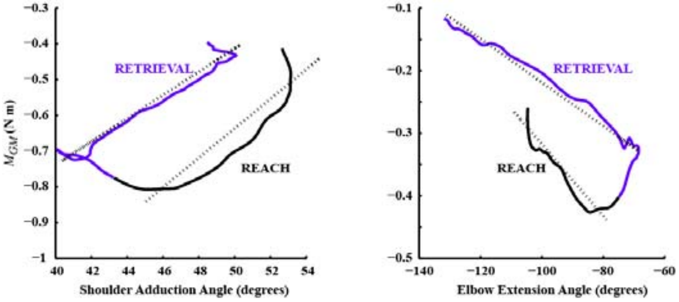

Figure 3. Relationship between M_{GM} and angle for shoulder adduction (left) and elbow extension (right). Data from all trials were normalized in time to the mean duration of reach and retrieval phases of motion across all trials. Resulting normalized time series were averaged for each monkey, and then averaged across monkeys (black traces or solid lines). Dotted lines represent least-squares linear fits to averaged data.

Nearly reciprocal reach and retrieval movements could be accomplished with minor modifications to joint stiffness parameters. Retrieval, involving elbow flexion, actually involved lower flexion moments than reach (Fig. 3). The transition from reach to retrieval involved a 45% decrease in elbow joint stiffness, but no significant change in shoulder joint stiffness. Shoulder and elbow torque offsets were 30% and 50% lower magnitude, respectively, during retrieval.

Fundamentally different interaction moments contributed to the lower-magnitude joint moments observed during retrieval. During reach, interaction moments (M_{INT}) at the elbow and shoulder were of the same sign as gravitational moments (M_{GRAV}), requiring higher muscle moments than would be required to resist gravity alone (Fig. 4). During retrieval, interaction moments opposed gravity, resulting in lower required muscle moments. Minor decreases in shoulder stiffness parameters resulted in upper arm adduction. Resulting interaction moments contributed to elbow flexion despite reduced elbow moment.

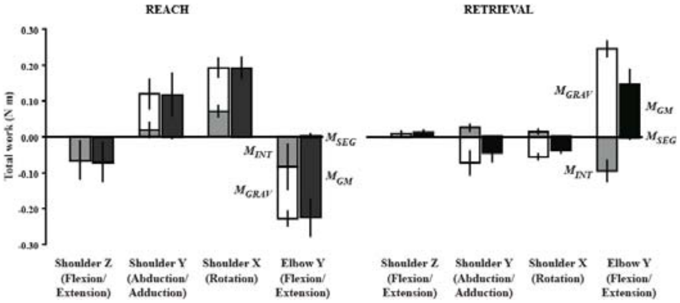

Figure 4. Net work by components of net moment averaged across all monkeys for reach (left) and retrieval (right) phases of movement. Segment work was small for all degrees of freedom. During reach, interaction and gravitational moments were of the same sign, whereas during retrieval interaction moments counteracted the moments necessary to resist gravity. The shoulder generated positive work in abduction/adduction and external rotation during reach, whereas the elbow absorbed energy. Retrieval showed the opposite pattern.

CONCLUSIONS

- Gravity dominated both reach and retrieval movements.
- Joint stiffness control represents a simple strategy that allows appropriate movements to evolve in gravity.
- The transition from reach to retrieval involved minor changes to joint stiffness parameters.
- Upper arm adduction during retrieval allowed interaction torques to contribute to elbow flexion despite reduced flexor moments.

REFERENCES

1. Hollerbach JM, Flash T (1982) Dynamic interactions between limb segments during planar arm movement. Biol. Cybern. 44: 67-77
2. Hogan N (1985) The mechanics of multi-joint posture and movement control. Biol. Cybern. 52: 315-331
3. Gottlieb GL, Song Q, Almeida GL, Hong D, Corcos D (1997) Directional control of planar

PASSIVE SENSITIVITY DETERMINES GOAL-LEVEL VARIABILITY IN A SHUFFLEBOARD TASK

[1] Joby John, [2] Jonathan B. Dingwell, [1] Joseph P. Cusumano
[1] Department of Engineering Science & Mechanics, Penn State University, State College, PA
[2] Nonlinear Biodynamics Lab, Department of Kinesiology, University of Texas, Austin, TX
[1] E-mail: jzj109@engr.psu.edu

INTRODUCTION

Variability is inherent in all human movement and has been posited to rise from a variety of sources ranging from the CNS, to being distributed in the peripheral motor system, to being a result of dynamic interaction of the moving and at-rest parts of the organism [1]. Regardless of the source of this variability, its effect on performance of skilled tasks is undeniable. This variability and its effect on performance manifests itself in repeated trials of a skilled task. We present a theoretical framework and modeling methodology that allows us to examine the mapping of this body-level variability to the goal level. We investigate this mapping and identify a totally passive property (independent of the control and internal variability) that affects goal-level performance, depending on the strategy adopted to perform the task. In light of this theoretical approach we analyze the variability that arises in a virtual shuffleboard experiment and present the results.

METHODS

To study the body-goal variability map we use a human-in-the-loop virtual shuffleboard task. This task consists of a subject actuating a linear low friction slider from which acceleration, velocity and position information are collected to simulate the physics in a virtual environment in real-time. The slider corresponds to a virtual cue that is used to push a virtual puck on level ground. When the contact force between the cue and the puck goes to zero, the puck is released and is decelerated by Coulomb friction on the ground. The goal of the task is for the puck to stop at a target that is a distance L from the datum. The subject is instructed to achieve the goal in every trial. Depending on his/ her error in a given trial, the subject corrects their strategy to get closer to the goal in the following trial.

At the core of the modeling framework are the concepts of *goal functions* and *goal equivalent manifolds (GEMs)* [2]. With a certain degree of generality we can represent the goal of a skilled task as a mathematical function of the form:

$$\mathbf{f}(\mathbf{x},\mathbf{y}) = \mathbf{0} \qquad (1)$$

where $\mathbf{f}$ is the function that captures the required interaction between the body states $\mathbf{x}$, the goal vector $\mathbf{y}$, the morphological and bio-mechanical constraints of the subject and the physics of the environment, such that the goal is perfectly achieved. The set of all body-states $\mathbf{x}$ that satisfies Eq.(1), typically has the structure of a manifold and defines the GEM. Repetitive attempts to perform the goal-oriented task can be viewed as attempts to converge onto this manifold. In the virtual shuffleboard game, since the final position of the puck is completely determined by the velocity and position of release, based on Newton's second law we obtain the goal-function as,

$$v^2 + 2\mu g(x - L) = 0, \qquad (2)$$

where v is the velocity of release of the puck, μ is the coefficient of friction, x is the position of release and L is the distance at which the target is located. Non-dimensionalizing the lengths by a constant R (the forearm length of the subject) and the velocity by $\sqrt{2gR}$ we can represent Eq. (2) as,

$$\tilde{v}^2/\mu + \tilde{x} - \tilde{l} = 0 \qquad (3)$$

where $\tilde{v} = v/R$, $\tilde{x} = x/R$ and $\tilde{l} = l/R$. The error at the target (e) due to small perturbations $[\xi, \zeta]$ to a state $[\tilde{x}^*, \tilde{v}^*]$ on the GEM can be represented using a Taylor series expansion of the goal function as $e = A\,[\xi, \zeta]^{\mathrm{T}}$ where $A = [\partial\tilde{f}/\partial\tilde{x}\,,\,\partial\tilde{f}/\partial\tilde{v}]$. We refer to the matrix A as the body-goal variability map. It is noted that only perturbations in the range space $\mathcal{R}$ of this body-goal variability matrix will result in any effect at the goal level. Perturbations

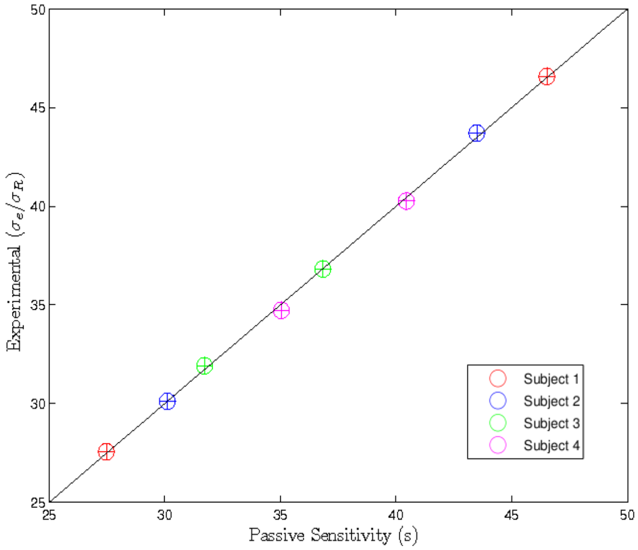

Figure.1. Plot of normalized performance (experimental) versus passive sensitivity s (theoretical) for 4 subjects at each of two μ values.

that lie in the null-space $\mathcal{N}$ of A i.e. tangent to the GEM have no effect at the target. The singular value s of this matrix A represents how the perturbations in the body-state on the GEM are amplified to produce the error at the target. In the shuffleboard example we can show that $s = \sqrt{1 + (2\tilde{v}/\mu)^2}$. It is seen that s depends on the coefficient of friction μ and the velocity of release $\tilde{v}$, and is independent of the control strategy used to achieve the goal in repetitive trials. We can further show that,

$$\sigma_e^2 = s^2 \sigma_{\mathcal{R}}^2, \tag{4}$$

where σ_e^2 is the variance of error at the target, s is the singular value of A, and $\sigma_{\mathcal{R}}^2$ is the component of body-level variance in the range space of A [2, 3]. Using Eq.(4) we can write,

$$\sigma_e / \sigma_{\mathcal{R}} = s \tag{5}$$

i.e. the performance at the target (σ_e) normalized against the standard deviation in the range space ($\sigma_{\mathcal{R}}$)will scale linearly with the passive sensitivity (s). In the shuffleboard task, we can change s by changing μ. We choose 8 different μ values such that the movement time of the puck (from $x = 0$) for a perfect trial (that ends right on the target at L =200 cms) would vary uniformly from 3 seconds to 5 seconds. To test the prediction of Eq.(5), we perform the shuffleboard task with 4 subjects performing 500 trials of the task for each of two randomly selected friction conditions.

RESULTS AND DISCUSSION

Figure.1 shows the experimentally estimated normalized performance ($\frac{\sigma_e}{\sigma_{\mathcal{R}}}$)against the theoretical value of passive sensitivity s. There was excellent agreement between the experimental value of $\sigma_e/\sigma_{\mathcal{R}}$ and the theoretical value of s. A regression performed on the data points had an $R^2 = 0.9993$ and mean-square fit error of 0.0329. Thus, whatever the effect of neuromotor control on $\sigma_{\mathcal{R}}$ (goal-relevant variabililty), it is amplified linearly according to the passive sensitivity s to produce performance (goal-level variability) σ_e. Integration of the passive sensitivity result (Eq.(4)) with stability measures that can quantify goal-relevant control effort will shed light on how subjects exploit features of the movement system (internal variability and stability) in tandem with the definition of the goal (goal-function and associated passive sensitivity) to generate goal-level performance.

CONCLUSIONS

We show how goal-level performance is affected by a totally passive property of the system. Further experiments will tell us if humans prefer/exploit strategies that *minimize* passive sensitivity and thus goal-level error. The excellent agreement of the experimental and theoretical values obtained from a linear fit imply that the effect of higher order terms is negligible. In related work, we have extended this modeling approach to study the inter-trial dynamics and associated stability properties of variability arising in such repetitive trials of goal-oriented tasks.

REFERENCES

1. Newell, K. and D. Corcos (eds.) (1993) *Variability and Motor Control,* Human Kinetics, Champaign, IL.
2. Cusumano, J.P, Cesari, P., *Bio. Cybern.*, **94**(5) , 367-379.
3. Golub, G. & Van Loan, C. (1996). *Matrix Computations*. Baltimore, MD: The John Hopkins University Press.

ACKNOWLEDGEMENTS

Partly funded by NIH grant # HD058942 (to JBD), and NSF grant #0625764 (to JJ and JPC).

AN ANATOMIC COORDINATE SYSTEM OF THE TRAPEZIUM USING CURVATURE

[1] Michael J Rainbow, [1]Joseph J Crisco
[1]Brown University / Rhode Island Hospital
email: michael_rainbow@brown.edu

INTRODUCTION

The carpometacarpal joint (CMC) can be described as a saddle joint formed by the articulation of the first metacarpal (MC1) and the trapezium (TPM). It has been reported that women are five to ten times more likely than men to develop osteoarthritis at this joint. In one *in vitro* morphological study, gender differences were found in curvature parameters of surfaces fit to the articular cartilage of the MC1 and TPM[1]. Kinematic studies have used skin mounted markers tracking to quantify motion of this joint. However, these methods are subject to skin movement artifact and do not account for articulation of the trapezium on the scaphoid. Accurate kinematics of the MC1, TPM, and scaphoid may be obtained through markerless bone tracking using computed tomography (CT). The description of CMC kinematics is contingent upon a coordinate system (ACS) that has anatomical meaning. Ateshian *et al*. described the principal directions of curvature of the articular surface of the trapezium as being oriented in the dorsovolar and radioulnar directions[1]. The purpose of this study was calculate an ACS using the principal directions of curvature of a polynomial surface that is fit in a least squares sense to the bone surface of the TPM acquired from *in vivo* CT scans. In addition, we test for the existence of gender differences in curvature parameters of the polynomial.

METHODS

After IRB approval and informed consent, the right wrist of 6 males and 6 females (mean age: 24.9, range 21-31 yrs.) were CT scanned. Each wrist was then segmented using Mimics 9.1 (Materialise, Leuven Belgium) generating tessellated 3-D bone surface models of the radius and ulna, all eight carpal bones, and all five metacarpals. The three principal axes of inertia, and centroid of the TPM were calculated according to previous methods and used to define an inertial coordinate system[2]. The cube root of the volume (V3) of the TPM was also calculated. The

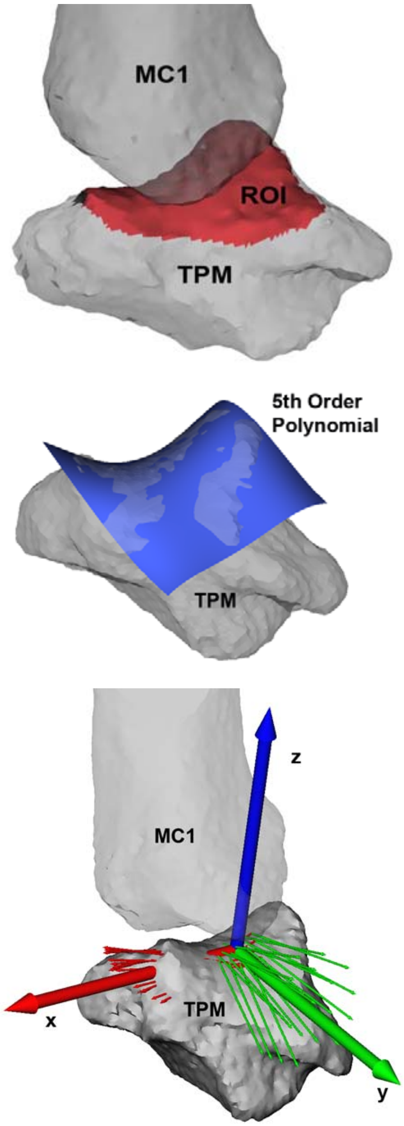

Figure 1: Top: The region of interest (ROI) is the trapezium (TPM) bone surface that articulates with the first metacarpal (MC1). Middle: A 5th order polynomial with all interaction terms is fit to the vertices of the ROI. Bottom: The origin of the anatomic coordinate system is placed at the centroid of the ROI at the surface. The x-axis is computed using the mean vector of the direction of maximum curvature averaged over a 28.27mm^2 area surrounding origin. The y-axis is derived similarly along the direction of minimum curvature.

bone surface of the TPM that corresponds to the cartilage that articulates with the MC1 was selected as the region of interest (ROI). The third principal axis of inertia happened to pierce the ROI. The ROI was transformed into inertial coordinates so that the convex and concave components of the ROI were oriented along the z-axis of the inertial coordinate system. A 5th order polynomial surface including all interaction terms was then fit to the vertex points of the ROI using custom code developed by John D'Errico in Matlab (Mathworks, Natick MA). The maximum and minimum curvature, Kmin and Kmax were found at each point as well as the principal directions of maximum and minimum curvature (**e1** and **e2**). The root mean squared curvature was also calculated at each point according to previous methods[1]. The values were then averaged across an area of 28.3mm^2 surrounding the centroid of the ROI. **e1** and **e2** were also averaged across this area. The direction of maximum curvature corresponded to the radioulnar axis and the direction of minimum curvature corresponded to the dorsovolar axis. The radioulnar axis was used as the x-axis of the ACS. The z-axis was created by taking the cross product of the x-axis and the averaged **e2**. The y-axis was created by taking the cross product of the z-axis and the x-axis. The origin of the ACS was placed at the centroid of the ROI moved to the surface using the 5th order polynomial equation. R^2 fit values and RMS error between the polynomial surface points and the vertex points of the ROI were calculated for all subjects.

Paired t-tests were used to test the hypothesis that V3, Krms, Kmin, and Kmax values differed with gender. The inter-subject variability of the ACS was tested by using a surface-based best-fit alignment algorithm in Geomagic (Raindrop Geomagic, Research Triangle Park, NC). TPMs of each subject were paired using all possible combinations. For each pair, one bone was scaled by volume to match the size of its partner. It was then fit to the partner bone and its ACS was moved using the same transformation. The angle between corresponding axes of the two ACSs were then computed.

RESULTS AND DISCUSSION

Mean V3 of male and female trapeziums was 12.89 ± 0.41 mm and 11.48 ± 0.56 mm respectively. While there was a significant difference in V3 between male and female trapeziums ($P<0.001$), there were no statistically significant differences in curvature parameters between male and females for Krms ($P=0.6643$), Kmin ($P=0.6726$), or Kmax ($P=0.7100$) (Table 1).

The mean angular deviations for the x-axis, y-axis, and z-axis of the ACS across all subjects was 10.54 ± 6.96º, 20.85 ± 12.56º, and 18.74 ± 13.52º respectively. This variation can be explained by differences in morphology of the entire trapezium as well as differences in curvature on the ROI. However, each subject's x-axis and y-axis corresponded to the radioulnar and dorsal volar axis respectively.

CONCLUSIONS

This study developed a consistent ACS that follows the principal curvatures of the saddle shaped articular surfaces of the TPM. The ACS will be used in measuring the kinematics of the MC1 with respect to the TPM as derived from markerless tracking of the CMC joint using serial CT scans. Gender differences in curvature parameters were also examined for a small area surrounding the origin of the ACS. Although gender differences have been found in previous studies of the corresponding articular cartilage, they were not found in the underlying bone in a young population.

REFERENCES

1. Ateshian GA, et al. *J. Biomech*, **25**, 591-607, 1992.
2. Coburn JC, et al. *J Biomech* **40**, 203-9, 2007.

Table 1: Curvature Parameters and Fit Values

	Krms (mm^{-1})	Kmin(mm^{-1})	Kmax(mm^{-1})	R^2	RMS-fit (mm)
Male	0.135 ± 0.015	-0.174 ± 0.021	0.069 ± 0.016	0.97 ± 0.02	0.31 ± 0.11
Female	0.142 ± 0.033	-0.182 ± 0.045	0.073 ± 0.018	0.95 ± 0.04	0.35 ± 0.25

GRIP FORCE FLUCTUATIONS ARE MORE THAN JUST NOISE

[1] Kornelius Rácz, [1,2]Francisco J. Valero-Cuevas
Brain-Body Dynamics Laboratory
[1]Department of Biomedical Engineering, Viterbi School, University of Southern California
[2]Division of Biokinesiology & Physical Therapy, University of Southern California
email: raths@usc.edu, web: http://bme.usc.edu/valero

INTRODUCTION

Statically grasping an object with three fingers is one of the most fundamental element of dexterous manipulation dexterous manipulation. Here we show that the sensorimotor system does not exhibit structured dynamical coordination among fingers only as the task becomes "complex", but quite to the contrary, such low-level coordinated activity also underlies static grasp. As in the case of isometric force production with a single finger [1], actively enforcing the equilibrium constraints of static grasp in the presence of unavoidable noise also requires structured dynamical coordination among fingers. This work, which extends techniques used to analyze other dynamical system such as postural stability or diffusive processes [2], opens a window into the previously undetected low-level dynamical control that underlies even the simplest of multi-finger tasks.

METHODS

The test device is a three-armed object (Fig. 1), whose arms lie in a plane and can rotate about a common center hinge. The relative angles of the arms were adjusted and locked in a configuration appropriate for a regular 3-finger grasp. A miniature 6-axis force transducer (ATI Nano 17) attached to the outer end of each arm served as the finger pad, giving each arm a total length of approx. 3 cm. The finger pads were covered with Teflon film. Various weights (50 g, 100 g or 200 g) were attached to the center hinge to change the total required grip force to hold the object statically while resting the wrists on a cushioned surface (Fig. 1). We sampled the forces and torques applied at each finger pad with 16-bit resolution at 400 Hz.

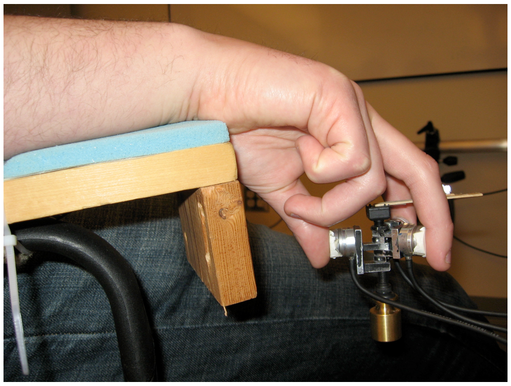
Figure 1: The test device with a 50 g weight attached to it

Five right-handed healthy male adults (ages: 24-43) participated in the experiment. Our 3x2 factorial design consisted of simply holding the object for 128 s, for each of the three weights both with and without visual feedback of the total grip force. The experiment was distributed over 2 days to preclude fatigue effects, and at least one minute of rest was provided between trials. On the first day visual feedback was not provided and subjects simply looked across the room, whereas on the second day feedback was provided and subjects were instructed to keep the cursors on a computer screen on a line representing the desired sum of normal forces applied to the object constant. We recorded three trials per weight, for a total of 9 trials per day.

For the data analysis, we focused on the normal forces, but the results are unaffected when looking at full 3D force vector magnitudes. We removed the first 8 seconds of each trial to prevent the influence of initial transients, and here we report the results of the subsequent 60 s of each trial. After determining that the power spectrum was flat beyond 10 Hz, we down-sampled the data to 40 Hz for computational efficiency. Given that the analysis used requires non-stationary data (i.e., constant mean and time-interval dependent autocorrelation), we transformed our data by using a Savitsky-Golay filter to compute first derivatives and remove trends [2].

The data are assumed to result from a noise process, which can be modeled by a Langevin equation $\dot{x} = f(x) + G(x)\xi$, where f(x) is a deterministic function of the state (normal force), G(x) is a tensor and ξ white noise. The time evolution of the associated state space probability density $\rho(x,t)$ can be described by the Fokker-Planck equation [4]:

$$\frac{\partial\rho(x,t)}{\partial t} = -\sum_i \frac{\partial D_i(x)\rho(x,t)}{\partial x_i} + \sum_{i,j} \frac{\partial^2 D_{ij}^{(2)}(x)\rho(x,t)}{\partial x_i \partial x_j}$$

where drift $D_i(x)$ and diffusion $D_{ij}^{(2)}(x)$ are the first and second moments of that distribution, respectively, both assumed to be time-independent. Roughly speaking, this formulation explicitly separates determinism – the mean behavior – from stochasticity – the variability. We calculated the moments in the following way [3]:

$$D_i(x) = \lim_{\Delta \to 0} \frac{1}{\Delta} \left\langle x_i(t+\Delta) - x_i(t) \right\rangle_{x(t)=x}$$

$$D_i^{(2)}(x) = \lim_{\Delta \to 0} \frac{1}{2\Delta} \left\langle (x_i(t+\Delta) - x_i(t))(x_j(t+\Delta) - x_j(t)) \right\rangle_{x(t)=x}$$

Where $\langle\ \rangle_x$ denotes the mean of data points in a sufficiently large neighborhood of x. We then fitted a line to the first moment and a parabola to the second moment to compare changes in the coefficients with respect to varying the task conditions. To this end, we performed a two-way ANOVA.

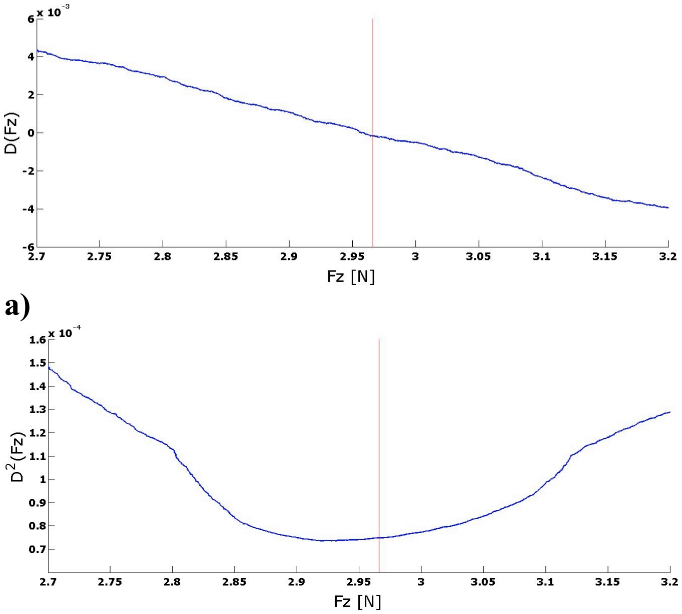

a)

b)

Figure 2: Sample drift (a) and diffusion (b) plots for thumb normal force. The vertical line indicates the mean force value: it coincides with the fix point (a) and a noise minimum (b).

RESULTS AND DISCUSSION

The two fundamental findings common to all subjects are: a) the system actively tries to maintain a force set point and b) the force set point coincides with a variability minimum.

The first finding is supported by the fact that the mean force level roughly coincided with a zero force change, i.e. was a fix point, while force changes scaled linearly in magnitude with deviation from and on average, in a direction towards that force level (Fig. 2 a), while the second finding is supported by the variability minimum being always close to the mean force level (Fig. 2 b). Again, variability scales with deviation, indicating an increased effort, which leads to an increase in noise. Adding visual feedback decreased the drift slope and offset significantly ($P < 0.01$), indicating that the drift truly reflects the controller effort. Weight only had an effect on the offset ($P < 0.01$), indicating an increased effort but unchanged sensitivity. Feedback also significantly increased the slopes of the diffusion parabola and its offset ($P < 0.01$). Since the feedback induces increased activity on the part of the subject, this finding shows that the diffusion reflects the variability increase with activity.

CONCLUSIONS

Despite the apparent simplicity of statically grasping and object, the analysis of the grip force fluctuations reveals determinism and thus the workings of a controller. By creating a stable force equilibrium point, this controller is able to maintain a desired force level even in the presence of unavoidable stochastic perturbations inherent in the sensorimotor system. Importantly, the controller’s effort to maintain this force level scales with the deviation from it. This work is the first to show, to our knowledge, the presence of a continuously active, low-level dynamic controller during static grasp; and opens up future research avenues to understand the fundamental neuromuscular components for the sensorimotor control of multi-finger manipulation, and its disability.

REFERENCES

1. Valero-Cuevas FJ, Venkadesan M, Todorov E. J Neurophys, in press, 2009.
2. Gottschall J, Peinke J, Lippens V, Nagel V. Phys Lett A. 373, 8-9, 811-816, 2008.
3. Friedrich R, Peinke J. Phys Rev Lett. 78, 863, 1997.
4. Haken H. Springer. 2004.

ACKNOWLEDGEMENTS

NIH AR-050520, AR-052345 and NSF EFRI-COPN to FVC.

Safety Margin in Ramp Torque Production Task with a Circular Object

Junfeng Huang, Jae Kun Shim
Department of Kinesiology, University of Maryland, College Park
email: jkshim@umd.edu, web: http://www.sph.umd.edu/KNES/faculty/jkshim/neuromechanics/

INTRODUCTION

Manipulation of circular objects such as doorknobs and jar lids is an essential part in everyday hand usage. Understanding the function of the hand in handling circular objects, especially multi-digit tasks that we commonly use in everyday manipulation tasks, is critical not only for improving our knowledge about the underlying neuromuscular mechanism but also for creating ergonomically optimal handles.

A previous study in maximum voluntary torque task shows both normal force and tangential force sharing pattern in circular object is quite different from those in prismatic objects [1]. In order to prevent slippery, appropriate amount of normal force is necessary. However, it was found that human subjects tend to exert extra amount of normal force (safety margin [2]). The normalized safety margin is a measure of efficiency in grasping.

In this study, we employed an isometric multi-digit torque production with gradually increasing torque for a motor task. The purpose of the study was twofold; first we examined the effects of wrist position, torque direction, and number of digits on safety margin; second we investigated the synergic change under these conditions.

METHODS

Subjects: Ten right-handed subjects (males, age: 26.2±3.7 years old) participated the experiment after given informed consent. No history of neuromuscular disease or pathology was reported.

Experiment setup: An aluminum circular handle (radius: 4.5cm) was mechanically fixed on a tripod. Five 6D force/torque sensors (ATI, VA) were installed on the handle to record the forces and torques by individual digits. The relative positions of the sensors were decided through averaging measurements across subjects. The recorded data was conditioned, sampled (sampling frequency: 1000Hz, data acquisition card: NI6029, National Instrument, TX) and saved in a computer for data processing.

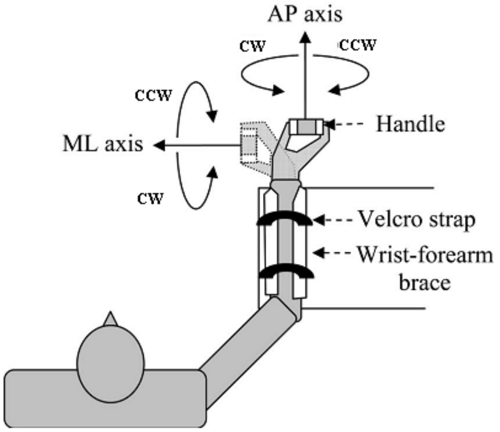

Figure 1: Experiment paradigm shows 2 of the 3 factors considered. DIGIT is not shown.

Procedure: Subjects sat on a chair, with right upper arms flexed ~20° in the sagittal plane and abducted ~45° in the frontal plane. The forearms were fastened on an arm trace by Velcro straps. Subjects held the handle with right hands and exerted isometric torque under a specific condition.

The experiment paradigm has 3 factors, each with 2 levels, including DIGIT (3-digit: thumb, middle, ring; 5-digit: all five digits), AXIS (ML: mediaolateral; AP: anteroposterial), and DIRECTION (NEG: counterclockwise (CCW) → clockwise (CW); POS: clockwise (CW) → counterclockwise (CCW)). Maximum voluntary contraction (MVC) in each combination condition was measured before the experiment. For each condition, 12 trials were performed.

When a trial started, subjects first produced 20% MVC in one direction, then in a period of 6 seconds, linearly reduced the torque to zero and increased to 20% MVC in the other direction. A computer monitor provided subjects with both the torque template and the real-time feedback.

Data analysis: The collected data was low pass filtered with a zero-phase shift filter in Matlab (Mathworks, CA). Regression analysis was performed for normal force versus torque in destabilizing and stabilizing period, respectively. Delta variance, the index of synergistic actions of the task fingers, was calculated using the previously used algorithm [5]. Repeated measure MANOVA was processed.

RESULTS

1. Safety margin in destabilization and stabilization

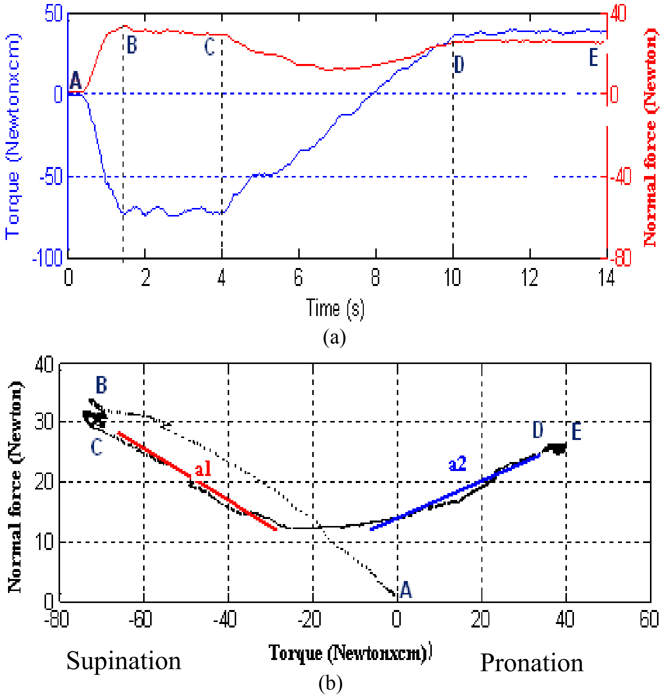

(a)

(b)

Figure 2: (a) the trajectories of normal force (red) and torque (blue) by a representative subject (b) phase portrait with regression lines

When torque changes direction, normal force also undergoes a U shape pattern. However, the minimal normal force occurs in a supination position.

It is found that the regression rate (a1) in destabilization is smaller than that (a2) in stabilization (F=8.295, $p<0.05$). In AP axis, subjects tended to grasp harder than along ML axis (F=16.938, $p<0.01$). The safety margin with 3-digit is slightly larger than with 5-digit, although the effect is not significant (F=4.058, $p<0.1$).

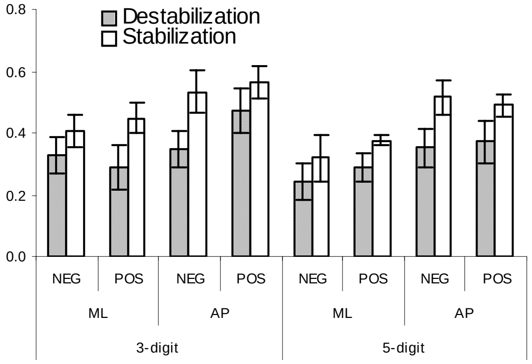

Figure 3: Regression line coefficients during destabilization and stabilization periods

2. Synergy during the transition

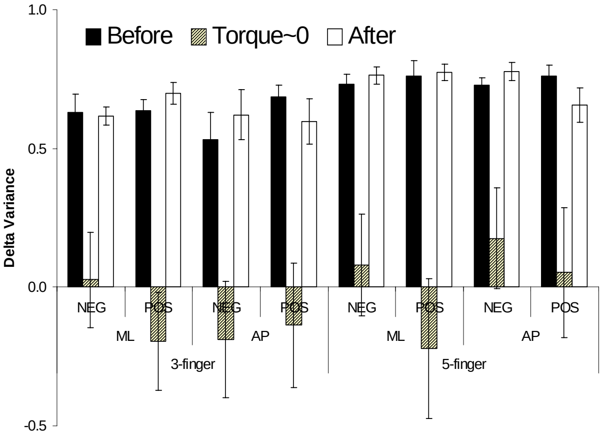

Figure 4: Delta variance among all digits involved in torque production task

The synergy starts from close to 1, decreases to zero when torque crosses 0, and returns to 1 again when stabilized in the other direction. This result confirms previous studies' findings.

CONCLUSIONS

Safety margin is smaller in destabilization stage than in stabilization stage regardless of factors considered here. Digit coordination is temporarily suppressed when torque reduces to zero.

REFERENCES

1. Shim JK, Huang J, et al. (2007) *Ergonomics* 50(5):660-75.
2. Fowler NK, Nicol AC (1999) *Clinical Biomechanics* 14:646-652
3. Shim JK, Olafsdottir H, et al. (2005) *Exp. Brain Res.* 164(2):260-270

Validity of Surface EMG Electrode Placement for Trunk Musculature

Rupal Mehta, Marco Cannella, David Ebaugh and Sheri Silfies
Rehabilitation Sciences Research Laboratories, Drexel University, Philadelphia
Email: rm335@drexel.edu web: http://www.drexel.edu/cnhp/rehab_sciences

INTRODUCTION

Surface Electromyography (sEMG) parameters such as trunk muscle timing and amplitude are commonly used to distinguish low back patients from pain free controls, and as an objective marker of change in clinical status. However, to detect small changes in these trunk muscle performance parameters, the variability in the sEMG signal must be low. This variability is introduced by a variety of factors (e.g., patient performance of the task, development of fatigue, the equipment, or the electrode positioning). To standardize sEMG measurements, guidelines have been drawn up for the positioning of sEMG electrodes for the trunk muscles. The purpose of this study is to evaluate the validity of standard sEMG electrode placement sites for trunk muscles.

METHODS

Validity of sEMG electrode placement was established by verifying placement using cadaver dissection and analysis of cross-correlation of sEMG signals across electrodes sites.

Cadaver Study: Eight cadavers were examined to validate the sEMG electrode placement on 7 muscles bilaterally. The placement sites were consistent with those cited in the literature [1,2]: internal oblique/transverse abdominus (IO/TrA) – 2 cm inferior-medial to anterior superior iliac spine (ASIS); external oblique (EO) -15 cm lateral to umbilicus; external oblique-2 (EO-2) - 5 cm supero-medial to EO placement; rectus abdominus (RA) - 3cm lateral to umbilicus; superficial lumbar multifidus (LM) - 2cm lateral to L5 spinous process; lumbar erector spinae (LES) -3cm lateral to L2 spinous process; and thoracic erector spinae (TES) -5cm lateral to T9 spinous process. These sites were marked on the cadavers and at each site the location of the underlying muscle was visually confirmed (see Fig 1 & 2).

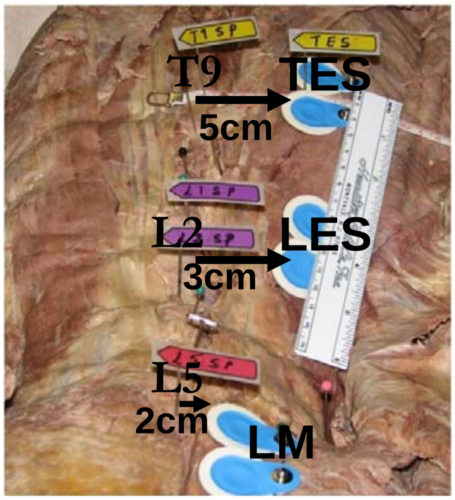

Figure 1. Digital photograph of the dissected extensor muscles with electrode placement and orientation of LM, LES & TES

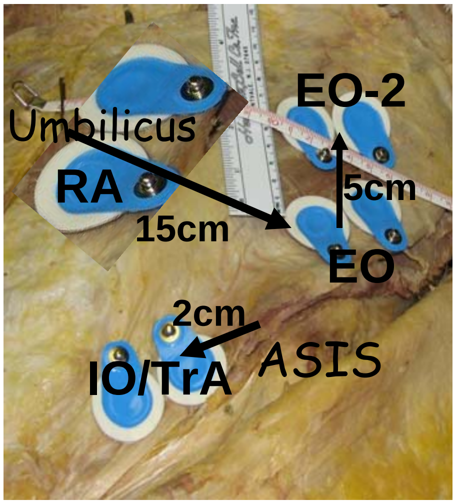

Figure 2. Digital photograph of the dissected abdominal wall with the electrode placement and orientation of RA, IO/TrA, EO & EO-2

Cross-correlation Analysis: Ten healthy subjects were recruited for this study. Pre-amplified electrode leads with snap Ag/Ag Cl surface electrodes were used in the study. The skin was lightly abraded and cleaned with alcohol swabs to lower the skin impedance. Electrodes were placed parallel to the muscle fibers with a 2 cm inter-electrode distance as previously described. Each subject performed 2 repetitions of isometric trunk flexion and extension in a semi-seated position. A reference target was set to 20% body weight. Post processing included removal of EKG signal using an algorithm adapted from Aminian et al. [3] and RMS filtering (80 data points). Prior to cross correlation the data were cut to 3 second epochs representing the most stable period of force production. Normalized cross-correlations (with respect to the autocorrelation of both signals at zero time lag) were then performed between each set of electrodes.

RESULTS AND DISCUSSION

From our anatomical observation of 8 cadavers, it was observed that the standard placement for each trunk muscle electrode site was valid. No significant difference was found in the maximum correlation between sides of the trunk for any of the comparisons, so we are reporting only left sided results. Table 2 presents the mean and 95% confidence interval of cross-correlation coefficient within abdominal and extensor muscle group. Cross-correlation of less than 0.30 represents low association between signals, between 0.30 and 0.70 represents a moderate relationship between the signals, and above 0.70 represents a strong relationship between the signals [4-6]. For the flexion task, moderate cross-correlation indexes were found between most of the abdominal muscles, whereas for extension task cross-correlation indexes were low.

Given that the tasks used to activate the trunk musculature would recruit all of the abdominal and extensor muscle groups simultaneously, we would expect that some of the correlation value would represent muscle co-activation. Considering this point, the low maximum cross-correlation values in the extensors indicate muscle activity specific to the recorded muscle groups. However, the ability to individually record surface EMG from the abdominal muscles may not be as accurate.

Table 1: Mean (95% Confidence Interval) Normalized Cross-Correlation Values

	Cross-Correlation Coefficient	
Flexion Task	Mean	95% CI
IO/TrA-EO	0.26	0.14 - 0.38
IO/TrA-EO2	0.33	0.20 - 0.46
IO/TrA-RA	0.47	0.35 - 0.59
EO-EO2	0.46	0.34 - 0.58
EO-RA	0.25	0.11 - 0.39
EO2-RA	0.37	0.22 - 0.52
Extension Task		
LM-LES	0.21	0.08 - 0.34
LM-TES	0.07	0.02 - 0.12
LES-TES	0.14	0.08 - 0.20

CONCLUSIONS

This study validated these surface electrode placement sites for commonly assessed trunk musculature.

REFERENCES

1. Cholewicki, J., Panjabi, M.M., et al. Stabilizing function of trunk flexor–extensor muscles around a neutral spine posture. *Spine* 22, 2207–2212, 1997.
2. Ng, J.K., Richardson, C.A. Reliability of electromyographic power spectral analysis of back muscle endurance in healthy subjects. *Arch. Phys. Med. Rehab* 77, 259–264, 1996.
3. Aminian, et al. *Med Biol Eng Comput.* **26**, 658-652, 1988.
4. C.J. De Luca, The use of surface electromyography in biomechanics. *Journal of Applied Biomechanics* 13, 135–163, 1997.
5. P. Vink, H.A.M. Daanen, A.J. Verbout. Specificity of surface- EMG of the intrinsic lumbar back muscles. *Human Movement Science* 8, 67–78, 1989
6. Marshall P. & Murhpy B. The validity and reliability of surface EMG to assess the neuromuscular response of the abdominal muscles to rapid limb movement. *Journal of Electromyography and Kinesiology* 13, 477–489, 2003.

ACKNOWLEDGEMENTS

Partial support provided by a grant from the NIH (K01HD053632)

JOINT-SPECIFIC POWER ABSORPTION DURING ECCENTRIC CYCLING

Steven Elmer, Matthew Madigan, and James Martin
Neuromuscular Function Lab, University of Utah
Email: steve.elmer@utah.edu

INTRODUCTION

Previous investigators [3,4] have used eccentric cycle ergometry (i.e., “negative work”) to increase muscle size, strength, and spring quality. These adaptations have desirable effects for athletes, individuals with orthopedic injuries (e.g., ACL reconstruction patients), and elderly populations who are trying to prevent/reverse disease related impairments (e.g., sarcopenia). Evidence from MRI suggests that the majority of individuals absorb eccentric work primarily using knee extensor muscles while some individuals utilize mostly hip extensor muscles. This variability in power absorption strategies could impact the outcome of a training/rehabilitation program. For example, an individual who is trying to strengthen quadriceps muscles but absorbs with hip extensor muscles may not experience the same localized benefits as an individual who absorbs with knee extensor muscles.

During concentric cycling muscles that span the ankle, knee, and hip contribute to the overall power produced at the pedal. Specifically, knee extensors are the dominate power producing muscles during submaximal cycling [1,7] whereas hip extensors muscles produce the most power during maximal cycling [5]. To our knowledge, biomechanical aspects of power absorption during eccentric cycling have not been reported. Thus, the purpose of this investigation was to quantify joint-specific power absorption during eccentric cycling.

METHODS

Eight eccentrically trained males (mass: 76±14kg, height: 177±6cm) participated in this study. Participants performed three practice sessions of eccentric cycling the week prior to the experimental data collection in order to become familiar with the ergometer and testing protocol. A five-horsepower motor was used to drive the flywheel and pedals of an isokinetic ergometer in the reverse direction. Participants resisted the reverse moving pedals at 60 rpm at a specified target power that was 20% of maximum concentric power. An SRM power meter displayed the instantaneous power that the participant was absorbing. During each trial, participants were given 30s to reach their target power and then maintained that target power for 30s. Seat position was standardized by measuring knee joint angle (170°, lateral malleolus to femoral condyle to greater trochanter) with a goniometer.

Pedal reaction forces were recorded with an instrumented pedal equipped with two 3-component piezoelectric force transducers and pedal and crank position were recorded using digital encoders. Joint kinematics were measured with an instrumented spatial linkage system [6]. Segmental masses, moments of inertia, and locations of centers of mass were estimated using the regression equations reported by de Leva [2]. Sagittal plane joint reaction forces and net joint moments were determined by using inverse dynamic techniques. Joint powers were calculated as the product of net joint moment and joint angular velocity and the power transferred across the hip (hip JRF) was calculated as the product of hip joint reaction force and linear velocity. Joint powers were averaged over the entire pedal cycle (complete revolution) and over the extension and flexion phases. A one-way ANOVA with subsequent Tukey post hoc analyses was used to asses differences in joint powers (alpha=.05).

RESULTS

During the eccentric trial the ankle, knee, and hip absorbed 10±1%, 58±3%, 29±3% of the total pedal power averaged over a complete revolution, respectively with 3±1% transferred across the hip to the pelvis (Figure 1). The knee and hip absorbed power mainly during the leg flexion phase (eccentric extension), whereas the hip also absorbed power during the leg extension phase (eccentric flexion; Figure 2). Knee flexion power was significantly greater (more negative) than ankle dorsi flexion, hip flexion, and hip JRF powers (Table 1, $p < .05$). Hip flexion power was greater ($p<.05$) than ankle dorsi flexion and hip JRF powers while ankle dorsi flexion and hip JRF powers were not different (Table 1). Hip extension power was significantly greater (p<.05) than ankle plantar flexion, knee extension, and hip JRF powers while none of the other three joint powers were different (Table 1).

DISCUSSION

These are the first data to document power absorbed during multi-joint eccentric actions. As has been reported for concentric cycling [1,4,7], eccentric cycling was performed with a combination of knee and hip actions including eccentric knee extension, eccentric hip extension, and eccentric hip flexion. Further, the relative contributions of joint-specific power absorbed during eccentric cycling (10% ankle, 57% knee, 30% hip, 3% hip transfer) mirror those contributions observed at a similar seat position, pedaling rate, and target power during concentric cycling (11% ankle, 55% knee, 25% hip, and 8% hip transfer, [7]). This suggests that the basic motor control strategies for producing and absorbing power during multi-joint movements are quite similar. Interestingly, two individuals absorbed power primarily with eccentric hip extension which highlights the individual variability in power absorption strategies. Muscle co-contractions may have been a factor in these two cases but EMG measurements are needed to confirm this. These findings have implications for physical therapists that use eccentric cycle ergometry as a rehabilitation and/or training tool. Specifically, when individuals are placed in an extended seat position both knee and hip extensor muscles will be targeted. Our next step is to determine if changes in seat position can alter the power absorption strategies used during eccentric cycling.

REFERENCES

1. Broker, J., Gregor, R. *Med. Sci. Sports. Exerc.* **26**, 64-74, 1994.
2. de Leva, P. *J. Biomech.*, **29**, 1223-1230, 1996.
3. LaStayo, P. et al. *J. Gerontol.*, **58**, 419-424, 2003.
4. Lindstedt, S. et al. *J. Exp. Biol.*, **205**, 2211-2216, 2002.
5. Martin, J., Brown, N. *J. Biomech.*, **42**, 474-479, 2009.
6. Martin, J. et al. *J. App. Biomech.*, **23**, 224-229, 2007.
7. Reiser, R. et al. *Biomed. Sci. Instr.*, ***38***, 209-214, 2002.

ACKNOWLEDGEMENTS

Supported by: Gatorade Sports Science Institute, International Society of Biomechanics, and Undergraduate Research Opportunities Program

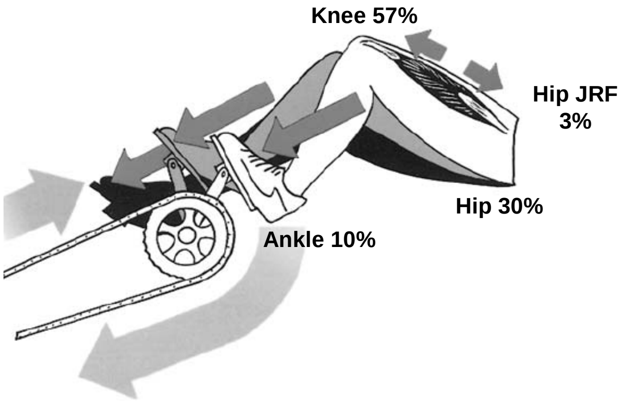

Figure 1: Relative contributions of joint-specific power absorbed over a complete crank revolution

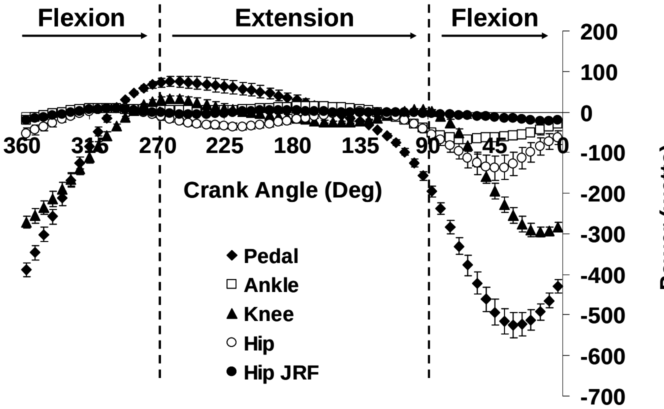

Figure 2: Instantaneous power absorbed throughout one complete crank revolution

Table 1: Joint-specific power absorbed during eccentric cycling. Mean ± SEM. * indicates different from all other joints (absorbed most power). ** indicates different than ankle and hip transfer.

Average Power (watts)	Pedal	Ankle	Knee	Hip	Hip JRF
Complete Revolution	-128 ± 6	-13 ± 2	-73 ± 2*	-38 ± 6**	-4 ± 1
Flexion	-234 ± 10	-21 ± 3	-139 ± 8*	-51 ± 11**	-7 ± 1
Extension	-22 ± 7	-4 ± 1	-7 ± 5	-25 ± 2*	-1 ± 1

EFFECT OF VIBROTACTILE TRUNK TILT FEEDBACK ON POSTURAL STABILITY IN OLDER ADULTS

[1]Daniel Ursu, [1]Liang-Ting Jiang, [1]Kathleen H. Sienko

[1]Dept. of Mechanical Engineering, Univ. of Michigan, Ann Arbor, MI, USA,
email: sienko@umich.edu, web: http://www-personal.umich.edu/~sienko/

INTRODUCTION

Single- and multi- axis vibrotactile feedback have been shown to significantly reduce the root-mean-square (RMS) tilt in subjects with vestibular loss during quiet standing and single- and multi-axis perturbations [1-3].

The goal of this pilot study was to assess the effectiveness of a vibrotactile sensory augmentation device in community-dwelling elderly who report losses of balance. A secondary aim of the study was to determine the effect of cognitive workload on postural stability both with and without the use of trunk-based vibrotactile feedback.

METHODS AND PROCEDURES

We have developed a multipurpose vibrotactile sensory substitution platform consisting of an off-the-shelf inertial measurement system (XSens), a vibrotactile display, customized control hardware, and a PC104 computer (Figure 1). Estimates of body tilt derived from the inertial measurement system are presented to the subject's trunk in the form of small vibrations by vibrotactile actuators (tactors) similar to pager motors. The tactors display the direction of the tilt.

Healthy elderly subjects ranging in age from 65 to 85, who report one or more losses of balance per week, were recruited from the Geriatrics Center's Human Subject and Assessment Core. Subjects were excluded if they were medically unstable, had a history of neurological disease that might affect balance, or had a BMI over 30 kg/m^2. The protocol consisted of a short training session (10 min.) followed by an experimental session comprising normal and tandem Romberg trials with combinations of the following conditions: device feedback OFF or ON, eyes open or closed, presence or absence of a secondary cognitive task (counting backwards by threes).

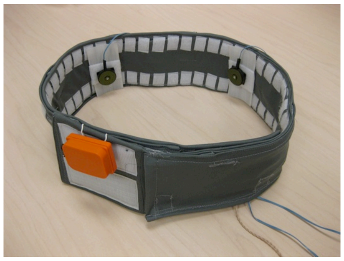

Figure 1. Trunk-based vibrotactile feedback display.

Tilt estimates were acquired from the motion sensor worn on the subject's lower back. Tilt magnitude, referred to as Phi tilt, was calculated as the square root of the squared sum of roll and pitch tilt components. The root-mean-square (RMS) tilt was calculated by taking the square root of the squared sum of the estimated tilt. The average of the baseline data (normal stance, eyes open, feedback OFF, no secondary task) was used for normalizing subsequent trials to facilitate comparisons across subjects. In order to capture the difference in trajectory area, the resultant two-axis tilt vector was fit with 95% confidence interval ellipses.

RESULTS AND DISCUSSION

The older adults involved in this study were able to use the vibrotactile feedback to significantly reduce their RMS sway and sway area in all but one of the normal stance conditions; there was no significant difference when subjects were asked to close their eyes and attend to a secondary task in the feedback ON versus OFF condition. The feedback had the greatest impact when subjects' eyes were closed. Figure 2 illustrates the sway area reduction when feedback was provided during normal stance with and without a concurrent secondary task.

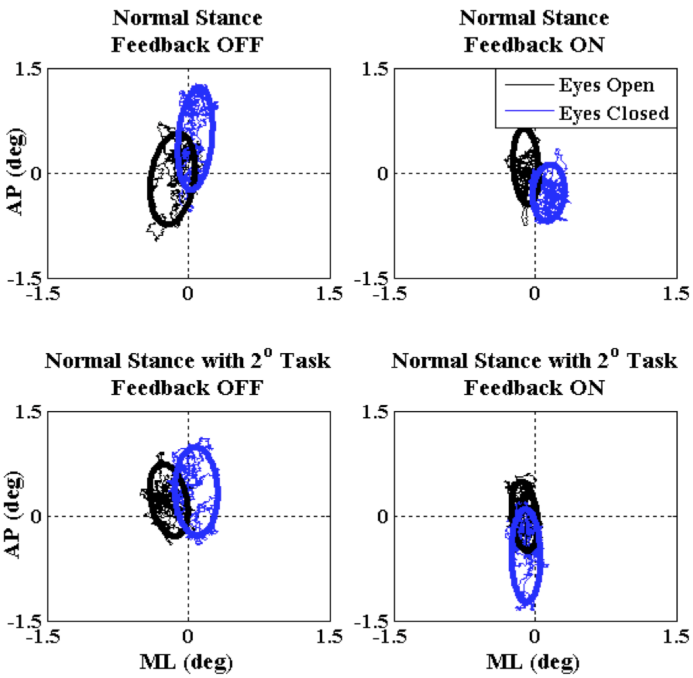

Figure 2. Sample elliptical fits of sway area for one subject during normal stance. Black and blue traces represent eyes open and closed conditions, respectively. The columns show the feedback OFF and ON results, respectively. The rows show the no secondary task and secondary task conditions, respectively.

Occasionally, in order to regain their balance, subjects stepped out of the stance to gain a more favorable footing. At that time, data collection was terminated for that specific trial. Some subjects, however, had fewer step outs and/or were able to maintain their balance for a longer period of time before stepping out when vibrotactile feedback was provided (Figure 3). The sway reduction observed in the tandem Romberg trials was inconsistent due to the challenging nature of the balance task and the large number of step outs. Increased statistical power is required for the tandem Romberg stance.

Trunk tilt feedback resulted in decreased Phi tilt for normal stance (Figure 3) and M/L tilt for tandem Romberg tasks. However, in the case of tandem Romberg, the difference was only significant for the eyes open trials with secondary task, and eyes closed trials without secondary task trials.

Subjects' baseline RMS sway and sway area values showed significant improvement at the end of the study compared with their initial baseline values measured prior to the start of the experiment. In addition, some improvement in baseline values was also seen after subjects underwent the short training session prior to the start of the experimental protocol. These findings suggest that repeated practice of specific stance exercises with vibrotactile feedback provides a short term learning effect to the user, leading to a reduction in sway. However, the effects of stance repetition alone (without feedback) need to be addressed in order to conclusively support this finding.

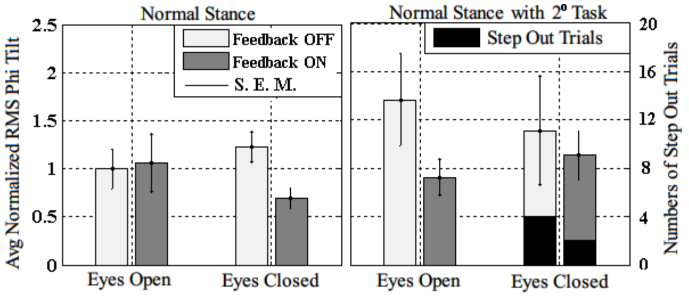

Figure 3. Average normalized RMS Phi tilt for normal stance.

CONCLUSIONS

In the elderly population described in this study, vibrotactile feedback significantly reduced subjects' RMS Phi tilt and sway area during normal stance with the eyes open and closed, as well as during tandem Romberg stance with eyes open and eyes closed. Moreover, vibrotactile feedback also reduced RMS Phi tilt and sway area during normal stance under increased cognitive workload conditions, when the performance of the trial conditions described above was coupled to a verbal secondary task.

REFERENCES

[1] Kentala, E. et. al, *Ann Otol Rhinol Laryngol, 2003.* ***112****(5): p. 404-9.*

[2] Wall, C., 3rd and E. Kentala, *J Vestib Res, 2005.* ***15****(5-6): p. 313-25.*

[3] Sienko, K. et. al, *J Vestib Res, in press.*

ACKNOWLEDGEMENTS

This study was supported by the Claude D. Pepper Older Americans Independence Center. We acknowledge Vivek Vichare for his device design contributions, Janet Kemp for subject testing assistance, Prof. James Ashton-Miller, Dr. Neil Alexander, and Takashi Furuya.

COMPENSATORY CHANGES IN THE UNINVOLVED KNEE AFTER GAIT TRAINING WITH REAL-TIME FEEDBACK IN ADULTS WITH KNEE OSTEO-ARTHRITIS

Bhupinder Singh1, NA Segal2, NF Johnston1, P Teran-Yengle1, JC Torner3, R Walace3, HJ Yack1
1Program in Physical Therapy & Rehabilitation Science
2Department of Orthopedics & Rehabilitation
3School of Public Health
The University of Iowa
Email: bhupindersingh@uiowa.edu

INTRODUCTION

A large contingent of patients with medial tibiofemoral osteoarthritis (OA) walk with larger knee adduction moments than normal subjects, resulting in increased medial compartment pressure. It has been suggested that patients with medial compartment knee OA may utilize medio-lateral trunk sway as a strategy to control the peak knee adduction moment [2]. By leaning over the affected knee and anterior tilting of the pelvis it has been demonstrated that OA patients can reduce the adductor moment at the diseased joint. While this leaning strategy is also sometimes seen as a naturally occurring compensation, the concern is that it will add to the stresses experienced by the contralateral knee. Such increased stress could potentially result in contralateral knee pathology.

Previously we showed that gait training with real-time biofeedback leads to reduction in knee adduction moments in the frontal plane [3]. We were concerned that the improvements in the most involved knee were not associated with detrimental compensatory changes at other joints including the uninvolved knee. The purpose of this study was to investigate whether reduction in knee adduction moment of involved knee leads to any compensatory changes in uninvolved knee joint.

METHODS

Fifteen subjects (9 female, 6 male; mean age 74.4 +/-6.9; mean weight 81.09 +/-14.11) with radiographic Kellgren Lawrence (KL) grade ≥ 2 and ipsilateral knee pain or stiffness on most days of the month, participated in this study. A physical and over-ground gait evaluation of all subjects was done during the first visit. The physical evaluation involved assessment of strength, flexibility, and range of motion of trunk, legs, and feet. During the gait evaluation subjects were asked to walk along an 8 m walkway at a speed of 1.12m/s. Evaluations were done using a three-dimensional motion analysis system (Optotrak, NDI; Kistler). Data was processed using Visual 3D software (C-Motion). Patient specific goals were established on the basis of gait and physical evaluations; with the possible addition of a home exercise program appropriate for correction of impaired flexibility and strength. Subjects participated in supervised treadmill gait training twice a week for 12 weeks. During gait training, subjects walked on an instrumented treadmill (Gaitway, Kistler) for three 8 minute intervals with adequate rest periods. They were provided with real-time biofeedback (Visual 3D) for correction of kinematic patterns that were thought to contribute to abnormal kinetics. Over ground kinetics and kinematics during walking were reassessed during the 8th (V2), 16th (V3), and 24th (V4) visits.

RESULTS & DISCUSSION

Results showed that the 1st peak external knee adduction moment of involved knee during gait was significantly ($p<0.01$) reduced by 29% from baseline (mean -.665 +/-.22) to third month of training (mean -.497 +/- .267) whereas the change on the uninvolved side was not significant ($p=0.56$) and reduced by 5.1 % from baseline (mean -.498 +/- 0.21) to third month (mean -.472+/- 0.243). The 2nd peak, considered to be associated with push off during the gait cycle, showed insignificant ($p=0.39$) change for the involved side decreasing by 6.2% from baseline (mean -.306+/- 0.126) to third month (mean -.287 +/- 0.151). On the Uninvolved side it increased significantly (p=0.034) by 22.3% from baseline (mean -.1894+/-0.146) to third month (mean -.231+/-0.1680). (Figure 1)

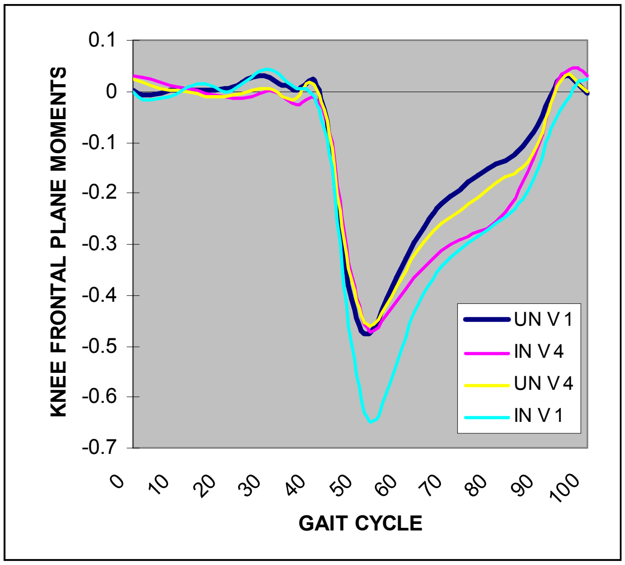

Figure 1: **Ensemble averaged frontal plane knee moments for all 15 subjects over one gait cycle (toe-off to toe-off) Comparison of adduction moment on the involved and uninvolved knee during baseline (V1), and 3rd month (V4) of gait training with real-time feedback.**

The results of this study indicate that reduction in knee frontal plane moment of the involved knee does not lead to any significant increase in adduction moment of the uninvolved knee. A greater external knee adduction moment has been shown to indicate greater loads in the medial than in the lateral compartment. Trunk lean motion in the frontal plane is often observed in patients with knee OA which shifts the body's mass toward the swing limb and increases the pressure across the medial compartment cartilage of the stance limb [1]. Andracchi, et. al, suggested that patients with knee OA utilize medio-lateral trunk sway as a strategy to control the peak knee adduction moment, but this strategy appears to be successful only in patients with less severe knee OA [2].Trunk lean to one side can potentially increase the knee moments of the unaffected knee, but the population of subjects we had showed trunk lean, both towards and away from the involved knee. Joint pain, weakness of hip abductor muscle strength and varus motion may influence this trunk motion during gait [1]. In our previous analysis of these subjects we showed a reduced knee adduction moment, but at what cost to the less involved side? There was an increase in knee adduction moment of the uninvolved side during second peak of the gait cycle, but the magnitude remained lower than the involved side. The feedback during gait training addressed abnormal kinematic patterns and led to subtle modifications to the frontal, transverse, and/or sagittal planes of trunk and pelvis movement. Thus, overall it seems that reduction in the adduction moment obtained with our gait training methods does not lead to any negative effects on the uninvolved side and further work is being done to see the compensatory effects at other joints.

CONCLUSIONS

Results of this study show that reduction of knee adduction moment following gait training with real-time biofeedback is not associated with any clinically significant change in knee adduction moment of the uninvolved knee joint. Thus this can be expected to be an effective treatment methodology for patients with knee osteoarthritis.

REFERENCES

1. K. Tanaka. *The Knee* **15** 2008 134–138.

2. A. Mundermann *Journal of Biomechanics* **41** 2008 165–170

3. P Teran-Yengle Abstract, Proceedings at GCMAS (2009)

ACKNOWLEDGEMENTS

This research was supported by the Beeson Career Development Award in Aging Program (NIH/NIA 1K23AG030945).

A SHOE-BASED METHOD FOR RANDOMLY PERTURBING THE STANCE PHASE OF GAIT AND ITS EFFECT ON STEP WIDTH

Hogene Kim, James K. Richardson, Joseph Nnodim, Hiroshi Takemura,James A. Ashton-Miller
Biomechanics Research Laboratory
University of Michigan, Ann Arbor, Michigan
Email: hogenek@umich.edu, Website: http://me.engin.umich.edu/brl/

INTRODUCTION

Many falls in the elderly occur while walking on an irregular surface [1]. It has been shown that an irregular surface increases the level of challenge during gait, as reflected by increased step width variability [2]. This step width (SW) variation may reflect the need to control stability in the frontal plane [3]. Recently a perturbation under the stance foot has been shown to cause a cross-over step whereby the first post-perturbation step crosses the midline in order to recover balance [4]. Rather than having to have patients walk on an uneven surface, which takes up too much room in the clinic, we developed a perturbing shoe to simulate the condition in which the swing foot lands on a small medially-located or laterally located pebble during gait on a flat surface. In this study, we tested the hypothesis that the perturbing shoe would significantly affect SW on the first post-perturbation step in healthy adults.

METHODS

As shown Figure 1, we developed and tested a special pair of sandals equipped with two hinged flippers concealed within the medial and lateral aspects of the shoe sole, just behind the metatarsal heads. When one of concealed flippers is deployed, the resultant medial-lateral inclination is 16^o, which corresponds to an 18 mm-high perturbation under the medial or lateral foot.

After 3 or more steps of normal gait, a flipper is covertly deployed during the swing phase. After heel strike of that swing foot the subject must then counter the effect of the perturbation during the stance phase (and subsequent steps).

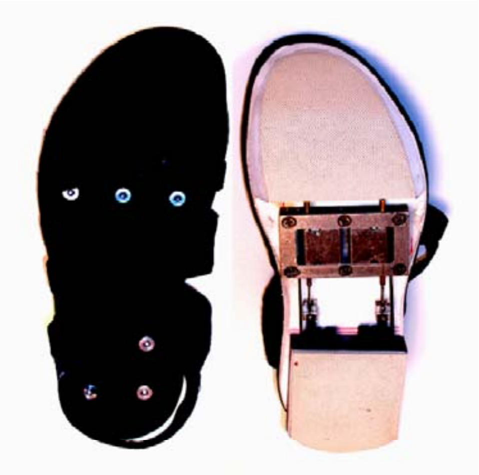

Figure 1. View of the perturbing shoe

The fulcrum is retracted during the next swing phase by an actuator hidden in the sole.

We recruited five males between the ages of 29 and 61 years. Subjects performed a total of 20 walking trials along a 6-m level walkway at a purposeful speed “as though they were going to mail a letter”. Four trials each were presented in randomized order with a right foot-medial, right foot-lateral, left foot-medial or a left foot-lateral perturbation. Subjects were told the perturbation would be deployed only once per gait trial. 3-D kinematics of foot, leg, pelvis and trunk (including ankle inversion angle, step length, and step width normalized by the subject’s mean unperturbed step width) were collected at 100 Hz in 3-D using optoelectric motion analysis cameras.

RESULTS AND DISCUSSION

Figure 2 shows the change in ankle inversion angle during the stance phase for medial, lateral, and unperturbed trials

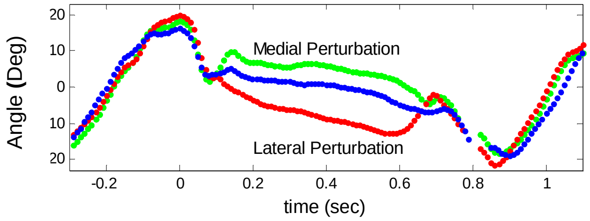

Figure 2. Change in stance phase ankle inversion angle in a sample unperturbed trial (middle line), medially-perturbed (upper line) and laterally-perturbed (lower line) trials. (+: inversion, 0: neutral posture, -: eversion)

A control chart (Figure 3; horizontal lines denote mean +/- 2*SD values of %SW) shows the effect on SW of a subject being medially or laterally perturbed during gait. In *both* cases, after the perturbation ("0" on x-axis), the SW of the first post-perturbation steps in these examples was substantially narrowed, being reduced by over two standard deviations from the mean of the unperturbed SW.

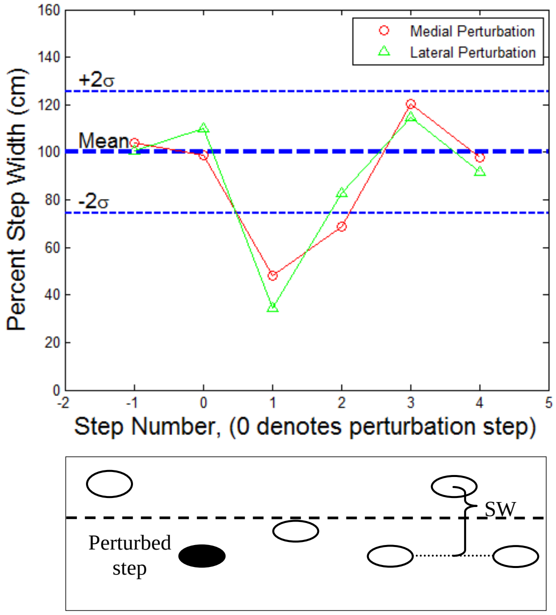

Figure 3. Control chart showing percent change in normalized step width of the first post-perturbation step following a medial or lateral perturbation.

Figure 4 shows box whisker plots with the median, upper and lower 25th centile quartiles, and 1.5*interquartile range of the normalized SW for medially and laterally perturbed trials. When the data from the four corresponding trials from each foot are lumped together, the SW with the largest deviation is shown for the medially- (triangles) and laterally- (diamonds) perturbed trials for each of the 5 subjects.

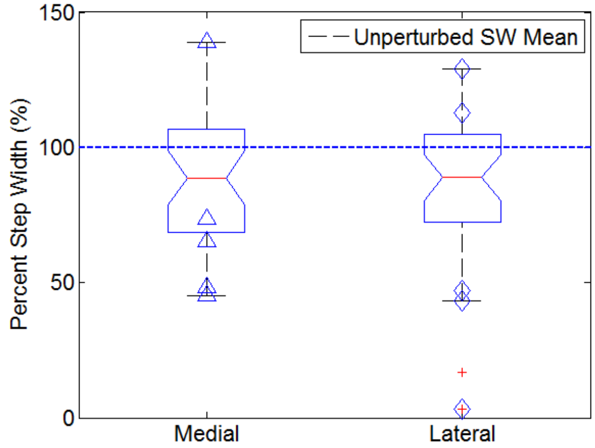

Figure 4. Box whisker plots and the largest SW deviations for the 5 subjects. (Δ: medially perturbed, ◊: laterally perturbed)

In both the medially- and laterally-perturbed trials, the SW of the first post-perturbation step was significantly different from the SW in the unperturbed trials (medial: $p = 0.0103$; lateral: $p = 0.0017$).

CONCLUSIONS

1) A shoe-based method for perturbing the stance phase of gait is an effective and safe method for challenging gait while walking.
2) Both medial and lateral mid-foot perturbations significantly reduce the post-perturbation step width.

REFERENCES

1. Berg et al., *Age and Aging*; **6**:2612-8, 1997
2. Thies et al., *Gait & Posture*, **22**:26-31, 2005
3. Bauby CE, et al., *J Biomech*, **33**:1433–40, 2000
4. Thies et al. *Gait & Posture*, **26**:156-160, 2007

ACKNOWLEDGEMENTS

PHS grants R01 AG 026569 & P30 AG 024824

A NOVEL PORTABLE VISUOMOTOR MANUAL REACTION TIME TEST

[1] Hogene Kim, [3]James T. Eckner, [3]James K. Richardson, [1,2]James A. Ashton-Miller
[1]Department of Biomedical Engineering, [2]Department of Mechanical Engineering
[3]Physical Medicine and Rehabilitation, University of Michigan Health System,
University of Michigan, Ann Arbor, Michigan
Email: hogenek@umich.edu, Website: http://me.engin.umch.edu/brl/

INTRODUCTION

There is a need for a simple, portable, and inexpensive clinical test of reaction time in at least two areas of medicine. In geriatrics manual simple reaction time (SRT) is significantly increased in elderly fallers [1]; and manual choice reaction time (CRT) differentiates between elderly fallers and non-fallers [2]. Similarly, the ability of the elderly to drive safely is predicted by their SRT and visual motion sensitivity [3]. In the area of sport-related concussion, the return-to-play issue is a current topic of concern: it is known that concussed football players and boxers have shown prolonged SRT compared to controls several days after complete symptom resolution [4]. Currently, SRT as well as CRT measurement typically involves a laptop and neuropsychological testing software that are too expensive to be widely available for testing younger athletes, who are the most prone of all athletes to sport-related concussion [5].

In high schools SRT has long been measured inexpensively via the “catch the ruler” test (asking a student to catch a ruler that is suddenly released, measuring the drop height and calculating the visuomotor SRT). We automated and extended this visuomotor manual SRT apparatus to measure SRT and CRT. We then used the method to test the null hypothesis that there is no gender difference in visuomotor SRT or CRT in young healthy adults.

METHODS

The apparatus is an elongated member equipped with LED for visual cues, an accelerometer, microcontroller and LCD display. The device can measure simple response time and choice response time (via a “Go - No Go” paradigm).

Twenty two healthy adults (12 females, 10 males, age: F: 23.9±7.7 years, M: 27.7±9.0 years; height: F: 169.4±7.4 cm, M: 179.3±6.9 cm; weight: F: 69.2±10.7 kg, M: 74±6.7 kg) were recruited for this study

The subjects stood with their dominant forearm resting on a horizontal surface with the wrist positioned at the edge of the surface. The examiner holds the device vertically and releases it after a random time interval for the subject to catch as quickly as possible using a pinch grip. This gives the Simple Response Time, henceforth termed SRT-D (where D denotes measured by the device, in ms). In the CRT test, the LED illuminates upon acceleration onset; the subject catches the device as quickly as possible if the LED illuminates, but lets it fall if the LED does not illuminate. The CRT, hence forth termed the Choice Response Time (CRT-D) is reported in ms units after each trial via the LCD display.

One optoelectric camera (Optotrak Certus) recorded the apparatus and finger kinematics at 500 Hz using one marker on the apparatus body and two markers on the tip of index finger and thumb. Electromyographic (EMG) activities in finger flexor muscles were sampled at 2 kHz to find the onset of EMG activity in target muscle group.

To validate the method the subject’s response was partitioned into three intervals using measurements independent of the device:

a) Pre-motor time (PMT): from the onset of device acceleration to the onset of agonist EMG activity.
b) Electromechanical delay (EMD): from the onset of depolarization of the agonist muscle group to the acceleration onset of the fingers
c) Movement Time (MVT): from acceleration onset of the finger to the first instant when device velocity returns to zero.

Technically, the sum of a) and b) are the reaction time, and the sum of a), b) and c) is the response time.

Finally, minimum response times were defined as the [mean-3.29*SD] point for the SRT data, and a similar point for the CRT-D data after logarithmic transformation of the skewed data and back-transformation to the original scale. The mean-3.29*SD corresponds to the minimum in one out of 1,000 trials.

RESULTS AND DISCUSSION

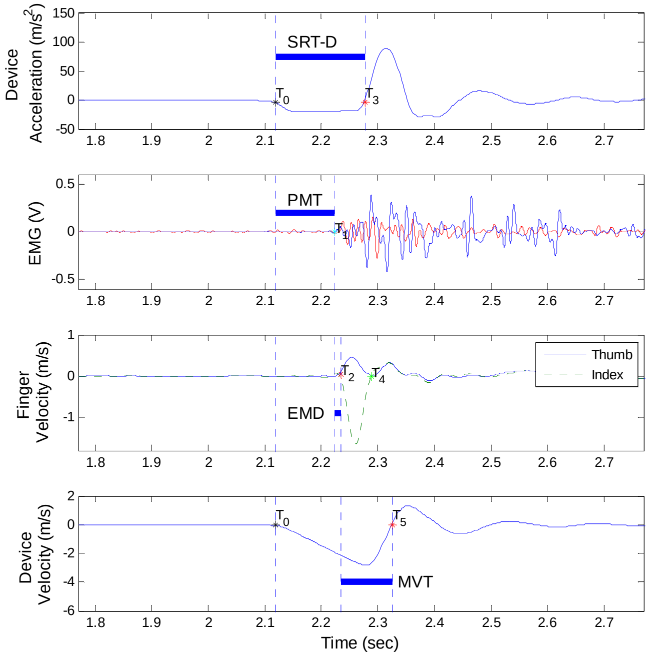

Figure 1. Simple Response Time Test – Sample device, finger kinematics, and finger flexor muscle activity for a female subject, showing SRT-D, PMT, EMD, and MVT.

SRT-D was within 5-10 ms of the sum of PMT+EMD+MVT showing construct validity. The difference was due to the use of the acceleration onset/offset by the device, and the device velocity onset/offset for the kinematic measurements.

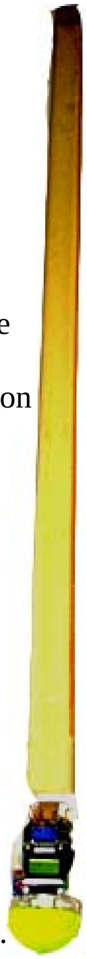

Table 1 summarizes results of SRT and CRT tests. There was no significant gender difference in SRT-D or CRT-D (effect size <0.23). A power analysis showed that sample sizes of 235 subjects would be needed in each group to demonstrate a significant gender difference. CRT-D was significantly longer than SRT-D (P<0.0001).

The estimated minimum response times for the SRT-D and CRT-D are found in Table 2.

The correlation between SRT-D and the reaction time (PMT+EMD) was 0.910.

Table 2. Minimum visuomotor estimated human visuomotor manual response times (in ms) by test

Group	**SRT-D**	**CRT-D**
Female	91.0	127.4
Male	90.0	122.7

CONCLUSIONS

1) No significant gender differences were found in SRT-D or CRT-D.
2) This inexpensive apparatus and method was validated using independent measures.

REFERENCES

1. Lord SR, et al. *J Am Geriatr Soc*.**39**:1194–1200, 1991
2. Lord SR, et al. *Gerontology*.**42**: 199–203, 1996
3. Wood, JM., *J Am Geriatr Soc* **56**:986–993, 2008.
4. Warden, DL, et al. *Neurology* **57**(3): 524-6. 2001
5. Theye, F. et al., *Clin Med Res* **2**(3):165-71. , 2004

ACKNOWLEDGEMENTS

Public Health Service grants: R01 AG 026569 & P30 AG 024824

Table 1. Summary of mean (SD) reaction and response times (in ms) for the SRT and CRT tests measured using the device as well as standard kinesiological techniques involving electromyography and kinematics.

Gender	**Simple Reaction Time (SRT) Test**				**Choice Reaction Time (CRT) Test**			
	PMT	**EMD**	**MVT**	**SRT-D***	**PMT**	**EMD**	**MVT**	**CRT-D****
Female	**118** (23)	**13** (7)	**46** (12)	**165** (25)	**180** (52)	**12** (12)	**57** (21)	**235** (54)
Male	**123** (24)	**11** (11)	**40** (9)	**162** (25)	**174** (48)	**15** (14)	**54** (23)	**230** (51)

* p-value = 0.236, **p-value = 0.1220

AGE-RELATED CHANGES IN DYNAMIC STABILITY AND AVOIDANCE STRATEGIES WHEN STEPPING OVER AN OBSTACLE IN A DUAL TASK PARADIGM

Maxime Paquette and Lori Ann Vallis
University of Guelph, Guelph, Canada
email: maxime@uoguelph.ca

Introduction: A large number of studies have investigated locomotor strategies in young and older adults for stepping over obstacles [e.g. 1, 2, 3]. Generally, findings indicate that older adults are more cautious and adopt safer stepping strategies to successfully step over an obstacle compared to young adults. Additionally, the effects of holding, carrying, or stabilizing an object during gait have also been studied [4, 5] but to our knowledge, no research has examined the influence of such tasks on gait parameters during obstructed walking. The purpose of the present study was to investigate how performance of an object stability task influences gait parameters in young and older adults when stepping over an obstacle in the travel path.

Methods: Young adults (YA; mean age: 22.8 ± 2.2 years) from the University of Guelph and older adults (OA; mean age: 75.2 ± 4.3 years) from a local retirement community were recruited to participate in this study. Participants completed a medical questionnaire to ensure they did not have any musculoskeletal disorders (e.g. osteoarthritis in lower limb), severe dizziness or vestibular loss and were not taking any medications that could affect balance. The Mini-Mental Status Exam (MMSE) and Timed up and Go test (TUG) were administered to all OA participants upon arrival at the laboratory. All scored higher than 24 on the MMSE and were therefore able to provide their informed consent to participate in the study. All older adults also successfully complete the Timed Up and Go test (TUG) in less than 12 seconds indicating an adequate level of mobility to be able to safely participate in the experimental protocol. This experiment was approved by the University of Guelph Research Ethics Board.

All participants were instrumented with infrared-emitting diode rigid body triads and anatomical points (e.g. heels, toes) were digitized for 3D kinematics data collection (Optotrak Motion Analysis system, 60 Hz, Model 3020, NDI, Inc). Subjects performed six unobstructed object stability trials, six obstructed walking trials and six obstructed object stability (dual-task) trials.

Obstructed experimental trials required participants to walk along a pathway and step over an obstacle (width: 1 m, depth: 1 cm) with a height normalized to 45% of lower leg length [3, 6]. Kinetic data of the walking trials was also acquired (240 Hz) via two force plates imbedded in the laboratory floor located before and after the obstacle (AMTI Model OR6-7). The object stability task (OS) required participants to stabilize a table tennis ball on an upside-down ultimate Frisbee disc. Before the dual task trials, participants were given simple instructions to complete both the obstacle avoidance task and the OS task to the best of their ability. Prior to each block of experimental trials, two to three practice trials were provided.

Average gait velocity (normalized to lower leg length) during the obstacle crossing step, horizontal heel landing distance from the trailing edge of the obstacle and, cumulative center of pressure path length in double support during obstacle crossing were calculated. The number of contacts the ball had with the edge of the disc were also recorded during OS trials. Age-related differences for all gait parameters were investigated and analyzed using a two-way MANOVA statistical test with age (young and older) and task condition (obstructed and obstructed OS) as independent factors and gait parameters as dependent factors. In addition, a statistical power analysis was performed for both analyses.

Results: Object stability task errors, or the number of ball contacts with edge of the disc, were recorded. Older adults produced more errors (Total = 11) compared to young adults (Total = 3) during the unobstructed OS trials. When task difficulty increased during the obstructed OS trials, OA produced even more errors (Total = 45) compared to YA (Total = 16). Landing distance revealed a main effect of age (F(1,140)=23.919, p=0.0001). In general, OA stepped closer to the trailing edge of the obstacle (0.157 m) compared to YA (0.209 m). In addition, landing distance also yielded a main effect of condition (F(1,140)=41.358, p=0.0001). For all participants, landing distance was decreased during the obstructed OS trials (0.149 m) compared to the obstructed only trials (0.217 m; Figure 1).

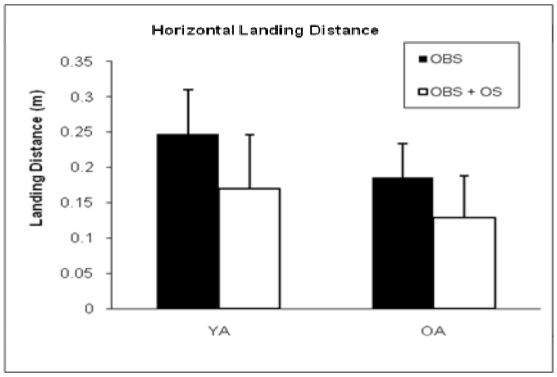

Figure 1. Horizontal landing distance of the lead heel

Path length indicated a main effect of age only (F(1,140)=25.673;p=0.0001). Across all conditions, OA produced larger cumulative COP path length values (30.6 m) compared to YA (22.2 m) indicating that OA had a greater sway magnitude. Normalized gait velocity during obstacle crossing revealed an interaction effect between age and condition (F(1,140)=7.956, p=0.005). Within the YA population, gait velocity was reduced for the obstructed OS task (0.977 m) compared to the obstructed only task (1.130 m). However, gait velocity was not changed in OA between the obstructed (0.936) and obstructed OS trials (0.974).

Discussion and Conclusions: In the present study, the ability of young and older adults to simultaneously complete a novel upper body stabilization task while stepping over an obstacle was investigated. Our results indicate that while OA generally stepped closer to the trailing edge of the obstacle, both YA and OA reduced landing distance during the obstructed OS trials compared to the obstructed only trials. Although stepping closer to the obstacle may increase the likelihood of hitting the obstacle, prior work [1] suggests that the risk of tripping would be more significant if the toe hit the obstacle during swing phase of gait. Similarly, Lowrey et al. [3] reported reduced landing distance in older adults compared to a younger population when stepping over an obstacle and observed that toe position in the step prior to obstacle crossing was not different between age groups. It appears that OA place a greater importance on trail toe location prior to obstacle crossing in order to ensure adequate toe placement and trajectory to successfully avoid the obstacle during swing phase. To better understand the implications of landing distance after the obstacle, investigation of toe-off location and toe clearance values will be necessary. Cumulative COP path length (CPL) was greater during double support for obstacle crossing in OA compared to YA. OA may produce larger CPL values in order to prevent reductions in gait stability by ensuring the COM remains within the base of support. Conversely, gait stability in OA may be reduced due to the challenging nature of the task and therefore, an increase in CPL may play an important role in controlling the COM within the base of support to regain dynamic stability. Further analyses investigating the COP and COM relationship will provide further insight into this interesting finding. It was expected to see a decrease in normalized gait velocity in both YA and OA during the obstructed OS trials. However, although YA reduced their gait velocity for those trials, OA did not. Interestingly, OA had significantly more object stability task errors than YA. Our findings suggest that OA prioritize the maintenance of gait velocity during obstacle crossing at the cost of object stability task performance and decreased landing distance.

References:

[1] Chen, Ashton-Miller, Alexander, Schultz (1991) *J of Gerontol* 46(6):196-203
[2] Chou and Draganich (1997) *J Biomech* 30(4):331-7
[3] Lowrey, Watson, Vallis (2007) *Exp Brain Res* 182: 289–299
[4] Bond, Morris (2000) *Arch Phys Med Rehab* 81(1): 110-6
[5] O'Shea, Morris, Iansek (2002) *Phys Ther* 82 (9) 888-897
[6] Chou, Kaufman, Hahn, Brey. (2003) *Gait Posture* 18: 125-133

GAIT TRAINING AND KNEE HYPEREXTENSION

P Teran-Yengle[1], NA Segal[2], NF Johnston[1], B Singh[1], JC Torner[3], R Walace[3], HJ Yack[1]
[1]Program in Physical Therapy & Rehabilitation Science
[2]Department of Orthopaedics & Rehabilitation
[3]School of Public Health
The University of Iowa
Email: patricia-teranyengle@uiowa.edu

INTRODUCTION

The health of articular cartilage is associated with appropriate stress occurring in appropriate regions (2). In the knee, abnormal arthokinematics can result in abnormal loading patterns that can potentially be detrimental to the integrity of the cartilage resulting in osteoarthritic changes (3). While knee hyperextension has been linked to a number of neuromuscular pathologies, the connection with osteoarthritis is less clear, but clinically evident (1). It is unclear if hyperextension contributes to the initiation of knee OA or if it evolves from compensatory strategies adapted by the patient.

Changing gait kinematics in order to correct for knee hyperextension is generally viewed as an appropriate goal when working with patients who have knee OA. The methods to accomplish this have typically been limited to taping, bracing, and/or muscle strengthening and have had only limited success. The purpose of this study was to investigate the use of gait training with real-time biofeedback in controlling knee hyperextension. This initial report provides data on three subjects who were part of a larger project studying interventions with knee OA patients.

METHODS

One female and two male patients with diagnosis of bilateral knee osteoarthritis underwent the gait training for correction of knee hyperextension. Knee hyperextension on these individuals was documented during their initial over-ground gait evaluation. The gait evaluation was conducted along an 8 m walkway using a three-dimensional motion analysis system (Optotrak, NDI; Kistler) with subjects walking at 1.12 m/s. Gait data were processed using Visual 3D software (C-Motion). The gait information in combination with the physical evaluation information was used to establish goals during gait training.

Subjects participated in supervised treadmill gait training twice a week for 12 weeks. Subjects walked on an instrumented treadmill (Gaitway, Kistler) at self selected walking speeds for 8 minute intervals with 3 to 5 minute rest periods. During the gait training, the subjects were provided with real-time biofeedback (Visual 3D) for correction of kinematic patterns representing knee hyperextension. Gait and physical evaluation were reassessed during the 8th, 16th, and 24th visits.

The objective with our participants was to progressively introduce real-time biofeedback to reduce and control knee hyperextension. First, the general body movement was shown using the skeleton model. Subjects then transitioned to using a running representation of their knee sagittal plane angle (Figure 1). Feedback was also provided during rest periods to reinforce corrected patterns over ground walking.

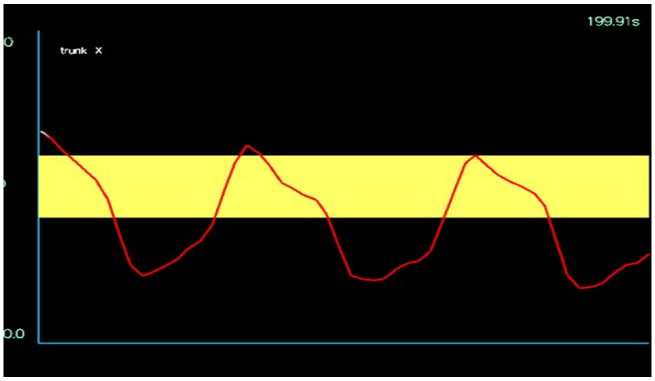

Figure 1: Example of single plane kinematic feedback used to provide subjects information on the position of their knee. Yellow area represents target region which was set at 5 degrees of knee flexion.

RESULTS & DISCUSSION

All three subjects responded positively to the gait training and showed improved control of knee hyperextension. Figure 2 shows ensemble of knee sagital plane range of motion for participant #3 for one gait cycle. The changes in range of motion for the knee in the sagittal plane are presented in Table 1. This table shows the improvements at the heel contact and forward progression of the involved knee for each subject.

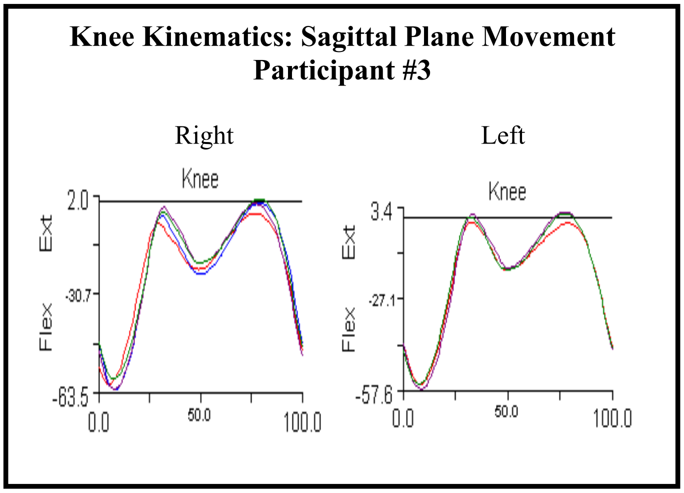

Figure 2: Example gait data showing ensemble averaged of knee sagittal plane range of motion for one gait cycle (toe-off to toe-off). Blue (Baseline); Red (After 1st month); Purple (after 2nd month) of gait training

At the initial evaluation, participant #3 showed 1.36 and 4.92 degrees of left knee hyperextension at heel contact and forward progression, respectively. After three months of training, the hyperextension was reduced to 0.88 and 2.05 degrees. Participant #10 showed reduction of left knee extension at the push off. This reduction was achieved along with a more stable pelvis during weight transfer. This particular subject demonstrated ability to carry over corrected gait patterns without visual feedback and referred improved awareness in knee alignment when standing and pain reduction at night. In regards to participant #11, she showed reduction of knee hyperextension at both heel contact and push off (Table 1), and reduction of knee adduction moment on both knees. Participant also referred improved ability to stand for longer periods of time without pain on either knee.

The gait training addressed modifications during the heel contact and forward progression to develop confidence in the stance-phase controlling for pelvic rotation, hip extension, and dorsiflexion range.

CONCLUSIONS

The gait training showed that knee sagittal plane kinematics can be influenced with dynamic gait training using real-time biofeedback.

REFERENCES

1. Fish D, Kosta Ch. *Genu Recurvatum: Identification of Three Distinct Mechanical Profiles. Journal of Prosthetics & Orthotics* 10(2):26-32, 1998.
2. Maly M. *Abnormal and Cumulative Loading in Knee Osteoarthritis. Current Opininion in Rheumatology*, 2008.
3. Andriacchi TP, Koo S, Scanlan S. *Gait Mechanics Influence Healthy Cartilage Morphology and Osteoarthritis of the Knee. J Bone Joint Surg Am.* 91:95-101, 2009.

ACKNOWLEDGEMENTS

This research was supported by the Beeson Career Development Award in Aging Program (NIH/NIA 1K23AG030945)

Knee Joint Angle (deg)	Pre Training		Post Training	
	HC	PO	HC	PO
Participant #3 (Left Knee)	1.36	4.92	0.88	2.05
Participant #10 (Left Knee)	1.28	5.65	4.80	-1.80
Participant #11 (Right Knee)	2.86	2.05	1.25	-0.46

Table 1: Involved knee join angles at heel contact (HC) and push off (PO) pre and post gait training

EFFECT OF TARGET SIZE ON WHOLE BODY INTER JOINT SYNERGIES: AN UNCONTROLLED MANIFOLD ANALYSIS

[1] Sohit Karol and [1, 2, 3] Jae Kun Shim
[1]Department of Kinesiology, University of Maryland, College Park
[2] Fischell Department of Bioengineering, University of Maryland, College Park
[3] Neuroscience and Cognitive Science (NACS) Program, University of Maryland, College Park
email: skarol@umd.edu

INTRODUCTION

The human body is a highly redundant system, and the framework within which the Central Nervous System (CNS) uses this redundancy is not been fully understood. This has also called the degrees of freedom problem in the motor control literature [1]. Although many earlier studies assumed that the redundant degrees of freedom pose a computational problem for the CNS, some recent studies, using the frame work of uncontrolled manifold analysis (UCM) have suggested that these redundant degrees of freedom might be acting in synergies to attain a better task performance [2].

The purpose of the present study was to investigate and compare the whole body inter joint kinematic synergies during a poking task, when subjects were presented with varied level of task constraints by changing the size of the target. Synergies were quantified using the Uncontrolled Manifold Analysis (UCM).

METHODS

33 healthy adult males, with no history of neurological disorders, participated in the study. Subjects were asked to hold a long stick (2.2 m) vertically with both the hands, and presented with a circular target, (0.8 m) above their head. Reflective markers were applied on the following landmarks: toe, ankle, knee, hip,, shoulder, elbow and wrist. Markers were also applied on the diameter of the circles, which was visible in the frontal plane, and the tip of the poking stick. Subjects were asked to repeat a sit to stand motion twenty times, look at the target and poke it. There were 20 repetitions for each of the 10 trials. Target size was varied to the following diameters: 1cm, 2 cm, 3 cm, 5 cm, 8 cm, 13cm. Synergies were quantified using the UCM analysis, which analyses the structure of joint angle variance in the vector space of the task (V_{UCM}) and orthogonal to the task (V_{ORTH}). A normalized index ΔV was calculated by subtracting V_{ORTH} from V_{UCM}, and then dividing the result by the total variability. Positive and greater values of ΔV imply greater inter joint synergies to attain the task demands (in this case, poking within the target range). Details of this method have been described elsewhere [3]. Within subjects ANOVA with Bonferroni corrections (α = 0.05) were used to compare the results.

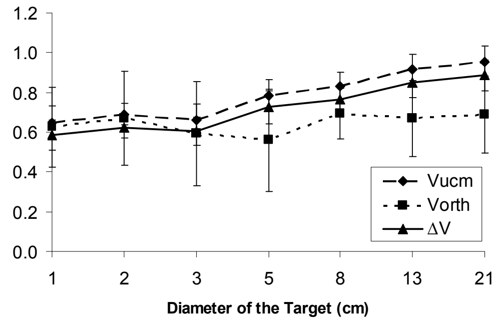

Figure 1: Mean (±SEM) joint configuration variance parallel to (V_{UCM}, dashed lines) and perpendicular (V_{ORTH}, dotted lines) to the linearized uncontrolled manifold (*UCM*) and ΔV (solid line) for hypotheses about controlling the location of the end point of the stick during poking.

RESULTS AND DISCUSSION

Changes in the components of variability, V_{UCM} and V_{ORTH}, and the index ΔV are shown in figure 1. For all target sizes, no significant differences were found in the index V_{ORTH} [$F_{6,32} = 0.89$, $p<0.05$]. However, significant effects of target size emerged in the component of variability V_{UCM} [$F_{6,32} = 15.73$, $p<0.05$] and for the index ΔV [$F_{6,32} = 13.72$, $p<0.05$]. Pair wise comparisons revealed a significant difference between the target sizes 21cm and 1 cm, 13cm and 1cm, 21cm and 2cm, 13cm and 2cm, 21cm and 3cm, and 13cm and 3cm.

The results suggest that the CNS controls the end point trajectory of the stick and uses the inter-joint variability for the large target sizes to attain these goals (13cm and 21cm). However, these results do no give any indication of a similar control strategy for smaller target sizes (1cm, 2cm, 3cm, 5cm and 8cm). It is to be noted that the value of V_{ORTH} does not change significantly with the target size. These results point to the fact that the error component of the variability remains consistent despite the size of the target. Increasing the target size (and hence making the task easier), only increases the non error component, which points towards the use of motor abundance, as opposed to motor redundancy [3].

It is also to be noted that for all the task conditions, there could be some other important performance variables that the CNS might need to stabilize, like the whole body center of mass, head position, acceleration etc], and the priority for stabilization of all these performance variables requires further analysis.

CONCLUSIONS

The purpose of the study was to investigate the effect of target size on multi joint synergies in a bimanual poking task. Preliminary findings using the uncontrolled manifold analysis [UCM] suggest that the error component of variability does not change with the size of the target. However, there is an increase in the non error component and multi joint synergy index (ΔV) as the target size increases. These results suggest that the inter joint synergies increase with the increase in target size, and the error variance is not affected at all, hence pointing towards the employment of the principle of abundance by the CNS.

REFERENCES

1.Turvey MT, *Am Pschol* **45(8)**, 938-953, 1990.
2. Schoner G, *Motor Control* **11(3)**, 259-275, 2007.
3.Latash M, *Motor Control* **4(3)**, 259-260, 2000.

DIFFERENCES OF TIBIOFEMORAL KINEMATICS BETWEEN ACL-INTACT AND ACL-DEFICIENT KNEES IN AN IN VITRO SIMULATED PIVOT LANDING

[1]Youkeun Oh, [2]Jennifer Kreinbrink, [2]Kathryn Antle, [2]Edward M. Wojtys and [1]James A. Ashton-Miller
Department of [1]Mechanical Engineering, [2]Orthopaedic Surgery, University of Michigan, Ann Arbor
email: youkeun@umich.edu web: http://me.engin.umich.edu/brl

INTRODUCTION

The role of the anterior cruciate ligament (ACL) in restraining tibial anterior translation is well documented. But the effect of the ACL on restricting tibial axial rotation remains controversial [1, 2]. The goal of this study was to quantify the role of the ACL in controlling tibial axial rotation by comparing, in a repeated measures design, the kinematics of ACL-intact and ACL-deficient cadaveric knees under compound impulsive loading. The primary hypothesis was that transecting the ACL would not affect peak tibial axial rotation under the simulated pivot landing.

METHODS

Twelve unembalmed cadaveric limbs were tested [mean (SD) age: 65.0 (10.5) years; 8 females]. Following the methods of Withrow et al. (2006) [4] lower extremities were cut 8 inches proximal and distal to the knee joint. Specimens were then dissected, leaving the ligamentous knee structures and the tendons of quadriceps, hamstrings, and gastrocnemius muscles intact. Each end of the specimen was potted using polymethylmethacrylate.

A custom testing apparatus was constructed to simulate the position of a single extremity as it strikes the ground while landing on one leg during a jump or pivot maneuver. The simulated quadriceps and two gastrocnemius muscles were represented by nylon cord (stiffness ~2 kN/cm) pretensioned to 180 N and 70 N, respectively. Two constant force springs (70 N each) were used to represent the hamstring muscle forces. In both cases, the simulated muscle unit was connected from the femur or tibia to the relevant tendons via cryoclamps through the anatomical lines-of-action, thereby representing the *in vivo* dynamic resistance of each muscle-tendon unit to sudden stretch. In all trials, an initial knee flexion angle of 15^{o} was used. A ground reaction force that reached its peak value at 50 ms was simulated by dropping a weight so as to apply a 2*BW (where BW is each donor's body-weight) impulsive force to the distal tibia. The linear momentum at impact was transformed into an axial compressive force and an impulsive axial torque component (peaked at 70 ms) by a specially-designed rotational device in series with the distal tibia. The peak axial torque was adjusted to reach a nominal value between 10 and 25 Nm.

Two 3-axis load cells (AMTI, Watertown, MA) measured the 3-D femoral forces and moments delivered to the construct, as well as the 3-D tibial reaction forces and moments. A 3-mm DVRT (Microstrain, Burlington, VT) was mounted on the anteromedial bundle of the ACL to record relative strain. Five 1-axis load cells (Transducer Techniques, Temecula, CA) measured muscle tensions. Impact forces, the five muscle forces and ACL strain data were recorded at 2 kHz using a 16-bit A/D board, while tibiofemoral kinematics was recorded at 400 Hz using an Optotrak Certus system (Northern Digital, Inc., Waterloo, Canada).

After five pre-baseline (compression force + flexion moment) trials (block 'A1'), three blocks of six trials were run on each ACL-intact specimen in an 'A1-B-C-A2' design, where 'B' and 'C' were randomized to be either an internally-directed or externally-directed axial torque combined with a compression force and a flexion moment, followed by the post-baseline trial block ('A2'). The ACL was then transected. Two blocks of six trials were then repeated on each ACL-deficient specimen in an 'A3-D' design, where 'A3' was the baseline trial for ACL-deficient specimens and 'D' was that of the peak axial torque trial that showed the larger ACL relative strain (per applied axial torque) in the 'B' and 'C' conditions.

A repeated measures ANOVA was used to examine the differences in kinematics between ACL-intact and ACL-deficient knees (with p<0.05 significant).

RESULTS AND DISCUSSION

Ten of the 12 specimens exhibited larger peak ACL relative strain per axially applied torque under the tibial internally-directed torque than the tibial externally-directed torque. According to the protocol, 10 out of 12 specimens were re-tested under the combination of the compression force, flexion moment, and tibial internal axial torque in the testing condition, 'D'. No significant difference in the peak tibial internal rotation angle was found when comparing the ACL-intact ('Int1') and ACL-deficient ('Int2') conditions (Fig. 1).

There were significant increases ($p<0.001$) in tibial anterior translation after transection of the ACL. However, there was no significant difference in the increments of tibial anterior translation (cf, d1 vs. d2, Fig. 2) due to tibial internal torque for ACL-intact vs. ACL-deficient knees.

The overall instantaneous center of rotation (ICR) [3] was calculated from impact to the time when the peak knee flexion angle occurred. The mean (SD) values for the trials of A2, A3, Int1, and Int2 were 73.58 (143.88) mm, 79.95 (174.08) mm, 49.14 (37.24) mm and 57.13 (71.81) mm, respectively. There were no significant differences when comparing the ACL-intact to ACL-deficient knees (Fig. 3).

Our findings corroborate previous studies [2,5], which show that the ACL does not play a role in resisting tibial internally-directed torque.

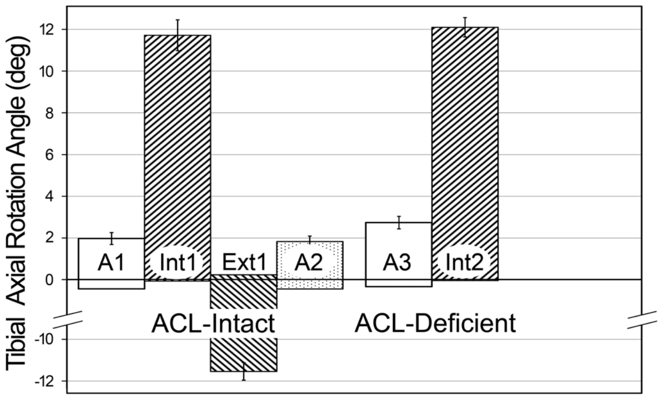

Figure 1: Peak tibial axial rotation angle (tibial internal rotation (+), tibial external rotation (-)). Error bars represent ±1 standard deviation

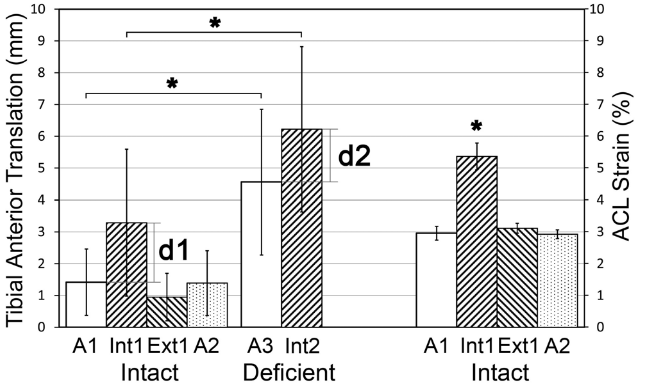

Figure 2: Tibial anterior translation (mm) and ACL strain (%). Significant differences are indicated by asterisks. Error bars represent ±1 standard deviation

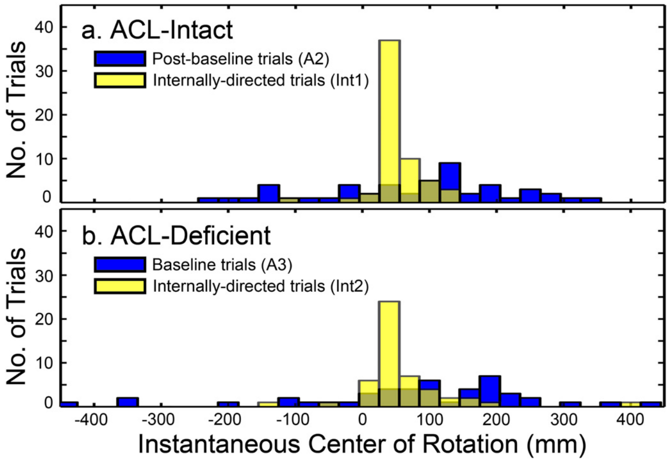

Figure 3: Histograms of the location of ICR. In the horizontal axis, positive and negative values represent the medial and lateral aspect of the tibial plateau, respectively.

CONCLUSIONS

In this first study of a knee preloaded by muscle forces and subjected to internally-directed torques applied to the distal tibia under compound impulsive end-loading conditions, the ACL does not provide meaningful resistance to a tibial internal rotation.

REFERENCES

1.Kanamori A, et al. *J Arthro* **16(6)**, 633-639, 2000.
2.Lo J., et al. *J Biomech* **41**, 1855-1861, 2008.
3.Koo S., et al. *J Biomech* **41**, 1269-1273, 2008.
4.Withrow TJ., et al. *AJSM* **34(2)**, 269-274, 2006.
5.Diermann N. et al. *Arch Orthop Trauma Surg* **129**, 353-358, 2009

ACKNOWLEDGEMENTS

PHS Grant R01 AR054821

MECHANICAL PROPERTIES OF AN ELASTOMER INSERT ANKLE FOOT ORTHOSIS

[1] Mukul Talaty, [2]Damani Seale and [2]Sorin Siegler
[1]MossRehab, Elkins Park, PA 19027, [2]Drexel University, Philadelphia, PA 19102
email: mctalaty@einstein.edu, web: http://einstein.edu/gaitlab

INTRODUCTION

Molded ankle foot orthosis (MAFOs) are an essential tool to assist walking function and thus independence to a large number of people with widely varying pathologies. The number of MAFO options and the process by which they are administered, however, contribute a great amount of variability to the final outcome. One piece of this variability stems from inadequate description of the material properties of MAFOs and how those mechanical properties contribute to the function of the brace. Ongoing research in our lab seeks to address these two issues by characterizing material properties and estimating the contribution of the brace to walking function.

In this abstract, we report the preliminary evaluation of the elastomer insert USS AFO component (UltraflexSystems, Inc. Pottstown, PA USA). Some components of this brace are relatively novel brace technology. In particular, we are interested in how the overall brace properties are affected by the elastomer as opposed to more conventional metal or silastic joint resistance. Furthermore, in more traditional MAFOs, the resistance or support provided by the brace stem from both the joint resistance and the brace structure (plastic shell – calf upright and foot plate portions – and the metal uprights, if used). We aimed to determine the extent to which the elastomer and the plastic contributed to the resistance in the USS AFO. Bench testing has become popular for AFO testing. Previous work has shown bench testing results can be sensitive to how the brace is constrained [1]. Finally, we were interested to characterize the designed hysteresis reported by the manufacturer.

METHODS

We used a bench testing approach fundamentally equivalent to existing bench testing methods [2, 3]. Briefly, loads were applied to deflect the brace into dorsiflexion while motion capture (Coda MPX30, Charnwood Dynamics, Ltd., UK) was used to assess its angular displacement. The applied loads were measures using forceplates (FP60120, Bertec, Inc. Columbus OH). The brace was secured in a vice by the forefoot section of the footplate. The vice was rigidly attached to long rails, which allowed all loads applied to the brace to be entirely within the base of support. The entire assembly rested atop the forceplate so no complex fixation methods or subsequent coupling loads were generated. To estimate brace stiffness, a least squares line of best fit was obtained from the applied moment – angular deflection plot. To evaluate results sensitivity to testing methods, we will repeat the tests in an instrumented spatial linkage as has been previously used to assess ankle flexibility in healthy and injured ankles [4]. Our characterization of brace hysteresis was exploratory as we have not evaluated this property in braces before.

RESULTS AND DISCUSSION

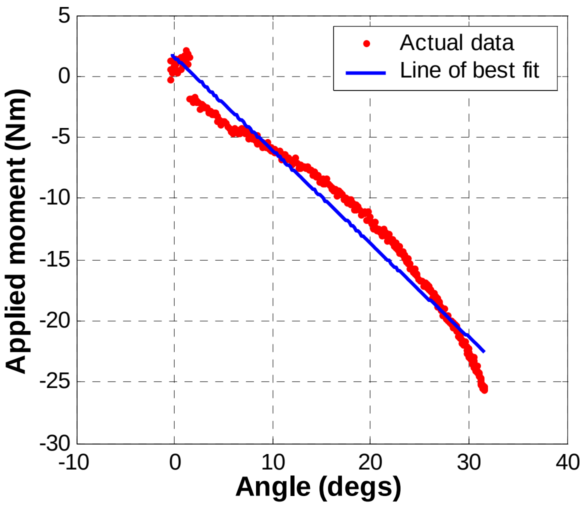

Figure 1: Loading arm only of load-deflection plot, including line of best fit (least squares) used to estimate brace stiffness. Data from single trial of the baseline testing condition.

A representative section of load-deformation plot used to estimate brace stiffness is shown in Figure 1. Brace stiffness estimates for three trials from all conditions are reported in Table 1. Figure 2 shows the plots used to characterize hysteresis.

Table 1. Brace stiffness across test conditions

Cond.	Trial 1	Trial 2	Trial 3	Average
Base	0.77	0.76	0.77	0.77
+8^{o} PF	0.92	1.04	1.11	1.02
+8^{o} DF	0.73	0.84	0.85	0.81

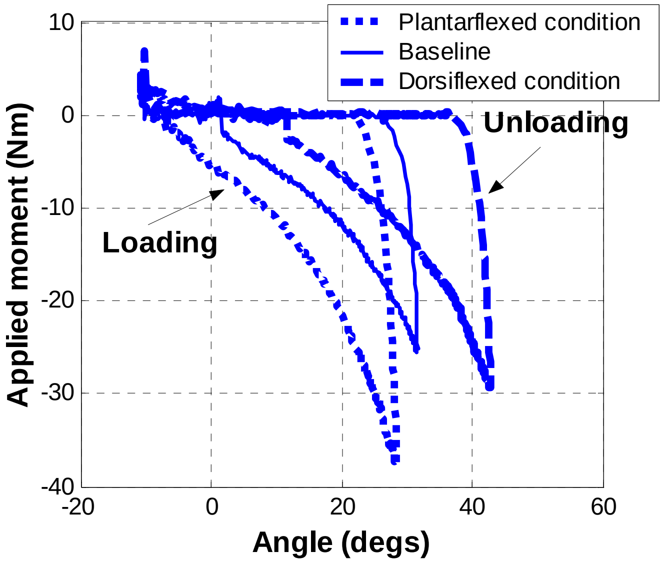

Figure 2: The entire load-deflection plot was used to characterize hysteresis.

Intercondition repeatability of the stiffness results (Table 1) suggests the testing methods were suitable for this particular brace. It was unexpected that the PF condition showed a higher stiffness (~25%) than that found in the baseline condition. The dorsiflexion response (i.e. testing the brace deflection into dorsiflexion as a load is applied) is dependent upon the compression of the elastomer in the anterior channel. Intuitively, it is thought this channel would be relatively uncompressed in a plantarflexed brace. It is unclear, at present, whether there is any interaction between the elastomer in the anterior and posterior channels, but this could help to clarify the nature of response. We have not consulted with the manufacturer yet to get their insights into this behavior, nor has the test been repeated to ensure there were no testing anomalies or errors. The similarity of the stiffness values in the baseline and dorsiflexed test conditions (0.77 vs. 0.81) suggest a uniform response of the elastomer column over the two deflection ranges encompassed by these two test conditions. Testing in the instrumented spatial linkage is ongoing and data are not reported here but will be presented at the meeting.

The hysteresis was found to exist, as stated by the manufacturer, in all test conditions. In general, the loading encompassed a brace deflection of approximately 30 degs where as the unloading returned only 5-7 degs. This response is likely also dependent on the settings of both anterior and posterior channels. In the present test conditions, the brace was ‘locked’ so that both channels were set to the same position. In this way, there was no free range of motion during which both elastomers were uncompressed. In the current testing paradigm, one channel was always compressed, and the other was at the threshold when the brace was unloaded. This represents a somewhat extreme case for how the brace may be used. How this hysteresis response changes when there is a free range present in the brace will also be assessed and reported.

In addition to the above, our further – and admittedly more interesting and useful – testing will center on evaluating the contribution of the brace support to components of movements during walking. To do this we will need estimates of the brace stiffness and assurances that these estimates reflect real-life walking conditions. This is the importance of the basic results reported here.

REFERENCES

[1] M. Talaty, Drexel University, Philadelphia, Doctoral Thesis 2002.
[2] P. Cappa, F. Patane, and R. G. Di, *J Biomech Eng*, vol. 127, pp. 1025-9, 2005.
[3] T. F. Novacheck, C. Beattie, A. Rozumalski, G. Gent, and G. Kroll, *Journal of Prosthetics and Orthotics*, vol. 19, pp. 98-103, 2007.
[4] W. LIu, S. Siegler, and L. Techner, *Clinical Biomechanics*, vol. 16, pp. 237-244, 2001.

ACKNOWLEDGEMENTS

The brace joint and partial funding for this work were graciously provided by UltraflexSystems, Inc. Pottstown, PA 19464. The funding mechanism was an unrestricted educational grant. The brace was graciously made by Allied Orthotics & Prosthetics, Philadelphia, PA.

EFFECT OF GOLF SWING STYLES ON RESULTANT JOINT MOMENTS OF LOW BODY JOINTS AND L4/L5

[1]Sunghoon Shin, and [2]Pilwon Hur
[1]Department of Kinesiology, and [2]Mechanical Science and Engineering
University of Illinois at Urbana-Champaign, IL, USA

E-mail: sshin27@uiuc.edu

INTRODUCTION

Recently, technical differences between one-plane and two-plane swing style are the most popular issues in golf swing coaching. One plane golf swing introduced by Jim Hardy [2] explains, the arms will be on the same plane as the shoulders at the top of the swing, whereas in a two plane swing the arms and shoulders are said to be on different planes, thus, creating two distinct movement patterns from the top of the swing through impact and follow through. However, there have been no investigations about the effect of two golf swing styles on the resultant joint moments of ankle, knee, hip, and L4/L5 which may imply golf injuries.

This study is to investigate the effect of two golf swing styles based on RMS deviation of the club head trajectory from swing plane (single-plane and multiple-plane swing styles) on the resultant joint moments in multiple lower body joints and L4/L5.

METHODS

In the previous study [3], RMS deviation of the club head trajectory from the swing plane was proved as an effective method to evaluate the swing plane. Therefore, RMS deviation of the club head trajectory from the swing plane was used to verify the group difference. There was significant difference in RMS deviation between two groups (single-plane group: 3.5±1.1 mm; multiple-plane group: 8.8±1.6 mm, $p < .01$).

Six right-handed professional golfers (Handicap 1 or lower) participated in the study: 3 subjects for single-plane group (height: 180.3±6.4cm; mass: 84.5±16.0; age: 29±8.5 years) and 3 subjects for multiple-plane group (height: 180.7±3.2cm; mass: 81.8±9.0; age: 37.3±16.1 years).

From attached reflective markers, nineteen markers (Left ASIS, Mid-PSIS, Left lateral thigh, left lateral epicondyle, left medial epicondyle, Left lateral shank, Left lateral malleolus, Left medial malleolus, Left heel, Left toe, Right ASIS, Right lateral thigh, Right lateral epicondyle, Right medial epicondyle, Right lateral shank, Right lateral malleolus, Right medial malleolus, Right heel, Right toe) were used in the analysis process as shown in the Figure1.

All subjects completed 3 trials of driver shots and the best one trial was analyzed. The resultant joint moments of left ankle, left knee, left hip and L4/L5 were computed by inverse dynamics. Resultant joint moments in multiple lower body joints and L4/L5 were assessed in a phase; from the address at ball to vertical club shaft position after impact. Modified Lariviere et al (1998)'s model was used for calculation of resultant joint moment of L4/L5 spine.

Eight digital cameras were used in 60 Hz each trial. AMTI OR6-5 force plate was used to collect force and moment data sampled at 100 Hz. Paired t-test was used to find if there was significant difference between two groups with SPSS v15.

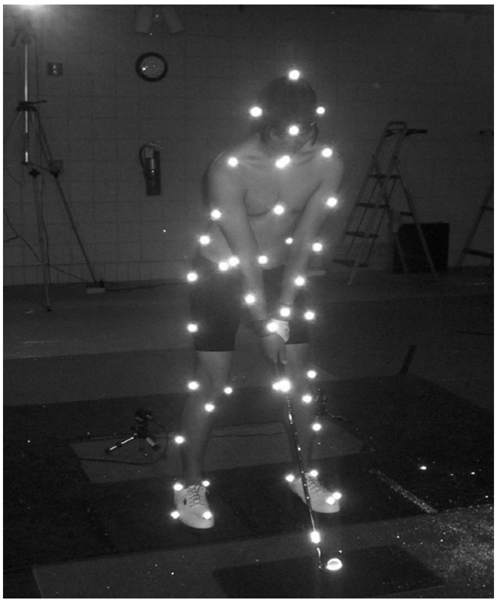

Figure 1. Marker positions

RESULTS AND DISCUSSION

The resultant joint moments of low body joints and L4/L5 for the each group are presented in Table1. Two golf swing styles have different mechanisms. Single-plane group used much greater joint moment in L4/L5, whereas multiple-plane group used much greater joint moment in left ankle. This may suggest that single-plane group is at much high risk of L4/L5 injury, whereas multiple-plane group is at much high risk of left ankle injury during golf swing of driver.

REFERENCES

1. Lariviere, C. and D. Gagnon. *Clinical Biomechanics*. 13:36-47, 1998.
2. Hardy, J., & Andrisani, J. (2004). The plane truth for golfers. New York: McGraw-Hill.
3. Sunghoon Shin, Jaffrey Casebolt, Christopher Lambert, Jae-Woong Kim and Young-Hoo Kwon, *proceedings of the International Society of Biomechanics in Sports*, South Korea, abstract 550,2008

Table1. Peak resultant joint moment normalized by body weight (N·m / N)

	Left ankle	**Left knee**	**Left hip**	**L4/L5**
Single-Plane Group(n=3)	0.0753±0.016	0.249±0.061	0.631±0.113	1.359±0.109
Multi-Plane Group (n=3)	0.177±0.075*	0.359±0.167	0.635±0.165	0.999±0.062*

* Significantly different from matching joint (p < .05)

BIOMECHANICS OF THE SIT TO STAND IN PEOPLE WITH MULTIPLE SCLEROSIS

Bradley Bowser, Sean O’Rourke, Lesley White and Kathy Simpson
University of Georgia Department of Kinesiology Biomechanics and Neuromuscular Physiology Laboratories   email: bowserbrad@gmail.com

INTRODUCTION

Rising from a seated position is one of the most common and functionally demanding activities of daily living and a prerequisite to other movements [1]. The-sit-to-stand (STS) requires balance, muscle strength, and coordinated contractions of the involved muscles [2]. People with multiple sclerosis (MS) often report symptoms of muscle weakness, disturbed balance and excess fatigue. However, the impact of such symptoms on daily activity performance remains less clear. Thus, the purpose of this study was to compare the kinematics and kinetics during STS transfers in a group of ambulatory individuals with relapsing remitting MS and a matched control group (CON).

METHODS

Thirty-three volunteers participated in the study (MS = 21; CON = 12). Individuals with MS (age=44±11.9 yrs, ht=166±6.9 cm, mass=79.1±19.8 kg) had physicians expanded disability status score (EDSS) of 6 or less. A group without MS, matched in age, height, and weight served as controls (CON) (age=42.8±11.8 yrs, ht=165.5±7.8 cm, mass=74.2±19.5 kg).

After obtaining informed consent, electromagnetic sensors were placed on the appropriate anatomical landmarks (sternum, sacrum, feet, shanks, thighs). Familiarization trials were performed. For the STS, participants began in standardized position with arms and hands folded across the chest, knee and ankle joints at 90˚, and each foot on a separate force platform in a fixed position. The participant rose to a standing erect posture at a self-selected speed. Kinematic (Flock of Birds®: 100 Hz; LP filter 5Hz) and ground reaction force (Bertec®: 1000Hz; LP filter 200Hz) data were collected during 5 STS trials. Data from the most affected limb in the MS group were compared to the non-dominant limb of CON. Independent sample t-tests were calculated for total STS rise and phase times, selected maximum (max) kinetic and kinematic magnitudes, and relative time to these events. Bonferoni adjustments were made to control family-wise error associated with multiple t-tests. Significance was accepted at $p<0.05$.

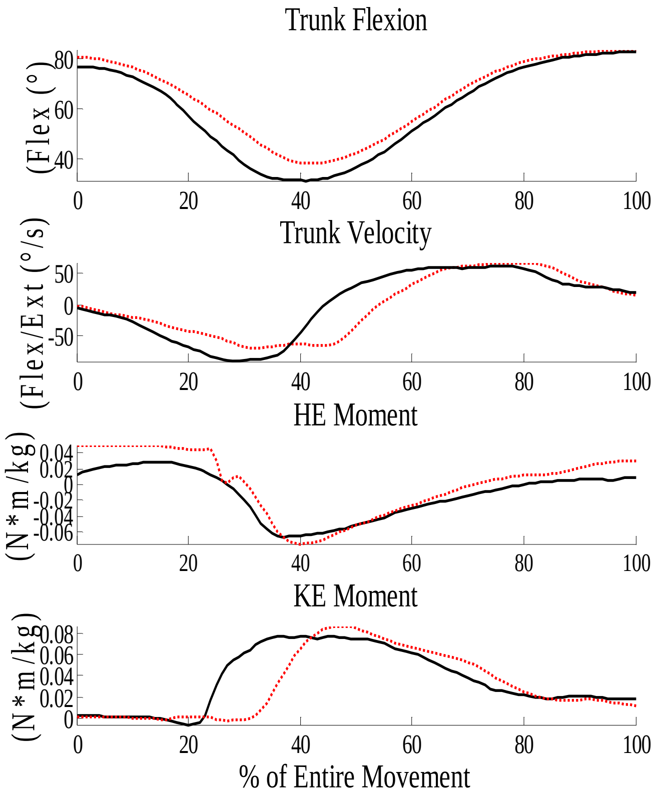

Figure 1. Representative trials of the CON (red dotted line) and MS (black solid line) groups for trunk angle, trunk velocity, HE and KE moments.

RESULTS AND DISCUSSION

Results are shown in Table 1 and displayed in Figure 1. Individuals with MS took longer to perform the STS task ($p<0.05$) as indicated by increased time during the deceleration phase (P3) ($p<0.01$). No group differences were observed for max knee extensor (KE) moments or velocities ($p>0.05$); however, relative to the entire STS movement, the max KE moment occurred earlier for the MS group ($p<0.05$). Similar results were found when examining the hip extensor (HE) moments.

Although no differences were found in max HE moments ($p>0.05$), a relatively earlier max HE moment ($p<0.01$) was found in the MS group. Additionally, the MS group displayed greater max trunk flexion, max trunk flexion velocity, and trunk extension displacement ($p<0.05$). No differences were found between groups for max KE velocity ($p>0.05$).

One possible explanation for the MS group having increased time in P3 (the phase made up of predominantly vertical motion) may be related to greater trunk extension displacement, which begins at max trunk flexion (shortly before P3 begins) and ends at the end of the movement. With no differences in max trunk extension velocity, it may take longer for the MS group to move the body through the larger range of motion to achieve the erect posture, thus resulting in a longer P3 time for the MS group. Another explanation for increased P3 time may be associated with reduced muscle function of the KE in MS during this phase. Concentric KE are the primary muscles used to raise the COM during P3 and largely determine the ability to perform STS [3]. Although no differences were found in the max KE moments, the earlier max KE moment in the MS group suggest less angular extension impulse generation from KE.

It appears that individuals with MS may use a compensatory movement strategy commonly displayed by individuals with lower extremity weakness and balance impairments, e.g., elderly, Parkinson patients [4, 5]. Although, the max HE moments were not significantly different between groups, the MS group exhibited increased max trunk flexion and max trunk flexion velocity when compared to controls ($p<0.05$). Increased trunk flexion places the COM of the body closer to the center of the base of support (which encompasses only the feet during P3) thereby increasing stability. Increasing trunk flexion velocity is also suggested to increase horizontal momentum to transfer to vertical momentum [6] and therefore, reduce the load on the KE. The increased trunk flexion momentum that creates the forward momentum of the body may explain the relatively earlier max KE and HE moments found in the MS group.

People with MS displayed movement strategies that were consistent with those who have compromised balance and leg extensor strength [4, 5]. As the KE muscles are major agonists to raise the body upwards research is needed to determine whether strength training these muscles would be effective at improving the ability to perform the STS task in ambulatory individuals with MS.

REFERENCES

1. Kralj A, et al. *J Biomech* **23**, 1123-1138, 1990.
2. Mak MK, et al. *Clin Biomech* **18**, 197-206, 2003.
3. Bohannon RW, *Physiotherapy Theory And Practice* **23**, 291-297, 2007.
4. Papa E, et al. *J Biomech* **33**, 1113-1122, 2000.
5. Inkster LM, et al. *Exp Brain Res* **154**, 33-38, 2004.
6. Pai YC, et al. *Med Sci Sports Exerc* **23**, 225-230.
7. White LJ et al. *Mult Scler* **10**, 668-674, 200

Table 1. Displays differences between the MS and CON groups (Mean±SD)

Variable	**MS**	**CON**
Total STS time (s)	2.06±0.39†	1.76±0.22
P3 time (s)	0.91±0.29†	0.64±0.12
Max trunk flexion angle (°)	39±14*	51±9
Max trunk flexion velocity (°/s)	-92±26*	-73±19
Trunk extension displacement (°)	51±14*	39±9
Max trunk extension velocity (°/s)	74±16	70±17
HE moment ($N \cdot m \cdot kg^{-1}$)	-0.067±0.02	-0.073±0.01
Rel. time to max HE moment (% of STS time)	34.5±6.8*	40.3±4.2
Max knee extension velocity (°/s)	116±27	138±30
Max KE moment ($N \cdot m \cdot kg^{-1}$)	0.086±0.02	0.089±0.01
Rel. time to max KE moment (% of STS time)	40.5±8.0*	46.6±5.0

†Significantly different between groups ($p<.01$). *Significantly different between groups ($p<.05$).

CAN AN EXTERNAL MUSCLE STIMULUS HELP THE LEARNING OF COMPLEX GROSS COORDINATE MOTION?

Insik Shin, Yonghyun Park and David O'Sullivan
Seoul National University,
e-mail: isshin@snu.ac.kr

INTRODUCTION

Demonstration, video analysis, practice in front of a mirror, working with a partner are just a few of the many various techniques used in mastering different sporting techniques [1]. What we want to investigate is the effectiveness of applying an external muscle stimulus to the learner to aid with the timing and coordination during complex motion or techniques. There are many questions that need to be answered before an evaluation of an external muscle stimulus; the timing of the stimulus, the stimulus duration, how strong should the stimulus be, et. In Braz's research using functional electrical stimulation (FES) the strategies are discussed.

According to Yamada [2], the key to a successful kip motion is the timing of hip flexion and extension, so ideally for this research the detailed examination of the kip movement is needed. Through the kinematic and EMG data the differences between the skilled and unskilled players kip movement on the high bar was analyzed and explained.

METHODS

After explaining the experimental procedure and receiving the signature of the subjects on the consent form the participant prepared for participation. The participant's warm up consisted of 10 minutes basic stretching and light jogging. After the attachment of reflective markers and electrodes (Kendal, Medi-trace Ag/AgCl) the EMG and kinematic data were recorded with Noraxon wireless EMG system(Noraxon, USA) at 1000Hz and 8 Oqus500 cameras(Qualysis, Sweden) at 100Hz respectively, while the subject performed kip movement. All EMG data were filtered with a band pass filter(10-500Hz), rectified and filter with a low pass filter at 3 Hz. The events are back the highest point in the back swing, the start when the COG is directly in line with the y coordinates of the pole and the top at the finish of the kip movement. The reversal pint is the point in the swing where the subject's COG reverses direction (highest forward position).

RESULTS AND DISCUSSION

After examining the EMG data from both the skilled and unskilled subjects it is evident that there is a different activation pattern. During the first phase from the starting point to the reversal point, the unskilled tend to kick upward much quicker and this is shown by the early activation of the rectus femoris and abdomen lower muscles. In the second phase, the skilled subjects co-activated the lumbar and gluteus maximus at the second kicking point. The unskilled subjects demonstrated uncoordinated muscle activation as they tended to use their lumbar muscles continuously while the unskilled only activated their muscles when needed, at the required time. During the final stage of the upward motion the unskilled subjects use their latissimus dorsi and pull themselves as opposed to the skilled subjects that use more momentum from the reverse kicking to swing their bodies upward.

For the kinematic analysis the trajectory of the subjects' center of mass, waist angle (relative angle between trunk and pelvis), right hip and shoulder angle was calculated and compared. As observed in figure 1 the skilled practitioner displayed a smoother transition from the RV (reversal point defined as the point where the subject's forward swing retarded and reversed direction) point to the finishing position in agreement with other kip movement research [2].

The maximum hip angle occurred quicker for the unskilled subjects which verified the EMG data showing the earlier activation of the flexors, lower abdominal muscles and rectus femoris. This early activation meant that the body gained a larger momentum and thus the unskilled subjects' trunk rises quicker and at the moment of the second kick their reaction force is not vertical but horizontal. In future research the investigation of using FES and what it's effects have on the kip movement will be done.

CONCLUSIONS

In conclusion, after the development of the functional electrical stimulation device the skilled EMG patterns will be used as guidelines for teaching the timing and order of muscle activation.

REFERENCES

1. Eccles DW, et al. *Psychology of Sport and Exercise*, 10, 96-107 (2009).
2. Yamada T, et al. *Proceedings of the ISBS Conference*, Spain, Abstract, 163-167, 2002.
3. Braz GP, et al. *Journal of Biomechanics*, April 5th, 2009.

ACKNOWLEDGEMENTS

This work was supported by the Korea Science and Engineering Foundation(KOSEF) grant funded by the Korea government(MOST) (No. R11-2007-028-02001-0).

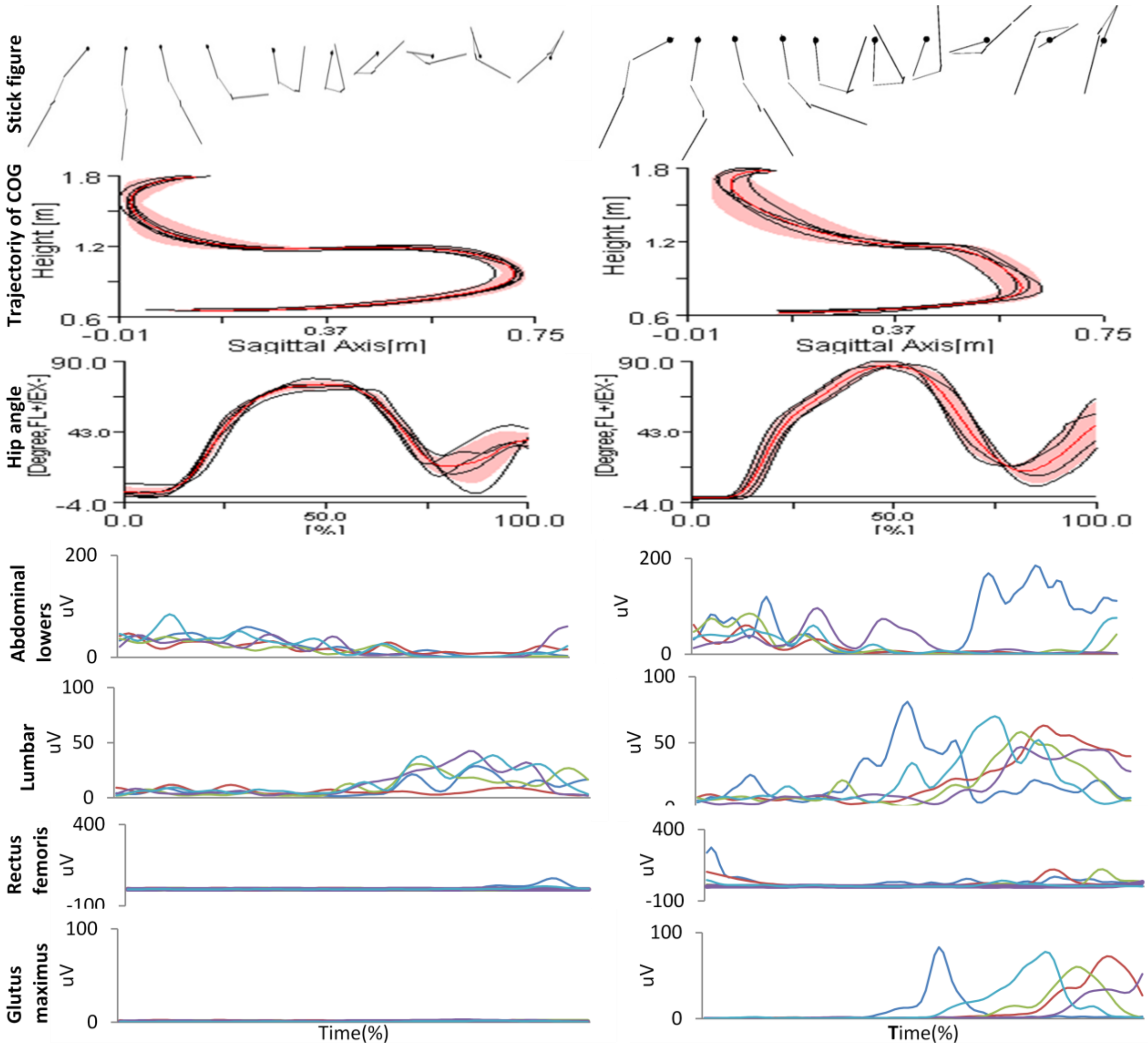

Figure 1: Left side data refers to skilled motion and the right side the unskilled motion. EMG signals in order from the top abdominal lowers, lumbar, rectus femoris and glutus maximus.

ASSESSMENT OF THE PRESSORE STEP^{TM} SYSTEM AS AN EXTENDED WEAR WEIGHTBEARING ACTIVITY MONITOR FOR USE WITH ORTHOPAEDIC PATIENTS

[1,2]Glenn Williams, [1]Eric Allen, [1]Jason Wu, [2]James Rudert, [2]Douglas Pedersen
[1]Physical Therapy & Rehabilitation Science, [2]Orthopaedics & Rehabilitation, University of Iowa
email: glenn-williams@uiowa.edu

INTRODUCTION

The typical weightbearing activity profiles of orthopaedic patients during the early period after knee joint injury and surgery are not well defined. Moreover, the effects of early weightbearing on cartilage, muscle, and patient outcomes are unclear and controversial. Therefore, research is needed that investigates these issues. Such research necessitates a valid and reliable method of monitoring weightbearing activity during daily life.

To be practical, a weightbearing activity monitor would ideally have the following characteristics: 1) ability to differentiate between full weightbearing, weightbearing as tolerated (~50% body weight), and partial weightbearing (~25% body weight) gait, 2) small enough size that the device can be worn during daily activities without impeding movement, 3) enough storage space to collect at least one week's weightbearing activity data, 4) inclusion of a compliance monitor capable of differentiating sedentary individuals from those who are non-compliant in use, 5) low cost in terms of the device and required orthoses or equipment modifications.

Although there are many commercially available activity monitors, few meet the requirements above. The Pressore Step^{TM} Activity and Compliance Monitoring System (CleveMed, Inc., Cleveland, Ohio, USA) reportedly has these characteristics.

The purpose of this abstract is to present our preliminary studies assessing the Pressore Step^{TM} System and some modifications we have made to facilitate its use as an extended wear weightbearing activity monitor for use with orthopaedic patients in the early period after knee injury and surgery.

METHODS

Pressore Step^{TM} System

The Pressore Step^{TM} Activity & Compliance Monitor consists of a small datalogger and a 0.5" diameter force sensing resistor (FSR; model 402, Interlink Electronics, Inc., Camarillo, CA, USA). The datalogger contains a thermistor that enables the device to monitor compliance by sensing body heat during wear. We elected to fix the sensor to the heel stirrup of an ankle brace typically used with patients who sustain ankle sprains (Aircast Air-Stirrup Universe, DJO, Inc., Vista, CA, USA). This approach was selected based on consideration of our target population (ACL patients), the desire to maximize compliance by allowing subjects to wear their preferred footwear, ease of application, ability to conceal the datalogger within the ankle brace (Figure 1), and cost. In accordance with Interlink's guidelines, the sensor was fixed to 1/16" polyurethane (PU) surface applied to the heel stirrup and a 1/32" PU "puck" was placed over the center of the sensor to promote consistent force distribution on the sensor.

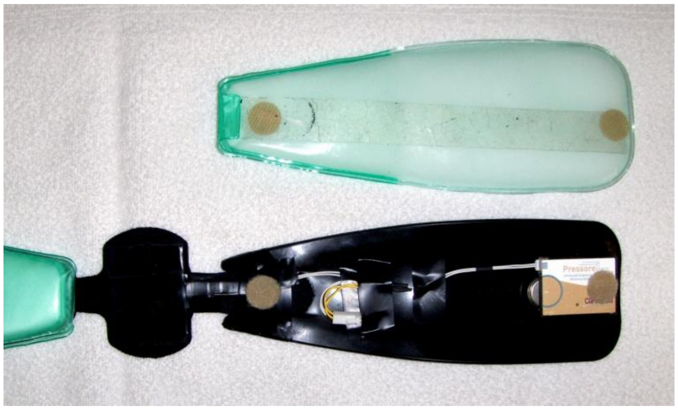

Figure 1: Pressore Step^{TM} System in ankle brace.

A series of tests were performed to examine the function of the sensor and datalogger and test the system's validty and reliability in both controlled and practical use. These tests included: 1) mechanical testing of sensor behavior and datalogger measurements using an MTS system, 2) assessment of measurements obtained from a subject applying load to a high precision physician scale through the heel with, 3) comparison of data obtained from a force plate and the monitor system during stance and in gait with varying degrees of weightbearing, and 4) assessment of reproducibility in double leg stance and in walking.

RESULTS AND DISCUSSION

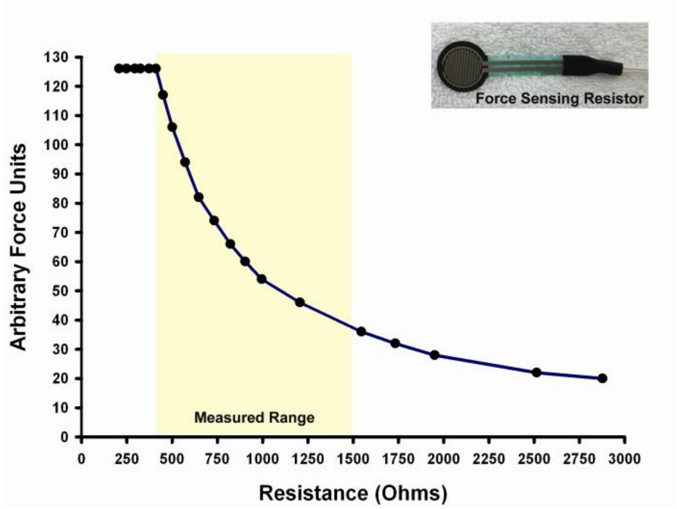

Figure 2: Results of MTS testing.

Testing of measurements from the sensor and datalogger while loads were applied with an MTS system demonstrated the nonlinear nature of the sensor output and that the datalogger records from a narrow range (~ 500 to 1500Ω). This nonlinearity is consistent with data provided by the manufacturer of the sensor.

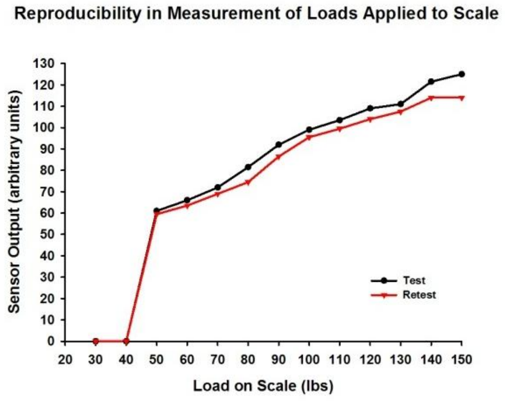

Figure 3: Results of testing with precision scale.

Data collected from the sensor while loads were applied to a precision scale yielded data that was consistent with the MTS test results (Figure 3).

Comparision of data obtained from a force plate and the Pressore Step^{TM} system during gait and stance demonstrated that the system has face validity and is responsive to type of weightbearing (Figure 4).

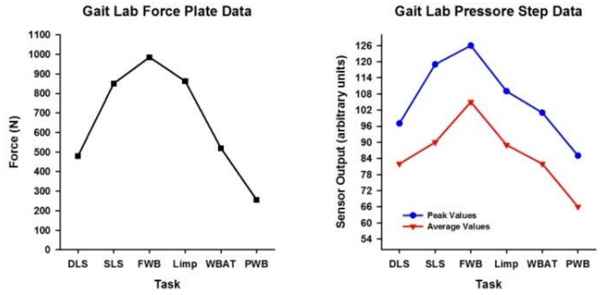

Figure 4: Comparison of force plate and monitor.

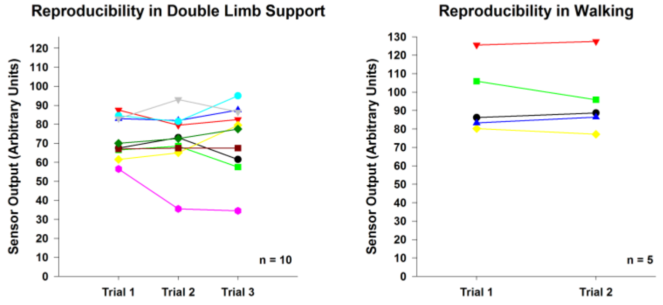

Figure 5: Reproducibility in stance and walking.

Data from reproducibility tests in double leg stance (ICC = 0.81) and walking (ICC = 0.96) demonstrate the device has satisfactory reproducibility when subjects have removed and replaced the monitoring system (day-to-day) as long as the effects sizes being considered are large. The mean percent error was about 4.5% in walking and about 10% in stance (↑ error attributed to shifts in weight distribution).

In addition, we noted that the device saturates in some users during walking and steps are often missed in partial weightbearing due to the narrow range of measurement. We have developed a tuning device that incorporates resistors in series and in parallel with the sensor to correct for this issue.

CONCLUSION

The Pressore Step^{TM} System demonstrates sufficient validity and reliability for use as an extended wear weightbearing monitor in the orthopaedic patient population. However, the system has some limitations that need to be taken into consideration.

ACKNOWLEDGEMENT: NIH-NIAMS Grant 1P50AR054090 supported this work.

TRANSFER OF DYNAMIC LEARNING ACROSS POSTURES

[1,2] Alaa Ahmed and [2]Daniel Wolpert
[1]Department of Integrative Physiology, University of Colorado at Boulder, USA,
[2]Department of Engineering, University of Cambridge, UK,
email: alaa@colorado.edu

INTRODUCTION

Skilled movement depends upon our ability to control for external dynamics and predict the consequences of that control. Our everyday movements generate forces upon the environment, as well as forces upon our own bodies. When these forces are predictable, voluntary movement is usually preceded by anticipatory postural adjustments (APAs). When learning difficult motor tasks, we frequently decompose them so that the control of individual body segments is practiced in isolation. But upon re-composition, the movement will result in novel complex internal forces between the body segments that were not experienced (or did not need to be compensated for) during isolated practice. But can the postural system immediately predict and compensate for these dynamics? In this study we investigated whether the whole-body postural adaptations learned to compensate for movement dynamics in one posture, would transfer to a novel whole-body posture, when performing the same arm reaching movement.

To investigate these questions we used a well-established experimental paradigm for dynamic adaptation of reaching movements. Participants made reaching movements while grasping the handle of a robotic force-generating manipulandum, which generates a force perturbation proportional to the handle velocity, and perpendicular in direction. The gradual adaptation of a sensorimotor map for arm control consistently observed in previous studies, allowed us to quantify any adaptation of related anticipatory postural adjustments (APAs). APAs specific to the perturbation. Furthermore, we also analysed the learning of novel arm dynamics in different supporting postures, and the ability to transfer these representations between postures.

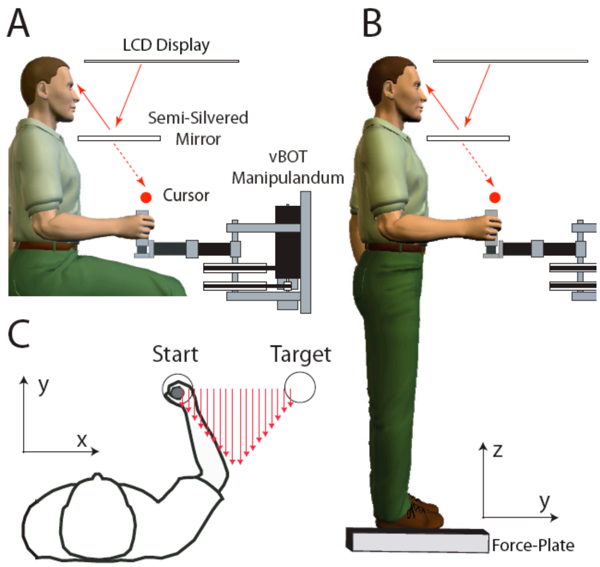

Figure 1: Experimental Setup; A: seated position; B: standing position; C: forces on FORCE trials.

METHODS

Thirteen right-handed participants (7M/6F) made planar reaching movements while in seated and standing postures. Experimental procedures were approved by the Local Ethics Committee.

Participants grasped the handle of a force-generating robotic manipulandum (vBOT) and moved a cursor to a target presented in the horizontal plane. Task relevant visual feedback was presented within the plane of movement via a semi-silvered mirror, reflecting the display of an LCD monitor suspended horizontally above (Figure 1A). When standing, participants stood with feet slightly apart on a 6-axis force-torque sensor (ATI Technologies, Apex, NC) (Fig. 1B).

Participants were randomly assigned to either the STAND (N=7) or SIT (N=6) group, named for the postural configuration in which the first FORCE trial was experienced. The STAND group initially performed 350 trials in the standing position. The first 50 were NULL trials, used to measure baseline performance (*Baseline*). The following 300 trials were FORCE trials (*Learning*). They then switched to a seated posture and performed 100 FORCE trials (*Transfer*), followed by 100 NULL trials to extinguish the adaptation (*Washout*). To quantify the transfer of the washout, participants then returned to the original standing configuration for another 100 NULL trials (*Transfer2*). In the SIT group, the order of postural configurations was reversed: 350 Sit trials; 200 Stand; 100 Sit. In FORCE trials, the robot generated a force upon the hand proportional to its velocity, and perpendicular (clockwise) to its direction, consistent with a viscous curl field (Fig. 1C). Catch trials were inserted randomly, (one in five trials) where a force channel was generated, restricting movement along a straight path directed towards the target by preventing motion in the perpendicular direction. Handle position, robot- generated forces, and forceplate forces were recorded at 500 Hz.

To assess learning of the dynamics in the seated condition we examined movement error on each trial, measured as the peak perpendicular deviation from the target vector (Fig 2A). To rule out the use of an impedance-based strategy, we examined the peak force generated into the force channel on catch trials as a measure of anticipatory control(Fig 2B). Transfer of learning in the standing position was measured as the velocity of the center of pressure prior to the onset of movement. Movement of the center of pressure in the direction of the impending perturbing force would indicate an anticipatory postural adjustment (Fig 2C). Appropriate anticipatory control should lead to minimal reactive control, measured as COP velocity after movement intitiation (Fig 2D).

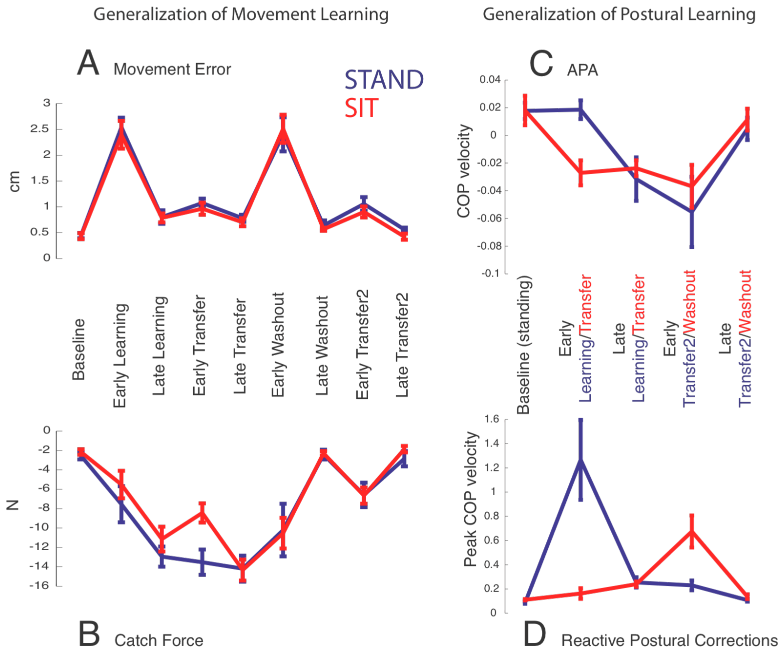

Figure 2: Results; A: Movement error; B: Anticipatory forces; C: Anticipatory postural adjustments; D: Reactive postural adjustments

RESULTS AND DISCUSSION

Movement performance, quantified as movement error and peak catch force produced, transferred from sitting to standing (SIT group) and from standing to sitting (STAND group) (Fig 2A,B, $p < 0.001$). Anticipatory postural adjustments specific to the arm perturbation gradually developed in the STAND group ($p < 0.001$, Fig 2C), and more slowly than the adaptation of movement control ($p<0.01$). APAs were immediately evident in the SIT group when they transferred to a standing position, even though they had not previously experienced the perturbation in that configuration (Fig 2C).

CONCLUSIONS

Subjects' arm movements were exposed to a novel dynamic environment, which resulted in an adaptation of the sensorimotor map for arm movement, as well as the map for postural control. Additionally, the flexibility of APAs observed in well-practiced movements, is also observed in movements involving recently learned dynamics. Finally, the CNS can immediately anticipate the effect of novel dynamics on different body postures. These results support the existence of separate mappings for posture and movement, which encode similar dynamics but are adapted independently. This novel paradigm lends itself to the simultaneous investigation of the nature of the dynamic representations underlying posture and movement control in a variety of unfamiliar, yet well-controlled environments. A greater understanding of their adaptability and flexibility will provide essential insights to guide the development of future rehabilitation techniques and interventions.

A STRAIN-ENERGY APPROACH TO SIMULATING SLOW FINGER MOVEMENTS AND CHANGES DUE TO LOSS OF MUSCULATURE

[1] Manish Kurse, [1,2]Francisco Valero-Cuevas
[1]Brain-Body Dynamics Lab, Department of Biomedical Engineering, Viterbi School of Engineering
[2]Division of Biokinesiology & Physical Therapy, University of Southern California, Los Angeles, CA
email: kurse@usc.edu, web: http://bme.usc.edu/valero

INTRODUCTION

The neuromuscular interactions that produce slow and accurate finger movements are not understood. The geometry of finger anatomy is such that a slow finger movement (i.e., sequence of joint rotations) completely defines the necessary excursions of all tendons. Given that muscle tone prevents tendons from becoming slack, all tendons must undergo eccentric or concentric excursions during functional finger movements. In this paper, we describe a novel computational solver to model slow finger movements, and report how the mathematics of strain-energy of over-constrained systems can predict the impairment in finger motion that accompanies partial paralyses.

METHODS

A slow moving finger is best modeled as a first order dynamical system having low mass and performing quasi-static motion (which is not the case for fast finger movements [1]). Our 3-D model consists of a kinematic 3-link mechanism with 2 degrees of freedom (ad-abduction and flexion-extension) at the metacarpophalangeal joint (MCP) and 1 degree of freedom (flexion-extension) at the proximal interphalangeal (PIP) and the distal interphalangeal (DIP) joints. All seven muscles of the index finger were included: *flexor digitorum profundus* (FDP), *flexor digitorum superficialis* (FDS), *extensor indicis proprius* (EIP), *extensor digitorum communis* (EDC), *first lumbrical* (LUM), *first dorsal interosseous* (FDI), and *first palmar interosseous* (FPI). The routing of the tendons across finger joints is represented by the moment arm matrix obtained from [2]. Our focus here is the computational engine, thus for now we have neglected the extensor mechanism, but its effects will be considered in subsequent work. Torsional springs at the joints simulate the known passive stiffness arising from skin and soft tissue. The muscles actuating the index finger are modeled as tunable linear elastic springs that only exert force in tension. Changing the latent resting length of a spring, l_0, results in a 'muscle force' that is proportional to the difference between its current and resting lengths. Therefore the "activation signal" to a muscle is simulated as a change in resting length, Δl_0 (Fig. 1). Here, we are only interested in understanding how finger movement arises from Δl_0, and simply assume that Δl_0 can arise from a neural command. A set of commanded resting lengths to all muscles defines the posture attained by minimizing the strain-energy of the finger at equilibrium: where the net joint torques produced by the muscles, τ_{ext}, are exactly balanced by the torques produced by joint-stiffness, τ_{in}.

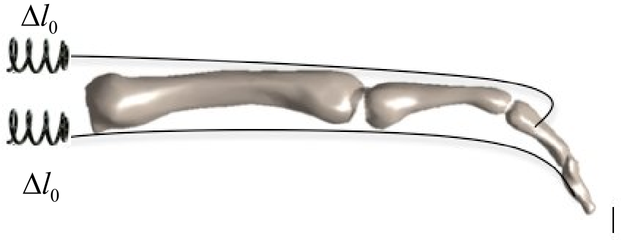

Figure 1: Model of the index finger being actuated by tunable springs.

$$\Delta s = R^T(\Delta\theta)$$
$$\tau_{ext} = RK_m(\Delta l_0 - \Delta s)$$
$$\tau_{in} = K_\theta(\Delta\theta)$$

where Δs is the change in tendon excursions, R is the moment arm matrix, K_m is the matrix of muscle spring constants, Δl_0 is the change in spring resting lengths, K_θ is the matrix of torsion spring constants at the joints and $\Delta\theta$ is the resulting change in joint angles.

Given that muscles behave like nonlinear springs that do not exert compressive force, there is an extra constraint defined by,

$$K_m \approx 0 \; if \; \Delta l_0 < R^T \Delta\theta$$

Also, we ensure that $\Delta l_0 > 0$ since muscle activation always leads to a net force greater than passive stretch force. We solve the forward kinematic problem iteratively using a Newton-Raphson iteration method.

As a first demonstration of our system, we simulated a simple quasi-static tapping motion by finding an appropriate trajectory of muscle resting length changes. The movement consisted of an initial retraction of the index finger followed by a downward flexion motion (Fig. 2). In addition, we simulated the resulting trajectory for acute radial, median and ulnar nerve palsies by removing the muscle commands to the i) two extensors, ii) the two flexors, and iii) the two interosseii and lumbrical, respectively and applying the same resting length change commands as before to the unaffected muscles. This simulates effects prior to neuromuscular adaptation (i.e., the robustness of finger trajectories to acute loss of some muscles). Note that the affected muscles continue to exert passive stretch forces even without the activation command.

RESULTS AND DISCUSSION

Not surprisingly, the fingertip deviates from the original trajectory when some muscle commands are removed. Some postures and directions of movement become impossible without the presence of specific muscles.

However, the value of these simulations is that they begin to explain the relative effect of different deficits and indicate which muscles are more or less critical to the execution of accurate and slow finger movements. In addition, finger movements are typically modeled using second order dynamics [3,4]. Here we are proposing that a simple quasi-static solver based on strain-energy equilibrium can model slow finger movements since mass and inertia properties of fingers are small. While muscle mechanics depends on neural activation and a muscle's force-length and force-velocity properties, the end product is a force command, which we generate by the adjustment of resting lengths of fictitious springs.

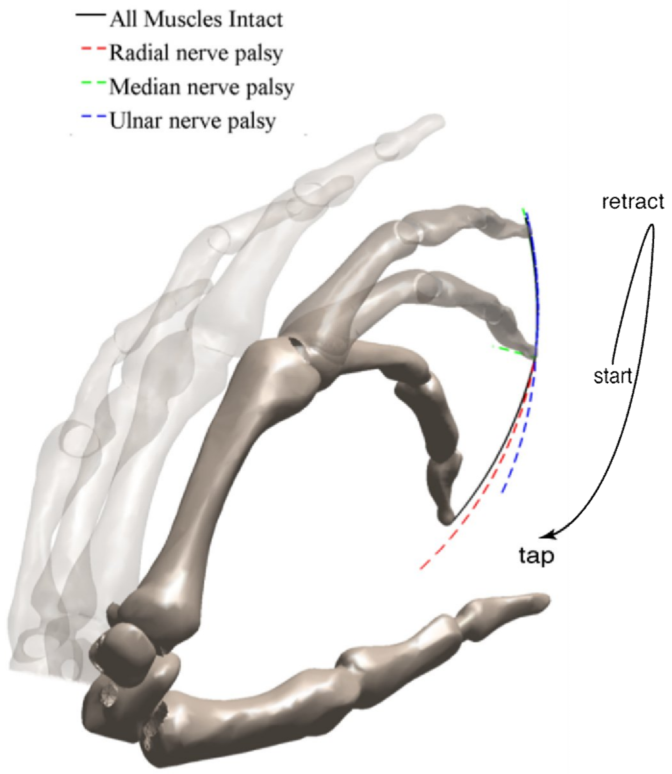

Figure 2. Fingertip trajectories for a simple tapping motion in unaffected and impaired cases.

Future work will incorporate tendon routing functions derived directly from cadaveric experiments to simulate more faithfully the extensor mechanism, as well as a more physiologically realistic muscle model.

REFERENCES

1. Darling WG and Cole KJ. (1990) J Neurophysiol 63: 1098-1108
2. An K. N., Y. Ueba, et al. (1983). J Biomech 16(6): 419-25.
3. Sueda S., Kaufman A., Pai D.K., (2008). ACM Transactions on Graphics, 27 (3)
4. Venkadesan, M. and F. J. Valero-Cuevas (2009). Phil Trans Roy Soc A 367(1891): 1163-79

ACKNOWLEDGEMENTS

NIH AR-050520, AR-052345 to FVC.

HAND FORCE ESTIMATION STRATEGIES FOR FIELD APPLICATION

[1] Joan Stevenson, [1]Susan Reid, [2]Alison Godwin and [1]Erin Sadler
[1]School of Kinesiology and Health Studies, Queen's University, Kingston, Ontario Canada
[2] School of Human Kinetics, Laurentian University, Sudbury, Ontario Canada
email:joan.stevenson@queensu.ca, web: http://www.phe.queensu.ca/ergbio/home.htm

INTRODUCTION

Linked segment modeling is used extensively in the field of Biomechanics and Ergonomics. Current development of Inertial Motion Units (IMU) based and other untethered motion capture systems is increasing the practicality of creating dynamic linked segment models using data recorded in field and workplace settings. Although motion capture technologies are beginning to mature, the challenge continues to automate determination of the magnitude, direction and timing of external forces.

Three strategies for automatically quantifying a load carried in the hands were developed and evaluated for potential use. Strategies were developed based on diverse input data including; a hand worn force sensor, EMG of torso, shoulder or upper arm muscles, and linear accelerations of body segments. Accuracy and the ability to determine force timing, magnitude and orientation of application, were compared.

METHODS

Strategies for estimating hand load were developed from data recorded for two studies that used three variant whole body lifting tasks.

Study 1: Fit adult males (n=12; 22.3 +/-3.5 years), performed multiple two handed stoop and squat box lifts from floor onto a waist height shelf. Box mass varied from ~ 0 to 20 kg in 5 kg increments. Lift order was randomized with three repeats at each load. Surface EMG and kinematic data were recorded simultaneously (Bortec® EMG, Polhemus Fastrak®). EMG were obtained from six muscles on the right side of the body: biceps, triceps, lateral deltoid, thoracic erector spinae (T9), lumbar erector spinae (L4) and external oblique. Only EMG data were used as input to the Parallel Cascade hand force estimation model developed.

Study 2: Fit adult males (n=13; 21.5 +/-1.5 years) performed two handed box lifts (mass ~ 0, 2.5, 5, 10, 15, 20 kg) and a single-handed right side pail lift from floor to waist height onto a horizontal shelf. Pail mass ranged from ~ 0 to 15 kg in 2.5 kg increments. Lift order was randomized. Three repeats were performed at each load. Surface EMG were obtained from the right side of the body for brachioradialis, biceps, triceps, lateral deltoid, thoracic erector spinae (T9), lumbar erector spinae (L4). EMG and kinematic data were recorded simultaneously (Bortec® EMG and XSens®, MTi attitude and heading trackers). MTi sensors were affixed to upper body segments; the sacrum, thorax (T9), head, right and left upper arms, and forearms immediately above the wrists. Subjects wore a fingerless glove with suede palm, with a 25x25mm conformable tactile pad (C500®, Pressure Profile Systems) over the third metacarpal head. Analogue switches on the handles and underside of the box or pail provided timing data for hand contact and lift.

Hand Sensor & Load Magnitude

C500 force sensor activation levels of an unloaded hand, at load liftoff and at load placement was determined by external switches. Activation levels were correlated to payload mass.

Hand Sensor & Lift Duration

External switches were used to mark lift onset and end. Using C500 data from 7 randomly selected subjects, a threshold activation level was set that minimized error in estimated lift duration. The optimization algorithm searched 300 samples (300ms) around lift onset. Lift end occurred when C500 activation dropped below this threshold. A parametric repeated-measures ANOVA evaluated differences in activation level across lift type and weight for each signal (C500, BEMG biceps, LEMG lumbar ES). Across subject performance of the threshold value was determined using remaining subject data.

EMG Muscle Activation & Load Magnitude

A forward regression analysis was performed using all muscle activation levels at lift off for the two handed box and single handed pail lift. Additionally an EMG based parallel cascade model for load classification was developed for the saggital plane squat lift.

EMG Muscle Activation & Lift Duration

Activation levels from the BEMG and LEMG, normalized against quiet resting, were used to set threshold activation levels using the method described previously.

Limb Kinetics & Load Magnitude

3D linear accelerations of the right wrist and thorax during up and down lifts were extracted from MTi data. Six parameters derived from duration and acceleration magnitude were used in a quadratic discriminate model (QDA) of the 0 and 15 kg single handed pail lifts. The 150 lifts were randomly assigned to training (120) or test (30) sets.

RESULTS AND DISCUSSION

Hand Sensor & Load Magnitude

In two handed lifts, a one-way ANOVA with post-hoc Scheffe test indicated significance for payloads differing by 10 kg (Δ5kg per hand). In single hand pail lifting significance was found for payloads differing by 10 kg. Average std. error of estimate was 5.6kg. Average failure to detect a load was 20.4% (+/-19%) for all loads and lifts.

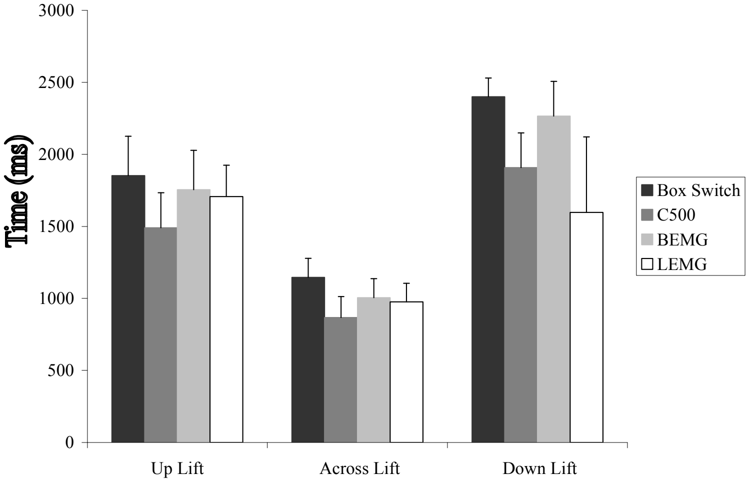

Figure1. Lift duration estimated using single threshold values.

Hand Sensor & Lift Duration

Using a C500 single threshold value resulted in a mean absolute error of 331 ms (Stdev 162 ms). At low loads, the C500 threshold failed to detect 36.9% (STD 36.7%) of lifts.

EMG Muscle Activation & Lift Duration

The mean absolute error in the duration estimated from the BEMG threshold analysis was 290 ms (STD 92 ms). Missed lifts varied from 26.7% at loads <5kg to 7% for >5kg). Average missed lifts across all loads was 14.9% (STD 24.5%).

EMG Muscle Activation & Load Magnitude

A forward regression with respect to the load lifted, using the activation level of all six muscles and the C500 returned the BEMG with an R^2 of 0.667. STD error of the estimate was 4.06 kg.

A nonlinear parallel cascade algorithm [1] was developed using the area, peak and mean of the erector spinae (L4 level) EMG LE, normalized by a zero load lift. This cascade gave a load lifted prediction with an error of ±1kg, for loads ranging from 5 to 25 kg.

Limb Kinetics & Load Magnitude

Six parameters were extracted and multiple QDA's were evaluated to select for best performance. QDA models, using 3 acceleration and one time parameter achieved misclassification rates of 5.34% (thorax) and 2.84% (wrist) while discriminating between 15 and 0 kg lifts.

CONCLUSIONS

Limb kinetics and EMG based load detection and classification schemes demonstrated better reliability and discrimination than a hand based sensor.

REFERENCES

1. Chan S, Morin EL, Stevenson JM *"The Use of EMG for Load Prediction during Manual Lifting"* Canadian Medical and Biological Engineering Society Proceedings 2007.
2. Korenberg, J.M. (1991). "Parallel Cascade Identification and Kernel Estimation for Nonlinear Systems", *Annals of Biomed Engineering* Vol. 19 pp429-455

ACKNOWLEDGEMENTS

The authors gratefully acknowledge S. Chan, K. Cassidy & B. McLeod of Queen's University, Kingston, Ontario Canada. Funding provided by the W.S.I.B. of Ontario, Canada

HIGH ACTUATOR GAINS ARE NECESSARY TO CONTROL A FAST FINGERT TAPPING MOTION OPTIMALLY

[1]Evangelos Theodorou, [1,2]Francisco Valero-Cuevas
[1]Brain-Body Dynamics Lab, Department of Biomedical Engineering, Viterbi School of Engineering
[2]Division of Biokinesiology & Physical Therapy, University of Southern California, Los Angeles, CA
University of Southern California, Los Angeles, CA
email: etheodor@usc.edu, web: http://bme.usc.edu/valero

INTRODUCTION

The nonlinearities of the neuromuscular plant and the large dimensionality of the state make understanding the neuromuscular control of the hand a challenging problem. Recent experimental and theoretical work [1] investigated the neural control of contact transition between motion and force during tapping with the index finger as a nonlinear optimization problem. Such transitions from motion to well-directed contact force are a fundamental part of dexterous manipulation, and the prior work suggests that such tasks are controlled optimally. To test this working hypothesis, we apply the framework of Iterative Linear Quadratic Regulator (ILQR). In addition this work is also the first to investigate the effects of torque delays on the controllability conditions to execute fast and accurate movements of the finger during a tapping motion.

METHODS

Iterative Linear Quadratic Regulator (ILQR).

The optimal control framework of iterative linear quadratic regulator was first introduced in [2, 3]. In the classical optimal control framework [4] the goal is to control a dynamical system while minimizing a cost-performance function. In the ILQR framework the objective is to minimize the performance criterion:

$$V = \frac{1}{2}\left(x(t_f) - x^*\right)^T Q_f \left(x(t_f) - x^*\right) + \frac{1}{2}\int_0^{t_f}\left(x^T Q x + u^T R u\right)dt \quad (1)$$

Under the dynamics constrains:

$$\dot{x} = F(x,\tau) \quad (2)$$

where the state x and the torques for a planar three-joint finger are defined as:

$$x = \left[\theta_{MCP}\ \theta_{PIP}\ \theta_{DIP}\ \dot{\theta}_{MCP}\ \dot{\theta}_{PIP}\ \dot{\theta}_{DIP}\right] \quad (3)$$

$$\tau = \left[\tau_{MCP}\ \tau_{PIP}\ \tau_{DIP}\ \right] \quad (4)$$

The matrix Q is the weight matrix associated with the state, R is the weight matrix associated with the controls *u* and Qf is the matrix which weights the errors with respect to a terminal state.

The locally optimal control is calculated iteratively. The equations of the iterative algorithm are summarized below:

$$\begin{aligned} \delta u_k &= -K\delta x_k - K_v v_{k+1} - K_u u_k \\ K &= \left(B_k^T S_{k+1} B_k + R\right)^{-1} B_k^T S_{k+1} A_k \\ K_v &= \left(B_k^T S_{k+1} B_k + R\right)^{-1} B_K^T, \\ S_k &= A_k^T S_{k+1}\left(A_k - B_k K\right) + Q, \\ v_k &= \left(A_k - B_k K\right)^T v_{k+1} - K^T R u_k + Q x_k \quad (5) \end{aligned}$$

With the boundary conditions:

$$\begin{aligned} S_N &= Q_f \\ v_N &= Q_f\left(x_N - x^*\right) \quad (6) \end{aligned}$$

We model the index finger by using the 2nd order triple pendulum forward dynamics

$$M(\theta)\ddot{\theta} + C(\theta,\dot{\theta}) = \tau \quad (7)$$

Where M is the inertia matrix, C is the coriolis matrix and τ is the torque vector. The task for the optimal controller is to bring the finger from an initial lifted posture to the target posture just before contact, i.e., a tapping movement.

In the first case of our computational work we assume that there are no delays in the delivery of the torques (i.e $\tau = u$). In the second case we investigate the effects of the delays intrinsic to the excitation-contraction dynamics of muscle. As in [1], we assume that the delays have the form of a first order differential equation

$$\dot{\tau} = A\tau + Bu \quad (8)$$

which increase the state vector by including the three torques.

Controllability

A system is controllable at time t1 if it is possible to find some input function u(t) that can transfer the system from an initial state x(t1) to a final state x(tf) in finite time tf-t1.

A measure of controllability for the case of discrete systems with state transition matrix Φ and control transition matrix Γ is given by the rank of the controllability matrix:

$$SVD\left[\Phi^{n-1}\Gamma \mid \ldots \mid \Phi\Gamma \mid \Gamma\right] \quad (9)$$

Where SVD stands for singular value decomposition. We can see from (9) that controllability depends on the state and control transition matrices. In the case where there is a zero singular value (i.e., a rank-deficiency system) the system is uncontrollable since in the eigendirection that corresponds to zero eigenvalue there is no control that can affect the state of the system.

RESULTS AND DISCUSSION

First we apply the ILQR framework for the case of no-delay toque control and generate the tapping movement. The sequence of postures is illustrated in Fig. 1.

Next we augment the state space model of forward dynamics with the delays imposed by the muscles (8) and apply ILQR to execute the same movement, Fig. 2. In this case the optimal control problem becomes more challenging since torques are not directly controlled but are driven by the equation (8). The additional delays might cause a failure of any optimization scheme to generate the desire movement.

To investigate the controllability characteristics we apply the controllability test (9) on the discretized version of equation (8). Our simulations show that in order for ILQR to generate the sequence of postures for the tapping task, the sub system (8) should not only be controllable but the singular values of the controllability matrix have to be relatively large (i.e., high control gains). The intuition is that with large singular values the sub-system (8) can deliver high torques in a short time. Thus, we have found a necessary condition for an optimal controller to perform this tapping movement. Therefore, this work specifies the research directions to follow in our future theoretical/experimental work to test the working hypothesis that the neuromuscular system controls fingers optimally. Future work must also include investigating how the interaction of the finger with objects and surfaces places additional requirements on the underlying control strategies.

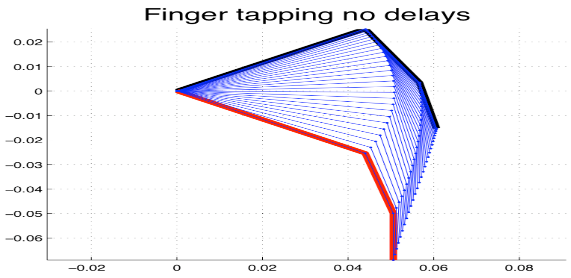

Fig. 1

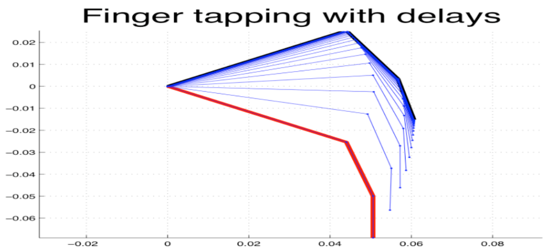

Fig. 2

REFERENCES

1. Venkadesan M, Valero-Cuevas FJ. Effects of neuromuscular lags on controlling contact transitions. Philosophical Transactions of the Royal Society A: 2008

2.Weiwei Li, E. Todorov, International Journal of Control. 80(9),1439 - 1453.

3. Weiwei Li, Valero-Cuevas FJ American Control Conference 2009.

4. R. Stengel, Optimal Control and Estimation. Dover Publications, New Work, 1993.

ACKNOWLEDGEMENTS

NIH AR-050520, AR-052345 and NSF EFRI-COPN to FVC.

THE INFLUENCE OF RUNNING SPEED ON THE EXTENSOR PARADOX OBSERVED IN ADULT RUNNERS

[1] Christopher Lambert, [2]Moon-Seok Kwon and [1]Young-Hoo Kwon
[1]Texas Woman's University, USA, [2]MSungkyunkwan University, Korea
email: CLambert@twu.edu

INTRODUCTION

It is well understood that proper coordination of muscle activity is necessary for efficient running [2]. While phasic activity of major muscle groups of the lower extremity has been thoroughly examined, there is still some controversy over the role of the hip and knee extensor muscles during running. Eccentric knee flexion following foot strike occurs to absorb the impact of the landing. Following mid-stance, the leg begins to extend with the onset of the propulsion phase until the foot leaves the ground. Previous research found knee extensor muscle activity diminished terminally with the onset of leg extension during the late stance phase of running [1,3]. This phenomenon became known as the "extensor paradox". One problem is that past studies subjectively determined the on/off status of the muscles. Further, only a single running speed was examined. The use of an objective assessment of the muscle activity is necessary to validate the existence of the extensor paradox. The effect of running speed on the extensor paradox must also be considered in order to better understand this phenomenon.

The purpose of this study was to objectively examine the electromyographic muscle activity of the superficial quadriceps during the stance phase of running and to determine the effect of running speed on the extensor paradox phenomenon.

METHODS

Twelve intercollegiate track athletes (4 male; 8 female) specializing in long distance running participated in this study on a voluntary basis. All participants (mean age = 20.6 yrs) had experience with treadmill running and had no recent history of injury.

Participants ran on a treadmill (zero inclination) at three different speeds (3, 4, & 5 m/s) while kinematic and electromyographic data were collected. The four speeds represent the middle of the speed range used in previous literature. Following a warm-up, participants began walking on the treadmill while the speed was gradually increased to the desired setting. A stabilization period of at least thirty seconds was provided in order to ensure the participants had established a consistent pace.

Knee extensor muscle activity during the stance phase of running was examined using electromyography. Surface EMG (Noraxon Myosystem 900, Scottsdale, AZ) from the rectus femoris, vastus lateralis, and vastus medialis of the dominant leg was collected by disposable 20-mm disc electrodes (Noraxon Ag/AgCl). The electrodes were fixed over the muscle belly with an inter-electrode distance of approximately 25 mm. A reference electrode was placed on the tibial tuberosity of the same leg. All electrode cables were secured to prevent electrode detachment and induced artifact during running activities. Preamplified EMG signals were amplified (x 1000), bandpass filtered (15 Hz-400 Hz), and sampled at 1000 Hz.

Two-dimensional video analysis (100Hz) captured the right and left sagittal plane motion of the upper and lower body while running. Kinematic data was processed and analyzed using Kwon3DXP (Visol Inc., Korea). Video analysis was used to compute knee angles and stance phase events. Events during stance phase included foot contact (FC), maximum knee flexion (MKF), and toe-off (TO). Late stance phase was defined in this study as the period from maximum knee flexion to toe off.

Ten-second samples were collected during each trial for all running speeds to allow for a minimum of six complete gait cycles by each participant. Two trials at each speed were recorded and processed resulting in twelve full gait cycles at each speed for all participants. A TTL signal was introduced during each trial allowing for synchronization of the kinematic and EMG signals. The phasic activity of all three muscles was examined during each period of stance. All stance phase subperiods were compared to a threshold to determine the on/off status of the muscles. A baseline signal was recorded for each muscle prior to running. The threshold was calculated as the standard deviation of the range of the baseline signal (100-ms) multiplied by a factor of 8. A muscle signal that fell below the threshold for more than 50-ms was considered "Off".

RESULTS AND DISCUSSION

All stance phases for each muscle were subjected to threshold analysis based on their respective baseline signals (Figure 1A, B, & C). The existence of the extensor paradox was not confirmed at any of the three running speeds. The relatively high baseline multiplication factor of 8 was chosen due to the noise-free nature of modern amplifiers. However, visual inspection of the three quadriceps (Figure 1D) shows a clear trend of diminishing muscle activity following maximum knee flexion. This is perhaps the method used to identify the extensor paradox in previous studies, but is not objectively valid.

An increase in the magnitude of the multiplication factor for the baseline SD will eventually result in termination of knee extensor activity. It is the determination of the appropriate threshold which appears to be the key issue in validating the existence of the extensor paradox.

Further examination of the role hip extensors, knee flexors, and plantar flexors play in the trend of knee extensor decline during the late stance phase of running is in process. Also, the process for better determination of the appropriate threshold levels based on running speed is being examined.

This study shows that the existence of the extensor paradox is based on the threshold settings, and can be manipulated when viewed subjectively. Regardless, the trend of declining knee extensor activity throughout late stance phase of running is apparent.

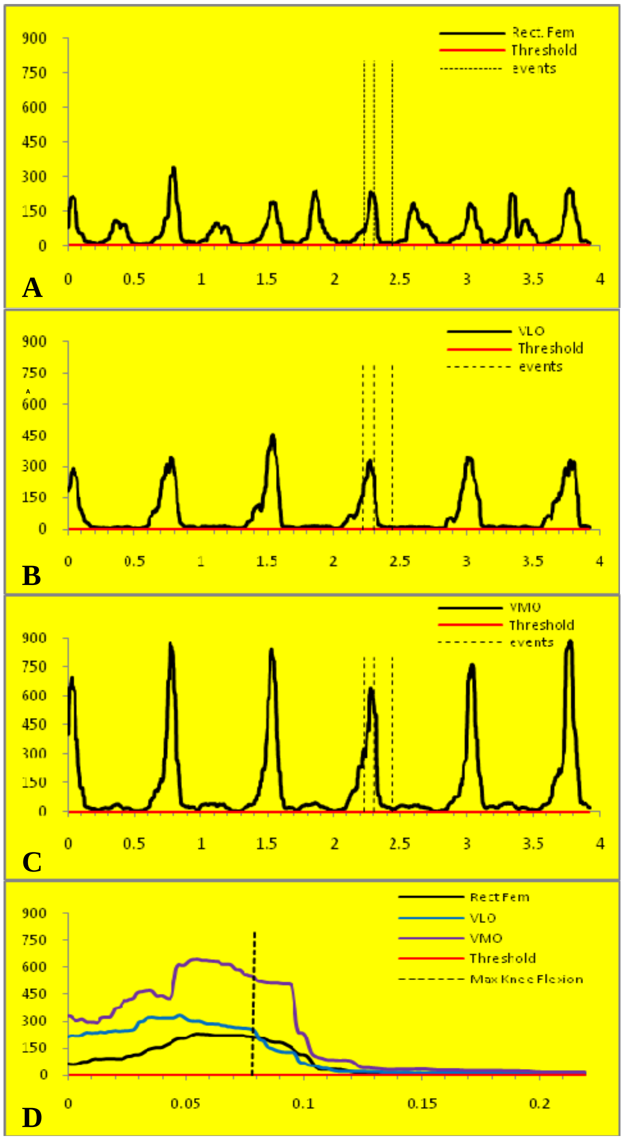

Figure 1: EMG and threshold for three muscles (A, B, C) over six stance phases at 4m/s, and single stance period in higher resolution (D).

REFERENCES

1. Brandell, B.R. (1973) An analysis of muscle coordination in walking and running gaits. *Medicine & Sport: Biomechanics III* (p. 278-287). Basel, Switzerland: Karger.
2. Elliot et al. *Medicine & Science in Sports* **11**, 322-327, 1979.
3. McClay et al. (1990). Muscle activity in running. *Biomechanics of Distance Running* (pp. 165-185). Champaign: Human Kinetics.

MULTI-MUSCLE SYNERGIES IN A DUAL TASK

Miriam Klous, Alessander Danna dos Santos, Mark L Latash
Department of Kinesiology, Pennsylvania State University, USA
miriam@psu.edu

INTRODUCTION

In several recent studies (Latash et al, 2007; Robert et al, 2008) it has been suggested that multi-muscle control of vertical posture is based on a hypothetical hierarchical scheme. At the lower level, muscles are organized in groups, called muscle modes (M-modes). At the upper level, the gains at muscle modes are manipulated to produce required actions. M-modes can form the basis for a multi-M-mode synergy that ensures stability of an important performance variable. In the current study we asked a question whether a set of M-modes can stabilize two performance variables at the same time.

METHODS

Eleven subjects participated in the study. Subjects were standing on the force plate with their feet in parallel at hip width and performed continuous voluntary sway at 0.5 Hz in the anterior-posterior direction. Three different loads (1.8 kg, 3.2 kg, and 6.1 kg) were attached at the ankle level via a pulley system such that they produced a horizontal force acting forward or backward. There was also a no-load condition. During the trials, continuous visual feedback was provided on the moment of force around the frontal axis (M_y). The horizontal component of the reaction force in the anterior-posterior direction (F_x) and M_y were recorded using a force platform (AMTI). The surface muscle activity (EMG) of the following muscles were recorded: gastrocnemius lateralis (GL), gastrocnemius medialis (GM), tibialis anterior (TA), biceps femoris (BF), semitendinosus (ST), rectus femoris (RF), vastus lateralis (VL), vastus medialis (VL), lumbar erector spinae (ES), and rectus abdominis (RA).

For each condition, on average, 50 sways were used for data analysis. Further data analyses were performed using the uncontrolled manifold hypothesis framework as described in Danna-dos-Santos et al (2007), Robert et al (2008). Shortly, first, M-modes were defined using principal

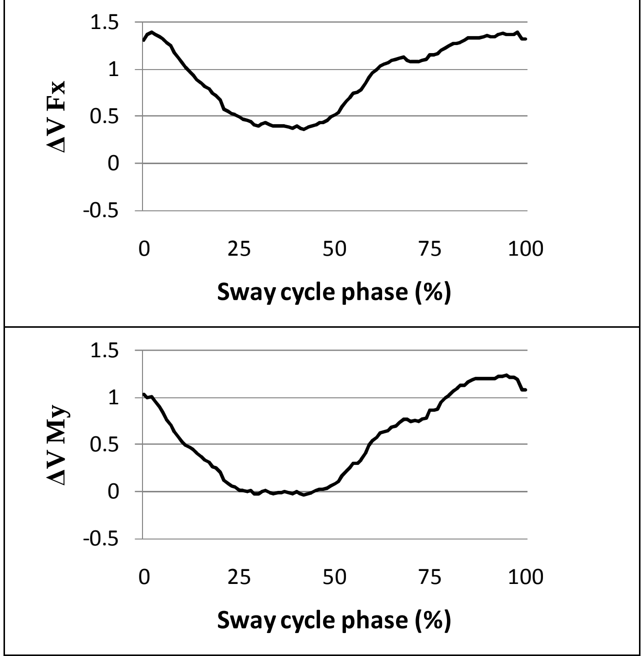

Figure 1: A typical example of the time profiles of ΔV for F_X (top) and M_Y (bottom) when a load of 1.8 kg was applied backwards

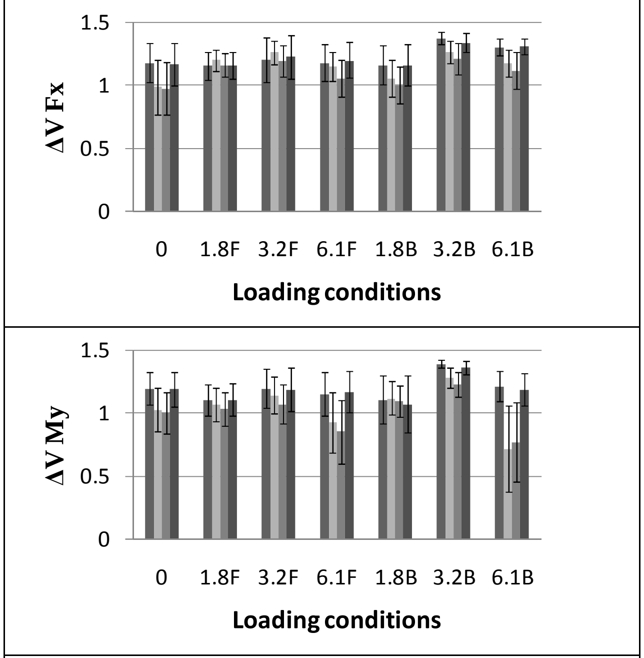

Figure 2: ΔV_{Fx} (top) and ΔV_{My} for each loading condition (F front, B back) for each of the four phases averaged across subjects

component analysis. Second, a Jacobian matrix was calculated using multiple regression defining the relations between small changes in the M-mode magnitudes and the performance variables ΔF_X and ΔM_Y. In the last step, the variance in the M-mode space across cycles was partitioned into a component that affected F_X (or M_Y) and the component that did not. A synergy index (ΔV) was computed as the normalized difference between the two variance indices such that positive ΔV values reflected a multi-M-mode synergy stabilizing F_X (or M_Y).

For statistical analysis, ΔV was z-transformed and quantified over the following four phases: 1) 95-100% and 1–5%, 2) 20%-30%, 3) 45%-55%, 4) 70%-80%. Average values for each of these intervals were calculated for each subject and each condition.

RESULTS AND DISCUSSION

All eleven subjects were able to show qualitatively similar 'sine-like' time profiles of M_Y across the seven load conditions. The activation profiles (EMGs) of all the ten muscles showed substantial modulation within the M_Y cycle. PCA allowed identifying three M-modes that, on average, accounted for 79% of the muscle activation variance. Fig. 1 shows a typical example of the time profiles of the synergy index ΔV for both performance variables F_X (top) and M_Y (bottom) when a load of 1.8 kg was applied in the backward direction.

Note the similar ΔV time profiles for F_x and M_y. Both show larger values at the beginning and end of the sway cycle and a drop between approximately 20% and 70% of the sway cycle. M_Y shows smaller ΔV values as compared to F_X, although $\Delta V > 0$ in both panels corresponding to multi-M-mode synergies stabilizing both F_X and M_Y over the whole cycle. Statistical analysis using the z-transformed values of ΔV_{Fx} and ΔV_{My} for all subjects confirmed that both ΔV_{Fx} and ΔV_{My} were significantly larger than zero ($p < 0.05$) and that ΔV for F_X was higher than for M_Y.

Fig. 2 shows the ΔV indices for each loading condition (F front, B Back), for each of the four phases, for F_X (top) and M_Y (bottom), averaged across subjects. Note that ΔV values are in general higher in Phases 1 and 4, and they show a drop in Phases 2 and 3. This was confirmed with a three-way ANOVA performed on the z-transformed values of ΔV_{Fx} and ΔV_{My}. The same ANOVA revealed that ΔV for F_X was higher for the 3.2 kg load as compared to the no-load condition and the 1.6 kg load condition. ΔV for M_Y was higher for the 3.2 kg load as compared to the 1.8 kg load.

DISCUSSION AND CONCLUSION

Results show that both performance variables F_x and M_y can be stabilized by a single set of muscle modes at the same time. Although feedback was given on the moment of force about the medio-lateral axis (M_y), the shear force (F_x) was better stabilized than M_y. This could be explained by the fact that the shear force is an essential variable to stabilize to be able to perform the task.

Furthermore, stabilization of the performance variables was not related to the time derivative of the movement, but to the direction of movement. Both performance variables were better stabilized when moving forward than when moving backward, likely because the subjects were more comfortable when moving in forward direction.

It can be concluded that the human body is able to stabilize more than one performance variables at the same time using the same muscle modes.

REFERENCES

1. Latash, ML et al. *Motor Control* **11,** 276-308, 2007.
2. Robert, T et al. *Experimental Brain Research* **187**, 237-253, 2008.
3. Danna-dos-Santos, A et al. *Experimental Brain Research* **179**, 533-550, 2007.

ACKNOWLEDGEMENTS

Supported in part by NIH grant NS-035032.

3-D INVERSE DYNAMICS ANALYSIS OF MARTIAL ARTS CIRCULAR KICK

[1] David Saxby and [2] D. Gordon E. Robertson
School of Human Kinetics, Faculty of Health Science, University of Ottawa, Ottawa, Ontario, Canada
Email: [1] dsaxb037@uottawa.ca, [2] dger@uottawa.ca

INTRODUCTION

This project investigated the kinetics of the lower limbs during the martial arts circular kick. Patterns of the net moments of force and powers were computed three-dimensionally. Due to the lack of three-dimensional kinetic investigations of the circular kick, this paper attempted to establish a basic outline of the recruitment patterns seen in this particular kick. The kinetic data were compared with similar powerful kicking activities from the literature such as soccer kicking [1] and *karate* front kicks [2]. Our hypothesis was that the circular kick requires similar kinetic patterns as other kicking modalities but possesses distinct features such as significant abductor power recruitment at the hip, limited pre-stretch and reduced follow-through.

METHODS

One subject performed a total of 15 trials of the circular kick delivered with maximal force into a stationary pad. The subject was an elite-level combat athlete competing internationally at 80 kg. A Vicon Motion Analysis system recorded the trajectories of 42 markers using seven MX-13 cameras at 200 Hz (see Figure 3). The marker coordinates were filtered using a Butterworth lowpass digital filter with cutoff of 6 Hz. Two Kistler force platforms measured the ground reaction forces of stance and kicking legs. Analog signals were filtered at 20 Hz. Visual3D computed the angular velocities, moments and powers for the ankle, knee and hip of both lower limbs using inverse dynamics. Only the kicking leg's results will be reported.

RESULTS AND DISCUSSION

Figure 1 holds the sagittal plane ensemble averaged (15 trials) angular velocities, moments and powers of the kicking leg's ankle, knee and hip joints. The results start 0.43 seconds before pad contact when some of the markers of the kicking leg become occluded. Negative values of the angular velocities and moments of force are plantiflexor at the ankle, flexor at the knee and extensor at the hip. Positive powers indicate the rate of work done by the associated moment of force.

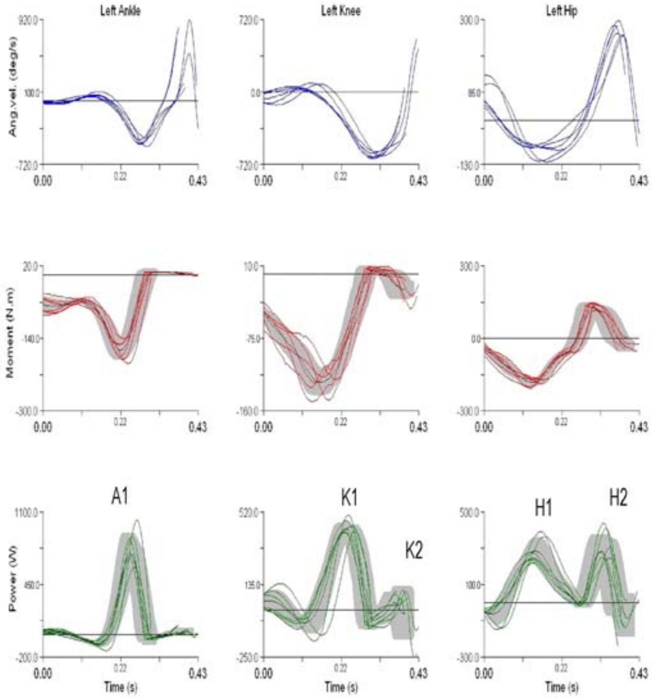

Figure 1: Flexor/extensor angular velocities (top), moments (mid) and powers (bottom) of ankle (left), knee (mid) and hip (right) of the kicking leg.

As the kicker begins the kicking motion, the hip extensors of the kicking limb (H1 in Figure 1) work positively to extend the hip until toe-off at *t*=0.28 s. After slight delays, both the ankle plantiflexors (A1) and knee flexors (K1) performed positive work to push away from the floor and simultaneously actively flex the knee, respectively.

After the leg is in swing (at *t*=0.28), the hip flexors acted to flex the hip (H2) and then immediately before contact the hip extensor moment dominated to stop hip flexion and extend the knee and foot towards the pad. In contrast, the knee flexors transition briefly to eccentric work to prevent hyperextension of the knee [*cf*. 2].

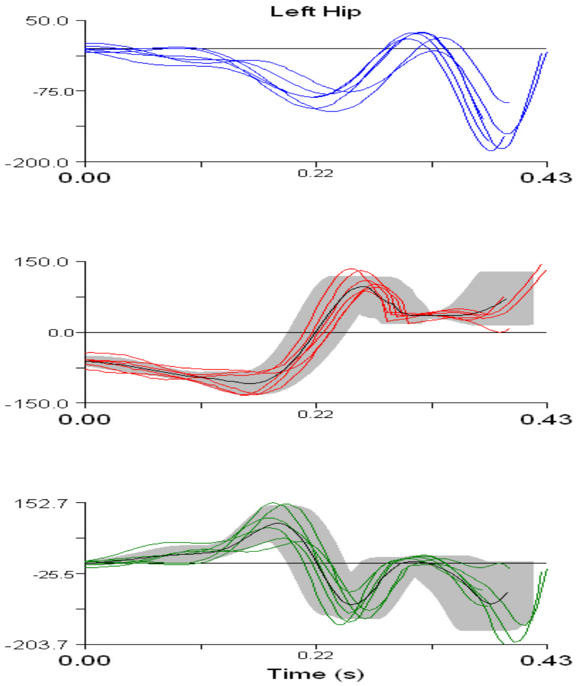

Figure 2: Ab/adductor angular velocities (top), moments (mid) and powers (bottom) of the hip of the kicking leg.

Figure 2 holds the frontal plane ensemble averaged (15 trials) angular velocities, moments and powers for the hip of the kicking leg. Negative velocities and moments indicate abduction.

Notice in Figure 2 the abductor moment is initially acting isometrically. The abductor moment quickly begins positive work to elevate the kicking limb to the maximum kicking height. Then, the adductor moment works eccentrically to stop the elevation of the limb. Prior to impact, the adductors briefly act isometrically and then eccentrically to control the rates of abduction. Note prior to impact, the kicker is rotating towards the pad on the stance leg. As well, the trunk is substantially hyperextended as the kick is delivered.

This circular kick did not exhibit identical recruitment patterns as soccer kicking or the *karate* front kick. The circular kick differs from a soccer kick because it is delivered from a stationary stance, has no approach run and has no follow-through. As well, martial arts kicks are delivered so an opponent cannot anticipate the time of execution. As result, the pre-stretch–while it does occur–is not as dramatic or pronounced as in soccer kicking where a large wind-up precedes a maximal kick. It appears being fast and accurate with the circular kick is more valuable than maximal power. Additionally, soccer kicks and *karate* front kicks use different surfaces for contact with the ball or opponent. In the circular kick, the athlete uses the anterior surface of the tibia as the contact surface; whereas, soccer kicking uses the instep and the *karate* front kick uses the ball of the foot. As a result, the knee flexor moment of the circular kick activates earlier in the motion to resist extension of the knee and to ensure that proper contact is made with the pad. This accounts from the lower hip extensor activity compared to soccer and *karate* front kicks.

CONCLUSIONS

The martial arts circular kick exhibited pre-stretching, large concentric flexor and extensor hip powers, large ankle plantiflexor power at push-off, substantial hip abductor and adductor moments and powers as well as protective or breaking behavior at the knee joint. These results demonstrate the martial arts circular kick has distinctly different kinetic characteristics than either the soccer kick or the *karate* front kick.

REFERENCES

1. Nunome H, *et al*. *Med Sci Sport and Exercise*, **34**: 2028-2036, 2002.
2. Robertson DGE, Mosher RE. Biomechanics IX-B. Human Kinetics: Champagne, IL, 1985.

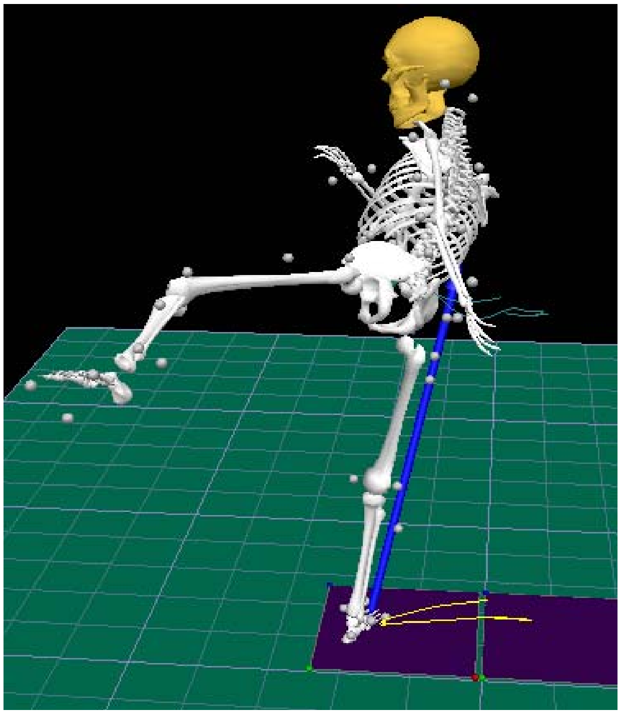

Figure 3: Model immediately before impact.

AN ERGONOMIC INVESTIGATION OF SPEED FASTENING WORK RATES

Chad E. Gooyers and Joan M. Stevenson
School of Kinesiology & Health Studies, Queen's University, Kingston, Ontario, Canada
email: 6ceg@queensu.ca

INTRODUCTION

Present day manufacturing assembly relies extensively on a variety of fasteners for the assembly of sub-systems, components and trim. Speed fastening (SF) is one commonly used non-structural assembly fastening method. The primary limitation of this process is a lack of the continuous feed of rivets. One path to productivity improvement for SF is the development of a continuously feed rivet gun that eliminates reloading from the work cycle. This proactive ergonomic investigation was carried out to examine differences in muscle activation, ratings of perceived exertion and body discomfort across three different work rates (7, 14 and 21 fasteners / min) for a simulated SF task performed both at shoulder and waist height (*See Figure 1*). The SF hand tool used in this investigation had a mass of 1.5kg.

METHODS

Twelve healthy female subjects (23.6±1.8 years, 60.9±10.8 kg, 1.7±0.09 m) participated in this investigation. Data collection was completed over four test sessions. The first test session was used for subject familiarization with the SF tasks as well as the data collection protocol. Subsequent test days (scheduled at least 24 hours apart) were block randomized to one of three work rates (7, 14 and 21 fasteners/min.) with subjects required to complete 120 minutes of simulated SF with a 50% work to rest duty cycle. Each 120 minute work session was divided into 60 x 2 minute trials that were fully randomized for working height.

Surface electromyography (EMG) from eight muscles including: the biceps brachii, lateral head of the triceps, anterior deltoid, upper trapezius, flexor carpi radialis longus (FCRL), flexor carpi ulnaris (FCU), extensor carpi radialis (ECR) and extensor carpi ulnaris were recorded using bipolar pairs of electrodes (2.5cm center-to-center distance) from the subjects' preferred working side. EMG electrodes were interfaced with a Bortec AMT-8 amplifier system (Bortec Biomedical, Calgary, AB) and a 16-bit analog to digital converter (NIDAQ USB-6211, National Instruments, Texas, USA). Raw data were acquired at 2048 Hz , differentially amplified and band passed from 10Hz – 1kHz. and stored on personal computer using a custom program created in Labview 8.6 (National Instruments, Texas, USA). Linear envelopes for each muscle site were created using a dual-pass 2nd order Butterworth filter with a 3Hz cut-off frequency, followed by normalization to a maximum voluntary isometric contraction (MVIC) and conversion to Amplitude Probability Distribution Functions (APDF).

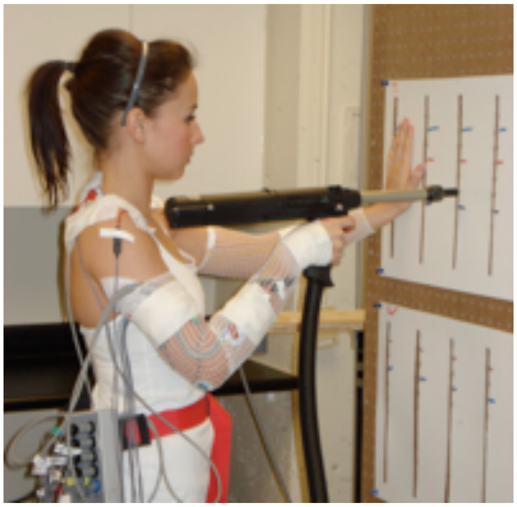

Figure 1: Sample work trial at shoulder height.

In addition to sEMG data, ratings of perceived exertion (RPE) were collected from subjects using the Borg 6-20 scale after every two minute working trial. At the end of each test session, measures of anatomical pain and discomfort were collected using a body discomfort map that had subjects rank their discomfort on a scale from 1 to 9.

RESULTS

The data used in this investigation were taken from the last 10 trials (20 minutes of work) completed at both shoulder and waist height from each test session. Separate repeated measures ANOVA ($p < .05$) were used for statistical analysis of EMG, RPE discomfort data. No significant differences were found in the 10th, 50th and 90th percentile activation of sEMG data across work rates, however significant differences were found between working heights. A significant interaction effect between work rate and working height was found for all muscles. The ensemble averaged 50th percentile muscle activation at both waist and shoulder height (normalized to MVIC) can be seen in *Figure 2*.

Significant differences were also found in RPE scores across each of the three work rates, as well as between working heights. One interesting point to note however is that even at shoulder height for the fastest work-rate (21 fasteners/min.) the mean RPE scores was still very sub-maximal (< 12 on the Borg scale). For body discomfort scores no significant differences were found across any of the work rates.

DISCUSSION

In 1997, NIOSH published a comprehensive literature review on musculoskeletal disorders (MSDs) which concluded that there was strong evidence for causal relationships between MSDs of several bodies regions and repetitive motion, sustained exertion, awkward posture and vibration [1]. Manual SF assembly exposes operators to all of these known risk factors.

It is hypothesized that no differences were seen in muscle activation or discomfort scores because although the number of fasteners broached across all three work rates varied, even at the slowest work rate subjects were not able to rest their arm between the insertion of each individual cycle. For this reason subjects were required to support the weight of the hand tool (approximately 1.5 kg) for same duration of time (30 seconds / minute) across all work rates. From this it could be speculated that the only real difference that occurred across work rates was the number of times the trigger was actuated.

The results of this study demonstrate that to adequately provide muscular rest for employees who work with hand tools, the entire mass of the tool needs to be taken out of the hand. Failing to do so will require sustained muscular contraction to support the tool over the entire duration of a work shift. This type of muscular loading is a known risk factor for the development of musculoskeletal injury.

SUMMARY

Muscle activation for the simulated SF task was not significantly affected by work rate. It was however affected by working height. RPE measures, were significantly affected by both work rate and working height. No differences were seen in the amount of reported discomfort across work rates.

REFERENCES

1. Bernard B et al. (1997). NIOSH Pub No 97-141. Cincinnati, OH.

ACKNOWLEDGEMENTS

This research was supported by the Auto21 Network Centre of Excellence.

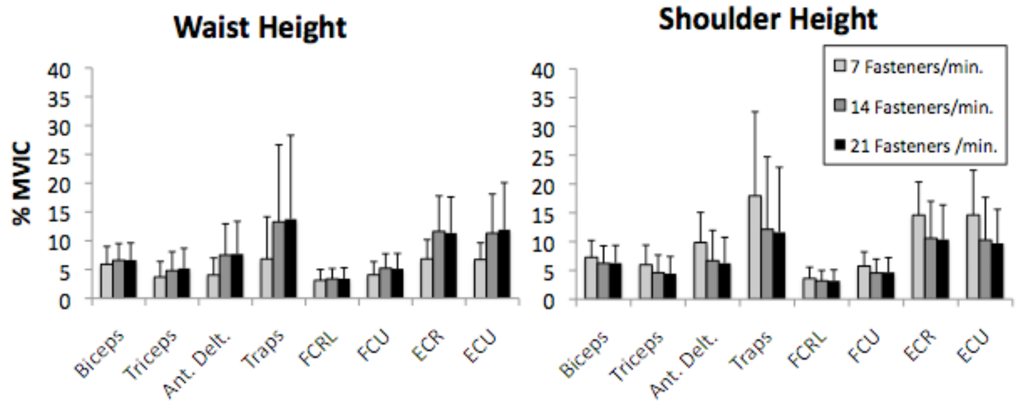

Figure 2. Ensemble averaged 50th percentile muscle activation (+SD).

MOTOR ASYMMETRY REDUCTION IN OLDER ADULTS REVEALED BY INTERLIMB TRANSFER

Kati Wuebbenhorst [1] and Robert L. Sainburg [1]
[1] Deptartment of Kinesiology, The Pennsylvania State University, University Park, PA, USA,
email: *rls45@psu.edu*

INTRODUCTION

We have previously described substantial asymmetry in the transfer of final position accuracy and movement direction between the arms, following adaptation to novel visuomotor transformations in young adults [1]. These findings were consistent with our Dynamic Dominance Model of motor lateralization, which attributes non-dominant hemisphere specialization to control of steady state position, and dominant hemisphere specialization to control of movement trajectory [1]. Interestingly, several brain-aging studies have demonstrated that hemispheric asymmetries for cognitive and perceptual tasks become reduced as a result of the normal aging process, which has lead to the HAROLD model (hemispheric asymmetry reduction in older adults) [2]. However, this model has not been examined for motor asymmetries. We now hypothesize that motor asymmetry reductions in older adults should result in more symmetrical interlimb transfer of final position and initial direction than that shown for young adults.

METHODS

Our subjects were split in two groups, Right-Left (RL) and Left-Right (LR), each with 3 neurologically intact right-handed men aged from 65 to 79 years old. The participants were adapted to a 30° counterclockwise visual motor rotation (vmr) during a center-out reaching to targets task. The eight direction targets positioned 15 cm from the start. Half the subjects performed the multidirectional reaching task with the nondominant arm first (LR) and then the dominant arm, while the other half (RL) performed with the dominant arm first and then the nondominant (Table 1).

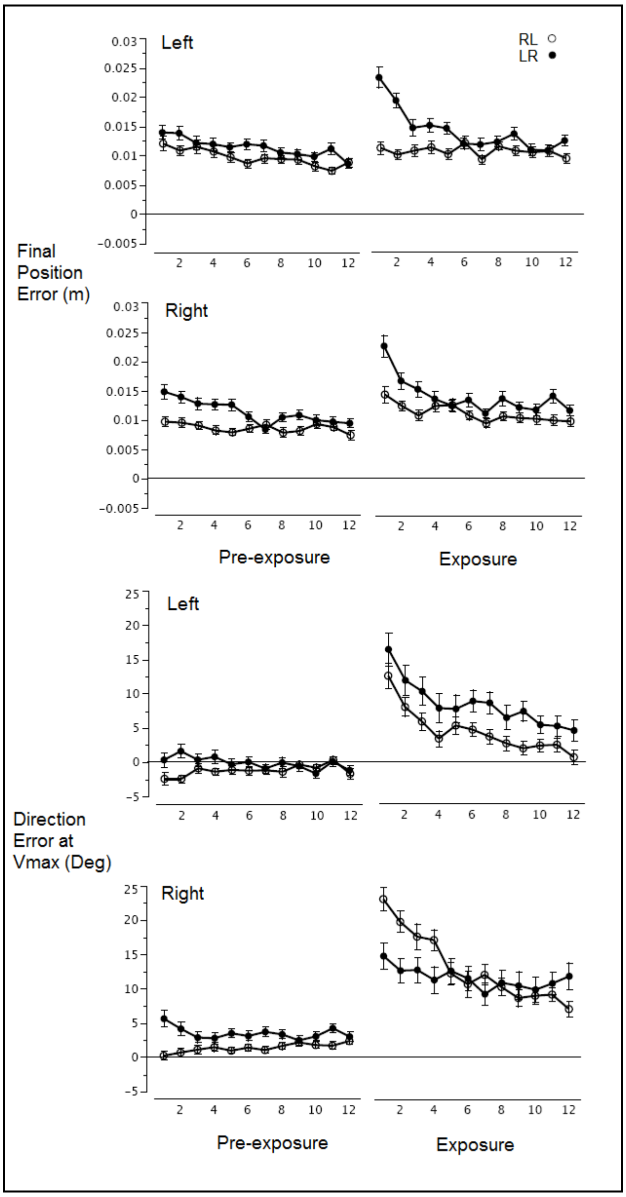

Figure 1: Mean performance measures, final position error (top) and direction error at Vmax (bottom) are shown for left and right arms separately. Every data point shown on the X-axis represents the average of two consecutive cycles across all subjects (mean ± SE). Performance measures for the LR group (filled circles) and RL group (open circles) are shown separately.

RESULTS AND DISCUSSION

Figure 1 shows final position errors and direction errors at peak tangential hand velocity for left and right arm movements of the pre-exposure and exposure sessions.

Transfer was assessed with following opposite arm adaptation trials. When the first exposure cycle was compared between naïve and opposite arm adapted conditions, both final position error and trajectory direction transferred in both directions (right to left arm, and left to right arm). However, asymmetry in the amplitude of this effect remained, such that transfer of final position information, from right to left arms was greater than vice versa. Consistent with the examples shown in Figure 1 (top) the comparison of means for left (LR 0.023±0.002, RL 0.011±0.001) and right (LR 0.022±0.002, RL 0.014±0.001) arm movements proved significant (left P=0.008, right P=0.003). Similarly, opposite arm transfer of initial direction was greater for the right than the left arm. The differences shown in Figure 1 (bottom) were significant for right (P=0.001) but not for left arm movements (P=0.229).

CONCLUSIONS

These results support the extension of the HAROLD model of hemispheric reduction in older adults to include a reduction in motor asymmetry. However, in our subjects, this asymmetry reduction was not complete, which may either reflect the age range that we studied, the limited number of subjects, thus far recruited, or a limit to asymmetry reduction in the motor skills of older adults.

REFERENCES

1. Sainburg RL, et al. *Exp Brain Res* **145**, 437-447, 2002.
2. Cabeza R, *Psychology & Aging* **17**, 85-100, 2002.

ACKNOWLEDGEMENTS

This study was supported by the NIH NICHD: National Center for Medical Rehabilitation Research, Grant #: 5R01HD039311

Table 1: Experimental design.

Session	**Pre-exposure**		**Exposure**	
	192 Baseline Trials	192 Baseline Trials	192 Rotation Trials	192 Rotation Trials
Group LR	Left	Right	Left	Right
Group RL	Right	Left	Right	Left

INTERLIMB COORDINATION DIFFERENCES IN LEFT- AND RIGHT-HANDERS.

[1] Andrzej Przybyla, [1, 2, 3]Robert L Sainburg
Departments of [1]Kinesiology and [2]Neurology, [3]The Penn State Neuroscience Institute, The Pennsylvania State University, University Park, PA

INTRODUCTION

We previously detailed interlimb asymmetries in coordination patterns providing evidence for motor lateralization in right-handed individuals. The right dominant arm shows advantages in intersegmental coordination as indicated by more efficient torque strategies and, often, straighter movements with smaller initial direction errors. The left non-dominant arm was consistently found to be more proficient in stabilizing limb posture [1, 2]. Handedness Inventory [3] and neural activation profiles recorded during unilateral movements [4] provide evidence that left-handers tend to be less lateralized. We ask whether left-handers show the same intersegmental coordination advantages for the left dominant arm, as do right-handers for their right dominant arm. If so, the differences in interlimb coordination should be reversed with the left dominant arm being specialized for movement dynamics. Furthermore, the reduced degree of handedness in left-handers should be reflected in interlimb asymmetries in these coordination patterns.

METHODS

Young neurologically intact right- (n=13) and left-handers (n=13) signed the consent form approved by the Institutional Review Board of the Pennsylvania State. Subjects sat in the virtual reality environment setup with arms covered and supported on the air sleds to minimize gravity and friction (see Figure 1). 180 rapid reaching movements (0.7-1.2m/s) were performed with cursor (d=1.6cm) representing the tip of the index finger (veridical display) and hand being exchanged every 18 trials. Three targets (d=2.8cm) were presented in sudo-randomized order to exert 20° elbow extension with shoulder flexion of 0, 10 or 20° to increase intersegmental requirements respectively. The starting position (d=2cm) was set for 90° elbow extension with 30° shoulder flexion. To encourage performance, subjects were awarded 10, 5, 3 or 0 points depending on final accuracy. Points were not awarded if finger tangential velocity was out of range (0.7-1.2m/s). Feedback about velocity was provided after each trial in the form of horizontal bar rising to the indicated limits. All trials were 1 sec in duration and recordings were pre triggered 250 ms prior to trial initiation indicated with a single beep as a go signal. Both limbs were set to two-segment planar reaching by restraining all joints distal to the elbow that was leveled to shoulder height. A six-degree of freedom (6-DOF) electromagnetic movement tracking system Flock of Birds (FOB) (Ascension Technology, USA) configured with four sensors was used to sample position of the index finger, the elbow and the shoulder at the rate of 103 Hz. FOB sensors were firmly attached approximately at the centre of each arm segment and relative anatomical landmarks were digitized: the tip of index finger, the lateral epicondyle of the humerus, and the acromion, directly posterior to the acromio-clavicular joint. Note that these anatomical landmarks relations to corresponding sensors reminded constant during testing thus the centre and both ends of each segment were recorded. Data collection and settings of interactive display were controlled via custom made stand alone application programmed in REAL BASIC™ (REAL Software, Inc., USA). Data stored in text format were processed in IgorPro 6.0 (WaveMetrics, Inc., USA) to return peak tangentional velocity, error in movement direction at time of peak velocity, movement linearity defined as minor/major axis of movement path, absolute and variable final position accuracy. ANOVAs were then performed in JMP 7.0 (JMP, USA).

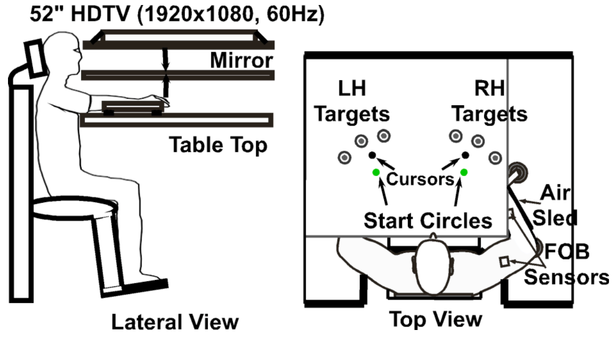

Figure 1: Experimental setup.

RESULTS AND DISCUSSION

According to extended Handedness Inventory, our left-handed subjects were significantly less lateralized in functional tasks than right-handers, with handedness scores being on average 50% for lefties and 80% for righties. Although handedness score is based on functional tasks, our later statistical analysis showed that it was not a good predictor of interlimb asymmetries, as measured by our tasks.

As previously shown, movement velocities varied across targets, such that medial directions were slowest. Nevertheless, velocities were matched for each target across subjects and hands. Examples of typical hand paths are shown in Figure 2.

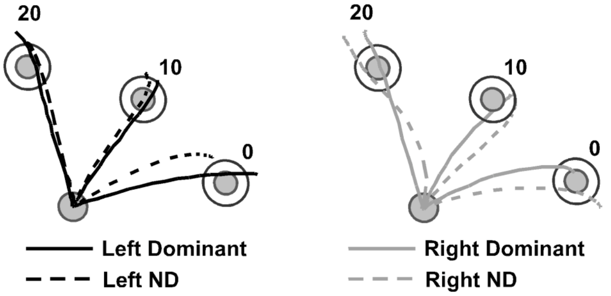

Figure 2: A typical hand paths for dominant (solid) and non-dominant (dashed) arms of right- (light) and left-handers (dark).

Left-handers (red) showed little differences between arms in initial directions for multi joint movements, while right handers showed substantial differences (blue) (Figure 3, top). As previously reported, the non-dominant arm in right-handers showed much more curvature than the dominant arm for the most medial target. These differences are substantially smaller in left-handed subjects with the non-dominant arm following the pattern of the dominant side (Figure 3, bottom).

There were no significant interactions in final position accuracy, but there was a trend to increase error for the more complex movements to medial targets (Figure 4). Overall, right-handers' dominant arm shows the best accuracy in final positions across targets.

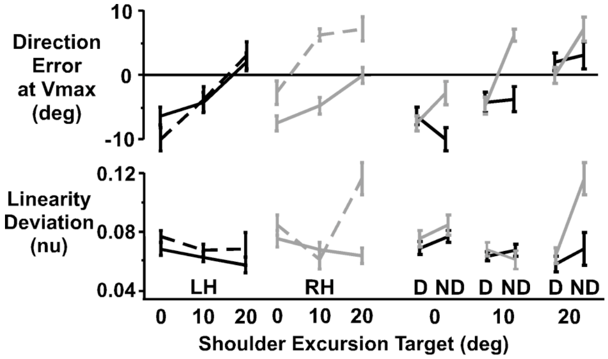

Figure 3: Direction error and linearity across targets for dominant (solid) and non-dominant (dashed) arm of right- (light) and left-handers (dark).

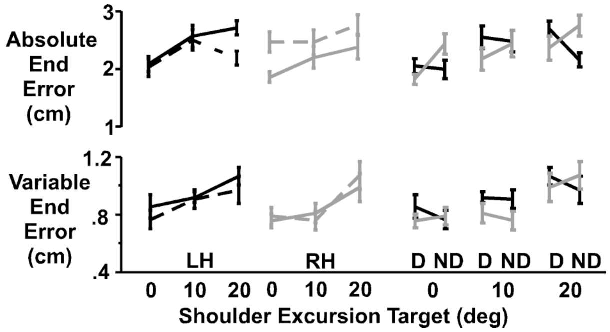

Figure 4: Absolute and variable error in final position across targets. Legend as above.

CONCLUSIONS

In this task that stresses intersegmental coordination, left-handers are less lateralized, as reflected by less differences in initial direction, curvature, and accuracy between the arms. Interestingly, the more lateralized right handers showed greater accuracy in these measures, suggesting that lateralization imparts a coordination advantage.

REFERENCES

1. Sainburg RL and Kalakanis D, *J Neurophysiol* **83**, 2661-2675, 2000.
2. Bagesteiro LB and Sainburg RL, *J Neurophysiol* **88(5)**, 2408-2421, 2002.
3. Oldfield RC, *Neuropsychologia* **9**, 97-113, 1971.
4. Verstynen T, et al. *J Neurophysiol* **93(3)**, 1209-1222, 2005

ACKNOWLEDGEMENTS

This work was supported by grant #R01 HD39311 from the National Institutes of Health (NIH): NICHD and approved by the Pennsylvania State University's Institutional Review Board.

WHIPLASH INJURY PREVENTION WITH ACTIVE HEAD RESTRAINT

[1] Paul C. Ivancic, [2] Daohang Sha, and [1] Manohar M. Panjabi
[1] Biomechanics Research Laboratory, Department of Orthopaedics and Rehabilitation, Yale University School of Medicine, New Haven, CT, USA; email: paul.ivancic@yale.edu
[2] Center for Clinical Epidemiology and Biostatistics, University of Pennsylvania School of Medicine, Philadelphia, PA, USA.

INTRODUCTION

Previous epidemiological studies observed that a gap greater than 10 cm between the head restraint and back of the head was associated with higher neck injury risk and greater incidence of chronic symptoms in whiplash patients [1]. Active neck injury prevention systems, such as the active head restraint and energy absorbing seat, have been developed for some automobiles. However, their implementation is without thorough understanding of their injury prevention mechanisms.

The goals of this study were to develop a new Human Model of the Neck (HUMON) for whiplash simulation, consisting of a neck specimen mounted to the torso of a rear impact dummy and carrying an anthropometric head, and to use the model to investigate the relation between the active head restraint (AHR) position and whiplash injuries.

METHODS

HUMON (**Figure 1**) consisted of a neck specimen mounted to the torso of BioRID II and carrying an anthropometric head stabilized with muscle force replication. HUMON was seated and secured in a Kia Sedona seat with AHR on a sled. The AHR was activated by HUMON's momentum pressing into the seatback during whiplash and rotated forward via a pivoting mechanism between it and the seatback. Whiplash was simulated with the AHR in the each of the five positions immediately prior to impact (**Figure 2**): minimum gap and height (AHR 1), midrange gap and maximum height (AHR 2), maximum gap and height (AHR 3), midrange gap and minimum height (AHR 4), and midrange gap and height (AHR 5). Subsequently, whiplash was simulated without the AHR. The impacts were first performed at a maximum measured horizontal sled acceleration of 7.1 g and subsequently at 11.1 g.

Peak spinal motions were contrasted with physiologic ranges obtained from intact flexibility tests. Significant reduction ($P<0.05$) in the spinal motion peaks with the AHR, as compared to without, were determined. Linear regression analyses identified correlation between head/AHR gap and peak biomechanical parameters ($R^2>0.3$ and $P<0.001$).

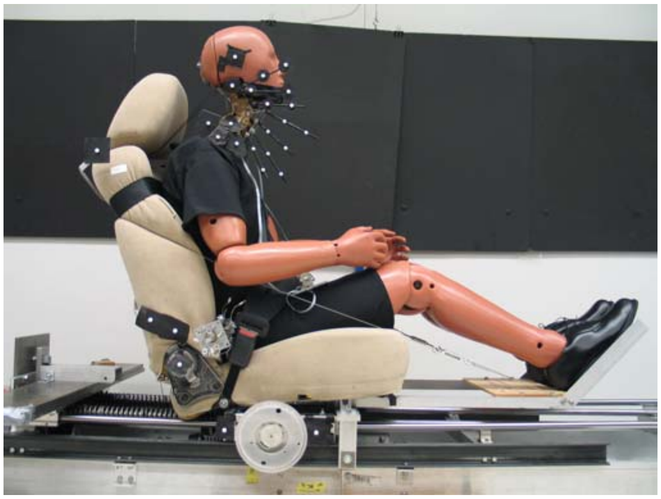

Figure 1. Photograph of the Human Model of the Neck (HUMON) and rear impact apparatus.

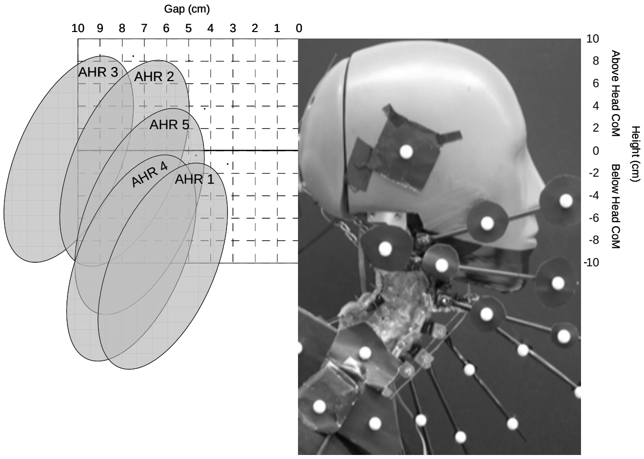

Figure 2. Schematic of the average active head restraint (AHR) position immediately prior to impact for each of the five positions studied.

RESULTS AND DISCUSSION

The AHR significantly reduced average peak spinal motions throughout the middle and lower cervical spine, however these peaks exceeded the physiologic range in flexion at head/C1 and in extension at C4/5, C6/7, and C7/T1. The AHR position with the smallest gap generally allowed the least motion in excess of physiologic. Correlation was observed between the head/AHR gap and extension peaks at C4/5 and C5/6 (**Figure 3**). Based upon these correlations, motion beyond the *in vivo* physiologic range may occur at C5/6 and C4/5 due to head/AHR gaps in excess of 9.2 and 9.6 cm, respectively, causing extension injuries. These results are consistent with previous epidemiological studies which observed higher neck injury risk [1] and greater incidence of chronic symptoms for a head restraint gap larger than 10 cm.

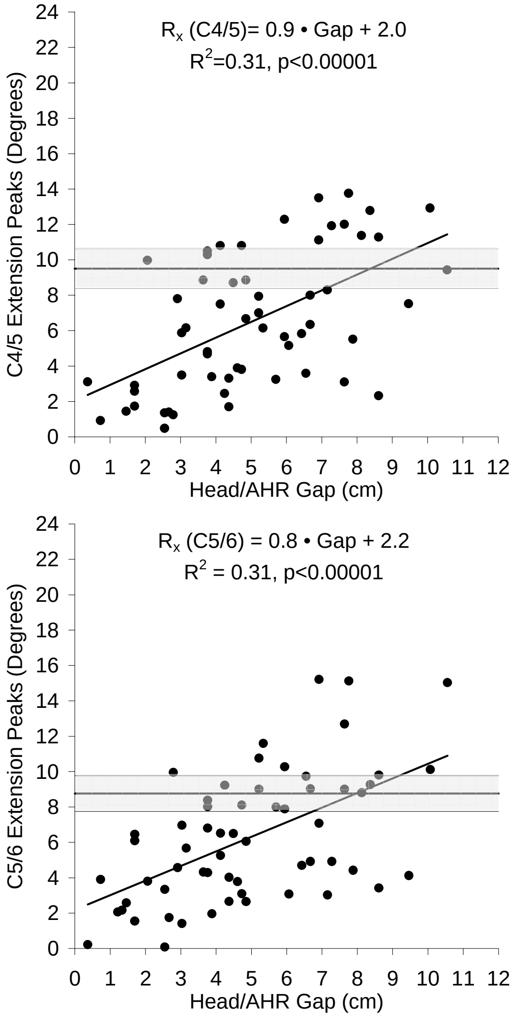

Figure 3. Correlation between head/AHR gap and C4/5 and C5/6 extension peaks. The *in vivo* physiologic rotation range is indicated in grey shading.

CONCLUSIONS

1. A new, novel Human Model of the Neck (HUMON) for whiplash simulation was developed consisting of a neck specimen mounted to the torso of BioRID II and carrying an anthropometric head. The model was used to investigate the relation between active head restraint (AHR) position and whiplash injury.

2. The AHR significantly reduced the average peak spinal motions throughout the middle and lower cervical spine, as compared to no AHR, however these peaks exceeded the physiologic range in flexion at head/C1 and in extension at C4/5, C6/7, and C7/T1.

3. Correlation was observed between head/AHR gap and extension peaks at C5/6 and C4/5. Based upon these relations, motion beyond the *in vivo* physiologic range may cause injury at these spinal levels due to head/AHR gaps in excess of 9.2 and 9.6 cm, respectively.

4. The AHR may not be fully activated at the time of peak spinal motions, thus reducing its protective effect.

5. Improved understanding of the whiplash prevention mechanisms may lead to improved injury prevention systems and reduced neck injury risk.

REFERENCES

1. Olsson I, et al. An in-depth study of neck injuries in rear end collisions. *Proceedings of IRCOBI*. Bron, France, 1990.

ACKNOWLEDGEMENTS

This research was supported by grant 5R01CE001257 from the Centers for Disease Control and Prevention (CDC).

EFFECT OF ACTIVE HEAD RESTRAINT ON RESIDUAL NECK INSTABILITY DUE TO REAR IMPACT

[1] Paul C. Ivancic, [2] Daohang Sha, [1] Brandon D. Lawrence, and [1] Fred Mo
[1] Biomechanics Research Laboratory, Department of Orthopaedics and Rehabilitation, Yale University School of Medicine, New Haven, CT, USA; email: paul.ivancic@yale.edu
[2] Center for Clinical Epidemiology and Biostatistics, University of Pennsylvania School of Medicine, Philadelphia, PA, USA.

INTRODUCTION

Rear automotive crashes commonly result in injurious neck strains and whiplash injuries. These strains lead to clinically observed symptoms of neck, shoulder, and back pain, headache, dizziness, paresthesias, and vertigo. Multiple epidemiological studies have reported that traditional passive head restraints and standard seat designs have been ineffective or provided up to only 20% effectiveness in preventing neck injuries. While previous studies have indicated potential benefits of active injury prevention systems, including the active head restraint (AHR), no studies have evaluated their effects on residual neck instability due to whiplash. The goals of the present study were to determine residual neck instability due to simulated rear impacts of a new Human Model of the Neck (HUMON). The impacts were performed with and without the AHR at two impact severities.

METHODS

The experimental protocol is outlined in **Figure 1**. The whole cervical spine specimen was used for flexibility testing while intact and following rear impacts with and without the AHR. HUMON (**Figure 2**) was used to simulate rear impacts and consisted of the cervical spine specimen mounted to the torso of a rear impact dummy and carrying an anthropometric head, stabilized with muscle force replication. The muscle force replication was deactivated prior to flexibility testing. Pure flexion-extension moments were applied to the occipital mount of the whole cervical spine specimen in four equal steps up to peak loads of 1.5 Nm. To allow for viscoelastic creep, 30-second wait periods were given following each load application. Two preconditioning cycles were performed and data were recorded on the third loading cycle using a digital. From the resulting load displacement curves, the flexibility parameters of total (flexion plus extension) neutral zone (NZ) and total range of motion (RoM) were determined for all spinal levels.

Single factor, repeated measures ANOVA and pair-wise Bonferonni post-hoc tests were used to determine significant differences ($p<0.05$) in the flexibility parameters among the test conditions for each spinal level. Linear regression analyses were performed to identify correlation ($R^2>0.3$; $P<0.001$) between the flexibility parameter increases measured following impact and the high-speed spinal rotation peaks measured during impact with and without the AHR for both the 7.1 and 11.1 g impacts combined.

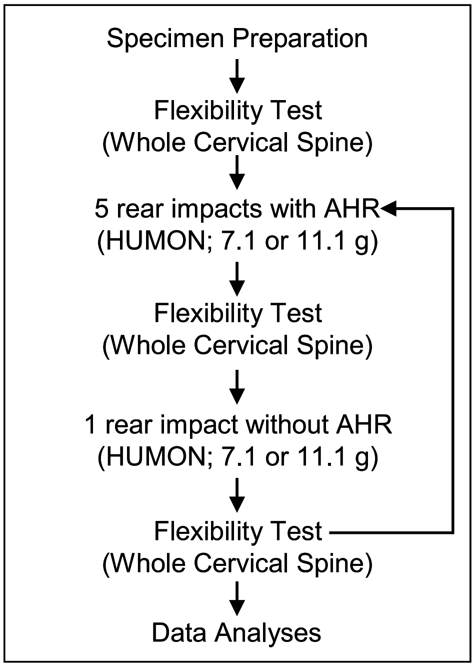

Figure 1. The experimental protocol in which flexibility testing was performed following each rear impact of the Human Model of the Neck (HUMON). Impacts were performed with and without the active head restraint (AHR).

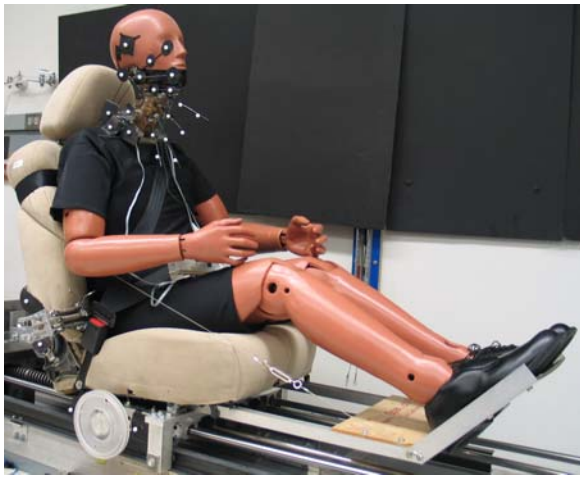

Figure 2. Photograph of the Human Model of the Neck (HUMON) used to simulate rear impacts.

RESULTS AND DISCUSSION

Our results indicated significant increases in the average flexibility parameters, up to 3.1°, at C2/3, C3/4, and C5/6 due to 7.1 g rear impacts even in the presence of the AHR. Subsequently, increases in the flexibility parameters progressed and spread to head/C1 and to the inferior spinal levels following the 11.1 g impacts. Correlation was observed between the C7/T1 extension peaks measured during impact and the flexibility parameter increases measured following impact (**Figure 3**). The flexibility parameter increases were generally larger due to the impacts without, as compared to with the AHR. Extrapolation of our results indicated that every 1° of extension beyond the physiologic limit during whiplash contributed approximately 0.5° of residual neck rotation following whiplash. The present results underscore the importance of neck injury prevention systems in minimizing spinal rotations during whiplash to reduce the resulting residual instability, pain, and chronic symptoms.

CONCLUSIONS

1. The present study determined residual neck instability due to simulated rear impacts with and without the AHR using HUMON.
2. Our results indicated residual neck instability, up to 3.1°, due to rear impact even in the presence of the AHR. Increased neck flexibility was initially observed at C2/3, C3/4, and C5/6 due to 7.1 g impacts with the AHR, and subsequently progressed and spread to head/C1 and the lower cervical spine at the higher impact severity.
3. Assuming that the present correlation between the C7/T1 extension peaks and resulting residual instability may be applied throughout the middle and lower cervical spine, then every 1° of extension beyond the physiologic limit during whiplash may contribute approximately 0.5° of residual rotation.
4. Greater residual neck instability was generally observed due to rear impacts without, as compared to with the AHR.
5. The present data underscored the protective effect of the AHR in reducing residual neck instability due to whiplash.

ACKNOWLEDGEMENTS

This research was supported by grant 5R01CE001257 from the Centers for Disease Control and Prevention (CDC).

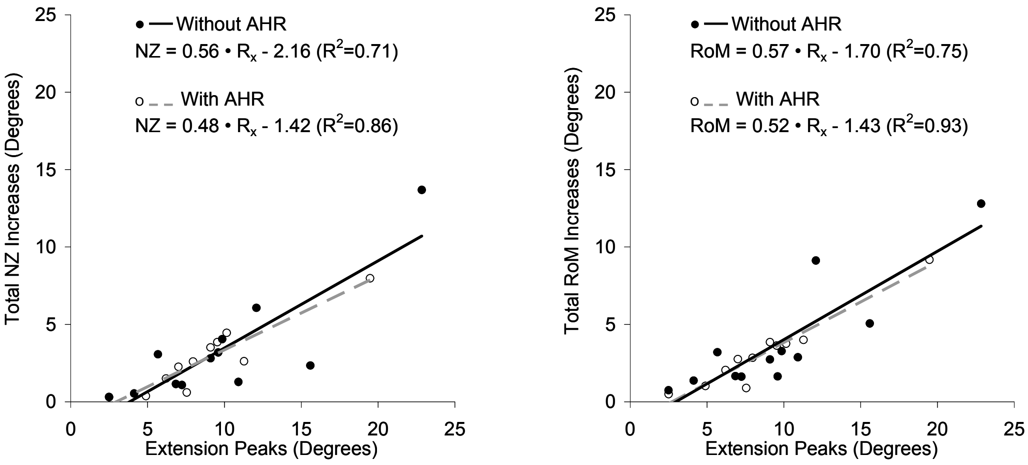

Figure 3. Correlation between the C7/T1 neutral zone (NZ) and range of motion (RoM) increases following impact and the high-speed spinal extension peaks during the impacts with and without the active head restraint (AHR). Data from the 7.1 and 11.1 g impacts were combined.

3D Kinetic Synergies in Handwriting

[1,2,3]Jae Kun Shim, [1]Alexander W Hooke, [1]Sohit Karol, [1]Jaebum Park

[1]Department of Kinesiology, [2]Fischell Department of Bioengineering, [3]Neuroscience and
Cognitive Science Program, University of Maryland, College Park, MD 20742, USA
e-mail: jkshim@umd.edu, web: http://www.sph.umd.edu/KNES/faculty/jkshim/neuromechanics

INTRODUCTION

The seemingly simple act of handwriting is one of many marvels of the central nervous system (CNS). Previous handwriting studies have focused exclusively on handwriting kinematics rather than its kinetics due to the technical difficulties to record pen-hand contact forces in three dimensions (3D). Our group has recently developed Kinetic Pen, which is capable of recording 3D forces/ moments at all pen-hand contacts (Hooke et al. 2008). The purpose of this study was to investigate central nervous system strategies for controlling multi-finger forces in 3D space during a writing task. This study specifically investigates the synergistic actions of finger forces in three orthogonal dimensions (i.e., radial, tangential, and vertical) for circle drawing. Four hypotheses were tested: 1) Kinetic synergies between the pen-hand contact forces exist in all three dimensions. 2) The radial and tangential components yield stronger synergies than the vertical component. 3) Synergies exist in both CW and CCW directions and the synergy strengths do not differ between them. 4) The self-pacing yields stronger synergies than the external pacing.

METHODS

Twenty-four subjects drew 30 discrete concentric circles using Kinetic Pen (Fig. 1) for each experimental condition, which included two directions (clockwise, CW vs. counter-clockwise, CCW) and two pacing (self-paced vs. external-paced). For the external-paced condition, subjects drew circles while following metronome beeps. The 3D contact forces and moments of force between the hand and the pen were calculated from recordings of the miniature 3D force/moment sensors (Nano-17, ATI) embedded in the barrel of the pen (Hooke et al, 2008). The pen-hand contacts included thumb, index finger, middle finger, and webbing between thumb and index finger.

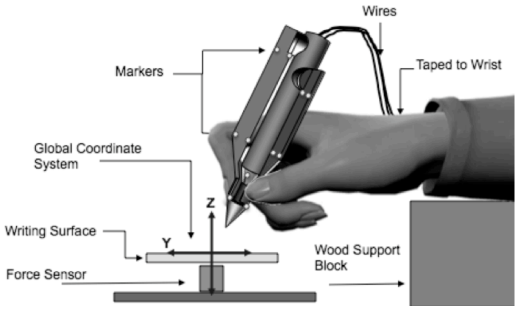

Figure 1: Schematic of experimental setting showing a subject holding the Kinetic Pen with reflective markers attached.

The 3D position of the pen was recorded using a Vicon motion capture system. The 3D position/orientation of the pen was used to transform the local sensor refrence frames into the global reference frame. Uncontrolled Manifold Analysis (Scholz & Schöner 1999; Shim et al. 2008) was used to quantify the index of kinetic synergy, $\Delta V(t)$ (Shim et al. 2008) in three orthogonal dimensions: a *radial* component that dictates the pen's motion from the circle edge towards its center, a *tangential* component that dictates the pen's motion tangent to the curvature of the circle, and *vertical* component that dictates the pen's motion perpendicular the writing surface. The total variance [$V_{TOT}(t)$] of four-dimensional (i.e., index, middle, ring, and web) space across the circles was resolved into two components. The vectors F(t) were broken into their projection on, and orthogonal to, the null space (UCM) of Eq. 1. The variance within the UCM per degree of freedom [$V_{UCM}(t)$] was calculated. This component of total variance causes no change in the kinematics of the pen. The variance orthogonal to the UCM [$V_{ORTH}(t)$] was also calculated. This component causes change in the kinematics of the pen from the average kinematics (i.e., kinematic errors). Note that $V_{UCM}(t)$ and $V_{ORTH}(t)$ represent CNS abilities to utilize the redundant degrees-of-freedom and to reduce kinematic errors. ΔV(t), the index of synergistic action between pen-hand contact forces was calculated (Eq. 2).

$$[U]\begin{bmatrix}\vec{F}(t)_{thumb}\\ \vec{F}(t)_{index}\\ \vec{F}(t)_{middle}\\ \vec{F}(t)_{web}\end{bmatrix}=\left[m\vec{a}(t)_{COM}-\vec{F}(t)_{tip}\right] \qquad \text{Eq. 1}$$

$$\Delta V(t)=\left(\frac{V_{UCM}(t)}{3}-\frac{V_{ORT}(t)}{1}\right)\Big/\left(\frac{V_{UCM}(t)+V_{ORT}(t)}{4}\right) \qquad \text{Eq. 2}$$

RESULTS AND DISCUSSION

Kinetic synergies existed across all three dimensions and were significantly stronger in the radial and tangential components than vertical component (Fig 2). This suggests that the CNS utilizes kinetic synergies that are not only task dependent but also able to prioritize components within a task to optimize the handwriting performance. The kinetic synergies of radial and tangential forces were much stronger than those found during simple grasping tasks used in previous studies. This may have been caused by the high precision of the manual dexterity necessary to write words, where errors on the scale of millimeters can render script illegible. It is also to be noted that high kinetic synergy existed also in vertical component (ΔV>0) although precise control of vertical forces is not required for the optimally drawn shape of circles. The findings were supported by the repeated-measures ANOVA on time-averaged ΔV, which showed significant ($p<.05$) effects of Direction, Component, Direction x Component, Direction x Component x Pace.

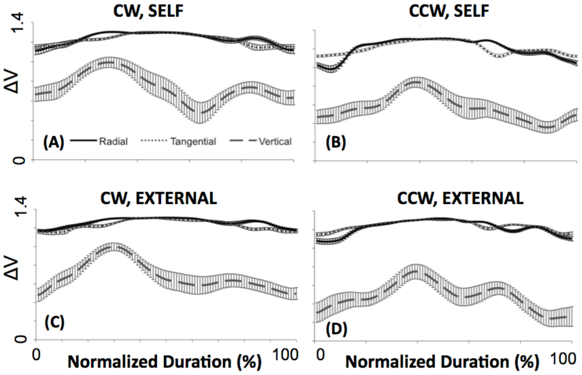

Figure 2: Synergy strength, measured by ΔV, for radial, tangential, and vertical force components.

SUMMARY/CONCLUSIONS

The results of this study suggest that the CNS controls pen-hand contact forces synergistically during handwriting so that the pen's kinematic outputs can be consistent for circle drawing tasks. The kinetic synergy is stronger for the force components, radial and tangential, which are critical for shaping the desired kinematic handwriting outputs, although vertical force component also showed synergistic actions of pen-hand contact forces.

REFERENCES

Hooke AW & Shim JK (2008) *J Biomch* **41**: 2060-2064.

Scholz & Schöner (1999) *Exp Brain Res* **126**: 289-306.

Shim JK, et al. (2005) *J Neurophysiol.* **93**: 3649-3658.

Shim JK, et al. (2008) Motor Control **12**: 311-329.

AN ANALYTICAL APPROACH TO EVALUATING UNCEMENTED TOTAL HIP REPLACEMENT INTRAOPERATIVE PROXIMAL FEMUR FRACTURE RISK

[1]Walter Schmidt, [1]William Shields, [1]James Fuchs, [1]Joseph Racanelli and [1]Aiguo Wang
[1]Stryker Orthopaedics, Mahwah, NJ
email: walter.schmidt@stryker.com, web: www.stryker.com

INTRODUCTION

Intraoperative proximal femoral fracture during uncemented femoral stem insertion is a recognized complication during primary total hip arthroplasty, with published fracture rates reported as high as 20% [1] in clinical studies.

Uncemented, proximally filling, porous-coated femoral components, along with associated reamers and broaches, must be designed with both an optimized level of press-fit and with sufficient manufacturing precision. An optimized press-fit level ensures adequate stem support for short-term stability, promotes bone in-growth in the short to medium term, and minimizes stem subsidence in the long term. Manufacturing tolerances which are overly generous can lead to an inconsistent stem seating depth. If the stem appears proud under a typical stem insertion sequence, there may be a temptation to drive the stem deeper into the bone with additional mallet blows risking femoral fracture. If too little force is exerted in driving the stem to its ideal seating depth, it may be an indicator of a lack of press-fit and stem subsidence in the long term.

In this study, an analytical approach to assess intraoperative femoral fracture risk of uncemented THR design concepts (prior to implant approval and use) is proposed.

METHODS

Finite element models of a predicate device and three design concepts, used in conjunction with a numerically identical proximal femur model, were generated using the following protocol:

Femoral Stem Modeling: 3D CAD models of a predicate device (Secur-Fit™ Plus HA Cementless Hip Stem, Stryker Orthopaedics) and 3 design concepts (referred to hereafter as design concepts A, B, and C) were developed. A consistent, midrange stem size was selected for all design evaluations.

Proximal Femoral Bone Modeling: An individual CT scan was selected from a CT scan database whose left proximal femur accommodated the femoral stem size being investigated. The CT scan was generated using a 1.0mm slice thickness. Both outer cortical and cortical-to-cancellous bone boundaries were segmented out of the CT scan, exported as STL files, and converted to IGES files. Next, a CAD assembly model containing component models of the cortical and cancellous bone, surgical reamer and broach was prepared. Virtual surgery was then performed to prepare the bone as per surgical protocol. The assembly model generation and virtual surgery steps are repeated for each design concept utilizing mathematical duplicates of the bone model. A reference FEM model of the intact, proximal third of the proximal femur was also exported. Each finite element within the cancellous bone of the reference model was mapped with unique elastic modulus properties [2], while the cortical bone was mapped with a uniform elastic modulus of 12GPa [3]. Refer to Figure 1.

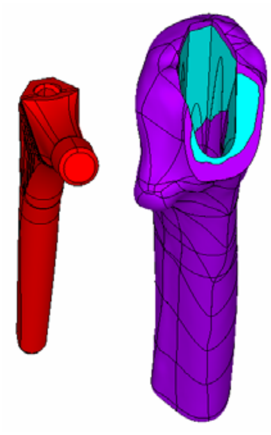

Figure 1:
Predicate CAD Model

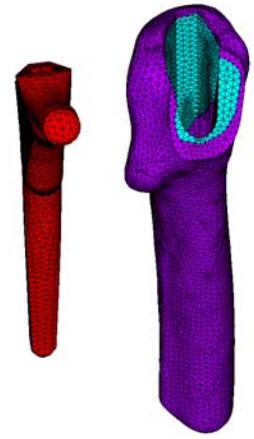

Figure 2:
Predicate FEA Model

Femoral Stem Finite Element Model Generation: A finite element model of each femoral stem was generated within ANSYS v11 (ANSYS Inc, Canonsburg, PA) with a variable mesh size varying from 0.5 to 2.5mm. Material properties pertaining to each stem was supplied.

Resected Proximal Femur Finite Element Model Generation: A finite element model for the resected, proximal third of four numerically identical femura, each prepared per the surgical protocol of each associated stem, was also generated within ANSYS v11. A variable mesh size from 1 to 5mm was utilized. Bone material properties, using the material properties from the intact reference model, were mapped onto the resected bone model. Refer to Figure 2.

Analysis Sequence: Each stem was seated into the bone from a 1mm proud to 1mm recessed position in 0.5mm displacement increments.

RESULTS

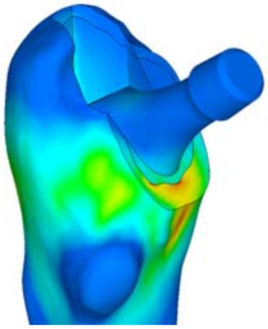

Figure 3: Predicate Model Hoop Strain

The cortical bone maximum circumferential (hoop) strains (Figures 3 & 4) and insertion force necessary to generate the imposed displacement (Figure 4) were extracted and plotted for each insertion step.

The cortical bone maximum circumferential (hoop) strains (Figures 3 & 4) and insertion force necessary to generate the imposed displacement (Figure 4) were extracted and plotted for each insertion step.

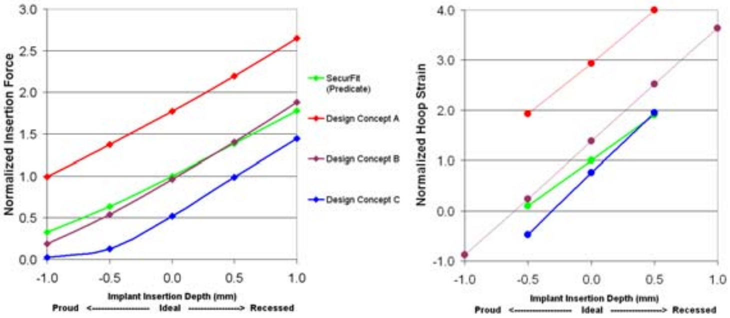

Figure 4: Normalized Insertion Force & Hoop Strain as a Function of Insertion Depth

A qualitative ranking of the design concepts and predicate device was generated and subsequently validated by independent evaluations using physical sawbones [4] and cadaveric testing [5], preparing the bone test/cadaveric samples per the equivalent surgical protocol.

DISCUSSION

An analytical method for comparing cortical bone hoop strains and implant insertion forces between proposed uncemented femoral stem designs to a predicate device has been developed.

In this study, design concept B was the best match to the predicate from an insertion force perspective, while design concept C was the best match from a hoop strain perspective. The slope of the insertion force and hoop strain versus insertion depth curves provides additional insight as to the "level of forgiveness" of the design to over or under reaming.

This method is currently limited to providing a qualitative ranking due to the use of elastic material properties for the bone. As a result, this method tended to overestimate the ultimate strain and insertion force values, but from a qualitative perspective, predicted comparative behavior accurately, as validated by sawbones and cadaveric testing [4,5]. The addition of nonlinear bone material properties for a better quantitative evaluation represents the basis for future work.

Although this study was performed using nominal tolerances, it is recommended to perform additional comparative evaluations using MMC (maximum material condition) and LMC (least material condition) tolerance conditions.

REFERENCES

1. Jasty MJ, et al. *JOA*, **8**, No 5, 479-487, 1993.
2. Rho JY, et al. *Med Eng Phys*, **17**, No 5, 347-355, 1995.
3. Evans FG, *Mechanical Properties of Bone*, Charles C Thomas Publisher, Springfield, IL, 107-108, 1973.
4. Fuchs J, et al. *Impact Load Test Model for Femoral Press-Fit Design Optimization in Uncemented THA*, presented at the 55th Annual Meeting of the ORS (2009).
5. Shields W, et al. *The Strengths and Weaknesses of a Cadaveric Model for Femoral Press-fit Design Optimization in Uncemented THA*, presented at the 55th Annual Meeting of the ORS (2009).

Temporal and frequency characteristics of trunk and hip muscle activity patterns in early walkers with and without cerebral palsy.

[1]Laura Prosser, [2,3]Samuel Lee, [1]Mary Barbe, [1]Ann VanSant and [1,3]Richard Lauer
[1]Physical Therapy, Temple University; [2]Physical Therapy, University of Delaware; [3]Research Department, Shriners Hospital for Children
email: lprosser@temple.edu

INTRODUCTION

Cerebral palsy (CP) is the most common neuromuscular disorder in children, with a high economic cost and negative impact on quality of life. Poor control of postural muscles is often considered a primary impairment in CP, which causes compensation by other muscles to assist in maintaining upright posture, and thus limiting those muscles from functioning effectively as primary movers of the extremities. Information on how the trunk and gluteal muscles function during walking will assist in understanding their role to maintain upright posture during walking and facilitate the development of interventions to address deficits in their function.

The objective of this project was to investigate differences in trunk and hip muscle activation patterns during the early stages of walking in children with spastic CP compared to children with typical development (TD).

METHODS

Participants. Thirty-one children (15 CP, 16 TD) were included in this study. All participants had 0.5-60 months of walking experience, with an average of 28.5±18.1 months in both groups. The children with CP also had a GMFCS level of II or III.[1] All procedures were approved by the Temple University Hospital IRB. Parental consent was obtained prior to participation and assent was obtained from participants 7 years of age or older.

Procedures. Surface electromyographic (EMG) data were acquired bilaterally from the trapezius, erector spinae, rectus abdominus, external oblique, gluteus maximus and gluteus medius (Myomonitor III, Delsys Inc., Boston, MA). EMG data were collected at 1200 Hz, preamplified, and bandpass filtered from 20-450 Hz. Children walked barefoot down an instrumented walkway (GAITRite®, CIR Systems,

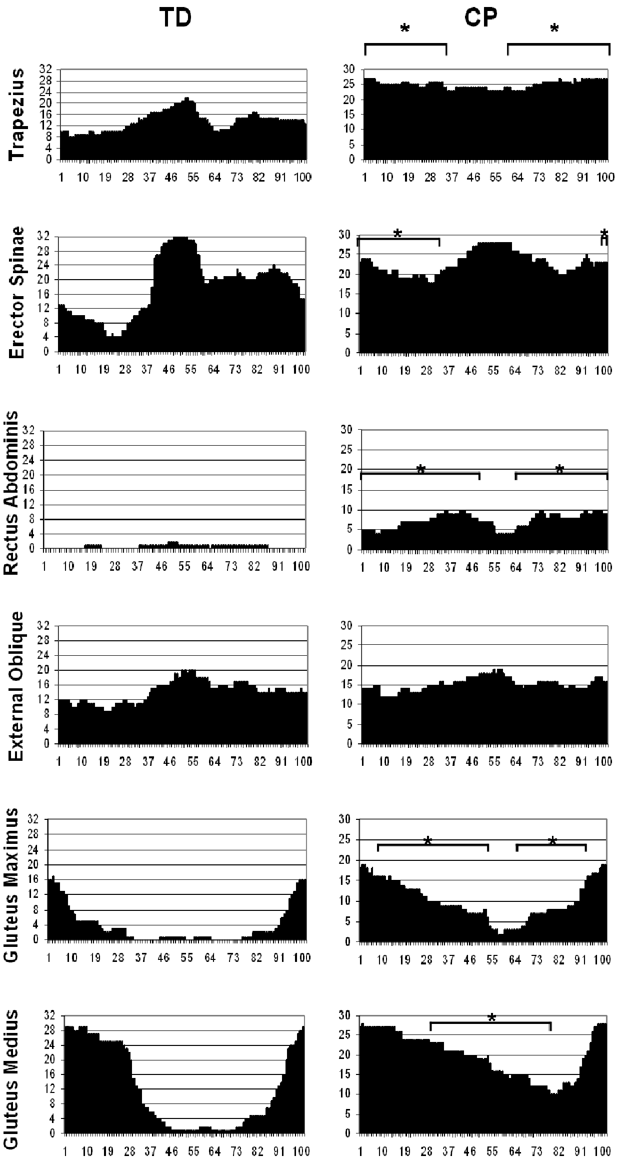

Figure 1: Histograms for number of children with muscle activity at each point in gait cycle in TD and CP groups. Left and right sides were counted individually. Asterisks (*) indicate periods of activity where the CP group has significantly more children with muscle activation than the TD group.

Havertown, PA) at a self-selected pace to collect time-synchronized footfall data used to identify initial foot contact.

Data analysis. Ten gait cycles (5 left, 5 right) were selected for analysis. EMG data were processed using custom-written programs in MATLAB (The Mathworks Inc., Natick, MA). All signals were normalized to 1000 points, representing the gait cycle from 0 to 100% in 0.1% increments. The timing of muscle activity onset was determined in reference to a static baseline using the Teager-Kaiser Energy (TKE) operator.[2] The number of children in each group who had activity in the muscle at each point in the gait cycle was determined. The chi square test, χ^2, was performed at each point in the gait cycle to determine if significant differences ($p<0.05$) existed between groups in the number of children who had activity in the particular muscle.

Additionally, a time-frequency pattern for each muscle was generated using the continuous wavelet transform.[3] A functional principal component analysis (PCA) was used to identify variability in the instantaneous mean frequency (IMNF) curves between the groups. The four PCA output weights were tested using a Welch statistic to determine if the differences existed between the groups.

RESULTS AND DISCUSSION

The CP group had significantly more children with activation than the TD group for all muscles except the external oblique. Locations of differing activity during the gait cycle are indicated by asterisks in Figure 1.

The CP group also had higher mean frequency throughout the gait cycle for all muscles (Figure 2). Higher IMNF can result from increased rates of motor unit firing, increased number of recruited motor units, or decreased synchrony of motor units [4], and may contribute to muscle fatigue in children with CP.[5] Limitations of the study include the use of an assistive device by some children in the CP group, and the potential influence of recording activity from adjacent deep trunk muscles.

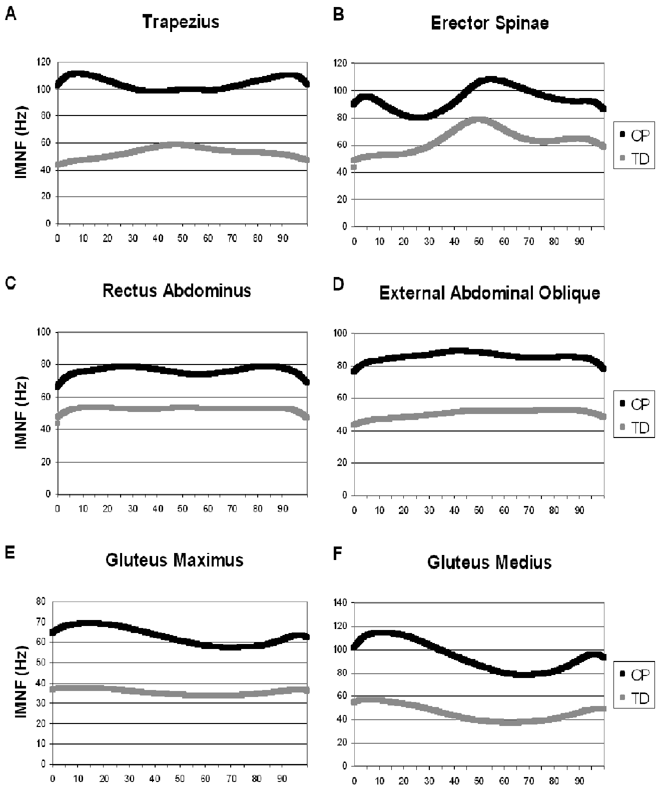

Figure 2. IMNF curves in CP and TD groups. All muscles were significantly different between groups for each principal component (p<0.000). The four PCA harmonics accounted for over 97% of the variability for each muscle.

CONCLUSIONS

Children with spastic CP demonstrate greater activity in the trunk and hip muscles than children with TD. Postural muscle training during the early stages of walking in CP should be investigated to encourage the development of more functional and efficient movement strategies in these children.

REFERENCES

1. Palisano R, et al. *Dev Med Child Neurol* **39**, 214-223, 1997.
2. Li X, et al. *Ann Biomed Eng* **35**, 1532-1538, 2007.
3. Lauer RT, et al. *Gait Posture* **26**, 420-427, 2007.
4. Hermens HJ, et al. *J Electromyogr Kinesiol* **2**, 15-25, 1992.
5. Lam WK, et al. *Gait Posture* **22**, 189-197, 2005.

ACKNOWLEDGEMENTS

This study was funded by the American Physical Therapy Association Section on Pediatrics, and NINDS R03NS048875.

STUDY OF MUSCLE TORQUE SHARING PATTERNS IN ISOMETRIC PLANTAR FLEXION BY AN EMG-DRIVEN BIOMECHANICAL MODEL

[1] Liliam F. Oliveira, [2] Luciano L. Menegaldo
[1]Physical Education and Sports school, Federal University of Rio de Janeiro
[2]Military Institute of Engineering, Rio de Janeiro
e-mail: liliam@eefd.ufrj.br, lmeneg@ime.eb.br

INTRODUCTION

Skeletal muscles are usually simulated with mechanical models for estimating the force produced by individual muscles in different motor tasks [1,2]. Although it is usual to discuss motor control strategies based on EMG recordings, a coherent relationship between neuromuscular activation and its respective biomechanical effect must be sought. The aim of this study was comparing the excitation from EMG and individual muscle force patterns in isometric plantar flexions. A modified version of the classical Zajac contraction dynamics model (Figure 1) was used to find forces from the excitations.

METHODS

A group of 13 male subjects laid prone on a Norm/Cybex™ Dynamometer, with the knee extended and the ankle at neutral (90°) position. The protocol consisted of two steps of submaximal loads of 20% (low) and 60% (medium/high) MVC, separated by 10 seconds of relaxing time. A feedback display of actual force output was provided to the subject. Torque signal and surface EMG from *gastrocnemius medialis* (**gm**), *gastrocnemius lateralis* (**gl**), *soleus* (**sol**) and *tibialis anterior* (**ta**) muscles were synchronously collected. Raw EMG signal initially band-pass filtered (15 – 350 Hz), rectified and low-pass filtered with a 2th order Butterworth filter (2Hz cut-off frequency). Input excitation signal u(t) for the muscle model (Figure 1) was found by normalizing the processed step EMG with MCV EMG. The torque output was found by the sum of each simulated muscle force multiplied by its respective ankle angle moment arm, using polynomial regression equations [3]. The difference between simulated and dynamometer measured torque was calculated as the mean square error between the two curves and expressed relative to the maximal measured torque (%RMSE). Man-Whitney test was applied to assess significant changes of the muscle individual estimated torque and excitation function between the two intensities levels. Significant difference was set as a p value of 0.05.

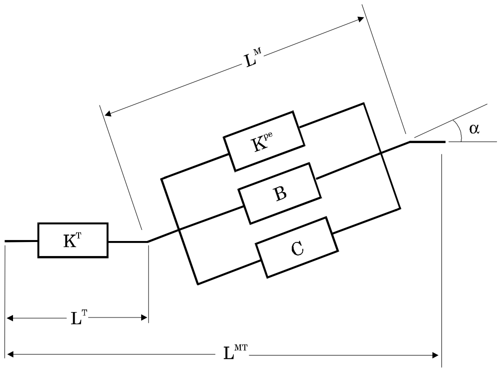

Figure 1: Adimensional Zajac model [5] with added parallel elastic and damping elements .

K^T = stiffness of the tendon
K^{pe} = stiffness of the parallel elastic element
B = damping element
C = contractile element
L^T = length of the tendon
L^M = length of the contractile element
L^{MT} = length of muscle-tendon complex
α = penation angle

RESULTS AND DISCUSSION

The %RMSE was significantly higher for the low intensity level (23.0 ± 10.8%) compared to the medium/high (18.1 ± 11.1 %), showing that the model is less accurate for low contractions. A typical result of the individual muscle torques, total torque and dynamometer-measured torques are shown in Figure 2. From Table 1 the torques generated by each muscle revealed greater contribution of the **sol** muscle followed by the **gm**, similarly for both effort intensities. The **gl** contributed less, although showing a significant increase from the low to the medium/high excitation u(t). Very little co-contraction from **ta** observed. As expected, all muscle activation levels significantly increased to overcome the medium effort, with different rates. However, for the low intensity step, the contribution of **sol** and **gm** were similar, while **gl** contributed significantly less. To attend the torque demands at the medium effort step, **gl** neural contribution increased approximately four times, while the relative participation of both **sol** and **gm** increased approximately twice. Apparently, for this particular task, by increasing the effort level, the SNC keeps a more or less similar torque sharing contribution from each muscle, by changing the relative input contribution from each one.

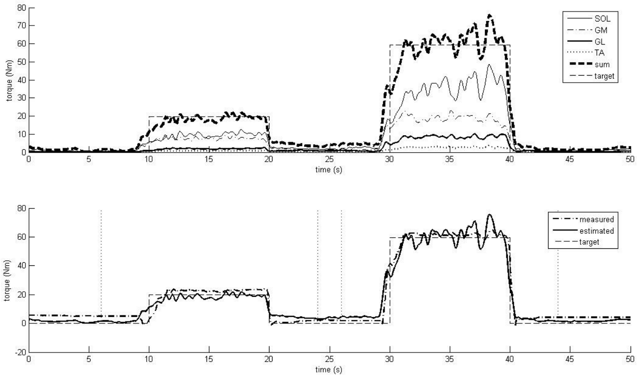

Figure 2: Torque contribution curves from each muscle and total torque, showing also the test protocol (above), for one example subject. Total torque generated by the model and measured by dynamometer (below). The thin dotted vertical lines represents the time limits (before and after the 20% and 60% MVC.

REFERENCES

1. Piazza S.J., Delp S.L.,The influence of muscles on knee flexion during the swing phase of gait. *Journal of Biomechanics,* 29, 723-733, 1996.
2. Manal K., Buchanan T.S., One-parameter neural activation to muscle actication model: estimating isometric joint moments from electromyograms. *Journal of Biomechanics,* 36, 1197-1202, 2003.
3. Menegaldo L.L., Fleury, A. T. Weber H. I., Moment Arms and Musculotendon Lengths Estimation for a three-dimensional Lower-limb Model, *Journal of Biomechanics,* Vol. 37, pp.1447-1453, 2004.
4. Zajac, F.E., Muscle and Tendon: properties, Models, Scaling and Application to Biomechanics and Motor Control, *CRC Critical Reviews in Biomedical Engineering*, Vol.17, No.4, pp. 359-411, 1989.

ACKNOWLEDGEMENTS

The authors are gratefully acknowledged to CAPES Foundation of the Brazilian Education Ministry, and to the Physical Education School of the Brazilian Army, Rio de Janeiro.

Table 1 . Mean ± stand deviation of the normalized excitation function u(t) and relative individual torque contribution to the final torque estimation M(t), for low (20%MVC) and medium/high (60%MVC) contraction intensities. * p<0.05 between contraction intensities.

	Intensity	**SOL**	**GM**	**GL**	**TA**
u(t)	**low**	8.73 ± 2.98%	11.29 ± 3.53%	5.71 ± 2.93%	1.20 ± 0.62%
	medium	23.37± 6.48% *	27.76 ± 6.77% *	22.73 ± 7.04 % *	3.60 ± 1.40% *
M(t)	**low**	58.17 ± 12.40%	35.43 ± 10.36%	8.63 ± 4.04%	2.24 ± 0.96%
	medium	57.14 ± 7.10%	32.07 ± 5.84%	13.62 ± 2.36 % *	2.83 ± 1.23%

AUTOMATIC DETECTION OF SLIP-INDUCED BACKWARD FALLS

[1]Jian Liu and [2]Thurmon E. Lockhart
[1]Department of Health and Human Performance, University of Houston, [2]Department of Industrial and Systems Engineering, Virginia Tech
email: jliu30@uh.edu, web: http://hhp.uh.edu/

INTRODUCTION

Falls are the leading cause of injury deaths among people 65 years and older. The National Safety Council reported that in 2005, 17,700 Americans met their death by falling, and of these deaths, the majority (over 80%) were people over 65 years of age [1]. It is certainly desirable to avoid the fall accidents altogether through developing a comprehensive fall prevention program [2]. However, in case of unavoidable falls, an effective injury-prevention technology is critical to minimize/reduce fall-related physical injuries. Recently, the concept of wearable airbag [3] emerged as one viable and promising injury-prevention approach.

Being able to detect fall events unambiguously and reliably is the key for the practical implementation of wearable airbag technology. Consequently, fall event detection has attracted several research attentions since early 2000s [4-7]. Despite the continuous efforts, existing fall detection technology still requires much research. First of all, previous fall detection methods have been exclusively evaluated with falling from a static posture (i.e., standing). It is unknown whether and to what extent these methods can be applied to more realistic scenarios (i.e., falls during dynamic movement). Second, previous methods have been tested with the younger adults only. Considering the age-related motion feature differences, fall detection performance evaluation has to involve the elderly who are the most likely users for this type of technology. To address these two issues, it is desirable to develop and evaluate the fall detection methods with the elderly during walking.

Therefore, the purpose of this study was to evaluate a novel fall detection algorithm in differentiating slip-induced backward falls from activities of daily living (ADLs). It was hypothesized that the new algorithm would have better performance than the existing algorithm [7] in terms of higher specificity and sensitivity.

METHODS

Participants. Ten elderly participants (> 65 years old) were recruited from the local community for this study. Their anthropometric information was summarized as: age (mean = 75 years, SD = 6.0 years), weight (mean = 74.1 kg, SD = 9.1 kg), height (mean = 1.74 m, SD = 0.08 m). They were required to be in generally good physical health. Informed Consent (Virginia Tech IRB #07-628) was approved by the IRB committee at Virginia Tech and obtained from the participants prior to any data collection.

Apparatus and Procedures. A detailed description of the experiment protocol for normal walking and slip-induced backward falls has been published previously [8]. Briefly, participants were instructed to walk at a normal pace on a linear walkway with the protection of an overhead harness system. Unexpected slips were induced by changing the dry floor surface into slippery surface (covered with 3:1 KY-Jelly and water mixture) without participants' awareness. One inertial measurement unit (IMU, Inertia-Link, MicroStrain Inc., USA) was placed close to the sternum. This IMU is capable of measuring 3D orientation, 3D acceleration, and 3D angular velocity at a sampling rate of 100Hz. The slippery surface was introduced repeatedly until three slip perturbation trials were obtained from each participant. After each trial with the slippery surface, participants were encouraged to walk continuously as normal as possible at a normal pace for 5 to 10 minutes before the next slippery trial. The participants had no knowledge regarding the exact timing of the floor surface change.

Each participant was instructed to perform the 5 types of daily activities according to randomized sequence. The activities include lying down on a bed, bending over to pick up an object from the ground, sitting down on a regular chair, sitting down into a rocking chair, and sitting into a bucket seat. At the beginning and the end of each trial, they were required to maintain the static posture for 1 second. All the timing information was provided to the participants via auditory cues by the experimenter.

Fall event detection. All of the participants were randomly assigned into two groups. The data from the first group (4 participants) were used as the training dataset to construct the new detection algorithm. The data from the second group (6 participants) were used as the validation dataset to validate the performance of the new algorithm. The quadratic form of discriminant analysis was performed on the training dataset in order to derive the discriminant function, *F(a,w)*. The optimal detection threshold was determined based on the relationship between detection thresholds and sensitivity/specificity. The baseline algorithm was formulated based on the literature [7]. The associated discriminate function, *F(w)*, took the threshold as 130°/s. Receiver Operating Characteristic (ROC) curves [9] were used to quantify the overall discrimination performance of the new algorithm and the baseline algorithm. Sensitivity and specificity associated with the specific detection thresholds were computed. Discriminant function and ROC curves were constructed in MATLAB (MathWorks, USA).

RESULTS

Training dataset includes 69 ADL trials and 6 slip-induced fall trials. The discriminant function for the new algorithm is shown below:

$$F(\alpha,\omega) = -0.5251 + \begin{pmatrix}\alpha\\ \omega\end{pmatrix} \cdot \begin{pmatrix}-0.0586\\ -0.0070\end{pmatrix} + \begin{pmatrix}\alpha\\ \omega\end{pmatrix} \cdot \begin{pmatrix}0.0246 & -0.0010\\ -0.0010 & -0.0004\end{pmatrix} \cdot \begin{pmatrix}\alpha\\ \omega\end{pmatrix}^{-1}$$

where a specific data trial was detected as fall if *F(a,w)* < -4.994.

The validation dataset including 105 ADL trials and 7 slip-induced fall trials was processed by the new algorithm and the baseline algorithm. The overall discrimination performance was illustrated in Figure 1. The performance of the new algorithm (AUC = 1.0) was slightly higher than the baseline algorithm (AUC = 0.9743). With the specific detection thresholds, the new algorithm achieved higher sensitivity (100% vs. 85.71%) and higher specificity (95% vs. 90%) compared to the baseline algorithm.

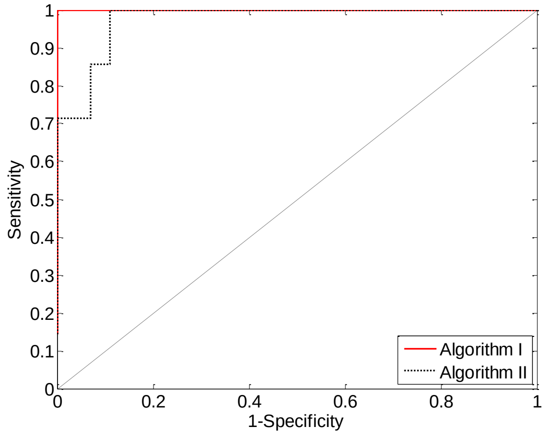

Figure 1 – ROC curves of new algorithm (I) and baseline algorithm (II)

DISCUSSIONS

(Due to space limitation, discussions will be presented in full paper.)

REFERENCES

1 **National Safety Council, *Report on Injuries in America (Unintentional death)*. 2006.**

2 **Bell, J.L., et al., *Evaluation of a comprehensive slip, trip and fall prevention programme for hospital employees.* Ergonomics, 2008. 51(12): p. 1906-25.**

3 **Fukaya, K. and M. Uchida, *Protection against impact with the ground using wearable airbags.* Industrial Health, 2008. 46(1): p. 59-65.**

4 **Lindemann, U., et al., *Evaluation of a fall detector based on accelerometers: a pilot study.* Medical & Biological Engineering & Computing, 2005. 43(5): p. 548-551.**

5 **Karantonis, D.M., et al., *Implementation of a real-time human movement classifier using a triaxial accelerometer for ambulatory monitoring.* Ieee Transactions on Information Technology in Biomedicine, 2006. 10(1): p. 156-167.**

6 **Bourke, A.K., J.V. O'Brien, and G.M. Lyons, *Evaluation of a threshold-based tri-axial accelerometer fall detection algorithm.* Gait & Posture, 2007. 26(2): p. 194-199.**

7 **Nyan, M.N., et al., *Distinguishing fall activities from normal activities by angular rate characteristics and high-speed camera characterization.* Medical Engineering & Physics, 2006. 28(8): p. 842-849.**

8 **Liu, J. and T.E. Lockhart. *Aging effect on joint moment generation strategy in successful reactive-recovery from unexpected slips*. in *Human Factors and Ergonomics Society 49th Annual Meeting*. 2005. Orlando, FL.**

9 **Zweig, M.H. and G. Campbell, *Receiver Operating Characteristic (Roc) Plots - a Fundamental Evaluation Tool in Clinical Medicine (Vol 39, Pg 561, 1993).* Clinical Chemistry, 1993. 39(8): p. 1589-1589.**

THE EFFECT OF LUMBOPELVIC POSTURE ON PELVIC FLOOR MUSCLE ACTIVATION AND INTRAVAGINAL PRESSURE GENERATION IN CONTINENT WOMEN

Angela C Capson, Joseph Nashed, Linda McLean
School of Rehabilitation Therapy, Queen's University
email: mcleanl@queensu.ca

INTRODUCTION

This study was undertaken to determine the effect of changing standing lumbopelvic posture on pelvic floor muscle (PFM) activity and resultant intravaginal pressure.

Recruitment of the PFMs is essential in stabilizing the urethra and enhancing urethral closure to maintain continence and in supporting the pelvic organs. It is also believed that the PFMs play an important role in spinal stabilization during postural perturbations and may enhance the stability of the sacroiliac (SI) joints by generating stiffness of the joint through force closure [1,2]. Because of their synergy with the abdominal muscles and their attachments to the lumbopelvic structures, dysfunction of the PFMs may increase the likelihood of lumbopelvic injury by impairing spinal and pelvic stability mechanisms during postural tasks that require spinal stiffness.

It has recently been suggested that lumbopelvic posture may influence the ability of the PFMs to contract effectively [3]. The PFMs have anatomical connections on the pelvis and coccyx, and PFM fibres cross the SI joints, making them susceptible to stretch or shortening during changes in lumbopelvic posture. Accordingly the length-tension relationship of the PFMs may be affected by postural adjustments. The aim of this study was to determine whether postural changes (1) induce differences in the contractile activity of the PFMs in response to postural or other perturbations, and (2) result in differences in vaginal closure force produced by the PFM contraction.

METHODS

Nulliparous, continent women between the ages of 22 and 40 years were recruited and provided written informed consent. Each participant performed two sets of five tasks (quiet standing, maximal effort cough, Valsalva maneuver, maximum voluntary contraction (MVC) of the PFMs, and a standardized load-catching task) in three different standing postures (normal lumbopelvic posture, hyperlordosis, and hypolordosis). During the first set, electromyographic activity was recorded from the PFMs bilaterally using a Periform^{TM} vaginal probe coupled to Delsys^{TM} D.E.2.1 electrodes and Bagnoli-8 EMG amplifiers. During the second set, intravaginal pressure was recorded using a Peritron^{TM} perineometer. During both sets, pelvic angle was recorded simultaneously with EMG or intravaginal pressure using an Optotrak^{TM} 3D motion analysis system to ensure that subjects maintained the required posture throughout the three trials of each task.

All data were filtered using a moving 200ms RMS window with 199ms overlap, and peak values were determined for each trial and each task after removing baseline activation levels. One-way repeated measures analyses of variance (ANOVAs) were performed on the peak PFM EMG and intravaginal pressure amplitudes to determine the effect of posture. One way ANOVAs were also performed on the lumbopelvic angles to ensure that the three postures were significantly different during all tasks.

RESULTS AND DISCUSSION

Sixteen women participated, with mean age 27.1 (5.48) years and mean body mass index 22.8 (1.57) kg/m^2. The women were generally active, the majority reporting 5-10 hours of physical activity performed per week. None of the women had signs or symptoms of incontinence.

There was significantly higher resting PFM activity in the hypolordosis as compared to the normal and hyperlordotic postures. During the MVC (Figure

1), coughing, Valsalva, and load-catching tasks, subjects generated significantly more PFM EMG activity when in their normal posture than when in hyper- or hypolordotic postures ($p<0.05$ in all cases). Conversely, higher peak intra-vaginal pressures were generated in the hypolordotic posture for all tasks ($p<0.05$ in all cases). The lumbopelvic angles were significantly different between the three postures for all tasks ($p < 0.001$).

It is postulated that the contractility of the pelvic floor is affected by postural changes due to alterations in the length-tension relationship of the PFM fibres. Creating a hyper- or hypolordosis distorts the PFMs by changing the orientation their attachments to the sacrum, coccyx, pubic symphysis and ligamentous structures. An anterior pelvic tilt (hyperlordosis) is thought to cause a posterior rotation of the coccyx relative to the pubic bones and produce stretch on the PFMs, thereby lengthening the muscle fibres. A posterior pelvic tilt (hypolordosis) causes an anterior rotation of the coccyx and creates a shortening of the muscle fibres. Both of these distortions decrease the ability of the PFMs to generate maximum contractility.

Despite maximal PFM EMG activation in the neutral posture, this posture is not the ideal position for intra-vaginal pressure generation. It is hypothesized that higher pressures are produced in a hypolordotic position due to the orientation of the pelvic floor musculature relative to the vagina. In hypolordosis, the PFMs are oriented approximately parallel to the vaginal canal. Although the PFMs are not contracting as strongly in this position, intra-vaginal pressure may be maximized due to optimal closure pressure created whereby the vagina (and urethra) are effectively pinched closed between the pelvic floor and the pubic symphysis. In a normal or hyperlordotic posture, the PFMs are oriented obliquely relative to the vagina, creating lower resultant closure forces.

These results have important implications for individuals with urinary incontinence, as postural interventions may decrease urine leakage during increases in intra-abdominal pressure by utilizing positions of maximal squeeze pressures (ie hypolordosis). Conversely, deviations from normal standing postures may adversely affect spinal stability. Maximal PFM contractility will generate the greatest force closure at the sacroiliac (SI) joints and provide the strongest base for the abdominal cavity, through which intra-abdominal pressure and the resultant spinal stability are produced. This supports the idea that function is maximized and the risk of injury is minimized when tasks are performed in a neutral spine position [4].

CONCLUSIONS

The results of this study suggest that the contractility of the PFMs is dependent on lumbopelvic posture and that postural intervention may be an important adjunct therapy in the treatment of stress urinary incontinence in women. Conversely, postural changes (both anterior and posterior pelvic tilt) may impede the ability of the PFMs to generate maximum intra-abdominal pressure for spinal stability and maximum closure force at the sacroiliac joints.

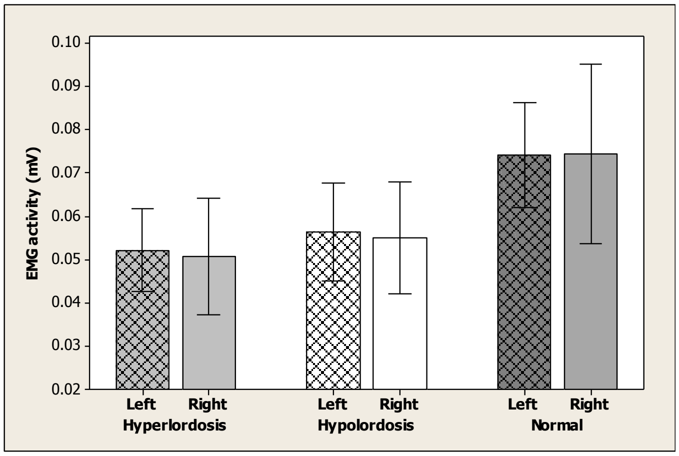

Figure 1: EMG activity of the PFMs during MVC.

REFERENCES

1. Smith MD, Coppieters MW, Hodges PW. *Int Urogynecol J*. **18**: 901-911, 2007.
2. Snijders, C.J., Vleeming, A., Stoeckart, R. *J Clin Biomech*. **8**:285–294, 1993.
3. Sapsford RR, Richardson CA, Maher CF, Hodges PW. *Arch Phys Med Rehabil*. **89**:1741-7, 2008.
4. Oxland TR, Panjabi MM. *J Biomech*. **25**(10):1165-1172, 1992.

EFFECTS OF SEATED WHOLE-BODY VIBRATION ON SPINAL STABILITY CONTROL: STIFFNESS & REFLEX

Gregory P. Slota[1,2], Michael L. Madigan[1]
[1]Kevin P. Granata Musculoskeletal Biomechanics Lab, Virginia Tech
[2]Biomechanics Lab, Kinesiology Dept, Penn State
email: GSlota@psu.edu, web: www.biomechanics.esm.vt.edu

INTRODUCTION

Whole-body vibration (WBV) is a risk factor for low back disorders, but the neuromuscular, biomechanical, and/or physiological mechanisms responsible for this increased risk are unclear. The neuromusculoskeletal system that contributes to the control of spinal stability can be thought of as three subsystems: passive tissue stiffness, active muscular stiffness, and neuromuscular reflexes [1]. The purpose of this study was to measure the effect of seated whole-body vibration on these subsystems. By understanding the changes in these subsystems of spinal stability control simultaneously, the results can elucidate the link between WBV and LBDs.

METHODS

Twenty healthy subjects (10 males, 10 females, age 24.8±6.2 years, height 171.5±8.8 cm, mass 69.0±10.6 kg) provided informed consent and completed two experimental sessions approved by the Virginia Tech Institutional Review Board. Both sessions involved exposure to a series of pseudorandom force perturbations to flex the trunk (Figure 1a) before and after an intervention. The intervention for one session involved exposure to seated WBV (2–20 Hz bandwidth and 1.15 m/s^2 root-mean-squared amplitude) for 30 minutes (Figure 1b). The intervention for the other session involved quiet sitting (QS) for 30 minutes.

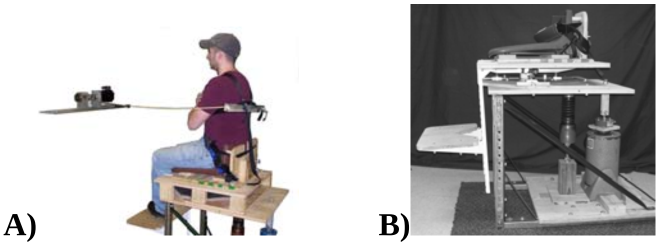

Figure 1: Experimental setup: A) Trunk perturbations, B) Vibration seat

During force perturbations, data was sampled from a torque cell measuring the force of the perturbations, a digital encoder on the motor monitoring displacement, and bilateral pairs of electrodes on the erector spinae (ES) and the rectus abdominus (RA) muscles. These data were used with system identification techniques to quantify total trunk stiffness, ES reflex delay and gain, and RA activity (to assess co-contraction involvement) [2]. A two-way repeated measures ANOVA was used to investigate the effect of time (before an after intervention) and intervention (WBV and QS) on trunk stiffness, muscle reflex gain and delay, and muscle co-contraction.

RESULTS and DISCUSSION

Exposure to 30 minutes of seated WBV decreased trunk stiffness by 12.5±15.4% (*P*=0.005, Figure 2a), did not affect RA activity (*P*=0.983, Figure 2b), decreased reflex gain by 11.5±26.6% (*P*=0.033, Figure 2c), and did not affect reflex delay (*P*=0.999, Figure 2d). Exposure to 30 minutes of QS resulted in no significant changes in measures of trunk stiffness (*P*=0.776), RA activity (*P*=0.112), reflex gain (*P*=0.596), or reflex delay (*P*=0.617).

The results of this study found that 30 minutes of WBV exposure reduced trunk stiffness and reflex gain, suggesting that spinal stability control was impaired. The measured reduction in total trunk stiffness incorporated the combined effects of passive stiffness, active stiffness, and reflexes. Active stiffness is controlled through co-contraction of the trunk muscles, and was monitored by the activity of the RA muscles which were unchanged with WBV exposure. This indicates that co-contraction (and therefore active stiffness) was not affected by WBV and did not contribute to the reduction in total trunk stiffness. Reflex gain decreased after both interventions, but was not significant within either WBV or QS. This indicates that a decrease in reflex gain did not contribute significantly to the decrease in total stiffness with WBV. These results also suggest that the decrease in trunk stiffness was due, at least in part, to a decrease in passive stiffness. The passive tissues, such as intervertebral discs and paraspinal ligamentous tissues, may have experienced creep deformation with WBV, which can result in reduced stiffness [1]. This leads to the conclusion that the decrease in total trunk stiffness with seated WBV was due to the combination of reduced passive stiffness (due to vibration) and reduced muscle reflexes (due to sitting).

Two possibilities that can explain the changes in muscle utilization in stabilizing the spine are muscular fatigue or changes in the sensory information used in feedback control. It has been shown that seated WBV can cause fatigue in muscles [3], however, the findings of the current study showed no significant changes to muscle reflex delay, a common effect of fatigue, which may suggest that the muscles were not fatigued. While there were no significant changes to muscle reflex delay, the gain of the muscle reflex response was reduced after WBV exposure. This is likely a result of changes in the sensory organs which elicit muscle reflexes becoming impaired with WBV exposure. Consistent with this, changes in the system of proprioception were used to explain an increase in maximum torso flexion angle in response to sudden loadings [4]. This result was coupled with the analysis that the position sense error of the torso increased 1.58 fold after 5 Hz WBV exposure. Disruption of the proprioceptive system can create errors is position, velocity, and force control and is attributed to changes in muscle reflex behavior.

CONCLUSIONS

In conclusion, 30 minutes of seated WBV reduced the stiffness of the trunk and decreased reflex gain without compensation from increased reflex gain or co-contraction recruitment. These effects can impair spinal stability and increase the risk of a low back injury. By understanding the effects of WBV on the subsystems of spinal stability control, this information can contribute to the development of interventions to help prevent LBDs.

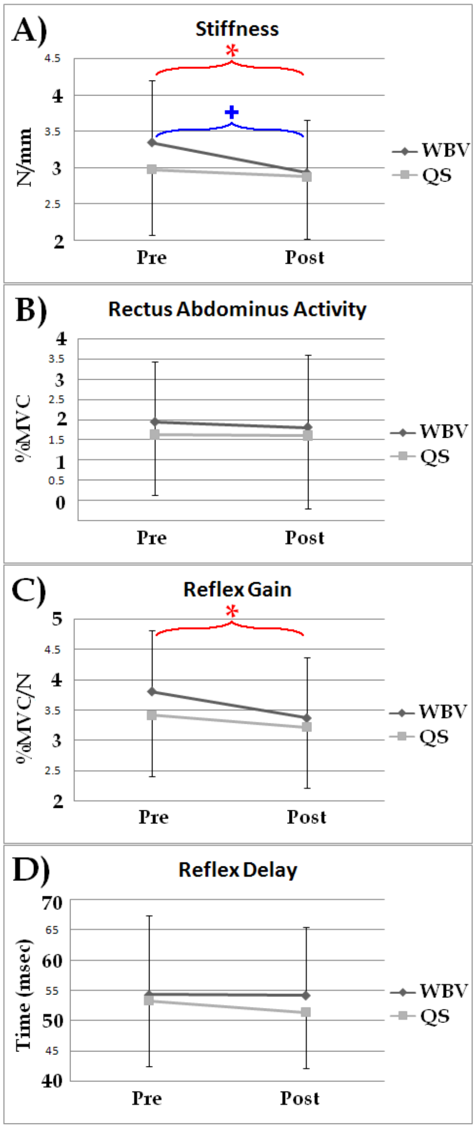

Figure 2: Results of the dependent measures with respect to exposure to WBV and quiet sitting for a) total trunk stiffness, b) RA activity, c) ES reflex gain, d) ES reflex delay. * indicates significant main effect of time ($P<0.05$); + indicates simple effect of WBV ($P<0.05$).

REFERENCES

1. Panjabi MM. *J Spinal Disord*, 5, 390-6, 1992.
2. Moorhouse KM. et al. *J Biomech*, 40, 1058-65, 2005
3. Wilder DG. et al. *Spine*, 21, 2628-39, 1996
4. Li, L. et al. *Int J of Ind Ergo*, 38,792-800, 2008

ACKNOWLEDGEMENTS

The project described was supported, in part, by Grant Number R01 AR046111 from the National Institute of Arthritis and Musculoskeletal and Skin Diseases.

MECHANICAL LOADING OF IN SITU CHONDROCYTES IN A LAPINE RETROPATELLAR CARTILAGE AFTER ANTERIOR CRUCIATE LIGAMENT TRANSECTION

[1,2] Sang Kuy Han, [2] Ruth Seerattan and [1,2]Walter Herzog
[1]Department of Mechanical & Manufacturing Engineering, University of Calgary, Canada,
[2]Human Performance Laboratory, University of Calgary, Canada
email: shan@ucalgary.ca, web: http://kin.ucalgary.ca/hpl/

INTRODUCTION

Early osteoarthritis (OA) changes the structural integrity of articular cartilage and results in softening, swelling, fibrillation and fissuring of the tissue [1]. These changes are thought to alter the mechanical environment of chondrocytes, thereby affecting chondrocyte mechanical response [2]. Although chondrocyte mechanics and biology have been studied in early OA, these studies were performed in isolated chondrocytes or for *in situ* cartilage preparations using histological analyses [3, 4]. Chondrocyte mechanics in OA tissue have not been measured in intact articular cartilage in real time. Therefore, the purpose of this study was to quantify chondrocyte mechanics in intact articular cartilage in healthy and early OA tissue.

METHODS

Patellar cartilage from twelve knees of 15 months old, skeletally mature female New Zealand white rabbits was used for chondrocyte mechanics analysis. Four knees were harvested nine weeks following Anterior Cruciate Ligament (ACL) transection, and the corresponding intact contralateral controls were harvested at the same time. Four additional knees were harvested from normal (ACL intact) rabbits. Retropatellar cartilages were grouped according to experimental (ACL-transected, n =4) and control (contralateral, n =4 and normal controls, n =4), and were harvested with the intact patellae. Fluorescein conjugated dextran (excitation: 488nm, emission: 500nm. Molecular Probes, OR, USA) was suspended in DMEM (Dulbecco's Modified Eagle's Medium, Gibco, OR, USA) at a concentration of 0.8 mg/ml (0.26 mM). The patella was incubated in the dextran solution for 4-8 hours at 4°C prior to fluorescent confocal imaging.

Two MPa surface pressure was applied to the mid region of the medial side of the retro-patellar cartilage using a round glass indentor (diameter = 2 mm) at an average speed of 6 μm/s. Once the desired pressure was reached, the indentor displacement was held constant for 20 min when a steady state was reached [4]. Optical sections were recorded at before and after loading using a spacing of 0.5 μm in the z (optical) direction. The indentation system based on confocal microscope was developed specifically for the purpose of quantifying chondrocyte mechano-biology in the intact cartilage and has been described in detail previously [5] (Figure 1).

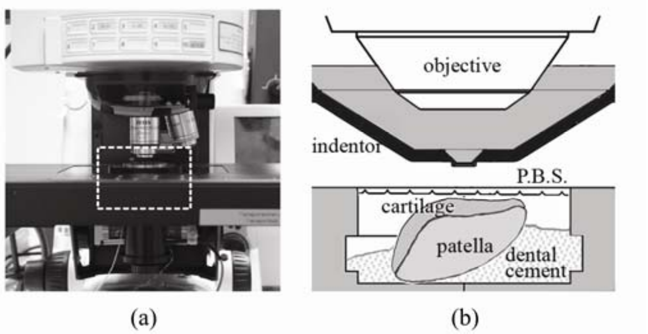

Figure 1: Custom-designed indentation system; (a) indentation system on confocal microscope, (b) schematic illustration for the area marked with the dashed line in (a).

Twelve cells from each patella (for a total of 48 cells each from experimental, contralateral and normal joints) were used for cell morphology analysis. Cells were located in the superficial zone of the rabbit retropatellar cartilage between the articular surface and 40μm depth. Cell widths and depths were defined along the major and minor axis of the cross section taken perpendicular to the cell height, respectively.

After indentation testing, retropatellar cartilages in all three groups were assessed by histological analysis and graded according to the Mankin scoring system.

RESULTS AND DISCUSSION

Gross Morphology: Experimental joints showed symptomatic signs of early OA. Mankin scores for the proximal region of the retropatellar surface were significantly greater for the experimental compared to the contralateral and normal control tissues ($P < 0.05$), while they were not different for the middle and distal regions. Average cartilage thickness in the experimental joints (803 ± 139 μm) was significantly greater than the contralateral (674 ± 47 μm) and normal joints (646 ± 79 μm) ($P < 0.05$).

Tissue Deformation: Average compressive tissue strains for 2 MPa surface pressure loading were similar for the experimental (16 ± 7%), contralateral (16 ± 3%) and normal tissue (17 ± 6%). However, average axial local extracellular matrix (ECM) strains were significantly greater for the experimental tissue (38 ± 8%) than the contralateral (27 ± 10%) and normal tissues (28 ± 8%) (Figure 2, $P < 0.05$). The average axial local ECM strains were also greater than the average cell strains in all experimental group tissues (Figure 2, *** $P < 0.005$). Average transverse ECM strains were also greater for the major and minor directions (14 ± 6% and 4 ± 4%, respectively) in the experimental compared to the contralateral (8 ± 6% and 0 ± 2%, respectively) and normal tissues (5 ± 4% and 1 ± 2%, respectively) (Figure 2, $P<0.05$).

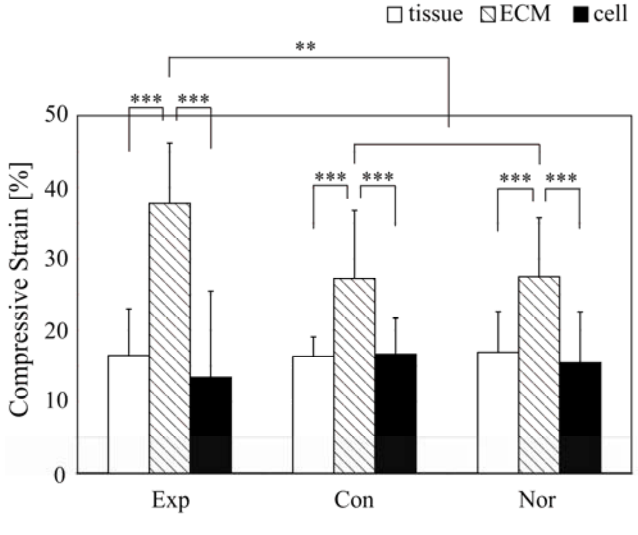

Figure 2: Compressive nominal tissue strains, extracellular matrix strains, and cell strains for retropatellar cartilage from experimental, contralateral and normal knees ($n = 4$, ** $P<0.05$, *** $P<0.005$).

Cellular Deformation: There was no significant difference in the average axial cell strains for the 2 MPa load application between the experimental (13 ± 12%), contralateral (17 ± 5%) and normal groups (15 ± 7%). However, average increases in cell width were greater in the experimental (13 ± 10%) than the contralateral (7 ± 13%) and normal joint cartilages (6 ± 6%) ($P<0.05$, $P<0.005$, respectively). Cell depth changes were similar in all three groups: 8 ± 13%, 7 ± 14% and 6 ± 6% for the experimental, contralateral, and normal tissues, respectively. Following loading, average cell volumes increased in the experimental joints (8 ± 24%, $P < 0.005$), while they decreased in the contralateral (-8 ± 10%, $P < 0.005$) and normal joints (-8 ± 8 %, $P < 0.05$).
Before loading, average cell volumes in the experimental (352 ± 88 μm^3) and contralateral joints (349 ± 66 μm^3) were significantly greater than those observed in the normal joints (302±73 μm^3) ($P < 0.005$). Following loading, average cell volumes increased in the experimental joints (8 ± 24%, $P < 0.005$), while they decreased in the contralateral (-8 ± 10%, $P < 0.005$) and normal joints (-8 ± 8 %, $P < 0.05$).

CONCLUSIONS

Based on the results of this study, we conclude that chondrocyte deformations following controlled loading of retropatellar cartilage differs qualitatively and quantitatively between normal and early OA cartilages.

REFERENCES

1. Seedholm BB, et al. *Ann Rheum Dis* **38,** 307-316, 1979.
2. Korhonen and Herzog. *J Biomech* **41**, 480-485, 2008.
3. Alexopoulos L, et al. *J Biomech Eng* **125,** 2003.
4. Clark A, et al. *Osteoarthritis Cartilage* **13**, 1100-1114, 2005.
5. Han S-.K., et al. *Med Eng & Phys* Under revision, 2008.

ACKNOWLEDGEMENTS

The Canada Research Chair Programme for Molecular and cellular Biomechanics and the Alberta Ingenuity Fund.

ROBOTIC OUTCOMES IN PERSONS WITH ROTATOR CUFF TEARS

[1,2] Margaret Finley, [2]Susan Conroy, [2,3] Lauren Jones-Lush, [2]Christopher Bever

[1]University of Indianapolis, Krannert School of Physical Therapy [2]Baltimore Veterans Administration Medical Center, [3]University of Maryland Dept Of Physical Therapy and Rehabilitation Science
email: finleym@uindy.edu http://pt.uindy.edu/

INTRODUCTION

Rotator cuff tears are one of the most common causes of pain and disability of the upper extremity[1]. Impaired motor control and biomechanics of the shoulder girdle with concomitant instability often exists prior to any surgical procedure. In this patient population clinical measures are limited, with questionable reliability and validity[2].

The MIT-MANUS robotic device has been found to be a reliable tool for of a patient's self generated motions, quantifying different features of motor performance (e.g. accuracy, speed, coordination, smoothness, etc) [3,4,5]. Robot generated outcome measures have demonstrated the ability to detect significant improvements in motor performance even when the clinical measures revealed only small changes[4,5]. The device can provide means to quantify aspects that have traditionally relied exclusively on qualitative observation, such as smoothness of movement[5]. Therefore, robotic measurement of patient unconstrained movements could be employed as the primary outcome in patients with rotator cuff tears. The purpose of this study was to evaluate the capability of the MIT-MANUS to detect movement differences between extremities with a rotator cuff and without tears. A secondary purpose was to determine if a relationship exists between self-reported functional outcomes, clinical motion measures and robotic generated variables.

METHODS

Twelve individuals (age=58.9±.7.9yrs) with physician diagnosed rotator cuff tears completed the self-report functional status measures of the Shoulder Pain and Disability Index (SPADI) and the American Shoulder and Elbow Surgeons Standardized Assessment (ASES) followed by performance of a planar reaching robotic evaluation with their involved extremity followed by their non-involved limb. The evaluations were performed on the highly-backdriveable low friction MIT-MANUS[6]. Backdriveable robots have low endpoint impedance insuring a gently compliant behavior of the robot when interacting with the subject. Therefore, the machine does not interfere with motion and allows the individual to move freely. The robot reaching evaluation required the subject to reach from the center target to eight peripheral targets evenly distributed on a circle with radius of 14cm and moving clockwise, without movement assistance. For all robot tasks the subjects were seated in a chair, centered in front of the robot support table. A waist strap with vertical straps anterior-medial the shoulders was applied during all training and evaluation sessions to limit/prevent forward trunk compensation without impeding scapular motions.

Outcome variables assessed for the reaching task were aiming error (mean absolute angle between actual direction and a straight line between start and target), mean speed (total displacement traveled over total movement duration), peak speed, mean-to-peak speed ratio (mean speed divided by the peak speed is a metric of movement smoothness[5] and movement duration.

Paired t-tests evaluated if a difference could be detected between involved and uninvolved extremities ($p \leq 0.05$) while Pearson correlation evaluated the relationship between the robotic outcomes and the self-report functional scales (($p \leq 0.05$). Correlation was defined as moderate ($r=0.50$ -0.69), high ($r=0.70$ -0.89) or as very high ($r>0.90$).

RESULTS

The MIT-MANUS detected a difference in mean speed (p=0.026), movement smoothness (p=0.003), and movement duration (p=0.031) between involved and uninvolved extremities in persons with rotator cuff tears (Table 1).

Significant moderate correlation were found between the ASES total and robotic outcomes of mean speed (r=0.58, p=0.05). Mean speed also had significant moderate correlation to SPADI pain (r = -0.69, p = 0.014), SPADI disability (r = -0.63, p=0.028) and SPADI total (r = 0.-67, p = 0.016). High correlation was found between movement duration and SPADI pain (r = 0.81, p = 0.001), SPADI disability (r = -0.72, p = 0.009) and SPADI total (r = 0.78, p = 0.003)

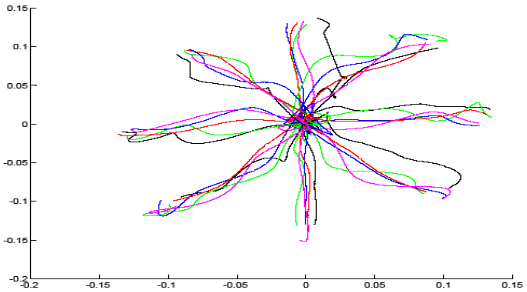

Figure 1: Reaching task output from a representative participant with rotator cuff tear.

CONCLUSIONS

This study provides the first evidence that planar robot outcomes may provide objective measures of motor control in patients with shoulder impairments quantifying biomechanical profiles and perhaps provide insights into recovery more distinctly than clinical measures. Goal-directed, quantifiable rehabilitation outcomes measuring redevelopment of function through improved range of motion, strength and motor control are lacking in patients with musculoskeletal impairments. A moderate to strong relationship exists among the SPADI self-report functional outcome and speed and duration of movement on the planar robot evaluation. The MIT-MANUS derived robotic metrics are sensitive to bilateral differences and, therefore, potentially able to determine changes, potentialy in advance of clinical measures. Since the clinical scales for orthopedic impairments are limited and these robot outcome measures are shown to be reliable and sensitive, they can be utilized in future investigations as primary outcomes to evaluate patients with orthopedic conditions.

REFERENCES

1. Ejnisman B, et al. Interventions for tears of the rotator cuff in adults In: The Cochran Library, 2004.
2. Cook KF, et al. *Arch Phys Med Rehabil* 2001;82(11):1558-65.
3. Finley,M.A.,et al *J. Applied Biomech* (in press). (Epub ahead of print, 2008).
4. Finley, MA, et al. *J Rehabil Res Develop*, 42(5), September/October 2005, 683-92.
5. Rohrer B, et al. , 2002;22(18):8297-304.
6. Krebs HI, et al. *IEEE Trans Rehabil Eng* 1998;6(1):75-87

ACKNOWLDEGEMENTS

Funding was provided by the Career Development Grant #B3827V from the VA Rehabilitation and Development Service

Table 1: Robotic outcomes in involved and uninvolved extremities (mean, std error).
***** indicates significant difference between extremities

	Involved limb	Uninvolved limb	p-value
Aiming Error (rad)	2.02 (0.04)	1.95 (0.05)	0.402
Mean speed (m/sec)	0.10(0.01)	0.12(0.01)	0.026*****
Peak speed (m/sec)	0.23(0.02)	0.26(0.01)	0.165
Smoothness (mean speed:peak speed)	0.45 (0.01)	0.47(0.01)	0.003*****
Movement duration (sec)	1.81(0.15)	1.48(0.07)	0.015*****

ORDERLY RECRUITMENT OF MOTOR UNITS BY OPTICAL STIMULATION IN TRANSGENIC MICE

Michael E. Llewellyn, Kimberly R. Thompson, Karl Deisseroth, and Scott L. Delp

Department of Bioengineering. Stanford University.
Email: llewellm@stanford.edu   Web: http://nmbl.stanford.edu/

INTRODUCTION

The principle of orderly recruitment states that small fatigue-resistant motor units are recruited before large fatigable motor units [1]. Here we show that it is possible to control motor activity directly with optical stimulation by using a light-sensitive cation channel (channelrhodopsin-2) genetically inserted into the membranes of motor axons that open with millisecond precision and high fidelity in response to blue light (470 nm) [2]. By measuring several indices of motor unit recruitment order, we also show evidence that optical stimulation recruits motor units in their normal physiologic order in transgenic mice. This technology could become the first viable alternative to electrical stimulation in limb re-animation projects, and may allow the possibility of fine motor control and fatigue resistance with optically-based prosthetics.

METHODS

We implanted LED-based optical or bipolar electrical cuffs around the exposed sciatic nerves of anesthetized transgenic mice (Thy1-ChR2). The mouse's body temperature was maintained with an isothermal pad and heat lamp. The sciatic nerve was severed proximal to the cuff prior to experimentation and kept moist with mammalian Ringer's solution. We simultaneously recorded stimulation intensities, measured by rectified integrated EMG, in both lateral gastrocnemius and soleus during single muscle twitches elicited by both electrical and optical stimulation. Optical power at the surface of the peripheral nerve was estimated with the Kubelka-Munk model [3]. The number and size of myelinated motor axons innervating each individual muscle were measured using confocal microscopy in a cross-section of sciatic nerve by use of a retrograde dye (fast blue) injected into each muscle.

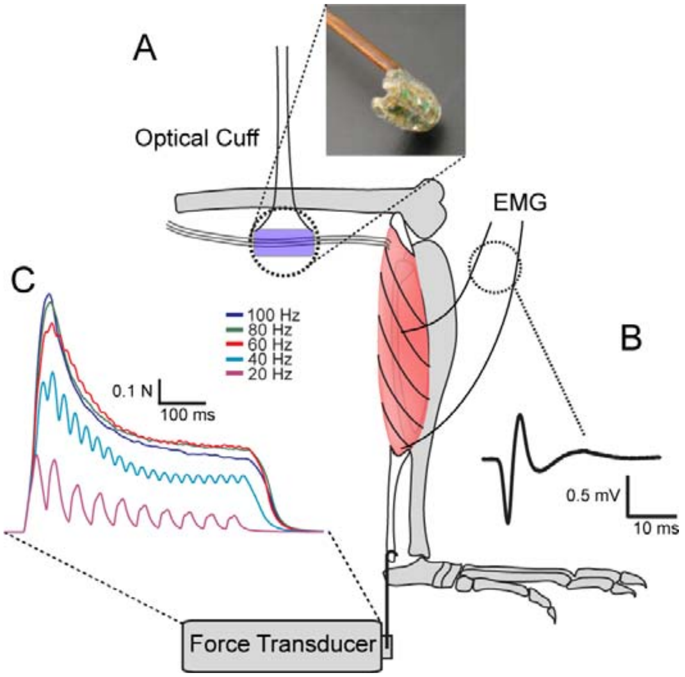

Figure 1: Optical stimulation setup. **A.** An LED-based optical or electrical cuff is implanted around the sciatic nerve of an anesthetized transgenic (Thy1-ChR2) mouse. The optical cuff is 4x2 mm and contains 16 LEDs (468 nm) arranged in a concentric perimeter facing the peripheral nerve in the center, an example is shown. **B.** Fine wire differential EMG are inserted into the muscle belly and near the muscle-tendon junction to record the electrical response of the subject muscle(s). A sample EMG induced by optical stimulation is shown; note the absence of an electrical stimulation artifact. **C.** A force transducer attached to the Achilles tendon by a thin steel hook records the contractile response of the muscle(s). Muscles not being recorded are cut from their attachment to the Achilles tendon. Samples of contractile responses from the medial gastrocnemius using varying frequencies of optical stimulation are displayed.

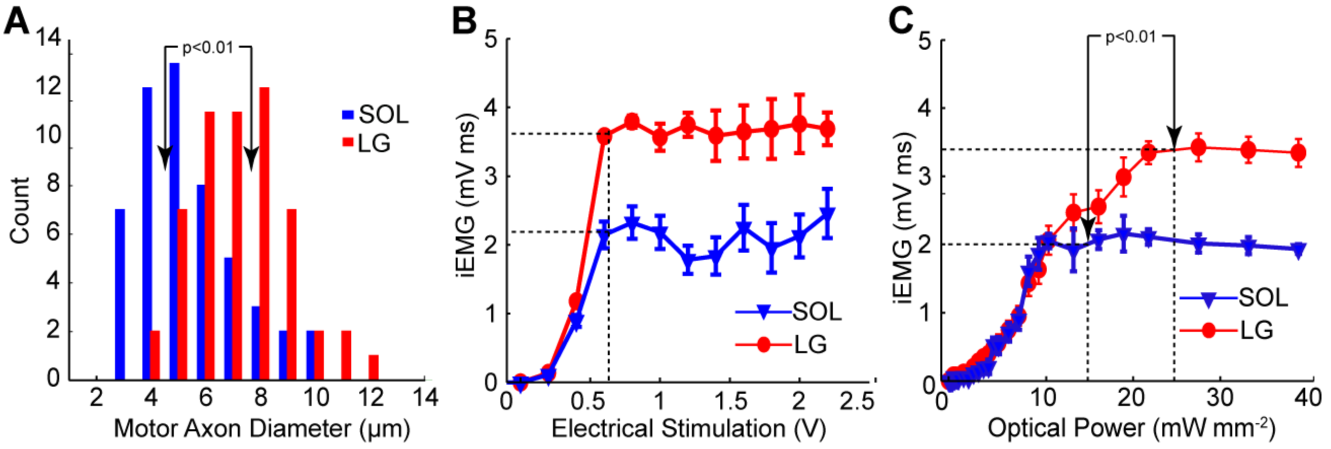

Figure 2: Evidence of orderly recruitment. **A.** Soleus muscle contains an equivalent number of motor units, but has on average significantly smaller motor axons than lateral gastrocnemius. This implies that, on average, soleus contains smaller motor units than lateral gastrocnemius. **B.** Using electrical stimulation both lateral gastrocnemius and soleus reach maximal stimulation at the same electrical stimulation intensity (~0.6 V). **C.** Using optical stimulation, however, soleus reaches maximal stimulation at a significantly lower value of optical stimulation intensity (14 mW mm^{-2}) than lateral gastrocnemius (22 mW mm^{-2}). Since soleus has smaller motor units than lateral gastrocnemius; smaller motor units are recruited at a lower optical power, which is consistent with orderly recruitment.

RESULTS AND DISCUSSION

Our experiments demonstrated the feasibility of using optical stimulation to control skeletal muscle activity. We show the ability to elicit single muscle twitches and tetani, without an electrical stimulation artifact on EMG. The peak muscle force evoked by optical stimulation is comparable to that by electrical stimulation; and is not due to heat or electric field effects produced by the optical cuff as demonstrated in non-transgenic control animals (results not shown).

Our results provide evidence of orderly recruitment by optical stimulation in Thy1-ChR2 mice. We have found that mouse soleus is innervated by equivalent numbers of motor units that are significantly smaller than those innervating lateral gastrocnemius (Figure 2A). Also, we have found that soleus reaches maximal excitation at a significantly lower value of optical power (Figure 2C). This evidence suggests that smaller motor units are recruited prior to larger motor units with increasing optical stimulation intensity which is consistent with orderly recruitment. We found no evidence of orderly recruitment using electrical stimulation (Figure 2B).

Electrical stimulation is generally non-optimal for limb re-animation projects because it recruits large volumes of fatigable muscle. For the first time, we demonstrate an alternative to electrical stimulation that possibly recruits motor units in the normal physiological order. Also unlike electrical stimulation, the use of a transgenic channel allows for specific cell-type targeting and alteration of the channel properties (i.e. kinetics, light sensitivity) for unprecedented control of muscle activity.

REFERENCES

1.Henneman, E. (1957). "Relation between size of neurons and their susceptibility to discharge." Science **126**(3287): 1345-7.
2.Zhang, F., L. P. Wang, et al. (2006). "Channelrhodopsin-2 and optical control of excitable cells." Nat Methods **3**(10): 785-92.
3.Aravanis, A. M., L. P. Wang, et al. (2007). "An optical neural interface: in vivo control of rodent motor cortex with integrated fiberoptic and optogenetic technology." J Neural Eng **4**(3): S143-56.

ACKNOWLEDGEMENTS

We thank the Stanford BioX program and Stanford Medical Scientist Training Program for support.

OPTIMIZATION OF MUSCLE WRAPPING OBJECTS USING SIMULATED ANNEALING

Christopher J. Gatti and Richard E. Hughes*
Laboratory for Optimization and Computation in Orthopaedic Surgery
University of Michigan, Ann Arbor, MI 48109
*email: rehughes@umich.edu, web: http://www-personal.umich.edu/~rehughes/index.html

INTRODUCTION

Musculoskeletal models often use wrapping objects, such as cylinders and spheres, to constrain muscle paths from passing through anatomical obstacles. However, the selection of wrapping object parameters is typically a time-consuming process, which consists of iteratively and manually changing parameters and comparing model-predicted moment arms to experimental data. The purpose of this study was to develop a method for efficiently determining wrapping object parameters that predict moment arms that match experimental literature.

METHODS

The SIMM Holzbaur shoulder model [1] was used to demonstrate the ability of a data-driven optimization to determine wrapping object parameters. Wrapping parameters were determined for two cases: 1) modeling the triceps moment arm at the elbow using a cylindrical wrapping object, and 2) modeling the middle deltoid using a spherical wrapping object. Experimentally-measured muscle moment arms were obtained from the literature and combined to create goal data sets for the optimizations. For the triceps optimization, experimental data consisted of elbow flexion moment arms from 0°-140° of elbow flexion [2-6]. For the middle deltoid optimization, experimental data consisted of elevation moment arms in three different planes (frontal, scapular, saggital) from 0°-100° of arm elevation [7-9], thus this optimization had to simultaneously match three data sets.

The kinematics of the Holzbaur shoulder model and the cylinder- and sphere-wrapping algorithms were programmed in Matlab. Muscle origins and insertions were unchanged from the original Holzbaur shoulder model. Muscle via points that were close to the wrapping object were moved slightly away from the joint center to allow for a larger wrapping parameter space to be searched which resulted in continuous moment arm curves. Simulated annealing [10] was used to determine optimal wrapping object parameters for each optimization. The objective function of the optimization was composed of two parts:

$$Min\ f(\mathbf{x}) = \sum_{i=1}^{r}\left[w_i \sqrt{\sum_{j=1}^{n}\left(m(\Theta_{ij},\mathbf{x}) - g(\Theta_{ij})\right)^2 \Big/ n}\right] + P(\mathbf{x})$$

The first part consisted of the root mean square (RMS) error between the model-predicted moment arms $m(\Theta_{ij},\mathbf{x})$ and the experimental moment arm data (i.e., goal) $g(\Theta_{ij})$, where Θ_{ij} is the set of joint angles for the simulated joint motion i with postures j, and $\mathbf{x} = (x_1,\ldots,x_k)$ which is the vector of wrapping parameters to be optimized. In the case of the middle deltoid optimization, the RMS error for each action was weighted by w_i to produce similar errors for the different actions. The second part of the objective function consisted of penalty functions, $P(\mathbf{x})$, which penalized wrapping parameters corresponding to unrealistic moment arms and muscle paths.

The cylinder wrapping object was defined by 7 parameters: x-, y-, and z-locations of the origin; x-, y-, and z-components of the vector defining the orientation of the long axis; and the radius. The sphere wrapping object is defined by 4 parameters: x-, y-, and z-locations of the origin; and the radius. All of the respective wrapping object parameters were used as optimization variables. The optimal wrapping parameters were then used to compute muscle moment arms for each action in the optimizations, and these values were compared to the experimental data as well as those from the original Holzbaur shoulder model.

RESULTS AND DISCUSSION

It was found that an optimization algorithm could be used to determine wrapping object parameters which produced moment arms that were similar to experimental data (Fig. 1 and 2). The triceps and middle deltoid optimizations required

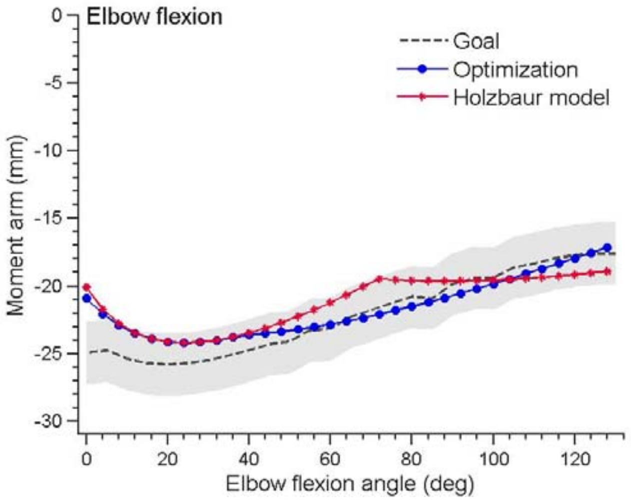

Figure 1. Triceps elbow flexion moment arms from experimental data (Goal, ± 1 stdev), optimal cylinder wrapping object parameters (Optimization), and Holzbaur shoulder model (Holzbaur model).

approximately 6 and 29 seconds, respectively, and these values represent average values for each respective optimization. Additionally, this method improved the moment arm predictions of the Holzbaur shoulder model. However, it should be recognized that the goal data used in this study were not likely the same data used to develop the Holzbaur shoulder model, although these data should be similar. The greatest benefit of this method is the efficiency at which model parameters were determined, thus eliminating much of the time required to manually refine the wrapping objects.

REFERENCES

1. Holzbaur KRS, et al. *Ann Biomed Eng* **33**:829-840, 2005.
2. An KN, et al. *J Biomech* **14**:659-669, 1979.
3. Gerbeaux M, et al. *J Biomech* **29**:171-180, 1996.
4. Pigeon P, et al. *J Biomech* **29**:1365-1370, 1996.
5. Murray WM, et al. *J Biomech* **35**:19-26, 2002.
6. Ettema GJC, et al. *Hum Movement Sci* **17**:201-220, 1998.
7. Liu J, et al. *Clin Biomech* **12**:32-38, 1997.
8. Kuechle DK, et al. *J Shoulder Elb Surg* **6**:429-439, 1997.
9. Ackland DC, et al. *J Anat* **213**:383-390, 2008.
10. Kirkpatrick S, et al. *Science* **220**:671-680, 1983.

ACKNOWLEDGEMENTS

Funding was provided by grant R41HD53886 from the National Institutes of Health.

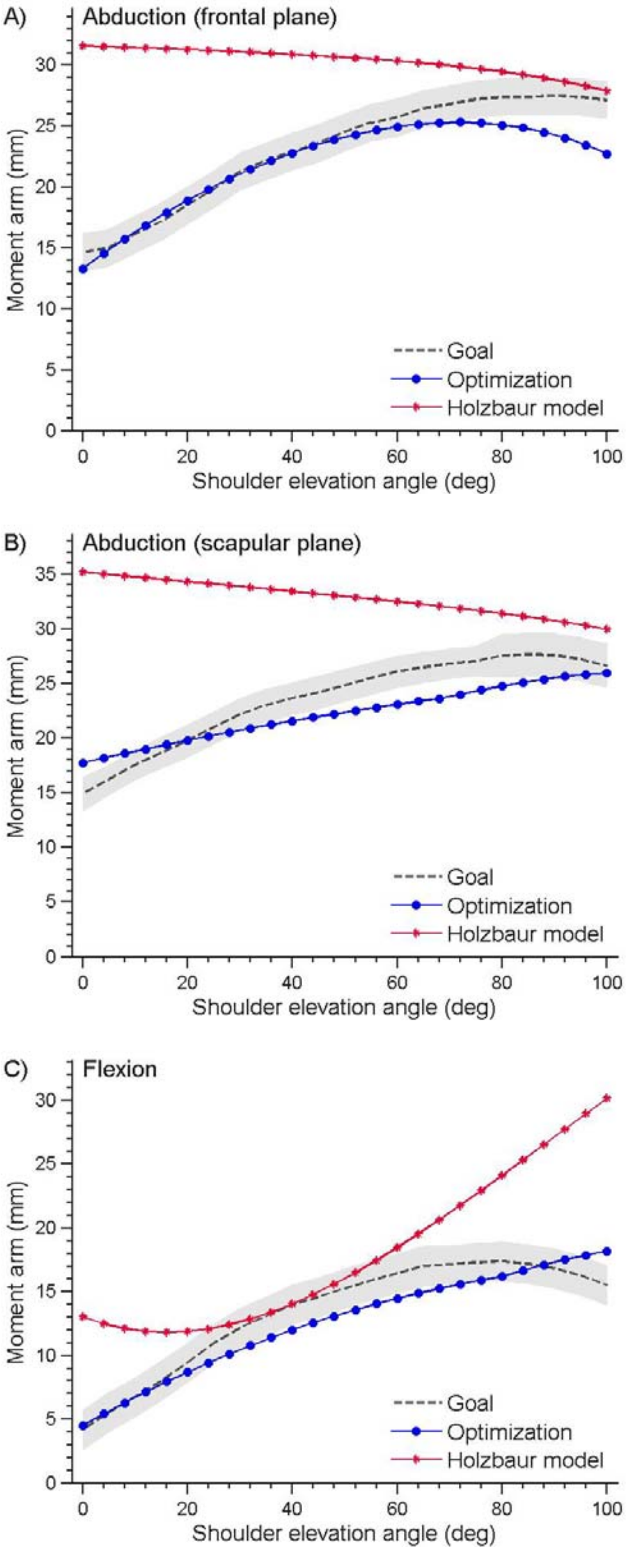

Figure 2. Middle deltoid moment arms from experimental data (Goal, ± 1 stdev), optimal sphere wrapping object parameters (Optimization), and Holzbaur shoulder model (Holzbaur model) for (A) abduction in the frontal plane, (B) abduction in the scapular plane, and (C) flexion.

CENTER OF PRESSURE SWAY PARAMETERS CONSIDERED JOINTLY BETTER DIFFERENTIATE OLDER ADULT FALLERS FROM NON-FALLERS

[1,2]Kimberly Edginton Bigelow and [2]Necip Berme
[1]University of Dayton, Department of Mechanical and Aerospace Engineering, Dayton, OH, USA
[2]The Ohio State University, Department of Mechanical Engineering, Columbus, OH, USA
email: Kimberly.Bigelow@udayton.edu

INTRODUCTION

Posturography has the potential to help identify older adults at high-risk of falling due to balance deficits, but this potential is limited by lack of standardization in testing methodology [1]. With over 35% of older adults falling each year, it is imperative that fall-risk screening become clinically routine so that proactive fall prevention strategies can be employed for those who would benefit the most [2].

The use of a force-measuring platform to quantitatively measure information about an individual's sway has the promise to offer a quick clinical screen that overcomes limitations of subjectivity, space and time requirements of common functional balance tests. This use of posturography has currently been hindered because of the large number of possible sway parameters, both traditional and non-traditional, that can be reported [1]. It is currently unknown what parameters best differentiate fallers and non-fallers and whether a group of parameters might reveal more than a single sway measure [1].

The aim of this study was to determine what postural sway parameter(s) best differentiated older adults who had fallen from those who had not, allowing for the development of a posturography protocol that could be used clinically.

METHODS

One hundred and fifty older adults self-reported their fall history for the past year. Those who reported at least two falls in the past year were classified as fallers. There were 21 fallers (13 females, 8 males; mean age: 83.6 ± 7.6; mean height: 164.3 ± 9.3 cm; mean weight: 72.5 ± 17.5 kg). The remaining 129 subjects were classified as non-fallers (97 females, 32 males; mean age: 81.1 ± 7.9; mean height: 163.2 ± 10.5 cm; mean weight: 72.4 ± 17.4 kg).

Subjects performed four quiet-standing tasks in a randomized order on a force-measuring platform (Model BP5050, Bertec Corporation, Columbus, Ohio): eyes open with feet comfortable, eyes closed with feet comfortable, eyes open with feet together, and eyes closed with feet together. All trials were 60 seconds long and data was collected at 1000 Hz.

From the center of pressure data the following traditional sway measures were calculated: A/P Sway Range, M/L Sway Range, Mean Sway Velocity, RMS, 95% Confidence Ellipse Area, Angular Deviation from A/P, Mean Frequency, and M/L Sway Velocity. Additionally, Detrended Fluctuation Analysis was performed to calculate the fractal measures. DFA plots revealed novel two-region findings, as shown in Figure 1. A/P and M/L Short-Term and Long-Term Scaling Exponents, as well as Crossover Point were thus found.

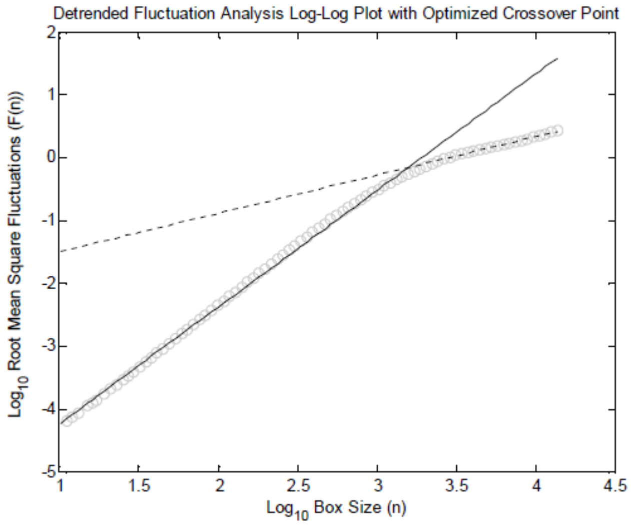

Figure 1. Representative DFA plot of 60 second COP data, revealing novel multiple scaling regions (short-term region, solid line; long-term, dashed).

Stepwise logistic binary regression with forward selection ($\alpha=0.15$) was used for each testing condition, using all postural sway parameters above, as well as several personal demographics. Fall status was defined as the response variable. For each resulting logistic regression model, the Somers' D value was calculated, a statistical measure of goodness-of-fit of the model, with a value of 1 representing the best fit.

RESULTS AND DISCUSSION

The logistic regression model associated with the eyes closed, feet comfortable condition yielded the highest Somer's D value, 0.715. The resulting parameters included in the model for this testing condition are shown in Table 1.

Table 1. Parameters, in order of significance, to best differentiate fallers from non-fallers in the eyes closed, feet comfortable condition.

Logistic Regression Model Parameters
M/L Velocity
A/P Short Term Scaling Exponent
M/L Short Term Scaling Exponent
Mean Frequency
BMI
Age

Medial-lateral center of pressure velocity was identified as the most significant parameter to differentiate fallers from non-fallers in the eyes closed, feet comfortable condition. It was found that individuals who swayed faster were more likely to fall. This sway parameter also showed strong significance in the differentiation of individuals based on fall risk for the other testing conditions that had models of lower Somers' D values. This finding is in agreement with Maki and others who identified M/L stability as important in the prevention of falls [3,4]. It has been suggested that inability to control M/L stability may indicate loss of cutaneous sensation in the feet [3,4]. This was not tested in the current study.

As shown in Table 1, differentiation ability was best when multiple parameters were considered jointly. Fractal measures were found to be important to include in this group. This suggests that there is a need to jointly consider both traditional and non-traditional measures in differentiating individuals based on fall risk. This finding is significant, especially as groups strive to show that non-linear analyses reveal more than traditional analyses, but do not attempt to describe how these measures might work in combination [5]. It may be true that non-linear analyses reveal certain characteristics about an individual's sway that traditional analyses do not, but this alone is not sufficient.

The resulting logistic regression model was used to calculate probability that each individual had fallen at least twice in the past year. Past fall history has been found to correlate well to future fall-risk [1]. Older adults often report fall history incorrectly, though, making the use of the described protocol an important clinical tool. Results demonstrated that non-fallers were correctly identified as having low likelihood of falls (7.3% ± 10.8%), whereas most fallers were identified as having a relatively high likelihood of falling (40.0% ± 33.9%). Those fallers with low calculated likelihood of falling were most commonly those who had fallen due to problems not related with balance (i.e. falls caused by foot drop while walking). From a clinical perspective, this suggests that a simple fall risk screening of only 60 seconds could allow physicians to identify many patients at risk of falling due to balance deficits.

CONCLUSION

To enhance clinical usage of posturography, it is recommended that the eyes closed, comfortable stance condition be performed and the measures listed in Table 1 be examined. Future work is needed to further develop and validate the logistic regression model so that it may be more usable for predicting falls in the clinical environment.

REFERENCES

1.Raymakers JA, et al. *Gait Posture*, **21**, 48-58, 2005.
2.AGS, BGS and AAOS. *JAGS* **49**, 664-672, 2001.
3.Maki BE, et al. *J Gerontol* **49**, M72-M84, 1994.
4.Melzer I, et al. *Age Ageing* **33**, 602-607, 2004.
5. Norris JA, et al. *J Biomech* **38,** 1263-1272, 2005.

ACKNOWLEDGEMENTS

The authors thank Haluk Ay, Thomas A. Adams II, and Chris Bigelow.

THE RELATIONSHIP BETWEEN INTRAVAGINAL AND URETHRAL PRESSURE DURING VOLUNTARY CONTRACTION AND DURING COUGHING IN CONTINENT WOMEN

[1] Linda McLean, [2]Stephanie Madill
[1]Queen's University, School of Rehabilitation Therapy, Canada
email: mcleanl@queensu.ca; web: www.rehab.queensu.ca

INTRODUCTION

Vaginal pressure is frequently used as a measure of pelvic floor muscle (PFM) function and as a surrogate measure for urethral closure pressure in physiotherapy research and practice [1]. Vaginal pressure measurements during dynamic activities such as PFM contraction or coughing have not been compared with urethral pressure measurements to determine if they do, in fact, provide a valid representation. We hypothesized that pressure increases recorded in the vagina would reflect the functional outcome of PFM contraction as it pertains to increases in urethral closure pressure and would accurately reflect intra-urethral pressure generated during coughing. Due to its closer proximity to the urethra, pressure recorded adjacent to the anterior vaginal wall was hypothesized to be more strongly correlated with urethral pressure than is pressure recorded adjacent to the posterior vaginal wall.

METHODS

This was a cross-sectional observational study. Women without neurological or rheumatological diagnoses, diabetes, prolapse ≥ POP-Q stage II or previous pelvic surgery were recruited. All participants provided informed, written consent. Demographic data were recorded and volunteers completed the Urogenital Distress Inventory (UDI). The women were taught how to correctly perform a PFM contraction, confirmed by vaginal palpation and observation. Urethral pressure was measured using a saline-filled, 8 French triple lumen catheter interfaced with a Becton Dickinson DTX^{TM} Plus DT-12 pressure transducer. The catheter opening was positioned in the urethra at the point where the transducer recorded the highest pressure values during both a PFM contraction and a cough. Vaginal pressure data were recorded adjacent to the anterior and posterior vaginal walls using two air-filled, 10 French rectal balloons mounted on the anterior and posterior surfaces of a vaginal probe, which were interfaced with Motorola MPX5010 Integrated Silicon pressure transducers. Data were recorded using Delsys EMGWorks^{TM} Acquisition software at a sampling rate of 1000 Hz while, in supine the volunteers performed three maximum voluntary PFM contractions (PFM MVCs) and in standing they performed three PFM MVCs and three maximum effort coughs.

All data were dual filtered using a third order, 5Hz low pass Butterworth filter. The filtered mean of the first 100 data points was subtracted from each data file. The peak pressure was determined for each pressure recording site during each repetition of each task. The peak pressures were compared among the pressure recording sites and tasks using a repeated measures analysis of variance (ANOVA) ($\propto=0.05$). For each task, the peak pressures were compared among pressure recording sites by calculating the regression of the peak urethral versus peak vaginal pressure curves. Cross-correlation functions were computed among the urethral, anterior vaginal, and posterior vaginal pressure curves. Lastly, ensemble averaged urethral pressure versus vaginal pressure curves were created during the rising phase of urethral pressure during each task.

RESULTS AND DISCUSSION

Eleven women participated. The sample had a median (range) age of 42 (29 to 68) years, body mass index of 26.7 (18.9 to 29.7) kg/m^2, UDI score of 3/19 (0 to 8), and had 2 (0 to 4) children and had 2 (range 0 to 2) vaginal deliveries.

The peak urethral pressure was higher during coughing than during either the supine or the standing PFM MVCs ($p<0.001$ for both). There was no difference between the peak urethral pressure generated during the supine and standing PFM MVCs ($p=1.00$). There was no difference in peak intravaginal pressure among the three tasks for either the anterior or the posterior pressure recording site (p=1.00 for both). Peak urethral pressure was linearly related to peak intravaginal pressure (slopes= 3.53 to 3.66 for the PFM MVCs and 6.89 for the cough; p<0.001 for all tasks). The cross-correlation coefficients between urethral and vaginal pressure and between anterior and posterior vaginal pressure were all high (r>0.96). The relationship between the generation of urethral pressure and the generation of intravaginal pressure is presented in Figure 1. The rise in urethral pressure was highly correlated with that of anterior (slope= 0.768 ±0.030, p<0.001) and posterior (slope= 0.772 ±0.092, p<0.001) vaginal pressure recorded during coughing. The relationship between urethral and vaginal pressure was also linear during the standing PFM MVCs, but the slopes were much lower (anterior slope=0.252 ± 0.049, p<0.001, posterior slope=0.321 ±0.043,p<0.001) and more variable. The relationship between urethral pressure and vaginal pressure was curvilinear during the supine PFM MVCs.

It appears that women do not generate maximal urethral closure pressure when performing a PFM MVC, however the difference in peak urethral pressure between PFM MVC and coughing was not reflected in the intravaginal pressure measurements. Peak pressure recorded using the anterior vaginal transducer was not different from that recorded using the posterior vaginal transducer, and there was no difference in the ensemble averaged urethral pressure versus anterior and posterior vaginal pressure curves for any of the three tasks. As such, the location of the pressure transducers within the vagina (anteriorly or posteriorly) appears to be of no consequence on experimental results.

Based on the urethral vs vaginal pressure curves, it appears that pressure generated from a PFM MVC is evident in the vaginal pressure before it is evident in the pressure measurements. This delay may be related to the electromechanical delay between muscle activation and force output and/or due to time required to take up slack in the pelvic supporting tissues before pressure can be transmitted to the urethra. Coughing, which is a more explosive task, appears to demonstrate more rapid transmission of forces from the vagina to the urethra, but these forces are more likely related to the abrupt rise in intra-abdominal pressure rather than pressure induced by PFM contraction.

CONCLUSIONS

While it must be recognized that urethral pressure includes components generated by the urethral sphincters and passive tissue stiffness that do not contribute to intravaginal pressure, this study has demonstrated that intravaginal pressure recorded adjacent to both the anterior and posterior vaginal walls is strongly correlated with urethral pressure and can be used as a surrogate for urethral pressure measures in biomechanical studies of the continence system and as a functional outcome measure in physiotherapy.

REFERENCES

1. Bø, K. and M. Sherburn, Phys Ther, 2005. 85:269-282.

ACKNOWLEDGEMENTS

Funding for this research was provided by the National Sciences and Engineering Research Council of Canada (NSERC).

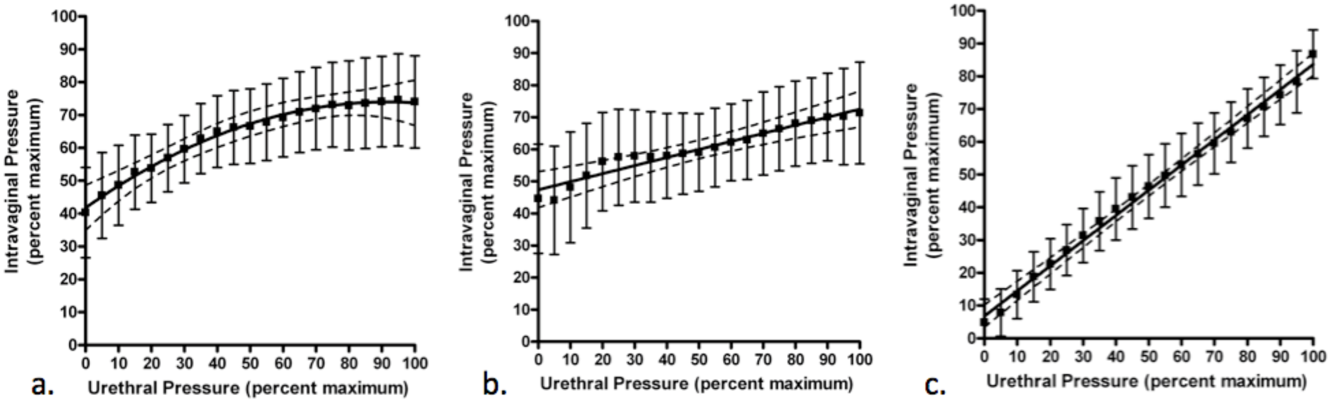

Figure 1: Ensemble average curves for urethral pressure versus anterior vaginal pressure during a. PFM MVC performed in supine, b. PFM MVC performed in standing, c. Maximal effort cough performed in standing.

History effects of antagonist coactivation at constant muscle length

Huub Maas and Peter A. Huijing
Faculteit Bewegingswetenschappen, *Vrije* Universiteit Amsterdam, The Netherlands
email: h.maas@fbw.vu.nl, web: http://www.move.vu.nl/members/huub-maas/

INTRODUCTION

We have shown previously that forces can be transmitted between synergistic and antagonistic muscles [for a recent review see 1]. These mechanical interactions are mediated by connective tissues surrounding muscles. Up to this point, the effects of such epimuscular pathways on muscular force transmission were tested predominantly during simultaneous excitation of synergistic and antagonistic muscles. Many *in vivo* tasks require simultaneous activity of multiple muscles, including antagonists, but often with different timing of burst onsets and offsets. For example during a ballistic movement, the synergistic muscle group is excited first followed by coactivation of antagonistic muscles in the final phase of the movement, to decelerate the joint. It is hypothesized that force transmission to the tendon of an agonistic muscle is affected by the timing of onset of antagonist muscle activity.

Therefore, the aim of this study was to assess the acute effects of antagonist coactivation during agonist activity on isometric muscle forces.

METHODS

In deeply anesthetized Wistar rats (n = 5, 302 ± 16 g, male), the distal tendons of flexor carpi ulnaris (FCU), palmaris longus (PL) and extensor carpi ulnaris (ECU) muscles were transected and connected to force transducers. Connective tissues enveloping the muscle bellies in the antebrachium were left intact. The ulnar/median (U/M) nerve complex and the radial (R) nerve were dissected, cut proximally and each placed on a pair of silver electrodes. The ulnar and median nerves innervate all palmar muscles of the antebrachium ('wrist and digit flexors'), including synergistic FCU and PL. The radial nerve innervates all dorsal muscles of the antebrachium ('wrist and digit extensors'), including ECU. PL and ECU were kept at reference length, corresponding to a neutral wrist position and the elbow joint at approximately 90°. Optimum FCU length (l_o) was determined during simultaneous stimulation of U/M and R nerves. For selected FCU lengths (approximately l_o+0.5 mm, l_o-1.5 mm and l_o-3.5 mm), effects of three different stimulation protocols (Figure 1) on forces exerted at the three hooked up tendons were assessed. (*i*) Simultaneous stimulation of U/M and R nerves; (*ii*) Stimulation of the U/M nerve adding R nerve stimulation after 500 ms while U/M nerve stimulation is continued; and (*iii*) the same as in *ii*, but starting with R nerve stimulation. FCU reference length is located 1.9 ± 0.7 mm below optimum length.

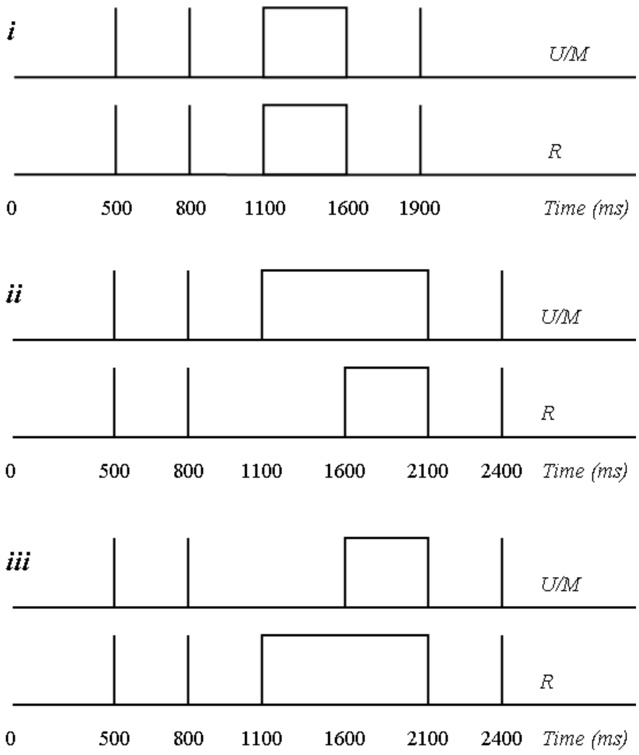

Figure 1: Schematic representation of the different nerve stimulation protocols used. Vertical lines indicate twitches and rectangles indicate pulse trains at 100 Hz.

RESULTS AND DISCUSSION

Figure 2 shows superimposed force waveforms of FCU tested at high length for two nerve stimulation protocols (*i* and *ii*). If R nerve was stimulated after the onset of U/M nerve stimulation, an initial steep increase in force was observed followed by and exponential decay. Other important observations are: (a) mean FCU force at the end of nerve stimulation was substantially higher (3.60 N) than mean FCU force (3.14 N) following synchronized onset of U/M and R nerve stimulation, (b) FCU force during stimulation of U/M nerve exclusively (t = 1100-1600 ms) was lower (2.95 N) than if R nerve was stimulated simultaneously with U/M. If the order of nerve stimulation onset was reversed (protocol *iii* in Figure 1), FCU force was lower (3.01 N, data not shown) than following simultaneous onset of U/M and R nerves (3.14 N).

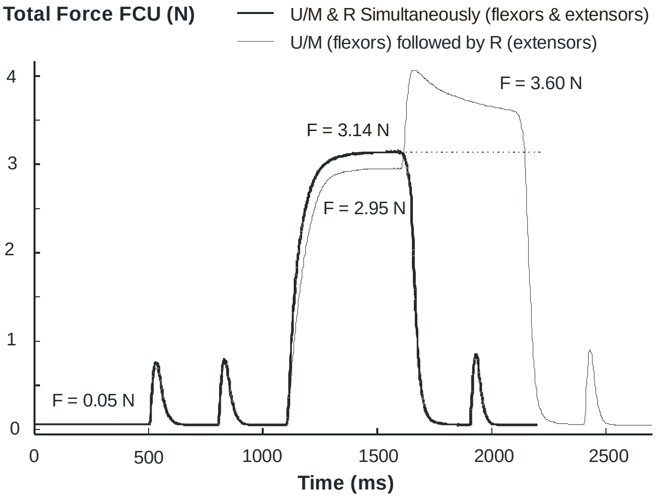

Figure 2. Typical force waveforms during two different nerve stimulation protocols (protocol *i* and *ii* in Figure 1) for FCU kept at constant high muscle length (l_0 + 0.9 mm).

Mean tetanic FCU forces (n = 5) at the end of nerve stimulation for the different protocols are shown in Fig. 3. ANOVA indicated a significant main effect of stimulation protocol at high FCU length. Note that active FCU force found for U/M followed by R stimulation (3.89 ± 0.33 N) was higher than optimal active force found for the synchronized onset of U/M and R nerve stimulation (3.60 ± 0.27 N). No significant effects were found for the other two lengths tested.

We conclude that distal force of FCU kept at a constant high length is co-determined by the activity of antagonistic muscles as well as the order of nerve stimulation.

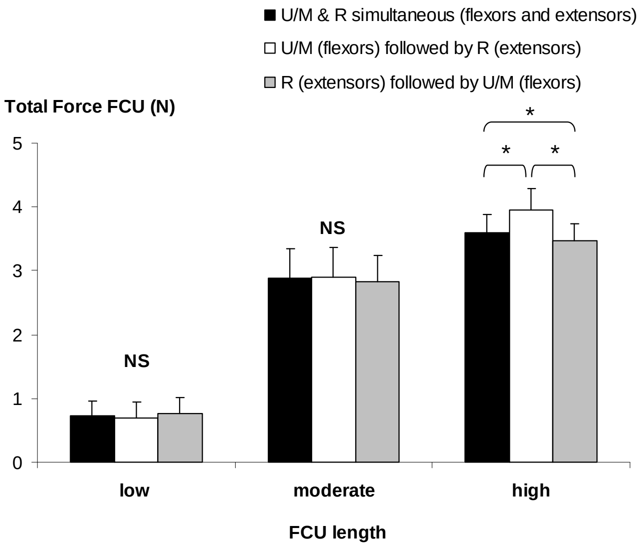

Figure 3. Mean (n = 5) effects of the timing of nerve stimulation onset on FCU forces during stimulation of U/M and R nerves for the three FCU lengths tested. * $p < 0.05$.

Our results may be explained by a different distribution of fiber mean sarcomere length [2] at mechanical equilibrium. A higher force can be the result of a decrease in the distribution of fiber mean sarcomere length (and vice-versa).

The present data are also compatible with residual force enhancement after lengthening and residual force depression after shortening [3]. Note that our results were obtained during contractions at a constant muscle-tendon complex length, but shortening and/or lengthening contractions are expected locally. Further studies are needed to assess if local length changes of sufficient magnitude are feasible during the muscle conditions used here.

REFERENCES

1. Huijing PA. *J Electromyo Kinesiol* **17**: 643, 2007.
2. Huijing PA. *Hum Mov Sci* **14**: 443-486, 1995.
3. Herzog W. *Hum Mov Sci* **23**: 591–604, 2004.

ACKNOWLEDGEMENTS

Guus Baan for technical support. Supported by EU Marie Curie International Reintegration Grant MIRG-CT-2007-203846.

AN HEIRARCHICAL VISCOELASTIC LIGAMENT FAILURE MODEL

[1]Scott R. Lucas, [2]Robert S. Salzar and [2,3]Cameron R. Bass
[1]Exponent, Inc., [2]University of Virginia, [3]Duke University
email: slucas@exponent.com, web: www.exponent.com

INTRODUCTION

Most existing microstructure-based ligament models assume that collagen fibrils or fascicles behave linear elastically, [c.f. 1,2] in contrast with the information on fascicles that has suggested viscoelastic behavior [3,4]. Ligament failure models have been proposed [5-7]; however, to the authors' knowledge, there exist no viscoelastic ligament failure models that are based on fascicle material and failure properties determined experimentally. The motivation for the viscoelastic failure model in this study was to improve the failure models of uni-axially-oriented ligaments.

METHODS

Probabilistic distributions were used to describe both fascicle recruitment and failure behaviors. Three distribution types (normal, Weibull, and exponential) were investigated. The failure distribution was based on experimental fascicle failure tests [4]. Previous failure testing on eight human cervical posterior longitudinal ligaments (PLL) [7] were used to develop the recruitment distribution parameters and to validate the model. The ligament failure response was governed by the fascicle viscoelastic and failure behavior and the probabilistic manner in which they are recruited and then failed.

Cross-sectional areas of the ligament (CSA_L) and fascicles (CSA_F) and the fascicle volume fraction (VF) were quantified, and the number of fascicles (N) in the ligament was calculated as:

$$N = VF\left(\frac{CSA_L}{CSA_F}\right) \tag{1}$$

A probability density function (PDF) was assigned to represent fascicle recruitment and fascicle failure. The recruitment PDF parameters were optimized by fitting the model to the PLL failure data. The number of fascicles recruited (dN) at each ligament strain increment were calculated as:

$$dN[\varepsilon_L(t)] = N \cdot PDF \cdot d\varepsilon_L \, . \tag{2}$$

where ε_L is the ligament Lagrangian strain.

Once recruited, the individual fascicle force (F_F) was governed by quasi-linear viscoelasticity in terms of fascicle Lagrangian strain (ε_F) [3]. The ligament force ($\tilde{F}_L$) was then calculated which included all recruited fascicles at each strain increment. A cumulative density function ($CDF_{F,f}$) was fit to the fascicle failure Lagrangian strain data [3] and the number of fascicles failed at each ligament strain increment was calculated:

$$CDF_{F,f}^{(i)} = dN \cdot CDF_{F,f} \, . \tag{3}$$

Finally, the ligament force during the tensile failure test (F_L) was calculated by subtracting the force response of the failed fascicles from the original ligament force response ($\tilde{F}_L$),

$$F_L(\varepsilon_L, t) = \tilde{F}_L(\varepsilon_L, t) - CDF_{L,f}(\varepsilon_L) \cdot \tilde{F}_L(\varepsilon_L, t) \tag{4}$$

where $CDF_{L,f}$ is the $CDF_{F,f}$ normalized by N.

Using the initial recruitment distribution found from the model development, the failure distribution found from fascicle experimental failure test data, and the average number of fascicles in each ligament, the model was developed and used to predict the force response corridors from previous human spine ligament testing [8]. For each ligament type, these corridors were calculated as the average (± one standard deviation) force-time response from eight human PLLs, eleven anterior longitudinal ligaments (ALL), and six ligamentum flavums (LF).

RESULTS AND DISCUSSION

The normal distribution ($A^2 = 0.35$, $p > 0.25$) best fits the fascicle failure strain data. The resulting fascicle failure strain CDF and 95% confidence intervals are shown, Figure 1.

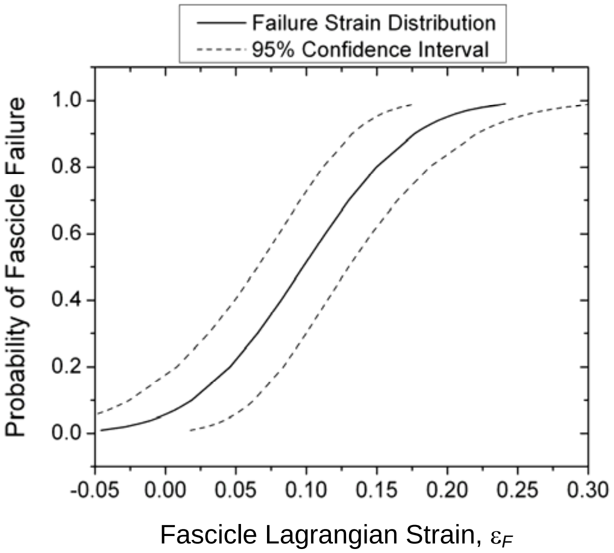

Figure 1. Fascicle failure strain distribution as a normal cumulative distribution function (solid line) with 95% confidence intervals (dotted lines).

Regarding recruitment, the model with the normal recruitment distribution PDF best fit the experimental data from PLL failure tests ($R^2 = 0.76 \pm 0.12$). The average (± one standard deviation) force response and model force prediction is shown for the PLL in Figure 2. The model represented the average PLL force very well from the recruitment portion of the force response until the peak force. Although the model did not follow the average PLL force after the peak PLL force, it remained within one standard deviation of the average force, with exception of a small portion of the curve at approximately 0.39 to 0.50 strain.

The collagen in the ALL and PLL is dense and predominately aligned in a superior-inferior orientation. Therefore, the model was a reasonable predictor of the ALL and PLL failure force responses. The collagen in the LF is less dense, but is also predominately aligned in a superior-inferior orientation between the adjacent lamina. The model overestimated the average LF failure force response; however, it remained within one standard deviation. This suggests that the calculated number of fascicles was incorrect, the recruitment or failure distribution differed from the average respective distribution, there were other factors that limited the response of the LF collagen fascicles, or a combination of all of these reasons. Further research is necessary to identify these delineating factors.

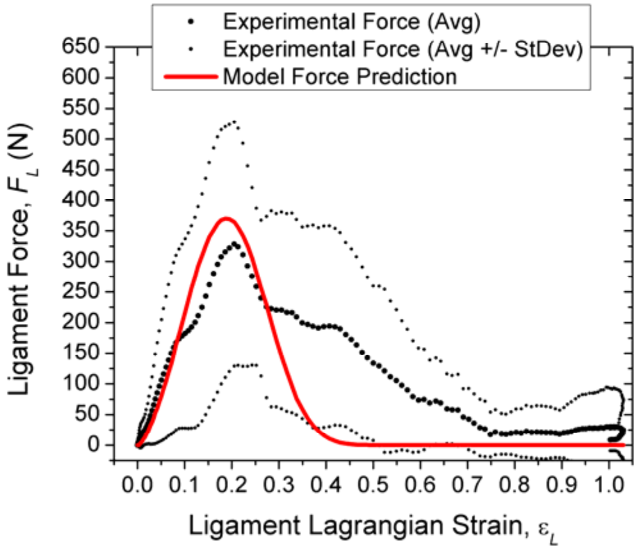

Figure 2. Microstructural model force prediction of average PLL experimental force. The experimental force was averaged from eight PLL tensile failure tests. The model force was calculated using the average distribution parameters (recruitment and failure).

CONCLUSIONS

This paper presented a ligament failure model that included fascicle material and failure properties obtained from experimental data at fast strain rate deformations. It was demonstrated that the resulting force prediction was close to the average force response for each ligament.

REFERENCES

1.Kastelic J, et al. *J Biomech* **13**, 887-893, 1980.
2.Lanir Y, *J Biomech* **16**, 1-12, 1983.
3.Elliot D, et al., *Annals Biomech Eng* **31**: 599-605, 2003.
4.Lucas SR, et al., *Biomech Mod Mechanobiology* **in press**.
5.Liao H and Belkoff SM, *J Biomech* **32**: 183-188, 1999.
6.Wren TAL and Carter DR, *J Biomech Eng* **120**: 55-61, 1998.
7.De Vita R and Slaughter WS, *Biomech Mod Mechanobiology* **6**: 189-193, 2006.
8.Bass CR, et al. *Spine* **32**: E7-E13, 2007.

ACKNOWLEDGEMENTS

This research was supported by the US Office of Naval Research, the Naval Air Systems Command (contract number N00421-06-C-0048) and the University of Virginia School of Engineering and Applied Science.

GROUND CONTACT TIME IN STEEPLECHASE HURDLING

Jenny Willis & Iain Hunter
Brigham Young University, Provo, UT
email: iain_hunter@byu.edu   web: http//biomech.byu.edu

INTRODUCTION

The origin of the steeplechase can be traced back to over 150 years ago when it began as a horse race in England. It has become a competitive track and field event for both men and women. The event was first introduced as an Olympic event for women in 2008. The steeplechase is a 3000 meter race requiring endurance, power, coordination and flexibility.

The challenges confronted during the race make steeplechase a unique event. During the race, runners confront 28 barriers in addition to 7 water jumps. Each lap the runners hurdle five barriers. One of these barriers is followed by a 3.66m water pit. All of the barriers over which the runners hurdle are 0.914m for men and 0.768m for women. Unlike hurdles, the barriers do not tip over upon impact. The rigid nature of the barrier combined with the distance of the race, give steeplechase hurdling distinguishable traits when compared to sprint hurdling.

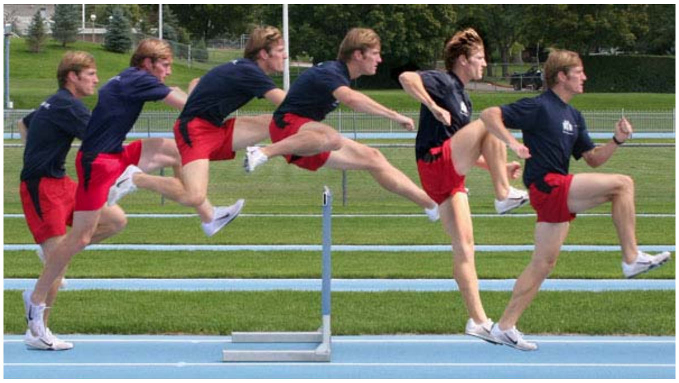

Figure 1: The movement pattern used in steeplechase hurdling.

In sprint hurdling, running speed is much greater. As a result, sprinters experience a greater forward lean of the trunk when hurdling [1]. In steeplechase hurdling, there is a greater focus on running economy. Additionally, in sprinting, individuals have less ground contact time due to a much quicker turnover than steeplechasers [2]. The distance between barriers also sets steeplechase apart from sprint hurdling. Steeplechase barriers are separated by approximately 80 meters, which allows each approach at a barrier to be analyzed as a unique event.

Shorter ground contact time leads to improved running speed [3]. In sprinting, those who have less ground contact time maintain a faster velocity. In longer distance events such as the 3000 meter, an ideal ground contact time has yet to be determined.

This study investigated how takeoff ground contact time in steeplechase hurdling relates to horizontal velocity over the barrier. Our purpose was to determine whether ground time during the takeoff step led to a greater horizontal flight velocity. Additionally, take off distance, was analyzed to determine its relationship to horizontal velocity.

METHODS

A high-speed camera running at 200Hz was placed perpendicular to the backstretch of the track at the 2008 Olympic Trials for the men's 3000m steeplechase. A 6m section of the track was visible within the camera view. The camera was placed 12m from lane 1 on the infield of the track. A 4m horizontal scaling was completed. Adjustments were made according to the lane position of each runner as they crossed the camera view.

The top 9 male runners in the finals of the 2008 Olympic Trials were analyzed. Ground time was determined by subtracting initial foot contact times from the point of takeoff in the step preceding the barrier. Horizontal velocity of the left hip was calculated 0.1s prior to when the hip was directly above the barrier until 0.1s after the hip passed the barrier using Dartfish ProSuite 4.5 (Dartfish Corp, Alpharetta, GA). Takeoff distance was measured horizontally, from takeoff toe to the front edge of the barrier.

Flight velocity was normalized by race time to account for running speed differences. A simple linear regression determined the correlation between flight velocity and takeoff ground time after accounting for race time.

RESULTS AND DISCUSSION

As take-off ground time increases, horizontal flight velocity decreases even after accounting for differences in average race pace ($p<0.01$, Figure 2).

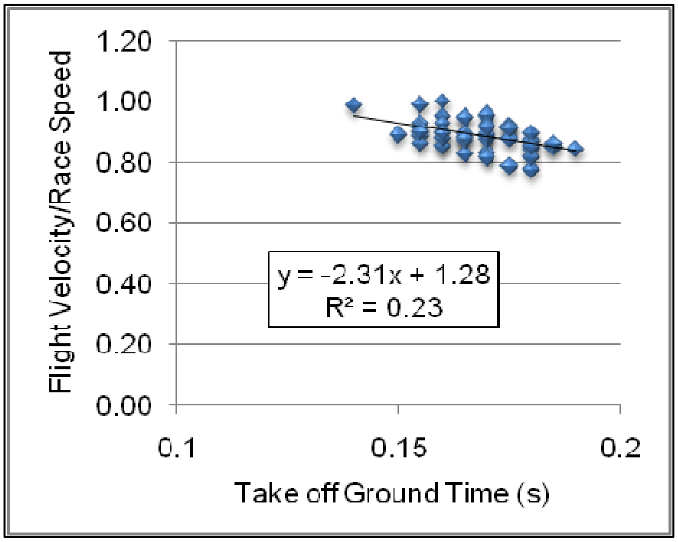

Figure 2: The relationship between horizontal flight velocity and take off ground time after accounting for average race speed.

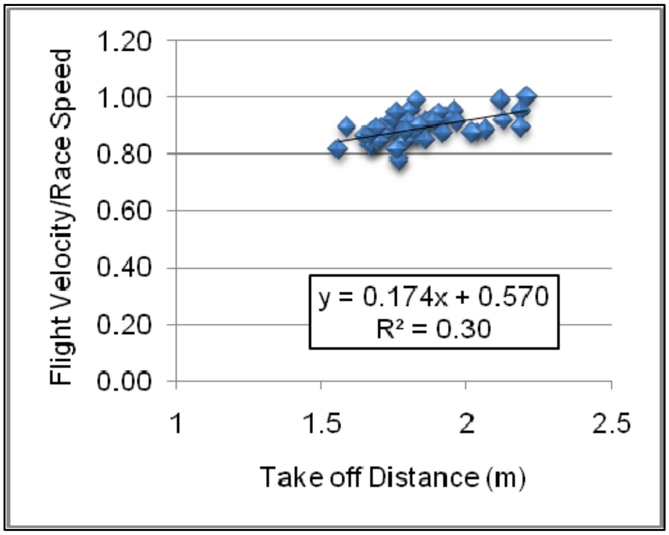

Figure 3: Flight velocity divided by average race speed versus take off distance.

When steeplechasers take off close to the barrier, they need to convert more of their horizontal velocity into vertical to avoid hitting the barrier with their lead leg. Additionally, lower flight velocities require the athlete to jump higher to avoid hitting the barrier on the way up or down since they must be in the air for a greater time. This was confirmed with greater take off distances leading to greater horizontal flight velocities ($p<0.01$, Figure 3). Along with the decreased velocity when takeoff occurs to close to the barrier, there is also a concern with the extra energy required to complete these higher jumps.

SUMMARY/CONCLUSIONS

There are many factors to consider in determining how a runner best maintains velocity over the barrier. However, it appears that takeoff ground time is an important variable to consider. Those who spent less time on the ground at takeoff demonstrated greater velocities over the barrier. Athletes who find ways to decrease ground contact time in the take-off step for steeplechase hurdling come closer to maintaining their race pace. This improvement may be possible through plyometric training specific to steeplechase hurdling.

REFERENCES

1. McDonald C, Dapena J. *Medicine and Science in Sports Exercise* **23**, 1392-1402, 1991.
2. Bushnell TD, Hunter I. *Sports Biomechanics* **6**, 261-268, 2007.
3. Mero A, et al. *Sports Medicine* **13**, 276-392, 1992.

ACKNOWLEDGEMENTS

Thank you to USA Track and Field for funding this study

REPEATABILITY OF ANKLE JOINT KINEMATIC DATA AT HEEL STRIKE USING THE VICON PLUG-IN GAIT MODEL

Cynthia J. Wright, Amee L. Seitz, Brent L. Arnold and Lori A. Michener
Virginia Commonwealth University, Richmond, VA
email: wrightcj@vcu.edu

INTRODUCTION

The Vicon Plug-In Gait (PiG) model is a commercially available biomechanical model for calculating joint kinematics using the Newington-Helen Hayes marker set. The PiG has been criticized by some for its simplistic marker set based on anatomic landmarks, which may increase the negative effect of soft tissue artifact and marker placement error on the accuracy and reliability of model output. Despite this criticism, the PiG is widely used in clinical gait analysis and has been shown to have moderate to good intra- and inter-tester repeatability using coefficients of multiple determination (CMD) to test waveform similarity [1,2]. CMDs are useful for some applications, but they do not capture the model's ability to measure joint kinematics at a discrete time point. While Schwartz et al. [3] reported reliability of discrete measures at the hip and knee using the PiG model, its reliability to measure ankle angles at a discrete point in all 3 anatomical planes is unknown.

As our laboratory specializes in ankle instability, reliable measurement of ankle joint kinematics was of particular interest. Heel strike (HS) was the discrete point of interest because previous research has found kinematic differences between individuals with ankle instability and healthy controls at HS [4,5]. Thus, the objective of this study was to assess the repeatability of ankle joint angles at HS in the sagittal, frontal and transverse planes using the PiG model.

METHODS

Eight healthy adults (3 males, 5 females, 25.63 ± 3.50 yrs, 1.69 ± 0.07 m, 66.69 ± 10.08 kg) were tested in our Sports Medicine Research Laboratory. All subjects had no history of lower extremity fracture or surgery, ankle sprain, or acute injury.

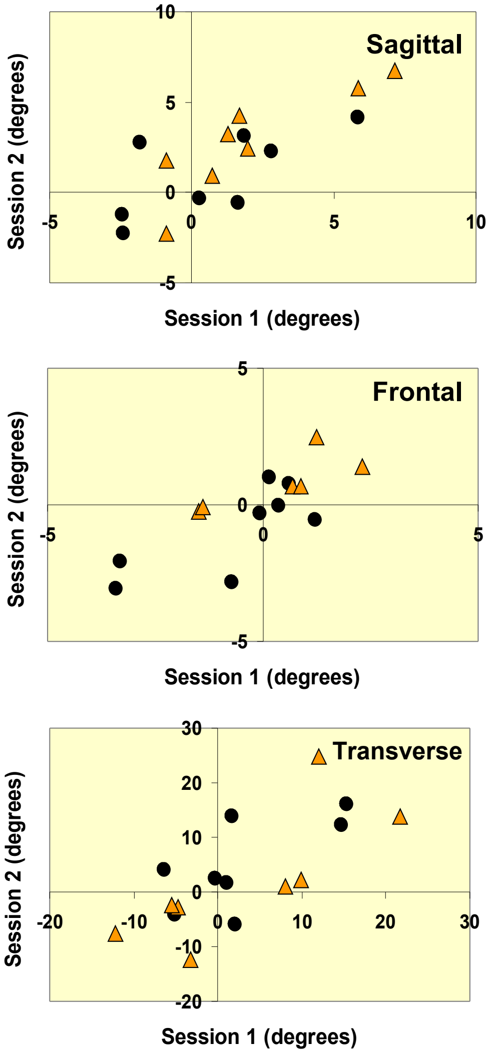

Figure 1: Between session intra-examiner agreement of ankle angles at heel strike for all 3 anatomic planes.

Each subject was tested during a single visit. During this visit, 2 examiners recorded 2 sessions each. For each session subject anthropometric measurements were obtained, the PiG marker set was applied, 5 practice trials were given, and 10 trials were recorded at 100Hz using a 12-camera infra-red motion analysis system. A trial consisted of walking across the capture space with HS of each foot occurring on a force plate (Bertec Corp., Columbus, Ohio). Markers were removed between each session, and adhesive residue cleaned off to prevent visual clues for marker re-placement.

Data was captured, Woltring filtered, and processed using Vicon Nexus 1.3 software (OMG, Oxford, UK). HS was defined as onset of ground reaction force >20N. Data was exported to a custom Matlab program which identified ankle joint ankle in each plane at HS. Data from 3 trials per session were averaged for analysis. Intraclass correlation coefficients ($ICC_{2,k}$) and standard error of the measurement with 90% confidence bounds (SEM_{90}, $SEM_{90} = 1.64 * SD * \sqrt{1-ICC}$), were calculated to assess intra- and inter-examiner reliability and error of ankle joint angle at HS separately for left and right ankles, in the 3 anatomical planes.

RESULTS AND DISCUSSION

Results for intra- and inter-examiner reliability and SEM_{90} are reported in Table 1. Intra-examiner ICCs ranged from acceptable to good in all planes, however error was only acceptable in the sagittal and frontal planes. The intra-examiner repeatability of ankle joint angle between sessions for each subject is shown in Figure 1. Inter-examiner ICCs were acceptable in the sagittal plane only. Low between-subject variability, as well as inter-examiner error, may have contributed to low inter-examiner ICCs.

Our results were similar to previous work using the PiG model, in that sagittal and frontal planes were the most reliable, whereas transverse plane motion had the lowest repeatability [1-3]. Previous ankle instability research has reported between group differences in ankle joint kinematics of 1-6 degrees [4,5]. The PiG model may not have sufficient precision to detect differences at the lower end of this scale.

CONCLUSIONS

Overall the PiG model shows good intra-examiner reliability and acceptable levels of error for ankle joint kinematics at HS in the sagittal and frontal planes, but not the transverse. Inter-examiner reliability and error were good for the sagittal plane only, suggesting only one examiner should be used for data collection. A more reliable and precise model would increase the ability to detect small differences in joint kinematics.

REFERENCES

1. Kadaba MP, et al. *J Orthop Res* **7**(6), 849-60, 1989.
2. Westhoff B, et al. *Sportverletzung Sportschaden* **18**(2), 76-9, 2004.
3. Schwartz MH, et al. *Gait Posture* **20**(2), 196-203, 2004
4. Delahunt E, et al. *Am J Sports Med* **34**(12), 1970-6, 2006.
5. Monaghan K, et al. *Clin Biomech* **21**(2), 168-74, 2006.

ACKNOWLEDGEMENTS

Funded in part by The Foundation for Physical Therapy.

Table 1: Intra- and Inter-examiner Reliability of the Average of 3 trials: Mean, SD, ICC, & SEM_{90}.

Comparison	Plane	Side	Mean angle ± SD (º)	ICC (95% CI)	SEM_{90} (º)
Intra-tester	Sagittal	Left	1.27 ± 2.70	0.77 (-0.29-0.95)	2.14
		Right	2.04 ± 0.93	0.93 (0.18-0.99)	1.24
	Frontal	Left	0.56 ± 2.67	0.89 (0.45-0.98)	1.49
		Right	-0.10 ± 1.53	0.86 (0.27-0.97)	0.94
	Transverse	Left	-3.15 ± 13.92	0.84 (0.28-0.97)	9.10
		Right	1.41 ± 8.30	0.88 (0.37-0.98)	4.80
Inter-tester	Sagittal	Left	0.54 ± 3.53	0.83 (0.23-0.96)	2.38
		Right	1.52 ± 2.92	0.86 (0.38-0.97)	1.79
	Frontal	Left	0.22 ± 2.76	0.34 (-3.46-0.88)	3.68
		Right	-0.05 ± 1.87	0.61 (-0.98-0.92)	1.92
	Transverse	Left	-1.48 ± 13.29	0.26 (-0.41-0.86)	18.75
		Right	0.99 ± 10.51	0.70 (-0.51-0.94)	9.44

PRESSURES APPLIED TO ANATOMICAL LANDMARKS OF THE KNEE WHILE IN KNEELING POSTURES

Moore, Susan M.; Porter, William L.; Mayton, Alan G.
National Institute for Occupational Safety and Health (NIOSH), Pittsburgh, PA, USA
Email: SMMoore@cdc.gov, Web: http://www.cdc.gov/NIOSH/Mining/

INTRODUCTION

According to the Mine Safety and Health Administration (MSHA) injury database, 227 knee injuries were reported in underground coal mining in 2007 [1]. Low-seam coal mines are those with extremely low working heights (≤42”). Gallagher et. al [2] found that the average cost per knee injury in low-seam coal operations was $13,121.29. Thus, it can be estimated that the financial burden of knee injuries was nearly three million dollars in 2007. Pressure applied to the knee while kneeling and crawling is likely a risk factor. Typically, mine workers utilize kneepads to better distribute the pressures at the knee; however, their ability to reduce the stresses at the knee is unknown. The objective of this study was to determine the pressure applied to the knee during static postures used in low-seam mining while not wearing kneepads and while wearing two kneepads commonly used in the industry (one articulated and one non-articulated).

METHODS

Ten subjects (7 male, 3 female) with an average age of 34±17 years (19 to 60 years) and an average weight and height of 683±98 N and 168.7±8.0 cm, respectively, participated. The subjects simulated postures utilized in low-seam mines: kneeling in full flexion; kneeling at 90° of knee flexion; and kneeling on one knee. These postures were simulated with working heights of 38” and 48” except for kneeling at 90°. This posture was performed only in 48”, since it is nearly impossible for adults at 38”. These postures were simulated for three kneepad states: no kneepads, non-articulated kneepads, and articulated kneepads. Testing order was randomized.

A custom-made capacitive pressure sensor[1] was used that was pre-shaped to the knee when it was at 90° of flexion. With the sensor affixed to the knee, a researcher palpated around the patella, patellar tendon (PT), and tibial tubercle (TT) identifying the sensing units associated with each structure. The sensor was zeroed in non-weight bearing conditions with the subject’s knee in 90° of knee flexion (for kneeling on one knee and kneeling at 90° of knee flexion) or when they were in a squat (for kneeling in full flexion). This ensured that the pressure measurements taken while the subject was in the assigned posture were only a result of the pressure applied directly to the knee by the floor and not due to pressure being applied to the sensor by the knee itself.

The subject assumed each of the five different postures and data were collected for 10 seconds. During analysis, the PT and TT data were combined due to their small individual size (~2 in.^{2}). The ratio of the pressure applied to the patella and the combined PT and TT was then determined for each point in time and the average of these ratios was taken to obtain a mean pressure ratio. For the patella and combined PT and TT, the maximum pressure at each point in time was then calculated and the average of these values taken to obtain the mean of the maximum pressure on each structure.

---

[1] Included 196 individual sensing units; Pressure Profile Systems, CA TactArray

A priori orthogonal contrasts were developed. Contrasts for kneepad states included comparisons of no kneepad state to wearing kneepads and comparing the non-articulated to articulated kneepads. All contrasts were tested using a T statistic using an alpha = 0.05

RESULTS

The majority (>60%) of the pressure was on the combined PT and TT for all postures (Figure 1). No difference was detected between the no kneepad and kneepad states, but a difference was detected between the articulated and non-articulated states. The presence of kneepads significantly reduced the mean of the maximum pressure applied to the combined PT and TT (Figure 2). The mean maximum pressure on the patella was much lower and ranged from 1.3 ± 1.1 psi to 27.1± 17.2 psi between postures. The pressure on the patella was sometimes higher with kneepads compared to the no kneepad state.

DISCUSSION

The pressure applied to the patella and combined PT and TT was determined for postures associated with low-seam mining. The majority of the pressure was transmitted to the knee via the combined PT and TT. While the kneepads did decrease the maximum pressure experienced at the combined PT and TT, pressures of greater than 25 psi were still experienced. At this time, it is unknown how this external pressure affects the internal stabilizing structures of the knee. The kneepads performed similarly despite significant differences in their material make-up. Some new kneepad designs in the industry have focused on eliminating the pressure at the patella. These data suggest that future kneepad designs should focus on redistributing the pressure at the combined PT and TT to other areas such as the shin.

REFERENCES

1. Mine Safety and Health Administration, *Injury and Illness Database*. 2007.
2. Gallagher, S., S. Moore, and P. Dempsey, *An Analysis of Injury Claims in Low-Seam Coal Mines.* Journal of Safety Research (submitted), 2008.

ACKNOWLEDGEMENTS

This work was funded by the National Institute for Occupational Safety and Health.

DISLCAIMER

The findings and conclusions in this study are those of the authors and do not represent the views of the National Institute for Occupational Safety and Health.

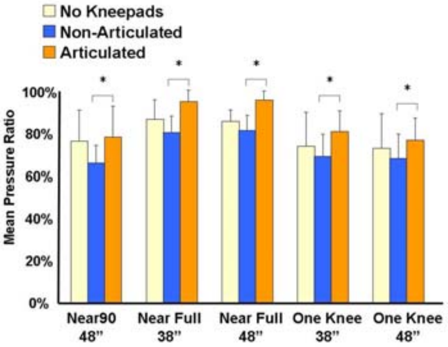

Figure 1. Mean pressure ratio at the combined PT and TT. *p<0.05

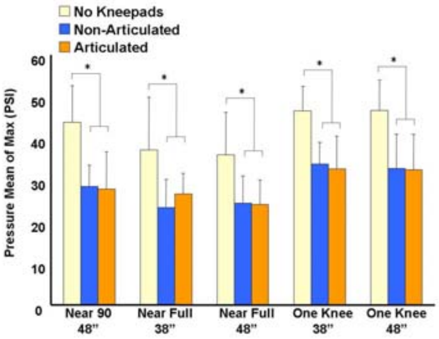

Figure 2. Mean of the maximum pressure at combined PT and TT. *p<0.05

THEORETICAL ANALYSIS OF THE MUSCLE LOADING IN A THUMB IN RESPONSE TO INCREASED JOINT STIFFNESS

[1]John Z. Wu, [2]Zong-Ming Li, [1]Robert G. Cutlip, and [3]Kai-Nan An
[1]National Institute for Occupational Safety and Health, Morgantown, WV, USA
[2]University of Pittsburgh, Pittsburgh, PA, USA
[3]Mayo Clinic College of Medicine, Rochester, MN, USA
Email: jwu@cdc.gov

INTRODUCTION

The development of osteoarthritis (OA) in the hand is associated with difficulties in gripping activities [1]. Previous studies indicated that OA in the hand results in increased joint stiffness [2], which in turn affects the grip strength. The biomechanics underlying the interactions between the muscular loading and joint stiffness variations due to OA has not been investigated. Since it is not convenient to experimentally measure the muscle forces in a finger under physiological conditions, biomechanical models of the hand and fingers are useful for studying such problems. The goal of the present study is to theoretically analyze the muscle force in a thumb in response to increased joint stiffness.

METHODS

The thumb was modeled as a linkage system consisting of a trapezium, a metacarpal bone, proximal and distal phalanges (Fig. 1). These four bony sections were linked via three joints: interphalangeal (IP), metacarpophalangeal (MCP), and carpometacarpal (CMC) joints. The IP joint was modeled as a hinge with one DOF (degree-of-freedom), while the MP and CMC joints were modeled as universal joints with two DOFs. Nine muscles were included in the proposed model: flexor pollicis longus (FPL), extensor pollicis longus (EPL), extensor pollicis brevis (EPB), abductor pollicis longus (APL), flexor pollicis brevis (FPB), abductor pollicis brevis (APB), the transverse head of the adductor pollicis (ADPt), the oblique head of the adductor pollicis (ADPo), and opponens pollicis (OPP). The thumb model was developed on the platform of the commercial software package AnyBody (version 3.0).

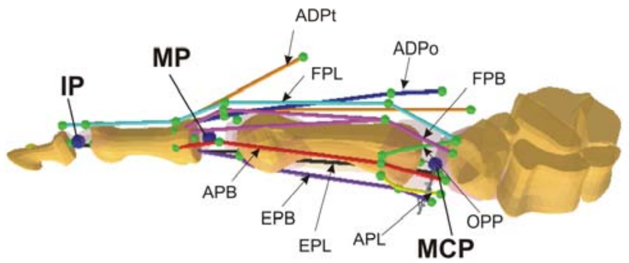

Figure 1: Schematics of the proposed thumb model developed using AnyBody.

The joints were assumed to have a linear stiffness [3]. The joint stiffness was simulated by adding a joint moment (M_r) that was proportional to the joint angular displacement (θ) from its neutral position (θ_0) and in opposite direction to the joint motion: $M_r = k(\theta - \theta_0)$. The normal joint stiffness (k) was assumed to be 0.05, 0.10, and 0.15 Nm/rad for the IP, MCP, and CMC joint, respectively. The joint stiffness was assumed to increase by 50% and 100%, simulating the early stage of OA. Numerical tests were performed using an inverse dynamic approach. The joint was prescribed to an angular motion at one degree-of-freedom (DOF) each time with all other DOFs of the joints being mechanically constrained, while the muscles forces in response to the joint motions were predicted. The joints were moving from their prescribed extreme positions within a time period of 10 s and at constant speeds.

RESULTS AND DISCUSSION

The predicted forces in EPL and FPL muscles in response to the IP, MCP, and CMC joint extension/flexion motions are shown in Fig. 2. The maximal muscle forces in EPL and FPL (in response to IP motion) for the joint with increased stiffness were found to increase by approximately 70% and 100%, respectively, compared with those for the normal joint. The increased joint stiffness also induced increased muscle forces in all other muscles in response to other joint motions (results not shown).

The predicted relationships between the joint motion and extrinsic muscle (FPL, EPL, APL, and EPB) activities are generally consistent with those observed in the experimental measurements [4] (results not shown).

CONCLUSIONS

Our simulations indicated that the increase in the joint stiffness - a biomechanical consequence in the early stage of OA in the fingers - induces a substantial increase in muscle forces, especially in EPL and FPL muscles in response to the IP, MCP, or CMC extension/flexion motions. Because the strength of the muscles in the fingers is limited, the muscles will not be able to overcome the joint resistance and to move the joints in the entire range of motion, if the joint stiffness is increased to a certain limit. This explains, in part, why the OA patients suffer a reduced range of motion [5].

REFERENCES

1. Chaisson, C. E., Zhang, Y., Sharma, L., Felson, D. T. *Osteoarthritis Cartilage* **8** Suppl A, S29-32. 2000.
2. Herzog, W., Clark, A., Longino, D. *Novartis Found Symp* **260**, 79-95. 2004.
3. Li, Z. M., Davis, G., Gustafson, N. P., Goitz, R. J. *J Orthop Res* **24** (3), 407-15. 2006.
4. Li, Z. M., Tang, J., Chakan, M., Kaz, R. *J Orthop Res* **26** (9), 1289-95. 2008.
5. Petersson, I. F., Jacobsson, L. T. *Clin Rheumatol* **16** (5), 741-60. 2002.

DISCLAIMER

The content of this publication does not necessarily reflect the views or policies of the National Institute for Occupational Safety and Health (NIOSH), nor does mention of trade names, commercial products, or organizations imply endorsement by the U.S. Government.

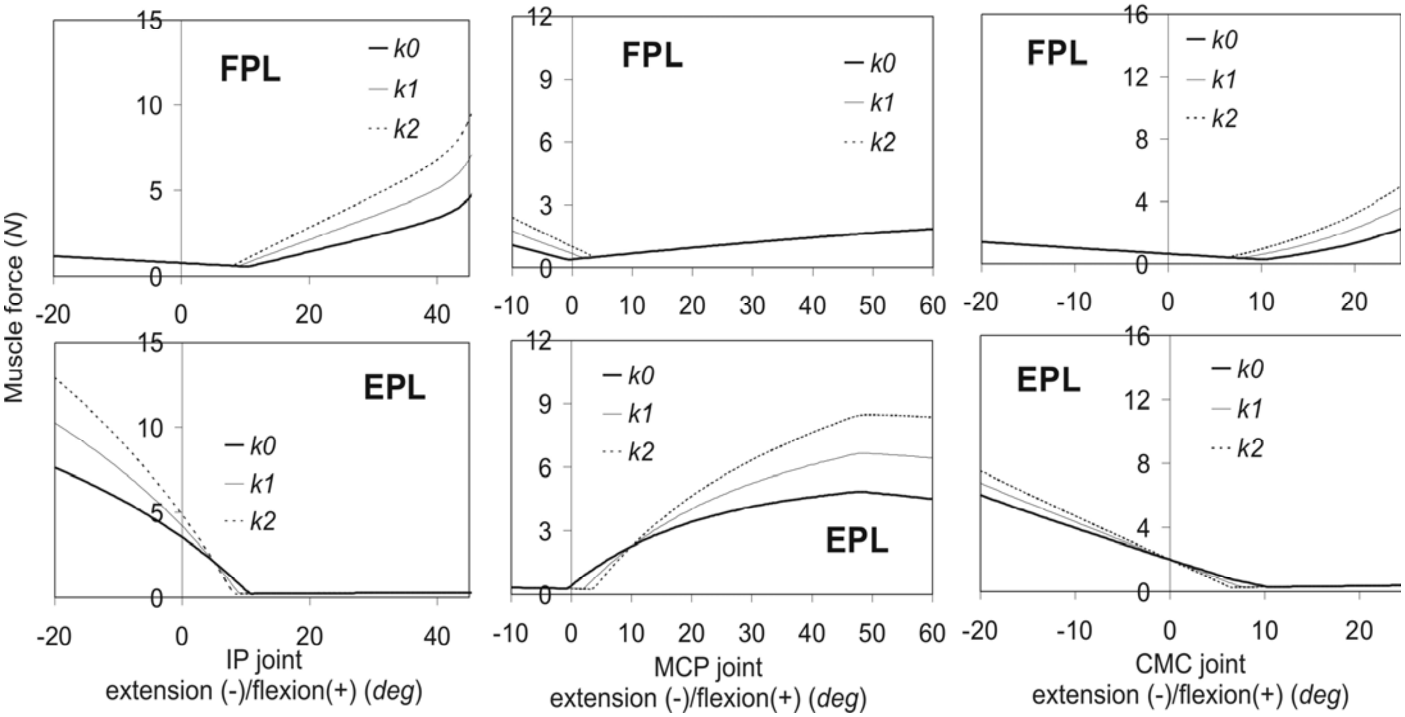

Figure 2: Predicted forces in FPL and EPL muscles in response to IP, MCP, and CMC joint extension/flexion motions. k_0, k_1, and k_2 are the stiffness for the normal joint and the joints with 50% and 100% increased stiffness, respectively.

AN ANALYSIS OF THE FINGER JOINT MOMENTS IN A HAND AT THE MAXIMAL ISOMETRIC GRIP: EFFECTS OF FRICTION AND CYLINDER DIAMETER

John Z. Wu, Ren G. Dong, Thomas W. McDowell, and Daniel E. Welcome
National Institute for Occupational Safety and Health, Morgantown, WV, USA
Email: jwu@cdc.gov

INTRODUCTION

The interaction between a handle and a hand affects the comfort and safety of the operator in operating a tool or a machine. In most of the previous studies, the investigators considered only the normal contact forces [1]. The effect of friction on the joint moments in fingers has not been sufficiently analyzed. Furthermore, the observed contact forces have not been linked to the internal musculoskeletal loading in previous experimental studies. In the current study, we develop an inverse dynamic model of a hand on the basis of the experimental data reported in [2]. Our hypotheses are that the dependence of the joint moments in the fingers on the diameter of the cylindrical handle is consistent in trend with those observed in the gripping forces reported in [2], and that the effects of friction on the distal interphalangeal (DIP) joint are different from those on proximal interphalangeal (PIP), and metacarpophalangeal (MCP) joints.

METHODS

For the time being, only four fingers -- index, long, ring, and little finger – were included in the model. The anatomical structure of each finger comprised four phalanges -- distal, long, proximal, and metacarpal phalange. These four phalanges were connected by three joints [3]: DIP, PIP, and MCP joints. The DIP and PIP joints were considered as hinges with one degree of freedom (DOF), simulating flexion/extension motion; whereas the MCP joint was modeled as a universal joint with two DOFs, simulating adduction/abduction and flexion/extension motions. The hand model was developed on the platform of the commercial software package AnyBody (version 3.0) (Fig. 1).

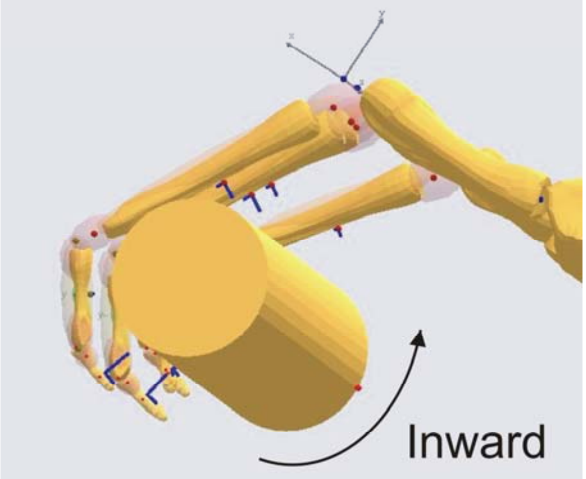

Figure 1: The hand model developed on the platform of the commercial software package AnyBody.

The simulations were performed using an inverse dynamics technique. The joint angles and the normal contact forces on each finger section reported in [2] were used as input, while the joint moments of each finger were predicted. The friction effects on the joint moments were simulated by applying tangential forces to each finger section. The magnitudes of the frictional forces were calculated by multiplying the normal contact forces by a friction coefficient. By varying the directions of the frictional forces, the effects of the torque direction can be simulated.

RESULTS AND DISCUSSION

The predicted joint moments in each of the four fingers as a function of cylinder diameter are shown in Fig. 2. The central column shows the results for the "frictionless grip", whereas the left and right columns show the results for the grip with a friction coefficient of 0.25 when rotating outward and inward, respectively. The theoretical results show that the descending order for the magnitude of the maximal joint moments in DIP and PIP in the fingers is: long, index, ring, and little finger. For the MCP joint, the trends in the joint moment for a large cylinder (D > 39 mm) are the same as in DIP and PIP joints, while that for a small cylinder (D < 31 mm) the descending order for the magnitude of

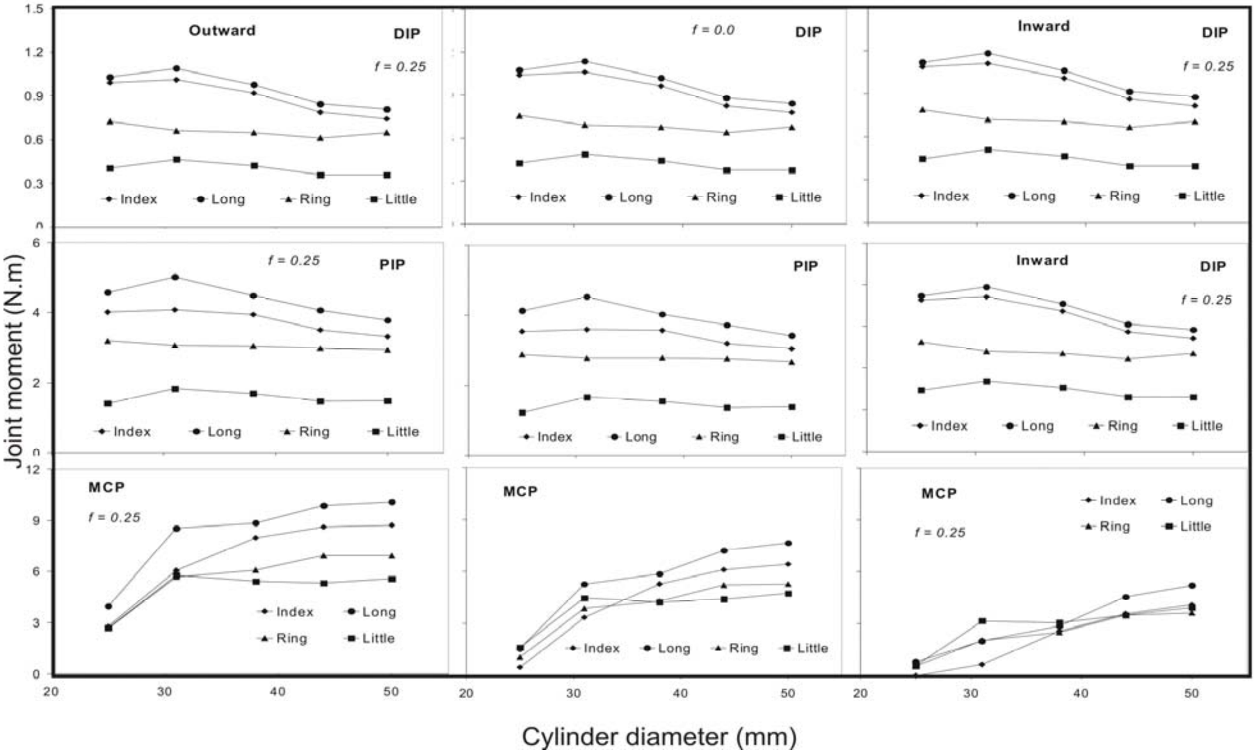

Figure 2: Simulated effects of the cylinder diameter and friction on the finger joint moments. The central column: the frictionless grip; the left and right columns: the grip with a friction coefficient 0.25 when rotating outward and inward, respectively.

the maximal joint moments changes to: long, little, ring, and index finger. For the DIP and PIP joints, the maximal joint moment as a function of cylinder diameter reaches the maximum at a cylinder diameter of about 31 mm, while the maximal MCP joint moment increases with an increasing cylinder diameter. The friction and torque directions do not vary the general trends of the dependence of the joint moments on cylinder diameter.

Our results show that the DIP and PIP joint moments reach their maximums at a handle diameter of about 31 mm, which is consistent with the trend of the finger contact forces measured in the experiments [2]. However, in the experimental study, the observed contact forces were not linked to the internal musculoskeletal loading. In the current study, we have confirmed that the contact forces on the fingers are associated with the PIP and DIP joint moments. Assuming that the DIP and PIP joint moments are predominant when gripping a cylinder, subjects should be able to apply the maximum gripping force at a cylinder diameter of about 31 mm.

CONCLUSIONS

In the current study, we proposed a universal model of a hand with four fingers to simulate grasping tasks. One of the most important advantages of the current approach over the previous studies is that the current model is developed with a commercially available software package (AnyBody) such that researchers and bioengineers can apply it as a universal tool for solving practical problems. The proposed approach will be useful for simulating musculoskeletal loading in the hand for occupational activities, thereby optimizing tool designs.

REFERENCES

1. Kong, Y. K., Freivalds, A. *Int J Indus Ergonomics* **32**, 13–23, 2003.
2. Lee, J. W., Rim, K. *J Biomed Eng* **13**(2), 152–62, 1991.
3. An, K. N., Chao, E. Y., Cooney, W. P., Linscheid, R. L. *J Biomech* **12**(10), 775–88, 1979.

DISCLAIMER

The content of this publication does not necessarily reflect the views or policies of the National Institute for Occupational Safety and Health (NIOSH), nor does mention of trade names, commercial products, or organizations imply endorsement by the U.S. Government.

THE RELATIONSHIP BETWEEN MUSCLE STRENGTH AND GAIT ASYMMETRY IN UNILATERAL, TRANS-TIBIAL AMPUTEES

Chandra H. Lloyd[1] and Todd D. Royer[2]
[1]Faculty of Kinesiology, University of Calgary, Canada
[2]Department of Health, Nutrition, and Exercise Sciences, University of Delaware, USA
email: chlloyd@ucalgary.ca, web:http://www.udel.edu/HNES

INTRODUCTION

Persons with unilateral, trans-tibial amputation (TTA) have an increased risk of developing osteoarthritis (OA) in the knee of their intact limb [1]. Several OA risk factors, such as peak knee external adduction moment and vertical ground reaction force load rate, have been found to be greater on the intact limb in TTAs [2]. Between-side strength discrepancies observed in TTAs [3] may be associated with an asymmetrical gait which relies heavily on the intact limb. This gait asymmetry may, over time, lead to a greater risk of developing OA in the intact limb. Therefore, the purpose of this study was to investigate the relationship between strength and gait asymmetry in TTAs. It was hypothesized that: (1) TTAs would be more asymmetrical than controls for gait and strength variables, and (2) muscle strength asymmetry would positively correlate with both gait asymmetry and intact side gait variables associated with knee OA risk.

METHODS

Eight individuals (7 male, 1 female; age 43±13 years; BMI 30.3±1.7 kg/m^2) with a unilateral transtibial amputation and eight able-bodied age, gender, and BMI matched controls (7 male, 1 female; age 45±13 years; BMI 31.0±3.4 kg/m^2) participated in this study.

Gait Analysis: To collect 3D gait data, retro-reflective markers were attached to each subjects' legs and pelvis using a modified Helen Hayes marker set. For TTA subjects, shank and foot markers on the prosthesis were approximated to match the intact side. Subjects then walked down a 10 meter runway at a self-selected pace over two force plates sampling at 480 Hz until five successful trials were captured for each limb. Eight digital cameras captured marker trajectory data at 60Hz. Three kinetic variables were calculated via inverse dynamics: peak knee external adduction moment (KEAMp), KEAM load rate (KEAMlr), and vertical ground reaction force load rate (GRFlr).

Strength Testing: Knee extensor (KEXT), knee flexor (KFLEX), and hip abductor (HABD) maximum isometric strength was measured using a handheld dynamometer with a static strap providing resistance. TTA subjects were tested with their prosthesis in place. For KEXT and KFLEX, the dynamometer head was placed on the distal shank or as distally as possible over TTA subjects' remnant limb within the prosthetic socket. HABD was tested with the subject side-lying, the dynamometer placed over the lateral femoral condyle. The highest force value measured out of three maximal efforts was used for analysis after being normalized to lever arm length (dynamometer head to joint line) and body mass.

Statistical Analysis: A symmetry index (SA) [4] was calculated for each variable to define asymmetry between limbs, with zero equaling perfect symmetry. Differences in asymmetry between groups were compared using a non-parametric t-test (hypothesis 1). All variables found to be more asymmetrical in TTAs as defined by $P \leq 0.05$ or effect size (ES) ≥ 0.70 were further analyzed to determine the relationship between strength asymmetry and OA risk variables. Spearman's Rank Correlations were performed between strength SA and gait variable SA, as well as between strength SA and intact side gait variables in TTAs (hypothesis 2). A rho of less than 0.5 was considered weak, 0.5 to 0.7 moderate, and 0.7 or greater a strong relationship.

RESULTS AND DISCUSSION

KEXT, KFLEX, and vGRFlr were significantly more asymmetrical in the TTA group ($P < 0.05$, ES= 4.21, 2.39, and 1.52, respectively) (Fig. 1). KEAMlr and KEAMp were not statistically significant, but had strong effect sizes at ES= 1.10

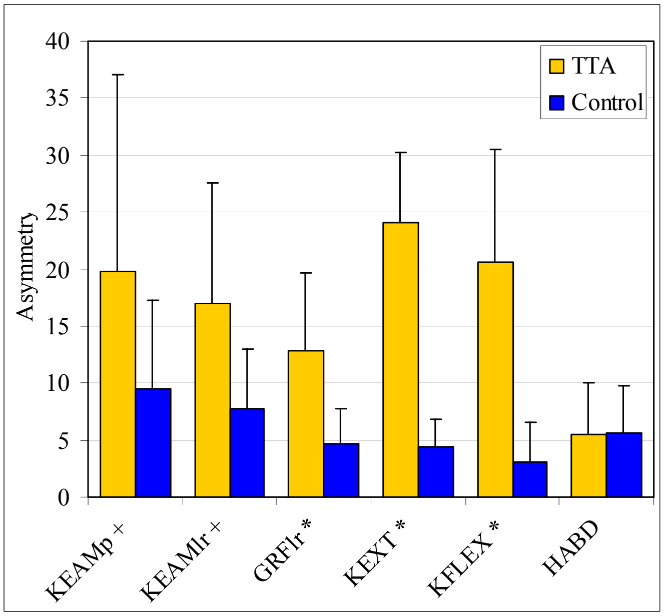

Figure 1: Asymmetry between TTA and control groups for the 6 variables. 0= perfect symmetry, increasing values indicate greater asymmetry. * =*P*<0.05, + =ES>0.7 between TTAs and controls.

and ES= 0.76, respectively. Thus the expectation that TTAs would be more asymmetrical than controls was supported. This is in agreement with previous literature [2,3]. HABD was not more asymmetrical in TTAs. Good symmetry between sides in TTAs indicates that the role of the hip abductors is not affected following a trans-tibial amputation. Muscles at the joint closest to the level of amputation, in this case the knee flexors and extensors, therefore appear more likely to be influenced by TTA gait adaptations.

For the correlations between strength asymmetry and gait variables, KEAMlr SA had a strong correlation with KEXT SA (rho=0.714, p<0.05), and a moderate correlation with KFLEX SA (rho=0.500). We propose that TTAs walk in such a way as to avoid large moments of force at the stump/socket interface. TTAs typically maintain a more extended knee on the prosthetic side during the stance phase of walking [5]. Greater knee extension would decrease joint moments and limit demands on the musculature of that limb, allowing the muscles on the prosthetic side to weaken.

Intact side GRFlr was moderately correlated with KFLEX SA (rho=0.643). Knee flexor strength asymmetry may have been related to the vGRFlr on the intact side because the knee flexors are used to provide forward propulsion in the absence of plantarflexors [6]. Weak knee flexors on the prosthetic side limb would prevent that limb from producing adequate propulsion. The intact limb would then have to weight itself more quickly in order to pull the body forward, resulting in a greater load rate on the intact limb.

KEAMp was not related to any of the strength symmetry measures. Strength asymmetry in TTAs appears to be more strongly related to loading rates during gait, rather than peak moments of force. It has been suggested that high loading rates during gait are one of the main causes for the initiation and progression of OA in the able-bodied population [6]. It may therefore be beneficial to investigate in greater detail the effects of muscle strength discrepancies on high loading rates in TTAs. Additionally, this relationship between strength asymmetry and OA risk has important rehabilitation implications in the TTA population.

CONCLUSIONS

Strength asymmetry of the knee extensors and flexors is related to OA risk variables, particularly loading rates, in individuals with a trans-tibial amputation. Strength asymmetry measures may therefore be useful in indicating problematic gait patterns in this population.

REFERENCES

1. Norvell D. et al. *Arch Phys Med Rehabil* **86,** 487-493, 2005.
2. Royer T and Wasilewski C. *Gait and Posture* **23,** 303-306, 2006.
3. Isakov E et al. *Clin Biomech* **11**, 233-235, 1996.
4. Zifchock R et al. *Gait and Posture* **27**, 361-367, 2007.
5. Powers C et al. *Gait and Posture* **8**, 1-7, 1998
6. Mundermann A et al., Arthritis Rheum **52**, 2835-2844, 2005.

ACKNOWLEDGEMENTS

This study was funded through the ASB Student Grant-In-Aid Award.

DOES A UNILATERAL RESTRICTION IN ANKLE MOBILITYAFFECT TRUNK KINEMATICS AND LOW-BACK LOADING DURING MANUAL LIFTING TASKS?

[1]Tyson A.C. Beach, [2]Jessica M. Clark, [3]Monica R. Maly, [1]Jack P. Callaghan
[1]Department of Kinesiology, University of Waterloo, Waterloo, ON, Canada, tbeach@uwaterloo.ca, callagha@uwaterloo.ca
[2]School of Physical Therapy, University of Western Ontario, London, ON, Canada, jclar59@uwo.ca
[3]School of Rehabilitation Science, McMaster University, Hamilton, ON, Canada, mmaly@mcmaster.ca

INTRODUCTION

Pain or mobility limitation in any area of the body could influence the trunk kinematics of workers. Davis and Seol [1] found that individuals who had previously injured upper or lower extremity joints moved their trunk differently when lifting than did individuals without previous injuries. Interestingly, previously injured segments or joints most distal to the low-back (e.g., hands/wrists and feet/ankles) had a greater influence on trunk kinematics than more proximal joints (e.g., shoulder). Because low-back loading patterns and trunk kinematics are tightly coupled, it is possible that distal joint dysfunction (e.g., injury-induced deficits in joint mobility) could alter the potential for low-back injury associated with occupational task performance. The purpose of this study was to determine if low-back loading during manual lifting tasks could be altered by a unilateral loss of ankle joint mobility.

METHODS

Eight male university students who had a mean age of 25 yrs (SD = 3.9 yrs), a mean stature of 1.84 m (SD = 0.06 m), and a mean mass of 88.5 kg (SD = 9.5 kg) participated in this study.

Together with force platform data, 3D kinematics of the trunk, pelvis, thighs, shanks, and feet were collected from study participants while they performed 18 permutations of a laboratory-based manual lifting task. Participants lifted two masses (light = 3.72 kg; heavy = 12.73 kg) from three different origins to three different destinations (Figure 1) at a self-selected pace. All lifts were performed both with and without the presence of a custom right ankle restraint; three repetitions of each lifting permutation were performed. An off-the-shelf support (T1 brace, Active Ankle Systems Inc., Jefferson, IN, United States) was modified to restrict ankle dorsiflexion in addition to limiting inversion and eversion.

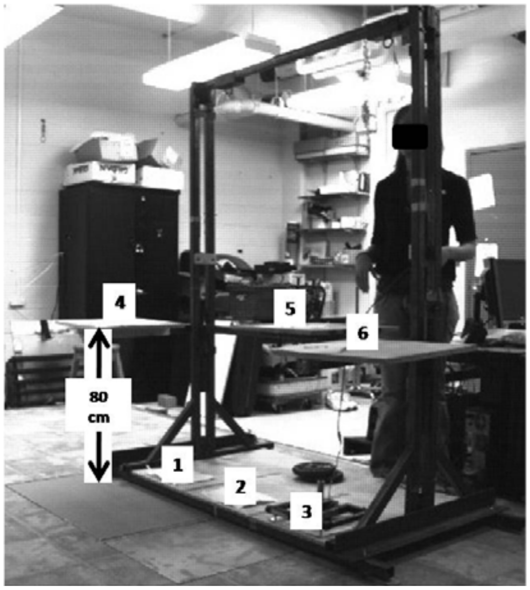

Figure 1. Configuration of experimental set-up. Lift origins (1,2,3) and destinations (4,5,6) are labeled.

Using measured anthropometrics, kinematic, and force platform data as inputs, a 3D inverse dynamics link segment model (LSM) of the lower body and trunk was created for each participant using commercial software (Visual3D, C-Motion, Inc., Germantown, MD, United States). From the LSM, orthogonal components of a net reaction moment about the low-back were calculated and subsequently input into a regression model [2] to yield estimates of L4/L5 joint compressive forces while lifting. No attempt was made to quantify L4/L5 joint shear forces, although anterior/posterior (A/P) and medial/lateral (M/L) shear components of net L4/L5 reaction forces were calculated based on the LSM.

Dependent variables were calculated as the mean of three “peak” values garnered from selected kinetic (L4/L5 load magnitudes) and kinematic (trunk and ankle angles) time-series data associated with each lifting permutation. Within-participant statistical comparisons were made using a general linear model ANOVA ($\alpha = 0.05$).

RESULTS

Significantly less ankle joint motion was permitted during lifting when the ankle restraint device was worn by study participants ($p < 0.0398$). Ankle dorsiflexion was most restricted, as losses of over 20 degrees were documented in some participants.

Qualitatively, various compensatory movement strategies were exhibited when ankle motion was restrained during lifting (Figure 2). Participants typically elected to flex their trunk by about 2 to 5 degrees more when the ankle restraint was present, although differences were not always statistically significant and were often greater when loads were lifted from the affected side. No statistically significant differences in trunk lateral bend or axial twist angles were observed when the ankle restraint was present ($p > 0.05$).

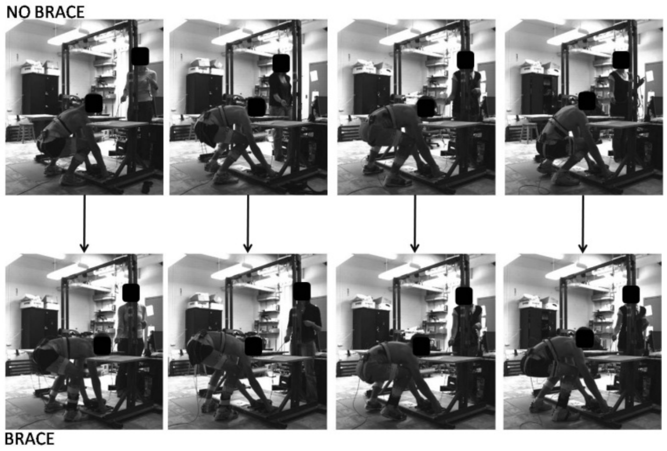

Figure 2. Various compensatory movements were exhibited in response to a unilateral restriction in ankle joint mobility.

Associated with compensatory lifting strategies, the L4/L5 reaction shear forces were altered in the A/P and M/L directions when ankle motion was restrained (Figure 3). As participants adapted their movement patterns in response to decreased ankle mobility, low-back loading patterns differed significantly from those observed when no deficits were imposed in ankle motion during lifting. In many cases, L4/L5 shear loads were of greater magnitude when the ankle was restrained, especially in the A/P direction. However, L4/L5 shear loading responses in the M/L direction were dependent on the external task demands (i.e., lift origins and destinations). L4/L5 joint compressive forces were unaffected by unilateral ankle joint motion restriction regardless of the specific external task constraints (Figure 3).

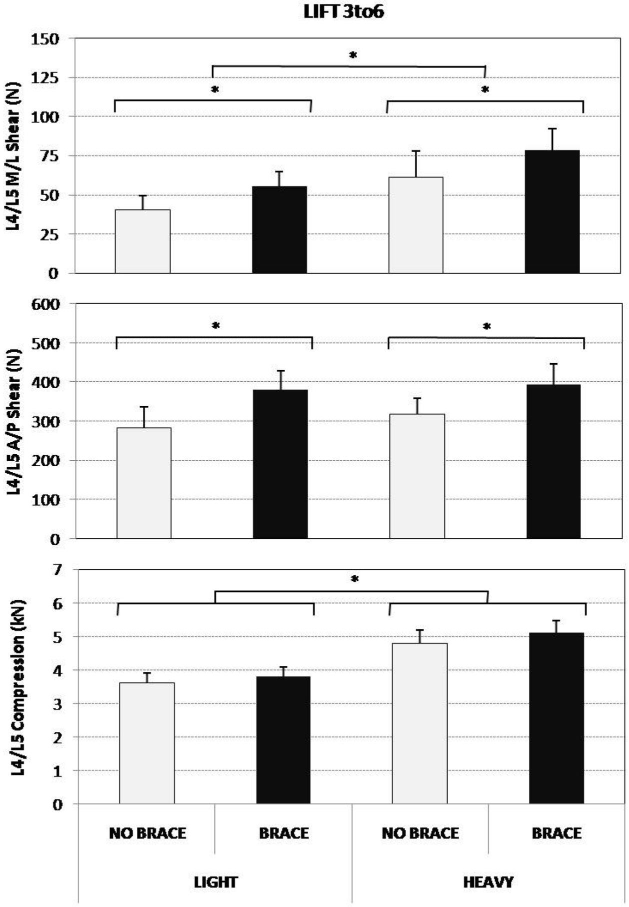

Figure 3. Low-back loading response of participants when they lifted light and heavy loads from positions 3 to 6 with and without restricted ankle mobility.

DISCUSSION AND CONCLUSIONS

Gross limitations in distal joint mobility can alter the way in which individuals move and load their low-backs when lifting. These altered loading patterns may increase the risk for low-back pain reporting [3] and therefore more work is necessary to track low-back pain incidence after peripheral joint injury. Given the complex changes observed in L4/L5 reaction kinetics, future attempts to incorporate trunk muscle activation patterns into the computation of low-back joint loads under similar conditions are warranted.

REFERENCES

1. Davis KG, Seol H. *Ergonomics* **48**, 135-149, 2005.
2. McGill SM, et al. *Ergonomics* **39**, 1107-1118, 1996.
3. Norman R, et al. *Clin Biomech* **13**, 561-573, 1998.

ACKNOWLEDGEMENTS

Funding for this project was provided by the *Centre of Research Expertise for the Prevention of Musculoskeletal Disorders* (CRE-MSD).

THE MAGNITUDE AND THE TIME DEPENDENT STRUCTURE OF FORCE FLUCTUATIONS ARE NOT MUSCLE-LENGTH DEPENDENT

[1] Samantha L. Winter and [2]John H. Challis
[1]Aberystwyth University, and [2]The Pennsylvania State University
email: sbw@aber.ac.uk, web: http://www.aber.ac.uk/sportexercise

INTRODUCTION

The force fluctuations produced during sustained isometric contractions have important implications for successful movement performance and the accurate control of muscle force. These fluctuations have been examined for different muscle groups, age groups, and for subjects before and after strength training (e.g., Enoka et al. [1]). However there has been no systematic evaluation of the effect of muscle length on the fluctuations in force during an isometric contraction. It is reasonable to suppose that aspects of the force fluctuations may be different for different muscle lengths since there is evidence that the optimal stimulation pattern of muscle is different for different muscle lengths [2]. In order to effectively study the relationship between the nature of the force fluctuations and muscle length in vivo, abduction of the index finger was studied as it caused by only one muscle, the First Dorsal Interosseus (FDI) [3].

The purpose of this study was to quantify the magnitude and time dependent structure of the fluctuations in force during sustained isometric contractions for different effort levels, at different muscle lengths in the FDI. It was hypothesized that length dependent differences in the neural recruitment strategy would show up as differences in these measures.

METHODS

Twelve subjects, five females and seven males were recruited; mean age 26 ± 6 years, mean mass 72.5 ± 16.7 kg, mean height 1.72 ± 0.1 m. All subjects provided written informed consent before participating and the Institutional Review Board at The Pennsylvania State University approved all procedures. A custom built rig was used to restrain the thumb at an 80 degree angle to the index finger and the wrist was restrained using Velcro straps at a 45 degree angle to the hand. A uni-axial force transducer (PCB 208-C01) was placed against the distal phalangeal head of the proximal phalanx of the index finger in order to measure the force due to isometric index finger abduction. Care was taken to align the axis of the transducer with the line of action of the force applied by the finger.

Subjects performed familiarization contractions then performed maximal isometric finger abduction contractions in three finger positions: long FDI muscle length, medium FDI muscle length, and short FDI muscle length. Neuromuscular stimulation was delivered during one of the maximum efforts in each finger position (square wave percutaneous stimulation applied at a frequency of 100 Hz to the motor point using a Sys Stim 270A stimulator at a level that was tolerable for the subject, but that produced a rapid finger abduction movement on application of the

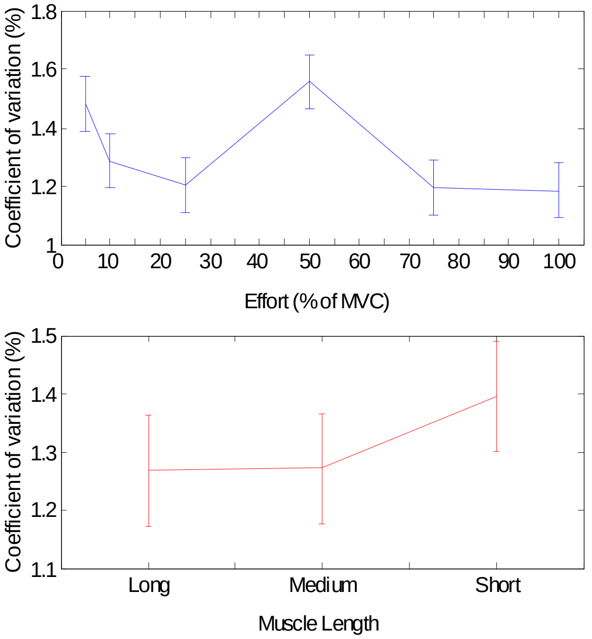

Figure 1: Mean coefficient of variation (bars show standard error) for a) each effort level where means are taken across all muscle lengths and subjects; and, b) for each muscle length where means are taken across all effort levels and subjects.

stimulation). Subjects then produced isometric contractions at long, medium and short muscle lengths at 5%, 10%, 25%, 50%, 75% and 100% of the maximum in each finger position by targeting a force displayed on a computer monitor in a Labview 8.2 environment. A one minute rest was given between each effort and five minutes rest was given between finger positions. The force signal was sampled at 160Hz and low pass filtered at 40Hz. A minimum variance criterion was used to select a window for further analysis from the force record. The magnitude of the fluctuations was quantified using the coefficient of variation (CV) (the standard deviation of force divided by the mean force). The fractal scaling index, alpha, was calculated using the Detrended Fluctuation Analysis (DFA) algorithm [4]. A surrogate analysis of the data showed that the DFA results were due to signal properties, not measurement system noise. Statistical comparisons on the DFA and CV response variables were performed using a three way ANOVA.

RESULTS AND DISCUSSION

While the neuromuscular stimulation was at a level sufficient to increase force if the subjects were not able to fully recruit the muscle voluntarily, all subjects were able to fully recruit the muscle in at least one of the finger positions. A Chi-Square test showed no association between finger position, and therefore muscle length, at which subjects were not able to fully activate the muscle (p=0.937).

The magnitude, as quantified by CV, of the fluctuations in force was significantly increased at short muscle lengths (p=0.012) (Figure 1). The DFA indicated different scaling behavior for short muscle lengths (Figure 2) that was statistically significant (p=0.010). This may be due to different motor unit firing characteristics required to achieve full activation at short muscle lengths.

The relationship between CV and effort level, and between alpha and effort level, may be due to the relative contributions of motor unit recruitment and rate coding to force gradation in the FDI.

CONCLUSIONS

The results showed that there was no systematic inability to maximally activate the FDI at short muscle lengths, as evidenced by the lack of increase in force when a maximal effort was supplemented by neuromuscular stimulation. However, there was a statistically significant increase in the magnitude of the force fluctuations, quantified by the CV, of force, and a statistically significant change in the time dependent structure of the force fluctuations, quantified by the alpha value, of the fluctuations. Taken together the results indicate that full activation of the FDI is possible at short muscle lengths, but that an alternative recruitment strategy is necessary to achieve this. These findings have implications for the accurate control of movement and force production.

REFERENCES

1.Enoka RM, et al. *J Electromyogr Kinesiol,* **13**, 1-12, 2003.

2.Mela P, et al. *IEEE Trans Neural Syst Rehabil Eng*, **10**, 85-93, 2002.

3.Masquelet AC, et al. *Rev Clin Radiol Anat*, **8**, 19-28, 1968.

4.Peng, C-K, et al. *Phys Rev E*, **49**, 1685-1689, 1994.

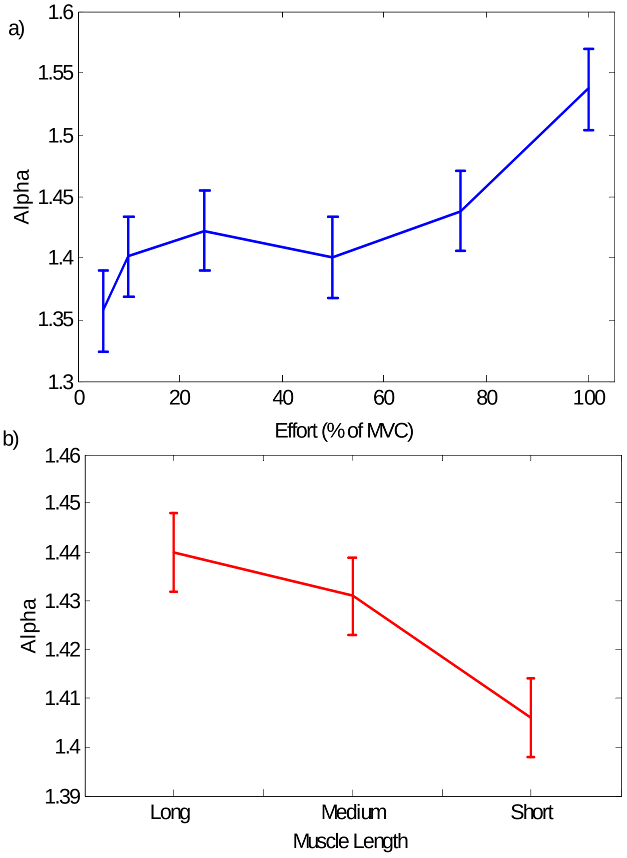

Figure 2: Mean alpha value (bars show standard error) for a) each effort level where means are taken across all muscle lengths and subjects; and, b) for each muscle length where means are taken across all effort levels and subjects.

THIGH-CALF AND HEEL-GLUTEUS CONTACT FORCES IN HIGH FLEXION (EXPERIMENTAL RESULTS)

Jonisha P. Pollard
National Institute for Occupational Safety and Health, Pittsburgh Research Laboratory, Pittsburgh, PA, USA
email: JPollard@cdc.gov, web: http://www.cdc.gov/niosh/mining

INTRODUCTION

In restricted vertical working heights such as low-seam coal mines, workers are forced to assume kneeling or squatting postures to perform work. These postures are associated with increased risks for the development of significant knee pathologies such as meniscal tears and osteoarthritis [1,2].

Previous research has shown an increased applied knee flexion moment when kneeling in high flexion [3]. However, these models have been applied to flexion up to 140° which neglects contact between the thigh and calf which occurs beyond 140°. In addition to thigh-calf contact, when kneeling near full flexion there may be additional contact between the heel and gluteal muscles.

To the author's knowledge, heel-gluteus contact has not been previously investigated, but thigh-calf contact has received some attention. Zelle (2007) reported thigh-calf contact forces up to 30% bodyweight (BW) [4]. Zelle (2009) reported decreased knee forces when accounting for thigh-calf contact [5]. Caruntu (2003) reported erroneous force and moment estimations when thigh-calf contact was neglected from models to determine muscle and ligament forces [6].

In this study thigh-calf and heel-gluteus contact forces were quantified to determine their effect on the externally applied flexion moment in high flexion.

METHODS

Ten subjects were recruited (7 male; age: 34 ± 17 years; weight: 683 ± 98 N; height 169 ± 8 cm) from the National Institute for Occupational Safety and Health in Pittsburgh, PA. No subjects had a history of knee pathologies.

Subjects were instructed to stand while a clinical seating pressure assessment system (ClinSeat®, Tekscan Inc., South Boston, Massachusetts, USA) was placed along their lower right leg from the popliteal to the heel. They were then instructed to squat and pressure data was collected for 5 seconds. (Figure 1) Next, the subject kneeled on the floor at 90° flexion. The pressure sensor was again laid across their lower right leg. They then went into full flexion while data were collected for 5 seconds. During data collection, the distance from the top of the sensor to the lateral epicondyle of the femur was measured and recorded. Subjects were given no specific instructions on kneeling, and therefore assumed postures which they felt caused the least discomfort.

The supplied software (Advanced ClinSeat, Tekscan Inc., South Boston, Massachusetts, USA) was used to record the pressure distributions and calculate the centers of pressure and total forces at the thigh-calf and heel-gluteus contact areas.

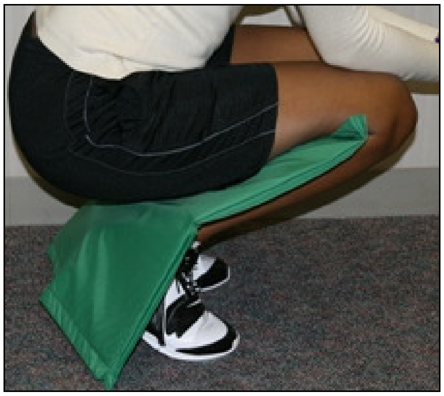

Figure 1: Experimental data collection

RESULTS AND DISCUSSION

In all subjects, thigh-calf contact forces when squatting were at least 20% BW, with a mean of 39 ± 14% BW (Figure 2). Thigh-calf contact in full flexion was less than squatting with a mean of 28 ± 13% BW (Figure 3). The centers of pressure were

6.6 and 6.1 inches inferior of the epicondylar axis for squatting and kneeling near full flexion, respectively. In 7 of the 10 subjects, kneeling near full flexion resulted in heel-gluteus contact. These contact forces were less than the thigh-calf contact forces, with a mean of 11 ± 6% BW and a center of pressure 16.3 inches inferior of the epicondylar axis; approximately at the subject's heel.

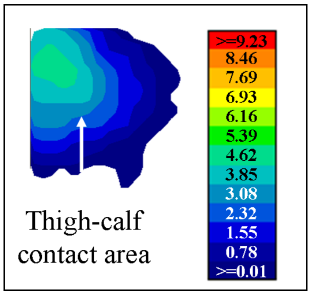

Figure 2: Typical pressure distribution (psi) for squatting.

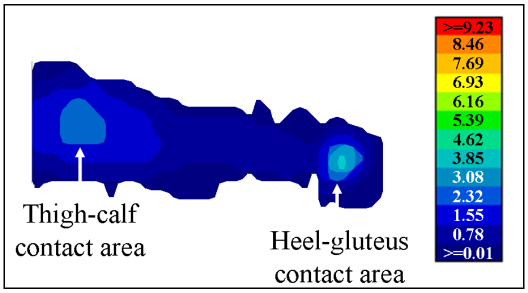

Figure 3: Typical pressure distribution (psi) for kneeling near full flexion.3

Thigh-calf and heel-gluteus contact forces created extension moments about the knee. Mean thigh-calf contact moments when squatting and kneeling near full flexion were 4% BW*Ht and 3% BW*Ht, respectively. The mean heel-gluteus contact moment was 3% BW*Ht.

The forces and moments generated by thigh-calf contact have been shown to greatly affect the muscle and ligament forces as well as the stresses in knee structures. Caruntu and colleagues (2003) found that when accounting for thigh-calf contact, quadriceps forces decreased by 700 N and medial collateral ligament forces increased by 50% [6]. Zelle (2009) found reductions in compressive knee forces by 1.99 times BW when thigh-calf contact was included. Contact stresses on the tibial post of polyethylene knee replacements also decreased by 21.2 MPa when including thigh-calf contact [5]. Having a comparable moment contribution to thigh-calf contact, it is expected that heel-gluteus contact will have similar affects on the forces and stresses in the internal knee structures.

CONCLUSIONS

Thigh-calf and heel-gluteus contact forces act in the anterior direction of the shank, thereby extending the knee and reducing the applied flexion moment. These forces act to stabilize the knee in high flexion and may significantly affect calculations in computational knee models.

Traditionally, segment contact forces have been neglected from biomechanical models. The complexity of modeling tissue deformation and pressure distributions may discourage researchers from considering these inputs. However, the magnitude of these forces were shown to be quite large, >30% BW and the moments produced by these contact forces may decrease externally applied flexion moments by as much as 9% BW*Ht.

In the future, biomechanical models should account for the thigh-calf and heel-gluteus contact as neglecting these forces may result in erroneous force and moment estimations.

REFERENCES

1. Anderson JJ, Felson DT. *Am J Epidemiol* **128**, 179-189, 1988.
2. Sharrard WJW, Lidell FDK. *Brit J Industr Med* **19**, 195-202, 1962.
3. Nagura T, et al. *J Orthop Res* **20,** 881-886, 2002
4. Zelle J, et al. *Clin Biom* **22**, 821-826, 2007.
5. Zelle J, et al. *J Biomech,* 2009.
6. Caruntu DI, et al. *Summer Bioengineering Conference*, Key Biscayne, Florida, 2003.

DISCLAIMER

The findings and conclusions in this paper are those of the author and do not necessarily represent the views of the National Institute for Occupational Safety and Health.

IS MUSCLE CO-ACTIVATION A PREDISPOSING FACTOR FOR LOW BACK PAIN DEVELOPMENT DURING STANDING?

Erika Nelson-Wong and Jack P. Callaghan
Department of Kinesiology, University of Waterloo, Waterloo, ON
email: enelsonw@uwaterloo.ca

INTRODUCTION

Occupations involving static postures such as prolonged standing have been associated with low back pain (LBP) development [1]. While trunk muscle co-activation has been found in people with LBP compared with healthy controls [2], it is unknown whether these differences preceded the development of the LBP problem. Therefore, it cannot be determined whether the muscle co-activation is an adaptation to LBP or a predisposing factor.

Previous work [3] has found muscle co-activation to be associated with LBP development in previously asymptomatic individuals. The purpose of this study was to investigate whether muscle co-activation is a predisposing versus adaptive factor in standing-induced LBP. A multifactorial approach including clinical assessment tools and psycho-social questionnaires was used to enhance the clinical relevance of the work.

METHODS

43 volunteers, 22 male and 21 female, with no history of LBP were enrolled. Following a clinical examination by a physical therapist, 16 channels of continuous electromyography (EMG) from the trunk and hip were collected during 2-hrs of standing. Participants were instructed to ‘stand in their usual style’ as they completed light occupational tasks. Participants rated LBP on a 100 mm visual analog scale (VAS) every 15 min. Participants who exhibited increases of LBP > 10 mm were considered to be pain developers (PD).

Muscle co-activation was quantified with co-contraction index [4] (CCI). Three-way general linear models (group, gender and time) were used for statistical analyses with $p<0.05$ for significance.

RESULTS

Participants clearly separated into two groups with 40% of participants being classified as PD (Figure 1). There were no gender differences in pain development, gluteus medius or trunk flexor/extensor co-activation as quantified by CCI.

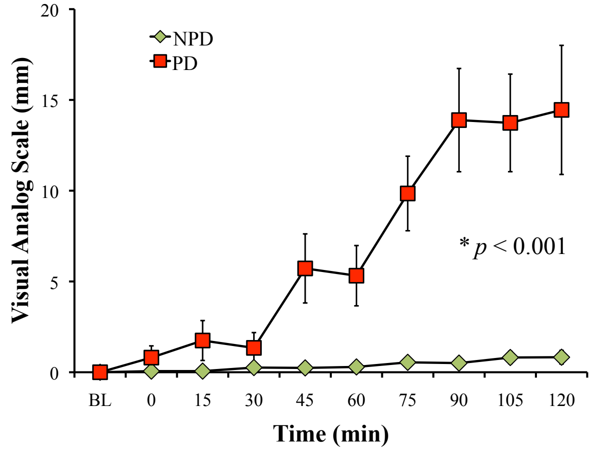

Figure 1: PD and NPD were clearly separated based upon VAS scores during the 2-hours of standing.

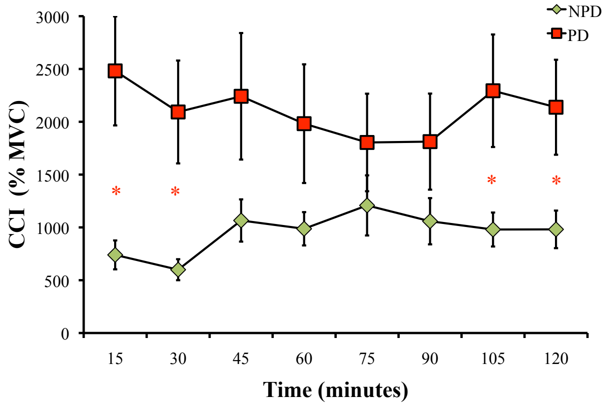

Figure 2: PD demonstrated higher gluteus medius muscle CCI than NPD, especially during early and late stages of standing (*$p < 0.05$).

The only clinical assessment tool that predicted PD was a novel Active Hip Abduction (AHAbd) test ($p < 0.05$) [5]. Bilateral gluteus medius and trunk flexor/extensor CCI values were higher in PD versus NPD during the initial and final stages of standing (Figure 2).

PD and NPD groups demonstrated different modulation of co-contraction throughout the standing period. PD had a decrease in both trunk and gluteus medius co-contraction during the middle portion of standing, corresponding to the period of acute pain development (Figure 3), while the NPD group had an overall increase in their co-contraction levels during the same time period (Figure 4).

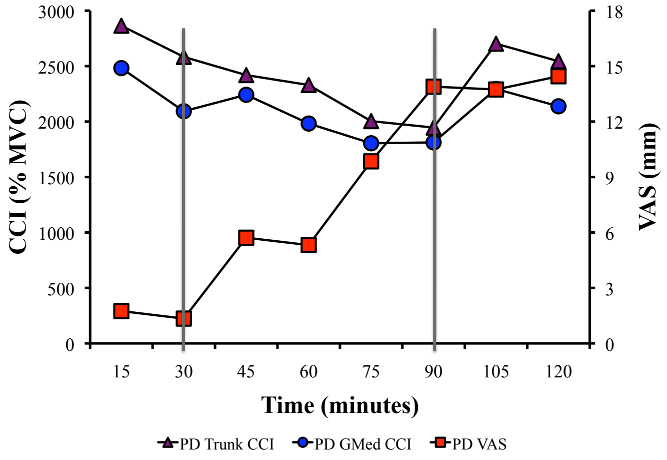

Figure 3: Pain Developers had a decrease in both trunk and gluteus medius CCI during time period of greatest pain development (30-90 minutes).

DISCUSSION

Low back pain developers had increased co-contraction prior to any subjective reports of pain, leading us to conclude muscle co-activation is a predisposing rather than adaptive factor for LBP development during this task. PD also demonstrated decreased frontal plane control and reported more difficulty in performance during the AHAbd clinical test. Muscle co-activation during standing in this group may be present as a compensatory motor control pattern for an underlying deficiency in trunk control that has not yet manifested with clinical LBP symptoms. A combination of the above findings could be useful in early identification of individuals who are at-risk for LBP, especially those exposed to occupational tasks involving prolonged standing.

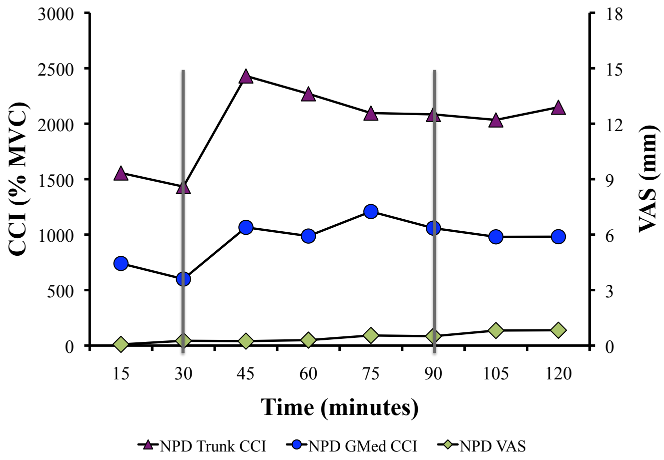

Figure 4: Non-Pain Developers had a general increase in both trunk and gluteus medius CCI during the same time period (30-90 minutes).

CONCLUSIONS

Individuals who develop LBP during standing demonstrate different muscle activation patterns than individuals who do not develop LBP. Differences exist prior to pain development, and therefore may be a predisposing factor for LBP during standing. Some increase in muscle co-activation during a relatively static, prolonged task, may provide some protection against LBP development.

REFERENCES

1. Kim J, et al. *Appl Ergon* **25** (1), 9-34, 1994.
2. Van Dieen J, et al. *Journal of Electromyography and Kinesiology* **13**, 333-351, 2003.
3. Nelson-Wong E, et al. *Clinical Biomechanics* **23**, 545-553, 2008.
4. Lewek, M, et al. *Osteoarthritis and Cartilage* **12** (9), 745-751, 2004.
5. Nelson-Wong, et al. *J Orthop & Sports Physical Therapy*, submitted in revision, 2009.

ACKNOWLEDGMENTS

The authors wish to acknowledge the Natural Sciences and Engineering Research Council of Canada. Dr. Nelson-Wong is also supported through a PODS II scholarship, Foundation for Physical Therapy, American Physical Therapy Association.

EFFECT OF MODULATION OF THE INTERNAL FORCES ON DIGIT COORDINATION DURING MULTI-FINGER OBJECT PREHENSION

Joel Martin, Mark Latash, Vladimir Zatsiorsky
Department of Kinesiology, The Pennsylvania State University, University Park, PA 16802
email: jrm496@psu.edu

INTRODUCTION

Holding an object statically in the air requires subjects to co-vary finger forces such that a synergy [1] exists between the fingers in order to satisfy the three basic equations of equilibrium. Ultimately, these equations signify that the controller needs to coordinate finger forces to account for (a, b) horizontal and vertical translations of the object and (c) orientation of the object (torque). During prehension the forces exerted on an object can be divided into manipulation and internal forces. Manipulation forces cause a disturbance to the equilibrium of an object while internal forces do not disturb equilibrium, internal forces cancel each other out. The purpose of this study was to investigate how finger forces change when subjects were instructed to increase specified internal forces in a self-paced, ramp-like manner while statically holding an object.

METHODS

Ten young, healthy, male subjects participated in the experiment. The main testing apparatus consisted of an aluminum handle with four six-component force/moment transducers for each finger and one imitation transducer for the thumb (Figure 1). Attached to the base of the handle was a horizontal bar so that a mass could be positioned at five locations (L2, L1, M, R1, R2) to generate different external torques.

The subjects were instructed to grasp the handle and perform three tasks without allowing any movement of the handle to occur. The tasks were: 1) grasp the handle stronger, i.e. slowly increase the finger normal forces (SQZN), 2) slowly spread (abduct) fingers tangentially (SPDT), and 3) slowly squeeze (adduct) fingers tangentially (SQZT). Subjects were asked to increase the instructed forces in a smooth ramp-like manner at a self-timed pace. The tasks required subjects to manipulate internal forces while keeping manipulation forces constant. For each subject five trials were recorded at each task for each external torque. The total number of trials was 75 (5 trials x 5 torques x 3 tasks = 75 total trials).

The main focus of the analysis was on the change in normal and tangential forces during the trials at both the individual (IF) and virtual finger (VF) level. (A virtual finger is an imaginary finger that has the same net mechanical effect as the sum of the four fingers' effects.) Three- and two-way repeated measure ANOVAs were performed at the IF and VF levels, respectively.

RESULTS

The results are organized by the three tasks. We were most interested in force changes in the non-instructed direction (i.e. normal force changes for SPDT and SQZT; tangential force changes for SQZN) as well as any similar patterns of finger interaction common across subjects. The average vectors produced by each finger, acting on the force sensors, at the end of each trial are shown in figure 2.

SQZN: As required by the task the normal forces all showed significant increase during the trials. Tangential forces showed significant changes as well ($p < 0.001$, IF and VF levels), the VF force changes were in the negative direction, i.e. downward. The magnitude of change increased as the external load moved in the right direction, i.e. produced lower pronation or higher supination torques.

SPDT: Both the changes in normal and tangential forces were significantly different from zero ($p < 0.01$, IF and VF levels). The normal forces of all fingers, and thus VF, showed fairly large increases during the trials. Note that this increase was not prescribed by the instruction. The I-finger showed the largest positive tangential force change, across all torques. The M- and R-fingers showed minimal change and the L-finger showed a negative change in tangential force, across all trials. The averaged VF tangential force change was positive for all torques.

SQZT: Similar to SPDT, both the normal and tangential forces showed changes that were significantly different from zero ($p < 0.005$, IF and VF levels). However, the direction of change and pattern of change were different than SPDT. The direction of the tangential force change matched that required of the task. I-finger showed tangential force change in the opposite direction. M-finger showed minimal change and R- and L-fingers showed a change in tangential force in the prescribed direction. The VF tangential force change was downward and the VF normal force change was increased, for all torques.

DISCUSSION

The results show that instructed force changes in one direction also induced force changes orthogonal to the instructed direction. This is not totally unexpected. In order to maintain rotational equilibrium of the handle force changes in one direction may necessitate forces in the opposite direction to also change, since both contribute substantially to the total moment of force. This finding agrees with those of Niu et al. [2] in a study in which subjects were asked to double their grasping force, which was defined as the total normal force exerted on a similar handle. Positive change in normal forces for SPDT and SQZT may have been necessary to prevent slipping of the fingers off the forces sensors. However, the change in tangential force did not scale with change in normal force across the fingers.

The pattern of change in tangential fingers forces for SPDT and SQZT agree with those published by Pataky et al. [3]. In that study subjects were asked to maximally squeeze and spread fingers. The results showed that in both directions the I-finger showed the largest changes, followed by the L-finger. R- and M-fingers showed the smallest changes in tangential force. For both tasks the I-finger produced force opposite to that by M-, R-, and L-fingers. This may signify that the CNS controls finger spread and squeezing by representing the I-, M-, R-, and L-fingers as two virtual fingers so that it effectively only needs to send two sets of commands, as opposed to four. This may be one strategy utilized by the CNS in solving the motor redundancy problem.

REFERENCES

1. Latash ML. *Synergy*. Oxford University Press, New York, 2008.
2. Niu X, et al. *Exp Brain Res* **194**, 115-129, 2009.
3. Pataky TC, et al. *J of Hand Therapy* **21**, 377-385, 2008.

ACKNOWLEDGEMENTS

This study was funded by NIH grants AG-018751, NS-035032, and AR-048563.

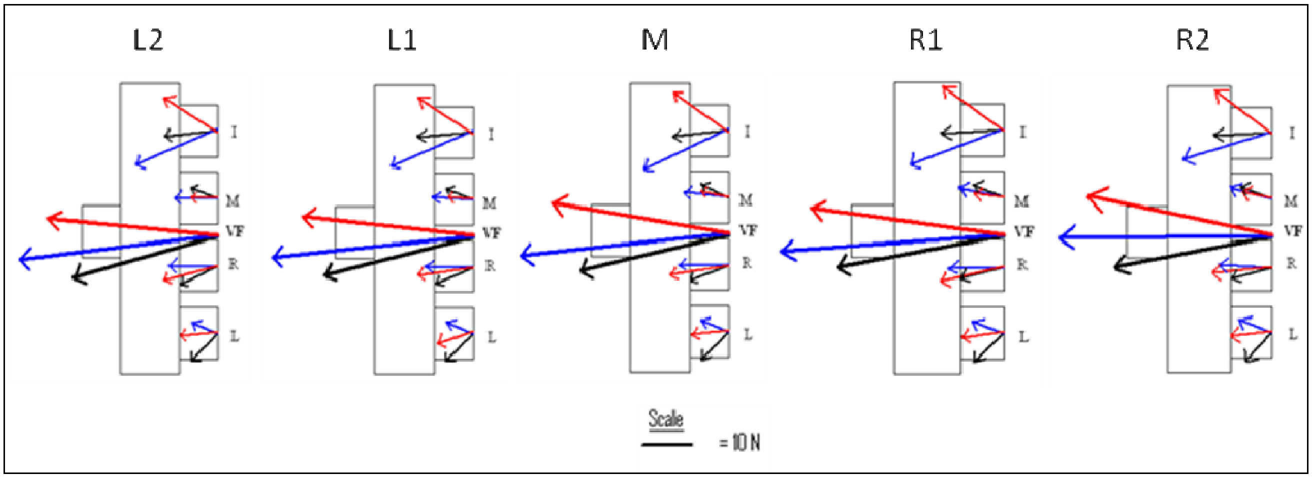

Figure 2: Force vector representation of each finger (I, M, R, L,VF) acting on the handle, at end of each task. Black, red, and blue vectors represent the tasks SQZN, SPDT, and SQZT, respectively.

ARE ULTRASOUND MEASURES OF MUSCLE THICKNESS REPRESENTATIVE OF MUSCLE ACTIVATION IN THE ABDOMINAL WALL?

[1,2]Stephen H. M. Brown, [1]Stuart M. McGill
[1]Department of Kinesiology, University of Waterloo, Waterloo, ON, Canada, and [2]Current address: Department of Orthopaedic Surgery, University of California San Diego
email: s5brown@ucsd.edu

INTRODUCTION

Ultrasound (US) imaging is a valuable tool which, when applied appropriately, has the potential to provide significant insight into abdominal muscle contraction. Typically, changes in muscle thickness are obtained and interpreted. However, the link between ultrasound measures of muscle thickening and electromyographic (EMG) measures of activation is not clear. Abdominal bracing and hollowing are two widely used clinical training and rehabilitation exercises designed to re-educate faulty motor patterns and ensure sufficient spine stability. They have been shown to recruit the abdominal wall muscles in quite different manners, with abdominal hollowing focusing on the isolated recruitment of the transverse abdominis (TrA) and, to a lesser extent, the internal oblique (IO) [1], and abdominal bracing focusing on a more balanced recruitment across the entire torso musculature [2]. This study employed abdominal hollowing and bracing as two different means of recruiting the abdominal muscles, in order to compare interpretations of activation between US and EMG measures.

METHODS

Five healthy males, with no history of back pain or abdominal injury, volunteered for this study.

Ultrasound images were obtained in B-Mode (MicroMaxx, Sonosite Inc., Bothell, WA) with a 38-mm linear transducer (6-13 MHz). All images were taken with the probe at the level of the umbilicus on the left side of the body, with the lateral position adjusted to allow a clear view of the three layers of the abdominal wall musculature. The three probe orientations were: 1) horizontal along the transverse plane; 2) angled 35 degrees inferior-laterally (along the approximate line of the IO fibres; 3) angled 60 degrees superior-laterally (along the approximate line of the EO fibres). The mid-point of the probe was positioned in the same location for each of the three orientations.

Participants were taught how to properly perform the abdominal brace and hollow maneuvers. All contractions were performed in a modified sit-kneel position, designed to keep the spine in a neutral posture. For the comparison of bracing and hollowing techniques, participants performed six abdominal hollow and six abdominal brace conditions, two at each of three orientations of the ultrasound probe.

Additionally, each participant then performed four isometric ramped torque contractions, two producing a net flexor muscle moment, and two producing a net extensor muscle moment. During these contractions ultrasound images were recorded solely with the probe oriented at the 35 degree angle (IO fibre line of action).

For all contractions, the thickness of the IO and external oblique (EO) was measured in both the relaxed state and at maximum contraction (Figure 1). The difference between these two measures was quantified, and divided by the rest thickness, to obtain a relative change in muscle thickness. Additionally, surface EMG of the IO and EO muscles was recorded on the right side of the body, throughout each contraction, and subsequently linear enveloped and normalized to the peak voltage obtained during standardized isometric contractions designed to elicit maximal activation from the muscles.

RESULTS AND DISCUSSION

Neither the IO nor EO muscle demonstrated any definitive relationship between ultrasound thickness change measures and EMG activation measures during the abdominal bracing and hollowing contractions, and displayed even further discrepancies during the ramped flexor and extensor torque contractions. Figure 2 displays a scatterplot of ultrasound and EMG measures across all conditions and participants for the IO muscle.

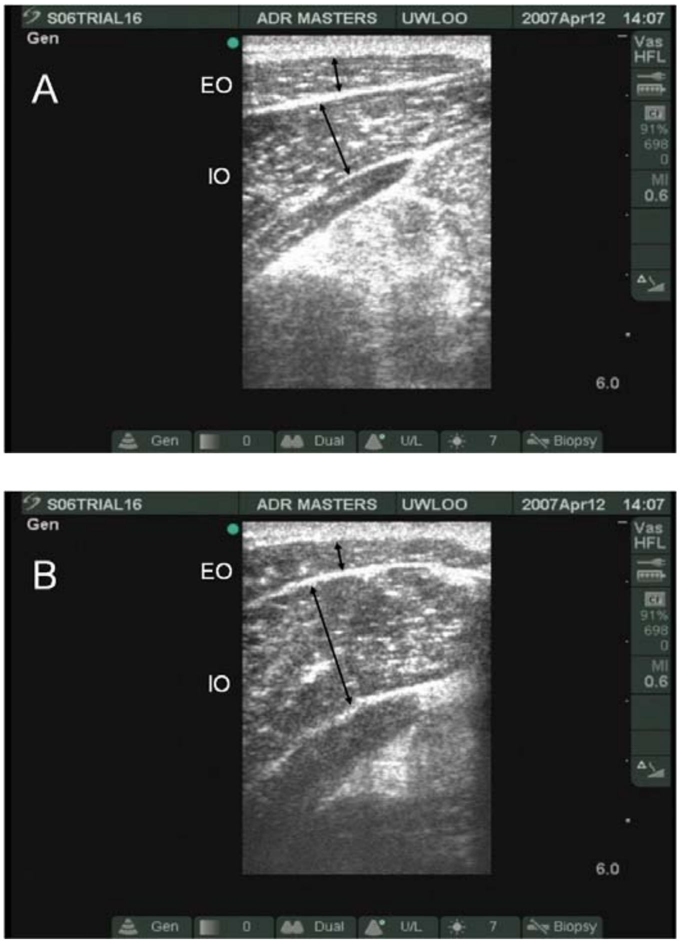

Figure 1. Example of an ultrasound image captured for an abdominal brace trial during relaxation (A) and contraction (B). Arrowed lines indicate measures of the thickness of each muscle. The medial side of the body is to the right of the image.

CONCLUSIONS

It appears that there are very complex dynamics between abdominal wall muscles during different strategies of contraction. This is most likely due to the wall forming a mechanical composite with the fibres of one layer adhered transversely to an adjoining layer through an intervening sheet of connective tissue. This is akin to a “plywood-like” architecture. These connective tissues have the ability to transmit force between the layers, thus providing a distinct mechanical linkage [3]. This composite nature of the abdominal wall muscles acts such that contraction in one layer will cause forces to be transmitted through the intervening connective tissue attachments to adjacent muscle layers, which can directly affect the amount of thickening that that muscle will experience. This severely limits the ability to assess muscle effort and/or force production from ultrasound measures of muscle thickness alone. Thus, it is not surprising that there is little relationship between activation (via EMG amplitude) and thickening (via US) measured in muscles of the abdominal wall.

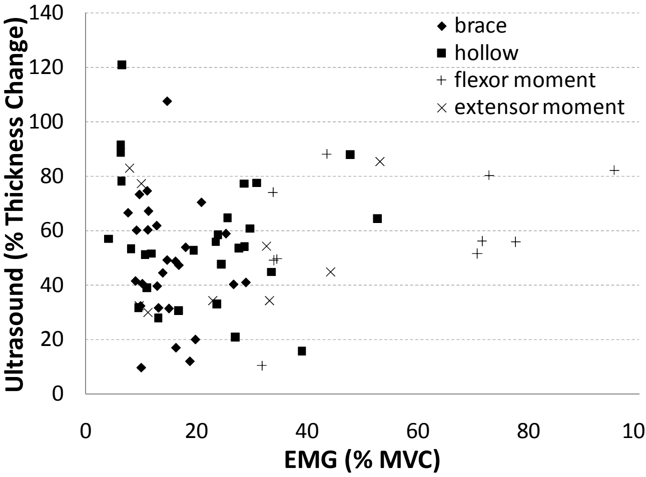

Figure 2. Scatterplot of internal oblique EMG muscle activation levels versus ultrasound muscle thickness percent changes during each of the abdominal brace, abdominal hollow, flexor moment and extensor moment contractions.

REFERENCES

1. Richardson CA, Jull GA. *Manual Therapy* **1**, 2-10, 1995.
2. Kavcic N et al. *Spine* **20**, 2319-2329, 2005.
3. Brown SHM, McGill SM. *Spine* **34**, E70-E75, 2009.

ACKNOWLEDGEMENTS

The authors thank the Natural Sciences and Engineering Research Council (NSERC), Canada, for financial support.

DYNAMIC POSTURAL STABILITY IN PREGNANT FALLERS, NON-FALLERS, AND NON-PREGNANT CONTROLS

[1,2]Jean L. McCrory, [2]April J. Chambers, [2]Ashi Daftary, and [2]Mark S. Redfern
[1]West Virginia University, [2]University of Pittsburgh
email: jmccrory@hsc.wvu.edu

INTRODUCTION

Approximately 27% of pregnant women report a fall during their pregnancies [1]. Pregnant women undergo numerous anatomical, physiological, and hormonal changes that may be related to the increased risk of falling. Studies of static balance in pregnant women reveal increased anterior-posterior center of pressure (COP) movement during pregnancy [2-4]. Dynamic postural control of pregnant women has not been investigated. It is unknown if pregnant women who have fallen have impaired postural control when compared to pregnant women who have not fallen or to non-pregnant women. Moreover, the effect of exercise on the incidence of falls has not been explored. The **purpose** of this study was to compare dynamic postural stability in pregnant women who have fallen during their pregnancies with those who have not and to a group of non-pregnant women. A second purpose was to examine the effect of exercise on fall incidence in our cohort.

METHODS

Forty one pregnant women (age: 29.5±4.9 yrs, hgt: 1.7±0.7 m, 2nd trimester mass: 74.7±12.1 kg, 3rd trimester mass: 81.6±11.0 kg) and 40 non-pregnant controls (age: 26.5±6.4 yrs, hgt: 1.7±0.6 m, mass: 66.0±8.9 kg) participated. Data were collected on the pregnant women in the middle of their 2nd and 3rd trimesters and on the control women in the week following menses.

After obtaining consent, pregnant subjects were surveyed about previous pregnancies, current exercise participation, current employment, and history of falls while pregnant. Dynamic postural stability data were collected on all subjects using an Equitest system (NeuroCom Inc., Clackamas, OR). Subjects wore a chest and hip harness to protect against a fall. A battery of small, medium, and large fore-aft translation perturbations was delivered to each subject. The magnitude of each was based on the subjects' height. Three trials of each condition were performed. COP data were collected at 100 Hz. The translation velocity was 15.2 cm/sec. The durations of the small, medium, and large perturbations were 250 ms, 300 ms, and 400 ms, respectively. Reaction time, initial sway, sway velocity, and total sway were determined for each trial. Reaction time was calculated as the time from translation onset until the COP moved independently of the force plates. Initial sway was defined as the maximum fore-aft COP movement immediately following translation. Sway velocity was calculated as the initial sway divided by the time from the onset of COP movement to the time of the initial sway. Total sway was defined as the total fore-aft movement of the COP. A mixed-model ANOVA was performed on each of the four variables (α=0.05). Subject was designated as a random factor while fall group (pregnant non-faller, pregnant faller, or control), direction (forward, backward) and magnitude (small, medium, and large) were designated as fixed factors. Tukey post-hoc tests were performed if the ANOVA found differences between subject groups or perturbation magnitudes (α=0.05). Finally, a Chi square analysis was performed to examine the effect of exercise on fall-risk in the pregnant women (α=0.05).

RESULTS AND DISCUSSION

Eighteen of the pregnant subjects reported falling at least once. A total of 28 falls were reported. Twelve pregnant women withdrew from the study between their 2nd and 3rd trimesters (8 because of medical reasons and 4 for unknown reasons). Therefore, these 18 women who reported falling represent 56% of the sample. No falls required hospitalization, although three required medical care. No subject delivered prematurely because of a fall.

Reaction time was not different between pregnant fallers (124.8±17.7 ms), pregnant non-fallers (126.8 ±25.9 ms), and non-pregnant controls (124.1±18.6

ms) ($p = 0.09$). Reaction time did not differ between perturbation directions ($p=0.487$), but was less for the large perturbations when compared to the medium and the small trials ($p=0.018$).

Initial sway was less in the pregnant fallers when compared to the pregnant non-fallers and controls ($p < 0.001$). No differences were noted between the latter two groups. Initial sway differed between the small, medium, and large perturbations ($p < 0.001$), but not between the forward and backward perturbations ($p = 0.131$). Sway velocity and total sway were less in the pregnant fallers when compared to their non-faller counterparts and the control participants (both p-values < 0.001). Similarly, both the sway velocity and total sway were significantly different between the forward and backward perturbations as well as the small, medium, and large slides ($p<0.05$). Initial sway, sway velocity, and total sway data for the pregnant fallers, pregnant non-fallers, and non-pregnant controls are shown in Table 1.

Table 1: COP movement variables for the pregnant fallers, pregnant non-fallers, and non-pregnant controls. Data are shown as mean (std dev).

	Pregnant Fallers*	Pregnant Non-Fallers	Non-Pregnant Controls
Initial Sway (cm)	4.03 (1.81)	4.56 (1.81)	4.47 (1.96)
Sway Velocity (cm/s)	23.8 (13.2)	30.0 (13.1)	29.9 (14.2)
Total Sway (cm)	5.97 (2.97)	7.04 (2.81)	7.11 (3.38)

*On each variable, pregnant fallers differed from other groups ($p < 0.05$).

The pregnant fallers demonstrated increased rigidity, as evidenced by the lack of sway following the perturbation. Anthropometric factors most likely did not play a role in whether or not the subject fell. There were no differences in pregnant mass, weight gain during pregnancy, or waist circumference between the fallers and the non-fallers ($p > 0.10$), nor was there a significant interaction between the trimester and fall incidence for any of the variables ($p > 0.80$). The altered response in the pregnant fallers may be due to factors not assessed in this study, such as muscle strength.

Thirty-one pregnant participants reported regular exercise during their pregnancies, while 10 reported no exercise at all. Walking, prenatal yoga, and Pilates were the most common exercises reported. Of the 32 pregnant women for whom we have complete fall and activity data, 18 were categorized as fallers and 25 as exercisers. The distribution of pregnant fallers vs non-fallers and exercisers vs non-exercisers is shown in Table 2. The Chi-square for the fall categorization was 0.50 ($p = 0.480$). The Chi-square for the exercise categorization was 10.125 ($p = 0.001$), meaning that non-exercisers were more likely to fall than those who participated in regular exercise.

Table 2: Categorization of the 32 pregnant subjects based on fall and exercise history. Chi-square = 10.125 ($p = 0.001$).

		Exerciser?	
		No	**Yes**
Faller?	**No**	0	14
	Yes	7	11

CONCLUSIONS

Pregnant women who have fallen exhibit altered dynamic postural stability compared to those who have not fallen as well as non-pregnant women. COP movement was markedly limited in the pregnant fallers. The pregnant women who have not fallen demonstrate similar COP movement patterns to the non-pregnant women.

Exercise participation may play a role in reducing fall risk. All of the sedentary pregnant women in our study experienced a fall during their pregnancies. Further investigation of the efficacy of exercise in fall prevention in this population is warranted.

REFERENCES

1. Dunning K et al. *Am J Indus Med* **44**, 664-672, 2003
2. Butler EE et al. *Am J Obstet Gynecol* **195**, 1104-8, 2006.
3. Davies J et al. *Anesthesiology* **97**, 1576-81, 2002.
4. Jang J et al. *Clin Biomech* **23**, 468-76, 2008.

ACKNOWLEDGEMENTS

We would like to thank Kristen Berger and Leah Enders for their work on this project. This research was supported by NIOSH K01 OH8548.

INFLUENCE OF AUTOMOBILE SEAT LUMBAR SUPPORT PROMINENCE ON SPINE AND PELVIS POSTURES: A RADIOLOGICAL INVESTIGATION

Diana E. De Carvalho [1], Jack P. Callaghan [1]
[1]Department of Kinesiology, University of Waterloo, Waterloo, ON
email: ddecarva@uwaterloo.ca

INTRODUCTION

Sitting in a vehicle has been identified as a cause of mechanical low back pain in the literature [1]. In sitting, the pelvis rotates posteriorly and the lumbar lordosis flattens. This places increased pressure on the posterior aspects of the intervertebral discs and is recognized as a risk factor for disc herniation [1]. Maintaining the lumbar lordosis of the low back with a built in lumbar support has been suggested to decrease injury risk and relieve low back pain associated with sitting in a car seat. It is presently unknown whether this intervention actually causes a change at the level of the spine. While past studies in the literature have presented radiographic data in sitting, to date only one has investigated lumbar spine radiographic measures in the automobile seat specifically [2]. Hazard and Reinecke [2] found that a pneumatic continuous passive motion lumbar support was able to cycle lumbar lordosis angle between 21° and 41° for two participants sitting in an automobile seat. In this study, plain film radiographs are used to measure changes in lumbar spine and pelvic posture between standing and sitting in an automobile seat with varying amounts of lumbar support. The prototype lumbar support used in this study provides a horizontal excursion of 4.0cm, twice the current industry standard of 2.0cm. The study received ethics approval from both the University of Waterloo and the Canadian Memorial Chiropractic College.

METHODS

Eight male subjects, recruited from a student population, were included in this study. Participants were radiographed in four postures: standing, sitting in an automobile seat with 0% lumbar support prominence (LSP), 50% LSP and 100% LSP. In all conditions, shoulder angle was kept constant by having the participants lightly grip a steering wheel at the 10 o’clock and two o’clock positions. Subjects maintained each posture for two minutes to ensure a consistent adaptation time before exposures were taken. Radiographs were taken by radiology technicians at the Canadian Memorial Chiropractic College and average exposure values were 100 KVP and 40 MAS. Digital copies of the plain film radiographs were made with a high resolution scanner (Kodak LS75 Film Digitizer, Eastman Kodak Co., Rochester, NY). Radiographic measures of lumbar lordosis, intervertebral disc angles L1/L2 – L5/S1, lumbosacral angle, lumbosacral lordosis and sacral tilt were completed using eFilm Workstation™ software (Merge Healthcare, Milwaukee, USA). A 1-way ANOVA (standing/seated condition) with a value for significance of $p \leq 0.05$ were conducted. Tukey’s Studentized Range Test post hoc was used on all significant effects.

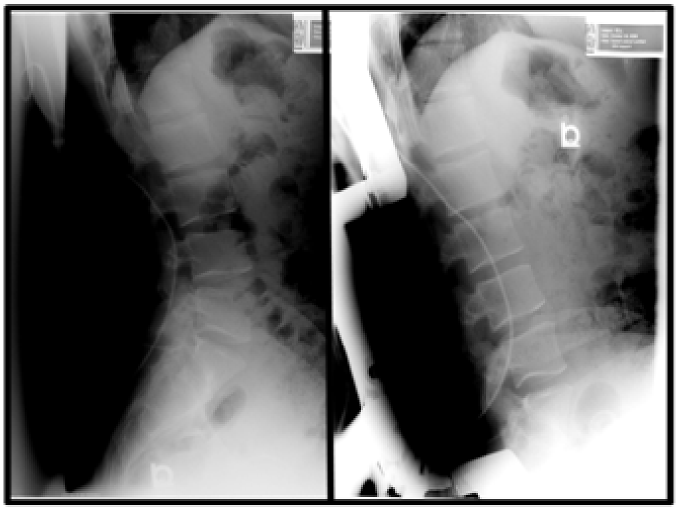

Figure 1: Lateral lumbar radiographs of the same participant standing (left) and sitting in an automobile seat with 0% LSP (right).

RESULTS

All measures, with the exception of the L5/S1 intervertebral disc angle, were significantly different between standing and sitting with 0% LSP (L1/L2 angle $p=0.045$ all else $p<0.001$). Lumbar lordosis angle decreased by an average of 63° (SE 5°) from standing to sitting with 0% LSP indicating an increase in lumbar flexion.

Intervertebral joint angles, which normally become larger and more lordotic (extended) throughout the lumbar spine (on average 5° at L1/L2 increasing to 14° at L5/S1), all decreased in sitting with 0% LSP. Specifically the intervertebral angles decreased to neutral or even -1° (kyphotic or flexed) from L1/2 to L4/5 with 10° of extension remaining at L5/S1. Intervertebral joint angles at L5/S1 were not significantly different between all postures tested.

Pelvic measures indicated posterior rotation in sitting with respect to standing with the lumbosacral angle decreasing from 40° to 13° and sacral tilt decreasing from 43° to -2°.

Two measures specifically, intervertebral joint angles between L1/L2 and L2/L3 were returned to angles not significantly different from standing with both 50% and 100% LSP ($p=0.044$ and $p<0.001$ respectively). All other radiographic angles demonstrated a return towards standing angles in response to increasing levels of lumbar support from 0% LSP to 100% LSP (Table 1).

DISCUSSION AND CONCLUSIONS

The radiograph measures in this study provide a comprehensive summary of the effect of sitting in an automobile seat with varying amounts of lumbar support. The results of this study suggest that the prototype lumbar support tested is capable of affecting spine posture, especially at the upper lumbar segments. Increasing lumbar support from the current industry standard of 2cm to 4cm resulted in a trend of returning radiographic measures closer to standing values. While these improvements may be slight, it is possible that the change imparted is enough to minimize injury risk and discomfort.

The significant differences in radiographic measures from standing to sitting presented in this paper further emphasize the range of motion experienced at different vertebral levels in car seat sitting and the importance of returning the spine and pelvis to a less flexed posture with a lumbar support. Further investigation will determine if these postural changes are enough to reduce risk of injury and low back discomfort during a prolonged driving situation.

REFERENCES

1. Porter JM and Gyi DE. 2002. The prevalence of musculoskeletal troubles among car drivers. *Occupational Medicine* **52**;1:4-12.
2. Hazard RG and Reinecke SM. Lumbar continuous passive motion: radiographic measurement. *Journal of the Neuromusculoskeletal System*. 1995;**3**(4):192-196.

ACKNOWLEDGEMENTS

AUTO21**,** CIHR, FCER and Schukra of North America.

Table 1: Radiographic lumbar spine and pelvis measures resulting from the four conditions tested.

Average Angle in Degrees (Standard Error of the Mean)

	Lumbar Lordosis	IVD L1/L2	IVD L2/L3	IVD L3/L4	IVD L4/L5	IVD L5/S1	Lumbosacral Lordosis	Lumbosacral Angle	Sacral Inclination
Standing	63 (5)	5 (1)	6 (1)	8 (1)	13 (1)	14 (1)	150 (3)	40 (5)	43 (4)
0% LSP	20 (5)	0 (1)	-1 (1)	0 (1)	0 (1)	10 (3)	171 (2)	13 (2)	-2 (1)
50% LSP	25 (5)	2 (1)	1 (5)	1 (0)	1 (1)	7 (3)	170 (1)	12 (2)	1 (3)
100% LSP	30 (5)	3 (1)	3 (5)	3 (1)	2 (1)	9 (2)	167 (1)	8 (2)	3 (3)

THE EFFECT OF APPROACH IN VOLLEYBALL SPIKE JUMP FOR FEMALE ATHLETES

ChengTu Hsieh
California State University, Chico, Chico, CA
Email: cthsieh@csuchico.edu

INTRODUCTION

Jump height is a crucial factor for being successful in many sports such as volleyball. Numerous studies have investigated the factors that contribute to jump height. These studies indicated that arm swing, countermovement, and approach each have an essential effect on jump height [e.g. 3, 5, 9, 13]. Other than segmental factors, studies also identified several kinematic and kinetic variables which have significant association with jump height such as force, power, velocity, etc. [e.g. 2, 14].

Dusault (1986) showed that approach velocity had a positive relationship with jump height. Additionally, Khayambashi (1986) pointed that male volleyball players used more steps in approach that resulted in greater jump height but not for female players. Studies have also indicated that after maximizing the approach velocity, the horizontal velocity and motion were minimized during takeoff phase [1, 11]. Consequently, Shahbazi et al. (2008) confirmed that there was no positive relationship between horizontal velocity and jump height during takeoff phase.

Although these studies indicated that approach is one of the crucial factors for volleyball spike jump performance, few of them have extended the examination toward the effect of approach in this particular sport performance. Therefore, the purposes of present study were to investigate the effect of approach for jump height and the relationship between the jump height and kinematic variables.

METHODS

Ten female volleyball players (mean body height = 1.78 ± 0.09 m; mean body mass = 66.4 ± 7.4 kg) were recruited from a highly competitive team (NCAA Division I). All policies and procedures for the use of human subjects were followed and approved by the local Institutional Review Board.

Each subject was required to warm-up for at least 5 minutes by stretching all major muscle groups for jump performance and practicing several normal spike jumps in front of a net and camera. All subjects performed a maximum of 10 volleyball spike jumps (VBSJ) and 10 countermovement jumps with arm swing (VJA). Each subject took a 5 minute break between the two types of jumps and a half minute break between each trial.

Two-dimensional coordinate data from the left side of the body were obtained with a 60-Hz video camera in conjunction with a motion analysis system (Vicon Motus: 9.2). Reflective markers were placed on acromion, greater trochanter, lateral femoral epicondyle, lateral malleolus, 5th metatarso-phalangeal joint, later humerus epicondyle, and ulnar styloid process (Figure 1).

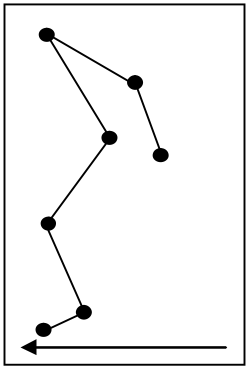

Figure 1. Experimental set-up showing the location of land markers and the direction of approach for VBSJ.

Data were collected from 10 frames before the movement onset until 10 frames after the peak of the jump. Jump height was determined from the height of COM at takeoff to the peak of the jump. The kinematics variables of preparation and propulsive phases for VBSJ and VJA were calculated. These variables included the duration (time) and velocity in horizontal (x) and vertical direction (y). Preparation phase started form the feet plantation to the lowest COM. The propulsive phase started from the lowest COM to the takeoff. Paired t-test was performed to compare the kinematic variables. Holm's correction was applied to adjust *P*-value for controlling both type I and II errors [8, 10]. Zero-order correlation coefficients were calculated to examine the association between jump height and kinematic variables in VBSJ and VJA.

RESULTS AND DISCUSSION

Results of paired t-tests, means and standard deviations for all the variables are presented in Table 1. Table 2 shows the associations between jump heights and kinematic variables. The findings of the present study indicated that the jump height of VBSJ (0.35 ± .07 m) was significantly greater ($p < 0.008$) than the jump height of VJA (0.31 ± .06 m). This is consistent with several studies that the jump height can be enhanced with the facilitation of approach in different type of jumping performance such as run-up jump with one leg takeoff [e.g. 14]. Additionally, the decreased of horizontal velocity from preparation phase to propulsive phase is similar to the findings of Ciapponi et al. (1995) and Prsala (1982) who found that participants were takeoff with minimal horizontal velocity after approach.

However, the results of zero-order correlation showed that there are no significant associations between horizontal velocity and jump height in both types of jumping which is similar to the findings of Shahbazi et al. (2008). This indicated that the approach may not have a direct contribution to the jump height. On the other hand, approach may have significant contribution toward force or power production since the vertical velocity and time in preparation and propulsive phases imply that acceleration is greater in VBSJ for both phases (see Table 1). Therefore, future research should be completed to identify and isolate the effects of approach for volleyball spike jump performance.

REFERENCES

1. Ciapponi et al. *Proc Annu Meet, 13th Int Symp on Biomech in Sports,*1995.
2. Dowling, J. & Vamos, L. *J Appl Biomech*, **9**, 95-110, 1993.
3. Dusault, C. *C.V.A. Volleyball Tech J*, **8**(2), 33-41, 1986
4. Feltner, ME et al. J. *J Sports Sci*, **17**, 449-466, 1999.
5. Hara, M. et al. *Hum Movement Sci*, **27**, 636-648, 2008.
6. Harman, EA et al. *Med Sci Sports Exerc*, **22**, 825-833, 1990.
7. Khayambashi, K. *Snipes J*, 9, 1-7, 1986.
8. Knudson, D. *Sports Biomech*, **8**(1), 96-104, 2009.
9. Lees, A. et al. *J of Biomech*, **37**, 1929-1940, 2004.
10. Lundbrook, J. *Clin Exp Pharmacol Physiol*, 25, 1032-1037, 1998.
11. Prsala, J. *C.V.A. Volleyball Tech J*, **7**(2), 57-64, 1982.
12. Shahbazi et al. *Proc Annu Meet, 25th Int Symp on Biomech in Sports*, 2008.
13. Walsh, M.S. et al. *J of Strength Cond Res*, **21**, 362-366, 2007.
14. Young, W. et al. *J Sport Med Phys Fit*, **39**, 285-293, 1999.

Table 1: Means, standard deviations, and paired t-test results. Pre and Pro represents the preparation and propulsion phase, respectively. * ($p <$ new adjusted critical level)

	Height (m)	Pre X (m/s)	Pre Y (m/s)	Pre T (s)	Pro X (m/s)	Pro Y (m/s)	Pro T (s)
VJA	0.31 ± .06	-0.57 ± .12	-1.54 ± .32*	0.54 ± .10*	0.66 ± .21	2.86 ± .23	0.33 ± .05*
VBSJ	0.35 ± .07*	-2.76 ± .55*	-1.32 ± .23	0.28 ± .03	-1.66 ± .31*	2.91 ± .33*	0.20 ± .03

Table 2: Zero-order correlation between jump height and kinematic variables. * ($p < 0.05$)

	Pre X	Pre Y	Pre T	Pro X	Pro Y	Pro T
VJA Ht	.157	-.492*	-.193	.188	.911*	-.437*
VBSJ Ht	-.130	-.482*	-.147	.060	.715*	-.336*

FEATURE BASED ALL HEXAHEDRAL MESH GENERATION IN ORTHOPAEDIC BIOMECHANICS

[1] Kiran H. Shivanna, [1,2]Srinivas C. Tadepalli, [1,2,4]Vincent A. Magnotta and [1,2,3]Nicole M. Grosland
[1]Center for Computer Aided Design, [2]Department of Biomedical Engineering, [3]Department of Orthopaedics and Rehabilitation, [4]Department of Radiology.
The University of Iowa, Iowa City, IA
E-mail: kiran-shivanna@uiowa.edu, web: http://www.ccad.uiowa.edu/mimx/

INTRODUCTION

Numerical simulation using finite element analysis (FEA) is widespread in biomechanics research. One of the crucial steps in an FEA is mesh generation, as it affects the solution accuracy. Three-dimensional meshes generally contain tetrahedral and/or hexahedral elements. Due to superior numerical performance and the need for fewer elements, hexahedral elements are typically preferred over tetrahedral elements. In contrast to the favorable numerical quality of hexahedral meshes, mesh generation often poses a challenge.

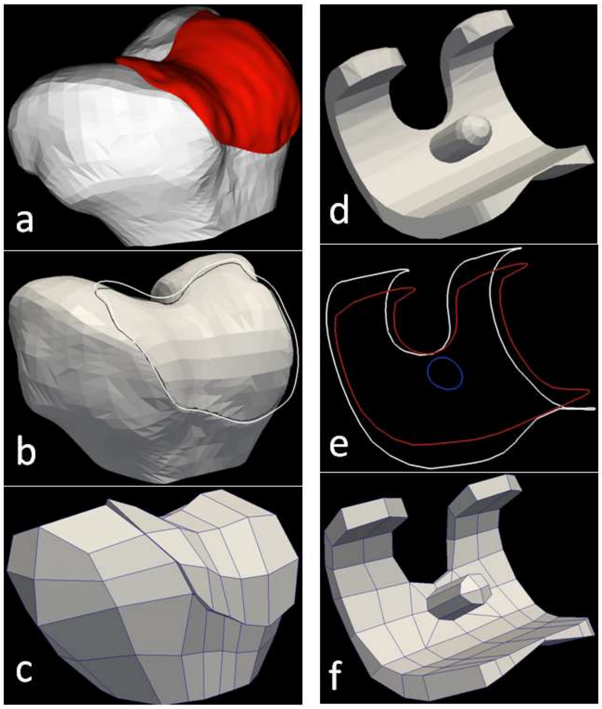

Figure 1: Surfaces, feature edges and building blocks. The distal femur: a) femur and cartilage surfaces, b) feature edges extracted from the cartilage, c) building block structure for mesh generation. A femoral TKA component: d) the triangulated surface, e) feature edges extracted, and f) corresponding building block structure.

For orthopaedic applications, often the anatomical region of interest is segmented from a three-dimensional CT dataset. A surface is then generated from this region of interest. Two methods have been developed to generate a hexahedral mesh from the surface based representation. The first method is a mapped mesh approach where a template mesh is mapped onto the surface definition [1]. The second approach projects a multiblock based rectilinear hexahedral mesh, with the surface of the blocks conforming to the anatomical surface [2]. With the multiblock method, element size, distribution and orientation can be closely controlled.

The above mentioned characteristics make the multiblock approach an attractive option for meshing structures with feature boundaries. To preserve these features in the resulting mesh, it is important to align nodes and/or elements along these boundaries. This helps in capturing effect of local features on the final solution obtained. In this work a feature can either be a triangulated surface or an edge/line about which the elements should be aligned during mesh generation. Instances of multiple features in orthopaedics include the cartilage, cortical shell and cancellous bone definitions, and implants.

METHODS

The key to an effective multiblock method is the generation of the block structure, mimicking closely the shape of the anatomy to be meshed. To that end, interactive tools have been devised to ease the process of block generation. The ability to extract feature edges from the triangulated surface representation enables nodes to be distributed along a feature edge and thus better capture the features of interest.

Two examples have been chosen to demonstrate the application of incorporating feature edges into the meshing process: (1) The distal femur and corresponding cartilage definition (Figure 1a,b,c) and (2) a femoral total knee arthroplasty (TKA) component (Figure 1d,e,f). Each mesh initiates with a triangulated surface representation of the structure of interest. A building block structure is interactively created about the surface. If the two vertices belonging to the edge of a building block are within a specified tolerance from the feature of interest, then all nodes on that edge are projected onto that feature. Feature edges take precedence over surfaces for node projection. Similarly, if all four vertices of a building block face lie within the specified tolerance of a surface, all the nodes belonging to the face are projected onto the surface. After all the edges and faces are projected/computed, the interior nodes are computed. Once the mesh is established, the mesh quality is further improved using optimization based mesh smoothing techniques [3].

RESULTS AND DISCUSSION

Figure 2 shows the results of the method applied to the distal femur (Figure 2a) and the femoral TKA component (Figure 2b). The number of elements in the distal femur and TKA meshes is 4872 and 7034, respectively. The meshes were smoothed by optimizing the scaled Jacobian across the mesh. The scaled Jacobian was selected because it is independent of element size. During mesh optimization, the minimum scaled Jacobian for the algorithm was fixed at 0.1.

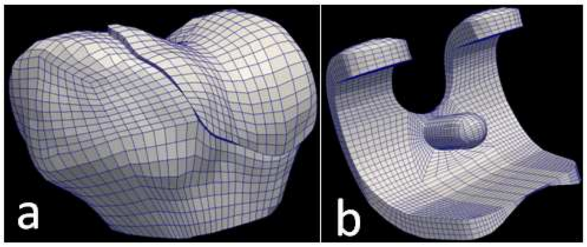

Figure 2: Finite element meshes: a) The distal femur and cartilage, and b) the femoral TKA component.

The proposed method captures the features (Figure 1b,e) by distributing the nodes and elements along the features. The meshes shown (Figure 2) were generated in matter of minutes. The most time consuming part in the meshing process is the generation of the building block structure. But the interactive editing tools developed as part of IA-FEMesh [2] ease the process. Following the mesh quality improvement, all elements in the mesh have a positive Jacobian value, thus making them suitable for analysis.

While other methods are available to mesh irregular geometries, rarely do the existing methods consider discrete triangulated surfaces as a starting point as well as integrate feature boundaries into the mesh generation process. Most methods use geometric data such as splines and bezier surfaces or convert the existing triangulated data into geometric data [4]. Hence, the methods are cumbersome for meshing the triangulated data while retaining the features of interest. Even if the existing methods were used to mesh the discrete surfaces, the time required would be on the order of hours. This would preclude their use in the studies involving a large number of datasets. The meshes generated using the multi-block feature edge and surface projection techniques can be generated in a matter of minutes.

Currently, the decision of projecting an edge or a face is dependent on how close the building block vertices are to a given feature. In the future, user will have the option of overriding the projection decisions.

CONCLUSIONS

The multiblock method, initially designed for meshing a single discrete surface, has been extended to mesh multiple surfaces with feature edges. Mesh generation initiates with discrete surfaces, making it an ideal method for generating meshes for anatomic structures. The meshes are generated in a matter of minutes, making the method suitable for a large number of datasets.

REFERENCES

1. Grosland NM, et al. *Comput Meth Biomech Biomed Eng* **12(1)**, 35-43, 2009.
2. Grosland NM, et al. *Comput Meth Prog Biomed* **94(1)**, 96-107, 2009.
3. Shivanna KH, et al. ASME Summer Bio Eng Conference, Lake Tahoe, USA, 2009.
4. Schonning A, et al. *Comput Aided Des*, (Article in Press).

A BIOMECHANICAL COMPARISON OF THE SIDE-TO-SIDE AND PULVERTAFT TENDON TRANSFER REPAIR TECHNIQUES

[1]Stephen H. M. Brown, [1]Eric Hentzen, [1]Alan Kwan, [2]Samuel R. Ward, [3]Jan Fridén, [1]Richard L. Lieber
Departments of [1]Orthopaedic Surgery and [2]Radiology, University of California San Diego, [3]Department of Hand Surgery, Sahlgrenska University Hospital, Gothenburg, Sweden
email: s5brown@ucsd.edu, web: http://muscle.ucsd.edu

INTRODUCTION

The primary goal of tendon transfer surgery is to restore lost function. Strong tendon repairs are required to facilitate rehabilitation by allowing early mobility, preventing adhesions and promoting strengthening and motor learning [1,2]. Prerequisite for early return to activity is a strong and stiff repair that enables efficient transfer of load, through the repair, across the joint(s) of interest and into the bony insertion. The side-to-side (SS) suture repair technique was developed to meet these aims. The purpose of this paper was to quantify the strength and stiffness of the SS repair technique compared to the classic Pulvertaft (PT) suture repair technique.

METHODS

Flexor digitorum profundus (FDP) and flexor digitorum superficialis (FDS) tendons were harvested fresh from four cadaveric forearms. All repairs were carried out with the FDS tendon serving as the donor and the FDP tendon as the recipient. Seven SS transfers and 6 PT transfers were performed by an experienced hand surgeon (Figure 1). The length of the overlap region was standardized at 30 mm to permit comparison between methods.

All mechanical tests were carried out using an Instron (Model 1122) material testing machine. Clamps secured the tendons on either side of the repair, and were mounted vertically and immersed in phosphate-buffered saline solution throughout the tests. Slack length of the overall structure was established as the length just prior to the initiation of load resistance. Repairs were tested in tension at a displacement rate of 10 mm/min. First, repairs were conditioned with 5 consecutive cycles of 5% clamp-to-clamp displacement. At the end of the conditioning cycles, repairs were allowed to relax for approximately 25 seconds, and were then elongated to failure.

Deformation of the repair was quantified by tracking elastin dye lines placed on the tendons on either side of the repair region.

Variables measured were: peak load at each of the five conditioning cycles, load of first failure (first detectable drop of force during the failure test), ultimate load (highest force achieved during the failure test), and repair stiffness (slope of the linear region of the load-deformation curve). Comparisons between the SS and PT repair techniques were made using non-paired t-tests with an alpha level of 0.05.

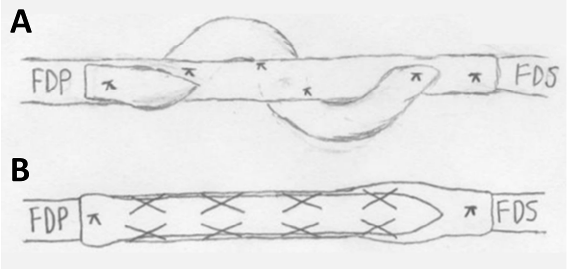

Figure 1. A) Pulvertaft (PT) repair consists of the FDS weaving through 3 incisions in the FDP, and 6 locking sutures; B) Side-to-side (SS) repair consists of the FDS inserting through 1 incision in the FDP, 4 cross-stitch running sutures back and forth down both sides, and 2 locking sutures.

RESULTS AND DISCUSSION

All failures occurred in the repair region, rather than at the clamps or within the tendon substance. Thus, the repair is, in fact, the “weak link” of this construct. It was observed that PT repairs failed at the sutures followed by the FDS tendon pulling through the FDP tendon; SS repairs failed by shearing of fibers within the FDS, whereby fibers that were locked down with the running sutures stayed attached to the FDP, and adjacent, non-locked down fibers sheared away with the FDS.

There were no statistically significant differences in the cross-sectional areas (p=0.99) or initial lengths (p=0.93) between SS and PT repairs. Therefore, all comparisons can be made between un-normalized loads and deformations.

Load at each of the conditioning displacement cycles (range p = 0.011 to p = 0.013), load at first failure (p = 0.001, Figure 2), ultimate load (p < 0.001, Figure 2), and repair stiffness (p = 0.016, Figure 3) were all significantly greater for the SS compared to the PT technique.

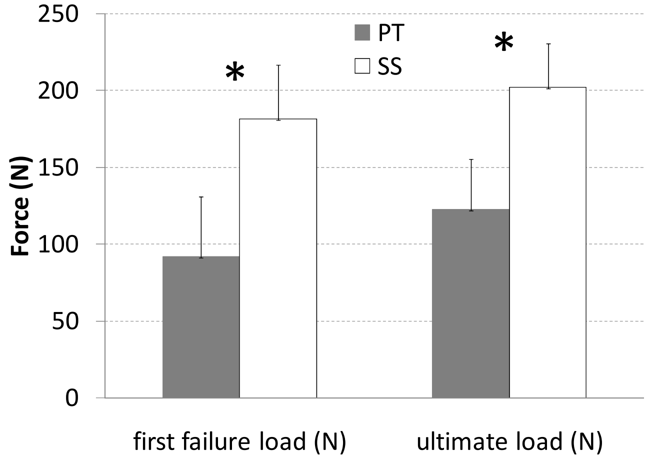

Figure 2. A statistically significant difference (*) was found between the SS and PT repair techniques for both the first failure load and ultimate load. Means and standard deviations are shown.

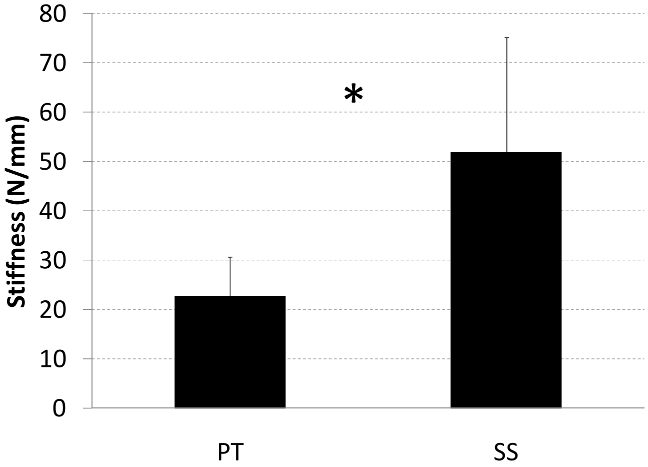

Figure 3. A statistically significant difference (*) in stiffness was found between the SS and PT repair techniques. Means and standard deviations are shown.

CONCLUSIONS

The SS repair technique was significantly stronger and stiffer compared to the standard PT technique. This could permit patients to return to activity sooner after surgery. Ultimately, this will result in greater function and fewer complications. The mean failure loads for both repair techniques were greater than the estimated average maximum isometric force that can be generated by the FDS muscle [3], thus indicating that acute failure of the repair would not be a primary concern post-surgery. However, it is known that tendon repair ultimate stress decreases transiently after repair, and should be considered. A stiffer repair may be beneficial as it enables a more efficient transfer of load from the donor muscle to the recipient tendon, and ultimately to the site of bony insertion. An ideal tendon transfer would deform minimally across the repair site, leaving length changes to occur within the tendons and muscles themselves, which are designed to shorten/lengthen across joints. The SS tendon transfer repair was much stiffer than the PT repair, and will thus transfer muscular loads under smaller deformations and with less absorbed energy. This should enable the SS repair to function better and undergo less cumulative deformation during the healing process, thus facilitating an earlier return to activity post-surgery.

REFERENCES

1. Doi K, et al. *Plast Surg Reconstr* **121**, 2037-2045, 2008.
2. Friden J, et al. *Scand J Surg* **97**, 341-346, 2008.
3. Ward SR, et al. *J Neurophysiol* **96**, 2815-2818, 2006.

ACKNOWLEDGEMENTS

The authors acknowledge Mr. Robert Healey for help with the data collection, Prof. David Amiel for the use of equipment, NSERC Canada for funding a Post-doctoral Fellowship for S.H.M. Brown, Swedish Research Council grant 11200, and NIH grant HD050837.

A COMPARISON OF BASE RUNNING TECHNIQUES IN BASEBALL

Travis Ficklin, Jesus Dapena, and Alex Brunfeldt
Department of Kinesiology, Indiana University, Bloomington, IN, USA
email: tficklin@indiana.edu

INTRODUCTION

Safe arrival at a base in baseball requires covering the distance between bases in a short time. Often it also requires stopping at the base, typically using head-first (HF) or feet-first (FF) sliding techniques. Previous research has found no time differences between these two techniques [1,2]. The purpose of this study was to compare the effectiveness of the two sliding techniques to running through the base (RT) and to running to a stop on the base (RS).

METHODS

Nine collegiate baseball players executed maximum effort runs from a lead-off position 13 ft (3.96 m) ahead of first base to second base using RT, HF, FF, and RS techniques. A video camera shooting at 60 Hz taped the entire run. The last 10 m of each run were also taped with two HD (1080i) cameras shooting at 50 Hz, and the 3D coordinates of 21 body landmarks were calculated using DLT. Landmark locations in the last 10 m were filtered with a 12 Hz cutoff frequency; center of mass (c.m.) locations were then calculated from the landmark locations.

The start of the run was defined as the instant when the trail foot left the ground. The times for the entire 22.90 m run (t_{total}), the first 12.90 m (t_{1290}) and the final 10 m (t_{10}) were measured using video analysis.

In all trials, the c.m. was still short of the base at the instant of contact. Because of this, two velocities were computed for the last 10 m: effective velocity (v_{eff}) and actual velocity (v_{cm}), using the formulas $v_{eff} = 10\text{ m} / t_{10}$ and $v_{cm} = \Delta S_{cm10} / t_{10}$, where ΔS_{cm10} was the horizontal distance traveled by the c.m. between the instant when the c.m. reached a point 10 m from second base and the instant of first contact with the base. The difference between v_{eff} and v_{cm} represented a theoretical velocity gain (v_{bonus}) achieved by touching the base with a point of the body located at a certain distance ahead of the c.m. (“final reach”, d_{bonus}).

Average velocity of the c.m. was calculated for meter-long intervals in the last 10 meters prior to the base in each condition, from the interval 10-9 m away from the base to the interval 3-2 m away from the base. This yielded 8 interval velocities for each player in each condition.

Times and velocities were compared across conditions using repeated measures ANOVA. Tukey post-hoc tests were used to identify specific differences between means ($\alpha = .05$).

RESULTS AND DISCUSSION

No significant time differences were found between any of the conditions in the first 12.90 m of the run.

Comparisons between the four conditions for total time in the entire run and for time and effective velocity in the last 10 m showed that the RT condition was faster than FF and RS, but no significant differences were found between RT and HF nor between HF and FF. RS was slower than all other conditions. (See t_{total}, t_{10} and v_{eff} in Table 1.)

In regard to the actual velocity of the c.m. over the last 10 m, RT was the fastest condition, and RS the slowest; there were no significant differences between HF and FF. (See v_{cm} in Table 1.)

The bonus velocity was linked to the reach distance. The HF condition produced the largest reach distance and bonus velocity in the samples, followed by FF, RS and RT, in that order. (See d_{bonus} and v_{bonus} in Table 1.) Statistically, the values were larger in HF than in RS and RT, and larger in FF than in RT.

The velocity of the RT condition showed a slightly increasing trend during the last 10 m, while the other three conditions showed constant velocity followed by a marked slowing down in the last 3-7 m. (See Figure 1.) In the 10th meter prior to the base, the c.m. velocities of the four conditions showed no significant differences. In the 8th or 7th meter prior to the base, there were still no significant differences between RT and HF, between HF and FF, and between FF and RS, but RT was significantly faster than FF and RS, and HF was significantly faster than RS. (See the diagrams at the top of Figure 1.) In the 5th meter prior to the base, RS became significantly slower than all the other conditions, while the interrelationships between RT, HF and FF remained the same as before, with RT faster than FF, but no significant differences between RT and HF nor between HF and FF. In the 4th or 3rd meter prior to the base, RT became the fastest condition, RS remained the slowest, and there was still no significant difference between HF and FF. HF and FF showed no significant c.m. velocity differences in any of the one-meter intervals.

The RT condition produced a larger average c.m. velocity than the HF condition in the last 10 m. However, the larger final reach of the HF condition closed some of the velocity gap. Thus, the effective velocity was not significantly larger in RT than in HF (although it approached significance, and was in fact detectable by paired t-test with $p < .01$).

The FF condition had smaller c.m. velocity, final reach and effective velocity than HF, but the differences were not statistically significant. However, the effective velocity in the FF condition was significantly slower than in the RT condition.

The RS condition suffered the disadvantage of the smallest c.m. velocity and a small final reach. This combination produced a slower effective velocity for RS than for any other condition.

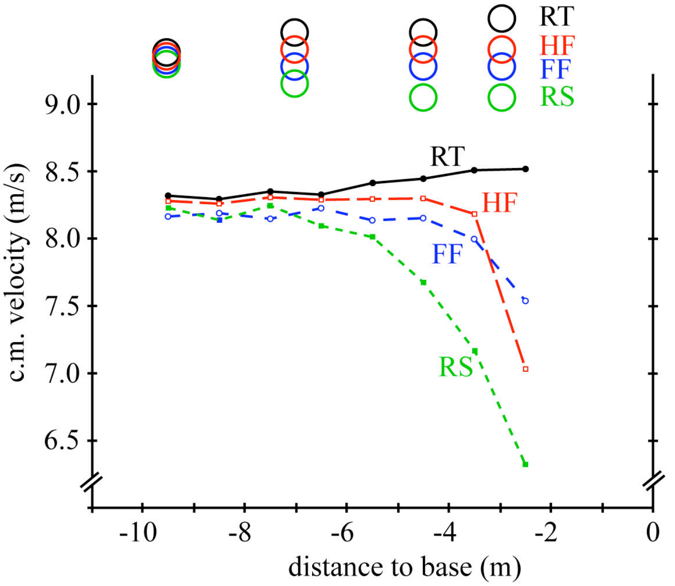

Figure 1. Average c.m. velocities in one-meter increments prior to the base. The diagrams at the top show when the velocities of the various conditions became statistically different from each other.

The times and effective velocities in the last 10 m clearly showed that the running through, feet-first, and run to a stop conditions are ranked in that order in regard to the time required for reaching the base, while the head-first condition is probably intermediate between the running-through and feet-first conditions. However, it is important to keep in mind that minimizing travel time between bases is not the only factor to be considered. Before deciding which technique to use, the player has to take into account the possible need to stop at the base, the need to avoid the baseman's tag, keeping options open for possible further immediate play, and minimizing the risk of injury.

REFERENCES

1. Hosey, RG, Mattacola, CG and Shapiro, R. *Clin J Sport Med* **13**: 242-244, 2003.
2. Kane, SM, House, HO and Overgaard, KA. *Am J Sports Med* **30**: 834-836, 2002.

Table 1.

Condition	t_{total} (s)	t_{1290} (s)	t_{10} (s)	v_{eff} (m/s)	v_{cm} (m/s)	v_{bonus} (m/s)	d_{bonus} (m)
RT	3.275 ± .090	2.144 ± .051	1.131 ± .044	8.85 ± .35	8.42 ± .16	.44 ± .22	.48 ± .23
HF	3.330 ± .104	2.142 ± .043	1.188 ± .069	8.44 ± .49	7.63 ± .40	.81 ± .11	.96 ± .09
FF	3.401 ± .083	2.177 ± .055	1.224 ± .071	8.20 ± .46	7.54 ± .37	.65 ± .12	.79 ± .12
RS	3.478 ± .062	2.159 ± .052	1.319 ± .048	7.59 ± .27	7.11 ± .23	.49 ± .07	.63 ± .08

RELATIONSHIPS BETWEEN SPASTCITY OF THE KNEE EXTENSORS AND MUSCLE MASS IN CHILDREN WITH CEREBRAL PALSY

[1, 2] Samuel Pierce, [3]Laura Prosser, [3]Samuel Lee, and [4]Richard Lauer
[1]Widener University, [2]Shriners Hospitals for Children Philadelphia,
[3]University of Delaware, [4]Temple University
email: srpierce@mail.widener.edu

INTRODUCTION

Cerebral palsy (CP) is a heterogeneous collection of non-progressive motor disorders of the developing brain that may occur antenatally or postnatally up to the age of two years [1]. Spasticity is often found in children with CP. Spasticity has been most commonly defined as a "velocity dependent increase in tonic stretch reflexes (muscle tone) with exaggerated tendon jerks, resulting from hyperexcitability of the stretch reflex' [2]. Traditionally, physical therapists have viewed spasticity as being primarily reflexive. But, researchers often found no increase in reflexes during the assessment of spasticity and theorized that the passive stiffness of a muscle caused spasticity [3]. In addition, the role of muscle mass in spasticity has not been investigated in children with CP. The purpose of this study was to examine the relationship between spasticity, reflex activity, co-activation, and muscle mass during the assessment of spasticity of knee extensors in children with CP.

METHODS

A retrospective sample of 8 children with CP (mean age = 10.4 years, SD = 1.8, range 8.0-13.6) was analyzed. One limb was tested and two surface EMG electrodes were placed on the child's leg. One electrode was placed on the vastus lateralis (VL) and medial hamstrings (MH). Signal conditioning electrodes with a parallel bar arrangement (contact area 1 x 10 mm, 10 mm interelectrode distance) were used to detect electrical activity of the muscles. Additional filtering and amplification of the EMG signal were completed using the Bagnoli 4-channel EMG system which has a band pass filter between 20-450 Hz and the gain set at 1000. EMG signals were sampled at a rate of 1.2kHz. Baseline EMG data were collected for at least five seconds. One set of three continuous passive movements at a velocity of 5°/s was collected for gravity correction calculation of the limb's weight during data processing. One set of ten continuous passive movements from 90 degrees of knee flexion to 15 degrees of knee flexion was completed at 180°/s with a return speed of 5°/s to assess knee extensor spasticity.

A custom Matlab program was used for post processing and analysis of the torque and EMG data. The gravity corrected knee extensor peak resistive torque was calculated once the limb was moving at a constant velocity. The maximum passive resistive torque of the ten movement repetitions was identified as the peak torque. EMG data were full wave rectified and processed using a second order Butterworth 10 Hz low pass filter with phase correction to create a linear envelope. EMG onset and offset was defined as muscle activity which was three standard deviations above baseline and occurred for a minimum of 50 ms. Reflexive muscle activity was defined as the presence of EMG activity of the either the MH or VL during passive movement. Co-contraction was defined as simultaneous EMG activity of both the MH and VL during passive movement.

Magnetic resonance imaging (MRI) was used to measure the maximum muscle anatomical cross-sectional area (CSA) and muscle volume of the knee extensors. All imaging procedures were performed in a clinical 1.5 Tesla magnet (GE Medical Systems, Waukesha, WI, USA). Images were acquired using a standard thoracic coil. Sequential scans acquired 3D data from the most proximal to the most distal part of the quadriceps femoris (QF) using a standard spoiled gradient-echo sequence. The imaging protocol was conducted as follows: (1) Coronal T1-weighted (TR/TE =

500/20) spin-echo localizing scans were obtained with a field of view of 24 cm and (2) transverse 3D spoiled gradient-echo images (flip angle = 30) were obtained with a TR of 22.5 ms, and minimum TE was automatically determined by the imaging software (typically 1.7 ms). The images were acquired with an encoding matrix of 256 x 256 x 28. A field of view of 12 to 27 cm was used depending on the size of the patient's leg, and slice thickness was 7 mm. Chemically-selective fat suppression was used to enhance definition between muscle groups.

Images obtained from the MRI scans were de-identified and analyzed by a blinded associate to determine the fat free CSA of each image slice using an interactive computer program, EXTRACTOR, and a correction algorithm. Individual segments of each head of each muscle were analyzed and then summed to determine the CSA of each slice. Maximum CSA was defined as the slice with the highest summed CSA of the component muscle heads. Volume was calculated by summing the products of the CSA of each slice.

Data was analyzed for normality and found not to be normally distributed. Spearmen correlation coefficients were complete to determine the relationship between measurements of knee extensor muscle mass (maximum CSA, muscle volume, CSA normalized to patient weight, and volume normalized to patient weight) and knee extensor spasticity (peak passive torque, reflex activity of the MH and VL, and co-contraction.)

Table 1: Correlation matrix for measures of QF muscle mass and knee extensor spasticity. An asterisk (*) indicates p<0.05.

	Peak Knee Extensor Passive Torque	MH EMG Percentage On	VL EMG Percentage On	Co-contraction EMG Percentage On
Max CSA	.619	.732*	.735*	.786*
Volume	.738*	.845*	.831*	.896*
CSA/weight	.071	.282	.374	.270
Volume/weight	.405	.374	.735*	.516

RESULTS AND DISCUSSION

Table 1 presents the correlation matrix examining relationships between measures of muscle mass of the QF and knee extensor spasticity. Significant positive correlations were found between the percentage of the passive range of motion with MH activation, VL activation, maximum CSA, and muscle volume ($p<0.05$). There were also significant positive correlations between peak knee extensor passive torque and muscle volume as well as muscle volume normalized to weight and VL activation ($p<0.05$).

Interestingly, the QF muscle mass (CSA and volume) is positively correlated with MH and VL reflex activity and co-contraction of these two opposing muscle groups. These findings suggest that the quadriceps muscle mass is greater in the lower extremities with higher levels of spasticity and co-activation, however, the specific mechanisms for the cause of the greater muscle mass cannot be determined from the retrospective nature of the present study. Postulated mechanisms for having greater muscle mass include having greater levels of neural drive directly to the quadriceps related to elevated VL reflex activity or indirectly by the quadriceps requiring greater neural drive to over come high levels of MH reflex activity and co-contraction. Additional research is needed to confirm these findings and examine alternative hypotheses for the relationship between spasticity and muscle mass. The results of this study should be interpreted cautiously due to the small sample size used in the investigation. It is unknown if the results of this study would generalize to other muscle groups and age ranges in children with spastic CP.

REFERENCES

1. Lin JP. The cerebral palsies: a physiological approach. J *Neurol Neurosurg Psychiatry*, **74 Suppl 1**:i23-i29, 2003
2. Lance JW. The control of muscle tone, reflexes, and movement: Robert Wartenberg Lecture. *Neurology*, **30(12)**:1303-1313, 1980
3. Dietz V, et al. Normal and impaired regulation of muscle stiffness in gait: a new hypothesis about muscle hypertonia. *Exp Neurol,* **79(3):**680-687, 1983

ACKNOWLEDGEMENTS

This study was funded by the National Institutes of Health Grants 1R03-NS048875 and R01-HD043859

MAXIMIZING VELOCITY IN THE HAMMER THROW

Iain Hunter, Carrie Robinson, and Travis Clyde
Brigham Young University, Provo, UT
email: iain_hunter@byu.edu   web: http//biomech.byu.edu

INTRODUCTION

Hammer throwing dates back as far as 1800 B.C. in Ireland. Today, men throw a 7.26 kg implement while women throw 4.00 kg. The event was included in the 1900 Olympic Games for men and began in 2000 for women. The hammer throw is one of the more technical events in track and field that requires a unique combination of power, stability, and coordination. The required technique for positioning the body and applying the torques to increase angular momentum of the hammer-thrower system must be nearly perfect for a successful hammer throw due to the large centripetal forces.

Figure 1: Technique of the hammer throw. The mass of 7.26 kg with a radius of approximately 1.4 m creates enormous centripetal forces.

As with most throwing events in track and field, maximizing the magnitude of release velocity is the primary focus [1]. With the complexity of the movement, determining which characteristics of technique apply best to increasing release velocity can be difficult. In angular motion, a change in one variable often has a meaningful effect on another variable. However, it is clear that the larger the torque the athlete can generate will lead to greater changes in angular momentum of the hammer-thrower system [2].

During the double support phase of each turn (when both feet are on the ground) large torques can be generated. The rotation of the trunk along with the action of the lower body may relate to the amount of torque exerted. This study investigated whether the angular range during double support between the shoulder and hip lines from a longitudinal axis related to the distance thrown. Since the time the torque is applied also determines the changes in angular momentum, an analysis of the timing of foot placements was also completed.

METHODS

Two digital camcorders (Canon Elura 60, Lake Success, NY) were placed perpendicular to each other and zoomed in to view the entire movement of the thrower and hammer. Peak Motus 8.5 was used to digitize and calculate three-dimensional coordinates of the hammer head, shoulders, and hips for every throw at the 2008 Mt SAC Relays, 2008 BYU High Performance Meet, and the 2008 US Olympic Trials. Altogether, 80 throws were digitized from the men's and women's events at these meets.

Throwing distance, timing of double and single support phases, and positioning of the hips relative to the hammer head at the beginning of double and single support were measured and recorded.

Linear regressions were performed to determine any factors that were related to throwing distance.

RESULTS AND DISCUSSION

The angular range of the shoulder to hip angle during double support was significantly related to throwing distance during the second turn, but not any other turns ($R^2=0.33$, $p<0.01$ and $R^2=0.15$, $p<0.04$ for women and men respectively, Figure 1). However, there was a large variability in the angular range showing that there are other factors of great importance to consider (mean±SD = 27±15 deg for women and 41±15 deg for men).

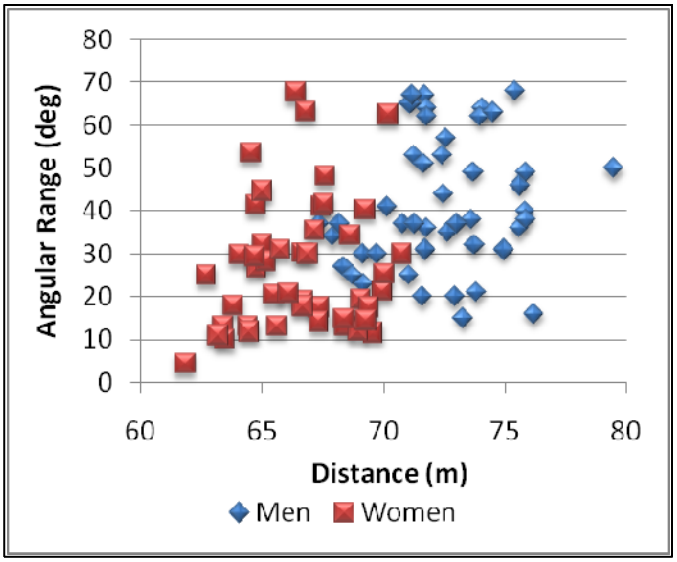

Figure 1: The relationship between angular range of the shoulder to hip angle versus distance for men and women during the second turn.

Another factor we measured was timing of single and double support phases. A surprising finding occurred. Significance only showed up in the second turn, similar to the angular range data. The ratio of double to single support for women was a predictor of distance ($R^2=0.29$, $p=0.04$) with less time in double support relating to greater throwing distance. For men, less time spent in double support led to greater throwing distances ($R^2=0.33$, $p=0.03$). The greater range of motion in a shorter amount of time demonstrates large increases in angular momentum being generated during double support of the second turn.

All significant findings occurred during turn two. Major increases in linear velocity of the hammer occur during double support [2]. While the movement patterns and torques generated in other turns must be of importance, it seems that the second turn is critical in effective hammer throwing.

However, the observed trends were difficult to detect since much variability shows up comparing person to person. Since clear trends with these variables failed to show strong correlations, there must be other major factors that predict throwing distance better. The torques that a hammer thrower generates to build up angular momentum were not measured in this study. This is likely the main factor to consider in the future. The larger the torque regardless of the positions used, the greater the change in angular momentum. One other factor to consider is due to the nature of manual digitizing, some variability is to be expected.

SUMMARY/CONCLUSIONS

This study showed that during turn two, the best throws occur when a large range of motion occurs in trunk rotation during double support during a relatively short amount of time. Coaches and athletes should focus on improving the range of motion through the trunk and other methods for producing large torques that shorten the time spent in double support. This is especially important during turn two, but the other turns should not be ignored since there are clearly other factors of importance in hammer throwing that this study did not detect.

REFERENCES

1. Hunter I, Killgore G. *Track Coach* **162**, 5180-5182, 2003.
2. Dapena J, Mcdonald C. Med Sci in Sports and Exer **21**, 206-220, 1989.

ACKNOWLEDGEMENTS

Thank you to USA Track and Field for funding this study.

Development of an analytical model for rotator cuff repairs

[1, 2] Amit Aurora, MS, [1] Antonie J. van den Bogert, PhD and [1] Kathe Derwin, PhD
[1] Orthopedic Research Center, Dept of Biomedical Engg, Lerner Research Institute, Cleveland, OH
[2] Dept of Chemical and Applied Biomedical Engg, Cleveland State University, Cleveland, OH
Email: auroraa@ccf.org web: http://www.lerner.ccf.org/bme/derwin/

INTRODUCTION

Currently, surgical repair of the rotator cuff tears is the gold standard for the treatment of these injuries. However, these repairs have a high retear rate of 20-90% due to factors not restricted to tear size, chronicity of the repair and rehabilitation protocol [1, 2]. Hence, there remains a critical need for a repair strategy that is both biologically stimulating and improves the mechanical performance of these repairs. This has led to a surge in the development of synthetic and biologic scaffolds over the last decade [3]. Despite, these advances very little is known of the role these scaffolds play in load sharing and in the biomechanics of the repair. The objective of the present study was to develop and validate analytical models of a primary and augmented tendon repair. We intend to use these models to investigate the mechanical role of the various components of the tendon repair.

MATERIALS AND METHODS

A. Model for primary and augmented repairs: The primary and augmented repairs were modeled using springs. The primary repair had two springs in series (Figure 1a): the bone-suture-tendon interface (spring#1) and the tendon (spring#2). The augmented repair had a total of five springs (Figure 1b). The tendon (spring#2) was divided in two springs, spring#2' and spring#2”. The bone-scaffold-suture component (spring#3) and the scaffold-suture-tendon interface (spring#4) were in series with each other and together in parallel with the primary repair (spring 1 and 2’). The entire repair model was then placed in series with the other half tendon spring#2”.

B. Spring mechanical properties: The properties of the individual springs were obtained experimentally using male cadaveric canine shoulders (~30kgs).

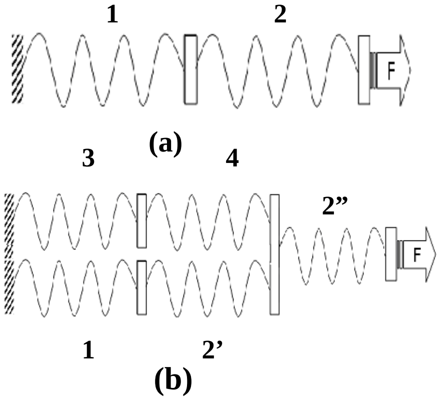

Figure 1: Schematic representation of (a) primary and (b) augmented rotator cuff repair.

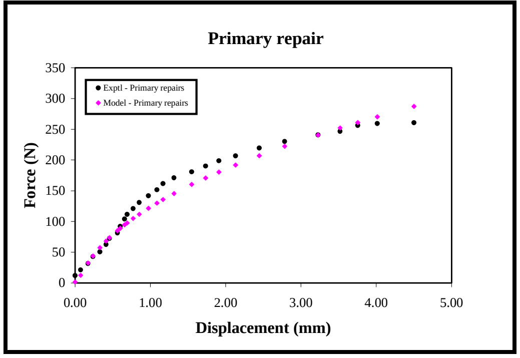

Figure 2: Load displacement plots for model predicted and experimental primary repair

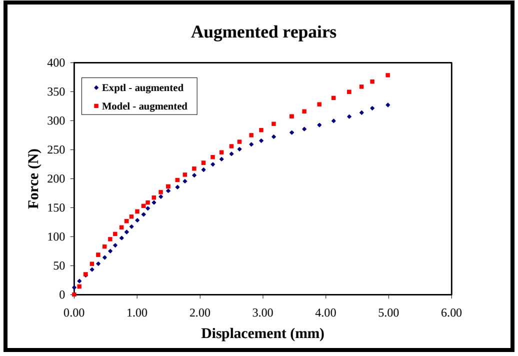

Figure 3: Load displacement plots for model predicted and experimental augmented repair

Spring#1 & Spring#2: Canine shoulders (n=5) had their infraspinatus (IFT) tendon released and repaired to the greater tuberosity using two transosseous Mason Allen sutures. The IFT muscle was freeze clamped and the repair was cycled between 5-100N for 100 cycles @ 0.25Hz and subsequently loaded to failure at 30mm/min. Optical markers were placed on the tendon near the insertion site and the tendon midsubstance to determine the properties of the spring#1 & #2. *Spring#3:* Woven PLLA devices (n=3) were screwed to a saw bone on one end and sutured with 3 simple stitches to a rod on the other end. The devices were preloaded to 5N and subsequently loaded to failure @ 30mm/min.

Spring#4: Three Mason Allen sutures were placed in isolated canine IFT tendons (n=5) and secured over a rod. The IFT muscle was frozen and the suture-tendon interface was cycled between 5-30N for 20 cycles @ 0.25Hz followed by load to failure at 30mm/min. The load-displacement properties of spring#3 & #4 were determined using actuator displacements.

C.Repair mechanical properties: For *primary repair constructs* the IFT tendons of five canine shoulders were released and repaired to the greater tuberosity. For *augmented repair constructs* IFT tendons of five canine shoulders were released and repaired to the greater tuberosity followed by augmentation with a woven PLLA device screwed to the bone. The surgical & testing protocol was similar to the respective individual springs described above.

D. Curve fitting*:* The average experimental data for each spring was fitted to a power law [F = A(x) ^b] up to the yield load, defined as the first maximum load attained by the specimen. The parameters A and b were determined using the Curve fitting toolbox in MATLAB (Mathworks, Natick, MA).

D. Model development and validation: A system of equations was developed for both, primary and augmented repair constructs, using the average curve-fit data from the individual component testing. The models were solved under static equilibrium conditions using the optimization toolbox in MATLAB. To validate the models, the model generated load (output) was obtained for a given displacement (input) and was compared to experimental data. The average RMS difference of the predicted versus experimental data was computed.

RESULTS

The RMS value for the primary model (13.8N) was 6% of the average experimental yield load (235.3±39N) (Figure 2). The RMS value for the augmented repair model (22.8N) was 7% of the yield load of the average experimental yield load (327±46.5N) (Figure 3). Experimentally no significant difference (ttest, $p>0.05$) was seen between the stiffness of the primary (132±27.5N/mm) and augmented (121±23.3N/mm) repair constructs. However, the model predicted stiffness of the augmented repair construct (122N/mm) was higher than the model predicted stiffness for the primary repair construct (92N/mm). The model also predicted that the augmentation component (springs #3 and #4) carries 25% of the yield load of the augmented repair construct.

DISCUSSION

The goal of this study was to develop a simple analytical model for primary and augmented tendon repair constructs. RMS below 10% suggests that developing a model using a spring analogy can predict the mechanical behavior of both the repair constructs with reasonable accuracy up to the point of maximum (yield) load. However, the model appears to predict an increase in stiffness with augmentation, which the experimental data does not support. We are currently computing the confidence intervals for our model predictions, in an effort to determine if this apparent difference in stiffness is statistically significant. One limitation of our model is that the parameters were obtained from failure testing of samples that were first subjected to a cyclical loading protocol. Hence, the model cannot be used to predict the biomechanical performance of the repairs upon the very first onset of mechanical load. Further, our model cannot be used to predict failure loads (complete rupture) as the model was developed only up to and including the point of maximum (yield) load. Finally, compared to the clinical scenario, the experimental repairs used to develop this model are greatly simplified. Hence the model is limited to making only general observations about the mechanical roles of the various components of a tendon repair.

CONCLUSIONS

In summary, we present here a simple, accurate model to estimate the mechanical behavior of primary and augmented tendon repair. We believe that the model will be useful for identifying the relative contributions of the various components of the repair construct and suggesting improvements to current repair strategies.

REFERENCES

1.Galatz LM, et al, JBJS 86A, 219-224, 2004.
2.Gaizelly DF, et al, COR, 304, 43-53, 2004.
3.Aurora A, et al, JSES, 16(Suppl 5), 171-8, 2007

ACKNOWLEDGEMENTS

Molecular Medicine Fellowship - Cleveland State University

THE IMMEDIATE BILATERAL EFFECTS OF UNILATERAL KNEE BRACING FOR THE TREATMENT OF KNEE OSTEOARTHRITIS: PRELIMARY RESULTS

Becky Avrin Zifchock, Sherry Backus, Eric Bogner, Helene Pavlov, Lisa Mandl, Chris Chen, Glenn Garrison, Allison Brown, Frank Cordasco, Riley Williams, David Hunter, Asheesh Bedi, Howard Hillstrom
Hospital for Special Surgery, New York, NY
email: zifchockr@hss.edu

INTRODUCTION

Knee osteoarthritis (OA) is a disease that affects more than 20 million adults in the US, with direct healthcare costs estimated to be $7.9 billion and growing [1]. Some of these costs can be attributed to the fact that many people affected by the disease in one joint, subsequently have additional joints affected, contributing to additional health care costs. If the disease were the result of systemic risk factors alone, bilateral decline would occur at similar rates. However, many patients initially present with unilateral OA, and subsequently exhibit symptoms in the contralateral limb. Studies by Shakoor et al. [2] and Spector et al. [3] reported that, following hip or knee replacement, patients typically required joint replacement in the same joint in their contralateral limb within two years. While it is unclear why this progression occurs, it is important to assess whether treatment of the involved limb inadvertently increases the rate of progression in the uninvolved limb.

Knee bracing is a commonly used conservative treatment for patients with mild to moderate knee OA. Studies have shown that knee bracing can relieve the pain associated with the disease, and that it has positive effects on function including reducing the knee abduction moment [4]. In terms of medial knee OA, a varus posture of the knee, along with large abductory moments are likely to indicate abnormal loading of the medial compartment. Characterizing the effects of a knee brace on static alignment, as well as dynamic knee kinetics and kinematics is important for understanding the potential benefits of the brace. This study sought to measure the effects of unilateral knee bracing on loading in both knees. The purpose of this study was to examine the immediate effects of unilateral knee bracing on pain levels, joint alignment, and knee kinetics and kinematics of both the involved and uninvolved sides of patients with unilateral, medial knee OA. It was hypothesized that there would be side-to-side differences, as well as differences between a braced and unbraced condition.

METHODS

As part of an ongoing longitudinal study, the first four of twenty subjects (all male; 66 years ±9; 81±7 kg; 1.8±0.1m) with unilateral medial knee osteoarthritis were studied. All subjects were K-L grade 2 or 3 in the involved knee, as assessed by radiograph, and were asymptomatic on their uninvolved knee. Subjects were fit with a custom unloader valgus knee brace (Ossur Unloader One; Aliso Viejo, CA) and allowed a one-week accommodation period. Instrumented gait analyses were performed at baseline (without the brace) and after a one-week brace accommodation period (with the brace). The analyses were conducted in a data collection volume containing a 12-camera system (Motion Analysis Corp; Santa Rosa, CA) sampling at 100Hz and four forceplates (AMTI; Watertown, MA and Bertec; Columbus, OH) sampling at 1000Hz. The gait analyses were performed in a barefoot condition, although all research subjects were also provided with standardized footwear (New Balance 576; Boston, MA) to wear in conjunction with the knee brace outside of the lab. Subjects walked overground at a self-selected pace. Kinetics and kinematics were assessed in both the involved and uninvolved knees. Peak stance-phase knee adduction angles and (internal) abduction moments were measured from each of a minimum of 8 gait cycles per subject. At each measurement session, subjects were asked to rate their pain levels on a 100mm visual analog scale following the performance of each of three tasks: walking 50ft at a comfortable pace, walking 50ft at a fast pace, ascending and descending 5 stairs.

Radiographs of both knees were obtained at baseline with and without the knee brace applied to the involved limb. From these, the minimum medial joint space and the tibio-femoral angle were measured. A two-way repeated-measures ANOVA was carried out to compare each dependent variable between the braced and unbraced conditions, and between the involved and uninvolved limbs. Additionally, effect sizes were calculated for the effect of both condition and limb. Due to the preliminary nature of these results, a p-value < 0.10 was considered significant, and an effect size > 0.7 was considered large.

RESULTS AND DISCUSSION

Kinematic and kinetic results are shown in Table 1. These data showed no interaction between limb and condition, nor were there differences between baseline (unbraced) and one-week (braced) conditions. However, there were significant differences between the involved and uninvolved limbs. Conversely, as shown in Table 2, the results indicated a significant interaction between limb and condition for the pain scores for all three tasks. The brace significantly reduced the pain in the braced limb, but had virtually no effect on pain in the uninvolved limb. It is likely that this occurred because baseline scores were low in the contralateral limb, potentially limiting the ability to detect a treatment effect. Radiographic measurement results are shown in Table 3. There were no statistical differences between the involved and uninvolved limbs or between the braced and unbraced conditions. However, the large effect size (> 0.7) suggests a difference between the limbs for both parameters. This difference may become statistically significant with the addition of the remaining subjects.

CONCLUSIONS

The results to date suggest that there is a difference between the involved and uninvolved sides of patients with medial knee OA. There do not appear to be any immediate (one-week) effects on the functional or structural factors measured in this study. However, the brace had a significant clinical effect in that it reduced pain in the involved limb. In light of the expectation that the brace would affect structure and function, the lack of changes for these factors is surprising. However, these findings represent only four subjects, and the differences may be more pronounced at the short-term (4-month) or long-term (12-month) follow-up.

REFERENCES

1. Prevention, CFDC; Arthritis: The Nation's Leading Cause of Disability. 2007
2. Shakoor et al. *Arthritis Rheum* **46**(12) 3185-9, 2002.
3. Spector et al. *Ann Rheum Dis* **53**(9) 565-8, 1994.
4. Pollo et al. *Am J Sports Med* **30**(3) 414-21, 2002.

ACKNOWLEDGEMENTS

The authors gratefully acknowledge New Balance for providing the footwear for our subjects, and Ossur for providing the braces and an unrestricted educational grant that helped to support this study.

Table 1: The effects of bracing on knee kinematics and kinetics (knee adduction is positive)

Variable	Baseline (Unbraced) Condition		1-Week (Braced) Condition		Effect of Condition, p-value (Effect Size)	Effect of Limb, p-value (Effect Size)
	Involved	Uninvolved	Involved	Uninvolved		
Knee Add Angle, deg	6.5 (4.4)	2.7 (4.2)	6.5 (2.0)	2.4 (4.3)	0.84 (0.1)	0.06 (1.1)
Knee Abd Mom, N-m/kg	-0.5 (0.1)	-0.4 (0.1)	-0.6 (0.1)	-0.4 (0.1)	1.00 (0.3)	0.03 (1.9)

Table 2: The effects of bracing on pain scores (0 = No Pain and 100 = Worst Pain)

Variable	Baseline (Unbraced) Condition		1-Week (Braced) Condition		Interaction Between Condition and Limb, p-value
	Involved	Uninvolved	Involved	Uninvolved	
Stairs	61.7 (21.2)	1.3 (2.3)	31.3 (24.3)	3.7 (6.4)	0.08
50' Comfortable Walk	62.7 (5.1)	1.3 (1.5)	19.3 (21.4)	0.0 (0.0)	0.05
50' Fast Walk	58.0 (17.3)	1.0 (1.7)	17.3 (9.8)	0.0 (0.0)	0.04

Table 3: The effects of bracing on radiographic measures in a braced and unbraced condition at baseline

Variable	Unbraced Condition		Braced Condition		Effect of Condition, p-value (Effect Size)	Effect of Limb, p-value (Effect Size)
	Involved	Uninvolved	Involved	Uninvolved		
TF Angle, deg (varus +)	2.3 (4.6)	-1.4 (5.2)	1.4 (3.9)	-2.2 (4.7)	0.17 (0.2)	0.26 (0.8)
Joint Space, mm	1.7 (3.4)	4.1 (2.5)	2.0 (3.4)	4.5 (2.3)	0.11 (0.1)	0.14 (0.8)

INJURY PREVENTION TRAINING RESULTS IN BIOMECHANICAL CHANGES CONSISTENT WITH DECREASED KNEE LOADING IN FEMALE ATHLETES DURING LANDING

Christine D. Pollard, Susan M. Sigward and Christopher M. Powers
Jacquelin Perry Musculoskeletal Biomechanics Research Laboratory
Division of Biokinesiology and Physical Therapy
University of Southern California, Los Angeles, CA, USA
email: cpollard@usc.edu, web: www.usc.edu/go/mbrl

INTRODUCTION

Tears of the anterior cruciate ligament (ACL) are one of the most common knee injuries sustained by females who engage in athletics and recreational activities. As a result, numerous injury prevention training programs designed to reduce the incidence of non-contact ACL tears have been reported in the literature [1-3]. Most of these programs attempt to alter knee joint loading through some form of strengthening and/or neuromuscular training. Although the success of these prevention programs is encouraging, it is not known if ACL injury prevention training alters lower extremity mechanics in a way that reduces knee loading. The purpose of this study was to investigate whether an ACL injury prevention training program previously shown to reduce the incidence of ACL injury alters knee joint mechanics in female soccer athletes during landing.

METHODS

Subjects consisted of 30 female club soccer players (age range: 11 to 17 years) with no history of knee injury and no history of participating in a formal ACL injury prevention training program. Three-dimensional kinematics (eight camera Vicon motion analysis system, 250 Hz) and ground reaction forces (AMTI, 1500 Hz) were collected while each subject performed a drop landing task from a height of 36 cm (3 trials). Data were obtained prior to and immediately following participation in a previously described injury prevention training program [2]. The training program was implemented 2 times a week for 10 weeks (20 minutes per session) as part of the normal in-season soccer practice schedule. The program included stretching, strengthening, plyometric exercises, and agility activities. Visual3D™ software (C-Motion, Inc., Rockville, MD, USA) was used to quantify three-dimensional kinematics and internal net joint moments (inverse dynamics equations) of the dominant limb (i.e. the limb used to kick a ball) during the deceleration phase of landing. Sagittal plane joint power was computed as the scalar product of angular velocity and net joint moment. All kinetic data were normalized to body mass.

Variables of interest included peak knee valgus angle, average knee adductor (valgus) moments, average knee extensor moments, average hip extensor moments, knee energy absorption, and hip energy absorption. To further explore the relationship between the knee and hip load distribution during landing, we examined the knee to hip extensor moment ratio (average knee extensor moment/average hip extensor moment) and the knee to hip energy absorption ratio (knee energy absorption/hip energy absorption). Using this ratio, a value greater than “1” indicated increased knee extensor moments compared to hip extensor moments or increased knee energy absorption compared to hip energy absorption while a value of less than “1” would indicate increased hip extensor moments compared to knee extensor moments or increased hip energy absorption compared to knee energy absorption.

Differences between pre and post-training were evaluated using paired t-tests. Statistical analyses were performed using SPSS statistical software (Chicago, IL). Significance levels were set at $P \leq 0.05$.

RESULTS

Following training, subjects demonstrated decreased knee extensor moments (1.18 ± 0.25 Nm/kg vs. 1.30 ± 0.29 Nm/kg; *P* = 0.03) and increased energy absorption at the hip (150.8 ± 47.6 Watts/kg vs. 129.8 ± 45.8 Watts/kg; *P* = 0.04). Furthermore, subjects exhibited a decrease in the knee/hip extensor moment ratio (1.8 ± 0.9 vs. 2.3 ± 1.8; *P* = 0.05; Figure 1) and knee/hip energy absorption ratio (2.6 ± 1.8 vs. 3.2 ± 1.3; *P* = 0.03; Figure 2). No differences were found in the frontal plane knee moments or angles.

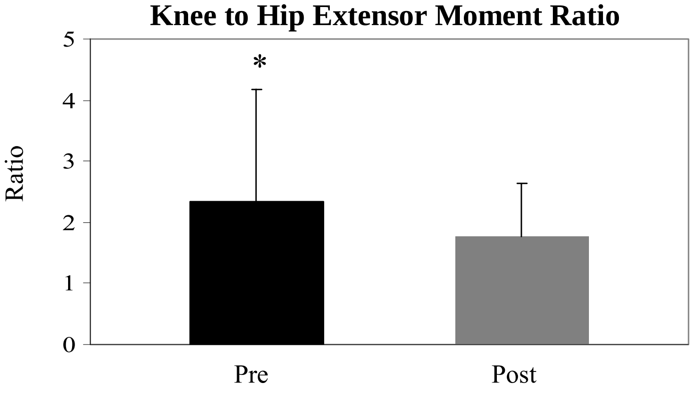

Figure 1: Knee to hip extensor moment ratio pre- and post-training during the deceleration phase of landing. *Indicates significant differences ($P \leq 0.05$).

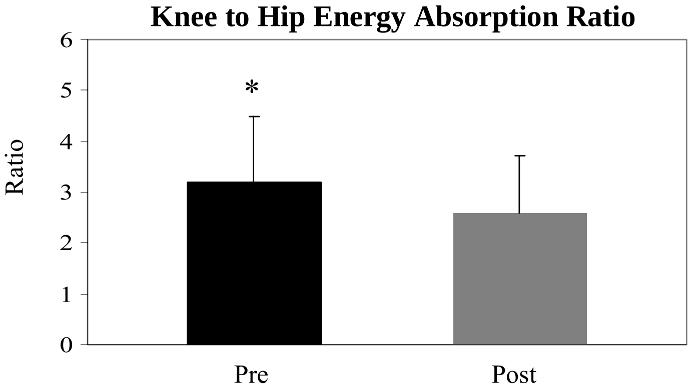

Figure 2: Knee to hip energy absorption ratio pre- and post-training during the deceleration phase of landing. *Indicates significant differences ($P \leq 0.05$).

DISCUSSION

Participation in an injury prevention training program previously shown to reduce ACL injury was effective in altering lower extremity mechanics in female athletes. In particular we observed a distinct change in the strategy used to attenuate impact forces. More specifically, we found that training increased utilization of the hip extensors resulting in a decrease in the reliance on the knee musculature to decelerate the body center of mass during landing. This change in behavior was best illustrated by the post-training “shift” in the knee/hip extensor moment ratio and the knee/hip energy absorption ratio. Our findings are particularly compelling in that the training program that was used in our study has been shown to reduce the incidence of ACL injuries in female athletes. As such, our results point to the modification of biomechanical and/or neuromuscular risk factors as being a possible mechanism by which injury prevention programs are successful in decreasing ACL tears.

CONCLUSIONS

Following participation in a 10-week ACL injury prevention training program, female subjects exhibited a change in their landing strategy that was reflective of decreased knee loading. We propose that this training program may reduce the risk for ACL injury by improving utilization of the hip musculature which then promotes shared control of the body center of mass during landing.

REFERENCES

1. Hewett TE, et al. *Am J Sports Med* **24**, 699-706, 1999.
2. Mandelbaum BR, et al. *Am J Sports Med* **33**, 1003-1010, 2005.
3. Myklebust G, et al. *Clin J Sports Med.* **13,** 71-78, 2003.

ACKNOWLEDGEMENTS

This study was funded by the National Institutes of Health (R01 AR053073-02).

THE EFFECTS OF GENDER AND OBESITY ON TRUNK INERTIAL PARAMETERS IN OLD AND ELDERLY ADULTS

April J. Chambers[1], Alison L. Sukits[1], Jean L. McCrory[2,3], Rakié Cham[1]
[1]Bioengineering, University of Pittsburgh, Pittsburgh, PA, USA
[2]Health and Physical Activity, University of Pittsburgh, Pittsburgh, PA, USA
[3]Human Performance and Applied Exercise Science, West Virginia University, Morgantown, WV, USA
email: ajcst49@pitt.edu, web: http://www.hmbl.bioe.pitt.edu

INTRODUCTION

Anthropometry is a necessary aspect of research in the elderly, especially in biomechanics and injury prevention research [1-4]. Typically, body segment parameters are derived from regression equations or models based on cadaveric studies [5] or imaging [6]. A major limitation of these predictive equations is their lack of incorporating gender, age, race or body type [1]. As a result, the use of these parameter estimates has been shown inaccurate in various populations including children [7] and older adults [1]. Unfortunately, there is little inertial anthropometric information available on the elderly [1-3,8-10].

Body segment parameter inaccuracies may be due to gender-specific variations in tissue density within and between body segments as well as age-related redistribution of mass [8]. The effect of obesity may be another reason for the inaccuracies associated with traditional body segment parameter estimations [1,4]. Dual energy x-ray absorptiometry (DXA) has been validated as a reliable in-vivo method to derive body segment parameters that includes tissue density, age, gender and obesity [1,7]. The aim of this study was to report trunk inertial parameters in older adults (aged 65 years and older) and to investigate the impact of aging, gender and obesity.

METHODS

Eighty-three healthy older adults, screened for metal implants, were divided into 8 subgroups based on gender (Female and Male), obesity determined from body mass index (BMI) ($BMI \leq 30$, non-obese and $BMI > 30$, obese) and age (≤ 75 yrs, old and >75 yrs, elderly). Each participant underwent a whole body DXA scan (Hologic QDR 1000/W) lying supine. For each DXA scan, trunk segment boundaries were identified as the shoulder joint center (estimated as the acromion) and the hip joint center [5,6].

Segment mass as a percent of body mass (SM), segment length as a percent of body height (SL), distance from the center of mass to the proximal end of the segment as a percent of segment length (COM), and frontal plane radius of gyration as a percent of segment length (Rg) were determined [1,7]. These dependent variables were each entered individually in a mixed-factor repeated measures analysis of variance (ANOVA). The independent factors were gender, obesity and age group. Analyses included main effects, two-way and three-way interactions. Post hoc analyses included comparisons using a Student's t-test. Statistical significance was set at 0.05.

RESULTS AND DISCUSSION

The accuracy of body segment parameters presented here was acceptable and consistent with values reported in the literature [1,6,8-10]. No significant effects were noted in trunk SL. A vertical resolution of 1.30 cm (same resolution as in [7]) may have limited the analysis of SL.

Trunk SM accounted for a significantly greater percent of body mass in obese compared to non-obese individuals (Figure 1). Increases in trunk SM agree with previous literature stating that increased BMI is highly correlated to increases in waist circumference and abdominal fat [2,11,12]. Males had greater SM than females. Males have previously reported with higher trunk segment mass compared to females [8,12]. These gender trends seem to carry into older adults and the elderly. Two-way interaction effects with obesity and age group were also found in trunk SM. In general, obese elderly adults had significantly higher trunk SM than non-obese elderly and all older adults. An increase in factors that would contribute to increased trunk SM has been previously noted with increasing age and obesity [2,9]. It should be of health concern that obese elderly adults have significantly higher trunk SM. Certain waist anthropometry, not just BMI, have been implicated as important predictors of health, obesity and mortality risk in the elderly [2,8].

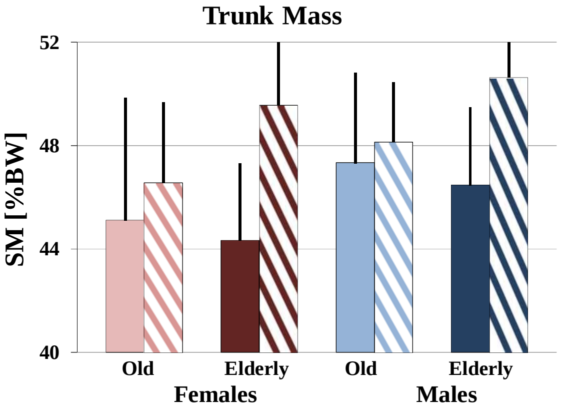

Figure 1: Mean trunk SM. Non-obese shown as solid bars and obese as hashed bars. Standard errors are provided.

Gender and obesity effects were also found in COM and Rg. Males had a more proximal trunk COM compared to females (Figure 2). A more distal trunk COM in the female group may seem counterintuitive. However, Okada reported significantly larger mass ratio of the lower trunk and smaller mass ratio of the upper trunk in elderly females compared to males [12]. An increased mass in the lower trunk and less in the upper trunk would translate into a more distal trunk COM in elderly females. Finally, non-obese individuals had a greater trunk Rg than obese. This is interesting since a decrease in Rg was noted in segments with weight loss [4].

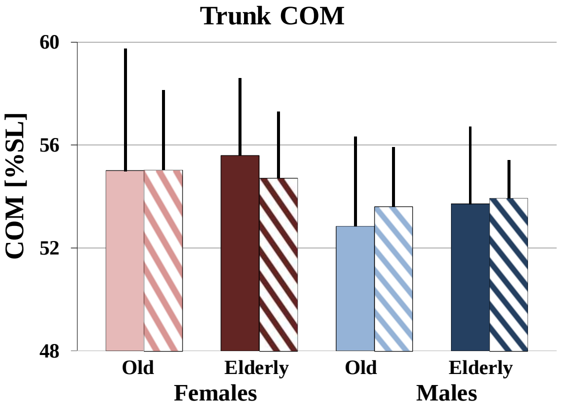

Figure 2: Mean trunk COM. Non-obese shown as solid bars and obese as hashed bars. Standard errors are provided.

In general, there is little reported in the literature on the effect of obesity on body segment parameters, especially COM and Rg. However, Durkin & Dowling reported large differences within both young and middle-aged male and female body segment parameters. The authors acknowledge that these variations might be attributed to variations in body type or obesity [1].

CONCLUSIONS

In conclusion, age, obesity and gender have a significant impact on trunk SM, COM and Rg in older and elderly adults. The data presented here can be used to accurately represent trunk anthropometrics of an aging population. This study underlines the need to consider age, obesity and gender when utilizing anthropometric data sets.

REFERENCES

1. Durkin JL, et al. J Biomech Eng 125, 515-22, 2003.
2. Hughes VA, et al. Am J Clin Nutr 80, 475-82, 2004.
3. Kuczmarski MF, et al. J Am Diet Assoc 100, 59-66, 2000.
4. Matrangola SL, et al. J Biomech 41, 3278–81, 2008.
5. Dempster, WT. WADC TR, 55-159, 1955.
6. de Leva P. J Biomech 29, 1223-30, 1996.
7. Ganley KJ, et al. Gait & Posture 19, 133-40, 2004.
8. Jensen RK, et al. J Biomech 27, 89-96, 1994.
9. Muri J, et al. J Biomech 41, 1809-12, 2008.
10. Pearsall DJ, et al. Ann Biomed Eng 24, 198-210 1996.
11. Janssen I, et al. Int J Obes 30, 1223-8, 2006.
12. Okada H, et al. Biomechanism 13, 125–139, 1996.

ACKNOWLEDGEMENTS

Pittsburgh Claude D. Pepper Older Americans Independence Center - Grant #: P30 AG024827
Special thanks to the CTRC, Dr. S. Greenspan & Donna Medich.

QUADRICEPS ACTIVATION AT DIFFERENT HIP AND KNEE JOINT ANGLES

[1] Samantha L. Winter and [1]Mark Burnley
[1]Aberystwyth University
email: sbw@aber.ac.uk, web: http://www.aber.ac.uk/sportexercise

INTRODUCTION

The method of Herzog and ter Keurs [1] permits the reconstruction of the force-length curve of bi-articular muscles for individual subjects. This method assumes that for a bi-articular muscle crossing two joints, A and B, the variation in the output at Joint A in response to a change in the angle of Joint B can only be due to the force-length properties of the bi-articular muscle since the contribution of mono-articular muscles crossing Joint A would be constant. This method is useful in understanding the extent of variability in the expressed section of the force-length relationship as it allows the determination of the force-length relationship for individual subjects rather relying on the averaging of data across subjects. Such inter-individual variation is important since it may have an influence on the quality of movement and muscle co-ordination.

An important assumption of the method of Herzog and ter Keurs [1] is that the activation of the mono-articular and bi-articular muscles is constant across different joint configurations. Previous work using a muscle model to validate the method of Herzog and ter Keurs [1] has shown that the method is robust to random and systematic errors arising from incomplete activation of up to 20% of the maximum joint moment for a given position [2]. Nevertheless, if it could be shown that the degree of quadriceps activation across different hip and knee joint configurations were reasonably consistent, this would provide additional support for the reliability of the method. The purpose of this study was to measure the degree of quadriceps activation across different hip and knee joint angle configurations using doublet interpolation [3].

METHODS

Five subjects (mean ± standard deviation age: 30.8 ± 3.8 years; mass: 72.7 ± 13.9 kg; height: 1.77 ± 0.10 m) were familiarized with the procedures and provided written informed consent. The University Ethics Committee for Research Procedures at Aberystwyth University approved all procedures. Subjects performed a five minute cycle ergometer warm-up and then performed maximal isometric knee extension contractions using the right leg in a Biodex III dynamometer (Biodex Medical Systems, Shirley, NY) in the following hip and knee angle configurations (full hip and knee joint extension being defined as 0 degrees): a 0 hip angle and a 10, 90 and 110 degree knee angle, a 55 degree hip angle and a 10 and 90 degree knee angle, and an 85 degree hip angle and a 10, 90 and 110 degree knee angle. These positions were chosen to reflect a range of vasti and rectus femoris muscle lengths. Subjects were asked to perform two maximal efforts in each position. The order of presentation of the joint configurations was randomized for each subject. Care was taken to correctly align the dynamometer axis with the lateral femoral condyle in each position before each trial. The lower leg was firmly attached to the lever arm above the ankle using a padded Velcro strap, and straps secured firmly across the waist and both shoulders. Before each contraction a baseline recording was taken to account for any passive torque, this was subtracted from the Biodex record. The Biodex output was

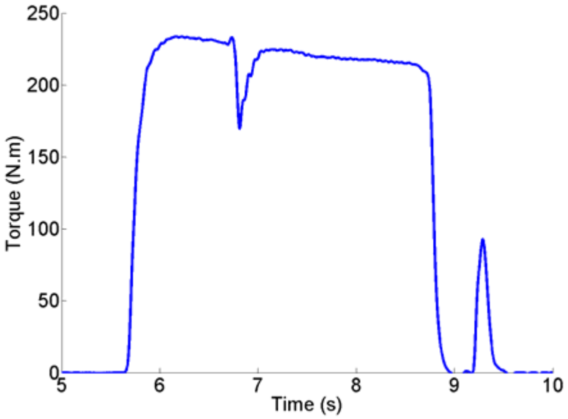

Figure 1: Example of a torque profile recorded during a maximum voluntary contraction with a superimposed doublet and subsequent potentiated doublet torque.

sampled at 1,000Hz and was low pass filtered using a zero lag fourth order Butterworth filter with a cut off of 40Hz.

Carbon rubber electrodes (12 x 10 cm, EMS Physio, Oxfordshire, UK) coated in conductive gel were placed on the anterior thigh and secured using elastic Velcro bandages. The cathode was placed on the midline of the thigh at 30% of thigh length measured in the seated position from the anterior superior iliac spine to the superior border of the patella, the anode was positioned 8 cm proximal to the superior border of the patella over the vastus medialis. A constant-current, variable-voltage stimulator (Digitimer DS7AH, Welwyn Garden City, UK) was used to deliver doublet stimuli (100-µs pulses, 10-ms interval) at 400 V. During a familiarization visit, the current was increased in steps of 10 mA from 100 mA until no further increase in potentiated doublet torque occurred. The current was then increased by a further 10 mA (range utilized, 310–430 mA). These stimuli were tolerated without discomfort. The superimposed doublet and the potentiated doublet measured after the contraction of interest (Figure 1) were used to compute voluntary activation as a percentage of maximal activation. The potentiated doublet torque was calculated as the peak torque achieved following the doublet stimuli delivered 1 s after the contraction, and the superimposed doublet torque was calculated as the increase in torque immediately following the stimuli delivered 1.5 s after the start of the contraction.

The highest activation achieved in each joint configuration was used in the statistical analysis. The Freeman and Tukey [4] transformation was applied to the percentage activation results in order to transform the percentages to a normal distribution. A one-way repeated measures ANOVA with alpha set at 0.05 was performed on the transformed results to determine whether significant differences in the degree of voluntary activation existed between joint configurations.

RESULTS AND DISCUSSION

Data from six contractions was rejected since the doublet had not successfully been delivered during the maximum part of the contraction. The mean activation in each joint angle configuration was above 90% (Table 1) and there was no significant effect of joint position on the degree of activation (p=0.096, power=0.806). The variation in activation across joint configurations for all subjects was within the level of noise simulated in the model-based validation of the method [2].

CONCLUSIONS

These results provide evidence that the degree of quadriceps activation is consistent across different hip and knee joint angle configurations. This suggests that the assumption of consistent activation at different knee and hip joint positions is reasonable and provides further evidence that the method of Herzog and ter Keurs [1] is reliable in determining the section of the force-length relationship that different subjects operate over.

REFERENCES

1. Herzog W and ter Keurs HE. *Pflugers Arch*, **411**, 637-641, 1988.
2. Winter SL and Challis JH. *J Appl Biomech* **24**, 207-214, 2008.
3. Suter E and Herzog W. *J Appl Physiol*, **90**, 1036-1040.
4. Freeman MF and Tukey JW. *Ann Math Statist*, **21**, 607-611.

Table 1: Mean and standard error (SE) percentage activation in the different joint configurations (0 degrees represents full hip or knee extension).

Hip Angle (degrees)	0	0	0	55	55	85	85	85
Knee Angle (degrees)	10	90	110	10	90	10	45	90
Mean % Activation	96.2	91.3	94.1	96.8	91.6	98.3	92.7	95.0
SE % Activation	1.7	2.8	1.7	1.6	2.7	1.3	1.9	2.5

THE EFFECT OF PROLONGED VIBRATION EXPOSURE ON THE TENSILE MECHANICAL PROPERTIES OF SINGLE LAYERS OF THE ANNULUS FIBROSUS

Diane E. Gregory and Jack P. Callaghan
Department of Kinesiology, University of Waterloo, Waterloo, Ontario, Canada
email: dgregory@uwaterloo.ca

INTRODUCTION

Disc herniation is an injury to the annulus fibrosus (AF) of the intervertebral disc. It is characterized by the posterior migration of the nucleus pulposus through the AF tissue. The migration progresses through clefts in the layers of the AF that have formed as a result of cyclic tension in the posterior annular layers. Exposure to vibration may increase the risk of herniation. In particular, vibration has been shown to reduce proteoglycan synthesis in the AF [1, 2], which in turn may reduce the strength of the tissue, making it more susceptible to cleft formation. Further, cyclic loading has resulted in decreased strength in ligament tissue [3] and could plausibly have a similar effect on AF tissue. The purpose of this investigation was to determine any differences between the mechanical properties of single AF layers harvested from discs that were exposed to prolonged axial vibration versus control discs.

METHODS

Thirty-two single layer AF tissues were harvested from porcine intervertebral discs obtained from the cervical spine levels C34 and C56. Sixteen of these tissues were harvested from discs subjected to two hours of vibration and the remaining 16 tissues from control discs. The intervertebral discs that were vibrated were subjected to 1400N of axial compressive load that was cyclically loaded to +/- 10% load (140N) at a rate of 5Hz. The control discs were subjected to 1400N of static axial compressive load for two hours.

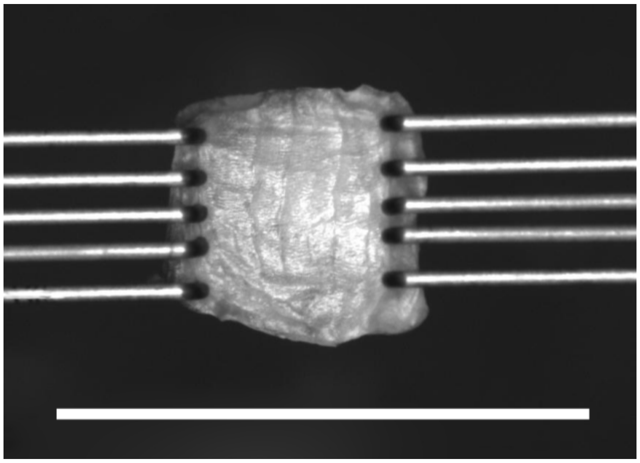

Figure 1: Single layer annulus fibrosus tissue mounted via rakes in strain-control testing apparatus. Note the vertically aligned collagen fibres. White horizontal bar represents 10 mm.

The 32 single layer tissues were obtained from the anterior and posterior AF as well as from both superficial and deep sections. Each tissue sample was mounted in a custom biaxial tensile testing system (BioTester 5000, CellScale, Waterloo Instruments Inc, Ontario, Canada), such that strain was applied perpendicular to the orientation of the collagen fibres (Figure 1). Tissues were preconditioned with three repeats of 10% strain at a rate of 1% strain/sec and subsequently strained at 2% strain/sec until failure. Variables of interest obtained from the stress-strain curve were maximum stress, strain at maximum stress, elastic modulus, length of toe region (% strain), and stress at the end of the toe region. A 4-way ANOVA was used to determine the effect of condition (2 levels: vibrated versus control); cervical level (2 levels: C34 versus C56); tissue depth (2 levels: superficial versus deep); and tissue location (2 levels: anterior versus posterior). A significance level of 0.05 was used.

RESULTS AND DISCUSSION

The tissues harvested from discs that were subjected to vibration did not demonstrate differences in the elastic modulus, maximum stress, and strain at maximum stress (Table 1). Vibrated tissues did, however, have significantly larger toe regions, with a mean toe region of 50% strain (S.D. 33%) as compared to control tissues which had a mean toe region of 31% strain (S.D. 15%) (p = 0.027). The stress at the end of the toe region was not significantly different between the control and vibrated tissues (Table 2).

No significant effect of spinal level, tissue depth, or tissue location was observed.

It is generally accepted that the toe region of the stress-strain curve of connective tissues occurs as a result of collagen fibre uncrimping. However, due to the perpendicular orientation of these tissues, it is unlikely that the toe region seen here can be explained by such fibre reorientation. Rather, it is more likely that the toe region represents strain in the matrix that connects collagen fibres to one another in parallel. A larger toe region may therefore represent initial damage in this matrix. This initial damage may eventually result in the ability for the nucleus pulposus to migrate through each layer of the AF with greater ease and therefore increase the risk of disc herniation. Further, an increased toe region may be indicative of increased laxity and altered joint mechanics in the intervertebral disc as a whole.

CONCLUSIONS

This study suggests that prolonged axial vibration may potentially result in the initiation of injury to the AF, specifically to the inter-collagen matrix. This damage has the potential to transcribe into an increased risk of sustaining disc herniation by allowing the nucleus pulposus to migrate through the layers of the AF with greater ease.

Further research is required to assess the effect of vibration on the complete intact intervertebral disc and to determine if vibration does increase the risk of disc herniation.

REFERENCES

1. Yamazaki S, et al. *Spine* **2**, 415-20, 2004.
2. Ishihara H, et al. *Spine* **17,** S7-S12, 1992.
2. Weisman G, et al. *Am J Sports Med* **8**, 24-30, 1980.

Table 1: Average (standard deviation) values collapsed across cervical level (C34 and C56), tissue depth, and tissue location for the control tissues and the vibrated tissues. For each variable between control and vibrated tissues, the p-value was greater than 0.05 (not statistically significant).

	Elastic Modulus (MPa)	**Maximum Stress (MPa)**	**Strain at Max Stress (%)**
Control (n=16)	3.41 (2.61)	1.44 (1.26)	117 (50)
Vibrated (n=16)	2.91 (2.06)	1.62 (1.63)	115 (43)

Table 2: Average (standard deviation) values obtained from toe region of the stress-strain graph collapsed across cervical level (C34 and C56), tissue depth, and tissue location for the control tissues and the vibrated tissues. Only the toe region length was significantly different between the control and vibrated tissues (p=0.027).

	Toe Region Length (% Strain)	**Stress at End of Toe Region (MPa)**
Control (n=16)	31 (15)	0.33 (0.24)
Vibrated (n=16)	50 (33)	0.59 (0.63)

SURGICAL RECESSION OF THE GASTROCNEMIUS DOES NOT INFLUENCE PLANTAR PRESSURE

[1] Nicole Chimera, [2]Mike Castro and [1]Kurt Manal
[1]Center for Biomedical Engineering Research, University of Delaware, Newark, DE,
[2]Center for Orthopedic Research & Education, Phoenix, AZ
email: manal@udel.edu, web: www.cber.udel.edu

INTRODUCTION

Isolated gastrocnemius contracture (IGC) has been defined as normal ankle dorsiflexion with the knee flexed and less than 5° of dorsiflexion with the knee fully extended [1]. Individuals with IGC can not attain sufficient gastrocnemius length for knee extension and ankle dorsiflexion to occur at the same time during mid-stance. A proposed compensatory strategy for IGC is early heel rise, which could result in increased pressure on the fore-foot [2]. Although the effect of this theory is unknown, early heel rise may increase cumulative fore-foot loading and thus result in foot pathology. Patients with IGC often present with disabling foot pathologies that impact their ability to perform activities of daily living without pain.

Gastrocnemius recession surgery is an infrequently used surgical option to treat painful overuse foot pathologies. Further surgical recession is a means to increase ankle joint range of motion, and therefore may normalize time to heel off [3]. This allows the vertical load to be distributed over a greater proportion of the foot and for a longer duration [2,4]. The purpose of this study was to evaluate the effect of IGC and subsequent gastrocnemius recession surgery on time to heel rise and peak fore-foot plantar pressure. We hypothesized that patients with IGC would exhibit early heel rise and have elevated fore-foot peak plantar pressure and fore-foot pressure time integral compared to control subjects, and that following surgery these values would normalize.

METHODS

7 legs clinically diagnosed with IGC were matched for gender, age, weight, and height with healthy control subjects from a database of 35 subjects recruited from the local area. IGC was defined as

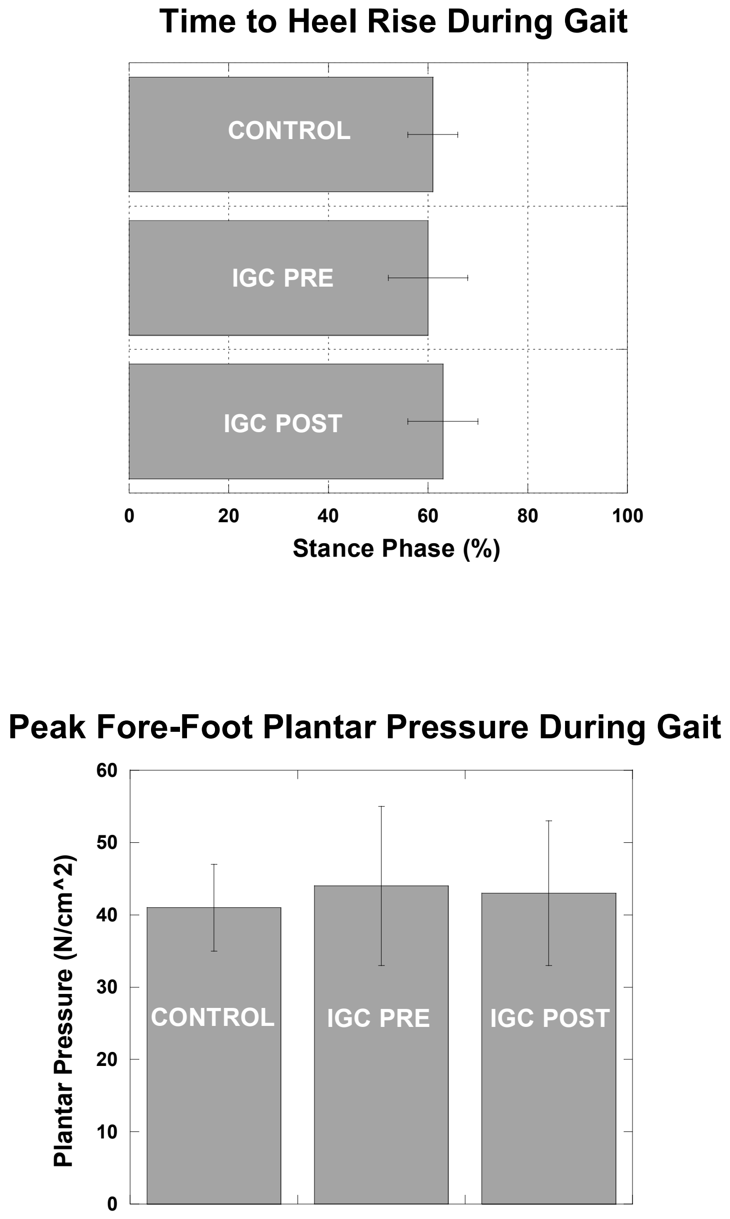

Figure 1: Time to heel rise and peak fore-foot plantar pressure for CONTROL and IGC subjects. There were no significant differences between or within groups.

less then 0° of passive ankle dorsiflexion with the knee in full extension. Control subjects had normal ankle range of motion. IGC subjects were tested prior to surgery and 3 months post-operatively. Control subjects were tested only once. A bi-plane goniometer was used to measure dorsiflexion range of motion.

The Tekscan HR Mat was used to assess plantar pressure during the stance phase of gait. Data were collected at 50 Hz. Five self-selected speed walking trials were collected. Walking speed was monitored using a photoelectric timing unit. A trial was not accepted if the subject altered their stride or visually targeted the pressure mat.

Data from the pressure mat was passed through a PC interface board to a desktop computer and stored for off-line analysis. Time to heel rise and peak fore-foot plantar pressure were obtained from the HR Mat System Software and used for comparison between groups. The fore-foot pressure time integral was exported and analyzed in a custom Lab View program.

Wilcoxen signed rank and Mann-Whitney U exact tests were used to compare between and within subjects, respectively. An alpha level of $p < 0.05$ was used to identify statistical significance for demographic variables, walking speed, time to heel rise, peak fore-foot plantar pressure, and fore-foot pressure time integral.

RESULTS AND DISCUSSION

There were no differences in group demographics or walking speed (Table 1). Time to heel rise, peak fore-foot plantar pressures (Figure 1), and the pressure time integral (11.3 ± 3.0 vs. 10.0 ± 1.2 N/cm^2*s) were not different between IGC and control subjects. Further, gastrocnemius recession surgery did not affect any of these plantar pressure measures.

CONCLUSIONS

In contrast to our hypotheses, subjects with IGC did not exhibit early heel rise or have elevated peak fore-foot plantar pressures or pressure time integrals compared to the control subjects. This was an unexpected finding and may be related to compensations occurring elsewhere along the kinetic chain. For example, the gastrocnemius is a bi-articulate muscle and therefore an alternate strategy could have been to increase knee flexion during mid-stance as suggested by Majacic et al. [5]. Although we had a limited number of subjects in our study, we suggest that patients with IGC do not exhibit early heel rise, elevated peak plantar pressure or pressure time integrals during natural cadence walking. Additional research is necessary to assess the lower extremity joint kinematics associated with IGC and is the focus of ongoing work.

REFERENCES

1.DiGiovanni CW, et al. *J Bone Joint Surg.* .**84A**, 962-70, 2002.
2.Subotnick SI, et al. *J Am Podiatry Assoc* **61**, 423-7, 1971
3.Johanson MA, et al. *J Athl Train* **41**, 159-65, 2006.
4.Cornwall MW & McPoil TG. *J Am Podiatr Med Assoc* **89**, 272-7, 1999.
5.Matjacic ZA, et al. *J Biomech* **39**, 255-66, 2006

ACKNOWLEDGEMENTS

Synthes, Inc.

Table 1: Average group demographics**.** There were no significant differences between or within groups.

	Gender	**Age** years (SD)	**Height** m (SD)	**Weight** kg (SD)	**Speed** m/s (SD)
IGC PRE	♀ = 6; ♂ = 1	50.6 (2.1)	1.7 (.07)	83.8 (6.8)	1.35 (.22)
IGC POST	SAME	51.3 (1.7)	SAME	83.6 (6.7)	1.36 (.07)
CONTROL	♀ = 6; ♂ = 1	49.4 (5.5)	1.7 (.11)	76.1 (10.5)	1.53 (.28)

SAME indicates IGC POST is unchanged from IGC PRE

ISOKINETIC PLANTAR FLEXION TORQUE INCREASES AFTER OPEN GASTROCNEMIUS RECESSION

[1] Nicole Chimera, [2]Mike Castro and [1]Kurt Manal
[1]Center for Biomedical Engineering Research, University of Delaware, Newark, DE,
[2]Center for Orthopedic Research & Education, Phoenix, AZ
email: manal@udel.edu, web: www.cber.udel.edu

INTRODUCTION

The amount of force developed by a muscle is related to many factors including where the muscle operates on its length-tension curve. It is well documented that placing the triceps surae muscle group in a lengthened state (i.e.: near maximal dorsiflexion) elicits maximum plantar flexion torque [1, 2]. Isolated gastrocnemius contracture (IGC) is characterized by limited dorsiflexion with the knee extended [3], and thus patients with IGC may exhibit plantar flexion strength deficits as a consequence of their reduced range. The ability to generate sufficient torque at the ankle and at the appropriate time is important for normal gait.

Increased range of motion, and thus triceps surae length can be achieved through surgery. Gastrocnemius recession is a surgical procedure in which the gastrocnemius tendon is incised; however the effect that this procedure has on plantar flexion torque generation is not known. The purpose of this study was to evaluate plantar flexion strength in patients with IGC pre and post open gastrocnemius recession surgery. We hypothesized that pre-operative plantar flexion strength would be less than healthy controls. Further, we hypothesized that gastrocnemius recession surgery would increase dorsiflexion range of motion and because of this increased range patients would be stronger compared to pre-operative plantar flexion torque. However post-operative plantar flexion would still be less than healthy control subjects.

METHODS

7 legs clinically diagnosed with IGC were matched for gender, age, weight, and height with healthy control subjects from a database of 35 subjects recruited from the local area. IGC was defined as less then 0° of passive ankle dorsiflexion with the

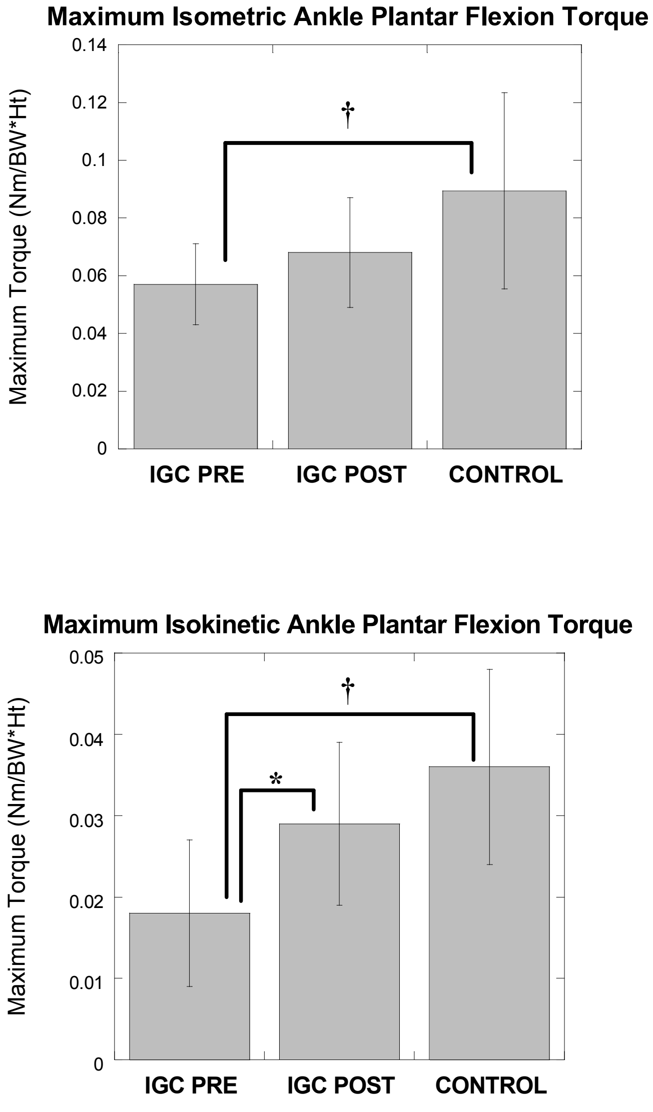

Figure 1: Peak isometric and isokinetic plantar flexion torques PRE and POST surgical recession compared to control subjects.
* IGC PRE significantly different from IGC POST
† IGC PRE significantly different from CONTROL

knee in full extension. Control subjects had normal ankle range of motion. IGC subjects were tested prior to surgery and 3 months post-operative. Control subjects were tested only once. A bi-plane goniometer was used to measure dorsiflexion range of motion.

The Biodex was used to measure maximal isometric and isokinetic (60°/sec) ankle plantar flexion force production. Three trials of isometric and isokinetic plantar flexion contractions were performed with maximum ankle dorsiflexion while the knee was placed in full extension.

The trial which elicited the peak isometric and isokinetic ankle plantar flexion torques were used for comparison. The torque signal was passed through a moving average window in a custom Lab View program, and the peak was calculated after limb weight, foot plate weight, and the passive moment were taken into account. Torque was normalized to body weight and height to account for strength differences known to occur between people of different sizes.

Wilcoxen signed rank and Mann-Whitney U exact tests were used to compare between and within subjects, respectively. An alpha level of $p < 0.05$ was used to identify statistical significance for dorsiflexion range of motion, peak isometric plantar flexion torque, and isokinetic plantar flexion torque.

RESULTS AND DISCUSSION

Dorsiflexion range of motion significantly improved following gastrocnemius recession surgery; there were no differences in group demographics (Table 1). Peak isometric and isokinetic plantar flexion torque were significantly lower for pre-surgical IGC subjects compared to controls (Figure 1). Isokinetic plantar flexion torque increased significantly post-surgically. Although not statistically different, isometric plantar flexion strength also increased post-operatively.

CONCLUSIONS

Gastrocnemius recession surgery restored normal dorsiflexion range of motion in our group of subjects. It also allowed for increased plantar flexion torque, presumably a result of the muscle working on a more favorable portion of the length tension curve. Plantar flexion torque increases with increased ankle dorsiflexion while the Achilles tendon moment arm decreases [4]; therefore increased torque is likely associated with improvements along the length-tension curve. Post-operative plantar flexion torque however was still less than control subjects. We suggest that post-operative strength training would be ideal for these subjects.

REFERENCES

1. Fugl-Meyer A, et al. *Acta Physiol Scand* **107**, 47-56, 1979.
2. Sale D, et al. *J Appl Physiol* **52**, 1636-42, 1982.
3. Silfverskiold N. *Acta Chir Scand* **56**, 315-330, 1924.
4. Magnaris CN, et al. *Eur J Appl Physiol* **83**(4-5), 363-369.

ACKNOWLEDGEMENTS

Synthes, Inc.

Table 1: Average group demographics and dorsiflexion range of motion.

	Gender	**Age** years (SD)	**Height** m (SD)	**Weight** kg (SD)	**DF ROM** ° (SD)
IGC PRE	♀ = 6; ♂ = 1	50.6 (2.1)	1.7 (.07)	83.8 (6.8)	-1 (1)* †
IGC POST	SAME	51.3 (1.7)	SAME	83.6 (6.7)	13 (5)
CONTROL	♀ = 6; ♂ = 1	49.4 (5.5)	1.7 (.11)	76.1 (10.5)	14 (8)

SAME indicates IGC POST is unchanged from IGC PRE
* IGC PRE significantly different from IGC POST
† IGC PRE significantly different from CONTROL

FOOT STRIKE CONTACT LOCATION AND FOOT LOADING DURING THE DEVELOPMENT OF RUNNING IN CHILDREN AGE 3 TO 11 YEARS

Martine I.V. Mientjes, Jeff C. Pisciotta and Mario A. Lafortune
Nike Sport Research Lab, Beaverton, OR, USA
E-mail: Martine.Mientjes@nike.com

INTRODUCTION

Foot plantar loading contributes key knowledge toward the understanding of the development of running in children. Foot loading during walking has been studied extensively [1,7,4,6]. Only one study was found that examined foot loading in children during running [5]. The purpose of the current study, the Kids Global Research Project, was to examine the development of running in children from 4 different countries: Germany, Japan, USA and Brazil. This abstract presents the USA foot pressure data. The purpose of the research was to determine foot strike contact location and to quantify foot loading during running in children age 3 to 11 years. It was hypothesized that during the development of running, younger children would land flatfooted or on their forefoot and older children would land on their heel. It was also hypothesized that forefoot loading, after taking body weight into account, would increase over age due to an increase in muscle strength and an improvement in coordination.

METHODS

Healthy active boys and girls were recruited at the age of 3, 5, 7 and 9 years (resulting in 4 groups). After obtaining the informed parental consent they visited the lab once a year for 3 consecutive years. Data of sixty-one children were included resulting in 183 data sets over the 3 years (Table 1). Children ran barefoot on a foam runway at a self-selected speed. The foam runway (Peak G 15.9) surrounded, but did not cover, an EMED pressure sensing plate (Novel GmbH, Germany; 4 sensors/cm^2, 50Hz). Timing gates were used to record running speed. A minimum of 5 trials per child were collected. Of these 5 trials, 3 consistent trials were selected for further analysis. Foot strike location was determined for each trial using the initial coordinates of the center of pressure (COP). A foot strike was classified as “heel strike” when the COP started in the rear 1/3 of foot length [2].

The foot was divided into 4 anatomical areas to quantify loading: hindfoot, midfoot, forefoot, and toes. Foot loading was computed by integrating pressure over area. Absolute peak force (N) and peak force normalized to body weight (% BW) were extracted from the data. A repeated measures ANOVA was used to compare absolute foot loading, normalized foot loading and self-selected running speed within and between groups ($p<0.05$).

RESULTS and DISCUSSION

At the younger ages, 80% or more of the children landed on their heel (Table 1). By the age of 6 most children were heel strikers (> 93.3%). In a large sample of elite adult distance runners, 74.9% were heel strikers [3]. Either, the percentage of heel strikers in our sample of children is greater than that of elite adult runners, or the elite adult runners ran at a relatively faster speed. It is also possible that elite runners have modified their foot strike location due to training.

Table 1. The age, number of children, mean body mass and the percentage of heel strikers is shown.

Age (yrs)	Number of children	Mean body mass (kg)	Heel strike (%)
3	15	14.5	86.7
4	15	16.7	80.0
5	34	19.5	82.4
6	19	22.8	100.0
7	31	25.6	93.5
8	12	29.2	100.0
9	27	31.2	96.3
10	15	33.2	93.3
11	15	37.4	100.0

Absolute peak force increased over age in all 4 anatomical foot areas ($p<0.001$; Figure 1). The largest increase was seen under the forefoot followed by the hindfoot. Once normalized to body weight, the peak force under the forefoot increased with age (p<0.026) whereas the peak force under the hindfoot and toes did not change over age (Figure 2). Some changes in normalized peak force under the midfoot were found over age which may be attributed to arch development. These findings indicate that body weight is a leading contributor to the magnitude of foot loading during running in children age 3 to 11.

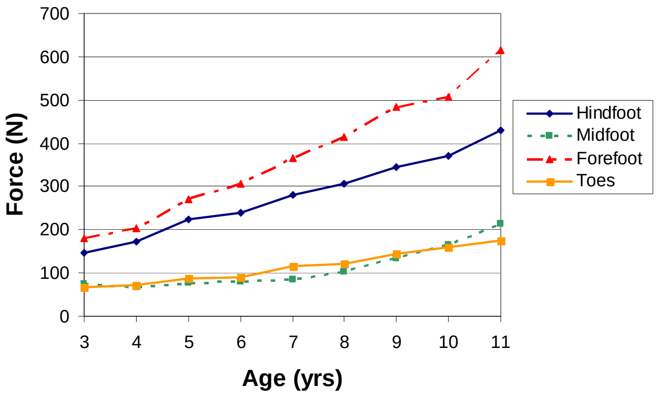

Figure 1. Absolute peak force under each anatomical area is shown over age.

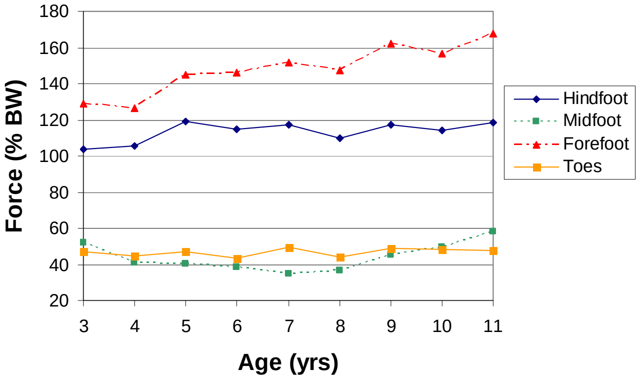

Figure 2. Normalized peak force under each anatomical area is shown over age.

The increase in normalized peak force under the forefoot can be explained by an increase (p<0.001) in self-selected running speed with age (Figure 3). Normalized peak force under the forefoot and running speed are highly correlated (R^2=0.86). Other potential factors increasing normalized forefoot loading over age are an increase in muscle strength and an improvement in coordination.

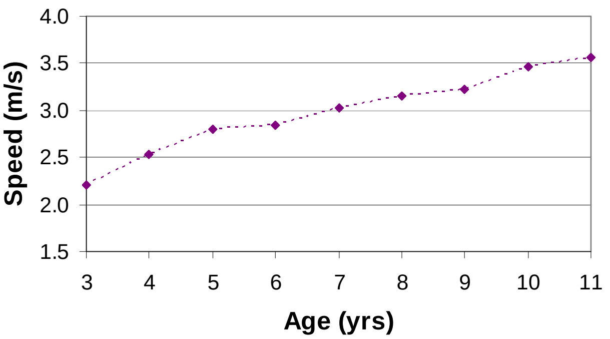

Figure 3. Self-selected running speed is shown over age.

CONCLUSIONS

Our hypothesis that during running the younger children in our study would land flatfooted or on their forefoot did not hold. The majority of children over the entire age range examined, ages 3 to 11, were heel strikers.

Foot loading was largely influenced by body weight. As hypothesized, normalized forefoot foot loading did increase over age and can be explained by an increase in running speed. An increase in muscle strength and an improvement in coordination with age may also play a role in the increase in foot loading over age. These findings have implications for footwear design.

REFERENCES

1. Bosch K, et al. *Gait Posture* **26**, 238- 247, 2007.
2. Cavanagh P, Lafortune, M. *J Biomechanics* **13**, 397-406, 1980.
3. Hasegawa H, et al. *J Strength Con Res* **21**, 888-893, 2007.
4. Hallemans A, et al. *Foot Ankle Int* **24**, 444-453, 2003.
5. Henning E, Rosenbaum D. *Foot Ankle* **11**, 306-311, 1991.
6. Kellis E. *Gait Posture* **14**, 92-97, 2001.
7. Mickle K, et al. *Int J Pediatr Obes* **1**, 183-188, 2006.

ACKNOWLEDGEMENTS

Data collection: L Bloomer, A Medellin & C Kvamme. Subject recruitment: J Botsford. Manuscript reviewer: J Bishop.

POWER GRIP FORCE IS MODULATED IN DYNAMIC ARM MOVEMENT

[1]Fan Gao, [3]Y.J. Lin and [2]T. Scott Marzilli

[1]Department of Allied Health Sciences, University of Texas Southwestern Medical Center, Dallas, TX USA
[2]Department of Health and Kinesiology, University of Texas at Tyler, Tyler, TX USA
[3]Department of Mechanical Engineering, University of Texas at Tyler, Tyler, TX USA
E-mail: fangao2000@gmail.com

INTRODUCTION

During hand precision grip both grip force (normal to the contact surface) and load force (tangential to the contact surface) are needed and a strong coupling between these two forces has been well documented under various conditions ranging from lifting an object to performing rapid arm movement (Gao et al. 2005). Though precision grip is very useful in our daily lives, power grip is often used in work settings. Power grip force could be evaluated using hand dynamometer and this has been standardized in ergonomics and hand rehabilitation. Though most of job activities, such as food processing, construction, need power gripping coupled with dynamic arm movement only few studies have been done to evaluate the power grip force in dynamic condition. The objective of this study is to examine the modulation of power grip force under dynamic arm movement and its relationship to muscle activities and potential risk related to musculoskeletal injury. We hypothesize that the power grip force will be modulated with the dynamics of arm movement. Specifically, with the increase in speed of arm movement the physical demanding will be increased as indicated by an increase of EMG activities. The increase in muscle activities may be related to a higher risk of musculoskeletal injury incurred in the working sites.

METHODS

Six subjects voluntarily participated in the pilot study. Subject was standing erect and instructed to hold a digital dynamometer with three different levels of grip forces (low, medium and strong, corresponding to 20%, 40% and 60% of the maximum grip force respectively) and perform cyclic arm movement in the sagittal plane at three different speeds (slow, self-paced, fast) with upper arm held by side.

BIOPACK MP150 system (Aero Camino, Goleta, CA 93117, USA) with accelerometer (±5 g), EMG and hand dynamometer (.315 kg, Isometric range: 0-100 Kg) modules were used for hand acceleration, muscle activity and grip force recording. Hand acceleration, muscle activity (sEMG) and grip force were recorded using AcqKnowledge software at a rate of 1,000 Hz. Before each task the subject was asked to practice and be familiar with the speed and force level prescribed. The data collection was started as soon as the subject was ready to keep the grip force and arm movement. The subject was instructed to keep the grip force and arm movement rate for about 30 s. Initially, the elbow was flexed at 90 degrees with forearm pronated. In total, subject performed 9 tasks. Each task lasted ~30 second and a one min break was provided to avoid fatigue. For each task, surface Electromyography on major elbow flexors (Biceps Brachii), elbow extensors (Triceps Brachii) and finger flexor muscles were recorded (Figure 1).

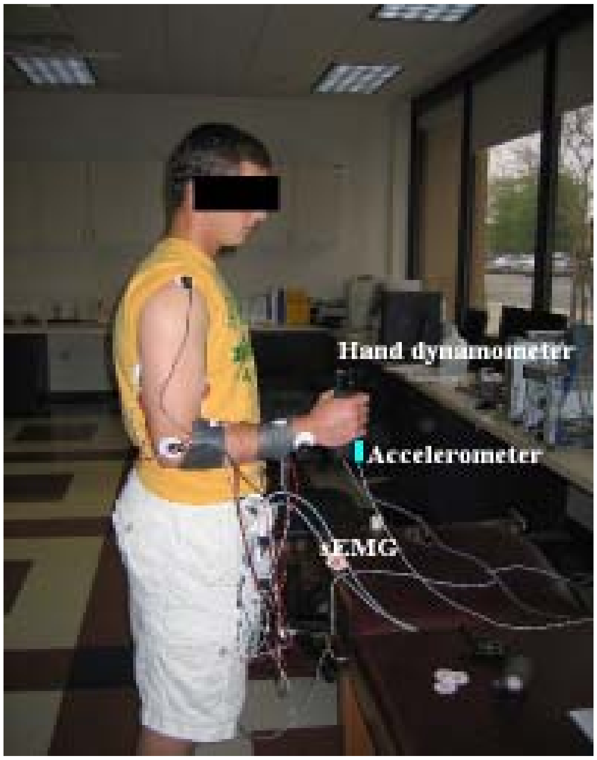
[redacted]

Figure 1. Experimental setup

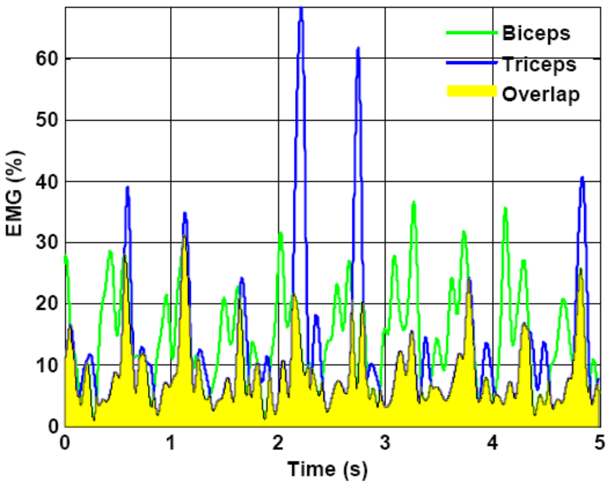

Figure 2. Quantification of muscle co-contraction

Raw sEMG signals were processed with bias removal, full-wave rectification and low pass filtering (5 Hz cut-off frequency) and then normalized with respect to the largest value of activation obtained in each muscle group. Muscle co-contraction was quantified using the method proposed by Frost et al. (1997). However, in this study a 5 second window was used in stead (Figure 2). Averaged normalized EMG signals within 5 seconds were used to quantify the muscle activities. Grip force was high pass filtered to remove the baseline drift and standard deviation was calculated to quantify the modulation of grip force with respect to arm movement. Statistics including t-test and one-way ANOVA were conducted using SPSS (SPSS Inc., Chicago, IL, USA).

RESULTS and DISCUSSION

In general, the cyclic movement frequencies were consistent across subjects, ranging from 1.6±.15 to 4.27±.15 Hz with self-paced frequency at 2.27±.46 Hz. With the increase of cyclic movement speed ($P<0.05$) and grip force level ($P<0.05$) the deviation of normalized grip force increased. In addition, the corresponding grip index, characterized as the normalized EMG activity, increased with the increase of both grip force levels ($P<0.05$) and cyclic movement speed ($P<0.05$). The index of co-contraction of elbow muscles also increased as either grip force level ($P<0.05$) or cyclic movement speed increased ($P<0.05$). Using a simple model based on harmonic motion the elbow joint stiffness was found to be proportional to the square of cyclic movement frequency and the moment inertia of the forearm and hand-held object.

CONCLUSION

In summary, the increase of co-contraction of elbow muscles with the increase of arm movement frequencies (dynamics) could be attributed to the increase of elbow joint stiffness and hence will facilitate the fast arm movement. The increased physical demand will result in higher muscle activities and potential risk of repetitive musculoskeletal injuries. The results of this study could provide recommendation for workers who will experience both power grip and dynamic arm movement. Based on the pilot study we recommend that power grip force coupled with fast arm movement should be avoided or reduced in the working sites and if needed arm movement should be performed at a self-paced or even lower rate.

REFERENCES

1. Gao, F. et al., *Exp Brain Res*, **165**(1), 69-83, 2005
2. Frost, G., et al., *J Electromyogr Kinesiol*, **7**(3), 179-186, 1997

DYNAMIC ARCH DEVELOPMENT: MIDFOOT CONTACT AREA AND LOADING DURING RUNNING IN CHILDREN AGE 3 TO 11 YEARS

Martine I.V. Mientjes, Jeff C. Pisciotta and Mario A. Lafortune
Nike Sport Research Lab, Beaverton, OR, USA
E-mail: Martine.Mientjes@nike.com

INTRODUCTION

The formation of the longitudinal arch is one of the major changes in foot shape during healthy growth and development. The majority of studies evaluating dynamic arch development have been done with children under the age of 3 years [6,4] or under the age of 5 ¼ years [2]. These studies all confirmed arch development over age as measured during standing or walking. Only one study was found that evaluated dynamic arch development between age 6 and 10 years [5]. In this older age range, no changes were found in arch development during walking. The purpose of the present study was to quantify dynamic arch development in boys and girls over a wider age range than previous work, from age 3 to 11 years. This study is part of the Kids Global Research Project, a large study evaluating the development of running in children from 4 countries: Germany, Japan, USA and Brazil. This abstract presents USA data.

METHODS

Healthy active boys and girls were recruited at the age of 3, 5, 7 and 9 years (resulting in 4 groups). After obtaining the informed parental consent they visited the lab once a year for 3 consecutive years. Data of sixty-one children were included resulting in 183 data sets over 3 years (Table 1). Children ran barefoot on a foam runway at a self-selected speed. The foam runway surrounded, but did not cover, an EMED pressure sensing plate (Novel GmbH, Germany; 4 sensors/cm^2, 50Hz). Timing gates were used to record running speed. A minimum of 5 trials per child were collected. Of these 5 trials, 3 consistent trials were selected for further analysis. Data analysis was limited to heel strikers because our analysis method requires that all regions of the foot make contact with the floor at some time during the stance phase.

The foot was divided into 6 anatomical areas: hindfoot, midfoot, medial midfoot, lateral midfoot, forefoot, and toes. The contact area of these individual regions was determined for each selected trial. Individual contact areas were normalized to the entire foot contact area. Foot loading was computed by integrating pressure over area. Peak forces under the individual areas were normalized to body weight. A repeated measures ANOVA was used to compare normalized contact area, normalized peak force and self-selected running speed within and between groups ($p<0.05$).

Table 1. The age, number of girls and boys and their mean body mass is shown.

Age (yrs)	Girls #	Boys #	Girls mass (kg)	Boys mass (kg)
3	10	5	14.0	15.3
4	10	5	16.1	17.5
5	20	14	18.9	20.3
6	10	9	21.8	23.9
7	17	14	25.1	26.1
8	7	5	29.7	28.6
9	16	11	31.9	30.4
10	9	6	34.5	31.6
11	9	6	38.9	35.4

RESULTS and DISCUSSION

A decrease in normalized midfoot contact area (Figure 1), due to a decrease in the medial midfoot contact area ($p<0.001$), occurs between age 3 and 7 for boys and girls. This change in medial midfoot geometry is illustrated in figure 2. The reduction in medial midfoot contact area is an indication of arch development. The decrease in normalized midfoot contact area at the younger ages is in agreement with previous work showing that the development of the longitudinal arch begins as soon as the child learns to stand and walk [1] and further develops up to the age of 5 ¼ years [2]. A decrease up to the age of 7 was unexpected based upon work of Henning *et al.* (1994) that showed no changes in arch development during walking in children between age 6 and 10. Interestingly, the present study shows changes in midfoot contact area between age 9 and 11. This is due to an increase in lateral midfoot contact area ($p<0.026$) and may be a result of an increase in normalized peak loading under the lateral midfoot between age 9 and 11 ($p<0.003$; Figure 3). This increase in lateral midfoot loading is illustrated in figure 2 by the change in color. An increase in loading may cause the midfoot to flatten, resulting in a greater contact area. The increase in normalized peak loading under the lateral midfoot may be due to an increase in self-selected running speed ($p<0.001$), enhancements in muscle strength or changes in coordination over age.

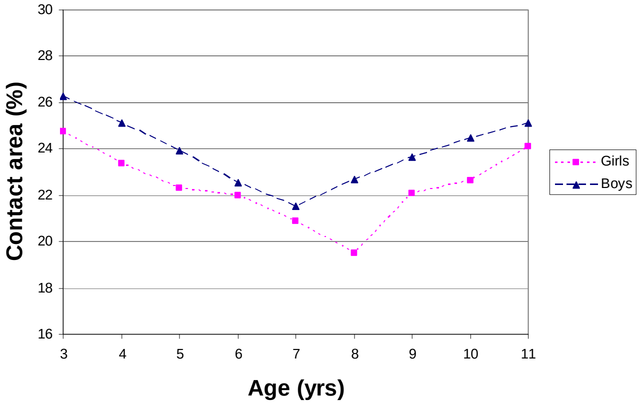

Figure 1. Normalized midfoot contact areas are shown over age by gender.

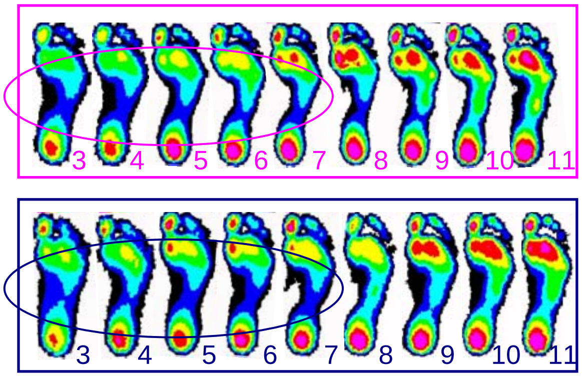

Figure 2. Pressure maps for girls (top) and boys (bottom) are shown over age. The blues are the lowest pressures, green and yellow are medium pressures and red and pink are the highest pressures.

Unger *et al*. (2004) reported a broader midfoot in boys than girls under the age of 3 years during walking. Although not statistically significant ($p<0.14$), the results in our study consistently show that boys have a broader midfoot than girls during running over the entire age range examined. This cannot be explained by body weight since boys were not consistently heavier than girls (Table 1), nor did normalized loading under the midfoot show a gender trend.

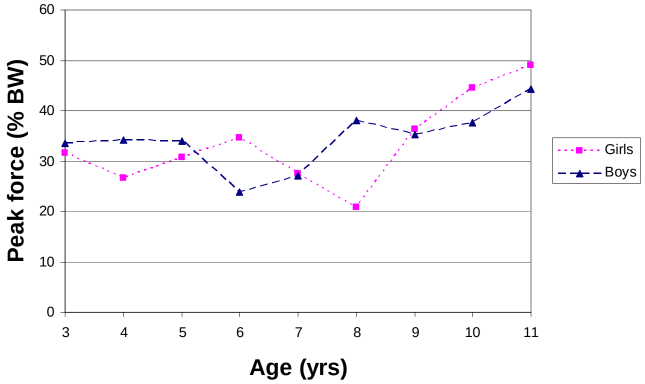

Figure 3. Normalized peak forces under the lateral midfoot are shown over age by gender.

CONCLUSIONS

The current study shows that the dynamic arch during running continues to develop until age 7. Increased loading, possibly due to increases in running speed, muscle strength or coordination, may affect midfoot contact area. Furthermore, boys have a greater midfoot contact area than girls over the entire age range examined, age 3 until 11. These findings have implications for footbed design.

REFERENCES

1. Bertsch C, et al. *Gait Posture* **19**, 235-242, 2004.
2. Bosch K, et al. *Gait Posture* **26**, 238-247, 2007.
3. Cavanagh P, et al. *Foot Ankle* **7**, 262-276, 1987.
4. Henning E, Rosenbaum D. *Foot Ankle* **11**, 306-311, 1991.
5. Henning E, et al. *Foot Ankle* **15**, 35-40, 1994.
6. Unger H, Rosenbaum D. *Foot Ankle* **25**, 582-587, 2004.

ACKNOWLEDGEMENTS

Data collection: L Bloomer, A Medellin & C Kvamme. Subject recruitment: J Botsford. Document reviewer: J Bishop.

THE EFFECT OF LOWER LIMB INSTRUMENTATION ON KINETICS AND KINEMATICS DURING STAIR CLIMBING

Andrew S. Beath, Jennifer L. Durkin
Department of Kinesiology, University of Waterloo, Waterloo, ON
Email: abeath@uwaterloo.ca

INTRODUCTION

The level of instrumentation applied to the lower limb may influence 3D joint kinetics and kinematics during stair ambulation. The purpose of this study was to determine these effects by manipulating the number of active motion capture markers applied to the thigh, lower leg and foot during a stair climbing task. A secondary purpose was to determine whether these effects were related to movement speed.

METHODS

Nine healthy subjects completed 3 stair ambulation trials at 2 speeds (self selected and 1Hz timed) while motion capture (Northern Digital, Waterloo, ON) and ground reaction force (AMTI, Watertown, MA) data were collected at 64 Hz and 1024 Hz, respectively. The force platform was mounted in the second step of a custom staircase. Three motion capture marker setups were collected in a randomized order. These included a setup with skin markers over bony landmarks, a setup with only rigid marker clusters attached to the lower limbs, and a third setup combining the first two. Lower limb kinetics and kinematics were determined using Visual3D (C-motion, Kingston ON). Moments of force were normalized to body mass, all trials were normalized to 100% of contact time and ensemble averaged. Key variables that were included in the analysis were: contact time, ankle and knee minimum, maximum angles and range of motion, and ankle and knee minimum and maximum moments of force, during stair ascent and descent. Two-way repeated measures ANOVAs (α=0.05) followed by Tukey HSD post hoc analyses were run on the data.

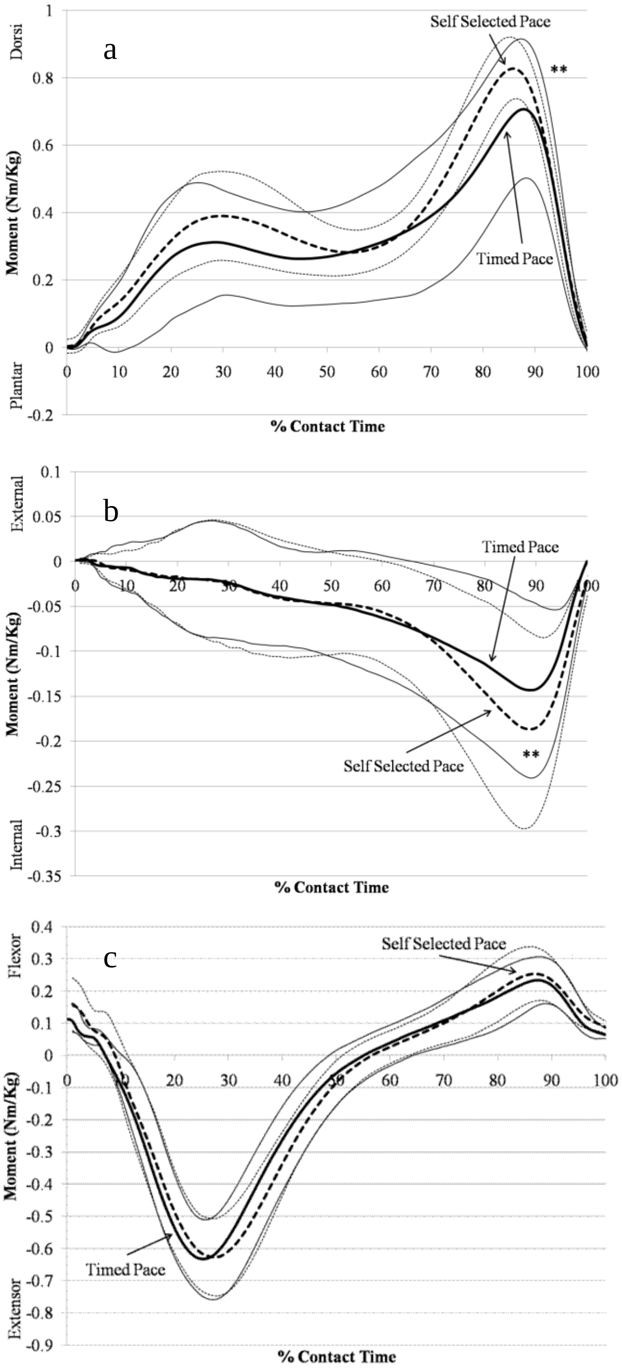

Figure 1: a) Ankle F/E moment b) Ankle I/E moment c) Knee F/E moment. ** indicates where significance occurred.

RESULTS

Statistically significant differences between marker setup and speed are displayed in Tables 1-2. Participant contact time with the force plate was shorter for the self selected pace compared to the timed pace ($p<0.0005$). There was no difference in pace between the marker setups ($p>0.05$). No significant differences were found for stair descent ($p>0.05$). During stair ascent, pace affected peak ankle dorsiflexor moment ($p<0.01$), peak ankle eversion moment ($p<0.05$), peak knee flexor moment ($p<0.05$), and peak knee abductor moment ($p<0.05$). Figure 1 shows the peaks occurred at the same instance for both ankle moments but a significant difference in time to peak moment was found for the knee moments. During stair ascent, marker setup affected peak knee abduction angle ($p<0.01$), and the range of knee motion in the frontal plane ($p<0.01$).

DISCUSSION

Movement speed significantly affected ankle and knee joint peak moments during stair ascent. This is a well-known effect [1], however instrumentation did not affect self-selected walking speed as interaction effects were not found. The number of markers applied to the lower limb affected ankle and knee joint angles during stair climbing. This could be due to the number of markers applied to the lower limb, soft tissue artifact [2], or due to the methods of securing the plates to the leg segments using tensor bandages. The results show that the skin-mounted marker setup was significantly different from both the rigid plates and the combination setups. Since the rigid plates and combination setups both involved the use of an underwrapping method to secure the rigid plates, this likely caused the differences in kinematics seen. Similar methods of securing rigid plates to the lower limbs is common and should be carefully considered in future research [3]. Further, the effect of active motion capture markers in addition to other data recording devices such as EMG on natural motion should considered whenever possible [4].

REFERENCES

1. Lelas, J.L. et al. (2003). *Gait and Posture* **17(2)**; p. 106-112.
2. Cappozzo, A. et al (1996) *Clinical Biomechanics* **11(2)**; p. 90-100
3. Manal, K. et al (2000) *Gait and Posture* **11;** p. 38-45
4. Frigo, C. and Crenna, P. (2008). *Clinical Biomechanics,* In Press.

ACKNOWLEDGEMENTS

The authors wish to thank the Natural Sciences and Engineering Research Council for financial support of this study.

Table 1. Main effects for marker setup. Values with dissimilar letters (A,B) are statistically different.

Stair Ascent	Skin-Mounted	Rigid Plates	Both
Ankle Range of Motion (^{o})	33.2 (3.2)^{A}	35.3 (3.5)^{B}	34.4 (3.7)^{AB}
Knee Abduction Angle (^{o})	-2.3 (4.2)^{A}	2.2 (5.2)^{B}	2.2 (5.5)^{B}
Knee Abd/Add ROM (^{o})	6.4 (2.8)^{A}	10.3 (2.6)^{B}	9.7 (2.3)^{B}
Stair Descent			
Ankle Inversion Angle (^{o})	16.1 (7.1)^{A}	13.9 (6.6)^{B}	14.4 (6.7)^{B}

Table 2. Main effects for movement speed. Peak moments are compared.

Stair Ascent	Self-Selected	Timed
Contact Time (s)	0.99 (0.14)	1.24 (0.07)
Ankle Dorsiflexion Moment (Nm/kg)	0.84 (0.09)	0.76 (0.07)
Ankle Eversion Moment (Nm/kg)	0.16 (0.05)	0.14 (0.05)
Knee Extension Moment (Nm/kg)	0.29 (0.06)	0.25 (0.07)
Knee Abduction Moment (Nm/kg)	0.03 (0.02)	0.02 (0.02)
Stair Descent		
Contact Time (s)	0.93 (0.14)	1.21 (0.07)

THE INTERACTION BETWEEN POSTURE AND COGNITION DURING A MANUAL FITTING TASK

Jessica M. Seaman, Katelyn C. Ponto, Ashley E. Keough, Joong Hyun Ryu & Jeffrey M. Haddad

Motor Development Laboratory, Department of Health and Kinesiology, Purdue University,
jmseaman@purdue.edu

INTRODUCTION

An increasing amount of research has demonstrated that postural fluctuations (sway) are modulated based on the constraints of a concurrent suprapostural task [1, 2] For example, when performing a suprapostural precision manual [3] or visual fixation task [1], individuals reduce their postural sway below quiet standing baseline conditions. This reduction aids the completion of the task because any extraneous postural movements impede accuracy or visual acuity. Although a reduction in postural sway sometimes aids the completion of a suprapostural task, some degree of postural sway can be functional [4]. Specifically, postural sway can be exploratory in that it generates sensory information regarding the environmental landscape over which movements are or will be occurring [5]. It therefore appears that the expression or suppression of sway in a healthy postural system is dependent on the constraints and goals of a suprapostural task.

Research has also shown that performing a concurrent cognitive task while standing influences the dynamics of postural sway. For example, when performing a digit memorization task, participants systematically reduce postural sway as the number of digits to be memorized increases [6].

Although both cognition and the constraints of a suprapostural task can influence postural sway, to date there has been little research examining how postural sway is affected when both a cognitive and manual task are simultaneously performed. This is important because many tasks performed in everyday life have both a manual and cognitive component. It is possible that performing a cognitively demanding task reduces the ability of the postural system to appropriately modulate postural sway based on the constraints of the suprapostural task. The purpose of this study was therefore to examine changes in postural dynamics as participants performed a precision manual fitting task while simultaneously performing a digit memorization task. It was hypothesized that as individuals performed a concurrent memorization task, they would be less able to modulate postural movements based on the constraints of the manual precision task.

METHODS

Participants (8 males and 7 females; aged 18-25) were required to fit a block (88.9mm X 88.9mm) through either a large (130mm) or small (100mm) opening while memorizing 0, 2, 4, 6 or 8 digits (Figure 1). The order in which the small and large opening trials were presented was counterbalanced between participants. Within each large and small opening block, the number of digits to be memorized was presented in a random order. Each trial was performed five times (50 total trials).

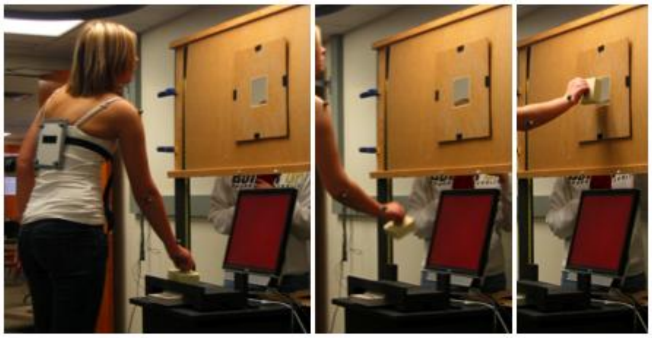

Figure 1: Example of a participant fitting the block through the small opening. The sequence of numbers to be memorized was displayed on the computer screen below the fitting board.

During each trial the participant memorized digits that were displayed on a computer screen for 10 seconds. After ten seconds, the computer screen turned red and the participant was required to accurately fit the block through the opening. Once the block was through the opening, the computer produced a “ring” sound and the participant repeated the digits they had memorized. Postural stability over the course of each trial (the time between when the block was first picked up until it passed through the opening) was analyzed by calculating postural time-to-contact from the center of pressure (CoP) time series (collected at 120Hz from an AMTI force platform). Postural TtC is a measure that calculates the time it would take for the CoP to reach the base of support (boundaries of the feet) given its instantaneous position, velocity and acceleration [7]. Since the coordinates of the base of support are used in the TtC calculation, it is well suited for measuring postural stability during dynamic tasks where the CoP shifts within the base of support.

RESULTS AND DISCUSSION

The first conclusion to emerge from the results was that postural TtC increased (posture became more stabilized) when fitting through the small opening compared to when fitting through the large opening (p<.05). This was especially true in the later parts of the fit cycle (as the block is being fit through the opening) when the precision requirements of the task were greater (Figure 2). The systematic increase in postural TtC across the duration of the fitting cycle suggests that individuals are capable of modulating postural stability based on the instantaneous precision demands of the task. When the precision requirements were more difficult (e.g. towards the end of the fitting movement), posture became more stabilized. This may have been due to a suppression of exploratory postural movements. However, when the precision constraints of the fit were less demanding, posture was not as stabilized. This may be because the postural system allowed some exploratory postural movements to be expressed.

The second conclusion to emerge from the results was that performing a concurrent memorization task did not appear to influence postural stability as the participant performed a manual fitting task (Figure 2; p>.05). This finding was counter to the original hypothesis that performing a memorization task would interfere with the ability of the postural system to exhibit constraint-specific modulations in postural stability. This result was surprising because previous research has shown that during quiet standing paradigms postural sway decreases when individuals are asked to memorize a series of numbers [6]. The methodologies were virtually identical between our research and previously published research, with the exception that our participants performed a fitting task while memorizing numbers. It is possible that performing a manual fitting task while memorizing a series of numbers may draw attention away from the task of maintaining upright stance. Whereas, participants focus more attention on stance when instructed to stand and memorize numbers (causing a decrease in postural sway). Future work will examine if simultaneously performing a cognitive and manual task impedes the ability of the postural system to modulate postural sway in elderly subjects. It is possible that such multitasking is more difficult in elderly subjects compared to the current pool of college-aged individuals.

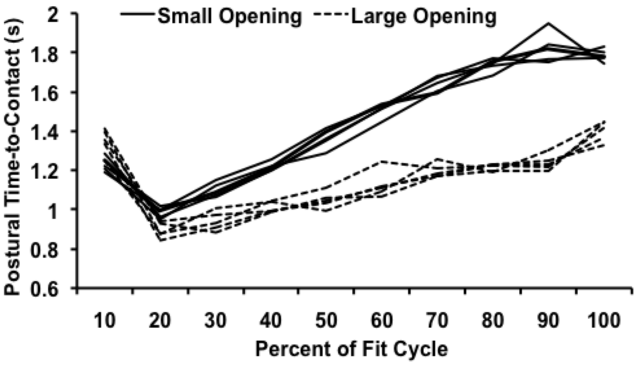

Figure 2: Postural time-to-contact over the reach cycle when fitting through the small (solid lines) and large (dotted lines) opening. Larger numbers represent a greater degree of postural stabilization. Each line represents one of the cognition levels.

REFERENCES

1. Stoffregen TA, et al. *J Exp Psy: HPP* **25,** 1641-1658, 1999.
2. Mitra S, & Frazier EV. *Hum Mov Sci* ***23,*** *1-20, 2004.*
3. Balasubramaniam et al. *Gait Posture* **11,** 12-24, 2000.
4. Riccio GE. *Variability and Motor Control, 317-358,* 1993.
5. Hamill J, et al. *Movement System Variability,* 153-165, 2006.
6. Riley MA et al. *Brain Res Bul* **62,** 191-195, 2003.
7. Haddad JM, et al. *J App Biomech* **22,** 155-161, 2006.

KINEMATIC DESCRIPTION OF THREE TYPES OF SOFTBALL PITCHES USING A UNIQUE GLENOHUMERAL MODEL

Laura Miller, James Richards, Thomas Kaminski and Todd Royer
Department of Health, Nutrition, Exercise Sciences, University of Delaware, Newark, DE
Email: lauraatc@udel.edu

INTRODUCTION

Clinical application of upper extremity joint angle calculations have proven challenging in biomechanics. Kinematic descriptions of joint angles provide the clinician the position of the joint during response to various stresses. It is therefore critical that joint angle calculations are both clinically applicable and accurate.

Various dynamic motions have been described in the upper extremity. Clinical application of a glenohumeral kinematic model necessitates acknowledgement of both Codman's paradox and the issue of gimbal lock [1]. Euler angles are one common method for calculation of joint angles; however, the sequence-dependent nature of those calculations can cause discrepancies, particularly at the glenohumeral joint. Consequently, caution must be exercised when interpreting Euler angles for clinical application [1,2]. Helical (screw) axis calculations are time-dependent, describing instantaneous rotation and translation about a single axis [1]. However, besides requiring the rotation axis to be appropriately localized into an anatomical coordinate system before being clinically applied [2], Helical motion is limited to defining distinct motion consistent with clinical articulations [1]. When combinations of motion, such as circumduction in the glenohumeral or hip joint are present, Helical motion is inefficient at distinguishing paths of motion. The spherical rotation coordinate system proposed by Cheng [2] also provides a model for the glenohumeral joint. However, implementation of this algorithm resulted in mathematically similar results to the International Shoulder Group (ISG) recommendation for calculating glenohumeral joint angles: the Euler YZY (Abduction/Internal Rotation/Abduction) sequence. For overhead shoulder motion, the Euler sequence of YZY is a common method for calculating kinematic data. This rotation sequence commonly used to examine baseball pitching. Softball pitching, however, presents a motion that is not well-defined by current methods of joint angle calculation. The windmill motion of the softball pitch requires full circumduction of the humerus, with varying degrees of internal and external rotation depending on pitch type. The circumduction motion of the humerus lends itself to errors during calculations using standard Euler and Helical models. The aim of this communication is to describe a unique kinematic model to calculate glenohumeral joint angles during a ballistic motion: the softball pitch; while also providing clinically useful measures of joint angles not previously reported in the literature.

METHODS

Eleven subjects (age= 15.4 ± 1.2 yr. old; height= 159.2 ± 10.8 cm; mass= 55.9 ± 8.4 kg) participated in this study. The protocol was institutionally approved and all subjects provided written assent with corresponding parental consent. All subjects were right-handed pitchers.

Eleven Eagle Digital cameras (Motion Analysis Corporation, Santa Rosa, CA), recording at 240 Hz, were used to record the displacements of reflective markers during collection. EVaRT 5.1.1 software was used for determination of the 3-D coordinates for each of the markers. After proper warm-up, subjects were fitted with a reflective marker set representing a modified version of the International Shoulder Group (ISG) recommendations for biomechanical analysis of the upper extremity. These points included: suprasternal notch, sternal body, acromioclavicular joint, medial and lateral epicondyles of the humerus, radial styloid, ulnar styloid, head of third metacarpal, and the dorsal surface of C7 and T8. Five trails were collected for each subject.

Markers were tracked using EVaRT 5.1.1 software to correctly identify position in the volume. A custom software program developed using Lab View 8.21 (National Instruments, Austin, TX) was developed and used to calculate all kinematic data.

RESULTS AND DISCUSSION

Planar deviations described the position of the upper arm relative to anatomical planes of motion positioned at the glenohumeral joint center. The internal/external rotation motion was described using a Helical calculation.

Shoulder motion during the windmill pitch is poorly described using conventions of Euler and Helical calculations. Neither Helical nor Euler calculations provided clinically useful descriptions of the motion. The flexion/horizontal flexion/internal rotation (XZY) Euler rotation appeared to be the likely candidate for describing shoulder motion. The flexion priority rotation was chosen because the primary motion at the shoulder during the windmill pitch is flexion with the critical phase being the acceleration or delivery component prior to ball release.

The flexion/extension curve in the Euler XZY sequence, when the gimbal lock is corrected, demonstrates logical description of shoulder motion during the pitch. At the start of the pitch, the shoulder is forward flexed approximately 25°. The curve continues to increase as the shoulder is flexed toward the head, with maximum flexion occurring at about 176°. It is at this point that the gimbal lock occurs. When mathematically correcting for the gimbal lock, the curve then demonstrates an expected decline in shoulder flexion as the arm begins a downswing to prepare for ball release. However, the internal/external rotation does not explain the motion seen three-dimensionally. Furthermore, correcting for the gimbal lock is not a perfect solution as the discontinuity initiates in advance of the point of error and continues for a number of frames after resolution. Therefore, due to the discontinuity seen in the flexion/extension and abduction/adduction curves and also given the misrepresentation of internal/external rotation, the XZY Euler rotation was not an appropriate convention to describe the entire windmill pitch.

A planar deviation model was created to describe shoulder motion during a windmill pitch. The position of the arm at any point of time could then be described by three values corresponding to orientation from the frontal, sagittal, and transverse planes of the glenohumeral joint. The curves for these calculations offered no discontinuities and demonstrate three motions of the shoulder with accuracy to three-dimensional movements. However, this model does not include internal/external rotation motion. Internal/external rotation of the shoulder during the acceleration phase was isolated independent of other arm motions. This was accomplished by comparing a vector locked to the elbow to a plane fit to the path of motion of the humerus relative to the trunk. When compared to the Helical calculations it appears that while Helical misrepresents abduction/adduction and horizontal flexion/extension, it provides a reasonable estimate of internal/external rotation.

CONCLUSIONS

While it is not customary to utilize separate methods to explain kinematic data, the windmill pitch presents complications that require this practice. This model was also unique in describing shoulder motion without conventional Euler rotation sequences.

REFERENCES

1. Hill AM, et al. *Gait & Posture*, **27**, 177-188, 2008
2. Cheng PL. *Ann Biomed Eng* **28,** 1381-1392, 2000

MUSCLE RECRUITMENT ORDER IN VARIOUS REACTION TIME TESTS

Matt Pain, Yanjia Gu and Mike Hiley
SSES, Loughborough University, UK
email: m.t.g.pain@lboro.ac.uk; web: www.lboro.ac.uk/departments/sses/

INTRODUCTION

Reaction time is dependent on several factors: arrival of the stimulus at the sensory organ, conversion by the sensory organ to a neural signal, neural transmissions and processing, muscular activation, soft tissue compliance, and the selection of an external measurement parameter. The contribution of stages such as, afferent and efferent conduction times and the delay between the onset of muscle action potentials and contraction have been considered in investigations of reflexes [1].

The different conduction times and muscle fibre activation times have a marked effect on the duration of reflexes. Little research has evaluated reaction times involved with different muscle groups. It would appear reasonable to assume that the distance an action potential must travel and the properties of the muscles it is innervating play an important aspect in a similar way to reflexes.

This study aimed to evaluate RTs and activation patterns between various muscles groups in a variety of RT tests.

METHODS

Seven healthy adults gave informed consent (age 27 ± 4 years). Surface EMG was recorded from 7 upper body muscles: deltoideus p. acromialis (DPA), deltoideus p. scapularis (DPS), pectoralis major (PEC), biceps brachii (BB), triceps (TB), flexor carpus ulnaris (FCU), interosseus (INT), whilst the subjects performed simple RT tests.

Seven different conditions were utilized, each designed to use a different muscle group as the primary agonist in each test. Examples of 6 tests are shown in Figure 1. DPS was similar to DPA except the elbow was pushed backwards onto the transducer. For each trial an LED was randomly activated with a remote control within a 10 second period following a warning. The response was measured with a force transducer. EMG, force and LED trigger data were collected through a common ADC at 1000 Hz.

Force and EMG onset were determined automatically when the value exceeded 3 standard deviations of the resting level. A simple computer RT test was also included with 10 trials per subject. T-test and ANOVA with a post hoc test were used to determine significance differences in reaction times and gradients, p = 0.05.

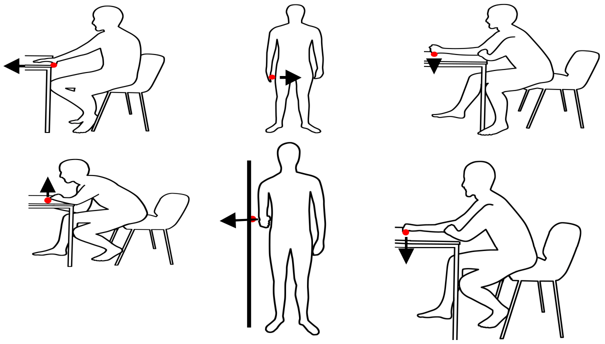

Figure 1: Illustration of movements to test specific muscles (top left clockwise: INT, PEC, TB, FCU, DPA, BB)

RESULTS AND DISCUSSION

The standard deviation of mean RTs within subject muscle group trials was on average 35 ms (not presented in Table 1). Variability, Stdev in Table 1, was significantly greater between the same muscle groups for different subjects than different muscle groups for an individual subject. Three subjects had significant differences between reaction times determined with different upper body muscle groups.

There was generally no correlation, $R^2 < 0.2$ between the force RTs and the computer tests, although for INT Vs computer $R^2 = 0.3$.

More athletic subjects, (1-3, self reported) had the lowest average force measured RTs and these were lower than the computer test times. For the other subjects the computer tests gave lower RTs than the average of the force tests. It is possible that this is partly due to the increased rate of force development that would be expected in more athletic individuals. However, this increased rate of force development should also lead to a quicker movement time which is included in the determination of computer reaction time test.

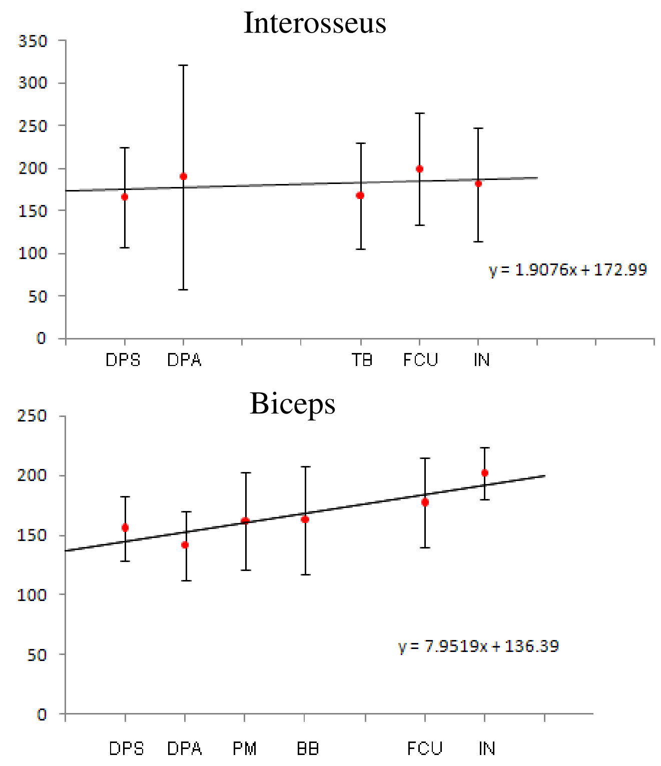

Figure 2. Activation time Vs. muscle group for the interosseus and the biceps conditions.

For each movement of each subject the EMG onset time was regressed against muscle, in a proximal to distal order, once the primary antagonist had been removed. Across all subjects INT and FCU movements generally had flat profiles while the larger muscles typically had obvious positive gradients. The average gradient values for INT and FCU across subjects were significantly lower than the average gradient values for the other muscle groups (an example of two muscle groups from one subject is given in Figure 2).

This variation in activation pattern with preferred primary agonist could indicate that a stabilizing sequence of events occurred with larger muscle groups that was not required for the well supported movements of the hand. It would also appear that the more athletic subjects were able to coordinate, or accommodate, this during the reaction time tests allowing them to produce relatively shorter/quicker RT than the computer test, for the large muscle group actions.

CONCLUSIONS

Reaction time tests using standard keyboard presses or finger based clicking activities have generally indicated that athletes do not have quicker reaction times than healthy age matched individuals.

The results of this study suggest that the inference of RT in athletic activities from computer tests may not be wholly justified as different muscles have different reaction times and coordination patterns. From this data it is apparent that the differences in activation pattern with RT and athleticism require further quantifying.

REFERENCES

1. Holmes, O. *Human Physiology,* London: Chapman & Hall, 1993.

Table 1: Mean reaction times (n=10) for all muscle groups and the computer tests of each subject.

Reaction times (milliseconds)

Subject	PEC	DPA	DPS	BB	TB	FCU	INT	Ave	Stdev	Comp
1	**210**	**157**	**180**	**162**	**170**	**172**	**170**	*174*	*17*	**231**
2	**173**	**214**	**203**	**186**	**188**	**184**	**165**	*188*	*17*	**188**
3	**231**	**251**	**X**	**209**	**196**	**203**	**212**	*217*	*20*	**242**
4	**231**	**191**	**221**	**216**	**227**	**210**	**224**	*217*	*13*	**199**
5	**229**	**252**	**225**	**217**	**X**	**214**	**203**	*223*	*17*	**219**
6	**277**	**253**	**221**	**208**	**252**	**248**	**209**	*238*	*26*	**186**
7	**340**	**330**	**322**	**329**	**304**	**232**	**209**	*308*	*37*	**256**
Ave	*242*	*235*	*229*	*218*	*223*	*209*	*212*			*217*
Stdev	*53*	*55*	*49*	*53*	*49*	*26*	*44*			*27*

QUANTIFYING HUMAN KNEE ANTHROPOMETRIC DIFFERENCES BETWEEN ETHNIC GROUPS AND GENDER USING SHAPE ANALYSIS TECHNIQUES

[1]Walter Schmidt, [2]Mauricio Reyes, [3]Felix Fischer, [4]Ruud Geesink, [2]Lutz Nolte, [1]Joseph Racanelli, [3]Nils Reimers
[1]Stryker Orthopaedics, Mahwah, NJ, USA,
[2]ARTORG Center for Biomedical Eng. Research, Bern, Switzerland,
[3]Stryker Osteosynthesis, Kiel, Germany, [4]University Hospital, Maastricht, Netherlands
email: Mauricio.Reyes@artorg.unibe.ch , web: www.stryker.com

INTRODUCTION

Optimal restoration of normal knee anatomy is one of the primary objectives for successful total knee arthroplasty (TKA). Total knee replacements have their design basis of some form of "averaged" knee anthropometry, although the population group and sample size over which the averaged anatomic data is obtained varies between total knee replacement manufacturers. Orthopaedic surgeons have reported either insufficient implant bone coverage or implant overhang in designs across the industry as a result of sub-optimum implant fit [1].

Although there is evidence to suggest that there are gender differences in the anteroposterior to mediolateral dimension aspect ratios of the femoral condyle [2], the actual anatomical differences between gender may be more complex than this simple relationship. This is also true for ethnic group variations, as concluded in a study published for a generally smaller-sized, south Asian Indian population [3]. More rigorous knee anthropometry data mining is necessary to more precisely assess global knee morphological variations.

Recent advances in quantitative computed tomography (CT) image processing have enabled researchers in this study to develop a comprehensive "virtual bone database" (VBD). Using the VBD, in conjunction with shape analysis techniques, a systematic methodology was established to consistently measure distal femur and proximal tibia anatomic dimensions between Asian and Caucasian population groups and then between males and females within those ethnic groups.

Statistical comparisons between these groups were then made to establish their statistical significance and what role these differences should play in next generation knee prosthesis designs.

METHODS

Landmark dimension selection: Figure 1 presents the anatomical landmarks dimensions which were measured in this study.

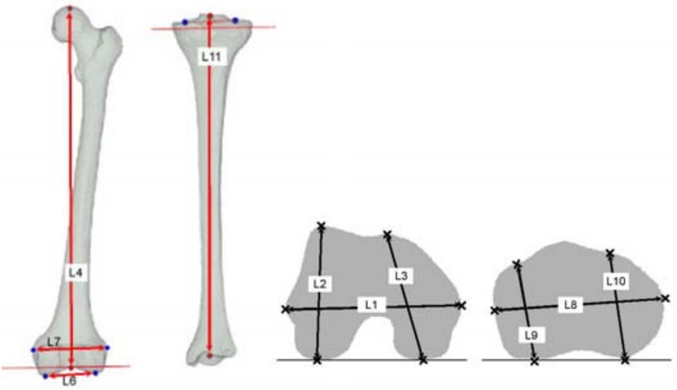

Figure 1: Anatomic landmark measurement locations

Landmarks L1-L3 apply to the distal femur and are measured from a virtual cutting plane which is normal to the mechanical axis, 8mm above the medial point between the femoral condyles.

Landmark L4 correponds to the femoral length, while Landmark L5 corresponds to the overall anterior posterior dimension of the distal femur as measured in the sagittal view.

Landmark 6 corresponds to the M/L width of the most distal points of the femoral condyles when viewed from the frontal plane, while Landmark 7 corresponds to the transepicondylar line length.

Landmarks L8-L10 apply to the proximal tibia and are measured from a virtual cutting plane which is normal to the mechanical axis, 6mm below the sulcus of the tibial condyles, while Landmark 11 corresponds to the tibial length.

Population selection: A total of 65 right femura and 57 right tibiae, processed from CT scans of slice thicknesses ranging from 0.7 to 1.5mm, were randomly selected from the VBD. These patients range in age from 19 to 85 years.

The dataset was further divided by gender and by ethnic group (i.e.; East Asians and Caucasians), as presented in Tables 1-4.

Dimension processing methodology: CT scan image segmentation was performed in a semi-automatic fashion to extract the outer cortical surface profiles of the femur and tibia.

After image segmentation, reference bone images were selected for the femur and tibia and a combined affine and non-rigid image registration approach [4] is employed to establish corresponding anatomical points across the images. Given a point x in the reference image, we target a corresponding point x′ such that $x' = A^{-1}(\varphi'^{-1}(x))$, where A and φ are the affine and non-rigid transformations needed to morph every bone image onto the reference bone image. The affine transformation allows for large scale deformations, whereas the non-rigid transformation captures the local shape variations.

Anatomic landmarks are selected interactively by mouse clicking on locations on the reference bone using a graphical user interface in which the reference bone is viewed and can be rotated in 3D space. The positions identified on the reference bone are transformed to the equivalent position on the clinical bone images, from which dimensional data is extracted and stored. The landmark selection process was later enhanced to allow for landmarks to be defined on specific cutting planes.

RESULTS

The results of the statistical evaluation (using the Mann-Whitney U-Test) are presented in Tables 1-4.

DISCUSSION and CONCLUSIONS

A statistically significant difference in the distal femur and proximal tibia dimensions was found between males and females, but not between Asian and Caucasian groups.

The automated algorithm for anatomical landmark dimensioning facilitates the ability to measure and analyze large datasets quickly and consistently, circumventing slower, error prone manual measurement techniques previously implemented.

Ongoing work includes increasing the sample size, extending anatomical landmarks dimensions to other measurements including radii (e.g.; femoral head diameters and femoral bow) and angles (e.g.; femoral neck angle). The processing will also be enhanced to include automatic first order statistical analysis for the output data sets.

Table 1: Femoral Dimensions by Ethnic Group, mm (n=65)

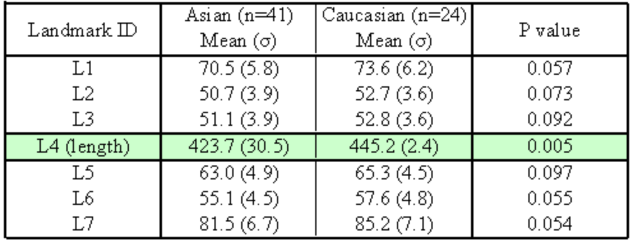

Landmark ID	Asian (n=41) Mean (σ)	Caucasian (n=24) Mean (σ)	P value
L1	70.5 (5.8)	73.6 (6.2)	0.057
L2	50.7 (3.9)	52.7 (3.6)	0.073
L3	51.1 (3.9)	52.8 (3.6)	0.092
L4 (length)	423.7 (30.5)	445.2 (2.4)	0.005
L5	63.0 (4.9)	65.3 (4.5)	0.097
L6	55.1 (4.5)	57.6 (4.8)	0.055
L7	81.5 (6.7)	85.2 (7.1)	0.054

Table 2: Femoral Dimensions by Gender, mm (n=65)

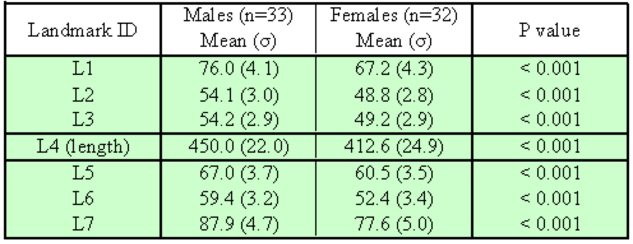

Landmark ID	Males (n=33) Mean (σ)	Females (n=32) Mean (σ)	P value
L1	76.0 (4.1)	67.2 (4.3)	< 0.001
L2	54.1 (3.0)	48.8 (2.8)	< 0.001
L3	54.2 (2.9)	49.2 (2.9)	< 0.001
L4 (length)	450.0 (22.0)	412.6 (24.9)	< 0.001
L5	67.0 (3.7)	60.5 (3.5)	< 0.001
L6	59.4 (3.2)	52.4 (3.4)	< 0.001
L7	87.9 (4.7)	77.6 (5.0)	< 0.001

Table 3: Tibial Dimensions by Ethnic Group, mm (n=57)

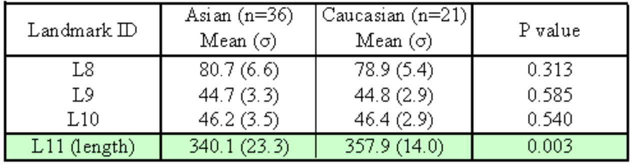

Landmark ID	Asian (n=36) Mean (σ)	Caucasian (n=21) Mean (σ)	P value
L8	80.7 (6.6)	78.9 (5.4)	0.313
L9	44.7 (3.3)	44.8 (2.9)	0.585
L10	46.2 (3.5)	46.4 (2.9)	0.540
L11 (length)	340.1 (23.3)	357.9 (14.0)	0.003

Table 4: Tibial Dimensions by Gender, mm (n=57)

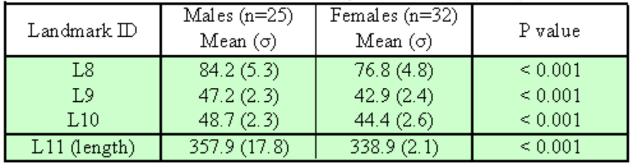

Landmark ID	Males (n=25) Mean (σ)	Females (n=32) Mean (σ)	P value
L8	84.2 (5.3)	76.8 (4.8)	< 0.001
L9	47.2 (2.3)	42.9 (2.4)	< 0.001
L10	48.7 (2.3)	44.4 (2.6)	< 0.001
L11 (length)	357.9 (17.8)	338.9 (2.1)	< 0.001

REFERENCES

1. Chin, KR, et al. *Intraoperative Measurements of Male and Female Distal Femurs During Primary Total Knee Arthroplasty*, J Knee Surg, **15**, 213-217, 2002.
2. Hitt, K, Shurman, JR, et al. *Anthropometric Measurements of the Human Knee: Correlation to the Sizing of Current Knee Arthroplasty Systems*, J Bone Joint Surg Am, **85**, 115-122, 2003.
3. Vaidya SV, Ranawat, et al. *Anthropometric Measurements to Design Total Knee Prostheses for the Indian Population*, JOA, **15**, No 1, 79-85, 2000.
4. Vercauteren, T, et al. *Non-parametric Diffeomorphic Image Registration with the Demons Algorithm*, Medical Image Computing & Computer-Assisted Intervention 2007, pp. 319-326, 2007.

REDUCTIONS IN STRETCH SHORTEN CYCLE FORCE ENHANCEMENT WITH INCREASED COUPLING TIME DURING MAXIMAL KNEE EXTENSIONS

[1]Matt Pain, [2]Mickael Begon, and [3]Steph Forrester
[1]SSES, Loughborough University, [2]Université de Montréal, [2]STI, Loughborough University,
email: m.t.g.pain@lboro.ac.uk; web: www.lboro.ac.uk/departments/sses/

INTRODUCTION

The Stretch Shorten Cycle (SSC) occurs when an active musculotendinous unit is forcibly stretched before it shortens, giving rise to increased levels of force production during the shortening. There are a number of mechanisms suggested for this phenomenon (discussed in a review edition of the Journal of Applied Biomechanics, Issue 4 volume 13, 1997) but the exact contribution to overall performance is still equivocal. Introducing a delay, Coupling Time (CT), between the eccentric and concentric actions in a SSC reduces the force enhancement in an exponential manner [1].

Previous experiments that varied the CT used compound actions such as bench pressing, squatting or jumping. These motions present: variable rather than maximal activation throughout the SSC; often occur over short time frames; and have large changes in velocity. All these contribute to the difficulty in comparing their results with those from *in vitro* and *in situ* studies that are normally performed under far more controlled stretch and hold conditions or stretch and shorten conditions.

The aim of this research is to examine the effect of CT on SSC enhancement during well controlled pseudo-isovelocity conditions with maximal voluntary activation.

METHODS

Seven athletic subjects (5 male, 2 female, age 22.4 ± 0.6 years; height 178 ± 12 cm; weight 79.8 ± 8.7 kg) gave informed consent in accordance with Loughborough University ethical committee. Two sets of maximum voluntary knee extensions were conducted on a CON-TREX dynamometer (CMV AG, Switzerland).

The first set were maximum effort eccentric-isometric-concentric contractions. These were performed for six isometric coupling times (CT) (0.07, 0.3, 0.6, 1, 2, 4 s) and three velocities ($30°s^{-1}$, $60°s^{-1}$ and $100°s^{-1}$). Initial knee angle was set to 10° of flexion and subjects were asked to maximally resist forced flexion through a 70° range of motion (to 80° of flexion) and to continue pushing maximally throughout the isometric and concentric phases. The second set were maximum effort isometric-concentric contractions. These employed the same isometric angle (80° of flexion) (held for 2 s) and concentric velocities as in the first set of trials.

The torque at 10°, 20° and 30° into the concentric movement was evaluated for each trial and normalised based on the values for the shortest coupling time (0.07 s) at the same velocity.

RESULTS AND DISCUSSION

In the eccentric-isometric-concentric trials normalised concentric torque appeared to decrease exponentially with increasing isometric coupling time (Figure 1, Eqn. 1) with a half life of 0.7 seconds.

$$\frac{T}{T_{ct=0.07}} = 0.759 + 0.259\exp(-1.002ct) \qquad \text{Eqn. 1}$$

This half life is comparable with the half life of 0.85 s determined by [1] during bench pressing, but shorter than half lives seen in the some lower limb compound movement experiments, which have claimed half lives to up to 4 seconds [2]. This value is also falls within the range of values found for the half life of active force enhancement decay. This tends to have a range between 0.5 to 1.1 s, determined from muscle fibre experiments [3] and in situ whole muscle experiments [4]. It would appear that the longest half lives determined from older data during compound lower body movements are not the norm. We have also previously determined half lives between 0.8 and 1.1 s for SSC enhancement decay during countermovement jumps [5].

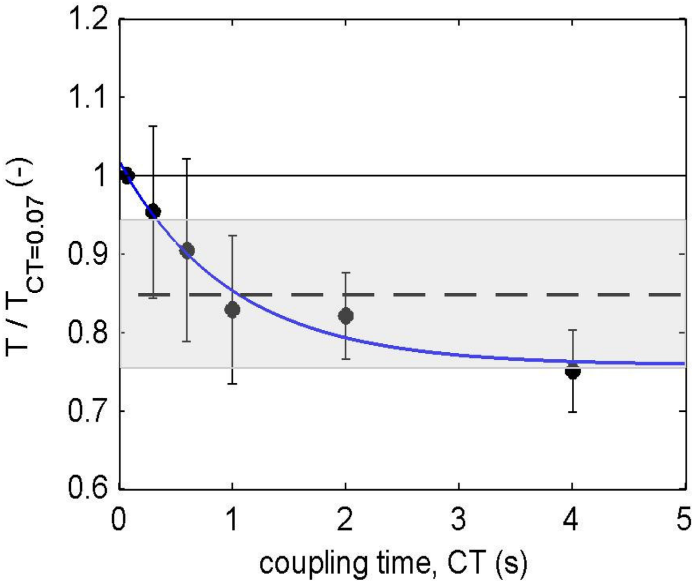

Figure 1: Normalised concentric torque (normalised to 0.07 s CT value) versus CT. Black circles are mean ± SD from eccentric-isometric-concentric trials averaged over all velocities, all concentric positions and all subjects. Solid blue line is the exponential fit. Dashed line and shaded region are the mean ± SD from isometric-concentric trials averaged over the same conditions.

As other studies have shown [6], the improvement in SSC performance is not as great when compared to isometric preload as when compared to purely concentric contractions. The SSC performance was only significantly better than the isometric-concentric performance for the shortest coupling times and was worse at the longest CT. This would support the idea that a significant proportion, but not all, of the improvement from the SSC can be accounted for by the increased time to increase activation prior to the start of the concentric contraction. Here, when more time is allowed in the form of an extended isometric hold performance dropped back to that of a pure isometric fore-period illustrating a distinct dynamic contribution to the concentric force enhancement.

It may also warrant consideration, given the relatively small number of points used in various studies to fit the exponential decay, that the exponential decay could be an artifact of choosing a single function to fit the data. This could arise with the results in Figure 1 due to the first 2 or 3 data points decreasing in value as a short term stretch related enhancement dropped off; points 3, 4 and 5 being constant and approximately equal to the isometric-concentric trials; and the last point dropping off due to greater fatigue within the SSC trials. Maximal effort in the SSC trials would have been required for up to 7 seconds but only for up to 3 seconds in the isometric-concentric trials.

These results suggest that improvements due to the active stretching last no longer than 1 s. However, the exact load at the start of the concentric phase has not been explicitly accounted for and the EMG activity of the quadriceps also needs quantifying.

CONCLUSIONS

Torque appears to decay exponentially with increasing CT. The half life seen in this experiment was similar to the active force enhancement decay, seen in muscle fibre experiments [2] and in situ whole muscle experiments [3].

A SSC for maximum voluntary knee extensions can have a significant advantage over isometric preload on the concentric torque generation, but only for low CT. This supports the idea that a high proportion of the improvement from the SSC can be accounted for by the increased time to develop pre-activation prior to the start of the concentric contraction. However, it also highlights that a distinct dynamic component is present which decreases with increasing CT.

REFERENCES

1.Wilson et al. *Med Sci Sport Exerc* **23**, 364-370, 1991.
2.Shorten *Med Sci Sport* **25**, 1-18, 1987.
3.Edmann et al. *J Gen Physiol* **80**, 769-784, 1982.
4.Schachar et al. *J Biomech* 35, 1299-1306, 2002.
5.Pain et al. *Proceedings of the 5th World Congress of Biomechanics* Munich, 2006
6.Walshe et al. *J Appl Physiol* **84**, 97-106, 1998.

ACKNOWLEDGEMENTS

Tom Beaumont for his assistance in data collection.

MAXIMAL KNEE EXTENSION STRETCH SHORTEN CYCLES ON AN ISOVELOCITY DYNAMOMETER TO EXAMINE ACTIVE FORCE EHANCEMENT

[1] Matt Pain, [2]Mickael Begon and [3]Steph Forrester
[1]SSES, Loughborough University, UK [2]Université de Montréal, Canada, [3]STI, Loughborough University
email: m.t.g.pain@lboro.ac.uk; web: www.lboro.ac.uk/departments/sses/.

INTRODUCTION

Force enhancement following muscle stretch has been widely observed in electrically stimulated muscle [1]. It has also been observed in voluntarily activated human muscle, but only for the adductor pollicis and the ankle joint muscles [2], not for larger muscles such as the quadriceps femoris [3]. These studies using isolated joint motions, have been limited to stretch and hold they have not followed the hold with a controlled concentric contraction.

In contrast, studies examining the stretch shorten cycle *in vivo* have focussed on compound actions such as countermovement jumps. Investigations of force enhancement within a stretch shorten cycle in a controlled *in vivo* environment, such as used in the studies of paragraph one, would seem a useful intermediary.

This study aimed to measure *in vivo* force enhancement following muscle stretch on the subsequent hold and concentric action for maximum voluntary contractions of the human quadriceps femoris.

METHODS

Seven athletic subjects (5 male, 2 female, age 22.4 ± 0.6 years; height 178 ± 12 cm; weight 79.8 ± 8.7 kg) gave informed consent in accordance with Loughborough University ethical committee. Three sets of maximum voluntary knee extensions were conducted on a CON-TREX dynamometer (CMV AG, Switzerland).

The first set were maximum effort eccentric-isometric-concentric (EIC) contractions. These were conducted for six isometric coupling times (CT) (0.07, 0.3, 0.6, 1, 2, 4 s) and three velocities ($30°s^{-1}$, $60°s^{-1}$ and $100°s^{-1}$). Initial knee angle was set to 10° of flexion and subjects were asked to maximally resist forced flexion through a 70° range of motion (to 80° of flexion) and to continue pushing maximally throughout the isometric and concentric phases. The second set were maximum effort eccentric-isometric contractions. These employed the same eccentric velocities and isometric angle (80° of flexion) as in the first set of trials. In all trials the isometric contraction was held for 4 s. Finally, subjects also performed an isolated maximum effort isometric contraction again using a knee angle of 80° of flexion.

For the first two sets of trials, mean torque over consecutive 100 ms time intervals throughout the isometric contraction was determine. These torques were normalised based on the isolated isometric value to enable comparisons across subjects.

RESULTS AND DISCUSSION

Some subjects were unable to perform the required EIC task. They failed to achieve eccentric torque or isometric torque as high as in the isolated isometric trial and were inconsistent during the subsequent hold and concentric contractions (Figures 1(b) and 1(d)). However, other subjects produced more consistent performances. Eccentric torque exceeded the isolated isometric value then progressively dropped off during the hold and concentric contractions (Figures 1(a) and 1(c)) as has been reported previously for the quadriceps [3].

Consequently, pooling results to give the group average voluntary torque profile during the isometric hold section of the EIC contractions gave poor agreement with *in vitro* observations and a force decrement throughout the hold phase (Figure 2(a)). This is consistent with many previous studies showing the inability of subjects to maximally activate large muscles during eccentric contractions [4]. Where force enhancement in individuals was found it was small and decayed, roughly exponentially, to isometric levels after 1 s.

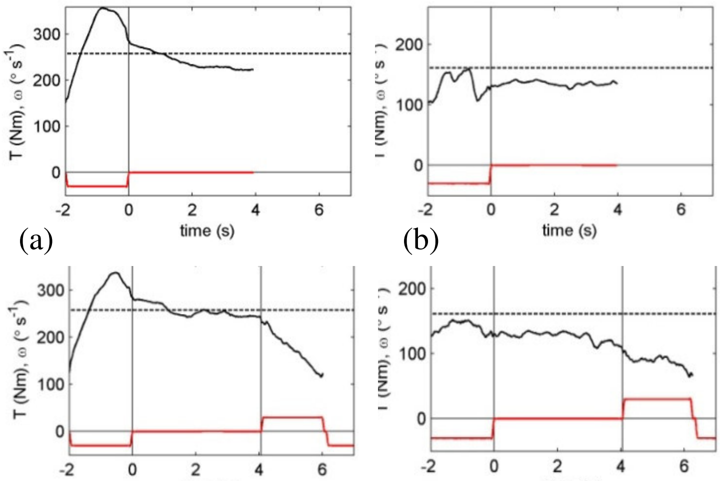

Figure 1. Torque vs. time and velocity vs. time profiles from eccentric-isometric trials and EIC trials: (a) and (c) subject 6 at 30°s^{-1}; (b) and (d) subject 3 at 30°s^{-1}. Horizontal dashed line is the isolated isometric torque.

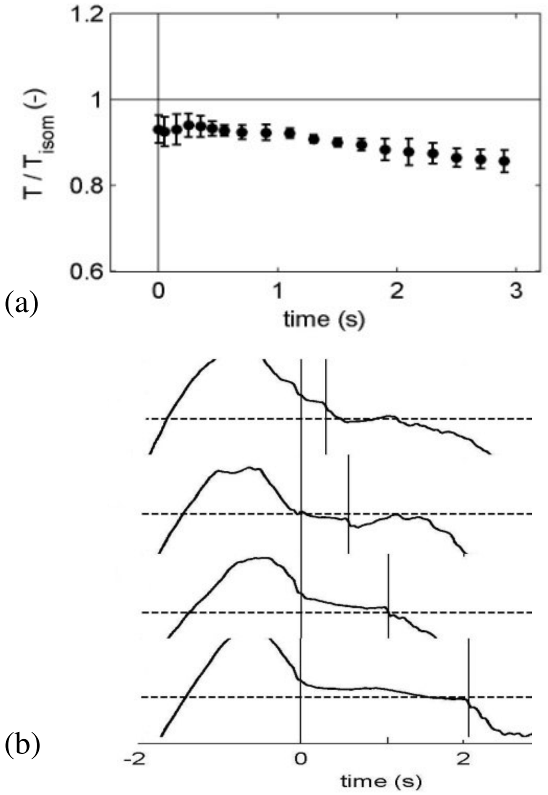

Figure 2. (a) Normalised isometric torque (to isolated isometric value) in EIC trials (mean ± SD all subjects and velocities); (b) EIC torque for subject 6, and CT = 0.3, 0.6, 1 and 2 s. 1st line is isometric onset, 2nd line is concentric onset. ashed line is isolated isometric torque.

For those subjects who achieved eccentric torques above the isometric value, a small drop in torque was observed at the start of the concentric contraction that appeared to be independent of the torque level and CT (Figure 2(b)). Also, the concentric contraction could start at a higher torque value than the isolated isometric torque and continue above this level for a brief period. However, whether this was due to errors in the true isometric level, increased activation at onset of concentric contraction, or some force enhancement not being negated as soon as the contraction starts, has not been determined.

CONCLUSIONS

During experiments involving voluntary maximal eccentric activation, the between subjects variability in torque profiles and force enhancement was large. Some subjects were unable to reach isometric levels during eccentric contractions, despite being active and regularly participating in sport. Some were also unable to reach isometric torques levels despite an extended time to achieve this during an isometric contraction following stretch.

In subjects who showed limited force enhancement the following concentric contraction could start at higher than the isolated isometric torque and remain above this level for a brief period. However, the reason for this enhanced force is undetermined.

The inability of subjects to produce maximal activation can be a limiting factor in experiments designed to investigate fundamental *in vivo* muscle properties.

REFERENCES

1. Edman KA, et al., *J Physiol* **281**, 139-155, 1978.
2. Lee E-J, & Herzog W, *J Physiol* **545**, 321-330, 2002.
3. Hahn D, et al., *Eur J Appl Physiol* **100**, 701-709, 2007.
4. Westing SH, et al., *Eur J Appl Physiol* **62**, 104-108, 1991.

ACKNOWLEDGEMENTS

Tom Beaumont for his assistance in data collection.

EFFECTS OF AGE AND WALKING SPEED ON COACTIVATION DURING GAIT

[1,2]Daniel S. Peterson MS, [1,3]Philip E. Martin PhD
[1]Pennsylvania State University, University Park, PA [2]Steadman Hawkins Research Foundation, Vail, CO
[3]Iowa State University, Ames, IA; *dspeterson8@gmail.com

INTRODUCTION

Metabolic cost of walking (C_w) is higher for the elderly than for young adults across a range of walking speeds[1]. The underlying mechanism for this difference, however, is not fully understood. Recent studies have examined coactivation during dynamic activities[1,2,4], but few have also incorporated metabolic measures to determine the relationship between coactivation and C_w[1].

The purposes of this study were to determine 1) the effects of age on coactivation during gait, and 2) the relationship between coactivation and C_w during gait at several walking speeds.

METHODS

Subjects: Fourteen young (20-30 yrs) and 14 older (65-80 yrs) healthy active adults participated in this study.

Experimental Design: Participants walked on a treadmill for seven minutes at each of four speeds (0.89, 1.12, 1.34, and 1.57 $m \cdot s^{-1}$) in random order. Electromyography (EMG) data were collected from tibialis anterior (TA), gastrocnemius medialis (GM), lateral soleus (SOL), vastus lateralis (VL), semitendionsus (ST), and biceps femoris (BF) for 30 seconds during each condition. Expired air was also collected during each trial to determine C_w.

Data Analysis: Four antagonist pairs of muscles, two for the shank (TA–SOL, TA–GM) and two for the thigh (VM–BF, VM–ST), were identified. EMG data were normalized to the average EMG amplitude during the 1.12$m \cdot s^{-1}$ trial. A coactivation index (CI) was defined as the area of overlap between the agonist and antagonistic EMG signals[3] (Equation 1; Figure 1):

$$CI = 2 \cdot \left(\frac{\int \min(EMG_{ag}, EMG_{antag})}{\int EMG_{ag} + \int EMG_{antag}} \right) * 100 \qquad \text{(Eq. 1)}$$

CI about the thigh and shank (CI_{TH}, CI_{SH}) were determined by averaging pairs of coactivation indices about each segment. Total CI (CI_{TOT}) was also determined as the sum of CI_{TH} and CI_{SH}. To determine when coactivation occurred during each stride, the area of overlap between antagonist musculature was also calculated for 10% increments over each stride.

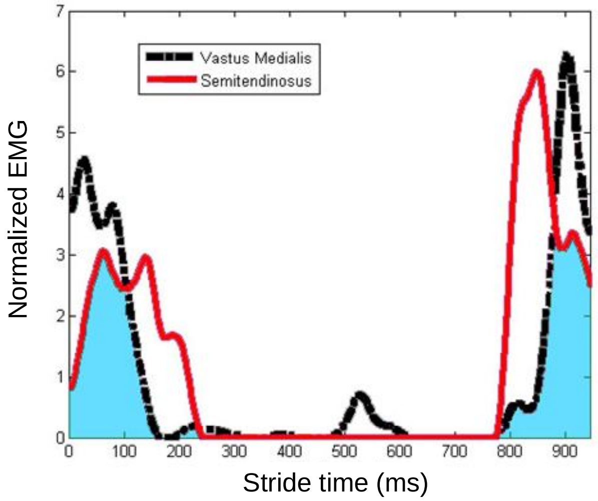

Figure 1: Example of CI_{TH} quantification for one stride. Shaded region represents coactivation (t_0 = heel strike).

RESULTS

C_w was 23% higher for older adults with respect to young when averaged across walking speeds ($F_{1,26}$=29.86, p<0.001). Older adults also reflected significantly higher CI_{TH} than young adults ($F_{1,26}$=16.36, p<0.001), but not CI_{SH} ($F_{1,26}$=0.29, p=0.60; Figure 2). CI_{TOT} was larger for old ($F_{1,26}$=13.57, p<0.001). When CI was calculated over 10% stride intervals, an age by interval interaction was shown for CI_{TH} ($F_{9,234}$=6.21; p<0.001), with older adults experiencing higher CI_{TH} near heel strike than young (Figure 3).

Collapsing across age, statistically significant positive relationships were found between C_w and CI_{TH} (all speeds; r=0.39-0.46), CI_{SH} (speeds 0.89, and 1.12 $m \cdot s^{-1}$; r=0.40 and 0.40, respectively), and CI_{TOT} (all speeds; r=0.46-0.57; Figure 4).

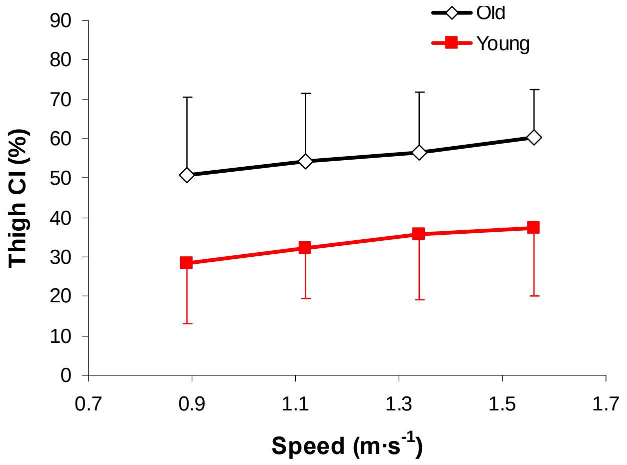

Figure 2: CI_{TH} was significantly greater for older adults at all walking speeds.

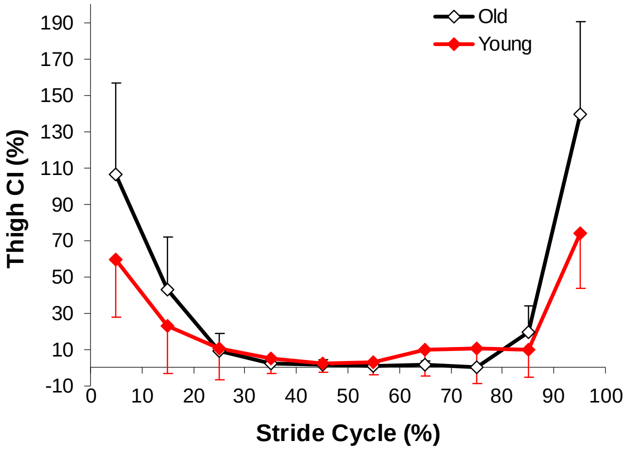

Figure 3: CI_{TH} was greater for older adults just prior to and after heel strike, which is represented at 0 and 100% of the stride cycle.

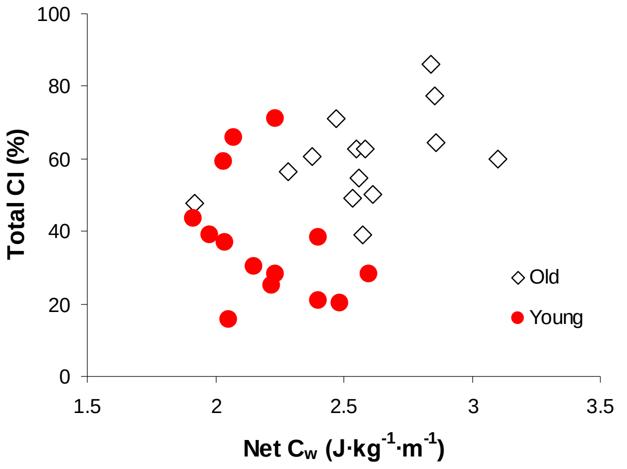

Figure 4: CI_{TOT} vs. net C_w at 1.57 $m \cdot s^{-1}$ (r=0.51 for all subjects, r=0.55 for only the older adults)

Separate correlation analyses were carried out between C_w and coactivation for each age group. Positive correlations persisted, although primarily in older individuals. Specifically, older adults showed positive correlations between C_w and CI_{SH} (0.89, and 1.12 $m \cdot s^{-1}$; r=0.55 and 0.67, respectively), and between C_w and CI_{TOT} at 1.12 (r=0.55) and 1.57 (r=0.55) $m \cdot s^{-1}$.

DISCUSSION

Older adults exhibited higher coactivation about the thigh and higher C_w when compared to young adults.

The age-related differences in coactivation for the thigh may be due in part to a greater need for active muscular stabilization of the knee in older adults with respect to young. Hortobagyi and DeVita[4] suggested decrements in strength and neurological function may cause older adults to increase coactivation to stabilize and stiffen joints during dynamic tasks. In the current study, the higher CI_{TH} exhibited by older adults was generally focused on the 10% of stride before and 10% after heel strike, indicating older adults may rely more on active muscular stabilization than young to control knee motion during heel strike (Figure 3).

Unlike coactivation about the thigh, coactivation about the shank was distributed relatively evenly throughout the stride. Further, these responses were similar for young and older subjects indicating higher coactivation was not used to a greater degree in older adults to actively stabilize the ankle.

Pooling data for older and young participants, C_w was shown to have a modest positive correlation to CI_{TOT}, indicating higher C_w was associated with higher levels of antagonist muscle coactivation. These results combined with previous literature[1,2,4] suggest that coactivation does contribute to the higher C_w seen in older adults.

REFERENCES

1. Mian OS et al. (2006). *Acta Physiol [Oxf].* **186**(2):127-39.
2. Hortobagyi et al. (2009). *Gait Posture.* doi:10.1016/j.gaitpost.2008.12.007
3. Winter DA (1990). *Biomechanics and Motor Control of Human Movement*. New York: Wiley.
4. Hortobagyi T & DeVita P (2000). *J Electromyogr Kinesiol.* **10**(2):117-26.

PRELIMINARY INVESTIGATION OF SLIP AND TRIP PROPENSITY IN OVERWEIGHT AND NORMAL WEIGHT ADULTS

Sara L. Matrangola, Dennis E. Anderson, Michael L. Madigan
Virginia Polytechnic Institute and State University, Blacksburg, VA, USA
E-mail: smatrang@vt.edu, Web: http://www.biomechanics.esm.vt.edu/

INTRODUCTION

Slips, trips, and falls account for approximately 21% and 13% of disabling [1] and fatal [2] occupational injuries, respectively. In addition, obese individuals fall almost twice as often compared to non-obese individuals [3] and falls were identified as the most common cause of injuries in the obese (~36% of all injuries) [4]. This is of concern because over 66% of adults in the United States are considered overweight or obese [5], and this percentage is increasing. Between 1980 and 2002, for example, obesity prevalence doubled among adults and overweight prevalence tripled among children [5]. However, the influence of being overweight on slip and trip propensity has yet to be investigated.

Therefore, the goal of the current study was to investigate differences in slip and trip propensity between overweight and normal weight adults. We hypothesized that due to the reported increased risk of falls in obese individuals, overweight subjects will exhibit an increased slip and trip propensity compared to normal weight subjects.

METHODS

Eight subjects (59.4 ± 26.8 years), including four overweight (body mass index, or BMI, = 28.9 ±1.7 kg/m^2) and four normal weight (BMI = 19.6 ±1.3 kg/m^2) participated in the study. A medical screening was performed to exclude participants with any self-reported neurological, cardiac, respiratory, otological, or musculoskeletal disorders, or a history of multiple falls within the past year.

Subjects walked along a walkway at two prescribed gait speeds: 1.2 m/s (Slow) and 1.5 m/s (Fast). Three trials were completed at each speed. During each trial, the position of selected anatomical landmarks was sampled at 100 Hz using a Vicon 460 motion analysis system (Vicon Motion Systems Inc., Lake Forest, CA), and ground reaction forces were sampled at 1000 Hz using a force platform (Bertec Corporation, Columbus, OH).

Required coefficient of friction (RCOF), the ratio of anterior-posterior shear to normal foot forces generated during gait, was used to quantify slip propensity [6]. A higher RCOF implies that a greater shear force is needed to keep the foot from slipping. Minimum toe clearance, defined as the lowest vertical position of the foot during the swing phase of gait, was used to quantify trip propensity. A smaller toe clearance value implies an increased risk of tripping [7].

A Wilcoxon Rank-Sum test was used to investigate differences in slip and trip propensity between overweight and normal weight groups within each gait speed. This test was used due to small sample size and non-normal distributions. Statistical analysis was performed using JMP v7 (Cary, North Carolina, USA).

RESULTS AND DISCUSSION

The overweight group exhibited a higher RCOF than the normal weight group ($p<0.05$) for both gait speeds (Figure 1). No significant differences were found between the overweight and normal weight group for minimum toe clearance.

A higher RCOF for the overweight group indicates that overweight subjects require more frictional resistance and are more likely to initiate a slip than the normal weight group. Fall risk is dependent upon the number of fall initiating events and balance recovery capability [8]. Our results indicate that overweight individuals may be at an increased risk of falls due to an increased propensity for fall initiating events (i.e. slipping).

Contrary to our hypothesis, the overweight group did not exhibit smaller toe clearance values. These results imply that the overweight group does not have an increased propensity for initiating a trip. However, being overweight or obese causes alterations in gait, such as smaller strides and longer periods of double support, and it has been suggested that these alterations are an attempt to be more stable during gait [9]. It is possible that these alterations in gait also result in a decreased risk of tripping. To our knowledge, this has not been addressed in previous studies. Though being overweight does not appear to influence the propensity to trip, it may still decrease balance recovery capability from a trip, and thereby increase fall risk.

One limitation to this study was the relatively large range of subject ages. However, studies have found that RCOF and minimum toe clearance are not significantly different between young and older adults [10, 11]. Another limitation is that the small sample size limits the statistical power of our results. It is important to note that even with a small sample size, significant differences were still found for our slip propensity measure, RCOF. Third, our measures were used as a surrogate measure of slip and trip propensity, and the relation between these variables and risk of falls has not been quantified.

CONCLUSIONS

In conclusion, the overweight group was found to have a greater risk for slips, but not for trips, compared to the normal weight group. Future studies should also investigate differences in slip and trip recovery between normal weight, overweight, and obese individuals to help understand the biomechanical mechanisms behind the increased risk of falling in the obese.

REFERENCES

1. Courtney TK, et al. *Ergonomics* **44**, 1118-37, 2001.
2. *MMWR Morb Mortal Wkly Rep* **56**, 297-301, 2007.
3. Fjeldstad C, et al. *Dyn Med* **7**, 4, 2008.
4. Matter KC, et al. *Obesity (Silver Spring)* **15**, 2384-90, 2007.
5. Ogden CL, et al. *Jama* **295**, 1549-55, 2006.
6. Buczek FL, et al. *International Symposium on Slip Resistance - the Interaction of Man, Footwear, and Walking Surfaces* 353-358, 1995.
7. Rietdyk S, et al. *Clin Biomech (Bristol, Avon)* **20**, 1085-93, 2005.
8. Robinovitch SN, et al. *J Neurophysiol* **88**, 613-20, 2002.
9. Spyropoulos P, et al. *Arch Phys Med Rehabil* **72**, 1065-70, 1991.
10. Lockhart TE, et al. *Ergonomics* **46**, 1136-60, 2003.
11. Mills PM, et al. *Hum Mov Sci* **20**, 427-46, 2001.

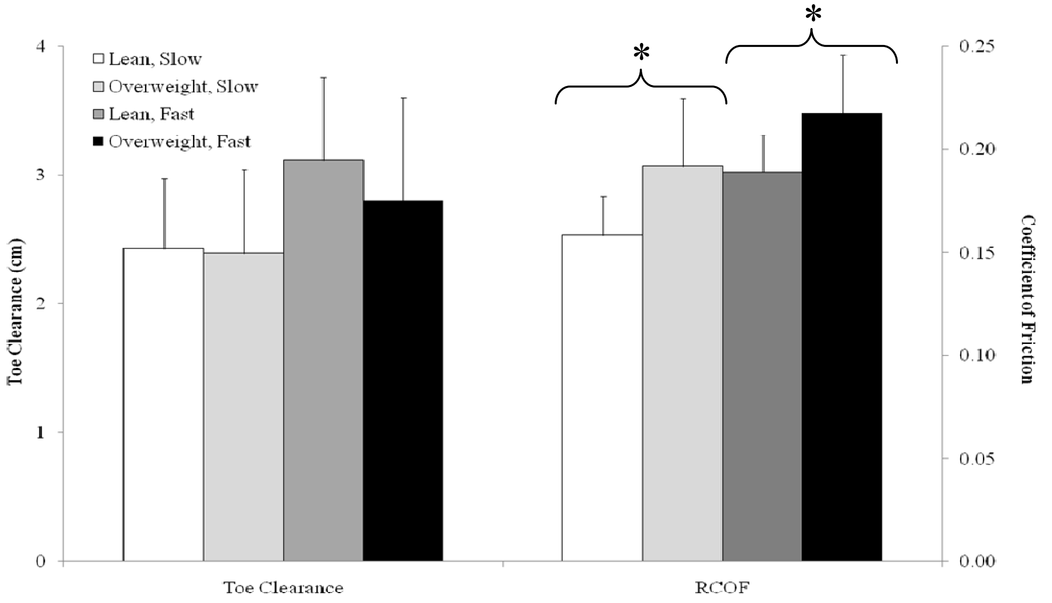

Figure 1: Slip and Trip Propensity Measures for Slow and Fast Gait Speeds. * indicates p-value <0.05

THE VALIDITY OF DIFFERENT OCCLUSAL INDICATORS.

[1] Steph Forrester, [2]Matt Pain, [3]Andy Toy and [4]Ron Presswood
[1]STI, Loughborough University, UK; [2]SESS, Loughborough University, UK; [3]Gorse Covert Dental Practice, Loughborough, UK; [4]8801 Gaylord, Houston, Texas 77024, USA.
email: s.forrester@lboro.ac.uk; web: www.sports-technology.com/.

INTRODUCTION

Occlusal indicators are widely used to obtain information on tooth contacts during occlusion in the fitting of prosthetic devices [1]. A wide range of indicators exist ranging from articulating ribbons through to the T-Scan pressure measurement system. These devices differ not only in their measurement characteristics but also in their material properties such as thickness and plasticity. Previous studies on the performance of occlusal indicators have focused on comparing their sensitivity, reliability, validity and practical utility (benefit versus cost) from a marking perspective [1,2]. No study has investigated whether the presence of an indicator affects muscle function during occlusion. This represents a further threat to validity since changes in muscle function may affect the contact properties of the occlusion, in which case the recorded information would not represent what occurs under natural dentition conditions.

This study aimed to determine whether four commonly used indicators (Parkell ribbon, articulating silk, T-Scan and articulating paper) affected neuromuscular function during occlusion.

METHODS

Eighteen healthy subjects (12 male, 6 female, age 27 ± 7 years) performed three trials onto the four indicators (Table 1) and onto their natural dentition. In the first trial they slowly brought their teeth together to form a stable occlusion and then performed a strong bite onto the indicator / their teeth. The second and third trials were maximum clenches held for 3 – 5 seconds. The subjects performed a bite onto cotton rolls between each indicator to give a common staring point in terms of prior proprioception and muscle activation. The order of indicators was randomised between subjects and the indicators were applied by a dental nurse using standard clinical procedures. The same procedure was used for T-Scan as for the remaining three indicators to avoid any differences in neuromuscular function being attributed to the more obtrusive T-Scan mounting system.

Table 1. Indicator thickness.

Indicator	Parkell (PK)	Silk (SK)	T-Scan (TS)	Paper (PA)
Thickness (μm)	24	60	96	202

Note: Measurements were obtained using a Sylvac system (www.sylvac.ch) with accuracy of 0.1 μm.

Surface EMG were recorded bilaterally from the temporalis anterior (TA) and superficial masseter (MS). The filtered and root mean square averaged (50 ms) EMG signals were normalised to the global maximum amplitude recorded across all trials for that subject. Maximum and mean amplitude and mean anterior-posterior coefficient (APC; a measure of the ratio of total masseter to total temporalis activity [4]) were obtained. A questionnaire after each indicator asked the subject to rate each indicator on four parameters (effect on bite, comfort, texture and toughness) on a scale from -3 to +3.

Indicator effects on EMG parameters were assessed using repeated measures ANOVA with Bonferroni post-hoc analysis. Comparisons to natural dentition were conducted using paired samples t-tests. Indicator effects in the questionnaire responses were tested using Freidman. All statistical tests assumed a significance level of $p = 0.05$.

RESULTS AND DISCUSSION

Comparing each indicator to natural dentition, significant differences were obtained for T-Scan in MS maximum amplitude and both T-Scan and articulating paper in mean APC ($p = 0.018$, 0.050 and 0.048 respectively; Figures 1 – 2 and Table 2).

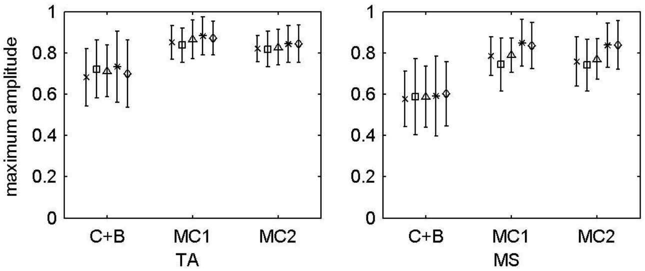

Figure 1: Maximum amplitude of the TA and MS in the contact and bite (C+B) and maximum clenches (MC1 and MC2) for each indicator and natural dentition (see Figure 2 for key).

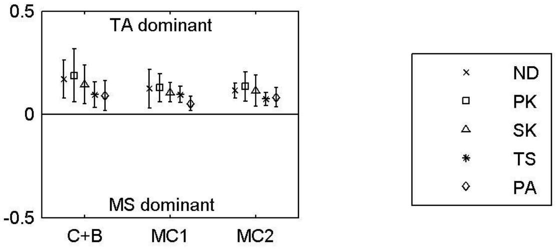

Figure 2: Mean APC in the contact and bite (C+B) and maximum clenches (MC1 and MC2) for each indicator and natural dentition.

The results indicate that the two thickest indicators, T-Scan and articulating paper, give different neuromuscular function during occlusion compared to natural dentition. In comparison, the two thinnest indicators, Parkell and silk ribbon, show no difference to natural dentition. Hence, the thickest indicators may not give a valid recording of the occlusal contacts that occur under natural dentition conditions. Indeed, their neuromuscular response shows some similarity to that reported for clenching onto cotton rolls [4].

There was a significant indicator effect for MS maximum amplitude and mean APC. The T-scan and articulating paper had higher MS amplitude and less TA dominance than the Parkell and silk ribbons (p = 0.026 and 0.013 respectively). A significant indicator effect was also observed in the questionnaire results between the same indicator pairs; T-scan and paper versus Parkell and silk (Table 2).

The similarity in neuromuscular response between T-Scan and paper suggests that it is not only indicator thickness that affects neuromuscular response but also material properties. T-Scan was less than half the thickness of paper and closer to silk in this regard (Table 1). However, it was far more plastic than the other indicators and was also much stiffer in compression, reducing its ability to conform to the occluded surface. It may have been these properties, in combination with thickness that generated the observed response.

CONCLUSIONS

T-Scan and articulating paper significantly influence neuromuscular function during occlusion and therefore may not represent valid means of identifying occlusal contacts that occur under natural dentition conditions. In comparison, Parkell and silk ribbon do not affect neuromuscular function and, in this regard, represent more valid means of identifying occlusal contacts that occur under natural dentition conditions.

REFERENCES

1. Babu RR & Nayar SV, *J Indian Prosthodont Soc* **7**:170-174, 2007.
2. Saracoglu A & Ozpinar B, *J Prosthet Dent* **88**:522-526, 2002.
3. Baba K, et al., *J Prosthet Dent* **83**:83-89, 2000.
4. Ferrario VF, et al., *Man Ther* **12**:372-379, 2007.

ACKNOWLEDGEMENTS

Work funded by grants from the British Society of Occlusal Studies and Mrs Marion E Mundy, Houston, Texas.

Table 2. Significant differences in the EMG parameters and perception questions in the maximum clenches for: (i) indicator versus natural dentition; and (ii) between indicators.

	EMG parameters			Perception questionnaire			
	Max amplitude TA	Max amplitude MS	mean APC	effect on bite	comfort	texture	toughness
(i) Indictor vs ND	-	TS > ND (p = 0.018)	TS,PA < ND (p = 0.049)				
(ii) Between indicators	-	PK,SK < TS,PA (p = 0.026)	PK,SK > TS,PA (p = 0.013)	SK > PA	SK > TS, PA	PK > TS	PK,SK > TS

EVALUATION OF ASYMMETRY IN GROUND REACTION FORCES AND MUSCLE ACTIVITY DURING THE STANCE PHASE OF GAIT IN ASYMPTOMATIC SUBJECTS

[1,2]David R. Burnett, MS, [1,2]Naira H. Campbell-Kyureghyan, PhD, [3]Julia Kar, MS, [3]Peter M. Quesada, PhD
[1]Department of Industrial Engineering; [2]Center for Ergonomics; [3]Department of Mechanical Engineering
University of Louisville
email: drburn02@louisville.edu

INTRODUCTION

Walking is a fundamental and universal activity of daily living for humans [1]. Still, conflicting results have been reported regarding the inherent symmetry or asymmetry of biomechanical gait parameters such as ground reaction force (GRF) and electromyography (EMG) in asymptomatic subjects, perhaps due to unclear definitions or using only a single gait variable [1]. Determining whether biomechanical differences exist between the non-dominant (ND) and dominant (D) sides of the body is critical [2] as gait asymmetry may indicate a potential biomechanical susceptibility toward the development of other joint pathologies. The objective of this study is to quantify symmetry of GRF and EMG variables between the ND and D sides of the body in asymptomatic subjects during the stance phase of gait. The research is specifically aimed at determining ranges of symmetry that can be used as criteria for comparisons of healthy and impaired individuals.

METHODS

8 male and 4 female subjects, with an average age of 23.7 years, participated in the study. In order to be included in the study, subjects could not be experiencing any joint pain which would potentially alter their natural gait. Average (±SD) height and weight of the subjects was 173.1 (±11.6) cm and 75.9 (±18.6) kg, respectively. 11 of the 12 subjects were right-handed. All subjects voluntarily agreed to participate in the study and signed the IRB approved consent form prior to participation.

Subjects walked 10-12 meters at a self selected pace and contacted a force plate (Bertec Corp.) approximately midway through the trial. 3 trials were conducted with the ND foot contacting the force plate, and 3 trials were collected with the D foot contacting the force plate. GRF data was sampled at 1000 Hz and normalized to subjects' height and weight. The peak vertical component of the ground reaction force (VGRF) during heelstrike (HS) and toe-off (TO) was determined. Additionally, EMG activity from 4 bilateral muscle groups: erector spinae (ES), rectus abdominis (RA), rectus femoris (QUAD), and hamstring (HAM) was collected using bipolar, 10 mm surface electrodes (Noraxon, U.S.A. Inc.). Electrode placement and collection of maximum voluntary contractions (MVC) for normalization purposes was conducted according to Cram et al. [3] (Table 1). Raw EMG signals were sampled at 1000 Hz and preamplified (10 MΩ). Post-processing of the EMG signal included a series of 3rd order Butterworth band pass (10-450 Hz) and band stop (58-62 Hz) filters. The EMG signal was normalized to the peak MVC value. RMS amplitude during the stance phase was calculated for each muscle.

A symmetry index (SI) of VGRF and RMS measures was calculated by dividing the value for the ND side by the value for the D side (Table 1) and statistical differences were determined with a paired t-test at an alpha level of 0.05. A value of 1 would indicate perfect symmetry while positive values would indicate a gait pattern that favors the ND side. Acceptable ranges of the SI were determined by taking the mean ± 2 SD. Additionally, intra-subject standard deviations (ISSD) were calculated to assess the reliability of the VGRF and RMS as measures of symmetry.

RESULTS AND DISCUSSIONS

There were no statistical differences between the ND and D peak VGRF values at HS ($p = 0.83$) or TO ($p= 0.17$). The average (± SD) of SI_1 (HS) and SI_2 (TO) were 0.999 (±0.063) and 0.971 (± 0.091), respectively. Thus, the acceptable range of VGRF SI at the commencement and completion of stance phase would be 0.845 – 1.097 and 0.789 – 1.153, respectively (Figure 1). Essentially, neither the ND nor D leg was preferably used with respect to VGRF in asymptomatic subjects, and based on this variable asymptomatic subjects maintain a rather symmetric gait, presumably throughout the entire stance phase. Additionally, the average ISSD for SI_1 and SI_2 were quite small (0.049 & 0.074, respectively) which indicate that the SI for these particular variables is reliable and appropriately used in symmetry analysis of human gait. Utilizing a different formula for SI, Herzog et al. [4] reported similar findings in which normal subjects showed less than 4% deviation from perfect symmetry for a number of gait variables associated with VGRF.

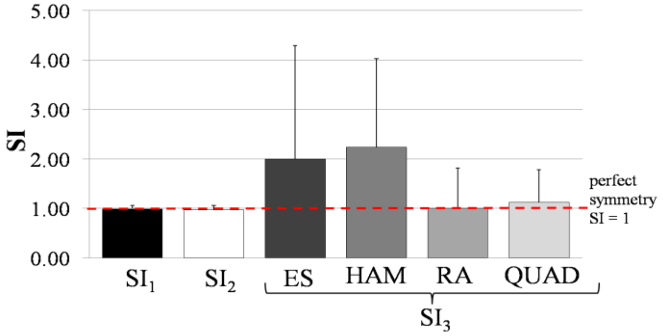

	AVG	SD	Acceptable Range	ISSD	p
SI_1	0.999	0.063	(0.873, 1.125)	0.048	0.83
SI_2	0.971	0.091	(0.789, 1.153)	0.074	0.17
ES	2.000	2.295	(0, 6.590)	0.896	0.98
HAM	2.238	1.794	(0, 5.826)	0.758	*0.01*
RA	1.008	0.808	(0, 2.624)	0.230	0.08
QUAD	1.121	0.659	(0, 2.439)	0.443	0.63

Figure 1: Summary of symmetry evaluation of VGRF (SI_1 & SI_2) and RMS (SI_3)

As can also be seen from Figure 1, the average SI values for the RA and QUAD muscle pairs are approximately equal to 1, indicating symmetry between the ND and D sides of the body. Differences in RMS during stance were not significant ($p > 0.05$), and average ISSD values demonstrate reliability of these measures between subjects. However, ES and HAM average SI values show greater muscle activation of the ND side relative to the D side, with the HAM RMS differences being significant ($p = 0.01$). Still, the increased average ISSD values indicate that intra-subject reliability may be questionable for these parameters. A brief discussion of several previous studies involving EMG analysis of the back and lower extremities during gait may be useful in partially explaining these findings. First, Thorstensson et al. [5] concluded that the main function of the ES is the restriction of unnecessary trunk motion while hamstring activity was greatest during deceleration in the swing phase [6] and thus, may not be as useful for quantifying symmetry during stance as was postulated in the current study. Conversely, a recent study by Sherburne et al. [7] found that the quadriceps were the primary contributors to support and stabilization of the knee during forward propulsion which may explain to some degree the symmetry between the ND and D limbs in the current study.

CONCLUSIONS

Asymptomatic subjects showed high levels of symmetry during stance phase with respect to VGRF at HS and TO. Symmetry between the ND and D QUAD muscles was also found. Acceptable ranges of asymmetry were established, and future research will consider the application of similar methodologies among symptomatic subjects.

REFERENCES

1. Sadeghi H, et al., *Gait and Posture.* **12:**34-45, 2000.
2. Teichtahl AJ, et al., *Arch Phys Med Rehabil.* **90:** 320-324, 2009.
3. Cram JR, et al., *Intr. to sEMG.* 336-369, 1998.
4. Herzog W, et al., *Med. Sci. Sports Exerc.* **21:** 110-114, 1989
5. Thorstensson A, et al., *Acta Physiol Scand.* **116:** 13-20, 1982
6. Dubo HI, et al., *Arch Phys Med Rehab.* **57:** 415-420, 1976
7. Sherburne KB, et al., *J Orth. Res.* **24:** 1983-1990, 2006

Table 1: Description of symmetry indices, electrode placement, and MVC tasks

GRF		EMG			
HS Symmetry Index (SI_1)	**TO Symmetry Index (SI_2)**	**Symmetry Index (SI_3)**	**Muscle**	**Electrode Placement**	**MVC**
$\frac{\text{Peak VGRF}_{\text{ND, HS}}}{\text{Peak VGRF}_{\text{D, HS}}}$	$\frac{\text{Peak VGRF}_{\text{ND, TO}}}{\text{Peak VGRF}_{\text{D, TO}}}$	$\frac{\text{RMS}_{\text{ND, stance}}}{\text{RMS}_{\text{D, stance}}}$	**RA**	3 cm apart, 2 cm lateral from the umbiculus over the muscle belly	resisted torso flexion
			ES	Parallel to the spine, 2 cm apart, 2 cm from the spine over the muscle mass	resisted torso extension
			QUAD	2 cm apart, approx. half the distance between the knee and iliac spine	resisted knee extension
			HAM	3 cm apart, approx. half the distance from the gluteal fold to the back of the leg	resisted knee flexion

SPECIFICITY IN THE STRENGTH AND POWER PROFILES OF ELITE ATHLETES

[1] Steph Forrester and [2]Matt Pain
[1]STI, Loughborough University, UK; [2]SSES, Loughborough University, UK
email: s.forrester@lboro.ac.uk; web: www.sports-technology.com.

INTRODUCTION

The strength and power requirements to optimize athletic performance are sport-specific. Previous studies comparing the strength and power characteristics of athletes from different sports have generally focused on single isolated movements, e.g. 1 RM squat, bench press, maximum jump height [1]. The subject-specific nature of the strength – speed relationship [2] indicates that care is required when extrapolating single measurements to more realistic conditions. Nevertheless, assessing how well adapted the strength – speed relationship of an athlete is to the specific demands of their sport may have implications in talent identification and athlete development.

This study aimed to determine whether there are significant differences in the strength – speed and power – speed profiles of five elite athletes from different sports. This was based on measurements of maximum voluntary torque over a range of speeds for knee and hip, extension and flexion. A further aim was to qualitatively assess how well their profiles matched sport-specific demands.

METHODS

Five elite male athletes (Table 1) gave informed consent in accordance with the Loughborough University ethics board. Maximal effort contractions were conducted on a Cybex NORM dynamometer. Measurements were taken for extension and flexion of the knee and hip. For each joint action five isometric trials and eight eccentric-concentric trials covering the range of velocities 50° to 400° s^{-1} were performed using an existing protocol [3]. Maximum torque for each isometric trial and maximum isovelocity torque for each eccentric and concentric velocity were obtained from the dynamometer data.

A seven parameter strength model, which included the effects of involuntary neural inhibition, was fitted to the maximum torque – velocity data for each joint [3]. To assess whether there were significant differences between these subject-specific strength models, the root mean square (RMS) difference between the model and experimental torque – velocity data was computed based on: (i) the subject's model; and (ii) each of the other subjects' models. This was done for both absolute and normalised torque values (normalised to maximum isometric torque) to allow differences in the shape of the curves to be differentiated from those due purely to absolute strength. The RMS differences were compared using one-sided independent samples t-tests with significance set at $p = 0.05$.

Table 1. Characteristics of the five elite athletes

Subject	Sport	Age	Height (m)	Mass (kg)
TJ	Triple jump	22	1.82	72.6
HJ	High jump	24	1.89	81.9
TC	Track cycling	25	1.83	86.0
GY	Gymnastics	19	1.78	78.5
KA	Karate	30	1.75	89.3

RESULTS AND DISCUSSION

The strength and power characteristics indicated qualitative and statistically significant differences between athletes (Figure 1 and Table 2). In every case, based on both absolute and normalized torques, the fit of the experimental data to an athletes' own model was significantly better than the fit to any of the others. These results support previous observations [2] on the subject-specific nature of the strength – speed and power – speed relationships.

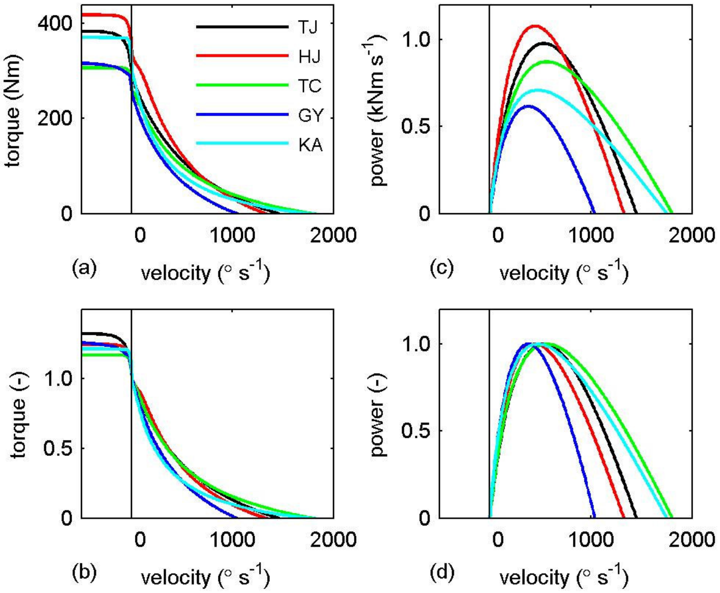

Figure 1: Knee extension results for the five elite athletes: (a) maximum voluntary torque – velocity; (b) normalised torque – velocity; (c) power – velocity; and (d) normalised (to the peak value) power – velocity.

Examining the results in more detail, a number of trends in the data that qualitatively support the profiles to reflect the sport-specific demands for each athlete can be identified (Table 2):

- HJ, TJ and GY require eccentric extensor strength for landing (high T_{ecc}/T_o; I).
- TC requires concentric speed and strength and is in one of few sports that actively focuses on knee flexion (low ω_c/ω_{max}, high ω_{max} and high $\omega(P_{max})$; II, III and V).
- GY does not require high absolute (lower body) strength or speed (low ω_{max}, low P_{max}, low $\omega(P_{max})$; III, IV and V).
- KA requires speed and the maintenance of power at high velocitie rather than pure strength and kicking is a predominately unloaded action (low ω_c/ω_{max}, and high ω_{max} ; II and III).

It would be of interest to assess to what degree the subject-specific nature of these strength and power curves are genetic and to what degree they are trainable. Such a differentiation would suggest whether strength and power measurements have a stronger role in talent identification (genetic) or athlete development (trainable). Differentiation is not possible from the present results, and a longitudinal study would be required to provide such insight.

CONCLUSIONS

The strength and power characteristics of the knee and hip extensors and flexors for five elite athletes from different sports were all significantly different. Furthermore, these differences generally reflected the specific demands of their sports. This held for both absolute and normalised strength and power values, and indicated measurable differences in the expressed torque – velocity curves between athletes. The role of such measures in talent identification and athlete development requires further investigation.

REFERENCES

1. Izquierdo M, et al. *Eur J Appl Physiol* **87**, 264-271, 2002.
2. Baker D, et al., *Eur J Appl Physiol* **104**, 350-355, 1994.
3. Yeadon MR, et al., *J Biomech* **39**, 476-482. 2006.

Table 2. Key parameters describing the strength model for the five elite athletes.

Subject	Knee Extension					Knee Flexion					Hip Extension					Hip Flexion				
	I	II	III	IV	V	I	II	III	IV	V	I	II	III	IV	V	I	II	III	IV	V
TJ	**1.28**	0.46	25.3	0.98	9.3	1.25	0.42	24.6	0.84	8.8	1.25	*0.50*	*18.2*	1.08	*6.8*	1.20	0.30	*18.0*	0.36	5.9
HJ	1.24	0.32	23.1	**1.08**	7.8	*1.10*	**0.24**	*18.0*	*0.36*	*5.6*	1.17	**0.16**	32.1	0.62	8.7	1.39	0.34	**23.4**	0.68	**7.8**
TC	*1.17*	0.24	**31.5**	0.87	**9.8**	**1.28**	*0.50*	**36.0**	**1.24**	**13.3**	*1.12*	0.40	34.0	**1.78**	**12**	**1.40**	0.45	*18.0*	0.39	6.4
GY	**1.28**	*0.50*	*18.1*	*0.62*	*6.6*	1.26	0.37	*18.0*	0.37	6.3	**1.37**	*0.50*	19.1	*0.50*	7.0	*1.15*	**0.16**	*18.0*	*0.22*	*4.8*
KA	1.22	**0.16**	30.5	0.71	8.3	1.23	0.33	30.1	0.61	10.1	1.36	**0.16**	**36.0**	1.02	9.8	1.18	*0.50*	20.6	**0.72**	7.6

I. T_{ecc}/T_o (-) ratio of maximum voluntary eccentric to maximum voluntary isometric torque; II. ω_c/ω_{max} (-) curvature of the concentric hyperbola, range from 0.15 (high) to 0.5 (low); III. ω_{max} (rad s^{-1}) maximum angular velocity; IV. P_{max} (kW) maximum power; V. $\omega(P_{max})$ (rad s^{-1}) angular velocity at maximum power.

CONTROL OF SUBMAXIMAL CENTER OF PRESSURE MOVEMENTS IN HEALTHY WOMEN: EFFECTS OF AGE AND MOVEMENT TYPE

[1] Manuel Hernandez, [1,2,4]James Ashton-Miller and [3,4,5]Neil Alexander
[1]Department of Biomedical Engineering, [2]Department of Mechanical Engineering, [3]Department of Internal Medicine, Division of Geriatric Medicine, [4]Institute of Gerontology, University of Michigan; [5]VA Ann Arbor Health Care System Geriatric Research, Education and Clinical Center, Ann Arbor, Michigan. email: manueleh@umich.edu

INTRODUCTION

Movement of the center of pressure (COP) is commonly used by the central nervous system to control the location of the whole body center of mass during upright stance. As indicated by standing postural sway, COP movements increase with age [1]. Volitional movements of the COP have been recently studied in young adults [2]. However, little is known about the speed-accuracy trade-off characteristics of COP movements of older adults during bipedal stance.

In this study, the effects of target size and movement type were assessed separately to explore their relative interaction with age, leading to the following hypotheses: First, (H1) in comparison to young adults, healthy older adults will exhibit an increase in COP movement time, number of submovements, and ratio of peak-to-average COP velocity, across all speed-accuracy tasks. Second, (H2) in comparison to reciprocal movements, discrete movements will lead to increased movement time, number of submovements, and ratio of peak-to-average COP velocity.

METHODS

Subjects. Healthy young (mean±SD, age 23±3, N = 13) and healthy older females (age 76±6, N=12) were recruited from the local community. Young women were taller (164±6 cm versus 159±5 cm), but did not differ in weight, body mass index, or foot length.

Protocol. While standing on a force platform, subjects performed accuracy-constrained COP movements 'as fast and as accurately as possible' with a fixed movement amplitude (6 cm) and varying target size (2, 3, and 4 cm). Participants performed two movement types as prompted by an auditory cue: 1) *discrete trials*, moving their COP to the target and then in the alternate direction upon cuing; or 2) *reciprocal trials*, participants leaned their body back-and-forth for 30 sec. Data was

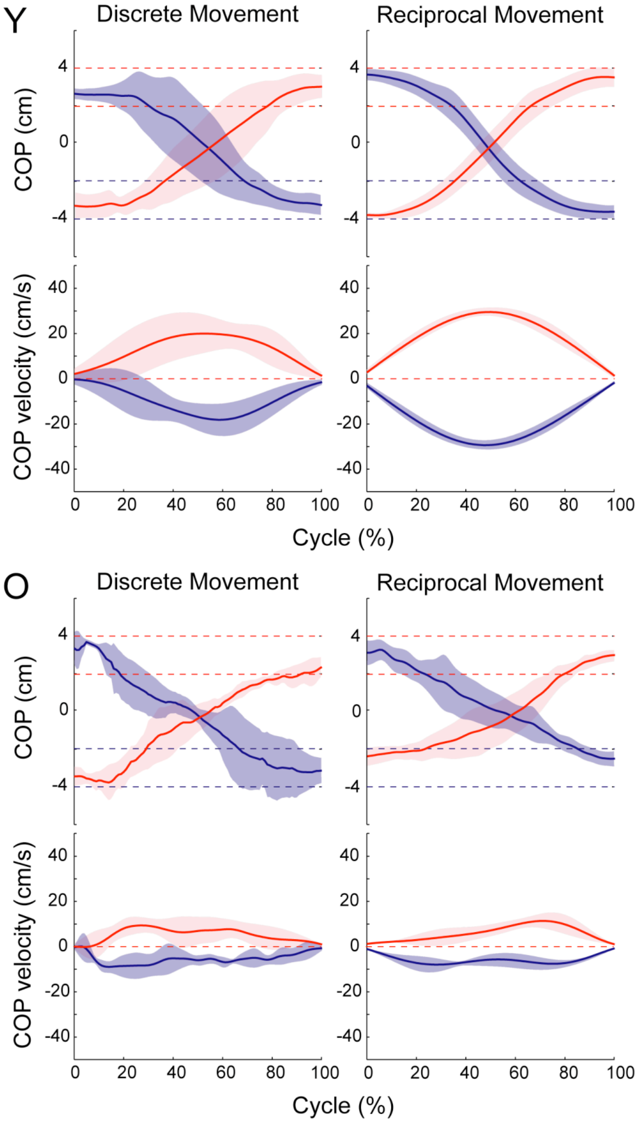

Figure 1: COP position and velocity data illustrating the mean (solid line) and standard deviation (shaded area) of anterior (red) and posterior (blue) movements. Y: Young; O: Old.

collected over three separate test sessions, but to minimize practice effects only data from the final visit are presented below.

Data Analysis. Repeated measures analysis of variance was used to examine the effect of age, movement type (i.e., reciprocal vs. discrete), and target size, as well as their interactions. To examine group or within-subject differences, post-hoc tests were carried out using Hochberg's step-up method to correct for multiple comparisons. P < 0.05 was considered statistically significant. Similar trends in movement type and target size were observed in anterior and posterior movements, so COP characteristics from both movement directions were combined for each age group.

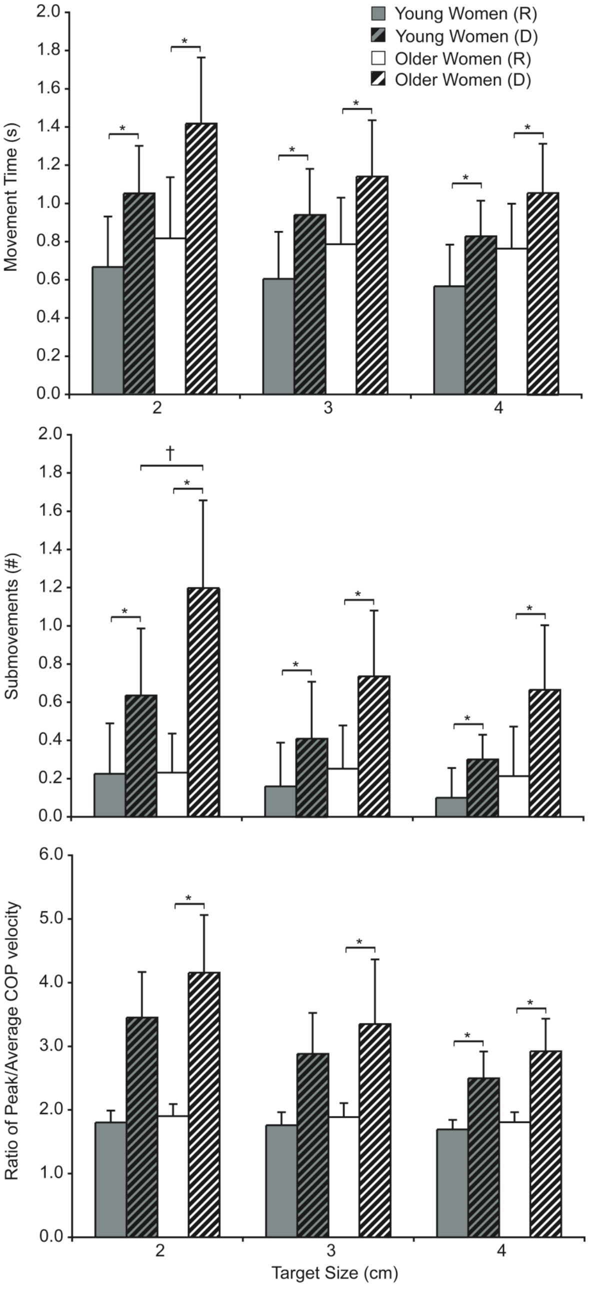

Figure 2: Influence of target size and movement type (reciprocal (R) or discrete (D)) on mean (SD) movement time, number of submovements, and ratio of peak over average COP velocity. Hochman's step-up post hoc test results for age and movement type are designated by † and *, respectively (p < .003).

RESULTS AND DISCUSSION

Exemplar movements are seen in Figure 1 for young and older women. Overall, older women had longer movement times (p < .05), more submovements (p < .005), and a higher ratio of peak-to-average COP velocity (p < .05) than young women under all conditions (Figure 2), consistent with a significant role of neuromotor noise in determining movement time and submovements [3].

Compared to reciprocal movements, discrete movements resulted in increased COP movement time, number of submovements, and ratio of peak-to-average velocity (Figure 2), consistent with previous studies [4]. A decrease in target size affected all outcomes during discrete, but not during reciprocal, trials (p<0.05). Compared to young, older women had a disproportionate increase in discrete COP submovements (age x movement type, p < .01).

CONCLUSIONS

When required to move their COP accurately, older adults, when compared to young, move more slowly and less smoothly, particularly in a discrete movement task.

REFERENCES

1. Prieto TE, et al. *IEEE Trans Biomed Eng* **43**, 956-966, 1996.
2. Duarte M, Freitas SM. *Motor Control* **9**, 180-196, 2005.
3. Meyer DE, et al. *Psychol Rev*, **95**, 340-370,1988.
4. Smits-Engelsman BC, et al. *Exp Brain Res* **145**, 222-230, 2002.

ACKNOWLEDGEMENTS

We thank members of the Mobility Research Center for their assistance with recruitment and data collection. We are grateful to the National Institutes of Health for their support of this project (NRSA Grant Number 1 F31 AG024689-01).

BARRIER CLEARANCE IN THE 3000M STEEPLECHASE

Sarah Ingebretsen, Iain Hunter, Ruthann Cunningham, & Jenny Willis

Brigham Young University, Provo, UT
E-mail: iain_hunter@byu.edu Web: biomech.byu.edu

INTRODUCTION

The steeplechase is a 3000 meter track race consisting of 28 barriers and 7 barriers followed by a water pit. The water pit is 3.66m long. Each lap the runners hurdle four barriers followed by a water jump. Barrier heights for men are 0.914m (36 in) and barrier heights for women are 0.762m (30in).

One of the goals for steeplechase athletes is to minimize the loss of running speed while hurdling the barriers. Many coaches believe this can be accomplished by accelerating during the approach and minimizing jump height while still safely clearing the barrier [1]. Men should take off between 1.2 and 1.5 meters before the barrier. The landing should be around 1 meter past the barrier [2]. These values differ for women due in part to slower running speeds and lower barrier heights [3]. It has also been suggested that body clearance of 3 to 6 cm, keeping the lead leg slightly bent and leaning forward with the trunk at the point of hurdle clearance will help decrease time spent over the hurdle [1].

Previous studies have looked at speed but not body positioning in steeplechase hurdling. For the water jump, accelerating during the approach to the barrier resulting in a relatively long landing distance helps maintain race pace [3]. As the steeplechase race progresses, men and women hurdle the barriers with greater step lengths and speeds while race pace remains the same [3].

In order to effectively coach steeplechase hurdling, the optimal body positioning and movement must be determined. This study investigated how barrier clearance related to the percent loss of horizontal velocity during steeplechase hurdling between men and women. Other characteristics of technique were measured to help explain barrier clearance findings.

METHODS

Two Canon Elura 60 digital video cameras were placed around the third barrier at the 2007 USA Track and Field Nationals men's and women's steeplechase finals. A survey pole calibration was performed to obtain three-dimensional body positioning for every lap of the top 8 finishers. We were unable to digitize every lap due to other athletes or photographers blocking camera views. However, a total of 20 jumps for the women and 33 for the men were analyzed. Barrier clearance was defined as the height of the center of mass relative to barrier height when the athlete was at the high point of the jump. Two linear regressions were performed (one each gender) of clearance height relative to the percent loss of velocity from the penultimate step to the first step after landing.

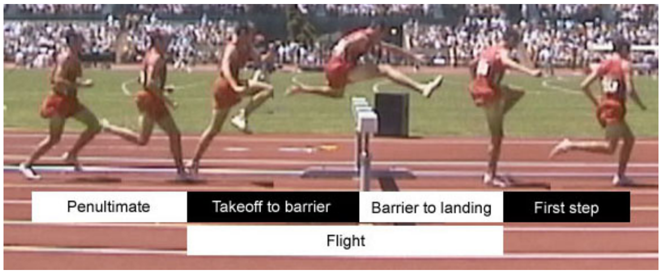

Figure 1: Step definitions.

RESULTS AND DISCUSSION

Barrier clearance was closely related to the percent of velocity lost among men ($R^2 = 0.57$, $p < 0.01$), but not among women ($R^2 = 0.08$, $p < 0.25$) (Figure 2).

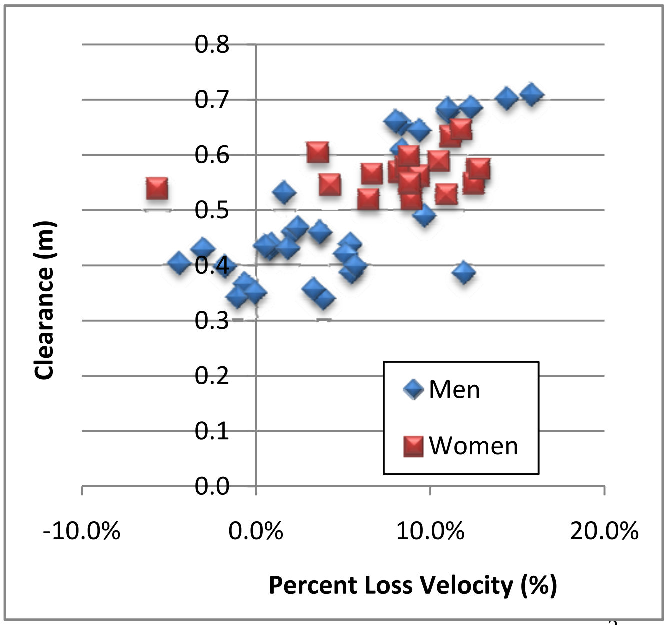

Figure 2: Results of the regression analyses ($R^2 = 0.57$, $p < 0.01$ for men; $R^2 = 0.08$, $p < 0.25$ for women).

Men jump higher, relative to the ground, but have a lower clearance, due to the greater barrier height. During the take-off, horizontal kinetic energy is partly transferred into vertical kinetic energy. Greater jump heights require more horizontal energy to be transferred, resulting in a greater loss of horizontal velocity.

To help minimize the need to jump higher, the vertical separation between the hip and knee of the trail leg when the center of mass is at its peak height is less among men (0.25m for men, 0.32m for women, $p<0.01$).

Women can safely clear the barrier without the need to jump as high off the ground as men do since the barriers are 0.152 m (6 in) lower. Figure 2 shows a small range of clearance heights among women, which shows there are other factors relating to the percent loss of velocity. When considering characteristics such as: take-off and landing distance, hip and knee angles, and heights of trail and lead legs, the high variability made any meaningful conclusions difficult to make.

When coaching steeplechase athletes, it is imortant to take into consideration the differences between men and women. In order to minimize loss of running speed, men should be taught to minimize clearance height. This can be accomplished by leveling out their trail leg when it is directly above the hurdle. This will bring the trail leg closer to the height of the center of mass, minimizing hurdle clearance. More research needs to be done in order to determine what causes women to lose speed over the hurdles.

SUMMARY/CONCLUSIONS

Men lose horizontal velocity when they hurdle with a greater clearance. So, they must work on movement patterns and takeoff distances that will help minimize hurdle clearance. However, a similar relationship was not observed among women. There are other factors not measured in this study that relate to what leads to lost velocity among women. This study only focused on velocity. The effect of various techniques on economy must also be considered as coaches and athletes modify technique.

REFERENCES

1. Popov T. *Modern Athlete & Coach* **21**, 17-18, 1983.
2. Griak R. *Track & Field Q Rev* **82**, 41, 1982.
3. Hunter I. *J Sport Sci & Med* **5**, 318-322, 2006.

ACKNOWLEDGEMENTS

Thank you to USA Track and Field for funding part of this study.

THE EFFICACY OF STABILITY BALL ACCOMMODATION TRAINING ON TRUNK POSTURE, MUSCLE ACTIVATION LEVELS AND DISCOMFORT RATINGS DURING SEATED OFFICE WORK

Jennie Jackson, Diane Gregory, Priyanka Banerjee, Jack P. Callaghan
University of Waterloo, Waterloo, Ontario, Canada
e-mail: ja2jacks@uwaterloo.ca

INTRODUCTION

Dynamic or 'active' sitting involving frequent postural adjustments has been proposed to be beneficial if prolonged muscle loading is avoided and periodic rest occurs in muscle fibres to prevent fatigue [1,2]. Further, active sitting may benefit spinal tissues if compression magnitude is varied by the dynamic movements such that nourishment occurs of both muscles [3] and the intervertebral disc (IVD) itself [4]. Sitting on a stability ball chair may promote dynamic sitting. Previous studies did not find favourable changes in muscle activity levels or spinal postures as compared to sitting on an office chair [5,6], however, neither study examined the effect of an accommodation training period for ball sitting, as per manufacturer recommendation.

The purpose of this study was to determine the impact of an accommodation protocol on postural, muscle activation and comfort reporting variables in males and females sitting on a stability ball. The secondary purpose of the study was to determine whether a gender effect was evident in postural, muscle activation and comfort reporting variables.

METHODS

Twelve subjects (6 males and 6 females) performed a two hour standardized typing and mousing task while sitting on a stability ball (Evolution Chair™, Posture Perfect Solutions Ltd., North Vancouver, British Columbia, Canada). The task was repeated after a nine day break during which half the subjects followed an accommodation training protocol while the other half had no exposure to stability ball sitting. The accommodation training involved a gradual increase in the amount of time spent working on the ball each day (Table 1). Muscle activation levels and spine angles were collected in 14 minute blocks throughout the task and discomfort ratings were taken after each block.

Table 1: Posture Perfect Solutions Accommodation Training Schedule

Day	Duration on Stability Ball
1	15 min
2	20 min
3	30 min
4	40 min
5	1 hour
6	1 hour 15 min
7	1 hour 30 min
8	1 hour 45 min
9	2 hours

Surface EMG was collected bilaterally from: external oblique (EO), internal oblique (IO), thoracic erector spinae (TES) and, lumbar erector spinae (LES). For each of the 8 muscles and all 8 of the 14 minute working blocks from the two hour work exposure average EMG, probability of rest and the total number and length of EMG gaps were calculated. Amplitude probability distribution function (APDF) [1] analyses were utilized to determine the probability of a muscle being at rest (defined as 0% MVC activation) during each block.

Trunk and upper arm motion data were recorded using active markers and Optotrak Certus position sensors (Northern Digital Inc., Waterloo, Ontario, Canada). Single markers were placed on bony landmarks at the distal end of the 2nd metacarpal, ulnar styloid process, lateral epicondyle, glenohumeral joint and tragus on the right body side to permit the calculation of sagittal plane joint angles. Rigid fins with three non-collinear markers were applied to the skin above the spinous process of vertebrae C7, T12 and atop the sacrum to facilitate the calculation of three-dimensional lumbar and thoracic trunk angles. Changes in spinal flexion posture were determined using a shifts analysis [7] and the time spent in different postures was determined from APDF analyses.

Perceived discomfort ratings recorded on a visual analog scale (VAS) were measured on the following body areas: upper back, lower back, buttocks, and for overall discomfort.

RESULTS

A significant four-way interaction ($p < 0.05$) was found between gender, group, day and block for discomfort ratings of the upper back, lower back, buttocks and overall discomfort. All variables demonstrated the same interaction patterns: both control and experimental groups showed decreased discomfort on day two, but the magnitude in decrease differed between the groups. The final piece of the interaction was the opposite pattern in gender response for VAS score changes between days by group – where accommodation group females demonstrated larger decreases in scores between days, in males, control group subjects demonstrated this pattern. Discomfort scores from the lower back are presented in Figure 1 by group and gender.

No significant changes were found in muscle activation levels between days for either the control or the experimental group. Muscle activity levels during the seated work tasks were low: average ES EMG across 1 hour work task 2.4 – 5.0% MVC (individual subject range, 0.4% to 13.9 % MVC) and average abdominal EMG 2.0 – 3.2% MVC (individual range 0.5 to 8.3% MVC).

The mean lumbar flexion posture adopted across the two hour working period did not change significantly between days for either the control, 59.6% maximum flexion angle ($Flex_{max}$) and 58.7% $Flex_{max}$ respectively, or experimental group participants, 55.2% $Flex_{max}$ and 56.7% $Flex_{max}$, respectively. Further, no differences were found in trunk postures between genders, nor were interactions found at any level.

Two significant interactions independent of the accommodation training were found which showed differences between male and female oblique EMG amplitude response. Most notably, females showed a continuous increase in left side EO EMG amplitude across the two hour sitting task, while males showed relatively constant EO activation amplitudes.

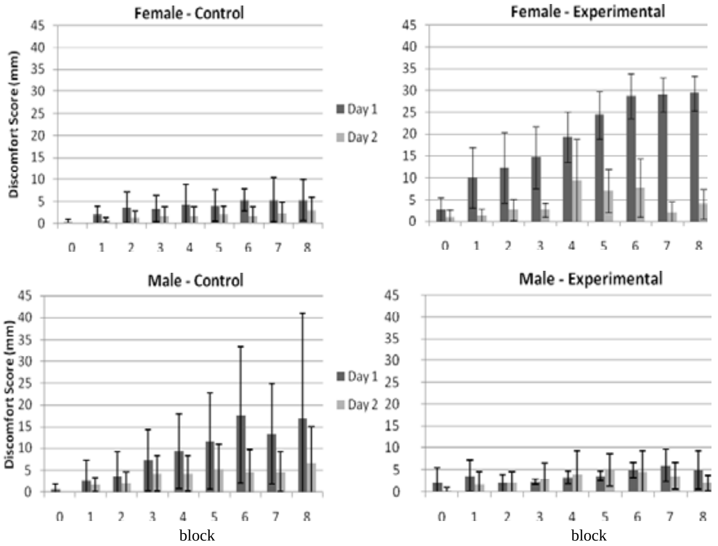

Figure 1: Low back discomfort scores

DISCUSSION

No significant changes were found in any of the biomechanical variables considered, namely, muscle activity, number of EMG gaps, mean posture or the number of postural shifts, indicating that the accommodation training was ineffective in modulating postural or muscle activation variables.

A significant four-way interaction between experimental group, gender, day and block was found for all reported discomfort variables and further investigation showed female accommodation group subjects demonstrated a considerable decrease in discomfort scores following the training, but males showed no change.

ACKNOWLEDGEMENTS

This study was funded, in part, by Posture Perfect Solutions Ltd. (North Vancouver, British Columbia, Canada)

REFERENCES

1.Jonsson B. *Electroencephalogr Clin Neurophysiol Suppl* **34**, 417-28, 1978.
2. Veiersted, KB et al. *Int Arch Occup Environ Health* **62**, 31-41, 1990.
3. Visser, B. *JEK* **16**, 1-16, 2006.
4. Holm, S et al. *Spine* **8**, 866-874, 1983.
5. Gregory, DE et al. *Hum Fac* **48**, 142-153, 2006.
6. Kingma, I et al. *Appl Ergon* **40**, 199-205, 2009.
7. Gregory, DE et al. *Gait Posture* **28**, 86-92, 2008.

USING FORWARD DYNAMIC SIMULATIONS OF HIGH SPEED RUNNING TO ASSESS HAMSTRING STRAIN INJURY POTENTIAL

Elizabeth S. Chumanov[1], Bryan C. Heiderscheit[2], and Darryl G. Thelen[1]

[1]Department of Mechanical Engineering, University of Wisconsin-Madison Madison, WI
[2]Department of Orthopedics and Rehabilitation, University of Wisconsin-Madison Madison, WI
E-mail: easchmerr@wisc.edu Web: http://www.engr.wisc.edu/groups/nmbl/

INTRODUCTION

The hamstrings are the most commonly injured muscle among athletes, with injuries tending to occur during high speed running [1]. However, the phase of the gait cycle when injury actually occurs is still debated. It is plausible that injury may occur during late swing when the hamstrings are active, stretched and decelerating the limb [2, 3]. Alternatively, others have speculated that contact forces during early stance may overload the hamstrings and give rise to injury [4, 5]. A more recent study suggested that the hamstrings may be susceptible to injury when undergoing a lengthening contraction during late stance [6].

Our objective for this study was to use forward dynamic simulations to systematically investigate the influence of speed on hamstring kinetics during the stance and swing phases of high speed running. We tested the hypothesis that 1) peak hamstring loads during swing would exceed those during stance at maximal running speeds 2) negative work done by the lengthening hamstrings would increase with speed, and primarily be done during swing phase.

METHODS

Ten athletes (age 20-34 yrs) participated, each capable of sprinting at speeds in excess of 7.0 m/s (2 females) or 8.0 m/s (8 males). Each subject ran at speeds ranging from 80-100% of maximum on a high-speed instrumented treadmill that monitored 3D ground reactions (2000Hz). An optical motion capture system was used to record whole body kinematics (200Hz), and surface electromyography was used to measure lower extremity muscle activities (2000Hz). A 14 segment, 31 degree of freedom (DOF) linked-segment model was first scaled to each subject, and then used to compute joint kinematic trajectories from the measured motion. Fifty-two musculotendon actuators (26 on each limb) crossing the hip and knee were included in the model, with each actuator represented by a Hill-type lumped parameter model [2]. Computed muscle control was then used to derive excitations that drove the model to closely track measured sagittal hip and knee angles (Fig. 1). Other DOF's followed prescribed trajectories. Hamstring musculotendon force, power and work quantities were then extracted from the simulations. A repeated measures ANOVA was used to evaluate the influence of speed and phase on these measures.

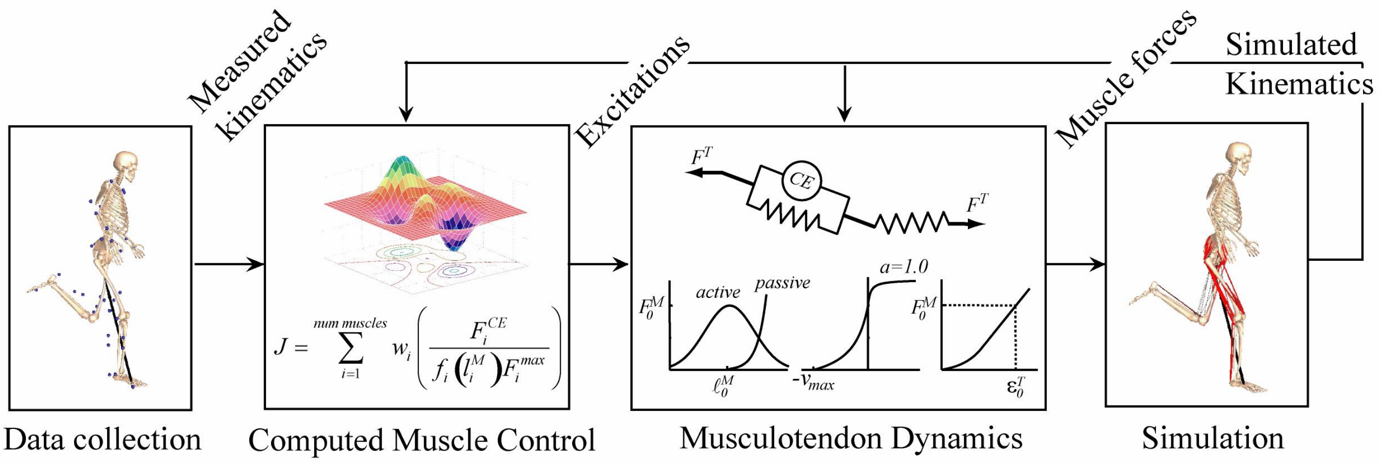

Figure 1. A brief summary of the methodology to go from experimental kinematic data (3D motion and 3D forces) to a muscle actuated simulation that predicts muscle forces and powers.

RESULTS

Table 1. Peak biceps femoris long head forces (N/kg) and net musculotendon work.

	Sprinting Speed		
	80%	90%	100%
$^+$*Peak force (N/kg)*			
Stance phase	12.1	11.8	11.6
*Swing phase	10.3	11.8	11.9
$^+$*Work (J/kg)*			
*Net positive work	0.36	0.38	0.43
*Net negative work	0.31	0.36	0.46

*Indicates significant speed effect

$^+$Indicates speed by gait cycle phase interaction

The simulations closely replicated the experimental kinematics when the hamstrings were active; with average RMS tracking errors of 2º and 3º at the hip and knee, respectively. Computed hamstring excitations were also consistent with the timing of measured EMG activities. Hamstring loading exhibited distinct peaks during late swing and early stance (Fig. 2). A significant speed by phase interaction was found for peak hamstring forces ($p<0.001$), with the peak forces during swing phase increased significantly with speed while those during stance remained consistent (Table 1). Negative work was performed by the hamstrings only during swing, with most of it done between 70 and 90% of the gait cycle (Fig. 2). Positive work was done by the hamstring musculotendons from late swing throughout all of stance. Negative work increased significantly with speed, and exceeded the positive work done by the hamstrings at the fastest speed (Table 1).

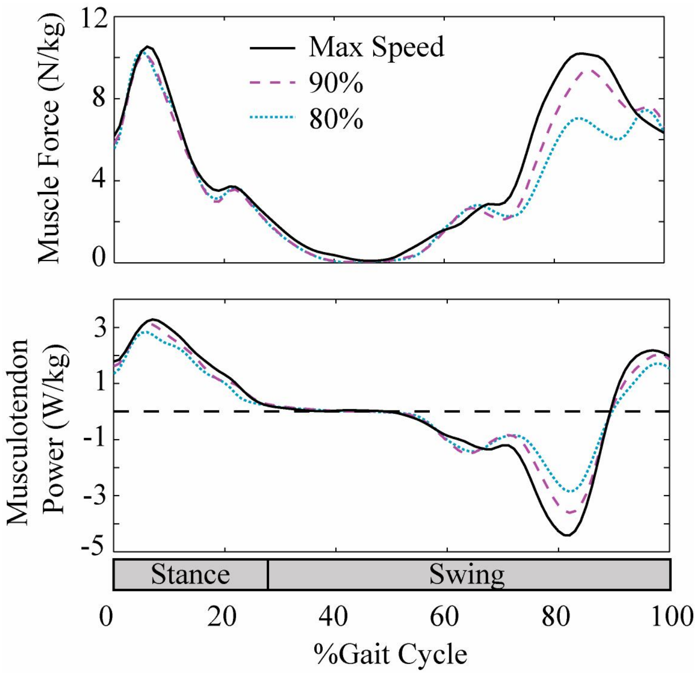

Figure 2. Biceps femoris long head muscle force and musculotendon power throughout the sprinting gait cycle.

DISCUSSION

Muscle injuries are linked with active lengthening contractions [7], with the degree of injury associated the magnitude of negative work done by a maximally activated muscle [8]. Our results suggest that the hamstring musculotendons are substantially loaded during both the stance and late swing phases of high speed running. However, the hamstrings are only lengthening during swing phase, such that the negative work done at the musculotendon level is constrained to this phase. While it is possible for muscle fibers to lengthen when the musculotendon is shortening [9], we do not see evidence of lengthening at the musculotendon level during stance [6]. We conclude that the biomechanical demands placed on the hamstrings during the late swing phase of sprinting appear most consistent with acute musculotendon injury mechanisms.

REFERENCES

1. Gabbe, B. J., et al. *Br J Sport Med*, **39**, 106-110, 2005.
2. Chumanov, E., et al. *J Biomech*, **40**, 3555-3562, 2007.
3. Jonhagen, S., M. O. Ericson, et al. *Scan J Med Sci Sports*, **6**, 15-21, 1996.
4. Mann, R. and Hagy. J *Am J Sports Med*, **8**, 345-350, 1980.
5. Orchard, J. and T. M. Best *Clinical J Sport Med*, **12**, 3-5, 2002.
6. Yu, B, et al. *J Biomech*, **41**, 3121-3126, 2008.
7. Lieber, R. L. and J. Friden. *J Phy Med Rehab*, **81**(11 Suppl), S70-9, 2002.
8. Brooks, S.V., et.al. *J Appl Phys*, **91**, 661-666, 2001.
9. Fukunaga, T., et al. *Ex Sport Sci Rev*, **30**, 106-110, 2002.

ACKNOWLEDGEMENTS

We acknowledge support from AAUW, NIH AR 56201 and NFL Charities.

FORCE MEASUREMENT DURING ICE HOCKEY FORWARD SKATING

[1]TJ Stidwill, [1]David Pearsall, [1]Phil Dixon, [1]René Turcotte
[1] Department of Kinesiology and Physical Education, McGill University, Montreal, Quebec, Canada
E-mail: rene.turcotte@mcgill.ca, web: http://icehockeyscience.mcgill.ca

INTRODUCTION

Given the technical challenges of measuring force during ice skating, not much is known of the dynamics involved with this unique form of locomotion. Previously, the group of Lamontagne, Gagnon, and Doré completed the only known studies attempting to directly determine forces on-ice specifically for ice hockey skating [1,2]. In addition to sophisticated 3D measures to determine skate orientation, they demonstrated the feasibility of using strain gauge transducers attached to the blade of a hockey skate to estimate forces while performing a parallel stop. No information of this kind has been obtained using modern skate designs. Thus, the aim of this study was to build an accurate, practical, and portable instrumented system to enable the measurement of forces during ice hockey skating while maintaining the integrity of the skate's construction.

METHODS

The system consisted of three strain gauge sets affixed to an ice hockey skate's blade holder with wire leads connected to a microprocessor controlled data acquisition device carried in a backpack worn by the skater (<1 kg). The recorded signals indicated the compressive and/or tensile deformation of the skate blade holder between the skate boot and skate blade (Figure 1).

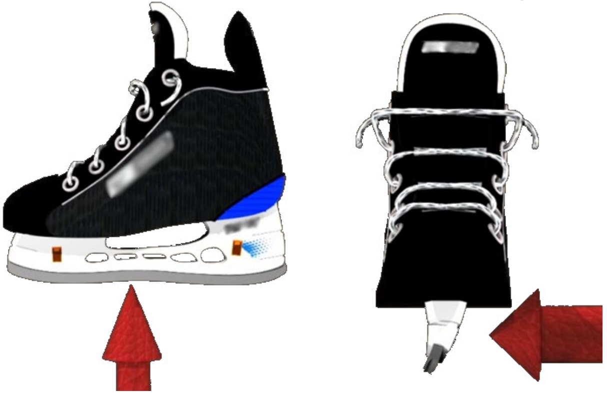

Figure 1 – Exaggeration of deformation caused by vertical loading (left) and deformation caused by lateral loading (right).

One gauge was used to measure the vertical strain (V), and was oriented along the longitudinal axis (transverse plane) of the blade holder's beam element. Two pairs of gauges were used to measure medial-lateral (ML) strain and were oriented parallel to the vertical axis of the blade holder along the front and back posts. Given the complex geometric configuration of the nylon blade holder as well as varied junctions with different materials (i.e. metal blade below, epoxy foot plate above), an extensive dynamic validation process was conducted of both the V and ML strain to force relationships by loading in three orthogonal directions against a force plate.

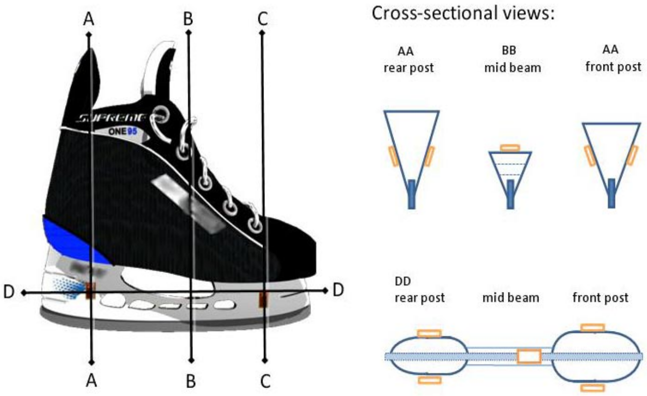

Figure 2 – Strain gauge placement.

V force calibration was performed by having a subject wearing an instrumented hockey skate step onto the force plate with varied loads and rates. Three vertical loading rates were assessed: 280 N/s, 850 N/s, and 3000 N/s, with 30 separate trials of loads ranging from 0 to 850 N (the equivalent of one body weight). The testing of strain gauge response to forces in the ML plane was performed by placing the skate blade longitudinally along the force plate with the medial/lateral side of the skate facing downwards, followed by downward loads ranging from 0 to 400 N (approximately one half body weight). Lastly, to demonstrate the practical feasibility of using this system in the cold environment of an ice arena, an experienced skater performed several trials of forward skating on ice.

RESULTS AND DISCUSSION

The configuration of the strain gauges simultaneously determined the V and ML force components experienced by the blade holder, up to a theoretical maximum of 7440 N, with a resolution accuracy of 1.9 N and an RMS error of ± 68 N (coefficient of variation = 9.2). The V loading tests yielded correlations of the voltage reading (strain gauge) to force (measured on the force plate) for slow, medium and fast loading rates ranging from r = 0.94 to 0.99. V loadings showed a minimal (less than 40 N) response in the ML gauges (i.e. minimal false or cross-talk signals). Correlations for ML loading tests ranged from r = 0.95 to 0.99. ML loading tests showed a small response in the V gauge (less than 40 N). The current configuration of strain gauges has also been shown to be able to determine simultaneously and independently the V and/or ML force components experienced by the blade holder. In order to demonstrate the functional usefulness of the measurement system, a subject performed a forward skating task on ice with the right skate instrumented.

Figure 3 shows force-time curves of the total force (summation of V and ML), as well as V and ML component forces for a representative skating trial on-ice of the right skate (note: for conceptual display the left skate forces were approximated by replicating the right skate's data, offset temporally by 50%). Descriptive parameters from these force-time patterns can be obtained; for examples, contact time, stride time, and force maximums. In this sample trial shown, clear dynamic differences are evident between step order, with a transition from short duration (0.31 s), single force peaks (200 % BW) in the 3rd step to longer duration (0.38 s), and bimodal force peaks (120 and 180 % BW) by the 6th step. This pattern was consistently recorded, with trial-to-trial coefficient of variation ranging between 3.9 and 12.5 for steps 2 through 6 in peak force and coefficient of variation ranging between 2.8 and 10.0 in contact time estimates for each respective step.

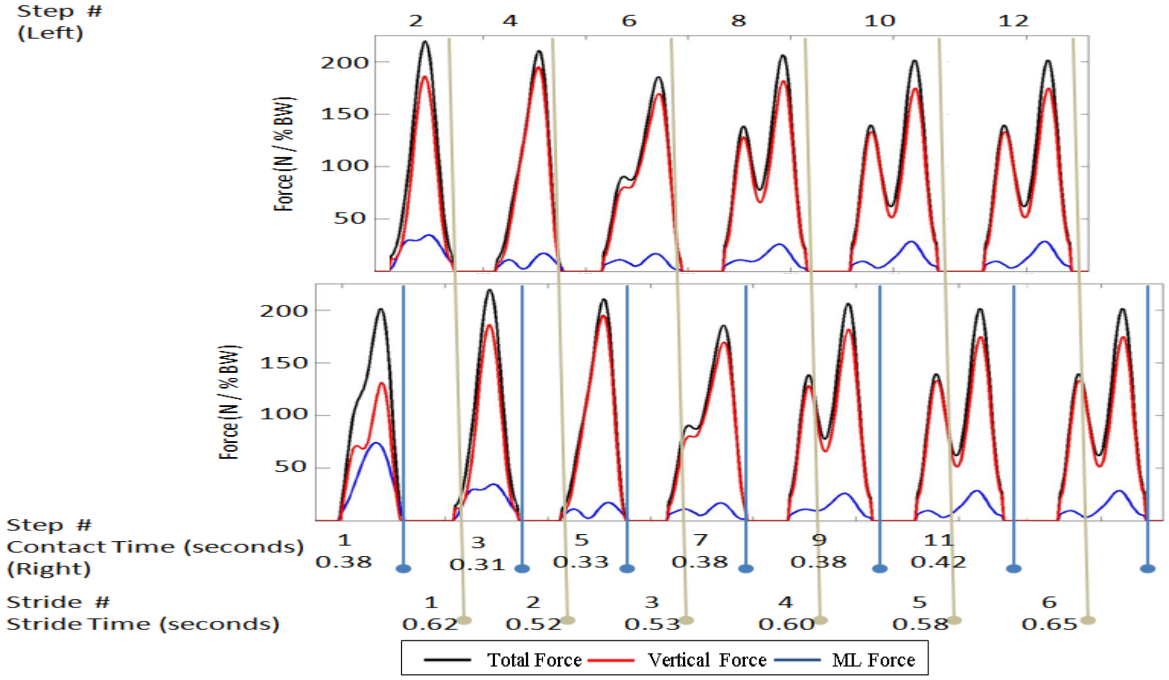

Figure 3 – Representative trial of a subject; right skate (bottom) and approximated left skate (top) force-time profiles, as well as contact time and stride time information.

CONCLUSION

With conventional skate models, it is possible to use strain gauges to estimate both vertical and transverse forces in real time and on-ice. The practicality and accuracy of this testing approach has many applications, such as a quantitative tool for skating power assessment to aid athletes and coaches.

ACKNOWLEDGEMENT

The authors would like to thank Bauer Hockey Inc. for their significant financial and in-kind contributions to the study, and NSERC for their support.

REFERENCES

1. Gagnon, M, et al. *Research Q for exercise and sport* 54(2) 136-143, 1983.
2. Lamontagne, M, et al. *Cdn J of Sport Sciences* **6(3)**, 169-183, 1983.

LONGITUDINAL SEX DIFFERENCES IN KNEE ABDUCTION IN YOUNG ATHLETES

[1,2]Kevin R. Ford, [2]Robert Shapiro, [1]Gregory D. Myer, [3]Antonie J. van den Bogert
and [1,2]Timothy E. Hewett
[1]Cincinnati Children's Hospital, [2]University of Kentucky and [3]Cleveland Clinic
email: kevin.ford@cchmc.org, web: http://cincinnatichildrens.org/sportsmed/

INTRODUCTION

Neuromuscular risk factors likely underlie the higher rate of anterior cruciate ligament (ACL) injuries in female compared to male athletes. Specifically, altered movement patterns, such as dynamic knee abduction (valgus), may increase ACL injury risk in female athletes [1,2] Increases in these neuromuscular risk factors may coincide with rapid adolescent growth that leads to divergent levels of neuromuscular control between sexes [3]. Hence, the adolescent pubertal growth spurt may be the optimal phase of growth and development to investigate related sex differences in ACL injury risk.

The primary purpose of this study was to determine if the specific timed onset of neuromuscular risk factors related to abnormal movement patterns increased in females, but not males, during the adolescent growth spurt. We hypothesized that during adolescent growth, pubertal females would demonstrate longitudinal increases in knee abduction moments and motion compared to pubertal males. We also hypothesized that following the adolescent growth spurt, post-pubertal females would have significantly greater knee abduction moments and motion compared to post-pubertal males.

METHODS

Using a nested cohort design (total sample = female n=709; male n=250), a subset of 315 subjects met the inclusion criteria for this study (based on 2 consecutive year samples and maturational status). Subjects were classified into two separate maturational groups: pubertal female (PF) n = 145, pubertal male (PM) n = 37, post-pubertal female (PPF) n = 120, post-pubertal male (PPM) n = 13. Each subject participated in two testing sessions approximately one year apart (mean 365.7 ± 14.7 days). Three trials of a drop vertical jump (DVJ) were collected from a 31 cm box. They were instructed to drop directly down off the box and

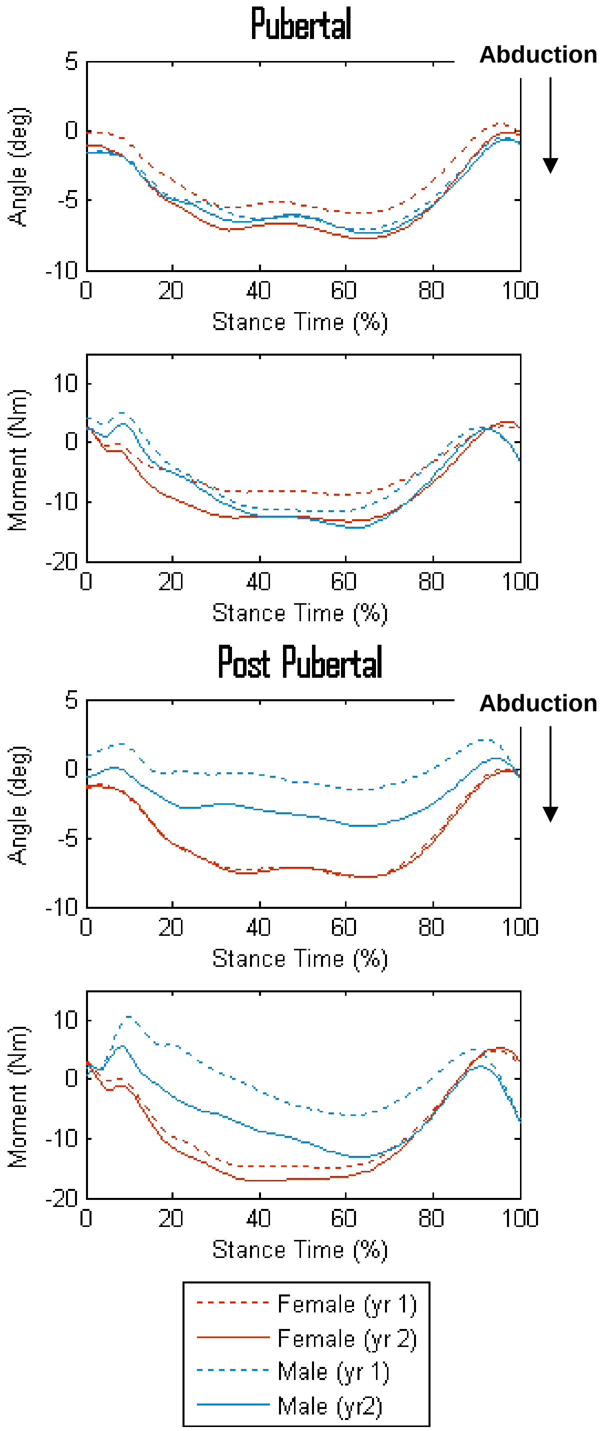

Figure 1: Knee abduction angle and moment for pubertal (top two plots) and post-pubertal athletes during stance phase.

immediately perform a maximum vertical jump, raising both arms, jumping for a basketball rebound. 3D knee joint angles were calculated according to the cardan rotation sequence (i.e. flexion/extension, abduction-adduction and internal-external rotation). Kinematic data were combined with force data to calculate knee joint moments using inverse dynamics. Maximum abduction angle and external moments were calculated during the DVJ deceleration phase. Two between group independent variables of sex (female, male) and maturation level (pubertal, post-pubertal), in addition to the within subject independent variable (year 1, year 2), were analyzed in a 2X2X2 ANOVA. An $\alpha \leq 0.05$ was used to indicate statistical significance.

RESULTS AND DISCUSSION

The mean difference in stature between the two testing years was 4.8±2.4 cm in PF and 6.6±2.8 cm in PM compared to 1.0±2.6 cm and 1.6±2.2 cm in PPF and PPM, respectively. This indicates that the pubertal group experienced rapid adolescent growth. There was a significant three-way interaction with peak knee abduction angle (p=0.029, Table 1, Figure 1). Post hoc analyses identified a significant longitudinal increase in peak abduction angle in PF (p<0.001), but no change in PM (p=0.90). PPF had significantly greater overall peak abduction angle following adolescent growth compared to PPM (female -9.3±5.7°; male -3.6±4.6°; p<0.001). Peak knee abduction moment increased from the first year to the second year in all subjects (main effect of year p<0.001). A two-way interaction between sex and maturation group was identified (p=0.013). Post-hoc analysis indicated that PPF had significantly greater peak knee abduction moment compared to PPM (female:-21.9±13.5 Nm; male:-13.0±12.0 Nm; p=0.017). Sex differences in knee abduction moment were not observed in pubertal subjects (p>0.05). Similar results were found with body-mass normalized knee abduction moments. PPF landed with significantly greater normalized knee abduction moment compared to males (female -0.37 ± 0.23 Nm/kg; male -0.18 ± 0.16 Nm; p = 0.002).

CONCLUSIONS

This study identified, through longitudinal analyses, that knee abduction angle was significantly increased in pubertal females during rapid adolescent growth compared to males. In addition, knee abduction motion and moments were significantly greater for consecutive years in young female athletes, following rapid adolescent growth, compared to males. A puberty and sex interaction was found with greater knee abduction moment in PF compared to PPF. In contrast, knee abduction moment was significantly lower in PM compared to PPM. The combination of longitudinal, sex and maturational group differences indicate that early puberty appears to be a critical phase related to the divergence of increased ACL injury risk factors. Injury prevention programs that focus on neuromuscular training may be beneficial to help address the development of ACL injury risk factors that occur in female athletes during maturation.

REFERENCES

1. Hewett TE, et al. *Am J Sports Med.* **33**, 492-501, 2005.
2. Griffin LY, et al. *Am J Sports Med.* **34**,1512-1532, 2006.
3. Hewett TE, et al. *J Bone Joint Surg Am.* **86-A**, 1601-1608, 2004.

ACKNOWLEDGEMENTS

This work was supported by NIH/NIAMS
Grant R01-AR049735.

Table 1: Mean (±SD) peak knee abduction angle and moment for pubertal and post-pubertal subjects.

		Pubertal		**Post-Pubertal**	
Variable	**Test Session**	**Female**	**Male**	**Female**	**Male**
Knee Abduction Angle (deg) [a,b]	Year 1	-7.7 ± 6.1	-8.2 ± 5.8	-9.3 ± 5.7	-2.6 ± 4.4
	Year 2	-9.3 ± 6.2	-8.3 ± 6.2	-9.4 ± 5.6	-4.6 ± 4.8
Knee Abduction Moment (Nm)[b]	Year 1	-14.4 ± 10.9	-16.4 ± 12.3	-20.6 ± 13.7	-9.6 ± 9.4
	Year 2	-19.2 ± 12.1	-19.4 ± 15.0	-23.2 ± 13.4	-16.3 ± 14.7

[a]Denotes interaction of year, sex, maturation, [b]Denotes interaction of sex and maturation. (p<0.05)

FINITE ELEMENT ANALYSIS BASED DESIGN OPTIMIZATION FOR PROSTHETIC SOCKET

[1]Fan Gao, [2]Zhigang Wang and [2]Xin Lei

[1]Department of Allied Health Sciences, University of Texas Southwestern Medical Center, Dallas, TX USA
[2]BioCAX LLC., 1411 Chirsta CT, Sewickley, PA USA
E-mail: fangao2000@gmail.com, wang@biocax.com, lei@biocax.com

INTRODUCTION

Historically, the design and fabrication of a prosthetic socket are done manually by prosthetists. The entire process is usually subject to the prosthetist's experience and expertise. Inconsistencies during measurement and rectification significantly impact the patient's satisfaction of the final product. Prosthetic socket serves as a human-device interface between the residual limb and the prosthesis and its function and comfort are of the most important design considerations. Functionally, the socket transmits load from the human body to the prosthesis, maintains stability of the prosthesis on the residual limb and delivers sufficient control over the prosthesis when the amputee stands and walks. Prosthetic socket design is essential for the performance of the prosthesis.

Recently with the introduction of hand-held laser scanning, integration of CAD with rapid prototyping (RP) the socket design and fabrication process can be dramatically expedited with high precision. In addition, finite element analysis (FEA) has been shown to be a powerful tool in studying the interface stress distribution, which is highly associated with patient's comfort. Based on anatomical structures either pressure-tolerant or pressure-relief zone can be identified and consequently rectification of the socket profile that is guided by optimizing the interface pressure distribution is preferred. FEA can simulate the stress distribution of the limb-socket system with reasonable accuracy and the numerical result matched well with experimental data. The objective of this study is to propose a new prosthetic design methodology, which integrates the patient-specific FEA and multiple-objective optimization algorithm to achieve optimal prosthetic socket design based on quantified stress metrics.

METHODS

The anatomical structure of the residual limb is subject-dependent and hence a custom socket design is desired. The transverse scans of the stump will be obtained using either CT or MRI. The image slices can be merged into a 3D model consisting of bone, muscles and skin. Mechanical properties of the tissues can be obtained from laboratory test using indentation method or from previous publication. The model will be pre-processed and meshed for finite element analysis. FEA simulation will predict the pressure distribution and identify the pressure concentration especially around the pressure-relief zone on the interface (Figure 1).

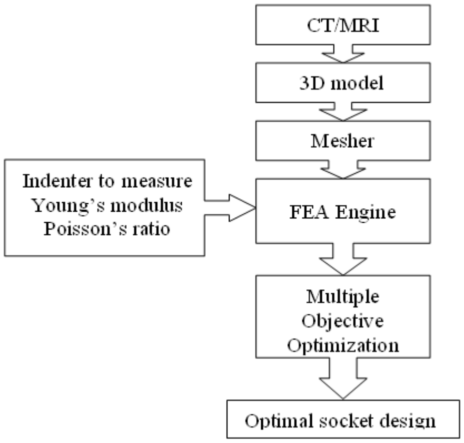

Figure 1. Flow of socket design optimization

The prosthetic socket design process is formulated as a multi-objective optimization problem (MOOP). We propose a cost function system to capture the socket design performance metrics allowing an automatic optimization. It is based on the clinical data and FEA simulation of the stump-socket system. The cost function consists of the following quantitative factors: pressure on pressure-relief areas (based on pain tolerance pressure threshold), pressure gradient on pressure-relief areas, shear stress on stump surface, pressure on the inner surface of distal bone and soft tissue and displacement of distal bone.

In the process of conventional manual rectification the PR areas on the prosthetic socket will be shaved off to relieve pain and intrusion will be added around PT areas for the purpose of load-bearing. The shape modification is simulated using second order smooth B-spline functions. The prosthetic socket design space is defined by the geometrical neutral surface which exactly reflects the stump shape and variances of characteristic PT/PR areas. The 3D geometrical neutral surface is extracted from the CT/MRI. The PT/PR areas of the specific patient are determined based on the anatomical characteristics and eight PT/PR areas' are identified as independent design variables: anterior lateral surface, patella tendon, popoliteal fossa, calf muscle, tibia crest, tibia end, fibular head and fibular end.

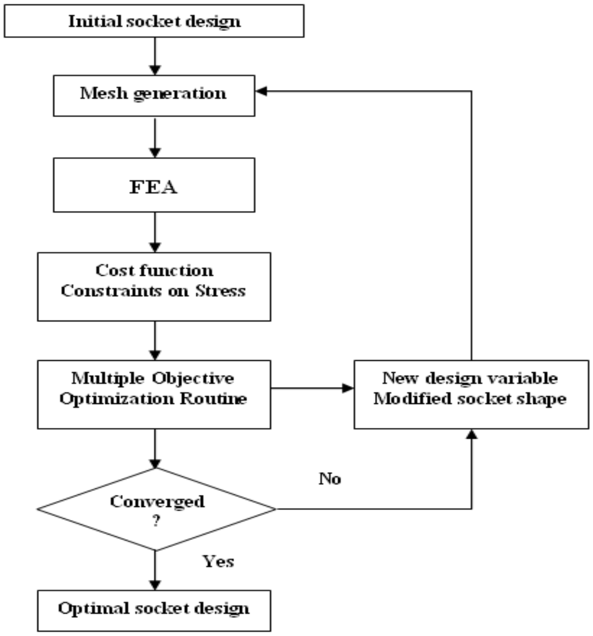

Figure 2 Design optimization flow

As shown in Figure 2, the optimization flow begins with an initial socket design that is a 100% match on the stump geometry but yet an optimal one. The socket is first meshed to 3D FEA mesh for simulation and then the stress distribution of the limb-socket system is used to evaluate the cost function for optimization routine. Many non-linear multiple optimization algorithms can be selected to generate the next design parameter set for optimization iteration. The optimal socket design will be achieved as soon as the cost function converges. Among these, conjugated gradient method, BFGS and Powell-Brent method will be good candidates for optimization due to computational efficiency. The disadvantage is, however, that they can be easily trapped into the local minimum. To overcome this, global optimization method, like genetic algorithm and simulated annealing, could be used. Their performance is superior but the cost is usually high. In each optimization iteration significant amount of calculation including meshing and FEA is involved therefore a balance between optimum and performance should be pursued. The final step of optimal socket design is to export the STL/IGES file to CAM system for rapid prototyping and experimental data will be used to evaluate the performance of the automated design.

RESULTS and DISCUSSION

The comfort level of a prosthesis user is directly linked to the mechanical interactions between the residual limb and the prosthetic socket. Among many, the stresses at the interfaces, e.g. the socket-limb interface and the bone-tissue interface, are the most critical factors that are served as either design objectives or constraints during socket optimization. However, such interfacial information is complex since multiple parts, i.e., bones, muscles, skin, liner and socket, are involved. They have different structural characteristics such as shapes, mechanical behaviors and frictional properties, which often change with different loading conditions. Although finite element analysis has proven to be a powerful tool to reveal the distribution of pressure and shear stress at the socket-limb and bone-tissue system, it is still a challenge to integrate finite element analysis into a patient-specific optimization due to a high demand in computational resources. However, with the rapid development in information technology, the seemingly costly computation can now be handled easily even using a home-based desktop PC. We believe the success of implementing the proposed optimal design will dramatically increase the productivity of prosthetists and comfort for patients.

REFERENCES

1. Fuh, J.Y.H. et al. *Proceedings of Advanced Manufacturing Technology for Medical Applications*, 207-226 2006.
2. Linder-Ganz, E., et al., *Ann Biomed Eng*, **37**(2), 387-400, 2009
3. Portnoy, S., et al., *Ann Biomed Eng*, **35**, 120-135, 2007
4. Marler, R. *Structural and Multidisciplinary Optimization*, **26**(2) 369-395, Apr.1996
5. Nocedal, J. et al., "*Numerical Optimization*" 1999, 194-202

VISUAL FEEDBACK CONTROL OF BODY POSITION IS IMPAIRED BY INTENSIVE JUMPING

Erika Zemková, Dušan Hamar
Faculty of Physical Education and Sport, Comenius University, Bratislava, Slovakia
email: zemkova@yahoo.com, web: http://www.fsport.uniba.sk

INTRODUCTION

The study evaluates the effect of maximal rebound jumps on a sensorimotor task based on visual feedback control of body position.

METHODS

A group of 14 PE students (age 23.7 ± 2.6 y, height 178.6 ± 9.2 cm, and weight 70.6 ± 11.4 kg) had to hit the target randomly appearing in one of the corners of the screen by horizontal shifting of COM in appropriate direction prior to and after each of six 60-seconds maximal jumps (Figure 1, 2). Each test consisted of 60 responses. Time, distance, and velocity of COP trajectory between stimulus appearance and its hit by visually guided COM movement on the screen were registered by means of the system FiTRO Sway Check based on dynamometric platform (Figure 3). During serial jumps the power in the concentric phase of take off was registered using the PC based system FiTRO Jumper. Its calculation is based on contact and flight times measured by the contact mattress with accuracy of 1 ms.

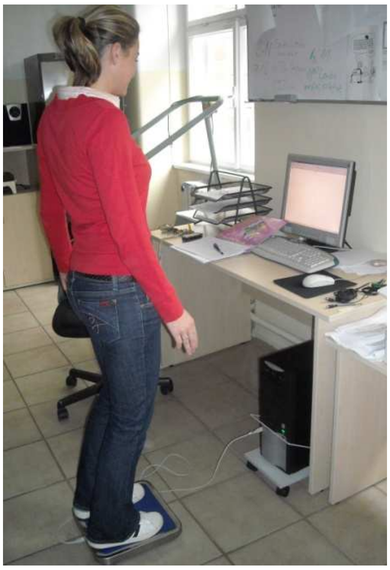

Figure 1: Diagnostic system FiTRO Sway Check (www.fitronic.sk)

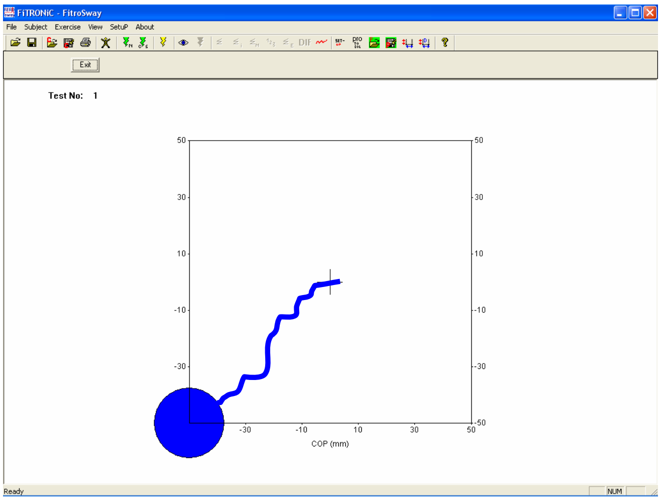

Figure 2: On-line display of task execution

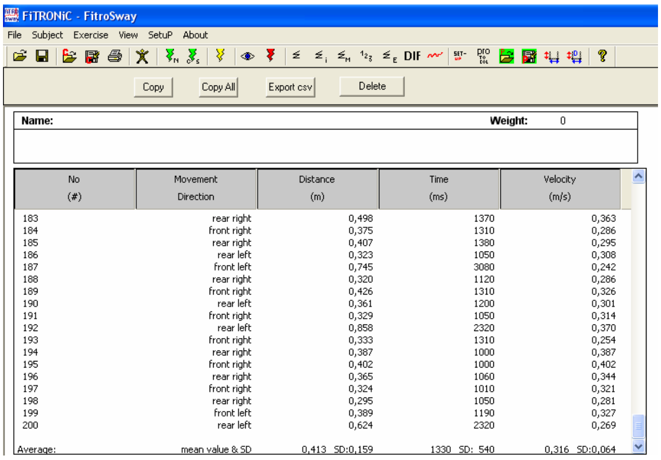

Name:

Weight: 0

No (#)	Movement Direction	Distance (m)	Time (ms)	Velocity (m/s)
183	rear right	0,498	1370	0,363
184	front right	0,375	1310	0,286
185	rear right	0,407	1380	0,295
186	rear left	0,323	1050	0,308
187	front left	0,745	3080	0,242
188	rear right	0,320	1120	0,286
189	front right	0,426	1310	0,326
190	rear left	0,361	1200	0,301
191	front right	0,329	1050	0,314
192	rear left	0,858	2320	0,370
193	front right	0,333	1310	0,254
194	rear right	0,387	1000	0,387
195	front right	0,402	1000	0,402
196	rear right	0,365	1060	0,344
197	front right	0,324	1010	0,321
198	rear right	0,295	1050	0,281
199	front left	0,389	1190	0,327
200	rear left	0,624	2320	0,269
Average:	mean value & SD	0,413 SD:0,159	1330 SD: 540	0,316 SD:0,064

Figure 3: Summary report of sensorimotor parameters

RESULTS AND DISCUSSION

Results showed (Figure 4) that after jumping (about 110 jumps in each set) mean response time significantly ($p \leq 0.05$) increased from an initial value of 1616 ± 506 ms to 1825 ± 562 ms after 4th set with no further increase toward 6th set. Similarly, mean distance of COP covered during response time increased significantly ($p \leq 0.05$) from pre-exercise values of 0.449 ± 0.298 m to 0.550 ± 0.295 m after 4th set and followed by plateau toward 6th set. On the other hand, no significant change in mean COP velocity was detected.

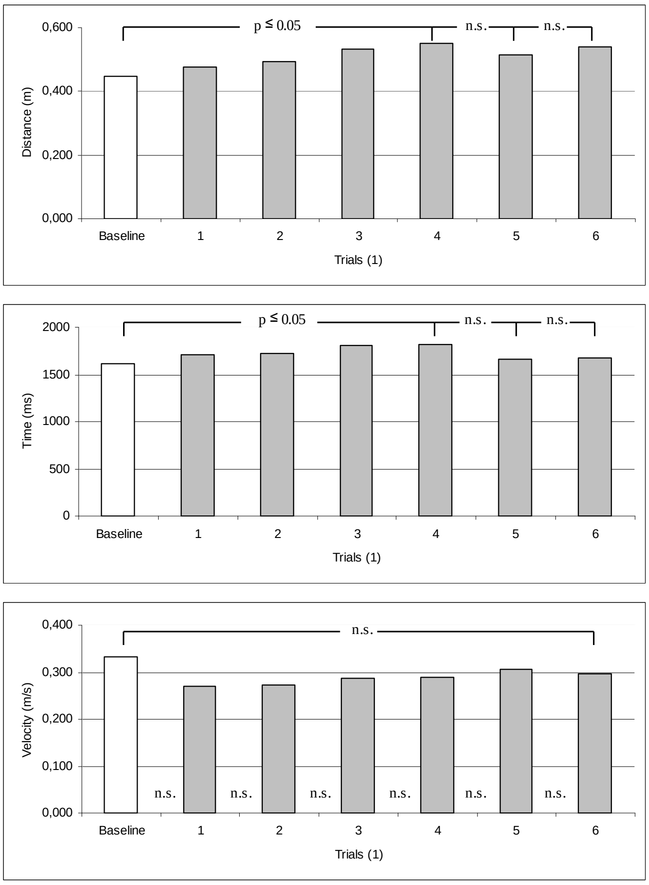

Figure 4: Distance, response time, and velocity of COP trajectory prior to and after each of six 60-seconds maximal jumps

Theoretically the impairment of sensorimotor parameters after maximal rebound jumps may be attributed to a deterioration of both the motor and the sensory function. Involvement of impairment of the motor side may be assumed from decrease in the power in the concentric phase of take off (from the first to last series of jumps by 10.3 % in an initial and by 5.3% in the last 5 seconds of jumping). However, such an assumption is questioned by results of studies providing no correlations between postural sway amplitude and ankle joint pronator muscle strength [1] and maximum inversion and eversion moments [2]. On the other hand, a fatigue induced delay in rate of force development has been associated with an increase in unilateral postural sway amplitude [3]. So one has to admit that this mechanism played a role in the deterioration of visually-guided sensorimotor task. It is also possible that the sensory system was affected, namely at the peripheral level through a change in the spindle excitation threshold of the fatigued muscles. Muscle fatigue induces a depression in the spindle afferent fibers discharge, possibly due to a decrease in the γ-motoneurone activation. The gamma system is known to facilitate the alpha motoneurons that control slow-twitch fibres. Assuming by correlation between the activity of soleus muscle and the COP displacement [4], these fibres are involved in control of body position. However, besides impairment of muscle spindles function also decreased sensitivity of joint receptors and cutaneous mechanoreceptors on the sole due to their intensive stimulation during jumping may be taken in account. Resulting partial reduction of afferent impulses utilized in proprioceptive feedback of body control might also contribute to less precise perception of COM position and regulation its movement. However, this effect was observed only from 1st to 4th set of 60-seconds jumping, after which no further increase in response time and distance of COP movement occurred. This finding may be explained by lower susceptibility of already impaired proprioceptors to further mechanical stimulation in the final 2 sets of jumping. A further reduction of proprioceptive acuity in fatigued legs might be also compensated for by alternative sensory inputs from different body segments, namely trunk and upper-leg muscles.

CONCLUSION

Intensive repeated jumping negatively affects visual feedback control of body position. However, after reaching some level of deterioration of proprioceptive function, there is no further impairment of sensorimotor parameters.

REFERENCES

1. Tropp H. *Int J Sports Med*, **7**, 291-4, 1986.
2. Lentell GL, Katzman LL, Walters MR. *J Orthop Sports Phys Ther*, **11**, 605-11, 1990.
3. Lundin TM, Feuerbach JW, Grabiner MD. *J Appl Biomech*, **9**, 191-201, 1993.
4. Nardone A, Tarantola J, Galante M, Schieppati M. *Arch Phys Med Rehabil*, **79**, 920-4, 1998.

ACKNOWLEDGEMENT

This study was supported through a Scientific Grant Agency of the Ministry of Education of Slovak Republic and the Slovak Academy of Sciences (No. 1/4504/07).

THE ASSOCIATIONS BETWEEN BIOMECHANICAL IMPAIRMENTS AND HAND FUNCTION IN PEOPLE WITH RHEUMATOID ARTHRITIS

Nancy A. Baker, and Joan C. Rogers
University of Pittsburgh, email: nab36@pitt.edu

INTRODUCTION

People with rheumatoid arthritis (RA) often experience significant limitations in hand function such as buttoning buttons and handling coins. RA is a form of polyarticular synovitis which can cause fixed structural deformities of the wrist, hand, and fingers, such as volar subluxation of the carpal bones on the radius, metacarpophalangeal joint ulnar deviation, metacarpophalangeal palmar subluxation, and swan neck deformities [1] (Figure 1). These deformities can lead to pain, stiffness, and restricted movement in the affected joints.

Healthcare professionals frequently measure biomechanical deficits, such as range of motion (ROM), grip strength, and dexterity as a method of quantifying hand function limitations. This study examined the association between biomechanical outcomes (ROM, grip, and dexterity) and functional hand use.

METHODS

45 people with RA were recruited from the University of Pittsburgh Medical Center (UPMC) Arthritis Network Disease Registry. Subjects had to have a primary diagnosis of RA, be between 18 and 65 years old, and report some limitations in hand use. Participants completed two hand performance tests: The Arthritis Hand Function Test (AHFT) [2] and the Keitel Hand Function Index (KHFI) [3].

Instruments: The AHFT measures both biomechanical outcomes and hand tasks. It consists of pure and applied tasks: 2 pure biomechanical outcomes (grip and 9-hole peg test), 4 bilateral applied dexterity tasks (lacing shoe, buttons, cutting “meat,” and manipulating coins) and 2 bilateral applied strength tasks (lifting cans and pouring water). The KHFI consists of 11 performance test items that measure active ROM of the thumb, fingers, wrists, forearms and elbows.

In addition to measuring performance, visible structural deformities were identified and listed by a Certified Hand Therapist. From these a total number of hand problems score was developed.

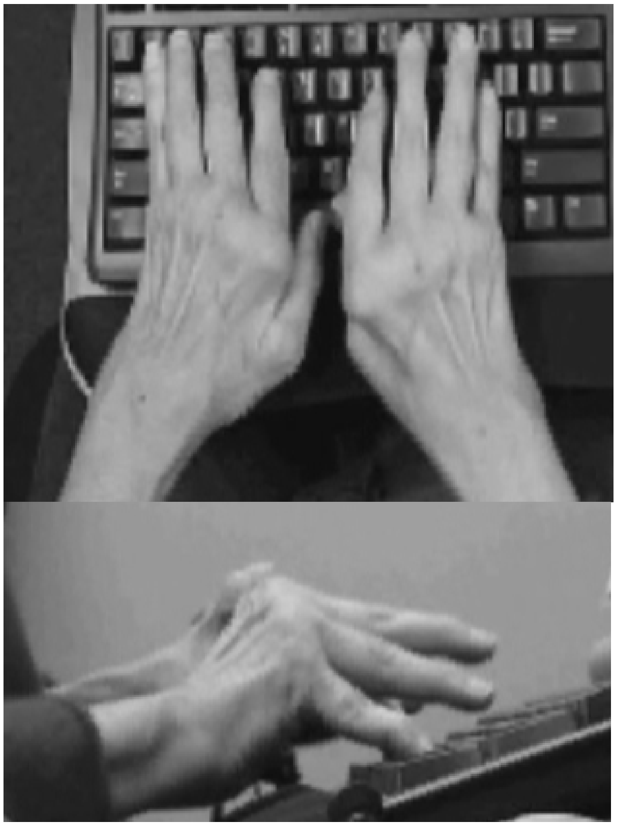

Figure 1: Examples of structural deformities of the hands in RA. A – metacarpophalangeal joint ulnar deviation; B – volar subluxation of the carpal bones on the radius, metacarpophalangeal palmar subluxation, swan neck deformities (R 3rd and 5th digits).

Data processing: Total grip and total dexterity scores were developed by summing the right and left scores for each outcome. Each applied tasks AHFT raw score was transformed into a categorical impairment score (“severe,” “moderate,” “mild,” and “effective” [4]). These scores were summed to develop a Total Applied AHFT score which ranged from 6 to 24, with a higher score indicating greater hand function. Total Keitel scores range from 4 to 52, with higher scores indicating greater impairment in active ROM.

Statistical Analysis: Backward stepwise multiple regression models with each applied hand task as the outcome measure and the biomechanical variables (total grip, total dexterity, total Keitel), as well as the total problems, and age as the predictor variables were used to determine which biomechanical variables were most strongly associated with hand function.

RESULTS AND DISCUSSION

Subjects were 56.2 (±8.5) years and primarily female (84%). They had had RA for a mean of 16.7 (±10.3) years. The median of the total number of problems score was 2 problems and ranged from 0 to 15. The mean total grip strength score was 366.8 (±160.3) mmHg. The mean total dexterity score was 51.2 (±11.2) seconds. The mean Total Keitel score was 21.8 (±10.8).

All models were significant except for Coins (Table 1). Grip was most often associated with hand function, playing a significant part in 4 of the 6 models. Dexterity, too, was an important predictor of hand function. Number of problems had only limited associations with hand function, and pure active range of motion, as represented by the Keitel, was not significant in any model.

For tasks which required strength rather than precision, such as cutting meat or lifting items, strength had the strongest association. For tasks requiring manipulation, such as doing buttons or tying laces, dexterity became more important. Overall hand function, as represented by the AHFT score, was more strongly associated with dexterity, suggesting that for many tasks, the ability to manipulate items is a better predictor of function than basic strength. Interestingly, manipulating coins, which involved picking up coins and manipulating them in the hand, was not significantly associated with any biomechanical skill. The ability to perform in-hand manipulation tasks may require a set of skills not measured by current dexterity tasks.

CONCLUSIONS

Number of problems is a poor predictor of hand function, as is overall ROM for people with RA. Grip and/or dexterity, however, can provide a good index of overall hand performance for functional tasks regardless of age and structural deformity. Biomechanists should identify whether a hand task is more reliant on grip or dexterity to determine which of these variables to measure.

REFERENCES

1. Biese J. Arthritis. In: Cooper C, ed. *Fundamentals of Hand Therapy*. St. Louis, MO: Mosby, Inc.; 2007.
2. Backman C, et al. *Occup Ther J Res* **11**, 245-255, 1991.
3. Eberl DR, et al. *Arthrit Rheum* **19**, 1278-1286, 1976.
4. Backman C, et al. *Arthritis Hand Function Test: Test Manual (research edition),* Vancouver, BC: Canada: The University of British Columbia, 1997.

ACKNOWLEDGEMENTS

Funding for this project was provided by the American College of Rheumatology Research and Education, Health Professional Investigator Award. Subjects were recruited from the UPMC Arthritis Network Disease Registry which was funded by the St. Margaret Memorial Hospital Foundation.

Table 1 – Regression models predicting hand function from biomechanical variables

		partial *r*					
	Mean (SD)	age	problem	Keitel	grip	dexterity	R^2
Shoe	49.9 (15.5)	.38	--	--	-.45	.60	.65
Button	30.3 (14.7)	--	.45	--	--	.41	.37
Cutting	48.4 (29.8)	--	--	--	-.59	--	.35
Coins	16.3 (14.2)	--	--	--	--	--	--
Lifting	10.6 (2.7)	--	--	--	.55	--	.30
AHFT	13.6 (3.6)	--	--	--	-.41	.64	.79

Shoe – Lacing/tying a shoe lace (secs); Button – fastening/unfastening 4 buttons (secs); Cutting – cutting “meat” with a knife (secs); Coins – manipulating and inserting 4 coins (secs); Lifting – lifting tray with up to 12 cans (# of cans); AHFT – Total AHFT score; -- - variable did not significantly contribute to the model

PROACTIVE BALANCE CONTROL: KINEMATIC ANALYSIS OF A REACH TASK

Anuradha Mukherjee, Charles Armstrong
Motion Analysis Laboratory, Dept. of Kinesiology, The University of Toledo
email: anuradha.mukherjee@utoledo.edu

INTRODUCTION

Feed-forward or proactive balance control mechanisms represent a neurological control strategy which involves activation of the balance system in anticipation of a perturbing force(s). A conventional method to study this is with voluntarily initiated, commonly experienced internal perturbations such as reaching tasks. While numerous studies have addressed various aspects of proactive balance control, these studies have typically utilized a forward reaching task which introduces a sagittal plane perturbation. Few studies have employed non-sagittal plane perturbations, or considered the implications of such in describing the associated balance control mechanisms. Thus, the purpose of this research was to examine the peak center of pressure excursion distance (COP) and maximum trunk lean angles in sagittal and frontal planes in a maximum arm's length reach task, and to determine if these were influenced by the subject's gender. Insight into the balance control mechanisms of healthy human adults may be of particular relevance in the treatment of populations such as the elderly and those with compromised balance due to injury or disease.

METHODS

Twenty healthy volunteers (10 males, 23.7±3.23 years, 76.3±14.2kg, 172.7±8.93cm and 10 females (21.7±3.62 years, 61.1±6.57 kg, 164.4±6.84cm) from the University of Toledo campus with no prior history of limb or low back injury, were recruited for the study. The participants were moderately active and physically fit. Individuals with a history of any condition that may have compromised balance were excluded from participating in this study. All subjects provided written informed consent, as approved by the Human Subjects Research Review Committee at The University of Toledo.

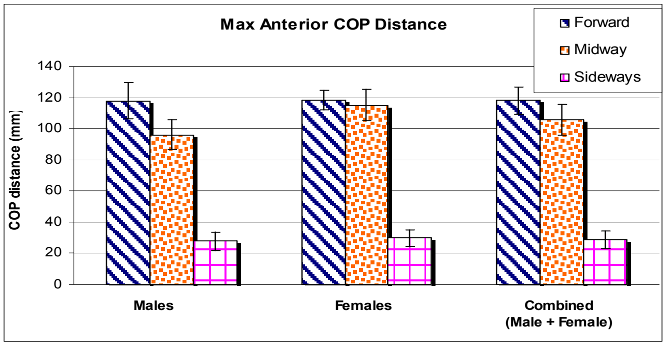

Figure 1 Max. ACOP excursion in males, females & group

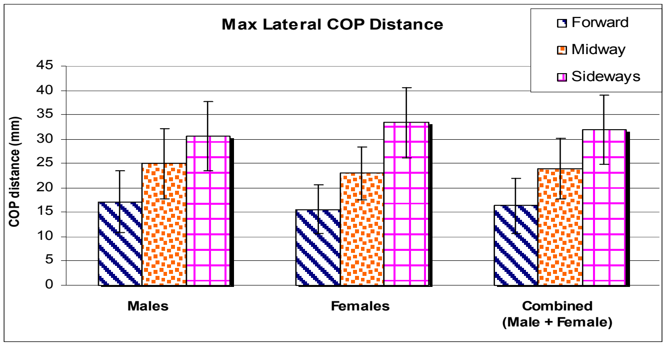

Figure 2 Max. LCOP excursion in males, females & group

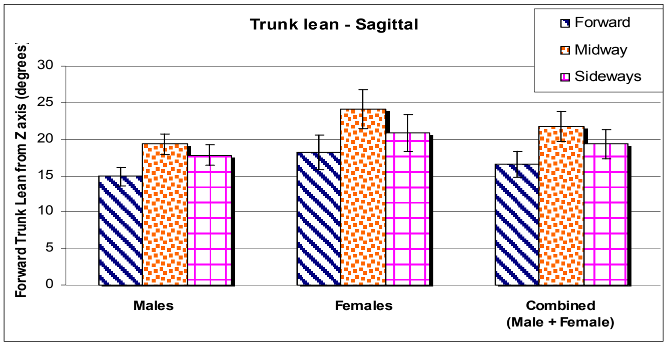

Figure 3 Max. sagittal trunk lean in males, females & group

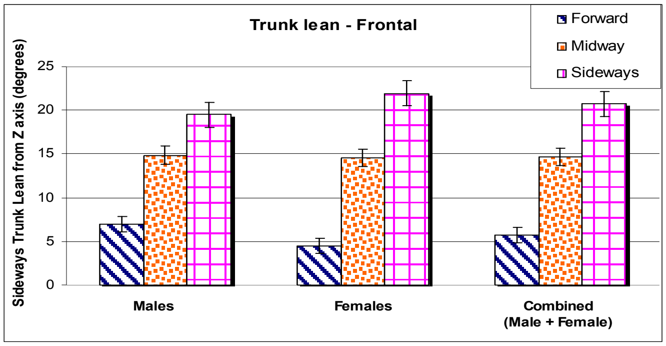

Figure 4 Max. frontal trunk lean in males, females & group

Participants were asked to stand barefoot on a force platform (AMTI, Newton, MA), and, upon an auditory cue, reach for targets kept at their previously measured maximum arm's length distance, in three different reach directions - forward, midway, sideways. There were fifteen randomized trials for each participant, including five in each of the three directions.

Kinematic assessment of the subject's movement was done via a 3D Motion Analysis system (Motion Analysis Inc., CA). Thirty three reflective markers were used to create a kinematic model. Video data was collected at 60Hz while force data was collected at 960Hz. KinTrak 6.2.3 software (Motion Analysis Inc., CA) was used to measure the dependent variables for each trial, which were then averaged across trials and subjects.

Multiple two way repeated measures ANOVA were performed using SPSS 14.0. A priori significance level was set at $p \leq 0.05$, and Tukey post-hoc test performed for pair wise comparisons, to study the effects of reach direction and gender on COP distances and trunk lean angles.

RESULTS AND DISCUSSION

Upon statistical analysis, both sagittal plane COP, i.e. ACOP ($F_{1,18} = 135.40$, $p < 0.001$, $\eta^2 = 0.88$, $1-\beta > 0.99$) and frontal plane i.e. LCOP ($F_{1,18} = 4.24$, $p < 0.022$, $\eta^2 = 0.19$, $1-\beta = 0.7$) demonstrated significant main effects. No significant gender differences were found. Maximum trunk angle leans, in both planes also showed significant main effects - sagittal plane, ($F_{2,36} = 7.176$, $p = 0.002$, $\eta^2 = 0.285$, $1-\beta = 0.912$), and frontal plane, ($F_{2,36} = 84.619$, $p < 0.001$, $\eta^2 = 0.825$, $1-\beta > 0.99$). However, there was considerable inter-subject variability.

In observing sagittal plane trunk lean, the greatest amount occurred in the midway reach 21.7 ± 6.9^0, followed by sideway reach 19.3 ± 6.5^0 and lastly forward reach 16.5 ± 6^0 (Figure 3). And, as was expected, trunk angle in the frontal plane (Figure 4), was the greatest in the sideway reach task 20.7 ± 4.6^0. We found that females appeared to have greater trunk lean in both planes for all three directions, though differences were not statistically significant ($p=0.133$). An interesting observation was the oppositely directed COP shift at the beginning of every task across all participants, which has been reported in several other studies (1,2). The posterior displacement of the COP appears to be an anticipatory adjustment that is intended to create a distance between the COP and the center of mass location, which defines the moment arm for sagittal plane rotation of the body. The ability of the plantarflexors to create a sagittal plane stabilizing torque allows for greater COP motion in the A-P direction than in the M-L direction. Greater trunk lean angles among females suggest a relationship between anthropometric factors and both COP displacement and amount of trunk lean. Further research is needed to gain insight into these important relationships.

CONCLUSIONS

Collectively, the results of this study generate far more questions than they answer. However, they provide support for the theory that, when faced with a movement that challenges balance, the CNS proactively employs strategies that appear to be intended to minimize the destabilizing effects of this challenge. And, that the characteristics of these strategies are influenced by the nature of the destabilizing challenge. Balance control mechanisms are highly dynamic and complex phenomenon and hence, they should be examined by taking into consideration the cognitive as well as the perceptual nature of a particular task, along with the vestibular, vision and somatosensory aspects.

REFERENCES

1. Kaminski T.R, et al. *Exp Brain Res* **136,** 439-446 2001.
2. Tyler A, et al. *Gait and Posture* **20**,126-133 2004.

CERVICAL LAMINOPLASTY CONSTRUCT STABILITY: EXPERIMENTAL AND FINITE ELEMENT INVESTIGATION

[1, 2] Srinivas C Tadepalli, [1, 2] Anup A Gandhi, [3] Douglas C Fredericks,
[3] Joseph D Smucker, [1, 2, 3] Nicole M Grosland
[1]Department of Biomedical Engineering, [2]Center for Computer Aided Research, [3]Department of Orthopaedics and Rehabilitation.
The University of Iowa, Iowa City, IA
Email: nicole-grosland@uiowa.edu, web: http://www.ccad.uiowa.edu/mimx

INTRODUCTION

Cervical laminoplasty is one of the modern techniques utilized in the management of cervical spondylotic myelopathy (CSM). Cervical laminoplasty was developed to increase the spinal canal diameter and area without permanently removing the dorsal elements of the spine, thereby maintaining cervical alignment and stability. There have been a number of technique-related innovations such as the use of sutures, autograft, allograft, ceramic spacers and mini-plates [1]. The single-hinge (open door) laminoplasty technique consists of opening the lamina from either the left or right side, with the contra lateral side acting as a hinge. It remains unclear as to what loads the posterior bone can tolerate before the failure of the laminoplasty construct. The main aim of this study was to evaluate the biomechanical stability of single vertebral segments in the cervical spine after open door laminoplasty via the use of human cadaveric specimens and a finite element (FE) model.

METHODS

Experimental study

A total of 16 human cervical vertebrae (C3-C6) were obtained from 6 cadaveric spines (age 68-91 years, mean 85 years). All specimens were scanned using CT to make sure they were free from major pathological defects. CT image data was imported into Image-J [2] for pre-operative measurements of the sagittal canal diameter and spinal canal area. In preparation for the experimental testing, the vertebrae were dissected to remove all surrounding soft tissues. Of the 16 individual vertebrae, 4 were without any surgical intervention and the remaining 12 were implanted with either an open door (OD) plate or a graft plate. Each vertebra was randomly assigned to one of the following groups: OD plate, graft plate or intact vertebrae. After the surgery, detailed digital photographs were taken and imported into Image-J [2] for post-operative measurements of the spinal sagittal canal diameter, canal area and laminar opening. Each vertebra was potted using Bondo (Bondo Corp, Atlanta, GA) and tested in one of two modes of loading; namely, direct compression and parasagittal compression. In the direct compression loading mode, the vertebral body was potted so that the posterior surface of the body was parallel to the potting surface. An indenter of circular cross section (9 mm in diameter) was used to compress the vertebra. In the parasagittal compression loading mode, the vertebra was potted such that the spinous process of the vertebra was at an angle of approximately 45° to the base of the loading fixture. Also a special fixture of rectangular cross section (15mm X 5mm) was designed to apply a uniform compressive load on the lamina thereby preventing slippage.

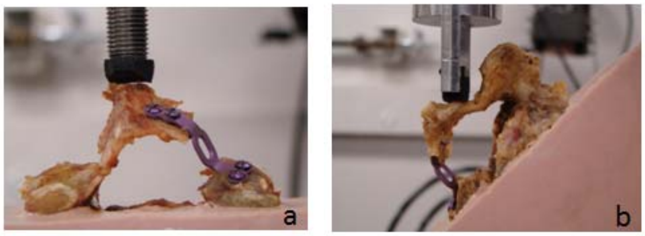

Figure1: Implanted cervical spine. a) Direct compressive loading. b) Parasagittal compressive loading.

All potted specimens were mounted on an 858 MTS Mini Bionix II (MTS, Eden Prairie, MN) via a custom designed fixture. The specimens were loaded to failure at the rate of 1mm/min. Cross head displacements and the corresponding reaction force throughout the test were recorded to determine the failure loads. The data was analyzed for statistical significance using an independent sample one tailed t-test assuming equal variance. A confidence interval of 95% (p = 0.05) was used to analyze all the data.

Finite element study

The effect of failure loads on the biomechanical behavior of the posterior bone and the laminoplasty implants were studied using the finite element (FE) method. A previously developed 3D nonlinear FE model of a C5 vertebra was used in this study [3]. A mesh convergence study was performed to ensure the accuracy of the model. Frictional contact boundary conditions were incorporated between the bone-plate, plate-screw and screw-bone interfaces to accurately capture the interface phenomena. A series of nodes of the vertebra were completely fixed in all the directions so as to simulate the experimental potting conditions. The FE analysis was performed in two steps. In the first step, the lamina was opened so as to accommodate the 10mm laminoplasty plate. This enabled the stresses developed in the posterior bone during laminar opening to be applied as the initial conditions in the FE analysis. In the second step, failure loads obtained from the experiments were applied to the FE model to investigate the biomechanical behavior of the posterior bone and the laminoplasty plates.

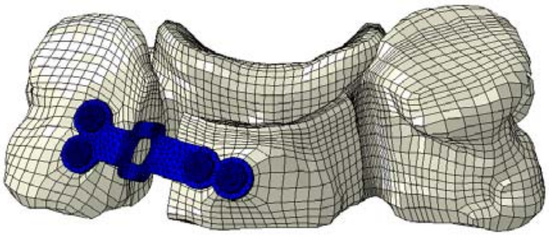

Figure 2: FE model of the C5 cervical vertebrae with the laminoplasty plate and screws.

RESULTS AND DISCUSSION

A substantial increase in the sagittal canal diameter and the spinal canal area was observed for all specimens. The sagittal canal diameter on average increased by 29% while the canal area increased by 38%. Statistically there was a significant difference in the failure loads of the intact and the implanted (graft plate and OD plate) specimens under both direct compression and parasagittal compression. There was not a statistical significant difference in the failure loads observed between the specimens implanted with the graft plate and OD plate under both direct and parasagittal loading conditions. The failure loads of the implanted specimens were significantly less than the intact specimens. It was evident that introduction of the hinge reduces the strength of the lamina by 5-9 fold depending on the direction of loading conditions. Neither screw pullout nor the failure of the implants were observed during experimental testing.

The FE model predicted similar results in both direct compression and parasagittal compression loading conditions. The stresses in the hinge region exceeded the yield strength of the cortical bone indicative of failure. Stresses in the laminoplasty implants (plates and screws) were below the yield strength of titanium alloy.

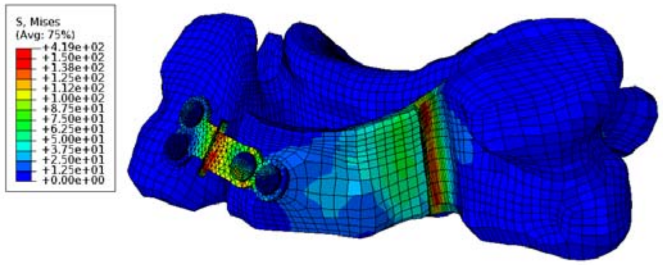

Figure 3: FE model illustrating the stresses (MPa) in the implant and posterior bone

CONCLUSIONS

To our knowledge this is the first attempt at evaluating the failure loads of the lamina via the use of experimental testing coupled with a finite element analysis. The FE method is an ideal tool to determine the biomechanical response of the instrumented cervical spine. Our novel modeling techniques provide a means to capture the complex irregular geometry of cervical spine on a specimen-specific basis. Moreover, experimentally validated FE models help to better understand the behavior of the instrumented cervical spine. Our goal is to simulate a multilevel laminoplasty procedure in a multi-segment model of the cervical spine and perform stability tests.

REFERENCES

1.Steinmetz, et al. *The Spine Journal* 6(1), 2006.
2.Image-J, www.rsweb.nih.gov.
3.Tadepalli SC, et al. *ASME SBC* 2008.

STAND-TO-SIT MOVEMENT AFTER BI-COMPARTMENTAL KNEE REPLACEMENT

[1] He Wang, [1]Eric Dugan, [1]Jeff Frame, and [2]Lindsey Rolston
[1]Ball State University, [2]Henry County Orthopedic Center, New Castle, IN
email: hwang2@bsu.edu

INTRODUCTION

Total knee replacement is a common method of treating pain and dysfunction associated with knee osteoarthritis (OA). However, cartilage degeneration is often confined in the medial and patellofemoral compartments [1]. The Journey Deuce system (Smith & Nephew Inc.) is a bi-compartmental knee replacement (BKR) system used to treat knee OA by replacing the medial and patellofemoral compartments while preserving the cruciate ligaments and lateral compartment. To date, there is very little information regarding functional outcomes after BKR surgery. It is not known if sparing the cruciate ligaments and lateral compartment of the knee could help patients maintain knee stability during daily activities requiring lowering the body, e.g. stand to sit.

The purpose of the study is to compare frontal plane knee mechanics and EMG of hamstring muscles during stand-to-sit movement of the surgical and contra-lateral limbs of patients post BKR surgery and the limbs of healthy control subjects. It was surmised that the BKR system with the preserved lateral compartment would result in normal frontal plane mechanics and help knee joint maintain medio-lateral stability. It was also hypothesized that the preserved ACL would function normally to control the tibia anterior translation without requiring increased hamstring co-activation.

METHODS

10 healthy control subjects and 8 unilateral BKR patients (post-op: 14 ± 4 months) participated in the study. 3D kinematic, kinetic, and EMG analyses were conducted during stand-to-sit movement. The following variables were analyzed: peaks of knee varus/valgus moments and knee varus/valgus angular displacements during stand-to-sit, mean hamstrings (BF, ST) root mean squared (RMS) EMG during trunk flexion and extension phases of the stand-to-sit. Paired Student's t-tests were used to determine the differences in the BKR group (BKR vs. non-BKR limbs). One way MANOVA was used to determine the differences between the limbs of BKR and control groups, $\alpha = 0.05$.

RESULTS AND DISCUSSION

There were no differences of peak knee varus/valgus angle and moment among the three limbs ($P > 0.05$) (Table 1). There were no differences of RMS EMG of hamstring muscles among the three limbs ($P > 0.05$) (Table 1).

Individuals with medial knee OA typically exhibit increased peak knee varus angle and knee varus moment when compared to non-OA subjects. In this study, no differences were found in peak knee varus angle and moment between the three limbs. It appears that normal frontal plane knee mechanics were restored after BKR knee surgery. In addition, unlike many TKA patients who often had mid-flexion instability and showed greater varus/valgus angular displacement when lowering the body from a standing position [2], the normal varus/valgus angular displacement associated with the BKR knee indicates that the medio-lateral knee stability is well maintained during stand-to-sit.

ACL-deficient knees exhibit increased hamstring co-activation during knee flexion/extension movement [3]. The greater hamstring co-activation is used to compensate the missing or reduced function of the ACL [3,4]. As the BKR surgery retains cruciate ligaments, it was expected that the BKR knee would have a normal ACL function and would not exhibit increased hamstring co-activation during stand-to-sit. This hypothesis was supported. In this study, the BKR limbs demonstrated similar level of hamstring co-activation EMG to the non-BKR and control limbs. The normal level hamstring co-activation EMG indicates that the ACL of the BKR knee can provides adequate constrain to anterior translation of tibia relative to femur when lowering the body.

CONCLUSIONS

BKR knees demonstrated normal frontal plane knee mechanics during stand-to-sit movement. The normal level of hamstring co-activation EMG reflects a normal ACL function during the stand-to-sit movement.

REFERENCES

1.McAlindon, T. E., et al. *Br J Rheumatol* 31(3): 189-92, 1992.
2.Wang H, et al. *Clinical Biomechanics* 20, 428-433, 2005.
3.Solomonow M, et al. *Am J Sports Med* 15:207-213, 1987
4.Baratta R, et al. *Am J Sports Med* 16(2):113–122, 1988.

ACKNOWLEDGEMENTS

BSU SEET Fund 2008.

Table 1: Knee frontal plane mechanics and hamstring RMS EMG of the BKR, non-BKR, and control limbs during stand-to-sit.

Variables	BKR limb	Non-BKR limb	Control limb
Knee Mechanics			
Min varus/valgus moment (Nmm/kg)	-208 ± 86	-207 ± 224	-230 ± 170
Max varus/valgus moment (Nmm/kg)	70 ± 44	139 ± 94	115 ± 82
Min varus/valgus angle (deg)	4 ± 3	3 ± 3	2 ± 3
Max varus/valgus angle (deg)	18 ± 8	15 ± 6	17 ± 7
Hamstring RMS EMG during Phase I			
BF	0.227 ± 0.136	0.241 ± 0.136	0.211 ± 0.176
ST	0.351 ± 0.291	0.181 ± 0.06	0.318 ± 0.427
Hamstring RMS EMG during Phase II			
BF	0.222 ± 0.126	0.241 ± 0.149	0.220 ± 0.194
ST	0.391 ± 0.395	0.199 ± 0.09	0.303 ± 0.454

Catch-like property in human adductor pollicis muscle

[1,2] Rafael Fortuna, [1] Marco Aurélio Vaz, and [2] Walter Herzog
[1]School of Physical Education, Federal University of Rio Grande do Sul, Porto Alegre, RS, Brazil
[2]Faculty of Kinesiology, The University of Calgary, Calgary, AB, Canada;
email:rfortuna@kin.ucalgary.ca

INTRODUCTION

The "catch-like property" of skeletal muscle is the dramatic increase in force when a single stimulus is added at the onset of a sub-tetanic low-frequency stimulation train (Binder-Macleod, 2005). This property has been observed in single motor units, whole animal muscles and human muscles, and is intrinsic to muscle cells. It is not related to changes in the neuromuscular junction or increased motor unit recruitment. Despite an abundance of observations on the catch-like property, its origin remains a matter of intense debate.

The aim of the present study was to induce the catch-like property in human adductor pollicis and identify the possible origin of the increase in force with an additional activation pulse (catch inducing train or CIT) compared to a reference contraction without an additional pulse (constant frequency train or CFT).

METHODS

Subjects: Twelve normal subjects (♂=6; ♀=6; 23±4 years of age), with no history of neuromuscular disease, gave free written informed consent to participate in this study.

Force: The forearm was placed on a custom-designed apparatus to measure thumb adduction forces and carpometacarpal joint angles, as described previously (Lee et al., 2002). A rotary stepper motor was connected to a rod via gears. The rod was attached perpendicular to the plane of the gear through a length adjustable rail arm. Calibrated strain gauges were mounted on the end of the rod to measure adduction force via an auxiliary piece for thumb placement and fixation. Angle measurements were obtained through an analogue encoder connected to the apparatus.

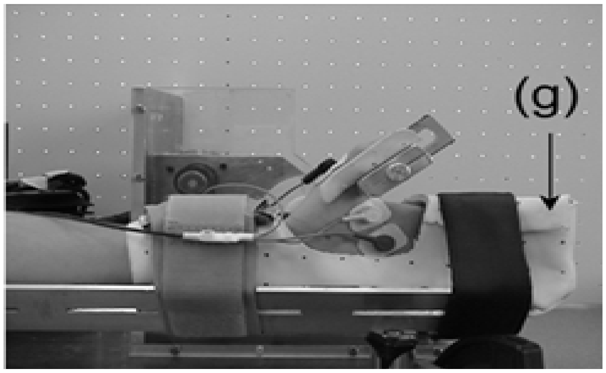

Full adduction was defined as 0 degree and abduction angles were defined as positive. Thumb movements were controlled by rotation of the motor and moving the rod using defined programs through a digital controller.

Stimulation: The ulnar nerve, which innervates the adductor pollicis muscle, was stimulated with a Grass S8800 stimulator, a SIU8T isolation unit and two carbon-impregnated rubber electrodes (4 x 4,5cm). Stimulation pulses were 800µs and the stimulation train lasted for three seconds. A 10 Hz train was used for the constant frequency reference train (CFT) with an extra pulse (8ms) added after the first stimulation pulse for the catch inducing train (CIT).

Protocol: Three levels of stimulation (low, medium and high) were used for all subjects to test if the catch-like property is associated preferably with one fibre type. All testing was performed at two muscle length (10º and 30º) to test if length dependent calcium sensitivity might affect the catch property. In order to determine if potentiation might be responsible for the catch property, three single stimuli were given 5,10, and 15s before and at 5,10 and 15s after the CIT and CFT tests. Just prior to deactivation, stiffness of the muscle in the CIT and CFT trains was assessed using a quick stretch of small magnitude (Lee et al., 2002). Every test was repeated three times and the order of testing (stimulation strength and muscle length) was randomized. A minimum of 1 min rest was provided between tests and five minutes of rest was strictly enforced prior to potentiation testing.

RESULTS AND DISCUSSION

Force was systematically increased for the CIT compared to the reference CFT tests for both muscle length (10º and 30º) (Fig. 1). The catch-like effect was more pronounced at the low stimulation voltage, when predominantly fast-twitch fibers were recruited (Fig. 2). The catch-like property was independent of muscle length, was not affected by potentiation and did not produce different stiffness compared to the reference tests (results not shown).

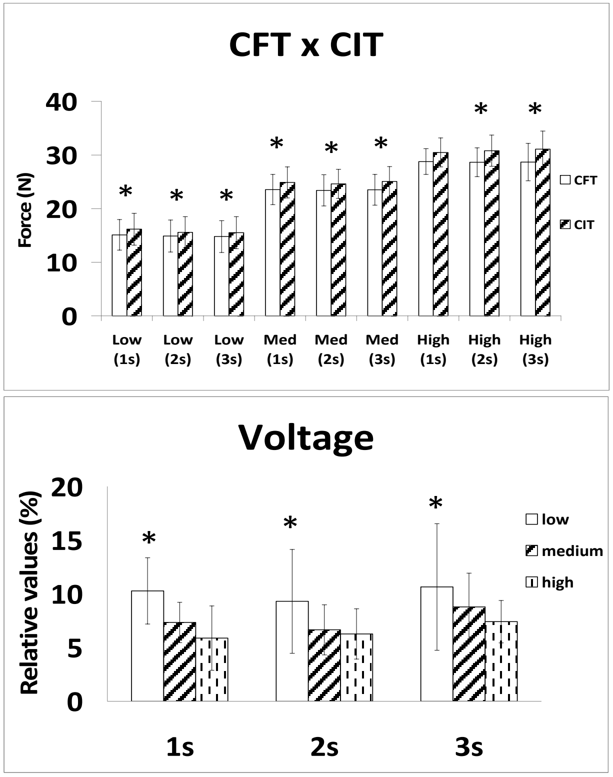

Figure 1-2: 1- Force increase of the CIT compared to CFT at 30º for low, medium and high voltage stimulation of the ulnar nerve evaluated 1, 2 and 3s following the onset of stimulation; 2- Relative force increase (%) of the CIT over CFT for the low, medium and high voltage stimulation tests evaluated at 1, 2 and 3s following the onset of stimulation (angle of 30º).

CONCLUSIONS

There is a distinct increase in force of about 10% with a single additional stimulation pulse in the CIT compared to the reference CFT tests. The catch-like property is more pronounced at low compared to high stimulation levels, suggesting that the effect is higher in fast- compared to slow-twitch fibers. There is no length effect and potentiation does not seem to play a role in the catch-like property of human adductor pollicis. Stiffness was the same in the CIT and the reference CFT tests suggesting that the increase in force associated with the catch-like property is not associated with an increased proportion of attached cross-bridges, but rather with an increased average force per cross-bridge (Huxley and Ford, 1981). Based on these results, we suggest that a single additional stimulation pulse early in a sub-maximal stimulation train increases the average force per cross-bridge in an as of yet undetermined way. This increase in cross-bridge force might be associated with a transition of weakly to strongly bound cross-bridge states mediated by the doublet nature of the additional stimulation pulse used in the CIT tests.

REFERENCES

Binder-Macleod S, et al., *Muscle Nerve*. 31:681-693,2005

Lee, H. D., et al, Journal of physiology. 545:321-330,2002

ELASTIC LEG EXOSKELETON REDUCES THE METABOLIC COST OF HOPPING

[1] Alena M Grabowski and [1] Hugh Herr
[1]Massachusetts Institute of Technology
email: alenag@mit.edu web: http://web.media.mit.edu~alenag

INTRODUCTION

During bouncing gaits such as hopping and running, the overall mechanics of the musculoskeletal system have been well characterized and predicted using a spring-mass model [1,2]; whereby the compliant musculoskeletal structures of the leg, primarily tendons, greatly reduce metabolic costs by facilitating elastic energy storage and return. However, muscles must generate force during each stretch-shorten cycle to compensate for energy losses due to damping, and thus accrue a metabolic cost.

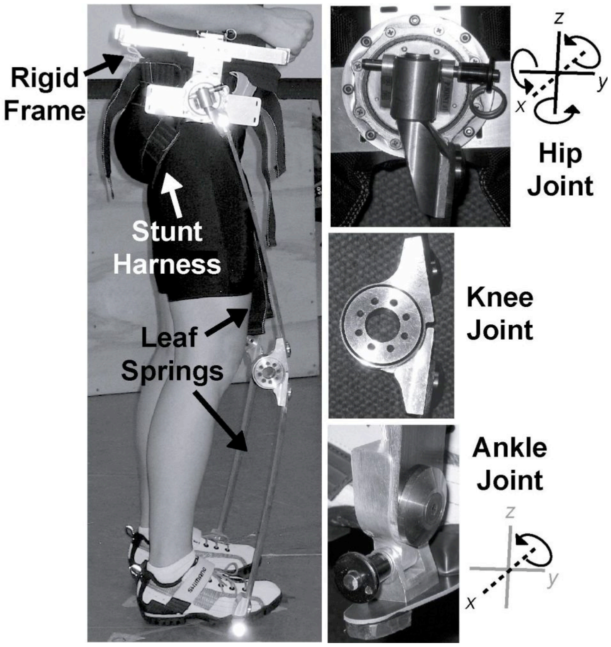

Figure 1: Elastic leg exoskeleton with 3 degree of freedom "hip" joint, fixed "knee" joint and 2 degree of freedom "ankle" joint.

While hopping or running on compliant surfaces, humans utilize the rebound of the surface, alter leg stiffness, and maintain linear spring-like mechanics of the leg and in-series surface combination [3]. Because changes in leg stiffness require hoppers and runners to adjust the rate and amount of muscle force generation, the metabolic energy required for the task is also altered.

We posit that if elastic energy can be efficiently stored and returned in an exoskeleton positioned in parallel to the human leg, rather than in the musculoskeletal system, wearing this exoskeleton could augment human hopping performance by reducing metabolic cost.

We designed an elastic exoskeleton that acts in parallel to the wearer's legs, and transmits the weight of the body through the exoskeleton directly to the ground (Fig. 1). We hypothesized that while hopping on both legs, hoppers would 1) adjust their leg stiffness while wearing an exoskeleton so that the combination of the hopper and exoskeleton would behave as a linear spring-mass system; achieving the same total stiffness as during normal hopping, and 2) require less metabolic energy while wearing an exoskeleton compared to normal hopping likely due to a decreased rate and amount of muscular force generated by their legs.

METHODS

Nine healthy recreational runners [5 F, 4 M, age 27.3 (6.0), mass 71.58 kg (13.83), leg length 0.929 m (0.055)] stood and then hopped in place at 2.0, 2.2, 2.4, and 2.6 Hz with and without an exoskeleton while we measured ground reaction forces, exoskeletal compression, and metabolic rates. All trials were 5 minutes long with rest given between trials. Before beginning each experimental session, we instructed subjects to hop in place on both feet, leave the ground between hops, and match the beat of a metronome.

We custom-made each exoskeleton such that it's initial stiffness approximated an *a priori* calculated leg stiffness assuming a 2.0 Hz hopping frequency and spring-mass mechanics with a non-zero aerial phase. The overall exoskeletal spring stiffness was non-linear; as it was compressed, the exoskeleton was initially stiff and then softened. The average weight of each exoskeleton was 62.2 N.

We collected 10 sec of ground reaction force data (1080 Hz) between minutes 3-5 of each trial (AMTI Inc.; Watertown, MA), and then processed this data using a customized Matlab program (MathWorks; Natick, MA). Raw force data were filtered with a 4th order zero-lag Butterworth Filter that had a 30 Hz cut-off. We then calculated peak vertical displacement of the center of mass during stance according to Cavagna, 1975 [4].

Before each experimental session, we measured the vertical force and displacement of each exoskeleton using an Instron materials testing machine (Instron 5580, Norwood, MA). Then, we combined this data with motion capture data (Vicon 512 system; Oxford, UK) collected during each trial to infer the force delivered by the exoskeleton. During all hopping trials with the exoskeleton, we determined exoskeletal compression from the distance between a reflective marker placed at the top of the thigh leaf spring segment and a reflective marker placed on the exoskeletal "ankle" joint. Marker position data were captured at 120 Hz simultaneously with the GRF data.

We measured rates of oxygen consumption and carbon dioxide production using a portable system (Cosmed K4b^2, IT). We averaged steady-state rates between minutes 2.5-4.5 and then calculated metabolic cost in Watts using a standard equation. We calculated net power by subtracting standing from gross metabolic power. We did not normalize metabolic power to weight because we sought to determine how the exoskeleton affected metabolic cost irrespective of it's added weight.

RESULTS AND DISCUSSION

Hoppers adjusted their biological leg stiffness while hopping in an exoskeleton so that the combination of the hopper and exoskeleton behaved as a linear spring with a total stiffness similar to that of normal hopping at the same frequency. There were no significant differences in hopping frequency, contact time, or hopping height between hopping with or without an exoskeleton, thus our efforts to maintain amplitude (asking subjects to jump with an aerial phase) and frequency (matching the beat of a metronome) appeared to be successful.

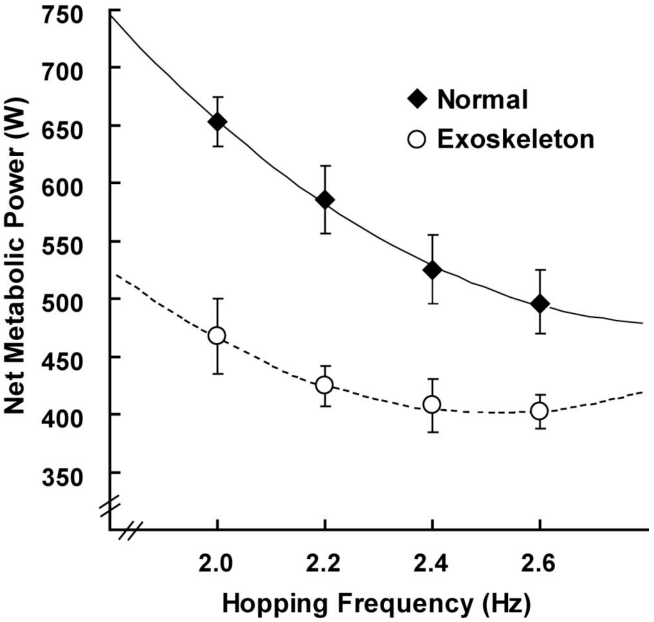

Figure 2: Average net metabolic power (error bars ± S.E.M.) to hop at 2.0 – 2.6 Hz normally (solid diamonds), and with a parallel leg exoskeleton (open circles). Hopping with an exoskeleton demanded significantly less metabolic power at all hopping frequencies ($p < 0.005$) compared to normal hopping.

Our results are similar to results from previous research, which show that hoppers maintain linear spring-mass dynamics when hopping on a wide range of elastic and damped surfaces placed in series with the hopper's legs. Our findings also support the idea that maintaining linear spring-mass dynamics of the center of mass, by dramatically altering biological leg mechanics in the presence of series or parallel impedance perturbations to the leg, may be a primary neuromuscular control strategy during bouncing gaits.

We found that hopping with an exoskeleton required substantially less metabolic energy than hopping normally (Fig. 2); net metabolic power was 24% less on average. Our leg exoskeleton likely decreased the metabolic demands of human hopping by effectively and efficiently transferring the weight of the wearer through an exoskeleton to the ground instead of this force being completely borne by the hopper's legs.

REFERENCES

1. McMahon TA, and Cheng GC. *J Biomech*, **23**, 65-78, 1990.
2. Blickhan R. *J Biomech* **22**, 1217-1227, 1989.
3. Moritz CT and Farley CT. *J Exp Biol* **208**, 939-949, 2005.
4. Cavagna GA. *J Appl Physiol* **39**, 174-179, 1975.

PERFORMANCE OF A HIP PROTECTOR DEPENDS ON ITS POSITION DURING A FALL

[1] Woochol J. Choi, [1]Joaquin A. Hoffer and [1,2]Stephen N. Robinovitch

[1]Dept. of Biomedical Physiology and Kinesiology, Simon Fraser University, Burnaby, BC, Canada
[2]School of Engineering Science, Simon Fraser University, Burnaby, BC, Canada
email: woocholc@sfu.ca

INTRODUCTION

Hip protectors are designed to attenuate and redistribute the force applied to the hip region during a fall, and thereby reduce risk for hip fracture [1]. However, little information exists on the effectiveness of hip protectors in achieving these goals, and how this is altered by displacement of the hip protector relative to the greater trochanter (GT). In the current study, we tested these issues.

METHODS

Biomechanical impact tests were conducted with a hip impact simulator. The surrogate hip was dropped onto a dual arrangement of an 2D pressure distribution plate (RSscan International) and a force plate from fall heights of 5 cm, 10 cm and 20 cm. Trials were acquired without a hip protector, and with three different soft shell hip protectors: 14 mm and 16 mm thick horseshoe-shaped pads (SafeHip, Tytext A/S), and a 16 mm thick continuous pad (Hipsaver). For each drop height, each protector was tested in nine positions: located centrally in its intended location over the GT, and displaced by either 2.5 cm or 5 cm in the superior, posterior, inferior, and anterior directions (Figure 1b). Three trials were acquired for each condition.

During each trial, we collected total hip impact force, pressure distribution and trochanteric force. All measures were acquired with a 500 Hz sampling rate. The RSscan plate had 4096 pressure sensors (64 by 64 array), a resolution of 0.01 kPa, range of 3 to 1270 kPa and accuracy (maximum error between the actual applied pressure and the value measured by RSscan plate) of 0.37 kPa, based on in-house calibration.

Our main outcome variables were the magnitude and location of peak pressure, trochanteric force and forces applied to four defined hip regions. We defined four C-shaped regions over the hip centered about the GT, and named the central area (area A) the ‘danger zone’ since it represented direct impact on the GT and femoral diaphysis (Figure 1a). We calculated the integrated force applied to each region by summing the product of sensor area multiplied by pressure measured by each sensor within the area of interest.

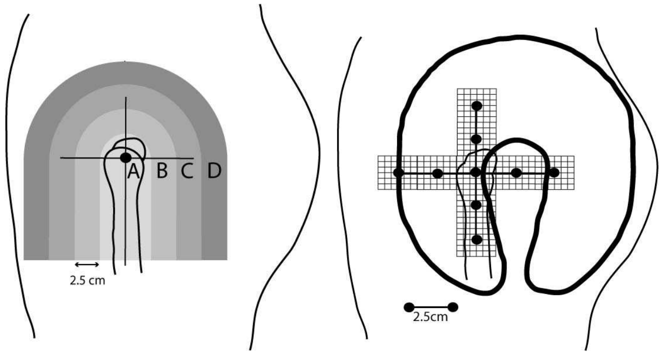

a

b

Figure 1 **a:** definition of four different areas over the hip region: area A, danger zone (light gray) consisted of a C-shaped region of width 5 cm (sum of a half-circle of radius 2.5cm centered at GT and a 16 cm long rectangle extending distally from the GT); areas B, C, and D (progressively darker gray) consisted of C-shaped hollow regions of width 10 cm, 15 cm, and 20 cm each **b:** pad displaced 2.5 cm in the posterior direction

Randomized group ANOVA was used to test whether each of our outcome variables was associated with drop height (3 levels), hip protector type (4 levels), and pad displacement (9 levels). The significance level in all tests was set to $\alpha = 0.05$, and all analyses were conducted in SPSS 16.0.

RESULTS AND DISCUSSION

The integrated force that impacted on the danger zone (area A) was associated with drop height ($p < 0.0005$), hip protector type ($p < 0.0005$) as well as hip protector displacement condition ($p < 0.0005$). For 20 cm drops, 83 % of the total force was applied to the danger zone in the unpadded condition, but the percent force was reduced to 34 % and 19 % with 14 mm and 16 mm horseshoe protectors, and to 40 % with the 16 mm continuous protector (Figure 2). The force distribution to areas B, C and D was also associated with fall height ($p < 0.0005$), hip protector type ($p < 0.0005$) and hip protector displacement condition ($p < 0.0005$). For 20 cm drops, hip protectors redistributed the forces applied on the hip region by lowering and deflecting much of the force away from the danger zone and onto adjacent soft tissue areas B, C and D. This protective effect was reduced when the hip pads were displaced away from their optimal location.

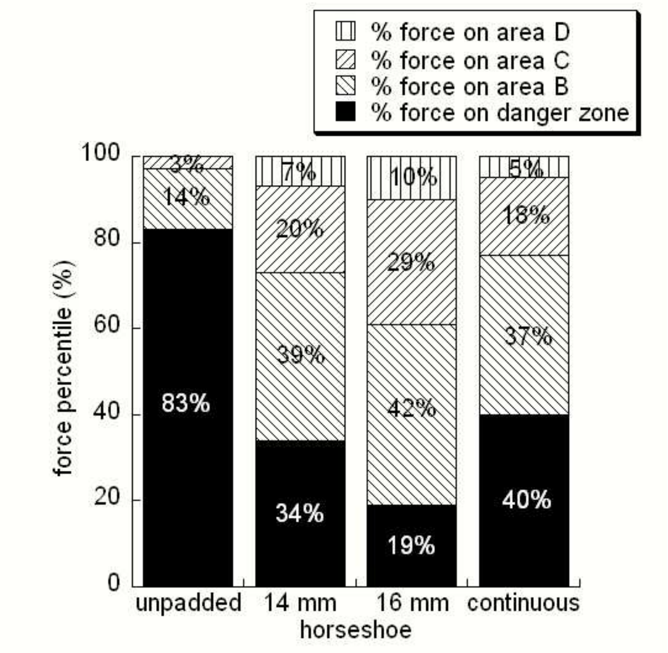

Figure 2 Force distribution to four different areas over the hip.

The trochanteric impact force was also associated with fall height ($p < 0.0005$), hip protector type ($p < 0.0005$) and hip protector displacement condition ($p < 0.0005$). For 20 cm falls with hip protectors centrally placed, trochanteric force averaged 45 % lower with the 16 mm horseshoe protector, 38 % lower with the 14 mm horseshoe, and 30 % lower with the 16 mm continuous protector, compared to the unpadded condition (Figure 3). The trochanteric force was 29 % higher for 5 cm pad displacement in the anterior direction, compared to centrally placed pads. There was a significant interaction between hip protector and displacement condition, indicating that both the 14 mm and 16 mm thick horseshoe pad protectors outperformed the 16 mm continuous protector in all but 3 displacements conditions.

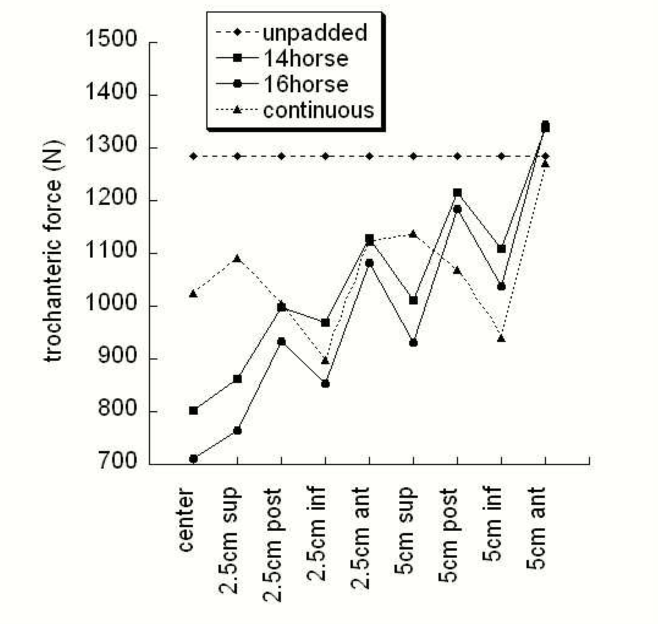

Figure 3 Effect of protector placement on the trochanteric force.

The peak pressure was reduced and shunted outside the danger zone by the optimally placed hip protectors, but the effectiveness declined when the protectors were displaced.

CONCLUSIONS

All three soft shell hip protectors we tested showed protective effects against external impact when optimally positioned in their intended location over the proximal femur. However, the horseshoe shaped protectors we tested provided superior protective benefit when compared to the continuous protector, and the 16 mm thick horseshoe protector performed better than the 14 mm horseshoe protectors. Furthermore, the protective effect was strongly dependent on correct placement of the protector with respect to the GT. Our findings are informative for developing more efficacious hip protectors and garments.

REFERENCE

1. Robinovitch SN, et al. *J Biomech Eng*. Nov;117(4):409-13, 1995

ACKNOWLEDGEMENT

This research experiment was funded in part by NSERC operating grant (grant # RGPIN239735).

GLENOHUMERAL JOINT CONTACT FORCES DURING WHEELCHAIR ACTIVITIES

Melissa M.B. Morrow, Kai-Nan An, and Kenton R. Kaufman
Biomechanics and Motion Analysis Laboratories, Division of Orthopedic Research,
Mayo Clinic, Rochester, MN 55906 USA
email: kaufman.kenton@mayo.edu

INTRODUCTION

Manual wheelchairs users rely on their upper extremities for mobility and activities of daily living. The glenohumeral joint is poorly designed for weight bearing, and the upper extremity (UE), with its small musculature, is not efficient for ambulating. This places manual wheelchair users at a high risk of upper extremity injury limiting not only their ambulation, but all areas of function. Therefore, a complete understanding of wheelchair activities is of particular importance in addressing the shoulder dysfunction in this population.

Direct measurement of propulsive handrim forces during propulsion has yielded useful information. However, this approach does not specifically describe the internal muscle and joint forces. Only five studies have examined the muscle force distribution problem at the shoulder joint during wheelchair propulsion [1]. Level propulsion has been shown to result in small glenohumeral contact forces leaving room for other activities to be responsible for pain and pathology at the shoulder. The purpose of this study was to estimate the joint contact forces in high demand wheelchair activities beyond level propulsion. We hypothesized that the weight relief condition would result in the highest glenohumeral joint contact forces.

METHODS

Twelve manual wheelchair users were recruited for this study. Subjects performed three trials of two propulsion tasks (level, 1:12 ramp) and a weight relief task. Kinematics were recorded with a 10-camera system (Motion Analysis Corp.). Three dimensional handrim forces and moments were collected with bilateral SmartWheels (Three River Holdings, LLC). Intersegmental forces and moments were calculated using inverse dynamics.

Glenohumeral joint contact forces for each wheelchair activity were determined using an optimization algorithm developed in MATLAB (Mathworks, Inc.). A Hill-type musculoskeletal model was used consisting of thirteen muscle bundles crossing the shoulder complex. Model input variables included intersegmental forces and moments calculated in Visual3D (C-motion, Inc.), muscle parameters from the literature [2], and muscle orientations for known joint orientations (SIMM, Musculographics, Inc.). The model was validated with EMG recordings.

The optimization algorithm utilized two optimal criteria [1,3]: (1) minimization of the neuromuscular activation, α; and (2) minimization of the sum of the muscle stress cubed, subject to constraints:

$$\sum_{i=1}^{m} \left| \boldsymbol{F}_i^M \right| \boldsymbol{\tau}_i + \boldsymbol{F}^J = \boldsymbol{F}^P$$

$$\sum_{i=1}^{m} \left| \boldsymbol{F}_i^M \right| (\boldsymbol{r}_i \times \boldsymbol{\tau}_i) = \boldsymbol{M}^P$$

$$0 \le F_i^M \le (\alpha * \bar{F}_i^a + \bar{F}_i^p) * PCSA_i * \sigma; i = 1, m.$$

where m = number of muscles; $\boldsymbol{F}_i^M$ = muscle force of ith muscle; $PCSA_i$ = physiological cross-sectional area of ith muscle; $\boldsymbol{\tau}_i$ = unit muscle force direction vector of ith muscle; $\boldsymbol{F}^J$ = joint constraint force; $\boldsymbol{F}^P$, $\boldsymbol{M}^P$ = intersegmental force and moment due to the external force system; $\boldsymbol{r}_i$ = insertion of ith muscle; σ = muscle stress limit; and $\bar{F}_i^a, \bar{F}_i^p$ = normalized muscle active and passive force, respectively.

The maximum joint contact forces for each activity were identified for the study cohort using each optimal criterion. A one-way ANOVA with three repeated measures (level, ramp and weight relief) was performed for each peak contact force. When significant main effects were identified (α = .05), post hoc Bonferroni-adjusted pair wise comparisons were performed.

RESULTS AND DISCUSSION

Ramp propulsion and weight relief resulted in significantly greater anterior, medial and superior forces when compared to level propulsion (Table 1). When compared to the weight relief condition, ramp propulsion was greater only in the medial force direction. The magnitude of the resultant joint contact force for ramp propulsion (3448 N) was more than 3X greater than that of level propulsion (1010 N) and moderately greater than weight relief (2767 N) (Figure 1). This highlights the potential injurious nature of the weight relief maneuver and ramp propulsion. These high demand activities might contribute to impingement and joint degeneration.

When comparing these results to intersegmental forces and moments determined from the same study cohort [4], slightly different conclusions are drawn. The inverse dynamics results point to both the weight relief and ramp propulsion, but do not clearly single out the ramp as the activity creating the highest joint loading.

CONCLUSIONS

The results of this study provide two important findings. First, estimated intersegmental joint forces and moments do not provide a complete interpretation of injury potential associated with wheelchair activities. More complex modeling is necessary to assess loading within the glenohumeral joint. Second, while weight relief has been shown previously to cause high loading in the glenoid, ramp propulsion has not been studied. This work shows that ramp propulsion creates extraordinary joint loads and should be avoided by manual wheelchair users when possible.

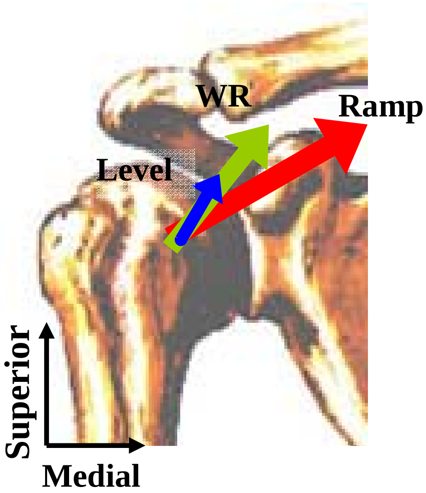

Figure 1. Frontal view of relative maximum resultant glenohumeral joint contact forces for three activities. Blue arrow represents level propulsion, green arrow represents weight relief, and the red arrow is the ramp condition. The length of each arrow is proportional to the magnitude of the joint contact force.

REFERENCES

1. Erdemir A, et al. *Clin Biomech* **22,** 131-154, 2007.
2. Langenderfer J, et al. *Clin Biomech* **19**, 664-670, 2004.
3. Kaufman KR, et al. *Neuroscience* **40**, 781-792, 1991.
4. Morrow MMB, et al. *J Elect Kines* 2009.

ACKNOWLEDGEMENTS

Work supported by NIH Grant Number R01 HD 48781.

Table 1. Maximum Glenohumeral Joint Contact Forces

Activity	Objective Function	Max Anterior Force (N) (mean ±std)	Max Medial Force (N) (mean ±std)	Max Superior Force (N) (mean ±std)
Level	*min α*	460 ± 143	648 ± 170	624 ± 145
	min stress	486 ± 127	631 ± 156	601 ± 134
Ramp	*min α*	1054 ± 230[1]	2702 ± 609[1,2]	1866 ± 423[1]
	min stress	933 ± 175[1]	2642 ± 506[1,2]	1826 ±490[1]
Weight Relief	*min α*	885 ± 42[1]	1987 ± 513[1]	1711 ± 436[1]
	min stress	890 ± 50[1]	1997 ± 540[1]	1709 ± 422[1]

[1] Forces significantly higher than level ($p<.05$), [2] Forces significantly higher than weight relief ($p<.05$)

THE EFFECTS OF LATERAL LIGAMENT SECTIONING ON THE STABILITY OF THE ANKLE AND SUBTALAR JOINT

[1]Stacie I. Ringleb, [1]Ajaya Dhakal, [2]CAPT Claude D. Anderson, [1]Sebastain Bawab, [1]Rajesh Paranjape,
[2]CAPT Marlene DeMaio
[1]Mechanical Engineering, Old Dominion University, [2]Department of Orthopaedic Surgery, Naval Medical Center Portsmouth
email: SRingleb@odu.edu

INTRODUCTION

The frequency of subtalar joint instability is 10 to 25% in patients with chronic lateral functional hindfoot instability [1]. The majority of patients are initially diagnosed with lateral ankle joint instability, therefore the diagnosis of subtalar joint instability is often made by the process of elimination.

The physical examination cannot reproducibly determine whether the instability is at the ankle or subtalar joint. Stress radiography cannot provide a three dimensional picture of subtalar joint kinematics, and the image depends on the direction from which radiograph is taken. MRI takes longer to perform and the results are difficult to quantify, as damaged ligaments do not always indicate functional instability. A better understanding of the hindfoot kinematics when subtalar joint is present may lead to a clinically relevant technique to diagnose subtalar joint instability. Therefore, the purpose of this study was to investigate the effects of ligament sectioning on subtalar joint instability and the kinematics of the ankle and subtalar joint under multiple manual loading conditions.

METHODS

Eight fresh-frozen cadaveric lower extremities sectioned at the midpoint of the shank were obtained (5 left, 3 right; mean age 74.3 years; 6 female, one male, one unspecified). X-rays were obtained to ensure that each specimen had no evidence of coalitions, severe arthritis, fusion, or other disorders that might affect motion. Each specimen was placed into a custom six degree-of-freedom positioning and loading device. Kinematic data were collected from the tibia, talus and calcaneus with a Polhemus Liberty (Polhemus, Colchester, VT) and The MotionMonitor (Innovative Sports Training, Chicago, IL). Two trials of data were collected throughout the complete range of motion in plantarflexion/ dorsiflexion, inversion/eversion, internal/ external rotation, supination/pronation, anterior/posterior drawer and inversion/ eversion while the ankle was held in dorsiflexion. Loads were applied by a specialty trained foot and ankle surgeon. These motions were collected when the ligaments were intact and the following ligaments were serially sectioned: anterior talofibular ligament (ATFL), calcaneofibular ligament (CFL), cervical ligament and interosseous talocalcaneal ligament. Euler angle data were exported from the MotionMonitor for all conditions, except for anterior/posterior drawer where the change in magnitude of the relative position of the bones was analyzed. A custom program written in Matlab (The Mathworks, Natick, MA) further reduced the data for analysis. A within-subjects repeated measure ANOVA was used to analyze the difference in joint motion when each ligament was sectioned using SPSS (SPSS Inc., Chicago, IL). The coefficient of repeatability between two sets of data was calculated [2].

RESULTS AND DISCUSSION

The coefficient of repeatability was ± 5.5°, ± 5° and ±4.4° for the hindfoot (calcaneus relative to tibia), ankle and subtalar joint, respectively. Significant changes in motion occurred at the ankle when the ATFL and CFL were sectioned and at the subtalar joint when interosseous ligament was sectioned (Table, Figure).

The interosseous ligament is the most significant ligament in stabilizing subtalar joint [3]. In an *in vitro* study, the subtalar joint became unstable when it was sectioned in isolation [3]. Statistically and clinically significant increases in subtalar joint motion were observed when the interosseous ligament was sectioned. This study examined the effect of the interosseous ligament with the ATFL, CFL and cervical ligament, which were sectioned before the interosseous ligament.

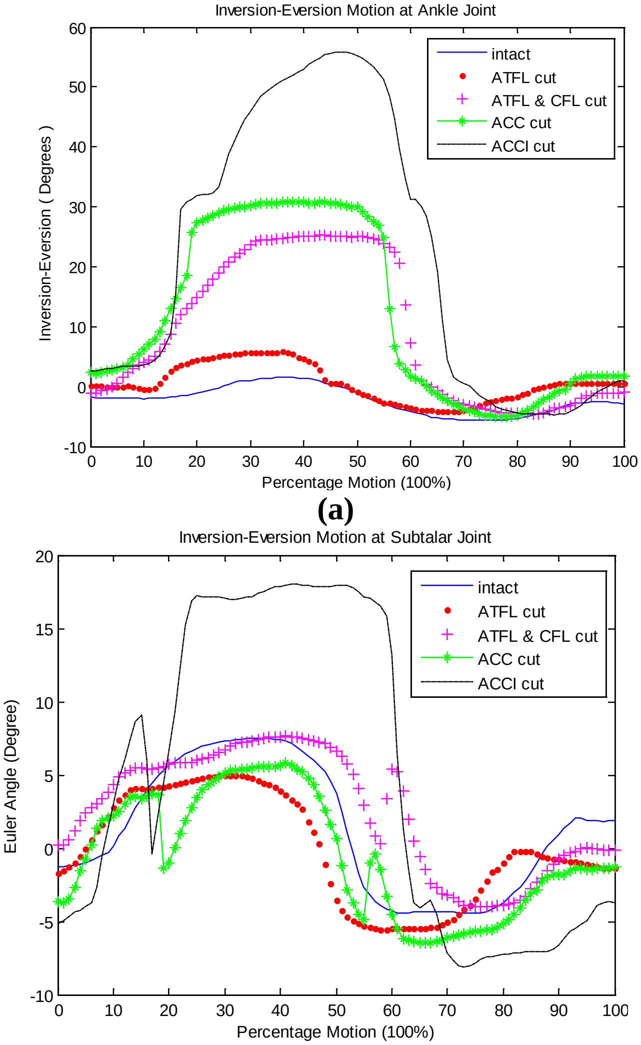

(a)

(b)

Figure: Sample curve of inversion-eversion at the a) ankle and b) subtalar joint.

Another proposed support structure for the subtalar joint is the calcaneofibular ligament [4]. In the present study, a statistically significant increase (1.78°, p=0.008) was noticed when external rotation was applied when the CFL was sectioned. While this finding was not clinically significant or within the experimental error range, it suggests that the role of the CFL in subtalar joint stability should be further investigated.

Previous studies [5] and clinical knowledge have shown that the ATFL and CFL have a significant role in stabilizing ankle. The findings in this study support this during the application of anterior translation and internal rotation after the ATFL was sectioned and during inversion-eversion and after the CFL was sectioned. While most studies examine the kinematics of the hindfoot during anterior drawer to identify ATFL insufficiencies [5] and inversion to identify CFL insufficiencies, internal rotation at ankle was found to increase significantly (p=0.0003, 8.8°) after sectioning ATFL.

REFERENCES

1. Karlsson J, et al. *Scandinavian Journal of Medicine & Science in Sports* 8,191-7, 1998.
2. Bland MJ and Altman D. *The Lancet* 327,307-10, 1986.
3. Kjærsgaard-Andersen, et al. *The American Journal of Sports Medicine* 16,512-6, 1988.
4. Laurin CA, et al., *Can J Surg* 11,270, 1968.
5. S.I. Ringleb, et al. *J Orthopaedic Research* **23**,743-749, 2005.

ACKNOWLEDGEMENTS

This research was funded by American Orthopaedic Foot and Ankle Society.

IRB Approved Study NMCP2007.0069

The views expressed in this article are those of the author(s) and do not necessarily reflect the official policy or position of the Department of the Navy, Department of Defense or the United States Government

Table: Significant Changes in Ankle and Subtalar Joint Rotations/Translations

Motion	Joint	Ligament	Change in rotation/translation	p-value
Inversion	Ankle	ATFL	4.28°	0.004
		CFL	8.56°	0.007
	Subtalar	interosseous	13.45°	0.004
internal rotation	Ankle	ATFL	8.80°	0.0003
supination	Subtalar	interosseous	9.45°	0.012
anterior drawer	Ankle	ATFL	4.53 mm	0.027

COMPARISON OF USE OF BACKREST AND FOREARM SUPPORT WITH A STANDARD WORKSTATION AND A WORKSTATION WITH A BOARD ATTACHMENT

Sohaila El Sagheir and Geneviève Dumas
Department of Mechanical and Materials Engineering, Queen's University, Kingston, Ontario
e-mail: elsagheir@me.queensu.ca

INTRODUCTION

Lower back pain and upper extremity disorders are commonly associated with computer work. Forearm support on the work surface has been considered as a strategy to prevent these problems[1]. A commercial workstation board attachment (Life with Ease), previously known as the Butterfly Board, is claimed to promote use of back rest and forearm support. The objective of this study was to monitor this usage for the Butterfly Board and compare it to a standard workstation.

METHODS

Twelve participants (females, age 18-45) with no previous history of musculoskeletal diseases were tested on two workstation setups: (A) standard workstation with adjustable chair and desk height, (B) workstation with the Butterfly attachment board. Both workstations were ergonomically adjusted according to Canadian Guidelines[2]. Three Novel^{TM} Pressure mats (Novel, Munich, Germany) were attached to the chair back and participant's forearms. Each participant performed a standard task involving mouse and keyboard use for 20 minutes on each setup (order alternated between participants). Participant's motion was captured by a synchronized video camera. Amplitude Probability Density Function (APDF) for peak pressure were determined at levels 10%, 50% and 90% by recording the frequency of occurrence of the maximum pressure values(peak pressure) at each time frame and determining the percentage of occurrence of zero pressure values per setup (Figures 1-5). Area of contact with the pressure mats and center of pressure path length were also compared. Center of pressure trajectory patterns were visually compared between the 2 setups.

RESULTS AND DISCUSSION

For the ***Back***, the backrest was used most of the time with both set-ups (A: 84%, B: 98%) but slightly more with the Butterfly Board ($p<0.05$).The mean peak pressure was also larger with the Butterfly Board ($p=0.04$). There was no significant difference in area of contact or in center of pressure path length during the task between the two set-ups.

For the ***Forearms***, there was no significant difference in resting time between the twoo set-ups. Peak pressure was significantly higher with the standard workstation for both the right ($p=0.02$) and the left ($p=0.004$) forearms. There was no significant difference in the mat area of contact for either forearm and for the center of pressure path length for the right forearm. Center of pressure path length was larger while using setup B for left forearm ($p=0.01$).

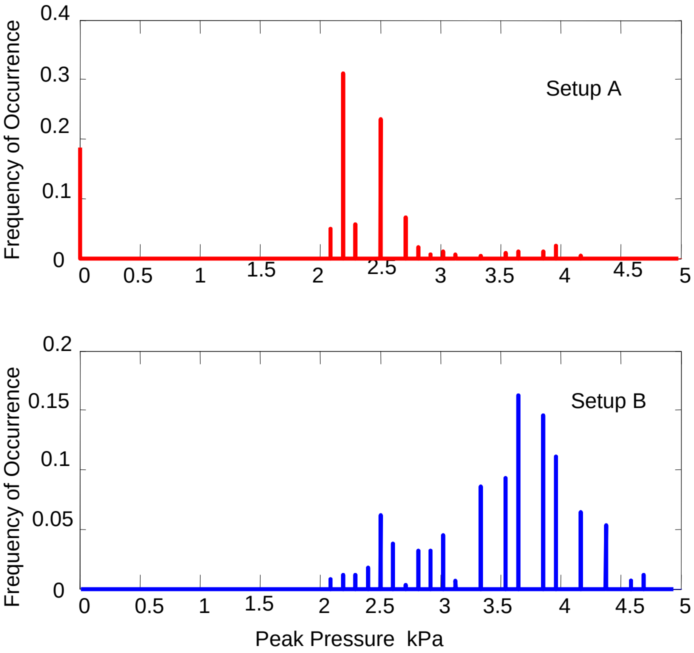

Figure 1: Frequency of occurrence (%) of Peak pressure for the back-Participant (4)

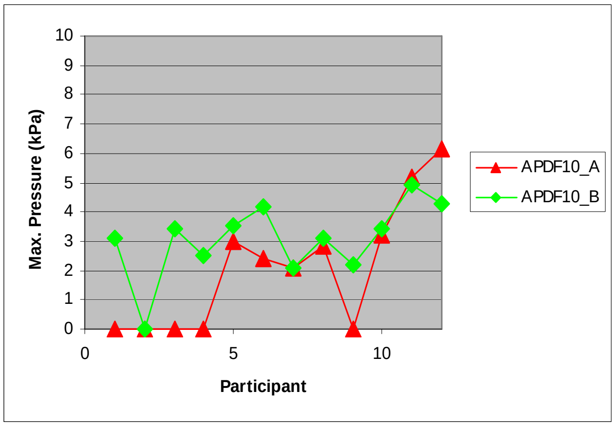

Figure 2: APDF 10% for the back-P(max)

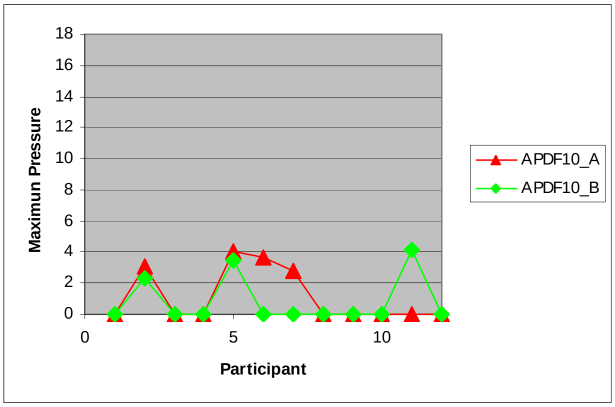

Figure 3: APDF 10% for the Left forearm-P(max)

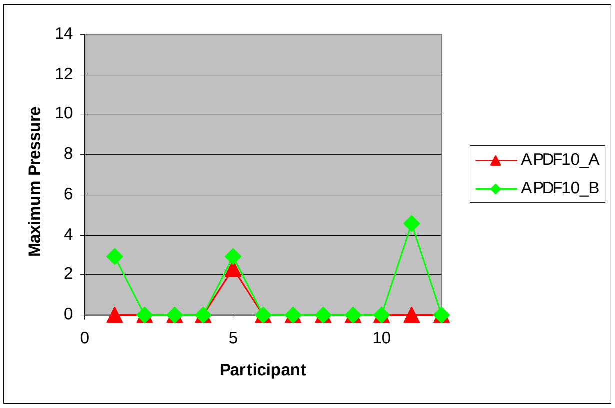

Figure 4:APDF 10% for the right forearm-P(max)

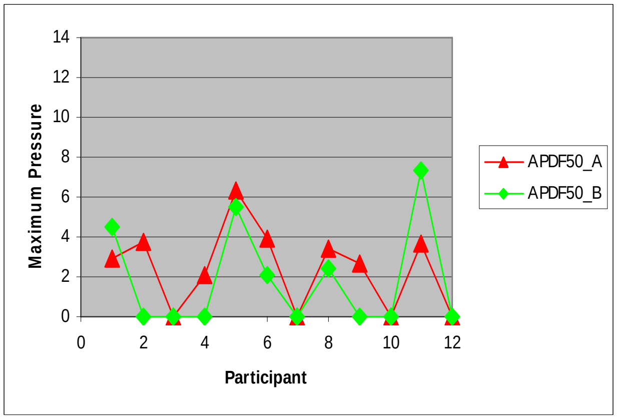

Figure 5:APDF 50% for the right forearm-P(max)

Forearm data were also analyzed with video motion analysis, to account for the resting location by choosing a certain frame on the pliance software that represents peak pressures exerted by both forearms then comparing it to the same frame number cut from the video (frame to frame analysis) to determine the pattern of resting and its location. This was done for the same task for each setup as shown in figures 5 and 6. The participants were found resting on the desk with their wrist while using setup (A), they were found utilizing the forearm support while using setup (B).

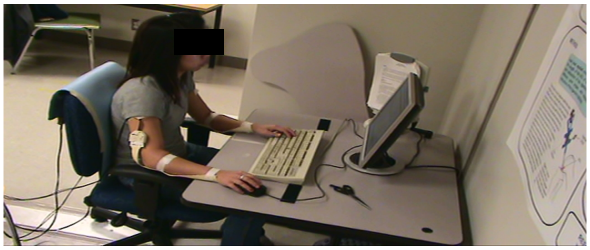

Figure 6: Video motion analysis-setup (A)

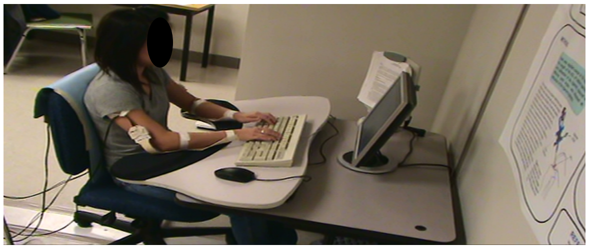

Figure 7: Video motion analysis-setup (B)

CONCLUSIONS

The results demonstrated significantly higher usage of back rest with the Butterfly board though the difference was small. From video and pressure data analysis, the Butterfly board seemed to reduce points of excessive pressure at the wrist and elbow areas during computer work, but not to provide longer resting time. The results are consistant with EMG annd posture data of a previous study of the same set-ups [3].

REFERENCES

[1] Feng Y. et al. *Ergonomics* **40,** 834-848 1997.
[2] Guidelines on Office Ergonomics. *CSA-Z412 International* (2006).
[3] Dumas G.A. et al. *Ergonomics* **51,** 1735-1756, 2008.

ACKNOWLEDGEMENTS

This study was funded by NSERC grant A6858.

AN EMG ASSISTED BIOMECHANICAL MODEL OF LUMBAR SPINE WITH PASSIVE COMPONENTS

[1] Yu Shu, [1]Judith M. Burnfield, [2]Gary A. Mirka
[1]Madonna Rehabilitation Hospital, Lincoln, NE,
[2]Department of Industrial and Manufacturing Systems Engineering, Iowa State University, Ames, IA
email: yshu@madonna.org, web: http://www.madonna.org/research_institute

INTRODUCTION

In order to accurately predict the load on the spine during manual lifting exertions, a biomechanical model must realistically represent the complicated interactions between various spinal components such as active muscles, ligaments, inter-vertebral discs, and abdominal pressure. Different methods can be used to describe these components - thus electromyography (EMG) assisted, optimization and finite element models have been developed. However, each of these techniques has its own advantages and disadvantages. For example, EMG-assisted biomechanical models are able to capture complicated co-activation patterns of the agonist and antagonist muscles of the trunk. However, models based exclusively on EMG activity are unable to estimate the load from passive components of the extensor mechanism which play a significant role in the net extensor moment, especially near or at full trunk flexion posture. On the other hand, finite element models can precisely simulate the viscoelastic behavior of the passive components of the spine, but estimations of active muscle forces are usually based on assumptions and may not represent the wide range of possible activation patterns in real lifting exertions. The current study demonstrates a novel method to combine these approaches to create a new EMG assisted biomechanical model that includes passive components of the spine.

METHODS

Eighteen subjects voluntarily participated in this study. They performed repetitive controlled and free dynamic lifting and lowering exertions at different combination of speed and load conditions. In the first experiment, six subjects were secured in an isokinetic dynamometer which restrained the pelvis and lower extremity and they performed isokinetic flexion/extension exertions at the speed of 10°/s, 20°/s and 30°/s with 10%, 20% and 30% of their maximum extension force. During the second experiment, twelve subjects slowly lifted and lowered a load weighted 10%, 20% and 30% of the subjects maximum lifting capacity from a squat (bent knee) and stoop (straight knee) posture. In all of these trials, the subjects were asked to reach their full trunk flexion posture. The EMG activity of the major trunk muscles (erector spinae, latissimus dorsi, rectus abdominis, external obliques and internal obliques) and the kinematics of the trunk movements were recorded.

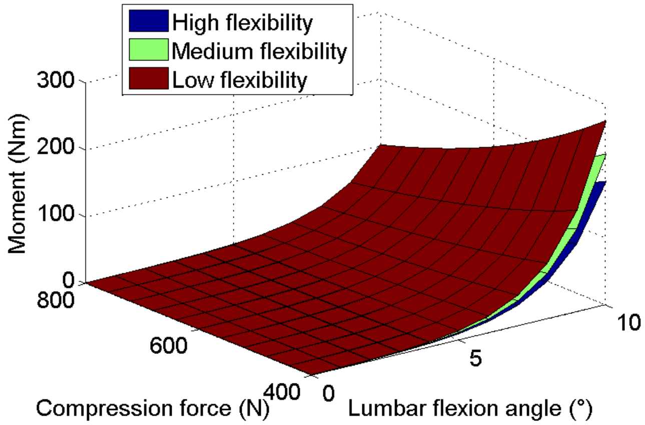

Figure 1: Illustration of the 3D surface of passive moment vs. load and lumbar flexion angle

Passive tissue forces were estimated through the use of a finite element model of the lumbar region [1]. A 3-dimensional response surface of net moment from passive components (Figure 1) was first constructed based on compression force, lumber flexion angle, and subject's flexibility conditions. The estimated value of the instantaneous passive contribution during the extension/flexion exertion was determined by the instantaneous compression force from active muscles and trunk flexion angle. The forces from active muscles were estimated from normalized EMG activities (multiplied by the estimated cross-sectional area of the muscles and the maximum muscle stress value). The origin and insertion of the muscles were estimated from the anthropometric data of the subjects [2] and were used to calculate the moment arms for active muscles. The total internal moments from both passive components and active muscles were compared with the measured net external moment to validate the model. Two different EMG-assisted models (Model 1: muscle only, without passive components; Model 2: muscle with passive components) were compared with the measured net external moment to provide insight into the utility of the inclusion of these passive tissue forces. Coefficient of correlation (r^2) values between measured and model predicted sagittal moments of the two models in different conditions were calculated to quantitatively assess the difference.

RESULTS AND DISCUSSION

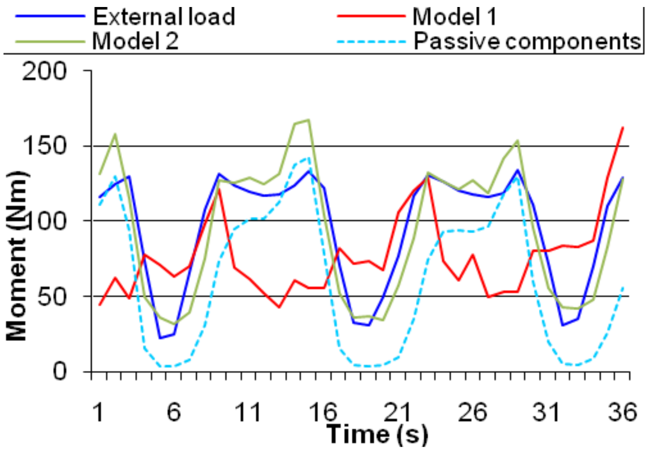

Figure 2: Measured sagittal moment vs. model predicted sagittal moment in three free dynamic lifting/lowering exertions

The sagittal moment relative to L5/S1 joint in three lifting/lowering exertions from one subject is presented in Figure 2. The subject started from a fully flexed posture, lifted the load to the upright posture (about 7 seconds), lowered the load (about 13 seconds), and repeated the lifting motion two more times. The trace from the model 1 (muscle only) showed the flexion relaxation phenomenon with the muscle activity diminishing as the subject reached the full flexion posture. At this posture, passive components generated the majority of the restorative moment to support the trunk. Model 2 (with passive components) correctly predicted the net internal moment by including the moments from passive components.

The necessity of considering the moments generated by passive components in trunk exertions at or near full flexion postures is obvious from the improvement of r^2 values illustrated in Table 1. Additionally, the consistency of these values in different experimental setups indicated the model with passive components was robust across various load, speed, pelvis restraint and knee posture conditions.

CONCLUSIONS

This study introduced a new method for including the effects of passive components of the spine in an EMG-assisted biomechanical model and demonstrated significant improvements in predicting the spinal load at or near full flexion postures.

REFERENCES

1. Shin G, et al. *Clinical Biomechanics* **22**(9):965-71, 2007.
2. Marras WS, et al. *Spine* **20**(13): 1440-1451, 1995.

Table 1: Comparison of r^2 values between measured external sagittal moments and model predicted internal moments for model 1 (muscle only) and model 2 (with passive components)

	Controlled (pelvis restrained)						**Free**	
	Load			**Speed**			**Knee posture**	
	10%	**20%**	**30%**	**10°/s**	**20°/s**	**30°/s**	**Bend**	**Straight**
Model 1	.47±.15	.34±.25	.28±.20	.38±.22	.40±.22	.32±.20	.12±.13	.12±.11
Model 2	.68±.16	.68±.16	.63±.12	.69±.14	.70±.11	.61±.17	.76±.9	.74±.11

BIOMECHANICAL CHARACTERISTICS OF DROP LANDING ON AN INVERTED SURFACE WITH ANKLE BRACE

Songning Zhang, Qingjian Chen, and Michael Wortley
Biomechanics/Sports Medicine Lab, The University of Tennessee, Knoxville, TN, USA
email: szhang@utk.edu web: web.utk.edu/~Esals/resources/biomechanics_laboratory.html

INTRODUCTION

The most commonly used testing protocol to investigate ankle sprain mechanisms and ankle braces is an inversion drop on a trapdoor platform [1, 2]. Only until recently that landing has been incorporated in such applications [3, 4]. Only few studies incorporated landing on an inverted surface [4]. However, no studies have shown biomechanical differences of landing on an inverted surface in comparison to landing on a flat surface. Furthermore, the effects of ankle braces restricting ankle inversion on an inclined surface in landing have not been fully examined. Therefore, the purpose of this study was to examine biomechanical characteristics of drop landing on an inclined surface with an ankle brace.

METHODS

Eleven healthy subjects (6 females and 5 males, age: 24.6 ± 3.5 years, height: 1.70 ± 0.10 m, mass: 65.6 ± 14.9 kg) with no current ankle injury and no history of major lower extremity injuries participated in the study. A seven-camera motion analysis system (240 Hz, Vicon, UK) was used to collect 3D bilateral lower extremity kinematic data. Two force platforms (1200 Hz, AMTI, USA) were used to measure the ground reaction forces (GRF) simultaneously with the 3D kinematics. An inverted surface [45.72 cm (L) × 22.86 cm (W) × 11.43 cm (H)] with a 25° inversion slope was mounted on top of the right force platform with double sided tapes along with a flat surface [40 cm (L) × 40 cm (W) × 4 cm (H)] mounted on the top of the left force platform during drop landing conditions. The subjects performed five drop landing trials from a 0.45 m height on the flat surface without (LF_NB) and with (LF_BR) a semi-rigid ankle brace (Element, DeRoyal Industries, Inc.) and the inverted surface without (LS_NB) and with (LS_BR) brace.

Visual3D (C-Motion, Inc., USA) was used to compute 3D kinematic variables for the right lower extremity. A customized computer program (VB_V3D) was used to determine critical events and values of the computed variables from Visual3D. Surface effects during landing on the flat and slant surfaces were examined using a 2 × 2 (brace × surface) repeated measures ANOVA for selected variables with an alpha level of 0.05 (SPSS 15.0, SPSS Inc., Chicago, IL).

RESULTS AND DISCUSSION

The statistical results showed a significantly higher 1st (F1_Z) and 2nd (F2_Z) peak vertical GRFs in flat surface landing compared to the inverted landing (Table 1). The brace caused higher 1st (F1_X) peak lateral GRFs in the flat surface landing and lower 1st peak lateral GRFs in the inverted surface landing. Furthermore, the slant surface caused a significant decrease in the 1st and 2nd (F2_X) peak lateral GRFs. The maximum inversion angle was significantly increased from the flat surface landing to the inverted surface landing (Table 1). Landing on the flat surface imposed an eversion motion after contact whereas landing on the inverted surface caused inversion movement. The brace did not cause any significant changes in peak inversion or range of motion (ROM) in frontal plane, but a reduced dorsiflexion ROM (ROM_DF).

The greater 1st peak vertical GRF seen in the flat surface landing was initially thought to be associated with a toe-heel landing strategy. A closer examination of ankle sagittal kinematics showed that subjects initially exhibited similar contact angles in both landing conditions. However, significantly less dorsiflexion ROM was observed compared to the flat surface landing indicating a stiffer landing strategy adopted by the subjects during inclined surface landing compared to the flat surface landing. The ankle joint is constrained by the laterally sloped surface resulting in the reduced ROM and therefore the reduced peak GRFs. This stiffer strategy and the eliminated eversion motion commonly associated with landing on a flat surface place the ankle and the rest of the lower extremity in an unfavorable position for impact attenuation.

We expected to see an increase in the horizontal GRF due to the increased surface slope in inverted landing but the results showed reduced peak lateral GRFs. Landing on inverted surface requires greater friction between the shoe and surface to avoid slip (with sand papers on the slope) which may cause greater energy dissipation therefore reduced peak GRFs. Furthermore, the more inverted contact ankle angle places the lateral ankle ligament complex under a tighter and stretched state thus allowing this ligament complex to contribute more to impact attenuation in the inverted landing.

CONCLUSIONS

Landing on an inverted surface causes a reduced peak GRFs but resulted in a stiffer landing with decreased dorsiflexion ROM. The inverted slope places the ankle in a compromised position and may predispose it to inversion sprains. Under the high inversion loading introduced during the landing condition, the ankle brace does not seem to offer significant protection.

REFERENCES

1. Alt, W., et al. (1999). *Foot Ankle Int,* **20**, 238-245.
2. Cordova, M. L., et al. (2007). *Scand J Med Sci Sports*, **17**, 216-222.
3. Ubell, M. L., et al. (2003). *Am J Sports Med*, **31**, 935-940.
4. Venesky, K., et al. (2006). *J Athl Train,* **41**, 239-244.

ACKNOWLEDGEMENTS

Ankle braces were provided by DeRoyal Industries, Inc.

Table 1. Average GRFs and frontal plane ankle kinematic variables: mean ± STD.

Cond	F1_Z (BW)	F2_Z (BW)	FMin1_X (BW)	FMin2_X (BW)	Max_Inv (deg)	ROM (deg)	ROM_DF (deg)
LF_NB	1.28±0.25 [b]	3.20±0.64 [b]	-0.23±0.06 [b]	-0.31±0.08 [b]	5.2±3.9 [b]	-6.7±3.1 [b]	44.4±7.9 [a,b]
LF_BR	1.32±0.25	3.38±0.73	-0.26±0.08	-0.28±0.08	1.8±4.8	-4.0±3.1	35.2±5.1
LS_NB	0.95±0.22	2.86±0.55	-0.09±0.06	-0.21±0.07	25.2±3.9 [1]	13.5±5.1	35.3±5.1
LS_BR	0.85±0.25	2.69±0.56	-0.02±0.07	-0.23±0.11	22.6±5.2	14.4±4.7	28.1±6.2

[a]: significantly different between NB and BR ($p<0.05$) & [b]: significantly different between flat and inverted surfaces ($p<0.05$).

THE EFFECT OF TFCC INJURY ON ECU FUNCTION AND FRICTION

[1]Zac Domire,[1]Furkan Karabekmez, [1]Ahmet Duymaz, [2]Timothy Rutar, [1]Peter Amadio, [1]Steven Moran
[1]Mayo Clinic, Rochester, MN, [2]Washington State University, Pullman, WA
email: Domire.Zachary@mayo.edu

INTRODUCTION

Injury to the triangular fibrocartilage complex (TFCC) is a frequently occurring wrist injury. Treatment options following injury vary widely, but, it has been proposed that extensor carpi ulnaris (ECU) function is an important consideration when making surgical decisions about TFCC repair. Tang et al. [1] showed that the TFCC acts as a retinacular component for the ECU tendon, and that injury to the TFCC increases the moment arm of the ECU by nearly 30 percent.

Increasing the moment arm of the ECU will adversely effect force production by increasing muscle excursion and velocity for any given movement. However, muscle function is determined not by muscle force, but by muscle moment, which increased moment arm may enhance. It is unclear how the decrease in muscle force will balance with the increased mechanical advantage. The following study will examine the effects of increasing the moment arm of the ECU on moment producing capacity using a simple musculoskeletal model. It is also possible that TFCC injury may increase friction acting on the ECU tendon. This increased friction may cause additional wear on the surface of the tendon, which would further increase friction. The resulting vicious cycle of tendon damage could lead to tendonitis, tendon injury and pain. The following study will also examine the effects of TFCC injury on ECU tendon friction by using a cadaveric model.

METHODS

Isometric and isokinetic joint strength curves were simulated for the ECU in both injured and non-injured states. The ECU was modeled as a hill type, muscle like actuator. The muscle had force-length and force-velocity properties and was connected in series with an elastic element representing the tendon. The moment arm and muscle length of the ECU was changed in the injured simulation based on data from Tang et al. [1]. Muscle model parameters were taken from the literature [2,3].

Six human cadaveric wrists were studied. Frictional testing was performed by applying a constant load to the proximal tendon and measuring the load at the distal tendon while moving through a range of motion. A custom made motorized apparatus was used to move the specimens. Three cycles of motion were completed for both radio/ulnar deviation and flexion/extension. The range of motion was from 35˚ extension to 40˚ flexion and 15˚ radial to 35˚ ulnar deviation. The speed was 5˚/s for each test. Force at the distal tendon was measured throughout the motion at 45 Hz.

To create a TFCC injury, a 2 cm longitudinal incision was made over the volar side of the ulnocarpal joint. The attachment to the TFCC to the fovea and peripheral margin of ulna was separated with a scalpel. The ulnolunate ligament and the ulnotriquetral ligament, the palmar and dorsal radio-ulnar ligaments were also incised. The horizontal portion of the TFC was divided to the ulnar styloid but ulnar styloid was left intact. To complete the injury the TFCC's dorsal edge which mingles with the fibrous sheet of the ECU was separated carefully to avoid any damage to the ECU tendon. Following the creation of the injury, friction was tested repeating the same procedure as above.

Before calculation of friction the force data were smoothed using a fourth order bi-directional Butterworth filter with a cutoff of 4Hz. From the filtered force data, friction was calculated at each position. This was done by calculating the difference between the recorded force and the dead weight force for each direction of movement and then averaging the absolute value of this difference for each direction. The mean friction was calculated across all three cycles of motion. Friction was compared between the intact and the injured condition using a paired t-test. The level of significance was set at 0.05.

RESULTS AND DISCUSSION

The ECU force was reduced following injury (Figure 1). The difference increased with the amount of wrist extension and with increasing velocity. The largest decrease in force was seen at 60˚ of extension at 300˚/s. The difference in force here was less than 4 N. The ECU moment producing capacity was increased following injury (Figure 2). The difference decreased with the amount of wrist extension and with increasing velocity. The smallest increase in moment was seen at 60˚ of extension at 300˚/s. The difference in moment here was nearly 30 Nmm.

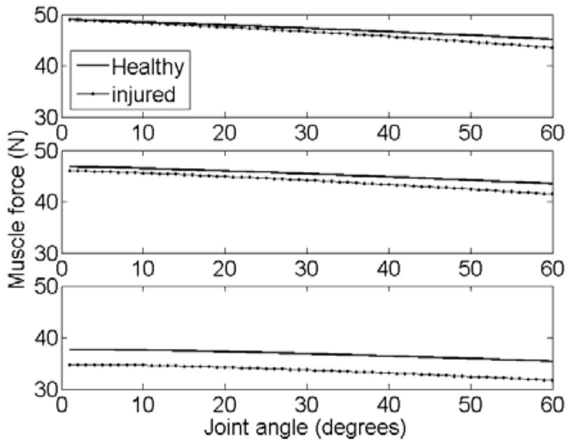

Figure 1: ECU force plotted against joint angle. Top – Isometric. Middle – Isokinetic at 60˚/s. Bottom – Isokinetic at 300˚/s.

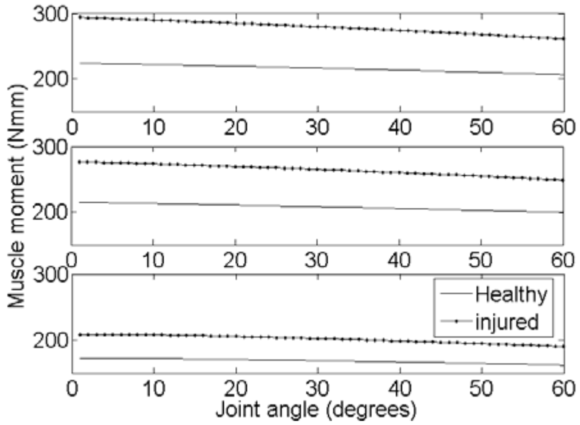

Figure 2: ECU moment plotted against joint angle. Top – Isometric. Middle – Isokinetic at 60˚/s. Bottom – Isokinetic at 300˚/s.

Friction during flexion/extension was slightly decreased following TFCC injury. The difference was small in absolute terms, but was statistically significant and was seen in all six specimens. Friction was unchanged following TFCC injury for radio/ulnar deviation (Table 1).

Table 1: Mean friction

	Intact	Injury
Flex./Ext.*	0.18 ± 0.11 N	0.13 ± 0.09 N
R/U Dev.	0.21 N ± 0.10 N	0.21 ± 0.13 N

Note - * indicates significant difference

The reason behind the small force decrease following TFCC injury is related to the ratio of the optimum fiber length to the moment arm of the muscle. This ratio has been previously identified as an important factor in muscle function [4]. This ratio is very large (12.77) for the ECU. Consequences of a high optimum fiber length to the moment arm ratio are very flat relationships between muscle force and joint angle or angular velocity. While injury to the TFCC does decrease this ratio, it is still large (9.75) following injury.

CONCLUSIONS

While injury to the TFCC does result in decreased ECU force producing capacity, moment producing capacity is increased. Additionally, as a result of TFCC injury, the friction acting on the ECU tendon was decreased during flexion/extension movements and unchanged during radio/ulnar deviation. There are many valid reasons for deciding to perform a TFCC repair, including pain and instability; however, neither ECU function nor friction should be a consideration when deciding on TFCC repair.

REFERENCES

1.Tang JB, et al. *J Hand Surg [Am]* **23**, 986-91, 1998.
2.Challis JH. *J Strength Cond Res* **18**, 803-9, 2004.
3.Loren GJ and Lieber RL. *J Biomech* **28**, 791-9, 1995
4.Zajac FE. *J Hand Surg [Am]* **17**, 799-804, 1992.

ACKNOWLEDGEMENTS

This study was supported by a grant from the Mayo Foundation.

We would like to thank Lawrence Berglund and Chunfeng Zhao for their technical assistance.

EFFECT OF INITIAL METHOTREXATE CONCENTRATION ON THE ELUTION AND MECHANICAL PROPERTIES OF VERTEBROPLASTIC BONE CEMENT

John A Handal, Jacob F. Schulz, Joshua M. Pahys, Eric A. Williams, Simon Kwok, and
Solomon P. Samuel
Department of Orthopedic Surgery, Albert Einstein Medical Center, Philadelphia, PA 19141
Email: samuelsp@einstein.edu

INTRODUCTION

Pathologic bone fractures and other lesions caused by cancer metastases can be currently managed with the injection of bone cements to relieve pain and restore the structural integrity of the bone. Chemotherapeutic agents can be added to these bone cements to reduce the need for additional systemic chemotherapy or radiation therapy [1-2].

Even though antibiotic eluting bone cements are successfully used in orthopedic practice, adding chemotherapy drugs to bone cement pose a different set of problems. This is mainly due to the toxicity concerns associated with the use of chemotherapy agents. To avoid local or systemic toxicity, the drug elution profile of a particular bone cement/drug concentration need to be determined. The drug elution profile depends on many factors including initial drug concentration, mixing conditions, surface area of the bone cement implant, etc. In this study, the effect of initial methotrexate amount on bone cement elution was measured.

It is our hypothesis that the relationship between clinically relevant initial drug concentration and amount of methotrexate eluted is not linear. The aim of this experiment is to measure *in vitro* drug elution from bone cement (Vertebroplastic radiopaque resinous material) containing four different initial methotrexate amounts. In addition, the effect of initial methotrexate concentration on the flexural properties of post cured bone cement was determined.

METHODS

Vertebroplastic radiopaque resinous material was kindly provided by DePuy Spine Inc., MA. Methotrexate was obtained from Bedford laboratories, Bedford, OH.

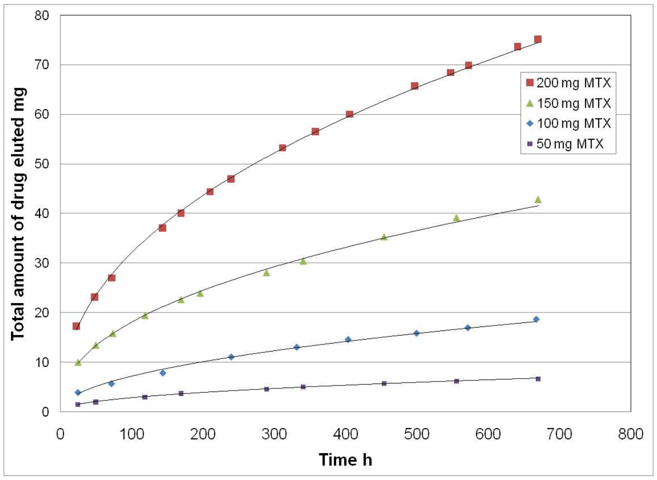

Figure 1: Comparison of methotrexate elution. The drug elution increased at least four times when the initial concentration doubled from 100 mg to 200 mg.

Preparation of experimental bone cement mixtures: The bone cement used in this study is a two part system containing 22.5 g of powder (methylmethacrylate polymer and barium sulfate) and 9.1 ml liquid monomer (methylmethacrylate monomer). The powder component (2.5 g) of the bone cement was first mixed thoroughly with methotrexate (50 or 100 or 150 or 200 mg). The liquid monomer (1 ml) was then added to the prepared powder and mixed well. The resulting chemotherapeutic bone cement mixture was used within 5 minutes to prepare the elution and mechanical test specimens.

Preparation of *in vitro* test specimens: Glass vials were used as molds to prepare the cylindrical specimens. The prepared methotrexate/bone cement mixtures were poured into the glass vials and were allowed to harden for 24 h at 37^{o} C. The polymerized cylindrical bone cement specimens were then taken out of the glass molds by breaking the glass molds carefully. Three cylindrical elution test specimens were prepared in each group.

***In vitro* elution experiment:** The cylindrical bone cement specimens were placed in vials containing 20 ml saline. The vials were placed in an incubator maintained at 37^o C. Methotrexate elution was measured at different time points for 670 h. The eluted methotrexate concentration was measured in triplicates using a micro-plate reader (Spectramax 190, Molecular devices, CA) at a wavelength of 405 nm. The elution media was replaced whenever the methotrexate concentration was measured.

Three-point bending test: 2 x 2 x 40 mm rectangular test bars were prepared by injecting bone cement mixtures into square borosilicate glass tubes (Friedrich & Dimmock, Milvile, NJ). The post cured specimens were soaked in 50 ml saline for 20 days. Flexural strength and modulus of the bone cement specimens after soaking was determined by a 3-point bending test. The specimens were loaded to failure by using an electromechanical testing machine (800LE4 Dynamic Test System, Test resources Inc., Shakopee, MN) at a crosshead speed of 1 mm/min. The distance between the support beams of the three point test jig is 28 mm.

The flexural strength (in MPa) for a three point bend test was calculated by the following formula

$\sigma = 3lF/2BH^2$ ---------- (2)

where l is the distance between the supports in mm, F is the failure load (N), B is the width, and H is the height of the beam in mm.

The flexural modulus (E in GPa) for a three point bend test was calculated from

$E = (F/D)\,(l^3/4BH^3)$ ---------- (3)

where l is the distance between the supports in mm, B and H are the specimen width and height respectively in mm, and F/D is the slope in the linear region of the load-displacement curve.

RESULTS AND DISCUSSION

The results indicate that the relationship between initial methotrexate amount and methotrexate elution is non-linear. Methotrexate elution increased four fold when the initial methotrexate amount was increased from 100 to 200 mg. This may be due to the drastic changes in pore structure and interconnectivity caused by the addition of 200 mg methotrexate. The effect of changes in pore structure on the mechanical properties of bone cement was evaluated using a three point bending test. Addition of methotrexate decreased the flexural strength of vertebroplastic bone cement. However, the flexural modulus (dry control specimens) was not affected by the addition of methotrexate. The mechanical properties decreased after soaking in saline for 20 days (Table 1). It should be noted that the stiffness and strength of bone cement is usually very high when compared to the properties of cancellous bone [3]. Therefore, the decrease in mechanical properties of this experimental chemotherapeutic bone cement after soaking should not in anyway compromise the mechanical stability of the fracture construct. Due to the potential local toxicity to surrounding vital organs, the surgeons should be careful in determining the initial amount methotrexate added.

CONCLUSIONS

The results showed that Vertebroplastic bone cement is suitable for use with chemotherapeutic agents. Initial methotrexate amount seems to play a major role in the pore structure formation. This should be kept in mind to avoid any local drug toxicities to adjacent healthy tissues.

REFERENCES

1. Roodman (2004) N Engl J Med 350:1655-64.
2. Handal *et al* (2007) Clinical Orthopaedics and Related Research. 459: 105-109
3. Boger *et al* (2005) European Cells and Materials. Vol. 10, S1

ACKNOWLEDGEMENTS

Authors would like to thank Depuy Spine, MA for their financial support and bone cement.

Table 1: Mechanical properties of bone cement pre and post elution. Control did not contain any methotrexate.

	Flexural Strength (MPa)	Flexural Modulus (MPa)
Before soaking		
Control	55.6 ± 2.9	2408.6 ± 62.5
100 mg MTX	47.7 ± 2.8	2589.6 ± 178.1
200 mg MTX	39.4 ± 2.7	2540 ± 76.5
After soaking for 20 days		
Control	43.7 ± 2.8	1839.3 ± 51.4
100 mg MTX	30.3 ± 3.4	1438.8 ± 55.1
200 mg MTX	28.9 ± 1.8	1391.4 ± 94.9

FEMALES EXHIBIT SHORTER PARASPINAL REFLEX LATENCIES THAN MALES

[1] Emily M. Miller, [1]Gregory P. Slota and [1,2]Michael L. Madigan
[1]Virginia Tech-Wake Forest SBES, [2]Virginia Polytechnic Institute and State University ESM
email: millerem@vt.edu, web: www.biomechanics.esm.vt.edu

INTRODUCTION

Females suffer low back disorders (LBD) at a higher rate and with greater severity than males [1]. The reasons for gender differences are unclear, but they may relate to paraspinal reflexes as they contribute to spinal stability control [2]. In fact, LBD patients exhibit altered paraspinal reflexes compared to healthy controls [3], and gender differences have been reported in the paraspinal reflex response [4,5]. However, studies reporting gender differences in reflexes were confounded by factors such as an experimental condition (e.g. rehabilitation, prolonged flexion, or an extension preload) or differences in trunk kinematics secondary to differences in trunk mass.

Due to the confounding factors within these studies, our goal was to investigate gender differences in paraspinal reflex latency while accounting for gender differences in kinematics. Since reflex latency in the knee musculature was reported to be shorter in females in response to perturbations scaled by body weight [6], it was hypothesized that females would exhibit shorter paraspinal reflex latencies than males.

METHODS

Force perturbations were applied to the trunks of 10 males (mass: 73.4 ± 1.5 kg, age: 22.6 ± 2.8 yr) and 10 females (mass: 65.0 ± 1.4 kg, age: 27.2 ± 7.8 yr). While in an upright stance, participants were restrained from the pelvis down and attached to a pendulum via Kevlar cable and a harness (Figure 1). The weighted pendulum swung down and away from the participants to elicit a brief flexion moment at the instant when the pendulum reached vertical and the cable became taut. Five perturbations were applied at each of five levels, presented in random order and resulting in impulses averaging 3.97 ± 0.22, 5.96 ± 0.32, 7.67 ± 0.70, 9.00 ± 0.66, and 10.21 ± 0.59 N·s. Levels were set by adjusting the height of the weight on the pendulum. Participants were instructed to close their eyes, cross their arms, relax prior to the perturbation, and calmly return to an upright position following the perturbation. Real-time EMG was monitored to ensure no anticipatory stiffening of the trunk musculature in extension or with co-contraction.

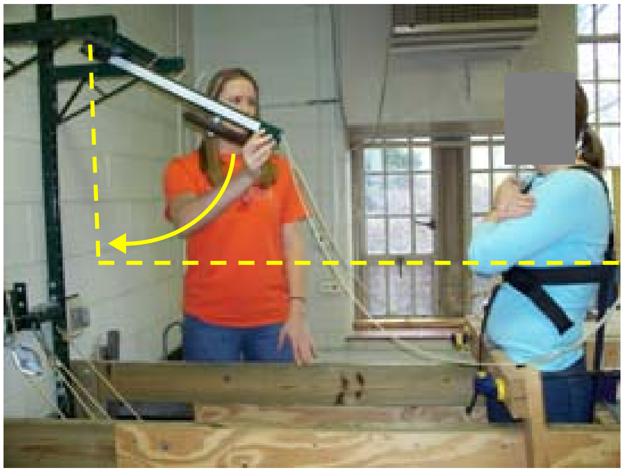

Figure 1. Experimental set-up. The vertical dotted line represents the final pendulum position when the cable is taut, shown as the horizontal dotted line.

Muscle activity was sampled at 1000 Hz with bipolar surface EMG electrodes (Measurement systems Inc., Ann Arbor, Michigan) placed on the erector spinae and rectus abdominus, band-pass filtered between 40 and 500 Hz, rectified, and integrated with a 25 Hz low-pass filter. Trunk rotation was sampled at 100 Hz with a tri-axial angle sensor (X-sens Motion Technologies, Netherlands) placed at the T6-T8 level of the spine and low-pass filtered at 20 Hz. Tension forces in the cable were sampled at 1000 Hz with an in-line load cell (Interface SSM-500, Scottsdale, Arizona) and low-pass filtered at 20 Hz.

Reflex latency was determined as the time delay between force onset in the cable and EMG onset in the erector spinae, up to 120 ms to exclude voluntary responses [5]. Onset times were found when a baseline mean, from 50-250 ms prior to each perturbation, was exceeded by two standard deviations. Trunk kinematics in response to the perturbations were quantified using the maximum trunk flexion velocity between force onset and the time of maximum flexion. Regression analyses were conducted to determine the effects of gender on reflex latency with respect to the recorded impulses and maximum flexion velocities.

RESULTS AND DISCUSSION

Reflexes were detected in 94% of the perturbations. Regressing reflex latency with respect to impulse (Figure 2a), reflex latency was shorter in females than males (p=0.036) and did not vary by impulse (p=0.325). However, maximum trunk flexion velocity (Figure 2b) was faster (p=0.013) in females compared to males and increased with impulse (p<0.001). This may have been due to smaller whole body (and therefore trunk) mass in females compared to males (p<0.001). Regressing reflex latency with respect to maximum trunk flexion velocity (Figure 2c), reflex latency remained shorter in females (p=0.037) and was not affected by maximum trunk flexion velocity (p=0.154). Prior to each perturbation, baseline EMG as a percentage of maximum voluntary contraction did not vary by gender (p=0.264) or impulse (p=0.277).

These findings reveal that reflex latency was shorter in females in response to the force perturbations applied to the trunk when accounting for gender differences in trunk kinematics. This does not match previous paraspinal findings of either longer female reflex latencies or no gender differences [4,5]. However, the former was concluded from a rehabilitation study, after which males decreased reaction time more dramatically than females [5], and the latter was found during an extension preload or following static flexion, both of which could alter reflex characteristics [4]. Our gender differences were consistent with shorter reflex latencies of the quadriceps in females [6].

The injury mechanism for LBD remains unclear. If impaired reflexes contribute directly to LBD, then the shorter latencies in females found here appear to be inconsistent with the longer latencies found in patients with LBD [3]. Additional research is needed to elucidate the role of paraspinal reflexes in LBD and to understand the causes for gender differences in LBD. Investigating other aspects of neuromuscular reflexes may help explain these gender differences in LBD.

REFERENCES

1.MacDonald MJ, et al. *J Occup Environ Med* **39**, 35-43, 1997.
2.Panjabi MM. *J Spinal Disord* **5**, 383-389, 1992.
3.Radebold A, et al. *Spine* **26**, 724-730, 2001.
4.Granata KP, et al. *Clin Biomech* **20**, 16-24, 2005.
5.Wilder DG, et al. *Spine* **21**, 2628-2639, 1996.
6.Shultz SJ, et al. *J Athl Train* **36**, 37-43, 2001.

ACKNOWLEDGEMENTS

This research was funded by 2 RO1 AR046111.

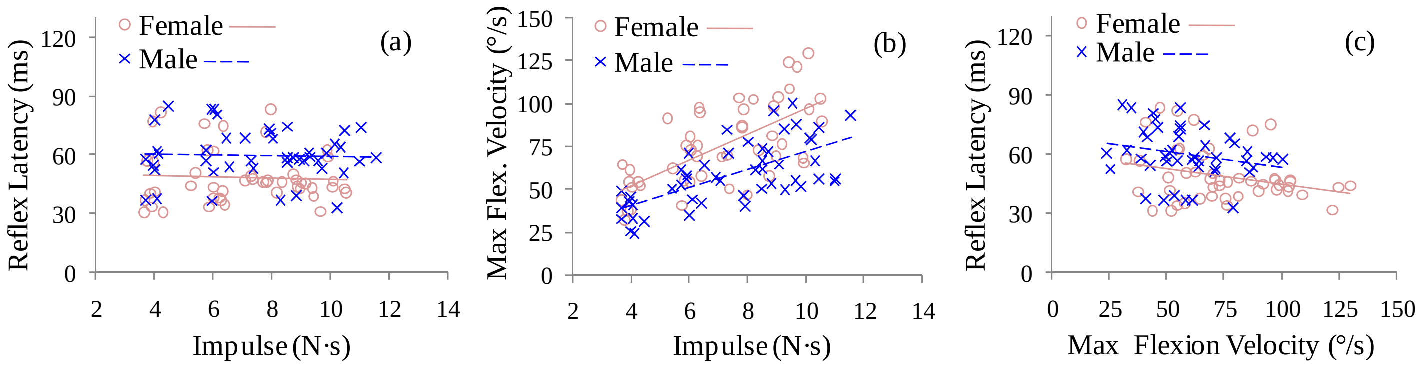

Figure 2. Responses to the force perturbations: a) reflex latency with respect to impulse, b) maximum trunk flexion velocity with respect to impulse, and c) reflex latency with respect to maximum trunk flexion velocity.

RELIABILITY OF MUSCLE FIBRE CONDUCTION VELOCITY IN THE TIBIALIS ANTERIOR

Kyle C. McIntosh and David A. Gabriel
Electromyographic Kinesiology Laboratory, Brock University
e-mail: dgabriel@brocku.ca

INTRODUCTION

Recent efforts directed at using muscle fibre conduction velocity (MFCV) to assess neuromuscular disorders have had difficulty in achieving high test-retest reliability across multiple sessions, as assessed by the intraclass correlation coefficient (ICC). Previous studies have produced mixed results. Merletti et al. (3) examined the tibialis anterior with an electrode array ($ICC = 0.11$) while Farina et al. (1) studied the biceps with an electrode grid ($ICC = 0.75$). Grid electrodes improved the reliability estimates but not enough for clinical work (2).

The lower reliability in both studies was attributed to differences in electrode replacement across test sessions, and electrode misalignment with respect to the muscle fibres which resulted in an overestimation of MFCV. The purpose of this study was to determine if MFCV methodology could be refined sufficiently to improve its test-retest reliability while using an array electrode. The establishment of a reliable electrode placement method with an array electrode would facilitate the widespread use of MFCV in both clinical and research laboratories.

METHODS

Eighteen college-aged individuals participated in this study. There were three days of testing with at least 48 hours between each test day. Each session began with skin preparation, identification of the motor point(s), and placement of a 4-bar surface electrode. A series of evoked potentials (M-waves) in the tibialis anterior were elicited by stimulating the deep peroneal nerve with a handheld probe. The resulting M-waves were used to evaluate the similarity of potentials across recording surfaces, and to angle the electrode to maximize the delay between subsequent potentials. Subjects then performed five-second isometric actions of the dorsiflexors at 30 and 100% of maximal voluntary contraction (MVC). There were at least three minutes between each contraction.

The sEMG signals were band-passed (3-1000 Hz) and amplified (Grass P511, Astro-Med Inc., West Warwick, RI) to maximize their resolution on the 16-bit analogue-to-digital converter (NI PCI-6052E, National Instruments, Austin, TX). The force (JR3 Inc., Woodland, CA) and sEMG signals were then sampled at 5 kHz using a computer-based data acquisition system (DASYLab, DASYTEC National Instruments, Amherst, NH). The data were stored on a Celeron PC for off-line processing (Dell, Round Rock, TX). Force, root-mean-square (RMS) sEMG amplitude and MFCV were calculated on a 1-second segment window of data located in the first half of the contraction (MATLAB, The Math Works, Natick, MA).

To calculate MFCV, the sEMG signals were first up-sampled to 25 kHz in increase the time resolution (see Figure 1). The stability of the MFCV estimate was not improved by a higher sampling rate. The cross-correlation function $R_{xy}(t)$ was then calculated for adjacent bipolar signals $x(t)$ and $y(t)$, detected 1 cm apart:

$$R_{xy}(t) = \int_{\infty}^{\infty} x(\tau)y(t+\tau)\,dt$$

The time-shift (τ) associated with the maximum correlation was used as the delay in the calculation of MFCV. To ensure the similarity in signals, the cross-correlations were always greater than 0.80 (see Figure 2).

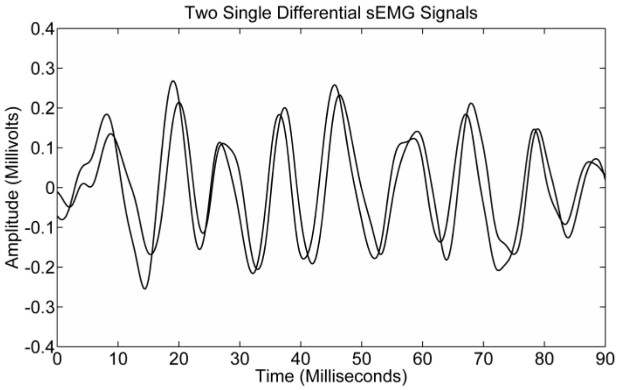

Figure 1. Two sEMG waveforms to illustrate a distinct time difference between the signals.

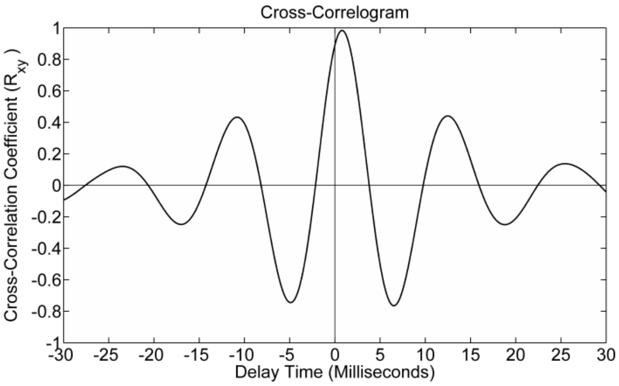

Figure 2. The cross-correlation between the sEMG signals depicted in Figure 1.

RESULTS

The test-retest reliability of 30% MVC force was better than 100% MVC force (see Table 1). The opposite was true for RMS sEMG amplitude. However, the test-retest reliability of MFCV for the two conditions was comparable. The means, standard deviations, and reliability coefficients for the criterion measures at the 100% MVC condition are consistent with other studies (1,3,4). However, the reliability coefficients are greater than previously reported (1,3).

CONCLUSIONS

Using M-waves to evaluate the similarity of potentials across recording surfaces, and to angle the electrode to maximize the delay between successive potentials, resulted in very good test-retest reliability for MFCV in the tibialis anterior. Further, the results were obtained with a 4-bar electrode array and commercial amplifiers, suggesting that it is possible to obtain reliable data using commonly available equipment.

REFERENCES

1. Farina D, et al. *J Neurosci Meth* **115,** 1-12, 2002.
2. Kimura J. *J Neurol Neurosurg Psyciatry* **71**, 427-430, 2001.
3. Merletti R, et al. *J Electromyogr Kinesiol* **5, 2,** 67-80, 1995.
4. Patten C, Kamen G. *Eur J Appl Physiol* **83**, 128-143.

ACKNOWLEDGEMENTS

Funding provided by the Natural Sciences and Engineering Research Council of Canada (NSERC).

Table 1. Means (M), standard deviations (SD), and intraclass correlation coefficients (ICC) for force, muscle fiber conduction velocity (MFCV), and root-mean-square (RMS) amplitude at 30 and 100% of maximal voluntary contraction (MVC).

	100% MVC Condition			**30% MVC Condition**		
	Force (N)	MFCV m/s	RMS (mV)	Force (N)	MFCV m/s	RMS (mV)
Mean (SD)	165.52 ± 16.46	5.02 ± 0.74	0.20 ± 0.04	51.66 ± 6.66	4.46 ± 0.60	0.04 ± 0.01
ICC	0.72	0.86	0.93	0.91	0.84	0.65

MISSTEPPING AND HIP FRACUTES IN THE OSTEPOROTIC ELDERLY

Mehmet Uygur, James G. Richards, Slobodan Jaric, Paulo B. de Freitas and David A. Barlow
Department of Health, Nutrition and Exercise Sciences, University of Delaware
Email: muygur@udel.edu

INTRODUCTION

Hip fractures are one of the most detrimental health problems among the elderly. It has been believed that most of the hip fractures are fall related. However, it could be speculated that excessive loading of the lower extremity throughout an unexpected level change during locomotion (i.e., an unforeseen curb while walking or miscounting the number of stairs during stair descent) may represent an underestimated reason of this devastating problem. Therefore, we hypothesized that the forces acting on the hip joint throughout missteps may occur within the range of theoretically necessary values leading to hip fractures in the osteoporotic elderly.

METHODS

A customized platform and a box, 17.8 cm high, were placed end to end with the box set on top of a force plate. Fourteen healthy young adults (age, mass and height were (mean ± SD) 24 ± 3.9 years, 173 ± 8.4 cm, and 72.3 ± 15.5 kg, respectively) completed the following four experimental conditions:

1. Participants stood upon the elevated platform and were asked to take two steps forward initiated with the right foot and finishing on the box bringing both feet together. This stepping action was repeated four times and was referred to as *regular stepping forward (RSF).*
2. Participants were then blindfolded and repeated the first procedure up to 12 times. This task was referred to as *blindfolded stepping forward (BSF).*
3. In a randomly selected trial between the 4th and 12th conditions of *BSF,* the box over the force plate was unexpectedly removed. Therefore, participants took a right step forward and landed on the force plate which was positioned 17.8 cm lower than the height of the platform. This trial was collected once and referred to as *misstep*.
4. The blindfold was thereafter removed and participants were asked to take one step forward and one step down on the force plate with their left foot. This action was repeated 4 times and referred to as *regular stepping down (RSD).*

Kinetics of all four conditions were recorded at a rate of 1 920 s^{-1} using an AMTI force plate, while the kinematics of the lower extremities was simultaneously recorded by 8 CCD cameras operating at 240 Hz. Inverse dynamics were applied to the collected data. Sagittal plane joint angles were analyzed at the foot contact and at the peak ground reaction force (GRF). Peak vertical forces of the proximal thigh segment (PrxTF) in the local coordinate system and its loading rate (PrxTF/ time to peak forces) were also calculated.

RESULTS AND DISCUSSION

No differences were found among the selected kinematic (Figure 1) and kinetic (Figure 2) variables between RSF and BSF which indicated that the methodological approach to induce missteps was successful. In addition, results showed that the missteps resulted in an altered joint positioning in the ankle and knee at both the foot contact and peak GRF when compared to RSD. Moreover, missteps caused markedly larger peak vertical proximal thigh forces (PrxTF), and greater loading rates when compared to other stepping conditions.

When the misstep condition was compared to RSF and BSF, no differences were found in the plantar-flexion angle of the ankle at foot contact and also in the knee flexion angle at peak GRF ($p>.05$). Both PrxTF and its loading rate was greater ($p<.001$) during missteps when compared to RSD (Figure 2). GRF range during misstep was found to be between 2005-3908 N, whereas during RSD the same forces were 803-1440 N.

The joint angles during RSD at the time of foot contact were found to be similar to the previously reported for normal stair descent (1). During stair descent, plantarflexed position of the ankle plays a crucial role during the dissipation and absorption of the energy among lower extremity joints. However, the ankle was found to be in dorsiflexed position during missteps at the time of foot contact and was similar to those occurring in stepping forward conditions. Therefore the necessary pre-programmed joint positioning that is required for RSD was lacking in missteps. Moreover, the lower extremity was in a more upright position during misstep when compared to RSD at peak GRF which might be important factor in transmitting the impact forces to the proximal femur.

To evaluate whether the forces acting upon the hip joint during misstep would be sufficient to cause possible hip fractures in the elderly, we compared our PrxTF with the ultimate strength of the proximal femur previously reported in in-vitro studies. The PrxTF range in our study (1610-3082 N) occurred within the range for fractures reported in previous in-vitro studies representing vertical loading (933-7000 N) (2) and stair descent (942-5281 N) (3).

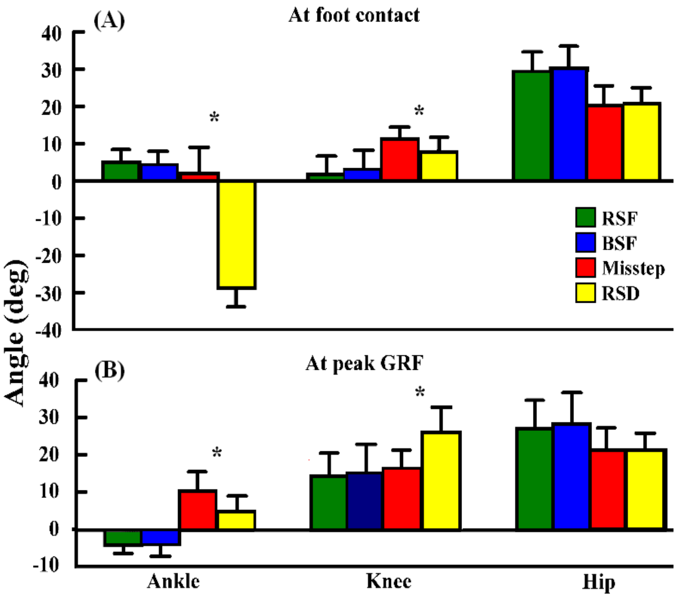

Figure 1. Sagittal plane joint positioning (means and SD error bars): (A) at foot contact, and (B) at peak GRF. Positive values indicate dorsiflexion for ankle, flexion for knee and hip (* indicate significant difference ($p<.05$) between misstep and RSD)

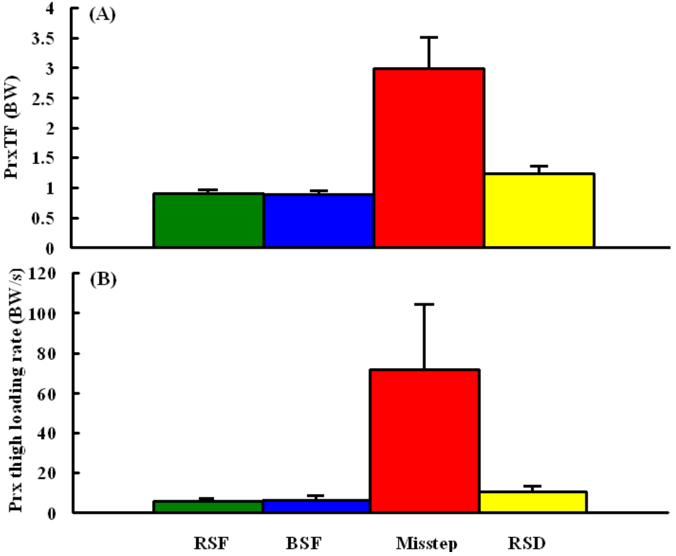

Figure 2. Kinetic variables (means and SD error bars) showing (A) peak vertical proximal thigh segment force, and (B) proximal thigh segment's loading rate.

CONCLUSIONS

As a result of the altered joint positioning, uncommonly high and rapidly loading acting upon the lower extremity were found during missteps. Furthermore, the forces acting on the proximal thigh segment during missteps were within the range of theoretical force values reported in the literature that may lead to hip fractures. Therefore, missteps could be an underestimated reason for hip fractures of the osteoporotic elderly. To reduce this vulnerability in elderly populations, efforts to attenuate high impact loading situations should be made. This could be accomplished by designing more appropriate shock attenuating footwear or walking surfaces, as well as by making necessary architectural adjustments to the physical environment.

REFERENCES

1. Andriacchi TP, et al. *J Bone Joint Surg Am* **62**, 749-757, 1980.
2. Lochmuller EM, et al. *Osteoporosis International* **8(6)**, 591-598, 1998.
3. Michaeli DA, et al. *Skeletal Radiology* **28(2)**, 90-95, 1999.

TEST-RETEST RELIABILITY OF IN-SHOE LATERAL HEEL PRESSURE MEASUREMENTS DURING GAIT

[1]Kristyn M. Leitch, [1]Trevor B. Birmingham, [1]J. Robert Giffin, [1]Ian C. Jones and [1]Thomas R. Jenkyn
Wolf Orthopaedic Biomechanics Laboratory, University of Western Ontario: London, Ontario, Canada
email: kleitch@uwo.ca

INTRODUCTION

Lateral heel wedges (LHW) provide a potential non-invasive and low cost means of decreasing knee joint loads and pain in individuals with medial compartment knee osteoarthritis (OA). Although there is some evidence to suggest that LHWs decrease the external knee adduction moment (EKAM) during gait and improve symptoms, previous studies have produced inconsistent results [1, 2]. Further investigation into the mechanisms of LHW is warranted. It has been suggested that wedging causes a change in foot pressures that directly affect the knee adduction moment [3, 4]. However, the measurement of foot pressures during walking is a relatively new aspect of quantitative gait analysis that has not yet undergone rigorous reliability testing, particularly under the conditions used to test the effects of LHWs. The purpose of this present study was to examine the test re-test reliability of the lateral heel pressure (LHP) during gait with a LHW intervention

METHODS

Twenty-eight participants (9 male, 17 females, mean age 44 ± 8 yrs.) completed two separate test occasions, at least 24 hours apart and within one week. After giving written consent in accordance with the Institutional Review Board, each participant underwent three-dimensional gait analysis, using 8 high speed high resolution digital cameras and a floor mounted force plate, while instrumented with the Novel Pedar-X in-shoe plantar pressure measurement system (Novelelectronics Inc., St.Paul, MN, USA). During testing, participants were exposed to three LHW conditions in random order: standardized footwear (SF) (no wedge condition), or SF with 4°, and 8° wedge, placed underneath the insole on the lateral side of the participants dominate leg. Kinematic and kinetic data were combined to calculate the first peak EKAM normalized to body size (%BW x Height). The foot was divided into four quadrants and the lateral heel quadrant was used to determine LHP at the moment first peak EKAM occurred. The same area of pressure cells was analyzed for visit 1 and visit 2 for each participant. Statistical analysis was confined to the limb receiving the LHW intervention. To graphically assess agreement between measures, Bland and Altman plots were constructed. Intra class correlation coefficients (ICCs) (type 2, 1) and standard error of measurement (SEM) were then calculated to evaluate reliability of the measurements [5, 6, 7]. The ICC provided an indication of how well the measures distinguished among patients (relative reliability), while the SEM provided an expression of the measurement error in original units (absolute reliability).

RESULTS AND DISCUSSION

Bland and Altman plots for day 1 and day 2 show a strong agreement and a systematic bias between days 1 and 2 (Figure 1). This bias indicates a possible learning effect. The ICCs with 95% CIs and the SEMs are reported in Table 1. The ICCs for LHP were consistently high (0.79-0.83). The SEM allows us to interpret the lateral heel pressure measurements within a certain amount of measurement error. For example, if a participant reported a lateral heel pressure measurement of 120kPA we could be 95% confident that the participant's true value range from 97.38 kPa to 142.62 kPa.

CONCLUSIONS

The present reliability estimates are only generalizable to participants with characteristics similar to those in this study, as well as to similar

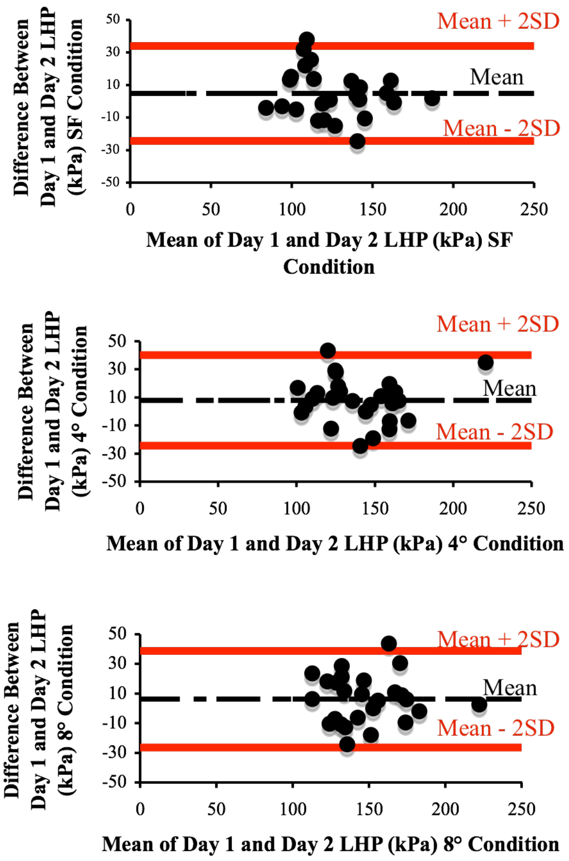

Figure 1: Bland and Altman Plots for day 1 and day 2 LHP during SF, 4 and 8 wedge condition

testing equipment and procedures. It should also be kept in mind that no studies were found with comparable participant demographics and testing procedures, and therefore, it is not possible to directly compare the results of this study to those in the current literature. It is encouraged that further investigation into the effect of lateral heel wedges on similar gait parameters be conducted.

REFERENCES

1.Butler RJ, et al. *J Orthp Res* **9**, 1121-1127, 2007.
2.Rubin R, et al. *J Am Podiatr Med Assoc* **95**, 347-352, 2005.
3.Erhart JC, et al. *J Biomech* **41**, 2989-2994, 2008.
4.Maly MR, et al. *J Clinical Biomech* **17**, 603-610, 2002.
5.Birmingham TB, et al. *Arthr Rheum* **15**, 1012-1017, 2007
6.Shrout PE, et al. *Psychol Bull* **86**, 420-428, 1979.
7.Stratfor PW, et al. *Phys Ther* **77**, 745-755, 1997.

Table 1: Test Re-Test Reliability Statistics For Lateral Heel Pressure

	ICC*	**95% CI***	**SEM***
		Min, max	
Lateral Heel Pressure kPa			
Standardized Footwear	0.83	0.65, 0.92	10.33
4° Wedge	0.81	0.58, 0.91	11.39
8° Wedge	0.79	0.58, 0.90	11.54
*ICC= Intraclass Correlation Coefficients, SEM = Standard Error of Measurement, CI = Confidence Interval			

INVERSE OPTIMIZATION OF DIGIT FORCES IN MULTI-FINGER PREHENSION BASED ON ANALYTICAL DETERMINATION OF THE OBJECTIVE FUNCTION

[1, 3] Xun Niu, [1]Alexander V. Tereknov,
[2]Yakov B. Pesin, [1]Mark L. Latash and [1]Vladimir M. Zatsiorsky

[1]Department of Kinesiology, [2]Mathematics Department, [3]Department of Statistics
The Pennsylvania State University, University Park, PA,
email: xun100@psu.edu

INTRODUCTION

The problem of inverse optimization consists of finding a cost function that is being optimized by the central controller in a given motor task. A common approach to this problem is to 'guess and check': a researcher selects a set of likely candidate cost functions, e.g. the sum of the squared or cubed values of the muscle forces or digit forces, etc, and applies these functions to the obtained experimental data. The cost function that better fits experimental data is accepted as the function most probably used by the central controller (see [1] for the review).
This approach was recently challenged by attempts not to guess the cost function but to determine it analytically from the experimental data [2, 3]. In this study, a new method of Analytical Inverse Optimization [3] was applied in human multi-finger prehension (grasping) study.

METHODS

Experiment. Eight male subjects were instructed to stabilize in the air a vertically oriented instrumented handle using a prismatic grasp. The forces and moments of force exerted by individual digits were recorded with six ATI 6-component sensors. Four loads, 0.25, 0.5, 0.75, and 1.0 kg were attached at different points along the horizontal bar attached to the handle, thus generating four external torques of 0.2 Nm, 0.4 Nm clockwise and counterclockwise plus zero torque. There were a total of 20 different load/torque conditions in the experiment. The experiment had two phases: calibration and force exertion at the target level. First, the subjects were instructed to hold the handle vertically with minimal normal (grip) force. The computer recorded the forces and then set a target force level at a specified percentage of the calibration force 100%, 125%, 150% and 175%. Visual feedback on the grip force and target force was provided on the computer screen. Subjects were instructed to squeeze the handle and to match the target force level. Each trial lasted 10 seconds.

Optimization. The objective function for this experiment was assumed to be an unknown additive function J of unknown scalar differentiable functions g_i. The mathematical method of finding such a function(s) that includes also a proof of the Uniqueness Theorem is described in [3]. Two linear equality constraints were assumed.

Minimize:

$$J(F_1, F_2, F_3, F_4)=g_1(F_1)+ g_2(F_2)+ g_3(F_3)+ g_4(F_4)$$

subject to constraints of total force and moment:

$$\begin{pmatrix} 1 & 1 & 1 & 1 \\ Y_1 & Y_2 & Y_3 & Y_4 \end{pmatrix} F = \begin{pmatrix} \frac{1}{2} F_{total} \\ M^n \end{pmatrix}$$

where g_i is an unknown scalar differentiable function with $g'(\cdot)>0$ in the feasible region, F_i is the individual finger normal force, Y_i is the average coordinate of the center of force application (CFA) of each finger with respect to the thumb, F is the normal force vector, F_{total} is the total normal force magnitude, M^n is the moment generated by the normal force. The matrix at the left hand side of the linear constraints is C.

The pivotal idea in finding the objective function J is to minimize the angle between the subspace formed by the main principal components of the matrix of experimental data and the plane $\breve{C}KF = 0$, where $\breve{C} = I - C^T(CC^T)^{-1}C$ and K is a 4×4 orthogonal matrix composed of the coefficients of the highest order terms in the objective function J. There are an infinite number of objective functions to yield the same optimal solution. However, the method allows finding a solution which is essentially similar to J up to unknown linear terms (Uniqueness Theorem [3]).

RESULTS AND DISCUSSION

The data points from 80 trials by each subject dispersed around a plane in a four-dimensional space (corresponding to the four normal finger forces), which could be determined by the PCA (94.04±0.41% variance explained by the first two principal components).

The angle between the reconstructed plane $\breve{C}KF = 0$, and the principal components was 2.53±0.74 degree. The new plane contained 93.76±0.37% of the raw data variance.

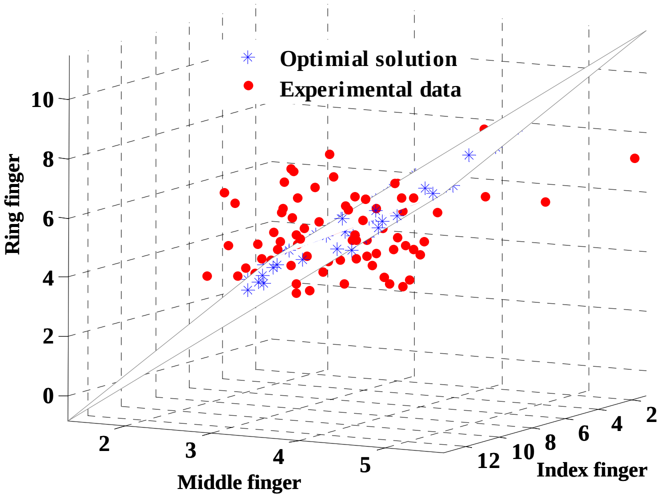

Figure 1: The two-dimensional surface of finger forces projected onto the three-dimensional space: Ring finger-Index finger-Middle finger. Red dots represent the observed experimental data; Blue stars represent the optimal solution obtained from the optimization procedure.

The Analytical Inverse Optimization procedure estimated the formulation of the objective function for each subject in the experiment. An exemplary objective function generated for subject #1 was

$$J = \frac{1}{2}(F_1^2 + 2.64F_2^2 + 2.13F_3^2 + 6.35F_4^2) - 1.91F_1 + 1.43F_2 + 2.92F_3 - 2.45F_4$$

For all subjects, the formulation of objective function showed positive coefficients of the second order term which agreed with the assumption of minimizing the objective function; otherwise the optimal solution could not be obtained since the objective function had an infinite minimal value.

The experimental data and the optimal solution projected onto a three-dimensional space are illustrated in figure 1. The experimental data were scattered around the plane; all the optimal solutions from the estimated objective function were located on the reconstructed plane. The errors of normal force sharing percentage in virtual finger (an imagined finger with the same mechanical effect as all four fingers) between the experimental data and the predicted values were less than 6% over all fingers and subjects (Table 1). To see the random error of sharing percentage due to the trial-by-trial error, subject #1 did a ten-day experiment (load: 0.5 Kg; torque: 0.4 Nm) with 12 trials every day. The random errors were 3.0%, 3.5%, 4.6% and 4.0% for the index, middle, ring and little finger. The optimization and random errors were very close.

The absolute error value between the experimental data and optimization results were 0.36±0.04 N, 0.49±0.04 N, 0.44±0.01 N and 0.35±0.02 N for the index, middle, ring and little finger across subjects.

CONCLUSIONS

The suggested method was successful in finding an objective function that satisfied well the experimental data.

REFERENCES

1. Prilutsky BI, Zatsiorsky VM. *Exerc Sport Sci Rev* **30**: 32-38, 2002.
2. Bottasso CL, et al. *Multibody Syst Dyn* **16**:123-154, 2006.
3. Terekhov VA, Pesin YB, Niu X, Latash ML, Zatsiorsky VM. Submitted to *J Math Biol*

ACKNOWLEDGEMENTS

The study was partially supported by NIH grants AG-018751, NS-035032, and AR-048563 and NSF grant DMS-0503810.

Table 1: The RMS differences between the observed normal force sharing percentages and the values predicted from optimization (in **%** of the VF normal force). The data are for eight subjects.

Note: the values in the table are very close to the random error (trial-by-trial error) observed in the experiment

Subject #	1	2	3	4	5	6	7	8
Index finger	1.8	2.36	2.66	2.85	2.76	2.37	4.54	4.38
Middle finger	2.85	3.68	3.68	3.54	3.56	2.82	5.9	4.91
Ring finger	4.13	3.82	3.22	3.24	3.5	3.43	3.63	4.46
Little finger	2.47	2.73	2.54	2.58	2.8	2.29	4.05	3.96

AN ANALYSIS OF CHARACTERISTICS OF GROUND RECATION FORCES ACCORDING TO CIRCLE MOTION IN GYMNASTICS THE POMMEL HORSE

^{1}Daegeun Kim, ^{2}Kwangdong Park, ^{3}Kyoungkyu Jeon
^{1}Dankook University, ^{2}Dankook University, ^{3}Dankook University
email: kdg0933@empal.con

INTRODUCTION

The pommel horse is a gymnastic apparatus which consists of a horse 105 centimeters high, 160 centimeters long, and 35 centimeters wide and two knobs on it (FIG 2008).

In order to perform more balanced motion from aspects of other components as well as knobs, gravity and forces which result from the apparatus are conveyed to the upper part of the body and legs of a gymnast by means of his hands and perform a motion. A gymnast's forces of pressing according to ground reaction force and his hand's frictional force are essential factors for performing a desirable motion.

So, this research aims to examine the mechanism of a circle motion, a basic one of the pommel horse competition, by analyzing factors of changes in performing the motion from a viewpoint of motor mechanics and to provide an efficient method of training for the competition.

METHODS

To achieve these purposes, this research adopts four gymnasts with a 10-year career as a scope. Their physical characteristics and details are shown in Table 1.

Table 1: The Physical Characteristics of Study Subjects

Subject	Age	Training	Weight	Height
4	22.25±0.5	11.75±0.5	62.25±1.26	167.25±2.99

This research uses two motion master 100 IR cameras and two ground reaction force instruments (AMTI ORG-6 Model) for setting up an event.
Event is defined, as shown in Figure 1.
The intensity of ground reaction force and the trace of circle motion are determined by Kwon 3D XP Program and divided into each body weight of the four subjects by means of Dowling & Vamos's (1993) equation for standardization.

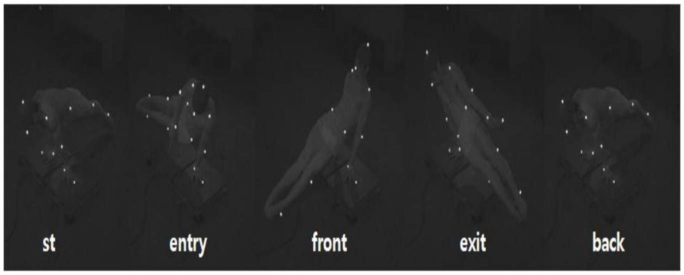

Figure 1: Circle Event

RESULTS and DISCUSSION

1. Change of time according to motion
Mean values and standard deviations of events at circle motion are shown in Table 2.
The four subjects are much alike in the time average required to make a turn of circle motion: 0.85 ± 0.04 seconds. The distance between entry and front is greatest in the locomotive section. A lot of time is required to reduce the speed of revolution and to keep the balance of the centroid because the body is not extended at performing motions.

Table 2: Reqyired Time by Section Unit: sec

	entry	front	exit	back
M±SD	0.21±0.02	0.44±0.02	0.65±0.02	0.85±0.04

2. Ground reaction forces
Data analysis is made on the intensity and direction of ground reaction forces which result from the main motion event and values of the intensity and direction of the four subjects are compared; values of Fx, Fy, and Fz stand for values of direction of interior (-) and exterior (+), direction of front (-) and rear (+), and direction of horizon (+), respectively.

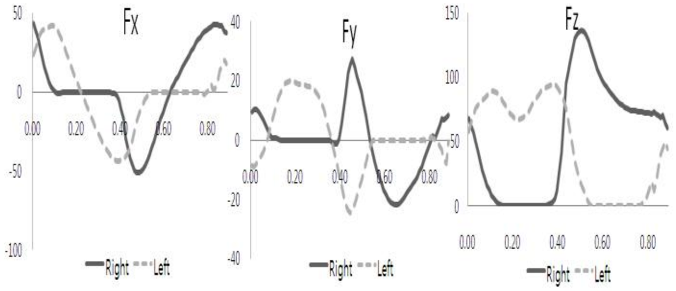

Figure 1: Values of ground reaction forces

Values of ground reaction forces of the left hand and the right hand are shown in Table 3 and Figure 2. The values of ground reaction forces at performing the main motion indicate that the right hand's force is bigger than the left one. The locomotion of weight is observed when the right hand is turned to the left, and the ground reaction force in at the end of the motion is bigger than the force in the beginning of the motion. This result is inferred from that the motion is performed while a gymnast is revolving on an axis.

Fy refers to ground reaction force at moving back and forth. The force which pushes the body backward is called braking force, and the force which pushes forward, and move backward, the body is called propulsion force. The motion at entry does not affect ground reaction forces because it is performed by left finger ends which push the front surface and thrust the body forward by means of the propulsive force of the left hand. It is observed that right finger ends transmit force to the front surface and turn the body in the direction of motion and that the palm of the light hand takes the locomotive balance by means of the braking force.

In vertical ground reaction forces, bigger are values of the right side compared to values of the left side. This means that there is a delicate coordination between the body and of segments of two legs on the axis of the hand and that the right hand pushes the apparatus strong to support the movement of the upper part of the body and raise the hip and the center of the body while the body being turned to the left

CONCLUSIONS

So far, this research adopted three gymnasts as a scope, utilized ground reaction force instruments, and analyzed factors of changes in performing the motion from the angle of a motor mechanics. The results of analysis are as follows.

Greatest is the time required to make a turn of circle motion between entry and front in the locomotive section. This is because the left hand touches the ground reaction force instrument and keeps the balance of the centroid.

Values of Fx, Fy, and Fz from ground reaction force instruments suggest that the circle motion encounters a difficulty in taking the balance due to the small surface of the front and the reduction of the frictional force and that it takes the balance to turn the right hand and the left hand outward and the strong sustainment of the right hand enables a gymnast to perform naturally the next motion.

This research suggests that analyses of electromyogram and kinematic analysis are to be made in order to draw more meaning conclusion. This research leaves this as a future study.

REFERENCES

1. Dowling, J. J. Vamos, L. *Journal of applied biomechanics*, Vol.9 No.2. 1993

2. Federation of International Gymnastics. *International Code of point-man Artistic Gymnastics*. 2008

3. Park, Y.H., Youm, C.H, et al. *Korean Journal of Sport Biomechanics*, Vol.17, No. 1, pp. 1-8. 2007

Table 3: Values of ground reaction forces

Left	entry	front	exit	back	Right	entry	front	exit	back
Fx	2.40	-34.65	0	22.36	Fx	0	-37.10	6.00	36.45
Fy	19.66	-23.38	0	-5.08	Fy	0	22.48	-23.36	9.65
Fz	69.13	66.00	0	53.94	Fz	0	94.20	83.35	61.69

KINEMATIC ANALYSIS ON THE MOTION OF JUMP LOTUS KICK 540° IN WUSHU

[1] Youngseok Kang , [2]Kwangdong Park and [3]Kyoungkyu Jeon
[1]Dankook University, [2]Dankook University, [3]Dankook University
email: kysws1@nate.com, web: http:// www.dankook.ac.kr

INTRODUCTION

Wushu a world-wide sport originated from traditional Chinese martial arts.

Wushu is divided into two competitions: 'taolu' (forms) and 'sanda' (sparring). This research focuses on the degree of difficulty of the 'taolu' competition. The purposes of this research are threefold. The first one is to explore scientifically a system of technique of the Wushu sport. The second one is to suggest a strategy for developing the ability of the 'taolu' competition players and raising the ratio of success of their performance. The third one is to provide a systematic methodology for training of Wushu. To achieve these purposes, this research makes a quantitative analysis on kinematic factors of the 540° motion of Jump lotus kick in the 'taolu' competition by using the three-dimensional image technology.

METHODS

This research adopts as a scope three subjects with a ten-sport-player-career. They won a prize in national competitions and are eligible to successfully perform the 540° motion of Jump lotus kick. This research utilized three digital cameras; cameras 1 to 3 are respectively installed in front, at an angle of 45 degrees of the left, and at an angle of 45 degrees of the left, on the basis of the direction of proceed motion. The crank speed is set up as frames/sec, and the speed of shutter as 1/250sec. Values of Fx, Fy, and Fz stands for values of front and rear, values of upper and lower, and values of left and right, based on the direction of proceed motion.

Utilized is The Dig-4 Porgram of APAS (Ariel Performance Analysis System, USA). Smoothing was conducted to eliminate outcomes and errors rom the DLT (DirectLinear Transformation) technique. The cut-off frequency is set up as 10.0Hz.

Figure 1: Action of jump lotus kick 540°

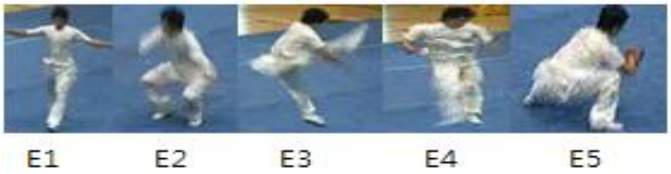

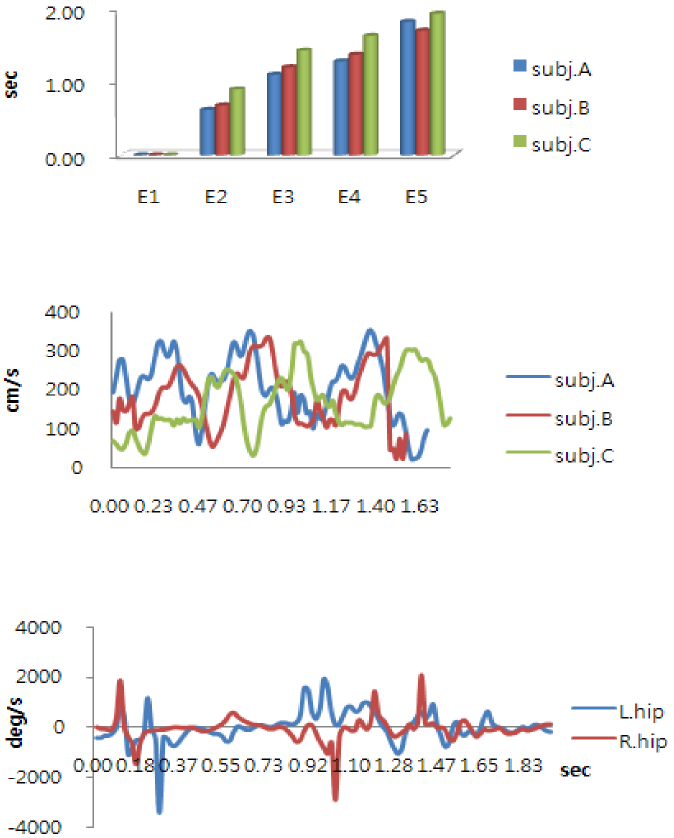

Figure 2: Time required, Velocity at the center of body and Change of vertical angular velocity

RESULTS and DISCUSSION

1. Time required

In the average of the time required, E2, E3, E4, and E5 are 0.73sec, 1.24 sec, 1.43sec, and 1.82sec, respectively. E2 refers to the section of stamping feet and it indicates the quick time required in the order of A to C. It is inferred from this that at the time of approach run the weight is not quickly moved to the direction of proceed motion. E4 stands for the section of kicking lotus kick and A represents the quickest time required in this section. This is because a big swing motion enables the weight to rise vertically for the weight's vertical jump in the sections E2 and E3. The sections E4 and E5 are sections in which the weight rotates in a 540-degree arc. The required time of A is longest in these sections: 0.54 sec. This means that a high jump supplies the subjective long duration of flight and enables him or her to land leisurely after posing a complete motion.

2. Velocity at the center of body

In E1, speeds of centroid of A to C are 223.47cm/s, 100.44cm/s, and 124.68cm/s, respectively. In E2, speeds of centroid A to C are 59.31 cm/s, 54.78cm/s and 31.73cm/s, respectively. Here, A indicates the quickest speed. This is because in the section of E3, A increases most quickly as 194.02cm/s quantity of motion to which transferred is the centroid by raising quickly the centroid after lowering the centroid by means of the quick movement of weight. Kang & Park (2007) argue that it is desirable to raise a vertical speed and to perform a high kick motion by turning the leg's segments around. A projects momentum high in the vertical upper direction by means of raising the speed of center as 220.36cm/s on the peak of E4, and then he or she lands safely in E5 by enlarging the trace of rotational motion.

3. Angular velocity of hip joint

In E2, values of the left and the right of Y axis are -1412.11 deg/s and -673.05 deg/s, respectively. This is because the left leg and the right leg enlarge the semi-diameter of rotation by increasing angular velocity of hip joint by means of bending left hip joint and right ones when these legs use a reaction on the ground.

In E3 and E4, Y axis indicates the peak. The angular velocity of the centroid which is quickly raised to the peak is increased to the direction of the proceed motion. E3 is the time point in which a subjective kicks lotus kick. In E3, values of the left and the right of Z axis are 407.14 deg/s and 564.50deg/s. Here, a kick increases a moment arm in the peak and pauses a swing motion by means of the trace of a large circular motion.

CONCLUSIONS

The results of the analysis on the 540° motion of Jump lotus kick are as follows. First, it is important to shorten the required time for standing on tiptoe and to move quickly moment weight forward. Second, it is desirable to raise the vertical velocity of the centroid for securing the height and to perform the motion by using inner and outer rotations with segments of left legs and right hands on the long axis on the peak. Finally, it is desirable to bend left hip joint and right ones for maximizing their use of a reaction, to project the transferred momentum high to the peak, and to enlarge the trace of the motion of Jump lotus kick

REFERENCES

1. Bae, KH, *Korean journal of sports science*,12(4) 94-105,2000.
2. Kang, YS, & Park, KD, *Journal of Biomechanics* ,40, s613,2007.

Table 1: Mean values of angular velocity of hip joint

Hip joint(deg/s)			E1	E2	E3	E4	E5
Mean	A	L	421.46	150.58	382.73	580.48	-71.81
		R	269.84	-284.82	-313.58	7.54	-687.9
	B	L	97.08	-1412.11	1010.78	-1707.81	-349
		R	708.28	-673.05	414.48	-1563.46	630.41
	C	L	-1267.61	27.93	407.14	111.86	344.57
		R	-570.22	576.57	564.5	204.74	-39.81

FATIGABILITY OF TRUNK MUSCLES WHEN SIMULATING PUSHING MOVEMENT DURING TREADMILL WALKING

Yi-Ling Peng[1], Yang-Hua Lin[1], Hen-Yu Lien[1] and Wen-Ke Chiou[2]
[1] Graduate Institute of Rehabilitation Science, Chang Gung University, Taoyuan, Taiwan
[2] Graduate Institute of Industrial Design, Chang Gung University, Taoyuan, Taiwan
email: pongpong0223@yahoo.com.tw

INTRODUCTION

Pushing is a common movement in moving objects, and it also related to about 9% to 20% low back injuries occurrence [1]. During pushing, not only different pushing handle heights and pushing weights would influence the trunk muscle activity and lumbar spine compression force [2] [3], but also poor muscle endurance is a possible cause of low back pain.

In order to provide a clinical guideline of endurance test and fatigability in trunk muscles during pushing movement, the purpose of the present study was to demonstrate the effect of continuous pushing movement on trunk muscles' activity and fatigability.

METHODS

Thirty healthy young adults would be expected in this program to perform treadmill walking with simulating pushing and without simulating pushing movement. Volunteers first perform walking with simulating pushing until reaching subjective assessment of trunk muscle fatigue by Borg CR-10 Scale, and at least a week later, return to carry out walking without pushing movement. In the walking with simulating pushing condition, volunteers are asked to pushing with their maximum pushing force, and visual and verbal feedback are provided to maintain the hand force.

The electromyography signal of erector spinea (ES), multifidus (MF), rectus abdominis (RA) and external oblique (EO) muscles at both sides are collected by surface electrodes. Median frequency (MDF) and root-mean-square (RMS) are calculated in the initial, middle and final periods of both walking with and without simulating pushing conditions. Pushing force of both dominate and non-dominate hands are recorded by load cells, and Borg's scale are also noted in every thirty seconds.

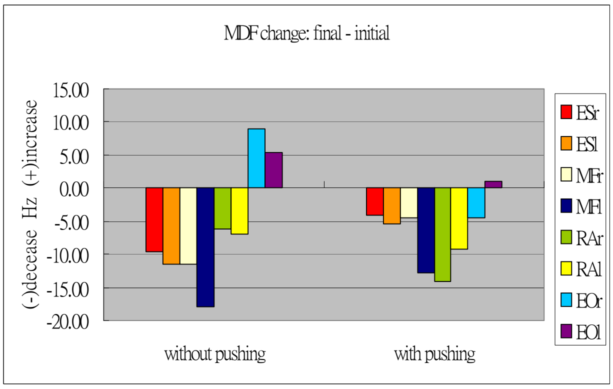

Figure 1: Median frequency (MDF) change in with pushing and without pushing conditions during treadmill walking.

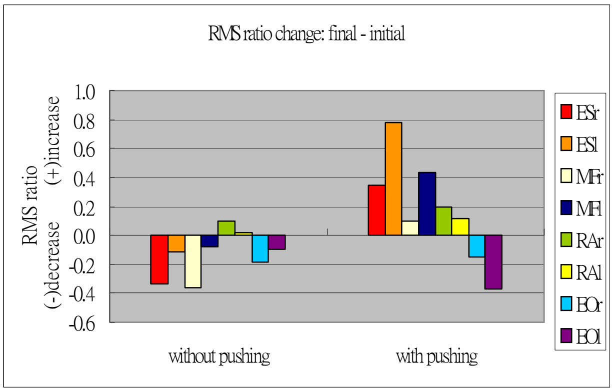

Figure 2: Root-mean-square (RMS) change in with pushing and without pushing conditions during treadmill walking.

Two-way repeated measure ANOVA is used to compare the differences of MDF and RMS between the two conditions in three periods. The difference of pushing force between initial and final periods is calculated by paired-t test.

RESULTS AND DISCUSSION

At present, MDF of ES, MF and RA decrease in both walking with and without simulating pushing conditions (figure 1). Time is a main factor of MDF in back extensors. MDF of ES (*p*=0.039) and MF (*p*=0.006) decrease with exercise time. However, condition is a main factor of MDF in trunk flexors. MDF of RA (*p*=0.004) and EO (*p*=0.047) is higher in walking without pushing than with pushing condition (table 1).

RMS of ES, MF and RA increase only in simulating pushing condition (figure 2). There is no interaction or main effect of time and condition in all trunk muscles, rectus abdominus and external oblique (*p*>0.05) (table 2).

MDF of trunk extensors decreased with time demonstrated muscle fatigue. RMS increased in trunk flexors in walking with simulating pushing condition indicated more muscle activities involved at the final period.

CONCLUSIONS

MDF and RMS changes showed different trends in walking with and without pushing conditions. Besides, there were different factors to affect MDF on trunk flexors and extensors. Time is a main factor of MDF in back extensors and condition is a main factor of MDF in trunk flexors.

REFERENCES

1. Hoozemans MJ, et al. Pushing and pulling in relation to musculoskeletal disorders: a review of risk factors. *Ergonomics* **41**, 757-81, 1998.
2. Hoozemans MJ, et al. Mechanical loading of the low back and shoulders during pushing and pulling activities. *Ergonomics* **47**, 1-18, 2004.
3. Lee PJ and Granata KP. Interface stability influences torso muscle recruitment and spinal load during pushing tasks. *Ergonomics* **49**, 235-48, 2006.

ACKNOWLEDGEMENTS

This work was supported by National Science Council (NSC96-2314-B-182-024)

Table 1: Mean and SD of MDF in tree periods of walking with pushing and without pushing conditions.

	Condition with pushing			Condition without pushing			Main effect	
	MDF (Hz)			MDF (Hz)			Condition	Time
	Initial	Middle	Final	Initial	Middle	Final	*p*	*p*
Trunk extensors								
ES	134.56±15.06	131.72±13.81	129.78±16.11	139.62±6.04	132.18±4.07	129.01±11.12	*p*=0.685	*p*=0.039
MF	134.42±23.18	132.45±19.78	125.73±15.92	145.15±20.73	139.65±13.75	130.36±17.40	*p*=0.192	*p*=0.006
Trunk flexors								
RA	140.22±17.52	134.30±17.97	128.48±21.91	158.01±14.92	146.86±36.47	151.42±23.56	*p*=0.004	*p*=0.230
EO	109.80±11.82	107.20±8.82	108.08±6.94	113.91±10.48	117.88±9.88	121.02±6.28	*p*=0.047	*p*=0.063

Table 2: Mean and SD of RMS in tree periods of walking with pushing and without pushing conditions.

	Condition with pushing			Condition without pushing			Main effect	
	RMS			RMS			Condition	Time
	Initial	Middle	Final	Initial	Middle	Final	*p*	*p*
Trunk extensors								
ES	1.481±1.178	1.577± 1.443	2.046± 2.210	1.352±0.841	1.295±0.804	1.130±0.865	*p*=0.301	*p*=0.681
MF	1.581±1.196	1.666±1.231	1.846±1.689	1.556±1.099	1.441±0.732	1.338±0.911	*p*=0.528	*p*=0.975
Trunk flexors								
RA	0.410±0.373	0.648±0.495	0.563±0.246	0.121±0.058	0.339±0.472	0.180±0.148	*p*=0.075	*p*=0.077
EO	0.820±0.670	0.769±0.240	0.557±0.164	0.518±0.189	0.463±0.228	0.379±0.159	*p*=0.09	*p*=0.117

ARM MOTION COUPLING DURING LOCOMOTION-LIKE ACTIONS: AN EXPERIMENTAL STUDY AND A DYNAMIC MODEL

[1,2]Shapkova E.Yu., [1,3]Terekhov A.V., [1]Latash M.L.

[1]Department of Kinesiology, the Pennsylvania State University, University Park, PA 16802, USA
[2]Institute of Phthisiopulmonology, Ministry of High Medical Technologies of Russia, St.Petersburg 193036, Russia, eys3@psu.edu
[3]Institute of Mechanics, Moscow State University, Moscow 119192, Russia

INTRODUCTION

Arm swinging during human locomotion has been viewed as a consequence of coupling between hypothetical pattern generators for the lower and upper extremities [5,6]. Stable patterns of modulation of the upper and lower extremity muscles are also observed in standing subjects when they rhythmically swing their arms [1,2]. *The aim* of our study has been to explore the interactions between rhythmic motor patterns produced by a hypothetical neural oscillator and a voluntary motor command unrelated to the ongoing rhythmic action, such as stopping one of the arms voluntarily. We expected that effects of the command for the discrete voluntary action on the rhythmic action of the other arm could be described with a new constraint on the neural oscillator without a change in the coupling between the arms.

METHODS AND PROCEDURES

Eight healthy right-handed subjects performed an out-of-phase arm-swinging task while stepping in place or while standing (STEP and STAND *Task*) at individually defined Natural (0.9-1 Hz) and Fast (1-1.1 Hz) *Speed*. The subjects stopped the right or left arm (*Side*) in response to an auditory signal while trying to keep the rest of the movement pattern unchanged. Eight blocks of 15 trails (24 s each) corresponding to the *Task* x *Speed* x *Side* design, were performed randomly. A four-camera ProReflex motion analysis system was used to capture the position of six passive reflective markers placed over the shoulder, elbow, and wrist joints at 240 Hz. The amplitude and cycle duration of arm swing during 3 cycles before and after STOP (*Pre-Stop, Post-Stop*) were quantified. Standard methods of parametric statistics were used.

RESULTS AND DISCUSSION

After the voluntary STOP of one arm movement, the continuing arm showed an increase in its amplitude in all the subjects, for both arms, during both STEP and STAND tasks, and under both natural and fast speeds (Fig.1).

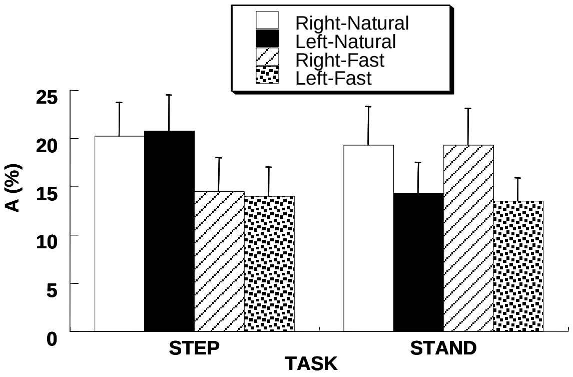

Figure 1: An increase in the amplitude of arm movement (A, in % to the pre-stop arm amplitude) after the other arm stopped swinging. Averaged across subjects data with standard error bars are plotted.

The increase in amplitude (ΔA) between the pre-STOP and post-STOP was, on average, 16.9±2.9%. A four-way ANOVA with the factors *Period (Pre-Stop, Post-Stop), Task (Stand, Step), Side (Right, Left),* and *Speed (Normal, Fast)* on A showed significant effects of *Period, Task,* and *Side* ($F_{[1,115]} > 14$; $p < 0.001$) without other effects. There was higher A after the stop as compared to prior to the stop, during standing as compared to stepping, and in the left arm as compared to the right arm. The cycle duration showed only a significant effect of *Task* ($F_{[1,116]}= 9.8$, $p < 0.01$): On average, the arm cycle duration during stepping was about 5% lower than during standing.

Mathematical Model. Each arm motion was modeled with a single Van der Pol oscillator:

$$\begin{aligned}\ddot{x}_1 + \nu_1\dot{x}_1\left((x_1^2+\dot{x}_1^2/\omega_1^2)-A_1^2\right)+\omega_1^2 x_1 &= f_1(x_1,\dot{x}_1,x_2,\dot{x}_2)\\ \ddot{x}_2 + \nu_2\dot{x}_2\left((x_2^2+\dot{x}_2^2/\omega_2^2)-A_2^2\right)+\omega_2^2 x_2 &= f_2(x_1,\dot{x}_1,x_2,\dot{x}_2)\end{aligned} \quad (1)$$

Here x_1 and x_2 are α_{ARM} angles of the two upper extremities, ω_1 and ω_2 are prescribed frequencies and A_1 and A_2 are amplitudes parameters. Parameters ν_1 and ν_2 determine the strength of mechanisms stabilizing the desired oscillatory pattern. To make anti-phase oscillation of x_1 and x_2 stable and functions f_1 and f_2 symmetrical with respect to x_1 and x_2 we used the coupling functions from the Haken-Kelso-Bunz model [3], and simplified it by reducing the number of free parameters:

$$\begin{aligned}f_1(x_1,\dot{x}_1,x_2,\dot{x}_2) &= -b_1\dot{x}_1(x_1-x_2)^2\\ f_2(x_1,\dot{x}_1,x_2,\dot{x}_2) &= -b_2\dot{x}_2(x_2-x_1)^2\end{aligned} \quad (2)$$

Here parameters b_1, and b_2 determine the properties of the coupling between the two arms. Different values of ω_1 and ω_2 in (1) may lead to significant desynchronization [3]. For simplicity we assumed that the prescribed frequencies are set by the CNS to equal values, $\omega_1=\omega_2=\omega$. All other parameters were allowed to differ for the two limbs. The final equations are:

$$\begin{aligned}\ddot{x}_1 + \nu_1\dot{x}_1\left((x_1^2+\dot{x}_1^2/\omega_1^2)-A_1^2\right)+\omega_1^2 x_1 &= -b_1\dot{x}_1(x_1-x_2)^2\\ \ddot{x}_2 + \nu_2\dot{x}_2\left((x_2^2+\dot{x}_2^2/\omega_2^2)-A_2^2\right)+\omega_2^2 x_2 &= -b_2\dot{x}_2(x_2-x_1)^2\end{aligned} \quad (3)$$

The model (3) was capable to produce cyclic changes of the x_1 and x_2 similar to the experimental data (Fig.2).

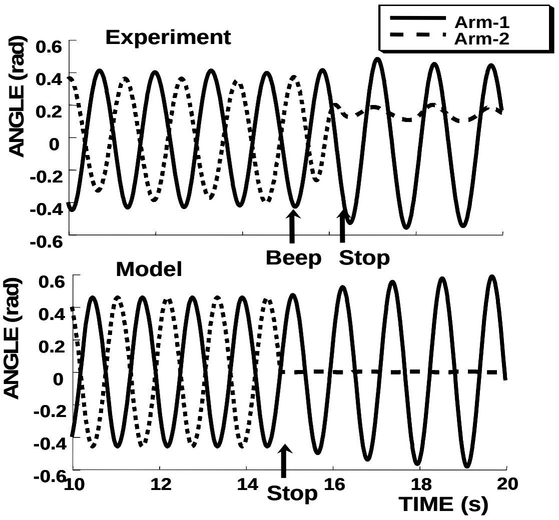

Figure 2: ***Experiment:*** a representative example of the arm sway trajectory. The arrows show the Beep and Stop moments. ***Model:*** Results of the simulation with the parameters defined using the average experimental values. The arrow shows the time of introducing the constraint $x_2 = 0$. *Note the increase in the amplitude of the continuing arm motion in both panels.*

Our experiments have shown strong coupling effects between the two arms. This effect was nearly symmetrical between the left and right arms. It was similar in magnitude in the tasks that did and did not involve simultaneous rhythmic leg movement (marching in place). We were able to model the effect using a simple dynamic model with two coupled non-linear oscillators, similar to the one suggested by Haken et al. (1985).

REFERENCES

[1] Abe and Yamada (2001). *Exp Brain Res* **139,** 120-125
[2] Danna-Dos-Santos et al. (2009). *Exp Brain Res* 193, 565–579
[3] Fuchs et al. (1996). *Biol Cybern* **74,** 21-30
[4] Haken et al. (1985). *Biol Cybern* **51,** 347-356
[5] Ustinova et al. (2006). **96,** 1124-1134
[6] Zehr et al. (2008). *J Physiol* **582,** 209-227

ACKNOWLEDGEMENTS

Suppoorted by NIH grant NS-035032.

THE RELATIONSHIP BETWEEN LIMB LOADING ASYMMETRY AND KNEE FUNCTION PRIOR TO TOTAL KNEE ARTHROPLASTY

Cory L Christiansen and Jennifer E Stevens-Lapsley

Department of Physical Medicine & Rehabilitation, Physical Therapy Program,
University of Colorado Denver, Aurora, CO, USA
email: cory.christiansen@ucdenver.edu

INTRODUCTION

Lower limb loading asymmetry, characterized by preferential unloading of the involved limb during weight bearing activity, is typical for patients with knee osteoarthritis (OA) prior to and following unilateral total knee arthroplasty (TKA) [1-3]. If loading asymmetry is linked to functional limitation and quadriceps strength asymmetry, pre-surgical interventions targeting symmetrical weight-bearing may be an avenue for improving functional outcome after TKA. However, if loading asymmetry is directly related to pain level, promoting symmetrical loading may be detrimental.

The purpose of this study was to test for limb loading asymmetry in people with end-stage OA, scheduled to undergo TKA, during transitions between sitting and standing. In addition, the relationships between loading asymmetry and clinical measures of functional performance were evaluated.

METHODS

Twenty-five people with knee OA, scheduled for unilateral TKA, participated (age: 64.2 ± 9.1 years; mass: 85.9 ± 18.3 kg; height: 1.68 ± 0.10 m; sex: 14 women and 11 men). Participants performed a Five Times Sit-to-Stand Test (FTSST) involving a timed sequence of transfers between sitting and standing. During the test, peak vertical ground reaction force (v-GRF) and vertical impulse were measured with two force platforms (PASCO scientific, Roseville, CA) located under participants' right and left feet. Pain level was assessed immediately following the FTSST using a Visual Analog Scale (VAS) from 0 = no pain to 10 = very severe pain.

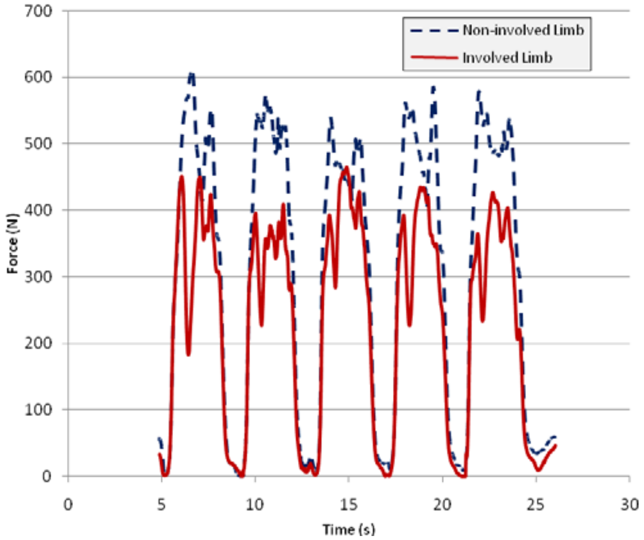

Figure 1: Vertical ground reaction force during the Five Times Sit to Stand Test for involved and non-involved limb of a representative participant.

In addition to the FTSST, a Timed-Up-and-Go (TUG) test and stair climbing test (SCT) were used as measures of functional activity performance. The TUG measured the time it took to rise from an arm chair (seat height of 46 cm), walk 3 meters, turn, and return to sitting in the same chair without physical assistance. The SCT measured the time to ascend and descend one stair flight (12 steps). Time for all three functional measures was collected using a manual stop-watch and participants were instructed to move as "quickly and safely" as they could.

Maximum isometric knee extension torque was measured with an electromechanical dynamometer (CSMI, Stoughton, MA) as participants were seated with hips flexed to 85° and knees flexed to 75°. Participants were instructed to provide a maximum effort knee extension and peak torque values were recorded. Strength testing was performed separately for both limbs.

Limb loading asymmetry was assessed as the ratio of involved to non-involved limb peak v-GRF during the FTSST. Quadriceps strength asymmetry was assessed as the ratio of involved to non-involved peak knee extension torque. A student t-test was used to compare involved to non-involved peak v-GRF and vertical impulse during the FTSST. Pearson correlations were used to assess the relationship of limb loading asymmetry with FTSST time, TUG time, SCT time, quadriceps strength asymmetry, and pain score.

RESULTS AND DISCUSSION

Figure 1 provides representative involved and non-involved limb v-GRF tracings during the FTSST. During the FTSST, differences were present ($p<0.05$) between involved and non-involved limbs for peak v-GRF (6.04 ± 0.92 and 6.99 ± 0.55 N/kg, respectively) and vertical impulse (41.16 ± 14.2 and 49.24 ± 20.2 Ns/kg, respectively). The ratio of involved to non-involved limbs for peak v-GRF was 0.87 ± 0.13 (all values are mean ± SD). Twenty-two of the 25 participants had lower peak v-GRF values on the involved limb.

Outcome values and correlations between loading asymmetry and all other variables are presented in Table 1. No significant correlation was found between pain and loading asymmetry during the FTSST. Correlations of loading asymmetry with functional measures and quadriceps strength asymmetry were low to moderate.

It has been suggested that lower limb loading asymmetry following TKA is a response to pain [4], quadriceps weakness [2], and/or habitual unloading [1] of the involved limb. The mechanism of unloading may partly depend on the time prior to or following TKA. For example, quadriceps muscle weakness has been correlated with involved limb unloading at 3 months post-TKA [2]. However, loading asymmetry during sit-to-stand transfers has been measured 16 months post-TKA, in the absence of quadriceps weakness or significant pain [1].

Our findings indicate strength asymmetry is positively correlated with limb loading asymmetry prior to TKA. However, pain may not play a prominent role in loading asymmetry during transfers between sitting and standing, based on the lack of relationship between these variables. In addition, negative correlations between loading asymmetry and functional measures indicate loading asymmetry may negatively influence functional performance prior to unilateral TKA.

CONCLUSIONS

Limb loading asymmetry is present during transfers between sitting and standing for individuals with OA, prior to TKA. Asymmetrical quadriceps strength is positively related to this loading asymmetry. In addition, loading asymmetry has low to moderate correlation with timed functional activity performance for these individuals.

REFERENCES

1. Boonstra MC, et al. *Knee* **15**, 390-395, 2008.
2. Mizner RL & Snyder-Mackler L. *J Orthop Res* **23**, 1083-1090, 2005.
3. Rudolph KS, et al. *Phys Ther* **87**, 1422-1432, 2007.
4. Hurwitz DE, et al. *J Orthop Res* **18**, 572-79, 2000.

ACKNOWLEDGEMENTS

Funding: American College of Rheumatology New Investigator Award, Arthritis Foundation New Investigator Award. Research assistance: Tasia Robertson, Jackie Balter, Michael Bade.

Table 1: Outcome measurements and Pearson product moment correlations between limb loading asymmetry and outcome measurements.

	FTSST	TUG	SCT	STRENGTH ASYM	PAIN
Mean ± SD	12.2 ± 3.0 s	8.2 ± 1.6 s	18.3 ± 6.8 s	0.83 ± 0.29	3.0 ± 2.6
Correlation with LOADASYM (*r*)	-0.36*	-0.42*	-0.50*	0.49*	-0.19

LOADASYM = Loading asymmetry represented by the ratio of involved to non-involved peak v-GRF during the FTSST, FTSST = Five Times Sit to Stand Test, TUG = Timed Up and Go test, SCT = Stair Climb Test, STRENGTH ASYM = Strength asymmetry represented by the ratio of involved to non-involved peak knee extension torque, PAIN = Pain rating from the Visual Analog Scale during sit-to-stand testing. * $p < 0.05$.

Gait strategy changes with walking speed to accommodate biomechanical constraints

Hyunmin Kang, Jin Yeom and Sukyung Park
Biomimetics Lab, Mechanical Engineering Dept. KAIST, Korea,
email: sukyungp@kaist.ac.kr, web: biomt.kaist.ac.kr

INTRODUCTION

Steady state human locomotion at level ground needs compensatory energy input against impulsive energy loss during heel strike. Ground push-off by the stance leg right before the onset of double support phase appeared to be four times energy efficient than the an active hip torque generation during the swing phase [1]. However, if there is biomechanical constraint applied to the maximum allowable ankle push-off, despite its cost effectiveness, the nervous system may need to employ active hip torque to compensate heel strike energy loss to maintain steady state walking, as similar to the postural strategy changes from ankle to hip strategy to accommodate biomechanical constraints in response to backward perturbation [2]. In this study, we hypothesized that the gait strategy changes from ankle strategy (that compensates heel strike energy loss mostly by the ankle joint push-off impulse) to hip strategy (that generates additional energy input using active hip joint torque during the swing phase) to accommodate biomechanical constraints at ankle joint torque.

METHODS

Eight healthy male volunteers aged 23-27 participated in this study after signing informed consent approved by KAIST IRB. Subjects walked along the 10m walkway with randomly ordered five different gait frequencies given by the auditory cues while having almost constant step lengths. The uniform interval of gait frequencies was obtained by the one third of gait frequency difference between the self-selective and maximum gait frequency. To examine whether the required increase in push-off impulse can be controlled by the nervous system, subjects also performed added inertia trials with weighted backpack of 15~20% of their body mass. Ground reaction forces of each foot and joint kinematics were measured by dual force plates and optical motion capture system, respectively.

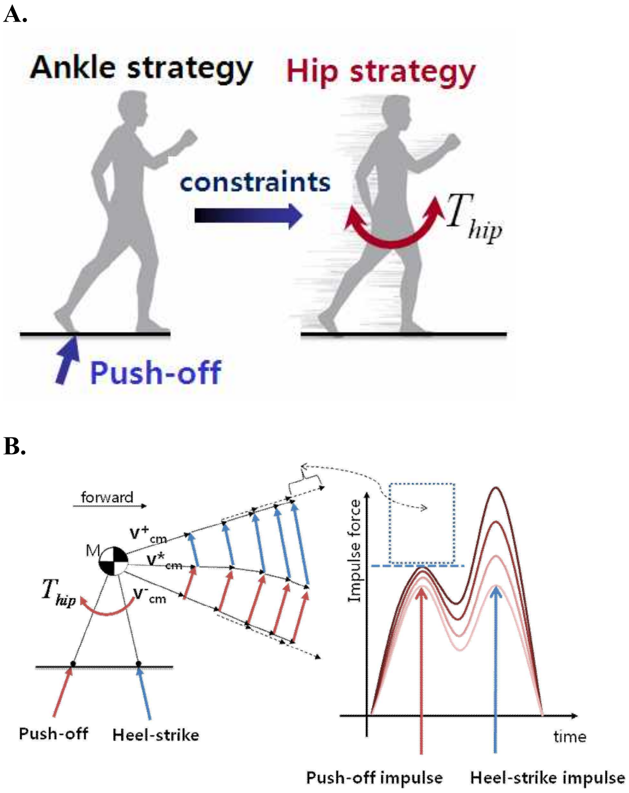

Figure 1: (A) Hypothesis of gait strategy change to accommodate biomechanical constraints of the ankle. (B) Push-off impulsive force is saturated while heel strike impulsive force is still increasing with walking speed.

Both push-off and heel strike impulses are calculated by integrating impulsive ground reaction forces measured from the force platform over the duration of impulsive forces. Several methods are considered to define the duration of impulsive force – COM velocity hodograph, COM work (power), and vertical ground reaction forces [3]. COM hodograph shows vertical and forward component of COM velocity, and the points where the maximum angular excursion of COM velocity occurs are defined as upper or lower limits of the duration. Work done by push-off impulse shows positive power during the step-to-step transition (double support) phase, while work done by heel strike collision shows negative power. The time duration of overlapped positive and negative power is used to define the duration of impulse. We chose another method which uses vertical ground reaction forces. The peak values of the push-off and heel strike impulsive forces are defined as start and end point of each impulsive force, respectively.

Mechanical energy was calculated by the sum of potential and the kinetic energy of the center of mass using a sacral marker.

RESULTS AND DISCUSSION

Peak impulsive force of both push-off and heel strike were not significantly different in magnitudes at slow step frequency, but push-off impulsive forces appeared to saturate for the higher step frequency trials. The magnitudes of the impulse were almost similar with each other at slower gait speed while the push off impulse was significantly smaller than the heel strike impulse at higher step frequency due to the saturated push off impulsive forces. The differences in the mechanical energy between the beginning and the end of the swing phase were negligible at slower step frequency, while they monotonically increased with step frequency. With added inertia, the constraint on ankle plantar flexion becomes active at slower gait speed than the control trials.

Biomechanical constraints on ankle joint torque was demonstrated by the saturated ankle joint push-offs. Increased mechanical energy during the swing phase implies that the nervous system employs active hip torque to compensate heel strike energy loss to maintain steady state walking despite its higher energy cost than the ankle push-offs. As was observed in the postural strategy change [2], the results suggest that biomechanical constraints induce gait strategy change from ankle to hip strategy.

CONCLUSIONS

Biomechanical constraints on ankle joint torque was demonstrated by the saturated ankle joint push-offs. Observed limitation on push-off propulsion force at higher gait speed would attribute to intrinsic muscle properties [4], while the heel strike impulsive force, which does not involve active muscle shortening but mostly involves passive muscle components, showed monotonic increase. Deficiency of push-off impulsive pre-compensation against collision loss at high gait speed is complemented by hip torque actuation during the swing phase. Increased mechanical energy during the swing phase implies that the nervous system employs active hip torque to compensate heel strike energy loss to maintain steady state walking despite its higher energy cost than the ankle push-offs. We also suggest that biomechanical constraints induce gait strategy change from ankle to hip strategy, as was observed in the postural strategy change [2].

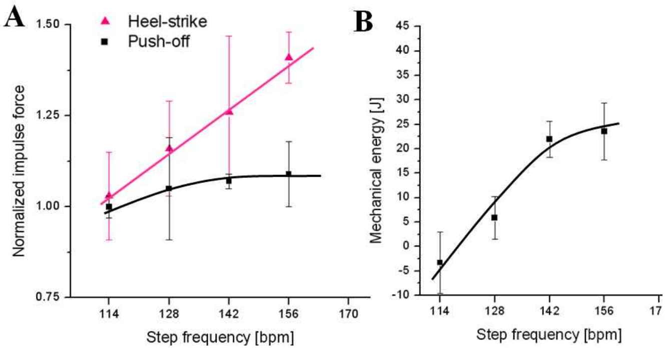

Figure 2: (A) Impulsive force of the ankle push-off and heel strike at double support phase. (B) Increase of mechanical energy during swing phase.

Appropriate collision compensation by the combination of push-off propulsion and hip torque actuation would serve as an assessment of gait performance. We expect that the elderly who could not maintain steady state gait in response to the perturbation that requires gait strategy change, such as the increased inertia, walking on an inclined surface, and/or faster gait speed, may show inappropriate complementary hip torque engagement though their plantar flexor is significantly limited.

ACKNOWLEDGEMENTS

The work was supported by the Basic research fund of UTRC of the Agency for Defense Development, Korea and the second stage of the Brain Korea 21 Project.

REFERENCES

1. Kuo, AD, *J Biomech Eng*. **124**, 113-20, 2002.
2. Park, S., et al. *Exp Brain Res*. **154**, 417-27, 2004.
3. Adamczyk and Kuo, submitted to *J Exp Biol*.
4. Cunningham et al. *Eur J Appl Physiol* **56**, 24-29, 1987

BIOMECHANICAL EVALUATION OF THE CHANGE IN THUMB EXTENSION FOLLOWING RELOCATION OF THE EXTENSOR POLLICIS LONGUS TENDON

Suzanne H. Nicewonder[1], George D. Chloros[2], Ethan R. Wiesler[2], and Martin L. Tanaka[1,2]

[1] Virginia Tech – Wake Forest University School of Biomedical Engineering and Science (SBES).
[2] Wake Forest University School of Medicine (Department of Orthopaedic Surgery).
Email: snicewon@vt.edu

INTRODUCTION

Surgical procedures to treat rheumatoid arthritis, wrist tenosynovitis, and other distal radioulnar conditions resulting in wrist reconstruction require an incision in the back of the wrist to access the bones and structures within. As part of this surgical procedure, the Extensor Pollicis Longus (EPL) tendon is relocated from the ligamentous sheath that guides it around Lister's tubercle. Since the EPL no longer follows its natural path, the mechanical pulley effect provided by engagement with Lister's tubercle is lost. Consequently, the effective length of the tendon is increased. Clinical evidence shows that EPL relocation often reduces thumb function and range of motion: patients with compromised thumb motion may be unable to use scissors or perform other tasks requiring thumb extension.

The purpose of this study was to evaluate the effect of EPL relocation on thumb extension. Based on wrist and hand anatomy, a rigid body mathematical model was developed to simulate thumb extension. A cadaveric experiment was also conducted and the results were used to calibrate and verify the model.

METHODS

Mathematical Model

A biomechanical model of the system was created based on anatomic geometry (Fig. 1). The model consisted of five rigid body segments representing the distal phalange, proximal phalange, first metacarpal, and two carpal (wrist) segments. Torsional springs were placed at each joint to represent joint stiffness due to elasticity of the joint capsule, ligaments, and other passive tissues spanning the joint. The spring constant (*k*) at each joint (*i*) was selected to be proportional to the joint size, allowing for the calculation of torque at each involved joint, $T_i = -k_i \theta_i$.

Equilibrium equations were calculated for each segment. This resulted in 15 equilibrium equations similar to the three shown below for the distal phalange segment:

$$\sum M_{P5} = T_5 + EPL_x r_5 (\sin\theta_5) + EPL_y r_5 (\cos\theta_5) = 0 \quad (1)$$

$$\sum F_x = F_{5x} - EPL_x = 0 \quad (2)$$

$$\sum F_y = -F_{5y} + EPL_y = 0 \quad (3)$$

The system was modeled using MATLAB software (MathWorks; Natick, MA). Forces were applied to the EPL and the corresponding thumb extension angles were calculated. The model was calibrated by adjusting the torsional spring constants based on measured experimental and anatomical data.

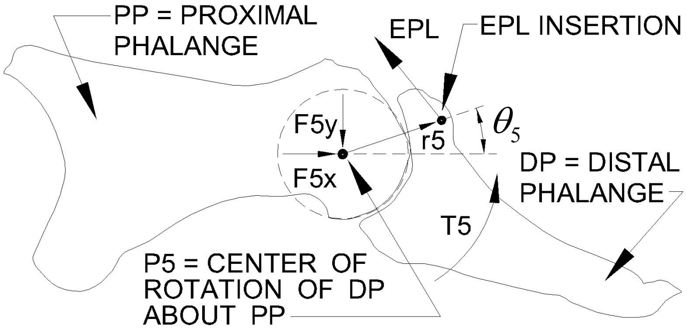

Figure 1: Model of distal thumb segments. Applying force to the EPL tendon results in thumb extension, as the distal phalange rotates about P5, the DIP joint.

Experiment

Twelve cadaveric forearms were dissected and an external fixator was installed to immobilize the wrist in a neutral position. The limb was secured to a test frame and two Kirschner wire (K-wire) pins were installed: one through Lister's tubercle and one through the distal interphalangeal (DIP) joint of the thumb (Fig. 2). The EPL tendon was exposed in its natural position. A suture was secured to the tendon and force was applied using known weights. The applied force, EPL displacement, and thumb extension angle were recorded. After each measurement the force was removed to minimize mechanical creep. Upon completion of the experiment in the natural position, the EPL was surgically relocated (radial to Lister's tubercle) and the experimental procedure was repeated.

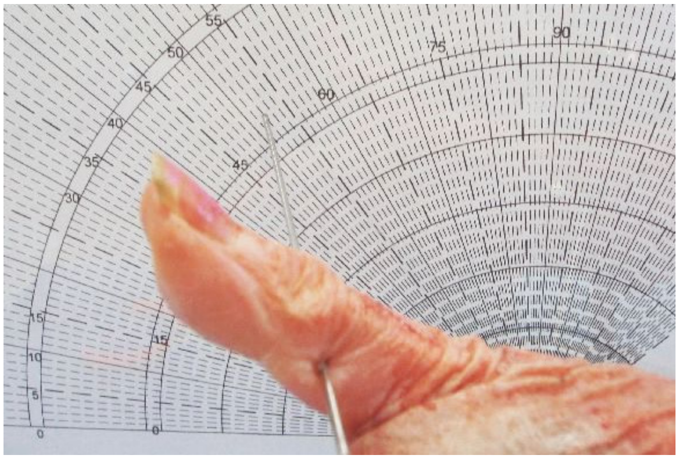

Figure 2: A K-wire through the DIP Joint (P5) was used in the experiment to measure thumb extension angle.

RESULTS AND DISCUSSION

For the natural cadaveric thumb, the mean range of motion in extension (min, max) was 47.7° (14.0°, 94.7°). This range of motion is consistent with other published findings [1]. Following EPL relocation, the mean range of motion decreased to 31.1° (10.7°, 80.7°). This result supports clinical evidence that thumb motion is reduced after relocation. The mathematical model coordinates well with the experimental data for the naturally positioned EPL. Following relocation, the model also follows the general trend of the experimental results, but not as accurately (Fig. 3). Model accuracy may be improved through further model calibration and accounting for additional parameters that may affect the movement.

The nonlinearity of the thumb motion suggests that the thumb extension angle may be dependent on multiple parameters including the force applied to the tendon, the unique resistance of each joint, and the geometrical path through which the EPL travels. Although the configuration is naturally 3-dimensional (3D), thumb extension activity is primarily dominated by 2D motion. Therefore, a planar analysis was performed in order to reduce the complexity. The range of thumb motion observed in this experiment parallels other studies [2] that use a similar projected planar analysis of motion.

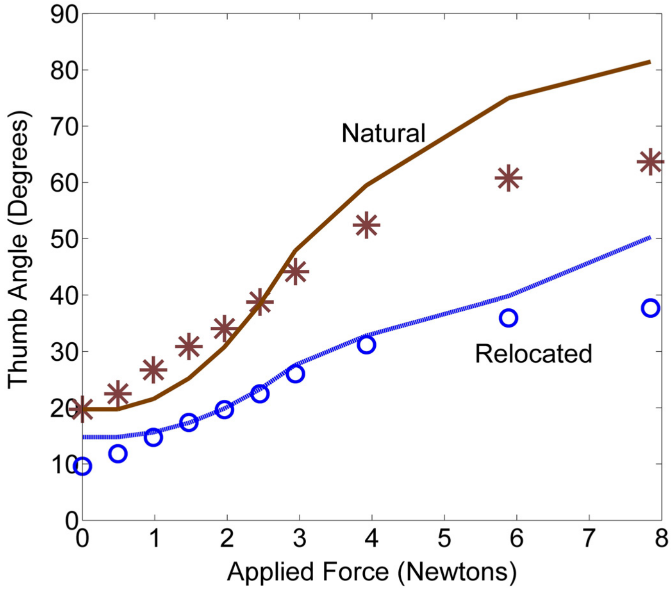

Figure 3: Mathematical model of the natural extension of the thumb (solid) correlates well with the experimental data (stars). Likewise, the modeled relocated results (dashed) correlate well with the measured data (circles).

This study suggests that it may be possible to preoperatively predict thumb extension for surgical procedures involving EPL relocation. Clinically this information may be applied to improve function of the post-surgery thumb. The model suggests that removing excess EPL tendon length may improve thumb extension performance.

CONCLUSIONS

The calibrated mathematical model correlated well with experimental data. Together they provide new information on the biomechanical relationship between EPL tendon motion and thumb extension, both before and after EPL relocation. They also lay a foundation to guide ongoing research targeted at improving EPL tendon surgery outcomes. In the future, these results may be used to assist in surgical planning for EPL relocation, with the goal of improved thumb function and patient quality of life.

REFERENCES

1. Imaeda T, An KN, and Cooney WP. *Hand Clinics*, **8**, 9–15, 1992.
2. Tang J, Zhang X, and Li Z. *Ergonomics*, **51:**7, 1109 -1118, 2008.

A Theoretical Study of the Effect of Elbow Muscle Co-Contraction Level on Forearm Steadiness

Mark T. Gordon[1] and James A. Ashton-Miller[1,2]
[1]Department of Mechanical Engineering, [2]Department of Biomedical Engineering, Institute of Gerontology, and Internal Medicine, University of Michigan, Ann Arbor
email: mtgordon@umich.edu, web: http:// me.engin.umich.edu/brl/

INTRODUCTION

Some older adults struggle to perform everyday tasks requiring fine motor skills. These include precise movements such as buttoning shirts, tying shoes, feeding themselves, using phones, or inserting a key in a lock. The performance of many of these tasks is frustrated by a lack of hand steadiness. The literature suggests that older adults have less hand steadiness than younger adults [1] as well as higher amounts of co-contraction [2].

Upper extremity steadiness has been quantified as the variation in hand position both for static tasks [2] and for reaching tasks [3]. Increased co-contraction is associated with lower inter-movement trajectory variability within same subjects [4]. No association was found between co-contraction and acceleration variability between subjects [2]. However, the effect of co-contraction on within-subject positional variability within a given single movement or task, which is closely related to steadiness, has not been studied.

The goal of this research, therefore, was to determine if the additional co-contraction exhibited by older adults is a compensatory action to steady the hand or if it is a source of additional positional variability. Our working hypothesis is that, in the healthy individual, elbow muscle co-contraction level largely determines the steadiness of the forearm. Our primary hypothesis is that there exists an optimum co-contraction level that maximizes forearm steadiness. The secondary hypothesis is that an age-related decrease in muscle contractile strength leads to decreased optimal steadiness.

METHODS

We developed a planar model of the upper and lower arm complete with four major agonist and four major antagonist muscles of the elbow (Figure 1). The moment and stiffness developed by each muscle was considered a function of muscle cross-sectional area, moment arm, and activation level. The muscles develop a net moment about the joint, along with a rotational resistance to internal or external perturbing moments that is based upon the short range muscle resistance to stretch (but not compression, of course). We assumed the normal variability (SD) in the magnitude of each muscle force to be a function of muscle cross-sectional area and activation level [5]. The variation in each muscle force contributes to variability in the net joint moment as well as net joint stiffness. The stiffness was then used to calculate the positional variability of the forearm, assuming the upper arm was grounded.

Given the external moment applied to the joint and the co-contraction level of the muscles, a MATLAB algorithm solved for the muscle activation pattern that minimizes the positional variability of the elbow. The co-contraction level was then varied to determine the effect of co-contraction on forearm steadiness and test the primary hypothesis.

We next varied the muscle properties of the model muscles to simulate how these might affect the steadiness of the forearm in younger and older adults. The simulation was then used to find the optimum co-contraction level that maximized the steadiness of the hand for both the younger adult model and the older adult model. The secondary hypothesis was then tested.

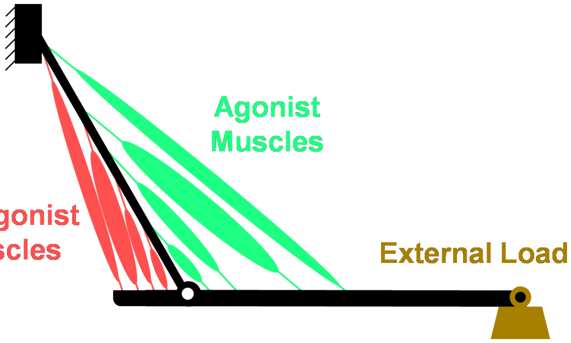

Figure 1: Simple Elbow Joint Model

RESULTS AND DISCUSSION

The simulation results demonstrated an optimum co-contraction level that maximizes forearm steadiness supporting the primary hypothesis (Figure 2). Higher levels of co-contraction were associated with more variability. This finding is contrary to studies which examined the variability *between* movements and then applied the same reasoning to a single movement [3,4].

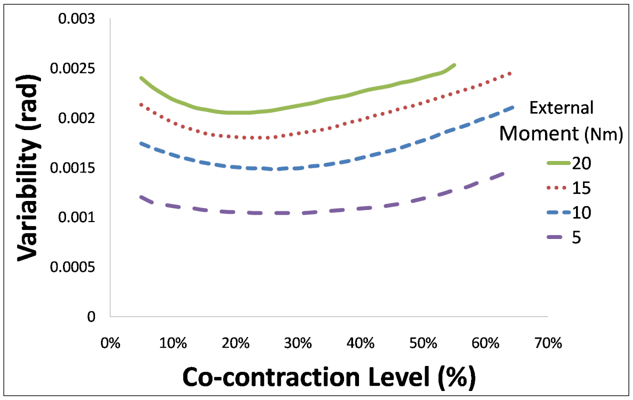

Figure 2: Simulation Data Showing Optimal Co-Contraction Levels for Varying External Moments

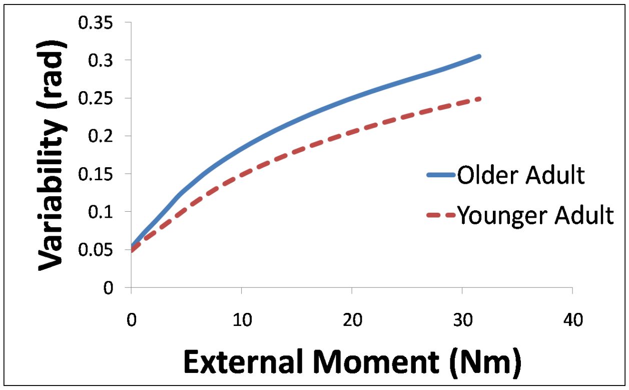

Figure 3: Simulation Data Suggesting Older Adults have Higher Variability

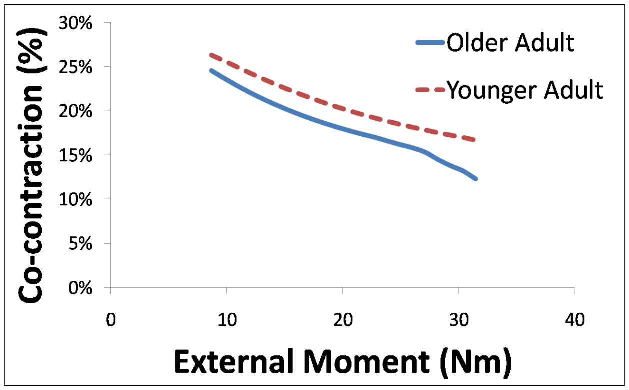

Figure 4: Simulation Data Suggesting Older Adults have Lower Optimal Co-Contraction Levels than Younger Adults

The simulation results suggest that people with weaker muscles, such as many older adults, will show a decrease in steadiness supporting the secondary hypothesis (Figure 3). This corroborates findings of manual steadiness in older subjects [1]. While muscle strength is not the only change that occurs with age, the model was sufficiently sensitive to this parameter to replicate the aging effect on steadiness.

The simulation also suggests that older adults have lower optimal co-contraction levels when exerting the same external moment as younger adults. This result suggests that the higher level of co-contraction seen in older adults is not to increase steadiness. Since co-contraction decreases the effect of internal or external disturbances, the elderly may be favoring joint stiffness over steadiness. If these modeling predictions were to be validated by experiment, then future interventions might target co-contraction levels in older adults.

CONCLUSIONS

The results suggest that elbow muscle co-contraction level plays a significant role in forearm steadiness. Positional variability is predicted to be increased at the greatest co-contraction levels which is contrary to current dogma. The simulation also predicts reduced steadiness in older adults based solely on the decrease in muscle cross-sectional area associated with aging.

REFERENCES

1. Ranganathan, VK, et al. *J Am. Geriatr Soc,* **49**, 1478-1484, 2001.
2. Laidlaw, DH, et al. *J Appl Physiol* **93**, 1400-1410, 2002.
3. Gribble, PL, et al. *J Neurophysiol*, **89**, 2396-2405, 2003
4. Faisal, AA, et al. *Nature Neuroscience*, **9**, 2008
5. Hamilton, AFC, et al. *Exp Brain Res*, **157**, 417-430.

ACKNOWLEDGEMENTS

NIA Training Grant AG000114

THEORETICAL PREDICTIONS OF HUMAN UPPER EXTREMITY BUCKLING BEHAVIOR UNDER IMPULSIVE END-LOADING: EFFECTS OF GENDER AND EXTENSOR MUSCLE STRETCH BEHAVIOR

Yunju Lee and James A. Ashton-Miller
Biomechanics Research Laboratory, Department of Mechanical Engineering, University of Michigan,
Ann Arbor, Michigan, U.S.A.
email: yunjulee@umich.edu, web: http://me.engin.umich.edu/brl/

INTRODUCTION

Falls are a leading cause of injury in the population. When an upper extremity is used to arrest a fall to the ground, the impulsive end-load at the wrist can reach one body-weight (1*BW) or more [1]. If the upper extremity gives way or buckles under such a load then there is a risk of the head striking the ground to cause traumatic brain injury. We have reported pilot simulation results on the effects of age and gender on the magnitude of the distal end load under which an adult upper extremity might collapse [2]. However, a limitation of that study included linear elastic and damping stretch behavior for the arm extensor muscles, as well as invariant muscle moment arms. In this paper we explore the effect of non-linear muscle stretch responses [3, 4] and elbow angle-dependent triceps moment arm [5] on the load-displacement behavior of the upper extremity axially end-loaded by an impulsive load.

METHODS

A planar, two-link, lumped parameter, musculo-skeletal model of the adult upper extremity was developed using Adams 2008 R3 engineering software. Frictionless revolute joints were assumed at the wrist, elbow and shoulder. Segment anthropometric, mass and inertial properties and ground surface stiffness were taken from [6]. The resistance of the precontracted elbow extensor muscles to forced flexion was modeled with a rotational spring and damper at the elbow and shoulder identified from impulsive measurements in eight adults. The short range muscle resistance to stretch was first assumed to vary linearly with muscle stretch force, but then the effects of non-linear relationships were systematically explored for larger stretches (inset, Figure 1, bottom right). The maximum volitional isometric shoulder flexor muscle strength, rotational stiffness and viscous coefficients were assumed to be 1.5-times those for the elbow extensor muscles in healthy males and females, respectively. Body weight (BW) and stature were assumed to be 713 N and 1.73 m in each gender group. The slightly flexed model limb was end loaded by an axial impulsive load which was systematically varied between 400 N and 2.4 kN [6]. At impact, the arm extensor muscles were considered to be isometrically precontracted at 70% of their maximum volitional activity [1]. Female gender was simulated by scaling male muscle stiffness and damping behavior by the *gender* factor *g*, where $g = 0.69$ to reflect the decrease in muscle stiffness and damping coefficients relative to size-matched young males [6]. Simulations were run for four initial pre-impact elbow flexion angles: 5^o, 10^o, 15^o and 20^o (where 0^o denotes elbow extension) [6].

The sensitivity of arm load-deflection behavior to changes in extensor muscle responses to large stretches were examined as follows: (a) both stiffness and damping coefficients decreased non-linearly with muscle force [curve ‘4’, Figure 1 inset], (b) a ‘softening’ relationship [3] with a breakpoint occurring after the muscle had been lengthened by 14% (equivalent to 20^o of elbow deflection) of its normal range of motion [curve ‘5’], (c) a bilinear relationship, with the change in slope at 20^o of elbow flexion, [curve ‘6’] and (d) a linear-exponential relationship [4], respectively [curve ‘7’]. These four ‘softening’ relationships were modulated by the 30% decrease in triceps moment arm from 20^o to 80^o flexion [5]. We also examined the effect of changing arm extensor muscle pre-activation level by multiplying the male muscle stiffness value of 1 by the *muscle* preactivation ratio, *m*. We also examined model sensitivity to changing the ratio of resistance provided by the elbow and the shoulder, respectively.

Model outcomes included the increase in elbow angle, defined as the maximum change under load from the initial elbow angle. The extremity was considered to have "collapsed" when elbow deflection angle reached 140^{o}, and a head might strike the ground. OpenSim was used to estimate the triceps muscle sarcomere length and thence how much elbow flexion corresponded to the range of short range muscle stiffness.

RESULTS AND DISCUSSION

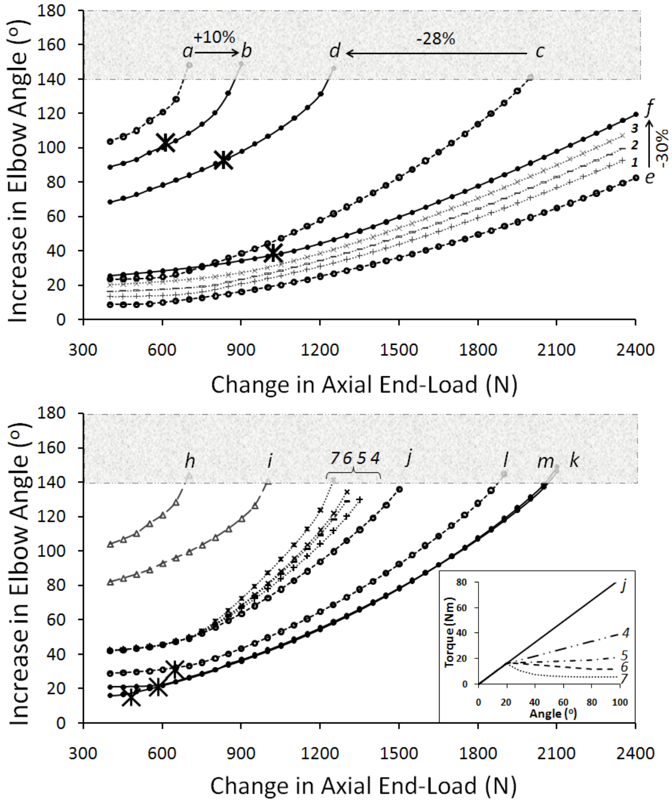

Figure 1: Predicted elbow deflection behavior as a function of the impulsive increase in axial end-load, muscle tensile properties, and initial elbow angle in the Young Male (upper) and Young Female (bottom) limb. The shaded region denotes limb collapse. See text for abbreviations.

In the young male model (upper graph), each curve in the upper Figure is labeled with letter *a-f* which correspond to 6 different initial conditions. Curve set *(a, c, e,* shown as dotted lines) are based on initial elbow angles of 20^{o}, 10^{o}, 5^{o} and values of the product *r,* where $r = g \times m$, with values of 0.55, 0.75, 0.81, respectively. Curve set *(b, d, f,* shown as solid lines) show how much *m* had to be modified by a multiplier to fit DeGoede's experimental data ([1], the "✱"points). For example, for an initial 5^{o} elbow angle, *m* had to be modified from 0.81 to 0.57 (*e* → *f*), equivalent to a 30% decrease in both model elbow and shoulder stiffness. Likewise, a 28% decrease *(m = 0.74 → 0.53)* was needed to modify line *c* to *d,* and a 10% increase to modify line *a* to *b (m = 0.55 → 0.61)*. The effect of differentially reducing elbow rotational resistance relative to the shoulder resistance from that in curve *e*, can be seen in the gray dotted lines *(1, 2, 3),* where the elbow and shoulder reductions were 0% & 60%, 10% & 50%, 20% & 40%, respectively. Therefore, the buckling load is more sensitive to elbow than shoulder muscle stiffness. Buckling behavior was very sensitive to initial elbow angle at impact; increasing the angle, *f*(5^{o}) → *d*(10^{o}) → *a*(20^{o}), caused the limb collapse load to decrease ~4-fold from ~2,400 N to 1,250 N to 700 N.

In the young female (lower graph), the three "✱" data points are mean experimental data for young 5 females. In the curve set (*j, k, l, m*), a 45% increase in *m* was needed to modify curve *j* to *k* so it passed through the correct data point; likewise a 12% increase (*l* → *m*). The curve set *(4, 5, 6, 7)* are the results of how softening relationships (see Methods & Figure inset) modify the *j* curve which had an initial angle of 15^{o} and stiffness ratio of 0.69 to reduce the load for collapse in the young female. Curves *h* & *i* represent the loading cases in which the initial elbow angles were 15^{o} & 20^{o} with r = 0.55.

CONCLUSIONS

1. Upper extremity collapse is likely to occur in:
   a) Males when landing with excessive initial elbow flexion (>20^{o}) or inadequate elbow muscle pre-activation (<53% MVC).
   b) Females when landing with excessive initial elbow flexion (>20^{o}), too little shoulder extensor muscle preactivation (<30%), or elbow extensor muscle weakness (<58% MVC).
2. The model suggests women pre-activate and stiffen their shoulder muscles more than males.

REFERENCES

1.DeGoede KM, et al. *J Biomech* **35**, 843-848, 2002.
2.Lee Y, et al. *NACOB*, Ann Arbor, USA, Abstract 136, 2008.
3.Grover JP, et al. *C Biomech* **22**, 360-368, 2007.
4.Malamud JG, et al. *J Neurophysiol* **76**, 2280-2289, 1996.
5.Murray WM, et al. *J Biomech* **28**, 513-525, 1995.
6.DeGoede KM, et al. *J Biomech* **36**, 413-420, 2003.

TRANSMISSION OF WHOLE BODY VIBRATION IN CHILDREN WHILE STANDING

Eadric Bressel, Gerald Smith, and Jaimie Branscomb
Biomechanics Laboratory, Utah State University, Logan UT, USA
email: eadric.bressel@usu.edu

INTRODUCTION

Whole body vibration has recently been used as a therapeutic intervention for the treatment of children with disabling conditions [1,2]. Researchers of these studies have observed encouraging results in terms of improved mobility and bone strength. However, the use of whole body vibration in children raises an important question regarding its safety as it is not clear how children attenuate vibration while standing. Occupational assessments while seated [3] indicate that children absorb less vibration than adults (i.e., 12-86% less) suggesting that adult vibration parameters while standing (e.g., 1 mm amplitude at 30 Hz) are not applicable to children and may produce different physiological effects. The purpose of this present study was to determine if children transmit vibration differently than adults while standing on a vibration platform. It was hypothesized that the transmissibility would be greater in children than adults. That is, children would display greater amplitudes of vibration (mm) in the upper and lower body when compared to adults.

METHODS

Twelve healthy children (age = 7.2 ± 3.1 yrs; mass = 22.6 ± 14.4 kg) and ten healthy adults (age = 25.9 ± 5.5 yrs; mass = 73.1 ± 10.0 kg) with no reported musculoskeletal injuries participated in the study. The experimental protocol required each participant to stand on a commercially available vibration platform (i.Tonic International B.V., Netherlands) with progressively greater frequencies of 28, 33, and 42 Hz. Participants stood on the platform for approximately 10 s at each frequency with no shoes and knees slightly bent (i.e., 10-25º; Figure 1). The transmissibility of vibration oscillation was assessed with a high speed motion analysis system (Vicon Motion Systems). Seven cameras sampling at 500 Hz tracked low mass reflective markers placed on the vibration platform and on the skin over the following bony landmarks: Lateral malleolus (ankle), tibial tuberosity (tibia), anterior superior iliac spine (ASIS), sternum, and anteromedial frontal bone (forehead; Figure 1).

The Vicon system was calibrated according to manufacturer guidelines and its accuracy for tracking markers was assessed using a ‘spot checking’ technique described by Delia Croce and Cappozzo [4]. Three-dimensional position data from each reflective marker were computed from direct linear transformations and then exported to a Microsoft Excel spreadsheet for post analyses. The vertical amplitude of oscillation (z; Figure 1) for 20 cycles of data were computed and averaged between limbs. The mean amplitude for each marker was compared between groups (children and adults), across frequencies (28, 33, & 42 Hz) and markers using a repeated measures analysis of variance (ANOVA) with follow-up multiple comparisons: Type I error set at 0.05.

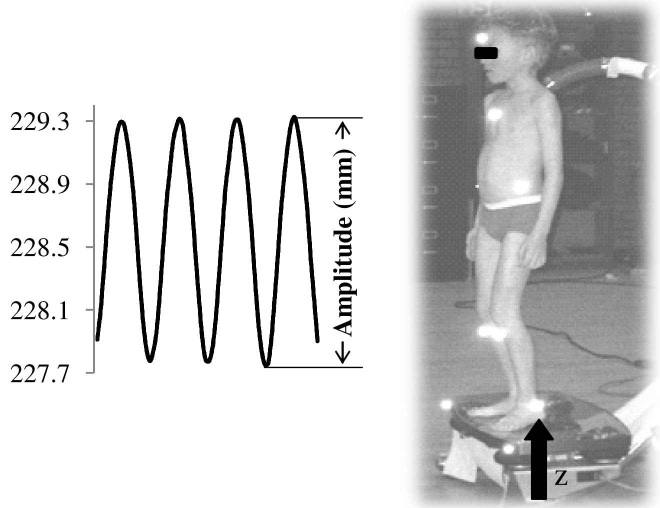

Figure 1. Vibration platform set-up and representative vertical (z) vibration waveform. Amplitude was calculated from peak to peak.

RESULTS AND DISCUSSION

No significant interactions were observed among factors (p = 0.06 – 0.40) indicating that children and adults respond similarly across vibration frequencies and marker positions. Figure 2 illustrates that platform vibrations were not substantially attenuated in the lower body since ankle and tibia markers were on average 53% greater than ASIS, sternum, and forehead markers (p = 0.01-0.08).

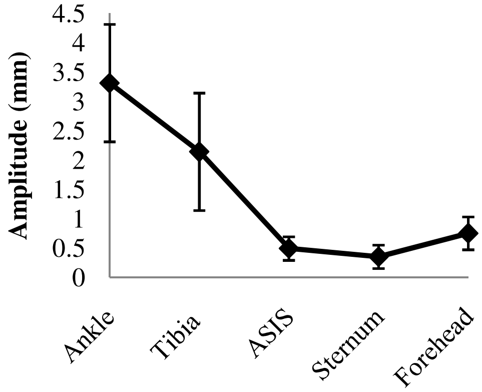

Figure 2. Pattern of vibration transmission from the ankle to forehead.

Regarding between group comparisons, markers on the tibia and ASIS of children were 171% and 86% greater respectively, than values for the adults (Table 1). Conversely, marker amplitudes on the vibration platform were 23% greater for the adults than children (Table 1).

The physiological effects of whole body vibration while standing are often based on how the platform is adjusted in terms of amplitude, frequency, and duration [1,2]. However, factors that include joint kinematics and body mass determine how the vibration is transmitted from the platform through the body [5]. Because children have less tissue mass to dampen the vibration and they display different structural organization of bone and other tissues, the transmissibility is likely different from adults, which was observed in this study. However, the original findings of this study are that despite differences in mass and structural organization of tissues, children are able to use other mechanical factors (e.g., muscle activity level) to attenuate vibration by the time it reaches the upper body and head as evidenced by forehead amplitude values (Table 1). These findings are important from a safety perspective as excessive head vibration may have deleterious effects.

CONCLUSIONS

It may be concluded that children display greater amplitudes of vibration in the tibia and ASIS when compared to adults, despite the platform amplitude being uncontrollably lower for children (Table 1). In contrast to occupational assessments while seated [3], amplitudes of vibration in the upper body are similar between children and adults while in standing.

REFERENCES

1. Semler O. et al. (2008). *Clin Rehab* **22**, 387-394. **22**, 676-685.
2. Ward K. et al. (2004). *J Bone Miner Res* **19**, 360-369.
3. Giacomin J. (2005). *Clin Biomech **20**, 372-380.*
4. Delia Croce U. & Cappozzo A. (2000). *Med Biol Eng Comput **38**, 260-266.*
5. Cardinale M. & Wakeling J. (2005). *Br J Sports Med* **39**, 585-589.

ACKNOWLEDGEMENTS

This study was supported by a research catalyst grant from Utah State University.

Table 1: Marker amplitudes (mm) for adults and children standing on the vibration platform at 33Hz.

	Platform	Ankle	Tibia	ASIS	Sternum	Forehead
Adults	1.78 ±0.16	3.68 ±1.97	1.15 ±0.46	0.31 ±0.09	0.35 ±0.10	0.76 ±0.22
Children	1.45 ±0.26*	2.94 ±1.40	3.12 ±2.53*	0.67 ±0.39*	0.34 ±0.19	0.74 ±0.33

*Significantly different from adults, p = 0.03-0.01

EFFECT OF TACTILE PAVING ON GAIT PARAMETERS IN OLDER ADULTS

[1,2] Sibylle B. Thies, [1]Laurence Kenney and [1]Dave Howard
[1] Institute for Health & Social Care Research, University of Salford, Manchester, UK
[2] Institute for the Built & Human Environment, University of Salford, Manchester, UK
email: s.thies@salford.ac.uk, web: http://www.ihscr.salford.ac.uk/

INTRODUCTION

Fall-related injuries in older people are associated with loss of independence [1], morbidity [2] and death [3], and walking on uneven ground has been reported as a leading activity in which fallers were engaged at the time of a fall [4]. A number of studies have identified relationships between biomechanical variables (speed, gait variability) measured during walking on smooth and irregular surfaces and fear of falling and fall risk [5-7].

Tactile blister paving has been developed in order to provide warning and guidance for blind and visually impaired people and is used at critical points such as pedestrian crossings. Each 40x40 cm paving slab contains blisters ("domes") protruding 5mm above the surrounding pavement. These slabs are laid over a distance of up to 2.4m up to the curb of the street [8]. Such paving may be considered manmade uneven ground, yet despite the known effects of uneven surfaces on gait and balance a search with Web of Science resulted in only one study on healthy young subjects that investigated the effects of tactile pavement on the biomechanics of gait [9] and no reports of the effects on older people.

It was our objective to design a laboratory platform resembling a pedestrian crossing and to investigate gait parameters in older adults walking on smooth and tactile paving. We hypothesized that tactile pavement, as compared to smooth pavement, would result in increased gait variability and decreased speed in older adults.

METHODS

Test platform: in this study the test platform was configured according to the UK's Department for Transport guidelines [8]. The length of the pavement area was 2.4m and the slope leading to the curb of the street was 1:12. A pedestrian traffic light and three pairs of timing gates were integrated with a motion analysis system so that the state changes of the light could be synchronized with the marker data.

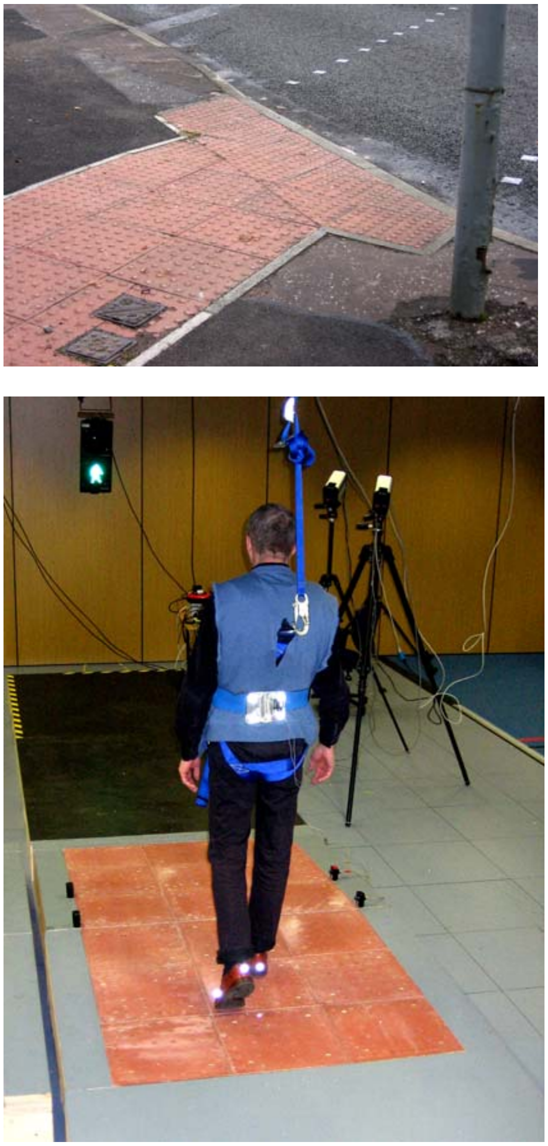

Figure 1: Controlled pedestrian crossing: real world (top) and laboratory set up (bottom).

Test Protocol: 20 older adults (10 with a history of falling) were randomly allocated into either group A or B. Group A began with walking trials on tactile paving, followed by trials on smooth paving; group B proceeded through the study in the reverse order. Participants then carried out, in a randomized order, a series of walks at self-selected speed along the walkway for both paving types. The 30 walking trials, half of them on tactile paving, comprised i) continuous walking, in which the participant proceeds along the walkway uninterrupted; ii) walking & stopping at curb after an early trigger of the traffic light; iii) walking & stopping at curb after a late trigger of the light. Their presentation was random. This paper only discusses the results for condition (i).

Data collection & analysis: reflective markers were placed on both shoes and on a rigid plate attached to a waist belt. Heel and toe markers were used to first calculate heel strike and toe-off [10] and subsequently to obtain step time and step width & length during dual support (Figure 2). A waist marker was used to obtain speed. Parameter variability was characterized by the standard deviation and paired t-tests were used for comparison of the two paving conditions.

RESULTS AND DISCUSSION

This is the first study to report on gait parameters obtained for a scenario that closely resembles crossing of the street. Ten steps per subject per pavement condition were recorded. No changes in step width and step length variability or speed were obtained. However, step time variability significantly increased from the smooth to the tactile paving condition ($p=0.01$) indicating that subjects exhibited a less rhythmic gait pattern when walking on tactile paving. This has been associated with an elevated falls risk [5-7]. Given the “domes” of blister pavement we will next determine the minimum toe-clearance on both surfaces and evaluate the probability of tripping [11]. Moreover, we will evaluate the effect of pavement type on successful stopping for conditions ii & iii and will analyze data of fallers and non-fallers separately.

CONCLUSIONS

Safe ambulation in the community is crucial to older adults’ independence & quality of life and gait analysis may support good urban design: our results show less regular gait on tactile than on smooth paving and this may reflect an increase in falls risk. Further analysis is required to confirm our findings.

REFERENCES

1. Dunn JE, et al. *Am J Public Health* **82**, 1263-1267, 1992.
2. Gryfe CI, et al. *Age Ageing* **6**, 201-210, 1977.
3. Sattin RW. *Annu Rev Public Health* **13**, 489-508, 1992.
4. Berg WP, et al. *Age Ageing* **26**, 261-268, 1997.
5. Maki BE. *J Am Geriatr Soc* **45**, 313-320, 1997.
6. Hausdorff JM, et al. *Arch Phys Med Rehabil* **82**, 1050-1056, 2001.
7. DeMott TK, et al. *Am J Phys Med Rehabil* **86**, 125-132, 2007.
8. www.dft.gov.uk/transportforyou/access/peti/guidanceontheuseoftactilepav6167
9. Kobayashi Y, et al. *IEEE Trans Neural Sys Rehabil Eng* **13**, 53-59, 2005.
10. O’Connor CM, et al. *Gait Posture* **25**, 469-474, 2007.
11. Best R, et al. *J Biomech* **41**, 1147-1151, 2008.

ACKNOWLEDGEMENTS

UK Engineering & Physical Science Research Council.

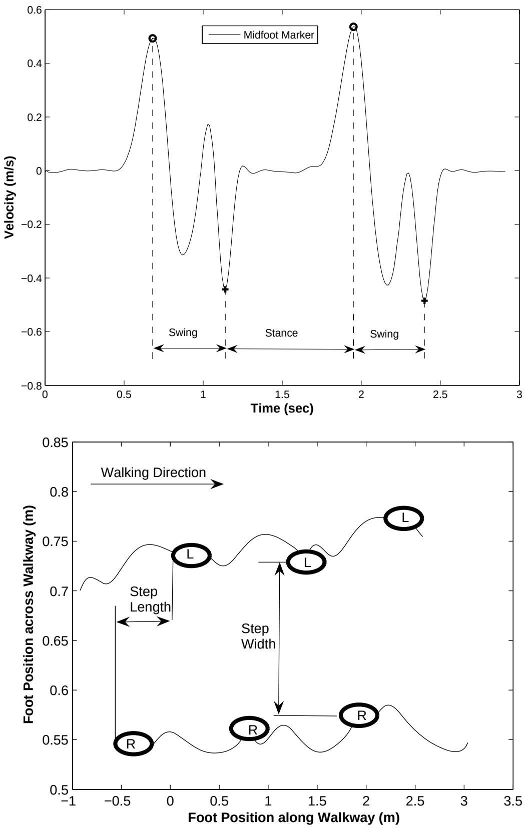

Figure 2: Kinematic data of heel strike, ‘+’, and toe-off, ‘o’, (top) and definition of step width & length (bottom).

IMPACT FORCES DURING BALLET: IMPLICATIONS FOR INJURY

[1] Rhonda Boros and [2]Lindsey Skelton
[1]Biomechanics Lab, Health, Exercise & Sport Sciences, Texas Tech University
[2]Department of Sociology, Anthropology, and Social Work, Texas Tech University
email: RL.BOROS@TTU.EDU, web: http://www.hess.ttu.edu/rboros

INTRODUCTION

Pre-professional high school and professional ballet dancers are at extremely high risk for mild and severe lower extremity injury [1,2]. A 26 to 51% lifetime injury prevalence in collegiate and professional dancers has been reported [1]. This high injury risk is cause for concern, as the study of ballet is typically initiated at an extremely young age, and young dancers spend a great deal of time in the dance hall training and practicing [1].

Dance related injuries in ballet have often been associated with high magnitude landing impacts. However, there is a lack of scientific research describing the ground reaction forces associated with common ballet skills [1,3], and only a few select skills, including the grand plie, demi plie, passé, grand jete and aerobic dance have been analyzed biomechanically to any extent [1,4,5,6,7]. Comparative ground reaction forces during isolated ballet skills versus skills performed as part of a dance routine are also lacking.

The main purposes of this study, therefore, were to 1) determine the relative ground reaction forces during the performance of five basic ballet skills (grand plie, arabesque, cabriole, changement, entrecht) and compare them with those of more common locomotion skills (vertical jump, hop, walk, jog); and 2) determine any changes in ground reaction forces that occur when the ballet skills are performed as part of a dance routine.

METHODS

Six female ballet dancers from pre-professional and collegiate dance programs in the Lubbock, TX area, (mean+/-SD age 19.7+/-2.7yr, mass 60.8+/-5.0kg, height 1.642+/-0.025m) participated as subjects. Each subject was informed of the study purpose and signed an informed consent prior to participation. Subjects wore their own ballet slippers for all trials. Two AMTI force plates sampling at 1000 Hz were used to determine body mass normalized ground reaction forces (N/kg body mass).

Following an individual warm-up, each subject performed five counter-movement vertical jumps (CMJ) starting and landing on the same force plate. To control arm swing hands were clasped behind the head. Following the jump trials, two trials each of hopping, walking, and jogging were performed. Four trials each of the ballet skills (grand plie, changement, entrecht, arabesque, and cabriole) were subsequently performed for comparison with the more everyday locomotion skills.

Finally, dancers performed a dance routine consisting of two changements, two entrechts (all leaving and landing on a single force plate), followed by two balonetes moving forward off the plate, followed by one pique arabesque into a one step tour jete with the final landing occurring back on the original force place. The main purpose of this routine was to allow the comparison of ground reaction forces incurred during dance skills performed in isolation with the same or similar skills performed as part of a dance routine. Statistical comparisons were made via paired t-tests, with a significance level set at 0.05.

RESULTS AND DISCUSSION

Normalized vertical ground reaction forces (nVGRF) were similar to those previously reported for aerobic dance [6,7] and traveling leaps [4,5,6]. Mean and standard deviation results for the locomotion and dance trials are presented in Figure 1, and statistically significant differences ($p<0.05$) between the locomotion and ballet skills are noted.

During the CMJ, dancers were instructed to jump as high as possible, thus attempting to develop a maximal effort impulse to propel their bodies vertically in the air. Landing nVGRF of the entrecht and cabriole were similar to those of the CMJ, suggesting that the dancers needed to create as much vertical force as possible (near maximum effort perhaps) to achieve the desired image and technical characteristics of the skills.

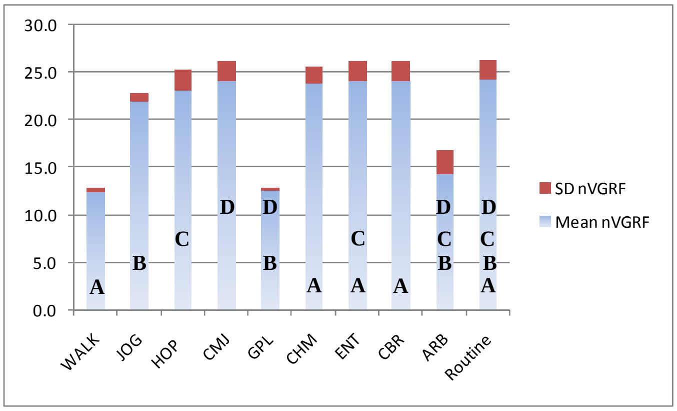

Figure 1: nVGRF (N/kg) during locomotion and ballet skills. Letters denote significant differences ($p<0.05$) between locomotion and ballet skills.

The changement impact forces were similar to those of hopping, perhaps demonstrating that the dancers only needed to generate and absorb moderate amounts of force to perform this skill properly. Arabesque and grand plie nVGRF were similar to those of walking, suggesting that these forces are of low impact and hence deliver minimal stress to the lower extremity.

The highest ground reaction forces occurred during the dance routine (~2.3BW). An interesting finding was that the peak forces during the dance routine were experienced during the consecutive changements and entrechts, rather than during the final tour jete. This result is somewhat unexpected, as the tour jete involved a greater horizontal distance traveled and thus would be expected to result in a greater impact peak [4,5]. A possible explanation for our observation is that the performance of the four sequential changement and entrecht jumps required stiffer lower extremity control compared with the same skills in isolation, resulting in relatively larger nVGRF. The final tour jete, in contrast, was the final landing in the routine after which the dancers simply stepped through and off the plate. Had the dancers been required to stick this final landing, the impact forces would have likely been much greater. This latest result has huge implications for injury considering the incredible number of hours young ballerinas spend training and perfecting their technique and performance.

CONCLUSIONS

Results of the present study demonstrate that many ground impact forces experienced during ballet jumps are statistically significantly greater than those of measured walking, hopping and even jogging locomotor patterns. Repeated or sequenced contacts in dance were shown to produce greater impact forces compared with isolated skills. Considering pre-professional high school ballet dancers have been reported to train over five hours a day [1], there is some cause for concern that these repeated impacts may play a critical role in acute and chronic lower extremity injury.

The present study did not account for the foot contact area absorbing the impacts nor joint kinematics associated with these skill performances. Considering female ballet landings are performed primarily en pointe (i.e., on the toes) [8], further research is needed to determine the true foot pressures and lower extremity joint forces and moments realized during isolated and sequential ballet landing impacts.

REFERENCES

1. Hincapie CA, et al. *Arch Phys Med Rehabil*, **89**, 1819-1829, 2008.
2. Bronner S, et al. *Am J Sports Med*, **31**, 365-373, 2003.
3. Tuckman AS, et al. *Foot & Ankle*, **13**, 220-223, 1992.
4. Simpson KJ and Kanter L. *Med Sci Sports Exerc*, **29,** 916-927, 1997.
5. Simpson KJ and Pettit M. *Med Sci Sports Exerc*, **29**, 928-936, 1997.
6. Michaud TJ, et al. *J. Sports Med Physical Fit*, **33**, 359-366, 1993.
7. Ricard MD and Veatch S. *J Applied Biomech*, **10**, 14-27, 1994.
8. Miller CD, et al. Foot & Ankle, 11, 97-100, 1990.

ACKNOWLEDGEMENTS

We would like to thank the student assistants in the Biomechanics Lab at Texas Tech, especially Brent Carter for his ballet expertise and assistance with data collection and processing.

BIOMECHANICAL PARAMETERS AND MILE PERFORMANCE

Jesse Tukuafu, Iain Hunter, Ruthann Cunningham, & Jenny Willis
Brigham Young University, Provo, UT
email: iain_hunter@byu.edu web: http//biomech.byu.edu

INTRODUCTION

Track and cross-country races can be decided by less than a tenth of a second. With such a small time differential, every aspect of running is important. Elite sprinters emphasize proper technique to maximize their power and speed. Middle distance runners rely upon a balance of proper technique and running economy. Distance runners focus on economy of movement to maintain a given speed for extended periods.

Increased lower leg muscle-tendon stiffness has been found to improve running economy [1]. The leg acts as a spring during the stance phase of running. The spring model of the leg is associated with the effective vertical stiffness of the center of mass. Runners with higher effective vertical stiffness have an inverse relationship with aerobic demand [2].

The ability of the lower leg to act as a spring is identified by the range of motion of the leg during the stance phase and more specifically the degree of knee flexion/extension during certain points of the stance phase. Faster runners will optimize the range of motion and degree of knee flexion/extension during the stance phase to maximize running economy.

Distance runners choose a stride length and stride frequency that is most economical [3]. Sprinters have been shown to differ significantly from distance runners in these characteristics and ground contact time while running at the same pace [4]. Faster distance runners may be able to spend less time on the ground when compared to slower runners at the same speed. This would indicate the ability of the faster runners to increase speeds while balancing aerobic demand.

This study investigated the biomechanical differences among females running at 5.94 m/s (4:30 min/mile pace). The purpose of the study was to determine whether faster runners exhibit biomechanical differences when running at competition level speeds. The hypothesis of this study is that faster one-mile runners will experience a smaller range of motion during the stance phase and less time on the ground.

METHODS

Thirty-nine female NCAA Division I Track and Cross Country athletes voluntarily participated in the study. Participants were free of injuries at the time of testing. Racing flats (Nike® Zoom Waffle Racer™ 2005 and 2007) were used during the running trial. After a five-minute warm-up, each participant performed a running trial on a treadmill set at 5.94 m/s for 11 strides or 22 steps.

Trials were recorded using a six camera Vicon Nexus software system (Vicon Motion Systems Ltd, Lake Forest, CA). Each camera was calibrated at 75 Hz and running trials were recorded at 240 Hz. Hip, knee and ankle angular positions were recorded using 35 infrared markers and Vicon's PlugIn Gait module. Hip, knee and ankle angles were measured at certain points of the running stride for both sides of the body. Center of mass vertical oscillation, stride rate, stride length and ground contact time were also recorded.

The collegiate coach for all 39 participants provided information regarding one-mile personal records (PR). Hip, knee and ankle angles for both sides of the body were averaged. A stepwise linear regression was used to determine the correlations between one-mile PR and average hip, knee and ankle angles at certain points in the stride. Correlations between one-mile PR and center of mass oscillation, stride rate, stride length and ground contact time were also performed.

RESULTS AND DISCUSSION

Linear regression showed a positive correlation between one-mile PR and average knee touchdown angle (R^2=0.18, p<0.05). The correlation showed that the faster the mile time the closer knee touchdown angle was to full extension.

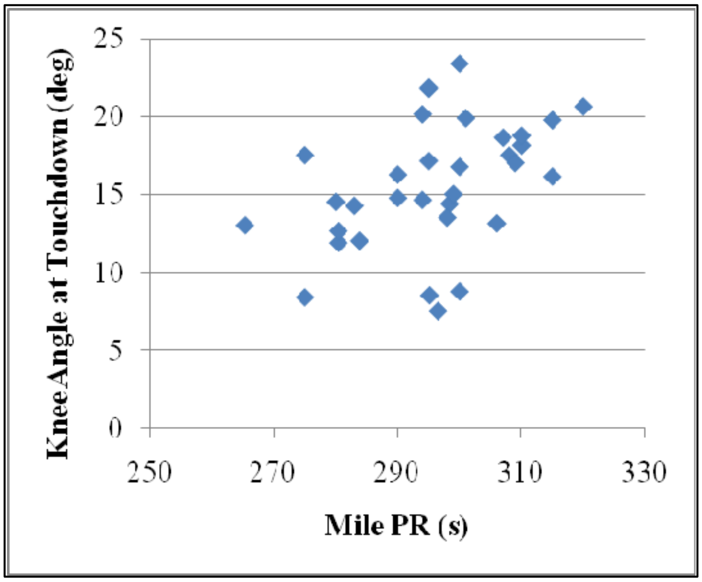

Figure 1: Knee angle at touchdown versus mile personal record (Knee angle = 1.346 x Mile PR + 274.7). Zero degrees represents full extension.

Only a small indication of the hypothesis was observed. The straighter knee angle at touchdown indicates a stiffer landing, but the knee range of motion from touchdown to maximum knee flexion during stance was non-significant. No other characteristics were statistically significant with mile PRs. Many characteristics of running technique were measured here with little statistical significance. This implies that there are other factors going into performance that must be considered. Physical conditioning is the most likely factor related to mile run performance. This does fit with previous findings of improved running economy with greater vertical stiffness in running [2]. When a muscle is conditioned to handle greater force production, it can react to the ground with a greater stiffness. However, this does not appear to be showing up in any large degree in kinematical measurements.

In order to increase vertical stiffness and running economy, previous studies show plyometric training to be effective. In this cross-sectional study, it appears that kinematics are only slightly related to performance. However, the small trend that was observed fits with the idea of increased vertical stiffness that leads to greater running economy.

CONCLUSIONS

Kinematical factors play only a small relationship in determining mile run performance. Physical conditioning is the primary factor worth considering. Through plyometric training, ground forces can be altered and running economy can be improved. Supplementing traditional training techniques with plyometric training will likely give the greatest performance improvements.

REFERENCES

1.Heise G, Martin P. *Medicine and Science in Sports Exercise* **30**, 750-754, 1998.
2.Spurs R, Murphy A, Watsford M. *Eur J Appl Physiol* **89,** 1-7, 2003.
3.Cavanagh P R, Kram R. *Medicine and Science in Sports and Exercise* **21,** 467-479, 1989.
4.Bushnell TD, Hunter I. *Sports Biomechanics* **6**, 261-268, 2007.

ACKNOWLEDGEMENTS

Thank you to the Brigham Young University Women's Track and Cross Country Team.

FRICTIONAL PROPERTIES OF THE HAND SKIN

Mehmet Uygur, Paulo B. de Freitas and Slobodan Jaric
Department of Health, Nutrition and Exercise Sciences, University of Delaware
email: muygur@udel.edu

INTRODUCTION

A common approach in evaluation of hand function has been based on force coordination. To hold and manipulate a hand-held object one has to apply a certain magnitude of force perpendicularly to the object (i.e., grip force; GF) to avoid slippage caused by the tangential force (load force; LF) acting at the hand-object contact area. However, applying a too high GF could be detrimental to the task performance and also could cause fatigue or crash a fragile object. The magnitude of GF needed to prevent slippage depends on both the magnitude of LF and the coefficient of friction (COF) acting between the hand skin and the object surface.

Having in mind importance of friction in manipulation activities (1, 2), as well as the importance of hand function *per se*, it is surprising that COF of different hand skin areas has remained mainly unexplored. Therefore, we aimed to investigate COF of various hand segments that are both commonly used (and, therefore, ‘specialized’) and ‘non-specialized’ for grasping. We hypothesized that the specialized skin areas (i.e., tips of the digits and palm) would have higher COF than the non-specialized areas that are virtually never used for grasping (i.e., fist and wrist).

METHODS

Sixteen healthy volunteers aged between 19 and 33 participated in the experiment. The experimental device (weight 5 N) consists of two parallel grasping surfaces connected with a single-axis force transducer measuring GF, and a multi-axis transducer measuring LF, placed underneath it (Figure 1F).

Participants performed the tasks under 2 coatings (high friction rubber and low friction acetate) employing 5 different grasps that involved different hand skin areas (see Fig. 1). COF was tested by using the method known as ‘slip ratio’ measurement (1, 2). This method allows for detection of the minimum GF necessary to avoid slippage.

The participants were instructed to hold the device and gradually decrease GF until the device slips. The ratio of the GF recorded just before slippage and the weight of the handle provided the slip ratio which was used to calculate COF [COF= 1/(2*slip ratio)]. Five trials were performed under each grasping and coating conditions and last 3 were used for calculating both the reliability and the average value of COF.

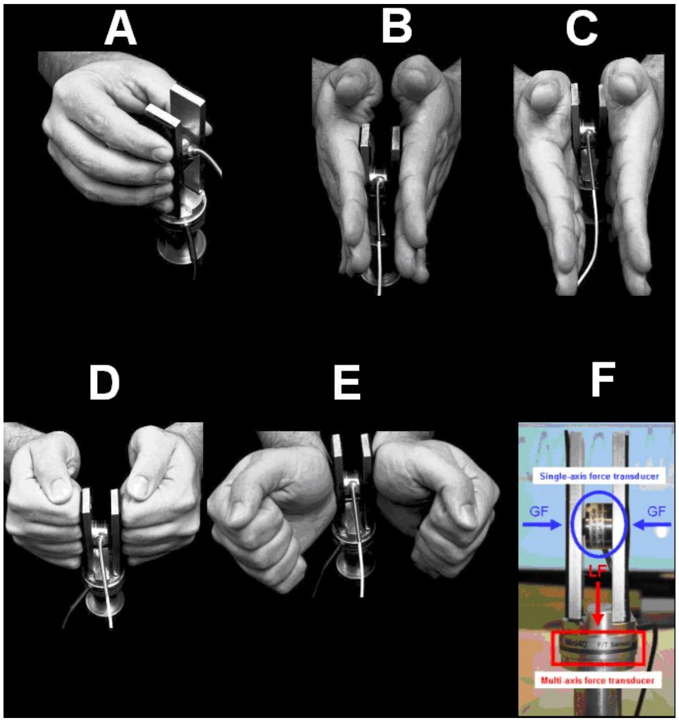

Figure 1. Illustration of the applied grasping techniques (A - tip of the digits; B - distal palm; C - proximal palm, D - fist, E - wrist) and the experimental device (F).

RESULTS AND DISCUSSION

The data revealed high intra-class correlation coefficients (ICC>.8) and no systematic bias among consecutive trials, suggesting therefore a high reliability of the assessed slip ratio.

Regarding the COF, the results suggested not only the expected main effect of coating (p<.001; COF higher for the rubber than for the acetate coating), but also of grasping (p<.001), and grasping*coating interaction (p<.001). Simple effect analyses demonstrated that there was a significant effect of skin hand area on COF for both coating. For rubber coating, the COF of the tips of the digits was significantly lower than of the distal palm (p<.01), but higher than of the fist (p<.001) and wrist skin areas (p<.001). COF was also higher in the proximal palm than in the fist (p<.01) and wrist areas (p<.01). No differences were found between the proximal palm and distal palm (p>.05), and between the tips of the digits and proximal palm grasp (p>.05). For the acetate coating, there were no differences in COF among the tips of the digits, distal, and proximal palm areas, but the COF of these areas were all significantly higher than in the fist and wrist areas (p>.05). Finally, the results also suggest a high across subject variability regarding COF of the same skin areas (see the error bars in Fig. 2).

Note that a high COF is important when manipulating heavy objects since it requires lower GF, and therefore, causes less fatigue and allows for a better control of the manipulated objects. From that perspective, a higher COF found in the palm and digits (which are commonly used in various types of grasping) should not be surprising. The interaction observed the coating and grasping techniques suggests that the observed differences in COF of various skin areas could be coating specific. Currently, it could only be speculated that the friction related advantages of the hand segments could be more specific when grasping 'natural materials' (e.g., wood, stone, bone) than non-natural ones (e.g., rubber, acetate, metal). This may give us possible evidence regarding a potentially important aspect of the evolutionary development of human hand.

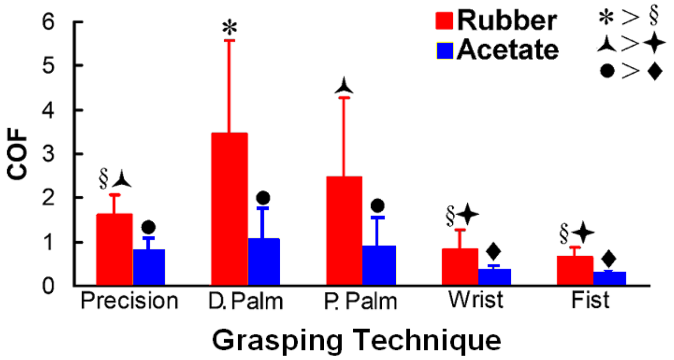

Figure 2. Coefficients of friction (COF) obtained from the various grasping techniques. Error bars represent SDs.

CONCLUSIONS

The results support the hypothesis regarding the higher COF of the specialized than in the non-specialized hand skin areas. Moreover, the COF differences between hand segments could be coating specific. Taking also into account a prominent differences in COF across participants, our findings strongly emphasize the importance of taking COF into account in the future biomechanical, ergonomic and motor control studies of manipulation activities.

REFERENCES

1. de Freitas et al., Experimental Brain Research, in press, 2009.
2. Johansson RS et al. Experimental Brain Research G 56, 550-564, 1984.

THE EFFECT OF ATORVASTATIN CALCIUM ON THE CORTICAL BONE STRENGTH OF CORTICOSTEROID TREATED RABBITS

[1]John A. Handal, [1]Thomas K. John, [1]Rashad Booker, [2]Jasvir S Khurana, [1]Minn Saing, [1]Solomon P. Samuel
[1]Department of Orthopedic Surgery, Albert Einstein Medical Center, Philadelphia, PA 19141,
[2]Pathology, Temple University Hospital, Philadelphia, PA 19140
Email: samuelsp@einstein.edu

INTRODUCTION

Corticosteroid therapy is a well known etiological factor for the development of osteoporosis (“secondary” osteoporosis) and femoral head osteonecrosis. Recently, HMG-CoA reductase inhibitors (popularly known as statins) have been suggested as a treatment option to prevent the development of corticosteroid induced femoral head osteonecrosis [1-2]. The exact mechanism by which statins prevent the development of osteonecrosis is unknown. Patients on corticosteroids may also develop hyperlipidemia and require treatment with statins.

Although statins have been shown to have an anabolic effect on bones [3], the effect of the combination of corticosteroid and statin treatment on cortical bones is unknown. In this study, the effect of atorvastatin calcium on the mechanical strength of corticosteroid treated rabbit femurs was evaluated. The results of the mechanical testing were also compared with bone histology sections.

METHODS

25 New Zealand white rabbits were used for this study. The animal protocol was approved by IACUC. Six rabbits were used as controls; the other nineteen rabbits received a weekly 2-3 mg/kg intramuscular injection of methylprednisolone acetate (Depo Medrol). Ten of these nineteen rabbits also received a daily 10 mg oral dose of powdered atorvastatin calcium (Lipitor, Pfizer Inc., NY) mixed with a teaspoon of baby food. The control rabbits also received a teaspoon of baby food daily. The rabbits were sacrificed at the end of 10 weeks.

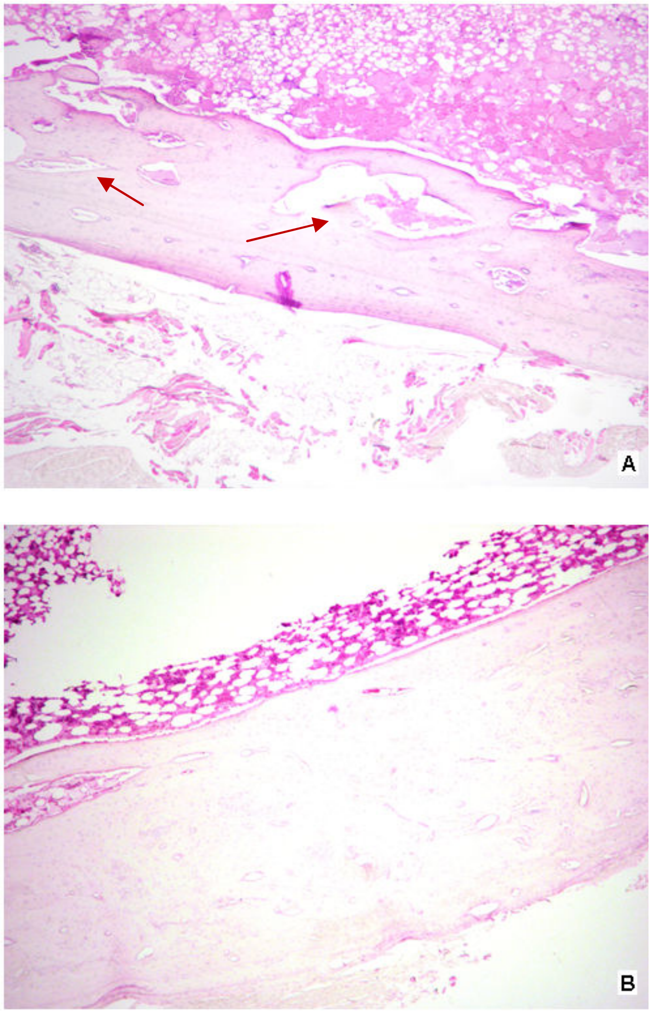

Figure 1: Most of the corticosteroid treated rabbits exhibited excessive cortical tunneling (A) when compared to the control rabbits (B).

After removing the surrounding soft tissues, the harvested femurs were wrapped in saline soaked gauze and stored at –20° C until further use. The femurs were tested in 3-point bending mode using an electro mechanical testing machine (800LE4 Dynamic Test System, Test Resources Inc., Shakopee, MN) at a crosshead speed of 1 mm/min until failure. The load-deformation curve and anatomic data was used to calculate the flexural strength and modulus [4]. The flexural strength and modulus of contralateral limbs were averaged before analyzing the differences between the treatment groups. ANOVA was used to analyze the differences between the treatment groups. After mechanical testing and anatomic measurement, one femur from each rabbit was fixed in buffered formalin, decalcified and processed for histology.

RESULTS AND DISCUSSION

The results showed that the average flexural strength and modulus of femurs decreased with corticosteroid treatment (Table 1). However, surprisingly the flexural strength of femurs in the corticosteroid plus statin treated rabbit group was significantly lower when compared to just the corticosteroid treatment group ($p<0.05$). Both the flexural strength and modulus differences were statistically significant between control and corticosteroid plus statin treated rabbit group ($p<0.05$) but was not statistically significant between control and corticosteroid treatment group ($p>0.05$). A very similar trend was seen in the tibias too (results not shown).

The histology slides showed extensive cortical thinning and tunneling of the cortex by fibroblasts and osteoclasts in all the corticosteroid treated bones (Figure 1). There was some reduction in hematopoetic marrow cells and foci of fat necrosis. There was some reduction in hematopoetic marrow cells and foci of fat necrosis. Although the cortical thickness was maintained in corticosteroid plus statin treated rabbits, the strength was nevertheless lower.

It is well known that rabbits are more susceptible to the adverse effects of corticosteroid treatment than other animal species. For example, corticosteroid treated rabbits are more prone to severe weight loss, muscle atrophy, infection, elevated lipid levels and elevated glucose levels. Therefore, the results of this study needs to be taken in perspective. Even though statins seems to maintain cortical thickness, it somehow affects the bone quality of these rabbits. More studies are needed to evaluate the micro-architecture and collagen quality of the corticosteroid plus statin treated rabbit femurs. The study results also warrant at least a retrospective chart review to make sure that the same trend does not happen in human patients.

CONCLUSIONS

Our findings suggest that the introduction of statins in corticosteroid treated rabbits may actually decrease bone strength despite the current impression that statins usually improve bone strength (or at least bone mineral density) when given alone through their anabolic effect. If this finding is substantiated on other species and humans the results can extremely important given the prevalence of steroid and statin use in the general population.

REFERENCES

1.Belmont *et al* (2004) Arthritis and Rheumatism 50(9):S597-S598.
2.Pritchett JW (2001) Clinical Orthopaedics and Related Research (386):173-178.
3.Mundy *et al* (1999) Science, 286:1946 - 1949.
4.Turner and Burr (1993) Bone, 14, 595–608.

ACKNOWLEDGEMENTS

Funding for this study was provided by Albert Einstein Society of Philadelphia.

Table 1: The flexural strength and modulus of femurs (average ± SD) from each treatment group measured using 3-point bending test. The number of animals used per group is shown in brackets.

	Flexural Strength MPa	**Flexural modulus GPa**
Control	149 ± 12 (6)	15.98 ± 1.95
Corticosteroid	130.4 ± 22.8 (9)	13.4 ± 3.2
Corticosteroid + Atorvastatin	109.4 ± 17.5 (10)	11.8 ±1.9

KNEE POSITIONING INFLUENCES WHOLE BODY 3-D VIBRATION TRANSMISSION

Gerald Smith, Eadric Bressel, Jaimie Branscomb, and Eric Snyder
Biomechanics Laboratory, Utah State University, Logan UT, USA
email: Gerald.Smith@usu.edu

INTRODUCTION

Whole body vibration has in recent years become a commonly used addition to training and therapy and is thought to positively stimulate muscle and bone. While numerous studies have evaluated both positive and negative physiological responses to vibration [1, 2, 3], few have provided more than cursory description of the vibration instrumentation involved or have discussed differing responses resulting from mechanical designs which produce unique vibration characteristics (see [4] for one instrumentation comparison). In most studies, accelerometers attached to a vibration plate and over anatomical landmarks are used to determine responses. Rarely have three-dimensional responses been evaluated; vertical vibration has typically been assumed to be of prime importance.

Motion analysis instrumentation has only recently gained sufficient speed and resolution to be capable of reliably detecting high frequency, low amplitude vibration. Applied to human vibration response, such high-speed motion analysis can help map the vibration transmission characteristics from vibration platform to various landmarks of the skeleton in three-dimensions. In this paper, a 3-D motion analysis approach to vibration was used to examine the effect of standing knee position on transmission of vibration from feet to head.

METHODS

Two vibration platforms were used in this study. The FreeMotion iTonic platform allows user control of frequency (nominal settings of 25 Hz, 30 Hz and M) as well as high and low amplitudes. A second instrument was included in the study because of its distinctly different surface movement pattern. The Pneu-Vibe Pro vibration platform from PneuMex Inc. has user control of frequency with continuous variable settings ranging between 20 and 60 Hz. Amplitude is also adjustable between high and low. For the study, both platforms were set to low amplitude with nominal frequencies of 30 Hz. Actual frequencies were about 33 Hz and 25 Hz, respectively. Sagittal plane movement pattern of each plate is illustrated in Figure 1. Horizontal and vertical movements of the platform were in-phase for the iTonic but out-of-phase for Pneu-Vibe resulting in an oval motion of that platform surface.

A seven camera Vicon MX motion analysis system with Nexus software driving T-20 cameras operating at 500 Hz was used to record vibrational responses. Low mass retro-reflective markers were placed on the corners of each platform plus over subject skeletal landmarks (lateral malleolus, tibial tuberosity, anterior-superior iliac spine (ASIS), T12 and C7 vertebrae, sternum, and forehead). Peak-to-peak displacement of each marker was determined for each condition. Mean of 20 cycles was analyzed for each subject and condition.

Ten healthy adults (25.9 ± 5.5 yrs; 73.1 ± 10.0 kg) participated in the study. For each platform, vibration response was recorded with extended knees and with flexed knees. Knee flexion was determined by subject comfort and ranged between about 10 and 25 degrees.

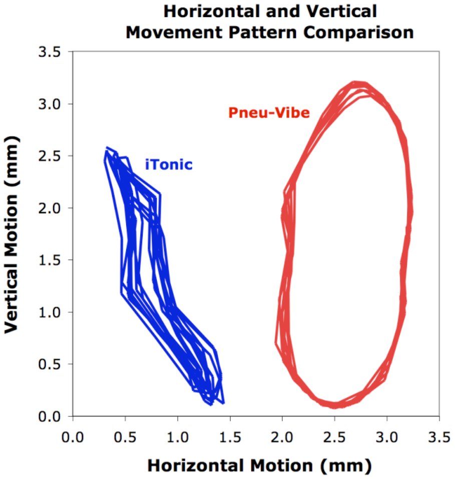

Figure 1. Movement pattern for iTonic and Pneu-Vibe machines at nominal frequencies of 30 Hz. Significantly greater horizontal motion occurred with the Pneu-Vibe machine ($p < 0.001$).

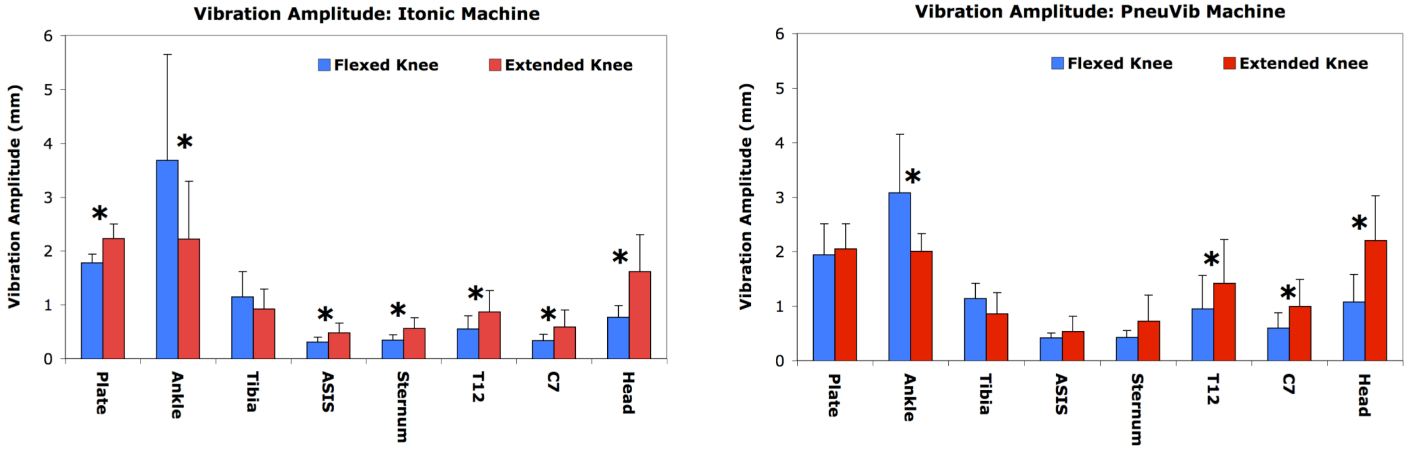

Figure 2. Peak-to-peak amplitude of vibration in the vertical direction for the Freemotion iTonic platform (left) and the PneuMex Pneu-Vibe Pro platform (right). Plate vibrations in the vertical direction were about 2 mm in each case. Vibration was attenuated as it was transmitted from foot to the rest of the body.
* $p < 0.05$ for paired t-test comparison of flexed vs. extended vibration amplitude.

RESULTS AND DISCUSSION

Vibration platform peak-to-peak amplitudes were about 2 mm for each machine in the low amplitude setting (Figure 2). In the A-P (anterior-posterior) direction, amplitudes were different for the iTonic and Pneu-Vibe machines (0.8 ± 0.1 mm and 1.1 ± 0.1 mm, $p < 0.001$). In the medio-lateral direction, vibration amplitudes were very small (about 0.2 to 0.3 mm) and not different between conditions.

With a flexed knee, substantially increased vibration amplitude was observed at the ankle. More proximal points on the leg as well as trunk landmarks experienced vibration at reduced amplitudes in each direction. At the head, vibration amplitude was greater than any trunk landmark. This suggests that the head may experience a resonance stimulated by the vibration of the trunk.

Knee flexion clearly influenced vibration amplitude for most skeletal landmarks in both vertical and A-P directions. At the head, vertical vibration nearly doubled for the extended knee condition, similar to accelerometer assessed head vibrations [4]. In addition, A-P vibration of the head was about 1 mm for the flexed knee condition but more than 1.6 mm with an extended knee (for both platforms). The significantly different A-P movements of the platform surfaces did not result in vibrational differences at the head.

The use of high-speed motion analysis with skin mounted reflective markers introduces a new methodology for evaluation of vibration transmission through the human body. Transmissions observed in this study were similar to previous studies using accelerometry [5, 6]. At 500 Hz sampling frequency, the system can adequately sample a cycle of typical vibration data from many landmarks simultaneously without the challenges of multiple accelerometers and cables. Precision of such systems when carefully calibrated are better than 0.1 mm and easily detected very low amplitude vibrations of trunk markers.

REFERENCES

1. Cardinale M & Wakeling J. *Brit J Sports Med* **39**, 585-589, 2005.
2. Dolny D & Reyes GFC. *Curr Sports Med Rep* **7**, 152-157, 2008.
3. Jordan MJ et al. *J Strength Cond Res* **19**, 459-466, 2005.
4. Abercromby AFJ *Med Sci Sports Exerc* **39**, 1794-1800, 2007.
5. Rubin C et al. *Spine* **28**, 2621-2627, 2003.
6. Kiiski J et al. *J Bone Min Res* **23**, 1318-1325, 2008.

ACKNOWLEDGEMENTS

Funding for this project was provided by a Research Catalyst grant from Utah State University to E.B.

FINGER ENSLAVING IN A THREE-DIMENSIONAL PRESSING TASK

Shweta Kapur, Jason Friedman, Vladimir M. Zatsiorsky, Mark L. Latash
Department of Kinesiology, Pennsylvania State University
email: suk212@psu.edu

INTRODUCTION

Various studies have looked at the unintended force production (enslaving) and force sharing patterns in multifinger pressing tasks (e.g, [2]). Only one study has looked at the enslaving and sharing of finger forces in tasks which involve finger force production in directions orthogonal to natural pressing [4]. This work explores indices of finger interaction in multi-directional pressing tasks. We describe the differences in enslaving matrices when pressing in different directions, and under different types of feedback.

METHODS

Eight subjects (4 males and 4 females) participated in the study. The subjects had to press in five different directions – down (under two instructions, to keep the force in the right – left direction zero and to keep the force in the forward - backward direction zero), down and right, down and left, down and forwards, and down and backwards. The forces and moments exerted by individual digits were recorded with 6-component sensors (ATI Industrial Automation, Garner, N.C.). The sensor surface was covered by P-100 sand paper. The transducer placement was such that force down was along the –Z axis, right force was along +X, and forward force was along the +Y axis. The experiment consisted of two parts: one finger pressing tasks and four finger pressing tasks. Maximum voluntary downward force (MVC) was recorded using unidirectional sensors. The targets were set at 22.5% MVC for down force production tasks, 3.75% MVC for the right–left force production tasks, and 10% MVC for forward–backward force production tasks. The feedback was shown on the computer screen, only for the task finger for one finger pressing trials. The subjects had to move the cursor in the instructed direction, along a straight line following a moving target. For the one-finger pressing task, subjects were instructed to "focus only on the task finger" but not to lift any fingers off the sensors at any time.

Enslaving matrices and indices of enslaving along the three axes were computed over the one-finger pressing tasks. A four-by-four enslaving matrix was constructed for enslaving in each direction for each of the six pressing tasks. In this matrix, forces produced by the other fingers, when one finger was instructed to produce force, were divided by the force magnitude produced by the task finger. It was calculated as follows:

$$\mathbf{E} = \begin{bmatrix} \frac{\Delta f_{I,I}}{\Delta F_I} & \frac{\Delta f_{I,M}}{\Delta F_M} & \frac{\Delta f_{I,R}}{\Delta F_R} & \frac{\Delta f_{I,L}}{\Delta F_L} \\ \frac{\Delta f_{M,I}}{\Delta F_I} & \frac{\Delta f_{M,M}}{\Delta F_M} & \frac{\Delta f_{M,R}}{\Delta F_R} & \frac{\Delta f_{M,L}}{\Delta F_L} \\ \frac{\Delta f_{R,I}}{\Delta F_I} & \frac{\Delta f_{R,M}}{\Delta F_M} & \frac{\Delta f_{R,R}}{\Delta F_R} & \frac{\Delta f_{R,L}}{\Delta F_L} \\ \frac{\Delta f_{L,I}}{\Delta F_I} & \frac{\Delta f_{L,M}}{\Delta F_M} & \frac{\Delta f_{L,R}}{\Delta F_R} & \frac{\Delta f_{L,L}}{\Delta F_L} \end{bmatrix}$$

where f_{jk} is force produced by finger j when k is the task finger and F_k is the total force produced by the task finger. The enslaving index $|\mathbf{E}|$ was calculated as the sum of all non-diagonal entries of the enslaving matrix.

Sharing of forces among the four fingers was calculated for the four finger pressing trials. The forces were expressed in percent of the MVC.

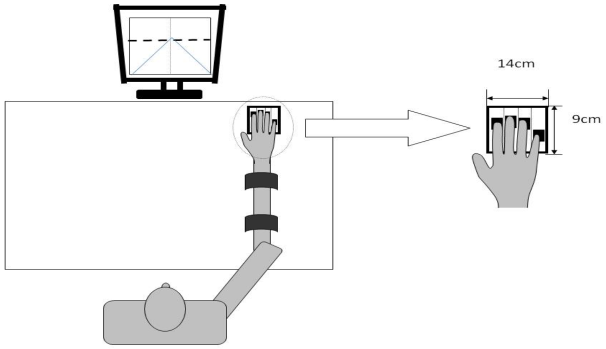

Figure 1: Experimental setup used for the study

RESULTS AND DISCUSSION

RMS of the force vector angle (root mean square of the instructed force direction minus the actual angle of the force vector, averaged over time and repetitions, and then across subjects; see Table 1) shows a difference in the performance of subjects across tasks. Subjects performed worse in the Down-back as compared to the Down-left and Down-right tasks, which was supported by ANOVA ($p < 0.001$). However, the performance was almost similar when required to press down and stabilize the forward/back force component at zero and when stabilizing the left/right force component at zero.

Negative entries were found for enslaving in non-down force production tasks (i.e., non-task fingers acted in an opposite direction to the task direction). The enslaving index in the X direction for the Down-right task was much higher than that for the Down-left task (see Table 2). This was supported by a t-test ($p < 0.01$). This suggests that enslaving in the X (right-left) direction is asymmetrical. In contrast, the enslaving index in the Y direction was more symmetrical, with the enslaving measure for the Down-back task not significantly different from that for the Down-forward task ($p > 0.4$).

For the downward (Z-axis) pressing tasks, the enslaving in Z direction did not vary significantly for the three different feedback conditions – no feedback about force produced in X or Y directions, feedback about force produced in X direction and feedback about force produced in Y direction ($p > 0.1$).

Table 1: RMS of the force vector angle (average ± standard error) for pressing tasks in different directions in four-finger pressing tasks.

Condition	*RMS angle (degrees)*
Down (stabilizing L/R)	2.20 (±2.17)
Down (stabilizing F/B)	4.25 (± 2.04)
Down left	3.39 (± 2.92)
Down Right	3.16 (± 1.31)
Down front	5.78 (± 1.78)
Down back	8.60 (± 2.92)

Table 2: |E| (enslaving index) for different task conditions averaged across all subjects

Condition	**$\|E\|_x$**	**$\|E\|_y$**	**$\|E\|_z$**
Down	----	----	1.43 (± 0.29)
Down (stabilize L/R)	-1.44(± 1.37)	----	2.19 (± 0.61)
Down (stabilize F/B)	----	0.56 (± 0.87)	2.65 (± 0.78)
Down right	4.30 (± 2.30)	----	2.47 (± 0.68)
Down left	0.11 (± 0.29)	----	1.68 (± 0.44)
Down forward	----	1.80 (±0.42)	2.23 (± 0.57)
Down back	----	1.22 (± 0.35)	1.88 (± 0.42)

Additionally, ANOVA (Task × Finger) showed that the sharing of forces among the four finger pressing tasks was not significantly different in the down pressing tasks with different feedbacks.

CONCLUSIONS

Some of the results can be naturally interpreted as a combination of two effects, enslaving in the task force direction and synergic finger force adjustments. In particular, an earlier study of abduction-adduction tasks [3] showed a synergic force production by the ulnar and radial finger pairs in opposite directions. This tendency might have contributed to the negative enslaving indices in the X direction. Enslaving indices in the downward direction have shown consistency across tasks and feedback conditions in addition to earlier observations of consistent enslaving over a broad range of forces [2]. The marked asymmetry of enslaving along the X axis is an unexpected finding that requires further investigation as well as the relative role of neural and peripheral factors in the observed effects.

REFERENCES

1. Kang N. et al. *Exp Brain Res,* **157,** 336-350, 2004.
2. Li ZM. et al. *Exp Brain Res,* **119**, 276-289, 1998.
3. Pataky TC. et al *Ergonomics*,**47**, 8,876-889, 2004.
4. Pataky TC. et al *Exp Brain Res,* **179**, 301-312, 2007.

ACKNOWLEDGEMENTS

This work was supported in part by NIH grants AR-048563, AG-018751 and NS-035032

MODULATING STEP LENGTH DURING WALKING BY YOUNG AND OLD ADULTS

Paul DeVita, Tim Copple, Jonathan Patterson, Patrick Rider, Ben Long, Ken Steinweg & Tibor Hortobagyi. East Carolina University, Greenville, NC email: devitap@ecu.edu

INTRODUCTION

Step length (SL) is a fundamental component of locomotion and has been widely reported as a descriptive quantity. It is well known for example that SL is shorter in old vs young adults [1]. Despite its importance the underlying factors that control SL in any population or those factors that lead to varied SLs across populations remain unknown because, to our knowledge, few studies have investigated the biomechanical causes of SL. The small amount of literature on this topic includes the removal of ankle muscles through a tibial nerve block and the subsequent reduction in SL [6]. However, removing muscle through nerve blocks alters other gait mechanics and may not provide a true assessment of muscle function in the natural state [4].

Walking gaits are produced by coordinated power and work from lower limb muscles. Since muscle work is quantified by joint powers [2,7] we presume that each gait element such as SL is controlled by the particular joint power profiles. We also propose that SL in walking can be controlled by the positive hip power in early swing (i.e. pulling the limb forward) and by positive powers at all three lower limb joints during stance (i.e. pushing the body forward). Further, the distal to proximal shift in joint powers in walking in old vs young adults [1,3,5] provides the basis for a preliminary hypothesis about the biomechanical causes of SL in both age groups. We hypothesize old relative to young adults control SL by primarily modulating hip joint work and less so by modulating knee and ankle joint work. The purpose of the study was to identify the relationships among lower limb joint powers and SL in healthy, highly mobile young (age: 21 ± 2 yrs, height: 1.73 ± 0.11 m, n=13) and old adults (79 ± 3 yrs, height: 1.69 ± 0.09 m, n=6).

METHODS

SLs and joint powers were derived from 3d lower limb kinematics and ground reaction forces from ~18 walking trials per subject, all at 1.50 m/s ± 5%. Each subject used self selected SLs ranging from ~0.50 m to the maximum length they could readily walk at the set speed. Positive hip work in early swing, positive work at each joint during stance and the sum of the stance work across joints were derived from joint powers and correlated with SL for each age group (over all subjects & trials) as a population based assessment of SL control. These variables were also correlated with SL within each individual subject (over trials) and the r values were then averaged across subjects within each age group using Fisher transformation. These results were used to see if individuals manipulated SL similarly (i.e. the population results accurately described individuals' performance). We assumed that since work from joint powers is the underlying cause of walking, correlations relating joint work and SL would reveal cause and effect outcomes. SL was strongly correlated with SL normalized to height (all subjects, r=0.98) thus, SL is shown in m.

RESULTS AND DISCUSSION

SLs ranged from 0.54 m to 1.23 m and 0.55 m to 1.02 m in young and old subjects indicating that both groups used similarly short SLs but old subjects could not step as far as young at the test pace. Relationships among all work variables were stronger in young vs. old adults in both population and individual analyses (Table 1). Stance work at all joints for the populations was significantly related to SL in young whereas stance work at knee and ankle but not hip were related to SL in old adults. Correlations based on individuals were stronger than for populations. We interpret this result as showing that each subject selected a control strategy more consistently than the populations values indicated. This was particularly true for old subjects who had larger differences than young between population and individual values. Thus young adults manipulated SL more consistently as individuals and as a population whereas old adults manipulated SL consistently on an individual basis but had greater variation in SL control strategies among individuals within the population. This interpretation is shown in the summed joint work results (figure 1). Summed work in young adults strongly predicted SL in population and individual analyses whereas it was a weak predictor for the old population yet a strong predictor for individual old adults. Summed work had the strongest relationship with SL in young and old individuals indicating that both groups manipulated SL primarily by manipulating total work output from the lower extremities as opposed to relying more so on precise work production at each joint. Young but not old adults also changed SL by modulating swing phase hip work suggesting they alter SL by not only controlling their pushing effort but also by controlling the work used to pull the swing limb forward.

CONCLUSIONS

Both groups controlled SL by primarily modulating total joint work from the lower limb. Most surprisingly, old adults manipulated SL more so by modulating ankle and knee joint work than hip joint work. This observation refuted the hypothesis, is novel, and is generally conflicts with previous aging work showing the preferential use of proximal hip vs. more distal knee and ankle musculature in the biomechanical process of walking [1,3,5].

REFERENCES

1. DeVita P, et al. *J Appl Physiol*, **88**, 1804-1811, 2000.
2. Elftman H. *Am. J. Physiol.* **125**, 357-366, 1939.
3. Karamanidis K, et al. *Annals Biomed Eng*, **37**, 467-476, 2009.
4. Neptune R, et al. *J Biomech*, **34**, 1387–1398, 2001.
5. Silder A, et al. *J Biomech,* **41,** 1520–1527, 2008.
6. Sutherland D, et al. J Bone Jt Surg, **62**, 354-363, 1980.
7. Winter D, *Clin Orthop Relat Res,* **175,** 147-154, 1983.

Figure 1. Summed joint work vs. SL.

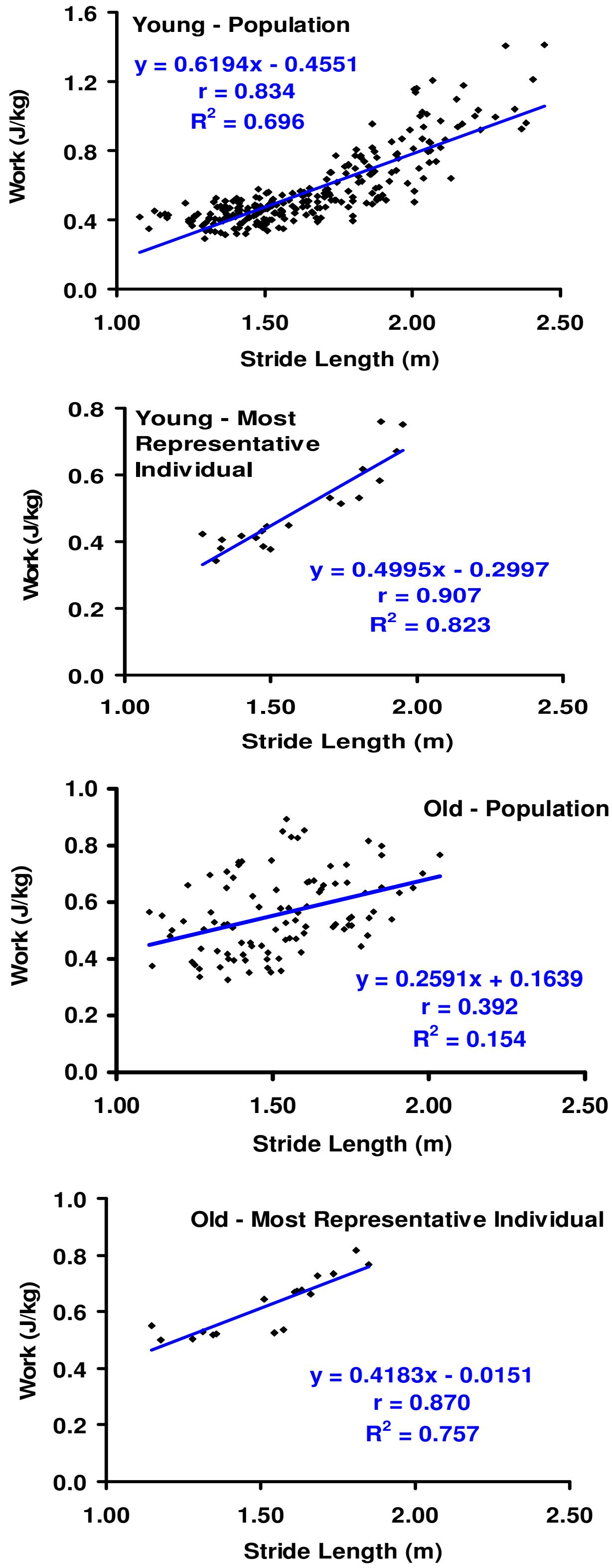

Table 1: Correlation coefficients among SL and work variables. **Bold values** significantly different from zero, $p<0.05$.

	Stance Phase				Swing Phase
Young	Hip	Knee	Ankle	Summed	Hip
Population	**0.459**	**0.762**	**0.677**	**0.834**	**0.341**
Individual	**0.720**	**0.872**	**0.871**	**0.912**	**0.514**
Old					
Population	-0.035	**0.355**	**0.589**	**0.392**	0.137
Individual	**0.377**	**0.763**	**0.792**	**0.880**	0.006

BIOMECHANICS OF TRANSPORT OF A FRAGILE OBJECT

Stacey L. Gorniak, Vladimir M. Zatsiorsky, Mark L. Latash
Department of Kinesiology; The Pennsylvania State University, University Park
Email: slg220@psu.edu

INTRODUCTION

Recent studies of multi-finger prehension have focused on the coordination of fingertip forces and moments of force during the handling (in both static and dynamic tasks) of rigid objects that do not deform easily [1-3]. While this is the case for some of the objects we encounter in everyday life, we also manipulate objects that are fragile and deformable. Currently, it is not known how finger forces and moments change during manipulation of a fragile object. The aim of the current study is to investigate kinetic and kinematic patterns during vertical transport of fragile and non-fragile objects.

METHODS

Right-handed subjects (n = 14) sat in a chair with both arms unsupported while facing a table. Subjects were instructed to grasp the instrumented object using one of three different finger configurations: with the digits of the right hand; with the digits of the left hand; and with the index, middle, ring, and little fingers of the right hand in opposition to the index finger of the left hand. In tasks involving only one hand, the non-involved hand rested on the subject's lap. In two-hand tasks, the two hands of the subject were not permitted to touch each other at any point during recording. The object was instrumented with five 6-component force /torque sensors to measure digit forces. An accelerometer and a set of passive markers were used to record object kinematics. The object could "collapse" meaning motion of one of the side panels by 3 mm. The force of collapse (fragility) was controlled by the current through a solenoid that resisted motion of the side panel.

Once the object was grasped, subjects lifted it to a height of 0.1 m above the surface of the table, indicated by a visual target. Subjects were asked to maintain the orientation and location of the object without deviations from the vertical axis, using the bulls-eye level as a feedback device. When subjects indicated that they were ready to start a trial, data collection began. Subjects were instructed to move the object quickly and accurately 0.3 m vertically to a new visual target without the object collapsing. Subjects were instructed to remain in this final location until the end of the trial; total trial duration was 5 seconds.

The grip forces corresponding to the fragility indices (FR-indices) tested in this experiment can be found in Table 1. FR-index was calculated as the quotient of the minimum grip force required to maintain the object (total weight 7.2 N) in static equilibrium (F^{GRIP} min = 7.5 N) divided by the grip force needed to collapse the object. As the object became more rigid, FR-index decreased. After a change in the FR-index, the subjects lifted the object and squeezed it slowly until it "collapsed". Hence, they were aware of permissible forces in all conditions.

FR-index	**F^{GRIP} collapse (N)**
0.45	16.7
0.37	20.2
0.24	30.8
0.15	50.2

Table 1: FR-indices tested with corresponding F^{GRIP} required for object collapse.

RESULTS

As FR-index increased (object became more fragile), maximum object acceleration decreased and movement time increased ($p < 0.001$). Further investigation has shown that grip force (F_G) was strongly correlated with object acceleration (A) from the onset of movement to the time of maximum acceleration ($R^2 = 0.99$; $p < 0.001$). Movements with the right hand (and two hands together) showed higher correlation between grip force and acceleration compared to movements with the left hand ($p < 0.05$; ANOVA on z-transformed R^2 values). Both the force intercept (b) and regression coefficient (k) in the regression equation $F_G = b+k*A$ decreased for higher FR-indices.

Mean squared jerk values decreased by 71% as FR-index increased. In contrast, normalized jerk (mean squared jerk normalized by movement time and object displacement) increased by 9% as the FR-index increased ($p < 0.001$).

As FR-index increased, both grip force and safety margin (the amount of grip force exerted beyond what is required to prevent object slip) decreased by 37% ($p < 0.001$). The two-hand condition resulted in the lowest values of safety margin compared to the one-hand cases ($p < 0.001$).

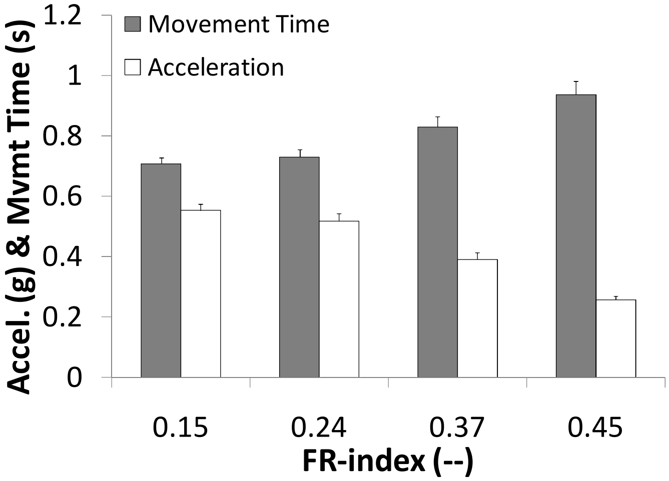

Figure 1: Average movement time and maximum acceleration data across all subjects (+ standard errors) for the tested FR-indices.

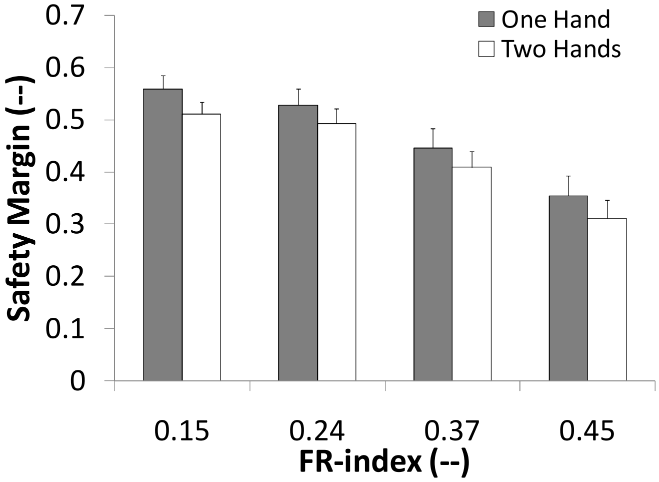

Figure 2: Average safety margin (+ standard errors) across all subjects for one- and two-hand tasks for the tested FR-indices.

ACKNOWLEDGEMENTS

NIH Grants: AG-018751, NS-035032, AR-048563, and M01 RR-1073.

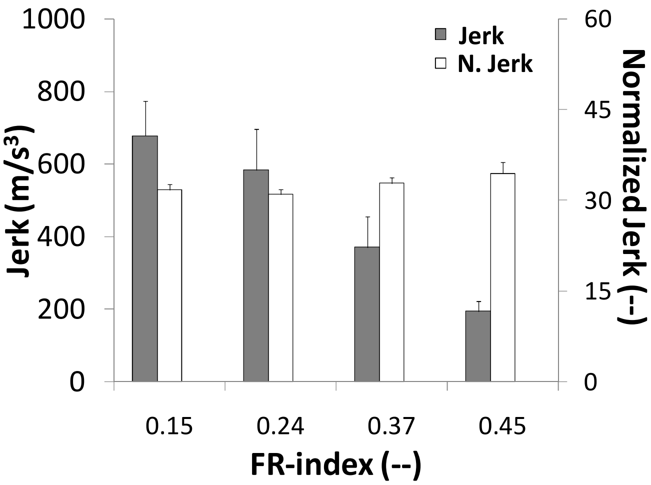

Figure 3: Average jerk and normalized jerk values (+ standard errors) across all subjects for the tested FR-indices.

DISCUSSION & CONCLUSIONS

We observed adjustments in both movement kinematics and kinetics with changes in the FR-index. When moving more fragile objects, subjects used smaller acceleration and mean squared jerk magnitudes, while movement time increased. Notably, although the mean squared jerk index dropped, this change was not seen for the normalized jerk index. This result provides further support for the universal nature of minimum-jerk criterion [4].

Very high correlation coefficients between grip force and object acceleration suggest that the feed-forward coupling between the two represents a universal mechanism of grip force adjustment with expected changes in the load force [5], a mechanism that is common across objects of different fragility. However, a decrease in the modulation of grip forces with acceleration during movement of non-fragile objects was unexpected. Further evidence of a drop in safety margin in bimanual tasks, compared to unimanual tasks, has been confirmed for both fragile and non-fragile objects [6].

REFERENCES

1. Burstedt et al. (1997). *Exp Brain Res* 117: 67-79.
2. Shim et al. (2005). *J Neurophysiol* 93: 766-776.
3. Zatsiorsky et al. (2003). *Exp Brain Res* 148: 77-87.
4. Hogan and Flash (1987). *Trends Neurosci* 10: 170-174.
5. Gao et al. (2005). *Exp Brain Res* 165: 69-83.
6. Gorniak et al. (2009). *Exp Brain Res* 193: 615-631.

ON THE APPROPRIATENESS OF ESTIMATING INTRAMUSCULAR MYOELECTRIC SIGNALS FROM SURFACE ELECTRODES FOR THE ROTATOR CUFF

[1]Rebecca L. Brookham, [1]Danielle L. Waite and [1*]Clark R. Dickerson
[1]University of Waterloo, Waterloo, Ontario, Canada
*email: cdickers@uwaterloo.ca

INTRODUCTION

Surface electrodes are commonly used in recording electromyographic (EMG) signals as surrogates of muscle force. Surface electrodes are inexpensive, easy to use and non-invasive; but are only useful for monitoring superficial muscles, and their large (non-specific) pick-up volume can result in frequent signal cross-contamination. Intramuscular (fine wire) electrodes are less commonly used due to their cost, required insertion-expertise, and invasiveness to participants. Due to the small size and depth of the rotator cuff musculature, their accessibility for surface recordings is difficult, and in the case of the subscapularis, impossible. Previous studies have compared simultaneous signals from surface and intramuscular recordings to determine if surface electrodes approximate the activity of deep muscles [1-5]. To our knowledge, no reported data exists that systematically compares surface and indwelling EMG activity levels for the rotator cuff musculature. Thus, the purpose of this study was to quantify the nature of the relationship between surface and intramuscular recordings of the rotator cuff muscles (excluding subscapularis), in order to assess if the surface electrodes can be used to predict intramuscular electrode activity. It was hypothesized that surface measurements would overestimate intramuscular values, and that the identified relationships would depend on exertion type and arm posture.

METHODS

12 right-hand dominant males [mean: 20.7 years, 76.7 kg] participated after providing informed consent. Exclusion criteria included a history of upper limb or low back injury in the past 6 months, or known neuromuscular, cardiovascular or metabolic conditions. Bipolar intramuscular electrodes (27 gauge needles, 44 gauge wires) were inserted into the supraspinatus, infraspinatus and teres minor [6]. Bipolar Ag/AgCl surface electrodes were placed on the skin surface over the supraspinatus and infraspinatus. Subjects performed two maximal voluntary contractions (MVCs) specific to each of the recorded muscles, followed by 20 maximal isometric exertions: shoulder flexion and abduction at 45º and 90˚ elevation, and a reference position (0º elevation - arm at side), with force being directed from the hand on the palmar and dorsal aspects of the hand and radial and ulnar aspects wrist. These 20 exertions were organized into groups based on hand *force direction* (palmar, dorsal, radial, ulnar) and *posture* (neutral, 45° and 90° humeral flexion, 45° and 90° humeral abduction). Exertion duration was 6 seconds, with 2 minutes rest between exertions. EMG was linear enveloped (single pass, low-pass Butterworth filter, 3 Hz cutoff), and normalized for each subject and each muscle (Figure 1). Mean normalized EMG was then calculated during a 2 second window (time 2 - 4 seconds). Linear least squares best fit regressions (unconstrained, and constrained with zero intercept) were used to compare: supraspinatus intramuscular and surface signals; infraspinatus intramuscular and surface signals; and intramuscular teres minor and surface infraspinatus signals. The intramuscular signals were considered the true representation of muscle activity. Variance explanation (r^2) was calculated to determine how linearly related the

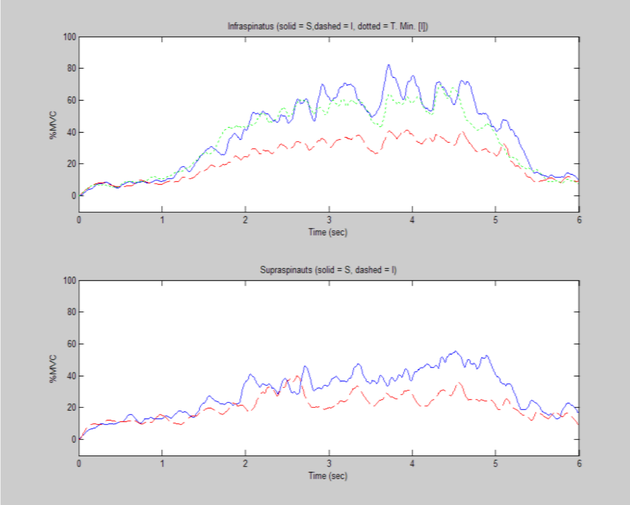

Figure 1: Normalized EMG: [Top] surface infraspinatus (solid), intramuscular infraspinatus (dashed), intramuscular teres minor (dotted); [Bottom] surface supraspinatus (solid) and intramuscular supraspinatus (dashed).

signals were. These relationships were further examined using *force direction* and *posture* as additional model effects in the linear regression; post hoc analysis (Student's t test) indicated significant differences between variables within groups. Trials containing signal artifact (identified visually) were excluded from analyses.

RESULTS

These comparisons resulted in the equations listed in Table 1, and indicated the following for traditional and zero intercept fit lines, respectively:

- Surface supraspinatus electrode overestimated the intramuscular electrode by 88.7% MVC (+ bias), and 81.8% MVC (eq'ns 1-2; Figure 2).
- Surface infraspinatus electrode overestimated the intramuscular electrode by 185.7% MVC (+ bias), and 156.4% MVC (eq'ns 3-4).
- Surface infraspinatus electrode overestimated the intramuscular teres minor electrode by 270.4% MVC (+ bias), and 244.8% MVC (eq'ns 5-6).

Post hoc analysis indicated there was a significant difference between *force direction* for supraspinatus ($p < 0.01$) and infraspinatus ($p < 0.01$) signals, however, as inclusion of this model effect only improved the explained variance by 3%, a more parsimonious model (without this model effect) was preferred. There was no significant difference found between *postures* in any comparisons.

Table 1: Linear least squares best fit regressions

	Regression Equations	**r^2**
1	$EMG_{S,FW} = 20.32 + 0.53*EMG_{S,SF}$	0.73
2	$EMG_{S,FW} = 0.55* EMG_{S,SF}$	0.73
3	$EMG_{I,FW} = 18.33 + 0.35* EMG_{I,SF}$	0.40
4	$EMG_{I,FW} = 0.39* EMG_{I,SF}$	0.40
5	$EMG_{TM,FW} = 21.01 + 0.27* EMG_{I,SF}$	0.61
6	$EMG_{TM,FW} = 0.29* EMG_{I,SF}$	0.61

Note: S = supraspinatus, I = infraspinatus, TM = teres minor, FW = fine wire, SF = surface

DISCUSSION

Quantifying the relationship between rotator cuff surface and intramuscular electrodes proved our first hypothesis to be correct: surface electrodes overestimated their respective intramuscular electrode signals during maximal exertions. However, explanation of these relationships did not markedly change when *posture* was considered, and was only minimally altered when *force direction* of task was considered. Explanations of variance for supraspinatus and teres minor intramuscular predictions were good (greater than 60%), suggesting that these surface electrodes may be used for estimating intramuscular activations in these muscles, albeit with an sizeable offset as defined by multiplicative coefficients (Table 1) to correct for overestimations. Conversely, explanation of variance was low for infraspinatus intramuscular predictions (perhaps due to differences in recorded fiber orientations), suggesting that the use of surface infraspinatus electrodes to estimate intramuscular signals may be problematic. Past works have shown good agreement between surface and intramuscular signals [1-3], while others have shown slightly better agreement between adjacent (rather than underlying) muscles ($r^2 = 0.8$ vs. $r^2 = 0.6$) [4]. Further research is needed to test these relationships for the shoulder in other force directions and postures, and during submaximal exertions, which are partly responsible for the large offsets in our equations. These findings could potentially simplify experimental measurement of shoulder muscle activity, at least for supraspinatus and teres minor.

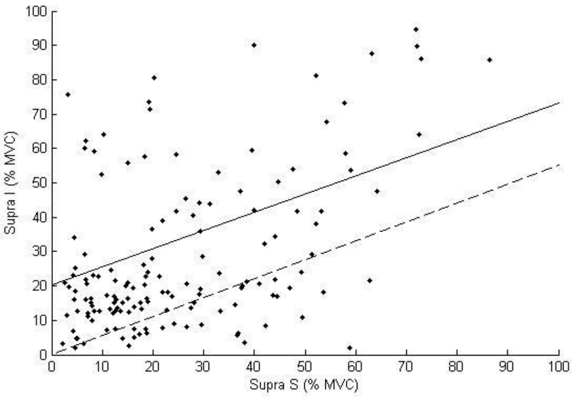

Figure 2: Prediction of supraspinatus intramuscular via surface electrode. [Best fit line (solid) and forced-zero intercept line (dotted)]

REFERENCES

1. Giroux B & Lamontagne M. *Electromyogr Clin Neurophysiol*, **30**, 397-405, 1990.
2. Jacobson WC, et al. *J Electromyogr Kinesiol*, **5**(1), 37-44, 1995.
3. M^{c}Gill S, et al. *J Biomech*, **29**(11), 1503-1507, 1996.
4. Stokes IAF, et al. *Clin Biomech*, **18**, 9-13, 2003.
5. Byrne CA, et al. *J Electromyogr Kinesiol*, **15**(6), 564-575, 2005.
6. Delagi E & Perotto A. *Anatomic guide for the electromyographer*. 2nd Ed., 1980.

THE ROLE OF TIBIALIS POSTERIOR ON FOOT KINEMATICS DURING WALKING

Michael B Pohl, Melissa Rabbito and Reed Ferber
The Running Injury Clinic, Faculty of Kinesiology, University of Calgary, Calgary, AB, Canada
email: mbpohl@ucalgary.ca, web: www.runninginjuryclinic.org

INTRODUCTION

Many overuse injuries of the lower extremity are associated with excessive/prolonged pronation of the foot during gait. Pronation is a complex motion and its quantification during gait has mainly been limited to rearfoot motion. However, foot pronation also occurs across the more distal joints of the foot. Thus it is pertinent to quantify both rearfoot and forefoot motion when assessing pronation. In vitro studies suggest that the tibialis posterior muscle may play a role in preventing collapse of the medial longitudinal arch, contribute to rearfoot inversion, and adduct the forefoot [1]. In addition, patients with posterior tibial tendon dysfunction (PTTD) demonstrate increased rearfoot eversion along with increased dorsiflexion and abduction of the forefoot [2]. These studies suggest that the tibialis posterior function is important in controlling both the rearfoot and forefoot mechanics associated with pronation.

One method of assessing the role of tibialis posterior on foot mechanics may be through exercise-induced fatigue of this muscle. A decrease in power output of the muscle due to fatigue could result in altered foot mechanics, specifically in the form of excessive or prolonged pronation. However, this paradigm has only been investigated for the combined foot invertors and only rearfoot motion was measured [3]. Therefore, the aim of this study was to compare rearfoot and forefoot mechanics during walking both before and immediately after fatiguing exercise of tibialis posterior. It was hypothesized that muscle fatigue will lead to greater and prolonged rearfoot eversion and forefoot dorsiflexion, along with greater forefoot abduction.

METHODS

The data are part of an ongoing study to understand the relationship between anatomical structure, muscular function and biomechanics of the foot. To date, eight females and three males have participated in this study (age 23.8 ± 6.9 yrs, mass 62.4 ± 10.2 kg). All subjects were free from lower extremity injury and had a static standing rearfoot angle within normal limits [4]. Retroreflective markers were attached to the forefoot, rearfoot (Figure 1) and shank of the right limb.

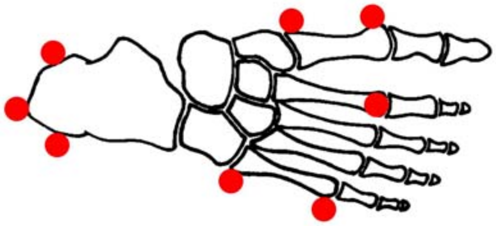

Figure 1: Foot marker placement.

After a standing calibration trial, subjects walked at 1.2 ms^{-1} on a treadmill while baseline (PRE) kinematic data was captured at 120Hz. Then the subject's maximum isometric contraction (MIC) was determined during isolated foot adduction using a custom built device containing a dynamometer (Figure 2). This movement was chosen as MRI studies have demonstrated the tibialis posterior is activated most selectively and effectively during foot adduction [5]. Subjects then performed multiple sets (50 reps) of fatiguing foot adduction exercises at 50% MIC. Maximum isometric contractions were measured after every two sets and subjects continued to perform fatiguing exercise until their MIC dropped below 70% of the baseline measure. A post-fatigue (POST) treadmill walking trial was subsequently collected.

Three-dimensional kinematics were calculated for the forefoot (relative the rearfoot) and rearfoot (relative to the shank). Wilcoxen signed-rank tests were used to compare PRE and POST values for the following variables: peak rearfoot eversion (Pk RF EV), forefoot dorsiflexion (Pk FF DF) and abduction (Pk FF ABD); time to peak rearfoot eversion (time RF EV) and forefoot dorsiflexion (time FF DF); and forefoot abduction at toe-off (FF ABD @TO).

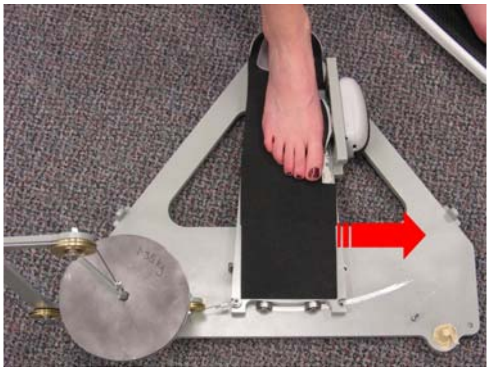

Figure 2: Custom device for performing foot adduction and assessing strength.

RESULTS AND DISCUSSION

Upon completion of the fatiguing protocol for tibialis posterior, the MIC strength dropped to 65.2% ± 8.7% of the PRE value.

A comparison of PRE and POST kinematic variables are presented in Table 1. In terms of rearfoot eversion, both the peak value and the time to the peak value were unchanged following the fatiguing exercises. This suggests that a 20-30% reduction in force production of tibialis posterior was insufficient to alter rearfoot kinematics. However, this is not to say that tibialis posterior does not play a role in controlling rearfoot motion. Other muscles such as the gastrocnemius and soleus may also assist in rearfoot inversion and have small inversion moment arms. Thus, it is possible that other muscles may compensate to control rearfoot motion in the absence of adequate tibialis posterior function.

Only one of the forefoot kinematic variables, peak forefoot abduction, was statistically different following the fatiguing protocol. Although peak forefoot abduction increased in 9 out of 12 patients, it is questionable whether this small 0.4° mean increase is clinically relevant. As with the rearfoot, the failure to alter forefoot kinematics may be due to compensatory strategies by other muscles.

The results imply that tibialis posterior fatigue was not successful in systematically altering either forefoot or rearfoot kinematics associated with excessive or prolonged pronation of the foot. The findings contradict the results of Ness et al. [2] who reported that patients with advanced PTTD had greater rearfoot eversion, forefoot dorsiflexion and forefoot abduction compared to controls. However, the patients in the former study had progressed to the stage of a fixed pes planus deformity of the foot, where tibialis posterior was completely deficient. It is unclear whether weakness of the tibialis posterior muscle or anatomical malalignment leads to excessive pronation of the foot. It is feasible that the contribution of muscular function in controlling pronation may differ depending on foot structure. It is envisioned that this relationship will be elucidated as this study progresses.

CONCLUSIONS

A reduction in force production of the posterior tibialis muscle following fatiguing exercise did not alter rearfoot or forefoot kinematics during walking.

REFERENCES

1. Thordarson DB, et al. *Clin Orthop Rel Res* **316**, 165-172, 1995.
2. Ness ME, et al. *Gait Posture* **27**, 331-339, 2008.
3. Christina KA, et al. *Hum Mov Sci* **20**, 257-276, 2001.
4. Cornwall MW, et al. *Foot* **14**, 133-138.
5. Kulig K, et al. *Med Sci Sports Exe* **36**, 862-867, 2004.

Table 1: Mean (SD) kinematic measures prior to (PRE) and following (POST) fatiguing exercise.

	Pk RF EV (°)	Time RF EV (%stance)	Pk FF DF (°)	Time FF DF (%stance)	Pk FF ABD (°)	FF ABD @TO (°)
PRE	**2.5** (3.0)	**44** (8)	**4.0** (2.6)	**68** (8)	**10.1** (5.6)	**2.8** (6.1)
POST	**2.6** (2.9)	**43** (10)	**3.6** (2.1)	**64** (11)	**10.5** (5.4)	**2.7** (5.6)
p-value	0.154	0.253	0.319	0.091	0.039*	0.438

* Indicates a significant difference between PRE and POST measures ($p < 0.05$).

MOTION EFFECTS OF MANUAL MANIPULATION ON CERVICAL LATERAL FLEXION

[1]B. Rutledge, [2]J. Vorro, Ph.D., [3]S. Gorbis, D.O., F.A.A.O., [1]T.R. Bush, Ph.D.
Michigan State University, East Lansing, Michigan, USA
[1]Department of Mechanical Engineering, [2]Department of Family and Community Medicine,
[3]Department of Osteopathic Manipulative Medicine
email: rutled36@msu.edu, reidtama@msu.edu, web: www.egr.msu.edu/bdrl

INTRODUCTION

It has been estimated that neck pain in Western populations is prevalent in 70% of individuals at some time in their lives [1]. Although there is no single solution to cervical spine impairments, there are several techniques used by physicians to improve a patient's cervical mobility and relieve pain. Manual manipulation, which can be conducted in many forms, is a noninvasive technique used to improve function of the cervical region [2]. Currently there are no scientifically accepted means of quantifying the effects of manipulation on the cervical region. Of particular interest to clinicians is the magnitude of motion change resulting from treatment and the duration of treatment effects. The objective of this experiment was to quantify the effects of manual manipulation, applied in the form of muscle energy, on ranges of cervical spine lateral flexion (side-bending).

METHODS

Four subjects, all exhibiting signs of cervical dysfunction as identified by a clinical examination participated in the experiment. Subjects were asked to return 24 hours, 48 hours and 7 days from the initial test day. Prior to testing, all volunteers completed an informed consent procedure, a Visual Analog Pain Scale (VAS) as well as a Neck Pain and Disability Questionnaire. After completion of these forms, an osteopathic physician with over 20 years of experience performed a palpatory diagnostic examination of cervical lateral flexion, during which he recorded the nature of the patient's cervical range and quality of motion. For this exam, the subject was instructed to sit in an erect posture on a stool with his or her eyes closed and arms crossed. Positioning himself behind the subject, the examiner placed one hand on the top of the subject's head and the other at the base of their neck. Starting from a neutral position the head was guided to the right until an end-range of motion was determined, followed by a return to the neutral position and a guided motion to the left.

The diagnostic exam was then repeated three consecutive times in front of a five-camera motion capture system where three-dimensional kinematic data were recorded (Qualisys™, Gothenburg, Sweden) for a 35-60 second period. To obtain the kinematic data sets, three markers were placed on the subject's head, and a triad of markers was attached to the sternum.

Within 30 minutes of the collection of the kinematic data the physician performed a muscle-energy treatment on the subject. Muscle-energy treatment involves the voluntary contraction of a patient's muscles in a precisely controlled direction to relax shortened muscles that restrict motion. Upon completion of the treatment, another set of kinematic data were recorded. These data were collected within 30 minutes of treatment and were used to document effects of the treatment.

Subjects were asked to return 24 hours and 48 hours post treatment, as well as 7 days post-treatment. During the 24 hour and 48 hour tests, both kinematic and pain assessments were executed as well as a repeat of the first day's diagnostic procedure. Day 7 protocol was identical to the first test session: diagnosis of cervical lateral flexion, kinematic data collection, treatment, and a second kinematic data collection.

From the three-dimensional position data acquired, angles were computed for the head relative to the neck. Each test consisted of three trials of cervical lateral flexion, each with three cycles of right to left cervical flexion, resulting in nine end-range values per subject per assessment. The data were normalized with regard to time, and then the full cervical range of motion was analyzed on a per cycle basis. Full range of motion was defined as the total angular displacement from right maximum lateral flexion to left maximum lateral flexion, as shown in Figure 2. Statistical analysis included paired t-tests conducted at a 95% confidence level to determine whether significant kinematic changes occurred for cervical ranges of motion between pre and post-treatment.

RESULTS AND DISCUSSION

When examining the range of motion data, all participants demonstrated an increase between pre and post-treatment cervical range of motion (both on Day 1 and Day 7). Statistical analysis indicated a significant increase ($p < 0.001$) in full range of motion immediately following treatment. This is demonstrated in Figure 3 with a linear analysis of the range of motion for a subject pre and post-treatment. When comparing the linear regression lines of the two data sets, it can be observed that on average the cervical range of motion was greater post-treatment over the nine cycles.

The average increase in full range of motion over these trials was 4.53 degrees. Also, for the two subjects able to participate in the 24 hour post-treatment evaluation, a decrease in range of motion was observed from the Day 1 post-treatment examination to the 24 hour assessment. A further, but less substantial, decrease in these two patients range of motion occurred 48 hours post treatment.

These statistical findings suggest that positive effects from muscle-energy treatment are immediate. This effect is most likely due to the mechanical nature of soft tissues. The tissues appear to be able to achieve a higher strain at the same stress than that produced prior to treatment. An increase in strain is due to a percent elongation in the tissue due to muscle-energy therapy, thus extending the subjects range of motion. A confounding issue in this study is that the motions were passively guided. Although the examiner had years of experience and performs this task on a daily basis in a clinical setting, the possibility exists that the examiner was not consistent in the loading placed on the head to guide it to the end range. Further quantification of the examiner's technique is necessary.

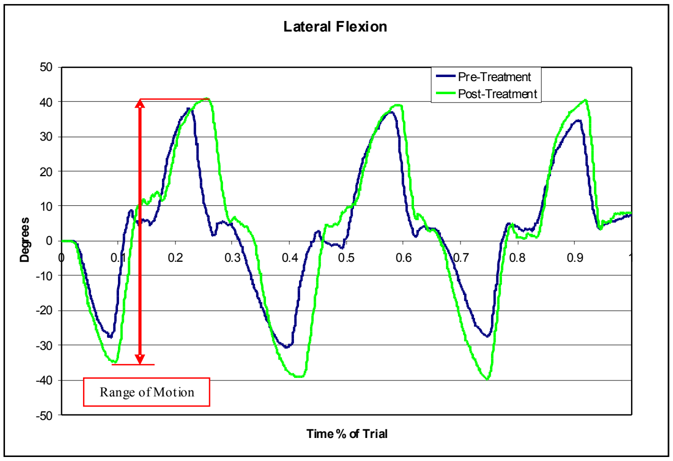

Figure 1. Lateral flexion plots of a subject pre and post-treatment for the initial day of testing.

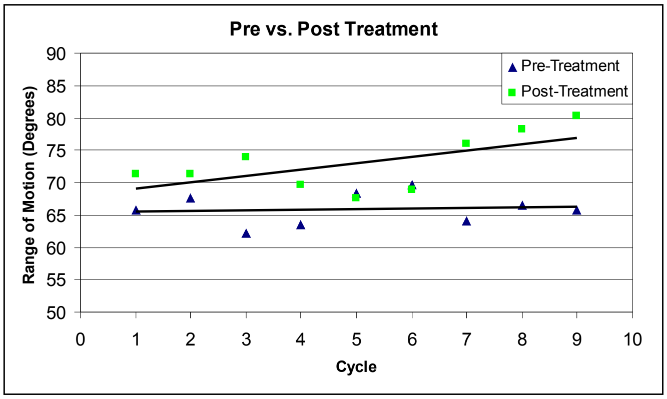

Figure 2. Linear analysis of range of motion for cervical lateral flexion for a single subject over all nine cycles: comparisons between pre and immediately post-treatment.

REFERENCES

1. Bovim G, et al. *Spine* **19**, 1307-1309, 1994.
2. Johnston W, et al. *Functional Methods*. Indianapolis: American Academy of Osteopathy, 2005

CORRELATION BETWEEN BONE MINERAL DENSITY AND FIXATION STRENGTH OF ORTHOPEDIC BONE PLATES

[1]Jacob Cartner, [1]Yanming Zheng, [2]William Ricci and [3]Paul Tornetta
[1]Smith & Nephew, Inc., [2]Washington University School of Medicine, [3]Boston University School of Medicine
Email: Jacob.Cartner@smithnephew.com

INTRODUCTION

Fracture fixation stability for orthopedic bone plates is dependent upon bone mechanical integrity. Locked plates have shown theoretical advantages in poor quality bone when compared to traditional non-locked plates, since the locked interface functions to mechanically unite all of the screws to the plate and form a single beam. Dual Energy X-Ray Absorptiometry (DEXA) scanning yields defined bone quality parameters, but how bone mineral density (BMD) correlates to fixation strength during the period of fracture healing may be construct dependent. In this study, we sought to evaluate the effect of BMD on the strength of locked and non-locked plate constructs using a cadaveric distal femoral fracture model.

METHODS

Thirty-two human cadaveric femora (16 matched pairs) were harvested for this study. DEXA screening was performed on all bones to obtain BMD. An extra-articular metaphyseal 3cm gap was then created to simulate a comminuted distal femur supracondylar fracture. All bones were instrumented using distal femur locking plates (Smith & Nephew, Memphis, TN). The left and right femurs of matched pairs were randomly assigned to either locked or non-locked diaphyseal fixation. Metaphyseal fixation in all specimens was accomplished with five bicortical cannulated locking screws. Diaphyseal fixation was with four bicortical screws, either locked or non-locked. All specimens were potted and subjected to an axial cyclic compressive bending load of 50/500 N with a physiological varus moment at 2 Hz for 500,000 cycles. After 500,000 cycles, a constant load was applied until failure. Failure was defined as plate breakage or deformation, screw loosening, or bone fracture.

RESULTS AND DISCUSSION

DEXA results indicated a BMD range of 0.27–1.19 g/cm^2 for the bones utilized. Locked constructs showed no correlation between strength and BMD (R^2=0.01), whereas there was a clear demonstration that BMD moderately correlated to non-locked construct strength (R^2=0.50). The intersection of trendlines occured just above 0.65-0.70 g/cm^2 (Fig 1), a range below which has been described as indicative of osteopenia onset [1]. These results indicate a patient with osteopenia may benefit from a locked plate, whereas a patient with healthy bone may benefit from a non-locked orthopedic plate.

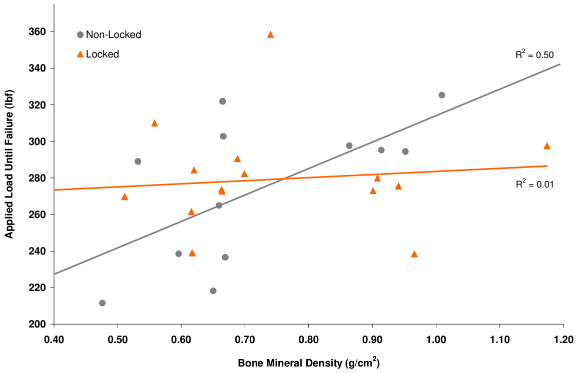

Figure 1: BMD and strength of locked or non-locked constructs after fatigue loading.

CONCLUSIONS

For low BMD bone, locked plates have shown to be stronger after fatigue when compared to non-locked plates. In higher BMD bone, non-locked plates may provide superior compressive capabilities, which improves fixation strength during fatigue. Thus, maintenance of fixation stability during rehabilitation is not only dependent upon BMD, but construct type should also be considered. These results provide a scientific basis to guide surgeons when deciding when locked screws are indicated for fracture fixation.

REFERENCES

1. Orwoll ES and Bliziotes M. *Osteoporosis Pathophysiology and Clinical Management.* Humana Press, Totowa, NJ.

ACHIEVING GREATER BONE-PLATE COMPRESSIVE FORCES IN FRACTURE FIXATION
An Investigation Into Screw Thread Form Effects

[1]Jacob Cartner, [2]William Ricci and [3]Paul Tornetta
[1]Smith & Nephew, Inc., [2]Washington University School of Medicine, [3]Boston University School of Medicine
Email: Jacob.Cartner@smithnephew.com

INTRODUCTION

Conventional cancellous screws have proven purchase in healthy bone, but may be prone to loosening in osteoporotic bone. We hypothesized that optimizing screw thread form may improve purchase into poor quality bone and enhance bone-plate compressive forces. The purpose of this study was to evaluate the mechanical characteristics of a cancellous bone screw with a high major to minor diameter ratio using two osteopenic models.

METHODS

Twelve ‘osteopenia’ bone screws (major to minor diameter ratio of 1.85) were inserted through a thin B-type straight plate into a pre-drilled pilot hole to a depth of 20mm per ASTM recommendations [1]. Testing media included two groups: low density (10 pcf) solid rigid polyurethane foam blocks (*n* = 6) (Pacific Research Laboratories, Vashon, WA) and osteopenic fresh-frozen femoral diaphyseal cadaver (*n* = 6) (femur bone mineral density < 0.60 g/cm^2).

Rotational loading was applied manually using a hex driver until torque reached a peak value, which was denoted as stripping torque. The amount of compression gained between plate and bone was also measured using Tekscan (Boston, MA, USA) across a range of possible clinical insertion torques. This same procedure was used for twelve traditional cancellous bone screws (major to minor diameter ratio of 1.60), which were inserted through a conventional straight plate into both test medias.

RESULTS AND DISCUSSION

There was a linear relationship between applied torque and compressive force generation for both screws. General trends in data were consistent across both test medias. The ‘osteopenia’ bone screws showed a 34% increase in torque in foam block testing before stripping occurred ($p << 0.01$), and they were able to gain greater compression against bone across a range of insertion values as compared to conventional bone screws (Figure 1). Thus, these screws may provide better fracture reduction and lagging capabilities in the clinical situation. Greater compression may lead to enhanced mechanical stability over time during cyclical loading of the healing process.

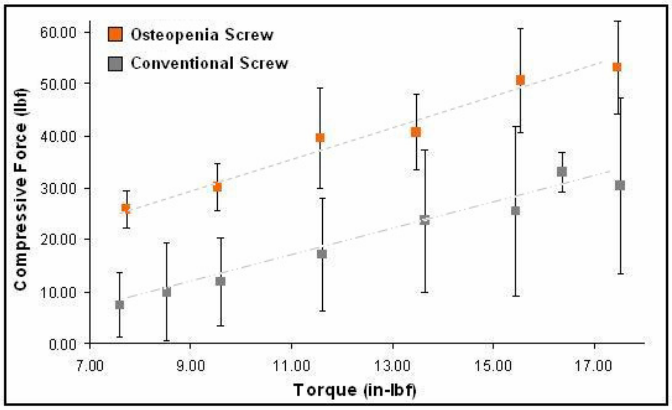

Figure 1: Plate-bone compression forces in an osteopenic cadaveric bone model. Correlation coefficient, $R^2 = 0.97$ for both screws.

CONCLUSIONS

When tested in surrogate foam and cadaveric bone models, bone screws with a higher major to minor diameter ratio provided superior stripping torque and compressive forces as compared to conventional cancellous bone screws. While tested in a clinically appropriate scenario, it is also recognized that one potential limitation is the comparison of two constructs of different plate design. However, this study was able to demonstrate a consistent difference in bone-plate compressive forces associated with two screw thread form designs. These findings indicate that the use of a specialized non-locked osteopenia screw may be advantageous in poor quality bone.

REFERENCES

1. ASTM F 543 07. Standard Specification and Test Methods for Metallic Medical Bone Screws.

USING A ROBOTIC TREADMILL TRAINER TO MEASURE CHANGES IN RAT LOCOMOTION FOLLOWING SPINAL CORD INJURY

[1] Nathan D. Neckel, [1]Haining Dai, [1]Justin Laracy and [1]Barbara Bregman
[1]Georgetown University Dept of Neuroscience, Washington D.C.
email: ndn3@georgetown.edu

INTRODUCTION

The Rodent Robotic Motor Performance System (RRMPS, Robomedica Inc, Irvine CA) is a commercially available device designed to provide body weight supported treadmill training to neurologically impaired rodents. The device also employs two programmable robotic manipulators which attach above the ankle of the hindlimbs of the test subject to record the position in the parasagittal plane. Current techniques to analyze this position data are based off of the bipedal stepping of thoracically transected rats [1]. When different types of injuries or postures are studied, more appropriate algorithms should be used. Presented here is a method of step detection for use with rats walking in a quadrapedal posture following a cervical over-hemisection. With this method the changes in rat stride length and duration of step cycle can be measured following spinal cord injury (SCI).

METHODS

9 healthy adult female Sprague-Dawley rats were pre-trained on the RRMPS for 9 days before baseline recordings of hindlimb positions were made as the rats walked for 2 minutes at 8 cm/s. The animals then received a right C4-5 over-hemisection injury which bilaterally ablates the dorsal corticospinal pathway, and unilaterally ablates the contralateral rubrospinal (and other descending) pathways leaving the forelimbs more impaired than the hindlimbs, and the right limbs more impaired than the left limbs. After one week of recovery the locomotor performance of the animals was recorded with the RRMPS, and then again every week for 6 weeks.

To analyze the locomotor changes of the animals, the position data was broken into steps, and then the steps were divided into swing and stance phases. All raw data was initially low-pass filtered (85Hz cutoff frequency) by the RRMPS device, but the horizontal trajectory was re-filtered with a 4th-order Butterworth filter with 5Hz cutoff frequency in custom software (MATLAB) (Fig 1A). Possible steps were defined as regions of local minima (black circles), followed by a local maxima (black squares), and then returning to a local minima. Toe

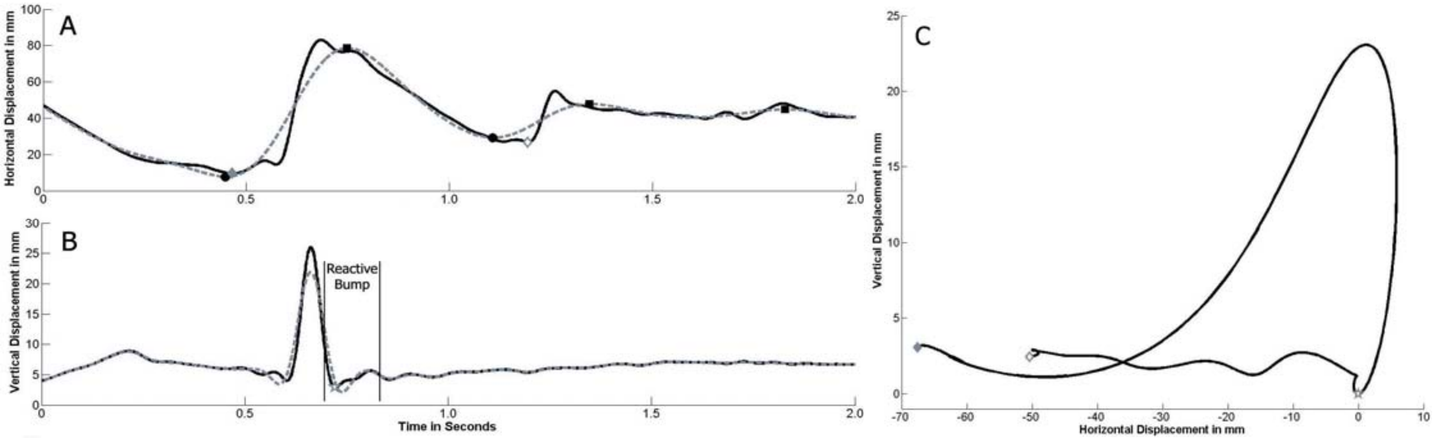

Figure 1: A: Horizontal position (solid black line) was filtered (dashed gray line) to find local minima (black circle) and maxima (black square), step start (solid gray diamond) and end (hollow gray diamond). B: Vertical position (solid black line) was filtered (dashed gray line) to find a reactive bump when the limb strikes the treadmill (gray star). C: The parasagital deviations from paw strike of a representative injured rat as it passes from toe off, to paw strike, and ends when the position is closest to the toe off position.

off was defined as the minima of the original horizontal trajectory that was within a 500 ms window centered on the local minima of the filtered trajectory (solid gray diamond). Some possible steps were the last step in a sequence, and therefore were ended not with the start of a subsequent step, but when the ankle returned nearest to the starting position (hollow gray diamond). Possible steps were excluded if they were quicker than 0.2 seconds, higher than 5 cm, progressed in a counter-clockwise motion or did not start and stop in the lower rear third of the traveled path. Previous studies with the RRMPS define the initiation of stance as the change from positive to negative horizontal velocity, but that is not an accurate enough definition for animals in the posture tested here. Remaining steps were once again filtered (4th order Butterworth, 10 Hz cutoff) and the region of the vertical trajectory after the horizontal velocity changed from positive to negative was screened for rapid changes in vertical velocity from negative to positive. The earliest instance of this indicated a reactive “bump’ with the treadmill (Fig 1B). The original vertical minima of this “bump” was taken as the initial contact with the treadmill (gray star) and the beginning of stance phase.

From this algorithm we extracted several parameters from each individual step, including stride length (horizontal distance from toe off to heal strike) and cycle time (duration from toe off to step end). For each animal all step parameters were averaged for that week. Differences between weeks after injury and healthy values for all animals were computed with a student t-test. Differences between left and right hindlimbs for all animals in a given week were computed with a single factor ANOVA.

RESULTS AND DISCUSSION

With the novel algorithm presented here we were able to define the steps patterns of rats as they walked in a quadrapedal posture before and after a right C4-5 over-hemisection SCI. Table 1 shows the changes in stride length and cycle time over the course of the experiment. It is of no surprise that the stride length and cycle time of the left hindlimb did not change following injury, for it is only mildly impaired following this type of injury. It is also characteristic of the injury to see slower steps in the right hindlimb. What is of particular interest is that at 18 days post injury the left hindlimb begins to take shorter, slower steps. This may be due to the development of a compensatory strategy where the animal spends more time on the left hindlimb and less time moving it forward, in an effort to use the other more impaired limbs less.

CONCLUSIONS

The development of a novel algorithm was important to appropriately characterize the behavior of rats as they walk in the RRMPS in a quadrapedal posture. The ability to apply this algorithm to both healthy and injured rats allows us to identify and quantify the locomotor deficits following SCI. These techniques will be vital in our further investigations into quantifying the effects of robotic gait training following SCI in rodent models.

REFERENCES

1. Timoszyk WK, et al. *Brain Res* **19**;1050(1-2):180-9,2005.

Table 1: Average stride length and cycle time of the left and right hindlimb of rats before and after SCI. Standard deviation in parentheses and significant differences (p<0.05) from healthy values are shaded. For a given week no significant differences between left and right hindlimbs were found.

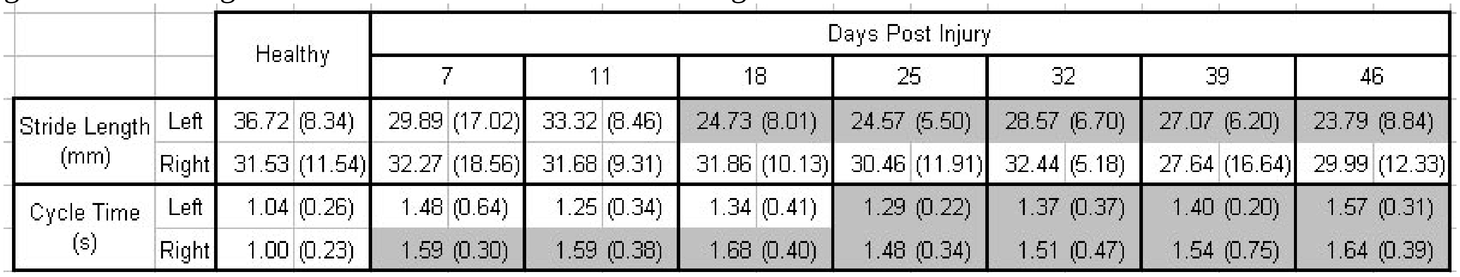

		Healthy	Days Post Injury						
			7	11	18	25	32	39	46
Stride Length (mm)	Left	36.72 (8.34)	29.89 (17.02)	33.32 (8.46)	24.73 (8.01)	24.57 (5.50)	28.57 (6.70)	27.07 (6.20)	23.79 (8.84)
	Right	31.53 (11.54)	32.27 (18.56)	31.68 (9.31)	31.86 (10.13)	30.46 (11.91)	32.44 (5.18)	27.64 (16.64)	29.99 (12.33)
Cycle Time (s)	Left	1.04 (0.26)	1.48 (0.64)	1.25 (0.34)	1.34 (0.41)	1.29 (0.22)	1.37 (0.37)	1.40 (0.20)	1.57 (0.31)
	Right	1.00 (0.23)	1.59 (0.30)	1.59 (0.38)	1.68 (0.40)	1.48 (0.34)	1.51 (0.47)	1.54 (0.75)	1.64 (0.39)

USE OF A GEARED WHEELCHAIR WHEEL FOR FACILITATING MANUAL RAMP ASCENT: EFFECTS ON TRUNK MUSCULAR DEMAND

[1]Samuel J. Howarth, [2]Jan M. Polgar, [1]Clark R. Dickerson, [1]Jack P. Callaghan
1. Department of Kinesiology, University of Waterloo, Waterloo, ON
2. School of Occupational Therapy, University of Western Ontario, London, ON
E-mail: sjhowart@uwaterloo.ca

INTRODUCTION

During wheelchair propulsion, trunk muscle activity is necessary for maintaining an upright posture as well as providing a stable base for upper limb propulsion [1]. While much research has been completed on the upper extremity demands during propulsion on both level and inclined surfaces [2,3], there is yet to be a study of trunk muscular effort during ramp ascent.

The primary goal of the current study was to document the activation required from trunk muscles during wheelchair propulsion on an inclined surface. Secondly, the influence of a geared wheel on trunk muscle activation was also investigated. It was hypothesized that the activation demand from the trunk musculature would increase with ramp grade. Furthermore, the use of a geared wheel would reduce the muscular effort during ramp ascent.

METHODS

Thirteen healthy participants (6 male – age = 23.5 ± 3.5 years, height = 1.73 ± 0.08 m, mass = 77.4 ± 6.4 kg, shank length = 0.45 ± 0.03 m; 7 female – age = 23.4 ± 3.3 years, height = 1.66 ± 0.06 m, mass = 63.3 ± 6.7 kg, shank length = 0.45 ± 0.03 m) without any neurological impairments and no prior history of low-back pain were recruited from a student population. Participants signed an informed consent document approved by the Office of Research Ethics at the University of Waterloo prior to beginning the study.

Participants performed manual wheelchair ramp ascent of four ramp grades (1:12, 1:10, 1:8, 1:6) using three different wheelchair wheels (standard pneumatic wheel (S), MAGICWHEELS® (Seattle, WA, USA) in (G) and out (NG) of gear). Ramp ascent was performed at a self-selected pace.

Electromyographic (EMG) recordings were obtained bilaterally from the rectus abdominis (RA), external oblique (EO), internal oblique (IO), latissimus dorsi (LD) and upper erector spinae (ES) during all ramp ascent trials. Unilateral kinematics of the right upper limb were collected using a 9 camera motion capture system (MX20+, Vicon, Los Angeles, CA, USA). Reflective markers were also affixed to the top and bottom on each side of the ramp and to the anterior frame of the wheelchair. The beginning and end of ramp ascent were defined respectively as the instances when the markers placed on the wheelchair intersected with the markers at the bottom and top of the ramp. Raw EMG data were collected at a rate of 3000 Hz while kinematic data were collected at 50 Hz.

Instances corresponding to the push phase as well as the recovery phase for each propulsive stroke during ramp ascent were extracted from the kinematic patterns of the second metacarpal. EMG data collected during ramp ascent were full wave rectified, low-pass filtered using a single pass Butterworth digital filter with a cutoff frequency of 2.5 Hz and normalized as a percentage to the maximum activity elicited from a maximal voluntary isometric contraction (MVIC). Peak and integrated activities for each muscle were determined separately for the push and recovery phases during ramp ascent. The temporal locations of peak activity within the push and recovery phases were also calculated for each muscle as a percentage of the respective phase duration.

Statistical differences between wheel and ramp conditions were analyzed with a two-factor analysis of variance. Tukey's post-hoc tests were performed for statistically significant main effects while

Scheffe’s method was used to analyze statistically significant interactions. The level of significance was set to $p < 0.05$ for all analyses.

RESULTS AND DISCUSSION

Integrated muscular effort during a single propulsive stroke increased with ramp grade for each muscle ($p < 0.05$). Peak trunk muscle activity during ramp ascent was higher than previously reported muscle activation levels during level propulsion [1].

RA and EO peak activation during the push phase did not increase with ramp grade during the G wheel condition (Figure 1, $p < 0.05$).

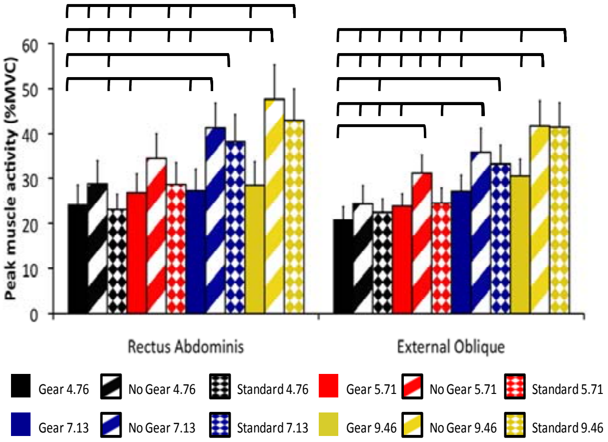

Figure 1 – Peak activity of the RA and EO for the push phase of wheelchair propulsion during ramp ascent.

Use of a geared wheelchair wheel was able to prevent increased activation requirements from the abdominal musculature during ascent of steeper ramp grades. The peak activity of the RA and EO during ascent of the two steepest ramps with the G wheel condition was reduced by 34% and 24% relative to the NG and S wheel conditions respectively ($p < 0.05$).

Peak activity of the abdominal muscles occurred closer to the end of the push phase as ramp grade increased (Figure 2, $p < 0.05$).

The geared wheels utilized in this investigation were heavier than the standard wheel by 2.2 kg. However, peak activity of the trunk muscles during the NG condition was not statistically larger than the S wheel condition despite the larger mass of the geared wheel. This is an effect of redistributing the mass on the geared wheel to achieve a similar rotational inertia between the NG and S conditions.

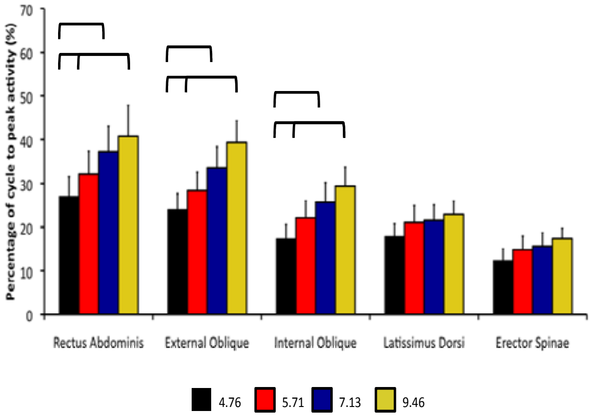

Figure 2 – Location of peak activity within the push phase during ramp ascent.

Independence of manual wheelchair users (MWUs) is often predicted by muscular strength and sufficient motor control of the upper limb and trunk [4]. Reducing the demand from the torso musculature by using a geared wheel may allow MWU’s with impaired trunk muscle control or activation capacity to manually propel their wheelchair over longer distances and steeper inclines.

CONCLUSIONS

Trunk muscular effort increased with ramp grade during ascent. Use of a geared wheel produced decreases in activation demands of the abdominal musculature during the push phase. The geared wheel may enhance MWU ability to navigate terrains that require higher muscular demands.

REFERENCES

1. Yang YS, et al. *Clin Biomech* **21**, 1032-1041, 2006.
2. Mulroy et al., *Arch Phys Med Rehab* **77**, 187-193, 1996.
3. Chow JW, et al. *Arch Phys Med Rehab* **90**, 271-278, 2009.
4. Dallmeijer et al. *J Rehabil Res Dev* **42**, 55-63, 2005.

DESIGN AND DEVELOPMENT OF A DYNAMIC KNEE SIMULATOR FOR IN-VITRO KNEE BIOMECHANICS RESEARCH

Karla Cassidy, Abra Ens and Naveen Chandrashekar
University of Waterloo, Waterloo, ON, Canada
email: nchandra@uwaterloo.ca

INTRODUCTION

The knee is one of the most important and complex joints in the human body. Knee ligament injuries are common among the younger generation due to the amateur and professional sports they are involved in. Among older generation, osteoarthritis at the knee joint is a major problem.

Both in-vivo and in-vitro techniques are used to study the biomechanics of human knee joint. In-vivo techniques are used to study knee kinematics during various activities while in-vitro technique is used to study primarily the mechanical properties of various ligament structures. However, strains in the knee ligaments during various activities are very difficult to measure. Both knee kinematics (which can be measured from outside the body) and internal muscle forces (impossible to measure) affect the knee ligament strain during various activities. Further it is ethically impossible to instrument the knee of a live person and measure the strain in real time.

To this end, we designed an electromechanical system which can be used to simulate knee kinematics and muscle forces on a cadaver knee. Using this system, one can measure the ligament strain and other parameters of interest while the knee is forced to undergo the type of loading that occurs during various activities.

METHODS

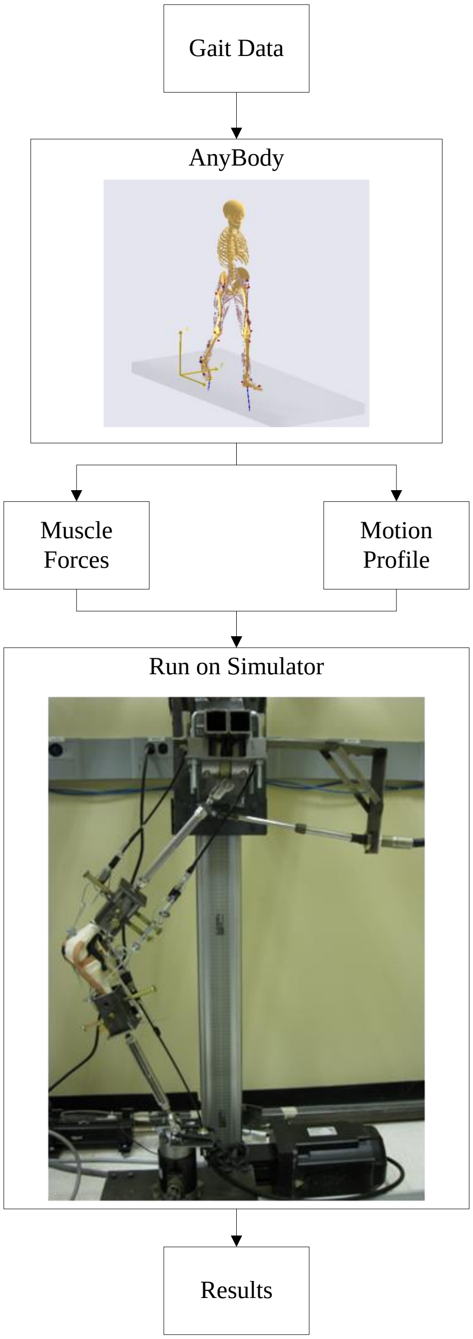

Figure 1: Dynamic Knee Simulator Process

The dynamic knee simulator (Fig. 1) is designed on the principle that the internal forces in the knee (joint reaction force and ligament strain) is directly related to knee kinematics and muscle forces in the lower limb. Accordingly, two set of high-speed actuators, one each at ankle and hip joint are responsible for relative vertical positioning of the hip and relative horizontal positioning of the ankle. The design restricts the lower limb in the adduction/abduction motion, leaving all other joint DOF free to move as prescribed by the actuator reactions. Two exceptions are at the ankle and hip joints, active restraints are used in the internal/external rotation at the hip and the pronation/supination at the ankle. These restraints are to mimic the natural restrictions in these planes of motion from ligament influence. Four other actuators are responsible for applying the muscle forces; Quadriceps, Hamstrings, Calf and flexion moment at the hip. These actuators can be connected to the knee joint using control cables. All these actuators are controlled by a computerized multi-axis motion control system.

To test the feasibility of simulating simple knee mechanics using this system, simple gait was simulated on a polymer knee model. The knee joint was mounted through the femur and tibia to the mechanical hip and ankle connections. Published gait data[1] was input into the Anybody modeling system (Anybody Technology, Alaborg, Denmark). This software gives individual muscle forces during gait based on marker data by running an optimization algorithm. The hip and ankle coordinate data was input into the corresponding actuators and the knee kinematics was simulated. Simultaneously, the muscle forces were applied during this gait by the corresponding actuators run in force controlled mode. These muscle forces were based on the data obtained by the Anybody modeling system. Owing to the fragility of the polymer knee model, only 1/10th of the actual muscle forces were applied and the gait speed was reduced to 1/10th of the actual speed. The muscle forces applied were measured using a data acquisition system and compared to the muscle forces output by the Anybody modeling system.

RESULTS AND DISCUSSION

The simulator successfully simulated the knee kinematics during the gait. As shown in Fig. 2 the applied muscle force profile closely resembled the profile calculated by the Anybody modeling system. The results show good correlation between actual loads on the knee and what it actually experiences in the simulator. This validation shows that the system has the potential to mimic true muscle reactions and motion profiles.

CONCLUSIONS

It is possible to simulate complicated knee kinematics on cadaver knees with realistic muscle forces. Our design is for a wide range of possible lower limb motions; proven by a simple gait. This validation shows the capabilities of the actuators to follow gait pattern and actual muscle force profiles. The actuators have the capability to go above and beyond the forces and speeds required to simulate forces causing knee injury. Our dynamic knee simulator can be a very useful for research in knee biomechanics. The system also has the expansion capability to incorporate the motion profile in lateral direction.

REFERENCES

1. CL Vaughan (1992). *Dynamic of Human Gait*. Cape Town, South Africa: Kiboho Publishers.

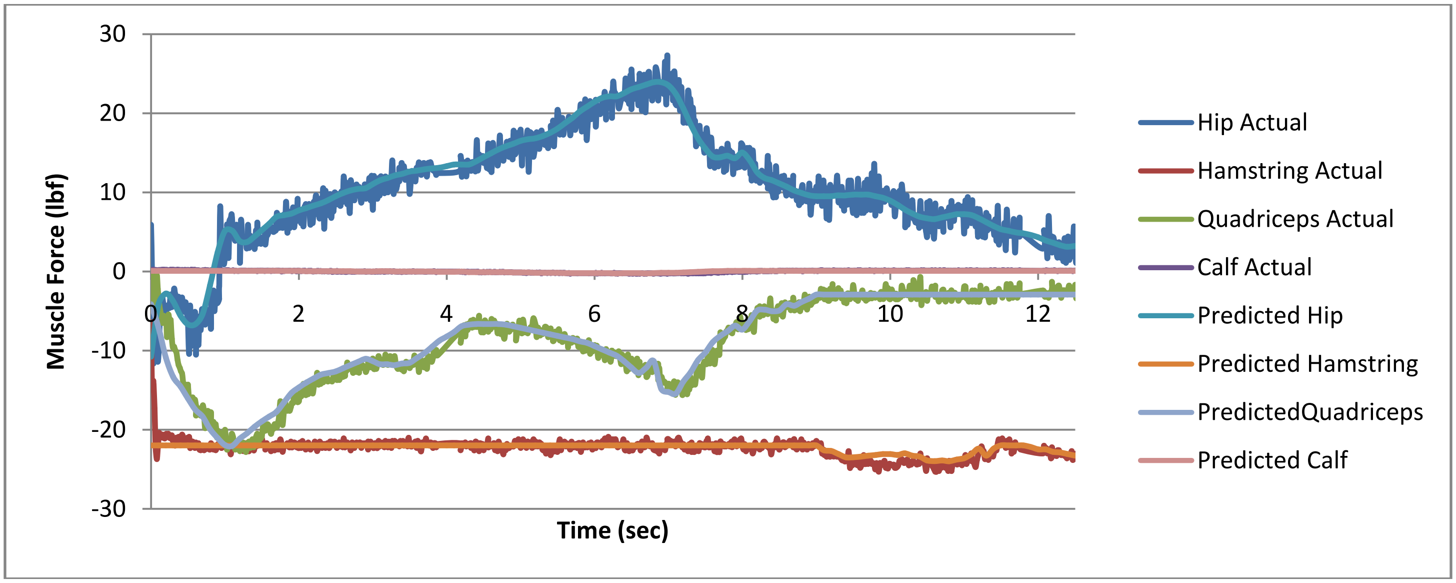

Figure 2: Comparison between required muscle forces and actual muscle forces (negative force is muscle contraction). In case of hip, the graph shows force causing the flexion moment.

EFFECTS OF EXERCISE IN TRABECULAR AND CORTICAL BONE OF OSTEOPENIC RATS: A BIOMECHANICAL STUDY

Ariane Zamarioli, Priscila Simões, Patrícia Chagas, José Batista Volpon, Antônio Carlos Shimano
Laboratory of Biomechanics – Faculty of Medicine of Ribeirão Preto
email: arianezamarioli@usp.br

INTRODUCTION

Osteoporosis bone loss occurs most frequently in postmenopausal women and in the elderly. Primary osteoporosis occurs in both genders; it often follows menopause in women and occurs later in men [1].

Estrogen deficiency after menopause is the primary cause of increased bone turnover and progressive reduction in bone mass and strength in women [2, 3]. Current strategies for the prevention of osteoporotic fractures focus on minimizing bone loss after menopause, normalizing bone turnover and even increasing bone mass [4].

The risk of fracture is greater at skeletal where trabecular bone is predominant. The most common fractures sites are in the head of the femur, vertebrae and distal radius [1].

The prevention and treatment of osteoporosis would be facilitated considerably if nonpharmacological modifiable lifestyle strategies could prove to be effective [5]. Exercises are one of these strategies, that are currently used and whose effects mau be positive on bones.

The purpose of this study was to evaluate the effects of exercise in trabecular and cortical bone of osteopenic rats.

METHODS

This study was approved by our Institutional Review Board: Ethical Committee in Animals Experiment.

Forty-eight three-month-old female Wistar rats were randomly assigned to six groups (n=8/group): (1) control, (2) osteopenic and sedentary, and (3) osteopenic and exercised animals.

The experimental period lasted 140 days and animals from group three were submitted to a treadmill running exercise two months after ovariectomy, after osteopenia installation [6, 7].

Physical exercise program consisted of running on a flatbed treadmill. Rats ran four days a week, one hour per day during 12 weeks, at a speed of 15 m/min from the beginning of the training until the sixth week. Then the speed was increased to 19 m/min during the remaining six weeks.

At the end of the experiment, femurs and tibias were tested in an universal testing machine (EMIC® DL 10000, Brazil) (Figure 1).

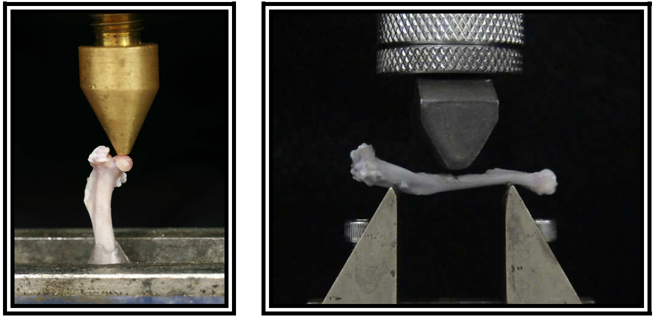

Figure 1. Mechanical testing of femur and tibia: flexion compression test and three-point ventral bending test, respectively.

Data were analyzed using analysis of covariance - ANOVA One Way Analysis of Variance to test the differences between groups. The level of significance was set at 5%.

RESULTS AND DISCUSSION

Successful ovariectomy was confirmed at necropsy as uterus atrophy. Uteri mass of ovariectomized rats was significantly lower than uteri mass in control groups (p<0.0001).

The mean values of ultimate load in femurs were: 1 (126.3 ± 7.1) N; 2 (106.9 ± 20.1) N and 3 (113.6 ±

13.7) N. There was statistical difference between groups 1 and 2 ($p<0.02$) (Graph 1). It shows that, exercise could return the ultimate load of trabecular bone to its original state.

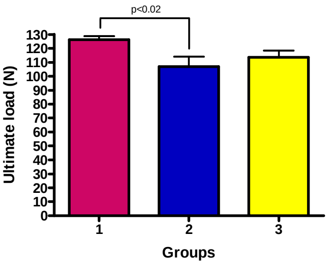

Graph 1. Mean and standard deviation values of ultimate load in femurs.

The mean values of stiffness in femurs were: 1 (323.3 ± 13.1) 10^3N/m; 2 (271.8 ± 47.9) 10^3N/m and 3 (303.6 ± 32.5) 10^3N/m. There was statistical difference between groups 1 and 2 ($p<0.04$) and 2 and 3 ($p<0.05$) (Graph 2). This result shows that exercise could return the stiffness of trabecular bone to its original state. Same behavior was found in ultimate load.

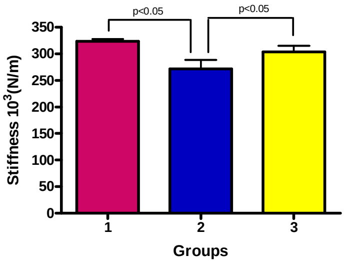

Graph 2. Mean and standard deviation values of stiffness of femurs.

The mean values of ultimate load in tibias were: 1 (54.5 ± 18.5) N; 2 (31.0 ± 20.6) N and 3 (37.2 ± 13.1) N. There was a statistical difference between groups 1 and 2 ($p<0.001$) and 1 and 3 ($p<0.02$) (Graph 3). It shows that, exercise could improve the ultimate load of tibia, but was not able to return the bone to its initial state.

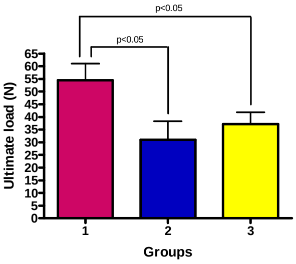

Graph 3. Mean and standard deviation values of ultimate load of tibias.

The mean values of stiffness in tibias were: 1 (516.6 ± 62.0) 10^3N/m; 2 (442.5 ± 87.3) 10^3N/m and 3 (501.4 ± 68.5) 10^3N/m. There was statistical difference between groups 1 and 2 ($p<0.05$) (Graph 4). This finding shows that exercise could return the stiffness of tibias to its original state.

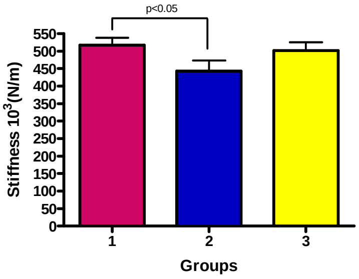

Graph 4. Mean and standard deviation values of stiffness of tibias.

After osteopenia installation, the ultimate load and stiffness of femurs returned to its normal state by means of exercise practice. In tibias, the stiffness also returned to its normal state with exercise, but not ultimate load.

CONCLUSIONS

Data from our study suggest that an exercise program may recuperate bony resistance, which was decreased by osteopenia. Thus, we found that trabecular bones are more sensitive in response to exercise after osteopenia installation.

REFERENCES

1. McDonnel PM, et al. *Annals of Biomedical Engineering*, **35**, 170-189, 2006.
2. Fuchs RK et al. *Bone*, **31**, 290-296, 2007.
3. Iwamoto et al. *Journal of Orthopaedics Science*, **3**, 257-263, 1998.
4. Iwamoto J et al. *Journal Bone of Mineral Metabolism*, **22,** 26-31, 2004.
5. Drysdale IP et al. *Journal Clinical Densitometry*, **10,** 179-182, 2007.
6. Kalu DN. *Endocrinoly*, **124,** 7-16, 1991.
7. Thompson DD. *Guidelines and animal models for osteoporosis Bone*. **17,** 125-133, 1995.

ACKNOWLEDGEMENTS

This project was funded by the FAPESP (*Fundação de Apoio à Pesquisa do Estado de São Paulo*).

SOURCES OF TWO COMPONENTS OF VARIANCE IN MULTIFINGER CYCLIC FORCE PRODUCTION TASKS

Varadhan SKM, Jason Friedman, Vladimir M. Zatsiorsky, Mark L. Latash
Department of Kinesiology, Penn State University, University Park, PA 16802
Email: vxs921@psu.edu

INTRODUCTION

In a multifinger cyclic force production task, finger force variance measured across trials can be decomposed into two components, one that affects the combined force output (“bad variance”), and one that does not (“good variance”). Previous studies have shown that "bad variance" and force rate are approximately linearly related. Based on this finding and a model of multifinger force production, we hypothesized that the “bad variance” during cyclic force production will increase monotonically with the rate of force change, both within-a-cycle, and across trials at different frequencies. Alternatively, “bad variance” could be related to task frequency, not force rate.

METHODS

Eight healthy right-hand dominant volunteers, (4M:4F, mean ± s.d.: age 26 ± 4 years, weight 69.5 ± 8.0 kg, height 1.68 ± 0.010 m) participated in the study. There were three types of tests, maximal voluntary contraction (MVC) tests, single-finger ramp tests, and cyclic force production tests. The cyclic force production task involved producing patterns of finger forces to targets by pressing on one-dimensional force sensors (model 208C02; PCB Piezotronic Inc.), at a frequency set by a metronome. Four different frequencies were used, 0.67 Hz, 0.9 Hz, 1.1 Hz and 1.33 Hz. The targets were set at 10% and 30% MVC for all the four frequencies. For the 0.9 Hz frequency, an additional set of targets, 10% MVC and 40% MVC was used. The task was performed either with only the index finger or with all four fingers. Subjects were instructed to make crests and troughs lie within a given target range, as indicated by dashed target lines on the monitor, and to make the changes in force magnitude between these target ranges smooth (like in a sine wave). Additionally, a computer-generated metronome indicated when the peak or trough should take place.

The data from the cyclic force production task were analyzed within the framework of the uncontrolled manifold (UCM) hypothesis. According to this hypothesis, the neural controller works in a space of elemental variables and creates in that space a sub-space corresponding to a desired value of a particular performance variable (the UCM). Further, the controller limits variability orthogonal to the UCM (“bad variability”, V_{ORT}) while allowing relatively high variability within the UCM (“good variability”, V_{UCM}).We computed V_{UCM} and V_{ORT} components of variance in the space of commands to individual fingers (“modes”).

To test the hypothesis that V_{ORT} is dependent on force rate, a repeated measures ANOVA was performed. To test whether V_{ORT} increases with force amplitude, another repeated-measures ANOVA was performed. This ANOVA was performed only for the 0.9 Hz conditions.

We also performed linear regression analysis between the two components of variance (V_{UCM} and V_{ORT}) and the task characteristics such as total force magnitude (F_{TOT}) and its rate of change (dF_{TOT}/dt) as suggested in an earlier study (Latash et al 2002):

$$V_{UCM} = a_1 * F_{TOT} + c_1 \qquad (1)$$

$$V_{ORT} = a_2 * F_{TOT} + b_2 * | dF_{TOT}/dt | + c_2 \qquad (2)$$

RESULTS AND DISCUSSION

There was an approximately linear relationship between the mean force and V_{UCM}. V_{ORT} shows a similar dependence on the force rate, dF/dt. The two components of the variance are plotted against force in Figure 1 (the means across subjects). Note the similar $V_{UCM}(F)$ *slopes*,for the different frequencies with the same amplitude. The time profiles of V_{ORT} are similar to those of the force rate, but the magnitudes of V_{ORT} do not scale with task frequency (and hence force rate), rather, their magnitudes show large variation along the cycle but little variation across task frequencies.

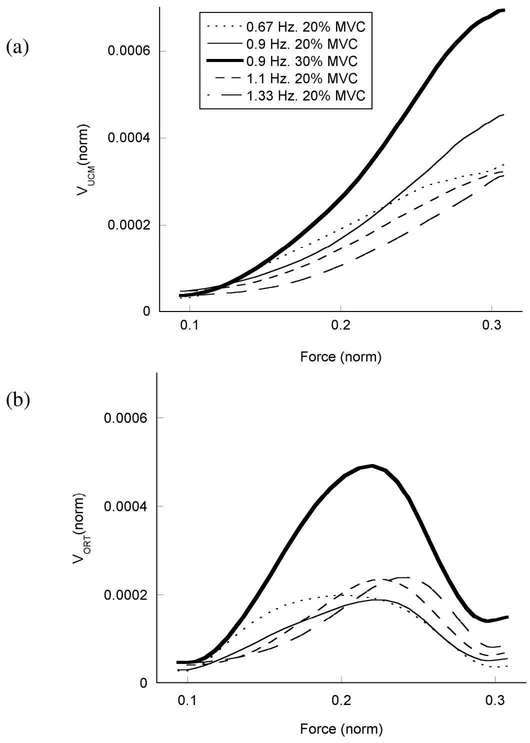

***Figure 1**. (a) V_{UCM} and (b) V_{ORT} for the force increase half-cycle, for the different frequency / amplitude combinations, averaged across subjects.*

For V_{ORT}, repeated measures ANOVA showed significant effects for *Time* ($F_{(2.4,142.9)} = 6.38$, $p < 0.005$) and interactions *Time × Direction* ($F_{(2.4,142.9)} = 9.31$, $p < 0.0001$) and *Time × Frequency* ($F_{(2.4,142.9)} = 4.51$, $p < 0.01$). Other effects were not statistically significant. In particular, there was not a main effect for *Frequency*, meaning that V_{ORT} did not increase with increased frequency.

The second repeated measures ANOVA showed a significant main effect for *Amplitude* ($F_{(1,28)} = 22.75$, $p < 0.0001$), with larger V_{ORT} for the 30% amplitude compared to the 20% amplitude. Interaction effects were significant for *Time × Direction* ($F_{(2.3,66.2)} = 6.02$, $p < 0.005$) and for *Time × Amplitude* ($F_{(2.3,66.2)} = 5.35$, $p < 0.01$). The other effects were not statistically significant.

The linear regressions showed very good fits. However, at least one of their coefficients (b_2 in Eq. 2) changed across the tasks in an unexpected way. Namely, an increase in task frequency led to a drop in b_2 such that, despite the associated change in the force rate, the amount of V_{ORT} remained unchanged across the different frequencies. So, the natural increase in *dF/dt* as the frequency increased was nearly perfectly matched by a reduction in the scaling of V_{ORT} on *dF/dt*. This effect persisted over all five frequencies explored in the experiment. Note that when a similar scaling of *dF/dt* was achieved by a change in force amplitude while keeping the frequency constant, V_{ORT} increased significantly, as it could be expected if the regression coefficient b_2 stayed unchanged.

These relations are summarized in Figure 1b and Figure 2. While the force rate increases with increasing frequency (see Figure 2), V_{ORT} does not (see Figure 1b).

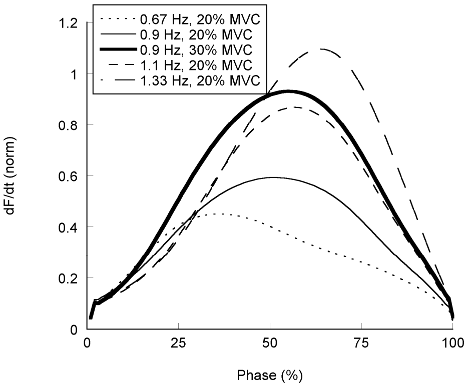

***Figure 2.** Changes in force rate (dF/dt) with changes in frequency / amplitude, averaged across subjects.*

These findings are consistent with the hypothesis that the two components of variance, V_{UCM} and V_{ORT} arise from two different sources (Goodman et al 2005). According to these authors, two parameters are set before each trial, namely an amplitude parameter β and a timing parameter τ. This model predicts that V_{UCM} is largely defined by variance in setting β, while V_{ORT} is largely defined by variance in setting τ. Our data suggests that variance of τ is modulated as a function of frequency, probably by increasing the relative timing accuracy as the frequency increases. This has the effect of maintaining approximately constant total force variance despite changes in frequency and force rate.

REFERENCES

1. Goodman et al. *Exp Brain Res* 163: 75-85, 2005

2. Latash et al *Exp Brain Res* 146: 412-432, 2002

ACKNOWLEDGEMENTS

The study was in part supported by NIH grants AG-018751, NS-035032, and AR-048563

ASSESSING THE FIT OF CONSTITUTIVE MODELS TO EXPERIMENTAL STRESS-STRAIN DATA

[1,2]Duane A Morrow, [2]Tammy L Haut Donahue, [2]Gregory M Odegard, and [1,2]Kenton R Kaufman
[1]Mayo Clinic, [2]Michigan Technological University
email: kaufman.kenton@mayo.edu

INTRODUCTION

The accuracy of a constitutive model is tied directly to the ability of that model to be well-characterized with experimental data. When characterizing a constitutive model, consideration must be given to the method for handling several data sets. This is especially important for biological materials in which the constitutive equations can be relatively complex and the amount of observed variability between samples can be substantial.

Constitutive model parameters can be determined through optimization-based curve-fitting techniques, either simultaneously fitting all available stress-strain data from multiple samples or fitting data curves from individual samples and averaging resultant model parameters. It remains unclear, however, which method, if any, is preferable for this class of materials.

The goal of this study was to examine the differences in methods that can be used to determine the coefficients of a material model and provide a framework for determining the most accurate data characterization.

METHODS

Stress-strain data was obtained from uniaxial material tests of twelve fresh-frozen extensor digitorum longus muscles of skeletally-mature New Zealand White rabbits, performed with institutional approval. Each specimen was deformed in either longitudinal extension (LE, n=4), transverse extension (TE, n=4), or longitudinal shear (LS, n=4) (Fig. 1). Full details on experimental setup are available in Morrow et al, 2009 [1].

The muscle was modeled as incompressible and transversely isotropic. A polynomial expansion of the I_1, I_2, and I_4 invariants was used for the strain energy function [2]:

$$\boldsymbol{W} = \sum_{i=1}^{3} a_i (I_1 - 3)^i + \sum_{j=1}^{3} b_j (I_2 - 3)^j + \sum_{k=2}^{6} c_k (I_4 - 3)^k$$

Model parameter coefficients were determined using unconstrained nonlinear optimization in MATLAB (Mathworks, Inc., Natick, MA). Best-fit model parameters were found using two different methods of curve fitting: data was curve-fitted using all data simultaneously as a single data set (ALL method), and alternatively, obtaining model parameters iteratively using one trial from each of the test directions (LE, TE, and LS) and averaging the four sets of model coefficients (EACH method). Best-fit parameters were determined for the 45 combinations of the constitutive model, varying between one and three I_1 terms, one and three I_2 terms, and one and five I_4 terms. References to model formulations are specified in the form of *a*-*b*-*c*, where there are *a* I_1 terms, *b* I_2 terms, and *c* I_4 terms).

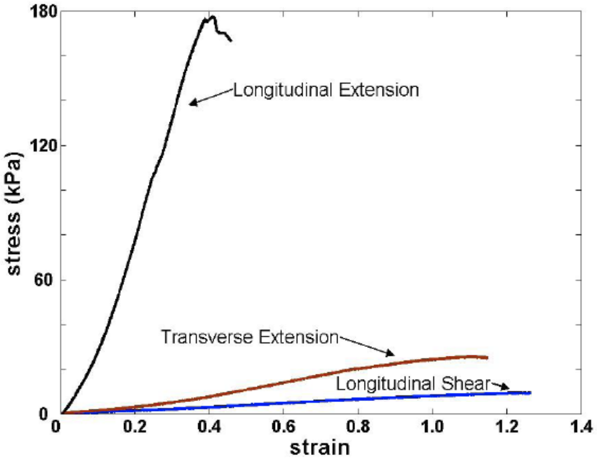

Figure 1. Representative stress-strain curves for longitudinal extension, transverse extension, and longitudinal shear.

Curve-fits were assessed using the root mean squared error (RMSE) to compare each of the twelve stress-strain curves, grouped by test direction, against derived models. A two-tailed, pairwise Student's t-test was used to determine if there is any difference in the RMSE between the ALL and EACH methods for each material test direction, with significance set at $p \leq 0.05$.

RESULTS AND DISCUSSION

The mean RMSEs for models characterized using the ALL method were found to be significantly lower than those characterized using the EACH method (p < 0.001) (Table 1).

Table 1. Summary RMSE data for ALL and EACH test methods by material test direction

	ALL		EACH	
	Mean	SD	Mean	SD
LE	8.57	1.66	12.50*	5.01
TE	2.22	0.46	2.60*	1.11
LS	0.48	0.24	0.49	0.21

* indicates significant difference from ALL (p<0.001). Data given in kPa.

The effect of polynomial terms was assessed by examining RMSE values for the LE, TE, and LS against the total number of terms in the various ALL models (Figure 2). These plots reveal the presence of two or three striations, or mean levels, of RMSE for the available combination of terms. Observing the patterns of the LE and TS RMSE (Figure 2) indicate that lower RMSEs for those directions can be attained using only four variables. Examination of the TE RMSE, however, reveals that a minimum of five variables was necessary to reduce the RMSE.

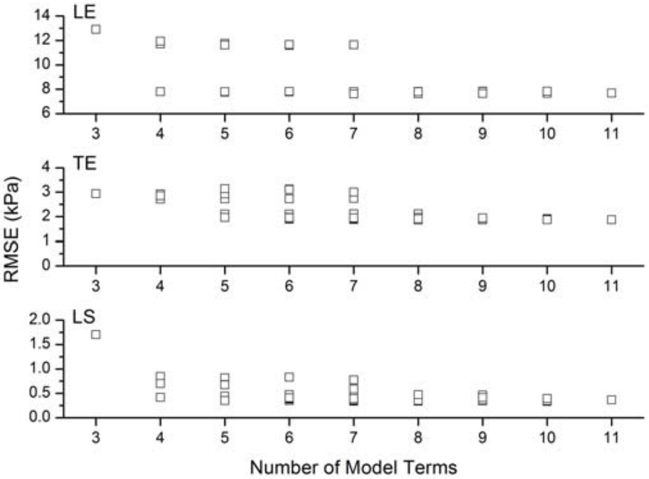

Figure 2. Plot of RSME by direction for LE (top), TE (middle), and LS (bottom) by number of constitutive model terms.

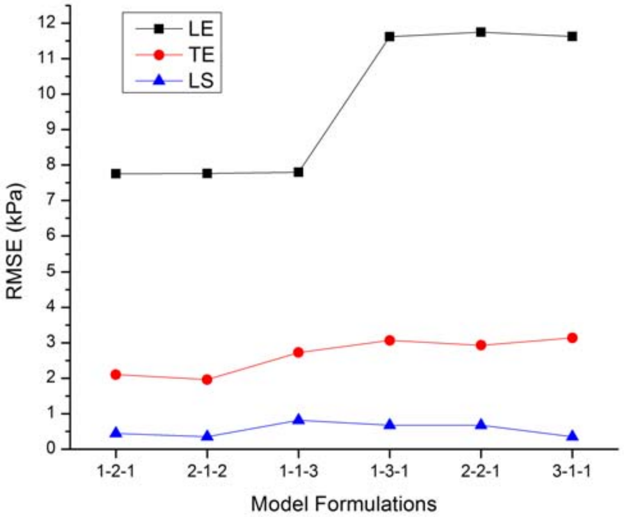

Figure 3. Plot of RMSE for all five-term models.

To find which combination of five terms gave the closest fit to the experimental data, RMSE was plotted by direction for each five-term model (Figure 3). It is clear from the figure that the *1-2-1* and *2-1-2* models (the left-most points of Figure 3) have the smallest overall RMSEs when considering all three directions of testing. To further determine whether one model is superior, plots of the model against the experimental data are examined. Visual inspection revealed that the fit of LE, TE, and LS data for the *2-1-2* model all follow the general tenor of their respective experimental data better than the *1-2-1* model, making it a good fit from both RMSE and visual inspection standpoints.

CONCLUSIONS

When fitting a material model to experimental data from multiple trials, a better fit is obtained by fitting all data simultaneously. While RMSE can be used to find which combination of terms in a polynomial constitutive formulation most closely characterizes experimental data, visual inspection should still be performed to ensure that the resulting model has an appropriate general shape and inflection points.

REFERENCES

1. Morrow DM, et al. *J Mech Behav Biomed Mater,* In Press, 2009.
2. Holzapfel GA. *Nonlinear Solid Mechanics* John Wiley & Sons, Ltd., 2000.

ACKNOWLEDGEMENT

Funding provided by NIH grant HD31476.

PREHENSION STRATIGIES FOR GRASPING OBJECTS WITH COMPLEX GEOMETRY

Gregory Slota[1], Mark Latash[2], Vladimir Zatsiorsky[1]
[1]Biomechanics Lab, [2]Motor Control Lab; Pennsylvania State University
email: GSlota@psu.edu, web: www.biomechanics.psu.edu/

INTRODUCTION

The study of redundant (or abundant) systems is of importance when trying to understand the different control mechanisms the CNS uses in daily life. When grasping and manipulating objects with a hand, forces and moments of force are generated with each of the fingers in order to hold the object and maintain a desired position and orientation. Different constraints are imposed on the net forces of the system; however there still exist numerous possible combinations of individual finger forces. There is a two tier hierarchical control of prehension: 1) thumb & virtual finger, 2) individual fingers [1]. Within these two levels, the CNS will control force patterns based on optimization of a particular cost function(s) [2]. The purpose of this study was to measure finger forces and patterns of co-variation while investigating the use of mechanical advantage of a finger as a control mechanism when dealing with objects of different geometries.

METHODS

Twelve subjects (6 males, 6 females, age 28.6 ± 5.2 yr) provided informed consent and participated in the experiment which was approved by the Office of Research Protection at Penn State. The subjects had their forearm supported and strapped onto a platform. Each trial consisted of grasping the handle with the thumb opposing the four fingers and the fingertips positioned on their corresponding sensor. Subjects were instructed to grasp the handle with minimal effort required to keep the handle from slipping. Additionally, the handle was to be held steady and level, using a spot-level as guidance. Once equilibrium was achieved, data were sampled for 10 seconds at 500 Hz. Each condition was repeated three times. Post processing and data reduction provided average values per trial and then per condition.

The test apparatus used consisted of a handle instrumented with five Nano-17, 6-DoF, sensors (Figure 1). The four fingers (index:*I*, middle:*M*, ring:*R*, little:*L*) were spaced vertically 3 cm apart with the thumb located at the midline. The thumb and fingers were spaced 3 cm laterally from the midline. This configuration is used as the baseline grip condition (G0). Changes in the grip condition consisted of increasing the lateral position of the index finger by 1 cm (G1), 2 cm (G2), & 3 cm (G3). Additionally, a mass was positioned along a horizontal beam to generate an external moment of force on the handle: L2= –8 cm (–0.403 Nm), L1= –4 cm (–0.202 Nm), C0= centered (0 Nm), R1= 4 cm (0.202 Nm), R2= 8 cm (0.403 Nm). Data were calculated for the thumb and each finger (*IMRL*) as well as the virtual finger (*Vf* = sum{*IMRL*}). Forces and moments were calculated in terms of the normal force (*Fn*), vertical tangential force (*Ft*), and their corresponding moments (*Mn,Mt*) generated about a horizontal axis passing through the center of the handle.

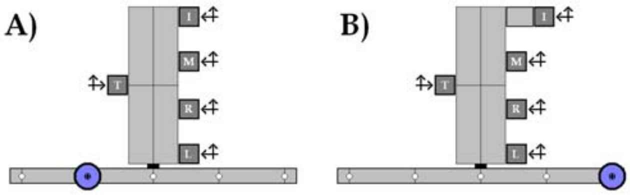

Figure 1: Handle configuration with 6-DoF sensors for each finger contact point: A) Normal grip, B) Index finger sensor displaced. Also shown are changes in external moments A) L1, B) R2.

RESULTS and DISCUSSION

The results of this study are summarized in Table 1. As the grip spacing increased from G0 to G3, the *Ft* significantly increased 146% for the index finger, decreased 47.0% and 12.7% for the middle and little fingers, while not affecting the ring finger (Figure 2a). The net effect was for the *Ft* for the virtual finger to significantly decrease 10.6% and the thumb to increase 14.0% (Figure 2b). The only finger in which *Fn* changed significantly was the index finger with a 24.0% increase. The overall effect of changes in forces resulted in a 151% decrease in the total *Mt* and a 184% increase in total *Mn* magnitude (Figure 2c).

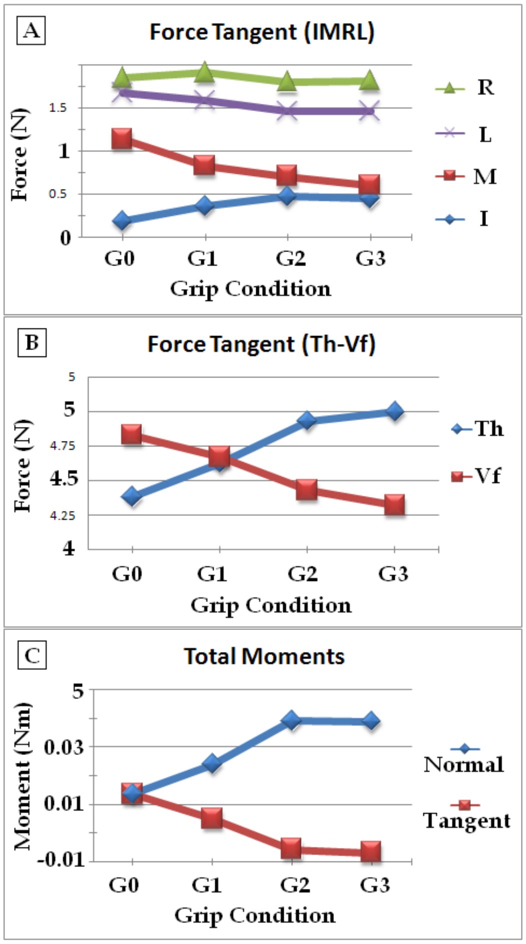

Figure 2: Finger forces with changes in grip configuration. A) *Ft* –I,M,R,L. B) *Ft*-Th,*Vf*, C) Total Moments: *Mn*, *Mt*

With the increase in the lateral displacement of the index finger sensor there was an increase in both the *Ft* and *Fn* generated by that finger. For the index finger, an increase in both forces increased their moment of force in the same direction. In order to balance the total moment of force on the handle, the net *Mt* was changed by a shift of the *Ft* balance from the *Vf* to the thumb via decreased *Ft* of the middle and little fingers.

As to the mechanisms involved in the increased *Fn* and *Ft* of the index finger, this can include the central controller utilizing the handle's geometry or changes in anatomical geometry increasing muscle force generation.

In terms of the hierarchy of control employed by the system, maintenance of the total moment of force was achieved at the thumb-*Vf* level. While there was an increase in the *Mt* generated by the index finger, the total *Mt* of the *Vf* was unchanged. The increased *Mn* of the *Vf* was counter balanced by the changed *Mt* generated by the thumb.

CONCLUSIONS

Results showed that the index finger increased its force involvement (*Ft*,*Fn*) while also generating greater moments of force (*Mt*,*Mn*) where it had a mechanical advantage, but the understanding behind this process requires further research.

REFERENCES

1.Zatsiorsky, VM, et al. *Exp Brain Res*, **148**, 77-87, 2003
2.Zatsiorsky, VM, et al. *Biol Cybern*, **87**, 40-9, 2002

ACKNOWLEDGEMENTS

The study was in part supported by NIH grantsAG-018751, NS-035032, and AR-048563.

Table 1: Significance of forces and moments due to increased grip spacing of the index finger

	Forces & Moments							
Finger	Δmag	**Ft**	Δmag	**Fn**	Δmag	**Mt**	Δmag	**Mn**
I	↑	**$P=0.024$**	↑	**$P<0.001$**	↑	**$P=0.041$**	↑	**$P=0.002$**
M	↓	**$P<0.001$**	~	$P=0.487$	↓	**$P<0.001$**	↓	**$P=0.014$**
R	~	$P=0.755$	~	$P=0.886$	~	$P=0.748$	~	$P=0.254$
L	↓	**$P=0.045$**	~	$P=0.053$	↓	**$P=0.047$**	↓	**$P=0.038$**
Vf	↓	**$P=0.003$**	~	$P=0.460$	~	$P=0.957$	↑	**$P=0.031$**
Th	↑	**$P<0.001$**	~	$P=0.415$	↑	**$P<0.001$**		*N/A*
(**Bold** signifies $P<0.05$)				**Total Moment**	↓	**$P=0.046$**	↑	**$P=0.031$**

ACTIVATION OF THE SHOULDER MUSCULATURE DURING A SUSTAINED SUB-MAXIMAL ABDUCTION ISOMETRIC CONTRACTION.

Mark Timmons, Ryan Adler and Andrew Boguszewski
Department of Kinesiology, The University of Toledo, Toledo, OH
email: mark.timmons@utoledo.ed

INTRODUCTION

Fatigue of the musculature of the shoulder girdle has been associated with an increase in shoulder pain and dysfunction [1]. Muscular fatigue reduces the dynamic stability of the shoulder girdle [2]. Muscle fatigue at sub-maximal contraction intensities has been shown to increase the magnitude of the surface electromyography (EMG) signal as motor unit recruitment increases [3,4]. The objective of this investigation was to determine the effect of a sustained sub-maximal isometric abduction contraction on activation of the scapular rotator and deltoid muscles as well as any apparent differences between the sexes in muscle activation during sustained sub-maximal isometric contractions.

METHODS

A one between three within mixed repeated measures design was used for this investigation. Ten males (20.8±0.98yrs, 80.2±15.1Kg, 178.6±2.6cm) and 10 females (21.2±0.41yrs, 65.1±0.8.4Kg, 165.5±0.7.7cm) participated in this investigation. All subjects were healthy physically active and without a history of shoulder, back or neck pathology.

Subjects performed five shoulder abduction isometric maximal voluntary contractions (MVC) and one sustained contraction at 30% MVC on a Biodex isokinetic dynamometer. The sustained sub-maximal isometric contraction was concluded when the subject could not maintain an abduction torque at 30% of their MVC. Contractions were performed at 45° and 90° arm abduction in the plane of the scapula. Contractions at each arm abduction angle were performed on different days, separated by one week.

During each contraction, surface EMG signals were collected from the deltoid (DEL), upper trapezium (UT), lower trapezium (LT) and serratus anterior (SA) muscles at 2000Hz. The EMG signals were bandpass filtered (20-500Hz) and fullwave rectified. The integrated EMG (IEMG) value was calculated during 3 second time epochs throughout the entire sub-maximal contraction, time epochs overlapped by 1.5 seconds. The sub-maximal IEMG values were normalized to the IEMG calculated during a 3 second analysis window during the MVC trials.

The IEMG values at 10-100% of the contraction duration were entered into to a mixed repeated measures (muscle x sex x arm abduction angle x time) analysis of variance. Statistical significance was determined at $p<0.05$.

RESULTS AND DICUSSION

Male subjects held the contraction for a longer duration (81.3±14.1sec) than the female subjects (71.2± 5.3sec) ($F_{1,36} = 4.632$, $p = 0.038$), differences in contraction duration between arm abduction angles were not significantly different. Significant main effects for muscle ($F_{3,1520} = 21.168$, $p<0.001$), sex ($F_{1,152} = 9.639$, $p = 0.002$), arm angle ($F_{1,152} = 4.156$, $p = 0.043$), and time ($F_{10,1520} = 64.679$, $p<0.001$) were found. The IEMG across all time intervals from the SA (0.835 ± 0.053) and UT (0.760 ± 0.053) were significantly higher than the DEL (0.552 ± 0.053) and LT (0.474 ± 0.053). Females (0.704 ± 0.024) displayed greater IEMG values than males (0.596 ± 0.025). IEMG values increased throughout the entire sub-maximal contraction (0.529 ± 0.324 to 0.747 ± 0.420). The arm x time interaction was significant ($F_{10,1520} = 1.964$, $p=0.034$) A greater increase in IEMG was seen at 45° than 90° arm abduction (Figure 1). The muscle by time interaction was significant ($F_{30,1520} =$

2.977, p<0.001) (Figure 2). The LT demonstrated no change in IEMG throughout the contraction duration (0.487±0.27 to 0.575±0.072). The greatest increases in IEMG were shown by the SA (0.540 ±0.027 to 1.118±0.072) and UT (0.4676±0.027 to 0.973±0.072). A smaller increase in IEMG was shown by the DEL (0.400±0.027 to 0.672 ± 0.079). All three and four way interactions were not statistically significant.

The results of this investigation show that a sustained isometric abduction contraction of the shoulder has a greater effect on the scapular rotator musculature than the deltoid muscle. This is in contrast to Minning *et al* that reported a greater fatigue in the DEL then the scapular rotators [5]. The difference in findings can be explained due to a difference in contraction intensity. During the current study subjects performed 30% MVC contraction as opposed to a 50% MVC in the Minning *et al* study. Even though males showed greater muscle activation, no apparent differences were seen between males and females in increase in the activation of the shoulder musculature during the sustained contraction. These findings suggest that there is no difference between the sexes in recruitment of muscle fiber during fatigue producing activities. As well these findings emphasize the importance of the scapular rotators to the healthy function of the shoulder girdle.

REFERENCE

1. McQuade KJ, *et al.*, *JOSPT*, **24**, 57-65, 1998

2. Ludewig PM, *et al.*, *JOSPT*, **28**, 74-80, 1996

3. Bigland-Ritchie B, *et al.*, *Acta Physiol Scand*, **128**, 137-148, 1986

4. Deluca, CJ, *et al*, *J of Physiol*, **329**, 113-128, 1982

5. Minning S, *et al.*, *J Electromyogr Kinesiol*, **17,** 153-159, 2007

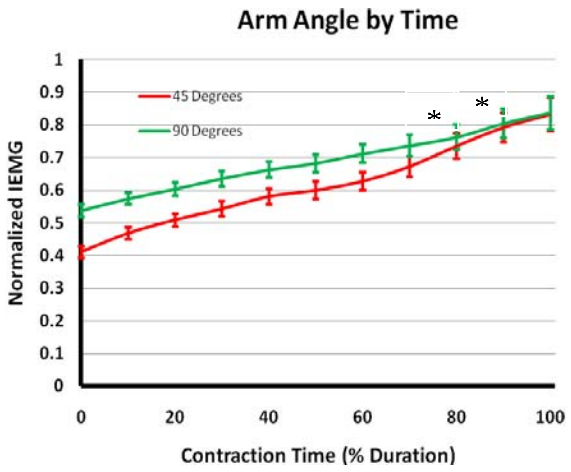

Figure 1: The arm angle by time interaction, (*) signifcantly greater increases in IEMG between 70% - 80% and 80% - 90% contraction duriation at 45° than 90° arm abduction.

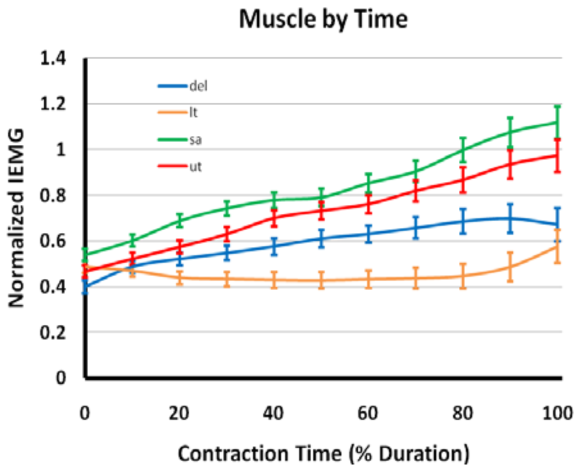

Figure 2: Muscle by time interaction, significantly greater increases in IEMG throughout the contraction duration in the SA and UT muscles than the DEL and LT muscles.

MECHANICAL PROPERTIES OF THE ANTERIOR CRUCIATE LIGAMENT AFTER CORTICOSTEROID ADMINISTRATION

Rodrigo Okubo, Ariane Zamarioli, Maurício José Falcai, José Batista Volpon and Antônio Carlos Shimano
School of Medicine of Ribeirão Preto, University of São Paulo, Brazil
email: rokubo@usp.br

INTRODUCTION

Intra-articular corticosteroid injections became widely used by sports medicine physicians to treat professional athletes. Physicians continue to use corticosteroid injections to treat a wide range of musculoskeletal disorders [1,2]. However, local injections of corticosteroids are associated with numerous adverse effects (eg, articular cartilage damage, tendon rupture, skin depigmentation, and so forth) [1]. Then, the purpose of this study was to investigate the effects of an intra-articular administered slightly soluble corticosteroid on the mechanical properties of anterior cruciate ligament (ACL) of rats.

METHODS

This study was approved by the Institutional Animal Care and Use Committee of our institution (CETEA). Fifteen male Wistar rats (University of São Paulo, Ribeirão Preto, SP, Brazil), weighting approximately 250 g were used in this study.

Rats were randomly assigned to five groups (n=5 per group): Group 1 – Control group that consisted in animals with no interventions. Group 2 – Saline group, that consisted in animals which received one intra-articular injection of saline 9% into both knees. The animals were killed two weeks after the injection. Group 3 – two-weeks-corticosteroid group, that consisted in animals which were submitted to corticosteroid injection in knees, bilaterally. The animals were killed two week after the injection.

In the corticosteroid-treated groups (3), a dexamethasone phosphate – Dexagil (Marjan Farma, São Paulo, Brazil) was injected into articular cavity of rat's knees. The dosage was 0,1ml, approximately 10 times an equivalent human dose on a mass basis. This schedule of drug administration was selected to provide similar conditions applied in humans.

A meticulous injection technique was used to ensure placement of the corticosteroid within the knee joint and avoid infection. No anesthesia was used during this procedure.

At the end of the experiment, the animals were killed under anaesthesia. Furthermore, the anatomical structures involving knee joint femur, ACL and tibia were harvested (Figure 1), removed and kept in saline 9% until performance of mechanical test.

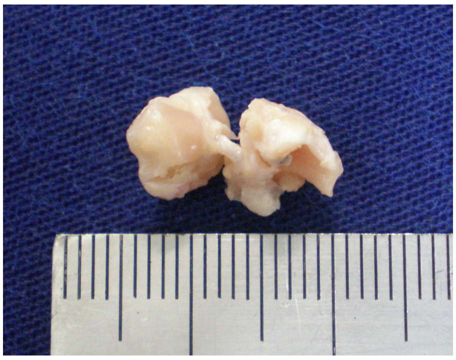

Figure 1: View of anatomical structures involving knee joint; femur and tibia extremities and the ACL.

For the mechanical test, the dissected specimens were rigidly mounted in 45 degrees of flexion on a test fixture, which was designed so that relative motion, which could occur between the tibia and the femur, was a linear displacement nearly parallel to the axis of the ligament. The tests were performed in a Universal Testing Machine (EMIC®, Brazil) from Laboratory of Bioengineering of Faculty of Medicine of Ribeirão Preto – USP. ACL was submitted to traction test (Figure 2) using a load cell of 500 N, a preload of 3 N with accommodation time of 30 seconds and speed of 10 mm/min. During tests graph load versus displacement was plotted and ultimate load and stiffness were evaluated.

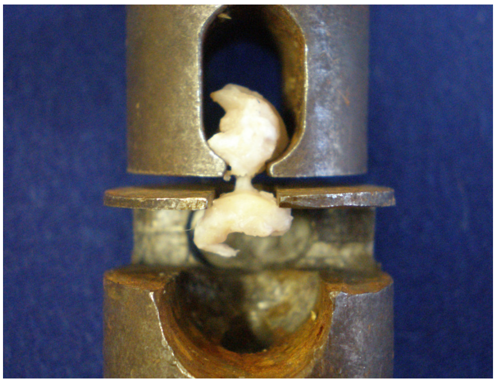

Figure 2: The placement of ACL in universal testing machine during mechanical test of traction.

Data were analyzed using analysis of covariance - ANOVA One Way Analysis of Variance to test the differences between groups. The level of significance was set at 5%.

RESULTS AND DISCUSSION

The group submitted to treatment with corticosteroid showed a significantly lower ultimate load when compared to both control and saline group ($p<0.05$) (Figure 3).

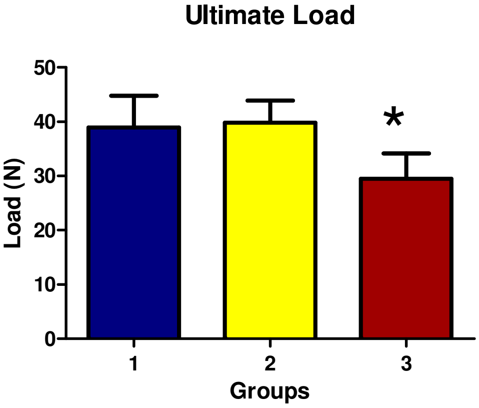

Figure 3: Graph representing values of the mean of ultimate loads. Asterisk indicates significant statistical differences.

We observed similar significant difference among groups concerning stiffness (Figure 4).

We found that corticosteroid injection in anterior cruciate ligament provide a significant decrease on mechanical properties such as reduction in ultimate load and stiffness.

Kennedy and Willis [3] showed a decrease in the tensile strength in the Achilles tendon of rabbits two and seven days after a single injection of corticosteroids.

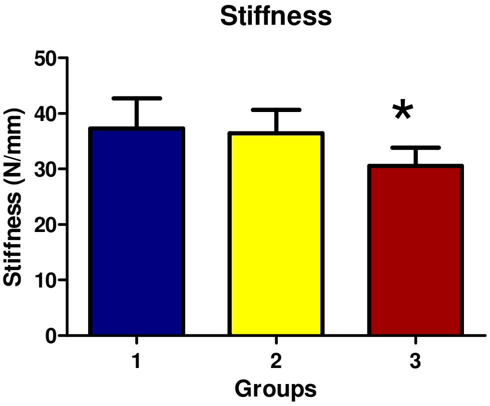

Figure 4: Graph representing values of the mean of stiffness. Asterisk indicates significant statistical differences.

Previous studies have shown that intra-articular administration of corticosteroids reduces the mechanical properties of ligaments by up to 20% after fifteen weeks of application [4]. In our study we confirmed previous observations that injection of corticosteroid decline mechanical properties of ligaments, although the magnitude of the strength reduction in the present study was considered larger (by up to 23%) than in previous studies.

CONCLUSIONS

The present study demonstrated the deleterious effects of a short-term corticosteroid administration on the mechanical resistance of anterior cruciate ligament.

REFERENCES

1. Nichols AW. Complications Associated With the Use of Corticosteroids in the Treatment of Athletic Injuries. *Clin J Sport Med*. 2005;**15**:370.
2. Hill JJ, Trapp RG, Colliver JA. Survey on the use of corticosteroid injections by orthopaedists. *Contemp Orthop*. 1989;**18**:39–45.
3. Kennedy JC, Willis RB. The effects of local steroid injections on tendons: a biomechanical and microscopic correlative study. *Am J Sports Med.* 1976:**4:**11–21.
4. Noyes FR, Grood ES, Nussbaum NS, Cooper SM. Effect of intra-articular corticosteroids on ligament properties: a biomechanical and histological study in rhesus knees. *Clin Orthop Relat Res.* 1977:197–209.

LOW STRESS TENDON FATIGUE: MECHANICAL AND STRUCTURAL FINDINGS

Gabriel Parent and Eve Langelier
PERSÉUS Research Group, Mechanical Engineering Department, Université de Sherbrooke
Email: Eve.Langelier@USherbrooke.ca, website: http://www.eureka.gme.usherb.ca/perseus/

INTRODUCTION

Micro-damage accumulation has been proposed as a source of mechanical degradation in tendons. Recently, Fung et al conducted high stress fatigue testing on tendons [1]. They observed: a triphasic pattern of tissue strain increase, an initial increase in tissue stiffness followed by an extended period of relative stability and then, a rapid decline before rupture. Under light microscopy (PMMA embedding), they characterized damage at low to moderate fatigue levels by increasing kinked fibre deformation patterns, while at higher fatigue levels, they observed dissociation, discontinuities and fibre rupture.

A better understanding of tendon fatigue progression would help improve the prevention and treatment of tendinopathy, a common health problem. The objective of the present study is to examine the mechanical and structural bases of low stress fatigue.

METHODS

Forty tendons were isolated from five rat tails within an hour of resection. Following isolation, the tendons' cross-sectional areas (A_0) were evaluated using an optical micrometer. The tendons were then washed five times. All these manipulations were performed in D-PBS containing an antibiotic-antimycotic agent. The tendons were then divided into four groups, all kept in D-PBS with antibiotic-antimycotic and protease inhibitors (1µg/ml Aprotinin, 1µg/ml Leupeptin, 1µg/ml Pepstatin A, 1mM PMSF). In the first group, the tendons were used as controls (no fatigue – 0% strain). In the other groups, the tendons were subjected to low stress fatigue loading (sine wave pattern, 1.5MPa, 1Hz) up to 4% strain (group 2), 8% strain (group 3) or rupture (group 4) at 37°C.

For mechanical characterization and loading, the tendons were transferred into a bioreactor. After temperature stabilization, the resting length (L_0) of the specimen was defined by achieving a tension load of 0.75MPa at equilibrium. Thereafter, the loading protocol began.

During fatigue loading, force (F) and tissue length (L) were recorded in a series of 10-second long time segments. Strain (ε) and stress (σ) were calculated as:

$\varepsilon(t) = \dfrac{L(t) - L(0)}{L(0)}, \sigma(t) = \dfrac{F(t)}{A_0}$. The compliance ($J$) was calculated as: $J(\tau) = \sqrt{\dfrac{\text{psd}\{\varepsilon'\}(1\text{Hz})}{\text{psd}\{\sigma'\}(1\text{Hz})}}$, where $\varepsilon' = det\,rend\{\varepsilon(\tau : \tau + 10\,sec)\}$, $\sigma' = det\,rend\{\sigma(\tau : \tau + 10\,sec)\}$ and *psd* stands for the power spectral density of the signal evaluated in each time segment (*detrend* is a Matlab function that removes linear trends.)

For structural characterization, biopsies taken from control and loaded tendons were prepared either for brightfield microscopy (longitudinal sections coloured with H&E), scanning electron microscopy (longitudinal sections prepared with a method adapted from Provenzano et al. [2]) or transmission electron microscopy (transverse sections). In the latter case, collagen fibril density was evaluated. The images were morphologically bottom-hat filtered (Matlab, Mathworks, Natick, MA, USA). Then, the pixel intensity was separated into two categories: fibril and background. The density was then calculated as:

$\rho = \dfrac{\#\,pixels \rightarrow fibril}{\#\,pixels \rightarrow image}$. The densities of all groups were compared using the Kruskal-Wallis test with Dunn's post-hoc test (GraphPad v5.0b, Prism Software, San Diego, CA). Statistical significance was established at $p < 0.05$.

RESULTS AND DISCUSSION

Mechanical characterization showed strain increase in a triphasic pattern as observed for high stress fatigue [1]. Tissue compliance followed a "U-shaped curve" as it decreased initially, remained relatively stable for an extended time period and increased before rupture. This U-shaped compliance curve is consistent with the stiffness observed during high stress fatigue [1].

Brightfield microscopy of fatigued tissue showed a lower collagen fibril density with increased fibril disorganization and waving. Observations differ somewhat from those obtained during high stress fatigue [1], possibly because of differences in the preparation protocol. PMMA embedding seems to preserve structural integrity of fatigued tissues and highlight local defects better than paraffin embedding, which appears to highlight an overall decrease in radial cohesion between fibrils. Scanning electron microscopy showed a greater number of local defects with fatigue. However, with increased fatigue, specimens became more difficult to cut longitudinally. Therefore, processing may have emphasized damages. Finally, density measured on transmission electron micrographs decreased with fatigue, which is coherent with other microscopic observations.

REFERENCES

X. Fung DT et al. *J Orthop Res* **27**, 264–273, 2009.
X. Provenzano PP et al. *Connect Tissue Res* **42**,123-133, 2001.

ACKNOWLEDGEMENTS

G. Parent received a scholarship from the IRSST. This research was supported by the NSERC.

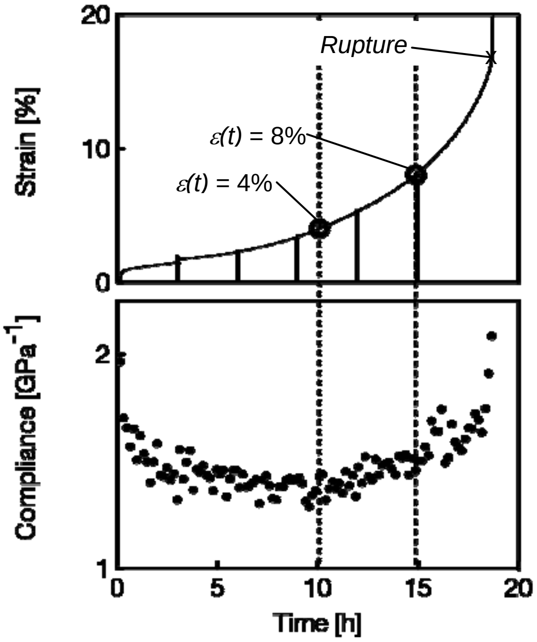

Figure 1: Results of mechanical characterization

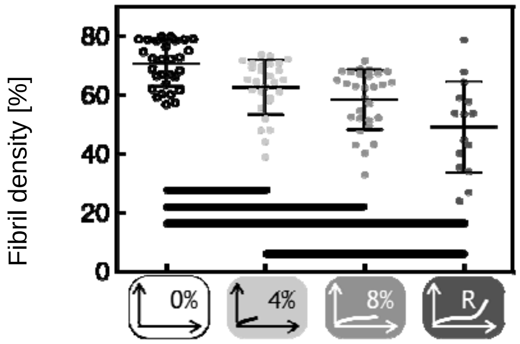

Figure 2: Fibril density from transmission electron micrographs. Bars indicate significant differences.

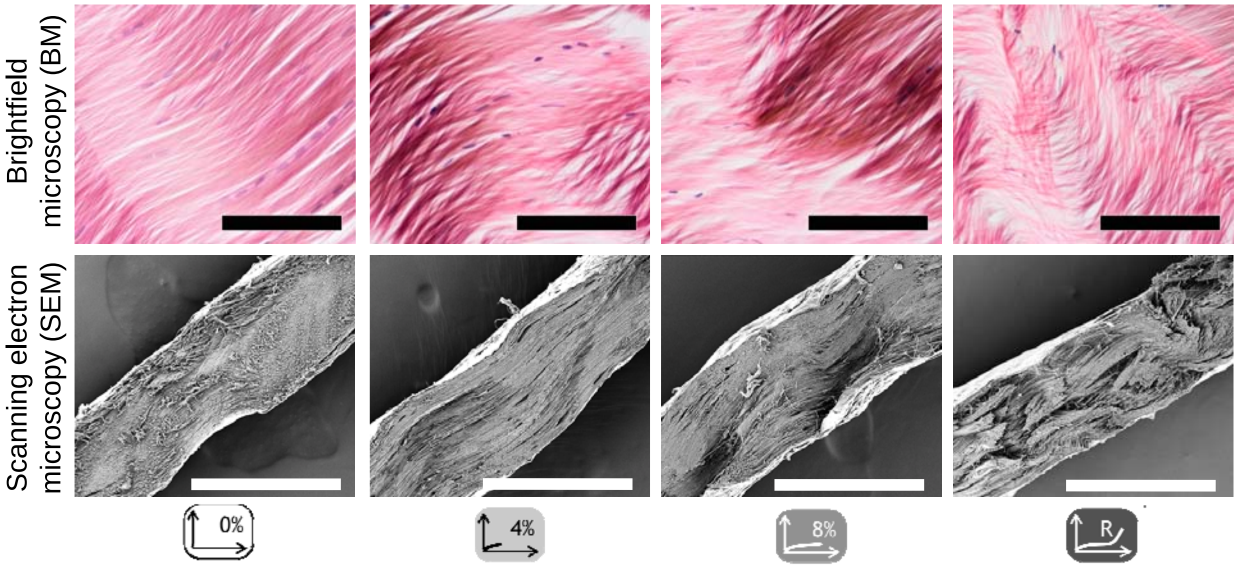
Brightfield microscopy (BM)
Scanning electron microscopy (SEM)
0%
4%
8%
R

Figure 3: Qualitative structural characterization. Bar = 100µm for BM and 200µm for SEM.

CHANGES IN MUSCLE-SKELETAL SYSTEM AFTER SPINAL CORD INJURY: A BIOMECHANICAL STUDY IN PARAPLEGIC RATS

Ariane Zamarioli, Daniel Maranho, Rodrigo Okubo, Maurício José Falcai, José Batista Volpon and
Antônio Carlos Shimano
Laboratory of Biomechanics – Faculty of Medicine of Ribeirão Preto
email: arianezamarioli@usp.br

INTRODUCTION

Spinal cord is a chronic affliction, with high incidence, that causes permanent and irreversible functional consequences in patients [1]. This disease has many complications that reduces life quality and increases morbidly and mortality [2, 3]. The complications may affect urologic, cardiologic, circulatory, respiratory and muscle-skeletal system [4, 5]. Concerning the muscle-skeletal system, the most common alteration due to spinal cord injury are spasticity and atrophy of muscle [6] and bone loss (osteopenia and osteoporosis) [8].

Previous studies have shown, experimentally, the spinal cord in experimental animals [1, 9, 10]. However, few studies concern the loss of muscle resistance.

The purpose of this preliminary study was to investigate the loss of muscle resistance in spinal cord injured rats. We also investigated this changes according by time post lesion.

METHODS

All animal procedures were approved by our Institutional Review Board.

Thirty three-month-old male Wistar rats were randomly assigned to two groups (n=15/group): (1) control animals (CONT) and (2) spinal cord injured animals (SCI). Each group was divided into three subgroups according to the follow-up of animals (n=5/subgroup): (2w) 2 weeks, (4w) 4 weeks and (8w) 8 weeks post lesion. The groups were compared in relation to the experimental period (i.e. 1w sham x 1w SCI).

Animals from group SCI were submitted to a experimental spinal cord injury. The lower thoracic cord of rats in the SCI group was exposed by a laminectomy in T10 and then the cord was completely sectioned (Figure 1).

Daily care was taken to the animals in order to avoid infections, ulcers and other complications due to paraplegia and surgical procedure.

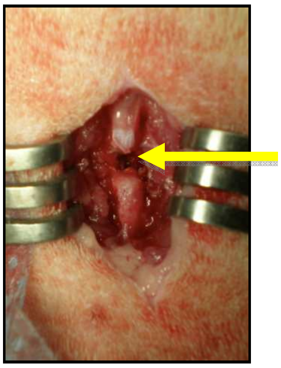

Figure 1: Arrow shows the point where spinal cord was sectioned.

At the end of the experiment (varying according by subgroup), gastrocnemius were dissected, measured by a Paquimeter Mitutoyo® and tested by traction in an universal testing machine (EMIC® DL 10000, Brazil), where ultimate load and stiffness were recorded (Figure 2).

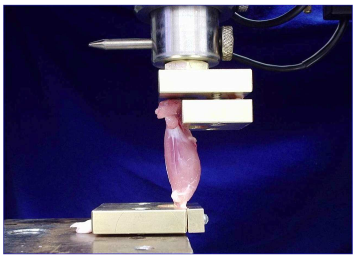

Figure 2: Gastrocnemius during mechanical test.

RESULTS AND DISCUSSION

Our results were based on 24 rats. There were 6 dropouts (SCI group) during the course of the study because of deaths whose reasons were: deep venous thrombosis, urinary and renal infections and autotomy.

Successful complete spinal cord lesion was confirmed at: gait analysis in a special treadmill, sensitive and motor assessment and at necropsy, when the cord was dissected and analyzed by histology.

Macroscopic analysis

The results concerning macroscopic measures are given in table 1. Figure 3 illustrates the significant difference between the muscles of control and spinal cord injured groups.

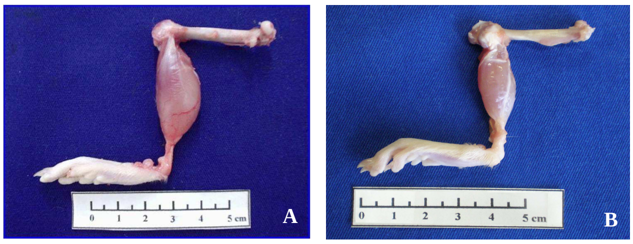

Figure 3: Gastrocnemius of control (A) and spinal cord injured groups (B).

Mechanical analysis

2 w (two weeks)

The mean values of ultimate load were: CONT (42.65 ± 12.43) N and SCI (18.91 ± 4.80) N. The ultimate load of spinal cord injured animals was 55.7% lower than in control group.

The mean values of stiffness were: CONT (4.72 ± 0.30) N and SCI (3.64 ± 0.11) N. The stiffness of spinal cord injured animals was 22.9% lower than in control group.

4 w (four weeks)

The mean values of ultimate load were: CONT (55.27 ± 2.84) N and SCI (20.55 ± 0.93) N. The ultimate load of spinal cord injured animals was 62.8% lower than in control group.

The mean values of stiffness were: CONT (5.94 ± 0.49) N and SCI (4.19 ± 0.78) N. The stiffness of spinal cord injured animals was 29.5% lower than in control group.

8 w (eight weeks)

The mean values of ultimate load were: CONT (63.30 ± 2.17) N and SCI (32.2 ± 2.15) N. The ultimate load of spinal cord injured animals was 49.1% lower than in control group.

The mean values of stiffness were: CONT (7.05 ± 0.23) N and SCI (5.98 ± 0.13) N. The stiffness of spinal cord injured animals was 15.2% lower than in control group.

CONCLUSIONS

Our preliminary study allowed a quantitative analysis of muscle loss after spinal cord lesion. There was an expressive decrease in macroscopic measures of the gastrocnemius in animals with spinal cord injury. In addition, the gastrocnemius of spinal cord injured animals showed a significant loss of muscle resistance and its loss was time-dependent. Further studies must be conducted in order to investigate procedures that may minimize this loss.

REFERENCES

1.Santos-Benito FF, et al. *J Neurotrauma*, **23,** 521-536, 2006.

2. Groat WC. *Urology*, **50,** 36-56, 1997.

3. Toosi KK et al. *Annals of Biomedical Engineering*, **36,** 1470-1480, 2008.

4. Christopher P, et al. The *Journal of Spinal Cord Medicine*, **30,** 307-308, 2007.

5. Bauman WA, et al. *Spinal Cord*, **46,** 466-476, 2008

6.Boncompagne S, et al. *Proceedings of the National Academy of Sciences of the United States of America*, **104,** 19339-19344, 2007.

7. Sheffler LR, et al. *Muscle & Nerve*, **35,** 562-590, 2007.

8.Reiter AL. *Eur Spine J*, **16,** 771-776, 2007.

9.Jiang LS, Et al. *Calcified Tissue International*, **80,** 167-175, 2007.

10.Sugawara H, et al. *The Journal of Spinal Cord Medicine*, **21,** 302-308, 1998

Table 1: Values of macroscopic measures of gastrocnemius in both control and spinal cord injured groups.

Groups	Subgroups	P P (mm)	M P (mm)	D P (mm)
CONT	**2 w**	26.4 ± 2.70	34.0 ± 2.12	23.8 ± 0.84
	4 w	30.6 ± 1.34	35.2 ± 1.48	26.6 ± 2.07
	8 w	33.4 ± 1.34	43.6 ± 2.41	28.6 ± 1.14
SCI	**2 w**	26.0 ± 1.41	26.5 ± 0.71	20.5 ± 0.71
	4 w	15.5 ± 0.71	17.0 ± 1.41	13.0 ± 1.41
	8 w	23.0 ± 0.57	25.0 ± 0.63	19.0 ± 1.03

PP=proximal perimeter; MP=middle perimeter and DP=distal perimeter

THE EFFECT OF GENDER AND PERCEIVED THREAT ON THE REACTION AND MOVEMENT TIMES OF YOUNG ADULTS PERFORMING A SIMULATED SPORT-PROTECTIVE RESPONSE

David B. Lipps, James T. Eckner, James K. Richardson, and James A. Ashton-Miller
University of Michigan, Ann Arbor, MI, USA
email: dlipps@umich.edu, Web: me.engin.umich.edu/brl

INTRODUCTION

The upper extremities are used to protect the head and body from impact with an object or the ground. Previous work has shown age, gender, and perceived threat significantly affected movement times in seated subjects blocking an approaching object at head level [1]. Reaction time and movement time both play an important role in determining the safety of athletes on the playing field. For example, baseball and softball pitchers have at most 420 ms to respond to a ball batted directly at them, when failure to block it could lead to catastrophic injury and/or death [2]. This study tested the null hypothesis that neither gender nor perceived threat will affect the reaction time or movement times of young adults when blocking a foam ball projectile aimed directly at their face.

METHODS

Nineteen healthy young adults (8 male, 11 female; mean age 27.5 years; mean height 173.3 cm; mean weight 71.8 kg) participated in this study. Subjects were equipped with a protective mask and chest protector. An air cannon located at head height directly in front of the subject fired a bright yellow foam tennis ball directly toward the subject's head at 21 m/s. The distance between the end of the cannon and the subject was incrementally decreased (61 cm increments) to increase task difficulty. The subjects started with both hands on their hips and moved both hands up to protect their face after the ball was fired. The subjects indicated when they were prepared for the cannon to fire. The air cannon fired the projectile after a random time delay of up to three seconds. Subjects underwent at least 4 trials at a distance of 8.25 m to become comfortable with the experiment ('low threat'). Subjects were then moved progressively closer to the cannon until they reached a distance (4–6 m) where they failed to block at least 4 of the 8 trials ('high threat').

Data collection began when the projectile cleared a light gate at the muzzle of the air cannon. An Optotrak Certus (Northern Digital, Waterloo, Ontario, Canada) motion capture system was used to measure forearm kinematics at 1 kHz. Optoelectronic markers were placed over the ulnar styloid on the left wrist and across the horizontal plane through the sternoclavicular joints. The initiation of protective motion was defined as the instant where the acceleration of the forearm exceeded 3*SD of the mean acceleration at rest. The completion of the protective motion was defined as the instant the forearm broke the sternoclavicular reference plane. Myoelectric measurements were recorded at 2 kHz from the infraspinatus, middle deltoid, brachioradialis, and extensor capri ulnaris muscles. The onset of myoelectric activity was defined by identifying the points at which the myoelectric activity was 5% and 10% above baseline noise levels and thence, via linearly extrapolation, back to baseline noise level.

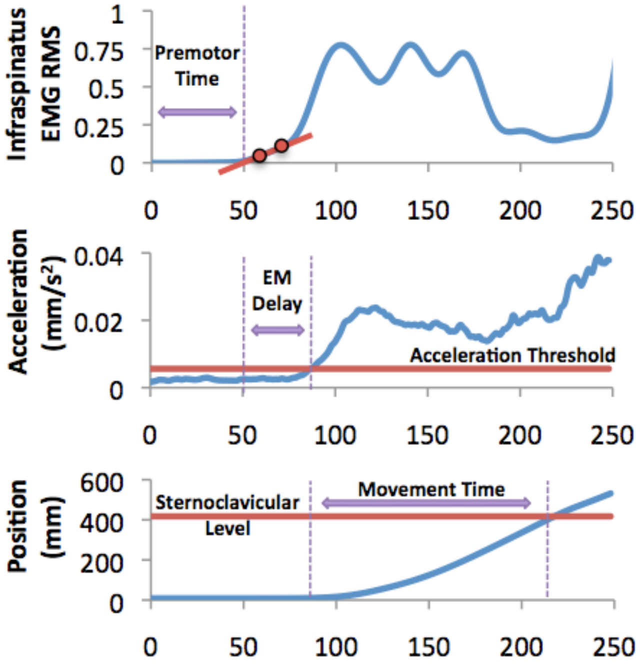

Figure 1. Illustration of premotor time, EM delay, and movement time for a typical trial.

Premotor time was the interval between the projectile breaking the light gate plane until the first onset of myoelectric activity. Electromechanical (EM) delay was the interval from the first onset of myoelectric activity to the initial acceleration of the forearm. Reaction time was the sum of premotor time and EM delay. Movement time was the interval from the initial acceleration of the forearm until the ulnar marker broke the horizontal sternoclavicular plane. These measurements are illustrated in Figure 1. A two-way ANOVA was used to test the effects of perceived threat and gender on reaction and movement time and $P<0.05$ was considered significant.

RESULTS AND DISCUSSION

Reaction time and movement time both differed significantly with gender ($p<0.001$) and perceived threat ($p<0.001$), but the interactions of perceived threat X gender did not reach significance for either measurement. Males had a 27% reduction in mean reaction time and a 19% reduction in mean movement time with increasing perceived threat levels, while females showed a 21% reduction in mean reaction time and a 14% reduction in mean movement time with increasing perceived threat levels (Figure 2). The blocking accuracy for all subjects was 94% at the ‘low threat’ level and 39% for the ‘high threat’ level.

The use of an air cannon for measuring reaction time simulates an athletic response time similar to blocking a baseball or softball coming directly at the head. These results show that subjects blocking a ball aimed directly at their face from relatively close (‘high threat’ level) have a mean response time below 420 ms (Men: 250 ms, Women: 288 ms).

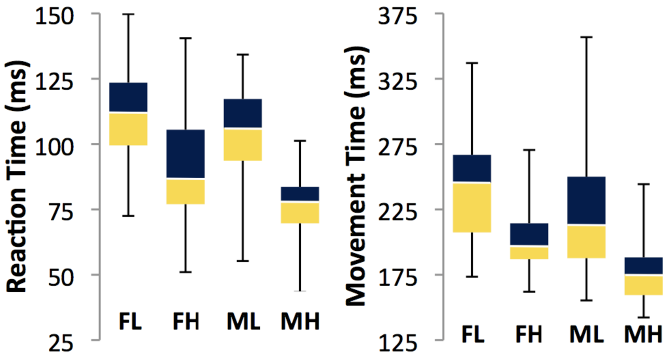

Figure 2. Box plots for reaction time and movement time. Boxes represent quartiles and the tails represent the max and min values. (F=Female, M=Male, L=Low Threat, and H=High Threat)

The fact that females had slower reaction times than males may be due to physiological or motivational factors. Gender differences have indeed been noted in simple and choice reaction times in healthy adults [3], and females sprinters had significantly slower simple reaction times than did male sprinters at the Beijing Olympics [4]. However, gender differences in speed-accuracy tradeoff could still be responsible: in aiming tasks, for example, males emphasize speed; females emphasize accuracy [5].

A limitation of our study is that an auditory cue preceded the visual stimulus by a small amount. A microphone mounted on one subject‘s helmet showed that sound was detected 5–17 ms before the ball reached the end of the cannon, depending on the distance the subject was from the cannon. However, since the sound was detected at a consistent time for each distance, it does not invalidate the overall study findings.

CONCLUSIONS

Both gender and perceived threat significantly affect reaction and movement time in young adults protecting their face from an approaching ball.

REFERENCES

1. DeGoede KM, et al. *J Gerontol* **56A**, M584-M588, 2001.
2. McDowell M and Ciocco MV. *Br J Sports Med* **39**, 223-225, 2005.
3. Der G and Deary IJ. *Psychol Aging* **21**, 62-73, 2006.
4. Lipps DB et al. Submitted *Am Soc Biomech,* 2009.
5. Rohr LE. *J Mot Behav* **38**, 431-437, 2006.

ACKNOWLEDGEMENTS

We would like to acknowledge funding from the NDSEG Graduate Fellowship, Foundation for PM&R New Investigator Award, and the UM-BJIPRC Pilot Grant, the work of Hogene Kim, Trina DeMott and Nick LeCursi, and equipment from Dr. Lloyd Smith.

ANALYSIS OF THE INTERNAL STRESSES IN INTERVERTEBRAL DISC L4-L5 USING THE PHOTOELASTICITY

Antônio Carlos Shimano[1], Sarah Fakher Fakhouri[1], Ariane Zamarioli[1], Rodrigo Okubo[1], Cleudmar Amaral Araújo[2], Helton L. A. Defino[1]
[1]Laboratory of Biomechanics – Faculty of Medicine of Ribeirão Preto
[2]School of Mechanical Engineering of Federal University of Uberlândia
email: ashimano@fmrp.usp.br

INTRODUCTION

The discal hernias have been pointed as one of the main structures involved to etiology of low back pain [1]. These diseases affect mainly the intervertebral disc L4 and L5, due to highest load [2, 3].

The discal cells are sensitive to mechanical involvements, being directly influenced by hydrostatical pressure and compressive load [4, 5].

Photoelastic is a science that studies physical effects by light due to action of tensions or deformations in transparent elastic bodies and, it has been one of the techniques available for determining and evaluating the distribution of internal stress in structural systems [6, 7, 8]. It is an experimental technique that allows a qualitative and quantitative analysis of state of internal stress of materials by means of view of optical effects [9].

The purpose of this study was analyze the inner stress in intervertebral discs between L4 and L5 vertebrae when submitted to compression load using the technique of photoelasticity of plane transmission.

METHODS

Two sagittal cutts were performed, two in each area: central and lateral of L4 and L5 vertebral bodies of polyurethane (Nacional™), for obtaining two experimental models. The were performed unilaterally because vertebral bodies are symmetric. The distance between the cutts was 16.0 mm (Figure 1).

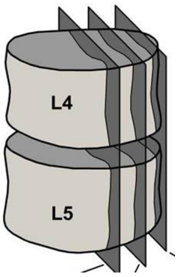

Figure 1. Schematic drawing showing of experimental models of vertebral bodies L4-L5.

By these cutts we obtained the geometry of central and lateral intervertebral discs. Anterior part of disc hat 10.0 mm of height and posterior 7.0 mm.

Experimental models obtained were used as mold for its confection in acrylic resin T208, mixed with monomer of styrene and catalyzer. For each 40.0 ml of resin were mixed 3.2 ml of monomer and 0.8 ml of catalyzer. Experimental models in acrylic were positioned in respective mold of Teflon®, where it was add the flexible photoelastic resin epoxy (Polipox™) between them for modeling the intervertebral discs. This resin has elasticity modulus of 4.51MPa and Poisson Coefficient of 0.4 and, for confection of photoelastic models it was used a proportion of 2.2 ml of resin for 1.0 ml of catalyzer.

We confectioned four photoelastic models from each experimental model (central and lateral). Photoelastic model from central experimental model had 39.4 mm of width and from lateral 26.7 mm. All models had 60.0 mm of length and 8.0 mm of thickness (Figure 2).

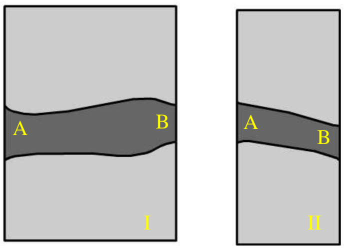

Figure 2. Schematic draw of the photoelastic models with emphases for anterior (A) and posterior (B) area of intervertebral discs of central (I) and lateral (II) experimental models.

In quantitative analysis we observed the point of beginning and highest concentration of stress. For quantitative analysis we applied a load of 2.3 Kgf registered by using load cell Kratos™, with capacity of 10 Kgf. The shear stress were calculated in a standard way in 16 points, respective to central and lateral models, based on contour of intervertebral disc (Figure 3).

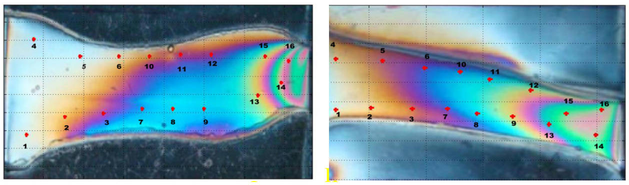

Figure 3. Distribution of analyzed points in central (I) and lateral (II) models.

RESULTS AND DISCUSSION

By means of qualitative analysis we observed the stress started in posterior part of disc and in there it reached the highest concentration.

Quantitative analysis was used to quantify stress in each area of discs. In central models the posterior area of disc, located in points 13 to 16 showed a mean of (57.74 ± 17.20)kPa. The anterior area, points 1 to 6, had lower stress concentration with mean of (20.30 ± 11.24)kPa. Medial area of disc, points 7 to 12, showed a stress concentration higher than in anterior area, but lower than in posterior, with mean of (31.97 ± 3.77)kPa.

In lateral models the posterior area, points 13 to 16, showed a mean of (75.77 ± 2.10)kPa. Anterior area, points 1 to 6, had a lower inner stress with a mean of (32.06 ± 17.12)kPa. Medial area, points 7 to 12, had an intermediated stress of (43.86 ± 2.79)kPa.

The photoelasticity showed to be an efficient technique. However, some authors related, using different techniques, the posterior area is the area of disc with the highest pressure, making easier the appearance of disc degeneration [2, 4, 10, 11].

CONCLUSIONS

The photoelastic analysis showed the posterior area of intervertebral disc has the highest concentration stress, being probably more susceptible to diseases as low back pain, disc degeneration and disc hernia.

REFERENCES

1. Kuslich SD, et al. *Orthopedic Clinic of North America* **22,** 181-187, 1991.
2. Adams MA, et al. *Spine* **13,** 1625-1636, 2000.
3. RANNOU F, et al. *Joint Bone Spine* **68**, 543-546, 2001.
4. Guehring T, et al. *European Spine Journal* **15,** 597-604, 2006.
5. Handa, T, et al. *Spine* **22**, 1085-1091, 1997.
6. Dally JW, et al. Experimental stress analysis, 1978.7. DOYLE JF, et al. Manual on Experimental Stress Analysis, 1978.
8. Mahler DB, et al. Journal of Dental Research **34**, 831-838, 1955.
9. Hirokawa S, et al. *IEEE transactions on rehabilitation engineering* **6**, 300-308, 1998.
10. Iatridis JC, et al. *Spine* **24,** 996-1002, 1999.
11. Kroeber M et al. *Spine* **30**, 181-187, 2005.

VALIDATION OF AN EXPERIMENTAL DEVICE SIMULATING THE STANCE PHASE OF A CANINE HINDLIMB AT TROT: AN *IN VITRO* KINEMATICS STUDY

[1]Bertrand Lussier,[2-3-4]Julien Clément, [2-3-4]Emna Jaafar, [2-3-4]Yvan Petit and [2-3-4]Nicola Hagemeister.
1)Faculty of veterinary medicine, University of Montreal; 2) École de technologie supérieure ;
3)Laboratoire de recherche en imagerie et orthopédie ; 4) Hôpital du Sacré-Cœur de Montréal
email : bertrand.lussier@umontreal.ca

INTRODUCTION

Rupture of the cranial cruciate ligament (RCCL) is the most common orthopedic disorder afflicting dogs [1]. It modifies the kinematics and internal loads of the stifle and invariably leads to the development of osteoarthritis. Several surgical techniques developed for correction of the CCL-deficient stifle have been reported, but none are able to restore the kinematics of an intact stifle [2]. The outcome of surgical correction of RCCL has so far been conducted by anecdotal reports, retrospective studies, evaluation of limb function by the use of ground reaction forces (GRF), clinical studies, theoretical models of stifle biomechanics and *in vitro* biomechanical cadaver studies. In the past years, the use of *in vitro* models simulating weight bearing has gained popularity. Most *in vitro* studies analyzing kinematics of the canine stifle were made in 2D under low static loads. Gait implies a displacement of the load application at the hip from caudal to cranial, modifying the moments applied to the stifle. Such a motion is qualified as isotonic. To our knowledge, no testing device allows the simulation of this condition. Our goal was to design an experimental device simulating a quasi-dynamic model of the stance phase at trot of the canine hind limb under near physiologic conditions. Our hypotheses are as follows: 1) the device allows reliable measurements with low intra-specimen and inter-specimen variability; 2) the kinematics generated by the device are representative of reported *in vivo* 3D kinematics [3]; 3) peak vertical forces generated by the loaded limbs in the device will be similar to those recorded in the literature for a walking dog during the stance phase [4].

METHODS

A theoretical model of the canine hind limb was developed in order to calculate relative motion of the femur and tibia during the stance phase. An experimental device was built from this model. Six paired (left + right) hind limbs were harvested from 3 adult large breed dogs euthanatized for reasons unrelated to this study. The dogs were similar in age, size and body weight (range, 29.5-31 kg). Clinical and radiographic stifle examinations were performed to exclude any pathology. The limbs were prepared and mounted on the device. Each limb was submitted to vertical loading (9 kg) to the artificial hip joint. The gait was simulated with a computerized sequence using a linear actuator and a rotational motor inducing the artificial ankle's anterior-posterior and flexion-extension respectively. The stance phase of the gait at walk was simulated three times on each hind limb based on previously published sagittal plane kinematics of the ankle, knee and hip in dogs [5]. Kinematics of

Figure 1: Schematic view of the custom made testing rig of the rig (Catia V5 software, IBM corp. USA).

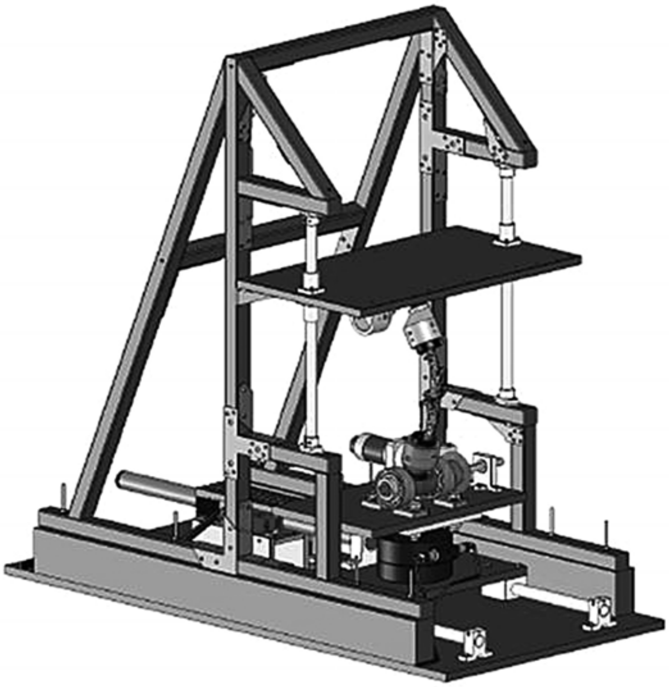

the tibia and femur was measured with an optoelectronic system (Optotrak 3020, Norton Digital inc., Waterloo, ON). Kinematics' curves were generated using Euler angles with the method of Grood and Suntay [6]. Vertical ground reaction forces were measured with a 2.5 kN axial/torsion force transducer (MTS Corp., Minneapolis MN). Validation consisted in evaluating intra and inter-specimen variability of the 3D kinematics' curves of the stifle. Amplitude of motion and peak ground reaction forces as well as the general shape of kinematics' curves were also compared with *in vivo* curves described in the literature [3,4].

RESULTS AND DISCUSSION

Data recorded during *in vitro* simulations highlighted average intra-specimen variability less than 0.8° and 0.7 mm for the three rotations and translations of the stifle respectively, compared with 5.8° and 1.3 mm for the inter-specimen variability. The comparison of the six average curves of motion collected on the tested stifles to those from *in vivo* trials reveals similar patterns in every case. However, amplitude of is slightly greater on *in vivo* curves [5]. Peak vertical forces measured in the device (138+/-2N) were also similar to *in vivo* trials reported in the literature [4]

CONCLUSIONS

Results show that the device generates reliable motion on a loaded limb which is representative of the *in vivo* 3D kinematics reported in the literature. This model could be used to evaluate the effects of cranial cruciate ligament rupture. Moreover, it could be used evaluate different surgical techniques, to determine which surgical procedures have the potential to re-establish normal stifle kinematics. The tools developed in this study might also lead to the design and evaluation of new surgical techniques. Finally, this model could be adapted and used with the human knee

REFERENCES

1. Johnson JA et al. *Vet Comp Orthop Traumatol* 1994;**7**:56–697.
2. Brinker WO, et al. In: Brinker WO, et al, eds. *Handbook of small animal orthopedics and fracture treatment*. Philadelphia: WB Saunders, 1990:341
3. Korvick DO et al. *J Biomech* 1994. **27**: 77-874.
4. Voss K et al. Vet Comp Orthop Traumatol 2007; **20**: 299–304
5. DeCamp CE., et al. AJVR 1996. **57**(1): 120-126.
6. Grood ES and W.J Suntay. *J Biomech Eng* 1983., **105**,136-144

ACKNOWLEDGEMENTS

We would like to acknowledge the Natural Science and Engineering Council (NSERC), the Fonds Québécois de Recherche en Nature et Technologies (FQRNT), the Canadian Foundation for Innovation (CFI) and the Fonds en santé des animaux de compagnie (FSAC) for funding this study and Annie Levasseur for technical assistance.

A COMBINATORIAL APPROACH TO AUTOMATED PATIENT-SPECIFIC FINITE ELEMENT MESHING

[1,2]Austin J. Ramme, [1,2,3]Vincent A. Magnotta, and [1,2,4]Nicole M. Grosland
[1]Center for Computer-Aided Design, [2]Department of Biomedical Engineering,
[3]Department of Radiology, [4]Department of Orthopaedics and Rehabilitation
The University of Iowa, Iowa City, IA
email: austin-ramme@uiowa.edu, web: http://www.ccad.uiowa.edu/mimx/

INTRODUCTION

Medical imaging technologies have allowed for *in vivo* exploration of the human musculoskeletal system. With advances in the resolution of acquired images and computing power, patient-specific orthopaedic model development is becoming a reality. The finite element (FE) method is often employed to investigate stress and strain patterns exerted on cartilage, bones, and implants [1]. The development of FE models in orthopaedics provides a means to evaluate the musculoskeletal system in health, injury, and disease. It also provides a quantitative means to evaluate new surgical methods and implant design. However, relatively few FE studies have been performed on a patient-specific basis due to the extensive manual labor involved in the 3D mesh generation required for the analysis. Most modern orthopaedic finite element research incorporates a baseline model that is modified for the researcher's subject of interest.

In the future, patient-specific FE analysis will help to ensure optimal implant choice and positioning in surgical planning. IA-FEMesh is an open-source software package designed to facilitate patient-specific FE mesh generation for orthopaedic applications derived from a medical imaging dataset [2]. Currently, IA-FEMesh's meshing protocol relies on manual building block placement around 3D surfaces. As the complexity of the surface increases (e.g. phalanx versus cervical vertebrae), the number of required blocks increases and hence the time required to create the block structure increases. In this work, we evaluate the ability of a surface based analysis to automatically place the building blocks and a combinatorial look-up table approach to construct a usable building block structure for meshing.

METHODS

Before the automated building block placement process, a 3D model of the region of interest was generated from CT images. Once 3D geometry was established, surface feature identification was achieved by first computing the Gaussian curvature at each vertex of the surface [3]. Regions of particularly high (convex or concave) Gaussian curvature corresponded to regions of complex geometry; moreover, based on experience these represent locations where the blocks are typically positioned manually. A statistical analysis of the curvature calculations was used to retain the vertices with the greatest absolute curvature. Finally, a distance constraint was incorporated to prevent redundant identification of a given region and to allow the user to control the density of the defined building blocks. The final filtered dataset contains a set of unique points corresponding to regions of complex geometries.

Once the points of interest were defined on the surface, the next step involved segmenting the surface with respect to the already identified features. The Vascular Modeling Toolkit (VMTK) has allowed for medial axis analysis, centerline generation, and surface segmentation with respect to the already identified surface feature seed points [4]. Building blocks were defined based on the bounding box for each component of the segmented surface regions.

However, this raw building block structure was unusable due to block overlap and lack of connectivity between the blocks. A combinatorial look-up table was developed to modify the 729 potential cases of overlapping blocks. After the building block structure had been untangled, a variety of other modifications were made to the block structure including: removal of empty and zero volume blocks, ensuring one-to-one face correspondence between blocks, and establishing connectivity between adjacent blocks. Using this process, a valid building block structure appropriate for mesh generation in IA-FEMesh was created.

RESULTS AND DISCUSSION

Figure 1 demonstrates sample results from each of the steps involved in generating a patient specific finite element mesh for a proximal phalanx. First, a subject is imaged and the images were segmented to generate three dimensional surfaces of the region of interest (Figure 1A-D). These surfaces then entered the automated building block process. Figure 1E demonstrates the Gaussian curvature values calculated from the surface where blue represents negative curvature and red represents positive curvature. Figure 1F demonstrates the Gaussian curvature feature identification of regions of complex geometry after using the filtering technique previously described. Figure 1G and 1H demonstrate the VMTK functionality to establish centerlines and segment the surface. Figure 1I demonstrates building blocks defined simply by the segmented region's extents. Figure 1J shows the output from combinatorial block untangling. Figure 1K demonstrates the final building block structure after establishment of one to one face correspondence and block connectivity. The automated building block process allows the user to modify distance and clustering constraints to allow flexibility in variable geometries. We have applied our algorithm to the proximal, medial, and distal phalanx bones and have seen promising results.

CONCLUSIONS

We have developed an algorithm to automatically define building blocks using a combinatorial look-up table based on statistical analysis of surface curvature and medial axis calculations. We are currently in the process of developing three dimensional models of various bones from the human musculoskeletal system to continue to validate this algorithm. Future improvements to the algorithm will include a method to ensure that minimum volume building blocks are assigned to a given model regardless of the model's orientation in relation to the global origin. The automation of building block definitions for mesh generation will help to enable orthopaedic finite element analysis to be applied to better understand the musculoskeletal system in health, injury, and disease on a patient-specific basis.

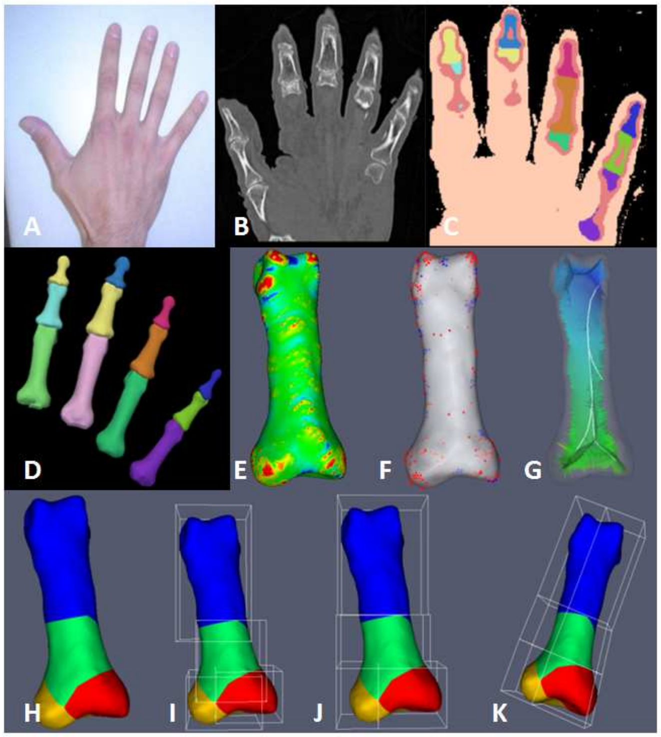

Figure 1: An example (proximal phalanx) of the process used to develop patient specific meshes for finite element analysis. A/B.) Imaging of a region of interest. C.) Segmentation of the image dataset. D.) 3D model generation. E.) Surface Gaussian curvature calculations. F.) Surface feature landmark identification. G.) VMTK medial axis centerline generation. H.)VMTK surface segmentation. I.) Building block structure defined by region extents. J.) Untangled building block structure. K.) Final building block structure for finite element mesh generation.

REFERENCES

1. Ratner BD, et al. *Biomaterials science: An introduction to materials in medicine*, 851, 2004.
2. Grosland, N.M. et al. *Computer Methods Programs in Biomedicine*, **94**, 96-107, 2009.
3. Subburaj K. et al. *Computer-Aided Design & Applications*, **5**, 153-160, 2008.
4. Antiga, L et al. *Med Biol Eng Comput*, **46**, 1097-1112, 2009.

VALIDATION OF AN EXPERIMENTAL DEVICE SIMULATING THE STANCE PHASE OF A CANINE HINDLIMB AT TROT IN THE CRANIAL CRUCIATE DEFICIENT STIFLE: AN *IN VITRO* KINEMATICS STUDY

[1]Bertrand Lussier, [2-3-4]Julien Clément, [2-3-4]Emna Jaafar, [2-3-4]Yvan Petit and [2-3-4]Nicola Hagemeister.
1) Faculty of veterinary medicine, University of Montreal; 2) École de technologie supérieure ; 3) Laboratoire de recherche en imagerie et orthopédie ; 4) Hôpital du Sacré-Cœur de Montréal
email : bertrand.lussier@umontreal.ca

INTRODUCTION

Rupture of the cranial cruciate ligament (RCCL) is the most common orthopedic disorder afflicting dogs [1]. It modifies the kinematics and internal loads of the stifle and invariably leads to the development of osteoarthritis. Several surgical techniques developed for correction of the CCL-deficient stifle have been reported, but none are able to restore the kinematics of an intact stifle [2]. In the past years, the use of *in vitro* models simulating weight bearing has gained popularity. Most *in vitro* studies analyzing kinematics of the canine stifle were made in 2D under low static loads. Gait implies a displacement of the load application at the hip from caudal to cranial, modifying the moments applied to the stifle. Such a motion is qualified as isotonic. To our knowledge, no testing device allows the simulation of this condition. Our goal was to use a validated experimental device simulating a quasi-dynamic model of the stance phase at trot of the canine hind limb under near physiologic conditions in the cranial cruciate ligament deficient stifle (CCLDS). Our hypotheses are as follows: 1) the device allows reliable measures with low intra-specimen and inter-specimen variability; 2) the kinematics generated by the device are representative of reported *in vivo* 3D kinematics in dogs with CCLDS [3]; 3) peak vertical forces generated by the loaded limbs in the device will be similar to those recorded in the literature for a walking dog during the stance phase [4].

METHODS

Six paired hind limbs were harvested from 3 adult large breed dogs euthanazied for reasons unrelated to this study. The dogs were similar in age, size and body weight (range, 29.5-31 kg). Clinical and radiographic stifle examinations were performed to exclude any pathology. The limbs were prepared and mounted on a previously validated experimental device. Each limb was submitted to vertical loading (9 kg) to the artificial hip joint. The gait was simulated with a computerized sequence using a linear actuator and a rotational motor inducing the artificial ankle's anterior-posterior motion and flexion-extension respectively. The stance phase of the gait at walk was simulated three times on each hind limb. Then, with the limbs still mounted in the device, the cranial cruciate ligament (CCL) was transected through a small medial arthrotomy which was closed using a simple continuous pattern. A positive drawer sign confirmed complete transection of the CCL. Kinematics of the tibia and femur was measured in the 2 situations (intact and CCLDS) with an optoelectronic system. Kinematics' curves were generated using Euler angles with the method of Grood and Suntay [5]. Vertical ground reaction forces were measured with a 2.5 kN axial/torsion force transducer. Validation consisted in evaluating intra and inter-specimen variability of the 3D kinematics' curves of the stifle. Amplitude of motion and peak ground reaction forces as well as the general shape of kinematics curves were also compared with *in vivo* curves described in the literature [3, 4]

RESULTS AND DISCUSSION

The comparison of the six average curves of motion collected on the tested stifles to those from *in vivo* trials reveals similar patterns [3]. Data recorded during *in vitro* simulations in CCLDS highlighted the following changes between intact and CCLDS: an increase in flexion (4^o), abduction (2^o), internal rotation (3^o), cranial translation (4mm), medial translation (1,5mm) and proximal displacement (3mm) of the tibia were recorded. These changes are compatible with to those reported in vivo [3].

However, the amplitude of changes is slightly greater on *in vivo* curves. Peak vertical forces measured in the device (138+/-2N) were also similar to *in vivo* trials reported in the literature [4].

CONCLUSIONS

Results show that the device generates reliable motion on a loaded limb which is representative of the *in vivo* 3D kinematics in CCLDS reported in the literature. This model could be used to evaluate the impact of surgical correction of CCLDS and compare different surgical techniques. It could also be used to determine which surgical procedures have the potential to re-establish normal stifle kinematics. The tools developed in this study might also lead to the design and evaluation of new surgical techniques. Finally, this model could be adapted and used with the human knee.

REFERENCES

1. Johnson JA et al. *Vet Comp Orthop Traumatol* 1994; **7**:56–697.
2. Brinker WO, et al. In: Brinker WO, et al, eds. *Handbook of small animal orthopedics and fracture treatment*. Philadelphia: WB Saunders, 1990:341
3. Korvick DO et al. *J Biomech* 1994. **27**: 77-874
4. Voss K et al. Vet Comp Orthop Traumatol 2007; **20**: 299–3045
5. Grood ES and W.J Suntay. *J Biomech Eng* 1983., **105**,136-144.

ACKNOWLEDGEMENTS

We would like to acknowledge the Natural Science and Engineering Council (NSERC), the Fonds Québécois de Recherche en Nature et Technologies (FQRNT), the Canadian Foundation for Innovation (CFI) and the Fonds en santé des animaux de compagnie (FSAC) for funding this study and Annie Levasseur for technical assistance.

JOINT MOMENT CONTRIBUTIONS TO SWING KNEE EXTENSION ACCELERATION DURING GAIT IN SUBJECTS WITH SPASTIC HEMIPLEGIC CEREBRAL PALSY

[1]Evan Goldberg, [2]Philip Requejo and [1]Eileen Fowler
[1]Center for Cerebral Palsy, Department of Orthopaedic Surgery, University of California, Los Angeles, Los Angeles, California, USA
[2]Rancho Los Amigos National Rehabilitation Center, Downey, California, USA
egoldberg@mednet.ucla.edu

INTRODUCTION

Inadequate peak knee extension during the swing phase of gait is a major deficit in patients with spastic cerebral palsy (CP), leading to a shorter stride length and decreased walking velocity. Our laboratory has shown that the ability to extend the knee during swing is dependent on the selective voluntary motor control (SVMC) of the subject. Subjects with good SVMC are more capable of extending the knee while flexing the hip during swing than subjects with poor SVMC [1]. The biomechanical mechanisms responsible for knee extension have not been thoroughly evaluated in CP.

Arnold et al. [2] used induced acceleration analysis (IAA) to examine muscle contributions to terminal-swing knee extension in nondisabled subjects and found that the swing limb vasti and hip extensors and stance limb hip extensors and abductors accelerate the swing knee toward extension. However, IAA results are dependent on body segment orientation; therefore, contributions to knee extension acceleration may differ in CP due to altered gait kinematics. The purpose of this study was to compare the contributions of lower extremity joint moments and gravity to swing phase knee extension acceleration in the hemiplegic and non-hemiplegic limbs in participants with spastic CP.

METHODS

Six participants with spastic hemiplegic CP were recruited for this study. Each participant was evaluated for his or her lower extremity SVMC using the Selective Voluntary Motor Control Assessment of the Lower Extremity tool (SCALE). A total score between 0 and 10 (0 = poor, 10 = normal) was given for each limb. Gait data were collected using an eight-camera system (Motion Analysis Corp.).

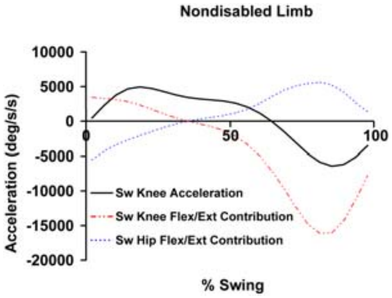

Figure 1: Swing hip and knee flexion/extension moment contributions to swing knee acceleration in an exemplar nondisabled subject.

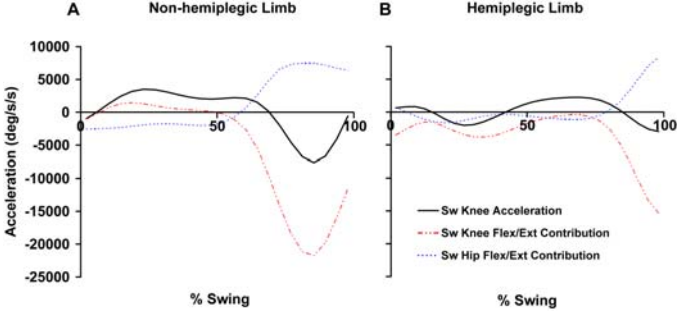

Figure 2: Swing hip and knee flexion/extension moment contributions to swing knee acceleration in a participant with CP for the A) non-hemiplegic limb and B) hemiplegic limb.

The most representative trial for each limb was selected. Kinematic and kinetic data were calculated from the experimental data. A biomechanical model described by Kepple et al. [3] was used. IAA was performed using the Induced Acceleration Analysis Module in Visual 3D (C-Motion, Inc.) to calculate the contributions of bilateral joint moments and gravity to swing knee acceleration [3]. The model was configured at each frame according to the experimental data. All joint moments and gravity were set to zero, and one joint moment (or gravity) was entered into the model at a time. The resulting knee acceleration of the swing limb was calculated for the input at each frame. The input moment was then set back to zero and all other joint moments and gravity were sequentially entered into the model. Joint moment and gravity contributions were averaged during the extension phase of swing, and contributions to swing knee acceleration in the hemiplegic and non-hemiplegic limbs were compared using paired t-tests.

RESULTS AND DISCUSSION

When comparing IAA results in the hemiplegic and non-hemiplegic limbs, the largest differences were found in the swing limb, specifically sagittal plane hip and knee moment contributions. In a typical nondisabled subject, the non-synergistic action of swing hip and knee sagittal plane moments is evident when assessing their contributions to swing knee acceleration (Fig. 1). Immediately following toe-off, a knee moment accelerates the knee toward extension while a hip moment accelerates the knee toward flexion. Approximately halfway through the extension phase of swing, the actions of these moments reverse, and the knee moment accelerates the knee toward flexion while the hip moment accelerates the knee toward extension.

In the non-hemiplegic limb of an exemplar participant (SCALE = 8), contributions to swing knee acceleration from the swing hip and knee sagittal plane moments are similar in their general pattern to that of a nondisabled subject (Fig. 2A). In the hemiplegic limb (SCALE = 4), both the knee and hip moments accelerate the knee into flexion for most of the extension phase, which indicates a synergy pattern, resulting in a substantially smaller swing knee acceleration compared to the non-hemiplegic limb (Fig. 2B).

For all participants, a significant difference was found between the negative contributions to swing knee extension from the swing limb joint moments of the hemiplegic limb and the non-hemiplegic limb with the hemiplegic limb having a greater magnitude of acceleration (Table 1). Significant differences were also found between the hemiplegic and non-hemiplegic limbs for the average knee acceleration, and differences approached significance for the average stance limb ankle joint moment contributions and average swing limb knee joint moment contributions (Table 1). On the stance limb, strategies varied by subject and limb; however, total stance limb contributions only differed by ~2% between limbs. No significant difference was found between limbs (Table 1).

CONCLUSIONS

While previous studies suggest that inadequate terminal-swing knee extension in subjects with CP may be caused by muscle weakness [2], our results do not support this concept. A greater contribution by the non-hemiplegic limb during stance to swing phase hemiplegic knee acceleration was not found. These stance phase contributions were similar for both limbs. In contrast, a significant difference was found between negative (or flexor) contributions from the swing limb of the hemiplegic and non-hemiplegic limbs. A greater average flexor acceleration was provided by the hemiplegic limb. These excessive negative contributions may be caused by impaired SVMC and/or spasticity. Treating the spasticity of the swing limb may improve swing knee extension, depending on SVMC ability [1]; however, strengthening specific muscle groups alone (e.g., the hip muscles) may not improve terminal knee extension in CP.

REFERENCES

1. Fowler EF and Goldberg EJ. *Gait Post* **29**, 102-107, 2009.
2. Arnold AS, et al. *J Biomech* **40,** 3314-3324, 2007.
3. Kepple TM, et al. *Gait Post* **6**, 1-8, 1997.

Table 1

	Non-hemiplegic	Hemiplegic	Mean Difference	95% Confidence Interval
Average Swing Knee Acceleration (in deg/s^2)	2226 ± 823	1471 ± 954	756	157 to 1355*
Average Contribution from:				
Gravity	336 ± 369	170 ± 246	166	-142 to 475
Stance Muscles	2183 ± 628	2219 ± 675	-37	-267 to 194
Stance Hip	809 ± 508	449 ± 294	360	-133 to 852
Stance Knee	70 ± 559	161 ± 300	-91	-900 to 717
Stance Ankle	1304 ± 491	1609 ± 566	-305	-661 to 51**
Swing Muscles	-1384 ± 658	-2147 ± 637	763	355 to 1170*
Swing Hip	-1425 ± 342	-997 ± 825	-428	-1579 to 723
Swing Knee	224 ± 813	-789 ± 990	1013	-264 to 2290**
Swing Ankle	-184 ± 201	-361 ± 445	177	-94 to 448

*indicates $p < 0.05$, **indicates $p < 0.10$, positive indicates extension accelerations (negative = flexion)

Postural feedback scaling describes the postural abnormality of Parkinsonian patients

[1]Seyoung Kim, [2]Fay B. Horak, [2]Patricia Carlson-Kuhta and [1]Sukyung Park
[1]Department of Mechanical Engineering, KAIST, Daejeon, Korea
[2]Neurological Sciences Institute, Oregon Health & Science University, Portland, OR, USA
email: sukyungp@kaist.ac.kr, web: http://biomt.kaist.ac.kr

INTRODUCTION

We investigated whether the postural responses of young subjects, elderly subjects, and subjects with Parkinson's disease (PD) can be described as a continuous feedback control system, and whether the balance impairment of the subjects with PD can be described as abnormal scaling of postural feedback gain. Although various forms of univariate analysis methods have been used to assess postural control of the elderly and patients with PD, results are not consistent. We hypothesize that the balance impairment of subjects with PD can be quantified as abnormal scaling of postural feedback gain with increases in perturbation magnitude. Our results show that multivariate, linear feedback model simulations of postural responses to a range of surface perturbations are consistent with continuous feedback control and that postural kinematic strategy of subjects with PD could be explained by abnormal hip and ankle gains and inflexible selection of feedback gain.

METHODS

Seven healthy young (mean age 24±3 yrs), 7 healthy elderly (63±7 yrs) subjects, and 7 age-matched patients with PD (64±9 yrs) participated. The healthy subjects reported no history of balance disorder. All PD subjects have medication (on levadopa) prior to the test and were evaluated to be moderate (23.8±10.2) Parkinsonism according to the Total Motor Score of the Unified Parkinson Disease Rating Scale (UPDRS).

Seven subjects in each group experienced backward perturbations with 7 different backward translation magnitudes ranging from 3~15 cm with a constant duration of 275msec. The magnitude of perturbation was designed to induce significant postural strategy change from ankle to hip strategy [1,2]. Subjects were instructed to stand upright with their arms crossed over their chests, and to recover to their initial upright posture in response to the perturbation without stepping or lifting their heels if possible.

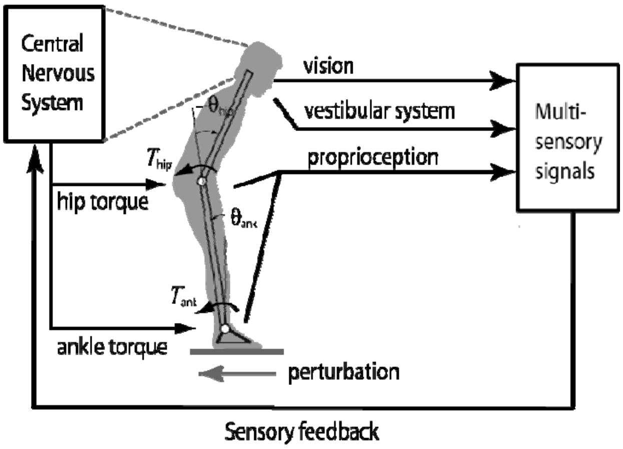

Figure 1: Schematics of postural feedback control model by the central nervous system (CNS). Sensory information of body postural coordination are measured by vision, vestibular organ and muscle spindles, and then sent to the CNS to be processed. Based on the estimate of body kinematics, appropriate control plans are selected and then motor commands are produced as joint torques.

Postural responses were quantified with ground reaction forces and joint kinematics. A full-state, 2-segment feedback model was used to quantify how the nervous system generates compensatory joint torques (Figure 1). Feedback control gain is written as a form of coefficient that relates joint kinematics and joint torques as follows,

$$\begin{bmatrix} T_{ank} \\ T_{hip} \end{bmatrix} = \underbrace{\begin{bmatrix} k_{11} & k_{12} & k_{13} & k_{14} \\ k_{21} & k_{22} & k_{23} & k_{24} \end{bmatrix}}_{\mathbf{K}} \cdot \begin{bmatrix} \theta_{ank} \\ \theta_{hip} \\ \omega_{ank} \\ \omega_{hip} \end{bmatrix}$$

where T_{ank}, T_{hip} are ankle joint and hip joint torque, $\boldsymbol{K}$ is a 2 by 4 feedback gain matrix of multiple gain components, θ_{ank}, θ_{hip} are ankle and hip joint angle, and ω_{ank}, ω_{hip} are ankle and hip angular velocity, respectively. Multiple gains represent that the coupled contribution of other joint kinematics to generate a specific joint torque. For convenience, we defined ‘ankle gain’ and ‘hip gain’ as the gain components that correspond to an ankle joint angle feedback to an ankle joint torque (k_{11}), and hip joint angle feedback to the hip joint torque (k_{22}), respectively. Feedback control gain was obtained from an optimization that minimizes the fitting error between the data and the model simulation.

RESULTS AND DISCUSSION

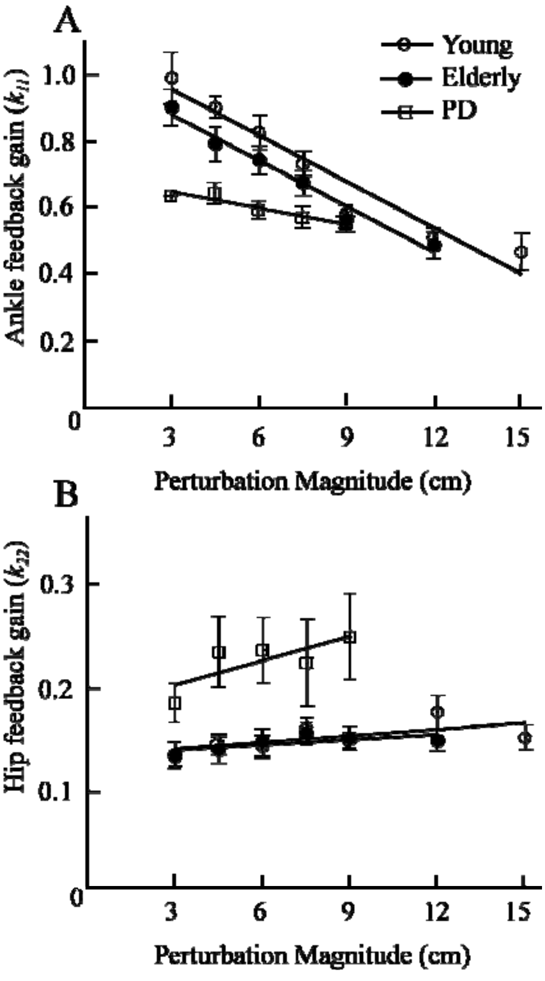

Figure 2: Averaged gain parameters that correspond to (A) ankle angle feedback to ankle torque and (B) hip angle feedback to hip torque of three subject groups.

All three subject groups showed gradual scaling of feedback gains as a function of perturbation magnitudes (Figure 2), and the scaling started even before the maximum allowable ankle torque was reached. This implies that the postural control can be interpreted as a feedback process that takes into account body dynamics and biomechanical constraints [2].

While the young and elderly groups showed similar gain parameter distributions across translation magnitudes, PD subjects significantly larger hip joint angle feedback gains (k_{12}, k_{22}), than young or age-matched controls, leading to stiffer hip joints so that overall postural sway resembles an inverted pendulum and displays significantly smaller hip joint motion. Therefore, unusually small postural responses of the PD subjects can be ascribed to larger than normal hip joint angle feedback gain, while the early violation of the flat-foot constraint could be accounted for by inadequate ankle gain scaling.

The current, postural feedback gain scaling model provides a quantitative understanding of neural control of posture. Unlike conventional gain parameters which usually describe how the postural response magnitude changes across perturbation magnitudes [1], the feedback gain of the current model describes the long-loop gain of the automatic postural control system by the CNS. While the slope of the change of postural responses describes the ability of the CNS to generate the initial motor command trajectory, the feedback gain quantifies how the nervous system makes use of sensory feedback to generate compensatory motor commands [1,2]. In conclusion, our feedback control gain model quantitatively described the postural abnormality of the patients with PD as reduced ability to modify postural feedback gain with changes in perturbation magnitude.

REFERENCES

1. Horak FB, et al. *J Neurophysiol*. **75**, 2380, 1996.
2. Park S, et al. *Exp Brain Res*. **154**, 417-27, 2004.

ACKNOWLEDGEMENTS

This work has been supported by a Basic Research Fund of the Korea Institute of Machinery and Materials, the second stage of the Brain Korea 21 Project, and NIH grants AG06457 from NIA.

Mechanical properties of orbital fat and its encapsulating connective tissue

[1] Kinon Chen and [1]James D. Weiland
[1]Department of Ophthalmology, University of Southern California, Los Angeles, CA
email:kinonche@usc.edu, JWeiland@doheny.org

INTRODUCTION

Orbital fat (OF) and its encapsulating connective tissue (CT) (abbr. OFCT) have recently been found to play a significant role in orbital biomechanics. Some studies have reported that OFCT prevent anterior globe displacement in trauma, which provide an important mechanism of eye stability, and the injury mechanism of trauma was caused principally by the dynamics of OFCT relating to both the rotation and the increased intraocular pressure of the globe [1,2]. Other studies have suggested that OFCT play an important role in supporting eye movements. It was found that OFCT displace and deform proportionally in the same direction at significant level as the extraocular muscles and optic nerve during the eye movements, and this action helps in stabilizing the muscle paths [3,4,5].

The aim of the present study is to characterize the mechanical properties of OFCT.

METHODS

A total of 20 pig eyes and 20 human eyes will be obtained to complete this study. We have performed experiments on 8 pig eyes so far. The pig eyes were obtained from a local slaughterhouse within 4 hours of death of the animals, and the human eyes will be obtained from an eye bank within 48 hours of death of the donors.

One OFCT sample was obtained from each eye. The sample was dissected in either superior-inferior or nasal-temporal direction in the posterior region adjacent to the optic nerve head. Samples were consistently 1.5 mm in width by using a 1.5-mm-wide customized twin-blade cutting tool in the dissection. Dissected sample was placed in a custom clamp instrument that predefined the sample length to be 1.0 mm. Thickness of each sample was measured under a microscope. Though it would be ideal to measure the individual properties of the OF and CT. Separating them without damaging the integrity is impossible.

The clamp instrument with the secured sample was transported to our mechanical testing system (Bose® ElectroForce® 3100, Eden Prairie, Minnesota) and was submerged in a 37 ± 1 ^{o}C saline chamber. Displacement was applied to pull the sample linearly at 1 mm/sec by the machine. The reaction force was recorded during the testing.

Engineering stress was calculated from dividing the

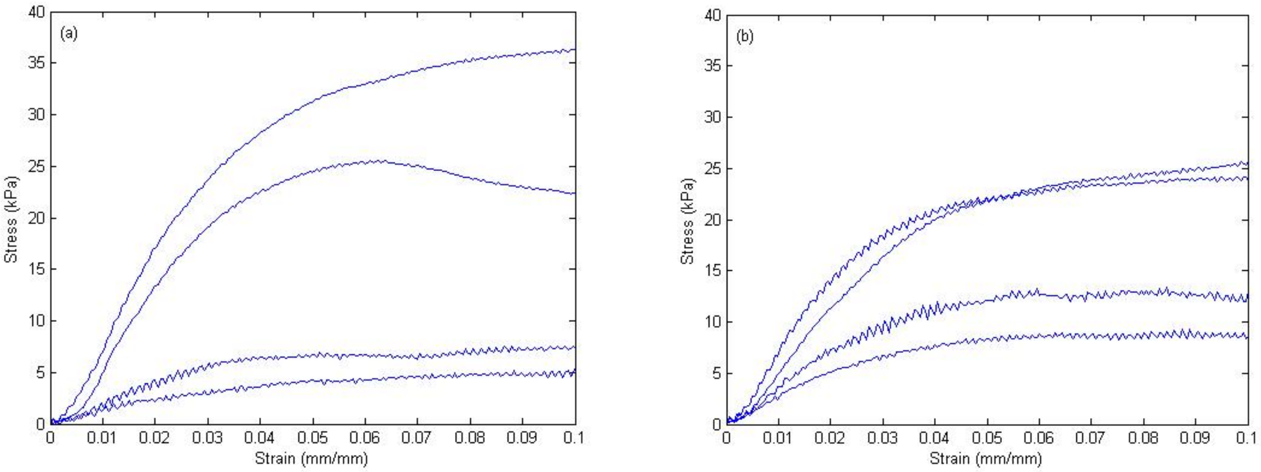

Figure 1: Stress-strain relationship of pig orbital fat and its encapsulating connective tissue from uniaxial experiment. Samples in (a) superior-inferior and (b) nasal-temporal direction (n = 4).

reaction force by the initial area. Strain was obtained from dividing the applied displacement by the initial length. The stress-strain relationship was approximated linear before deformation reached plasticity (Figure 1), and this region was defined to be the elastic region of the samples. The elastic stress-strain relationship was best-fitted into a linear curve.

Statistical analysis using the two-sided rank sum test was performed to evaluate the difference of the yield stress, yield strain, and Young's modulus between the samples in superior-inferior and nasal-temporal direction. The significance level was set to be 5 %. All data processing was done in MATLAB®.

RESULTS AND DISCUSSION

The yield stress, yield strain, and Young's modulus of the samples are reported in Table 1. Although the nasal-temporal samples in average had an 86 % and 83 % higher yield stress and Young's modulus than the superior-inferior samples had, our statistical analysis found that there was no significant difference between the samples in these directions.

The samples in average had a 1.5 % yield strain (Table 1), which is relatively small in soft tissues in general. When the samples were stretched beyond the elastic region, they did not fail completely. After the elastic region, the stress-strain relationship showed a long plateau region, which indicates that OFCT had a long plastic deformation characteristic (Figure 1). Future simulation study is required to understand how such mechanical characteristic may play a role in orbital biomechanics.

This is the first time the yield stress, yield strain, and Young's modulus of OFCT are reported in the literature. We are continuing this study on both pig and human eyes, and we believe that these data are valuable to help us to understand the mechanical properties of OFCT and also to build a realistic computer model of the eye in the future.

REFERENCES

1. Cirovic S, et al. *Br J Ophthalmol* **90**, 778-783, 2006.
2. Cirovic S, et al. *Comput Methods Biomech Biomed Engin* **8**, 1-6, 2005.
3. Schutte S, et al. *Vision Res* **46**, 1724-1731, 2006.
4. Botha CP, *Visualization in Medicine and Life Sciences*, Springer-Verlag Berlin Heidelberg, New York, pp. 221-233, 2007.
5. Schoemaker I, et al. *Invest Ophthalmol Vis Sci* **47**, 4819-4826, 2006.

ACKNOWLEDGEMENTS

The authors would like to thank the financial support from the Department of Energy's Office of Science (grant no. DE-FC02-04ER63735), W.M. Keck Foundation, and Clarence and Estelle Albaugh Trust.

Table 1: Mean and standard deviation of the yield stress, yield strain, and Young's modulus of the pig orbital fat and its encapsulating connective tissue samples in superior-inferior and nasal-temporal direction (n = 4).

	Superior-Inferior	**Nasal-Temporal**
Yield stress (kPa)	2.9 ± 2.5	5.4 ± 2.5
Yield strain (mm/mm)	0.015 ± 0.001	0.015 ± 0.001
Young's modulus (kPa)	302.4 ± 258.5	552.3 ± 266.7

COMPARISON OF TESTING PROTOCOLS OF ANKLE SPRAIN MECHANISM: INVERSION DROP TEST AND LANDING ON AN INVERTED SURFACE

Qingjian Chen, Songning Zhang , Micheal Wortley, Clare Milner and Divia Bhaskaran
Biomechanics/Sports Medicine Lab, The University of Tennessee, Knoxville, TN, USA
email: qchen4@utk.edu, web: web.utk.edu/~Esals/resources/biomechanics_laboratory.html

INTRODUCTION

The ankle is the most injured joint in sports and accounts for 10 - 30% of all sports injuries [1]. Of those ankle injuries, a lateral ankle sprain is the most common. A majority of studies has used an inversion drop platform to induce ankle inversion movement to study lateral ankle sprains. However, this testing method only induces the inversion movement and not the plantarflexion movement or sufficient vertical loading commonly seen in an ankle sprain suffered on the field. A very limited number of studies employed drop landing in their experimental protocol to study the lateral ankle sprain mechanism [2,3]. Therefore, the objective of the study was to investigate kinematics of two ankle brace testing protocols: drop landing on an inverted surface and inversion drop test with and without an ankle brace. The hypothesis was that drop landing on an inverted surface would better replicate the movement associated with ankle sprain.

METHODS

Eleven healthy subjects (6 females and 5 males, age: 24.6 ± 3.5 years, height: 1.70 ± 0.10 m, mass: 65.6 ± 14.9 kg) with no current ankle injury and no history of major lower extremity injuries participated in the study. A seven-camera motion analysis system (240 Hz, Vicon, UK) was used to collect 3D bilateral lower extremity kinematic data. Two force platforms (1200 Hz, AMTI, USA) were used to measure the ground reaction forces (GRF) simultaneously with the 3D kinematics. An inverted surface (Figure 1a) with a 25° inversion slope was mounted on top of the right force platform along with a flat surface (Figure 1a) mounted on top of the left force platform during drop landing conditions. A customized inversion drop trapdoor platform [91.5 cm (L) x 46 cm (W) x 20 cm (H)] (Figure 1b) was used in an inversion drop test to attempt to invert the ankle to 25° during testing conditions. The subjects performed five trials each of landing on the inverted surface without (LS_NB) and with (LS_BR) a semi-rigid ankle brace (Element, DeRoyal Industries, Inc.) and inversion drop without (ID_NB) and with (ID_BR) the brace.

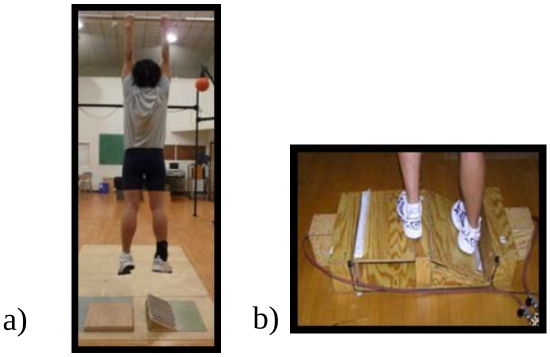

Figure 1. Landing on a) inverted landing surface and inversion drop on b) inversion drop platform.

3D kinematic variables were calculated using Visual 3D (C-Motion Inc.) for the right side lower extremity. Selected variables were analyzed using 2 × 2 (brace × movement) repeated measures ANOVAs ($p < 0.05$).

RESULTS AND DISCUSSION

The results of the two testing protocols showed that the time to the peak inversion angle (TMax_Inv) for the inverted surface landing occurred significantly sooner than in the inversion drop on the trapdoor (Table 1). Significantly higher contact and maximum inversion (Max_Inv_V) velocity and less time to maximum inversion velocity (TMax_Inv_V) were also found in the inverted surface landing compared to the inversion drop test. No significant difference was found for the contact plantarflexion angle between the two testing protocols, however the inverted surface landing produced significant higher dorsiflexion range of motion (ROM_DF) and maximum dorsiflexion velocity in the drop landing compared the inversion drop. These results implied that the landing protocol introduced greater inversion loading than the inversion drop.

For the brace effect, the results showed that there was a significant brace x movement interaction for peak inversion angle (Max_Inv) showing a greater inversion angle in inversion drop without brace compared to the landing conditions (Table 1). The dorsiflexion ROM significantly decreased while wearing the ankle brace in both movement conditions. The brace reduced the contact and peak inversion velocities and increased TMax_Inv_V during the inversion drop. However the brace increased the contact and peak inversion velocities and reduced TMax_Inv_V in landing on the inverted surface compared to the inversion drop. These results demonstrated that the ankle brace was more effective in reducing inversion loading in the inversion drop than in the landing protocol.

CONCLUSIONS

The results indicate that the inverted surface landing provides greater inversion velocity and loading and therefore simulates the ankle sprain mechanism better than the inversion drop protocol. The effectiveness of ankle brace in reducing inversion velocity and loading is diminished in the inversion landing protocol but it provides greater restriction in sagittal plane movement than the inversion drop protocol.

REFERENCES

1. Fong, D. T., et al. (2007). *Sports Med*, **37**, 73-94
2. Hodgson, B., et al. (2005). *Journal of Sport Rehabilitation*, **14**, 301-312.
3. Venesky, K., et al. (2006). *J Athl Train*, **41**, 239-244.

ACKNOWLEDGEMENTS

Ankle braces were provided by DeRoyal Industries, Inc.

Table 1. Average frontal plane and sagittal plane ankle kinematic variables: mean ± STD.

Cond	Max_Inv* (deg)	TMax_Inv (s)	ROM_DF (deg)	Cont_V (deg/s)	Max_Inv_V * (deg/s)	TMax_Inv_V * (s)
LS_NB	25.2±3.9 [1]	0.060±0.011 [2]	35.3±5.1 [1,2]	163.9±128.0 [1,2]	273.8±156.0 [2]	0.027±0.009 [1,2]
LS_BR	22.6±5.2	0.055±0.010	28.1±6.2	256.7±119.7	373.1±121.1	0.021±0.007
ID_NB	27.7±6.1	0.239±0.046	16.7±5.2	-26.8±78.6	166.5±67.9	0.173±0.060
ID_BR	22.0±4.8	0.241±0.050	6.2±5.2	-17.2±50.6	69.1±59.7	0.245±0.085

[1]: significantly different between NB and BR in inverted surface and inversion drop conditions ($p<0.05$)
[2]: significantly different between inverted surface landing and inversion drop conditions ($p<0.05$)
[*]: significant brace × movement interaction in the inverted surface landing and inversion drop ($p<0.05$)

THE INFLUENCE OF TURNING STRATEGY ON DYNAMIC POSTURAL STABILITY IN PERSONS WITH EARLY STAGE PARKINSON'S DISEASE

[1]Jooeun Song, [1]Abbie Ferris, [1]Susan Sigward, [1, 2]Beth Fisher, [1, 2]Giselle Petzinger, [1]Megan Parent, and [1,2]George J. Salem
Jacquelin Perry Musculoskeletal Biomechanics Research Laboratory
[1]Division of Biokinesiology & Physical Therapy
[2]Department of Neurology, Keck School of Medicine
University of Southern California, Los Angeles, CA, USA
email:jooeunso@usc.edu, web: www.usc.edu/go/mbrl

INTRODUCTION

Two main strategies for turning have been identified in healthy young adults: the step turn and the spin turn. [1,2] Adaptations during turning are influenced by both the phase of turning and the turning strategy.

Persons with *early stage* Parkinson's disease (EPD) typically demonstrate minimal levels of functional impairment and disability, yet often report difficulty with turning tasks. [3,4] Difficulty turning is thought to be associated with 1) impaired postural control and 2) the inability to adjust the type of turning strategy in response to the demands of the task. To date, most of the studies evaluating turning in persons with PD have focused on those in advanced stages of the disease; little is known in regard to persons with EPD. Therefore, the purpose of this study was to: 1) compare turning preferences between persons with EPD and healthy control (HC) participants, and 2) determine the influence of EPD on dynamic postural stability during turning.

METHODS

Fifteen persons with EPD, diagnosed within 3 yrs, and 10 HC subjects participated. All EPD participants were tested in the "on" medication state (i.e., fully responding to their PD medications). At the time of testing, none of the participants exhibited dyskinesia, dystonia, or other signs of involuntary movement.

Three-dimensional kinematics (8 camera, VICON Motion System, 60 Hz) and segment inertial parameters were used to calculate the whole body center of mass (COM). Center of pressure (COP) was determined from force plate measures during single and double limb stance (AMTI force plate 1.2m x 1.2m, 1560Hz).

Participants walked 4 meters to a designated location and turned to the right at a 90° angle. Ten trials were collected. An equal number of trials were completed starting with the right and left foot to control for the influence of the start foot.

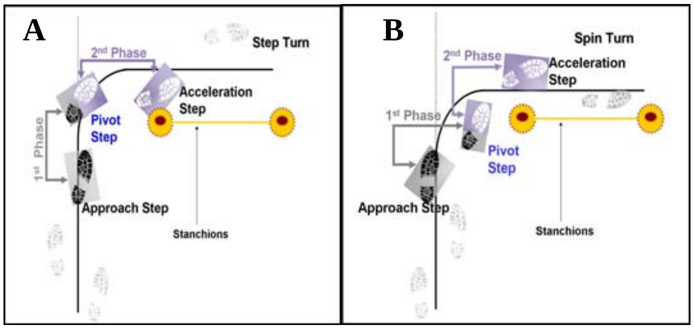

Figure 1. Schematic representation of steps during the step turn (A) and the spin turn (B).
1st phase: from approach step to pivot step; 2nd phase: from pivot step to acceleration step

The turn includes three consecutive steps: the *approach* step, the *turn* step, and the *acceleration* step. Turn strategies were defined as either step, when the change in direction was to the *opposite* side of the pivot foot (Figure 1A) or spin, when the change in direction was to the *same* side of the pivot foot (Figure 1B). [1,2] The number of step and spin turns were recorded for each participant.

Dynamic postural stability was quantified during three successful trials, using the method previously described by Hof [5], as the distance between the COP and extrapolated COM (eCOM). The eCOM was calculated using COM position and velocity. Greater postural stability was indicated by shorter COP-eCOM distances in the direction of initial forward progression (DIFP) and the direction of the turn (DOT). Two phases of turning were considered; Phase 1 was defined from the heel strike of the approach step to the heel strike of the pivot step. Phase 2 was defined from the heel strike of the pivot step to the heel strike of the acceleration step.

A Mann-Whitney U test was used to determine the difference in the ratio of the number of step versus spin turns between groups. Independent t-tests were used to determine the difference in peak dynamic postural stability in the DIFP and DOT between groups for each phase of turning ($p<0.05$).

RESULTS

The step/spin ratio was significantly greater in persons with EPD indicating that they used the step turn strategy more frequently than the spin turn when compared to HC subjects. All subsequent analyses were performed on step turns.

In the first phase of turning, approach to pivot step, there was no difference between groups in the DIFP; whereas, persons with EPD demonstrated a significantly shorter COP-eCOM distance in the DOT compared to HC participants (Figure 2A). In the second phase of turning, pivot to acceleration step, significantly shorter distances in both DIFP and DOT were seen in persons with EPD when compared to HC participants (Figure 2B).

DISCUSSION

Persons with EPD preferred the step turn strategy 1.4 times more often than the spin turn strategy during turning.

Analysis of the COP-eCOM distances indicated that persons with EPD demonstrated increased postural stability during step turning. These findings suggest that persons with EPD may preferentially adopt a more cautious postural-control strategy, in an attempt to ensure safety.

CONCLUSIONS

Persons with EPD demonstrated greater postural control during the step turn compared to HC participants. This strategy may be an effort to maintain balance and prevent falls.

REFERENCES

1. Taylor MJD, et al. *Hum Mov Sci* **24**, 558-73, 2005.
2. Hase K, Stein RB. *J Neurophysiol* **81**, 2914-22, 1999.
3. Bloem BR, et al. *J Neurol* ***248***, 950-58, 2001.
4. Stack EL, et al. *Parkinsonism Relat Disord* **12**, 87-92, 2006.
5. Hof AL, et al. *J Biomech* **38**, 1-8, 2005.

ACKNOWLEDGEMENTS

Supported by the Magistro Family Foundation Research Grant

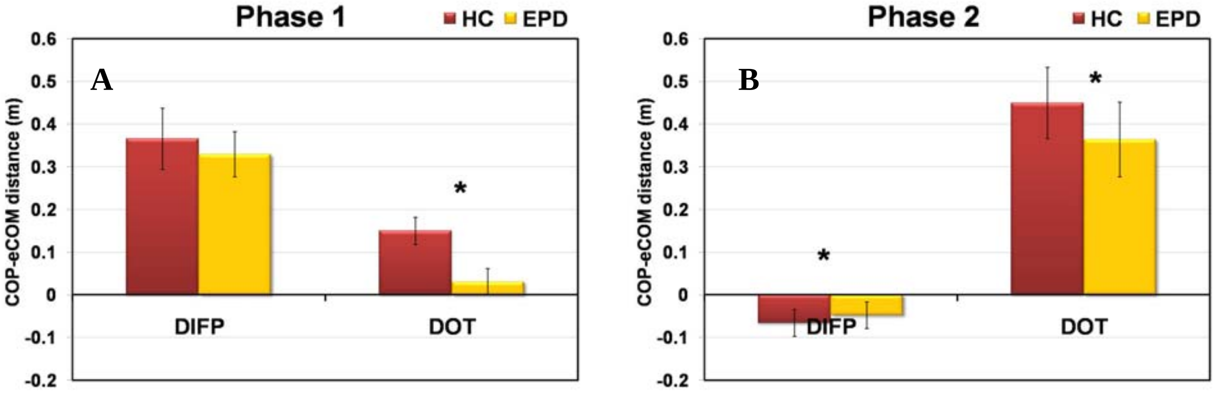

Figure 2. The COP-eCOM distances between groups in the 1st Phase (A) and 2nd Phase (B) *****$p<0.05$

A COMPARISON OF PRODISC AND CHARITE TDR DESIGNS UNDER ALTERNATIVE WEAR TESTING STANDARDS

+Goreham-Voss, C M; Brown, T D
University of Iowa Orthopaedic Biomechanics Research Laboratory.
2172 Westlawn, University of Iowa, Iowa City, IA 52242.
curtis-voss@uiowa.edu

INTRODUCTION

Total disc replacements (TDRs) are an alternative treatment for degenerative disc disease which, unlike fusion, preserve mobility of the functional spinal unit. Polyethylene wear in TDRs has not been fully characterized, due to their relatively recent introduction to US markets and to the difficulty in determining and replicating their motion in vivo. However, given the younger patients typically indicated for TDRs, and the dire complications associated with any sort of revision, understanding the long-term wear characteristics of TDRs is of very high importance.

In this study, a recent numerical wear model [1] was used to characterize the wear of the first two TDRs to receive FDA approval in the US: the ProDisc (Synthes Spine), and the Charite (Depuy Spine). Each of the implant designs was tested under three consensus wear testing standards for lumbar TDRs: (1) ASTM F2423, (2) ISO 18192, and (3) ISO 18192 alternative loading conditions (listed in Appendix D.3 of the standard).

METHODS

Finite element models of the ProDisc and Charite TDRs were created in Abaqus (Figure 1). For both models, endplates were modeled as rigid analytical surfaces, while the (insert) polyethylene cores were modeled with linear brick elements having an elastic modulus of 1,400 MPa and a Poisson's ratio of 0.3. For the ProDisc, the inferior surface of the polyethylene insert was assumed to be rigid. The endplates were each controlled through reference points located at the centers of curvature of the contacting surfaces. Rotational inputs were applied to the superior endplate (which was fixed in translation), while the axial load was applied to the inferior endplate of the Charite and to the insert of the Prodisc (which were free to translate).

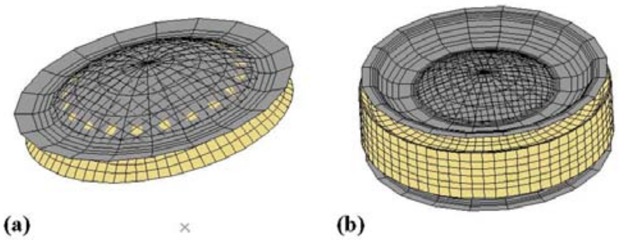

Figure 1. Finite element model of the (a) ProDisc, and (b) Charite TDRs.

Wear was incorporated through Abaqus' adaptive meshing algorithm and the UMESHMOTION subroutine. At the end of each motion cycle, UMESHMOTION was called for each node on the polyethylene contact surfaces. The history of the node's contact pressure (σ) and sliding distance (d) were used to calculate the linear wear depth (w) according to the Archard formulation:

$$w = k(CS) * \sigma * d \qquad (1)$$

where k(CS) is the wear coefficient as a function of cross-shear ratio (CS). For this study, it was assumed that polymer chains align preferentially in the direction of the dominant frictional work, thereby establishing a principal molecular orientation (PMO). In the wear algorithm, this was implemented by assigning a PMO to each node, for each motion cycle, in the direction that would minimize the frictional work performed perpendicular to that PMO. With the PMO thus established, CS was defined (as per Kang et al. [2]) as the fraction of the total frictional work that was performed in a direction perpendicular to the PMO. The wear coefficient curve was also based on that described by Kang et al., scaled to recover wear rates similar to those found by Rawlinson et al. [3] for the Prodisc TDR. At the end of each motion cycle, the wear depth for each node was scaled by 250,000 cycles, and the surface nodes on the polyethylene cores were updated accordingly.

Abaqus' adaptive meshing adjusted interior nodes to preserve a high quality mesh. Forty such update intervals were performed, resulting in a 10 million cycle simulation.

The ASTM and ISO standards were implemented as recommended, with the exception of not including the 10 degree incline recommended by the ISO standard. The ASTM inputs were applied concurrently (the standard also allows for applying each motion separately), with the flexion-extension rotation 90 degrees out of phase from the axial rotation and lateral bending, resulting in nearly circular motion loci. The ISO standard results in elliptical motion loci, and the alternate ISO loading results in a 'fish-shaped' motion loci with two discrete stopping points during the motion [4].

RESULTS

Figure 2 shows the gravimetric wear and wear rate for each of the six test cases. The computed wear for the Prodisc under ASTM loading becomes invalid after 6 million cycles, as the material loss was so severe that impingement would have occurred if the full endplate geometry had been included in the model.

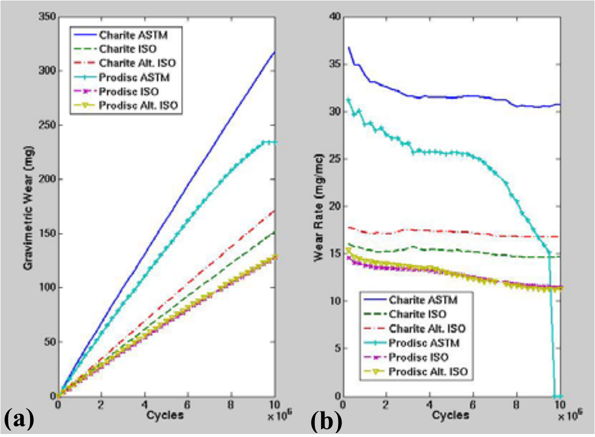

Figure 2. (a) Wear, and (b) wear rate for two TDRs under 3 loading conditions.

The significant differences seen in total wear are also reflected in the linear wear depth distributions seen in Figure 3. The ASTM standard clearly results in far more wear than the ISO variants. Also of note is the strong imbalance of wear between the superior and inferior surfaces of the Charite polyethylene core.

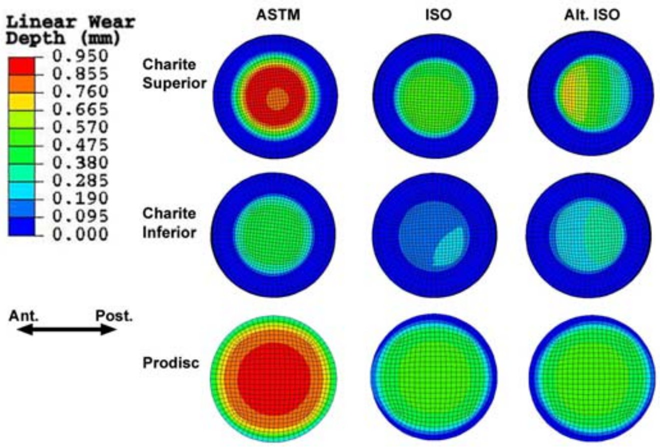

Figure 3. Linear wear depth distributions.

DISCUSSION

The results presented here demonstrate the differences in wear behavior between different implant designs and wear standards. The superior surface of the Charite appears to behave very similarly to the Prodisc. Although most of the articulation is taken up in the superior surface, over time there is increasing relative motion of the inferior surfaces, causing the total wear of the Charite to be 20% to 30% higher than the Prodisc under the same input. The significantly increased wear of both implant designs under the ASTM standard is likely due to the increased range of motion: 15 degree range in F/E for ASTM versus 9 degrees for ISO. In addition, the difference between the constant 1,200 N load prescribed by ASTM and the sinusoidal 600N-2000N load prescribed by ISO may contribute to the differing wear response. There is clearly a need for additional testing to determine which wear standards will most accurately reflect in vivo conditions, as well as how different implant designs will influence wear testing results.

REFERENCES

1. Goreham-Voss, CM & Brown, TD NACOB. Ann Arbor, MI, Abstract 72, 2008
2. Kang, L et al. *J Biomech* **41**, 340-6, 2008.
3. Rawlinson, JJ et al. *J Neurosurg Spine* **24,** 165-73, 2007.
4. Goreham-Voss, CM et al. ORS, Las Vegas, NV, Abstract 2357, 2009.

ACKNOWLEDGEMENTS

This study was supported by a grant from the NIH (AR052653).

DIFFERENCES IN WEAR RESULTING FROM PERTURBATIONS OF THE ISO STANDARD FOR TOTAL DISC REPLACEMENT

+Goreham-Voss, C M; Brown, T D
University of Iowa Orthopaedic Biomechanics Research Laboratory.
2172 Westlawn, University of Iowa, Iowa City, IA 52242.
curtis-voss@uiowa.edu

INTRODUCTION

Polyethylene wear in total disc replacements (TDRs) is an ongoing clinical, design, and research concern. Consensus standards for wear testing allow correlation of testing results across different laboratories and across the vastly different contemporary implant designs. A necessary early step for these standards, given the difficulty of determining the in vivo kinematics of TDRs and the variability inherent in any such measures, is to determine the sensitivity of an implant's wear to perturbations of the proposed testing parameters. Numerical wear models provide an ideal vehicle for such a purpose due to their quick set-up and short runtimes. In this study, a recent numerical wear model incorporating cross-shear [1] was used to explore perturbations of the ISO standard for TDR wear (18192-1), for the case of the ProDisc implant.

METHODS

A finite element model of the Prodisc TDR was created in Abaqus CAE (Figure 1a). The superior endplate was modeled as a rigid analytical surface, while the polyethylene insert was modeled with linear brick elements having an elastic modulus of 1,400 MPa and a Poisson's ratio of 0.3. The inferior surface of the polyethylene insert was assumed to be rigid. The superior endplate and the rigid surface of the insert were each controlled through reference points located at the center of curvature of the contacting surfaces. Rotational inputs were applied to the insert (which was fixed in translation), while the axial load was applied to the superior endplate (which was free to translate). Contact was defined between the superior endplate and the insert, with a coefficient of friction of 0.08.

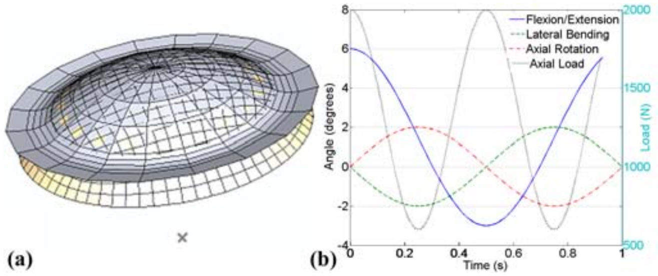

Figure 1. (a) Finite element model, and (b) baseline input waveforms for ISO testing of the Prodisc TDR.

Wear was incorporated through Abaqus' adaptive meshing algorithm and the UMESHMOTION subroutine. At the end of each motion cycle, UMESHMOTION was called for each node on the polyethylene contact surface. The history of the node's contact pressure (σ) and sliding distance (d) were used to calculate the linear wear depth (w) according to the Archard formulation:

$$w = k(CS) * \sigma * d \qquad (1)$$

where k(CS) is the wear coefficient as a function of cross-shear ratio (CS). For this study, it was assumed that polymer chains align preferentially in the direction of the dominant frictional work, thereby establishing a principal molecular orientation (PMO). In the wear algorithm, this was implemented by assigning a PMO to each node, for each motion cycle, in the direction that would minimize the frictional work performed perpendicular to that PMO. With the PMO thus established, CS was defined (as per Kang et al. [2]) as the fraction of the total frictional work that was performed in a direction perpendicular to the PMO. The wear coefficient curve was also based on that described by Kang et al., scaled to recover wear rates similar to those found by Rawlinson et al. [3] for the Prodisc TDR. At the end of each motion cycle, the wear depth for each node was scaled by 250,000 cycles, and the surface nodes on the polyethylene core were updated accordingly. Abaqus' adaptive meshing adjusted interior nodes to preserve a high quality mesh. Forty such update intervals were performed, resulting in a 10 million cycle simulation.

The input recommended by ISO standard 18192-1 for lumbar implants was applied as a baseline case (Figure 1b). Following this, 13 perturbations of the recommended input parameters were tested: the amplitude of each rotational input was halved (Low), doubled (High), and set to zero (Null); the axial load amplitude was halved (Low) and doubled, with a 110 N offset in the mean to prevent complete unloading (High); and the axial load waveform was adjusted to dwell approximately 3 times longer in the lower range than in the higher (Low) and vice versa (High).

RESULTS

Figure 2 shows the wear distribution, volumetric wear and wear rate for the baseline case. The general spatial pattern of wear did not vary appreciably for the above perturbations.

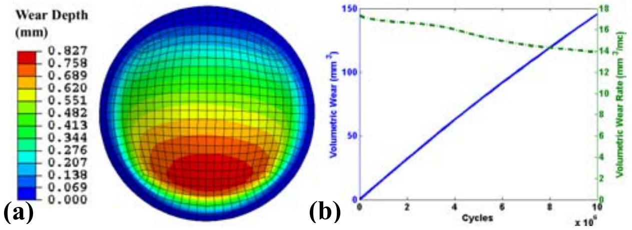

Figure 2. (a) Linear wear distribution, and (b) volumetric wear and wear rate for baseline case.

The magnitudes of the wear rate did change significantly, however, in response to several of the perturbations, as shown in Figure 3. Axial rotation and axial load amplitude had minimal influence on wear behavior, whereas flexion/extension amplitude had a major effect.

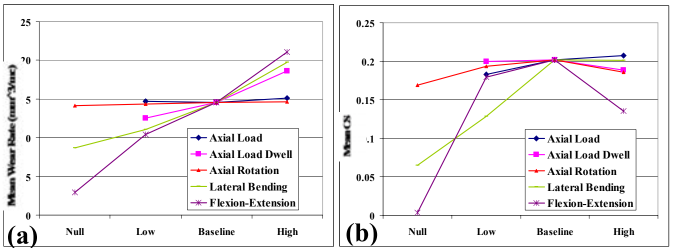

Figure 3. Variation in (a) mean wear rate, and (b) mean CS, as input waveforms were varied.

DISCUSSION

Clearly, altering the inputs of the ISO standard can create a striking difference in wear behavior of the Prodisc TDR. The most surprising of the results was from changing the lateral bending input, which resulted in a factor-of-two difference in wear rate, despite the relatively small ($\pm 2^{\circ}$) excursion involved. This may be associated with the concomitant increase in CS. The effects of altering the flexion and extension range, on the other hand, appear to stem primarily from increasing or decreasing the total sliding distance involved. The negligible effect of changing the axial load waveform is likely due to the temporal mean load remaining unchanged.

The results presented here would have been burdensomingly time-consuming to obtain via physical testing. The numerical model makes these comparisons (and many others) practicable, as each analysis took less than 4 hours (on a 3 GHz Intel Xeon with 16 GB RAM) and required no user intervention during the run time. Such tests can supplement standardized physical testing, to provide a broad backdrop of wear sensitivity to testing parameters. The framework developed here can be readily adapted to more complex descriptions of wear, as may be necessitated by further physical testing and material development.

REFERENCES

1. Goreham-Voss, CM & Brown, TD NACOB. Ann Arbor, MI, Abstrac 72, 2008.
2. Kang, L et al. *J Biomech* **41**, 340-6, 2008.
3. Rawlinson, JJ et al. *J Neurosurg Spine* **24**, 165-73, 2007.

ACKNOWLEDGEMENTS

This study was supported by a grant from the NIH (AR052653).

COMPARAISON OF TOTAL HIP ARTHROPLASTY AND A HIP RESURFACING DURING QUIET STANDING

Vicky Bouffard[1, 4], Marc Therrien[1], Julie Nantel [1,4] Martin Lavigne[3], Pascal-André Venditolli[3]
François Prince[1, 2, 4]

[1]Gait and Posture Laboratory, Marie Enfant Rehabilitation Center, Montreal, Qc, Canada
[2]Department of Surgery, Faculty of Medicine, University of Montreal, Montreal, Qc, Canada
[3]Orthopaedic Department, Maisonneuve – Rosemont Hospital, Montreal, Qc, Canada
[4]Department of Kinesiology, University of Montreal, Montreal Qc, Canada
vicky.bouffard@umontreal.ca

INTRODUCTION

Since younger patients are now more frequently affected by osteoarthritis (OA) [1] expectations from hip arthroplasty had changed. Indeed, patients do not only want to be relieved from pain and stiffness but they wish also to return as soon as possible to a high level of physical activities [2].

The main type of hip replacement is the total hip arthroplasty (THA). Over the years, this prosthesis has proved its worthiness and is now recognized as an effective, reproducible and frequently used therapeutic option [3]. A second type is the surface replacement arthroplasty (SRA). In SRA, the femoral head is shaped and bones are preserved, which are the major advantages of this prosthesis [4].

In their study, Nantel et al., (2008) [5] found a difference between the two prostheses (THA vs. SRA), for the range of the center of pressure (COP) in the medio-lateral (M/L) direction, during a quiet standing task. They supposed that the size of the femoral head might have an impact and may be a key point in postural control after hip arthroplasty.

During the past few years, a variation of the THA has been developed. This prosthesis uses a large diameter femoral head (32mm) (LD-THA). Therefore, the aim of this study is to compare patients undergoing hip replacement (LD-THA or SRA) postural control at 12 months post surgery.

METHODS AND PROCEDURES

All patients were diagnosed with hip OA and had a surgical intervention using a posterior approach. A control group was used for comparison. Goroups' characteristics are shown in Table 1.

Table 1. Means (SD) of the group's characteristics.

	THA (n=18)	SRA (n=20)	Control (n=12)
Age (y)	50.2 (6.4)	49.1 (6.8)	44.4 (9.2)
Gender	6 F/12 M	9 F/11 M	4 F/8 M
Weight (kg)	78.1(13.8)	78.9(15.0)	77.0(13.8)
Height (m)	1.68(.06)	1.68(.07)	1.72(.07)
BMI(kg/m^2)	27.4(3.7)	27.7(3.6)	26.0(3.4)

All patients were performing two postural tasks on an AMTI force platform. At first, they were asked to stand still for 2 minutes with their eyes open (EO) and then with eyes closed (EC). During the second task, the patients had to maintain a one leg stance position for 10 s for the operated (OL) and sound limb (SL). The abductors muscles' strength was also tested using a Penny and Giles hand-held dynamometer. The peak vertical force of the OL was calculated as a percentage of the peak vertical force of the SL.

COP relative data were extracted, analysed and filtered using a second-order, low pass Butterworth filter with a cut-off frequency fixed at 10 Hz. From those data, the range (max-min), root-mean-square (RMS) amplitude and the velocity of the COP (V_{COP}) were calculated in the ML and antero-posterior (AP) directions. The results were then averaged for each task and analysed using a 3-way ANOVA. The results were then further analysed if necessary, with Tukey post-hoc test and paired t-tests. All analyses were done with a level of signification set at 0.05.

RESULTS AND DISCUSSION

No difference has been observed for the sociodemographic data.

During quiet standing, the statistical analyses (Tables 2 and 3) revealed no main effect between the two prostheses. However results revealed a main effect for different vision conditions for the V_{COP} in both directions. Subjects have a better postural control in EO compared to EC condition. During the one leg stance, the results demonstrated a significant difference between the OL and SL for the V_{COP} in the AP direction. No interaction between the factors was found for all variables. No main effect was found for the abductor strength ratio.

Table 2. Mean (SD) of COP velocity (cm/s)* Significant difference between eyes open and closed.

	Eyes Open	Eyes Closed
V_{COP} ML *	0.43 (0.10)	0.45 (0.15)
V_{COP} AP *	0.69 (0.16)	0.93 (0.31)

Table 3. Mean (SD) of COP velocity (cm/s)*Significant difference between operated and sound limb.

	Operated limb	Sound limb
V_{COP} ML	3.9 (1.2)	3.8 (1.1)
V_{COP} AP *	3.6 (1.4)	3.6 (1.5)

Table 4. Mean (SD) of abductors strength ratio.

	LD-THA	SRA	Controls
Abd strength ratio (%)	89.4 (16.2)	92.6 (9.9)	87.6 (7.6)

The absence of a statistical difference between the two prostheses and the control subjects during a simple task (quiet standing), demonstrates that the patients restore their muscular strength and endurance needed to maintain a good postural control, especially with the abductor/adductor muscles controlling the stability in the ML direction [6]. On the other side, the presence of a significant difference during a more complex task (one leg stance) suggests that the recovery is not completed and may interfere in daily living activities [7] such as walking, turning climbing stairs dressing, etc. There is no significant difference in the abductor ratio. However, a rehabilitation program may be helpful to improve the recovery post surgery.

Besides, the significantly increase of the V_{COP} during the EC condition suggests that subjects with a hip arthroplasty react similarly to the control group, where their postural control is disrupted without visual inferences. Their surgical intervention seems to not have impaired their proprioception functions.

SUMMARY

After 12 months, patients undergoing hip arthroplasty (SRA or LD-THA) seems to have difficulties to accomplish complex quiet standing tasks. A rehabilitation program could be an option in order to improve the recovery post surgery.
Taken together these results showed that despite the design differences between SRA and LD-THA, the large femoral head seems to be the key point in restoring the hip joint biomechanics and improve postural stability.

REFERENCES

1. Loeser RF.*Osteoarthritis cartilage*, in press, 2009.
2. MacKichan ,F., Wylde, C., Dieppe, P. *Rheum Dis Clin North Am.*, **34**, 311-330, 2008.
3. Vendittoli, PA et al. *Hip Int.*, **16**, S73-81, 2006.
4. Mont, MA. *J. Arthroplasty*, **22**, 100-8, 2006
5. Nantel, J., Termoz, N., Centomo, H., Lavigne, M, Vendittoli, PA., Prince, F. *Clin. Biomech.*, **23**, 402-407, 2008.
6. Winter,DA et al. *J. Neurophysiol.*, **75**, 2334-2343, 1996.
7. Jonsson, E., Seiger, A., Hirscheld, H. *Clin. Biomech.*, **19**, 688-694, 2004

ACKNOWLEDGEMENTS

This research was funded by th CIHR (NRF 82453). We would like to thanks the CIHR-MENTOR training program and the FRSQ for their financial and scholarship supports. The study was also funded (unrestricted grant) by Zimmer, Warsaw, USA.

ELECTROMYOGRAPHIC RESPONSES TO AGING IN CHILDREN WITH CEREBRAL PALSY

[1] Richard Lauer, [2]Samuel Pierce, [1]Carole Tucker, [1]Mary Barbe, and [1]Laura Prosser
[1]Temple University, [2]Widener University,
email: rlauer2@temple.edu

INTRODUCTION

The use of surface electromyography (sEMG) recorded during the performance of a functional activity, such as gait, has provided valuable insight into motor development and changes with age in the pediatric population. [1] Muscle activation changes with age have not been reported for children with cerebral palsy (CP). A strong correlation between muscle activity and function in children with CP, as well as a decline in ambulatory status as children with CP mature into adults, has been demonstrated in previous studies [2]. Thus, changes in the sEMG indicative of such alterations in muscle activation patterns would be expected. In typically developing (TD) children, it has been reported that there are no changes in the onset and offset times of muscle activation patterns over the age of 3 years [1]. However, more detailed analysis has not been reported. Changes in signal amplitude and frequency with age should be investigated in both children with TD and with CP.

The purpose of this study was to examine age-related changes in muscle activity (time-frequency components) using established wavelet analysis techniques in a group of children with CP and a group of children with TD. It was hypothesized that changes in the age-related sEMG time-frequency characteristics would be evident in both groups, and that change in the time-frequency characteristics would be evident depending on a diagnosis of TD or CP.

METHODS

A retrospective analysis of sEMG data collected from two different study protocols was performed. In both studies, the parents of all the children signed a university institutional review board (IRB) approved consent form, and the children gave verbal assent, or written assent if over the age of seven. The data was divided into four groups, representing either an older (above the age of 7) or younger (below the age of seven) age group with either CP or TD. Data were analyzed from 24 children with TD, 16 in the younger age group (mean age 3.4, range: 1 to 6 years, 9 females and 7 males) and 8 in the older age group (mean age: 11.2, range 8 to 13 years, 5 females and 3 males). Data were also available for 26 children with CP, 14 in the younger age group (mean age 4.9, range: 2 to 7 years, 5 females and 9 males) and 12 in the older age group (mean age: 10.8, range 8 to 14 years, 6 females and 6 males). In both studies, children with CP were classified as Level II (impaired ambulation over distances) or Level III (use of assistive devices) on the Gross Motor Function Classification Scale.

The two studies from which the sEMG data were pooled both involved the analysis of the sEMG signals during gait, but focused on different sets of muscles. However, both studies had sEMG data available from the rectus femoris (RF) and the medial hamstring (MH) muscles bilaterally. For the older children, the sEMG data was acquired with the Motion Lab Systems MA-310 surface EMG recording system (Baton Rouge LA). The sEMG signals were collected at a sampling rate of 1.2 kHz, with a preamplifer gain of 20 and bandpass filtering between 20 and 350 Hz. For the younger children, the Myomonitor III (Delsys Inc., Boston, MA) was used with a sampling rate of 1.2 kHz, and a preamplifier gain of 10, and bandpass filtering between 20 and 450 Hz.

The sEMG data from the muscles were processed in MATLAB (The MathWorks Inc., Natick MA, USA). Before any analysis was performed, all raw data were low passed filtered using a 2nd order Butterworth filter with phase correction and a cutoff of 350 Hz. This was done to match the frequency ranges of the sEMG signals between the two studies. A time-frequency analysis was then performed on the sEMG data using the continuous wavelet transform (CWT) [4]. The three dimensional scalogram output of the CWT was reduced to a time-frequency curve by calculating the instantaneous mean frequency (IMNF) for each 0.1% cycle interval. A functional principal component analysis (PCA) was completed using the IMNF curves from all gait cycles to assess if the muscle IMNF curves across the four groups differed, and at what points in the gait cycle. Overall differences between groups pre and post surgery were tested using a Welch statistic, while individual groups differences were assessed using Tamhane's T2 multiple comparison test ($\alpha = 0.05$).

RESULTS AND DISCUSSION

Figure 1 shows the comparison in activation between the RF and MH muscles in the four groups. The PCA was able to account for 97 to 99% of the variability between groups. The IMNF curves for the RF muscle were statistically different between all groups ($p<0.001$). The IMNF curves for the MH muscle were statistically different between all groups ($p<0.001$) except for the CP young and old group comparison, which indicated no difference ($p > 0.285$)

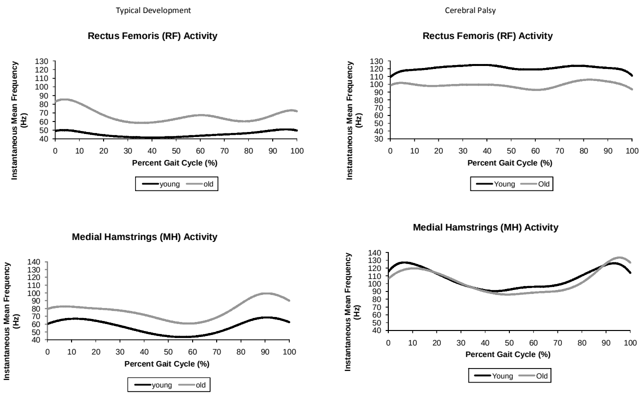

Figure 1 - Comparison of RF and MH activity for the children with CP and TD in the young and old age groups

As a function of age, the older children with TD for the RF and MH muscles exhibited an increase in the IMNF curve, with less variable activation times. This may represent increased rate coding of motor unit activation, or increased number of motor units recruited. These activation characteristics would most likely result in a larger magnitude muscle force generated which would be required to move or stabilize the older child's larger body segments during gait. This is in contrast to the RF muscle in the child with CP, where it appeared that at a younger age the objective was to activate the muscle maximally and continuously, and that with learning and maturation a relatively more synchronous pattern was developed, but was still less synchronous than the TD patterns. This would need to be explored further in a longitudinal study with the same group of individuals.

The MH muscle, in contrast to the RF, exhibited a fairly consistent pattern of activation in the child with CP regardless of age. In addition, the activation level was much higher in children with CP than the child with TD regardless of age. Given the well-documented finding of spasticity in the hamstrings in children with CP, the muscle's force generating capabilities may be impacted and greater activation necessary to offset the relative mechanical inefficiency or increased co-contraction of antagonist muscle groups in children with CP. Further, the higher activation levels may mask or negate measureable age-related changes in activation patterns of this muscle.

One limitation of this study is that the EMG data for the two groups were collected with two different systems, and although off line corrections were made to the data to allow for frequency comparisons, the possibility still exists that the systems used influenced the results. In addition, the results of this study need to be taken with caution given the retrospective nature of this study. A prospective study of these muscles in a group of children with a wider age range, and using the same data collection system is warranted to determine if the trends reported here remain.

REFERENCES

1. Sutherland DH, et al. The development of mature gait. *J Bone Joint Surg Am*, **62(3):**336-353, 1980.
2. Rosenbaum P, et al. A report: the definition and classification of cerebral palsy April 2006. *Dev Med Child Neurol Suppl*, **109**:8-14, 2007.
3. Lauer RT, et al. A time-frequency based electromyographic analysis technique for use in cerebral palsy. *Gait Posture*, **26(3):** 420-427, 2007.

ACKNOWLEDGEMENTS

This study was funded by the National Institutes of Health Grant # R03-NS048875 and the American Physical Therapy Association Section on Pediatrics.

TELESCOPING ACTION IMPROVES THE FIDELITY OF AN INVERTED PENDULUM MODEL IN DIPLEGIC CEREBRAL PALSY GAIT

[1, 2] Frank L Buczek, [2] Kevin M Cooney, [3] Matthew R Walker, [4] Michael J Rainbow, [5] James O Sanders
[1] National Institute for Occupational Safety & Health, Morgantown WV, [2] Shriners Hospitals for Children, Erie PA, [3] York University, Toronto, Ontario, [4] Brown University, Providence RI, [5] University of Rochester Medical Center, Rochester NY, email: fbuczek@cdc.gov

INTRODUCTION

An inverted pendulum (IP) model of human gait is a useful construct to understand the role of gravity in propulsion. Dynamic walking models, both analytical [1,2] and experimental [3], have shown that human-like gait can be achieved on downward slopes through gravity alone. However, additional sources of propulsion are needed for level gait. Particularly useful is work done by the trailing leg to redirect the body center-of-mass (COM) just prior to foot contact by the leading leg [4]. Such an analytical finding was supported by inverse dynamics of a telescoping IP directly applied to normal gait [5]. Here, pendulum radial kinematics (telescoping) improved the prediction of ground reaction forces (GRF). When radial kinematics were set to zero, GRF predictions deviated significantly from actual values, and these deviations occurred during power bursts at the hip, knee, and ankle joints. We hypothesized that these findings would extend to patients with diplegic cerebral palsy, despite common mobility disabilities (e.g., weakness, spasticity, poor motor control, etc.).

METHODS

After informed consent, nine pediatric patients diagnosed with diplegic cerebral palsy, referred to the laboratory for instrumented gait analysis, were enrolled in the study. They walked without assistive devices, with the least involved having true equinus, and most involved having crouch gait. Kinematic data were collected at 120 Hz using a ten camera Vicon 612 system, and low-pass filtered (6 Hz cutoff). A thirteen-segment, full-body model was implemented in Visual3D (C-Motion Inc.), and the instantaneous location of the full-body COM was calculated. Horizontal and vertical GRF (*Fh*, *Fv*) were collected at 1560 Hz using three AMTI force plates, and center-of-pressure (COP) coordinates were averaged across single support, consistent with Eqs. (1) and (2) derived for a stationary pendulum pivot [5]. (Here, m is body mass, g is gravitational acceleration, r is pendulum length, and θ, ω, α are the pendulum angular position, velocity, and acceleration, respectively.) Subtracting coordinates of the average COP from those of the instantaneous COM provided a telescoping IP [5]. Radial and angular kinematics of this pendulum were calculated using central difference techniques, and input to Eqs. (1) and (2). Setting radial kinematics ($\dot{r}, \ddot{r}$) to zero removed the telescoping action. Inverse dynamics in Visual3D provided associated lower extremity joint powers. Five separate repeated measures ANOVAs detected differences ($p \leq 0.05$) among actual and predicted minima and maxima in *Fh* and *Fv*, with and without telescoping. Root mean square (RMS) errors were also calculated across ensemble averages to quantify differences between actual and predicted *Fh* and *Fv*.

$$Fh = m\left[\left(\ddot{r} - r\omega^2\right)\cos\theta - \left(r\alpha + 2\dot{r}\omega\right)\sin\theta\right] \tag{1}$$

$$Fv = m\left[\left(\ddot{r} - r\omega^2\right)\sin\theta + \left(r\alpha + 2\dot{r}\omega\right)\cos\theta\right] + mg \tag{2}$$

RESULTS AND DISCUSSION

Changes in pendulum length (telescoping action) averaged 2.1 cm over single support. GRF were predicted best when this telescoping action was included (Figure). RMS errors for *Fh* increased from 3.1%BW to 7.7%BW when telescoping was removed, as the predicted force diverged from actual values in early and late single support. RMS errors for *Fv* increased from 9.3%BW to 24%BW, and the double peak pattern was lost, when telescoping was removed. Significant differences were found for all comparisons involving the no telescoping condition, apart from a local minimum in *Fv* near 50% single support (Table). In every case, deviations from actual data were worse when telescoping was removed, and these deviations were greatest during lower extremity power bursts calculated for these patients. We conclude that, despite their mobility disabilities, telescoping contributes to *Fh* and *Fv* during single support for these diplegic cerebral palsy patients, and reflects changes in hip, knee, and ankle angles modulated by joint powers.

REFERENCES

1. Kuo AD. *J Biomech Engr* **123**, 264-269, 2001.
2. Mochon S, McMahon TA. *J Biomechanics* **13**, 49-57, 1980.
3. McGeer T. *Intl J Robotics Research* **9**, 62-82, 1990.
4. Kuo AD, et al. *Exerc Sport Sci Rev* **33**, 88-97, 2005.
5. Buczek FL, et al. *Clin Biomech* **21**, 288-296, 2006.
6. Winter DA. 1991. *Biomechanics and Motor Control of Human Gait, 2nd Edition*, University of Waterloo Press, Waterloo, Ontario CA.

ACKNOWLEDGEMENTS & DISCLAIMER

Much of this study was performed when the authors were employed at Shriners Hospitals for Children, Erie PA. The opinions expressed in this abstract are those of the authors and do not necessarily reflect the views of the National Institute for Occupational Safety and Health.

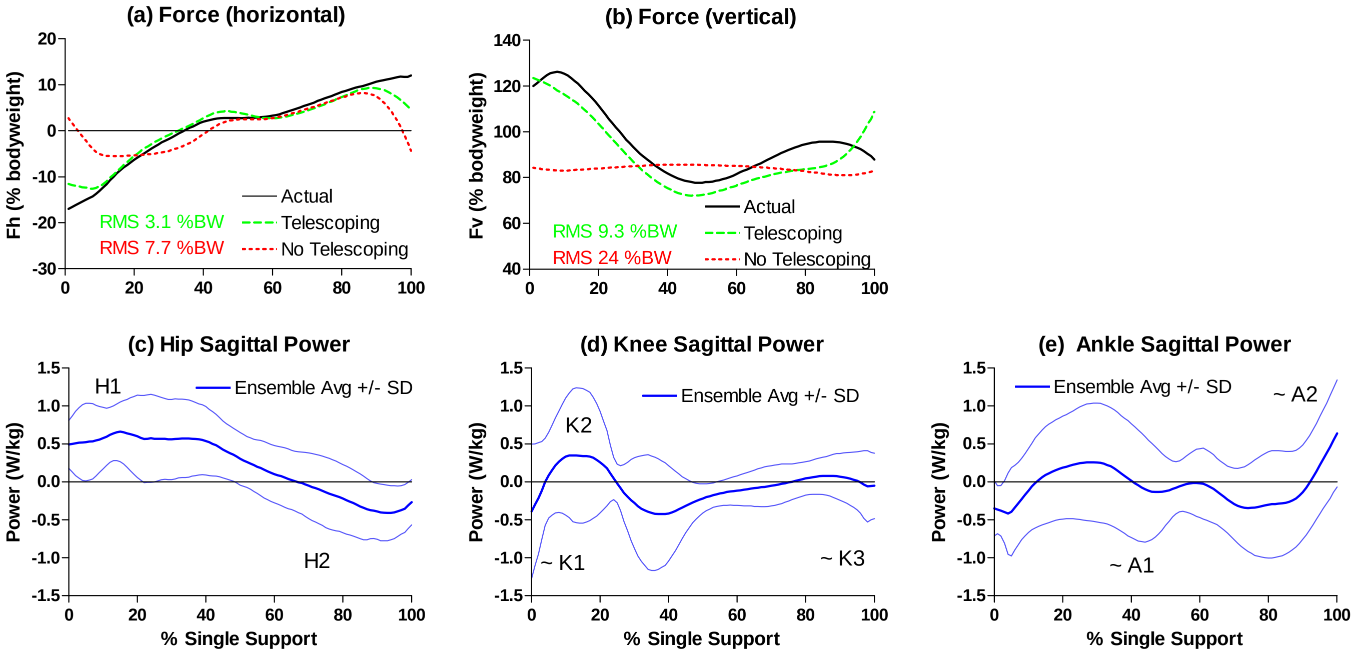

Figure. Relationship between ground reaction forces and joint powers. For all panels, one walking trial for each of nine diplegic cerebral palsy patients were averaged across single support. Panels (a) and (b) include actual (solid), predicted with telescoping (dashed), and predicted without telescoping (stippled) horizontal and vertical ground reaction forces; RMS errors are also indicated as % bodyweight. Panels (c) – (e) include means (± one standard deviation) for joint powers at the hip, knee, and ankle. Typical power bursts for normal gait (e.g., H1, H2, K1, K2, etc.) are indicated after Winter [6, pp. 47-48].

Table. Statistical results for inverse dynamics (repeated measures ANOVAs, Tukey Honest Significant Difference *post hoc* tests)

				P values		
Variable	**ACT**	**TEL1**	**TEL0**	**ACT v TEL1**	**ACT v TEL0**	**TEL1 v TEL0**
$F_{h\ min}$ (%BW)	-17.5 (10.8)	-12.0 (8.2)	1.8 (11.0)	0.469265	0.001920*	0.021382*
$F_{h\ max}$ (%BW)	13.1 (3.7)	7.1 (4.8)	-1.3 (10.9)	0.151730	0.000788*	0.037437*
F_{vmax1} (%BW)	133.5 (33.8)	125.9 (30.0)	83.6 (4.8)	0.704633	0.000330*	0.001069*
$F_{v\ min}$ (%BW)	67.1 (18.0)	70.5 (26.0)	85.5 (4.1)	0.860166	0.029574*	0.081056
F_{vmax2} (%BW)	102.5 (10.2)	94.7 (14.0)	82.6 (5.6)	0.102520	0.000261*	0.009949*

For each kinetic variable, maxima and minima in actual data were compared with inverse dynamics data predicted by Eqs. (1) and (2) at the same relative time (i.e., percent of single support). ACT = actual data, TEL1 = inverse dynamics with telescoping, TEL0 = inverse dynamics without telescoping, BW = bodyweight. Data are means and (standard deviations) with n = 9. (*) indicates significant at $P \leq 0.05$.

CHILDREN WITH CEREBRAL PALSY REQUIRE MORE STRIDES TO DISSIPATE DISTURBANCES PRESENT IN THEIR WALKING PATTERN

[1] Max J. Kurz, Brad Corr and Wayne Stuberg
[1]Munroe-Meyer Institute for Genetics and Rehabilitation, University of Nebraska Medical Center,
Omaha Nebraska
email: mkurz@unmc.edu, web: http://www.unmc.edu/dept/mmi/

INTRODUCTION

Cerebral palsy (CP) is a neurologic disorder that is a result of a defect or lesion in the immature brain. Although the brain lesion does not progressively worsen, there is often an accumulation of musculoskeletal impairments that result in insufficient muscular force generation, contractures, spasticity, and skeletal deformations. These musculoskeletal problems can create disturbances in the voluntary control of the walking pattern, and are one of the main reasons that children with CP stop walking or seek new surgical and rehabilitative treatments [2]. If the disturbances present in their walking pattern are not alleviated, they may cause a loss of balance and falls. A high frequency of falls may result in bodily harm, a reduction in physical activity, and a diminished social acceptance by the child's peers [2]. Although the clinician readily acknowledges these factors, limited investigations have been conducted to quantify the nature of the disturbances present in the walking patterns of these children. This scientific knowledge is necessary for shaping the current surgical and rehabilitative trends that are directed toward restoring walking function and balance in these children. The specific aim of this investigation was to provide the initial framework for quantifying the disturbances present in the walking patterns children with CP.

METHODS

Eight children with spastic diplegic CP (Age= 7.8 ± 2.8 yrs.), and seven typically developing children (Age = 8.0 ± 2.4 yrs.) walked on a treadmill for two minutes. The walking speed used by all the participants was based on the Froude number for children with CP who are community ambulators [3]. The children with CP had a Gross Motor Function Classification (GMFC) level between 1 and 2, and walked on the treadmill while wearing their prescribed ankle-foot-orthoses [4]. None of the children had surgical interventions or Botox injections within the last two years.

A motion capture system (120Hz) was used to determine the three-dimensional angular rotations of the lower extremity joints. The position data for all markers were filtered using a zero-lag Butterworth filter with a 6 Hz cut-off.

A state vector (S) was created for each of the respective lower extremity joints (Eq 1.)

$$S(t) = [\theta \quad \phi \quad \psi \quad \dot{\theta} \quad \dot{\phi} \quad \dot{\psi}] \qquad \text{Eq 1.}$$

where θ is flexion-extension, ϕ is abduction-adduction, ψ is internal-external rotation, and $\dot{\theta}$, $\dot{\phi}$, $\dot{\psi}$ are the respective derivatives. The state space data were partitioned into their respective strides and were normalized to 101 samples. Poincare maps were created for every sample of the stride, and the Floquet multipliers (FM) were calculated for each map [1]. The FM quantified the rate of dissipation of small disturbances that were present in the joint's movement pattern. It was assumed that the mean of the limit cycle trajectories (S*) represented the preferred joint movement pattern, and deviations away from this limit cycle from one stride (S_n) to the next (S_{n+1}) represented disturbances in the joint's kinematics (Eq 2).

$$[S_{n+1} - S^*] = J(S^*)[S_n - S^*] \qquad \text{Eq 2.}$$

The rate of change in the joint's movement from one stride to the next was quantified by the Jacobian ($J(S^*)$). The FM were the eigenvalues of the Jacobian. The largest FM across the stride was used to quantify the dissipation rate of the disturbances present in the joint's pattern. A FM that was further away from zero signified that it took longer to

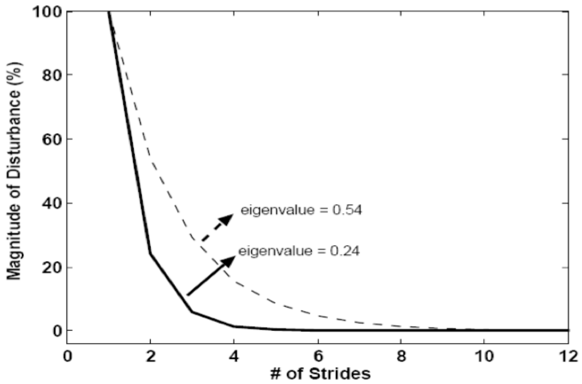

Figure 1: The smaller eigenvalue (0.24) indicates that disturbances dissipate at are faster rate while the larger eigenvalue (0.54) dissipates disturbances at relatively slower rate. According to Floquet theory, the faster rate at which disturbances are dissipated, the more stable the walking pattern.

dissipate disturbances present in the joint's movement pattern (Figure 1). A mixed ANOVA design was used to discern differences in the FM for the lower extremity joints of children with CP and the typically developing children.

RESULTS AND DISCUSSION

There was a significant between group main effect for the largest FM ($p<0.0001$), indicating the aggregate of the joints' FM for the children with CP (0.71±0.1) was significantly larger than the aggregate of the joints' FM for the typically developing children (0.58±0.1). This indicated that children with CP required more strides to dissipate the disturbances present in their gait pattern. Furthermore, this suggests that the children with CP had poorer walking balance and may be more susceptible to a fall. This notion concurs with clinical gross motor function balance tests of children with CP, and the high prevalence of falls noted in these children [2,5].

Although the FM values for all the respective joints were larger for the children with CP (Figure 2), no significant joint by group interaction was found ($p>0.05$). We suspect that the lack of significant differences may be due to where the musculoskeletal impairments were in the leg for each individual child. For this investigation, we did not recruit our subjects based on a specific joint musculoskeletal abnormality. Rather the children were recruited based on a GMFC level. We are optimistic that if we narrow our focus to certain types of joint musculoskeletal impairments (*e.g.*, skeletal torsions, joint contractures, foot deformities, *etc*.) that we will be able to further quantify the disturbances seen in the joint movement patterns of the various CP clinical classifications.

CONCLUSIONS

Children with CP require more strides to dissipate the disturbances present in their walking pattern. Most likely the inability to dissipate these disturbances is related to the lower extremity neuro-musculoskeletal impairments that often accompany CP. Further studies are warranted to quantify the musculoskeletal tenants that may be augmenting these gait disturbances and hindering their dissipation. This scientific knowledge will help to shape the current surgical and rehabilitation treatments that are aimed at restoring walking function and balance in children with CP.

REFERENCES

1. Arellano C, et al. *MSSE* **41(3)**: 620-7, 2009.
2. Bottos M & Gericke C. *Dev Med Child Neurol* **45**:786-790, 2003.
3. Abel MF & Damiano DL. *J Ped Orthop* 16(6):753-758, 1996.
4. Palisano R, et al. *Dev Med Child Neurol* **39**:214-223, 1997.
5. Kembhavi G, et al. *Ped Phys Ther* **14**:92-99, 2002.

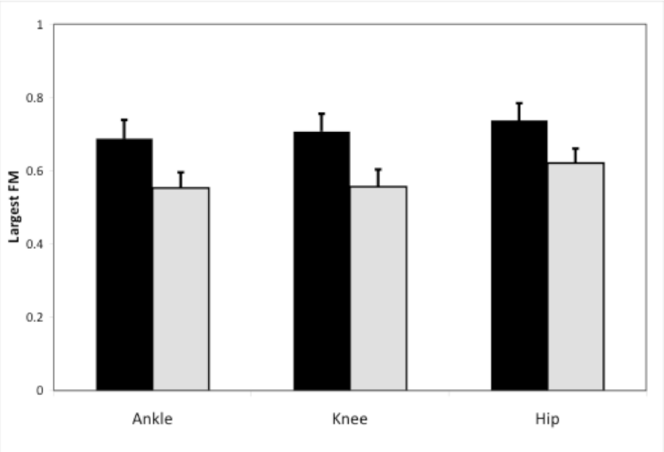

Figure 2: Mean (±SEM) FM for the respective lower extremity joints. The black bars are the FM for the children with CP and the grey bars are the FM for the typically developing children.

NON-UNIFORM DISTRIBUTION OF SARCOMERE LENGTHS ALONG A MUSCLE FIBER

Benjamin W. Infantolino and John H. Challis

Biomechanics Laboratory, Department of Kinesiology, The Pennsylvania State University,
University Park, PA, USA
E-mail: bwi100@psu.edu

INTRODUCTION

Sarcomere length is an important parameter that can be used to determine where a muscle will operate on its force-length curve *in vivo* (3). Sarcomere lengths have been estimated by counting the number of sarcomeres for a given length of a whole fiber and dividing by the distance that encompasses those fibers (7) or by measuring sarcomere length for a portion of the whole fiber using laser diffraction (3). Both methods assume a Gaussian sarcomere length distribution within the sarcomere. Evidence exists to suggest that sarcomere lengths differ significantly along a muscle fiber, with shorter lengths appearing at either end (1). The purpose of this study was to determine whether the sarcomere lengths along whole single muscle fibers follow a Gaussian distribution. If sarcomere lengths follow this distribution then methods that compute an average sarcomere length (i.e., laser diffraction) will produce accurate sarcomere length results.

METHODS

Muscle fascicles from the first dorsal interosseous muscle were removed and placed in a solution of 20% nitric acid to digest the connective tissue surrounding the muscle fibers. Whole muscle fibers were removed using a dissecting stereomicroscope and fine forceps. Six whole fibers were removed in total. Each fiber was placed on a microscope slide and checked to ensure that it was indeed an entire fiber. Once it was determined that the fiber was single, complete, and intact, the microscope was focused at 200x magnification. The whole fiber was imaged in sections. Beginning at one end of the fiber, a stage driver was used to advance the fiber a repeatable distance to ensure that no portion of the muscle fiber would be missed or double counted. Digital images of the fiber were obtained along the entire length of the fiber (Figure 1).

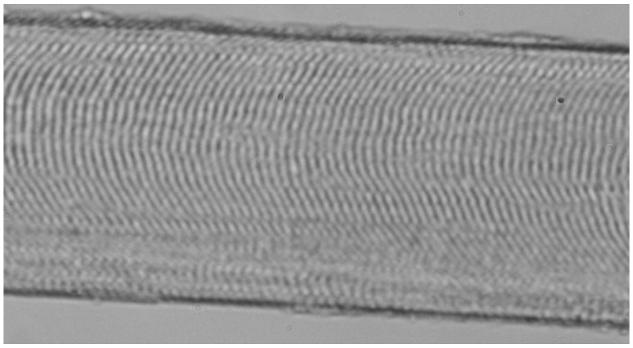

Figure 1: Muscle fiber at 200x magnification.

Custom MATLAB code was used to measure each individual sarcomere length along the fiber for the six complete fibers. The program has been previously validated for accuracy and repeatability.

The sarcomere lengths from each fiber were used to produce a normality plot. In addition the, detrended fluctuation analysis (DFA) was used to determine if long-range correlations existed in the sarcomere lengths along a single fiber (5). Values between 0.5 and 1 indicate long-range correlations while values between 1 and 1.5 indicate 1/f noise.

DFA results were not due to random noise as shown by surrogate analysis.

RESULTS

Each fiber clearly demonstrated a non-Gaussian distribution of sarcomere lengths based on a 95% confidence interval (Figure 2).

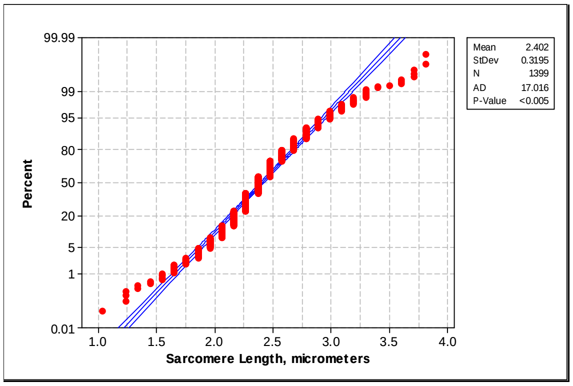

Figure 2: Representative normal probability plot with 95% confidence interval

In addition, the DFA produced an average value of 0.80 ± 0.08, indicating that long-range correlations existed in the samples. Surrogate DFA analysis indicated that the long-range correlations were due to the particular arrangement of sarcomeres in each fiber, not measurement noise.

DISCUSSION

Huxley and Peachey (1) described differences in average sarcomere length measured at different locations along a fiber. The current findings support these results. Non-uniform sarcomere length distribution has been used to explain the existence of various phenomena in muscle, for example an increase in muscle force after stretch, tension creep, and the ability to work on the descending limb of the force-length curve of muscle (2, 4).

Limitations to this study are the use of fixed cadaver tissue and the ability of the measuring program to detect the sarcomeres. Fixation does not appear to change the sarcomere length (e.g., 6) so the distributions seen in the fibers can be assumed to be indicative of an *in vivo* situation. The sarcomere measuring program produced a red dot where it detected each sarcomere which allowed confirmation of the program for accurate identification of each sarcomere.

This study demonstrated that sarcomere lengths are distributed non-uniformly along a muscle fiber. This finding has implications for the measurement of sarcomere lengths for use in musculoskeletal models, for example in surgical simulations. Laser diffraction techniques cannot capture this subtlety within muscle fibers, and therefore should be used with caution when the non-uniformity of sarcomere lengths could have an effect on the results of the investigation.

REFERENCES

1. Huxley, A.F., et al., *J Physiol*, 1961. **156**: p. 150-65.

2. Julian, F.J., et al., *J Physiol*, 1979. **293**: p. 379-92.

3. Lieber, R.L., et al., *Clin Orthop Relat Res*, 2004(419): p. 267-79.

4. Morgan, D.L., *Biophys. J*, 1990. **57**(2): p. 209-21.

5. Peng, C.K., et al., *Phys. Rev. E*, 1994. **49**(2): p. 1685-9.

6. Ward, S.R., et al., *J Biomech*, 2009. **42**(2): p. 193-6.

7. Wickiewicz, T.L., et al., *Clin Orthop Relat Res*, 1983. **179**: p. 275-283.

Kinematics estimation using a global optimization with closed-loop constraints

[1]Mickaël Begon, [2]Vincent Fohanno and [2]Floren Colloud
[1]Université de Montréal (Canada), [2]LMS Université de Poitiers (France)
email: mickael.begon@umontreal.ca, web: http://www.kinesio.umontreal.ca

INTRODUCTION

The global optimization of a chain model has shown many interests to estimate the joint kinematics: the mediolateral rotation of the thigh is improved [2], the data are directly usable for simulation [1] and the kinematics can be accurately reconstructed using a small number of markers or marker occlusions [1]. The reconstruction is feasible while the Hessian matrix remains of full rank. For some activities (*e.g.* kayaking and rowing) the number of degrees-of-freedom (*dof*) is reduced due to closed-loops; in this case fewer makers should be required or the redundancy should increase the accuracy of the reconstruction.

The purpose of this study was to compare a standard algorithm of global optimization with a new algorithm with closed-loop constraints to reconstruct a paddling kinematics.

METHODS

A kayaker performed setup movements for locating the joint centres using a functional approach [3] and six trials of paddling on an ergometer. The kinematics were acquired using a 10-camera motion analysis system at 300 Hz (T40, Vicon - Oxford, UK). A 17-segment, 42-*dof* chain model was developed in the *HuMAnS* toolbox and its parameters (i.e. segment lengths and marker locations with respect to the respective body segment) were determined using 94 reflective markers.

Three marker sets (A, B, C) shown in Fig. 1 (n_A=88, n_B=46, n_C=29 markers) and two algorithms of global optimization were used to reconstruct the joint kinematics. The first one (*algo1*) corresponded to a Newton–Gauss non-linear least square algorithm. The configuration $\mathbf{q}$ was iteratively adjusted $(\mathbf{q} = \mathbf{q} + d\mathbf{q})$:

$$\begin{cases} \min\limits_{dq} \frac{1}{2} d\mathbf{q}^{\mathrm{T}} \mathbf{J}^{\mathrm{T}} \mathbf{J}\, d\mathbf{q} + \left[\mathbf{J}^{\mathrm{T}}\left(\mathrm{Tags}(\mathbf{q}) - \mathbf{T}_{obs}\right)\right]^{\mathrm{T}} d\mathbf{q} \\ \mathbf{q}_{\min} - \mathbf{q} \le d\mathbf{q} \le \mathbf{q}_{\max} - \mathbf{q} \end{cases} \quad (1),$$

where $J_{i,j} = \dfrac{\partial \mathrm{Tags}_i(\mathbf{q})}{\partial q_j}$ for i=1…n and j=1…42.

The second algorithm (*algo2*) was based on a quadratic programming with a weighting matrix and constraints to ensure the closed-loops of the lower-limbs (feet strapped on the footrest) and the upper-limbs with the paddle. The constraints $\mathrm{Task}(\mathbf{q})$ were introduced on the augmented Jacobian matrix $\mathbf{J}_A = \left[\mathbf{J} \;\vdots\; \dfrac{\partial\, \mathrm{Task}(\mathbf{q})}{\partial \mathbf{q}}\right]^{\mathrm{T}}$:

$$\begin{cases} \min\limits_{dq} \frac{1}{2} d\mathbf{q}^{\mathrm{T}} \mathbf{J}_A^{\mathrm{T}} \mathbf{W} \mathbf{J}_A\, d\mathbf{q} + \left[\mathbf{J}_A^{\mathrm{T}} \mathbf{W} \begin{pmatrix} \mathrm{Tags}(\mathbf{q}) - \mathbf{T}_{obs} \\ \mathrm{Task}(\mathbf{q}) \end{pmatrix}\right]^{\mathrm{T}} d\mathbf{q} \\ \mathbf{q}_{\min} - \mathbf{q} \le d\mathbf{q} \le \mathbf{q}_{\max} - \mathbf{q} \end{cases} \quad (2).$$

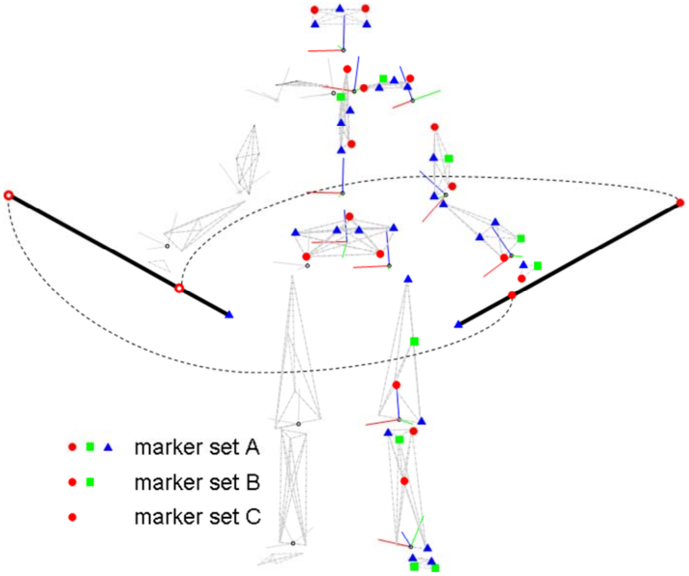

Figure 1: Paddler model with the three marker sets. The markers on the right limbs are similar to those on the left limbs. Two half-paddles are modeled with two markers that should coincide.

The global error of reconstruction was calculated as:

$$E = \frac{1}{F}\sum_{f=1}^{F}\sqrt{\frac{1}{3\times N_f - 42}\sum_{n=1}^{N_f}\left(\mathrm{Tags}(\mathbf{q}) - \mathbf{T}_{obs}\right)^2}\ ,$$

where F is the number of frames and N_f the number of visible markers for frame f.

The kinematics reconstructed using all the markers and *algo1* was the reference and root mean square differences (RMSd) were calculated between the reference and the other kinematics for the upper-limbs, lower-limbs and trunk *dof*.

RESULTS AND DISCUSSION

Fig. 2 shows an example of the reconstruction of the initial posture and the error in location between the observed markers and those obtained by the optimal chain model configuration.

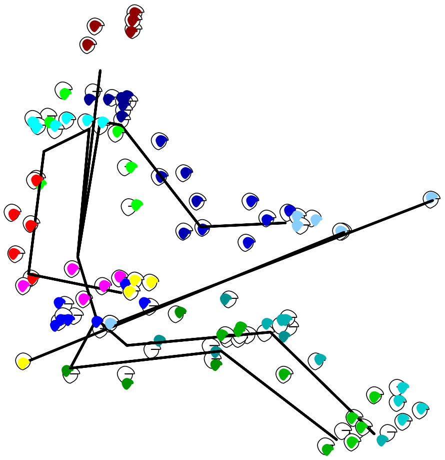

Figure 2 The dots represent the observed markers and the circles are the markers associated with the chain model.

The standard algorithm did work with the marker set *C* because the Hessian calculated as $\mathbf{J}^T\mathbf{J}$ in Eq. (1) was not of full rank. The ankle *dof* could not be determined because no marker was on the feet. The other combinations algorithm-marker set gave a mean error of about 10 mm (Table 1).

Table 1: Reconstruction error (in meters)

Marker set	A	B	C
algo1	0.010	0.010	--
algo2	0.008	0.011	0.016

With the decreased redundancy, the kinematics is less smooth because the random errors (e.g. skin movement artefact) are not compensated for; moreover the RMS difference increased (Table 2). With marker set B (46 markers for a 42-*dof* model), the RMS difference was up to 3º. This difference was slightly modified by the closed-loop constraints (*algo2*B *versus* *algo1*B). The RMS difference increased of 3º when 17 additional markers were removed.

Table 2: Root mean square differences (in degrees) [upper-limbs, lower-limbs, trunk+head]

	A	B	C
algo1	reference	[2.1, 2.3, 2.5]	--
algo2	[1.7, 0.2, 0.1]	[3.4, 2.1, 2.5]	[6.2, 4.0, 4.8]

The markers were removed from an *a priori* knowledge of the skin movement artefact. Further analyses will be performed to select the minimal marker set that minimizes the RMS differences.

This study helps in determining a minimal marker set for on-water experiments (in a towing tank) where the kayaker will be followed by a moving motion analysis system [4]. In this case a limited number of markers can be reconstructed because (*i*) the lower-limbs and the pelvis are partially hidden in the boat and (*ii*) the 3D reconstruction will be less accurate than a reconstruction in laboratory conditions due to vibrations and water reflections. The marker set *C* composed of a few markers (e.g. no marker on the feet, the back of the pelvis) placed as far as possible to each other took into account these limitations. The second algorithm highlights that closed-loop constraints can be introduced in a global optimization to improve the reconstruction of the joint kinematics.

ACKNOWLEDGEMENTS

The financial support of Région Poitou-Charentes and EU (CPER 2007-2013) is gratefully acknowledged.

REFERENCES

1. Begon M, et al. *J Biomech* 41: 581-586, 2008
2. Lu TW, et al. J. *J Biomech* 32, 129–134, 1999
3. Ehrig RM, et al., *J Biomech* 39, 2798–2809, 2006
4. Colloud F, et al., *J Biomech* 41, S57, 2008

RECOVERY GAIT FOLLOWING AN UNEXPECTED SLIP

Elizabeth A. Timcho, April J. Chambers, Rakié Cham
Department of Bioengineering, University of Pittsburgh, Pittsburgh, PA, USA
Email: eat18@pitt.edu, web: www.hmbl.bioe.pitt.edu

INTRODUCTION

Falls due to slipping are a major cause of injury. The incidence of falls results in high economic and societal costs including medical care and lost productivity. In 2000, approximately 11.6 million fatal and nonfatal incidences of falls were reported and total lifetime costs of injury due to falls were estimated at $81 billion.[1] Falls often result from a loss of balance that can be attributed to slipping.[2] Thus it is important to study response to slips and quantify biomechanics in order to improve workplace environments and decrease the number of slips and falls.

One variable commonly evaluated when studying the biomechanics of slips is the required coefficient of friction (RCOF), defined as the ratio of shear force to normal force.[2] Most slips occur due to a high ratio of shear force to normal force applied on a floor surface immediately following heel contact.[2,3] Previous studies have shown that subjects adjust their gait on potentially slippery surfaces, which often results in a reduction in their peak RCOF as subjects reduce the relative shear force applied at heel contact.[2] However, it has not been determined how quickly a subject's gait returns to normal patterns following a slip.

The purpose of this study is to determine whether gait returns to normal baseline conditions after an unexpected slip by analyzing peak RCOF values before and after a slip.

METHODS

Ten young subjects (20-35 yrs,) screened for neurological and orthopedic abnormalities, were instructed to walk at a self-selected pace across a vinyl tile walkway, while ground reaction forces and whole body motion were sampled at 1080 and 120 Hz, respectively. Subjects were informed the first few trials would be dry, 'baseline dry' (BD). Without the subjects' knowledge, a glycerol solution (glycerol-water ratio of 75:25) was applied at the left/leading foot-floor interface, generating an 'unexpected slip'. Subjects were then told that the next few trials would be dry, 'recovery dry' (RD). Fifteen trials were collected on a dry floor.

Table 1: Subject characteristics, mean (SD).

	Male (n=5)	Female (n=5)	Total (n=10)
Age (years)	23.6 (1.34)	24.8 (4.49)	24.2 (3.19)
Height (cm)	178.0 (8.28)	165.9 (5.42)	172.0 (9.18)
Weight (kg)	80.8 (11.77)	65.4 (15.92)	73.1 (15.50)

Ground reaction force data was time normalized with respect to stance time for each foot with 0% = heel contact (HC) and 100% = toe off (TO). RCOF was calculated using the ratio of force in the anterior-posterior direction to the normal force.[2] The maximum RCOF value during 10-30% of the stance was selected for analysis.[2] Within subject repeated measures ANOVAs were conducted on the peak RCOF using condition (BD/RD) and trial number nested with condition as independent variables. Significance level was set at 0.05. A post-hoc analysis was performed when necessary.

RESULTS AND DISCUSSION

Mean peak RCOF values for all subjects during the RD trials for right foot and left foot are displayed (Figures 1 and 2). Subjects had a mean BD peak RCOF of 0.193 ± 0.029 and 0.199 ± 0.030 for the right foot and left foot, respectively.

The results for the right foot showed no statistically significant difference in peak RCOF values between BD and RD conditions (p=0.4918). As such, RD trial was not significantly different either (p=0.1709). However, the peak RCOF values for the left (previously slipped) foot displayed a significant difference in condition (p=0.0278). In addition, RD trial number was also significant for the left foot (p=0.0003). The post-hoc analysis revealed that mean peak RCOF values for RD trials 1, 2, 3, 4 and 6 were different than the mean BD peak RCOF values. Therefore it took approximately

5-6 RD trials for the left (previously slipped) foot to return to mean BD conditions.

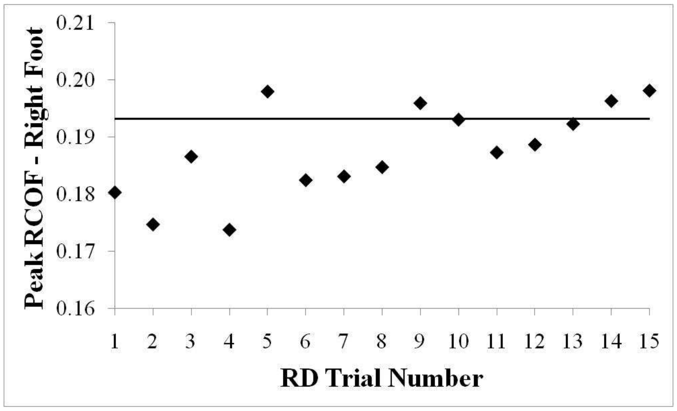

Figure 1: Mean peak RCOF during RD trials on right foot. Black horizontal line represents mean peak RCOF at BD. No individual RD trials were significantly different from mean BD peak RCOF values.

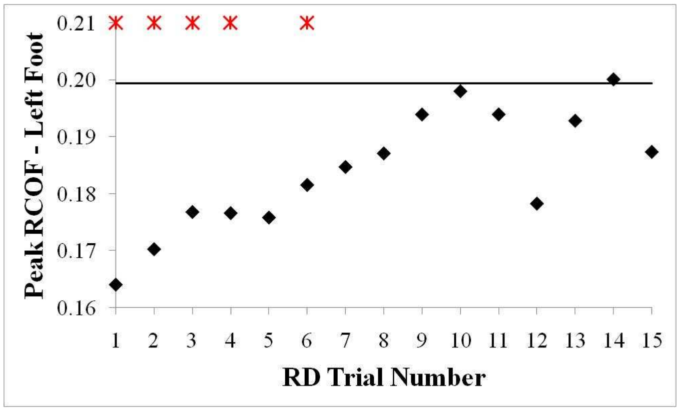

Figure 2: Mean peak RCOF during RD trials on left (previously slipped) foot. Black horizontal line represents mean peak RCOF at BD. Red asterisks denote RD trial number is significantly different from mean BD peak RCOF values.

After experiencing a slip, subjects significantly reduced their peak RCOF even though they were informed that the remaining trials would be dry. A reduction in peak RCOF has been shown to decrease slip risk and was present when subjects were warned that there was potential for a slip.[2,3] Reduced peak RCOF was present in the first few trials following the slip for both feet, suggesting that subjects were walking with more caution. However, the peak RCOF values for the right foot showed no significant difference between BD and RD conditions or trial effect. The peak RCOF values for the left (previously slipped) foot were significantly different from BD immediately following a slip and then gradually increased to the mean BD peak RCOF value. This suggests that subjects eventually ‘relax’ and return to their baseline gait in which they are no longer anticipating a slip. According to the data presented here this occurs after the sixth RD trial immediately following a slip. It is possible that with a larger subject pool this trial number would be later based on Figure 2. Additionally, the directions or warning conditions provided by the researcher could impact this ‘relaxation’ effect. If subjects do in fact return to baseline values, it may be possible to generate an additional ‘unexpected slip’.

Previous research has shown that young adults only adjust their gait on the foot that would be slipping.[3] This could explain the differences found between the right foot and left foot. It was also found that older adults required an additional step before a potentially slippery surface to adjust their gait.[3] Therefore, it is possible that older adults would exhibit similar behavior on their right foot as on their left foot.

CONCLUSIONS

The left (previously slipped) foot displayed significant differences between peak RCOF values in BD and RD trials, while the right foot did not show any significant difference. In addition, it appears that after 6 RD trials, young adults ‘relax’ and peak RCOF values return to BD values for the left (previously slipped) foot. These results show that subjects are initially anticipating a slippery floor regardless of verbal instruction. Also, this implies that it may be possible to generate more than one ‘unexpected slip’ in young adults.

REFERENCES

1. Corso P, et al. *Injury Prevention* **12**, 212-218, 2006.
2. Cham R, Redfern MS. *Gait & Posture* **15**, 159–171, 2002.
3. Lockhart TE, et al. *Gait & Posture* **26**, 142-149, 2007.

ACKNOWLEDGEMENTS

Funding source: NIOSH R01 OH007592
Neurological screening: Dr. Joseph Furman

Flexion-Withdrawal Reflexes in the Upper-Limb Adapt to the Position of the Limb.

[1] Zachary A. Riley, [1]Eileen T. Krepkovich, [1]Elizabeth C. Mayland,
[1,2,3,4]Wendy M. Murray, and [1,2,3]Eric J. Perreault
[1]Sensory Motor Performance Program, Rehabilitation Institute of Chicago, Chicago, IL
Departments of [2]Biomedical Engineering and [3]PM&R, Northwestern University, Chicago, IL
[4]VA Hines, Hines, IL
Email: z-riley@northwestern.edu

INTRODUCTION

Noxious electrical stimulation of the fingers produces a coordinated reflex response in upper limb muscles that results in the withdrawal of the limb, analogous to removing the hand from touching a hot stove [1, 2]. In general, the upper limb withdrawal is accomplished by a proximal-distal progression of shoulder extension, elbow flexion, and wrist extension [1]. However, exceptions to coordinated withdrawal movement patterns have been observed. For example, some stimulation sites in the lower limb make the leg extend rather than flex [3]. The response of the upper limb has not been studied in the same detail as the lower limb; however, it has been shown that the reflex response can modulate with the phase of movement, as occurs with reaching tasks in the upper limb [4]. The cutaneous afferent feedback (Aδ, C-fiber) responsible for the withdrawal reflex does not make direct connections onto motor neurons in the spinal cord. This suggests that these complex neural circuits would be mutable under different task conditions, operating in the best manner to remove the limb from the painful environment. The purpose of the present experiment was to test the flexibility of the flexion-withdrawal reflex and torque responses by observing the behavior of the limb when it is in different positions. We hypothesized that the flexion-withdrawal response would coordinate to match the limitations placed on the arm due to positioning.

METHODS

Ten healthy adults (28.6 ± 3.9 yrs) participated in the experiments and provided informed consent through Northwestern University. Each subject was tested with the arm in three different positions (Table 1). Noxious electrical stimulation was delivered through ring electrodes placed on the index finger (Digit II). Constant current stimulus trains (20 ms duration) consisting of 10 pulses at a rate of 300 Hz were delivered at random intervals for a total of 8 stimuli in each of the arm positions. The typical stimulus intensity to evoke a painful response was 40—50 mA, and was at least 30—40 X perceptual threshold. Electromyograms (EMGs) were recorded from the brachioradialis (BRD), biceps brachii lateral head (BIC), triceps brachii lateral head (TRI), anterior deltoid (AD), and posterior deltoid (PD) muscles. The subject's forearm was secured to a 6-DOF load cell (JR-3) with an orthosis and the torso was restrained in a chair.

Table 1. Arm Configurations

	Elbow Flexion	Shoulder Flexion	Shoulder Abduction
FLEX	128.2°	28.4°	80.0°
MID	87.7°	49.1°	67.2°
EXT	41.8°	73.9°	78.9°

Reflex responses in the upper-limb muscles were quantified by recording the mean of the rectified EMG for a time window between 60—120 ms for the shoulder muscles and 80—140 ms for the arm muscles (consistent with the onset times of the reflexes), averaged across all 8 trials in each arm position. Resultant endpoint force vectors in the transverse plane were calculated by taking the mean of the endpoint forces for a 20 ms window following force signal onset, defined as the point when the signal exceeded 2 standard deviations above the mean of the force before stimulation. The 20 ms time window was chosen to avoid later, voluntary force changes. Paired t-tests were used to compare EMGs as well as the angle of the vectors and the magnitudes of the vectors in the x- and y-directions.

RESULTS AND DISCUSSION

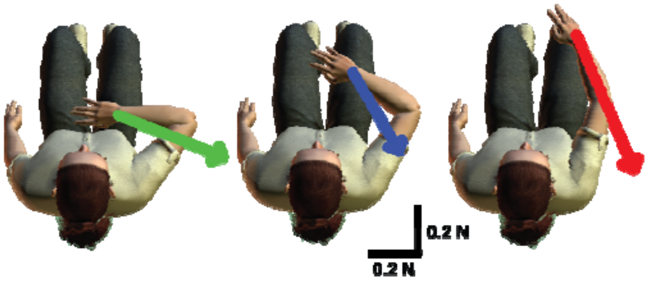

Figure 1. Representative figure displaying the flexed, middle, and extended arm positions. The arrows indicate the resultant force vectors after stimulation in each position.

The results of the current study demonstrated the flexibility the nervous system has in choosing the appropriate motor action following a painful stimulus to the index finger. For example, when the arm was flexed into the chest (FLEX) the response was to pull the arm across the body (Fig.1, Left). Alternatively, when the arm was extended (EXT) in front of the body the reflex response was to withdraw the arm backwards, closer to the midline of the body (Fig.1, Right). There were significant differences in the angle of the resultant vector between FLEX and both MID and EXT positions (both, $P<0.001$), and the magnitude of the vector was significantly greater in the lateral direction in the FLEX position ($P=0.002$ and $P<0.001$, MID and EXT, respectively). Posture-dependent changes in muscle activation were consistent with the measured endpoint forces. EMG activity in the upper limb muscles during the reflex period was generally greater when the arm was in the flexed position. Specifically, reflex responses in biceps brachii ($P=0.03$) and posterior deltoid ($P=0.03$) were greater when the arm was flexed (Fig. 2, right). The latencies for the reflex responses were not different between arm positions; however, the latencies were consistently shorter in the posterior deltoid (62.5±2.3 ms) than in either of the elbow flexor muscles (BRD 81.5 ± 4.3 ms, $P<0.001$, BIC 84.1 ± 3.5 ms, $P<0.001$). This is consistent with the progression of shoulder extension followed by elbow extension [1].

CONCLUSIONS

The present study examined posture-dependent changes of the flexion withdrawal reflex in the human arm. The first position, with the arm flexed close to the body, resulted in the subject drawing the arm across the body to remove it from the stimulus. Importantly, even though a potential strategy would be to push the arm in the anterior direction since it is limited in moving in the posterior direction, we observed no extension reflexes in any of the conditions, as is observed under certain conditions in the lower limb [2]. Alternatively, when the arm is furthest from the body, the strategy is to pull the arm back closer to the midline. The differences in withdrawal movements could reflect the flexibility of these reflexes in performing a motor action that can protect the system. Another potential explanation for the results is that the different withdrawal force directions are due to changes in the biomechanics of the limb when altering arm positions. This possibility is currently being explored with upper limb musculoskeletal modeling.

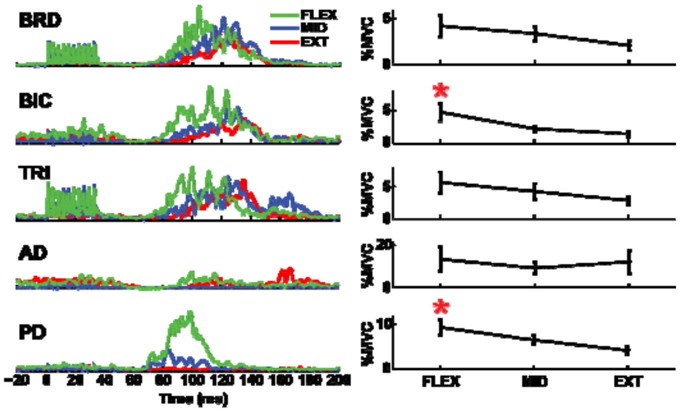

Figure 2. Left, Representative EMG from one subject following stimulation. Right, Average EMG for a 60 ms period following stimulation for all subjects. * indicates significance ($P < 0.05$).

REFERENCES

1. Dewald, J.P., et al., Muscle Nerve, 1999. **22**(9): p. 1209-21.
2. Floeter, M.K., et al., Muscle Nerve, 1998. **21**(5): p. 591-8.
3. Hagbarth, K.E., J Neurol Neurosurg Psychiatry, 1960. **23**: p. 222-7.
4. Serrao, M., et al., J Neurosci, 2006. **26**(13): p. 3505-13.

ACKNOWLEDGEMENTS

The work has been supported by an award from the Craig H. Nielsen Foundation to W.M.M. and an NIH award (R01 NS053813) to E.J.P.

PRELIMINARY INVESTIGATION OF BALANCE RECOVERY FROM A TRIP IN OVERWEIGHT AND NORMAL WEIGHT OLDER ADULTS

Sara L. Matrangola, Kathleen A. Bieryla, Michael L. Madigan
Virginia Polytechnic Institute and State University, Blacksburg, VA, USA
E-mail: smatrang@vt.edu, Web: http://www.biomechanics.esm.vt.edu/

INTRODUCTION

Obesity is a major health concern in the United States (US). Over one billion people worldwide are considered overweight, and of those, 300 million are considered obese [1]. In addition to numerous health conditions, obesity is associated with an increased risk of falls and subsequent injury. Obese individuals fall almost twice as often (27% vs. 15%) compared to non-obese individuals [2] and falls were identified as the most common cause of injuries in the obese (~36% of all injuries) [3]. Overweight or obese older adults would seem to be at an even higher risk for falls. A larger mass will require the person to generate increased torques to control the trunk, but the muscles generating this torque are weakened by sarcopenia [4]. However, the influence of overweight or obesity on balance recovery from a trip in older adults has yet to be investigated.

Therefore, the goal of the current study was to examine the effect of being overweight on balance recovery from a trip in older adults. We hypothesized that due to a higher torque demand for recovery and decreased ability to generate that torque from sarcopenia, being overweight will have a negative effect on balance recovery from a trip.

METHODS

Eight participants (73.9 ± 6.9 years), four overweight and four normal weight, were used in the study. Body mass index (BMI) was used to determine inclusion into the overweight group (28.8 ± 2.4 kg/m^2) or normal weight (20.8 ± 2.4 kg/m^2) group. A medical screening was performed to exclude participants with any neurological, cardiac, respiratory, otological, or musculoskeletal disorders, or a history of multiple falls within the past year. The study was approved by the Virginia Tech Institutional Review Board, and written consent was obtained from all participants.

Participants walked repeatedly along a 9 m walkway at a self-selected pace while looking straight ahead. They were informed that a trip might occur in any trial and were instructed to, upon tripping, regain their balance and continue walking. After a minimum of 20 walking trials, a 7.6 cm (3 in.) high pneumatically driven obstacle embedded in the floor was triggered manually to elicit a trip in the mid-to-late swing phase of gait. Two nonfunctional dummy obstacles were placed in the walkway so that participants were unaware of where the trip would occur (Figure 1). Also, participants wore a full body harness for the duration of the experiment to prevent a fall to the ground in the event of an unsuccessful trip recovery.

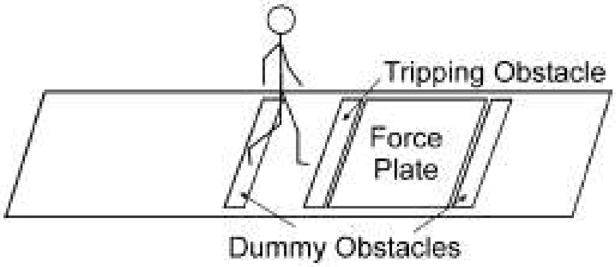

Figure 1: Experimental setup with tripping obstacle, two dummy obstacles, and force plate.

Whole body kinematics, ground reaction forces, and force applied to the harness were recorded. Reflective markers were placed bilaterally over selected anatomical landmarks on the head, arms, trunk, and lower extremities. Marker data were sampled at 100 Hz using a Vicon 460 motion analysis system (Vicon Motion Systems Inc., Lake Forest, CA). Ground reaction forces were sampled at 1000 Hz using a force platform (Bertec Corporation, Columbus, OH) and were used to determine the time of foot contact after the trip.

Trip recovery performance was quantified using maximum trunk flexion angle, maximum trunk angular velocity, and time to maximum trunk flexion angle from trip onset. These measures were selected based upon their importance in successful trip recovery [5, 6].

A Wilcoxon Rank-Sum test was used to analyze differences in trip recovery measures between overweight and normal weight groups. This test was used due to small sample size and non-normal distributions. In addition, effect size was calculated using Cohen's *d,* the mean overweight value subtracted from the mean normal weight value, divided by the standard deviation of the normal weight value. Statistical analysis was performed using JMP v7 (Cary, North Carolina, USA).

RESULTS AND DISCUSSION

Time to maximum trunk angle from trip onset was 49.5% higher in overweight older adults (p=0.043) compared to normal weight adults. Maximum trunk angle and maximum trunk angular velocity were 68.3% and 49.2% higher in overweight adults, but these differences did not reach statistical significance (p=0.083; see Table 1).

Reducing trunk flexion and trunk flexion velocity is crucial to recovering balance after a trip [7]. In this study, the overweight group had larger values for all measures calculated. This indicates that the overweight group has decreased ability to arrest forward trunk movement during a trip and will be more likely to fall. More specifically, the overweight group took longer to reach their larger maximum trunk flexion. This indicates that being overweight increases the amount of time the center of mass is outside the base of support, and thereby decreasing the ability to recover balance.

Several limitations warrant discussion. First, we did not account for differences in recovery strategy (elevating vs. lowering) between participants. Second, the small sample size limits our statistical power. Third, participation requirements (medical screening) may preclude the generalization of our results to non-healthy older adults. Finally, it is unclear if results from this study transfer to trips outside of the laboratory setting.

CONCLUSIONS

In conclusion, the overweight older adults exhibited significantly longer time to maximum trunk angle compared to the normal weight group. The overweight group also exhibited trends toward larger values of trunk flexion and trunk flexion velocity. These results suggest that being overweight negatively affects balance recovery after tripping in healthy older adults, and may help to explain the increased risk of falling in these individuals.

REFERENCES

1. *WHO Consultation on obesity* 1998.
2. Fjeldstad C, et al. *Dyn Med* **7**, 4, 2008.
3. Matter KC, et al. *Obesity (Silver Spring)* **15**, 2384-90, 2007.
4. Baumgartner RN. *Ann N Y Acad Sci* **904**, 437-48, 2000.
5. Bieryla KA, et al. *Gait Posture* **26**, 208-13, 2007.
6. Pavol MJ, et al. *J Gerontol A Biol Sci Med Sci* **56**, M428-37, 2001.
7. Grabiner MD, et al. *J Gerontol* **48**, M97-102, 1993.

Table 1: Trip recovery measures.

	Normal Weight	Overweight	Effect Size (p-value)
Maximum Trunk Angle (deg)	30.6±12.0	51.5±20.4	-1.76 (0.083)
Maximum Trunk Angular Vel. (deg/s)	111.7±33.9	166.6±27.8	-1.62 (0.083)
Time to Maximum Trunk Angle (s)	0.49±0.10	0.73±0.10	-2.46 (0.043)

INDIVIDUAL LIMB WORK IS INFLUENCED BY ANKLE-FOOT-ORTHOTICS WORN BY CHILDREN WITH CEREBRAL PALSY

[1] Max J. Kurz, Wayne Stuberg and Glen Ginsburg
[1]Munroe-Meyer Institute for Genetics and Rehabilitation, University of Nebraska Medical Center, Omaha Nebraska
email: mkurz@unmc.edu, web: http://www.unmc.edu/dept/mmi/

INTRODUCTION

Cerebral palsy (CP) is a neurologic disorder that results from a defect or lesion in the immature brain. Children with CP develop muscular impairments and skeletal deformities of the ankle-foot complex as they mature. Consequences of these impairments may include an equinus foot posture, and inconsistent modulation of the ankle joint throughout the gait cycle. To treat these ankle joint abnormalities, clinicians frequently prescribe an Ankle-Foot-Orthosis (AFO) that prevents excessive plantarflexion during the stance and swing phase (Figure 1). Quite often the prescribed AFO results in positive improvements in gait kinematics during single support, and an improvement in the child's walking efficiency [3].

The external work performed by the limbs during the double support phase of gait has recently received considerable attention because it requires a coordinated effort by the trailing and leading legs to redirect the center of mass [2]. For this redirection to occur properly, the trailing leg must produce a sufficient amount of positive external work to balance the amount of negative external work produced by the leading leg on the center of mass. An imbalance in the amount of work performed by the legs may alter the redirection of the center of mass [2]. Limited efforts have been made to determine the influence of current AFOs designs on the double support phase. It is possible that they may influence the external work performed by the individual legs on the center of mass. The specific aim of this investigation was to evaluate the influence of AFOs on the external work performed by the individual legs of children with CP.

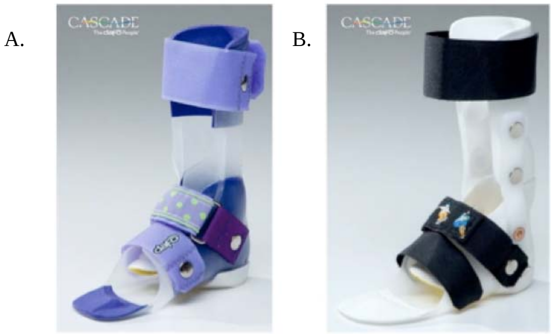

Figure 1. Exemplary solid AFO with a pre-tibial strap (A) and a hinged AFO (B).

METHODS

Eleven children that were diagnosed as having CP with spastic diplegia (Age = 9.1 ± 2; Mass = 31.6 ± 13 kg) participated in this investigation. The participants were independent walkers, and had Gross Motor Function Classification levels between 1 and 2 [4]. Three of the children wore solid AFOs with a pre-tibial strap (Figure 1A), and eight wore hinged AFOs (Figure 1B). The hinged AFO design limited ankle plantarflexion, but allowed for full dorsiflexion throughout the gait cycle. The solid AFO limited ankle plantarflexion and dorsiflexion.

Each participant walked at a self-selected pace along a 16-meter walkway while barefoot, and while wearing his or her prescribed AFOs. We collected individual limb ground reaction forces from four AMTI force platforms (120 Hz) that were mounted in series, and evaluated three steps from each participant. The individual limb ground reaction force components were summed to determine the acceleration of the center of mass. Each component of the acceleration was integrated to determine the instantaneous velocity of the center of mass [1]. We calculated the external mechanical work performed by the lead and trail limbs from the dot products of the respective individual limb forces and the velocity of the center of mass [2]. The amount of external work performed by each of the respective limbs was quantified by integrating the power curve, and the work values were normalized by the participant's body mass. We evaluated the amount of positive (W^+_{DS}) and negative limb work (W^-_{DS}) performed during double support, the difference in the amount of work performed by the individual limbs during double support (W_{DIFF}), and the amount of positive work (W^+_{SS}) performed during single support. Repeated measures ANOVA was used to discern differences in the amount of external limb work performed while barefoot and while wearing an AFO.

We additionally used the center of pressure profiles from the respective force platforms to determine changes in the step length and width while barefoot and while wearing AFOs.

RESULTS AND DISCUSSION

The children with CP walked at a significantly faster speed while wearing AFOs (AFO = 1.1±0.04 m/s; Barefoot = 1.0±0.04 m/s; p=0.0046), and used a significantly (p=0.004) longer step length (AFO = 53.4 ± 6 cm; Barefoot= 48.6 ± 5 cm). Although the mean step width was larger while walking barefoot, there were no significant differences (p = 0.13) between the two conditions (AFO= 11.1 ± 5 cm; Barefoot= 12.7 ± 6 cm).

The children with CP performed significantly more negative work by the lead leg during double support (p < 0.0001), and significantly less positive work by the trail leg (p = 0.01) while wearing AFOs (Figure 2). The work performed by the individual legs was more balanced while walking barefoot (W_{DIFF} = 0.004 ± 0.1 J/kg), and had a significantly (p<0.0001) more work performed by the lead limb while walking with AFOs (W_{DIFF} = -0.17 ± 0.1 J/kg). These results imply that the AFO may influence the external limb work that is necessary for the redirection of the center of mass during double support. This notion is further supported by the fact that the children did not have a larger amount of positive work performed by the trail leg while wearing AFOs even though they selected a longer step length.

Significantly (p = 0.02) less positive work was performed on the center of mass during single support while wearing AFOs. We speculate that the reduced amount of work performed during single support may be the reason that children with CP have an improved metabolic cost while wearing AFOs [3]. Taken together, we suspect that the metabolic cost of walking in children with CP may have a large dependence on the amount of limb work performed for the support and control of the body's weight during single support.

CONCLUSIONS

AFOs influence the amount of external limb work performed on the center of mass of children with CP. Although AFOs appear to influence the redirection of the center of mass during double support, they reduce the amount of work performed on the center of mass during single support. The results presented here suggest that new AFO designs are necessary to improve double support phase dynamics. It is possible that the different types of AFOs worn by the children may have had different effects on the amount of external limb work performed on the center of mass. We are currently evaluating if the results presented here extend to the various AFO designs (*i.e.*, hinged, solid, leaf-spring, *etc*.).

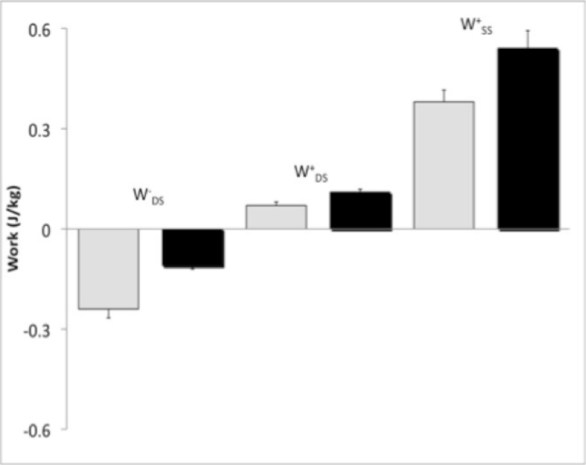

Figure 2. Mean (± SEM) external limb work values for double and single support. The black bars are for walking barefoot, and the grey bars are for walking with an AFO.

REFERENCES

1. Cavagna GA (1975). *J Appl Physiol* **39**:174-179.
2. Donelan JM et al. (2002). *J Exp Biol* **205**:3717-3727.
3. Figueiredo EM et al. (2008). *Ped Phys Ther* **20**:207-223.
4. Palisano R, et al. *Dev Med Child Neurol* **39**:214-223, 1997.

TRIP RECOVERY STRATEGY SELECTION IN YOUNGER AND OLDER ADULTS AND THE ASSOCIATED PHYSICAL DEMANDS

[1] Paulien Roos, [2]Polly McGuigan and [2]Grant Trewartha
[1]Nonlinear Biodynamics Laboratory, Department of Kinesiology, The University of Texas at Austin,
USA, [2]School for Health, University of Bath, UK
email: PERoos@mail.utexas.edu

INTRODUCTION

About one third of older adults fall at least once a year, with tripping as the main cause [1]. There are two main strategies that people use to prevent falling due to a trip: an elevating and a lowering strategy [2]. Strategy selection depends on the timing of the trip stimulus within the swing phase of the walk [3]. Early swing perturbations result in elevating and late swing perturbations result in lowering strategy recoveries [3]. Around mid-swing, there will be a 'strategy overlap' phase where strategy selection is not mechanically obvious. Previous studies showed that older adults more often adopt a lowering strategy than younger adults [4], but it is not understood why. The older adults may become incapable or unwilling to use an elevating strategy as this strategy may be more demanding when perturbed later in swing. The aim of this study was to investigate whether an elevating strategy recovery becomes more demanding when perturbed later in swing.

METHODS

A combined experimental and simulation modelling approach was used. Experimental methods were similar to those described previously [5]. Briefly, female participants were recruited into a 'younger' (n=8) or an 'older' group (n=7). Trips were induced in random walking trials at varying points during the swing phase. Kinematic data were collected at 200 Hz with a CODA CX1 system (Charnwood Dynamics Ltd., UK). Kinematic data were processed as described in [5]. The percentage of the swing phase at which trips were induced ($\%_{swing}$) was calculated relative to the average swing duration of all walking trials. The recovery limb angle at contact was calculated (α_{exp}, defined like α in Fig. 1).

An inverted pendulum model of trip recovery (Fig. 1) was developed to investigate how timing of the trip stimulus and placement of the recovery limb influenced the force required by the recovery limb for successful recovery using an elevating strategy. The model was developed in Simmechanics (Mathworks Natick, MA) and comprised a rigid segment with a mass (m_{body}=61 kg). A rotational spring, with stiffness K_{rot}, at the base simulated the reduction of the body's forward angular momentum by the initial stance limb. A massless linear spring, with stiffness K_{lin}, attached to the rigid segment by a fixed hinge joint (hip) at an angle α, simulated the reduction of the body's forward angular momentum by the recovery limb during the first recovery step. It was assumed that at a trip the linear momentum of walking (at 1.7 m/s) would be directly translated into angular momentum. Recovery was successful when the angular momentum was reversed ($\dot{\theta}<0°/s$). A fall occurred when $\theta>90°$.

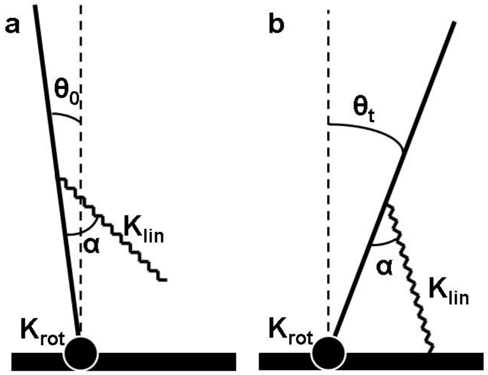

Figure 1: Structure of the inverted pendulum trip recovery model, a) at the instant of the trip stimulus and b) at ground contact of the recovery limb.

Perturbations were initiated with $\%_{swing}$ between 30% and 90% (corresponding to $\theta_0 = -8°$ and $\theta_0 = 16°$), and α between 0° and 90°. When perturbed later in swing the swing limb will be further in front of the body; however there will be less time available for placement of the recovery limb.

We therefore expected recovery step length (and therefore α) to vary with $\%_{swing}$. K_{lin} and K_{rot} were estimated from experimental trials (15 kN/m and 1850 Nm/rad, respectively).

Outcome measures indicated whether successful recovery was possible, as well as the maximum force in the linear spring during the contact phase (F_{max}).

RESULTS AND DISCUSSION

$\%_{swing}$ was calculated for 61 trip trials of the younger adults (59% elevating strategies) and 89 trials of the older adults (20% elevating strategies). Both younger and older adults used an elevating strategy when perturbed in early swing ($\%_{swing}$<40%), and almost always used a lowering strategy when perturbed in late swing ($\%_{swing}$>80%); subjects used both strategies when perturbed in early mid-swing ($\%_{swing}$: 40-60%) (Table 1). Responses to perturbations in late mid-swing ($\%_{swing}$: 60-80%) differed between younger and older adults; older adults always adopted a lowering strategy, while younger adults also adopted elevating strategies (Table 1).

Table 1: The percentage use of elevating strategy recoveries by younger and older adults in response to perturbations in different phases of swing.

	Younger	**Older**
Early swing	100%	100%
Early mid-swing	86%	54%
Late mid-swing	26%	0%
Late swing	0%	6%

Younger adults showed a positive correlation (r = 0.706, p=0.002) between α_{exp} and $\%_{swing}$ during elevating strategy recoveries, which means subjects took larger recovery steps when perturbed later in swing. This correlation was not present in the older adults (r = -0.208, p = 0.516).

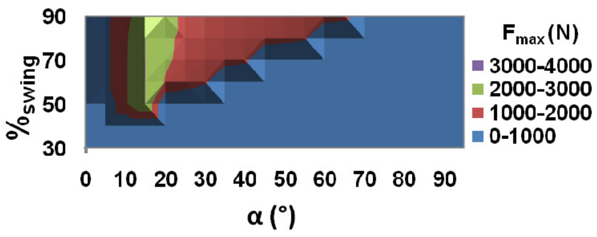

Figure 2: F_{max} for varying α and $\%_{swing}$.

The simulations showed that an increased F_{max} (maximum force in the recovery limb) was required to recover successfully when perturbed later in swing (increasing $\%_{swing}$). An increased recovery step (increased α), like the younger adults showed when perturbed later in swing, reduced the F_{max} value required to recover successfully. (Fig. 2)

In summary, we showed that the shift to adopting a lowering strategy instead of an elevating strategy is made earlier for older (%swing ≈ 60%) than for younger adults (%swing ≈ 80%). We propose that an elevating strategy would be more effective but more difficult than a lowering strategy recovery when individuals are perturbed later in swing. This is based on the assumptions that for an elevating strategy: (1) there is more time available to counteract the forward angular momentum by the initial stance limb, as described by [6]; and (2) the recovery limb is lifted over the obstacle and placed more anterior relative to the body center of mass (CM), providing a larger moment arm to reduce the body's forward angular momentum [6]. It becomes however more difficult to elevate the swing limb over an obstacle when perturbed later in swing, as the body CM moves more anterior to the center of pressure. This may be why the older adults did not increase α_{exp} with $\%_{swing}$. The simulations confirmed that an elevating strategy recovery becomes more difficult later in swing, as larger forces were required in the recovery limb.

CONCLUSIONS

Older adults did not use an elevating strategy when perturbed during late mid-swing (60-80%), while younger adults adopted either an elevating or a lowering strategy. Simulations with an inverted pendulum model showed that recovery limb strength and step length may be the limiting factor for the use of an elevating strategy in mid and late swing. This suggests that strengthening of the appropriate muscle groups is essential in fall prevention practice.

REFERENCES

1. Tinetti ME, et al. *New Engl J Med* **319**, 1701-7, 1988.
2. Eng JJ, et al. *Exp Brain Res* **102**, 339-49, 1994.
3. Schillings AM, et al. *J Neurophysiol* **83**, 2093-102, 2000.
4. Pavol MJ, et al. *J Gerontol A-Biol* **56**, M428-M37, 2001.
5. Roos PE, et al. *Gait Posture* **27**, 352-6, 2008.
6. Pijnappels M, et al. *J Biomech* **37**, 2004.

Evidence for passive stabilization during single-limb stance in Flamingos

Lena Ting[1] and Young-Hui Chang[2]*
[1] Department of Biomedical Engineering, Emory University and Georgia Tech, Atlanta, GA, USA
[2] School of Applied Physiology, GeorgiaTech, Atlanta, GA, USA
*E-mail: yh.chang@ap.gatech.edu *Web: http://www.ap.gatech.edu/chang/CNLhome.html

INTRODUCTION

Standing on one leg is a challenge to postural control and metabolic cost, yet many birds do so with little effort. No group better epitomizes this remarkable balancing act than the flamingos (*Phoenicopteridae)* with their unusually long, thin legs [1]. Passive mechanisms are suggested to lock the ankles [2, 3], but little is known about the knee and hip. The femur is oriented horizontally and likely requires large torques for joint stability (Fig 1). We hypothesized that passive mechanisms contribute significantly to the postural control dynamics in flamingos. We performed morphological and kinematics analyses in dead specimens, and tested postural sway in live birds to obtain anatomical and functional evidence of passive postural stability.

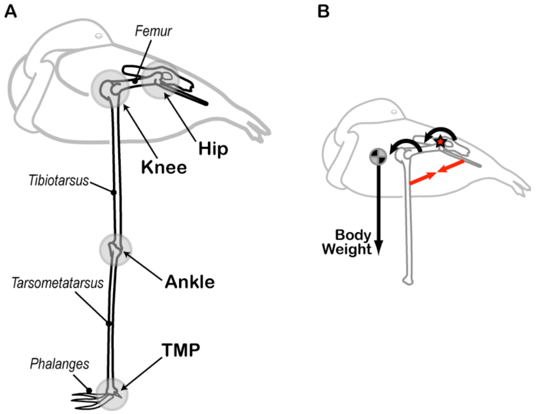

Fig. 1. (**A**) Pelvic limb anatomy of a sleeping flamingo. Femur is horizontally oriented, short, and close to the body. (**B**) Passive mechanisms (red arrows and star) for resisting knee extensor and hip flexor torques (black arrows) generated by body weight during quiet stance to stabilize proximal limb.

METHODS

To identify possible anatomical mechanisms for passive joint stabilization, we studied *ex vivo* kinematics. Two adult Caribbean flamingos (*Phoenicopterus ruber*) were euthanized for veterinary reasons, frozen, and donated by the Birmingham Zoo (Birmingham, AL). We performed all dissections and analyses on fully thawed specimens. To evaluate passive stability of knee and hip joints during one-legged postural control, we held the carcass upright by supporting the ankle and tilted the tibiotarsus forward and backward in the sagittal plane. We measured knee and hip joint angles (Dartfish, Atlanta, GA) until the prep became unstable.

We also measured postural sway in live juvenile Chilean flamingos (*P. chilensis)* at Zoo Atlanta (Atlanta, GA). We collected ground reaction forces and moments (AMTI HE6X6, Watertown MA) during one- and two-legged stance from 8 birds over 3 months (2-11 weeks old). Birds ranged from 0.25-1.4 kg and had hip-to-ground leg lengths of 17-40 cm. Birds often fell asleep on one leg or adopted sleeping postures during trials that could last up to 20 minutes at a time.

We analyzed center of pressure (COP) movements as a 2-D random walk using Stabilogram Diffusion Analysis (SDA). Short-term and long-term regions of the stabilogram diffusion plot suggest open-loop and closed-loop postural control strategies, respectively [4].

RESULTS

We observed full joint range of motion with little resistance during dissection: 63° in knee and 60° in hip. With some exceptions, flamingo pelvic limb anatomy is similar to other birds [5]. In flamingos, several muscles and ligaments originate from the pelvic ischium and insert directly onto proximal tibiotarsus (Fig 1B, red arrows). Even without any muscle activation, this soft tissue chain mechanically limited knee extension. We discovered unique cartilaginous structures at the hip joint that we could not find described in the literature (Fig 1B, red star). With a fully protracted femur, an acetabular protuberance and femoral hook engage and lock to limit sagittal and frontal plane hip motion.

When supported at the distal tibiotarsus, the specimen maintained upright and stable posture similar to behaving birds. In this configuration, knee and hip joints were fully protracted but could be easily retracted through manipulation. With a light downward pressure applied near the tail the body pitched upward relative to the leg, whereas little movement occurred when downward pressure was applied at the shoulders. Notably, the joints remained immobile even when the tibiotarsus was tilted backwards 72° (Fig 2). In forward tilts, the preparation became unstable at 47° due to a large turning moment in the transverse plane, but no changes in knee and hip angle were observed up to this point.

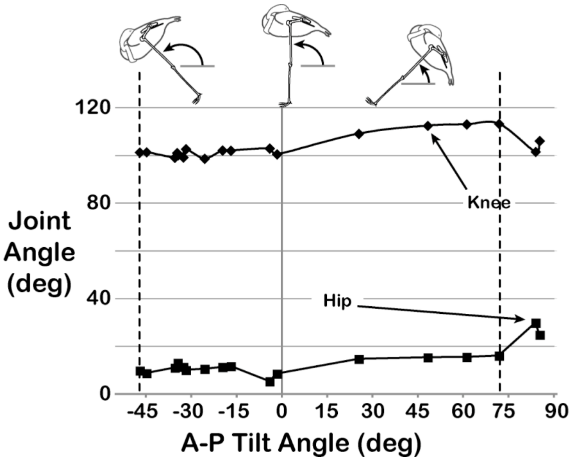

Fig. 2. Knee and hip angles vs. tibiotarsus (A-P tilt) angle in a flamingo specimen. Joints remained stable in forward and backward tilts between dashed lines.

Although their feet cover more than 16 cm^2, juvenile flamingos maintained their COP within a ~1 cm^2 area even when alert and grooming. The initial slope region of the SDA plot indicated a persistent diffusive motion of the COP for time intervals of 0.5-2s, similar to humans (~1s) [4]. With head tucked and eyes closed, however, the COP area was further reduced (Fig 3A) and the timescale of persistent diffusive motion reached as much as 5s (Fig 3B).

DISCUSSION

The anterior location of the flamingo's center of mass provides a biomechanical bias that functionally locks knee and hip joints in a stable postural configuration, even in the absence of muscle activity. As in other birds, the flamingo center of mass is anterior to the knee joint such that the force of gravity generates an extensor torque at the knee and a flexor torque at the hip during quiet stance. The specialized structures of the flamingo limb lock the knee and hip in protraction and adduction with little resistance to retraction (see Fig. 1B). Since the joints are free to move in one direction, this passive stability would not impede the actions of any muscle activity for postural control or escape.

Our behavioral data also confirm our anatomical findings. They demonstrate that closed-loop feedback control of posture acts at extremely long time intervals when birds are quiescent, but on timescales comparable to humans when alert.

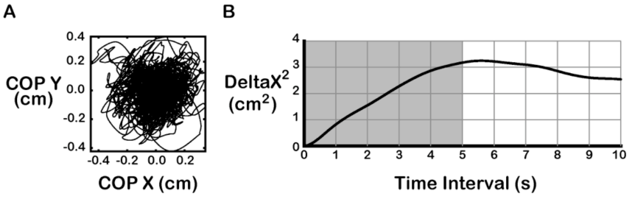

Fig. 3. (**A**) COP movements in an adult sleeping bird remained within a 0.64cm^2 area. (B) SDA from same bird shows ~5s time interval in the short-term region (shaded) suggesting a key role for open-loop control.

CONCLUSIONS

Passive mechanisms for joint stabilization at the knee and hip joints may provide an economical way for flamingos and possibly other birds to maintain a stable one-legged stance for extended periods such as during sleep.

REFERENCES

1. Zeffer A, et al. *Biol J Linnean Soc*, **79**, 461-484, 2003.
2. Necker R. J Comp Physiol A, **192,** 439-448, 2006.
3. Stanley E. *A familiar history of birds. Their nature, habits, and instincts*, London: Parker, 1835.
4. Collins JJ and De Luca CJ. *Exp Brain Res*, **95**, 308-318, 1993.
5. Vanden Berge JC. *The American Midland Naturalist*, **84**, 289-364, 1970.

ACKNOWLEDGEMENTS

We thank Cindy Pinger, Matt Runnells and Clay Hilton, DVM of the Birmingham Zoo; James Ballance, Sprina Liu and Christina Davis at Zoo Atlanta; Jay Bauman for dissection help; Hosnieh Sharafi for help with video analysis; and, Keith Van Antwerp for force platform customization.

RECOVERY LIMB POSITIONING AND TRIP RECOVERY SUCCESS

[1] Paulien Roos, [2]Polly McGuigan and [2]Grant Trewartha
[1]Nonlinear Biodynamics Laboratory, Department of Kinesiology, The University of Texas at Austin, USA, [2]School for Health, University of Bath, UK
email: PERoos@mail.utexas.edu

INTRODUCTION

About 30% of people aged over 65 fall at least once a year, with tripping as the main cause [1]. Most studies investigating biomechanical aspects of trip recovery have focused on response time [2], lower limb strength [3] and muscle activation [4]. The aim of this study was to investigate the force required by the recovery limb to recover successfully in more challenging trip situations. To be able to better control the trip conditions a simulation modelling approach was used.

METHODS

An inverted pendulum model of trip recovery (Fig. 1) was developed to investigate how walking velocity and recovery limb placement influenced the force required by the recovery limb for a successful elevating strategy recovery. The model was developed in Simmechanics (Mathworks Natick, MA) and comprised a rigid segment with a mass (m_{body}=61 kg). A rotational spring, with stiffness K_{rot}, at the base of the rigid segment simulated the reduction of the body's forward angular momentum by the initial stance limb. A massless linear spring, with stiffness K_{lin}, attached to the rigid segment by a fixed hinge joint (hip) at an angle α, simulated the reduction of the body's forward angular momentum by the recovery limb during the first recovery step. The initial body inclination (θ_0) was set to 8°. Perturbations were initiated with initial walking velocities (v_{walk}) between 0.5 and 3.0 m/s, and α between 0° and 95°. To simulate perturbations of different magnitudes v_{walk} was varied. A larger initial walking velocity results in a larger initial angular momentum, which corresponds to a larger perturbation. To simulate different recovery limb placements α was varied.

K_{lin} and K_{rot} were estimated from previously collected experimental trials [5] (15 kN/m and 1850 Nm/rad, respectively). Recovery was successful when the angular momentum was reversed ($\dot{\theta}<0°/s$) and a fall occurred when $\theta>90°$.

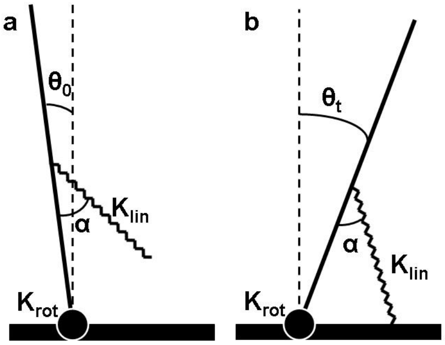

Figure 1: Structure of the inverted pendulum trip recovery model, a) at the instant of the trip stimulus and b) at ground contact of the recovery limb.

Outcome measures indicated whether successful recovery was possible, as well as the maximum force in the linear spring during the contact phase (F_{max}).

An analysis was performed to investigate the sensitivity of the maximum force required for successful recovery (F_{max}) to variations in α and v_{walk}. F_{max} for mid-range values of α and v_{walk} (35° and 0.75 m/s) was compared to F_{max} values one standard deviation (SD) away from this (9° and 0.2 m/s). To increase the moment arm to reverse the body angular momentum and therefore reduce the required recovery effort, α was increased by one SD from the mid-range value. As a slower initial walking velocity would result in a smaller body angular momentum after the trip perturbation and reduce the required recovery effort, v_{walk} was decreased by one SD from the mid-range value.

RESULTS AND DISCUSSION

Simulation results are shown in a surface plot (Fig. 2) with α on the horizontal axis, v_{walk} on the vertical axis and F_{max} (the maximum force in the recovery limb) on the surface. The surface is white where simulations resulted in a fall. This occurred for the smaller α values (corresponding to a smaller recovery step). F_{max} was 0 N when successful recovery was achieved prior to recovery limb ground contact, i.e. the rotational spring at the rigid segment reversed the angular momentum before the linear spring contacted the ground.

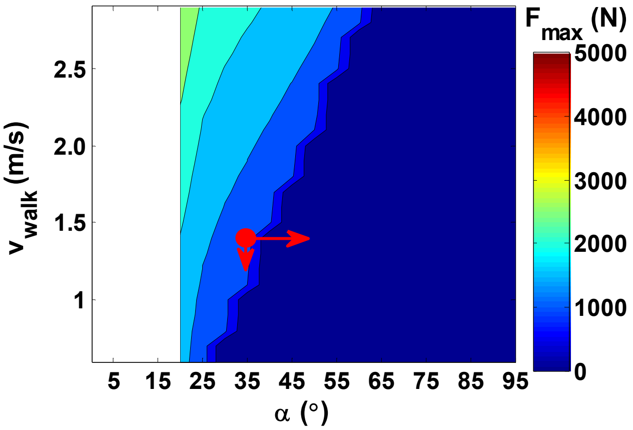

Figure 2: F_{max} for different α and v_{walk} values. The red arrows indicate deviations of one standard deviation in α and v_{walk} from a set mid-range value.

For the medium α values an increased v_{walk} resulted in an increased F_{max}. For large α values successful recovery was possible before the recovery limb contacted the ground (F_{max} = 0 N). As a larger α corresponds to a more forward placement of the recovery limb, there was more time available to reduce the forward angular momentum of the body before ground contact of the recovery limb, resulting in a lower F_{max}.

Table 1: F_{max} for mid-range α and v_{walk}, and for a one SD increase in α or v_{walk} from this mid-range.

	F_{max} (N)	
mid-range value	α + 9°	v_{walk} -0.2 m/s
1260	0	1141

The maximum force required for successful recovery (F_{max}) was more sensitive to a one SD increase in α (larger recovery step length) from the mid-range value than to a one SD decrease of v_{walk} (Fig. 2, Table 1). A one SD increase in α resulted in an F_{max} of 0 N. Therefore successful recovery was achieved prior to recovery limb ground contact and no force was required in the recovery limb.

These results suggest that a combination of recovery limb force and recovery limb placement limits successful recovery. Recovery limb placement is influenced by the reduction of the body forward angular momentum by the initial stance limb [6], response time and recovery limb movement velocity. The simulation results showed that recovery limb positioning influences the force required to recover successfully from a trip. They also showed that appropriate recovery limb positioning is essential to recover successfully in situations close to the limits of successful trip recovery. When interpreting the simulation modelling outcomes it has to be kept in mind that the model is a simplification of reality. The simulations predict only trends of trip recovery behavior.

CONCLUSIONS

Simulations with an inverted pendulum model showed that the force required in the recovery limb to recover successfully from a trip is more sensitive to recovery limb positioning than to walking velocity.

Recovery success is often limited in older adults, as they generally have a small recovery limb force potential, and therefore cannot generate high F_{max} values. In addition, older adults are limited in their recovery limb movement speed and therefore cannot achieve the highest α values. Our simulations imply that older adults would benefit most from a faster response time and increased limb movement speed in order to achieve a sufficiently large recovery step length.

Some studies have shown that slip and trip recovery responses may be improved by training [7]. The results of this study suggest that trip training should focus on both speed and strength aspects of tripping responses.

REFERENCES

1.Tinetti ME, et al. *New Engl J Med* **319**, 1701-7, 1988.
2. Bogert van den AJ, et al. *J Biomech* **35**, 199-205, 2002.
3. Pavol MJ, et al. *J Gerontol A-Biol* **56**, M428-M37, 2001.
4. Pijnappels M, et al. *Gait Posture* **21,** 388-94, 2005.
5. Roos PE, et al. *Gait Posture* **27**, 352-6, 2008.
6. Pijnappels M, et al. *J Biomech* **37**, 2004.
7. Bieryla KA, et al. *Gait Posture* **26,** 208-13, 2007.

INTRADISCAL PRESSURE CHANGES WITH POSTERIOR LUMBAR DYNAMIC STABILIZATION SYSTEMS: UNIVERSAL CLAMP AND WALLIS

[1]Miranda N. Shaw, [2]Brice Ilharreborde, [1]Lawrence J. Berglund, [1]Kristin D. Zhao, [1,3]Ralph E. Gay, and [1]Kai-Nan An
[1]Biomechanics Laboratory, Division of Orthopedic Research, Mayo Clinic, Rochester, MN
[2]Department of Pediatric Orthopedic Surgery, Robert Debré Hospital, Paris 7 University, France
[3]Department of Physical Medicine and Rehabilitation, Mayo Clinic, Rochester, MN
email: an.kainan@mayo.edu

INTRODUCTION

One cause of chronic low back pain is damaged or degenerated intervertebral discs. This condition is sometimes treated by fusing the symptomatic level. However, accelerated adjacent level degeneration is a well established risk. Implants that stabilize the symptomatic motion segment while preserving motion and allowing disc loading have become available.

The aim of this study was to quantify pressure changes in the intervertebral disc (IVD) due to the application of two nonfusion, dynamic stabilization systems: Universal Clamp (UC) and the Wallis device.

METHODS

Nine fresh frozen human lumbar spines (L1-sacrum) were obtained from the Mayo Anatomical Bequest Program following IRB approval. Specimens were thawed, kept moist with saline, and all non-ligamentous soft tissues were removed. Specimens were potted with the sacrum oriented in neutral position. Prior to experimentation, the UC bands were placed at L3 and L4. Placement of these devices did not interfere with testing procedures.

Potted specimens were attached to a custom spine testing apparatus previously described [1] (Figure 1) and tested to +/- 7.5 N-m torque for range of motion in flexion/extension (F/E), left/right lateral bending (LB), and left/right axial rotation (AR). Three-dimensional kinematic measurements were obtained using an Optotrak™ Certus optoelectric data acquisition system (Northern Digital Inc., Ontario, Canada) and accompanying software (The Motion Monitor™, Innovative Sports Training, Chicago, IL, USA). Active Optotrak marker triad sensors were rigidly fixed to each vertebral body.

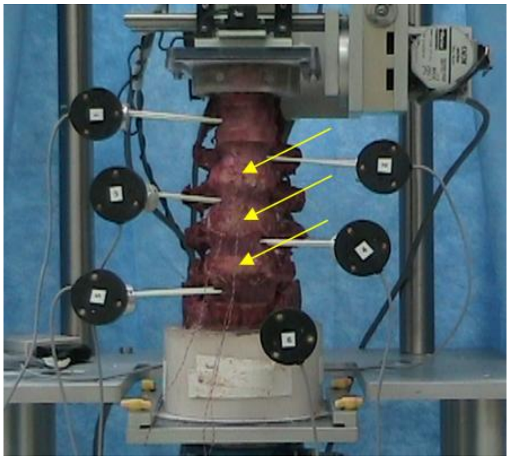

Figure 1: Spine testing apparatus with arrows indicating the pressure transducer IVD entrance.

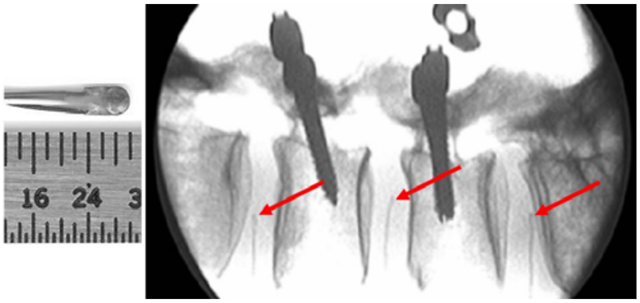

Figure 2: Pressure transducer and fluoroscopic image demonstrating transducer positioning.

A single miniature pressure transducer (Model 060s, Precision Measurement Company, Ann Arbor, MI) was inserted into the nucleus of each instrumented L3/L4 disc and the two adjacent discs (L2/L3, L4/L5). Positioning within the central IVD was verified by fluoroscopy (Figure 2). Insertion was accomplished by a telescoping needle arrangement that facilitated placement without injury to the transducer or wire interface. Pressure readings were amplified, filtered, and recorded simultaneously during range of motion measurements using the MotionMonitor™ software. Each transducer was calibrated in an air chamber prior to use.

Each spine was tested using the same protocol, while instrumented at L3/L4: (1) intact, (2) bilateral sublaminar Universal Clamps (UC), (3) UC system connected by a transverse rod (UCTR), and (4) Wallis. During conditions (1), (2), and (3), the UC bands remained attached to the specimen. For conditions (3) and (4), the L3/L4 supra- and interspinous ligaments were transected. When Wallis was tested (4), the UC bands were removed.

RESULTS AND DISCUSSION

Six specimens were removed from the analysis due to degenerated and/or dehydrated disc conditions that rendered the output data uninterpretable. Therefore, only results from three specimens are reported. Representative pressures for each specimen are shown in Figure 3.

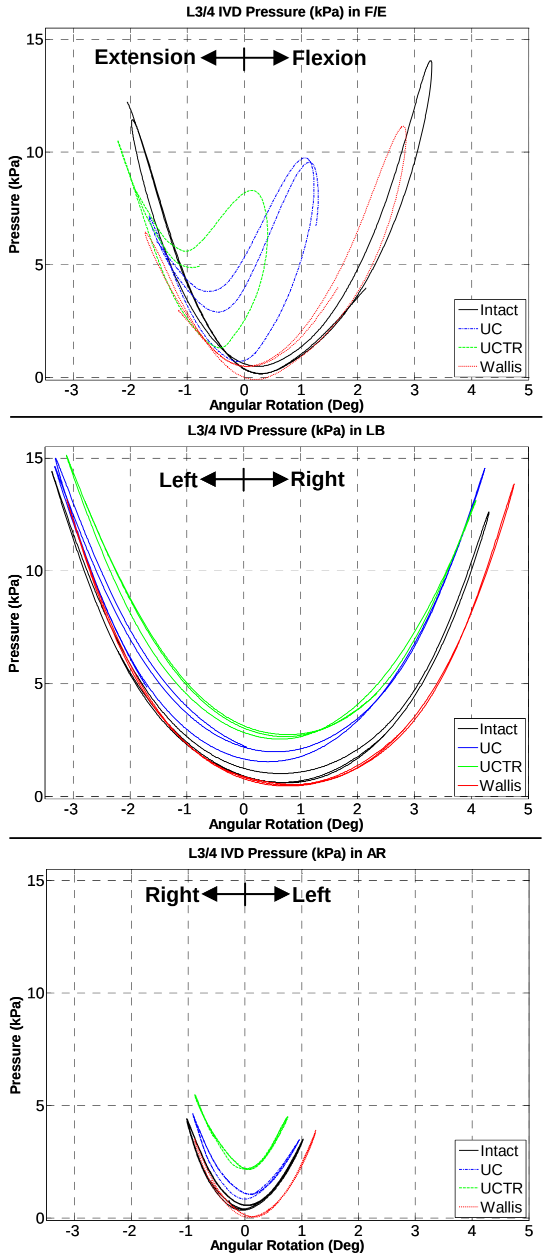

Figure 3: Representative pressure (kPa) in the IVD during dynamic testing.

Only total pressure range changes are reported here. At the instrumented level, L3/L4, pressure decreased in F/E with the UC (15%) and UCTR (31%) and increased with the Wallis (31%), as compared to intact. In LB, all devices resulted in an increase in pressure from that of intact (UC:9%, UCTR:2%, Wallis:1%). Pressure decreased with the UC (16%) and UCTR (15%) and increased with the Wallis (15%) in AR.

At the adjacent levels, similar pressure changes were found as at L3/L4. The largest pressure changes were exhibited in the L4/L5 discs, especially in AR. The UC decreased pressure by 10% and pressure increased with UCTR (32%) and Wallis (26%) in AR.

CONCLUSIONS

Each of the dynamic stabilization systems resulted in change of intradiscal pressure as compared to intact. However, the pressure trends, to increase as the spine moves into maximum range of motion, were similar for all devices. In general, the UCTR resulted in the smallest change in total pressure and Wallis the largest.

This study had several limitations. Disc pressure is very sensitive to axial loading. Only pure moment loading was applied in this study and not axial loading. Therefore, the actual pressure values recorded were due to the bending moment rather than internal disc pressure. Discal pressure is also sensitive to disc health and hydration. Since this was a human cadaver study, many discs were dehydrated or degenerated. Thus, the pressure transducers were often damaged due to the fibrous nature of the degenerated disc or there was inconsistent data due to dehydration.

REFERENCES

1. Gay RE, et al. *Clin Biomech* **23**, 1-7, 2008.

ACKNOWLEDGEMENTS

This study was funded by a contract with Abbott Spine, Bordeaux, France.

INFLUENCE OF MICROSTRUCTURE ON THE MECHANICAL PROPERTIES OF VERTABRAL BONE ASSESSED BY QUANTITATIVE COMPUTED TOMOGRAPHY – STUDY ON SYNTHETIC MODEL-

[1]Annie Levasseur, [2]Heidi-Lynn Ploeg and [1, 3]Yvan Petit
[1]LIO, Hôpital du Sacré de Montréal, Montreal, Canada,
[2]University of Wisconsin-Madison, Madison, USA;
[3]École de technologie supérieure, Montreal, Canada.; email: gog92@hotmail.com

INTRODUCTION

Assessment of bone mechanical properties from quantitative computed tomography (QCT) and predictive relationships is commonly used to personalize biomechanical finite element analyses (FEA). Such models are then used to predict bone mechanical behaviour under various loading conditions.

Results of previous studies revealed important discrepancies between mechanical behaviour predicted from QCT and experimental results [1-2]. Our hypothesis is that bone microstructure is an important biomechanical parameter for the establishment of predictive relationships of bone properties, which is usually not considered in QCT-based methods. The purpose of this study was to investigate the influence of microstructure on vertebral bone's apparent structural response.

METHODS

Sixty compression specimens (dia 19.05 mm x 25.40 mm) and twelve synthetic vertebrae were fabricated out of acrylonitrile butadiene styrene by an additive fabrication process (Prodigy Plus, Stratasys, MN, USA). Three structural parameters were controlled (Figure 1): spacing between filaments (air gap), layer orientation and raster orientation.

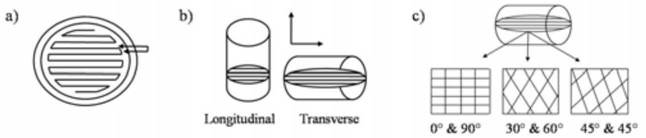

Figure 1: Structural parameters controlled during fabrication: (a) air gap, (b) layer orientation and (c) raster orientation.

Two sets of predictive relationships were established between the QCT density (ρ) and the measured elastic modulus (E) of the compression specimens: one taking into account all structural parameters and the second confounding some or all parameters. Structural parameters were considered when defining relationships by regrouping together compression specimens with the same structural parameter. Apparent elastic moduli within CT-scanned vertebrae were estimated using all derived E-ρ relationships and utilised to define the mechanical properties of vertebral FEAs. The overall structural stiffness of vertebrae predicted with the FEA was then compared to the mechanical behaviour obtained from compressive tests.

RESULTS AND DISCUSSION

Second order polynomial relationships were found between the density and the elastic modulus of the test specimens (Table 1). Higher coefficients of determination were obtained when structural parameters were considered into the relationships.

Table 1: Predictive relationships and coefficient of determination (R^2) between density and elastic modulus

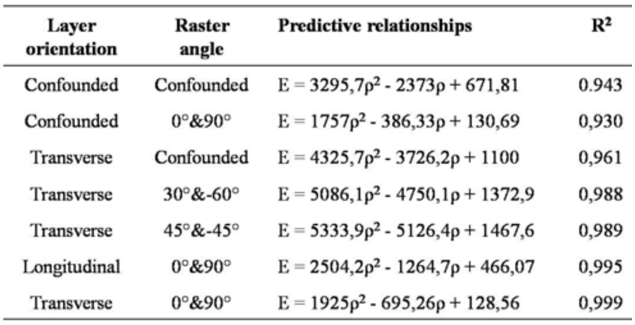

Layer orientation	Raster angle	Predictive relationships	R^2
Confounded	Confounded	$E = 3295,7\rho^2 - 2373\rho + 671,81$	0.943
Confounded	0°&90°	$E = 1757\rho^2 - 386,33\rho + 130,69$	0,930
Transverse	Confounded	$E = 4325,7\rho^2 - 3726,2\rho + 1100$	0,961
Transverse	30°&-60°	$E = 5086,1\rho^2 - 4750,1\rho + 1372,9$	0,988
Transverse	45°&-45°	$E = 5333,9\rho^2 - 5126,4\rho + 1467,6$	0,989
Longitudinal	0°&90°	$E = 2504,2\rho^2 - 1264,7\rho + 466,07$	0,995
Transverse	0°&90°	$E = 1925\rho^2 - 695,26\rho + 128,56$	0,999

Figure 2 compares the stiffness measured experimentally with the prediction using the FEA. The difference between the model's prediction and the experimental data was significantly smaller (p=0.04, Wilcoxon test) when mechanical properties of vertebrae were estimated considering the structural parameters (7 ± 4% compared to 13 ± 9%).

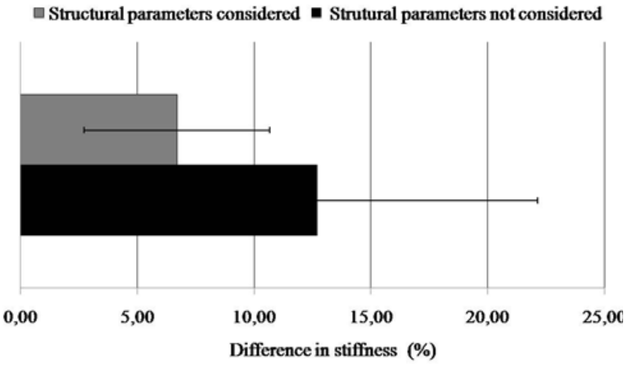

Figure 2: Percentage of stiffness difference between experimental data and predicted values.

CONCLUSIONS

Results suggest that considering structural parameters significantly improves the predicted mechanical behaviour of vertebrae using FEA. Therefore, microstructure is important to take into account for the prediction of bone's apparent structural response.

REFERENCES

1.Liebschner MA, et al. *Spine* **28**, 559-565, 2003.
2.Silva MJ, et al. *J. Orthop. Res.* **16**, 300-308, 1998.

ACKNOWLEDGEMENTS

This research was funded in part the Canadian Institutes of Health Research (CIHR) and Canadian Foundation for Innovation (FCI). The authors wish to thank Karine Dupuis and Yan Bourgeois for their technical support.

AN IN-VITRO BIOMECHANICAL EVALUATION OF POSTERIOR LUMBAR DYNAMIC STABILIZATION SYSTEMS: UNIVERSAL CLAMP AND WALLIS

[1]Miranda N. Shaw, [2]Brice Ilharreborde, [1]Lawrence J. Berglund, [1]Kristin D. Zhao, [1,3]Ralph E. Gay, and [1]Kai-Nan An
[1]Biomechanics Laboratory, Division of Orthopedic Research, Mayo Clinic, Rochester, MN
[2]Department of Pediatric Orthopedic Surgery, Robert Debré Hospital, Paris 7 University, France
[3]Department of Physical Medicine and Rehabilitation, Mayo Clinic, Rochester, MN
email: an.kainan@mayo.edu

INTRODUCTION

Chronic low back pain due to intervertebral disc degeneration is often treated by fusing the symptomatic level. Yet many risks and problems are still associated with this procedure. Recently, more treatment options for degenerative lumbar spine conditions have become available and include motion preservation devices. These devices, often referred to as ‘dynamic stabilization’ devices, are designed to provide stabilization while retaining some physiologic spinal motion.

The purpose of this study was to compare the relative range of motion differences of two nonfusion, dynamic stabilization systems: Universal Clamp (UC) and Wallis.

METHODS

Nine fresh frozen human lumbar spines (L1-sacrum) were obtained from the Mayo Anatomical Bequest program after IRB approval. Specimens were thawed at room temperature prior to experimental testing. All non-ligamentous soft tissues were removed and the specimens were kept moist with normal saline soaked toweling. Specimens were potted in fixtures designed to integrate with a custom spine simulator apparatus with the sacrum oriented in neutral position. Prior to experimentation, the UC bands were placed at L3 and L4. Placement of these devices did not interfere with testing procedures.

Potted specimens were attached to a custom spine testing apparatus previously described [1] (Figure 1) and tested to +/- 7.5 N-m torque for range of motion in flexion/extension, left/right lateral bending, and left/right axial rotation. Three-dimensional kinematic measurements were obtained using an Optotrak™ Certus optoelectric data acquisition system (Northern Digital Inc., Ontario, Canada) and accompanying software (The MotionMonitor™, Innovative Sports Training, Chicago, IL, USA). Active Optotrak marker triad sensors were rigidly fixed to each vertebral body.

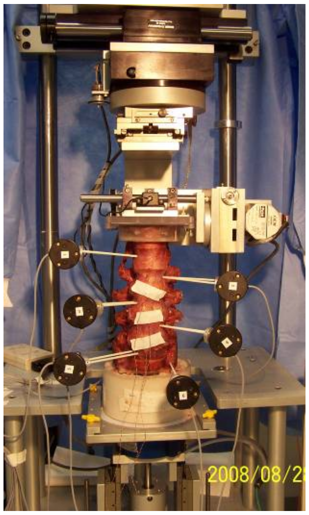

Figure 1: Spine testing apparatus.

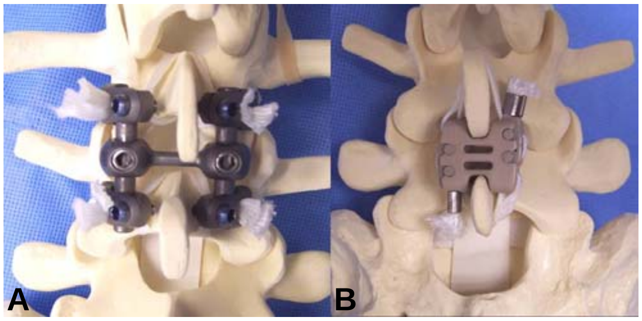

Figure 2: **A**: Universal Clamp with Transverse Rod; **B**: Wallis.

Each spine was tested with the same regime: (1) intact, (2) L3-L4 dynamic stabilization with bilateral sublaminar Universal Clamps (UC), (3) L3-L4 UC system connected by a transverse rod (UCTR) (Figure 2A), and (4) L3-L4 dynamic posterior stabilization with the Wallis device

(Figure 2B). During conditions (1), (2), and (3), the UC bands remained attached to the specimen. For conditions (3) and (4), the L3-L4 supra- and interspinous ligaments were transected. When Wallis was tested (4), the UC bands were removed.

Angular motions at +/-7.5 N-m at the instrumented level, L3-L4, and adjacent levels for each device were compared to intact. Data were compared with one-way repeated measures ANOVA (P<0.05). Pairwise comparisons were tested with Tukey (95% confidence) between levels of instrumentation.

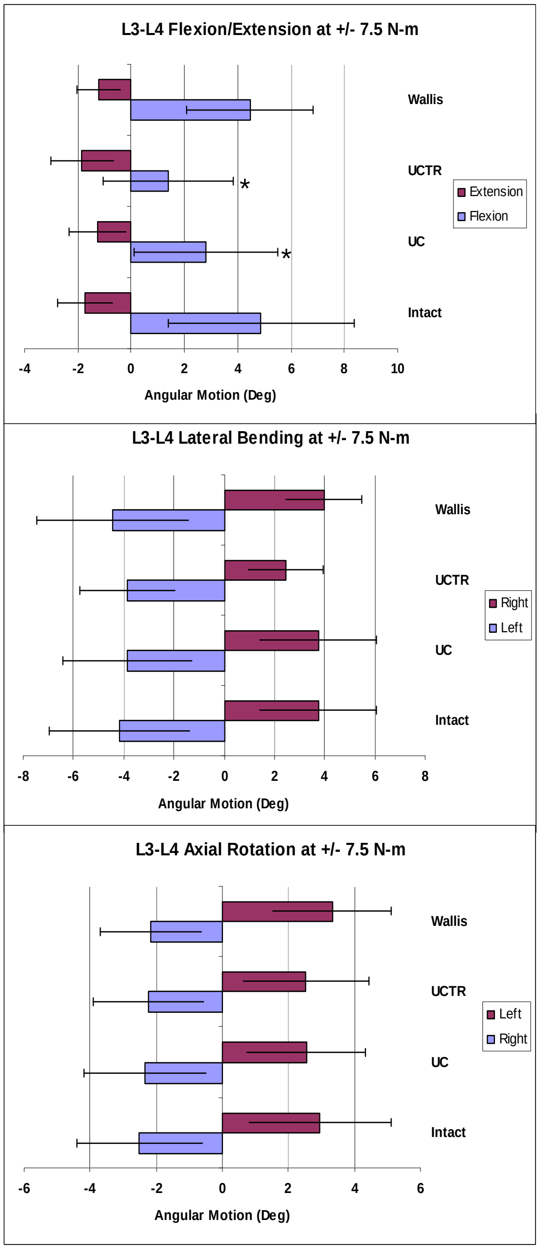

Figure 3: Angular motion of the instrumented level, L3-L4. * Significance at P<0.05

RESULTS AND DISCUSSION

The change in the range of motion due to surgical intervention from the intact condition is our main interest. Thus, results reported here are based on the pairwise analyses between the intact condition and each intervention.

At the adjacent levels, L2-L3 and L4-L5, there was no significant change in range of motion due to instrumentation. The range of motion at the instrumented level, L3-L4, is shown in Figure 3. There was no significant difference in extension. However, in flexion the range of motion decreased 44% with the UC and 76% using the UCTR system, as compared to the intact condition. These decreases in motion were significant with P<0.05. No significance was found in lateral bending or axial rotation.

CONCLUSIONS

Changes in range of motion associated with three posterior dynamic stabilization systems were evaluated: Universal Clamp, Universal Clamp with transverse connector, and Wallis. These devices significantly changed motion of the instrumented level in flexion, but not in extension, lateral bending, or axial rotation. The dynamic stabilization systems did not significantly affect adjacent level kinematics.

Posterior dynamic stabilization systems such as the ones investigated here are designed to stabilize degenerated spinal levels while allowing some motion of the diseased spine. The Universal Clamp and Wallis designs provided motion similar to intact at the instrumented level.

REFERENCES

1. Gay RE, et al. *Clin Biomech* **23**, 1-7, 2008.

ACKNOWLEDGEMENTS

This study was funded by a contract with Abbott Spine, Bordeaux, France.

UPPER EXTREMITY KINETIC MODEL OF FUNCTIONAL ARM REACHING IN STROKE

Wei Liu[1], Mary Rodgers[1], Sandra McCombe Waller[1], Thomas Kepple[2] and Jill Whitall[1]
[1]Dept. of Physical Therapy & Rehabilitation Science, University of Maryland School of Medicine, Baltimore, MD
[2]Dept. of Health, Nutrition and Exercise Sciences, University of Delaware, Newark, DE
Email: wliu@som.umaryland.edu, Web: www.pt.umaryland.edu

INTRODUCTION

Currently, few biomechanical kinetic models are available to quantify the kinetics of upper extremities (UE) during the functional arm-reaching task in individuals with stroke. Although UE kinematics of individuals with stroke has been extensively studied [1], the kinetics of UE has only been limited to either isometric contractions (static) [2], or reaching with gravity eliminated [2, 3]. The purpose of this study was to develop a three-dimensional (3-D) kinetics model for functional arm reaching that includes gravitational force in individuals with stroke.

METHODS

An UE kinetics model was developed that included 7 rigid body segments: trunk, left/right upper arm, left/right forearm and left/right hand. There are a total of 14 degree of freedoms (DoF) in this model, including three degree-of-freedom shoulder joints and two degree-of-freedom elbow and wrist joints at each side. The trunk is treated as ground with reference to the lab coordinate system (global system). UE kinematics were calculated by using Euler angles following X-Y-Z rotation sequence (Figure 1). Joint moments were determined by using simplified Newton-Euler approach [4].

Application of the model was accomplished in a pilot study that included three right-handed subjects with hemiparesis (ages: 63±4 years) and three non-disabled adults (age: 34±7 years). After informed consent, subjects were seated at a table and reached with one arm toward the side of a box located in front of them at their maximum reach distance from the edge of the table. Unilateral reaching tasks were completed at preferred speed with restricted trunk movement. The Motionmonitor^{TM} magnetic

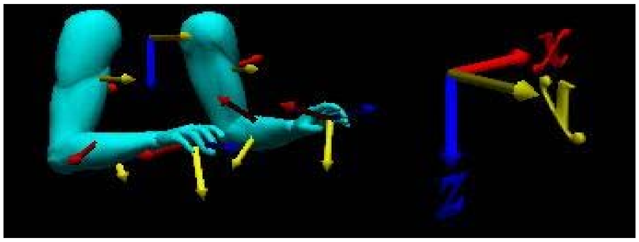

Figure 1: Global and local coordinate system set up

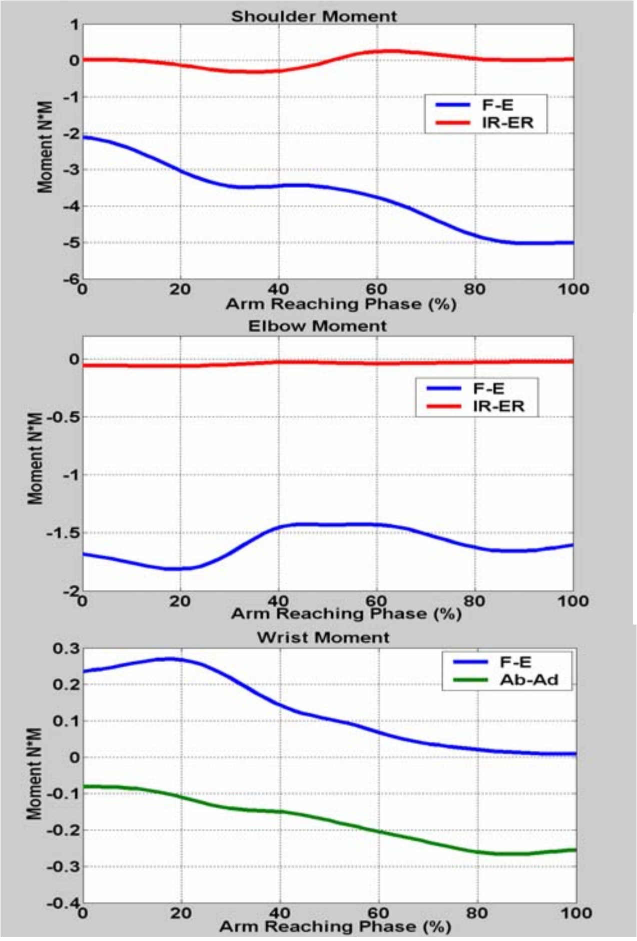

Figure 2: Mean joint moments of shoulder, elbow and wrist of non-disabled subjects (n=3). Positive direction (+): E (Extension), Ad (Adduction), ER (External Rotation); Negative direction (-): F (Flexion), Ab (Abduction), IR (internal Rotation). Profiles are the average of three trials for the three subjects.

tracking system (Chicago, IL) was used to collect position data (50 Hz) from seven sensors attached to the trunk, bilateral upper arms, forearms and hands. Joint moment profiles were compared between the paretic arm of individuals with stroke and the right arm of non-disabled adults.

RESULTS AND DISCUSSION

Shoulder and elbow moments in the non-disabled adults were mainly flexor for this unilateral reaching task. Wrist moments were mainly extensor associated with increasing wrist abductor because supination of the elbow caused gravity to pull the wrist joint into adduction (Figure 2). In contrast, the kinetics profile of the subjects with stroke during the arm reaching showed different movement control strategy in which impairment of the hand prevented wrist moments from counteracting gravity during reaching when the elbow supinates (Figure 3). This kinetic model allowed us to detect a clear movement control strategy in individuals with stroke. Future kinetics analysis will determine how kinetics produces the desired arm-reaching trajectory and enables accurate assessment of the efficacy of physical rehabilitation interventions.

REFERENCES

1. Levin MF et al. *Exp Brain Res*. **143**, 171-180, 2002.
2. Ellis MD et al. *Muscle Nerve*. **32**, 170-178, 2005.
3. Sainburg RL etal. *Exp Brain Res*. **142**, 241-258, 2002.
4. Winter DA. *Biomechanics and Motor Control of Human Movement*, **Third Edition**, John Wiley & Sons, New York, 2004.

ACKNOWLEDGEMENTS

This study was supported by NIA Claude D. Pepper Older Americans Independence Center P60-AG12583; NICHD R21HD047756.

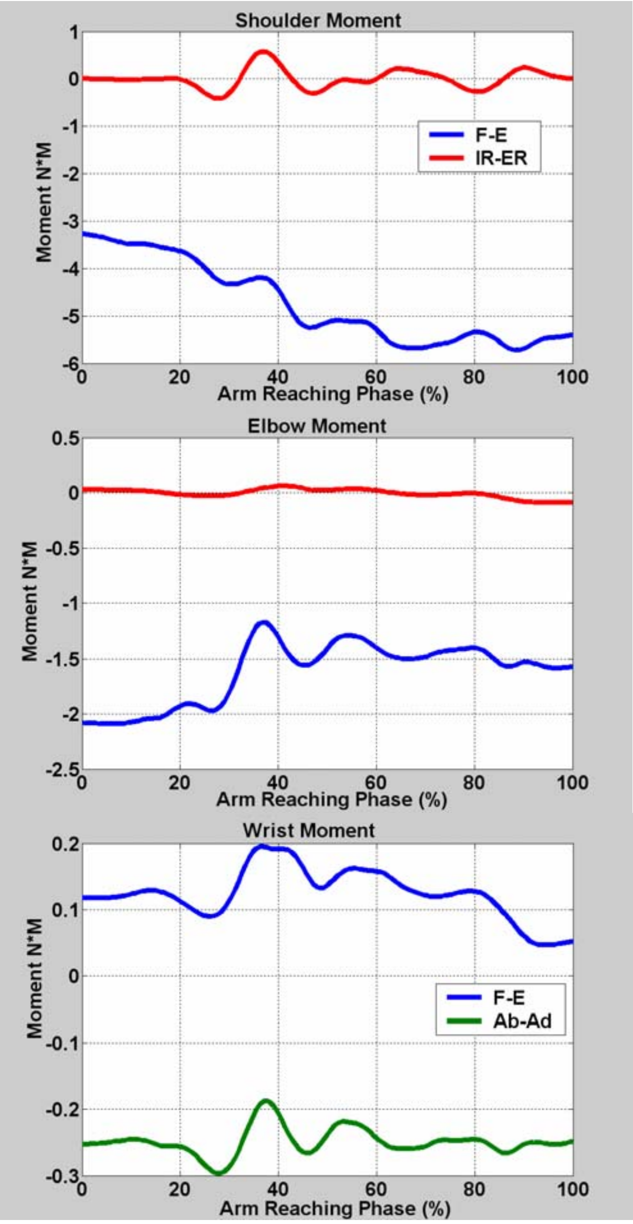

Figure 3: Mean joint moments of shoulder, elbow and wrist of subjects with stroke (n=3). Positive direction (+): E (Extension), Ad (Adduction), ER (External Rotation); Negative direction (-): F (Flexion), Ab (Abduction), IR (internal Rotation). Profiles are the average of three trials for the three subjects.

MODULATION OF FORCE STRUCTURE VIA VISUAL SCALING OF FAST TIME SCALE PROCESSES

Xiaogang Hu and Karl M. Newell
Department of Kinesiology, The Pennsylvania State University
Email: xxh120@psu.edu

INTRODUCTION

Long-range temporal correlations (i.e. 1/f processes) have been observed in human motor behaviors (e.g. isometric force control [1]). It has been shown that control of the high frequency components of force output is degraded, possibly due to the latency of sensorimotor feedback, tremor, and visual information scaling (i.e. smaller visual scaling in high frequency force components [2]).

This study investigated whether selectively increasing the visual scaling of the high frequency force components enhances the control of the faster time scale processes under different force targets. A related question was whether and how the control of the low frequency force components will be changed. Thus, we examined the hypothesis that increased visual scaling in the high frequency components improves the control of high frequency force bandwidth but the effect of this manipulation on the control of the low frequency components was more open.

METHODS

Eleven right handed young healthy individuals participated in this study. They gave informed consent that was approved by the University IRB. Participants were seated in a chair facing a LCD monitor, with their right dominant hand pronated on the table. Through isometric abduction, the lateral side of the index finger pressed on a load cell. The force was sample at 40 Hz.

The Maximum Voluntary Contraction (MVC) was recorded. The participants were instructed to adjust their force to match a red target waveform displayed on the monitor. A yellow trajectory representing their force was displayed in real time to the subjects. Four types of waveforms were used as force targets: 1) straight line; 2) 0.8 Hz sine wave; 3) pink noise; 4) brown noise. The mean amplitude of the force target was 20% of participant's MVC and the amplitude was ±5% of MVC.

During the experiment, the high frequency components of the force feedback were amplified by a scaling (scaling = 0, 2, 4, 6, 8). Two frequency ranges (4-8 Hz and 8-12 Hz) were separately manipulated with scaling. The experiment consisted of 4 blocks of trials, with one type of force target in each block. Each block contained 10 conditions (5 Scaling × 2 Frequency ranges), the order of which was randomized across subjects. Participants had 3 consecutive 20 s trials at each condition.

RESULTS AND DISCUSSION

The force structure was assessed by using a spectral slope analysis, where a linear regression was performed on the logarithmic power spectrum (Fig. 1). In the constant target condition, statistical analysis revealed that the slope decreased with

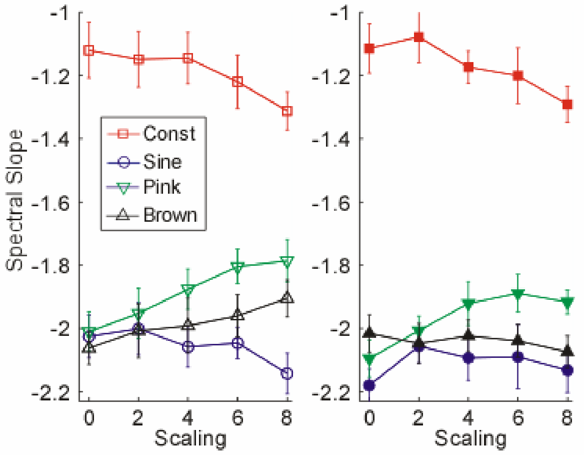

Figure 1: Spectral slope. Left panel: the 4-8 Hz bandwidth amplification condition, and the mean slopes are represented by open symbols. Right panel: the 8-12 Hz bandwidth amplification condition, and the mean slopes are represented by solid symbols. Error bars represent standard error across participants.

increasing scaling [$p = 0.001$]. In contrast, in the pink noise target condition, the slope increased when scaling increased [$p = 0.001$]. In the brown noise target, the slope increased significantly in 4-8 Hz bandwidth amplification condition [$p = 0.015$]. No significant change of slope was found in the sine wave target condition [$ps > 0.05$].

The sum of normalized power (SoP) of three frequency bandwidths covering 4 Hz range (0-4 Hz, 4-8 Hz, and 8-12 Hz) was calculated to provide more detailed information concerning where in the frequency range the changes occurred (see Fig 2). In the constant target condition, statistical analysis showed that the SoPs of 0-4 Hz in the 4-8 bandwidth amplification condition decreased with increasing scaling [$p = 0.004$]. The SoPs of 4-8 Hz and 8-12 Hz frequency ranges also decreased when scaling increased [$ps < 0.05$]. In the pink noise target, the SoPs of 0-4 Hz decreased significantly with increasing scaling [$p = 0.002$]. However, no significant change of SoPs in any of the 4-8 Hz and 8-12 Hz frequency ranges was found [$ps > 0.05$].

In the constant target condition, the larger ratio of decrease in the higher frequency force resulted in a higher proportion of power in the lower frequency, which lead to a steeper spectral slope. However, in the pink noise target, the increased slope with increasing scaling was mainly contributed by a decrease of power in 0-4 Hz. The amplification of power in high frequency ranges in visual feedback had no significant effect on changes of SoP in the sine wave and brown noise targets.

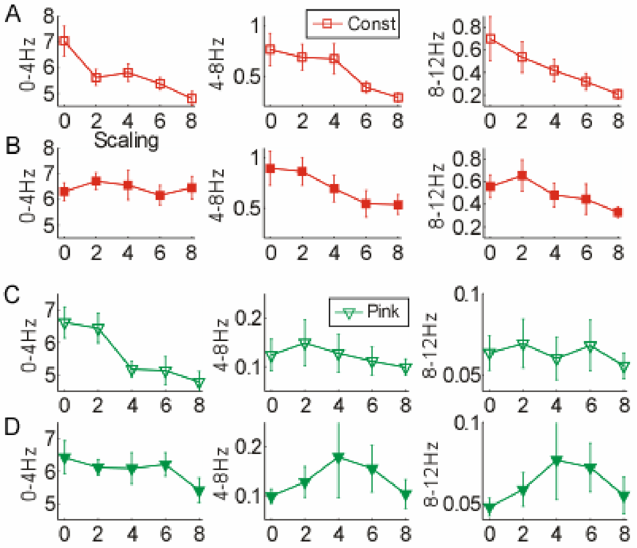

Figure 2: Sum of power (SoP) of three frequency ranges. The left column: the SoP of 0-4 Hz, the middle column: the SoP of 4-8 Hz, and the right column: the SoP of 8-12 Hz. Open symbols represent 4-8 Hz bandwidth amplification condition (Panel A & C), solid symbols represent 8-12 Hz bandwidth amplification condition (Panel B & D).

The results showed that increased visual scaling in the high frequency components facilitated the control of high frequency force (i.e. reduced power in high frequency force in the constant target condition) and that the control of the low frequency force bandwidth was also changed (i.e. decreased power in 0-4 Hz in the constant target and the pink noise target conditions).

The visual scaling manipulations in the sine wave and brown noise target conditions had no effect on the force structure. This result may be explained by the fact that the slower time scales dominate the force output (steeper slope), therefore, the fast time scales have less effect during the force control.

CONCLUSIONS

This study showed that increased visual scaling in high frequency bandwidth facilitated the control of force within the frequency bandwidth as well as in the neighboring bandwidths. Depending on the task constraints, the findings reveal that the amplification of the fast time scales feedback information can be utilized to enhance force control but this scaling modulation becomes less effective as the force frequencies increase. It is speculated that a control model based on frequency modulated error feedback mechanism may be able to predict the multi-time scale behaviors in force control.

REFERENCES

1. Sosnoff JJ, Newell KM. *Percept Psychophys* **67**, 335-344, 2005.
2. Sosnoff JJ, et al. *J Exp Psychol Hum Percept Perform* **35**, 439-446, 2009.

ACKNOWLEDGEMENTS

This study was supported by NSF 0518845

THE EFFECTS OF ANTERIOR SHEAR DISPACEMENT RATE ON THE VISCOELASTIC PROPERTIES OF THE PORCINE CERVICAL SPINE

Kaitlin M. Gallagher, Samuel J. Howarth, Jack P. Callaghan
Department of Kinesiology, University of Waterloo, Waterloo, ON, Canada
email: kgallagh@uwaterloo.ca

INTRODUCTION

Load rate has been shown to influence ultimate failure loads and failure patterns of the porcine cervical spine under anterior shear loading [1,2]. Higher load rates have been used to produce acute anterior shear failure of the porcine cervical spine with higher ultimate loads [2]. Pars interarticularis fractures were shown to occur at lower anterior shear load rates while combined pars interarticularis fractures with endplate avulsions occurred with higher load rates [2].

While tissue-specific viscoelastic properties of the spine are well understood, it is unclear whether the viscoelastic properties are consistent for the vertebral joint structure. For example, soft tissue injuries have been shown to be load rate dependent, whereas hard tissue injuries were shown to not be load rate dependent [1]. The primary purpose of this study was to investigate the effects of displacement rate on the properties of the porcine cervical spine exposed to anterior shear failure under a controlled compressive load. It was hypothesized that higher displacement rates will result in higher load rates and evidence of viscoelastic properties. A secondary purpose of this study is to determine preliminary acute anterior shear failure limits with changes in displacement rate.

METHODS

Thirty porcine cervical functional spinal units (FSU) were tested in this study (C3/4 n=15, C5/6 n=15). Width and depth of each FSUs exposed endplates were measured to estimate endplate area of the FSUs intervertebral disc. An x-ray, in the horizontal plane, of each FSU was taken to quantify facet angles and tropism (Table 1).

Each FSU was secured into a set of aluminum cups with a combination of steel wire, screws, and dental plaster (Denstone, Miles, IN, USA) and placed into a servohydraulic materials testing machine (Instron 8872, Instron Canada, Burlington, ON, Canada). Initially, a compressive 300N preload was applied to the FSU for 15 minutes. Following the initial preload, flexion/extension and anterior/posterior shear passive tests were performed to quantify their respective neutral zones. Shear displacement was applied via two linear actuators (Tolomatic Inc., Hamel, MN, USA) that were driven by two brushless servomotors (Kollmorgen/Danaher Motion Inc., Radford, VA, USA). Applied shear forces were measured using two load cells (Transducer Technologies, Temecula, CA, USA) mounted in series with the linear actuators.

Each FSU was randomly assigned to one of three shear displacement rates (1, 4, or 16mm/s) for the acute shear failure protocol. A constant 1600N compressive load was applied simultaneously throughout acute shear failure. Flexion/extension and anterior/posterior shear passive tests were performed following the acute failure protocol to quantify changes after failure. Following the post-failure passive tests, x-rays of the FSU were taken and injuries were documented.

Ultimate anterior shear load, displacement, average stiffness, and energy to failure were determined for each FSU from the anterior shear load-displacement curve during acute failure. Initial load rate and stiffness over the first 0.5 seconds of the failure test were also calculated.

Table 1: Mean (standard deviation) facet and disc geometries.

	FSU Level	
	C3/4	**C5/6**
Disc Area (mm^2)	646 (64)	691 (66)
Left Facet Angle (deg)	43.9 (4.2)	47.2 (2.8)
Right Facet Angle (deg)	44.0 (3.4)	49.8 (3.8)

One-way analyses of variance (SAS, Cary, NC, USA) were performed on each of the outcome measures. Tukey's post hoc tests were performed for all significant main effects. The level of statistical significance was $p < 0.05$ for all analyses.

RESULTS AND DISCUSSION

Initial load rate for C3/4 and C5/6 FSUs was highest for the 16 mm/s displacement rate ($p < 0.0013$) (Figure 1). The 1 mm/s and 4 mm/s displacement rates did not produce load rates that were significantly different from one another (C3/4 $p = 0.1207$; C5/6 $p = 0.6200$). Ultimate load of the C5/6 FSUs was higher for the 16 mm/s group than both the 1 mm/s ($p = 0.033$) and 4mm/s ($p = 0.027$) groups (Figure 2). Significant differences were not found between the displacement rates for ultimate load at the C3/4 level. The remaining dependent variables (ultimate displacement, average stiffness, and energy) showed no significant differences between displacement rates at either level.

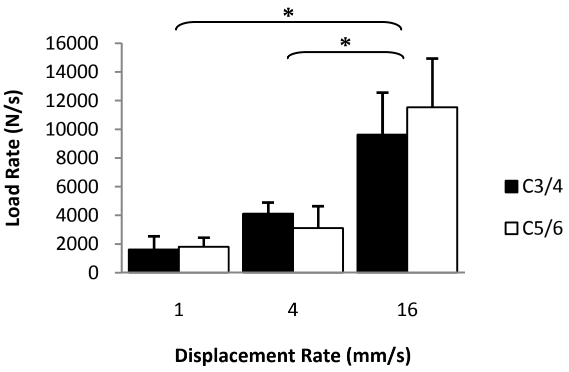

Figure 1: Initial load rate for each displacement rate. An asterisk (*) denotes significant differences across displacement rates.

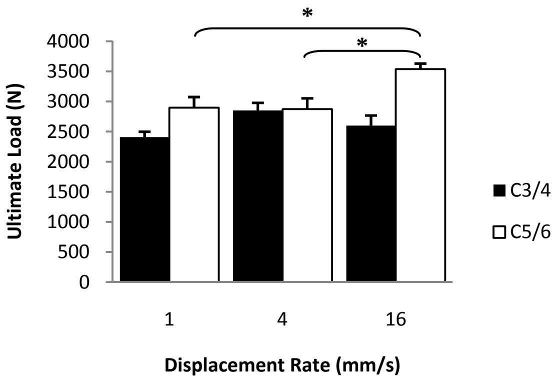

Figure 2: Ultimate anterior shear load for each displacement rate. An asterisk (*) denotes significant differences across displacement rates for the C5/6 FSUs.

The significant main effect of displacement rate on ultimate anterior shear load that was evident for the C5/6 FSUs and not the C3/4 FSUs. This may have been due to anatomical differences between the two levels, such as lordosis and an increase in facet contact area. The C5/6 FSUs are more lordotic than the C3/4 FSUs. Previous studies have shown the facet joints of the lower three lumbar vertebrae withstand larger compressive loads than the facet joints of the upper two lumbar vertebrae [3]. This is particularly apparent when there is a loss of disc height and increased extension [3]. As well, there is an increase in facet surface contact area with a more extended posture and loss of disc height [4]. These two anatomical features could possibly play a role in modulating the viscoelastic properties of the FSUs and could explain the differences found between the levels given a similar lordosis change between C3/4 and C5/6 in the porcine spine.

CONCLUSIONS

The current study looked to investigate the effects of displacement rate on the viscoelastic properties of the porcine cervical spine and define preliminary acute anterior shear failure limits under a controlled compressive load condition. The absence of a significant increase in ultimate anterior shear load for the C3/4 FSUs demonstrates that the expected increase in mechanical properties at higher load rates due to a viscoelastic response did not hold, despite a significant increase in load rate at the higher displacement rates.

REFERENCES

1. Cripton P, et al. *Symposium: Injury Prevention Through Biomechanics*, 111-126, 1995.
2. Yingling VR, et al. *Spine* **24,** 1882-1889, 2004.
3. Adams MA, et al. *J Bone Jt Surg* **62-B**, 358-362, 1980.
4. Dunlop RB, et al. *J Bone Jt Surg* **66-B**, 706-710, 1984.

RECOVERY OF SCAPULA KINEMATICS AND SHOULDER MUSCLE ACTIVATION FOLLOWING AN ISOMETRIC FATIGUE TASK

[1]John Borstad, [1]Nick Kynyk, [1]Mark Lower, [1]Matt Sellers, [2]Kimberly Szucs, and [3]Anand Navalgund
[1]Physical Therapy Division; [2]School of Allied Medical Professions; [3]Biomedical Engineering: The Ohio State University, Columbus, OH
email: borstad.1@osu.edu

INTRODUCTION

Subacromial impingement syndrome (SIS) of the shoulder is the third most frequent musculoskeletal complaint requiring physician visits. SIS results from mechanical compression of the rotator cuff tendons and/or subacromial bursa between the humeral head and acromion and over time, this compression results in tissue inflammation and pain in the shoulder during arm elevation and often interrupts sleep.

Alterations in the direction and magnitude of 3-dimensional scapulothoracic kinematics in those with SIS have been described [1]. Others have described alterations in activation of the muscles that move the scapula on the thorax [2]. However, it is unknown whether these alterations cause SIS, or if they are in response to the pain experienced with SIS. For this reason, discovery of mechanisms leading to scapula movement or muscle activation alterations may improve prevention and treatment of SIS.

Muscle fatigue is a proposed mechanism for biomechanical alterations because prevalence rates of SIS are high in groups that use their arms overhead repetitively, such as workers or throwing athletes. Our prior work demonstrated both scapula kinematic and muscle activation alterations immediately following an isometric fatigue task [3]. For this experiment, we asked if kinematics and muscle activation levels return to pre-fatigue levels after rest. We hypothesized that kinematics and muscle activation would return to pre-fatigue values after six minutes.

METHODS

Ten healthy male subjects participated. 3-dimensional scapula kinematics and surface electromyographic (EMG) data were collected during scapular plane arm elevation and lowering in standing at four time points: pre-fatigue, immediately post-fatigue, and three and six minutes post-fatigue. Kinematics of the scapula, humerus, and thorax were collected with an electromagnetic motion capture system at 100 Hz per sensor. EMG data from the serratus anterior, upper trapezius, and lower trapezius were collected at 1000 Hz. The fatigue task was an isometric push-up plus with the feet elevated 23cm, held until the subject voluntarily quit.

Muscle fatigue was determined by calculating the percent decline in Median Power Frequency (MPF) over the duration of the fatigue task. **S**capula orientations relative to the trunk during arm elevation/lowering were determined using a Z, Y’, X’’ Euler sequence. EMG data during arm elevation/lowering were bandwidth filtered from 5 to 500Hz, RMS processed, averaged over 0.1 sec intervals and normalized. Mean orientation and normalized muscle activation at 60°, 90°, 120° of humerus elevation relative to the trunk (Z, Y’, Z’’) were analyzed during arm elevation and lowering separately with a two-factor (time by angle) repeated measures ANOVA with $p<0.05$ established for statistical significance.

RESULTS and DISCUSSION

The MPF of all three muscles declined during the fatigue task: Serratus Anterior 29.5%; Upper Trapezius 27.6%; and Lower Trapezius 33.6%. There were no statistically significant interaction effects between time and angle during arm elevation or lowering for any of the dependent variables.

During arm elevation, there was a statistically significant effect of time on all three scapula orientations and on lower trapezius activation. Scapula internal rotation angle was greater at all three post-fatigue time points; scapula upward rotation angle was greater at 6 minutes; and scapula anterior tilting angle was greater at post-task than at pre-task (Figure 1). Normalized activation of the lower trapezius was greater at 3 and 6 minutes than it was immediately post-fatigue (Figure 3: Blue Bars).

Figure 1.

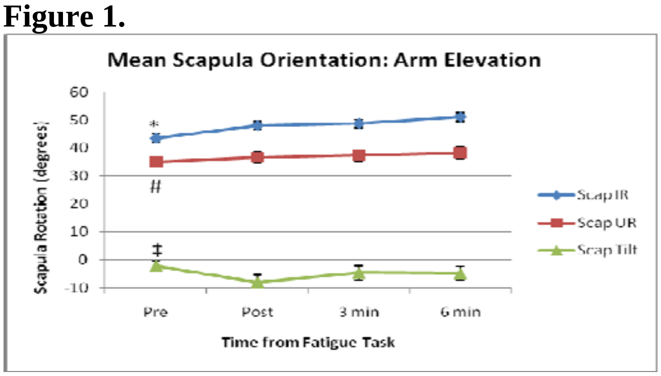

* Pre < Post, 3 min, and 6 min.
# Pre < 6 min.
‡ Pre < Post.

During arm lowering, there was a statistically significant effect of time on all three scapular rotations. Scapula internal rotation angle was greater at all three post-fatigue time points; scapula upward rotation angle was greater at 6 minutes; and scapula anterior tilting angle was greater at post-task than at pre-task (Figure 2). There was also a statistically significant effect of time on serratus anterior activation with higher activation at 6 minutes than at post-fatigue (Figure 3: Red Bars).

Figure 2.

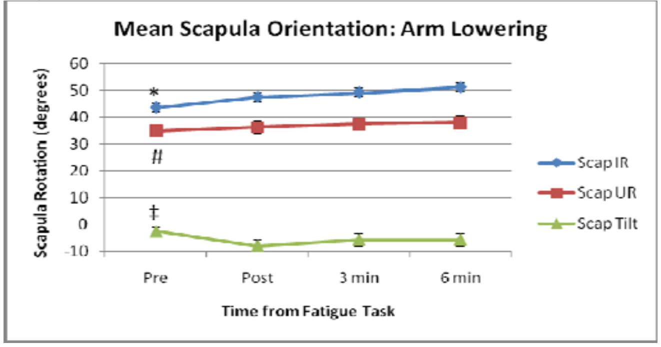

* Pre < Post, 3 min, and 6 min.
# Pre < 6 min.
‡ Pre < Post.

The isometric task resulted in decreased MPF, indicating acute muscle fatigue. In contrast, the higher muscle activation levels that were expected at post-task were not demonstrated [4].

Figure 3.

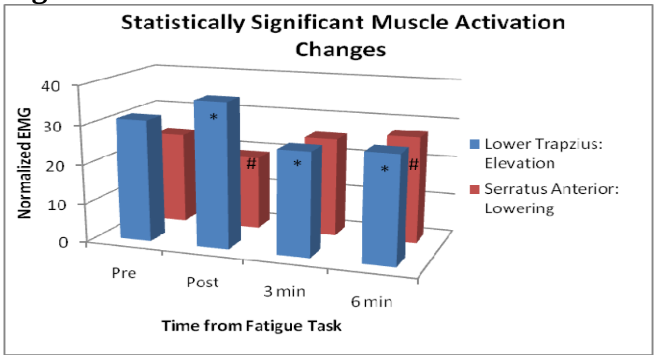

* Post > 3 min and 6 min.
# Post < 6 min.

Scapula internal rotation remained increased for 6 minutes, perhaps related to maintaining scapular protraction during the task or to decreased lower trapezius activation. Increased scapula internal rotation may decrease the subacromial space [5] and increase the potential for SIS. Scapula anterior tilting was increased at post-task but was not significantly different from pre-task levels at 3 and 6 minutes. Although not statistically different, post-task serratus anterior activation was lower than pre-task which may explain the increased anterior tilt. Increased internal rotation and anterior tilt of the scapula due to acute fatigue may make overhead workers or athletes susceptible to SIS.

CONCLUSIONS

Fatigue-induced biomechanical alterations did not fully recover even after 6 minutes of rest. In particular, scapula internal rotation remained increased relative to baseline during both arm elevation and lowering. Muscle activation changes do not fully explain the kinematic alterations.

REFERENCES

1. Ludewig PM and Cook T. *Phys Ther* **80**, 276-291, 2000.
2. Cools A et al. *Am J Sports Med* **31**, 542-549, 2003.
3. Szucs K et al. *Med Biolog Eng Comp* In Press.
4. Enoka RM and Duchateau J. *J Physiol* **586**, 11-23, 2008.
5. Solem-Bertoft E et al. *Clin Orthop Rel Res* **296**, 99-103, 1993.

QUANTIFYING COORDINATION DURING RECOVERY FROM A TRIPPING TASK

Noah Rosenblatt, Christopher Hurt and Mark D. Grabiner
Clinical Biomechanics Laboratory, University of Illinois at Chicago
email: nrosenbl@uic.edu, web: www.uic.edu/ahs/biomechanics

INTRODUCTION

Given the high cost and ramifications of falls by older adults, much attention has focused on identifying clinically modifiable risk factors associated with their falling. Using an overground tripping protocol, variables such as longer response time, increased trunk flexion angle and velocity at recovery foot ground contact, and decreased recovery step length have all been associated with failed recovery [1]. Similar failure mechanisms have been observed when disturbances are induced by a motorized treadmill. In many cases subjects who initially fail learn quickly to successfuly recover on subsequent attempts [2]. Collectively, this suggests that repeated exposure to these disturbances may be useful in training subjects to recover following anteriorly-directed trips. However, the mechanisms of failed recovery provide insight into biomechanics only at specific temporal events, i.e. toe-off and foot strike. Thus the purpose of this study was to quantify training-related changes in lower extremity and trunk coordination, during the *entire* recovery step, following the onset of a large postural disturbance delivered by a motorized treadmill.

METHODS

Fourteen healthy, community dwelling women (age: 64±8 yrs), participated in this study which was part of a larger study on falling. Training consisted of four one-hour sessions. A motorized treadmill (Simbex, Lebanon NH) was used to deliver postural disturbances to subjects who wore a safety harness to prevent a fall. Motion capture was conducted at 60Hz using an eight-camera system (Motion Analysis, Santa Rosa, CA). Training began with a "standard disturbance", during which the treadmill was accelerated to 0.89 m/s in ~150 ms [2], followed by 30-50 disturbances during which a 0.5s initial acceleration of magnitude 1.5-6.5m/s^2 was followed by a deceleration. After the final session (day 4) subjects were again presented with the "standard disturbance". One week following the final session subjects returned to the lab and a trip was induced during gait [1]. Failure during both training and forward trip occurred when subjects were completely supported by the harness.

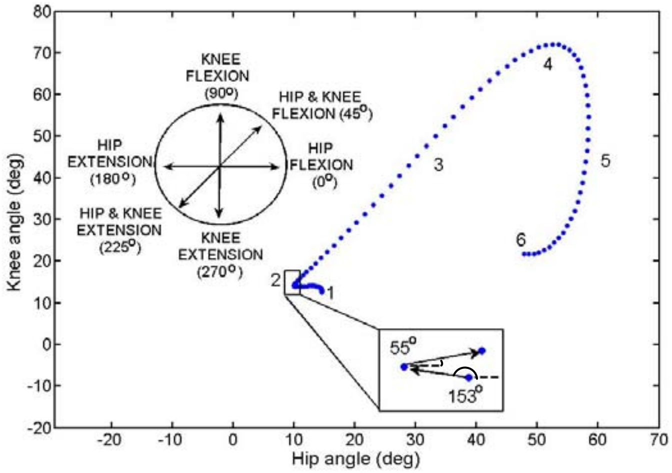

Figure 1: Angle-angle plot of a representative subject. Numbered regions (same in Figure 2) correspond to: 1-passive hip extension at disturbance onset 2-transition from hip extension to hip & knee flexion 3- hip & knee flexion 4-transition from hip & knee flexion to extension 5- rapid knee extension 6-rapid hip extension before contact. *Lower right:* Hip-knee Coupling angle (θ) is calculated as the angle between the horizontal and the vector connecting adjacent points. *Top left:* θ can be associated with particular motions i.e. θ=45° when both the knee & hip flex together (region 3).

Relative hip and knee sagittal plane angles and the trunk angle relative to the vertical, during the standard disturbances on day 1 and day 4 were analyzed. Coordination was quantified based on a vector-coding technique [3, 4], in which all angles during the recovery step, from disturbance onset to foot ground contact, were interpolated to 100 data points. Angle-angle plots were created to visualize the relative motion of two joints simultaneously (Figure 1). Step initiation (SI), determined by piecewise curve fitting, was defined as when curves transitioned from region 1 to 2. For all data points, coupling angles (θ) were determined (Figure 1 – *Lower right*). At each point of the interpolated recovery step time series (percent), cosθ and sinθ was calculated and the average cos and sin was taken across all subjects ($\cos\bar{\theta}$ and $\sin\bar{\theta}$). At each percentage, the degree of concentration (DoC), a measure of intersubject variability (Figure 2-*Bottom*) was calculated as $0 \le \sqrt{(\cos\bar{\theta})^2 + (\sin\bar{\theta})^2} \le 1$ [3], whereby larger values of DoC correspond with smaller values of intersubject variability. Similar analysis was performed for hip-trunk coupling. Reported p-values are based on paired samples t-tests between successful trials on day 1 and 4.

RESULTS AND DISCUSSION

Successful recoveries were associated with a series of time-dependent transitions from initial flexion of the knee & hip (Figure 1- regions 2, 3) to extension (regions 4, 5, 6) before recovery foot ground contacts. Simultaneously, the trunk transitions from passive flexion to active extension. Thus if, and when, these transitions occur seems to be important. SI, expressed as a % of recovery step from disturbance onset, decreased from day 1 to day 4 (28.3±6.4% vs. 22.7±4.5%, p=0.08, Figure 2), and in turn the transitions from hip & knee flexion to extension (region 3 to 5) and hip & trunk flexion to extension both occur earlier on day 4 compared to day 1 (75.8±4.3% vs. 66.2±3.1% for hip & knee, p<0.01, Figure 2; 85.8±4.2 vs. 77.8±5.1 for hip & trunk, p<0.01), allowing for greater hip, knee and trunk extension at recovery foot ground contact. As a result both hip-knee and hip-trunk angles at recovery foot strike are greater on day 4 compared to day 1 ($\theta =$ 202.6±20.7 vs. 239.7 ± 18.5 for hip-knee, p=0.03; θ=170.7±28.7 vs. 196.8±6.6 for hip-trunk, p=0.04). In contrast to day 4 recoveries, over half of the subjects who recovered on day 1 did not transition the hip-knee coupling angle into region 6 (i.e. hip extension that could prevent limb buckling at ground contact), nor the hip-trunk angle into a region corresponding to trunk extension ($\theta >$ 180°). This is also true for the six subjects that failed day 1. With training, subjects independently converged on similar solutions to successful recovery. Intersubject variability throughout the recovery phase was lower (i.e. higher DoC) on day 4 than on day 1 (Figure 2), particularly during the last 20% of the recovery step. Subjects that failed on day 1 showed the greatest intersubject variability, but after repeated exposure to the disturbances converged on a solution similar to other subjects.

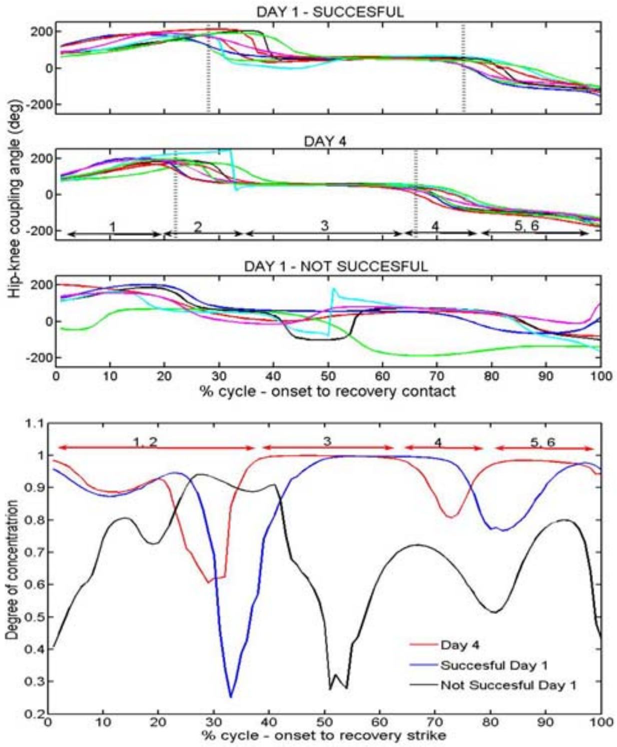

Figure 2: *Top*: Hip-knee coupling angle during recovery Successful subjects on day 1 shown in same color on day 4. Angles arbitrarily + and - for continuity. From the left, vertical dotted grey lines represent SI and transition from hip & knee flexion to extension, respectively *Bottom*: Intersubject variability during recovery step. Larger DoC represents less intersubject variability in the coupling angle curves. DoC was lowest for those that failed on day 1 and highest for all subjects on day 4. The large troughs correspond to variability in SI (region2) and transitions from flexion to extension (region 4), which are smaller and occur sooner on day 4.

In summary, after training, SI and the transitions from hip, knee and trunk flexion to extension occurred earlier in the recovery step. Together, these kinematics could contribute to the successful recovery – i.e. lead to an increased recovery step length, and decreased trunk flexion angle and velocity at recovery foot strike [2]. Transfer of this motor program could explain why none of the trained subjects fell during the forward trip. To our knowledge this is the first time that this vector coding technique has been used to quantify changes in coordination during training to reduce trip-related fall risk. We believe this measure has clinically utility since, unlike relative phase, it is easily interpreted directly in terms of joint angles.

REFERENCES

1. Pavol MJ, et al. *J Gernetol* **56**, M428-437, 2001.
2. Owings T, et al. *Clin Biomech* **16**, 813-819, 2001.
3. Field-Fote EC, et al. *Phys Ther* **82**, 707-715, 2002.
4. Sparrow WA, et al. *J Motor Behav* **19**, 115-129, 1987.

DIFFERENCES IN FRONTAL PLANE STABILITY DURING TREAMDILL AND OVERGROUND WALKING

Noah J. Rosenblatt and Mark D. Grabiner
Clinical Biomechanics Laboratory, University of Illinois at Chicago
email: nrosenbl@uic.edu, web: www.uic.edu/ahs/biomechanics

INTRODUCTION

Given the consequences of falling to the side by older adults, attention has focused on identifying gait-related variables associated with increased lateral stability and decreased fall risk. Step-width (SW) and step-width variability (SWV) have traditionally been associated with frontal plane stability [1, 2]. Recently the "margin of stability" (MOS) has also been adopted for this purpose [3]. Since its calculation includes both center of mass (COM) position and velocity relative to the foot it may better describe stability during locomotion.

Frontal plane stability may be influenced by the conditions during which gait occurs. In contrast to sagittal plane variables that vary little between treadmill and overground walking [4], Stolze et al. [5] showed a significant difference in SW between the two conditions. To the best of our knowledge the work by Stolze et al is the only within-subject study to describe SW during treadmill and overground walking. However, SWV and MOS were not considered.

The purpose of this study was to determine the extent to which overground and treadmill walking differ in regard to frontal plane stability of healthy, young subjects. We hypothesized that SW would increase during treadmill walking. We also tested the null that SWV would not differ between conditions Lastly, we hypothesized that MOS would increase, in parallel, with SW, during treadmill walking.

METHODS

Ten healthy young subjects (age 24.4±4.5 yr) participated. Subjects walked at a comfortable, self-selected speed, both overground and on a treadmill (Marquette Electronics, Marquette, WI). Treadmill walking lasted for 10 consecutive minutes. For each of 30 overground walking trials, subjects walked 8 m across the lab floor, while a Polaris electronic wireless timer (FarmTek Inc, Wylie, TX) recorded walking speed, the values of which were averaged across all trials.

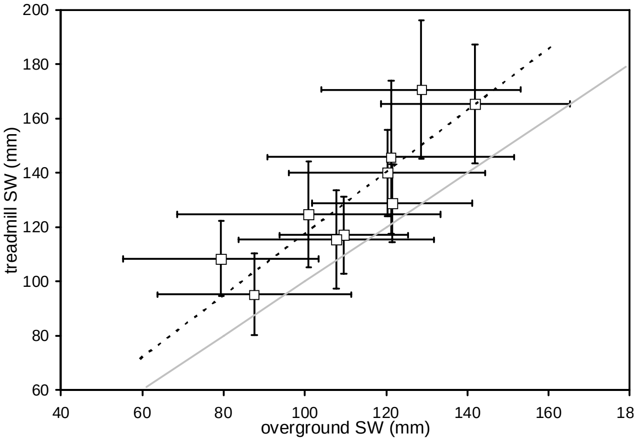

Figure 1: Overground SW significantly correlates with treadmill SW. Subject data points fell to the left of the line of unity (grey), suggesting subjects consistently walked with greater SW on the treadmill. Error bars represent SWV, which is significantly larger during overground walking. The best fit line (dotted black) has a slope of 1.13 and R^2=0.79

SW, SWV and MOS were computed from the motions of 23 passively reflective markers placed over specific body landmarks, and tracked using an eight camera motion capture system operating at 60 Hz (Motion Analysis, Santa Rosa, CA). SW was determined as the distance between the centroid of each foot segment at successive mid-stances. For each subject, SW was separately averaged over all left and right step. The standard deviations were used to represent SWV. MOS was measured as the distance between the extrapolated center of mass (XCOM) and the lateral border of the base of support (BOS_{lat}): $MOS=BOS_{lat}-XCOM$, where $XCOM=COM+\dot{COM}/\omega_0$, $\dot{COM}$ is the velocity of the COM, ω_0 is the natural frequency of a pendulum with length 1.34 times trochanteric height [3], and BOS_{lat} is approximated from the position of markers over the metatarsal and heels. MOS was calculated from heel strike to contralateral toe-off. The minimum value of MOS is reported (MOS_{min}). The more positive MOS_{min} the more stable the gait.

Walking speeds for the conditions were compared using a paired t-test. If a significant correlation existed between SW, SWV or MOS_{min}, and walking speed for both conditions then walking speed would be used as a covariate in the between-condition analyses. Between-condition analyses were performed using 2 (left vs. right limb) by 2 (overground vs. treadmill) repeated measures analyses of variance (ANOVA) for SW, SWV and MOS_{min}. For each main effect, a Pearson correlation was determined between the subject-specific values of the variable for the two cases. Analyses were performed using SPSS software (SPSS, Inc, Chicago, IL) with significance given for $p<0.05$.

RESULTS AND DISCUSSION

Walking speed was significantly larger for overground compared to treadmill walking (1.41±0.16 m/s vs. 1.09±0.17 m/s, $p<0.01$), and the correlation between the two values was significant ($r=0.69$, $p=0.028$). However the correlations between walking speed and SW, SWV or MOS_{min} were not significant. As a result walking speed was excluded from subsequent analyses.

Across all steps, SW during treadmill walking was ~15% larger than that during overground walking (131.2±24.3 mm vs. 111.8±18.9 mm, $p=0.001$). The correlation between treadmill and overground SW was significant ($p=0.001$, $r=0.884$; Figure 1). Between limb differences were not significant.

Across all steps, SWV during treadmill walking was about ~23% smaller than that of overground walking (24.2±4.7 mm vs. 18.7 ±5.1 mm, $p=0.001$; Figure 1). However the correlation between SWV during the two conditions was not significant. Between-limb differences were also not significant.

MOS_{min} was invariant between overground and treadmill walking (66.3±8.9 mm and 62.9±10.0 mm, respectively), but significantly correlated ($p<0.002$, $r=0.90$; Figure 2). Between-limb differences were not significant, although they were quite obvious for two of the subjects (Figure 2).

The constant MOS_{min} during conditions in which SW varied significantly suggests that during unperturbed overground walking, foot placement is chosen with the goal of attaining a desired value [3]. Alternatively, given the consequences of stepping off a raised, moving treadmill belt, it is possible that subjects voluntarily increase SW to potentially increase lateral stability. However, paradoxically, a larger SW is associated with increased trunk acceleration. The net result therefore can be an invariant MOS_{min}. In either case, the decreased SWV during treadmill walking reflects increased precision of foot control.

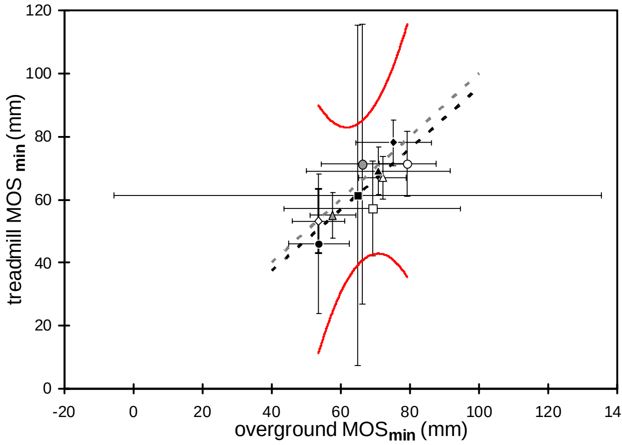

Figure 2: MOS_{min} is not affected during treadmill and overground walking. The best fitting straight line (dotted grey) to the data (subject means ± SD) has a slope of 0.96, $R^2=0.738$, and a line of unity (dotted black) falls within the 95% confidence interval for the best fit line (red curved lines). Although on average there is little between-limb difference in MOS_{min} one subject had an approximately eight-fold between-limb difference for both conditions, resulting in large SD when the limbs were pooled together.

CONCLUSION

Kinematic parameters associated with frontal plane stability, particularly SW and SWV are significantly different, but meaningfully correlated, during treadmill and overground walking. However, MOS_{min} was insensitive to whether walking was on the treadmill or overground. Thus measures of SW and SWV only partially reflect frontal plane dynamic stability. The larger, more precise SW during treadmill walking may reflect an end goal of the central nervous system, to maintain a constant average MOS_{min}, regardless of the walking tasks.

REFERENCES

1. Shrager MA, et al. *Gait Posture* ***28***, 466-471, 2008.
2. Owings TA, et al. *J Biomech* **37**, 935-938, 2004.
3. Hof AL, et al. *J Biomech* **38**, 1-5, 2005.
4. Lee SJ, et al. *J Appl Physiol* **104**, 747-755, 2008.
5. Stolze H, et al. *Electroencephalogr Clin Neurophysiol* **105**, 490-497, 1997.

ON GENDER DIFFERENCES IN THE REACTION TIMES OF SPRINTERS AT THE 2008 BEIJING OLYMPICS

David B. Lipps, James T. Eckner, James K. Richardson, Andrzej Galecki, and James A. Ashton-Miller
University of Michigan, Ann Arbor, MI, USA
email: dlipps@umich.edu, Web: me.engin.umich.edu/brl

INTRODUCTION

The International Association of Athletics Federations (IAAF) rules stipulate that a reaction time of less than 100 ms constitutes a false start for sprinters. Mero and Komi showed the mean reaction time from the gun signal to 10% force production on the starting block in eight national-level Finnish male sprinters was 119 ms [1]; the reaction time of female sprinters was not measured. Gender differences have been noted in reaction times in other sports such as handball [3]. In this paper we address three questions. Q1: Is there a gender difference in the reaction times of world-class sprinters? Q2: What is the absolute minimum reaction time that is humanly possible for elite male and female sprinters? Q3: How do those minimum reaction times compare with the 100 ms IAAF threshold criterion? To answer these questions, we used published reaction time data from the 2008 Beijing Olympics and tested the null hypothesis that no gender difference exists in the reaction time of world-class sprinters.

METHODS

The reaction time data were collected from the official results website for the 2008 Beijing Olympics for men and women's 100 m, 200 m, 400 m, and 100/110 m hurdles. Reaction times from the heats, quarterfinals, semifinals, and finals were included in the analysis as a 'round' factor. Since sprinters (always identified by the same bib number) could participate in multiple individual races or advance in a race to participate in multiple rounds of an individual race, we could not consider such data to be independent. Therefore, simple statistical analyses such as a t-test or ANOVA without repeated measures are not appropriate.

The statistical analysis was performed using SPSS 16.0 (SPSS Inc., Chicago, IL). Since the data are right skewed, they were power-transformed and normality was then confirmed with the Shapiro-Wilk test. A linear mixed model was then used to analyze the transformed reaction time data. Gender was treated as a fixed factor, and Race(Bib ID) and Round(Race) were treated as random factors. The random factors allowed our statistical model to handle the lack of independence in the reaction time data. A type III test of fixed effects was used to investigate the gender effect. We defined the minimum simple reaction time (SRT) that is humanly possible for an Olympic sprinter to achieve in 1 out of 100 races to be the [mean-2.576*SD] value, a value that was found for each gender by using a Taylor expansion while back-transforming to the original temporal scale.

RESULTS AND DISCUSSION

The reaction times for male and females sprinters are shown in a histogram in Figure 1. The linear mixed model showed the fixed effect of gender was significant ($p<0.001$). Analysis of the random factors showed different races and different rounds accounted for 29% and 33% of the variability in the mean reaction time.

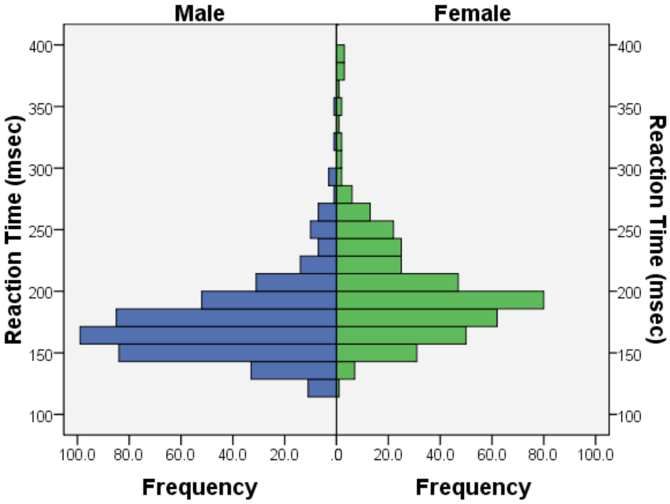

Figure 1. Population pyramid showing reaction times for male and female sprinters (original scale).

The estimated marginal mean for male sprinters was 168 ms with a 95% confidence interval of 160 ms to 178 ms. The estimated marginal mean for female sprinters was 191 ms with a 95% confidence interval of 180 ms to 205 ms. The estimated absolute minimum SRT value was 124 ms for males and 130 ms for females, values. Interestingly, male sprinters had 25 false starts in Beijing, while females only had 4 false starts, reflecting their 6 ms larger margin identified in this paper.

A previous study used reaction time from the official results of international sprinting competitions [3] and showed the mean reaction time for male sprinters increased as a function of the race length and decreased as they advanced through the heats to the finals. Furthermore, there was no difference in the reaction time in less experienced sprinters. Despite these findings, their study had major limitations. First potential gender differences were not examined. Second, a Gaussian distribution for the reaction time data was unfortunately assumed (Figure 1). Lastly, independence of data points was assumed (via use of a one-way ANOVA), an incorrect assumption for this data set.

Our results show a strong gender difference in sprinters participating in the 2008 Beijing Olympics. Another previous study showed a gender difference in the reaction times of sprinters in the 100/110m sprint events at the 2004 Olympics [4]. However, that study focused on lane position effects rather than gender in their statistical model. Multiple measurements were used from the same athlete as long as they were in different lane positions for each race. The use of an analysis of variance without data transformation is not as robust a statistical model for investigating gender differences as the present linear mixed model using transformed data.

This is the first time that an accurate estimate of the 6 ms gender difference in the minimum SRT of elite world-class sprinters has been reported. This result suggest that the criterion for a false start may need to be raised from the present 100 ms for female sprinting competitions to account for inherent gender differences in reaction time between males and females. A potential explanation for the gender difference may be a difference in how the central nervous system of each sex deals with stressful time-critical situations. For example, healthy young adult females have also shown significantly longer upper extremity reaction times than males when manually raising the arms to block a foam ball projected directly at their face at a high speed [5].

The consequences of false starts are greater for sprinters in the Olympics than for the sprinters in the Mero and Komi study. This helps explain why the present mean male reaction time is longer than theirs.

The limitations to our statistical analyses include the point that we only examined gender as a fixed factor. We could include age as another factor, but previous work showed no age difference [3] and including the age factor would have lowered statistical power. We did not included height and weight as covariates because these data are not publically available online. Finally, the Taylor expansion used in the minimum SRT analysis is only an approximation; a bootstrapping method might be a superior approach.

CONCLUSIONS

1) There is a significant gender difference in the mean reaction time for elite sprinters.
2) The minimum (humanly) possible reaction times for world-class male and female sprinters are 124 ms and 130 ms, respectively.
3) These minimum possible reaction times are as much as 24 ms (24%) and 30 ms (30%) longer than the official IAAF 100 ms criterion.
4) There should be different false start criteria for men and women.
5) False start criteria should be based on data from world-class athletes taken in actual competition.

REFERENCES

1. Mero A and Komi PV. *Eur J Appl Physiol* **61**, 73-80, 1990.
2. Dane S and Erzurumluoglu A. *Intern J Neurosci* **113**, 923-929, 2003.
3. Collet, C. *Percept Mot Skills* **88**, 65-75, 1999.
4. Brown et al. *Med Sci Sports Exerc* **40**, 1142-1148, 2008.
5. Lipps DB et al. Submitted *Am Soc Biomech,* 2009.

COMPARISON OF TIBIAL TRANSLATIONS DURING SOFT AND STIFF LANDINGS IN HEALTHY ADULTS: A BIPLANE FLUOROSCOPY STUDY

*Daniel Peterson, Jake Krong, Erik Giphart, Kevin Shelburne, J Richard Steadman, and Michael Torry
Steadman Hawkins Research Foundation, Vail, CO 81657; *dspeterson8@gmail.com

INTRODUCTION

Many anterior cruciate ligament (ACL) injuries occur by non-contact mechanisms marked by sudden deceleration of the center of mass, as in the case of landing from a jump. Previous landing studies have traditionally defined landing techniques in terms of *soft* or *stiff* according to the degree of maximal knee flexion angle attained during the landing phase[1]. It has been hypothesized that stiffer landings may place individuals at a higher risk of ACL injury due to increased ground reaction force and altered tibio-femoral kinetics[2].

The purpose of this study was to measure the tibio-femoral kinematics of soft and stiff landings using biplane fluoroscopy. Since the primary function of the ACL is to prevent anterior translation of the tibia (ATT) relative to the femur, we hypothesized that stiff landings would induce greater ATT compared to soft landings

METHODS

Seven healthy subjects (6M, 1F; age 28±6.3yrs) completed 5 stiff and 5 soft drop landings from a height of 40cm within the boundaries of a biplane fluoroscopy system (Fig 1). Subjects also completed a seated, unloaded knee extension task from approximately 0 to 90 degrees of knee flexion. Fluoroscopy images were collected for one soft landing, one stiff landing, and the extension task, and were digitized at 100 Hz. Fluoroscopy data was tracked using MBRSA (Medis Specials, Leiden, Netherlands, Fig 2).

The origin of the femoral coordinate system was placed between the medial and lateral femoral condyles on the center line of a cylinder fitted to the medial and lateral posterior condyles. The neutral position of the tibia was defined as the position of the tibia at full extension in the knee extension trial (Fig 3). Knee kinematics were calculated using methods described by Grood & Suntay (1983)[3].

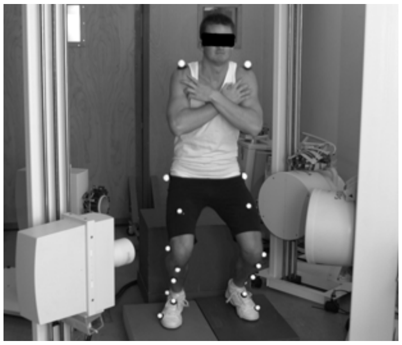

Figure 1: Biplane fluoroscopic set-up

Knee translation data from soft and stiff landing tasks were expressed relative to the knee extension kinematics by subtracting knee extension translation data at corresponding knee flexion angles. Referencing translation data during landing tasks to a low ACL load activity such as knee extension provides a consistent way to measure translations straining the ACL[4].

Simultaneous with fluoroscopy data, traditional motion capture techniques were utilized to measure 3D body segment kinematics and ground reaction forces, and to calculate joint kinetics[5] for all collected trials. Motion analysis data were collected at 120 Hz.

RESULTS

Motion Analysis: Stiff landings produced larger maximal ground reaction force (MaxGRF; p=0.001), and smaller maximum knee flexion (MaxKneeFlex; p=0.001) angle with respect to soft landings. Maximal knee extension torque (MaxKneeTorque) was similar between soft and stiff landings (Table 1).

Biplane Fluoroscopy: Maximum relative ATT (MaxRAntTib), internal rotation (MaxRIntRot), and valgus (MaxRValg) angles were all similar between soft and stiff landings (Table 1; Fig 4).

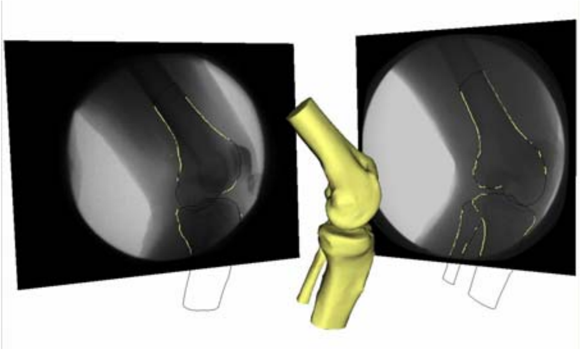

Figure 2: Tracking analysis of one frame during a landing. Bone geometries reconstructed from CT scans are automatically matched onto calibrated fluoroscopy images after their contours are detected semi-automatically.

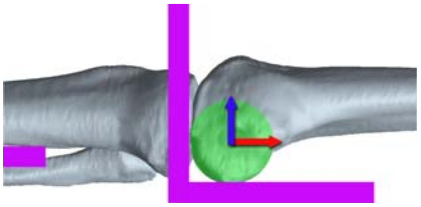

Figure 3: Example of femur coordinate system

Table 1: Dependant variables

	Stiff	Soft
MaxKneeFlex (deg)*	47.63 (11.97)	81.58 (9.05)
MaxGRF (N/kg)*	27.26 (5.19)	17.31(1.22)
MaxKneeTorque (Nm/kg)	1.79 (0.39)	1.73 (0.18)
MaxRAntTib (mm)	4.42 (1.60)	4.42 (1.22)
MaxRIntRot (deg)	6.06 (5.15)	5.91 (6.38)
MaxRValg (deg)	0.56 (0.90)	1.18 (1.06)

* $p<0.005$

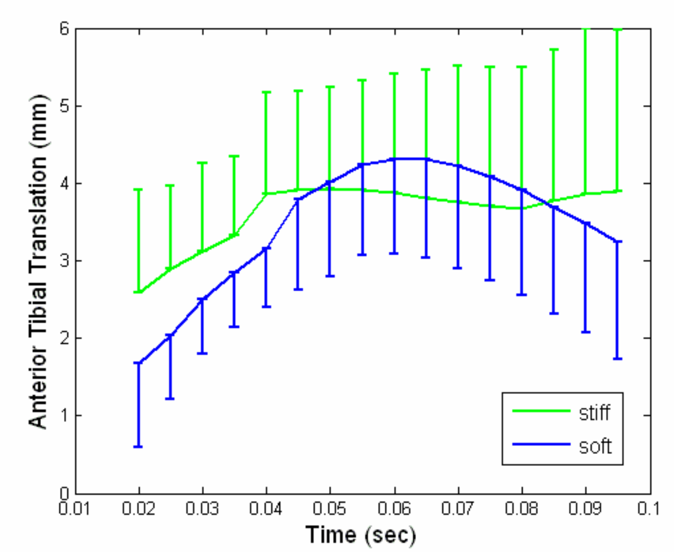

Figure 4: Relative anterior tibial translation plotted against time during soft and stiff landing.

DISCUSSION

Despite the higher GRF and lower knee flexion angles observed in stiff landings with respect to soft landings, relative anterior tibial translation, external rotation, and valgus angles were similar across both landing tasks. These results indicate that in this controlled setting, ATT, internal rotation, and valgus angles in healthy subjects are similar across a range of landing techniques. Further, these results suggest that load in the ACL during these tasks were similar.

Peak knee extension torque was similar between soft and stiff landings. This may be due to the fact that in addition to higher GRF seen in stiff landings, subjects also landed with less knee flexion, reducing the GRF moment arm about the knee. Future studies specifically manipulating GRF and knee extension moment should be carried out to determine these variables' effects on tibio-femoral kinematics, as they have been identified as potential determinants of ACL strain during landing[6].

Previous literature has suggested that subjects who land more upright, or stiff, are more prone to ACL injury[1]. Results from the current study suggest that stiffer landings alone do not make the knee more prone to ACL injury as defined by greater ATT, internal rotation, or valgus angles. However, the landings measured in the current study were executed in a controlled laboratory setting. It is possible that in uncontrolled, or in unanticipated conditions, stiffer landings may produce loads that increase the risk of ACL injury.

REFERENCES

1. DeVita P & Skelly W (1992). *Med Sci Sport & Exer*. **24**(1):108-15.
2. Chappell JD et al. (2007). *Am J Sports Med*. **35**(2):235-41.
3. Grood ES & Suntay WJ (1983). *J Biomech Eng*. **105**(2):136-44.
4. Ishibashi Y et al (1997). *Arthroscopy.* **13**(2):177-82.
5. Kernozek et al. (2008) *Am J Sports Med.* **26**(3):554-65.
6. Pflum MA et al. (2004). *Med Sci Sports Exerc*. **36**(11):1949-58.

GROUND REACTION FORCE IS A TEMPORAL PREDICTOR OF ANTERIOR TIBIAL TRANSLATION DURING DROP LANDINGS IN HEALTHY ADULTS

*Daniel Peterson, Jake Krong, Erik Giphart, J Richard Steadman, Michael Torry, and Kevin Shelburne
Steadman Hawkins Research Foundation; Vail, CO 81657; *dspeterson8@gmail.com

INTRODUCTION

The anterior cruciate ligament (ACL) is the primary restraint to anterior translation of the tibia relative to the femur. Thus, ACL load at the knee is mainly determined by the net anterior shear force applied to the tibia. This shear force is determined by external loads, such as ground reaction force (GRF), and the internal forces such as muscles and contact forces between the bones of the knee. Of these determinants, only external loads can be measured in the laboratory setting. It has been suggested that GRF during highly dynamic activities such as landing from a jump predict load in the ACL[1]. Until recently, this anterior tibial translation (ATT) was too small to reliably measure in vivo during dynamic activity. However, using a recently developed biplane fluoroscopy system, we can reliably measure ATT with submillimeter accuracy.

The purposes of this study were to 1) use biplane fluoroscopy to determine the timing of ATT during drop landing, and 2) to determine whether the timing of GRF predicts timing of ATT.

METHODS

Seven healthy subjects (6M, 1F; age 28±6.3yrs) completed 5 drop landings from a height of 40cm inside a biplane fluoroscopy system (Fig 1). Subjects also performed a seated, unloaded knee extension task from approximately 0 to 90 degrees of knee flexion. Fluoroscopy images were captured at 100 Hz for one soft landing and the knee extension task. Bone geometries reconstructed from CT scans were automatically matched onto the calibrated fluoroscopy images after their contours were detected semi-automatically (Medis Specials, Leiden, Netherlands, Fig 2).

The origin of the femoral coordinate system was placed between the medial and lateral femoral condyles on the center line of a cylinder fitted to the medial and lateral posterior condyles. The neutral position of the tibia was defined as the position of the tibia at full extension in the knee extension trial. Knee kinematics were calculated using the methods described by Grood & Suntay (1983)[3].

ATT during landing was expressed relative to knee extension ATT by subtracting knee extension ATT at corresponding knee flexion angles of the landing data to yield relative ATT (RATT). Referencing translation data during landing tasks to a low ACL load activity such as knee extension provides a consistent way to measure translations straining the ACL[4].

Simultaneous with fluoroscopy data, traditional motion capture techniques were utilized to measure 3D body segment kinematics and GRF and to calculate joint kinetics for all collected trials[5]. Motion analysis data was collected at 120 Hz. Timing of RATT and GRF were determined for each trial individually.

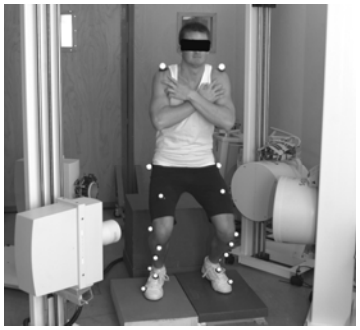

Figure 1: Biplane fluoroscopy set-up.

RESULTS

For all subjects the tibia was translated anterior relative to the femur at ground contact and as the knee flexed during the first moments of the landing (Fig 3a). Maximum RATT was 4.42 (±1.2) mm, showing a parabolic curve from 0.02 to 0.1 seconds after ground contact (Fig 3b). Maximal GRF occurred at 0.067 (±0.015) sec (Fig 3b), and was not different than time of maximum RATT (0.063 ±0.007; p=0.52).

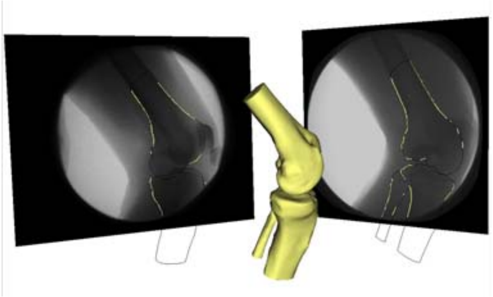

Figure 2**:** Tracking analysis of one frame during a landing.

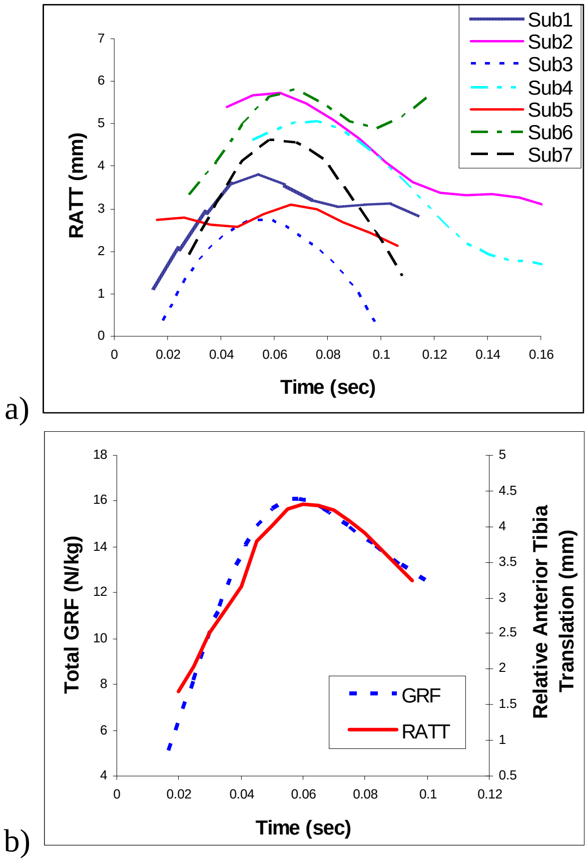

Figure 3: Relative anterior tibial translation for all subjects (a) and average RATT plotted with average GRF (b) (t_0=ground contact).

DISCUSSION

Timing of maximal RATT was similar to timing of maximal GRF. A potential explanation for the congruence between GRF and ATT may be due to the relationship between GRF, knee extensor torque, and tibio-femoral load. The modeling study by Pflum et al.[6] indicated that tibial femoral contact force, and the anterior force produced by the quadriceps were the two major contributors to anterior force on the tibia during landing. Authors showed that when the femur loads the tibia, the downward slope of the tibia forces the femur to slide backwards down the tibial slope. This study further reported tibial-femoral force to be temporally associated with GRF. In addition, GRF is a key determinant of extensor torque, and thus the force generated by the quadriceps muscles. A number of studies have shown that quadriceps force at low angles of knee flexion produces anterior shear of the tibia. Thus, tibial translation experienced shortly after ground contact is likely due to the compressive force of the femur onto the tibia, and the force in the quadriceps muscles, both of which are related closely to GRF. The temporal association between GRF and tibial translation is also supported by a recent in vivo ACL strain study[1], which showed that during a hopping task, maximal ACL strain occurred near the time of peak GRF.

Although this study provides some insight into determinants of timing of maximal RATT, future studies should be carried out which specifically manipulate factors which have been suggested to contribute to anterior tibial translation and ACL strain, such as GRF and knee extensor torque.

CONCLUSION

Timing of maximal GRF and relative anterior tibial translation were related, implying that GRF may be an important factor in the timing of maximal tibial translation.

REFERENCES

1. Chappell JD et al. (2007). *Am J Sports Med.* **35**(2):235-41.
2. Grood ES & Suntay WJ (1983). *J Biomech Eng.* **105**(2):136-44.
3. Kernozek et al. (2008) *Am J Sports Med.* **26**(3):554-65.
4. Ishibashi Y et al (1997). *Arthroscopy.* **13**(2):177-82.
5. Pflum MA et al. (2004). *Med Sci Sports Exerc.* **36**(11):1949-58.
6. Cerulli G et al (2003). *Knee Surg Sports Traumatol Arthrosc.* **11**(5):307-11.

A METHOD TO DETERMINE WHETHER A MUSCULOSKELETAL MODEL CAN RESIST ARBITRARY EXTERNAL LOADINGS WITHIN A PRESCRIBED RANGE

Alan Chu and Richard E. Hughes*
Laboratory for Optimization and Computation in Orthopaedic Surgery
University of Michigan, Ann Arbor, MI 48109
*email: rehughes@umich.edu, web: http://www-personal.umich.edu/~rehughes/index.html

INTRODUCTION

Musculoskeletal models often use mathematical representations of the anatomy to compute muscle lengths and moment arms [1]. It is possible to create a model that will not satisfy mechanical conditions of equilibrium for a set of external loading conditions. Such a model would be "unloadable." A model that has a solution for any externally applied force that lies in a prescribed range will be termed "loadable" here. The purpose of this project is to develop an efficient method for testing whether a musculoskeletal model geometry is loadable.

METHODS

Consider a static musculoskeletal model with joints and muscles, along with an external force **F** applied to the model. Static equilibrium for the model can be written in the standard matrix notation

$$\begin{aligned} \mathbf{Ax} &= \mathbf{b} \\ \mathbf{x} &\geq \mathbf{0} \end{aligned} \qquad (1)$$

where **A** is a matrix whose columns each correspond to unit torque for each muscle, **x** is a vector containing force magnitudes for each muscle, and **b** is a vector containing the torque generated by the external force **F** and the torques from the masses of the appendages. Additional rows are added to **A** for the degrees of freedom provided by additional joints in the model. The system is considered arbitrarily loadable if there exists a solution **x** to (1) for any arbitrary **F**.

In order to determine the loadability of a model for a specific and continuous range of forces, the user can specify an arbitrary number of vectors $\mathbf{h}_k$ so that these vectors describe the boundary of a convex hull of externally applied force vectors. Every force vector **F** that lies in the convex hull can be written as a non-negative linear combination of the vectors $\mathbf{h}_k$:

$$\mathbf{F} = \sum_{k=1}^{q} \lambda_k \mathbf{h}_k \qquad (2)$$

$$\sum_{k=1}^{q} \lambda_k = 1 \quad \text{and} \quad \lambda_k \geq 0 \ \ (k = 1, 2, ..., q)$$

where λ_k is an arbitrary non-negative scalar multiplier, the $\mathbf{h}_k$ vectors specify the boundary of the user-chosen convex hull of external forces, and q is the number of $\mathbf{h}_k$ vectors.

The system is determined to be loadable for all vectors that lie in the convex hull if one or more solutions, $\mathbf{y}_k$, to the following equations

$$\begin{aligned} \mathbf{Ay}_k &= \beta_k \\ \mathbf{y}_k &\geq \mathbf{0} \qquad (k = 1, 2, ..., q) \end{aligned} \qquad (3)$$

exist, where $\boldsymbol{\beta}_k$ is a vector containing the torque generated by each $\mathbf{h}_k$ vector as the external force, along with torques from the masses of the appendages. In other words, each equation in (3) is the same as in (1), except that $\mathbf{h}_k$ is used for the externally applied force vector. Note that (3) actually consists of q equations, each using a different $\boldsymbol{\beta}_k$. By solving (3) for each $\boldsymbol{\beta}_k$, loadability is determined for all the possible force vectors that lie in the convex hull specified by the $\mathbf{h}_k$ vectors. If one or more solutions to (3) do not exist, the system is unloadable since the equations in (3) are merely using each $\mathbf{h}_k$ as the external force vector.

However, for the purposes of determining loadability of a musculoskeletal model, only the feasibility of a solution $\mathbf{y}_k$ to (3) needs to be ascertained. If there are p degrees of freedom in the model, feasibility can be determined by solving the linear program:

$$\begin{aligned} &\text{minimize} \quad \sum_{j=1}^{p} \mathbf{u}_j + \sum_{j=1}^{p} \mathbf{v}_j \\ &\text{subject to} \quad \mathbf{Ay}_k + \mathbf{u} - \mathbf{v} = \boldsymbol{\beta}_k \\ &\mathbf{y}_k \geq \mathbf{0}, \mathbf{u} \geq \mathbf{0}, \mathbf{v} \geq \mathbf{0} \qquad (k = 1, 2, ..., q) \end{aligned} \qquad (4)$$

The formulation in (4) can be solved using the revised simplex method [2], a matrix-based implementation of the generalized simplex method [3]. Each formulation in (3) has a solution if and only if each one in (4) has a solution with **u** = **v** = **0**. Consequently, solutions to (4) with **u** = **v** = **0** are necessary and sufficient for loadability of the model.

RESULTS AND DISCUSSION

The method of determining loadability was applied to two examples involving a three-dimensional shoulder model: one example that was determined to be loadable, and one that was determined to be unloadable. The shoulder model (Figure 1) was constructed using Repository 6.2 of the AnyBody Modeling System™ version 3.0, and the loadability method and resulting analysis was implemented in MATLAB.

The AnyBody Modeling System uses inverse dynamic analysis to determine the muscle configuration of its models [4]. For a given posture and externally applied force, the software produces a matrix similar to **A** in (1), and a vector similar to **b** in (1). The appropriate entries of this matrix and vector were used to solve for muscle force activity using (4). The static posture used in the analysis is shown in Figure 1, and consists of a glenohumeral abduction angle of $\pi/6$, an elbow flexion angle of $\pi/2$, and an elbow pronation angle of $5\pi/18$. The convex hull of externally applied forces is specified by three vectors applied medially to the elbow, in addition to the zero vector applied at the elbow, as shown in Figure 1. The AnyBody global coordinate convention is such that $+x$ is forward from the body, $+y$ is up, and $+z$ is lateral to the right of the body. The three non-zero vectors describing the convex hull are at angles of $\pi/6$ to the z-axis.

Since the external forces are producing adduction of the shoulder, removing all the deltoid and supraspinatus muscles may cause the model to be unloadable since those muscles are the major abductors. The method described by (4) was applied, and it was determined that the shoulder model without the deltoid and supraspinatus muscles was in fact loadable. Although only the existence of solutions to (3) is necessary to determine loadability for the convex hull, a solution was solved for each of the three non-zero force vector vertices of the convex hull. The solution for each of these vertices used an infraspinatus segment, a triceps (medial head) segment, and a pronator teres caput humeral segment to provide the necessary abductive force. Each solution used a different amount of force for each of those muscles, but all three solutions activated those same muscles. Since the model specified by (1) does not impose an upper limit on the amount of force each muscle can produce, our mathematical method found a solution to resist the convex hull of external forces by utilizing weaker shoulder abductors such as the infraspinatus combined with the triceps. The pronator teres muscle was activated in order to maintain the elbow flexion angle of $\pi/2$, and elbow pronation angle of $5\pi/18$ in the model posture. Hence, this model was determined to be loadable for the specified convex hull of forces.

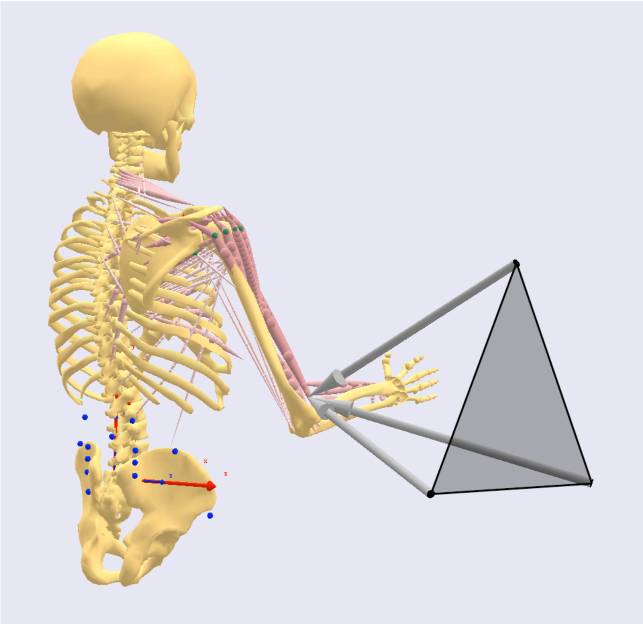

Figure 1. Anybody shoulder model used in the examples.

Next, in addition to taking out all the deltoid and supraspinatus muscles, all the infraspinatus muscles and the medial heads of the triceps muscles were removed. After applying the loadability algorithm, solutions to (4) with $\mathbf{u} = \mathbf{v} = \mathbf{0}$ could not be found for each vector defining the vertices of the convex hull. Since (4) could not be solved with $\mathbf{u} = \mathbf{v} = \mathbf{0}$, the shoulder model was determined to be unloadable. Removing these additional muscles eliminates all muscles with an abduction moment, and the shoulder is not able to abduct against the external forces.

REFERENCES

1. Dickerson CR, et al. *Comput Methods Biomech Biomed Engin* **10**, 389-400, 2007.
2. Dantzig G, et al. *Mathematical Tables and Other Aids to Computation* **8**, 64-67, 1954.
3. Dantzig G, et al. *Pacific Journal of Mathematics* **5**, 183-195, 1955.
4. Damsgaard M, et al. *Simulation Modelling Practice and Theory* **14**, 1100-1111, 2006.

UPPER EXTREMITY MOTION SEQUENCE IN JAVELIN THROWING

[1] Hui Liu, [2]Steve Leigh and [2]Bing Yu
[1]Beijing Sport University, [2]University of North Carolina at Chapel Hill
email: liuhuibupe@163.com

INTRODUCTION

A proximal-to-distal (P-D) sequence employed for upper extremity motions during the delivery of the javelin throwing is believed to be critical for obtaining great release speed in javelin throwing [1]. This belief was based on the fact that the upper extremity joint center linear velocities reached their maximums in a P-D sequence during the delivery of javelin throwing. The sequence of occurrences of joint center maximum linear velocities, however, does not necessarily represent the sequence of segment or joint motions. The purpose of this study was to examine the sequence of the upper extremity joint and segment angular motions in javelin throwing. We hypothesized that elite javelin throwers' upper extremity joint and segment angular motions followed a P-D sequence, and that this sequence of upper extremity motions was the same for both genders. The results of this study should provide significant information for technical training in the javelin throwing.

METHODS

The subjects were 32 female and 30 male right handed elite javelin throwers who competed in 2007 and 2008 USATF National Championships. The best trail of each subject was used in this study.

Two high definition video camcorders were used to record each subject's performance from the last cross step to the release of the javelin at a frame rate of 60 frames/second. The DLT method was used to estimate real-life 3-D coordinates of 21 critical body landmarks and 3 landmarks on javelin. The estimated real-life 3-D coordinates were filtered through a Butterworth low-pass digital filter at an estimated optimal cut-off frequency of 7.14 Hz.

The shoulder, elbow and wrist joint angles, and the upper trunk rotation angle were reduced for analysis. Shoulder joint angles were defined as the Euler angles of upper arm reference frame relative to a trunk reference frame in an order of rotation of horizontal adduction-abduction, adduction-abduction, and internal-external rotation. The elbow angle was defined as the inclination angle between the longitudinal axes of the upper arm and forearm while the wrist angle was defined as the inclination angle between the longitudinal axes of the hand and forearm. Upper trunk rotation angle was defined as the angle between the line connecting the left and right shoulder joints and the line connecting the left and right hip joints about the axis through the midpoints of the two lines.

The beginning times of 6 upper extremity motions that would accelerate the javelin relative to the time of the right foot landing of the last cross step were identified for each subject. These times were normalized to the time duration between the right foot landing of the last cross step and the release.

Two-way analysis of variance (ANOVA) with mixed design were performed to determine the effects of motion and gander on the sequence of the beginning of selected upper extremity joint and segment angular motions. Post-hoc Student-Newman-Keul tests were performed to locate the time differences between every two adjacent motions if the ANOVA revealed significant main effect of motion. A Type I error rate of 0.05 was used as the indication of overall statistical significance in the ANOVA.

RESULTS AND DISCUSSION

ANOVA detected significant a significant interaction effect of motion and gender ($P = 0.001$). One-way ANOVA with repeated measures, therefore, was performed for each gender to determine the effect of motion on beginning time. One-way ANOVAs showed significant effect of motion on the beginning time for both genders ($p < 0.001$). Post-hoc tests showed that the upper extremity motions in javelin throwing can be divided into 5 groups for male javelin throwers (Table 1) and 4 groups for female javelin throwers (Table 2), respectively ($p < 0.001$).

Table 1. Sequence of upper extremity motions of elite male javelin throwers ($p < 0.05$).

	Motion	Beginning time (%)
1	Upper trunk forward rotation	-14.7 ± 33.0
2	Shoulder horizontal adduction	68.4 ± 9.4
3	Shoulder abduction	77.9 ± 8.5
4	Elbow extension	82.5 ± 3.5
	Shoulder internal rotation	85.5 ± 4.6
5	Wrist flexion	97.2 ± 3.1

Table 2. Sequence of upper extremity motions of elite female javelin throwers ($p < 0.05$).

	Motion	Beginning time (%)
1	Upper trunk forward rotation	-12.4 ± 26.9
2	Shoulder abduction	70.9 ± 13.4
3	Shoulder horizontal adduction	77.7 + 9.4
	Elbow extension	81.9 ± 3.8
	Shoulder internal rotation	82.8 ± 4.8
4	Wrist flexion	97.0 ± 3.0

The results of the present study partially support our hypothesis that elite javelin throwers started their upper extremity motions with upper trunk forward rotation and ended their upper extremity motions with wrist flexion, which appeared to be in a P-D sequence. However, the elite male javelin throwers started their elbow extension and shoulder internal rotation essentially at the same time (Table 1) while the elite female javelin throwers started their shoulder horizontal adduction, elbow extension, and shoulder internal rotation essentially at the same time (Table 2). These results demonstrated a reverse of the P-D sequence of upper extremity motions at the shoulder and elbow in javelin throwing. These results were consistent with the literature. The literature showed that the shoulder internal rotation motion was started after elbow extension was started in baseball pitching [7], which was similar to that in the penalty throwing in water polo [3]. Studies on throwing arm joint torques and muscle activities in baseball pitching also showed that throwing arm joint angular motions did not necessarily follow a P-D sequence for maximum release speed of the baseball [2, 4]. Studies on the upper extremity motions in tennis serving demonstrated that starting shoulder internal rotation after the elbow starts extension may be an effective way to obtain maximum final speed of the tennis racquet [5].

The results of the present study do not support the P-D sequence of upper extremity motions in javelin throwing reported in literature [1, 6], which is main because the present study used the beginning times of joint angular motions to represent the sequence of upper extremity motions while the literature used the time of peak joint center linear velocities. The sequence of peak joint center linear velocities does not represent the sequence of joint angular motions, and thus provide little information for javelin throwing training.

The results of this study do not support our hypothesis that elite male and female javelin throwers used the same sequence of upper extremity motions in javelin throwing. The gender difference in the sequence of upper extremity motions in javelin throwing may reflect the gender difference in javelin throwing techniques due to gender differences in physical conditions.

CONCLUSIONS

Elite javelin throwers accelerated the javelin using a certain sequence of upper extremity motions during the delivery, which is not a P-D sequence. Male and female javelin throwers used different sequence of upper extremity motions.

REFERENCES

1. Best RG, et al. *J Sports Sci* **11**, 315-328, 1993.
2. Feltner ME, et al. *Int J Sport Biomech* **2**, 235-259, 1986.
3. Feltner ME, et al. *J Appl Biomech* **12**, 359-382, 1996.
4. Hirashima M, et al. *J Sports Sci* **20**, 301-310, 2002.
5. Marshall RN, et al. *J Sports Sci* 18, 247-245.
6. Mero A, et al. *J Appl Biomech* **10**,166-177, 1994.
7. Sakurai S, et al. *J Appl Biomech* **9**, 47-65, 1993.

ACKNOWLEDGEMENTS

This study was financially supported by USA track and Field, the Graduate School at the University of North Carolina Chapel Hill, and the International Society of Biomechanics.

PELVIC AND SHOULDER ROTATIONS OF IDIOPATHIC SCOLIOTIC ADOLESCENTS DURING WALKING

[1]Marie-Michèle Briand, [1]Mathieu Charbonneau, [2-3]Hubert Labelle and [1-2]François Prince

[1]Department of kinesiology, University of Montreal, Montreal, QC, Canada,
[2]Department of surgery, University of Montreal, Montreal, QC, Canada,
[3]CHU Sainte-Justine Research Center, Montreal, QC, Canada
Emails: mm.briand@umontreal.ca, francois.prince@umontreal.ca

INTRODUCTION

Scoliosis is a 3D deformation of the spine and thoracic cage. Female adolescents are mostly affected by this pathology and major changes occur during rapid growth periods and affect bones, ligaments as well as muscles [1,2]. These changes have consequences on gait pattern. Kinematics have been largely studied but most researchers reported angular displacement only in the sagittal plane. It is believed that asymmetric trunk rotations during walking could be a detrimental factor related to scoliosis. Therefore, the purpose of this study is to quantify pelvic and shoulder rotations in coronal and frontal planes in both idiopathic scoliotic patients (ISP) and control adolescents (CTRL). Asymmetry and coordination will be compared.

METHODS

Ten control adolescents and nine ISP walked at a comfortable speed for ten trials on a 10m walkway. Table 1 shows the mean age, height and weight (with standard deviation) for both control and ISP groups. Kinematics were extracted from 18 reflective markers attached bilaterally on the lower limbs and acromions and 6 on different levels of the spine. Data were collected at 60Hz from 8-cameras VICON motion analysis system (Oxford Metrix, UK).

Table 1: Mean (SD) age, height and weight for both control and idiopathic scoliotic patients.

	CTRL	ISP
Age (years)	14.4 (0.9)	15.0 (0.9)
Height (cm)	161.2 (9.7)	158.0 (7.6)
Weight (kg)	55.0 (9.5)	51.5 (9.8)

Shoulder and pelvic angles were calculated, for a gait cycle, using the equation ($\theta = \arctan(\Delta y / \Delta x)$) and the right side was used as a reference. Asymmetry was determined by the ratio between rotation angles of left and right gait cycles. This was calculated for both planes and separately for pelvis and shoulders. Statistical analyses included Student-t test for paired (left/right) and unpaired (CTRL/ISP) subjects. To evaluate coordination between the pelvis and shoulders, cross-correlations were used to compare groups and a Student-t test was also used.

RESULTS AND DISCUSSION

Control adolescents walked at a slightly but not statistically significant faster speed than ISP. No other tendency is reported for cadence, stride length, stance and double support phase durations. Table 2 presents angular measurements of both groups first in the coronal plane and second, the frontal plane. The only variable that reached the level of signification was the right vs. left pelvic angle in coronal plane for the control group ($p = 0.01$).

Table 2: Mean (+/-1SD) pelvic and shoulder range of motion in CTRL and ISP subjects.

	Coronal Plane			
	Pelvis		Shoulders	
	L	R	L	R
CTRL(°)	8.3 (2.6) *	7.7 (2.4)	7.0 (2.4)	7.1 (2.2)
ISP(°)	6.1 (3.0)	6.3 (3.0)	6.1 (1.6)	5.7 (2.5)
	Frontal Plane			
CTRL(°)	8.5 (2.4)	8.3 (2.4)	2.5 (1.0)	2.5 (1.0)
ISP (°)	7.0 (2.4)	7.0 (1.7)	2.1 (0.5)	2.1 (0.6)

*p=0.01between control group left and right cycles.

To compare coordination between pelvis and shoulders, cross-correlations were used. This statistical tool was used to show whether the pelvic and shoulder rotations were in phase or out of phase. Figure 1 gives examples of rotation angles in the frontal plane.

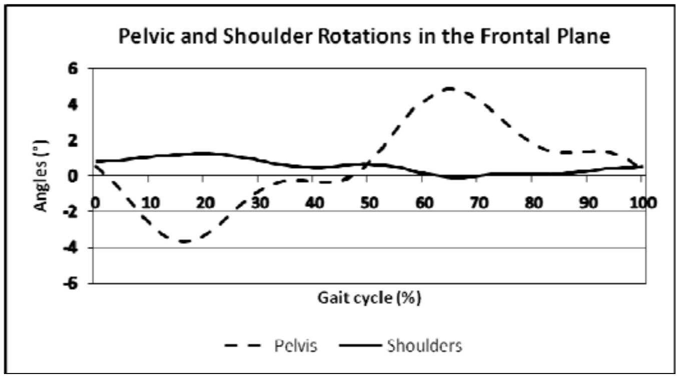

Figure 1: Pelvic and shoulder rotations angles in frontal plane.

Cross-correlation is presented in Table 3. Significant differences were found between CTRL and ISP groups in the frontal plane.

Control and ISP subjects were not different for range of motion. Angle values were similar to those found previously in literature [3,4]. However, in this study, ISP Cobb's angles were 15 degrees or less. At this point, the deformation may not be significant enough to modify the walking pattern. It did however have an influence on the coordination between the pelvis and the shoulders. With higher cross-correlation coefficients, the pelvis and shoulders of the control group appeared to be more synchronized than those in the ISP group in the frontal plane only.

Table 3: Cross-correlation results.

	Cross-correlation coefficients			
	CL	CR	FL	FR
CTRL	-0.74	-0.71	-0.69	-0.66
ISP	-0.68	-0.65	-0.64	-0.63
p value	0.02*	0.01*	0.06	0.12

C = coronal, F = frontal, L = left, R = right
p: Student-t test between CTRL and ISP, *: $p \leq 0.05$.

CONCLUSIONS

Pelvic and shoulder rotations of ISP and CTRL subjects were not statistically different in frontal plane or in coronal plane during normal walking. ISP have shown less asymmetry and their coordination was significantly poorer than the CTRL group.

REFERENCES

1. Burwell RG. *Pediatr Rehabil* **6**, 137-170, 2003.
2. Reamy BV, Slakey JB. *Am Fam Physician,* **64**, 111-116, 2001.
3. Rose J, Gamble JG. (1994). *Human Walking 2nd Edition*, Williams & Wilkins Press, Baltimore, MD.
4. Stokes VP et al. *J Biomech,* **22**, 43-50, 1989.

ACKNOWLEDGEMENTS

We would like to acknowledge the Canadian Institutes of Health Research (CIHR) and MENTOR program for their financial support. We also wish to acknowledge the Fonds de recherche en santé du Québec (FRSQ) for scholarship awarded to FP.

THE PROBABILITY FOR TIBIAL STRESS FRACTURE INCREASES WITH RUNNING SPEED DESPITE A REDUCTION IN THE NUMBER OF LOADING CYCLES

[1] W. Brent Edwards, [2] David Taylor, [1] Thomas J. Rudolphi, [1] Jason C. Gillette, and [1] Timothy R. Derrick
[1] Iowa State University, Ames, IA,
[2] Trinity College Dublin, Dublin 2, Ireland
email: edwards9@iastate.edu web: www.kin.hs.iastate.edu

Introduction

Stress fractures are common overuse injuries among runners that result from the mechanical fatigue of bone. The failure of materials subjected to mechanical fatigue is dependent on both loading magnitude and loading exposure. Reducing speed is one potential mechanism of load reduction during running [1]. However, a reduction in running speed is associated with an increased number of loading cycles for a given mileage (assuming a positive relationship between stride length and speed). It is therefore unclear if these increased loading cycles are detrimental to skeletal health despite reductions in loading magnitude.

The purpose of this study was to determine the influence of running speed on the probability of tibial stress fracture. We hypothesized that reducing running speed would decrease tibial strain sufficiently enough to negate the detrimental increase in loading cycles associated with a given running mileage. This would lead to a reduction in the probability of tibial stress fracture with a corresponding decrease in running speed.

Methods

Ten male subjects ran overground at three prescribed speeds (2.5, 3.5, and 4.5 m/s). Force platform (1600 Hz) and kinematic data (160 Hz) were collected synchronously. Average stride frequency was recorded. Cardan joint and segment angles were calculated. Joint moments and reaction forces were determined for the hip, knee, ankle, and subtalar joint using standard inverse dynamics.

A SIMM musculoskeletal model, containing 43 lower-extremity muscles, was used to obtain maximum dynamic muscle forces (adjusted for muscle length and velocity), muscle moment arms, and muscle orientations. This information was used in a static optimization routine to estimate individual muscle forces during stance. The cost function to be minimized was the sum of squared muscle stresses. Six moments were used to constrain the optimization including the three orthogonal components at the hip, the flexion-extension moment at the knee and ankle, and the subtalar moment. Contact forces acting on the distal tibia were calculated as 90% the vector sum of the ankle reaction force and muscle forces crossing the ankle joint (the fibula bears 10% of the load) [2]. Peak instantaneous contact force served as input to a finite element model to estimate tibial strains during stance. A separate model was created for each subject that was scaled to the individual's leg length.

Stress fracture probability at each speed was determined using a probabilistic model of bone damage, repair, and adaptation [3]. The stress fracture model used the Weibull approach, a common procedure in fatigue mechanics used to determine the probability of failure when there is considerable scatter in a material's fatigue behavior (e.g., cortical bone). The model began with a modified Weibull equation that accounted for stressed volume:

$$P_f = 1\text{-}\exp[-(V_s/V_{so})(t/t_f)^w]$$

where V_{so} is the reference stressed volume, t_f is the reference time until failure at the applied strain level and number of loading cycles/day, and w expresses the degree of scatter in the material. These constants were derived from experimental fatigue testing literature and allowed the researcher to predict the cumulative probability of failure P_f for a specimen having stressed volume V_s from time zero to t. Bone repair was incorporated into the model with a second Weibull equation:

$$P_r = 1\text{-}\exp[-(t/t_r)^v]$$

where t_r is the reference time until repair and v expresses the degree of scatter in repair (i.e., variability in the time for a basic multicellular unit to tunnel through and remove a microcrack). By determining the probability that bone will not repair itself ($1-P_r$) and multiplying it by the instantaneous probability that failure will take place (time differential of P_f), we obtained an instantaneous probability that accounted for failure and repair; integrating with respect to time gave the cumulative probability of failure with repair (P_{fr}). For adaptation, we assumed a rate of 4 µm/day of bone deposition on the periosteal surface. Standard beam theory was then used to determine the change in strain over time t. This change in strain was converted to a single equivalent strain using a weighted average procedure. The equivalent strain was utilized within the "failure" Weibull equation P_f to determine the probability of failure with repair and adaptation (P_{fra}).

Cumulative P_{fra} was determined for a running regimen of 3 miles/day over the course of 100 days. Differences in peak P_{fra} as a function of running speed were compared using a repeated measures ANOVA ($\alpha=0.05$) with Bonferroni adjusted post-hoc comparisons ($\alpha=0.05/3=0.017$).

Results

Peak P_{fra} occurred after approximately 40 days of training (Fig. 1). Decreasing running speed from 4.5 to 3.5 m/s reduced the likelihood for tibial stress fracture by 4% (p=0.01; Table 1). Decreasing running speed from 3.5 to 2.5 m/s reduced the likelihood for tibial stress fracture by 12% (p=0.01).

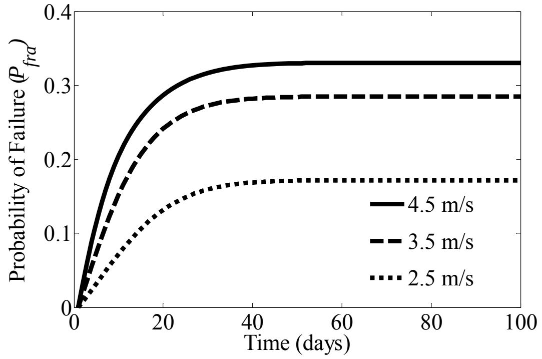

Figure 1. Group ensemble P_{fra} over 100 days for each running speed.

Table 1. Mean peak P_{fra} (SD) across running speeds. Significant differences were observed between all speeds (p<0.017).

2.5 m/s	3.5 m/s	4.5 m/s
0.17 (0.21)	0.29 (0.29)	0.33 (0.30)

Discussion

The purpose of this study was to determine the effects of running speed on the probability of tibial stress fracture. Our hypothesis was supported by the results of this study in that a linear reduction in running speed resulted in a corresponding non-linear reduction in peak P_{fra}. Therefore, runners wanting to reduce their probability for tibial stress fracture may benefit from a decrease in running speed. This finding was a direct result of the reduced joint contact forces and therefore reduced strains associated with slower running speeds. Because a reduction in running speed was also associated with an increase in the number of loading cycles for a given running mileage, it appears that stress fracture development is more dependent on loading magnitude rather than loading exposure. This statement is of course specific to the parameters investigated in this study and may therefore not apply to different running velocities and mileages.

Conclusions

For a given mileage, a decrease in running speed reduces the likelihood for tibial stress fracture. Strain magnitude may play a more important role in stress fracture development than the total number of loading cycles.

References

1. Keller, TS. et al. *Clin Biomech* **11**, 253-259, 1996.
2. Sasimontonkul, S. et al. *J Biomech* **40**, 3503-3509, 2007.
3. Taylor, D. et al. *J Orthop Res* **22**, 487-494, 2004.

LOSS OF ISOMETRIC TENSION IN MYOFIBRILS UNDERGOING ACTIVATED STRETCHES

Appaji Panchangam and Walter Herzog
Human Performance Laboratory, University of Calgary, Calgary
email: apanchangam@kin.ucalgary.ca

INTRODUCTION

Stretching of activated skeletal muscle fibers results in immediate loss of isometric tension and focal sarcomere disruption [1]. Loss of tension has been thought to be a direct consequence of the loss of tension generating units, the sarcomeres [2] and the disruption itself was explained with a theoretical model [3]. These two effects, *viz.*, loss of tension and sarcomere disruption, seem to be concurrent on most tissue levels. However, stretch experiments on isolated myofibrils showed evidence neither for sarcomere disruption [4,5], nor for reduction in isometric tension. Consequently, the question whether sarcomere disruption is necessary or not for loss of isometric tension following stretch, remained untested at the myofibril level. We stretched activated myofibrils of rabbit psoas muscles to test the hypothesis that loss of tension following activated stretches does not require sarcomere disruption.

METHODS

Rabbits were euthanized by an intravenous injection of sodium pentobarbital solution (240 mg/ml), a protocol approved by the University of Calgary Animal Care and Ethics Committee. Small strips of psoas muscle were dissected and stored in 50% rigor and 50% glycerol (v/v) solution at −20°C for 10 days.

On the day of the experiment, a small sample of the tissue was cut and subsequently blended in a rigor solution. A small amount of the blended mixture was placed in a fluid exchange chamber mounted on an inverted microscope (Zeiss, Axiovert 200M, Germany) and myofibrils were allowed to settle at the bottom of the chamber for ~5 min. Then, myofibrils in suspension were washed away by replacing the bathing solution with a relaxing solution leaving only the myofibrils that had settled at the bottom of the chamber.

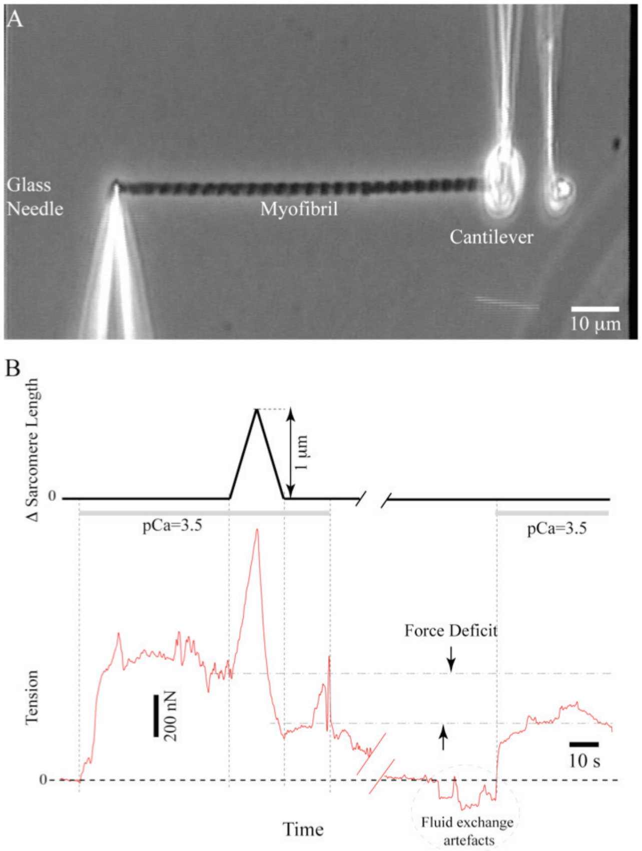

Figure 1: *A*. A Sample myofibril preparation (magnification, 100x). *B*. Myofibrils were stretched and released at constant speed (top). The tension response of a representative myofibril to the stretch-release cycle is shown in the bottom trace. Force deficit was estimated from the isometric tension measurements before and after the stretch.

Myofibrils were mounted (Figure 1A) with one end fixed to the tip of a glass micro needle and the other end attached to a silicon nitride cantilever of known stiffness. The cantilever movement was tracked by projecting it onto a linear CCD array (10,680 elements) to estimate the tension in the myofibril.

Myofibrils were maximally activated by replacing the bathing solution with a high-[Ca^{2+}] activating solution (pCa=3.5). At peak isometric tension, myofibrils were subjected to a single stretch-release cycle of magnitude, 1 µm sarcomere^{-1} and speed, 0.1 µm s^{-1} sarcomere^{-1}. Myofibrils were subsequently relaxed and re-activated to estimate the isometric tension following the stretch-release protocol. Force deficit, the percentage loss in maximum isometric tension, was estimated from the two isometric tension measurements before and after the stretch-release cycle (Figure 1B). Control myofibrils were simply activated twice, but not stretched. All experiments were videotaped throughout the experimental protocol to note any sarcomere disruption.

RESULTS AND DISCUSSION

At maximal activation, myofibrils produced a peak isometric tension of 157 ± 37 kN m^{-2} (mean ± SD; n=4) at an average sarcomere length of 2.61 ± 0.1 µm. During the stretch-release cycle, myofibrils reached a peak sarcomere length of 3.3 ± 0.1 µm resulting in 28.4 ± 5.6 % strain. Isometric tension immediately following the stretch-release cycle was significantly lower when compared to that before the cycle, and closely matched with the peak isometric tension during the second activation. The stretch-release cycle resulted in a force deficit of 44 ± 3 %, whereas the control myofibrils showed only a 4 ± 18 % (n=3) decrease in isometric force from the first activation to the second activation. Even with such large force deficits, the sarcomeres appeared to be stable and remained intact throughout the experimental protocol (Fig. 2).

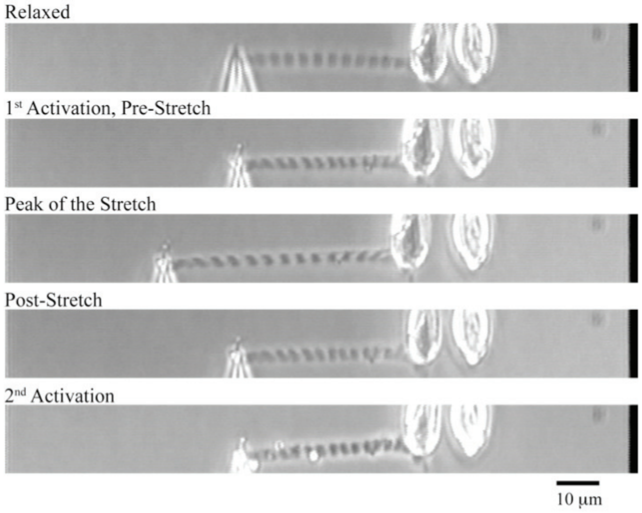

Figure 2: A Representative myofibril at 5 different stages of the experiment. Sarcomeres within myofibrils were intact throughout the stretch protocol. No rapid lengthening of sarcomeres was observed.

Previous experiments [4,5] involving activated stretches of single myofibrils did not show evidence of sarcomere disruption or loss of tension and damage. In contrast, we produced a 44 % reduction in tension, an indication of severe damage, yet without any visible sarcomere disruption. The loss in tension could not be due to force depression [6], because such history-dependent effects should have been abolished by the relaxation and re-activation procedure [6,7].

CONCLUSIONS

The observation, that activated stretching of myofibrils results in loss of tension without any sarcomere disruption, contradicts the commonly held view that loss of tension is a direct consequence of sarcomere disruption. We conclude that the mechanism for loss of tension in stretched muscles arises mostly from within the sarcomere.

We speculate that activated stretching permanently alters the interaction between active and passive force-transmission mechanisms thereby reducing the isometric tension.

REFERENCES

1. Macpherson PC et al. *J. Physiol.* 500.2:523-533, 1997.
2. Talbot JA & DL Morgan. *J. Muscle Res. Cell Motil.* 17:261-268, 1996.
3. Morgan DL. *Biophys. J.* 57:209-221, 1990.
4. Telley IA et al. *J. Physiol.* 573:173-185, 2006.
5. Rassier DE et al. *Proc. R. Soc. Lond. B.* 270:1735-1740, 2003.
6. Abbott BC & Aubert XM, J. Physiol. 117:77-86, 1952
7. Herzog W & TR Leonard. *J. Biomech.* 30(9):865-872, 1997.

ACKNOWLEDGEMENTS

Canadian Institutes of Health Research (CIHR), The Canada Research Chair Programme, and the Natural Sciences and Engineering Research Council (NSERC) of Canada

Changes in Ankle Kinematics to Preserve an Invariant Roll-over Shape

[1]Charles Wang and [1,2]Andrew Hansen
[1]Northwestern University, [2]Jesse Brown VA Medical Center
e-mail: a-hansen@northwestern.edu

INTRODUCTION

The roll-over shape (ROS), which is the effective rocker that the ankle-foot system conforms to from heel contact to opposite heel contact, may be a useful tool for design and evaluation of lower limb prostheses because it has been shown to be invariant to changes in walking speed, added weight to the torso, and heel height during able-bodied walking [1-3]. However, it is uncertain whether ankle kinematics also remain unchanged during this part of the gait cycle (GC) or whether they adapt to preserve the same ROS. By studying able-bodied persons walking on rocker shoes of different radii, we could invalidate the idea of ankle kinematics invariance, ROS invariance, or both. We hypothesized that ankle flexion during single support of walking would change in response to different shoe rocker radii in order to maintain an invariant roll-over shape radius. Based on a model that assumes ROS invariance, we also hypothesized that for decreasing shoe rocker radius, the difference in ankle flexion angle between the end and the beginning of single support would decrease.

METHODS

Ten able-bodied subjects were asked to walk in four different pairs of rocker shoes at three different speeds (Figure 1). The rockers added to the bottom of the shoes had radii of 25%, 40%, and 55% of the subject's leg length. The fourth shoe had a flat elevated bottom. These were coded R25, R40, R55, and FLAT. The three speeds were freely self-selected speed, 30% faster, and 30% slower. Data were collected at the VA Chicago Motion Analysis Research Lab, equipped with six force platforms and an eight-camera motion analysis system. A modified Helen Hayes marker system [4] was used to monitor joint kinematics during gait. We also measured the subjects' ground reaction forces (GRF) as they walked on the force plates. The data collected were first processed with commercial software, EVA Realtime and Orthotrak, yielding ankle kinematics and joint center coordinates.

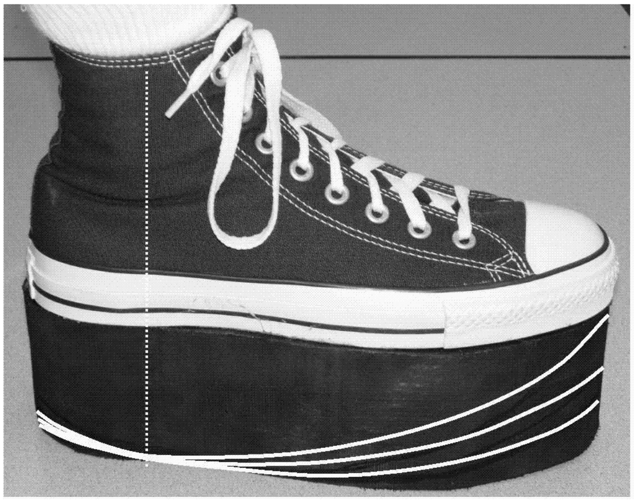

Figure 1: High top canvas shoe with stiff crepe material attached. Different radii were obtained by cutting along the lines drawn on the sole (lines in the picture are not drawn to scale).

Custom MATLAB scripts were used to overlay trials with different shoes but at the same walking speed. Range of motion (ROM) of the ankle, defined as the ankle flexion at opposite heel strike (50% GC) subtracted by that at opposite toe off (10% GC), was measured and compared for different shoes and walking speeds. Knee flexion, hip flexion, and pelvic obliquity curves were visually inspected as a function of the GC. Another script was used to transform the center of pressure of the GRF under the shoe from a lab-based to a shank-based coordinate system, yielding the roll-over shape [5]. This curve was fitted to a circular arc to find its radius and center to aid in the comparison of the different conditions.

SPSS was used to perform a 3x4 two-way repeated measures ANOVA to see if there were significant differences in ankle flexion range of motion and ankle-foot-shoe roll-over shape radius between the three walking speeds and four shoe rocker radii. Additionally, pairwise comparisons were performed for statistically significant factors.

RESULTS AND DISCUSSION

The results shown are data collected from one subject, representative of the entire pool, at freely self-selected speed. Ankle kinematics were not affected by walking speed ($p = 0.65$), but they were clearly changed by the shoes (Figure 2). The differences in ankle ROM between the four rocker shoes at each speed were highly significant ($p < 0.001$). At freely self-selected speed, the ROM (mean ± SD deg) for all the subjects were 24.2 ± 4.0, 14.7 ± 2.9, 10.5 ± 3.1, and 5.7 ± 3.4 for FLAT, R55, R40, and R25, respectively. The data showed a consistent decrease in ROM with decreasing shoe rocker radius, supporting our hypothesis. Based on the pairwise comparisons, each rocker shoe resulted in a significantly different ankle ROM from each other ($p < 0.04$ for all comparisons).

On the other hand, the ankle-foot-shoe roll-over shapes were remarkably invariant, independent of walking speeds ($p = 0.38$) and shoe rocker radii ($p = 0.37$) (Figure 3). The ROS radius (mean ± SD) of all twelve conditions for the ten subjects was 17.7 ± 2.4% of height or 33.4 ± 4.6 % of leg length. This radius agrees with previous studies [6] and is in the range of the radii of rocker shoes we made. Since, the other joint kinematics analyzed were almost unaffected by the changing rocker radii, it can be concluded that ankle kinematics adapted to preserve an invariant ankle-foot-shoe roll-over shape.

This ankle adaptation may indicate a neurological goal to maintain an ideal roll-over shape, regardless of changing walking conditions. Understanding the ideal ROS for able-bodied gait can improve prosthetic and orthotic designs that may enable their users to achieve gaits closer to able-bodied gait.

REFERENCES

1. Hansen AH, et al. *Clin Biomech* **19**, 407-414, 2004.
2. Hansen AH, et al. *JRRD* **42** 3, 381-390, 2005.
3. Hansen AH, et al. *JRRD* **41** 4, 547-554, 2004.
4. Kadaba MP, et al. *J Orthop Res* **8**, 383-392, 1990.
5. Fatone S, et al. *JRRD* **44** 1, 11-20, 2007.
6. Hansen AH, *PhD Dissertation,* Northwestern University, 2002.

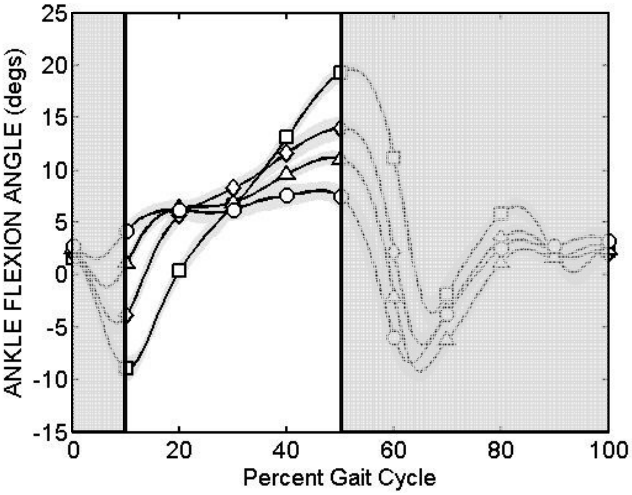

Figure 2: Ankle flexion over the entire gait cycle (GC) of a subject's right foot at freely self-selected speed. During single support (10%~50% GC), the ankle range of motion fluctuates significantly ($p < 0.001$) between rocker shoe conditions. (Note: square = FLAT, diamond = R55, triangle = R40, circle = R25.)

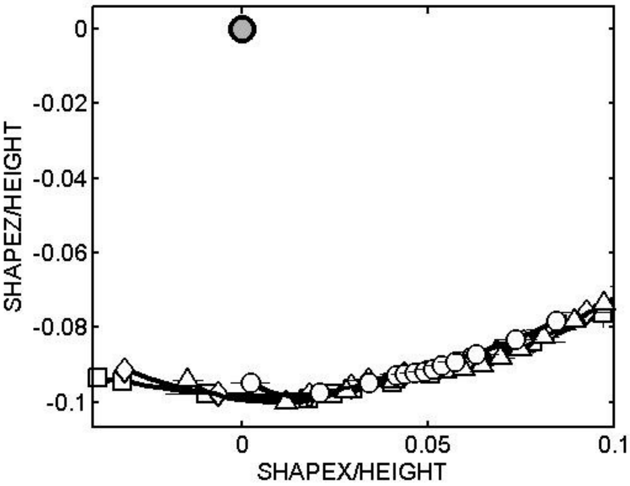

Figure 3: Ankle-foot-shoe roll-over shape (normalized by height) of a subject's right foot at freely self-selected speed. The curves are almost identical for all shoe conditions. The mean roll-over shape radius of all the subjects was 17.7 ± 2.4% of height or 33.4 ± 4.6 % of leg length. (Note: square = FLAT, diamond = R55, triangle = R40, circle = R25; (0,0) is the ankle center.)

ACKNOWLEDGEMENTS

The authors would like to thank Rebecca Stine and Kathy Waldera for their assistance. This work was supported by NIH Grant # R03 HD050428-01A2.

Effective Rocker Shapes for Walking, Swaying, and Standing

[1]Charles Wang and [1,2]Andrew Hansen
[1]Northwestern University, [2]Jesse Brown VA Medical Center
e-mail: a-hansen@northwestern.edu

INTRODUCTION

The roll-over shape (ROS), which is the effective rocker that the ankle-foot system conforms to from heel contact to opposite heel contact in walking, may be a useful tool for design and evaluation of lower limb prostheses. During many activities of daily living, however, standing and swaying are also important. Walking ROSs have been found to be nearly circular in shape and unchanged with variations in walking speed, added weight to the torso, and shoe heel height [1-3]. However, it is unclear what the effective rocker shapes are for able-bodied persons during gentle swaying or quiet standing. We hypothesized that the effective shapes of swaying and standing would be flatter than walking ROSs, providing an inherently stable base.

METHODS

Ten able-bodied subjects were asked to walk at their freely self-selected speed, sway gently, and stand quietly. During swaying, the subjects were asked to perform low amplitude, low frequency sways, trying not to lift their heels or toes off the ground. All subjects wore Converse canvas sneakers provided by the lab because this shoe has a flat sole and does not restrict ankle motion.

Data were collected at the VA Chicago Motion Analysis Research Lab, equipped with six force plates and an eight-camera motion analysis system. A modified Helen Hayes marker system [4] was used to monitor joint kinematics. We also measured ground reaction forces (GRF) as they walked, swayed, and stood on the force plates. Commercial software, EVA Realtime and Orthotrak, was used to yield ankle kinematics and joint center coordinates.

A custom Matlab script was used to transform the center of pressure (COP) of the GRF under the shoe from a lab-based to a shank-based coordinate system, yielding the effective rocker shape [5]. Walking and swaying shapes were fit with second order polynomials:

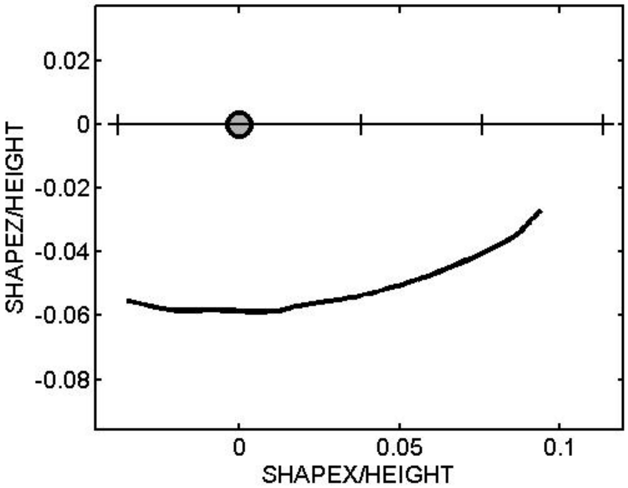

Figure 1: Walking roll-over shape (normalized by height) of a subject's right foot. The curve can be fitted to a circle and the mean ± SD radius for all the subjects was 16.1 ± 2.5% of height or 30.4 ± 4.6% of leg length. The arc length was 13.2 ± 1.0% of height or 86.7 ± 6.8% of foot length (FL). The horizontal line is a FL and the ankle center (0,0) is at ~25% FL.

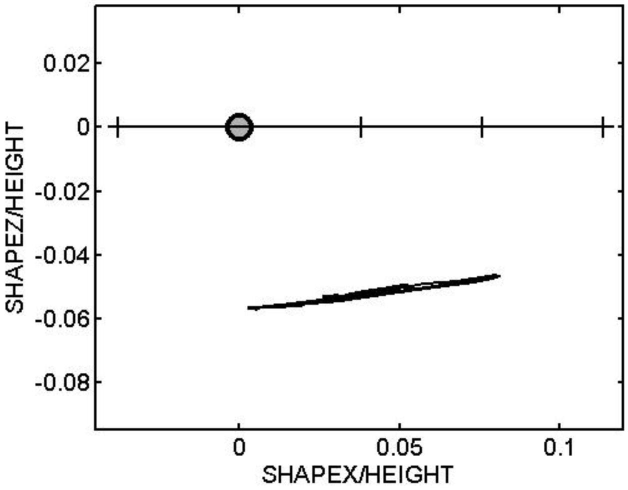

Figure 2: Swaying effective shape (normalized by height) of a subject's right foot. The curve is flat with a length of 7.2 ± 1.3% of height or 47.2 ± 8.4% of foot length (FL). The horizontal line is a FL and the ankle center (0,0) is at ~25% FL.

$$Z = a_2 X^2 + a_1 X + a_0 \qquad (1)$$

where X and Z were the anterior and proximal components, respectively, of the effective rocker shapes. The hypothesis was that the a_2 coefficient would be reduced for swaying effective shapes compared with walking shapes, indicating a reduction in curvature. A one-tailed paired T-test was performed in SPSS to test this hypothesis. The arc length of the walking shape was calculated from its best-fit circle, using L = radius * central angle. The lengths of the flat shapes were calculated using $L = [(x_1-x_2)^2+(y_1-y_2)^2]^{1/2}$, where (x_1,y_1) and (x_2,y_2) are the coordinates of the ends of the shapes.

RESULTS AND DISCUSSION

The results shown are data collected from one subject, representative of the entire pool. Visual inspection shows that the walking ROS was circular and that the effective rocker shapes of swaying and standing were flatter, as hypothesized (Figures 1-3). The mean a_2 coefficient of all the subjects (Table 1), which is proportional to curvature, for the swaying shapes is significantly lower than those for walking ($p < 0.001$). The mean arc length (Table 1) indicate that the subjects utilized almost 87% of their foot length while walking, but kept their COP around the middle 50% of their feet while swaying and around the middle 5% while standing. Swaying keeps the COP within reported functional stability limits [6]. The standing COP is near the center of the functional stability limits and likely chosen to react to unexpected forward or backward perturbations.

Understanding standing and walking patterns of able-bodied gait can be important for prosthetic and orthotic designs. For example, the "flat" region in some prosthetic feet may be useful for prosthesis users with poor balance. The length of the "flat" region may determine the appropriate compromise between stability and mobility for each user. These results may also be applicable to walking casts/boots and rockers for total contact casts. Additionally, the development of bi-modal ankle-foot prostheses that provide a curved effective shape during walking and a flat effective shape during standing may be warranted.

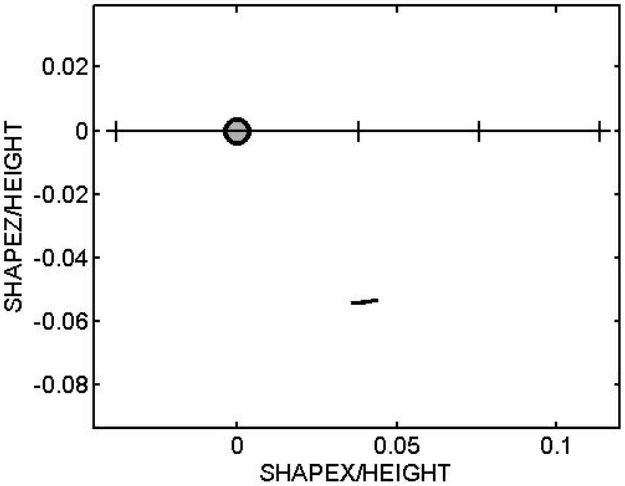

Figure 3: Standing effective shape (normalized by height) of a subject's right foot. The curve is flat with a length of 0.7 ± 0.3% of height or 4.9 ± 1.9% of foot length (FL). The horizontal line is a FL and the ankle center (0,0) is at ~25% FL.

REFERENCES

1. Hansen AH, et al. *Clin Biomech* **19**, 407-414, 2004.
2. Hansen AH, et al. *JRRD* **42** 3, 381-390, 2005.
3. Hansen AH, et al. *JRRD* **41** 4, 547-554, 2004.
4. Kadaba MP, et al. *J Orthop Res* **8**, 383-392, 1990.
5. Fatone S, et al. *JRRD* **44** 1, 11-20, 2007.
6. Holbein-Jenny MA, et al. *Ergonomics* **50** 5, 631-646, 2007.

ACKNOWLEDGEMENTS

The authors would like to thank Rebecca Stine and Kathy Waldera for their assistance. This work was supported by NIH Grant # R03 HD050428-01A2.

Table 1: Characteristics of the three effective rocker shapes. The arc lengths show that the subjects used most of their feet during walking, about half during swaying, and only about 5% while standing. The a_2 coefficients show that swaying shapes were significantly flatter than walking shapes ($p < 0.001$).

Measurement	*Walking*	*Swaying*	*Standing*
Arc Length	13.2 ± 1.0% H	7.2 ± 1.3% H	0.7 ± 0.3% H
	86.7 ± 6.8% FL	47.2 ± 8.4% FL	4.9 ± 1.9% FL
a_2 Coefficient	3.53 ± 0.44	0.43 ± 0.31	N/A

Note: All values displayed are mean ± SD of all ten subjects. H = height, FL = foot length.

DEVELOPING AN EMPIRICAL SPATIAL SHOULDER MUSCLE ACTIVITY MAP

Alicia L. Belbeck, Amy Y. Chow, Clark R. Dickerson
Department of Kinesiology, University of Waterloo, Waterloo, Ontario, Canada
email: cdickers@uwaterloo.ca

INTRODUCTION

Although both empirical [1] and mathematical [2] approaches have been used to quantify shoulder muscle activity during task performance, these efforts have either focused on a few constrained tasks or lack extensive validation. Additional attempts to estimate shoulder exposures for work tasks have focused on identifying comfort levels [3] and strength requirements [4], and thus did not explore the physical consequences of performing work throughout a reach envelope. Unfortunately, these shortcomings compromise the practicality of their general adoption for ergonomic design applications, particularly for virtual environments.

The aim of this study was to establish a spatial (3-D positional) sensitivity of 14 shoulder muscles within a right-handed work envelope. The results will help develop a priori estimates of muscle forces and stresses, thus enabling proactive ergonomic designs to be evaluated for muscular loading. Additionally, the results provide extensive empirical evaluation data for existing mathematical shoulder muscle force prediction models.

METHODS

Fourteen university-aged males with no history of shoulder pain participated (age 22.0 ± 2.0 years). Bipolar surface electrodes were placed on 14 different sites on the right upper extremity (anterior, middle and posterior deltoid, biceps, triceps, infraspinatus, supraspinatus, pectoralis major sternal and clavicular insertions, latissimus dorsi, serratus anterior, and upper middle and lower trapezius). Muscle activity was recorded at 1500 Hz with a T2000 EMG system (Noraxon, Arizona, USA).

One hundred and forty 40N ramped directional seven second push tasks were performed (70 up; 70 down) within a right-handed reach envelope at specific locations spaced 20 cm apart along three axis: x (frontal plane -40 to 60 cm); y (saggital plane -10 to 50 cm); and z (coronal plane -20 to 60 cm). The origin of these axes was located at the center of the trunk at umbilical level. A Motoman HP50N (West Carrollton, OH, US) positioned the handle. Hand force was recorded with an MSA-6 transducer (AMTI, Watertown, MA, USA), and force feedback was provided to participants via custom LabView software (National Instruments, Texas, USA).

Exertion-specific muscle activity data were linear enveloped using a 4 Hz cutoff and normalized to activity levels recorded during three maximal voluntary contractions (MVC) for each muscle. Three-second central windows for each push task were evaluated for each muscle during each trial.

Two directional (up, down) 3-way ANOVAs were used for data analysis using the x, y and z positions as factors. Further, multiple linear regression was used to create predictive equations for each muscle for upward exertions to determine normalized muscle activity values.

RESULTS AND DISCUSSION

In both force directions, muscle myoelectric activity varied with spatial location (x, y, z). Significant ($p<0.05$) differences existed for all muscles, though specific muscles had variable spatial sensitivity that corresponded to their primary function. Many of these relationships were nonlinear.

Table 1-Prediction equations and variance explanation of several shoulder muscles for upward exertions.

Muscle	r^2	Prediction Equation
Pec. Sternal	0.81	$= 8.29 – 0.028(x) – 0.0003(z)^2 + 0.0072(x–22.09)^2 + 0.0008[(x–22.09)(z–27.41)]$
Supraspinatus	0.74	$= 2.13 + 2.11(x) + 0.14(y) + 0.12 (z) + 0.022(x-22.09)^2 + 0.0031(y-20.84)^2 – 0.002(z-37.41)^2 – 0.0012[(x-22.09)(z-27.41)] – 0.0013[(x – 22.09)(y-20.84)] – 0.00032(x-22.094)^3$
M. Deltoid	0.73	$= -5.55 + 0.16(x) + 0.21(y) + 0.16 (z) + 0.005(x-21.96)^2 + 0.0062(y-20.87)^2 + 0.0014(y-20.87)*(z-27.46)$
Lat. Dorsi	0.72	$= 6.78 + 0.023(x) + 0.034(y) + 0.019(z) + 0.001(x–22.09)^2 + 0.0017(y–20.84)^2 + 0.0011[(y–20.84)(z-27.41)]$
Upper Trap.	0.67	$= -1.022 + 0.083(x) + 0.16(y) + 0.2(z) + 0.003(x-22.09)^2 + 0.0033(y-22.84)^2 – 0.0014[(x-22.09)(z-27.41)]$
Lower Trap.	0.65	$= 3.74 + 0.17(x) + 0.024(y) + 0.045(z) + 0.0024(x-22.09)^2 + 0.004(y-20.84)^2 – 0.0019(z-27.41)^2$
Serratus Ant.	0.64	$= -3.47 + 0.081(x) + 0.24(y) + 0.23(z) + 0.005(x-22.09)^2 + 0.004(y-20.84)_2 + 0.0023[(y-20.84)(z-27.41)]$

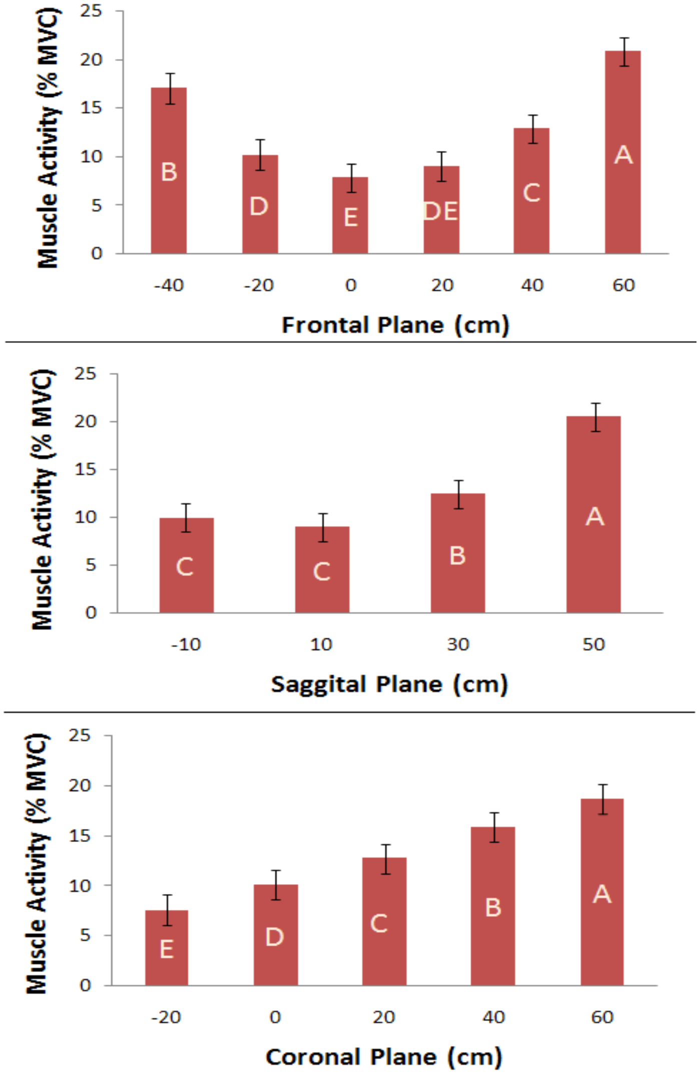

Figure 1 – Spatial variation effect on middle deltoid muscle activity for upward tasks. Different letters denote significantly different activity levels.

In general, muscle activation increased when exertions were performed further away from the system origin. In some cases values exceeded recommended limits for extended work [5]. Results reflecting these general findings are shown for a representative muscle, the middle deltoid (Figure 1).

Multiple linear regression produced spatially-based prediction equations for normalized muscle activity for each muscle (examples in Table 1). The variance explanation achieved by these equations exceeded 0.6 for all but three of the muscles monitored (posterior deltoid, lower trapezius, and biceps). With these equations, predictions of muscle activity for any location in the reach envelope are possible (an upward 40N push middle deltoid example on a 60cm surface is shown in Figure 2.

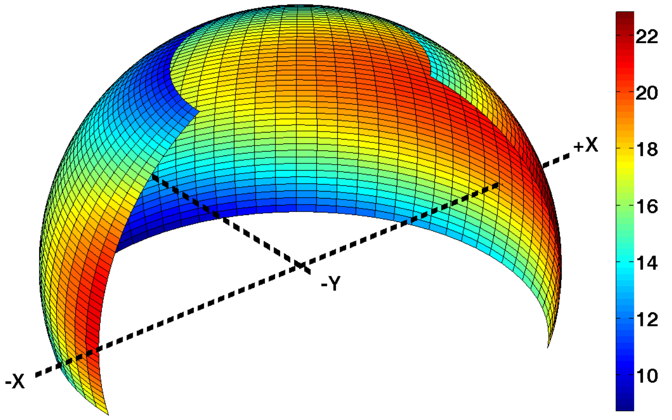

Figure 2 – Example of predicted muscle activity for middle deltoid on a 60 cm work surface Note the nonlinear shifts with spatial location of the exertion, which reflect the prediction equations generated.

CONCLUSIONS

Spatially dependent trends for all 14 muscles tested existed. They largely confirmed heuristic understanding of muscle function for specific exertion directions (i.e. arm elevators were more active as well as more accurately predicted during upward trials). In addition, we identified significant differences in activity level for each muscle between tested locations along each axis. More importantly, the results provide the research community with a previously unavailable, extensive dataset of shoulder muscle activity levels for multiple muscles throughout a large reach envelope.

The 3-D prediction equations created revealed interactions between axes and muscle activity for many shoulder muscles for upward exertions. This provides the foundational work for an advanced tool to evaluate the consequences on tissue-level loading of the spatial positioning of work demands. These initial equations will inform the expansion of predictive ability to include multiple hand force levels as well as additional exertion directions and evaluation of predictive model performance for interpolative and extrapolative situations.

REFERENCES

1. Soechting et al. *J Bmech Eng* 119:93-102, 1997.
2. Dickerson et al. *Comp Meth Biomech & Biomed Eng*, 10(**6**):389-400, 2007.
3. Das, et al. *Hum Factors*, 40 (**4**): 633-646, 1998.
4. Strasser et al. *Indust Ergo* 23:339-347, 1999.
5. Jonsson, *Cont Clin Neurophys*, S34:417-428, 1978.

A METHOD FOR PREDICTION OF SEATED SPINAL CURVATURE

Sam Leitkam, Tamara Reid Bush, PhD
Michigan State University Department of Mechanical Engineering
email: leitkams@msu.edu, reidtama@msu.edu

INTRODUCTION

The ergonomics of seating require knowledge of both the seat and the human that is interacting with that seat. To fully understand the interaction between these two separate bodies, it is necessary to be able to quantify and measure each. While it is possible to design and build seats that will move and conform to a wide array of spinal articulations, the ability to quantify these articulations while in a seat, such as an office chair, is still an open and unsolved problem.

Several viable methods exist for quantifying spinal curvature of some or all of the human back [1,2,3], but these primarily rely on the use of technology that is not feasible for use in an ergonomic related study. For example, X-Rays provide static images, which are not adequate for the study of dynamic seated environments. Also, the equipment required for MRI or CT scans creates an environment that is not conducive to extended seated tasks and wide ranges of movement.

The purpose of this research was to develop a method that can be used to quantify spinal articulation while seated. A future goal of this work is to utilize these methods to collect data that will support the development of a mathematical model for spinal curvature prediction in a seated environment.

METHODS

The presented method employed the use of a three-dimensional motion capture system (Qualisys, Gothenburg, Sweden) to quantify the position of visible body landmarks and used these to predict the position and orientation of the spine. Specifically, the positions of the thorax and the pelvis were measured because these two rigid bodies directly affect spinal curvature. The relative orientations of these two structures were used to calculate an "openness" angle [4]. A larger openness angle corresponded to tilting the sternum rearward, rolling the top of the pelvis forward, and thus producing a lordotic curvature in the lumbar spine. Conversely, a smaller openness angle corresponded to tilting the sternum forward, rolling the top of the pelvis rearward, and producing a kyphotic curvature in the spine.

Six subjects with no reported back pain or spinal injuries volunteered to participate in the research. Each subject was informed of the process and signed consent to participate.

To develop the methodology and assess the relationship between "openness" and spinal articulation, all subjects were seated on a stool. While seated, the subjects were asked to assume four different static positions. Each subject was measured in maximum lordotic and maximum kyphotic lumbar positions, as well as a self-selected "natural" position and a position where the subject was asked to sit as "straight and tall" as possible. The first two were used as the extreme cases of lordotic and kyphotic postures, while the "comfortable", and "straight and tall" positions served as intermediate points within the range of normal motion.

Retro-reflective markers were affixed to each subject at key anatomical landmarks. Markers were located on the sternum, anterior superior iliac spines (ASIS), lateral femoral condyles and seventh cervical vertebra (C7), twelfth thoracic vertebra (T12), and one midway between the posterior superior iliac spines (Mid PSIS). Additionally, between C7 and T12, and between T12 and the Mid PSIS, markers were placed with a spacing of approximately 1 inch along the spinal column as seen in Figure 1.

The openness angle (θ) was calculated based on the markers affixed to the sternum, C7 and the pelvis, also seen in Figure 1. A thoracic vector was calculated with the marker on the sternum as the origin and pointing posteriorly to a marker affixed over the spinous process of the C7 vertebra. The pelvis vector was calculated with an origin at the midpoint between the right and left hip joint centers (HJC) [5] and passing through the subject's midpoint of the ASIS positions. These two vectors were then projected onto a sagittal plane and the angle between them was calculated as the openness angle.

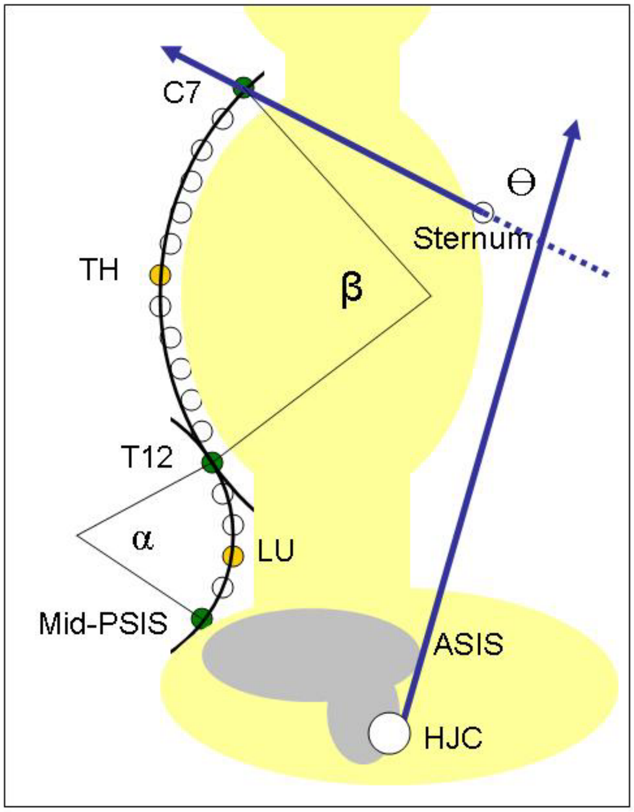

Figure 1. Definition of Curves and Angles

The curvature of the spine was quantified by two arcs. First, the primary (kyphotic) curvature was defined as an angle (β) of an arc passing through the markers at C7, T12 and the most posterior marker between the two (TH). Similarly, the secondary (lordotic) curvature was defined as an angle of an arc (α) passing through the markers at T12, Mid PSIS, and the most eccentric (anterior for lordotic curvature, posterior for kyphotic curvature) marker between those two (LU).

RESULTS AND DISCUSSION

A linear regression analysis between the openness angle and the lumbar angle across the 4 different positions, resulted in an average r^2 value for the six subjects of 0.886. An example regression plot for a single subject can be seen in Figure 2.

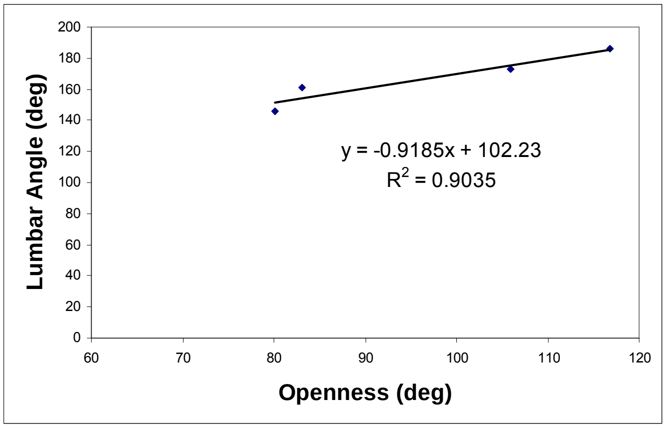

Figure 2. Sample Regression Analysis of Openness vs. Lumbar Angle for a single subject.

Figure 2 also shows the expected trend that as the openness angle gets larger, so does the lumbar angle. Physically, as the thorax tilts rearward and the pelvis rotates forward, the openness angle grows and a lordotic curvature is accentuated. Lordotic curvature corresponds with a smaller radius of curvature, and thus a larger overall angle in the lumbar region. The inverse case also holds.

CONCLUSIONS

Data demonstrated that a linear relationship existed between the openness angle and lumbar curvature. This method has the potential to be used to predict the posterior lumbar angle based on the relative positions of the thorax and pelvis. This work allows further characterization of the body seat interface on commercial seats without modification of the seat or interfering with the user/seat contact.

REFERENCES

1. Li G, et al. *Ergonomics* **42**, 674 – 695,1999
2. Janik TJ, et al. *Journal of Orthopaedic Research* **16**, 766-770, 1998
3. Harrison DE, et al. *Eur Spine J* **11**, 287-293, 2002
4. Bush TR, et al. *Human Factors* **50**, 629-642, 2008
5. Bush TR, et al. *J Biomech* **36**, 1739-1743, 2003

THE ROLE OF JUXTA-ARTICULAR BONY COMPLIANCE ON INTRA-ARTICULAR IMPACT STRESSES

Curtis M. Goreham-Voss*, Yuki Tochigi, M. James Rudert, Thomas D. Brown
University of Iowa Orthopaedic Biomechanics Research Laboratory.
*2172 Westlawn, University of Iowa, Iowa City, IA 52242.
curtis-voss@uiowa.edu

INTRODUCTION

It has been well established that excessive loading of articular cartilage can lead to degeneration of the cartilage and eventual osteoarthritis in the joint. This phenomenon is often studied in the laboratory through the use of small, rigid impactors on a cartilage and bone explant. However, such models do not account for the additional compliance of a second cartilage layer or the supporting bone that is present in physiologic intra-articular impacts. In this study, a finite element model of tibio-talar impact was created, with the goal of better understanding the role of cartilage and bone layers in the distribution and attenuation of impact stresses. Recent impact-to-fracture studies of cadaveric human ankles provide a basis for the simulation design.

METHODS

Three-dimensional talar and distal tibial subchondral bone surfaces were segmented from CT scans of a whole joint. Using TrueGrid (XYZ Scientific, Livermore, CA), three different finite element models were created (Figure 1): (a) cartilage only, in which a 1.5 mm layer of cartilage was extruded from the CT surface, and was considered rigidly backed; (b) local bone backing, in which the cartilage layers were backed by a 1 mm shell of subchondral bone and approximately 2 cm of cancellous bone; and (c) long "full" bone, similar to (b) but where a linear spring (k = 3.7 N/m) is also included behind the distal tibia to simulate 15 cm of tibial shaft, approximately the length of bone left intact for the cadaveric impact. For each of these models, the tibia and talus were controlled by reference points located, respectively, above and below the meshes. The talar reference point was constrained in all degrees of freedom, while the tibial reference point was constrained in all degrees of freedom except axial translation. For the long bone model, the spring is between the reference point and the local distal tibia bone mesh.

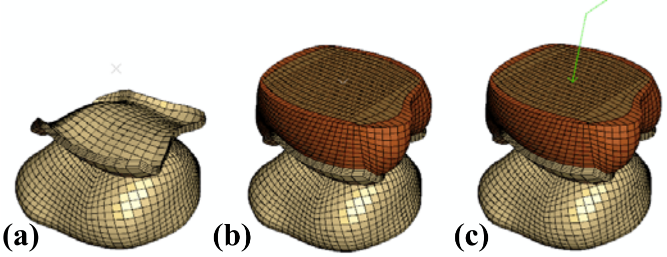

Figure 1. Finite element meshes for (a) cartilage only, (b) bone backing, and (c) long bone models.

An impact similar to the cadaveric impact was simulated using Abaqus Explicit. A 4.54 kg point mass was attached to the tibia reference point and given an initial velocity of -2.28 m/s, corresponding to a drop height of 26.5 cm and an impact energy of 11.8 J. Simulation times of 5 ms were able to capture the full loading and unloading of the joint. Cartilage was modeled with a previously validated impact-specific material [1] using first-order Ogden hyperelasticity (μ=1MPa, α=7.5) and viscoelasticity defined with a Prony series expansion (g1=0.75, τ=0.001 s). The subchondral and cancellous bone had elastic moduli of 19.8 GPa and 760.3 MPa, respectively, and Poisson's ratios of 0.4 [2, 3].

RESULTS

Peak contact pressures on the talus decreased dramatically as additional (bony) compliance was added (Figure 2). The subchondral bone was found to carry a large portion of the load in the distal tibia model. The long bone spring played a major role in reducing cartilage stress, by compressing over 2 mm and reducing both the peak stresses and stress rates.

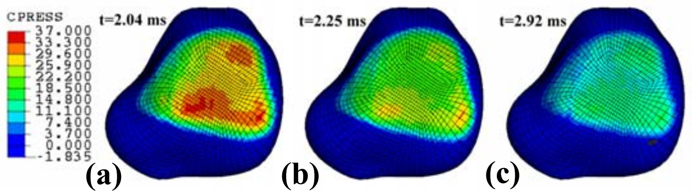

Figure 2. Peak contact stress and time of occurrence in (a) cartilage only, (b) bone backing, and (c) long bone models.

The effect of bony compliance can also be seen by comparing the time histories of the displacement of the point mass throughout the simulations. As shown in Figure 3, the presence of the long bone in particular significantly lengthens the impact time, thereby reducing stress rates.

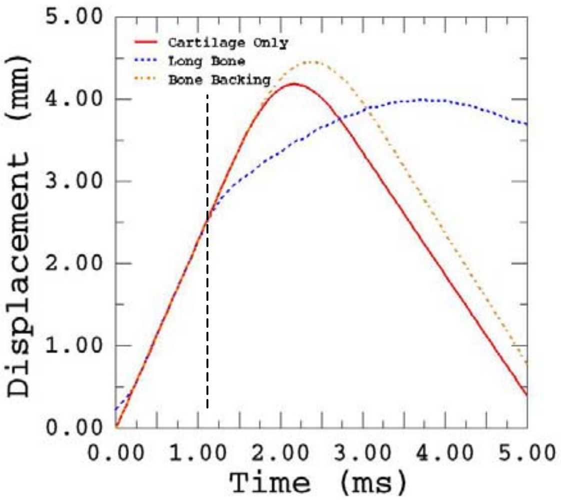

Figure 3. Displacement histories of point mass during impact simulation. The vertical line indicates the start of impact. The mass is in freefall prior to that point.

DISCUSSION

Clearly, the supporting bone structure of the tibio-talar joint plays an important, and perhaps under-appreciated, role in absorbing and diffusing intra-articular impacts. This observation is an important consideration when evaluating the results of a rigid impactor-on-cartilage drop tower experiments and extrapolating those results to physiologic systems. Furthermore, the apparent effect of bony compliance helps to explain the results of cadaver joint impacts (Figure 3), which have shown relatively low cell-death rates despite fracture-producing impact levels.

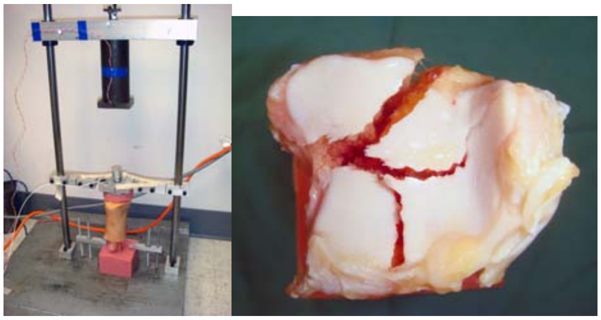

Figure 3. Experimental setup and resulting fracture of cadaver tibio-talar impact.

The results presented in this study indicate a need for further testing to understand how impact energy is transmitted through joints, and how that transmission may differ from impact administered directly to cartilage. The finite element model used here can assist in evaluating and comparing impact between alternative of cartilage impaction protocols.

REFERENCES

1. Goreham-Voss, CM et al. Orthopaedic Research Society, San Francisco, CA, Abstract 0634, 2009.
2. Li, B & Aspden, RM. *Ann. Rheum. Dis.*, **56**, 247-254, 1997.
3. Anderson, IA et al. *J Mater. Sci. Mater. Med.*, **11**, 743-749, 2000.

ACKNOWLEGEMENTS

Supported by a grant from the NIH
(5 P50 AR055533).

THE USE OF SUBJECT-SPECIFIC ANATOMIC PARAMETERS IN AN EMG-DRIVEN MUSCULOSKELETAL MODEL RESULTS IN IMPROVED KNEE JOINT MOMENT PREDICTIONS WHEN COMPARED TO GENERIC AND SCALED MODELS

Liang-Ching Tsai and Christopher Powers

Jacquelin Perry Musculoskeletal Biomechanics Research Laboratory
Division of Biokinesiology and Physical Therapy
University of Southern California, Los Angeles, CA, USA
email: liangcht@usc.edu; URL: pt.usc.edu/labs/mbrl

INTRODUCTION

When estimating muscle forces and moments using an EMG-driven model, 3 modeling approaches are commonly employed: 1) use of a generic musculoskeletal model; 2) rescaling of a generic musculoskeletal model; and 3) use of MRI-based anatomic parameters to create a subject-specific model [4]. The purpose of this study was to compare the accuracy of each approach in estimating the sagittal plane moment at the knee. We hypothesized that an EMG-driven knee joint model that uses direct measures of subject-specific physiological cross-sectional areas (PCSA) and lever arms of the lower extremity musculature would result in improved knee joint moment predictions when compared to generic and scaled musculoskeletal models.

METHODS AND PROCEDURES

Two male and 2 female subjects performed 3 trials of a drop-landing task and isokinetic knee extension exercise (60°/sec; 75°-15° of knee flexion) on a Kin-Com dynamometer. Lower extremity kinematics and ground reaction forces during drop-landing were recorded using a VICON motion analysis system (250 Hz) and AMTI force platforms (1500 Hz). The net sagittal-plane knee moment was calculated using inverse dynamics equations. The Kin-Com dynamometer was used to directly measure the knee extensor moment during the isokinetic knee extension task.

Muscle activation levels during the two tasks were recorded from the vastus lateralis (VL), vastus medialis (VM), rectus femoris (RF), semitendinosis (ST), biceps femoris long head (BFL), medial gastrocnemius (MG), and lateral gastrocnemius (LG) using surface electrodes. Three maximum voluntary isometric contractions (MVIC) were collected for each muscle group. Raw EMG signals were band-pass filtered (35-500 Hz), smoothed (6-Hz low-pass filter), and normalized to the maximum EMG value recorded during testing (i.e. during either the MVIC, drop-landing, or isokinetic knee extension tasks). Muscle activation of the vastus intermedius (VI) was estimated as the average of the VM and VL EMG. Semimembranosis (SM) was assumed to have the same activation as ST; and the biceps femoris short head (BFS) was assumed to have the same activation as BFL [3]. A 40-ms electro-mechanical delay was used to adjust for the time difference between EMG and force output.

Sagittal and axial magnetic resonance (MR) images of the lower extremity were obtained from each subject using a 3T MR system. For each muscle used in the model, the cross sectional area was measured from each axial image to calculate the total muscle volume. The total muscle volume was combined with the muscle pennation angle and fiber length [2] to yield the PCSA for each muscle. Lever arms (perpendicular distance from muscle tendon to knee joint center) of the quadriceps, medial and lateral hamstrings, and MG and LG were measured from the sagittal MR images at 0, 15, 30, 45, and 60° of knee flexion. A second order polynomial curve fitting procedure was used to estimate lever arm from 0 to 90° of knee flexion.

SIMM software [1] was used to create a generic anatomical knee joint model. The model included 10 musculotendon actuators: VL, VI, VM, RF, ST, SM, BFL, BFS, MG, and LG. Muscle EMG and joint kinematics were used as input variables to estimate muscle forces and the net knee moment. To create a scaled subject-specific knee model, the dimensions of the femur, tibia, patella, and ankle and foot complex of the generic SIMM model were rescaled based on the distance from hip to knee joint center, the distance from knee to ankle joint center, patella thickness, and foot length, respectively. The PCSA of each muscle was rescaled based on the power of 2/3 of the body mass for each subject [4,5]. Knee sagittal-plane moments were calculated using the generic SIMM model, the scaled SIMM model, and the model with subject-specific PCSA and lever arm data measured from MR images.

Knee joint moments estimated by the 3 models were compared to gold-standard knee moment measurements obtained from inverse dynamics equations (drop-landing) and the Kin-Com dynamometer (isokinetic knee extension). Coefficient of multiple correlation (CMC) and mean absolute difference (MAD) were calculated for each task to examine the accuracy of each model in predicting the sagittal-plane knee joint moment.

RESULTS

The sagittal-plane knee joint moments during drop-landing and isokinetic knee extension are shown in Figure 1 and Figure 2. For both tasks, the model with subject-specific PCSA and lever arm data measured from MRI had a higher CMC value and a smaller MAD when compared to the generic and scaled SIMM models, indicating better agreement with gold-standard joint moment measurements (Table 1). The scaled SIMM model had a lower CMC and a greater MAD than the generic SIMM model, indicating that the moment prediction did not improve when rescaling a generic model based on the segment size and body mass of the subject (Table 1).

DISCUSSION

The results of this study demonstrate that moment predictions can be improved when subject-specific anatomic parameters are used. Creating a subject-specific model by rescaling a generic model did not result in improved moment predictions compared to the generic model. Given that the net joint moment is the sum of the individual muscle moments, it stands to reason that direct measures of the anatomic parameters would lead to more accurate muscle force predictions and muscle moment estimations.

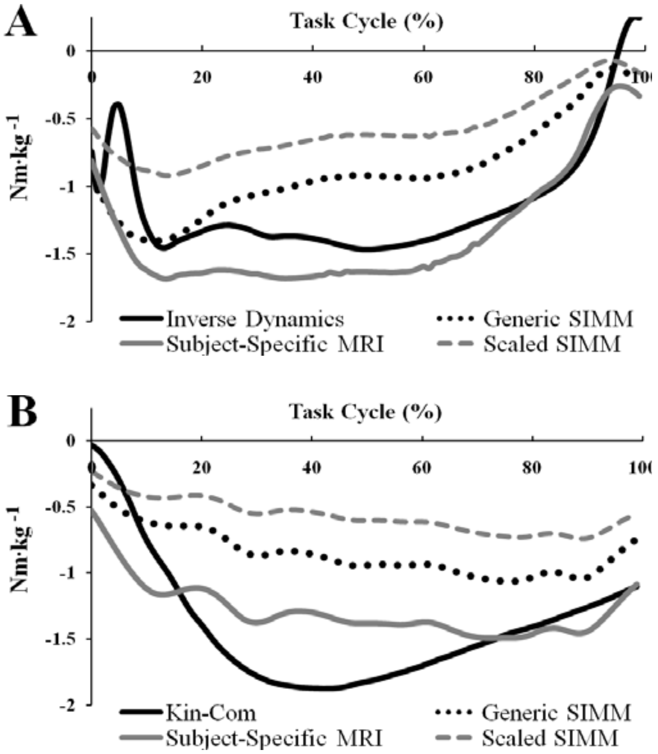

Figure 1. Knee extensor moments during drop-landing (A) and isokinetic knee extension (B).

Table 1. CMC value and MAD (Nm·kg^{-1}) for the three EMG-driven knee joint models.

	Landing		Isokinetic	
	CMC	MAD	CMC	MAD
Generic Model	0.68	0.57	0.50	0.72
Scaled Model	0.55	0.69	0.32	0.89
MRI Model	0.84	0.34	0.67	0.47

REFERENCES

1. Delp, SL et al. *IEEE Trans Biomed Eng* **37**, 757-767, 1990.
2. Friederich, JA and Brand, RA. *J Biomech* **23**, 91-95, 1990
3. Lloyd, DG and Besier, TF. *J Biomech* **36**, 765-776, 2003.
4. Scheys L et al. *Gait Posture* **28**, 640-648, 2008.
5. Zoeller RF et al. *Med Sci Sports Exerc* **104**, 701-710, 2008.

INDIVIDUALS WITH PATELLOFEMORAL PAIN DEMONSTRATE HIGHER PATELLOFEMORAL JOINT STRESSES COMPARED TO THOSE WHO ARE PAIN-FREE: EVALUATION USING FINITE ELEMENT ANALYSIS

Shawn Farrokhi and Christopher M. Powers
Jacquelin Perry Musculoskeletal Biomechanics Research Laboratory
Division of Biokinesiology and Physical Therapy
University of Southern California, Los Angeles, CA, USA
Email: farrokhi@usc.edu, web: www.usc.edu/go/mbrl

INTRODUCTION

Patellofemoral pain (PFP) is a common and debilitating condition affecting individuals of all ages. Despite the high incidence of PFP in society, the underlying pathomechanics are not clearly understood [1]. Currently, the most accepted hypothesis regarding the etiology of PFP is related to increases in patellofemoral joint stress and subsequent cartilage wear. The purpose of the current study was to test the hypothesis that individuals with PFP demonstrate higher joint stress profiles compared to persons who are pain-free.

METHODS AND PROCEDURES

Seven females with PFP and seven gender, age, and activity matched pain-free controls participated. Each subject completed two phases of testing: 1) magnetic resonance (MR) imaging, and 2) biomechanical assessment. Data gathered from the MR assessment and biomechanical testing were subsequently used as input parameters into a finite element (FE) model of the patellofemoral joint for stress analysis [2]. Subject-specific input parameters into the FE model included: 1) joint geometry, 2) quadriceps muscle forces, and 3) weight-bearing patellofemoral joint kinematics (Figure 1).

Subject-specific patellofemoral joint geometry was created from sagittal plane MR images of the knee. Each set of images were segmented to create 3-D rigid body models of the femur, tibia, and patella. The articular cartilage of the femur and patella were modeled as linear elastic elements with material properties consistent with that of human cartilage.

Following the MR assessment, subjects were instrumented for biomechanical analysis. Data obtained from the biomechanical testing (knee kinematics, net knee joint moment, knee flexor EMG), and MRI assessment (quadriceps moment arms and physiological cross-sectional area) were used to estimate the force of the quadriceps utilizing a 3-D static optimization force model previously created in our laboratory. The individual quadriceps forces estimated by the model were subsequently applied to the FE model.

To determine the weight-bearing orientation of the knee, loaded MR images were acquired at 15 and 45 degrees of knee flexion using a custom made non-ferromagnetic loading device providing a resistance of 25% of subject's body weight. The position of the rigid body representation of the femur, patella, and tibia was then registered to the position of the boney surfaces from the weight-bearing images of each respective structure.

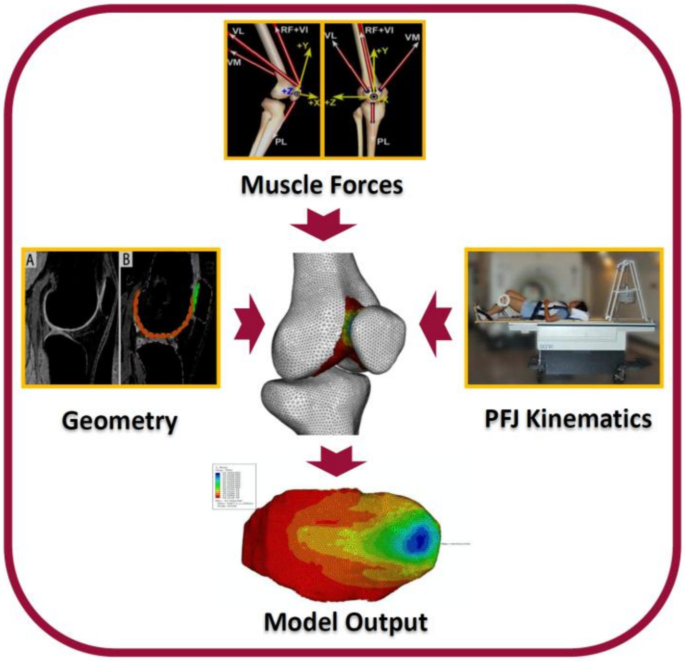

Figure 1. Subject-specific input parameters used to create the finite element model of the patellofemoral joint.

Finally, using a nonlinear finite element solver, quasi-static loading simulations were performed to calculate peak cartilage hydrostatic pressure and octahedral shear stress at 15 and 45 degrees of knee flexion during a static squat (Figure 2). During model simulations, the femur and the tibia were fixed in space relative to their position determined from the weight-bearing images. Since soft tissue constraints of the patellofemoral joint (i.e. the patellofemoral joint ligaments and the peripatellar retinaculum) were not included in the model, the rotational degrees of freedom for patella were constrained. However, the patella was allowed to translate in its remaining 3 degrees of freedom in response to the magnitude and direction of pull of the quadriceps force.

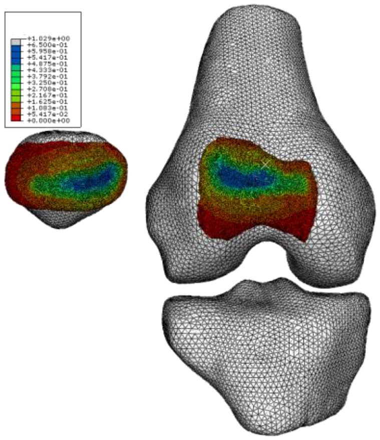

Figure 2. Representative finite element model of the patellofemoral joint stress distribution.

RESULTS

At 15 degrees of knee flexion, the peak hydrostatic pressures were 61% greater for the patellar cartilage and 51% greater for the femoral cartilage in the PFP group compared to their pain-free counterparts (Figure 3). Similarly, the peak octahedral shear stresses were 35% and 91% higher in the PFP group for the patellar and femoral cartilage, respectively.

At 45 degrees of knee flexion, the peak hydrostatic pressures were 44% greater in the patellar cartilage and 38% greater the femoral cartilage in the PFP group compared to their pain-free counterparts (Figure 4). Similarly, the peak octahedral shear stresses were 29% and 17% higher in the PFP group for the patellar and femoral cartilage, respectively.

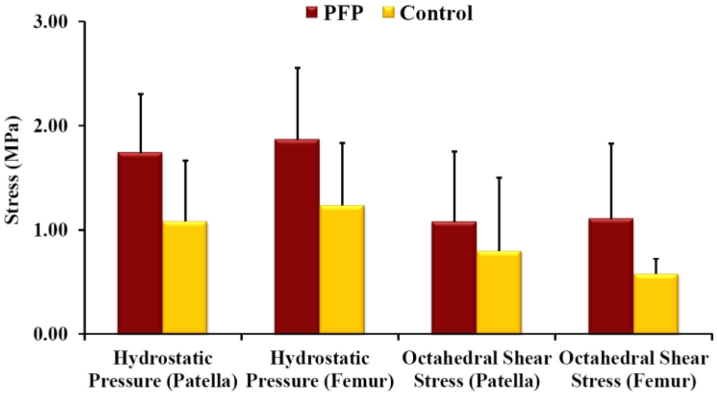

Figure 3. Peak patellofemoral joint stress profile at 15 degrees of knee flexion.

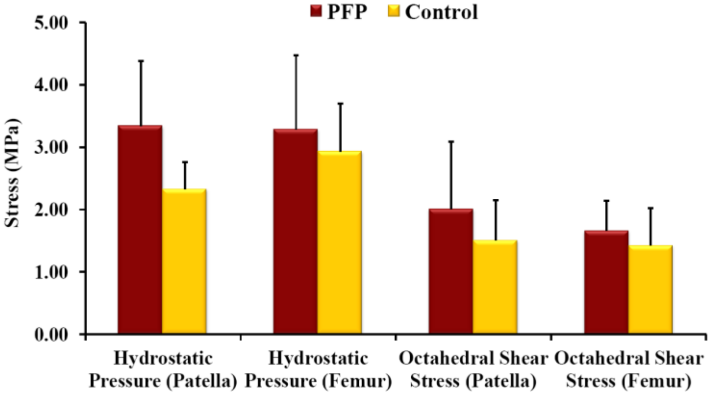

Figure 4. Peak patellofemoral joint stress profile at 45 degrees of knee flexion.

DISCUSSION

On average, the peak hydrostatic pressures and octahedral shear stresses were consistently higher for the individuals with PFP compared to the pain-free controls at 15 and 45 degrees of knee flexion. The combined findings of elevated hydrostatic pressure and octahedral shear stress in this population support the premise that PFP is related to abnormal patellofemoral joint stress. Therefore, it stands to reason that treatments aimed at decreasing patellofemoral joint stress may be beneficial in this patient population.

REFERENCES

1. Powers, CM. *J. Orthop Sports Phys Ther* **28**, 345-354, 1998.
2. Besier, TF. *Med. Sci. Sports Med* **37**, 1924-1930, 2005.

ACKNOWLEDGEMENTS

This study was funded by the Foundation for Physical Therapy (PODSI & PODSII).

IS THERE A LOW BACK COST TO HIP-CENTRIC EXERCISE? EXAMINING THE L4/L5 JOINT COMPRESSION DURING MOVEMENTS PRESCRIBED TO OVERLOAD THE HIPS

David M. Frost, Tyson A.C. Beach, Chad M. Fenwick, Jack P. Callaghan and Stuart M. McGill
Department of Kinesiology, University of Waterloo, Waterloo, Ontario
email: d3frost@uwaterloo.ca

INTRODUCTION

Recent evidence suggests that the musculature of the hips, and more specifically the gluteals, may play a critical role in the prevention and rehabilitation of lower extremity injury and the enhancement of athletic performance [1,2]. For example, increasing gluteus maximus activity may assist in the prevention of ACL injury via a reduction in knee valgus [2,3], or aid in the development of greater hip power during athletic activities [1]. Consequently, clinicians and performance coaches alike have begun experimenting with training methods believed to challenge the hip musculature. Gluteal (re-)education or integration is emphasized, via the use of specific coaching cues, movement patterns, or modalities; however rarely is there consideration given to the implications of such training methods on joints proximal or distal to the hips. Depending on the movement pattern or point of application of the external load (i.e., knees), eliciting greater gluteal activity may actually come with a cost by increasing the potential for injury at another joint. The objective of this investigation was to quantify the joint compression (JC) at L4/L5 while using two commonly prescribed modalities (sled towing and elastic bands) to overload the hip musculature.

METHODS

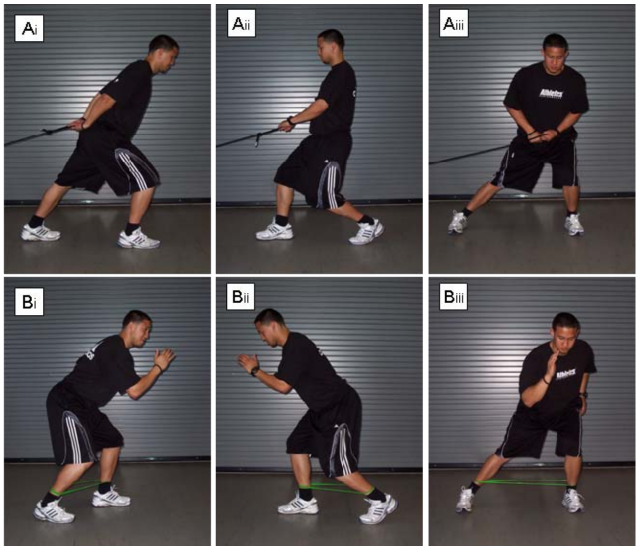

Figure 1: A) sled; and B) band resisted movements, moving i) forwards; ii) backwards; and iii) laterally.

Nine healthy men with no history of lower limb or lower back injury were asked to perform a total of 18 ‘walking’ trials using two modalities: 1) sled towing with an external load applied to the hands at the level of the navel (Figure 1A); and 2) elastic bands (Perform Better, RI) placed around the ankles (Figure 1B). Each participant completed forward, backward and lateral trials (Figure 1) with three separate loads. Sleds were loaded with 20%, 50% and 80% bodyweight, and the bands had stretch coefficients of approximately 310 (blue), 200 (green) and 150 (yellow) N/m. All trials were performed with bent knees.

Surface EMG was recorded bilaterally from 8 sites (rectus abdominis, external oblique, internal oblique, latissimus dorsi, upper and lower erector spinae, gluteus maximus, gluteus medius), lumbar spine motion was monitored with an electromagnetic measurement system (Isotrak), and hand forces (sled only) were estimated via a load cell placed in series with the sled’s rope handle. All analog data were sampled simultaneously at 2400 Hz and synchronized with digital video recorded from the sagittal and frontal planes (30 Hz).

EMG signals were rectified, low pass filtered (2.5 Hz) and normalized to a maximum voluntary contraction (MVC). Processed EMG and lumbar spine motion data were entered into an anatomically detailed model of the lumbar spine [4] to provide an estimate of the muscle compressive force applied to the L4/L5 joint. The 3D reaction forces and external moments about L4/L5 were estimated from the video files and the hand forces (3DMatch, University of Waterloo). The EMG-force relationship was ‘fixed’ for each subject by computing the least squared error between the internal (EMG model) and external moment of all trials. The L4/L5 joint compressive force was calculated as the sum of the gained muscle compressive force and the joint reaction force. One stride was analyzed (right toe off to right toe off).

Peak EMG (gluteus medius and maximus) and peak L4/L5 joint compression for each condition were compared using a 3-way (condition, direction, load) repeated measures ANOVA with Holm-Sidak post hoc comparisons. Only the between-load comparisons are presented in detail.

RESULTS AND DISCUSSION

Both gluteal activity and JC for the sled and band conditions were found to be load dependent; however, the differences were also direction specific (Figure 2). Increasing the load/elastic resistance was unable to elicit a significant change in peak compression or gluteal activity when participants moved in a forward direction (Figure 2A). During the backward trials, JC was significantly increased by 20% and 13% for the sled and band conditions respectively, when participants were exposed to the largest load/resistance (Figure 2B). Gluteal activity was unaffected by an increase in elastic stiffness, however both LGMD and LGMX were significantly different with the heaviest sled load (48% and 30% increases for LGMD and LGMX respectively). As observed in the forward direction, increasing the elastic stiffness had no effect on the JC or gluteal activity when participants moved laterally (Figure 2C). Higher sled loads, however, did prompt an increase in JC (16% and 32% for loads 2 and 3 respectively). The largest sled load also resulted in the greatest LGMX activity, although interestingly, LGMD was significantly higher during the 50% trial (40% versus 9% increase from load one).

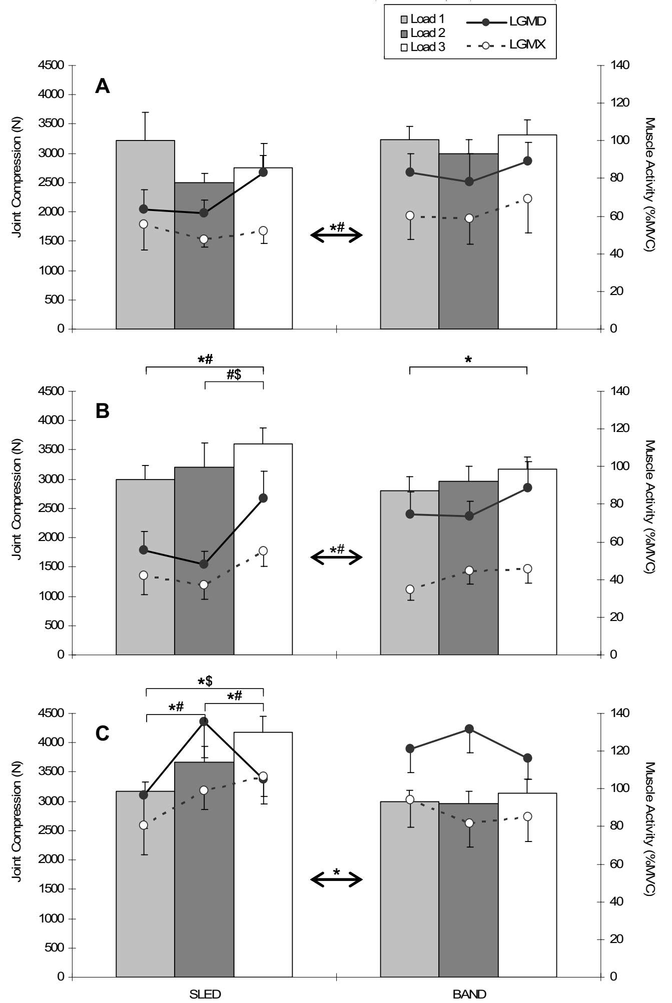

Figure 2: Peak L4/L5 joint compression (N) and peak gluteus medius (LGMD) and maximus (LGMX) activity (%MVC) for the A) forward; B) backward; and C) lateral conditions. Three loads are presented. Error bars signify standard error. The *, $^{\#}$ and $^{\$}$ represent significant differences for L4/L5 compression, LGMD and LGMX respectively.

Significant differences were also noted in LGMD between the sled and band conditions when participants walked forwards or backwards. JC was significantly different between the two conditions for each direction tested (Figure 2).

Although it was hypothesized that each subsequent increase in band stiffness would provide greater overload to the hip musculature, LGMD and LGMX activity was unaffected by the increases to the elastic stiffness. In fact, the only significant change was an increase in peak L4/L5 compression. Increasing the sled load did elicit higher gluteal activity when participants moved backwards and laterally; however such a change was not without an increase in JC, and the activity was not significantly higher than using an elastic band.

IMPLICATIONS

Prior to employing novel methods for preventative, rehabilitative or performance enhancing purposes, potential benefits should be weighed against ‘costs’ to neighboring segments and joints.

REFERENCES

1. Robertson DGE, et al. *J Appl Biomech* **24**, 333-339, 2008.
2. Hollman JH, et al. *J Sport Rehab* **18**, 104-117, 2009.
3. Hewett TE, et al. *Am J Sports Med* **33**, 492-501, 2005.
4. McGill SM, et al. *Spine* **11**, 666-678, 1986.

ACKNOWLEDGEMENTS

We would like to acknowledge the financial support of NSERC.

THE INFLUENCE OF GENDER AND MATURATION ON LANDING STRATEGIES: IMPLICATIONS FOR ACL INJURY

Susan M. Sigward, Christine D. Pollard, Wei-Cheng Cheng, Szu-Ping Lee, and Christopher M. Powers
Jacquelin Perry Musculoskeletal Biomechanics Research Laboratory
Division of Biokinesiology and Physical Therapy
University of Southern California, Los Angeles, CA, USA
email: Sigward@usc.edu, web: www.usc.edu/go/mbrl

INTRODUCTION

Non-contact anterior cruciate ligament (ACL) injury rates are 3-8 times greater for female athletes when compared to their male counterparts. [1] Injury bias has been attributed to gender related difference in performance. Studies examining gender differences in lower extremity biomechanics have consistently reported that females perform athletic maneuvers with decreased knee and hip flexion, increased knee extensor moments, decreased hip extensor moments, increased knee valgus angles, and increased valgus moments when compared to males. Taken together, this biomechanical profile is thought to put females at an increased risk for ACL injury.

It has been hypothesized that females utilize a strategy that limits the amount of knee and hip flexion during dynamic tasks, and instead, rely more on their passive restraints in the frontal plane (i.e. ligaments) to decelerate the body center of mass.[2] In addition, it has been suggested that females favor use of the knee extensors over the hip extensors to attenuate impact forces during athletic tasks. Although this biomechanical pattern has been generalized to females, it is not known at what age this pattern emerges.

The purpose of this study was to 1) examine gender differences in sagittal plane loading strategies and knee frontal plane loading during landing and 2) to determine if differences exist between athletes across various stages of maturation.

METHODS

Subjects consisted of 119 athletes (59 male, 60 females) ages 9 to 22. Subjects were divided into groups based on maturation; pre-pubertal, pubertal, post-pubertal and young adult. Classification was based on the Pubertal Maturation Observational Scale [3] and a self-report of Tanner stages.

Visual3D™ software (C-Motion, Inc., Rockville, MD, USA) was used to quantify three-dimensional kinematics and internal net joint moments (inverse dynamics equations) of the dominant limb (i.e. the limb used to kick a ball) during the deceleration phase of landing. Sagittal plane joint power was computed as the scalar product of angular velocity and net joint moment. All kinetic data were normalized to body mass.

The dependent variables included average knee adductor moments, average knee extensor moment/average hip extensor moment ratio and knee energy absorption/hip energy absorption ratio during the deceleration phase of landing.

To determine differences in landing strategies existed between gender and maturation levels, 2 x 4 (group x maturation level) ANOVA's were performed for each variable. In the event of a significant main effect for maturation LSD post-hoc testing was performed ($P < 0.05$). Statistical analyses were performed using SPSS software (Chicago, IL). Significance was set at $P \leq 0.05$.

RESULTS

Significant main effects for gender and maturation were found for average knee to hip extensor moment ratio (Figure 1), knee to hip sagittal plane energy absorption ratio (Figure 2), and average knee adductor moments (Figure 3). No gender x maturation interactions were found for any variable.

The ratio of knee to hip extensor moments and knee to hip absorption were greater in females when compared to males. Females also demonstrated significantly greater knee adductor moments compared to males.

No significant differences between pre-pubertal and adult athletes or between pubertal and post-pubertal athletes were found for any variable. When collapsed across gender, pubertal and post-pubertal athletes had greater knee to hip extensor moment and energy absorption ratios than the pre-pubertal and young adult athletes (Figures1 & 2). Post-pubertal athletes exhibited greater knee adductor moments than young adult athletes (Figure 3).

Figure 1.

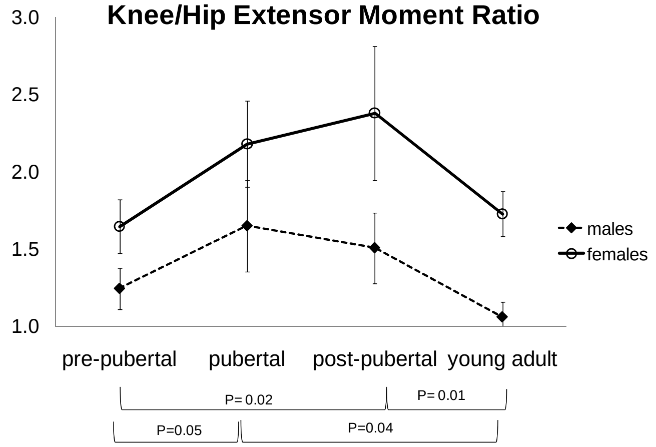

Figure 2.

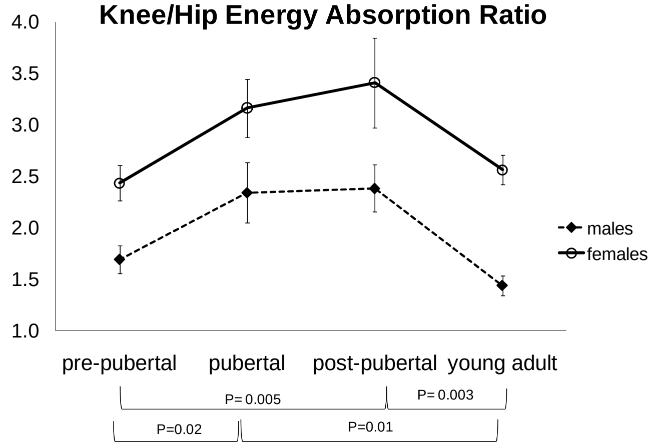

Figure 3.

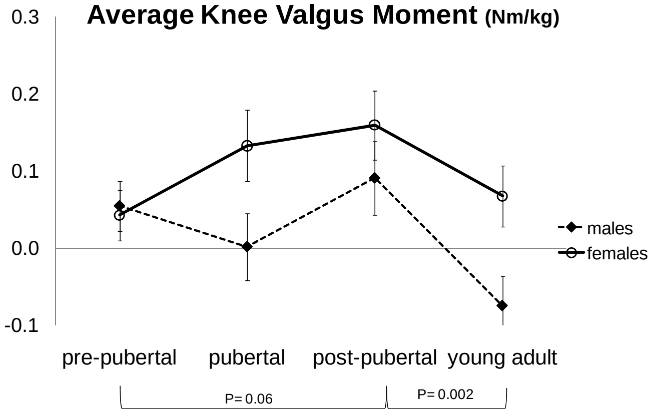

DISCUSSION

In general, females exhibited a strategy that relied more on their knee extensors relative to the hip extensors to attenuate impact forces during landing. This was illustrated by the higher sagittal plane moments and greater energy absorption at the knee relative to the hip. In contrast, males attenuated impact forces through a more equal utilization of the knee and hip extensors. Given the importance of the hip extensors in modifying landing stiffness, [4] the diminished hip kinetics in the female group is suggestive of impaired sagittal plane shock absorption.

Apart from the differences in the sagittal plane, females also exhibited higher knee valgus moments when compared to males. We propose that the higher knee valgus moments representative of a strategy aimed at attenuating impact forces that should ideally be absorbed at the hip.

The greater knee to hip ratios occur during periods of maturation associated with in the greatest changes in growth (pubertal and post-pubertal). The effect of maturation appears to be similar between males and females as no interaction was noted between gender and maturation for any variable. These data indicate that athletes undergoing rapid growth may be more susceptible to developing patterns of impaired sagittal plane shock absorption.

CONCLUSIONS

The disproportionate use of the knee extensors observed in females reflects a biomechanical pattern that places greater mechanical loads on the knee joint and perhaps the ACL. Interestingly, the tendency to favor the use of the knee extensors relative to the hip extensors varied across different stages of maturation similarly for males and females suggesting that the development of a sagittal plane landing strategy may be influenced by growth.

REFERENCES

1. Agel J, et al. *J Ath Train* 42, 270-77, 2005
2. Hewett TE, et al. *Clin Orthop* 402, 76-94,2002
3. Davies PL. *Occup Ther Pediatr* 20, 19-24, 2000
4. Decker MJ, et al C*lin Biomech* 18, 662-69, 2003

ACKNOWLEDGEMENTS

This study was funded by the National Institutes of Health (R01 AR053073-02).

INFLUENCE OF GLENOID INCLINATION ON ROTATOR CUFF MOMENT ARMS: A COMPUTATIONAL STUDY

[1]Joseph E. Langenderfer, [2]Mark A. Baldwin, [2]Paul J. Rullkoetter
[1]Central Michigan University, Mt. Pleasant, MI, [2]University of Denver, Denver, CO
email: lange1je@cmich.edu

INTRODUCTION

Glenoid inclination has been associated with rotator cuff tears [1, 2]. A more inferiorly facing glenoid has been shown to reduce superior translation of the humerus during abduction in experimental studies of normal cadavers [3] and with arthroplasty components [4]. Decreased glenoid inclination (inferiorly facing glenoid) results in a more normal, inferior position of the humerus during abduction even in the presence of simulated rotator cuff tear [3], and as such, the deltoid is able to act as a more powerful abductor via an increased moment arm. Glenoid [5] and humeral [5,6] component positioning has been shown to affect abduction kinematics and range of motion. Similarly, superior placement of the humeral component reduces rotator cuff abduction moment arms [6]. However, the influence of glenoid inclination on rotator cuff moment arms has not been previously investigated. Therefore, the purpose of this study was to utilize a previously developed finite element model of the glenohumeral (G-H) joint to investigate how glenoid inclination angle affects moment arms of the rotator cuff. The hypothesis was that rotator cuff abduction moment arms are increased with a more inferiorly facing glenoid.

METHODS

A previously described three-dimensional finite element model [7] of the G-H joint was used to calculate rotator cuff moment arms with the glenoid normally oriented, rotated superiorly (+5°), and inferiorly (-5°) (Figure 1). Geometry was extracted from cryosection images of the male Visible Human right shoulder (NLM, NIH, Bethesda, MD). Bone and cartilage were modeled as rigid with a pressure-overclosure relationship defined for G-H contact. Cuff tendons were modeled as non-linear springs embedded in a ground matrix with stiffness matching tendon mechanical properties, e.g. [8].

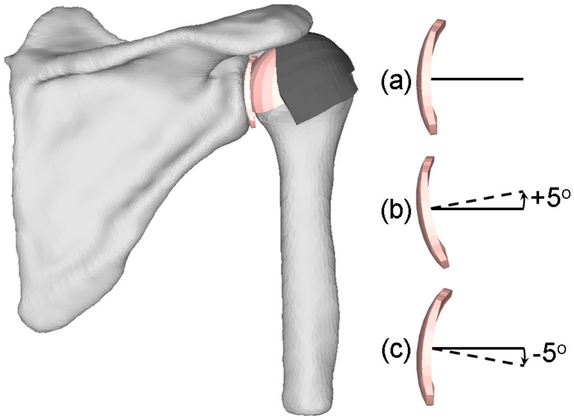

Figure 1: G-H model with glenoid: (a) normal, (b) inclined +5° (superiorly facing) and (c) inclined -5° (inferiorly facing).

Each simulation was performed in Abaqus/Explicit 6.7-3 (Abaqus, Inc., Providence, RI), with the same boundary conditions replicating a cadaveric experiment in which the scapula is fixed and the humerus is free to translate and rotate while rotator cuff tendon excursions and joint angle was measured. Simulations were performed with an initial settling step whereby forces were applied to connector elements distributed across the cuff tendons to bring the articular surfaces into contact [7], and then during a subsequent step, kinematic boundary conditions were applied to rotate the humerus about an anatomical axis [9] from 0º to 60º of G-H scapular plane abduction. Abduction angle and connector elements lengths were measured during the abduction motion. Tendon excursions were calculated from the connector lengths and abduction moment arms were calculated by differentiating 3rd order polynomials fit to the excursion vs. abduction angle data.

Simulations were performed with the glenoid in the anatomic (normal) orientation and with the glenoid cartilage rotated +/- 5° about an anterior-posterior axis through the glenoid centroid (Figure 1). Moment arms calculated for the inclined glenoids were compared to normal moment arms.

RESULTS

During the initial phase of motion (from 0^o to ≈20^o abduction), moment arms increased when the glenoid was inferiorly facing (-5 degrees) and decreased when the glenoid was superiorly facing (+5 degrees) (Figure 2). With the glenoid inferiorly facing, the average increase in moment arm during the initial phase was 4.8% for supraspinatus and 11.6% for infraspinatus, with smaller increases for subscapularis and teres minor. For the later phase of motion (after ≈ 30° of abduction), moment arms did not demonstrate as consistent a trend and for many regions the trend was opposite as for the initial phase.

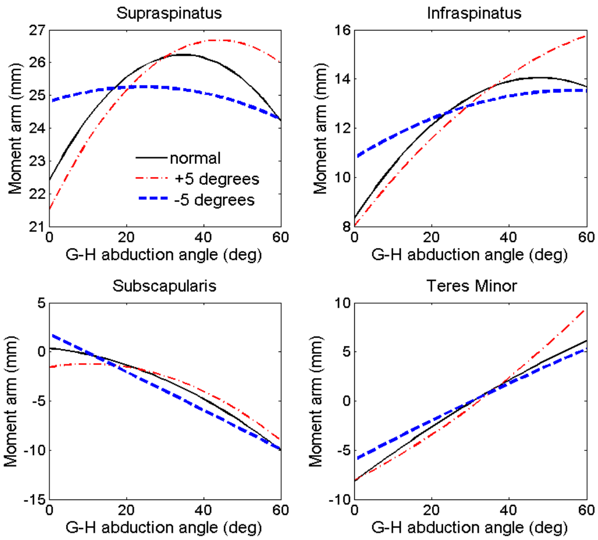

Figure 2: Rotator cuff abduction moment arms for normal glenoid, and glenoid inclined +/-5^o.

DISCUSSION

This study demonstrated the use of a computational model of the G-H joint to calculate changes in cuff moment arms associated with glenoid inclination and found moment arms were increased when the glenoid was more inferiorly facing. Prior studies have described alterations in the ability of the deltoid to generate abduction torque with changes in inclination angle [3], but this is the first study to describe similar alterations for the rotator cuff. These results have implications for understanding how variations in normal inclination angle and component placement affect G-H joint strength and stability in healthy subjects and post-arthroplasty patients, respectively. Additionally, with cuff tear, alteration of the inclination angle, in lieu of tendon transfer [10], might allow some restoration of strength especially in the initial phase of abduction when the cuff plays an important role.

There are several limitations of this study that should be noted and might influence the results of the current model. One factor is that moment arms were calculated with the tendon excursion method which is affected by humeral head translation. However, if the moment arm calculations were erroneously influenced by superior translation of the humerus, one would expect moment arms to be increased for the +5^o inclination condition rather than decreased as calculated here. Additionally, it is worth noting that moment arms were also calculated as the orthogonal distance from the tendon line-of-action and an instantaneous helical axis and similar trends were found. Other factors affecting the results are the kinematic boundary conditions applied to the model that were derived from the literature [9], and that the model was developed from geometry of a single specimen.

In summary, this study demonstrated that rotator cuff moment arms are affected by glenoid inclination. This *in silico* study could be replicated *in cadavera*, and the model could be improved by incorporating *in vivo* measured kinematics and geometry from the same subject, and then ultimately from multiple subjects.

REFERENCES

1. Hughes, RE, et al. *Clin Orthop* **407**, 86-91, 2003.
2. Tetreault, P, et al. *J Orthop Res* **22**, 202-707, 2004.
3. Konrad, GG, et al. *Clin Biomech* **21**, 942-948, 2006.
4. Oosterom, R, et al. *Clin Biomech* **19**, 1000-1008, 2004.
5. Favre, P, et al. *Clin Biomech* **23**, 175-183, 2008.
6. Nyffeler, RW, et al. *JBJS* **86-A**, 575-580, 2004.
7. Adams, CR, et al. *J Biomech* **40**, 3373-3380, 2007.
8. Itoi, E, et al. *J Orthop Res* **13**, 578-584, 1995.
9. Veeger, HEJ, *J Biomech* **33**, 1711-1715. 2000.
10. Nakajima, T, et al. *Clin Biomech* **14**, 265-270, 1999.

ACKNOWLEDGEMENTS

This work was supported via the Central Michigan University President's Research Investment Fund.

OPTIMISING BALLET FLOOR DESIGN TO ASSIST IN INJURY PREVENTION

Paul Fleming (abstract 890)
STI, Loughborough University,
email: p.r.fleming@lboro.ac.uk; web: www.lboro.ac.uk/departments/cv/

INTRODUCTION

There are no published authoritative guidelines on acceptable values, or variability, for the performance of ballet floors. To overcome some of the limitations of variability in venue floors the Birmingham Royal Ballet (BRB) Company have utilized a portable floor system, comprising prefabricated panels, transported and assembled for each show. However, concerns were raised over the best design of the portable floor and this study aimed to evaluate and evolve a portable floor system to optimize performance and safety.

The Company's clinical director was looking to understand and control the floor system better as part of a long-term injury tracking project. It was clear that shock absorbency was a key parameter to provide comfort to the dancers, and to control the magnitude and uniformity. Dancer anecdotes had indicated the large range of surface 'hardness' they experienced around the country, borne out by a series of fieldwork measurements. Research has identified the shock absorbency of a sport surface can be linked to lower limb injuries, particularly from overuse [1]. For athletic performance, energy return [2] is also attributed to reduce fatigue and potentially susceptibility to injury. Ballet is an extreme example of prolonged athletic performance, especially in many maneuvers for control of the lower limbs during landing and take off.

There were no precedents found, however, in the literature for Ballet for typical loading, load duration or injury studies relating to surface behavior. The study thus required the selection of an appropriate test methodology and assessment criteria, against which to assess floor behavior and acceptable limits for impact protection.

EVALUATION METHODOLOGY

The standard method for measuring 'shock absorbency' of a sport surface is the 'Artificial Athlete' (AA) test, often known as the 'Berlin Athlete', and more recent version known as the Advanced AA or AAA. It is currently specified for soccer, rugby, hockey, tennis and sports hall floors. The AA measures the peak force, via accelerometer, of a controlled impact (fixed mass, drop height and spring damper). The peak force is expressed as 'Force Reduction', which is expressed as a % when compared to rigid concrete (standard = 6600N).

In the UK guidance for 'Floors for Indoor Sports' [3] suggests a suitable range for Force Reduction of 45 to 75% for 'combined elastic' floors (combined means floor bending and deformable support at the ground surface contact points). Based on the author's own research [4], a difference of 5% in FR is 'significant', and perceptible to users.

The study as a whole assessed the field venues. It also assessed a series of 'elastic' supports for a series of floor designs. The main focus was to design the portable floor system for the BRB.

Figure 1 shows the floor undercarriage system of the BRB original portable floor comprising rubber pads, in a pattern replicated for all boards, attached to the longitudinal wooden batons which in turn support the transverse batons to which the floor board is attached (size 2.5 by 1.2m).

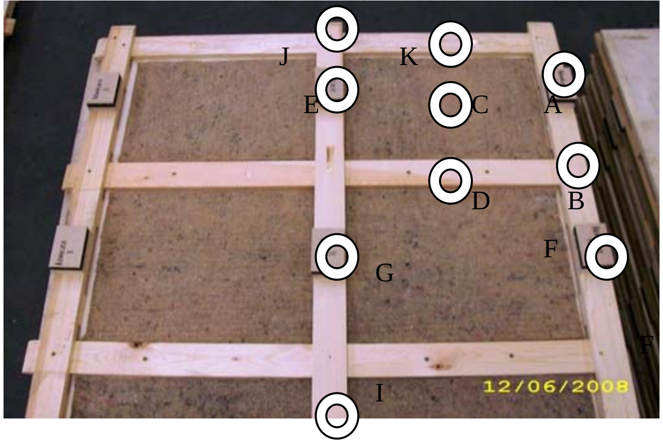

Figure 1: Original Floor System undercarriage(Test locations A, F, E and G are on pad positions, the space between batons create 'panels')

The locations of the AA tests was carefully chosen. To measure the variation in support across the floor system and the anticipated interaction of the components. In addition, all testing was undertaken with 6 panels fitted together to reduce boundary effects, with the middle panel assessed. Ten clear variations in support were identified (by observation), later modified to thirteen because of the varying load transfer across panels.

The development of the modified floor system focused on selection of the most appropriate rubber pad, and an iterative redesign of the baton sub-structure. Other modifications to the floor panel thickness (and hence stiffness) and to the baton thickness were discounted to reduce the number of variables and for cost reasons. A schematic of the final design is shown in Figure 2.

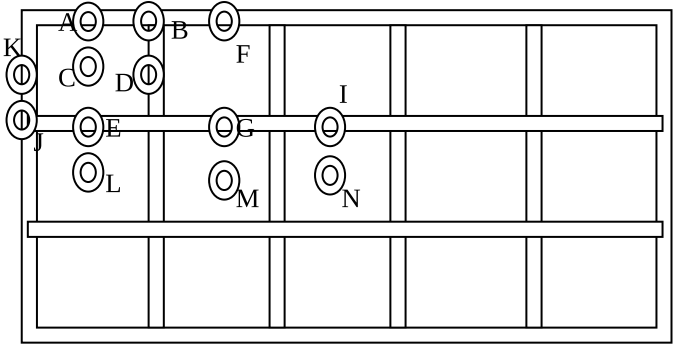

Figure 2. Modified Floor system, showing test positions similar to those in Figure 1.

RESULTS AND DISCUSSION

The force reduction behavior of the system is relatively complex. This is a combination of factors, including: the pad size, thickness, stiffness, and spacing; the board and baton size, weight and stiffness, area of unsupported 'panels' created by the baton spacing, the depth of baton creating space for the floor board to bend on its own, and the use of any stiffening supports to assist the interlocking of adjacent panels. In addition, clearly the rate and magnitude of (point) loading applied, though this is a constant for the AA test method. Modelling this behavior is complex, although it was demonstrated empirically – sufficiently to design the new system.

Figure 3 shows the modified floor system versus the original. Prior to modification the portable floor system generated a Force Reduction response in the range 38-65. The general effect of adding in the extra baton was to slightly stiffen the mid-panel response (see positions C and K). In addition, the mid-span supports to the batons were removed, lowering the stiffness of the pad support position and increasing FR (positions A, B, F and G). Positions A and F show an increased improvement in FR due to a 'half' pad being utilized overcoming the original design problem that adjacent panels had effectively 'double pads' where the edge located pads butted together. These modifications provided a much greater uniformity across the whole floor section. Further modifications to positions G and I to stiffen it back up appear warranted, however.

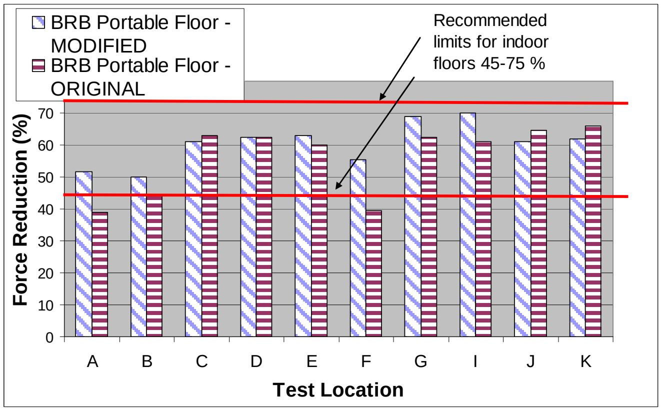

Figure 3. Comparison of FR between floor systems

Energy recovery was, in general, similar between the two systems, in the range 55-70%. Floor panel bending or pad resilient deformation generally gave the higher energy recovery response.

Feedback to date on the new system is positive from the ballet dancers. It is being trialed at venues and further fieldwork is planned.

CONCLUSIONS

The methodology, data and design modifications provide important benchmarking for ongoing studies into ballet dancer injuries. Few studies have previously identified the variation caused by the construction of the dance floor and shown the benefit of changes in design from mechanical testing.

REFERENCES

1.Nigg, B. M., Sports Medicine 2, 367-379, 1985
2.Nigg, B.M., et al. Medicine and Science in Sport
3.Sport England, 'Floors for Indoor Sports', 2002, (http://www.sportengland.org/) 08/04/09.
4. Fleming P, etc al, 1st Int. Conference on Sport Surfaces, CD-ROM, Loughborough University, 2007.

ACKNOWLEDGEMENTS

Birmingham Royal Ballet Company, for permission to publish this work. Luke Hopper, visiting researcher from for sharing his data.

MRI-COMPATIBILE LOADING DEVICES FOR MEASUREMENT OF TENDON AND MEDIAN NERVE MOTION WITHIN THE CARPAL TUNNEL

[1]Jessica E Goetz, [1]Thomas E Baer, [1]Nicole M Jensen, [2]Daniel R Thedens,
[1]Ericka A Lawler, and [1]Thomas D Brown
[1]Department of Orthopaedics & Rehabilitation, University of Iowa, Iowa City IA, [2] Department of Radiology, University of Iowa, Iowa City IA
email: jessica-goetz@uiowa.edu web: http://poppy.obrl.uiowa.edu/

INTRODUCTION

Carpal tunnel syndrome (CTS) is the most commonly encountered peripheral neuropathy. It results from mechanical insult to the median nerve as it passes through the carpal tunnel among the digital flexor tendons (Figure 1). While a substantial body of work has focused on variations in carpal tunnel fluid pressure associated with CTS [1], newer work addresses the effects of impingement of the flexor tendons on the median nerve [2].

It is well known that the digital flexor tendons move significantly in the longitudinal direction through the tunnel during various hand activities [3]. Less understood, however, is how the tendons move transversely in response to various CTS-provocative activities. This work describes the development of a suite of MRI-compatible instruments designed for imaging the contents of the carpal tunnel during controlled functional activity. Images collected while using these specialized loading devices demonstrate dramatic transverse tendon and nerve movement, providing evidence to support the importance of tendon impingement studies in CTS research.

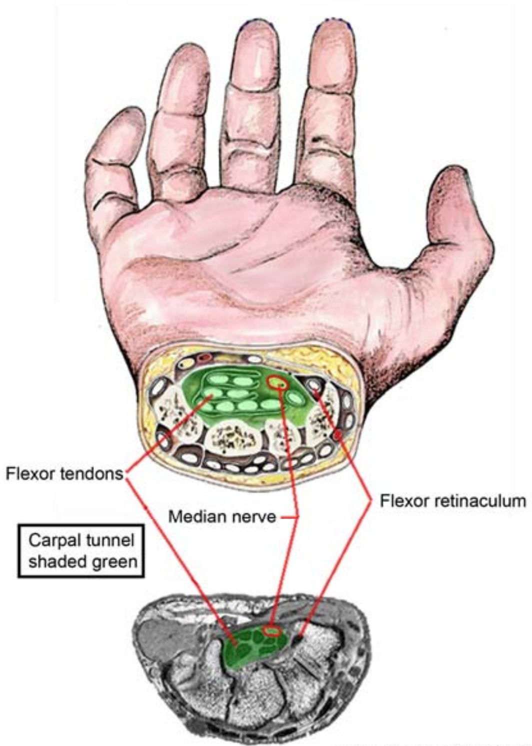

Upper figure from D'Arcy C & McGee S JAMA. 2000;283:3110-3117

Figure 1: Illustration of carpal tunnel location (top) and MRI of carpal tunnel cross-section (bottom).

METHODS

Four CTS-provocative hand activities were chosen for study: squeeze grip, single-finger key press, and volar press with fingers either straight or bent. Fixtures were constructed from MRI-compatible materials (acetal, acrylic, nylon and polypropylene) to position a subject's hand in a specific position while holding a predefined isometric load. Each loading device included a purpose-built switch to provide the subject with audio feedback when the load was within a predetermined range. During the MRI scan, the subject was instructed to maintain the load on the device so that a buzzer remained active.

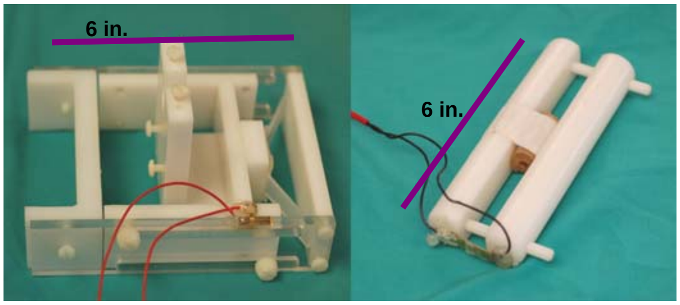

Figure 2: Device for volar flat and bent finger press and single finger key press (left). Squeeze grip device (right).

The loading fixtures were used in conjunction with a splinting system that held the wrist in a specific flexed or extended position. Two subjects were scanned while using the loading devices. Each subject was splinted at wrist angles ranging from 45° of flexion to 45° of extension with the carpal tunnel positioned centrally within a transmit/receive lower extremity coil for MR imaging. Three-dimensional images of the tunnel and wrist were acquired using a Dual Echo Steady State (DESS) pulse sequence with water excitation. The resolution was 0.3mm x 0.3mm x 0.8mm over an 8cm x 6cm x 7.5cm field of view (FOV) for the resting state scan and 0.4mm x 0.4mm x 1.0mm over the same FOV for imaging under load. The slight reduction in resolution reduced the scan duration to 90 seconds, allowing the subjects to remain still during the specified loading tasks.

RESULTS AND DISCUSSION

The loading devices allowed MRI capture of the movements of the digital flexor tendons and their interaction with the median nerve associated with changes in wrist angle and hand loading activities. No visible artifact resulted from having the loading devices in the magnet.

The tendons and the nerve demonstrated dramatic transverse movement during changes in wrist position (Figure 3). The tendons and the nerve demonstrated noticeable, although somewhat less pronounced, changes when moving from an unloaded to a loaded condition. The loads assigned to the activities were sufficient to cause a deviation from the unloaded tendon/nerve geometries and stacking arrangements, but not so large as to prevent the subject from remaining still while maintaining the load through the 1.5 minute scan.

CONCLUSIONS

The strikingly large transverse motions and deformations of the tendons and, most importantly, of the nerve itself offer a compelling imaging-based argument for further research to better understand median nerve insults from tendinous impingement as a key factor potentially contributing to carpal tunnel syndrome. The work described here addresses the problem of measuring soft tissue deformation *in vivo* during normal loading activities.

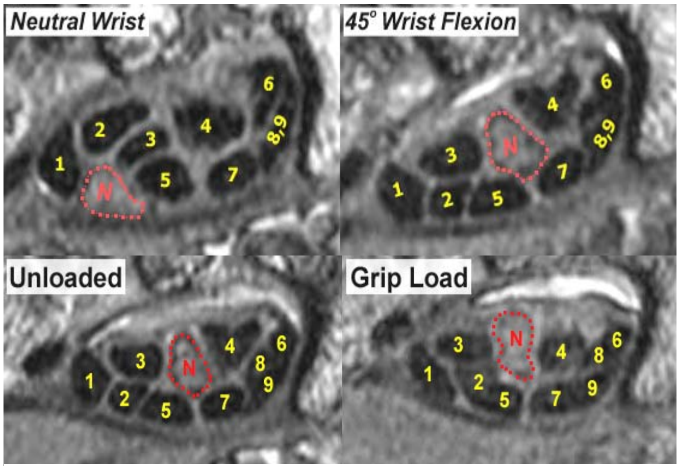

Figure 3: MR images of a single longitudinal section of the carpal tunnel during hand motion. Moving the unloaded wrist from straight to 45° of flexion caused the median nerve to extrude through the tendons (top). Movement from a relaxed to a squeeze grip loading caused changes in tendon and nerve shapes (bottom).

REFERENCES

1. Rempel D. *Repetitive Motion Disorders of the Upper Extermity*, Rosemont, IL, AAOS, 1994.

2. Ko C & Brown TD. *Comput Methods Biomech Biomed Engin,* **10**(5), 343-9, 2007.

3. Szabo RM, et al. *J Hand Surg*, **19A**, 901-6, 1994.

ACKNOWLEDGEMENTS

Funding provided by NIH AR0553899.

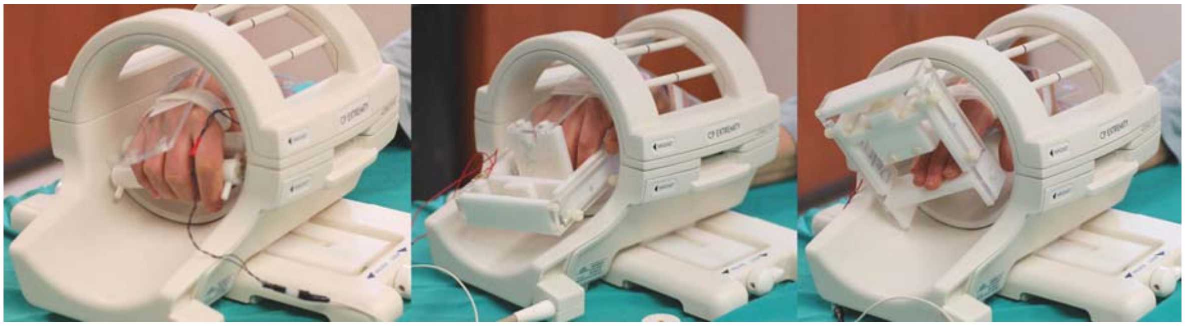

Figure 4: The squeeze grip (left), the volar press with bent fingers (center), and the volar press with straight fingers (right) demonstrated inside the MR coil. During scanning, the subjects were stabilized to reduce movement artifact with additional padding which was removed here for clarity of the loading devices.

THE NEED FOR A BAIL-OUT PLAN: SCREW OPTIONS FOR OSTEOPOROTIC BONE

[1]Zane Hartsell and [2]Paul Cooper MD
[1]Smith & Nephew, Inc [2]Georgetown University Hospital
Email: Zane.Hartsell@smithnephew.com

INTRODUCTION

Cortical screws have been proven to gain adequate purchase and achieve sufficient insertion torque in healthy bone. However, in osteoporotic bone or poor metaphyseal bone as seen in the foot, screw stripping can occur prior to generation of a sufficient torque for fracture fixation. This is particularly applicable to the geriatric population and diabetic charcot bone. In this study it was hypothesized that a screw with a larger major/minor diameter ratio, an osteopenia screw, would provide improved bone purchase as compared to conventional screws. Thus, this type of screw could be used as a bail-out measure for screw stripping in osteoporotic bone, or as a primary choice for fixation with plates in cases of midfoot and hindfoot arthrodesis. This study was designed to evaluate the stripping torque and pullout strength of an osteopenia screw, in both bail-out and preemptive manner, as compared to a standard cortical screw.

METHODS

Testing groups for this experiment were as follows: cortical screws ((5) 2.7 mm cortical bone screws), osteopenia screws in bail-out manner ((4) 4.0mm osteopenia screws inserted into a hole stripped by a 2.7 mm screw), and osteopenia screws used in a preemptive manner ((4) 4.0mm osteopenia screws).

For the stripping torque test, screws were inserted through a ¼ tubular plate into a block of foam with a 2.0mm predrilled through hole. A 25.4mm thick low density (10 pcf) solid rigid polyurethane foam blocks (n = 4) (Pacific Research Laboratories, Vashon, WA) were used to simulate osteoporotic bone. Stripping torque was defined as maximum insertion torque reached by the screw before the screw began to spin freely in the foam. This torque was measured by a Himmelstein 50 in-lb torque cell (Hoffman Estates, IL) and recorded by LabView 8.0 (National Instruments Corporation, Austin, TX).

Pullout tests were conducted on screws inserted to a depth of 20mm into the same test media with a 2.0mm predrilled hole. Axial pull-out testing was then conducted on a MTS testing frame (Eden Prairie, MN). A Jacob's chuck was used to apply a tensile load to the screws at a rate of 0.2 in/min along its longitudinal axis while a data acquisition system recorded the maximum pull-out force.

For both tests, the screws were inserted by a custom screw testing machine at a rate of 5RPM and an axial load of 2.5 lbs, to retain screw driver engagement.

RESULTS AND DISCUSSION

The results of the testing agreed with the hypothesis that the bail-out screw (4.0mm osteopenia screw inserted after a stripped 2.7mm screw) would provide superior stripping torque and pullout strength as compared to the 2.7mm cortical screw. The bail-out screw showed a 57% increase in stripping torque ($p<<0.01$) (Figure 1) and a 76% increase in pullout strength ($p<<0.01$) (Figure 2) when compared to the 2.7mm cortical screw. Additionally, the bail-out screw only showed minor decrease in both stripping torque (6 %, $p=0.45$) (Figure 1) and pullout strength (11%, $p<<0.01$) (Figure 2) when compared to the osteopenia screw tested in preemptive manner.

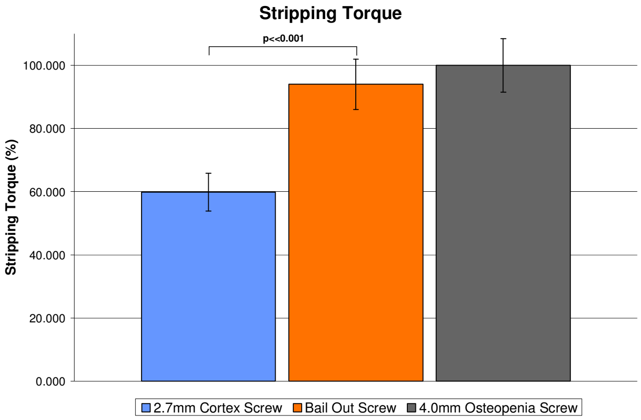

Figure 1: Stripping torque of the three testing groups in simulated osteoporotic bone

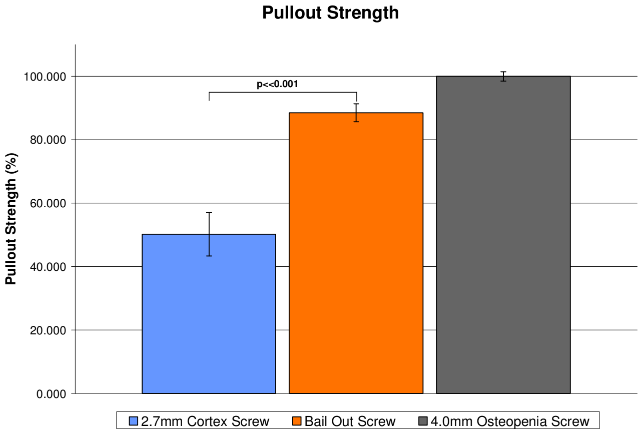

Figure 2: Pullout strength of the three test groups on simulated osteoporotic bone

CONCLUSIONS

The osteopenia screw when used as a bail-out screw achieved superior stripping torque and pullout strength when compared to a standard cortical screw. The stripping torque of the osteopenia screw was not significantly influenced when used in the bail-out manner as compared to that in the preemptive manner; however, the pullout out strength reduction was minimal. The results of this study indicate that the osteopenia screw of larger major/minor diameter ratio could be an effective bail-out option for screw stripping associated with osteoporotic fracture fixation, or in cases where elective fusions require optimal plate fixation and stability.

THE EFFECTS OF SINGLE- VS. DOUBLE-ROW SUPRASPINATUS SURGICAL REPAIR ON CYCLIC AND FAILURE LOADING

[1]Danny M. Pincivero, [2]Kelly R. Marbaugh, [3]Jason L. Levine, [3]Nicholas Iagulli, [3]Jason Rabenold,
[3]Salvatore Frangiamore, [2,3]Vijay K. Goel
[1]Human Performance and Fatigue Laboratory, Department of Kinesiology, [2]E-CORE, Department of Bioengineering, [3]Department of Orthopedic Surgery, The University of Toledo
Email: danny.pincivero@utoledo.edu

INTRODUCTION

The objectives of this study were to examine tissue elongation and static failure differences between two different surgical repair techniques for a simulated supraspinatus muscle tendon injury.

METHODS

Twenty fresh-frozen human cadaveric shoulder specimens (right and left matched pairs) were initially obtained from a tissue bank. One matched pair and two other specimens were excluded from testing due to severe osteoarthritic degeneration of the humeral head, and technical issues related to specimen preparation. The resulting number of specimens was 7 right and 9 left shoulders (mean ± SD, age = 66.0 ± 15.1 years, range = 46 to 94 years, 7 men and 2 women). The humerus was first cut mid-shaft and the specimen was allowed to thaw. All skin and subcutaneous fat was removed, followed by the deltoid and trapezius muscles. Subperiosteol dissection was used to remove the subscapularis from the proximal humerus, which allowed better access to the supraspinatus footprint and articular margin. Using a 10-blade scalpel, the anterior 20 mm portion of the supraspinatus footprint was dissected from the articular margin of the humerus to simulate a full-thickness tear. The specimens were then randomly assigned to one of two different surgical repair techniques: modified single-, and double-row repair.

Surgical repair

For the modified single-row repair, the cortical bone at the anteromedial footprint was tapped, just lateral to the bone trough created at the anterior articular margin. A Smith and Nephew Twin-Fix double loaded suture anchor was placed at a 45 degree angle. The first suture was passed through the tendon in a horizontal mattress fashion in a posteromedial position. The second suture was passed through the cuff as a single suture configuration in the lateral portion of the rotator cuff. The horizontal mattress suture was tied first using a modified Roeder knot with three overlying and alternating half-hitches. The lateral suture was then tied in similar fashion using the same knot construct.

Specimens randomly assigned to the double-row repair group were first tapped at two sites of the supraspinatus footprint. The medial anchor was placed just lateral to the bone trough created at the anterior articular margin. The lateral anchor was placed 1 cm lateral to the medial anchor. Two Smith and Nephew Twin-fix single loaded suture anchors were placed at 45 degree angles, one medially and one laterally. The medial anchor suture was passed in a horizontal mattress fashion. The lateral anchor suture was passed in a single suture fashion through the lateral cuff. The medial anchor suture was tied first using a modified Roeder knot with three overlying alternating half-hitches. The lateral anchor suture was then tied in similar fashion using the same knot construct.

Experimental testing

Following the surgical repair, the coracoacromial arch, rotator cuff (excluding the supraspinatus muscle), and glenohumeral capsule were incised. The supraspinatus muscle-tendon complex was carefully removed from the bony attachment within the supraspinous fossa and elevated laterally until it was completely dissociated from the scapula, leaving the muscle and humerus intact. The humerus was anchored to an aluminum plate, via a U-bolt and two threaded screws placed through the bone (Figure 1A). The supraspinatus muscle belly was frozen to a custom designed cryogenic clamp, via the deposition of dry ice into the clamp pockets (Figure 1B).

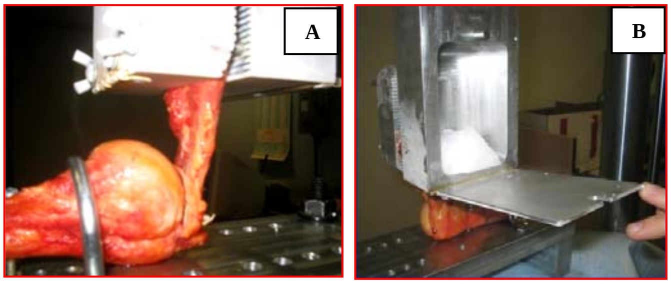

FIGURE 1: Supraspinatus muscle-humerus specimen preparation for cyclic and static loading. (A) Humerus and muscle fixation to the aluminum plate and clamp, respectively. (B) Deposition of dry ice into the muscle clamp.

Axial loading was applied to the supraspinatus muscle on a servo-controlled hydraulic materials testing machine equipped with a 2.5 kN load cell (MTS Corp., Eden Prairie, MN). When the specimen was semi-thawed, the muscle was transected proximal to the myotendinous junction. A digital image of the muscle cross-sectional area was manually traced using an imaging software program (ImageJ, NIH), and was multiplied by 30 N/mm^2 to estimate the force generating capacity of the muscle. The first experimental procedure involved cyclic loading (1000 cycles, 1 Hz) between a pre-load of 10 N and 50% of the estimated force generating capacity of each specimen (mean ± SD, 61.8 ± 23.9 N). The resulting viscoelastic induced deformation (mm) of the specimen was determined as the difference between the first and last peak lengthening cycles (Figure 2). Following the cyclic protocol, each specimen was loaded to failure at 1 mm/s. The stiffness of was calculated along the linear region of the load-deformation curve, while the failure load occurred at the terminal point of the linear region.

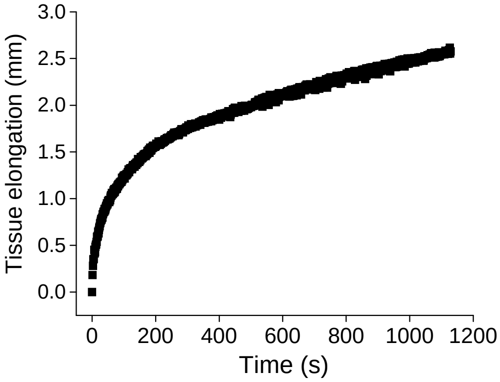

FIGURE 2: Tracing of cyclic loading of a sample specimen illustrating time-dependent lengthening.

RESULTS AND DISCUSSION

The results demonstrated no significant differences ($t_{14} = -0.57$, $p = 0.58$) in viscoelastic deformation across the 1000 cycles (single-row group = 2.05 ± 0.25 mm, double-row group = 1.79 ± 0.29 mm). No significant differences between the single and double-row repairs for specimen stiffness (mean ± SD, 40.3 ± 6.6 and 37.0 ± 4.2 N/mm, respectively) and failure loads (mean ± SD, 248.1 ± 64.3 and 193.8 ± 28.9 N, respectively) were observed.

Comparing the biomechanical properties of the single-row repair with the modified suture configurations and double-row repair may be of great value, especially if double-row repair requires longer surgical time, leads to higher implant cost, and is technically more demanding (1). The findings of the present study found no significant differences between the two constructs in terms of static failure loads or cyclic displacement, thereby suggesting a viable alternative approach for supraspinatus tendon repair. As the present investigation, however, is the first such study involving the modified single-row procedure, caution is warranted in extrapolating the results to a direct clinical application.

CONCLUSIONS

The major findings of the current investigation present evidence that a modification to the standard single-row technique of repairing full-thickness supraspinatus tendon tears appears comparable to the double-row procedure. It is recommended that future studies addressing clinical outcome measures following the modified single-row technique be incorporated to validate treatment efficacy.

REFERENCES

1. Ma CB, et al. *J Bone Joint Surg* 88, 403-410, 2006.

ACKNOWLEDGEMENTS

The authors wish to acknowledge the assistance of David Dick, M.S., Aaron Matyas, M.S., and Nathan Patrick, B.S. for their assistance with specimen preparation and mechanical testing.

KNEE EXTENSOR TORQUE REDUCTION DURING CONSTANT PERCEIVED EXERTION ISOMETRIC CONTRACTIONS

[1]Anuradha Mukherjee, [1]Danny M. Pincivero
[1]Human Performance and Fatigue Laboratory, Department of Kinesiology, The University of Toledo
Email: danny.pincivero@utoledo.edu

INTRODUCTION

The quality of motor performance relies heavily upon the sensation of force/exertion that accompanies a muscular contraction. When producing a muscular contraction to a constant level of perceived exertion, a reduction in the generated torque naturally ensues (1). However, the magnitude of this decrease in muscle generated torque, as a function of perceived exertion level, is yet to be conclusively established. The objective of the present study was to evaluate knee extensor torque and activation during sub-maximal voluntary contractions guided by perceived exertion.

METHODS

Forty-eight healthy young adults (23 men, 22.8 ± 2.6 years, 80.1 ± 13.4 kg, 176.0 ± 7.0 cm, and 25 women 21.9 ± 3.6 years, 64.6 ± 7.7 kg, 166.9 ± 7.1 cm) with no history of lower leg injury, neurological or cardiopulmonary conditions participated.

Subjects participated in two evaluation sessions, separated by approximately 1 week. All subjects were assessed for knee extensor torque during five brief (5 s) maximal voluntary contractions (MVC), during both sessions at a fixed knee angle (90^o) on an isokinetic dynamometer (Biodex Medical Inc, Shirley, NY). During the second session, subjects performed, in addition to and following the MVC's, 9 sub-maximal contractions to 10-90% MVC (10% increments, random order). The subjects were provided visual feedback from a computer monitor and were required to match a target line for 5 seconds. The visual feedback of their torque production was then removed, and the subjects were instructed to continue contracting their knee extensors to maintain a constant level of perceived exertion for 10 seconds. A minimum rest period of 2 minutes separated all sub-maximal contractions. Immediately following each sub-maximal contraction (total duration = 15 s), subjects were asked to provide a numerical rating of their perceived exertion from the Borg category-ratio scale (CR-10).

Surface electromyograms (EMG) were recorded (1000 Hz, 20-500 Hz bandpass filtered) from the vastus medialis (VM), rectus femoris (RF) and vastus lateralis (VL) muscles. Following full wave rectification of the raw signals, EMG activity was integrated (IEMG) over the middle 3 seconds of each contraction. The EMG's from the sub-maximal contractions were normalized to the MVC's. Following the removal of the visual feedback, the change in knee extensor torque across the 10 s contraction was examined by the slope, normalized to the three highest (averaged) MVC's ($\%MVC \bullet s^{-1}$).

RESULTS AND DISCUSSION

The results demonstrated a significant increase ($F_{8,368}$ = 407.7, $p<0.001$) in ratings of perceived exertion across the sub-maximal contraction intensities, and no gender main effect ($F_{1,46}$ = 0.28, p=0.60) or contraction intensity by gender interaction ($F_{8,368}$ = 0.86, p=0.55) (Figure 1).

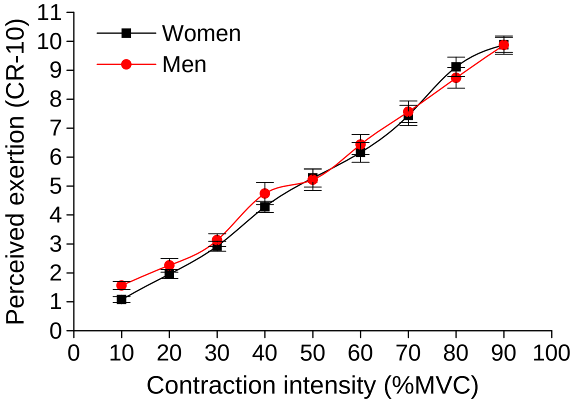

Figure 1: Ratings of perceived exertion following the sub-maximal isometric contractions, illustrating the close correspondence between the subjective rating and relative target level.

The normalized IEMG data demonstrated a significant increase with sub-maximal contraction intensity ($F_{8,368}$ = 1,238.3, p<0.001), while VL activity was significantly greater than RF and VM IEMG ($F_{8,368}$ = 407.7, p<0.001) (Figure 2). The relatively greater levels of normalized IEMG activity of the VL, over the VM and RF muscles, is consistent with previous studies (1-3) suggesting the possibility of a greater activation weighting in favor of stronger individual muscles within synergistic groups.

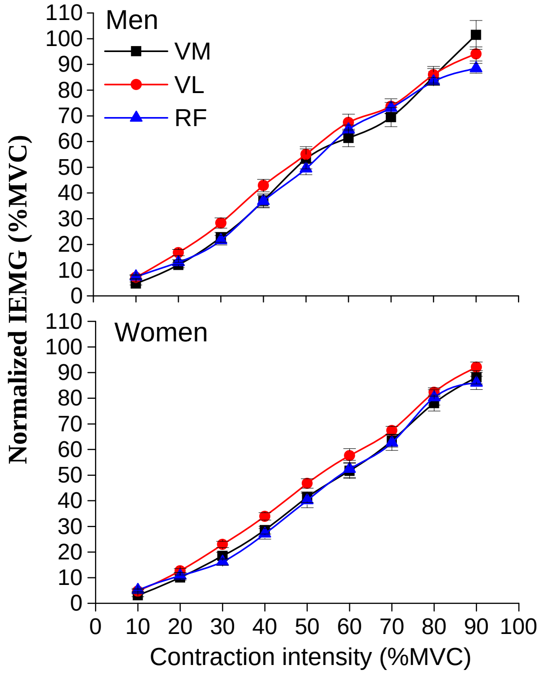

Figure 2: Normalized IEMG of the VM, VL, and RF muscles in men and women during sub-maximal (10-90% MVC) isometric knee extension contractions.

Following the removal of the concurrent visual feedback regarding torque level matching, a linear decline in knee extensor torque was observed at most sub-maximal contraction intensities, while subjects maintained the same level of perceived exertion. The results demonstrated a significant contraction intensity main effect ($F_{8,368}$ = 76.1, p<0.001), and no significant gender main effect ($F_{1,46}$ = 3.10, p=0.09) or interactions ($F_{8,368}$ = 0.90, p=0.52). Illustrated in Figure 3, it was observed that the reduction in knee extensor torque following visual feedback removal was dependent on the initial sub-maximal contraction intensity target. Specifically, the reduction in normalized knee extensor torque significantly increased at greater sub-maximal contraction intensities.

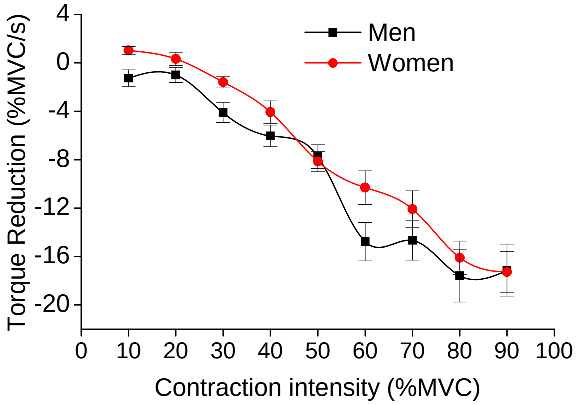

Figure 3: Reduction in normalized knee extensor torque during sub-maximal contractions following visual feedback removal.

The modulation of muscle-produced torque in order to maintain a constant level of exertion is a concomitant mechanism accompanying a reduction in force generating ability, due to fatigue processes. A similar pattern of a muscle force decrease was observed over a prolonged contraction period (100 s) at a single initial sub-maximal target (4), partially confirming the results of the present study.

CONCLUSIONS

The major findings of the present study demonstrated that during sustained isometric knee extensor contractions, healthy young adults maintain a constant rating of perceived exertion through modifications in torque generation. Although the constant perceived exertion contractions were relatively brief (i.e., 10 s), it is suggested that physiological mechanisms related to muscle fatigue contributed to the torque reduction at greater sub-maximal contraction intensities.

REFERENCES

1. Alkner BA, et al. *Med Sci Sports Exerc*, **32**, 459-463, 2000.
2. Pincivero DM, et al. *Muscle Nerve*, **28**, 54-61, 2003.
3. Pincivero DM & Coelho AJ. *Muscle Nerve*, **23**, 393-398, 2000.
4. Plaskett CJ & Cafarelli E. *J Appl Physiol*, **91**, 1535-1544, 2001.

Evaluation of lumbar lordosis with and without high-heeled shoes

[1, 2] Brent Russell, [1] Kimberly Muhlenkamp, and [1] Kathryn Hoiriis
[1] Life University, College of Chiropractic, [2] Georgia State University
email: brussell@life.edu, web: http://www.life.edu

INTRODUCTION

Some women complain of low back pain (LBP) from wearing high-heeled shoes. Many doctors and therapists believe that these shoes cause increased lumbar lordosis as the source of the pain. For example, the American Physical Therapy Association has cautioned that, "Walking in high heels forces the back to arch and the chest to thrust forward. Basically, high heels cause the neck and back to hyperextend." [1] In contrast, six of the seven published studies on this topic found either decreased lordosis or no effect from heels; but, some mixed results, small subject groups, and questionable methods have left the issue unclear. Considering both LBP and the wearing of high-heeled shoes are common, clinicians may be wasting time and effort with incorrect assumptions. The purpose of this project was to evaluate the effect of high-heeled shoes on lumbar lordosis using a more reliable method and larger sample size.

METHODS

We recruited 61 university students, faculty, and staff who reported no significant structural or neurological abnormalities. We included men as well as women, as had some previous studies. For measurement we used a Spinal Mouse (idiag AG, Fehraltorf, Switzerland; see below), previously shown to be reliable for assessment of lumbar lordosis and sacral angle [2]. After barefoot evaluation, each person wore high-heeled shoes for a ten-minute adaptation (four cycles of walking, sitting & standing up, carrying a box of office supplies, standing), after which a second lordosis measurement was done with shoes still on. All shoes had heel heights between 7.5–10 cm. Participants provided information for age, height and weight, frequency per week and number of years wearing high-heeled shoes, and whether the shoes caused them LBP. Our project was approved by the Life University IRB.

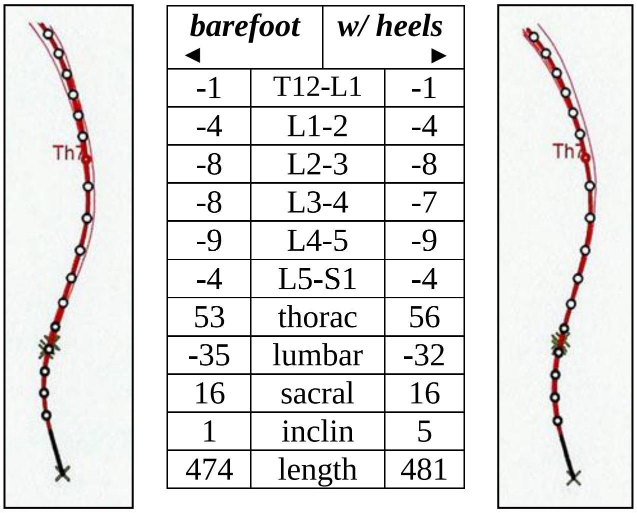

barefoot ◄		*w/ heels* ►
-1	T12-L1	-1
-4	L1-2	-4
-8	L2-3	-8
-8	L3-4	-7
-9	L4-5	-9
-4	L5-S1	-4
53	thorac	56
-35	lumbar	-32
16	sacral	16
1	inclin	5
474	length	481

Figure 1: SM angles for one subject. The lumbar angle (absolute value) is decreased with heels, indicating decreased lordosis.

The Spinal Mouse (SM) is a hand-held device designed to roll down either side of the spine to detect angular change of position during scans from C7 to the third sacral segment. Rotation around its medial-lateral axis generates positive values in areas of kyphosis ("thorac" and sacral regions, Figure 1), and negative values in areas of lordosis (lumbar region and intersegmental angles). The bold lines in the figure are means of four individual paraspinal scans (thin lines), which vary with surface contour asymmetry and measurement inconsistency. The lumbar angle, representing the region from T12 to S1, was our main outcome measure, but we also monitored scan length for consistency between conditions; the sacral angle, representing pelvic tilt (part of the clinical perception of lordosis), was a secondary measure; and we did not analyze thoracic or spinal inclination angles ("inclin", Figure 1) in this study. We used an Excel document for dependent *t*-tests of group means; however we excluded from analysis one subject with a lumbar kyphosis, two for scan length inconsistency (>5% barefoot-to-heels differences), and lost data for three from equipment malfunction.

RESULTS AND DISCUSSION

Lumbar lordosis and sacral angles for static standing in high-heeled shoes were slightly decreased from barefoot standing, but statistically insignificant, for our participant group (Table 1: degrees are absolute values). Only 31 subjects (all female) reported wearing heels previously, and only seven of them admitted to LBP from their shoes.

Some individuals did have an increase in lordosis. To examine them for shared characteristics, we separated subjects into two subgroups (Table 2) according to increased or decreased lordosis, and we considered "clinically significant change" to be magnitudes equal to or greater than the mean change plus one standard deviation ($\geq$5 degrees). It is unlikely that changes smaller than this would be clinically detectable by visual or manual examination. Only four subjects with increased lordosis met this criterion; we believe it possible that clinicians are seeing these few and assuming the same effect for everyone. In our study they were somewhat younger and had a shorter history of wear, but did not otherwise appear much different, from the six subjects with a significantly decreased lordosis.

Some limitations: validity of Spinal Mouse sagital plane measurement has not been established; in the main study of reliability, Mannion [2] felt there was no "suitable gold standard" for validity but found its measurements comparable to other surface contour devices. We relied upon Mannion's [2] findings of reliability and did not use a control group of repeated measurements of barefoot subjects; but our mean barefoot lordosis and sacral angles were much smaller than Mannion's 32 and 21 degrees, respectively [2]. A further limitation was that many participants were chiropractic students and faculty already familiar with the popular heels-cause-increased-lordosis belief. We let them know of the conflicting opinions and were careful not to suggest a desired outcome; we had no indications of anyone attempting to influence their results. Finally, one could question whether our adaptation time was adequate. Previous studies with results similar to ours used adaptation periods ranging from one minute to three hours [3]; there is no evidence that longer adaptation makes a difference.

CONCLUSIONS

It appears that high-heeled shoes do not have any significant effect on lumbar lordosis for most people. Low back pain attributed to heels likely is caused by some factor other than increased lordosis.

REFERENCES

1. American Physical Therapy Association: http://www.apta.org/AM/Template.cfm?Section=Home&CONTENTID=26185&TEMPLATE=/CM/ContentDisplay.cfm. Accessed 2009 March 30.
2. Mannion AF, et al. *European Spine Journal* **13**, 122-36, 2004.
3. Opila-Correia KA. *Archives of Physical Medicine and Rehabilitation*, **71**, 905-9, 1990.

ACKNOWLEDGEMENTS

Thank you to Drs. Mark Geil and Jerry Wu of the Georgia State University Biomechanics Lab, and Dr. Ekaterina Malakhova of Life University.

Table 1. Lumbar lordosis and sacral angles in wearing high-heeled shoes and standing barefoot (n=55)

lordosis mean (SD)	sacral angle mean (SD)	scan length mean (SD)	gender age: mean (SD), range
bare 22.9° (7.8) heels 22.3° (7.4), P=.873	bare 10.4° (6.3) heels 9.9° (6.2), P=.830	bare 472 mm (34) heels 475 mm (35), P=.977	35 F / 20 M 33.3 y (10.8), 21 – 62y

Table 2. Subjects sorted by increased (↑) or decreased (↓) lordosis (* 3 subjects had no change)
† "clinically significant change" defined as $\geq$ subgroup mean change + 1 SD
‡ only includes data for subjects who normally wear high-heeled shoes

* subgroups ↓ or ↑ mean change (SD)	† clinically signif. mean change (SD)	gender, age: mean (SD)	‡ wear /wk, ‡ yrs wear mean (SD), range
n=20 ↑ 3.1° (2.0)	n=4 ↑ 6.5° (0.6)	3 F / 1 M 24.5 y (2.52)	n=3, 1.3/wk (0.6), 1 -2/wk 9.3 y (1.2), 8 – 10 y
n=32 ↓ 3.1° (2.0)	n= 6 ↓ 6.5° (1.6)	5 F / 1 M 36.0 y (12.4)	n=5, 3.0 /wk (1.8), 0.25 – 5/wk 16.2 y (12.0), 8 – 37 y

SEMI-AUTOMATED TENDON IDENTITY TRACKING IN MR IMAGES

[1]Nicole M Jensen, [1]Jessica E Goetz, [2]Daniel R Thedens,
[1]Thomas E Baer, [1]Ericka A Lawler, and [1]Thomas D Brown
[1] Department of Orthopaedics & Rehabilitation University of Iowa, Iowa City IA,
[2] Department of Radiology, University of Iowa, Iowa City IA
email: nicole-jensen@uiowa.edu web: http://poppy.obrl.uiowa.edu/

INTRODUCTION

Carpal tunnel syndrome (CTS) is a commonly encountered compressive peripheral neuropathy. There is increasing evidence that CTS may be caused at least in part by impingement on the median nerve by the digital flexor tendons. Finite element (FE) analysis offers an attractive means to provide definitive information about mechanical insult to the median nerve. However, to provide useful data, these models must be driven with realistic anatomic motion [1]. Due to inter-subject variability of tendon “stacking” and the unpredictability of tendon deformation, the identification of respective segmented tendons within the tunnel is indeterminate [2], and the nine individual digital flexor tendons can be reliably distinguished only at a distal location within the hand (Figure 1). Therefore, a method has been developed using a region-growing technique to track tendon identities from the hand through the carpal tunnel in a MR image series, starting from a more distal location where identities are unambiguous. This in turn allows for tracking individual tendons’ transverse motions within the carpal tunnel.

METHODS

An MRI section within the hand in which each tendon is easily distinguished is used as the starting image for the region-growing technique. Each tendon on the starting image is identified and traced. The area within this boundary is calculated and used as a growth limitation parameter to ensure that one tendon does not merge into another. The centroid of the initially traced area is used as the center of a 3x3 seed region for growth on the next proximal image in the series. Each tendon region is grown using a 4-connected neighborhood comparison scheme, with a pixel being added to the tendon region if the absolute value of the difference between its intensity and the mean gray value of the seed region is less than 50% that of the seed value. The tendon region continues to grow until either there are no remaining candidate boundary pixels or its area has reached the area growth limitation parameter. The centroid of the resulting region is then used to define the 3x3 seed region to grow the tendon region on the subsequent proximal image, and so forth. The tendon tracking process is complete once the slice-by-slice region growing has propagated to one of the previously segmented tunnel images.

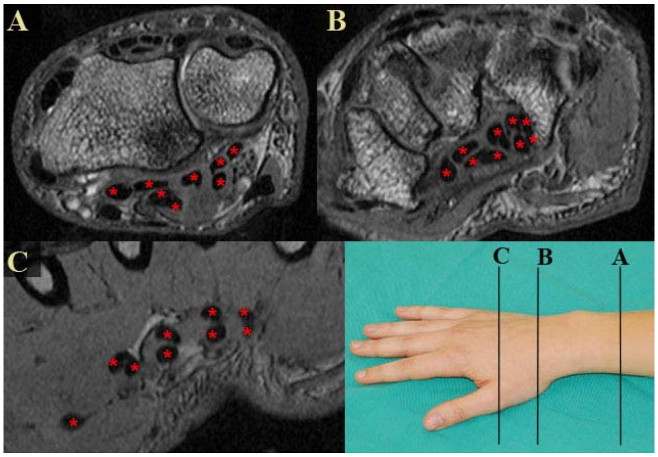

Figure 1: MR images, with flexor tendons identified by red dots within (B) and on either side of (A&C) the carpal tunnel. Only in the distal image in the hand (C), where the tendons align in pairs going to each finger (one to the thumb) and in two layers (deep and superficial), is tendon positive identification possible.

The known tendon identities are then continued through the series of segmented slices, by determining in which segmented region the centroid of an identified tendon lies. When this process is complete, each segmented tendon in the tunnel has a unique anatomic identifier. This identifier will be assigned to the same tendon in any image series processed with this method, thereby allowing for assessment of tendon movement with wrist motion.

RESULTS AND DISCUSSION

Three-dimensional magnetic resonance images of the wrist of a male subject were acquired using a transmit/receive lower-extremity coil and a ninety second Dual Echo Steady State (DESS) pulse sequence with water excitation. The acquired resolution was 0.4mm x 0.4mm x 1.0mm over an 8cm x 6cm x 7.5cm field of view. Wrist positions ranged from 55 degrees of flexion to 55 degrees of extension. For each scan, the nine flexor tendons, the median nerve, and the carpal tunnel boundary were segmented on images spanning the length of the carpal tunnel.

Dramatic transverse motions of the flexor tendons and nerve were observed as the wrist moved from extension to flexion (Figures 2 & 3). Excursion of the nerve from the volar to the dorsal side of the tunnel was apparent as the wrist moved from neutral into flexion. Large deformations of the tendons are also visible as the wrist moved (e.g., tendon 5 in Figure 2). The positively identified tendon segmentations allowed generation of a 3D model of the carpal tunnel including both the tendons and nerve (Figure 3). Tracking the excursions of the flexor tendons and the median nerve during wrist movement is necessary for driving realistic FE models.

CONCLUSIONS

The close proximity of the tendons in the carpal tunnel, their substantial transverse motion during functional activities, and individual "stacking" variability contribute to the difficulty of positively identifying each tendon in an image of the carpal tunnel. The work described herein addresses the development of a semi-automated method for section-to-section tracking of the identity of each tendon in the carpal tunnel using a region-growing technique.

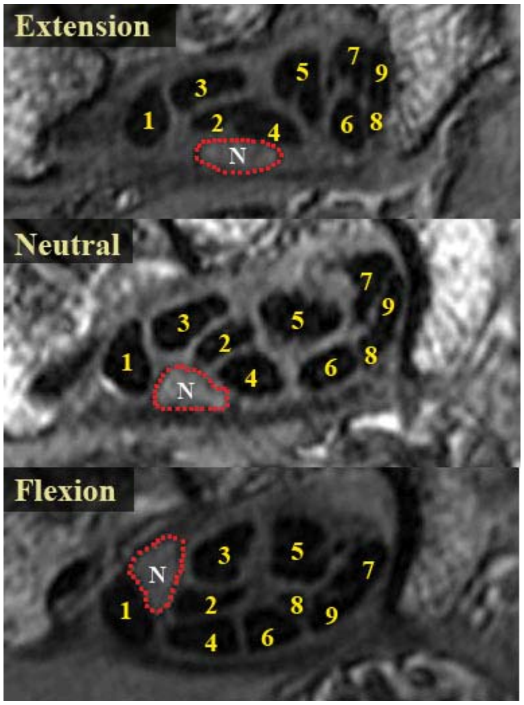

Figure 2: Identified tendons in extension (Top), neutral (Middle), and flexion (Bottom). N represents the nerve; 1 corresponds to the FPL (thumb); 2,4,6,8 to the superficial tendon of each finger (index to little); and 3,5,7,9 to the deep tendon of each finger.

REFERENCES

1. Keir PJ, et al. *Clin Biomech*, **14**, 635-645, 1999.
2. Valverde FL, et al. *Computer Methods and Programs in Biomedicine*, **73**, 233-247, 2004.

ACKNOWLEDGEMENTS

Funding provided by NIH AR053899.

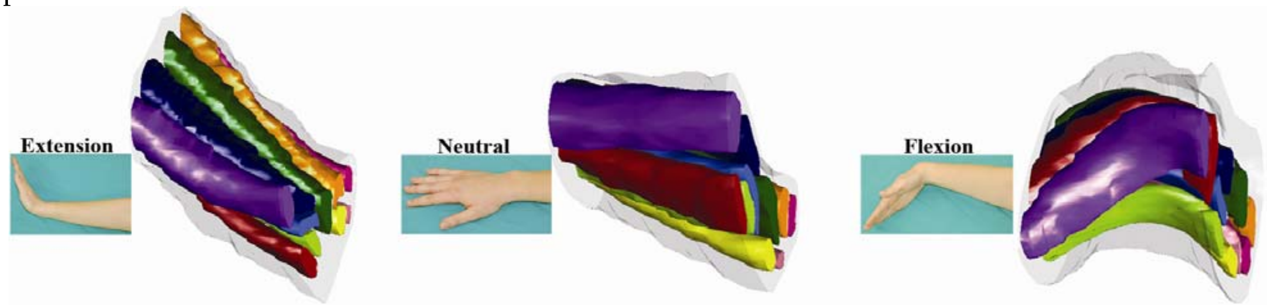

Figure 3: Isosurface of carpal tunnel segmentations in extension (Left), neutral (Middle), and flexion (Right). After identification with the region-growing techniques, the individual tendons can be compared in different wrist positions. Purple corresponds to the flexor pollicis longus (thumb) tendon; red to the nerve, dark colors to deep finger tendons, light colors to superficial finger tendons, and opaque gray to the carpal tunnel boundary.

The Influence of Cricket Leg Guards on Running Times and Stride Parameters.

James Webster and Jonathan Roberts
Sports Technology Institute, Loughborough University
email: J.M.F.Webster@lboro.ac.uk, web: http://www.sports-technology.co.uk

INTRODUCTION

Professional sport has become increasingly competitive over the past two decades, resulting in professional teams, governing bodies and equipment manufacturers constantly striving to maximize performance. Equipment design has been highlighted as an area which can have a significant affect on performance, which could ultimately be the difference between winning and loosing. Within the majority of sports, research has focused on maximizing athlete performance, however, for protective equipment (PPE) in sport a greater emphasis has been placed on preventing injury , as a result, traditional PPE is often cumbersome and ill fitting and in sports such as cricket, where large amounts of PPE are worn, there is an opportunity to improve performance without sacrificing protection through the development of new equipment. Previous work by Webster and Roberts (2009) has demonstrated that cricket leg guards are perceived by the player to have a negative influence on running performance. An earlier study by Looke *et al.* (2006) found that different batting pads did not affect running and turning speed relative to each other, but this study did not consider their influence on running speed compared to running without leg guards. Therefore, this study aims to determine if batting pads have detrimental affects on performance, and whether this is predominantly caused by the added mass to the legs of the athlete or as a result of changes in running gait.

METHODS

This study analyzed the effect of cricket leg guards on running and turning speeds, as well as stride characteristics across five conditions, including 3 different types of batting leg guards (P1, P2 and P3) weighing 500g, 740g and 900g per leg guard respectively, a weighted comparison (where a 900g weight was attached to each leg), and a no pad condition. The initial study measured running and turning times through SMART speed timing gates placed at each

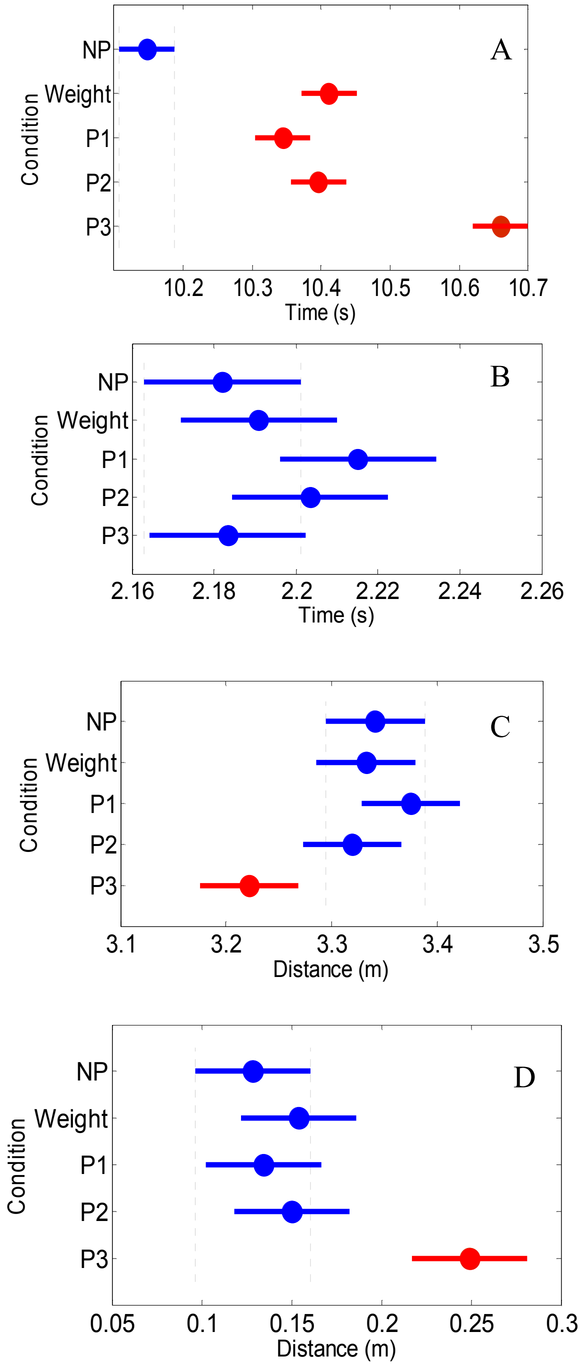

Figure 1: Mean ± one standard deviation for A) overall time, B) time taken to turn, C) stride length and D) stride width for the 5 conditions of no pads (NP), weighted comparison (900g), pad type 1 (P1) (500g), pad type 2 (P2) (740g) and pad type 3 (P3) (900g).

crease and 5 meters before the crease to calculate turning time, individual splits and total time. Ten male subjects were used for this initial study with a mean age of 19.8 ±1.3 years, and all played county 1st or 2nd team level or equivalent. Each participant completed 4 sets of 3 runs for each condition, with a 15 minute rest between conditions. Condition order was randomized to prevent any order affects.

A secondary study was conducted to analyze running stride parameters utilizing a CODA CX1 4 camera system, with 2 integrated force plates (Kistler 9281C) to determine heel strike and toe off. A full lower body marker set was used to capture the running motion, and was analyzed using Visual 3D to allow stride width and length to be calculated. For this secondary study, 9 cricketers were used with a mean age of 19.4 ±1.1 years and again all played county level cricket or equivalent.

RESULTS AND DISCUSSION

Within the initial study a set of repeated measures ANOVAs were used to determine if different batting leg guards affect running times and whether any detrimental affects could be solely attributed to additional weight. From the results it was identified that all three pads (P1, 2 and 3) and the weighted comparison significantly impeded running performance ($P<0.05$) increasing time taken to run 3 runs by 0.2s, 0.25s, 0.53s and 0.28s respectively when compared to running without pads, which at top speed could equate to as much as 3.5m of ground covered. It was also determined that P3 was significantly ($P<0.01$) more detrimental to performance than P1, P2 and the weighted comparison (Figure 1A). These results suggest that although weight does influence running speed it is not solely accountable for the increase in time, as P3 was equal in weight to the weighted comparison. Turn times were also analyzed through a repeated measures ANOVA but no significant differences between conditions ($P>0.05$) were found with the maximal difference in time of 0.029s (Figure 1B), suggesting the difference in times is due to negative affects on straight line running.

The second study focused on determining if different pads directly affected the stride parameters of cricketers when compared to running without pads. The results of the ANOVA suggest that there is no significant differences in stride length caused by P1, P2 or the weighted comparison, however, P3 does appear to significantly decrease stride length by an average of 0.014m ($P<0.05$) as shown in Figure 1C. P3 was also found to have a significant affect on stride width, resulting in players running with a wider gait, whereas no significant difference were found between the other conditions as illustrated in Figure 1D.

CONCLUSIONS

Overall this study has identified that cricket leg guards do have a detrimental affect on running times. This increase in time taken to complete three runs can be attributed to differences in straight line running speed rather than time taken to change direction. A proportion of this increase in running time can be attributed to the added mass of the leg caused by the leg guards, however, this does not fully account for the negative affect on running time caused by P3. The results suggest that heavy bulky leg guards can increase stride width and decrease stride length which can significantly affect running speeds. These findings have practical implications when designing cricket leg guards demonstrating that pads need to be as light and closely fitting as possible to minimize impedance on stride parameters such as width and length.

REFERENCES

1. Loock, N et al. *Sports Biomechanics,* **5**(1), 15-22 2006.
2. Webster J. M. and Roberts, J. *J Sports Engineering and Technology* **223**, In Press, 2009.

ACKNOWLEDGEMENTS

The authors would like to thank the Sports Technology Institute at Loughborough University for providing facilities and technical staff that enabled this study to be completed. Sincere appreciation is extended to the cricketers who donated their time within the testing.

IMPROVING DYNAMIC STABILITY DURING THE COMPENSATORY STEPPING RESPONSE OF A TRANSFEMORAL AMPUTEE

[1] Jeremy R. Crenshaw, [2] Kenton R. Kaufman, and [1] Mark D. Grabiner
[1]Department of Kinesiology and Nutrition, University of Illinois at Chicago, Chicago, IL
[2]Department of Orthopaedic Surgery, Mayo Clinic, Rochester, MN
email: jcrens2@uic.edu, web: http://www.uic.edu/ahs/biomechanics

INTRODUCTION

Over one year, 66% of individuals with a transfemoral amputation (TFA) reported falling [1]. This high incidence of falls indicates a need for preventative interventions. For older adults, another population with a high incidence of falls, practicing a compensatory stepping response (CSR) has yielded beneficial results. After one training session, older adults improved recovery kinematics after a treadmill disturbance [2] and an overground trip [3]. To the best of our knowledge, CSR training has not been applied to individuals with a TFA.

We hypothesized that training would improve the CSR of a transfemoral, amputee subject by:

- decreasing the incidence of falls.
- limiting the use of a single-limb hopping strategy [4].
- increasing step length (L_{step}), decreasing step time (t_{step}), and decreasing trunk inclination angle (θ_{trunk}) at recovery step completion [2,3].
- increasing the anteroposterior (AP) margin of dynamic stability at foot strike (MOS_{AP}) [5].

METHODS

One female subject with a TFA (27 years, 165 cm, 62.5 kg, 3.5 years after traumatic TFA) and one female subject with intact limbs (21 years, 177 cm, 85.7 kg) participated in this study. The prosthesis consisted of a microprocessor knee (C-Leg®, Otto Bock, Minneapolis, MN) and a dynamic response foot. The amputee and non-amputee subjects participated in six and one days of CSR training, respectively.

The training protocol consisted of a progressively challenging sequence of CSR trials. For each trial, the subjects stood on a custom treadmill (Active Step™, Simbex, Lebanon, NH), and posteriorly-directed treadmill accelerations necessitated an anterior-directed CSR of multiple steps. The initial belt accelerations lasted 0.5 sec, and ranged from 1.5 m/s^2 to 6.5 m/s^2. After the initial acceleration, the treadmill decelerated at a constant rate of -0.375 m/s^2. For small disturbances (≤ 2.25 m/s^2), peak treadmill velocity was maintained so that the minimum belt displacement was 2 m.

The amputee subject performed two series of CSRs each day, once with the initial step with the non-prosthetic limb (NPL), and once with the initial step with the prosthetic limb (PL). The subject with no amputations performed one series of CSRs, stepping with the self-preferred limb. For all trials, three-dimensional position data were recorded by motion capture at 120 Hz. L_{step}, t_{step}, θ_{trunk}, and MOS_{AP} were calculated at foot strike of the first six steps following the disturbance. The equation for MOS_{AP} was modified from previous literature [5] to consider the treadmill belt velocity as follows:

$$MOS_{AP} = BOS_{AP} - \left(x_{COM} + \frac{(v_{COM} - v_{belt})}{\sqrt{\frac{g}{l}}} \right)$$

in which:

- BOS_{AP}: AP position of the base of support (toe marker) of the stepping foot
- x_{COM}, v_{COM}, and v_{belt}: AP position and velocity of the overall body center of mass and velocity of the treadmill belt, respectively.
- g: acceleration of gravity (9.81 m/s^2)
- l: distance between the stepping ankle center to the body COM mass in the sagittal plane.

Trials of the amputee from the first and sixth day were compared to assess a training effect. Comparisons were made using disturbances common to both subjects and initial stepping limbs, i.e., those with an initial belt acceleration of 2.75-3.5 m/s^2.

RESULTS AND DISCUSSION

The CSRs of the amputee improved with training:

- The amputee fell on day 1 (initial acceleration of 4.5 m/s^2, NPL initial step), but successfully recovered from the same disturbance on day 6.
- The amputee decreased the use of a hopping strategy from day 1 (5 of 25 trials) to day 6 (1 of 34 trials).
- MOS_{AP} improved with training, especially at the 2nd or 3rd step when performed with the PL (Figure 1).
  - 2nd step with PL
    - Day 1 = -0.179 ± 0.118 m
    - Day 6 = -0.082 ± 0.094 m
  - 3rd step with PL
    - Day 1 = -0.220 ± 0.147 m
    - Day 6 = -0.049 ± 0.021 m
- Improvements in MOS_{AP} coincided with increased L_{step} and decreased θ_{trunk} (Figure 1 & Table 1). These changes occurred without altering t_{step}.

Although the MOS_{AP} and kinematics of the trained amputee more closely approximated those of the non-amputee, the trained amputee demonstrated smaller MOS_{AP} after the 2nd step. This difference may be due to greater θ_{trunk}, despite greater L_{step}.

Table 1. Mean L_{step} and θ_{trunk} of the initial 3 steps.

	L_{step} (m)	θ_{trunk} (deg)
Day 1	0.759 ± 0.123	8.28 ± 7.63
Day 6	0.941 ± 0.096	4.03 ± 3.64
Non-Amputee	0.940 ± 0.152	1.03 ± 4.28

CONCLUSIONS

CSR training by a transfemoral amputee was associated with increased step length and decreased trunk flexion following large postural disturbances. The resulting improvements in dynamic stability may reduce trip-related fall-risk.

REFERENCES

1. Miller WC, et al. *Arch Phys Med Rehabil* **82**, 1031-1037, 2001.
2. Owings T, et al. *Clin Biomech* **16**, 813-819, 2001.
3. Bieryla K, et al. *Gait Posture* **26**, 208-213, 2007.
4. Crenshaw J, et al. *Proceedings of NACOB*, Ann Arbor, MI, 257, 2008.
5. Hof AL, et al. *J Biomech* **38**, 1-8, 2005.

ACKNOWLEDGEMENTS

Funding by Otto Bock U.S.A., Minneapolis, MN.

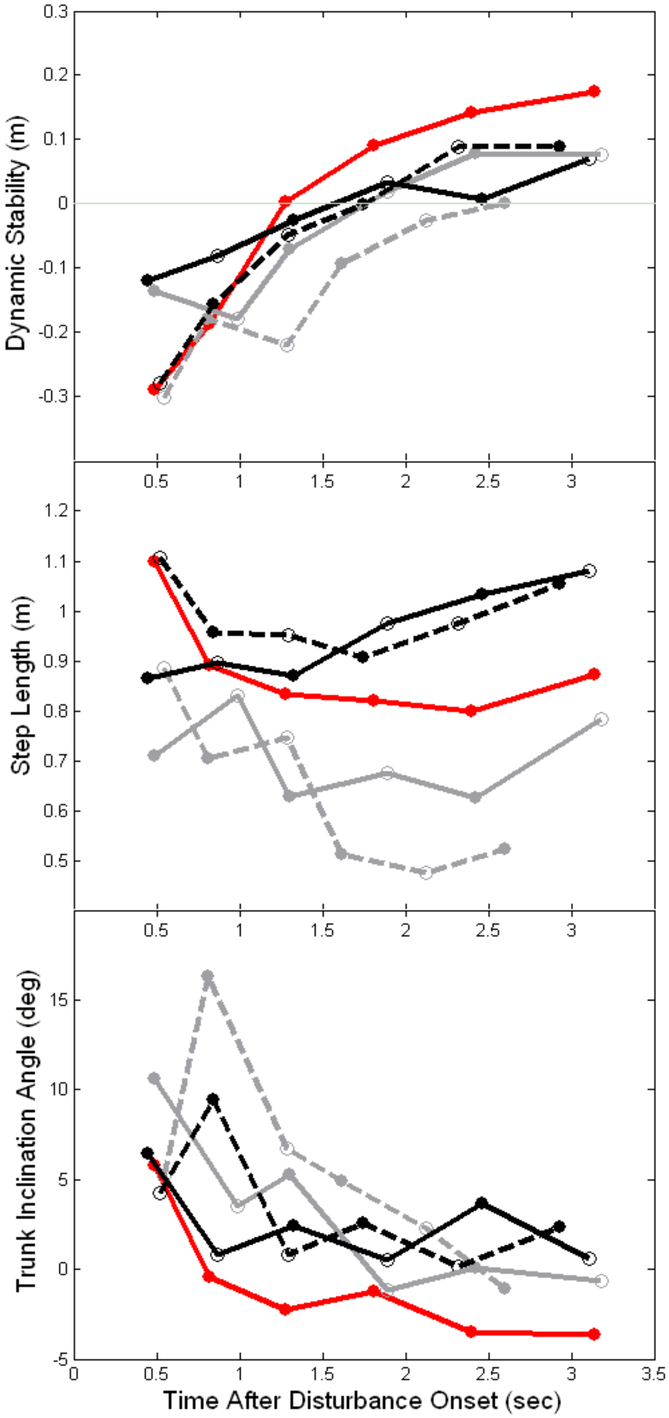

Figure 1. Mean MOS_{AP}, L_{step}, and θ_{trunk} (0° is upright, positive denotes forward tilt) for each heel strike after disturbance onset (initial belt acceleration of 2.75-3.5 m/s^2). Solid lines denote an initial step with the NPL, and dashed lines represent an initial step with the PL. Solid circles represent steps with the NPL, and hollow circles represent steps with the PL. Grey lines represent data from day 1. Black lines represent data from day 6. Red lines denote data from the non-amputee subject.

PREHENSION SYNERGY: THE CHANEGES IN SYNERGISTIC DIGIT ACTIONS UNDER SYSTEMATCIALLY MANIPULATED CONDITIONS OF TASK CONSTRAINTS

Jaebum Park, You-Sin Kim, and Jae Kun Shim
Department of Kinesiology, University of Maryland, College Park
email: jbpark@umd.edu web: http://www.hhp.umd.edu/KNES/faculty/jkshim/

INTRODUCTION

In order to maintain a stable static grasp of hand-held objects, the central nervous system (CNS) needs to satisfy a set of external static constraints. In many of human grasping tasks, multiple fingers are involved in static grasping tasks and the CNS needs to control a set of finger forces and moments to satisfy the static constraints. When the number of forces and moments the CNS must control is greater than the number of constraints, infinite finger force and moment combinations can produce exactly the same motor outcomes. This problem has been known as motor redundancy in human movement science. In order to solve the motor redundancy problem, the CNS needs to make decisions on the combinations of finger forces and moments that will be used for a given motor task. It has been known that individual fingers (i.e., elemental variables) are coordinated to generate a desired task-specific outcome during multi-digit manipulation tasks, and this phenomenon has been called multi-digit synergy [1, 2]. Compared to a large number of studies on multi-digit synergies of fixed object pressing (i.e., constraints free condition) and free object grasping, little has been investigated about synergic actions among elemental variables (i.e., digits forces and moments) which are affected by different combinations of static task constraints (i.e., mechanical constraints). The aim of this study is to investigate how the systematic changes of static task constraints affect the synergic actions among individual digits forces and moments during multi-digit prehension task.

METHODS

Equipment: Five six-component (three force and three moment components) transducers were attached to an aluminum handle (5.0mm × 85.0mm × 7mm), and one six-component (three position and three angle components) magnetic tracking device as mounted to the top of the handle in order to provide real-time feedback as linear and angular translations of the handle.

Experimental Procedure: There were four levels of task constraints by three levels of external torques (i.e., -0.70Nm, 0Nm, and +0.70Nm). The four levels of task constraints included rotation constraint only (R), horizontal translation + rotation constraints (HR), vertical translation + rotation constraints (VR), and horizontal translation + vertical translation + rotation constraints (HVR). Pronation and supination efforts were required under the positive (+0.70Nm) and negative external torque (-0.70Nm) conditions, respectively. The task for the subjects was to hold the handle while maintaining the handle in equilibrium (i.e., quasi-static grasping) by watching computer screen which provided a feedback of real-time linear and angular position of the handle. For a given condition, twenty five consecutive trials were performed.

Model: The following three task constraints (i.e., mechanical constraints) exist for a static prehension regarding digits forces and moments in a two-dimensional grasping plane.

$$-F_{th}^{n} = F_{i}^{n} + F_{m}^{n} + F_{r}^{n} + F_{l}^{n} \qquad (1)$$

$$F_{th}^{t} + F_{i}^{t} + F_{m}^{t} + F_{r}^{t} + F_{l}^{t} = -w \qquad (2)$$

$$\sum_{k} (M_{k}^{n} + M_{k}^{t}) = -Tq, k = \{th, i, m, r, l\} \qquad (3)$$

F and M represent the force and moment; n and t refer to the normal and tangential force component; w and Tq represent the weight of the object and external torques; subscripts *th, i, m, r*, and *l* indicate the thumb, index, middle, ring and little finger, respectively. Eq.1, 2, and 3 refer to the task constraints of horizontal translation (H), vertical translation (V), and rotation (R), respectively. Hence, the number of required task constraints was varied according to given conditions.

Uncontrolled Manifold (UCM) analysis: Two variances (i.e., variance along the UCM and the variance orthogonal to UCM) were calculated in five-dimensional forces or moments space and divided by the number of degrees of freedom for each variance. Note that the variance along the UCM (V_{UCM}) does not change the resultant force or moment (i.e., good variance) while the variance orthogonal to the UCM (V_{ORT}) reflects the controlled space which changes the total force or moment resulting in the increases of performance error (see [3] for details). Two variances are orthogonal to each other so that the total variance (V_{TOT}) is the sum of V_{UCM} and V_{ORT}. ΔV was calculated in order to examine the variance per dimension (Eq. 4). The ΔV was normalized by the total variance per dimension ($V_{TOT}/5$) because the total variances were varied across the subjects.

$$\Delta V = \frac{(V_{UCM} / 4) - V_{ORT}}{(V_{TOT} / 5)} \qquad (4)$$

RESULTS AND DISCUSSION

Positive values of ΔV would reflect synergistic actions among elemental variables in order to stabilize the performance variables. In contrast, negative values of ΔV would imply that the elemental variables contribute to a variation of the performance variables resulting in destabilization of the performance variables.

Normal force stabilization: It was obvious that positive values of ΔV_{Fn} indices were shown in the HR and HVR condition in which horizontal translation was constrained (Fig. 1A). However, positive values of ΔV_{Fn} were also shown even when the horizontal translation was not constrained (i.e., R and VR conditions) (Fig. 1A). ΔV_{Fn} in HR and HVR condition were greater than that in R and VR condition.

Tangential force stabilization: The sum of digits' tangential forces should be equal and opposite to the weight of the object when the vertical translation is constrained (Eq.2). It was clearly shown that ΔV_{Ft} indices were positive in VR and HVR condition. However, ΔV_{Ft} indices were negative when the vertical translation was not constrained (i.e., R and HR conditions).

Moment of force stabilization: In general, ΔV_M indices increased systematically with the number of task constraints. In other words, HVR condition contained three task constraints (i.e., horizontal, vertical translation, and rotation constraints), and ΔV_M was the greatest in this condition. In particular, ΔV_M indices were positive for all conditions except the rotation constraint (R) condition (Fig.1C).

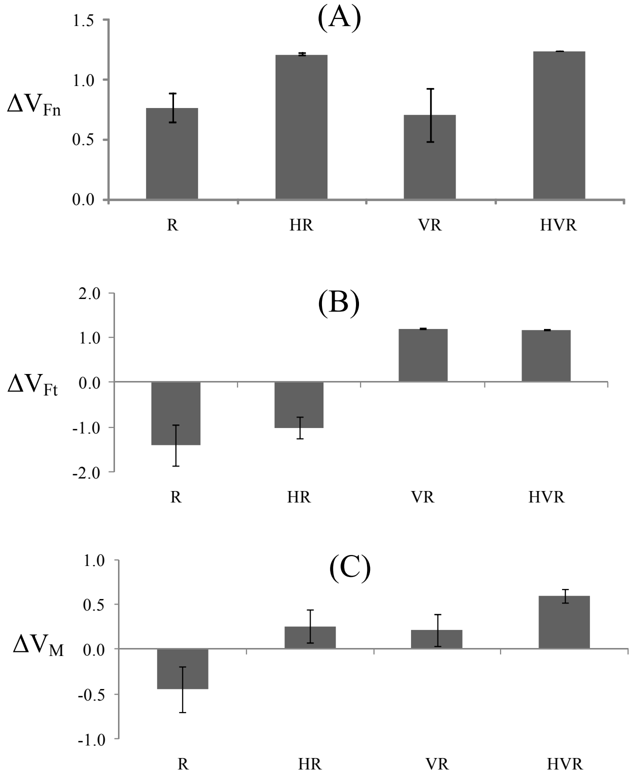

Figure 1. ΔV indices computed for (A) the total normal force (ΔV_{Fn}), (B) total tangential force (ΔV_{Ft}), and (C) total moment (ΔV_M) stabilization under four combinations of mechanical constraints (i.e., R, HR, VR, and HVR). Averaged across subjects (*n* = 4) and three external torque conditions data are presented with standard error bars.

CONCLUSIONS

The resultant normal force was stabilized even when the horizontal translation was not constrained. Meanwhile, the resultant tangential force was stabilized only when the vertical constraint was constrained in the prehension tasks. The synergy strength (ΔV) of moment of force increased systematically with the number of static constraints in the prehension task.

REFERENCES

1. Li ZM, et al. *Exp Brain Res* **119,** 276-86, 1998.
2. Zatsiorsky VM, et al. *Exp Brain Res* **148,** 77-87, 2003.
3. Latash ML, et al. *Exp Brain Res* **141,** 153-65, 2001.

GREATER TROCHANTER REATTACHEMENT: EXPERIMENTAL EVALUATION OF CABLE TENSION AND DISPLACEMENT DURING WALKING

[1,2] Kajsa Duke, [1]G Yves. Laflamme, [2]Vladimir Brailovski, [1,2]Yan Bourgeois, [1]Charles Toueg,
[1]Annie Levasseur and [1, 2]Yvan Petit
[1]Sacre Coeur Hospital, Montreal, Canada,
[2]Ecole de technologie supérieure, Montréal, Canada; email: Yvan.Petit@etsmtl.ca

INTRODUCTION

During hip revision surgeries an osteotomy of the greater trochanter (GT) is often performed. Biomechanical analysis of GT reattachement began in the late 1970's when only wires were used [1]. More recently, cables and cable plate systems are being employed. Hersh et al [2] compared the stiffness of wire, cable and a short Dall Miles Two Cable Grip system (Howmedica, Rutherford, NJ). The cable grip system was found to be the stronger and more rigid of the three [2]. Even with recent improvements, a relatively high failure rate is still reported [3]. More modern cable grip type systems that extend down the lateral diaphysis of the femur have yet to be investigated. Variability in cable tension is also not well understood. The objective of this study is to evaluate the change in cable tension and displacement of the GT during loading similar to walking.

METHODS

A 4th generation Sawbones composite femur (Pacific Research Laboratories Inc. Vashon, WA) was osteotomised and implanted with a femoral stem and the GT was then reattached with a 4 cable system (Cable-Ready®, Zimmer, Warsaw, IN). The cable tension was monitored with a through hole compression load cell (Omega, Stamford, CT) and were tightened starting with the upper (most proximal) cable and subsequently tightened down the shaft. The first through fourth cables were then retightened as recommended by the manufacturer. Cable tension was set to either 178, 356 or 534 N (356 N or 80 lb is recommended by the manufacturer.)

A custom made frame (Figure 1) applied quasi static load on the head of the femoral stem implant (2340 N) and abductor pull (667 N) on the GT in order to simulate walking. This loading was applied three times (steps) to evaluate the effect of repeated loads. The entire experiment was then repeated three times, in random order, for each cable tension configuration to assess the reproducibility of measurements.

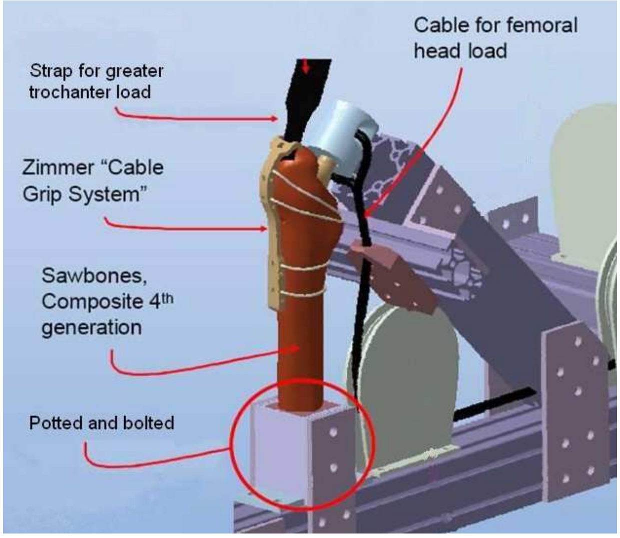
Cable for femoral head load
Strap for greater trochanter load
Zimmer "Cable Grip System"
Sawbones, Composite 4th generation
Potted and bolted

Figure 1: Schematic of loading frame

Femur and GT displacement was measured with an Optotrack system (Northern Digital inc., Canada). A custom calibration procedure was used to animate a 3-D CAD femur model and measure relative gap and shear displacement of the GT.

RESULTS AND DISCUSSION

Cable tightening was analyzed determine any drop in cable tension as subsequent cables were tightened. The first cable dropped an average of 45%, the second 13% and no significant loss was observed in the third cable. All cables were retightened to the desired tension within an error of 9.8 N. Because a large drop in cable tension was observed, as seen in Figure 2, it was important to properly retighten the cables before locking the set screws as suggested by the manufacturer.

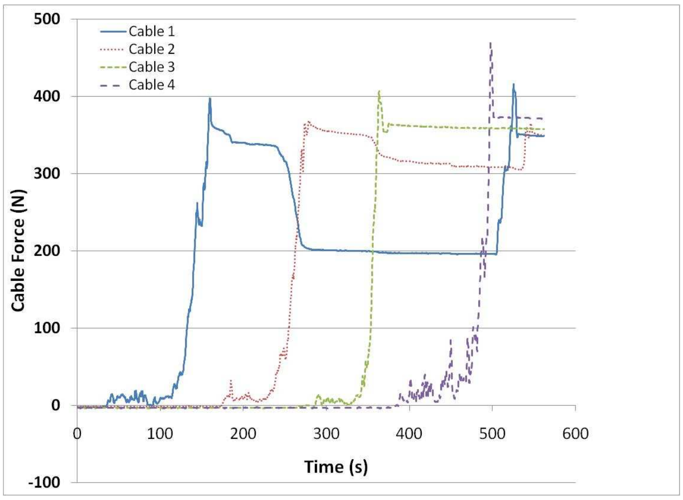

Figure 2: Cable tension during subsequent cable tightening

Cable tension was continuously monitored during loading to analyze any potential cable loosening. All cables loosen after testing with the exception of the first and fourth cable when tensioned to 178 N. With the manufacturer's recommended initial tension, the cables lost on average 23 N (7%) of tension. The second cable observed the greatest loss (60 N or 17%). This suggests that the cables slack considerably during the first few steps. However, this test was unable to show the long term effect of cyclic loads or bone remodeling around the cables.

GT displacement, relative to the femur, was monitored during loading. The gap measured was 0.39±0.14, 0.46±0.02 and 0.42±0.08 mm for 178, 356 or 534 N initial cable tightening respectively. The shear, or sliding, of the GT was more variable and was greatest at 0.89±0.3 mm when tension was only 178 N. The shear was only 0.24±0.06 and 0.26±0.11mm for the 356 N and 534 N initial cable tensions respectively.

CONCLUSIONS

A drop in cable tension was observed when tightening subsequent cables. Therefore, retightneing of the cables, as reccomended by the manufacturer, is very important. Loss in cable tension is measured after the simulation of only three steps. The effect of cyclic loading will be analyzed in future studies.

More variability in the displacement and greater shear was observed when the cables were only tensioned at 178 N (50% of the manufacturer recommended tension). Reducing the tension is not recommended. However, there appears to be no difference between the shear and gap when cables are tensioned at 356 N or 534 N. This suggests avoiding excessive tightening of the cables as it may increase stress in the bone.

REFERENCES

1. Markolf KL, et al. *Clin Ortho Rel Res*, **141**:111-21, 1979
2. Hersh CK, et al., *Clin Ortho Rel Res*, **329**:317-25, 1996
3. Barrack RL & Butler RA, *Clin Ortho Rel Res*, **441**:237-42, 2005

ACKNOWLEDGEMENTS

Funded by NSERC
Thank-you to Yannick Baril and Michel Drouin

A QUANTITATIVE ANALYSIS OF THE RELATIONSHIP BETWEEN SCAPULAR ORIENTATION AND SHOULDER STRENGTH

Bryan R. Picco, Steven L. Fischer, Clark R. Dickerson
Department of Kinesiology, University of Waterloo, Waterloo, ON
email: bpicco@uwaterloo.ca

INTRODUCTION

There is an increasing emphasis on reducing scapular protraction as a preventative measure to decrease injury risk in both rehabilitative and workplace settings [1]. However, few studies have examined the influence of scapular orientation on functional shoulder measures such as maximum hand force production, or strength. Protracted and retracted scapula positions are known to reduce isometric shoulder flexion force, but no research has examined this relationship in other force directions, such as shoulder extension and abduction. This study examined the influence of scapular orientation on shoulder strength with four hand force exertion directional exertions. We hypothesized that as the shoulder deviates from a neutral position, maximal isometric force decreases in all exertion directions.

METHODS

Ten university-aged males without shoulder pain performed twelve maximal isometric efforts while standing with their right arm flexed to 90° and elbow fully extended. Exertions were conducted in for each combination of force direction (up, down, medial, lateral) and scapular orientation (neutral, protracted, or retracted). Hand force was measured using a MC3A force cube (ATMI, MA, USA), and 3-D motion was recorded by tracking 12 reflective markers using a using an 8 camera motion analysis system (Vicon, Oxford, UK), using a previously described acromion marker cluster method [2] to determine scapular orientation.

A two factor (exertion direction, scapular orientation) repeated measures ANOVA was used to compare force magnitudes across the exertions ($\alpha<0.05$). Recorded neutral scapula orientation values were averaged within subjects across all force directions to establish a reference value. All orientations for individual exertions are expressed relative to this subject specific average neutral orientation.

RESULTS AND DISCUSSION

Direction of force application had the greatest influence on strength (Figure 1). Strength decreased progressively from down, up, to horizontal force directions (medial and lateral were not different).

Scapular orientation influenced strength for vertical force exertions (Figure 1). Upward strength was significantly reduced with the scapula retracted (99.6 ± 22.0 N) compared to a neutral posture (109.9 ± 27.0 N). Strength was not significantly reduced with protracted postures (97.1 ± 26.3 N). When applying force in the downward direction, strength was significantly increased with a retracted scapula (171.3 ± 43.0 N) compared to protracted (143.0 ± 29.5 N) postures, but not neutral (160.0 ± 35.0 N) postures. No strength differences existed for horizontal force exertions (lateral or medial).

For exertions with the scapula retracted, average relative retraction angle was -7.7° from neutral (average neutral = 0°). For protraction trials, average relative scapula protraction was 7.6° from neutral. Force direction did not influence scapular orientation (Figure 2). Average relative scapular angles were significantly different from each other for the three orientation conditions. The average scapula range of motion documented in this study (15.3°) is within the maximal range of motions found by Sheikhzadeh et al. in previous studies [3].

Our study is the first to provide insight into the influence scapular orientation has on isometric shoulder strength in the downward, left, and right directions in a healthy population. Although the direction of force exertion influences maximal isometric shoulder strength more than scapular orientation, orientation nonetheless significantly modulated strength. This was seen only in vertical force application directions. Decrements observed in maximal isometric shoulder elevation force with retracted scapula positions in the current study are similar to previous findings [1]. However, we did not find similar significant reductions with protracted scapula positions. Also, contrary to past findings, a retracted posture increased downward force in our study, possible as a consequence of positioning the shoulder adductors in a more favorable length to generate force. The average absolute isometric elevation force measured here was less than in forces measured previously [1].

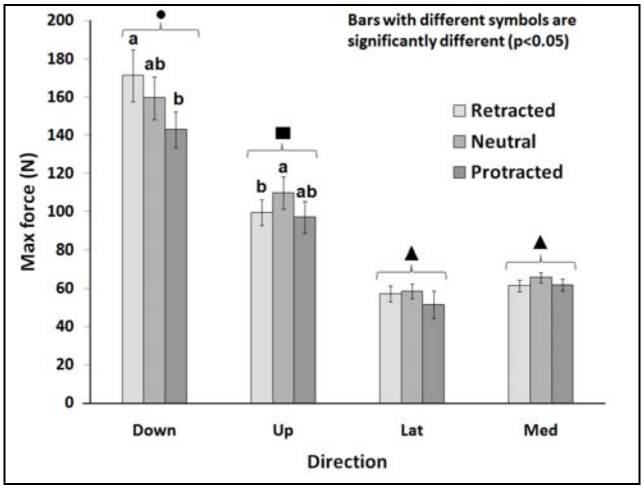

Figure 1: Maximal isometric shoulder force in 4 directions in 3 scapular postures; shoulder forward-flexed to 90°, elbow fully extended

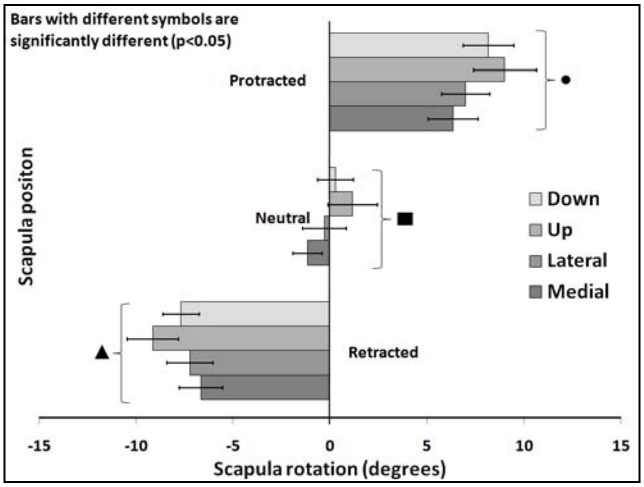

Figure 2: Scapular orientation for 3 scapular postures and 4 applied force directions; shoulder forward-flexed to 90°, elbow fully extended

Discrepancies in our findings from previous studies could be due to experimental set-up. Participants in this study gripped a force transducer handle rather than exerting a force on a transducer attached to the wrist [1]. Our intentional measurement of functional strength, in terms of hand force producible, undoubtedly affected absolute force values. This experimental decision increased the degrees of freedom in the arm system, which added an increased requirement, which was to maintain wrist joint stiffness in order to transmit force to the gripped handle. The more distal measurement location also increased the distance to the point of force application, thus also increasing moment loads. Participants were standing upright, where previous studies used a seated test posture. Again, this choice was done in order to more realistically simulate standing work that is commonplace in industry, but may have reduced hand force generation due to whole-body balance limitations.

The quantification of scapula orientation using the acromion marker cluster method [2] is advanced beyond previous efforts to monitor the influence of scapular orientation on strength. The three scapula orientations were significantly different on a common scale within each force direction. Indeed, when looking at individual scapular orientations, they did not significantly change across direction (Figure 2). This indicates that participants assumed correct, consistent scapula postures for each trial.

Our findings support existing wisdom regarding reducing industrial reach distances that result in abnormal scapular orientations, particularly those that require vertical forces, where differences were greatest. Neutral scapula postures consistently generated higher force than protracted postures that commonly occur with increased reach lengths. The additional influence of scapular orientation is also expected to be seen in shoulder muscular activity levels, which were concomitantly measured as a part of this strength study, as well as in submaximal exertions at the same positions. This will reveal any tissue demand variations associated with similar task performance in different scapular postures.

REFERENCES

1. Smith J, et al. *Archive Physical Medicine Rehabilitation* **83**, 367-70, 2002.
2. Van Andel C, et al. *Gait and Posture* **29**, 123-128, 2009.
3. Sheikhzadeh et al. *Journal of Shoulder and Elbow Surgery* **17**, 936-942.

ACKNOWLEDGEMENTS

NSERC of Canada partially funded this research.

A New Device for Measuring Flexor Tendon Forces and Grip Force: A Cadaver Model

[1] Shihyun Park, [1] Andris Freivalds, [1] Neil A. Sharkey, [2] Brian D. Lowe
[1] Pennsylvania State University, University Park, PA, 16801 USA
[2] National Institute for Occupational Safety and Health, Cincinnati, OH 45226 USA
email: shpark@psu.edu,

INTRODUCTION

Failure to properly consider tendon forces in designing a tool and excessive use of hand tools can have harmful effects on users. These effects may range from minor discomfort and fatigue to work related disorders or cumulative trauma disorders (CTDs) of the finger, hand and forearm [1]. From the solutions of force / moment equili-brium equations of Kong (2001), for an external load of P, 9.05P and 2.83P were reported for the flexor digitorum profundus (FDP) and flexor digitorum superficialis (FDS) in the gripping task, respectively [2]. The most reliable assessment of the effects of external loading conditions on tendon forces is obtained by directly measuring tendon forces. However, no method has solved the force rate between the tendon forces and the external forces in the power grip with hand tools, and simultaneously applied tension to tendons to study the muscle coordination necessary to produce two-dimensional gripping force. The objective of this study was to develop a hand motion simulator (HMS) as a method that is capable of simultaneously measuring both flexor tendon (internal) forces and a grip (external) force with simulating a power grip hand motion with different tendon force ratios in a cadaver arm.

METHODS

The hand motion simulator was built to simulate a grasp motion of a cadaver hand with a grip force generated by pulling flexor tendons connected with linear actuators. This new device was composed with a testing frame, Force Delivery Unit (FDU), Data Acquisition (DAQ), and Vision system for motion capturing, and a custom developed software (Figure 1). The FDU consists of two stepper motors driven linear actuator in series with a force transducer for force feedback control. Each force transducer is attached to a cable connected to a freeze clamp in the line of force of each muscle [3]. The DAQ system was designed for measuring internal & external forces coupled with force feedback control system. External forces are defined as grip force measured from a force transducer in a handle, and internal forces are determined as tendon forces taken by force transducers in line with force delivery units. In addition, 16 ch. force sensitive resistors were attached on each phalange to measure finger force

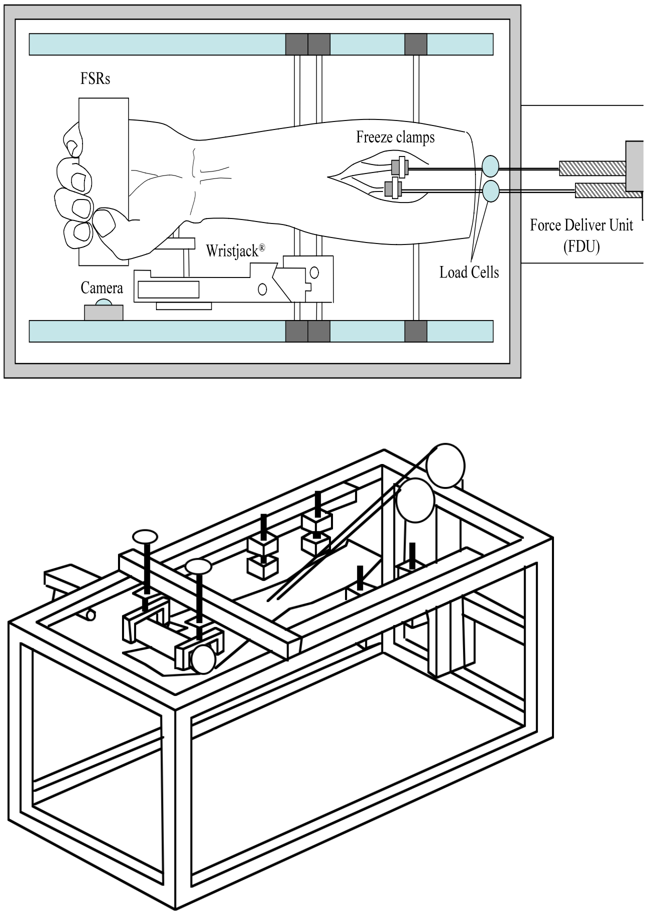

Figure 1: Schematic of the Hand Motion Simulator showing the muscle delivery unit and force transducers with a cadaver arm.

distributions for a power grip motion. For finger motion capturing, a CCD camera was attached on the side of the frame to capture finger joint angles in lateral view. Captured images represented static grip postures of each condition. As the post process, the custom Labview software analyzes captured images to measure finger joint angles. One human cadaver forearm was used to demonstrate the utility of the device for measuring tendon forces and a grip force. The entire forearm was mounted into the testing frame with Schanz screws to secure the specimen. The flexor digitorum profundus (FDP) and the flexor digitorum superficialis (FDS) were the main finger flexor muscles to control finger postures for grasping motion. The activities of the FDP and FDS were each demonstrated by a separate force delivery unit activated by a motion controller. To control muscle forces, the motion controller implemented a force-feedback control loop in order to keep the actual force, F_A, in each FDU cable measured by each load transducer equal to the target force, F_T, desired force to grasp a handle.

RESULTS

The hand motion simulator showed very stable motions and data acquisition with a cadaver forearm. In the validation test of the force feedback control system, the HMS generated 98.98±0.41 N for 100 N target forces. The error between F_A and F_T was 1.02±0.41N and it showed the reliability of the system (Figure 2). Figure 3 shows sample data plots of tendon forces (FDP and FDS) measured by force transducers in line with the force delivery units and grip forces recorded by a handle.

DISCUSSION

The new device presented in this study dose has some limitations. Intrinsic muscles were not considered in our research, because effects of these muscles on the finger flexion could be neglected. However, pulling the FDP and FDS muscles was limited to control metacarpophalangeal (MCP) joint regardless of the motion of proximal and distal interphalangeal joints. We believe that the strengths of this study outweigh the weakness. Although we cannot make firm conclusions based on only one specimen being tested, we believe that this new testing device will provide new and useful information on the source of direct measurement of tendon forces.

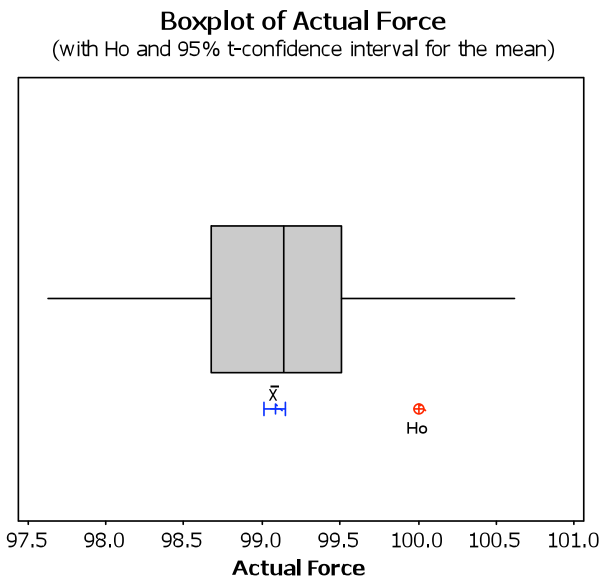

Figure 2: Average Actual force generated by the HMS for 100 N Target Force

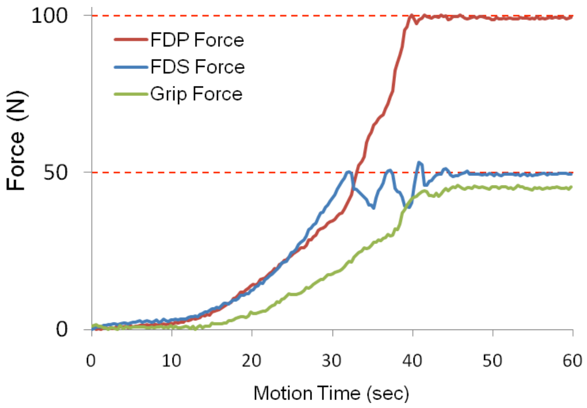

Figure 3: Sample data plots of tendon forces and a grip force measured by the HMS

REFERENCES

1.NIOSH, Musculoskeletal Disorders and Workplace Factors. *Report 97-141*. Cincinnati, OH, NIOSH, 1997.

2.Kong, Y.K., Optimum Design of Handle Shape through Biomechanical Modeling of Hand Tendon Forces, *Ph.D. dissertation*, University Park, PA: Pennsylvania State University, 2001

3.Sharkey, N.A., Smith T.S., Lundmark D.C., "Freeze clamping musculo-tendinous junctions for in vitro simulation of joint mechanics." *Journal of biomechanics* 28(5): 631-635, 1995.

SEQUENTIAL DISRUPTION OF THE CRURAL FASCIA RESULTS IN LOSS OF STABILITY DURING LOCOMOTION

[1]Victoria A. Stahl, and [2]T. Richard Nichols
[1]Biomedical Engineering, [2]Applied Physiology, Georgia Institute of Technology
email: victoria.stahl@bme.gatech.edu web: http://www.ap.gatech.edu/Nichols

INTRODUCTION

Medial-lateral stability of the limb during locomotion has been examined in insects[1], humans[2] and cats[3]. In all cases the focus of the studies has been on the neuromuscular system while the fascial connections between muscles and the skeletal system have been mostly ignored. The crural fascia, in particular, connects the hamstring muscles to the calcaneus, and surrounds the triceps surae muscles. We hypothesize that this anatomical connection plays a role in passively stabilizing the distal limb during level walking and therefore controls the extent of paw circumduction during the swing phase.

METHODS

Three-dimensional kinematics were recorded from the spontaneously stepping, premammillary cat under four, consecutive fascia disruption conditions: 1) intact – no manipulations to the crural fascia; 2) split – longitudinally split over the gastrocnemius muscles; 3) medial band cut – a horizontal cut through the fascia to medial side of the medial band; 4) lateral band cut – a horizontal cut through the fascia to the lateral side of the lateral band. A minimum of three trials were recorded under each fascia condition; a trial is defined as a consistent, spontaneous period of walking for at least 20 seconds at a treadmill speed of 0.6-0.7 m/s

Markers were placed on the right leg at the iliac crest, greater trochanter, upper shank (to calculate the virtual knee), lateral malleolus, meta-tarsal phelangeal joint (mtp) and toe. The data was collected using six Vicon cameras at 125 Hz (one cat was collected and processed using Peak Motus at the same data collection settings). Paw contact (pc) and paw off (po) were demarked post-hoc by video analysis of the animal walking.

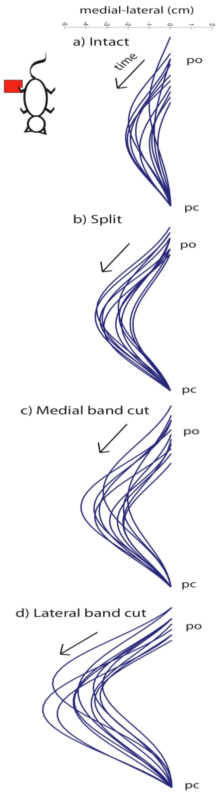

Figure 1: Excursion of the mtp marker on the right leg of cat 1 during swing in one trial under different fascia conditions. Note the increased circumduction and variability of the trajectories. The arrow represents the direction of time.

The data were analyzed using custom Matlab scripts and each marker was low pass filtered at 6Hz. In order to evaluate the circumduction of the paw the trajectory of the mtp in the medial-lateral direction was used. Data from nine steps in each trial were calculated and then averaged together under each condition for each animal. The swing phase of each trial was examined. In order to calculate the area the pc and po were set to 0 in the medial-lateral direction (Figure 1). The area was then averaged for each trial and the variance was determined. Three trials for each cat were averaged together and presented in Table 1.

RESULTS AND DISCUSSION

Figure 1 depicts the nine steps from a trial under the four fascia conditions in one cat. This figure shows the increase in circumduction area as well as highlights the increased variance of the swing under the different fascia cut conditions. In three out of four cats the area of circumduction increased and in all cats the variance of the trajectory increased (Table 1). When averaged across all cats the area of circumduction increased post fascia cutting by 46.25% and the variance by 216.5%. The circumduction and variance tends to increase sequentially upon further fascia disruption implying a greater loss of control of the paw during swing.

These results are consistent regardless of collection time or weight support of the animal.

CONCLUSIONS

Completely disrupting the crural fascia results in an increase in paw circumduction and variance. Therefore the crural fascia acts to limit movement of the paw during the swing phase by reducing the degrees of freedom in the limb.

REFERENCES

1. Wickramasuriya, A. et al. *J. Theoretical Biology*, **256**, 414-427.
2. Hyun, G. et al. *J Biomech* **41**, 2899-2905, 2008.
3. Misiaszek, JE. *J. Neurophysiol*, **96**, 1816-1828, 2006.

ACKNOWLEDGEMENTS

Data collection would not have been possible without the assistance of Claire Honeycutt, PhD, Inez Falcon and Chris Tuthill. Research funded by HD 32571 and NS 20855.

Table 1: Area and variance of average paw excursion across the different fascia disruption conditions.

Experiment	**Average Area of Paw Excursion (cm^2)**			
	Intact	**Split**	**Medial band cut**	**Both bands cut**
Cat 1	18.09	32.83	35.07	43.53
Cat 2	27.09	29.17	27.44	35.90
Cat 3	22.07	23.12	28.05	31.02
Cat 4	59.83	74.01	63.85	44.91

Experiment	**Average Variance of Paw Excursion**			
	Intact	**Split**	**Medial band cut**	**Both bands cut**
Cat 1	216.00	506.85	608.91	1206.20
Cat 2	117.87	100.41	257.02	146.56
Cat 3	36.40	183.65	427.72	610.88
Cat 4	352.14	1516.78	1181.33	1153.53

Are feedback related adjustments to step width affected by performance of the Stroop Test?

Christopher P. Hurt[1] Noah Rosenblatt[1] Mark D. Grabiner[1]
[1]Department of Kinesiology and Nutrition, University of Illinois at Chicago, Chicago, IL, USA
churt2@uic.edu, URL:http://www.uic.edu/ahs/biomechanic

INTRODUCTION

The attentional demand of walking increases as one ages [1]. This may reflect an interaction between age-related decreases in the fidelity of sensorimotor information [2] and the dynamic stability requirements of gait [3]. Reduced ability to concurrently attend to both attentional and motor tasks may increase fall risk [4].

Maintenance of frontal plane dynamic stability while walking is largely dependent on swing foot placement, which is commonly measured as step width (SW). Step-by-step control of SW is related to trunk kinematics at the previous midstance in both young and older adults [5]. Thus, some of the attentional component of walking may be allocated towards monitoring trunk kinematics and adjusting step width.

Two studies have independently shown that in young adults, SW variability (SWV) and trunk velocity variability decrease while performing the Stroop test, an attention demanding task [6,7]. The decreased variability reported in these studies may be related on a step-by-step basis thus suggesting that the feedback related control of SW is unaffected by the performance of an attentional task.

The purpose of the current study was to test whether the relationship between trunk kinematics and the subsequent SW is affected by the performance of an attention demanding task. We hypothesized that the relationship between trunk kinematics and the subsequent step width would not be affected in younger adults while performing the Stroop test. Due to an increased attentional demand of walking in older adults we further hypothesized that superimposing an attentional task while the older adults walked would have an effect on the step-by-step relationship.

METHODS

Twelve healthy young adults (6 males 6 females, age 25± 3.3 years) and eleven healthy older adults (4 males 7 females, age 61±5.6 years) participated in this study. Each subject walked on a motorized treadmill at a self-selected speed for 10 min during two randomly ordered tasks of simply walking and walking while performing the Stroop test. The Stroop test involved verbally identifying the color of the text used in a projection of the name of one of four colors. The text was not necessarily the name of the color. The projected images changed at a frequency of 1 Hz.

Kinematics were captured using an eight camera motion capture system (Motion Analysis, Santa Rosa, CA). SW and frontal plane position and acceleration of the trunk center of mass (COM) were identified using custom MATLAB software. The trunk COM was estimated from the positions of the shoulder and pelvis markers and extracted at midstance, which was defined as the instant at which the frontal plane velocity of the trunk was zero. This instant represents a time point after which the frontal plane COM motion is directed toward the swing limb and thus may be critical to SW adjustment. SW was calculated as the difference between successive left to right foot centroids at midstance.

Statistics:

The step-by-step relationship between trunk kinematics and SW for younger and older adults was quantified using a mixed regression model [8]. The mixed model was utilized to account for individual differences of subjects across conditions and was of the form:

$$SW = \beta_0 + \beta_1 position + \beta_2 acceleration.$$

Dummy variables were coded into the model to evaluate whether the control and Stroop test conditions affected how position and acceleration were regressed onto SW. Finally a term was included into the model to account for how stepping limb affected this relationship. Between-condition differences in the descriptive statistics of each group were tested using dependent t-tests.

RESULTS AND DISCUSSION

Younger adults performed the Stroop with generally fewer errors than older adults while walking (95% vs. 84% p=0.07). SWV was significantly different between conditions in younger adults. ($p<0.05$, Table 2). Variability of younger adults decreased 14%, 6%, and 14% for SWV, trunk position variability and trunk acceleration variability, respectively, while performing the Stroop. Variability of the same measures in older adults decreased only 3%, 5%, and 1%.

Performance of the Stroop did not affect the relationship between trunk kinematics and subsequent SW in younger adults. The interaction terms, i.e., position×task and acceleration×task were not significant (Table 1). This suggests that performance of the Stroop test did not interfere with younger adults ability modify SW in response to trunk kinematics at midstance on a step-by-step basis.

In contrast, performance of the Stroop test affected the relationship between trunk kinematics and subsequent step widths in older adults. Significant position×task and acceleration×task effects were found (Table 1). Despite minimal differences in the descriptive statistics the attentionally demanding task altered the relationship between trunk kinematics and subsequent step widths on a step-by-step basis in older adults. Previous studies have shown that the performance of an attentional task decreased older adult's ability to modify their step [4].

Table 1. Unstandardized beta coefficients for position and acceleration of the trunk COM are listed with task and the interaction terms ± standard error. *p<0.05

Younger Adults	**β**	**S.E.**	**p-value**
Position	**1.152 ***	**0.021**	**<0.001**
Acceleration	**0.024 ***	**0.002**	**<0.001**
Condition	**-4.270**	**4.485**	**0.349**
Position x Condition	**0.034**	**0.021**	**0.100**
Acceleration x Condition	**-0.003**	**0.002**	**0.149**

Older Adults	**β**	**S.E.**	**p-value**
Position	**1.185 ***	**0.018**	**<0.001**
Acceleration	**0.025 ***	**0.001**	**<0.001**
Condition	**6.042**	**0.958**	**0.123**
Position x Condition	**0.060 ***	**0.023**	**0.009**
Acceleration x Condition	**-0.007***	**0.002**	**<0.001**

CONCLUSIONS

In younger adults the general decrease in the variability of trunk kinematics at midstance and SW appeared to be related on a step-by-step basis. This suggests that the relationship between trunk kinematics and subsequent SW's was insensitive to performance of the Stroop test by younger adults. However, for older adults this relationship was altered by performing the attentionally demanding task. This further suggests that the attentional demand of treadmill walking is greater in older adults. The potential deleterious affect of attentionally demanding tasks on the step width-trunk kinematic relationship may compromise, to some extent, frontal plane dynamic stability of older adults.

REFERENCES

1. Lajoie Y, et al. *Exp Aging Res*, **22**, 185-198, 1996.
2. Kuo A. *IEEE*. **54**, 1919-1926, 2007.
3. Kuo A, *Int J. Robot Res.* **18**:917-930 1999.
4. Chen H et al. *J Gerontol: Med Sci* . **51A,** M116-22, 1996.
5. Hurt C. et al. *Gait and Posture* in revision
6. Grabiner M, & Troy K. *J Neuroeng Rehab,* **2**, 2005.
7. Dingwell J et al. *J Neuroeng Rehab,* **5**, 2008.
8. Hedeker D. & Gibbons R., *Longitudinal Data Analysis,* John Wiley & sons, Hoboken, New Jersey, 2006

Table 2: Kinematic variables of older and younger adults during the No Stroop (NS) and Stroop condition ± standard deviation *p<0.05 between task condition in the younger adults

Task	**Step Width(mm)**	**Step Width Variability**	**Trunk Position (mm)**	**Trunk Position Variability**	**Trunk Acceleration (mm/s^2)**	**Trunk Acceleration Variability**
Older NS	142.7 ± 30.0	23.2 ± 3.9	43.0 ± 13.8	12.3 ± 2.0	642.9 ± 155.2	137.5 ± 43.3
Older Stroop	137.7 ± 30.5	22.6 ± 4.1	41.9 ± 15.0	11.7 ± 2.4	616.2 ± 141.6	136.2 ± 39.3
Younger NS	124.9 ± 29.5	28.3 ± 6.4*	33.9 ± 11.6	24.74 ± 8.1	555.4 ±114.2	157.6 ± 54.9
Younger Stroop	128.0 ± 30.4	24.4 ± 5.0	36.1 ± 13.1	23.3 ± 8.2	578.0 ± 142.8	135.32 ± 39.1

RETHINKING MAXIMUM VOLUNTARY EXERTION TECHNIQUES TO AVOID MUSCLE FATIGUE WHILE REDUCING EXPERIMENTAL SETUP TIME: A SHOULDER EXAMPLE

Jaclyn N. Chopp, Steven L. Fischer and Clark R. Dickerson
Department of Kinesiology, University of Waterloo, Waterloo, ON
email: jchopp@uwaterloo.ca

INTRODUCTION

Normalized surface electromyography magnitude (EMG), expressed as a percentage of a maximum voluntary exertion (MVE), is commonly used to study the muscular loading implications of performing upper extremity intensive work. However, little research has addressed the importance of defining and standardizing the MVEs used. The purpose of a MVE is to produce the maximum voluntary amplitude of myoelectric activity for a muscle. In normalization, the level of EMG measured during an experimental or field task analysis, is expressed a percentage of the maximum capacity as defined by the MVE values [1]. If the selected MVE does not elicit maximal activity, then the corresponding normalized values will be disproportionately higher due to an underestimated maximum value (the denominator), therefore inflating the intensity of muscle load relative to its capacity. This may cascade into falsely identifying a task as hazardous or problematic. By defining standardized test contractions that reliably elicit maximum activity, we can avoid misidentifying problematic tasks while also providing an improved representation of how a muscle performs relative to its maximum voluntary capacity.

In the shoulder, a universal standardized MVE protocol is emerging, but not finalized. Specifically, two studies have attempted to determine a set of contractions that elicit maximal activity from various shoulder muscles [2-3]. These foundational studies have are somewhat limited due to intrinsic factors including data processing techniques, few repetitions of test contractions and an approach that did not select tested postures systematically throughout a range of motion.

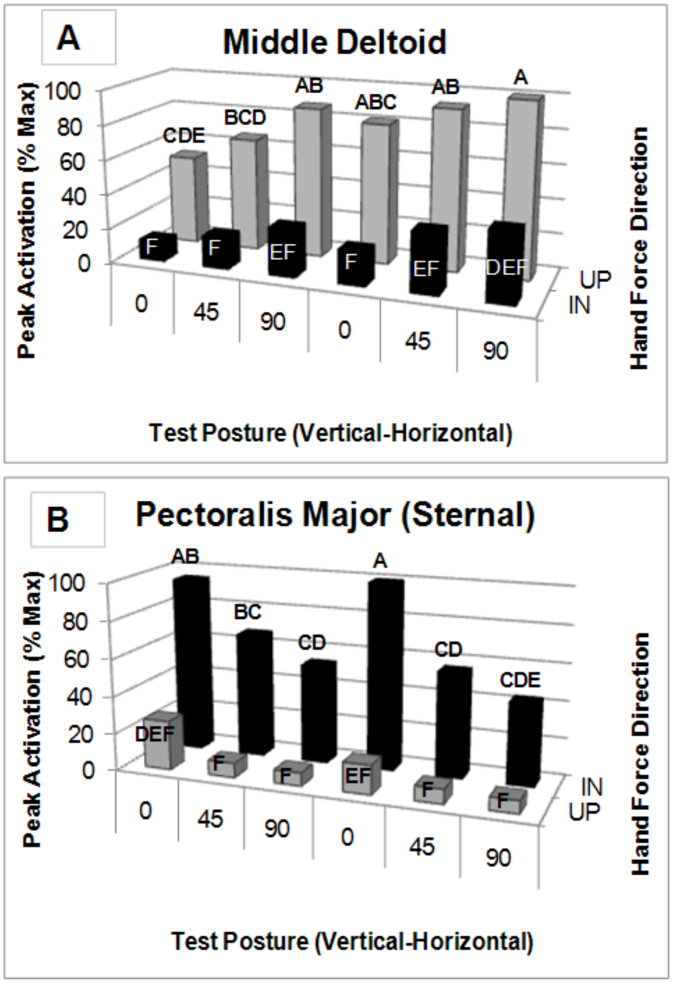

Figure 1: Peak activation for the middle deltoid (A), and pectoralis major: sternal insertion (B) taken as a percentage of the maximal activation. Mean values were calculated across all participants for each MVE tested and normalized to the maximal activation; significance ($p<0.05$) is indicated by different letters.

There were two major objectives in this study: to determine (1) which test MVE(s) elicited maximal activity for each muscle tested and (2) whether specific test MVEs produced maximal muscle activity from more than one muscle. To minimize fatigue effects due to multiple MVE trials, while still evaluating a sufficient range of test postures, our study focused on evaluating two muscle groups.

METHODS

Sixteen right-hand dominant participants (8 male, 8 female) were included in this study. Bi-polar Ag-

AgCl Noraxon dual surface electrodes with a fixed 2cm spacing (Noraxon, Arizona, USA) were placed over four different right upper extremity muscle sites: anterior and middle deltoid, and pectoralis major: both clavicular and sternal insertions. Muscle activity for these sites was recorded using the Noraxon T2000 EMG system (Noraxon, Arizona, USA). EMG signals were bandpass filtered from 10-500Hz, and differentially amplified (common-mode rejection ratio >100 dB at 60Hz, input impedance 100MΩ) to generate maximum signal (in the range of the A/D board). EMG signals were A/D converted at 1500 samples/second using a 16 bit A/D card with a ±3.5V range. Participants completed 36 maximal exertions during a single experimental session. The postures tested were six combinations of shoulder flexion (45˚ and 90˚) and horizontal abduction (0˚, 45˚, 90˚). Hand forces were applied in two directions for each of the six arm postures: upward (with respect to gravity) and inward (medially across the body). Each test exertion condition was performed three times, resulting in 36 overall exertions. Subjects applied a power grip on a 2.5cm diameter handle mounted to a stationary pole. Each ramped exertion was five seconds long. Recorded muscle activity was linear enveloped, then a 500 msec moving average was applied, and a peak value was obtained from the resulting curve. A two-way repeated measures ANOVA was used to determine the effects of test position (angles of shoulder flexion and horizontal abduction) and test contraction direction (upwards or inwards) on peak muscle activity. A p-value of 0.05 was used to determine significant differences.

RESULTS AND DISCUSSION

Each muscle had significantly different peak muscle activity for multiple test MVEs. Additionally, each muscle achieved maximal activity in more than one tested exertion, meaning that two or more tested MVEs produced non-dissimilar maximal activities. Maximal activity occurred in the deltoid during several MVEs that incorporated upward force (Figure 1A) and in the pectoralis major for multiple MVEs that included inward force (Figure 1B).

Test exertions found to elicit maximal activity were similar to previous findings [2-3]. The test exertions that were found to obtain maximal activity from the deltoid in this research included the "90-90-UP" MVE which approximated the "full can" test; which elicited maximal activity from the deltoid in previous research [2]. However, this more systematic investigation determined that maximal activation can be achieved at intermediate locations as well as those determined in previous research. Additionally, these intermediate locations obtained maximal activity from more than one muscle. Thus, less test contractions were needed.

The motivation behind combining MVEs to get information for multiple muscles centers on fatigue avoidance. A lower number of test contractions minimize both subject discomfort and alterations in EMG signal (such as increased amplitude) that can be modulated by muscular fatigue [3]. As well, research has confirmed associations between fatigue and perceived pain and discomfort during endurance tasks [4]. Additional research is needed in this area to determine standard normalization postures for other muscles of the shoulder, which we did not evaluate. Although postures determined by the current study, as well as past research, may be adequate for obtaining maximal activity, the current lack of standardization when reporting results inhibits the comparison of specific magnitudes between studies.

CONCLUSIONS

It was determined that:

(1) statistically indifferent maximal activity levels existed for each muscle for multiple MVEs and

(2) that test exertions exist that can obtain maximal activity from multiple muscles.

The consistency of the postures found to maximize the electromyographic signal in our study with those suggested by previous research confirmed that various exertions elicit maximal activity levels. The possibility of extending this approach to reduce the number of MVEs performed exists if additional muscle combinations are examined.

REFERENCES

1.Bao S, et al. *J Electromyogr Kines,* **5**, 251–7, 1995.
2.Boettcher CE, et al. *J Orthopaed Res*, **26**, 1591-7, 2008.
3.Kelly BT, et al. *J Orthopaed Res,***14**, 647–53, 1996.
4.Garg A, et al. *Int J Ind Ergonom*, **30**, 103-113, 2002.

ACKNOWLEDGMENTS

NSERC of Canada partially funded this research.

A DEVICE TO QUANTIFY CYCLIC COMPRESSIVE LOADS APPLIED TO SOFT TISSUE FOR IN-VIVO ANIMAL MODELS

Thomas J. Cunningham[1], Timothy A. Butterfield[2]
[1]Department of Kinesiology and Health Promotion, College of Education, [2]Division of Athletic Training, College of Health Sciences, University of Kentucky, Lexington, KY
tim.butterfield@uky.edu

INTRODUCTION

Application of cyclic compressive loads during the manipulation of soft tissues, a primary characteristic of therapy generally referred to as massage, has been utilized as a clinical therapeutic technique for many years. An emerging area of interest concerns the application of compressive cyclic loads to exercised muscle tissue. Manipulation of this soft tissue during *in-vivo* animal trials has given some insight as to the potential acute effects of massage techniques when extrapolated to varying human conditions. Devices utilized in previous research to administer these loads [1,2] have been beneficial for uncovering these relationships. However, more accurate, reliable and versatile methods for force delivery and measurement are needed to address previous devices' limitations and further advance this line of research. A device is presented that can accurately quantify and replicate an entire spectrum of normal forces and frequencies typically seen in a multitude of clinical tissue manipulation techniques for *in-vivo* animal research.

METHODS

A spring loaded strut mechanism was designed to allow a cylinder to roll horizontally over a contoured mass of tissue. The cylinder displaced vertically in response to the normal force exerted upwards from the tissue during an oscillating movement, similar in concept to the actions of a suspension system in an automobile. Vertical displacement of the roller was resisted by two identical compressive springs which were attached to the struts suspending the roller's axle. The amount of preloaded force was adjusted by altering the initial deformation length of the springs using a rigidly fixed micrometer head with a stroke length of 25 mm and a resolution of .01 mm (MCLN12, Misumi, Addison, IL). A force transducer (SLB-25, Transducer Techniques, Temecula, CA) was mounted in series between the micrometer head and compression spring loading mechanism, allowing continuous readings of the normal force applied to the roller (Figure 1). The horizontal position of the roller system and subsequently the contact point of the roller was controlled using a linear actuator with a stroke length of 120 mm (402XET02, Parker Hannafin, Rohnert Park, CA) driven by a servo motor (BE232, Parker Hannafin, Rohnert Park, CA). Limitations of the system concerning positioning error and range of obtainable massage frequencies were considered negligible considering the capabilities of the equipment used. An isometric view of the total assembly can be seen in Figure 2A.

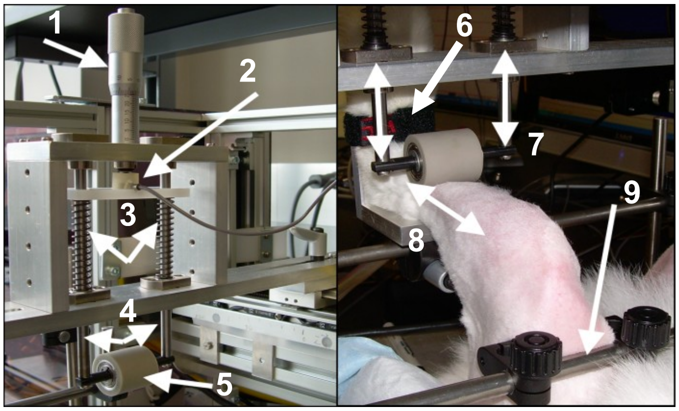

Figure 1: Spring loaded roller mechanism of the massage device (left) with anesthetized rabbit hindlimb (right). Mechanism's key aspects:

1. Vertically mounted micrometer
2. Force transducer mounted is series between the micrometer head and compressive springs (3)
4. Struts rigidly attached to the roller's axle and distal end of compressive springs
5. 25 mm diameter roller with Urethane coating of Asker C Hardness of 90 (type of roller adjustable)
6. Distal attachment pedal of the animal's hindlimb
7. Vertical movement constraint of the struts via flanged bearings
8. Horizontal movement of roller across the hindlimb
9. Proximal hindlimb positioning clamp.

Calibration of the spring loaded roller mechanism involved displacing the roller using a V-block mounted to a digital force gauge directly below the mechanism. (Figure 2A) The micrometer was incrementally adjusted 0.5mm throughout its full stroke range and the output voltage of the transducer and visual reading of the force gauge at each position was recorded.

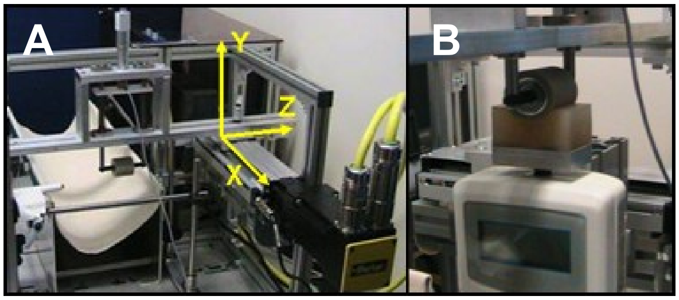

Figure 2: A) Isometric view of the entire device assembly. Movements for a given cycle are modeled as: $X(t) = A\sin((2\pi/T)t)$, $Z(t) = C$, $F(y(t)) = 2k(y_0 + y(t)) - mg - uF_y$ where A, C and T are constants. B) Calibration of strut assembly using a mounted digital force gauge.

An example of a typical data collection was conducted to demonstrate the force readings of the proposed device. The long axis of the tibialis anterior of a rabbit hindlimb was positioned and secured in the path of the oscillating roller. The roller oscillated over the muscle belly at a frequency of 0.5 Hz with an amplitude of 25 mm and initial force set at 7 Newtons (N) and progressing to 19 N at 2 N increments. Instantaneous forces during each cycle were collected at 1000 Hz and presented for qualitative comparisons.

RESULTS AND DISCUSSION

The springs used during this collection were determined to have a *k* value of 1.0478 N/mm and the minimum measureable force of the machine was 1.41 N (r=1). This minimum force limitation was due to the weight of the roller strut assembly (1.23 N) and the friction produced between the vertical struts and the flanged bearings. The device was considered capable of administering and measuring all desirable massage forces noting previous literature has shown a nominal force of 11.4 N has produced promising effects [3]. Data collected using one NZW rabbit can be seen in figure 3.

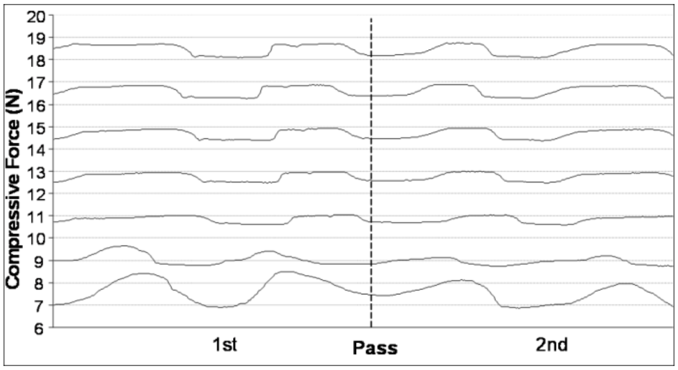

Figure 3: Forces administered to the rabbit's tibialis anterior muscle during two consecutive oscillations at 0.5 Hz.

A deviation of force was consistent at certain points during each cycle. This was attributable to the contours of the hindlimb being compressed in its secured position. Fluctuations were greater for cycles set at a relatively lower force. In this case, the roller was driven upwards over the muscle rather than at a heavier load where the roller compressed the soft tissue and fluctuated minimally. Care was taken when positioning the animal to assure the long axis of the limb was perpendicular to the axis of the roller. This limited the influence of rigid tissue such as bone and minimized undesirable spring deflection. Inherent in this system are fluctuations about a nominal force. The most observed range was 1.5 N in the lowest force setting. Not present was movement artifact at end positions. Both characteristics are substantial improvements of previously reported limitations [1,2].

These results indicate that the device presented has the ability to quantify compressive loads to soft tissues during cyclic motions. This device has addressed some of the previous challenges seen in similar research protocols. Future research involving this device will be able to more accurately evaluate the effects of force and frequency during massage movements in a variety of animal models.

REFERENCES

1. Butterfield TA, et al. *Med. Sci. Sports Exerc*. **40**, 1289-1296, 2008
2. Zeng H, et al. *J. Med. Devices* **2**,041003 1-8, 2008
3. Best TM, et al. *Clin J Sport Med* **18**, 446-460, 2008

CHANGES IN POSTURE DO NOT AFFECT THE FUNCTIONAL RANGE OF MOTION FOR THE PORCINE CERVICAL SPINE UNDER SHEAR LOADING

Samuel Howarth, Kaitlin Gallagher and Jack P. Callaghan
Department of Kinesiology, University of Waterloo, Waterloo, ON
E-mail: sjhowart@uwaterloo.ca

INTRODUCTION

The neutral zone of a vertebral joint for rotational loading (e.g. flexion-extension) has been defined as a region of minimal stiffness and can be an indicator of passive tissue injury [1]. Existence and quantification of a neutral zone under anterior/posterior shear loading remains unknown. Moreover, flexed and extended postures have been shown to change the size of facet gaps and stiffness properties of the vertebral joint [2,3] and may influence the shear neutral zone size, should one exist.

The goal of this study was to develop an objective method for quantifying the shear neutral zone as well as document the influence on the neutral zone length and stiffness of flexed and extended postures.

METHODS

Fifteen C34 and fifteen C56 osteoligamentous functional spinal units (FSUs) consisting of the intervertebral disc, the two vertebrae and all passive structures were excised from fifteen porcine cervical spines. Endplate cross-sectional area was calculated from measurements of the endplate depth and width while facet angles were quantified from an x-ray taken in the transverse plane (Table 1). Specimens were secured prior to testing in a custom set of aluminum cups with a combination of steel wire, screws and dental plaster (Denstone, Miles, IN, USA).

Table 1: Mean (standard deviation) disc cross-sectional area and facet angles.

	Level	
	C34	**C56**
Disc Area (mm^2)	646 (64)	691 (66)
Left Facet Angle (deg)	43.9 (4.2)	47.2 (2.8)
Right Facet Angle (deg)	44.0 (3.4)	49.8 (3.8)

A compressive preload of 300 N was applied with a servohydraulic material testing system (8872, Instron Canada, Burlington, ON, Canada) for 15-minutes while the external moments on the joint were minimized to define the specimen's neutral position. Following the preload, a flexion-extension passive test was performed to determine each specimen's neutral zone about the flexion-extension axis. Neutral position and the flexion and extension angles at the limits of the linear region from the neutral zone were the three postures used during subsequent passive anterior shear testing in random order.

A constant 300 N compressive load was applied throughout each shear passive test. Shear force applied to the inferior vertebra was measured during the passive tests by two uniaxial load cells (Transducer Technologies, Temecula, CA, USA) that were mounted in series with a pair of linear actuators (Tolomatic Inc., Hamel, MN, USA) driven by brushless servomotors (Danaher Motion Inc., Radford, VA, USA). Linear actuator displacement rate was controlled at 0.2 mm/sec for each passive shear test. Shear force and displacement were sampled at a rate of 7 Hz.

Each passive shear test began by setting the specimen's posture about the flexion-extension axis. Once the posture was set, the linear actuators were driven outwards (anterior shear) at the prescribed displacement rate. Applied shear force was continuously uploaded to a display that was monitored by the investigators. The target force was ±400 N for all passive tests that was approximately 14% of the ultimate shear failure load. Actuator velocity was reversed after achieving the target force and the specimen was then loaded to the target force in the opposite polarity (posterior shear). Five continuous cycles of anterior and posterior shear displacement to the target forces were performed.

The final three cycles were isolated and used for further analysis.

The point of minimum stiffness was determined by symbolically differentiating a 4th order polynomial fitted to the force-displacement relationship [4]. Endpoints of the neutral zone were defined as the displacement values corresponded to the inflection point stiffness and represented a change in stiffness of 4.5 N/mm from the inflection point stiffness. Neutral zone range and average stiffness across the neutral zone and hysteresis over the entire loading and unloading cycle were calculated.

A single factor (POSTURE) repeated measures analysis of variance (ANOVA) was conducted (SAS, Cary, NC, USA) following exclusion of any significant effects of vertebral level (C34 versus C56) on each of the dependent measures. Least significant difference post-hoc analyses were performed for any significant effect of posture. The level statistical significance was defined as $p < 0.05$.

RESULTS AND DISCUSSION

Average anterior shear neutral zone length was 1.33 mm and was not significantly influenced by posture ($p = 0.1485$, Figure 1). Hysteresis was not altered when the flexion-extension posture was changed ($p = 0.9864$).

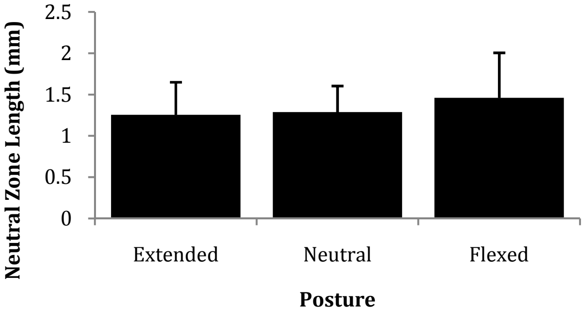

Figure 1: Neutral zone length in each posture.

A region on the shear force versus displacement relationship of nearly zero stiffness was not identifiable in any of the postures. The region isolated within the current investigation is better defined as a functional range of minimized resistance to anterior shear loading.

Passive tests performed in an extended posture produced higher stiffness within the functional range than tests performed in either the neutral or flexed postures ($p < 0.0227$, Figure 2). This is consistent with previous findings and is a consequence of increased facet contact area and decreased facet gap [2,5].

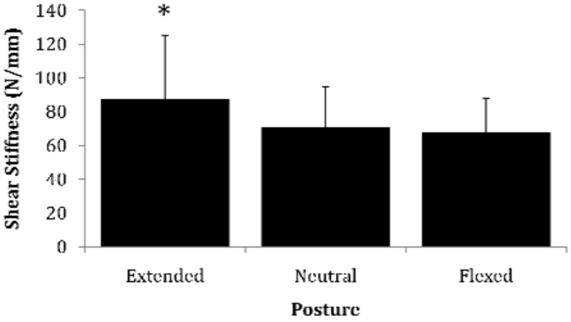

Figure 2: Average anterior shear stiffness within the region of minimized stiffness. The asterisk indicates that shear stiffness was largest in an extended posture.

CONCLUSIONS

A neutral zone consistent with a region of minimal stiffness (i.e. nearly zero) did not exist for shear loading of the porcine FSU. However, a range of motion was identified around a minimum point of stiffness that was not influenced by either flexed or extended postures. Stiffness across the functional range was larger in extended postures and is attributable to increased facet contact area and reduced facet gap. Future investigations should investigate changes in the shear functional range of motion with passive tissue injury in the spine.

REFERENCES

1. Oxland TR & Panjabi MM. *J Biomech* **25**, 1165-1172, 1992.
2. Yingling VR & McGill SM. *Spine* **24**, 1882-1889, 1999.
3. Drake JD, et al. *Spine* **33**, E728-E734, 2008.
4. Thompson RE, et al. *Clin Biomech* **18**, 89-98, 2003.
5. Dunlop RB, et al. *J Bone Jt Surg* **66B**, 706-710, 1984.

Endurance Time is Joint-Specific: A Modeling and Meta-Analysis Investigation

[1] Keith Avin, [2]Laura Frey Law
Graduate Program in Physical Therapy and Rehabilitation Science
The University of Iowa, Iowa City, IA

INTRODUCTION

Muscle fatigue is defined as "any exercise-induced reduction in the ability to exert muscle force or power, regardless of whether or not the task can be sustained" (1). This highly complex phenomenon has been the focus of countless investigations over several decades. However, little attention has been given to whether fatigue varies systematically between muscles about a given joint.

As contraction intensity increases, often standardized to maximum voluntary contraction (%MVC), endurance time (ET) decreases in a curvilinear fashion. This intensity-ET relationship is frequently referred to as Rohmert's curve (2). Despite the plethora of research on ETs for a static muscle contraction, this vast array of data has not been systematically analyzed to investigate 1) between-joint differences or 2) validate static intensity-ET models. Thus, the goals of this study were to: 1) perform a thorough systematic review of the literature to obtain all data related to sustained static contractions and their associated ET; 2) calculate empirically-derived models that demonstrate the negative decay which best fit the static fatigue ET and contraction intensity data; and 3) use these models to make joint-level comparisons, validated using traditional statistical meta-analysis comparisons. This information may prove beneficial for future applied fatigue research, ergonomic applications of digital human modeling, as well as clinical interventions of appropriate therapeutic dosing parameters.

METHODS

The authors performed a two-stage systematic review of literature pertaining to sustain static contraction until volitional failure in healthy, human subjects with a mean reported age between 18-50 years. Power and exponential functions were fit with their respective 95% Confidence Interval to the entire data set (generalized model), for each of the specific joints (i.e., ankle, back, grip, elbow, knee, and shoulder), and for specific joint torque directions (e.g. ankle plantar- and dorsi-flexion).

RESULTS AND DISCUSSION

The literature search resulted 180 articles meeting the inclusion criteria from a total of 15,210 potential publications. The numbers of studies per joint are as follows: Ankle (17), Back (20), Hand/Grip (38), Elbow (52), Knee (54), are Shoulder (11). The total sample sizes for each joint range from 32 to 834, and mean sample sizes ranged from 10.4 to 22.8 subjects per study, with a total of 349 data points.

The power function explained a greater portion of the data variance in all of the 7 models ($R^2 > 0.73$)(Fig.1). All 15 pairwise joint model comparisons were significant (standardized overlap < 0.59 between 95% CIs for joint-specific models, Fig 2).

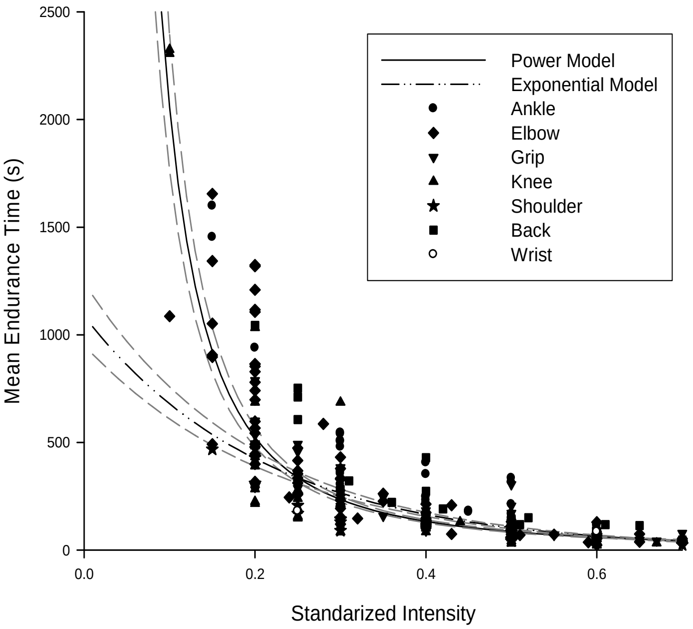

Figure 1: The general power (R^2 = 0.81) and exponential (R^2 = 0.78) static fatigue models are shown with their 95% confidence intervals (CIs) along with the entire data set (N=180 studies, 349 task intensities).

Although ET differences varied with intensity, the ankle was most fatigue-resistant, followed by the back, elbow, knee, and finally the shoulder was the most fatigable (Fig 2). Large effect sizes (> 0.8) were observed across 11 joint pairs, in particular for comparisons with the ankle (the most fatigue-resistant) and the shoulder (least fatigue-resistant). Ankle dorsiflexion and plantarflexion were not significantly different throughout the intensity range. Elbow flexion and extension models were only significantly different below 28% MVC, with flexion more fatigue resistant than extension. No other within-joint comparisons were performed due to lack of data available.

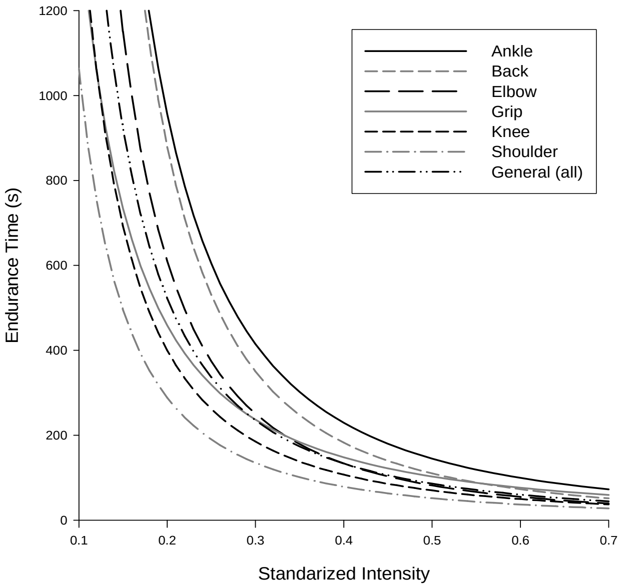

Figure2. Each joint-specific power fatigue model is plotted to demonstrate relative differences in fatigue resistance (ET) between each joint model as a function of contraction intensity (% MVC):

This is the first study to systematically compile data related to sustained static contractions to determine ET models as a function of intensity level, and compare them across joints and torque directions. The primary findings of this investigation are: 1) the compilation of studies reporting ETs for static contractions resulted in the power function being best able to predict 74-91% of the variance in the reported fatigue data across all intensities;
2) the joint-specific models indicate ET varies significantly between joints (e.g. ankle, back, elbow, grip, knee, and shoulder) as a function of contraction intensity; 3) statistical between-joint comparisons of the pooled fatigue data generally validate these model conclusions; and 4) the with-in joint antagonist comparisons (e.g. elbow flexion vs extension) were not able to consistently show significant differences in fatigue-resistance.

Future studies are warranted to better characterize model differences with specific population categories, such as males versus females, young versus old, and endurance-trained versus untrained individuals. Although these characterizations were beyond the scope of this work, they may have influenced the final models, as the distribution between each potential population category was not necessarily balanced (with the exception of no older adult populations included). For example, of the 115 fatigue data points for the elbow, 60 involved only men, 1 involved solely women, and 54 were mixed, including both men and women. Thus the resulting fatigue curves are likely to be influenced to a greater extent by men than women.

CONCLUSIONS

In summary, the power curves resulted in consistently higher R^2 values and a single generalized fatigue model does not adequately represent most individual joints. The underlying mechanisms contributing to these differences are not clear, but likely multifactorial. These findings may impact applied sciences such as rehabilitation and ergonomics, as well as future investigations of muscle fatigue. Indeed, fatigue development at one joint may not be representative of fatigue across all joints. Future studies on specific fatigue mechanisms may benefit from replication at multiple joints.

REFERENCES

1. Bigland-Ritchie B, and Woods JJ. *Muscle Nerve* **7**, 691-699, 1984.
2. Rohmert W. *Int Z angew Physiol einschl Arbeitsphysiol* **18**: 123-164, 1960.

ACKNOWLEDGEMENTS

Funding for this study provided in part by NIH NRSA 1 F31 AR056175-01 (K.A.), K12 HD055931 (L.F.L.), and USCAR, Dearborn, MI (L.F.L., K.A.).

Sensitivity Analysis of Loading Conditions on Mechanical Stiffness Measurements of a Passive Dynamic Ankle Foot Orthoses

[1] Kota Takahashi and [1] Steven Stanhope
[1]Human Performance Laboratory, Biomechanics and Movement Science, University of Delaware
email: ktaka@udel.edu

INTRODUCTION

Passive Dynamic Ankle Foot Orthoses (PD-AFO) are spring-like braces prescribed for patients with various gait impairments, including children with cerebral palsy, and patients recovering from stroke.

Using a novel automated fabrication method, McLucas et al. developed a PD-AFO consisting of footplate, strut, and cuff components (Figure 1). These AFOs can serve several functions: 1) help prevent foot drop during first rocker phase of gait, 2) store elastic energy during the second rocker phase as the subject's shank applies a force to the cuff surface, 3) release the stored energy to aid in forward propulsion during the third rocker phase.

The rate and magnitude of elastic energy storage supplied by the PD-AFO are influenced by the mechanical stiffness properties. Ultimately, the mechanical properties may predict the effectiveness of the orthotic during gait. Therefore, developing an accurate and reliable method for experimental stiffness measurements will be essential for adequate PD-AFO prescription.

Traditional assessment of AFO stiffness involves a linear approximation of the ratio of the externally applied moment to the angular deformation. Previous evaluations have been performed by various methods of external loading applications. These include a manual loading via custom-made apparatus [2], an automated loading about all three planes by a robotic device [3], and a loading by a muscle training device while a person's limb was fitted into an AFO [4]. Yet, there are no definitive methods for the most accurate and reliable methods.

The accuracy and reliability of stiffness estimates may depend on the ability to replicate loading conditions when a subject walks with the AFO. It is unknown whether certain loading techniques can influence the AFO stiffness.

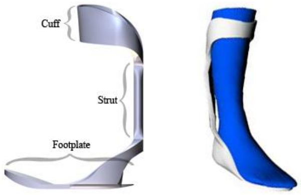

Figure 1: The PD-AFO components consist of footplate, strut, and cuff.

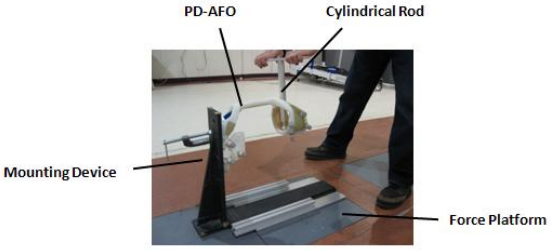

Figure 2: The footplate of AFO is mounted onto a vertical base plate. The entire mounting device is above a force platform. A cylindrical rod with a spherical tip is used to apply a force to the cuff surface, deforming the AFO into dorsiflexion.

The purpose of this study was to examine the sensitivity of different loading angles on the reliability of stiffness measurements. Specifically, the study analyzed the effects of altering the angle of force applied to the cuff on estimates of PD-AFO stiffness.

METHODS

A PD-AFO described by McLucas et al. was used for the stiffness analysis. The footplate of the AFO was mounted to a vertical base plate that was placed over a force platform (Figure 2). A custom-made cylindrical rod with a spherical end tip was used to manually apply a slow continuous force to the inner surface of the cuff, deforming the AFO into dorsiflexion. Retroreflective markers were placed on the cuff and the footplate, and the movement of the markers was measured using a motion capturing system. Under the assumption of rigid body segments, a three-dimensional angular deformation of footplate relative to cuff was measured using a Cardan X-Y-Z sequence (X-axis represents the flexion-extension axis). By subtracting the initial weight of the AFO and the mounting device, the ground reaction force signified the reaction force supplied by the AFO. The AFO moment about the X-axis was estimated using inverse dynamics under the assumption of static equilibrium. The stiffness was calculated by the slope of the linear fit of the sagittal plane components of the moment versus angular deformation (from 0 to 10 degrees) graph (Figure 3). A total of 17 trials were performed. For each trial, the load angle (angle of the force applied relative to the cuff segment) was varied to alter the amount of shear forces in the sagittal plane. The average load angle for each trial was calculated by measuring the angle of the ground reaction force relative to the cuff surface in the sagittal plane for the duration of the trial. The load angle is indicative of the magnitude of shear forces relative to the normal force. The load angle is 90 degrees when the applied force is purely normal to the cuff segment. An increase in shear forces directed away from the ankle joint center will result in an increase of the load angle, while an increase in shear forces directed towards the ankle joint center will result in a decrease of load angle.

RESULTS AND DISCUSSION

The experimental stiffness values of PD-AFOs are sensitive to the load angles. The AFO stiffness was as high as 3.20 Nm/deg, and was as low as 2.41 Nm/deg, depending on the load angles (Figure 4). The presence of shear forces directed towards the ankle joint center decreased the AFO stiffness, while shear forces directed away from the ankle joint center increased the stiffness.

Using the linear regression model shown on Figure 4, the stiffness when the load angle is 90 degrees can be estimated as 2.71 Nm/deg. For every one degree of deviation from 90 degrees, there is a 1.0% error in the AFO stiffness.

CONCLUSIONS

Our results indicate that altering the load angle on the cuff can modify the experimentally derived AFO stiffness. These results give valuable insights into designing a device for accurate and reliable stiffness measurements of PD-AFOs. Our goal is to devise an experimental method that replicates congruent loads and congruent deformations induced while a person walks with the AFO, such that the experimental stiffness values equate the stiffness supplied by the AFO during gait.

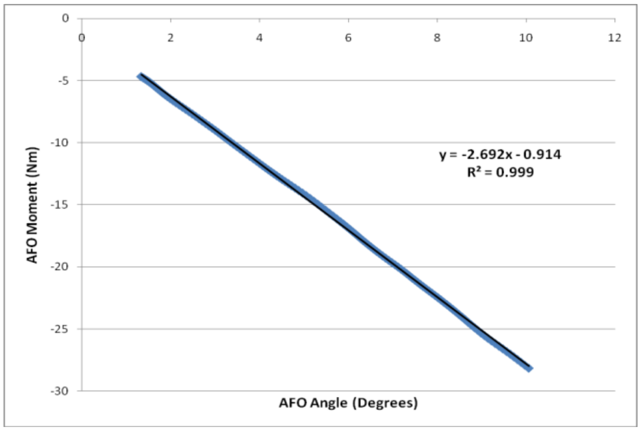

Figure 3: The stiffness of AFO is calculated by finding the linear best fit of the Moment vs Angle curve. Negative moment signifies a plantarflexion moment. Analysis was restricted to the sagittal plane.

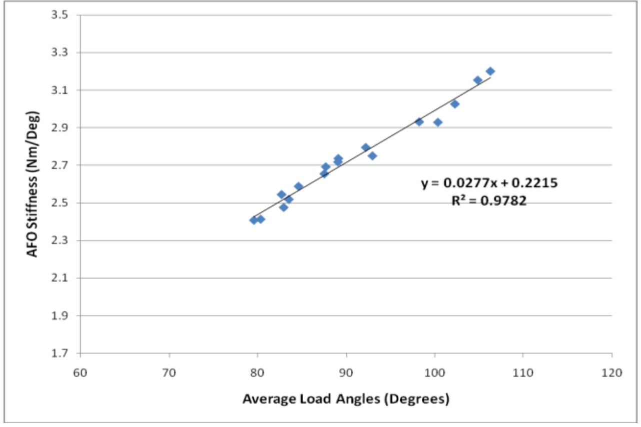

Figure 4: The effects of Load Angles on AFO Stiffness. As the Load Angle is increased (the force is directed more distally away from the Ankle Joint Center), the magnitude of stiffness increases.

REFERENCES

1. McLucas JL, et al. *The 12th World Congress of ISPO*, 2007.
2. Sumiya T, et al. *Prosthetic and Orthotics International* **20**, 132-137, 1996.
3. Cappa P, et al. *Journal of Biomechanical Engineering* **127**, 1025-1029, 2005.
4. Yamamoto S, et al. *Journal of Prosthetic and Orthotic* **5**, 59-64, 1993

CAPTURING WHEELCHAIR PROPULSION KINEMATICS USING INERTIAL SENSORS

Alexander W. Hooke, Melissa M.B. Morrow, Kai-Nan An, Kenton R. Kaufman
Biomechanics and Motion Analysis Laboratories, Division of Orthopedic Research
Mayo Clinic, Rochester, MN, 55906
E-mail: kaufman.kenton@mayo.edu

INTRODUCTION

Biomechanical assessments of wheelchair propulsion have largely occurred on a level, laboratory surface or on a stationary dynamometer enabling propulsion to be studied under standardized conditions. However, the most realistic method of assessing variables associated with wheelchair propulsion is to test users in their own wheelchair configuration while pushing in their natural environment. Dependence on camera-based motion capture systems has prevented previous studies from assessing upper extremity (UE) kinematics in the user's natural environment. With recent advances in kinematic measurement technologies, it is now possible to collect motion data outside the laboratory setting via inertial measurement units (IMUs). The IMU sensors comprised of an accelerometer, magnetometer, and gyroscope whose signals are fused together, yielding the 3D orientation of the sensor in space. IMUs are gaining popularity during the brief history since their inception, largely for the purpose of ambulatory motion capture [1, 2]. The goal of this study was to identify whether IMUs are capable of independently capturing accurate UE kinematics. This was done by comparing the joint angles calculated based on measurements recorded by the IMUs to those recorded by a camera based system (considered to be the gold standard).

METHODS

Three able-bodied subjects were recruited for this study. A total of 4 IMUs (XSens Technologies, NL) were mounted to each subject in the following locations: sternum, lateral-posterior right upper arm, distal, flat surface of right forearm, and distal, flat surface of right hand. Sensors were attached using double sided tape and foam athletic wrap with sensor alignment on each segment following the recommendations of Cutti, et al. (Figure 1) [1]. A marker set and model previously shown to capture accurate UE kinematics during wheelchair propulsion was also used as a kinematic gold-standard [3].

Anatomical systems of reference for the thorax and proximal humerus used ISB recommendations to describe humero-thoracic kinematics. Anatomical systems of reference for the distal humerus, forearm, and hand were defined functionally based on the flexion-extension and pronation-supination axes of the elbow and forearm and were used to describe elbow and wrist kinematics [4]. Joint angles between segments were calculated using Euler angle decomposition following ISB recommendations.

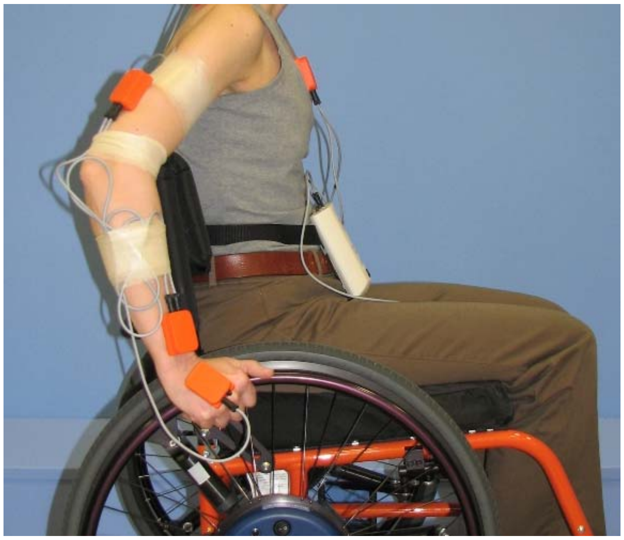

Figure 1: Experimental setup: IMUs are placed on the hand, forearm, upperarm, and thorax segments to measure UE kinematics. Reflective markers not shown.

The testing protocol consisted of collecting a 10 second static trial in which subjects sat upright in a wheelchair with arms at their sides. Functional tasks at the elbow were then performed. Subjects were instructed to flex-extend the elbow up to 130° five times while maintaining a constant pronation-supination angle with the humerus in neutral position. They were then instructed to fully pronate-supinate the forearm, keeping the elbow flexed at 90° and humerus in neutral position. Subjects then performed 3 trials of propelling the wheelchair approximately 10m through the lab's motion capture volume while kinematics from both systems were recorded. All data was normalized for a single wheelchair propulsion cycle.

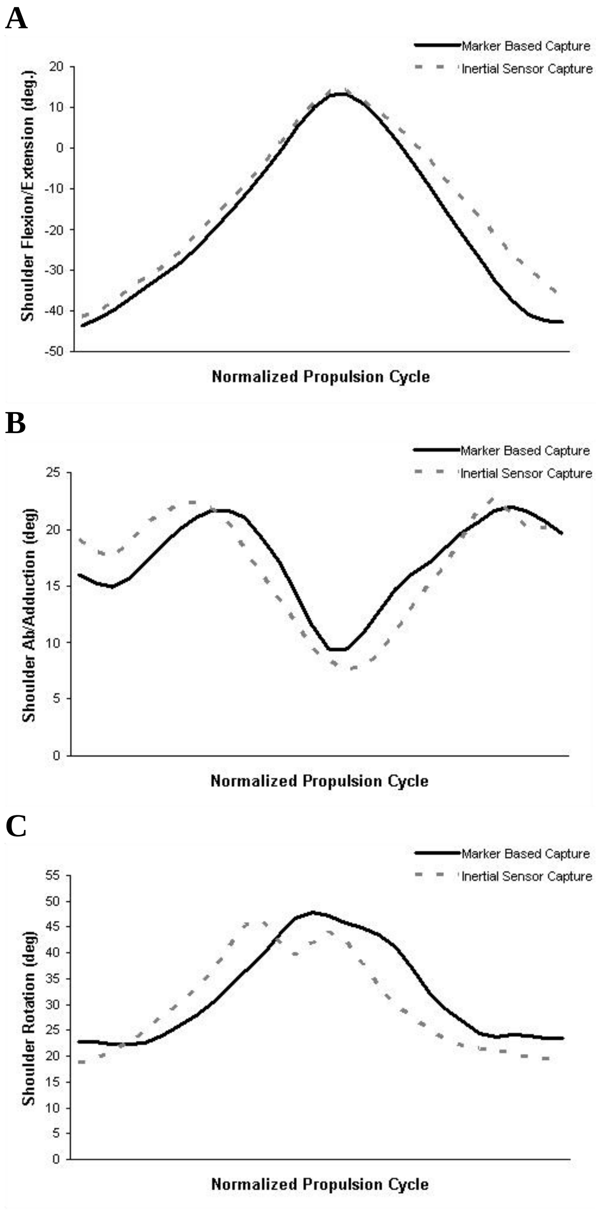

Figure 2: Comparison of shoulder intersegmental kinematics using camera-based and IMU capture systems during wheelchair propulsion across a level surface. A) Flexion/Extension B) Ab/Adduction C) Rotation

RESULTS AND DISCUSSION

The validity of the UE kinematics captured using the IMU system was compared to the UE kinematics captured by the camera-based system (Figure 2). The RMS error values for the shouder, elbow, and wrist joint were less than 5 degrees (Table 1).

Joint	Axis	RMS Error (°)
Shoulder	Flex/Ext	3.97 (1.83)
	Ab/Adduction	2.88 (1.58)
	Int/Ext Rotation	3.6 (1.83)
Elbow	Flex/Ex	4.72 (2.19)
	Pro/Supination	3.54 (1.58)
	Carry	3.78 (1.62)
Wrist	Flex/Ext	4.11 (1.99)
	Ab/Adduction	5.23 (3.00)

Table 1: RMS error (standard error) of IMU motion capture system for UE kinematics during wheelchair propulsion

CONCLUSIONS

There are differences in UE kinematics when using an IMU compared to a passive camera-based system. However, these errors are not clinically significant. This indicates that with further development, an IMU system shows promise for community-based kinematic data collection.

REFERENCES

1. Cutti, A.G., et al. *Med Biol Eng Comput* **46**, 169-178. 2008.
2. Zhou, H. and H. Hu. *Sensor Review*, **27**, 151-158. 2007.
3. Morrow, M.M., et al. *J Electromyogr Kinesiol* **In press**, 2009.
4. Woltring, H.J., et al. *J Biomech* **27,**1415-32,1994.

ACKNOWLEDGEMENTS

Work supported by NIH Grant Number R01 HD 48781.

INFLUENCE OF FOOT-FLOOR FRICTION COEFFICIENT ON THE PASSIVE RESPONSE TO SLIP DURING WALKING

[1]Arash Mahboobin, [1]Rakié Cham, and [2]Stephen J. Piazza
[1]University of Pittsburgh, Pittsburgh, PA, [2]Pennsylvania State University, University Park, PA
Email: arm19@pitt.edu

INTRODUCTION

Falls initiated by slips and trips are a serious health hazard to older adults. Experimental studies have provided important descriptions of postural responses to slipping, but the causes of failed recovery attempts are difficult to determine from experiments alone. Computational modeling and simulation techniques can complement experimental approaches to identify both the causes of falling and fall recovery strategies.

In moderate and severe slips that occur at or shortly after heel contact of the stance leg, an active response generated in the leading/slipping leg is needed to prevent a fall [1]. This response consists of a flexion moment and an extension moment at the knee and hip, respectively, and these corrective moments are in general triggered about 150 to 200 ms after heel contact [1].

The purpose of this study is to determine the impact of a systematic reduction in the foot-floor friction coefficient (μ) on the kinematics of walking shortly after heel contact (150 ms after heel contact), i.e. when the effects of the active corrective moments previously mentioned do not play a major role in the dynamics of walking. The relevance of the potential findings of this work is at least two-fold. First, the findings may provide insights into the active corrective moments needed to prevent a fall. Specifically, it is expected that as μ is reduced, body kinematics will diverge from normal/slip-resistant gait. A greater difference in the body kinematics between the dry and slip simulations implies a greater need for an early and larger corrective response to prevent a fall. Second, the data generated in these simulations may have important implications in safety-related research, specifically in the design of slip-resistant shoe and flooring environments.

METHODS

Normal walking kinematics and bilateral ground reaction forces were collected for a healthy male subject (age=25 yrs., mass=69 kg, height=170 cm). Following the normal walking, a glycerol solution was applied onto the floor to generate an unexpected slip at heel contact of the left foot (leading/slipping leg).

A 2-D musculoskeletal model was developed in OpenSim [2] and used to obtain a kinematically-consistent set of joint angles and moments of normal gait using the measured motions and ground reaction forces. The model was composed of 10 segments: torso, pelvis, left/right thigh, left/right shank, left/right rear-foot, and left/right toe. The model was constrained to the sagittal plane, and incorporated 12 degrees-of-freedom (DOF).

Forward-dynamic simulations incorporating foot-floor interaction were created using SIMM/Dynamics Pipeline (MusculoGraphics, Inc.) and SD/FAST. Contact between the feet and the floor was modeled using the spring-based contact that is based on the scheme described by Neptune et al. [3] and which includes friction. A quasi-Coulomb friction model was used in which highly viscous damping was applied when sliding velocities were small and friction forces proportional to normal forces ($F_f = \mu N$) were applied otherwise. A hard-sole shoe used in our experiments was scanned and incorporated in the model to aid in spring placement. Contact elements (46 per foot), spaced 2 cm apart, were placed along the plantar surface of each foot segment.

A parameter optimization was performed in which the set of joint moments was found that minimized the squares of the differences between measured and simulated joint rotations and measured ground reaction forces. The optimization was accomplished using a hybrid of particle swarm [4] and Nelder-Mead downhill simplex [5] methods. Finally, after establishing a simulation that satisfactorily tracked normal walking, slip was simulated by reducing the frictional forces applied to the leading foot (i.e., by reducing μ). The applied joint moments remained the same as in the normal (dry) gait simulation.

RESULTS AND DISCUSSION

As expected, during the early stance period (~150 ms) following heel contact, the difference in walking kinematics between the normal gait and slip simulations increased with smaller μ values (Figure 1). Specifically, applying the required joint moments needed in normal/dry walking in simulations with values of $\mu \geq 0.25$ resulted in only a minor deviation in gait kinematics from the dry condition, based on the RMS error (computed from 0-150 ms) of 1.7º and 3.5º for the hip and knee angles of the leading leg, respectively. In contrast, the simulation findings indicate that walking with normal/dry joint moments in environments characterized by μ values less than 0.25 will result in body kinematics that will be significantly different from normal/dry gait patterns (RMS error > 5º). Additionally, as μ is reduced, the slip simulations will result in earlier perturbed gait kinematics in stance (Figure 1). These findings imply the need for early and appropriate active corrective responses to prevent a fall, especially in slippery environments with μ values less than 0.25. Experimentally, it has been shown that the required friction for non-slip gait ranges from 0.17 to 0.22 [6]. Our simulation findings nicely agree with these results.

Implementation of physiologically relevant controllers to generate active corrective responses [1] to external perturbations will be addressed in our future work.

REFERENCES

1.Cham R and Redfern MS. *J Biomech* **34**, 1439-45, 2001.
2.Delp SL, et al. *IEEE T Bio-Med Eng* **54**, 1940-1950, 2007.
3.Neptune RR, et al. *Comput Meth Biomech Biomed Eng* **3**, 321-34, 2000.
4.Kennedy J and Eberhart, R. *Proceedings of the IEEE International Conference on Neural Networks*, Piscataway, NJ, 1995.
5.Press WH, et al. *Numerical Recipes in C: The Art of Scientific Computing*. Cambridge University Press, Cambridge, 1988.
6.Redfern MS, et al. *Ergon* **44**, 1138-1166, 2001.

ACKNOWLEDGEMENTS

Funding provided by NIOSH (R01OH007592).

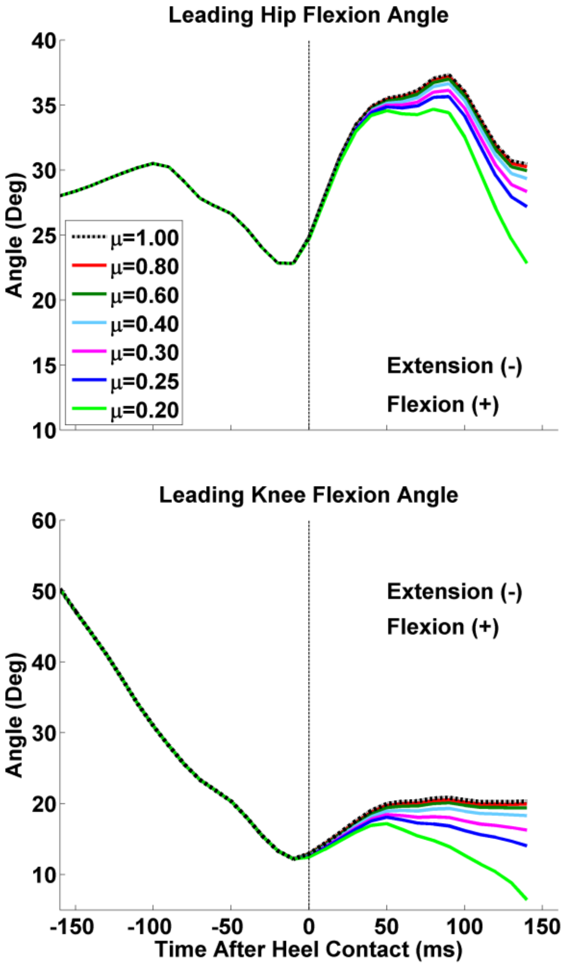

Figure 1: Leading/slipping hip and knee flexion angle comparisons between dry (dotted-dashed line) and slip simulations. The vertical line at 0 ms indicates onset of heel contact. Note that for values of $\mu \geq 0.25$, the model is capable of producing consistent gait patterns that are similar to the dry condition, only utilizing normal gait moments. At the later stages of stance, the kinematics on slippery floors diverge from the dry condition (not plotted here), indicating the need for active corrective moments.

THE EFFECTS OF MORTON'S EXTENSION INSERTS ON PLANTAR LOADING PATTERNS, PAIN, AND FUNCTION IN INDIVIDUALS WITH HALLUX RIGIDUS

[1] Kristin K. Morris, [1]Josh M. Tome, [2]Amar Patel, [2]Judith F. Baumhauer, [1]Deborah A. Nawoczenski
[1]Ithaca College Movement Analysis Lab, Center for Foot and Ankle Research
[2]Strong Orthopaedics Foot and Ankle Clinic
email: dnawoczenski@ithaca.edu

INTRODUCTION

Hallux rigidus (HR) is characterized by a progressive loss of motion at the first metatarsophalangeal (MTP) joint secondary to osteoarthritic changes and proliferative bony response. Hallux rigidus is the second most common disorder of the great toe and affects one in 45 people over the age of 50[1]. Aside from osteoarthritic changes and a loss of motion, patients with hallux rigidus demonstrate altered kinematics and plantar loading patterns, increased pain, and decreased function [2-4]. While surgical outcomes have been favorable, conservative care is the first line of treatment. Conservative care may include steroid injections, non-steroidal anti-inflammatory drugs, modalities, and activity modification, shoe adjustments, and most often orthoses [5]. Although the most common of interventions, the mechanisms by which orthoses are effective have not been well documented. Morton's extension inserts are one type of orthosis that include a characteristic rigid extension of the footplate beneath the great toe, which purportedly reduces pain and inflammation by altering motion and plantar loading patterns.

The first purpose of this study is to determine what loading patterns are characteristic of subjects with HR when compared to age and BMI matched controls. The second purpose is to determine the effect of a Morton's extension insert on plantar loading patterns, pain, and function in persons with hallux rigidus.

METHODS

All procedures were approved by Ithaca College and University of Rochester Institutional Review Boards. Thirty-two subjects participated in this study; 16 patients diagnosed with stages I-III HR (age 57.2 ± 7.7 years, BMI 25.8 ± 4.2) were recruited from the Foot and Ankle Clinic at Strong Orthopaedics and matched for age and BMI with 16 control subjects without foot pathology. Maximum mean pressure (MMP) and pressure time integrals (PTI) were collected with the Pedar® in-shoe pressure measurement device as subjects walked in his/her personal footwear. For the subjects with HR, the Foot Function Index- Revised (FFI-R) was used to document pain and function before and after a six week intervention wearing the Morton's extension. Repeated collection of pressure data was performed at the six week follow up. Appropriate t-tests and ANOVA with Bonferroni adjustment were used to compare regional loading patterns between controls and subject with HR, as well as to assess the effect of the orthotic condition on regional loading distribution between lateral metatarsals (MT3-5) relative to medial metatarsals (MT1-2), as well as the hallux relative to MT1-2 for each of the dependent variables.

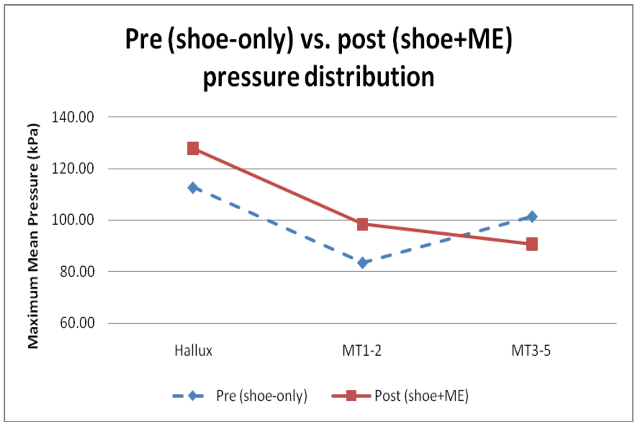

Figure 1: Demonstrates shift of maximum mean pressure (MMP) medially after six week intervention. ME=Morton's extension

RESULTS AND DISCUSSION

Significant differences in plantar loading patterns were found between subjects with HR and matched controls. Subjects with HR demonstrated reductions in MMP under MT1-2 (83.5 and 102.3 kPa, HR and control respectively, p=.03); additionally, MMP was increased under the lateral metatarsals in relationship to the medial metatarsals (MT3-5:MT1-2) when compared to the control group (1.3 and 0.9 HR and control respectively, p<.01). No significant differences were seen under the hallux (p=.56).

The 6-week intervention with the Morton's inserts resulted in significant changes in FFI-R scores. Subjects with HR reported a reduction in the pain subscale (pre 37.9, post 28.6, p<.01), disability subscale (pre 40.1, post 31, p=.02), and total score (pre 32.8, post 26.7, p<.05) of the FFI-R. Plantar loading patterns indicated a medial shift after wearing the insert when compared to pre intervention, shoe-only condition (Table 1). MMP and PTI were significantly increased under MT1-2 and hallux regions. Although the magnitude of reduction of the MMP under MT3-5 was not significant (p=.07), the loading distribution between adjacent forefoot regions MT3-5:MT1-2 indicated a significant shift of pressures to MT1-2 (P<.001) (Figure 1). It is interesting to note that the pressure distribution shifted medially to resemble that of the control group.

The alteration of loading patterns that appear to normalize following use of the Morton's extension insert may be helpful in preventing secondary complications of the knee and hip frequently observed in this patient population.

CONCLUSIONS

When compared to control subjects, subjects with HR demonstrate a loading pattern of decreased medial and increased lateral forefoot pressure. This finding is similar to that found in a study by Van Geluwe, who examined individuals with asymptomatic static and functional hallux limitus [4]. However, unlike their subjects, ours with symptomatic HR did not demonstrate an increase in loading of the hallux relative to the medial forefoot. After using the Morton's extension insert, our subjects demonstrated a medial shift of plantar pressures. They also showed improvements of approximately 25% in FFI-R pain and disability subscales, which may be secondary to differences in loading patterns seen after intervention with the Morton's extension.

To our knowledge, this is the first case series to evaluate the plantar loading and functional changes following use of an orthotic intervention for subjects with HR. The Morton's extension is an inexpensive, over-the-counter intervention, and therefore may be a viable conservative treatment alternative to surgical intervention. Further studies are under way to assess the longer term benefits of this intervention.

REFERENCES

1. Shereff M, et al. *J Bone Jt Surg* **80-A**(6), 898-908, 1998.
2. Canesco K, et al. *J Orthop Res* **26,** 419-427, 2008.
3. Nawoczenski DA, et al. *Foot Ankle Int* **29**(3), 265-272, 2008.
4. Van Gheluwe B, et al. *J Am Podiatr Med Assoc* **96**(5), 428-436, 2006.
5. Grady J, et al. *J Am Podiatr Med Assoc* **92**(2), 102-108, 2002.

ACKNOWLEDGEMENTS

This work is supported in part by the American Orthopaedic Foot and Ankle Society.

Table 1: Group mean ± standard deviation in each region. P<.05 significant. ME=Morton's extension

	MMP (kPa)			PTI [(kPa)*s]		
	Pre (shoe-only)	Post (shoe+ME)	P value	Pre (shoe-only)	Post (shoe+ME)	P value
MT1-2	83.5±21.1	98.4±24.3	0.00	43.1±15.9	53.8±16.7	0.00
MT3-5	101.4±24.7	90.7±18.2	0.07	63.1±19.2	56.9±16.1	0.04
Hallux	112.6±35.9	127.9±39.7	0.01	49.2±15.6	65.1±26.5	0.00
MT3-5:MT1-2	1.3±0.3	1.0±0.2	0.00	1.6±0.6	1.1±0.1	0.00
Hallux:MT1-2	1.4±0.5	1.4±0.8	0.82	1.2±0.5	1.3±0.6	0.73

DIMENSIONAL ACCURACY OF AN AUTOMATED ANKLE FOOT ORTHOSIS FIT AND MANUFACTURING PROCESS

[1]Elisa Schrank and [2,1]Steven Stanhope
[1]Department of Mechanical Engineering, University of Delaware,
[2]Department of Health, Nutrition and Exercise Sciences, University of Delaware
email: schranke@udel.edu

INTRODUCTION

Passive-dynamic ankle foot orthoses (PD-AFOs) constitute a class of ankle braces that provide plantar flexion assistance by replicating a patient's muscle function via a spring-like action. Traditionally, customized PD-AFOs are fabricated by an orthotist through a laborious process that involves creating a negative mold of the patient's foot and shank, generating a positive mold, manually fabricating the AFO around the positive mold, and finally refining and fitting the AFO by hand.

Computer aided design (CAD) enables the virtual modeling, analysis, and design modification of physical parts. CAD models can be fabricated via selective laser sintering (SLS), a rapid freeform manufacturing technique [2]. Parameterization of a CAD model can be used for the automated size and shape (fit) and function customization of parts. Darling et al. reported a semi-automated orthosis customization process that drove a parameterized orthosis model with patient-specific imaging data [1]. However, this design was primarily scaled to accommodate the subject size and shape and lacked the organic shape characteristics typically associated with manually fabricated orthotics.

We have developed the framework of an automated fully-customized PD-AFO design process (Figure 1), which describes a method for rapidly customizing and manufacturing a fit- and function-customized PD-AFO. This paper focuses on a sub-method within that process. Our automated fit customization and manufacturing method, which is driven by palpable anatomical landmark locations, utilizes the power of CAD and CAD-integrated parameterization to rapidly customize the fit characteristics of a PD-AFO.

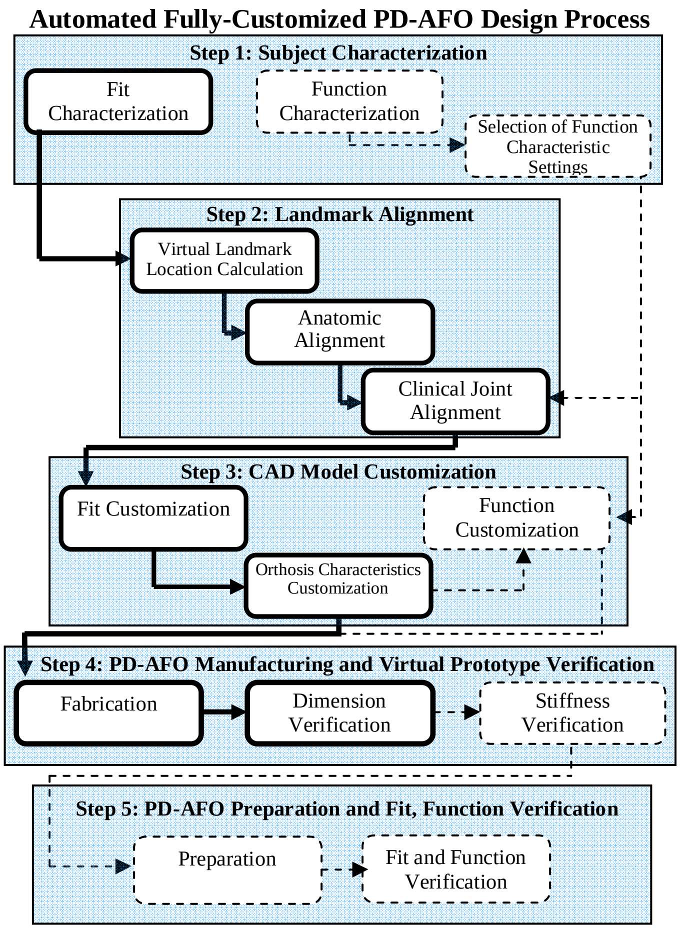
Automated Fully-Customized PD-AFO Design Process
Step 1: Subject Characterization
Fit Characterization
Function Characterization
Selection of Function Characteristic Settings
Step 2: Landmark Alignment
Virtual Landmark Location Calculation
Anatomic Alignment
Clinical Joint Alignment
Step 3: CAD Model Customization
Fit Customization
Function Customization
Orthosis Characteristics Customization
Step 4: PD-AFO Manufacturing and Virtual Prototype Verification
Fabrication
Dimension Verification
Stiffness Verification
Step 5: PD-AFO Preparation and Fit, Function Verification
Preparation
Fit and Function Verification

Figure 1: Automated fully-customized PD-AFO design process flow chart with the automated fit customization and manufacturing method in bold.

METHODS

The automated fit customization and manufacturing method consisted of eight steps (Figure 1, bold outlines). Completion of the process resulted in a dimension-verified PD-AFO with fit-customized footplate, cuff and strut components (Figure 2a).

Fit characterization: The standing subject (height 1.77m; mass 71.8kg) was instructed to remain motionless while the 3D locations of 44 landmarks were digitally acquired, or digitized, using a 3D

Fusion FaroArm (±.036mm accuracy; FARO Technologies Inc., Lake Mary, FL) and recorded in Geomagic Studio 9 (Geomagic, Inc., Research Triangle Park, NC). Three ground landmarks established a ground plane coincident with the foot's plantar surface. Seventeen anatomical landmarks were identified by palpation. Twenty-four cuff landmarks were identified by a cuff template scaled based on shank length and circumference and positioned by a clinician.

Virtual landmark location calculation: The 3D locations of three virtual landmarks (ankle and knee joint center, ankle joint projection onto ground plane) that could not be digitized were calculated and virtually created.

Anatomic alignment of landmarks: The digitized and virtual landmarks were transformed from the world coordinate system, automatically established during digitization, to an anatomically-relevant joint coordinate system, based on the foot and shank.

Clinical joint alignment of landmarks: Custom-written MATLAB® (The MathWorks, Inc., Natick, MA) scripts were used to calculate the 3D angular deviations of the ankle joint from an anatomically neutral ankle position and then used to rotate the landmarks to into a desired position (neutral).

CAD model fit and orthosis characteristics customization: The parameterized PD-AFO CAD model was constructed in Autodesk Inventor Professional v11 (Autodesk, Inc., San Rafael, CA). The 3D locations of the clinically-aligned landmarks served as the initial parameters used to customize the model's three major components. A footplate profile made of 2D splines that connected the digitized anatomical landmarks on the foot perimeter controlled the footplate shape. The interior cuff surface was formed by 4 rows of lofted 3D splines connecting the digitized cuff landmarks. The strut was sized as a function of shank length and shaped by 11 parallel, lofted, 2D profiles. The footplate, cuff, and strut were connected by a set of lofted upper and lower spans. Additional customization included footplate and cuff thicknesses, footplate and cuff padding offsets, and a strut offset. Finally, strategically-located 3mm hemispherical dimples were added to the model to enable subsequent dimension verification.

PD-AFO fabrication and dimension verification: Four PD-AFOs with varying build orientations were fabricated via SLS. The FaroArm, with a 3mm spherical-tipped probe, was used to measure 11 select inter-dimple distances (centroid to centroid) on the fabricated PD-AFOs. Dimension measurements were averaged over the four PD-AFOs and compared to the CAD model dimensions. The maximum difference, mean difference, and standard deviation were calculated.

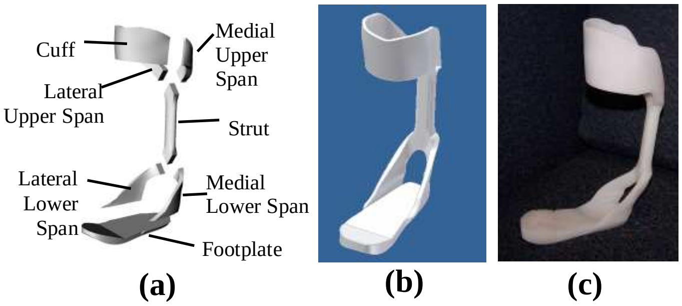

Figure 2: (a) PD-AFO components. (b) Fit-customized PD-AFO CAD model. (c) Fabricated PD-AFO.

RESULTS AND DISCUSSION

A PD-AFO CAD model was customized for a healthy male subject (Figure 2b). The landmarks were rotated 3.1°, 1.7° and 4.5° in the plantar flexion, valgus, and adduction directions, respectively, to align the ankle joint into the neutral position. The PD-AFOs were fabricated in less than 24 hours and had excellent dimensional accuracy (max difference = 0.975mm; mean difference = 0.284mm; SD = 0.280mm) (Figure 2c).

This study demonstrates excellent dimensional accuracy of the ankle foot orthosis fit and manufacturing process. In addition to fit customization, the automated fully-customized PD-AFO design process incorporates customization and tuning of PD-AFO function characteristics.

REFERENCES

1. Darling AL, et al. *Appl Bion Biomech* **3(2)**, 93-9, 2006.
2. Faustini MC, et al. *IEEE Trans Biomed Eng*, **55(2)**, 784-90, 2008.

ASSOCIATIONS BETWEEN FORCE STEADINESS AND TESTS OF HAND FUNCTION ACROSS THE ADULT LIFE SPAN

Adam R. Marmon, Michal A. Pascoe and Roger M. Enoka
University of Colorado, Boulder; Department of Integrative Physiology

INTRODUCTION

As older adults are usually weaker [1, 3, 4] and less steady than young adults [1, 2, 5], measures of strength and steadiness are frequently used as indices of motor function. However, there are relatively few studies about the associations between these indices and performance on functional hand tests. The aim of the study was to evaluate the relations among measures of isometric hand strength, force steadiness, and hand function.

METHODS

Seventy-five healthy men and women (30 men; 19 - 89 yrs) were assigned to one of three groups; young (19-36 yrs), middle-aged (41- 59 yrs), and old (66-89 yrs). Each subject performed 3 strength measures, 2 force steadiness tasks, and 4 functional hand tests with the dominant and non-dominant hands. The strength measures comprised maximal voluntary contractions during index finger abduction, precision pinch, and handgrip. The steadiness measures involved isometric contractions during which hand muscles exerted an abduction force with the index finger and a precision pinch with the index finger and thumb (Figures 1A and B). The target force for the steadiness tasks was 5% of maximum and the contraction was held for 60 s. Subjects received intermittent visual feedback during each 60-s trial (5 s with, 5 s without). The functional tests included manipulating small metal pegs into a board with holes cut out (Grooved Pegboard Test), removing small plastic pieces from a game board using tweezers (Operation^{TM}), a scissor task (Star Cutout), and tracing a 4-revolution spiral with a pen (Archimedes Spirals) (Figures 1C- F).

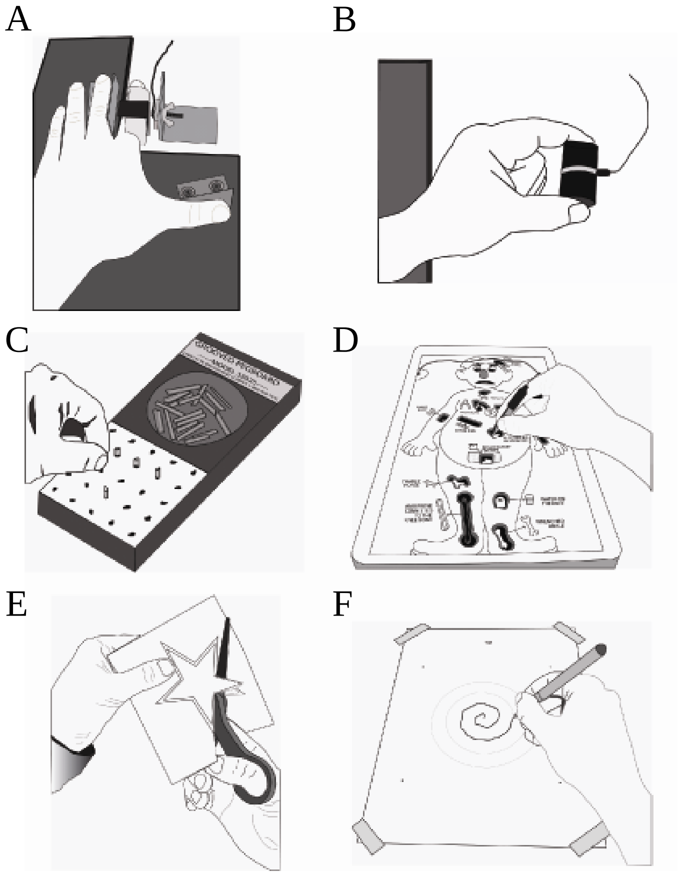

Figure 1. Experimental set-ups for hand steadiness and function. Steadiness; index finger abduction (A) and precision pinch (B). Function; Grooved Pegboard (C), Operation^{TM} (D), Star cutout (E), and Archimedes Spirals (F).

RESULTS AND DISCUSSION

Significant differences were observed between young and old adults for all strength, steadiness and functional tests (Table 1). Middle-aged and old adults differed for grip strength, both steadiness measures with feedback provided, and all functional tests except the errors in matching the Archimedes Spirals. Middle-aged and young adults only differed significantly for grip strength, pinch steadiness, and Grooved Pegboard ($p < 0.05$).

Multiple regression models and partial correlations were calculated using strength and steadiness measures to predict functional performance (Table 2). The strongest associations were found between steadiness and performance on both the Grooved Pegboard test and the game Operation^{TM}. Significant regression models for the Grooved Pegboard showed performance time could be predicted by index finger steadiness and grip strength (R^2= 0.36; p< 0.001). Performance on the game Operation^{TM} was significantly predicted by pinch steadiness, grip strength, and index finger steadiness (R^2= 0.40; p< 0.001).

CONCLUSIONS

These findings indicate that the physiological mechanisms responsible for differences in performance on some tests of hand function are related to the steadiness of submaximal isometric contractions. However, only about 36% of the variability in performance on the Grooved Pegboard and 40% of the variability in performance in the game of Operation^{TM} were related to measures of hand strength and steadiness.

REFERENCES

1. Galganski M, et al. *J Neurophysiol* **69,** 2108-15, 1993.
2. Graves AE, et al. *J Neurophysiol* **83**, 2030-39, 2000.
3. Klein CS, et al. *Muscle Nerve* **28**, 62-8, 2003.
4. Porter MM, et al. *Can J Appl Physiol* **20**, 429-39, 1995.
5. Tracy BL and Enoka RM. *J Appl Physiol* **92**, 1004– 12, 2002.

ACKNOWLEDGEMENTS

Supported by NIA AG09000.

Table 1. Descriptive statistics for the measures of strength, steadiness, and function for the three groups of subjects.

	Young	Middle-aged	Old
Age (yrs)	25.8 ± 4.3	50.6 ± 5.5	74.5 ± 6.2
Grip strength (N)	350 ± 90	297 ± 98	*244 ± 73
Pinch strength (N)	49.5 ± 12.3	43.5 ± 16.3	*40.6 ± 11.4
FDI strength (N)	32.4 ± 9.6	30.1 ± 10.5	*26.0 ± 7.9
Pinch steadiness (%)	1.4 ± 0.4	1.8 ± 0.7	†*2.2 ± 0.8
FDI steadiness (%)	2.2 ± 0.9	2.7 ± 1.1	†*4.7 ± 2.9
Archimedes spiral (mm)	0.40 ± 0.09	0.49 ± 0.21	*0.71 ± .84
Operation^{TM} (score)	9.24 ± 1.8	8.52 ± 2.0	†*6.08 ± 2.1
Pegboard (s)	59.3 ± 6.0	*65.7 ± 8.6	†*88.9 ± 15.7
Star cutout (errors)	1.72 ± 2.3	1.84 ± 2.0	†*3.0 ± 2.6

Data are mean ± SD. The two steadiness measurements correspond to coefficients of variation for force (%). * p< 0.05 compared with young adults. † p< 0.05 compared with middle-aged adults.

Table 2. Multiple regression predictions of two measures of hand function (Pegboard and Operation^{TM}).

		Strength			Steadiness	
	Overall Prediction	Grip	Pinch	FDI	Pinch	FDI
Pegboard	0.36	**-0.34**	-0.20	-0.25	0.46	**0.57**
Operation ^{TM}	0.40	**0.45**	0.36	0.39	**- 0.57**	**-0.47**

The data indicate the overall prediction (R^2) of each equation (row) and the relative associations (r; part correlations) of the significant predictors for the performance on the Grooved Pegboard and Operation^{TM} tests (p< 0.001). The variables used in the multiple regression models to predict functional performance are bolded.

PATELLOFEMORAL JOINT KINETICS DURING FORWARD STEP-UP, LATERAL STEP-UP AND FORWARD STEP-DOWN EXERCISES

[1] Chatchada Chinkulprasert, [2] Roongtiwa Vachalathiti, [3] Christopher M Powers

[1, 2] Faculty of Physical Therapy and Applied Movement Science, Mahidol University, Salaya, Phuttamonthon, Nakhon Pathom, THAILAND, [3] Jacquelin Perry Musculoskeletal Biomechanics Research Laboratory, Division of Biokinesiology and Physical Therapy, University of Southern California, Los Angeles, CA, USA

email: chatcha@swu.ac.th, chinkulp@usc.edu

INTRODUCTION

Stepping exercises are commonly prescribed exercises for persons with patellofemoral pain (PFP) [1,2,3]. Appropriate rehabilitation exercises for persons with PFP should emphasize appropriate lower extremity muscle training without increasing symptoms. To that end, specific exercises for PFP should minimize patellofemoral joint loading and stress.[2, 4] To date, few studies [5-7] have investigated patellofemoral stress during various rehabilitation exercises (i.e. squatting and non-weight bearing knee extension). The purpose of this study was to characterize patellofemoral joint kinetics during forward step-up (FSU), lateral step-up (LSU) and forward step-down (FSD) exercises in healthy individuals.

METHODS

Three-dimensional lower extremity kinematics and electromyographic (EMG) activity of the knee muscles were obtained from 19 healthy young adults while they performed forward step-up, lateral step-up and forward step-down exercises with the same step height. The step height for each subject was standardized allowing a knee flexion angle of 45° for each condition. Each subject randomly performed each stepping exercise (3 trials of 5 repetitions) at a fixed rate using a metronome (1 second up and 1 second down). Knee joint moments were computed using visual 3D software and normalized by body mass. Data obtained from the 3 trials were averaged. Muscle EMG and joint kinematics were used as input variables into a musculoskeletal model (SIMM) to estimate the net knee extensor moment.

A previously described biomechanical model was used to estimate patellofemoral joint stress [8]. Briefly this model uses subject input variables (i.e. knee joint kinematics, net knee joint moment) as well as variables from the literature (i.e. knee moment arms, quadriceps force/patella ligament force ratios and joint contact area). Model output was the patellofemoral reaction force and patellofemoral joint stress followed as figure 1.

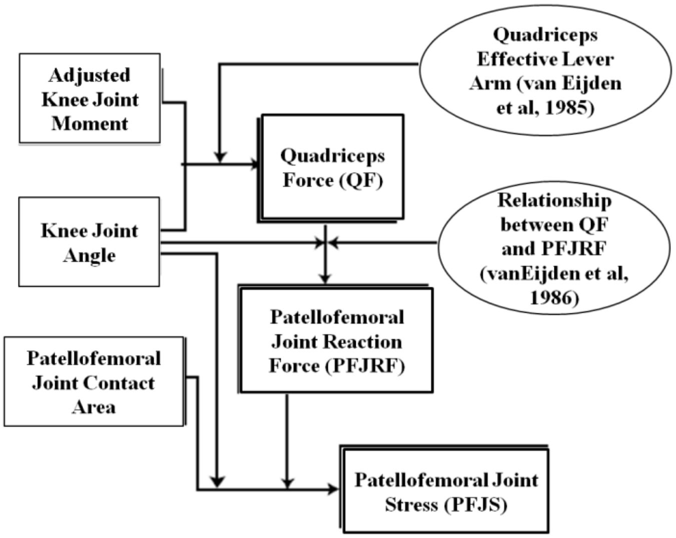
Adjusted Knee Joint Moment
Knee Joint Angle
Patellofemoral Joint Contact Area
Quadriceps Effective Lever Arm (van Eijden et al, 1985)
Quadriceps Force (QF)
Relationship between QF and PFJRF (vanEijden et al, 1986)
Patellofemoral Joint Reaction Force (PFJRF)
Patellofemoral Joint Stress (PFJS)

Figure 1. Flow chart of patellofemoral joint model.

Differences in peak patellofemoral joint reaction force and stress were compared across stepping exercises using a one-way ANOVA with repeated measures. Separate ANOVA's were conducted for the concentric and eccentric phases of each exercise. The Bonferroni adjustment was used in post hoc multiple comparisons for both phases. All significance levels were set at p<0.05.

RESULTS

Patellofemoral Joint Reaction Force (PFJRF): For both concentric and eccentric phases, peak PFJRF was significantly different among 3 stepping exercises (*p=0.004 and p=0.028 respectively)*. Post hoc analysis indicated that peak PFJRF during FSD was significantly greater than LSU (*p=0.006*) during the concentric phase (Fig. 2A). During the eccentric phase, peak PFJRF during FSD was greater than LSU (*p= 0.019*).

Patellofemoral Joint Stress (PFJS): For both concentric and eccentric phases, peak PFJS was significantly different among the 3 stepping exercises (*p=0.001, p=0.004*). Post hoc analysis indicated that peak PFJS produced during the FSD was greater than LSU (*p=0.001*) and FSU (*p=0.004*) during the concentric phase (Fig. 2B). During the eccentric phase, peak PFJS during FSD was greater than LSU *(p= 0.007)* and FSU *(p=0.02)*.

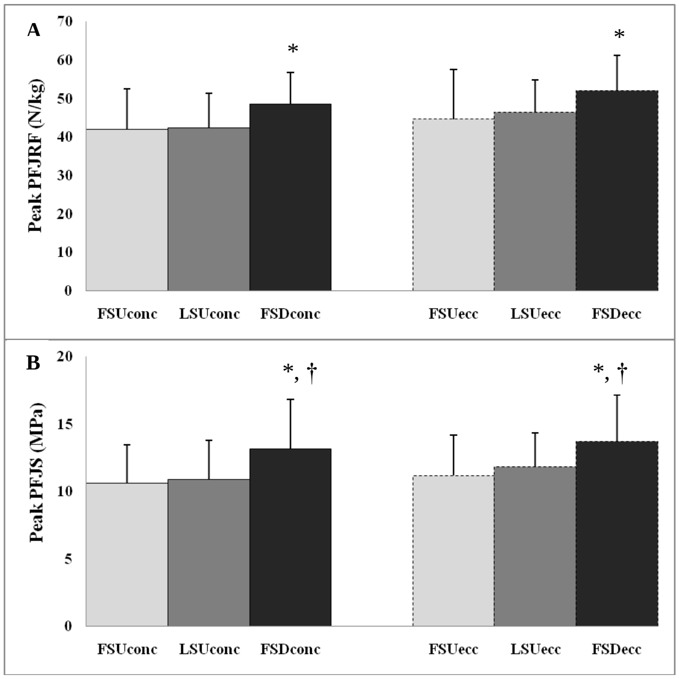

Figure 2. PFJRF for both concentric and eccentric (A). PFJS for both concentric and eccentric (B) among FSU, LSU and FSD) *Indicates significant differences ($P \leq 0.05$) between FSD and LSU for both phases. †Indicates significant differences ($P \leq 0.05$) between FSD and FSU for both phases.

DISCUSSION

Our data revealed that peak PFJS during the FSD was greater significantly than the LSU and FSU. The increased peak PFJS during the FSD was the direct result of an increase in the PFJRF. The fact that the PFJRF is mainly driven by the knee extensor moment, suggests that there is a greater quadriceps demand during FSD than LSU and FSU activities. This finding was consistent for both the concentric and eccentric phases.

CONCLUSIONS

FSD places increasing stress on patellofemoral joint when compared to LSU and FSU. Clinicians may want to avoid using the FSD exercises to minimize patellofemoral joint loading during the rehabilitation of persons with PFP.

REFERENCES

1. Witvrouw E, et al. *Am J Sports Med* **28**, 687-694, 2000.
2. Witvrouw E, et al. *Am J Sports Med* **32**, 1122-1130, 2004.
3. Westfall DC, et al. *J Sport Rehibil* **1**, 317-325, 1992.
4. Shelton GL, et al. *J Orthop Sports Phys Ther* **14**, 243-249, 1991.
5. Steinkamp LA, et al. *Am J Sports Med* **21**, 438-444, 1993.
6. Wallace DA, et al. *J Orthop Sports Phys Ther* 32, 141-148, 2002.
7. Salem GJ, et al. *Clin Biomech* 16, 424-430, 2002.
8. Brechter JH, et al. *Gait Posture* 16, 115-123, 2002.

ACKNOWLEDGEMENTS

The Commission on Higher Education, Thailand.

COMPARISON OF GLENO-HUMERAL KINEMATICS OBTAINED USING BONE PINS AND SKIN MOUNTED MARKERS – A PRELIMINARY VALIDATION STUDY

[1,2]S Rao, [5]A Miana, [2]M Lenhoff, [2] S Backus, [7]B Vanadurongwan [4]N Chen, [2]A Brown,[4]S Coleman, [4]F Cordasco,
[4]D Altchek, [2]S Fealy, [3]C Imhauser, [6]A Karduna,[4]R Warren, [3]T Wright, [2]R Zifchock, [2]H Hillstrom
[1]New York University, New York, USA; [2]Leon Root Motion Analysis Lab, [3]Biomechanics Department,
[4]Orthopedics Department, Hospital for Special Surgery, New York, USA; [5]Instituto Vita, Sao Paulo, Brazil;
[6]University of Oregon, Eugene, USA; [7]Siriraj Hospital, Mahidol University, Bangkok, Thailand
email: smita.rao@nyu.edu

INTRODUCTION

Accurate and valid characterization of glenohumeral kinematics plays a critical role in facilitating our understanding of pathology at the shoulder joint. *In vivo* strategies to quantify glenohumeral kinematics have used two main techniques: 1) use of skin mounted sensors, [1] 2) use of a skin mounted jig.[2] The purpose of this study was to compare glenohumeral kinematics obtained using bone pins to those obtained using skin mounted markers and a skin mounted jig, using a cadaver model. The null hypothesis was that no differences exist in glenohumeral kinematics between the three different tracking methods.

METHODS

One cadaver (two upper limbs) with no known musculoskeletal pathology was mechanically grounded to a vertical steel stanchion, allowing unrestrained motion of the upper extremities.

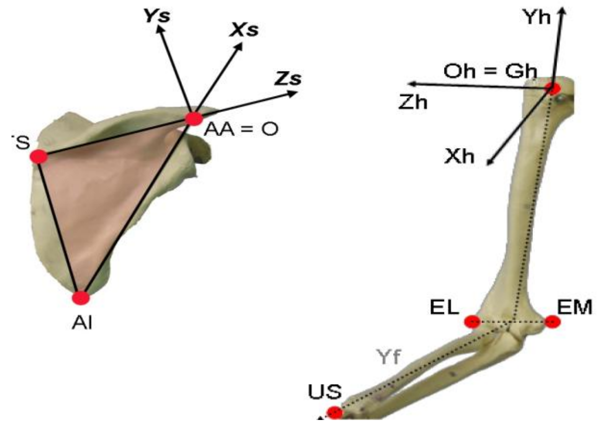

Figure 1. Scapula (viewed from rear) and humerus coordinate systems

The scapula and humerus were instrumented with one Steinmann pin each. A cluster of four retroreflective markers was affixed to each bone pin. Four retroreflective markers were secured to the skin overlying the scapula and the humerus, and over a scapula-tracking device, designed to conform to the midportion of the scapular spine [2]. Anatomical coordinate systems were defined, according to ISB recommendations, [3] for the scapula and humerus with a digitizing pointer. (Coordinate systems depicted in Fig. 1)

Kinematic data were collected at 100 Hz using a 10-camera system (Motion Analysis Inc, Santa Rosa CA) during three tasks (glenohumeral flexion, abduction and external rotation) and two conditions (elbow flexed and elbow extended). Data were analyzed using Visual 3D (C-motion Inc, MD). The following segments were defined: bone pin humerus, skin marker humerus, bone pin scapula, skin marker scapula and scapular jig. Euler angles were defined using a y-x'-z'' sequence of rotations, where y is the supero-inferior axis, x is the anterior-posteior axis and z is the medial-lateral axis.[1]

RESULTS

Representative data are depicted in Figure 2. Differences between bone pin and skin mounted marker tracking methods are expressed in terms of Root Mean Square Error (RMSE) and summarized in Tables 1 and 2 below.

	Specimen L	**Specimen R**
	Elbow extended	
Flexion	13.6°	6.1°
Abduction	2.4°	2.1°
Ext Rtn	2.9°	7.3°
	Elbow flexed	
Flexion	17.6°	10.0°
Abduction	3.2°	5.9°
Ext Rtn	4.5°	5.5°

Table 1. Average RMSE (degrees) glenohumeral kinematics between bone pin and skin marker tracking methods.

	Specimen L	**Specimen R**
	Elbow extended	
Flexion	6.3°	2.0°
Abduction	4.4°	2.1°
Ext Rtn	3.4°	3.0°
	Elbow flexed	
Flexion	8.3°	5.3°
Abduction	3.0°	5.0°
Ext Rtn	4.8°	11.5°

Table 2. Average RMSE (degrees) in glenohumeral kinematics between bone pin and scapula tracking methods.

DISCUSSION AND CONCLUSIONS:

Preliminary results from two upper extremities indicate that skin tracking methods of characterizing glenohumeral kinematics are accompanied by an RMSE of less than 10° in abduction and external rotation, when compared to methods using bone-pins. Greatest RMSEs were noted with flexion greater than 90° with good agreement when below 90°. (Figure 2). Altering elbow position (elbow extended versus elbow flexed) did not influence RMSE in flexion, abduction or external rotation. These results are in agreement with previous reports. [2, 4]

Additional analyses are underway to examine the effect of Euler rotation sequence [5], and the use of improved tracking methods such as a humerus shell. Shoulder joint coordinate system development to minimize the RMSE while assessing glenohumeral kinematics is in progress.

REFERENCES

1. Ludewig PM et al. *Phys Ther* **80**, 276-291, 2000.
2. Karduna AR et al. *J Biomech Eng* **123**, 184-90, 2001.
3. Wu G et al. *J Biomech* **38**, 981-992, 2005.
4. Ludewig PM et al. *J Bone Joint Surg Am* **91,** 378-89, 2009.
5. Karduna, AR et al. *J Biomech* **33**, 1063-1068, 2000.

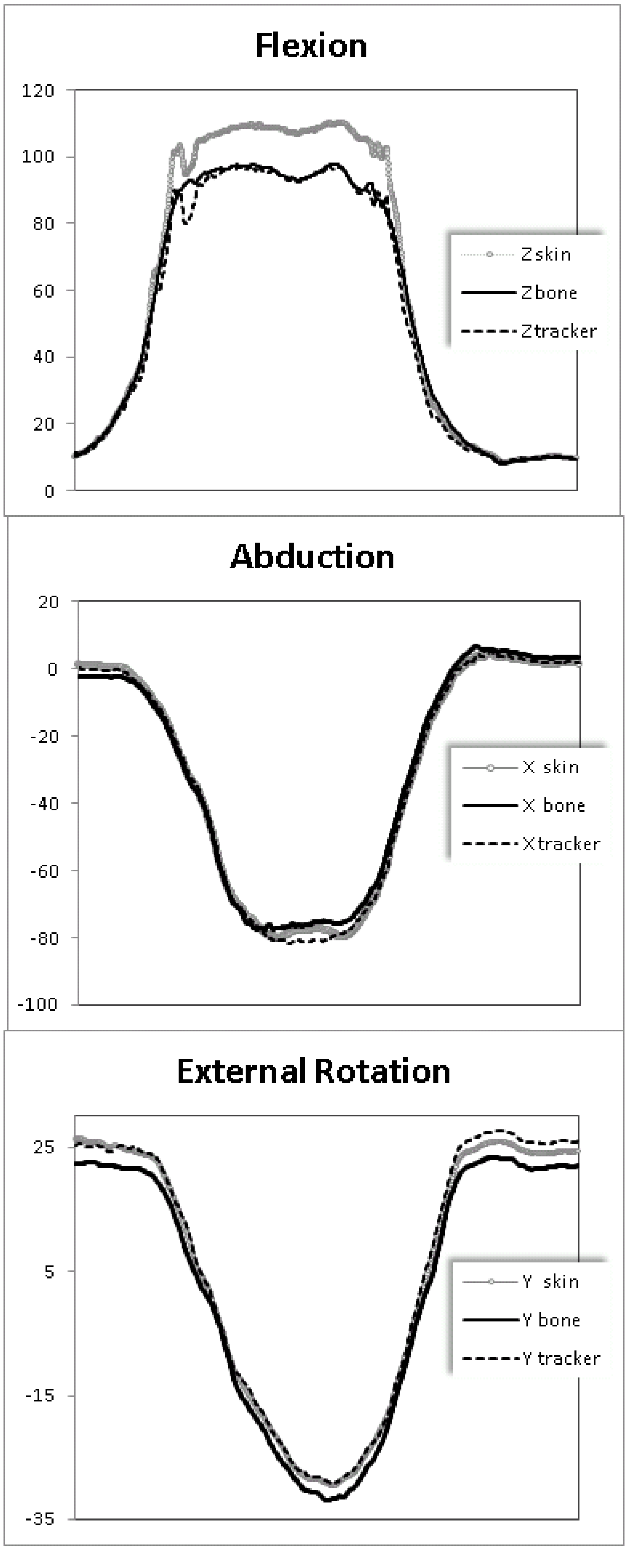

Figure 2. Comparison of tracking methods used to capture gleno-humeral kinematics

ACKNOWLEDGEMENTS:

David Adar from the Psychomotor Skill Laboratory at Hospital for Special Surgery for assistance with the cadaveric specimen.

USING ANKLE, KNEE, AND HIP PEAK ANGULAR VELOCITIES TO PREDICT LOWER EXTREMITY WORK DURING DROP LANDINGS

Lindsay Barlow, Jacob Gardner, Steven T. McCaw
School of Kinesiology and Recreation, Illinois State University, Normal IL
email: lnbarlo@ilstu.edu

INTRODUCTION

A kinetic and energetic analysis is useful for determining the relative joint contributions to skill performance, but remains a relatively time and labor intensive method of assessment despite the availability of commercial software. Additionally, the clinical applications and interpretations of such biomechanical analyses are often not fully understood [1]. Kinematic data, including joint angular velocity evaluated qualitatively, has long been proposed as a biomechanical "tool" to effectively evaluate performance [3].

During the absorption phase of landing, the rapidly flexing joints of the lower extremity are brought to rest by eccentric activity of the appropriate muscles. The angular version of the work-energy relationship (Equation 1) suggests that, as angular velocity (ω) increases, greater angular work is required to bring the rotating body to rest:

$$\mathcal{T}\theta = \frac{1}{2} I \left(\omega_f - \omega_i\right)^2 \qquad \text{(Eq. 1)}$$

This study examined the relationship between peak ω and mechanical work at the ankle, knee and hip joints during drop landings. We looked at both soft and stiff landings while wearing a variety of different ankle braces. We hypothesized that there would be a strong positive correlation between peak dorsiflexion/flexion ω and negative work during the landing, as could be predicted with the angular analog of the work-energy relationship.

METHODS

Sixteen female university students (age, 20.6 ± 1.0 y; ht, 1.66 ± 0.07m; mass, 66.5 ± 10.8 kg) volunteered as participants. All were free of injury for 6 months prior to data collection and were experienced in landing as determined by a questionnaire. Participants performed two-legged landings off a 0.32-m platform onto a force platform as in previous research [2]. Only the right leg was analyzed.

Five soft and five stiff landings were performed in five bilateral ankle stabilizer conditions (no stabilizer, standard taping, lace-up boot, hinged boot, and stirrup style), for a total of fifty trials per subject. Stabilizers and style conditions were randomized across participants, and conveniently provided greater ranges in the peak ω and negative work data for establishing correlations.

Ankle, knee and hip kinematics, joint moment of force and energetics were calculated using standard inverse dynamic techniques combining an optotrak system (200 Hz), force platform (1000Hz), anthropometics. Joint work was calculated as the integral of the mechanical power-time curve from contact until $\omega_{\text{joint}} = 0$.

Pearson correlation coefficients were calculated between peak ω and negative work at each joint. A stepwise multiple regression was performed between total work (Σhip+knee+ankle work) and the peak ω of the three joints.

RESULTS AND DISCUSSION

Figure 1 presents grand ensemble mean curves by each condition for joint ω and joint mechanical power, and a scattergram of peak joint ω and joint mechanical work.

There was a statistically significant positive correlation between peak angular velocity and negative work at each joint. The r values ranged from .94 at the hip to .53 at the knee joint, reflecting strong to moderate relationships, respectively.

The statistically significant ($p<0.001$) multiple regression equation computed was

$$Work_{total} = -.287 + 0.006\,\omega_{hip} + .002\omega_{ankle}$$
(r^{2}= 0.630, standard error of estimate =.425).

CONCLUSIONS

The moderate to strong correlations between peak ω and joint work suggest that peak angular velocity can be used to qualitatively assess the negative work performed at the joints of the lower extremity during a landing. Since calculating joint ω is less labor and calculation intensive than calculating joint kinetics and energetics (primarily work and power) analyzing joint ω provides a simpler method of describing energy absorption by the lower extremity. This could provide a starting point for the teaching of joint energetics in the undergraduate sports medicine curriculum.

Changes in peak ω do not account for all the work done in the work-energy relationship. Fluctuations in joint moments can also contribute to work variability. Therefore, the next step to developing a qualitative “tool” for lower extremity performance assessment is to investigate the relationships among the joint moment, peak ω_{joint} and joint work.

REFERENCES

1. Brand, RA. Can biomechanics contribute to clinical orthopaedic assessments? *Iowa Ortho. J.* **9**:61-64, 1988.
2. McCaw, ST and Cerullo, JF Prophylactic ankle stabilizers affect ankle joint kinematics during drop landings. *Med. Sci. Sports Exer.* **31**:702-707,1999.
3. Norman, R. W. K. How to use biomechanical knowledge. *How to be an effective coach.* Taylor, J. W. (Ed.). Toronto: Coaching Association of Canada, 92-111,1975.

ACKNOWLEDGEMENTS

This study was supported by a *Jump Rope for Heart* grant from the Illinois Association for Health, Physical Education, Recreation and Dance.
DonJoy and AirCast generously donated the ankle supports.
Special thanks to Justin Stanek, ATC for assistance

Figure 1: Lower extremity grand ensemble curves and correlations. From left to right, peak ω flexion/dorsiflexion, negative mechanical power, and correlations between peak ω flexion/dorsiflexion and work.

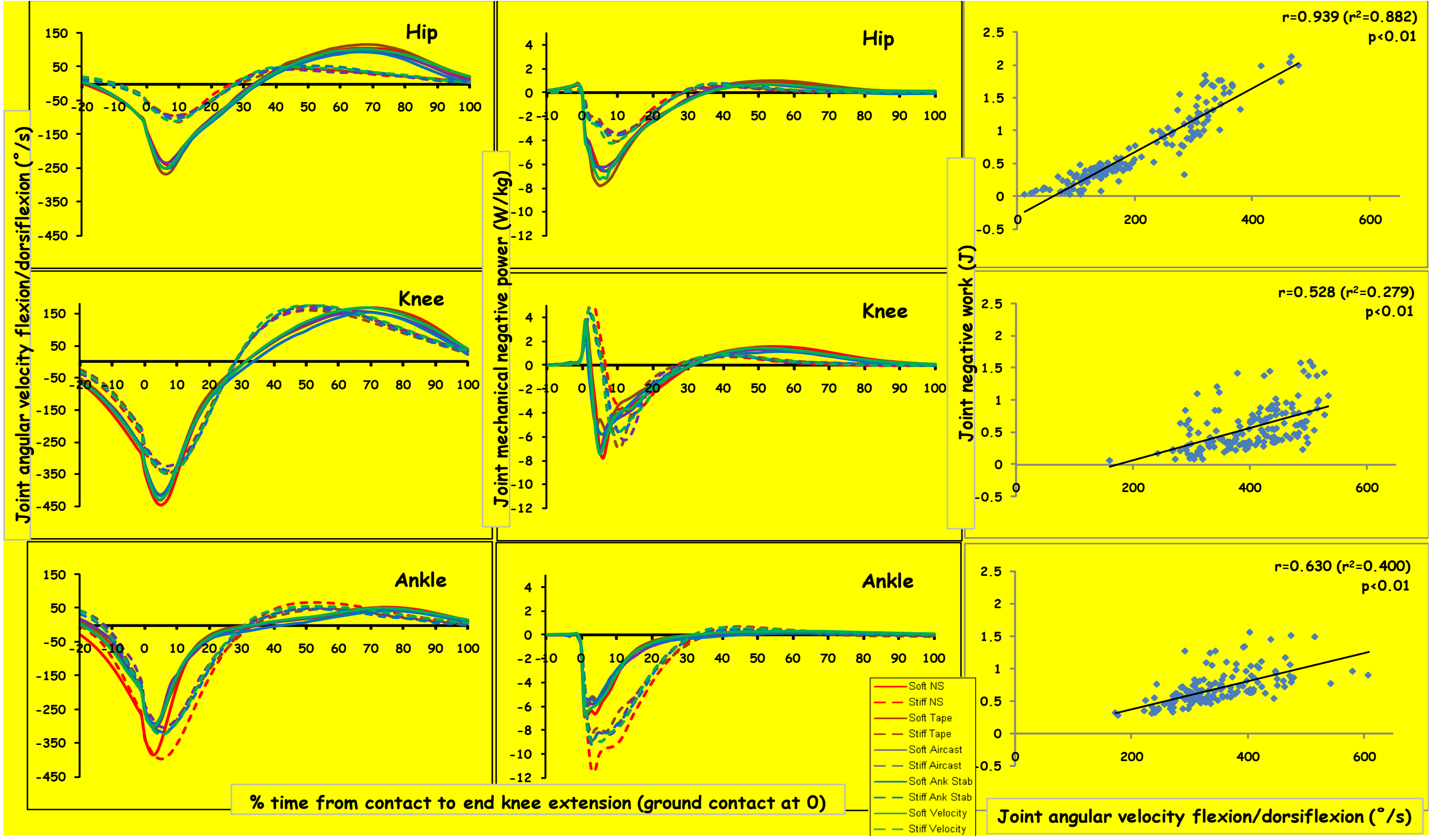

PILOT STUDY OF GAIT SYMMETRY EFFECTS FOLLOWING HIP FRACTURE REHABILITATION

[1] Mary Rodgers, [1]Paula Geigle and [2]Ram Miller
[1]Dept. Physical Therapy & Rehabilitation Science, [2]Div. Gerontology, Dept. Epidemiology & Preventive Medicine, University of Maryland School of Medicine
email: mrodgers@umaryland.edu, web: http://pt.umaryland.edu

INTRODUCTION

The impact of hip fracture in our country is substantial, with more than 350,000 persons over age 65 predicted to fracture a hip in the United States during the coming year [1]. Early rehabilitation has been shown to reduce hospital length of stay, however, these patients have significant muscular atrophy and weakness on the side of fracture that can persist for months after fracture with mobility deficits remaining for a number of years [2]. While exercise programs have been shown to improve physical function in patients with total hip replacement surgery, these programs require patients to travel to centers for participation since direct supervision is needed [3]. Studies of home-based exercise programs post hip replacement surgery have reported increases in walking speed, however, none have included more detailed information about gait parameters and symmetry.

The purpose of this pilot study was to investigate the effects of a 16-week home-based exercise program, beginning 2 months post hip fracture on lower extremity function as shown in the 6-minute walk and gait parameters. The hypothesis was that this moderate intensity home exercise intervention would improve gait function in older adults post hip fracture.

METHODS

Four participants met the following inclusion criteria for this pilot study: 1) diagnosis of hip fracture (ICD-0 codes 820.0 to 820.9); 2) age 65 or older; 3) living in the community at time of fracture; 4) hospitalization within 4 days of the fracture; 5) successful fixation (partial or total hip replacement or open reduction internal fixation) of a hip fracture; 6) non-pathological fracture; 7) minimal trauma fracture; and 8) ambulating without human assistance pre-fracture.

After informed consent, the four participants were tested before and after a 16-week home-based physical therapy program beginning two months post hip fracture (after traditional rehabilitation had ended). The exercise training program included lower extremity strengthening with a mini shuttle (see figure) and cardiovascular conditioning. For the aerobic component, the goal intensity of the training was 65% to 75% of age-predicted maximal heart rate. The resistive component targeted strengthening for the bilateral hip extensors hip abductor, knee extensor, and plantar flexor muscle groups.

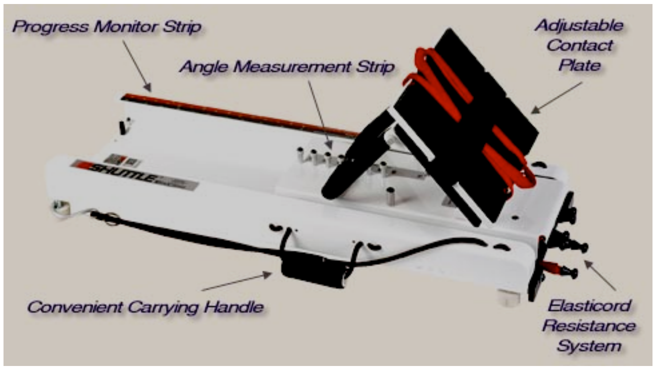

Figure 1. Resistance Training Device (Shuttle Systems, Glacier WA)

Before and after the 16-week exercise program, data were collected for the 6-minute walk distance. Gait parameters were also collected for three trials at walking preferred speed using a GaitRite® gait mat (CIR Systems, Havertown, PA) to measure selected spatio-temporal parameters. A symmetry index (SI) was used to quantify fracture and nonfracture percent stance symmetry in gait [4]:

$$SI = \frac{V_{fracture} - V_{nonfracture}}{\tfrac{1}{2}\left(V + V\right)} \times 100$$

Where V*f* is fracture side percent stance and V*n* is nonfracture side percent stance. A symmetry index equaling zero corresponds to perfect symmetry.

RESULTS AND DISCUSSION

The 6 minute walk distance increased in three of the four subjects following training as shown in Figure 2. Gait parameters results for each subject are shown in Table 1. Velocity and cadence increased for three of the four subjects. Symmetry was improved in three of the four subjects following training (Figure 3).

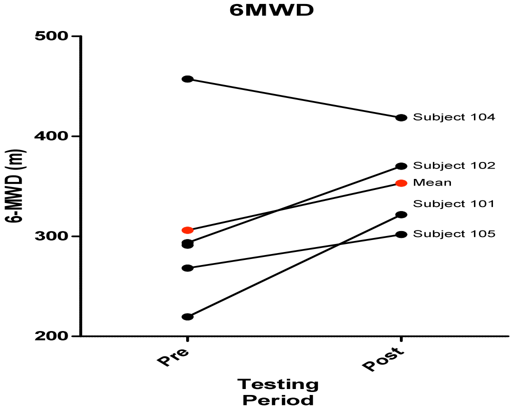

Figure 2. Six minute walk distances for each subject before and after the 16 week training intervention.

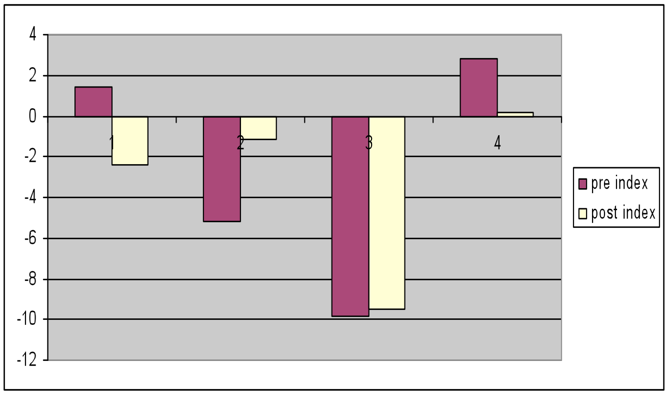

Figure 3. Symmetry index for each subject where zero represents perfect symmetry.

CONCLUSIONS

This pilot study demonstrated that a moderate intensity home exercise intervention improved gait function as shown in three of the four older adults post hip fracture tested. This pilot data provides a basis for future investigation into effective intervention for individuals post hip fracture.

REFERENCES

1. Magaziner, et al. *Am J Epidemiol* **157,** 1023-1031, 2003.
2. Mangione KK, et al. *Physiother Can* **59**, 10-18, 2007.
3. Palombaro et al. *Phys Ther* **86**, 809-816, 2006.
4. Galea MP, et al. *Arch Phys Med Rehabil* **89**, 1442-1447, 2008.

ACKNOWLEDGEMENTS

Funding provided by a pilot study from the Baltimore Claude D. Pepper Older Americans Independence Center (P50 AG2874-01, Goldberg, PI).

Subject	**Velocity (cm/s)**		**Cadence (steps/m)**		**Double Support (%)**		**Stride Length (cm)**		**Symmetry Index**	
	pre	**post**	**pre**	**post**	**Pre**	**Post**	**pre**	**post**	**pre**	**post**
101	**60.9**	**88.7**	**95.7**	**113.5**	**37.5**	**30.9**	**76.0**	**94.0**	**1.5**	**-2.4**
102	**90.4**	**110.2**	**123.0**	**124.5**	**37.5**	**27.7**	**88.5**	**106.0**	**-5.2**	**-1.2**
104	**112.5**	**111.8**	**111.0**	**110.0**	**31**	**31.5**	**123.3**	**122.3**	**-9.8**	**-9.5**
105	**79.0**	**91.7**	**97.0**	**102.0**	**33.8**	**30.1**	**98.0**	**108.0**	**2.8**	**0.2**

Table 1: Gait parameters for each subject during preferred speed walking trials (mean of three trials).

RELATIONSHIPS BETWEEN SELECTED JAVELIN TECHNIQUE VARIABLES AND THROWING PERFORMANCE

Steve Leigh[1], Hui Liu[2], and Bing Yu[1]
[1]Center for Human Movement Science, Division of Physical Therapy
The University of North Carolina at Chapel Hill; [2]Beijing Sports University
email: stvleigh@email.unc.edu

INTRODUCTION

The javelin throw is one of four Olympic throwing events, where a javelin is thrown for maximum distance. Flight distance is the major partial distance contributing to long throws, and is mainly dependent on a great release speed. The javelin is the most aerodynamic of all the Olympic throwing implements, so aerodynamic distance is a significant factor in throwing far. It is necessary to carefully control the release to optimize aerodynamic factors. Simultaneously maximizing release speed and controlling the release is technically demanding.

The purpose of this study is to explore the relationships between throwing technique and throwing performance.

METHODS

Two high-definition digital camcorders were used to record the javelin throw competitions at the 2007 USA Track and Field National Outdoor Championships, 2008 US Olympic Team Trials, and 2008 UNC/Nike Elite Meet. The camcorders were aligned so their optical axes were perpendicular and operated at 60 frames/second. The longest throws by the 30 female and 32 male competing athletes were subsequently analyzed. Twenty-one body landmarks, and the tip, tail, and center of mass of the javelin were manually digitized in both camcorder views for each throw [1]. Three-dimensional coordinate data were obtained using the Direct Linear Transformation procedure [2].

For each trial, the release parameters of release speed, height, and angles, and the partial distances were reduced. These variables represent throwing performance. Kinematic variables of joint and segment angles and positions were reduced at the final stride critical instants of right foot touchdown, left foot touchdown, and release. The whole body speeds and times between the critical instants were also reduced. These variables represent throwing technique, and are known as technical parameters.

Statistical analyses were performed to explore the relationships between throwing performance and throwing technique. Female and male javelin throwers were assessed separately. Statistical significance was set a priori at $\alpha = 0.1$. Bivariate Pearson correlation coefficients were calculated between the technical parameters and the official distance, release speed, and aerodynamic distance. Multiple regression equations were calculated to determine the effect of select technical parameters on release speed and aerodynamic distance. The technical parameters were the independent variables and release speed and the official distance were the dependent variables. The three technical parameters with the strongest bivariate correlation with the independent variable were chosen for entry into the multiple regression.

RESULTS AND DISCUSSION

For female javelin throwers greater official distances were associated with: greater hip-shoulder separations at right foot touchdown, smaller right elbow flexion angles at right foot touchdown, greater whole body speeds at left foot touchdown, smaller left leg angles at left foot touchdown, and shorter times spent in double support.

A linear combination of whole body speed at left foot touchdown (mean = 4.4 m/s; $b = 0.97$; $p = 0.07$) and time spent in double support (mean = 0.14 sec; $b = -15.21$; $p = 0.03$) accounted for a significant amount of release speed variability ($R^2 = 0.23$; $F = 4.12$; $p = 0.03$). A linear combination of right elbow flexion angle at right foot touchdown (mean = 23°; $b = -0.08$; $p = 0.01$), right shoulder adduction angle at right foot touchdown (mean = -8°; $b = -0.10$; $p = 0.05$), and javelin inclination angle at release (mean = 41°; $b = -0.27$; $p = 0.04$) accounted for a significant amount of aerodynamic distance variability ($R^2 = 0.32$; $F = 4.00$; $p = 0.02$).

Our data suggest that female javelin throwers utilize a high runway speed with minimal braking during ground contact in the final stride to achieve great release speeds. Release speed is the most important factor for throwing long official distances. Using runway speed to achieve great release speeds is a method commonly taught by coaches. Our data also suggest that female javelin throwers control their release of the javelin with their throwing arm to keep the inclination of the javelin low. By keeping the javelin low, drag forces are minimized and aerodynamic distance can be increased. These results show that female javelin throwers use different strategies to achieve great release speeds and long aerodynamic distances.

For male javelin throwers greater official distances were associated with: greater right shoulder external rotation angles at right foot touchdown, smaller right shoulder horizontal adduction angles at right foot touchdown, shorter times spent in single support, lower javelin inclinations at left foot touchdown, greater trunk forward tilts at left foot touchdown, greater right shoulder adduction angles at left foot touchdown, smaller right shoulder horizontal adduction angles at left foot touchdown, greater trunk forward tilts at release, greater hip-shoulder separations at release, smaller right elbow flexion angles at release, and javelin center of mass positions in front of the right shoulder at release.

A linear combination of right shoulder external rotation angle at left foot touchdown (mean = 52°; $b = -0.05$; $p = 0.07$), right shoulder adduction angle at release (mean = -7°; $b = 0.08$; $p = 0.02$), and right shoulder horizontal adduction angle at release (mean = 5°; $b = -0.15$; $p < 0.01$) accounted for a significant amount of release speed variability ($R^2 = 0.31$; $F = 4.28$; $p = 0.01$). A linear combination of right knee angle at left foot touchdown (mean = 140°; $b = 0.74$; $p = 0.08$), right shoulder adduction angle at release (mean = -7°; $b = -0.38$; $p = 0.03$), and right shoulder horizontal adduction angle at release (mean = 5°; $b = 0.45$; $p = 0.03$) accounted for a significant amount of aerodynamic distance variability ($R^2 = 0.31$; $F = 4.10$; $p = 0.02$).

Our data suggest that male javelin throwers mainly use arm motion to generate great release speed and to control their release for long aerodynamic distances. The regression equations contain the same technical parameters with opposite sign regression weights for release speed and aerodynamic distance. This suggests that an increase in release speed is associated with a decrease in aerodynamic distance, and these technical parameters must be optimized. Our data also suggest that male javelin throwers utilize high runway speeds with minimal braking and low javelin inclinations to throw long official distances. The influence of these strategies, however, is secondary to arm motion and of less importance compared with female javelin throwers.

CONCLUSIONS

Release speed and aerodynamic distance are important factors for throwing a javelin long distances. Technique affects both of these factors. It is important for a javelin thrower to use an optimal combination of technical parameters to achieve a high release speed and a long aerodynamic distance to throw long official distances.

REFERENCES

1. Abdel-Aziz YI and Karara HM. *ASP Symposium on Close Range Photogrammetry*, ASP, Falls Church, VA, 1971.
2. Hay JG and Yu B, *J Sports Sciences*, **13**, 125-140, 1995.

ACKNOWLEDGEMENTS

This study was financially supported by USA Track and Field, the Graduate School at the University of North Carolina at Chapel Hill, and the International Society of Biomechanics.

FOOT-STRIKE PATTERN SELECTION TO MINIMIZE MUSCLE ENERGY EXPENDITURE DURING RUNNING: A COMPUTER SIMULATION STUDY

Ross H. Miller, Elizabeth M. Russell, Allison H. Gruber, and Joseph Hamill
Department of Kinesiology, University of Massachusetts, Amherst, MA, USA
Email: rhmiller@kin.umass.edu Web: http://www.umass.edu/biomechanics

INTRODUCTION

While the majority of recreational runners strike the ground with their heel first, a greater proportion of elite competitive runners strike the ground with their midfoot first [1]. It is generally unknown why different runners naturally select different foot-strike patterns. However, there is a growing movement in the running community to train natural recreational heel-strike runners to instead strike the ground with their midfoot first (e.g. ChiRunning and the Pose Method).

A primary rational behind these training programs is the suspicion or assumption that midfoot striking is more metabolically efficient than heel striking. Regarding the metabolic cost of running, two potential problems with a converted foot-strike pattern are: (1) there is no strong scientific evidence that heel striking is more energetically costly than other strike patterns, and (2) naturally-selected stride parameters tend to incur lower oxygen costs than prescribed parameters [2]. In addition, running shoe designs generally focus on heel rather than midsole cushioning, suggesting that running with a midfoot strike could incur greater injury risks by not taking advantage of a shoe's protective features [3].

To evaluate the efficacy of these training programs, it is therefore important to gain a greater understanding of the relationship between metabolic cost and foot-strike pattern selection in runners. Measuring subtle changes in metabolic cost on human subjects can be difficult due to experimental and equipment limitations, and because human runners may optimize their performances on criteria other than metabolic cost. With a computer modeling and simulation approach, researchers can have more precise control over these factors.

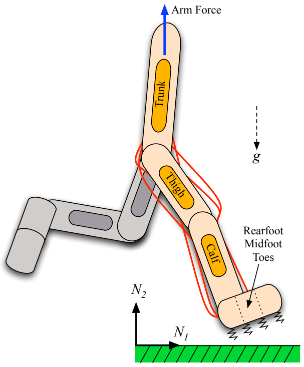

Figure 1: The computer model used in the simulations. The knee flexor and digitorum muscle models are not shown.

Therefore, the purpose of the study was to determine the foot-strike pattern selected in a computer simulation of a running human when the model is instructed to minimize its metabolic cost.

METHODS

Forward dynamics simulations of one full step of running were performed using a two-dimensional bipedal computer model (Fig. 1). Each leg was actuated by 12 Hill-based muscle models. Ground contact was modeled by viscoelastic frictional elements on the foot that were parameterized to represent shod human feet [4].

The muscle model included a sub-model of human muscle energy expenditure [5]. The energy rate of a muscle was the sum of the activation, maintenance, and lengthening/shortening heat rates and the mechanical work rate of the contractile component.

To allow the model free selection over the foot-strike pattern, the simulation began at the initiation of the right leg's swing phase and ended at the initiation of the left leg's swing phase. The simulation thus had to contain one full stance phase of the left leg, but no constraints were directly imposed on the kinematics of this phase. Initial kinematic conditions were derived from a human subject running at 4.0 m/s. The objective function of the simulation was to minimize the total muscle energy expended per distance traveled, while closely matching the initial kinematics of the right leg with the final kinematics of the left leg, and vice-versa. The control variables were the muscle model excitation signals and the initial segment angular positions and velocities. The initial kinematics were allowed to vary within the ranges exhibited by the subject when running at this speed with heel, midfoot, and forefoot strike patterns. The optimal control variables were found using a parallel simulated annealing algorithm.

RESULTS AND DISCUSSION

Over the time of the simulated step (363 ms), the model ran at an average speed of 3.95 m s^{-1}, with a stride frequency of 1.38 Hz and a stride length of 2.86 m. The speed and stride parameters were within 5% of the performance of the subject from whom the simulation's initial conditions and the model's parameters were derived.

The simulation spent 15.9 W kg^{-1} to run at this speed, which is close to the rate of 16.1 W kg^{-1} predicted from the oxygen cost vs. speed relationship for trained human runners [6]. When running with this energy rate, the simulation exhibited a distinct heel-first foot-strike pattern when initiating ground contact (Fig. 2). A follow-up simulation with kinematic constraints forcing the model to land on its midfoot used an increased energy rate of 16.9 W kg^{-1} to run at the same speed.

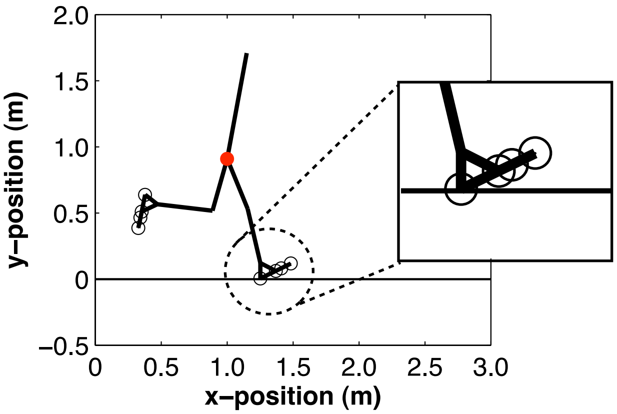

Figure 2: The posture of the model at the first instance of foot contact (vertical ground reaction force > 0).

CONCLUSIONS

A variety of other factors not considered here (e.g. running speed, anthropometry, muscle mechanical properties, footwear, three-dimensional motion) could influence the selection of a foot-strike pattern and the metabolic cost of running. However, under these particular simulated conditions, a heel-first strike pattern was selected when the goal was to minimize the metabolic cost of a step of running. Since the simulated running performance was minimally constrained by input experimental data, we conclude that the heel-first strike pattern was less metabolically costly than other strike patterns that could have been chosen instead. If another foot-strike pattern was less costly, it should have been chosen as the optimal solution.

If the simulation is assumed to be a reasonable analog of the mechanical and metabolic aspects of the human subject's running performance, the results demonstrate an example where converting to an unnatural midfoot strike pattern increased the energetic cost of running at a given speed. Further experimental and simulation-based work is needed to investigate the relationship between foot-strike pattern and the energetics of human running. Training programs that advocate an improvement in metabolic efficiency through the adoption of a midfoot strike pattern may not necessarily confer this improvement to all runners.

REFERENCES

1. Hasegawa H, et al. *J Strength Cond Res* **21**, 888-893, 2007.
2. Gutman AK, et al. *J Exp Biol* **209**, 622-632, 2006.
3. Cavanagh PR and Lafortune MA. *J Biomech* **13**, 397-406, 1980.
4. Aerts P and de Clercq D. *J Sports Sci* **11**, 449-461, 1993.
5. Umberger BR, et al. *Comp Meth Biomech Biomed Engr* **6**, 99-111, 2003.
6. Mayhew JL. *Br J Sports Med* **11**, 116-121, 1977.

CAN RISK FACTORS FOR KNEE INJURY DURING LANDING BE REDUCED BY SIMPLE VERBAL INSTRUCTION?

Clare E. Milner, Abhaya Srivatsan, Songning Zhang & Jeffrey T. Fairbrother
University of Tennessee, Knoxville, TN, USA. Email: milner@utk.edu

INTRODUCTION

Knee injuries are very common during sports activities, particularly those which involve jumping and landing. Anterior cruciate ligament (ACL) tears are a particular cause for concern, and the majority of these occur via non-contact mechanisms [1]. In recent years, several preventative programs have been developed in an attempt to address this issue and reduce the number of ACL tears occurring during landing from a jump. It has been suggested that future research in this area should focus on identifying which components of these programs are contributing directly to modifying the biomechanics of jump landings [2]. Proposed biomechanical risk factors for ACL injury include: increased frontal plane knee abduction motion; reduced knee flexion, high peak ground reaction force, and interlimb asymmetry [3].

Therefore, the aim of this study was to determine whether simple verbal instructions altered landing performance in female recreational athletes. In particular, frontal and sagittal plane knee mechanics, peak vertical ground reaction force, and interlimb symmetry were compared among control (CTRL), soft landing (SOFT), knees over toes (KOT), and equal weight (EQWT) conditions.

METHODS

Twelve young, healthy female recreational athletes aged between 18 and 35 years were recruited into the study (mass 57.3 ± 9.5kg; height 1.62 ± 0.05m; age 25.6 ± 2.0y). All subjects provided informed consent to participate. Lower extremity position and force data were recorded using an optoelectronic motion capture system and synchronized force platforms. Participants performed maximal effort countermovement jumps following simple verbal instructions in a control condition and three counterbalanced intervention conditions. Standardized instructional statements were used in all conditions. Practice trials were used to familiarize the participants with each condition, and five good trials were recorded.

The following variables were calculated for the dominant limb from ground contact to peak knee flexion: peak vertical ground reaction force; peak knee flexion angle; peak knee abduction angle; knee abduction excursion (from initial contact to peak abduction). Symmetry index of peak vertical ground reaction force was calculated using both limbs. One way repeated measures MANOVA and post-hoc tests were used to compare biomechanical variables in the dominant limb among the four conditions. One way repeated measures ANOVA and post-hoc tests were used to compare SI among conditions ($p \leq 0.05$).

RESULTS AND DISCUSSION

Peak vertical ground reaction force was different across groups ($p = 0.013$). In particular, it was reduced in the SOFT condition compared to all three other conditions, as expected (Table 1). It was similar among the other three conditions. Significant differences were also found in peak knee flexion angle across conditions ($p = 0.001$). In particular, more knee flexion was observed in the SOFT and KOT condition compared to the CTRL condition. Increased knee flexion in the SOFT condition compared to the CTRL was expected, since knee flexion is the major shock absorbing mechanism in the lower extremity. This ties in with the lower peak vertical ground reaction force observed in the SOFT condition. Similar reductions in ground reaction force and increases in knee flexion have been reported previously with other instructional protocols [e.g. 4,5]

Greater peak knee flexion was found in KOT compared to all three other conditions. Additionally, both peak knee valgus (p = 0.724) and knee valgus excursion (p = 0.346) were similar across conditions. These results were unexpected and may be related to the participants' interpretation of the instruction given (land with knees over toes). If this was interpreted in the sagittal rather than the frontal plane, it may have resulted in increased knee flexion to place the knee vertically above the toes. Including a demonstration of the desired technique has been successful in reducing knee valgus [5], and should be included in future studies.

As expected, participants were more symmetrical (lower SI) in the EQWT condition compared to the other conditions (p = 0.045). Notably, peak vertical ground reaction force was similar in the dominant limb in the EQWT condition compared to the CTRL condition. Therefore, the improvement in symmetry in the EQWT condition was achieved without an increase in peak force.

The benefit of these verbal instructions is that they are simple and do not require specialized equipment, such as video, for incorporation into an activity program. Further work is required to determine whether these performance changes can be retained over the longer term.

SUMMARY

Two simple verbal instructions were successful in reducing biomechanical risk factors for ACL injury during a single session: 'land softly' reduced peak ground reaction force and increased peak knee flexion; 'equal weight on both feet' improved interlimb symmetry of peak vertical ground reaction force. The 'knees over toes' instruction had no effect on frontal plane knee kinematics (although peak knee flexion angle was increased).

REFERENCES

1. Boden BP, et al. *Orthop* **23**, 573-578, 2000.
2. Hewett TE, et al. *Am J Sports Med* **34**, 490-498, 2006.
3. Hewett TE, et al. *Am J sports Med* **33**, 492-501, 2005.
4. Cowling EJ, et al. *Br J Sports Med* **37**, 126-130, 2003.
5. Mizner RL, et al. *J Orthop Sports Phys Ther* **38**, 573-561, 2008.

Table 1: Knee angles and ground reaction force in different instruction conditions, mean (sd)

	Peak vertical GRF (BW)	Peak knee flexion (°)	Peak knee abduction (°)	Knee abduction excursion (°)	Symmetry Index
CTRL	1.989 (0.651)	87.1 (19.9)	-10.5 (4.1)	7.7 (3.4)	21.1 (18.4)
SOFT	1.509 (0.214)	94.6 (17.2)	-9.9 (3.9)	8.5 (3.2)	16.5 (10.6)
KOT	1.792 (0.400)	101.4 (18.9)	-10.4 (6.26)	9.0 (4.1)	19.9 (13.5)
EQWT	1.899 (0.584)	91.7 (22.3)	-10.7 (4.2)	8.7 (3.5)	10.6 (7.8)

THE INFLUENCE OF PRIOR HAMSTRING INJURY ON MUSCULOTENDON MORPHOLOGY AND MUSCLE CONTRACTION MECHANICS

[1]Amy Silder and [1,2,3]Darryl Thelen
Departments of [1]Biomedical Engineering, [2]Mechanical Engineering, and [3]Orthopedics and Rehabilitation, University of Wisconsin - Madison
email: silder@wisc.edu

INTRODUCTION

Hamstring strain injuries are extremely common among sprinters and typically involve the proximal musculotendon junction (MTJ) of the biceps femoris long head (BFLH) [1,2]. These injuries frequently occur in the latter half of the swing phase of sprinting, when the hamstrings undergo a lengthening contraction to decelerate the limb prior to foot contact [3]. We previously found that scar tissue at the site of prior injury persists for many months after an athlete returns to sport [2]. This altered morphology may adversely affect local tissue mechanics and contribute to the high re-injury rates (~30%, [1]) seen in these individuals. For this study, we used dynamic magnetic resonance (MR) imaging to measure in-vivo mechanical strains within the BFLH during lengthening contractions performed by two previously injured and four healthy control subjects. We hypothesized that regions of high localized strain would exist adjacent to the site of prior injury.

METHODS

Static and dynamic MR images were obtained from the right limbs of four healthy athletes and the previously injured left limbs of two athletes. All scans were conducted on a GE 1.5T MR scanner (General Electric Healthcare, Milwaukee, WI). High resolution images were first obtained to evaluate bilateral differences in tendon/aponeurosis volume and to visualize muscle fiber directions [2,4] (Fig. 1A, 2A). We then used cine phase contrast (PC) imaging to measure tissue velocities within a coronal-oblique imaging plane that bisected the long axis of the biceps femoris (Fig. 1B). Subjects were positioned prone on a MR-compatible device that was designed to guide the limb through cyclic knee flexion-extension, while using an inertial load to induce a lengthening contraction in the hamstrings (~20% of max strength) [5]. Three trials were conducted, each lasting 1min 39s. Scanning parameters were: voxel size = 1.4x1.4x6mm, VENC = 5cm/s, 256×256 matrix, TR/TE = 21.6/7.1ms, 2 lines of k-space/cycle, and 40 reconstructed frames/cycle.

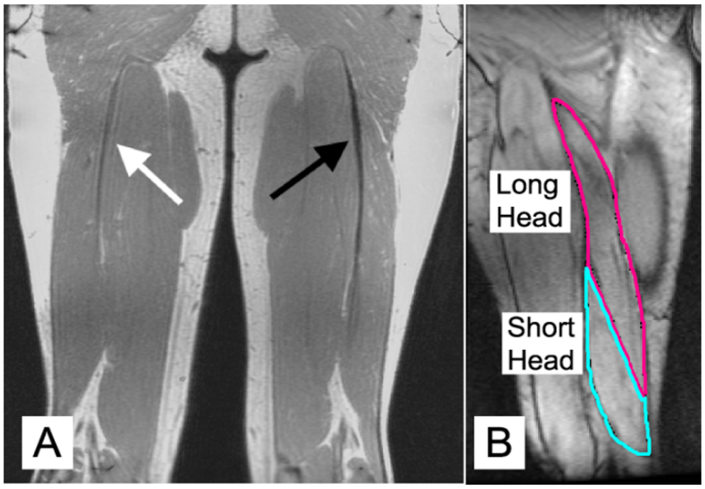

Figure 1. (A) The two previously injured subjects presented with substantial scarring adjacent to the site of prior injury (black arrow). (B) The coronal-oblique dynamic imaging plane bisected the long axis of the biceps femoris, encompassing both the long and short heads.

Velocity images were analyzed using a mesh based tracking approach [6]. A mesh of triangular elements (edge length of ~6mm) was first generated over a region that enclosed the entire BFLH. Element shape functions were used to express the pixel velocities within each element as a linear function of nodal velocities. Forward-backward and Fourier tracking [6] were subsequently used to integrate velocities, producing estimates of the nodal trajectories throughout the cyclic motion. These were then coupled with the element shape functions to compute the Lagrangian finite strain tensor, **E**, for each element, with respect to the muscle's configuration in a shortened state. The first principal strain, E_1, and direction were computed and defined by the most positive eigenvalue and corresponding eigenvector of **E**.

RESULTS

MR imaging and clinical examination at the time of initial injury indicated that both subjects' injuries occurred along the proximal MTJ of the left BFLH. The proximal tendon/aponeurosis volumes for these subjects were 49% and 139% larger that the uninjured limb, compared to an average difference of 12% between limbs in the healthy subjects.

Tissue displacement profiles and principal strain directions at the time of peak knee extension were similar for all healthy and injured subjects. The largest motion was observed along the lateral border of the BFLH, adjacent to the distal aponeurosis (Fig 2B). In the proximal muscle tissue, E_1 was consistently oriented laterally and downward (Fig. 2C), and generally aligned with the muscle fiber direction (Fig. 2A). The magnitude of E_1 varied somewhat throughout the muscle tissue for the healthy subjects, with slightly larger tensile strains observed in the proximal BFLH (Fig. 3A). Such differences were exaggerated in the two previously injured subjects, who exhibited more non-uniform and localized strain concentrations in this same area (Fig. 3B).

DISCUSSION

This study provides important new insights into the ways in which post-injury remodeling can alter both musculotendon morphology and mechanics. Notably, both previously injured subjects exhibited enlarged proximal tendon/aponeuroses and greater principal strains in the proximal muscle tissue during low-load lengthening contractions.

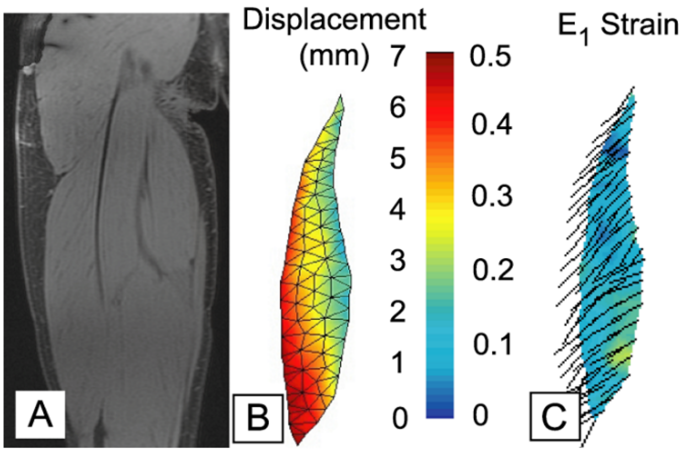

Figure 2. (A) Water-recontructed IDEAL images were used to visualize muscle fiber directions [4]. (B) Tissue motion was largest along the lateral region of the BFLH and (C) was generally aligned with the fiber direction.

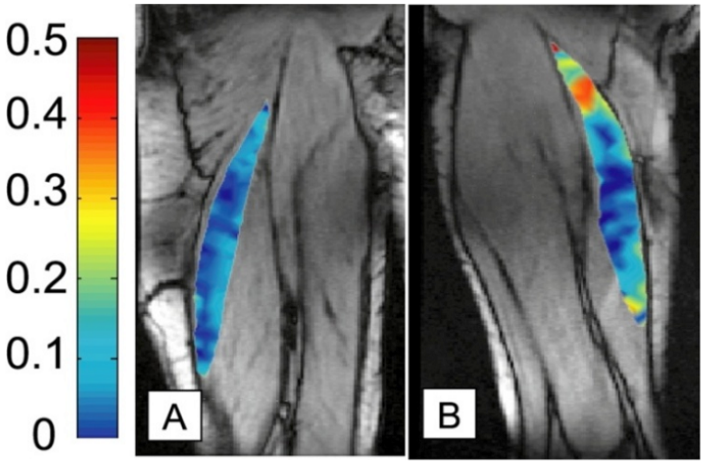

Figure 3. Larger strains were measured within a 2-3cm region surrounding the proximal MTJ boundary of the two injured subjects (B, left limb) compared to the healthy subjects (A, right limb).

The inertial loads used in this study require the proximal tendon to stretch during knee extension [7]. It is feasible that scar tissue is stiffer than the contractile tissue it replaces, and hence may have necessitated greater mechanical strain in the adjacent muscle tissue. Alternatively, scarring can alter lateral force transmission paths [8], which may also contribute to localized strain concentrations. The inclusion of additional injured subjects and a comparison of these measures with computational models is warranted to more definitively understand the underlying factors associated with injury risk. Nevertheless, these results suggest that long-term changes in morphology can alter lengthening contraction mechanics in a way that may contribute to the high risk for re-injury seen in these athletes. Such information is relevant for scientifically establishing effective rehabilitation programs for preventing re-injury.

REFERENCES

1. Orchard J and Best TM, *Clin J Sport Med*, **12**, 3-5, 2002.
2. Silder A, et al., *Skeletal Radiol*, **37**, 1101-9, 2008.
3. Thelen DG, et al., *MSSE*, **37**, 1931-8, 2005.
4. Reeder SB, et al., *Magn Reson Med*, **54**, 636-44, 2005.
5. Westphal CJ et al., *Proceedings of the North American Congress on Biomechanics*, Ann Arbor, MI, 2008.
6. Zhu Y and Pelc NJ, *IEEE Trans Med Imag*, **18**, 557-569, 1999
7. Silder A et al., *Proceedings of the North American Congress on Biomechanics,* Ann Arbor, MI, 2008.
8. Trotter JA, *Comp Biochem Physiol A*, **133**, 1127-33, 2002.

ACKNOWLEDGEMENTS

NIH AR 56201, NFL Charities, Christopher Westphal, Bryan Heiderscheit, Marc Sherry, and Silvia Blemker

THE EFFECTS OF DETRAINING ON STABILOMETRIC PERFORMANCE IN VOLLEYBALL PLAYERS

Boyi Dai, Christopher J. Sorensen and Jason C. Gillette
Department of Kinesiology, Iowa State University, Ames, IA, USA
email: daiboyi@iastate.edu, web: http://www.kin.hs.iastate.edu/

INTRODUCTION

Ankle sprain (AS) is a common sports related injury, especially for activities that largely involve landing from a jump such as basketball rebounding and volleyball blocking [1].

Stabilometry is a method for study of postural equilibrium. Decreased stabilometric performance (SP) has been associated with ankle instability and AS. Studies showed that coordination training and orthoses could enhance SP and decrease AS through improved neuromuscular control and mechanical support respectively [2,3].

However, the effects of detraining on SP haven't been studied. Detraining can be induced by injuries which can cause athletes to be absent from normal training from several days to years [4]. Training duration and intensity is often lower during off season than during competition season also resulting in detraining effects. It is important to know the effects of detraining on the ability of dynamic posture control in order to develop effective AS prevention training programs for rehabilitated athletes after detraining and for healthy athletes after an off season. The purpose of this study was to investigate how one month detraining could influence SP in collegiate volleyball players. It was hypothesized that the SP would decrease after the detraining.

METHODS

Twelve NCAA Division I female volleyball athletes (Before detraining: age 19.3 ± 1.2 yrs, height 1.78± 0.07 m, mass 71.2 ± 5.7 kg) took SP tests at the completion of one competition season and took SP tests again after one month season interval. Subjects were asked to record self-selected training workouts and duration during the season interval. In a SP test, each subject performed 4 SP trials in which the subject stood upright on right leg with eyes closed, left knee flexed at about 90 degrees without contact with the support limb, and arms folded in front of the chest. The duration of each trial was set at 20 sec during which force plate data were collected at 160 Hz and times of losing balance were recorded.

Center of pressure (COP) was calculated from force and moment data obtained from force plate. COP sway area; mediolateral (M/L), anterioposterior (A/P), and overall COP standard deviation (SD); M/L, A/P, and overall COP velocity were also calculated.

Standing time was calculated by the time duration from the start of each trail to subjects losing their balance or reaching 20 seconds. COP sway area was calculated by using convhull function in MATLAB (Figure 1). COP standard deviation was calculated by taking standard deviation of COP. Average COP velocity was calculated by taking the mean value of rectified COP velocity. All calculations were performed in MATLAB 7.4.0.

Wilcoxon Signed-Rank Test was used in SPSS 16.0 to compare dependent variables between pre-detraining and post-detraining SP tests. A Type I error rate of 0.05 was selected as indication of statistical significance.

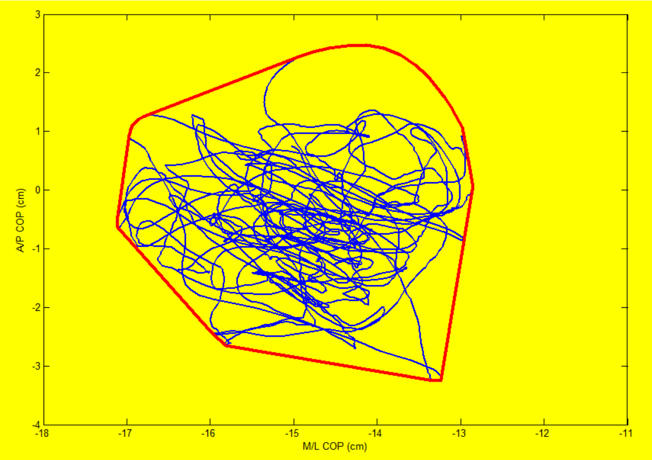

Figure 1: COP sway trajectory and sway area (outer border) calculated by convhull function.

RESULTS AND DISCUSSION

During competition season, the training time was 20 hours/week (14 practice & 6 game competition). During the one month season interval, athletes performed self-selected training and the training duration was 2.8±1.7 hours/week. No significant differences were found in height and weight before and after detraining ($p>0.05$).

No significant differences were found in standing time, COP area, and COP SD ($p>0.05$) (Table 1). Significant increases were observed in M/L velocity ($p=0.03$), A/P velocity ($p=0.05$), and overall velocity ($p=0.02$) after detraining (Table 1).

The hypothesis was supported by the significant increase in COP velocity parameters after one month detraining. Raymakers et al. [5] suggested that COP velocity information showed the most consistent differences between test situations, health conditions and age ranges. The results indicated that after one month detraining, although the standing time and COP displacement parameters remained similar, subjects needed a relatively faster postural sway pattern to maintain balance.

Tropp et al. [2,3] suggested that coordination training improved functional stability and postural control, whereas an orthoses provides mechanical support. Both of them were effective in the prevention of ankle joint injuries. On the other hand, 3-8 weeks detraining was shown to be enough to change muscular characteristics [6]. Twenty days bed-rest could significantly increased mean velocity of COP during quiet standing [7]. For current study, athletes were exposed to 20 hours training per/week during competition season and the training included strength training, balance training, volleyball practice, and game competition. However, subjects' training hours dropped to 2.8 hours/week during season interval for one month. It was postulated that during competition season, athletes' control patterns of postural stability were largely strengthened by intense training from both strength and proprioception aspects. After one month detraining, subjects' strength and proprioception abilities both may have decreased and resulted in decreased posture controlling ability. However, one month detraining was a relative short time, and decreases in balance control were detected by the more sensitive COP velocity information rather than standing time and COP SD information.

CONCLUSIONS

One month detraining results in significant decrease in the stabilometric performance and potential increase in the risk for ankle sprain injuries in volleyball players. Balance training should be implemented for athletes after detraining to prevent ankle sprain injuries.

REFERENCES

1. Bahr R, et al. *Am J Sports Med* **22**, 595–600, 1994.
2. Tropp H, et al. *Am J Sports Med* **12**, 185-188, 1984.
3. Tropp H, et al. *Am J Sports Med* **13**, 259-262, 1985.
4. Lynch SA and Renström PA. *Sports Med* **27**, 61-71, 1999.
5. Raymakers JA, et al. *Gait Posture* **21**, 48-58, 2005.
6. Mujika I, and Padilla S. *Med Sci Sports Exerc* **33**, 1297-303, 2001.
7. Kouzaki M, et al. *Acta Physiol* **189**, 279-292, 2007.

Table 1: SP parameters before and after detraining (Average and Standard deviation, * $p \leq 0.05$)

	Standing time (s)	COP Area (cm^2)	M/L SD (cm)	A/P SD (cm)	Overall SD (cm)	M/L Velocity (cm/s)	A/P Velocity (cm/s)	Overall Velocity (cm/s)
Before detraining	13.8 (4.5)	35.3 (11.1)	1.4 (0.2)	1.7 (0.5)	1.4 (0.2)	6.4* (1.5)	7.1* (1.4)	10.1* (1.4)
After detraining	13.1 (4.5)	37.6 (8.2)	1.5 (0.2)	1.8 (0.3)	1.5 (0.2)	7.1* (1.3)	8.2* (1.5)	11.5* (1.2)

SEAT TUBE ANGLE AFFECTS RECTUS FEMORIS ACTIVATION WHEN RIDING IN AN AERODYNAMIC POSITION

[1]Amy Silder, [2]Kyle Gleason, and [1,2,3]Darryl Thelen
Departments of [1]Biomedical Engineering, [2]Mechanical Engineering, and [3]Orthopedics and Rehabilitation, University of Wisconsin - Madison
email: silder@wisc.edu

INTRODUCTION

Triathlon specific bike frames have steeper seat tube angles (STA) than traditional road bikes. A steep STA translates and rotates the pelvis forward, facilitating a more aerodynamic riding position. Prior studies have found that these frames can also provide physiological and performance benefits in the early stages of a run performed after a fatiguing cycling bout [1]. Various hypotheses have been raised regarding the specific factors that may influence subsequent running performance. It is thought that the steeper STA may produce a more extended hip, which then facilitates longer stride length after cycling [1]. Additionally, a steeper STA may increase hamstring and gluteus activity in cycling, thereby diminishing quadriceps fatigue prior to running [1,2]. The purpose of this study was to investigate lower extremity joint angles, muscle lengths, and activation patterns when cycling at three STAs. We hypothesized that a steeper STA would result in a more extended hip and greater hamstring activity. To gain additional insights into factors that may affect the bike-to-run transition during triathlons, we also measured muscle activities and kinematics during running.

METHODS

Ten volunteers participated in this study (6 male, 4 female, age 32±9y, height 1.78±0.08m, mass 70±10kg). Cycling and running efforts were based on each subject's race pace for the 40k bike and 10k run portions of an Olympic distance triathlon. These were self-reported as 33.5±2.2km/hr and 3.8±0.4m/s, respectively. Cycling speed was converted into a power output for use during testing [3]. Cycling was performed on an adjustable stationary bicycle that was initially configured to replicate each subject's own bike set-up. We then varied STA (73°, 76°, 79°) while maintaining the radial distance between the crank and saddle, and between the crank and handlebars. Subjects biked at 90 revolutions per minute (rpm) using aerobars attached to the bike frame (Fig. 1). Data were collected for ~15s per configuration. Following cycling, each subject ran on an instrumented treadmill (Bertec) at 70, 80, 90, 100 and 110% of 10k pace. Full body kinematics and muscle activities were recorded during all cycling and running tasks. Muscle activities were measured on the right limb for the vastus lateralis (VL), rectus femoris (RF), biceps femoris (BF), medial hamstrings (MH), tibialis anterior (TA), medial gastrocnemius (GAS), and soleus (SOL).

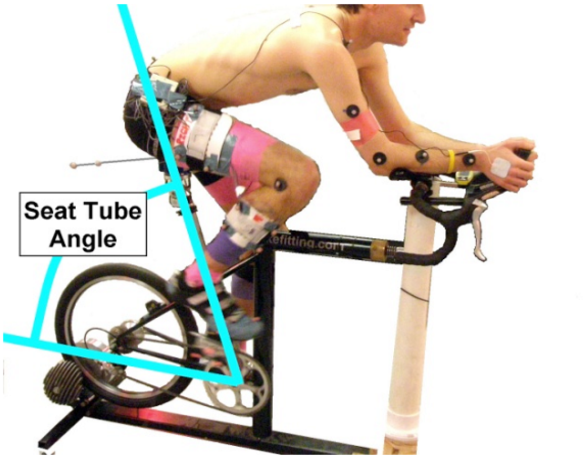

Figure 1: STA is the angle of the seat tube relative to the horizontal crank axis. Aerobars are typically used during triathlon training and racing.

Scaled musculoskeletal models [4] were created of each subject, and used to compute 3D joint angles and estimate musculotendon lengths. Electromyographic (EMG) signals were post-processed and onset, offset, and duration of muscle activity were then determined. The magnitude of muscle activity was estimated for each subject by finding the root-mean-square (RMS) value for each crank or gait cycle, and then averaged across cycles. Peak joint angles, musculotendon lengths, muscle activation timing, and RMS EMG activities were compared between cycling conditions and across running speeds using repeated measures ANOVAs ($\alpha=0.05$).

RESULTS

Anterior pelvic tilt increased significantly with STA, rotating forward an average of 3° for each 3° seat tube rotation. However, there were no significant differences in peak hip, knee, and ankle angles across STAs, with the exception of a slight increase (~1°) in knee extension. At the musculotendon level, there were significant increases in SOL, TA, MH, VL, and RF muscle excursions as STA increased. All muscle length excursions and peak lengths were significantly greater during running than cycling (Fig. 2).

The duration and magnitude of muscle activity was similar across all STAs, with the exception of a significant increase in RF muscle activity with STA (Fig. 3). This change was substantial, with an average 43% increase in activity between the 73° and 79° STAs. Muscle activity was significantly less during cycling compared to running, for all muscles except the RF and VL.

DISCUSSION

This study demonstrates that a steep STA increases pelvic tilt, but has minimal effect on peak lower extremity joint angles. Hence, the hypothesis that a steeper STA allows for a more extended hip is not supported, at least in the case where the handle bars are rotated simultaneously with the STA. There were some significant increases in muscle excursions (1-2mm) as STA increased, suggesting that a slightly greater range of motion was used. However, it is noteworthy that the absolute muscle lengths were substantially different between cycling and running (Fig. 2), such that the relatively small influence of STA on muscle excursions, in itself, may not affect the bike-to-run transition.

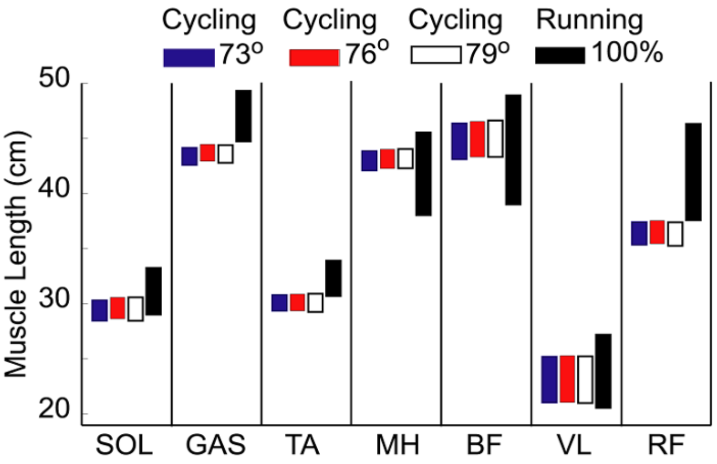

Figure 2: Though significant, the effect of STA on muscle excursions during cycling is minor compared to the absolute difference in length between cycling and running.

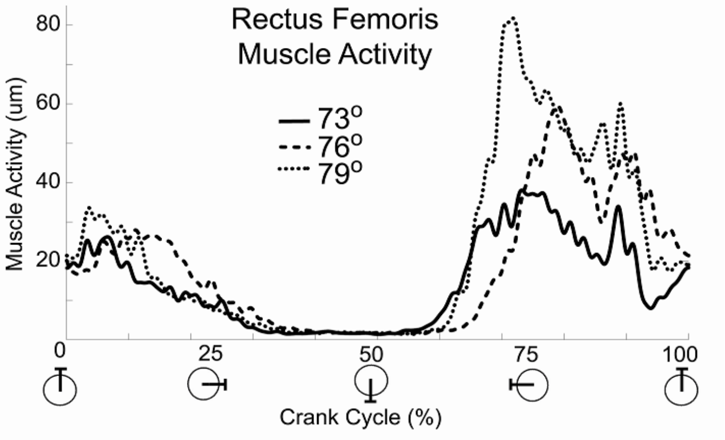

Figure 3: Rectus femoris activity increased with steeper STA during the upstroke of the crank cycle.

Despite the similarity in joint motion, there were changes in neuromuscular coordination with STA. Contrary to our hypothesis, we saw no evidence of increased reliance on hamstring activity at a steeper STA. However, RF activity increased with STA, with the major burst of activity occurring during the upstroke of the crank cycle. The RF normally functions as a top transition and extensor muscle during cycling [5], implying that coordination of this phase of the pedal stroke may be altered with STA. Hence, these results suggest that improved running performance after cycling on a steep STA [1] would more likely arise from a change in coordination than from a change in muscle lengths.

REFERENCES

1. Garside I and Doran DA *Journal of Sports Sciences*, **18**, 825-833, 2000.
2. Heil DP, et al. *MSSE*, **27**, 730-735, 1995.
3. Martin JC, et al. *Journal of Applied Biomechanics*, **14**, 276-291.
4. Delp SL, et al. *IEEE Trans BiomedEng*, **37**, 757-767, 1990.
5. Neptune RR, et al. *J Biomechanics*, **30**, 1051-1058.

ACKNOWLEDGEMENTS

Rick Neptune, PhD

Ankle Shock While Running on a Treadmill: A Requisite Stride Number

[1]Dwight E. Waddell, [1]Christi L. Brewer and [2]Jane M. Cappaert
[1]University of Mississippi, Department of Exercise Science, [2] Schering-Plough Consumer HealthCare
email: waddell@olemiss.edu

INTRODUCTION

Methodological considerations when measuring kinematics on a treadmill have recently been considered answering the question, “how many steps are enough?’ [1] Shock measures at the ankle using accelerometers have been reported for many years describing parameters ranging from energy and peak shock to spectral characteristics due to impact. The number of reported strikes used for these calculations varies, and no specific number has been reported as “enough”. The purpose of this study was to determine how many strides were necessary to characterize the peak shock and temporal response of the ankle of subjects while running at their preferred speed on a typical laboratory treadmill (Quinton Series Q4500).

METHODS

Thirteen subjects (8 male, 5 female, age range 18-24 years old) participated in this University IRB approved protocol. Subjects wore the same brand canvas-top sport shoe within gender (male = Airwalks, female = Cherokee). Subjects ran at their preferred running speed for 8-10 minutes, and accelerometry data were recorded in a 2 minute portion of each run after treadmill acclimatization. A two dimensional, 10G accelerometer (Noraxon U.S.A. Inc.) was tightly wrap-mounted (at the limit of subjects’ comfortability) at the base of the tibia. Heel strike sensors (Noraxon U.S.A. Inc.) were mounted on the outside of shoes to time mark heel strikes. Peak shock as well as an ensemble average of the integral of the power spectral density (PSD, frequency range from 12-25 Hz) associated with heel strike and stance phase were calculated with in-house programs (Matlab, The MathWorks, Inc., Natick MA). A Repeated Measures ANOVA was employed to determine at which point an additional 5 heel strikes no longer significantly altered the mean of both the peak shock and integrated PSD. A total of 60 strides were included, therefore comparisons were made at 5, 10, 15, 20 etc. up to 60 heel strikes.

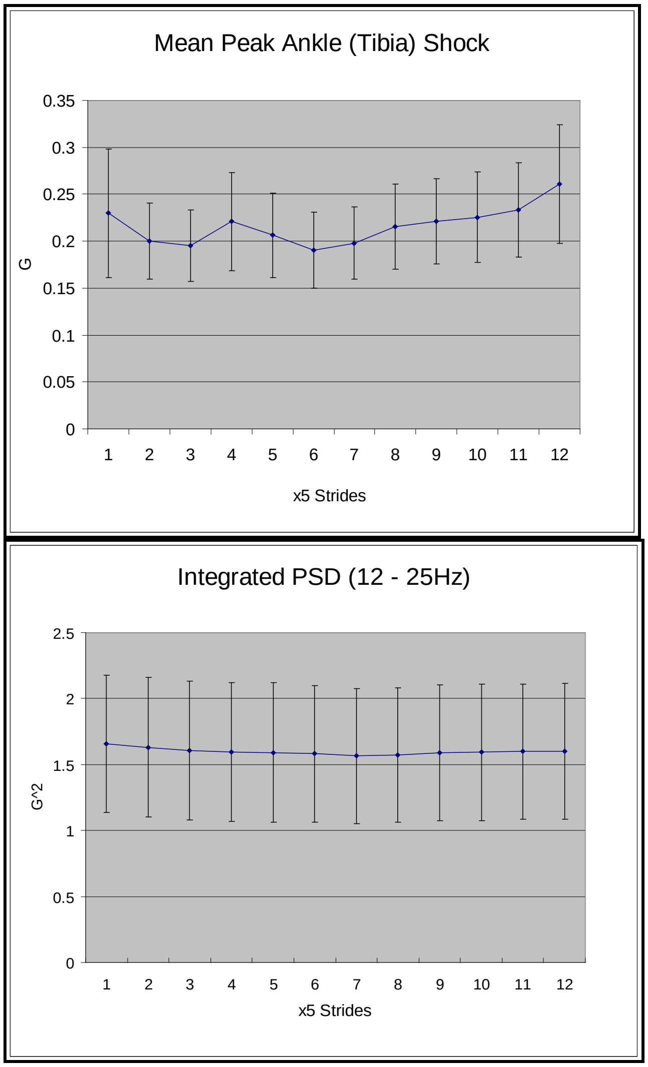

Figure 1: top - mean peak ankle shock at heel strike across x5 strides, bottom – average integrated PSD (12-25 Hz) across x5 strides during stance phase.

RESULTS AND DISCUSSION

Figure 1. shows the results of the repeated measures calculations across the 12 levels of dependent variables. There were no significant differences for either shock or integrated PSD with the inclusions of additional groups of 5 strides ($p > .05$).

CONCLUSIONS

Much like kinematic and kinetic gait data, it appears five consecutive strides are sufficient to characterize the mean of spatial and temporal accelerometry data at the ankle. The variance of these measures is now being considered. There are statistical issues looking at repeated measures of variances and a more complicated analysis will be called for in order to determine if 5 strides will be sufficient to characterize accelerometry variance at the ankle.

REFERENCES

1. Owings, TM & Grabiner, MD. Measuring step kinematics on an instrumented treadmill: how many steps are enough. *Journal of Biomechanics*, **36** (2003) 1215-1218.

SAFE PATIENT HANDLING: A KINEMATIC ANALYSIS OF DEVICE-ASSISTED VERSUS NO DEVICE SIT-TO-STAND MOTION

[1,2]Michaela M. McBride, [1,2]Aaron M. Hueftle, [1,2]Megan E. Krause, [1]Thad W. Buster, [1,2]Judith M. Burnfield, [2]Gregory R. Bashford, [1]Adam P. Taylor
[1]Madonna Rehabilitation Hospital, Institute for Rehabilitation Science and Engineering, Lincoln, NE
[2]Biological Systems Engineering and Biological Sciences, University of Nebraska – Lincoln, Lincoln, NE
email: jburnfield@madonna.org, web: http://madonna.org/research_institute

INTRODUCTION

Workplace injuries in the rehabilitation environment are of significant concern due to their impact on patient care. One common activity that leads to injuries is transferring from one surface to another (e.g., bed to chair) [1]. Mechanical devices have been developed to assist with transfers and to reduce the risk of injury. To date, no research has systematically compared the extent to which patient movements within these devices simulate normal transfer motions. Knowledge of the biofidelity of these movement patterns could help guide clinical use of select devices within therapeutic treatment programs aimed at enhancing patients' independent transfer skills. The purpose of this study was to compare sagittal plane trunk, pelvis and lower extremity kinematics recorded during sit-to-stand movements with and without a transfer device.

METHODS

Ten young, healthy adults participated (5 males, 5 females). Sagittal plane kinematics were recorded using a 12-camera motion analysis system (Qualisys Motion Analysis System, Gothenburg, Sweden) to determine trunk, pelvis and thigh positions relative to vertical and knee and ankle joint angles. A Vancare VeraLift power-assisted sit-to-stand device was used for the device-assisted trials. Each participant performed three sit-to-stand trials with no device (ND) and six device-assisted sit-to-stand trials: three giving their best effort to assist the device (DA-BE) and three offering no effort to assist the device (DA-NE). Separate, one-way analyses of variance (3x1 ANOVA) identified key differences in INITIAL (0% movement cycle; seated) and FINAL (100% movement cycle; standing) positions between ND, DA-BE and DA-NE. The coefficient of multiple correlations (CMC) [2] quantified similarities in kinematic profiles between ND and DA-BE and ND and DA-NE.

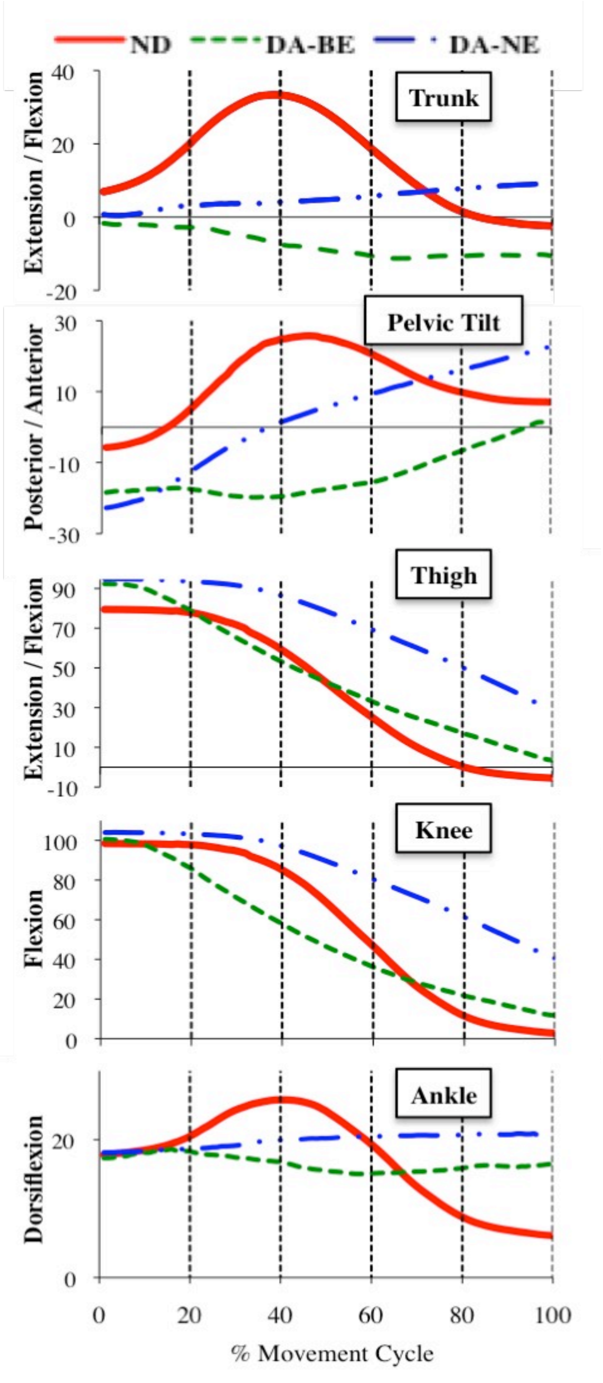

Figure 1: Mean sagittal plane joint angles recorded during sit-to-stand motion.

RESULTS AND DISCUSSION

The mean ensemble plots arising from performance of the three conditions are provided in Figure 1. Table 1 identifies significant differences in INITIAL and FINAL positions across conditions. CMC values comparing movement profiles across the three conditions are presented in Table 2.

Table 1: Comparison of initial and final joint postures during the three transfer conditions.

Region	Phase	Significant Main Effect ($P < 0.00625$)
Trunk	INITIAL	ND>DA-BE
	FINAL	DA-NE>ND>DA-BE
Pelvis	INITIAL	ND>DA-BE, DA-NE
	FINAL	DA-NE>ND, DA-BE
Thigh	INITIAL	DA-BE, DA-NE>ND
	FINAL	DA-NE>DA-BE, ND
Knee	INITIAL	NS (p=0.139)
	FINAL	DA-NE>DA-BE, ND
Ankle	INITIAL	NS (p=0.916)
	FINAL	DA-NE, DA-BE>ND

The trunk began and ended in significantly more flexion in the ND condition compared to DA-BE. DA-NE had greater trunk flexion than ND only at the end. The pelvis began in significantly more posterior tilt in DA-BE and DA-NE compared to ND. Final pelvis position was significantly more anteriorly tilted during DA-NE compared to other conditions. The thigh started in greater flexion in DA-BE and DA-NE compared to ND. The end thigh position was more flexed in DA-NE compared to other conditions. While the starting knee posture did not differ across conditions, DA-NE demonstrated significantly greater flexion at cessation compared to DA-BE and ND. The overall arc of ankle movement was limited in device-assisted movement. Initial ankle postures were similar across conditions; however, ND posture was significantly less dorsiflexed at cessation compared to device-assisted movement.

CONCLUSIONS

A key goal for many rehabilitation patients is to learn to independently transfer between positions. When profound weakness and balance prevent the patient from safely performing this task, external human and/or device assistance is often required. Device-assisted movement patterns that simulate normal transfers could enable clients to transfer safely and to practice the activity they seek to relearn. The current study focused on the movement patterns occurring in one sit-to-stand transfer device frequently used in rehabilitation settings. DA-BE movement patterns in the VeraLift most closely emulated normal sit-to-stand movements at the thigh and knee as evidenced by the high CMC values. CMC values for these same anatomic regions dropped notably during the no effort condition. The lowest CMC values between the device-assisted conditions and normal sit-to-stand movements occurred at the trunk, pelvis and ankle.

The current study represents a first step in exploring the biofidelity of device-assisted sit-to-stand movement patterns. Further research is required to explore movement patterns (joint motions and muscle activation patterns) in other devices frequently used in rehabilitation settings; as well as to identify the impact patient pathology has on the clinician's ability to facilitate optimal movement and muscle activation patterns.

REFERENCES

1. Schoen, D.C., *Low Back Pain, Orthopaedic Nursing* **23,** 154-157, 2004.
2. Kadaba, M.P., et al. *Journal of Orthopedic Research,* **7,** 849-860, 2005

ACKNOWLEDGEMENTS

The authors would like to thank the Undergraduate Creative Activities and Research Experiences (UCARE) Program (MMM, AMH) and the Agricultural Research Division Undergraduate Fellowship (MEK) for funding this project.

Table 2: Coefficients of multiple correlation (CMC) values comparing kinematic profiles during each device-assisted condition to the no device condition at the trunk, pelvis, thigh, knee and ankle.

	Trunk	Pelvis	Thigh	Knee	Ankle
Device-assisted: best effort	0.49 ± 0.11	0.35 ± 0.11	0.97± 0.02	0.95 ± 0.03	0.69 ± 0.11
Device-assisted: no effort	0.56 ± 0.09	0.75 ± 0.12	0.83 ± 0.04	0.86 ± 0.07	0.58 ± 0.10

CONTRIBUTIONS OF LEG MUSCLES TO THE AXIAL KNEE JOINT CONTACT FORCE DURING NORMAL WALKING

[1] Kotaro Sasaki and [2] Richard R. Neptune
[1] Department of Mechanical and Biomedical Engineering, Boise State University, Boise ID USA
[2] Department of Mechanical Engineering, University of Texas at Austin, Austin, TX USA
email: kosasaki@boisestate.edu

INTRODUCTION

Joint contract forces developed during dynamic motor activities can be significantly influenced by muscle forces [1, 2]. However, individual muscle force contributions to joint contact forces are not fully understood. Previous studies using inverse dynamics-based analyses have estimated joint forces during walking, typically by computing the sum of the contributions from the intersegmental joint forces and muscle forces that cross the joints of interest [3]. However, muscles can contribute to forces in joints that they do not cross through dynamic coupling [4], and therefore these approaches may neglect important contributions from specific muscles.

In contrast, muscle-actuated forward dynamics simulations are governed by the dynamic equations of motion, and therefore have the ability to quantify the contribution of every muscle to every joint force (e.g., [5]). The specific objective of this study was to use a muscle-driven forward dynamic simulation to identify individual muscle contributions to the knee joint force during normal walking, which has important implications for understanding the development and progression of osteoarthritis and other joint disorders in the knee.

METHODS

Muscle-driven forward simulation of walking

A sagittal-plane forward dynamics simulation of walking was generated using a musculoskeletal model (SIMM: MusculoGraphics) and deriving the equations of motion using SD/FAST (PTC). The model consisted of a trunk and two legs with 13 degrees-of-freedom and 25 Hill-type musculotendon actuators per leg (combined into nine functional groups). The tibiofemoral joint was modeled as a planar joint, with the position and orientation of the tibia being prescribed as functions of knee flexion angle [6]. Visco-elastic elements were attached to each foot segment to model foot-ground contact [7]. Dynamic optimization was performed to fine-tune the muscle excitation patterns such that the simulation reproduced experimental kinematics and ground reaction forces (GRFs) over a full gait cycle (i.e., heel-strike to the subsequent ipsilateral heel-strike) [5]. Constraints on muscle excitation timing were imposed in the optimization to be consistent with experimental electromyography (EMG) to assure that muscles were generating force at the appropriate time in the gait cycle.

Experimental data

Previously collected experimental data (kinematics, GRFs and EMG) during walking at 1.2 m/s on an instrumented treadmill were used (n=10, age 29.6±6.1 years old, [8]). Kinematics, GRFs and surface EMG from 7 muscles were collected at 120, 480 and 1200 Hz, respectively, for 15 seconds. Low-pass filtered kinematic and GRF data (6 and 20 Hz cut-off frequencies, respectively) and EMG linear envelope were time-normalized to the gait cycle, averaged within and then across the subjects to obtain a group average.

Muscle contributions to knee joint force

The axial knee joint force (the force component parallel to the longitudinal axis of the tibia) over the gait cycle was determined from the system equations of motion using SD/FAST. Individual muscle contributions to the axial knee joint force were obtained using a joint force decomposition technique [4].

RESULTS AND DISCUSSION

The maximum axial knee joint force was ~3 times body weight (one BW is equivalent to 736 N), which occurred during weight acceptance in early stance phase (Fig. 1: ~15% gait cycle). The magnitude was comparable to previous *in vivo* knee joint force measurements of ~2.8 BW [9]. The quadriceps (rectus femoris and vastus muscles), hamstrings and gluteus maximus contributed substantially to the peak knee joint force during weight acceptance (Fig. 2: 0-20% gait cycle). The plantar flexors (soleus and gastrocnemius) also contributed to the knee joint force from mid- to late stance, with the gastrocnemius being the primary contributor (Fig. 2: ~20-55% gait cycle). The pronounced quadriceps and gastrocnemius contributions in this study are consistent with previous simulation work [10].

The simulation results highlighted that in addition to the major muscles crossing the knee joint (i.e., the quadriceps, hamstrings and gastrocnemius), muscles that do not cross the knee joint (e.g., soleus, gluteus maximus) can potentially be significant contributors to the knee joint force. These muscles are also among the primary contributors to ground reaction forces in walking [5], and thereby, contribute to knee joint force via dynamic coupling.

The results of simulation studies such as these have the potential to provide much insight into specific characteristics of pathological gait affected by joint diseases, such as knee osteoarthritis. For example, reduced knee extensor moment in early stance and reduced plantar flexor moment in late stance are often observed in knee osteoarthritis patients [11, 12], and may be related to the patients' desire to reduce their knee joint forces during walking. However, a challenging aspect of modeling-based joint loading studies is validation of the results as joint loading is difficult to measure *in vivo* during dynamic tasks such as walking. However, instrumented implants have provided important validation data [9, 13], and combining such data with detailed models is a promising area for future work.

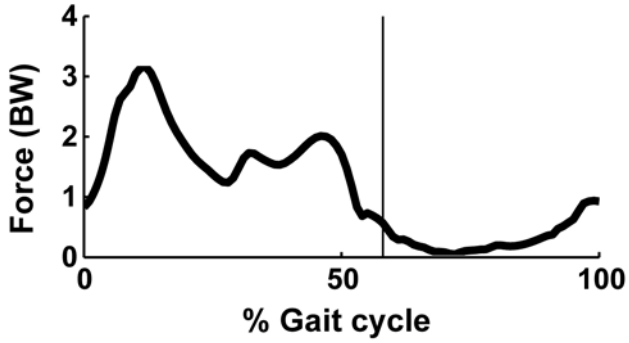

Figure 1: The axial knee joint force over the gait cycle. The vertical line represents toe-off.

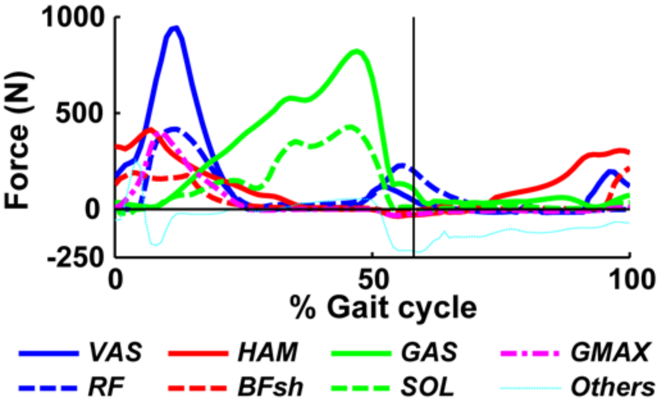

Figure 2: Individual muscle contributions to the axial knee joint force over the gait cycle. The vertical line represents toe-off. **VAS:** vastus muscles, **RF:** rectus femoris, **HAM:** hamstrings, **BFsh:** biceps femoris short head, **GAS:** gastrocnemius, **SOL:** soleus, **GMAX:** gluteus maximus, **Others:** all other muscles combined.

REFERENCES

1. Lu TW, et al. *J Biomech* **30**, 1101-1106, 1997.
2. Glitsch U and Baumann W. *J Biomech* **30**, 1123-1131, 1997.
3. Hardt DE. *J Biomech Eng* **100**, 72-78, 1978.
4. Zajac FE, et al. *Gait Posture* **17**, 1-17, 2003.
5. Neptune RR, et al. *Gait Posture* **19**, 194-205, 2004.
6. Yamaguchi GT and Zajac FE. *J Biomech* **22**, 1-10, 1989.
7. Neptune RR, et al. *Comp Meth Biomech Biomed Eng* **3**, 321-334, 2000.
8. Neptune RR and Sasaki K. *J Exp Biol* **208**, 799-808, 2005.
9. Heinlein B, et al. *Clin Biomech* **24**, 315-326, 2009.
10. Shelburne KB, et al. *J Orthop Res* **24**, 1983-1990, 2006.
11. Kaufman KR, et al. *J Biomech* **34**, 907-915, 2001.
12. Astephen JL, et al. *J Biomech* **41**, 868-876, 2008.
13. D'Lima DD, et al. *J Biomech* **40** (Suppl 1), S11-S17, 2007.

EFFECTS OF NOVEL PHYSIOLOGICAL-BASED FUNCTIONAL ELECTRICAL STIMULATION PATTERNS ON POST-STROKE GAIT

[1] Trisha Kesar, [2] Ramu Perumal, [1,2]Darcy Reisman,
[1,2]Katherine Rudolph, [1]Jill Higginson, [1,2]Stuart A. Binder-Macleod
[1]Biomechanics and Movement Science Program, [2]Department of Physical Therapy, University of Delaware, Newark, DE, USA. Email: kesar@udel.edu

INTRODUCTION

Foot drop, caused by paresis of the ankle dorsiflexor muscles, is a common post-stroke gait impairment. Foot drop makes swing limb foot clearance difficult, and contributes to decreased endurance and increased incidence of falls.

Functional electrical stimulation (FES) is an intervention that delivers electrical stimulation to ankle dorsiflexor muscles during the swing phase of gait to correct foot drop [1]. The arrangement or pattern of pulses within the train can be varied to control motion during FES [2] (Fig.1). It has been well documented that the stimulation patterns traditionally used during FES, i.e., constant-frequency trains or CFTs, can contribute to limitations such as imprecise control of force and rapid muscle fatigue [2]. Previous studies have also shown that novel stimulation patterns, called variable-frequency trains (VFTs), enhance isometric muscle performance compared to CFTs (Fig. 1) [2]. VFTs include a high-frequency burst of 2-3 pulses within the stimulation train. The nervous system delivers similar high-frequency bursts of pulses during physiological contractions [2].

Although VFTs can enhance skeletal muscle performance during FES, VFTs have never been used during FES for gait. Thus, the aim of this study was to compare the effects of delivering dorsiflexor FES using VFTs versus CFTs on post-stroke gait. We hypothesized that VFTs would produce better correction of foot drop compared to CFTs.

METHODS

Twelve subjects (49 to 72 years; 9 males) with post-stroke hemiparesis provided informed consent approved by the IRB to participate in this study.

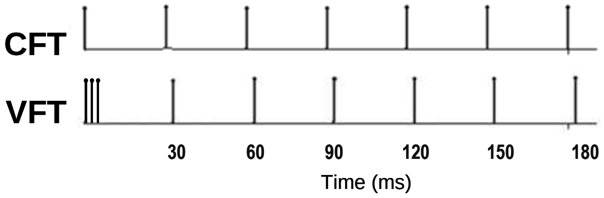

Figure 1. Schematic depicting the 2 stimulation patterns used in this study. CFTs consisted of single pulses (300-µs pulse duration) separated by 33-ms inter-pulse intervals. VFTs included a 200-Hz high-frequency burst at the start of a CFT with 33-ms inter-pulse intervals.

Electrical stimulation was delivered surface electrodes (TENS Products, CO) using a Grass S8800 stimulator (Grass Instruments, MA). With subjects seated, the stimulation intensity was set by gradually increasing the amplitude of a 300-ms long stimulation train until a neutral ankle joint position (0º) was achieved. Two compression closing foot switches (Motion Lab Systems Inc., LA) were attached to the soles of each subject's shoes. A customized, real-time FES system (CompactRIO, National Instruments, TX) was used to deliver FES to the paretic ankle dorsiflexor muscles during the paretic swing phase based on footswitch signals. *Instrumented gait analysis* was performed as subjects walked on a split-belt treadmill instrumented with two force platforms (AMTI, Watertown, MA). Marker data were captured at 100-Hz using an 8-camera motion analyses system (Vicon 5.2, Oxford, UK). Force platform, footswitch, and stimulation channel data were sampled at 2000-Hz. Outcome variables were computed using commercial software (Visual 3D; C-Motion, MD).

Three *walking conditions* were compared: (1) walking without FES (noFES), (2) walking with dorsiflexor muscle FES using CFTs (FES-CFT), and (3) walking with dorsiflexor FES using VFTs

(FES-VFT). All 3 walking conditions were tested at the subjects' self-selected over ground walking speed.

RESULTS AND DISCUSSION

Gait variables of interest and joint angle data are presented in Table 1 and Figure 2 respectively.

Table 1. Gait Variables of Interest (N=12)

		No FES	FES CFT	FES VFT
Ankle Angle (°)	Swing	-2.9	0.3 (*)	2.2 (†)
	At IC	-8.5	-3.0 (*)	-1.0
	At Toe-off	-9.2	-5.2 (*)	-3.1 (†)
Knee Flexion (°)	Swing	44.1	42.6 (*)	40.8 (†)

Positive ankle angles represent dorsiflexion.* Significant difference from noFES. † Significant difference from FES-CFT.

As anticipated, we observed significantly greater ankle dorsiflexion during swing and at initial contact (IC) during dorsiflexor FES versus noFES. Also, as hypothesized, during dorsiflexor FES, VFTs produced enhancements in all outcome variables compared to CFTs.

Interestingly, dorsiflexor FES resulted in reduced ankle plantarflexion at toe-off, which is a previously unreported 'adverse effect' of dorsiflexor FES on post-stroke gait. Detailed analysis of our data revealed that because foot switches were used to trigger FES during gait, dorsiflexor FES started a little earlier than 'true' toe-off (as determined using vertical ground reaction forces). Similar to the present study, most FES systems for foot drop start dorsiflexor FES between heel-off and toe-off, which may result in adverse effects on ankle kinematics at toe-off, as demonstrated in our study.

Another novel finding of our study was a reduction in peak swing phase knee flexion observed during dorsiflexor FES compared to noFES. Interestingly, forward dynamic simulations of post-stroke gait predict reduced swing phase knee flexion as an effect of dorsiflexor FES, consistent with our findings [3].

CONCLUSIONS

We demonstrated the feasibility and advantages of using physiological-based stimulation patterns (VFTs) during FES for post-stroke gait. The use of VFTs to improve post-stroke gait performance during FES, as presented for the first time in our study, is an example of the successful translation of research evidence from animal literature [4] to isometric human studies [2], and finally, to a clinical application. Also, we demonstrated that dorsiflexor FES can adversely affect ankle angles at toe-off and swing phase knee kinematics. Our systematic analysis of the effects of FES on post-stroke gait revealed that the accurate timing of delivery of FES during gait is critical, and merits further investigation.

REFERENCES

1. Liberson WT et al. *Arch Phys Med Rehabil* **42**, 101-5, 1961.
2. Binder-Macleod S & Kesar T. *Muscle Nerve* **31**, 681-93, 2005.
3. Higginson JS et al. *ASME Summer Bioengineering Conference*, 2007.
4. Burke RE et al. *Science* **168,** 122-4, 1970.

ACKNOWLEDGEMENTS

NIH Grant R01 NR010786, NIH Shared Instrumentation Grant S10 RR022396-01, DOD Grant W911NF-05-1-0097 University of Delaware Dissertation Fellowship

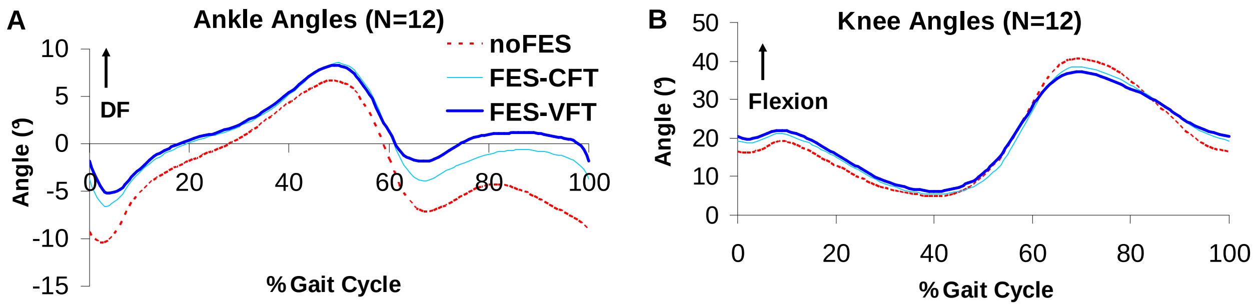

Figure 2. Sagittal plane (A) ankle angles (dorsiflexion = DF = positive) and (B) knee angles (flexion = positive)

IN-VITRO ESTIMATION OF FINGER JOINT REACTION FORCES DURING ISOMETRIC FORCE GENERATION

[1]Sang Wook Lee and [1,2]Derek G. Kamper
[1]Rehabilitation Institute of Chicago, [2]Illinois Institute of Technology
e-mail: sanglee2@northwestern.edu

INTRODUCTION

Osteoarthritis (OA), the most common form of arthritis, is one of the leading causes of disability among the elderly in Caucasian populations [1]. Although the importance of mechanical factors such as high joint loading in the etiology of OA has been emphasized [2], few studies have actually estimated joint force/pressure in the finger joints during common manual tasks, such as pinch or power grasp. Previous studies largely relied on the measurement of geometric variables such as tendon locations, to solve the force and moment equilibrium equations used to estimate the joint contact forces resulting from loading of tendons [3]. Thus, various kinetic components in finger dynamics (e.g. frictional loss of tendon force and passive joint dynamics) and their effects on resultant joint reaction forces were not considered.

In this study, we present a novel method to estimate finger joint reaction forces produced by the flexor digitorum profundus (FDP) tendon, a major extrinsic flexor tendon of the hand. Fingertip force and moment data under tendon loading were measured in cadavers and incorporated with a normative model of the hand [4]. This model was employed to estimate the joint reaction forces resulting from applied loading of the FDP tendon. The transmission of tendon force to joint reaction force was examined across different finger postures in order to examine the effects of grip type and object size.

METHODS

Two fresh-frozen cadaveric hands were tested to estimate the joint reaction forces at three finger joints, i.e. distal phalangeal (DIP), proximal interphalangeal, and metacarpophalangeal (MCP) joints, under tendon force application. The distal tendon of the FDP muscle was exposed and sutured to nylon cord to allow tendon loading. Each specimen was mounted on a fixation device (Agee-Wristjack, Hand Biomechanics Lab, Sacramento, CA), and its index fingertip was secured to a 6 degree-of-freedom load cell (JR3, Inc., Woodland, CA). For each specimen, a set of six postures, i.e. two pairs of proximal and distal interphalangeal (PIP, DIP) joint angles (IP1: (30°, 20°) and IP2: (45°, 30°)) explored at each of three metacarpophalangeal (MCP) joint angles (MCP1: 0°, MCP2: 30°, MCP3: 60°), were tested in order to examine the effects of different grip types or different object sizes on the joint reaction forces. For example, a small object size would correspond to large finger flexion angles.

The six-dimensional fingertip output vector (force and moment) was first recorded without tendon loading. Then, approximately 25% of the maximal force of the FDP (11.8N) was applied. In order to eliminate the effects of passive joint stiffness/damping on the fingertip output vector, only the change in the fingertip force and moment values due to tendon loading were incorporated into the force and moment equilibrium equations. These equations were derived based on the finger tendon-pulley geometry described by a normative finger model [4]. At each posture, potential tendon force loss due to mechanical factors, such as friction, was set to an independent variable, and obtained from an optimization process that minimizes the least-square errors in the force/moment equilibrium equations at all joints. Then, from these equilibrium equations, magnitudes and directions of joint reaction forces at all three joints were computed.

Also, joint reaction force vectors applied onto the proximal end of the distal and middle phalanges (i.e. DIP and PIP joints), which are specifically vulnerable to OA (i.e. Heberden's and Bouchard's nodes) were decomposed into two components, compression force (parallel to the proximal segment) f_c and shear forces (orthogonal to the segment) f_s. From the estimated force components, the corresponding joint shear force angle α, which can indicate the high pressure location within the joint, was calculated

$$\alpha = \tan^{-1}\left({f_s}/{f_c} \right) \qquad (1)$$

RESULTS AND DISCUSSION

Resultant joint loading was generally larger at DIP joint than at other joints (Fig. 1). Joint reaction forces at the DIP and PIP joints were increased along with the increase in both IP and MCP joint angles, while MCP joint force remains relatively constant across different postures. As the contact areas of the DIP and PIP joints are smaller than that of the MCP joint, the results of this analysis confirm the increased risk of these joints to the development of OA (i.e. DIP: Heberden's node, PIP: Bouchard's nodes).

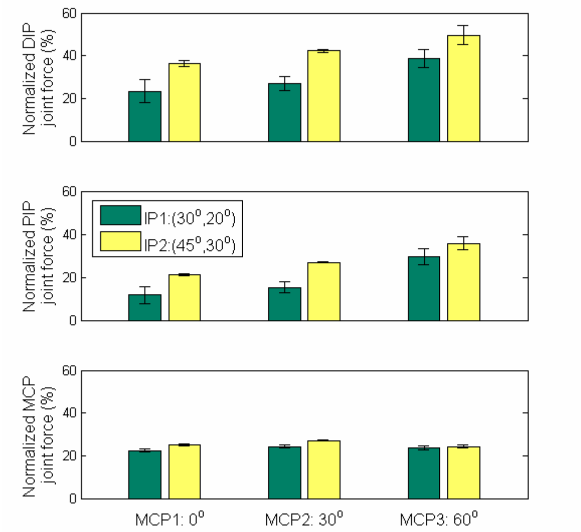

Figure 1: Mean (SD) magnitudes of the joint reaction forces normalized by the applied tendon force across different postures.

Joint shear force angle α values, which represent the shear force vs. compression force ratio, were generally higher at DIP joints (Table 1). At DIP joints, α values decreased along with the increase in the IP and MCP joint angles, which indicates that higher shear force at DIP joint can be generated in smaller IP and MCP angles, in other words, when interacting with large objects. On the other hand, at the PIP joint, the joint shear force angle values increased in more flexed postures (i.e. larger IP/MCP angles). Note that positive α values (>0) indicate increased localized high pressure on the volar aspect of the joint. This may be associated with the predominant palmar articular cartilage loss commonly observed in DIP/PIP joints affected by OA [5].

Table 1: Mean joint shear force angles (unit: °)

	DIP		PIP	
	IP1	IP2	IP1	IP2
MCP1	45	40	8	27
MCP2	39	36	15	27
MCP3	24	30	15	28

* Here, note that 0° indicates pure compression force, 90° pure palmar shear force, and -90° dorsal shear force.

The results of this study indicate that both magnitude and direction of finger joint reaction forces are complex functions of grip strength (i.e. tendon force), object size, and other postural effects that affect finger joint angles, such as personal preference. Thus, careful consideration of these factors should be taken when the risk of developing certain musculoskeletal diseases (e.g. OA) involved in specific tasks is to be assessed.

Applicability of these findings to the general population is limited by the small sample size (n = 2). Further testing with more specimens will be needed to examine the effects of potential anatomical variability on the estimated tendon force – joint force relationship. In addition, some discrepancy between the actual tendon location of the specimens and those obtained from the normative model may exist. Future studies should examine the relationship between other major finger tendons and joint reaction forces, thereby enabling more accurate estimation of finger joint force in manual tasks, which usually require concurrent activation of multiple muscles.

REFERENCES

1. Felson D. *Rheum Dis Clin North Am* **19**, 607-615, 1993.
2. Brandt KD, et al. *Rheum Dis Clin North Am* **34**, 531-559, 2008.
3. Cooney WP and Chao EY. *J Bone Joint Surg Am* **59**, 27-36, 1977.
4. An et al. *J Biomech* **12**, 775-788, 1979.
5. Tan et al. *Arthritis Rheum* **52**, 2355-2365, 2005.

Effects of Increased Task Difficulty on Performance Variable Stabilization during Human Locomotion

Arick Auyang[1], Young-Hui Chang[1,2]
[1]Comparative Neuromechanics Lab, School of Applied Physiology, GeorgiaTech, Atlanta, GA, USA
Email: arick.auyang@gmail.com
http://www.ap.gatech.edu/chang/CNLmission.html

INTRODUCTION

Evidence for the simplification of motor control of kinematic performance variables during human locomotion exists in areas of biomechanics, neurophysiology, computational neuroscience, and robotics[1,3,4,6]. Human hopping in place is the simplest form of a human bouncing gait that can be modeled as a spring-mass system [2,5]. We recently showed that leg length and orientation are stabilized (i.e., decreased variance) through the purposeful structuring of joint angle variance during human hopping[1]. Our data showed that overall leg length stabilization increased as hopping frequency increased while leg orientation stabilization showed no change (**Fig. 1**). Hopping at non-preferred frequencies likely created a more difficult task that required increase stabilization of leg length. As the index of difficulty (ID) for an upper extremity task increases, local variable variance becomes increasingly structured to stabilize the performance variables in local variables [8]. The purpose of this study is to test more directly whether greater task difficulty during locomotion causes increased structuring of variance to meet the increased demands of stabilizing leg orientation.

The Uncontrolled Manifold (UCM) analysis allows us to analyze whether segment angle variance is structured to exploit motor redundancy and stabilize a kinematic performance variable [7]. We investigated 2.2Hz one-legged human hopping in place with increased demands for foot placement precision to study the use of motor abundance in stabilizing leg length and leg orientation. Increased foot placement precision requires a smaller margin of error for take-off and landing leg orientation but should have little effect on leg length demands. We hypothesized that a task with a higher ID for foot placement precision will result in increased structure of joint angle variance to stabilize leg orientation but not leg length.

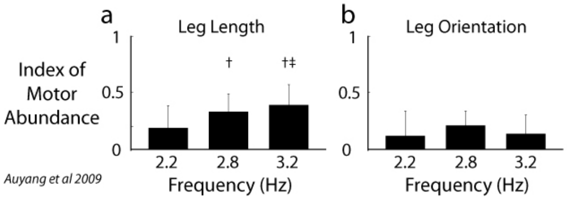

Auyang et al 2009

Fig. 1. Average Index of Motor abundance (IMA) shows selective stabilization of **(a)** leg length and **(b)** leg orientation at three hopping frequencies. Data are average IMA ±1 standard deviation (n=10). †denotes significant difference from 2.2 Hz ($p<0.01$). ‡ denotes significant difference from 2.8 Hz ($p<0.01$).

METHODS

Subjects hopped on their dominant leg at 2.2Hz on three different target sizes (88, 213, and $466 mm^2$) while 3-D lower body kinematics data were collected. Target sizes constrained foot placement thus requiring increased precision. Target sizes were determined using Fitts' Law which describes a relationship between the distance traveled of the end effector and the target size, where smaller targets correspond to greater ID. Sagittal plane segment angles (Vicon) were calculated using Matlab. We ran the UCM analysis for each performance variable (leg length and leg orientation) at 1% bins over the entire hopping cycle for all hops (~62 hops per condition). The UCM analysis tells us whether motor redundancy is used to stabilize the performance variables leg length and orientation by selecting a certain set of goal oriented joint kinematic combinations. We calculated an Index of Motor Abundance (IMA, [1]) at each time point to test whether subjects selectively utilized motor redundancy in the joints to stabilize each performance variable, indicated by an IMA greater than 0. IMA was averaged across 100% of the hopping cycle for Fig. 1 and 3.

RESULTS

Preliminary data from 2 subjects showed that as the index of difficulty (ID) increased (i.e., smaller targets), the average total variance of the four segment angles (foot, shank, thigh, pelvis) also increased (**Fig. 2**). Overall variance of leg orientation, however, decreased (**Fig. 3**) as ID increased. UCM results of both subjects showed higher ID resulted in increased coordination of segment angles to stabilize leg orientation (**Fig. 4b**) but not leg length (**Fig. 4a**).

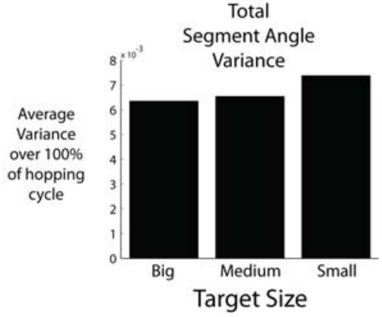

Fig. 2. Average total segment angle variance over 100% of the hopping cycle for leg orientation when hopping with increased ID i.e. smaller targets. Representative subject.

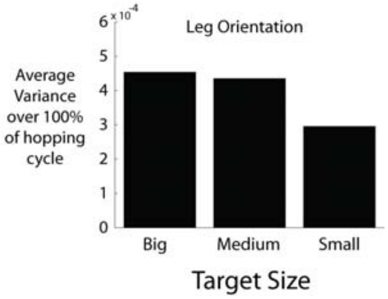

Fig. 3. Average variance over 100% of the hopping cycle for leg orientation when hopping with increased ID i.e. smaller targets. Representative subject.

DISCUSSION

Preliminary results support our hypothesis that utilization of motor redundancy can be appropriately and selectively up regulated to meet increased locomotor task demands. By constraining the target landing area, landing and take-off angle of the leg become increasingly important to completing the task. The average variance over 100% of the hopping cycle reveals that as difficulty of the task increases, leg orientation variance decreases despite increases in total segment angle variance. Furthermore, our results from a UCM analysis show that as task difficulty increases, IMA for leg orientation also increases while IMA for leg length does not (**Fig. 4**). These results explain how a lower leg orientation variance in a more difficult locomotor task (**Fig. 3**) can be achieved through increased interjoint coordination (**Fig. 4b)**.

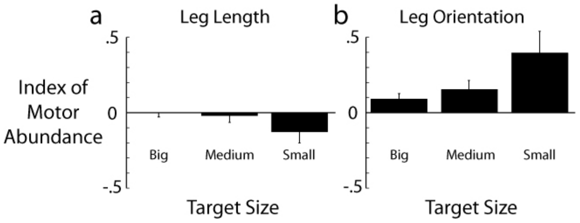

Fig. 4. Average Index of Motor abundance (IMA) ±1 standard deviation **(a)** for leg length and **(b)** leg orientation at three target sizes. Preliminary data for 2 subjects.

Our preliminary findings suggest that as task performance is increasingly constrained, the locomotor system responds with greater exploitation of motor redundancy by both increasing use of those joint kinematics combinations that meet the performance goal and decreasing combinations that do not meet the performance goal. This also shows evidence for how interjoint coordination might be used to stabilize performance variables when presented with real world task constraints caused by different gait pathologies and neuromuscular injuries.

REFERENCES

1. Auyang A, Yen J, and Chang Y.H. (2009). *Exp Brain Res*. 192, 253-64.
2. Blickhan, R. (1989). *J Biomech*. 22, 1217-27.
3. Bosco G, Poppele RE and Eian J (2000). *J Neurophysiol*. 83: 2931-2945.
4. Farley CT and Morgenroth DC (1999). *J Biomech.* 32: 267-273.
5. McMahon, T.A. and G.C. Cheng. (1990). *J Biomech*. 23, 65-78.
6. Raibert MH, Brown HB and Murthy SS (1984). *International Journal of Robotics Research* 3: 75-92.
7. Scholz, J.P. and G. Schoner. (1999). *Exp Brain Res*. 126, 289-306.
8. Tseng YW and Scholz JP. (2003). *Exp Brain Res.* 149, 276-88

UPPER LIMB MUSCLE VOLUME CHARACTERIZATION IN OLDER ADULT SUBJECTS

[1,2] Meghan Vidt, [1,2] Melissa Daly, [1,2] Anthony Marsh and [1,2] Katherine Holzbaur
[1]Wake Forest University, Winston-Salem, NC USA
[2]Virginia Tech – Wake Forest University School of Biomedical Engineering and Sciences
email: mvidt@wfubmc.edu, web: http://www.sbes.vt.edu/kholzbau/MoBL/index.html

INTRODUCTION

Previous studies have shown that isometric strength is directly correlated with muscle volume [1, 2]. It has also been observed that muscle atrophy and reduced strength occur with aging [3]. Upper extremity muscle volumes have previously been measured in young adults (age 24-37) [1, 2]. It was shown that individual muscle volume, as a percentage of total muscle volume, was consistent across test subjects. Furthermore, strength in the upper limb was significantly correlated with muscle volume. However, there are no comparable data for older adults. The objective of this study was to characterize the distribution of upper limb muscle volume and upper limb strength in a group of older adults (age 65 and older) and to compare these assessments to the existing data of young adults.

METHODS

Six ostensibly healthy subjects (3 females and 3 males) were evaluated (age: 72-80 years; body mass: 54.4-90.7 kg; height: 160-181.6 cm). All participants gave written informed consent. Subjects were imaged supine in a 1.5 T MRI scanner (GE Healthcare, Milwaukee, WI) with a series of spoiled gradient (SPGR) scans. The body coil was used to obtain images of the shoulder and upper arm, with a scan time of approximately 10 minutes. A flexed array long bone coil (Invivo, Orlando, FL) was used to image the upper limb in two successive scans, each approximately 14 minutes in duration.

The MR images were manually segmented (3D Doctor, Able Software Corp., Lexington, MA) to produce a three dimensional reconstruction of the muscles of interest. A reproducibility study, in which each muscle was segmented twice, showed repeatability within 5% muscle volume. Representative muscles for the major functional groups in the shoulder, elbow, and wrist were chosen for characterization (deltoid, pectoralis major, biceps brachii, triceps, extensor carpi radialis and flexor carpi radialis).

Maximum isometric joint moment at the wrist (flexion, extension), elbow (flexion, extension) and shoulder (adduction, abduction) joints were assessed using a KIN-COM isokinetic dynamometer (Isokinetic International, Harrison, TN). Mean muscle volume of each muscle was determined as a percent of the total muscle volume of the 6 muscles investigated. A Student's t-test was used to evaluate differences between individual muscle volumes and percent of total muscle volume in young and older adults. A regression analysis was used to determine the relationship between the maximum isometric moment at each joint and the muscle volume of the representative muscle crossing the joint.

RESULTS AND DISCUSSION

For each of the 6 muscles, the mean volume for the older adults was, on average, 20.9 ± 8.6 percent smaller than the mean for the young adults, despite comparable height and body mass ranges in both groups (young adult height 171.5 ± 9.3 cm and body mass 69.2 ± 15.8 kg [1]; older adult height 168.9 ± 10.2 cm and body mass 74.0 ± 13.5 kg). However, these differences did not reach significance in this subject sample. Each muscle volume was normalized by the total muscle volume for the 6 muscles studied. The volume of biceps expressed as a percentage of the total volume of the six muscles was significantly greater in older compared to younger adults (Figure 1).

For the 6 older adults, over 50% of the variation in maximum isometric joint moment was accounted for by variation in muscle volume. At the shoulder joint, 58% of the variation in abduction was accounted for by the volume of the deltoid muscle (p = 0.076) (Figure 2). Likewise, 83% of the variation in shoulder adduction was accounted for by the pectoralis major muscle volume (p = 0.011) (Figure 3). In addition, the relationship between joint moment and muscle volume was consistent with that observed previously for younger adults. For example, the slope for the relationship between abduction joint moment and deltoid volume for the older adults fell within the 95% confidence interval for the young adults. Similarly, the relationships between muscle volume and flexion and extension strength at the wrist and elbow joints for the elderly adults fell within the 95% confidence interval for the relationship observed for the young adults.

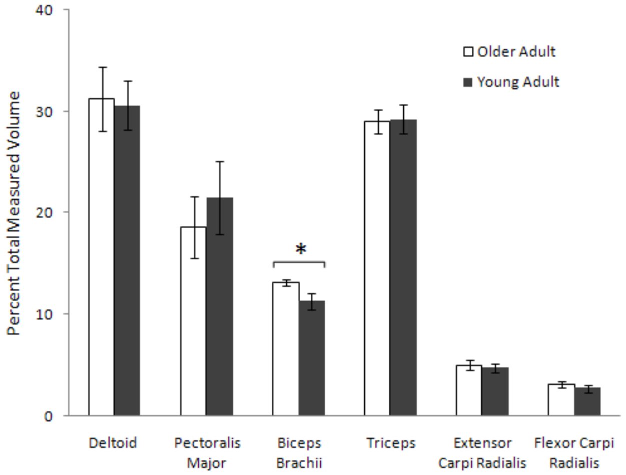

Figure 1: Mean muscle volume as a percent of total measured muscle volume ± SD for older and young adults; * indicates significant difference.

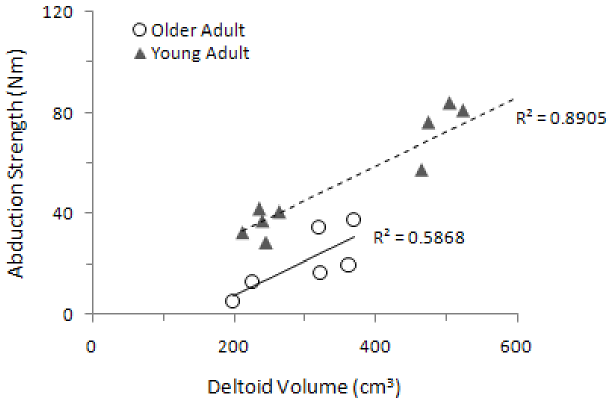

Figure 2: Isometric shoulder abduction joint moment compared to deltoid muscle volume.

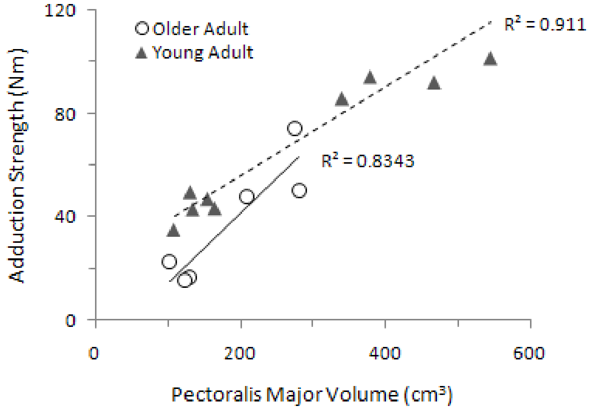

Figure 3: Isometric shoulder adduction joint moment compared to pectoralis major muscle volume.

CONCLUSIONS

We conclude that, with the exception of biceps, the distribution of muscle volume remains consistent between young and older adults. The relationship between isometric joint moment generating capacity and muscle volume is maintained when compared to young adults, despite the overall reduction in muscle volume in this subject sample.

This small sample of 6 subjects represents a portion of a larger study of 20 older adults, in which the upper limb strength, function, and muscle volume is being characterized and evaluated. The analyses described here will ultimately include this larger group, which may provide additional insight into whether changes with age exist in the relationship between muscle volume and joint moment. In addition, this larger study incorporates an upper limb training protocol to identify changes in muscle volume and coordination with strength training in older adults.

REFERENCES

1. Holzbaur KR, et al. *J Biomech* **40**, 2442-2449, 2007.
2. Holzbaur KR, et al. *J Biomech* **40**, 742-749, 2007.
3. Klein CS, et al. *J Appl Physio* **91**, 1341-1349, 2001.

ACKNOWLEDGEMENTS

Funding for this project was provided by the Wake Forest University Science Research Fund and Cross-Campus Collaborative Research Fund.

MUSCLE FORCES IN THE LOWER LIMB
PREDICTED BY STATIC AND DYNAMIC OPTIMIZATION

Ross H. Miller, Brian R. Umberger, and Graham E. Caldwell
Department of Kinesiology, University of Massachusetts, Amherst, MA, USA
Email: rhmiller@kin.umass.edu Web: http://www.umass.edu/biomechanics

INTRODUCTION

The estimation of individual muscle forces during movements has long been a topic of interest in biomechanics and motor control. To resolve the mechanical indeterminacy of the musculo-skeletal system, many researchers have resorted to mathematical optimization techniques [1,2].

Static optimization is a common approach for model-based estimation of muscle forces. One of the most popular objective functions is the minimization of the sum of cubed muscle stresses. Crowninshield and Brand [1] posed a physiological rational for this function for unimpaired walking, based on empirical and theoretical considerations of maximizing muscular endurance.

The Crowninshield and Brand [1] criterion has also been used to predict muscle forces during other movements, such as fast running [3] and jumping [4]. However, it is unlikely that the nervous system adopts an endurance-maximizing muscle activation strategy for these movements. Validating muscle force predictions by any method is difficult since no *in vivo* "gold standard" data are available. However, force predictions can be compared and evaluated against muscle forces from forward dynamics simulations, where the exact muscle forces actuating the model are known [2].

Therefore, the purpose of the study was to compare muscle forces obtained by minimizing cubed muscle stresses via static optimization for walking, sprinting, and jumping, to those predicted from forward dynamics simulations of these movements. It was hypothesized that muscle forces predicted by static optimization and by dynamic optimization of the forward dynamics simulations would be similar for walking, but not for sprinting or jumping.

METHODS

Forward Dynamics Simulations

Simulations of walking, sprinting, and jumping were generated using a 2D computer model comprised of a trunk and two legs (Fig. 1). Each leg was actuated by 12 Hill-based muscle models. A vertical sinusoidal force on the trunk represented the effect of arm swing during locomotion.

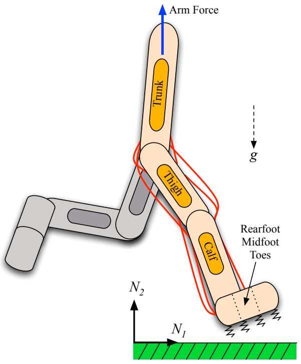

Figure 1: The computer model used in the forward dynamics simulations. The knee flexor and digitorum muscles are not shown.

The locomotion simulations began at initial foot contact and ended after one step. The jumping simulation began in a static squat and ended at the peak height. Dynamic optimization was used to find muscle model excitations that minimized the muscle energy expended per distance traveled (walking), maximized the average horizontal speed (sprinting), or maximized peak height (jumping).

Static Optimization

The same model (Fig. 1) was used to estimate the muscle forces using static optimization. At each time step, muscle forces that minimized the sum of cubed muscle stresses [1] were sought:

$$J = \sum_{m=1}^{12} \left(\frac{F_m}{PCSA_m} \right)^3$$

where F_m and $PCSA_m$ are the force and the physiological cross-sectional area of muscle *m*. Values for $PCSA_m$ were those used in the forward dynamics simulations, drawn from the literature.

The muscle forces were constrained to be tensile and beneath a maximum force, and were required to generate the net active muscle moments from the forward dynamics simulations within 0.001 Nm.

Muscle forces from static and dynamic optimization were deemed similar if: (1) the RMS difference was ≤ 15% of the maximum isometric muscle force (F_o), and (2) the cross-correlation coefficient was ≥ 0.85.

RESULTS AND DISCUSSION

The model's sprinting speed (7.33 m/s) and jumping height (43 cm) were both within 5% of recorded performance by the human subject from whom the model's parameters were derived. The model walked at the same speed as the subject (1.6 m/s) but spent 14% more energy (6.4 vs. 5.6 W/kg).

Seven muscle forces met both similarity criteria for walking, compared to four for sprinting and only one for jumping (Table 1). RMS differences averaged 12% F_o (125 N) for walking, 24% F_o (235 N) for sprinting, and 39% F_o (431 N) for jumping. Force timing, quantified by the cross-correlation coefficient, averaged 0.73 for walking, 0.78 for sprinting, and 0.39 for jumping.

Table 1. RMS differences (D, in % F_o) and cross-correlation coefficients (r) between the muscle forces predicted by static and dynamic optimization.

	Walking		Sprinting		Jumping	
Muscle Model	**D**	**r**	**D**	**r**	**D**	**r**
Iliopsoas	17	0.42	30	0.91*	74	0.40
Glutei	7*	0.97*	10*	0.95*	58	0.82
Rectus femoris	12*	0.76	19	0.77	81	0.11
Lateral hams.	19	0.12	21	0.96*	58	0.24
Medial hams.	11*	0.87*	25	0.62	65	0.48
Knee flexor	5*	0.16	51	0.15	42	0.35
Vasti	5*	0.89*	11*	0.88*	9*	0.98*
Gastrocnemius	9*	0.86*	5*	0.97*	24*	0.08
Soleus	5*	0.95*	8*	0.98*	14*	0.82
Tibialis anterior	11*	0.88*	21	0.63	13*	0.13
Extensor dig.	22	0.86	49	0.91*	20	0.14
Flexor dig.	15*	0.97*	41	0.65	10*	0.18

* = met similarity criterion

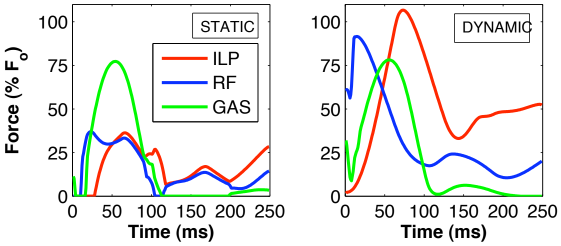

Figure 2. Muscle force predicted by static (left) and dynamic (right) optimization for sprinting.

Figure 2 shows muscles with high (iliopsoas), moderate (rectus femoris), and low (gastrocnemius) RMS differences for sprinting. Temporal patterns in force were qualitatively similar for most muscles, but peak forces differed by up to 70% of F_o.

CONCLUSIONS

Muscle forces predicted by static and dynamic optimization compared better for walking than for sprinting or jumping. If we assume that forward dynamics simulations are reasonable analogs of human movement actuated by reasonably realistic muscle forces, the Crowninshield and Brand [1] criterion appears to predict accurate muscle forces for low-intensity, cyclical motions like walking [2]. This finding was supported by the present results.

The present results suggest that the accuracy of muscle forces predicted using the Crowninshield and Brand [1] criterion may be compromised to varying degrees for high-intensity cyclical (e.g. sprinting) and discrete (e.g. jumping) motions. In these cases, where maximizing endurance likely does not dominate muscle coordination, static optimization and stress minimization may not be an appropriate framework, and researchers should consider other options for estimating muscle forces.

REFERENCES

1. Crowninshield RD and Brand RA. *J Biomech* **14**, 793-801, 1981.
2. Anderson FC and Pandy MG. *J Biomech* **34**, 153-161, 2001.
3. Glitsch U and Baumann W. *J Biomech* **11**, 1123-1131, 1997.
4. Czaplicki A, et al. *Comp Meth Biomech Biomed Engr* **9**, 45-54, 2006.

DIFFERENCES IN UPPER BODY POSTURE AND POSTURAL MUSCLE ACTIVATION IN FEMALES WITH LARGER BREAST SIZES

[1]Mindy Bennett, [1]Seth Kuhlman, [1]Michelle Sabick, [1]Ronald Pfeiffer, [2] Steve Laverson
[1]Boise State University, Boise,ID. [2]Feel Beautiful Plastic Surgery, Encinitas, CA
email: mindy.bennett@gmail.com

INTRODUCTION

Breast hypertrophy is a common medical condition whose morbidity has increased over recent decades. Symptoms of breast hypertrophy often include musculoskeletal pain in the neck, back and shoulders, painful shoulder grooves from bra straps, and numerous psychosocial health burdens. It is postulated that the size and weight of hypertrophic breasts alters the body's center of gravity, leading to secondary effects on the musculoskeletal system [1].

While numerous prospective studies to date have provided subjective evidence of the health burdens of breast hypertrophy, limited studies have been performed examining the quantitative effects of excess breast tissue mass on spine biomechanics and cervico-thoracic muscle activation. To date, reduction mammaplasty is the only treatment shown to significantly reduce the severity of the symptoms associated with breast hypertrophy. However, due to a lack of sound scientific evidence in the medical literature justifying the medical necessity of reduction mammaplasty, insurance companies often deny requests for coverage of this procedure. Therefore, the purpose of this study is to investigate biomechanical differences in the upper body of women with larger breast sizes in order to provide scientific evidence of the musculoskeletal burdens of breast hypertrophy to the medical community.

METHODS

22 female subjects (average age 25.90, ± 5.47 years) who have never undergone or been approved for breast augmentation surgery, were recruited to participate in this study. Kinematic data of the head, thorax, pelvis and scapula was collected during static trials and during each of four different tasks of daily living. Surface EMG (sEMG) data from the Midcervical (C-4) Paraspinal, Upper Trapezius, Lower Trapezius, Serratus Anterior, and Erector Spinae muscles were recorded in the same activities. Maximum voluntary contractions (MVC) were used to normalize the sEMG data, and %MVC during each task in the protocol was analyzed. Kinematic data from the tasks of daily living were normalized to average static posture data for each subject.

Subjects were divided into groups of control subjects (n=12, reported bra-cup size A, B, or C) or hypertrophy subjects (n=10, reported bra-cup size D or larger) [2]. To compare results between the groups, a two-tailed independent t-test was performed for each dependent variable with significance set at $\alpha=0.05$.

RESULTS AND DISCUSSION

Significant differences in torso flexion were found between the control group and the hypertrophy group during both the pencil activity (p=0.054) and the step up activity (p=0.001). There were also significant differences in lower trapezius muscle activation during the static trial (p=0.051). Average static posture data is shown in Figure 1. Although not significant, women in the hypertrophy group also tended to exhibit greater head flexion, pelvic tilt and torso flexion under static conditions, and also exhibited increased muscle activation in all five muscles under the same conditions.

Despite the relatively few significant differences in static posture alignment found in this study, it is important to note that the hypertrophy group did tend to present with greater amounts of cervical lordosis (head flexion), forward shoulder position (shoulder protraction), thoracic kyphosis (torso flexion) and lumbar lordosis (pelvic tilt) than women in the control group. These findings are supported by postulations by Letterman et al [1], who postulated that the types of structural changes we saw are a direct result of a change in the body's center of gravity to compensate for the weight and position of hypertrophic breasts [1].

While the muscle activation differences between the two groups were not significant, higher levels of muscle activation exhibited by hypertrophy subjects during both static posture and tasks of daily living may be related to the altered static postural alignment exhibited by these same subjects. Changes in the direction of muscle pull as a result of an altered static skeletal alignment may affect the amount of muscle tension required to maintain a static position[3], thus possibly explaining chronic musculoskeletal weakness and pain experienced by women with breast hypertrophy.

CONCLUSIONS

Results of this study provide scientific information regarding the effects of breast hypertrophy on the musculoskeletal system. Of greatest interest, are the slight differences in both upper body posture and muscle activation seen in women with larger breast sizes under static conditions.

While none of the postural alterations seen in women with large breasts were significantly different from those seen in women with smaller breasts, the data presented shows a trend towards altered musculoskeletal alignment due to the size and weight of larger breasts. However, future research should involve a larger sample population in order to see true statistical differences between the two groups.

Therefore, results of this study provide scientific evidence of the physical burdens placed on the musculoskeletal system in the case of breast hypertrophy, and should be considered when determining the medical necessity of reduction mammaplasty.

REFERENCES

1. Letterman, G., and M. Schurter. *Annals of Plastic Surgery* **5**, 425-431, 1980.

2. Kerrigan, C., et al. *Plastic and Reconstructive Surgery* **108,** 1591-1599, 2001.

3.Braun, B.L., and Amundsun, L.R. *Archives of Physical Medicine and Rehabilitation* **70**, 322-329, 1989.

ACKNOWLEDGEMENTS

Special thanks to Mikaela Boham for generously giving her time to help complete the data collection for this study.

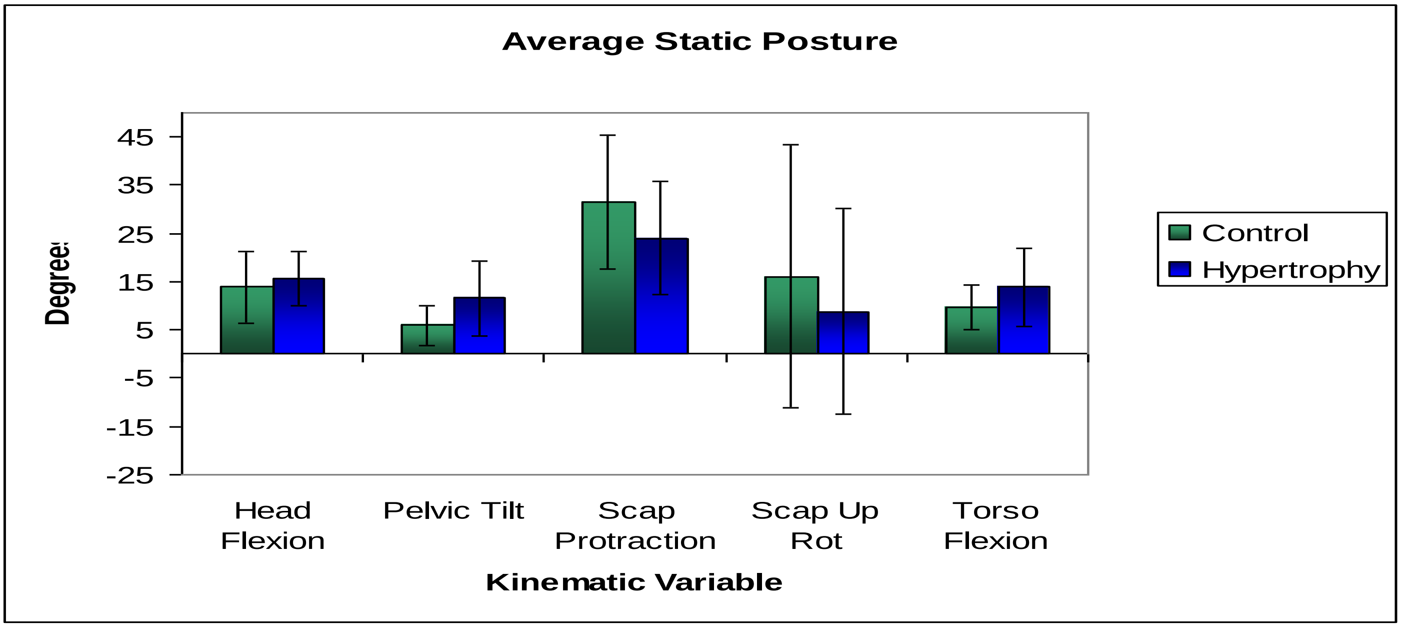

Figure 1. Average Static Posture Data

BALANCE ADJUSTMENT DURING OBSTACLE CROSSING IN PATIENTS WITH TOTAL HIP ARTHROPLASTY

Shiu-Ling Chiu and Li-Shan Chou
Department of Human Physiology, University of Oregon, Eugene, Oregon 97403, USA.
email: chou@uoregon.edu, web: http://biomechanics.uoregon.edu

INTRODUCTION

Total hip arthroplasty (THA) is a common surgery for a deteriorated hip joint to effectively regain its functions. Approximately 250,000 THA were performed in the United States every year [1]. THA surgical approach has been identified as a major factor for post surgery joint stability and functions [2]. Patients undergoing THA are found to have higher risks of falls due to the residual deficits in balance control and joint functions [3]. However, the differences between anterior and lateral surgical approaches have not been well addressed, and studies analyzing the obstacle crossing performance, which challenges the balance [4] and joint stability [5], have not been conducted in THA patients. The purpose of this study is to investigate the effect of anterior and lateral surgical approaches on the balance control for obstacle crossing in patients undergoing THA.

METHODS

Thirty-one adults were recruited and divided into three groups in this study. There were 12 subjects undergoing THA with anterior approach (7 men, 5 women, age = 56.9 ± 3.3 yrs, BMI = 31.98 ± 5.13 kg/m^2), 9 subjects undergoing THA with lateral approach (8 men, 1 woman, age = 55 ± 6.5 yrs, BMI = 31.31 ± 3.9 kg/m^2) and 10 control subjects (5 men, 5 women, age = 59.9 ± 5.3 yrs, BMI = 26.3 ± 3.9 kg/m^2). Pre-surgery Harris hip scores of hip joint function were 52.8 ±12.7 and 58.7 ±11.8 for the anterior and lateral groups, respectively. All patients received the same un-cemented Zimmer hip implants and followed the same physical therapy regimens during the study period. THA patients were tested three times at pre-surgery, 6-weeks and 16-weeks post surgery. Control subjects were tested twice with one month apart.

An eight-camera motion analysis system (Motion Analysis Corp., Santa Rosa, CA) was used to collect the whole body motion during level walking and crossing an obstacle corresponding to 10% of individual's body height. A total of 29 reflective markers were placed on bony landmarks. Two force plates (Advanced Mechanical Technology Inc., Watertown, MA) were placed in series at the center of a 10-m walkway. The surgical limb of THA patient, or the dominate limb of the control subject, was instructed to cross the obstacle as the trailing limb.

Ranges of motion of the antero-posterior (AP) and medio-lateral (ML) CoM-CoP inclination angles during a gait cycle were calculated to assess balance control [6]. All variables obtained during obstacle crossing condition were then presented as percentage of changes from level walking performance to quantify adjustments needed for obstacle negotiation. Paired t-test was used to compare the variable differences between obstacle crossing and level walking, and a mixed-model analysis of repeated measures was used to analyze the effects of groups and time. Significance level was set at 0.05.

RESULTS AND DISCUSSION

Gait velocity decreased significantly in all subjects when stepping over an obstacle (Table 1). Significant group differences were detected between the control and anterior groups at pre-surgery and 6-week post surgery, and between controls and lateral group at 6-week post surgery. Compared to pre-surgery, significant time effects were detected in THA patients at 16-week post surgery. Obstacle crossing also induced a significant increase in the AP CoM-CoP inclination angles for all three groups (Table 1). Both THA patient groups walked with a significantly reduced inclination angle than their controls at pre-surgery and 6-week post surgery. Similarly, significant time effects were detected in THA patients at 16-week post surgery. The ML CoM-CoP inclination angles were generally decreased during obstacle crossing for all three groups. However, no significant differences between obstacle crossing and level walking conditions were detected. In general, all THA patients walked slower with a smaller AP but greater ML CoM-CoP inclination angle. No significant group differences were detected between the anterior and lateral THA groups.

When stepping over an obstacle of 10% body height, control subjects exhibited approximately a 13% reduction in gait velocity (Fig. 1), 14% increase and 1.3% reduction in AP and ML CoM-CoP inclination angles, respectively (Figs. 2 and 3). Our data demonstrated a trend that gait and balance control of THA patients could be affected by the presence of obstacle to a greater extent than their controls, especially prior to the surgery (Figs 1, 2 & 3). There is also a tendency for these obstacle-induced differences being normalized after THA surgery.

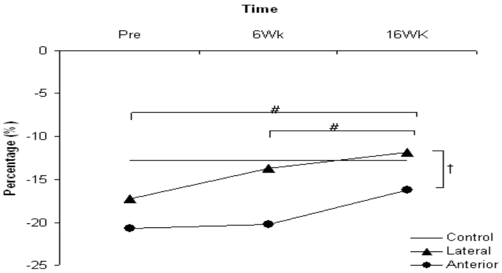

Figure 1: Changes in gait velocity (% level walking values; † group effect; $^{\#}$ time effect)

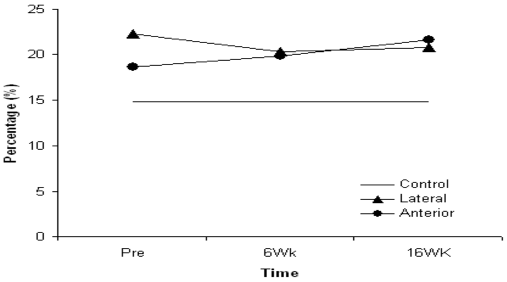

Figure 2: Changes in AP CoM-CoP inclination angles (% level walking values)

CONCLUSIONS

Stepping over an obstacle induced changes in the CoM-CoP inclination angles. These changes tended to be greater in THA patients, which could imply a greater balance perturbation. Both THA surgical approaches improve patients' ability to accommodate changes in balance control during obstacle crossing. However, the small sample size could limit the findings of this study.

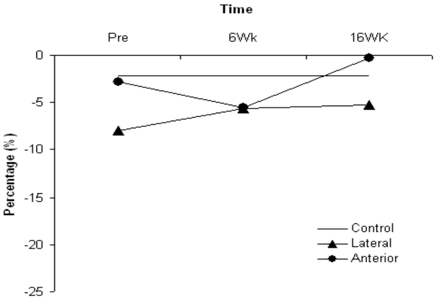

Figure 3: Changes in ML CoM-CoP inclination angles (% level walking values)

REFERENCES

1. Lindemann, U., et al. *Clin Rehabil* **20**, 413-20, 2006.
2. Masonis, J.L., et al. *Clin Orthop Relat Res* **405**, 46-53, 2002
3. Majewski, M., et al. *J Bone Joint Surg [Br]* **87**, 1337-1343, 2005.
4. Hahn, M.E. and L.S. Chou. *J Biomech* **37**, 837-844, 2004.
5. Chou, L.S. and L.F. Draganich. *J Biomech* **30**, 331-337, 1997.
6. Lee, H.J. and L.S. Chou. *Arch Phys Med Rehabil* **87**, 569-575, 2006

ACKNOWLEDGEMENTS

The assistance from Vipul Lugade is greatly appreciated.

Table 1: Gait velocity and CoM-CoP inclination angles and during obstacle crossing and level walking

	Controls		**Anterior THA**						**Lateral THA**					
			Pre-surgery		6-week post surgery		16-week post surgery		Pre-surgery		6-week post surgery		16-week post surgery	
	OB	Level	OB	Level	OB	Level	OB	Level	OB	Level	OB	Level	OB	Level
Gait Velocity (m/s)	1.11*	1.28	0.88*†	0.94	0.87*†	1.08	0.99*$^{\#}$	1.19	0.97*	1.18	0.96*†	1.07	1.09*$^{\#}$	1.23
	(0.12)	(0.17)	(0.09)	(0.26)	(0.20)	(0.2)	(0.17)	(0.17)	(0.16)	(0.1)	(0.13)	(0.14)	(0.15)	(0.09)
Antero-posterior (°)	29.96*	26.33	24.77*†	20.65	24.27*†	20.49	27.03*$^{\#}$	22.41	27.64*†	22.75	24.97*†$^{\#}$	20.18	27.82*$^{\#}$	23.12
	(3.17)	(4.02)	(1.61)	(2.44)	(3.37)	(3.82)	(3.83)	(4.03)	(3.43)	(3.16)	(3.09)	(2.59)	(2.71)	(2.72)
Medio-lateral (°)	7.09	7.18	8.81	10.14	8.37$^{\#}$	8.9	8.78	8.89	8.58	9.37	8.09$^{\#}$	8.60	8.13	8.60
	(1.87)	(0.83)	(1.43)	(3.32)	(2.04)	(1.8)	(1.98)	(2.09)	(1.91)	(2.19)	(2.08)	(1.52)	(1.66)	(1.28)

* Significant differences when comparing obstacle crossing to level walking; † group effect; $^{\#}$ time effect.

CHANGES IN JOINT KINEMATICS AND ASYMMETRY THROUGHOUT A RUN TO FATIGUE IN HEALTHY FEMALE RUNNERS

[1]Allison M. Brown, PT, MA, [1]Rebecca A. Zifchock, PhD, [2]Andreia Miana, MSc, and [1]Howard J. Hillstrom, PhD
[1]Leon Root MD, Motion Analysis Laboratory, Hospital for Special Surgery, New York, NY
[2]Instituto Vita, São Paulo, Brazil
email: brownal@hss.edu.

INTRODUCTION

Running is a popular form of physical exercise due to its cardiovascular and weight control benefits. It is, however, a high-impact and repetitive activity that results in an annual injury rate of nearly 50% of its participants [1].

A large portion of running injury studies focus on the analysis of data collected in a fresh state. However, it is likely that any injury-related effects are not present until a runner becomes fatigued. Kinematic alterations as a result of fatigue may also result in a more asymmetrical gait, and thus, injury susceptibility on one side. Gait asymmetries have been linked to injuries in both runners [2] and non-runners [3]. However, the link between asymmetry, injury, and fatigue is unclear. Previous studies, which suggest that injury-susceptible runners are not more asymmetrical than runners who remain uninjured [2], where conducted in a fresh state.

The effects of fatigue on lower extremity kinematics have been well documented. Literature has shown changes in lower extremity kinematics following an exhaustive treadmill run [4]. However, no studies have looked at what point during the run are kinematic changes likely to occur. Documenting the progression of changes that occur in normal, healthy runners with fatigue is important for comparison to injured populations.

Therefore, this study looks to examine changes in joint kinematics and kinematic asymmetry that occur over the course of a run to exertion. It is hypothesized that kinematics and asymmetry values would change over time.

METHODS

As part of a normative running database, data from the first six of 100 healthy female runners (32.5years ±7.5, 1.58m ± 0.9, 56.7kg ± 4.7) were included in this study. All runners were rearfoot strikers, free from injury and running a minimum of 15 miles/week.

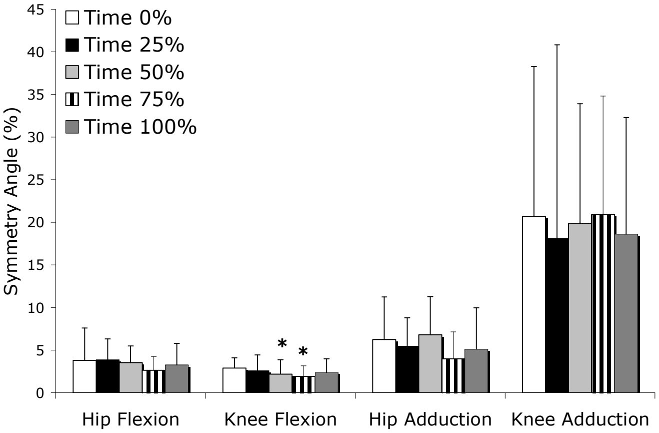

Figure 1: SA values at 0%, 25%, 50%, 75% and 100% of a run to exertion. Significant differences between baseline and a time interval are indicated by (*).

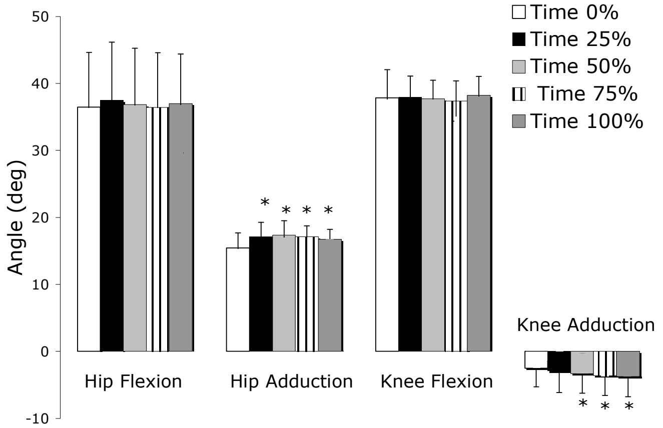

Figure 2: Loading response peak hip and knee angles at 0%, 25%, 50%, 75% and 100% of a run to exertion. Significant differences between baseline and a time interval are indicated by (*).

Instrumented gait analysis was performed while participants performed a run to exertion on a treadmill. Video data were collected at 120Hz. All runners wore a laboratory-provided neutral running shoe (New Balance 1062; Boston, MA) with holes cut out of the heel to allow for marker placement directly on the skin over the calcaneus.

The run to exertion (23.5 minutes ±5.8) was performed at the individuals' self-selected 5K race pace. Runners were considered exerted when they reached a rating of 17/20 on the Borg Rating of Perceived Exertion Scale. Data were collected every three minutes over the course of the run. Video data were smoothed with a low-pass fourth order Butterworth filter.

Peak hip flexion, peak hip adduction, peak knee flexion and peak knee adduction were measured during the loading response phase of stance. Loading response was defined as the period of time from initial contact to first peak knee flexion. Data from the dominant limb were used for analysis of kinematics. Data from both limbs were used to calculate asymmetry values: the symmetry angle (SA), as described by Zifchock et al [5] was used to quantify asymmetry. An SA value of 0% indicated perfect symmetry, while increasing values were indicative on increasing asymmetry. Peak joint angles and SA values calculated at 0%, 25%, 50%, 75% and 100% of the run were used for this analysis. A one-way repeated measures ANOVA was used to test for differences across time. A significant ANOVA was followed up with post-hoc testing that compared each time period to baseline (0%). Due to the preliminary nature of the study, significance was set at $p \leq 0.10$.

RESULTS AND DISCUSSION

SA value data are shown in Figure 1. There were no significant changes in hip flexion, hip adduction or knee adduction SA values over time. However, there was a significant change in knee flexion asymmetry ($P = 0.067$). Post-hoc testing revealed significant changes between times 0% and 50% ($P=0.099$) and 0% and 75% ($P=0.039$). Other than at 100% of the run, SA values tended to decrease. These findings are contrary to the expectation that asymmetry levels would increase. In fact, SA values at the knee demonstrated decreased knee flexion asymmetry.

Kinematic data are included in Figure 2. These data show significant changes in frontal plane hip ($P=0.012$) and knee ($P=0.002$) angles over the course of the run to exertion. During loading response, runners demonstrated significantly increased hip adduction between times 0% and 25% ($P=0.033$), 0% and 50% ($P=0.019$), 0% and 75% ($P=0.062$), and 0% and 100% ($P=0.033$). Knee abduction angles increased between times 0% and 50% ($P=0.05$), 0% and 75% ($P=0.062$) and 0% and 100% ($P=0.017$). No significant change in knee abduction angle was seen between time 0% and time 25%. There were no significant changes in peak hip and knee flexion angles during loading response. These findings differ from previous research [4] that found increased stance phase peak knee flexion angles following a run to exertion. However, it is unclear whether these changes have occurred as a result of muscular fatigue, or as a means to prevent injury by absorbing shock and minimizing impact forces.

CONCLUSIONS

In healthy runners, there was significantly decreased knee flexion asymmetry throughout a run to exertion. There were no significant changes in sagittal or frontal plane hip asymmetry nor were there significant changes in frontal plane knee asymmetry throughout a run to exertion. Additionally, this study demonstrates that healthy runners had increasingly larger peak hip adduction and knee abduction angles throughout a run to exertion. Future studies will focus on joint kinematic changes and asymmetry changes as a result of exertion in an injured population.

REFERENCES

1. Macera CA et al. *Arch Intern Med* **149**, 2565-2568, 1989.
2. Zifchock RA et al. *J Biomech* **39**, 2792=2797, 2006.
3. Ferber R et al. *Clin Biomech* **18**, 132-141, 2003.
4. Derrick TR et al. *Med Sci Sports Exerc* **34**, 998-1002, 2002.
5. Zifchock RA et al. *Gait Posture* **27**, 622-627, 2008.

ACKNOWLEDGEMENTS

The authors wish to thank New Balance for providing the footwear used to carry out this study.

A METHOD TO QUANTIFY THE INFLUENCE OF RADIAL HEAD FRACTURE LOCATION ON ELBOW KINEMATICS

[1]Laurel Kuxhaus, [2]Mandy Brogdon, [1,3]Michael J. Druschel, [2]Patrick J. Schimoler, [1]Jeffrey S. Marchessault, [1]Mark E. Baratz, and [2]Mark Carl Miller
[1]Allegheny General Hospital, [2]University of Pittsburgh, [3]Case Western Reserve University
email: mcmiller@wpahs.org

INTRODUCTION

Radial head fracture is a common injury, occurring in 33% of all elbow fracture cases. [1] The Mason system classifies the type of fracture based on the amount of the articulating surface involved and the amount the fragment is displaced. [2] For a Mason Type II fracture, 30% of the articulating surface is disrupted and the displacement is less than 2 mm. The clinical treatment for these fractures is unclear – is surgery required to prevent loss of elbow motion? Evidence suggests that there may be a decrease in range of pronation/supination motion if left untreated, [3] yet some patients recover complete range of motion without surgical treatment. The inspiration for the development of this technique was the hypothesis that the fracture location influences the range of motion. This work presents an innovative method to perform such tests and includes a demonstration of its feasibility and results.

METHODS

The overall approach was to replace the native radial head in a cadaver elbow specimen with a geometrically-accurate replica that has been precisely fractured. By making multiple radial head replicas, the influence of different fracture locations can be quantified in the same cadaver specimen, eliminating the confounding factor of interspecimen variability. Another advantage is the ability to create a more precise fracture than one could physically create with the native radial head.

A CT scan (VolumeZoom, Siemens, New York, NY) of a fresh-frozen cadaver elbow was performed at Allegheny General Hospital. The slice thickness was 1 mm. The DICOM image files generated were then manipulated in Mimics (Materialise, Leuven, Belgium). The radial head was isolated, including the bicepital tuberosity, and exported as a solid model to SolidWorks (DS Solidworks, Concord, MA). In SolidWorks, the radial head fracture was created. Six different fractures were created, each in its own replica radial head. A stereolithography machine was used to manufacture the fractured radial head replicas. Figure 1 shows five replicas with the native head. Each fracture disrupted 30% of the articulating surface of the radial head and the fractures were equispaced around the circumference of the head itself. The solid model of each radial head was modified to accept the insertion of a 6.35 mm-diameter rod, concentric with the intramedullary canal of the radius. The rod had crosslock pins to ensure fixation with both the replica radial head and the native radius bone. The bone fragment created by the fracture was modified to accommodate a screw that could affix it to the radial head in prescribed longitudinal displacements. Stepped surfaces on both the radial head and fragment prevented rotation around the screw itself. A 2 mm thick washer inserted between the bone fragment and radial head around the same fixation screw permitted the creation of a 2mm radial displacement. (Figure 2) To prevent rotation of the bone fragment, a straight pin was added.

These replica radial heads were designed for insertion with the preservation of the annular ligament. To insert them as such, an osteotomy of the humerus was necessary to gain access to the native radial head and permit the insertion of the fractured radial head replicas.

One cadaver specimen was used to demonstrate the feasibility of this method. Two replica radial heads were inserted in turn. Each was inserted with the fracture closed and with a 2 mm radial displacement. The osteotomy was closed with screw fixation after each insertion and the specimen was inserted in to the AGH Elbow Simulator. [4]

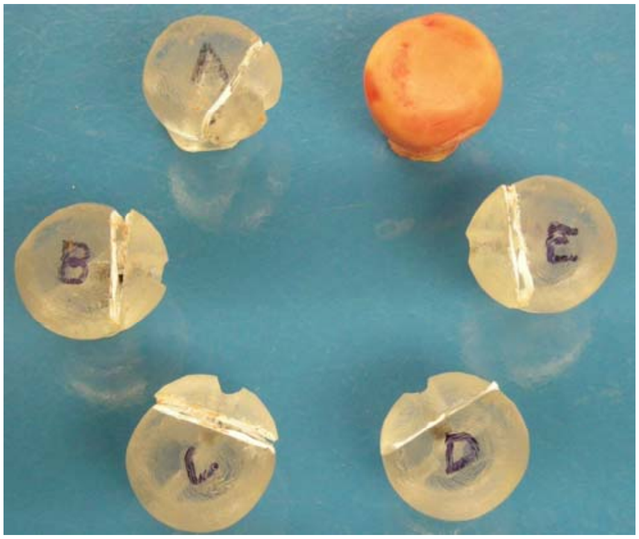

Figure 1: Five fractured and displaced replica radial heads. The intact (native) head is also shown.

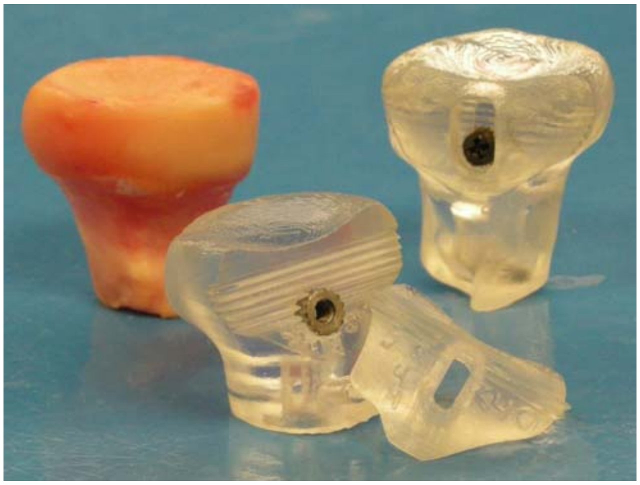

Figure 2: Replica radial heads illustrating the fractured bone fragment.

Table 1: Range of motion with different radial head conditions.

	A		B	
Disp.	**0 mm**	**2 mm**	**0 mm**	**2 mm**
ROM	120.7°	104.6°	123.3°	118.3°

By means of the simulator which used a PID controller, the specimen was pronated and supinated with a constant flexion angle of 90°. A potentiometer (P1701, Novotechnik, Southborough, MA) and inclinometer (X3Q, US Digital, Vancouver, WA) monitored pronation/supination and flexion/extension angle, respectively. The muscle forces and motions were recorded. Three trials of each type were performed and the results were averaged.

RESULTS AND DISCUSSION

The insertion of the fractured radial head replicas into the cadaver specimen proved feasible. Table 1 shows the range of motion with each plastic head. Note that the total range of motion decreases with the radial displacement of the bone fragment. The range of motion of the two heads with 0 mm displacement (simulating the intact native head) was similar. These preliminary results indicate that the decrease in range of motion caused by 2 mm of fracture displacement changes with the fracture location.

CONCLUSIONS

This work has demonstrated the feasibility of a method to evaluate the influence of fracture location and displacement on the kinematics of the elbow joint. Future work will include additional kinematic testing of the specimens with more fracture locations in the AGH Elbow Simulator to precisely quantify the motion deficits induced by Mason Type II radial head fractures.

REFERENCES

1. Morrey, *The Elbow and its Disorders*, 2000.
2. Mason, *Br J Surg*, **42**, 123-32, 1954.
3. Herbertssohn *et al.*, *JBJS*, **86A,** 569-74, 2004.
4. Kuxhaus et al., *J Med Dev*, In Press, 2009.

ACKNOWLEDGEMENTS

The authors thank Dr. Walter Song for his clinical guidance and assistance with the concept design.

DEEP HIP MUSCLE ACTIVATION DURING A SQUAT EXERCISE

Mike Decker, Jake Krong, Dan Peterson, Tyler Anstett, Michael Torry, Erik Giphart, Kevin Shelburne,
Marc Philippon
Steadman-Hawkins Research Foundation, Biomechanics Laboratory, Vail, CO
E-mail: michael.decker@shsmf.org, Web: www.shsmf.org

INTRODUCTION

Hip joint function during a squat has recently received increased clinical attention due to the growing awareness of femoroacetabular impingement (FAI) [1]. During a squat, patients with FAI demonstrate restricted pelvic motion and hip flexion, internal rotation and abduction due to inappropriate contact of the femur and acetabulum [2]. Muscular dysfunction of the pectineus, iliopsoas, gluteus medius and piriformis muscles in concert or isolation may enhance this irregular mechanical relationship but diminutive information is available regarding their function.

The purpose of this study was to describe the activation of the pectineus, iliopsoas, gluteus medius and piriformis muscles during a squat.

METHODS

Ten healthy individuals (1.72 ± 0.04 m; 674.17 ± 43.3 N; 28.70 ± 2.00 y) participated in this study. All participants provided written consent prior to participation, in accordance with the Vail Valley Medical Center's Institutional Review Board.

The participants performed a squat similar to a rehabilitation exercise (~2/3 of maximum squat). The squat exercise was performed at a pace of 0.5 Hz. Indwelling electrodes were used to record (1200 Hz) muscle activation from the pectineus, iliopsoas, gluteus medius and piriformis muscles. The electrodes were ultrasound guided to assure correct placement into the muscle and for patient safety. Electrode placement was confirmed via inspection of the digital ultrasound pictures by a radiologist that was blinded to the study.

All EMG data (Bagnoli-8, DelSys, Boston, MA, USA) were processed with a 50 ms, root-mean-squared (RMS) moving window (1 ms increments) with custom software (MATLAB, Natick, MA, USA). The EMG data were scaled to maximum EMG reference values measured during the MVC trials and represented 100% MVC.

Fifty-three retro-reflective, spherical markers (diameter =1.0 cm) were attached to select anatomical landmarks. A ten-camera motion analysis system (Motion Analysis, Cortex 1.1.4, Santa Rosa, CA, USA) was used to capture three-dimensional hip motions at a frequency of 120 Hz. The marker trajectories were low pass filtered at 10 Hz with a fourth order Butterworth filter.

Three-dimensional hip and pelvis kinematics were calculated with a commercial software package (Motion Monitor, Version 7.0, Innovative Sports Training, Chicago, IL, USA). Joint angles were determined using a YXZ sequence as proposed by Grood and Suntay [3] such that sagittal joint motion was represented as rotations about the y-axis, frontal plane motion represented by rotations about the x-axis and transverse plane motion as rotations about the z-axis.

RESULTS

When rising from a squatted position, the hip joint progressively extended from 54.8 ± 3.6° of hip flexion to 4.4 ± 2.8° of hip flexion; abducted from 0.5 ± 2.5° of hip adduction to 2.3 ± 1.5° of hip abduction; and externally rotated from 0.8 ± 1.7° of hip internal rotation to 4.1 ± 1.4° of hip external rotation. The pelvis rotated posterior from 19.2 ± 3.0° of anterior pelvic tilt to 5.9 ± 1.9° of anterior pelvic tilt. The lowering phase demonstrated equal and opposite hip and pelvic motions.

The ensemble EMG time series data are located in Figure 1. The EMG amplitude values ranged between 2.3 ± 7.1 %MVC and 33.4 ± 10.1 %MVC.

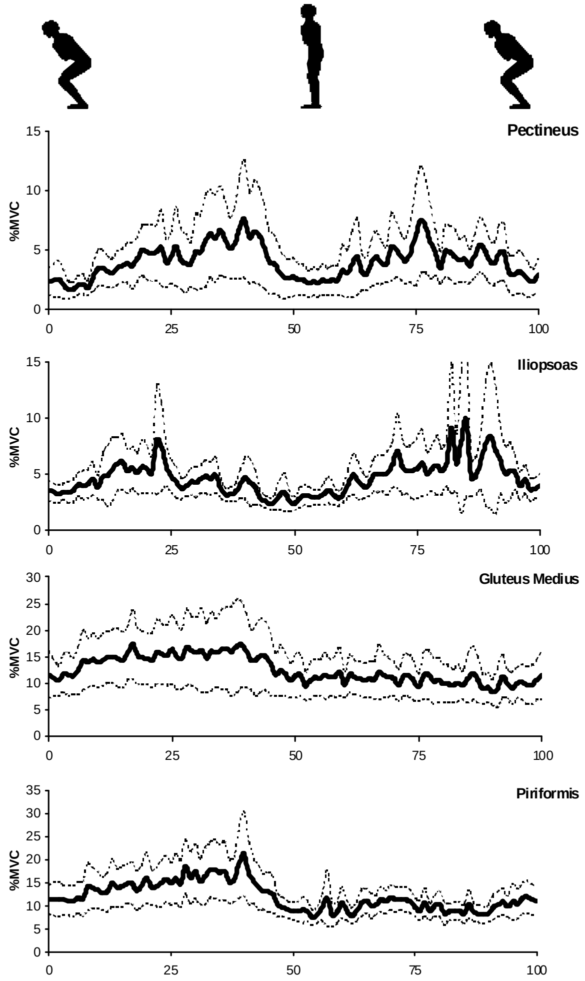

Figure 1. Mean (±SE) ensemble EMG activation patterns for the pectineus, iliopsoas, gluteus medius and piriformis muscles during a squat when rising (0-49%) and lowering (50-100%).

DISCUSSION

It is believed that the deep muscles of the hip may provide fine control of hip joint stability, acting as the "rotator cuff" of the hip joint [4]. Because of the inherent difficulties in inserting fine wire electrodes in these muscles, little knowledge is available to support these claims.

The functional interpretations of the EMG patterns found in the current study are based on the changing moment arms of the muscles that occur during hip flexion [5]. The internal/external rotation and adduction moment arms of the iliopsoas muscle are small relative to its hip flexion and pelvic tilt moment arms. Thus, it is likely that the iliopsoas acted mainly as an antagonist to the gluteal muscles to control pelvic tilt.

Pectineus activation was low during maximum hip flexion because it has an internal rotation moment arm similar to the gluteal muscles. However, the moment arms of the gluteal muscles change from internal rotation at deep flexion to external rotation as the hip approaches neutral extension in stance. The pectinueus muscle has an internal rotation moment arm thus activation becomes antagonist to the gluteal muscles as the body rises to standing. Thus, pectineus muscle activation increases as the gluteal muscles switch from internal rotation to external rotation but then diminishes near stance as the gluteal muscles relax.

The piriformis and gluteus medius muscles have moment arms that change from internal rotation at deep flexion to external rotation in stance. Thus these muscles performed as gluteal synergists during the squatting activity, acting concentrically during rising and eccentrically during lowering.

CONCLUSIONS

The piriformis and gluteus medius muscles are recruited to aid in hip extension during the squatting exercise. The activation of these muscles promotes posterior pelvic tilt and hip external rotation and abduction. To limit these accessory motions, the pectineus and iliopsoas muscles are recruited to produce anterior pelvic tilt, hip adduction and internal rotation. Thus, the deep muscles of the hip may have functioned as the "rotator cuff" of the hip joint to finely control pelvic and hip motions.

REFERENCES

1. Lamontagne, M. et al. (2008). *Clin Orthop Rel Res*, **467**, 645-650.
2. Kubiak-Langer, M. et al. (2007). *Clin Orthop Rel Res*, **458**, 117-124.
3. Grood, ES, Suntay WJ (1983). *J Biomech Eng*, **105**, 136-144.
4. Torry, M. et al. (2006). *Clin Sports Med*, **25**, 179-197.
5. Delp, SL. et al. (1999). *J Biomech*, **32**, 493-501.

METHOD FOR VERIFYING MECHANICAL PROPERTIES OF PROXIMAL TIBIA TRABECULAR BONE DERIVED FROM CT DATA

[1]Vincent Alipit, [1]Joe Racanelli
[1]Stryker Orthopaedics
email: vincent.alipit@stryker.com

INTRODUCTION

To develop more representative finite element models of human bone for use in finite element analysis (FEA), computer tomography (CT) data is used as a basis of mechanical properties and bone geometry. Individual element properties are mapped from the CT data through a series of processing steps that impact the finite element model material properties. A high level evaluation of the mapped properties relative to published physical test data can provide increased confidence in the process. This study provides a method for verifying that a CT scan derived proximal tibia finite element model will have mapped mechanical properties of trabecular bone supported by published data

METHODS

A lower limb CT scan from a patient aged 63, weighing 74 kg, and measuring 175 cm tall was taken in 1mm slices. Published data used as a basis for comparison was taken from mechanical testing done by Goldstein et al [1] on five cadaveric specimens from ages 50-70 years, described as average height and weight.

The patient's CT scan was imported into Simpleware's [2] Scan IP software. The tibia was segregated by thresholding. This technique selects pixels in the CT scan's slices above a certain Hounsfield Unit (HU) value. A HU is an X-ray attenuation unit used to interpret CT scan data, where a value of 0 is water and -1000 is air [3]. In this case a HU of 600 was chosen to represent the lower value for cortical bone to bound the trabecular volume [4]. Based on previous experience, a portion of trabecular bone may have the same apparent density as soft tissue surrounding the tibia, thus it is not feasible to threshold for HU less than cortical. The trabecular bone is selected after the cortical boundary has been defined by filling in the inner cavity of the cortical bone. The combined selection constitutes the complete tibia geometry.

The model was meshed with higher order tetrahedral elements using a second Simpleware module; Scan FE. The element size was based on the CT scan's native slice resolution of 1mm x 1mm with a thickness of 1mm. Mechanical properties were calculated based on established correlations between bone density and elasticity [4]. The Scan FE software calculated these values using the following equations from Rho et al [1]: $\rho = 114 + 0.916 * HU$ *and* $E = 0.06 * \rho^{1.55}$, where ρ is the density and E is elastic modulus. Each element in the finite element model was assigned a calculated elastic modulus based on a HU value that corresponded to the element's location in the CT scan. A Poisson's ratio of 0.3 was assigned globally.

The FE model was imported into ANSYS 11.0 [5]. A cutting plane was created in accordance with reference 1 protocol for the initial tibial plane resection.

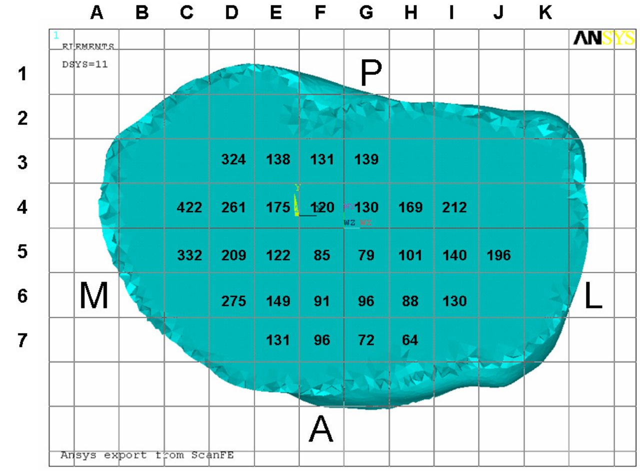

Figure 1: Resection with averaged elastic moduli values

A second cutting plane was developed 10mm distal to the initial tibial plateau resection resulting in a representative 10mm thick proximal tibia section. A 7mm square grid was superimposed on the resected surface to allow for sub-segregation of the mapped data. 7mm diameter cylinders were cut out of each grid square in each section. The moduli of elements inside each cylinder were averaged. Figure 1 shows the resection surface of the FE bone model with average elastic modulus values. The resulting average values were then compared to values obtained from Goldstein et al shown in Figure 2.

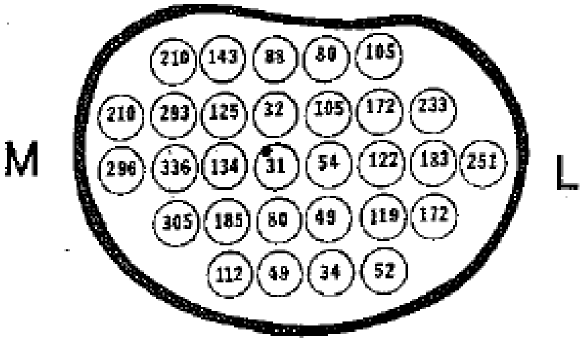

Figure 2: Elastic Moduli map from Goldstein et al.

RESULTS AND DISCUSSION

Figure 3 (A & B) summarizes elastic modulus data from the FE model compared to published data from ref 1 for the first 10mm of resected proximal tibia per the grid if Figure 1. 19 of the 30 regions moduli values fell within one standard deviation (sd) of ref 1 data. 26 of 30 regions fell within 2 sd and 29 of 30 regions fell within 3 sd.

Ensuring FE model material property accuracy is critical to the model development. Due to the number of steps and tools that may be used in the process of developing a FE model from CT data, a high level property verification tool can be used to ensure the model is representative. Although the CT scan patient data was outside the published physical test specimen group, 70% of the FE model's elastic modulus values fell within 1 sd, 86% fell within 2sd and 97% fell within 3sd with similar location trending. Comparative result differences are expected due in part to gender, age, ethnicity and weight and should be considered when comparing results.

This method will be further developed in future work comparing matched data from mechanical testing of cadaver specimens with matched CT scan data, eliminating potential variability between patients

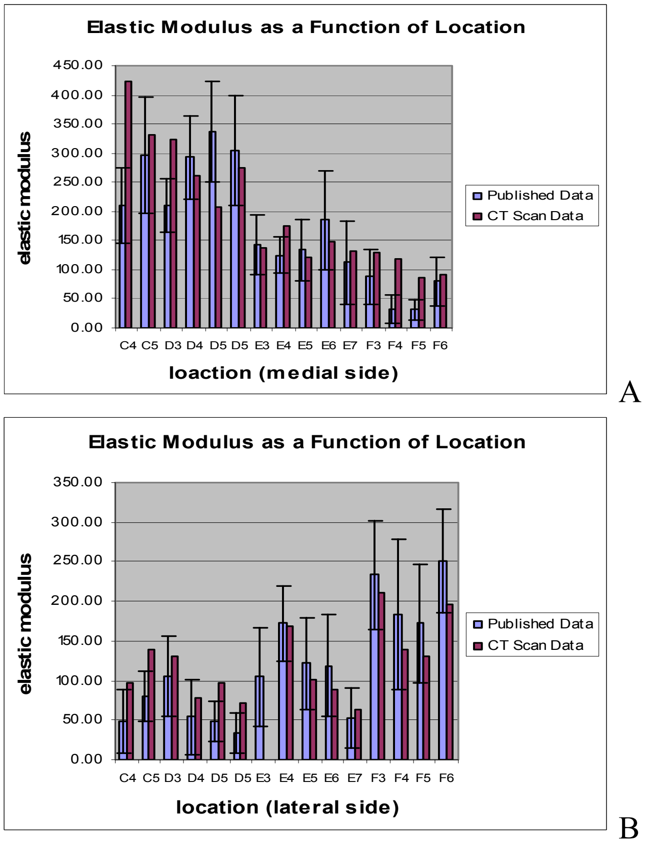

Figure 3: Elastic Modulus as a Function of Location from Figure 1, A represents the medial side and B the lateral side.

REFERENCES

1. Goldstein, et al. *J. Biomechanics* **16**, 965-969, d1983.
2. Simpleware Ltd. Exeter, England.
3. Rho, et al. *Med. Eng. Phys* **7**, 347-355, 1995.
4. Aamodt, et al. *JBJS (Br)* **81,** 143-147, 1999
5. Ansys, Inc. Canonsburg, PA.

ADAPTIVE SURROGATE MODELING FOR COST-EFFECTIVE DETERMINATION OF NONLINEAR TISSUE PROPERTIES

[1] Jason P. Halloran, [1]Jason D. Frampton, and [1]Ahmet Erdemir
[1]Department of Biomedical Engineering, The Cleveland Clinic, Cleveland, OH
email: hallorj@ccf.org

INTRODUCTION

Computational predictions of tissue mechanics, from evaluating intervention strategies for pressure relieving footwear to assessing the effects of anterior cruciate ligament reconstruction on cartilage stress, require not only accurate geometric representation but patient and/or specimen specific tissue deformation characteristics. Successful material models addressing patient specificity have been developed but these highlighted a possibly large computational cost dictated by iterative optimization using nonlinear finite element (FE) models [1,2]. Hence, the goal of this study was to assess the potential benefits of implementing an adaptive surrogate modeling framework to decrease this computational cost. Optimization of nonlinear-elastic material parameters using an inverse FE model of the heel pad plantar tissue was conducted for illustration purposes. The adaptive surrogate modeling framework utilizes previous FE results to interpolate a desired output and bypasses the need to rely solely on computationally expensive FE simulations and thus, has the potential to save significant computational costs.

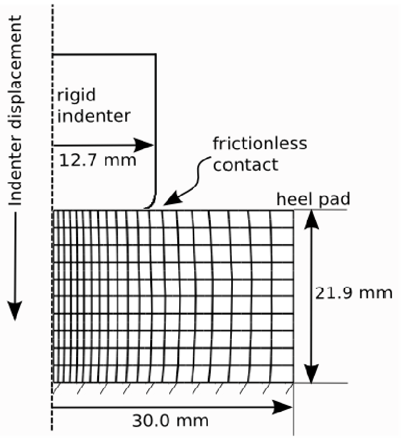

Figure 1. FE model

METHODS

In vivo displacement-load data from indentation testing of heel pad plantar tissue was used to drive the optimization. Data was obtained from a custom experimental apparatus designed to hold a subject's foot in place while a 25.4 mm indenter compressed the heel pad to ~50% thickness of the unloaded state at a rate of 5.7 mm/s. Ultrasound images and force were recorded during the testing [1].

A displacement driven axi-symmetric **FE model** of the indenter and heel pad tissue was used [1] (Fig 1). Heel thickness was tailored to the subject and the indenter was modeled as rigid. The soft tissue utilized an incompressible Ogden material model [3], where material coefficients μ and α defined the hyperelastic behavior. Boundary conditions were specified to recreate the experimental kinematic conditions. Indenter force was monitored and compared with experimental results.

For given Ogden material coefficient values (μ and α), the **surrogate model** utilized local, linear regression on a database of FE solutions to estimate the model versus experimental squared error result. The Lazy Learning toolbox [4] was utilized. The squared error was calculated from 10 evenly spaced time points, from zero displacement up to the maximum. A leave-one-out cross validation error (CVE) is also predicted by the surrogate model. For CVE values less than the prescribed tolerance of 10 N, squared error values were returned by the surrogate model. If the CVE was above the tolerance, an FE simulation was conducted and the results were saved to the database.

Optimization was performed to minimize the difference between model and experimental displacement-load results. Material parameters (μ and α) were the control variables and both simulated annealling (SA), a global search method, and sequential quadratic programming (SQP, fmincon, available in Matlab, Mathworks, Inc, Natick, MA), a gradient based approach, were implemented. Test cases included optimization routines with and without the surrogate model included. Routines utilizing the surrogate model actively populated the database (initially empty) as the solution proceeded. Results were compared between all simulations for relative accuracy, computational expense and utilization of the surrogate model.

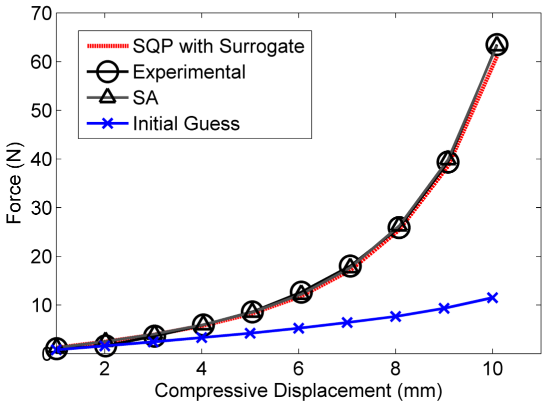

Figure 2. Compressive displacement versus force for the best fit, simulated annealing (SA) optimization, as well as the lowest achieved RMS error, sequential quadratic programming with the surrogate model (SQP with Surrogate). Experimental values and starting point results (Initial Guess) for the SQP optimizations are also included.

RESULTS

Surrogate modeling reduced the computation time of the SA optimization from 7 to under 2 hours (on an Intel® 2.0 GHz Xeon processor with 2 GB of RAM). The approach reduced the number of FE calls by 73.1% (538 vs 2000). Material coefficients were similar between surrogate and non-surrogate simulations (Table 1). SQP realized the same trend where the surrogate model reduced computation time by 70%, from 13 minutes to approximately 4 minutes. Coefficient values were functionally consistent for all analyses with the highest RMS error value of ~1 N (less than 1.5% of max. indentation force) for the SQP optimization with the surrogate model (Table 1).

DISCUSSION

Overall, implementation of the surrogate model resulted in marked improvements in computational expense for both global, SA, as well as the SQP optimizations. For this application, a slight sacrifice in accuracy was realized, as measured by the RMS error results, for the SQP with surrogate optimization but overall displacement-load behavior was obviously retained (Fig 2). Reasonable initial guess values were utilized for this controlled study but additional analyses demonstrated the robustness of the global, SA method over the SQP approach. For larger, more feature rich models a local minimum solution can be a concern and bringing a global method, such as SA, down to a feasible computational cost is worthwhile. In practice, surrogate tolerance values require insight into the behavior of the underlying structure and were set using previously developed methods [5]. The presented 2D application not only allowed for a test bed to accurately assess the benefits of the surrogate model but also demonstrated the effectiveness of the method to efficiently solve for subject specific tissue properties. Additionally, this approach is well suited to handle other computationally expensive, iterative processes such as a musculoskeletal or probabilistic study [5].

REFERENCES

[1] Erdemir, et al. J Biomech. 2006;39(7):1279-86.
[2] Lei, and Szeri. J Biomech. 2007;40(4):936-940.
[3] Twizell, and Ogden. J Aus Math Soc. 1986;B,24:424-444.
[4] Atkeson, et al. Artif Intell Rev. 1997;11:11-73.
[5] Halloran, et al. J Biomech Eng. Feb;131(1):011014.

ACKNOWLEDGEMENTS

This work was financially supported by NIH grant 1R01 EB006735 and NIH grant 5T32AR050959-05

Table 1: Summary of results for: simulated annealing (SA), SA with the surrogate model (SA – Surrogate), sequential quadratic programming (SQP) and SQP with the surrogate model (SQP – Surrogate). RMS error represents the difference between FE and experimental values.

	SA	SA – Surrogate	SQP	SQP – Surrogate
μ (kPa)	8.10	8.48	8.05	7.90
α	10.89	10.71	10.92	10.85
Time (min.)	420	110	13	4
RMS error (N)	0.42	0.55	0.42	0.97

SHOULDER ROTATOR MUSCLE FATIGUE AND EMG DURING REPEATED MAXIMAL EFFORT EXERCISE

[1]Nicholas Hess, [1]Shawn Calhoun, [1]Danny M. Pincivero
[1]Human Performance and Fatigue Laboratory, Department of Kinesiology, The University of Toledo
Email: danny.pincivero@utoledo.edu

INTRODUCTION

Previous studies have demonstrated a greater magnitude of voluntary muscle force production and a lower rate of muscle fatigue development in women, as compared to men (1,2). With respect to shoulder rotation, little information exits regarding muscle fatigue patterns between men and women. The objectives of the present study were to examine shoulder rotator muscle fatigue and activation, via the electromyogram (EMG), during maximal effort contractions between healthy young adult men and women.

METHODS

Subjects for this study consisted of 10 healthy men (mean ± SD, age = 21.3 ± 3.9 years, height = 178.4 ± 3.9 cm, mass = 75.8 ± 8.5 kg) and 10 healthy women (age = 22.0 ± 2.7 years, height = 165.4 ± 6.47 cm, mass = 65.8 ± 9.3 kg) who were all right hand dominant. Subjects performed three sets of 30 reciprocal, concentric maximal-effort shoulder internal (IR) and external (ER) rotation at a pre-set angular velocity of 3.14 rad•s^{-1} on the Biodex Isokinetic Dynamometer. Values for shoulder IR and ER peak torque (PT) were calculated for each repetition. The single highest repetition value for shoulder internal and external rotation PT was then converted to body mass-relative (N•m•kg^{-1}) and allometric-scaled (N•m•kg^{-n}) units. The rate of shoulder internal and external muscle fatigue was calculated by a fatigue index (% reduction in torque) and the slope of each isokinetic variable from the single highest repetition value through the 30th repetition.

Electromyograms of the pectoralis major (PM), latissimus dorsi (LD), infraspinatus (IN), and posterior deltoid (PD) muscles were sampled with surface electrodes (2000 Hz, 20-500 Hz band-pass filtered). All EMG signals were full-wave rectified and integrated over the middle 1.05 rad angular displacement of each repetition, and normalized to the single-highest repetition value throughout each 30 repetition set.

RESULTS AND DISCUSSION

Single highest peak torque

The single highest PT value generated within each set decreased significantly more across the 3 sets for the men than women ($F_{2,36} = 4.22$, p=0.023, Figure 1). Men displayed significantly ($F_{1,18} = 22.9$, $p<0.001$) greater PT for IR than ER, while the opposite pattern was observed for women. When corrected for body mass in relative and allometric-scaled units, men generated significantly greater IR and ER PT (Table 1).

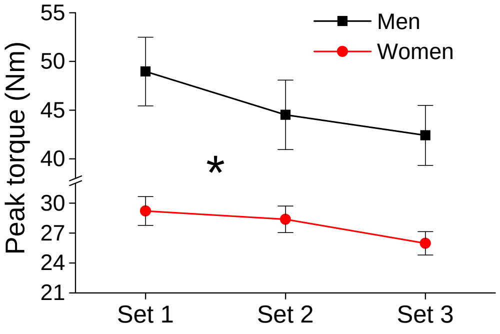

FIGURE 1: Single highest PT within each set, collapsed across IR and ER.

Peak torque and EMG fatigue

The decrease in ER and IR PT for the men and women are depicted in Figure 2. The results demonstrated a significant set main effect ($F_{2,36} = 9.26$, $p<0.001$) and a direction by set interaction ($F_{2,36} = 3.68$, $p<0.001$) for the peak torque fatigue index. The interaction was specifically observed to occur between sets 1 and 3 ($F_{1,18} = 8.01$, p=0.01), as a significantly greater increase in the fatigue index across these sets occurred for internal, than external, rotation. There were no significant direction or gender main effects, or other interactions. The peak torque fatigue slope demonstrated significant direction ($F_{1,18} = 4.46$, p=0.049) and gender ($F_{1,18} = 13.07$, p=0.002) main effects, and a significant direction by gender interaction ($F_{1,18} = 4.79$, p=0.04). The interaction indicated that the men experienced a significantly greater fatigue slope of the internal, than external rotator muscles, whereas the women displayed the opposite pattern.

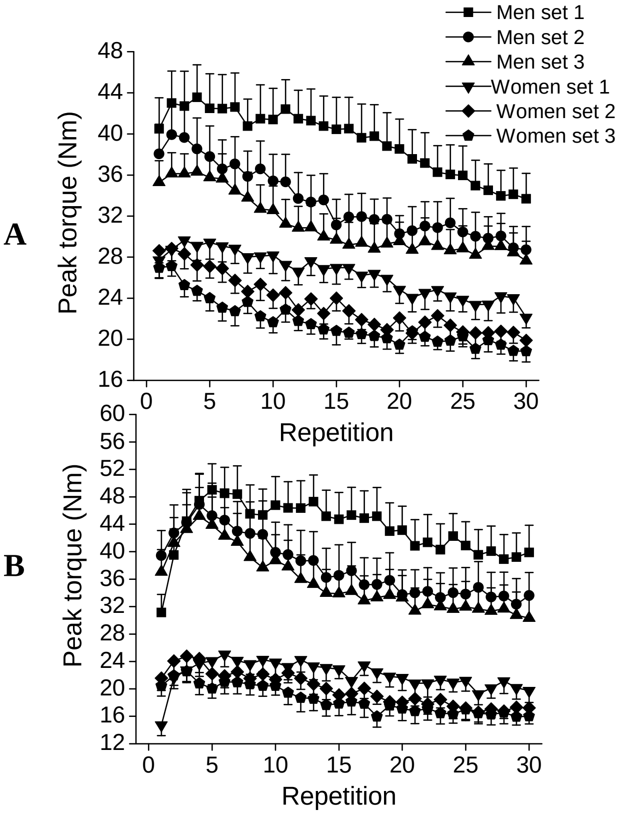

FIGURE 2: Muscle fatigue tracings for healthy young men and women for ER (A) and IR (B) PT.

With respect to IEMG, the results demonstrated significantly ($F_{1,16} = 15.43$, p=0.001) greater PM activity than the LD muscle, when collapsed across all repetitions and sets, while a significant increase was observed only across the first 4 repetitions (Figure 3, $F_{29,464} = 13.53$, p<0.001). Infraspinatus IEMG activity was significantly ($F_{1,18} = 7.11$, p=0.02) greater than the PD, when averaged across all sets and repetitions. A significant ($F_{29,522} = 6.37$, p<0.001) increase in IEMG activity across the first 2 repetitions of all sets (averaged) was observed, followed by no significant changes.

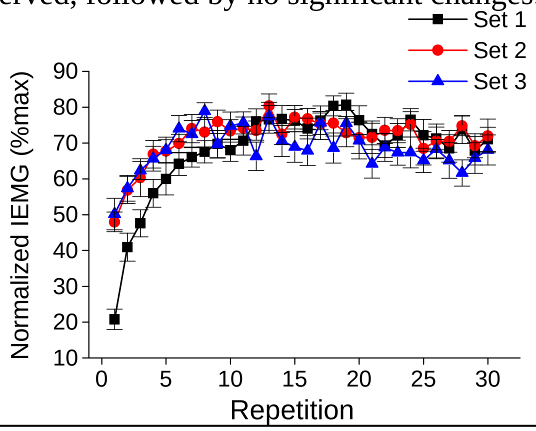

FIGURE 3: Normalized IEMG of the PM collapsed across men and women.

CONCLUSIONS

The major findings of the present study confirm previous results regarding the greater inherent voluntary force generating capacity of men with less fatigue resistance, than women (1,2). It is also concluded that despite clear patterns in the deterioration of voluntary muscle generating torque, the behavior of the surface EMG during maximal-effort fatiguing contractions initially increases followed by a plateau.

REFERENCES

1.Hunter SK & Enoka RM. *J Appl Physiol*, **91**, 2686-2694, 2001.
2.Pincivero DM, et al. *Eur J Appl Physiol*, **89**, 134-141, 2003.

TABLE 1: Mean (± SD) for the single-highest PT in absolute (N•m), relative (N•m•kg^{-1}), and allometric-scaled (N•m•kg^{-n}) units for isokinetic internal and external shoulder rotation in men and women.

	Internal rotation		External rotation	
	Men	**Women**	**Men**	**Women**
Absolute PT	52.14 ± 13.47*	27.07 ± 5.07	45.79 ± 10.17*	31.34 ± 5.03
Relative PT	0.68 ± 0.13*	0.42 ± 0.07	0.60 ± 0.09*	0.48 ± 0.04
Allometric PT	0.54 ± 0.10*	0.33 ± 0.06	0.22 ± 0.05*	0.13 ± 0.02
Fatigue index				
Set 1	20.10 ± 10.46	20.64 ± 8.26	21.46 ± 6.35	21.12 ± 8.24
Set 2	26.62 ± 8.55	29.38 ± 8.47	23.72 ± 4.33	26.90 ± 5.79
Set 3	29.74 ± 8.20	26.42 ± 8.02	21.89 ± 4.32	24.91 ± 5.72

MECHANICAL LOADING CAUSES AN ACUTE AND TEMPORARY DECREASE IN THE STIFFNESS OF MOUSE TIBIAE

[1] Varun A. Bhatia, [1,2]Karen L. Troy
[1]Bioengineering Department, University of Illinois at Chicago
[2]Department of Kinesiology and Nutrition, University of Illinois at Chicago
email: vbhati2@uic.edu, web: http://www.uic.edu/ahs/biomechnics

INTRODUCTION

Bone is a dynamic tissue that adapts to best resist its loading environment by remodeling, the process by which micro-damage is repaired and micro and macro structure may be altered. Animal models have been valuable tools for understanding this process and have been studied with the long-range goal of developing mechanical loading-based interventions to improve bone strength in aging humans.

Our previous work with a human model of bone adaptation has shown that young women experience an acute and temporary decrease in bone mineral content (BMC) approximately three months after initiating a regular novel mechanical loading regime [1]. We believe this may be a reflection of increased remodeling space within the bone. The degree to which bone strength may be decreased due to this change in BMC is unknown. The purpose of this study is to quantify the changes in BMC and mechanical stiffness during the initial remodeling phase in a mouse tibia loading model. Our hypothesis is that, similar to humans, mice will show a temporary decrease in BMC. Along with this decrease in BMC, we also hypothesize that a decrease in mechanical stiffness and strength of the bone will occur.

METHODS

With protocols approved by the Institutional Animal Care and Use Committee, 26 female C57BL/6J mice (age: 18 weeks) were divided into five loading groups: 3-day (6 mice), 7-day (4 mice), 10-day (6 mice), 14-day (6 mice) and 21-day (4 mice). Prior to any mechanical loading and after sacrifice, both tibiae were scanned using a small animal DEXA (pDXA, Norland Stratec, Ft. Atkinson, WI) to measure the BMC. Prior to the start of the experiment, a strain gage was affixed to the mid-diaphysis of the tibiae of two euthanized mice and used to identify the force required to produce surface strains of 1000-1200$\mu\varepsilon$. Based on the strain gage data a peak compressive load of 8N was chosen.

A custom fabricated loading apparatus was used to axially compress the left tibia of each mouse for 50 cycles a day at 0.5Hz (Figure 1), three days per week (Monday, Wednesday, Friday) for the respective number of days. For example, the 10-day group was loaded on Mon/Weds/Fri/Mon and sacrificed on the following Wednesday. Based on previous data indicating that a rest period between loading cycles can be osteogenic [2], a 15 second rest period was inserted between each loading cycle. The right tibia acted as a within-subject control.

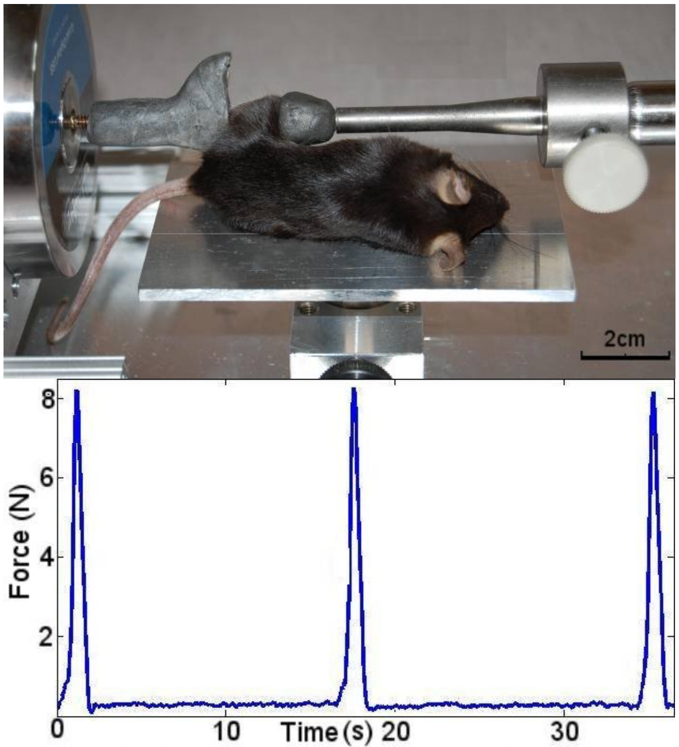

Figure 1 (top) Mouse tibia loading device (bottom) tibia loading wave form, recorded during an experimental trial.

After sacrifice, the loaded and the contra-lateral tibiae were dissected out for mechanical testing. Whole-bone stiffness was measured in axial compression by applying a ramped load up to 12 N at about 400 με/s. Stiffness was calculated as the average slope of 6 cycles. Tibiae from one mouse per group were reserved for histological analysis and the remaining bones were tested to failure at the same strain rate to determine the yield and ultimate force.

Planned comparisons included paired t-tests for post-loading BMC and stiffness (contra-lateral versus loaded) for each group and single sample t-tests of the percent change in BMC from pre-to post-loading for each group.

RESULTS AND DISCUSSION

The loaded limb of the 10-day group showed a 6.2% decrease in BMC compared to the contra-lateral limb (Table 1). This difference disappeared at 14 days and by 21 days the loaded limb's BMC was 3.8% larger than the contra-lateral limb.

The 3-day group's loaded limb stiffness was decreased 13.5% compared to the contra-lateral limb (Table 1). This difference disappeared by 10 days and at 21 days there was a trend towards the loaded limb being stiffer than the contra-lateral limb. Pre/post test comparisons for percent change BMC showed the same results, with a significant 6.5% decrease in BMC (p=0.007) in the loaded limb at 10 days.

Table 1: Mean (SD) of BMC and Stiffness of left and right tibiae of 3 day, 7 day, 10 day, 14 day and 21 day groups. L=loaded limb, R=contra-lateral limb

Group	BMC (mg)	Stiffness (N/mm)
3 day	**L** 26.8 (3.21) **R** 26.4 (1.39) p= 0.822	**L** 54.4 (4.7) **R** 63.8(4.3) p=0.003
7 day	**L** 21.67 (2.26) **R** 21.67 (1.53) p= 1.0	**L** 56.4 (9.9) **R** 60.8 (8.9) p=0.454
10 day	**L** 25.53 (1.51) **R** 27.22 (0.25) p= 0.035	**L** 58.3 (8.7) **R** 52.4 (10) p=0.051
14 day	**L** 25.28 (2.91) **R** 26.36 (1.82) p= 0.263	**L** 53 (8.9) **R** 52.5 (9.5) p=0.576
21 day	**L** 27.00 (1.83) **R** 26.00 (1.63) p= 0.092	**L** 54.8 (11.9) **R** 42.9 (4.3) p=0.276

The data support our hypotheses that both BMC and stiffness transiently decrease in response to mechanical loading. Interestingly, the decrease in stiffness preceded any detectable change in BMC (Figure 2). It is possible that the initial decrease in stiffness results from micro-damage to the bone (we would not expect the strains imposed here to cause gross damage). The micro-damage initiates a remodeling response that results in removal of damaged bone and apposition on the bone surfaces. Initially, this manifests as a decrease in BMC as bone is removed. Longer-term loading results in increased BMC and probably in geometrical changes in bone structure.

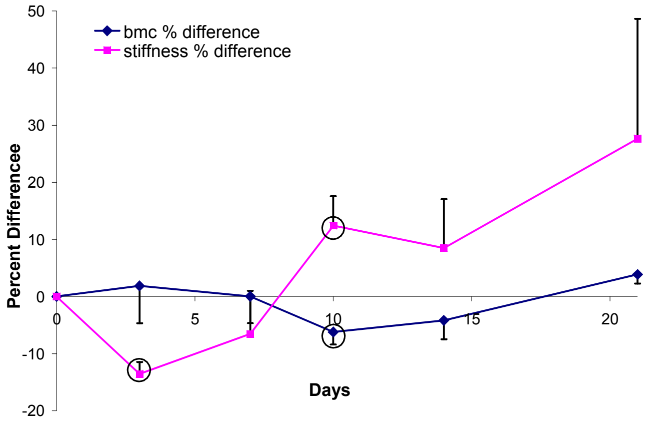

Figure 2: Percent difference in BMC and stiffness, between loaded and contra-lateral tibiae with respect to time. Error bars show standard error. 'O' indicates p<0.06. Zero percent difference is assumed at day zero.

At 6 weeks other groups have shown increases in BMC and in maximum cross sectional moment of inertia (I_{max}) [3]. The increase in I_{max} reflects increased strength. Though not statistically significant, the 21-day group shows a trend towards increased BMC and stiffness of the loaded limb. An increase in the number of mice in the group may result in statistical significance. Decreased stiffness may correspond to a decrease in failure strength of the bone. The decrease in BMC and stiffness in mice due to loading in the short term may have serious implications on fracture risks. However, the degree to which this phenomenon puts humans at risk for fracture after commencing a novel loading regime is yet to be determined.

REFERENCES

1. Troy KL, et al. Proceedings of the Orthop. Res. Soc. #1181, 2008
2. Srinivasan S, et al. J Bone Miner Res **17**, 1613-1620, 2002.
3. Fritton JC, et al. Bone **36**, 1030-1038, 2005.

FORCE-LENGTH PROFILES FOR THE TRICEPS BRACHII

Nicholas J. Fiolo, Jessica L. Kutz, Benjamin W. Infantolino and John H. Challis
Biomechanics Laboratory, Department of Kinesiology, The Pennsylvania State University,
University Park, PA, USA
E-mail: njf5042@psu.edu

INTRODUCTION

The force-length curve of muscle is an important factor in many musculoskeletal models (e.g., Zajac [1]). For certain muscles it is feasible to determine the force-length properties *in vivo*, for example by exploiting the fact that some muscles are biarticular [1, 2]. Many models of the musculoskeletal system assume that each muscle acts at or near the plateau of its force-length curve [3]. While this assumption may be correct for some muscles Herzog et al. [2] demonstrated that is not the case for the Rectus Femoris. Their study demonstrated that speed skaters and cyclists used different portions of their force-length curve than runners for the Rectus Femoris. If such variability can exist it cannot always be valid to assume muscles act on the plateau region of the force-length curve. Using *in vivo* methods to determine muscle force-length properties will help guide in model formulation.

Although the Triceps consists of three distinct heads in many musculo-skeletal models they are functionally lumped together (e.g., 5, 6). Given this assumption the *in vivo* operating range of the Triceps was assessed. Therefore, the purpose of this study was to investigate the variability of the force-length curve of the Triceps Brachii.

METHODS

Six male subjects (mean height: 148 ± 8 cm, mass: 75 ±13 kg, age: 22 ±2 years) volunteered and provided informed consent for this study. Each subject performed isometric elbow extensions using their dominant arm. The testing protocol consisted of a five second maximum contraction at the specific elbow angle, followed by a thirty second rest period. After five contractions at the specific elbow angle, a one minute rest was given before proceeding to the next elbow angle. Subjects performed contractions at 0, 30, 60, 90, and 120 degrees of elbow flexion.

All testing was performed in a Biodex dynamometer. The participant's flexion/extension shoulder angles were standardized at 45 degrees, and the forearm was held in a neutral position. Subjects were secured to the Biodex using lap and shoulder straps, to stabilize the subject and minimize unwanted movement during contractions. The elbow joint center was aligned with the axis of rotation of the Biodex.

The moment produced by the subjects for each trial was sampled at 1000 Hz using LabView (National Instruments, Texas, USA). The mean of the three highest moments recorded at each joint angle were averaged to determine the maximum moment. The moment data was converted into tendon force data using the non-linear equation described in Ramsay et al. [7].

For each subject tendon force-joint angle plots were determined. These curves were then analyzed using the method of Winter and Challis [2]. This method distinguishes between force-length curves as acting of the ascending, descending, or plateau region of the force-length curve. Throughout this analysis elbow joint angle is assumed to reflect muscle length.

RESULTS

The force-joint angle (length) profiles for the six subjects demonstrated differences with regards to the section of the force-length curve that they operated on (Figure 1). Three of the six subjects operated on the ascending limb of the force-length curve, two on the plateau, and one on the descending limb.

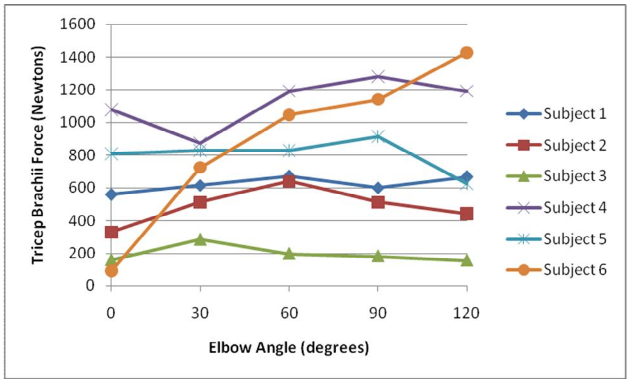

Figure 1: The Triceps force elbow joint angle curves for the six subjects.

If the force-joint angle curves are normalized with respect to the greatest force in the curve this is an indication of variability between subjects (Figure 2). The subjects whose Triceps Brachii operates on the asceding limb of the force-length curve would produce increasing force through a longer range of motion then those subjects who operate on the plateau of the force-length curve.

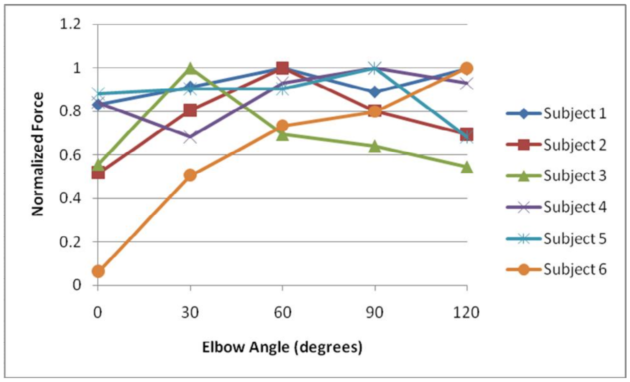

Figure 2: The Triceps force elbow joint angle curves for the six subjects.

DISCUSSION

The purpose of this study was to investigate the variability of the force-length curve of the Triceps Brachii. There some variability between the subjects which reflect patterns seen in other muscles [2, 3]. This variability indicates the problems that can arise in musculoskeletal models, where between subject variability may not be accounted for. The procedure to collect data for estimating the force-length curves took approximately 20 minutes to complete; a short time considering the potential applications of musculoskeletal models.

There are a number of assumptions in this study. The Triceps has three heads all of which may behave different to their net effect. But for the subjects with descending force-length curves at least one of these heads must be operating on the same portion of the force-length curve as determined in this study. Joint angle was used as a surrogate for muscle length, and while this is a non-linear relationship as the elbow angle increases this corresponds to Triceps length increases. Finally the tendon of the Triceps would stretch as muscle force is applied to it, so for those muscles operating on the ascending limb of the force-length curve as muscle force increases with increasing joint angle the tendon would be stretched more by the increase in force thus deminishing the length change in the muscle fibers.

REFERENCES

1. Zajac FE. *Crit Rev Biomed Eng* **17**, 359-411, 1989.
2. Winter SL and Challis JH. *J Appl Biomech* **23**, 207-214, 2008.
3. Herzog W, et al. *Med Sci Sports Exerc* **23**, 289-296, 1991.
4. Pierrynowski, MR and Morrison JB. *Math Biosci* **23**, 1289-1296, 1985
5. Alexander RM. *Biol Cybern* **76,** 97-105, 1997.
6. Lan N. *IEEE Trans Neural Syst Rehabil Eng* **10**, 249-259, 2002.
7. Ramsay JW, et al. *J Biomech* **42**, 436-473, 2009.

AN EVALUATION OF FUNCTIONAL ASYMMETRY AT NON-PREFERRED WALKING SPEEDS

Rodney S. Smith, John R. Rice, and Matthew K. Seeley
Brigham Young University, Provo, UT, USA
email: rodneysmith83@gmail.com

INTRODUCTION

The idea of functional asymmetry has been used to explain documented bilateral asymmetries for various biomechanical measures during normal gait [1]. According to this idea, the non-dominant and dominant legs, considered as whole entities, contribute asymmetrically to support (upward center of mass acceleration) and propulsion (forward center of mass acceleration). It was believed that the non-dominant leg contributes more to support, while the dominant leg contributes more to propulsion [1]. We recently demonstrated, however, that the non-dominant and dominant legs contribute similarly to support and propulsion during preferred-speed walking, but the dominant leg contributes 7% more to propulsion than the non-dominant leg during walking at a speed that is 20% greater than preferred [2]. This indicates that functional asymmetry may not exist during preferred-speed gait, but it may occur while walking at a speed that is greater than preferred.

The purpose of this study was to further investigate the potential relationship between functional asymmetry and non-preferred walking speeds. We formulated three hypotheses that were based upon the idea that functional asymmetry may be influenced by walking speed: (1) As walking speed increases, contributions to propulsion (measured via impulse due to the forward-directed ground reaction force; GRF) would increase at a greater rate for the dominant leg than for the non-dominant leg; this was expected because propulsive requirements increase as walking speed increases. (2) Contributions to propulsion would be significantly greater for the dominant leg, relative to the non-dominant leg for walking speeds that are greater than preferred. (3) Contributions to support (measured via impulse due to the vertical GRF) would be bilaterally symmetrical at various walking speeds, because support requirements are relatively constant across different walking speeds, due to the constancy of gravity.

METHODS

Bilateral GRFs were observed for 20 healthy subjects (age = 23 ± 2 yrs; height = 1.74 ± 0.09 m; mass = 71.4 ± 13.1 kg) who walked at nine different speeds (Table 1). Informed consent was obtained prior to data collection. Five trials were performed for both legs at each speed. Walking speed was measured with an optoelectronic timing device and reported immediately to subjects. If the speed was not within ± 2.5% of the target speed, the trial was performed again. Impulse due to vertical GRF (support) was calculated as the time integral of the vertical GRF during stance. Propulsive impulse was calculated as the time integral of the anterior-posterior GRF, while this force was oriented in the forward direction (approximately the second half of stance). Impulses were normalized to the product of: 1) body weight and 2) the square root of limb length/gravity [3].

Two repeated measures ANOVA (p = 0.05) were used to evaluate the influence of leg and speed on both dependent variables: support and propulsive impulse. A potential leg × speed interaction was tested for each dependent variable. If an interaction was detected, *post hoc* tests were used to compare

Table 1. Mean walking speeds (m/s) for the present study: the preferred speed (PS) and other speeds that were relatively slower (-) or faster (+). *P* values for bilateral comparisons of support and propulsive impulses are also indicated; there was no significant between-leg difference at any of the observed speeds.

Target Speed	**-40%**	**-30%**	**-20%**	**-10%**	**PS**	**+10%**	**+20%**	**+30%**	**+40%**
Actual Speed	0.94 ± 0.1	1.09 ± 0.1	1.25 ± 0.2	1.41 ± 0.3	1.56 ± 0.3	1.71 ± 0.3	1.88 ± 0.3	2.03 ± 0.4	2.20 ± 0.4
Support (*p*)	0.76	0.78	0.68	0.64	0.74	0.84	0.87	0.80	0.83
Propulsive (*p*)	0.89	0.89	0.73	0.56	0.20	0.20	0.07	0.34	0.42

the dependent variables at each speed. Alpha levels were adjusted using the false discovery rate procedure for multiple comparisons [4].

RESULTS AND DISCUSSION

A significant leg × speed interaction was detected for support ($p = 0.01$) and propulsive ($p = 0.04$) impulse (Figure 1). *Post hoc* comparisons revealed no significant bilateral differences for any of the dependent variables at any walking speed (Table 1).

Overall, the data were inconclusive regarding the idea that walking speed affects functional asymmetry. The first hypothesis was supported, but the second and third were not. The observed leg × speed interaction for propulsive impulse was predicted and in the expected direction. As speed increased, the dominant leg contributed disproportionately more to propulsion (Figure 1B), supporting the idea that functional asymmetry is related to walking speed and more prevalent at increased speeds. A lack of statistical bilateral difference for propulsive impulse at any of the increased walking speeds contradicted the second hypothesis. A qualitative view, however, of the propulsive impulse data (Figure 1B) indicates that whole-leg contributions to support do vary in a manner that fits with the idea that functional asymmetry is influenced by walking speed. Lastly, the observed leg × speed interaction for support impulse contradicted the third hypothesis. Speculating, it appears that dominant leg contributions to support decrease disproportionately, relative to non-dominant leg contributions as walking speed increases (Figure 1A); this observation also fits with the idea that functional asymmetry is more prevalent at increased walking speeds.

CONCLUSIONS

Although our data failed to support two of the three hypotheses, support of the first hypothesis and other trends in the data indicate that functional asymmetry may be related to walking speed.

REFERENCES

1. Sadeghi H et al., *Gait Post* 12, 34-45, 2000.
2. Seeley MK et al., *Gait Post* 1, 24-28, 2008.
3. Hof A, *Gait Post*, 4, 222-223, 1996.
4. Curran-Everett D, *Am J Physiol*, 279, R1-R8, 2000.

ACKNOWLEDGEMENTS

This project was supported by funding from the Brigham Young University College of Health and Human Performance.

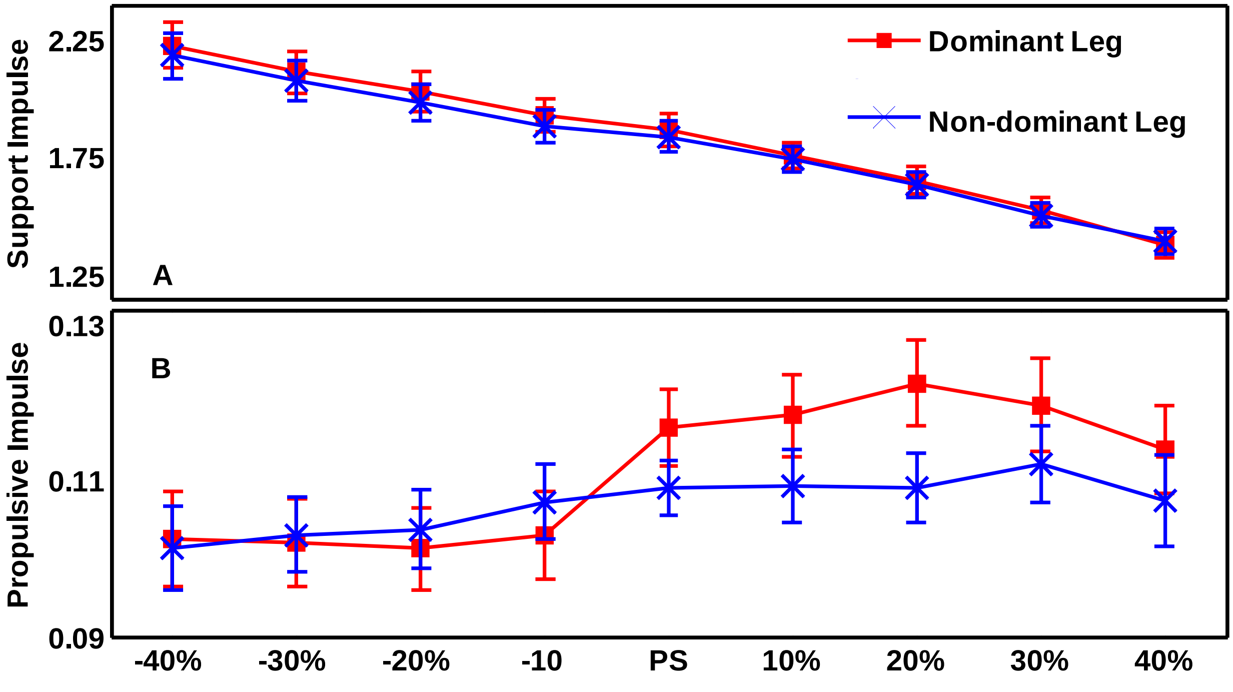

Figure 1. Means and standard errors for support (A) and propulsive (B) impulse for walking at nine different speeds. Normalized impulse is on the vertical axis. Walking speed is on the horizontal axis: preferred speed (PS) is in the middle, and slow (-) and fast (+) speeds are on the left and right, respectively.

STRAIN IN THORACOLUMBAR SPINE DURING CYCLIC LOADING AT TWO FREQUENCIES

[1, 2]Sai Vikas Yalla, [1]Naira H Campbell-Kyureghyan, [1]Patricia Cerrito and [1]Michael J Voor
[1]University of Louisville, Louisville, KY 40292
[2]email: s0yall01@louisville.edu

INTRODUCTION

A systematic review of epidemiological studies between 1980 to 1997 revealed a strong association between repetitive lifting, Manual Material Handling (MMH) tasks, and low back pain [1]. Later studies found that the number of lifts per minute, along with velocity during MMH tasks, were risk factors leading to fatigue fractures, and hence injuries, of the lower back [2,3]. Even with the presence of lifting limits and guidelines, low back injuries still remain the single largest category of work related injuries, comprising 27% of non fatal occupational injuries [4].

While typical MMH tasks were found to have lifting rates ranging from 1 to 15 lifts per minute [5], material testing for fatigue failure in previous studies was tested at lifting rates ranging from 15 to 120 lifts per minute [6]. The effect of lift frequency was analyzed measuring accumulated strain in terms of number of cycles as a failure criterion in most of the prior studies. In order to better assess the effect of loading frequency, the current study investigates accumulated strain with respect to duration over a period of 8 hours at two different frequencies.

METHODS

38 fresh thoracolumbar spine motion segments were dissected from 12 human cadavers whose age ranged from 53 to 91 years. Motion segments were positioned at Harrison angles to account for their natural alignment [7] utilizing a specially designed loading fixture. A compressive preload of 350 N was applied for 15 minutes to reduce postmortem effects and simulate torso load. 18 segments were monotonically tested for compressive failure, defined as a drop in sustained force, at a rate of 4 mm/hr. Cyclic testing was performed on two randomized groups of 10 segments. Each group was tested at two frequencies, 0.1 and 0.2 Hz, representing 6 and 12 lifts per minute respectively, for a period of 8 hours. Cyclic load magnitude for each segment was set at 50% of the monotonic failure stress from the same spine monotonic compressive failure test. A nested model, which is a special case of a mixed model, was used for statistical analysis at $\alpha=0.05$.

RESULTS

Accumulated strain was calculated as percentage deformation of the intervertebral disc with respect to the initial disc height. 60% of the 8-hour accumulated strain occurred during the first hour of cyclic loading. A gradual decrease in the strain rate was observed over the remaining 7 hours (Figure 1). A significant ($p<0.05$) 64% increase in strain was observed at the end of the 8 hour period when the loading frequency increased from 0.1 Hz to 0.2 Hz.

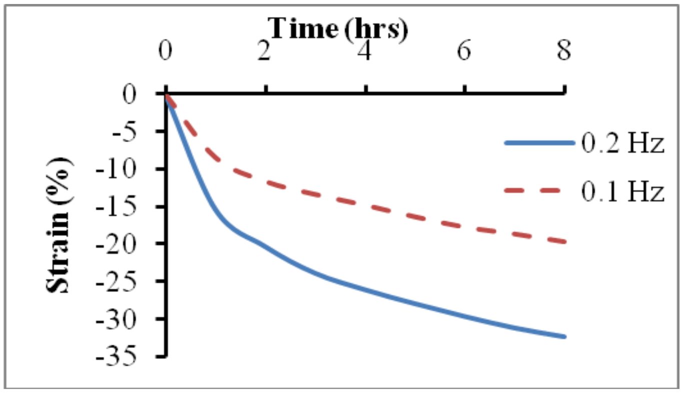

Figure 1: Accumulated strain (%) at 0.1 and 0.2 Hz over an 8 hour period.

Strain rate is defined as the slope of the accumulated strain from Figure 1. High rates were observed during the first 2 hours, where strain rate at 0.2 Hz was 5%/hr compared to 3.2%/hr at 0.1 Hz, a 56% ($p<0.05$) increase in strain rate from 0.1 Hz to 0.2 Hz... As the loading continued, strain rate at both 0.1 Hz and 0.2 Hz gradually decreased, becoming fairly constant and similar for the two frequencies (Figure 2).

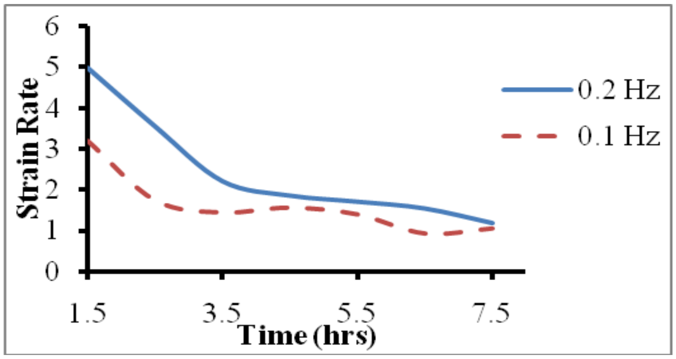

Figure 2: Rate of change of strain (%/hr) over 8 hour period at 0.1 and 0.2 Hz

The percentage increase in strain with increased loading frequency from 0.1 Hz to 0.2 Hz was examined. The strain at 0.2 Hz rapidly diverged from the 0.1 Hz strain, showing an increase of 82% after approximately 1 hour, but slowly decreasing after that time to 64% at the end of the 8-hour loading period (Figure 3).

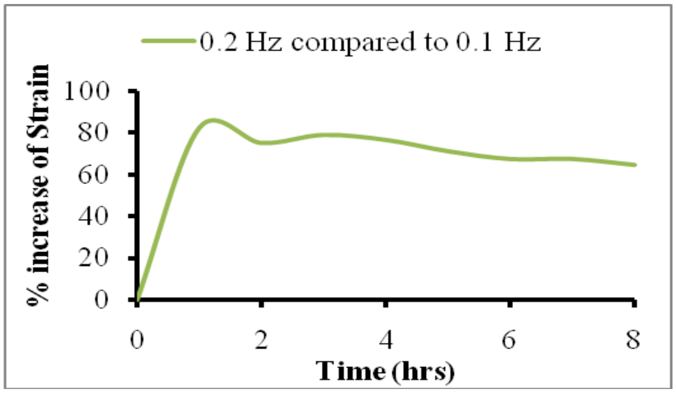

Figure 3: Increase in accumulated strain from cycling at 0.2 Hz compared to 0.1 Hz in terms of percentage over 8 hour period.

Since the specimens loaded at 0.2 Hz experienced twice the number of cycles over a given time period, strain was also compared with respect to number of cycles. For 2000 loading cycles, 5.6 and 2.8 hours for 0.1 and 0.2 Hz respectively, a significant ($p<0.05$) 32% increase in strain was observed for the 0.2 Hz loading compared to the 0.1 Hz loading.

DISCUSSION

Doubling the loading frequency from 0.1 Hz to 0.2 Hz resulted in higher loading velocity and doubles the number of cycles, which lead to a 56% increase in strain rate and an 82% increase in total strain during the initial stages of loading. Rapid increase in disc stiffness during the initial stages was also found in an earlier study for cycling at 0.5 Hz [8]. However, as the loading continues, the disc stiffens and the strain rate decreases, resulting in a logarithmic ($R^2>0.90$) accumulation of strain over the entire 8 hour period. Eventually the stiffness, and hence strain rate, becomes relatively constant and the disc starts to exhibit saturation of strain.

8 hours of cyclic loading at 0.2 Hz requires 5760 cycles to complete, while requiring only 2880 cycles at 0.1 Hz. Comparing accumulated strain for the same number of cycles shows a 32% increase due to the higher loading rate. This difference is due to the increased loading velocity at 0.2 Hz and the viscoelastic nature of the disc. While the velocity effect is important, ignoring the actual number of cycles performed over a given time period, as in most prior studies, can underestimate the total effect of increased loading frequency.

CONCLUSIONS

Spine motion segment testing at frequencies of 0.1 and 0.2 Hz produced evident differences in accumulated strain. The number of cycles is not a sufficient indicator of risk since they do not account for load changes or for the duration of exposure to cyclic loads, thereby possibly underestimating the effect of frequency. Strain, although eliminating some of the problems associated with other damage measures, is susceptible to saturation over time and, in isolation, might not be a good damage measure.

REFERENCES

1. Kuiper JI, et al., *International Journal of Industrial Ergonomics* **24**, 389-404, 1999.
2. Fathallah FA, et al., *Spine* **23**, 1035, 1998.
3. Marras WS, et al., *Ergonomics* **43**, 1866-1886, 2000.
4. BLS, *US Department of Labor: http://www. bls. gov/cpi*, 2006.
5. Marras WS, et al., *Spine* **18**, 617-628, 1993.
6. Gallagher S, et al., *Spine* **32**, 1832, 2007.
7. Harrison DE, et al., *Spine* **26**, e235, 2001.
8. Hansson TH, et al., *Journal of Orthopaedic Research* **5**, 479-487, 1987.

FIVE-TOED SOCKS DECREASE STATIC POSTURAL CONTROL AMONG HEALTHY INDIVIDUALS AS MEASURED WITH TIME-TO-BOUNDARY ANALYSIS

Junji Shinohara, Phillip Gribble
Athletic Training Research Laboratory, University of Toledo, Toledo, OH, USA
Email: Junji.Shinohara11@utoledo.edu

INTRODUCTION

Receiving accurate sensory information is critical for effective motor control during any physical activity. It is especially necessary during dynamic sports activities that require stable standing and accurate ball control, such as baseball, golf and tennis. Orthotics and ankle braces have been believed to enhance the proprioceptive [1] and cutaneous [2] afferent inputs to the central nervous system (CNS); assumedly generating improved efferent inputs for enhanced motor control. While orthotics and ankle braces are commonly used for pathological conditions, such as foot and ankle injuries, a unique pair of athletic socks called five-toed socks has become popular in Japan for healthy active individuals marketed to enhance their athletic ability by increasing postural stability.

There are claims that the five-toed socks improve postural control by separating the toes, potentially increasing the proprioceptive and cutaneous inputs to the CNS, thereby enhancing the perception of the ground and provide a better grip. While the five-toed socks are becoming more popular in Japan, no scientific research has been performed to examine these theories or study the effectiveness of the socks. Therefore, the purpose of this study was to assess the effect of the five-toed socks on static postural control during single-limb balance tests with eyes open and closed.

METHODS

Twenty healthy subjects (11 males, 9 females; 25.5±2.6yrs; 170.8±10.3cm; 74.0±14.3kg) were asked to complete three testing sessions, separated by approximately one week, to measure static postural control. The subjects were tested under three conditions: wearing five-toed socks, wearing regular socks, and wearing no socks (Figure 1). For each condition, static postural control was assessed on a force plate (model 4060NC; Bertec Corp Inc., Columbus, OH) with the subject in a single-limb stance with their hands on their iliac crests, with eyes open (EO) and eyes closed (EC). During the EO trial, subjects were instructed to focus their vision on a large “X” on the wall 3.5 m in front of them and 1.5 m from the floor. The subjects were instructed to keep the non-test limb off the ground in a comfortable position without the limb touching the ground. The test limb was determined as the limb the subject would choose to stand on while kicking a ball. The subjects were instructed to stand as still as possible for 15 seconds. If the subjects hopped on the test limb or touched the ground with the non-test limb, the trial was discarded and repeated. Center of pressure (COP) data were sampled at 50Hz. The subjects completed three 15-second trials with a one-minute rest between trials. Sock conditions were randomized.

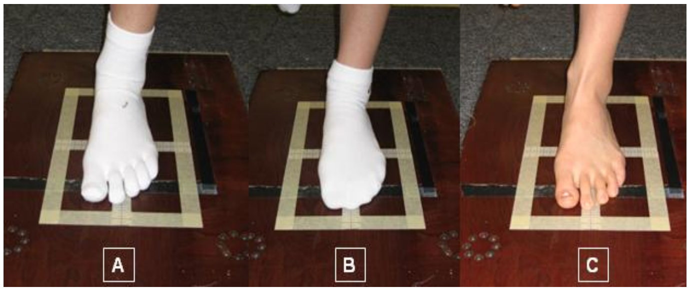

Figure 1: Sock Conditions with single-limb balance tests. A) Five-toed sock condition, B) Regular sock condition, and C) No sock condition.

For each condition, the COP data were averaged for the three test trials, both for EO and for EC trials. The Motion Monitor software (Innovative Sports Training, Inc., Chicago, IL) collected COP data during the single-limb balance testing. MATLAB software (The Mathworks Inc., Natick, MA) was utilized to calculate the Time-to-Boundary (TTB) variables in both the anteroposterior (TTBAP) and mediolateral (TTBML) directions.

The TTB dependent variables, calculated for TTBAP and TTBML separately for EO and EC trials, were the TTB absolute minimum and mean of the TTB minima [3,4]. The independent variable was sock conditions (wearing five-toed socks, wearing regular socks, and wearing no socks). For each dependent variable, a one-way repeated measures ANOVA was performed. Significance was set a priori at $p<0.05$.

RESULTS and DISCUSSION

The five-toed sock condition showed significantly lower TTB values than the no sock condition in the TTBML absolute minimum samples during EO trials ($F_{2,17}=4.075$; $P=0.025$) (Figure 2a) and the mean of the TTBML minima samples during EC trials ($F_{2,17}=3.919$; $P=0.048$) (Figure 2b), indicating that the five-toed condition was associated with decreased static postural stability when compared to the no sock condition. There were no other significant differences among the sock conditions in either TTBAP or TTBML directions.

The current study demonstrated that the five-toed socks did not improve static postural control among healthy individuals in both anteroposterior and mediolateral directions during EO and EC trials, measured with TTB analysis. Further, in the TTBML absolute minimum during EO trials and the mean of the TTBML minima during EC trials, the five-toed sock condition seemed to impair the postural control when compared to the no sock condition, contrasting the claims that are associated with these socks.

With the five toed-sock condition, individually wrapped toes potentially increase proprioceptive and cutaneous inputs by enhancing tactile sensations and providing pressure to the skin between the toes. However, it is possible that most of the subjects have not experienced this enhanced sensation around the toes before, and this novel sensation may have interrupted the concentration of the subjects during the single-limb balance testing. Future study should include at least a one week adaptation period for subjects to become accustomed to the enhanced sensation around the toes before the data collection is conducted. Additionally, assessing static postural control may not be the most sensitive or applicable measure of the effectiveness of five-toed socks therefore investigation using measures of dynamic postural control may be warranted. Future study also should include comparisons between healthy and pathological conditions such as chronic ankle instability.

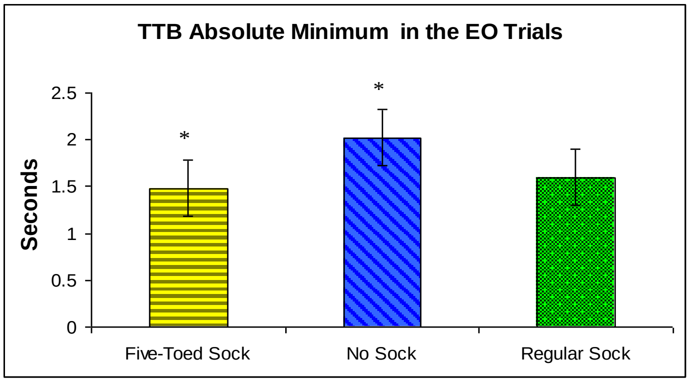

Figure 2a: TTBML absolute minimum in the EO trails ($F_{2, 17}=4.075$; $P=0.025$).

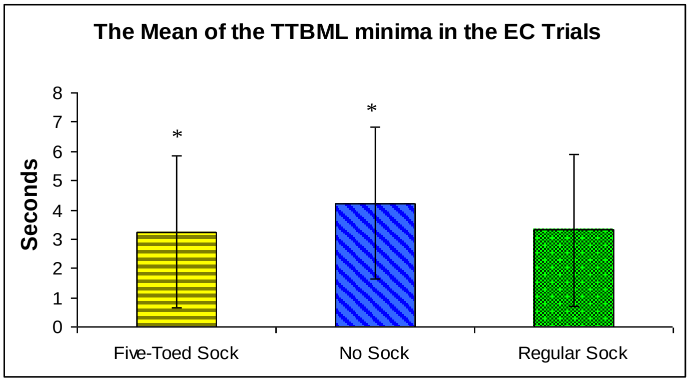

Figure 2b: The mean of the TTBML minima in the EC trials ($F_{2, 17}=3.919$; $P=0.048$).

CONCLUSION

Single-limb balance testing using measures of TTB revealed that the five-toed sock condition negatively influenced static postural control when compared to the no sock condition among healthy individuals. Further study should include the adaptation period for subjects to become used to the enhanced sensations around the toes before the data collection is conducted.

REFERENCES

1. Jerosch J, et al. *Knee Surg Sports Traumatol Arthrosc* **3**, 39–46, 1995.
2. Kavounoudias A, et al. *Neuroreport* **9**, 3247–3252, 1998.
3. Van Wegen, et al. *Human Movement Science* **21**(1), 61-84, 2002.
4. Hertel J, et al. *Gait Posture* **25**, 33-39, 2007.

BIOMECHANICAL EVALUATION AND REDESIGN OF AN ACCESSORY UNIT FOR EXERCISE IN MANUAL WHEELCHAIR USERS

Christine N. Hofmann[1] and Karen L. Troy[1]
[1]Department of Kinesiology and Nutrition, University of Illinois at Chicago, Chicago IL
Email: klreed@uic.edu   web: http://www.uic.edu/ahs/biomechanics

INTRODUCTION

Manual wheelchair users are at high risk for injuries to the upper extremity due to activities of daily living such as wheelchair propulsion and transfers [2]. Evidence suggests that manual wheelchair users who regularly exercise experience a decrease or even complete resolution of shoulder pain [5]. However, most fitness equipment cannot accommodate a wheelchair. A proof of concept unit that attaches to a stationary cycle was designed to allow a wheelchair user to produce a rowing motion (Figure 1). This type of activity may benefit wheelchair users by strengthening the posterior shoulder stabilizers and improving cardiovascular fitness.

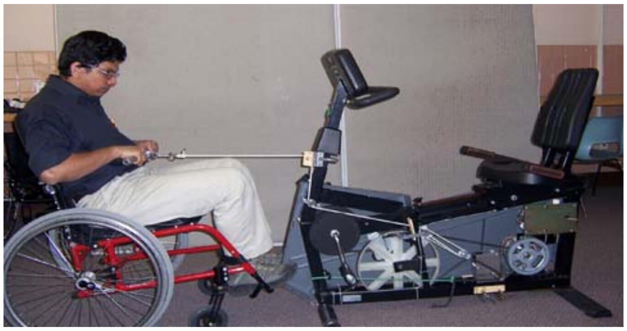

Figure 1 A manual wheelchair user exercising with the accessory unit

The purpose of this study was to identify design changes that should be made to the accessory unit to improve overall usability, comfort, and exercise biomechanics. To accomplish this we compared the biomechanics of the trunk and upper extremities during exercise to known injury thresholds [1,3,4,6] and solicited feedback from wheelchair users.

METHODS

Four healthy manual wheelchair users (2 males, age 22-47, height 155-178 cm, mass 50-73 kg) volunteered to participate in this institutionally reviewed and approved study. Eleven passive reflecting markers were placed on the torso and dominant upper extremity of each subject. These were used to define a four-segment model (hand, forearm, upper arm, and torso) consistent with standards recommended by ISB [7]. A small load cell placed in series with the handle bar was used to calculate the force with which a subject pulled during exercise. Each subject was instructed in proper exercise technique and then performed three sets of 20 repetitions of rowing. Marker motions were collected at 60Hz using an 8-camera Motion Capture system (Motion Analysis, Santa Rosa, CA).

Data consisted of: the wrist kinematics (extension, ulnar deviation), shoulder kinematics (plane of elevation and elevation angle), peak rowing force, and kinematics at the instant of peak rowing force.

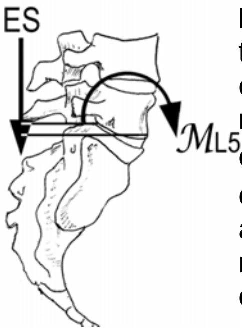

Figure 2 Free-body diagram of the lumbar spine showing the erector spinae force (ES) and moment about L5 due to the exercise ($\mathcal{M}_{L5}$). ES force was calculated assuming a moment arm from either the anterior (69 mm) or posterior (39 mm) aspect of the vertebral body

Peak compressive and sheer forces at each subject's L5 were calculated based on a quasi-static model (Figure 2). The fulcrum was assumed to be either the anterior or posterior aspect of the vertebral body, yielding two possible solutions that represent a maximum and minimum force required for equilibrium. Wrist position and L5 forces were compared to published injury thresholds.

RESULTS AND DISCUSSION

The average peak wrist radial and ulnar deviation was 1 ± 4° and 8 ± 2° respectively (Figure 3, top). Because repetitive motion injury to the wrist has been linked to activities with non-neutral wrist positions [1], we recommend that the straight handle bar be angled 4° on each side to radially deviate the wrists. We expect the average peak radial and ulnar deviations with the modified handle bar to be 4-5°. Alternatively, separate grips could be used for each hand, allowing the wrists to move independently throughout the cycle. In addition, since some subjects had difficulty gripping the handlebar we recommend the addition of wrist loops to facilitate this.

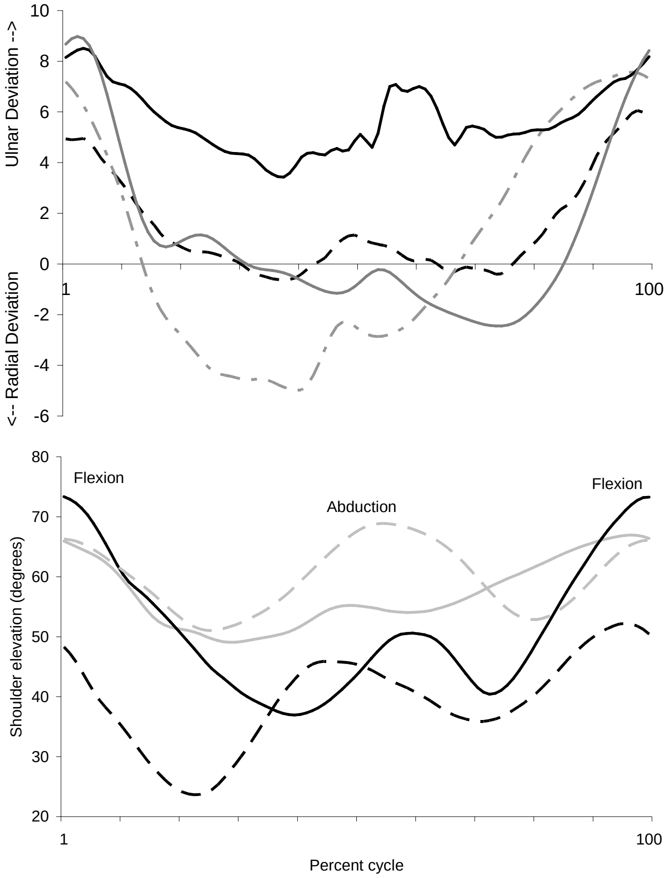

Figure 3 Mean radial/ulnar deviation (top) and shoulder elevation angle (bottom) for all four subjects during a complete (100%) exercise cycle

Peak shoulder elevation angle (65±9°) occurred at the beginning and end of each rowing cycle when subjects' arms were extended anteriorly (Figure 3, bottom). Based on recommendations that reaching tasks be neither above shoulder height nor so low as to make a subject pull from low to high [1], the height of the pulley system should be adjustable. This would allow the participant to place the pulley at a central position that is most comfortable.

Some subjects had difficulty controlling the motion of their trunk during exercise. Providing an optional restraining strap to help keep a participant from sliding in his or her wheelchair would help to alleviate this problem.

The average peak rowing force was 130±21N approximately horizontally directed. Even subjects who exercised quite intensely only produced forces as high as 190 N; this is due to the momentum of the flywheel that provides resistance in the stationary cycle. Based on the peak rowing force and measured moment arms, the computed compressive force at L5 ranged from 100-264 N (minimum) to 149-585 N (maximum). Compared to the injury threshold of 3400 N [3] we conclude that the accessory unit can be used without fear of repetitive motion injury to the lumbar spine.

The large range of values seen especially in L5 force was primarily due to the height of subjects' hands during exercise. One subject, whose upper extremity function was noticeably more impaired than the other subjects, was able to complete the exercise but only with difficulty. This subject had higher elbow flexion and less shoulder motion than the others, causing larger moments about the lumbar spine. Even so, the forces and moments he generated were well below the injury threshold.

SUMMARY

Based on observation the measured kinematics and feedback from users, the following changes are recommended to the accessory unit: (1) angle the handle bar to minimize radial/ulnar deviation, (2) add wrist loops on the handle bar to make gripping easier, especially in populations with diminished grip strength, (3) make pulley height adjustable, (4) provide a restraining belt to prevent trunk motion relative to the wheelchair, especially in populations with little trunk control.

ACKNOWLEDGEMENTS

Funding provided by NIDRR H133E070029

REFERENCES

[1] Bridger, R.S., (1995). *Introduction to Ergonomics*.McGraw Hill

[2] Davis, J.L.et al.. *J Rehabil Res Dev*. 1998; 35(1):61-72.

[3] Granata, K.P. and Marras, W.S. *Ergonomics*. 1999; 42(9):1187-1199.

[4] Kelsey, K.L.et al. 1984, *J Orthop Res*, 2, 61-66.

[5] Nawoczenski DA et al. *Phys Ther*. Dec 2006;86(12):1604-1618.

[6] Punnet, L et al. 1991 *Scand J Work Env Health,* 17, 337-346.

[7] Wu et al 2005 *J Biomech* 38, 981-992

POSTURAL SWAY DYNAMICS AND FALLS RISK IN TYPE 2 DIABETES

S., Morrison[1], S., Colberg[2], H.K., Parson[3], A.I Vinik[3],
[1]School of Physical Therapy, Old Dominion University, [2]Exercise Science Department, Old Dominion University, [3] Strelitz Diabetes Institute, Eastern Virginia Medical School
Email: smorriso@odu.edu

INTRODUCTION

Age-related diseases like Diabetes are commonly associated with a general loss of system complexity and related functional capacity that impairs health, well being, and independent living. The decline that occurs in diabetic individuals can be observed across a broad spectrum of performance measures. For example, older individuals with type 2 diabetes often exhibit impaired balance and altered gait dynamics and, as a result, are at an increased risk of falling [4]. This increased risk of falling is often the result of the older diabetic individual having to compensate for both age- and disease-related factors that can impact on balance and stability. For example, in addition to such age-related changes as a loss of lower limb muscle strength, power, and slower reaction times [2], the diabetic individual also has to compensate for those factors associated with the disease process such as possibility of neuropathy [4,5]. Consequently, the older diabetic individual is often at an even greater risk of falling when compared to age matched, healthy individuals given the range of factors which can contribute to a loss of stability.

One common factor which contributes to the decline in postural stability is a reduction in physical activity – a factor which is also a precursor to increased falls risk [2]. Given that regular activity have been shown to improve postural stability in healthy older individuals [1] the aims of this study were 1) to determine the falls risk and postural sway characteristics of a group of older individuals with type 2 diabetes and 2) to examine the effect of six-week strength/balance training on the postural stability of this same group.

METHODS

Sixteen individuals with type 2 diabetes and 21 age-matched controls participated (50-75 yrs). The falls risk of all subjects was ascertained using the Physiological Profile Assessment test [3] which incorporates measures of simple reaction time (RT) from the hand and foot, sensation, proprioception and lower limb strength to produce an overall falls risk score (range -2 to +4).

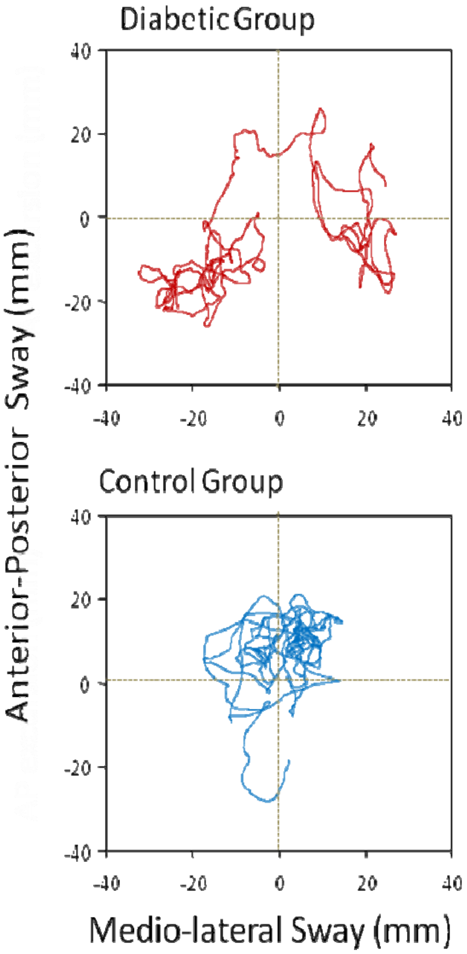

Figure 1: Representative examples of AP and ML COP excursions for a healthy older and a diabetic individual. Traces were attained during the eyes closed condition.

The postural stability of each subject was also assessed while they stood on a Bertec balance plate. Changes in each subject's center of pressure (COP) were assessed as a function of different support surfaces (firm, foam) and vision (eyes open, closed). Differences in the range, variability and structure (using approximate entropy, ApEn) of the COP outputs were measured. After these assessments, all subjects participated in a six weeks of balance/low level resistance training after which they were re-assessed using the falls screen and postural tests.

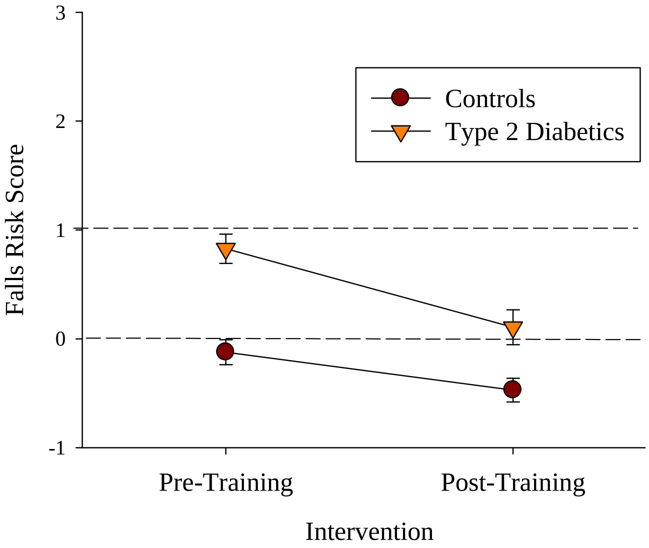

Figure 2: Difference in mean falls risk score between the two groups as a function of the exercise intervention.

RESULTS AND DISCUSSION

As illustrated in figure 2, prior to the intervention, the diabetic group had a significantly higher falls risk score (0.77±0.13) compared to controls (-0.12±0.11; $F_{1,35} = 20.32$; $p<0.05$). The diabetic group also exhibited evidence of neuropathy, and had significantly slower RT's for both the hand and foot.

Evaluation of the COP data showed that the diabetic group exhibited increased postural sway (increased COP excursion) compared to controls (see Figure 1). This was particularly evident during the eyes closed and foam surface conditions compared to controls. During these conditions, the COP output of the diabetic group was also less variable (decreased SD) and more regular (decreased ApEn) than that observed for the controls.

Following the balance training, the diabetic group had a significant reduction in their falls risk score (0.10±0.16; $F_{1,30} = 33.01$; $p<0.05$). A decrease was also observed in the overall falls risk score for the control group but this change was not significant.

For the diabetic group, this improvement in overall balance was characterized by significant increases in lower limb strength, proprioception, sensation and faster reaction times for both the hand and foot. The COP measures of the diabetic group post-exercise also showed significant changes, with the resultant output exhibiting increased signal complexity and increased variability compared to their pre-exercise values.

CONCLUSIONS

Overall, the results of this study show that balance training has wide-spread positive effects on physiological function for older individuals with Type 2 diabetes. In particular, decreased risk of falling and altered postural sway dynamics were observed. Interestingly, the COP output of the Diabetic group became more similar in terms of complexity/variability to that seen in the age-matched controls, which may reflect that the exercise intervention resulted in increased variability of postural dynamics.

REFERENCES

1. Buchner, DM, et al., (1997). The effect of strength and endurance training on gait, balance, fall risk, and health services use in community-living older adults. *J Gerontol A Biol Sci Med Sci*. **52A**(4): p. M218-224.
2. Close, JCT, et al, (2005). What is the role of falls? *Best Practice & Research Clinical Rheumatology*. **19**(6): p. 913-935.
3. Lord, SR, et al., (2003). A physiological profile approach to falls risk assessment and prevention. *Physical Therapy*. **83**(3): p. 237-252.
4. Maurer, MS, et al., (2005). Diabetes mellitus is associated with an increased risk of falls in elderly residents of a long-term care facility. *J Gerontol A Biol Sci Med Sci*. **60**(9): p. 1157-1162.
5. Richardson, JK, Hurvitz, EA, (1995). Peripheral neuropathy: A true risk factor for falls. *J Gerontol A Biol Sci Med Sci*. **50A**(4): p. M211-215.

ARCHITECTURAL PARAMETERS OF THE TRICEP BRACHII DURING ISOMETRIC CONTRACTIONS

Jessica L. Kutz, Nicholas J. Fiolo, Benjamin W. Infantolino and John H. Challis
Biomechanics Laboratory, Department of Kinesiology, The Pennsylvania State University, University Park, PA, USA
E-mail: jlk5268@psu.edu

INTRODUCTION

Measures of muscle architecture such as muscle thickness, pennation angle, and muscle fascicle length are used to describe a muscle's function (e.g., 1). In musculoskeletal models, muscle thickness is assumed to remain constant [2] and the force a muscle fascicle transmits to its tendon is a function of its location on the force-length curve and the cosine of the pennation angle. In complex muscles such as the Tricep Brachii, multiple muscle heads may complicate this relationship. Blazevich et al. [1] described enough muscle architecture variability in the four quadriceps muscles, such that one or two measures could not be used to predict the architecture of the entire knee extensor complex. The purpose of this study was to determine the architecture of the long head of the Triceps Brachii muscle during isometric muscle contractions throughout its range of motion.

METHODS

Six male subjects (mean height: 148 ± 8 cm, mass: 75 ±13 kg, age: 22 ±2 years) completed a maximal isometric contraction test following the protocol of a Biodex machine similar to that of Hatze [3]. All subjects voluntarily gave informed consent. Subjects were strapped to the Biodex machine over their chest and waist in order to minimize unwanted movements. Subjects were asked to perform maximal isometric contractions of the Tricep Brachii five times for each of the five different elbow flexion angles (0, 30, 60, 90, and 120 degrees). Shoulder angles were held constant at 45 degrees and the forearm was held in a neutral position for all subjects. The subjects were asked to hold their maximal contractions for five seconds during which ultrasound images were taken of the long head of the Tricep Brachii using a frame grabber board (LG-3, Scion Image) and ultrasound machine (SSD-900, ALOKA, USA) with 7.5 MHz linear probe operating in B-mode. Biodex data were sampled at 100 Hz using LabView (National Instruments, Texas, USA). Subjects were given a thirty second rest period to reduce effects of fatigue between each contraction and a one minute rest between elbow angles.

Following subject testing, a custom written MATLAB(version 7.4.0, The MathWorks, Natick, USA) program was used to analyze the data. The mean of the three highest moments recorded at each joint angle were averaged to determine the maximum moment.

Ultrasound images of the trials with the highest moments were digitized for each joint angle by a trained operator. They were digitized in Scion Image, and measurements made of pennation angle and muscle thickness. Means for each subject were calculated for the pennation angles and muscle thicknesses for each elbow angle.

Based on a planimetric model of pennated muscle [2], the fascicle lengths of the long head of the Triceps were computed by dividing each muscle thickness by the sine of its respective pennation angle (Figure 1).

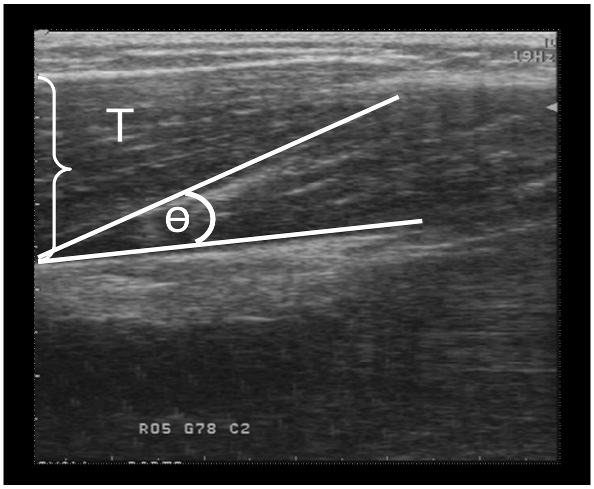

Figure 1: Ultrasound image showing for the long head of the Triceps Brachii muscle the thickness (T) and pennation angle (Θ).

RESULTS AND DISCUSSION

Muscle thickness remained relatively constant throughout the range of motion for all subjects, with a mean coefficient of variation of 6.5 ± 1.8%. This corresponds to the primary assumption in the planimetric model of muscle used here [2].

At zero degrees elbow flexion the pennation angle was 12.9 ± 0.5 degrees, which is smaller than values reported in the literature [4]. The trend was for pennation to decrease with increasing joint angle and therefore increasing muscle length. A regression line fit to these data indicated a negative slope (-0.03 ± 0.02) which averaged across all subjects corresponded to a 3.3 degree change in pennation angle through the range of joint motion examined

The trend was for fascicle length to increase with increasing joint angle (Figure 2). In some of the subjects this increase was not monotonic, yet with this would be anticipated based on muscle force-length properties. The fiber length in only one of the three heads of the Triceps was tracked, albeit the one with largest physiological cross-sectional area [4]. If the fascicles of the long head of the Triceps Brachii shorten, then the tendons attached to the Triceps Brachii must presumably be stretched by the a change in force of one or both of the other heads of the Triceps. This would suggest that the force-length curves for the three heads are not synchronous, either because of different expressions of the force-length properties of three heads or differences in activation patterns.

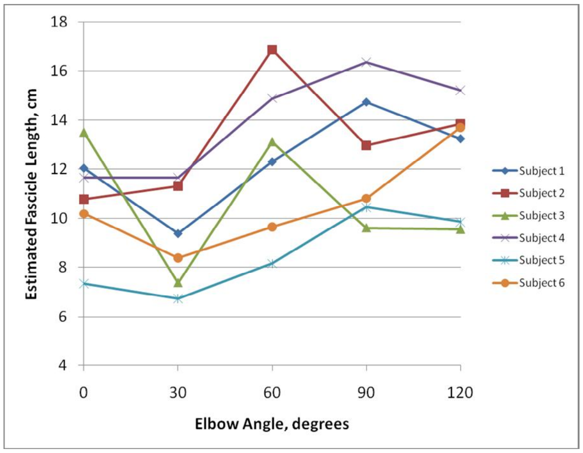

Figure 2: Estimated fascicle length versus elbow angle for the Triceps Brachii.

This complexity in the interaction between architecture and muscle function illustrates the need to measure all the architectural parameters of a muscle and not to rely on one or two parameters to describe a muscle's function.

REFERENCES

1. Blazevich AJ, et al. *J Anat* **209**, 289-310, 2006.
2. Otten E. *Exerc Sport Sci Rev* **16**, 89-137, 1988.
3. Hatze H. *Eur J Appl Physiol* **46**, 325-328, 1981.
4. Veeger HEJ, et al. *J Biomech* **30**, 647-652, 1997.

ACKNOWLEDGEMENTS

The support of ALOKA, USA in the execution of some of this work is gratefully acknowledged.

Conservation of Limb Function after Peripheral Nerve Injury in Rat Locomotion

Jay M. Bauman* and Young-Hui Chang
Comparative Neuromechanics Lab, School of Applied Physiology, Georgia Tech, Atlanta, GA
*email: jbauman3@mail.gatech.edu, web: http:www.ap.gatech.edu/chang/CNLhome.html

Introduction

The capacity for locomotion persists after neuromuscular injury to the limbs via the principle of compensation--a change in some local properties such that a greater goal may continue to be met. Yet there is a dearth of knowledge on general compensation mechanisms and how they relate to specific neuromuscular pathologies. The elucidation of common features in locomotor compensation and their correlation to different injuries could yield insights into general limb control strategies during healthy and impaired locomotion.

Though rodents have emerged as the overwhelming model of choice for spinal cord and peripheral nerve injury studies, current locomotor assays in rats lack the resolution to study subtle motor deficits associated with recovery from nerve injury. Investigators typically characterize rat locomotion with subjective survey tools (e.g. BBB locomotor rating scale), or by spatio-temporal stride parameters (e.g. Sciatic Function Index) [4]. Unfortunately these methods cannot provide data on interjoint compensation or kinematics of the proximal joints, and have been demonstrated to incorrectly imply full recovery despite visual evidence of motor impairment [5].

Joint kinematics provides more comprehensive understanding of limb function and recovery, but optical kinematics derived from skin markers are not accurate due to skin movement relative to the underlying joints [6]. We have built a high-speed x-ray video system to directly measure accurate whole limb kinematics from bone positions. Our previous results revealed errors in knee angle as large as 40° at foot contact compared to optical methods. This system permits us to comprehensively examine basic compensation mechanisms to a variety of peripheral nerve injuries.

We denervated major ankle plantarflexor muscles in rats to quantify specific locomotor deficits and patterns of interjoint coordination over the time course after injury. Muscle-specific changes were observed in similar surgeries on cats depending on the multiarticular character of the involved muscles [1,2]. Asymmetries in stride parameters such as duty factor have also been observed [3]. Peripheral nerve cut injuries clearly disrupt local variables such as joint angle trajectories, but this may be a necessary condition such that the values of other limb properties can be conserved from the pre-injured state. We hypothesized that the locomotor deficits observed after muscle denervation would correspond to a stabilization of leg length and leg orientation as global variables for walking in rats.

Methods

Surgical denervations were performed on three male Sprague-Dawley rats under aseptic conditions. Incisions were made in the posterior popliteal area of the left hindlimb and the branches of the tibial nerve leading to the selected ankle extensor muscles were isolated with retractors. Then the nerves were cut close to the muscle and as large a section as possible was completely removed. This peripheral nerve injury protocol removed innervation to the entire triceps surae group (lateral gastrocnemius, medial gastrocnemius, and soleus) and plantaris.

We captured sagittal plane x-ray video images of the rats at 200 Hz as they walked on a treadmill at 40 cm/s. Data were collected from each rat on PID (post-injury day) 7, 10, 14, 21, and 28. Distal limb joints were tracked using custom Matlab software (T. Hedrick, UNC-Chapel Hill) with radio-opaque tantalum markers due to minimal skin movement, whereas the hip knee and pelvis were manually digitized from bony landmarks. Analyses consisted of calculating joint angle trajectories, interjoint coordination patterns, toe-to-hip leg length and orientation, and stride parameters of the injured hindlimb. The data were then compared to data from four healthy control rats at the same speed.

Results and Discussion

Joint angle trajectories from all three injured rats on PID 7 show that the ankle and MTP joints were notably altered after denervation (>50° difference from control data for most of the cycle, **Fig. 1**). Knee and hip joint trajectories were moderately altered with increased extension (~20-40º).

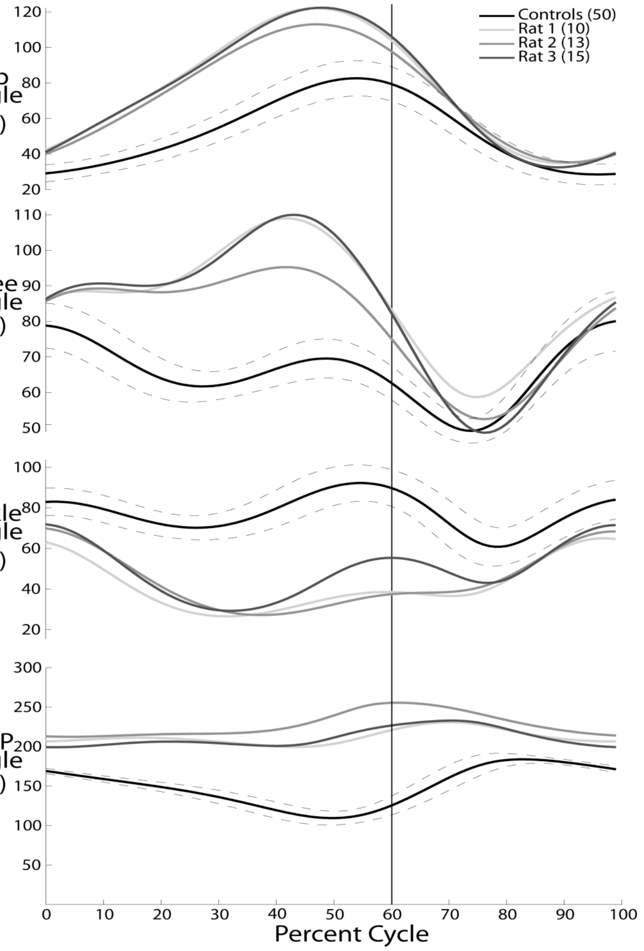

Fig. 1: Mean joint angle trajectories at PID 7 versus mean of all controls. Dashed lines are ±1SD of control, #step cycles in parentheses. Vertical line indicates end of stance phase.

In contrast, preliminary results for the same rats indicate leg length and orientation trajectories were unchanged (**Fig. 2**), confirming our hypothesis. There were no significant differences in mean values of leg length and leg orientation between the injured and control rats over the entire normalized gait cycle ($p<0.01$). The new joint configurations from injured animals taken together are consistent, or goal-equivalent, with a limb configuration that preserves leg length and orientation trajectories from the pre-injured state. Interjoint compensation patterns were visibly disrupted except for hip-knee coordination, which maintained the same shape over greater ranges.

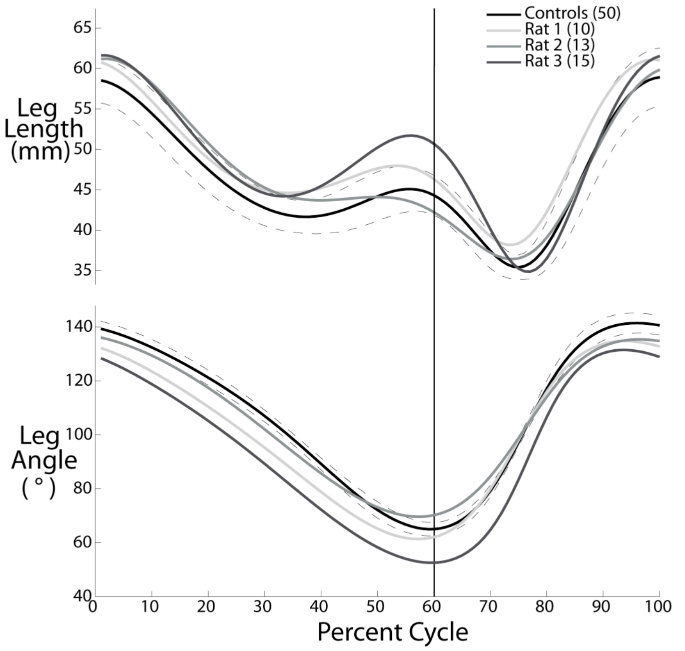

Fig. 2: Mean leg length and orientation trajectories for 3 rats at PID 7 versus mean of all controls. Legend is same as Fig. 1

Conclusion

Surgical denervation of all four ankle plantarflexor muscles resulted in an expected large-scale disruption of joint angles and stride parameters. Notably, values of leg length and orientation were indistinguishable from controls after injury, despite paralysis of all major ankle extensors. Along with the results of this study, a systematic mapping of compensation patterns to different nerve injuries will ultimately yield a valuable baseline for evaluating the efficacy of reinnervation (nerve repair) surgeries, as well as provide insights into basic principles of locomotor compensation.

References

1. Abelew TA, et al. *Journal of Neurophysiology*, **84**, 2709-2714, 2000.
2. Chang YH, et al. *Integrative and Comparative Biology*, **43**, 987-987, 2003.
3. Yu P, et al. *Muscle & Nerve*, **24,** 231–239, 2001.
4. Bain JR, et al. *Plastic and Reconstructive Surgery*, **83**, 129–138, 1989.
5. Varejao ASP, et al. *Muscle & Nerve*, **27**, 706-714, 2003.
6. Muir GD and AA Webb *European Journal of Neuroscience*, **12**, 3079-3086, 2000.

Acknowledgements

We thank Dr. Tyson Hedrick (UNC-Chapel Hill) for use of his custom motion tracking code. This study was supported by NIH 1R21AR054760-01.

AFFERENT REGULATION OF LOCOMOTOR CPG CONTRIBUTES TO MOVEMENT STABILIZATION: A SIMULATION STUDY

[1]Alexander Klishko, [2]Sergey Markin, [2]Natalia Shevtsova, [2]Michel Lemay, [2]Ilya Rybak, [1]Boris Prilutsky
[1]Georgia Institute of Technology, Atlanta, [2] Drexel University College of Medicine, Philadelphia
email: aklishko3@gatech.edu, web: http://www.ap.gatech.edu/Prilutsky/

INTRODUCTION

It is commonly accepted that the locomotor rhythm in mammals is generated by a spinal locomotor central pattern generator (CPG) and that the muscle length- and tendon force-sensitive afferents regulate the CPG operation and adjust it to limb biomechanical characteristics and locomotor conditions (e.g., McCrea, 2002; Ekeberg and Pearson, 2005). Specifically, the activities of spindles and Golgi tendon organs from flexors and extensors were shown to control the duration of flexion/swing and extension/stance phases and the timing of phase transitions (Ekeberg and Pearson, 2005).

In this study we asked whether the above afferent feedback can also stabilize locomotor behavior following mechanical perturbations like tripping or stepping in a hole?

To answer this question, we have developed a neuromusculoskeletal model that describes a half-center neural CPG controlling a simple biomechanical system consisting of one rigid body segment and two muscles. The motion-dependent length- and force-feedback from both muscles provides afferent control of the CPG. Behavior of the model was investigated by applying mechanical perturbations during swing and stance phases.

METHODS

Model. The developed neuromusculoskeletal model of the locomotor CPG controlling a one-segment leg with two muscles is shown in (Fig. 1). The two-level CPG consists of a half-center rhythm generator (RG) and pattern formation (PF) circuits and generates a basic “locomotor” rhythm while receiving tonic “supra-spinal” drive (derived from Rybak et al., 2006). The simplified musculoskeletal limb model simulated by a pendulum is forced to oscillate by two antagonistic muscles, flexor (F) and extensor (E), the gravitational force, and the ground reaction force (GRF). The GRF is applied during the “stance” phase, when pendulum moves counterclockwise (angular velocity $\dot{q} ? 0$). Muscles were described by a Hill-type model with the force-length and force-velocity properties (Harischandra and Ekeberg, 2008). The muscles are activated by the corresponding motoneurons (Mn-F and Mn-E), which in turn receive phasic excitation from the CPG (PF level). The muscles provide length-dependent (Ia and II afferents) and force-dependent (Ib afferents from the extensor) feedback controlling both the timing of phase transitions (flexion-extension and extension-flexion) in the CPG (at the RG level) and the activity of motoneurons via the PF circuit and disynaptic excitation of Mn-E during extension.

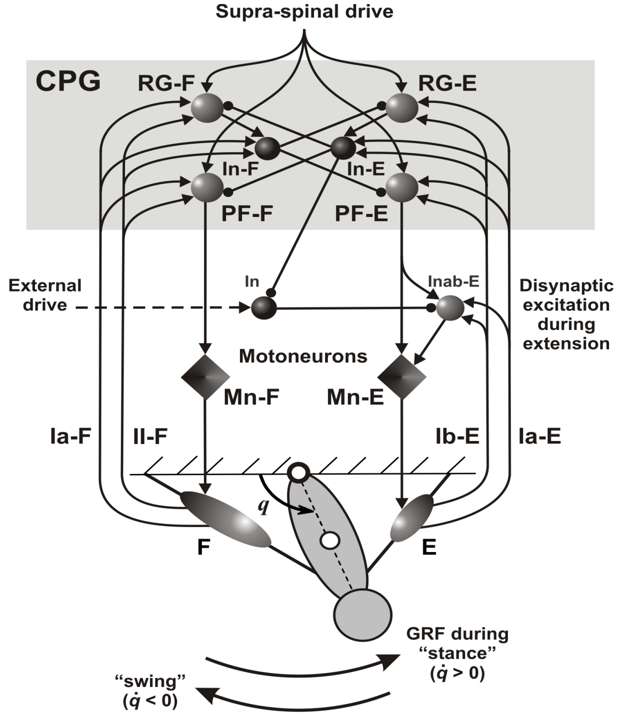

Figure 1: Neuromusculoskeletal model

Model parameters have been adjusted to reproduce experimentally observed changes of the swing and stance phase durations with locomotor speed in the cat.

Perturbations. Tripping during swing phase was simulated as an external force applied for 50 ms. Stepping in a hole during stance was modeled by setting the GRF to zero for the rest of the current stance phase. Perturbations were applied throughout stance or swing with the time step of 50 ms.

To evaluate stability of the system we determined the time during which the system returns to the unperturbed regime after perturbation (Return time) and the difference in phase before perturbation and after return (Phase shift). We have also evaluated how these characteristics depend on the gain of each afferent feedback type.

RESULTS AND DISCUSSION

Our simulations have shown that after perturbations the system typically returns to a stable periodic regime with the same angle range of motion and cycle duration as before perturbation but with a phase shift. The Phase shift and the Time of return depended on the perturbation onset, cycle phase and feedback gain. Changes in Phase shift and Return time obtained at different perturbation Onset times and different gains of group II, Ib, and Ia afferents are shown in Figs. 2, 3, and 4, respectively.

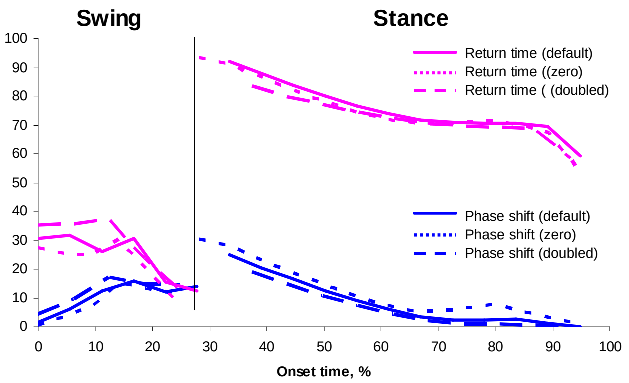

Figure 2: Phase shift (blue) and Return time (magenta) as a function of Onset perturbation time (in %) at different gains (default, zero, doubled) of group II afferent feedback.

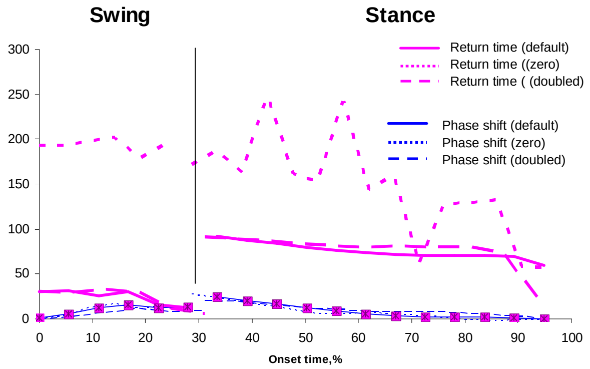

Figure 3: Phase shift (blue) and Return time (magenta) as a function of Onset perturbation time (in %) at different gains (default, zero, doubled) of group Ib afferent feedback.

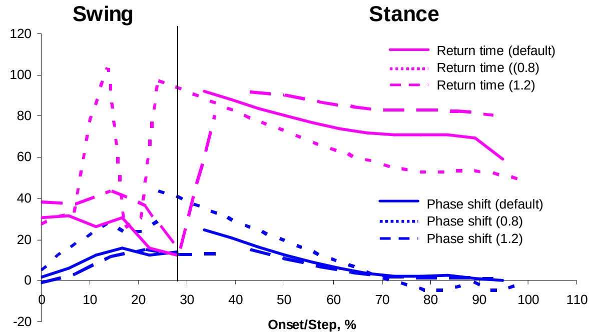

Figure 4: Phase shift (blue) and Return time (magenta) as a function of Onset perturbation time (in %) at different gains (default, 0.8, 1.2) of group Ia afferent feedback.

CONCLUSIONS

Our simulations have shown that feedback signals from primary and secondary afferents are sufficient to return the system to its stable regime after the applied perturbations within 1-2 step cycles.

The stability of system behavior under conditions of applied perturbations was stronger dependent on Ia afferent feedback than on other afferents.

REFERENCES

1. Ekeberg O, Pearson K. *J Neurophysiol* **94**: 4256-4268, 2005.
2. Harischandra N, Ekeberg O. *Biol Cybern* **99,** 125-138, 2008.
3. McCrea DA. *J Physiol* **533**, 41-50, 2001.
4. Rybak IA et al., *J Physiol* **577**, 617-639, 2006.

ACKNOWLEDGEMENTS

Supported by NIH grants HD032571 and NS048844 and by the Center for Human Movement Studies at Georgia Tech.

EXTENSOR STRENGTH, SURGICAL TENSIONING, AND PINCH FORCE FOLLOWING BRACHIORADIALIS TO FPL TENDON TRANSFER: A SIMULATION STUDY

[1]Jeremy P.M. Mogk, [2]M. Elise Johanson, [2]Vincent R. Hentz,
[3]Katherine R.S. Holzbaur, and [1,4,5]Wendy M. Murray
[1]SMPP, Rehabilitation Institute of Chicago, [2]VA Palo Alto Health Care System, [3]Dept of Biomedical Engineering, Wake Forest University Health Sciences, [4]Depts of Biomedical Engineering and Physical Medicine & Rehabilitation, Northwestern University, [5]Edward Hines, Jr. VA Hospital
email: j-mogk@northwestern.edu, http://www.smpp.northwestern.edu/Murray/index.shtml

INTRODUCTION

Following cervical spinal cord injury (SCI), loss of hand function presents a challenge for autonomy. Functional independence can be greatly improved with surgical restoration of lateral pinch function, which involves transfer of the non-paralyzed brachioradialis muscle (BR) to the flexor pollicis longus (FPL) tendon. Computer simulations suggest that the surgeon's intraoperative "tensioning" of the BR-FPL transfer can have a marked effect on post-operative outcome, since the surgeon chooses the muscle attachment length, and force production varies with length [1]. These simulations assumed both non-impaired muscle strength and maximal activation of the transferred BR post-operatively. However, experimental data show that activation of the transferred BR is significantly lower during maximum lateral pinch efforts than resisted elbow flexion, with a more pronounced deficit in patients with weak elbow extension [2].

We used a biomechanical simulation approach to examine the effects of (i) muscle strength, and (ii) surgical attachment length on predictions of post-operative pinch force, based on recorded activation patterns.

METHODS

We integrated biomechanical simulations with MRI, EMG, dynamometric, and goniometric data. We augmented a model of the upper limb [3] to incorporate the BR-FPL transfer [1], and derived a Jacobian to enable pinch force calculation [4]. We included eight additional muscles that often remain under voluntary control after cervical SCI: two wrist extensors (ECRB and ECRL), three elbow extensors (all three heads of the triceps, TRI), and three elbow flexors (brachialis, BRA, and both heads of the biceps, BIC). The remaining muscles were "paralyzed" by setting their active force-generating capacity to zero.

All simulations utilized EMG and joint posture data recorded from four individuals with tetraplegia and BR-FPL transfers during maximal lateral pinch force exertions. EMG recorded from the BIC, TRI and ECRB defined the activation levels of the modeled elbow flexors, as well as elbow and wrist extensors. The simulations computed the highest BR-FPL activation (act^{BR}), and the resultant lateral pinch force, for which (i) the elbow flexor moment was not larger than the extensor moment (i.e. BR-FPL + BRA + BIC ≤ TRI), and (ii) the wrist flexor moment was not larger than the extensor moment (i.e. BR-FPL ≤ ECRB + ECRL). Wrist and elbow moments were balanced about the flexion-extension axes only, and included posture-dependent inertial moments as well as passive moments produced by both active and paralyzed muscles. In this context, act^{BR} represents the proportion of posture-specific active BR muscle force that could be exerted without generating a net flexion moment at either joint. Test postures were defined by goniometric data. In these simulations, the shoulder was abducted (90°) and transversely flexed (30°) [2], and the elbow and wrist were extended.

Simulations were repeated at different strength levels and attachment lengths. "Non-impaired strength" assumed healthy muscle volumes [5] (and thus, force- and moment-generating capacity) in the tetraplegic limb. "Scaled strength" adjusted muscle volumes based on a combination of patient-specific wrist and elbow torque measurements and BR volume data (measured via MRI). Three surgical attachment lengths were also examined [1].

RESULTS AND DISCUSSION

Given the levels of elbow and wrist muscle co-activation recorded during maximum effort lateral pinch, our simulations suggest that strength influences both act^{BR} and pinch force. Simulations based on the BIC, TRI, and ECRB activations observed in two subjects illustrate limitations imposed by muscle weakness (Fig. 1). When we assumed non-impaired strength, calculated activations levels (1.0) and pinch forces (35.9 N) were maximized (and the same) for both patients because non-impaired extensor strength was sufficient to balance the flexor moments produced by BR-FPL and the elbow flexors. When strength was scaled, both act^{BR} and pinch force decreased substantially, yet uniquely, to accommodate for patient-specific elbow and wrist extensor weakness.

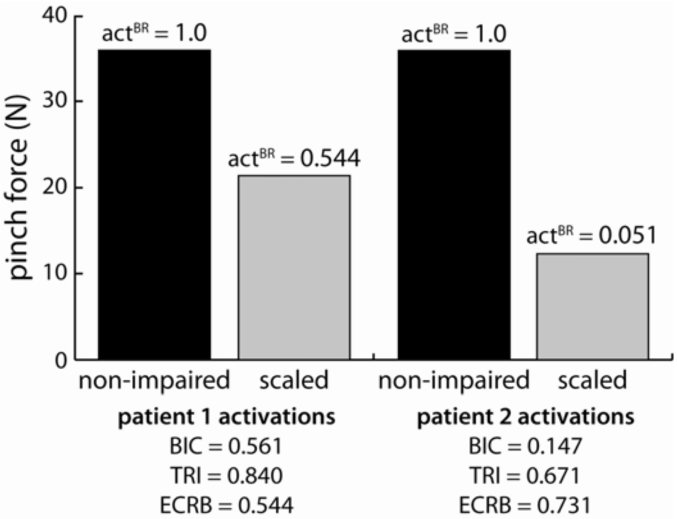

Figure 1. Pinch force and act^{BR}, calculated assuming non-impaired and scaled strength levels, given co-activation of elbow and wrist muscles from two patients.

Because act^{BR} was limited by weak elbow and wrist extensors in the simulations using patient-specific scaled strength levels, resultant pinch forces were less sensitive to surgical tensioning compared with those calculated using non-impaired strength (Fig. 2). For example, we calculated comparable pinch forces under “loose” (i.e. transferred length = 80% of original length) and “resting” (original length) tensioning conditions when we simulated patient strength levels, despite the fact that loose tensioning optimizes transferred BR force-length properties for extended elbow and wrist postures [1]. This occurred because calculated act^{BR} was less than 1.0 and varied with tensioning condition. In contrast, non-impaired extensor strength was sufficient for $act^{BR} = 1.0$ for both tensioning conditions. The significantly different ($p < 0.005$) forces calculated in the non-impaired strength simulations reflect muscle force-length properties. For scaled strength, the pinch force predicted for each tension differed primarily in the relative contributions of active and passive force (i.e. looser tension = more active force), rather than force magnitude.

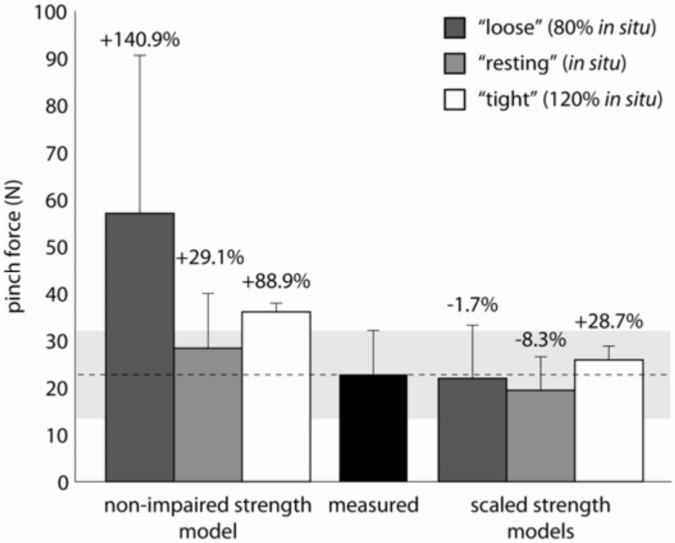

Figure 2. Comparison of measured and predicted pinch force (average of 11 trials; n = 4), with the mean % error shown above each bar.

Importantly, incorporation of patient-specific data led to results that were comparable to measured data (Fig. 2, black bar). Simulation results for the passive component of BR-FPL pinch force were larger than typically measured, and will be evaluated further.

CONCLUSIONS

Rehabilitation strategies that focus on strength training of the elbow and wrist extensors would benefit post-operative function of the surgically reconstructed tetraplegic limb.

REFERENCES

1. Murray WM, et al. *J Bone Joint Surg* **88A**, 2009-2016, 2006.
2. Johanson ME, et al. *J Hand Surg* **31A**, 747-753, 2006.
3. Holzbaur KR, et al. *Ann Biomed Eng* **33**, 829-840, 2005.
4. Goehler CM and Murray WM. *Proc ASME SBC,* Lake Tahoe, United States, 2009.
5. Holzbaur KR, et al. *J Biomech* **40**, 742-749, 2007.

ACKNOWLEDGEMENTS

NIH 5 R01 HD 46774 and VA A3741R.

KINETICS OF A WEIGHTED CHALLENGE IN INDIVIDUALS WITH KNEE OSTEOARTHRITIS

Andrew Kubinski[1] and Jill S. Higginson[1]
[1]Center for Biomedical Engineering Research, University of Delaware
Email: higginson@udel.edu

INTRODUCTION

The far reaching impact of knee osteoarthritis (OA) is well known. Biomechanical studies have indicated that individuals with OA walk more slowly [1], with less knee excursion [2], and with a higher knee adduction moment [1] compared to age-matched controls. Individuals with knee OA also use different strategies when challenged by different walking conditions. Walking while carrying a weighted backpack has been used to study the gait adaptations of adolescents [3], and young adults [4], as well as to assess physical performance gains in older adults [5]. The objective of our study was to investigate adaptations used by adults with knee OA during a weighted challenge. We hypothesized that there would be no differences in ground reaction forces (GRF), or hip, knee, and ankle moments, suggesting that healthy and OA subjects use similar strategies to carry load.

METHODS

Subjects were recruited from the community and gave written informed consent to participate in the study. Eight healthy subjects (age: 64.4 ± 5.9yrs, BMI: 23.7 ± 3.8) and seven knee OA subjects (age: 63.6 ± 7.0yrs, BMI: 31.1 ± 3.5, K/L score ≥ 2) were analyzed. Subjects walked at 1.0 m/s on an instrumented, split-belt treadmill (1080 Hz, Bertec Corp., Columbus, OH). The weighted challenge was implemented using a front and back loaded weight vest equal to 1/6th body weight.

To measure joint and limb positions, we used 23 retroreflective markers of the Helen Hayes marker set and a six camera motion capture system (60 Hz, Motion Analysis, Santa Rosa, CA). Five gait cycles were averaged for each subject to get one single curve that represents their gait pattern. Kinetic data were processed using a 4th order, phase corrected, Butterworth filter with a cutoff of 6 Hz. The kinetic data were normalized to the total weight (person alone for unweighted or person + load for weighted) taken from a static standing trial on one force plate. Paired t-tests were used to determine within subject statistical significance and student's t-tests were used to determine statistical significance between the groups for the following variables of interest: peak A/P and VERT GRFs, and peak hip, knee and ankle moments. Statistical significance was set at $p < 0.05$.

RESULTS AND DISCUSSION

During unweighted walking, the knee OA group had significantly lower first and second peaks in their VERT GRF (p=0.03 and p=0.004) compared to the healthy group (Figure 1). This agrees with previous work that studied the biomechanics of walking with a diseased knee [6]. During the weighted challenge, the knee OA group had a significant decrease in the valley of their VERT GRF (p=0.012) and a significant increase in their peak braking force (p=0.02) compared to their unweighted condition. Knee OA subjects exhibit significantly smaller propulsive forces (p=0.012) compared to the healthy group during the weighted challenge.

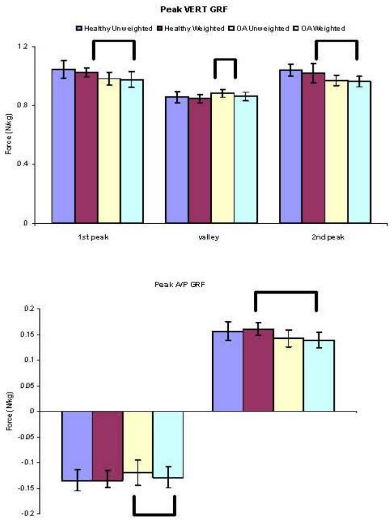

Figure 1. Peak VERT and A/P GRF.
Brackets: $p<0.05$

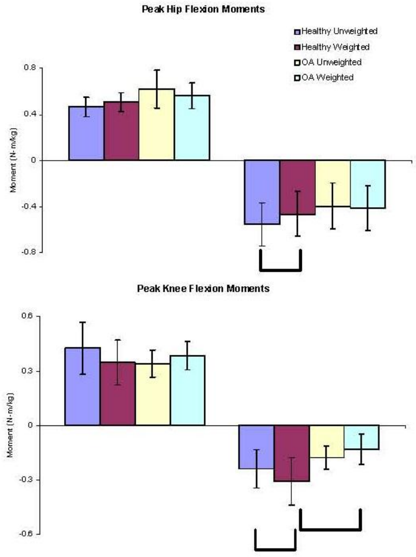

Figure 2. Peak knee and hip flexion moments. Brackets: $p<0.05$

In the healthy weighted condition, peak hip extension moment was significantly decreased ($p=0.018$) and the peak knee extension moment significantly increased ($p=0.022$) compared to their unweighted condition. The transferring of the moment from the hip to the knee could be a detrimental kinetic strategy when challenged with a weighted condition because it could lead to more knee joint loading during propulsion. The comparison between the healthy and knee OA groups during the weighted condition only led to a finding of significantly decreased knee extension moment in the knee OA group ($p=0.007$). This decrease in peak knee extension moment combined with the decrease in the propulsive force could be a strategy to decrease terminal joint loading to alleviate knee pain.

This is the first study looking at the effect of carrying weight in healthy vs. knee OA subjects. By normalizing kinetics to total weight carried, we can determine if different subject groups use similar kinetic patterns. Our data suggests slight changes in the kinetic strategy within subjects and between subjects when challenged with carrying a load while walking at a controlled speed. Hip, knee, and ankle angles associated with these peaks in kinetics as well as knee joint excursions may also be of interest. Previous work in our research group has shown that individuals with knee OA walk with less knee excursion and more stiffness [2].

Study limitations include differences in demographics between the two groups. Specifically, the BMI of the healthy group is significantly lower ($p=0.002$) than OA subjects, but data are normalized to body weight plus load carried. However, the actual percentage of body weight added was significantly larger for the healthy group ($p=0.046$) with 17.7% ± 1.9 for the healthy group and 15.8% ± 1.4 for the knee OA group. We used the subjects' self-reported weight in order to load them, and was not always consistent with the weight obtained during data collection on the instrumented treadmill.

In the future, we plan to fully analyze the kinematic, kinetic, and spatiotemporal variables of this challenged walking condition within and between a knee OA group and an age-matched healthy control group to identify compensatory strategies that may influence OA progression.

REFERENCES

1. Mündermann A, et al. *Arthritis Rheum* **50**, 1172-1178, 2004.
2. Zeni & Higginson *Clin Biomech* In Press.
3. Cottalorda J, et al. *J Pediatr Orthop B* **12**, 357-364, 2003.
4. Knapik JJ, et al. *Mil Med* **169**, 45-56, 2004.
5. Bean J, et al. *J Am Geriatr Soc* **50**, 663-670, 2002.
6. Stauffer RN, et al. *Clin Orthop Rel Res* **126**, 246-255, 1977.

ACKNOWLEDGMENTS

This work was completed thanks to the help of Dr. Joseph Zeni Jr., PT, Ph.D and funding from NIH P20-RR16458.

REPEATABILITY OF IN-VIVO MOTION ANALYSIS:
OPTICAL vs. ELECTROMAGNETIC TRACKING SYSTEMS

Chu Jui Chen, Masahiro Fujimoto, Sue Ewers, Tal Amasay, Jun San Juan, Vipul Lugade,
Carl Erickson, Li-Shan Chou, Andy Karduna
Department of Human Physiology. University of Oregon. Eugene, Oregon 97403. USA.
email: cchen1@uoregon.edu, web: http://biomechanics.uoregon.edu

INTRODUCTION

Studies have been conducted to test the performance of optical [1] and electromagnetic (EM) tracking systems [2]. Hassan et al. (2007) reported direct comparisons between the two systems [3]. However, these studies measured the system performance using pendulums or rigid objects. Inaccuracies during the in-vivo testing may occur due to rigid body assumptions, skin motion artifact and complex dynamic motions. To the best of our knowledge, there are no published in-vivo studies comparing the performance these systems under dynamic conditions.

The purpose of the present study is to measure and compare the intra- and inter-day repeatability of 3-D kinematic motion using optical and EM systems.

METHODS

Twelve young healthy adults (6 female, 6 male, mean age = 25.6 ± 5.3 years) were recruited for this study. The body motion was captured with an 8-camera optical system (Motion Analysis Corp., Santa Rosa, CA) and an EM system (Polhemus Liberty, Colchester, VT). The sampling rate was 120 Hz for both systems. A total of 29 reflective markers were placed on the subject's bony landmarks [4]. Each marker was precisely marked with four points to allow for digitization by the EM system so that the coordinate frames of the two systems could be aligned. Seven EM sensors were attached to the following locations: the spinous process of the 5th lumbar vertebra, the lateral aspect of the right and left thigh, the lateral aspect of the right and left shank (leg), and the top of the right and left foot (tarsal bones).

The subjects performed a sit to stand task with self selected pace and feet placement while sitting on a 46 cm high chair for a total of three trials. Data from another three trials were collected after 15 minutes of resting. Finally, participants were asked to repeat the testing on the next day with three more sit-to-stand trials performed.

Sagittal plane hip, knee, ankle joint angles during all sit to stand trails were calculated using the same laboratory written Matlab program (MATLAB Version 7.0; The Mathworks Inc., Natick, MA) from data collected with both systems. Representative joint angle curves are shown in Figure 1. The sit-to-stand motion began at the first discernible hip flexion (more than 0.025^o between two consecutive frames). The end of the sit-to stand motion was defined by the last noticeable hip flexion motion (less than 0.025^o) [5].

Coefficient of multiple correlation (CMC) of the intra-day and inter-day repeatability were calculated for hip, knee, and ankle joint angle curves during sit-to-stand [6]. A Paired t-test examined the

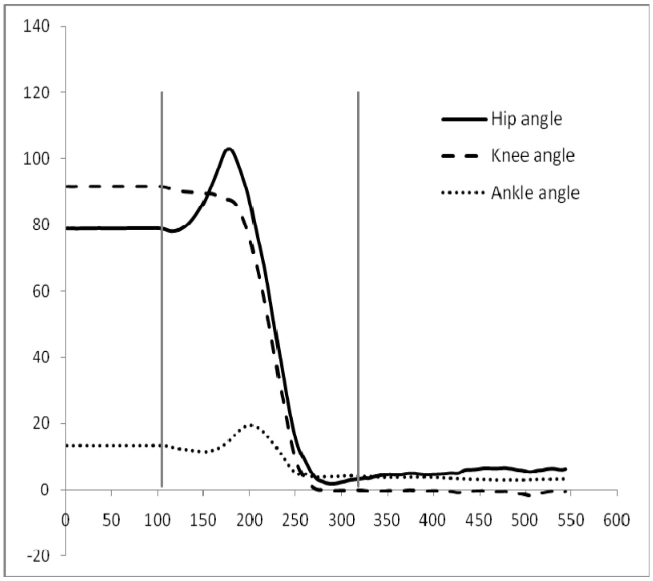

Figure 1: The hip, knee, ankle joint angle curve during the sit-to-stand.

difference of CMCs between optical and EM system at an alpha level of 0.05.

RESULTS AND DISCUSSION

The patterns of the hip, knee, ankle joint curves during a sit to stand motion were similar to those reported previously [7]. Mean ranges of motion of hip, knee and ankle joints from sit to stand are 82.3 ± 10.2, 87.3 ± 10.3, and 17.6 ± 12.0 degrees , for the optical system and 83.9 ± 12.3, 87.0 ± 11.5, and 15.9 ± 13.3 degrees for the EM system.

The mean and standard deviation of CMC representing intra-day and inter-day repeatability for all the subjects are shown in Table 1. For both the EM and optical systems, the repeatability of joint angle motion at the hip, knee, and ankle were high, with an average CMC value of 0.965, for both within day as well as between days. Furthermore, the optical system demonstrated significantly higher intra-day and inter-day CMCs than the EM system at the hip joint. For the ankle joint, the inter-day CMC of the optical system was significantly greater than the EM system, but not the intra-day CMC.

The CMC values for the ankle joint are lower and have larger standard deviation when compared to the hip and knee joint for both systems. These may be because the subjects' feet placement was not controlled between trials.

A single well-trained investigator placed markers and performed digitization on both testing days. Although the points for digitization were precisely marked on each marker, it was difficult to digitize the exactly same four points every time. In addition, skin motion artifact for the thigh and shank EM sensors cannot be neglected. These limitations could have affected the inter-day repeatability of the EM system.

CONCLUSIONS

For both systems, there was high intra-day and inter-day repeatability during a sit to stand task. The optical system provided a slightly better between day repeatability than the EM system during a dynamic movement setting, but the biomechanical and clinical importance of these differences remains to be determined.

REFERENCES

1. Chiari, L, et al. *Gait and Posture* **21**, 197-211, 2005.
2. McQuade, KJ, et al. *Journal of Applied Biomechanics* **18** (2): 171-179 2002.
3. Hassan, EA, Jenkyn, T.R., Dunning, C.E. *Journal of Biomechanics* **40**, 930-935, 2007.
4. Hahn, M.E., Chou, L.S. *Journal of Biomechanics* **37**, 837-44, 2004
5. Pamela J. et al. *Arch Phys Med Rehabil* **73**, 609-617, 1992.
6. Kadaba, MP, et al. *Journal of Orthopaedic Research* **7**, 849-860, 1989.
7. Kralj, A, et al. *Journal of Biomechanics* **23**, 1123-1138, 1990.

ACKNOWLEDGEMENTS

The assistance from Lucas Ettinger in data collection and Mika Naito in data processing are greatly appreciated.

Table 1: Mean and standard deviation of the coefficient of multiple correlation (CMC): hip, knee and ankle joint angle motion during sit-to-stand.

Joint Angle (deg)	Coefficient of multiple correlation (CMC)				
	Intra-day		Inter-day		
	EM	Optical	EM	Optical	*p*-value
Hip	0.981 ± 0.019	0.990 ± 0.005	0.966 ± 0.016	0.980 ± 0.012	$p_1 = 0.020$ $p_2 = 0.003$
Knee	0.990 ± 0.010	0.993 ± 0.004	0.982 ± 0.010	0.986 ± 0.008	$p_1 = 0.265$ $p_2 = 0.087$
Ankle	0.941 ± 0.072	0.951 ± 0.030	0.885 ± 0.090	0.935 ± 0.055	$p_1 = 0.550$ $p_2 = 0.030$

p_1: intra-day comparison; p_2: inter-day comparison

VARUS KNEE TORQUES IN HIGH-HEELED STAIR DESCENT

Catherine A. Stevermer, Nicole L. Nelsen and Jason C. Gillette
Department of Kinesiology, Iowa State University, Ames, IA
e-mail: ktsteve@iastate.edu; http://www.kin.hs.iastate.edu/

INTRODUCTION

Previous gait research has suggested altered knee joint loads in high-heeled shoes may be associated with knee osteoarthritis (OA) [1]. During level ground gait, increased external knee flexor and varus torques (14-26%) have been identified in moderately- to high-heeled footwear [1,2]. The elevated varus loads suggest magnified compressive forces through the medial compartment of the knee joint [3], which is the typical site for knee OA.

High-heeled footwear alters the loads placed on the lower extremities by shifting weight-bearing to the forefoot and moving the center of mass forward. High-heeled footwear is inherently more unstable as the ankle is in a plantarflexed position and reduces the base of support during single-limb support [4,5]. Mediolateral force excursions are less with high-heeled shoes during gait [4]. Therefore, the knee joint may be the compensatory mechanism for stability.

As females attempt to maintain stability in high-heeled footwear, they may experience difficulty while descending stairs [6]. Negotiating stairs is a daily aspect of community ambulation, so high-heel wearers may modify their descent strategy to maintain stability by making adjustments in the frontal and transverse planes.

Previous research determined that wearing high-heeled shoes produced higher torques in the frontal plane for young adults at the hip, knee and ankle than low-heeled shoes when climbing stairs [5]. The purpose of the current project was to determine the effect of high-heeled shoes on frontal plane torques while descending stairs. The expected results were that females would exhibit reduced mediolateral center of pressure (COP) excursions and higher varus knee torques in high-heeled footwear compared to the low-heel footwear.

METHODS

Seven young adult females (age 23.6 ± 5.5 yrs; 1.7 ± 0.1 m; 62.4 ± 10.4 kg) participated in this project. An eight-camera video system (Vicon, Englewood, CO) was used to track 28 reflective markers placed bilaterally on each subject. Landmarks for tracking included: cervicale, acromion, ASIS, PSIS, sacrum, greater trochanter, mid-femur, fibular head, lateral femoral condyles, mid-tibia, medial and lateral malleolus, calcaneus, 5th metatarsal head and great toe. Kinematic data were captured at 160 Hz using Vicon Nexus software.

A three-step wooden stair module without rails (step height = 19 cm; tread depth = 28 cm) was used for this project. Two portable force platforms (AMTI; Watertown, MA) were placed on the second and third tread to collect ground reaction forces. A third platform was located at the base of the module.

Participants performed stair descent in self-selected low-heel footwear (< 2 cm) and high-heeled footwear (avg. 6.9 ± 1.0 cm). The order of performance was balanced across subjects. Participants performed the stair descent task with arms freely moving at their sides. Participants descended the steps at a self-selected pace. Beginning at the top of the staircase, individuals descended three steps to floor level and walked an additional two meters, coming to a stop with their feet side-by-side. Each participant completed two trials leading with the right foot and two trials leading with the left in each type of footwear, for a total of eight trials.

Inverse dynamics was used to calculate joint angles, joint forces and joint torques in three dimensions. Center of pressure variables were also analyzed. Joint torques were normalized for body mass and are reported as Nm/kg.

Right and left side trials were collapsed into "low-heel" and "high-heeled" conditions. A multivariate analysis of variance (MANOVA) was conducted to determine condition differences for kinetic variables and gait speed. Bonferroni correction was utilized for the multiple (10) comparisons; statistical significance was defined at $p<0.005$.

RESULTS AND DISCUSSION

While descending stairs in high-heeled shoes, participants walked 8% slower compared to low-heel footwear ($p<0.001$). Participants walked at 0.66 ± 0.06 m/s in low-heel footwear, while in high-heeled shoes individuals moved at 0.61 ± 0.05 m/s. The slower velocity is an effective strategy for maintaining stability in high-heeled footwear.

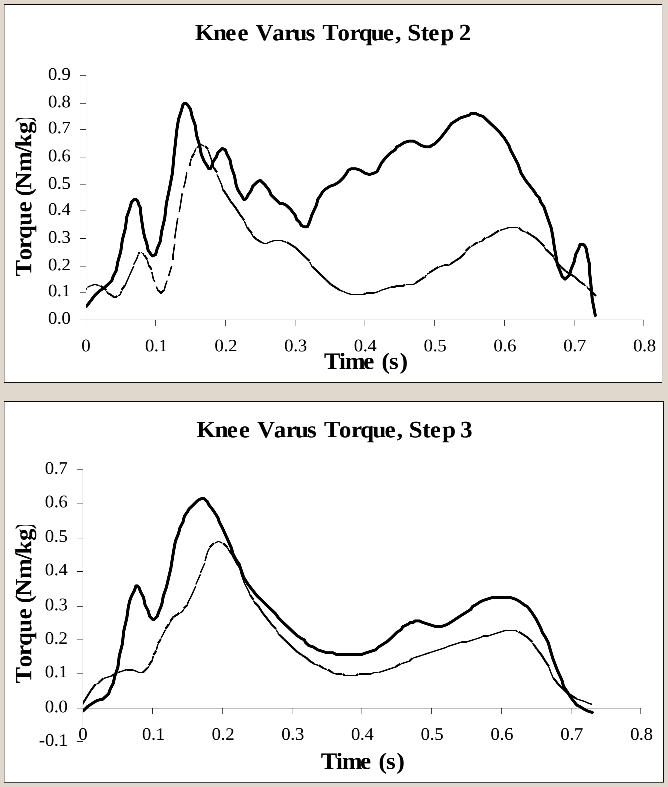

Figure 1: Knee varus torques during stair descent for the second and third steps. Torque values are presented for high-heel footwear (solid) and low-heel footwear (dashed) in Nm/kg over duration (in seconds).

The hypothesis regarding the COP excursion was not supported by the data. The mediolateral COP excursion appeared to be reduced in the high-heeled condition (4.51 ± 1.74 cm) compared to the low-heeled condition (5.72 ± 1.48 cm) on the first step, however the result was not significant ($p=0.009$) when the Bonferroni correction was made. The other two steps did not approach statistical significance due to high variability.

The other expected result was supported. Peak knee varus torques were higher in high-heeled footwear than in low-heel footwear (Figure 1) during the stance phase while descending stairs ($p<0.001$). On the second step, varus knee torque was elevated in high-heeled footwear (0.78 ± 0.19 Nm/kg) compared to low-heel footwear (0.56 ± 0.13 Nm/kg). On the final (or third) step, the high-heeled condition was also higher than the low-heel condition (0.55 ± 0.18 Nm/kg and 0.41 ± 0.08 Nm/kg, respectively.)

Previous researchers have indicated that frontal plane knee torques were higher with high-heeled footwear (0.41 ± 0.23 Nm/kg) compared to low-heel footwear (0.29 ± 0.22 Nm/kg) during stair ascent in young adults [4]. Based on the current findings, it appears varus torques may be higher during stair descent compared to stair ascent.

Stair descent appears to be a task that produces elevated varus torques in females, as values during stair descent in low-heel footwear were higher than reported varus torques (0.39 ± 0.06 Nm/kg) for level ground gait in high-heeled footwear [1]. As females have a higher incidence of medial knee OA, this association may warrant further investigation.

CONCLUSIONS

The current findings suggest descending stairs in high-heeled footwear produces increased varus torques at the knee. Resulting medial compressive forces may potentially increase the risk of knee OA in the medial compartment. Individuals also appear to reduce their velocity of descent to maintain stability in high-heeled footwear.

REFERENCES

1. Kerrigan DC, et al. *The Lancet* **357**, 1097-1098, 2001.
2. Kerrigan DC, et al. *Arch Phys Med Rehabil* **86**, 871-875, 2005.
3. Sharma L, et al. *Arth & Rheum* **41**, 1233-1240, 1998.
4. Ebbeling CJ, et al. *JOSPT* **19(4)**, 190-196, 1994.
5. Hsue BJ & Su FC. *J Electromyogr & Kines* (In Press), 2008.
6. Nagata H. *Safety Sci* **21**, 37-49, 1995.

Comparison of Functional and Isokinetic Fatigue Protocols: Injury Research Implications

[1] Al T. Douex and [1] Thomas W. Kaminski
[1]Health, Nutrition and Exercise Sciences, Human Performance Laboratory, University of Delaware
email: adouex@udel.edu, web: http://www.udel.edu/HNES/AT/Site/research.html

INTRODUCTION

Within the sport disciplines, there is a plethora of epidemiological evidence that contends that 54 – 71% of all injuries occur late in competitions or practices [1, 2]. Equally important is the notion that 58% of these injuries are caused by some noncontact mechanism [2]. The deleterious outcomes elicited by fatigue are typically related to altered biomechanics or motor control strategies [3]; however, studies predicting such effects may use inadequate techniques to fatigue subjects relative to author's conclusions. Perhaps, future studies could be refined by understanding differences in fatigue methodology. The purpose of this study was to compare the effects of intense exercise-induced fatigue on quadriceps/hamstring torque production and EMG using a functional fatigue protocol (FFP) and an isokinetic fatigue protocol (IFP).

METHODS

Twenty healthy subjects (10 male, 10 female; age: 21.4±3.5 yrs.; height: 169.8±7.3 cm; mass: 72.0±18.8 kg) volunteered for the two sessions comprising this investigation. Inclusion criteria were: (1) subject deemed healthy by the *Physical Activity Readiness Questionnaire*; (2) subject was free from illness/injury; and (3) subject was physically able to complete the FFP/IFP.

In both sessions, subjects completed isokinetic strength testing for knee flexion (KF) and extension (KE) on the KinCom 125AP Dynamometer. Both concentric (CON) and eccentric (ECC) actions were recorded at a rotational velocity of 180°/sec. Simultaneously, surface EMG was recorded from Vastus Medialis (VM), Vastus Lateralis (VL), Biceps Femoris (BF) and Semitendinosus (ST).

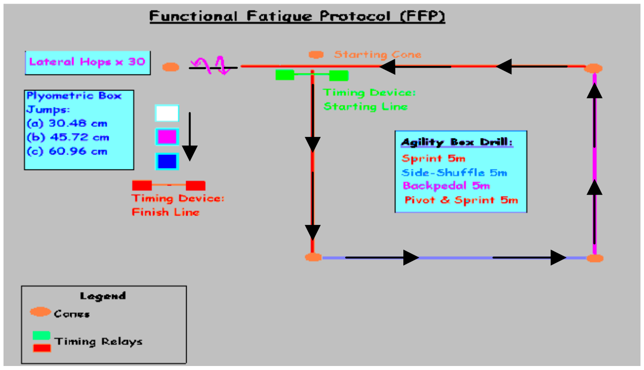

Figure 1: The Functional Fatigue Protocol (FFP) involved a 5 m x 5 m agility box drill, followed by 30 2-legged lateral hops over a 10.16 cm barrier, concluding with a series of plyometric box jumps.

In the first session, subjects were fatigued using the FFP (Figure 1), which consisted of a series of timed sprinting, cutting, and jumping tasks. For each repetition, subjects were asked to perform at maximal effort and render a Borg Rating of Perceived Exertion (RPE) score at the end. After a one month washout period, subjects reported for the second session incorporating the IFP. In the IFP, subjects performed CON KF and CON KE at various velocities, starting at 240°/sec and decreasing by 30°/sec intervals. Subjects continued to exercise in either fatigue protocol with intermittent 20-second rest periods until the termination criteria were met. Upon conclusion, subjects were immediately re-tested for isokinetic strength.

RESULTS AND DISCUSSION

Isokinetic peak torque (PT) and average torque (AT) data were extracted for both CON- and ECC-KF and KE. Root Mean Square Amplitude (RMS) and Median Spectral Frequency (F_{med}) values were extracted from EMG data for each muscle. All data were visually inspected and analyzed using custom software. Comparisons were made using a mixed-model repeated measures analysis of variance (ANOVA) where ($P<0.05$).

There were statistically significant differences in both PT and AT for the KE muscle group pre- to post-fatigue for the FFP and IFP (see figure 2). Interestingly, for the KF muscle group, significant decreases in PT and AT were only evident pre- to post-fatigue for the FFP (see Figure 3). The FFP appeared to universally target the musculature of the lower extremity, while the IFP did not. It is perceived as easier to pull with the line of gravity while on the dynamometer; hence subjects may not have been contracting their hamstrings with maximal intensity during the down phase of the IFP.

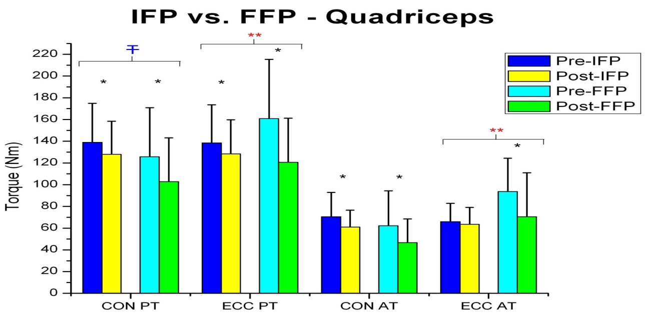

Figure 2: Quadriceps (KE) data prior to and following both the FFP and the IFP. * P<0.05; Significant decreases occurred from pre- to post-fatigue strength measures. ** P<0.05; Significant differences in change scores occurred between the IFP and FFP. ∓ P= 0.064; Trend towards significance for concentric peak torque change scores between the IFP and FFP.

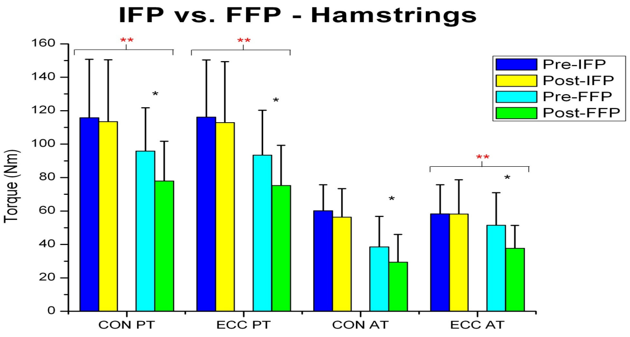

Figure 3: Hamstrings (KF) data prior to and following both the FFP and IFP. * P<0.05; Significant decreases occurred from pre- to post-fatigue strength measures. ** P<0.05; Significant differences in change scores occurred between the IFP and FFP.

The EMG data yielded mixed results. For the KE muscle group, there were significant differences in F_{med} across protocols. VL CON and VL ECC yielded changes where P<0.0001 and P=0.002 respectively and VM CON yielded changes where P<0.0001. VM ECC trended towards significance where P=0.059. The quadriceps yielded no significant changes across any EMG RMS variables. The KF muscle group also exhibited significant changes across protocols in $F_{med.}$, ST CON and ST ECC rendered changes where P=0.008 and P=0.011 respectively and BF CON and BF ECC both yielded changes where P=0.001. EMG RMS for ST CON and ST ECC also showed a significant change where P=0.003 and P=0.004 respectively. Follow up t-tests revealed that more pronounced changes were evident for KE following the FFP where F_{med} decreased in VM CON (pre-/post-IFP: 20.67±11.12 to 20.25±10.84; pre-/post-FFP: 38.47±5.32 to 33.87±2.83; P=0.007), VM ECC (pre-/post-IFP: 26.22±12.89 to 32.06±19.11; pre-/post-FFP: 36.02±5.01 to 33.78±3.96; P=0.039) and VL ECC (pre-/post-IFP: 37.08±20.62 to 39.33±21.15; pre-/post-FFP: 57.48±15.12 to 50.17±14.27; P=0.021).

The reductions in EMG F_{med} confirm that fatigue was achieved in the observed muscle groups. Other authors have demonstrated a left-hand shift in medial spectral frequency following exhaustive exercise [4]. It appears as though the FFP had a greater effect on the quadriceps than the IFP. In general, the data did render the changes in EMG RMS values consistent with fatigue; research suggests that RMS Amplitude values decrease following fatigue when maximal contractions are performed [5], however only the ST data demonstrated significance.

CONCLUSIONS

While both fatigue protocols caused a similar effect on the quadriceps' force production, the FFP had a greater effect on the hamstrings. Additionally, the deficits in quadriceps and hamstring activation evident with the FFP are suggestive of a more proximal (central) fatigue mechanism. Since greater forces are needed under dynamic conditions to avoid noncontact injuries, it is important to appropriately address methodology in the application of the results of fatigue studies. This FFP is a valid protocol for use in research targeting sports biomechanics.

REFERENCES

1. Agel J, et al. *J Athl Train* **42**, 241-248, 2007.
2. Hawkins RD, et al. *Br J Sports Med* **35**, 43-47, 2001.
3. Kellis E and Kouvelioti V. *J Electromyog Kinesiol* **19**, 55-64, 2009.
4. Kallenberg LAC and Herman HJ. *J Electromyog Kinesiol* **18**, 780-788, 2007.
5. Bigland-Ritchie B, et al. *J Physiol* **340**, 335-346, 1983.

COMPARING KNEE KINEMATICS DURING GAIT USING BIPLANE FLUOROSCOPY AND OPTICAL MARKER-BASED METHODS

Jake Krong, Daniel Peterson, Erik Giphart, Kevin Shelburne and Michael Torry
Steadman-Hawkins Research Foundation, Biomechanics Laboratory, Vail, CO
E-mail: jacob.krong@shsmf.org, Web: www.shsmf.org

INTRODUCTION

Motion sensor and optical marker camera systems are commonly used to measure tibio-femoral kinematics. There are inherent errors in these systems, such as inconsistent marker placement on anatomical landmarks and soft tissue movement artifact incurred during dynamic trials [1]. These errors are typically magnified when attempting to measure translations between the femur and tibia [2]. Markers attached to bone pins provide greater accuracy, but are invasive and may cause discomfort for subjects [3]. Biplane fluoroscopy is a potentially more accurate way of understanding knee motion. However, this device is relatively new to the field of gait analysis and there are no comparative studies showing the relationship of the data derived by biplane fluoroscopy and traditional motion capture methods. Comparative studies are needed to facilitate greater understanding of this device's capabilities and limitations. The purposes of this study were to: 1) describe knee rotations during gait using biplane fluoroscopy, and 2) compare this to similar data derived from traditional optical marker techniques. We hypothesized that while knee rotation angles would be similar between the two systems, there would be less variability between subjects using biplane fluoroscopy.

METHODS

Five healthy male subjects (29.8 ± 7.5yrs, 1.8 ± 0.1m, 84.0 ± 8.1kg) completed a walking trial while biplane fluoroscopic images were collected at 100 Hz by two high-speed cameras (Phantom V5.1, Vision Research, Wayne, NJ) interfaced with two BV Pulsera fluoroscopy systems (Philips Medical Systems, Best, Holland). Optical marker data was collected by Eagle cameras (Motion Analysis Corp., Santa Rosa, CA) at 120 Hz. Fluoroscopy images were collected during the loading portion of stance phase, while optical data was collected during the entire gait cycle.

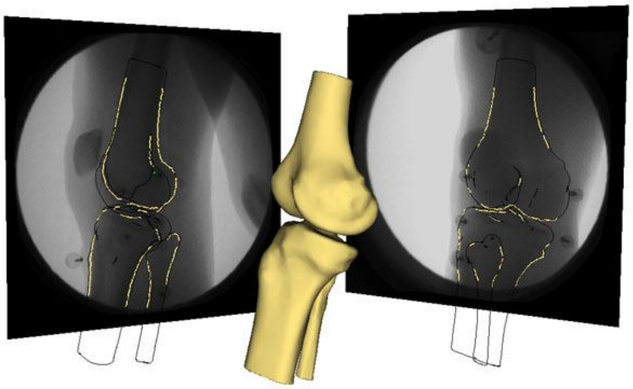

Figure 1: 3D models of the femur and tibia were matched to fluoroscopy images

A CT scan was acquired using an Aquilion 64 (Toshiba America Medical Systems, Tustin, CA). Three dimensional models of the femur and tibia were reconstructed from the CT images (0.5mm slices with a 512x512 pixel resolution) in Mimics software (Materialise, Inc, Ann Arbor, MI). Fluoroscopy images were tracked in Model-Based RSA software (Medis Specials, Leiden, Netherlands) by selecting manually selecting automatically detected bone contours. An 6DOF optimization algorithm calculated the 3D pose and orientation of the models in space (Figure 1). Optical data was collected and tracked in Cortex (Motion Analysis Corp., Santa Rosa, CA) and post-processed using The MotionMonitor (Innovative Sports Training, Chicago, IL).

Coordinate systems were applied to the femur and tibia models as follows: The origin of the femoral coordinate system was placed between the medial and lateral femoral condyles on the center line of a cylinder fitted to the medial and lateral posterior condyles (Figure 2). The tibial coordinate system was placed at the tibial spine and aligned with the femoral coordinate system. Using these coordinate systems, translations and rotations of the tibia with respect to the femur were determined by methods described by Grood and Sunday [4]. For the optical marker kinematics, coordinate systems were created using a modified Helen Hayes model [5] and calculations followed the conventions of Grood and Suntay [4].

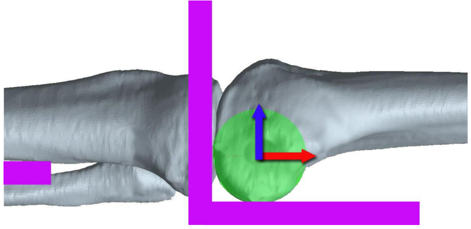

Figure 2: Example of femur coordinate system.

RESULTS AND DISCUSSION

Knee rotations for each data collection system are shown in Figure 3. The optical marker system displayed larger values in flexion and external rotation, and smaller values in adduction. Peak values, however, were not significantly different: flexion (p=0.059), adduction (p=0.352), external rotation (p=0.599).

Coefficient of Variation ($c_v = \frac{\sigma}{\mu}$) among the subjects was generally lower at peak values for biplane fluoroscopy compared to the marker-based technique (Table 1). The coefficient of variation was lower in biplane fluoroscopy for adduction and external rotation. In flexion, the coefficient of variation was higher in biplane fluoroscopy.

CONCLUSIONS

Biplane fluoroscopy is a novel way of measuring highly accurate 3D rotations about the knee. The results of this study compare favorably with traditional methods of measuring knee kinematics. For comparing cohorts of subjects, marker methods appear to be sufficient to compare rotations. In the future, this method can be applied to other joints, whose complexity and lack of bony landmarks make using marker-based optical systems difficult, and more dynamic motions such as jumping, where error due to marker motion and soft tissue artifact is increased.

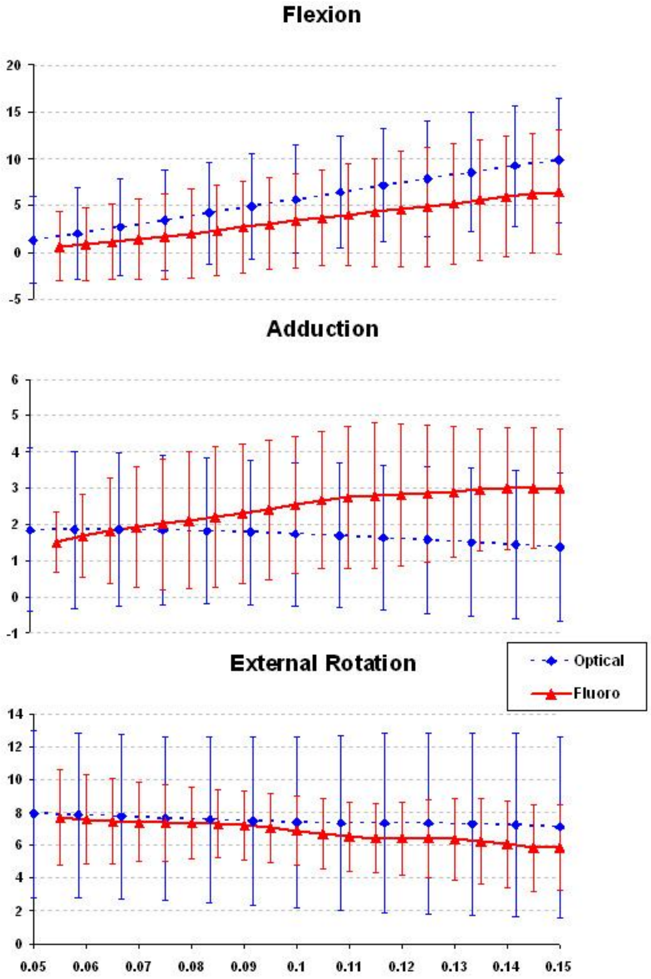

Figure 3: Knee rotations (degrees) measured using optical and biplane fluoroscopy techniques. The x-axis represents time after heel strike (seconds). Standard deviations for the entire group are shown.

Table 1: Coefficient of Variation

	Fluoroscopy	Optical
Flexion	1.02	0.67
Adduction	0.55	1.49
Internal Rotation	0.44	0.78

REFERENCES

1. Gao B and Zheng N. *J Biomech* **41**: 3189-3195, 2008.
2. Garling EH et al. *J Biomech* **40**: 518-524, 2007.
3. LaFortune MA et al. *J Biomech* **25**: 347-357, 1992.
4. Grood ES and Suntay WJ. *J Biomech Eng* **105**: 136-144, 1983.
5. Cappozzo A et al. *Gait and Posture* **21**: 186-196, 2005.

BIPLANE FLUOROSCOPY ANALYSIS OF KNEE KINEMATICS DURING GAIT

Jake Krong, Daniel Peterson, Erik Giphart, Kevin Shelburne and Michael Torry
Steadman-Hawkins Research Foundation, Biomechanics Laboratory, Vail, CO
E-mail: jacob.krong@shsmf.org, Web: www.shsmf.org

INTRODUCTION

Optical marker camera systems and electromagnetic sensors are commonly used to measure lower limb kinematics with the important goal of attempting to identify gait adaptations after injury, surgery, or rehabilitation. There are inherent errors in these systems, such as inconsistent marker placement on anatomical landmarks and soft tissue movement artifact during dynamic trials [1]. It is important to accurately measure tibio-femoral translations and rotations to understand and estimate stresses being placed on ligaments serving to stabilize the knee [2].

Biplane fluoroscopy is a novel and potentially more accurate way of understanding 6DOF tibio-femoral kinematics. Despite increasing use of this device, there is a paucity of normative data. The purpose of this study was to describe knee rotations and translations during gait using biplane fluoroscopy. We hypothesized that while knee rotation angles would be similar to what had previously been reported in the literature, translations would have less total excursion during stance phase.

METHODS

Five healthy male subjects (29.8 ± 7.5yrs, 1.8 ± 0.1m, 84.0 ± 8.1kg) completed a walking trial at 2.75 mph while biplane fluoroscopic images were collected at 100 Hz (Figure 1) by two high-speed cameras (Phantom V5.1, Vision Research, Wayne, NJ) interfaced with two fluoroscopy systems (Philips Medical Systems, Best, Holland). Fluoroscopy images were collected during the loading portion of stance phase.

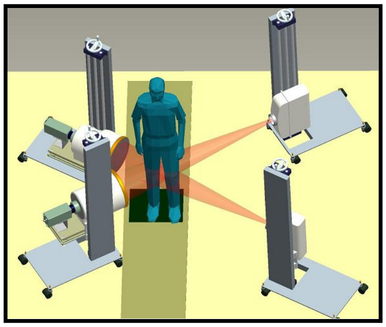

Figure 1: Biplane fluoroscopy collection area

A CT scan was acquired using an Aquilion 64 (Toshiba America Medical Systems, Tustin, CA). Three dimensional models of the femur and tibia were reconstructed from the CT images (0.5mm slices with a 512x512 pixel resolution) in Mimics software (Materialise, Inc, Ann Arbor, MI). Fluoroscopy images were tracked in Model-Based RSA software (Medis Specials, Leiden, Netherlands) by selecting manually selecting automatically detected bone contours. An 6DOF optimization algorithm calculated the 3D pose and orientation of the models in space (Figure 2).

Coordinate systems were applied to the femur and tibia models as follows: The origin of the femoral coordinate system was placed between the medial and lateral femoral condyles on the center line of a cylinder fitted to the medial and lateral posterior condyles (Figure 2). The tibial coordinate system was placed at the tibial spine and aligned with the femoral coordinate system. Using these coordinate systems, translations and rotations of the tibia with respect to the femur were determined by methods described by Grood and Sunday [3].

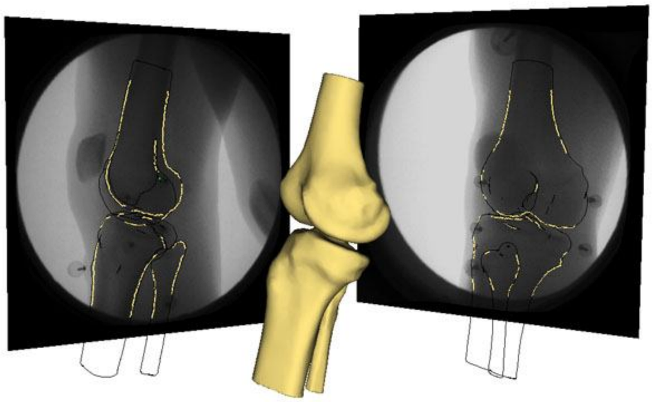

Figure 2: 3D models of the femur and tibia were matched to fluoroscopy images

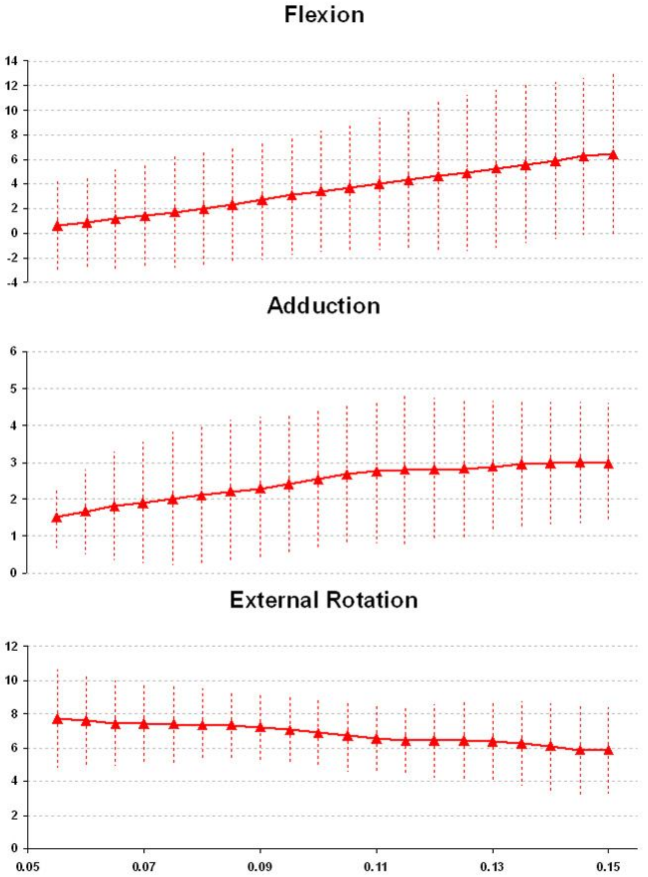

Figure 2: Knee rotations (degrees) and standard deviations. The x-axis represents time after heel strike (seconds).

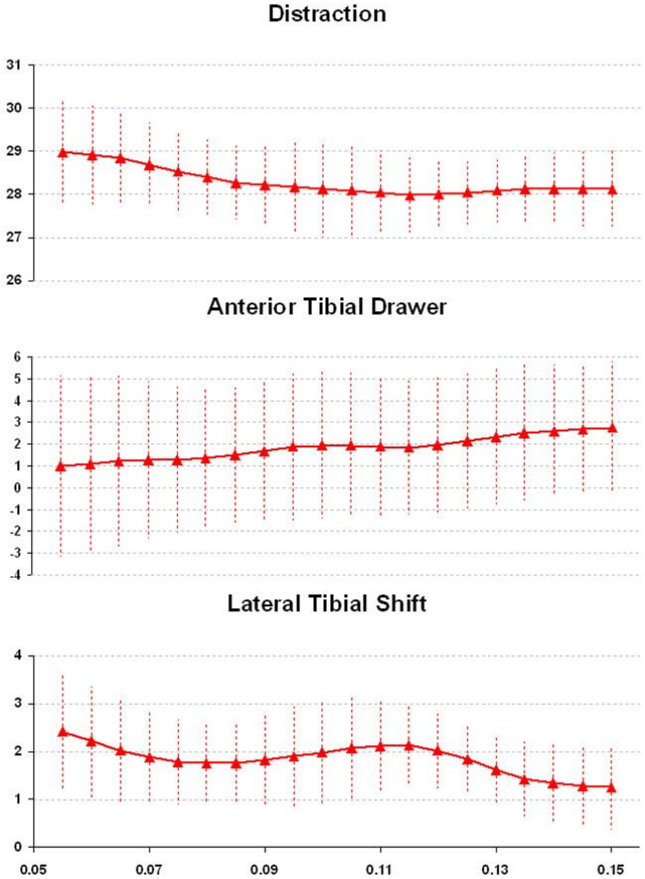

Figure 3: Knee translations (mm) and standard deviations. The x-axis represents time after heel strike (seconds).

RESULTS AND DISCUSSION

During the loading portion of stance phase, the tibio-femoral joint became more flexed, the tibia was adducted between 1.5º and 3º, and the tibia was initially externally rotated, but began to internally rotate by about 2 º (Figure 2). As the knee was flexing, the tibia moved anterior to the femur by 2mm and medial to the femur by 1mm (Figure 3).

The magnitudes of translations are lower than what has been reported in bone pin studies and using marker-based systems such as the point cluster techniques [4]. In those studies, translational excursions during loading phase were on the order of a centimeter, while our results show excursions of a few millimeters. Our results also compare favorably to other biplane fluoroscopy studies analyzing gait [5].

CONCLUSIONS

Tibiofemoral rotations in biplane fluoroscopy are similar to what has been previously reported in bone pin studies. The advantage of fluoroscopy is that it is less painful for the subject. Lower translational displacements indicate that optical techniques may overestimate the strain being placed on knee ligaments during dynamic trials. Biplane fluoroscopy is a useful and highly accurate method for identifying gait pathologies.

REFERENCES

1. Garling EH et al. *J Biomech* **40**: 518-524, 2007.
2. Woo SLY et al. *J Orthop Surg Res* **1**: 2, 2006.
3. Grood ES and Suntay WJ. *J Biomech* **105**: 136-144, 1983.
4. Andriacchi TP et al. *J Biomech Eng* **120**: 743-749, 1998.
5. Komistek RD et al. *Clin Orthop Relat Res* **410**: 69-81, 2003.

SEX DIFFERENCES IN POSTURE AND KINEMATICS OF THE HUMAN HEAD AND NECK

[1]Liying Zheng, [2]Jessica Jahn and [1,2]Anita Vasavada

[1]School of Mechanical and Materials Engineering; [2]Voiland School of Chemical Engineering and Bioengineering
Washington State University, Pullman, WA, USA; Email: liying_zheng@wsu.edu

INTRODUCTION

Many studies have shown that females are more likely to experience neck injury and neck pain, particularly whiplash injuries in rear-end collisions [1, 2]. The intrinsic sex differences in the neck skeleton may be one of the possible reasons for higher incidence in females. Generally, males' bones are larger than females', and the skull is one of the most reliable skeletal predictors of sex [3]. Even in men and women who were matched for height and neck length, females had significantly smaller head and vertebral size [4].

In addition to size, posture and kinematics can affect neck strength and the potential for injury. The long-term goal of this work is to build gender-specific computational models to quantify how much those skeletal sex differences affect neck strength. The specific goal of this study is to investigate sex differences in posture and kinematics of the head and neck region, especially for those parameters which are incorporated into neck models (e.g., range of motion (ROM), intervertebral motion distribution and intervertebral instantaneous axis of rotation (IAR)). Further, the hyoid bone and associated muscles may play a role in neck flexion [5]. However, no studies have quantified the kinematics of the hyoid bone or any possible sex differences. This study will try to answer not only if there is a difference in posture and kinematics between women and men, but also what causes the differences? Are they related to the skeletal geometry?

METHODS

Sixteen females and sixteen males with a broad height distribution were recruited (the height ranged from the 3rd to the 97th percentile female height and from < 1st to the 98th percentile male height). All the subjects underwent lateral X-rays at five different postures (Fig. 1). The subjects' height, weight and other anthropometric data were measured. Lateral radiographs were digitized to calculate vertebral dimensions and to obtain the size- and/or posture-related parameters (Fig. 1).

Cervical curvature was defined similar to a study by Tecco [6]: the vertebral body centers and midpoints of superior and inferior endplate (from C2 to C7) were fit using a second order polynomial function ($X=P2*Y^2+P1*Y+P0$) (Fig. 2A). The second order coefficient (P2) indicates the curvature of the cervical spine. The correlations between P2 and other posture and size parameters were studied.

The overall ROM was defined by the difference in head angle (with respect to the first thoracic vertebra) from maximum extension to maximum flexion. The intervertebral motion distribution was defined by normalizing the segmental ROM [7] (Fig. 2B) by the overall ROM. The absolute intervertebral IAR was determined by the classic Rouleaux method [8] and normalized by the height and depth of the lower vertebra.

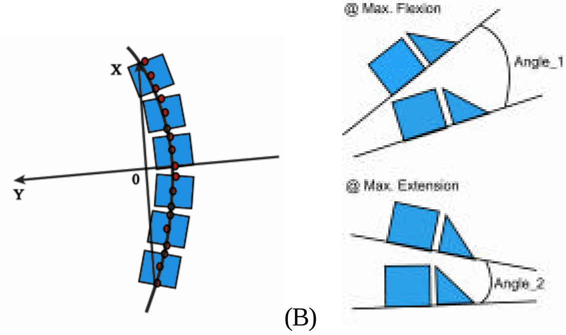

(A) (B)

Fig. 2 (A) Cartesian axis references used for measurement of the cervical curve, where X axis was superimposed on a line connecting the midpoint of C2 superior endplate and that of C7 inferior endplate, the origin was at the midpoint of this line, and Y axis was perpendicular to the X axis through the origin; (B) Segmental ROM = Angle_1 – Angle_2

We investigated whether the hyoid bone motion could be defined as a function of other bone motions. The correlations between the position of hyoid bone (coordinates and angle of hyoid bone) and different posture-related parameters were calculated.

Sex differences in kinematic values between males and females (i.e. overall ROM, intervertebral motion distribution and IAR) were evaluated using unpaired t-tests. In the regressions of the cervical curvature and hyoid bone position, the sex difference was analyzed using analysis of covariance (ANCOVA), where the independent variables (predictors) were used as covariates.

RESULTS AND DISCUSSION

The cervical curvature (P2) was a function of head angle: $P2=-0.001*HeadAngle+0.0193$, ($R^2=0.87$). However, there was no significant difference between women and men ($p=0.1$).

According to the results of cervical curvature, the head angle could be a predictor of the posture of head and neck system. Furthermore, it indicated that women and men may have the similar postures when the head angles are same.

Overall ROM was similar between females and males ($p= 0.93$). There were no significant sex differences for normalized intervertebral IAR (for x coordinates: $0.13<p<0.79$; for y coordinates: $0.20<p<0.69$) or the intervertebal motion distribution (normalized segmental ROM) (Fig.3).

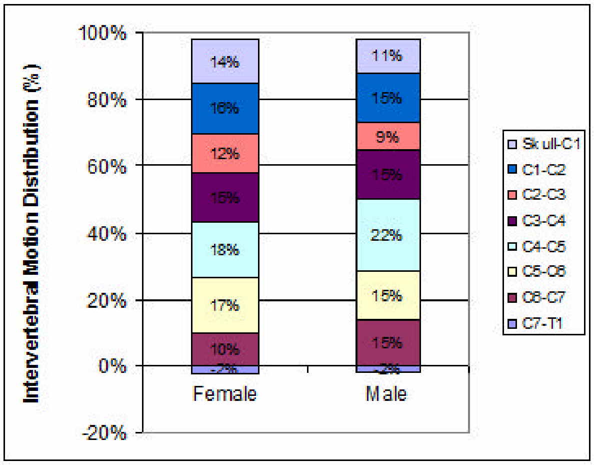

Fig. 3: Intervertebal motion distribution, where the sex difference was not significant for each level ($0.2<p<0.9$).

The position of the hyoid bone had a strong correlation with position of either the skull, jaw or C3. There was a significant sex difference in the linear regression of hyoid bone with respect to the position of C3 ($p<=0.05$), but not to the skull or jaw. (Fig.4)

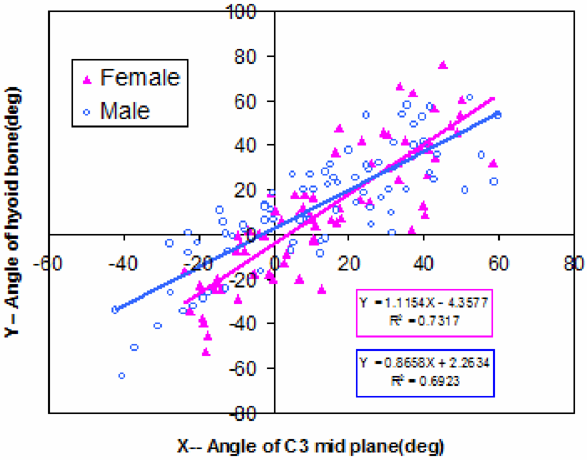

Fig. 4: Regressions of hyoid bone angle, where females had significantly different regression compared to males ($p=0.01$)

CONCLUSIONS

The size of the neck skeletal structure might be a surrogate of sex differences in skeletal kinematics, since most kinematical parameters show no significant sex difference after being normalized by vertebral size or controlling the covariates.

Therefore, for further analysis of sex differences in neck musculoskeletal biomechanics, the kinematics in female and male models will be adjusted mainly according to skeletal size. However, the kinematics of hyoid bone may need to reflect sex difference.

REFERENCES

1. Berglund A, et al. *Ann Epidemiol* **13**, 66-72, 2003.
2. Spitzer WO, et al. *Spine* **20**, 1S-73S, 1995.
3. Shipman P, et al. *The Human Skeleton*, Harvard University Press, 270-7, 1985
4. Vasavada AN, et al. *J Biomech* **41**, 114-21, 2008
5. Siegmund GP, et al. *J Biomech Eng* **129**, 66-77, 2007
6. Tecco S, et al. *Eur J Orthod* **29**, 204-9, 2007
7. Simpson AK, et al. *Spine* **33**, 183-6, 2008
8. Panjabi MM, et al. *J Biomech* **12**, 911-20, 1979

ACKNOWLEDGEMENTS

Funded by NSF (CBET #0748303)

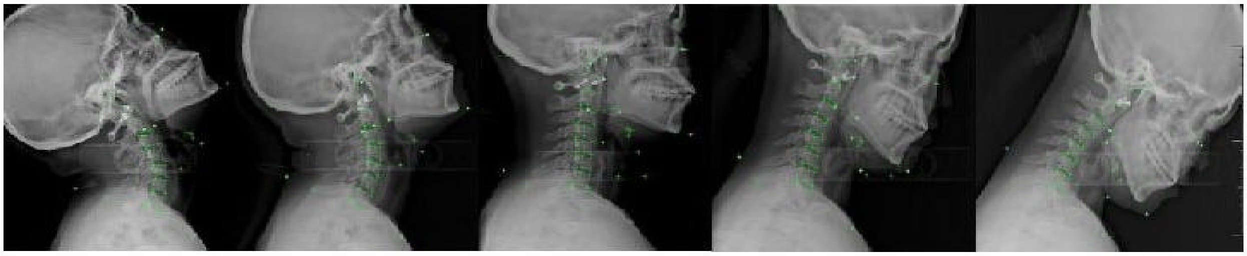

Fig. 1: Lateral X-rays of a subject at five postures (from voluntary maximum extension to maximum flexion).

QUIET STANDING AND QUIET SITTING IN YOUNG CHILDREN WITH AUTISM SPECTRUM DISORDERS.

Kimberly Fournier, Krestin Radonovich, Jacquelyn Selbst, Hope Benefield and Chris Hass
The University of Florida, Gainesville, FL
email: kfournier@hhp.ufl.edu

INTRODUCTION

Motor control deficits appear to be common co-morbid symptoms in children with autism spectrum disorders (ASD) [1]. Specifically, preliminary research indicates that individuals with ASD may have delayed and/or impaired postural control [2, 3, 4]. Unfortunately, postural control is typically evaluated with tasks that can be demanding on cognition, communication and attention. Due to these constraints, individuals with ASD may have difficulty performing conventional tasks such as quiet standing due to distractedness. As a result, our ability to further define motor impairments in postural control using standard tasks has proved challenging. Thus, we propose using an alternative task of attention directed quiet sitting. Here in, we evaluated postural control in children with ASD and typically developing (TD) children during both quiet standing and attention directed quiet sitting tasks to assess the potential of using sitting as an alternative measure for postural control in individuals with ASD.

METHODS

During quiet standing trials, 7 children diagnosed with ASD (5.4 ± 2.2 yrs; 1.1 ± 0.1 m; 19.8 ± 2.7 kg) and 11 TD children (5.4 ± 2.2 yrs; 1.1 ± 0.1 m; 19.8 ± 2.7 kg) were asked to stand with their feet comfortably apart (self–selected stance width). Foot positioning was marked on the initial trial and used for all subsequent trials. Children were asked to stand “as still as possible” for 20 s with their arms comfortably at their side. Children performed 4 experimental trials. During quiet sitting trials, children were asked to sit quietly while watching a video segment with engaging images and sounds (Baby Einstein Mozart, The Baby Einstein Company, LLC). Four, 120 s experimental trials were collected and 20 s time intervals were averaged and used in subsequent analyses.

Ground reaction forces were recorded (360 Hz) while children stood on a forceplate (Type 4060–10, Bertec Corp., Columbus, OH) embedded level with the floor. Ground reaction forces and moments collected from the forceplate were processed and the location of the center of pressure (COP) was calculated. Once the COP was calculated, the peak displacements in the mediolateral (ML Range) and anteroposterior (AP Range) directions were determined and the sway area was calculated for all trials. Trials with a COP sway area greater than 200 cm^2 were considered to contain voluntary movements beyond those of typical postural adjustments during quiet standing or quiet sitting and were therefore excluded from statistical analyses.

An individual’s data from the 4 experimental trials in each condition were averaged to provide one representative datum for each dependent variable. The representative datum was then submitted for statistical analyses. In addition, an individual’s data from the 4 standing trials, sorted in ascending order according to the sway area were correlated to sorted data from their 4 sitting trials, as a preliminary assessment of the relationship between the two tasks.

RESULTS

A one way MANOVA performed for COP measures during quiet standing and quiet sitting revealed a significant multivariate effect of group (p=0.01). Follow up univariate tests revealed that children with ASD exhibited significantly larger ML Range, AP Range and Sway Area values during quiet standing (p<0.01, p<0.01, p<0.01 respectively) and ML Range, AP Range and Sway Area values during quiet sitting (p<0.01, p<0.05, p<0.01 respectively) when compared to age-matched TD children (Table 1.)

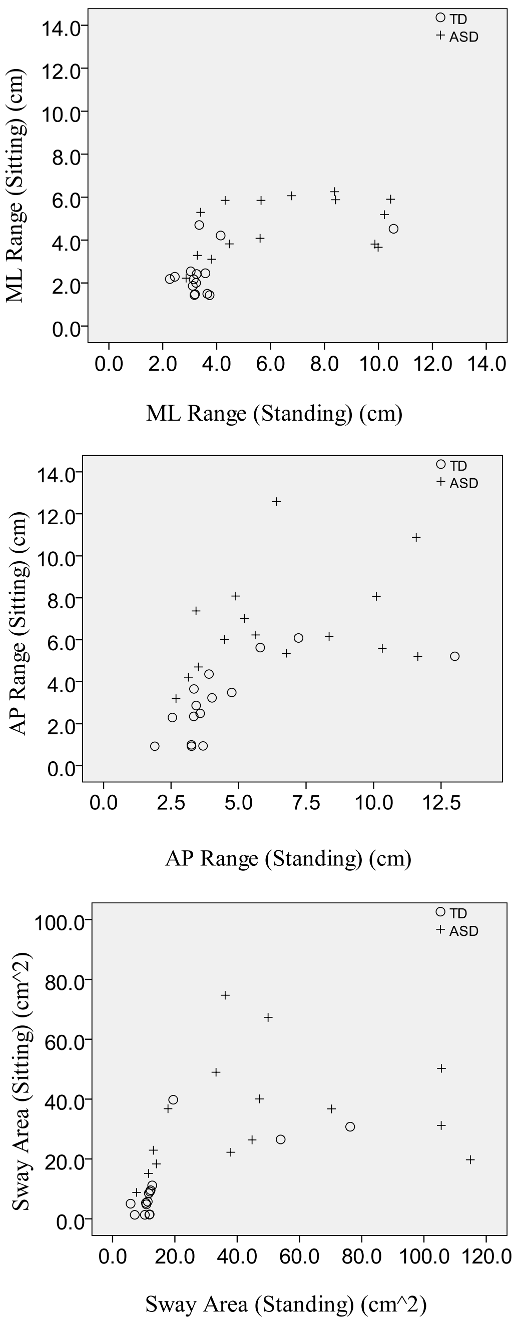

Figure 1: Scatter plots for quiet standing and quiet sitting COP measures.

COP measures were observed to be significantly, positively correlated for ML Ranges (Pearson ***r***=0.595, ***p***<0.00), AP Ranges (Pearson ***r***=0.530, ***p***<0.00) and Sway Areas (Pearson ***r***=0.492, ***p***<0.00) for quiet standing and quiet sitting trials (Figure 1).

DISCUSSION

Our results support previous reports that children with ASD have deficits in postural control. Children with ASD were observed to have increased COP movements in the ML and AP directions and consequently had larger sway areas during quiet standing when compared to TD children. When using an attention demanding task to assess postural control, it appears differences observed between groups were not reduced. Similarly to quiet standing, children with ASD had increased COP movements for all three measures during quiet sitting. Sway areas for children with ASD were 240% larger during quiet standing and 220% larger during quiet sitting. Therefore, it appears postural control deficits observed in children with ASD during quiet standing may not be due to constraints associated with the task but rather, are indeed representative of altered control of posture during quiet conditions.

CONCLUSIONS

Preliminary results suggest that postural control during quiet standing and quiet sitting are related and yield similar group differences for postural control assessment of young children with ASD and TD children. Results suggest that quiet sitting may be used as an alternative task when children with ASD are unable to comply with the constraints associated with quiet standing.

REFERENCES

1. Green, D. et al. (2009). *[Epub ahead of print]*.
2. Gepner, B. (1995). *Neuroreport*, ***6***, 1211-14.
3. Kohen-Raz, R. (1992). *Journal of Autism and Developmental Disorders*, ***22***, 419-32.
4. Minshew, N. J. (2004). *Neurology*, ***63***, 2056-61.

ACKNOWLEDGEMENTS

Autism Speaks #CH/1964/01-201007-065-00-00-01

Table 1. Descriptive Statistics (M±SD) for COP measures during quiet standing and quiet sitting.

	Standing			**Sitting**		
	ML Range (cm)	**AP Range (cm)**	**Sway Area (cm^2)**	**ML Range (cm)**	**AP Range (cm)**	**Sway Area (cm^2)**
TD (n=11)	3.6 ± 1.0	4.3 ± 1.6	16.7 ± 11.8	2.6 ± 1.4	3.7 ± 2.2	13.3 ± 14.6
ASD (n=7)	7.5 ± 2.1	7.0 ± 2.8	56.9 ± 32.1	5.5 ± 1.9	7.3 ± 1.7	43.9 ± 21.5

METABOLIC RESPONSE IN FUNCTIONAL ELECTRICALLY STIMULATED PEDALING WITH THE LOWER LEG MUSCLES

[1]Nils A. Hakansson and [2]Maury L. Hull
[1]Department of Mechanical Engineering, University of Delaware, Newark, DE, USA
[2]Department of Mechanical Engineering, University of California, Davis, CA, USA
email: nilsh@udel.edu

INTRODUCTION

Functional electrical stimulation (FES) pedaling with the muscles of the upper leg can provide cardiorespiratory benefit to spinal cord injured (SCI) individuals [1-2]. Activation of the lower leg muscles could further enhance the benefit of FES pedaling by increasing the metabolic response to the exercise [1-2]. The objective of this study was to determine whether FES pedaling with the upper and lower leg muscles and a fixed ankle joint would enable an individual with SCI to achieve increased metabolic responses than pedaling with the upper leg muscles alone.

METHODS

A forward dynamic model of FES pedaling crank was used to compute electrical stimulation on and off times that minimized the sum of the area under the muscle stress-time curve for each muscle and the difference between the areas of the muscle stress-time curves of the quadriceps (QUADS), gluteus maximus (GMAX), and hamstrings (HAMS) muscle sets (referred to as Stim3) and the QUADS, GMAX, and HAMS plus the triceps surae (TRI) and tibialis anterior (TA) muscles sets (referred to as Stim5) (Figure 1) [3].

Experimental data were collected as 7 subjects (1 female; mean age 25 ± 7 years; mean height 1.74 ± 0.10 m; mean weight 67 ± 13 kg) with a complete spinal cord injury between level T6 to T12 at least 1 year prior to the 4-week study pedaled an ERGYS 2 (Therapeutic Alliances, Inc., Dayton, OH, USA) FES ergometer to assess their response to metabolic responses to Stim3 and Stim5. Testing sessions were divided into two 2-week time blocks. The order of the electrical stimulation timing patterns, Stim3 and Stim5, was randomly assigned during the first 2-week time block and was then reversed during the second 2-week time block [4]. The testing protocol consisted of pedaling at 50 rpm with no applied workload for 7 minutes and a 0.06 Kp (approximately 3 W at 50 rpm) workload increases after every 7-minute period thereafter until the pedaling rate dropped below 35 rpm. Blood lactate concentrations and breath-by-breath $\dot{V}O_2$ data were collected over the final minute of each 7-minute period.

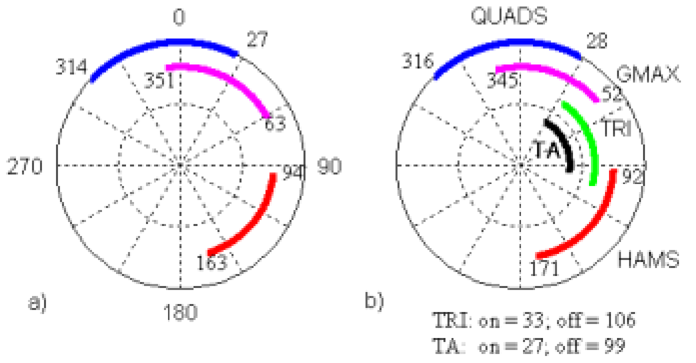

Figure 1. Plot of muscle electrical stimulation on and off timing as a function of crank angle for a) Stim3 and b) Stim5. Top-dead-center indicates 0 degrees and the beginning of the crank cycle.

Two-factor one-tailed repeated measures ANOVA tests were used to test the hypothesis that Stim5 would enable an individual with SCI to increase the two metabolic measures, $\dot{V}O_2$ and blood lactate concentration [5]. The two factors in these analyses were the electrical stimulation timing patterns at two levels (Stim3 and Stim5) and the 2-week time blocks. The dependent variables in these analyses were the 1-minute averaged $\dot{V}O_2$ (taken over the same minute across all sessions for an individual subject and corresponded to the last minute of highest 7-minute period reached by the subject in all of his or her experimental testing sessions) and the blood lactate concentration. The criterion level of significance was $p<0.05$.

RESULTS

The electrical stimulation timing patterns did not have a significant effect on $\dot{V}O_2$ ($p = 0.1176$)

(Figure 2). The average $\dot{V}O_2$ for pedaling with Stim3 was 441 ± 231 mL/min and for Stim5 was 473 ± 213 mL/min. The electrical stimulation timing patterns did have a significant effect on blood lactate concentration ($p = 0.0049$) (Figure 3). The average blood lactate concentration for Stim5 was (6.8 ± 2.3 mmoles/L) and for Stim3 was (5.9 ± 2.3 mmoles/L). The interactions between the electrical stimulation timing patterns and the time blocks were not significant for either the $\dot{V}O_2$ ($p = 0.4864$) or the blood lactate concentration ($p = 0.1306$).

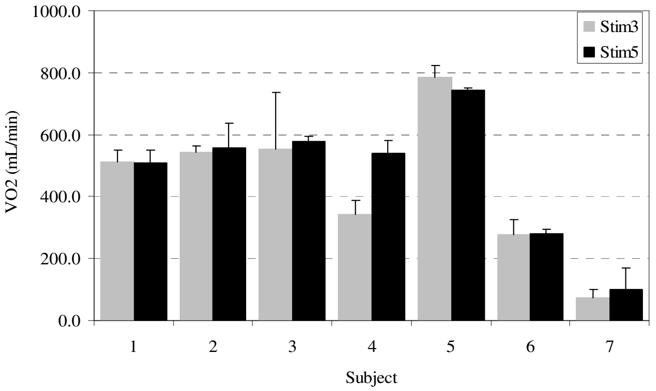

Figure 2. Subjects' rate of oxygen consumption ($\dot{V}O_2$) averaged over the two time blocks for Stim3 and Stim5. Error bars denote 1 S.D.

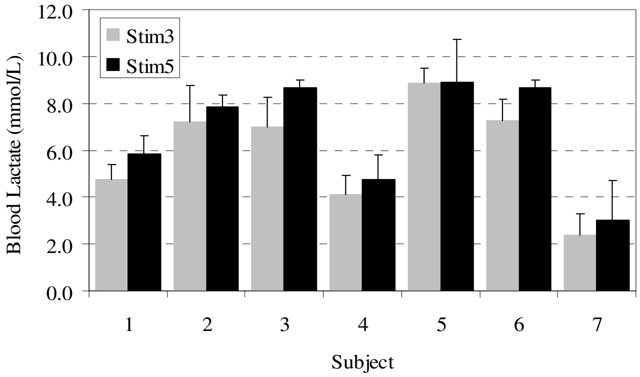

Figure 3. Subjects' blood lactate concentrations averaged over the two time blocks for Stim3 and Stim5. Error bars denote 1 S.D.

DISCUSSION

An unanticipated result was the lack of a difference in the measured rate of oxygen consumption for the subjects pedaling with the Stim3 and Stim5. The maximum stimulation amplitude was the same and the stimulation on and off timing for the upper leg muscles was nearly identical for Stim3 and Stim5 (Figure 1). Therefore, the 32 ml/min difference in the average $\dot{V}O_2$ measured for Stim3 (441 ml/min) and Stim5 (473 ml/min) would have been due to the lower leg muscle metabolic activity. Because of muscle atrophy, fiber type conversion associated with disuse from the spinal cord injury, and the non-physiological recruitment of muscle fibers with surface electrical stimulation, the rate of oxygen consumption by the lower leg muscles was too low to register a statistically significant difference.

Activation of the lower leg muscle sets in FES pedaling caused the blood lactate concentration to increase for 6 of the 7 subjects (Figure 3). More muscle sets were activated and surface electrical stimulation of muscles is associated with the recruitment of type II fibers and, consequently, anaerobic metabolism. Considering that the blood lactate measures were taken over the same minute completed for all trials by that subject, it can be concluded that the lower leg muscle sets activated with Stim5 were the source of the increased blood lactate concentration.

The result that blood lactate concentration increased with Stim5 signifies the potential for more muscle mass to benefit from the training effects of the exercise. The incorporation of more muscles in the exercise would increase the number of muscle fibers activated and presumably allow the benefits of FES training to be realized in more muscles of the leg. There were no negative effects associated with the incorporation of the lower leg muscles in the exercise. The results indicate that stimulating the lower leg muscles in FES pedaling could lead to enhanced exercise outcomes over time.

REFERENCES

1. Glaser RM, et al. *Proceedings RESNA,* Washington DC, pp. 279-281, 1996.
2. Janssen TWJ, et al. *Proceedings RESNA,* Washington DC, pp. 288-290, 1996.
3. Hakansson NA and Hull ML. *IEEE Trans Biomed Engr.*, in press, 2009.
4. Hakansson NA, *PhD Dissertation*, 2008.
5. Trumble, DR, et al., *Basic and Appl Myology,* **11**, 91-98, 2001.

ACKNOWLEDGEMENTS

This work was supported by the National Institute on Disability and Rehabilitation Research (NIDRR) (Award Number H133G0200137).

THE ROBOTIC GAIT SIMULATOR: THE EFFECT OF EMG TO FORCE ESTIMATION

[1,2]Patrick M. Aubin and [1,3,4]William R. Ledoux
[1]VA RR&D Center of Excellence for Limb Loss Prevention and Prosthetic Engineering, Seattle, WA 98108, and Departments of [2]Electrical and [3]Mechanical Engineering, and [4]Orthopaedics & Sports Medicine, University of Washington, Seattle, WA 98195
email: wrledoux@u.washington.edu, web: http://www.amputation.research.va.gov/

INTRODUCTION

Cadaveric models are useful to further our understanding of foot and ankle function, biomechanics, and pathology. There are significant challenges however in accurately recreating *in vitro* the complex foot and ankle kinematics, musculotendinous forces, and ground reaction forces that occur during gait. To address these challenges we have developed the robotic gait simulator (RGS) by employing a 6-DOF parallel robot and nine force control tendon actuators. The inputs into the RGS are the stance phase tibial kinematics, electromyography (EMG) of nine extrinsic lower limb muscles, and the vertical ground reaction force (vGRF). We created a set of heuristics to manually adjust the vGRF until it matches normative *in vivo* gait data. Results from three cadaveric specimens each performing three gait trials are presented. Comparing the temporal characteristics of the *in vitro* and *in vivo* Achilles tendon force and vGRF reveals the limitations of a common EMG to force estimation method.

METHODS

Ten healthy subjects were recruited and asked to perform five gait trails each after providing informed consent for this Institutional Review Board approved study. A 12-camera Vicon motion analysis system sampled kinematic data at 250Hz while a Bertec force plate sampled kinetic data at 1500Hz.

The RGS consists of an R2000 parallel robot with a mobile Kistler force plate, nine force control tendon actuators and load cells in series with each tendon, a tibia mounting frame, and a six-camera Vicon motion analysis system (Figure 1). To simulate gait the tibia is fixed while the R2000 moves the force plate, i.e. the “ground,” to recreate the relative tibia to ground motion.

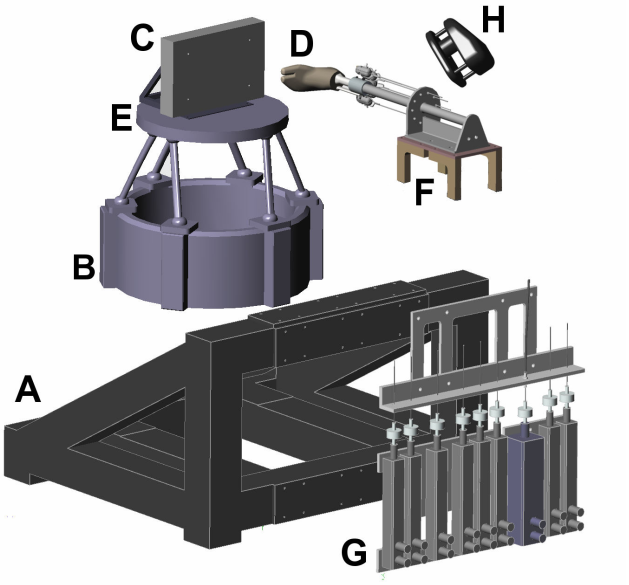

Figure 1: An exploded view of the Robotic Gait Simulator (RGS) with surrounding frame (A), the R2000 (B), mobile force plate (C), cadaveric foot (D), mobile platform (E), tibia mounting frame (F), tendon actuation system (G) and motion analysis system (H).

The force requirements for the nine extrinsic tendons were estimated from each muscle’s physiological cross sectional area (*PCSA* cm^2), the maximum specific isometric tension (*MST* N/cm^2), the EMG activity during gait (EMG % of maximum voluntary contraction) [1] and a gain (*G*) (eq. 1).

$$F_T = G \cdot PCSA \cdot MST \cdot EMG \qquad \text{eq. 1}$$

Three fresh frozen cadaveric right feet each performed three trials. The simulation from heel strike to toe off was scaled to 1/15th of physiological velocity. The vGRF and non-Achilles tendon forces were scaled to one half of the *in vivo* forces to minimize the chances of failing frail cadaveric specimens. During the simulation the vGRF and tendon forces were recorded at 1000Hz.

In order to achieve the desired vGRF two parameters were manually adjusted iteratively between gait simulations, namely, the trajectory of the mobile force plate along the superior-inferior tibial axis and the Achilles tendon gain, *G* (eq. 1). The superior-inferior offset was used to affect the first peak of the vGRF while adjustments to the Achilles tendon gain G were used to affect the second peak of the vGRF. Gait simulations were repeated iteratively while manually tuning these two parameters until the magnitude of the first and second peak of the simulated vGRF approximated the *in vivo* vGRF peaks. No attempt was made to control the temporal characteristics.

RESULTS AND DISCUSSION

The vGRF from the nine *in vitro* gait simulations reached peak magnitudes similar to the *in vivo* vGRF scaled to one half body weight (0.5BW) (Figure 2). The average % error across all trials between the *in vivo* and *in vitro* vGRF was 9.4% for the first peak and 3.1% for the second peak. The average RMS errors across all trials between the target and actual *in vitro* tendon force for the eight non-Achilles extrinsic tendons were between 2.8N and 8.5N RMS (Table 1). The Achilles tendon had the highest average RMS error at 20.3N, but its RMS error as a percent of peak force was the smallest at 2.3% (Table 1).

Inspection of the temporal characteristics of the *in vitro* vGRF and Achilles tendon force during late stance demonstrated some of the limitations of our *in vivo* muscle force estimate based on EMG. After heel rise the Achilles tendon force strongly dictates the vGRF. The early decrease in the *in vitro* vGRF indicates an underestimation of Achilles tendon force between 75% and 100% of the stance phase. This is confirmed by comparing our estimated Achilles tendon force derived from EMG measurements to those obtained *in vivo* using a fiber optic measurement technique [2] (Figure 2). Ishikawa *et al.*'s *in vivo* measurement of Achilles tendon force has a peak occurring at approximately 75% of stance phase compared to a peak at approximately 65% for the Achilles tendon force estimate derived from EMG (Figure 2). Our EMG-scaled model (eq. 1) used to estimate muscle force does not include muscle activation or deactivation first order dynamics, nor does it account for the parallel passive element present in a Hill-based muscle model. Including the electromechanical delay (EMD) into our model would delay the time at which peak Achilles tendon force occurs and the rate at which it decreases in late stance. Similarly, passive force developed in response to a lengthened muscle-tendon unit exists late in the stance phase [2]. Bogey *et al.*'s EMG to force estimation method which models the passive force production and EMD of soleus and gastrocnemius has temporal characteristics similar to the *in vivo* force data [3]. These findings have motivated us to use *in vivo* measurements of Achilles tendon force or more sophisticated EMG to force models to estimate the target tendon forces for future RGS simulations.

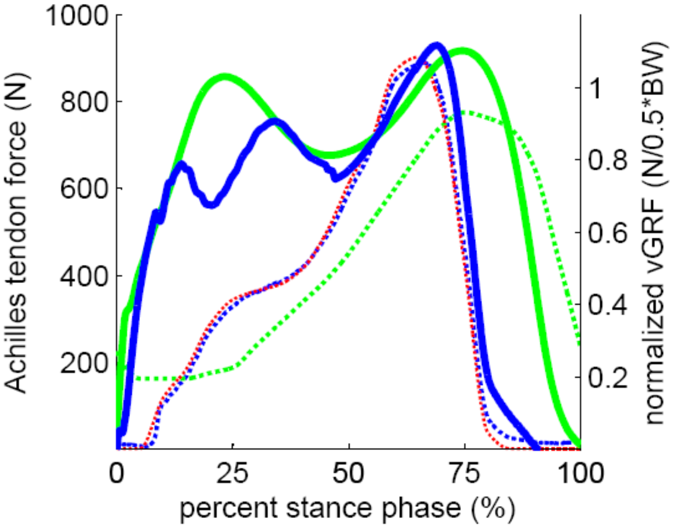

Figure 2: *In vitro* simulation results compared to *in vivo* gait data. The thick solid lines are mean *in vivo* (green) and *in vitro* (blue) vGRF (N/0.5BW). Mean Achilles tendon forces (N) are shown as the thin dotted lines with the EMG based estimate in red, *in vitro* simulation results in blue and Ishikawa *et al.*'s *in vivo* fiber optic measurement in green.

REFERENCES

1. Blackman, A.J. *et al.*, JOR, in revision.
2. Ishikawa, M. *et al.*, J Appl Physiol 99, 603-8 (2005).
3.Bogey, R.A *et al.*, IEEE Trans Neural Syst Rehabil Eng 13, 302-10 (2005).

ACKNOWLEDGEMENTS

This research was supported in part by the VA RR&D, grant A3923.

Table 1: Tendon force tracking RMS error expresses as newtons (N) and percent of peak force (%).

	Ach	EDL	EHL	PL	PB	FHL	FDL	TP	TA
N	20.3	4.8	4.7	5.6	5.0	7.8	2.8	8.5	6.8
%	2.3	16.4	35.7	11.7	27.9	15.1	13.4	11.4	10.9

PASSIVE RESISTANCE TO KNEE MOTION FOLLOWING TOTAL KNEE ARTHROPLASTY

[1] Jeannette M. Byrne, [2]Stephen D. Prentice
[1]School of Human Kinetics and Recreation, Memorial University of Newfoundland
[2]Department of Kinesiology, University of Waterloo
email: jmbyrne@mun.ca

INTRODUCTION

Numerous studies have found complaints of knee stiffness in individuals post knee replacement surgery [1]. When patients complain of joint stiffness, from a biomechanical perspective, what they may be experiencing is an increase in passive resistance to knee motion. This passive resistance to motion, or passive moment, has not been quantified in this population. The focus of the current research was, therefore, to quantify passive knee resistance in Total Knee Arthroplasty (TKA) patients. Results of this work will help determine if mechanical stiffness underlies patient complaints of knee stiffness. Additionally, as the passive moment contributes to the net moment at a joint, better understanding of the effects of TKA on passive knee resistance may add to current understanding of knee moment changes in this population.

METHODS

Six individuals, an average of 32 months post TKA (range: 19 – 72 months; age: 70.67 ±10.5 years), were examined in this study. Their results were compared to 6 age matched controls (age: 69.7 ±4.4 years) with no history of lower limb arthritis or serious lower extremity injury.

Passive knee moment data were collected using a protocol modified from that of Reiner and Edrich [2]. With subjects in a seated position the experimenter slowly moved the knee from a flexed position to full extension and back again. The force required to move the knee through range was recorded using a loadcell attached just above the ankle malleoli using a custom designed ankle brace. The loadcell was mounted such that it measured forces exerted perpendicular to the long axis of the shank. Three trials were collected in two different hip positions: 90º flexion (sitting) and 180º (supine lying).

Three-dimensional knee joint kinematics were recorded during this motion using an Optotrak (NDI, Waterloo, ON) active marker system. The kinematics of a 2-segment (shank and thigh) lower limb model were determined using marker data from rigid plates that were affixed to both the shank and thigh. Each plate held three infrared emitting diodes securely fastened at mid-segment level. Singular value decomposition was employed during processing to reduce error due to skin movement artifact. Electromyography (EMG) was used to monitor quadriceps and hamstrings muscle activity during the motion to ensure motion was truly passive in nature.

Force and kinematic data were combined as per Reiner and Endrich [2], to determine the passive moment at the knee during the motion. The moment calculated using the force data consisted primarily of moment due to gravity and passive moment (inertial effect could be ignored due to the slowness of the motion). The equation below was used to separate these components and determine the passive moment.

$$\mathrm{M}_{\mathrm{pas}} = Fl - mgl_{CoG}\cos(\theta)$$

Where g is acceleration due to gravity, and θ is the angle between the shank and the left horizontal. Resulting passive moment curves were spline fit so they could be averaged over similar joint angles. A fourth order polynomial was then fit to these moment-angle curves. This polynomial was then differentiated to determine the passive knee stiffness at each of the two hip angles tested.

RESULTS and DISCUSSION

Excessive EMG during the flexion portion of the passive motion meant only the extension phase was analysed. As patients and controls varied with respect to the range of knee motion covered, all data were truncated (15º-55º). Patients and controls exhibited similar trends in passive knee moment, with greater resistance to knee extension while in a seated position and greater resistance to knee flexion when supine. Generally, however, passive moment values for patients were biased toward the flexor moment portion of the curve. The average passive knee moment – angle relationship at the two hip angles examined is illustrated in Fig 1. Analysis of stiffness values showed no significant differences in stiffness between patients and controls over the knee range examined.

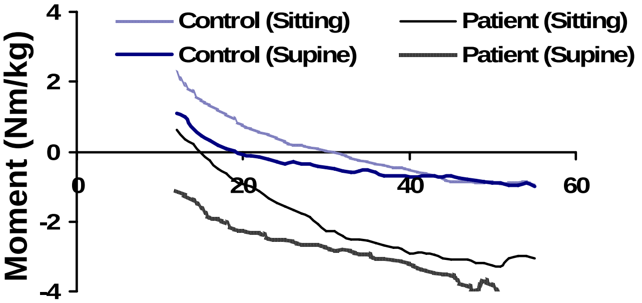

Figure 1: Passive moment for patients and controls. Horizontal axis represents examined knee range of motion (15º-55º of knee flexion). Average data based on data from all patient or control trials in the seated or supine position. (+ moment is flexion).

The current study represents the first attempt to quantify *in vivo* passive knee stiffness in this population. Results showed that the passive moment-angle relationship for both patients and controls followed expected patterns, suggesting no dramatic changes in the passive characteristics of replaced joints. For the small group tested, however, there does appear to be some difference in the magnitude of passive resistance following joint replacement.

One trend of interest was that, at both hip angles tested, patients exhibited greater passive knee moment than controls. The primary resistance to motion during knee motion was extensor in origin. Two possible sources of this extensor resistance exist: either it was produced by muscle activation or it came from passive tissues. Since EMG activity was monitored to ensure that minimal activation occurred, the latter reasoning is most likely true. There are several possible factors that may contribute to this increased midrange resistance. All patients in the study exhibited deficits in active knee flexion (107º ± 10º). While this degree of knee flexion enabled participants to perform the tasks examined, it was substantially less then typical maximum knee flexion (~140º). While patient characteristics (i.e. preoperative knee range and adherence to post-operative physiotherapy programs) can affect post-operative knee flexion, the factor which seems to have received the most attention is post-operative tibio-femoral kinematics [3,4]. Many investigations have determined that tibio-femoral kinematics differ post knee replacement. While the specifics of these differences vary depending on the type of prosthesis used, Victor and Bellemans [3] suggest that abnormalities in femoral rollback, femoral external rotation and posterior condylar offset can all result in decreased knee flexion post-TKA. It could be argued that alterations in tibio-femoral kinematics would invariably affect resistance to knee motion. It was hypothesized that this was the case in the current study, and that the increased resistance to motion observed in patients in the 15º to 55º range of knee flexion was due to alteration in tibio-femoral joint kinematics. Alternatively the increased passive resistance could also have been due to tension in passive tissues. This was unlikely, however, because in this range of knee motion, there would be minimal stress placed on passive tissues [5].

Due to the limited knee range of motion tested and small subject numbers, further research is needed to confirm the findings of this research. At this point, however, the current work provides a firm basis on which to build additional studies of this nature.

.REFERENCES

1. Moffet et al *Archives of Physical Medicine and Rehabilitation*, 85, 546-556. 2004
2. Reiner and Edrich. *J Biomech* 32, 539 – 544. 1999
3. Victor and Bellemans 2006 *Clin Orthop Relat Res*. 452:53-58. 2006
4. Dennis et al *The Journal of Arthroplasty*.13,748-752. 1998
5. McFaull and Lamontagne. *Human Movement Science.* 17: 139 – 165.1998

ACKNOWLEDGEMENTS

Funding to JM Byrne provided by a CIHR post-doctoral fellowship. SD Prentice funding from NSERC.

ACCURACY OF OPTICAL AND ELECTROMAGNETIC TRACKING SYSTEMS DURING DYNAMIC MOTION

Vipul Lugade, Carl Erickson, Masahiro Fujimoto, Chu Jui Chen, Jun San Juan, Andy Karduna, Li-Shan Chou
Department of Human Physiology. University of Oregon. Eugene, Oregon 97403. USA.
email: vlugade@uoregon.edu, web: http://biomechanics.uoregon.edu

INTRODUCTION

While biomechanics laboratories have to choose between electromagnetic (EM) and optical tracking systems when conducting research, relatively few studies have provided information comparing the accuracy of each system. Utilizing a mechanical articulator to mimick elbow motion, Hassan and colleagues found that both systems were appropriate for measuring upper extremity kinematics and deviations occurred mostly at smaller angles [1].

Several studies have investigated the accuracy of different camera based systems, and comparisons have been made between optical systems in the past [1,2], but few direct comparisons of an optical and a EM system to a gold standard under pre-defined dynamic motion has been conducted. The purpose of this study was to assess the accuracy of both an EM and optical system when compared to our gold standard during dynamic motions. The gold standard used in the study was a cleanroom robot programmed to manipulate a carbon fiber beam through pre-defined motions in two planes within the capture volume of both the EM and optical systems.

METHODS

A LR Mate 200iB cleanroom robot (FANUC Robotics America Inc., Rochester Hills, MI) manipulated a rigid carbon fiber beam attached to the most distal segment of the robot. The beam was moved through a range of -20 to 70 degrees of flexion-extension at each 15 degree increment in the transverse plane between -45 and 45 degrees. The robot was controlled through a known range of motion at three different speeds: 30 deg/sec, 45 deg/sec and 60 deg/sec.

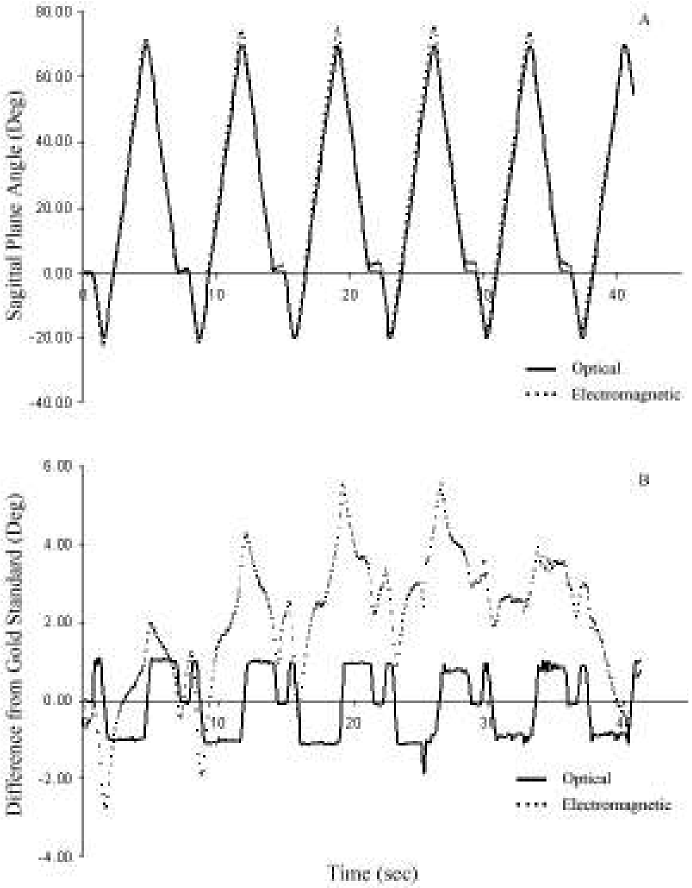

Figure 1: Sample trial at 30deg/sec for sagittal plane angles (A) and each systems difference from the gold standard (B).

Three non co-linear reflective markers were placed on the rigid beam, with an additional three markers placed on a rigid table, to be used as the reference for kinematics analysis. Each optical marker was precisely marked at four points to allow for digitization by the EM system. EM sensors were also placed at the center of the rigid beam and table. Marker trajectories were captured simultaneously by an EM (Liberty Electromagnetic Tracker, Polhemus Inc., Burlington, VT) and an optical system (8-camera Eagle System, Motion Analysis Corp., Santa Rosa, CA), both sampling at 120 Hz. Both tracking systems were triggered and synchronized with the robot using a laptop which was controlling the motion of the robot.

All data were filtered using a 4th order lowpass Butterworth filter with a 6Hz cutoff frequency. Angles in the sagittal and transverse planes were calculated using a Y-X-Z Euler sequence, with Y representing the superior-inferior axis, X the anterior-posterior axis and Z the medio-lateral axis. The accuracy of each system to the gold standard was assessed using the RMS error throughout the trial.

RESULTS AND DISCUSSION

Sagittal plane angles (Figure 1A) and transverse plane angles demonstrated that both systems tracked the motion of the robot. When compared to the robot, the optical system showed consistent differences across time, while the EM system demonstrated greater differences when approaching 0 degrees in the transverse plane (Figure 1B). The optical system demonstrated greater RMS error at higher speeds, while slight increases in error were demonstrated by the EM system. The EM system had approximately 2 degrees greater RMS error than the optical system at all speeds (Table 1).

In the transverse plane, the calculated RMS error of the EM system was approximately 3 degrees greater than the optical system at all speeds. Slight differences in the transverse plane RMS values were demonstrated by both the optical and EM system when the angular speed was increased from 30 deg/sec to 60 deg/sec.

The accuracy of the EM system was susceptible to metal interference and the distance from the sensors to the receiver, though metal objects such as force plates were removed from the immediate vicinity. The majority of the motion of the rigid beam was confined to the center of the capture volume of both the optical system and EM system, though movement to the end ranges of motion might have influenced the greater error for the EM system at those points. All collections were performed on a single day with calibration, marker placement and digitization procedures performed for the optical and EM systems by experienced investigators.

CONCLUSIONS

Results showed that an optical system had greater accuracy than an EM system during dynamic motion at varying speeds in two planes when compared to a gold standard. While both systems are capable of providing accurate kinematic data, researchers need to properly access the amount of interference and type of movement that is to be collected before choosing an appropriate motion capture system.

REFERENCES

1. Hassan EA, et al., *J Biomech* **40**, 930-935, 2007.
2. Richards JG., *Human Movement Sci* **18**, 589-602, 1999.

ACKNOWLEDGEMENTS

The authors would like to thank Robert Catena, Sue Ewers, Tal Amasay and Lucas Ettinger for their assistance in this study.

Table 1: RMS errors for the optical and EM systems when compared to the gold standard.

Joint Angle (Deg)	**30 deg/sec**		**45 deg/sec**		**60 deg/sec**	
	Optical	**EM**	**Optical**	**EM**	**Optical**	**EM**
Sagittal Plane	0.74	2.69	0.94	2.90	1.22	2.99
Transverse Plane	1.70	5.10	1.93	5.15	2.15	4.56

A NEW METHOD DESIGNED TO QUANTIFY SENSORIMOTOR INTEGRATION IN THE LOWER EXTREMITY

[1]Mark A. Lyle, [1,2]Francisco J. Valero-Cuevas and [2]Christopher M. Powers
Jacquelin Perry Musculoskeletal Biomechanics Research Laboratory
[1]Division of Biokinesiology & Physical Therapy, University of Southern California, Los Angeles, CA
[2]Brain-Body Dynamics Lab, Department of Biomedical Engineering, Viterbi School of Engineering
email: mlyle@usc.edu, web: http://pt.usc.edu/labs/mbrl

INTRODUCTION

Sensorimotor integration (SMI) can be defined as the process by which multi-modal sensory signals are transformed into, or affect, motor commands. SMI is essential for coordinated movement and is particularly relevant in sport [1]. For example, sport maneuvers often require sudden deceleration and change of direction that necessitate time-sensitive interactions between sensory and motor signals. Because lower extremity injuries are most commonly associated with self-initiated quick, transitional movements [2], it stands to reason that these injuries may be a result of inappropriate SMI. Currently, no test method is available to quantify lower extremity SMI. A test to quantify SMI for the thumb and fingers has recently been developed [3,4], which we have adapted for the lower extremity to test hypotheses that relate SMI to risk of injury. Here, we introduce the novel method and report on its repeatability and precision.

METHODS

The test device consists of a helical compression spring prone to buckling mounted on a stable base (i.e. fixed end) with a 20x30 cm platform affixed to the free end (Figure 1a). The compression spring parameters are as follows: free length=25.4 cm, mean diameter=3.08 cm, wire diameter=0.04 cm, total coils=28.7, material=hard drawn wire (#850, Century Spring Corp., Los Angeles, CA). The test device was placed on an in-ground force plate to record the vertical ground reaction force at 1500 Hz (AMTI, Waterton, MA).

Six healthy adults (4 males, 2 females; mean age: 29 years) performed the test where leg function was isolated from trunk motion. Subjects held an upright partially seated posture on a bicycle saddle, were supported at the trunk by leaning forward against a seatbelt at the level of the xiphoid process, and rested the non-dominant foot on a step with light pressure allowed for balance (Figure 1b). The test limb was positioned with the foot on the device platform in a standardized posture (i.e. 60° of hip and knee flexion). A computer monitor directly in front of the participant provided real-time visual force feedback of the vertical compression force (Figure 1b).

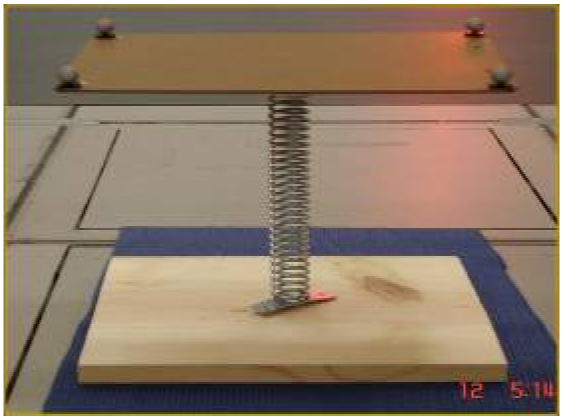

a)

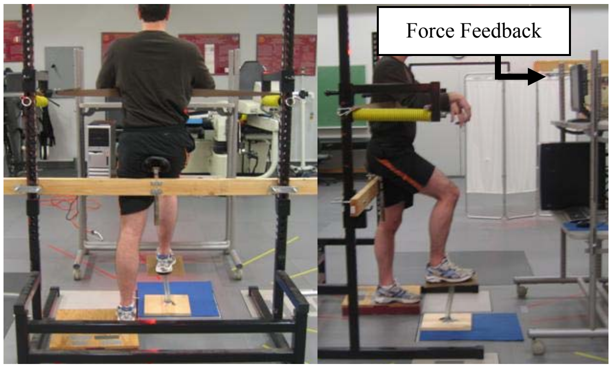

b)

Figure 1: Test method a) device and b) position.

The instability of the helical spring (i.e. tendency to buckle) increases with compression force [3,4], thus the highest sustained compression force achieved during the task is representative of the maximal neuromuscular ability to stabilize the leg in contact with the unstable ground. The stiffness and slenderness of the spring were chosen such that buckling required low forces.

Participants were instructed to compress the spring with their foot with the goal of making the force feedback line as high as possible (i.e. maximize vertical compression force) and sustain the highest force during each 15 s trial without letting the foot slip on the platform. Individuals completed 20 trials on each of two consecutive days. The dependent variable of interest was the maximal mean compressive force during the sustained hold as determined by a 10-second moving average. The compression force was considered to be sustained if the coefficient of variation was ≤10%. The moving average and maximum trial value was determined using a custom MATLAB (The Mathworks, Natick, MA) program. Intraclass correlation coefficient (ICC) and standard error of the measurement (SEM) were used to determine the repeatability and precision of the vertical compression force in each subject. The mean of participants' best three trials were used from each day.

RESULTS AND DISCUSSION

Across subjects, the average sustained vertical compression force ranged from 112-114 N. Although strength was not assessed in this study, these maximal compression forces (only ~17% of body weight) show that strength was not a primary determinant for task performance. This is in agreement with findings from the original method where task performance was not correlated with thumb strength [3].

The mean vertical compression force was similar across days for individual subjects (Figure 2) and demonstrated strong test-retest reliability ($ICC_{(2,3)}=0.94$, $p=0.001$) and high precision (SEM=2.06 N). The stability of the measure combined with the low SEM suggests that this test may be capable of detecting differences in sensorimotor function among groups of subjects (e.g., males vs. females) or changes in response to training.

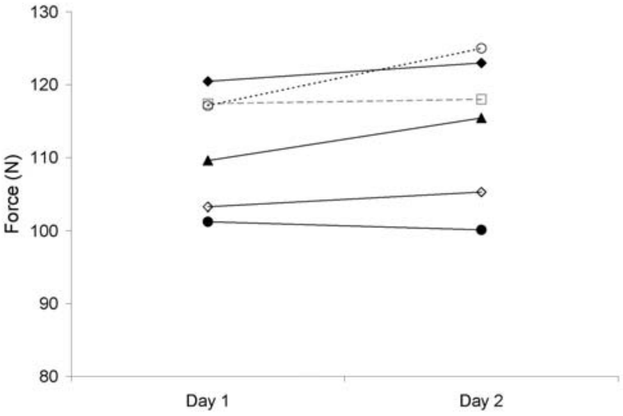

Figure 2: Vertical compression force for individual subjects was similar on Day 1 and Day 2.

CONCLUSIONS

Despite the challenging task of compressing an unstable spring, performance was consistent across days. Future studies can now focus on establishing test validity under conditions thought to influence sensorimotor integration (e.g., pathology, training and rehabilitation) in the context of theories relating SMI and lower extremity injury. An advantage of the test method described here is that strength does not appear to be a variable relevant to performance. In addition, the test method is designed to test only the limb of interest. These inherent advantages are in contrast to commonly used whole body movements (i.e. cutting and landing) that are often used to infer movement control strategies.

REFERENCES

1.Nielsen JB. *J Appl Physiol.* **96**, 1961-1967, 2004.
2.Olsen OE, et al. *Am J Sports Med.* **32**, 1002-1012, 2004.
3. Valero-Cuevas FJ, et al. *J Biomech*. **36**, 265-270, 2003.
4. Venkadasen M, et al. *J Biomech*. **40**, 1653-1661, 2007.

ACKNOWLEDGEMENTS

This study was supported by the Foundation for Physical Therapy (PODS I) Scholarship.

EFFECT OF BALANCE RECOVERY TASK DIFFICULTY ON STEPPING VELOCITIES FOR FORWARD, SIDEWAYS AND BACKWARD LOSS OF BALANCE DIRECTIONS

Alessandro Telonio and Cécile Smeesters
Research Center on Aging, Sherbrooke QC, Canada
Human Performance and Safety Research Group (PERSEUS), Sherbrooke QC, Canada
Department of Mechanical Engineering, Université de Sherbrooke, Sherbrooke QC, Canada
e-mail: Cecile.Smeesters@USherbrooke.ca web: http://www.usherbrooke.ca/gmecanique

INTRODUCTION

Several studies have shown that both age and loss of balance direction affect balance recovery following small and medium postural perturbations [1]. However, it is only recently that this has also been shown for large postural perturbations at the threshold of balance recovery where avoiding a fall is not always possible.

We demonstrated that the maximum lean angles from which participants could be suddenly released and still recover balance using a single step were 32% greater for younger (YA) than older (OA) adults [2]. Maximum lean angles were also 23% and 31% greater for forward leans than for sideways and backward leans, respectively. Finally, the age related reduction in maximum lean angles was 41% smaller for backward leans compared to the other lean directions.

More importantly, we demonstrated that knee extension power (r^2=63-72%) was the best clinical predictor of the maximum lean angles in all three directions [3]. Similarly, the best experimental predictors of the maximum lean angles in all three directions were mean (r^2=62-84%) and maximum (r^2=63-84%) step velocities at the maximum lean angles [4]. However, these strong associations do not show a true cause and effect relationship.

If declines in lower extremity muscle power and stepping velocities are responsible for this decreased ability to recover balance with age and lean direction, stepping velocities should increase as the balance recovery task becomes more difficult. The purpose of this study was thus to determine the effect of the incremental initial lean angles on the mean and maximum step velocities for forward, sideways and backward loss of balance directions.

METHODS

Data from 16 YA (22.9±3.1yrs) and 16 OA (68.1±5.8yrs), who participated in experiments to determine the maximum forward, sideways and backward lean angles from which participants could be suddenly released and still recover balance using a single step, were used [2].

Using 3 force platforms (OR6-7, AMTI, Newton MA), 2 load cells (FD-2 and MC3A, AMTI, Newton MA) and 3 optoelectronic position sensors (Optotrak, NDI, Waterloo ON), we obtained initial lean angles, mean step velocities (step length divided by step time) and maximum step velocities (maximum first derivative of foot position).

Unconditional growth linear regression models [5], which take into account both intra and inter individual variances, were used to determine the effect of initial lean angle on mean and maximum step velocities for each lean direction.

RESULTS AND DISCUSSION

As expected, both mean and maximum step velocities increased with the incremental initial lean angles in all three lean directions (Figure 1):

- For mean step velocity, the linear regression analyses resulted in model R^2 explaining 72-92% of the variability.
- For maximum step velocity, the linear regression analyses resulted in model R^2 explaining 68-92% of the variability.
- Linear regression analyses grouping all lean directions together resulted in model R^2 explaining 75% and 74% of the variability for mean and maximum step velocities, respectively.

CONCLUSIONS

Therefore, in healthy adults, stepping velocities did increase as the balance recovery task became more difficult for forward, sideways and backward loss of balance directions. The association between declines in lower extremity muscle power, declines in stepping velocities and the decreased ability to recover balance with age and loss of balance direction is thus very strong.

However, to truly confirm a cause and effect relationship, one would have to determine if an intervention aimed at improving lower extremity muscle power could improve stepping velocities and thus improve forward, sideways and backward maximum lean angles. Alternatively, one could determine if a lack of intervention would result in a natural decline in lower extremity muscle power, an associated decline in stepping velocities and thus a decline in forward, sideways and backward maximum lean angles.

REFERENCES

1. Maki BE, et al. *J Biomech* **29**(3), 343-353, 1996.
2. Telonio A and Smeesters C. 31st Annu Meet Am Soc Biomech, Stanford CA, Aug 22-25 2007.
3. Telonio A, et al. 4th N Am Congr Biomech, Ann Arbor MI, Aug 5-9 2008.
4. Telonio A and Smeesters C. 4th N Am Congr Biomech, Ann Arbor MI, Aug 5-9 2008.
5. Singer JD and Willett JB. *Applied longitudinal data analysis: modeling change and event occurrence*, Oxford University Press, New York NY, 2003.

ACKNOWLEDGEMENTS

We gratefully acknowledge the assistance of Mathieu Hamel, Geneviève Plante-Pellerin and Lise Trottier along with the support of the Junior I Research Fellow Grant of an FRSQ Centre 6391 and 5393 from the Research Centre on Aging.

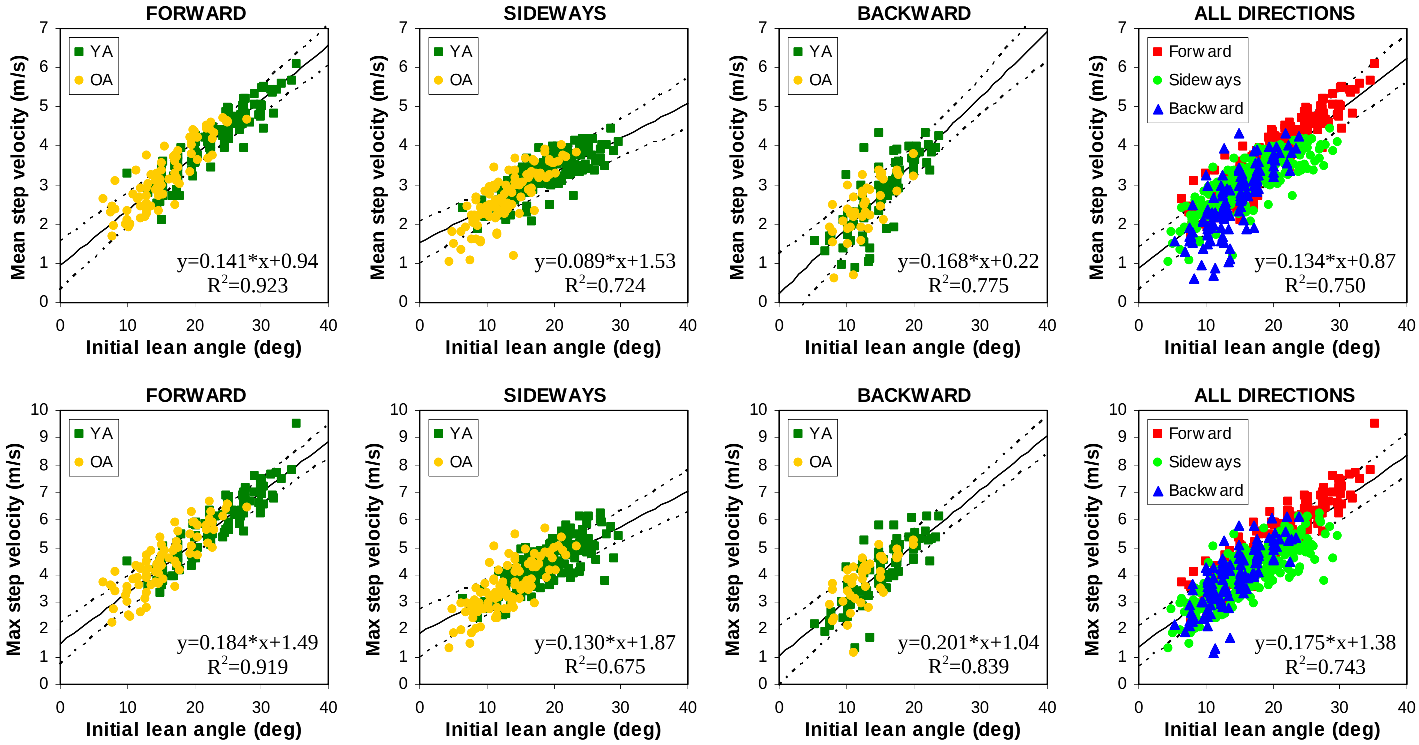

Figure 1: Effect of the forward, sideways and backward incremental initial lean angles on the mean and maximum step velocities for younger (YA) and older (OA) adults. Mean ± standard deviation regression lines are shown for each lean direction and for all lean directions together.

USE OF DESIGN OF EXPERIMENT APPROACH TO PREDICT FORCE - DISPLACEMENT RELATIONSHIP FOR THE SUBJECT-SPECIFIC MODEL OF LATERAL MENISCUS

[1]Mohammad Kia, [1]Trent M. Guess, [2]Meenashki Mishra , and [2]Ganesh Thiagarajan
[1]Musculoskeletal Biomechanics Research Lab,[2]Computational Mechanics Lab
University of Missouri – Kansas City

INTRODUCTION

The menisci play an important biomechanical role in the human knee. They protect the knee joint articular cartilage, provide joint lubrication, and increase stability of the knee joint [1]. They also act as shock absorbers by spreading contact forces over the articular surface. However, menisci representations are often ignored in multibody computational knee models. In the multibody framework, the menisci can be represented as discrete bodies connected by springs and dampers, but determining the properties of these connecting springs is not straightforward. The aim of this study was to develop a systematic method to determine mechanical properties for a multibody model of a lateral meniscus. A design of experiment approach was used to estimate the mechanical properties by matching the force-displacement relationship of the multibody model of lateral meniscus to a transverse isotropic finite element (FE) model of the same geometry.

METHODS

The lateral meniscus geometry of a subject-specific model was obtained from Magnetic Resonance Image (MRI) of a cadaver knee (78 year old female, right knee). 3D Slicer (www.Slicer.org) was used to convert the MR images into a three-dimensional geometry. A macro was written in MSC/ADAMS software (MSC Software Corporation, Santa Ana, CA), to automatically divide the menisci geometries into 32 discrete rigid elements (Figure 1). Individual geometries interacted with neighboring geometries through field elements. The field element can apply a translational and rotational action-reaction force between two parts by adding a 6x6 matrix of stiffness coefficients representing the meniscus properties. In this study, the stiffness matrix parameters were implemented as design factors, which include nine variables [2]. To determine the values of the stiffness matrix parameters, a FE model and multi-body model of the lateral meniscus were compared under the same loading conditions. In this step, the lateral meniscus was fixed at two ends and a load of 100 N was applied in the lateral direction. Maximum lateral displacement was defined as an objective function.

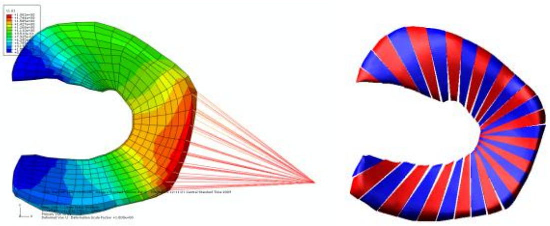

Figure 1: Comparing finite element and multi-body model of the lateral menisci

The FE model of the meniscus used a hexahedral mesh generated in TRUEGRID and then imported into ABAQUS (Abaqus Inc., Providence, RI) for analysis. The meniscus was defined as a transverse isotropic and linear elastic material with the following properties: E_1=150 MPa, E_2=20 MPa, E_3=20 MPa, ν_1=0.2, ν_2=0.2, ν_3=0.3, G_1=G_2=G_3=57.7 MPa, where suffix 1 denotes circumferential direction, 2 radial and 3 axial directions respectively [3]. Nodes, where force is to be applied, were tied to a single point (N) using beam elements. The properties given to beam elements were E=415 MPa and ν=0.33. Point N was constrained to move only in the lateral direction and a force of 100N was applied to it in the lateral direction. The maximum displacement produced at point N was 1.896 mm.

Two-level fractional factorial design, including nine base factors was constructed as a screening algorithm. A total number of 32 simulation runs were made to determine which factors were statistically effective on meniscus displacement. Finally, based on significant factors, a higher order plan (quadratic model) was designed to find the best possible value for each factor.

RESULTS AND DISCUSSION

All statistical analysis was done using ADAMS/Insight. After the screening process, results indicate that only the stiffness in the circumferential direction K_θ, stiffness in the radial direction K_r, and torsional stiffness about z axis T_r are statistically significant in the response (Figure 2). In order to measure the appropriate objective function, a new simulation plan with all significant factors at three variation levels was designed (3^2, three-level full factorial design). As a result, a non-linear model best fit the new simulation plan (Table 1). It also showed that the effect of all three important factors plus all of the interaction terms and quadratic terms should be considered in this model. During the optimization process, ADAMS/Insight automatically changes the factor values so that the resulting response comes as closely as possible to the specified target value, in this case 1.896 mm (Table 2). After parameter optimization and updating the stiffness matrix with new values, the difference between the multibody and FE model on the meniscus displacement was 0.005 mm.

CONCLUSIONS

In this study, a FE model and multibody model of a lateral meniscus were developed under the same dynamic loading conditions. Design of Experiment methods were used to match the final displacement of the meniscus to the FE prediction. It has been shown that we could predict behavior of the FE model fairly well by only adjusting three factors: circumferential stiffness, radial stiffness, and torsion. Limitations of the current study includes constraining the displacement to a single degree of freedom and using an objective function that only counts the displacement at the end of simulation. In the future more loading scenarios such as compression will be considered.

Table 1: Goodness of fit for the prediction model

Model	**SS**	**df**	**MS**	**F**	**P**
Regression	61.6	9	6.84	68.65	0.00
Residual	0.056	17	0.0033		
Total	61.6	26			
R^2	0.99				
R^2_{adj}	0.99				

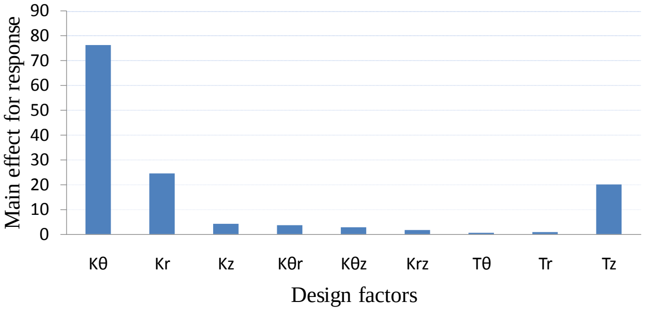

Figure 2: Main effect of each design factor for the meniscus lateral displacement

REFERENCES

1. H.H Lindner, *Clinical Anatomy a LANGE medical book* **49**, pp. 615-616.
2. Kia M, Guess TM. *Summer Bioengineering Conference*, Marco Island, Florida, 2008.
3. Donahue TL, et al. *Journal of Biomechanical Engineering* **124**,273-280, 2002.

ACKNOWLEDGEMENTS

This research was funded by the National Science Foundation, Grant Number 506297, under the IMAG program for Multi-scale Modeling.

Table 2: Objective function response to the design factors for the nominal and optimized cases

	Kθ N/mm	**Kr N/mm**	**Tz N-mm/deg**	**Displacement (mm)**
Nominal	250	250	25	3.234
Prediction	500	494	31.25	1.896
Multi-body	500	494	31.25	1.901
FE	-	-	-	1.896

PREDICTING AN IMMINENT FALL USING 3D TRUNK ACCELERATION

[1]Julie B. Cain, [1]Jeremy R. Crenshaw, [2]Kenton R. Kaufman, and [1]Mark D. Grabiner
[1]Department of Kinesiology and Nutrition, [1]University of Illinois at Chicago, Chicago IL, [2]Department of Orthopedic Surgery, [2]Mayo Clinic, Rochester, MN
email: jcain2@uic.edu, web: www.uic.edu/ahs/biomechanics

INTRODUCTION

Falls are the leading cause of trauma related deaths and injuries in adults 65 years and older [1]. Fall prevention interventions have reduced fall-related morbidity and mortality in the United States only incrementally over the past 20 years [2,3]. This may reflect that the extent to which falls by older adults can be reduced is limited. An alternative to fall prevention is to limit the injury potential of an imminent fall, that is, predict a fall before it happens. A prerequisite to this approach is the ability to sensitively and rapidly use instantaneous system states to categorize conditions as “imminent fall” or “no imminent fall”.

Previous work has revealed the significance of trunk kinematics in discriminating falls from recoveries by older adults following a laboratory-induced trip [4] and large postural disturbances delivered by a motorized treadmill [5]. The present study was conducted to determine the extent to which trunk kinematics could discriminate falls from recoveries following delivery of large postural disturbances that required compensatory stepping responses to avoid falling, and to determine how long after the onset of the disturbance such discrimination could be made. We hypothesized that the trunk acceleration signatures of compensatory stepping responses that led to falls and recoveries would differ significantly from one another and that a combination of discrete time-related values from each signature would sensitively and rapidly discriminate the outcomes.

METHODS

Fifteen healthy young adults (8 males age 22.9±2.9 years, 7 females age 21.9±2.8 years) volunteered to participate and provided written informed consent. Whole body kinematics were measured using an 8-camera motion capture system operating at 60Hz.

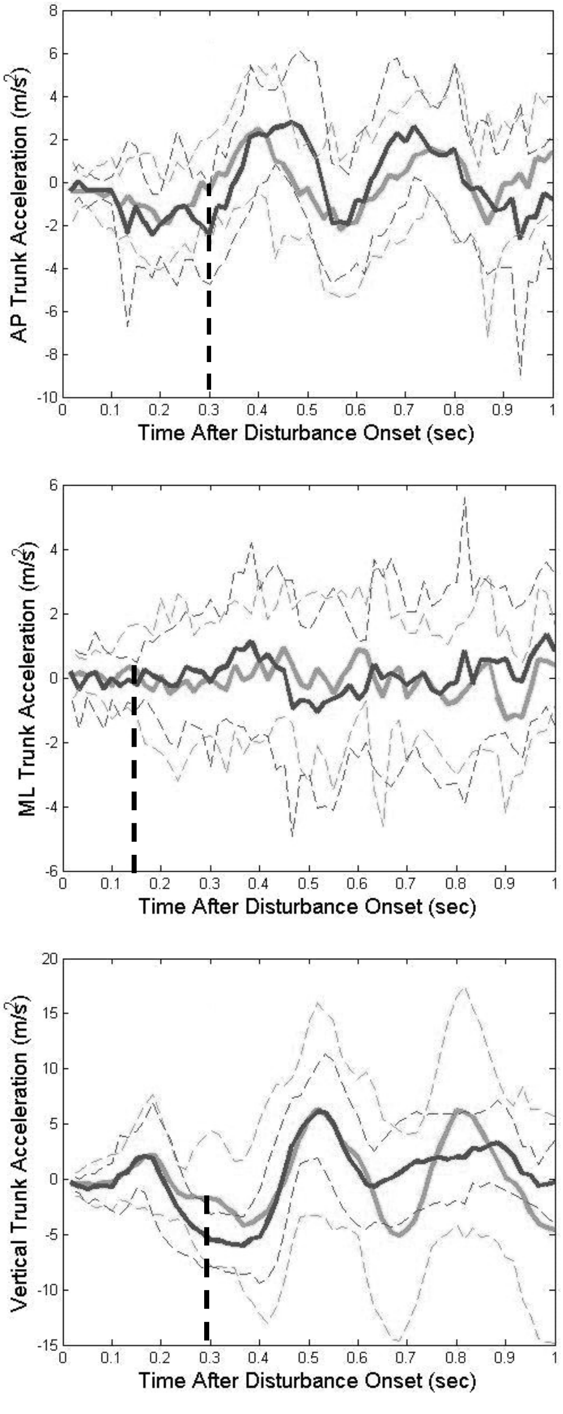

Figure 1: Anteroposterior (X), mediolateral (Y), and vertical (Z) accelerations of the trunk COM for 1000 ms after the disturbance onset. Black lines represent falls and gray lines represent recoveries. Standard deviations are presented by the dotted lines. Vertical dashed lines represent the time points selected by the discriminant analysis.

Postural disturbances were delivered to subjects, who were supported by a safety harness, by a custom motorized platform (Active Step™, Simbex, Lebanon, NH). Following an acclimatization period, a standardized postural disturbance was delivered that accelerated from 0.0 to 6.5m/s^2 in 0.5s. All subjects were unable to restore dynamic stability. Subjects were then progressed through a series of postural disturbances, the magnitude of which first increased and then decreased (3.0 - 6.25m/s^2). Subsequently, the standardized postural disturbance was again delivered. All subjects were able to restore dynamic stability.

Anteroposterior (X), mediolateral (Y), and vertical (Z) linear acceleration time series of the trunk center of mass (COM) were computed. From these time series, the acceleration values at 50, 100, 150, 200, 250, 300 and 350 ms following the onset of the postural disturbance were extracted. These data were analyzed using stepwise discriminant analysis.

RESULTS AND DISCUSSION

Three variables, measured in the anteroposterior (X), mediolateral (Y), and vertical (Z) directions at 300, 150 and 300 ms following the onset of the disturbance, respectively, were included in the final discriminant function (Wilks'Lamda = 0.57, p = 0.002, Table 1). Pearson correlations between the variables revealed their independence (all -0.13 < r < -0.27, all p ≥0.15)

Table 1: Means±standard deviations of acceleration values included in the final discriminant function

Category	$A_{X@300}$	$A_{Y@150}$	$A_{Z@300}$
fall	-2.4±2.32	-0.24±0.71	-5.5±2.4
recovery	-0.4±2.5	0.24±1.44	-1.7±6.1

The sensitivity and specificity of the discriminant function was 80% and 87% respectively. Using a cross-validation technique, the function correctly classified 80% of subjects.

CONCLUSIONS

Although promising, these results are preliminary, having been collected on young healthy adults, to whom large postural disturbances were delivered only in the sagital plane, causing an anteriorly-directed motion of the body (simulating a trip) and from an initial quasi-static condition. Further work, using disturbances that simulate a slip and disturbances delivered in the frontal plane, are necessary to further confirm the utility of this method to detect imminent multi-directional falls. In addition, additional work using older adults will be necessary. Nevertheless, the results suggest that it may be possible to sensitively detect multi-directional and imminent falls using biomechanical data and, further, that the time required to do so may be fast enough to serve as a trigger to deploy injury prevention strategies.

REFERENCES

1. Stevens et al. *Journal of Safety Research*, **36:**409–411, 2005.
2. National Center for Health Statistics. *Healthy People 2000 Final Review*, Hyattsville, Maryland, Public Health Service, 2001.
3. Centers for Disease Control and Prevention and The Merck Company Foundation. *The State of Aging and Health in America 2007*, Whitehouse Station, NJ: The Merck Company Foundation, 2007.
4. Pavol et al. *J Gerontology*, 56A:M428-M437, 2001.
5. Owings et al. *Clin Biomechanics*, 16:813-819, 2001.

THE STUDY OF MENISCI EFFECT ON TIBIO-FEMORAL KINEMATICS IN A COMPUTATIONAL KNEE JOINT

Mohammad Kia, Trent M. Guess, and Gavin C. Paiva
Musculoskeletal Biomechanics Research Lab, University of Missouri – Kansas City

INTRODUCTION

The menisci are important knee structures that are often ignored in computational models of the knee. Previous work on this project has shown that representation of the menisci significantly reduces the contact forces and pressures on the articulating surfaces of the tibia and femur [1]. The purpose of this study was to examine the significance of the menisci on tibio-femoral kinematics. Improvements were made to a previously developed multi-body model of the meniscus by dividing meniscus geometries into smaller pieces in the circumferential direction. The effects of the menisci on knee kinematics were then examined by inserting the menisci models into a validated dynamic 3-D computational model of a knee loaded in a dynamic knee simulator (Kansas Knee Simulator, University of Kansas, Lawrence, KS). The predicted tibia-femur kinematics of the knee model with (w) menisci and without (wo) menisci were compared to experimental data during simulated squat and walking profiles.

METHODS

In the present study, knee geometries (tibia, femur, patella, articular cartilage, medial and lateral meniscus, and ligaments) of the subject specific model were derived from Magnetic Resonance Images (MRI) of a cadaver knee (78 year old female, right knee). 3D Slicer (www.Slicer.org) was used to convert the MR images into three-dimensional geometries. The knee geometries as well as ligament insertion/origin points were aligned in MSC.ADAMS (MSC Software Corporation, Santa Ana, CA) using acquired experimental data.

Six one-dimensional spring elements were used to simulate the knee ligaments including the anterior cruciate ligament (anterior and posterior bundles), posterior cruciate ligament (anterior and posterior bundles), lateral collateral ligament, and medial collateral ligament. Because the menisci remained intact during the experimental tests, previous studies suggested that representation of the menisci model might improve our prediction of tibio-femoral kinematics [2].

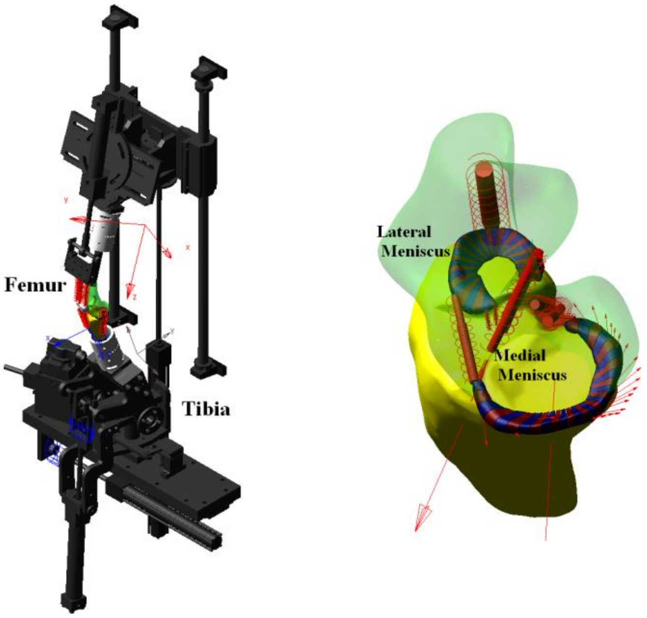

Figure 1: Knee model with menisci in ADAMS/View

Previously, a macro was written to automatically divide the menisci geometries into 4x4 mm discrete rigid elements. Since meniscus fibers are oriented circumferentially, several studies treated the menisci as a linearly elastic and transversely isotropic material [3]. In view of that, we modified the macro to divide menisci geometries in the circumferential direction (Figure 1). This new version of the macro also assigns mass properties, links the geometries, and automatically defines deformable contacts between the menisci, femur, and tibia. Hertzian contact theory was used to determine the parameters of the compliant contact force model based on cartilage material properties and contact geometry [1]. The menisci geometries interact through field elements which are represented by a 6x6 matrix of stiffness coefficients.

Matrix elements were estimated from matching the force-displacement relationship of an individual multi-body model of lateral meniscus to an isotropic FE model of the same geometry of meniscus in ABAQUS (Abaqus Inc., Providence, RI).

The lateral and medial menisci were attached to the tibia plateau with eight linear springs, representing horn attachments of the menisci. The insertions for the horn attachment were located on the anterior and posterior of each meniscus and on the tibia plateau. The transverse ligament was also modeled as a one-dimensional spring element. The resulting stiffness of all ligaments were similar to our previous study [1].

Simulation inputs to the computational model included the measured forces and torques produced by the actuators of the knee simulator. During testing, the femur and tibia position and orientation were measured using an Optotrak 3020 system with respect to the camera coordinate. To facilitate data comparison, all experimental data was transformed to the femur coordinate. Finally, in order to study the effects of the menisci, the root mean square error (RMSE) of predicted tibio-femur kinematics with and without menisci were compared to experimental data of the loaded cadaver knee during a walk and squat cycle.

RESULTS AND DISCUSSION

RMS errors of predicted position and orientation for simulation with and without the menisci are shown in Table 1. The position and orientation of the tibia were represented in the femoral coordinate system as Cartesian XYZ and Euler 123 coordinates. The maximum knee (hip) flexion angle in the squat test was 110 (55) degrees. During the squat a simulated body load was applied at the hip, but no out-of-sagittal -plane forces were applied at the ankle. The walking profile replicates knee loading and motion of ISO specification 14243-1. Results indicate that during the simulated squat exercise, the menisci improve the kinematics error for some orientations, but not all. The result of the walking profile shows that adding the menisci to the knee model generally decreases RMS errors. This may be explained by the fact that the menisci play a more significant role during the walk which has significant non-sagittal plane activity than the simulated sagittal plane profile like the squat.

CONCLUSIONS

In this study, a macro was developed that automated the process of creating a multi-body meniscus model from its MRI derived geometry. In addition, tibio-femoral kinematics were determined from tracking the positions and orientations of the tibia relative to the femur during a simulated walk and squat exercise. The limitation of this study includes the use of Hertzian contact theory to determine the parameters of the deformable contact model. It is believed that the extra lateral shift (x) on tibia kinematics of model with menisci was because of the simplification to define the contact force. Our current results suggest examining the effect of menisci on the tibio-femoral kinematics while each cruciate ligament is transected. In the future we will be considering more complex dynamic activities, such as squatting profiles with transected ACL/PCL. Also a design of experiment approach will be used to improve our calculation of parameters for the deformable contact force model.

REFERENCES

1. Kia M, Guess TM. *Summer Bioengineering Conference,* Marco Island, Florida, 2008.
2. Weimer KA, et al. 6th *Combined meeting of the Orthopaedic Research Societies,* Honolulu, Hawaii, Abstract 95, 2007.
3. Donahue TL, et al. *Journal of Biomechanical Engineering* **124**,273-280, 2002.

ACKNOWLEDGEMENTS

This research was funded by the National Science Foundation, Grant Number 506297, under the IMAG program for Multi-scale Modeling.

Table 1: RMS errors between model and experimental kinematics for model with (w) and without (wo).

RMSE	**Orientation(deg) and position (mm)**					
	Body 1	**Body 2**	**Body 3**	**X**	**Y**	**Z**
Squat (wo menisci)	1.47	2.31	9.95	17.19	6.41	6.10
Squat (w menisci)	1.49	3.70	10.90	23.01	6.05	6.40
Walk (wo menisci)	1.33	2.71	6.22	11.98	6.21	2.82
Walk (w menisci)	1.13	2.49	6.72	12.99	4.89	2.73

CLAVICLE KINEMATICS FOLLOWING CHANGE IN LENGTH OF THE STERNOCLAVICULAR LIGAMENTS

[1]Kimberly A. Szucs, [1,2]John D. Borstad
[1]School of Allied Medical Professions; [2]Physical Therapy Division: The Ohio State University,
Columbus, OH email: kim.szucs@osumc.edu

INTRODUCTION

Shoulder motion is achieved through synchronous movement of the humerus, scapula, and clavicle. Clavicle rotations relative to the thorax occur at the sternoclavicular joint and include elevation/ depression, protraction/retraction, and long-axis rotation (Figure 1). Scapula rotations are a combination of sternoclavicular (SC) and acromioclavicular (AC) joint rotations. Limited motion at either the SC or AC joint may alter scapula motion. Altered scapula rotations have been demonstrated in persons with subacromial impingement syndrome, though the mechanism for these changes is not known [1]. As normal shoulder motion is dependent upon coordinated movement of the humerus, scapul and clavicle, it is important to understand clavicle rotations in relationship to the other segments in normal and pathologic conditions.

The SC joint has three ligaments that stabilize the joint: the anterior and posterior sternoclavicular ligaments, and the costoclavicular ligament. The anterior and posterior sternoclavicular ligaments limit translation of the sternal end of the clavicle in the transverse plane [2]. It has been suggested that the costoclavicular ligament limits axial rotation, though this relationship has not been previously demonstrated [3]. If the length of the SC ligaments is altered, clavicle rotations may be altered, which may affect motion of the shoulder complex.

The purpose of this study was to determine if changes in the length of the anterior sternoclavicular and costoclavicular ligaments resulted in altered 3-dimensional motion of the clavicle. The posterior sternoclavicular ligament was not included due to inability to access this ligament in the cadaver without disrupting other joint structures. We hypothesized that shortening these two ligaments would result in decreased clavicle rotations and cutting the ligaments would increase clavicle rotations.

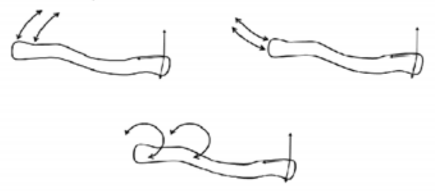

Figure 1: Clavicle Rotations: elevation, retraction, posterior rotation

METHODS

Data were collected from 10 cadaver shoulders. The shoulders were randomly assigned to test either the anterior sternoclavicular ligament (n= 4) or the costoclavicular ligament (n= 6). The cadavers were male, with a mean age of 78.5 years.

3-dimensional kinematic data of the thorax, humerus, and clavicle were captured with the Flock of Birds electromagnetic system. An 8 mm sensor was taped to the skin overlying the specimen's sternum. Sensors for the clavicle and humerus were secured in non-ferrous housing and inserted into the bone with a screw. The clavicle sensor was inserted at the midpoint of the bone, and the humeral sensor near the insertion of the deltoid muscle (Figure 2). Specimens were tested in an upright position, with the shoulder free to move. Clavicle rotations relative to thorax were described with a Z, Y', X" sequence, with retraction around the superiorly directed thoracic Z, elevation around an anteriorly directed Y', and posterior rotation around a laterally directed X".

3-dimensional kinematic data were recorded as the specimen's arm was passively elevated five times in the coronal plane (normal condition). Then the SC joint was dissected to access the joint ligaments. For shoulders assigned to the anterior SC ligament group, the ligament was first cut, and kinematic data collected (cut condition). The ligament was then sutured in a shortened position to collect data in the short condition. The costoclavicular ligament was shortened by clamping a hemostat across the width of the ligament (short condition). The ligament was then cut and data collected in the cut condition. The order of the conditions was constrained by the available resting lengths of the ligaments.

For each ligament, mean clavicle rotations in each ligament condition (normal, short, cut) were compared at every 15° of arm elevation. A repeated measures ANOVA was run with arm elevation angle and ligament condition as within subjects factors. Elevation and lowering phases of arm motion were compared separately.

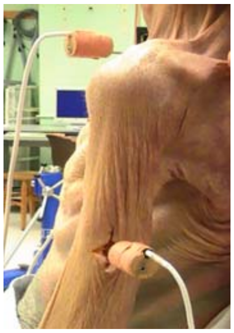

Figure 2: Insertion of the bone screws and sensors.

RESULTS and DISCUSSION

For the costoclavicular ligament, there were no main effects of ligament condition for any dependent variable in the elevation or lowering phases. There were also no interaction effects between arm angle and ligament condition for the dependent variables during either phase.

For the anterior SC ligament, there was a statistically significant main effect of ligament condition for clavicle retraction in the elevation phase ($p=.033$). Mean clavicle retraction was greater in the cut condition than in the short condition (Figure 3). In the lowering phase, the main effect of ligament condition for clavicle retraction neared statistical significance ($p=.0051$), with the cut condition demonstrating an increase in retraction compared to normal and short conditions. There were no interaction effects between arm angle and ligament condition of the anterior SC ligament for any dependent variable in either phase.

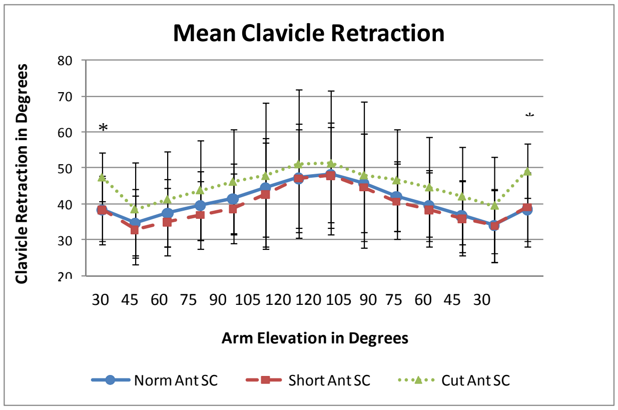

Figure 3: ***=** Cut > Normal, Short condition

Altering the length of the anterior sternoclavicular ligament resulted in changes in clavicle rotation. It was anticipated that a shortened anterior SC ligament would decrease clavicle retraction, however this relationship was not demonstrated. During clavicle retraction at the SC joint, the concave sternal end of the clavicle rolls and slides posteriorly on the convex surface of the manubrium. This causes the anterior sternoclavicular ligament to become taut. By cutting this ligament, the clavicle was able to move more on the manubrium, resulting in an increase in clavicle retraction.

Altering the length of the costoclavicular ligament did not produce changes in any of the three clavicle rotations. This suggests that the costoclavicular ligament has a limited role in influencing the motion of the clavicle. It is possible that clamping the ligament did not provide a sufficient length change to alter motion of the clavicle.

An increase in clavicle retraction, as observed in the cut condition of the anterior SC ligament, may alter the kinematics of the shoulder complex as a whole. In response to increased clavicle retraction, scapula motion may be altered. Understanding this relationship between clavicle and scapula rotations may provide improved insight into the pathology of shoulder disorders.

REFERENCES

1.Ludewig PM, et al. *Phys Ther* **80**, 276-291, 2000.
2.Spencer EE, et al. *J Shoulder and Elbow Surg* **11**, 43-47, 2002.
3.Rajaratnam S, et al. *Clin Anat* **15**, 108-111, 2002.

KINEMATIC RESPONSES TO GALVANIC STIMULATION OF THE HUMAN VESTIBULAR SYSTEM DURING LOCOMOTION

Daniel P. Steed, Jennica L. Roche and Mark S. Redfern
Department of Bioengineering, University of Pittsburgh, Pittsburgh, PA, USA
email: DPSteed@gmail.com, web: http://hmbl.bioe.pitt.edu

INTRODUCTION

Balance is controlled through the integration of vestibular, visual, and proprioceptive senses. The primary aim of this project is to understand the impact of vestibular signals in the maintenance of balance during walking. Galvanic vestibular stimulation (GVS) was used to evoke internal perturbations of the human balance system.

GVS causes perceived head accelerations depending upon the polar orientation of the electrodes. This perception results in postural responses to counteract the perceived acceleration. Typically, GVS is used to cause postural deviations during stance [1,2]. GVS has also been employed to perturb the balance system during gait. Vision has been shown to dominate over the other types of sensory information that dictate the control of movement [3]. Thus, the responses to GVS are present, yet diminished during gait with normal vision [4]. Without vision, subjects involuntarily deviate laterally away from their planned trajectory towards the anodal side [4].

METHODS

Nine healthy young adults (2F, 7M; mean age 25 ± 3.7 years) were screened to be free of neurological and vestibular disorders. Subjects wore tight fitting clothing and standardized rubber-soled shoes as well as a safety harness to protect from ground contact injuries. Before the start of the testing session, subjects were informed that they may or may not experience GVS during any trial.

The skin over the subjects' mastoid processes was abraded (NuPrep^{TM} gel), cleansed using an alcohol swab, and coated (TENS Clean-Cote® whipe) to decrease skin resistance as well as aid in the adherence of the electrodes. Self-adhering Superior Silver® stimulating electrodes (3.17cm diameter) were fixed over each mastoid process (binaural-bipolar configuration). The galvanic current duration was eleven seconds in total (linear stimulus isolator, model A395R-A, World Precision Instruments, Inc.). Subjects were exposed to two separate five second mock-square waves of alternating polarity (1mA), separated by one second of rest within each GVS trial (Figure 1). Trials with anode towards the subjects' right first (such as displayed in Figure 1) are denoted R^+. Trials with anode towards the subjects' left first are denoted R^-. For any trial where the GVS was applied, only data from the first five seconds of the ±1mA current were analyzed.

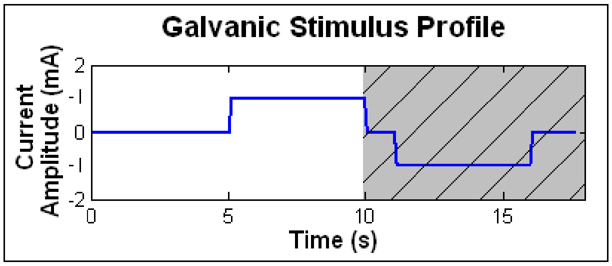

Figure 1: Schematic representation of the galvanic stimulus. The shaded gray area was not analyzed.

Motion capture data (Vicon 612 / M2 camera system) was recorded (120Hz) to collect full-body kinematic responses to GVS. Membrane footswitches were adhered to the sole of the shoes for precise temporal determination of heel contact of both the right and left foot.

A total of twenty-one gait trials (7 conditions, repeatability of 3) were collected using seven types of trials composed of: three GVS conditions (none/R^+/R^-), two eye conditions (open [EO]/closed [EC]), and two GVS trigger conditions (heel contact [HC]/mid-stance [MS]). The trigger condition is relative to the HC of the right foot.

RESULTS AND DISCUSSION

An overall cyclical pattern exists in the ML translation of the sternum and mid-pelvis during gait irrespective of the presence of vision or GVS. Greater maximum ML deviations from control trajectories (EO, no GVS) were observed for the head ($p<0.0001$), thorax ($p<0.0001$), and pelvis ($p<0.0001$) during trials with EC and/or GVS (Figure 2).

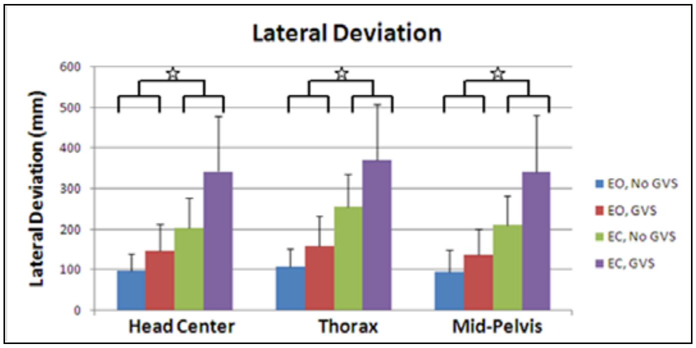

Figure 2: The effect of vision and GVS on lateral deviation (standard deviation displayed) of the head, sternum, and pelvis. The absolute value of the maximum lateral deviation was used to combine GVS R^+ and R^- conditions. Statistical significance denoted with a star.

Furthermore, when examining conditions with EC only, the head ($p<0.02$), sternum ($p<0.01$), and pelvis ($p<0.02$) experienced greater maximum lateral deviations when first exposed to a condition as compared to the second or third exposure to the same condition (Figure 3).

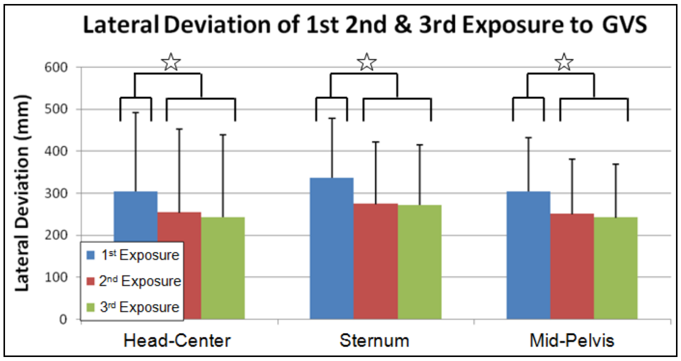

Figure 3: Lateral deviation (standard deviation displayed) due to GVS with EC for the 1st (blue), 2nd (red), and 3rd (green) exposure to GVS collapsed across trigger time and direction. The absolute value of the maximum lateral deviation was used to combine GVS R^+ and R^- conditions. Statistical significance denoted with a star.

The position of the mid-pelvis was obtained at each of the six HCs following the GVS trigger (where GVS activation was at the HC or MS of step 1). GVS significantly altered the position of the mid-pelvis at steps 3 ($p<0.02$) and 4 ($p<0.02$) with EO and at steps 3 ($p<0.01$), 4 ($p<0.01$), 5 ($p<0.01$), and 6 ($p<0.01$) with EC.

Consistent with literature, all subjects deviated towards the anodal side during stimulation. The onset of the response to GVS was observed approximately one stride after GVS trigger with EC. Hlavacka et al. showed that the first whole-body biomechanical signs of a galvanic current during stance are observed approximately one second after the trigger [5]. Our subjects walked at a self-selected pace of approximately 1.2 seconds per stride. Thus, the responses to GVS during stance and gait are temporally consistent, suggesting that the delay seen in GVS responses are due to some neural processing for postural control as opposed to a delay due to the phases of gait.

Current literature states that no “learning” or adaptation exists in response to GVS; no signs of “turning back” towards the original gait target had been observed [4]. Learning was indeed present in this current study. Greater maximum ML deviations were experienced during the first exposure to a specific GVS trial condition. Slip severity, a measure of biomechanical responses to external perturbations, has been shown to lessen after first exposure [6]. It is possible that similar mechanisms adapt to lessen the effect of unexpected internal perturbations, such as GVS, as well as the effects of unexpected external perturbations, such as a slip.

CONCLUSIONS

The aim of this project was to examine the biomechanical responses to GVS during locomotion. Lateral deviations increased during gait without vision. Furthermore, GVS increased the lateral deviation of whole-body movement towards the anodal side during gait with GVS; this effect was exaggerated with EC. Future works will continue to examine the learning effects of GVS, the effects of segmental tilting during gait, and the overall role of the vestibular system during gait.

REFERENCES

1. Fitzpatrick et al. *J Appl Physiol* **96**, 2301-2316, 2004.
2. Day et al. *J Physiol* **500.3**, 479-399, 2007.
3. Kennedy et al. *Exp Brain Res* **153**, 113-117, 2003.
4. Bent et al. *Neurosci Lett* **279**, 157-160, 2000.
5. Hlavacka et al. *Brain Res Bull* **40**, 431-435, 1996.
6. Chambers et al. *Gait Posture* **25**, 565-572, 2007.

ACKNOWLEDGEMENTS

Subjects were screened at the Eye & Ear Institute, University of Pittsburgh Medical Center. Partial funding was provided by Robert Bosch LLC.

PARTITIONING GAIT DATA INTO TEMPORAL AND INTENSITY DIFFERENCES

[1]Nathaniel E. Helwig, [1]Sungjin Hong, [2]Elizabeth T. Hsiao-Wecksler
[1]Department of Psychology, University of Illinois at Urbana-Champaign
[2]Department of Mechanical Science and Engineering, University of Illinois at Urbana-Champaign
email: nhelwig2@illinois.edu, web: mechse.illinois.edu/research/hsiao-wecksler/

INTRODUCTION

Despite the well-known need for the time-normalization of gait data trajectories differing in length, little is discussed about partitioning and quantifying temporal (timing) from intensity (amplitude) differences within gait cycle data. We present a method for quantifying both temporal and intensity deviations from normative behaviors within gait data trajectories. Applying this method to joint angle trajectories, we show that diagnostic recognition of individuals can be meaningfully improved when both temporal and intensity deviation patterns are utilized concurrently.

METHODS

For our analysis, we focused on joint angle trajectories collected from the right and left legs of 10 young (21 ± 2 years) male subjects. (Note: this technique applies to other 1D gait data trajectories as well). Subjects ambulated on a treadmill under two conditions: 1) non-braced (normal) walking, and 2) knee-braced walking such that right knee motion was completely restricted by a brace (DonJoy, Vista, CA). Kinematic data were collected using a six camera motion analysis system at 120 Hz (Vicon, Oxford, UK; Model 460).

Data were segmented into gait cycles from heel strike to heel strike. The time axis of each cycle was linearly transformed from the experimentally-recorded time units to a time axis representing percentage of the gait cycle, such that each cycle contained 100 points (Figure 1). Consensus angle trajectories were created for both the ankle and knee by averaging non-braced data over cycles, legs, and subjects.

Using piecewise dynamic time warping (PDTW; a modification of DTW[1] that we have devised), we temporally aligned the four joint angle trajectories

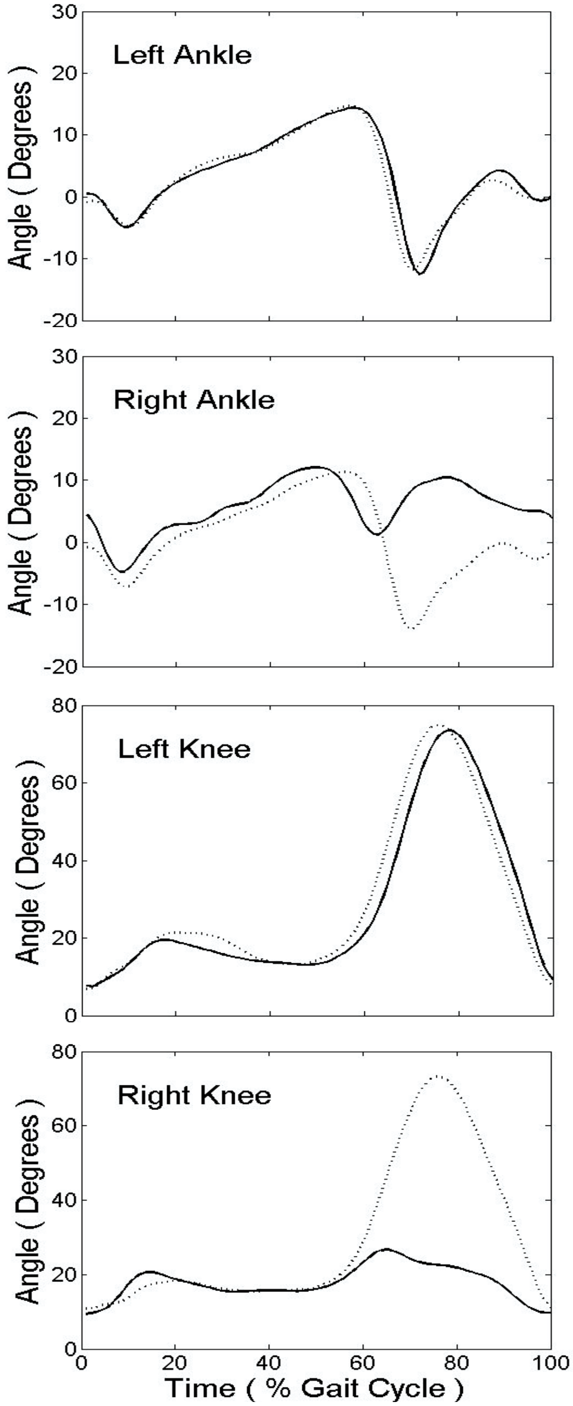

Figure 1: Sample joint angle trajectories during normal walking (dotted) and walking with a knee brace on the right knee (solid).

(leg [left, right] × joint [ankle, knee]) from each gait cycle (non-braced or knee-braced) with the given joint's consensus trajectory. Temporal deviation from normality was defined as the average time shift needed to align each data point of the given trajectory with the consensus trajectory. Intensity deviation from normality was defined as the Euclidean distance between the given trajectory and the consensus (after alignment by PDTW).

After removing arbitrary scale differences between the temporal and intensity deviations, the values were combined to form an 8-element (leg [left, right] × joint [ankle, knee] × parameter [temporal, intensity]) deviation pattern vector for the cycle.

Deviation pattern centroids were determined for each subject-condition combination (e.g., subject 01 with knee brace) by averaging deviation pattern vectors over gait cycle replications. Each cycle was then classified as the subject-condition combination whose deviation pattern centroid was closest (based on minimum Euclidean distance) to the cycle's deviation pattern vector. Classification success was evaluated using only intensity deviation patterns (which aligns with current practice), as well as using intensity plus temporal information with different weightings on either component.

RESULTS AND DISCUSSION

The rate of correct classification was calculated for each condition (Table 1). A cycle was considered successfully classified if the appropriate subject-condition combination was correctly identified.

For the non-braced condition, 73.3% of the cycles were correctly classified even before PDTW was applied (i.e., using only intensity deviation patterns). After alignment by PDTW, the classification rate dropped slightly when only intensity deviations were considered (71.4%). However, the rate of correct classification rose to 81.4% when both temporal and intensity data were used optimally (weighted such that the intensity deviations were three times more influential than the temporal deviations).

In the knee-braced condition, temporal and intensity differences were confounded before temporal alignment, such that none of the cycles were correctly classified. After alignment by PDTW, the classification rate improved to 68.6% using only intensity deviations. The rate improved even further to 87.1% when intensity and temporal deviations were considered (this time weighted such that intensity deviations were twice as influential).

CONCLUSIONS

The proposed method partitions gait data in terms of both temporal and intensity deviations from normative behavior. These deviation patterns can be used to classify movement data from different individuals and experimental conditions.

This ability to separately quantify temporal and intensity deviations from normal gait behavior could meaningfully improve diagnostic recognition and be relevant to injury recovery research. Gait data trajectories from injured individuals likely contain both temporal and intensity differences from healthy movement patterns. By separately quantifying the temporal and intensity deviations from healthy behavior, it may be possible to relate certain deviation patterns to specific stages of the rehabilitation process.

REFERENCES

1. Sakoe H & Chiba S. *IEEE Trans. on Acoustics, Speech, and Signal Processing*, **26**, 43–49, 1978.

ACKNOWLEDGEMENTS

This work was funded by the NSF (#0540834).

Table 1: Percentage of gait cycles for which the subject-condition was correctly classified a) using length-normalized curves before PDTW, and b) using curves aligned by PDTW.

a)	**Only Intensity**	**Equal Weighting**	**Optimal Weighting**
No Brace	73.3%	N/A	N/A
Knee Brace	0.0%	N/A	N/A

b)	**Only Intensity**	**Equal Weighting**	**Optimal Weighting**
No Brace	71.4%	64.8%	81.4%
Knee Brace	68.6%	80.0%	87.1%

TIME-NORMALIZATION TECHNIQUES FOR GAIT DATA

[1]Nathaniel E. Helwig, [1]Sungjin Hong, [2]Elizabeth T. Hsiao-Wecksler
[1]Department of Psychology, University of Illinois at Urbana-Champaign,
[2]Department of Mechanical Science and Engineering, University of Illinois at Urbana-Champaign
email: nhelwig2@illinois.edu, web: mechse.illinois.edu/research/hsiao-wecksler/

INTRODUCTION

Given natural variation in walking behavior, segmenting data into gait cycles almost always results in gait cycle data of differing lengths. To compare data (e.g., ankle angle trajectories) within or between individuals, it is necessary to use some time-normalization technique so that a point-by-point comparison of intensity information between the data trajectories is possible.

A method commonly used to “time-normalize” gait data (here referred to as linear length normalization [LLN]) is to linearly convert the trajectory’s time axis from the experimentally-recorded time units to an axis representing percentage of the gait cycle. However, other time-normalization techniques are also possible, such as dynamic time warping [DTW][1] and derivative dynamic time warping [DDTW][2]. DTW shifts the time index of each data point in a test trajectory to minimize the distance between the test and consensus trajectories. DDTW is a modification of DTW that minimizes the difference in the first derivatives of the trajectories.

In this paper, we compare the performance of LLN, DTW, and DDTW for aligning gait data trajectories and present the benefits of two new methods (piecewise linear temporal alignment [PLTA] and piecewise dynamic time warping [PDTW]). PLTA segments trajectories at points of interest (i.e., prominent maxima and minima) and applies LLN to align corresponding segments in the test and consensus trajectories. PDTW is a modification of DTW where trajectories are segmented at points of interest and classical DTW is used to align corresponding intensity-normalized segments.

METHODS

For our analysis, we focused on joint angle trajectories collected from the right and left legs of 10 young (21 ± 2 years) male subjects. (Note: these techniques can be used to temporally align other 1D gait data trajectories as well). Subjects ambulated on a treadmill under two conditions: 1) non-braced (normal) walking, and 2) knee-braced walking such that right knee motion was completely restricted by a brace (DonJoy, Vista, CA). Kinematic data were

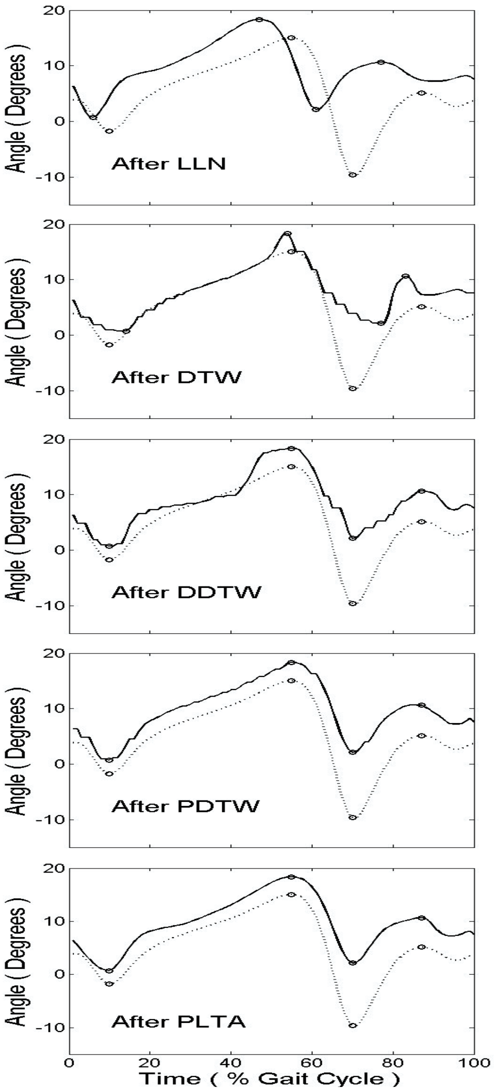

Figure 1: Ankle angle trajectory for consensus non-braced data (dotted) and a right ankle angle during knee-braced condition after the given time-normalization technique is applied (solid).

collected using a six camera motion analysis system at 120 Hz (Vicon, Oxford, UK; Model 460).

Consensus angle trajectories were created for both the ankle and knee by averaging LLN-adjusted non-braced data over cycles, legs, and subjects. Each trajectory (non-braced or knee-braced) was then aligned with the appropriate non-braced consensus by all of the time-normalization methods (Figure 1). To evaluate the effectiveness of the temporal alignment techniques, we calculated the difference in the first derivatives (i.e., rate-of-change) between the test and consensus trajectories after alignment.

RESULTS AND DISCUSSION

As expected, when aligning the non-braced data, temporal and shape pattern differences from the consensus were minimal after LLN was applied. Compared to LLN, DTW and DDTW increased the average shape dissimilarity (i.e., squared difference in the first derivatives) between the test trajectories and the consensus (Figure 2). In contrast, both PDTW and PLTA reduced the shape dissimilarity (compared to LLN) for the ankle data, and PLTA reduced the dissimilarity for the knee data.

Results from the braced condition illustrate the systematic temporal and shape pattern differences caused by the knee brace (Figure 2). For the right ankle, all time-normalization techniques were able to remove (compared to LLN) some of the systematic temporal differences caused by the brace (with PDTW and PLTA performing best). For the right knee, DDTW increased (compared to LLN) the shape dissimilarity between the aligned trajectories and the consensus, whereas the other techniques reduced the dissimilarity (with PDTW and PLTA providing the best alignment).

CONCLUSIONS

Our results demonstrate that different methods used to temporally align gait data can produce rather different alignment results (Figure 1).

LLN makes gait data trajectories length-comparable but does nothing to address localized temporal differences within the trajectories. DTW is able to address localized temporal differences but is inappropriate when natural intensity differences exist in localized segments of the data trajectories (which is true of most gait data).

In contrast, DDTW, PDTW, and PLTA are able to effectively align points of interest in gait data trajectories, regardless of intensity differences. We have found that PLTA and PDTW produce smoother, more natural looking curves than DDTW. Thus, we recommend the use of PLTA or PDTW to temporally align (and to quantify temporal differences within) gait data trajectories.

REFERENCES

1. Sakoe H & Chiba S. *IEEE Trans. on Acoustics, Speech, and Signal Processing*, **26**, 43–49, 1978.
2. Keogh EJ & Pazzani MJ. *First SIAM International Conference on Data Mining*, Chicago, United States, Abstract 1, 2001.

ACKNOWLEDGEMENTS

This work was funded by the NSF (#0540834).

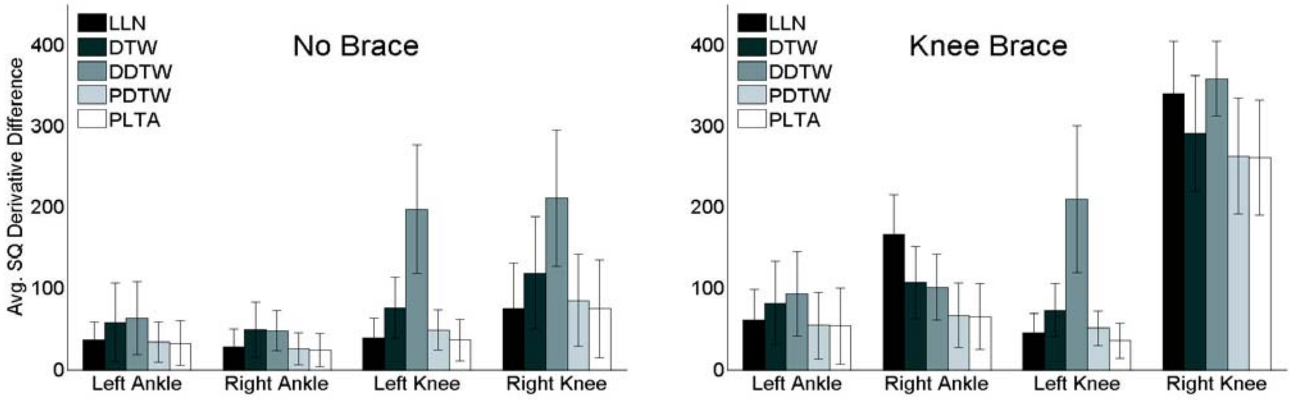

Figure 2: Average squared difference in the first derivatives of the consensus angle trajectory and the aligned trajectory after each time-normalization method.

VALIDATION OF A SINGLE CAMERA 3D MOTION TRACKING SYSTEM

[1]Kristian M. O’Connor, [2]Brian S. R. Armstrong, [1]Joshua Weinhandl,
[2]Todd P. Kusik, and [2]Robb T. Barrows

[1] Department of Human Movement Sciences
[2] Department of Electrical Engineering
University of Wisconsin-Milwaukee, Milwaukee, WI, USA
E-mail: krisocon@uwm.edu Web: www.chs.uwm.edu/neuromechanics

INTRODUCTION

Three-dimensional kinematics of the lower limb during dynamic activities have been shown to be predictive of ACL injury [1]. Motion tracking outside of a laboratory environment is a critical next step in applying ACL research findings to the general population. The Retro-Grate Reflector (RGR) is a new technology that allows for 3-D motion capture using a single camera [2]. An RGR target is constructed by applying artwork on the front and back of a transparent substrate, such as a glass or plastic plate (Figure 1).

Figure 1: RGR target. Moiré patterns change as orientation of target changes.

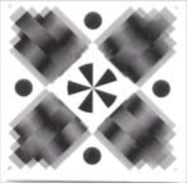

The three-layer structure of substrate and artwork produces moiré patterns, which are seen as light and dark fringes. The moiré patterns respond to changes in orientation. Small rotations produce moiré-pattern displacements that are visible to the eye. With the out-of-plane rotations revealed by the moiré patterns, the RGR system is able to determine 6-DOF pose from a single camera image. Armstrong et al. [2] reported ±0.0082 deg RMS error over a 54° measurement range. O’Connor et al. [3] compared the orientation and position information recorded by the RGR system with data recorded with a traditional multi-camera system. The six degree-of-freedom pose data correlated greater than 0.99 between systems. That study used a series of static poses, and the technology has since been refined to record moving pose information from multiple RGR targets at a sampling rate adequate for assessment of human movement. Therefore, the purpose of this study was to compare motion data for standard athletic movements recorded simultaneously with the RGR and multi-camera (Motion Analysis Eagle) systems.

METHODS

Nine subjects performed three single-leg land-and-cut maneuvers from a 35 cm high box. Thigh and shank three-dimensional kinematics were collected with the RGR and Eagle camera systems simultaneously at 100 Hz. Plates with four reflective spheres were attached to the thigh and shank, and an RGR target was mounted to the center of the plate (Figure 2).

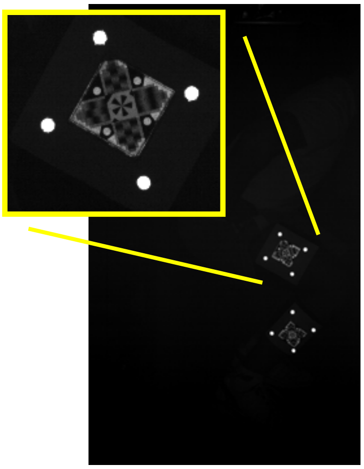

Figure 2: Camera image at maximum knee flexion. Inset provides greater detail of target and marker mounting.

Prior to data collection, the coordinate systems of the two measurement systems were co-registered using a sequence of 30 static poses of a four marker plate with an RGR target rigidly attached. The

RMS errors between RGR-target and Eagle-based pose information were calculated from the static poses. The RMS error for pitch, roll, and yaw were 0.57°, 0.68°, and 0.79°, respectively. The spatial RMS errors were 4.2, 6.0, and 3.9 mm. During the cutting task, thigh and shank pose information was recorded simultaneously by a Motion Analysis 7-camera Eagle system (Santa Rosa, CA) and a Basler A501k (Ahrensburg, Germany) 1.3 MPixel camera. After attaching the plates, a standing trial was recorded and all kinematic information were reported relative to the standing orientation. All raw kinematic data were filtered at 12 Hz. The six-degree-of-freedom pose of the thigh and shank were calculated for the Eagle-based measurements using a standard cross product approach. Segment poses were also calculated based on the information intrinsic to the RGR target. Knee angles in the three planes were calculated using a joint coordinate system approach [4]. Touchdown and peak angles were compared using a dependent t-test (p<.05).

RESULTS AND CONCLUSIONS

The time series of the knee angles in the sagittal, frontal, and transverse planes matched closely (Figure 3). There were no differences in the kinematic variables between the Eagle and RGR measurements in any plane (Table 1). In addition, most dependent variables correlated strongly between the two systems. The only discrepancies appeared in the frontal plane, where there was trend suggesting a difference in peak angles and a moderate correlation in touchdown angles. The way in which the segment local coordinate systems were defined was based on the assumption that subjects were perfectly aligned with the room coordinate system. It is likely that this was a false assumption, which would lead to cross talk between planes. Any small differences in Eagle and RGR measurements may have been magnified by this effect. In summary, these results strongly support the ability to use the RGR technology as a valid 3-D motion capture system.

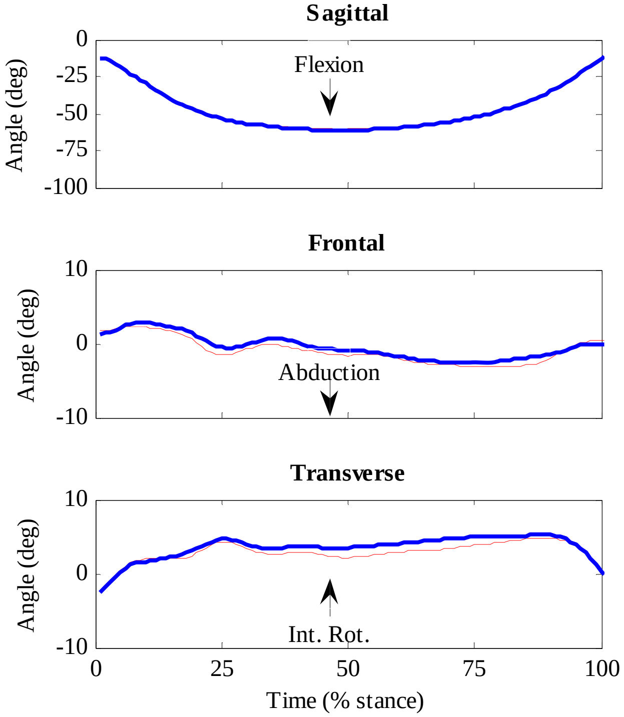

Figure 3: Joint angles in all three planes. The thick blue line represents the RGR measurements and the thin red line represents the Eagle measurements.

REFERENCES

1.Hewett, TE et al. *Am J Sports Med*, **33**, 492-501, 2005.
2.Armstrong, BSR. In *Proc. 2002 Int. Conf. on Robotics and Automation*. IEEE, 2002.
3.O'Connor et al.*Proceedings of the American Society of Biomechanics*, Stanford, CA, 2007.
4.Grood & Suntay. *J Biomech Eng*, **105**, 136-144, 1983.

ACKNOWLEDGEMENTS

The authors would like to thank the UWM Research Growth Initiative and the NIH (1R15AR056117-01) for their financial support of this project.

Table 1. Comparison of knee joint kinematics collected with the Eagle and RGR systems.

	Sagittal		**Frontal**		**Transverse**	
	TD	Peak	TD	Peak	TD	Peak
Eagle	-13.9 (7.6)	-68.4 (13.6)	1.9 (2.1)	-6.8 (6.8)	-2.6 (4.9)	7.7 (4.7)
RGR	-14.0 (7.6)	-68.9 (13.8)	1.4 (2.8)	-5.6 (7.7)	-2.7 (5.9)	8.6 (5.8)
Difference	0.1	0.5	0.5	-1.2	0.1	-0.9
p-value	0.411	0.096	0.238	0.053	0.440	0.102
r	0.97	0.99	0.57	0.97	0.94	0.95

PROPHYLACTIC ANKLE STABILIZERS AFFECT ANKLE BUT NOT KNEE OR HIP JOINT ENERGETICS DURING DROP LANDINGS

Jacob Gardner, Lindsay Barlow, Steve McCaw
School of Kinesiology and Recreation, Illinois State University, Normal, IL
email: jkgardn@ilstu.edu

INTRODUCTION

Lateral ankle sprains are one of the most common athletic injuries in sports involving jumping and landing. Many athletic coaches and trainers require their athletes to wear ankle support to reduce the risk of excessive inversion. However, the use of ankle stabilizers has been shown to restrict sagittal plane measures of dosiflexion [3] with potential interference to the ankle's contribution of energy absorption. Recent changes in stabilizer design and materials are intended to provide support to the lateral ankle joint without restricting sagittal plane motion.

This study compared the effects of 4 ankle stabilizers on ankle, knee, and hip joint kinetics and energetics during soft and stiff landings. We hypothesized that wearing ankle stabilizers would alter the relative contribution of individual lower extremity joints to energy absorption.

METHODS

Sixteen female college students (age: 20.6 ± 1.0 y; ht: 1.66 ± 0.07m; mass: 66.5 ± 10.8kg) volunteered as participants. All were free of chronic or acute lower extremity injury for 6 months and were experienced in landing (volleyball or basketball).

Five soft and five stiff landings were performed in five bilateral ankle stabilizer conditions (no stabilizer, standard taping, lace-up boot, hinged boot, and stirrup style (total = 50 trials per subject). Stabilizers and style conditions were randomized across participants. Participants performed two-legged landings off a 0.32m platform. The right foot landed fully on a force platform. Ankle, knee and hip joint moments of force and energetics were calculated using standard inverse dynamic techniques combining an optotrak system (200 Hz), force platform (1000Hz) and anthropometrics. Both kinematic and GRF data were smoothed at 20 Hz [2]. Energy absorbed at a joint was calculated as the integral of the joint power time curve from initial contact until joint angular velocity = 0.

Each participant's five-trial mean value of the negative work at the ankle, knee and hip joints and the total work (∑hip+knee+ankle) for each landing style/stabilizer condition was entered into a two-way repeated measures ANOVA ($\alpha=0.05$).

RESULTS AND DISCUSSION

Total work by the limb was, on average, ~ 2x greater in the soft landing conditions than in the stiff landing conditions (Table 1). Except for the hinged brace condition, total work was significantly decreased with ankle stabilization, but not to the extent of the change in landing style.

The amount of negative work at the ankle was greater in stiff than in soft landings. Work at the ankle was significantly reduced in all stabilizer conditions except for the hinged brace compared to the non-stabilized condition (Figure 1 & Table 1).

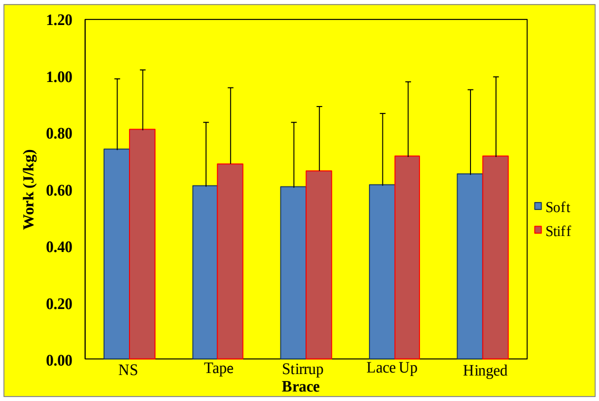

Figure 1: Negative work at the ankle joint.

There was a significant brace by style interaction at the knee for negative work. Knee work in the tape support was significantly less than the no support condition, but only during soft landings. There was a main effect of style but not stabilizer at the hip (Table 2).

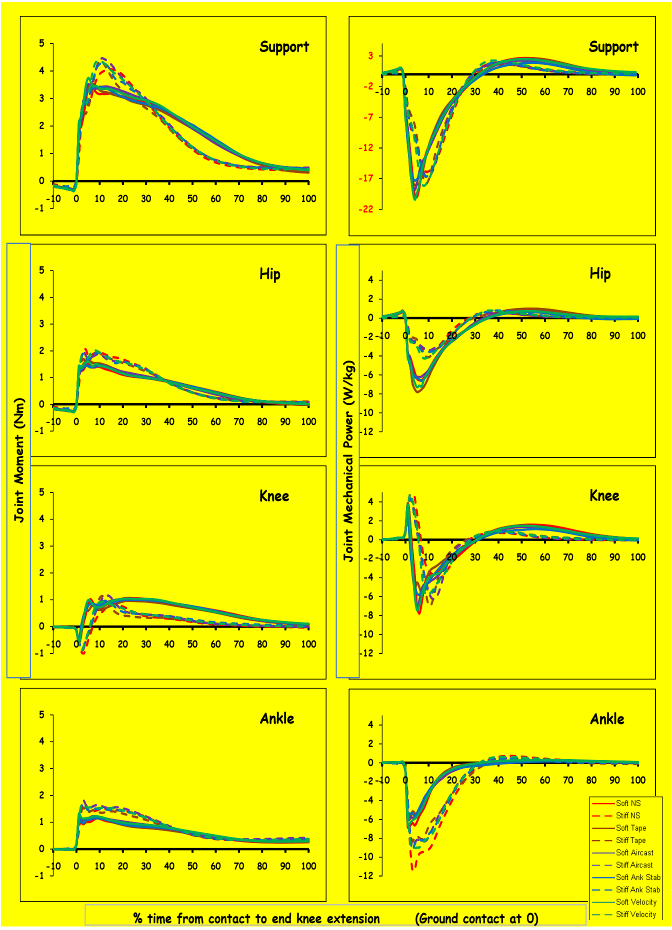

Figure 2: Grand ensemble (mean only) joint moments and powers for the stabilizer/landing style conditions.

Although the moment and power time-curves of our data differ from [2], most likely because of data-smoothing differences [1], the relative contribution of the joints still differed between soft and stiff landings, as in [2]. Although the negative work at the ankle was ~8 J•kg^{-1} greater in stiff than soft landings, the relative ankle contribution to total work was approximately double. However, in stabilized conditions, the relative contribution of the ankle joint was reduced relative to the no stabilizer condition. When stabilized, the ankle performed about 3.4% less work than the non-stabilized condition in the soft landing and about 6.3% less work than the non-stabilized condition in the stiff landing (Table 1). There was not a consistent increase in work at the knee or hip to make up for the reduced negative work at the ankle.

CONCLUSIONS

Despite changes in the materials and design, the use of ankle stabilizers adversely affects energy absorption by the ankle during drop landings. This supports our hypothesis that wearing ankle stabilizers would alter the relative contribution of individual lower extremity joints to energy absorption.

REFERENCES

1. Bisseling R & Hof A. *J Biomechanics*, 39:2438-2444.
2. Devita P and Skelly W, *Med. Sci.Sports Exerc.*, 24:108-115, 1992.
3. McCaw ST & Cerullo J, *Med. Sci. Sports Exerc.*, 31: 702-707, 1999.

ACKNOWLEDGEMENTS

This study was supported by a *Jump Rope for Heart* grant from the Illinois Association for Health, Physical Education, Recreation and Dance. The brace manufacturers generously donated the ankle stabilizers. Special thanks to Justin Stanek, ATC.

Table 1: Means and SDs of work and relative joint contribution to total work by the leg during landing

	NS		**Tape**		**Stirrup**		**Lace Up**		**Hinged**	
Impact Phase Powers	**Soft**	**Stiff**	**Soft**	**Stiff**	**Soft**	**Stiff**	**Soft**	**Stiff**	**Soft**	**Stiff**
Total Work	**-2.61 ± 0.44** **100.00%**	**-1.41 ± 0.21** **100.00%**	**-2.44 ± 0.45** **100.00%**	**-1.35 ± 0.28** **100.00%**	**-2.42 ± 0.59** **100.00%**	**-1.32 ± 0.34** **100.00%**	**-2.58 ± 0.41** **100.00%**	**-1.38 ± 0.24** **100.00%**	**-2.55 ± 0.52** **100.00%**	**-1.39 ± 0.28** **100.00%**
Work at Hip	**-1.03 ± 0.49** **39.28%**	**-0.29 ± 0.15** **20.55%**	**-1.16 ± 0.51** **47.37%**	**-0.32 ± 0.15** **24.16%**	**-1.01 ± 0.57** **41.56%**	**-0.29 ± 0.16** **21.96%**	**-1.10 ± 0.51** **42.79%**	**-0.32 ± 0.12** **23.25%**	**-1.09 ± 0.52** **42.95%**	**-0.33 ± 0.16** **23.37%**
Work at Knee	**-0.85 ± 0.39** **32.37%**	**-0.30 ± 0.16** **21.88%**	**-0.67 ± 0.26** **27.61%**	**-0.33 ± 0.13** **24.72%**	**-0.81 ± 0.32** **33.27%**	**-0.36 ± 0.19** **27.41%**	**-0.86 ± 0.30** **33.31%**	**-0.34 ± 0.15** **24.68%**	**-0.80 ± 0.34** **31.35%**	**-0.35 ± 0.10** **25.34%**
Work at Ankle	**-0.74 ± 0.25** **28.34%**	**-0.81 ± 0.21** **57.56%**	**-0.61 ± 0.23** **25.01%**	**-0.69 ± 0.27** **51.13%**	**-0.61 ± 0.23** **25.16%**	**-0.66 ± 0.23** **50.64%**	**-0.62 ± 0.25** **23.90%**	**-0.72 ± 0.27** **52.07%**	**-0.65 ± 0.31** **25.70%**	**-0.71 ± 0.28** **51.29%**

Mean and SD values are calculated from individual trials for each subject; work values are in J·kg-1

LOWER BODY KINEMATICS WHILE WALKING ACROSS A SLOPED SURFACE

[1] Scott P. Breloff, [2]Chip R. Wade and [3]Dwight E. Waddell
[1]Univeristy of Oregon, Department of Human Physiology, [2]Auburn University Department of Industrial and Systems Engineering, [3]Univerisy of Mississippi, Department of Exercise Science
email: breloff@uoregon.edu web: http://biomechanics.uoregon.edu/MAL/index.html

INTRODUCTION

Level surface walking has been well researched [1], with recent work investigating up and down slope walking [2,3]. Research has suggested Individuals are more likely to fall when walking on a sloped when compared to that of a level surface [4] Mechanisms for the increased likelihood of falling have been described as the proactive/reactive mechanisms of the balance control system [5] and the larger sheer forces due to an increasing angle of the surface [6]. The purpose of this study was to investigate if lower body kinematics will change as a function of slope and determine if a difference exists not only between conditions, but individual feet.

METHODS

Ten healthy male subjects (18-25 years) participated in the study. A roof segment 8.53m long and 2.44m wide with a 6\12 pitch (26.50^0 slope) was constructed. The roof segment was shingled with commonly used shingles and according to proper installation methods. Subjects completed two walking sessions on non-consecutive days. The initial session; subjects walked on a level surface which mimicked the length and width of the sloped surface. The second session; subjects walked along the sloped roof segment. Five to ten successful trials were incorporated in the analysis. Feet were analyzed separately and classified as the upslope or downslope foot. Ankle, knee and hip angles (Figures 1 & 2) were analyzed at two peaks in the gait cycle corresponding to weight acceptance (first 45% of stride) and propulsion second 45% of stride). Paired T-tests were used to calculate difference in conditions. Sloped data (upslope and downslope) were compared individually for changes. Alpha was set at 0.05.

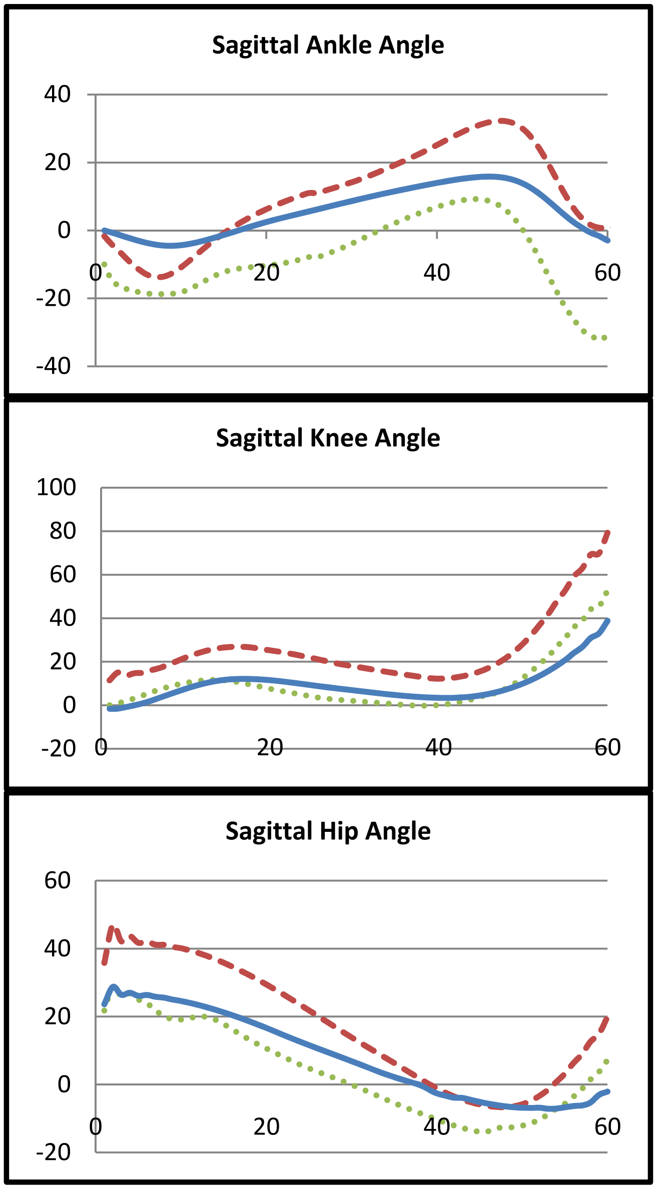

Figure 1: Sagittal plane lower body kinematics. Dashed line is upslope, solid is level and dotted line is downslope.

RESULTS AND DISCUSSION

The kinematic data from each subject was ensemble averaged and peaks were chosen using a custom excel program. Peaks angles about the ankle, knee and hip were compared for level and sloped walking.

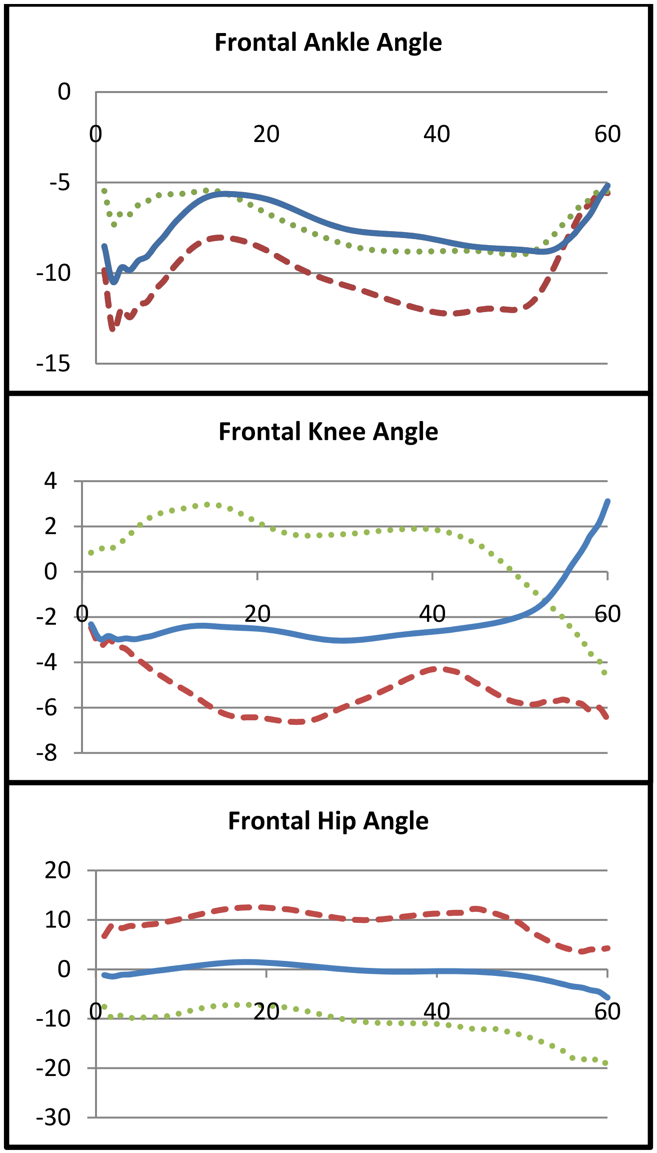

Figure 2: Frontal plane lower body kinematics. Dashed line is upslope, solid is level and dotted line is downslope.

Paired T-tests (alpha = .05) indicated a statistically significant change in several peak angles about the ankle, knee and hip in both the frontal and sagittal planes.

CONCLUSIONS

There is a serious need for research to prevent falls from roofs, both by improving the existing work practices, and by developing new approaches, methods and systems for fall preventions and protection.

A change in lower body kinematic variables during cross sloped walking might indicate an increased likelihood for falling while on a sloped surface and chronic injuries. By determining the changes in gait related performance during locomotion on a sloped surface (i.e. roof), safety measures and engineering controls could be developed and implemented to reduce the risk of falls on and from sloped surfaces.

REFERENCES

1. Winter, D. (2005). Biomechanics of motor control of human movement 3rd edition. . New Jersey, John Wiley & Sons, Inc..

2. Redfern, M., DiPasquale, J. (1997). "Biomechanics of descending ramps." Gait & Posture **6**: 119-125.

3. Lay, L., Hass, C., Gregor, R. (2006). "The effect of sloped surface on locomotion: A kinematic and kinetic analysis." Journal of Biomechanics **39**: 1621-1628.

4. Hsiao, H., Simeonov, P. (2001). "Preventing falls from roofs: a critical review." Ergonomics **44**(5): 537-561.

5. Woollacott, M. H., Tang, P. F. (1997). "Balance control during walking in the older adult: research and its implications." Physical Therapy77:646-660.

6. Harper, F. C., Warlow, W. J., Clarke, B. L. (1967). "The forces applied to the floor by the foot in walking. II. Walking on a slope." National Building Studies Research Paper **32**: 1-8.

Joint Angle (deg)	**Kinematic Peaks (Degrees)**					
	Level HS	**Level TO**	**UpSlope HS**	**UpSlope TO**	**DownSlope HS**	**DownSlope TO**
Ankle Flexion/ Extension	-4.5 ± 1.8	15.8 ± 1.7	-13.7 ± 1.2*	32.2 ± 1.58*	-18.7 ± 0.8*	9.1 ± 1.1*
Knee Flexion/ Extension	12.14 ± 4.8	38.8 ± 4.6	26.8 ± 0.78*	79.3 ± 1.25*	11.6 ± 0.99	52.7 ± 1.8*
Hip Flexion/ Extension	28.7 ± 11.0	-7.1 ± 11.1	46.9 ± 0.51*	-6.6 ± 0.74	28.6 ± 1.0	-13.9 ± 1.8
Ankle Inversion/ Eversion	-10.4± 0.60	-8.8 ± 0.58	-13.2 ± 0.22*	-12.6 ± 0.57*	-7.7± 0.13*	-8.9 ± 0.27
Knee Abduction/ Adduction	-2.9 ± 4.1	3.1 ± 4.1	-6.6 ± 0.83	-6.5 ± 0.66	2.9 ± 0.42*	-4.8 ± 0.31
Hip Abduction/ Adduction	1.4 ± 12.2	-5.7 ± 12.4	12.5 ± 0.70*	12.1 ± 0.96*	-10.0 ± 0.49*	-19.3 ± 1.3*

Table 1: Peaks of lower body kinematics during level and sloped walking conditions. *Denotes significant change from level.

INFLUENCE OF THONG FLIP-FLOPS ON RUNNING KINEMATICS IN PRESCHOOLERS

Justin F. Shroyer, Leah E. Robinson, and Wendi Weimar
Department of Kinesiology, Auburn University
email: shroyjf@auburn.edu, web: http://www.auburn.edu

INTRODUCTION

Footwear is important in human movement because it is the interface between the foot and the ground in shod activities. The foot is the first and sometimes only interaction with the ground and plays a key role in the regulation of normal walking gait patterns [1]. There is a plethora of research on varying types of footwear, but a type that has not been thoroughly investigated is thong style flip-flops. With casual observation of an increase in the wearing of flip-flops by children and the anecdotal evidence provided by podiatrists that flip-flops are poor footwear choices, the effects of wearing flip-flops on gait mechanics warrants investigation. Therefore, the purpose of this study was to determine if thong style flip-flops have an effect on the movement patterns of preschool-age children while running when compared to athletic sneakers.

METHODS

Twelve (8 F and 4 M) preschool-age children (age 56.27 mos ± 3.32) were used for this study. Two participants at a time reported to the Auburn University's Sport Biomechanics Laboratory for testing. The athletic shoes used in the study were the TT Jetstream (for males) and TT Pandora (for females) by Stride Rite® (Figure 1). The flip-flops were generic flip-flops purchased at a local department store (Figure 2).

Figure 1: Stride Rite® TT Pandora and TT Jetstream

Figure 2: Generic flip-flop

Upon arriving to the lab for testing, the children were randomly assigned to a footwear order (flip-flops or sneakers first). Retroreflective markers were then placed on four anatomical locations on both lower extremities: (1) greater trochanter of the femur, (2) lateral epicondyle of the femur, (3) lateral malleolus of the fibula, and (4) distal portion of the fifth metatarsal. For the athletic shoe condition, the foot was palpated through the shoe and the marker was placed on the shoe above the distal portion of the fifth metatarsal. A researcher then demonstrated the task of running to the participants. Each participant ran through the capture volume at a self-selected pace for a distance of 7.6 m. Participants were encouraged to run as fast as they could. For the capture volume, a Canon 3CCD Digital Video Camcorder was placed perpendicular to the sagittal plane of the motion, 5.8 m away. This process was repeated for the other participant. After the successful completion of data collection for both participants, the participants footwear was switched and the data collection procedures were repeated.

The kinematic variables of interest were stride length (SL), average hip velocity in the x direction (V_{HX}), and peak ankle dorsiflexion during the swing phase of the non support leg (θ_{DSW}). Digital video was digitized post data collection using Ariel Dynamics APAS v12.2.0.1. SL was determined using the lateral malleolus marker from initial contact of the right foot until initial contact of the ipsilateral limb. θ_{DSW} was calculated as the angle between the lower leg (as determined by the line from the lateral epicondyle of the femur to the lateral malleolus) and the foot (as determined by the line from the lateral malleolus to the distal end of the fifth metatarsal). Data were analyzed with a one-way ANOVA with repeated measures for each dependent variable, SL, V_{HX} and θ_{DSW}.

RESULTS AND DISCUSSION

The result of this study show a significant main effect of footwear on SL. Specifically, the flip-flops resulted in shorter stride length than athletic shoes (Table 1). The findings align with previous research that demonstrates a decreased stride length in adults who wore flip-flops [2]. A possible explanation for the decreased stride length is the decreased mass of the flip-flop, which would decrease the inertia of the foot during the swing phase [3]. Another explanation could be that the children take a shorter stride to decrease the swing phase in an attempt to keep the flip-flop on the foot. Therefore, the child may want to (a) get the foot back to the ground to take advantage of the assistance of the ground and/or (b) strike the ground with foot in a more horizontal position. This phenomenon was noted by DeWit and colleagues (2000), in a study comparing barefoot versus shod conditions. This study resulted in shorter step lengths and larger step frequencies in the barefoot condition, and they attributed the results to a different "touch down" geometry [4].

Surprisingly, there was not a significant main effect of footwear on V_{HX} (Table 1). Particularly in light of the significant stride length difference. The combination of these two outcomes (stride length and velocity) indicate that even though the children had longer strides, when they wore athletic shoes, they did not have an increased velocity in the x direction. It is hypothesized that the lack of significance was due to the relatively few number of participants and not the mean difference of .27 ms^{-1}.

It was hypothesized that there would be a decreased dorsiflexion angle due to the implied moment at the ankle from the toe flexors trying to "grip" the flip-flop; however, no differences were observed at the ankle during the swing phase (Table 1).

CONCLUSIONS

There is an abundance of literature of the effects of footwear type, design, or modification on gait mechanics; however, it is lacking in the area of the effects of flip-flops on gait mechanics. This study illustrates that thong style flip-flops do alter the performance of the task of running in preschool-age children as seen in the decreased stride length, while wearing flip-flops. Whether the result of a decreased stride length is a direct result of altered mechanics to keep the flip-flop on the foot or because of the mass differences in the footwear is still in debate.

In conclusion, there was a difference in stride length in preschoolers while wearing thong flop-flops when compared to athletic sneakers. There were no differences in dorsiflexion angle or hip velocity.

REFERENCES

1. Nurse, M.A. and B.M. Nigg, *The effect of changes in foot sensation on plantar pressure and muscle activity.* Clinical Biomechanics (Bristol, Avon), 2001. **16**(9): p. 719-27.
2. Shroyer, J., et al., *Influence of sneakers versus flip-flops on attack angle and peak vertical force at heel contact.* Medicine & Science in Sports & Exercise, 2008. **40**(5): p. S333.
3. Majumdar, D., et al., *Temporal spatial parameters of gait with barefoot, bathroom slippers and military boots.* Indian J Physiol Pharmacol, 2006. **50**(1): p. 33-40.
4. De Wit, B., D. De Clercq, and P. Aerts, *Biomechanical analysis of the stance phase during barefoot and shod running.* Journal of Biomechanics, 2000. **33**(3): p. 269-78.

ACKNOWLEDGEMENTS

The authors would like to thank the Stride Rite® Corp. for their donation of footwear for this project.

Table 1: Effect of footwear on SL, V_{HX}, and θ_{DSW} **(**$p \le .05$). Significance noted*

	Footwear	N	Mean	SD	*F*	*p*	η^2	*Power*
SL (m)*	Flip-flops	12	1.3921	.159	9.366	.011	.460	.795
	Sneakers		1.6723	.340				
V_{HX} (ms^{-1})	Flip-flops	12	2.7102	.458	2.773	.124	.201	.331
	Sneakers		2.9819	.521				
θ_{ASW} (°)	Flip-flops	12	102.83	5.23	.608	.452	.052	.110
	Sneakers		104.99	8.92				

BIOMECHANICAL ASYMMETRY BEFORE AND AFTER TOTAL KNEE ARTHROPLASTY IN SUBJECTS WITH AND WITHOUT BACK PAIN

[1, 2] Naira H Campbell-Kyureghyan, [1]David R. Burnett, [1]Robert V. Topp, [1]Peter M. Quesada
[1]University of Louisville, Louisville, KY 40292
[2]email: nhcamp01@louisville.edu

INTRODUCTION

Studies estimate that 54 million Americans suffer from low back pain (LBP) [1] and 21 million have osteoarthritis (OA), which commonly affects the weight bearing joints of the lower extremities [2]. Total knee arthroplasty (TKA) is a commonly used surgical intervention for knee OA in which the OA diseased joint is replaced by a prostetic device. To date, limited research exists on the relationship between TKA and LBP, and biomechanical relationships between the development and progression of knee OA and LBP are unclear. Specific symptoms of LBP that are suspected to be risk factors for knee OA resulting in TKA include strength and biomechancial asymmetry. The objective of this study is to quantify knee strength and biomechanical asymmetry among TKA patients either with or without LBP.

METHODS

8 subjects (2 male, 6 female) who had reported LBP were included in Group 1 and 7 subjects (2 male, 5 female) who did not report LBP were included in Group 2. All subjects have undergone TKA and signed the IRB approved informed consent form. Data collection occurred 8 weeks prior to and 12 weeks after TKA (T1 & T4, respectively). Reflective markers were placed in a modified Helen Hayes arrangement and marker spatial coordinates were obtained at 100 Hz with a Hawk Motion Tracking System (Motion Analysis Corp.). A force plate (Bertec Corp.) simultaneously recorded ground reaction force (GRF) at 1000 Hz. Subjects performed a single sit-to-stand repetition with the non-operated leg on the force plate followed by a 30 second trial with the operated leg on the force plate. Knee strength measurements were subsequently obtained using a Biodex Isokinetic Dynamometer. Five outcome measures (Table 1) are presented in this paper. Differences between these outcome measures at T1 and T4 were determined using student t-tests with $p < 0.05$ considered to be significant.

RESULTS

Knee strength, as measured by PTBW, significantly increased by 104% for the non-operated leg and by 38.9% for the operated leg for Group 2 ($p = 0.01$ & 0.02, respectively). For Group 1 however, PTBW increased by only 14.9% for the non-operated leg and 4.5% for the operated leg (Fig 1a).

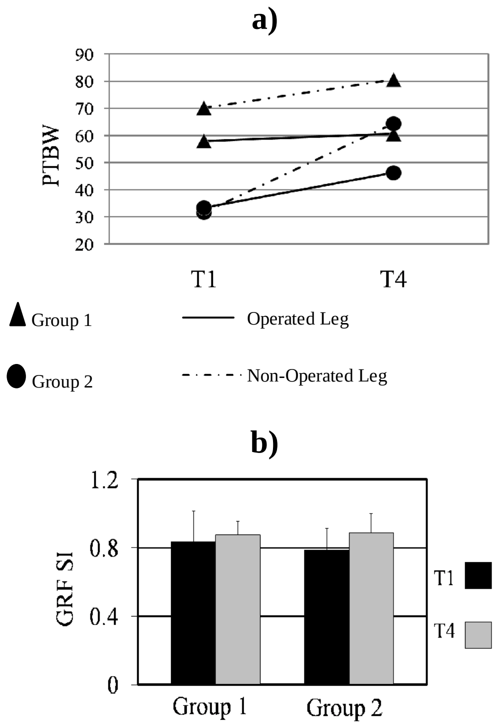

Figure 1: a) Comparison of PTBW during knee extension; b) Comparison of GRF SI during sit-to-stand

GRF SI values for Group 2 increased significantly ($p=0.02$) from 0.79 at T1 to 0.88 at T4 (Fig 1b).

Improvements in GRF SI between T1 and T4 were not seen for Group 1 (GRF SI = 0.88).

Although not statistically significant, subjects in both groups displayed smaller or comparable values for LSD, MLPS, and MLTL at T4 compared to T1 (Table 2). Additionally, subjects without LBP exhibited less trunk kinematic asymmetry at both sessions than subjects with LBP.

Table 2: Average trunk kinematic parameters for Group 1 and Group 2 at T1 and T4

	LSD (mm)		**MLPS (mm)**		**MLTL (^{o})**	
	G1	**G2**	**G1**	**G2**	**G1**	**G2**
T1	23.7	8.57	35.05	28.64	5.17	3.08
T4	17.2	10.59	32.14	26.90	4.37	3.84
p	0.22	0.35	0.31	0.39	0.15	0.15

DISCUSSION

Both groups showed significant differences in PTBW changes before and after TKA. Non-LBP subjects (Group 2) exhibited large increases in PTBW while increases for subjects with LBP (Group 1) were much smaller. These findings are in agreement with a previous study that concluded that chronic LBP or reduced endurance of the spinal musculature was associated with significant inhibition of knee extensors [3]. The increase in GRF SI for non-LBP subjects (Group 2) after TKA was not seen in LBP subjects (Group 1). These results indicate that subjects in Group 1 may have developed certain compensatory mechanisms to minimize pain in the surgically repaired knee as well as the lower back, and these compensatory methods were still apparent even after TKA.

CONCLUSIONS

Quantitative biomechanical data collected 8 weeks prior to and 12 weeks after TKA was evaluated for subjects with and without LBP. TKA patients without LBP showed significant improvements in knee extension strength and biomechanical asymmetry during sit-to-stand tasks. Similar trends were not observed in a group of TKA patients with LBP.

ACKNOWLEDGEMENTS

This study was supported by a grant from the NIH (NINR) R01 R008135-01A2

REFERENCES

1. Deyo R, et al., *Spine*. **31**:2724-2727, 2006.
2. Felson DT, et al., *Arth & Rheum*. **41**:1343-1355, 1998.
3. Suter E, et al., *Spine*. **26**:361-366, 2001.

Table 1: Description of outcome measures used in the study

Outcome Measure	**Description**
Vertical GRF Sym Index (SI)	Peak GRF operated leg/peak GRF non-operated leg
Lateral Seat Displacement	Center shift of the shoulders and ankles while seated prior to sit-stand
Max Lateral Pelvic Shift (MLPS)	Max displacement between centers of pelvis and ankles during sit-stand
Max Lateral Trunk Lean (MLTL)	Angular disp between centers of shoulders and ankles during sit-stand
Peak Torque/Body Wt (PTBW)	Knee flexion/extension strength for operated and non-operated leg

OCCUPANT KINEMATICS IN LOCOMOTIVE LOW-SPEED IMPACTS

[1]Elaine R. Serina, [2]Foster J. Peterson, [1]Kirsten White, [1]Daniel M. Desautels
[1] Talas Engineering, Inc., [2] Full Service Railroad Consulting, Inc.
email: eserina@talasinc.com, web: www.talasinc.com

INTRODUCTION

During the operation of a train, the locomotive engine experiences a varying acceleration environment. Impulses are transmitted to the locomotive during coupling (joining railcars together) and slack action (stretching or compressing the train). These forces act primarily in the longitudinal direction and occur frequently during locomotive operation. Subjective descriptions of these impact events range from "minor" to "hard" jolts, and injuries have been claimed by the locomotive cab occupants (e.g. engineer and conductor) as a result of these impacts.

The occupants of the locomotive cab in these low-speed impacts experience frontal or rear forces on their bodies, depending on their seated orientation. The effects of low-speed locomotive impacts on the occupant kinematics and forces on the occupants have not been investigated in the research literature. However, the effect on the human body of low-speed automobile impacts has been studied extensively. Therefore, the purpose of this study is to characterize the motion and forces on the locomotive and occupant during low-speed locomotive impacts and draw comparisons to the research literature on automobile impacts.

METHODS

A series of 24 locomotive impact tests were conducted. A 1978 GP-9 locomotive engine (1750 hp, ~250,000 lb) was coupled to a group of 10-12 stationary empty railroad tank cars (~70,000 lbs each) (Figure 1). The locomotive engine speed at impact was approximately 1-5 mph. Impacts at these speeds produced longitudinal accelerations similar to typical coupling and slack action events. Twelve tests were performed with the locomotive traveling forward into the railroad tank cars (frontal impact) and twelve in reverse (rear impact).

During each test, a healthy male subject (35 years, 6'1", 275 lb) sat in the engineer's seat while operating the locomotive. Immediately prior to impact, the operator assumed a neutral seating position, facing directly forward.

Accelerations of the locomotive engine, engineer's seat, and subject's head were recorded simultaneously (Figure 2). Tri-axial accelerometers (Silicon Designs, Inc., Measurement Specialties) were mounted on the locomotive frame, in a seat pad on the engineer's seat underneath the ischial tuberosities, and on the engineer's seat frame. The subject wore custom headgear with two accelerometers (Measurement Specialties) rigidly attached to measure head CG accelerations in a head reference coordinate system (fore-aft and vertical, in the neutral seated position). Occupant data was recorded at 500 Hz (DataBRICK) and videotaped.

Figure 1: Locomotive engine and railcars.

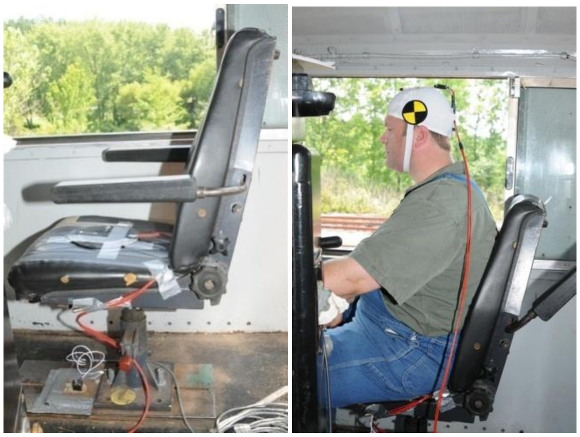

Figure 2: Instrumented seat and subject

RESULTS AND DISCUSSION

In general, the peak accelerations measured at the seat pad and head increased with increasing locomotive acceleration, and the peak locomotive acceleration increased with increasing impact speed. Peak accelerations are presented in Table 1. The data is presented as +*x* forward, +*y* right, -*z* up. Representative acceleration time histories are shown for a single rear impact test (Figure 3).

	Frontal Impact	*Rear Impact*
Locomotive (x)	0.08-1.26	0.24-0.84
Seat Pad (x)	0.08-0.73	0.24-0.79
Seat Pad (-z)	0.05-0.49	0.05-0.33
Head Resultant	0.13-0.75	0.20-0.93

Table 1: Range of peak acceleration measured (g)

The subject's body did not move excessively during any of the tests. Neither hyperflexion nor hyperextension of the neck or back occurred. During the rear impact tests the subject's upper body moved rearward relative to the seat. The acceleration measured at the head lagged the acceleration at the seat pad. The head did not contact the seat back in any test. During the frontal impact tests, there was little relative motion between the head and torso, so minimal neck flexion occurred. This was also observed in simulated automotive frontal impact tests with unbelted volunteers up to velocity changes of 3.5 mph [3]. The subject did not slide forward in his seat nor contact the structures in front of him. The subject sustained no injuries and reported no symptoms following each test or after the completion of the test series.

The seat pad peak vertical accelerations measured in the -z direction were examined for all tests as axial compression tends to be a significant factor in causing intervertebral disc injuries. The results suggest that the compression in the lumbar spine during these impacts is very low. Significantly higher compressive forces are generated during common daily activities [4].

The peak locomotive accelerations measured in our tests were comparable to accelerations in automotive impacts with changes in velocity of 1-2 mph [1,2]. However, the peak resultant head accelerations in those automobile impacts were greater than those found in these locomotive impacts. This can be explained by the significantly longer duration over which the locomotive longitudinal acceleration oscillates after the initial pulse (range: 0.35-0.9 sec) as compared to the acceleration pulse in low-speed automobile impacts. The initial locomotive acceleration pulse duration (range: 0.063-0.174 sec) was shorter but comparable to reported impulse durations for low-speed automobile impacts.

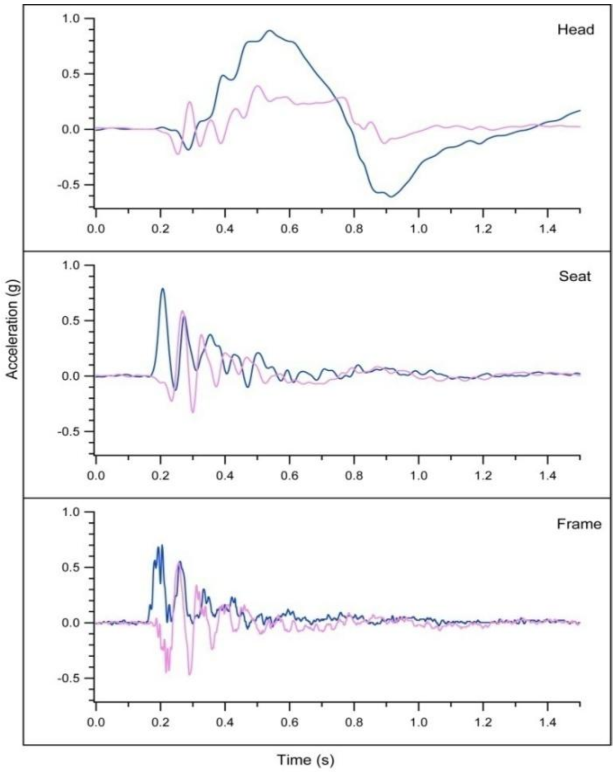

Figure 3: Sample results, rear impact: x —, z —

CONCLUSIONS

While the peak locomotive accelerations and initial pulse durations measured are comparable to low-speed automotive impacts in the research literature, the longer acceleration pulses result in lower head accelerations. The accelerations and forces experienced by an occupant in a low-speed locomotive impact are low, less than many non-injurious volunteer automobile impact studies and less than those experienced during activities of daily living.

REFERENCES

1. Welcher JB, et al. *SAE* 2001-01-0899, 2001.
2. West DH, et al., *Accid Reconst J*, 5, 22-26, 1993
3. Matsushita T, et al. *SAE* 942208, 1994.
4. Girvan DS, Serina ER *4th WCB*, Calgary, 2002.

LOWER EXTREMITY JOINT MOMENTS DURING CARRYING TASKS IN CHILDREN

[1]Jason Gillette, [1]Catherine Stevermer, [2]Ross Miller, [1]Brent Edwards and [3]Charles Schwab
[1]Dept. of Kinesiology, Iowa State University, [2]Dept. of Kinesiology, University of Massachusetts,
[3]Dept. of Agricultural & Biosystems Engineering, Iowa State University, email: gillette@iastate.edu

INTRODUCTION

Farm youth perform tasks that are often designed for adults, resulting in children carrying asymmetric loads that are proportionally large and/or heavy. Field measurements indicate lifting and carrying tasks performed by farm children are equivalent to industrial manual materials handling tasks that pose high injury risks [1]. Differences in gait mechanics between children and adults would be expected to contribute to age-related differences during carrying tasks. Adult-like kinetic gait patterns have been observed by 5 years of age, except that ankle plantarflexion moments are reduced in children below 9 years of age [2]. Changes in characteristics of the carrying task such as load amount, symmetry, and size would be expected to contribute to task-related differences. For example, maximum normalized hip abduction, hip internal/external rotation, knee extension, and ankle plantarflexion moments have been shown to increase when adolescent girls carried loaded backpacks [3].

Upper body joint moments are dependent upon load amount and symmetry for bucket carrying tasks. Increasing unilaterally carried loads from 10% to 20% body weight (BW) or carrying the same load amount unilaterally as compared to split bilaterally increases shoulder flexion/abduction/external rotation and L5/S1 lateral bending/axial rotation moments [4]. It is unknown whether the increases in upper body joint moments are also reflected in lower body joint moments. Bucket carrying requires balancing external loads in the frontal plane, so it was hypothesized that hip abduction and adduction moments would increase when increasing carried loads from 0% to 20% BW. Increases in normalized upper/lower body joint moments for children may indicate increased risk of injury. When considering frontal plane challenges combined with potentially reduced ankle moment generating capacity in children, it was also hypothesized that 8-10 year olds would have increased ankle inversion and eversion moments as compared to adults.

METHODS

Thirty-five participants in three age groups (8-10 years, 12-14 years, adult) participated in the study (gender distribution, average age, height, mass):

- 6/3 M/F, 8.8±1.0 year, 1.37±0.08 m, 33±7 kg,
- 9/5 M/F, 12.4±0.9 year, 1.56±0.06 m, 51±11 kg,
- 7/5 M/F, 24.0±1.7 year, 1.76±0.07 m, 72±13 kg.

Two sizes of buckets were carried: large (18.9 L, 36.8 cm high, 30 cm diameter) and small (3.8 L, 19.5 cm high, 16.7 cm diameter). The buckets were filled using sealed bags of lead shot amounting to three levels of load based on body weight: 0%, 10%, and 20% BW. Unilateral carrying tasks were performed with both large and small buckets, while bilateral carrying tasks were only performed with small buckets. Buckets were carried unilaterally with the self-selected dominant hand, and the load was evenly split between the buckets during the bilateral conditions. In total, three repetitions of the nine conditions (3 loads x 3 bucket/symmetry combinations) were completed.

Participants carried buckets 6 m while reflective markers placed on the lower extremities and pelvis were tracked by an eight optical camera system. Ground reaction forces were measured by a force platform at the halfway point of the walking path. Using inverse dynamics, lower extremity joint moments were calculated during the stance phase on the side of the body where unilateral loads were carried. Maximum ankle plantarflexion/dorsiflexion, ankle inversion/eversion, knee flexion/extension, hip flexion/extension, hip abduction/adduction, and hip internal/external rotation moments were calculated for each carrying trial, normalized by BW·height, and averaged across trials. Multivariate ANOVA was used to test for main effects of age group, carrying condition, and their interactions (significance $p<0.05/6=0.0083$ with Bonferroni correction). When significant main effects were found, post-hoc Scheffe comparisons were determined at a significance level of $p<0.05$.

Table 1. Maximum normalized joint moments as a function of age (* children significantly greater than adults, # adults significantly greater than children).

Moment (%BW·ht)	**8-10 years**	**12-14 years**	**Adults**
Ankle			
Plantarflex	0.82±0.11	0.87±0.12*	0.81±0.12
Dorsiflexion	0.20±0.07*	0.14±0.06	0.11±0.04
Inversion	0.17±0.07*	0.14±0.06*	0.12±0.03
Eversion	0.08±0.06*	0.07±0.08*	0.05±0.04
Knee			
Flexion	0.21±0.09	0.24±0.08*	0.19±0.05
Extension	0.39±0.13	0.39±0.11	0.48±0.17#
Hip			
Flexion	0.73±0.16	0.71±0.17	1.01±0.16#
Extension	0.58±0.12*	0.68±0.18*	0.43±0.10
Abduction	0.34±0.15	0.42±0.15	0.43±0.15
Adduction	0.25±0.11*	0.19±0.08	0.19±0.08
Int. rotation	0.41±0.11	0.42±0.08	0.41±0.09
Ext. rotation	0.27±0.07	0.33±0.09*	0.25±0.06

Table 2. Maximum normalized joint moments as a function of carrying task (* weight effect: 20% BW > 0% BW, # weight reverse effect: 0% BW > 20% BW, ** symmetry effect: unilateral > bilateral, ## symmetry reverse effect: bilateral > unilateral).

Moment (%BW·ht)	**Unilateral Large 0% BW**	**Unilateral Large 10% BW**	**Unilateral Large 20% BW**
Ankle			
Plantarflex	0.77±0.10	0.83±0.11	0.89±0.13*
Hip			
Abduction	0.42±0.13#	0.34±0.14	0.25±0.12
Adduction	0.18±0.08	0.23±0.09	0.29±0.11*
	Unilateral Small 0% BW	**Unilateral Small 10% BW**	**Unilateral Small 20% BW**
Ankle			
Plantarflex	0.76±0.11	0.83±0.11	0.90±0.10*
Hip			
Abduction	0.44±0.12#	0.40±0.13	0.32±0.14
	Bilateral Small 0% BW	**Bilateral Small 10% BW**	**Bilateral Small 20% BW**
Ankle			
Plantarflex	0.77±0.11	0.84±0.10	0.90±0.11*
	Bilateral Small 20% BW	**Unilateral Small 20% BW**	
Hip			
Abduction	0.54±0.13##	0.32±0.14	
Int. rotation	0.38±0.09	0.48±0.09**	

RESULTS AND DISCUSSION

Maximum joint moments were dependent upon age (Table 1) and carrying task (Table 2), but not their interaction. For age effects, ankle inversion, ankle eversion, and hip extension moments were greater for children age groups than for adults. In contrast, knee extension and hip flexion moments were greater for adults than for both children age groups. For load amount, ankle plantarflexion moments were greater when carrying unilateral large, unilateral small, and bilateral small buckets at 20% as compared to 0% BW. Hip adduction moments were greater when carrying a unilateral large bucket at 20% BW than at 0% BW, while the opposite effect was seen for hip abduction moments. For symmetry effects, internal hip rotation moments were greater when carrying a unilateral small bucket than for bilateral small buckets at 20% BW, while hip abduction moments showed the opposite effect. There were no significant differences for bucket size effects.

The first hypothesis was not supported because while hip adduction moments increased with load amount, hip abduction moments actually decreased. In general, hip abduction moments decreased in tasks involving higher load amounts and unilateral carrying. Hip abduction moments may be less effective during these challenging tasks, with individuals instead utilizing upper body postural adjustments such as generating L5/S1 lateral bending moments [4]. The second hypothesis was supported since ankle inversion and eversion moments were greater for 8-10 years olds than for adults. This is of practical concern for ankle sprains, especially in rough and/or muddy terrain beyond idealized lab conditions. Children also appear to rely more on hip extension moments, while adults rely more on knee extension and hip flexion moments. Overall, carrying 20% BW loads that increase moments in the low back and shoulders also increase moments in the ankles, particularly in children.

REFERENCES

1. Allread WG, et al. *J Agric Safety Health* **10**, 257-273, 2004.
2. Chester VL, et al. *Clin Biomech* **21**, 726-732, 2006.
3. Chow DHK, et al. *Med Eng Phys* **28**, 430-437, 2006.
4. Gillette JC, et al. *J Appl Biomech*, In press, 2009.

EFFECTS OF AGE AND INSTRUCTIONS LIMITING THE NUMBER OF STEPS ON THE THRESHOLD OF BALANCE RECOVERY

Marc-André Cyr and Cécile Smeesters
Research Center on Aging, Sherbrooke QC, Canada
Human Performance and Safety Research Group (PERSEUS), Sherbrooke QC, Canada
Department of Mechanical Engineering, Université de Sherbrooke, Sherbrooke QC, Canada
e-mail: Cecile.Smeesters@USherbrooke.ca web: http://www.usherbrooke.ca/gmecanique

INTRODUCTION

We have recently demonstrated that instructions limiting the number of steps did not affect the threshold of balance recovery in younger adults (YA) [1,2]. Indeed, results showed that the effect of using only a single step, no more than 2 steps or no limit on the number of steps on the maximum forward lean angle as well as on kinematic [1] and kinetic [2] performance measures was too small to be pertinent. However, experimental evidence has shown that older adults (OA) are more likely than YA to take more than one step to recover balance following small and medium postural perturbations [3]. The purpose of this study was thus to determine if the threshold of balance recovery was also not affected by limits on the number of steps in OA.

METHODS

As with our 28 YA (24.8±2.6yrs), we determined the maximum forward lean angles from which 10 OA (68.4±3.0yrs) could be suddenly released and still recover balance using: i) only a single step, ii) no more than two steps and iii) no limit on the number of steps. Balance recovery was considered unsuccessful if a participant recovered balance using more steps then allowed (stepping failure) or if more than 20% of body weight was supported by the safety harness cable (harness failure).

Using 3 force platforms (OR6-7, AMTI, Newton MA), 2 load cells (FD-2 and MC3A, AMTI, Newton MA) and 4 optoelectronic position sensors (Optotrak, NDI, Waterloo ON), the following performance measures were obtained: maximum lean angle (θ_{max}) and reaction time (RT) as well as weight transfer time (WTT), stride time (ST), stride velocity (SV) and stride length (SL) of all the steps taken by the participants.

One-way repeated measures analyses of variance (rm-ANOVA) were used to separately determine the effect of limits on the number of steps in YA [1] and OA. Two-way rm-ANOVA were then used to determine the effect of age and its interaction with the three limits on the number of steps.

RESULTS AND DISCUSSION

Effect of age on the performance measures: OA demonstrated a poorer ability to recover balance to avoid a fall than YA (Table 1). OA had smaller θ_{max}, longer WTT1 and WTT2, slower SV1 and SV2, and shorter SL1 than YA.

Effects of limits on the number of steps on θ_{max}: Instructions limiting the number of steps significantly affected θ_{max} in both age groups (Table 1). However, the effect was larger in OA ($\Delta\theta_{2\text{-}1}$=2.7deg, $\Delta\theta_{N\text{-}1}$=4.1deg) than in YA ($\Delta\theta_{2\text{-}1}$=1.0deg, $\Delta\theta_{N\text{-}1}$=1.0deg).

Effects of limits on the number of steps on the other performance measures: At θ_{max}, limits on the number of steps also significantly affected RT ($\Delta RT_{2\text{-}1}$=4ms), WTT1 ($\Delta WTT1_{2\text{-}1}$=-9ms), SV1 ($\Delta SV1_{N\text{-}1}$=-18cm/s), SL1 ($\Delta SL1_{2\text{-}1}$=-9cm, $\Delta SL1_{N\text{-}1}$=-8cm) and SV2 ($\Delta SV2_{N\text{-}2}$=-69cm/s) in YA (Table 1). However, they significantly affected ST1 ($\Delta ST1_{N\text{-}1}$=-38ms), SV1 ($\Delta SV1_{2\text{-}1}$=35cm/s) and SV2 ($\Delta SV2_{N\text{-}2}$=69cm/s) in OA. The strategy used to improve the ability to recover balance as more steps were allowed was thus different in the two age groups. YA used slower SV1 and SV2 and shorter SL1 as more steps were allowed, while OA used shorter ST1 and faster SV1 and SV2.

Number of steps taken at θ_{max}: For no more than two steps, 29% of YA used 1 step and 71% used 2 steps, whereas 50% of OA used 1 step and 50%

Table 1: Mean ± standard deviation results at the maximum lean angles for both younger [1] and older adults (N_{YA}=28 and N_{OA}=10).

	1 step		2 steps		No limit		p_{steps}		p_{age}
	YA	**OA**	**YA**	**OA**	**YA**	**OA**	**YA**	**OA**	
θ_{max} (deg)	29.7±2.3	19.8±6.0	30.7±2.8	22.5±5.4	30.7±2.9	23.9±4.6	**	***	***
RT (ms)	70±11	82±16	74±8	70±13	73±10	77±12	*		
First stride									
WTT1 (ms)	160±21	184±46	151±20	190±31	154±21	183±38	*		**
ST1 (ms)	195±23	213±35	182±28	190±32	185±26	176±17		*	
SV1 (cm/s)	506±51	361±83	490±44	396±74	488±50	394±70	*	**	***
SL1 (cm)	98±14	76±18	89±17	75±18	90±16	70±16	**		***
Second stride									
WTT2 (ms)	n/a	n/a	54±20	219±240	52±36	109±56			**
ST2 (ms)	n/a	n/a	272±54	358±75	347±165	414±196			
SV2 (cm/s)	n/a	n/a	423±98	235±130	354±138	304±136	**	**	*
SL2 (cm)	n/a	n/a	113±28	85±45	108±33	105±26			

θ_{max}: Maximum lean angle, RT: Reaction time, WTT: Weight transfer time, ST: Stride time, SV: Stride velocity, SL: Stride length.
* $p<0.05$, ** $p<0.01$, *** $p<0.001$.

used 2 steps. For no limit on the number of steps, 21%, 71% and 7% of YA used 1, 2 and 3 steps, respectively, whereas 20%, 30%, 10%, 10% and 30% of OA used 1, 2, 3, 4 and 5 steps, respectively. However, much less effort was put into these additional steps as they had slower SV and shorter StepL than the preceding steps.

Failure type above θ_{max}: For only a single step, 11% of YA had stepping failures and 89% had harness failures, whereas 60% of OA had stepping failures and 40% had harness failures. For no more than two steps, 4% and 96% of YA had stepping and harness failures, respectively, whereas 40% and 60% of OA had stepping and harness failures, respectively.

Correlations between limits on the number of steps: Despite all the significant effects stated above, θ_{max} and SV1 between the three limits on the number of steps were highly inter-correlated (Table 2).

CONCLUSIONS

In YA, the effect of instructions limiting the number of steps was considered too small to be pertinent. The additional steps did not help to increase θ_{max} by more than 1.0deg and the first step performance measures were nearly identical (Δ=±4-10%). In OA, however, the effect was larger. The additional steps increased θ_{max} by 4.1deg and the first step performance measures did change (Δ=±9-19%). OA were clearly able to use shorter ST1 and faster SV1 to improve their ability to recover balance as more steps were allowed. However, unlike YA, OA were either unable or unwilling to respect the instructions when only one or two steps were allowed. Nevertheless, the strong correlations between the three limits on the number of steps indicate that experiments at the threshold of balance recovery limiting the number of steps are still predictive of those not limiting the number of steps.

REFERENCES

1. Cyr MA and Smeesters C. *Gait Posture*, **29**(4), 628-633, 2009.
2. Cyr MA and Smeesters C. *J Biomech*, **40**(13), 2857-2864, 2007.
3. McIlroy WE and Maki BE. *J Gerontol* **51A**(6), M289-296, 1996.

ACKNOWLEDGEMENTS

Myriam Jbabdi, Pierre-Luc Martin and Mathieu Hamel for technical assistance and NSERC grant 298229-04 for financial support.

Table 2: Pearson correlation coefficients (r) between the three limits on the number of steps

	θ_{max}	SV1
1 step vs 2 steps	0.937	0.867
1 step vs No limit	0.893	0.881
2 steps vs No limit	0.903	0.892

θ_{max}: Maximum lean angle, SV: Stride velocity.

THE EFFECTS OF DIFFERENT FATIGUING PROTOCOLS ON LANDING MECHANICS AND KNEE KINESTHETIC SENSE

Mostafa Afifi and Richard Hinrichs
Arizona State University, Tempe, AZ, USA
e-mail: mostafa.afifi@asu.edu

INTRODUCTION

The fact that injuries tend to occur more frequently late in games has led to speculation that fatigue may be responsible (Pinto et al. 1999). Studying movements while fatigued may be a good way to understand mechanisms of injury. However there are many different ways to induce fatigue and it is not clear which is best to simulate what happens in an actual game situation. In jumping and landing fatigue may affect both the mechanics and the kinesthetics sense of the landing. Lattanzio et al. (1997) tested the effect of three different cycling general fatiguing protocols on knee joint position sense in both genders and found one of the protocols affected knee joint position sense in males only while the other two affected both genders. Gehring et al. (2009) found no change in knee mechanics and normalized ground reaction force (NGRF) following a leg press fatiguing protocol. However, Kernozek et al. (2008) found that after a squatting protocol both genders flexed the hips more after touchdown but only males flexed the knees more after touchdown. It remains unclear what the ideal protocol would be that simulates the effect of real game participation on landing mechanics and kinesthetic sense. The purpose of this study was to compare the effects of a running and a squatting general fatiguing protocol on landing mechanics and knee position sense to the effects of participating in a basketball game.

METHODS

Twelve active college students (6 males, 6 females) volunteered to participate in the study. Participants were excluded if they had any orthopedic condition that would prevent them from jumping.

Participants came on three different days to undergo the three fatiguing protocols. They performed three maximal vertical jumps on a force platform (1200 Hz, AMTI). They also underwent knee position sense testing during which they were asked to reproduce ten different knee positions. Participants then underwent three different fatiguing protocols. One protocol had participants perform repeated squats until they could no longer continue, a second had them run on a treadmill at 10 km/hr and 10% grade for 5 min, and a third had subjects participate in a 15-20 min full-court basketball game in which the winning team scored 12 baskets. After the fatiguing protocol the three maximal jumps and knee position sense testing were repeated.

The Wilcoxon signed-rank test was used to compare the peak knee flexion angle, peak NGRF, and sum of absolute errors in knee position reproduction in pre and post fatigue conditions for the three fatiguing protocols.

RESULTS AND DISCUSSION

The Wilcoxon signed-rank test showed peak knee flexion angle significantly increased as a result of fatigue from the run and squat protocols, $p<.05$ (Figure 1). There was a non-significant trend toward the same result following the basketball game ($p=.08$).
No changes in NGRF were observed after the basketball and running protocols, $p=1.0$ and $p= 0.81$, respectively; however, peak

NGRF significantly decreased post fatigue after the squat protocol, p<.05 (Figure 2).

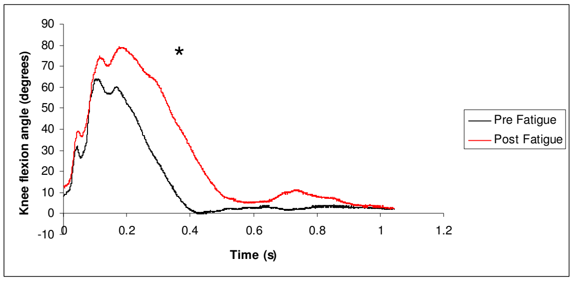

Figure 1. Knee flexion angle for the Squat condition
*Significant difference in peak between pre and post fatigue, p<.05

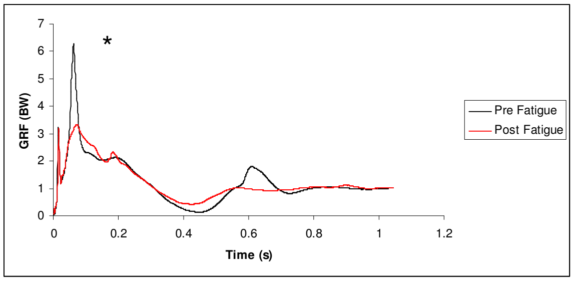

Figure 2. NGRF for the Squat condition
*Significant difference in peak between pre and post fatigue, p<.05

Our results are similar to Gehring et al. (2009) when it came to the basketball and running conditions. Although the running protocol produced a significant increase in peak knee flexion angle and the basketball protocol produced a non-significant increase in peak knee flexion angle, further observation revealed that knee flexion angles at peak GRF did not change. We did not initially look at that variable but results indicate it is a more important variable as its significant increase led to a reduction in NGRF in the squatting condition, which did not change for the basketball and running conditions. The significant changes observed following the squat condition are similar to those reported by Kernozek et al. (2008) suggesting the changes are task specific.

Both the basketball and running protocols led to a significant increase in absolute error when reproducing knee positions post fatigue, p<.05 (Figure 3). However the squatting protocol produced only a non-significant increase in absolute error, p=0.12.

Perhaps the changes in knee kinesthetic sense led to the changes observed in knee mechanics. Perhaps as knee kinesthetic sense decreased the body made other adjustments to reproduce similar landing mechanics as seen in the basketball and running conditions.

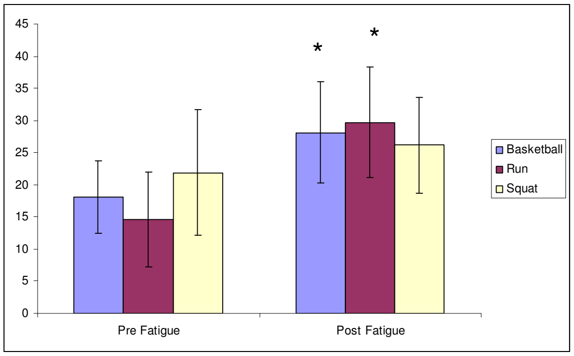

Figure 3. Mean sum of absolute errors in reproducing knee position for all conditions
*Significant difference between pre and post fatigue, p<.05

SUMMARY/CONCLUSIONS

This study compared the effects of running and squatting fatiguing protocols on landing mechanics and knee position sense to the effects of playing basketball on these variables. Although neither protocol showed identical changes to those after basketball, the running protocol produced similar changes in NGRF and knee position sense. Of the three fatiguing protocols tested here, the running protocol used in this study is the best choice for simulation of a real game situation.

REFERENCES

Gehring, D. et al. (2009). *Clin Biomech, 24,* 82-87.

Lattanzio, P.J. et al. (1997). *Clin J Sport Med, 7,* 22-27.

Kernozek, T.W. et al. (2008). *Am J Sports Med, 36,* 554-565.

Pinto, M. et al. (1999). *Clin J Sport Med, 9,* 70-74.

INFLUENCE OF INDENTER SIZE AND WRIST POSTURE ON TRANSVERSE CARPAL LIGAMENT STIFFNESS

[1]Michael W. Holmes, [2]Samuel J. Howarth, [2]Jack P. Callaghan and [1]Peter J. Keir
[1]Occupational Biomechanics Laboratory, McMaster University, Hamilton, ON, Canada,
[2]Department of Kinesiology, University of Waterloo, Waterloo, ON, Canada
Email: holmesmw@mcmaster.ca

INTRODUCTION

The carpal tunnel is formed by the carpal bones and enclosed on the volar side by the transverse carpal ligament (TCL). The TCL influences tendon and nerve movement, thus contributing to carpal tunnel mechanics as well as carpal stability. However, investigations of the role of the TCL in carpal stability have been equivocal [1,2].

Additionally, it has been proposed that manipulative treatment might be a therapeutic option for Carpal Tunnel Syndrome (CTS) rather than surgical release [3]. A better understanding of the material properties of the TCL is needed to clarify its role in carpal mechanics. Carpal tunnel compliance has been measured *in vivo* using a manual indentation apparatus [4]. For a neutral wrist posture, female carpal tunnels were found to be stiffer than males. This result was thought to provide insight into why females have a higher prevalence of CTS than males. Furthermore, it was also suggested that optimal TCL compliance is important for proper hand function [4].

The primary purpose of this study was to investigate the material properties of the intact cadaveric TCL by loading the structure in different wrist postures.

METHODS

Fresh-frozen cadaver arms, sectioned at the mid-humerus were tested. Specimens were thawed overnight prior to dissection. The TCL was exposed using a longitudinal incision in the palm followed by two horizontal incisions at the middle crease of the palm and proximal wrist crease. Skin and subcutaneous tissue was removed until the TCL and attachment sites were exposed. To associate load and motion, infrared-emitting diodes were attached to rigid light weight structures rigidly inserted into the pisiform and scaphoid. Three-dimensional motion of the proximal row was measured using the Optotrak Certus motion capture system (Northern Digital Inc., Waterloo, Canada) (Figure 1a).

Each specimen was positioned below the compressive actuator of a servo-hydraulic materials testing machine (8872, Instron Canada, Toronto, Canada). The actuator was equipped with a load cell to which a cylinder shaped indenter was affixed (Figure 1b). Four indenter sizes (5 mm, 10 mm, 20 mm and 35 mm diameters with bevelled edges) applied loading to the TCL in three wrist postures (30° extension, neutral and 30° flexion). Custom made splints secured the arm in the three postures.

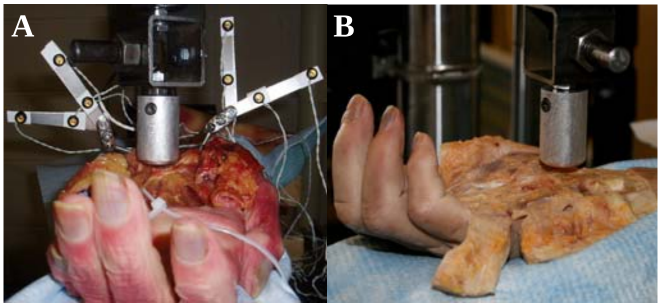

Figure 1: A) Markers inserted into pisiform and scaphoid; B) Specimen in neutral posture (20 mm indenter shown)

A maximum downward force of 50 N was applied at a rate of 5 N/second for each indentation test. Ten pre-conditioning cycles were performed followed by 3 loading cycles for each posture and indenter. Force, displacement and kinematics of the scaphoid and pisiform were sampled at a rate of 100 Hz. Each cycle was divided into loading and unloading phases and stiffness was calculated using custom software (MATLAB R2008a, Natick, MA, USA). Stiffness was measured as the slope of each cycle's force-displacement relationship [4].

Following indentation tests, the TCL was removed and a 5 mm x 5 mm sample from the distal region was mounted in a biaxial tensile system (BioTester 5000, CellScale, Waterloo Instruments Inc, Waterloo, Canada). The percent strain used for tensile tests were estimated from indenter trials. Strain was calculated from indenter size and displacement. Strain rate corresponded to the load rate for indentation tests. Samples were pre-conditioned with 3 trials of 5% strain over 5 seconds (1%/s). Samples were then tested with 3 trials at each calculated percent strain over 5 seconds. Finally, 3 trials were performed to 5% strain with different strain rates.

RESULTS AND DISCUSSION

Preliminary results from four cadaver wrists show the 5 mm indenter resulted in the lowest stiffness in extended and neutral postures (20.0 ± 5.3 N/mm, extension; 18.4 ± 4.4 N/mm, neutral) (Figure 2). During flexion, the 35 mm indenter had the lowest stiffness (22.0 ± 3.0 N/mm). The 20 mm indenter produced the greatest stiffness in extension and neutral (26.9 ± 8.3 N/mm, extension; 28.4 ± 10.8 N/mm, neutral). Overall, wrist extension resulted in the greatest stiffness (24.2 ± 3.0 N/mm). For 50 N loading, the 5 mm indenter showed the largest displacement (mean of all postures, 3.9 ± 0.2 mm). Wrist flexion had the greatest displacement (mean of all indenters, 3.5 ± 0.2 mm).

In extended and neutral postures, all indenters showed similar trends and stiffness was greatest with the 20 mm indenter. Considering anthropometric measures and indenter size, the largest indenter tends to cover the bony landmarks of the TCL. The neutral posture and 5 mm indenter produced values comparable to those found *in vivo* for females in a manual indentation study [4]. Preliminary analysis in the current study demonstrates that TCL stiffness from indentation testing is dependent upon the relative dimensions of the indenter and the carpal tunnel width. However, obvious methodological differences exist between the two studies making comparisons challenging.

Wrist extension demonstrated the greatest stiffness in our study. In an extended posture the carpal bones provide support to the flexor tendons, and the carpal bones rotate [5]. Carpal bone motion will cause the TCL to lengthen, resulting in increased stiffness, therefore, further analysis of carpal kinematics should prove important in this respect.

Investigations into the material properties of the TCL can help improve understanding of carpal tunnel mechanics. Preliminary results suggest measures from the current investigation were comparable to those found in an *in vivo* manual indentation study of neutral posture [4]. Understanding material properties of the TCL can influence manipulative treatment techniques and further examination of carpal kinematics and tensile loading should lead to insight into the TCL's role in carpal mechanics.

REFERENCES

1.Fisk GR. (1984). *Ann. Chir. Main*, **39**:297-299.
2.Garcia-Elias et al. (1989). *J Ortho Res*, **7**:705-712.
3.Sucher BM. (1998). *J Am Osteopath Assoc*, **98**:679-686.
4.Li ZM. (2005). *J Musculoskeletal Res*, **9**:153-159.
5.Moojen TM. (2002). *Clin. Biomech*, **17**:506-514.

ACKNOWLEDGEMENTS

This study was funded by CRE-MSD and NSERC (Canada) Discovery grant #217382-04. Thanks to Glenn Oomen for anatomical specimens and Diane Gregory for tensile testing help.

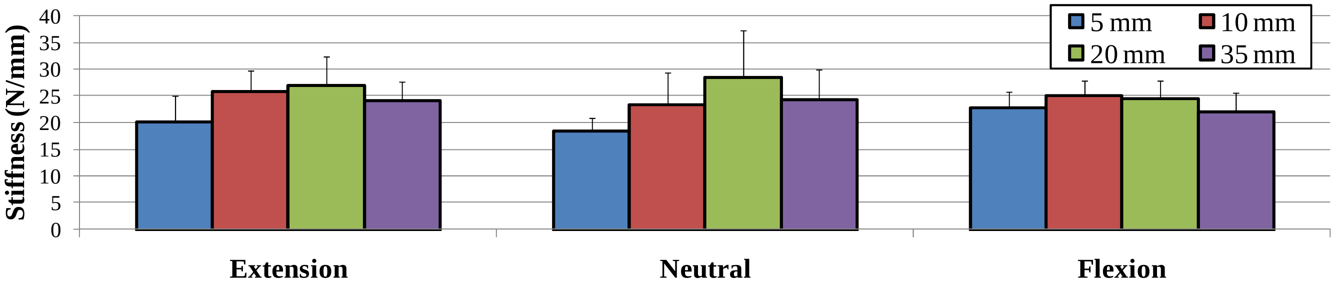

Figure 2: Mean stiffness plus SD for each indenter size and wrist posture (during the loading phase).

POSTURAL CONTROL RESPONSE TO STANCE ON A COMPLIANT SURFACE

Joshua Haworth, Adam Strang, Mathias Hieronymus, Mark Walsh
Miami University, Oxford, Ohio
email: hawortjl@muohio.edu

INTRODUCTION

Balance training is a common methodology used in rehabilitation and training settings, intended to enhance an individual's ability to maintain stability. Regularly, the use of a compliant surface is included in this training. It is implied that improvements in postural performance during interaction with a dynamic surface will translate to improved posture during stance on solid ground [1]. However, characterization of the postural control strategies used by the individual during interaction with a dynamic surface may serve to provide great insight to the control systems used to maintain posture during stance under any condition.

Center of pressure (COP) is a standard laboratory measure of stability, commonly collected and analyzed for characteristics such as sway range, velocity, and variability. Currently, there is a strong movement in the literature to consider the use of nonlinear statistics as ancillary measures for describing COP data [2].

The purpose of this study was to evaluate the postural sway performance of participants during quiet stance on a compliant surface, measured longitudinally throughout a balance training program. One of the goals of this evaluation includes determination of movement characteristics of postural sway during interaction with a movement responsive surface. Additionally, a nonlinear method of data processing was presented, along with traditional linear statistics, to serve as an effective movement descriptor.

METHODS

Eighteen healthy, physically active individuals (5 male, 13 female; age (yrs) = 20.24 ± .90; body mass (kg) = 66.05 ± 11.78), engaged in a six week balance training program (18 sessions) designed to target a variety of stance conditions. Each of these sessions lasted approximately 30 minutes and included a single trial of COP data collection followed by a series of eight training exercises (each including four levels of increasing difficulty) designed to maintain a safe but challenging experience during each exercise. COP was measured on a compliant surface, DynaDisc-Plus, placed atop a force plate (Bertec 60cm x 90cm).

Range, velocity, variability, and Lyapunov Exponent were calculated from each COP time series after separation into mediolateral and anterposterior components. Each variable was condensed by averaging the performance of all participants across 3 day groups to represent mean weekly performance. A one way repeated measure MANOVA was used to determine whether changes occurred across the six weeks. Paired t-tests were used *post hoc* to locate where these changes occurred throughout the six weeks. MANOVA and t-tests were performed using SPSS software v.16.0. Alpha level $p < 0.05$ was used for analyses

RESULTS AND DISCUSSION

Results of the repeated measures MANOVA indicate significant differences in each variable (range, variability, velocity, and LyE) across the six weeks of training, similar for both the ML and AP directions. Figure 1 presents the results in the mediolateral direction. In both directions, COP range (ML: $F_{5,85} = 4.065$, $P < 0.002$; AP: $F_{5,85} = 2.825$, $P < 0.021$) and variability (ML: $F_{4.185,71.145} = 4.789$, $P < 0.002$; AP: $F_{5,85} = 2.357$, $P < 0.047$) follow a quadratic trend, showing an initial (first two weeks) reduction followed by a return to pre-test values. This is interpreted as an initial attempt to reduce degrees of freedom, which is subsequently overcome by the added advantage to environmental searching and recognition associated with increased range and variability.

Figure 1: Week-wise analysis of variables in the ML direction;
A) COP Range, B) COP Velocity, C) COP Variability, and D) COP LyE.

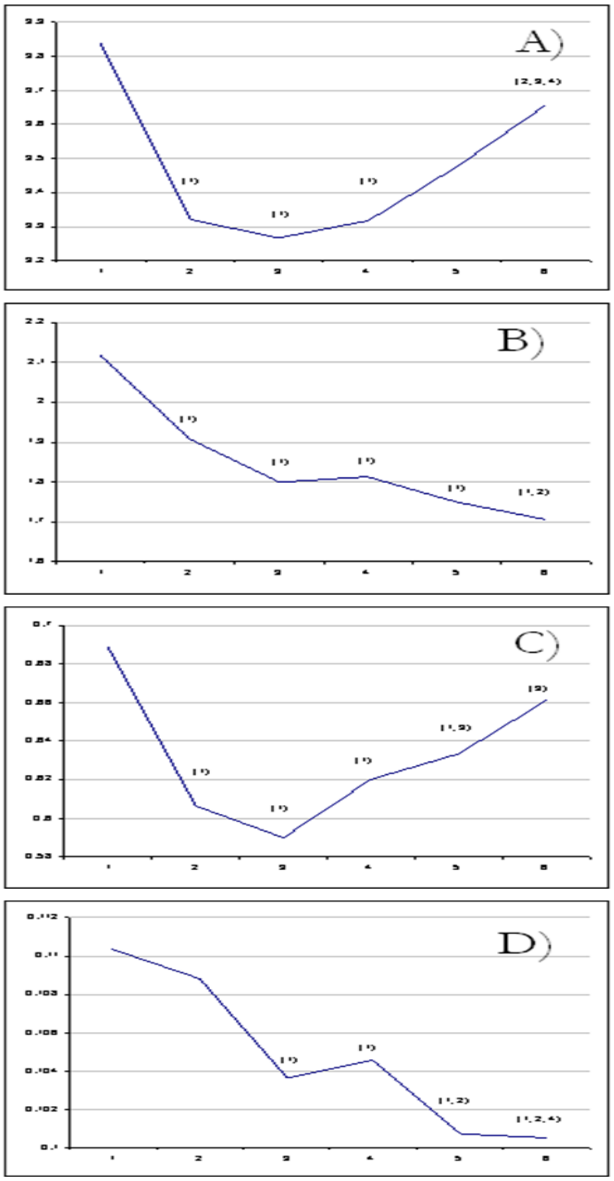

Weeks where difference is significant are listed in ( ), p< 0.05

Velocity (ML: $F_{5,85} = 8.366$, $P < 0.000$; AP: $F_{5,85} = 12.806$, $P < 0.000$) and LyE (ML: $F_{5,85} = 6.098$, $P < 0.000$; AP: $F_{3.211,54.593} = 5.886$, $P < 0.001$) follow a linear trend of continued reduction throughout the study. A Huyh-Feldt correction factor was used where Mauchly's test for sphericity indicated a violation of assumptions, as was the case for variability in the ML direction (Mauchly's $W = 0.154$; $\chi^2 = 28.26$, $P < 0.014$) and LyE in the AP (Mauchly's $W = 0.144$; $\chi^2 = 29.3$, $P< 0.010$). In both cases, the correction yielded significant results as presented above. Reduced LyE values indicate a more periodic (self-similar) structure within the COP path. It appears that the participants were able to develop a more calculated approach to the maintenance of balance by moving both more slowly and with a more regular movement pattern. It is argued that the slower and more regular movement pattern provides the performer with a strategic control over the behavior of the compliant surface, thus decreasing the complexity of the interaction task and allowing for a more stable postural experience, even in the face of a seemingly erratic environment.

CONCLUSIONS

This research has provided evidence that individuals do respond to balance training with changes in postural sway. Measures of range and variability were shown to decrease during the first two weeks of training, and then subsequently return to week one values. Measures of velocity and LyE were shown to decrease in a linear fashion throughout all six weeks of training. These changes in performance can be explained as a result of changing strategies enacted by the postural control system. At the outset, postural performance exhibits a developing rigidity in all four measured variables. In sum, individuals tend to move less within a smaller range, at a slower rate and with a more consistent pattern of movement. After two weeks of experience within the dynamic environment, training, the motor control system seems to become more relaxed in its control of range and variability. This is thought to occur due to the benefit to the system of increased exploratory movement within the environment, thus maximizing the information gathering capacity from which future movement is planned. At the same time, velocity continues to decrease as movement continues to become more self-similar. These qualities signify the benefit of increased processing time and planning of future movements. Slower movements result in slower response by the environment to those actions. More regular movement patterns elicit responses by the environment that are more predictable, and thus allow greater potential that the subsequently planned movement will be appropriate for the individual within the resulting environment.

REFERENCES

1. Hoffman, M., & Payne, V. G. (1995). The effects of proprioceptive ankle disk training on healthy subjects. *Journal of Orthopaedic & Sports Physical Therapy*, *21*(2), 90-93.
2. Stergiou N, ed. Innovative analyses of human movement. Champaign, IL: Human Kinetics, 2004.

SCAPULOTHORACIC MOTION AND MUSCLE ACTIVITY DURING THE RAISING AND LOWERING PHASE OF AN OVERHEAD REACHING TASK

D. David Ebaugh, PT, PHD [1] and Bryan A. Spinelli, PT, MS, OCS[1]
[1] Rehabilitation Sciences Research Laboratory, Drexel University, 245 North 15th Street MS 502, Philadelphia, PA, 19102
Email: debaugh@drexel.edu

INTRODUCTION

Scapulothoracic muscle activity is essential for the production and control of scapulothoracic motion as well as normal upper extremity function [1]. While previous research has furthered the understanding of scapulothoracic motion and muscle activity during the raising phase of motion, a gap exists with respect to the lowering phase. Clinically abnormal scapulothoracic motion (scapular dyskinesis) tends to be more pronounced, and patients note more pain when they lower their arm from a raised position [2]. Studies that investigate differences in scapulothoracic motion and muscle activity between arm raising and lowering in healthy individuals would provide a foundation for better understanding scapular dyskinesis in individuals with shoulder pain. The purpose of this study was to compare scapulothoracic motion and scapulothoracic muscle activity between the raising and lowering phases of an overhead reaching task.

METHODS

Twenty individuals (10 female and 10 male) without a history of shoulder pain or pathology volunteered to participate in the study (mean age = 22.5 years, SD = 3.4 years). Electromagnetic sensors on the scapula, humerus, and thorax were used to collect 3-D scapulothoracic and glenohumeral motion during the raising and lowering phases of scapular plane elevation. Surface electromyography (EMG) was used to simultaneously assess muscle activity from the upper trapezius, lower trapezius, and serratus anterior muscles. Scapulothoracic kinematic variables and EMG root mean square (RMS) values were the dependent variables. A 2-way repeated measures analysis of variance (ANOVA) with with-in factors of phase (raising and lowering) and arm angle (30°, 50°, 90°, 130°) was performed on each dependent variable. Post-hoc comparisons were conducted using paired t-tests with Bonferonni correction ($p=.01$).

RESULTS AND DISCUSSION

KINEMATICS: A significant phase by arm elevation angle interaction existed for scapular external rotation, clavicular elevation, and scapular posterior tilt ($p<.05$). During the lowering phase there was significantly more scapular external rotation (3.3°) and less clavicular elevation (1.7°) at 130° of arm elevation ($p <.01$). There was no significant difference in scapular posterior tilt between the raising and lowering phases at any of the selected arm elevation angles. There was a significant main effect of phase for clavicular retraction ($p <.05$). Collapsed across arm elevation angles, subjects demonstrated greater clavicular retraction (1.7°) during the lowering phase of motion. EMG: Significant main effects of phase and arm angle were noted for EMG activity of all muscles. Collapsed across arm elevation angles, there were significantly lower EMG RMS values during the lowering phase of motion for all muscles (Figure). During the lowering phase motion, there was 61%, 42%, and 39% reduction of EMG activity for the upper trapezius, lower trapezius, and serratus anterior muscles, respectively.

Overall, scapulothoracic motion was similar for the raising and lowering phases of the overhead reaching task with the largest difference between phases being 3.3°for scapular external rotation. These findings are in agreement with those of McClure et al. [3] who reported similar amounts of scapulothoracic motion (within 5°) during the raising and lowering phases of an overhead reaching task.

Conversely, significantly lower EMG amplitude values existed during the lowering phase across all muscles. The reduced EMG activity levels may partially be explained by gravities effect on the motion and the resultant loads imposed to the scapulothoracic musculature. During the raising phase, muscles contracted concentrically in order to overcome gravitational forces and elevate the arm. When the arm was lowered back to the side, gravity assisted the motion and less muscle activation was required. However, lower levels of muscle activation have been reported for eccentric contractions of the elbow flexor muscles during an elbow flexion/extension task performed in a gravity minimized position [4]. This suggests that factors other than gravity contribute to differences in muscle activation levels between eccentric and concentric contractions. We believe that lower levels of muscle activity during the lowering phase may reflect differing neuromuscular control strategies associated with eccentric and concentric contractions [5].

CONCLUSIONS

The findings from this study suggest that scapulothoracic muscle activation levels during eccentric contractions may be closer to an activation threshold below which their ability to control scapulothoracic motion may be compromised subsequently leading to scapular dyskinesis. This provides a possible explanation for why scapular dyskinesis is more notable during the lowering phase of motion.

REFERENCES

1. Ludewig PM, et al. *Journal of Orthopaedic and Sports Physical Therapy* **24**, 57-65, 1996.
2. Kibler WB and McMullen J. *Journal of the American Academy of Orthopaedic Surgeons* **11**, 142-51, 2003
3. McClure P, et al. *Journal of Shoulder and Elbow Surgery* **10**, 269-77**,** 2001.
4. Fang Y, et al. *Journal of Neurophysiology* **86**, 1764-72, 2001.
5. Enoka RM. *Journal of Applied Physiology* **81**, 2339-46, 1996.

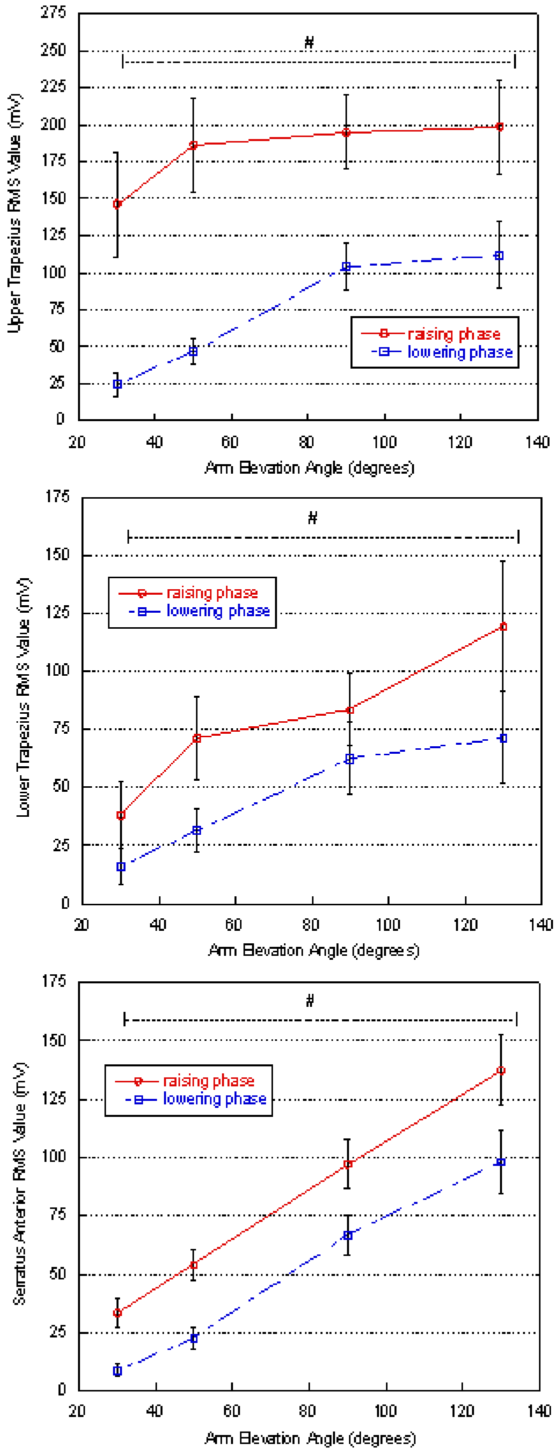

Figure: Mean and standard error of the mean for upper trapezius, lower trapezius, and serratus anterior muscle activity at select arm elevation angles for the raising and lowering phases of an overhead reaching task. Numeric symbol (#) indicates a significant main effect for phase (repeated-measures ANOVA; p<.05).

Effect of Walking Speed on Plantar Loading and Foot Kinematics in subjects with Stage II Posterior Tibial Tendon Dysfunction

[1]Christopher Neville, [3]A. Sam Flemister, [2]Jeff Houck
[1]SUNY Upstate Medical Center, Syracuse, NY; [2]Ithaca College-Rochester, Rochester, NY; [3]University of Rochester Medical Center, Rochester, NY
email: nevillec@upstate.edu

INTRODUCTION

Large forces are transmitted through the foot during walking.[1] The muscles and ligaments that cross the foot and ankle joints are responsible for producing and controlling these forces. In the presence of stage II Posterior Tibial Tendon Dysfunction (PTTD) weakness of the posterior tibialis muscle and failure of supporting ligaments (spring ligament) may alter the production and control of force.[2,3] Walking speed may effect force production and control, leading to changes in plantar loading patterns and foot kinematics.[4] Compensations for weakness may be possible at slower speeds but fail when walking faster. It remains unclear what effect walking speed may have on foot loading patterns and foot kinematics. It is hypothesized that, when walking fast, total loading in the foot and the distribution of loading under the foot will change as a sign of altered force production and control. Additionally, it is hypothesized that, when walking fast, altered medial longitudinal arch (MLA) kinematics will accompany changes in the loading patterns due to muscle weakness and failing support ligaments.

METHODS

Fourteen individuals with PTTD (6 male, 8 female; age=57.9 ± 12.4; body mass index = 31.6 ± 3.9) volunteered for this study. The arch height index, used to document the height of the MLA, was 0.311 ± .02 indicating a lower MLA and acquired flatfoot deformity.

An Optotrak Movement Analysis System (Northern Digital, Inc, Waterloo, CANADA) integrated with The Motion Monitor software (Innsport, Inc, Chicago, IL, USA) was used to measure movement from a multi-segment foot model during walking. The Pedar insole pressure system (Novel Inc, Germany) was used to collect plantar loading data during separate walking trials. Subjects were asked to walk at two speeds (1.0 m/s and 1.5 m/s) and speed was controlled using timing gaits. Plantar loading data was collected at 90 Hz and kinematic data at 60 Hz.

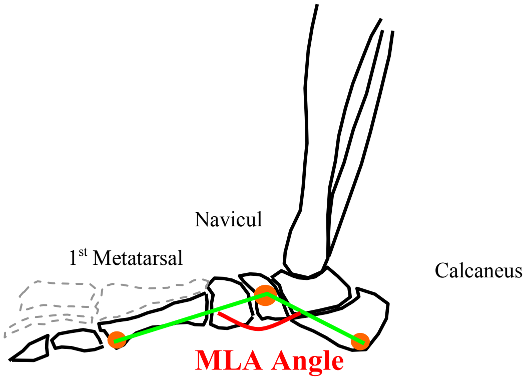

Figure 1: The medial longitudinal arch (MLA) angle was calculated using the dot product between two vectors created with the navicular tuberosity as the apex.

The multi-segment foot model was used to calculate a MLA angle (**Figure 1**). A minimum of five steps were averaged and the MLA angle was compared across stance with larger values indicating a lower MLA. The sub-talar neutral position was used as a zero reference position. The plantar loading data were also averaged from five steps and compared across the stance phase. Total loading under the foot as well as loading from two masks defined to correlate to loading posterior to the apex of the MLA and anterior to the apex of the MLA were examined. The heel segment consisted of pressure under the foot posterior to the navicular tuberosity (apex of the MLA in the kinematic model) while the forefoot mask was defined as an area of pressure anterior to the navicular tuberosity. A two-way repeated measure ANOVA model was used to compare walking speeds (1.0 m/s and 1.5 m/s) across three points in the stance phase of gait (heel rocker – 10%, ankle rocker – 50%, and toe rocker – 90%). The model was repeated for each dependent variable (total loading, heel loading, forefoot loading, MLA angle)

RESULTS

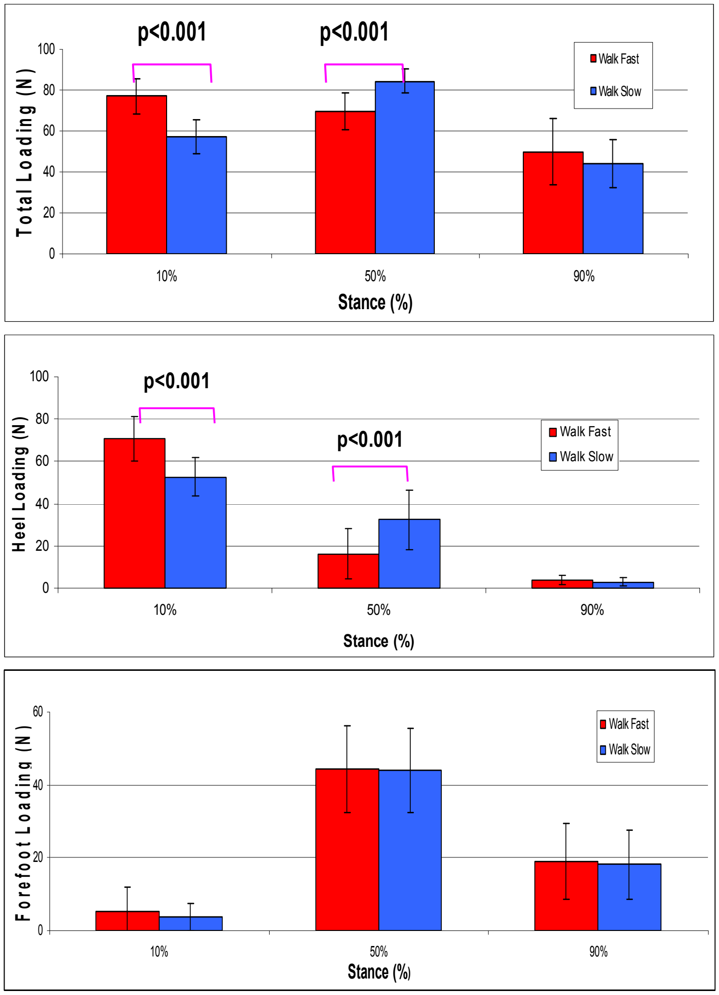

Figure 2. The total loading (top), heel loading (middle), and forefoot loading (bottom) for fast (red) and slow (blue) walking across three phases of stance. Significant differences are results of AVOVA pairwise comparisons between speeds.

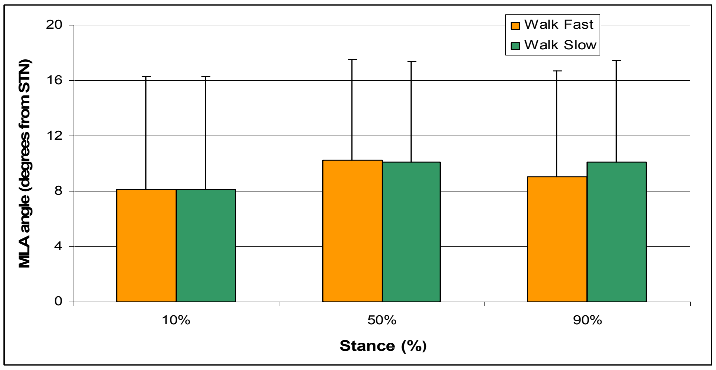

Figure 3. Kinematic measures of medial longitudinal arch angle comparing fast (orange) to slow (green) walking across three phases of stance. No differences were observed between walking speeds.

DISCUSSION

Despite altered plantar loading patterns in the foot suggesting a change in force transmission through the foot no change was observed in MLA angle. (**Figure 2 and 3**). The total plantar loading under the foot was larger at 10% of the stance and less at 50% of stance consistent with walking faster. Additionally, the heel loading was greater at 10% but less at 50% of stance suggesting an earlier heel rise and progression onto the forefoot when walking faster. However, no change in forefoot loading may imply the decrease in total load comes from unloading the heel without transferring load to the forefoot. This "lift off" pattern suggests a quicker transfer of weight to the opposite foot, possibly to unload the weaker, degenerative posterior tibialis tendon. These data suggests unloading when walking faster may serve as a compensatory mechanism as MLA kinematics were preserved when comparing walking speeds.

CONCLUSIONS

Walking faster alters the loading pattern in the foot in subjects with stage II PTTD. Evidence of unloading the foot when walking faster may serve to protect the midfoot as no change in MLA kinematics were observed.

REFERENCES

1. MacWilliams BA, Cowley M, Nicholson DE. Foot kinematics and kinetics during adolescent gait. *Gait & Posture*. 2003;17: 214-24.
2. Wacker J, Calder JD, Engstrom CM, Saxby TS. MR morphometry of posterior tibialis muscle in adult acquired flat foot. *Foot Ankle Int 26(9):671-4*. 2003;24:354-357.
3. Deland JT. The adult acquired flatfoot and spring ligament complex. Pathology and implications for treatment. *Foot Ankle Clin 8(3):637-45*. 2001;6:129-135.
4. Stoquart G, Detrembleur C, Lejeune T. Effect of speed on kinematic, kinetic, electromyographic and energetic reference values during treadmill walking. *Neurophysiol Clin*. 2008;38:105-116.

ACKNOWLEDGEMENTS

The authors are grateful for support from the National Institute of Arthritis and Musculoskeletal and Skin Diseases (Grant #: 1R15ARO54507-01A1)

GROUND REACTION FORCE MEASUREMENTS FOR MULTI-SEGMENT FOOT MODELS

[1,2]Dustin A. Bruening, [1]Kevin M. Cooney, [1,3]Frank L. Buczek
[1]Shriners Hospitals for Children, Erie PA, [2]University of Delaware, Newark DE, [3]National Institute for Occupational Safety & Health, Morgantown WV, email: dbruening@shrinenet.org

INTRODUCTION

Kinematic multi-segment foot models have been increasingly used in clinical gait analysis and human movement research. The addition of kinetics to multi-segment foot modeling, however, has been hampered by measurement difficulties. MacWilliams et al [1], for example, created a complex eight-segment foot model, measuring ground reaction forces (GRFs) using both a force platform and a pressure mat. Shear forces (f_{AP}, f_{ML}) and free moments (m) under each foot segment (i) were estimated by assuming that they were distributed proportionally to the vertical forces (f_V):

$$f_{APi} = (f_{Vi} / F_V) * F_{AP}$$
$$f_{MLi} = (f_{Vi} / F_V) * F_{ML} \qquad \text{(Method 1)}$$
$$m_i = (f_{Vi} / F_V) * M$$

In addition to relying upon an unproven proportionality theory, this method also cannot account for the possibility of opposing shear forces on separate foot segments (e.g. substantial collapse of the medial longitudinal arch in mid-stance or whole foot rotation). Giaccomozi and Macellari [2] suggested accounting for foot rotation by partitioning the overall free moment among the various segments and adjusting the shear values:

$$f_{APi} = (f_{Vi} / F_V) * F_{AP} - f_{Mi} * \sin(\alpha_i)\ x$$
$$f_{MLi} = (f_{Vi} / F_V) * F_{ML} + f_{Mi} * \cos(\alpha_i)\ y \qquad \text{(Method 2)}$$
$$m_i = d_i \times f_{Mi}$$
$$\text{And } f_{Mi} = f_{Vi} * (M / f_{Vi}{*}d_i)$$

Where d_i is the vector from the force plate center of pressure to each sensor, and α_i is the angle between d_i and the x-axis.

This method, however, is mathematically problematic, as $\sum f_i \neq F$. Not surprisingly, therefore, Yavuz et al.[3] found larger errors using method 2 than method 1 to predict peak shear stresses over the forefoot during gait. Both methods, though, showed RMS errors greater than 85 kPa.

The purposes of the present study were to: 1) measure the shear forces and free moments under a 3 segment foot model during normal gait, and 2) further evaluate the accuracy of the shear force proportionality assumption (using method 1).

METHODS

17 normal pediatric subjects (9M, 8F), representing a range of ages (7-18, mean 12.6) and foot sizes, were tested. Only the right foot was tested. Subjects first walked at a self-selected speed across a floor containing 2 adjacent AMTI OR6-7-100 force platforms. A minimum of 3 trials with full foot/plate contacts were collected. Next, the subject walked using a three-step targeting method, so that the rearfoot contacted one plate while the forefoot (and toes) contacted the adjacent plate. Foot placement was verified by two video cameras located on either side of the plate division. Finally, the same method was repeated, but with the hallux and toes on one plate and the rest of the foot on the adjacent plate. Subjects were instructed to walk as normally as possible and the starting position was adjusted until the appropriate placement, with a near normal gait pattern, was achieved. Trials were collected until at least three were identified with accurate foot placement (for each joint line).

Ground reaction force data was collected at 1560 Hz, low-pass filtered at 100 Hz, and threshold cutoff at 5N. Data processing was performed using Visual 3D software (C-motion, Inc). For the targeted trials, overall ground reaction forces were calculated by combining the outputs of the two force platforms to create a single virtual platform. Method 1 was then used to estimate the shear forces and moments on each platform from the virtual platform. All forces were then time-normalized to a complete gait cycle. A representative trial for each subject and each joint condition was chosen as the one with the smallest total RMS differences between its associated virtual GRFs and the mean GRFs from the initial, non-targeted trials. The representative trials were used to calculate a mean over all subjects (see Figure).

RESULTS AND DISCUSSION

With few exceptions, the measured and estimated forces were consistent, so that the group means are a reasonable representation (although not indicative of the full range of errors and particularly peak errors). RMS errors ranged from approximately 1% BW up to 6% BW in some cases, and were usually highest between the foot and toes in the AP direction.

Both ML and AP shear forces showed some small opposing actions between the rearfoot and forefoot in mid-stance. In early and mid-stance, the braking force by the rearfoot was underestimated, and a considerable portion of this force was falsely attributing to the forefoot. The greatest opposing actions occurred between the foot and the toe in the AP direction, as the toes 'flattened' in terminal stance. Method 1 markedly overestimated the propulsive contribution of the hallux and toes, and consequently underestimated the propulsive force of the forefoot. Besides periods of opposing shear forces, there are errors throughout the gait cycle, likely due to inaccuracies in the proportionality theory. Ironically, this theory was proposed for use in multi-segment foot models, yet it by definition assumes that the foot is a single, uniformly deforming, isotropic plantar surface.

The main limitation to this study is that the GRFs are based on targeted walking. However, the virtual GRFs from the chosen trials generally matched the initial non-targeting trials, consistent with Grabiner et al [4], who previously showed good agreement between targeted and non-targeted GRFs. Our methodology also limited force analysis to two segments at a time, but the salient information from each of these analyses occurs at time periods where the third segment is not a prominent factor. In fact, superposition of these curves may be possible so that all three separate segment forces can be estimated in a general sense.

In conclusion, this study has shown that although overall estimation errors can be relatively small, important information on segment function is lost using proportionality assumption methods to estimate shear forces.

(Disclaimer: The opinions expressed in this abstract are those of the authors and do not necessarily reflect the views of the National Institute for Occupational Safety and Health.)

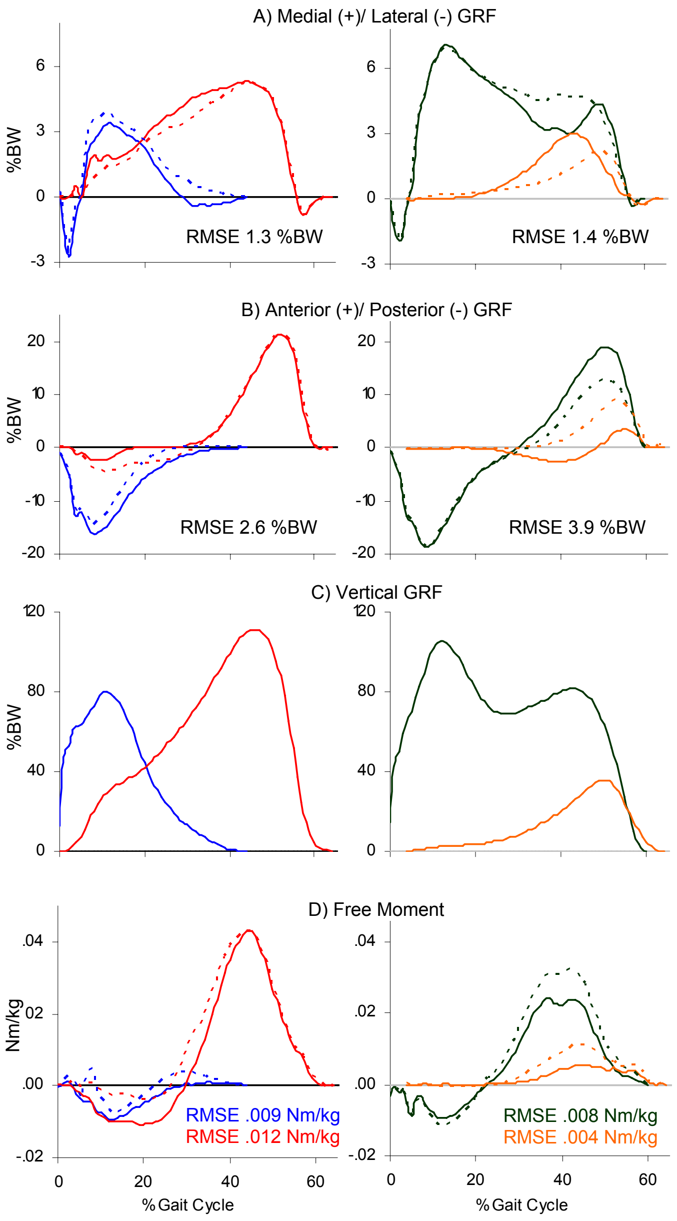

Figure. Mean measured and estimated, time normalized ground reaction forces under a 3-segment foot model during normal gait (N=17).

REFERENCES

1. MacWilliams, B.A., et al., Gait Posture, 2003. **17**(3): p. 214-24.
2. Giacomozzi, C. and V. Macellari, IEEE Trans Rehabil Eng, 1997. **5**(4): p. 322-30.
3. Yavuz, M., et al., J Biomech, 2007. **40**(13): p. 3045-9.
4. Grabiner, M.D., et al., J Biomech, 1995. **28**(9): p. 1115-7.

COMPARISON OF WARM-UP PERIODS FOR TREADMILL RUNNING

[1]Rebecca E Fellin, [1,2,3]Irene S Davis
[1]University of Delaware, Biomechanics and Movement Science Program, Newark, DE
[2]University of Delaware, Department of Physical Therapy, Newark, DE
[3]Drayer Physical Therapy Institute, Hummelstown, PA
email: fellin@udel.edu

INTRODUCTION

Treadmills are often used for the analyses of running mechanics. Prior to the collection of data, a warm-up period is typically provided so that the runner has a chance to accommodate to the treadmill (TM) and achieve his/her natural running style. The length of this warm-up period is typically between 3-5 minutes [1,6]. This time is fairly arbitrary, sometimes based upon the subject's report of running comfortably [6].

TM accommodation during walking has been more systematically studied [5,7]. Matsas and colleagues studied walking over a 14 minute period and found knee joint kinematics stabilized after 4 minutes of TM walking [5]. In another study knee joint variability during walking was monitored for 15 minutes [7]. These authors found no difference in this variability over the entire period. However, both of these studies were based upon discrete kinematic variables. It may also be important to examine the entire kinematic patterns during stance.

Trend symmetry (TS) is a quantitative measure of pattern similarity between waveforms [2]. This value is calculated using singular value decomposition of the angular rotation matrices. The ratio of the variability about and along the eigenvector is then computed. This method provides a unique approach to assess the similarity of angular patterns over stance at different points during a warm-up period.

Therefore, the purpose of this study was to determine when, during a typical 5 minute warm-up, that kinematic patterns become similar to those at the end of the warm-up. We hypothesized kinematic patterns at 3 and 4 minutes would be similar to those at the end of the 5 minute warm-up.

METHODS

17 individuals (24.8 ± 7.2 years, 9 males) running at least 10 miles per week were recruited for this study. All were rearfoot strikers and had to rate their treadmill comfort on a visual analog scale at ≥ 6/10 with zero being completely uncomfortable and 10 being totally comfortable. The reported values for TM comfort averaged 9.1 ± 1.2.

Retro-reflective markers were applied to the right lower extremity of each subject. Subjects then began running on the treadmill (Quinton Cardiology Inc, Bothell, WA, USA). The speed of the treadmill was set to the subject's self selected speed initially and slowly increased to 3.35 m/s. Data were then collected at 2, 3, 4 and 5 minutes, while subjects were running at the test speed. A VICON (Oxford Metrics, Oxford, UK) motion analysis system captured kinematic data at 120Hz. Five footstrikes at each time point were analyzed. Kinematic data were filtered at 12Hz.

Stance was identified kinematically as a force treadmill was not used [4]. Specifically, the distal heel marker change in velocity from negative to positive was used to identify footstrike. The time of peak knee extension was used to identify toe-off. For each trial, hip, knee and rearfoot angles during the stance phase were calculated for each subject in Visual 3D (C-motion, Germantown, MD, USA). Each subject's trials were then averaged using custom software. The trend symmetry (TS) value was calculated and used to compare the patterns [2]. TS values range from 0-1.0, with 1.0 indicating identical patterns and values ≥ 0.95 indicating similar patterns [2]. Within each subject, TS comparisons were made between minutes 2-5, 3-5, and 4-5 for each joint angle. The TS values for each joint angle were then averaged across subjects.

RESULTS AND DISCUSSION

Overall, the TS values were high, with the average across all joint angles being 0.96, 0.97 and 0.97 for 2, 3 and 4 minutes, respectively (Figure 1). TS values were lowest for knee adduction, ranging from 0.91 to 0.94. We thought this might be related to the subject's level of comfort with TM running. However, we found that the individuals with the lowest TM comfort scores reported high TS values (Figure 2). In addition, there were subjects with high TM scores and low TS values. Therefore, it does not appear that level of comfort with TM ambulation influenced joint angles.

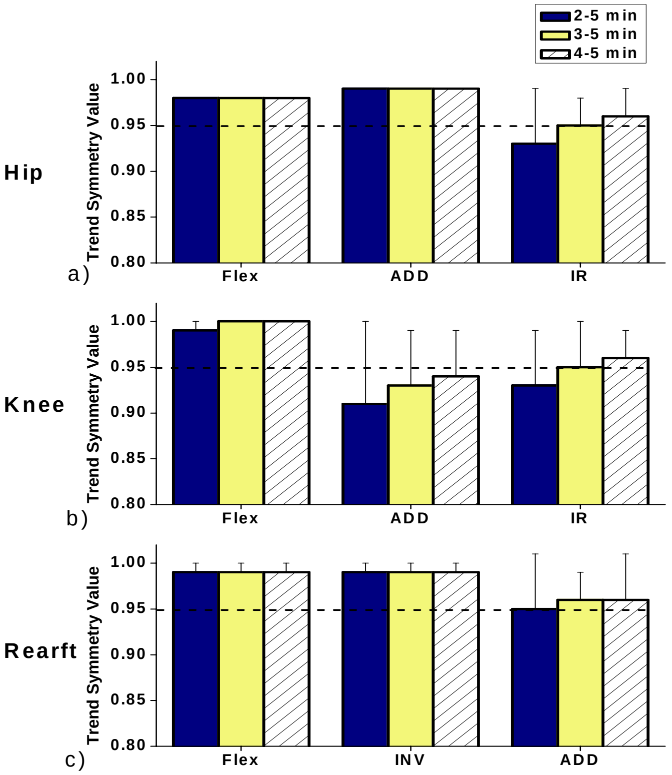

Figure 1: Trend symmetry values for the hip (a), knee (b) and rearfoot (c). The dotted line represents the TS value of 0.95, considered very good agreement between curves. Note that Y axis is truncated and starts at 0.80, and the SD=0.00 for some variables. Flex=flexion, INV=inversion ADD=adduction, and IR=internal rotation.

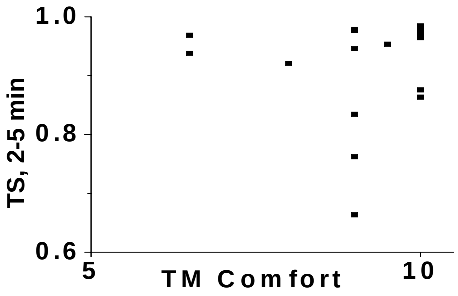

Figure 2: Scatterplot comparing knee adduction TS values between 2-5 minutes vs TM comfort. Note the some individuals with low TS scores demonstrated high TM comfort levels and vice versa.

Results for the 2-5 minute comparison were not consistent for all joint angles. The sagittal plane was the most similar across all joints. Additionally, the hip and rearfoot frontal plane curves were also similar between 2 and 5 minutes. TS values were ≥ 0.95 for these comparisons. However, the TS values for the 2-5 minute comparison were low for the transverse plane of hip and knee, as well as for the frontal plane of the knee.

The results for the 3-5 and 4-5 minute comparisions were similar to each other across joint angles. Aside from knee adduction, which was 0.93 and 0.94, all values were ≥ 0.95. These values indicated high similarity between the curves at 3 and 4 minutes with curves at 5 minutes.

Overall, 6/9 joint angles had TS ≥ 0.95 at 2 minutes. However, at 3 and 4 minutes, 8/9 curves had TS values ≥ 0.95. These results suggest that either a 3 or 4-minute warm-up would result in mechanics similar to those following a 5-minute warm-up.

It does not appear increasing TM warm-up beyond 3 minutes produced differences in joint angles. However, these data do not establish whether runners actually attained their natural running style by 5 minutes. Based upon the literature, most studies found mechanics had stabilized within this time frame. However, no other studies have examined the entire stance patterns of the hip, knee and rearfoot in all planes of motion.

CONCLUSIONS

Joint kinematics at 3 and 4 minutes appear to have similar patterns with those following a 5-minute warm-up period. Therefore, a warm-up of 3 minutes may be as valid as a 5-minute warm-up for examining joint kinematics during running.

REFERENCES

1. Baur H et al. *Isokinet Exerc Sci* **15**, 165-171, 2007.
2. Crenshaw SJ, Richards, JG. *Gait Posture* **24**, 515-21, 2006.
3. Fellin RE, Davis IS. *Med Sci Sports Exerc* **40**, S58, 2008.
4. Fellin RE, Davis IS. *Proceedings of the NACOB,* Ann Arbor, USA, 2008.
5. Matsas A, et al. *Gait Posture* **11**, 46-53, 2000.
6. Riley PO, et al. *Med Sci Sports Exerc* **40**, 1093-1100, 2008.
7. Van de Putte M, et al. *Biomed Mater Eng* **16**, 43-52, 2006.

ACKNOWLEDGEMENTS

This study was supported by NIH 1 S10 RR022396 and Drayer Physical Therapy Foundation.

MUSCLE FORCES DURING MASTICATION

[1] Miloslav Vilimek, [1]Tomas Goldmann
[1] Czech Technical University in Prague, Prague, Czech Republic
email: miloslav.vilimek@fs.cvut.cz, web: www.biomechanics.cz

INTRODUCTION

In order to perform true loading of temporo-mandibular joint and dental replacements, the loading of masticatory muscles during bolus processing was investigated. Input kinematic variables and mastication force were experimentally examined. The inverse dynamics approach and static optimization technique were used for solution of the redundant mechanism.

METHODS

First was the creation of mathematical 3D model of mandible and skull including 16 actuators for two temporo-mandibular (TM) joints. These actuators included two parts of masseter (deep and surface), two parts of temporalis (anterior and posterior), two parts of pterygoideus medialis (anterior and posterior) and two parts of pterygoideus lateralis (inferior and superior) for each left and right side. The model consist of mandible, skull and muscle attachments positions, and was symmetrical according to the medial plane. The mandible can move with 6 degrees of freedom against the skull and distance between both of TM joints is assumed invariable. Muscle attachments and muscle parameters as physiological cross-sectional area, pennation angle, muscle mass, optimum muscle lengths etc. were taken from literature [1].

The 3D mandible and skull motion was experimentally analyzed by three cameras and processed with APAS software (Ariel Dynamics Inc.) during bolus processing. Simultaneously with an experimental measurement of kinematic parameters was investigated a chewing force (Figure 1) during soft bolus mastication. The chewing force was measured by developed 3D force micro sensor. Force sensor was implanted into the specimen bolus side.

For the mandible were derived six equations of equilibrium. In these equations perform 16 unknowns of actuators forces and 2 unknown reactions in TM joints, each in three directions.

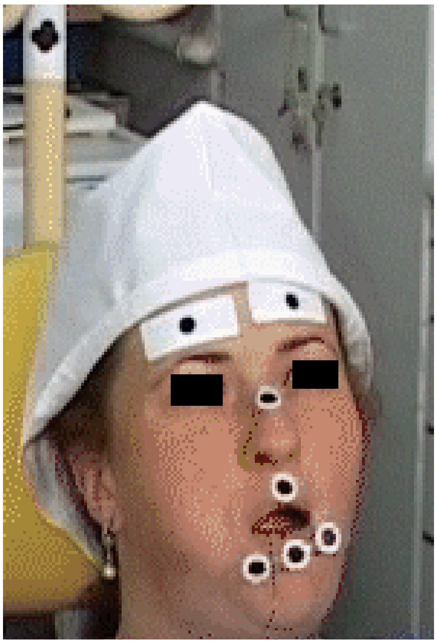

Figure 1: Experimental kinematic data and chewing force collection.

A representation of the musculotendon complex (Hill type model) using idealized mechanical objects is expressed in eq. (1). Disadvantages of these types of models include the assumptions associated with the input data, such as kinematic measurement of actuator length, and the muscle parameters of the model.

$$F = F_0^M \left[f_l^{act} \cdot f_v \cdot a(t) + f_l^{p} \right] \cos(\alpha(t)) \qquad (1)$$

Here is the basis for the physiological EMG-driven model [2,3] and it considers factors related to force-velocity f_v, force-length f_l^{act} and activation level $a(t)$ of the contractile muscle component, force-length relation of passive muscle component f_l^p, maximum isometric muscle force F_0^M, and pennation angle

$\alpha(t)$. This model corresponds with a full Hill type musculotendon complex.

EMG recording for activation signal estimation of all single and deep muscles is practically impossible. One potential method of addressing these discrepancies is to use an optimization scheme which assumes that EMGs are inherently imperfect, and the driven activation signal $a(t)$ (normalized EMG) is calculated by optimization method. So, in place of actuators forces the unknown variable is now activation (for each muscle).

This problem was solved with constrained static optimization technique. Optimization criteria were minimization of muscle activation, eq. (2), and minimization of TM joint reactions, eq. (3).

$$J = \sum_{i=1}^{n} a_i^2, \qquad (2)$$

$$J = \sum_{i=1}^{n} R_i^2, \qquad (3)$$

The function (1) was constrained so that all of the musculotendon forces were positive $F_i \geq 0$, because muscles can not produce compressive force. Next inequality constraints were $1 \geq a_i \geq 0$, for limitation of activation level.

RESULTS AND DISCUSSION

Chewing force (Figure 2) was measured only in one place, the most loaded tooth, on specimen bolus side even if in real situations the mandibles are contacting in multiple points. Has been examined, that chewing forces in both left-right and anterior-posterior directions are not insignificant.

The calculated TM joint forces are higher on the specimen balance side and smaller on the bolus side which is in conformity with [4]. By contrast, the calculated muscle forces are higher on the bolus side, for example masseter forces are shown on Figure 3. Inertia and mass properties of mandible have not significant influence in results because the mandible accelerations during our investigation was very small. The TM joint forces were investigated with smaller values than was published [5,6]. In our experiment was masticated soft bolus (bread), probably from this reason these force are smaller than published.

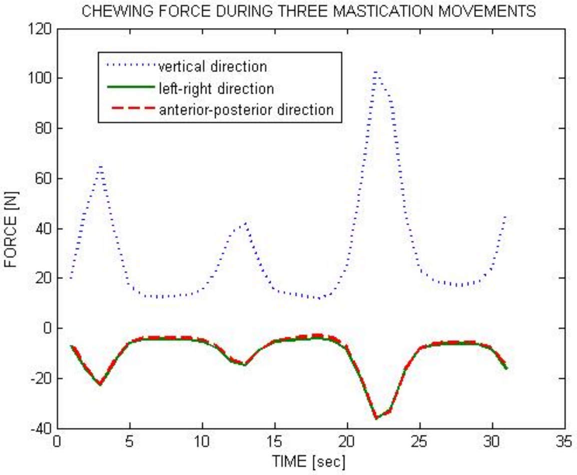

Figure 1: Experimentally collected chewing force on balance side.

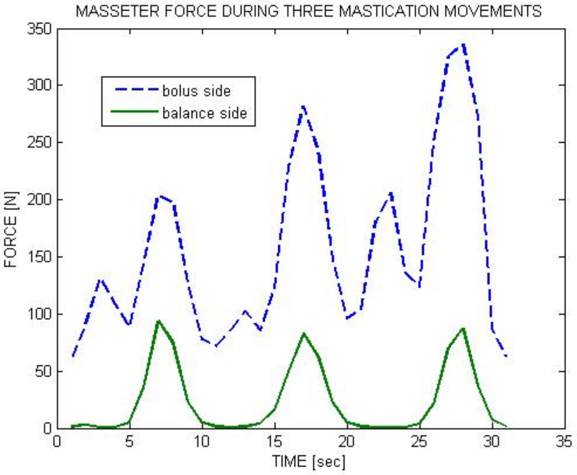

Figure 1: Calculated masseter forces on balance and bolus side.

REFERENCES

1. van Eijden TMGJ, et al. *Anat Rec* **248**, 464-474, 1997.
2. Lloyd, DG, et al. *J Biomech* **36**, 765-776, 2003.
3. Zajac, FE, *Crit Rev Biomed Eng* **17**, 359-411, 1989.
4. Koolstra JH, et al. *J Dent Res* **74**, 1564-1570, 1995.
5. Koolstra JH, et al. *J Biomech* **21**, 563-576, 1988.
6. May B, et al. *Clin Biomech* **16**, 489-495, 2001.

ACKNOWLEDGEMENTS

This research study was supported by grant MSM 6840770012.

GAIT RETRAINING TO REDUCE THE KNEE ADDUCTION MOMENT THROUGH REAL-TIME FEEDBACK OF DYNAMIC KNEE ALIGNMENT

Joaquin A. Barrios[1] and Irene S. Davis[1,2]
[1] University of Delaware, Newark, DE, USA
[2] Drayer Physical Therapy Institute, Hummelstown, PA, USA
E-mail: joaquin@udel.edu

INTRODUCTION

Varus knee alignment has recently been shown to be a risk factor for the development of medial knee osteoarthritis (OA) (1). This alignment is associated with high knee adduction moments (KEAM), which are also hallmark of medial knee OA. Therefore, a reduction in the KEAM in varus-aligned individuals with otherwise healthy knees may reduce their risk for developing OA. Retraining gait patterns to reduce dynamic knee alignment may reduce the KEAM. With habitual use of such a gait pattern, the onset of OA may be deterred.

Therefore, the purpose of this study was to investigate the effects of a gait retraining program using real-time feedback on reducing the KEAM in healthy, varus-aligned individuals without evidence of knee OA. It was expected that reductions in the KEAM would be associated with increases in hip adduction and internal rotation angles, and reduced knee adduction. We expected these changes to persist at a one month follow up. Further, it was expected that the new gait pattern would become more natural and require less effort with training.

METHODS

1 female and 7 male subjects (age 21.4 +/- 1.6 yrs) with varus knees were recruited for the study. The frontal plane mechanical axis of the tibia was measured using a caliper-inclinometer device (2) to determine knee alignment. A value of ≥ 11° from vertical was needed to qualify for the study. To determine knee joint function, all subjects completed the Sports and Recreational Activities subscale of the Knee Injury and Osteoarthritis Outcome Score Knee Survey (3). A score of ≤ 2/20 (where 20/20 means extreme symptoms) was needed to qualify. Finally, subjects had to rate their comfort for treadmill walking as > 8/10, with 10 being completely comfortable.

A baseline gait analysis was first conducted. 3D motion analysis was performed at a controlled speed at 1.46 m/s (± 2.5%) along a 25 m walkway. Kinematic data were captured using an 8-camera VICON motion analysis system (120 Hz), and kinetic data using a Bertec force platform (1080 Hz). Five usable trials were processed using Visual 3D and custom Labview software.

Subjects then underwent 8 sessions of gait retraining. Real-time kinematic feedback (Visual 3D, VICON) of knee adduction during stance was provided. Subjects were instructed to lower the stance-phase trace into a normative band, derived from a database of age-matched, healthy walkers (Figure 1).

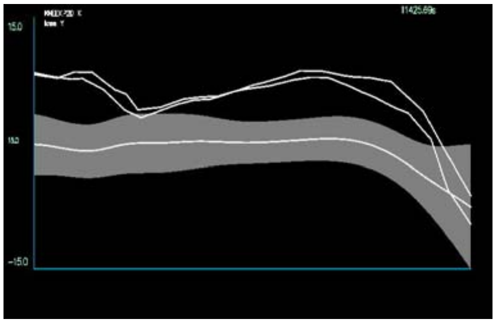

Figure 1. Actual screenshot of knee adduction angle data from two consecutive footstrikes and the target band of normative data presented to the subject.

The kinematic feedback was gradually removed in the later sessions using a fading feedback paradigm. At the end of each session, subjects were asked to rate the effort and naturalness of the gait modification on a verbal analog scale.

Immediately following the final training session, an overground gait analysis was conducted as in the baseline collection. All subjects returned for a one month follow up, again using the same overground methods.

RESULTS

Following the retraining, the peak KEAM was significantly reduced by 20% (p=0.027) (Figure 2) and knee adduction was decreased by 2° (p=0.071). These knee changes were accomplished through a 10° increase hip internal rotation (p=0.001) and a 3° increase in hip adduction (p=0.073). These mechanics were maintained at the one month follow-up.

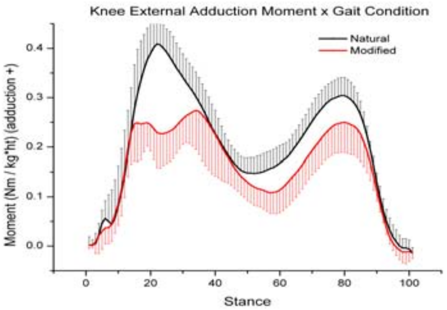

Figure 2. Comparison of baseline KEAM during natural walking to the modified gait pattern. Note that the KEAM was attenuated throughout stance.

The perceived effort associated with modified pattern decreased during the training protocol from 6.6/10 to 2.9/10 (p<0.001). Similarly, the pattern became more natural at the end of the protocol (7.1/10 to 3.9/10) (p=0.001).

DISCUSSION

This is the first systematic training study that demonstrates the effects of a gait retraining program on reducing the KEAM. The baseline KEAM value was similar to that of individuals with medial knee OA (4). This suggests the individuals in this study were at increased risk for developing OA. With the 20% reduction of KEAM, the value fell within the normal range. This was accomplished through a combination of hip internal rotation and adduction. These hip changes resulted in improved dynamic knee alignment. However the changes at the knee were smaller than those at the hip, likely due to the structural constraints of the knee. The reduction in KEAM seen in other interventions, such as laterally wedged foot orthoses, is approximately half of that seen with the retraining (4). This suggests that the training may be a more effective intervention.

With training, the modified pattern required less effort to execute, and felt more natural. Continued reinforcement of the pattern could lead to a pattern that is effortless and feel completely natural. This would be integral to a learned pattern becoming a preferred walking pattern over time.

Similar to ‘medial thrust’ gait (5), knee flexion excursion increased by ~10° in order to allow for a reduction in peak KEAM. This flexion may increase patellofemoral joint forces. While there were no complaints of pain over the course of the study, the long-term effects of this increased knee flexion are not known.

SUMMARY

The results of this suggest subjects with knee varus can reduce their KEAM, a likely precursor to knee OA, through gait retraining. The ability to perform this modified pattern was sustained at a one month follow-up.

REFERENCES

1. Brouwer et al. (2007). *Arth & Rheum*, 56:1204-1211.
2. Hinman et al. (2006). *Arthr & Rheum,* 55:306-313.
3. Roos et al. (1998). *JOSPT* 78(2): 88-96.
4. Butler RJ et al (2007). *J Orthop Res* 25:1121-11274.
5. Fregly et al. (2008). *I Trans Biom Eng*, 54:1687-95.

ACKNOWLEDGEMENTS

We would like to acknowledge the Grant-in-Aid Award from the American Society of Biomechanics, the Foundation for Physical Therapy, Drayer Sports Medicine Institute and NIH grant 1 S10 RR022396-01 and DOD grant W911NF-05-1-0097.